

PATENT

IN THE UNITED STATES PATENT AND TRADEMARK OFFICE

In re Application of: Ashkenazi et al.	Group Art Unit: 1647
Serial No.: 09/903,925	Examiner: Fozia Hamid
Filed: July 11, 2001	CERTIFICATE OF MAILING I hereby certify that this correspondence is being deposited with the United States Postal Service with sufficient postage as first class mail in an envelope addressed to: Assistant Commissioner of Patents, Washington, D.C. 20231 on 07/11/01.
For: SECRETED AND TRANSMEMBRANE POLYPEPTIDES AND NUCLEIC ACIDS	
	Date

DECLARATION OF AUDREY D. GODDARD, Ph.D UNDER 37 C.F.R. § 1.132

Assistant Commissioner of Patents
Washington, D.C. 20231

Sir:

I, Audrey D. Goddard, Ph.D. do hereby declare and say as follows:

1. I am a Senior Clinical Scientist at the Experimental Medicine/BioOncology, Medical Affairs Department of Genentech, Inc., South San Francisco, California 94080.
2. Between 1993 and 2001, I headed the DNA Sequencing Laboratory at the Molecular Biology Department of Genentech, Inc. During this time, my responsibilities included the identification and characterization of genes contributing to the oncogenic process, and determination of the chromosomal localization of novel genes.
3. My scientific Curriculum Vitae, including my list of publications, is attached to and forms part of this Declaration (Exhibit A).

Serial No.: *

Filed: *

4. I am familiar with a variety of techniques known in the art for detecting and quantifying the amplification of oncogenes in cancer, including the quantitative TaqMan PCR (i.e., "gene amplification") assay described in the above captioned patent application.

5. The TaqMan PCR assay is described, for example, in the following scientific publications: Higuchi *et al.*, Biotechnology 10:413-417 (1992) (Exhibit B); Livak *et al.*, PCR Methods Appl. 4:357-362 (1995) (Exhibit C) and Heid *et al.*, Genome Res. 6:986-994 (1996) (Exhibit D). Briefly, the assay is based on the principle that successful PCR yields a fluorescent signal due to Taq DNA polymerase-mediated exonuclease digestion of a fluorescently labeled oligonucleotide that is homologous to a sequence between two PCR primers. The extent of digestion depends directly on the amount of PCR, and can be quantified accurately by measuring the increment in fluorescence that results from decreased energy transfer. This is an extremely sensitive technique, which allows detection in the exponential phase of the PCR reaction and, as a result, leads to accurate determination of gene copy number.

6. The quantitative fluorescent TaqMan PCR assay has been extensively and successfully used to characterize genes involved in cancer development and progression. Amplification of protooncogenes has been studied in a variety of human tumors, and is widely considered as having etiological, diagnostic and prognostic significance. This use of the quantitative TaqMan PCR assay is exemplified by the following scientific publications: Pennica *et al.*, Proc. Natl. Acad. Sci. USA 95(25):14717-14722 (1998) (Exhibit E); Pitti *et al.*, Nature 396(6712):699-703 (1998) (Exhibit F) and Bieche *et al.*, Int. J. Cancer 78:661-666 (1998) (Exhibit G), the first two of which I am co-author. In particular, Pennica *et al.* have used the quantitative TaqMan PCR assay to study relative gene amplification of WISP and c-myc in various cell lines, colorectal tumors and normal mucosa. Pitti *et al.* studied the genomic amplification of a decoy receptor for Fas ligand in lung and colon cancer, using the quantitative TaqMan PCR assay. Bieche *et al.* used the assay to study gene amplification in breast cancer.

Serial No.: *

Filed: *

7. It is my personal experience that the quantitative TaqMan PCR technique is technically sensitive enough to detect at least a 2-fold increase in gene copy number relative to control. It is further my considered scientific opinion that an at least 2-fold increase in gene copy number in a tumor tissue sample relative to a normal (i.e., non-tumor) sample is significant and useful in that the detected increase in gene copy number in the tumor sample relative to the normal sample serves as a basis for using relative gene copy number as quantitated by the TaqMan PCR technique as a diagnostic marker for the presence or absence of tumor in a tissue sample of unknown pathology. Accordingly, a gene identified as being amplified at least 2-fold by the quantitative TaqMan PCR assay in a tumor sample relative to a normal sample is useful as a marker for the diagnosis of cancer, for monitoring cancer development and/or for measuring the efficacy of cancer therapy.

8. I declare further that all statements made herein of my own knowledge are true and that all statements made on information and belief are believed to be true. I declare that these statements were made with the knowledge that willful false statements and the like so made are punishable by fine or imprisonment, or both, under Section 1001 of Title 18 of the United States Code, and that such willful false statements may jeopardize the validity of the application or any patent issuing thereon.

Jan. 16, 2003

Date

Audrey D. Goddard

Audrey D. Goddard, Ph.D.

AUDREY D. GODDARD, Ph.D.

Genentech, Inc.
1 DNA Way
South San Francisco, CA, 94080
650.225.6429
goddarda@gene.com

110 Congo St.
San Francisco, CA, 94131
415.841.9154
415.819.2247 (mobile)
agoddard@pacbell.net

PROFESSIONAL EXPERIENCE

Genentech, Inc.
South San Francisco, CA

1993-present

2001 - present Senior Clinical Scientist
Experimental Medicine / BioOncology, Medical Affairs

Responsibilities:

- *Companion diagnostic oncology products*
- *Acquisition of clinical samples from Genentech's clinical trials for translational research*
- *Translational research using clinical specimen and data for drug development and diagnostics*
- *Member of Development Science Review Committee, Diagnostic Oversight Team, 21 CFR Part 11 Subteam*

Interests:

- *Ethical and legal implications of experiments with clinical specimens and data*
- *Application of pharmacogenomics in clinical trials*

1998 - 2001 Senior Scientist

Head of the DNA Sequencing Laboratory, Molecular Biology Department, Research

Responsibilities:

- *Management of a laboratory of up to nineteen –including postdoctoral fellow, associate scientist, senior research associate and research assistants/associate levels*
- *Management of a \$750K budget*
- *DNA sequencing core facility supporting a 350+ person research facility.*
- *DNA sequencing for high throughput gene discovery, - ESTs, cDNAs, and constructs*
- *Genomic sequence analysis and gene identification*
- *DNA sequence and primary protein analysis*

Research:

- *Chromosomal localization of novel genes*
- *Identification and characterization of genes contributing to the oncogenic process*
- *Identification and characterization of genes contributing to inflammatory diseases*
- *Design and development of schemes for high throughput genomic DNA sequence analysis*
- *Candidate gene prediction and evaluation*

1993 - 1998 Scientist

Head of the DNA Sequencing Laboratory, Molecular Biology Department, Research

Responsibilities

- *DNA sequencing core facility supporting a 350+ person research facility*
- *Assumed responsibility for a pre-existing team of five technicians and expanded the group into fifteen, introducing a level of middle management and additional areas of research*
- *Participated in the development of the basic plan for high throughput secreted protein discovery program – sequencing strategies, data analysis and tracking, database design*
- *High throughput EST and cDNA sequencing for new gene identification.*
- *Design and implementation of analysis tools required for high throughput gene identification.*
- *Chromosomal localization of genes encoding novel secreted proteins.*

Research:

- *Genomic sequence scanning for new gene discovery.*
- *Development of signal peptide selection methods.*
- *Evaluation of candidate disease genes.*
- *Growth hormone receptor gene SNPs in children with Idiopathic short stature*

Imperial Cancer Research Fund
London, UK with Dr. Ellen Solomon

1989-1992

6/89 –12/92 Postdoctoral Fellow

- *Cloning and characterization of the genes fused at the acute promyelocytic leukemia translocation breakpoints on chromosomes 17 and 15.*
- *Prepared a successfully funded European Union multi-center grant application*

McMaster University
Hamilton, Ontario, Canada with Dr. G. D. Sweeney

1983

5/83 – 8/83: NSERC Summer Student

- *In vitro* metabolism of β -naphthoflavone in C57BL/6J and DBA mice

EDUCATION

Ph.D.

"Phenotypic and genotypic effects of mutations in the human retinoblastoma gene."

Supervisor: Dr. R. A. Phillips

University of Toronto
Toronto, Ontario, Canada.
Department of Medical
Biophysics.

1989

Honours B.Sc

"The *in vitro* metabolism of the cytochrome P-448 inducer β -naphthoflavone in C57BL/6J mice."

Supervisor: Dr. G. D. Sweeney

McMaster University,
Hamilton, Ontario, Canada.
Department of Biochemistry

1983

ACADEMIC AWARDS

Imperial Cancer Research Fund Postdoctoral Fellowship	1989-1992
Medical Research Council Studentship	1983-1988
NSERC Undergraduate Summer Research Award	1983
Society of Chemical Industry Merit Award (Hons. Biochem.)	1983
Dr. Harry Lyman Hooker Scholarship	1981-1983
J.L.W. Gill Scholarship	1981-1982
Business and Professional Women's Club Scholarship	1980-1981
Wyerhauser Foundation Scholarship	1979-1980

INVITED PRESENTATIONS

Genentech's gene discovery pipeline: High throughput identification, cloning and characterization of novel genes. Functional Genomics: From Genome to Function, Litchfield Park, AZ, USA. October 2000

High throughput identification, cloning and characterization of novel genes. G2K:Back to Science, Advances in Genome Biology and Technology I. Marco Island, FL, USA. February 2000

Quality control in DNA Sequencing: The use of Phred and Phrap. Bay Area Sequencing Users Meeting, Berkeley, CA, USA. April 1999

High throughput secreted protein identification and cloning. Tenth International Genome Sequencing and Analysis Conference, Miami, FL, USA. September 1998

The evolution of DNA sequencing: The Genentech perspective. Bay Area Sequencing Users Meeting, Berkeley, CA, USA. May 1998

Partial Growth Hormone Insensitivity: The role of GH-receptor mutations in Idiopathic Short Stature. Tenth Annual National Cooperative Growth Study Investigators Meeting, San Francisco, CA, USA. October, 1996

Growth hormone (GH) receptor defects are present in selected children with non-GH-deficient short stature: A molecular basis for partial GH-insensitivity. 76th Annual Meeting of The Endocrine Society, Anaheim, CA, USA. June 1994

A previously uncharacterized gene, myl, is fused to the retinoic acid receptor alpha gene in acute promyelocytic leukemia. XV International Association for Comparative Research on Leukemia and Related Disease, Padua, Italy. October 1991

PATENTS

Goddard A, Godowski PJ, Gurney AL. NL2 Tie ligand homologue polypeptide. Patent Number: 6,455,496. Date of Patent: Sept. 24, 2002.

Goddard A, Godowski PJ and Gurney AL. NL3 Tie ligand homologue nucleic acids. Patent Number: 6,426,218. Date of Patent: July 30, 2002.

Godowski P, Gurney A, Hillan KJ, Botstein D, Goddard A, Roy M, Ferrara N, Tumas D, Schwall R. NL4 Tie ligand homologue nucleic acid. Patent Number: 6,413,770. Date of Patent: July 2, 2002.

Ashkenazi A, Fong S, Goddard A, Gurney AL, Napier MA, Tumas D, Wood WI. Nucleic acid encoding A-33 related antigen poly peptides. Patent Number: 6,410,708. Date of Patent: Jun. 25, 2002.

Botstein DA, Cohen RL, Goddard AD, Gurney AL, Hillan KJ, Lawrence DA, Levine AJ, Pennica D, Roy MA and Wood WI. WISP polypeptides and nucleic acids encoding same. Patent Number: 6,387,657. Date of Patent: May 14, 2002.

Goddard A, Godowski PJ and Gurney AL. Tie ligands. Patent Number: 6,372,491. Date of Patent: April 16, 2002.

Godowski PJ, Gurney AL, Goddard A and Hillan K. TIE ligand homologue antibody. Patent Number: 6,350,450. Date of Patent: Feb. 26, 2002.

Fong S, Ferrara N, Goddard A, Godowski PJ, Gurney AL, Hillan K and Williams PM. Tie receptor tyrosine kinase ligand homologues. Patent Number: 6,348,351. Date of Patent: Feb. 19, 2002.

Goddard A, Godowski PJ and Gurney AL. Ligand homologues. Patent Number: 6,348,350. Date of Patent: Feb. 19, 2002.

Attie KM, Carlsson LMS, Gesundheit N and Goddard A. Treatment of partial growth hormone insensitivity syndrome. Patent Number: 6,207,640. Date of Patent: March 27, 2001.

Fong S, Ferrara N, Goddard A, Godowski PJ, Gurney AL, Hillan K and Williams PM. Nucleic acids encoding NL-3. Patent Number: 6,074,873. Date of Patent: June 13, 2000

Attie K, Carlsson LMS, Gesundheit N and Goddard A. Treatment of partial growth hormone insensitivity syndrome. Patent Number: 5,824,642. Date of Patent: October 20, 1998

Attie K, Carlsson LMS, Gesundheit N and Goddard A. Treatment of partial growth hormone insensitivity syndrome. Patent Number: 5,646,113. Date of Patent: July 8, 1997

Multiple additional provisional applications filed

PUBLICATIONS

Seshasayee D, Dowd P, Gu Q, Erickson S, **Goddard AD** Comparative sequence analysis of the *HER2* locus in mouse and man. Manuscript in preparation.

Abuzzahab MJ, **Goddard A**, Grigorescu F, Lautier C, Smith RJ and Chernausk SD. Human IGF-1 receptor mutations resulting in pre- and post-natal growth retardation. Manuscript in preparation.

Aggarwal S, Xie, M-H, Foster J, Frantz G, Stinson J, Corpuz RT, Simmons L, Hillan K, Yansura DG, Vandlen RL, **Goddard AD** and Gurney AL. FHFR, a novel receptor for the fibroblast growth factors. Manuscript submitted.

Adams SH, Chui C, Schilbach SL, Yu XX, **Goddard AD**, Grimaldi JC, Lee J, Dowd P, Colman S., Lewin DA. (2001) BFIT, a unique acyl-CoA thioesterase induced in thermogenic brown adipose tissue: Cloning, organization of the human gene, and assessment of a potential link to obesity. *Biochemical Journal* **360**: 135-142.

Lee J, Ho WH, Maruoka M, Corpuz RT, Baldwin DT, Foster JS, **Goddard AD**, Yansura DG, Vandlen RL, Wood WI, Gurney AL. (2001) IL-17E, a novel proinflammatory ligand for the IL-17 receptor homolog IL-17Rh1. *Journal of Biological Chemistry* **276**(2): 1660-1664.

Xie M-H, Aggarwal S, Ho W-H, Foster J, Zhang Z, Stinson J, Wood WI, **Goddard AD** and Gurney AL. (2000) Interleukin (IL)-22, a novel human cytokine that signals through the interferon-receptor related proteins CRF2-4 and IL-22R. *Journal of Biological Chemistry* **275**: 31335-31339.

Weiss GA, Watanabe CK, Zhong A, **Goddard A** and Sidhu SS. (2000) Rapid mapping of protein functional epitopes by combinatorial alanine scanning. *Proc. Natl. Acad. Sci. USA* **97**: 8950-8954.

Guo S, Yamaguchi Y, Schilbach S, Wada T., Lee J, **Goddard A**, French D., Handa H, Rosenthal A. (2000) A regulator of transcriptional elongation controls vertebrate neuronal development. *Nature* **408**: 366-369.

Yan M, Wang L-C, Hymowitz SG, Schilbach S, Lee J, **Goddard A**, de Vos AM, Gao WQ, Dixit VM. (2000) Two-amino acid molecular switch in an epithelial morphogen that regulates binding to two distinct receptors. *Science* **290**: 523-527.

Sehl PD, Tai JTN, Hillan KJ, Brown LA, **Goddard A**, Yang R, Jin H and Lowe DG. (2000) Application of cDNA microarrays in determining molecular phenotype in cardiac growth, development, and response to injury. *Circulation* **101**: 1990-1999.

Guo S, Brush J, Teraoka H, **Goddard A**, Wilson SW, Mullins MC and Rosenthal A. (1999) Development of noradrenergic neurons in the zebrafish hindbrain requires BMP, FGF8, and the homeodomain protein soulless/Phox2A. *Neuron* **24**: 555-566.

Stone D, Murone, M, Luoh, S, Ye W, Armanini P, Gurney A, Phillips HS, Brush, J, **Goddard A**, de Sauvage FJ and Rosenthal A. (1999) Characterization of the human suppressor of fused; a negative regulator of the zinc-finger transcription factor Gli. *J. Cell Sci.* **112**: 4437-4448.

Xie M-H, Holcomb I, Deuel B, Dowd P, Huang A, Vagts A, Foster J, Liang J, Brush J, Gu Q, Hillan K, **Goddard A** and Gurney, A.L. (1999) FGF-19, a novel fibroblast growth factor with unique specificity for FGFR4. *Cytokine* **11**: 729-735.

Yan M, Lee J, Schilbach S, **Goddard A** and Dixit V. (1999) mE10, a novel caspase recruitment domain-containing proapoptotic molecule. *J. Biol. Chem.* **274**(15): 10287-10292.

Gurney AL, Marsters SA, Huang RM, Pitti RM, Mark DT, Baldwin DT, Gray AM, Dowd P, Brush J, Heldens S, Schow P, **Goddard AD**, Wood WI, Baker KP, Godowski PJ and Ashkenazi A. (1999) Identification of a new member of the tumor necrosis factor family and its receptor, a human ortholog of mouse GITR. *Current Biology* **9**(4): 215-218.

Ridgway JBB, Ng E, Kern JA, Lee J, Brush J, **Goddard A** and Carter P. (1999) Identification of a human anti-CD55 single-chain Fv by subtractive panning of a phage library using tumor and nontumor cell lines. *Cancer Research* **59**: 2718-2723.

Pitti RM, Marsters SA, Lawrence DA, Roy M, Kischkel FC, Dowd P, Huang A, Donahue CJ, Sherwood SW, Baldwin DT, Godowski PJ, Wood WI, Gurney AL, Hillan KJ, Cohen RL, **Goddard AD**, Botstein D and Ashkenazi A. (1998) Genomic amplification of a decoy receptor for Fas ligand in lung and colon cancer. *Nature* **396**(6712): 699-703.

Pennica D, Swanson TA, Welsh JW, Roy MA, Lawrence DA, Lee J, Brush J, Taneyhill LA, Deuel B, Lew M, Watanabe C, Cohen RL, Melhem MF, Finley GG, Quirke P, **Goddard AD**, Hillan KJ, Gurney AL, Botstein D and Levine AJ. (1998) WISP genes are members of the connective tissue growth factor family that are up-regulated in wnt-1-transformed cells and aberrantly expressed in human colon tumors. *Proc. Natl. Acad. Sci. USA.* **95**(25): 14717-14722.

Yang RB, Mark MR, Gray A, Huang A, Xie MH, Zhang M, **Goddard A**, Wood WI, Gurney AL and Godowski PJ. (1998) Toll-like receptor-2 mediates lipopolysaccharide-induced cellular signalling. *Nature* **395**(6699): 284-288.

Merchant AM, Zhu Z, Yuan JQ, **Goddard A**, Adams CW, Presta LG and Carter P. (1998) An efficient route to human bispecific IgG. *Nature Biotechnology* **16**(7): 677-681.

Marsters SA, Sheridan JP, Pitti RM, Brush J, **Goddard A** and Ashkenazi A. (1998) Identification of a ligand for the death-domain-containing receptor Apo3. *Current Biology* **8**(9): 525-528.

Xie J, Murone M, Luoh SM, Ryan A, Gu Q, Zhang C, Bonifas JM, Lam CW, Hynes M, **Goddard A**, Rosenthal A, Epstein EH Jr. and de Sauvage FJ. (1998) Activating Smoothed mutations in sporadic basal-cell carcinoma. *Nature.* **391**(6662): 90-92.

Marsters SA, Sheridan JP, Pitti RM, Huang A, Skubatch M, Baldwin D, Yuan J, Gurney A, **Goddard AD**, Godowski P and Ashkenazi A. (1997) A novel receptor for Apo2L/TRAIL contains a truncated death domain. *Current Biology.* **7**(12): 1003-1006.

Hynes M, Stone DM, Dowd M, Pitts-Meek S, **Goddard A**, Gurney A and Rosenthal A. (1997) Control of cell pattern in the neural tube by the zinc finger transcription factor *Gli-1*. *Neuron* **19**: 15-26.

Sheridan JP, Marsters SA, Pitti RM, Gurney A., Skubatch M, Baldwin D, Ramakrishnan L, Gray CL, Baker K, Wood WI, **Goddard AD**, Godowski P, and Ashkenazi A. (1997) Control of TRAIL-Induced Apoptosis by a Family of Signaling and Decoy Receptors. *Science* **277** (5327): 818-821.

Goddard AD, Dowd P, Chernaused S, Geffner M, Gertner J, Hintz R, Hopwood N, Kaplan S, Plotnick L, Rogol A, Rosenfield R, Saenger P, Mauras N, Hershkopf R, Angulo M and Attie, K. (1997) Partial growth hormone insensitivity: The role of growth hormone receptor mutations in idiopathic short stature. *J. Pediatr.* **131**: S51-55.

Klein RD, Sherman D, Ho WH, Stone D, Bennett GL, Moffat B, Vandlen R, Simmons L, Gu Q, Hongo JA, Devaux B, Poulsen K, Armanini M, Nozaki C, Asai N, **Goddard A**, Phillips H, Henderson CE, Takahashi M and Rosenthal A. (1997) A GPI-linked protein that interacts with Ret to form a candidate neurturin receptor. *Nature*. **387**(6634): 717-21.

Stone DM, Hynes M, Armanini M, Swanson TA, Gu Q, Johnson RL, Scott MP, Pennica D, **Goddard A**, Phillips H, Noll M, Hooper JE, de Sauvage F and Rosenthal A. (1996) The tumour-suppressor gene patched encodes a candidate receptor for Sonic hedgehog. *Nature* **384**(6605): 129-34.

Marsters SA, Sheridan JP, Donahue CJ, Pitti RM, Gray CL, **Goddard AD**, Bauer KD and Ashkenazi A. (1996) Apo-3, a new member of the tumor necrosis factor receptor family, contains a death domain and activates apoptosis and NF-kappa β . *Current Biology* **6**(12): 1669-76.

Rothe M, Xiong J, Shu HB, Williamson K, **Goddard A** and Goeddel DV. (1996) I-TRAF is a novel TRAF-interacting protein that regulates TRAF-mediated signal transduction. *Proc. Natl. Acad. Sci. USA* **93**: 8241-8246.

Yang M, Luoh SM, **Goddard A**, Reilly D, Henzel W and Bass S. (1996) The bglX gene located at 47.8 min on the Escherichia coli chromosome encodes a periplasmic beta-glucosidase. *Microbiology* **142**: 1659-65.

Goddard AD and Black DM. (1996) Familial Cancer in Molecular Endocrinology of Cancer. Waxman, J. Ed. Cambridge University Press, Cambridge UK, pp.187-215.

Treanor JJS, Goodman L, de Sauvage F, Stone DM, Poulson KT, Beck CD, Gray C, Armanini MP, Pollocks RA, Hefti F, Phillips HS, **Goddard A**, Moore MW, Buj-Bello A, Davis AM, Asai N, Takahashi M, Vandlen R, Henderson CE and Rosenthal A. (1996) Characterization of a receptor for GDNF. *Nature* **382**: 80-83.

Klein RD, Gu Q, **Goddard A** and Rosenthal A. (1996) Selection for genes encoding secreted proteins and receptors. *Proc. Natl. Acad. Sci. USA* **93**: 7108-7113.

Winslow JW, Moran P, Valverde J, Shih A, Yuan JQ, Wong SC, Tsai SP, **Goddard A**, Henzel WJ, Hefti F and Caras I. (1995) Cloning of AL-1, a ligand for an Eph-related tyrosine kinase receptor involved in axon bundle formation. *Neuron* **14**: 973-981.

Bennett BD, Zeigler FC, Gu Q, Fendly B, **Goddard AD**, Gillett N and Matthews W. (1995) Molecular cloning of a ligand for the EPH-related receptor protein-tyrosine kinase Htk. *Proc. Natl. Acad. Sci. USA* **92**: 1866-1870.

Huang X, Yuang J, **Goddard A**, Foulis A, James RF, Lernmark A, Pujol-Borrell R, Rabinovitch A, Somoza N and Stewart TA. (1995) Interferon expression in the pancreases of patients with type I diabetes. *Diabetes* **44**: 658-664.

Goddard AD, Yuan JQ, Fairbairn L, Dexter M, Borrow J, Kozak C and Solomon E. (1995) Cloning of the murine homolog of the leukemia-associated PML gene. *Mammalian Genome* **6**: 732-737.

Goddard AD, Covello R, Luoh SM, Clackson T, Attie KM, Gesundheit N, Rundle AC, Wells JA, Carlsson LMTI and The Growth Hormone Insensitivity Study Group. (1995) Mutations of the growth hormone receptor in children with idiopathic short stature. *N. Engl. J. Med.* **333**: 1093-1098.

Kuo SS, Moran P, Gripp J, Armanini M, Phillips HS, **Goddard A** and Caras IW. (1994) Identification and characterization of Batk, a predominantly brain-specific non-receptor protein tyrosine kinase related to Csk. *J. Neurosci. Res.* **38**: 705-715.

Mark MR, Scadden DT, Wang Z, Gu Q, **Goddard A** and Godowski PJ. (1994) Rse, a novel receptor-type tyrosine kinase with homology to Axl/Ufo, is expressed at high levels in the brain. *Journal of Biological Chemistry* **269**: 10720-10728.

Borrow J, Shipley J, Howe K, Kiely F, **Goddard A**, Sheer D, Srivastava A, Antony AC, Fioretos T, Mitelman F and Solomon E. (1994) Molecular analysis of simple variant translocations in acute promyelocytic leukemia. *Genes Chromosomes Cancer* **9**: 234-243.

Goddard AD and Solomon E. (1993) Genetics of Cancer. *Adv. Hum. Genet.* **21**: 321-376.

Borrow J, **Goddard AD**, Gibbons B, Katz F, Swirsky D, Fioretos T, Dube I, Winfield DA, Kingston J, Hagemeijer A, Rees JKH, Lister AT and Solomon E. (1992) Diagnosis of acute promyelocytic leukemia by RT-PCR: Detection of *PML-RARA* and *RARA-PML* fusion transcripts. *Br. J. Haematol.* **82**: 529-540.

Goddard AD, Borrow J and Solomon E. (1992) A previously uncharacterized gene, *PML*, is fused to the retinoic acid receptor alpha gene in acute promyelocytic leukemia. *Leukemia* **6 Suppl 3**: 117S-119S.

Zhu X, Dunn JM, **Goddard AD**, Squire JA, Becker A, Phillips RA and Gallie BL. (1992) Mechanisms of loss of heterozygosity in retinoblastoma. *Cytogenet. Cell. Genet.* **59**: 248-252.

Foulkes W, **Goddard A.** and Patel K. (1991) Retinoblastoma linked with Seascale [letter]. *British Med. J.* **302**: 409.

Goddard AD, Borrow J, Freemont PS and Solomon E. (1991) Characterization of a novel zinc finger gene disrupted by the t(15;17) in acute promyelocytic leukemia. *Science* **254**: 1371-1374.

Solomon E, Borrow J and **Goddard AD.** (1991) Chromosomal aberrations in cancer. *Science* **254**: 1153-1160.

Pajunen L, Jones TA, **Goddard A**, Sheer D, Solomon E, Pihlajaniemi T and Kivirikko KI. (1991) Regional assignment of the human gene coding for a multifunctional peptide (P4HB) acting as the β -subunit of prolyl-4-hydroxylase and the enzyme protein disulfide isomerase to 17q25. *Cytogenet. Cell. Genet.* **56**: 165-168.

Borrow J, Black DM, **Goddard AD**, Yagle MK, Frischauf A.-M and Solomon E. (1991) Construction and regional localization of a *NotI* linking library from human chromosome 17q. *Genomics* **10**: 477-480.

Borrow J, **Goddard AD**, Sheer D and Solomon E. (1990) Molecular analysis of acute promyelocytic leukemia breakpoint cluster region on chromosome 17. *Science* **249**: 1577-1580.

Myers JC, Jones TA, Pohjolainen E-R, Kadri AS, **Goddard AD**, Sheer D, Solomon E and Pihlajaniemi T. (1990) Molecular cloning of 5(IV) collagen and assignment of the gene to the region of the X-chromosome containing the Alport Syndrome locus. *Am. J. Hum. Genet.* **46**: 1024-1033.

Gallie BL, Squire JA, **Goddard A**, Dunn JM, Canton M, Hinton D, Zhu X and Phillips RA. (1990) Mechanisms of oncogenesis in retinoblastoma. *Lab. Invest.* **62**: 394-408.

Goddard AD, Phillips RA, Greger V, Passarge E, Hopping W, Gallie BL and Horsthemke B. (1990) Use of the RB1 cDNA as a diagnostic probe in retinoblastoma families. *Clinical Genetics* **37**: 117-126.

Zhu XP, Dunn JM, Phillips RA, **Goddard AD**, Paton KE, Becker A and Gallie BL. (1989) Germline, but not somatic, mutations of the RB1 gene preferentially involve the paternal allele. *Nature* **340**: 312-314.

Gallie BL, Dunn JM, **Goddard A**, Becker A and Phillips RA. (1988) Identification of mutations in the putative retinoblastoma gene. In Molecular Biology of The Eye: Genes, Vision and Ocular Disease. UCLA Symposia on Molecular and Cellular Biology, New Series, Volume 88. J. Piatigorsky, T. Shinohara and P.S. Zelenka, Eds. Alan R. Liss, Inc., New York, 1988, pp. 427-436.

Goddard AD, Balakier H, Canton M, Dunn J, Squire J, Reyes E, Becker A, Phillips RA and Gallie BL. (1988) Infrequent genomic rearrangement and normal expression of the putative RB1 gene in retinoblastoma tumors. *Mol. Cell. Biol.* **8**: 2082-2088.

Squire J, Dunn J, **Goddard A**, Hoffman T, Musarella M, Willard HF, Becker AJ, Gallie BL and Phillips RA. (1986) Cloning of the esterase D gene: A polymorphic gene probe closely linked to the retinoblastoma locus on chromosome 13. *Proc. Natl. Acad. Sci. USA* **83**: 6573-6577.

Squire J, **Goddard AD**, Canton M, Becker A, Phillips RA and Gallie BL (1986) Tumour induction by the retinoblastoma mutation is independent of N-myc expression. *Nature* **322**: 555-557.

Goddard AD, Heddle JA, Gallie BL and Phillips RA. (1985) Radiation sensitivity of fibroblasts of bilateral retinoblastoma patients as determined by micronucleus induction *in vitro*. *Mutation Research* **152**: 31-38.

RESEARCH

SIMULTANEOUS AMPLIFICATION AND DETECTION OF SPECIFIC DNA SEQUENCES

Russell Higuchi*, Gavin Dollinger¹, P. Sean Walsh and Robert GriffithRoche Molecular Systems, Inc., 1400 53rd St., Emeryville, CA 94608. ¹Chiron Corporation, 1400 53rd St., Emeryville, CA 94608. *Corresponding author.

We have enhanced the polymerase chain reaction (PCR) such that specific DNA sequences can be detected without opening the reaction tube. This enhancement requires the addition of ethidium bromide (EtBr) to a PCR. Since the fluorescence of EtBr increases in the presence of double-stranded (ds) DNA an increase in fluorescence in such a PCR indicates a positive amplification, which can be easily monitored externally. In fact, amplification can be continuously monitored in order to follow its progress. The ability to simultaneously amplify specific DNA sequences and detect the product of the amplification both simplifies and improves PCR and may facilitate its automation and more widespread use in the clinic or in other situations requiring high sample throughput.

Although the potential benefits of PCR¹ to clinical diagnostics are well known^{2,3}, it is still not widely used in this setting, even though it is four years since thermostable DNA polymerases⁴ made PCR practical. Some of the reasons for its slow acceptance are high cost, lack of automation of pre- and post-PCR processing steps, and false positive results from carryover-contamination. The first two points are related in that labor is the largest contributor to cost at the present stage of PCR development. Most current assays require some form of "downstream" processing once thermocycling is done in order to determine whether the target DNA sequence was present and has amplified. These include DNA hybridization^{5,6}, gel electrophoresis with or without use of restriction digestion^{7,8}, HPLC⁹, or capillary electrophoresis¹⁰. These methods are labor-intensive, have low throughput, and are difficult to automate. The third point is also closely related to downstream processing. The handling of the PCR product in these downstream processes increases the chances that amplified DNA will spread through the typing lab, resulting in a risk of

"carryover" false positives in subsequent testing¹¹.

These downstream processing steps would be eliminated if specific amplification and detection of amplified DNA took place simultaneously within an unopened reaction vessel. Assays in which such different processes take place without the need to separate reaction components have been termed "homogeneous". No truly homogeneous PCR assay has been demonstrated to date, although progress towards this end has been reported. Chehab, et al.¹², developed a PCR product detection scheme using fluorescent primers that resulted in a fluorescent PCR product. Allele-specific primers, each with different fluorescent tags, were used to indicate the genotype of the DNA. However, the unincorporated primers must still be removed in a downstream process in order to visualize the result. Recently, Holland, et al.¹³, developed an assay in which the endogenous 5' exonuclease assay of *Taq* DNA polymerase was exploited to cleave a labeled oligonucleotide probe. The probe would only cleave if PCR amplification had produced its complementary sequence. In order to detect the cleavage products, however, a subsequent process is again needed.

We have developed a truly homogeneous assay for PCR and PCR product detection based upon the greatly increased fluorescence that ethidium bromide and other DNA binding dyes exhibit when they are bound to dsDNA¹⁴⁻¹⁶. As outlined in Figure 1, a prototypic PCR

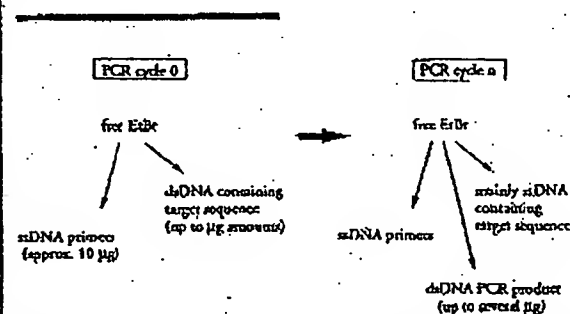


FIGURE 1 Principle of simultaneous amplification and detection of PCR product. The components of a PCR containing EtBr that are fluorescent are listed—EtBr itself, EtBr bound to either ssDNA or dsDNA. There is a large fluorescence enhancement when EtBr is bound to DNA and binding is greatly enhanced when DNA is double-stranded. After sufficient (n) cycles of PCR, the net increase in dsDNA results in additional EtBr binding, and a net increase in total fluorescence.

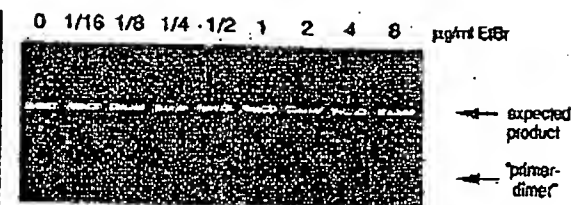


FIGURE 2 Gel electrophoresis of PCR amplification products of the human nuclear gene, HLA DQα, made in the presence of increasing amounts of EtBr (up to 8 μg/ml). The presence of EtBr has no obvious effect on the yield or specificity of amplification.

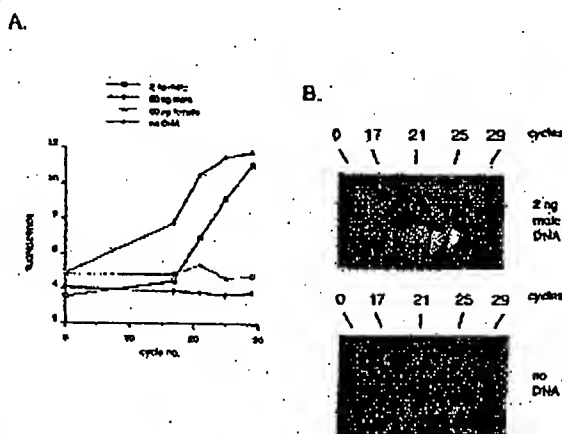


FIGURE 3 (A) Fluorescence measurements from PCRs that contain 0.5 μg/ml EtBr and that are specific for Y-chromosome repeat sequences. Five replicate PCRs were begun containing each of the DNAs specified. At each indicated cycle, one of the five replicate PCRs for each DNA was removed from thermocycling and its fluorescence measured. Units of fluorescence are arbitrary. (B) UV photograph of PCR tubes (0.5 ml Eppendorf-style, polypropylene micro-centrifuge tubes) containing reactions, those starting from 2 ng male DNA and control reactions without any DNA, from (A).

begins with primers that are single-stranded DNA (ss-DNA), dNTPs, and DNA polymerase. An amount of dsDNA containing the target sequence (target DNA) is also typically present. This amount can vary, depending on the application, from single-cell amounts of DNA¹⁷ to micrograms per PCR¹⁸. If EtBr is present, the reagents that will fluoresce, in order of increasing fluorescence, are free EtBr itself, and EtBr bound to the single-stranded DNA primers and to the double-stranded target DNA (by its intercalation between the stacked bases of the DNA double-helix). After the first denaturation cycle, target DNA will be largely single-stranded. After a PCR is completed, the most significant change is the increase in the amount of dsDNA (the PCR product itself) of up to several micrograms. Formerly free EtBr is bound to the additional dsDNA, resulting in an increase in fluorescence. There is also some decrease in the amount of ssDNA primer, but because the binding of EtBr to ssDNA is much less than to dsDNA, the effect of this change on the total fluorescence of the sample is small. The fluorescence increase can be measured by directing excitation illumination through the walls of the amplification vessel

before and after, or even continuously during, thermocycling.

RESULTS

PCR in the presence of EtBr. In order to assess the effect of EtBr in PCR, amplifications of the human HLA DQα gene¹⁹ were performed with the dye present at concentrations from 0.06 to 8.0 μg/ml (a typical concentration of EtBr used in staining of nucleic acids following gel electrophoresis is 0.5 μg/ml). As shown in Figure 2, gel electrophoresis revealed little or no difference in the yield or quality of the amplification product whether EtBr was absent or present at any of these concentrations, indicating that EtBr does not inhibit PCR.

Detection of human Y-chromosome specific sequences. Sequence-specific, fluorescence enhancement of EtBr as a result of PCR was demonstrated in a series of amplifications containing 0.5 μg/ml EtBr and primers specific to repeat DNA sequences found on the human Y-chromosome²⁰. These PCRs initially contained either 60 ng male, 60 ng female, 2 ng male human or no DNA. Five replicate PCRs were begun for each DNA. After 0, 17, 21, 24 and 29 cycles of thermocycling, a PCR for each DNA was removed from the thermocycler, and its fluorescence measured in a spectrofluorometer and plotted vs. amplification cycle number (Fig. 3A). The shape of this curve reflects the fact that by the time an increase in fluorescence can be detected, the increase in DNA is becoming linear and not exponential with cycle number. As shown, the fluorescence increased about three-fold over the background fluorescence for the PCRs containing human male DNA, but did not significantly increase for negative control PCRs, which contained either no DNA or human female DNA. The more male DNA present to begin with—60 ng versus 2 ng—the fewer cycles were needed to give a detectable increase in fluorescence. Gel electrophoresis on the products of these amplifications showed that DNA fragments of the expected size were made in the male DNA containing reactions and that little DNA synthesis took place in the control samples.

In addition, the increase in fluorescence was visualized by simply laying the completed, unopened PCRs on a UV transilluminator and photographing them through a red filter. This is shown in figure 3B for the reactions that began with 2 ng male DNA and those with no DNA.

Detection of specific alleles of the human β-globin gene. In order to demonstrate that this approach has adequate specificity to allow genetic screening, a detection of the sickle-cell anemia mutation was performed. Figure 4 shows the fluorescence from completed amplifications containing EtBr (0.5 μg/ml) as detected by photography of the reaction tubes on a UV transilluminator. These reactions were performed using primers specific for either the wild-type or sickle-cell mutation of the human β-globin gene²¹. The specificity for each allele is imparted by placing the sickle-mutation site at the terminal 3' nucleotide of one primer. By using an appropriate primer annealing temperature, primer extension—and thus amplification—can take place only if the 3' nucleotide of the primer is complementary to the β-globin allele present.²²

Each pair of amplifications shown in Figure 4 consists of a reaction with either the wild-type allele specific (left tube) or sickle-allele specific (right tube) primers. Three different DNAs were typed: DNA from a homozygous, wild-type β-globin individual (AA); from a heterozygous sickle β-globin individual (AS); and from a homozygous sickle β-globin individual (SS). Each DNA (50 ng genomic DNA to start each PCR) was analyzed in triplicate (3 pairs

mmocy.

ess the
HLA
cent at
occen-
lowing
e 2, gel
ic yield
Br was
ndicat-

Se se-
nent of
ries of
primers
human
either
DNA.
After 0,
or each
is fluo-
plotted
of this
case in
DNA is
umber.
re-fold
ontain-
increase
her no
DNA
fewer
in fluo-
f these
the ex-
taining
in the

ualized
n a UV
h a red
as that
VA.

-globin
sch has
etection
Figure
ications
graphy
These
for ci-
human
nparted
rial 3'
primer
has am-
c of the
ent 1.22
nsists of
the (left
Three
zygous,
ozygous
ozygous
genomic
(3 pairs

of reactions each). The DNA type was reflected in the relative fluorescence intensities in each pair of completed amplifications. There was a significant increase in fluorescence only where a β -globin allele DNA matched the primer set. When measured on a spectrofluorometer (data not shown), this fluorescence was about three times that present in a PCR where both β -globin alleles were mismatched to the primer set. Gel electrophoresis (not shown) established that this increase in fluorescence was due to the synthesis of nearly a microgram of a DNA fragment of the expected size for β -globin. There was little synthesis of dsDNA in reactions in which the allele-specific primer was mismatched to both alleles.

Continuous monitoring of a PCR. Using a fiber optic device, it is possible to direct excitation illumination from a spectrofluorometer to a PCR undergoing thermocycling and to return its fluorescence to the spectrofluorometer. The fluorescence readout of such an arrangement, directed at an EtBr-containing amplification of Y-chromosome specific sequences from 25 ng of human male DNA, is shown in Figure 5. The readout from a control PCR with no target DNA is also shown. Thirty cycles of PCR were monitored for each.

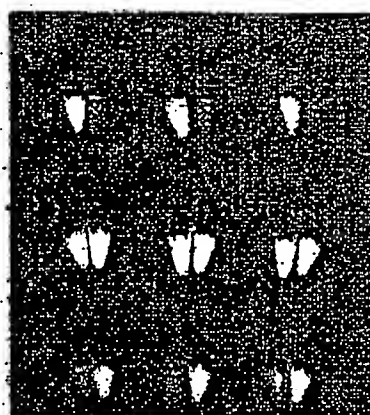
The fluorescence trace as a function of time clearly shows the effect of the thermocycling. Fluorescence intensity rises and falls inversely with temperature. The fluorescence intensity is minimum at the denaturation temperature (94°C) and maximum at the annealing/extension temperature (50°C). In the negative-control PCR, these fluorescence maxima and minima do not change significantly over the thirty thermocycles, indicating that there is little dsDNA synthesis without the appropriate target DNA, and there is little if any bleaching of EtBr during the continuous illumination of the sample.

In the PCR containing male DNA, the fluorescence maxima at the annealing/extension temperature begin to increase at about 4000 seconds of thermocycling, and continue to increase with time, indicating that dsDNA is being produced at a detectable level. Note that the fluorescence minima at the denaturation temperature do not significantly increase, presumably because at this temperature there is no dsDNA for EtBr to bind. Thus the course of the amplification is followed by tracking the fluorescence increase at the annealing temperature. Analysis of the products of these two amplifications by gel electrophoresis showed a DNA fragment of the expected size for the male DNA containing sample and no detectable DNA synthesis for the control sample.

DISCUSSION

Downstream processes such as hybridization to a sequence-specific probe can enhance the specificity of DNA detection by PCR. The elimination of these processes means that the specificity of this homogeneous assay depends solely on that of PCR. In the case of sickle-cell disease, we have shown that PCR alone has sufficient DNA sequence specificity to permit genetic screening. Using appropriate amplification conditions, there is little non-specific production of dsDNA in the absence of the appropriate target allele.

The specificity required to detect pathogens can be more or less than that required to do genetic screening, depending on the number of pathogens in the sample and the amount of other DNA that must be taken with the sample. A difficult target is HIV, which requires detection of a viral genome that can be at the level of a few copies per thousands of host cells⁶. Compared with genetic screening, which is performed on cells containing at least one copy of the target sequence, HIV detection requires both more specificity and the input of more total



Homozygous
AA

Heterozygous
AS

Homozygous
SS

FIGURE 4 UV photograph of PCR tubes containing amplifications using EtBr that are specific to wild-type (A) or sickle (S) alleles of the human β -globin gene. The left of each pair of tubes contains allele-specific primers to the wild-type alleles, the right tube primers to the sickle allele. The photograph was taken after 30 cycles of PCR, and the input DNAs and the alleles they contain are indicated. Fifty ng of DNA was used to begin PCR. Typing was done in triplicate (3 pairs of PCRs) for each input DNA.

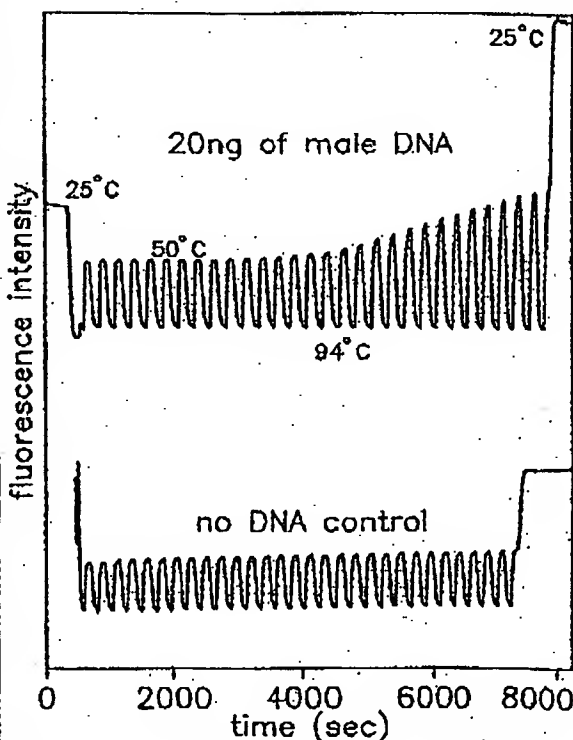


FIGURE 5 Continuous, real-time monitoring of a PCR. A fiber optic was used to carry excitation light in a PCR in progress and also emitted light back to a fluorometer (see Experimental Protocol). Amplification using human male-DNA specific primers in a PCR starting with 20 ng of human male DNA (top), or in a control PCR without DNA (bottom), were monitored. Thirty cycles of PCR were followed for each. The temperature cycled between 94°C (denaturation) and 50°C (annealing and extension). Note in the male DNA PCR, the cycle (time) dependent increase in fluorescence at the annealing/extension temperature.

DNA—up to microgram amounts—in order to have sufficient numbers of target sequences. This large amount of starting DNA in an amplification significantly increases the background fluorescence over which any additional fluorescence produced by PCR must be detected. An additional complication that occurs with targets in low copy-number is the formation of the "primer-dimer" artifact. This is the result of the extension of one primer using the other primer as a template. Although this occurs infrequently, once it occurs the extension product is a substrate for PCR amplification, and can compete with true PCR targets if those targets are rare. The primer-dimer product is of course dsDNA and thus is a potential source of false signal in this homogeneous assay.

To increase PCR specificity and reduce the effect of primer-dimer amplification, we are investigating a number of approaches, including the use of nested-primer amplifications that take place in a single tube³, and the "hot-start", in which nonspecific amplification is reduced by raising the temperature of the reaction before DNA synthesis begins²³. Preliminary results using these approaches suggest that primer-dimer is effectively reduced and it is possible to detect the increase in EtBr fluorescence in a PCR instigated by a single HIV genome in a background of 10^3 cells. With larger numbers of cells, the background fluorescence contributed by genomic DNA becomes problematic. To reduce this background, it may be possible to use sequence-specific DNA-binding dyes that can be made to preferentially bind PCR product over genomic DNA by incorporating the dye-binding DNA sequence into the PCR product through a 5' "add-on" to the oligonucleotide primer²⁴.

We have shown that the detection of fluorescence generated by an EtBr-containing PCR is straightforward, both once PCR is completed and continuously during thermocycling. The ease with which automation of specific DNA detection can be accomplished is the most promising aspect of this assay. The fluorescence analysis of completed PCRs is already possible with existing instrumentation in 96-well format²⁵. In this format, the fluorescence in each PCR can be quantitated before, after, and even at selected points during thermocycling by moving the rack of PCRs to a 96-microwell plate fluorescence reader²⁶.

The instrumentation necessary to continuously monitor multiple PCRs simultaneously is also simple in principle. A direct extension of the apparatus used here is to have multiple fiber optics transmit the excitation light and fluorescent emissions to and from multiple PCRs. The ability to monitor multiple PCRs continuously may allow quantitation of target DNA copy number. Figure 3 shows that the larger the amount of starting target DNA, the sooner during PCR a fluorescence increase is detected. Preliminary experiments (Higuchi and Dollinger, manuscript in preparation) with continuous monitoring have shown a sensitivity to two-fold differences in initial target DNA concentration.

Conversely, if the number of target molecules is known—as it can be in genetic screening—continuous monitoring may provide a means of detecting false positive and false negative results. With a known number of target molecules, a true positive would exhibit detectable fluorescence by a predictable number of cycles of PCR. Increases in fluorescence detected before or after that cycle would indicate potential artifacts. False negative results due to, for example, inhibition of DNA polymerase, may be detected by including within each PCR an inefficiently amplifying marker. This marker results in a fluorescence increase only after a large number of cycles—many more than are necessary to detect a true

positive. If a sample fails to have a fluorescence increase after this many cycles, inhibition may be suspected. Since, in this assay, conclusions are drawn based on the presence or absence of fluorescence signal alone, such controls may be important. In any event, before any test based on this principle is ready for the clinic, an assessment of its false positive/false negative rates will need to be obtained using a large number of known samples.

In summary, the inclusion in PCR of dyes whose fluorescence is enhanced upon binding dsDNA makes it possible to detect specific DNA amplification from outside the PCR tube. In the future, instruments based upon this principle may facilitate the more widespread use of PCR in applications that demand the high throughput of samples.

EXPERIMENTAL PROTOCOL

Human HLA-DQ α gene amplifications. containing EtBr. PCRs were set up in 100 μ l volumes containing 10 mM Tris-HCl, pH 8.3; 50 mM KCl; 4 mM MgCl₂; 2.5 units of *Taq* DNA polymerase (Perkin-Elmer Cetus, Norwalk, CT); 20 pmole each of human HLA-DQ α gene specific oligonucleotide primers GH26 and GH27¹⁹ and approximately 10^3 copies of DQ α PCR product diluted from a previous reaction. Ethidium bromide (EtBr; Sigma) was used at the concentrations indicated in Figure 2. Thermocycling proceeded for 20 cycles in a model 480 thermocycler (Perkin-Elmer Cetus, Norwalk, CT) using a "step-cycle" program of 94°C for 1 min, denaturation and 60°C for 30 sec, annealing and 72°C for 30 sec, extension.

Y-chromosome specific PCR. PCRs (100 μ l total reaction volume) containing 0.5 μ g/ml EtBr were prepared as described for HLA-DQ α , except with different primers and target DNAs. These PCRs contained 15 pmole each male DNA-specific primers Y1.1 and Y1.2²⁰, and either 60 ng male, 60 ng female, 2 ng male, or no human DNA. Thermocycling was 94°C for 1 min, and 60°C for 1 min using a "step-cycle" program. The number of cycles for a sample were as indicated in Figure 3. Fluorescence measurement is described below.

Allele-specific, human β -globin gene PCR. Amplifications of 100 μ l volume using 0.5 μ g/ml of EtBr were prepared as described for HLA-DQ α above except with different primers and target DNAs. These PCRs contained either primer pair HGP2/HB14A (wild-type globin specific primers) or HGP2/HB14S (sickle-globin specific primers) at 10 pmole each primer per PCR. These primers were developed by Wu et al.²¹. Three different target DNAs were used in separate amplifications—50 ng each of human DNA that was homozygous for the sickle trait (SS), DNA that was heterozygous for the sickle trait (AS), or DNA that was homozygous for the w.t. globin (AA). Thermocycling was for 30 cycles at 94°C for 1 min, and 55°C for 1 min, using a "step-cycle" program. An annealing temperature of 55°C had been shown by Wu et al.²¹ to provide allele-specific amplification. Completed PCRs were photographed through a red filter (Wratten 23A) after placing the reaction tubes atop a model TM-36 transilluminator (UV-products, San Gabriel, CA).

Fluorescence measurement. Fluorescence measurements were made on PCRs containing EtBr in a Fluorolog-2 fluorometer (SPEX, Edison, NJ). Excitation was at the 500 nm band with about 2 nm bandwidth with a OG 435 nm cut-off filter (Melles Griest, Inc., Irvine, CA) to exclude second-order light. Emitted light was detected at 570 nm with a bandwidth of about 7 nm. An OG 530 nm cut-off filter was used to remove the excitation light.

Continuous fluorescence monitoring of PCR. Continuous monitoring of a PCR in progress was accomplished using the spectrofluorometer and settings described above as well as a fiberoptic accessory (SPEX cat. no. 1950) to both send excitation light to, and receive emitted light from, a PCR placed in a well of a model 480 thermocycler (Perkin-Elmer Cetus). The probe end of the fiberoptic cable was attached with "5 minute-epoxy" to the open top of a PCR tube (a 0.5 ml polypropylene centrifuge tube with its cap removed) effectively sealing it. The exposed top of the PCR tube and the end of the fiberoptic cable were shielded from room light and the room lights were kept dimmed during each run. The monitored PCR was an amplification of Y-chromosome-specific repeat sequences as described above, except using an annealing/extension temperature of 50°C. The reaction was covered with mineral oil (2 drops) to prevent evaporation. Thermocycling and fluorescence measurement were started simultaneously. A time-base scan with a 10 second integration time

was used and the emission signal was ratioed to the excitation signal to control for changes in light-source intensity. Data were collected using the dm3000f, version 2.5 (SPEX) data system.

Acknowledgments

We thank Bob Jones for help with the spectrofluorometric measurements and Heatherbell Fong for editing this manuscript.

References

- Mullis, K., Faloona, F., Scharf, S., Saiki, R., Horn, G. and Erlich, H. 1986. Specific enzymatic amplification of DNA *in vitro*: The polymerase chain reaction. *CSHQB* 51:263-275.
- White, T. J., Arnheim, N. and Erlich, H. A. 1989. The polymerase chain reaction. *Trends Genet.* 5:185-189.
- Erlich, H. A., Gelfand, D. and Sninsky, J. J. 1991. Recent advances in the polymerase chain reaction. *Science* 252:1643-1651.
- Saiki, R. K., Gelfand, D. H., Stoffel, S., Scharf, S. J., Higuchi, R., Horn, G. T., Mullis, K. B. and Erlich, H. A. 1988. Primer-directed enzymatic amplification of DNA with a thermostable DNA polymerase. *Science* 239:487-491.
- Saiki, R. K., Walsh, P. S., Levenson, C. H. and Erlich, H. A. 1989. Genetic analysis of amplified DNA with immobilized sequence-specific oligonucleotide probes. *Proc. Natl. Acad. Sci. USA* 86:6230-6234.
- Kwok, S. Y., Mack, D. H., Mullis, K. B., Fieresz, B. J., Ehrlich, C. D., Blair, D. and Friedman-Kien, A. S. 1987. Identification of human immunodeficiency virus sequences by using *in vitro* enzymatic amplification and oligomer cleavage detection. *J. Virol.* 61:1690-1694.
- Chehab, F. F., Doherty, M., Cai, S. P., Kan, Y. W., Cooper, S. and Rubin, E. M. 1987. Detection of sickle cell anemia and thalassemia. *Nature* 329:203-204.
- Horn, G. T., Richards, B. and Klinger, K. W. 1989. Amplification of a highly polymorphic VNTR segment by the polymerase chain reaction. *Nuc. Acids Res.* 16:2140.
- Katz, E. D. and Dong, M. W. 1990. Rapid analysis and purification of polymerase chain reaction products by high-performance liquid chromatography. *Biotechniques* 8:546-555.
- Helger, D. N., Cohen, A. S. and Karger, B. L. 1990. Separation of DNA restriction fragments by high performance capillary electrophoresis with low and zero crosslinked polyacrylamide using continuous and pulsed electric fields. *J. Chromatogr.* 516:33-48.
- Kwok, S. Y. and Higuchi, R. G. 1989. Avoiding false positives with PCR. *Nature* 339:237-238.
- Chehab, F. F. and Kan, Y. W. 1989. Detection of specific DNA sequences by fluorescence amplification: a color complementation assay. *Proc. Natl. Acad. Sci. USA* 86:9178-9182.
- Holland, P. M., Abramson, R. D., Watson, R. and Gelfand, D. H. 1991. Detection of specific polymerase chain reaction products by utilizing the 5' to 3' exonuclease activity of *Thermus aquaticus* DNA polymerase. *Proc. Natl. Acad. Sci. USA* 88:7276-7280.
- Markovits, J., Roques, B. P. and Le Pecq, J. B. 1979. Ethidium dimers: a new reagent for the fluorimetric determination of nucleic acids. *Anal. Biochem.* 94:259-264.
- Kapuscinski, J. and Sacz, W. 1979. Interactions of 4',6-diamidino-2-phenylindole with synthetic polynucleotides. *Nuc. Acids Res.* 6:3519-3534.
- Searle, M. S. and Embrey, K. J. 1990. Sequence-specific interaction of Hoechst 33258 with the minor groove of an adenine-trace DNA duplex studied in solution by ¹H NMR spectroscopy. *Nuc. Acids Res.* 18:3752-3762.
- Li, H. H., Gyllenstein, U. B., Cui, X. F., Saiki, R. K., Erlich, H. A. and Arnheim, N. 1988. Amplification and analysis of DNA sequences in single human sperm and diploid cells. *Nature* 336:414-417.
- Abbott, M. A., Pokor, B. J., Byrne, B. C., Kwok, S. Y., Salsky, J. J. and Erlich, H. A. 1988. Enzymatic gene amplification: qualitative and quantitative methods for detecting proviral DNA amplified *in vitro*. *J. Infect. Dis.* 158:1158.
- Saiki, R. K., Bugawan, T. L., Horn, G. T., Mullis, K. B. and Erlich, H. A. 1986. Analysis of enzymatically amplified β -globin and HLA-DQ α DNA with allele-specific oligonucleotide probes. *Nature* 324:163-166.
- Kogan, S. G., Doherty, M. and Gitchev, J. 1987. An improved method for prenatal diagnosis of genetic diseases by analysis of amplified DNA sequences. *N. Engl. J. Med.* 317:985-990.
- Wu, D. Y., Ugras, L., Pal, B. R. and Wallace, R. B. 1989. Allele-specific enzymatic amplification of β -globin genomic DNA for diagnosis of sickle cell anemia. *Proc. Natl. Acad. Sci. USA* 86:2757-2760.
- Kwok, S., Kellogg, D. E., McKinney, N., Spasic, D., Goda, L., Levenson, C. and Sninsky, J. J. 1990. Effects of primer-template mismatches on the polymerase chain reaction: Human immunodeficiency virus type 1 model studies. *Nuc. Acids Res.* 18:999-1005.
- Chou, Q., Russell, M., Birch, D., Raymond, J. and Bloch, W. 1992. Prevention of pre-PCR mis-priming and primer dimerization improves low-copy-number amplifications. *Submitted.*
- Higuchi, R. 1989. Using PCR to engineer DNA. p. 61-70. In: PCR Technology. H. A. Erlich (Ed.). Stockton Press, New York, N.Y.
- Haff, L., Atwood, J. G., DiCesare, J., Katz, E., Fionera, E., Williams, J. F. and Woudenberg, T. 1991. A high-performance system for automation of the polymerase chain reaction. *Biotechniques* 10:102-103, 106-112.
- Tamura, N. and Kahwa, L. 1989. Fluorescent EIA screening of monoclonal antibodies to cell surface antigens. *J. Immun. Med.* 11:59-63.

IBL

IMMUNO BIOLOGICAL LABORATORIES

sCD-14 ELISA

Trauma, Shock and Sepsis

The CD-14 molecule is expressed on the surface of monocytes and some macrophages. Membrane-bound CD-14 is a receptor for lipopolysaccharide (LPS) complexed to LPS-Binding-Protein (LBP). The concentration of its soluble form is altered under certain pathological conditions. There is evidence for an important role of sCD-14 with polytrauma, sepsis, burnings and inflammations. During septic conditions and acute infections it seems to be a prognostic marker and is therefore of value in monitoring these patients.

IBL offers an ELISA for quantitative determination of soluble CD-14 in human serum, -plasma, cell-culture supernatants and other biological fluids.

Assay features: 12 x 8 determinations (microtiter strips), precoated with a specific monoclonal antibody, 2x1 hour incubation, standard range: 3 - 96 ng/ml detection limit: 1 ng/ml CV: intra- and interassay < 8%

For more information call or fax

GESELLSCHAFT FÜR IMMUNCHEMIE UND -BIOLOGIE MBH
OSTERSTRASSE 86 · D-2000 HAMBURG 20 · GERMANY · TEL. +40/49100 61-64 · FAX +40/40 11 98

BIOTECHNOLOGY VOL 10 APRIL 1992

417

Oligonucleotides with Fluorescent Dyes at Opposite Ends Provide a Quenched Probe System Useful for Detecting PCR Product and Nucleic Acid Hybridization

Kenneth J. Livak, Susan J.A. Flood, Jeffrey Marmaro, William Giusti, and Karin Deetz

Perkin-Elmer, Applied Biosystems Division, Foster City, California 94404

The 5' nuclease PCR assay detects the accumulation of specific PCR product by hybridization and cleavage of a double-labeled fluorogenic probe during the amplification reaction. The probe is an oligonucleotide with both a reporter fluorescent dye and a quencher dye attached. An increase in reporter fluorescence intensity indicates that the probe has hybridized to the target PCR product and has been cleaved by the 5'→3' nucleolytic activity of *Taq* DNA polymerase. In this study, probes with the quencher dye attached to an internal nucleotide were compared with probes with the quencher dye attached to the 3'-end nucleotide. In all cases, the reporter dye was attached to the 5' end. All intact probes showed quenching of the reporter fluorescence. In general, probes with the quencher dye attached to the 3'-end nucleotide exhibited a larger signal in the 5' nuclease PCR assay than the internally labeled probes. It is proposed that the larger signal is caused by increased likelihood of cleavage by *Taq* DNA polymerase when the probe is hybridized to a template strand during PCR. Probes with the quencher dye attached to the 3'-end nucleotide also exhibited an increase in reporter fluorescence intensity when hybridized to a complementary strand. Thus, oligonucleotides with reporter and quencher dyes attached at opposite ends can be used as homogeneous hybridization probes.

A homogeneous assay for detecting the accumulation of specific PCR product that uses a double-labeled fluorogenic probe was described by Lee et al.⁽¹⁾ The assay exploits the 5'→3' nucleolytic activity of *Taq* DNA polymerase^(2,3) and is diagramed in Figure 1. The fluorogenic probe consists of an oligonucleotide with a reporter fluorescent dye, such as a fluorescein, attached to the 5' end; and a quencher dye, such as a rhodamine, attached internally. When the fluorescein is excited by irradiation, its fluorescent emission will be quenched if the rhodamine is close enough to be excited through the process of fluorescence energy transfer (FET).^(4,5) During PCR, if the probe is hybridized to a template strand, *Taq* DNA polymerase will cleave the probe because of its inherent 5'→3' nucleolytic activity. If the cleavage occurs between the fluorescein and rhodamine dyes, it causes an increase in fluorescein fluorescence intensity because the fluorescein is no longer quenched. The increase in fluorescein fluorescence intensity indicates that the probe-specific PCR product has been generated. Thus, FET between a reporter dye and a quencher dye is critical to the performance of the probe in the 5' nuclease PCR assay.

Quenching is completely dependent on the physical proximity of the two dyes.⁽⁶⁾ Because of this, it has been assumed that the quencher dye must be attached near the 5' end. Surprisingly, we have found that attaching a rhodamine dye at the 3' end of a probe still provides adequate quenching for the probe to perform in the 5' nuclease

PCR assay. Furthermore, cleavage of this type of probe is not required to achieve some reduction in quenching. Oligonucleotides with a reporter dye on the 5' end and a quencher dye on the 3' end exhibit a much higher reporter fluorescence when double-stranded as compared with single-stranded. This should make it possible to use this type of double-labeled probe for homogeneous detection of nucleic acid hybridization.

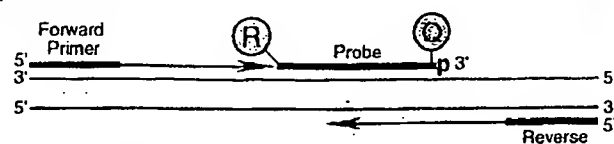
MATERIALS AND METHODS

Oligonucleotides

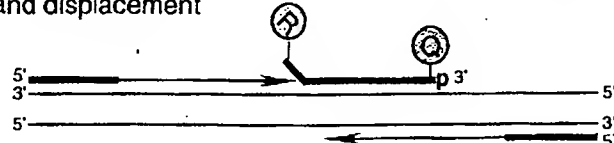
Table 1 shows the nucleotide sequence of the oligonucleotides used in this study. Linker arm nucleotide (LAN) phosphoramidite was obtained from Glen Research. The standard DNA phosphoramidites, 6-carboxyfluorescein (6-FAM) phosphoramidite, 6-carboxytetramethylrhodamine succinimidyl ester (TAMRA NHS ester), and Phosphalink for attaching a 3'-blocking phosphate, were obtained from Perkin-Elmer, Applied Biosystems Division. Oligonucleotide synthesis was performed using an ABI model 394 DNA synthesizer (Applied Biosystems). Primer and complement oligonucleotides were purified using Oligo Purification Cartridges (Applied Biosystems). Double-labeled probes were synthesized with 6-FAM-labeled phosphoramidite at the 5' end, LAN replacing one of the T's in the sequence, and Phosphalink at the 3' end. Following deprotection and ethanol precipitation, TAMRA NHS ester was coupled to the LAN-containing oligonucleotide in 250

Research

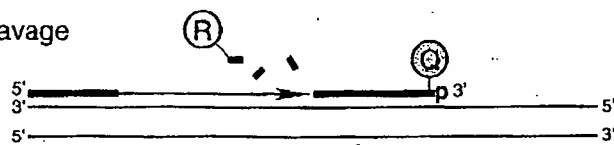
Polymerization



Strand displacement



Cleavage



Polymerization completed

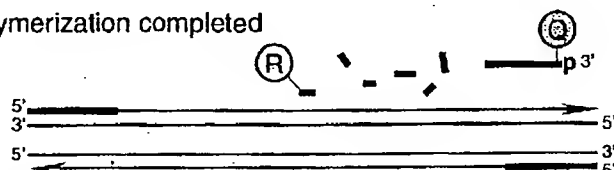


FIGURE 1 Diagram of 5' nuclease assay. Stepwise representation of the 5' → 3' nucleolytic activity of *Taq* DNA polymerase acting on a fluorogenic probe during one extension phase of PCR.

mm Na-bicarbonate buffer (pH 9.0) at room temperature. Unreacted dye was removed by passage over a PD-10 Sephadex column. Finally, the double-labeled probe was purified by preparative high-performance liquid chromatography (HPLC) using an Aquapore C₈ 220×4.6-mm column with 7-μm particle size. The column was developed with a 24-min linear gradient of 8–20% acetonitrile in 0.1 M TEAA (triethylamine acetate). Probes are named by designating the sequence from Table 1 and the position of the LAN-TAMRA moiety. For example, probe A1-7 has sequence A1 with LAN-TAMRA at nucleotide position 7 from the 5' end.

PCR Systems

All PCR amplifications were performed in the Perkin-Elmer GeneAmp PCR System 9600 using 50-μl reactions that contained 10 mM Tris-HCl (pH 8.3), 50 mM KCl, 200 μM dATP, 200 μM dCTP, 200 μM dGTP, 400 μM dUTP, 0.5 unit of AmpErase uracil N-glycosylase (Perkin-Elmer), and 1.25 unit of AmpliTaq DNA polymerase (Perkin-Elmer). A 295-bp segment from exon 3 of the human β-actin

gene (nucleotides 2141–2435 in the sequence of Nakajima-Iijima et al.⁽⁷⁾) was amplified using primers AFP and ARP (Table 1), which are modified slightly from those of du Breuil et al.⁽⁸⁾ Actin amplification reactions contained 4 mM MgCl₂, 20 ng of human genomic DNA, 50 nM A1 or A3 probe, and 300 nM each

primer. The thermal regimen was 50°C (2 min), 95°C (10 min), 40 cycles of 95°C (20 sec), 60°C (1 min), and hold at 72°C. A 515-bp segment was amplified from a plasmid that consists of a segment of λ DNA (nucleotides 32,220–32,747) inserted in the *Sma*I site of vector pUC119. These reactions contained 3.5 mM MgCl₂, 1 ng of plasmid DNA, 50 nM P2 or P5 probe, 200 nM primer F119, and 200 nM primer R119. The thermal regimen was 50°C (2 min), 95°C (10 min), 25 cycles of 95°C (20 sec), 57°C (1 min), and hold at 72°C.

Fluorescence Detection

For each amplification reaction, a 40-μl aliquot of a sample was transferred to an individual well of a white, 96-well microtiter plate (Perkin-Elmer). Fluorescence was measured on the Perkin-Elmer TaqMan LS-50B System, which consists of a luminescence spectrometer with plate reader assembly, a 485-nm excitation filter, and a 515-nm emission filter. Excitation was at 488 nm using a 5-nm slit width. Emission was measured at 518 nm for 6-FAM (the reporter or R value) and 582 nm for TAMRA (the quencher or Q value) using a 10-nm slit width. To determine the increase in reporter emission that is caused by cleavage of the probe during PCR, three normalizations are applied to the raw emission data. First, emission intensity of a buffer blank is subtracted for each wavelength. Second, emission intensity of the reporter is

TABLE 1 Sequences of Oligonucleotides

Name	Type	Sequence
F119	primer	ACCCACAGGAAGTATGATCACCACCTC
R119	primer	ATGTCGCGTTCCGGCTGACGTTCTGC
P2	probe	TCGCATTACTGATCGTTGCCAACCAGTp
P2C	complement	GTACTGGTTGGCAACGATCAGTAATGCGATG
P5	probe	CGGATTTCGTTGGTATCTATGACAAGGATp
P5C	complement	TTCATCCTTGTCTATAGATACCAGCAAATCCG
AFP	primer	TCACCCACACTGTGCCCATCTACGA
ARP	primer	CAGCGGAACCGTCATTGCCAATGG
A1	probe	ATGCCCTCCCCCATGCCATCCTGCGTp
A1C	complement	AGACGCAGGATGGCATGGGGAGGGCATACT
A3	probe	CGCCCTGGACTTCGAGCAAGAGATp
A3C	complement	CCATCTCTTGCTCGAAGTCCAGGGCGAC

For each oligonucleotide used in this study, the nucleic acid sequence is given, written in the 5' → 3' direction. There are three types of oligonucleotides: PCR primer, fluorogenic probe used in the 5' nuclease assay, and complement used to hybridize to the corresponding probe. For the probes, the underlined base indicates a position where LAN with TAMRA attached was substituted for a T. (p) The presence of a 3' phosphate on each probe.

A1-2 RAQGCCCTCCCCATGCCATCCTGGGTp
 A1-7 RATGCCCQCCCCATGCCATCCTGGGTp
 A1-14 RATGCCCTCCCCCAQGCCATCCTGGGTp
 A1-19 RATGCCCTCCCCATGCCAQCCTGGGTp
 A1-22 RATGCCCTCCCCATGCCATCCQGGGTp
 A1-26 RATGCCCTCCCCATGCCATCCTGGGQp

Probe	518 nm		582 nm		RQ ⁻	RQ ⁺	ΔRQ
	no temp.	+ temp.	no temp.	+ temp.			
A1-2	25.5 ± 2.1	32.7 ± 1.9	38.2 ± 3.0	38.2 ± 2.0	0.67 ± 0.01	0.86 ± 0.06	0.19 ± 0.06
A1-7	53.5 ± 4.3	395.1 ± 21.4	108.5 ± 6.3	110.3 ± 5.3	0.49 ± 0.03	3.58 ± 0.17	3.09 ± 0.18
A1-14	127.0 ± 4.8	403.5 ± 19.1	109.7 ± 5.3	93.1 ± 6.3	1.16 ± 0.02	4.34 ± 0.15	3.18 ± 0.15
A1-19	187.5 ± 17.9	422.7 ± 7.7	70.3 ± 7.4	73.0 ± 2.8	2.67 ± 0.05	5.80 ± 0.15	3.13 ± 0.16
A1-22	224.6 ± 9.4	482.2 ± 43.6	100.0 ± 4.0	96.2 ± 9.6	2.25 ± 0.03	5.02 ± 0.11	2.77 ± 0.12
A1-26	160.2 ± 8.9	454.1 ± 18.4	93.1 ± 5.4	90.7 ± 3.2	1.72 ± 0.02	5.01 ± 0.08	3.29 ± 0.08

FIGURE 2 Results of 5' nuclease assay comparing β-actin probes with TAMRA at different nucleotide positions. As described in Materials and Methods, PCR amplifications containing the indicated probes were performed, and the fluorescence emission was measured at 518 and 582 nm. Reported values are the average ± 1 S.D. for six reactions run without added template (no temp.) and six reactions run with template (+ temp.). The RQ ratio was calculated for each individual reaction and averaged to give the reported RQ⁻ and RQ⁺ values.

divided by the emission intensity of the quencher to give an RQ ratio for each reaction tube. This normalizes for well-to-well variations in probe concentration and fluorescence measurement. Finally, ΔRQ is calculated by subtracting the RQ value of the no-template control (RQ⁻) from the RQ value for the complete reaction including template (RQ⁺).

RESULTS

A series of probes with increasing distances between the fluorescein reporter and rhodamine quencher were tested to investigate the minimum and maximum spacing that would give an acceptable performance in the 5' nuclease PCR assay. These probes hybridize to a target

sequence in the human β-actin gene. Figure 2 shows the results of an experiment in which these probes were included in PCR that amplified a segment of the β-actin gene containing the target sequence. Performance in the 5' nuclease PCR assay is monitored by the magnitude of ΔRQ, which is a measure of the increase in reporter fluorescence caused by PCR amplification of the probe target. Probe A1-2 has a ΔRQ value that is close to zero, indicating that the probe was not cleaved appreciably during the amplification reaction. This suggests that with the quencher dye on the second nucleotide from the 5' end, there is insufficient room for Taq polymerase to cleave efficiently between the reporter and quencher. The other five probes exhibited comparable ΔRQ values that are

clearly different from zero. Thus, all five probes are being cleaved during PCR amplification resulting in a similar increase in reporter fluorescence. It should be noted that complete digestion of a probe produces a much larger increase in reporter fluorescence than that observed in Figure 2 (data not shown). Thus, even in reactions where amplification occurs, the majority of probe molecules remain uncleaved. It is mainly for this reason that the fluorescence intensity of the quencher dye TAMRA changes little with amplification of the target. This is what allows us to use the 582-nm fluorescence reading as a normalization factor.

The magnitude of RQ⁻ depends mainly on the quenching efficiency inherent in the specific structure of the probe and the purity of the oligonucleotide. Thus, the larger RQ⁻ values indicate that probes A1-14, A1-19, A1-22, and A1-26 probably have reduced quenching as compared with A1-7. Still, the degree of quenching is sufficient to detect a highly significant increase in reporter fluorescence when each of these probes is cleaved during PCR.

To further investigate the ability of TAMRA on the 3' end to quench 6-FAM on the 5' end, three additional pairs of probes were tested in the 5' nuclease PCR assay. For each pair, one probe has TAMRA attached to an internal nucleotide and the other has TAMRA attached to the 3' end nucleotide. The results are shown in Table 2. For all three sets, the probe with the 3' quencher exhibits a ΔRQ value that is considerably higher than for the probe with the internal quencher. The RQ⁻ values suggest that differences in quenching are not as great as those observed with some of the A1 probes. These results demonstrate that a quencher dye on the 3' end of an oligonucleotide can quench efficiently the

TABLE 2 Results of 5' Nuclease Assay Comparing Probes with TAMRA Attached to an Internal or 3'-terminal Nucleotide

Probe	518 nm		582 nm		RQ ⁻	RQ ⁺	ΔRQ
	no temp.	+ temp.	no temp.	+ temp.			
A3-6	54.6 ± 3.2	84.8 ± 3.7	116.2 ± 6.4	115.6 ± 2.5	0.47 ± 0.02	0.73 ± 0.03	0.26 ± 0.04
A3-24	72.1 ± 2.9	236.5 ± 11.1	84.2 ± 4.0	90.2 ± 3.8	0.86 ± 0.02	2.62 ± 0.05	1.76 ± 0.05
P2-7	82.8 ± 4.4	384.0 ± 34.1	105.1 ± 6.4	120.4 ± 10.2	0.79 ± 0.02	3.19 ± 0.16	2.40 ± 0.16
P2-27	113.4 ± 6.6	555.4 ± 14.1	140.7 ± 8.5	118.7 ± 4.8	0.81 ± 0.01	4.68 ± 0.10	3.88 ± 0.10
P5-10	77.5 ± 6.5	244.4 ± 15.9	86.7 ± 4.3	95.8 ± 6.7	0.89 ± 0.05	2.55 ± 0.06	1.66 ± 0.08
P5-28	64.0 ± 5.2	333.6 ± 12.1	100.6 ± 6.1	94.7 ± 6.3	0.63 ± 0.02	3.53 ± 0.12	2.89 ± 0.13

Reactions containing the indicated probes and calculations were performed as described in Material and Methods and in the legend to Fig. 2.

Research

fluorescence of a reporter dye on the 5' end. The degree of quenching is sufficient for this type of oligonucleotide to be used as a probe in the 5' nuclease PCR assay.

To test the hypothesis that quenching by a 3' TAMRA depends on the flexibility of the oligonucleotide, fluorescence was measured for probes in the single-stranded and double-stranded states. Table 3 reports the fluorescence observed at 518 and 582 nm. The relative degree of quenching is assessed by calculating the RQ ratio. For probes with TAMRA 6–10 nucleotides from the 5' end, there is little difference in the RQ values when comparing single-stranded with double-stranded oligonucleotides. The results for probes with TAMRA at the 3' end are much different. For these probes, hybridization to a complementary strand causes a dramatic increase in RQ. We propose that this loss of quenching is caused by the rigid structure of double-stranded DNA, which prevents the 5' and 3' ends from being in proximity.

When TAMRA is placed toward the 3' end, there is a marked Mg^{2+} effect on quenching. Figure 3 shows a plot of observed RQ values for the A1 series of probes as a function of Mg^{2+} concentration. With TAMRA attached near the 5' end (probe A1-2 or A1-7), the RQ value at 0 mM Mg^{2+} is only slightly higher than RQ at 10 mM Mg^{2+} . For probes A1-19, A1-22, and A1-26, the RQ values at 0 mM Mg^{2+} are very high, indicating a much

reduced quenching efficiency. For each of these probes, there is a marked decrease in RQ at 1 mM Mg^{2+} followed by a gradual decline as the Mg^{2+} concentration increases to 10 mM. Probe A1-14 shows an intermediate RQ value at 0 mM Mg^{2+} with a gradual decline at higher Mg^{2+} concentrations. In a low-salt environment with no Mg^{2+} present, a single-stranded oligonucleotide would be expected to adopt an extended conformation because of electrostatic repulsion. The binding of Mg^{2+} ions acts to shield the negative charge of the phosphate backbone so that the oligonucleotide can adopt conformations where the 3' end is close to the 5' end. Therefore, the observed Mg^{2+} effects support the notion that quenching of a 5' reporter dye by TAMRA at or near the 3' end depends on the flexibility of the oligonucleotide.

DISCUSSION

The striking finding of this study is that it seems the rhodamine dye TAMRA, placed at any position in an oligonucleotide, can quench the fluorescent emission of a fluorescein (6-FAM) placed at the 5' end. This implies that a single-stranded, double-labeled oligonucleotide must be able to adopt conformations where the TAMRA is close to the 5' end. It should be noted that the decay of 6-FAM in the excited state requires a certain amount of time. Therefore, what

matters for quenching is not the average distance between 6-FAM and TAMRA but, rather, how close TAMRA can get to 6-FAM during the lifetime of the 6-FAM excited state. As long as the decay time of the excited state is relatively long compared with the molecular motions of the oligonucleotide, quenching can occur. Thus, we propose that TAMRA at the 3' end, or any other position, can quench 6-FAM at the 5' end because TAMRA is in proximity to 6-FAM often enough to be able to accept energy transfer from an excited 6-FAM.

Details of the fluorescence measurements remain puzzling. For example, Table 3 shows that hybridization of probes A1-26, A3-24, and P5-28 to their complementary strands not only causes a large increase in 6-FAM fluorescence at 518 nm but also causes a modest increase in TAMRA fluorescence at 582 nm. If TAMRA is being excited by energy transfer from quenched 6-FAM, then loss of quenching attributable to hybridization should cause a decrease in the fluorescence emission of TAMRA. The fact that the fluorescence emission of TAMRA increases indicates that the situation is more complex. For example, we have anecdotal evidence that the bases of the oligonucleotide, especially G, quench the fluorescence of both 6-FAM and TAMRA to some degree. When double-stranded, base-pairing may reduce the ability of the bases to quench. The primary factor causing the quenching of 6-FAM in an intact probe is the TAMRA dye. Evidence for the importance of TAMRA is that 6-FAM fluorescence remains relatively unchanged when probes labeled only with 6-FAM are used in the 5' nuclease PCR assay (data not shown). Secondary effectors of fluorescence, both before and after cleavage of the probe, need to be explored further.

Regardless of the physical mechanism, the relative independence of position and quenching greatly simplifies the design of probes for the 5' nuclease PCR assay. There are three main factors that determine the performance of a double-labeled fluorescent probe in the 5' nuclease PCR assay. The first factor is the degree of quenching observed in the intact probe. This is characterized by the value of RQ^- , which is the ratio of reporter to quencher fluorescent emissions for a no template control PCR. Influences on the value of RQ^- include the particular reporter and quencher

TABLE 3 Comparison of Fluorescence Emissions of Single-stranded and Double-stranded Fluorogenic Probes

Probe	518 nm		582 nm		RQ	
	ss	ds	ss	ds	ss	ds
A1-7	27.75	68.53	61.08	138.18	0.45	0.50
A1-26	43.31	509.38	53.50	93.86	0.81	5.43
A3-6	16.75	62.88	39.33	165.57	0.43	0.38
A3-24	30.05	578.64	67.72	140.25	0.45	3.21
P2-7	35.02	70.13	54.63	121.09	0.64	0.58
P2-27	39.89	320.47	65.10	61.13	0.61	5.25
P5-10	27.34	144.85	61.95	165.54	0.44	0.87
P5-28	33.65	462.29	72.39	104.61	0.46	4.43

(ss) Single-stranded. The fluorescence emissions at 518 or 582 nm for solutions containing a final concentration of 50 nM indicated probe, 10 mM Tris-HCl (pH 8.3), 50 mM KCl, and 10 mM $MgCl_2$. (ds) Double-stranded. The solutions contained, in addition, 100 nM A1C for probes A1-7 and A1-26, 100 nM A3C for probes A3-6 and A3-24, 100 nM P2C for probes P2-7 and P2-27, or 100 nM P5C for probes P5-10 and P5-28. Before the addition of $MgCl_2$, 120 μ l of each sample was heated at 95°C for 5 min. Following the addition of 80 μ l of 25 mM $MgCl_2$, each sample was allowed to cool to room temperature and the fluorescence emissions were measured. Reported values are the average of three determinations.

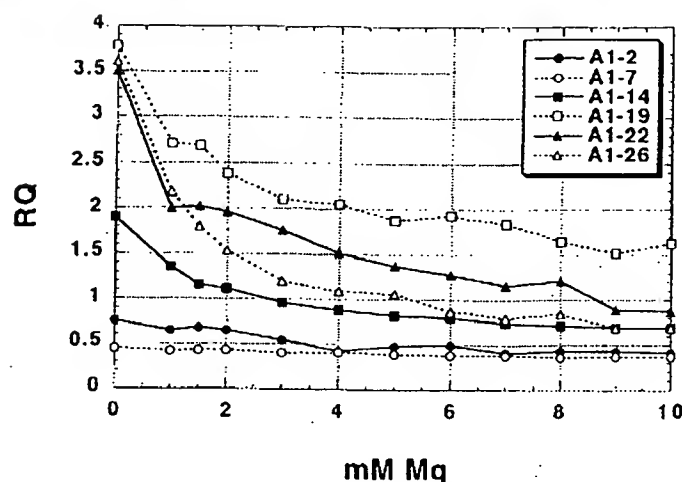


FIGURE 3 Effect of Mg^{2+} concentration on RQ ratio for the A1 series of probes. The fluorescence emission intensity at 518 and 582 nm was measured for solutions containing 50 nM probe, 10 mM Tris-HCl (pH 8.3), 50 mM KCl, and varying amounts (0–10 mM) of $MgCl_2$. The calculated RQ ratios (518 nm intensity divided by 582 nm intensity) are plotted vs. $MgCl_2$ concentration (mM Mg). The key (upper right) shows the probes examined.

dyes used, spacing between reporter and quencher dyes, nucleotide sequence context effects, presence of structure or other factors that reduce flexibility of the oligonucleotide, and purity of the probe. The second factor is the efficiency of hybridization, which depends on probe T_m , presence of secondary structure in probe or template, annealing temperature, and other reaction conditions. The third factor is the efficiency at which *Taq* DNA polymerase cleaves the bound probe between the reporter and quencher dyes. This cleavage is dependent on sequence complementarity between probe and template as shown by the observation that mismatches in the segment between reporter and quencher dyes drastically reduce the cleavage of probe.⁽¹⁾

The rise in RQ^- values for the A1 series of probes seems to indicate that the degree of quenching is reduced somewhat as the quencher is placed toward the 3' end. The lowest apparent quenching is observed for probe A1-19 (see Fig. 3) rather than for the probe where the TAMRA is at the 3' end (A1-26). This is understandable, as the conformation of the 3' end position would be expected to be less restricted than the conformation of an internal position. In effect, a quencher at the 3' end is freer to adopt conformations close to the 5' reporter dye than is an internally placed quencher. For the other three sets of

probes, the interpretation of RQ^- values is less clear-cut. The A3 probes show the same trend as A1, with the 3' TAMRA probe having a larger RQ^- than the internal TAMRA probe. For the P2 pair, both probes have about the same RQ^- value. For the P5 probes, the RQ^- for the 3' probe is less than for the internally labeled probe. Another factor that may explain some of the observed variation is that purity affects the RQ^- value. Although all probes are HPLC purified, a small amount of contamination with unquenched reporter can have a large effect on RQ^- .

Although there may be a modest effect on degree of quenching, the position of the quencher apparently can have a large effect on the efficiency of probe cleavage. The most drastic effect is observed with probe A1-2, where placement of the TAMRA on the second nucleotide reduces the efficiency of cleavage to almost zero. For the A3, P2, and P5 probes, ΔRQ is much greater for the 3' TAMRA probes as compared with the internal TAMRA probes. This is explained most easily by assuming that probes with TAMRA at the 3' end are more likely to be cleaved between reporter and quencher than are probes with TAMRA attached internally. For the A1 probes, the cleavage efficiency of probe A1-7 must already be quite high, as ΔRQ does not increase when the quencher is placed closer to the 3' end. This illus-

trates the importance of being able to use probes with a quencher on the 3' end in the 5' nuclease PCR assay. In this assay, an increase in the intensity of reporter fluorescence is observed only when the probe is cleaved between the reporter and quencher dyes. By placing the reporter and quencher dyes on the opposite ends of an oligonucleotide probe, any cleavage that occurs will be detected. When the quencher is attached to an internal nucleotide, sometimes the probe works well (A1-7) and other times not so well (A3-6). The relatively poor performance of probe A3-6 presumably means the probe is being cleaved 3' to the quencher rather than between the reporter and quencher. Therefore, the best chance of having a probe that reliably detects accumulation of PCR product in the 5' nuclease PCR assay is to use a probe with the reporter and quencher dyes on opposite ends.

Placing the quencher dye on the 3' end may also provide a slight benefit in terms of hybridization efficiency. The presence of a quencher attached to an internal nucleotide might be expected to disrupt base-pairing and reduce the T_m of a probe. In fact, a 2°C–3°C reduction in T_m has been observed for two probes with internally attached TAMRAs.⁽⁹⁾ This disruptive effect would be minimized by placing the quencher at the 3' end. Thus, probes with 3' quenchers might exhibit slightly higher hybridization efficiencies than probes with internal quenchers.

The combination of increased cleavage and hybridization efficiencies means that probes with 3' quenchers probably will be more tolerant of mismatches between probe and target as compared with internally labeled probes. This tolerance of mismatches can be advantageous, as when trying to use a single probe to detect PCR-amplified products from samples of different species. Also, it means that cleavage of probe during PCR is less sensitive to alterations in annealing temperature or other reaction conditions. The one application where tolerance of mismatches may be a disadvantage is for allelic discrimination. Lee et al.⁽¹¹⁾ demonstrated that allele-specific probes were cleaved between reporter and quencher only when hybridized to a perfectly complementary target. This allowed them to distinguish the normal human cystic fibrosis allele from the $\Delta F508$ mutant. Their probes had TAMRA attached to the seventh nucleotide from

Research

the 5' end and were designed so that any mismatches were between the reporter and quencher. Increasing the distance between reporter and quencher would lessen the disruptive effect of mismatches and allow cleavage of the probe on the incorrect target. Thus, probes with a quencher attached to an internal nucleotide may still be useful for allelic discrimination.

In this study loss of quenching upon hybridization was used to show that quenching by a 3' TAMRA is dependent on the flexibility of a single-stranded oligonucleotide. The increase in reporter fluorescence intensity, though, could also be used to determine whether hybridization has occurred or not. Thus, oligonucleotides with reporter and quencher dyes attached at opposite ends should also be useful as hybridization probes. The ability to detect hybridization in real time means that these probes could be used to measure hybridization kinetics. Also, this type of probe could be used to develop homogeneous hybridization assays for diagnostics or other applications. Bagwell et al.⁽¹⁰⁾ describe just this type of homogeneous assay where hybridization of a probe causes an increase in fluorescence caused by a loss of quenching. However, they utilized a complex probe design that requires adding nucleotides to both ends of the probe sequence to form two imperfect hairpins. The results presented here demonstrate that the simple addition of a reporter dye to one end of an oligonucleotide and a quencher dye to the other end generates a fluorogenic probe that can detect hybridization or PCR amplification.

ACKNOWLEDGMENTS

We acknowledge Lincoln McBride of Perkin-Elmer for his support and encouragement on this project and Mitch Winnik of the University of Toronto for helpful discussions on time-resolved fluorescence.

REFERENCES

1. Lee, L.G., C.R. Connell, and W. Bloch. 1993. Allelic discrimination by nick-translation PCR with fluorogenic probes. *Nucleic Acids Res.* **21**: 3761-3766.
2. Holland, P.M., R.D. Abramson, R. Watson, and D.H. Gelfand. 1991. Detection of specific polymerase chain reaction prod-

uct by utilizing the 5' to 3' exonuclease activity of *Thermus aquaticus* DNA polymerase. *Proc. Natl. Acad. Sci.* **88**: 7276-7280.

3. Lyamichev, V., M.A.D. Brow, and J.E. Dahlberg. 1993. Structure-specific endonucleolytic cleavage of nucleic acids by eubacterial DNA polymerases. *Science* **260**: 778-783.
4. Förster, V.Th. 1948. Zwischenmolekulare Energiewanderung und Fluoreszenz. *Ann. Phys. (Leipzig)* **2**: 55-75.
5. Lakowicz, J.R. 1983. Energy transfer. In *Principles of fluorescent spectroscopy*, pp. 303-339. Plenum Press, New York, NY.
6. Stryer, L. and R.P. Haugland. 1967. Energy transfer: A spectroscopic ruler. *Proc. Natl. Acad. Sci.* **58**: 719-726.
7. Nakajima-Iijima, S., H. Hamada, P. Reddy, and T. Kakunaga. 1985. Molecular structure of the human cytoplasmic beta-actin gene: Inter-species homology of sequences in the introns. *Proc. Natl. Acad. Sci.* **82**: 6133-6137.
8. du Breuil, R.M., J.M. Patel, and B.V. Mendelow. 1993. Quantitation of β -actin-specific mRNA transcripts using xeno-competitive PCR. *PCR Methods Applic.* **3**: 57-59.
9. Livak, K.J. (unpubl.).
10. Bagwell, C.B., M.E. Munson, R.L. Christensen, and E.J. Lovett. 1994. A new homogeneous assay system for specific nucleic acid sequences: Poly-dA and poly-A detection. *Nucleic Acids Res.* **22**: 2424-2425.

Received December 20, 1994; accepted in revised form March 6, 1995.

THIS MATERIAL MAY BE PROTECTED
BY COPYRIGHT LAW (17 U.S. CODE)

GENOMIC METHODS

Real Time Quantitative PCR

Christian A. Heid,¹ Junko Stevens,² Kenneth J. Livak,² and
P. Mickey Williams^{1,3}

¹BioAnalytical Technology Department, Genentech, Inc., South San Francisco, California 94080;

²Applied BioSystems Division of Perkin Elmer Corp., Foster City, California 94404

We have developed a novel "real time" quantitative PCR method. The method measures PCR product accumulation through a dual-labeled fluorogenic probe (i.e., TaqMan Probe). This method provides very accurate and reproducible quantitation of gene copies. Unlike other quantitative PCR methods, real-time PCR does not require post-PCR sample handling, preventing potential PCR product carry-over contamination and resulting in much faster and higher throughput assays. The real-time PCR method has a very large dynamic range of starting target molecule determination (at least five orders of magnitude). Real-time quantitative PCR is extremely accurate and less-labor-intensive than current quantitative PCR methods.

Quantitative nucleic acid sequence analysis has had an important role in many fields of biological research. Measurement of gene expression (RNA) has been used extensively in monitoring biological responses to various stimuli (Tan et al. 1994; Huang et al. 1995a,b; Prud'homme et al. 1995). Quantitative gene analysis (DNA) has been used to determine the genomic quantity of a particular gene, as in the case of the human *HER2* gene, which is amplified in ~30% of breast tumors (Slamon et al. 1987). Gene and genome quantitation (DNA and RNA) also have been used for analysis of human immunodeficiency virus (HIV) burden demonstrating changes in the levels of virus throughout the different phases of the disease (Connor et al. 1993; Platak et al. 1993b; Furtado et al. 1995).

Many methods have been described for the quantitative analysis of nucleic acid sequences (both for RNA and DNA; Southern 1975; Sharp et al. 1980; Thomas 1980). Recently, PCR has proven to be a powerful tool for quantitative nucleic acid analysis. PCR and reverse transcriptase (RT)-PCR have permitted the analysis of minimal starting quantities of nucleic acid (as little as one cell equivalent). This has made possible many experiments that could not have been performed with traditional methods. Although PCR has provided a powerful tool, it is imperative

that it be used properly for quantitation (Ragymaekers 1995). Many early reports of quantitative PCR and RT-PCR described quantitation of the PCR product but did not measure the initial target sequence quantity. It is essential to design proper controls for the quantitation of the initial target sequences (Pierre 1992; Clementi et al. 1993).

Researchers have developed several methods of quantitative PCR and RT-PCR. One approach measures PCR product quantity in the log phase of the reaction before the plateau (Kellogg et al. 1990; Pang et al. 1990). This method requires that each sample has equal input amounts of nucleic acid and that each sample under analysis amplifies with identical efficiency up to the point of quantitative analysis. A gene sequence (contained in all samples at relatively constant quantities, such as β -actin) can be used for sample amplification efficiency normalization. Using conventional methods of PCR detection and quantitation (gel electrophoresis or plate capture hybridization), it is extremely laborious to assure that all samples are analyzed during the log phase of the reaction (for both the target gene and the normalization gene). Another method, quantitative competitive (QC)-PCR, has been developed and is used widely for PCR quantitation. QC-PCR relies on the inclusion of an internal control competitor in each reaction (Becker-Andre 1991; Platak et al. 1993a,b). The efficiency of each reaction is normalized to the internal competitor. A known amount of internal competitor can be

³Corresponding author.

REAL TIME QUANTITATIVE PCR

RESULTS

PCR Product Detection in Real Time

added to each sample. To obtain relative quantitation, the unknown target PCR product is compared with the known competitor PCR product. Success of a quantitative competitive PCR assay relies on developing an internal control that amplifies with the same efficiency as the target molecule. The design of the competitor and the validation of amplification efficiencies require a dedicated effort. However, because QC-PCR does not require that PCR products be analyzed during the log phase of the amplification, it is the easier of the two methods to use.

Several detection systems are used for quantitative PCR and RT-PCR analysis: (1) agarose gels, (2) fluorescent labeling of PCR products and detection with laser-induced fluorescence using capillary electrophoresis (Fusco et al. 1995; Williams et al. 1996) or acrylamide gels, and (3) plate capture and sandwich probe hybridization (Mulder et al. 1994). Although these methods proved successful, each method requires post-PCR manipulations that add time to the analysis and may lead to laboratory contamination. The sample throughput of these methods is limited (with the exception of the plate capture approach), and, therefore, these methods are not well suited for uses demanding high sample throughput (i.e., screening of large numbers of biomolecules or analyzing samples for diagnostics or clinical trials).

Here we report the development of a novel assay for quantitative DNA analysis. The assay is based on the use of the 5' nuclease assay first described by Holland et al. (1991). The method uses the 5' nuclease activity of *Taq* polymerase to cleave a nonextendible hybridization probe during the extension phase of PCR. The approach uses dual-labeled fluorogenic hybridization probes (Lee et al. 1993; Bassler et al. 1995; Livak et al. 1995a,b). One fluorescent dye serves as a reporter (FAM (i.e., 6-carboxyfluorescein)) and its emission spectra is quenched by the second fluorescent dye, TAMRA (i.e., 6-carboxy-tetramethylrhodamine). The nuclease degradation of the hybridization probe releases the quenching of the FAM fluorescent emission, resulting in an increase in peak fluorescent emission at 518 nm. The use of a sequence detector (ABI Prism) allows measurement of fluorescent spectra of all 96 wells of the thermal cycler continuously during the PCR amplification. Therefore, the reactions are monitored in real time. The output data is described and quantitative analysis of input target DNA sequences is discussed below.

The goal was to develop a high-throughput, sensitive, and accurate gene quantitation assay for use in monitoring lipid mediated therapeutic gene delivery. A plasmid encoding human factor VIII gene sequence, pF8TM (see Methods), was used as a model therapeutic gene. The assay uses fluorescent Taqman methodology and an instrument capable of measuring fluorescence in real time (ABI Prism 7700 Sequence Detector). The Taqman reaction requires a hybridization probe labeled with two different fluorescent dyes. One dye is a reporter dye (FAM), the other is a quenching dye (TAMRA). When the probe is intact, fluorescent energy transfer occurs and the reporter dye fluorescent emission is absorbed by the quenching dye (TAMRA). During the extension phase of the PCR cycle, the fluorescent hybridization probe is cleaved by the 5'-3' nucleolytic activity of the DNA polymerase. On cleavage of the probe, the reporter dye emission is no longer transferred efficiently to the quenching dye, resulting in an increase of the reporter dye fluorescent emission spectra. PCR primers and probes were designed for the human factor VIII sequence and human β -actin gene (as described in Methods). Optimization reactions were performed to choose the appropriate probe and magnesium concentrations yielding the highest intensity of reporter fluorescent signal without sacrificing specificity. The instrument uses a charge-coupled device (i.e., CCD camera) for measuring the fluorescent emission spectra from 500 to 650 nm. Each PCR tube was monitored sequentially for 25 msec with continuous monitoring throughout the amplification. Each tube was re-examined every 8.5 sec. Computer software was designed to examine the fluorescent intensity of both the reporter dye (FAM) and the quenching dye (TAMRA). The fluorescent intensity of the quenching dye, TAMRA, changes very little over the course of the PCR amplification (data not shown). Therefore, the intensity of TAMRA dye emission serves as an internal standard with which to normalize the reporter dye (FAM) emission variations. The software calculates a value termed ΔR_n (or $\Delta R_{(2)}$) using the following equation: $\Delta R_n = (R_n^i) / (R_n^j)$, where R_n^i = emission intensity of reporter/emission intensity of quencher at any given time in a reaction tube, and R_n^j = emission intensity of re-

HUI ET AL

porter/emission intensity of quencher measured prior to PCR amplification in that same reaction tube. For the purpose of quantitation, the last three data points (ΔRn s) collected during the extension step for each PCR cycle were analyzed. The nucleolytic degradation of the hybridization probe occurs during the extension phase of PCR; and, therefore, reporter fluorescent emission increases during this time. The three data points were averaged for each PCR cycle and the mean value for each was plotted in an "amplification plot" shown in Figure 1A. The ΔRn mean value is plotted on the y-axis, and time, represented by cycle number, is plotted on the x-axis. During the early cycles of the PCR amplification, the ΔRn

value remains at base line. When sufficient hybridization probe has been cleaved by the *Taq* polymerase nuclease activity, the intensity of reporter fluorescent emission increases. Most PCR amplifications reach a plateau phase of reporter fluorescent emission if the reaction is carried out to high cycle numbers. The amplification plot is examined early in the reaction, at a point that represents the log phase of product accumulation. This is done by assigning an arbitrary threshold that is based on the variability of the base-line data. In Figure 1A, the threshold was set at 10 standard deviations above the mean of base line emission calculated from cycles 1 to 15. Once the threshold is chosen, the point at which

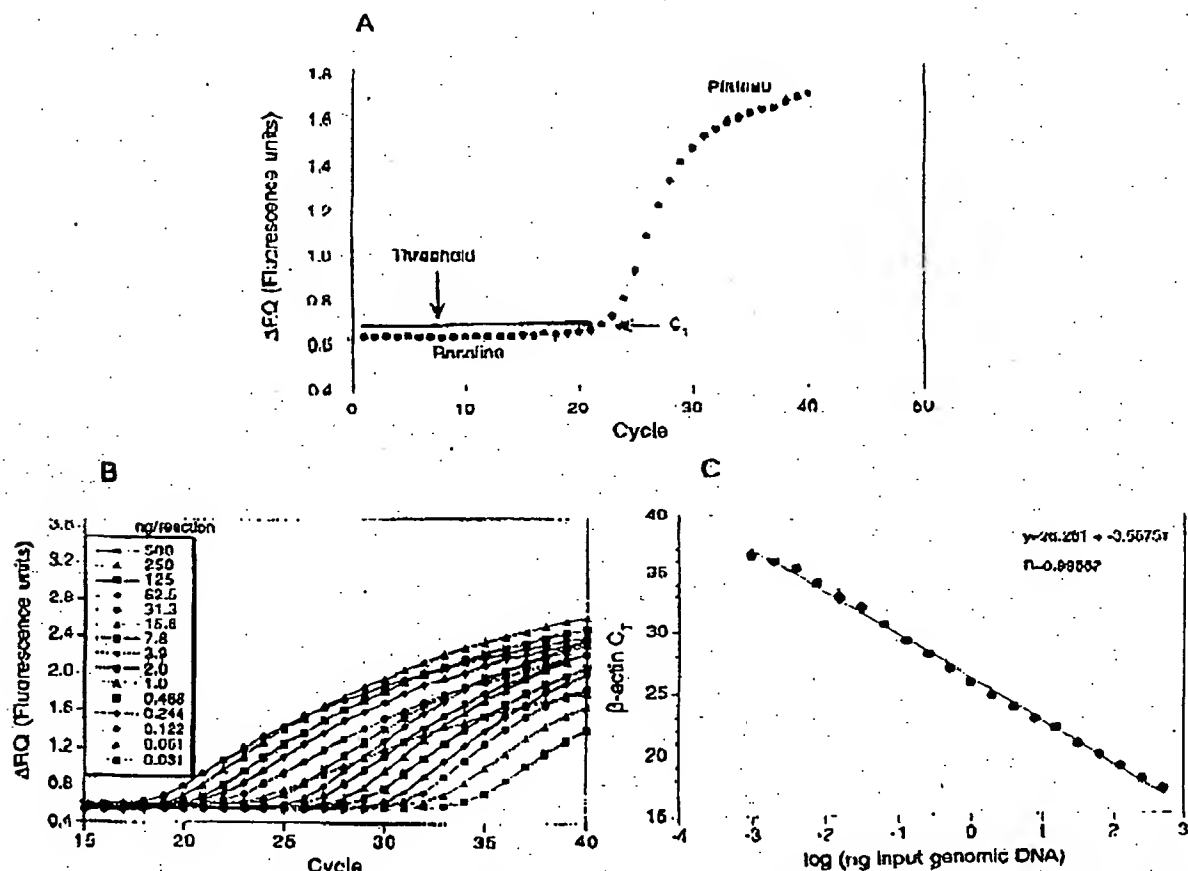


Figure 1 PCR product detection in real time. (A) The Model 7700 software will construct amplification plots from the extension phase fluorescent emission data collected during the PCR amplification. The standard deviation is determined from the data points collected from the base line of the amplification plot. C_T values are calculated by determining the point at which the fluorescence exceeds a threshold limit (usually 10 times the standard deviation of the base line). (B) Overlay of amplification plots of serially (1:2) diluted human genomic DNA samples amplified with β -actin primers. (C) Input DNA concentration of the samples plotted versus C_T . All

REAL TIME QUANTITATIVE PCR

the amplification plot crosses the threshold is defined as C_T . C_T is reported as the cycle number at this point. As will be demonstrated, the C_T value is predictive of the quantity of input target.

C_T Values Provide a Quantitative Measurement of Input Target Sequences

Figure 1B shows amplification plots of 15 different PCR amplifications overlaid. The amplifications were performed on a 1:2 serial dilution of human genomic DNA. The amplified target was human β actin. The amplification plots shift to the right (to higher threshold cycles) as the input target quantity is reduced. This is expected because reactions with fewer starting copies of the target molecule require greater amplification to degrade enough probe to attain the threshold fluorescence. An arbitrary threshold of 10 standard deviations above the base line was used to determine the C_T values. Figure 1C represents the C_T values plotted versus the sample dilution value. Each dilution was amplified in triplicate PCR amplifications and plotted as mean values with error bars representing one standard deviation. The C_T values decrease linearly with increasing target quantity. Thus, C_T values can be used as a quantitative measurement of the input target number. It should be noted that the amplification plot for the 15.6-ng sample shown in Figure 1B does not reflect the same fluorescent rate of increase exhibited by most of the other samples. The 15.6-ng sample also achieves endpoint plateau at a lower fluorescent value than would be expected based on the input DNA. This phenomenon has been observed occasionally with other samples (data not shown) and may be attributable to late cycle inhibition; this hypothesis is still under investigation. It is important to note that the flattened slope and early plateau do not impact significantly the calculated C_T value as demonstrated by the fit on the line shown in Figure 1C. All triplicate amplifications resulted in very similar C_T values—the standard deviation did not exceed 0.5 for any dilution. This experiment contains a >100,000-fold range of input target molecules. Using C_T values for quantitation permits a much larger assay range than directly using total fluorescent emission intensity for quantitation. The linear range of fluorescent intensity measurement of the ABI Prism 7700 Se-

ments over a very large range of relative starting target quantities.

Sample Preparation Validation

Several parameters influence the efficiency of PCR amplification: magnesium and salt concentrations, reaction conditions (i.e., time and temperature), PCR target size and composition, primer sequences, and sample purity. All of the above factors are common to a single PCR assay, except sample to sample purity. In an effort to validate the method of sample preparation for the factor VIII assay, PCR amplification reproducibility and efficiency of 10 replicate sample preparations were examined. After genomic DNA was prepared from the 10 replicate samples, the DNA was quantitated by ultraviolet spectroscopy. Amplifications were performed analyzing β -actin gene content in 100 and 25 ng of total genomic DNA. Each PCR amplification was performed in triplicate. Comparison of C_T values for each triplicate sample show minimal variation based on standard deviation and coefficient of variance (Table 1). Therefore, each of the triplicate PCR amplifications was highly reproducible, demonstrating that real time PCR using this instrumentation introduces minimal variation into the quantitative PCR analysis. Comparison of the mean C_T values of the 10 replicate sample preparations also showed minimal variability, indicating that each sample preparation yielded similar results for β -actin gene quantity. The highest C_T difference between any of the samples was 0.85 and 0.71 for the 100 and 25 ng samples, respectively. Additionally, the amplification of each sample exhibited an equivalent rate of fluorescent emission intensity change per amount of DNA target analyzed as indicated by similar slopes derived from the sample dilutions (Fig. 2). Any sample containing an excess of a PCR inhibitor would exhibit a greater measured β -actin C_T value for a given quantity of DNA. In addition, the inhibitor would be diluted along with the sample in the dilution analysis (Fig. 2), altering the expected C_T value change. Each sample amplification yielded a similar result in the analysis, demonstrating that this method of sample preparation is highly reproducible with regard to sample purity.

Quantitative Analysis of a Plasmid After

III ID F I AL

Table 1. Reproducibility of Sample Preparation Method

Sample no.	100 ng				25 ng			
	C _T	mean	standard deviation	CV	C _T	mean	standard deviation	CV
1	18.24 18.23 18.33	18.27	0.06	0.32	20.48 20.55 20.5	20.51	0.03	0.17
2	18.33 18.35 18.44				20.61 20.59 20.41			
3	18.3 18.3 18.42	18.37	0.06	0.32	20.54 20.6 20.49	20.54	0.11	0.54
4	18.15 18.23 18.32				20.44 20.48 20.38			
5	18.4 18.38 18.46	18.23	0.08	0.46	20.68 20.87 20.63	20.43	0.05	0.26
6	18.54 18.67 19				21.09 21.04 21.04	20.73	0.13	0.61
7	18.28 18.36 18.52	18.71	0.24	1.26	20.67 20.73 20.65			
8	18.45 18.7 18.73				20.98 20.84 20.75	20.68	0.04	0.2
9	18.18 18.34 18.36	18.63	0.16	0.83	20.46 20.54 20.48			
10	18.42 18.57 18.66				20.78 20.62 20.62	20.86	0.12	0.57
		18.29	0.1	0.55	20.48 20.79 20.78			
					20.78 20.62 20.62	20.51	0.07	0.32
Mean	(1-10)	18.42	0.17	0.90	20.66	20.73	0.1	0.16

for containing a partial cDNA for human factor VIII, pF8TM. A series of transfections was set up using a decreasing amount of the plasmid (40, 4, 0.5, and 0.1 µg). Twenty-four hours post-transfection, total DNA was purified from each flask of cells. β -Actin gene quantity was chosen as a value for normalization of genomic DNA concentration from each sample. In this experiment, β -actin gene content should remain constant relative to total genomic DNA. Figure 3 shows the result of the β -actin DNA measurement (100 ng total DNA determined by ultraviolet spectroscopy) of each sample. Each sample was analyzed in triplicate and the mean β -actin C_T values of the triplicates were plotted (error bars represent one standard deviation). The highest difference

between any two sample means was 0.95 C_T. Ten nanograms of total DNA of each sample were also examined for β -actin. The results again showed that very similar amounts of genomic DNA were present; the maximum mean β -actin C_T value difference was 1.0. As Figure 3 shows, the rate of β -actin C_T change between the 100 and 10-ng samples was similar (slope values range between 3.56 and 3.45). This verifies again that the method of sample preparation yields samples of identical PCR integrity (i.e., no sample contained an excessive amount of a PCR inhibitor). However, these results indicate that each sample contained slight differences in the actual amount of genomic DNA analyzed. Determination of actual genomic DNA concentration was accomplished

REAL TIME QUANTITATIVE PCR

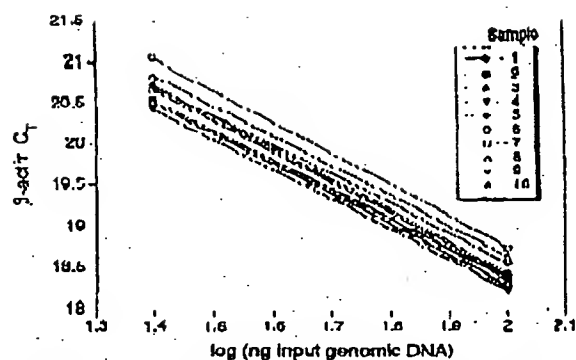


Figure 2 Sample preparation purity. The replicate samples shown in Table 7 were also amplified in triplicate using 25 ng of each DNA sample. The figure shows the input DNA concentration (100 and 25 ng) vs. C_T in the figure, the 100 and 25 ng points for each sample are connected by a line.

by plotting the mean β -actin C_T value obtained for each 100-ng sample on a β -actin standard curve (shown in Fig. 4C). The actual genomic DNA concentration of each sample, a , was obtained by extrapolation to the x-axis.

Figure 4A shows the measured (i.e., non-normalized) quantities of factor VIII plasmid DNA (pF8TM) from each of the four transient cell transfections. Each reaction contained 100 ng of total sample DNA (as determined by UV spectroscopy). Each sample was analyzed in triplicate

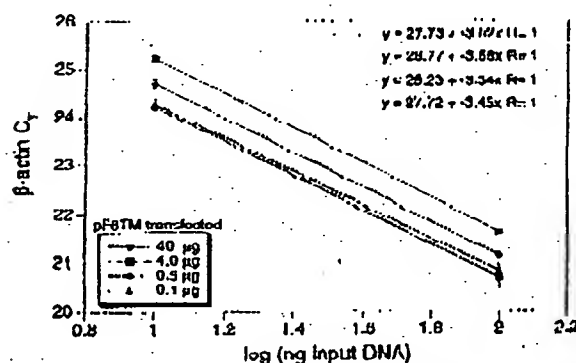


Figure 3 Analysis of transfected cell DNA quantity and purity. The DNA preparations of the four 293 cell transfections (40, 4, 0.5, and 0.1 μ g of pF8TM) were analyzed for the β -actin gene. 100 and 10 ng (determined by ultraviolet spectroscopy) of each sample were amplified in triplicate. For each amount of pF8TM that was transfected, the β -actin C_T values are plotted versus the total input DNA concentration.

PCR amplifications. As shown, pF8TM purified from the 293 cells decreases (mean C_T values increase) with decreasing amounts of plasmid transfected. The mean C_T values obtained for pF8TM in Figure 4A were plotted on a standard curve comprised of serially diluted pF8TM, shown in Figure 4B. The quantity of pF8TM, b , found in each of the four transfections was determined by extrapolation to the x-axis of the standard curve in Figure 4B. These uncorrected values, b , for pF8TM were normalized to determine the actual amount of pF8TM found per 100 ng of genomic DNA by using the equation:

$$\frac{b \times 100 \text{ ng}}{a} = \text{actual pF8TM copies per 100 ng of genomic DNA}$$

where a = actual genomic DNA in a sample and b = pF8TM copies from the standard curve. The normalized quantity of pF8TM per 100 ng of genomic DNA for each of the four transfections is shown in Figure 4D. These results show that the quantity of factor VIII plasmid associated with the 293 cells, 24 hr after transfection, decreases with decreasing plasmid concentration used in the transfection. The quantity of pF8TM associated with 293 cells, after transfection with 40 μ g of plasmid, was 35 μ g per 100 ng genomic DNA. This results in ~520 plasmid copies per cell.

DISCUSSION

We have described a new method for quantitating gene copy numbers using real-time analysis of PCR amplifications. Real-time PCR is compatible with either of the two PCR (RT-PCR) approaches: (1) quantitative competitive where an internal competitor for each target sequence is used for normalization (data not shown) or (2) quantitative comparative PCR using a normalization gene contained within the sample (i.e., β -actin) or a "housekeeping" gene for RT-PCR. If equal amounts of nucleic acid are analyzed for each sample and if the amplification efficiency before quantitative analysis is identical for each sample, the internal control (normalization gene or competitor) should give equal signals for all samples.

The real-time PCR method offers several advantages over the other two methods currently employed (see the Introduction). First, the real-time PCR method is performed in a closed-tube system and requires no post-PCR manipulation

HLID ET AL.

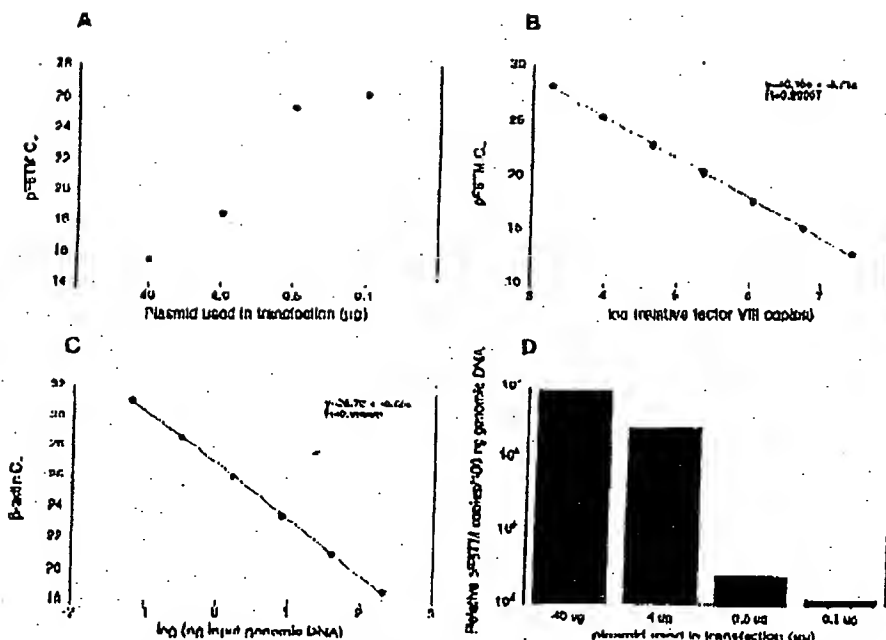


Figure 4. Quantitative analysis of pF8TM in transfected cells. (A) Amount of plasmid DNA used for the transfection plotted against the mean C_T value determined for pF8TM remaining 24 hr after transfection. (B, C) Standard curves of pF8TM and β-actin, respectively. pF8TM DNA (B) and genomic DNA (C) were diluted serially 1:5 before amplification with the appropriate primers. The β-actin standard curve was used to normalize the results of A to 100 ng of genomic DNA. (D) The amount of pF8TM present per 100 ng of genomic DNA.

of sample. Therefore, the potential for PCR contamination in the laboratory is reduced because amplified products can be analyzed and disposed of without opening the reaction tubes. Second, this method supports the use of a normalization gene (i.e., β-actin) for quantitative PCR or house-keeping genes for quantitative RT-PCR controls. Analysis is performed in real time during the log phase of product accumulation. Analysis during log phase permits many different genes (over a wide input target range) to be analyzed simultaneously, without concern of reaching reaction plateau at different cycles. This will make multi-gene analysis assays much easier to develop, because individual internal competitors will not be needed for each gene under analysis. Third, sample throughput will increase dramatically with the new method because there is no post-PCR processing time. Additionally, working in a 96-well format is highly compatible with automation technology.

The real-time PCR method is highly reproducible. Replicate amplifications can be analyzed

for each sample minimizing potential error. The system allows for a very large assay dynamic range (approaching 1,000,000-fold starting target). Using a standard curve for the target of interest, relative copy number values can be determined for any unknown sample. Fluorescent threshold values, C_T, correlate linearly with relative DNA copy numbers. Real time quantitative RT-PCR methodology (Gibson et al., this issue) has also been developed. Finally, real time quantitative PCR methodology can be used to develop high-throughput screening assays for a variety of applications [quantitative gene expression (RT-PCR), gene copy assays (Her2, ILV, etc.), genotyping (knockout mouse analysis), and immun-PCR].

Real-time PCR may also be performed using intercalating dyes (Higuchi et al. 1992) such as ethidium bromide. The fluorogenic probe method offers a major advantage over intercalating dyes—greater specificity (i.e., primer dimers and nonspecific PCR products are not detected).

METHODS

Generation of a Plasmid Containing a Partial cDNA for Human Factor VIII

Total RNA was harvested (RNAzol II from Tel Test, Inc., Friendswood, TX) from cells transfected with a factor VIII expression vector, pCIS2.8c251 (Eaton et al. 1986; Gorman et al. 1990). A factor VIII partial cDNA sequence was generated by RT-PCR (GeneAmp EZ RT/ RNA PCR Kit (part N808-0179, PE Applied Biosystems, Foster City, CA)) using the PCR primers F8for and F8rev (primer sequences are shown below). The amplicon was reamplified using modified F8for and F8rev primers (appended with *Hind*II and *Hind*III restriction site sequences at the 5' end) and cloned into pMTM-32 (Promega Corp., Madison, WI). The resulting clone, pF8TM, was used for transient transfection of 293 cells.

Amplification of Target DNA and Detection of Amplicon Factor VIII Plasmid DNA

(pF8TM) was amplified with the primers F8for 5'-CCCCGTCGCAAGAGTGAAGGTC-3' and F8rev 5'-AAACCTTCAACCTTGCATCTTACG-3'. The reaction produced a 422-bp PCR product. The forward primer was designed to recognize a unique sequence found in the 5' untranslated region of the parent pCIS2.8c251 plasmid and therefore does not recognize and amplify the human factor VIII gene. Primers were chosen with the assistance of the computer program Oligo 4.0 (National Biosciences, Inc., Plymouth, MN). The human β -actin gene was amplified with the primers β -actin forward primer 5'-TCACCCACACTCTTGCCTTACCA-3' and β -actin reverse primer 5'-CAGCGGAACCGCTTCAATGG-3'. The reaction produced a 295-bp PCR product.

Amplification reactions (50 μ l) contained a DNA sample, 10 \times PCR Buffer II (5 μ l), 200 μ M dATP, dCTP, dGTP, and 400 μ M dTTP, 4 mM MgCl₂, 1.25 Units AmpliTaq DNA polymerase, 0.5 unit Amplifase uracil *N*-glycosylase (UNG), 50 pmole of each factor VIII primer, and 15 pmole of each β -actin primer. The reactions also contained one of the following detection probes (100 nM each): F8probe 5'-(FAM)AGCTTCTCCACCTGCTTCTTCTCTTGCCTT(TAMRA)p 3' and β -actin probe 5'-(FAM)ATGCCCX(TAMRA)CCCCCATGCCATCp-3' where p indicates phosphorylation and X indicates a linker arm nucleotide. Reaction tubes were MicroAmp Optical Tubes (part number N801 0933, Perkin Elmer) that were frosted (at Perkin Elmer) to prevent light from reflecting. Tube caps were similar to MicroAmp Caps but specially designed to prevent light scattering. All of the PCR consumables were supplied by PE Applied Biosystems (Foster City, CA) except the factor VIII primers, which were synthesized at Genentech, Inc. (South San Francisco, CA). Probes were designed using the Oligo 4.0 software, following guidelines suggested in the Model 7700 Sequence Detector instrument manual. Briefly, probe *T_m* should be at least 5°C higher than the annealing temperature used during thermal cycling; primers should not form stable duplexes with the probe.

The thermal cycling conditions included 2 min at 50°C and 10 min at 95°C. Thermal cycling proceeded with

REAL TIME QUANTITATIVE PCR

reactions were performed in the Model 7700 Sequence Detector (PE Applied Biosystems), which contains a GeneAmp PCR System 9600. Reaction conditions were programmed in a Power Macintosh 7100 (Apple Computer, Santa Clara, CA) linked directly to the Model 7700 Sequence Detector. Analysis of data was also performed on the Macintosh computer. Collection and analysis software was developed at PE Applied Biosystems.

Transfection of Cells with Factor VIII Construct

Four T175 flasks of 293 cells (ATCC CRL 1573), a human fetal kidney suspension cell line, were grown to 80% confluency and transfected pF8TM. Cells were grown in the following media: 50% HAM'S #12 without G1T, 50% low glucose Dulbecco's modified Eagle medium (DMEM) without glycine with sodium bicarbonate, 10% fetal bovine serum, 2 mM L-glutamine, and 1% penicillin-streptomycin. The media was changed 30 min before the transfection. pF8TM DNA amounts of 40, 4, 0.5, and 0.1 μ g were added to 1.5 ml of a solution containing 0.125 M CaCl₂ and 1 \times HBPS. The four mixtures were left at room temperature for 10 min and then added dropwise to the cells. The flasks were incubated at 37°C and 5% CO₂ for 24 hr, washed with PBS, and resuspended in PBS. The resuspended cells were divided into aliquots and DNA was extracted immediately using the QIAamp Blood Kit (Qiagen, Chatsworth, CA). DNA was eluted into 200 μ l of 30 mM Tris-HCl at pH 8.0.

ACKNOWLEDGMENTS

We thank Genentech's DNA Synthesis Group for primer synthesis and Genentech's Graphics Group for assistance with the figures.

The publication costs of this article were defrayed in part by payment of page charges. This article must therefore be hereby marked "advertisement" in accordance with 18 USC section 1734 solely to indicate this fact.

REFERENCES

- Bassler, H.A., S.J. Flood, K.J. Livak, J. Marmaro, R. Kimm, and C.A. Hall. 1995. Use of a fluorogenic probe in a PCR-based assay for the detection of *Listeria monocytogenes*. *App. Environ. Microbiol.* 61: 3724-3729.
- Hecker-Andre, M. 1991. Quantitative evaluation of mRNA levels. *Meth. Mol. Cell. Biol.* 2: 189-201.
- Clement, M., S. Menzo, P. Bagnarelli, A. Manzini, A. Valenza, and P.E. Varaldo. 1993. Quantitative PCR and RT-PCR in virology. [Review]. *PCR Methods Applic.* 2: 191-196.
- Connor, R.I., H. Mohri, Y. Cao, and D.D. Ho. 1993. Increased viral burden and cytopathicity correlate temporally with CD4⁺ T-lymphocyte decline and clinical progression in human immunodeficiency virus type 1-infected individuals. *J. Virol.* 67: 1772-1777.
- Eaton, D.L., W.J. Wood, D. Eaton, P.E. Hays, P.

HFID LT AL

Venar, and C. Gionfrido. 1986. Construction and characterization of an active factor VIII variant lacking the central one third of the molecule. *Biochemistry* 25: 8343-8347.

Fusco, M.J., C.P. Treanor, S. Spivack, H.J. Tigge, and I.S. Kaminsky. 1995. Quantitative RNA-polymerase chain reaction-LNA analysis by capillary electrophoresis and laser-induced fluorescence. *Anal. Biochem.* 224: 141-147.

Perre, R. 1992. Quantitative or semi-quantitative PCR: Reality versus myth. *PCR Methods Applic.* 2: 1-9.

Furtado, M.R., L.A. Kingsley, and S.M. Winkler. 1995. Changes in the viral mRNA expression pattern correlate with a rapid rate of CD4+ T-cell number decline in human immunodeficiency virus type 1-infected individuals. *J. Virol.* 69: 2092-2100.

Gibson, U.E.M., C.A. Heid, and P.M. Williams. 1996. A novel method for real time quantitative competitive RT-PCR. *Genome Res.* (this issue).

Garman, C.M., D.R. Gies, and G. McCray. 1990. Transient production of proteins using an adenovirus transformed cell line. *DNA Prot. Engin. Tech.* 2: 3-10.

Higuchi, R., G. Dollinger, P.S. Walsh, and R. Griffith. 1992. Simultaneous amplification and detection of specific DNA sequences. *Biotechnology* 10: 413-417.

Holland, P.M., R.D. Abramson, R. Watson, and D.H. Gelfand. 1991. Detection of specific polymerase chain reaction products by utilizing the 5'-3' exonuclease activity of *Thermus aquaticus* DNA polymerase. *Proc. Natl. Acad. Sci.* 88: 7276-7280.

Huang, S.K., H.Q. Xian, T.J. Klein, G. Paciotti, H.G. Marsh, L.M. Lichtenstein, and M.C. Liu. 1995a. IL-13 expression at the sites of allergen challenge in patients with asthma. *J. Immunol.* 155: 2688-2694.

Huang, S.K., M. Yi, E. Palmer, and D.G. Marsh. 1995b. A dominant T cell receptor beta-chain in response to a short ragweed allergen. *Am J. Immunol.* 154: 6157-6162.

Kellogg, D.E., J.J. Shtinsky, and S. Kwak. 1990. Quantitation of HIV-1 proviral DNA relative to cellular DNA by the polymerase chain reaction. *Anal. Biochem.* 189: 202-208.

Lee, J.-G., C.R. Connell, and W. Bloch. 1993. Allelic discrimination by nick-translation PCR with fluorogenic probes. *Nucleic Acids Res.* 21: 3761-3766.

Livak, K.J., S.J. Flood, J. Maniara, W. Giusti, and K. Dettz. 1995a. Oligonucleotides with fluorescent dyes at opposite ends provide a quenched probe system useful for detecting PCR product and nucleic acid hybridization. *PCR Methods Applic.* 4: 357-362.

Livak, K.J., J. Maniara, and J.A. Todd. 1995b. Towards

fully automated genome-wide polymorphism screening. [Letter] *Nature Genet.* 9: 341-342.

Mulder, J., N. McKinney, C. Christopherson, J. Shtinsky, L. Greenfield, and S. Kwak. 1994. Rapid and simple PCR assay for quantitation of human immunodeficiency virus type 1 RNA in plasma: Application to acute retroviral infection. *J. Clin. Microbiol.* 32: 292-300.

Pang, S., Y. Koyanagi, S. Miller, C. Wiloy, H.V. Vinters, and I.S. Chen. 1990. High levels of unintegrated HIV-1 DNA in brain tissue of AIDS dementia patients. *Nature* 343: 85-89.

Platak, M.J., K.C. Luk, B. Williams, and J.D. Lifson. 1993a. Quantitative competitive polymerase chain reaction for accurate quantitation of HIV DNA and RNA species. *Aid Techniques* 14: 70-81.

Platak, M.J., M.S. Saag, L.C. Yang, S.J. Clark, J.C. Kappes, K.C. Luk, B.H. Hann, G.M. Shaw, and J.D. Lifson. 1993b. High levels of HIV-1 in plasma during all stages of infection determined by competitive PCR [see Comments]. *Science* 259: 1749-1754.

Prud'homme, G.J., D.H. Kono, and A.N. Theofilopoulos. 1995. Quantitative polymerase chain reaction analysis reveals marked overexpression of interleukin-1 beta, interleukin-1 and interferon-gamma mRNA in the lymph nodes of lupus-prone mice. *Mol. Immunol.* 32: 495-503.

Raczynski, L. 1995. A commentary on the practical applications of competitive PCR. *Genome Res.* 5: 91-94.

Sharp, P.A., A.J. Berk, and S.M. Herget. 1980. Transcription maps of adenovirus. *Methods Enzymol.* 65: 750-768.

Slanton, D.J., G.M. Clark, S.G. Wong, W.J. Levin, A. O'Brien, and W.L. McGuire. 1987. Human breast cancer: Correlation of relapse and survival with amplification of the HER-2/neu oncogene. *Science* 235: 177-182.

Southern, E.M. 1976. Detection of specific sequences among DNA fragments separated by gel electrophoresis. *J. Mol. Biol.* 98: 503-517.

Tan, X., X. Sun, C.F. Gonzalez, and W. Hsueh. 1994. PAF and TNF increase the precursor of NF-kappa B p50 mRNA in mouse intestine: Quantitative analysis by competitive PCR. *Biochim. Biophys. Acta* 1215: 157-162.

Thomas, P.S. 1980. Hybridization of denatured RNA and small DNA fragments transferred to nitrocellulose. *Proc. Natl. Acad. Sci.* 77: 5201-5205.

Williams, S., C. Scher, A. Krishnamo, C. Held, B. Karger, and P.M. Williams. 1996. Quantitative competitive PCR: Analysis of amplified products of the HIV-1 gag gene by capillary electrophoresis with laser induced fluorescence detection. *Anal. Biochem.* (in press).

Received June 3, 1996; accepted in revised form July 29, 1996.

WISP genes are members of the connective tissue growth factor family that are up-regulated in Wnt-1-transformed cells and aberrantly expressed in human colon tumors

DIANE PENNICA*†, TODD A. SWANSON*, JAMES W. WELSH*, MARGARET A. ROY‡, DAVID A. LAWRENCE*, JAMES LEE‡, JENNIFER BRUSH‡, LISA A. TANEYHILL§, BETHANNE DEUEL‡, MICHAEL LEW¶, COLIN WATANABE||, ROBERT L. COHEN*, MONA F. MELHEM**, GENE G. FINLEY**, PHIL QUIRKE††, AUDREY D. GODDARD‡, KENNETH J. HILLAN¶, AUSTIN L. GURNEY‡, DAVID BOTSTEIN†,‡‡, AND ARNOLD J. LEVINE§

Departments of *Molecular Oncology, ‡Molecular Biology, §Scientific Computing, and ¶Pathology, Genentech Inc., 1 DNA Way, South San Francisco, CA 94080; **University of Pittsburgh School of Medicine, Veterans Administration Medical Center, Pittsburgh, PA 15240; ††University of Leeds, Leeds, LS29JT United Kingdom; ‡‡Department of Genetics, Stanford University, Palo Alto, CA 94305; and §Department of Molecular Biology, Princeton University, Princeton, NJ 08544

Contributed by David Botstein and Arnold J. Levine, October 21, 1998

ABSTRACT Wnt family members are critical to many developmental processes, and components of the Wnt signaling pathway have been linked to tumorigenesis in familial and sporadic colon carcinomas. Here we report the identification of two genes, *WISP-1* and *WISP-2*, that are up-regulated in the mouse mammary epithelial cell line C57MG transformed by Wnt-1, but not by Wnt-4. Together with a third related gene, *WISP-3*, these proteins define a subfamily of the connective tissue growth factor family. Two distinct systems demonstrated *WISP* induction to be associated with the expression of Wnt-1. These included (i) C57MG cells infected with a Wnt-1 retroviral vector or expressing Wnt-1 under the control of a tetracycline repressible promoter, and (ii) Wnt-1 transgenic mice. The *WISP-1* gene was localized to human chromosome 8q24.1-8q24.3. *WISP-1* genomic DNA was amplified in colon cancer cell lines and in human colon tumors and its RNA overexpressed (2- to >30-fold) in 84% of the tumors examined compared with patient-matched normal mucosa. *WISP-3* mapped to chromosome 6q22-6q23 and also was overexpressed (4- to >40-fold) in 63% of the colon tumors analyzed. In contrast, *WISP-2* mapped to human chromosome 20q12-20q13 and its DNA was amplified, but RNA expression was reduced (2- to >30-fold) in 79% of the tumors. These results suggest that the *WISP* genes may be downstream of Wnt-1 signaling and that aberrant levels of *WISP* expression in colon cancer may play a role in colon tumorigenesis.

Wnt-1 is a member of an expanding family of cysteine-rich, glycosylated signaling proteins that mediate diverse developmental processes such as the control of cell proliferation, adhesion, cell polarity, and the establishment of cell fates (1, 2). Wnt-1 originally was identified as an oncogene activated by the insertion of mouse mammary tumor virus in virus-induced mammary adenocarcinomas (3, 4). Although Wnt-1 is not expressed in the normal mammary gland, expression of Wnt-1 in transgenic mice causes mammary tumors (5).

In mammalian cells, Wnt family members initiate signaling by binding to the seven-transmembrane spanning Frizzled receptors and recruiting the cytoplasmic protein Dishevelled (Dsh) to the cell membrane (1, 2, 6). Dsh then inhibits the kinase activity of the normally constitutively active glycogen synthase kinase-3 β (GSK-3 β) resulting in an increase in β -catenin levels. Stabilized β -catenin interacts with the transcription factor TCF/Lef1, forming a complex that appears in

the nucleus and binds TCF/Lef1 target DNA elements to activate transcription (7, 8). Other experiments suggest that the adenomatous polyposis coli (APC) tumor suppressor gene also plays an important role in Wnt signaling by regulating β -catenin levels (9). APC is phosphorylated by GSK-3 β , binds to β -catenin, and facilitates its degradation. Mutations in either APC or β -catenin have been associated with colon carcinomas and melanomas, suggesting these mutations contribute to the development of these types of cancer, implicating the Wnt pathway in tumorigenesis (1).

Although much has been learned about the Wnt signaling pathway over the past several years, only a few of the transcriptionally activated downstream components activated by Wnt have been characterized. Those that have been described cannot account for all of the diverse functions attributed to Wnt signaling. Among the candidate Wnt target genes are those encoding the nodal-related 3 gene, *Xnr3*, a member of the transforming growth factor (TGF)- β superfamily, and the homeobox genes, *engrailed*, *goosecoid*, *twist* (*Xtwn*), and *siamois* (2). A recent report also identifies *c-myc* as a target gene of the Wnt signaling pathway (10).

To identify additional downstream genes in the Wnt signaling pathway that are relevant to the transformed cell phenotype, we used a PCR-based cDNA subtraction strategy, suppression subtractive hybridization (SSH) (11), using RNA isolated from C57MG mouse mammary epithelial cells and C57MG cells stably transformed by a Wnt-1 retrovirus. Overexpression of Wnt-1 in this cell line is sufficient to induce a partially transformed phenotype, characterized by elongated and refractile cells that lose contact inhibition and form a multilayered array (12, 13). We reasoned that genes differentially expressed between these two cell lines might contribute to the transformed phenotype.

In this paper, we describe the cloning and characterization of two genes up-regulated in Wnt-1 transformed cells, *WISP-1* and *WISP-2*, and a third related gene, *WISP-3*. The *WISP* genes are members of the CCN family of growth factors, which includes connective tissue growth factor (CTGF), Cyr61, and *nov*, a family not previously linked to Wnt signaling.

MATERIALS AND METHODS

SSH. SSH was performed by using the PCR-Select cDNA Subtraction Kit (CLONTECH). Tester double-stranded

Abbreviations: TGF, transforming growth factor; CTGF, connective tissue growth factor; SSH, suppression subtractive hybridization; VWC, von Willebrand factor type C module.

Data deposition: The sequences reported in this paper have been deposited in the Genbank database (accession nos. AF100777, AF100778, AF100779, AF100780, and AF100781).

†To whom reprint requests should be addressed. e-mail: diane@gene.com.

The publication costs of this article were defrayed in part by page charge payment. This article must therefore be hereby marked "advertisement" in accordance with 18 U.S.C. §1734 solely to indicate this fact.

© 1998 by The National Academy of Sciences 0027-8424/98/9514717-6\$2.00/0 PNAS is available online at www.pnas.org.

cDNA was synthesized from 2 μ g of poly(A)⁺ RNA isolated from the C57MG/Wnt-1 cell line and driver cDNA from 2 μ g of poly(A)⁺ RNA from the parent C57MG cells. The subtracted cDNA library was subcloned into a pGEM-T vector for further analysis.

cDNA Library Screening. Clones encoding full-length mouse *WISP-1* were isolated by screening a λ gt10 mouse embryo cDNA library (CLONTECH) with a 70-bp probe from the original partial clone 568 sequence corresponding to amino acids 128–169. Clones encoding full-length human *WISP-1* were isolated by screening λ gt10 lung and fetal kidney cDNA libraries with the same probe at low stringency. Clones encoding full-length mouse and human *WISP-2* were isolated by screening a C57MG/Wnt-1 or human fetal lung cDNA library with a probe corresponding to nucleotides 1463–1512. Full-length cDNAs encoding *WISP-3* were cloned from human bone marrow and fetal kidney libraries.

Expression of Human *WISP* RNA. PCR amplification of first-strand cDNA was performed with human Multiple Tissue cDNA panels (CLONTECH) and 300 μ M of each dNTP at 94°C for 1 sec, 62°C for 30 sec, 72°C for 1 min, for 22–32 cycles. *WISP* and glyceraldehyde-3-phosphate dehydrogenase primer sequences are available on request.

In Situ Hybridization. ³²P-labeled sense and antisense riboprobes were transcribed from an 897-bp PCR product corresponding to nucleotides 601–1440 of mouse *WISP-1* or a 294-bp PCR product corresponding to nucleotides 82–375 of mouse *WISP-2*. All tissues were processed as described (40).

Radiation Hybrid Mapping. Genomic DNA from each hybrid in the Stanford G3 and Genebridge4 Radiation Hybrid Panels (Research Genetics, Huntsville, AL) and human and hamster control DNAs were PCR-amplified, and the results were submitted to the Stanford or Massachusetts Institute of Technology web servers.

Cell Lines, Tumors, and Mucosa Specimens. Tissue specimens were obtained from the Department of Pathology (University of Pittsburgh) for patients undergoing colon resection and from the University of Leeds, United Kingdom. Genomic DNA was isolated (Qiagen) from the pooled blood of 10 normal human donors, surgical specimens, and the following ATCC human cell lines: SW480, COLO 320DM, HT-29, WiDr, and SW403 (colon adenocarcinomas), SW620 (lymph node metastasis, colon adenocarcinoma), HCT 116 (colon carcinoma), SK-CO-1 (colon adenocarcinoma, ascites), and HM7 (a variant of ATCC colon adenocarcinoma cell line LS 174T). DNA concentration was determined by using Hoechst dye 33258 intercalation fluorimetry. Total RNA was prepared by homogenization in 7 M GuSCN followed by centrifugation over CsCl cushions or prepared by using RNazol.

Gene Amplification and RNA Expression Analysis. Relative gene amplification and RNA expression of *WISPs* and *c-myc* in the cell lines, colorectal tumors, and normal mucosa were determined by quantitative PCR. Gene-specific primers and fluorogenic probes (sequences available on request) were designed and used to amplify and quantitate the genes. The relative gene copy number was derived by using the formula $2^{-\Delta\Delta C_t}$ where ΔC_t represents the difference in amplification cycles required to detect the *WISP* genes in peripheral blood lymphocyte DNA compared with colon tumor DNA or colon tumor RNA compared with normal mucosal RNA. The Δ -method was used for calculation of the SE of the gene copy number or RNA expression level. The *WISP*-specific signal was normalized to that of the glyceraldehyde-3-phosphate dehydrogenase housekeeping gene. All TaqMan assay reagents were obtained from Perkin-Elmer Applied Biosystems.

RESULTS

Isolation of *WISP-1* and *WISP-2* by SSH. To identify Wnt-1-inducible genes, we used the technique of SSH using the

mouse mammary epithelial cell line C57MG and C57MG cells that stably express Wnt-1 (11). Candidate differentially expressed cDNAs (1,384 total) were sequenced. Thirty-nine percent of the sequences matched known genes or homologues, 32% matched expressed sequence tags, and 29% had no match. To confirm that the transcript was differentially expressed, semiquantitative reverse transcription-PCR and Northern analysis were performed by using mRNA from the C57MG and C57MG/Wnt-1 cells.

Two of the cDNAs, *WISP-1* and *WISP-2*, were differentially expressed, being induced in the C57MG/Wnt-1 cell line, but not in the parent C57MG cells or C57MG cells overexpressing Wnt-4 (Fig. 1A and B). Wnt-4, unlike Wnt-1, does not induce the morphological transformation of C57MG cells and has no effect on β -catenin levels (13, 14). Expression of *WISP-1* was up-regulated approximately 3-fold in the C57MG/Wnt-1 cell line and *WISP-2* by approximately 5-fold by both Northern analysis and reverse transcription-PCR.

An independent, but similar, system was used to examine *WISP* expression after Wnt-1 induction. C57MG cells expressing the *Wnt-1* gene under the control of a tetracycline-repressible promoter produce low amounts of Wnt-1 in the repressed state but show a strong induction of *Wnt-1* mRNA and protein within 24 hr after tetracycline removal (8). The levels of Wnt-1 and *WISP* RNA isolated from these cells at various times after tetracycline removal were assessed by quantitative PCR. Strong induction of Wnt-1 mRNA was seen as early as 10 hr after tetracycline removal. Induction of *WISP* mRNA (2- to 6-fold) was seen at 48 and 72 hr (data not shown). These data support our previous observations that show that *WISP* induction is correlated with Wnt-1 expression. Because the induction is slow, occurring after approximately 48 hr, the induction of *WISPs* may be an indirect response to Wnt-1 signaling.

cDNA clones of human *WISP-1* were isolated and the sequence compared with mouse *WISP-1*. The cDNA sequences of mouse and human *WISP-1* were 1,766 and 2,830 bp in length, respectively, and encode proteins of 367 aa, with predicted relative molecular masses of $\approx 40,000$ (M_r 40 K). Both have hydrophobic N-terminal signal sequences, 38 conserved cysteine residues, and four potential N-linked glycosylation sites and are 84% identical (Fig. 2A).

Full-length cDNA clones of mouse and human *WISP-2* were 1,734 and 1,293 bp in length, respectively, and encode proteins of 251 and 250 aa, respectively, with predicted relative molecular masses of $\approx 27,000$ (M_r 27 K) (Fig. 2B). Mouse and human *WISP-2* are 73% identical. Human *WISP-2* has no potential N-linked glycosylation sites, and mouse *WISP-2* has one at

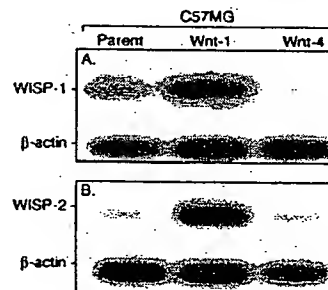


FIG. 1. *WISP-1* and *WISP-2* are induced by Wnt-1, but not Wnt-4, expression in C57MG cells. Northern analysis of *WISP-1* (A) and *WISP-2* (B) expression in C57MG, C57MG/Wnt-1, and C57MG/Wnt-4 cells. Poly(A)⁺ RNA (2 μ g) was subjected to Northern blot analysis and hybridized with a 70-bp mouse *WISP-1*-specific probe (amino acids 278–300) or a 190-bp *WISP-2*-specific probe (nucleotides 1438–1627) in the 3' untranslated region. Blots were rehybridized with human β -actin probe.

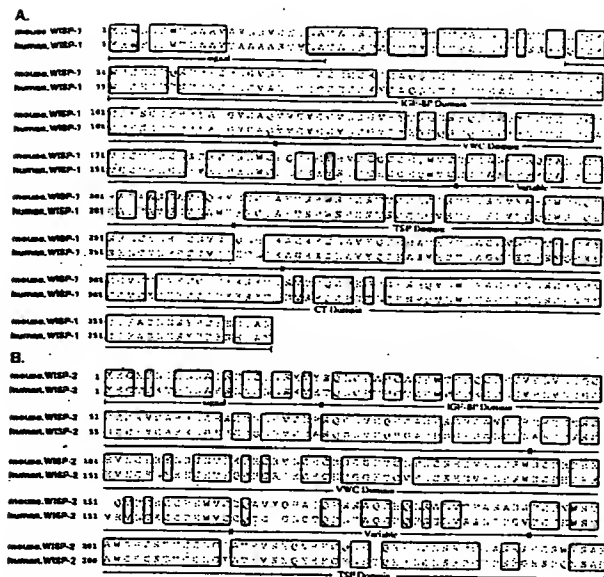


FIG. 2. Encoded amino acid sequence alignment of mouse and human *WISP-1* (A) and mouse and human *WISP-2* (B). The potential signal sequence, insulin-like growth factor-binding protein (IGF-BP), VWC, thrombospondin (TSP), and C-terminal (CT) domains are underlined.

position 197. *WISP-2* has 28 cysteine residues that are conserved among the 38 cysteines found in *WISP-1*.

Identification of *WISP-3*. To search for related proteins, we screened expressed sequence tag (EST) databases with the *WISP-1* protein sequence and identified several ESTs as potentially related sequences. We identified a homologous protein that we have called *WISP-3*. A full-length human *WISP-3* cDNA of 1,371 bp was isolated corresponding to those ESTs that encode a 354-aa protein with a predicted molecular mass of 39,293. *WISP-3* has two potential N-linked glycosylation sites and 36 cysteine residues. An alignment of the three human *WISP* proteins shows that *WISP-1* and *WISP-3* are the most similar (42% identity), whereas *WISP-2* has 37% identity with *WISP-1* and 32% identity with *WISP-3* (Fig. 3A).

***WISPs* Are Homologous to the CTGF Family of Proteins.** Human *WISP-1*, *WISP-2*, and *WISP-3* are novel sequences; however, mouse *WISP-1* is the same as the recently identified *Elm1* gene. *Elm1* is expressed in low, but not high, metastatic mouse melanoma cells, and suppresses the *in vivo* growth and metastatic potential of K-1735 mouse melanoma cells (15). Human and mouse *WISP-2* are homologous to the recently described rat gene, *rCop-1* (16). Significant homology (36–44%) was seen to the CCN family of growth factors. This family includes three members, CTGF, Cyr61, and the proto-oncogene *nov*. CTGF is a chemotactic and mitogenic factor for fibroblasts that is implicated in wound healing and fibrotic disorders and is induced by TGF- β (17). Cyr61 is an extracellular matrix signaling molecule that promotes cell adhesion, proliferation, migration, angiogenesis, and tumor growth (18, 19). *nov* (nephroblastoma overexpressed) is an immediate early gene associated with quiescence and found altered in Wilms' tumors (20). The proteins of the CCN family share functional, but not sequence, similarity to Wnt-1. All are secreted, cysteine-rich heparin binding glycoproteins that associate with the cell surface and extracellular matrix.

WISP proteins exhibit the modular architecture of the CCN family, characterized by four conserved cysteine-rich domains (Fig. 3B) (21). The N-terminal domain, which includes the first 12 cysteine residues, contains a consensus sequence (GCGC-CXXC) conserved in most insulin-like growth factor (IGF)-

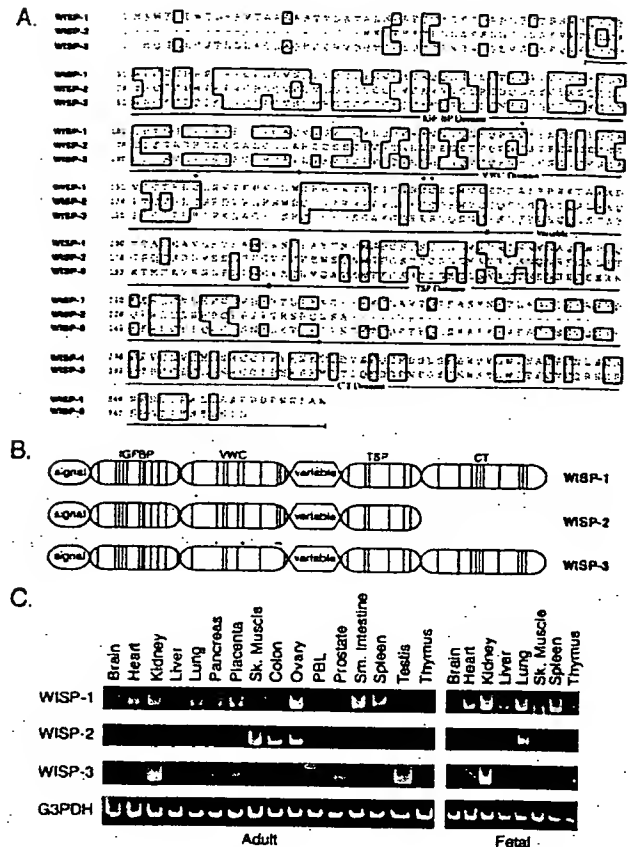


FIG. 3. (A) Encoded amino acid sequence alignment of human *WISPs*. The cysteine residues of *WISP-1* and *WISP-2* that are not present in *WISP-3* are indicated with a dot. (B) Schematic representation of the *WISP* proteins showing the domain structure and cysteine residues (vertical lines). The four cysteine residues in the VWC domain that are absent in *WISP-3* are indicated with a dot. (C) Expression of *WISP* mRNA in human tissues. PCR was performed on human multiple-tissue cDNA panels (CLONTECH) from the indicated adult and fetal tissues.

binding proteins (BP). This sequence is conserved in *WISP-2* and *WISP-3*, whereas *WISP-1* has a glutamine in the third position instead of a glycine. CTGF recently has been shown to specifically bind IGF (22) and a truncated *nov* protein lacking the IGF-BP domain is oncogenic (23). The von Willebrand factor type C module (VWC), also found in certain collagens and mucins, covers the next 10 cysteine residues, and is thought to participate in protein complex formation and oligomerization (24). The VWC domain of *WISP-3* differs from all CCN family members described previously, in that it contains only six of the 10 cysteine residues (Fig. 3A and B). A short variable region follows the VWC domain. The third module, the thrombospondin (TSP) domain is involved in binding to sulfated glycoconjugates and contains six cysteine residues and a conserved WSXCSXCG motif first identified in thrombospondin (25). The C-terminal (CT) module containing the remaining 10 cysteines is thought to be involved in dimerization and receptor binding (26). The CT domain is present in all CCN family members described to date but is absent in *WISP-2* (Fig. 3A and B). The existence of a putative signal sequence and the absence of a transmembrane domain suggest that *WISPs* are secreted proteins, an observation supported by an analysis of their expression and secretion from mammalian cell and baculovirus cultures (data not shown).

Expression of *WISP* mRNA in Human Tissues. Tissue-specific expression of human *WISPs* was characterized by PCR

analysis on adult and fetal multiple tissue cDNA panels. *WISP-1* expression was seen in the adult heart, kidney, lung, pancreas, placenta, ovary, small intestine, and spleen (Fig. 3C). Little or no expression was detected in the brain, liver, skeletal muscle, colon, peripheral blood leukocytes, prostate, testis, or thymus. *WISP-2* had a more restricted tissue expression and was detected in adult skeletal muscle, colon, ovary, and fetal lung. Predominant expression of *WISP-3* was seen in adult kidney and testis and fetal kidney. Lower levels of *WISP-3* expression were detected in placenta, ovary, prostate, and small intestine.

In Situ Localization of *WISP-1* and *WISP-2*. Expression of *WISP-1* and *WISP-2* was assessed by *in situ* hybridization in mammary tumors from Wnt-1 transgenic mice. Strong expression of *WISP-1* was observed in stromal fibroblasts lying within the fibrovascular tumor stroma (Fig. 4 A–D). However, low-level *WISP-1* expression also was observed focally within tumor cells (data not shown). No expression was observed in normal breast. Like *WISP-1*, *WISP-2* expression also was seen in the tumor stroma in breast tumors from Wnt-1 transgenic animals (Fig. 4 E–H). However, *WISP-2* expression in the stroma was in spindle-shaped cells adjacent to capillary vessels, whereas

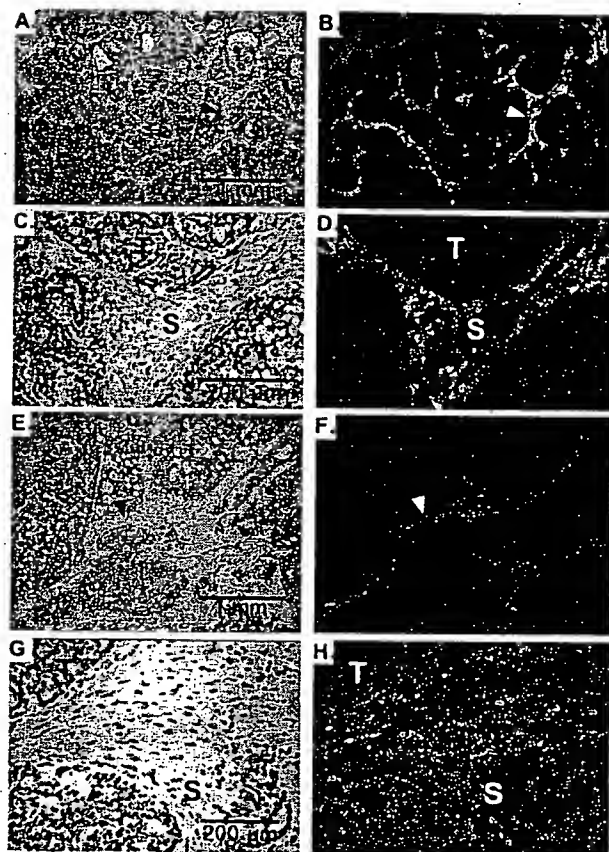


FIG. 4. (A, C, E, and G) Representative hematoxylin/eosin-stained images from breast tumors in Wnt-1 transgenic mice. The corresponding dark-field images showing *WISP-1* expression are shown in B and D. The tumor is a moderately well-differentiated adenocarcinoma showing evidence of adenoid cystic change. At low power (A and B), expression of *WISP-1* is seen in the delicate branching fibrovascular tumor stroma (arrowhead). At higher magnification, expression is seen in the stromal(s) fibroblasts (C and D), and tumor cells are negative. Focal expression of *WISP-1*, however, was observed in tumor cells in some areas. Images of *WISP-2* expression are shown in E–H. At low power (E and F), expression of *WISP-2* is seen in cells lying within the fibrovascular tumor stroma. At higher magnification, these cells appeared to be adjacent to capillary vessels whereas tumor cells are negative (G and H).

the predominant cell type expressing *WISP-1* was the stromal fibroblasts.

Chromosome Localization of the *WISP* Genes. The chromosomal location of the human *WISP* genes was determined by radiation hybrid mapping panels. *WISP-1* is approximately 3.48 cR from the meiotic marker AFM259xc5 [logarithm of odds (lod) score 16.31] on chromosome 8q24.1 to 8q24.3, in the same region as the human locus of the *novH* family member (27) and roughly 4 Mbs distal to *c-myc* (28). Preliminary fine mapping indicates that *WISP-1* is located near D8S1712 STS. *WISP-2* is linked to the marker SHGC-33922 (lod = 1,000) on chromosome 20q12–20q13.1. Human *WISP-3* mapped to chromosome 6q22–6q23 and is linked to the marker AFM211ze5 (lod = 1,000). *WISP-3* is approximately 18 Mbs proximal to CTGF and 23 Mbs proximal to the human cellular oncogene *MYB* (27, 29).

Amplification and Aberrant Expression of *WISPs* in Human Colon Tumors. Amplification of protooncogenes is seen in many human tumors and has etiological and prognostic significance. For example, in a variety of tumor types, *c-myc* amplification has been associated with malignant progression and poor prognosis (30). Because *WISP-1* resides in the same general chromosomal location (8q24) as *c-myc*, we asked whether it was a target of gene amplification, and, if so, whether this amplification was independent of the *c-myc* locus. Genomic DNA from human colon cancer cell lines was assessed by quantitative PCR and Southern blot analysis (Fig. 5 A and B). Both methods detected similar degrees of *WISP-1* amplification. Most cell lines showed significant (2- to 4-fold) amplification, with the HT-29 and WiDr cell lines demonstrating an 8-fold increase. Significantly, the pattern of amplification observed did not correlate with that observed for *c-myc*, indicating that the *c-myc* gene is not part of the amplicon that involves the *WISP-1* locus.

We next examined whether the *WISP* genes were amplified in a panel of 25 primary human colon adenocarcinomas. The relative *WISP* gene copy number in each colon tumor DNA was compared with pooled normal DNA from 10 donors by quantitative PCR (Fig. 6). The copy number of *WISP-1* and *WISP-2* was significantly greater than one, approximately 2-fold for *WISP-1* in about 60% of the tumors and 2- to 4-fold for *WISP-2* in 92% of the tumors ($P < 0.001$ for each). The copy number for *WISP-3* was indistinguishable from one ($P = 0.166$). In addition, the copy number of *WISP-2* was significantly higher than that of *WISP-1* ($P < 0.001$).

The levels of *WISP* transcripts in RNA isolated from 19 adenocarcinomas and their matched normal mucosa were

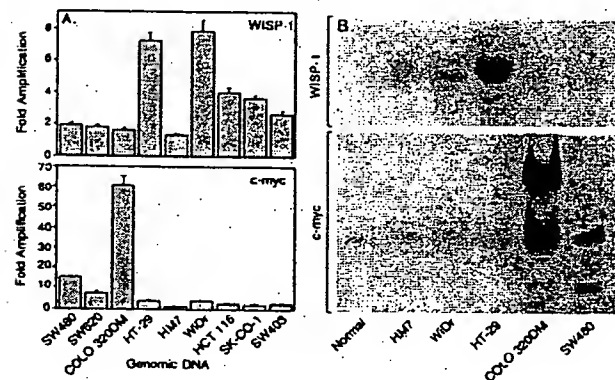


FIG. 5. Amplification of *WISP-1* genomic DNA in colon cancer cell lines. (A) Amplification in cell line DNA was determined by quantitative PCR. (B) Southern blots containing genomic DNA (10 μ g) digested with *Eco*RI (*WISP-1*) or *Xba*I (*c-myc*) were hybridized with a 100-bp human *WISP-1* probe (amino acids 186–219) or a human *c-myc* probe (located at bp 1901–2000). The *WISP* and *myc* genes are detected in normal human genomic DNA after a longer film exposure.

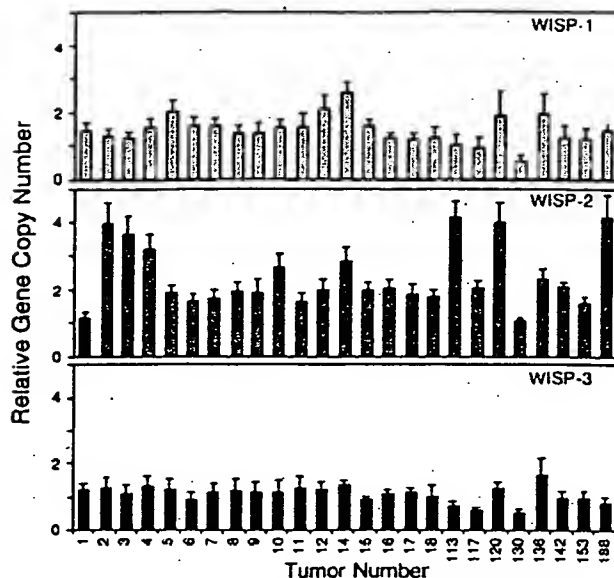


FIG. 6. Genomic amplification of *WISP* genes in human colon tumors. The relative gene copy number of the *WISP* genes in 25 adenocarcinomas was assayed by quantitative PCR, by comparing DNA from primary human tumors with pooled DNA from 10 healthy donors. The data are means \pm SEM from one experiment done in triplicate. The experiment was repeated at least three times.

assessed by quantitative PCR (Fig. 7). The level of *WISP-1* RNA present in tumor tissue varied but was significantly increased (2- to >25-fold) in 84% (16/19) of the human colon tumors examined compared with normal adjacent mucosa. Four of 19 tumors showed greater than 10-fold overexpression. In contrast, in 79% (15/19) of the tumors examined, *WISP-2* RNA expression was significantly lower in the tumor than the mucosa. Similar to *WISP-1*, *WISP-3* RNA was overexpressed in 63% (12/19) of the colon tumors compared with the normal

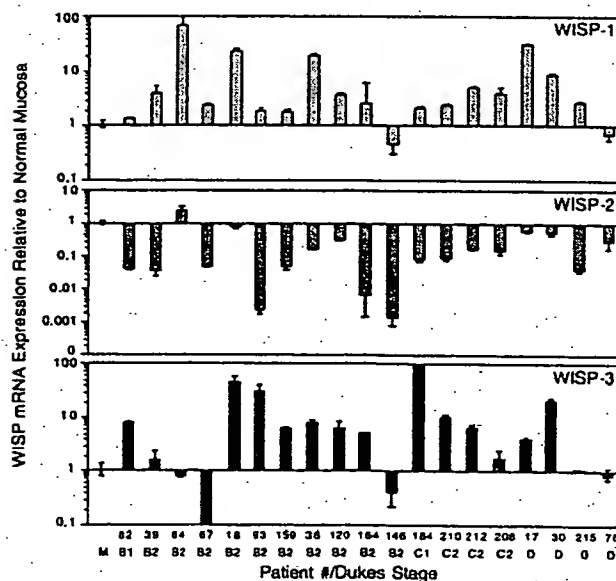


FIG. 7. *WISP* RNA expression in primary human colon tumors relative to expression in normal mucosa from the same patient. Expression of *WISP* mRNA in 19 adenocarcinomas was assayed by quantitative PCR. The Dukes stage of the tumor is listed under the sample number. The data are means \pm SEM from one experiment done in triplicate. The experiment was repeated at least twice.

mucosa. The amount of overexpression of *WISP-3* ranged from 4- to >40-fold.

DISCUSSION

One approach to understanding the molecular basis of cancer is to identify differences in gene expression between cancer cells and normal cells. Strategies based on assumptions that steady-state mRNA levels will differ between normal and malignant cells have been used to clone differentially expressed genes (31). We have used a PCR-based selection strategy, SSH, to identify genes selectively expressed in C57MG mouse mammary epithelial cells transformed by Wnt-1.

Three of the genes isolated, *WISP-1*, *WISP-2*, and *WISP-3*, are members of the CCN family of growth factors, which includes CTGF, Cyr61, and *nov*, a family not previously linked to Wnt signaling.

Two independent experimental systems demonstrated that *WISP* induction was associated with the expression of Wnt-1. The first was C57MG cells infected with a Wnt-1 retroviral vector or C57MG cells expressing Wnt-1 under the control of a tetracycline-repressible promoter, and the second was in Wnt-1 transgenic mice, where breast tissue expresses Wnt-1, whereas normal breast tissue does not. No *WISP* RNA expression was detected in mammary tumors induced by polyoma virus middle T antigen (data not shown). These data suggest a link between Wnt-1 and *WISPs* in that in these two situations, *WISP* induction was correlated with Wnt-1 expression.

It is not clear whether the *WISPs* are directly or indirectly induced by the downstream components of the Wnt-1 signaling pathway (i.e., β -catenin-TCF-1/Lef1). The increased levels of *WISP* RNA were measured in Wnt-1-transformed cells, hours or days after Wnt-1 transformation. Thus, *WISP* expression could result from Wnt-1 signaling directly through β -catenin transcription factor regulation or alternatively through Wnt-1 signaling turning on a transcription factor, which in turn regulates *WISPs*.

The *WISPs* define an additional subfamily of the CCN family of growth factors. One striking difference observed in the protein sequence of *WISP-2* is the absence of a CT domain, which is present in CTGF, Cyr61, *nov*, *WISP-1*, and *WISP-3*. This domain is thought to be involved in receptor binding and dimerization. Growth factors, such as TGF- β , platelet-derived growth factor, and nerve growth factor, which contain a cystine knot motif exist as dimers (32). It is tempting to speculate that *WISP-1* and *WISP-3* may exist as dimers, whereas *WISP-2* exists as a monomer. If the CT domain is also important for receptor binding, *WISP-2* may bind its receptor through a different region of the molecule than the other CCN family members. No specific receptors have been identified for CTGF or *nov*. A recent report has shown that integrin $\alpha_v\beta_3$ serves as an adhesion receptor for Cyr61 (33).

The strong expression of *WISP-1* and *WISP-2* in cells lying within the fibrovascular tumor stroma in breast tumors from Wnt-1 transgenic animals is consistent with previous observations that transcripts for the related CTGF gene are primarily expressed in the fibrous stroma of mammary tumors (34). Epithelial cells are thought to control the proliferation of connective tissue stroma in mammary tumors by a cascade of growth factor signals similar to that controlling connective tissue formation during wound repair. It has been proposed that mammary tumor cells or inflammatory cells at the tumor interstitial interface secrete TGF- β 1, which is the stimulus for stromal proliferation (34). TGF- β 1 is secreted by a large percentage of malignant breast tumors and may be one of the growth factors that stimulates the production of CTGF and *WISPs* in the stroma.

It was of interest that *WISP-1* and *WISP-2* expression was observed in the stromal cells that surrounded the tumor cells

(epithelial cells) in the Wnt-1 transgenic mouse sections of breast tissue. This finding suggests that paracrine signaling could occur in which the stromal cells could supply WISP-1 and WISP-2 to regulate tumor cell growth on the WISP extracellular matrix. Stromal cell-derived factors in the extracellular matrix have been postulated to play a role in tumor cell migration and proliferation (35). The localization of WISP-1 and WISP-2 in the stromal cells of breast tumors supports this paracrine model.

An analysis of WISP-1 gene amplification and expression in human colon tumors showed a correlation between DNA amplification and overexpression, whereas overexpression of WISP-3 RNA was seen in the absence of DNA amplification. In contrast, WISP-2 DNA was amplified in the colon tumors, but its mRNA expression was significantly reduced in the majority of tumors compared with the expression in normal colonic mucosa from the same patient. The gene for human WISP-2 was localized to chromosome 20q12-20q13, at a region frequently amplified and associated with poor prognosis in node negative breast cancer and many colon cancers, suggesting the existence of one or more oncogenes at this locus (36-38). Because the center of the 20q13 amplicon has not yet been identified, it is possible that the apparent amplification observed for WISP-2 may be caused by another gene in this amplicon.

A recent manuscript on *rCop-1*, the rat orthologue of WISP-2, describes the loss of expression of this gene after cell transformation, suggesting it may be a negative regulator of growth in cell lines (16). Although the mechanism by which WISP-2 RNA expression is down-regulated during malignant transformation is unknown, the reduced expression of WISP-2 in colon tumors and cell lines suggests that it may function as a tumor suppressor. These results show that the WISP genes are aberrantly expressed in colon cancer and suggest that their altered expression may confer selective growth advantage to the tumor.

Members of the Wnt signaling pathway have been implicated in the pathogenesis of colon cancer, breast cancer, and melanoma, including the tumor suppressor gene adenomatous polyposis coli and β -catenin (39). Mutations in specific regions of either gene can cause the stabilization and accumulation of cytoplasmic β -catenin, which presumably contributes to human carcinogenesis through the activation of target genes such as the WISPs. Although the mechanism by which Wnt-1 transforms cells and induces tumorigenesis is unknown, the identification of WISPs as genes that may be regulated downstream of Wnt-1 in C57MG cells suggests they could be important mediators of Wnt-1 transformation. The amplification and altered expression patterns of the WISPs in human colon tumors may indicate an important role for these genes in tumor development.

We thank the DNA synthesis group for oligonucleotide synthesis, T. Baker for technical assistance, P. Dowd for radiation hybrid mapping, K. Willert and R. Nusse for the tet-repressible C57MG/Wnt-1 cells, V. Dixit for discussions, and D. Wood and A. Bruce for artwork.

- Cadigan, K. M. & Nusse, R. (1997) *Genes Dev.* 11, 3286-3305.
- Dale, T. C. (1998) *Biochem. J.* 329, 209-223.
- Nusse, R. & Varmus, H. E. (1982) *Cell* 31, 99-109.
- van Ooyen, A. & Nusse, R. (1984) *Cell* 39, 233-240.
- Tsukamoto, A. S., Grosschedl, R., Guzman, R. C., Parslow, T. & Varmus, H. E. (1988) *Cell* 55, 619-625.
- Brown, J. D. & Moon, R. T. (1998) *Curr. Opin. Cell Biol.* 10, 182-187.
- Molenaar, M., van de Wetering, M., Oosterwegel, M., Peterson-Maduro, J., Godsave, S., Korinek, V., Roose, J., Destree, O. & Clevers, H. (1996) *Cell* 86, 391-399.
- Korinek, V., Barker, N., Willert, K., Molenaar, M., Roose, J., Wagenaar, G., Markman, M., Lamers, W., Destree, O. & Clevers, H. (1998) *Mol. Cell Biol.* 18, 1248-1256.
- Munemitsu, S., Albert, I., Souza, B., Rubinfeld, B. & Polakis, P. (1995) *Proc. Natl. Acad. Sci. USA* 92, 3046-3050.
- He, T. C., Sparks, A. B., Rago, C., Hermeking, H., Zawel, L., da Costa, L. T., Morin, P. J., Vogelstein, B. & Kinzler, K. W. (1998) *Science* 281, 1509-1512.
- Diatchenko, L., Lau, Y. F., Campbell, A. P., Chenchik, A., Moqadam, F., Huang, B., Lukyanov, S., Lukyanov, K., Gurskaya, N., Sverdlov, E. D. & Siebert, P. D. (1996) *Proc. Natl. Acad. Sci. USA* 93, 6025-6030.
- Brown, A. M., Wildin, R. S., Prendergast, T. J. & Varmus, H. E. (1986) *Cell* 46, 1001-1009.
- Wong, G. T., Gavin, B. J. & McMahon, A. P. (1994) *Mol. Cell Biol.* 14, 6278-6286.
- Shimizu, H., Julius, M. A., Giarre, M., Zheng, Z., Brown, A. M. & Kitajewski, J. (1997) *Cell Growth Differ.* 8, 1349-1358.
- Hashimoto, Y., Shindo-Okada, N., Tani, M., Nagamachi, Y., Takeuchi, K., Shiroishi, T., Toma, H. & Yokota, J. (1998) *J. Exp. Med.* 187, 289-296.
- Zhang, R., Averboukh, L., Zhu, W., Zhang, H., Jo, H., Dempsey, P. J., Coffey, R. J., Pardee, A. B. & Liang, P. (1998) *Mol. Cell Biol.* 18, 6131-6141.
- Grotendorst, G. R. (1997) *Cytokine Growth Factor Rev.* 8, 171-179.
- Kireeva, M. L., Mo, F. E., Yang, G. P. & Lau, L. F. (1996) *Mol. Cell Biol.* 16, 1326-1334.
- Babic, A. M., Kireeva, M. L., Kolesnikova, T. V. & Lau, L. F. (1998) *Proc. Natl. Acad. Sci. USA* 95, 6355-6360.
- Martinerie, C., Huff, V., Joubert, I., Badzioch, M., Saunders, G., Strong, L. & Perbal, B. (1994) *Oncogene* 9, 2729-2732.
- Bork, P. (1993) *FEBS Lett.* 327, 125-130.
- Kim, H. S., Nagalla, S. R., Oh, Y., Wilson, E., Roberts, C. T., Jr. & Rosenfeld, R. G. (1997) *Proc. Natl. Acad. Sci. USA* 94, 12981-12986.
- Joliet, V., Martinerie, C., Dambrine, G., Plassiat, G., Brisac, M., Crochet, J. & Perbal, B. (1992) *Mol. Cell Biol.* 12, 10-21.
- Mancuso, D. J., Tuley, E. A., Westfield, L. A., Worrall, N. K., Shelton-Inloes, B. B., Sorace, J. M., Alevy, Y. G. & Sadler, J. E. (1989) *J. Biol. Chem.* 264, 19514-19527.
- Holt, G. D., Pangburn, M. K. & Ginsburg, V. (1990) *J. Biol. Chem.* 265, 2852-2855.
- Voorberg, J., Fontijn, R., Calafat, J., Janssen, H., van Mourik, J. A. & Pannekoek, H. (1991) *J. Cell Biol.* 113, 195-205.
- Martinerie, C., Viegas-Pequignot, E., Guenard, I., Dutrillaux, B., Nguyen, V. C., Bernheim, A. & Perbal, B. (1992) *Oncogene* 7, 2529-2534.
- Takahashi, E., Hori, T., O'Connell, P., Leppert, M. & White, R. (1991) *Cytogenet. Cell Genet.* 57, 109-111.
- Meese, E., Meltzer, P. S., Witkowski, C. M. & Trent, J. M. (1989) *Genes Chromosomes Cancer* 1, 88-94.
- Garte, S. J. (1993) *Crit. Rev. Oncog.* 4, 435-449.
- Zhang, L., Zhou, W., Velculescu, V. E., Kern, S. E., Hruban, R. H., Hamilton, S. R., Vogelstein, B. & Kinzler, K. W. (1997) *Science* 276, 1268-1272.
- Sun, P. D. & Davies, D. R. (1995) *Annu. Rev. Biophys. Biomol. Struct.* 24, 269-291.
- Kireeva, M. L., Lam, S. C. T. & Lau, L. F. (1998) *J. Biol. Chem.* 273, 3090-3096.
- Frazier, K. S. & Grotendorst, G. R. (1997) *Int. J. Biochem. Cell Biol.* 29, 153-161.
- Wernert, N. (1997) *Virchows Arch.* 430, 433-443.
- Tanner, M. M., Tirkkonen, M., Kallioniemi, A., Collins, C., Stokke, T., Karhu, R., Kowbel, D., Shadravan, F., Hintz, M., Kuo, W. L., *et al.* (1994) *Cancer Res.* 54, 4257-4260.
- Brinkmann, U., Gallo, M., Polymeropoulos, M. H. & Pastan, I. (1996) *Genome Res.* 6, 187-194.
- Bischoff, J. R., Anderson, L., Zhu, Y., Mossie, K., Ng, L., Souza, B., Schryver, B., Flanagan, P., Clairvoyant, F., Ginther, C., *et al.* (1998) *EMBO J.* 17, 3052-3065.
- Morin, P. J., Sparks, A. B., Korinek, V., Barker, N., Clevers, H., Vogelstein, B. & Kinzler, K. W. (1997) *Science* 275, 1787-1790.
- Lu, L. H. & Gillett, N. (1994) *Cell Vision* 1, 169-176.

methods. Peptides AENK or AEQK were dissolved in water, made isotonic with NaCl and diluted into RPMI growth medium. T-cell-proliferation assays were done essentially as described^{20,21}. Briefly, after antigen pulsing (30 µg ml⁻¹ TTCF) with tetrapeptides (1–2 mg ml⁻¹), PBMCs or EBV-B cells were washed in PBS and fixed for 45 s in 0.05% glutaraldehyde. Glycine was added to a final concentration of 0.1M and the cells were washed five times in RPMI 1640 medium containing 1% FCS before co-culture with T-cell clones in round-bottom 96-well microtitre plates. After 48 h, the cultures were pulsed with 1 µCi of ³H-thymidine and harvested for scintillation counting 16 h later. Predigestion of native TTCF was done by incubating 200 µg TTCF with 0.25 µg pig kidney legumain in 500 µl 50 mM citrate buffer, pH 5.5, for 1 h at 37 °C. Glycopeptide digestions. The peptides HIDNEEDI, HIDN(N-glucosamine) EEDI and HIDNESDI, which are based on the TTCF sequence, and QQQHLFGSNVTDSCGNFCLFR(KKK), which is based on human transferrin, were obtained by custom synthesis. The three C-terminal lysine residues were added to the natural sequence to aid solubility. The transferrin glycopeptide QQQHLFGSNVTDSCGNFCLFR was prepared by tryptic (Promega) digestion of 5 mg reduced, carboxy-methylated human transferrin followed by concanavalin A chromatography¹¹. Glycopeptides corresponding to residues 622–642 and 421–452 were isolated by reverse-phase HPLC and identified by mass spectrometry and N-terminal sequencing. The lyophilized transferrin-derived peptides were redissolved in 50 mM sodium acetate, pH 5.5, 10 mM dithiothreitol, 20% methanol. Digestions were performed for 3 h at 30 °C with 5–50 mU ml⁻¹ pig kidney legumain or B-cell AEP. Products were analysed by HPLC or MALDI-TOF mass spectrometry using a matrix of 10 mg ml⁻¹ α-cyanocinnamic acid in 50% acetonitrile/0.1% TFA and a PerSeptive Biosystems Elite STR mass spectrometer set to linear or reflector mode. Internal standardization was obtained with a matrix ion of 568.13 mass units.

Received 29 September; accepted 3 November 1998.

- Chen, J. M. *et al.* Cloning, isolation, and characterization of mammalian legumain, an asparaginyl endopeptidase. *J. Biol. Chem.* 272, 8090–8098 (1997).
- Kembhavi, A. A., Buttle, D. J., Knight, C. G. & Barrett, A. J. The two cysteine endopeptidases of legume seeds: purification and characterization by use of specific fluorometric assays. *Arch. Biochem. Biophys.* 303, 208–213 (1993).
- Dalton, J. P., Holsa Jamsriska, L. & Bridley, P. J. Asparaginyl endopeptidase activity in adult *Schistosoma mansoni*. *Parasitology* 111, 575–580 (1995).
- Bennett, K. *et al.* Antigen processing for presentation by class II major histocompatibility complex requires cleavage by cathepsin E. *Eur. J. Immunol.* 22, 1519–1524 (1992).
- Riese, R. J. *et al.* Essential role for cathepsin S in MHC class II-associated invariant chain processing and peptide loading. *Immunity* 4, 357–366 (1996).
- Rodriguez, G. M. & Diment, S. Role of cathepsin D in antigen presentation of ovalbumin. *J. Immunol.* 149, 2894–2898 (1992).
- Hewitt, E. W. *et al.* Natural processing sites for human cathepsin E and cathepsin D in tetanus toxin: implications for T cell epitope generation. *J. Immunol.* 159, 4693–4699 (1997).
- Watts, C. Capture and processing of exogenous antigens for presentation on MHC molecules. *Annu. Rev. Immunol.* 15, 821–850 (1997).
- Chapman, H. A. Endosomal proteases and MHC class II function. *Curr. Opin. Immunol.* 10, 93–102 (1998).
- Fineschi, B. & Miller, J. Endosomal proteases and antigen processing. *Trends Biochem. Sci.* 22, 377–382 (1997).
- Lu, J. & van Halbeek, H. Complete ¹H and ¹³C resonance assignments of a 21-amino acid glycopeptide prepared from human serum transferrin. *Carbohydr. Res.* 296, 1–21 (1996).
- Fearon, D. T. & Locksley, R. M. The instructive role of innate immunity in the acquired immune response. *Science* 272, 50–54 (1996).
- Medzhitov, R. & Janeway, C. A. J. Innate immunity: the virtues of a nonclonal system of recognition. *Cell* 91, 295–298 (1997).
- Wyatt, R. *et al.* The antigenic structure of the HIV gp120 envelope glycoprotein. *Nature* 393, 705–711 (1998).
- Botarelli, P. *et al.* N-glycosylation of HIV gp120 may constrain recognition by T lymphocytes. *J. Immunol.* 147, 3128–3132 (1991).
- Davidson, H. W., West, M. A. & Watts, C. Endocytosis, intracellular trafficking, and processing of membrane IgG and monovalent antigen/membrane IgG complexes in B lymphocytes. *J. Immunol.* 144, 4101–4109 (1990).
- Barrett, A. J. & Kirschke, H. Cathepsin B, cathepsin H and cathepsin L. *Methods Enzymol.* 80, 535–559 (1981).
- Makoff, A. J., Ballantine, S. P., Smallwood, A. E. & Fairweather, N. F. Expression of tetanus toxin fragment C in *E. coli*: its purification and potential use as a vaccine. *Biotechnology* 7, 1043–1046 (1989).
- Lane, D. P. & Harlow, E. *Antibodies: A Laboratory Manual* (Cold Spring Harbor Laboratory Press, 1988).
- Lanzavecchia, A. Antigen-specific interaction between T and B cells. *Nature* 314, 537–539 (1985).
- Pond, L. & Watts, C. Characterization of transport of newly assembled, T cell-stimulatory MHC class II-peptide complexes from MHC class II compartments to the cell surface. *J. Immunol.* 159, 543–553 (1997).

Acknowledgements. We thank M. Ferguson for helpful discussions and advice; E. Smythe and L. Grayson for advice and technical assistance; B. Spruce, A. Knight and the BTS (Ninewells Hospital) for help with blood monocyte preparation; and our colleagues for many helpful comments on the manuscript. This work was supported by the Wellcome Trust and by an EMBO Long-term fellowship to B. M.

Correspondence and requests for materials should be addressed to C.W. (e-mail: c.watts@dundee.ac.uk).

Genomic amplification of a decoy receptor for Fas ligand in lung and colon cancer

Robert M. Pitti^{††}, Scot A. Marsters^{††}, David A. Lawrence^{††}, Margaret Roy^{*}, Frank C. Kischkel^{*}, Patrick Dowd^{*}, Arthur Huang^{*}, Christopher J. Donahue^{*}, Steven W. Sherwood^{*}, Daryl T. Baldwin^{*}, Paul J. Godowski^{*}, William I. Wood^{*}, Austin L. Gurney^{*}, Kenneth J. Hillan^{*}, Robert L. Cohen^{*}, Audrey D. Goddard^{*}, David Botstein[†] & Avi Ashkenazi^{*}

^{*} Departments of Molecular Oncology, Molecular Biology, and Immunology, Genentech Inc., 1 DNA Way, South San Francisco, California 94080, USA

[†] Department of Genetics, Stanford University, Stanford, California 94305, USA

^{††} These authors contributed equally to this work

Fas ligand (FasL) is produced by activated T cells and natural killer cells and it induces apoptosis (programmed cell death) in target cells through the death receptor Fas/Apo1/CD95 (ref. 1). One important role of FasL and Fas is to mediate immune-cytotoxic killing of cells that are potentially harmful to the organism, such as virus-infected or tumour cells¹. Here we report the discovery of a soluble decoy receptor, termed decoy receptor 3 (DcR3), that binds to FasL and inhibits FasL-induced apoptosis. The DcR3 gene was amplified in about half of 35 primary lung and colon tumours studied, and DcR3 messenger RNA was expressed in malignant tissue. Thus, certain tumours may escape FasL-dependent immune-cytotoxic attack by expressing a decoy receptor that blocks FasL.

By searching expressed sequence tag (EST) databases, we identified a set of related ESTs that showed homology to the tumour necrosis factor (TNF) receptor (TNFR) gene superfamily². Using the overlapping sequence, we isolated a previously unknown full-length complementary DNA from human fetal lung. We named the protein encoded by this cDNA decoy receptor 3 (DcR3). The cDNA encodes a 300-amino-acid polypeptide that resembles members of the TNFR family (Fig. 1a): the amino terminus contains a leader sequence, which is followed by four tandem cysteine-rich domains (CRDs). Like one other TNFR homologue, osteoprotegerin (OPG)³, DcR3 lacks an apparent transmembrane sequence, which indicates that it may be a secreted, rather than a membrane-associated, molecule. We expressed a recombinant, histidine-tagged form of DcR3 in mammalian cells; DcR3 was secreted into the cell culture medium, and migrated on polyacrylamide gels as a protein of relative molecular mass 35,000 (data not shown). DcR3 shares sequence identity in particular with OPG (31%) and TNFR2 (29%), and has relatively less homology with Fas (17%). All of the cysteines in the four CRDs of DcR3 and OPG are conserved; however, the carboxy-terminal portion of DcR3 is 101 residues shorter.

We analysed expression of DcR3 mRNA in human tissues by northern blotting (Fig. 1b). We detected a predominant 1.2-kilobase transcript in fetal lung, brain, and liver, and in adult spleen, colon and lung. In addition, we observed relatively high DcR3 mRNA expression in the human colon carcinoma cell line SW480.

To investigate potential ligand interactions of DcR3, we generated a recombinant, Fc-tagged DcR3 protein. We tested binding of DcR3-Fc to human 293 cells transfected with individual TNF family ligands, which are expressed as type 2 transmembrane proteins (these transmembrane proteins have their N termini in the cytosol). DcR3-Fc showed a significant increase in binding to cells transfected with FasL⁴ (Fig. 2a), but not to cells transfected with TNF⁵, Apo2L/TRAIL^{6,7}, Apo3L/TWEAK^{8,9}, or OPG/TRANCE/

RANKL¹⁰⁻¹² (data not shown). DcR3-Fc immunoprecipitated shed FasL from FasL-transfected 293 cells (Fig. 2b) and purified soluble FasL (Fig. 2c), as did the Fc-tagged ectodomain of Fas but not TNFR1. Gel-filtration chromatography showed that DcR3-Fc and soluble FasL formed a stable complex (Fig. 2d). Equilibrium analysis indicated that DcR3-Fc and Fas-Fc bound to soluble FasL with a comparable affinity ($K_d = 0.8 \pm 0.2$ and 1.1 ± 0.1 nM, respectively; Fig. 2e), and that DcR3-Fc could block nearly all of the binding of soluble FasL to Fas-Fc (Fig. 2e, inset). Thus, DcR3 competes with Fas for binding to FasL.

To determine whether binding of DcR3 inhibits FasL activity, we tested the effect of DcR3-Fc on apoptosis induction by soluble FasL in Jurkat T leukaemia cells, which express Fas (Fig. 3a). DcR3-Fc and Fas-Fc blocked soluble-FasL-induced apoptosis in a similar dose-dependent manner, with half-maximal inhibition at $\sim 0.1 \mu\text{g ml}^{-1}$. Time-course analysis showed that the inhibition did not merely delay cell death, but rather persisted for at least 24 hours (Fig. 3b). We also tested the effect of DcR3-Fc on activation-induced cell death (AICD) of mature T lymphocytes, a FasL-dependent process¹. Consistent with previous results¹³, activation of interleukin-2-stimulated CD4-positive T cells with anti-CD3 antibody increased the level of apoptosis twofold, and Fas-Fc blocked this effect substantially (Fig. 3c); DcR3-Fc blocked the

induction of apoptosis to a similar extent. Thus, DcR3 binding blocks apoptosis induction by FasL.

FasL-induced apoptosis is important in elimination of virus-infected cells and cancer cells by natural killer cells and cytotoxic T lymphocytes; an alternative mechanism involves perforin and granzymes¹⁴⁻¹⁶. Peripheral blood natural killer cells triggered marked cell death in Jurkat T leukaemia cells (Fig. 3d); DcR3-Fc and Fas-Fc each reduced killing of target cells from $\sim 65\%$ to $\sim 30\%$, with half-maximal inhibition at $\sim 1 \mu\text{g ml}^{-1}$; the residual killing was probably mediated by the perforin/granzyme pathway. Thus, DcR3 binding blocks FasL-dependent natural killer cell activity. Higher DcR3-Fc and Fas-Fc concentrations were required to block soluble FasL activity, which is consistent with the greater potency of membrane-associated FasL compared with soluble FasL¹⁷.

Given the role of immune-cytotoxic cells in elimination of tumour cells and the fact that DcR3 can act as an inhibitor of FasL, we proposed that DcR3 expression might contribute to the ability of some tumours to escape immune-cytotoxic attack. As genomic amplification frequently contributes to tumorigenesis, we investigated whether the DcR3 gene is amplified in cancer. We analysed DcR3 gene-copy number by quantitative polymerase chain

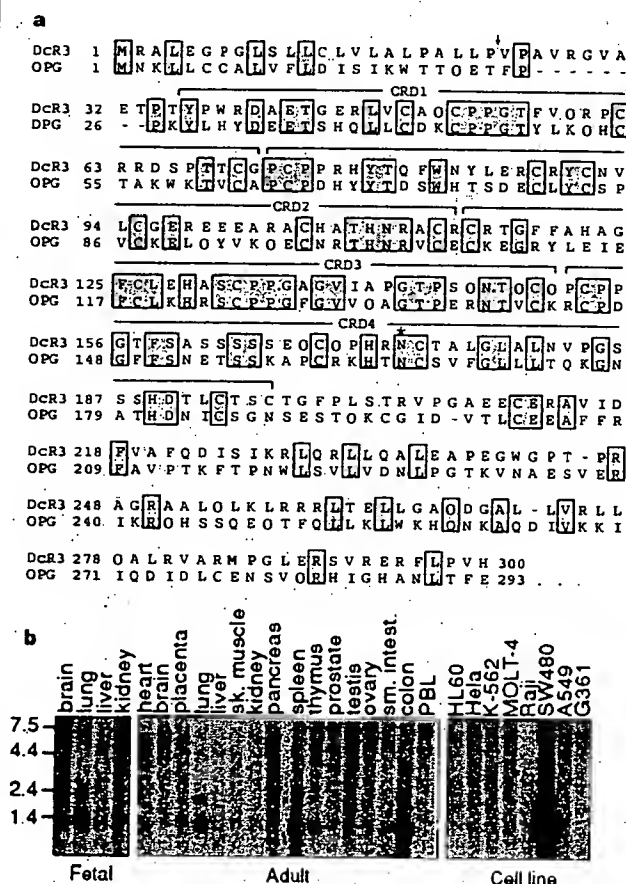


Figure 1 Primary structure and expression of human DcR3. **a**, Alignment of the amino-acid sequences of DcR3 and of osteoprotegerin (OPG); the C-terminal 101 residues of OPG are not shown. The putative signal cleavage site (arrow), the cysteine-rich domains (CRD 1-4), and the N-linked glycosylation site (asterisk) are shown. **b**, Expression of DcR3 mRNA. Northern hybridization analysis was done using the DcR3 cDNA as a probe and blots of poly(A)⁺ RNA (Clontech) from human fetal and adult tissues or cancer cell lines. PBL, peripheral blood lymphocyte.

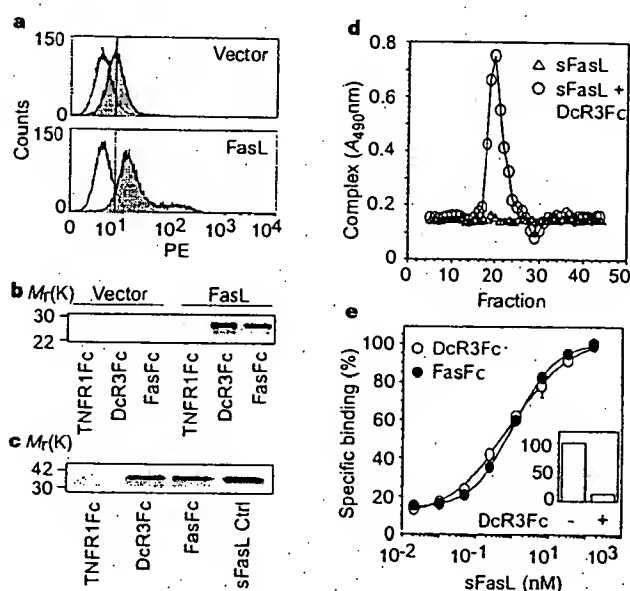


Figure 2 Interaction of DcR3 with FasL. **a**, 293 cells were transfected with pRK5 vector (top) or with pRK5 encoding full-length FasL (bottom), incubated with DcR3-Fc (solid line, shaded area), TNFR1-Fc (dotted line) or buffer control (dashed line) (the dashed and dotted lines overlap), and analysed for binding by FACS. Statistical analysis showed a significant difference ($P < 0.001$) between the binding of DcR3-Fc to cells transfected with FasL or pRK5. PE, phycoerythrin-labelled cells. **b**, 293 cells were transfected as in **a** and metabolically labelled, and cell supernatants were immunoprecipitated with Fc-tagged TNFR1, DcR3 or Fas. **c**, Purified soluble FasL (sFasL) was immunoprecipitated with TNFR1-Fc, DcR3-Fc or Fas-Fc and visualized by immunoblot with anti-FasL antibody. sFasL was loaded directly for comparison in the right-hand lane. **d**, Flag-tagged sFasL was incubated with DcR3-Fc or with buffer and resolved by gel filtration; column fractions were analysed in an assay that detects complexes containing DcR3-Fc and sFasL-Flag. **e**, Equilibrium binding of DcR3-Fc or Fas-Fc to sFasL-Flag. Inset, competition of DcR3-Fc with Fas-Fc for binding to sFasL-Flag.

reaction (PCR)¹⁸ in genomic DNA from 35 primary lung and colon tumours, relative to pooled genomic DNA from peripheral blood leukocytes (PBLs) of 10 healthy donors. Eight of 18 lung tumours and 9 of 17 colon tumours showed DcR3 gene amplification, ranging from 2- to 18-fold (Fig. 4a, b). To confirm this result, we analysed the colon tumour DNAs with three more, independent sets of DcR3-based PCR primers and probes; we observed nearly the same amplification (data not shown).

We then analysed DcR3 mRNA expression in primary tumour tissue sections by *in situ* hybridization. We detected DcR3 expression in 6 out of 15 lung tumours, 2 out of 2 colon tumours, 2 out of 5 breast tumours, and 1 out of 1 gastric tumour (data not shown). A section through a squamous-cell carcinoma of the lung is shown in Fig. 4c. DcR3 mRNA was localized to infiltrating malignant epithelium, but was essentially absent from adjacent stroma, indicating tumour-specific expression. Although the individual tumour specimens that we analysed for mRNA expression and gene amplification were different, the *in situ* hybridization results are consistent with the finding that the DcR3 gene is amplified frequently in tumours. SW480 colon carcinoma cells, which showed abundant DcR3 mRNA expression (Fig. 1b), also had marked DcR3 gene amplification, as shown by quantitative PCR (fourfold) and by Southern blot hybridization (fivefold) (data not shown).

If DcR3 amplification in cancer is functionally relevant, then DcR3 should be amplified more than neighbouring genomic regions that are not important for tumour survival. To test this,

we mapped the human DcR3 gene by radiation-hybrid analysis; DcR3 showed linkage to marker AFM218x7 (T160), which maps to chromosome position 20q13. Next, we isolated from a bacterial artificial chromosome (BAC) library a human genomic clone that carries DcR3, and sequenced the ends of the clone's insert. We then determined, from the nine colon tumours that showed twofold or greater amplification of DcR3, the copy number of the DcR3-flanking sequences (reverse and forward) from the BAC, and of seven genomic markers that span chromosome 20 (Fig. 4d). The DcR3-linked reverse marker showed an average amplification of roughly threefold; slightly less than the approximately fourfold amplification of DcR3; the other markers showed little or no amplification. These data indicate that DcR3 may be at the 'epi-centre' of a distal chromosome 20 region that is amplified in colon cancer, consistent with the possibility that DcR3 amplification promotes tumour survival.

Our results show that DcR3 binds specifically to FasL and inhibits FasL activity. We did not detect DcR3 binding to several other TNF-ligand-family members; however, this does not rule out the possibility that DcR3 interacts with other ligands, as do some other TNFR family members, including OPG^{2,19}.

FasL is important in regulating the immune response; however, little is known about how FasL function is controlled. One mechanism involves the molecule cFLIP, which modulates apoptosis signalling downstream of Fas²⁰. A second mechanism involves proteolytic shedding of FasL from the cell surface¹⁷. DcR3 competes with Fas for

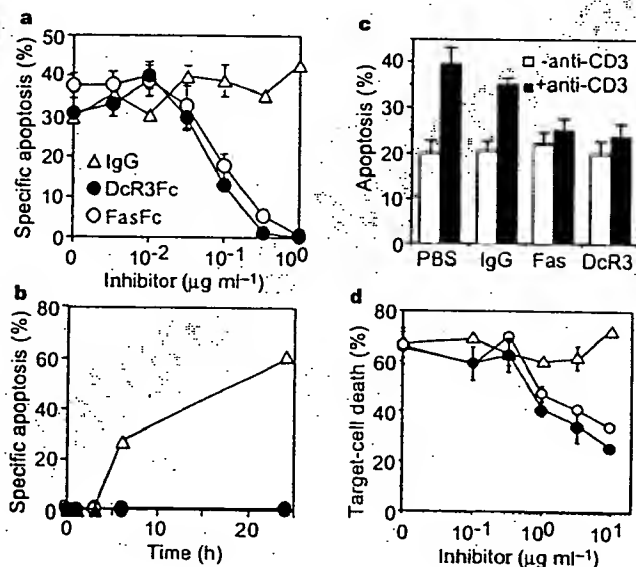


Figure 3 Inhibition of FasL activity by DcR3. **a**, Human Jurkat T leukaemia cells were incubated with Flag-tagged soluble FasL (sFasL; 5 ng ml⁻¹) oligomerized with anti-Flag antibody (0.1 μg ml⁻¹) in the presence of the proposed inhibitors DcR3-Fc, Fas-Fc or human IgG1 and assayed for apoptosis (mean ± s.e.m. of triplicates). **b**, Jurkat cells were incubated with sFasL-Flag plus anti-Flag antibody as in **a**, in presence of 1 μg ml⁻¹ DcR3-Fc (filled circles), Fas-Fc (open circles) or human IgG1 (triangles), and apoptosis was determined at the indicated time points. **c**, Peripheral blood T cells were stimulated with PHA and interleukin-2, followed by control (white bars) or anti-CD3 antibody (filled bars), together with phosphate-buffered saline (PBS), human IgG1, Fas-Fc, or DcR3-Fc (10 μg ml⁻¹). After 16 h, apoptosis of CD4⁺ cells was determined (mean ± s.e.m. of results from five donors). **d**, Peripheral blood natural killer cells were incubated with ⁵¹Cr-labelled Jurkat cells in the presence of DcR3-Fc (filled circles), Fas-Fc (open circles) or human IgG1 (triangles), and target-cell death was determined by release of ⁵¹Cr (mean ± s.d. for two donors, each in triplicate).

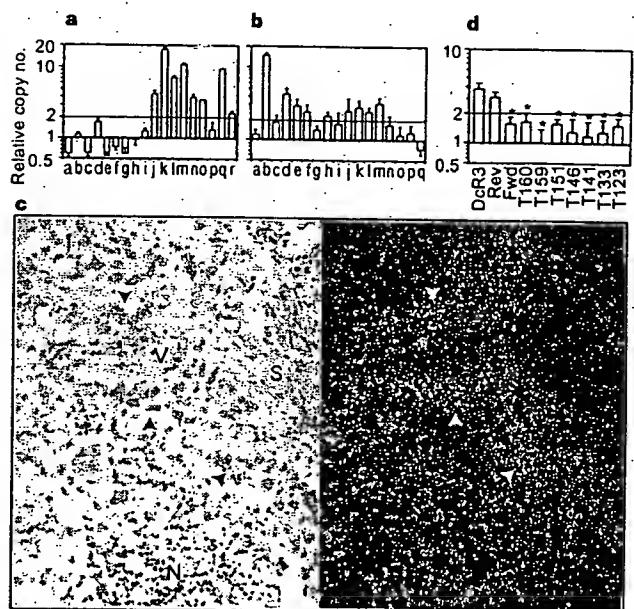


Figure 4 Genomic amplification of DcR3 in tumours. **a**, Lung cancers, comprising eight adenocarcinomas (c, d, f, g, h, j, k, r), seven squamous-cell carcinomas (a, e, m, n, o, p, q), one non-small-cell carcinoma (b), one small-cell carcinoma (i), and one bronchial adenocarcinoma (l). The data are means ± s.d. of 2 experiments done in duplicate. **b**, Colon tumours, comprising 17 adenocarcinomas. Data are means ± s.e.m. of five experiments done in duplicate. **c**, *In situ* hybridization analysis of DcR3 mRNA expression in a squamous-cell carcinoma of the lung. A representative bright-field image (left) and the corresponding dark-field image (right) show DcR3 mRNA over infiltrating malignant epithelium (arrowheads). Adjacent non-malignant stroma (S), blood vessel (V) and necrotic tumour tissue (N) are also shown. **d**, Average amplification of DcR3 compared with amplification of neighbouring genomic regions (reverse and forward; Rev and Fwd), the DcR3-linked marker T160, and other chromosome-20 markers, in the nine colon tumours showing DcR3 amplification of twofold or more (b). Data are from two experiments done in duplicate. Asterisk indicates P < 0.01 for a Student's t-test comparing each marker with DcR3.

FasL binding; hence, it may represent a third mechanism of extracellular regulation of FasL activity. A decoy receptor that modulates the function of the cytokine interleukin-1 has been described²¹. In addition, two decoy receptors that belong to the TNFR family, DcR1 and DcR2, regulate the FasL-related apoptosis-inducing molecule Apo2L²². Unlike DcR1 and DcR2, which are membrane-associated proteins, DcR3 is directly secreted into the extracellular space. One other secreted TNFR-family member is OPG³, which shares greater sequence homology with DcR3 (31%) than do DcR1 (17%) or DcR2 (19%); OPG functions as a third decoy for Apo2L¹⁹. Thus, DcR3 and OPG define a new subset of TNFR-family members that function as secreted decoys to modulate ligands that induce apoptosis. Pox viruses produce soluble TNFR homologues that neutralize specific TNF-family ligands, thereby modulating the antiviral immune response². Our results indicate that a similar mechanism, namely, production of a soluble decoy receptor for FasL, may contribute to immune evasion by certain tumours.

Methods

Isolation of DcR3 cDNA. Several overlapping ESTs in GenBank (accession numbers AA025672, AA025673 and W67560) and in Lifeseq™ (Incyte Pharmaceuticals; accession numbers 1339238, 1533571, 1533650, 1542861, 1789372 and 2207027) showed similarity to members of the TNFR family. We screened human cDNA libraries by PCR with primers based on the region of EST consensus; fetal lung was positive for a product of the expected size. By hybridization to a PCR-generated probe based on the ESTs, one positive clone (DNA30942) was identified. When searching for potential alternatively spliced forms of DcR3 that might encode a transmembrane protein, we isolated 50 more clones; the coding regions of these clones were identical in size to that of the initial clone (data not shown).

Fc-fusion proteins (immunoadhesins). The entire DcR3 sequence, or the ectodomain of Fas or TNFR1, was fused to the hinge and Fc region of human IgG1, expressed in insect SF9 cells or in human 293 cells, and purified as described²³.

Fluorescence-activated cell sorting (FACS) analysis. We transfected 293 cells using calcium phosphate or Effectene (Qiagen) with pRK5 vector or pRK5 encoding full-length human FasL⁴ (2 µg), together with pRK5 encoding CrmA (2 µg) to prevent cell death. After 16 h, the cells were incubated with biotinylated DcR3-Fc or TNFR1-Fc and then with phycoerythrin-conjugated streptavidin (GibcoBRL), and were assayed by FACS. The data were analysed by Kolmogorov-Smirnov statistical analysis. There was some detectable staining of vector-transfected cells by DcR3-Fc; as these cells express little FasL (data not shown), it is possible that DcR3 recognized some other factor that is expressed constitutively on 293 cells.

Immunoprecipitation. Human 293 cells were transfected as above, and metabolically labelled with [³⁵S]cysteine and [³⁵S]methionine (0.5 mCi; Amersham). After 16 h of culture in the presence of z-VAD-fmk (10 µM), the medium was immunoprecipitated with DcR3-Fc, Fas-Fc or TNFR1-Fc (5 µg), followed by protein A-Sepharose (Repligen). The precipitates were resolved by SDS-PAGE and visualized on a phosphorimager (Fuji BAS2000). Alternatively, purified, Flag-tagged soluble FasL (1 µg) (Alexis) was incubated with each Fc-fusion protein (1 µg), precipitated with protein A-Sepharose, resolved by SDS-PAGE and visualized by immunoblotting with rabbit anti-FasL antibody (Oncogene Research).

Analysis of complex formation. Flag-tagged soluble FasL (25 µg) was incubated with buffer or with DcR3-Fc (40 µg) for 1.5 h at 24 °C. The reaction was loaded onto a Superdex 200 HR 10/30 column (Pharmacia) and developed with PBS; 0.6-ml fractions were collected. The presence of DcR3-Fc-FasL complex in each fraction was analysed by placing 100 µl aliquots into microtitre wells precoated with anti-human IgG (Boehringer) to capture DcR3-Fc, followed by detection with biotinylated anti-Flag antibody Bio.M2 (Kodak) and streptavidin-horseradish peroxidase (Amersham). Calibration of the column indicated an apparent relative molecular mass of the complex of 420K (data not shown), which is consistent with a stoichiometry of two DcR3-Fc homodimers to two soluble FasL homotrimers.

Equilibrium binding analysis. Microtitre wells were coated with anti-human

IgG, blocked with 2% BSA in PBS. DcR3-Fc or Fas-Fc was added, followed by serially diluted Flag-tagged soluble FasL. Bound ligand was detected with anti-Flag antibody as above. In the competition assay, Fas-Fc was immobilized as above, and the wells were blocked with excess IgG1 before addition of Flag-tagged soluble FasL plus DcR3-Fc.

T-cell AICD. CD3⁺ lymphocytes were isolated from peripheral blood of individual donors using anti-CD3 magnetic beads (Miltenyi Biotec), stimulated with phytohaemagglutinin (PHA; 2 µg ml⁻¹) for 24 h, and cultured in the presence of interleukin-2 (100 U ml⁻¹) for 5 days. The cells were plated in wells coated with anti-CD3 antibody (Pharmingen) and analysed for apoptosis 16 h later by FACS analysis of annexin-V-binding of CD4⁺ cells²⁴.

Natural killer cell activity. Natural killer cells were isolated from peripheral blood of individual donors using anti-CD56 magnetic beads (Miltenyi Biotec), and incubated for 16 h with ⁵¹Cr-loaded Jurkat cells at an effector-to-target ratio of 1:1 in the presence of DcR3-Fc, Fas-Fc or human IgG1. Target-cell death was determined by release of ⁵¹Cr in effector-target cocultures relative to release of ⁵¹Cr by detergent lysis of equal numbers of Jurkat cells.

Gene-amplification analysis. Surgical specimens were provided by J. Kern (lung tumours) and P. Quirke (colon tumours). Genomic DNA was extracted (Qiagen) and the concentration was determined using Hoechst dye 33258 intercalation fluorometry. Amplification was determined by quantitative PCR¹⁸ using a TaqMan instrument (ABI). The method was validated by comparison of PCR and Southern hybridization data for the Myc and HER-2 oncogenes (data not shown). Gene-specific primers and fluorogenic probes were designed on the basis of the sequence of DcR3 or of nearby regions identified on a BAC carrying the human DcR3 gene; alternatively, primers and probes were based on Stanford Human Genome Center marker AFM218xe7 (T160), which is linked to DcR3 (likelihood score = 5.4), SHGC-36268 (T159), the nearest available marker which maps to ~500 kilobases from T160, and five extra markers that span chromosome 20. The DcR3-specific primer sequences were 5'-CTTCTTCGCGCAGCTG-3' and 5'-ATCAGCCGCGCACCAG-3' and the fluorogenic probe sequence was 5'-(FAM-ACACGATGCGTGCTCAAGCAG AAp-(TAMARA), where FAM is 5'-fluorescein phosphoramidite. Relative gene-copy numbers were derived using the formula 2^(ΔCT), where ΔCT is the difference in amplification cycles required to detect DcR3 in peripheral blood lymphocyte DNA compared to test DNA.

Received 24 September; accepted 6 November 1998.

- Nagata, S. Apoptosis by death factor. *Cell* 88, 355-365 (1997).
- Smith, C. A., Farrah, T. & Goodwin, R. G. The TNF receptor superfamily of cellular and viral proteins: activation, costimulation, and death. *Cell* 76, 959-962 (1994).
- Simonet, W. S. et al. Osteoprotegerin: a novel secreted protein involved in the regulation of bone density. *Cell* 89, 309-319 (1997).
- Suda, T., Takahashi, T., Golstein, P. & Nagata, S. Molecular cloning and expression of Fas ligand, a novel member of the TNF family. *Cell* 75, 1169-1178 (1993).
- Pennica, D. et al. Human tumour necrosis factor: precursor structure, expression and homology to lymphotxin. *Nature* 312, 724-729 (1984).
- Pitti, R. M. et al. Induction of apoptosis by Apo-2 ligand, a new member of the tumor necrosis factor receptor family. *J. Biol. Chem.* 271, 12687-12690 (1996).
- Wiley, S. R. et al. Identification and characterization of a new member of the TNF family that induces apoptosis. *Immunity* 3, 673-682 (1995).
- Marsters, S. A. et al. Identification of a ligand for the death-domain-containing receptor Apo3. *Curr. Biol.* 8, 525-528 (1998).
- Chicheportiche, Y. et al. TWEAK, a new secreted ligand in the TNF family that weakly induces apoptosis. *J. Biol. Chem.* 272, 32401-32410 (1997).
- Wong, B. R. et al. TRANCE is a novel ligand of the TNF family that activates c-Jun-N-terminal kinase in T cells. *J. Biol. Chem.* 272, 25190-25194 (1997).
- Anderson, D. M. et al. A homologue of the TNF receptor and its ligand enhance T-cell growth and dendritic-cell function. *Nature* 390, 175-179 (1997).
- Lacey, D. L. et al. Osteoprotegerin ligand is a cytokine that regulates osteoclast differentiation and activation. *Cell* 93, 165-176 (1998).
- Dhein, J., Walczak, H., Baumler, C., Debatin, K. M. & Krammer, P. H. Autocrine T-cell suicide mediated by Apo1(Fas/CD95). *Nature* 373, 438-441 (1995).
- Arase, H., Arase, N. & Saito, T. Fas-mediated cytotoxicity by freshly isolated natural killer cells. *J. Exp. Med.* 181, 1235-1238 (1995).
- Medvedev, A. E. et al. Regulation of Fas and Fas ligand expression in NK cells by cytokines and the involvement of Fas ligand in NK/LAK cell-mediated cytotoxicity. *Cytokine* 9, 394-404 (1997).
- Moretta, A. Mechanisms in cell-mediated cytotoxicity. *Cell* 90, 13-18 (1997).
- Tanaka, M., Imai, T., Adachi, M. & Nagata, S. Downregulation of Fas ligand by shedding. *Nature Med.* 4, 31-36 (1998).
- Gelmini, S. et al. Quantitative PCR-based homogeneous assay with fluorogenic probes to measure c-erbB-2 oncogene amplification. *Clin. Chem.* 43, 752-758 (1997).
- Emery, I. G. et al. Osteoprotegerin is a receptor for the cytotoxic ligand TRAIL. *J. Biol. Chem.* 273, 14363-14367 (1998).
- Wallach, D. Placing death under control. *Nature* 388, 123-125 (1997).
- Collotta, F. et al. Interleukin-1 type II receptor: a decoy target for IL-1 that is regulated by IL-4. *Science* 261, 472-475 (1993).

22. Ashkenazi, A. & Dixit, V. M. Death receptors: signaling and modulation. *Science* 281, 1305–1308 (1998).
23. Ashkenazi, A. & Chomow, S. M. Immunoadhesins as research tools and therapeutic agents. *Curr. Opin. Immunol.* 9, 195–200 (1997).
24. Marsters, S. *et al.* Activation of apoptosis by Apo-2 ligand is independent of FADD but blocked by CrmA. *Curr. Biol.* 6, 750–752 (1996).

Acknowledgements. We thank C. Clark, D. Pennica and V. Dixit for comments, and J. Kern and P. Quirke for tumour specimens.

Correspondence and requests for materials should be addressed to A.A. (e-mail: aa@gene.com). The GenBank accession number for the DcR3 cDNA sequence is AF104419.

Crystal structure of the ATP-binding subunit of an ABC transporter

Li-Wei Hung*, Iris Xiaoyan Wang†, Kishiko Nikaido†, Pei-Qi Liu†, Giovanna Ferro-Luzzi Ames† & Sung-Hou Kim*‡

* E. O. Lawrence Berkeley National Laboratory, † Department of Molecular and Cell Biology, and ‡ Department of Chemistry, University of California at Berkeley, Berkeley, California 94720, USA

ABC transporters (also known as traffic ATPases) form a large family of proteins responsible for the translocation of a variety of compounds across membranes of both prokaryotes and eukaryotes¹. The recently completed *Escherichia coli* genome sequence revealed that the largest family of paralogous *E. coli* proteins is composed of ABC transporters². Many eukaryotic proteins of medical significance belong to this family, such as the cystic fibrosis transmembrane conductance regulator (CFTR), the P-glycoprotein (or multidrug-resistance protein) and the heterodimeric transporter associated with antigen processing (Tap1–Tap2). Here we report the crystal structure at 1.5 Å resolution of HisP, the ATP-binding subunit of the histidine permease, which is an ABC transporter from *Salmonella typhimurium*. We correlate the details of this structure with the biochemical, genetic and biophysical properties of the wild-type and several mutant HisP proteins. The structure provides a basis for understanding properties of ABC transporters and of defective CFTR proteins.

ABC transporters contain four structural domains: two nucleotide-binding domains (NBDs), which are highly conserved throughout the family, and two transmembrane domains¹. In prokaryotes these domains are often separate subunits which are assembled into a membrane-bound complex; in eukaryotes the domains are generally fused into a single polypeptide chain. The periplasmic histidine permease of *S. typhimurium* and *E. coli*^{3–5} is a well-characterized ABC transporter that is a good model for this superfamily. It consists of a membrane-bound complex, HisQMP₂, which comprises integral membrane subunits, HisQ and HisM, and two copies of HisP, the ATP-binding subunit. HisP, which has properties intermediate between those of integral and peripheral membrane proteins⁶, is accessible from both sides of the membrane, presumably by its interaction with HisQ and HisM⁶. The two HisP subunits form a dimer, as shown by their cooperativity in ATP hydrolysis⁵, the requirement for both subunits to be present for activity⁴, and the formation of a HisP dimer upon chemical cross-linking. Soluble HisP also forms a dimer⁷. HisP has been purified and characterized in an active soluble form³ which can be reconstituted into a fully active membrane-bound complex⁴.

The overall shape of the crystal structure of the HisP monomer is that of an 'L' with two thick arms (arm I and arm II); the ATP-binding pocket is near the end of arm I (Fig. 1). A six-stranded β -sheet ($\beta 3$ and $\beta 8$ – $\beta 12$) spans both arms of the L, with a domain of α - plus β -type structure ($\beta 1$, $\beta 2$, $\beta 4$ – $\beta 7$, $\alpha 1$ and $\alpha 2$) on one side (within arm I) and a domain of mostly α -helices ($\alpha 3$ – $\alpha 9$) on the

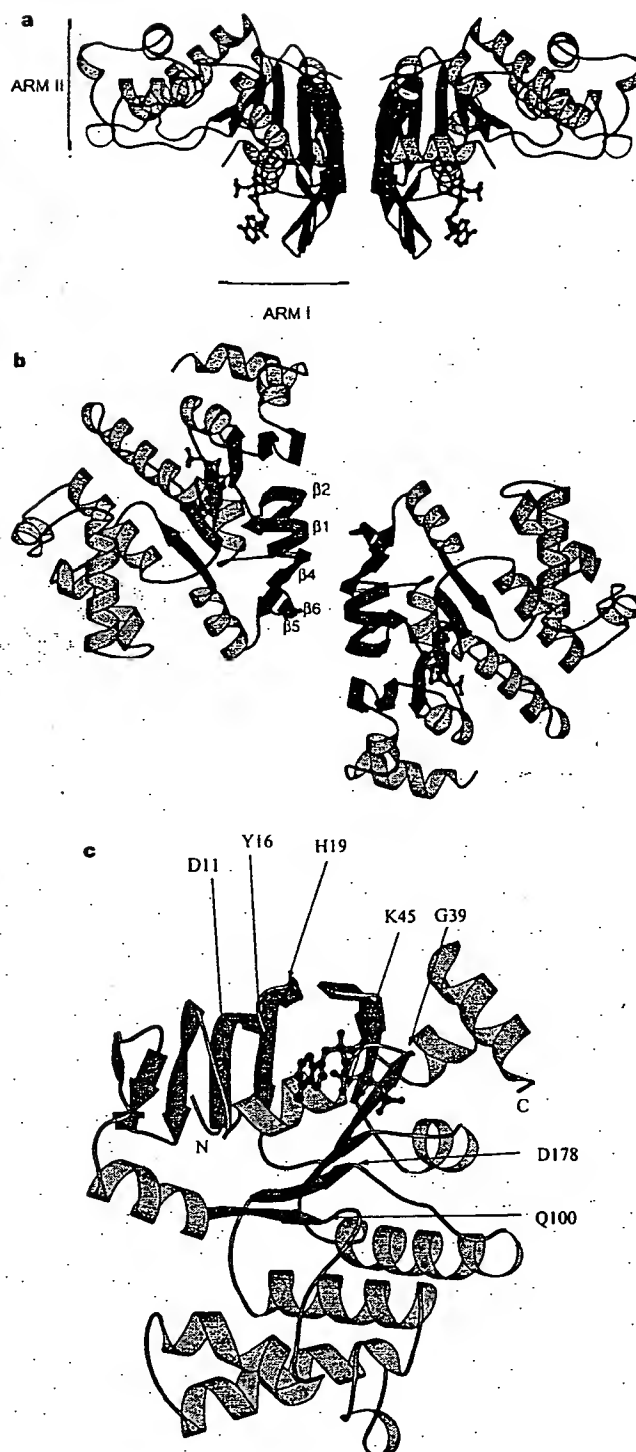


Figure 1. Crystal structure of HisP. **a**, View of the dimer along an axis perpendicular to its two-fold axis. The top and bottom of the dimer are suggested to face towards the periplasmic and cytoplasmic sides, respectively (see text). The thickness of arm II is about 25 Å, comparable to that of membrane. α -Helices are shown in orange and β -sheets in green. **b**, View along the two-fold axis of the HisP dimer, showing the relative displacement of the monomers not apparent in **a**. The β -strands at the dimer interface are labelled. **c**, View of one monomer from the bottom of arm I, as shown in **a**, towards arm II, showing the ATP-binding pocket. **a**–**c**, The protein and the bound ATP are in 'ribbon' and 'ball-and-stick' representations, respectively. Key residues discussed in the text are indicated in **c**. These figures were prepared with MOLSCRIPT⁸. N, amino terminus; C, C terminus.

NOVEL APPROACH TO QUANTITATIVE POLYMERASE CHAIN REACTION USING REAL-TIME DETECTION: APPLICATION TO THE DETECTION OF GENE AMPLIFICATION IN BREAST CANCER

Ivan BIÈCHE^{1,2}, Martine OLIVI¹, Marie-Hélène CHAMPÈME², Dominique VIDAUD¹, Rosette LIDEREAU² and Michel VIDAUD^{1*}

¹Laboratoire de Génétique Moléculaire, Faculté des Sciences Pharmaceutiques et Biologiques de Paris, Paris, France

²Laboratoire d'Oncogénétique, Centre René Huguenin, St-Cloud, France

Gene amplification is a common event in the progression of human cancers, and amplified oncogenes have been shown to have diagnostic, prognostic and therapeutic relevance. A kinetic quantitative polymerase-chain-reaction (PCR) method, based on fluorescent TaqMan methodology and a new instrument (ABI Prism 7700 Sequence Detection System) capable of measuring fluorescence in real-time, was used to quantify gene amplification in tumor DNA. Reactions are characterized by the point during cycling when PCR amplification is still in the exponential phase, rather than the amount of PCR product accumulated after a fixed number of cycles. None of the reaction components is limited during the exponential phase, meaning that values are highly reproducible in reactions starting with the same copy number. This greatly improves the precision of DNA quantification. Moreover, real-time PCR does not require post-PCR sample handling, thereby preventing potential PCR-product carry-over contamination; it possesses a wide dynamic range of quantification and results in much faster and higher sample throughput. The real-time PCR method, was used to develop and validate a simple and rapid assay for the detection and quantification of the 3 most frequently amplified genes (*myc*, *ccnd1* and *erbB2*) in breast tumors. Extra copies of *myc*, *ccnd1* and *erbB2* were observed in 10, 23 and 15%, respectively, of 108 breast-tumor DNA; the largest observed numbers of gene copies were 4.6, 18.6 and 15.1, respectively. These results correlated well with those of Southern blotting. The use of this new semi-automated technique will make molecular analysis of human cancers simpler and more reliable, and should find broad applications in clinical and research settings. *Int. J. Cancer* 78:661–666, 1998.

© 1998 Wiley-Liss, Inc.

Gene amplification plays an important role in the pathogenesis of various solid tumors, including breast cancer, probably because over-expression of the amplified target genes confers a selective advantage. The first technique used to detect genomic amplification was cytogenetic analysis. Amplification of several chromosome regions, visualized either as extrachromosomal double minutes (dmns) or as integrated homogeneously staining regions (HSRs), are among the main visible cytogenetic abnormalities in breast tumors. Other techniques such as comparative genomic hybridization (CGH) (Kallioniemi *et al.*, 1994) have also been used in broad searches for regions of increased DNA copy numbers in tumor cells, and have revealed some 20 amplified chromosome regions in breast tumors. Positional cloning efforts are underway to identify the critical gene(s) in each amplified region. To date, genes known to be amplified frequently in breast cancers include *myc* (8q24), *ccnd1* (11q13), and *erbB2* (17q12-q21) (for review, see Bièche and Lidereau, 1995).

Amplification of the *myc*, *ccnd1*, and *erbB2* proto-oncogenes should have clinical relevance in breast cancer, since independent studies have shown that these alterations can be used to identify sub-populations with a worse prognosis (Berns *et al.*, 1992; Schuurings *et al.*, 1992; Slamon *et al.*, 1987). Muss *et al.* (1994) suggested that these gene alterations may also be useful for the prediction and assessment of the efficacy of adjuvant chemotherapy and hormone therapy.

However, published results diverge both in terms of the frequency of these alterations and their clinical value. For instance, over 500 studies in 10 years have failed to resolve the controversy

surrounding the link suggested by Slamon *et al.* (1987) between *erbB2* amplification and disease progression. These discrepancies are partly due to the clinical, histological and ethnic heterogeneity of breast cancer, but technical considerations are also probably involved.

Specific genes (DNA) were initially quantified in tumor cells by means of blotting procedures such as Southern and slot blotting. These batch techniques require large amounts of DNA (5–10 µg/reaction) to yield reliable quantitative results. Furthermore, meticulous care is required at all stages of the procedures to generate blots of sufficient quality for reliable dosage analysis. Recently, PCR has proven to be a powerful tool for quantitative DNA analysis, especially with minimal starting quantities of tumor samples (small, early-stage tumors and formalin-fixed, paraffin-embedded tissues).

Quantitative PCR can be performed by evaluating the amount of product either after a given number of cycles (end-point quantitative PCR) or after a varying number of cycles during the exponential phase (kinetic quantitative PCR). In the first case, an internal standard distinct from the target molecule is required to ascertain PCR efficiency. The method is relatively easy but implies generating, quantifying and storing an internal standard for each gene studied. Nevertheless, it is the most frequently applied method to date.

One of the major advantages of the kinetic method is its rapidity in quantifying a new gene, since no internal standard is required (an external standard curve is sufficient). Moreover, the kinetic method has a wide dynamic range (at least 5 orders of magnitude), giving an accurate value for samples differing in their copy number. Unfortunately, the method is cumbersome and has therefore been rarely used. It involves aliquot sampling of each assay mix at regular intervals and quantifying, for each aliquot, the amplification product. Interest in the kinetic method has been stimulated by a novel approach using fluorescent TaqMan methodology and a new instrument (ABI Prism 7700 Sequence Detection System) capable of measuring fluorescence in real time (Gibson *et al.*, 1996; Heid *et al.*, 1996). The TaqMan reaction is based on the 5' nuclease assay first described by Holland *et al.* (1991). The latter uses the 5' nuclease activity of Taq polymerase to cleave a specific fluorogenic oligonucleotide probe during the extension phase of PCR. The approach uses dual-labeled fluorogenic hybridization probes (Lee *et al.*, 1993). One fluorescent dye, co-valently linked to the 5' end of the oligonucleotide, serves as a reporter [FAM (i.e., 6-carboxy-fluorescein)] and its emission spectrum is quenched by a second fluorescent dye, TAMRA (i.e., 6-carboxy-tetramethyl-rhodamine) attached to the 3' end. During the extension phase of the PCR

Grant sponsors: Association Pour la Recherche sur le Cancer and Ministère de l'Enseignement Supérieur et de la Recherche.

*Correspondence to: Laboratoire de Génétique Moléculaire, Faculté des Sciences Pharmaceutiques et Biologiques de Paris, 4 Avenue de l'Observatoire, F-75006 Paris, France. Fax: (33)1-4407-1754. E-mail: mvidauid@teaser.fr

Received 2 May 1998; Revised 30 June 1998

cycle, the fluorescent hybridization probe is hydrolyzed by the 5'-3' nucleolytic activity of DNA polymerase. Nuclease degradation of the probe releases the quenching of FAM fluorescence emission, resulting in an increase in peak fluorescence emission. The fluorescence signal is normalized by dividing the emission intensity of the reporter dye (FAM) by the emission intensity of a reference dye (i.e., ROX, 6-carboxy-X-rhodamine) included in TaqMan buffer, to obtain a ratio defined as the R_n (normalized reporter) for a given reaction tube. The use of a sequence detector enables the fluorescence spectra of all 96 wells of the thermal cycler to be measured continuously during PCR amplification.

The real-time PCR method offers several advantages over other current quantitative PCR methods (Celi *et al.*, 1994): (i) the probe-based homogeneous assay provides a real-time method for detecting only specific amplification products, since specific hybridization of both the primers and the probe is necessary to generate a signal; (ii) the C_t (threshold cycle) value used for quantification is measured when PCR amplification is still in the log phase of PCR product accumulation. This is the main reason why C_t is a more reliable measure of the starting copy number than are end-point measurements, in which a slight difference in a limiting component can have a drastic effect on the amount of product; (iii) use of C_t values gives a wider dynamic range (at least 5 orders of magnitude), reducing the need for serial dilution; (iv) The real-time PCR method is run in a closed-tube system and requires no post-PCR sample handling, thus avoiding potential contamination; (v) the system is highly automated, since the instrument continuously measures fluorescence in all 96 wells of the thermal cycler during PCR amplification and the corresponding software processes, and analyzes the fluorescence data; (vi) the assay is rapid, as results are available just one minute after thermal cycling is complete; (vii) the sample throughput of the method is high, since 96 reactions can be analyzed in 2 hr.

Here, we applied this semi-automated procedure to determine the copy numbers of the 3 most frequently amplified genes in breast tumors (*myc*, *ccnd1* and *erbB2*), as well as 2 genes (*alb* and *app*) located in a chromosome region in which no genetic changes have been observed in breast tumors. The results for 108 breast tumors were compared with previous Southern-blot data for the same samples.

MATERIAL AND METHODS

Tumor and blood samples

Samples were obtained from 108 primary breast tumors removed surgically from patients at the Centre René Huguenin; none of the patients had undergone radiotherapy or chemotherapy. Immediately after surgery, the tumor samples were placed in liquid nitrogen until extraction of high-molecular-weight DNA. Patients were included in this study if the tumor sample used for DNA preparation contained more than 60% of tumor cells (histological analysis). A blood sample was also taken from 18 of the same patients.

DNA was extracted from tumor tissue and blood leukocytes according to standard methods.

Real-time PCR

Theoretical basis. Reactions are characterized by the point during cycling when amplification of the PCR product is first detected, rather than by the amount of PCR product accumulated after a fixed number of cycles. The higher the starting copy number of the genomic DNA target, the earlier a significant increase in fluorescence is observed. The parameter C_t (threshold cycle) is defined as the fractional cycle number at which the fluorescence generated by cleavage of the probe passes a fixed threshold above baseline. The target gene copy number in unknown samples is quantified by measuring C_t and by using a standard curve to determine the starting copy number. The precise amount of genomic DNA (based on optical density) and its quality (i.e., lack

of extensive degradation) are both difficult to assess. We therefore also quantified a control gene (*alb*) mapping to chromosome region 4q11-q13, in which no genetic alterations have been found in breast-tumor DNA by means of CGH (Kallioniemi *et al.*, 1994).

Thus, the ratio of the copy number of the target gene to the copy number of the *alb* gene normalizes the amount and quality of genomic DNA. The ratio defining the level of amplification is termed "N", and is determined as follows:

$$N = \frac{\text{copy number of target gene (app, myc, ccnd1, erbB2)}}{\text{copy number of reference gene (alb)}}$$

Primers, probes, reference human genomic DNA and PCR consumables. Primers and probes were chosen with the assistance of the computer programs Oligo 4.0 (National Biosciences, Plymouth, MN), EuGene (Daniben Systems, Cincinnati, OH) and Primer Express (Perkin-Elmer Applied Biosystems, Foster City, CA).

Primers were purchased from DNAScience (Malvern, PA) and probes from Perkin-Elmer Applied Biosystems.

Nucleotide sequences for the oligonucleotide hybridization probes and primers are available on request.

The TaqMan PCR Core reagent kit, MicroAmp optical tubes, and MicroAmp caps were from Perkin-Elmer Applied Biosystems.

Standard-curve construction. The kinetic method requires a standard curve. The latter was constructed with serial dilutions of specific PCR products, according to Piatak *et al.* (1993). In practice, each specific PCR product was obtained by amplifying 20 ng of a standard human genomic DNA (Boehringer, Mannheim, Germany) with the same primer pairs as those used later for real-time quantitative PCR. The 5 PCR products were purified using MicroSpin S-400 HR columns (Pharmacia, Uppsala, Sweden) electrophoresed through an acrylamide gel and stained with ethidium bromide to check their quality. The PCR products were then quantified spectrophotometrically and pooled, and serially diluted 10-fold in mouse genomic DNA (Clontech, Palo Alto, CA) at a constant concentration of 2 ng/ μ l. The standard curve used for real-time quantitative PCR was based on serial dilutions of the pool of PCR products ranging from 10^{-7} (10^5 copies of each gene) to 10^{-10} (10^2 copies). This series of diluted PCR products was aliquoted and stored at -80°C until use.

The standard curve was validated by analyzing 2 known quantities of calibrator human genomic DNA (20 ng and 50 ng).

PCR amplification. Amplification mixes (50 μ l) contained the sample DNA (around 20 ng, around 6600 copies of disomic genes), $10\times$ TaqMan buffer (5 μ l), 200 μ M dATP, dCTP, dGTP, and 400 μ M dUTP, 5 mM MgCl_2 , 1.25 units of AmpliTaq Gold, 0.5 units of AmpErase uracil N-glycosylase (UNG), 200 nM each primer and 100 nM probe. The thermal cycling conditions comprised 2 min at 50°C and 10 min at 95°C . Thermal cycling consisted of 40 cycles at 95°C for 15 s and 65°C for 1 min. Each assay included: a standard curve (from 10^5 to 10^2 copies) in duplicate, a no-template control, 20 ng and 50 ng of calibrator human genomic DNA (Boehringer) in triplicate, and about 20 ng of unknown genomic DNA in triplicate (26 samples can thus be analyzed on a 96-well microplate). All samples with a coefficient of variation (CV) higher than 10% were retested.

All reactions were performed in the ABI Prism 7700 Sequence Detection System (Perkin-Elmer Applied Biosystems), which detects the signal from the fluorogenic probe during PCR.

Equipment for real-time detection. The 7700 system has a built-in thermal cycler and a laser directed via fiber optical cables to each of the 96 sample wells. A charge-coupled-device (CDD) camera collects the emission from each sample and the data are analyzed automatically. The software accompanying the 7700 system calculates C_t and determines the starting copy number in the samples.

Determination of gene amplification. Gene amplification was calculated as described above. Only samples with an N value higher than 2 were considered to be amplified.

RESULTS

To validate the method, real-time PCR was performed on genomic DNA extracted from 108 primary breast tumors, and 18 normal leukocyte DNA samples from some of the same patients. The target genes were the *myc*, *ccnd1*, and *erbB2* proto-oncogenes, and the β -amyloid precursor protein gene (*app*), which maps to a chromosome region (21q21.2) in which no genetic alterations have been found in breast tumors (Kallioniemi *et al.*, 1994). The reference disomic gene was the albumin gene (*alb*, chromosome 4q11-q13).

Validation of the standard curve and dynamic range of real-time PCR

The standard curve was constructed from PCR products serially diluted in genomic mouse DNA at a constant concentration of 2 ng/ μ l. It should be noted that the 5 primer pairs chosen to analyze the 5 target genes do not amplify genomic mouse DNA (data not shown). Figure 1 shows the real-time PCR standard curve for the *alb* gene. The dynamic range was wide (at least 4 orders of magnitude), with samples containing as few as 10^2 copies or as many as 10^5 copies.

Copy-number ratio of the 2 reference genes (*app* and *alb*)

The *app* to *alb* copy-number ratio was determined in 18 normal leukocyte DNA samples and all 108 primary breast-tumor DNA

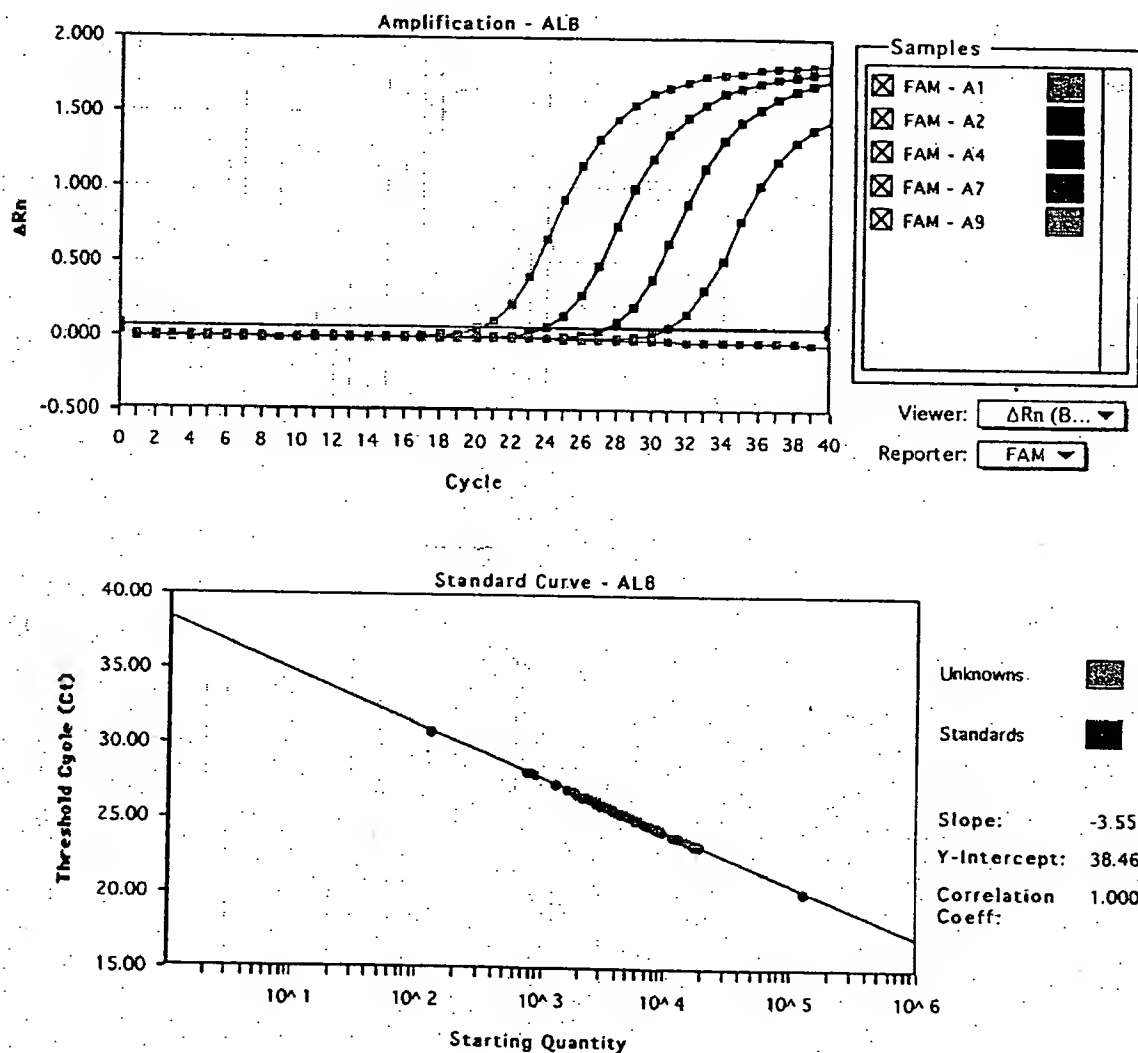


FIGURE 1 – Albumin (*alb*) gene dosage by real-time PCR. Top: Amplification plots for reactions with starting *alb* gene copy number ranging from 10^5 (A9), 10^4 (A7), 10^3 (A4) to 10^2 (A2) and a no-template control (A1). Cycle number is plotted vs. change in normalized reporter signal (ΔRn). For each reaction tube, the fluorescence signal of the reporter dye (FAM) is divided by the fluorescence signal of the passive reference dye (ROX), to obtain a ratio defined as the normalized reporter signal (Rn). ΔRn represents the normalized reporter signal (Rn) minus the baseline signal established in the first 15 PCR cycles. ΔRn increases during PCR as *alb* PCR product copy number increases until the reaction reaches a plateau. C_t (threshold cycle) represents the fractional cycle number at which a significant increase in Rn above a baseline signal (horizontal black line) can first be detected. Two replicate plots were performed for each standard sample, but the data for only one are shown here. Bottom: Standard curve plotting log starting copy number vs. C_t (threshold cycle). The black dots represent the data for standard samples plotted in duplicate and the red dots the data for unknown genomic DNA samples plotted in triplicate. The standard curve shows 4 orders of linear dynamic range.

samples. We selected these 2 genes because they are located in 2 chromosome regions (*app*, 21q21.2; *alb*, 4q11-q13) in which no obvious genetic changes (including gains or losses) have been observed in breast cancers (Kallioniemi *et al.*, 1994). The ratio for the 18 normal leukocyte DNA samples fell between 0.7 and 1.3 (mean 1.02 ± 0.21), and was similar for the 108 primary breast-tumor DNA samples (0.6 to 1.6, mean 1.06 ± 0.25), confirming that *alb* and *app* are appropriate reference disomic genes for breast-tumor DNA. The low range of the ratios also confirmed that the nucleotide sequences chosen for the primers and probes were not polymorphic, as mismatches of their primers or probes with the subject's DNA would have resulted in differential amplification.

myc, *ccnd1* and *erbB2* gene dose in normal leukocyte DNA

To determine the cut-off point for gene amplification in breast-cancer tissue, 18 normal leukocyte DNA samples were tested for the gene dose (N), calculated as described in "Material and Methods". The N value of these samples ranged from 0.5 to 1.3 (mean 0.84 ± 0.22) for *myc*, 0.7 to 1.6 (mean 1.06 ± 0.23) for *ccnd1* and 0.6 to 1.3 (mean 0.91 ± 0.19) for *erbB2*. Since N values for *myc*, *ccnd1* and *erbB2* in normal leukocyte DNA consistently fell between 0.5 and 1.6, values of 2 or more were considered to represent gene amplification in tumor DNA.

myc, *ccnd1* and *erbB2* gene dose in breast-tumor DNA

myc, *ccnd1* and *erbB2* gene copy numbers in the 108 primary breast tumors are reported in Table I. Extra copies of *ccnd1* were more frequent (23%, 25/108) than extra copies of *erbB2* (15%, 16/108) and *myc* (10%, 11/108), and ranged from 2 to 18.6 for *ccnd1*, 2 to 15.1 for *erbB2*, and only 2 to 4.6 for the *myc* gene. Figure 2 and Table II represent tumors in which the *ccnd1* gene was amplified 16-fold (T145), 6-fold (T133) and non-amplified (T118). The 3 genes were never found to be co-amplified in the same tumor. *erbB2* and *ccnd1* were co-amplified in only 3 cases, *myc* and *ccnd1* in 2 cases and *myc* and *erbB2* in 1 case. This favors the hypothesis that gene amplifications are independent events in breast cancer. Interestingly, 5 tumors showed a decrease of at least 50% in the *erbB2* copy number ($N < 0.5$), suggesting that they bore deletions of the 17q21 region (the site of *erbB2*). No such decrease in copy number was observed with the other 2 proto-oncogenes.

Comparison of gene dose determined by real-time quantitative PCR and Southern-blot analysis

Southern-blot analysis of *myc*, *ccnd1* and *erbB2* amplifications had previously been done on the same 108 primary breast tumors. A perfect correlation between the results of real-time PCR and Southern blot was obtained for tumors with high copy numbers ($N \geq 5$). However, there were cases (1 *myc*, 6 *ccnd1* and 4 *erbB2*) in which real-time PCR showed gene amplification whereas Southern-blot did not, but these were mainly cases with low extra copy numbers (N from 2 to 2.9).

DISCUSSION

The clinical applications of gene amplification assays are currently limited, but would certainly increase if a simple, standardized and rapid method were perfected. Gene amplification status has been studied mainly by means of Southern blotting, but this method is not sensitive enough to detect low-level gene amplification nor accurate enough to quantify the full range of amplification values. Southern blotting is also time-consuming, uses radioactive

reagents and requires relatively large amounts of high-quality genomic DNA, which means it cannot be used routinely in many laboratories. An amplification step is therefore required to determine the copy number of a given target gene from minimal quantities of tumor DNA (small early-stage tumors, cytopuncture specimens or formalin-fixed, paraffin-embedded tissues).

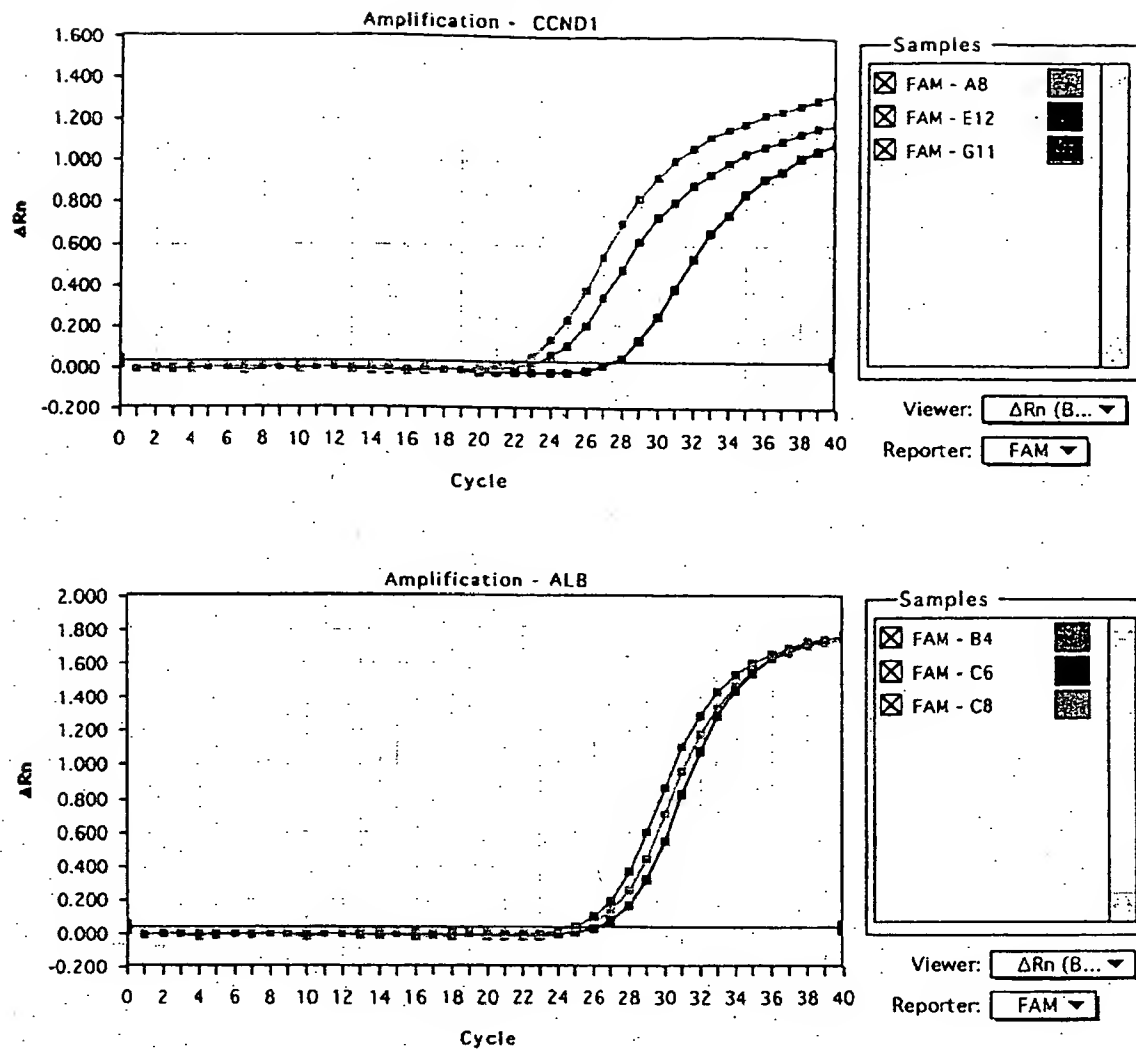
In this study, we validated a PCR method developed for the quantification of gene over-representation in tumors. The method, based on real-time analysis of PCR amplification, has several advantages over other PCR-based quantitative assays such as competitive quantitative PCR (Celi *et al.*, 1994). First, the real-time PCR method is performed in a closed-tube system, avoiding the risk of contamination by amplified products. Re-amplification of carryover PCR products in subsequent experiments can also be prevented by using the enzyme uracil N-glycosylase (UNG) (Longo *et al.*, 1990). The second advantage is the simplicity and rapidity of sample analysis, since no post-PCR manipulations are required. Our results show that the automated method is reliable. We found it possible to determine, in triplicate, the number of copies of a target gene in more than 100 tumors per day. Third, the system has a linear dynamic range of at least 4 orders of magnitude, meaning that samples do not have to contain equal starting amounts of DNA. This technique should therefore be suitable for analyzing formalin-fixed, paraffin-embedded tissues. Fourth, and above all, real-time PCR makes DNA quantification much more precise and reproducible, since it is based on C_t values rather than end-point measurement of the amount of accumulated PCR product. Indeed, the ABI-Prism 7700 Sequence Detection System enables C_t to be calculated when PCR amplification is still in the exponential phase and when none of the reaction components is rate-limiting. The within-run CV of the C_t value for calibrator human DNA (5 replicates) was always below 5%, and the between-assay precision in 5 different runs was always below 10% (data not shown). In addition, the use of a standard curve is not absolutely necessary, since the copy number can be determined simply by comparing the C_t ratio of the target gene with that of reference genes. The results obtained by the 2 methods (with and without a standard curve) are similar in our experiments (data not shown). Moreover, unlike competitive quantitative PCR, real-time PCR does not require an internal control (the design and storage of internal controls and the validation of their amplification efficiency is laborious).

The only potential disadvantage of real-time PCR, like all other PCR-based methods and solid-matrix blotting techniques (Southern blots and dot blots) is that it cannot avoid dilution artifacts inherent in the extraction of DNA from tumor cells contained in heterogeneous tissue specimens. Only FISH and immunohistochemistry can measure alterations on a cell-by-cell basis (Pauletti *et al.*, 1996; Slamon *et al.*, 1989). However, FISH requires expensive equipment and trained personnel and is also time-consuming. Moreover, FISH does not assess gene expression and therefore cannot detect cases in which the gene product is over-expressed in the absence of gene amplification, which will be possible in the future by real-time quantitative RT-PCR. Immunohistochemistry is subject to considerable variations in the hands of different teams, owing to alterations of target proteins during the procedure, the different primary antibodies and fixation methods used and the criteria used to define positive staining.

The results of this study are in agreement with those reported in the literature. (i) Chromosome regions 4q11-q13 and 21q21.2 (which bear *alb* and *app*, respectively) showed no genetic alterations in the breast-cancer samples studied here, in keeping with the results of CGH (Kallioniemi *et al.*, 1994). (ii) We found that amplifications of these 3 oncogenes were independent events, as reported by other teams (Berns *et al.*, 1992; Borg *et al.*, 1992). (iii) The frequency and degree of *myc* amplification in our breast tumor DNA series were lower than those of *ccnd1* and *erbB2* amplification, confirming the findings of Borg *et al.* (1992) and Courjal *et al.* (1997). (iv) The maxima of *ccnd1* and *erbB2* over-representation were 18-fold and 15-fold, also in keeping with earlier results (about

TABLE I - DISTRIBUTION OF AMPLIFICATION LEVEL (N) FOR *myc*, *ccnd1* AND *erbB2* GENES IN 108 HUMAN BREAST TUMORS

Gene	Amplification level (N)			
	<0.5	0.5-1.9	2-4.9	≥ 5
<i>myc</i>	0	97 (89.8%)	11 (10.2%)	0
<i>ccnd1</i>	0	83 (76.9%)	17 (15.7%)	8 (7.4%)
<i>erbB2</i>	5 (4.6%)	87 (80.6%)	8 (7.4%)	8 (7.4%)



Tumor	CCND1		ALB	
	C_t	Copy number	C_t	Copy number
■ T118	27.3	4605	26.5	4365
■ T133	23.2	61659	25.2	10092
■ T145	22.1	125892	25.6	7762

FIGURE 2 - *ccnd1* and *alb* gene dosage by real-time PCR in 3 breast tumor samples: T118 (E12, C6, black squares), T133 (G11, B4, red squares) and T145 (A8, C8, blue squares). Given the C_t of each sample, the initial copy number is inferred from the standard curve obtained during the same experiment. Triplicate plots were performed for each tumor sample, but the data for only one are shown here. The results are shown in Table II.

30-fold maximum) (Berns *et al.*, 1992; Borg *et al.*, 1992; Courjal *et al.*, 1997). (v) The *erbB2* copy numbers obtained with real-time PCR were in good agreement with data obtained with other quantitative PCR-based assays in terms of the frequency and degree of amplification (An *et al.*, 1995; Deng *et al.*, 1996; Valeron

et al., 1996). Our results also correlate well with those recently published by Gelmini *et al.* (1997), who used the TaqMan system to measure *erbB2* amplification in a small series of breast tumors ($n = 25$), but with an instrument (LS-50B luminescence spectrometer, Perkin-Elmer Applied Biosystems) which only allows end-

TABLE II - EXAMPLES OF *ccnd1* GENE DOSAGE RESULTS FROM 3 BREAST TUMORS¹

Tumor	<i>ccnd1</i>			<i>alb</i>			<i>Nccnd1/alb</i>
	Copy number	Mean	SD	Copy number	Mean	SD	
T118	4525	4603	77	4223	4325	89	1.06
	4605			4365			
	4678			4387			
T133	59821	61100	1111	9787	10137	375	6.03
	61659			10092			
	61821			10533			
T145	128563	125392	3448	7321	7672	316	16.34
	125892			7762			
	121722			7933			

¹For each sample, 3 replicate experiments were performed and the mean and the standard deviation (SD) was determined. The level of *ccnd1* gene amplification (*Nccnd1/alb*) is determined by dividing the average *ccnd1* copy number value by the average *alb* copy number value.

point measurement of fluorescence intensity. Here we report *myc* and *ccnd1* gene dosage in breast cancer by means of quantitative PCR. (vi) We found a high degree of concordance between real-time quantitative PCR and Southern blot analysis in terms of gene amplification, especially for samples with high copy numbers (≥ 5 -fold). The slightly higher frequency of gene amplification (especially *ccnd1* and *erbB2*) observed by means of real-time quantitative PCR as compared with Southern-blot analysis may be explained by the higher sensitivity of the former method. However, we cannot rule out the possibility that some tumors with a few extra

gene copies observed in real-time PCR had additional copies of an arm or a whole chromosome (trisomy, tetrasomy or polysomy) rather than true gene amplification. These 2 types of genetic alteration (polysomy and gene amplification) could be easily distinguished in the future by using an additional probe located on the same chromosome arm, but some distance from the target gene. It is noteworthy that high gene copy numbers have the greatest prognostic significance in breast carcinoma (Borg *et al.*, 1992; Slamon *et al.*, 1987).

Finally, this technique can be applied to the detection of gene deletion as well as gene amplification. Indeed, we found a decreased copy number of *erbB2* (but not of the other 2 proto-oncogenes) in several tumors; *erbB2* is located in a chromosome region (17q21) reported to contain both deletions and amplifications in breast cancer (Bièche and Lidereau, 1995).

In conclusion, gene amplification in various cancers can be used as a marker of pre-neoplasia, also for early diagnosis of cancer, staging, prognostication and choice of treatment. Southern blotting is not sufficiently sensitive, and FISH is lengthy and complex. Real-time quantitative PCR overcomes both these limitations, and is a sensitive and accurate method of analyzing large numbers of samples in a short time. It should find a place in routine clinical gene dosage.

ACKNOWLEDGEMENTS

RL is a research director at the Institut National de la Santé et de la Recherche Médicale (INSERM). We thank the staff of the Centre René Huguénin for assistance in specimen collection and patient care.

REFERENCES

- AN, H.X., NIEDERACHER, D., BECKMANN, M.W., GÖHRING, U.J., SCHARL, A., PICARD, F., VAN ROEYEN, C., SCHNÜRCH, H.G. and BENOER, H.G., *erbB2* gene amplification detected by fluorescent differential polymerase chain reaction in paraffin-embedded breast carcinoma tissues. *Int. J. Cancer* (Pred. Oncol.), 64, 291-297 (1995).
- BERNS, E.M.J.J., KLIN, J.G.M., VAN PUTTEN, W.L.J., VAN STAVEREN, I.L., PORTINGEN, H. and FOEKENS, J.A., *c-myc* amplification is a better prognostic factor than HER2/*neu* amplification in primary breast cancer. *Cancer Res.*, 52, 1107-1113 (1992).
- BIÈCHE, I. and LIDEREAU, R., Genetic alterations in breast cancer. *Genes Chrom. Cancer*, 14, 227-251 (1995).
- BORG, A., BALOETORP, B., FERNO, M., OLSSON, H. and SIGURDSSON, H., *c-myc* amplification is an independent prognostic factor in post-menopausal breast cancer. *Int. J. Cancer*, 51, 687-691 (1992).
- CELL, F.S., COHEN, M.M., ANTONARAKIS, S.E., WERTHEIMER, E., ROTH, J. and SHULDINER, A.R., Determination of gene dosage by a quantitative adaptation of the polymerase chain reaction (qPCR): rapid detection of deletions and duplications of gene sequences. *Genomics*, 21, 304-310 (1994).
- COURJAL, F., CUNY, M., SIMONY-LAFONTAINE, J., LOUASSON, G., SPEISER, P., ZEILLINGER, R., RODRIGUEZ, C. and THEILLET, C., Mapping of DNA amplifications at 15 chromosomal localizations in 1875 breast tumors: definition of phenotypic groups. *Cancer Res.*, 57, 4360-4367 (1997).
- DENG, G., YU, M., CHEN, L.C., MOORE, D., KURJUS, W., KALLIONIEMI, A., WALDMAN, F.M., COLLINS, C. and SMITH, H.S., Amplifications of oncogene *erbB-2* and chromosome 20q in breast cancer determined by differentially competitive polymerase chain reaction. *Breast Cancer Res. Treat.*, 40, 271-281 (1996).
- GELMINI, S., ORIANDO, C., SESTINI, R., VONA, G., PINZANI, P., RUOCO, L. and PAZZAGLI, M., Quantitative polymerase chain reaction-based homogeneous assay with fluorogenic probes to measure *c-erbB-2* oncogene amplification. *Clin. Chem.*, 43, 752-758 (1997).
- GIBSON, U.E.M., HEID, C.A. and WILLIAMS, P.M., A novel method for real-time quantitative RT-PCR. *Genome Res.*, 6, 995-1001 (1996).
- HEIO, C.A., STEVENS, J., LIVAK, K.J. and WILLIAMS, P.M., Real-time quantitative PCR. *Genome Res.*, 6, 986-994 (1996).
- HOLLAND, P.M., ABRAMSON, R.D., WATSON, R. and GELFANO, D.H., Detection of specific polymerase chain reaction product by utilizing the 5' to 3' exonuclease activity of *Thermus aquaticus* DNA polymerase. *Proc. nat. Acad. Sci. (Wash.)*, 88, 7276-7280 (1991).
- KALLIONIEMI, A., KALLIONIEMI, O.P., PIPER, J., TANNER, M., STOKKES, T., CHEN, L., SMITH, H.S., PINKEL, D., GRAY, J.W. and WALDMAN, F.M., Detection and mapping of amplified DNA sequences in breast cancer by comparative genomic hybridization. *Proc. nat. Acad. Sci. (Wash.)*, 91, 2156-2160 (1994).
- LEE, L.G., CONNELL, C.R. and BIOCH, W., Allelic discrimination by nick-translation PCR with fluorogenic probe. *Nucleic Acids Res.*, 21, 3761-3766 (1993).
- LONGO, N., BERNINGER, N.S. and HARTLEY, J.L., Use of uracil DNA glycosylase to control carry-over contamination in polymerase chain reactions. *Gene*, 93, 125-128 (1990).
- MUSS, H.B., THOR, A.D., BERRY, D.A., KUTE, T., LIU, E.T., KOERNER, F., CIRINCIONE, C.T., BUDMAN, D.R., WOOD, W.C., BARCOS, M. and HENGERSON, I.C., *c-erbB-2* expression and response to adjuvant therapy in women with node-positive early breast cancer. *New Engl. J. Med.*, 330, 1260-1266 (1994).
- PAULETTI, G., GODOLPHIN, W., PRESS, M.F. and SALMON, D.J., Detection and quantification of HER-2/*neu* gene amplification in human breast cancer archival material using fluorescence *in situ* hybridization. *Oncogene*, 13, 63-72 (1996).
- PIATAK, M., LUK, K.C., WILLIAMS, B. and LIFSON, J.D., Quantitative competitive polymerase chain reaction for accurate quantitation of HIV DNA and RNA species. *Biotechniques*, 14, 70-80 (1993).
- SCHUURING, E., VERHOEVEN, E., VAN TINTEREN, H., PETERSE, J.L., NUNNIK, B., THUNNISSEN, F.B.J.M., DEVILEE, P., CORNELISSE, C.J., VAN DE VIVER, M.J., MOOT, W.J. and MICHALIDES, R.J.A.M., Amplification of genes within the chromosome 11q13 region is indicative of poor prognosis in patients with operable breast cancer. *Cancer Res.*, 52, 5229-5234 (1992).
- SLAMON, D.J., CLARK, G.M., WONG, S.G., LEVIN, W.S., ULLRICH, A. and MCQUIRE, W.L., Human breast cancer: correlation of relapse and survival with amplification of the HER-2/*neu* oncogene. *Science*, 235, 177-182 (1987).
- SLAMON, D.J., GODOLPHIN, W., JONES, L.A., HOLT, J.A., WONG, S.G., KEITH, D.E., LEVIN, W.J., STUART, S.G., UDOLF, J., ULLRICH, A. and PRESS, M.F., Studies of the HER-2/*neu* proto-oncogene in human breast and ovarian cancer. *Science*, 244, 707-712 (1989).
- VALERON, P.F., CHIRINO, R., FERNANDEZ, L., TORRES, S., NAVARRO, D., AGUIAR, J., CABRERA, J.J., DIAZ-CHICO, B.N. and DIAZ-CHICO, J.C., Validation of a differential PCR and an ELISA procedure in studying HER-2/*neu* status in breast cancer. *Int. J. Cancer*, 65, 129-133 (1996).

IN THE UNITED STATES PATENT AND TRADEMARK OFFICE

Applicant : Ashkenazi et al.
App. No. : 09/903,925
Filed : July 11, 2001
For : SECRETED AND
TRANSMEMBRANE
POLYPEPTIDES AND NUCLEIC
ACIDS ENCODING THE SAME
Examiner : Hamud, Fozia M

Group Art Unit 1647

CERTIFICATE OF EXPRESS MAILING

I hereby certify that this correspondence is being deposited with the United States Postal Service with sufficient postage as first class mail in an envelope addressed to Commissioner of Patents, Washington D.C. 20231 on:

(Date)

Commissioner of Patents
P.O. Box 1450
Alexandria, VA 22313-1450

DECLARATION OF AVI ASHKENAZI, Ph.D UNDER 37 C.F.R. § 1.132

I, Avi Ashkenazi, Ph.D. declare and say as follows: -

1. I am Director and Staff Scientist at the Molecular Oncology Department of Genentech, Inc., South San Francisco, CA 94080.
2. I joined Genentech in 1988 as a postdoctoral fellow. Since then, I have investigated a variety of cellular signal transduction mechanisms, including apoptosis, and have developed technologies to modulate such mechanisms as a means of therapeutic intervention in cancer and autoimmune disease. I am currently involved in the investigation of a series of secreted proteins over-expressed in tumors, with the aim to identify useful targets for the development of therapeutic antibodies for cancer treatment.
3. My scientific Curriculum Vitae, including my list of publications, is attached to and forms part of this Declaration (Exhibit A).
4. Gene amplification is a process in which chromosomes undergo changes to contain multiple copies of certain genes that normally exist as a single copy, and is an important factor in the pathophysiology of cancer. Amplification of certain genes (e.g., Myc or Her2/Neu)

gives cancer cells a growth or survival advantage relative to normal cells, and might also provide a mechanism of tumor cell resistance to chemotherapy or radiotherapy.

5. If gene amplification results in over-expression of the mRNA and the corresponding gene product, then it identifies that gene product as a promising target for cancer therapy, for example by the therapeutic antibody approach. Even in the absence of over-expression of the gene product, amplification of a cancer marker gene - as detected, for example, by the reverse transcriptase TaqMan[®] PCR or the fluorescence *in situ* hybridization (FISH) assays - is useful in the diagnosis or classification of cancer, or in predicting or monitoring the efficacy of cancer therapy. An increase in gene copy number can result not only from intrachromosomal changes but also from chromosomal aneuploidy. It is important to understand that detection of gene amplification can be used for cancer diagnosis even if the determination includes measurement of chromosomal aneuploidy. Indeed, as long as a significant difference relative to normal tissue is detected, it is irrelevant if the signal originates from an increase in the number of gene copies per chromosome and/or an abnormal number of chromosomes.

6. I understand that according to the Patent Office, absent data demonstrating that the increased copy number of a gene in certain types of cancer leads to increased expression of its product, gene amplification data are insufficient to provide substantial utility or well established utility for the gene product (the encoded polypeptide), or an antibody specifically binding the encoded polypeptide. However, even when amplification of a cancer marker gene does not result in significant over-expression of the corresponding gene product, this very absence of gene product over-expression still provides significant information for cancer diagnosis and treatment. Thus, if over-expression of the gene product does not parallel gene amplification in certain tumor types but does so in others, then parallel monitoring of gene amplification and gene product over-expression enables more accurate tumor classification and hence better determination of suitable therapy. In addition, absence of over-expression is crucial information for the practicing clinician. If a gene is amplified but the corresponding gene product is not over-expressed, the clinician accordingly will decide not to treat a patient with agents that target that gene product.

7. I hereby declare that all statements made herein of my own knowledge are true and that all statements made on information or belief are believed to be true, and further that these statements were made with the knowledge that willful false statements and the like so

made are punishable by fine or imprisonment, or both, under Section 1001 of Title 18 of the United States Code and that such willful statements may jeopardize the validity of the application or any patent issued thereon.

By: Avi Ashkenazi
Avi Ashkenazi, Ph.D.

Date: 9/15/03

CURRICULUM VITAE

Avi Ashkenazi

July 2003

Personal:

Date of birth: 29 November, 1956
Address: 1456 Tarrytown Street, San Mateo, CA 94402
Phone: (650) 578-9199 (home); (650) 225-1853 (office)
Fax: (650) 225-6443 (office)
Email: aa@gene.com

Education:

1983: B.S. in Biochemistry, with honors, Hebrew University, Israel
1986: Ph.D. in Biochemistry, Hebrew University, Israel

Employment:

1983-1986: Teaching assistant, undergraduate level course in Biochemistry
1985-1986: Teaching assistant, graduate level course on Signal Transduction
1986 - 1988: Postdoctoral fellow, Hormone Research Dept., UCSF, and
Developmental Biology Dept., Genentech, Inc., with J. Ramachandran
1988 - 1989: Postdoctoral fellow, Molecular Biology Dept., Genentech, Inc.,
with D. Capon
1989 - 1993: Scientist, Molecular Biology Dept., Genentech, Inc.
1994 -1996: Senior Scientist, Molecular Oncology Dept., Genentech, Inc.
1996-1997: Senior Scientist and Interim director, Molecular Oncology Dept.,
Genentech, Inc.
1997-1990: Senior Scientist and preclinical project team leader, Genentech, Inc.
1999 -2002: Staff Scientist in Molecular Oncology, Genentech, Inc.
2002-present: Staff Scientist and Director in Molecular Oncology, Genentech, Inc.

Awards:

1988: First prize, The Boehringer Ingelheim Award

Editorial:

Editorial Board Member: Current Biology

Associate Editor, Clinical Cancer Research.

Associate Editor, Cancer Biology and Therapy.

Refereed papers:

1. Gertler, A., Ashkenazi, A., and Madar, Z. Binding sites for human growth hormone and ovine and bovine prolactins in the mammary gland and liver of the lactating cow. *Mol. Cell. Endocrinol.* 34, 51-57 (1984).
2. Gertler, A., Shamay, A., Cohen, N., Ashkenazi, A., Friesen, H., Levanon, A., Gorecki, M., Aviv, H., Hadari, D., and Vogel, T. Inhibition of lactogenic activities of ovine prolactin and human growth hormone (hGH) by a novel form of a modified recombinant hGH. *Endocrinology* 118, 720-726 (1986).
3. Ashkenazi, A., Madar, Z., and Gertler, A. Partial purification and characterization of bovine mammary gland prolactin receptor. *Mol. Cell. Endocrinol.* 50, 79-87 (1987).
4. Ashkenazi, A., Pines, M., and Gertler, A. Down-regulation of lactogenic hormone receptors in Nb2 lymphoma cells by cholera toxin. *Biochemistry Internatl.* 14, 1065-1072 (1987).
5. Ashkenazi, A., Cohen, R., and Gertler, A. Characterization of lactogen receptors in lactogenic hormone-dependent and independent Nb2 lymphoma cell lines. *FEBS Lett.* 210, 51-55 (1987).
6. Ashkenazi, A., Vogel, T., Barash, I., Hadari, D., Levanon, A., Gorecki, M., and Gertler, A. Comparative study on in vitro and in vivo modulation of lactogenic and somatotrophic receptors by native human growth hormone and its modified recombinant analog. *Endocrinology* 121, 414-419 (1987).
7. Peralta, E., Winslow, J., Peterson, G., Smith, D., Ashkenazi, A., Ramachandran, J., Schimerlik, M., and Capon, D. Primary structure and biochemical properties of an M2 muscarinic receptor. *Science* 236, 600-605 (1987).
8. Peralta, E., Ashkenazi, A., Winslow, J., Smith, D., Ramachandran, J., and Capon, D. J. Distinct primary structures, ligand-binding properties and tissue-specific expression of four human muscarinic acetylcholine receptors. *EMBO J.* 6, 3923-3929 (1987).
9. Ashkenazi, A., Winslow, J., Peralta, E., Peterson, G., Schimerlik, M., Capon, D., and Ramachandran, J. An M2 muscarinic receptor subtype coupled to both adenylyl cyclase and phosphoinositide turnover. *Science* 238, 672-675 (1987).

10. Pines, M., Ashkenazi, A., Cohen-Chapnik, N., Binder, L., and Gertler, A. Inhibition of the proliferation of Nb2 lymphoma cells by femtomolar concentrations of cholera toxin and partial reversal of the effect by 12-o-tetradecanoyl-phorbol-13-acetate. *J. Cell. Biochem.* 37, 119-129 (1988).
11. Peralta, E. Ashkenazi, A., Winslow, J., Ramachandran, J., and Capon, D. Differential regulation of PI hydrolysis and adenylyl cyclase by muscarinic receptor subtypes. *Nature* 334, 434-437 (1988).
12. Ashkenazi, A., Peralta, E., Winslow, J., Ramachandran, J., and Capon, D. Functionally distinct G proteins couple different receptors to PI hydrolysis in the same cell. *Cell* 56, 487-493 (1989).
13. Ashkenazi, A., Ramachandran, J., and Capon, D. Acetylcholine analogue stimulates DNA synthesis in brain-derived cells via specific muscarinic acetylcholine receptor subtypes. *Nature* 340, 146-150 (1989).
14. Lammare, D., Ashkenazi, A., Fleury, S., Smith, D., Sekaly, R., and Capon, D. The MHC-binding and gp120-binding domains of CD4 are distinct and separable. *Science* 245, 743-745 (1989).
15. Ashkenazi, A., Presta, L., Marsters, S., Camerato, T., Rosenthal, K., Fendly, B., and Capon, D. Mapping the CD4 binding site for human immunodeficiency virus type 1 by alanine-scanning mutagenesis. *Proc. Natl. Acad. Sci. USA.* 87, 7150-7154 (1990).
16. Chamow, S., Peers, D., Byrn, R., Mulkerrin, M., Harris, R., Wang, W., Bjorkman, P., Capon, D., and Ashkenazi, A. Enzymatic cleavage of a CD4 immunoadhesin generates crystallizable, biologically active Fd-like fragments. *Biochemistry* 29, 9885-9891 (1990).
17. Ashkenazi, A., Smith, D., Marsters, S., Riddle, L., Gregory, T., Ho, D., and Capon, D. Resistance of primary isolates of human immunodeficiency virus type 1 to soluble CD4 is independent of CD4-gp120 binding affinity. *Proc. Natl. Acad. Sci. USA.* 88, 7056-7060 (1991).
18. Ashkenazi, A., Marsters, S., Capon, D., Chamow, S., Figari, I., Pennica, D., Goeddel, D., Palladino, M., and Smith, D. Protection against endotoxic shock by a tumor necrosis factor receptor immunoadhesin. *Proc. Natl. Acad. Sci. USA.* 88, 10535-10539 (1991).
19. Moore, J., McKeating, J., Huang, Y., Ashkenazi, A., and Ho, D. Virions of primary HIV-1 isolates resistant to sCD4 neutralization differ in sCD4 affinity and glycoprotein gp120 retention from sCD4-sensitive isolates. *J. Virol.* 66, 235-243 (1992).

20. Jin, H., Oksenberg, D., Ashkenazi, A., Peroutka, S., Duncan, A., Rozmahel, R., Yang, Y., Mengod, G., Palacios, J., and O'Dowd, B. Characterization of the human 5-hydroxytryptamine_{1B} receptor. *J. Biol. Chem.* **267**, 5735-5738 (1992).
21. Marsters, A., Frutkin, A., Simpson, N., Fendly, B. and Ashkenazi, A. Identification of cysteine-rich domains of the type 1 tumor necrosis receptor involved in ligand binding. *J. Biol. Chem.* **267**, 5747-5750 (1992).
22. Chamow, S., Kogan, T., Peers, D., Hastings, R., Byrn, R., and Ashkenazi, A. Conjugation of sCD4 without loss of biological activity via a novel carbohydrate-directed cross-linking reagent. *J. Biol. Chem.* **267**, 15916-15922 (1992).
23. Oksenberg, D., Marsters, A., O'Dowd, B., Jin, H., Havlik, S., Peroutka, S., and Ashkenazi, A. A single amino-acid difference confers major pharmacologic variation between human and rodent 5-HT_{1B} receptors. *Nature* **360**, 161-163 (1992).
24. Haak-Frendscho, M., Marsters, S., Chamow, S., Peers, D., Simpson, N., and Ashkenazi, A. Inhibition of interferon γ by an interferon γ receptor immunoadhesin. *Immunology* **79**, 594-599 (1993).
25. Penica, D., Lam, V., Weber, R., Kohr, W., Basa, L., Spellman, M., Ashkenazi, A., Shire, S., and Goeddel, D. Biochemical characterization of the extracellular domain of the 75-kd tumor necrosis factor receptor. *Biochemistry* **32**, 3131-3138. (1993).
26. Barfod, L., Zheng, Y., Kuang, W., Hart, M., Evans, T., Cerione, R., and Ashkenazi, A. Cloning and expression of a human CDC42 GTPase Activating Protein reveals a functional SH3-binding domain. *J. Biol. Chem.* **268**, 26059-26062 (1993).
27. Chamow, S., Zhang, D., Tan, X., Mhtre, S., Marsters, S., Peers, D., Byrn, R., Ashkenazi, A., and Yunghans, R. A humanized bispecific immunoadhesin-antibody that retargets CD3⁺ effectors to kill HIV-1-infected cells. *J. Immunol.* **153**, 4268-4280 (1994).
28. Means, R., Krantz, S., Luna, J., Marsters, S., and Ashkenazi, A. Inhibition of murine erythroid colony formation in vitro by iterferon γ and correction by interferon γ receptor immunoadhesin. *Blood* **83**, 911-915 (1994).
29. Haak-Frendscho, M., Marsters, S., Mordenti, J., Gillet, N., Chen, S., and Ashkenazi, A. Inhibition of TNF by a TNF receptor immunoadhesin: comparison with an anti-TNF mAb. *J. Immunol.* **152**, 1347-1353 (1994).

30. Chamow, S., Kogan, T., Venuti, M., Gadek, T., Peers, D., Mordenti, J., Shak, S., and Ashkenazi, A. Modification of CD4 immunoadhesin with monomethoxy-PEG aldehyde via reductive alkylation. *Bioconj. Chem.* 5, 133-140 (1994).
31. Jin, H., Yang, R., Marsters, S., Bunting, S., Wurm, F., Chamow, S., and Ashkenazi, A. Protection against rat endotoxic shock by p55 tumor necrosis factor (TNF) receptor immunoadhesin: comparison to anti-TNF monoclonal antibody. *J. Infect. Diseases* 170, 1323-1326 (1994).
32. Beck, J., Marsters, S., Harris, R., Ashkenazi, A., and Chamow, S. Generation of soluble interleukin-1 receptor from an immunoadhesin by specific cleavage. *Mol. Immunol.* 31, 1335-1344 (1994).
33. Pitti, B., Marsters, M., Haak-Frendscho, M., Osaka, G., Mordenti, J., Chamow, S., and Ashkenazi, A. Molecular and biological properties of an interleukin-1 receptor immunoadhesin. *Mol. Immunol.* 31, 1345-1351 (1994).
34. Oksenberg, D., Havlik, S., Peroutka, S., and Ashkenazi, A. The third intracellular loop of the 5-HT₂ receptor specifies effector coupling. *J. Neurochem.* 64, 1440-1447 (1995).
35. Bach, E., Szabo, S., Dighe, A., Ashkenazi, A., Aguet, M., Murphy, K., and Schreiber, R. Ligand-induced autoregulation of IFN- γ receptor β chain expression in T helper cell subsets. *Science* 270, 1215-1218 (1995).
36. Jin, H., Yang, R., Marsters, S., Ashkenazi, A., Bunting, S., Marra, M., Scott, R., and Baker, J. Protection against endotoxic shock by bactericidal/permeability-increasing protein in rats. *J. Clin. Invest.* 95, 1947-1952 (1995).
37. Marsters, S., Penica, D., Bach, E., Schreiber, R., and Ashkenazi, A. Interferon γ signals via a high-affinity multisubunit receptor complex that contains two types of polypeptide chain. *Proc. Natl. Acad. Sci. USA.* 92, 5401-5405 (1995).
38. Van Zee, K., Moldawer, L., Oldenburg, H., Thompson, W., Stackpole, S., Montegut, W., Rogy, M., Meschter, C., Gallati, H., Schiller, C., Richter, W., Loetcher, H., Ashkenazi, A., Chamow, S., Wurm, F., Calvano, S., Lowry, S., and Lesslauer, W. Protection against lethal *E. coli* bacteremia in baboons by pretreatment with a 55-kDa TNF receptor-Ig fusion protein, Ro45-2081. *J. Immunol.* 156, 2221-2230 (1996).
39. Pitti, R., Marsters, S., Ruppert, S., Donahue, C., Moore, A., and Ashkenazi, A. Induction of apoptosis by Apo-2 Ligand, a new member of the tumor necrosis factor cytokine family. *J. Biol. Chem.* 271, 12687-12690 (1996).

40. Marsters, S., Pitti, R., Donahue, C., Rupert, S., Bauer, K., and Ashkenazi, A. Activation of apoptosis by Apo-2 ligand is independent of FADD but blocked by CrmA. *Curr. Biol.* 6, 1669-1676 (1996).
41. Marsters, S., Skubatch, M., Gray, C., and Ashkenazi, A. Herpesvirus entry mediator, a novel member of the tumor necrosis factor receptor family, activates the NF- κ B and AP-1 transcription factors. *J. Biol. Chem.* 272, 14029-14032 (1997).
42. Sheridan, J., Marsters, S., Pitti, R., Gurney, A., Skubatch, M., Baldwin, D., Ramakrishnan, L., Gray, C., Baker, K., Wood, W.I., Goddard, A., Godowski, P., and Ashkenazi, A. Control of TRAIL-induced apoptosis by a family of signaling and decoy receptors. *Science* 277, 818-821 (1997).
43. Marsters, S., Sheridan, J., Pitti, R., Gurney, A., Skubatch, M., Baldwin, D., Huang, A., Yuan, J., Goddard, A., Godowski, P., and Ashkenazi, A. A novel receptor for Apo2L/TRAIL contains a truncated death domain. *Curr. Biol.* 7, 1003-1006 (1997).
44. Marsters, A., Sheridan, J., Pitti, R., Brush, J., Goddard, A., and Ashkenazi, A. Identification of a ligand for the death-domain-containing receptor Apo3. *Curr. Biol.* 8, 525-528 (1998).
45. Rieger, J., Naumann, U., Glaser, T., Ashkenazi, A., and Weller, M. Apo2 ligand: a novel weapon against malignant glioma? *FEBS Lett.* 427, 124-128 (1998).
46. Pender, S., Fell, J., Chamow, S., Ashkenazi, A., and MacDonald, T. A p55 TNF receptor immunoadhesin prevents T cell mediated intestinal injury by inhibiting matrix metalloproteinase production. *J. Immunol.* 160, 4098-4103 (1998).
47. Pitti, R., Marsters, S., Lawrence, D., Roy, Kischkel, F., M., Dowd, P., Huang, A., Donahue, C., Sherwood, S., Baldwin, D., Godowski, P., Wood, W., Gurney, A., Hillan, K., Cohen, R., Goddard, A., Botstein, D., and Ashkenazi, A. Genomic amplification of a decoy receptor for Fas ligand in lung and colon cancer. *Nature* 396, 699-703 (1998).
48. Mori, S., Marakami-Mori, K., Nakamura, S., Ashkenazi, A., and Bonavida, B. Sensitization of AIDS Kaposi's sarcoma cells to Apo-2 ligand-induced apoptosis by actinomycin D. *J. Immunol.* 162, 5616-5623 (1999).
49. Gurney, A. Marsters, S., Huang, A., Pitti, R., Mark, M., Baldwin, D., Gray, A., Dowd, P., Brush, J., Heldens, S., Schow, P., Goddard, A., Wood, W., Baker, K., Godowski, P., and Ashkenazi, A. Identification of a new member of the tumor necrosis factor family and its receptor, a human ortholog of mouse GITR. *Curr. Biol.* 9, 215-218 (1999).

50. Ashkenazi, A., Pai, R., Fong, s., Leung, S., Lawrence, D., Marsters, S., Blackie, C., Chang, L., McMurtrey, A., Hebert, A., DeForge, L., Khoumenis, I., Lewis, D., Harris, L., Bussiere, J., Koeppen, H., Shahrokh, Z., and Schwall, R. Safety and anti-tumor activity of recombinant soluble Apo2 ligand. *J. Clin. Invest.* 104, 155-162 (1999).
51. Chuntharapai, A., Gibbs, V., Lu, J., Ow, A., Marsters, S., Ashkenazi, A., De Vos, A., Kim, K.J. Determination of residues involved in ligand binding and signal transmissiion in the human IFN- α receptor 2. *J. Immunol.* 163, 766-773 (1999).
52. Johnsen, A.-C., Haux, J., Steinkjer, B., Nonstad, U., Egeberg, K., Sundan, A., Ashkenazi, A., and Espevik, T. Regulation of Apo2L/TRAIL expression in NK cells – involvement in NK cell-mediated cytotoxicity. *Cytokine* 11, 664-672 (1999).
53. Roth, W., Isenmann, S., Naumann, U., Kugler, S., Bahr, M., Dichgans, J., Ashkenazi, A., and Weller, M. Eradication of intracranial human malignant glioma xenografts by Apo2L/TRAIL. *Biochem. Biophys. Res. Commun.* 265, 479-483 (1999).
54. Hymowitz, S.G., Christinger, H.W., Fuh, G., Ultsch, M., O'Connell, M., Kelley, R.F., Ashkenazi, A. and de Vos, A.M. Triggering Cell Death: The Crystal Structure of Apo2L/TRAIL in a Complex with Death Receptor 5. *Molec. Cell* 4, 563–571 (1999).
55. Hymowitz, S.G., O'Connel, M.P., Utsch, M.H., Hurst, A., Totpal, K., Ashkenazi, A., de Vos, A.M., Kelley, R.F. A unique zinc-binding site revealed by a high-resolution X-ray structure of homotrimeric Apo2L/TRAIL. *Biochemistry* 39, 633-640 (2000).
56. Zhou, Q., Fukushima, P., DeGraff, W., Mitchell, J.B., Stetler-Stevenson, M., Ashkenazi, A., and Steeg, P.S. Radiation and the Apo2L/TRAIL apoptotic pathway preferentially inhibit the colonization of premalignant human breast cancer cells overexpressing cyclin D1. *Cancer Res.* 60, 2611-2615 (2000).
57. Kischkel, F.C., Lawrence, D. A., Chuntharapai, A., Schow, P., Kim, J., and Ashkenazi, A. Apo2L/TRAIL-dependent recruitment of endogenous FADD and Caspase-8 to death receptors 4 and 5. *Immunity* 12, 611-620 (2000).
58. Yan, M., Marsters, S.A., Grewal, I.S., Wang, H., *Ashkenazi, A., and *Dixit, V.M. Identification of a receptor for BlyS demonstrates a crucial role in humoral immunity. *Nature Immunol.* 1, 37-41 (2000).

59. Marsters, S.A., Yan, M., Pitti, R.M., Haas, P.E., Dixit, V.M., and Ashkenazi, A. Interaction of the TNF homologues BLyS and APRIL with the TNF receptor homologues BCMA and TACI. *Curr. Biol.* 10, 785-788 (2000).
60. Kischkel, F.C., and Ashkenazi, A. Combining enhanced metabolic labeling with immunoblotting to detect interactions of endogenous cellular proteins. *Biotechniques* 29, 506-512 (2000).
61. Lawrence, D., Shahrokh, Z., Marsters, S., Achilles, K., Shih, D. Mounho, B., Hillan, K., Totpal, K. DeForge, L., Schow, P., Hooley, J., Sherwood, S., Pai, R., Leung, S., Khan, L., Gliniak, B., Bussiere, J., Smith, C., Strom, S., Kelley, S., Fox, J., Thomas, D., and Ashkenazi, A. Differential hepatocyte toxicity of recombinant Apo2L/TRAIL versions. *Nature Med.* 7, 383-385 (2001).
62. Chuntharapai, A., Dodge, K., Grimmer, K., Schroeder, K., Martsters, S.A., Koeppen, H., Ashkenazi, A., and Kim, K.J. Isotype-dependent inhibition of tumor growth in vivo by monoclonal antibodies to death receptor 4. *J. Immunol.* 166, 4891-4898 (2001).
63. Pollack, I.F., Erff, M., and Ashkenazi, A. Direct stimulation of apoptotic signaling by soluble Apo2L/tumor necrosis factor-related apoptosis-inducing ligand leads to selective killing of glioma cells. *Clin. Cancer Res.* 7, 1362-1369 (2001).
64. Wang, H., Marsters, S.A., Baker, T., Chan, B., Lee, W.P., Fu, L., Tumas, D., Yan, M., Dixit, V.M., *Ashkenazi, A., and *Grewal, I.S. TACI-ligand interactions are required for T cell activation and collagen-induced arthritis in mice. *Nature Immunol.* 2, 632-637 (2001).
65. Kischkel, F.C., Lawrence, D. A., Tinel, A., Virmani, A., Schow, P., Gazdar, A., Blenis, J., Arnott, D., and Ashkenazi, A. Death receptor recruitment of endogenous caspase-10 and apoptosis initiation in the absence of caspase-8. *J. Biol. Chem.* 276, 46639-46646 (2001).
66. LeBlanc, H., Lawrence, D.A., Varfolomeev, E., Totpal, K., Morlan, J., Schow, P., Fong, S., Schwall, R., Sinicropi, D., and Ashkenazi, A. Tumor cell resistance to death receptor induced apoptosis through mutational inactivation of the proapoptotic Bcl-2 homolog Bax. *Nature Med.* 8, 274-281 (2002).
67. Miller, K., Meng, G., Liu, J., Hurst, A., Hsei, V., Wong, W-L., Ekert, R., Lawrence, D., Sherwood, S., DeForge, L., Gaudreault, Keller, G., Sliwkowski, M., Ashkenazi, A., and Presta, L. Design, Construction, and analyses of multivalent antibodies. *J. Immunol.* 170, 4854-4861 (2003).

68. Varfolomeev, E., Kischkel, F., Martin, F., Wanh, H., Lawrence, D., Olsson, C., Tom, L., Erickson, S., French, D., Schow, P., Grewal, I. and Ashkenazi, A. Immune system development in APRIL knockout mice. Submitted.

Review articles:

1. Ashkenazi, A., Peralta, E., Winslow, J., Ramachandran, J., and Capon, D., J. Functional role of muscarinic acetylcholine receptor subtype diversity. *Cold Spring Harbor Symposium on Quantitative Biology*. **LIII**, 263-272 (1988).
2. Ashkenazi, A., Peralta, E., Winslow, J., Ramachandran, J., and Capon, D. Functional diversity of muscarinic receptor subtypes in cellular signal transduction and growth. *Trends Pharmacol. Sci.* Dec Supplement, 12-21 (1989).
3. Chamow, S., Duliege, A., Ammann, A., Kahn, J., Allen, D., Eichberg, J., Byrn, R., Capon, D., Ward, R., and Ashkenazi, A. CD4 immunoadhesins in anti-HIV therapy: new developments. *Int. J. Cancer* Supplement 7, 69-72 (1992).
4. Ashkenazi, A., Capon, and D. Ward, R. Immunoadhesins. *Int. Rev. Immunol.* **10**, 217-225 (1993).
5. Ashkenazi, A., and Peralta, E. Muscarinic Receptors. In *Handbook of Receptors and Channels*. (S. Peroutka, ed.), CRC Press, Boca Raton, Vol. I, p. 1-27, (1994).
6. Krantz, S. B., Means, R. T., Jr., Lina, J., Marsters, S. A., and Ashkenazi, A. Inhibition of erythroid colony formation in vitro by gamma interferon. In *Molecular Biology of Hematopoiesis* (N. Abraham, R. Shadduck, A. Levine F. Takaku, eds.) Intercept Ltd. Paris, Vol. 3, p. 135-147 (1994).
7. Ashkenazi, A. Cytokine neutralization as a potential therapeutic approach for SIRS and shock. *J. Biotechnology in Healthcare* **1**, 197-206 (1994).
8. Ashkenazi, A., and Chamow, S. M. Immunoadhesins: an alternative to human monoclonal antibodies. *Immunomethods: A companion to Methods in Enzymology* **8**, 104-115 (1995).
9. Chamow, S., and Ashkenazi, A. Immunoadhesins: Principles and Applications. *Trends Biotech.* **14**, 52-60 (1996).
10. Ashkenazi, A., and Chamow, S. M. Immunoadhesins as research tools and therapeutic agents. *Curr. Opin. Immunol.* **9**, 195-200 (1997).
11. Ashkenazi, A., and Dixit, V. Death receptors: signaling and modulation. *Science* **281**, 1305-1308 (1998).
12. Ashkenazi, A., and Dixit, V. Apoptosis control by death and decoy receptors. *Curr. Opin. Cell. Biol.* **11**, 255-260 (1999).

13. Ashkenazi, A. Chapters on Apo2L/TRAIL; DR4, DR5, DcR1, DcR2; and DcR3. Online Cytokine Handbook (www.apnet.com/cytokinereference/).
14. Ashkenazi, A. Targeting death and decoy receptors of the tumor necrosis factor superfamily. *Nature Rev. Cancer* 2, 420-430 (2002).
15. LeBlanc, H. and Ashkenazi, A. Apoptosis signaling by Apo2L/TRAIL. *Cell Death and Differentiation* 10, 66-75 (2003).
16. Almasan, A. and Ashkenazi, A. Apo2L/TRAIL: apoptosis signaling, biology, and potential for cancer therapy. *Cytokine and Growth Factor Reviews* 14, 337-348 (2003).

Book:

Antibody Fusion Proteins (Chamow, S., and Ashkenazi, A., eds., John Wiley and Sons Inc.) (1999).

Talks:

1. Resistance of primary HIV isolates to CD4 is independent of CD4-gp120 binding affinity. UCSD Symposium, HIV Disease: Pathogenesis and Therapy. Greenelefe, FL, March 1991.
2. Use of immuno-hybrids to extend the half-life of receptors. IBC conference on Biopharmaceutical Half-life Extension. New Orleans, LA, June 1992.
3. Results with TNF receptor Immunoconjugates for the Treatment of Sepsis. IBC conference on Endotoxemia and Sepsis. Philadelphia, PA, June 1992.
4. Immunoconjugates: an alternative to human antibodies. IBC conference on Antibody Engineering. San Diego, CA, December 1993.
5. Tumor necrosis factor receptor: a potential therapeutic for human septic shock. American Society for Microbiology Meeting, Atlanta, GA, May 1993.
6. Protective efficacy of TNF receptor immunoconjugate vs anti-TNF monoclonal antibody in a rat model for endotoxic shock. 5th International Congress on TNF. Asilomar, CA, May 1994.
7. Interferon- γ signals via a multisubunit receptor complex that contains two types of polypeptide chain. American Association of Immunologists Conference. San Francisco, CA, July 1995.
8. Immunoconjugates: Principles and Applications. Gordon Research Conference on Drug Delivery in Biology and Medicine. Ventura, CA, February 1996.

9. Apo-2 Ligand, a new member of the TNF family that induces apoptosis in tumor cells. Cambridge Symposium on TNF and Related Cytokines in Treatment of Cancer. Hilton-Head, NC, March 1996.
10. Induction of apoptosis by Apo2 Ligand. American Society for Biochemistry and Molecular Biology, Symposium on Growth Factors and Cytokine Receptors. New Orleans, LA, June, 1996.
11. Apo2 ligand, an extracellular trigger of apoptosis. 2nd Clontech Symposium, Palo Alto, CA, October 1996.
12. Regulation of apoptosis by members of the TNF ligand and receptor families. Stanford University School of Medicine, Palo Alto, CA, December 1996.
13. Apo-3: a novel receptor that regulates cell death and inflammation. 4th International Congress on Immune Consequences of Trauma, Shock, and Sepsis. Munich, Germany, March 1997.
14. New members of the TNF ligand and receptor families that regulate apoptosis, inflammation, and immunity. UCLA School of Medicine, LA, CA, March 1997.
15. Immunoadhesins: an alternative to monoclonal antibodies. 5th World Conference on Bispecific Antibodies. Volendam, Holland, June 1997.
16. Control of Apo2L signaling. Cold Spring Harbor Laboratory Symposium on Programmed Cell Death. Cold Spring Harbor, New York. September, 1997.
17. Chairman and speaker, Apoptosis Signaling session. IBC's 4th Annual Conference on Apoptosis. San Diego, CA., October 1997.
18. Control of Apo2L signaling by death and decoy receptors. American Association for the Advancement of Science. Philadelphia, PA, February 1998.
19. Apo2 ligand and its receptors. American Society of Immunologists. San Francisco, CA, April 1998.
20. Death receptors and ligands. 7th International TNF Congress. Cape Cod, MA, May 1998.
21. Apo2L as a potential therapeutic for cancer. UCLA School of Medicine. LA, CA, June 1998.
22. Apo2L as a potential therapeutic for cancer. Gordon Research Conference on Cancer Chemotherapy. New London, NH, July 1998.
23. Control of apoptosis by Apo2L. Endocrine Society Conference, Stevenson, WA, August 1998.
24. Control of apoptosis by Apo2L. International Cytokine Society Conference, Jerusalem, Israel, October 1998.

25. Apoptosis control by death and decoy receptors. American Association for Cancer Research Conference, Whistler, BC, Canada, March 1999.
26. Apoptosis control by death and decoy receptors. American Society for Biochemistry and Molecular Biology Conference, San Francisco, CA, May 1999.
27. Apoptosis control by death and decoy receptors. Gordon Research Conference on Apoptosis, New London, NH, June 1999.
28. Apoptosis control by death and decoy receptors. Arthritis Foundation Research Conference, Alexandria GA, Aug 1999.
29. Safety and anti-tumor activity of recombinant soluble Apo2L/TRAIL. Cold Spring Harbor Laboratory Symposium on Programmed Cell Death. . Cold Spring Harbor, NY, September 1999.
30. The Apo2L/TRAIL system: therapeutic potential. American Association for Cancer Research, Lake Tahoe, NV, Feb 2000.
31. Apoptosis and cancer therapy. Stanford University School of Medicine, Stanford, CA, Mar 2000.
32. Apoptosis and cancer therapy. University of Pennsylvania School of Medicine, Philadelphia, PA, Apr 2000.
33. Apoptosis signaling by Apo2L/TRAIL. International Congress on TNF. Trondheim, Norway, May 2000.
34. The Apo2L/TRAIL system: therapeutic potential. Cap-CURE summit meeting. Santa Monica, CA, June 2000.
35. The Apo2L/TRAIL system: therapeutic potential. MD Anderson Cancer Center. Houston, TX, June 2000.
36. Apoptosis signaling by Apo2L/TRAIL. The Protein Society, 14th Symposium. San Diego, CA, August 2000.
37. Anti-tumor activity of Apo2L/TRAIL. AAPS annual meeting. Indianapolis, IN Aug 2000.
38. Apoptosis signaling and anti-cancer potential of Apo2L/TRAIL. Cancer Research Institute, UC San Francisco, CA, September 2000.
39. Apoptosis signaling by Apo2L/TRAIL. Kenote address, TNF family Minisymposium, NIH. Bethesda, MD, September 2000.
40. Death receptors: signaling and modulation. Keystone symposium on the Molecular basis of cancer. Taos, NM, Jan 2001.
41. Preclinical studies of Apo2L/TRAIL in cancer. Symposium on Targeted therapies in the treatment of lung cancer. Aspen, CO, Jan 2001.

42. Apoptosis signaling by Apo2L/TRAIL. Weizmann Institute of Science, Rehovot, Israel, March 2001.
43. Apo2L/TRAIL: Apoptosis signaling and potential for cancer therapy. Weizmann Institute of Science, Rehovot, Israel, March 2001.
44. Targeting death receptors in cancer with Apo2L/TRAIL. Cell Death and Disease conference, North Falmouth, MA, Jun 2001.
45. Targeting death receptors in cancer with Apo2L/TRAIL. Biotechnology Organization conference, San Diego, CA, Jun 2001.
46. Apo2L/TRAIL signaling and apoptosis resistance mechanisms. Gordon Research Conference on Apoptosis, Oxford, UK, July 2001.
47. Apo2L/TRAIL signaling and apoptosis resistance mechanisms. Cleveland Clinic Foundation, Cleveland, OH, Oct 2001.
48. Apoptosis signaling by death receptors: overview. International Society for Interferon and Cytokine Research conference, Cleveland, OH, Oct 2001.
49. Apoptosis signaling by death receptors. American Society of Nephrology Conference. San Francisco, CA, Oct 2001.
50. Targeting death receptors in cancer. Apoptosis: commercial opportunities. San Diego, CA, Apr 2002.
51. Apo2L/TRAIL signaling and apoptosis resistance mechanisms. Kimmel Cancer Research Center, Johns Hopkins University, Baltimore MD. May 2002.
52. Apoptosis control by Apo2L/TRAIL. (Keynote Address) University of Alabama Cancer Center Retreat, Birmingham, Ab. October 2002.
53. Apoptosis signaling by Apo2L/TRAIL. (Session co-chair) TNF international conference. San Diego, CA. October 2002.
54. Apoptosis signaling by Apo2L/TRAIL. Swiss Institute for Cancer Research (ISREC). Lausanne, Switzerland. Jan 2003.
55. Apoptosis induction with Apo2L/TRAIL. Conference on New Targets and Innovative Strategies in Cancer Treatment. Monte Carlo. February 2003.
56. Apoptosis signaling by Apo2L/TRAIL. Hermelin Brain Tumor Center Symposium on Apoptosis. Detroit, MI. April 2003.
57. Targeting apoptosis through death receptors. Sixth Annual Conference on Targeted Therapies in the Treatment of Breast Cancer. Kona, Hawaii. July 2003.
58. Targeting apoptosis through death receptors. Second International Conference on Targeted Cancer Therapy. Washington, DC. Aug 2003.

Issued Patents:

1. Ashkenazi, A., Chamow, S. and Kogan, T. Carbohydrate-directed crosslinking reagents. US patent 5,329,028 (Jul 12, 1994).
2. Ashkenazi, A., Chamow, S. and Kogan, T. Carbohydrate-directed crosslinking reagents. US patent 5,605,791 (Feb 25, 1997).
3. Ashkenazi, A., Chamow, S. and Kogan, T. Carbohydrate-directed crosslinking reagents. US patent 5,889,155 (Jul 27, 1999).
4. Ashkenazi, A., APO-2 Ligand. US patent 6,030,945 (Feb 29, 2000).
5. Ashkenazi, A., Chuntharapai, A., Kim, J., APO-2 ligand antibodies. US patent 6,046,048 (Apr 4, 2000).
6. Ashkenazi, A., Chamow, S. and Kogan, T. Carbohydrate-directed crosslinking reagents. US patent 6,124,435 (Sep 26, 2000).
7. Ashkenazi, A., Chuntharapai, A., Kim, J., Method for making monoclonal and cross-reactive antibodies. US patent 6,252,050 (Jun 26, 2001).
8. Ashkenazi, A. APO-2 Receptor. US patent 6,342,369 (Jan 29, 2002).
9. Ashkenazi, A. Fong, S., Goddard, A., Gurney, A., Napier, M., Tumas, D., Wood, W. A-33 polypeptides. US patent 6,410,708 (Jun 25, 2002).
10. Ashkenazi, A. APO-3 Receptor. US patent 6,462,176 B1 (Oct 8, 2002).
11. Ashkenazi, A. APO-2LI and APO-3 polypeptide antibodies. US patent 6,469,144 B1 (Oct 22, 2002).
12. Ashkenazi, A., Chamow, S. and Kogan, T. Carbohydrate-directed crosslinking reagents. US patent 6,582,928B1 (Jun 24, 2003).

DECLARATION OF PAUL POLAKIS, Ph.D.

I, Paul Polakis, Ph.D., declare and say as follows:

1. I was awarded a Ph.D. by the Department of Biochemistry of the Michigan State University in 1984. My scientific Curriculum Vitae is attached to and forms part of this Declaration (Exhibit A).
2. I am currently employed by Genentech, Inc. where my job title is Staff Scientist. Since joining Genentech in 1999, one of my primary responsibilities has been leading Genentech's Tumor Antigen Project, which is a large research project with a primary focus on identifying tumor cell markers that find use as targets for both the diagnosis and treatment of cancer in humans.
3. I have read and understand the claims pending in the above-identified patent application, which are directed to a method of treating cancer in a mammal by administering to the mammal a therapeutically effective amount of an antibody that specifically binds to a polypeptide of SEQ ID NO: 2.
4. I have also read and understand the disclosure of WO 03/052119 A2, hereinafter referred to Baughn *et al.* Baughn *et al.* concerns polypeptides described as human transporters of ion channels and designated as "TRICH." One of the "TRICH" polypeptides, represented by SEQ ID NO:11, shows a 99.9% amino acid sequence identity to the polypeptide of SEQ ID NO:2 of the present application.
5. On page 59, line 9 – page 61, line 13, Baughn *et al.* states:

"TRICH appears to play a role in transport, neurological, muscle, immunological and cell proliferative disorders. In the treatment of disorders associated with increased TRICH expression or activity, it is desirable to decrease the expression or activity of TRICH. In the treatment of disorders associated with decreased TRICH expression or activity, it is desirable to increase the expression or activity of TRICH.

Therefore, in one embodiment, TRICH or a fragment or derivative thereof may be administered to a subject to treat or prevent a disorder associated with decreased expression or activity of TRICH. Examples of such disorders include, but are not limited to, a transport disorder such as akinesia, amyotrophic lateral sclerosis, ataxia telangiectasia, cystic fibrosis, Becker's muscular dystrophy, Bell's palsy, Charcot-Marie Tooth disease, diabetes mellitus, diabetes insipidus, diabetic neuropathy, Duchenne muscular dystrophy, hyperkalemic periodic paralysis, normokalemic periodic paralysis, Parkinson's disease, malignant hyperthermia, multidrug resistance, myasthenia gravis, myotonic dystrophy, catatonia, tardive dyskinesia, dystonias, peripheral neuropathy, cerebral neoplasms, prostate cancer, cardiac disorders associated with transport, e. g. , angina, bradyarrhythmia, tachyarrhythmia, hypertension, Long QT syndrome,

myocarditis, cardiomyopathy, nemaline myopathy, centronuclear myopathy, lipid myopathy, mitochondrial myopathy, thyrotoxic myopathy, ethanol myopathy, dermatomyositis, inclusion body myositis, infectious myositis, polymyositis, neurological disorders associated with transport, e. g. , Alzheimer's disease, amnesia, bipolar disorder, dementia, depression, epilepsy, Tourette's disorder, paranoid psychoses, and schizophrenia, and other disorders associated with transport, e. g. , neurofibromatosis, postherpetic neuralgia, trigeminal neuropathy, sarcoidosis, sickle cell anemia, Wilson's disease, cataracts, infertility, pulmonary artery stenosis, sensorineural autosomal deafness, hyperglycemia, hypoglycemia, Grave's disease, goiter, Cushing's disease, Addison's disease, glucose-galactose malabsorption syndrome, glycogen storage disease, hypercholesterolemia, adrenoleukodystrophy, Zellweger syndrome, Menkes disease, occipital horn syndrome, von Gierke disease, pseudohypoaldosteronism type I, Liddle's syndrome, cystinuria, iminoglycinuria, Hartup disease, Fanconi disease, and Bartter syndrome; a neurological disorder such as epilepsy, ischemic cerebrovascular disease, stroke, cerebral neoplasms, Alzheimer's disease, Pick's disease, Huntington's disease, dementia, Parkinson's disease and other extrapyramidal disorders, amyotrophic lateral sclerosis and other motor neuron disorders, progressive neural muscular atrophy, retinitis pigmentosa, hereditary ataxias, multiple sclerosis and other demyelinating diseases, bacterial and viral meningitis, brain abscess, subdural empyema, epidural abscess, suppurative intracranial thrombophlebitis, myelitis and radiculitis, viral central nervous system disease, prion diseases including kuru, Creutzfeldt-Jakob disease, and Gerstmann-Straussler-Scheinker syndrome, fatal familial insomnia, nutritional and metabolic diseases of the nervous system, neurofibromatosis, tuberous sclerosis, cerebelloretinal hemangioblastomatosis, encephalotrigeminal syndrome, mental retardation and other developmental disorders of the central nervous system including Down syndrome, cerebral palsy, neuroskeletal disorders, autonomic nervous system disorders, cranial nerve disorders, spinal cord diseases, muscular dystrophy and other neuromuscular disorders, peripheral nervous system disorders, dermatomyositis and polymyositis, inherited, metabolic, endocrine, and toxic myopathies, myasthenia gravis, periodic paralysis, mental disorders including mood, anxiety, and schizophrenic disorders, seasonal affective disorder (SAD), akathisia, amnesia, catatonia, diabetic neuropathy, hemiplegic migraine, tardive dyskinesia, dystonias, paranoid psychoses, postherpetic neuralgia, Tourette's disorder, progressive supranuclear palsy, corticobasal degeneration, and familial frontotemporal dementia; a muscle disorder such as cardiomyopathy, myocarditis, Duchenne's muscular dystrophy, Becker's muscular dystrophy, myotonic dystrophy, central core disease, nemaline myopathy, centronuclear myopathy, lipid myopathy, mitochondrial myopathy, infectious myositis, polymyositis, dermatomyositis, inclusion body myositis, thyrotoxic myopathy, ethanol myopathy, angina, anaphylactic shock, arrhythmias, asthma, cardiovascular shock, Cushing's syndrome, hypertension,

hypoglycemia, myocardial infarction, migraine, pheochromocytoma, and myopathies including encephalopathy, epilepsy, Kearns-Sayre syndrome, lactic acidosis, myoclonic disorder, ophthalmoplegia, acid maltase deficiency (AMD, also known as Pompe's disease), generalized myotonia, and myotonia congenita; an immunological disorder such as acquired immunodeficiency syndrome (AIDS), Addison's disease, adult respiratory distress syndrome, allergies, ankylosing spondylitis, amyloidosis, anemia, asthma, atherosclerosis, autoimmune hemolytic anemia, autoimmune thyroiditis, autoimmune polyendocrinopathy-candidiasis-ectodermal dystrophy (APECED), bronchitis, cholecystitis, contact dermatitis, Crohn's disease, atopic dermatitis, dermatomyositis, diabetes mellitus, emphysema, episodic lymphopenia with lymphocytotoxins, erythroblastosis fetalis, erythema nodosum, atrophic gastritis, glomerulonephritis, Goodpasture's syndrome, gout, Graves' disease, Hashimoto's thyroiditis, hyper eosinophilia, irritable bowel syndrome, multiple sclerosis, myasthenia gravis, myocardial or pericardial inflammation, osteoarthritis, osteoporosis, pancreatitis, polymyositis, psoriasis, Reiter's syndrome, rheumatoid arthritis, scleroderma, Sjögren's syndrome, systemic anaphylaxis, systemic lupus erythematosus, systemic sclerosis, thrombocytopenic purpura, ulcerative colitis, uveitis, Werner syndrome, complications of cancer, hemodialysis, and extracorporeal circulation, viral, bacterial, fungal, parasitic, protozoal, and helminthic infections, and trauma; and a cell proliferative disorder such as actinic keratosis, arteriosclerosis, atherosclerosis, bursitis, cirrhosis, hepatitis, mixed connective tissue disease (MCTD), myelofibrosis, paroxysmal nocturnal hemoglobinuria, polycythemia vera, psoriasis, primary thrombocythemia, and cancers including adenocarcinoma, leukemia, lymphoma, melanoma, myeloma, sarcoma, teratocarcinoma, and, in particular, cancers of the adrenal gland, bladder, bone, bone marrow, brain, breast, cervix, colon, gall bladder, ganglia, gastrointestinal tract, heart, kidney, liver, lung, muscle, ovary, pancreas, parathyroid, penis, prostate, salivary glands, skin, spleen, testis, thymus, thyroid, and uterus."

(Emphasis added.)

6. On page 61, lines 24-29, Baughn *et al.* state:

"In a further embodiment, an antagonist of TRICH may be administered to a subject to treat or prevent a disorder associated with increased expression or activity of TRICH. Examples of such disorders include, but are not limited to, those transport, neurological, muscle, immunological and cell proliferative disorders described above. In one aspect, an antibody which specifically binds TRICH may be used directly as an antagonist or indirectly as a targeting or delivery mechanism for bringing a pharmaceutical agent to cells or tissues which express TRICH."

(Emphasis added)

7. Thus, Baughn *et al.* suggest that TRICH polypeptides play a role in such diverse conditions as transport, neurological, muscle, immunological and cell proliferative disorders, including essentially any kind of cancer. They further suggest that such disorders can be prevented or treated either with TRICH polypeptides or with antagonists of TRICH polypeptides, such as antibodies which specifically bind TRICH. From other parts of the disclosure and the claims it appears that TRICH may be over- or under-expressed in such conditions, and in the case of under-expression, TRICH is used as a preventative or therapeutic agent, while in the case of over-expression, the treatment is performed with TRICH antagonists, such as antibodies which specifically bind TRICH. Baughn *et al.* have no data or other teaching indicating if the compound of SEQ ID NO: 11 is under- or over-expressed in any of these conditions.

8. Based on the disclosure discussed in paragraphs 5-7 above, in order to use antibodies that specifically bind the compound of SEQ ID NO: 11 for any therapeutic purpose, I would first need to determine if the polypeptide of SEQ ID NO: 11 is over-expressed or under-expressed in any transport, neurological, muscle, immunological or cell proliferative disorder. These broad classes of disorders include an extremely large number of diseases. Thus, for example, in addition to the cancer types (adenocarcinoma, leukemia, lymphoma, melanoma, myeloma, sarcoma, teratocarcinoma) and cancers (cancers of the adrenal gland, bladder, bone, bone marrow, brain, breast, cervix, colon, gall bladder, ganglia, gastrointestinal tract, heart, kidney, liver, lung, muscle, ovary, pancreas, parathyroid, penis, prostate, salivary glands, skin, spleen, testis, thymus, thyroid, and uterus) listed by Baughn *et al.*, cell proliferative disorders include a variety of other conditions, including actinic keratosis, arteriosclerosis, atherosclerosis, bursitis, cirrhosis, hepatitis, mixed connective tissue disease (MCTD), myelofibrosis, paroxysmal nocturnal hemoglobinuria, polycythemia vera, psoriasis, primary thrombocythemia, also listed by Baughn *et al.* Since Baughn *et al.* has no specific teaching about the involvement of the polypeptide of SEQ ID NO: 11 in any of such conditions, I would have no reason to prefer any type of disorders over other types, or any specific disease over any other.

9. Accordingly, in order to determine whether antibodies to the polypeptide of SEQ ID NO: 11 are useful in the treatment of any disease or disorder, I would need to investigate the involvement of the polypeptide of SEQ ID NO: 11 in a daunting number of transport, neurological, muscle, immunological and cell proliferative diseases until I find one where it seems to be involved, such as, under- or over-expressed. After finding a condition where the polypeptide of SEQ ID NO: 11 is over-expressed, I would need to examine whether the elevated expression levels of this polypeptide play a role in the pathology of the disease in question, and, if such role is confirmed, experimentally determine if antibodies specifically binding the polypeptide of SEQ ID NO: 11 are able to counteract such pathological role.

10. Anyone who has spent any time in a research laboratory, working on the identification of new drug targets and the development of drug candidates for the treatment of serious medical conditions would understand that the tasks outlined in paragraph 9 above would take more than a lifetime even for large groups of scientists. Accordingly, based on the disclosure of Baughn *et al.* I would not be able to use the

polypeptide of SEQ ID NO: 11 or an antibody specifically binding the polypeptide of SEQ ID NO: 11 for any therapeutic purpose, without a tremendous amount of experimentation, without any guarantee or even expectation that such experimentation would eventually yield a therapeutic use.

11. I hereby declare that all statements made herein of my own knowledge are true and that all statements made on information or belief are believed to be true, and further that these statements were made with the knowledge that willful false statements and the like so made are punishable by fine or imprisonment, or both, under Section 1001 of Title 18 of the United States Code and that such willful statements may jeopardize the validity of the application or any patent issued thereon.

Dated: 2-21-2007

By: Paul Polakis

Paul Polakis, Ph.D.

SV 2245898 v1

CURRICULUM VITAE

PAUL G. POLAKIS
Staff Scientist
Genentech, Inc
1 DNA Way, MS#40
S. San Francisco, CA 94080

EDUCATION:

Ph.D., Biochemistry, Department of Biochemistry,
Michigan State University (1984)

B.S., Biology. College of Natural Science, Michigan State University (1977)

PROFESSIONAL EXPERIENCE:

2002-present	Staff Scientist, Genentech, Inc S. San Francisco, CA
1999- 2002	Senior Scientist, Genentech, Inc., S. San Francisco, CA
1997 -1999	Research Director Onyx Pharmaceuticals, Richmond, CA
1992- 1996	Senior Scientist, Project Leader, Onyx Pharmaceuticals, Richmond, CA
1991-1992	Senior Scientist, Chiron Corporation, Emeryville, CA.
1989-1991	Scientist, Cetus Corporation, Emeryville CA.
1987-1989	Postdoctoral Research Associate, Genentech, Inc., South San Francisco, CA.
1985-1987	Postdoctoral Research Associate, Department of Medicine, Duke University Medical Center, Durham, NC

1984-1985

Assistant Professor, Department of Chemistry,
Oberlin College, Oberlin, Ohio

1980-1984

Graduate Research Assistant, Department of
Biochemistry, Michigan State University
East Lansing, Michigan

PUBLICATIONS:

1. Polakis, P. G. and Wilson, J. E. 1982 Purification of a Highly Bindable Rat Brain Hexokinase by High Performance Liquid Chromatography. **Biochem. Biophys. Res. Commun.** 107, 937-943.
2. Polakis, P.G. and Wilson, J. E. 1984 Proteolytic Dissection of Rat Brain Hexokinase: Determination of the Cleavage Pattern during Limited Digestion with Trypsin. **Arch. Biochem. Biophys.** 234, 341-352.
3. Polakis, P. G. and Wilson, J. E. 1985 An Intact Hydrophobic N-Terminal Sequence is Required for the Binding Rat Brain Hexokinase to Mitochondria. **Arch. Biochem. Biophys.** 236, 328-337.
4. Uhing, R.J., Polakis, P.G. and Snyderman, R. 1987 Isolation of GTP-binding Proteins from Myeloid HL60 Cells. **J. Biol. Chem.** 262, 15575-15579.
5. Polakis, P.G., Uhing, R.J. and Snyderman, R. 1988 The Formylpeptide Chemoattractant Receptor Copurifies with a GTP-binding Protein Containing a Distinct 40 kDa Pertussis Toxin Substrate. **J. Biol. Chem.** 263, 4969-4979.
6. Uhing, R. J., Dillon, S., Polakis, P. G., Truett, A. P. and Snyderman, R. 1988 Chemoattractant Receptors and Signal Transduction Processes in Cellular and Molecular Aspects of Inflammation (Poste, G. and Crooke, S. T. eds.) pp 335-379.
7. Polakis, P.G., Evans, T. and Snyderman 1989 Multiple Chromatographic Forms of the Formylpeptide Chemoattractant Receptor and their Relationship to GTP-binding Proteins. **Biochem. Biophys. Res. Commun.** 161, 276-283.
8. Polakis, P. G., Snyderman, R. and Evans, T. 1989 Characterization of G25K, a GTP-binding Protein Containing a Novel Putative Nucleotide Binding Domain. **Biochem. Biophys. Res. Commun.** 160, 25-32.
9. Polakis, P., Weber, R.F., Nevins, B., Didsbury, J. Evans, T. and Snyderman, R. 1989 Identification of the *ral* and *rac1* Gene Products, Low Molecular Mass GTP-binding Proteins from Human Platelets. **J. Biol. Chem.** 264, 16383-16389.
10. Snyderman, R., Perianin, A., Evans, T., Polakis, P. and Didsbury, J. 1989 G Proteins and Neutrophil Function. In ADP-Ribosylating Toxins and G Proteins: Insights into Signal Transduction. (J. Moss and M. Vaughn, eds.) Amer. Soc. Microbiol. pp. 295-323.

11. Hart, M.J., **Polakis, P.G.**, Evans, T. and Cerrione, R.A. 1990 The Identification and Characterization of an Epidermal Growth Factor-Stimulated Phosphorylation of a Specific Low Molecular Mass GTP-binding Protein in a Reconstituted Phospholipid Vesicle System. **J. Biol. Chem.** 265, 5990-6001.
12. Yatani, A., Okabe, K., **Polakis, P.** Halenbeck, R. McCormick, F. and Brown, A. M. 1990 ras p21 and GAP Inhibit Coupling of Muscarinic Receptors to Atrial K⁺ Channels. **Cell.** 61, 769-776.
13. Munemitsu, S., Innis, M.A., Clark, R., McCormick, F., Ullrich, A. and **Polakis, P.G.** 1990 Molecular Cloning and Expression of a G25K cDNA, the Human Homolog of the Yeast Cell Cycle Gene CDC42. **Mol. Cell. Biol.** 10, 5977-5982.
14. **Polakis, P.G.** Rubinfeld, B. Evans, T. and McCormick, F. 1991 Purification of Plasma Membrane-Associated GTPase Activating Protein (GAP) Specific for rap-1/krev-1 from HL60 Cells. **Proc. Natl. Acad. Sci. USA** 88, 239-243.
15. Moran, M. F., **Polakis, P.**, McCormick, F., Pawson, T. and Ellis, C. 1991 Protein Tyrosine Kinases Regulate the Phosphorylation, Protein Interactions, Subcellular Distribution, and Activity of p21ras GTPase Activating Protein. **Mol. Cell. Biol.** 11, 1804-1812
16. Rubinfeld, B., Wong, G., Bekesi, E. Wood, A. McCormick, F. and **Polakis, P. G.** 1991 A Synthetic Peptide Corresponding to a Sequence in the GTPase Activating Protein Inhibits p21^{ras} Stimulation and Promotes Guanine Nucleotide Exchange. **Internatl. J. Peptide and Prot. Res.** 38, 47-53.
17. Rubinfeld, B., Munemitsu, S., Clark, R., Conroy, L., Watt, K., Crosier, W., McCormick, F., and **Polakis, P.** 1991 Molecular Cloning of a GTPase Activating Protein Specific for the Krev-1 Protein p21^{rap1}. **Cell** 65, 1033-1042.
18. Zhang, K. Papageorge, A., G., Martin, P., Vass, W. C., Olah, Z., **Polakis, P.**, McCormick, F. and Lowy, D, R. 1991 Heterogenous Amino Acids in RAS and Rap1A Specifying Sensitivity to GAP Proteins. **Science** 254, 1630-1634.
19. Martin, G., Yatani, A., Clark, R., **Polakis, P.**, Brown, A. M. and McCormick, F. 1992 GAP Domains Responsible for p21^{ras}-dependent Inhibition of Muscarinic Atrial K⁺ Channel Currents. **Science** 255, 192-194.
20. McCormick, F., Martin, G. A., Clark, R., Bollag, G. and **Polakis, P.** 1992 Regulation of p21ras by GTPase Activating Proteins. **Cold Spring Harbor Symposia on Quantitative Biology.** Vol. 56, 237-241.
21. Pronk, G. B., **Polakis, P.**, Wong, G., deVries-Smits, A. M., Bos J. L. and McCormick, F. 1992 p60^{v-src} Can Associate with and Phosphorylate the p21^{ras} GTPase Activating Protein. **Oncogene** 7,389-394.
22. **Polakis P.** and McCormick, F. 1992 Interactions Between p21^{ras} Proteins and Their GTPase Activating Proteins. In Cancer Surveys (Franks, L. M., ed.) 12, 25-42.

23. Wong, G., Muller, O., Clark, R., Conroy, L., Moran, M., **Polakis, P.** and McCormick, F. 1992 Molecular cloning and nucleic acid binding properties of the GAP-associated tyrosine phosphoprotein p62. *Cell* 69, 551-558.
24. **Polakis, P.**, Rubinfeld, B. and McCormick, F. 1992 Phosphorylation of rap1GAP in vivo and by cAMP-dependent Kinase and the Cell Cycle p34^{cdc2} Kinase in vitro. *J. Biol. Chem.* 267, 10780-10785.
25. McCabe, P.C., Haubrauck, H., **Polakis, P.**, McCormick, F., and Innis, M. A. 1992 Functional Interactions Between p21^{rap1A} and Components of the Budding pathway of *Saccharomyces cerevisiae*. *Mol. Cell. Biol.* 12, 4084-4092.
26. Rubinfeld, B., Crosier, W.J., Albert, I., Conroy, L., Clark, R., McCormick, F. and **Polakis, P.** 1992 Localization of the rap1GAP Catalytic Domain and Sites of Phosphorylation by Mutational Analysis. *Mol. Cell. Biol.* 12, 4634-4642.
27. Ando, S., Kaibuchi, K., Sasaki, K., Hiraoka, T., Nishiyama, T., Mizuno, T., Asada, M., Nunoi, H., Matsuda, I., Matsuura, Y., **Polakis, P.**, McCormick, F. and Takai, Y. 1992 Post-translational processing of rac p21s is important both for their interaction with the GDP/GTP exchange proteins and for their activation of NADPH oxidase. *J. Biol. Chem.* 267, 25709-25713.
28. Janoueix-Lerosey, I., **Polakis, P.**, Tavitian, A. and deGunzberg, J. 1992 Regulation of the GTPase activity of the ras-related rap2 protein. *Biochem. Biophys. Res. Commun.* 189, 455-464.
29. **Polakis, P.** 1993 GAPs Specific for the rap1/Krev-1 Protein. in GTP-binding Proteins: the ras-superfamily. (J.C. LaCale and F. McCormick, eds.) 445-452.
30. **Polakis, P.** and McCormick, F. 1993 Structural requirements for the interaction of p21^{ras} with GAP, exchange factors, and its biological effector target. *J. Biol. Chem.* 268, 9157-9160.
31. Rubinfeld, B., Souza, B. Albert, I., Muller, O., Chamberlain, S., Masiarz, F., Munemitsu, S. and **Polakis, P.** 1993 Association of the APC gene product with beta- catenin. *Science* 262, 1731-1734.
32. Weiss, J., Rubinfeld, B., **Polakis, P.**, McCormick, F. Cavenee, W. A. and Arden, K. 1993 The gene for human rap1-GTPase activating protein (rap1GAP) maps to chromosome 1p35-1p36.1. *Cytogenet. Cell Genet.* 66, 18-21.
33. Sato, K. Y., **Polakis, P.**, Haubruck, H., Fasching, C. L., McCormick, F. and Stanbridge, E. J. 1994 Analysis of the tumor suppressor activity of the K-rev gene in human tumor cell lines. *Cancer Res.* 54, 552-559.
34. Janoueix-Lerosey, I., Fontenay, M., Tobelem, G., Tavitian, A., **Polakis, P.** and DeGunzburg, J. 1994 Phosphorylation of rap1GAP during the cell cycle. *Biochem. Biophys. Res. Commun.* 202, 967-975
35. Munemitsu, S., Souza, B., Mueller, O., Albert, I., Rubinfeld, B., and **Polakis, P.** 1994 The APC gene product associates with microtubules in vivo and affects their assembly in vitro. *Cancer Res.* 54, 3676-3681.

36. Rubinfeld, B. and Polakis, P. 1995 Purification of baculovirus produced rap1GAP. **Methods Enz.** 255,31
37. Polakis, P. 1995 Mutations in the APC gene and their implications for protein structure and function. **Current Opinions in Genetics and Development** 5, 66-71
38. Rubinfeld, B., Souza, B., Albert, I., Munemitsu, S. and Polakis P. 1995 The APC protein and E-cadherin form similar but independent complexes with α -catenin, β -catenin and Plakoglobin. **J. Biol. Chem.** 270, 5549-5555
39. Munemitsu, S., Albert, I., Souza, B., Rubinfeld, B., and Polakis, P. 1995 Regulation of intracellular β -catenin levels by the APC tumor suppressor gene. **Proc. Natl. Acad. Sci.** 92, 3046-3050.
40. Lock, P., Fumagalli, S., Polakis, P. McCormick, F. and Courtneidge, S. A. 1996 The human p62 cDNA encodes Sam68 and not the rasGAP-associated p62 protein. **Cell** 84, 23-24.
41. Papkoff, J., Rubinfeld, B., Schryver, B. and Polakis, P. 1996 Wnt-1 regulates free pools of catenins and stabilizes APC-catenin complexes. **Mol. Cell. Biol.** 16, 2128-2134.
42. Rubinfeld, B., Albert, I., Porfiri, E., Fiol, C., Munemitsu, S. and Polakis, P. 1996 Binding of GSK3 β to the APC- β -catenin complex and regulation of complex assembly. **Science** 272, 1023-1026.
43. Munemitsu, S., Albert, I., Rubinfeld, B. and Polakis, P. 1996 Deletion of amino-terminal structure stabilizes β -catenin in vivo and promotes the hyperphosphorylation of the APC tumor suppressor protein. **Mol. Cell. Biol.** 16, 4088-4094.
44. Hart, M. J., Callow, M. G., Sousa, B. and Polakis P. 1996 IQGAP1, a calmodulin binding protein with a rasGAP related domain, is a potential effector for cdc42Hs. **EMBO J.** 15, 2997-3005.
45. Nathke, I. S., Adams, C. L., Polakis, P., Sellin, J. and Nelson, W. J. 1996 The adenomatous polyposis coli (APC) tumor suppressor protein is localized to plasma membrane sites involved in active epithelial cell migration. **J. Cell. Biol.** 134, 165-180.
46. Hart, M. J., Sharma, S., elMasry, N., Qui, R-G., McCabe, P., Polakis, P. and Bollag, G. 1996 Identification of a novel guanine nucleotide exchange factor for the rho GTPase. **J. Biol. Chem.** 271, 25452.
47. Thomas JE, Smith M, Rubinfeld B, Gutowski M, Beckmann RP, and Polakis P. 1996 Subcellular localization and analysis of apparent 180-kDa and 220-kDa proteins of the breast cancer susceptibility gene, BRCA1. **J. Biol. Chem.** 1996 271, 28630-28635
48. Hayashi, S., Rubinfeld, B., Souza, B., Polakis, P., Wieschaus, E., and Levine, A. 1997 A Drosophila homolog of the tumor suppressor adenomatous polyposis coli

down-regulates β -catenin but its zygotic expression is not essential for the regulation of armadillo. **Proc. Natl. Acad. Sci.** 94, 242-247.

49. Vleminckx, K., Rubinfeld, B., **Polakis, P.** and Gumbiner, B. 1997 The APC tumor suppressor protein induces a new axis in *Xenopus* embryos. **J. Cell. Biol.** 136, 411-420.

50. Rubinfeld, B., Robbins, P., El-Gamil, M., Albert, I., Porfiri, P. and **Polakis, P.** 1997 Stabilization of β -catenin by genetic defects in melanoma cell lines. **Science** 275, 1790-1792.

51. **Polakis, P.** The adenomatous polyposis coli (APC) tumor suppressor. 1997 **Biochem. Biophys. Acta**, 1332, F127-F147.

52. Rubinfeld, B., Albert, I., Porfiri, E., Munemitsu, S., and **Polakis, P.** 1997 Loss of β -catenin regulation by the APC tumor suppressor protein correlates with loss of structure due to common somatic mutations of the gene. **Cancer Res.** 57, 4624-4630.

53. Porfiri, E., Rubinfeld, B., Albert, I., Hovanes, K., Waterman, M., and **Polakis, P.** 1997 Induction of a β -catenin-LEF-1 complex by wnt-1 and transforming mutants of β -catenin. **Oncogene** 15, 2833-2839.

54. Thomas JE, Smith M, Tonkinson JL, Rubinfeld B, and **Polakis P.**, 1997 Induction of phosphorylation on BRCA1 during the cell cycle and after DNA damage. **Cell Growth Differ.** 8, 801-809.

55. Hart, M., de los Santos, R., Albert, I., Rubinfeld, B., and **Polakis P.**, 1998 Down regulation of β -catenin by human Axin and its association with the adenomatous polyposis coli (APC) tumor suppressor, β -catenin and glycogen synthase kinase 3 β . **Current Biology** 8, 573-581.

56. **Polakis, P.** 1998 The oncogenic activation of β -catenin. **Current Opinions in Genetics and Development** 9, 15-21

57. Matt Hart, Jean-Paul Concordet, Irina Lassot, Iris Albert, Rico del los Santos, Herve Durand, Christine Perret, Bonnee Rubinfeld, Florence Margottin, Richard Benarous and **Paul Polakis.** 1999 The F-box protein β -TrCP associates with phosphorylated β -catenin and regulates its activity in the cell. **Current Biology** 9, 207-10.

58. Howard C. Crawford, Barbara M. Fingleton, Bonnee Rubinfeld, **Paul Polakis** and Lynn M. Matrisian 1999 The metalloproteinase matrilysin is a target of β -catenin transactivation in intestinal tumours. **Oncogene** 18, 2883-91.

59. Meng J, Glick JL, **Polakis P.**, Casey PJ. 1999 Functional interaction between Galpha(z) and Rap1GAP suggests a novel form of cellular cross-talk. **J Biol Chem.** 17, 36663-9

60. Vijayasurian Easwaran, Virginia Song, **Paul Polakis** and Steve Byers 1999 The ubiquitin-proteasome pathway and serine kinase activity modulate APC mediated regulation of β -catenin-LEF signaling. **J. Biol. Chem.** 274(23):16641-5.
- 61 **Polakis P**, Hart M and Rubinfeld B. 1999 Defects in the regulation of beta-catenin in colorectal cancer. **Adv Exp Med Biol.** 470, 23-32
- 62 Shen Z, Batzer A, Koehler JA, **Polakis P**, Schlessinger J, Lydon NB, Moran MF. 1999 Evidence for SH3 domain directed binding and phosphorylation of Sam68 by Src. **Oncogene.** 18, 4647-53
64. Thomas GM, Frame S, Goedert M, Nathke I, **Polakis P**, Cohen P. 1999 A GSK3- binding peptide from FRAT1 selectively inhibits the GSK3-catalysed phosphorylation of axin and beta-catenin. **FEBS Lett.** 458, 247-51.
65. Peifer M, **Polakis P**. 2000 Wnt signaling in oncogenesis and embryogenesis—a look outside the nucleus. **Science** 287,1606-9.
66. **Polakis P**. 2000 Wnt signaling and cancer. **Genes Dev**;14, 1837-1851.
67. Spink KE, **Polakis P**, Weis WI. 2000 Structural basis of the Axin-adenomatous polyposis coli interaction. **EMBO J** 19, 2270-2279.
68. Szeto, W., Jiang, W., Tice, D.A., Rubinfeld, B., Hollingshead, P.G., Fong, S.E., Dugger, D.L., Pham, T., Yansura, D.E., Wong, T.A., Grimaldi, J.C., Corpuz, R.T., Singh J.S., Frantz, G.D., Devaux, B., Crowley, C.W., Schwall, R.H., Eberhard, D.A., Rastelli, L., **Polakis, P.** and Pennica, D. 2001 Overexpression of the Retinoic Acid-Responsive Gene Stra6 in Human Cancers and its Synergistic Induction by Wnt-1 and Retinoic Acid. **Cancer Res** 61, 4197-4204.
69. Rubinfeld B, Tice DA, **Polakis P**. 2001 Axin dependent phosphorylation of the adenomatous polyposis coli protein mediated by casein kinase 1 epsilon. **J Biol Chem** 276, 39037-39045.
70. **Polakis P**. 2001 More than one way to skin a catenin. **Cell** 2001 105, 563-566.
71. Tice DA, Soloviev I, **Polakis P**. 2002 Activation of the Wnt Pathway Interferes with Serum Response Element-driven Transcription of Immediate Early Genes. **J Biol. Chem.** 277, 6118-6123.
72. Tice DA, Szeto W, Soloviev I, Rubinfeld B, Fong SE, Dugger DL, Winer J,

Williams PM, Wieand D, Smith V, Schwall RH, Pennica D, **Polakis P**. 2002 Synergistic activation of tumor antigens by wnt-1 signaling and retinoic acid revealed by gene expression profiling. **J Biol Chem**. 277,14329-14335.

73. **Polakis, P**. 2002 Casein kinase I: A wnt'er of disconnect. **Curr. Biol**. 12, R499.

74. Mao, W., Luis, E., Ross, S., Silva, J., Tan, C., Crowley, C., Chui, C., Franz, G., Senter, P., Koeppen, H., **Polakis, P**. 2004 EphB2 as a therapeutic antibody drug target for the treatment of colorectal cancer. **Cancer Res**. 64, 781-788.

75. Shibamoto, S., Winer, J., Williams, M., **Polakis, P**. 2003 A Blockade in Wnt signaling is activated following the differentiation of F9 teratocarcinoma cells. **Exp. Cell Res**. 29211-20.

76. Zhang Y, Eberhard DA, Frantz GD, Dowd P, Wu TD, Zhou Y, Watanabe C, Luoh SM, **Polakis P**, Hillan KJ, Wood WI, Zhang Z. 2004 GEPIs--quantitative gene expression profiling in normal and cancer tissues. **Bioinformatics**, April 8

SECOND DECLARATION OF PAUL POLAKIS, Ph.D.

I, Paul Polakis, Ph.D., declare and say as follows:

1. I am currently employed by Genentech, Inc. where my job title is Staff Scientist.
2. Since joining Genentech in 1999, one of my primary responsibilities has been leading Genentech's Tumor Antigen Project, which is a large research project with a primary focus on identifying tumor cell markers that find use as targets for both the diagnosis and treatment of cancer in humans.
3. As I stated in my previous Declaration dated May 7, 2004 (attached as Exhibit A); my laboratory has been employing a variety of techniques, including microarray analysis, to identify genes which are differentially expressed in human tumor tissue relative to normal human tissue. The primary purpose of this research is to identify proteins that are abundantly expressed on certain human tumor tissue(s) and that are either (i) not expressed, or (ii) expressed at detectably lower levels, on normal tissue(s).
4. In the course of our research using microarray analysis, we have identified approximately 200 gene transcripts that are present in human tumor tissue at significantly higher levels than in normal human tissue. To date, we have successfully generated antibodies that bind to 31 of the tumor antigen proteins expressed from these differentially expressed gene transcripts and have used these antibodies to quantitatively determine the level of production of these tumor antigen proteins in both human tumor tissue and normal tissue. We have then quantitatively compared the levels of mRNA and protein in both the tumor and normal tissues analyzed. The results of these analyses are attached herewith as Exhibit B. In Exhibit B, "+" means that the mRNA or protein was detectably overexpressed in the tumor tissue relative to normal tissue and "-" means that no detectable overexpression was observed in the tumor tissue relative to normal tissue.
5. As shown in Exhibit B, of the 31 genes identified as being detectably overexpressed in human tumor tissue as compared to normal human tissue at the mRNA level, 28 of them (i.e., greater than 90%) are also detectably overexpressed in human tumor tissue as compared to normal human tissue at the protein level. As such, in the cases where we have been able to quantitatively measure both (i) mRNA and (ii) protein levels in both (i) tumor tissue and (ii) normal tissue, we have observed that in the vast majority of cases, there is a very strong correlation between increases in mRNA expression and increases in the level of protein encoded by that mRNA.

6. Based upon my own experience accumulated in more than 20 years of research, including the data discussed in paragraphs 4-5 above and my knowledge of the relevant scientific literature, it is my considered scientific opinion that for human genes, an increased level of mRNA in a tumor tissue relative to a normal tissue more often than not correlates to a similar increase in abundance of the encoded protein in the tumor tissue relative to the normal tissue. In fact, it remains a generally accepted working assumption in molecular biology that increased mRNA levels are more often than not predictive of elevated levels of the encoded protein. In fact, an entire industry focusing on the research and development of therapeutic antibodies to treat a variety of human diseases, such as cancer, operates on this working assumption.
7. I hereby declare that all statements made herein of my own knowledge are true and that all statements made on information or belief are believed to be true, and further that these statements were made with the knowledge that willful false statements and the like so made are punishable by fine or imprisonment, or both, under Section 1001 of Title 18 of the United States Code and that such willful statements may jeopardize the validity of the application or any patent issued thereon.

Dated: 3-29-06

By: Paul Polakis

Paul Polakis, Ph.D.

DECLARATION OF PAUL POLAKIS, Ph.D.

I, Paul Polakis, Ph.D., declare and say as follows:

1. I was awarded a Ph.D. by the Department of Biochemistry of the Michigan State University in 1984. My scientific Curriculum Vitae is attached to and forms part of this Declaration (Exhibit A).
2. I am currently employed by Genentech, Inc. where my job title is Staff Scientist. Since joining Genentech in 1999, one of my primary responsibilities has been leading Genentech's Tumor Antigen Project, which is a large research project with a primary focus on identifying tumor cell markers that find use as targets for both the diagnosis and treatment of cancer in humans.
3. As part of the Tumor Antigen Project, my laboratory has been analyzing differential expression of various genes in tumor cells relative to normal cells. The purpose of this research is to identify proteins that are abundantly expressed on certain tumor cells and that are either (i) not expressed, or (ii) expressed at lower levels, on corresponding normal cells. We call such differentially expressed proteins "tumor antigen proteins". When such a tumor antigen protein is identified, one can produce an antibody that recognizes and binds to that protein. Such an antibody finds use in the diagnosis of human cancer and may ultimately serve as an effective therapeutic in the treatment of human cancer.
4. In the course of the research conducted by Genentech's Tumor Antigen Project, we have employed a variety of scientific techniques for detecting and studying differential gene expression in human tumor cells relative to normal cells, at genomic DNA, mRNA and protein levels. An important example of one such technique is the well known and widely used technique of microarray analysis which has proven to be extremely useful for the identification of mRNA molecules that are differentially expressed in one tissue or cell type relative to another. In the course of our research using microarray analysis, we have identified approximately 200 gene transcripts that are present in human tumor cells at significantly higher levels than in corresponding normal human cells. To date, we have generated antibodies that bind to about 30 of the tumor antigen proteins expressed from these differentially expressed gene transcripts and have used these antibodies to quantitatively determine the level of production of these tumor antigen proteins in both human cancer cells and corresponding normal cells. We have then compared the levels of mRNA and protein in both the tumor and normal cells analyzed.
5. From the mRNA and protein expression analyses described in paragraph 4 above, we have observed that there is a strong correlation between changes in the level of mRNA present in any particular cell type and the level of protein

expressed from that mRNA in that cell type. In approximately 80% of our observations we have found that increases in the level of a particular mRNA correlates with changes in the level of protein expressed from that mRNA when human tumor cells are compared with their corresponding normal cells.

6. Based upon my own experience accumulated in more than 20 years of research, including the data discussed in paragraphs 4 and 5 above and my knowledge of the relevant scientific literature, it is my considered scientific opinion that for human genes, an increased level of mRNA in a tumor cell relative to a normal cell typically correlates to a similar increase in abundance of the encoded protein in the tumor cell relative to the normal cell. In fact, it remains a central dogma in molecular biology that increased mRNA levels are predictive of corresponding increased levels of the encoded protein. While there have been published reports of genes for which such a correlation does not exist, it is my opinion that such reports are exceptions to the commonly understood general rule that increased mRNA levels are predictive of corresponding increased levels of the encoded protein.

7. I hereby declare that all statements made herein of my own knowledge are true and that all statements made on information or belief are believed to be true, and further that these statements were made with the knowledge that willful false statements and the like so made are punishable by fine or imprisonment, or both, under Section 1001 of Title 18 of the United States Code and that such willful statements may jeopardize the validity of the application or any patent issued thereon.

Dated: 5/07/04

By: Paul Polakis

Paul Polakis, Ph.D.

CURRICULUM VITAE

PAUL G. POLAKIS
Staff Scientist
Genentech, Inc
1 DNA Way, MS#40
S. San Francisco, CA 94080

EDUCATION:

Ph.D., Biochemistry, Department of Biochemistry,
Michigan State University (1984)

B.S., Biology. College of Natural Science, Michigan State University (1977)

PROFESSIONAL EXPERIENCE:

2002-present	Staff Scientist, Genentech, Inc S. San Francisco, CA
1999- 2002	Senior Scientist, Genentech, Inc., S. San Francisco, CA
1997 -1999	Research Director Onyx Pharmaceuticals, Richmond, CA
1992- 1996	Senior Scientist, Project Leader, Onyx Pharmaceuticals, Richmond, CA
1991-1992	Senior Scientist, Chiron Corporation, Emeryville, CA.
1989-1991	Scientist, Cetus Corporation, Emeryville CA.
1987-1989	Postdoctoral Research Associate, Genentech, Inc., South San Francisco, CA.
1985-1987	Postdoctoral Research Associate, Department of Medicine, Duke University Medical Center, Durham, NC

1984-1985

Assistant Professor, Department of Chemistry,
Oberlin College, Oberlin, Ohio

1980-1984

Graduate Research Assistant, Department of
Biochemistry, Michigan State University
East Lansing, Michigan

PUBLICATIONS:

1. Polakis, P. G. and Wilson, J. E. 1982 Purification of a Highly Bindable Rat Brain Hexokinase by High Performance Liquid Chromatography. **Biochem. Biophys. Res. Commun.** 107, 937-943.
2. Polakis, P.G. and Wilson, J. E. 1984 Proteolytic Dissection of Rat Brain Hexokinase: Determination of the Cleavage Pattern during Limited Digestion with Trypsin. **Arch. Biochem. Biophys.** 234, 341-352.
3. Polakis, P. G. and Wilson, J. E. 1985 An Intact Hydrophobic N-Terminal Sequence is Required for the Binding Rat Brain Hexokinase to Mitochondria. **Arch. Biochem. Biophys.** 236, 328-337.
4. Uhing, R.J., Polakis, P.G. and Snyderman, R. 1987 Isolation of GTP-binding Proteins from Myeloid HL60 Cells. **J. Biol. Chem.** 262, 15575-15579.
5. Polakis, P.G., Uhing, R.J. and Snyderman, R. 1988 The Formylpeptide Chemoattractant Receptor Copurifies with a GTP-binding Protein Containing a Distinct 40 kDa Pertussis Toxin Substrate. **J. Biol. Chem.** 263, 4969-4979.
6. Uhing, R. J., Dillon, S., Polakis, P. G., Truett, A. P. and Snyderman, R. 1988 Chemoattractant Receptors and Signal Transduction Processes in Cellular and Molecular Aspects of Inflammation (Poste, G. and Crooke, S. T. eds.) pp 335-379.
7. Polakis, P.G., Evans, T. and Snyderman 1989 Multiple Chromatographic Forms of the Formylpeptide Chemoattractant Receptor and their Relationship to GTP-binding Proteins. **Biochem. Biophys. Res. Commun.** 161, 276-283.
8. Polakis, P. G., Snyderman, R. and Evans, T. 1989 Characterization of G25K, a GTP-binding Protein Containing a Novel Putative Nucleotide Binding Domain. **Biochem. Biophys. Res. Commun.** 160, 25-32.
9. Polakis, P., Weber, R.F., Nevins, B., Didsbury, J. Evans, T. and Snyderman, R. 1989 Identification of the *ral* and *rac1* Gene Products, Low Molecular Mass GTP-binding Proteins from Human Platelets. **J. Biol. Chem.** 264, 16383-16389.
10. Snyderman, R., Perianin, A., Evans, T., Polakis, P. and Didsbury, J. 1989 G Proteins and Neutrophil Function. In ADP-Ribosylating Toxins and G Proteins: Insights into Signal Transduction. (J. Moss and M. Vaughn, eds.) Amer. Soc. Microbiol. pp. 295-323.

11. Hart, M.J., Polakis, P.G., Evans, T. and Cerrione, R.A. 1990 The Identification and Characterization of an Epidermal Growth Factor-Stimulated Phosphorylation of a Specific Low Molecular Mass GTP-binding Protein in a Reconstituted Phospholipid Vesicle System. *J. Biol. Chem.* 265, 5990-6001.
12. Yatani, A., Okabe, K., Polakis, P., Halenbeck, R., McCormick, F. and Brown, A. M. 1990 ras p21 and GAP Inhibit Coupling of Muscarinic Receptors to Atrial K⁺ Channels. *Cell* 61, 769-776.
13. Munemitsu, S., Innis, M.A., Clark, R., McCormick, F., Ullrich, A. and Polakis, P.G. 1990 Molecular Cloning and Expression of a G25K cDNA, the Human Homolog of the Yeast Cell Cycle Gene CDC42. *Mol. Cell. Biol.* 10, 5977-5982.
14. Polakis, P.G., Rubinfeld, B., Evans, T. and McCormick, F. 1991 Purification of Plasma Membrane-Associated GTPase Activating Protein (GAP) Specific for rap-1/krev-1 from HL60 Cells. *Proc. Natl. Acad. Sci. USA* 88, 239-243.
15. Moran, M. F., Polakis, P., McCormick, F., Pawson, T. and Ellis, C. 1991 Protein Tyrosine Kinases Regulate the Phosphorylation, Protein Interactions, Subcellular Distribution, and Activity of p21ras GTPase Activating Protein. *Mol. Cell. Biol.* 11, 1804-1812.
16. Rubinfeld, B., Wong, G., Bekesi, E., Wood, A., McCormick, F. and Polakis, P. G. 1991 A Synthetic Peptide Corresponding to a Sequence in the GTPase Activating Protein Inhibits p21^{ras} Stimulation and Promotes Guanine Nucleotide Exchange. *Internatl. J. Peptide and Prot. Res.* 38, 47-53.
17. Rubinfeld, B., Munemitsu, S., Clark, R., Conroy, L., Watt, K., Crosier, W., McCormick, F., and Polakis, P. 1991 Molecular Cloning of a GTPase Activating Protein Specific for the Krev-1 Protein p21^{rap1}. *Cell* 65, 1033-1042.
18. Zhang, K., Papageorge, A., G., Martin, P., Vass, W. C., Olah, Z., Polakis, P., McCormick, F. and Lowy, D. R. 1991 Heterogenous Amino Acids in RAS and Rap1A Specifying Sensitivity to GAP Proteins. *Science* 254, 1630-1634.
19. Martin, G., Yatani, A., Clark, R., Polakis, P., Brown, A. M. and McCormick, F. 1992 GAP Domains Responsible for p21^{ras}-dependent Inhibition of Muscarinic Atrial K⁺ Channel Currents. *Science* 255, 192-194.
20. McCormick, F., Martin, G. A., Clark, R., Bollag, G. and Polakis, P. 1992 Regulation of p21ras by GTPase Activating Proteins. *Cold Spring Harbor Symposia on Quantitative Biology*. Vol. 56, 237-241.
21. Pronk, G. B., Polakis, P., Wong, G., deVries-Smits, A. M., Bos J. L. and McCormick, F. 1992 p60^{v-src} Can Associate with and Phosphorylate the p21^{ras} GTPase Activating Protein. *Oncogene* 7, 389-394.
22. Polakis P. and McCormick, F. 1992 Interactions Between p21^{ras} Proteins and Their GTPase Activating Proteins. In Cancer Surveys (Franks, L. M., ed.) 12, 25-42.

23. Wong, G., Muller, O., Clark, R., Conroy, L., Moran, M., Polakis, P. and McCormick, F. 1992 Molecular cloning and nucleic acid binding properties of the GAP-associated tyrosine phosphoprotein p62. *Cell* 69, 551-558.
24. Polakis, P., Rubinfeld, B. and McCormick, F. 1992 Phosphorylation of rap1GAP in vivo and by cAMP-dependent Kinase and the Cell Cycle p34^{cdc2} Kinase in vitro. *J. Biol. Chem.* 267, 10780-10785.
25. McCabe, P.C., Haubrauck, H., Polakis, P., McCormick, F., and Innis, M. A. 1992 Functional Interactions Between p21^{rap1A} and Components of the Budding pathway of *Saccharomyces cerevisiae*. *Mol. Cell. Biol.* 12, 4084-4092.
26. Rubinfeld, B., Crosier, W.J., Albert, I., Conroy, L., Clark, R., McCormick, F. and Polakis, P. 1992 Localization of the rap1GAP Catalytic Domain and Sites of Phosphorylation by Mutational Analysis. *Mol. Cell. Biol.* 12, 4634-4642.
27. Ando, S., Kaibuchi, K., Sasaki, K., Hiraoka, T., Nishiyama, T., Mizuno, T., Asada, M., Nuno, H., Matsuda, I., Matsuura, Y., Polakis, P., McCormick, F. and Takai, Y. 1992 Post-translational processing of rac p21s is important both for their interaction with the GDP/GTP exchange proteins and for their activation of NADPH oxidase. *J. Biol. Chem.* 267, 25709-25713.
28. Janoueix-Lerosey, I., Polakis, P., Tavittian, A. and deGunzburg, J. 1992 Regulation of the GTPase activity of the ras-related rap2 protein. *Biochem. Biophys. Res. Commun.* 189, 455-464.
29. Polakis, P. 1993 GAPs Specific for the rap1/Krev-1 Protein. in GTP-binding Proteins: the ras-superfamily. (J.C. LaCale and F. McCormick, eds.) 445-452.
30. Polakis, P. and McCormick, F. 1993 Structural requirements for the interaction of p21^{ras} with GAP, exchange factors, and its biological effector target. *J. Biol. Chem.* 268, 9157-9160.
31. Rubinfeld, B., Souza, B., Albert, I., Muller, O., Chamberlain, S., Masiarz, F., Munemitsu, S. and Polakis, P. 1993 Association of the APC gene product with beta-catenin. *Science* 262, 1731-1734.
32. Weiss, J., Rubinfeld, B., Polakis, P., McCormick, F., Cavenee, W. A. and Arden, K. 1993 The gene for human rap1-GTPase activating protein (rap1GAP) maps to chromosome 1p35-1p36.1. *Cytogenet. Cell Genet.* 66, 18-21.
33. Sato, K. Y., Polakis, P., Haubruck, H., Fasching, C. L., McCormick, F. and Stanbridge, E. J. 1994 Analysis of the tumor suppressor activity of the K-ras gene in human tumor cell lines. *Cancer Res.* 54, 552-559.
34. Janoueix-Lerosey, I., Fontenay, M., Tobelem, G., Tavittian, A., Polakis, P. and DeGunzburg, J. 1994 Phosphorylation of rap1GAP during the cell cycle. *Biochem. Biophys. Res. Commun.* 202, 967-975.
35. Munemitsu, S., Souza, B., Mueller, O., Albert, I., Rubinfeld, B., and Polakis, P. 1994 The APC gene product associates with microtubules in vivo and affects their assembly in vitro. *Cancer Res.* 54, 3676-3681.

36. Rubinfeld, B. and Polakis, P. 1995 Purification of baculovirus produced rap1GAP. *Methods Enz.* 255,31
37. Polakis, P. 1995 Mutations in the APC gene and their implications for protein structure and function. *Current Opinions in Genetics and Development* 5, 66-71
38. Rubinfeld, B., Souza, B., Albert, I., Munemitsu, S. and Polakis P. 1995 The APC protein and E-cadherin form similar but independent complexes with α -catenin, β -catenin and Plakoglobin. *J. Biol. Chem.* 270, 5549-5555
39. Munemitsu, S., Albert, I., Souza, B., Rubinfeld, B., and Polakis, P. 1995 Regulation of intracellular β -catenin levels by the APC tumor suppressor gene. *Proc. Natl. Acad. Sci.* 92, 3046-3050.
40. Lock, P., Fumagalli, S., Polakis, P., McCormick, F. and Courtneidge, S. A. 1996 The human p62 cDNA encodes Sam68 and not the rasGAP-associated p62 protein. *Cell* 84, 23-24.
41. Papkoff, J., Rubinfeld, B., Schryver, B. and Polakis, P. 1996 Wnt-1 regulates free pools of catenins and stabilizes APC-catenin complexes. *Mol. Cell. Biol.* 16, 2128-2134.
42. Rubinfeld, B., Albert, I., Porfiri, E., Fiol, C., Munemitsu, S. and Polakis, P. 1996 Binding of GSK3 β to the APC- β -catenin complex and regulation of complex assembly. *Science* 272, 1023-1026.
43. Munemitsu, S., Albert, I., Rubinfeld, B. and Polakis, P. 1996 Deletion of amino-terminal structure stabilizes β -catenin in vivo and promotes the hyperphosphorylation of the APC tumor suppressor protein. *Mol. Cell. Biol.* 16, 4088-4094.
44. Hart, M. J., Callow, M. G., Sousa, B. and Polakis P. 1996 IQGAP1, a calmodulin binding protein with a rasGAP related domain, is a potential effector for cdc42Hs. *EMBO J.* 15, 2997-3005.
45. Nathke, I. S., Adams, C. L., Polakis, P., Sellin, J. and Nelson, W. J. 1996 The adenomatous polyposis coli (APC) tumor suppressor protein is localized to plasma membrane sites involved in active epithelial cell migration. *J. Cell. Biol.* 134, 165-180.
46. Hart, M. J., Sharma, S., elMasry, N., Qui, R-G., McCabe, P., Polakis, P. and Bollag, G. 1996 Identification of a novel guanine nucleotide exchange factor for the rho GTPase. *J. Biol. Chem.* 271, 25452.
47. Thomas JE, Smith M, Rubinfeld B, Gutowski M, Beckmann RP, and Polakis P. 1996 Subcellular localization and analysis of apparent 180-kDa and 220-kDa proteins of the breast cancer susceptibility gene, BRCA1. *J. Biol. Chem.* 1996 271, 28630-28635
48. Hayashi, S., Rubinfeld, B., Souza, B., Polakis, P., Wieschaus, E., and Levine, A. 1997 A Drosophila homolog of the tumor suppressor adenomatous polyposis coli

down-regulates β -catenin but its zygotic expression is not essential for the regulation of armadillo. *Proc. Natl. Acad. Sci.* 94, 242-247.

49. Vleminckx, K., Rubinfeld, B., Polakis, P. and Gumbiner, B. 1997 The APC tumor suppressor protein induces a new axis in *Xenopus* embryos. *J. Cell. Biol.* 136, 411-420.

50. Rubinfeld, B., Robbins, P., El-Gamil, M., Albert, I., Porfiri, P. and Polakis, P. 1997 Stabilization of β -catenin by genetic defects in melanoma cell lines. *Science* 275, 1790-1792.

51. Polakis, P. The adenomatous polyposis coli (APC) tumor suppressor. 1997 *Biochem. Biophys. Acta*, 1332, F127-F147.

52. Rubinfeld, B., Albert, I., Porfiri, E., Munemitsu, S., and Polakis, P. 1997 Loss of β -catenin regulation by the APC tumor suppressor protein correlates with loss of structure due to common somatic mutations of the gene. *Cancer Res.* 57, 4624-4630.

53. Porfiri, E., Rubinfeld, B., Albert, I., Hovanes, K., Waterman, M., and Polakis, P. 1997 Induction of a β -catenin-LEF-1 complex by wnt-1 and transforming mutants of β -catenin. *Oncogene* 15, 2833-2839.

54. Thomas JE, Smith M, Tonkinson JL, Rubinfeld B, and Polakis P., 1997 Induction of phosphorylation on BRCA1 during the cell cycle and after DNA damage. *Cell Growth Differ.* 8, 801-809.

55. Hart, M., de los Santos, R., Albert, I., Rubinfeld, B., and Polakis P., 1998 Down regulation of β -catenin by human Axin and its association with the adenomatous polyposis coli (APC) tumor suppressor, β -catenin and glycogen synthase kinase 3 β . *Current Biology* 8, 573-581.

56. Polakis, P. 1998 The oncogenic activation of β -catenin. *Current Opinions in Genetics and Development* 9, 15-21

57. Matt Hart, Jean-Paul Concordet, Irina Lassot, Iris Albert, Rico del los Santos, Herve Durand, Christine Perret, Bonnee Rubinfeld, Florence Margottin, Richard Benarous and Paul Polakis. 1999 The F-box protein β -TrCP associates with phosphorylated β -catenin and regulates its activity in the cell. *Current Biology* 9, 207-10.

58. Howard C. Crawford, Barbara M. Fingleton, Bonnee Rubinfeld, Paul Polakis and Lynn M. Matrisian. 1999 The metalloproteinase matrilysin is a target of β -catenin transactivation in intestinal tumours. *Oncogene* 18, 2883-91.

59. Meng J, Glick JL, Polakis P, Casey PJ. 1999 Functional interaction between Galpha(z) and Rap1GAP suggests a novel form of cellular cross-talk. *J Biol Chem.* 17, 36663-9

60. Vijayasunian Easwaran, Virginia Song, Paul Polakis and Steve Byers 1999 The ubiquitin-proteasome pathway and serine kinase activity modulate APC mediated regulation of β -catenin-LEF signaling. *J. Biol. Chem.* 274(23):16641-5.
61. Polakis P, Hart M and Rubinfeld B. 1999 Defects in the regulation of beta-catenin in colorectal cancer. *Adv Exp Med Biol.* 470, 23-32
62. Shen Z, Batzer A, Koehler JA, Polakis P, Schlessinger J, Lydon NB, Moran MF. 1999 Evidence for SH3 domain directed binding and phosphorylation of Sam68 by Src. *Oncogene.* 18, 4647-53
64. Thomas GM, Frame S, Goedert M, Nathke I, Polakis P, Cohen P. 1999 A GSK3- binding peptide from FRAT1 selectively inhibits the GSK3-catalysed phosphorylation of axin and beta-catenin. *FEBS Lett.* 458, 247-51.
65. Peifer M, Polakis P. 2000 Wnt signaling in oncogenesis and embryogenesis—a look outside the nucleus. *Science* 287,1606-9.
66. Polakis P. 2000 Wnt signaling and cancer. *Genes Dev*;14, 1837-1851.
67. Spink KE, Polakis P, Weis WI 2000 Structural basis of the Axin-adenomatous polyposis coli interaction. *EMBO J* 19, 2270-2279.
68. Szeto, W., Jiang, W., Tice, D.A., Rubinfeld, B., Hollingshead, P.G., Fong, S.E., Dugger, D.L., Pham, T., Yansura, D.E., Wong, T.A., Grimaldi, J.C., Corpuz, R.T., Singh J.S., Frantz, G.D., Devaux, B., Crowley, C.W., Schwall, R.H., Eberhard, D.A., Rastelli, L., Polakis, P. and Pennica, D. 2001 Overexpression of the Retinoic Acid-Responsive Gene Stra6 in Human Cancers and its Synergistic Induction by Wnt-1 and Retinoic Acid. *Cancer Res* 61, 4197-4204.
69. Rubinfeld B, Tice DA, Polakis P. 2001 Axin dependent phosphorylation of the adenomatous polyposis coli protein mediated by casein kinase 1 epsilon. *J Biol Chem* 276, 39037-39045.
70. Polakis P. 2001 More than one way to skin a catenin. *Cell* 2001 105, 563-566.
71. Tice DA, Soloviev I, Polakis P. 2002 Activation of the Wnt Pathway Interferes with Serum Response Element-driven Transcription of Immediate Early Genes. *J Biol. Chem.* 277, 6118-6123.
72. Tice DA, Szeto W, Soloviev I, Rubinfeld B, Fong SE, Dugger DL, Winer J,

Williams PM, Wieand D, Smith V, Schwall RH, Pennica D, Polakis P. 2002 Synergistic activation of tumor antigens by wnt-1 signaling and retinoic acid revealed by gene expression profiling. *J Biol Chem.* 277,14329-14335.

73. Polakis, P. 2002 Casein kinase I: A wnt'er of disconnect. *Curr. Biol.* 12, R499.

74. Mao, W., Luis, E., Ross, S., Silva, J., Tan, C., Crowley, C., Chui, C., Franz, G., Senter, P., Koeppen, H., Polakis, P. 2004 EphB2 as a therapeutic antibody drug target for the treatment of colorectal cancer. *Cancer Res.* 64, 781-788.

75. Shibamoto, S., Winer, J., Williams, M., Polakis, P. 2003 A Blockade in Wnt signaling is activated following the differentiation of F9 teratocarcinoma cells. *Exp. Cell Res.* 29211-20.

76. Zhang Y, Eberhard DA, Frantz GD, Dowd P, Wu TD, Zhou Y, Watanabe C, Luoh SM, Polakis P, Hillan KJ, Wood WI, Zhang Z. 2004 GEPIS—quantitative gene expression profiling in normal and cancer tissues. *Bioinformatics*, April 8

EXHIBIT B

	tumor mRNA	tumor IHC
UNQ2525	+	+
UNQ2378	+	+
UNQ972	+	-
UNQ97671	+	+
UNQ2964	+	+
UNQ323	+	+
UNQ1655	+	+
UNQ2333	+	+
UNQ9638	+	+
UNQ8209	+	+
UNQ6507	+	+
UNQ8196	+	+
UNQ9109	+	+
UNQ100	+	+
UNQ178	+	+
UNQ1477	+	+
UNQ1839	+	+
UNQ2079	+	+
UNQ8782	+	+
UNQ9646	+	-
UNQ111	+	+
UNQ3079	+	+
UNQ8175	+	+
UNQ9509	+	+
UNQ10978	+	-
UNQ2103	+	+
UNQ1563	+	+
UNQ16188	+	+
UNQ13589	+	+
UNQ1078	+	+
UNQ879	+	+

Impact of DNA Amplification on Gene Expression Patterns in Breast Cancer^{1,2}

Elizabeth Hyman,³ Päivikki Kauraniemi,³ Sampsa Hautaniemi, Maija Wolf, Spyro Mousses, Ester Rozenblum, Markus Ringnér, Guido Sauter, Outi Monni, Abdel Elkahloun, Olli-P. Kallioniemi, and Anne Kallioniemi⁴

Howard Hughes Medical Institute-NIH Research Scholar, Bethesda, Maryland 20892 [E.H.]; Cancer Genetics Branch, National Human Genome Research Institute, NIH, Bethesda, Maryland 20892 [E.H., P.K., S.H., M.W., S.M., E.R., M.R., A.E., O.K., A.K.]; Laboratory of Cancer Genetics, Institute of Medical Technology, University of Tampere and Tampere University Hospital, FIN-33520 Tampere, Finland [P.K., A.K.]; Signal Processing Laboratory, Tampere University of Technology, FIN-33101 Tampere, Finland [S.H.]; Institute of Pathology, University of Basel, CH-4003 Basel, Switzerland [G.S.]; and Biomedicum Biochip Center, Helsinki University Hospital, Biomedicum Helsinki, FIN-00014 Helsinki, Finland [O.M.]

ABSTRACT

Genetic changes underlie tumor progression and may lead to cancer-specific expression of critical genes. Over 1100 publications have described the use of comparative genomic hybridization (CGH) to analyze the pattern of copy number alterations in cancer, but very few of the genes affected are known. Here, we performed high-resolution CGH analysis on cDNA microarrays in breast cancer and directly compared copy number and mRNA expression levels of 13,824 genes to quantitate the impact of genomic changes on gene expression. We identified and mapped the boundaries of 24 independent amplicons, ranging in size from 0.2 to 12 Mb. Throughout the genome, both high- and low-level copy number changes had a substantial impact on gene expression, with 44% of the highly amplified genes showing overexpression and 10.5% of the highly overexpressed genes being amplified. Statistical analysis with random permutation tests identified 270 genes whose expression levels across 14 samples were systematically attributable to gene amplification. These included most previously described amplified genes in breast cancer and many novel targets for genomic alterations, including the *HOXB7* gene, the presence of which in a novel amplicon at 17q21.3 was validated in 10.2% of primary breast cancers and associated with poor patient prognosis. In conclusion, CGH on cDNA microarrays revealed hundreds of novel genes whose overexpression is attributable to gene amplification. These genes may provide insights to the clonal evolution and progression of breast cancer and highlight promising therapeutic targets.

INTRODUCTION

Gene expression patterns revealed by cDNA microarrays have facilitated classification of cancers into biologically distinct categories, some of which may explain the clinical behavior of the tumors (1-6). Despite this progress in diagnostic classification, the molecular mechanisms underlying gene expression patterns in cancer have remained elusive, and the utility of gene expression profiling in the identification of specific therapeutic targets remains limited.

Accumulation of genetic defects is thought to underlie the clonal evolution of cancer. Identification of the genes that mediate the effects of genetic changes may be important by highlighting transcripts that are actively involved in tumor progression. Such transcripts and their encoded proteins would be ideal targets for anticancer therapies, as demonstrated by the clinical success of new therapies against amplified oncogenes, such as *ERBB2* and *EGFR* (7, 8), in breast cancer and other solid tumors. Besides amplifications of known oncogenes, over

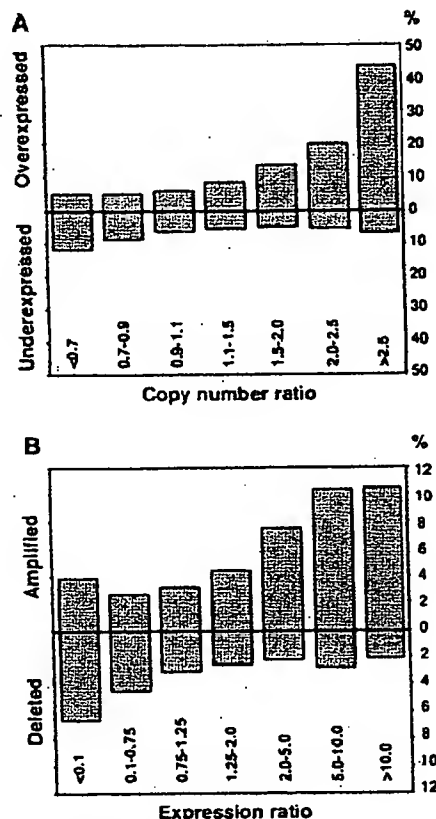


Fig. 1. Impact of gene copy number on global gene expression levels. A, percentage of over- and underexpressed genes (Y axis) according to copy number ratios (X axis). Threshold values used for over- and underexpression were >2.184 (global upper 7% of the cDNA ratios) and <0.4826 (global lower 7% of the expression ratios). B, percentage of amplified and deleted genes according to expression ratios. Threshold values for amplification and deletion were >1.5 and <0.7 .

20 recurrent regions of DNA amplification have been mapped in breast cancer by CGH⁵ (9, 10). However, these amplicons are often large and poorly defined, and their impact on gene expression remains unknown.

We hypothesized that genome-wide identification of those gene expression changes that are attributable to underlying gene copy number alterations would highlight transcripts that are actively involved in the causation or maintenance of the malignant phenotype. To identify such transcripts, we applied a combination of cDNA and CGH microarrays to: (a) determine the global impact that gene copy number variation plays in breast cancer development and progression; and (b) identify and characterize those genes whose mRNA expres-

Received 5/29/02; accepted 8/28/02.

The costs of publication of this article were defrayed in part by the payment of page charges. This article must therefore be hereby marked advertisement in accordance with 18 U.S.C. Section 1734 solely to indicate this fact.

¹ Supported in part by the Academy of Finland, Emil Aaltonen Foundation, the Finnish Cancer Society, the Pirkanmaa Cancer Society, the Pirkanmaa Cultural Foundation, the Finnish Breast Cancer Group, the Foundation for the Development of Laboratory Medicine, the Medical Research Fund of the Tampere University Hospital, the Foundation for Commercial and Technical Sciences, and the Swedish Research Council.

² Supplementary data for this article are available at Cancer Research Online (<http://cancerres.aacrjournals.org>).

³ Contributed equally to this work.

⁴ To whom requests for reprints should be addressed, at Laboratory of Cancer Genetics, Institute of Medical Technology, Lenkeitilijankatu 6, FIN-33520 Tampere, Finland. Phone: 358-3247-4125; Fax: 358-3247-4168; E-mail: anne.kallioniemi@uta.fi.

⁵ The abbreviations used are: CGH, comparative genomic hybridization; FISH, fluorescence in situ hybridization; RT-PCR, reverse transcription-PCR.

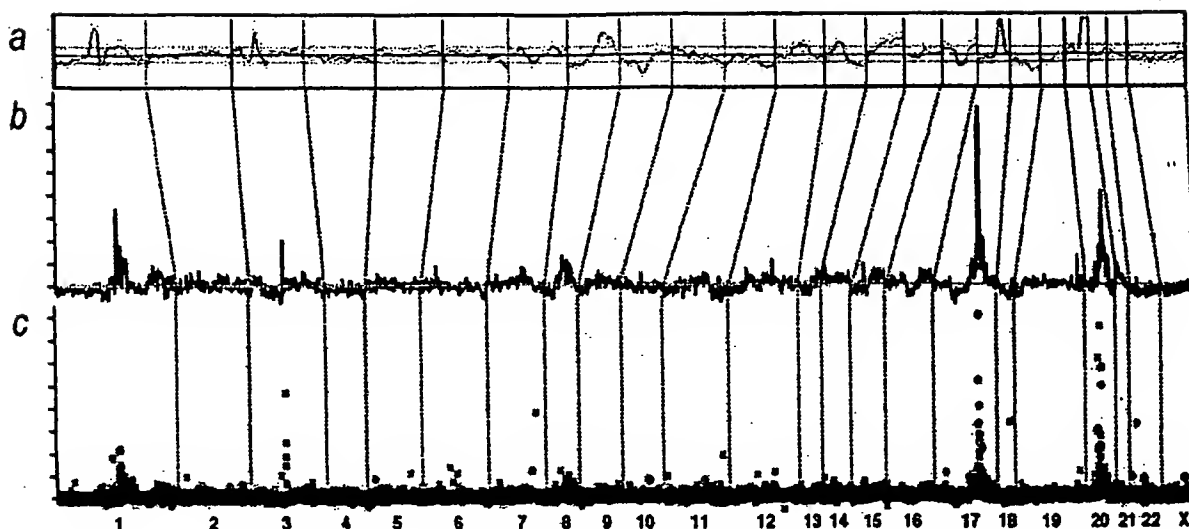


Fig. 2. Genome-wide copy number and expression analysis in the MCF-7 breast cancer cell line. A, chromosomal CGH analysis of MCF-7. The copy number ratio profile (blue line) across the entire genome from 1p telomere to Xq telomere is shown along with ± 1 SD (orange lines). The black horizontal line indicates a ratio of 1.0; red line, a ratio of 0.8; and green line, a ratio of 1.2. B-C, genome-wide copy number analysis in MCF-7 by CGH on cDNA microarray. The copy number ratios were plotted as a function of the position of the cDNA clones along the human genome. In B, individual data points are connected with a line, and a moving median of 10 adjacent clones is shown. Red horizontal line, the copy number ratio of 1.0. In C, individual data points are labeled by color coding according to cDNA expression ratios. The bright red dots indicate the upper 2%, and dark red dots, the next 5% of the expression ratios in MCF-7 cells (overexpressed genes); bright green dots indicate the lowest 2%, and dark green dots, the next 5% of the expression ratios (underexpressed genes); the rest of the observations are shown with black crosses. The chromosome numbers are shown at the bottom of the figure, and chromosome boundaries are indicated with a dashed line.

sion is most significantly associated with amplification of the corresponding genomic template.

MATERIALS AND METHODS

Breast Cancer Cell Lines. Fourteen breast cancer cell lines (BT-20, BT-474, HCC1428, Hs578t, MCF7, MDA-361, MDA-436, MDA-453, MDA-468, SKBR-3, T-47D, UACC812, ZR-75-1, and ZR-75-30) were obtained from the American Type Culture Collection (Manassas, VA). Cells were grown under recommended culture conditions. Genomic DNA and mRNA were isolated using standard protocols.

Copy Number and Expression Analyses by cDNA Microarrays. The preparation and printing of the 13,824 cDNA clones on glass slides were performed as described (11-13). Of these clones, 244 represented uncharacterized expressed sequence tags, and the remainder corresponded to known genes. CGH experiments on cDNA microarrays were done as described (14, 15). Briefly, 20 μ g of genomic DNA from breast cancer cell lines and normal human WBCs were digested for 14-18 h with *AluI* and *RsaI* (Life Technologies, Inc., Rockville, MD) and purified by phenol/chloroform extraction. Six μ g of digested cell line DNAs were labeled with Cy3-dUTP (Amersham Pharmacia) and normal DNA with Cy5-dUTP (Amersham Pharmacia) using the Bioprime Labeling kit (Life Technologies, Inc.). Hybridization (14, 15) and posthybridization washes (13) were done as described. For the expression analyses, a standard reference (Universal Human Reference RNA; Stratagene, La Jolla, CA) was used in all experiments. Forty μ g of reference RNA were labeled with Cy3-dUTP and 3.5 μ g of test mRNA with Cy5-dUTP, and the labeled cDNAs were hybridized on microarrays as described (13, 15). For both microarray analyses, a laser confocal scanner (Agilent Technologies, Palo Alto, CA) was used to measure the fluorescence intensities at the target locations using the DEARRAY software (16). After background subtraction, average intensities at each clone in the test hybridization were divided by the average intensity of the corresponding clone in the control hybridization. For the copy number analysis, the ratios were normalized on the basis of the distribution of ratios of all targets on the array and for the expression analysis on the basis of 88 housekeeping genes, which were spotted four times onto the array. Low quality measurements (*i.e.*, copy number data with mean reference intensity <100 fluorescent units, and expression data with both test and reference intensity <100 fluorescent units and/or with spot size <50 units)

were excluded from the analysis and were treated as missing values. The distributions of fluorescence ratios were used to define cutpoints for increased/decreased copy number. Genes with CGH ratio >1.43 (representing the upper 5% of the CGH ratios across all experiments) were considered to be amplified, and genes with ratio <0.73 (representing the lower 5%) were considered to be deleted.

Statistical Analysis of CGH and cDNA Microarray Data. To evaluate the influence of copy number alterations on gene expression, we applied the following statistical approach. CGH and cDNA calibrated intensity ratios were log-transformed and normalized using median centering of the values in each cell line. Furthermore, cDNA ratios for each gene across all 14 cell lines were median centered. For each gene, the CGH data were represented by a vector that was labeled 1 for amplification (ratio, >1.43) and 0 for no amplification. Amplification was correlated with gene expression using the signal-to-noise statistics (1). We calculated a weight, w_g , for each gene as follows:

$$w_g = \frac{m_{g1} - m_{g0}}{\sigma_{g1} + \sigma_{g0}}$$

where m_{g1} , σ_{g1} , and m_{g0} , σ_{g0} denote the means and SDs for the expression levels for amplified and nonamplified cell lines, respectively. To assess the statistical significance of each weight, we performed 10,000 random permutations of the label vector. The probability that a gene had a larger or equal weight by random permutation than the original weight was denoted by α . A low α (<0.05) indicates a strong association between gene expression and amplification.

Genomic Localization of cDNA Clones and Amplicon Mapping. Each cDNA clone on the microarray was assigned to a Unigene cluster using the Unigene Build 141.⁶ A database of genomic sequence alignment information for mRNA sequences was created from the August 2001 freeze of the University of California Santa Cruz's GoldenPath database.⁷ The chromosome and bp positions for each cDNA clone were then retrieved by relating these data sets. Amplicons were defined as a CGH copy number ratio >2.0 in at least two adjacent clones in two or more cell lines or a CGH ratio >2.0 in at least three adjacent clones in a single cell line. The amplicon start and end positions were

⁶ Internet address: http://research.nhgri.nih.gov/microarray/downloadable_cdna.html.

⁷ Internet address: www.genome.ucsc.edu.

Table 1 Summary of independent amplicons in 14 breast cancer cell lines by CGH microarray

Location	Start (Mb)	End (Mb)	Size (Mb)
1p13	132.79	132.94	0.2
1q21	173.92	177.25	3.3
1q22	179.28	179.57	0.3
3p14	71.94	74.66	2.7
7p12.1-7p11.2	55.62	60.95	5.3
7q31	125.73	130.96	5.2
7q32	140.01	140.68	0.7
8q21.11-8q21.13	86.45	92.46	6.0
8q21.3	98.45	103.05	4.6
8q23.3-8q24.14	129.88	142.15	12.3
8q24.22	151.21	152.16	1.0
9p13	38.65	39.25	0.6
13q22-q31	77.15	81.38	4.2
16q22	86.70	87.62	0.9
17q11	29.30	30.85	1.6
17q12-q21.2	39.79	42.80	3.0
17q21.32-q21.33	52.47	55.80	3.3
17q22-q23.3	63.81	69.70	5.9
17q23.3-q24.3	69.93	74.99	5.1
19q13	40.63	41.40	0.8
20q11.22	34.59	35.85	1.3
20q13.12	44.00	45.62	1.6
20q13.12-q13.13	46.45	49.43	3.0
20q13.2-q13.32	51.32	59.12	7.8

extended to include neighboring nonamplified clones (ratio, <1.5). The amplicon size determination was partially dependent on local clone density.

FISH. Dual-color interphase FISH to breast cancer cell lines was done as described (17). Bacterial artificial chromosome clone RP11-361K8 was labeled with SpectrumOrange (Vysis, Downers Grove, IL), and SpectrumOrange-labeled probe for *EGFR* was obtained from Vysis. SpectrumGreen-labeled chromosome 7 and 17 centromere probes (Vysis) were used as a reference. A tissue microarray containing 612 formalin-fixed, paraffin-embedded primary breast cancers (17) was applied in FISH analyses as described (18). The use of these specimens was approved by the Ethics Committee of the University of Basel and by the NIH. Specimens containing a 2-fold or higher increase in the number of test probe signals, as compared with corresponding centromere signals, in at least 10% of the tumor cells were considered to be amplified. Survival analysis was performed using the Kaplan-Meier method and the log-rank test.

RT-PCR. The *HOXB7* expression level was determined relative to *GAPDH*. Reverse transcription and PCR amplification were performed using Access RT-PCR System (Promega Corp., Madison, WI) with 10 ng of mRNA as a template. *HOXB7* primers were 5'-GAGCAGAGGGACTCGGACTT-3' and 5'-GCGTCAGGTAGCGATTGTAG-3'.

RESULTS

Global Effect of Copy Number on Gene Expression. 13,824 arrayed cDNA clones were applied for analysis of gene expression and gene copy number (CGH microarrays) in 14 breast cancer cell lines. The results illustrate a considerable influence of copy number on gene expression patterns. Up to 44% of the highly amplified transcripts (CGH ratio, >2.5) were overexpressed (i.e., belonged to the global upper 7% of expression ratios), compared with only 6% for genes with normal copy number levels (Fig. 1A). Conversely, 10.5% of the transcripts with high-level expression (cDNA ratio, >10) showed increased copy number (Fig. 1B). Low-level copy number increases and decreases were also associated with similar, although less dramatic, outcomes on gene expression (Fig. 1).

Identification of Distinct Breast Cancer Amplicons. Base-pair locations obtained for 11,994 cDNAs (86.8%) were used to plot copy number changes as a function of genomic position (Fig. 2, Supplement Fig. A). The average spacing of clones throughout the genome was 267 kb. This high-resolution mapping identified 24 independent breast cancer amplicons, spanning from 0.2 to 12 Mb of DNA (Table 1). Several amplification sites detected previously by chromosomal

CGH were validated, with 1q21, 17q12-q21.2, 17q22-q23, 20q13.1, and 20q13.2 regions being most commonly amplified. Furthermore, the boundaries of these amplicons were precisely delineated. In addition, novel amplicons were identified at 9p13 (38.65-39.25 Mb), and 17q21.3 (52.47-55.80 Mb).

Direct Identification of Putative Amplification Target Genes. The cDNA/CGH microarray technique enables the direct correlation of copy number and expression data on a gene-by-gene basis throughout the genome. We directly annotated high-resolution CGH plots with gene expression data using color coding. Fig. 2C shows that most of the amplified genes in the MCF-7 breast cancer cell line at 1p13, 17q22-q23, and 20q13 were highly overexpressed. A view of chromosome 7 in the MDA-468 cell line implicates *EGFR* as the most highly overexpressed and amplified gene at 7p11-p12 (Fig. 3A). In BT-474, the two known amplicons at 17q12 and 17q22-q23 contained numerous highly overexpressed genes (Fig. 3B). In addition, several genes, including the homeobox genes *HOXB2* and *HOXB7*, were highly amplified in a previously undescribed independent amplicon at 17q21.3. *HOXB7* was systematically amplified (as validated by FISH, Fig. 3B, inset) as well as overexpressed (as verified by RT-PCR, data not shown) in BT-474, UACC812, and ZR-75-30 cells. Furthermore, this novel

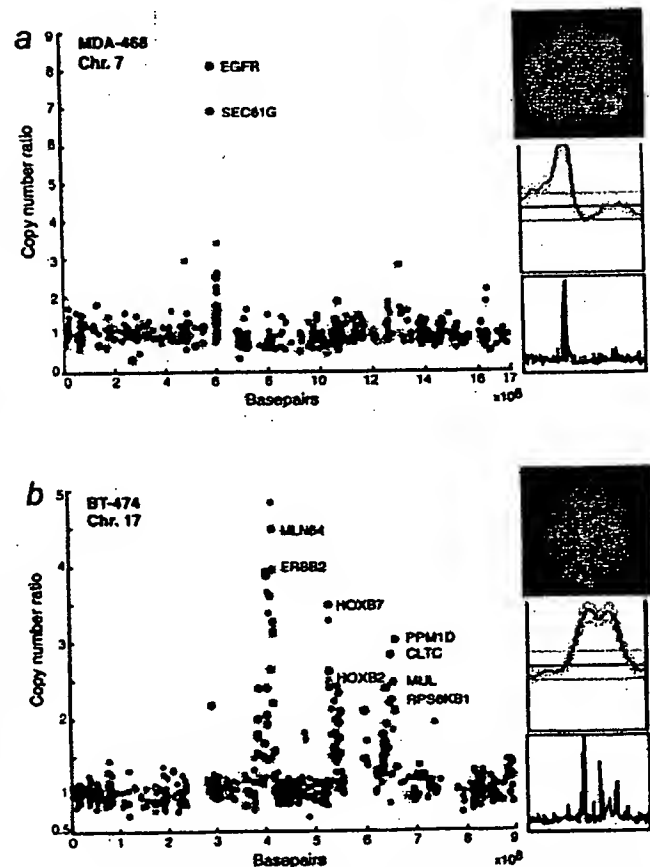
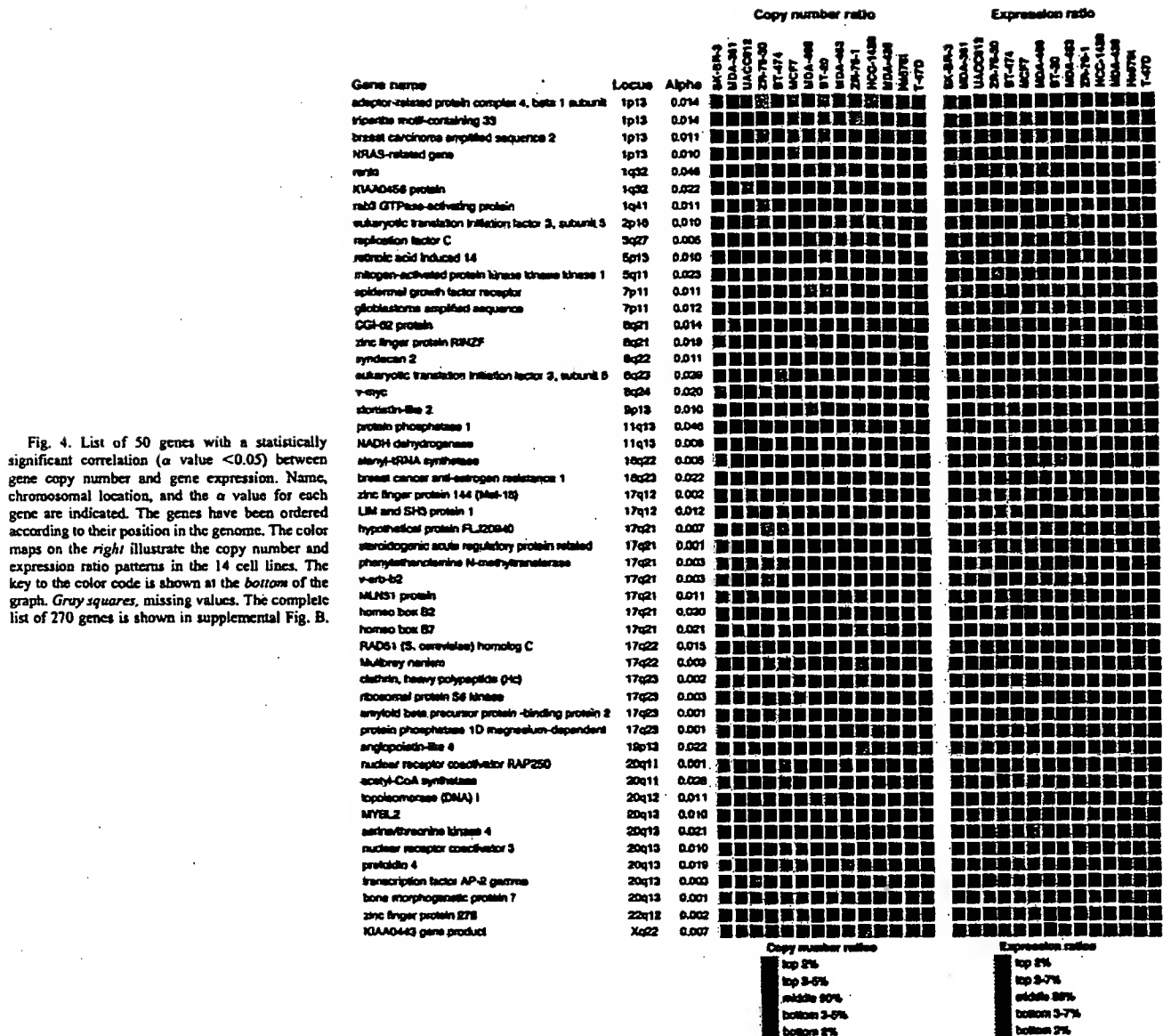


Fig. 3. Annotation of gene expression data on CGH microarray profiles. A, genes in the 7p11-p12 amplicon in the MDA-468 cell line are highly expressed (red dots) and include the *EGFR* oncogene. B, several genes in the 17q12, 17q21.3, and 17q23 amplicons in the BT-474 breast cancer cell line are highly overexpressed (red) and include the *HOXB7* gene. The data labels and color coding are as indicated for Fig. 2C. Insets show chromosomal CGH profiles for the corresponding chromosomes and validation of the increased copy number by interphase FISH using *EGFR* (red) and chromosome 7 centromere probe (green) to MDA-468 (A) and *HOXB7*-specific probe (red) and chromosome 17 centromere (green) to BT-474 cells (B).



amplification was validated to be present in 10.2% of 363 primary breast cancers by FISH to a tissue microarray and was associated with poor prognosis of the patients ($P = 0.001$).

Statistical Identification and Characterization of 270 Highly Expressed Genes in Amplicons. Statistical comparison of expression levels of all genes as a function of gene amplification identified 270 genes whose expression was significantly influenced by copy number across all 14 cell lines (Fig. 4, Supplemental Fig. B). According to the gene ontology data,⁸ 91 of the 270 genes represented hypothetical proteins or genes with no functional annotation, whereas 179 had associated functional information available. Of these, 151 (84%) are implicated in apoptosis, cell proliferation, signal transduction, and transcription, whereas 28 (16%) had functional annotations that could not be directly linked with cancer.

DISCUSSION

The importance of recurrent gene and chromosome copy number changes in the development and progression of solid tumors has been characterized in >1000 publications applying CGH⁹ (9, 10), as well as in a large number of other molecular cytogenetic, cytogenetic, and molecular genetic studies. The effects of these somatic genetic changes on gene expression levels have remained largely unknown, although a few studies have explored gene expression changes occurring in specific amplicons (15, 19–21). Here, we applied genome-wide cDNA microarrays to identify transcripts whose expression changes were attributable to underlying gene copy number alterations in breast cancer.

The overall impact of copy number on gene expression patterns was substantial with the most dramatic effects seen in the case of high-

⁸ Internet address: <http://www.geneontology.org/>.

⁹ Internet address: <http://www.ncbi.nlm.nih.gov/entrez>.

level copy number increase. Low-level copy number gains and losses also had a significant influence on expression levels of genes in the regions affected, but these effects were more subtle on a gene-by-gene basis than those of high-level amplifications. However, the impact of low-level gains on the dysregulation of gene expression patterns in cancer may be equally important if not more important than that of high-level amplifications. Aneuploidy and low-level gains and losses of chromosomal arms represent the most common types of genetic alterations in breast and other cancers and, therefore, have an influence on many genes. Our results in breast cancer extend the recent studies on the impact of aneuploidy on global gene expression patterns in yeast cells, acute myeloid leukemia, and a prostate cancer model system (22-24).

The CGH microarray analysis identified 24 independent breast cancer amplicons. We defined the precise boundaries for many amplicons detected previously by chromosomal CGH (9, 10, 25, 26) and also discovered novel amplicons that had not been detected previously, presumably because of their small size (only 1-2 Mb) or close proximity to other larger amplicons. One of these novel amplicons involved the homeobox gene region at 17q21.3 and led to the overexpression of the *HOXB7* and *HOXB2* genes. The homeodomain transcription factors are known to be key regulators of embryonic development and have been occasionally reported to undergo aberrant expression in cancer (27, 28). *HOXB7* transfection induced cell proliferation in melanoma, breast, and ovarian cancer cells and increased tumorigenicity and angiogenesis in breast cancer (29-32). The present results imply that gene amplification may be a prominent mechanism for overexpressing *HOXB7* in breast cancer and suggest that *HOXB7* contributes to tumor progression and confers an aggressive disease phenotype in breast cancer. This view is supported by our finding of amplification of *HOXB7* in 10% of 363 primary breast cancers, as well as an association of amplification with poor prognosis of the patients.

We carried out a systematic search to identify genes whose expression levels across all 14 cell lines were attributable to amplification status. Statistical analysis revealed 270 such genes (representing ~2% of all genes on the array), including not only previously described amplified genes, such as *HER-2*, *MYC*, *EGFR*, ribosomal protein S6 kinase, and *AIB3*, but also numerous novel genes such as *NRAS-related gene* (1p13), *syndecan-2* (8q22), and *bone morphogenic protein* (20q13.1), whose activation by amplification may similarly promote breast cancer progression. Most of the 270 genes have not been implicated previously in breast cancer development and suggest novel pathogenetic mechanisms. Although we would not expect all of them to be causally involved, it is intriguing that 84% of the genes with associated functional information were implicated in apoptosis, cell proliferation, signal transduction, transcription, or other cellular processes that could directly imply a possible role in cancer progression. Therefore, a detailed characterization of these genes may provide biological insights to breast cancer progression and might lead to the development of novel therapeutic strategies.

In summary, we demonstrate application of cDNA microarrays to the analysis of both copy number and expression levels of over 12,000 transcripts throughout the breast cancer genome, roughly once every 267 kb. This analysis provided: (a) evidence of a prominent global influence of copy number changes on gene expression levels; (b) a high-resolution map of 24 independent amplicons in breast cancer; and (c) identification of a set of 270 genes, the overexpression of which was statistically attributable to gene amplification. Characterization of a novel amplicon at 17q21.3 implicated amplification and overexpression of the *HOXB7* gene in breast cancer, including a clinical association

between *HOXB7* amplification and poor patient prognosis. Overall, our results illustrate how the identification of genes activated by gene amplification provides a powerful approach to highlight genes with an important role in cancer as well as to prioritize and validate putative targets for therapy development.

REFERENCES

- Golub, T. R., Slonim, D. K., Tamayo, P., Huard, C., Gaasenbeek, M., Mesirov, J. P., Coller, H., Loh, M. L., Downing, J. R., Caligiuri, M. A., Bloomfield, C. D., and Lander, E. S. Molecular classification of cancer: class discovery and class prediction by gene expression monitoring. *Science* (Wash. DC), 286: 531-537, 1999.
- Alizadeh, A. A., Eisen, M. B., Davis, R. E., Ma, C., Lossos, I. S., Rosenwald, A., Boldrick, J. C., Sabet, H., Tran, T., Yu, X., et al. Distinct types of diffuse large B-cell lymphoma identified by gene expression profiling. *Nature* (Lond.), 403: 503-511, 2000.
- Bittner, M., Meltzer, P., Chen, Y., Jiang, Y., Seftor, E., Hendrix, M., Radmacher, M., Simon, R., Yakhini, Z., Ben-Dor, A., et al. Molecular classification of cutaneous malignant melanoma by gene expression profiling. *Nature* (Lond.), 406: 536-540, 2000.
- Perou, C. M., Sorlie, T., Eisen, M. B., van de Rijn, M., Jeffrey, S. S., Rees, C. A., Pollack, J. R., Ross, D. T., Johnsen, H., Akslen, L. A., et al. Molecular portraits of human breast tumours. *Nature* (Lond.), 406: 747-752, 2000.
- Dhanasekaran, S. M., Barrette, T. R., Ghosh, D., Shah, R., Varambally, S., Kurchi, K., Pienta, K. J., Rubin, M. A., and Chinnaiyan, A. M. Delineation of prognostic biomarkers in prostate cancer. *Nature* (Lond.), 412: 822-826, 2001.
- Sorlie, T., Perou, C. M., Tibshirani, R., Aas, T., Geisler, S., Johnsen, H., Hastie, T., Eisen, M. B., van de Rijn, M., Jeffrey, S. S., et al. Gene expression patterns of breast carcinomas distinguish tumor subclasses with clinical implications. *Proc. Natl. Acad. Sci. USA*, 98: 10869-10874, 2001.
- Ross, J. S., and Fletcher, J. A. The *HER-2/neu* oncogene: prognostic factor, predictive factor and target for therapy. *Semin. Cancer Biol.*, 9: 125-138, 1999.
- Arteaga, C. L. The epidermal growth factor receptor: from mutant oncogene in nonhuman cancers to therapeutic target in human neoplasia. *J. Clin. Oncol.*, 19: 32-40, 2001.
- Knuutila, S., Björkqvist, A. M., Autio, K., Tarkkanen, M., Wolf, M., Monni, O., Szymanska, J., Larramendy, M. L., Tapper, J., Pere, H., El-Rifai, W., et al. DNA copy number amplifications in human neoplasms: review of comparative genomic hybridization studies. *Am. J. Pathol.*, 152: 1107-1123, 1998.
- Knuutila, S., Autio, K., and Aalto, Y. Online access to CGH data of DNA sequence copy number changes. *Am. J. Pathol.*, 157: 689, 2000.
- DeRisi, J., Penland, L., Brown, P. O., Bittner, M. L., Meltzer, P. S., Ray, M., Chen, Y., Su, Y. A., and Trent, J. M. Use of a cDNA microarray to analyze gene expression patterns in human cancer. *Nat. Genet.*, 14: 457-460, 1996.
- Shalon, D., Smith, S. J., and Brown, P. O. A DNA microarray system for analyzing complex DNA samples using two-color fluorescent probe hybridization. *Genome Res.*, 6: 639-645, 1996.
- Mousses, S., Bittner, M. L., Chen, Y., Dougherty, E. R., Baxevania, A., Meltzer, P. S., and Trent, J. M. Gene expression analysis by cDNA microarrays. In: F. J. Livesey and S. P. Hunt (eds.), *Functional Genomics*, pp. 113-137. Oxford: Oxford University Press, 2000.
- Pollack, J. R., Perou, C. M., Alizadeh, A. A., Eisen, M. B., Pergamenschikov, A., Williams, C. F., Jeffrey, S. S., Botstein, D., and Brown, P. O. Genome-wide analysis of DNA copy-number changes using cDNA microarrays. *Nat. Genet.*, 23: 41-46, 1999.
- Monni, O., Bärklund, M., Mousses, S., Kononen, J., Sauter, G., Heiskanen, M., Paavola, P., Avela, K., Chen, Y., Bittner, M. L., and Kallioniemi, A. Comprehensive copy number and gene expression profiling of the 17q23 amplicon in human breast cancer. *Proc. Natl. Acad. Sci. USA*, 98: 5711-5716, 2001.
- Chen, Y., Dougherty, E. R., and Bittner, M. L. Ratio-based decisions and the quantitative analysis of cDNA microarray images. *J. Biomed. Optics*, 2: 364-374, 1997.
- Bärklund, M., Forozan, F., Kononen, J., Bubendorf, L., Chen, Y., Bittner, M. L., Torhorst, J., Haas, P., Buecher, C., Sauter, G., et al. Detecting activation of ribosomal protein S6 kinase by complementary DNA and tissue microarray analysis. *J. Natl. Cancer Inst.*, 92: 1252-1259, 2000.
- Andersson, C. L., Hostetter, G., Grigoryan, A., Sauter, G., and Kallioniemi, A. Improved procedure for fluorescence *in situ* hybridization on tissue microarrays. *Cytometry*, 45: 83-86, 2001.
- Kauraniemi, P., Bärklund, M., Monni, O., and Kallioniemi, A. New amplified and highly expressed genes discovered in the ERBB2 amplicon in breast cancer by cDNA microarrays. *Cancer Res.*, 61: 8235-8240, 2001.
- Clark, J., Edwards, S., John, M., Flohr, P., Gordon, T., Maillard, K., Giddings, I., Brown, C., Bagherzadeh, A., Campbell, C., Shipley, J., Wooster, R., and Cooper, C. S. Identification of amplified and expressed genes in breast cancer by comparative hybridization onto microarrays of randomly selected cDNA clones. *Genes Chromosomes Cancer*, 34: 104-114, 2002.
- Varis, A., Wolf, M., Monni, O., Vakkari, M. L., Kakkola, A., Moshak, C., Frierson, H., Powell, S. M., Knuutila, S., Kallioniemi, A., and El-Rifai, W. Targets of gene amplification and overexpression at 17q in gastric cancer. *Cancer Res.*, 62: 2625-2629, 2002.
- Hughes, T. R., Roberts, C. J., Dai, H., Jones, A. R., Meyer, M. R., Slade, D., Burchard, J., Dow, S., Ward, T. R., Kidd, M. J., Friend, S. H., and Marton M. J.

- Widespread aneuploidy revealed by DNA microarray expression profiling. *Nat. Genet.*, 25: 333-337, 2000.
23. Virtaneva, K., Wright, F. A., Tanner, S. M., Yuan, B., Lemon, W. J., Caligiuri, M. A., Bloomfield, C. D., de La Chapelle, A., and Krahe, R. Expression profiling reveals fundamental biological differences in acute myeloid leukemia with isolated trisomy 8 and normal cytogenetics. *Proc. Natl. Acad. Sci. USA*, 98: 1124-1129, 2001.
24. Phillips, J. L., Hayward, S. W., Wang, Y., Vasselli, J., Pavlovich, C., Padilla-Nash, H., Pezullo, J. R., Ghadimi, B. M., Grossfeld, G. D., Rivera, A., Linchan, W. M., Cunha, G. R., and Ried, T. The consequences of chromosomal aneuploidy on gene expression profiles in a cell line model for prostate carcinogenesis. *Cancer Res.*, 61: 8143-8149, 2001.
25. Bärklund, M., Tirkkonen, M., Forozan, F., Tanner, M. M., Kallioniemi, O. P., and Kallioniemi, A. Increased copy number at 17q22-q24 by CGH in breast cancer is due to high-level amplification of two separate regions. *Genes Chromosomes Cancer*, 20: 372-376, 1997.
26. Tanner, M. M., Tirkkonen, M., Kallioniemi, A., Isola, J., Kuukasjärvi, T., Collins, C., Kowbel, D., Guan, X. Y., Trent, J., Gray, J. W., Meltzer, P., and Kallioniemi, O. P. Independent amplification and frequent co-amplification of three nonsyntenic regions on the long arm of chromosome 20 in human breast cancer. *Cancer Res.*, 56: 3441-3445, 1996.
27. Cillo, C., Faiella, A., Cantile, M., and Boncinelli, E. Homeobox genes and cancer. *Exp. Cell Res.*, 248: 1-9, 1999.
28. Cillo, C., Cantile, M., Faiella, A., and Boncinelli, E. Homeobox genes in normal and malignant cells. *J. Cell. Physiol.*, 188: 161-169, 2001.
29. Care, A., Silvani, A., Meccia, E., Mattia, G., Stoppacciaro, A., Parmiani, G., Peschle, C., and Colombo, M. P. HOXB7 constitutively activates basic fibroblast growth factor in melanomas. *Mol. Cell. Biol.*, 16: 4842-4851, 1996.
30. Care, A., Silvani, A., Meccia, E., Mattia, G., Peschle, C., and Colombo, M. P. Transduction of the SkBr3 breast carcinoma cell line with the HOXB7 gene induces bFGF expression, increases cell proliferation and reduces growth factor dependence. *Oncogene*, 16: 3285-3289, 1998.
31. Care, A., Felicetti, F., Meccia, E., Bottero, L., Parenza, M., Stoppacciaro, A., Peschle, C., and Colombo, M. P. HOXB7: a key factor for tumor-associated angiogenic switch. *Cancer Res.*, 61: 6532-6539, 2001.
32. Naora, H., Yang, Y. Q., Montz, F. J., Seidman, J. D., Kurman, R. J., and Roden, R. B. A serologically identified tumor antigen encoded by a homeobox gene promotes growth of ovarian epithelial cells. *Proc. Natl. Acad. Sci. USA*, 98: 4060-4065, 2001.

Microarray analysis reveals a major direct role of DNA copy number alteration in the transcriptional program of human breast tumors

Jonathan R. Pollack^{1,2}, Therese Sørlie³, Charles M. Perou⁴, Christian A. Rees^{1,2}, Stefanie S. Jeffrey^{1,2}, Per E. Lønning², Robert Tibshirani⁵, David Botstein¹, Anne-Lise Børresen-Dale⁶, and Patrick O. Brown^{1,2}

Departments of ¹Pathology, ²Genetics, ³Surgery, ⁴Health Research and Policy, and ⁵Biochemistry, and ⁶Howard Hughes Medical Institute, Stanford University School of Medicine, Stanford, CA 94305; ³Department of Genetics, Norwegian Radium Hospital, Montebello, N-0310 Oslo, Norway; ⁴Department of Medicine (Oncology), Haukeland University Hospital, N-5021 Bergen, Norway; and ⁵Department of Genetics and Lineberger Comprehensive Cancer Center, University of North Carolina, Chapel Hill, NC 27599

Contributed by Patrick O. Brown, August 6, 2002

Genomic DNA copy number alterations are key genetic events in the development and progression of human cancers. Here we report a genome-wide microarray comparative genomic hybridization (array CGH) analysis of DNA copy number variation in a series of primary human breast tumors. We have profiled DNA copy number alteration across 6,691 mapped human genes, in 44 predominantly advanced, primary breast tumors and 10 breast cancer cell lines. While the overall patterns of DNA amplification and deletion corroborate previous cytogenetic studies, the high-resolution (gene-by-gene) mapping of amplicon boundaries and the quantitative analysis of amplicon shape provide significant improvement in the localization of candidate oncogenes. Parallel microarray measurements of mRNA levels reveal the remarkable degree to which variation in gene copy number contributes to variation in gene expression in tumor cells. Specifically, we find that 62% of highly amplified genes show moderately or highly elevated expression, that DNA copy number influences gene expression across a wide range of DNA copy number alterations (deletion, low-, mid- and high-level amplification), that on average, a 2-fold change in DNA copy number is associated with a corresponding 1.5-fold change in mRNA levels, and that overall, at least 12% of all the variation in gene expression among the breast tumors is directly attributable to underlying variation in gene copy number. These findings provide evidence that widespread DNA copy number alteration can lead directly to global deregulation of gene expression, which may contribute to the development or progression of cancer.

Conventional cytogenetic techniques, including comparative genomic hybridization (CGH) (1), have led to the identification of a number of recurrent regions of DNA copy number alteration in breast cancer cell lines and tumors (2–4). While some of these regions contain known or candidate oncogenes [e.g., FGFR1 (8p11), MYC (8q24), CCND1 (11q13), ERBB2 (17q12), and ZNF217 (20q13)] and tumor suppressor genes [RB1 (13q14) and TP53 (17p13)], the relevant gene(s) within other regions (e.g., gain of 1q, 8q22, and 17q22–24, and loss of 8p) remain to be identified. A high-resolution genome-wide map, delineating the boundaries of DNA copy number alterations in tumors, should facilitate the localization and identification of oncogenes and tumor suppressor genes in breast cancer. In this study, we have created such a map, using array-based CGH (5–7) to profile DNA copy number alteration in a series of breast cancer cell lines and primary tumors.

An unresolved question is the extent to which the widespread DNA copy number changes that we and others have identified in breast tumors alter expression of genes within involved regions. Because we had measured mRNA levels in parallel in the same samples (8), using the same DNA microarrays, we had an opportunity to explore on a genomic scale the relationship between DNA copy number changes and gene expression. From

this analysis, we have identified a significant impact of widespread DNA copy number alteration on the transcriptional programs of breast tumors.

Materials and Methods

Tumors and Cell Lines. Primary breast tumors were predominantly large (>3 cm), intermediate-grade, infiltrating ductal carcinomas, with more than 50% being lymph node positive. The fraction of tumor cells within specimens averaged at least 50%. Details of individual tumors have been published (8, 9), and are summarized in Table 1, which is published as supporting information on the PNAS web site, www.pnas.org. Breast cancer cell lines were obtained from the American Type Culture Collection. Genomic DNA was isolated either using Qiagen genomic DNA columns, or by phenol/chloroform extraction followed by ethanol precipitation.

DNA Labeling and Microarray Hybridizations. Genomic DNA labeling and hybridizations were performed essentially as described in Pollack *et al.* (7), with slight modifications. Two micrograms of DNA was labeled in a total volume of 50 microliters and the volumes of all reagents were adjusted accordingly. "Test" DNA (from tumors and cell lines) was fluorescently labeled (Cy5) and hybridized to a human cDNA microarray containing 6,691 different mapped human genes (i.e., UniGene clusters). The "reference" (labeled with Cy3) for each hybridization was normal female leukocyte DNA from a single donor. The fabrication of cDNA microarrays and the labeling and hybridization of mRNA samples have been described (8).

Data Analysis and Map Positions. Hybridized arrays were scanned on a GenePix scanner (Axon Instruments, Foster City, CA), and fluorescence ratios (test/reference) calculated using SCANALYZE software (available at <http://rana.lbl.gov>). Fluorescence ratios were normalized for each array by setting the average log fluorescence ratio for all array elements equal to 0. Measurements with fluorescence intensities more than 20% above background were considered reliable. DNA copy number profiles that deviated significantly from background ratios measured in normal genomic DNA control hybridizations were interpreted as evidence of real DNA copy number alteration (see *Estimating Significance of Altered Fluorescence Ratios* in the supporting information). When indicated, DNA copy number profiles are displayed as a moving average (symmetric 5-nearest neighbors). Map positions for arrayed human cDNAs were assigned by

Abbreviation: CGH, comparative genomic hybridization.

To whom reprint requests should be addressed at: Department of Pathology, Stanford University School of Medicine, CCR Building, Room 3245A, 269 Campus Drive, Stanford, CA 94305-5176. E-mail: pollack1@stanford.edu.

**Present address: Zyomyx Inc., Hayward, CA 94545.

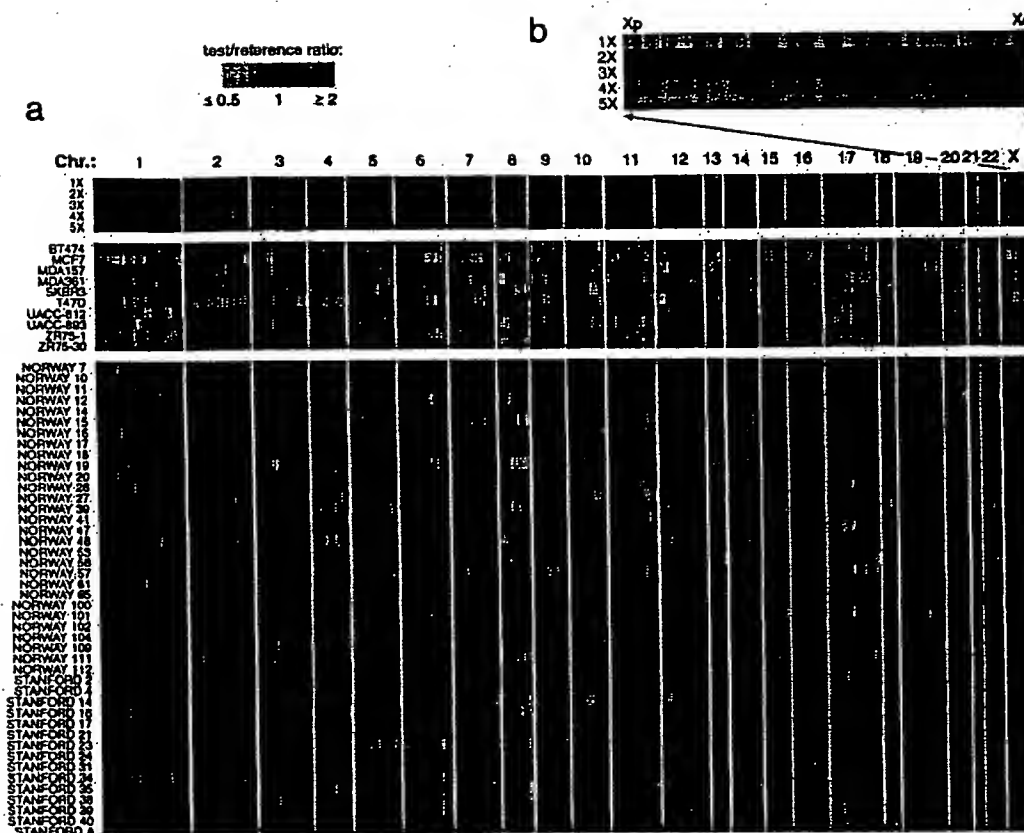


Fig. 1. Genome-wide measurement of DNA copy number alteration by array CGH. (a) DNA copy number profiles are illustrated for cell lines containing different numbers of X chromosomes, for breast cancer cell lines, and for breast tumors. Each row represents a different cell line or tumor, and each column represents one of 6,691 different mapped human genes present on the microarray, ordered by genome map position from 1pter through Xqter. Moving average (symmetric 5-nearest neighbors) fluorescence ratios (test/reference) are depicted using a log₂-based pseudocolor scale (indicated), such that red luminescence reflects fold-amplification, green luminescence reflects fold-deletion, and black indicates no change (gray indicates poorly measured data). (b) Enlarged view of DNA copy number profiles across the X chromosome, shown for cell lines containing different numbers of X chromosomes.

identifying the starting position of the best and longest match of any DNA sequence represented in the corresponding UniGene cluster (10) against the "Golden Path" genome assembly (<http://genome.ucsc.edu/>; Oct 7, 2000 Freeze). For UniGene clusters represented by multiple arrayed elements, mean fluorescence ratios (for all elements representing the same UniGene cluster) are reported. For mRNA measurements, fluorescence ratios are "mean-centered" (i.e., reported relative to the mean ratio across the 44 tumor samples). The data set described here can be accessed in its entirety in the supporting information.

Results

We performed CGH on 44 predominantly locally advanced, primary breast tumors and 10 breast cancer cell lines, using cDNA microarrays containing 6,691 different mapped human genes (Fig. 1a; also see *Materials and Methods* for details of microarray hybridizations). To take full advantage of the improved spatial resolution of array CGH, we ordered (fluorescence ratios for) the 6,691 cDNAs according to the "Golden Path" (<http://genome.ucsc.edu/>) genome assembly of the draft human genome sequences (11). In so doing, arrayed cDNAs not only themselves represent genes of potential interest (e.g., candidate oncogenes within amplicons), but also provide precise genetic landmarks for chromosomal regions of amplification and

deletion. Parallel analysis of DNA from cell lines containing different numbers of X chromosomes (Fig. 1b), as we did before (7), demonstrated the sensitivity of our method to detect single-copy loss (45, XO), and 1.5- (47,XXX), 2- (48,XXXX), or 2.5-fold (49,XXXXX) gains (also see Fig. 5, which is published as supporting information on the PNAS web site). Fluorescence ratios were linearly proportional to copy number ratios, which were slightly underestimated, in agreement with previous observations (7). Numerous DNA copy number alterations were evident in both the breast cancer cell lines and primary tumors (Fig. 1a), detected in the tumors despite the presence of euploid non-tumor cell types; the magnitudes of the observed changes were generally lower in the tumor samples. DNA copy-number alterations were found in every cancer cell line and tumor, and on every human chromosome in at least one sample. Recurrent regions of DNA copy number gain and loss were readily identifiable. For example, gains within 1q, 8q, 17q, and 20q were observed in a high proportion of breast cancer cell lines/tumors (90%/69%, 100%/47%, 100%/60%, and 90%/44%, respectively), as were losses within 1p, 3p, 8p, and 13q (80%/24%, 80%/22%, 80%/22%, and 70%/18%, respectively), consistent with published cytogenetic studies (refs. 2-4; a complete listing of gains/losses is provided in Tables 2 and 3, which are published as supporting information on the PNAS web site). The total

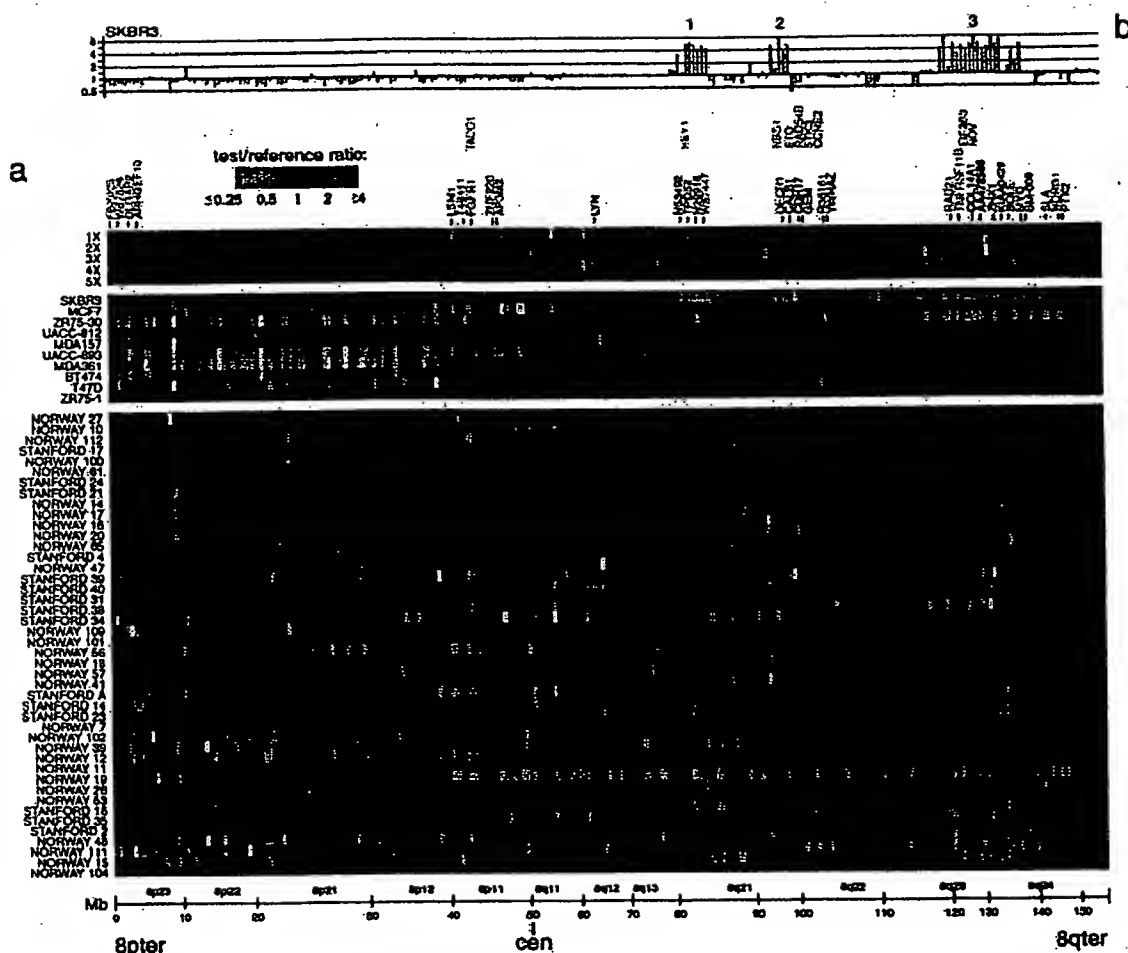


Fig. 2. DNA copy number alteration across chromosome 8 by array CGH. (a) DNA copy number profiles are illustrated for cell lines containing different numbers of X chromosomes, for breast cancer cell lines, and for breast tumors. Breast cancer cell lines and tumors are separately ordered by hierarchical clustering to highlight recurrent copy number changes. The 241 genes present on the microarrays and mapping to chromosome 8 are ordered by position along the chromosome. Fluorescence ratios (test/reference) are depicted by a log₂ pseudocolor scale (indicated). Selected genes are indicated with color-coded text (red, increased; green, decreased; black, no change; gray, not well measured) to reflect correspondingly altered mRNA levels (observed in the majority of the subset of samples displaying the DNA copy number change). The map positions for genes of interest that are not represented on the microarray are indicated in the row above those genes represented on the array. (b) Graphical display of DNA copy number profile for breast cancer cell line SKBR3. Fluorescence ratios (tumor/normal) are plotted on a log₂ scale for chromosome 8 genes, ordered along the chromosome.

number of genomic alterations (gains and losses) was found to be significantly higher in breast tumors that were high grade ($P = 0.008$), consistent with published CGH data (3), estrogen receptor negative ($P = 0.04$), and harboring TP53 mutations ($P = 0.0006$) (see Table 4, which is published as supporting information on the PNAS web site).

The improved spatial resolution of our array CGH analysis is illustrated for chromosome 8, which displayed extensive DNA copy number alteration in our series. A detailed view of the variation in the copy number of 241 genes mapping to chromosome 8 revealed multiple regions of recurrent amplification; each of these potentially harbors a different known or previously uncharacterized oncogene (Fig. 2a). The complexity of amplicon structure is most easily appreciated in the breast cancer cell line SKBR3. Although a conventional CGH analysis of 8q in SKBR3 identified only two distinct regions of amplification (12), we observed three distinct regions of high-level amplification (labeled 1–3 in Fig. 2b). For each of these regions we can define the

boundaries of the interval recurrently amplified in the tumors we examined; in each case, known or plausible candidate oncogenes can be identified (a description of these regions, as well as the recurrently amplified regions on chromosomes 17 and 20, can be found in Figs. 6 and 7, which are published as supporting information on the PNAS web site).

For a subset of breast cancer cell lines and tumors (4 and 37, respectively), and a subset of arrayed genes (6,095), mRNA levels were quantitatively measured in parallel by using cDNA microarrays (8). The parallel assessment of mRNA levels is useful in the interpretation of DNA copy number changes. For example, the highly amplified genes that are also highly expressed are the strongest candidate oncogenes within an amplicon. Perhaps more significantly, our parallel analysis of DNA copy number changes and mRNA levels provides us the opportunity to assess the global impact of widespread DNA copy number alteration on gene expression in tumor cells.

A strong influence of DNA copy number on gene expression is evident in an examination of the pseudocolor representations

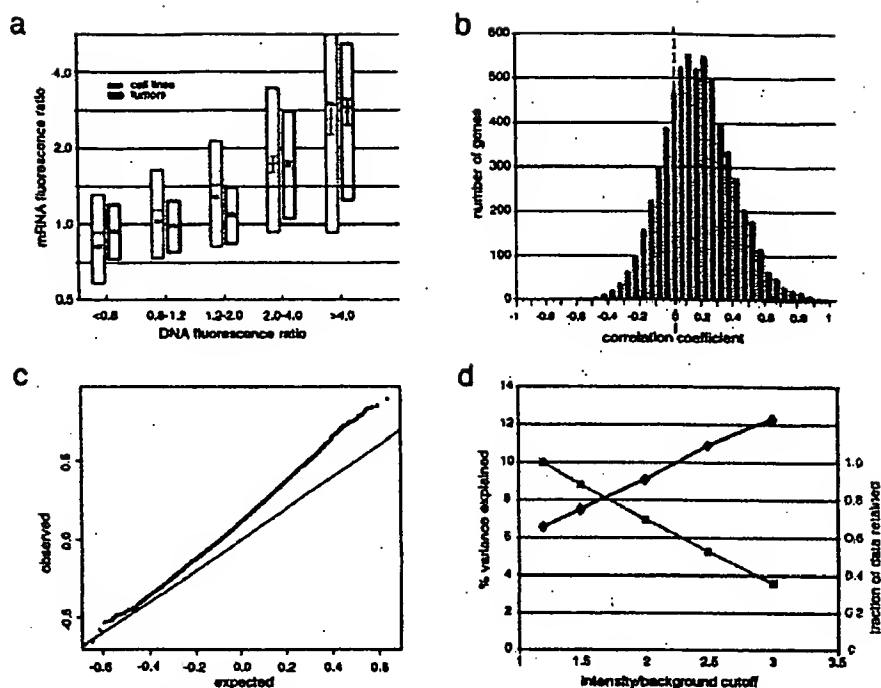


Fig. 4. Genome-wide influence of DNA copy number alterations on mRNA levels. (a) For breast cancer cell lines (gray) and tumor samples (black), both mean-centered mRNA fluorescence ratio (log₂ scale) quartiles (box plots indicate 25th, 50th, and 75th percentile) and averages (diamonds; Y-value error bars indicate standard errors of the mean) are plotted for each of five classes of genes, representing DNA deletion (tumor/normal ratio < 0.8), no change (0.8–1.2), low- (1.2–2), medium- (2–4), and high-level (>4) amplification. *P* values for pair-wise Student's *t* tests, comparing averages between adjacent classes (moving left to right), are 4×10^{-49} , 1×10^{-49} , 5×10^{-3} , 1×10^{-2} (cell lines), and 1×10^{-43} , 1×10^{-214} , 5×10^{-41} , 1×10^{-4} (tumors). (b) Distribution of correlations between DNA copy number and mRNA levels, for 6,095 different human genes across 37 breast tumor samples. (c) Plot of observed versus expected correlation coefficients. The expected values were obtained by randomization of the sample labels in the DNA copy number data set. The line of unity is indicated. (d) Percent variance in gene expression (among tumors) directly explained by variation in gene copy number. Percent variance explained (black line) and fraction of data retained (gray line) are plotted for different fluorescence intensity/background (a rough surrogate for signal/noise) cutoff values. Fraction of data retained is relative to the 1.2 intensity/background cutoff. Details of the linear regression model used to estimate the fraction of variation in gene expression attributable to underlying DNA copy number alteration can be found in the supporting information (see *Estimating the Fraction of Variation in Gene Expression Attributable to Underlying DNA Copy Number Alteration*).

tumors that could be attributed to underlying variation in DNA copy number. From this analysis, we estimate that, overall, about 7% of all of the observed variation in mRNA levels can be explained directly by variation in copy number of the altered genes (Fig. 4d). We can reduce the effects of experimental measurement error on this estimate by using only that fraction of the data most reliably measured (fluorescence intensity/background > 3); using that data, our estimate of the percent variation in mRNA levels directly attributed to variation in gene copy number increases to 12% (Fig. 4d). This still undoubtedly represents a significant underestimate, as the observed variation in global gene expression is affected not only by true variation in the expression programs of the tumor cells themselves, but also by the variable presence of non-tumor cell types within clinical samples.

Discussion

This genome-wide, array CGH analysis of DNA copy number alteration in a series of human breast tumors demonstrates the usefulness of defining amplicon boundaries at high resolution (gene-by-gene), and quantitatively measuring amplicon shape, to assist in locating and identifying candidate oncogenes. By analyzing mRNA levels in parallel, we have also discovered that changes in DNA copy number have a large, pervasive, direct effect on global gene expression patterns in both breast cancer

cell lines and tumors. Although the DNA microarrays used in our analysis may display a bias toward characterized and/or highly expressed genes, because we are examining such a large fraction of the genome (approximately 20% of all human genes), and because, as detailed above, we are likely underestimating the contribution of DNA copy number changes to altered gene expression, we believe our findings are likely to be generalizable (but would nevertheless still be remarkable if only applicable to this set of ~6,100 genes).

In budding yeast, aneuploidy has been shown to result in chromosome-wide gene expression biases (13). Two recent studies have begun to examine the global relationship between DNA copy number and gene expression in cancer cells. In agreement with our findings, Phillips *et al.* (14) have shown that with the acquisition of tumorigenicity in an immortalized prostate epithelial cell line, new chromosomal gains and losses resulted in a statistically significant respective increase and decrease in the average expression level of involved genes. In contrast, Platzer *et al.* (15) recently reported that in metastatic colon tumors only ~4% of genes within amplified regions were found more highly (>2-fold) expressed, when compared with normal colonic epithelium. This report differs substantially from our finding that 62% of highly amplified genes in breast cancer exhibit at least 2-fold increased expression. These contrasting findings may reflect methodological differences between the

studies. For example, the study of Platzer *et al.* (15) may have systematically under-measured gene expression changes. In this regard it is remarkable that only 14 transcripts of many thousand residing within unamplified chromosomal regions were found to exhibit at least 4-fold altered expression in metastatic colon cancer. Additionally, their reliance on lower-resolution chromosomal CGH may have resulted in poorly delimiting the boundaries of high-complexity amplicons, effectively overcalling regions with amplification. Alternatively, the contrasting findings for amplified genes may represent real biological differences between breast and metastatic colon tumors; resolution of this issue will require further studies.

Our finding that widespread DNA copy number alteration has a large, pervasive and direct effect on global gene expression patterns in breast cancer has several important implications. First, this finding supports a high degree of copy number-dependent gene expression in tumors. Second, it suggests that most genes are not subject to specific autoregulation or dosage compensation. Third, this finding cautions that elevated expression of an amplified gene cannot alone be considered strong independent evidence of a candidate oncogene's role in tumorigenesis. In our study, fully 62% of highly amplified genes demonstrated moderately or highly elevated expression. This highlights the importance of high-resolution mapping of amplicon boundaries and shape [to identify the "driving" gene(s) within amplicons (16)], on a large number of samples, in addition to functional studies. Fourth, this finding suggests that analyzing

the genomic distribution of expressed genes, even within existing microarray gene expression data sets, may permit the inference of DNA copy number aberration, particularly aneuploidy (where gene expression can be averaged across large chromosomal regions; see Fig. 3 and supporting information). Fifth, this finding implies that a substantial portion of the phenotypic uniqueness (and by extension, the heterogeneity in clinical behavior) among patients' tumors may be traceable to underlying variation in DNA copy number. Sixth, this finding supports a possible role for widespread DNA copy number alteration in tumorigenesis (17, 18), beyond the amplification of specific oncogenes and deletion of specific tumor suppressor genes. Widespread DNA copy number alteration, and the concomitant widespread imbalance in gene expression, might disrupt critical stoichiometric relationships in cell metabolism and physiology (e.g., proteasome, mitotic spindle), possibly promoting further chromosomal instability and directly contributing to tumor development or progression. Finally, our findings suggest the possibility of cancer therapies that exploit specific or global imbalances in gene expression in cancer.

We thank the many members of the P.O.B. and D.B. labs for helpful discussions. J.R.P. was a Howard Hughes Medical Institute Physician Postdoctoral Fellow during a portion of this work. P.O.B. is a Howard Hughes Medical Institute Associate Investigator. This work was supported by grants from the National Institutes of Health, the Howard Hughes Medical Institute, the Norwegian Cancer Society, and the Norwegian Research Council.

- Kallioniemi, A., Kallioniemi, O. P., Sudar, D., Rutovitz, D., Gray, J. W., Waldman, F. & Pinkel, D. (1992) *Science* 258, 818–821.
- Kallioniemi, A., Kallioniemi, O. P., Piper, J., Tanner, M., Stukke, T., Chen, L., Smith, H. S., Pinkel, D., Gray, J. W. & Waldman, F. M. (1994) *Proc. Natl. Acad. Sci. USA* 91, 2156–2160.
- Tirkkonen, M., Tanner, M., Karhu, R., Kallioniemi, A., Isola, J. & Kallioniemi, O. P. (1998) *Genes Chromosomes Cancer* 21, 177–184.
- Ferozan, F., Mahlamaki, E. H., Monni, O., Chen, Y., Veldman, R., Jiang, Y., Gooden, G. C., Ethier, S. P., Kallioniemi, A. & Kallioniemi, O. P. (2000) *Cancer Res.* 60, 4519–4525.
- Solinas-Toldo, S., Lampel, S., Stilgenbauer, S., Nickolenko, J., Benner, A., Dohner, H., Cremer, T. & Lichter, P. (1997) *Genes Chromosomes Cancer* 20, 399–407.
- Pinkel, D., Segreaves, R., Sudar, D., Clark, S., Poole, I., Kowbel, D., Collins, C., Kuo, W. L., Chen, C., Zhai, Y., *et al.* (1998) *Nat. Genet.* 20, 207–211.
- Pollack, J. R., Perou, C. M., Alizadeh, A. A., Eisen, M. B., Pergamenschikov, A., Williams, C. F., Jeffrey, S. S., Botstein, D. & Brown, P. O. (1999) *Nat. Genet.* 23, 41–46.
- Perou, C. M., Sorlie, T., Eisen, M. B., van de Rijn, M., Jeffrey, S. S., Rees, C. A., Pollack, J. R., Ross, D. T., Johnsen, H., Akslen, L. A., *et al.* (2000) *Nature (London)* 406, 747–752.
- Sorlie, T., Perou, C. M., Tibshirani, R., Aas, T., Geisler, S., Johnsen, H., Hastie, T., Eisen, M. B., van de Rijn, M., Jeffrey, S. S., *et al.* (2001) *Proc. Natl. Acad. Sci. USA* 98, 10869–10874.
- Schuler, G. D. (1997) *J. Mol. Med.* 75, 694–698.
- Lander, E. S., Linton, L. M., Birren, B., Nusbaum, C., Zody, M. C., Baldwin, J., Devon, K., Dewar, K., Doyle, M., FitzHugh, W., *et al.* (2001) *Nature (London)* 409, 860–921.
- Fejzo, M. S., Godfrey, T., Chen, C., Waldman, F. & Gray, J. W. (1998) *Genes Chromosomes Cancer* 22, 105–113.
- Hughes, T. R., Roberts, C. J., Dai, H., Jones, A. R., Meyer, M. R., Slade, D., Burchard, J., Dow, S., Ward, T. R., Kidd, M. J., *et al.* (2000) *Nat. Genet.* 25, 333–337.
- Phillips, J. L., Hayward, S. W., Wang, Y., Vasselli, J., Pavlovich, C., Padilla-Nash, H., Pezullo, J. R., Ghadimi, B. M., Grossfeld, G. D., Rivera, A., *et al.* (2001) *Cancer Res.* 61, 8143–8149.
- Platzer, P., Upender, M. B., Wilson, K., Willis, J., Lutterbaugh, J., Nosrati, A., Wilson, J. K., Mack, D., Ried, T. & Markowitz, S. (2002) *Cancer Res.* 62, 1134–1138.
- Albertson, D. G., Ylstra, B., Segreaves, R., Collins, C., Dairkee, S. H., Kowbel, D., Kuo, W. L., Gruy, J. W. & Pinkel, D. (2000) *Nat. Genet.* 25, 144–146.
- Li, R., Yerganian, G., Duesberg, P., Kraemer, A., Willer, A., Rausch, C. & Hehlmann, R. (1997) *Proc. Natl. Acad. Sci. USA* 94, 14506–14511.
- Rasnick, D. & Duesberg, P. H. (1999) *Biochem. J.* 340, 621–630.



TECHNICAL UPDATE

FROM YOUR LABORATORY SERVICES PROVIDER

HER-2/neu Breast Cancer Predictive Testing

Julie Sanford Hanna, Ph.D. and Dan Mornin, M.D.

EACH YEAR, OVER 182,000 WOMEN in the United States are diagnosed with breast cancer, and approximately 45,000 die of the disease.¹ Incidence appears to be increasing in the United States at a rate of roughly 2% per year. The reasons for the increase are unclear, but non-genetic risk factors appear to play a large role.²

Five-year survival rates range from approximately 65%-85%, depending on demographic group, with a significant percentage of women experiencing recurrence of their cancer within 10 years of diagnosis. One of the factors most predictive for recurrence once a diagnosis of breast cancer has been made is the number of axillary lymph nodes to which tumor has metastasized. Most node-positive women are given adjuvant therapy, which increases their survival. However, 20%-30% of patients without axillary node involvement also develop recurrent disease, and the difficulty lies in how to identify this high-risk subset of patients. These patients could benefit from increased surveillance, early intervention, and treatment.

Prognostic markers currently used in breast cancer recurrence prediction include tumor size, histological grade, steroid hormone receptor status, DNA ploidy, proliferative index, and cathepsin D status. Expression of growth factor receptors and over-expression of the HER-2/neu oncogene have also been identified as having value regarding treatment regimen and prognosis.

HER-2/neu (also known as c-erbB2) is an oncogene that encodes a transmembrane glycoprotein that is homologous to, but distinct from, the epidermal growth factor receptor. Numerous studies have indicated that high levels of expression of this protein are associated with rapid tumor growth, certain forms of therapy resistance, and shorter disease-free survival. The gene has been shown to be amplified and/or overexpressed in 10%-30% of invasive breast cancers and in 40%-60% of intraductal breast carcinoma.³

There are two distinct FDA-approved methods by which HER-2/neu status can be evaluated: immunohistochemistry (IHC, HercepTest™) and FISH (fluorescent in situ hybridization, PathVysion™ Kit). Both methods can be performed on archived and current specimens. The first method allows visual assessment of the amount of HER-2/neu protein present on the cell membrane. The latter method allows direct quantification of the level of gene amplification present in the tumor, enabling differentiation between low- versus high-amplification. At least one study has demonstrated a difference in

recurrence risk in women younger than 40 years of age for low- versus high-amplified tumors (54.5% compared to 85.7%); this is compared to a recurrence rate of 16.7% for patients with no HER-2/neu gene amplification.⁴ HER-2/neu status may be particularly important to establish in women with small (≤ 1 cm) tumor size.

The choice of methodology for determination of HER-2/neu status depends in part on the clinical setting. FDA approval for the Vysis FISH test was granted based on clinical trials involving 1549 node-positive patients. Patients received one of three different treatments consisting of different doses of cyclophosphamide, Adriamycin, and 5-fluorouracil (CAF). The study showed that patients with amplified HER-2/neu benefited from treatment with higher doses of adriamycin-based therapy, while those with normal HER-2/neu levels did not. The study therefore identified a sub-set of women, who because they did not benefit from more aggressive treatment, did not need to be exposed to the associated side effects. In addition, other evidence indicates that HER-2/neu amplification in node-negative patients can be used as an independent prognostic indicator for early recurrence, recurrent disease at any time and disease-related death.⁵ Demonstration of HER-2/neu gene amplification by FISH has also been shown to be of value in predicting response to chemotherapy in stage-2 breast cancer patients.

Selection of patients for Herceptin® (Trastuzumab) monoclonal antibody therapy, however, is based upon demonstration of HER-2/neu protein overexpression using HercepTest™. Studies using Herceptin® in patients with metastatic breast cancer show an increase in time to disease progression, increased response rate to chemotherapeutic agents and a small increase in overall survival rate. The FISH assays have not yet been approved for this purpose, and studies looking at response to Herceptin® in patients with or without gene amplification status determined by FISH are in progress.

In general, FISH and IHC results correlate well. However, subsets of tumors are found which show discordant results; i.e., protein overexpression without gene amplification or lack of protein overexpression with gene amplification. The clinical significance of such results is unclear. Based on the above considerations, HER-2/neu testing at SHMC/PAML will utilize immunohistochemistry (HercepTest®) as a screen, followed by FISH in IHC-negative cases. Alternatively, either method may be ordered individually depending on the clinical setting or clinician preference.

CPT code information

HER-2/neu via IHC

88342 (including interpretive report)

HER-2/neu via FISH

88271×2 Molecular cytogenetics, DNA probe, each

88274 Molecular cytogenetics, interphase in situ hybridization, analyze 25-99 cells

88291 Cytogenetics and molecular cytogenetics, interpretation and report

Procedural Information

Immunohistochemistry is performed using the FDA-approved DAKO antibody kit, Herceptest[®]. The DAKO kit contains reagents required to complete a two-step immunohistochemical staining procedure for routinely processed, paraffin-embedded specimens. Following incubation with the primary rabbit antibody to human HER-2/neu protein, the kit employs a ready-to-use dextran-based visualization reagent. This reagent consists of both secondary goat anti-rabbit antibody molecules with horseradish peroxidase molecules linked to a common dextran polymer backbone, thus eliminating the need for sequential application of link antibody and peroxidase conjugated antibody. Enzymatic conversion of the subsequently added chromogen results in formation of visible reaction product at the antigen site. The specimen is then counterstained; a pathologist using light-microscopy interprets results.

FISH analysis at SHMC/PAML is performed using the FDA-approved PathVysion[™] HER-2/neu DNA probe kit, produced by Vysis, Inc. Formalin fixed, paraffin-embedded breast tissue is processed using routine histological methods, and then slides are treated to allow hybridization of DNA probes to the nuclei present in the tissue section. The Pathvysion[™] kit contains two direct-labeled DNA probes, one specific for the alphoid repetitive DNA (CEP 17, spectrum orange) present at the chromosome 17 centromere and the second for the HER-2/neu oncogene located at 17q11.2-12 (spectrum green). Enumeration of the probes allows a ratio of the number of copies of chromosome 17 to the number of copies of HER-2/neu to be obtained; this enables quantification of low versus high amplification levels, and allows an estimate of the percentage of cells with HER-2/neu gene amplification. The clinically relevant distinction is whether the gene amplification is due to increased gene copy number on the two chromosome 17 homologues normally present or an increase in the number of chromosome 17s in the cells. In the majority of cases, ratio equivalents less than 2.0 are indicative of a normal/negative result, ratios of 2.1 and over indicate that amplification is present and to what degree. Interpretation of this data will be performed and reported from the Vysis-certified Cytogenetics laboratory at SHMC.

References

1. Wingo, P.A., Tong, T., Bolden, S., "Cancer Statistics", 1995;45:1:8-31.
2. "Cancer Rates and Risks", 4th ed., National Institutes of Health, National Cancer Institute, 1996, p. 120.
3. Slamon, D.J., Clark, G.M., Song, S.G., Levin, W.J., Ullrich, A., McGuire, W.L. "Human breast Cancer: Correlation of relapse and survival with amplification of the her-2/neu oncogene". Science, 235:177-182, 1987.
4. Xing, W.R., Gilchrist, K.W., Harris, C.P., Samson, W., Meisner, L.F. "FISH detection of HER-2/neu oncogene amplification in early onset breast cancer". Breast Cancer Res. And Treatment 39(2):203-212, 1996.
5. Press, M.F., Bernstein, L., Thomas, P.A., Meisner, L.F., Zhou, J.Y., Ma, Y., Hung, G., Robinson, R.A., Harris, C., El-Naggar, A., Slamon, D.J., Phillips, R.N., Ross, J.S., Wolman, S.R., Flom, K.J., "Her-2/neu gene amplification characterized by fluorescence in situ hybridization: poor prognosis in node-negative breast carcinomas", J. Clinical Oncology 15(8):2894-2904, 1997.

Provided for the clients of

PATHOLOGY ASSOCIATES MEDICAL LABORATORIES
PACLAB NETWORK LABORATORIES
TRI-CITIES LABORATORY
TREASURE VALLEY LABORATORY

*For more information, please contact
your local representative.*

Analysis of Genomic and Proteomic Data Using Advanced Literature Mining

Yanhui Hu, Lisa M. Hines, Haifeng Weng, Dongmei Zuo, Miguel Rivera,
Andrea Richardson, and Joshua LaBaer*

Institute of Proteomics, Harvard Medical School—BCMP, 240 Longwood Avenue, Boston, Massachusetts 02115

Received March 13, 2003

High-throughput technologies, such as proteomic screening and DNA micro-arrays, produce vast amounts of data requiring comprehensive analytical methods to decipher the biologically relevant results. One approach would be to manually search the biomedical literature; however, this would be an arduous task. We developed an automated literature-mining tool, termed MedGene, which comprehensively summarizes and estimates the relative strengths of all human gene–disease relationships in Medline. Using MedGene, we analyzed a novel micro-array expression dataset comparing breast cancer and normal breast tissue in the context of existing knowledge. We found no correlation between the strength of the literature association and the magnitude of the difference in expression level when considering changes as high as 5-fold; however, a significant correlation was observed ($r = 0.41$; $p = 0.05$) among genes showing an expression difference of 10-fold or more. Interestingly, this only held true for estrogen receptor (ER) positive tumors, not ER negative. MedGene identified a set of relatively understudied, yet highly expressed genes in ER negative tumors worthy of further examination.

Keywords: bioinformatics • micro-array • text mining • gene-disease association • breast cancer

Introduction

At its current pace, the accumulation of biomedical literature outpaces the ability of most researchers and clinicians to stay abreast of their own immediate fields, let alone cover a broader range of topics. For example, to follow a single disease, e.g., breast cancer, a researcher would have had to scan 130 different journals and read 27 papers per day in 1999.¹ This problem is accentuated with high-throughput technologies such as DNA micro-arrays and proteomics, which require the analysis of large datasets involving thousands of genes, many of which are unfamiliar to a particular researcher. In any microarray experiment, thousands of genes may demonstrate statistically significant expression changes, but only a fraction of these may be relevant to the study. The ability to interpret these datasets would be enhanced if they could be compared to a comprehensive summary of what is known about all genes. Thus, there is a need to summarize existing knowledge in a format that allows for the rapid analysis of associations between genes and diseases or other specific biological concepts.

One solution to this problem is to compile structured digital resources, such as the Breast Cancer Gene Database² and the Tumor Gene Database.³ However, as these resources are hand-curated, the labor-intensive review process becomes a rate-limiting step in the growth of the database. As a result, these

databases have a limited scale and the genes are not selected in a systematic fashion.

An alternative approach is automated text mining; a method which involves automated information extraction by searching documents for text strings and analyzing their frequency and context. This approach has been used successfully in several instances for biological applications. In most cases, it has been applied to extract information about the relationships or interactions that proteins or genes have with one another, in the literature or by functional annotation.^{3–7} Thus far, few publications have applied text-mining to examine the global relationships between genes and diseases. Perez-Iratxeta et al. automatically examined the GO (Gene Ontology) annotation of genes and their predicted chromosomal locations in order to identify genes linked to inherited disorders.⁸

To obtain a more global understanding of disease development, it would be valuable to incorporate information regarding all possible gene-disease relationships, including biochemical, physiological, pharmacological, epidemiological, as well as genetic. This information would enable comprehensive comparisons between large experimental datasets and existing knowledge in the literature. This would accomplish two things. First, it would serve to validate experiments by demonstrating that known responses occur as predicted. Second, it would rapidly highlight which genes are corroborated by the literature and which genes are novel in a given context. We have utilized a computational approach to literature mining to produce a

* To whom correspondence should be addressed: jlabae@tums.harvard.edu.

comprehensive set of gene-disease relationships. In addition, we have developed a novel approach to assess the strength of each association based on the frequency of citation and co-citation. We applied this tool to help interpret the data from a large micro-array gene expression experiment comparing normal and cancerous breast tissue.

Methods

MedGene Database. MedGene is a relational database, storing disease and gene information from NCBI, text mining results, statistical scores, and hyperlinks to the primary literature. MedGene has a web-based user interface for users to query the database (<http://hipseq.med.harvard.edu/MedGene/>).

Text Mining Algorithms. MeSH files were downloaded from the MeSH web site at NLM (National Library of Medicine) (<http://www.nlm.nih.gov/mesh/meshhome.html>) and human disease categories were selected. LocusLink files were downloaded from the LocusLink web site at NCBI (<http://www.ncbi.nlm.gov/LocusLink/>). Official/preferred gene symbol, official/preferred gene name, and gene alternative symbols and names, all relevant annotations and URLs for each LocusLink record, were collected. Gene search terms were used for literature searching and included all qualified gene names, gene symbols, and gene family terms. Primary gene keys, predominantly qualified gene family terms and gene official/preferred symbols, were used to index Medline records. If the official/preferred gene symbols did not meet the standards to be an index, then qualified gene official/preferred names were used. A local copy of Medline records (up to July, 2002) was pre-selected.

A JAVA module examined the MeSH terms and then indexed each Medline record with the appropriate disease terms. A separate JAVA module was used to examine the titles and abstracts for gene search terms and then to index the gene-related Medline records with the relevant primary gene key(s).

Statistical Methods. For every gene and disease pair, we counted records that were indexed for both gene and disease (double positive hits), for disease only (disease single hits), for gene only (gene single hits), and for neither gene nor disease (double negative hits) to generate a 2×2 contingency table. On the basis of the contingency table-framework, we applied different statistical methods to estimate the strength of gene-disease relationships and evaluated the results. These methods included chi-square analysis, Fisher's exact probabilities, relative risk of gene, and relative risk of disease¹⁰ (<http://hipseq.med.harvard.edu/MedGene/>). In addition, we computed the "product of frequency", which is the product of the proportion of disease/gene double hits to disease single hits and the proportion of disease/gene double hits to gene single hits. To obtain a normal distribution, we transformed all the statistical scores using the natural logarithm. We selected the log of the product of frequency (LPF) to validate MedGene and to use for the analysis with the micro-array data. Spearman rank-correlation coefficients were used to assess the linear relationship between LPF and micro-array fold change in expression level.

Global Analysis. Diseases with at least 50 related genes were selected for clustering analysis, and the LPF scores were normalized with total score for each disease. Hierarchical clustering was done with the "Cluster" software and the clustering result was visualized using "TreeView" (<http://rana.lbl.gov/EisenSoftware.htm>).

Breast Tissue Micro-Arrays. Eighty-nine breast cancer samples (79% ER-positive) and 7 normal breast tissue samples were selected from the Harvard Breast SPORC frozen tissue repository and were representative of the spectrum of histological types, grades, and hormone receptor immuno-phenotypes of breast cancer. Biotinylated cRNA, generated from the total RNA extracted from the bulk tumor, was hybridized to Affymetrix U95A oligo-nucleotide micro-arrays. These micro-arrays consist of 12,400 probes, which represent approximately 9000 genes. Raw expression values were obtained using CENE-CHIP software from Affymetrix, and then further analyzed using the DNA-Chip Analyzer (dChip) custom software.

Results

Automated Indexing of Medline Records by Disease and Gene. To study the gene-disease associations in the literature, we first compiled complete lists for human diseases and human genes. To index all Medline records that were relevant to human diseases, the Medical Subject Heading (MeSH) index of Medline records was utilized. MeSH is a controlled medical vocabulary from the National Library of Medicine and consists of a set of terms or subject headings that are arranged in both an alphabetic and an hierarchical structure. Medline records are reviewed manually and MeSH terms are added to each with software assistance.^{11,12} Twenty-three human disease category headings along with all of their child terms (see the Supporting Information, Supplemental Table 1, or visit http://hipseq.med.harvard.edu/MedGene/publication/s_Table1.html) were selected from the 2002 MeSH index creating a list of 4033 human diseases.

No index comparable to the MeSH index exists for genes, and thus, it was necessary to apply a string search algorithm for gene names or symbols found in Medline text. A complete list of genes, gene names, gene symbols, and frequently used synonyms were collected from the LocusLink database at NCBI,^{11,12} which contains 53,259 independent records keyed by an official gene symbol or name (June 18th, 2002). For the purposes of this study, no distinction was made between genes and their gene products. Authors often use the same name for both, differentiating the two only by the use of italics, if at all. For the intended use of this study, this lack of distinction is unlikely to have a large effect and may in fact be beneficial.

Initial attempts to search the literature using these lists revealed several sources of false positives and false negatives (Table 1). False positives primarily arose when the searched term had other meanings, whereas false negatives arose from syntax discrepancies necessitating the development of filters to reduce these errors. The syntax issues were readily handled by including alternate syntax forms in the search terms. The false positive cases, caused by duplicative and unrelated meanings for the terms, were more difficult to manage. Where possible, case sensitive string mapping reduced inappropriate citations. In many cases, however, this was not sufficient and the terms had to be eliminated entirely, thereby reducing the false positive rate but unavoidably under-representing some genes.

For the purposes of data tracking, a primary gene key was selected to represent all synonyms that correspond to each gene. Medline records were indexed with a primary gene key when any synonym for that key was found in the title or abstract. Case-insensitive string mapping was used for all searches except as noted above. No additional weight was

Table 1. Systematic Sources of False Positives and False Negatives in Unfiltered Data*

source of error	error type	example	filter solution
gene symbol/name is not unique	false positive	MAC—myelin associated glycoprotein MAC—malignancy-associated protein	eliminate this term
gene symbol is unrelated abbreviation	false positive	PA—pallid homologue (mouse), pallidin (also abbrev. for Pennsylvania)	eliminate this term
gene symbol/name has language meaning	false positive	WAS—Wiskott-Aldrich Syndrome (also the word "was")	case-sensitive string search
nonstandard syntax	false negative	BAG-1 instead of BAC1	add dash term
unofficial gene name/symbol	false negative	PSJ instead of TP53	add all gene nicknames
nonspecified gene name	false negative	estrogen receptor instead of Estrogen receptor 1	add family stem term

* In preliminary studies, Medline was searched for co-occurrence of genes and diseases and the resulting output was evaluated to identify error sources that were amenable to global filters. Each error source is categorized by the type of error it causes: false positives are suggested relationships that are not real and false negatives are real relationships that are underrepresented. The filter solutions used are indicated. Note that in some cases, the filter solution itself introduces error. In general, error rates maximized sensitivity, even at the expense of specificity if needed.

added for multiple occurrences of a term or the co-occurrence of multiple synonyms for the same gene key.

Medline records were searched with all qualified gene identifiers, such as the official/preferred gene symbol, the official/preferred gene name, all gene nicknames and all syntax variants. In situations where there are several members of a gene family or splice variants, some authors prefer to use a shortened gene family name, e.g., estrogen receptor instead of estrogen receptor 1 (*ESR1*), creating a source of false negatives. For this reason, gene family stem terms were created for all genes that have an alpha or numerical suffix (e.g., *IL2RA*, *TGFB*, *ESR1*, etc.) and then used to search the literature. The family stem terms were handled separately from the specific gene names so that it would be clear when linkages were made to the gene family versus a specific member in that family.

To improve performance and accuracy, some pre-selection was applied to the records that were scanned. First, review articles were eliminated to avoid redundant treatment of citations. Second, non-English journals were removed because the natural language filters were only relevant to English publications. Finally, journals unlikely to contain primary data about gene-disease relationships were also removed (e.g., *Int. J. Health Educ.*, *Bedside Nurse*, and *J. Health Econ.*). Together, these filters reduced the 12 198 221 Medline publications (July 2002) by 37%.

Ranking the Relative Strengths of Gene-Disease Associations. In total, there were 618 708 gene-disease co-citations, in which 16% (8297) of all studied genes had been associated to a disease and 96% (3875) of all diseases had been associated to at least one gene. To rank the relative strengths of gene-disease relationships, we tested several different statistical methods and examined the results. With the exception of the relative risk estimates, the methods provided similar results with respect to the rank order of the gene-disease association strengths. However, after comparing the results to other databases and after consulting disease experts, the log of the product of frequency (LPF) was selected for further analysis because it gave the best results overall.

Validation of MedGene. In developing this tool, it was important to minimize the number of missed genes (false negatives) and misclassified genes (false positives). However, in situations when these goals were in conflict, inclusiveness was prioritized. To determine the false negative rate in MedGene, breast cancer was used as a test case because it was associated with more genes than any other human disease and because

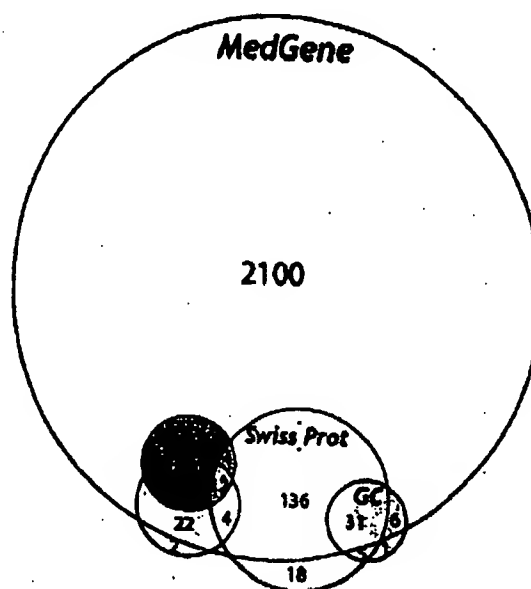


Figure 1. Estimation of the false negative rate by comparison with hand-curated databases. The breast cancer-related genes identified by MedGene were compared with those listed in several other databases including the Tumor Gene Database (TGD),² the Breast Cancer Gene Database (BCG),¹ GeneCards (GC)¹⁷ and Swissprot.¹⁸ Genes were considered false negatives if they were represented in at least one of these other databases and not in MedGene and their link to breast cancer was supported by at least one literature reference. All literature references were verified by manual review to confirm their validity. The number of genes in each database or shared by more than one database is indicated. The false negative rate was calculated by genes missed at MedGene (26)/total number of nonoverlapping genes in other databases (285).

there were several public databases that link genes to breast cancer. We compared the list of breast cancer-related genes from MedGene to these databases. Illustrated in Figure 1. Among the 285 distinct breast cancer-related genes that were supported by at least one literature citation in these hand-curated databases, 26 were absent from MedGene, suggesting a false negative rate of approximately 9%. To determine why these were missed, all literature references for these genes (80

papers) were reviewed manually (see the Supporting Information, Supplemental Table 2, or visit http://hipseq.med.harvard.edu/MedGene/publication/s_Table_2.html). Among these papers, most false negatives were caused by nonstandard gene terms or gene terms eliminated by our specificity filters. Few genes were missed because they were only mentioned in review papers (0.4%) or they appeared only in the body of the manuscript but not the abstract or title (1.1%). Of note, MedGene identified approximately 2000 additional breast cancer-related genes not listed in any other database.

To assess the false positive error rate, two complementary approaches were used: a detailed analysis of one disease and a global examination of 1000 diseases. The detailed approach examined the false positive error rate and its sources, whereas the global approach tested whether the overall results made biomedical sense.

Using the LPF, 1467 genes related to prostate cancer were assembled in rank order. We then retrieved approximately 300 Medline records each for the highest ranked 100 and the lowest ranked 200 genes and manually reviewed the titles and abstracts to determine the verity of the association. Nearly 80% of the highest ranked 100 genes fell into one of the five categories that reflect meaningful gene-disease relationships (see the Supporting Information, Supplemental Table 3, or visit http://hipseq.med.harvard.edu/MedGene/publication/s_Table_3.html). Among the lowest ranked 200 genes, approximately 70% reflected true relationships. Of the 600 records reviewed, there were only two in which the association between the gene and the disease was described as negative. Both were genes with very low scores. In both cases, the authors did not argue the absence of any relationship, but rather that a particular feature of the gene or protein was not shown to be related to human prostate cancer.^{13,14}

The coincidence of some gene symbols with medical abbreviations, chemical abbreviations and biological abbreviations resulted in most of the false positives (see the Supporting Information, Supplemental Table 4, or visit http://hipseq.med.harvard.edu/MedGene/publication/s_Table_4.html), emphasizing the importance of the filters that were added in the search algorithm (Table 1). Without the filters, the false positive rate more than doubled, and the false negative rate rose dramatically (data not shown). For example, among the papers about breast cancer, there were only 12 Medline records that referred to *ESR1* and 10 to *ESR2*, whereas almost 2000 papers mentioned estrogen receptor without specifying *ESR1* or *ESR2*; this latter group was detected by the family term filter.

To further validate these results, a global analysis of the gene-disease relationships described by MedGene was performed. For this experiment, it was reasoned that the more closely related the diseases are to one another, the more they will be related to the same gene sets. Thus, if the relationships defined by MedGene accurately reflected the literature, then an unsupervised hierarchical clustering of the gene data should group diseases in a manner consistent with common medical thinking. Conversely, if the clustered diseases do not make sense biologically or medically, it may reflect excessive false positives, false negatives, or inappropriate scoring of the data.

To execute this experiment, the gene sets and the corresponding LPF values for 1000 randomly selected diseases (each with at least 50 gene relationships) were used as a dataset for clustering the diseases. A review of the results showed that the resulting disease clusters were indeed logical based upon common medical knowledge (see the Supporting Information,

Supplemental Figure 1, or visit http://hipseq.med.harvard.edu/MedGene/publication/s_Figure_1.html). For example, in one such cluster shown in Figure 2, diabetes and its complications grouped together and were also closely linked to diseases associated with starvation states.

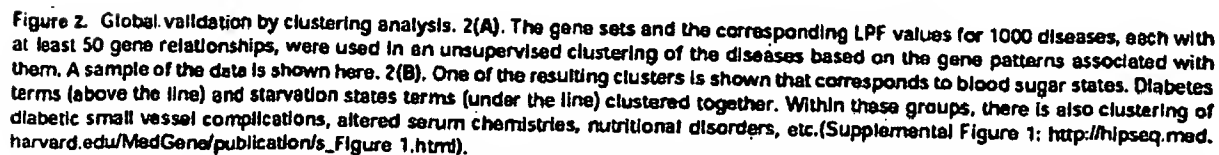
The number of genes associated with a given disease can be estimated by adjusting the MedGene number up by the false negative rate (~9%) and down by the false positive rate (~26% on average). Using this, the average disease has 103.7 ± 45.3 (mean \pm s.d.) genes associated with it, although the range is quite broad with 2359 genes related to breast cancer, 2122 genes related to lung cancer and no genes related to a number of diseases.

Applying MedGene to the Analysis of Large Datasets. Access to a comprehensive summary of the genes linked to human diseases provided an opportunity to analyze data obtained from a high-throughput experiment. We compared the MedGene breast cancer gene list to a gene expression data set generated from a micro-array analysis comparing breast cancer and normal breast tissue samples. Micro-array analysis identified 2286 genes that had greater than a 1-fold difference in mean expression level between breast cancer samples and normal breast samples. Using MedGene, we sorted the 2286 genes into four classes: 555 genes directly linked to breast cancer in the literature by gene term search (first-degree association by gene name); 328 genes directly linked by family term search (first-degree association by family term); 1021 genes linked to breast cancer only through other breast cancer genes (second-degree association); and 505 genes not previously associated with breast cancer. (See the Supporting Information, Supplemental Figure 2, or visit http://hipseq.med.harvard.edu/MedGene/publication/s_Figure_2.html.) Among the 505 previously unrelated genes, 467 were either newly identified genes or genes that had not previously been associated with any disease. Among the remaining 38 genes, 9 had been related to other cancers, specifically esophageal, colon, uterine, skin, and cervix.

To determine whether the genes highlighted by the micro-array analysis were more likely to have been previously linked to breast cancer in the literature, we created a two-dimensional plot of the fold change of expression level between breast cancer and normal tissue versus the literature score (LPF) (Figure 3A). There was a broad spread of expression changes among the genes directly linked to breast cancer ranging from less than 1-fold change (68%) to over 40-fold (0.3%). Notably, the majority of genes with greater than 10-fold expression changes were linked to breast cancer by first-degree association.

Among all 754 genes directly linked to breast cancer in the literature, there was no correlation between LPF and micro-array fold change ($r = 0.018$, p -value = 0.62). However, when we stratified the analysis based on the magnitude of the fold change, we observed an increasing trend in correlation (Figure 3B) suggesting that genes with a more substantial change in expression level were more likely to have a stronger association in the literature. For genes that had 10-fold change or more in expression level, the correlation increased to 0.41 (p -value = 0.05).

When we evaluated the micro-array data separately for ER positive and ER negative tumors, the trend in correlation between fold change and literature score was highly dependent on estrogen receptor status. Interestingly, there was a similar trend in correlation for ER positive tumors, but no trend in correlation for ER negative tumors.



disease unrelated to breast cancer. As expected, we did not observe an increasing trend in correlation for hypertension.

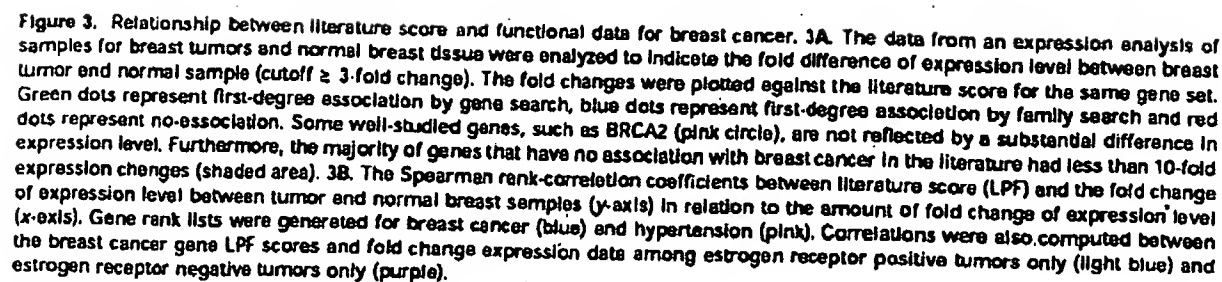


Table 2. Top 25 Genes Related to Selected Human Diseases*

breast neoplasms	hypertension	rheumatoid arthritis	bipolar disorder	atherosclerosis
estrogen receptor	<i>REN</i>	<i>RA</i>	<i>ERDA1</i>	apolipoprotein
<i>PCR</i>	<i>DBP</i>	<i>TNFRSF10A</i>	<i>SNAP29</i>	<i>APOE</i>
<i>ERBB2</i>	<i>LEP</i>	<i>CRP</i>	<i>PFKL</i>	<i>LDLR</i>
<i>BRCA1</i>	<i>AGT</i>	<i>AS</i>	<i>DRD2</i>	<i>ELN</i>
<i>BRCA2</i>	<i>INS</i>	<i>ESR1</i>	<i>TRH</i>	<i>ARC1</i>
<i>EGFR</i>	kallikrein	<i>HLA-DRB1</i>	<i>IMPA2</i>	<i>APOB</i>
<i>CYP19</i>	<i>ACE</i>	<i>DR1</i>	<i>HTR3A</i>	<i>APOA1</i>
<i>TFF1</i>	endothelin	interleukin	<i>DRD3</i>	<i>MSR1</i>
<i>PSEN2</i>	<i>S100A6</i>	<i>TNF</i>	<i>REM</i>	<i>LPL</i>
<i>TP53</i>	<i>BDK</i>	<i>IL6</i>	<i>KCNN3</i>	<i>PON1</i>
<i>CES3</i>	<i>DIAPH</i>	collagen	<i>DRD4</i>	plasminogen
<i>CEACAM5</i>	<i>SAR1</i>	<i>IL1A</i>	<i>HTR2C</i>	activator inhibitor
<i>ERBB3</i>	<i>PIH</i>	<i>ACR</i>	<i>RELN</i>	<i>PLG</i>
cydin	<i>CD59</i>	<i>TNFRSF12</i>	<i>DBH</i>	vascular cell
<i>COX5A</i>	<i>ALB</i>	<i>IL2</i>	<i>MAOA</i>	adhesion molecule
cathepsin	<i>CYP11B2</i>	<i>CHI3L1</i>	<i>COMT</i>	<i>ATOH1</i>
<i>ERBB4</i>	<i>MAT2B</i>	<i>IL8</i>	<i>HTR2A</i>	<i>VWF</i>
<i>TRAM</i>	angiotensin receptor	interleukin 1 matrix metalloproteinase	<i>SYNJ1</i>	<i>INS</i>
<i>CCND1</i>	<i>AGTR2</i>	interferon	<i>INPP1</i>	<i>ARG2</i>
<i>ECF</i>	<i>NPPA</i>	<i>CD68</i>	<i>NEDD4L</i>	<i>ABCA1</i>
<i>MUC1</i>	<i>LVM</i>	<i>IL4</i>	<i>FRA13C</i>	<i>OLR1</i>
insulin-like	<i>DBH</i>	<i>IL17</i>	transducer of	collagen
<i>BCL2</i>	<i>NPY</i>	<i>MMP3</i>	<i>ERBB2</i>	<i>MCP</i>
mucin	<i>POMC</i>	<i>SIL</i>	<i>BATF3</i>	lipoprotein
<i>FGF3</i>	neuropeptide		<i>ATP1B3</i>	<i>APOA2</i>
			<i>DRD5</i>	intercellular
				adhesion molecule
				<i>RAB27A</i>

* MedGene results for the top 25 genes associated with breast neoplasms, hypertension, rheumatoid arthritis, bipolar disorder, and atherosclerosis, respectively, ranked by LPP scores. The hyperlink to all the papers co-citing the gene and the disease is available at MedGene website (<http://hipseq.med.harvard.edu/MedGene/>).

Discussion

The Human Genome Project heralded a new era in biological research where the emphasis on understanding specific pathways has expanded to global studies of genomic organization and biological systems. High-throughput technologies can provide novel insight into comprehensive biological function but also introduces new challenges. The utility of these technologies is limited to the ability to generate, analyze, and interpret large gene lists. MedGene, a relational database derived by mining the information in Medline, was created to address this need. MedGene users can query for a rank-ordered list of human gene-disease relationships (Table 2) for one or more diseases. Each entry is hyperlinked to the original papers supporting each association and to other relevant databases.

MedGene is an innovative extension of previous text mining approaches. Perez-Iratxeta et al. used the GO annotation and their chromosomal locations to predict genes that may contribute to inherited disorders.⁸ MedGene takes a broader view and includes all diseases and all possible gene-disease relationships. Furthermore, MedGene utilizes co-citation to indicate a relationship rather than GO annotation, which is limited to the subset of genes that have GO annotation. Our approach is complementary to that taken by Chaussabel and Sher, who used the frequency of co-cited terms to cluster genes into a hierarchy of gene-gene relationships.⁹

A unique aspect of this tool is the ability to assess the relative strengths of gene-disease relationships based on the frequency of both co-citation and single citation. This presupposes that most co-citations describe a positive association, often referred to as publication bias¹³ and is supported by our observations

that negative associations are rare (Supplemental Table 3: http://hipseq.med.harvard.edu/MedGene/publication/s_Table3.html). Of course, relationships established by frequency of co-citation do not necessarily represent a true biological link; however, it is strong evidence to support a true relationship.

Another important feature of MedGene is the implementation of software filters that substantially reduced the error rate. We estimate that less than 10% of all associations were missed and at least 70% of even the weakest associations were real. For this study, all of the filters that we applied were general ones, e.g., expanding the list of all gene names to address the different syntax forms used by different journals, eliminating gene names that correspond to common English words, etc. The majority of the remaining search term ambiguities were idiosyncratic and difficult to identify systematically without causing a significant rise in false negatives. Alternative approaches, such as the examination of the nearest neighbor terms, need to be considered to further reduce the false positive rate.

It is not uncommon to see expression changes in microarray experiments as small as 2-fold reported in the literature. Even when these expression changes are statistically significant, it is not always clear if they are biologically meaningful. When comparing expression levels of disease to normal tissue, one expects an enrichment of known disease-related genes to appear in the altered expression group. MedGene provided a unique opportunity to test this notion in the context of existing knowledge on a novel breast cancer microarray dataset. For genes displaying a 5-fold change or less in tumors compared to normal, there was no evidence of a correlation between altered gene expression and a known role in the disease. This

Table 3. Genes with Large Expression Changes in ER- but Not in ER+ Breast Tumors

gene symbol	fold change (ER+)	fold change (ER-)
KRTHB1	1.0	610.8
BRS3	1.2	89.4
DKK1	1.2	69.8
ZIC1	1.9	59.6
TLR1	1.0	38.5
KIAA0680	2.6	33.2
CDKN3	1.0	30.6
EBI2	4.0	27.9
GZMB	3.8	21.9
STK18	4.7	18.6
GPR49	1.0	14.6
MYO10	1.6	14.4
LAD1	-1.0	13.5
POLE2	4.2	13.0
HMG4	4.4	12.9
BCL2L11	-1.2	12.3
LRP8	2.9	12.2
CCNB2	1.0	11.8
CCNE2	4.0	11.6
FCB	-4.3	11.1
KNLS6	2.9	10.9
HIF5	3.0	10.2
SERPINH2	4.6	10.2
YAP1	1.0	10.0
LPHB	-1.3	-10.4
TCEA2	-1.1	-10.8
TFF1	1.3	-11.4
COL17A1	-4.1	-15.7
POP5	1.1	-16.2
BPAC1	-4.6	-22.3
PDZK1	-1.1	-36.8
VEGFC	-2.8	-51.5
MUC6	-1.4	-64.9
SERPINA5	-1.0	-83.1
MEIS1	-1.6	-85.9
CA12	2.4	-150.3

Table 3. MedGene identified a set of relatively understudied, yet highly expressed genes in ER negative, but not ER positive breast tumors. All of these genes have either never been co-cited with breast cancer or have a weak association except those marked with an *.

reflects the many genes whose role in breast cancer may not involve large changes in expression in sporadic tumors (e.g., *BRCA1* and *BRCA2*) and genes whose modest changes in expression may be unrelated to the disease. Strikingly, among genes with a 10-fold change or more in expression level, there was a strong and significant correlation between expression level and a published role in the disease, providing the first global validation of the micro-array approach to identifying disease-specific genes.

The results derived from MedGene have two implications. First, a careful hunt for corroborating evidence of a role in breast cancer should precede any further study of genes with less than 5-fold expression level changes. Second, any genes with 10-fold changes or more are likely to be related to breast cancer and warrant attention. It is likely that this threshold will change depending on the disease as well as the experiment.

Interestingly, the observed correlation was only found among ER-positive tumors, not ER-negative. This may reflect a bias in the literature to study the more prevalent type of tumor in the population. Furthermore, this emphasizes that caution must be taken when interpreting experiments that may contain subpopulations that behave very differently. The MedGene approach identified a set of relatively understudied, yet highly expressed genes in ER-negative tumors that are worthy of further examination (Table 3).

In conclusion, we have developed an automated method of summarizing and organizing the vast biomedical literature. To our knowledge, the resulting database is the most comprehensive and accurate of its kind. By generating a score that reflects the strength of the association, it provides an important tool for the rapid and flexible analysis of large datasets from various high-throughput screening experiments. Furthermore, it can be used for selecting subsets of genes for functional studies, for building disease-specific arrays, for looking at genes common to multiple diseases and various other high-throughput applications. In the future, it will be possible to enhance the utility of the MedGene database by building links between genes and other MeSH terms as well as other biological processes and concepts, such as cell division and responses to small molecules.

Acknowledgment. We would like to thank P. Braun, L. Garraway, J. Pearlberg, and other members of our Institute for helpful discussion. Many thanks to the NLM (National Library of Medicine) for licensing of MEDLINE and the annotation effort of adding MeSH indexes for MEDLINE abstracts. This work was funded by grants from the Breast Cancer Research Foundation and an NHLBI PGA Grant (Vol HL65582-02).

Supporting Information Available: Twenty-three human disease category headings along with all of their child terms selected from the 2002 MeSH index (Supplemental Table 1); analysis of the causes of false negatives in MedGene (Supplemental Table); meaningful gene-disease relationships found in MedGene (Supplemental Table 3); causes for incorrect assignment of gene indexes (Supplemental Table 4); a review of the results, showing that the resulting disease clusters were indeed logical (Supplemental Figure 1); and a review of the results showing that among the 505 previously unrelated genes, 467 were either newly identified genes or genes that had not previously been associated with any disease (Supplemental Figure 2). This material is available free of charge via the Internet at <http://pubs.acs.org> and at the web sites mentioned in the text.

References

- (1) Baasiri, R. A.; Glasser, S. R.; Steffen, D. L.; Wheeler, D. A. *Oncogene* 1999, 18, 7958-7965.
- (2) Steffen, D. L.; Levine, A. E.; Yarus, S.; Baasiri, R. A.; Wheeler, D. A. *Bioinformatics* 2000, 16, 639-649.
- (3) Marcotte, E. M.; Xenarios, I.; Eisenberg, D. *Bioinformatics* 2001, 17, 359-363.
- (4) Ono, T.; Hishigaki, H.; Tanigami, A.; Takagi, T. *Bioinformatics* 2001, 17, 155-161.
- (5) Jernsen, T. K.; Laegreid, A.; Komorowski, J.; Hovig, E. *Nat. Genet.* 2001, 28, 21-28.
- (6) Chaussabel, D.; Sher, A. *Genome Biol.* 2002, 3, RESEARCH0055.
- (7) Gibbons, F. D.; Roth, F. P. *Genome Res.* 2002, 12, 1574-1581.
- (8) Perez-Iratxe, C.; Bork, P.; Andrade, M. A. *Nat. Genet.* 2002, 31, 316-319.
- (9) Funk, M. E.; Reid, C. A. *Bull. Med. Lib. Assoc.* 1983, 71, 176-183.
- (10) Humphrey, S. M.; Miller, N. E. *J. Am. Soc. Inf. Sci.* 1987, 38, 184-196.
- (11) Maglott, D. R.; Katz, K. S.; Scoupe, H.; Pruitt, K. D. *Nucleic Acids Res.* 2000, 28, 126-128.
- (12) Pruitt, K. D.; Maglott, D. R. *Nucleic Acids Res.* 2001, 29, 137-140.
- (13) Wadelius, M.; Andersson, A. O.; Johansson, J. E.; Wadelius, C.; Rane, E. *Pharmacogenetics* 1999, 9, 333-340.
- (14) Adam, R. M.; Borer, J. C.; Williams, J.; Eastham, J. A.; Loughlin, K. R.; Freeman, M. R. *Endocrinology* 1999, 140, 5866-5875.
- (15) Montori, V. M.; Smeja, M.; Guyatt, G. H. *Mayo Clin. Proc.* 2000, 75, 1284-1288.
- (16) Denenberg, V. H. *Statistics Experimental Design for Behavioral and Biological Research*; Wiley-Liss: New York, 1976.
- (17) Rebhan, M.; Chaila-Caspi, V.; Priusky, J.; Lancet, D. *Trends Genet.* 1997, 13, 163.
- (18) Bairoch, A.; Apweiler, R. *Nucleic Acids Res.* 2000, 28, 45-48. PR034027



An increased high-mobility group A2 expression level is associated with malignant phenotype in pancreatic exocrine tissue

N Abe^{*1}, T Watanabe², Y Suzuki¹, N Matsumoto¹, T Masaki¹, T Mori¹, M Sugiyama¹, G Chiappetta³, A Fusco⁴ and Y Atomi¹

¹First Department of Surgery, Kyorin University School of Medicine, 6-20-2, Shinkawa, Mitaka, Tokyo 181-8611, Japan; ²Department of Clinical Pathology, Kyorin University School of Medicine, 6-20-2, Shinkawa, Mitaka, Tokyo 181-8611, Japan; ³Istituto Nazionale dei Tumori Fondazione Senatore Pascalle, via M Semmola, Naples 80131, Italy; ⁴Dipartimento di Biologia e Patologia Cellulare e Molecolare, c/o Centro di Endocrinologia ed Oncologia Sperimentale del CNR, Università di Napoli Federico II, via Pansini, 5, Naples 80131, Italy

The altered form of the high-mobility group A2 (HMGA2) gene is somehow related to the generation of human benign and malignant tumours of mesenchymal origin. However, only a few data on the expression of HMGA2 in malignant tumour originating from epithelial tissue are available. In this study, we examined the HMGA2 expression level in pancreatic carcinoma, and investigated whether alterations in the HMGA2 expression level are associated with a malignant phenotype in pancreatic tissue. High-mobility group A2 mRNA and protein expression was determined in eight surgically resected specimens of non-neoplastic tissue (six specimens of normal pancreatic tissue and two of chronic pancreatitis tissue) and 27 pancreatic carcinomas by highly sensitive reverse transcriptase–polymerase chain reaction (RT–PCR) techniques and immunohistochemical staining, respectively. Reverse transcriptase–polymerase chain reaction analysis revealed the expression of the HMGA2 gene in non-neoplastic pancreatic tissue, although its expression level was significantly lower than that in carcinoma. Immunohistochemical analysis indicated that the presence of the HMGA2 gene in non-neoplastic pancreatic tissue observed in RT–PCR reflects its abundant expression in islet cells, together with its focal expression in duct epithelial cells. Intense and multifocal or diffuse HMGA2 immunoreactivity was noted in all the pancreatic carcinoma examined. A strong correlation between HMGA2 overexpression and the diagnosis of carcinoma was statistically verified. Based on these findings, we propose that an increased expression level of the HMGA2 protein is closely associated with the malignant phenotype in the pancreatic exocrine system, and accordingly, HMGA2 could serve as a potential diagnostic molecular marker for distinguishing pancreatic malignant cells from non-neoplastic pancreatic exocrine cells.

British Journal of Cancer (2003) 89, 2104–2109. doi:10.1038/sj.bjc.6601391 www.bjcancer.com

© 2003 Cancer Research UK

Keywords: HMGA2; pancreatic cancer; RT–PCR; immunostaining

The high-mobility group A (HMGA) family of proteins in mammals is composed of four proteins: HMGA1a, HMGA1b, HMGA1c, and HMGA2. The former three proteins are encoded by a single functional gene, that is, HMGA1 (formerly HMGI(Y)), while the last one is a product of a separate gene, that is, HMGA2 (formerly HMGI-C) (Manfioletti *et al*, 1991; Johnson *et al*, 1998). High-mobility group A2 has an approximately 50% amino-acid sequence homology with HMGA1, and features an internal 11 amino-acid deletion that characterises HMGA1 (Manfioletti *et al*, 1991; Tallini and Dal Cin, 1999). High-mobility group A2 proteins bind to the minor groove of AT-rich DNA sequences, thereby inducing a bend within the DNA (Thanos and Maniatis, 1992). They cannot initiate transcription, but they can enhance promoter binding of transcription factors (Thanos and Maniatis, 1992; Grosschedl *et al*, 1994; Mantovani *et al*, 1998).

High-mobility group A2 has been shown to be expressed abundantly during embryogenesis, but its expression is either

undetectable or remains at low levels in other normal adult tissues (Manfioletti *et al*, 1991; Zhou *et al*, 1995; Rogalla *et al*, 1996; Rommel *et al*, 1997; Hirning-Folz *et al*, 1998), suggesting that HMGA2 plays an important role (or roles) in cell proliferation and/or differentiation. Consistent with this, it has been demonstrated that HMGA proteins are phosphorylated in a cell-cycle-dependent manner (Reeves *et al*, 1991). Functionally, knocking out the HMGA2 gene in mice leads to the pygmy phenotype with characteristic hypoplasia of mesenchymal tissue, thereby confirming the important role(s) of HMGA2 in mammalian growth and development (Zhou *et al*, 1995).

The altered form of the HMGA2 gene, on the other hand, could somehow be related to the generation of human benign and malignant tumours. Rearrangements of the HMGA2 gene, for example, have been frequently observed in benign tumours of mesenchymal origin (Ashar *et al*, 1995; Schoenmakers *et al*, 1995). In such cases, the gene rearrangements were the consequence of chromosomal translocation involving regions 12q13–15, where the HMGA2 gene is located. The HMGA2 modifications consist of the loss of the carboxyl-terminal tail and its fusion with ectopic sequences (Ashar *et al*, 1995; Schoenmakers *et al*, 1995). The truncation of HMGA2, rather than its fusion with other genes, has

*Correspondence: Dr N Abe; E-mail: abent@kyorin-u.ac.jp

Received 17 February 2003; revised 14 July 2003; accepted 16 September 2003

also been shown to be responsible for cell transformation (Fedele *et al*, 1998). This was confirmed in transgenic mice carrying a truncated HMGA2, which developed a giant phenotype together with a marked expansion of the retroperitoneal and subcutaneous white adipose tissues (Bartista *et al*, 1999; Arlotta *et al*, 2000). Interestingly, most of these tumours related to the alteration in HMGA2 are of nonepithelial origin. In contrast, only a few data on the expression of HMGA2 in human malignant tumour originating from epithelial tissue are available (Rogalla *et al*, 1997). The overexpression of HMGA2 mRNA has been shown to be closely associated with high histologic grade in breast cancer (Rogalla *et al*, 1997), suggesting that the expression level of the HMGA2 protein/gene could be a potential clinicopathological marker with prognostic implications for a wide range of cancers. To test this possibility, we examined the HMGA2 expression in pancreatic cancers in the present study, and investigated whether alterations in HMGA2 are associated with the malignant phenotype of tumours in pancreatic tissue. To this end, HMGA2 mRNA expression was first analysed by highly sensitive reverse transcriptase-polymerase chain reaction (RT-PCR) techniques. Immunohistochemical detection of HMGA2 protein using a specific antibody was also attempted. Although relatively simple and easy to perform, immunohistochemistry is a potential method of examining whether the expression of a certain protein is specific to tumour cells, because it allows precise correlation of the protein expression with the phenotype of the cells on individual cell basis (Abe *et al*, 2000). In this sense, immunohistochemistry can provide more useful information than other assays by which proteins and/or mRNAs are extracted from tumours; possibly including a mixture of proteins from normal and irrelevant cells such as acinar cells or islet cells of the pancreas in the analysis (Abe *et al*, 2000). Based on the above considerations, we determined HMGA2 protein expression immunohistochemically on surgically resected specimens, normal pancreatic tissue, chronic pancreatitis tissue, and carcinomas of the pancreas.

MATERIALS AND METHODS

Tissue samples

The tissue samples were obtained at the time of surgery at the First Department of Surgery, Kyorin University Hospital, between October 1996 and August 2001. Specimens from 27 pancreatic carcinomas (20 primary carcinomas, four liver metastases, two peritoneal metastases, and one lymph node metastasis) and eight non-neoplastic tissues (six normal pancreatic and two chronic pancreatitis tissues) were obtained. In all, 27 carcinomas were histologically diagnosed as 12 well-differentiated tubular adenocarcinomas, six moderately differentiated tubular adenocarcinomas, seven poorly differentiated tubular adenocarcinomas, and two adenosquamous carcinomas (they were evaluated histologically according to the criteria of the Japan Pancreas Society). Normal pancreatic tissues were obtained from either patients who have undergone pancreatectomy due to pancreatic neoplasms or those with gastric cancer who have undergone pancreatectomy for lymph node dissection. In either case, specimens were obtained from a macroscopically healthy region distinct from the neoplastic lesion. All patients gave their informed consent prior to their inclusion in the study. Among the samples, those from 17 pancreatic carcinomas and six non-neoplastic pancreatic tissues were frozen on dry ice immediately after surgical resection for molecular investigation (RT-PCR), and stored at -80°C until use. All the tissue specimens were fixed for immunohistochemical analysis as soon as possible after surgical resection in 4% paraformaldehyde in phosphate-buffered saline (PBS) at 4°C for 14 h, followed by cryoprotection in a graded concentration series of sucrose in PBS. The specimens were then embedded in the OCT

HMGA2 expression in pancreatic carcinoma

N Abe *et al*

compound, frozen, and stored at -80°C until analysis. All the tissue specimens were histologically examined and pathological diagnoses were confirmed.

RT-PCR analysis

Reverse transcriptase-polymerase chain reaction for the HMGA2 expression was performed using a heminested PCR technique as described previously (Rogalla *et al*, 1996; Rommel *et al*, 1997). Total RNA was extracted by a modified guanidine thiocyanate method as described previously (Miyatani *et al*, 1986). cDNA was synthesised using the adapter primer (AP) AAG GAT CCG TCG ACA TC (T)17 and Superscript II reverse transcriptase (Gibco BRL, Gaithersburg, MD, USA). For the first and second rounds of the heminested PCR, the same lower primer (Rev) 5'-TCC TCC TGA GCA GGC TTC-3' (exon 4/5) was used. The forward primer 5'-CTT CAG CCC AGG GAC AAC-3' (exon 1) and the nested primer 5'-CAT CGC CTC AGA AGA GAG GAC-3' (exon 1) were used as upper primers. The PCR amplifications were both performed for 30 cycles (1 min at 94°C , 1 min at 53°C , and 2 min at 72°C). As a control reaction for intact RNA and cDNA, PCR amplification of the cDNA of the housekeeping gene β -actin was performed for all samples to exclude false-negative PCR results. Only those samples positive for β -actin were used for this study. The resulting PCR products were clearly visualised by gel electrophoresis on a 2% agarose-gel stained with ethidium bromide as bands at 220 base pairs (bp) for HMGA2 and at 154 bp for β -actin (Figure 1). The resulting bands were sequenced and their sequences were found to be identical to that of HMGA2.

Immunohistochemical analysis

Immunohistochemical examinations were performed by the avidin-biotin complex immunoperoxidase technique using an Avidin-Biotinylated Enzyme Complex kit (Vector Laboratories, Inc. CA, USA) as described previously (Abe *et al*, 1999, 2000, 2002). The HMGA2 protein expression was immunohistochemically analysed on surgically resected specimens, together with four pancreatic cancer cell lines (PANC-1, MIA PaCa-2, BxPC-3, and AsPC-1) using HMGA2-specific antibodies, raised in rabbit against the recombinant HMGA2 protein (Berlingieri *et al*, 1995). In brief, frozen sections 5 (5 m thick) were prepared, transferred onto poly-L-lysine-coated slides, air-dried, and then washed in PBS, followed by quenching of endogenous peroxidase activity with 0.3% hydrogen peroxide in methanol. After further rinsing with PBS, the sections were incubated with normal goat serum for 20 min at room temperature to block nonspecific binding, and then incubated with the primary anti-HMGA2 antibody (1:100 dilution) 14 h at 4°C . After another wash in 0.2% Triton X in PBS, the sections were further incubated with biotinylated anti-rabbit IgG for 30 min at room temperature, followed by washes in 0.2% Triton X in PBS. After the addition of streptavidin-biotin-conjugated peroxidase and incubation for 30 min at room temperature, the

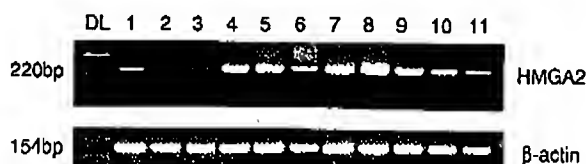


Figure 1 Reverse transcriptase-polymerase chain reaction products of HMGA2 after gel electrophoresis and ethidium bromide staining. Results show specific 220-bp bands. DL, DNA molecular weight marker; lane 1, positive control (hepatoma cell line HEP3B, which is known to express high level of HMGA2); lane 2, normal pancreas; lane 3, chronic pancreatitis; lane 4–11, pancreatic carcinomas.

sections were washed in 0.2% Triton X in PBS, and then the localisation of the HMGA2 protein was visualised by incubating the sections with 3,3'-diaminobenzidine. The slides were counterstained with Mayer's haematoxylin, dehydrated in a graded alcohol series, cleared in xylene, and mounted. Negative control staining was carried out by replacing the primary antibody with normal rabbit serum under the same experimental conditions. The immunostained slides were evaluated microscopically by a single investigator (NA) according to the criteria published previously (Abe *et al*, 1999, 2000) without prior knowledge of the clinical data for each case. The percentage of HMGA2-positive cells was scored by counting approximately 300–1000 tumour cells in three randomly selected fields (Abe *et al*, 1999, 2000, 2002). The immunohistochemical evaluation was considered positive when the HMGA2 nuclear immunoreactivity was detected in more than 20% of the cells according to the criteria published previously (Abe *et al*, 1999, 2000).

RESULTS

Expression of HMGA2 mRNA determined by RT-PCR

Among the six non-neoplastic tissue samples, five, including three normal tissues and two chronic pancreatitis tissues, gave rise to detectable HMGA2 bands, while one normal tissue sample showed no detectable HMGA2 band. The signal intensities of the HMGA2 band in chronic pancreatitis tissue samples were almost equivalent to those observed in the normal tissue samples. All the 17 samples of pancreatic carcinomas also showed HMGA2 bands by RT-PCR (Figure 1, Table 1). When the signal intensities of these HMGA2 bands were compared between non-neoplastic and carcinoma samples, the latter showed at least several fold more intense band than the former (Figure 1). Thus, an increased expression level of the HMGA2 mRNA is a distinct feature of pancreatic carcinoma.

Expression of HMGA2 protein determined by immunohistochemistry

To determine whether the altered HMGA2 mRNA expression observed in pancreatic carcinoma is associated with alterations in protein expression, we analysed the expression of the HMGA2 protein by immunohistochemistry. Its expression was first analysed in four pancreatic cancer cell lines. Intense multifocal or diffuse HMGA2 nuclear immunoreactivity was characteristically observed in these cell lines (Figures 2A–D). In both normal pancreas and chronic pancreatitis tissues, acinar cells did not exhibit any detectable HMGA2 immunoreactivity; however, a small proportion of duct epithelial cells showed faint HMGA2 immunoreactivity (Figure 3A). On the other hand, in the endocrine region, islet cells showed intense and diffuse HMGA2 immunoreactivity

(Figures 3B and F). In these cells, although HMGA2 immunoreactivity was localised mainly in the nuclei, faint staining was also observed within the cytoplasm. These results clearly indicated that the presence of the HMGA2 gene in non-neoplastic pancreatic tissue observed in the RT-PCR analysis reflects its expression in islet cells, together with its focal expression in duct epithelial cells. No significant difference in immunohistochemical findings was found between normal tissues and chronic pancreatitis tissues. When the expression of the HMGA2 protein in surgical specimens of carcinomas was then analysed, multifocally or diffusely distributed intense HMGA2 immunoreactivity was noted in all the pancreatic carcinoma specimens examined (Figures 3C–F). Intense nuclear staining was characteristically observed in the carcinoma cells. High-mobility group A2-positive carcinoma cells were observed regardless of the degree of differentiation (well/moderately or poorly differentiated tubular adenocarcinoma), histology type (tubular adenocarcinoma or adenosquamous carcinoma), or tumour site (primary or metastatic site). A strong correlation between HMGA2 overexpression and the diagnosis of carcinoma was noted (Fisher's exact probability, $P < 0.0001$, Table 1).

DISCUSSION

To evaluate the association between HMGA2 expression and the pathological diagnosis of pancreatic carcinoma, we investigated the expression of HMGA2 gene/protein in duct cell carcinoma and non-neoplastic tissue of the pancreas. High-mobility group A2 expression has been shown to be undetectable or to remain at low levels in normal adult tissues (Manfioletti *et al*, 1991; Zhou *et al*, 1995; Rogalla *et al*, 1996; Rommel *et al*, 1997; Hirning-Folz *et al*, 1998; Gattas *et al*, 1999). In the present study, however, a highly sensitive RT-PCR analysis revealed the expression of the HMGA2 gene in non-neoplastic pancreatic tissue, although its expression level was significantly lower than that in carcinoma. Immunohistochemical analysis indicated that the presence of the HMGA2 gene in non-neoplastic pancreatic tissue observed in the RT-PCR analysis reflects its abundant expression in islet cells together with its focal expression in duct epithelial cells. Thus, this study showed that the HMGA2 gene or protein is present even in normal pancreatic tissue. In HMGA2 immunohistochemical analysis, while only a small proportion of duct epithelial cells in the non-neoplastic tissue specimens showed HMGA2 immunoreactivity, a significantly higher proportion of carcinoma cells showed intense staining. In fact, a strong correlation between HMGA2 overexpression and the diagnosis of carcinoma was statistically verified. These findings indicate that an increased expression level of the HMGA2 protein is closely associated with the malignant phenotype in the pancreatic exocrine system, and accordingly, HMGA2 could serve as a potential diagnostic molecular marker for distinguishing pancreatic malignant cells from non-neoplastic pancreatic exocrine cells. A possible application of the results of the present study would be the determination of the HMGA2 gene and/or protein expression level in pancreatic juice collected at the time of endoscopic retrograde pancreatography. Using a sensitive and quantitative method such as competitive RT-PCR or immunoassay, the detection of even a small number of cancer cells could well be expected.

In order to evaluate the biological significance of the present results, it would be essential to understand the mechanisms by which the HMGA2 gene is involved in tumorigenesis, which unfortunately remain largely unclear. A clue to this issue was, however, provided by a recent report that transgenic mice carrying the HMGA2 gene developed pituitary adenomas (Fudcile *et al*, 2002). These findings indicate that the high HMGA2 expression level has a critical role in neoplastic transformation of cells. Another clue was also demonstrated when antisense HMGA2 RNA

Table 1 HMGA2 expression in pancreatic carcinoma

Histological type of pancreatic specimens	No. of positive specimens/no. of specimens analysed by RT-PCR	No. of positive ^a specimens/no. of specimens analysed by immunohistochemistry
Non-neoplastic tissue		
Normal pancreas	3/4 (75%)	0/6 (0%)
Chronic pancreatitis	2/2 (100%)	0/2 (0%)
Duct cell carcinoma	17/17 (100%)	27/27 (100%)

^aThe immunostained slides were scored as positive for immunohistochemistry when HMGA2 nuclear immunoreactivity was detected in more than 20% of the cells in the exocrine region.

HMGA2 expression in pancreatic carcinoma

N Abe et al

npj

2107

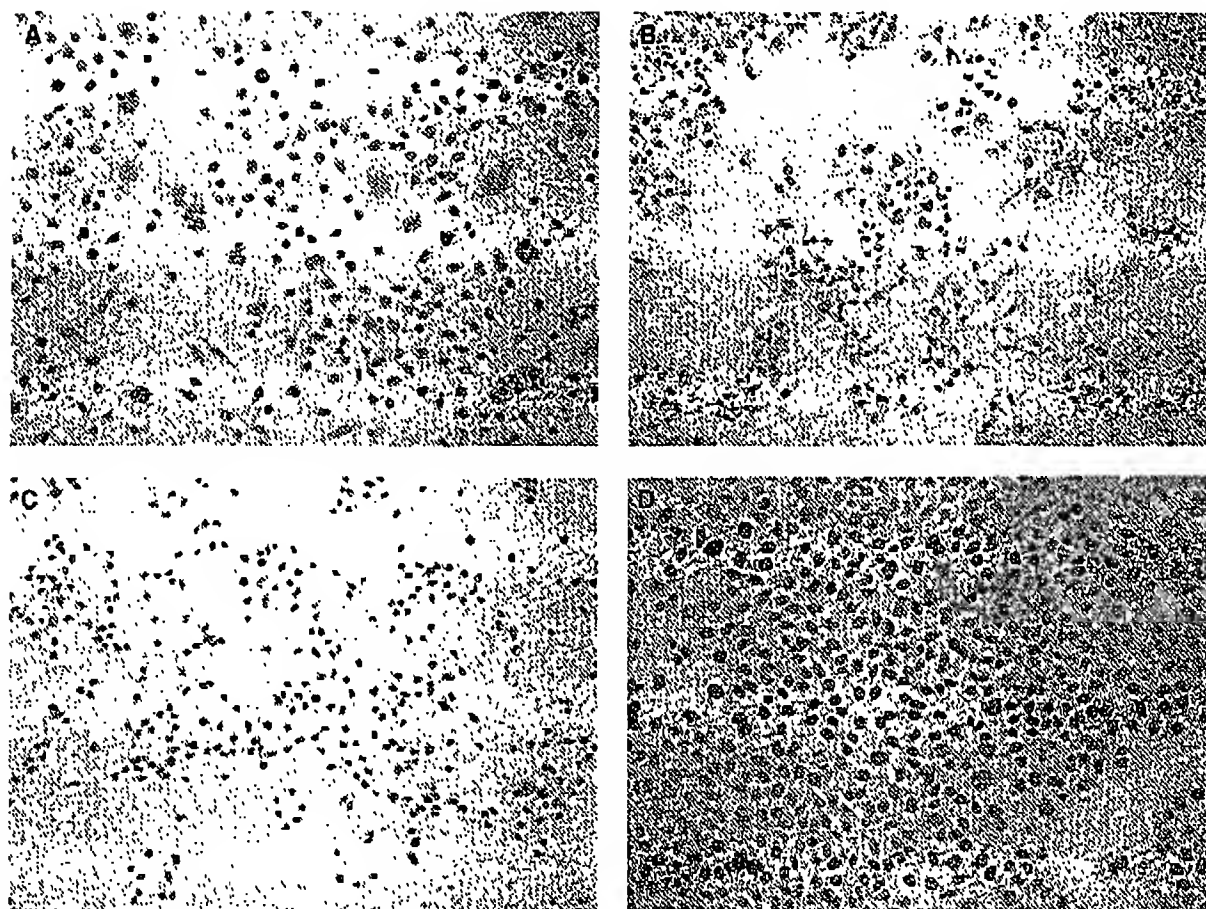


Figure 2 Immunohistochemical demonstration of the HMGA2 protein expression in pancreatic cancer cell lines. (A) AsPC-1 (Mayer's haematoxylin; original magnification $\times 200$). (B) PANC-1 (Mayer's haematoxylin; original magnification $\times 200$). (C) MIA PaCa-2 (Mayer's haematoxylin; original magnification $\times 100$). (D) BxPC-3 (Mayer's haematoxylin; original magnification $\times 200$). Intense multifocal or diffuse HMGA2 nuclear immunoreactivity (brown colour) was characteristically observed in cancer cells.

was shown to prevent retrovirally induced neoplastic transformation of rat thyroid cells *in vitro* (Berlingieri *et al*, 1995). The interaction between HMGA2 and the AP-1 transcriptional complex is considered to be responsible for the activation of genes whose expressions are associated with carcinogenesis (Vallone *et al*, 1997), since thyroid neoplastic transformation is associated with a drastic increase in AP-1 activity. This AP-1 activity is blocked by suppressing HMGA protein synthesis *in vitro* (Battista *et al*, 1998). The absence or decreased AP-1 transcriptional activity, which is directly or indirectly regulated by HMGA proteins, would inhibit the expression of AP-1-dependent genes, such as those of vascular endothelial growth factor (VEGF), collagenase I (matrix metalloproteinase-1; MMP-1), and stromelysin (MMP-3), which are essential for neoplastic transformation of cells (Vallone *et al*, 1997). In fact, significant downregulations of these mRNA expression levels were demonstrated in the retrovirally infected thyroid cell lines expressing the antisense HMGA2 (Vallone *et al*, 1997). Considering that the overexpression of the AP-1 (Tessari *et al*, 1999; Meggiato *et al*, 2003), VEGF (Seo *et al*, 2000), MMP-1 (Ito *et al*, 1999), and MMP-3 (Bramhall *et al*, 1996) has been demonstrated in human pancreatic cancer, together with our results, the interactions among these molecules may play an important role in pancreatic neoplastic transformation *in vivo*. Further studies, including the determination of expression levels of these molecules in tissue samples, have yet to be carried out to further clarify this issue. Conversely, the HMGA2 gene has recently

been shown not to be necessary for the malignant transformation of thyroid cells *in vivo* (Scala *et al*, 2001). This was demonstrated by comparing the frequency of radiation or papilloma virus E7 gene-induced thyroid carcinomas in mice carrying disrupted HMGA2 (pygmy mice) and that in mice carrying wild-type HMGA2 (Scala *et al*, 2001). Pygmy mice developed thyroid carcinomas with the same frequency as wild-type mice and furthermore, these two carcinomas generated in different mice showed no significant macroscopic and microscopic differences, indicating that HMGA2 is not sufficient for *in vivo* malignant transformation of thyroid cells (Scala *et al*, 2001). Several hypotheses could be considered to explain the discrepancy with the previous *in vitro* data, showing that HMGA2 is required for *v-mos*- and *v-ras*-Ki-induced cell transformations. One possible explanation would be that HMGA1, rather than HMGA2, may be required for thyroid cell transformation. This hypothesis is supported by the evidence that adenovirus carrying the HMGA1 gene in an antisense orientation induces programmed cell death in carcinoma cell lines derived from human thyroid, lung, colon, and breast cancers (Scala *et al*, 2000). We previously demonstrated that human pancreatic carcinoma expresses high HMGA1 levels (Abe *et al*, 2000, 2002), indicating that both HMGA2 and HMGA1 are overexpressed in this lesion. The expression of only one of the HMGA genes may be sufficient to lead epithelial cells of the pancreatic duct to exhibit the malignant phenotype. Further studies, such as the generation of HMGA1-knockout mice and

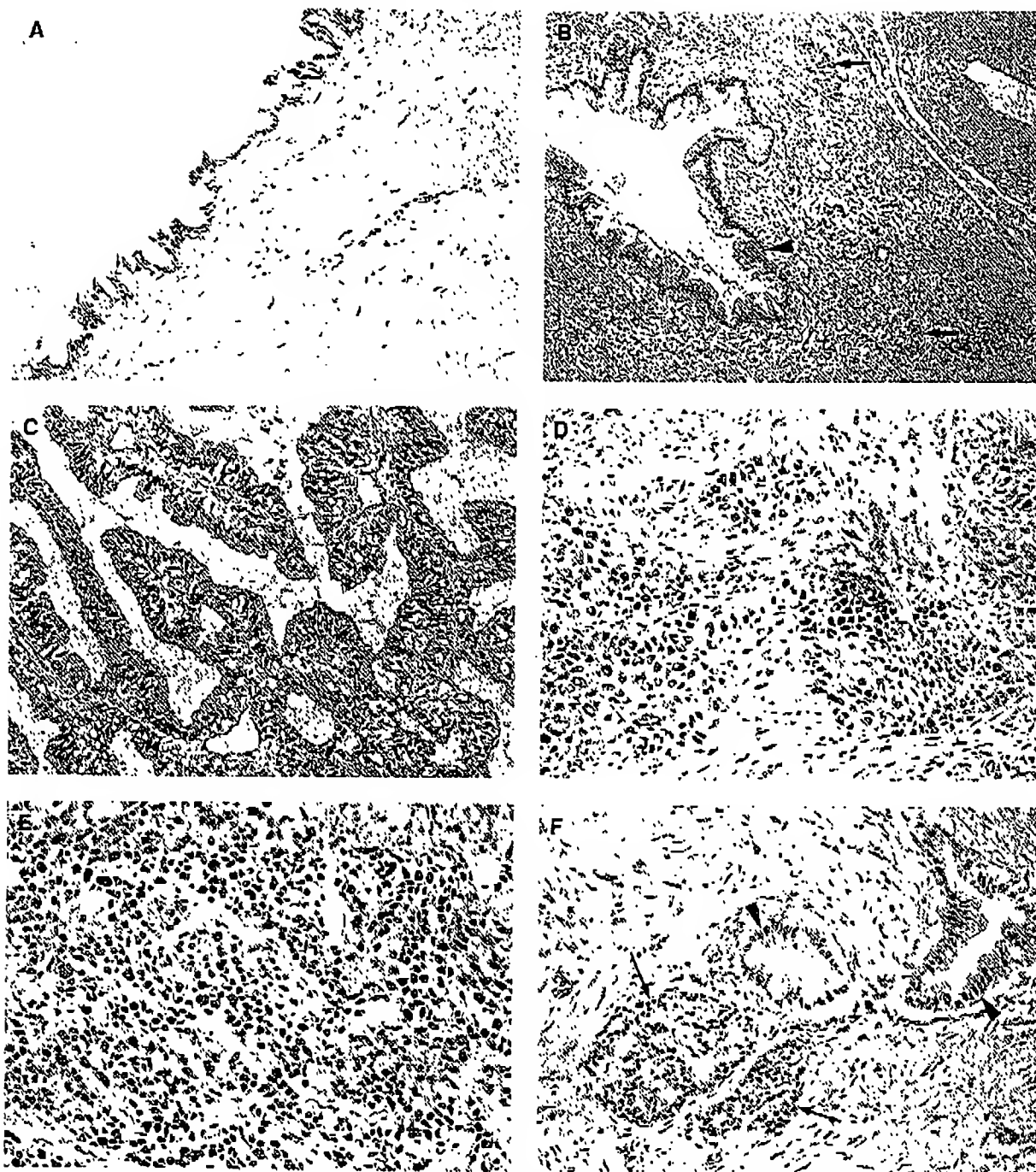


Figure 3 Immunohistochemical demonstration of the HMGA2 protein expression in surgically resected specimens of non-neoplastic pancreatic tissues and pancreatic carcinomas. (A) Non-neoplastic epithelial cells of the main pancreatic duct. A small proportion of duct epithelial cells show HMGA2 immunoreactivity (arrows). (Mayer's haematoxylin; original magnification $\times 200$). (B) Epithelial cells of branch pancreatic duct and islets in chronic pancreatitis tissue. Islet cells showed intense and diffuse HMGA2 immunoreactivity (arrows), while epithelial cells of the branch pancreatic duct did not exhibit any detectable HMGA2 immunoreactivity (arrowhead) (Mayer's haematoxylin; original magnification $\times 100$). (C) Primary pancreatic carcinoma exhibiting well-differentiated tubular adenocarcinoma (Mayer's haematoxylin; original magnification $\times 200$). (D) Primary pancreatic carcinoma exhibiting adenosquamous carcinoma (Mayer's haematoxylin; original magnification $\times 200$). (E) Metastatic lesion in the liver (Mayer's haematoxylin; original magnification $\times 200$). Intense and multifocal or diffuse HMGA2 immunoreactivity was noted in all the pancreatic carcinomas (C–E). (F) Section including both carcinoma cells and islet cells (Mayer's haematoxylin; original magnification $\times 200$). Islet cells showed intense and diffuse HMGA2 immunoreactivity (arrows), which was almost equivalent to that observed in carcinoma cells (arrowheads).

subsequent analysis of their susceptibility to developing malignancies, need to be carried out in order to clarify the role of a single HMGA gene in carcinogenesis in a wide variety of epithelial tissues.

In conclusion, this study has clearly demonstrated that an increased expression level of the HMGA2 gene/protein is closely associated with the malignant phenotype in pancreatic exocrine tissue, suggesting that HMGA2 could play a vital role in

tumorigenesis in the pancreatic exocrine system. The strong correlation between HMGA2 overexpression and the histological diagnosis of carcinoma indicates that the determination of the expression level of HMGA2 can be of great value in the diagnosis of pancreatic neoplasms.

REFERENCES

- Abe N, Watanabe T, Izumisato Y, Masaki T, Mori T, Sugiyama M, Chiappetta G, Fusco A, Fujioka Y, Atomi Y (2002) Diagnostic significance of high mobility group I(Y) protein expression in intraductal papillary mucinous tumors of the pancreas. *Pancreas* 25: 149-153
- Abe N, Watanabe T, Masaki T, Mori T, Sugiyama M, Uchimura H, Fujioka Y, Chiappetta G, Fusco A, Atomi Y (2000) Pancreatic duct cell carcinomas express high levels of high mobility group I(Y) (HMGI(Y)) proteins. *Cancer Res* 60: 3117-3122
- Abe N, Watanabe T, Sugiyama M, Uchimura H, Chiappetta G, Fusco A, Atomi Y (1999) Determination of high mobility group I(Y) expression level in colorectal neoplasias: a potential diagnostic marker. *Cancer Res* 59: 1169-1174
- Arlotta P, Tai AK, Manfioletti G, Clifford C, Jay G, Ono SJ (2000) Transgenic mice expressing a truncated form of the high mobility group I-C protein develop adiposity and an abnormally high prevalence of lipomas. *J Biol Chem* 275: 14394-14400
- Ashar HR, Fejzo MS, Tkachenko A, Zhou X, Fletcher JA, Weremowicz S, Morton CC, Chada K (1995) Disruption of the architectural factor HMGI-C: DNA-binding AT hook motifs fused in lipomas to distinct transcriptional regulatory domains. *Cell* 82: 57-65
- Battista S, de Nigris F, Fedele M, Chiappetta G, Scala S, Vallone D, Pierantoni GM, Megar T, Satoro M, Viglietto G, Verde P, Fusco A (1998) Increase in AP-1 activity is a general event in thyroid cell transformation *in vitro* and *in vivo*. *Oncogene* 17: 377-385
- Battista S, Fidanza V, Fedele M, Klein-Szanto AJ, Outwater E, Brunner H, Santoro M, Croce CM, Fusco A (1999) The expression of a truncated HMGI-C gene induces gigantism associated with lipomatosis. *Cancer Res* 59: 4793-4797
- Berlingieri MT, Manfioletti G, Santoro M, Bandiera A, Vlacotti R, Giancotti V, Fusco A (1995) Inhibition of HMGI-C protein synthesis suppresses retrovirally induced neoplastic transformation of rat thyroid cells. *Mol Cell Biol* 15: 1545-1553
- Bramhall SR, Stamp GWH, Dunn J, Lemoine NR, Neoptolemos JP (1996) Expression of collagenase (MMP2), stromelysin (MMP3) and tissue inhibitor of the metalloproteinases (TIMP1) in pancreatic and ampullary disease. *Br J Cancer* 73: 972-978
- Fedele M, Battista S, Kenyon L, Baldassarre G, Fidanza V, Klein-Szanto AJ, Parlow AF, Visone R, Pierantoni GM, Outwater E, Santoro M, Croce CM, Fusco A (2002) Overexpression of the HMGA2 gene in transgenic mice leads to the onset of pituitary adenomas. *Oncogene* 21: 3190-3198
- Fedele M, Berlingieri MT, Scala S, Chiariotti L, Viglietto G, Rippel V, Bullerdick J, Santoro M, Fusco A (1998) Truncated and chimeric HMGI-C genes induce neoplastic transformation of NIH3T3 murine fibroblasts. *Oncogene* 17: 413-418
- Gattas GF, Quade BJ, Novak RA, Morton CC (1999) HMGI-C expression in human adult and fetal tissues and in uterine leiomyomata. *Genes Chromosomes Cancer* 25: 316-322
- Grosschedl R, Giese K, Pagel J (1994) HMG domain proteins: architectural elements in the assembly of nucleoprotein structures. *Trends Genet* 10: 94-100
- Hirring-Folz U, Wilda M, Rippe V, Bullerdick J, Hameister H (1998) The expression pattern of the Hmgic gene during development. *Genes Chromosomes Cancer* 23: 350-357
- Ito T, Ito M, Shiozawa J, Naito S, Kanematsu T, Sekine I (1999) Expression of the MMP-1 in human pancreatic carcinoma: relationship with prognostic factor. *Mod Pathol* 12: 669-674
- Johnson KR, Lehn DA, Elton TS, Barr PJ, Reeves R (1998) Complete murine cDNA sequence, genomic structure, and tissue expression of the high mobility group protein HMGI(Y). *J Biol Chem* 263: 18338-18342
- Manfioletti G, Giancotti V, Bandiera A, Buratti E, Sautiewre P, Cary P, Crane-Robinson C, Coles B, Goodwin GH (1991) cDNA cloning of the HMGI-C phosphoprotein, a nuclear protein associated with neoplastic and undifferentiated phenotypes. *Nucleic Acids Res* 19: 6793-6797
- Mantovani F, Covaceuszach S, Rustighi A, Sgarra R, Heath C, Goodwin GH, Manfioletti G (1998) NF- κ B mediated transcriptional activation is enhanced by the architectural factor HMGI-C. *Nucleic Acids Res* 26: 1433-1439
- Mcggiato T, Calabrese P, De Cesare CM, Ballelo E, Valente M, Del Favero G (2003) C-JUN and CPP (CASPASE 3) in human pancreatic cancer: relation to cell proliferation and death. *Pancreas* 26: 65-70
- Miyatani S, Winkles JA, Sargent TD, Dawid IB (1986) Stage-specific keratins in *Xenopus laevis* embryos and tadpoles: the XK81 gene family. *J Cell Biol* 103: 1957-1965
- Reeves R, Langan TA, Nissen MS (1991) Phosphorylation of the DNA-binding domain of nonhistone high-mobility group I protein by cdc2 kinase: reduction of binding affinity. *Proc Natl Acad Sci USA* 88: 1671-1675
- Rogalla P, Drechsler K, Frey G, Hennig Y, Helmke B, Bonk U, Bullerdick J (1996) HMGI-C expression patterns in human tissues. Implications for the genesis of frequent mesenchymal tumors. *Am J Pathol* 149: 775-779
- Rogalla P, Drechsler K, Kazmierczak B, Rippe V, Bonk U, Bullerdick J (1997) Expression of HMGI-C, a member of the high mobility group protein family, in a subset of breast cancers: relationship to histological grade. *Mol Carcinog* 19: 153-156
- Rommel B, Rogalla P, Jox A, Kalle CV, Kazmierczak B, Wolf J, Bullerdick J (1997) HMGI-C, a member of the high mobility group family of proteins, is expressed in hematopoietic stem cells and in leukemic cells. *Leukemia Lymphoma* 26: 603-607
- Scala S, Portella G, Fedele M, Chiappetta G, Fusco A (2000) Adenovirus-mediated suppression of HMGI(Y) protein synthesis as potential therapy of human malignant neoplasias. *Proc Natl Acad Sci USA* 97: 4256-4261
- Scala S, Portella G, Vitagliano D, Ledent C, Chiappetta G, Giancotti V, Dumont J, Fusco A (2001) HMGI-C gene expression is not required for *in vivo* thyroid cell transformation. *Carcinogenesis* 22: 251-256
- Schoenmakers EFPM, Wanschura S, Moles R, Bullerdick J, Van den Berghe H, Van de Ven WJM (1995) Recurrent rearrangements in the high mobility group protein gene, HMGI-C, in benign mesenchymal tumours. *Nat Genet* 10: 436-444
- Sco Y, Baba H, Fukuda T, Takashima M, Sugimachi K (2000) High expression of vascular endothelial growth factor is associated with liver metastasis and a poor prognosis for patients with ductal pancreatic adenocarcinoma. *Cancer* 88: 2239-2245
- Tallini G, Dal Cin P (1999) HMGI(Y) and HMGI-C dysregulation: a common occurrence in human tumors. *Adv Anat Pathol* 6: 237-246
- Tessari G, Ferrara C, Poletti A, Giacon C, Mcggiato T, Martines D, Del Favero G, Naccarato R (1999) The expression of proto-oncogene c-jun in human pancreatic cancer. *Anticancer Res* 19: 863-867
- Thanos D, Maniatis T (1992) The high mobility group protein HMGI(Y) is required for NF- κ B dependent virus induction of the human IFN- β gene. *Cell* 71: 777-789
- Vallone D, Battista S, Pierantoni GM, Fedele M, Casalino L, Santoro M, Viglietto G, Fusco A, Verde P (1997) Neoplastic transformation of rat thyroid cells requires the junB and fra-1 gene induction which is dependent on the HMGI-C gene product. *EMBO J* 16: 5310-5321
- Zhou X, Benson KF, Ashar HR, Chada K (1995) Mutation responsible for the mouse pygmy phenotype in the developmentally regulated factor HMGI-C. *Nature* 376: 771-774

MOLECULAR BIOLOGY OF THE CELL

THIRD EDITION

**Bruce Alberts • Dennis Bray
Julian Lewis • Martin Raff • Keith Roberts
James D. Watson**



**Garland Publishing, Inc.
New York & London**

GARLAND STAFF

Text Editor: Miranda Robertson
Managing Editor: Ruth Adams
Illustrator: Nigel Orme
Molecular Model Drawings: Kate Hesketh-Moore
Director of Electronic Publishing: John M-Roblin
Computer Specialist: Chuck Bartelt
Disk Preparation: Carol Winter
Copy Editor: Shirley M. Cobert
Production Editor: Douglas Goertzen
Production Coordinator: Perry Bessas
Indexer: Maija Hinkle

Bruce Alberts received his Ph.D. from Harvard University and is currently President of the National Academy of Sciences and Professor of Biochemistry and Biophysics at the University of California, San Francisco. *Dennis Bray* received his Ph.D. from the Massachusetts Institute of Technology and is currently a Medical Research Council Fellow in the Department of Zoology, University of Cambridge. *Julian Lewis* received his D.Phil. from the University of Oxford and is currently a Senior Scientist in the Imperial Cancer Research Fund Developmental Biology Unit, University of Oxford. *Martin Raff* received his M.D. from McGill University and is currently a Professor in the MRC Laboratory for Molecular Cell Biology and the Biology Department, University College, London. *Keith Roberts* received his Ph.D. from the University of Cambridge and is currently Head of the Department of Cell Biology, the John Innes Institute, Norwich. *James D. Watson* received his Ph.D. from Indiana University and is currently Director of the Cold Spring Harbor Laboratory. He is the author of *Molecular Biology of the Gene* and, with Francis Crick and Maurice Wilkins, won the Nobel Prize in Medicine and Physiology in 1962.

© 1983, 1989, 1994 by Bruce Alberts, Dennis Bray, Julian Lewis, Martin Raff, Keith Roberts, and James D. Watson.

All rights reserved. No part of this book covered by the copyright hereon may be reproduced or used in any form or by any means—graphic, electronic, or mechanical, including photocopying, recording, taping, or information storage and retrieval systems—without permission of the publisher.

Library of Congress Cataloging-in-Publication Data

Molecular biology of the cell / Bruce Alberts . . . [et al.].—3rd ed.
p. cm.

Includes bibliographical references and index.

ISBN 0-8153-1619-4 (hard cover).—ISBN 0-8153-1620-8 (pbk.)

1. Cytology. 2. Molecular biology. I. Alberts, Bruce.

[DNLM: 1. Cells. 2. Molecular Biology. QH 581.2 M718 1994]

QH581.2.M64 1994

574.87—dc20

DNLM/DLC

for Library of Congress

93-45907
CIP

Published by Garland Publishing, Inc.
717 Fifth Avenue, New York, NY 10022

Printed in the United States of America

15 14 13 12 10 9 8 7 6 5 4 3 2 1

Front cover: The photograph shows a rat nerve cell in culture. It is labeled with a fluorescent antibody that stains its cell body and dendritic processes (yellow). Nerve terminals (green) from other neurons (not visible), which have made synapses on the cell, are labeled with a different antibody. (Courtesy of Olaf Mundigl and Pietro de Camilli.)

Dedication page: Gavin Borden, late president of Garland Publishing, weathered in during his mid-1980s climb near Mount McKinley with MBoC author Bruce Alberts and famous mountaineer guide Mugs Stump (1940–1992).

Back cover: The authors, in alphabetical order, crossing Abbey Road in London on their way to lunch. Much of this third edition was written in a house just around the corner. (Photograph by Richard Olivier.)

extracts. If these minor cell proteins differ among cells to the same extent as the more abundant proteins, as is commonly assumed, only a small number of protein differences (perhaps several hundred) suffice to create very large differences in cell morphology and behavior.

A Cell Can Change the Expression of Its Genes in Response to External Signals³

Most of the specialized cells in a multicellular organism are capable of altering their patterns of gene expression in response to extracellular cues. If a liver cell is exposed to a glucocorticoid hormone, for example, the production of several specific proteins is dramatically increased. Glucocorticoids are released during periods of starvation or intense exercise and signal the liver to increase the production of glucose from amino acids and other small molecules; the set of proteins whose production is induced includes enzymes such as tyrosine aminotransferase, which helps to convert tyrosine to glucose. When the hormone is no longer present, the production of these proteins drops to its normal level.

Other cell types respond to glucocorticoids in different ways. In fat cells, for example, the production of tyrosine aminotransferase is reduced, while some other cell types do not respond to glucocorticoids at all. These examples illustrate a general feature of cell specialization—different cell types often respond in different ways to the same extracellular signal. Underlying this specialization are features that do not change, which give each cell type its permanently distinctive character. These features reflect the persistent expression of different sets of genes.

Gene Expression Can Be Regulated at Many of the Steps in the Pathway from DNA to RNA to Protein⁴

If differences between the various cell types of an organism depend on the particular genes that the cells express, at what level is the control of gene expression exercised? There are many steps in the pathway leading from DNA to protein, and all of them can in principle be regulated. Thus a cell can control the proteins it makes by (1) controlling when and how often a given gene is transcribed (**transcriptional control**), (2) controlling how the primary RNA transcript is spliced or otherwise processed (**RNA processing control**), (3) selecting which completed mRNAs in the cell nucleus are exported to the cytoplasm (**RNA transport control**), (4) selecting which mRNAs in the cytoplasm are translated by ribosomes (**translational control**), (5) selectively destabilizing certain mRNA molecules in the cytoplasm (**mRNA degradation control**), or (6) selectively activating, inactivating, or compartmentalizing specific protein molecules after they have been made (**protein activity control**) (Figure 9-2).

For most genes transcriptional controls are paramount. This makes sense because, of all the possible control points illustrated in Figure 9-2, only transcriptional control ensures that no superfluous intermediates are synthesized. In the

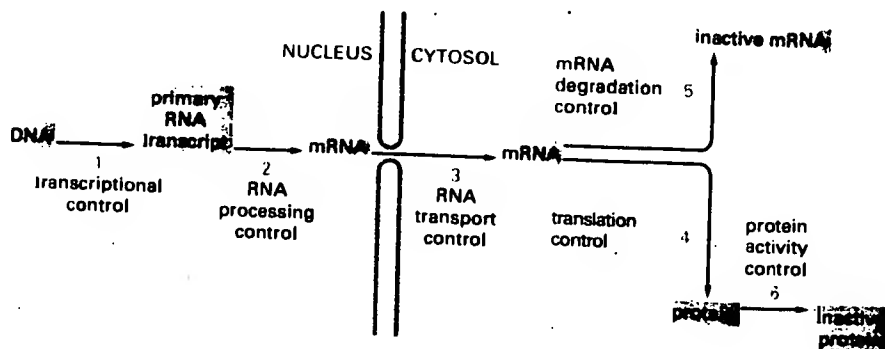


Figure 9-2 Six steps at which eucaryote gene expression can be controlled. Only controls that operate at steps 1 through 5 are discussed in this chapter. The regulation of protein activity (step 6) is discussed in Chapter 5; this includes reversible activation or inactivation by protein phosphorylation as well as irreversible inactivation by proteolytic degradation.

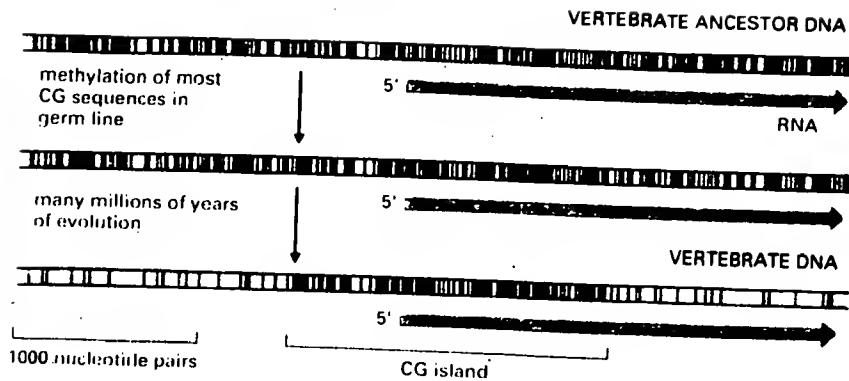


Figure 9-71 A mechanism to explain both the marked deficiency of CG sequences and the presence of CG islands in vertebrate genomes. A black line marks the location of an unmethylated CG dinucleotide in the DNA sequence, while a red line marks the location of a methylated CG dinucleotide.

Summary

The many types of cells in animals and plants are created largely through mechanisms that cause different genes to be transcribed in different cells. Since many specialized animal cells can maintain their unique character when grown in culture, the gene regulatory mechanisms involved in creating them must be stable once established and heritable when the cell divides, endowing the cell with a memory of its developmental history. Prokaryotes and yeasts provide unusually accessible model systems in which to study gene regulatory mechanisms, some of which may be relevant to the creation of specialized cell types in higher eucaryotes. One such mechanism involves a competitive interaction between two (or more) gene regulatory proteins, each of which inhibits the synthesis of the other; this can create a flip-flop switch that switches a cell between two alternative patterns of gene expression. Direct or indirect positive feedback loops, which enable gene regulatory proteins to perpetuate their own syntheses, provide a general mechanism for cell memory.

In eucaryotes gene transcription is generally controlled by combinations of gene regulatory proteins. It is thought that each type of cell in a higher eucaryotic organism contains a specific combination of gene regulatory proteins that ensures the expression of only those genes appropriate to that type of cell. A given gene regulatory protein may be expressed in a variety of circumstances and typically is involved in the regulation of many genes.

In addition to diffusible gene regulatory proteins, inherited states of chromatin condensation are also utilized by eucaryotic cells to regulate gene expression. In vertebrates DNA methylation also plays a part, mainly as a device to reinforce decisions about gene expression that are made initially by other mechanisms.

Posttranscriptional Controls

Although controls on the initiation of gene transcription are the predominant form of regulation for most genes, other controls can act later in the pathway from RNA to protein to modulate the amount of gene product that is made. Although these **posttranscriptional controls**, which operate after RNA polymerase has bound to the gene's promoter and begun RNA synthesis, are less common than *transcriptional control*, for many genes they are crucial. It seems that every step in gene expression that could be controlled in principle is likely to be regulated under some circumstances for some genes.

We consider the varieties of posttranscriptional regulation in temporal order, according to the sequence of events that might be experienced by an RNA molecule after its transcription has begun (Figure 9-72).

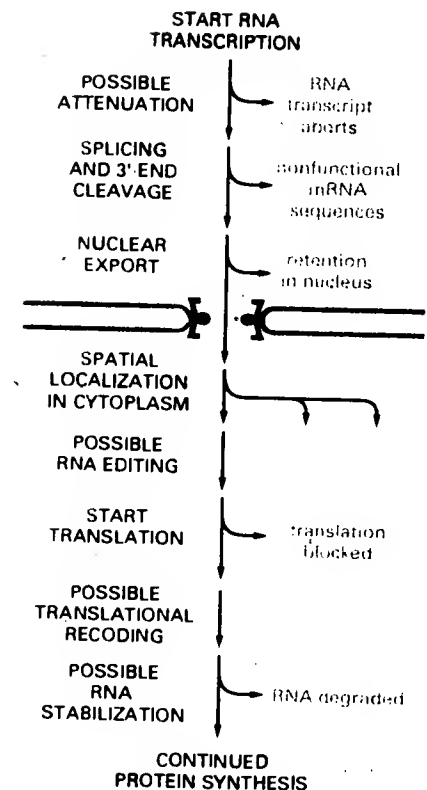


Figure 9-72 Possible post-transcriptional controls on gene expression. Only a few of these controls are likely to be used for any one gene.

MOLECULAR BIOLOGY OF
THE CELL

fourth edition

Bruce Alberts

Alexander Johnson

Julian Lewis

Martin Raff

Keith Roberts

Peter Walter

 **Garland Science**
Taylor & Francis Group

Garland

Vice President: Denise Schanck
Managing Editor: Sarah Gibbs
Senior Editorial Assistant: Kirsten Jenner
Managing Production Editor: Emma Hunt
Proofreader and Layout: Emma Hunt
Production Assistant: Angela Bennett
Text Editors: Marjorie Singer Anderson and Betsy Dilemnia
Copy Editor: Bruce Goatly
Word Processors: Fran Dependahl, Misty Landers and Carol Winter
Designer: Blink Studio, London
Illustrator: Nigel Orme
Indexer: Janine Ross and Sherry Granum
Manufacturing: Nigel Eyre and Marion Morrow

Cell Biology Interactive

Artistic and Scientific Direction: Peter Waller
Narrated by: Julie Theriot
Production, Design, and Development: Mike Morales

Bruce Alberts received his Ph.D. from Harvard University and is President of the National Academy of Sciences and Professor of Biochemistry and Biophysics at the University of California, San Francisco. **Alexander Johnson** received his Ph.D. from Harvard University and is a Professor of Microbiology and Immunology at the University of California, San Francisco. **Julian Lewis** received his D.Phil. from the University of Oxford and is a Principal Scientist at the Imperial Cancer Research Fund, London. **Martin Raff** received his M.D. from McGill University and is at the Medical Research Council Laboratory for Molecular Cell Biology and Cell Biology Unit and in the Biology Department at University College London. **Keith Roberts** received his Ph.D. from the University of Cambridge and is Associate Research Director at the John Innes Centre, Norwich. **Peter Walter** received his Ph.D. from The Rockefeller University in New York and is Professor and Chairman of the Department of Biochemistry and Biophysics at the University of California, San Francisco, and an Investigator of the Howard Hughes Medical Institute.

© 2002 by Bruce Alberts, Alexander Johnson, Julian Lewis, Martin Raff, Keith Roberts, and Peter Walter.

© 1983, 1989, 1994 by Bruce Alberts, Dennis Bray, Julian Lewis, Martin Raff, Keith Roberts, and James D. Watson.

All rights reserved. No part of this book covered by the copyright hereon may be reproduced or used in any format in any form or by any means—graphic, electronic, or mechanical, including photocopying, recording, taping, or information storage and retrieval systems—without permission of the publisher.

Library of Congress Cataloging-in-Publication Data

Molecular biology of the cell / Bruce Alberts ... [et al.]. -- 4th ed.
p. cm
Includes bibliographical references and index.
ISBN 0-8153-3218-1 (hardbound) -- ISBN 0-8153-4072-9 (pbk.)
1. Cytology. 2. Molecular biology. I. Alberts, Bruce.
IDNLM: 1. Cells. 2. Molecular Biology. I
QH581.2 .M64 2002
571.6--dc21

2001054471 CIP

Published by Garland Science, a member of the Taylor & Francis Group,
29 West 35th Street, New York, NY 10001-2299

Printed in the United States of America

15 14 13 12 11 10 9 8 7 6 5 4 3 2 1

Front cover Human Genome: Reprinted by permission from *Nature*, International Human Genome Sequencing Consortium, 409:860-921, 2001 © Macmillan Magazines Ltd. Adapted from an image by Francis Collins, NHGRI; Jim Kent, UCSC; Ewan Birney, EBI; and Darryl Leja, NHGRI; showing a portion of Chromosome 1 from the initial sequencing of the human genome.

Back cover In 1967, the British artist Peter Blake created a design classic. Nearly 35 years later Nigel Orme (illustrator), Richard Denyer (photographer), and the authors have together produced an affectionate tribute to Mr Blake's image. With its gallery of icons and influences, its assembly created almost as much complexity, intrigue and mystery as the original. *Drosophila*, *Arabidopsis*, Dolly and the assembled company tempt you to dip inside where, as in the original, "a splendid time is guaranteed for all." (Gunter Blobel, courtesy of The Rockefeller University; Marie Curie, Keystone Press Agency Inc; Darwin bust, by permission of the President and Council of the Royal Society; Rosalind Franklin, courtesy of Cold Spring Harbor Laboratory Archives; Dorothy Hodgkin, © The Nobel Foundation, 1964; James Joyce, etching by Peter Blake; Robert Johnson, photo booth self-portrait early 1930s, © 1986 Delta Haze Corporation all rights reserved, used by permission; Albert L. Lehninger, unidentified photographer) courtesy of The Alan Mason Chesney Medical Archives of The Johns Hopkins Medical Institutions; Linus Pauling, from Ava Helen and Linus Pauling Papers, Special Collections, Oregon State University; Nicholas Poussin, courtesy of ArtToday.com; Barbara McClintock, © David Micklos, 1983; Andrei Sakharov, courtesy of Elena Bonner; Frederick Sanger, © The Nobel Foundation, 1958.)

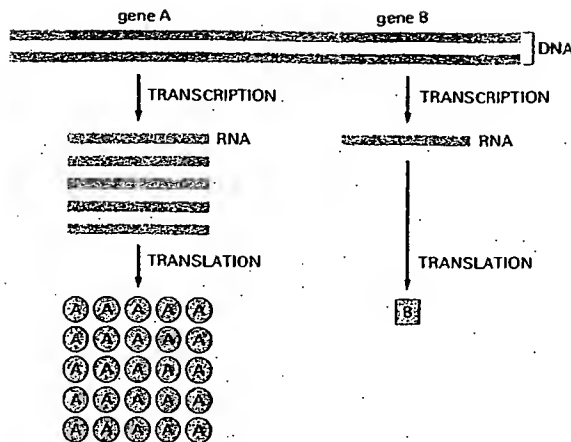


Figure 6-3 Genes can be expressed with different efficiencies. Gene A is transcribed and translated much more efficiently than gene B. This allows the amount of protein A in the cell to be much greater than that of protein B.

FROM DNA TO RNA

Transcription and translation are the means by which cells read out, or express, the genetic instructions in their genes. Because many identical RNA copies can be made from the same gene, and each RNA molecule can direct the synthesis of many identical protein molecules, cells can synthesize a large amount of protein rapidly when necessary. But each gene can also be transcribed and translated with a different efficiency, allowing the cell to make vast quantities of some proteins and tiny quantities of others (Figure 6-3). Moreover, as we see in the next chapter, a cell can change (or regulate) the expression of each of its genes according to the needs of the moment—most obviously by controlling the production of its RNA.

Portions of DNA Sequence Are Transcribed into RNA

The first step a cell takes in reading out a needed part of its genetic instructions is to copy a particular portion of its DNA nucleotide sequence—a gene—into an RNA nucleotide sequence. The information in RNA, although copied into another chemical form, is still written in essentially the same language as it is in DNA—the language of a nucleotide sequence. Hence the name **transcription**.

Like DNA, RNA is a linear polymer made of four different types of nucleotide subunits linked together by phosphodiester bonds (Figure 6-4). It differs from DNA chemically in two respects: (1) the nucleotides in RNA are *ribonucleotides*—that is, they contain the sugar ribose (hence the name *ribonucleic acid*) rather than deoxyribose; (2) although, like DNA, RNA contains the bases adenine (A), guanine (G), and cytosine (C), it contains the base uracil (U) instead of the thymine (T) in DNA. Since U, like T, can base-pair by hydrogen-bonding with A (Figure 6-5), the complementary base-pairing properties described for DNA in Chapters 4 and 5 apply also to RNA (in RNA, G pairs with C, and A pairs with U). It is not uncommon, however, to find other types of base pairs in RNA: for example, G pairing with U occasionally.

Despite these small chemical differences, DNA and RNA differ quite dramatically in overall structure. Whereas DNA always occurs in cells as a double-stranded helix, RNA is single-stranded. RNA chains therefore fold up into a variety of shapes, just as a polypeptide chain folds up to form the final shape of a protein (Figure 6-6). As we see later in this chapter, the ability to fold into complex three-dimensional shapes allows some RNA molecules to have structural and catalytic functions.

Transcription Produces RNA Complementary to One Strand of DNA

All of the RNA in a cell is made by DNA transcription, a process that has certain similarities to the process of DNA replication discussed in Chapter 5.

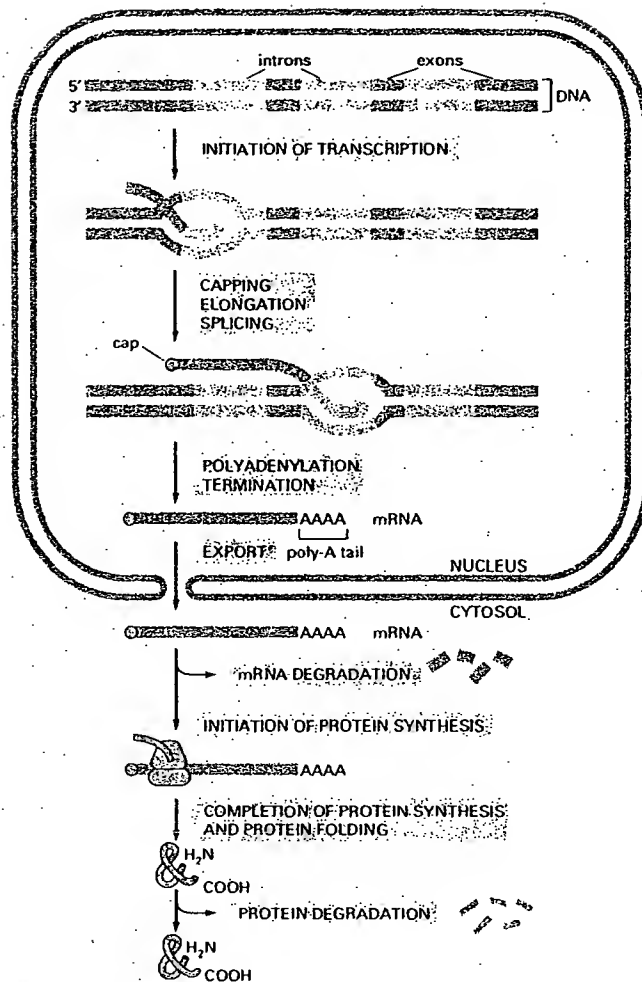


Figure 6-90 The production of a protein by a eucaryotic cell. The final level of each protein in a eucaryotic cell depends upon the efficiency of each step depicted.

ure 6-90) could be regulated by the cell for each individual protein. However, as we shall see in Chapter 7, the initiation of transcription is the most common point for a cell to regulate the expression of each of its genes. This makes sense, inasmuch as the most efficient way to keep a gene from being expressed is to block the very first step—the transcription of its DNA sequence into an RNA molecule.

Summary

The translation of the nucleotide sequence of an mRNA molecule into protein takes place in the cytoplasm on a large ribonucleoprotein assembly called a ribosome. The amino acids used for protein synthesis are first attached to a family of tRNA molecules, each of which recognizes, by complementary base-pair interactions, particular sets of three nucleotides in the mRNA (codons). The sequence of nucleotides in the mRNA is then read from one end to the other in sets of three according to the genetic code.

To initiate translation, a small ribosomal subunit binds to the mRNA molecule at a start codon (AUG) that is recognized by a unique initiator tRNA molecule. A large ribosomal subunit binds to complete the ribosome and begin the elongation phase of protein synthesis. During this phase, aminoacyl tRNAs—each bearing a specific amino acid bind sequentially to the appropriate codon in mRNA by forming complementary base pairs with the tRNA anticodon. Each amino acid is added to the C-terminal end of the growing polypeptide by means of a cycle of three sequential

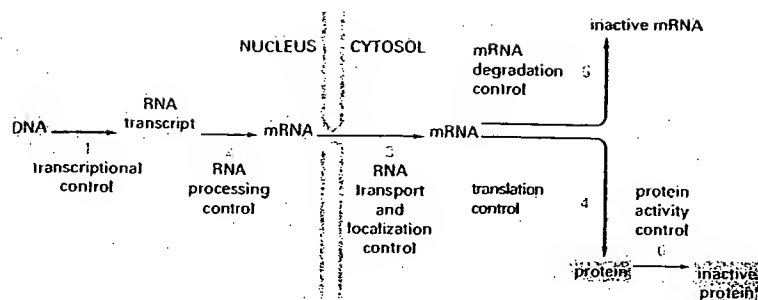


Figure 7-5 Six steps at which eucaryotic gene expression can be controlled. Controls that operate at steps 1 through 5 are discussed in this chapter. Step 6, the regulation of protein activity, includes reversible activation or inactivation by protein phosphorylation (discussed in Chapter 3) as well as irreversible inactivation by proteolytic degradation (discussed in Chapter 6).

Gene Expression Can Be Regulated at Many of the Steps in the Pathway from DNA to RNA to Protein

If differences among the various cell types of an organism depend on the particular genes that the cells express, at what level is the control of gene expression exercised? As we saw in the last chapter, there are many steps in the pathway leading from DNA to protein, and all of them can in principle be regulated. Thus a cell can control the proteins it makes by (1) controlling when and how often a given gene is transcribed (**transcriptional control**), (2) controlling how the RNA transcript is spliced or otherwise processed (**RNA processing control**), (3) selecting which completed mRNAs in the cell nucleus are exported to the cytosol and determining where in the cytosol they are localized (**RNA transport and localization control**), (4) selecting which mRNAs in the cytoplasm are translated by ribosomes (**translational control**), (5) selectively destabilizing certain mRNA molecules in the cytoplasm (**mRNA degradation control**), or (6) selectively activating, inactivating, degrading, or compartmentalizing specific protein molecules after they have been made (**protein activity control**) (Figure 7-5).

For most genes transcriptional controls are paramount. This makes sense because, of all the possible control points illustrated in Figure 7-5, only transcriptional control ensures that the cell will not synthesize superfluous intermediates. In the following sections we discuss the DNA and protein components that perform this function by regulating the initiation of gene transcription. We shall return at the end of the chapter to the additional ways of regulating gene expression.

Summary

The genome of a cell contains in its DNA sequence the information to make many thousands of different protein and RNA molecules. A cell typically expresses only a fraction of its genes, and the different types of cells in multicellular organisms arise because different sets of genes are expressed. Moreover, cells can change the pattern of genes they express in response to changes in their environment, such as signals from other cells. Although all of the steps involved in expressing a gene can in principle be regulated, for most genes the initiation of RNA transcription is the most important point of control.

How does a cell determine which of its thousands of genes to transcribe? As mentioned briefly in Chapters 4 and 6, the transcription of each gene is controlled by a regulatory region of DNA relatively near the site where transcription begins. Some regulatory regions are simple and act as switches that are thrown by a single signal. Many others are complex and act as tiny microprocessors, responding to a variety of signals that they interpret and integrate to switch the neighboring gene on or off. Whether complex or simple, these switching devices

Selective apoptosis of natural killer-cell tumours by L-asparaginase

Miki Ando,¹ Koichi Sugimoto,¹
Toshiyuki Kitoh,² Makoto Sasaki,¹
Kouichi Mukai,³ Jun Ando,¹ Motoki
Egashira,¹ Sheldon M. Schuster⁴ and
Kazuo Oshimi¹

¹Department of Haematology, Juntendo
University School of Medicine, Tokyo,

²Department of Paediatrics and Laboratory
Medicine, Shiga Medical Centre for Children;

Moriyama, ³Department of Pathology, Shiga
Medical Centre for Adults, Moriyama, Japan; and

⁴Keck Graduate Institute, Claremont, CA, USA

Summary

We examined the effectiveness of various anti-tumour agents to natural killer (NK)-cell tumour cell lines and samples, which are generally resistant to chemotherapy, using flow cytometric terminal deoxynucleotidyl transferase-mediated dUTP-biotin nick end-labelling (TUNEL) assay. Although NK-YS and NK-92 were highly resistant to various anti-tumour agents, L-asparaginase induced apoptosis in these two NK-cell lines. NK-cell leukaemia/lymphoma and acute lymphoblastic leukaemia (ALL) samples were selectively sensitive to L-asparaginase and to doxorubicin (DXR) respectively. Samples of chronic NK lymphocytosis, an NK-cell disorder with an indolent clinical course, were resistant to both drugs. Our study clearly separated two major categories of NK-cell disorders and ALL according to the sensitivity to DXR and L-asparaginase. We examined asparagine synthetase levels by real-time quantitative polymerase chain reaction (RQ-PCR) and immunostaining in these samples. At least in nasal-type NK-cell lymphoma, there was a good correlation among asparagine synthetase expression, *in vitro* sensitivity and clinical response to L-asparaginase. In aggressive NK-cell leukaemia, although asparagine synthetase expression was high at both mRNA and protein levels, L-asparaginase induced considerable apoptosis. Furthermore, samples of each disease entity occupied a distinct area in two-dimensional plotting with asparagine synthetase mRNA level (RQ-PCR) and *in vitro* L-asparaginase sensitivity (TUNEL assay). We confirmed rather specific anti-tumour activity of L-asparaginase against NK-cell tumours *in vitro*, which provides an experimental background to the clinical use of L-asparaginase for NK-cell tumours.

Keywords: natural killer cell tumour, L-asparaginase, chronic NK lymphocytosis, apoptosis, asparagine synthetase.

Received 7 March 2005; accepted for publication
27 June 2005

Correspondence: Koichi Sugimoto, MD,
Department of Haematology, Juntendo
University School of Medicine, 2-1-1 Hongo,
Bunkyo-ku, Tokyo 113-8421, Japan.
E-mail ksugimoto@med.juntendo.ac.jp

Natural killer (NK) cells are characterised by large granular lymphocyte morphology with CD3⁺ CD56⁺ phenotype, non-major histocompatibility complex-restricted cytotoxicity, and germ-line configuration of T-cell receptor genes (Hercend & Schmidt, 1988; Trinchieri, 1989; Robertson & Ritz, 1990). NK-cell disorders consist of two main categories: chronic NK lymphocytosis and NK-cell leukaemia/lymphoma. Chronic NK lymphocytosis is a rather benign disorder with persistent excess of mature NK cells (CD3⁺ CD16/CD56⁺) in the peripheral blood (Tefferi *et al*, 1994). In contrast, NK-cell leukaemia/lymphoma is a group of aggressive disorders, consisting of aggressive NK-cell leukaemia, nasal-type NK-cell lymphoma and blastic NK-cell lymphoma (Jaffe *et al*, 2001). Aggressive

NK-cell leukaemia takes a highly aggressive clinical course accompanied with fever and hepatosplenomegaly (Imamura *et al*, 1990; Chan *et al*, 1997; Kwong *et al*, 1997; Siu *et al*, 2002; Oshimi, 2003). Nasal-type NK-cell lymphoma occurs mainly in the nasal cavity with extensive necrosis and angioinvasion, and rapidly disseminates to various sites. Blastic NK-cell lymphoma, which may originate from the precursors of plasmacytoid dendritic cells, tends to involve multiple sites, including the skin (Chaperot *et al*, 2001; Feuillard *et al*, 2002). Poor outcome of these NK-cell leukaemia/lymphomas has been attributed not only to their rapid progression but also to the refractoriness to standard combination chemotherapy (Kwong *et al*, 1997). High expression of P-glycoprotein

Apoptosis of NK-cell Tumours by L-Asparaginase

(P-gp), which extrudes various cytotoxic agents, may contribute to their refractoriness to various anti-cancer agents (Yamamoto *et al*, 1993; Yamaguchi *et al*, 1995; Egashira *et al*, 1999). Some reports have recently shown that L-asparaginase, a commonly used agent for childhood acute lymphoblastic leukaemia (ALL), is effective against refractory and relapsed cases of NK-cell lymphoma (Matsumoto *et al*, 2003; Yong *et al*, 2003). As the agent depletes asparagine by its hydrolysis, tumour cells that depend on exogenous asparagine are sensitive to this agent (Clarkson *et al*, 1970; Ertel *et al*, 1979). Treatment with L-asparaginase induces apoptotic morphology in canine malignant lymphoma cells (Story *et al*, 1993). Flow cytometric terminal deoxynucleotidyl transferase-mediated dUTP-biotin nick end-labelling (TUNEL) assay confirmed that L-asparaginase induced G1 arrest and apoptosis in murine leukaemia cells (Ueno *et al*, 1997). In the present study, we applied the TUNEL assay to two NK-cell lines, NK-YS (Tsuchiyama *et al*, 1998) and NK-92 (Gong *et al*, 1994) derived from nasal-type NK-cell lymphoma and aggressive NK-cell leukaemia. Among various anti-tumour drugs, only L-asparaginase induced considerable amount of apoptosis in these NK-cell lines. Furthermore, considerable portion of NK-cell tumour samples was sensitive to *in vitro* treatment with L-asparaginase.

Materials and methods

Cell lines

Jurkat, K562, NK-92 and NK-YS cell lines were used. Jurkat and K562 were grown in Roswell Park Memorial Institute 1640 medium supplemented with 10% fetal calf serum (FCS), 100 U/ml penicillin and 100 µg/ml streptomycin. NK-92 and NK-YS, kindly provided by Dr Jiang-Hong Gong (University of British Columbia, Vancouver, Canada) and Dr Junjiro Tsuchiyama (Okayama University Medical School, Japan), respectively, were grown in Iscove's modified Dulbecco's medium supplemented with 10% FCS, 100 U/ml of interleukin-2 (Takeda, Osaka, Japan), 100 U/ml penicillin and 100 µg/ml streptomycin. The cells were split to keep the cell density at 2×10^5 to 1×10^6 cells/ml.

Patients and tumour samples

Eighteen patients with NK-cell disorders were entered into the study. Informed consent was obtained in all cases. T-cell receptor genes of all cases were all in germline configuration. Ten patients had chronic NK lymphocytosis, four nasal-type NK-cell lymphoma, two aggressive NK-cell leukaemia and two blastic NK-cell lymphoma. The percentages of CD56 or CD16 positive cells were more than 85% in eight patients, 60–85% in six, 50–60% in three and 30% in one. We also used ALL cells from six patients: two patients with T-ALL and four with B-ALL. Karyotypes of ALL samples were normal except for one which was t(9;22)(q34;q11).

Anti-cancer agents and drug treatment

We used doxorubicin (DXR), daunorubicin (DNR), vincristine (VCR), methotrexate (MTX), cytosine β-D-arabino-furanose (Ara-C) (all reagents were purchased from Sigma, St Louis, MO, USA), and L-asparaginase (Kyowa Hakkou, Tokyo, Japan). Logarithmically growing cells were treated for the indicated times with these drugs.

Cell fixation

Cells treated with the indicated conditions were harvested by centrifugation for 8 min at 4°C at 400 g, washed once with phosphate-buffered saline (PBS), and then fixed in 1% formaldehyde in PBS (pH 7.4) for 15 min on ice. After washing in PBS, cells were resuspended in 70% cold (–20°C) ethanol and immediately transferred to the freezer. The cells were stored at –20°C for 1 day before being subjected to the TUNEL assay.

Flow cytometric TUNEL assay

Cells were washed twice in PBS, resuspended in 50 µl of a cacodylate buffer containing 0.2 mol/l potassium cacodylate, 25 mmol/l Tris-HCl (pH 6.6), 2.5 mmol/l CoCl₂, 0.25 mg/ml bovine serum albumin, 5 U of terminal deoxynucleotidyl transferase (TdT) and 0.5 nmol of biotin-dUTP (all reagents were purchased from Boehringer Mannheim, Indianapolis, IN, USA). The cells were incubated in this solution at 37°C for 30 min, rinsed in PBS, resuspended in 100 µl of a solution containing 4 µl concentrated saline-sodium citrate buffer, 2.5 µg/ml fluoresceinated avidin (Boehringer Mannheim), 0.1% Triton X-100, and 5% (w/v) non-fat dry milk, and incubated in this solution for 30 min at room temperature in the dark. After incubation in the solution, the cells were rinsed in PBS containing 0.1% Triton X-100 and resuspended in 1 ml of PBS containing 5 µg/ml of propidium iodide (PI) and 200 µg/ml of RNase A (both from Sigma). This procedure essentially followed that of previous reports (Sugimoto *et al*, 1998, 2002).

Flow cytometry was performed on a CYTROM ABSOLUTE flow cytometer (Ortho, Raritan, NJ, USA). The PI signal of orange fluorescence and TUNEL-signal of green fluorescence of each cell were measured using linear and logarithmic amplifications of the standard optics of the CYTROM ABSOLUTE. Even without anti-tumour drug treatment, NK-cell samples often underwent apoptosis spontaneously in *in vitro* culture conditions. We thus evaluated the anti-tumour effect on NK-cell tumour and ALL samples using the corrected apoptotic cell percentage, which we defined as [drug-induced apoptosis (%) – spontaneous apoptosis (%)]/[100 – spontaneous apoptosis (%)].

Immunostaining

A monoclonal antibody 3G6 against asparagine synthetase was prepared by a standard hybridoma cell formation method

M. Ando *et al*

(Sheng *et al.* 1992; Hutson *et al.* 1997). As previously described, specimens of cell lines prepared using Cytospin 3 (Shandon, Pittsburgh, PA, USA) and bone marrow smears were fixed with a methanol and acetone mixture (1:1) for 90 s at 4°C using the EX-IHC automated immunohistochemistry system (Ventana Medical Systems, Tucson, AZ, USA). In lymphoma cases, formalin-fixed, paraffin-embedded tissue specimens were prepared. The slides were inhibited with H₂O₂, incubated with the primary monoclonal antibody against asparagine synthetase for 16 min at 37°C, and detected by the diaminobenzidine (DAB) Detection Kit (Ventana Medical Systems) (Itrino *et al.* 2004). The intensity of the asparagine synthetase signal was determined by inspection in comparison with the controls.

Real-time quantitative polymerase chain reaction assay of asparagine synthetase mRNA

Total RNA was isolated using RNA STAT-60 (Tel-Test, Inc.). First strand cDNA was synthesised from 1 µg of RNA using Super Script II (Gibco BRL, Carlsbad, CA, USA). Real-time quantitative polymerase chain reaction (RQ-PCR) was performed with the LightCycler FastStart DNA Master SYBR Green I kit, containing the SYBR Green I dye (Roche Molecular Biochemicals, Mannheim, Germany). For each sample, reactions were set up in capillaries with the following reaction mix: 2 µl of DNA template; 0.5 µl each of 10 µmol/l sense and antisense primers; 2.4 µl of 25 mmol/l MgCl₂; 2 µl of LightCycler-DNA Master SYBR Green I reaction mix; and 12.6 µl sterile water. The amplification conditions were 10 min at 95°C, followed by 40 cycles of denaturation at 95°C for 10 s, annealing at 60°C for 10 s and extension at 72°C for 6 s. All primers were purchased from TAKARA BIO Inc (Otsu, Japan). Primers for the amplification of asparagine synthetase cDNA were sense, 5'-CGGTAGTTGACCCGCTGTTG-3', and anti-sense, 5'-CACCATCCACTTIGGTCTGGTATTC-3'. The calculated number of transcripts of asparagine synthetase was normalised to the housekeeping gene glyceraldehydes-3-phosphate dehydrogenase (GAPDH).

Results

We examined apoptotic cell percentages of Jurkat and two NK-cell lines after treatment with various anti-cancer agents including VCR, MTX, Ara-C, DNR, DXR and L-asparaginase using flow cytometric TUNEL assay (Sugimoto *et al.* 1998, 2002). At first, we determined the treatment conditions (drug concentration and treatment duration), which caused 30–70% of apoptosis in Jurkat cells. NK-YS and NK-92 cells were extremely resistant to these drugs, and at most 10% of them were apoptotic. On the contrary, 84% of NK-YS and 67% of NK-92 cells underwent apoptosis after 48 h of incubation with 0.01 IU/ml of L-asparaginase, although the same treatment induced apoptosis only in 19% of Jurkat cells. Even at different concentrations and treatment durations, L-asparaginase in-

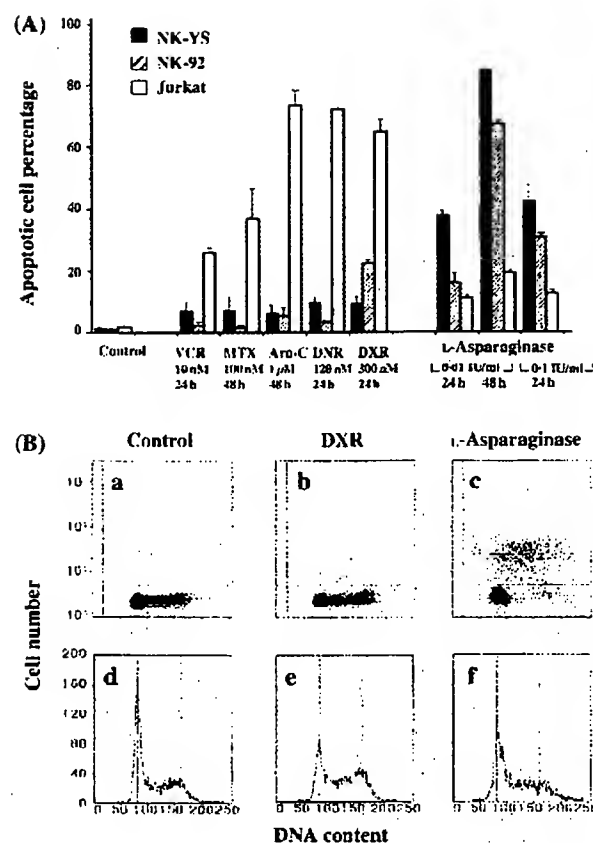


Fig 1. Apoptosis of NK-YS, NK-92 and Jurkat cells treated with various anti-tumour agents including L-asparaginase. (A) Apoptotic cell percentages of NK-YS, NK-92 and Jurkat cells treated with various anti-tumour agents were determined by flow cytometric TUNEL assay. Treatment conditions were as follows: 10 nmol/l of vincristine (VCR) for 24 h, 100 nmol/l of methotrexate (MTX) for 48 h, 1 µmol/l of cytosine β-D-arabino-furanose (Ara-C) for 48 h, 120 nmol/l of daunorubicin (DNR) for 24 h, 300 nmol/l of doxorubicin (DXR) for 24 h, 0.01 IU/ml of L-asparaginase for 24 and 48 h, and 0.1 IU/ml of L-asparaginase for 24 h. TUNEL assay was performed in triplicate for all cell lines. The arithmetic means and standard deviations were calculated with three values. NK-YS and NK-92 cells were selectively sensitive to L-asparaginase. (B) Cell cycle positions of apoptotic and non-apoptotic NK-YS cells determined by flow cytometric TUNEL assay. Untreated (a, d), treated with 300 nmol/l of doxorubicin for 24 h (b, e) and 0.01 IU/ml of L-asparaginase for 48 h (c, f). Most NK-YS cells at non-G1 cell cycle positions were apoptotic.

duced apoptosis rather specifically in those NK-cell lines (Fig 1A). Essentially the same results were obtained in four independent experiments. Among various anti-tumour agents tested here, only L-asparaginase was more effective to the two NK-cell lines than to Jurkat cells. As MTX and Ara-C, whose effects are known to be independent of P-gp status (Pastan & Gottesman, 1994), had little effect on these two NK-cell lines, high expression of P-gp cannot fully explain the refractoriness of NK-cell tumours to various anti-tumour agents. However, L-asparaginase was obviously effective to NK-cell tumour cell lines, regardless of any mechanisms of drug resistance. Figure 1B shows the results of flow cytometric TUNEL assay

Apoptosis of NK-cell Tumours by L-Asparaginase

on NK-YS cells. Treatment with 300 nmol/l of DXR for 24 h caused a small decrease in the G1 peak and small amount of apoptosis in NK-YS cells (b, c). Although treatment with L-asparaginase did not apparently change the cell cycle distribution of NK-YS (Fig 1B-c), most of the non-G1 cells underwent apoptosis (Fig 1B-f). Similar results were obtained in NK-92 cells (data not shown). We next examined the effectiveness of L-asparaginase to NK-cell tumour samples. Even without anti-tumour drug treatment, NK-cell samples often underwent apoptosis spontaneously in *in vitro* culture conditions. We thus evaluated the anti-tumour effect of L-asparaginase using the corrected apoptotic cell percentage, as indicated in the study design. Figure 2 shows the corrected apoptotic cell percentages of four nasal-type NK-cell lymphoma, two aggressive NK-cell leukaemia, two blastic NK-cell lymphoma, 10 chronic NK lymphocytosis and six ALL samples, treated with 450 nmol/l of DXR or with 10 IU/ml of L-asparaginase for 24 h. The corrected apoptotic cell percentages after DXR treatment were nearly 0% in chronic NK lymphocytosis, <10% in NK-cell tumours and about 40% in ALL. In contrast, L-asparaginase treatment caused corrected apoptotic cell percentages of 20–60% in NK-cell tumour

samples except one, and around 10% of apoptosis in chronic NK lymphocytosis and ALL samples. Therefore, our results showed that L-asparaginase was more effective than DXR not only to NK-cell lines but also to patient NK-cell tumour samples. On the contrary, ALL samples were more sensitive to DXR than to L-asparaginase. Chronic NK lymphocytosis was resistant to both agents. The characteristics, diagnosis, treatment regimen(s), survival duration of each patient are shown in Table I. According to the sensitivity to these two agents, ALL, NK-cell tumours, and chronic NK lymphocytosis could be clearly divided into three categories; i.e. DXR-sensitive, L-asparaginase-sensitive and resistant to both agents respectively (Fig 2).

As expression of asparagine synthetase is one known mechanism for resistance to L-asparaginase (Aslanian *et al*, 2001), we examined asparagine synthetase expression in the samples described above using RQ-PCR and immunostaining. Table II shows the normalised asparagine synthetase mRNA expression value (AS/GAPDH) of each sample. In nasal-type NK-cell lymphoma, asparagine synthetase mRNA levels of two samples were comparatively high (patients 1 and 2), and those of another two samples were low (patients 3 and 4). In this disease entity, asparagine synthetase mRNA levels inversely correlated with *in vitro* sensitivity to L-asparaginase. Although the sample number was relatively small, asparagine synthetase mRNA levels were high (>0.05) in two aggressive NK-cell leukaemia and two blastic NK-cell lymphoma cases. Expression of asparagine synthetase mRNA was high in almost all samples of chronic NK lymphocytosis. Then, we created a two-dimensional plot of asparagine synthetase mRNA expression and *in vitro* L-asparaginase sensitivity. Samples belonging to each disease entity occupied a distinct area in this scheme (Fig 3). In spite of comparatively low asparagine synthetase mRNA expression, ALL cells lacked sensitivity to L-asparaginase *in vitro*. All nine cases of chronic NK lymphocytosis that were resistant to L-asparaginase, had high expression levels of asparagine synthetase mRNA. On the contrary, although L-asparaginase induced considerable apoptosis in two aggressive NK-cell leukaemia and two blastic NK-cell lymphoma samples, asparagine synthetase mRNA expression of these samples was high. As for nasal-type NK-cell lymphoma, there was good correlation between the results of *in vitro* TUNEL assay and asparagine synthetase mRNA expression (Table II, Fig 3).

Figure 4 shows representative results of asparagine synthetase staining in NK-cell tumour cell lines and patient samples. Compared with the positive control (K562 cells; Fig 4A), NK-92, NK-YS (Fig 4B) and Jurkat cells were all negative for asparagine synthetase staining. As summarised in Table II, asparagine synthetase was detectable in one of four cases for nasal NK-cell lymphoma, two of two cases for aggressive NK-cell leukaemia and two of four cases of ALL. Although asparagine synthetase mRNA levels were relatively high in cases positive for asparagine synthetase immunostaining, high levels of asparagine synthetase mRNA expression did not always warrant the positive staining.

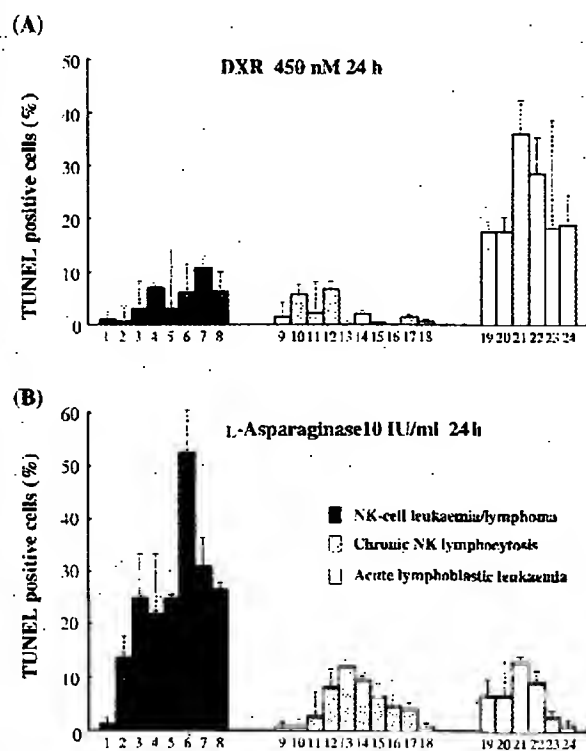


Fig 2. Selective effect of L-asparaginase to NK-cell leukaemia/lymphoma. (A) Corrected apoptotic cell percentages of NK-cell leukaemia/lymphoma, chronic NK lymphocytosis and acute lymphoblastic leukaemia (ALL) samples after the treatment with 450 nmol/l of doxorubicin for 24 h. TUNEL assay was performed in triplicate in all samples. (B) Corrected apoptotic cell percentages of the same samples as (A) after 10 IU/ml of L-asparaginase for 24 h treatment. TUNEL assay was performed in triplicate in all samples.

M. Ando *et al*

Table 1. Patient characteristics and clinical data.

Patient no.	Age (years)/sex	Diagnosis	In vitro response to		Clinical response		Survival from diagnosis	Positive cells (%)	
			L-Asp	DXR	L-Asp	Treatment		CD16	CD56
1	60/M	Nasal-type NK-cell lymphoma	R	R	NR	I(V)AM + L-asparaginase	4 months	1.2	94.6
2	66/F	Nasal-type NK-cell lymphoma	S	R	ND	CHOP	2 months	10	94
3	62/M	Nasal-type NK-cell lymphoma	S	R	CR	I(V)AM + L-asparaginase	>20 months	2.4	98.3
4	52/F	Nasal-type NK-cell lymphoma	S	R	CR	I(V)AM + L-asparaginase	>8 months	70	97.9
5	52/M	Aggressive NK-cell leukaemia	S	R	ND	PACCC, high dose MTX	6 months	4.1	29.3
6	22/M	Aggressive NK-cell leukaemia	S	R	CR	Hyper CVAD, L-asparaginase	3 months	ND	95.2
7	55/M	Blastic NK-cell lymphoma	S	R	ND	CHOP, MTX	17 months	ND	96.8
8	42/M	Blastic NK-cell lymphoma	S	R	ND	IVAM, allo-BMT	5 years	ND	56.1
9	50/M	Chronic NK lymphocytosis	R	R	ND	No treatment	>30 months	47	52
10	55/F	Chronic NK lymphocytosis	R	R	ND	No treatment	>10 years	59	79
11	18/F	Chronic NK lymphocytosis	R	R	ND	No treatment	>5 years	ND	64
12	41/F	Chronic NK lymphocytosis	R	R	ND	No treatment	>18 months	5.7	60.6
13	46/M	Chronic NK lymphocytosis	R	R	ND	No treatment	>5 years	66.1	8.4
14	58/F	Chronic NK lymphocytosis	R	R	ND	No treatment	>10 years	52	76
15	62/M	Chronic NK lymphocytosis	R	R	ND	No treatment	>5 years	ND	85
16	62/F	Chronic NK lymphocytosis	R	R	ND	No treatment	>10 years	94	95
17	34/M	Chronic NK lymphocytosis	R	R	ND	No treatment	>10 years	33	51
18	66/M	Chronic NK lymphocytosis	R	R	ND	No treatment	>10 years	78	6
19	30/F	T-ALL	R	S	NR	L17 M	6 months	2.6	4.9
20	75/M	T-ALL	R	S	ND	L17 M	2 months	2	3.3
21	56/F	B-ALL	R	S	NR	L17 M	4 months	0.3	0.3
22	30/F	B-ALL	R	S	ND	L17 M	>1 months	0.8	0.7
23	20/M	B-ALL	R	S	CR	L17 M, allo-PBSCT	>24 months	ND	ND
24	25/M	B-ALL	R	S	CR	L17 M	>6 months	1.2	4.4

Patient numbers are identical to those in Figs 2–4, and Table II.

Clinical response to L-asparaginase is shown as CR or NR. Complete remission (CR) means residual leukaemic blasts <5% in leukaemia cases, and complete resolution of signs and symptoms and normalisation of all imaging studies in lymphoma cases after L-asparaginase containing regimen. No response (NR) indicates more than 25% residual leukaemic blasts in leukaemia cases, and no reduction in measurable tumours in lymphoma cases after L-asparaginase containing regimen.

Discussion

As NK-cell leukaemia/lymphoma pursues an aggressive course with poor response and short survival with standard chemotherapy containing anthracycline, optimal treatment modalities need to be determined (Kwong *et al*, 1997). The present study clearly showed the effectiveness of L-asparaginase to NK-cell leukaemia/lymphoma *in vitro* using the TUNEL assay. Even at different concentrations and treatment durations, L-asparaginase induced apoptosis selectively in NK-cell lines. As previously reported for murine leukaemia cells, L-asparaginase induced G1 arrest and apoptosis rather specifically in the non-G1 population of NK cells (Ueno *et al*, 1997). There exist some immanent methodical limitations in *in vitro* L-asparaginase sensitivity assay. Ammonia released by hydrolysis of asparagine and glutamine, which is rapidly eliminated *in vivo*, might contribute to the cytotoxicity of *in vitro* L-asparaginase treatment (Wagner *et al*, 1999). In our experiments, however, culture medium containing phenolphthalein incubated with L-asparaginase was almost the same colour or even less red than the non-treated, rapidly growing control. This observation

may exclude the high concentration of ammonia in the L-asparaginase-containing medium. Furthermore, L-asparaginase is known to induce not only asparagine but also glutamine deprivation, the latter may cause cell shrinkage-dependent CD95 clustering, which leads to the activation of the receptor-mediated apoptotic pathway (Fumarola *et al*, 2001).

We next examined the effectiveness of L-asparaginase and DXR to NK-cell tumour samples. ALL, NK-cell leukaemia/lymphomas and chronic NK lymphocytosis correlated well with three categories of drug sensitivity; i.e. DXR-sensitive, L-asparaginase-sensitive and resistant to both agents respectively. Therefore, although L-asparaginase is commonly used for the treatment of adult ALL, NK-cell tumour samples were much more sensitive to this agent than ALL samples. Our results strongly indicate that L-asparaginase should be included in the treatment regimen for NK-cell leukaemia/lymphoma. The vast majority of the patients with chronic NK lymphocytosis have long-term survival without any treatment (Tefferi *et al*, 1994). Furthermore, our results showed poor response of chronic NK lymphocytosis to two representative anti-tumour agents of

Apoptosis of NK-cell Tumours by L-Asparaginase

Table II. Asparagine synthetase expression and *in vitro* sensitivity to L-asparaginase.

Patient no.	Diagnosis	AS mRNA (AS/GAPDH)	AS immunostaining	Apoptotic cell percentage after L-asp treatment (%)
1	Nasal-type NK-cell lymphoma	0.043	Positive	<15
2	Nasal-type NK-cell lymphoma	0.075	Negative	<15
3	Nasal-type NK-cell lymphoma	0.016	Negative	>25
4	Nasal-type NK-cell lymphoma	0.003	Negative	>25
5	Aggressive NK-cell leukaemia	0.054	Positive	>25
6	Aggressive NK-cell leukaemia	0.064	Positive	>25
7	Blastic NK-cell lymphoma	0.07	Negative	>25
8	Blastic NK-cell lymphoma	0.131	Negative	>25
9	Chronic NK lymphocytosis	0.075	Negative	<15
10	Chronic NK lymphocytosis	0.035	Negative	<15
11	Chronic NK lymphocytosis	ND	ND	<15
12	Chronic NK lymphocytosis	0.041	Negative	<15
13	Chronic NK lymphocytosis	0.086	Negative	<15
14	Chronic NK lymphocytosis	0.072	Negative	<15
15	Chronic NK lymphocytosis	0.074	Negative	<15
16	Chronic NK lymphocytosis	0.072	Negative	<15
17	Chronic NK lymphocytosis	0.028	Negative	<15
18	Chronic NK lymphocytosis	0.054	Negative	<15
19	Acute lymphoblastic leukaemia	0.031	ND	<15
20	Acute lymphoblastic leukaemia	0.062	Negative	<15
21	Acute lymphoblastic leukaemia	0.009	Negative	<15
22	Acute lymphoblastic leukaemia	0.008	Positive	<15
23	Acute lymphoblastic leukaemia	0.013	Positive	<15
24	Acute lymphoblastic leukaemia	0.029	Negative	<15
Cell line				
K562	Erythroblastic transformation from CML	0.968	Positive	<15
Jurkat	Acute lymphoblastic leukaemia	0.01	Negative	<15
NK-92	Aggressive NK-cell leukaemia	0.003	Negative	>25
NK-YS	Nasal-type NK-cell lymphoma	0.0002	Negative	>25

Asparagine synthetase mRNA expression level (AS/GAPDH), asparagine synthetase immunostaining, corrected apoptotic cell percentage of samples and apoptotic cell percentage of cell lines and apoptotic cell percentage of cell lines treated with 10 IU/ml of L-asparaginase for 24 h are shown. Apoptotic cell percentage was divided into two groups: <15% and >25%.

different mechanism of action. We should avoid anti-tumour treatment to patients with chronic NK lymphocytosis. High levels of asparagine synthetase mRNA expression in chronic NK lymphocytosis may cause the apparent L-asparaginase resistance.

Two-dimensional plotting with asparagine synthetase mRNA level and L-asparaginase sensitivity showed that each disease entity occupied a distinct region in the scheme (Fig 3). Samples of nasal-type NK-cell lymphoma were distributed in a rather elongated ellipse, which shows the inverse correlation between asparagine synthetase mRNA levels and *in vitro* L-asparaginase sensitivity in this disease entity. Furthermore, although the sample number was only four, these two parameters and asparagine synthetase immunostaining were interrelated with the clinical response to L-asparaginase. Indeed, patient 1, whose tumour cells were extremely resistant to L-asparaginase *in vitro* and showed high levels of asparagine synthetase mRNA and protein expression, responded very poorly to L-asparaginase, and the overall survival was only

4 months (Table I). ALL cells were resistant to *in vitro* L-asparaginase treatment in spite of relatively low asparagine synthetase mRNA levels. In aggressive NK-cell leukaemia and blastic NK-cell lymphoma, although asparagine synthetase mRNA levels were high, L-asparaginase induced considerable apoptosis *in vitro*. The two cases of aggressive NK-cell leukaemia were positive for asparagine synthetase immunostaining, which confirmed that asparagine synthetase expression is really high in these cases. We could explain the sensitivity of these samples to L-asparaginase by glutamine-deprived cell shrinkage-dependent apoptosis, which is independent of asparagine synthetase expression (Fumarola *et al*, 2001). Recent studies on paediatric ALL showed that asparagine synthetase mRNA expression is linked with L-asparaginase resistance only in TEL-AML1-negative but not -positive ALL (Remarkers-van Woerden *et al*, 2000; Stams *et al*, 2003, 2005). Therefore asparagine synthetase level alone should not determine sensitivity to L-asparaginase at least in some subtypes of haematological malignancies.

M. Ando et al

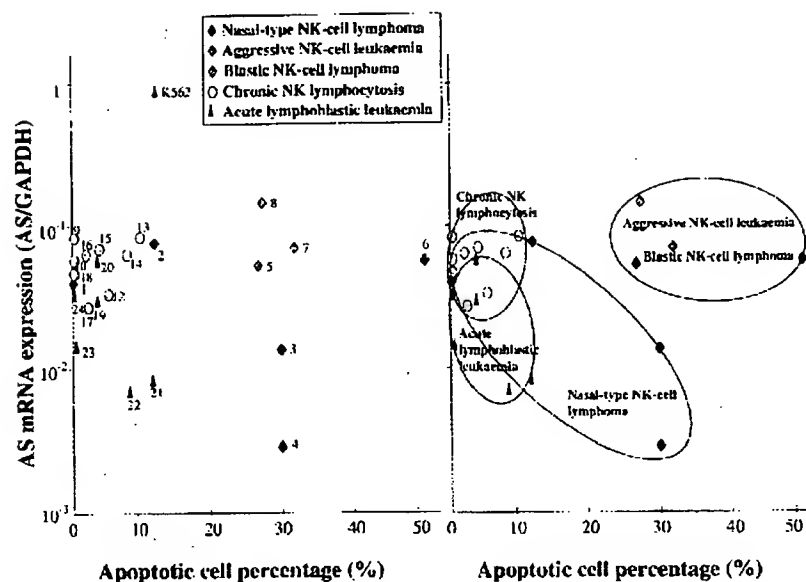


Fig 3. Asparagine synthetase mRNA expression versus *in vitro* L-asparaginase sensitivity in patient samples. Correlation between asparagine synthetase mRNA level and *in vitro* apoptotic cell percentage after treatment with 10 IU/ml of L-asparaginase for 24 h in NK-cell tumour, chronic NK lymphocytosis and ALL samples.

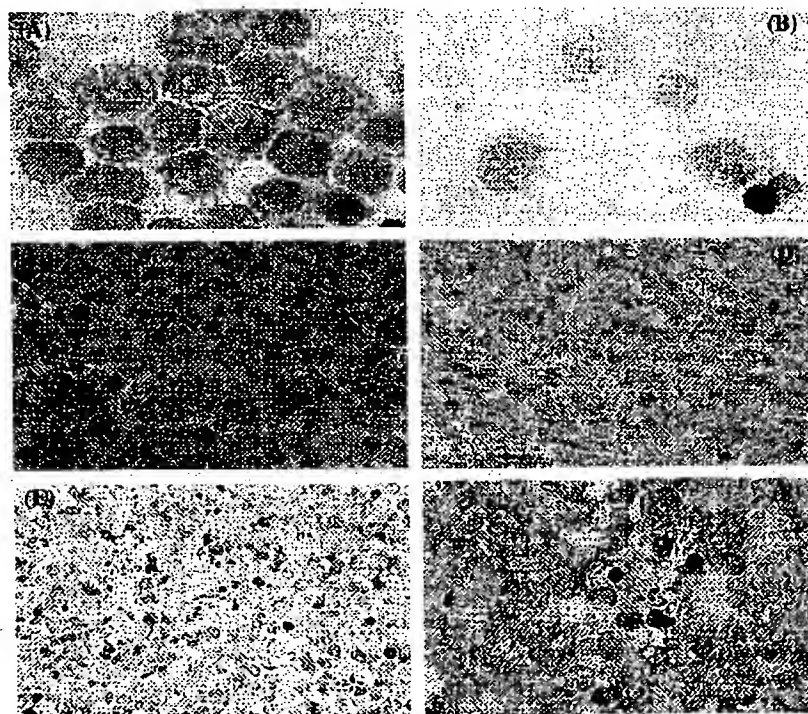


Fig 4. Immunohistochemical detection of asparagine synthetase protein in cell lines and NK-cell tumours. (A) Positive control (K562 cells), (B) negative control (NK-92 cells), (C) nasal-type NK-cell lymphoma (patient 1), (D) aggressive NK-cell leukaemia (patient 5), (E) nasal-type NK-cell lymphoma (patient 2), (F) blastic NK-cell lymphoma (patient 7). Original magnifications are $\times 400$ for A and B, and $\times 200$ for C-F.

In this report, we confirmed a rather specific anti-tumour activity of L-asparaginase against NK-cell tumours *in vitro*. This result provides an experimental background to the clinical use of L-asparaginase for NK-cell tumours. Furthermore,

during this study concerning L-asparaginase sensitivity, we made the following observations. (i) At least in nasal-type NK-cell lymphoma, there was a good correlation among asparagine synthetase expression, *in vitro* sensitivity and clinical response

Apoptosis of NK-cell Tumours by L-Asparaginase

to L-asparaginase. (ii) In aggressive NK-cell leukaemia, although asparagine synthetase expression was high, L-asparaginase induced considerable apoptosis *in vitro*. (iii) Each disease entity occupied a distinct area in the two-dimensional plot with RQ-PCR of asparagine synthetase and *in vitro* TUNEL assay. We expect to perform more detailed studies with larger number of samples to confirm these findings in the future.

References

- Aslanian, A.M., Fletcher, B.S. & Kilberg, M.S. (2001) Asparagine synthetase expression alone is sufficient to induce L-asparaginase resistance in MOLT-4 human leukaemia cells. *The Biochemical Journal*, **357**, 321–328.
- Chau, J.K.C., Sin, V.C., Wong, K.F., Ng, C.S., Tsang, W.Y.W., Chan, C.H., Cheung, M.M.C. & Lau, W.H. (1997) Nonnasal lymphoma expressing the natural killer cell marker CD56: A clinicopathologic study of 49 cases of an uncommon aggressive neoplasm. *Blood*, **89**, 4501–4513.
- Chaperot, L., Bendriss, N., Manches, O., Gressin, R., Maynadie, M., Trimoreau, F., Orfeuvre, H., Corront, B., Feuillard, J., Sotto, J.J., Bensa, J.C., Briere, F., Plumas, I. & Jacob, M.C. (2001) Identification of a leukemic counterpart of the plasmacytoid dendritic cells. *Blood*, **97**, 3210–3217.
- Clarkson, B., Krakoff, L., Burchenal, J., Karnofsky, D., Golbey, R., Dowling, M., Oettgen, H. & Lipton, A. (1970) Clinical results of treatment with E.coli L-asparaginase in adults with leukemia, lymphoma and solid tumors. *Cancer*, **25**, 279–305.
- Egashira, M., Kawamata, N., Sugimoto, K., Kaneko, T. & Oshimi, K. (1999) P-glycoprotein expression on normal and abnormally expanded natural killer cells and inhibition of P-glycoprotein function by cyclosporine A and its analogues, PSC833. *Blood*, **93**, 599–606.
- Ertel, J.J., Nesbit, M.E., Hammond, D., Weiner, I. & Sather, H. (1979) Effective dose of L-asparaginase for induction of remission in previously treated children with acute lymphocytic leukemia: a report from a children's cancer study group. *Cancer Research*, **39**, 3893–3896.
- Feuillard, J., Jacob, M.C., Valensi, F., Maynadie, M., Gressin, R., Chaperot, L., Arnould, C., Brignole-Baudouin, F., Drenou, B., Duchayne, E., Falkenrodt, A., Garand, R., Homolle, E., Husson, B., Kuhlein, E., Calvez, G.L., Sainty, D., Sotto, M.F., Trimoreau, F. & Bene, M.C. (2002) Clinical and biologic features of CD4⁺CD56⁺ malignancies. *Blood*, **99**, 1556–1563.
- Fumarola, C., Zerbini, A. & Guidotti, G.G. (2001) Glutamine deprivation-mediated cell shrinkage induces ligand-independent CD95 receptor signaling and apoptosis. *Cell Death and Differentiation*, **8**, 1004–1013.
- Gong, J.H., Maki, G. & Klingemann, H.G. (1994) Characterization of a human cell line (NK-92) with phenotypical and functional characteristics of activated natural killer cells. *Leukemia*, **8**, 652–658.
- Hercend, T. & Schmidt, R.E. (1988) Characteristics and uses of natural killer cells. *Immunology Today*, **9**, 291–293.
- Hutson, R.G., Kitoh, T., Moraga, D.A., Cosic, S., Schuster, S.M. & Kilberg, M.S. (1997) Amino acid control of asparagine synthetase: relation to asparaginase resistance in human leukemia cells. *American Journal of Physiology. Cell Physiology*, **272**, 1691–1699.
- Imamura, N., Kusunoki, Y., Kawa-Ha, K., Yonura, K., Hara, J., Oda, K., Abe, K., Dohy, H., Inada, T., Kajihara, H. & Kuramoto, A. (1990) Aggressive natural killer cell leukaemia/lymphoma: report of four cases and review of the literature: possible existence of a new clinical entity originating from the third lineage of lymphoid cells. *British Journal of Haematology*, **75**, 49–59.
- Iriao, T., Kitoh, T., Konmi, K., Kashima, T., Mukai, K., Takeuchi, E., Hongo, T., Nakahata, T., Schuster, S.M. & Osaka, M. (2004) Establishment of real-time PCR method for quantitative analysis of asparagine synthetase expression. *The Journal of Molecular Diagnostics*, **6**, 217–224.
- Jaffe, E.S., Harris, N.L., Stein, H. & Vardiman, J.W. (2001) *World Health Organization Classification of Tumours. Pathology and Genetics of Tumours of haematopoietic and lymphoid tissues*. IARC Press, Lyon.
- Kwong, Y.L., Chau, A.C.L., Liang, R., Chiang, A.K.S., Chim, C.S., Chau, T.K., Todd, D. & Ho, F.C.S. (1997) CD56⁺ NK lymphomas: clinicopathologic features and prognosis. *British Journal of Haematology*, **97**, 821–829.
- Matsumoto, Y., Nomura, K., Kanda, Y., Fujita, Y., Nakan, M., Ueda, K., Horiike, S., Yokota, S., Kusuzaki, K., Kitoh, T., Watanabe, A. & Taniwaki, M. (2003) Successful treatment with Ervinia L-asparaginase for recurrent natural killer/T cell lymphoma. *Leukemia & Lymphoma*, **44**, 879–882.
- Oshimi, K. (2003) Leukemia and lymphoma of natural killer lineage cells. *International Journal of Hematology*, **78**, 18–23.
- Pastan, I. & Gottesman, M.M. (1994) Multidrug resistance. *Annual Review of Medicine*, **42**, 277–286.
- Remakers van Woerden, N.L., Pieters, R., Loonen, A.H., Hubeek, L., Drunen, E., Beverloo, H.B., Slater, R.M., Harbott, J., Seyfarth, J., van Wering, E.R., Hahlen, K., Schmiegelow, K., Janka-Schaub, G.E. & Veerman, A.J.P. (2000) TEL/AML1 gene fusion is related to *in vitro* drug sensitivity for L-asparaginase in childhood acute lymphoblastic leukemia. *Blood*, **96**, 1094–1099.
- Robertson, M.J. & Ritz, J. (1990) Biology and clinical relevance of human natural killer cells. *Blood*, **76**, 2421–2438.
- Sheng, S., Moraga, D.A., Van Heeke, G. & Schuster, S.M. (1992) High-level expression of human asparagine synthetase and production of monoclonal antibodies for enzyme purification. *Protein Expression and Purification*, **3**, 337–346.
- Siu, L.L.P., Chan, J.K.C. & Kwong, Y.L. (2002) Natural killer cell malignancies: clinicopathologic and molecular features. *Histology and Histopathology*, **17**, 539–554.
- Stams, W.A.G., den Boer, M.L., Beverloo, B., Meijerink, J.P.P., Stigter, R.L., van Wering, E.R., Janka-Schaub, G.E., Slater, R. & Pieters, R. (2003) Sensitivity to L-asparaginase is not associated with expression levels of asparagine synthetase in t(12;21)⁺ pediatric ALL. *Blood*, **101**, 2743–2747.
- Stams, W.A.G., den Boer, M.L., Holleman, A., Appel, I.M., Beverloo, B., van Wering, E.R., Janka-Schaub, G.E., Evans, W.E. & Pieters, R. (2005) Asparagine synthetase expression is linked with L-asparaginase resistance in TEL-AML1-negative but not TEL-AML1-positive pediatric acute lymphoblastic leukemia. *Blood*, **105**, 4223–4225.
- Story, M.D., Voehringer, D.W., Stephens, L.C. & Meyn, R.E. (1993) L-Asparaginase kills lymphoma cells by apoptosis. *Cancer Chemotherapy and Pharmacology*, **32**, 129–133.
- Sugimoto, K., Yamada, K., Egashira, M., Yazaki, Y., Hirai, H., Kikuchi, A. & Oshimi, K. (1998) Temporal and spatial distribution of DNA topoisomerase II alters during proliferation, differentiation, and apoptosis in HL-60 cells. *Blood*, **91**, 1407–1417.
- Sugimoto, K., Tamayose, K., Sasaki, M., Hayashi, K. & Oshimi, K. (2002) Low-dose doxorubicin-induced necrosis in Jurkat cells and

M. Ando et al

- its acceleration and conversion to apoptosis by antioxidants. *British Journal of Haematology*, 118, 229-238.
- Tefferi, A., Li, C.Y., Witzig, T.F., Dhodapkar, M.V., Okuno, S.H. & Phyllis, R.L. (1994) Chronic natural killer cell lymphocytosis: a descriptive clinical study. *Blood*, 84, 2721-2725.
- Trinchieri, G. (1989) Biology of natural killer cells. *Advances in Immunology*, 47, 187-376.
- Tsuchiyama, J., Yoshino, T., Mori, M., Kondoh, E., Oka, T., Akagi, T., Hiraki, A., Nakayama, H., Shibuya, A., Ma, Y., Kawabata, T., Okada, S. & Harada, M. (1998) Characterization of a novel human natural killer-cell line (NK-YS) established from natural killer cell lymphoma/leukemia associated with Epstein-Barr virus infection. *Blood*, 92, 1374-1383.
- Ueno, T., Ohtawa, K., Mitsui, K., Kadera, Y., Hiroto, M., Matsushina, A., Inada, Y. & Nishimura, H. (1997) Cell cycle arrest and apoptosis of leukemia cells induced by L-asparaginase. *Leukemia*, 11, 1858-1861.
- Wagner, A., Hempel, G., Gumbinger, H.G., Jurgens, H. & Boos, J. (1999) Pharmacokinetics of anticancer drugs in vitro. *Advance in Experimental Medicine and Biology*, 457, 397-407.
- Yamaguchi, M., Kita, K., Miwa, H., Nishii, K., Oka, K., Ohno, T., Shirakawa, S. & Fukumoto, M. (1995) Frequent expression of P-glycoprotein/MDR1 by nasal T-cell lymphoma cells. *Cancer*, 76, 2351-2356.
- Yamamoto, T., Iwasaki, T., Watanabe, N., Oshimi, K., Naito, M., Tsuruo, T. & Kobayashi, Y. (1993) Expression of multidrug resistance P-glycoprotein on peripheral blood mononuclear cells of patients with granular lymphocyte-proliferative disorders. *Blood*, 81, 1342-1346.
- Yong, W., Zheng, W., Zhang, Y., Zhu, J., Wei, Y., Zhu, D. & Li, J. (2003) L-Asparaginase-based regimen in the treatment of refractory midline nasal/nasal-type T/NK-cell lymphoma. *International Journal of Hematology*, 78, 163-167.

Thyroid

VOLUME 7

NUMBER 5

OCTOBER 1997

CLINICAL RESEARCH

Levothyroxine Suppressive Therapy is Partially Effective in Treating Patients with Benign, Solid Thyroid Nodules and Multinodular Goiters.

NICOLAU LIMA, MEYER KNOBEL, HUMBERTO CAVALIERE,
CLAUDIA SZTEJNSZNAJD, EDUARDO TOMIMORI, and
GERALDO MEDEIROS-NETO

691

Is Percutaneous Ethanol Injection a Useful Alternative for the Treatment of the Cold Benign Thyroid Nodule? Five Years' Experience.

NADIA CARACCIO, ORLANDO GOLETTI, PIERO VINCENZO LIPPOLIS,
ARTURO CASOLARO, ENRICO CAVINA, PAOLO MICCOLI, and FABIO MONZANI

699

Value of Combined Technetium-99m Hydroxy Methylene Diphosphonate and Thallium-201 Imaging in Detecting Bone Metastases from Thyroid Carcinoma.

MD. SAYEEDUL ALAM, RYO TAKEUCHI, KANJI KASAGI, TAKASHI MISAKI,
SHINICHI MIYAMOTO, YASUHIRO IIDA, AKINARI HIDAKA, and JUNJI KONISHI

705

Human Thyroid Carcinoma Cell Lines and Normal Thyrocytes: Expression and Regulation of Matrix Metalloproteinase-1 and Tissue Matrix Metalloproteinase Inhibitor-1 Messenger-RNA and Protein.

G. AUST, A. HOFMANN, S. LAUE, A. ROST, T. KÖHLER, and W.A. SCHERBAUM

713

MUC1 Mucin Gene, Transcripts, and Protein in Adenomas and Papillary Carcinomas of the Thyroid.

IVAN BIÈCHE, EMMANUEL RUFFET, ALAIN ZWEIBAUM, FRANÇOISE VILDÉ,
ROSETTE LIDEREAU, and BRIGITTE FRANC

725

Incidence and Clinical Characteristics of Thyroid Carcinoma After Iodine Prophylaxis in an Endemic Goiter Country.

C. BACHER-STIER, G. RICCABONA, M. TÖTSCH, G. KEMMLER, W. OBERAIGNER,
and R. MONCAYO

733

Opposite Changes in Serum Soluble CD8 in Patients at the Active Stages of Graves' and Hashimoto's Diseases.

MIKIO WATANABE, NOBUYUKI AMINO, KAZUNORI HOCHITO,
KIYOSHI WATANABE, KANJI KUMA, and YOSHINORI IWATANI

743

Urinary Iodine Excretion During Normal Pregnancy in Healthy Women Living in the Southwest of France: Correlation with Maternal Thyroid Parameters.

PHILIPPE CARON, MADELEINE HOFF, SAMUEL BAZZI, ALAIN DUFOR,
GÉRARD FAURE, IMAD GHANDOUR, PATRICK LAUZU, YVAN LUCAS,
DOMINIQUE MARAVAL, FRÉDÉRIC MIGNOT, PASCAL RÉSSIGÉAC,
FRANÇOISE VERTONGEN, and VÉRONIQUE GRANGÉ

749

(continued)

Human Thyroid Carcinoma Cell Lines and Normal Thyrocytes: Expression and Regulation of Matrix Metalloproteinase-1 and Tissue Matrix Metalloproteinase Inhibitor-1 Messenger-RNA and Protein

G. AUST,¹ A. HOFMANN,² S. LAUE,² A. ROST,³ T. KÖHLER,³ and W.A. SCHERBAUM⁴

ABSTRACT

Matrix metalloproteinase-1 (MMP-1) and tissue matrix metalloproteinase inhibitor 1 (TIMP-1) play an important role in remodeling the extracellular matrix in normal and pathological processes. The effect of phorbol-myristate acetate (PMA), interleukin-1 (IL-1), and tumor necrosis factor- α (TNF- α) on MMP-1 and TIMP-1 expression was studied on highly purified thyrocytes and undifferentiated 8505 C, C 643, HTh 74, SW 1736 thyroid carcinoma cells compared with thyroid-derived fibroblasts. Messenger RNA (mRNA) levels were monitored by competitive semiquantitative reverse transcriptase polymerase chain reaction (RT-PCR) after 24 hours. Culture supernatants were assayed for free and/or complexed MMP-1 and TIMP-1 after 48 hours using enzyme-linked immunosorbent assay (ELISA) systems (detection limit: <2 ng/mL). MMP-1 and TIMP-1 mRNA were present in all cell types, although thyrocytes showed MMP-1 mRNA levels near the detection limit. 8505 C expressed MMP-1 mRNA levels of up to 10^6 times those of the other cells analyzed. PMA and IL-1 increased MMP-1 mRNA in most cell types. TIMP-1 mRNA increased after treatment with PMA in all cells except 8505 C, whereas only slight effects were shown after IL-1 stimulation. MMP-1 protein was undetectable in normal thyrocyte cultures, but was secreted spontaneously by all cell lines ([ng/mL]; C 643: 15 ± 7 ; HTh 74: 81 ± 1 ; SW 1736: 13 ± 2 ; 8505C: 2097 ± 320). There was a strong correlation between levels of MMP-1 mRNA and protein ($r = 0.99$, $p < .0001$). PMA and IL-1 increased MMP-1 secretion in all cell types after 48 hours. Fibroblasts ([ng/mL] 517 ± 55) and the cell lines (C 643: 142 ± 48 ; HTh 74: 115 ± 13 ; SW 1736: 202 ± 14 ; 8505 C: 120 ± 19) secreted TIMP-1 in unstimulated cultures, whereas only a trace amount was detected in thyrocyte cultures, even after PMA treatment. IL-1 upregulated TIMP-1 secretion after 48 hours in SW 1736, HTh 74, and C 643 cells. Our data suggest that in contrast to normal thyrocytes, dedifferentiated thyroid carcinoma cell lines are potential producers of MMP-1 as well as TIMP-1. High MMP-1 or MMP-1/TIMP-1 expression may play a role in tissue invasion of undifferentiated thyroid cancer cells.

INTRODUCTION

MATRIX METALLOPROTEINASES, (MMPs) constitute a family of structurally related proteolytic enzymes responsible for the proteolytic degradation of extracellular matrix (ECM) components. They are important participants in normal tissue remodeling and contribute to the phenotype of several pathological conditions that are associated with progressive ECM degradation. MMPs are highly regulated at different levels (1). At the transcriptional level, MMP expression can be directly induced or

suppressed on external stimulation, ie, with cytokines, phorbol 12-myristate 13-acetate (PMA), lipopolysaccharide (LPS), or retinoic acid (2,3). After secretion at post-transcriptional level, latent MMP proenzymes are regulated by proteolytic activation and interaction with tissue inhibitors of matrix metalloproteinase (TIMPs), their specific inhibitors. Any imbalance between the proteolytic MMPs activities and the TIMPs that could be influenced and caused by cytokines could potentially lead to pathological conditions (4).

MMP-1, although known as an interstitial collagenase,

¹Institut of Anatomy, ²Department of Internal Medicine III, and ³Institute of Clinical Chemistry and Pathobiochemistry, University of Leipzig, Germany. ⁴Department of Endocrinology, University of Duesseldorf.

is the only enzyme active at neutral pH that can degrade extracellular fibers comprised of collagen types I, II, and III. With this initial step, MMP-1 provides the cleavage products to other collagenase types (5). The major specific inhibitor of MMP-1 is TIMP-1, a 28.5-kd glycoprotein, which forms 1:1 stoichiometric complexes with the protease (6). Cytokines and growth factors have been shown to regulate the expression of both MMP-1 and TIMP-1 (1,7,8).

Although the participation of MMP-1 as the initial collagenase in tissue breakdown during tumor development is well documented (9–11), only one study has described the expression (12) but no study has as yet investigated the regulation of this enzyme in different thyroid tumors. Few studies have been published investigating the role of other MMPs in normal and pathological thyroid tissue by *in situ* hybridization and immunohistochemistry (13–16). Furthermore, tissue remodeling includes both the action of MMPs and their inhibitors; thus, these enzymes could be involved in autoimmune and other nonautoimmune thyroid diseases during morphological changes (17,18). It is still unknown whether or not thyrocytes are able to express MMPs and TIMPs. Although type IV collagenases (MMP-2 and MMP-9) were detected in various human epithelial cells of different tissue origin (19,20), only one study described the secretion of MMP-1 by epithelial cells (21).

Highly purified normal thyrocytes and four thyroid carcinoma cell lines were included in this study to investigate the involvement of these cells in MMP-1 and TIMP-1 production during thyroid tissue remodeling processes and in malignant thyroid neoplasms. MMP-1 and TIMP-1 expression were studied at both the mRNA and protein level by semiquantitative RT-PCR and ELISA measurement, respectively.

In unstimulated carcinoma cell lines both MMP-1 and TIMP-1 mRNA were expressed, partly at a high level, followed by the spontaneous secretion of the proteins. The various conditions for the stimulation of the different cell lines by cytokines and PMA were defined. In contrast to the cell lines, normal thyrocytes did not secrete MMP-1 and only trace amount of TIMP-1, even after stimulation with PMA.

MATERIALS AND METHODS

Preparation of tissues, thyroid-derived cells, and cell lines

Thyrocytes were prepared from surgical thyroid specimens from 3 patients (1 Graves' disease, 2 nontoxic goiter; mean age 54.3 ± 5.0 years). Fibroblasts were separated from thyroid tissue of 5 other patients (3 Graves' disease, 2 nontoxic goiter; mean age 43.6 ± 6.4 years). Graves' disease and nontoxic goiter were diagnosed on the strength of clinical, biochemical, and immunologic features as well as thyroid scintiscans.

Thyroid tissue was trimmed of fat and connective tissue immediately after surgery. Thyroid-derived cells were enriched after gradual enzymatic digestion of tissue and cultured over a period of 16 hours as described. Thyrocytes were obtained from the adherent fraction by incubating

the cell monolayer with phosphate buffered saline (PBS) without $\text{Ca}^{2+}/\text{Mg}^{2+}$ for 45 minutes (22). Residual fibroblasts were removed after subsequent incubation of the cells with the fibroblast-specific mab FibAS01 (22) and goat-anti-mouse IgG-DYNABEADS® M450 (DYNAL, Hamburg, Germany) according to the manufacturer's protocol.

Thyroid-derived fibroblasts were obtained after culturing small pieces of thyroid tissue in Dulbeccos's Modified Eagle's Medium (DMEM) with 10% fetal calf serum (FCS) and harvested in the 5th to 7th passage. The purity of the thyrocytes and fibroblasts was determined by using indirect immunofluorescence technique on a FACS-Scan (Becton Dickinson GmbH, Heidelberg, Germany) as described (22).

The following human anaplastic thyroid carcinoma cell lines were cultured in DMEM with 10% FCS: C 643 (23); SW 1736 (23); and HTh 74 (24). The cell line 8505 C (25) was purchased from the German Collection of Microorganisms and Animal Cell Cultures (DSM ACC219). This cell line was established from a primary thyroid tumor characterized histologically as a undifferentiated carcinoma that was partially composed of poorly differentiated papillary cells (25). This is a feature of a subgroup of anaplastic carcinoma (26). The majority of these coexistent better differentiated carcinoma foci in anaplastic carcinoma were papillary (26).

In vitro cultures

Using 24-well plates, 1×10^5 cells were cultured for 24 hours. The medium was aspirated and replaced with 500 μL OPTI-MEM (GIBCO BRL, Grand Island, NY) without FCS to eliminate possible stimulation of MMP-1 and TIMP-1 production by FCS. The medium contained the desired concentration of human IL-1 α (10 U/mL; Pepro Tech EC Ltd., London, UK), TNF- α (100 U/mL; Pepro Tech EC Ltd.), interferon- γ (IFN- γ) (500 U/mL; Pepro Tech EC Ltd.), or 10 ng/mL PMA (SIGMA).

Triplicate cultures of each stimulator were analyzed after 3, 6, and 24 hours at the mRNA and after 24 and 48 hours at the protein level. The supernatants were removed and stored at -80°C for further use. First, a collagenolytic assay based on the digestion of type I collagen was performed. This method showed direct evidence of free pro-MMP-1 enzyme in the cell culture supernatants of unstimulated and IL-1 α stimulated 8505 C, HTh 74, and C634 cells (data not shown). However, the method does not allow quantitation of MMP-1 enzyme activity. Thus, the cell culture supernatants were assayed for MMP-1, TIMP-1, and MMP1/TIMP-1 complex by ELISA (Amersham Life Sciences, Braunschweig, Germany). The MMP-1 assay (sensitivity: 1.7 ng/mL) detected only total human MMP-1, ie, free MMP-1 and MMP-1 complexed with inhibitors such as TIMP-1. It did not detect MMP-1 bound by the nonspecific protease inhibitor α_2 -macroglobulin. The MMP-1/TIMP-1 assay (sensitivity: 1.5 ng/mL) detected MMP-1/TIMP-1 complex, ie, activated MMP-1 that has been subsequently complexed with the specific MMP-1 inhibitor TIMP-1. It did not detect free active MMP-1, free TIMP-1, or pro-MMP-1. There was no cross-reactivity with active MMP-1 bound by the nonspecific protease inhibitor α_2 -macroglobulin. The TIMP-1 assay (sensitivity:

1.25 ng/mL) detected total human TIMP-1, ie, free TIMP-1 and that complexed with MMPs. The assay did not fully cross-react with TIMP-1 in complexes with other MMP. It did not cross-react with TIMP-2.

RNA extraction and cDNA synthesis

For gene expression studies, 5 mL RNAzol™ B (Biotex Laboratories Inc., Houston, TX) was added to the cell culture wells. The content of three wells of any cell type was pooled and then stored frozen for further mRNA analysis in liquid nitrogen. Total cellular RNA (cDNA) was isolated from the probes according to the manufacturer's protocol. RNA was fractionated on a denaturing 1.0% agarose gel and stained with ethidium bromide to confirm that spectrophotometric measurements were accurate and that the RNA had not been degraded. Five micrograms total RNA was reverse-transcribed to cDNA using the First-strand cDNA synthesis kit of Pharmacia (Uppsala, Sweden) in a total reaction volume of 15 μ L.

mRNA analysis by competitive RT-PCR

To correct for variations across different cDNA preparations, all samples were first adjusted to contain equal input glyceraldehyde-3-phosphate dehydrogenase (GAPDH) cDNA concentrations. Semi-quantitative GAPDH RT-PCR was used with a heterologous synthetic competitor fragment. The generation of the specific PCR products from the competitor and the cDNA with the GAPDH primers were published earlier (22,27).

We then estimated the MMP-1 and TIMP-1 cDNA in these adjusted samples. The primers were selected using the DNAsis computer program (Hitachi Software Engineering Co, Yokohama, Japan). The primer pairs span one or more introns to allow unambiguous discrimination between cDNA and unwanted contaminating genomic DNA. In quantitating MMP-1 and TIMP-1 cDNA, a rapid one-step method was introduced to synthesize an internal homologous competitor (plan diagram of procedure: Fig. 1, exemplary for MMP-1 [28]). A hybrid primer was synthesized (MMP-1hy) that consisted of two segments (seg₁, seg₂). It

had a length of 40 nucleotides, in which 20 nucleotides (seg₁) at the 3' end corresponded to the opposite strand of the target sequence a predetermined distance from primer MMP-1f, and 20 nucleotides at the 5' end (seg₂ = MMP-1r) that corresponded to the target sequence upstream from the segment seg₁. Amplification with the primers MMP-1f and MMP-1hy from the cDNA resulted in a 478-base pair (bp) (polymerase chain reaction (PCR) product. It was freed from excess primers and deoxynucleoside-triphosphates (dNTPs) using the Qiaquick Gel Extraction Kit (Qiagen GmbH, Hilden, Germany) and quantified. A known number of copies of the competitor was introduced in the GAPDH-adjusted samples and amplified with the primers MMP-1f and MMP-1r. With this approach, two products were generated, one derived from the cDNA (560 bp) and another, 82 bp smaller in size derived from the internal competitor (Fig. 1). PCR products were resolved by gel electrophoresis (1.5% agarose gel). The relative amounts of sample cDNA and competitor were quantified by measuring the intensity of ethidium fluorescence with a CCD image sensor and analyzing the data with the EASY program (Herolab, Wiesloch, Germany). The initial amounts of sample cDNA and competitor were assumed to be equal in those reactions where the ratio of the two products was judged to be equal. This was expressed in arbitrary units (AU) (22,29). One AU was defined as the lowest concentration of competitor yielding a detectable amplification product when added to PCR alone. For example, if equivalence between sample cDNA and competitor was reached using a 100-fold concentrated competitor the relative sample cDNA concentration was 100 AU. Thyrocytes and the cell lines were analyzed for the expression of thyroid-specific and cytokine receptor mRNAs in a simple RT-PCR. The sequences of the TPO and cytokine receptor primer pairs have been published by Watson et al. (30) and Tada et al. (31) and gave the following product sizes: TPO: 506 bp; IL-1R type I (p80): 300 bp; IL-1R type II (p68): 392 bp; TNF- α R (p75): 324 bp; TNF- α R (p55): 587 bp and IFN- γ R: 899 bp. The thyroglobulin (Tg) and thyroid stimulating hormone receptor (TSH-R) primer pairs were selected according to the published sequences using the DNAsis program (Table 1).

Each 25- μ L amplification reaction contained 2.5 μ L 10 \times concentrated PCR buffer (15 mM MgCl₂, Boehringer Mannheim, Germany), 0.3 U Taq DNA polymerase (Boehringer Mannheim, Germany), 100 μ M dNTPs (Perkin Elmer, Weiterstadt, Germany), 0.1 μ M of each primer (IMB, Jena, Germany), and 1 μ L cDNA and competitor in adjusted dilution. Furthermore, restriction mapping (restriction enzymes: Boehringer Mannheim GmbH, Germany) was carried out to confirm the originality of the PCR product (Fig. 1, Table 1).

Statistics

Protein levels of thyrocyte or fibroblast cultures from the different patients and of the thyroid carcinoma cell lines obtained from three separate experiments were presented as mean \pm SEM values. Statistical comparisons between unstimulated and stimulated cell cultures were performed by the alternate (Welch) t-test. The correlation between basal mRNA levels and the unstimulated protein secretion in all cell types was calculated according to the Spearman method.

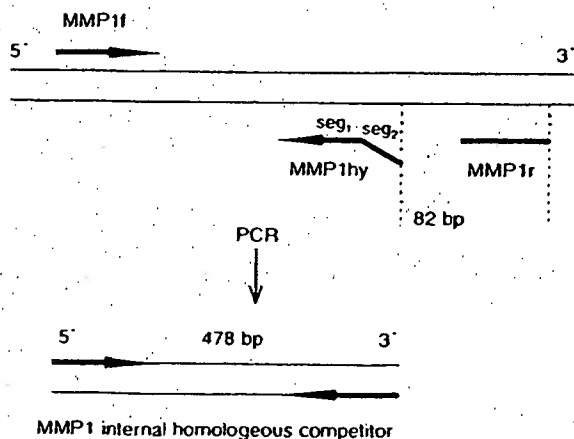


FIG. 1. General scheme for generating homologous competitors used for quantitative PCR.

TABLE 1. PRIMERS, LENGTH OF AMPLIFIED TEMPLATES, RESTRICTION MAPPING AND ASSAY CONDITIONS FOR RT-PCR

		Primer	Length of cDNA (bp)	Length of competitor (bp)	Annealing temperature	Number of cycles
Tg	forward	GCAGATCTTACTGAGTGGCT	416		60	35
	reverse	TGTCAGCACAGTGGCAATAC				
TSH-R exons 1-4	forward	ACTTGCTGCAGCTGGTGCT	354		65	35
	reverse	TGAGGGCATCAGGGTCTATG				
TSH-R exons 4-10	forward	GAAATTCGGAATACCAGGAACCTA ACT	896		53	35
	reverse	AATCATCGGACTTGGGGGTACA				
MMP-1	forward	TGGGAGCAAACACATCTGAC	560	478	64	33
	reverse	ATCACTTCTCCCGAATCGT				
	hybrid	ATCACTTCTCCCGAATCGT CCATATATGGCTTGGATGCC				
TIMP-1	forward	CTTAGGGGATGCCGCTGACA	351	274	64	30
	reverse	GGCAGGCAGGCAAGGTGACG				
	hybrid	GGCAGGCAGGCAAGGTGACG GGATGGATAAACAGGGAAAC				

Tg indicates thyroglobulin; TSH-R, thyroid stimulating hormone receptor; MMP-1, matrix metalloproteinase-1; TIMP-1, tissue inhibitor of metalloproteinase-1; bp, base pair.

RESULTS

Thyroid specific and cytokine receptor mRNA expression

Isolated thyrocytes as well as 8505 C cells expressed Tg and thyroperoxidase (TPO) mRNA, whereas transcripts of the TSH-R (exons 1-4, 354 bp, exons 4-10, 896 bp) were present only in the thyrocytes. The three anaplastic thyroid carcinoma cell lines SW 1736, C 634, and HTh 74 were completely negative for the Tg, TPO, and TSH-R mRNAs (Fig. 2). All cell lines and thyrocytes expressed IL-1R (type I and type II), TNF- α R (p75 and p55) and IFN- γ R mRNA (Fig. 2).

Basal MMP-1 and TIMP-1 mRNA and protein expression

In most stimulation experiments, mRNA levels did not increase until 24 hours of incubation. The 24-hour mRNA levels are shown in Figures 3 and 4. The 3- and 6-hour levels are demonstrated in those experiments where the mRNA levels reached their peak before 24 hours of stimulation. If not otherwise indicated, the MMP-1 levels were measured using the ELISA system, which recognizes free/complexed MMP-1.

MMP-1 and TIMP-1 mRNA were found during unstimulated culture in all investigated cell types, although the mRNA levels varied over a great range. 8505 C showed a basal MMP-1 mRNA level 20 times as high as those of the HTh 74 cells, 6×10^4 times as high as C 643, and 2×10^6 times as high as SW 1736 cells. In thyrocytes, MMP-1 mRNA levels were found near the detection limit (Figs. 3 and 4).

Generally, when analyzing the noted cell types, the measured basal MMP-1 or TIMP-1 mRNA levels correlated well with the basal protein expression (MMP-1: $r = 0.99$, $p < .0001$; TIMP-1: $r = 0.98$, $p < .002$). Corresponding to the high MMP-1 mRNA level, 8505 C cells secreted extremely high levels of MMP-1. No MMP-1 or TIMP-1 was

detected in unstimulated thyrocyte cultures at any timepoint examined. All other cell types showed a spontaneous MMP-1 and TIMP-1 secretion (Figs. 5 and 6). Thyroid-derived fibroblasts produced basal TIMP-1 levels of up to 4 times higher in the four carcinoma cell lines, which secreted nearly the same amounts of basal TIMP-1 protein. Nevertheless, TIMP-1 secretion of fibroblasts was found at lower levels than expected after TIMP-1 mRNA measurement in 4 of 5 analyzed patients. The results of the fibroblast cultures from patient five showing a higher TIMP-1 expression than those from the 4 other patients (basal 24 hour: 50 ± 2 ; PMA 24 hour: 90 ± 6 ng/mL TIMP-1) was omitted in Figure 6.

Comparing the basal amount of free/complexed and TIMP-1 complexed MMP-1 after 24 hours of stimulation, a significant level of MMP-1 was not complexed with TIMP-1 in 8505 C cultures, whereas in fibroblast cultures most of the MMP-1 activity was inhibited by TIMP-1. The anaplastic carcinoma cell line HTh 74 did not show such a great discrepancy between free/complexed and TIMP-1 complexed MMP-1 level as 8505 C cells (Fig. 7).

Effects of IL-1 α on MMP-1 and TIMP-1 mRNA and protein expression

Experiments were performed to determine whether human thyroid epithelial cells and thyroid carcinoma cell lines could produce or increase basal MMP-1 and TIMP-1 secretion after exposure to various stimuli. The results from these stimulation experiments are summarized in Figures 3 through 5. Generally, there was a delay in protein secretion level in comparison to the mRNA expression level. At the protein level, the cytokine-mediated stimulating or inhibiting effect is more distinct after 48 hours compared with 24 hours, even when the mRNA level had already decreased after 6 hours.

IL-1 upregulated MMP-1 mRNA in SW 1736 cells up to 100 times and, in thyroid-derived fibroblasts, up to 12 times after 24 hours of incubation (Fig. 3). This increased mRNA level was accompanied by a significantly enhanced

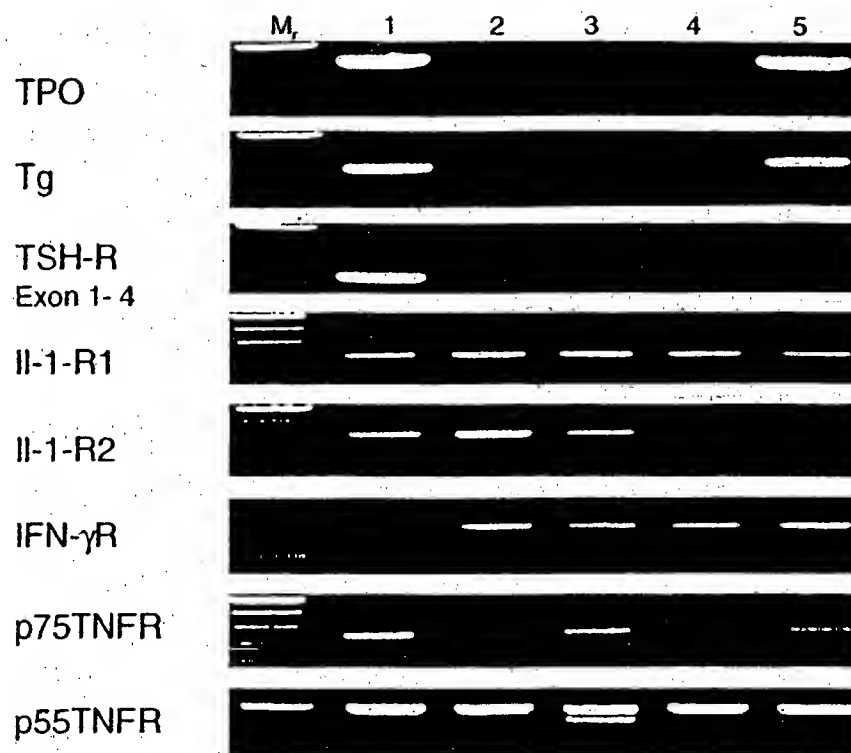


FIG. 2. Amplification of thyroid specific and interleukin-receptor mRNA in thyrocytes (1), SW 1736 (2), C 643 (3), HTh 74 (4) and 8505 C (5) cells using RT-PCR; M_r = 100-bp ladder (GIBCO).

MMP-1 secretion after 48 hours. Furthermore, IL-1 α increased MMP-1 mRNA expression in thyrocytes up to seven times after 6 hours, but no MMP-1 protein could be detected in thyrocyte cultures. IL-1 had no stimulatory effect on MMP-1 mRNA expression in C 643, HTh 74, and 8505 C cells after 24 hours, although a significant increase of MMP-1 secretion was found in HTh-74 and SW 1736 cells after 48 hours of incubation (Fig. 5). This discrepancy may be explained by a possible increase in MMP-1 mRNA level after 24 hours of stimulation. The same effect could also be observed in the IL-1 stimulated TIMP-1 at the mRNA as well as the protein level: the only slight effect of IL-1 on TIMP-1 mRNA expression in carcinoma cell lines after 24 hours was accompanied by a significant increase of TIMP-1 secretion in 8505 C and HTh 74 cells after 48 hours (Figs. 4 and 6).

Effects of TNF- α on both MMP-1/TIMP-1 mRNA and protein expression

In contrast to IL-1, TNF- α did not stimulate the MMP-1 and TIMP-1 mRNA and protein levels in all carcinoma cell lines and thyrocytes. Only thyroid-derived fibroblasts responded with a slight upregulation of MMP-1 and TIMP-1 mRNA expression after TNF- α stimulation, which was not accompanied by an increase of MMP-1 and TIMP-1 secretion.

Effects of PMA, and IFN- γ on MMP-1 and TIMP-1 mRNA and protein expression

PMA was included in our study as a positive control because it is known to upregulate or induce both MMP-1 and TIMP-1 secretion in various cell types (1,32). Indeed, PMA was able to induce or enhance MMP-1 mRNA levels in all cell types investigated, although the detected levels varied to a large extent (Fig. 3). This result is in good correlation with the significantly increased MMP-1 protein levels that were already detectable after 24 hours of stimulation (Fig. 5). PMA upregulated TIMP-1 mRNA levels by up to 20 times in C 643, and up to 2 times in SW 1736 and HTh 74 cells, fibroblasts and thyrocytes, but it did not change the TIMP-1 mRNA content in 8505 cells (Fig. 4). At the protein level, we found a significant stimulation of TIMP-1 secretion in C 643 and HTh 74 cells, as well as in thyroid-derived fibroblasts (Fig. 6).

In contrast to PMA, IFN- γ was without effect on stimulation or downregulation of MMP-1 and TIMP-1 mRNA or protein in any of the cell types investigated (Figs 5 and 6).

The main inhibitor of MMP-1 is TIMP-1, which forms 1:1 stoichiometric complexes with MMP-1, although some other inhibitors can also bind MMP-1. On the other hand, TIMP-1 can bind other MMP types.

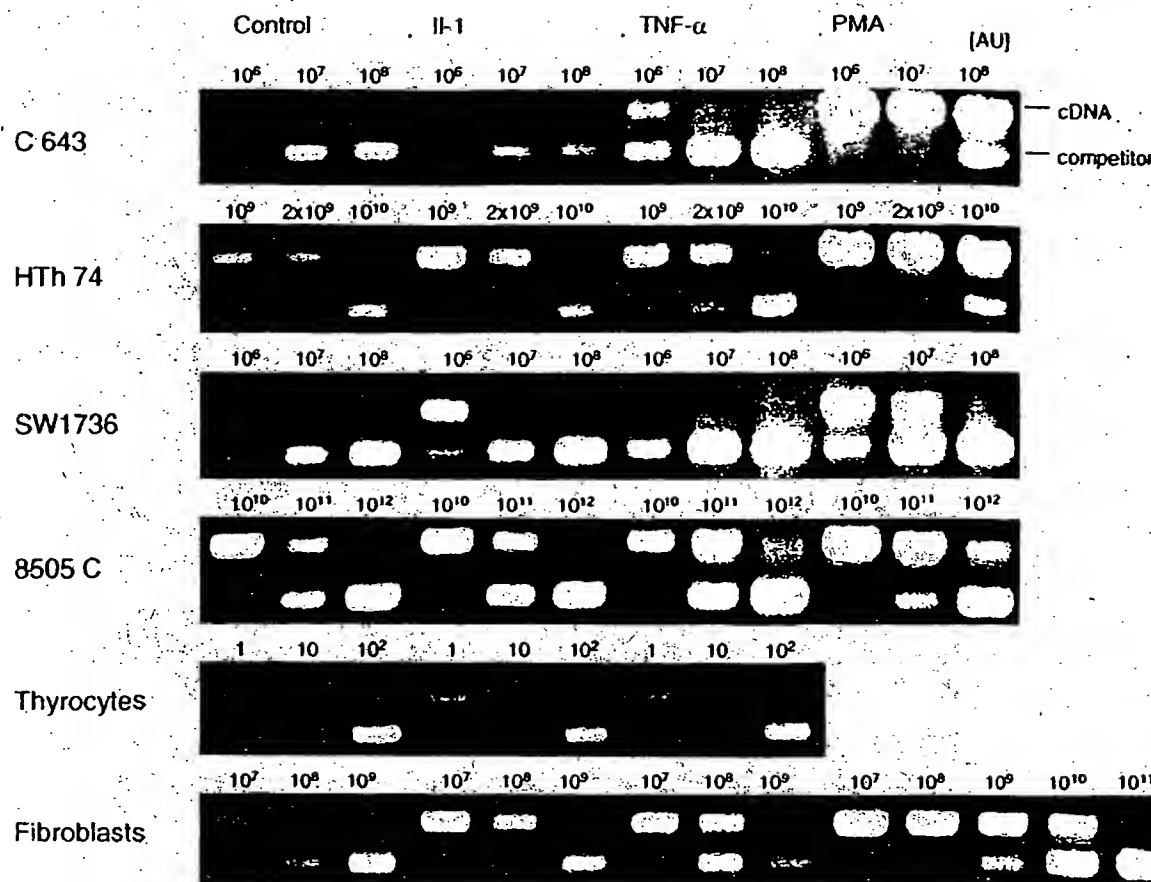


FIG. 3. Representative samples of competitive amplified MMP-1 mRNA of thyrocytes, thyroid-derived fibroblasts and thyroid carcinoma cell lines without stimulation (control) and after stimulation with 10 U/mL IL-1 α and 100 U/mL TNF- α and 10 ng/mL PMA after 24 hours. Serial dilutions of known amounts of the competitor fragment were coamplified with identical aliquots of cDNA. The 560-bp (cDNA) and 478-bp (competitor) PCR products were visualized by agarose gel electrophoresis and ethidiumbromide staining. The relative concentration of the added competitor was given in arbitrary units (AU) in the figure. One AU was defined as the lowest concentration of the competitor yielding a detectable amplification for MMP-1 mRNA. The ratio of competitor to cDNA fragments was determined by measuring the intensity of ethidium fluorescence with a CCD image sensor and analysis of data. Measured cDNA concentration can be expressed in AU.

DISCUSSION

Our findings demonstrate for the first time that thyroid carcinoma cell lines are able to express MMP-1 and TIMP-1 mRNA and protein at significant levels *in vitro*. The observation of spontaneous release of MMP-1 and TIMP-1 corresponds well with earlier studies covering the secretion of these proteins by several carcinoma cell lines (33,34).

However, in contrast to its clear physiological function in extracellular matrix breakdown, the role of MMP-1 in tumor growth and metastases is still controversial (9-11,35). Recently, Murray et al. (10) demonstrated that MMP-1 is associated with poor prognosis in colorectal cancer, and has a prognostic value independent of the Duke's stage. Therefore, MMP-1 could be a target for therapeutic intervention in such tumors. Furthermore, the hypothesis of whether or not cancer cells themselves are able to

produce MMP, or whether cancer cells stimulate the surrounding stromal cells to secrete MMP *in vivo*, is disputed. MMP-1 mRNA and protein were detected by both *in situ* hybridization and immunohistochemistry in stromal as well as tumor cells of head, neck, gastric, colorectal, and mammary carcinomas (9,10,36,37). In contrast, Kameyama (12) demonstrated by *in situ* hybridization that the MMP-1 mRNA was not expressed in the cancer cells but in the surrounding fibrous capsules of strongly differentiated papillary thyroid carcinoma tissue. Highly differentiated follicular carcinomas and follicular adenomas were depleted for MMP-1 transcripts. Undifferentiated follicular, papillary, and aggressive anaplastic carcinomas that showed poor prognosis and strong tumor invasive and metastatic potential and that can be compared in their morphological, genetic and growth features with undifferentiated thyroid carcinoma cell lines were not included this

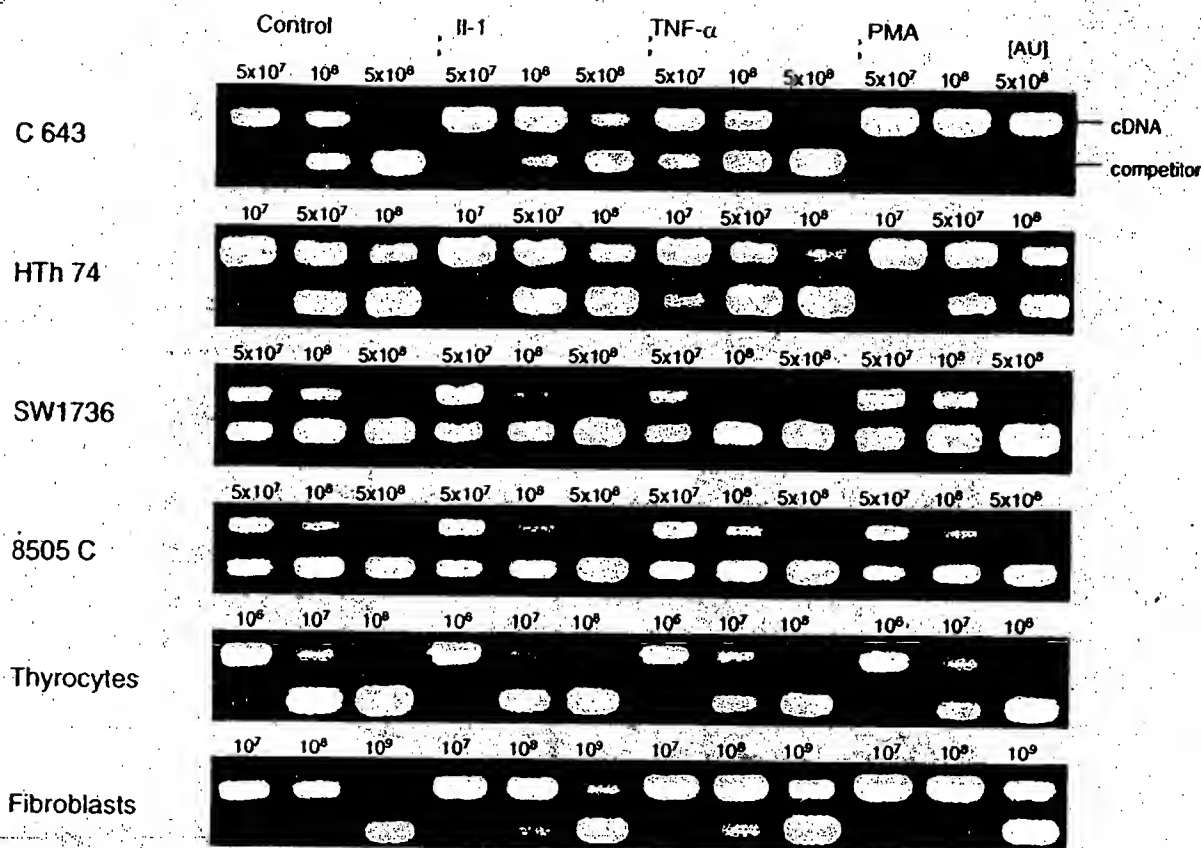


FIG. 4. Competitive TIMP-1 mRNA RT-PCR yielding a 351-bp (cDNA) and a 274-bp (competitor) PCR product. For further details see Figure 3.

study. However, the missing expression of MMP-1 by normal thyrocytes and the spontaneous secretion of this protein by highly malignant thyroid carcinoma cell lines, as demonstrated in our study, indicate the involvement of MMP-1 secretion of transformed thyrocytes in aggressive thyroid tumors.

Although all cell lines analyzed in our study spontaneously secreted MMP-1, we observed marked differences in the basal secretion capacity. The highest MMP-1 levels were determined in cultures of 8505 C cells. Only 8505 C cells expressed TPO and Tg mRNA that may be put down to residual differentiated components in the cell line (see *Materials*). However, none of the analyzed cell lines expressed TSH-R mRNA. The cell population doubling times were less than 40 hours. All cell lines had accumulations of multiple genetic events. These facts indicate the undifferentiated pathology of the studied lines. It is well known that anaplastic carcinoma cell lines well retain the malignant characteristics of their parental tumors (38–40).

Furthermore, we found a distorted proportion between MMP-1 and TIMP-1 mRNA/protein for carcinoma cell lines but not for normal thyroid-derived fibroblasts. The most disadvantageous constellation between MMP-1 and TIMP-1 was found in 8505 C cells. Similar to other studies (41), these results suggest the influence of an altered MMP/TIMP relation on tumor progression. However, it

should be mentioned that most studies, including the present one, do not take into consideration that a number of inhibitors distinct from TIMP-1 may regulate MMP-1 activity. Taking into account that the balance of active enzyme and TIMP-1 concentration strongly influence the extent of local matrix degradation, a number of studies showed unexpectedly high levels of TIMP-1 in malignant neoplasms (9,42,43). There is a great discussion as to whether the overall expression of MMP-1 and TIMP-1 or the amount of noncomplexed MMP-1 could be critical in aggressive tumor development. This fact underlines the nature of tissue breakdown, reflecting the complicated network of selective and coordinated production of individual proteinases and inhibitors under normal and pathophysiological conditions. Thus, the invasive and metastatic potential of thyroid tumors depends on the local net level of active MMPs.

The synthesis of MMP-1 and TIMP-1 is influenced by a variety of biochemical stimuli. The recent findings on MMP-1 and TIMP-1 gene promoters are useful in understanding the complex mechanisms implied in the regulation of MMP synthesis modulated by cytokines and tumor promoters (34,44,45). The promoter regions contain tumor promoter responsive elements (TRE) and binding motifs for the transcription factor PEA-3, which are recognized by proto-oncogenic transcription factors, such as the

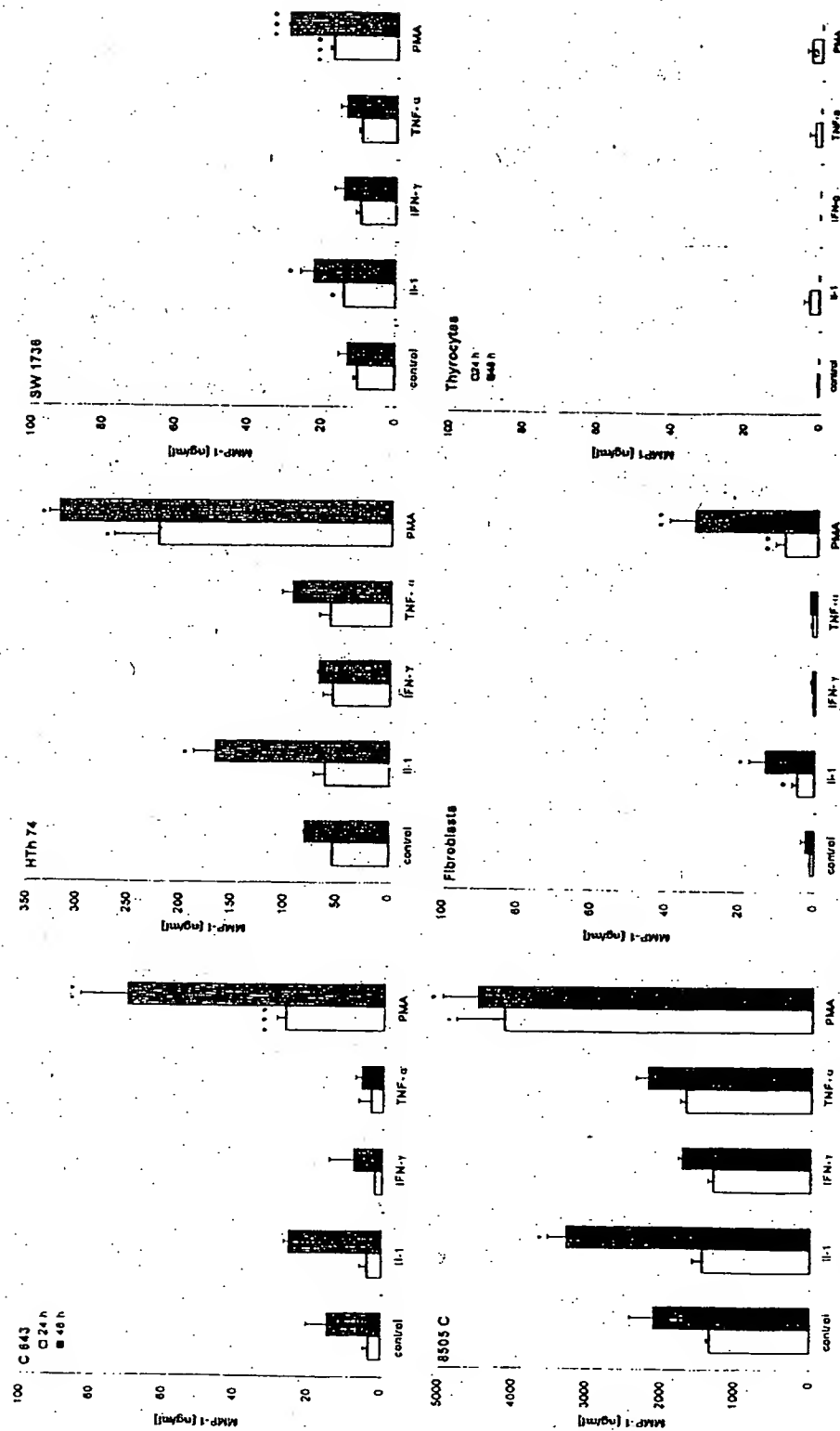


FIG. 5. MMP-1 protein levels (mean \pm SEM) in supernatants of unstimulated and stimulated cultures of thyroid carcinoma cell lines: 8505 C, SW 1736, C 643, HTh 74 ($n = 3$), thyroid-derived fibroblasts ($n = 4$) and the thyroid carcinoma cell lines: 8505 C, SW 1736, C 643, HTh 74 ($n = 3$) detected by MMP-1 ELISA, which recognizes total MMP-1, ie, free MMP-1 and that complexed with inhibitors such as TIMP-1, but not α_2 -macroglobulin. Cells were stimulated with 10 U/mL IL-1 α , 100 U/mL TNF- α , 500 U/mL IFN- γ , or 10 ng/ml PMA for 24 and 48 hours. For fibroblasts, each point represents the mean \pm SEM of four different donors, each experiment performed in triplicate. For thyroid carcinoma cell lines, each point represents the mean \pm SEM of three separate experiments each performed in triplicate. Significant differences between the basal and stimulated MMP-1 levels are indicated by asterisks (* $p < .05$; ** $p < .01$; *** $p < .005$). Please note the differences in scale between 8505 C, HTh 74, and the other cell types.

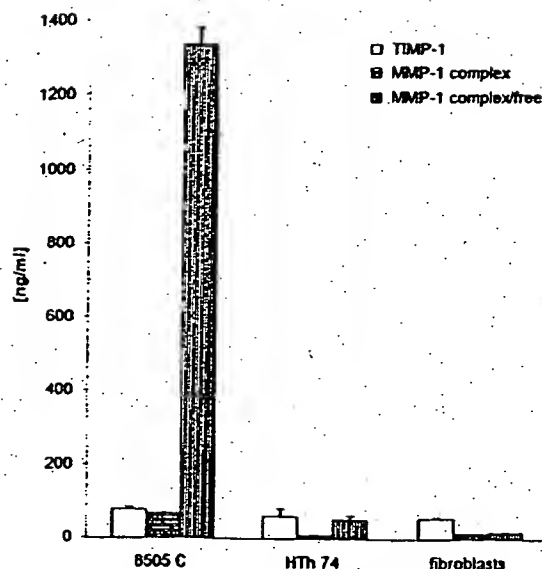


FIG. 7. Comparison between (i) free/complex and (ii) TIMP-1 complexed MMP-1 levels, and (iii) TIMP-1 levels in supernatants of unstimulated 8505 C and HTh 74 cells, and thyroid-derived fibroblasts after 24 hours using a (i) MMP-1 ELISA that recognizes total MMP-1 (see Figure 5). The (ii) MMP-1/TIMP-1 assay recognizes MMP-1/TIMP-1 complexes, ie, activated MMP-1 that has subsequently been complexed with the specific MMP inhibitor TIMP-1. The (iii) TIMP-1 ELISA recognizes total TIMP-1, ie, free TIMP-1 and that complexed with MMPs.

fos and *jun* family (45-47). IL-1, TNF- α , and PMA up-regulate proto-oncogenes like *fos* and *jun*, resulting in the stimulation of MMP-1 and TIMP-1 (45,48). The action of the cytokines is mediated by their specific receptors. In our study, IL-1R (type I and type II), TNF- α R (p75 and p55), and IFN- γ R mRNAs were demonstrated in all investigated cell types. PMA and IL-1 were shown to elevate MMP-1 and TIMP-1 in nearly all cell types investigated, thus confirming the results of several studies on other epithelial cells (reviewed in refs. 1,7,49). In the majority of experiments, we found a concordant expression of MMP-1 and TIMP-1 after stimulation, possibly achieved by the coordinated actions of the nuclear transcription factors, although MMP-1 and TIMP-1 expression can also be independently or even reciprocally regulated (1). The effect of TNF- α was not as distinct as in the case of PMA and IL-1, although several investigators found a pronounced effect of TNF- α particularly on TIMP-1 secretion (4,34). In contrast to studies performed with other cell types (863,864,819), IFN- γ did not influence MMP-1 and TIMP-1 expression in thyroid carcinoma cell lines. In summary, the involvement of the intrathyroidal physiological and pathological cytokine microenvironment in the regulation of MMP-1 and TIMP-1 induction activation and inhibition is strongly suggested.

Furthermore, the data demonstrate that regular human thyrocytes did not produce MMP-1, even after powerful stimulation with PMA. Investigating other mammalian epithelial cells, only one study revealed the production of

MMP-1 by rabbit corneal cells (21). It is yet not clear whether the MMP-1 mRNA detected in thyrocytes is due to a low level of constitutive transcription of the MMP-1 gene (illegitimate transcription), an existing pool of stable MMP-1 mRNA, or *in vitro* induction of MMP-1 mRNA. But it seems more likely that residual fibroblasts contained in the purified thyrocyte preparation (<0.2%) are responsible for the slightly positive RT-PCR results. Another explanation could be that thyrocytes are indeed MMP-1 producers, but the ELISA detection system used was not sensitive enough to measure extremely low MMP-1 secretion levels. Furthermore, the discrepancy between elevated TIMP-1 mRNA levels of thyrocytes and the extremely low TIMP-1 protein secretion by these cells is difficult to explain. Post-transcriptional regulatory events may be responsible for this confounding result.

Taken together, the present study suggests that the intrathyroidal cytokine microenvironment is involved in the regulation of MMP-1 and its inhibitor TIMP-1 in the thyroid, and that both proteins may be secreted by dedifferentiated thyroid carcinoma cells and involved in aggressive thyroid tumors *in vivo*.

REFERENCES

1. Ries C, Peindes PE 1995 Cytokine regulation of matrix metalloproteinase activity and its regulatory dysfunction in disease. *Biol Chem Hoppe Seyler* 376:345-355.
2. Pierce RA, Sandefur S, Doyle GA, Welgus HG 1996 Monocytic cell type-specific transcriptional induction of collagenase. *J Clin Invest* 97:1890-1899.
3. Pan L, Eckhoff C, Brinckerhoff CE 1995 Suppression of collagenase gene expression by all-trans and 9-cis retinoic acid is ligand dependent and requires both RARs and RXRs. *J Cell Biochem* 57:575-589.
4. Shingu M, Nagai Y, Isayama T, Naono T, Nobunaga M 1993 The effects of cytokines on metalloproteinase inhibitors (TIMP) and collagenase production by human chondrocytes and timp production by synovial cells and endothelial cells. *Clin Exp Immunol* 94:145-149.
5. Goldberg GI, Wilhelm SM, Kronberger A, Bauer EA, Grant GA, Eisen AZ 1986 Human fibroblast collagenase. Complete primary structure and homology to an oncogene transformation-induced rat protein. *J Biol Chem* 261:6600-6605.
6. Docherty AJ, Lyons A, Smith BJ, Wright EM, Stephens PE, Harris TJ, Murphy G, Reynolds JJ 1985 Sequence of human tissue inhibitor of metalloproteinases and its identity to erythroid-potentiating activity. *Nature* 318:66-69.
7. Mauviel A 1993 Cytokine regulation of metalloproteinase gene expression. *J Cell Biochem* 53:288-295.
8. Murphy G 1995 Matrix metalloproteinases and their inhibitors. *Acta Orthop Scand Suppl* 266:55-60.
9. Nomura H, Fujimoto N, Seiki M, Mai M, Okada Y 1996 Enhanced production of matrix metalloproteinases and activation of matrix metalloproteinase 2 (gelatinase A) in human gastric carcinomas. *Int J Cancer* 69:9-16.
10. Murray GI, Duncan ME, O'Neil P, Melvin WT, Fothergill JE 1996 Matrix metalloproteinase-1 is associated with poor prognosis in colorectal cancer. *Nat Med* 2:461-462.
11. Onisto M, Garbisa S, Caenazzo C, Freda MP, Di Francesco C, Nitti D, Liotta LA, Stetler-Stevenson WG 1993 Reverse transcription-polymerase chain reaction phenotyping of met-

- allopoteinases and inhibitors involved in tumor matrix invasion. *Diagn Mol Pathol* 2:74-80.
12. Kameyama K 1996 Expression of MMP-1 in the capsule of thyroid cancer—Relationship with invasiveness. *Pathol Res Pract* 192:20-26.
 13. Campo E, Merino MJ, Liotta L, Neumann R, Stetler-Stevenson W 1992 Distribution of the 72-kd type IV collagenase in nonneoplastic and neoplastic thyroid tissue. *Hum Pathol* 23:1395-1401.
 14. Demeure MJ, Damsky CH, Elfman F, Goretzki PE, Wong MG, Clark O 1992 Invasion by cultured human follicular thyroid cancer correlates with increased beta 1 integrins and production of proteases. *World J Surg* 16:770-776.
 15. Nakano T, Kusunoki T, Funasaka K, Murata K, Nishida S, Tomura T 1995 Study of type I and IV collagenase activity in human thyroid diseases. *Nippon Jibiinkoka Gakkai Kaiho* 98:937-941.
 16. Zedenius J, Stahle-Backdahl M, Enberg U, Grimelius L, Larsson C, Wallin G, Backdahl M 1996 Stromal fibroblasts adjacent to invasive thyroid tumors: expression of gelatinase A but not stromelysin 3 mRNA. *World J Surg* 20:101-106.
 17. Arai M, Niioka M, Maruyama K, Wada N, Fujimoto N, Nomiyama T, Tanaka S, Okazaki I 1996 Changes in serum levels of metalloproteinases and their inhibitors by treatment of chronic hepatitis C with interferon. *Dig Dis Sci* 41:995-1000.
 18. Nikkari ST, O'Brien KD, Ferguson M, Hatsukami T, Welgus HG, Alpers CE, Clowes AW 1995 Interstitial collagenase (MMP-1) expression in human carotid atherosclerosis. *Circulation* 92:1393-1398.
 19. Knowlden J, Martin J, Davies M, Williams JD 1995 Metalloproteinase generation by human glomerular epithelial cells. *Kidney Int* 47:1682-1689.
 20. Buisson AC, Zahm JM, Polette M, Pierrot D, Bellon G, Puchelle E, Birembaut P, Tournier JM 1996 Gelatinase B is involved in the in vitro wound repair of human respiratory epithelium. *J Cell Physiol* 166:413-426.
 21. Tao Y, Bazan HE, Bazan NG 1995 Platelet-activating factor induces the expression of metalloproteinases-1 and -9, but not -2 or -3, in the corneal epithelium. *Invest Ophthalmol Vis Sci* 36:345-354.
 22. Aust G, Heuer M, Laue S, Lehmann I, Hofmann A, Heldin N-E, Scherbaum WA 1996 Expression of TNA-alpha mRNA and protein in pathological thyroid tissue and carcinoma cell lines. *Clin Exp Immunol* 105:148-154.
 23. Mark J, Ekedahl C, Dahlenfors R, Westermarck B 1987 Cytogenetical observations in five human anaplastic thyroid carcinomas. *Hereditas* 107:163-174.
 24. Heldin NE, Cvejic D, Smeds S, Westermarck B 1991 Coexpression of functionally active receptors for thyrotropin and platelet-derived growth factor in human thyroid carcinoma cells. *Endocrinology* 129:2187-2193.
 25. Ito T, Seyama T, Hayashi Y, Hayashi T, Dohi K, Mizuno T, Iwamoto KS, Tsuyama N, Nakamura N, Akiyama M 1994 Establishment of two human thyroid carcinoma cell lines (8305C, 8505C) bearing p53 gene mutations. *International Journal of Oncology* 4:583-586.
 26. Wallin G, Backdahl M, Tallroth-Ekman E, Lundell G, Auer G, Lowhagen T 1989 Co-existent anaplastic and well differentiated thyroid carcinomas: a nuclear DNA study. *Eur J Surg Oncol* 15:43-48.
 27. Heuer M, Aust G, Ode-Hakim S, Scherbaum WA 1996 Different cytokine mRNA profiles in Graves' disease, Hashimoto's thyroiditis and non-autoimmune thyroid disorders determined by quantitative reverse transcriptase chain reaction (RT-PCR). *Thyroid* 6:97-106.
 28. Celi FS, Zenilman ME, Shuldiner AR 1993 A rapid and versatile method to synthesize internal standards for competitive PCR. *Nucleic Acids Res* 21:1047.
 29. Platzer C, Ode-Hakim S, Reinke P, Docke WD, Ewert R, Volk HD 1994 Quantitative PCR analysis of cytokine transcription patterns in peripheral mononuclear cells after anti-CD3 rejection therapy using two novel multispecific competitor fragments. *Transplantation* 58:264-268.
 30. Watson PF, Pickerill AP, Davies R, Weetman AP 1994 Analysis of cytokine gene expression in Graves' disease and multinodular goiter. *J Clin Endocrinol Metab* 79:355-360.
 31. Tada M, Diserens AC, Desbaillets I, de Tribolet N 1994 Analysis of cytokine receptor messenger RNA expression in human glioblastoma cells and normal astrocytes by reverse-transcription polymerase chain reaction. *J Neurosurg* 80:1063-1073.
 32. Nakano A, Tani E, Miyazaki K, Yamamoto Y, Furuyama J 1995 Matrix metalloproteinases and tissue inhibitors of metalloproteinases in human gliomas. *J Neurosurg* 83:298-307.
 33. Whitelock JM, O'Grady RL, Gibbins JR 1991 Interstitial collagenase (matrix metalloproteinase 1) associated with the plasma membrane of both neoplastic and nonneoplastic cells. *Invasion Metastasis* 11:139-148.
 34. Mackay AR, Ballin M, Pelina MD, Farina AR, Nason AM, Hartzler JL, Thorgeirsson UP 1992 Effect of phorbol ester and cytokines on matrix metalloproteinase and tissue inhibitor of metalloproteinase expression in tumor and normal cell lines. *Invasion Metastasis* 12:168-184.
 35. Urbanski SJ, Edwards DR, Maitland A, Leco KJ, Watson A, Kossakowska AE 1992 Expression of metalloproteinases and their inhibitors in primary pulmonary carcinomas. *Br J Cancer* 66:1188-1194.
 36. Polette M, Clavel C, Muller D, Abecassis J, Binniger I, Birembaut P 1991 Detection of mRNAs encoding collagenase I and stromelysin 2 in carcinomas of the head and neck by in situ hybridization. *Invasion Metastasis* 11:76-83.
 37. Clavel C, Polette M, Doco M, Binniger I, Birembaut P 1992 Immunolocalization of matrix metalloproteinases and their tissue inhibitor in human mammary pathology. *Bull Cancer (Paris)* 79:261-270.
 38. Boghaert ER, Ain K, Taylor K, Greenberg VL, Fowler C, Zimmer SG 1996 Quantitative and qualitative differences in growth, invasion and lung colonization of an anaplastic and a papillary human thyroid cancer cell line in vitro and in vivo. *Clin Exp Metastasis* 14:440-450.
 39. Asakawa H, Kobayashi T, Komoike Y, Yamagawa T, Takahashi M, Wakasugi E, Maruyama H, Tamaki Y, Matsuzawa Y, Monden M 1996 Establishment of anaplastic thyroid carcinoma cell lines useful for analysis of chemosensitivity and carcinogenesis. *J Clin Endocrinol Metab* 81:3547-3552.
 40. Viglietto G, Maglione D, Rambaldi M, Ceruti J, Romano A, Trapasso F, Fedele M, Ippolito P, Chiappetta G, Botti G, et al 1995 Upregulation of vascular endothelial growth factor (VEGF) and downregulation of placenta growth factor (PIGF) associated with malignancy in human thyroid tumors and cell lines. *Oncogene* 11:1569-1579.
 41. Nuovo GJ, MacConnell PB, Simsir A, Valea F, French DL 1995 Correlation of the in situ detection of polymerase chain reaction-amplified metalloproteinase complementary dnas and their inhibitors with prognosis in cervical carcinoma. *Cancer Res* 55:267-275.
 42. Naruo S, Kanayama H, Takigawa H, Kagawa S, Yamashita K, Hayakawa T 1994 Serum levels of a tissue inhibitor of

- metalloproteinases-1 (TIMP-1) in bladder cancer patients. *Int J Urol* 1:228-231.
43. Kossakowska AE, Urbanski SJ, Watson A, Hayden LJ, Edwards DR 1993 Patterns of expression of metalloproteinases and their inhibitors in human malignant lymphomas. *Oncol Res* 5:19-28.
44. Edwards DR, Rocheleau H, Sharma RR, Wills AJ, Cowie A, Hassell JA, Heath JK 1992 Involvement of AP1 and PEA3 binding sites in the regulation of murine tissue inhibitor of metalloproteinases-1 (TIMP-1) transcription. *Biochim Biophys Acta* 1171:41-55.
45. Schonthal A, Herrlich P, Rahmsdorf HJ, Ponta H 1988 Requirement for fos gene expression in the transcriptional activation of collagenase by other oncogenes and phorbol esters. *Cell* 54:325-334.
46. Gutman A, Wasylyk B 1990 The collagenase gene promoter contains a TPA and oncogene; responsive unit encompassing the PEA3 and AP-1 binding sites. *EMBO J* 9:2241-2246.
47. Wasylyk C, Gutman A, Nicholson R, Wasylyk B 1991 The c-Ets oncoprotein activates the stromelysin promoter through the same elements as several non-nuclear oncoproteins. *EMBO J* 10:1127-1134.
48. Brenner DA, O'Hara M, Angel P, Chojkier M, Karin M 1989 Prolonged activation of jun and collagenase genes by tumour necrosis factor-alpha. *Nature* 337:661-663.
49. Opdenakker G, Van Damme J 1992 Cytokines and proteases in invasive processes: molecular similarities between inflammation and cancer. *Cytokine* 4:251-258.

Address reprint requests to:
Dr. Gabriela Aust
Institute of Anatomy
University of Leipzig
Liebigstr. 13
Leipzig, D-04103, Germany

ARTICLE

Expression of Embryonic Fibronectin Isoform EIIIA Parallels α -Smooth Muscle Actin in Maturing and Diseased Kidney

Veronique L. Barnes, John Musa, Ronda J. Mitchell, and Jeffrey L. Barnes

Department of Medicine, Division of Nephrology, University of Texas Health Science Center, San Antonio, Texas (VLB,RJM,JLB); Medical Research Service, Audie Murphy Memorial Veterans Administration Hospital, San Antonio, Texas (JLB); and Department of Nephrology, Wilford Hall USAF Hospital, San Antonio, Texas (JM)

SUMMARY In this study we examined if an association exists between expression of an alternatively spliced "embryonic" fibronectin isoform EIIIA (Fn-EIIIA) and α -smooth muscle actin (α -SMA) in the maturing and adult rat kidney and in two unrelated models of glomerular disease, passive accelerated anti-glomerular basement membrane (GBM) nephritis and Habu venom (HV)-induced proliferative glomerulonephritis, using immunohistochemistry and in situ hybridization. Fn-EIIIA and α -SMA proteins were abundantly expressed in mesangium and in periglomerular and peritubular interstitium of 20-day embryonic and 7-day (D-7) postnatal kidneys in regions of tubule and glomerular development. Staining was markedly reduced in these structures in maturing juvenile (D-14) kidney and was largely lost in adult kidney. Expression of Fn-EIIIA and α -SMA was reinitiated in the mesangium and the periglomerular and peritubular interstitium in both models and was also observed in glomerular crescents in anti-GBM nephritis. Increased expression of Fn-EIIIA mRNA by in situ hybridization corresponded to the localization of protein staining. Dual labeling experiments verified co-localization of Fn-EIIIA and α -SMA, showing a strong correlation of staining between location and staining intensity during kidney development, maturation, and disease. Expression of EIIIA mRNA corresponded to protein expression in developing and diseased kidneys and was lost in adult kidney. These studies show a recapitulation of the co-expression of Fn-EIIIA and α -SMA in anti-GBM disease and suggest a functional link for these two proteins. (*J Histochem Cytochem* 47:787-797, 1999)

KEY WORDS
fibronectin
alternative splicing
smooth muscle actin
mesangium
glomerulonephritis
interstitial nephritis
fibrosis

ACTIVATION of mesenchymal cells has been associated with a switch to an α -smooth muscle actin (α -SMA) phenotype during proliferation and fibrosis in a variety of disease settings (Sappino et al. 1990; Johnson et al. 1991,1992; Kuhn and McDonald 1991; Alpers et al. 1992,1996; Jarnagin et al. 1994; Schmitt-Graff et al. 1994; Berndt et al. 1995; Boukhalfa et al. 1996; Tuchweber et al. 1996; Serini et al. 1998). In the kidney, it is well established that mesangial cells during glomerulonephritis and fibroblasts in interstitial nephritis are converted from a resting cell phenotype to

a myofibroblast-like cell during injury, acquiring the expression of α -SMA (Johnson et al. 1991; Alpers et al. 1992,1996; Johnson et al. 1992; Barnes et al. 1994a,1995b; Boukhalfa et al. 1996; El Nahas et al. 1996; Kliem et al. 1996; Tang et al. 1997). Factors involved in the phenotypic changes in mesenchymal cells remain unknown. However, prolonged culture and exposure to growth factors and extracellular matrix proteins activate the cells and elicit the expression of this cytoskeletal protein in several cell types such as liver fat-storing cells (Ito cells), breast stromal cells, fibroblasts, brain pericytes, and glomerular mesangial cells (Sappino et al. 1990; Elger et al. 1993; Jarnagin et al. 1994; Schmitt-Graff et al. 1994; Serini et al. 1998).

Recent interest has centered on a role for fibronectin (Fn), particularly an isoform containing an extra

Correspondence to: Jeffrey L. Barnes, PhD, Dept. of Medicine, Div. of Nephrology, University of Texas Health Science Center, 7703 Floyd Curl Drive, San Antonio, TX 78284.

Received for publication October 7, 1998; accepted January 12, 1999 (8A4801).

domain EIIIA (Fn-EIIIA), as a mediator of mesenchymal cell activation. The functions of the EIIIA domain are not known. However, its close proximity to the RGDS cell binding domain suggests that this isoform has specific functional roles (Schwarzbauer et al. 1985; Paul et al. 1986; Hynes 1990; Schwarzbauer 1991; ffrench-Constant 1995). The Fn-EIIIA variant is abundantly expressed during embryogenesis (ffrench-Constant and Hynes 1988,1989; Peters and Hynes 1996) and at the margins of healing wounds (ffrench-Constant et al. 1989; Brown et al. 1993), whereas this domain is spliced out of plasma Fn (derived from hepatocytes) and many tissue-specific cells in adult tissues (Peters et al. 1996), suggesting that it has important functions in remodeling (Paul et al. 1986; Schwarzbauer 1991; ffrench-Constant 1995). Functions for Fn-EIIIA have not been determined, but a close association with cells undergoing high rates of migration, proliferation, and differentiation suggests a role in cell activation (Schwarzbauer et al. 1985; ffrench-Constant and Hynes 1988,1989; ffrench-Constant et al. 1989; Hynes 1990; Schwarzbauer 1991; Brown et al. 1993; Barnes et al. 1994a,1995b; ffrench-Constant 1995; Peters and Hynes 1996).

Fn protein has been detected in glomeruli and the interstitium in developing kidney decreasing in intensity during maturation (Mounier et al. 1986; Peters and Hynes 1996; Peters et al. 1996). Similarly, α -SMA localizes in mesangial and peritubular structures during kidney development but is lost in adult kidney (Carey et al. 1992). Fn localizes in glomeruli and the peritubular interstitium in renal disease (Barnes et al. 1994a, 1995b; Yamamoto et al. 1994; Nicleleit et al. 1995; Alpers et al. 1996; El Nahas et al. 1996; Kliem et al. 1996), similar to areas of increased α -SMA expression during fibrosis, suggesting that these two proteins may be associated in tissues undergoing high rates of remodeling. However, the studies listed above examined localization of either Fn or α -SMA alone and did not examine if these two proteins co-localize or follow the same course of expression. Moreover, expression of Fn-EIIIA isoform in renal disease has been examined (Barnes et al. 1994a,b; Yamamoto et al. 1994; Nicleleit et al. 1995; Alonso et al. 1996), but correlations between this isoform and α -SMA expression have not been determined. Similarly, it is not known if the Fn-EIIIA isoform and α -SMA co-localize and follow the same course of expression during renal maturation. Because the Fn-EIIIA isoform may have an important role in cell activation in the kidney during nephrogenesis and remodeling, we examined the course of expression of Fn-EIIIA mRNA and the co-localization of these two proteins in embryonic, maturing, and adult kidney and in two unrelated models of renal disease characterized by mesangial cell proliferation, interstitial nephritis, and/or glomerular cres-

cents. The results showed that Fn-EIIIA and α -SMA co-localize and follow the same course of expression during kidney development and maturation and that a recapitulation of co-expression occurs in the mesangium and interstitium during renal disease.

Materials and Methods

Embryonic, Juvenile, and Adult Kidney

To examine the course of expression of Fn-EIIIA and α -SMA during kidney maturation, kidneys were obtained from 20-day embryos just before birth (rat gestation is 22 days), 7- (D-7) and 14-day (D-14) postnatal juveniles, and 6-8-week adult Sprague-Dawley rats (Charles River; Raleigh, NC). Kidney tissue was sliced and immediately frozen in liquid nitrogen, and stored in cryogenic tubes at -70°C for subsequent immunohistochemistry and in situ hybridization.

Induction of Anti-glomerular Basement Membrane (GBM) Nephritis

Anti-GBM Antibody. Glomeruli were isolated from Sprague-Dawley rat kidneys by differential sieving and GBM was purified according to the methods of Meezan et al. (1975). Rabbits were immunized with 100 μg GBM in complete Freund's adjuvant, followed 10 days later with an equal amount of antigen in Freund's incomplete adjuvant. The rabbits received periodic booster injections of 50-100 μg GBM in saline IV and were bled 10 days after each boost. All sera were pooled and an immunoglobulin fraction was obtained by 50% ammonium sulfate precipitation. The antibody was dialyzed against 0.02 M PBS pH 7.4, protein concentration quantified, sterile-filtered, and stored at -70°C until needed.

Protocol

An accelerated nephrotoxic nephritis was induced according to the methods of Lan et al. (1991). Nine rats were immunized with 5 mg rabbit IgG in Freund's complete adjuvant. Five days later the rats were divided into two groups, one challenged with 15 mg rabbit anti-GBM IgG in PBS ($n = 5$) IV and the other an untreated control group ($n = 4$). The rats were sacrificed at 3 weeks after the initial anti-GBM injection. At sacrifice, renal cortex was excised and frozen or fixed in 10% neutral buffered formalin for subsequent immunohistochemistry, in situ hybridization, and histological evaluation.

Proliferative Glomerulonephritis Induced by Habu Venom (HV)

To examine an association between Fn-EIIIA and α -SMA in lesions in a model of nonimmune glomerular disease, five rats were injected with HV as previously reported (Barnes 1989; Barnes and Abboud 1993; Barnes et al. 1994a,b, 1995b). Briefly, the rats were unilaterally nephrectomized to increase the incidence of subsequent glomerular lesions and 24 hr later they were injected with HV (*Trimeresurus flavoviridis*; Sigma Chemical, St Louis, MO) at a dose of 3.5 mg/kg IV. Seventy-two hr after injection of HV, the rats were

Fibronectin EIIIA Parallels α -Smooth Muscle Actin Expression

789

sacrificed and tissue was taken for subsequent morphological analysis, immunohistochemistry, and in situ hybridization. Lesions at 72 hr after HV are characterized by focal and segmental proliferative micronodules composed almost exclusively of mesangial cells (Barnes 1989; Barnes and Abboud 1993; Barnes et al. 1994b).

Immunohistochemical Localization of Fn-EIIIA and α -SMA Proteins

Localization of Fn-EIIIA and α -SMA was assessed by immunofluorescence and immunoperoxidase histochemistry using mouse monoclonal antibodies (MAbs) specific for the alternatively spliced extra domain (EIIIA) of cellular Fn (clones 3E2, Sigma and IST-9, Serotec; Harlan Bioproducts for Science, Indianapolis, IN). Mouse anti-human α -SMA MAb clone 1A4 was obtained from Sigma. Acetone-fixed frozen sections (6 μ m) were treated as previously described (Barnes 1989; Barnes and Abboud 1993; Barnes et al. 1994b). Sections were incubated with nonimmune IgG of the same species as the second antibody to block nonspecific binding, then with primary antibody followed by FITC- or biotin-labeled second antibodies [rat anti-mouse IgM MAb (Sigma) or donkey anti-mouse IgG MAb (Chemicon International; Temecula, CA)]. Second antibodies were adsorbed with IgGs of a variety of species (other than the primary) to avoid crossreactivity with endogenous rat IgG or to exogenous rabbit IgG administered to elicit anti-GBM nephritis. Sections employing the avidin-biotin complex (ABC; Vector Laboratories, Burlingame, CA) technique for immunoperoxidase were incubated with 0.6% hydrogen peroxide in methanol to block nonspecific peroxidase activity and 0.01% avidin, 0.001% biotin to block endogenous biotin activity. All incubations of primary and second antibody were for 30 min with three washes with PBS containing 0.1% bovine serum albumin (BSA), 5 min each between steps. Controls consisted of nonimmune mouse IgM, IgG, or PBS-BSA in place of primary antibody, followed by detection procedures as outlined above.

Dual Label Immunohistochemistry

To verify co-localization of EIIIA and α -SMA, dual label immunohistochemistry was employed utilizing two separate fluorescence tags. Tissue sections of representative kidneys of D-7 juveniles, anti-GBM, and 72-hr HV experiments were incubated with anti-Fn-EIIIA antibody followed by an affinity-purified FITC-labeled donkey anti-mouse IgG adsorbed with IgG derived from multiple species for dual labeling (Chemicon International). α -SMA was detected by direct immunostaining utilizing a Cy3-labeled mouse MAb (Sigma). Sections were washed with PBS-BSA between all antibody incubations. In addition, sections were incubated with normal nonimmune mouse IgG immediately before Cy3-anti- α -SMA to prevent potential binding of this labeled primary to the localized FITC-labeled second anti-mouse IgG antibody. Sections were viewed and photographed using an Olympus Research microscope equipped for epifluorescence using excitation and bandpass filters optimal for either FITC or Cy3. Sections incubated with anti-Fn-EIIIA and FITC-second antibody viewed with the Cy3 filter set and Cy3-anti- α -SMA viewed with the FITC filter set were negative, indicating effi-

cient barrier filtration of cross-illumination from the opposing fluorochromes.

In Situ Hybridization

Synthesis of riboprobe, tissue preparation, in situ hybridization and autoradiography were identical to methods used previously (Barnes et al. 1994a, 1995a,b). Briefly, cDNA probes containing a 160-bp alternatively spliced region EIIIA [generously provided by Dr. Richard O. Hynes, Massachusetts Institute of Technology (Paul et al. 1986)] and a 130-bp fragment derived from the 3'-untranslated rat α -SMA mRNA that is specific for α -SMA transcript (Kocher and Gabbiani 1987) (generously provided by Dr. Gabriel Gabbiani, University of Geneva) were used for generation of 35 S-labeled riboprobes to detect cellular localization of mRNA in sections of renal tissue. All experiments were performed simultaneously with the sense riboprobe as a negative control.

Preparation of Riboprobes

Linearized cDNA was transcribed in vitro using a Riboprobe system II kit (Promega; Madison, WI) according to the manufacturer's instructions. Either SP6 or T7 RNA polymerase and [35 S]-uridine-5'-(α -thio)-triphosphate (1300 Ci/mMol; New England Nuclear, Boston, MA) were included in the reaction mixture to generate [35 S]-labeled antisense and sense riboprobes. The reaction mixture was incubated for 60 min at 40°C, and then the DNA template was removed by digestion with 0.5 U RNase-free DNase, followed by removal of unincorporated nucleotides by phenol-chloroform extraction and ethanol precipitation. RNA probes (activity approximately 4×10^6 CPM/ μ l) were stored at -70°C and used within 3 days.

Tissue Preparation

Frozen sections (6 μ m) were cut and collected on aminosilane-glutaraldehyde-treated slides, then fixed for 20 min in 4% paraformaldehyde in 0.01 M PBS, pH 7.4. The sections were washed twice in PBS, dehydrated through a graded series of ethanols, air-dried, and used immediately for in situ hybridization.

Tissue Hybridization

In situ hybridization procedures were performed as previously described, involving prehybridization, hybridization, and removal of nonspecifically bound probe. Prehybridization steps included treatment with 0.2 N HCl, proteinase K (1 μ g/ml), and acetic anhydride to block background and enhance probe penetration. Twenty-five μ l of hybridization mixture containing 50% formamide, 10% dextran sulfate, 10 mM dithiothreitol, 0.1 M Tris-HCl, pH 7.5, 0.1 M NaPO₄, 0.3 M NaCl, 50 mM EDTA, 1 \times Denhardt's solution, 0.2 mg/ml yeast tRNA, and 2×10^5 cpm of 35 S-labeled riboprobe was applied to each section and covered with a siliconized coverslip. Hybridizations with EIIIA probes were performed in a sealed humid chamber for 18 hr at 50°C. α -SMA probes were very sticky, possibly due to a high content of G-C (75%) in the first half of the strand, and were

hybridized at 58°C. Excess probe was removed by washing slides in TE buffer, treatment with RNase A to decrease non-specific background activity, and rinsing in $2 \times$ SSC. Sections were dehydrated in graded ethanols, air-dried, and immersed in the dark in Kodak NTB-2 photographic emulsion (Eastman-Kodak; Rochester, NY). After air-drying the sections were exposed for 2–3 weeks at 4°C. The emulsion was developed and sections were stained with hematoxylin and eosin for subsequent bright- and darkfield microscopic analysis.

Results

Embryonic, Juvenile, and Adult Kidney

Expression of Fn-ElIIA and α -SMA is very similar in the renal parenchyma in the late embryo and early developing kidney, showing a nearly parallel localization of these two proteins in the glomerular mesangium and peritubular interstitium. Interstitial expression of both proteins also showed a parallel reduction of expression in the maturing and adult kidney, but glomerular α -SMA expression appeared to be preferentially reduced relative to Fn-ElIIA at the D-14 timepoint and beyond. Maturation of the metanephric parenchyma occurs in an outward direction from the interior towards the outer aspect of the cortex, with newly developing structures in the most peripheral aspect of the kidney and more mature structures deeper within the cortex. The pattern of expression of Fn-ElIIA and α -SMA protein followed this course, showing strongest intensity of staining in the peritubular and periglomerular interstitial mesenchymal cells and in the glomerular mesangium (Figures 1A and 1B) in developing cortex in 20-day embryos and in the outermost aspects of the cortex in D-7 kidneys (Figures 1C and 1D). Staining of Fn-ElIIA and α -SMA in more mature structures in the inner aspects of the cortex in D-7 kidneys showed less intensity of staining (Figures 1C, 1D, 2A, and 2B). Staining for both Fn-ElIIA and α -SMA in D-14 kidneys was substantially reduced and showed weak but evenly distributed staining of peritubular and periglomerular structures throughout the cortex (Figures 1E and 1F). Glomeruli expressed Fn-ElIIA and α -SMA in D-14 kidneys. However, staining intensity of α -SMA diminished, particularly in more mature glomeruli, towards the inner cortex. In adult kidneys, staining for Fn-ElIIA (Figure 1G) was lost in the peritubular and periglomerular interstitium, but the glomerular mesangium retained weak staining. Expression of α -SMA (Figure 1H) was entirely lost in the peritubular interstitium and glomerular mesangium throughout the kidney cortex in adult cortex. Dual labeling experiments verified a close correlation of Fn-ElIIA and α -SMA staining in peritubular and glomerular structures in maturing (D-7) kidney (Figures 2A and 2B). However, renal parenchyma destined to be-

come arterial and arteriolar structures in embryonic tissue, as well as arteries and arterioles in maturing and adult kidney, showed a departure from the parallel staining pattern and stained intensely for α -SMA but weakly for Fn-ElIIA (Figures 1C–1H).

Anti-GBM Nephritis

Anti-GBM nephritis was characterized by a mild mesangial proliferative glomerulonephritis, glomerular crescents, and focal areas of interstitial nephritis characterized by tubular atrophy and interstitial expansion. Expression of Fn-ElIIA and α -SMA protein was evident in all areas of disease and showed a distribution similar to that described for developing kidney, with strong staining in the periglomerular and peritubular interstitium and the mesangium (Figures 2C, 2D, and 3A–3D). Glomerular crescents also stained strongly for Fn-ElIIA and α -SMA (Figures 3A and 3B). Colocalization of Fn-ElIIA and α -SMA staining was verified by dual label immunofluorescence microscopy, showing a correlation between location, staining intensity, and severity of lesions in peritubular interstitium (Figures 2C and 2D) and glomeruli.

HV-induced Glomerulonephritis

Administration of HV results in an accelerated proliferative glomerulonephritis characterized by mesangiolysis, development of microaneurysms, and resulting in mesangial proliferative lesions by 72 hr after injection (Barnes 1989; Barnes and Abboud 1993; Barnes et al. 1994b, 1995a). In all kidneys studied, micronodules stained intensely for Fn-ElIIA and α -SMA (Figures 2E, 2F, 3E, and 3F). Periglomerular and peritubular structures stained weakly for Fn-ElIIA and α -SMA (Figures 2E, 2F, 3E, and 3F). Dual label immunofluorescence verified a co-localization of both proteins in all lesions examined (Figures 2E and 2F).

In Situ Hybridization

Expression of Fn-ElIIA and α -SMA mRNA corresponded to the localization of their respective proteins in embryonic, maturing, adult, and diseased kidneys (Figure 4). Message for Fn-ElIIA was observed in the interstitial mesenchyme and glomeruli, primarily in the deep cortex of 20-day embryos (Figure 4A). It became most concentrated in these same structures in the outer developing cortex of D-7 kidneys (Figure 4B) and was virtually lost in 2-week (Figure 4C) and adult rats. Similarly, Fn-ElIIA mRNA was detected in glomerular crescents and mesangium (Figure 4D) and in periglomerular and peritubular interstitium in areas of interstitial nephritis in anti-GBM rats (Figure 4E). Glomerular micronodules in kidneys from rats with HV-

Fibronectin EIIIA Parallels α -Smooth Muscle Actin Expression

791

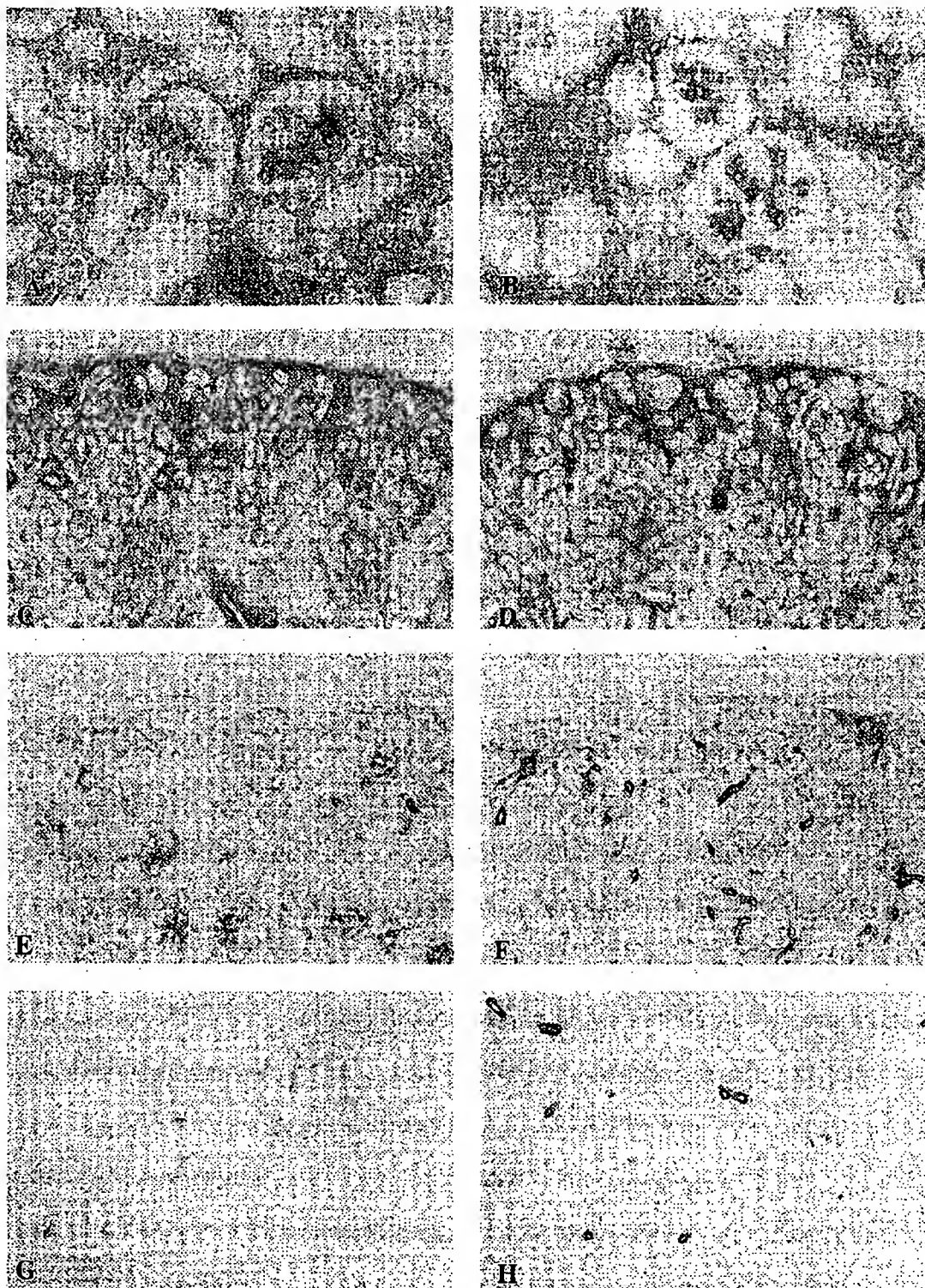


Figure 1 Immunoperoxidase localization of Fn-EIIIA (A,C,E,G) and α -SMA (B,D,F,H) in 20-day embryonic (A,B), D-7 (C,D) and D-14 (E,F) post-natal, and adult (G,H) rat kidneys. Expression of Fn-EIIIA and α -SMA appears to localize in identical structures and to follow the same course of expression during kidney maturation. Localization of both proteins is present in the glomerular mesangium and peritubular interstitium in 20-day embryo kidney and in the same structures in the newly developing outer cortex of D-7 kidneys. Except for arteries and arterioles, expression of both proteins is reduced in glomeruli and interstitium at 14 days and is largely lost in these areas in adult kidney.

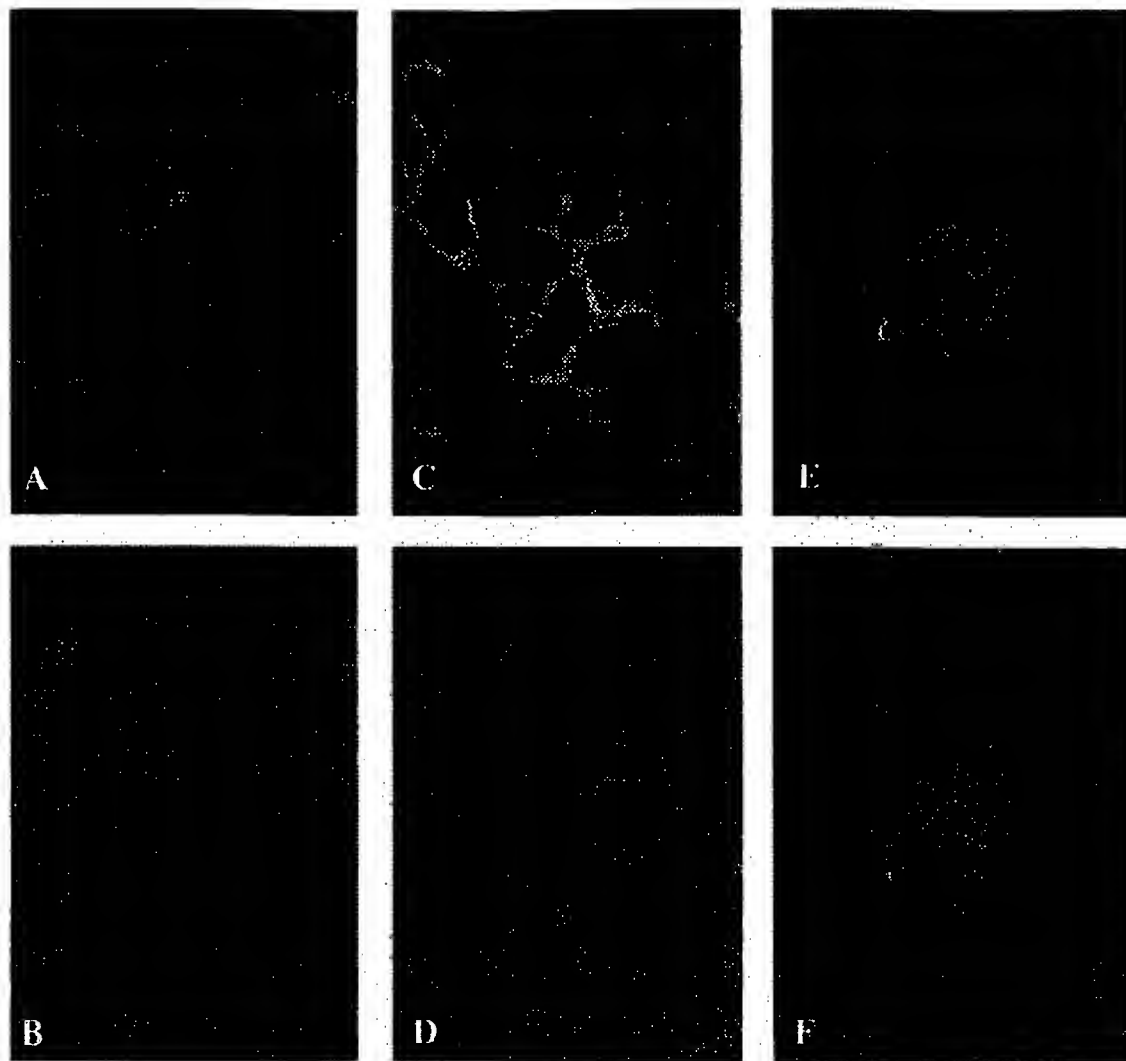


Figure 2 Dual label immunofluorescence verifying co-localization of Fn-EIIIA (A,C,E) and α -SMA (B,D,F) in the same sections in developing renal cortex of a D-7 post-natal rat (A,B) and in the interstitium (C,D) and a glomerulus (E,F) of rats treated with anti-GBM and HV, respectively. In all sections, Fn-EIIIA and α -SMA showed a very close correlation of expression by localizing in identical structures. Fn-EIIIA was detected by indirect immunofluorescence using a primary antibody and an FITC-labeled second antibody, and α -SMA was detected by direct immunofluorescence using Cy-3-labeled mouse anti- α -SMA (see Materials and Methods).

induced nephritis (Figure 4F) and, to a lesser extent, periglomerular and peritubular structures also showed enhanced expression of Fn-EIIIA mRNA. Sense controls showed negligible background staining.

Probes used for the detection of α -SMA mRNA were sticky (see Materials and Methods) and had a high degree of background staining, overshadowing the detail of peritubular expression of α -SMA message. However, specific message was detected above background in areas of high cellular activity, such as the outer aspect of the kidney cortex in D-7 postnatal kidney (Figure 4G), glomerular crescents (Figure 4H), and in HV-induced glomerular micronodules (Figure

4I), identical to areas of abundant expression of Fn-EIIIA mRNA and their respective proteins, as described above.

Discussion

These studies largely show a co-expression of Fn-EIIIA and α -SMA in embryonic and maturing rat kidneys and a recapitulation of expression in two unrelated models of renal disease. Expression of Fn-EIIIA and α -SMA was negligible or absent in adult renal parenchyma. However, a spatial and temporal association between these proteins was evident at sites of high cel-

Fibronectin EIIIA Parallels α -Smooth Muscle Actin Expression

793

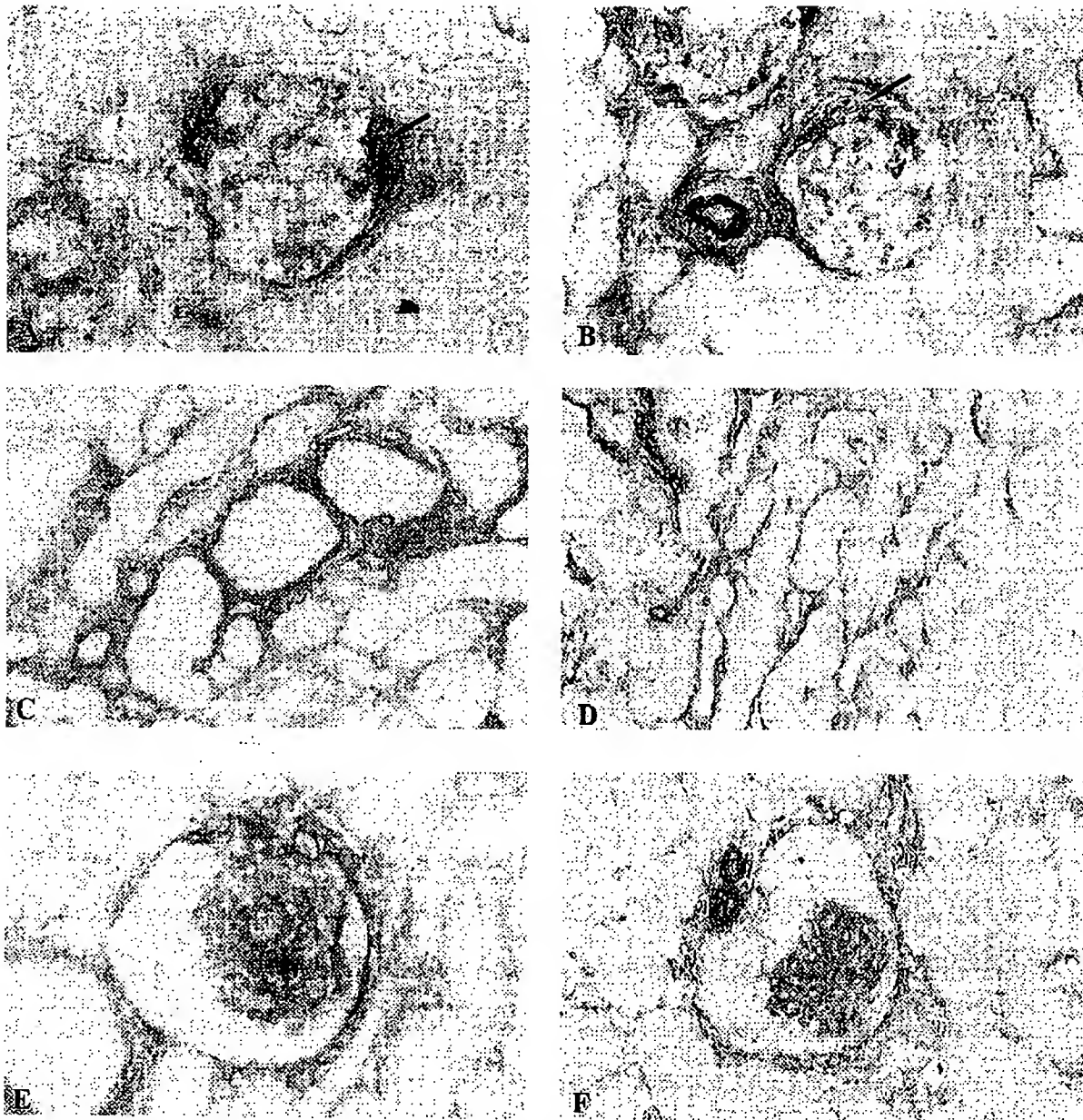


Figure 3 Immunoperoxidase localization of Fn-EIIIA (A,C,E) and α -SMA (B,D,F) in glomeruli (A,B) and interstitium (C,D) of an anti-GBM-treated rat and in glomeruli (E,F) of a rat treated with HV. EIIIA and α -SMA localize in the glomerular mesangium, crescents (arrows), and interstitium in kidney from rats treated with anti-GBM and in glomerular micronephrons and periglomerular and peritubule interstitium in HV-treated rats. Expression of both proteins appears to co-localize in the same structures in these two unrelated models of renal disease.

lular activity and activation during kidney development. Both proteins were expressed in the peritubular interstitium and glomerular mesangium, with staining intensity following the course of cortical development and a parallel reduction in expression during maturation. Fn-EIIIA mRNA was confined to the interstitium, in contrast to developing and maturing tubules, indicating that this Fn isoform is not synthesized by

the tubular epithelium and is not a component of mature tubular basement membrane. Instead, Fn-EIIIA may be expressed by mesangial cells and myofibroblasts or their precursors and as a provisional matrix for developing mesenchymal structures, and may be required for capillary growth and glomerulogenesis.

A recapitulation of Fn-EIIIA and α -SMA expression was observed during renal disease, with a co-

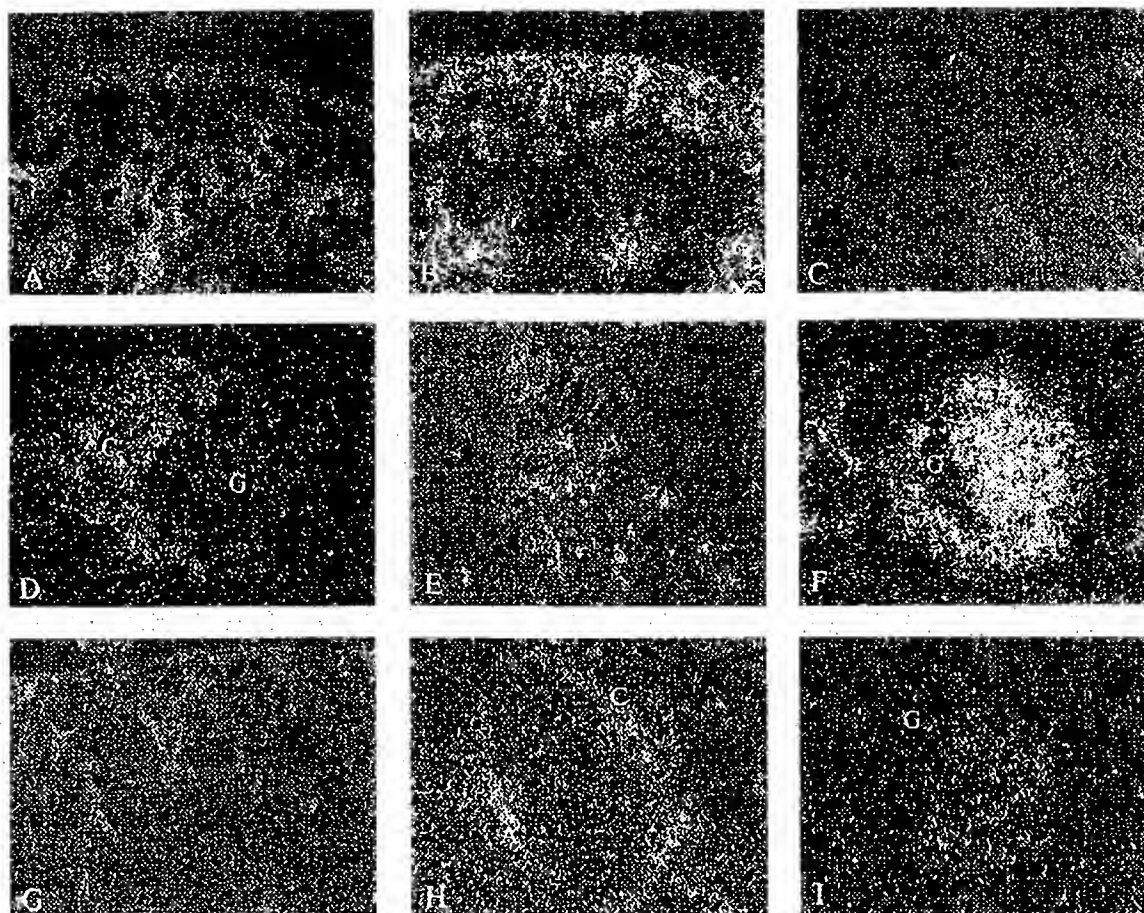


Figure 4 Darkfield localization of Fn-ELIIA mRNA (bright grains) by in situ hybridization in embryonic (A) and maturing D-7 (B) and D-14 (C) kidneys and in anti-GBM- (D,E) and HV- (F) induced nephritis. Message corresponds to the location and course of protein expression in kidney maturation. ELIIA mRNA is present in peritubular interstitial mesenchyme and in glomeruli in embryonic and D-7 juvenile kidney, and is lost in D-14 postnatal kidney. Similarly, α -SMA mRNA localizes in the outer cortex of a D-7 kidney (G) and in the glomerular mesangium and crescents and the interstitium in kidney of a rat with anti-GBM nephritis (H), as well as in a micronodule and in periglomerular structures in HV-induced proliferative glomerulonephritis (I). A, arteriole; C, crescents; G, glomerular capillary tuft.

expression of these proteins in the periglomerular and peritubular interstitium (by myofibroblasts) and in glomerular mesangium, similar to the areas of expression described during kidney development and maturation. A co-localization of Fn-ELIIA and α -SMA was also observed in glomerular crescents in anti-GBM nephritis. The cell types in crescents that may express α -SMA have not been identified but are believed to be myofibroblasts (Atkins et al. 1996) or transdifferentiated epithelial cells (Ng et al. 1998). The close association and course of dual expression of Fn-ELIIA and α -SMA in discrete tissue structures in three different conditions of cellular remodeling (nephrogenesis, proliferative glomerulonephritis, and interstitial disease) suggest that these two proteins are tightly linked and share common functional roles required for remodeling.

Activation of various mesenchymal cells is associated with a switch to an α -SMA-positive phenotype. Recent findings indicate that several cell types, such as liver fat-storing cells (Ito cells), breast stromal cells, fibroblasts, brain pericytes, and glomerular mesangial cells, do not express α -SMA in normal adult tissue or in primary culture. However, prolonged culture or exposure to growth factors activates these cells and elicits the expression of this cytoskeletal protein (Sappino et al. 1990; Johnson et al. 1991,1992; Elger et al. 1993; Schmitt-Graff et al. 1994; Serini et al. 1998). In addition, maintenance of Ito or mesangial cells on a surface that mimics normal basement membrane (i.e., Matrigel, an extract of Einglebroth-Holm-Swarm tumor) maintains cellular quiescence and downregulation of α -SMA expression, suggesting that extracellular matrix interactions are important in cell activation

(Rockey et al. 1992; DeLuca et al. 1993). Such cell-matrix interactions are supported by the observations that an Fn-EIIIA-enriched substratum induces fibroblast stress fiber formation and activation of a focal adhesion kinase (p125FAK), an important transmembrane signal transduction protein believed to be involved in cell activation (Xia and Culp 1995; Schlaepfer and Hunter 1996). Moreover, a role for Fn-EIIIA in cell activation has been reported in which Ito cells in normal liver and primary culture are α -SMA-negative but can be stimulated to express α -SMA when plated on Fn-EIIIA-fusion protein or endothelial cell-derived Fn-EIIIA, an interaction that could be inhibited by blocking with specific antibody to the EIIIA domain (Jarnagin et al. 1994). Interestingly, Ito cells during liver injury, fibroblasts in fibrotic lung disease, palmar fibromatosis, wound healing, interstitial nephritis, and mesangial cells during glomerulonephritis are converted from a resting cell phenotype to a myofibroblast-like cell during injury, and many of these mesenchymal cells are also associated with Fn-EIIIA during disease (Hynes 1990; Sappino et al. 1990; Kuhn and McDonald 1991; Barnes et al. 1994a, 1995b; Jarnagin et al. 1994; Schmitt-Gräff et al. 1994; Yamamoto et al. 1994, 1996; Berndt et al. 1995; Nickenleit et al. 1995; Alpers et al. 1996; Kliem et al. 1996; Tang et al. 1997; Serini et al. 1998). This study shows for the first time that Fn-EIIIA and α -SMA are temporally and spatially associated in kidney maturation and disease.

Other alternatively spliced isoforms, such as EIIIB, may also have functional roles in embryogenesis and disease (Schwarzbauer 1991; Nickenleit et al. 1995; Peters et al. 1996; Peters and Hynes 1996). Expression of Fn-EIIIA and Fn-EIIIB shows widespread co-distribution in embryonic tissues. However, it shows divergent tissue staining patterns in the adult mouse, suggesting variable functions for alternatively spliced Fn isoforms (Peters et al. 1996; Peters and Hynes 1996). Our previous studies showed a preferential enhancement of Fn-EIIIA mRNA and protein compared to Fn-EIIIB in late HV-induced glomerular lesions at a time when α -SMA was abundant (Barnes et al. 1995b), suggesting that a functional link between these two proteins is unique for the alternatively spliced EIIIA domain.

A functional role for Fn-EIIIA in cell activation and a switch to an α -SMA phenotype have not yet been defined. Remodeling during wound repair or after injury involves cellular behaviors including cell migration, proliferation, and synthesis of extracellular matrix, all of which Fn has been shown to influence (Hynes 1990; Schwarzbauer 1991; French-Constant 1995). Clues to the function of Fn-EIIIA in cell activation can be found in the observation that expression of α -SMA has been related to mesangial cell proliferation (Johnson et al. 1991; Elger et al. 1993) and hyper-

trophy (Glass et al. 1997) in vitro. Indeed, expression of α -SMA parallels mesangial and Ito cell proliferation and fibrogenesis (Johnson et al. 1991; Alpers et al. 1992, 1996; Johnson et al. 1992; Barnes et al. 1994a, 1995b; Jarnagin et al. 1994; Boukhalfa et al. 1996; Tuchweber et al. 1996). Mesangial cells in culture also require their own synthesis of Fn during migration and hillock formation (Glass et al. 1996). Mesangial cells in culture synthesize a matrix abundant in Fn-EIIIA (personal observations), unlike normal adult mesangial cells in vivo (Barnes et al. 1994a, 1995b; Peters et al. 1996; and this report). Therefore, Fn-EIIIA may also have some effect on mesangial cell migration.

We have previously characterized a model of proliferative glomerulonephritis, induced by HV, by a distinct temporal course involving mesangial cell migration, proliferation, and extracellular matrix synthesis (Barnes 1989; Barnes and Abboud 1993; Barnes et al. 1994a, 1995a, b). Our previous studies suggest that migrating mesangial cells do not require their own synthesis of Fn-EIIIA but may rely on exogenous sources of Fn isoforms derived from platelets and macrophages (Barnes et al. 1994a, 1995b), and agree with our in vitro studies (Barnes and Hevey 1991) showing a potent migratory mesangial cell response to platelet Fn, which is abundant in EIIIA (Paul et al. 1986; Peters et al. 1995). A switch to an α -SMA phenotype appeared to be related to mesangial cell synthesis of Fn-EIIIA and coincided with expression of α -SMA, proliferation, and matrix synthesis, suggesting that autocrine synthesis of Fn-EIIIA by mesangial cells has specific functions during the course of glomerular remodeling. Interestingly, Fn-EIIIA was expressed in early HV-induced glomerular lesions before mesangial cell expression of α -SMA (Barnes et al. 1994a); similar to a recent report by Serini et al. (1998) that ED-A (EIIIA) deposition precedes and then parallels α -SMA expression by fibroblasts during granulation tissue evolution in wound healing.

Serini et al. (1998) also showed that a functional ED-A domain is mandatory for α -SMA induction by transforming growth factor- β 1 (TGF- β 1). TGF- β 1 differentially regulates the expression of Fn-EIIIA in fibroblasts (Borsi et al. 1990) and induces expression of α -SMA in a variety of mesenchymal cells in culture (Desmouliere et al. 1993; Serini et al. 1998). Moreover, TGF- β 1 is frequently associated with a switch of fibroblast to a myofibroblast phenotype in liver, lung, and kidney disease (Sappino et al. 1990; Milani et al. 1991; Yamamoto et al. 1994; Zhang et al. 1995), and all three proteins frequently co-localize near myofibroblasts in these disease settings. Therefore, regulation of Fn-EIIIA synthesis by TGF- β 1 may provide a functional link for cell activation and α -SMA expression.

These studies show that Fn-EIIIA largely follows a parallel co-expression with α -SMA in several settings

of remodeling, including embryonic, maturing, and diseased kidney. An exact role for alternatively spliced Fn-IIIa in glomerular cell activation (expression of α -SMA) and cell function (migration, proliferation, matrix synthesis, and hypertrophy) has not been determined and remains the focus of current research.

Acknowledgments

Supported by NIH grant DK38758 from the National Institutes of Health (NIDDK), by the Office of Research and Development, Medical Research Service, Department of Veterans Affairs, and by the Southern Arizona Foundation.

We thank Dr George Henderson (Department of Medicine, UTHSCSA) for providing embryonic kidneys for this project. We also thank Drs Richard Hynes, and Gabriel Gabbiani for their generous gifts of cDNA probes to detect Fn-IIIa and α -SMA mRNA, respectively.

Literature Cited

- Alonso J, Gomez-Chiari M, Ortiz A, Seron D, Condom E, Lopez-Armada M, Largo R, Barar A, Egido J (1996) Glomerular up-regulation of EIIIA and V120 fibronectin isoforms in proliferative immune complex nephritis. *Kidney Int* 50:908-919
- Alpers CE, Hudkins KL, Gowu AM, Johnson RJ (1992) Enhanced expression of "muscle-specific" actin in glomerulonephritis. *Kidney Int* 41:1134-1142
- Alpers CE, Pichler R, Johnson RJ (1996) Phenotypic features of cortical interstitial cells potentially important in fibrosis. *Kidney Int* 49:S-28-31
- Atkins RC, Nikolic-Paterson DJ, Song Q, Lan HY (1996) Modulators of crescentic glomerulonephritis. *J Am Soc Nephrol* 7:2271-2278
- Barnes JL (1989) Glomerular localization of platelet secretory proteins in mesangial proliferative lesions induced by Habu snake venom. *J Histochem Cytochem* 37:1075-1082
- Barnes JL, Abboud HE (1993) Temporal expression of autocrine growth factors corresponds to morphological features of mesangial proliferation in Habu snake venom-induced glomerulonephritis. *Am J Pathol* 143:1366-1376
- Barnes JL, Hastings R, De La Garza MA (1994a) Sequential expression of cellular fibronectin by platelets, macrophages, and mesangial cells in proliferative glomerulonephritis. *Am J Pathol* 145:585-597
- Barnes JL, Hevey KA (1991) Glomerular mesangial cell migration: response to platelet secretory products. *Am J Pathol* 138:859-866
- Barnes JL, Hevey KA, Hastings RR, Bocanegra RA (1994b) Mesangial cell migration precedes proliferation in Habu snake venom-induced glomerular injury. *Lab Invest* 70:460-467
- Barnes JL, Mitchell RJ, Torres ES (1995a) Expression of plasminogen activator-inhibitor-1 (PAI-1) during cellular remodeling in proliferative glomerulonephritis in the rat. *J Histochem Cytochem* 43:895-905
- Barnes JL, Torres ES, Mitchell RJ, Peters JH (1995b) Expression of alternatively spliced fibronectin variants during remodeling in proliferative glomerulonephritis. *Am J Pathol* 147:1361-1371
- Berndt A, Kosmehl H, Mandel U, Gabler U, Luo X, Celeda D, Zardi L, Katnikamp D (1995) TGF β and bFGF synthesis and localization in Dupuytren's disease (nodular palmar fibromatosis) relative to cellular activity, myofibroblast phenotype and oncogenic variants of fibronectin. *Histochem J* 27:1014-1020
- Bursi L, Castellani P, Rizzo AM, Leprini A, Zardi L (1990) Transforming growth factor- β regulates the splicing pattern of fibronectin messenger RNA precursor. *FEBS Lett* 261:175-178
- Boukhalfa G, Desmouliere A, Rondeau E, Gabbiani G, Sraer JD (1996) Relationship between alpha-smooth muscle expression and fibrotic changes in human kidney. *Exp Nephrol* 3:241-247
- Brown LF, Dunin D, Lavigne I, Logan B, Dvorak HF, Van De Water L (1993) Macrophages and fibroblasts express embryonic fibronectin during cutaneous wound healing. *Am J Pathol* 142:793-801
- Carey AV, Carey RM, Gomez RA (1992) Expression of α -smooth muscle actin in the developing kidney vasculature. *Hypertension* 19:11-168-175
- DeLuca DJ, Konieczkowski M, Sedor JR (1993) α -smooth muscle cell actin and mesangial cell cytodifferentiation: matrix-adherent cells retain in vivo-like gene expression. *J Am Soc Nephrol* 4:649A
- Desmouliere A, Geinzz A, Gabbiani F, Gabbiani G (1993) Transforming growth factor- β 1 induces α -smooth muscle cell actin expression in granulation tissue myofibroblasts and in quiescent and growing cultured fibroblasts. *J Cell Biol* 122:103-111
- Elger M, Drenckhahn D, Nobiling R, Mundel P, Kriz W (1993) Cultured rat mesangial cells contain smooth muscle alpha-actin not found in vivo. *Am J Pathol* 142:497-509
- El Nahas AM, Muchanera-Kubarn EC, Zhang G, Adam A, Goumenos D (1996) Phenotypic modulation of renal cells during experimental and clinical renal scarring. *Kidney Int* 49:S-23-27
- ffrench-Constant C (1995) Alternative splicing of fibronectin—many different proteins but few different functions. *Exp Cell Res* 221:261-271
- ffrench-Constant C, Hynes RO (1988) Patterns of fibronectin gene expression and splicing during cell migration in chicken embryos. *Development* 104:369-382
- ffrench-Constant C, Hynes RO (1989) Alternative splicing of fibronectin is temporally and spatially regulated in the chicken embryo. *Development* 106:375-388
- ffrench-Constant C, Van De Water L, Dvorak HF, Hynes RO (1989) Reappearance of an embryonic pattern of fibronectin splicing during wound healing in the adult rat. *J Cell Biol* 109:903-914
- Glass WF, Karns LR, Haney LB (1997) Smooth muscle α -actin expression and hypertrophy in cultured human mesangial cells. *J Am Soc Nephrol* 8:515A
- Glass WF, Teng PR, Haney LB (1996) Extracellular matrix distribution and hillock formation in human mesangial cells in culture without serum. *J Am Soc Nephrol* 7:2230-2243
- Hynes RO (1990) *Fibronectins*. New York: Springer-Verlag
- Jarnagin WR, Rockey DC, Koteliensky VE, Wang S-S, Bissell DM (1994) Expression of variant fibronectins in wound healing: cellular source and biological activity of the EIIIA segment in rat hepatic fibrogenesis. *J Cell Biol* 127:2037-2048
- Johnson RJ, Floege J, Yoshimura A, Iida H, Couser WG, Alpers CE (1992) The activated mesangial cell: a glomerular "myofibroblast"? *J Am Soc Nephrol* 2:S190-197
- Johnson RJ, Iida H, Alpers CE, Majesky MW, Schwartz SM, Pritzl P, Gordon K, Gowu AM (1991) Expression of smooth muscle cell phenotype by rat mesangial cells in immune complex nephritis. Alpha-smooth muscle actin is a marker of mesangial cell proliferation. *J Clin Invest* 87:847-858
- Kliem V, Johnson RJ, Alpers CE, Yoshimura A, Couser WG, Koch KM, Floege J (1996) Mechanisms involved in the pathogenesis of tubulointerstitial fibrosis in 5/6-nephrectomized rats. *Kidney Int* 49:666-678
- Kocher O, Gabbiani G (1987) Analysis of α -smooth-muscle actin mRNA expression in rat aortic smooth-muscle cells using a specific cDNA probe. *Differentiation* 34:201-209
- Kuhn C, McDonald JA (1991) The roles of the myofibroblasts in idiopathic pulmonary fibrosis. Ultrastructural and immunohistochemical features of sites of active extracellular matrix synthesis. *Am J Pathol* 138:1257-1265
- Lan HY, Paterson DJ, Atkins RC (1991) Initiation and evolution of interstitial leukocytic infiltration in experimental glomerulonephritis. *Kidney Int* 40:425-433
- Meezan E, Hjelle T, Brendel K, Carlson EC (1975) A simple, versatile, nondisruptive method for the isolation of morphologically

Fibronectin EIIIA Parallels α -Smooth Muscle Actin Expression

797

- and chemically pure basement membranes from several tissues. *Life Sci* 17:1721-1732
- Milani S, Herbst H, Schuppan D, Stein H, Surrenti C (1991) Transforming growth factors β 1 and β 2 are differentially expressed in fibrotic liver disease. *Am J Pathol* 139:1221-1229
- Mounier F, Foidart J-M, Gubler M-C, Beziau A, Lacoste M (1986) Distribution of extracellular matrix glycoproteins during normal development of human kidney. An immunohistochemical study. *Lab Invest* 54:394-401
- Ng Y-Y, Fan J-M, Mu W, Nikolic-Paterson DJ, Huang T-P, Chang W-C, Atkins RC, Lan HY (1998) Involvement of glomerular epithelial-myofibroblast transdifferentiation (GEMT) in the development of glomerular crescents. *J Am Soc Nephrol* 9:505A
- Nickeleit V, Zagachin I, Nishikawa K, Peters JH, Hynes RO, Colvin RB (1995) Embryonic fibronectin isoforms are synthesized in crescents in experimental autoimmune glomerulonephritis. *Am J Pathol* 147:965-978
- Paul JI, Schwarzbauer JE, Tamkun JW, Hynes RO (1986) Cell-type-specific fibronectin subunits generated by alternative splicing. *J Biol Chem* 261:12258-12265
- Peters JH, Chen C, Hynes RO (1996) Fibronectin isoform distribution in the mouse. II. Differential distribution of the alternatively spliced EIIIB, EIIIA, and V segments in the adult mouse. *Cell Adhesion Commun* 4:127-148
- Peters JH, Hynes RO (1996) Fibronectin isoform distribution in the mouse. I. The alternatively spliced EIIIB, EIIIA, and V segments show widespread codistribution in developing mouse embryo. *Cell Adhesion Commun* 4:103-125
- Peters JH, Trevithick JE, Johnson P, Hynes RO (1995) Expression of the alternatively spliced EIIIB segment of fibronectin. *Cell Adhesion Commun* 3:67-89
- Rockey DC, Boyles JK, Gabbiani G, Friedman SL (1992) Rat hepatic lipocytes express smooth muscle actin upon activation in vivo and in culture. *J Submicrosc Cytol Pathol* 24:193-203
- Sappino A-P, Schurch W, Gabbiani G (1990) Differentiation repertoire of fibroblastic cells: expression of cytoskeletal proteins as marker of phenotypic modulations. *Lab Invest* 63:144-161
- Schlaepfer DD, Hunter T (1996) Signal transduction from the extracellular matrix—a role for the focal adhesion protein-tyrosine kinase FAK. *Cell Struct Funct* 21:445-450
- Schmitt-Grahl A, Desmouliere A, Gabbiani G (1994) Heterogeneity of myofibroblast phenotypic features: an example of fibroblastic cell plasticity. *Virchows Arch* 425:3-24
- Schwarzbauer JE (1991) Alternative splicing of fibronectin: three variants, three functions. *Bioessays* 13:527-533
- Schwarzbauer JE, Paul JI, Hynes RO (1985) On the origin of species of fibronectin. *Proc Natl Acad Sci USA* 82:1424-1428
- Serini G, Bochaton-Piallat M-L, Ropraz P, Geinoz A, Borsi L, Zardi L, Gabbiani G (1998) The fibronectin domain ED-A is crucial for myofibroblastic phenotype induction by transforming growth factor- β 1. *J Cell Biol* 142:873-881
- Tang WW, Van GY, Qi M (1997) Myofibroblast and α 1(III) collagen expression in experimental tubulointerstitial nephritis. *Kidney Int* 51:926-931
- Tuchweber B, Desmouliere A, Bochaton-Piallat ML, Bubbia-Brandt L, Gabbiani G (1996) Proliferation and phenotypic modulation of portal fibroblasts in the early stages of cholestatic fibrosis in the rat. *Lab Invest* 74:265-278
- Xia P, Culp LA (1995) Adhesion activity in fibronectin's alternatively spliced domain EDa (EIIIA): complementarity to plasma fibronectin functions. *Exp Cell Res* 217:517-527
- Yamamoto T, Noble NA, Cohen AH, Nast CC, Hishida A, Gold LI, Border WA (1996) Expression of transforming growth factor-beta isoforms in human glomerular diseases. *Kidney Int* 49:461-469
- Yamamoto T, Noble NA, Miller DE, Border WA (1994) Sustained expression of TGF- β 1 underlies development of progressive kidney fibrosis. *Kidney Int* 45:916-927
- Zhang D, Flanders KC, Phan SH (1995) Cellular localization of transforming growth factor- β expression in bleomycin-induced pulmonary fibrosis. *Am J Pathol* 147:352-361

BMI-1 Gene Amplification and Overexpression in Hematological Malignancies Occur Mainly in Mantle Cell Lymphomas¹

Silvia Beà, Frederic Tort, Magda Pinyol, Xavier Puig, Luis Hernández, Silvia Hernández, Pedro L. Fernández, Maarten van Lohuizen, Dolors Colomer, and Elias Campo²

The Hematopathology Section, Laboratory of Anatomic Pathology, Hospital Clinic, Institut d'Investigacions Biomèdiques "August Pi i Sunyer" (IDIBAPS), University of Barcelona, 08036 Barcelona, Spain (S. B., F. T., M. P., X. P., L. H., S. H., P. L. F., D. C., E. C.), and Division of Molecular Carcinogenesis, The Netherlands Cancer Institute, 1066 CX Amsterdam, Netherlands (M. v. L.)

Abstract

The *BMI-1* gene is a putative oncogene belonging to the Polycomb group family that cooperates with *c-myc* in the generation of mouse lymphomas and seems to participate in cell cycle regulation and senescence by acting as a transcriptional repressor of the *INK4a/ARF* locus. The *BMI-1* gene has been located on chromosome 10p13, a region involved in chromosomal translocations in infant leukemias, and amplified in occasional non-Hodgkin's lymphomas (NHLs) and solid tumors. To determine the possible alterations of this gene in human malignancies, we have examined 160 lymphoproliferative disorders, 13 myeloid leukemias, and 89 carcinomas by Southern blot analysis and detected *BMI-1* gene amplification (3- to 7-fold) in 4 of 36 (11%) mantle cell lymphomas (MCLs) with no alterations in the *INK4a/ARF* locus. *BMI-1* and *p16^{INK4a}* mRNA and protein expression were also studied by real-time quantitative reverse transcription-PCR and Western blot, respectively, in a subset of NHLs. *BMI-1* expression was significantly higher in chronic lymphocytic leukemia and MCL than in follicular lymphoma and large B cell lymphoma. The four tumors with gene amplification showed significantly higher mRNA levels than other MCLs and NHLs with the *BMI-1* gene in germline configuration. Five additional MCLs also showed very high mRNA levels without gene amplification. A good correlation between *BMI-1* mRNA levels and protein expression was observed in all types of lymphomas. No relationship was detected between *BMI-1* and *p16^{INK4a}* mRNA levels. These findings suggest that *BMI-1* gene alterations in human neoplasms are uncommon, but they may contribute to the pathogenesis in a subset of malignant lymphomas, particularly of mantle cell type.

Introduction

The *BMI-1*³ gene is a putative oncogene of the Polycomb group originally identified by retroviral insertional mutagenesis in Eμ-*c-myc* transgenic mice infected with the Moloney murine leukemia virus (1, 2). These animals had a rapid development of pre-B cell lymphomas showing frequent proviral insertions near the *BMI-1* gene. This integration resulted in *BMI-1* overexpression suggesting a cooperative effect between *C-MYC* and *BMI-1* genes in the development of these tumors (3, 4). Recent studies have indicated that the *BMI-1* gene may also participate in cell cycle control and senescence through the

INK4a/ARF locus by acting as an upstream negative regulator of *p16^{INK4a}* and *p14/p19^{ARF}* gene expression (5). The human *BMI-1* gene has been mapped to chromosome 10p13 (6), a region involved in chromosomal translocations in infant leukemias (7) and rearrangements in malignant T cell lymphomas (8, 9). More recently, high-level DNA amplifications of this region have been found by comparative genomic hybridization in NHLs and solid tumors (10, 11). However, the possible implication of the *BMI-1* gene in these alterations and its role in the pathogenesis of human tumors is not known. The aim of this study was to analyze the possible *BMI-1* gene alterations and expression in a large series of human neoplasms and to determine the relationship with *INK4a/ARF* locus aberrations.

Materials and Methods

Case Selection. A series of 262 human tumors, including 173 hematological malignancies and 89 carcinomas (Table 1), matched normal tissues from all carcinomas, 11 samples of normal peripheral mononuclear cells, and 5 reactive lymph nodes and tonsils, were selected based on the availability of frozen samples for molecular analysis.

DNA Extraction and Southern Blot Analysis. Genomic DNA was obtained using Proteinase K/RNase treatment. 15 μg were digested with *EcoRI* and *HindIII* restriction enzymes (Life Technologies, Inc., Gaithersburg, MD), for Southern blot analysis and hybridized with a 1.5-kb *PstI* fragment of the partial *BMI-1* cDNA (6).

RNA Extraction and Real-time Quantitative RT-PCR. Total RNA was obtained from 67 lymphoid neoplasms (10 CLLs, 27 MCLs, 8 FLs, and 22 LCLs) using guanidine/isothiocyanate extraction and cesium/chloride gradient centrifugation. One μg of total RNA was transcribed into cDNA using MMLV-reverse transcriptase (Life Technologies, Inc.) and random hexamers, following manufacturer's directions. Sequences of the *BMI-1* and the *p16* detection probes and primers were designed using the Primer Express program (Applied Biosystems, Foster City) as follows: *BMI-1* sense, 5'-CTGGTTGCCATTGACAGC-3'; *BMI-1* antisense, 5'-CAGAAATGAATGCCAG-CCA-3'; *p16* sense, 5'-CAACGCACCGAATAGTTACGG-3'; *p16* antisense, 5'-AAGCTTCGTCCTCCAGAGTCGC-3'. The probes *BMI-1*, 5'-CAGCTC-GCTTCAAGATGGCCGC-3', and *p16*, 5'-CGGAGGCCGATCCAGGTGG-GTA-3', were labeled with 6-carboxy-fluorescein as the reporter dye. The TaqMan-GAPDH Control Reagents (Applied Biosystems) were used to amplify and detect the *GAPDH* gene, as recommended by the manufacturer. The quantitative assay amplified 1 μl of cDNA in two to four replicates using the primers and probes described above and the standard master mix (Applied Biosystems). All reactions were performed in an ABI PRISM 7700 Sequence Detector System (Applied Biosystems). *GAPDH*, *BMI-1*, and *p16^{INK4a}* expression was related to a standard curve derived from serial dilutions of Raji cDNA. The RUs of *BMI-1* and *p16^{INK4a}* expression were defined as the mRNA levels of these genes normalized to the *GAPDH* expression level in each case.

Protein Analysis. Whole-cell protein extracts were obtained from additional frozen tissue available in 31 cases (7 CLLs, 12 MCLs, 8 FLs, and 4 LCLs), loaded onto a 10% SDS-polyacrylamide gel, and electroblotted to a nitrocellulose membrane (Amersham). Blocked membranes were incubated sequentially with the monoclonal antibody BMI-F6 (12), antimouse conju-

Received 10/16/00; accepted 1/29/01.

The costs of publication of this article were defrayed in part by the payment of page charges. This article must therefore be hereby marked advertisement in accordance with 18 U.S.C. Section 1734 solely to indicate this fact.

¹Supported by Grant SAF 99/20 from Comisión Interministerial de Ciencia y Tecnología, European Union Contract QLGI-CT-2000-689, the Asociación Española contra el Cáncer, and Generalitat de Catalunya 98SGR21. S. B. and F. T. were fellows supported by Spanish Ministerio de Educación y Cultura, and S. H. was supported by the Asociación Española contra el Cáncer and the Fundació Rius i Virgili.

²To whom requests for reprints should be addressed, at the Department of Pathology, Hospital Clinic, University of Barcelona, Villarroel 170, 08036-Barcelona, Spain. Phone: 34 93 227 5450; Fax: 34 93 227 5572; E-mail: campo@medicina.ub.es.

³The abbreviations used are: *BMI-1*, B cell-specific Moloney murine leukemia virus integration site 1; NHL, non-Hodgkin's lymphoma; CLL, chronic lymphocytic leukemia; FL, follicular lymphoma; LCL, large B cell lymphoma; MCL, mantle cell lymphoma; RT-PCR, reverse-transcription-PCR; RU, relative units.

Table 1 Hematological malignancies and solid tumor samples analyzed for BMI-1 gene alterations

Tissue samples	No. of cases
Hematological malignancies	
Hodgkin's disease	2
B cell lymphoproliferative disorders	
B-Acute lymphoblastic leukemia	14
CLL	29
Hairy cell leukemia	4
FL	15
MCL	36
LCL	40
T cell lymphoproliferative disorders	
T-Acute lymphoblastic leukemia	8
Large granular cell leukemia	4
Peripheral T-cell lymphoma	8
Myeloproliferative disorders	
Acute myeloid leukemia	7
Chronic myeloid leukemia	6
Solid tumors	
Colon carcinoma	26
Breast carcinoma	29
Laryngeal squamous cell carcinoma	34
Total	262

gated to horseradish peroxidase (Amersham), and detected by enhanced chemiluminescence (Amersham) according to the manufacturer's recommendations.

Statistical Analysis. Because of the non-normal distribution of the samples and the small size of some subsets of tumors, the statistical evaluation was performed using nonparametric tests (SPSS, version 9.0). Comparison between mRNA expression levels in the different groups of NHLs was performed using the Kruskal-Wallis Test, with a *P* for significance set at 0.05. For differences between particular groups, the conservative Bonferroni procedure was performed, and the *P* was set at 0.005. The remaining statistical analyses were carried out using the Mann-Whitney nonparametric *U* test (significance, *P* < 0.05). The comparison between BMI-1 and p16^{INK4a} quantitative mRNA levels was also performed using the Pearson's correlation coefficient.

Results

BMI-1 Gene Amplification. The BMI-1 gene was examined by Southern blot in a large series of human tumors and normal samples (Table 1). The cDNA probe used in the study detected three *Eco*RI fragments of 7.3, 3.8, and 2.6 kb and three *Hind*III fragments of 6.2, 4, and 3.5 kb. BMI-1 gene amplification (3- to 7-fold) was detected in 4 of 36 (11%) MCLs (Fig. 1). The amplifications were confirmed with both restriction enzymes. The amplified MCLs were two blastoid and two typical variants. No amplifications were observed in any of the solid tumors when compared with their respective matched non-neoplastic mucosa. No BMI-1 gene rearrangements were observed in any of the samples examined.

BMI-1 mRNA Expression. To determine the BMI-1 expression pattern in NHL we analyzed BMI-1 mRNA levels by real-time quantitative RT-PCR in 67 lymphomas (10 CLLs, 27 MCLs, 8 FLs, and 22 LCLs), including the four tumors with gene amplification. A distinct BMI-1 mRNA expression pattern was observed in the different types of lymphomas (Fig. 2; Kruskal-Wallis Test; *P* < 0.001). The BMI mRNA levels in CLLs (mean, 2.2 RU; SD, 1.3) and MCLs with no BMI-1 gene amplification (mean, 2.5 RU; SD, 2.3) were significantly higher than in FLs (mean, 0.9 RU; SD, 0.8) and LCLs (mean, 0.6 RU; SD, 0.4; Mann-Whitney nonparametric *U* test; *P* < 0.01). The 4 MCLs with BMI-1 gene amplification showed significantly higher levels of expression than all other groups of tumors (mean, 5.1 RU; SD, 1.6; *P* < 0.005). In addition, five typical MCLs with no structural alterations of the gene also showed very high levels of BMI-1 mRNA expression ranging from 4 to 9.8 RU, similar to cases with gene amplification (Fig. 2A).

BMI-1 Protein Expression. BMI-1 protein expression was examined by Western blot in 31 tumors (7 CLLs; 12 MCLs, including two

cases with BMI-1 gene amplification and 4 cases with mRNA overexpression and no structural alteration of the gene; 8 FLs, and 4 LCLs) in which additional frozen tissue was available. The monoclonal antibody against BMI-1 detected three closely migrating proteins of *M_r* 45,000–48,000 (2). The two more slowly migrating bands probably represent phosphorylated isoforms of the protein (12). The two MCLs with gene amplification and three of four cases with mRNA overexpression without amplification of the gene showed very high levels of protein expression. The remaining MCLs and CLLs showed intermediate levels of protein expression, whereas low- or no-expression signals were detected in the LCLs and FLs included in the study (Fig. 3). These results indicate that BMI-1 protein expression in NHL is concordant with the mRNA levels observed by real-time quantitative RT-PCR.

Relationship between BMI-1 and p16^{INK4a} Gene Alterations. The *INK4a/ARF* locus has been recently identified as a downstream target of the transcriptional repressing activity of the BMI-1 gene, suggesting that this gene may contribute to human neoplasias with wild type *INK4a/ARF* (5). Most of the lymphoproliferative disorders analyzed in the present study, including the four cases with BMI-1 gene amplification, had been previously examined for *p53* gene mutations and *INK4a/ARF* locus alterations, including gene deletions, mutations, hypermethylation, and expression (13, 14). The four MCLs with BMI-1 gene amplification and mRNA overexpression and the five tumors with BMI-1 mRNA overexpression with no structural alterations of the gene showed a wild-type configuration of the *INK4a/ARF* locus (13). However, one case with BMI-1 gene amplification and one case with mRNA overexpression with no alteration of the gene showed *p53* gene mutations associated with allelic deletions.

To determine the possible relationship between BMI-1 and p16^{INK4a} mRNA expression, p16^{INK4a} mRNA levels were evaluated by real-time quantitative RT-PCR in 50 tumors (10 CLLs, 27 MCLs, and 13 LCLs), including 6 cases with alterations in the *INK4a/ARF* locus (2 MCLs and 1 LCL with p16^{INK4a} gene deletion, 2 LCLs with p16 promoter hypermethylation, and 1 CLL with p16^{INK4a} gene mutation), and the 4 lymphomas with BMI-1 amplification. Negative or negligible levels of p16^{INK4a} were observed in the 6 tumors with *INK4a/ARF* locus alterations. These cases were not included in the comparisons between BMI-1 and p16^{INK4a} mRNA expression. The p16^{INK4a} expression levels were relatively similar in the different types of tumors. Only LCLs tended to have lower levels of expression, but the differences did not reach statistical significance (Fig. 2B). No differences were observed in the p16^{INK4a} mRNA levels between tumors with BMI-1 gene amplification and overexpression and lymphomas with germline configuration of the gene.

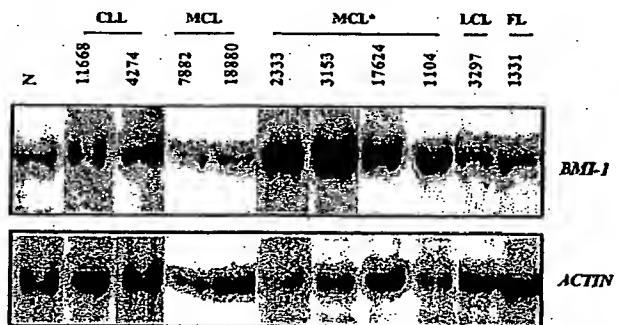


Fig. 1. Southern blot analysis of BMI-1 gene. Four MCLs (MCL*) showed BMI-1 gene amplification (3- to 7-fold) compared with non-neoplastic tissues (N) and other NHLs. No amplifications or gene rearrangements were detected in the remaining NHLs and carcinomas included in the study.

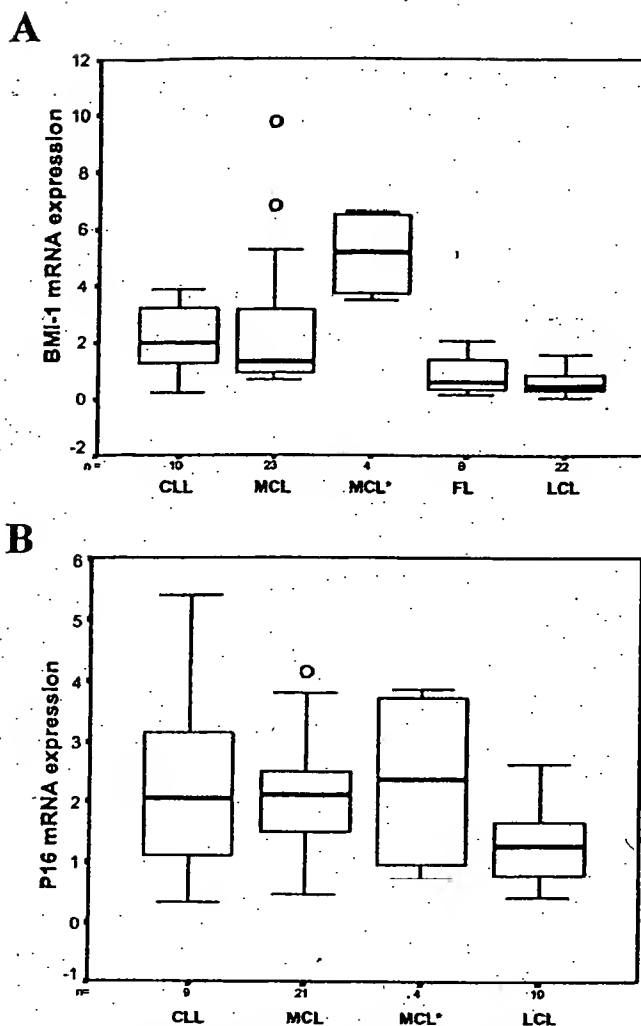


Fig. 2. A, quantitative BMI-1 mRNA transcript analysis (median and range) using real-time RT-PCR in a series of NHLs. MCLs with *BMI-1* gene amplification (MCL*) revealed significantly higher overall BMI-1 mRNA levels than all other types of NHLs, including MCLs with no structural alterations of the gene ($P < 0.005$). MCLs and CLLs expressed significantly higher levels than FLs and LCLs ($P < 0.001$). Results are depicted as the ratio of absolute BMI-1:GADPH mRNA transcript numbers (RU). Bars, SD. B, quantitative p16^{INK4a} mRNA transcript analysis (median and range) using real-time RT-PCR in a series of NHLs. Expression levels were relatively similar in the different types of tumors. Results are depicted as the ratio of absolute p16^{INK4a}:GADPH mRNA transcript numbers (RU). Bars, SD.

Discussion

In the present study, we have examined a large series of human tumors for the presence of gene alterations and mRNA expression of the *BMI-1* gene. Gene amplification was identified in four MCLs. These tumors showed significantly higher levels of mRNA and protein expression compared with other lymphomas with *BMI-1* in germline configuration. BMI-1 expression levels were also highly up-regulated in a subset of MCLs with no apparent structural alterations of the gene. No alterations were detected in any of the different types of carcinomas included in the study. *BMI-1* is considered an oncogene belonging to the Polycomb group family of genes. These proteins mainly act as transcriptional regulators, controlling specific target genes involved in development, cell differentiation, proliferation, and senescence. Different studies have shown the implication of BMI-1 overexpression in the development of lymphomas in murine and feline animal models (3, 4). The findings of the present study indicate

for the first time that *BMI-1* gene alterations in human neoplasms are an uncommon phenomenon, but they seem to occur mainly in a subset of NHLs, particularly of mantle cell type.

The human *BMI-1* gene has been mapped to chromosome 10p13. High-level DNA amplifications and gains in this region have been identified by comparative genomic hybridization in occasional solid tumors and NHLs (10, 11). Different chromosomal translocations involving the 10p13 region have also been identified in infant leukemias and T cell lymphoproliferative disorders (7, 8, 15). Most acute leukemias with this chromosomal alteration occur in children <12 months of age, whereas it seems to be extremely rare in adults. 10p translocations in T-cell lymphoproliferative disorders have been observed mainly in adult T cell leukemia/lymphomas and occasional cutaneous T cell lymphomas. In our study, we did not observe *BMI-1* rearrangements or amplifications in any of the acute leukemias or T cell lymphomas. However, all of the acute leukemias in this study were diagnosed in patients over 16 years, and no adult T cell leukemia/lymphomas or cutaneous lymphomas could be included in the series. Similarly, high-level DNA amplifications at the 10p13 region have been detected in head and neck carcinomas and other solid tumors. Although we found no evidence for *BMI-1* gene rearrangements or amplifications in a substantial set of carcinomas, this does not exclude the possibility of increased gene expression, or protein levels in these tumors. Additional studies are required to elucidate the possible involvement of *BMI-1* in these particular groups of human neoplasms.

In human hematopoietic cells, BMI-1 is preferentially expressed in primitive CD34+ bone marrow cells, whereas it is negative or very low in more mature CD34- cells (16). In peripheral lymphocytes, and particularly in follicular B cells, BMI-1 protein expression has been detected in resting cells of the mantle zone, whereas it is down-regulated in proliferating germinal center cells (17, 18). These observations indicate that BMI-1 expression in normal hematopoietic cells is tightly regulated in relation with cell differentiation in bone marrow and antigen-specific response in peripheral lymphocytes. BMI-1 expression in human tumors has not been examined previously. In this study, we have demonstrated that BMI-1 mRNA and protein expression show a distinct pattern in different types of lymphomas. Thus, BMI-1 levels were low in LCLs and FLs and significantly higher in MCLs and CLLs. These findings suggest that BMI-1 expression patterns in B cell lymphomas maintain in part the expression profile of their normal cell counterparts; because FLs and at least a subgroup of LCLs are considered lymphomas derived from follicular germinal center cells, whereas MCLs and CLLs are tumors mainly derived from naive pregerminal center cells. However, the four MCLs with *BMI-1* gene amplification expressed significantly higher mRNA levels than all other tumors. In addition, five MCLs with no structural alterations of the gene showed high mRNA levels similar to those observed in tumors with *BMI-1* gene amplification, suggesting that other mechanisms may be involved in up-regulation of the gene in these lymphomas. Different studies using animal models have shown a dose-dependent effect of *BMI-1* gene expression on skeleton development

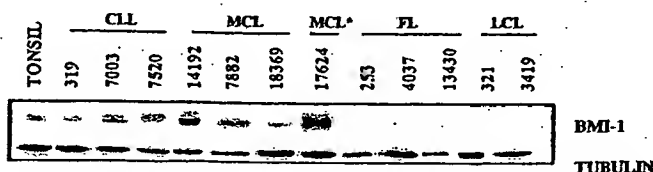


Fig. 3. Western blot analysis of BMI-1 protein in NHLs. The amplified MCL (17624) showed the highest BMI-1 protein levels, whereas other MCLs and CLLs had intermediate levels of expression. Very low or negative signal was observed in FLs and LCLs.

and lymphomagenesis (1, 3). These observations suggest that the high mRNA and protein levels detected in a subset of MCLs may play a role in the pathogenesis of these neoplasms.

Recent studies have identified the *INK4a/ARF* locus as a downstream target of the BMI-1 transcriptional repressor activity, suggesting that BMI-1 overexpression may contribute to human neoplasias that retain the wild-type *INK4a/ARF* locus (5). Interestingly, in our study, BMI-1 amplification and overexpression appeared in tumors with no alterations in *p16^{INK4a}* and *p14^{ARF}* genes. However, we could not detect differences in the expression levels of *p16^{INK4a}* in tumors with and without BMI-1 gene alterations. The reasons for this apparent discrepancy with experimental observations are not clear. One possibility may be that genes other than *INK4a/ARF* are the main targets of BMI-1 repressor activity in these tumors. Particularly, different genes of the HOX family are regulated by BMI-1 and may also be involved in lymphomagenesis (19, 20).

In conclusion, the findings of this study indicate that BMI-1 gene expression is differentially regulated in B cell lymphomas. Alterations of the gene seem to be an uncommon phenomenon in human neoplasms, but they may contribute to the pathogenesis in a subset of MCLs. Although, BMI-1 gene alterations occurred in tumors with wild-type *INK4a/ARF* locus, the possible cooperation between these genes and the oncogenic mechanisms of BMI-1 in human neoplasms require additional analysis.

Acknowledgments

The authors thank Iracema Nayach for her excellent technical assistance.

References

- Haupt, Y., Alexander, W. S., Barri, G., Klinken, S. P., and Adams, J. M. Novel zinc finger gene implicated as myc collaborator by retrovirally accelerated lymphomagenesis in E μ -myc transgenic mice. *Cell*, 65: 753-763, 1991.
- van Lohuizen, M., Verbeek, S., Sebeij, B., Wientjens, E., van der Gulden, H., and Berns, A. Identification of cooperating oncogenes in E μ -myc transgenic mice by provirus tagging. *Cell*, 65: 737-752, 1991.
- Alkema, M. J., Jacobs, H., van Lohuizen, M., and Berns, A. Perturbation of B and T cell development and predisposition to lymphomagenesis in E μ Bmi1 transgenic mice require the Bmi1 RING finger. *Oncogene*, 15: 899-910, 1997.
- Haupt, Y., Bath, M. L., Harris, A. W., and Adams, J. M. Bmi-1 transgene induces lymphomas and collaborates with myc in tumorigenesis. *Oncogene*, 8: 3161-3164, 1993.
- Jacobs, J. J., Kieboom, K., Marino, S., DePinho, R. A., and van Lohuizen, M. The oncogene and Polycomb-group gene *bmi-1* regulates cell proliferation and senescence through the *ink4a* locus. *Nature (Lond.)*, 397: 164-168, 1999.
- Alkema, M. J., Wiegant, J., Raap, A. K., Berns, A., and van Lohuizen, M. Characterization and chromosomal localization of the human proto-oncogene *BMI-1*. *Hum. Mol. Genet.*, 2: 1597-1603, 1993.
- Pui, C. H., Raimondi, S. C., Murphy, S. B., Ribeiro, R. C., Kalwinsky, D. K., Dahl, G. V., Crist, W. M., and Williams, D. L. An analysis of leukemic cell chromosomal features in infants. *Blood*, 69: 1289-1293, 1987.
- Berger, R., Baranger, L., Bernheim, A., Valensi, F., Flandrin, G., and Berbeim, A. T. Cytogenetics of T-cell malignant lymphoma. Report of 17 cases and review of the chromosomal breakpoints. *Cancer Genet. Cytogenet.*, 36: 123-130, 1988.
- D'Alessandro, E., Paterlini, P., Lo Re, M. L., Di Cola, M., Ligas, C., Quaglino, D., and Del Porto, G. Cytogenetic follow-up in a case of Sezary syndrome. *Cancer Genet. Cytogenet.*, 45: 231-236, 1990.
- Bea, S., Ribas, M., Hernandez, J. M., Bosch, F., Pinyol, M., Hernandez, L., Garcia, J. L., Flores, T., Gonzalez, M., Lopez-Guillermo, A., Piris, M. A., Cardesa, A., Montserrat, E., Miro, R., and Campo, E. Increased number of chromosomal imbalances and high-level DNA amplifications in mantle cell lymphoma are associated with blastoid variants. *Blood*, 93: 4365-4374, 1999.
- Knuutila, S., Björkqvist, A. M., Autio, K., Tarkkanen, M., Wolf, M., Monni, O., Szymanska, J., Larramendi, M. L., Tapper, J., Pere, H., el-Rifai, W., Hemmer, S., Wasenius, V. M., Vidgren, V., and Zhu, Y. DNA copy number amplifications in human neoplasms: review of comparative genomic hybridization studies. *Am. J. Pathol.*, 152: 1107-1123, 1998.
- Alkema, M. J., Bronk, M., Verhoeven, E., Otte, A., van't Veer, L. J., Berns, A., and van Lohuizen, M. Identification of Bmi1-interacting proteins as constituents of a multimeric mammalian polycomb complex. *Genes Dev.*, 11: 226-240, 1997.
- Pinyol, M., Hernández, L., Martínez, A., Cobo, F., Hernández, S., Bea, S., López-Guillermo, A., Nayach, I., Palacin, A., Nadal, A., Fernández, P., Montserrat, E., Cardesa, A., and Campo, E. *INK4a/ARF* locus alterations in human non-Hodgkin's lymphomas mainly occur in tumors with wild type *p53* gene. *Am. J. Pathol.*, 156: 1987-1996, 2000.
- Pinyol, M., Cobo, F., Bea, S., Jares, P., Nayach, I., Fernández, P. L., Montserrat, E., Cardesa, A., and Campo, E. *p16^{INK4a}* gene inactivation by deletions, mutations, and hypermethylation is associated with transformed and aggressive variants of non-Hodgkin's lymphomas. *Blood*, 91: 2977-2984, 1998.
- Foot, A. B., Oakhill, A., and Kitchen, C. Acute monoblastic leukemia of infancy in Klinefelter's syndrome. *Cancer Genet. Cytogenet.*, 61: 99-100, 1992.
- Lessard, J., Babán, S., and Sauvageau, G. Stage-specific expression of polycomb group genes in human bone marrow cells. *Blood*, 91: 1216-1224, 1998.
- Raaphorst, F. M., van Kemnade, F. J., Fieret, E., Hamer, K. M., Satijn, D. P., Otte, A. P., and Meijer, C. J. Cutting edge: polycomb gene expression patterns reflect distinct B cell differentiation stages in human germinal centers. *J. Immunol.*, 164: 1-4, 2000.
- Raaphorst, F. M., van Kemnade, F. J., Blokzijl, T., Fieret, E., Hamer, K. M., Satijn, D. P., Otte, A. P., and Meijer, C. J. Coexpression of *BMI-1* and *EZH2* polycomb group genes in Reed-Sternberg cells of Hodgkin's disease. *Am. J. Pathol.*, 157: 709-715, 2000.
- Gould, A. Functions of mammalian Polycomb group and trithorax group related genes. *Curr. Opin. Genet. Dev.*, 7: 488-494, 1997.
- van Oostveen, J., Bijl, J., Raaphorst, F., Walboomers, J., and Meijer, C. The role of homeobox genes in normal hematopoiesis and hematological malignancies. *Leukemia*, 13: 1675-1690, 1999.

Gene-expression profiles predict survival of patients with lung adenocarcinoma

DAVID G. BEER¹, SHARON L.R. KARDIA², CHIANG-CHING HUANG³, THOMAS J. GIORDANO⁴, ALBERT M. LEVIN², DAVID E. MISEK⁵, LIN LIN¹, GUOAN CHEN¹, TAREK G. GHARIB¹, DAFYDD G. THOMAS⁴, MICHELLE L. LIZYNESS⁴, RORK KUICK⁵, SATORU HAYASAKA³, JEREMY M.G. TAYLOR³, MARK D. IANNETTONI¹, MARK B. ORRINGER¹ & SAMIR HANASH⁵

Departments of ¹Surgery, ²Epidemiology, ³Biostatistics, ⁴Pathology and ⁵Pediatrics, University of Michigan, Ann Arbor, Michigan, USA

Correspondence should be addressed to D.G.B.; email: dgbeer@umich.edu.

Published online: 15 July 2002, doi:10.1038/nm733

Histopathology is insufficient to predict disease progression and clinical outcome in lung adenocarcinoma. Here we show that gene-expression profiles based on microarray analysis can be used to predict patient survival in early-stage lung adenocarcinomas. Genes most related to survival were identified with univariate Cox analysis. Using either two equivalent but independent training and testing sets, or 'leave-one-out' cross-validation analysis with all tumors, a risk index based on the top 50 genes identified low-risk and high-risk stage I lung adenocarcinomas, which differed significantly with respect to survival. This risk index was then validated using an independent sample of lung adenocarcinomas that predicted high- and low-risk groups. This index included genes not previously associated with survival. The identification of a set of genes that predict survival in early-stage lung adenocarcinoma allows delineation of a high-risk group that may benefit from adjuvant therapy.

Lung cancer remains the leading cause of cancer death in industrialized countries. Most patients with non-small cell lung cancer (NSCLC) present with advanced disease, and despite recent advances in multi-modality therapy, the overall 10-year survival rate remains a dismal 8–10%. However, a significant minority of patients (~25–30%) with NSCLC have stage I disease and receive surgical intervention alone. Although 35–50% of patients with stage I disease will relapse within 5 years^{2–4}, it is not currently possible to identify specific high-risk patients.

Adenocarcinoma is currently the predominant histological subtype of NSCLC (refs. 1,5,6). Although morphological assessment of lung carcinomas can roughly stratify patients, there is a need to identify patients at high risk for recurrent or metastatic disease. Preoperative variables that affect survival of patients with NSCLC have been identified^{7–10}. Tumor size, vascular invasion, poor differentiation, high tumor-proliferative index and several genetic alterations, including *K-ras* (refs. 11,12) and *p53* (refs. 10,13) mutations, have prognostic significance. Multiple independently assessed genes or gene products have also been investigated to better predict patient prognosis in lung cancer^{14–18}. Technologies that simultaneously analyze the expression of thousands of genes¹⁹ can be used to correlate gene-expression patterns with numerous clinical parameters—including patient outcome—to better predict tumor behavior in individual patients²⁰. Analyses of lung cancers using array technologies have identified subgroups of tumors that differ according to tumor type and histological subclasses and, to a lesser extent, survival among adenocarcinoma patients^{21,22}. Here we correlated gene-expression profiles with clinical outcome in a cohort of patients with lung adenocarcinoma and identified specific genes that

predict survival among patients with stage I disease. For further validation, we also show that the risk index predicted survival in an independent cohort of stage I lung adenocarcinomas.

Hierarchical profile clustering yields three tumor subsets

Using oligonucleotide arrays, we generated gene-expression profiles for 86 primary lung adenocarcinomas, including 67 stage I and 19 stage III tumors, as well as 10 non-neoplastic lung samples. Selected sample replicates showed high correlation among coefficients and reliable reproducibility. We determined transcript abundance using a custom algorithm and the data set was trimmed of genes expressed at extremely low levels, that is, genes were excluded if the measure of their 75th percentile value was less than 100. Although potentially resulting in the loss of some information, trimming in this manner decreased the possibility that the clustering algorithm would be strongly influenced by genes with little or no expression in these samples. Hierarchical clustering with the resulting 4,966 genes yielded 3 clusters of tumors (Fig. 1). All 10 non-neoplastic samples clustered tightly together within Cluster 1 (data not shown). We examined the relationships between cluster and patient and tumor characteristics (Fig. 1 and Supplementary Figure A online). There were associations between cluster and stage ($P = 0.030$) and between cluster and differentiation ($P = 0.01$). Cluster 1 contained the greatest percentage (42.8%) of well differentiated tumors, followed by Cluster 2 (27%) and Cluster 3 (4.7%). Cluster 3 contained the highest percentage of both poorly differentiated (47.6%) and stage III tumors (42.8%), yet contained 3 (14.3%) moderately differentiated and 1 (5%) well differentiated stage I tumor. Notably, 11 stage I tumors were present in Cluster 3, sug-

gesting a common gene-expression profile for this subset of stage I and stage III tumors.

For patients with stage I and stage III tumors, the average ages were 68.1 and 64.5 years and the percentage of smokers was 88.9% and 89.5%, respectively. Marginally significant associations between cluster and smoking history were observed ($P = 0.06$). A significant relationship between histopathological classification and cluster was only discernable for bronchioloalveolar adenocarcinomas (BAs), which were only present in Clusters 1 and 2 ($P = 0.0055$) and comprised 35.7% and 12.3% of tumors for Clusters 1 and 2, respectively.

We examined the heterogeneity in gene-expression profiles based on the trimmed data set among normal lung samples and stage I and stage III adenocarcinomas by calculating correlation coefficients between all pairs of samples. In contrast to normal lung samples that displayed highly similar gene-expression profiles (median correlation, 0.9); both stage I and III lung tumors demonstrated much greater heterogeneity in their expression profiles with lower correlation coefficients (median values, 0.82 and 0.79, respectively).

Northern-blot and immunohistochemistry analyses

Of the 4,966 genes examined, 967 differed significantly between stage I and III adenocarcinomas, a number in excess of that expected by chance alone (248 at alpha level (α) = 0.05). Three genes were arbitrarily selected to verify the microarray expression data. The mRNA from 20 of the normal lung and tumor samples was examined by northern-blot hybridization with probes for insulin-like growth factor-binding protein 3 (IGFBP3), cystatin C

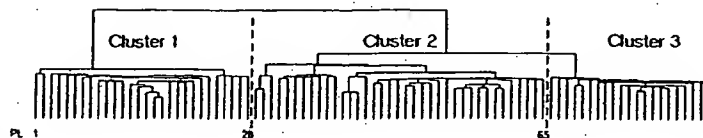


Fig. 1 Unsupervised classification analysis of lung adenocarcinomas. 3 classes of tumors identified by agglomerative hierarchical clustering of gene-expression profiles using the 4,966 expressed genes. Patient and histopathological information for each lung adenocarcinoma case by cluster designation and methods for *K-ras* 12/13th-codon mutational status and nuclear p53 protein accumulation are provided (Supplementary Figure A online). TN classification denotes information regarding patient tumor size and nodal involvement. Associations between cluster membership and patient or histopathological variables are indicated at significance level ($P \leq 0.05$).

and lactate dehydrogenase A (LDH-A) (Fig. 2a). Two gene probes not represented on the microarrays were used as controls, including histone H4, a potential index of overall cell proliferation, and 28S ribosomal RNA, a control for sample loading and transfer. The relative amounts of IGFBP3, cystatin C and LDH-A mRNA strongly correlated with microarray-based measurements (Fig. 2b). In both assays, IGFBP3 and LDH-A mRNA levels increased from stage I to stage III adenocarcinomas and were higher than those in normal lung. Cystatin C mRNA levels were more variable but relatively greater in normal lung than tumors. These results suggest that the oligonucleotide microarrays provided reliable measures of gene expression. The tumors showed slightly greater histone H4 expression than the normal lung, likely reflecting increased proliferation of tumor cells.

Immunohistochemistry was performed for IGFBP3, cystatin C and HSP-70 to determine whether mRNA overexpression was reflected by an increase of their corresponding proteins in tumors.

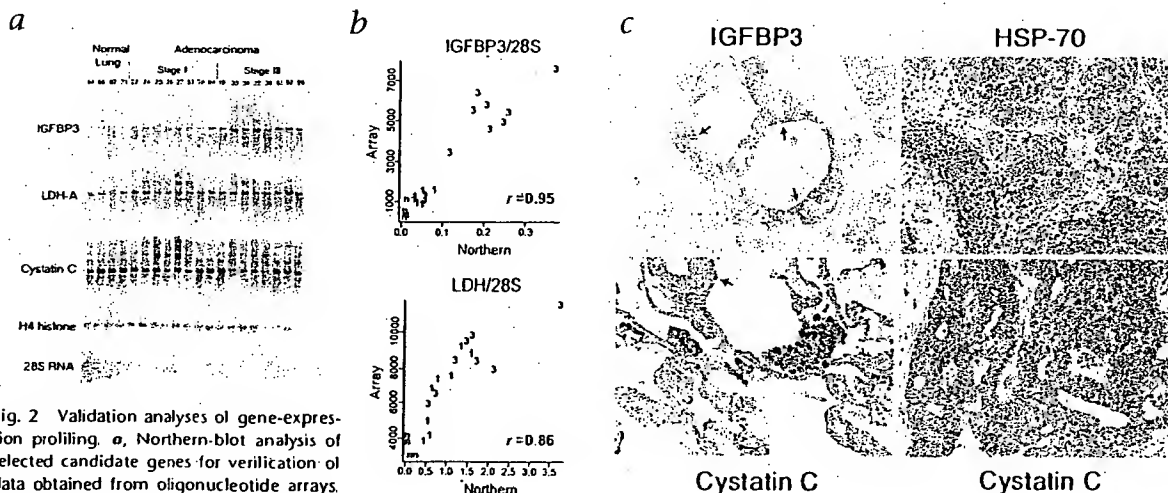


Fig. 2 Validation analyses of gene-expression profiling. **a**, Northern-blot analysis of selected candidate genes for verification of data obtained from oligonucleotide arrays. The same sample RNA for the 4 uninvolved lung, 8 stage I and 8 stage III tumors was used for the northern-blot and oligonucleotide array analyses. **b**, Correlation analysis of quantitative data obtained from oligonucleotide arrays and northern blots measured by integrated phosphorimager-based signals for the IGFBP3 and LDH-A genes. The ratio of IGFBP3, cystatin C and LDH-A mRNA to 28S rRNA was determined. The relative values for each gene from each sample are shown. n, non-neoplastic normal lung; 1, stage I tumors; 3, stage III tumors. **c**, Immunohistochemical analysis of IGFBP3, HSP-70 and cystatin C in lung and lung adenocarcinomas. Cytoplasmic IGFBP3 immunoreactivity in a neoplastic gland (tumor L22)

with prominent apical staining (blue reactant staining, arrow, upper left). Diffuse cytoplasmic HSP-70 immunoreactivity (tumor L27), yet stromal elements show no reactivity (upper right). Normal lung parenchyma (lower left) shows cytoplasmic cystatin C immunoreactivity in alveolar pneumocytes (arrow) and intra-alveolar macrophages but tumor (L90) shows diffuse cytoplasmic cystatin C immunoreactivity with prominent apical staining (lower right). Magnification, $\times 200$

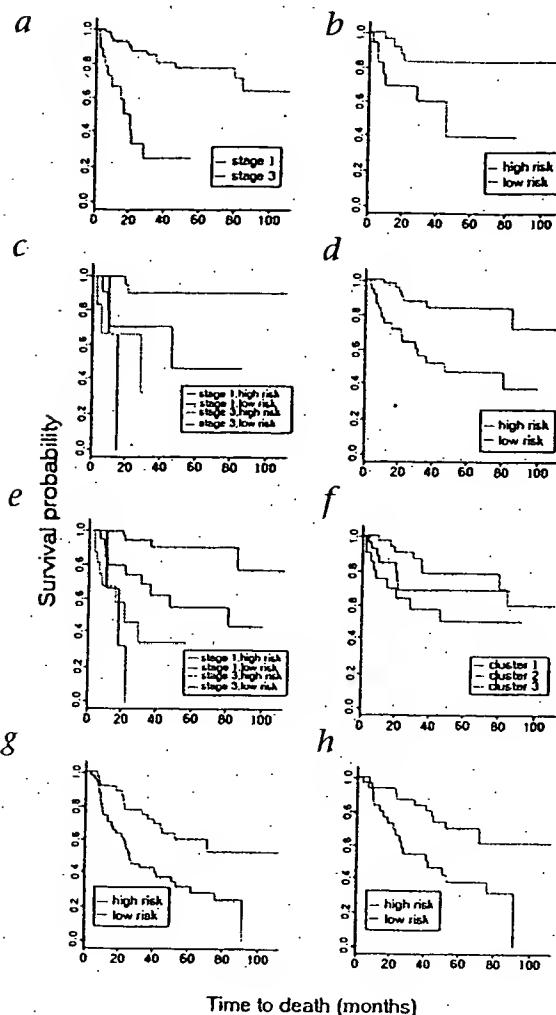


Fig. 3 Gene-expression profiles and patient survival. **a**, Relationship between tumor stage and patient survival (stage I and stage III differ significantly, $P < 0.0001$). **b**, Relationship between the survival in the 43 test samples and their risk assignments based on the 50-gene risk index estimated in the 43 training samples. The high- and low-risk groups differ significantly ($P = 0.024$). **c**, Relationship between patient survival and the risk assignments in test samples (in **b**) conditional for tumor stage. The high- and low-risk stage I groups differ significantly ($P = 0.028$), whereas stage III low- and high-risk groups did not ($P = 0.634$). **d**, Relationship between survival in the test cases and their risk assignments based on the 86 'leave-one-out' cross-validation of the 50-gene risk index. The high- and low-risk groups differ significantly ($P = 0.0006$). **e**, Relationship between test case's risk assignment and survival (in **d**) conditional on tumor stage. The high- and low-risk stage I lung adenocarcinoma groups differ significantly from each other ($P = 0.003$), whereas low- and high-risk stage III tumors do not. **f**, Relationship between tumor class identified by hierarchical clustering and patient survival. Survival for patients in Cluster 3 differed relative to the tumors in Cluster 2 ($P = 0.037$) and approached significance for Cluster 1 and 2 combined ($P = 0.06$). **g**, Analysis of the Michigan-based risk index using top cross-validated survival genes identify a low- and high-risk group in an independent cohort of 84 Massachusetts-based lung adenocarcinomas that are significantly different ($P = 0.003$). **h**, Among the 62 stage I lung adenocarcinomas in the Massachusetts sample, the high- and low-risk groups differed significantly ($P = 0.006$).

After conservatively choosing the 60th percentile cutoff point from the training set, we then applied this risk index and cutoff point to the testing set. The risk index of the top 50 genes correctly identified low- and high-risk individuals within the independent testing set ($P = 0.024$) (Fig. 3b and Supplementary Methods online). Notably, 11 stage I tumors were included in the high-risk subgroup. When this risk assignment was then conditionally examined for stage progression (Fig. 3c), low- and high-risk groups among stage I tumors were found to differ ($P = 0.028$) in their survival.

Identification of a robust set of survival genes

Although predictive of patient survival, a single training-testing set may not provide the most robust set of genes due to random sampling issues. Therefore, a 'leave-one-out' cross-validation approach was used to identify genes associated with survival from all 86-tumor samples. We first developed a 50-gene risk index in each training set, and then applied the risk index to the test case held out from the full set of tumors and assigned the held out tumor to the high- or low-risk groups (Fig. 3d). The high and low-risk subgroups determined in the test cases differed significantly in their overall survival ($P = 0.0006$). Among the larger group of stage I lung adenocarcinomas, the low-risk ($n = 46$) and high-risk ($n = 21$) groups had markedly different survival ($P = 0.003$) (Fig. 3e). Table 1 lists selected examples of the cumulative top 100 genes derived from this cross-validation procedure (complete list in Supplementary Table A online).

It was also noted that many of the stage I patients in the high-risk subgroup (Fig. 3e) were present in Cluster 3 (Fig. 1). Kaplan-Meier analysis (Fig. 3f) demonstrated a significantly worse survival ($P = 0.037$) for patients in Cluster 3 relative to patients in Cluster 2 and approaching significance for Cluster 1 and 2 combined ($P = 0.06$). This further indicates the important relationship between gene-expression profiles and patient survival, independent of disease stage.

Consistent with previous analyses of lung adenocarcinomas²³, 40% of stage I and 57.8% of stage III tumors had 12th or 13th codon *K-ras* gene mutations. Those patients with tumors containing *K-ras* mutations showed a trend of poorer survival, but

Immunoreactivity for both *IGFBP-3* and *HSP-70* (Fig. 2c) was detected in the cytoplasm of the adenocarcinomas, with little detectable reactivity in the stromal or inflammatory cells. Cystatin C was detected in alveolar pneumocytes and intra-alveolar macrophages in non-neoplastic lung parenchyma and also consistently in the cytoplasm of neoplastic cells.

Gene-expression profiles predict survival

As expected, Kaplan-Meier survival curves (Fig. 3a) and log-rank tests indicated poorer survival among stage III compared with stage I adenocarcinomas ($P = < 0.0001$). Two statistical approaches were used to determine whether gene-expression profiles could predict survival using the data set of 4,966 genes. In one approach, equal numbers of randomly assigned stage I and stage III tumors constituted training ($n = 43$) and testing ($n = 43$) sets. In the training set, the top 10, 20, 50 or 75 genes were used to create risk indices that were evaluated for their association with survival using the 50th, 60th or 70th percentile cutoff points to categorize patients into high or low groups. The results were similar across cutoff points but the 50-gene risk index had the best overall association with survival in the training set.



Table 1 Selected examples of the top 100 genes from cross-validation

Gene name	P (normal versus tumor t-test)	% Change in tumor	P (stage I versus stage III t-test)	% Change in stage III	Coefficient β	Unigene comment
CASP4	0.56	-6%	0.02	57%	0.0022	Apoptosis-related Caspase 4, apoptosis- related cysteine protease
P63	9.73E-04	37%	0.03	43%	0.0010	Transmembrane protein (63 kD), endoplasmic reticulum/ Golgi intermediate compartment
KRT7	8.02E-08	126%	0.11	55%	0.0003	Cell adhesion and structure Keratin 7
LAMB1	0.14	-20%	0.01	60%	0.0027	Laminin, β 1
BMP2	0.54	-21%	0.27	47%	0.0044	Cell cycle and growth regulators Bone morphogenetic protein 2
CDC6	1.31E-05	1070%	0.05	148%	0.0124	CDC6 (cell division cycle 6, <i>Saccharomyces cerevisiae</i> homolog)
S100P	2.10E-08	1572%	0.19	77%	0.0001	S100 calcium-binding protein P
SERPINE1	2.89E-03	72%	0.25	30%	0.0008	Serine (or cysteine) proteinase inhibitor, clade E (nexin)
STX1A	8.65E-08	54%	0.07	26%	0.0031	Syntaxin 1A (brain)
ADM	0.05	39%	0.04	117%	0.0016	Cell signaling adrenomedullin
AKAP 12	8.53E-03	-47%	0.05	214%	0.0010	A kinase (PRKA) anchor protein (gravin) 12
ARHE	0.06	-39%	0.05	87%	0.0092	ras homolog gene family, member E
GRB7	2.02E-03	38%	0.63	15%	0.0030	Growth factor receptor-bound protein 7
VEGF	6.50E-08	174%	0.02	85%	0.0013	Vascular endothelial growth factor
WNT10B	0.05	31%	0.48	20%	0.0022	Wingless-type MMTV integration site family, member 10B
HSPA8	0.36	8%	9.01E-04	51%	0.0008	Chaperones Heat-shock 70 kD protein 8
ERBB2	0.04	92%	0.37	120%	0.0013	Receptors v-erb-b2 avian erythroblastic leukemia viral oncogene homolog 2
FXD3	0.10	111%	0.31	73%	0.0046	FXD domain-containing ion transport regulator 3
SLC20A1	1.34E-03	58%	0.02	66%	0.0021	Solute carrier family 20 (phosphate transporter), member 1
CSTB	1.57E-04	50%	0.15	34%	0.0001	Enzymes, cellular metabolism Cystatin B (stefin B)
CTSL	0.48	-10%	0.03	67%	0.0007	Cathepsin L
CYP24	3.16E-06	N/A	0.97	2%	0.0008	Cytochrome P450, subfamily XXIV (vitamin D 24-hydroxylase)
FUT3	1.07E-07	114%	0.97	-1%	0.0033	Fucosyltransferase 3 (galactoside 3(4)-L- fucosyltransferase, Lewis blood group included)
MLN64	0.20	32%	0.42	80%	0.0007	Steroidogenic acute regulatory protein related
PDE7A	0.12	33%	0.01	-35%	-0.0187	Phosphodiesterase 7A
PLGL	0.04	-68%	0.35	-170%	-0.0011	Plasminogen-like
SLC1A6	0.07	-32%	0.12	86%	0.0069	Solute carrier family 1 (high-affinity aspartate/ glutamate transporter), member 6
COPEB	0.10	-33%	0.26	25%	0.0016	Transcription and translation Core promoter element binding protein
CRK	0.10	32%	0.03	48%	0.0098	v-crk avian sarcoma virus CT10 oncogene homolog
RELA	0.26	-7%	0.01	20%	0.0034	v-rel avian reticuloendotheliosis viral oncogene homolog A
KIAA0005	2.21E-04	40%	0.02	45%	0.0010	Unknown function KIAA0005 gene product
MGB1	0.27	125%	0.33	459%	0.0018	Mammaglobin 1

Bolded genes were also significant for survival in 43 tumor training set (Fig. 3b).

Table 1 Selected examples of the cumulative top 100 genes identified using training-testing, cross-validation of all 86 lung tumor samples. The percent change, as well as the direction, for the average values of the 10 non-neoplastic lung to all tumors, and for the 67 stage I to the 19 stage III tumors are shown. A positive coefficient β value is indicative of a relationship of gene expression to a

poorer patient outcome. The genes are listed in potential functional categories. Genes that were also present in the top 50 survival genes using the 43-tumor training set (Fig. 3b) are indicated in bold type. Complete listing of the gene probe sets and annotated gene and unigene identifiers can be found in the Supplementary Methods.



this difference did not reach statistical significance among all patients ($P = 0.25$), between patients within tumor clusters ($P = 0.41$) or when analyzed separately among stage I ($P = 0.22$) and stage III ($P = 0.53$) patients. Nuclear accumulation of p53 was detected in 17.9% stage I and in 22.2% stage III tumors. No significant relationship was observed for p53 staining and patient survival, cluster or tumor stage.

Confirmation using an independent set of adenocarcinomas

The robustness of our 50-gene risk index in predicting survival in lung adenocarcinomas was tested using oligonucleotide gene-expression data obtained from a completely independent (Massachusetts-based) sample of 84 lung adenocarcinomas (62 stage I, 14 stage II and 8 stage III; ref. 21, and dataset A at www.genome.wi.mit.edu/MPR/lung). To ensure equivalent power for testing and comparability of samples, the criteria for including tumors in the analysis were 40% or greater tumor cellularity, no mixed histology (that is, adenosquamous) and patient survival information. To obtain comparative gene-expression measures between the two data sets, gene sequences present on the U95A and HuGeneFL array were examined, and expression data for our top 50 cross-validation genes for all 84 Massachusetts samples were obtained and processed²⁴ (see also Supplementary Methods online). When we examined the risk assignment of these 84 samples, employing the identical cutoff point used for the 86 Michigan-based lung samples, we observed low- and high-risk groups (Fig. 3g; $P = 0.003$). Notably, among the 62 stage I tumors, high- and low-risk groups were observed that differed significantly ($P = 0.006$) in their survival (Fig. 3h).

Survival genes had graded and outlier expression patterns

A statistical and graphical analysis of the 100 survival-related

genes (Table 1) clustered against all 86 tumors revealed individual tumors with substantially elevated expression in both a limited and larger number of genes (Fig. 4a). Among these genes, we observed two distinct patterns of expression related to patient survival. One pattern, designated 'outlier', included genes showing substantially elevated expression (greater than five times the interquartile range among all samples), whereas the other pattern, designated 'graded', was characterized by continuously distributed expression with patient survival (Fig. 4b). The *erbB2* and *Reg1A* genes are examples of outlier expression patterns and *S100P* and *crk* genes of graded patterns. The number of outliers per person in the top 100 genes was identified and plotted according to survival times and events (Fig. 4c). Both stage I and stage III lung adenocarcinomas showed outlier gene patterns and 10 tumors contained 3 or more outlier genes.

Because gene amplification may result in increased gene expression, the nine genes with outlier expression patterns (*erbB2*, *SLC1A6*, *Wnt 1*, *MGB1*, *Reg1A*, *AKAP12*, *PACE*, *CYP24*, *KYNU*) and one gene with a graded expression pattern (*KRT18*) were examined using quantitative genomic PCR to evaluate genomic copy number (Fig. 5a). Gene amplification of *erbB2* (17q12) was detected in tumor L94, which had the highest *erbB2* mRNA expression (Fig. 4a). Gene amplification was not detected for any of the other seven tested genes in tumor L94, as well as in other tumors. The two genes most frequently demonstrating the outlier pattern in these lung adenocarcinomas were *KYNU* and *CYP24*, and were present in 10 and 9 tumors, respectively. *CYP24* has been described as a gene amplified and overexpressed in breast cancer²⁵, and these results indicate elevated expression in lung adenocarcinoma.

To determine whether the graded or outlier gene-expression patterns also occur at the protein-expression level, 10 of the 100

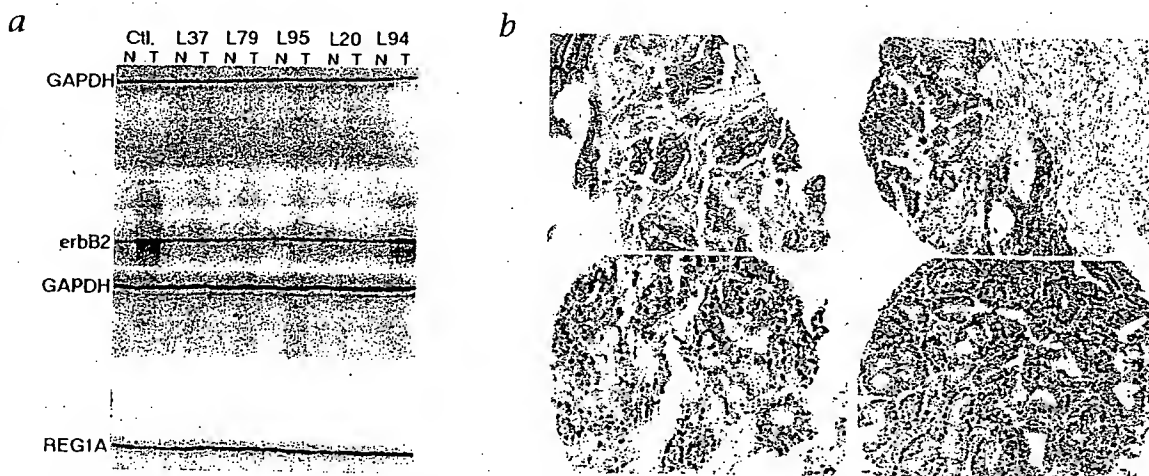


Fig. 5 Gene amplification and protein expression of survival-related genes. **a**, Analysis of potential gene amplification for 9 genes showing outlier expression patterns in the lung tumors (*erbB2*, *SLC1A6*, *Wnt 1*, *MGB1*, *Reg1A*, *AKAP12*, *PACE*, *CYP24* and *KYNU*) and examined using quantitative genomic PCR. A gene showing graded expression pattern (*KRT18*), and one gene (*PACE4*) with a similar chromosome location as *PACE*, were used as controls. Only *erbB2* and *Reg1A* are shown. An esophageal adenocarcinoma with known high-level genomic amplification of *erbB2* was used as a positive control and normal esophagus DNA was used as a negative control (C11). PCR fragments sizes were 343 bp for *GAPDH*, 166 bp for *erbB2* and 126 bp for

Reg1A. DNA is from normal lung (N) and tumor (T) from each patient (for example L37). **b**, Immunohistochemical analysis of survival related genes with lung adenocarcinoma microarrays using the tumors from this study. The transmembrane *erbB2* protein (top left) expression is substantially increased in tumor L94 containing the amplified *erbB2* gene (Fig. 4a and b). Expression of VEGF (top right) and S100P (bottom left) was located within the neoplastic cells and the pattern of immunoreactivity was consistent with the graded expression pattern demonstrated by their mRNA profiles. Expression of the oncogene *crk* (bottom right) was abundantly expressed in neoplastic lung cells. Magnification, $\times 400$ (*erbB2*); $\times 200$ (VEGF, S100P and *crk*).

top survival genes (Table 1) for which specific antibodies were available were chosen for immunohistochemical analysis using lung-tumor arrays from this study (Fig. 5b). Expression of membrane *erbB2* protein was substantially increased in the *erbB2*-amplified tumor L94 and very low levels of expression were present in other tumors, consistent with mRNA-expression measurements (Fig. 4a and b). CDC6 protein expression was also substantially higher in tumor L94, consistent with mRNA levels (data not shown). Expression of vascular endothelial growth factor (VEGF) and S100P (Fig. 5b), as well as cytokeratin 18 (KRT18), cytokeratin 7 (KRT7) and fas-associated death domain (FADD) protein (data not shown), was located within the lung tumor cells and consistent with the graded expression pattern of the mRNA profiles. The oncogene *crk* showed both graded mRNA as well as a graded protein-expression pattern with survival, and was abundantly expressed in the tumor cells (Fig. 5b). These results indicate that many survival-associated genes are expressed at the protein level and demonstrate similar mRNA and protein-expression patterns.

Discussion

We used several approaches for the analysis of gene-expression data related to clinicopathological variables and patient survival. One approach, hierarchical clustering, was used to examine similarities among lung adenocarcinomas in their patterns of gene expression. Previous studies of lung tumors^{21,22} have also used this method to describe subclasses of lung tumors. Here, we found three clusters that showed significant differences with respect to tumor stage and tumor differentiation. This suggests, as expected, that tumors with similar histological features of differentiation demonstrate similarities in gene expression. This feature also partly underlies the observed statistical association of tumor stage and cluster, as many of the higher-stage tumors, often poorly differentiated and previously associated with a reduced survival^{21,10}, were located in Cluster 3. Although this cluster contained the highest percentage of stage III tumors, it also contained a nearly equal mixture of stage I and stage III tumors and not all tumors were poorly differentiated. This indicates that a subset of stage I lung adenocarcinomas share gene-expression profiles with higher-stage tumors. Notably, 10 of the 11 stage I tumors found in Cluster 3 were the high-risk stage I tumors identified using the risk index in the 'leave-one-out' cross-validation.

In contrast to previous analyses of lung adenocarcinomas^{21,22}, we validated the expression data from the arrays. The strong correlation of northern-blot analysis and oligonucleotide-array data for gene expression in the same samples (Fig. 2b) indicates that these studies provide robust gene-expression estimates. Immunohistochemistry using the same tumor samples in tissue arrays demonstrates protein expression within the lung tumor cells. Together, these studies indicate that many of the genes identified using gene-expression profiles are likely relevant to lung adenocarcinoma. For example, *IGFBP3* gene expression is increased in lung adenocarcinomas (Fig. 2c). *IGFBP3* protein modulates the autocrine or paracrine effects of insulin-like growth factors, elevated *IGFBP3* expression is observed in colon cancer²⁶, and increased serum *IGFBP3* is associated with progression in breast cancer²⁷. Heat-shock protein 70 (HSP-70) is increased in lung adenocarcinomas of smokers²⁸ and is associated with increased metastatic potential in breast cancer²⁹. Increased serum lactate dehydrogenase is correlated with tumor stage and tumor burden³⁰, and cystatin C, a cysteine protease inhibitor ex-

pressed in human lung cancers³¹, is prognostic in some cancers³². The decreased expression of this protease inhibitor may affect the invasive properties of the tumor cell.

The cross-validation analytical strategy we used is particularly informative for these types of gene-expression analyses for disease outcome^{33,34}, and identification of cross-validated genes with a larger tumor cohort may help refine this risk index for use in a clinical setting. The gene-expression data also provide opportunities to observe overarching patterns that advance our understanding of associations between genes and disease. For example, the top 100 survival genes include those involved in signaling, cell cycle and growth, transcription, translation and metabolism. Expression of many of these genes is likely a function of increased proliferation and metabolism in the more aggressive tumors. Some genes, such as *erbB2* and *Reg1A* (Fig. 4a and b), were highly overexpressed in a few patients having poor survival. In one tumor, the *erbB2* gene was amplified (Fig. 5a), demonstrating that genomic changes may underlie the overexpression of a subset of these outlier genes. Immunohistochemistry confirmed protein overexpression in this patient's tumor (Fig. 5b). Notably, seven of the eight outlier genes were not amplified, indicating that other mechanisms underlie the increased mRNA expression of these survival-related genes.

Most genes showed a graded relationship between expression and patient survival. Genes such as that encoding VEGF, known to be strongly associated with survival in lung cancer^{35,36} were identified as related to patient survival in our study. VEGF demonstrated a graded expression pattern, as did the S100P and *crk* oncogene (Fig. 5b). S100P is a calcium-regulated protein not previously reported in lung cancer. The *crk* gene, the cellular homolog of the *v-crak* oncogene, is a member of a family of adaptor proteins involved in signal transduction and interacts directly with c-jun N-terminal kinase 1 (JNK1)³⁷. Although *crk* has not been shown to have a role in lung cancer, its role in the MAP-kinase pathway, which leads to activation of matrix metalloproteinase secretion and cell invasion³⁸, indicates potential involvement in the tumor cell invasion or metastasis of some lung adenocarcinomas. Among the many genes identified in this study, like *crk*, that may be causally involved in lung cancer progression (Table 1), some were related to survival in many patients, and others in only smaller subsets of patients. This result is consistent with the complex molecular architecture of tumors in general, the heterogeneity of lung adenocarcinomas in particular and the multiple mechanisms underlying tumor-cell survival, invasion and metastasis³⁹.

Our results demonstrate that a gene-expression risk profile—based on the genes most associated with patient survival—can distinguish stage I lung adenocarcinomas and differentiate prognoses. The particular genes that define the clusters, or are associated with survival, likely reflect the characteristics of the particular tumors included in the analysis. Current therapy for patients with stage I disease usually consists of surgical resection without adjuvant treatment⁴³. Clearly, the identification of a high-risk group among patients with stage I disease would lead to consideration of additional therapeutic intervention for this group, possibly leading to improved survival of these patients.

Methods

Patient population. Sequential patients seen at the University of Michigan Hospital between May 1994 and July 2000 for stage I or stage III lung adenocarcinoma were evaluated for this study. Consent was received and the project was approved by the local Institutional Review Board. Primary tumors and adjacent non-neoplastic lung tissue were obtained at the time of



surgery. Peripheral portions of resected lung carcinomas were sectioned, evaluated by a study pathologist and compared with routine H&E sections of the same tumors, and utilized for mRNA isolation. Regions chosen for analysis contained a tumor cellularity greater than 70%, no mixed histology, potential metastatic origin, extensive lymphocytic infiltration or fibrosis. Tumors were histopathologically divided into two categories based on their growth pattern: bronchial-derived, if they exhibited invasive features with architectural destruction, and bronchioloalveolar, if they exhibited preservation of the lung architecture. All stage I patients received only surgical resection with intra-thoracic nodal sampling and no other treatments. Stage III patients received surgical resection plus chemotherapy and radiotherapy.

Gene-expression profiling and K-ros mutation analysis. RNA isolation, cRNA synthesis and gene-expression profiling were performed as described²⁴. Details of gene annotation and K-ros mutation analysis are provided in supplementary information.

Northern-blot analysis. Total cellular RNA (10 µg) was separated in 1.2% agarose-formaldehyde gels and vacuum-transferred to Gene Screen Plus (NEN Life Science Products, Boston, Massachusetts). Hybridization conditions and probe labeling were as described²⁵. Individual sequence-validated cDNA image clones for human *IGF8P3* (clone 1407750), *LDH-A* (clone 2420241), *cystatin C* (*CT53*; clone 949938) were from Research Genetics (Huntsville, Alabama). The human histone H4 cDNA and the 28S ribosomal RNA 26-mer oligonucleotide probe were prepared and labeled as described²⁶.

Gene-amplification analysis. 11 genes were selected for the analysis of genomic alterations. Primers were designed using PrimerSelect 4.05 Windows 32 software (DNASTAR, Madison, Wisconsin), avoiding pseudogenes or potential homologous regions. Forward and reverse primers for the genes are provided (Supplementary Methods online). Quantitative genomic-PCR was then applied and analyzed as described²⁷.

Immunohistochemical staining. The H&E-stained slides of all primary lung tumors were used to identify the most representative regions of each tumor and a tissue microarray (TMA) block was constructed as described²⁸. Immunohistochemistry (IHC) was performed using both routine and sections from the TMA block as described²⁹. Detailed methods and the concentrations used for all antibodies are provided in the Supplementary Methods.

Statistical methods. *t*-tests were used to identify differences in mean gene-expression levels between comparison groups. Agglomerative hierarchical clustering³¹ was applied using the average linkage method to investigate whether there was evidence for natural groupings of tumor samples based on correlations between gene-expression profiles. To investigate the robustness of the clustering inference, gene-expression values were perturbed by adding random Gaussian error of magnitude obtained from a duplicate sample to each data point and then reclustered to determine concordance in the tumor's class membership. Pearson, χ^2 and Fisher's exact tests were used to assess whether cluster membership was associated with physical and genetic characteristics of the tumors.

To determine whether gene-expression profiles were associated with variability in survival times, 2 separate but complementary approaches were used. In the first approach, the 86 tumors were randomly assigned to equivalent training and testing sets consisting of equal numbers of stage I and III tumors in order to validate a novel risk-index function that captured the effect of many genes at once. In the second approach, cross-validation³² was used to more robustly identify the genes associated with survival. Briefly, a 'leave-one-out' cross-validation procedure in which 85 of the 86 tumors (the training set) was used to identify genes that were univariately associated with survival. The risk index was defined as a linear combination of the gene-expression values for the top genes identified by univariate Cox proportional-hazard regression modeling³³, weighted by their estimated regression coefficients. Kaplan-Meier survival plots and log-rank tests were then used to assess whether the risk-index assignment to high/low categories was validated in the test set. A more detailed description is provided (Supplementary Methods online).

Note: Supplementary information is available on the Nature Medicine website.

Acknowledgments

We thank D. Sonders for technical assistance; D. Sing for assistance with the figures; and G. Omenn for critical reading of this manuscript. This work was supported by National Cancer Institute grant: U19 CA-85953 and the Tissue Core of the University of Michigan Comprehensive Cancer Center (NIH CA-46952).

Competing interests statement

The authors declare that they have no competing financial interests.

RECEIVED 5 APRIL; ACCEPTED 14 JUNE 2002

1. Fry, W.A., Phillips, J.L. & Menck, H.R. Ten-year survey of lung cancer treatments and survival in hospitals in the United States. *Cancer* 86, 1867-1876 (1999).
2. Williams, D.E. et al. Survival of patients surgically treated for stage I lung cancer. *J. Thorac. Cardiovasc. Surg.* 82, 70-76 (1981).
3. Poirero, P.C. et al. Postsurgical stage I bronchogenic carcinoma: Morbid implications of recurrent disease. *Ann. Thorac. Surg.* 38, 331-338 (1984).
4. Naruke, T. et al. Prognosis and survival in resected carcinoma based on the new international staging system. *J. Thorac. Cardiovasc. Surg.* 96, 440-447 (1988).
5. Kaisermann, M.C. et al. Evolving features of lung adenocarcinoma in Rio de Janeiro, Brazil. *Oncol. Rep.* 8, 189-192 (2001).
6. Roggli, V.L. et al. Lung cancer heterogeneity: A blinded and randomized study of 100 consecutive cases. *Hum. Pathol.* 16, 569-579 (1985).
7. Gail, M.H. et al. Prognostic factors in patients with resected stage I non-small cell lung cancer: A report from the Lung Cancer Study Group. *Cancer* 54, 1802-1813 (1984).
8. Takise, A. et al. Histopathologic prognostic factors in adenocarcinomas of the peripheral lung less than 2 cm in diameter. *Cancer* 61, 2083-2088 (1988).
9. Ichinose, Y. et al. Is T factor of the TMN staging system a predominant prognostic factor in pathologic stage I non-small cell lung cancer. *J. Thorac. Cardiovasc. Surg.* 106, 90-94 (1993).
10. Harpole, D.H. et al. A prognostic model of recurrence and death in stage I non-small cell lung cancer utilizing presentation, histopathology, and oncoprotein expression. *Cancer Res.* 55, 51-56 (1995).
11. Rodenhuis, S. et al. Mutational activation of the K-ros oncogene: A possible pathogenic factor in adenocarcinoma of the lung. *N. Engl. J. Med.* 317, 929-935 (1987).
12. Slebos, R.J.C. et al. K-ros oncogene activation as a prognostic marker in adenocarcinoma of the lung. *N. Engl. J. Med.* 323, 561-565 (1990).
13. Horio, Y. et al. Prognostic significance of p53 mutations and 3p deletions in primary resected non-small cell lung cancer. *Cancer Res.* 53, 1-4 (1993).
14. Kern, J.A. et al. C-erbB-2 expression and codon 12 K-ros mutations both predict shortened survival for patients with pulmonary adenocarcinomas. *J. Clin. Invest.* 93, 516-520 (1994).
15. Ebina, M. et al. Relationship of p53 overexpression and up-regulation of proliferating cell nuclear antigen with the clinical course of non-small cell lung cancer. *Cancer Res.* 54, 2496-2503 (1994).
16. Mehdi, S.A. et al. Prognostic markers in resected stage I and II non-small cell lung cancer: an analysis of 260 patients with 5 year follow-up. *Clin. Lung Cancer* 1, 59-67 (1997).
17. Schneider, P.M. et al. Multiple molecular marker testing (p53; c-Ki-ros, c-erbB-2) improves estimation of prognosis in potentially curative resected non-small cell lung cancer. *Br. J. Cancer* 83, 473-479 (2000).
18. Herbst, R.S. et al. Differential expression of E-cadherin and type IV collagenase genes predicts outcome in patients with stage I non-small cell lung carcinoma. *Clin. Oncol. Res.* 6, 790-797 (2000).
19. Liotta, L. & Petricion, E. Molecular profiling of human cancer. *Nature Rev. Genet.* 1, 48-56 (2000).
20. Golub, T.R. Editorial: Genome-wide views of cancer. *N. Engl. J. Med.* 344, 601-602 (2001).
21. Bhattacharjee, A. et al. Classification of human lung carcinomas by mRNA expression profiling reveals distinct adenocarcinoma subclasses. *Proc. Natl. Acad. Sci. USA* 98, 13790-13795 (2001).
22. Garber, M.E. et al. Diversity of gene expression in adenocarcinoma of the lung. *Proc. Natl. Acad. Sci. USA* 98, 13784-13789 (2001).
23. Mills, N.E. et al. Increased prevalence of K-ros oncogene mutations in lung adenocarcinoma. *Cancer Res.* 55, 1444-1447 (1995).
24. Giordano, T.J. et al. Organ-specific molecular classification of lung, colon and ovarian adenocarcinomas using gene expression profiles. *Am. J. Pathol.* 159, 1231-1238 (2001).
25. Albertson, D.G. et al. Quantitative mapping of amplicon structure by array CGH identifies CYP24 as a candidate oncogene. *Nature Genet.* 25, 144-146 (2000).
26. Kansra, S. et al. IGF8P-3 mediates TGF β 1 proliferative response in colon cancer cells. *Int. J. Cancer* 87, 373-378 (2000).
27. Vadgama, J.V. et al. Plasma insulin-like growth factor-I and serum IGF-binding protein 3 can be associated with the progression of breast cancer, and predict the risk of recurrence and the probability of survival in African-American and Hispanic



ARTICLES

- women. *Oncology* 57, 330-340 (1999).
28. Volm, M., Mattern, J. & Stämmler, G. Up-regulation of heat shock protein 70 in adenocarcinoma of the lung in smokers. *Anticancer Res.* 15, 2607-2609 (1995).
29. Ciocca, D.R. *et al.* Heat shock protein hsp70 in patients with axillary lymph node-positive breast cancer: prognostic implications. *J. Natl. Cancer Inst.* 85, 570-574 (1993).
30. Rotenberg, Z. *et al.* Total lactate dehydrogenase and its isoenzymes in serum of patients with non-small cell lung cancer. *Clin. Chem.* 34, 668-670 (1988).
31. Krepela, E. *et al.* Cysteine proteases and cysteine protease inhibitors in non-small cell lung cancer. *Neoplasia* 45, 318-331 (1998).
32. Kos, J. *et al.* Cysteine proteinases and their inhibitors in extracellular fluids: Markers for diagnosis and prognosis in cancer. *Int. J. Biol. Markers* 15, 84-89 (2000).
33. Golub, T.R. *et al.* Molecular classification of cancer: Class discovery and class prediction by gene expression monitoring. *Science* 286, 531-537 (1999).
34. Hedenfalk, I. *et al.* Gene expression profiles in hereditary breast cancer. *N. Engl. J. Med.* 344, 539-548 (2001).
35. Ohta, Y. *et al.* Vascular endothelial growth factor and lymph node metastasis in primary lung cancer. *Br. J. Cancer* 76, 1041-1045 (1997).
36. Shibusa, T., Shijubo, N. & Abe, S. Tumor angiogenesis and vascular endothelial growth factor expression in stage I lung adenocarcinoma. *Clin. Cancer Res.* 4, 1483-1487 (1998).
37. Girardin, S.E. & Yaniv, M. A direct interaction between JNK1 and Crkl is critical for Rac1-induced JNK activation. *EMBO J.* 20, 3437-3446 (2001).
38. Liu, E. *et al.* The Ras-mitogen-activated protein kinase pathway is critical for the activation of matrix metalloproteinase secretion and the invasiveness in v-crk-transformed 3Y1. *Cancer Res.* 60, 2361-64 (2000).
39. Hanahan, D. & Weinberg, R.A. The hallmarks of cancer. *Cell* 100, 57-70 (2000).
40. Hanson, L.A. *et al.* Expression of the glucocorticoid receptor and K-ras genes in urethan-induced mouse lung tumors and transformed cell lines. *Exp. Lung Res.* 17, 371-387 (1991).
41. Lin, L. *et al.* A minimal critical region of the 8p22-23 amplicon in esophageal adenocarcinomas defined using STS-amplification mapping and quantitative PCR includes the GATA-4 gene. *Cancer Res.* 60, 1341-1347 (2000).
42. Kononen, J. *et al.* Tissue microarrays for high throughput molecular profiling of tumor specimens. *Nature Med.* 4, 844-847 (1998).
43. Johnson, R. & Wichern, D.W. *Applied Multivariate Statistical Analysis*. 543-578 (Prentice Hall, New Jersey, 1988).
44. Stone, M. Asymptotics for and against cross-validation. *Biometrika* 64, 29-38 (1977).
45. Cox, D.R. Regression models and life tables. *J.R. Stat. Soc.* 34, 187-220 (1972).





Journal of Immunological Methods 246 (2000) 79–90

JIM
Journal of
Immunological Methods
www.elsevier.nl/locate/jim

Rapid quantitation of proinflammatory and chemoattractant cytokine expression in small tissue samples and monocyte-derived dendritic cells: validation of a new real-time RT-PCR technology

Volker Blaschke^{a,*}, Kristian Reich^a, Sabine Blaschke^b, Sabine Zipprich^a,
Christine Neumann^a

^aDepartment of Dermatology, von-Siebold-Str. 3, D-37075 Goettingen, Germany

^bDepartment of Nephrology, Georg-August-University, Goettingen, Germany

Received 3 April 2000; received in revised form 21 August 2000; accepted 11 September 2000

Abstract

The analysis of cytokine profiles plays a central part in the characterization of disease-related inflammatory pathways and the identification of functional properties of immune cell subpopulations. Because tissue biopsy samples are too small to allow the detection of cytokine protein, the detection of mRNA by RT-PCR analysis is often used to investigate the cytokine milieu in inflammatory lesions. RT-PCR itself is a qualitative method, indicating the presence or absence of specific transcripts. With the use of internal or external standards it may also serve as a quantitative method. The most widely accepted method is quantitative competitive RT-PCR, based on internal shortened standards. Recently, online real-time PCR has been introduced (LightCycler[®]), which allows quantitation in less than 30 min. Here, we have tested its use for the analysis of cytokine gene expression in different experimental in vitro and ex vivo settings. First, we compared quantitative competitive RT-PCR with real-time RT-PCR in the quantitation of transcription levels of the CD4⁺ cell-specific chemoattractant Interleukin-16 during the maturation of monocyte-derived dendritic cells, and found a good correlation between both methods. Second, differences in the amounts of IL-16 mRNA in synovial tissue from patients with rheumatoid arthritis and osteoarthritis as assessed by real-time RT-PCR paralleled differences in the level of IL-16 protein in the synovial fluid. Finally, we employed real-time RT-PCR to study the cutaneous expression of several cytokines during experimental immunomodulatory therapy of psoriasis by Interleukin-10, and demonstrate that the technique is suitable for pharmacogenomic monitoring. In summary, real-time RT-PCR is a sensitive and rapid tool for quantifying mRNA expression even with small quantities of tissue. The results obtained do not differ from those generated by quantitative competitive RT-PCR. © 2000 Elsevier Science B.V. All rights reserved.

Keywords: Quantitative competitive RT-PCR; Real-time RT-PCR; LightCycler[®]; Interleukin-16; Interleukin-10 therapy; Rheumatoid arthritis; Psoriasis; Dendritic cell

Abbreviations: FCS, fetal calf serum; IFN γ , interferon- γ ; OA, osteoarthritis; PCR, polymerase chain reaction; PUVA, psoralene UVA; RA, rheumatoid arthritis; RT, reverse transcription; TNF α , tumour necrosis factor α

*Corresponding author. Tel.: +49-551-39-6410; fax: +49-551-39-8413.

E-mail address: vblasch@gwdg.de (V. Blaschke).

0022-1759/00/\$ – see front matter © 2000 Elsevier Science B.V. All rights reserved.
PII: S0022-1759(00)00304-5

1. Introduction

Recent studies have shown that several chronic inflammatory disorders are associated with specific changes in the balance between pro- and anti-inflammatory cytokines in affected compared to normal tissue. For example, in two types of chronic skin inflammation, psoriatic lesions are characterized by a preferential expression of Th1-type cytokines (Uyemura et al., 1993; Schlaak et al., 1994), whereas in early lesions of atopic dermatitis Th2-type cytokines have been observed (Sager et al., 1992; Neumann et al., 1996). However, the characterization of cytokine profiles is often hampered by the fact that only small amounts of tissue (typically punch biopsies) are available for investigation. Hence, quantitative investigations on the protein level are rarely undertaken, as detection methods such as ELISA are not sensitive enough and permit the analysis of only a limited number of factors from one sample. Therefore, expression analysis is often performed at the mRNA level by Northern blot analysis or RT-PCR. While Northern blot analysis requires considerable amounts of tissue material, RT-PCR is a highly sensitive method allowing the detection of mRNA transcripts from small quantities due to the exponential amplification process. RT-PCR is a qualitative method indicating the presence or absence of specific transcripts. Due to the exponential amplification and inter-sample variations in amplification efficiency, the amount of PCR product obtained does not provide a valid measure for the amount of a specific transcript present within the sample (Gilliland et al., 1990). By using external or internal standards, the amplification process can be controlled, allowing RT-PCR to be used quantitatively. The currently preferred method is quantitative competitive RT-PCR, where shortened constructs (internal standards) compete for the same sequence-specific primer pairs and are co-amplified in the same reaction tube (Gilliland et al., 1990). The wild-type and internal standard PCR products can afterwards be separated, e.g., by agarose gel electrophoresis, and subsequently quantified. To control for inter-sample variations, cytokine expression levels are standardized for a housekeeping gene, usually β -actin or GAPDH. This method is accurate, but tedious and time consuming. Recently, real-time PCR has become available, using

either labelled sequence-specific probes (e.g., TaqMan[®], Heid et al., 1996) or a fluorescent dye (e.g., SYBR Green, ethidium bromide, Higuchi et al., 1992) to monitor the formation of PCR products. However, since competitive and real-time RT-PCR use different approaches for quantitation (internal versus external standards), it has been unclear whether both techniques give identical results when quantifying cytokine expression. Therefore, in this study we have tested both methods for the quantitation of the CD4⁺ specific chemoattractant IL-16 during the maturation of monocyte-derived dendritic cells. Next, we investigated whether real-time RT-PCR could be used to quantify cytokine gene expression in small tissue samples. In patients with rheumatoid arthritis we compared IL-16 mRNA expression levels in synovial membrane tissue with protein expression in synovial fluid. Third, we used real-time RT-PCR to analyse the effects of subcutaneous IL-10 therapy on cutaneous proinflammatory cytokine pathways in psoriasis (Reich et al., 1998). We found that (i) quantitative competitive and real-time RT-PCR gave comparable results when quantitating IL-16 mRNA levels in monocyte-derived dendritic cells; (ii) the results of IL-16 mRNA quantitation by real-time RT-PCR from synovial membrane correlated well with IL-16 protein levels in the affected joints of rheumatoid arthritis and osteoarthritis patients; and (iii) real-time RT-PCR allowed the simultaneous detection of multiple disease-related cytokines in psoriasis and could be used for pharmacogenomic monitoring of experimental immunomodulatory therapy.

2. Materials and methods

2.1. Generation of dendritic cells

Dendritic cells were generated according to a modified protocol as previously described (Reich et al., 1999). Briefly, CD14⁺ (purity >85%) cells were positively selected from the peripheral blood mononuclear cells of healthy volunteers ($n=3$). Immature dendritic cells were obtained by incubation for 5 days in RPMI 1640/5% FCS, supplemented with 50 ng/ml rhIL-4 (Pharma Biotechnologie, Hanover, Germany) and 50 ng/ml rhGM-CSF (kindly pro-

vided by Schering-Plough Research Institute, Kenilworth, NJ, USA). Maturation of dendritic cells was induced by additional culture with 100 ng/ml TNF α (Pharma) and 50% (v/v) monocyte conditioned medium (Romani et al., 1996) for 3 days (Palucka et al., 1998). On day 8, mature dendritic cells were resuspended in medium/FCS and stimulated with TNF α (100 ng/ml) and IL-1 β (10 ng/ml, Strathmann Biotech, Hanover, Germany) or TNF α , IL-1 β and IL-10 (10 ng/ml, Strathmann). During culture, cells were harvested for RNA extraction on days 0, 2, 5, 7, 8 (before stimulation and 6 h after the addition of stimuli) and day 9. All donors in this study gave informed consent after the nature and possible consequences of the study had been fully explained.

2.2. Psoriasis patients and IL-10 therapy

Fourteen patients with chronic plaque psoriasis who had not received systemic immunosuppressive therapy including PUVA for at least 4 weeks or specific topical treatment for at least 2 weeks before study entry, were treated with rhIL-10 (4 μ g/kg body weight, ESSEX Pharma, Munich, Germany) subcutaneously as previously described (Reich et al., 1998). The clinical response to therapy was recorded as changes in the psoriasis activity and severity index (PASI) every week. Punch biopsies were obtained from the same marker plaque before and after 42 days of therapy and snap frozen in liquid nitrogen. Control biopsies were obtained from healthy volunteers ($n=5$).

2.3. Synovial samples

Synovial fluid was collected from patients with RA ($n=15$) or OA ($n=15$). Synovial membrane tissue (RA, $n=25$; OA, $n=10$) was obtained from patients undergoing synovectomy or arthroplasty.

2.4. ELISA procedure for IL-16

IL-16 was detected in synovial fluid by a solid-phase sandwich ELISA (Biosource, Ratingen, Germany) according to the instructions of the manufacturer. Fifty μ l of sample material were used per well,

and values were determined in duplicate. The sensitivity of the assay was 5 pg/ml.

2.5. RNA extraction and cDNA synthesis

Total RNA was prepared (RNeasy, Qiagen, Hilden, Germany), according to the instructions of the manufacturer, from synovial membrane, harvested dendritic cells ($0.5-1 \times 10^6$ cells) and cryostat sections ($30 \times 20 \mu$ m) from punch biopsies. After a DNase digestion step (FPLC-pure DNase I, Pharmacia, Freiburg, Germany), reverse transcription (Superscript II, Gibco, Eggenstein, Germany) was performed as previously described (Blaschke et al., 1999).

2.6. Generation of internal standards

Internal standards were generated as previously described (Blaschke et al., 1996, 1999). Briefly, the β -actin F/R (Genbank accession number X00351, β -actin F 5' \rightarrow 3': CCCAGCCATGTACGTTGCTAT; β -actin R 5' \rightarrow 3': GGGTGGCTTTTAGGATGGCAA, product size, 1047 bp, all oligonucleotide primers by MWG, Ebersberg, Germany) and IL-16 F/R (M90391, IL-16 F: CGAAGACTCAGCTGCAAAT; IL-16 R: GCCAGGCATGAATGTCATA, 1223 bp) PCR products were cloned into the *Sma*I restriction site of the transcription vector pBluescript (Stratagene, Heidelberg, Germany). Fragments of 224 bp (*Sau*I, *Pvu*MI) and 285 bp (*Bal*I, *Cel*II) were removed from the constructs by double restriction enzyme digestion, respectively. Afterwards, the free 5'- and 3'-ends were blunted by the Klenow fragment (Pharmacia), religated and recloned (now termed 'internal standards'). They were then linearized by restriction enzyme digestion with *Bam*HI in the polylinker region, quantified by densitometric comparison to λ -DNA/*Hind*III fragments (Gibco) and 10-fold dilution series were prepared in water. All PCR products used in this study were identified by cycle sequencing.

2.7. Quantitative competitive PCR

Two-fold dilution series starting with 2 μ l of cDNA in 11 μ l of water were prepared and 5- μ l aliquots were added to PCR reaction mixes con-

taining a constant known amount of the internal standard. After PCR, agarose gel electrophoresis was performed in the presence of ethidium bromide and the upper (representing wild-type cDNA) and lower (internal standard) bands were quantified by densitometry. After correcting for PCR product size, the ratios of the corresponding bands from the PCR reaction were used to quantify the molar amounts of β -actin or IL-16 cDNA molecules in the cDNA sample. Values were determined in duplicate. For each sample, the ratio of the molar amounts of IL-16 and β -actin per μ l cDNA was calculated.

2.8. Generation of external standards for real-time RT-PCR

Real-time RT-PCR on the LightCycler[®] (Roche Diagnostics, Mannheim, Germany) was performed in a total volume of 20 μ l in the presence of 2 μ l of 10 \times reaction buffer (Taq polymerase, dNTPs, MgCl₂, SYBR Green, Roche Diagnostics), and 2 μ l of cDNA (or water as negative control, which was always included). MgCl₂ was added to a final concentration of 4 mM, and 11.25 pmol of each oligonucleotide primer (Actin-LF: CCCAAGGCCA-ACCGCGAGAAGAT, product size, 219 bp; Actin-LR: GTCCCGGCCAGCCAGGTCCAG; IL16-LF: AAG-GGGCATCTCCAACATCATCAT, 332 bp; IL16-LR: CTCTGCCAAGCTGAACCCAAGAC; IL8-LF: CAGTTTTGCCAAGGAGTGCTAA, Genbank acc. no. X02910, 513 bp; IL8-LR: CCCGTGCAATATCTAGGAAAATC; TNF α -LF: GGCTCCAGGCGG-TGCTTGTTT, M28130, 409 bp; TNF α -LR: AG-ACGGCGATGCGGCTGATG; CXCR2-LF: GCCCT-GCCTGTCTTACTTTT, M73969, 509 bp; CXCR2-LR: TTGGCCAGCCTGATTTTCTTTT; IFN γ -LF: TTTGGGTTCTCTTGGCTGTTACT, M-29383, 418 bp; IFN γ -LR: CCTTTTTCGCTTC-CCTCTTTT) were added. Real-time PCR was performed in glass capillaries with an initial denaturation step of 30 s at 95°C, followed by 40 cycles of 0 s at 95°C, 5 s annealing temperature (β -actin, 66°C; IFN γ , 59°C; TNF α , 67°C; CXCR2, 58°C; IL-8, 55°C; IL-16, 62°C) and (product length (bp)/25) s 72°C. At the end of each cycle, the fluorescence emitted by the SYBR Green was measured. After completion of the cycling process, samples were subjected to a temperature ramp (from 5°C above

annealing temperature to 95°C at 2°C/s) with continuous fluorescence monitoring for melting curve analysis. Samples were loaded on an agarose gel, excised, quantified by densitometric comparison to λ -DNA/HindIII fragments (Gibco) and 10-fold dilution series prepared in water, ranging from 10 amol/ μ l to 0.0001 amol/ μ l (representing 6×10^6 to 60 copies/ μ l). For each PCR product, apart from primer-dimers, a single narrow peak was obtained by melting curve analysis at the specific melting temperature and only a single band of the predicted size was observed by agarose gel electrophoresis, indicating specific amplification without significant byproducts. Due to their high dilution factors, standard concentrations in the dilution series could not be measured directly. However, the fidelity of the dilution process could be assessed as a standard curve was generated (see below). By this method, the dilution series of the internal standards were also assessed after appropriate adaptation of the cycling parameters.

2.9. Quantitation of cDNA by real-time RT-PCR

From the melting curve, melting temperatures of the primer-dimer product and the specific PCR product were obtained. To exclude primer-dimer artefacts, fluorescence was not measured at the end of the extension step, but a separate detection step was added (2 s) at a temperature (β -actin, 87°C; IFN γ , 80°C; TNF α , 88°C; IL-8, 80°C; IL-16, 83°C; CXCR2, 85°C) above the melting point of primer-dimers and below the melting point of the specific PCR product. From the external standards, a calibration curve was automatically generated. Samples (determined in duplicate) were quantified accordingly (LightCycler[®] analysis software, version 3.39). As with quantitative competitive RT-PCR, samples were standardized for β -actin.

2.10. Statistics

All data groups were tested for Gaussian distribution. Statistical analysis was by the paired or unpaired *t*-test when applicable. Correlation between variables was analysed by Spearman's correlation coefficient. Variables are described by

mean \pm standard deviation (S.D.) or by median and range. Two-tailed P values <0.05 were considered as statistically significant. Statistical analysis was performed using the prism 2.01 software (GraphPad, San Diego, CA, USA).

3. Results

3.1. Quantitation of IL-16 production during maturation of dendritic cells by quantitative competitive RT-PCR

When wild-type cDNA and internal standard were co-amplified in the same tube, both competed for the binding of oligonucleotide primers according to their molar ratio, resulting in two distinct bands as observed by gel electrophoresis (Fig. 1). Bands were quantified by densitometry. After correcting for product size, the densitometric ratio of the corresponding bands was calculated for each lane. Given the amount of internal standard used for PCR and the dilution factor of the cDNA, the amount of IL-16 cDNA present in the sample could be calculated from each lane. Typically, four of the five lanes were suitable for analysis and were averaged. To allow for the comparison of different samples, results were standardized for β -actin. On day 0, there was a substantial expression of IL-16 in purified monocytes, which was markedly reduced on day 2. During dendritic cell maturation, IL-16 expression peaked in

immature day 5 dendritic cells and declined with final maturation (Fig. 2).

3.2. Quantitation of IL-16 in dendritic cell culture by real-time RT-PCR

Fluorescence in the capillary increased with PCR product formation in a linear fashion, although signals were found to arise not only from the specific PCR product, but also from primer-dimer products. Therefore, it was important to measure the specific fluorescence at a temperature above the melting temperature of the primer-dimer product, i.e., a temperature at which primer-dimers had completely melted into single strands. The melting temperature of primer-dimer products could be determined from the negative control sample, and similarly the specific target melting temperature could be obtained (Fig. 3A). Typically, melting temperatures of primer-dimer and specific target products were at least 5°C apart. Using an intermediate temperature for quantitation, no specific fluorescence could be detected in the negative control (Fig. 3B-D). The amount of standard was inversely proportional to the number of amplification cycles necessary to detect a significant fluorescent signal above background (threshold cycle, Fig. 3C). For data analysis, the fit-point method was used to manually set the threshold between background and significant fluorescence. Given the small numbers of target copies within the cDNA samples, this method proved superior to the second-derivative method offered by the analysis software. A standard curve was generated from plotting external standard concentrations against threshold cycle (Fig. 3D). The amount of target copies in the sample was calculated from the sample threshold cycle as compared to the standard curve. All samples were determined in duplicate, and variations were typically within 10%.

3.3. Correlation of quantitative competitive PCR and real-time RT-PCR

The results obtained by quantitative competitive RT-PCR and real-time RT-PCR for IL-16 gene expression during dendritic cell maturation (Fig. 2A,B) and after stimulation of mature dendritic cells

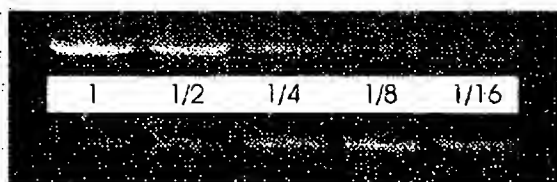


Fig. 1. Example of quantitative competitive RT-PCR. Two-fold dilution series of cDNA (1-1/16, upper bands) were coamplified with constant amounts of internal standard (lower bands). Band intensities were evaluated by densitometry and the ratio obtained from the lanes (typically four of five lanes were suitable) was used to calculate copy numbers.

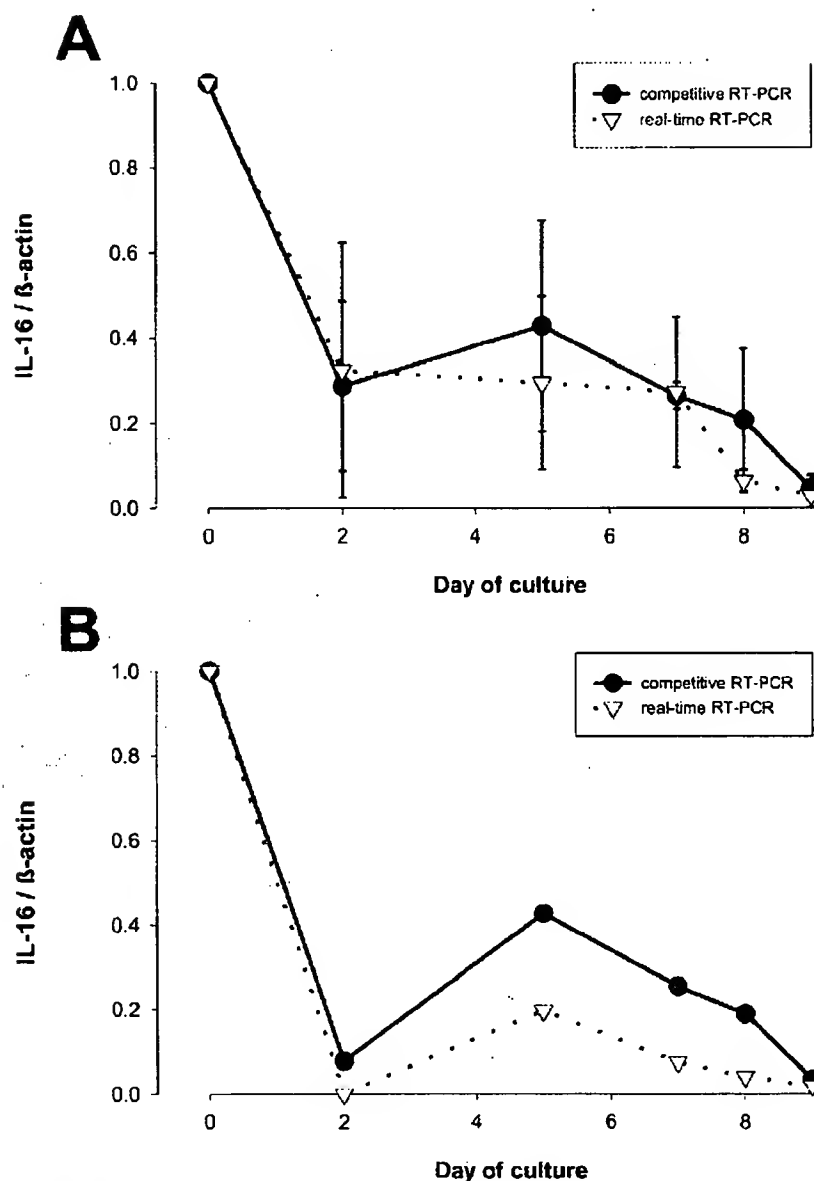


Fig. 2. IL-16 mRNA expression during dendritic cell maturation. Expression of IL-16 mRNA ($n=3$) was quantified by competitive quantitative RT-PCR and real-time RT-PCR. Results were standardized for day 0. (A) Results did not differ significantly between both methods (mean \pm S.D.). (B) A single, typical time course is shown.

with proinflammatory cytokines (data not shown) were similar. Thus, in a total of 27 samples quantified in parallel by both methods, we found a good correlation between both methods (Spearman $r=0.72$, $P<0.0001$).

3.4. IL-16 expression is increased in rheumatoid arthritis as compared to osteoarthritis

In synovial fluid from RA patients, IL-16 protein was significantly increased when compared to the

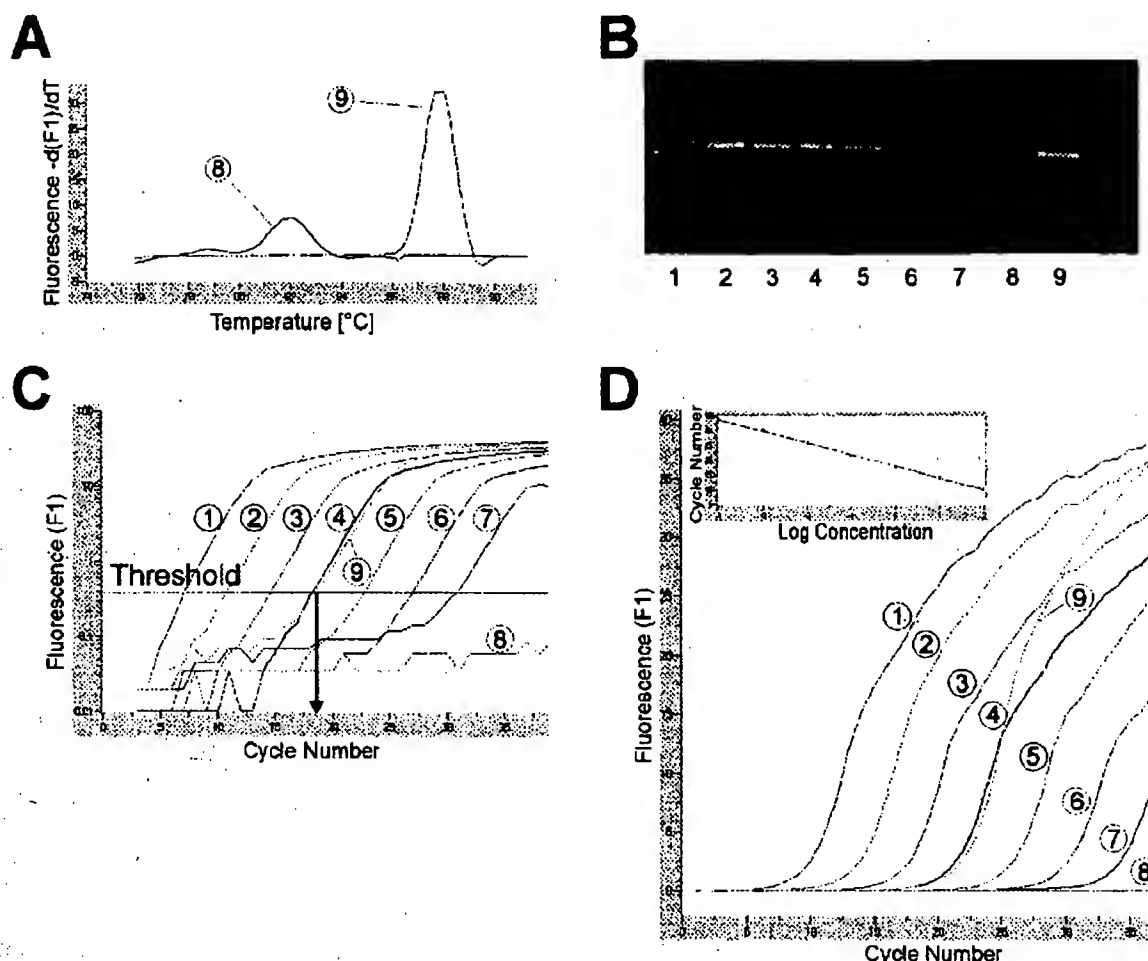


Fig. 3. Quantitation of CXCR2 by real-time RT-PCR. (A) Melting temperatures for the primer-dimer product (82°C, negative control, sample 8) and the specific target product (88°C) were determined in order to obtain the optimal temperature for fluorescence detection (85°C). (B) Ten-fold dilution series ranging from 100 amol/ μ l (sample 1) to 0.0001 amol/ μ l (sample 7), a negative control (sample 8) and a test sample (9) were subjected to real-time RT-PCR. By agarose gel electrophoresis, a single specific band was observed. (C) The threshold was set to a fluorescence intensity where all samples gave a detectable specific signal. The threshold cycle is defined by the point where sample fluorescence crosses the threshold (arrow). (D) A standard curve is generated (insert), allowing the test sample concentration to be determined. It is noteworthy that according to their respective threshold cycles, samples 4 and 9 contain similar amounts of target copies. From cycle 25 onwards, their specific fluorescence signals diverge and the final fluorescence emitted by sample 9 equals that of sample 2, which contains 100-fold more target copies. However, the threshold cycle is determined much earlier (see graph c). This indicates that end-point fluorescence detection is not a valid method for quantitation.

values in synovial fluid samples from OA patients (Fig. 4A). Similar results were obtained for mRNA levels (Fig. 4B) by real-time RT-PCR. Therefore, in this model, increased mRNA levels as detected by real-time RT-PCR coincide with increased protein expression as determined by ELISA.

3.5. Change in cytokine and cytokine receptor levels during IL-10 therapy of patients with psoriasis

Before the initiation of IL-10 therapy, levels of TNF α , IFN γ , IL-8 and its receptor CXCR2 were

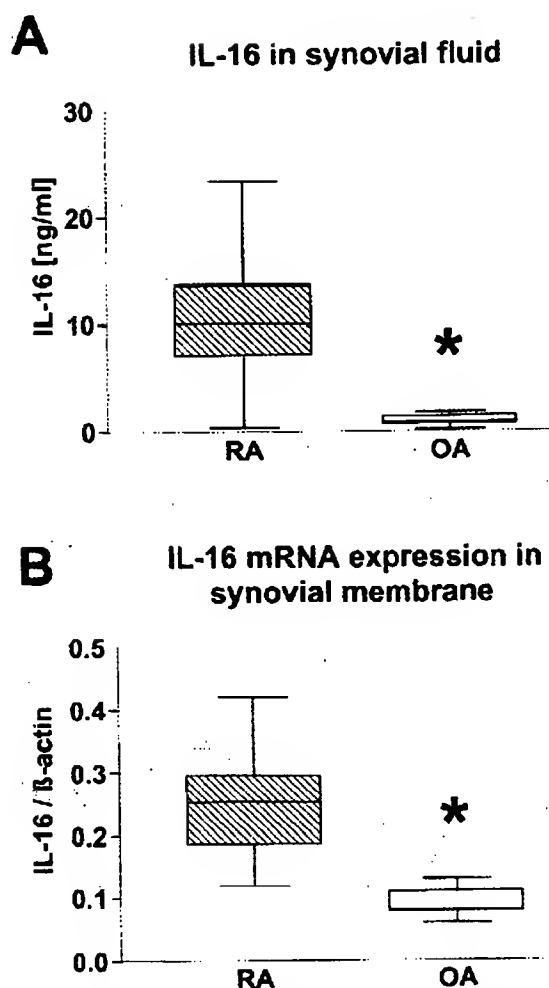


Fig. 4. IL-16 expression in rheumatoid arthritis. (A) IL-16 was quantified by ELISA in synovial fluid from patients with RA ($n=15$) and OA ($n=15$). (B) IL-16 mRNA expression was quantified in synovial membrane tissue (RA, $n=25$; OA, $n=10$) by real-time quantitative RT-PCR. Whiskers indicate data range, boxes extend from the 25-75th percentile and the horizontal lines indicate the median. Asterisks indicate significantly lower values in OA patients compared to RA patients ($P<0.05$).

markedly elevated in active psoriasis ($n=14$) when compared to normal skin ($n=5$), reflecting lesional inflammation. After 42 days of therapy, cutaneous levels of the proinflammatory cytokines and CXCR2 were significantly decreased (Fig. 5). This decrease was associated with a marked reduction in clinical disease severity as indicated by a decrease of the

PASI score from 22.4 to 8.4 at the end of treatment ($P<0.0001$, Wilcoxon signed rank test, Reich et al., submitted). However, cytokine levels at the end of therapy remained above those detected in normal skin, and a complete remission of clinical symptoms was not observed in any of the treated patients.

4. Discussion

In this study, we have evaluated the use of real-time quantitative RT-PCR technology for the detection of cytokine gene expression in cultured cells and small tissue samples. The validity of the method was studied using different experimental applications of RT-PCR in cytokine analysis. First, the results obtained for IL-16 gene expression by real-time RT-PCR in monocyte-derived dendritic cells were compared to those obtained by the currently preferred method, quantitative competitive RT-PCR. Second, mRNA levels of cytokines determined by real-time RT-PCR in synovial tissue from arthritis patients were correlated with protein expression in synovial fluid. Third, the effect of immunomodulatory therapy on cytokine gene expression in psoriatic skin lesions as determined by real-time RT-PCR was compared with the decrease of clinical symptoms. Our results clearly show that real-time RT-PCR is a useful method for quantifying even low level cytokine gene expression.

RT-PCR has proven to be a useful tool to study mRNA expression in small amounts of tissue, e.g., for the study of cytokines in the pathogenesis of disease. Although it is possible to homogenize fresh material for the quantitation of cytokines in the supernatant (Beck et al., 1996), the tools (such as ELISA) are not sensitive and permit only a very limited number of analyses. Since biopsy material is often paraffin embedded or cryopreserved, ELISA determinations may not be possible. From cryopreserved material, mRNA can be extracted for Northern blot analysis, but more than 10 μ g of total RNA may be needed for the detection of a single cytokine, which exceeds the yield from typical skin biopsies. Therefore, because of its high sensitivity, RT-PCR has increased in popularity. However, since target sequences are theoretically amplified some 2^{35} -fold, small variations in amplification efficiency may lead

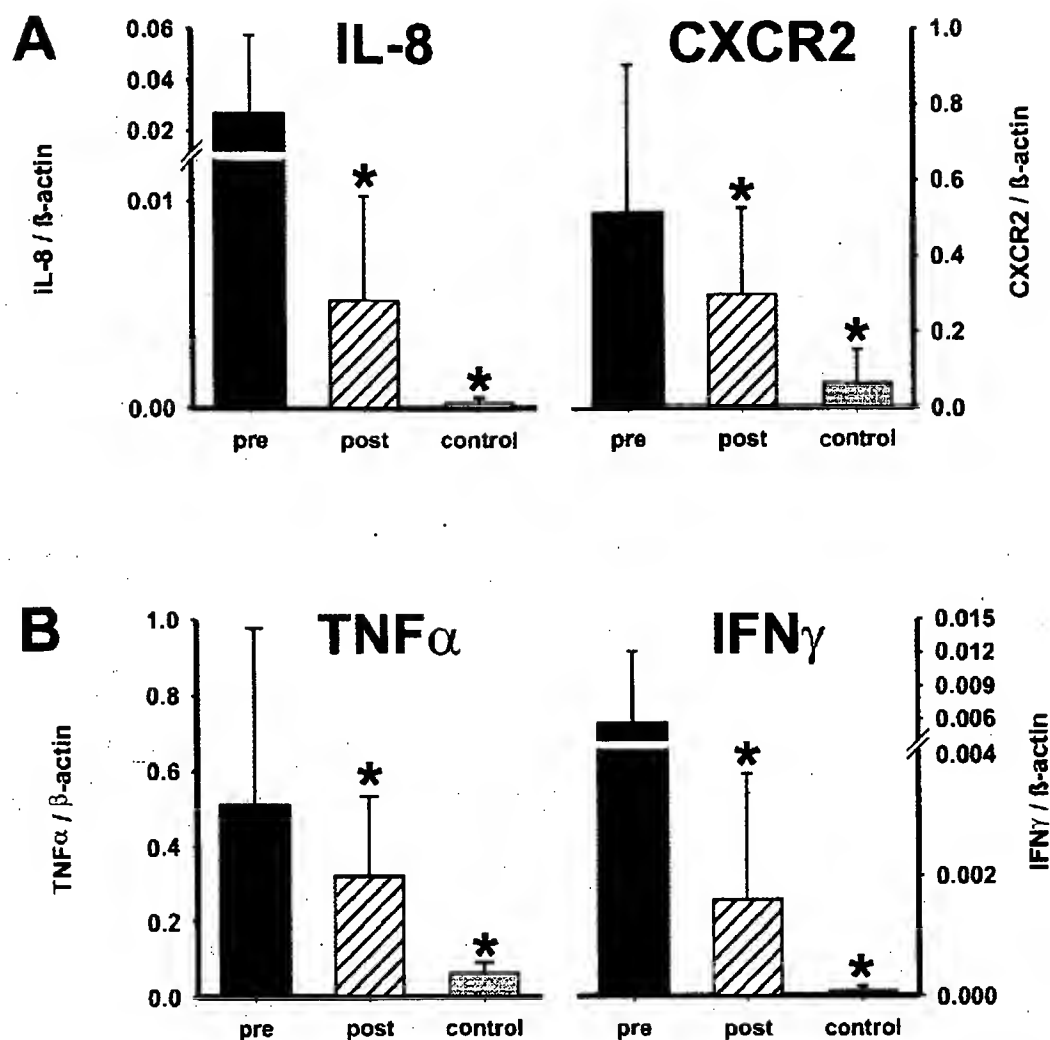


Fig. 5. Modulation of cytokine expression in psoriatic lesions by IL-10 therapy. Fourteen patients with chronic plaque psoriasis were treated subcutaneously with IL-10 for 42 days. Before and after therapy, cytokine expression within the marker lesion was quantified by real-time RT-PCR. (A) IL-8 and its receptor CXCR2. (B) TNF α and IFN γ . All post-treatment levels are significantly reduced as compared to pre-treatment levels, but still significantly elevated above normal skin (control). Mean \pm S.D., asterisks indicate significant inter-group differences for each cytokine and receptor ($P < 0.05$).

to significant changes in PCR product yield (Gilliland et al., 1990). The reason for inter-sample variations of amplification efficiency are poorly understood, but inhomogeneous heat distribution within common thermal block cyclers might play an important role. It is therefore generally agreed that quantitation by simple PCR product densitometry is obsolete. With the introduction of internal standards

into the amplification process, amplification efficiency can be monitored (Sieglings et al., 1994). To compare different samples, variations between samples, e.g., during reverse transcription, need to be controlled by quantifying a housekeeping gene (e.g., β -actin, Platzer et al., 1992), which is assumed to be equally expressed in the investigated tissues. However, the generation and coamplification of internal

standards, which usually consist of shortened PCR fragments, is difficult and time consuming. Therefore, in an alternative approach, dilution series of the target product are prepared as external controls and used to generate calibration curves (Heid et al., 1996). In the absence of internal controls it is necessary that all samples are amplified with the same efficiency. While common thermal block cyclers may not be suitable in this case, cyclers providing a homogeneous thermal distribution, such as the hot-air vent cyclers, could overcome this problem. In fact, as described in this study using the LightCycler® system (Roche Diagnostics), the inter-sample variation in amplification efficiency was small as results obtained from duplicate samples typically differed by less than 10%.

Quantitation by LightCycler® real-time RT-PCR is based on the threshold cycle method. For each sample, a determination is made of the cycle number at which the fluorescence related to the amount of double-stranded DNA is significantly elevated above background fluorescence. The more specific transcripts that are present, the less cycles are necessary to generate a significant signal (Heid et al., 1996). By using external standards, a calibration curve can be generated and samples can be quantified according to their threshold cycle. When hot air is used to heat or cool sample tubes, e.g., glass capillaries in this system, the cycling and subsequent analytical process may take as little as 30 min as compared to several hours with conventional PCR cyclers and agarose gel electrophoresis. In contrast to the common gel electrophoretic bands, which indicate successful and specific amplification of the specific PCR product, the LightCycler® system provides a melting curve analysis of the PCR products. With optimized cycling parameters, only the specific PCR product is obtained, resulting in a single narrow melting peak, which correlates with a single band by gel electrophoresis. During subsequent real-time PCR reactions, PCR product identity can routinely be ascertained by a melting curve analysis. As with ordinary RT-PCR, primer-dimer formation also occurred during real-time RT-PCR. However, in each case it was possible to select a temperature at which primer-dimers had completely melted, but at which the specific PCR product was not affected. Importantly, by using this temperature during fluorescence detection, no signals

were observed in negative control reactions. It is also noteworthy that because quantitation is performed early during PCR, it is independent of variations possibly occurring during late stages of the cycling process (compare Fig. 3). Analysis of the standard dilution series revealed that as little as 120 target copies could reliably be quantified with this method.

In this study, we used quantitative real-time RT-PCR to investigate the expression of IL-16, a chemoattractant specific for CD4-bearing cells. IL-16 is regarded as a proinflammatory cytokine since it has been shown to upregulate HLA-DR as well as CD25-expression (Parada et al., 1998). Recently identified cellular sources of IL-16 include T-cells, eosinophils and mast cells. In cutaneous inflammatory responses, e.g., in atopic and contact dermatitis, a strong CD4⁺ infiltrate is observed. We therefore speculated that IL-16 might be involved in recruiting the infiltrate and sustaining the inflammatory response. We focused on monocyte-derived dendritic cells since these resemble cutaneous dendritic cells, the most important antigen-presenting cells in human skin. During maturation of monocyte-derived dendritic cells we observed a strong expression shortly after monocyte purification. After 2 days of culture, IL-16 gene expression was markedly reduced. Although cells were purified by positive CD14 selection, we cannot exclude contamination with lymphocytes and granulocytes. It is therefore likely that the high initial expression of IL-16, followed by a dramatic decrease during the following 2 days, originated from contaminating cells which rapidly disappeared from the cultures. During culture of dendritic cells IL-16 expression peaked in immature dendritic cells (day 5) and declined with maturation. A similar expression pattern has recently been shown for IL-12, another proinflammatory cytokine with strong effects on T-cells (Kalinski et al., 1999). The decreased production of cytokines such as IL-12 and IL-16 in vitro may correspond to a reduced cytokine release from dendritic cells migrating from skin to regional lymph nodes in vivo. Such a mechanism would limit the effects of dendritic cell-derived cytokines to the site of initial antigen challenge.

Secondly, we have investigated the role of IL-16 in rheumatoid arthritis. In contrast to osteoarthritis patients, a significant CD4⁺ infiltrate is present in the affected joints of patients with rheumatoid arth-

ritis. In rheumatoid patients, elevated levels of IL-16 have been reported in the synovial fluid and the expression of IL-16 has been demonstrated by in situ hybridization in the synovial membrane (Franz et al., 1998). By real-time RT-PCR we found that IL-16 mRNA is expressed in lesional synovial membrane tissue at significantly higher levels than in OA. This observation was paralleled by the finding that in synovial fluid from RA patients IL-16 protein levels are significantly elevated when compared to OA patients. Therefore, it is possible that IL-16 could be involved in recruiting CD4⁺ cells to affected joints in RA.

Finally, we have used real-time RT-PCR to identify disease-related genes in psoriasis and to monitor the expression of these genes during experimental IL-10 therapy. Psoriasis is a chronic inflammatory skin condition of unknown origin. Enhanced keratinocyte proliferation is thought to be driven by cytokines such as TNF α and IFN γ released from infiltrating Th-1 cells. Neutrophils are also abundant in affected skin and may be attracted by chemotactic factors such as IL-8 that acts via the chemokine receptors CXCR1 and 2. By quantitative real-time RT-PCR we confirmed the important role of Th-1 and IL-8/CXCR2 pathways in psoriasis and were able to demonstrate a significant overexpression in lesional compared to normal skin. During therapy, we found significant reductions in the gene expression of the proinflammatory cytokines as well as CXCR2, paralleled by a clearing of clinical symptoms. Recently, a study involving IL-11 therapy reported similar results (Trepicchio et al., 1999) using sequence-specific probes for real-time RT-PCR. However, sequence-specific probes are expensive and have to be individually designed. Here, we show that SYBR Green-based real-time RT-PCR, which does not require sequence-specific probes, is a valid method for quantifying even low-level cytokine gene expression.

Real-time PCR has been employed to quantify minimal residual disease in hematological malignancies as a measure of therapeutic efficacy (Cassinat et al., 2000; Eckert et al., 2000). It may also prove to be a reliable tool for the detection of early relapse. Monitoring residual circulating malignant cells with both quantitative competitive and real-time RT-PCR using sequence-specific hybridization probes (Emig

et al., 1999; Wattjes et al., 2000) has demonstrated the applicability of the new method in this setting. The results of our study extend these findings and show that real-time RT-PCR is a rapid, reliable and valid method for the detection of cytokines and may be useful in various clinical applications, such as the identification of disease-related genes and pharmacogenomic monitoring. Since it is significantly less time consuming (30 min versus several hours) than the currently preferred method, quantitative competitive RT-PCR, it might become the method of choice within the near future.

Acknowledgements

We highly appreciate the skillful technical assistance of Ms. Karolin Zachmann and Mr. Thomas Juergens.

References

- Beck, L.A., Stellato, C., Beall, L.D., Schall, T.J., Leopold, D., Bickel, C.A., Baroudy, F., Bochner, B.S., Schleimer, R.P., 1996. Detection of the chemokine RANTES and endothelial adhesion molecules in nasal polyps. *J. Allergy Clin. Immunol.* 98, 766.
- Blaschke, V., Jungermann, K., Püschel, G.P., 1996. Exclusive expression of the Gs-linked prostaglandin E2 receptor subtype 4 mRNA in mononuclear Jurkat and KM-3 cells and coexpression of subtype 4 and 2 mRNA in U-937 cells. *FEBS Lett.* 394, 39.
- Blaschke, V., Reich, K., Middel, P., Letschert, M., Sachse, F., Harwig, S., Neumann, C., 1999. Expression of the CD4⁺ cell-specific chemoattractant interleukin-16 in mycosis fungoides. *J. Invest. Dermatol.* 113, 658.
- Cassinat, B., Zassadowski, F., Balitrand, N., Barbey, C., Rain, J.D., Fenaux, P., Degos, L., Vidaud, M., Chomienne, C., 2000. Quantitation of minimal residual disease in acute promyelocytic leukemia patients with t(15;17) translocation using real time RT-PCR. *Leukemia* 14, 324.
- Eckert, C., Landt, O., Taube, T., Seeger, K., Beyersmann, B., Proba, J., Henze, G., 2000. Potential of LightCycler technology for quantification of minimal residual disease in childhood acute lymphoblastic leukemia. *Leukemia* 14, 316.
- Emig, M., Saussele, S., Wittur, H., Weisser, A., Reiter, A., Willer, A., Berger, U., Hellmann, R., Cross, N.C., Hochhaus, A., 1999. Accurate and rapid analysis of residual disease in patients with CML using specific fluorescent hybridization probes for real time quantitative RT-PCR. *Leukemia* 13, 1825.
- Franz, J.K., Kolb, S.A., Hunzel, K.M., Lahrtz, F., Neidhart, M.,

- Aicher, W.K., Pap, T., Gay, R.E., Fontana, A., Gay, S., 1998. Interleukin-16, produced by synovial fibroblasts, mediates chemoattraction for CD4⁺ T lymphocytes in rheumatoid arthritis. *Eur. J. Immunol.* 28, 2661.
- Gilliland, G., Perrin, S., Blanchard, K., Bunn, H.F., 1990. Analysis of cytokine mRNA and DNA: detection and quantitation by competitive polymerase chain reaction. *Proc. Natl. Acad. Sci. USA* 87, 2725.
- Heid, C.A., Stevens, J., Livak, K.J., Williams, P.M., 1996. Real time quantitative PCR. *Genome Res.* 6, 986.
- Higuchi, R., Dollinger, G., Walsh, P.S., Griffith, R., 1992. Simultaneous amplification and detection of specific DNA sequences. *Biotechnology (NY)* 10, 413.
- Kalinski, P., Schuitmaker, J.H., Hilkens, C.M., Wierenga, E.A., Kapsenberg, M.L., 1999. Final maturation of dendritic cells is associated with impaired responsiveness to IFN-gamma and to bacterial IL-12 inducers: decreased ability of mature dendritic cells to produce IL-12 during the interaction with Th cells. *J. Immunol.* 162, 3231.
- Neumann, C., Gutesell, C., Fliegert, F., Bonifer, R., Herrmann, F., 1996. Comparative analysis of the frequency of house dust mite specific and nonspecific Th1 and Th2 cells in skin lesions and peripheral blood of patients with atopic dermatitis. *J. Mol. Med.* 74, 401.
- Palucka, K.A., Faquet, N., Sanchez-Chapuis, F., Gluckman, J.C., 1998. Dendritic cells as the terminal stage of monocyte differentiation. *J. Immunol.* 160, 4587.
- Parada, N.A., Center, D.M., Kornfeld, H., Rodriguez, W.L., Cook, J., Vallen, M., Cruikshank, W.W., 1998. Synergistic activation of CD4⁺ T cells by IL-16 and IL-2. *J. Immunol.* 160, 2115.
- Platzer, C., Richter, G., Uberall, K., Muller, W., Blocker, H., Diamantstein, T., Blankenstein, T., 1992. Analysis of cytokine mRNA levels in interleukin-4-transgenic mice by quantitative polymerase chain reaction. *Eur. J. Immunol.* 22, 1179.
- Reich, K., Bruck, M., Gräfe, A., Ventic, C., Neumann, C., Garbe, C., 1998. Treatment of psoriasis with interleukin-10. *J. Invest. Dermatol.* 111, 1235.
- Reich, K., Westphal, G., Schulz, T., Müller, M., Zipprich, S., Fuchs, T., Hallier, E., Neumann, C., 1999. Combined analysis of polymorphisms of the tumor necrosis factor-alpha and interleukin-10 promoter regions and polymorphic xenobiotic metabolizing enzymes in psoriasis. *J. Invest. Dermatol.* 113, 214.
- Romani, N., Reider, D., Heuer, M., Ebner, S., Kampgen, E., Eibl, B., Niederwieser, D., Schuler, G., 1996. Generation of mature dendritic cells from human blood. An improved method with special regard to clinical applicability. *J. Immunol. Methods* 196, 137.
- Sager, N., Feldmann, A., Schilling, G., Kreitsch, P., Neumann, C., 1992. House dust mite-specific T cells in the skin of subjects with atopic dermatitis: frequency and lymphokine profile in the allergen patch test. *J. Allergy Clin. Immunol.* 89, 801.
- Schlaak, J.F., Buslau, M., Jochum, W., Hermann, E., Girndt, M., Gallati, H., Meyer zum Büschenfelde, K.H., Fleischer, B., 1994. T cells involved in psoriasis vulgaris belong to the Th1 subset. *J. Invest. Dermatol.* 102, 145.
- Siegling, A., Lefmann, M., Platzer, C., Emmrich, F., Volk, H.D., 1994. A novel multispecific competitor fragment for quantitative PCR analysis of cytokine gene expression in rats. *J. Immunol. Methods* 177, 23.
- Trepicchio, W.L., Ozawa, M., Walters, I.B., Kikuchi, T., Gil- leaudeau, P., Bliss, J.L., Schwertschlag, U., Dorner, A.J., Krueger, J.G., 1999. Interleukin-11 therapy selectively downregulates type 1 cytokine proinflammatory pathways in psoriasis lesions. *J. Clin. Invest.* 104, 1527.
- Uyemura, K., Yamamura, M., Fivenson, D.F., Modlin, R.L., Nickoloff, B.J., 1993. The cytokine network in lesional and lesion-free psoriatic skin is characterized by a T-helper type 1 cell-mediated response. *J. Invest. Dermatol.* 101, 701.
- Wattjes, M.P., Krauter, J., Nagel, S., Heidenreich, O., Ganser, A., Heil, G., 2000. Comparison of nested competitive RT-PCR and real time RT-PCR for the detection and quantification of AML1/MTG8 fusion transcripts in t(8:21) positive acute myelogenous leukemia. *Leukemia* 14, 329.

Apoptosis 1997; 2: 518-528

Butyrate-induced reversal of dexamethasone resistance in autonomous rat Nb2 lymphoma cells

A. R. Buckley, J. S. Krumenacker, D. J. Buckley, M. A. Leff, N. S. Magnuson, J. C. Reed, T. Miyashita, G. de Jong and P. W. Gout

Department of Pharmacology and Toxicology, University of North Dakota School of Medicine and Health Sciences, Grand Forks, ND, USA (A. R. Buckley, J. S. Krumenacker, D. J. Buckley, M. A. Leff); Department of Microbiology and Immunology, Washington State University, Pullman WA, USA (N. S. Magnuson); The Burnham Institute, La Jolla, CA, USA (J. C. Reed, T. Miyashita); Departments of Medical Oncology (G. de Jong) and Cancer Endocrinology (P. W. Gout), British Columbia Cancer Agency, Vancouver, BC

The parental rat Nb2 lymphoma is a prolactin (PRL)-dependent T cell line. Exposure of a PRL-independent subline, Nb2-SFJCD1, to sodium butyrate (NaBT) causes transient reversal of their growth factor-independent proliferation in association with constitutive expression of protooncogenes *pim-1* and *c-myc*. In the present study, we investigated the effect of NaBT treatment on the sensitivity of Nb2-SFJCD1 cells to dexamethasone (DEX)-induced apoptosis. Pretreatment with NaBT (2 mM, 72 h) partially reversed resistance to apoptosis in Nb2-SFJCD1 cells exposed to DEX (100 nM) for 12 h, assessed by flow cytometric analyses of DNA fragmentation. However, the cytolytic effect of DEX was abrogated by PRL in a time- and concentration-dependent manner. Evaluation of apoptosis-associated gene expression in NaBT-pretreated cultures incubated with DEX or DEX+PRL indicated that the apoptosis resistance did not stem from altered *bcl-2* or *bax* expression. However, there was a strong correlation between the resistance to DEX-activated apoptosis and their enhanced expression of *pim-1* mRNA and protein. The results show that it is possible to reverse DEX-induced apoptosis of Nb2 pre-T cells and suggest the *pim-1* gene product has an important role as a suppressor of this process, perhaps functioning as a mediator of PRL action.

Key words: Apoptosis; Bcl-2; dexamethasone; Nb2 lymphoma; Pim-1; prolactin.

(Received 10 June 1997; accepted 7 August 1997)

Introduction

A primary challenge in the clinical treatment of cancer is presented by development in the neoplasms of progressively malignant changes. This tumour (or malignant) progression is manifested by, for example, an increased capacity of the cancers to invade adjacent tissues, metastasize to distant organs and resist drug therapy. New insight into methods to reverse drug resistance, hormonal or growth factor autonomy, and other phenotypic changes associated with malignant progression of cancers, may lead to novel therapeutic approaches of the disease.

A system of cultured rat cell lines, consisting of parent and subline 'Nb2 lymphoma' cells, has previously been developed as a paradigm for investigating the mechanisms underlying malignant progression of T cell cancers.¹⁻³ Comparative analysis of the genetically related cell lines can be used to identify cellular and molecular changes that underlie development of growth factor independence,^{2,4-8} metastatic ability¹ and resistance to dexamethasone (DEX)-induced apoptosis.^{9,10}

The original Nb2 lymphoma cell line, established

Supported in part by DK-44439 and CA-60181 from the NIH, RD-383 from the American Cancer Society, 95B089 from the American Institute for Cancer Research, 91-37206-6867 from the USDA, and the British Columbia Cancer Agency.

Correspondence to A. R. Buckley, Department of Pharmacology and Toxicology, University of North Dakota, School of Medicine and Health Sciences, 501 North Columbia Road, PO Box 9037, Grand Forks, ND 58202-9037 USA. Tel: (+1) 701 777-4293; Fax: (+1) 701 777-6124; email: abuckley@mail.med.und.nodak.edu

in culture from a malignant lymphoma which developed in the thymus/lymph of an oestrogen-treated Noble (Nb) rat,¹¹ has been found to morphologically and biochemically resemble T lymphocytes at an intermediate stage of development.¹² Early studies revealed that the cultured cells critically require the anterior pituitary hormone, prolactin (PRL) or other lactogens, for maintenance of growth and viability.¹¹ Lactogen deprivation of the Nb2 cells for 18–24 h results in their accumulation in the early G₁ phase of cell cycle. The sole addition of PRL to such quiescent cells leads to partially synchronous re-entry into the cell cycle.¹³ Consequently, the lactogen-dependent Nb2 cell line has provided a valuable tool for investigation of molecular mechanisms coupled to PRL-induced mitogenesis.¹⁴

Autonomous Nb2 sublines have been developed by prolonged culturing of the PRL-dependent cells in lactogen-deficient medium and subsequent cloning of surviving cells.¹ One such subline, designated Nb2-SFJCD1, is completely growth factor-independent. Importantly, the oncogenic behaviour of this subline is different from that of the parental Nb2-U17 line. Subcutaneous Nb2-SFJCD1 tumours in Nb rats rapidly disseminate to give rise to metastases in e.g., kidney and liver, in contrast to PRL-dependent Nb2-U17 tumours which are restricted to the injection site, even when fat advanced.³ Karyotypic analysis has demonstrated that the Nb2-SFJCD1 subline has the same chromosomal alterations as those identified in the parental line, plus several additional changes, indicating that it arose from the latter *via* clonal evolution.²

Another important distinction between Nb2-SFJCD1 and PRL-dependent Nb2 cells is their differential sensitivity to drug (glucocorticoid)-activated apoptosis. Exposure of PRL-dependent Nb2 cells to DEX, in the absence of PRL, activates cellular suicide mechanisms characterized by fragmentation of genomic DNA, a process which can be inhibited by addition of PRL.⁹ In contrast, Nb2-SFJCD1 cells resist DEX-activated apoptosis, even in the presence of suprapharmacological concentrations of the steroid.¹⁰ It is notable that Nb2-SFJCD1 cells constitutively express elevated levels of *pim-1*⁵ and *bcl-2*,⁷ two protooncogenes linked to suppression of apoptosis.^{15–18} This raises the possibility that the resistance of this subline to DEX-activated apoptosis stems from their constitutive expression

of these protooncogenes.

In previous studies, we demonstrated that treatment of Nb2-SFJCD1 cells with sodium butyrate (NaBT), a four carbon fatty acid acting as a differentiating agent, can transiently reverse their growth factor (PRL) independence. During a 72 h incubation with NaBT (2–3 mM) the cells became arrested in the G₁ phase of the cell cycle and, following removal of the fatty acid, transiently required PRL for proliferation.¹ Moreover, the levels of the protooncogenes, *c-myc* and *pim-1*, were significantly reduced as a result of the NaBT treatment and required PRL for activation, as observed in PRL-dependent Nb2 cells.⁸ In the present study, we show that pretreatment of Nb2-SFJCD1 cells with NaBT can reverse, at least in part, their resistance to DEX-activated apoptosis. The DEX sensitivity resulting from the NaBT treatment can be abrogated by addition of PRL. In addition, a role is suggested for the protooncogene, *pim-1*, as a suppressor of DEX-induced apoptosis and a mediator of the anti-apoptotic effect of PRL.

Materials and methods

Materials

Ovine PRL (NIDDK oPRL-20, AFP10677C) was obtained through the NIH Pituitary Hormone and Antisera Program (Rockville, MD, USA). A mouse (600 b.p. *XhoI/HindIII* probe) *bcl-2* complementary DNA (cDNA) was generously provided by Dr T. J. McDonnell (Houston, TX, USA). The mouse (600 b.p. *EcoRI* probe) *bax* cDNA and the anti-Bax antisera used have been previously characterized.⁷ Antiserum to Pim-1 protein was generated against a recombinant glutathione S-transferase-Pim-1 fusion protein, as described previously.⁵ Anti-Bcl-2 antiserum, which specifically recognizes mouse, rat and human Bcl-2, was obtained from Santa Cruz Biotechnology, Inc. (Santa Cruz, CA, USA; catalogue no. SC-492). Unless otherwise specified, all other reagents were of molecular biology grade, obtained from Sigma Chemical Co. (St. Louis, MO, USA).

Nb2 lymphoma cell cultures

The cloned, autonomous Nb2-SFJCD1 subline was

A. R. Buckley et al.

utilized. This cell line is completely PRL-independent, as shown by its rapid growth in lactogen-deficient, chemically defined culture medium, but still growth-responsive to PRL.^{1,8} Cultures were maintained at 37°C in Fischer's medium containing 10% horse serum (Bio Whittaker, Walkersville, MD, USA), 2-mercaptoethanol (2-ME; 10⁻⁴ M), penicillin (50 units/ml) and streptomycin (50 µg/ml) (maintenance medium) in a 5% CO₂/air atmosphere, as described previously.¹ Pretreatment with NaBT was carried out by incubating the cells in maintenance medium with 2 mM NaBT (Sigma) for 72 h. NaBT was then removed and the cells resuspended in maintenance medium containing 10% nonmitogenic gelding serum (ICN, Irvine, CA, USA) as the serum component (assay medium), for subsequent experimentation.⁸

Flow cytometric evaluation of DNA fragmentation

Apoptosis in cells was also assessed using flow cytometric analysis of cell nuclei stained with propidium iodide (PI; Sigma) to detect DNA fragmentation, as described by Nicoletti *et al.*¹⁹ Cells (1–2 × 10⁶) were fixed in cold (–20°C) 70% ethanol. The cells were washed, resuspended in RNase (1 mg/ml in PBS; Type 1-A, Sigma), and incubated for 60 min at 37°C. The cells were again washed, then resuspended in a hypotonic PI solution (50 µg/ml in PBS). Flow cytometric analysis was carried out using an Elite flow cytometer (Coulter Electronics, Hialeah, FL, USA) with the 488 nm line of an enterprise laser (Coherent, Palo Alto, CA, USA). Red fluorescence of the PI-stained cells was monitored through a 600 nm dichroic and a 610 LP filter and collected in a three-decade log histogram. Forward and side scatter were simultaneously measured. Time-of-flight measurement was used to exclude cellular debris and clumps. All samples were assessed using the same instrument settings. Results were expressed as per cent apoptotic cells of the total cell population.

Northern blotting procedures

Total RNA was isolated from 2 × 10⁷ Nb2-SFJCD1 cells cultured in 25-cm² flasks using RNeasy-L

(Tel-Test, Friendswood, TX, USA). The RNA was quantitated spectrophotometrically. For Northern analysis, RNA was denatured in formaldehyde and fractionated on 1% agarose gels, then transferred to GeneScreen Plus (DuPont, Wilmington, DE, USA). Equal loading per lane was verified by ethidium bromide staining of 18S and 28S ribosomal RNA, which was visualized and photographed under UV illumination. Membranes were hybridized with either *pim-1*, *bcl-2* or *bax* cDNA probes. Isolated inserts were labelled with [³²P]deoxy-CTP (DuPont NEN) using the random primer method of Feinberg and Vogelstein.²⁰ Hybridization and wash procedures were conducted using the methods of Church and Gilbert.²¹

Immunoprecipitation of [³⁵S]-methionine-labelled *Pim-1*

Cells were extensively washed free of extracellular methionine (MET), using MET-free RPMI 1640 medium (Gibco BRL, Gaithersburg, MD, USA) containing 2% dialyzed gelding serum. Cells (5 × 10⁶ cells/ml) were incubated with DEX (100 nM) or DEX + PRL (20 ng/ml) for various time periods. Two h prior to harvesting, cultures were pulse labelled with 100 µCi/ml of [³⁵S]-MET. The cells were disrupted in radioimmunoprecipitation assay (RIPA) buffer containing 50 mM Tris (pH 8.0), 250 mM NaCl, 2 mM EDTA, 1% NP40, 0.25% deoxycholate, 1 mM phenylmethylsulfonyl fluoride (PMSF), and 10 µg/ml each of chymostatin, aprotinin and leupeptin. The lysates were centrifuged for 20 min at 14,000 × g at 4°C. Sodium dodecyl sulfate (SDS) was added to the supernatants to a final concentration of 0.1%. The samples were pre-cleared by the addition of 6 µl of normal rabbit serum (Sigma) and 25 µl of recombinant protein G-agarose (Gibco) followed by incubation for 2 h at 4°C. After centrifugation, supernatant aliquots were precipitated with trichloroacetic acid and [³⁵S]-MET incorporation was determined by scintillation counting. Lysates [(1–1.5) × 10⁶ cpm] were incubated overnight at 4°C in the presence of 6 µl of anti-*Pim-1* antisera and 25 µl of protein G-agarose. The immunoprecipitates were washed 5 × with RIPA buffer, resuspended in SDS-sample buffer (containing 2-ME), and boiled for 10 min. Immunoprecipitated proteins were resolved by SDS

Reversal of apoptosis resistance

polyacrylamide gel electrophoresis (PAGE) using 10% gels. The gels were stained, incubated with Enhance (DuPont), dried and exposed to x-ray film for 1-3 days.

Immunoblotting of Bcl-2 and Bax proteins

Cells from experiments (2.5×10^7 cells/time point) were lysed in a buffer containing 10 mM Tris-HCl (pH 7.4), 0.15 M NaCl, 5 mM EDTA, 1% Triton X-100, 1 mM PMSF and 25 μ g/ml each of leupeptin and aprotinin, and then centrifuged for 10 min at $14,000 \times g$. Total protein content of the supernatants was determined using the Bradford reagent (BioRad, Richmond, CA, USA). Lysates (100 μ g protein/lane) were fractionated by SDS-PAGE using 10% gels and electrophoretically transferred to Immobilon membranes (BioRad). Membranes were blocked overnight at 4°C in 5% nonfat dried milk in Tris-buffered saline. Proteins were visualized by first incubating the membranes with anti-Bcl-2 (1/100) or anti-Bax (1/1,500) followed by chemiluminescence detection using a secondary antibody (1/3,000) coupled to alkaline phosphatase and a chemiluminescence substrate (BioRad). The membranes were exposed to x-ray film for 3-15 min.

Data analysis

Data are presented from experiments repeated three times unless otherwise noted. For Northern blotting procedures, equal RNA loading per lane was always verified by densitometric analysis of ethidium bromide-stained 18S and 28S ribosomal RNA. Where applicable, data are presented as the mean \pm SE. Statistically significant differences among treatment groups were evaluated by ANOVA followed by the student Newman Kucl's post-test for multiple comparisons.

Results

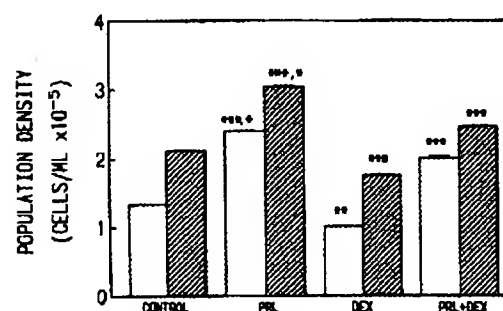
NaBT-Induced reversal of resistance to DEX-activated apoptosis

Witorsch *et al.* have reported that DEX substantially inhibited PRL-dependent mitogenesis of Nb2

lymphoma cells. In the absence of lactogen, DEX activated apoptosis which was abrogated by the addition of PRL.⁹ In contrast, DEX did not induce apoptosis in the PRL-independent Nb2-SFJCD1 cells in the absence of PRL, although it attenuated their replication.¹⁰ We have previously shown that treatment of Nb2-SFJCD1 cells with NaBT leads to growth arrest, transient reversals of their growth factor independence and constitutive expression of *pim-1*, a protooncogene implicated in the regulation of apoptosis.¹⁵

To investigate whether treatment with NaBT could also reverse the resistance of Nb2-SFJCD1 cells to DEX-activated apoptosis, experiments were first performed to determine the effects of the steroid on proliferation of untreated and NaBT-treated cells (2 mM NaBT, 72 h). As shown in Figure 1, untreated Nb2-SFJCD1 cells grew readily in the absence of PRL, but were growth-responsive to the hormone ($p < 0.001$). DEX (100 nM) partially inhibited replication of the untreated cells in the absence of PRL ($p < 0.001$); addition of the hormone significantly increased ($p < 0.001$ vs. control) proliferation albeit to a lesser extent ($p < 0.001$) compared with cultures treated with PRL alone. Following NaBT treatment the cells did not increase in number unless PRL had been added ($p < 0.001$). DEX treatment significantly reduced the

Figure 1. Effect of NaBT-pretreatment on the growth response of Nb2-SFJCD1 cell cultures to PRL and/or DEX. Nb2-SFJCD1 cells were incubated for 72 h with NaBT (2 mM, open bars) or without the fatty acid (control, cross-hatched bars), washed to remove NaBT and incubated with PRL (20 ng/ml), DEX (100 nM), or DEX+PRL. Initial cell concentrations: 1.5×10^5 cells/ml. At 48 h, cell counts were performed using an electronic cell counter. Data are presented as the means of triplicate values and represent results from four experiments. Standard error bars, when not visible, are obscured by symbols. *: $p < 0.001$ vs. PRL+DEX; **: $p < 0.01$ vs. control; ***: $p < 0.001$ vs. control.



A. R. Buckley et al.

number of NaBT-treated cells ($p < 0.001$), indicating that DEX-induced cytolysis had taken place. Addition of PRL (20 ng/ml) to the DEX-containing, NaBT-treated cultures increased cell numbers to a level nearly equivalent to that observed in NaBT-treated cultures containing only PRL ($p < 0.001$). These results confirm our previous observations that NaBT can induce PRL dependency in autonomous Nb2-SFJCD1 cells^{1,8} and suggest that the fatty acid-pretreated cultures were sensitive to DEX-initiated cytolysis which could be abrogated by PRL.

The cytolytic action of DEX in NaBT-pretreated Nb2-SFJCD1 cells was further examined for evidence of apoptosis by flow cytometric analysis. Cultures were incubated for 72 h with 2 mM NaBT, washed to remove the fatty acid and then further incubated with DEX (100 nM) for 12 h. Control cultures were treated identically but without NaBT. As shown in Figure 2, DEX (100 nM) was ineffective at inducing apoptosis in control Nb2-SFJCD1 cultures. However, pretreating the cultures with 2 mM NaBT for 72 h rendered the cells sensitive to

DEX; the glucocorticoid markedly increased the percentage of apoptotic cells. Notably, pretreatment with NaBT significantly increased the proportion of control cells undergoing apoptosis in the absence of DEX by nearly fivefold ($p < 0.05$). These results indicate that pretreatment of Nb2-SFJCD1 cells with NaBT can reverse the resistance of this subline to apoptotic action of glucocorticoids.

The anti-apoptotic effect of PRL was also evaluated. As shown in Figure 3, PRL reduced the levels of DEX-activated apoptosis in NaBT-pretreated Nb2-SFJCD1 cells in a concentration-dependent manner. This protective effect of the hormone is very similar to its concentration-dependent, mitogenic stimulation of PRL-dependent Nb2 cells¹¹ and NaBT-pretreated Nb2-SFJCD1 cells.⁸

It was also established how long the addition of PRL to DEX-treated cultures could be delayed without loss of its protective effect. NaBT-pretreated Nb2-SFJCD1 cells were incubated with DEX (100 nM) for a 12 h period for subsequent DNA fragmentation analysis; PRL (10 ng/ml) was added at 3, 6 or 9 h following addition of the steroid.

Figure 2. DEX-induced apoptosis in NaBT-pretreated Nb2-SFJCD1 cultures as a function of DEX concentration. NaBT-pretreated (2 mM, 72 h) and untreated cells were incubated for 12 h with DEX at the indicated concentrations for subsequent flow cytometric analysis of DNA fragmentation in PI-stained cell nuclei, as described in Materials and methods. Data are presented as the means \pm SEM of samples assessed in duplicate, and represent results from four experiments. a: $p < 0.05$ vs. untreated, control Nb2-SFJCD1 cells; b: $p < 0.01$ vs. NaBT-pretreated, control Nb2-SFJCD1 cells.

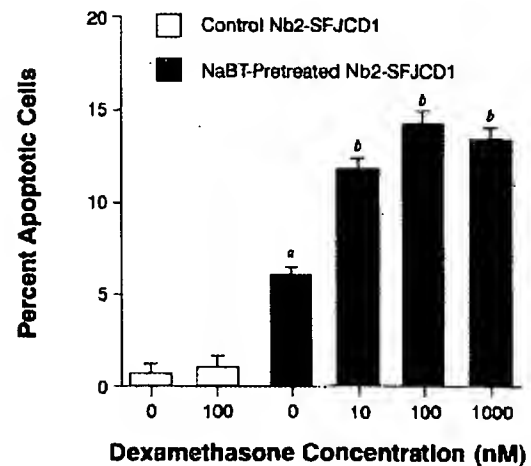
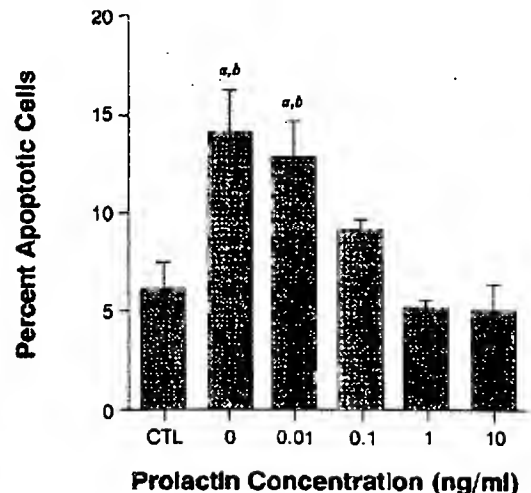
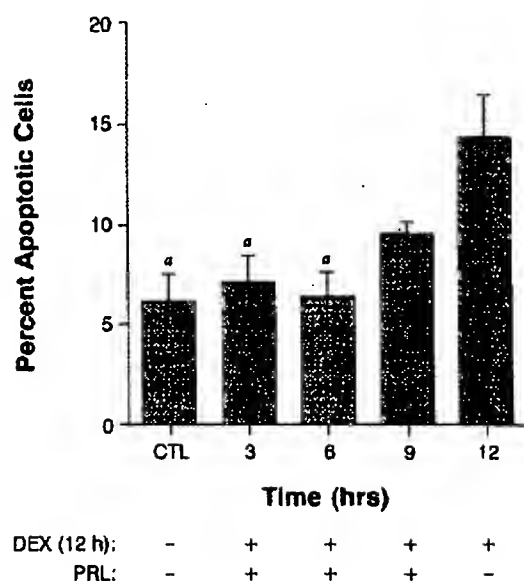


Figure 3. Anti-apoptotic effect of PRL as a function of its concentration. NaBT-pretreated (2 mM, 72 h) Nb2-SFJCD1 cells were incubated for 12 h with DEX (100 nM) plus PRL at the indicated concentrations. The percentage apoptotic cells in the cultures was determined using flow cytometric analysis of PI-stained cell nuclei, as described in Materials and methods. Data are presented as the means \pm SEM of samples assessed in duplicate and represent results from four experiments. a: $p < 0.01$ vs. CTL; b: $p < 0.01$ vs. 10 ng/ml PRL.



Reversal of apoptosis resistance

Figure 4. Anti-apoptotic effect of PRL added at various times after DEX administration. NaBT-pretreated (2 mM, 72 h) Nb2-SFJCD1 cells were incubated with DEX (100 nM) added at 0 h. PRL was added to cultures after 3, 6 or 9 h. The percentage of apoptotic cells in the cultures was evaluated by flow cytometry of PI-stained cell nuclei, as described in Materials and methods. Data are presented as means \pm SEM of samples evaluated in duplicate and represent results from four experiments. a: $p < 0.01$ vs. DEX only (12 h).

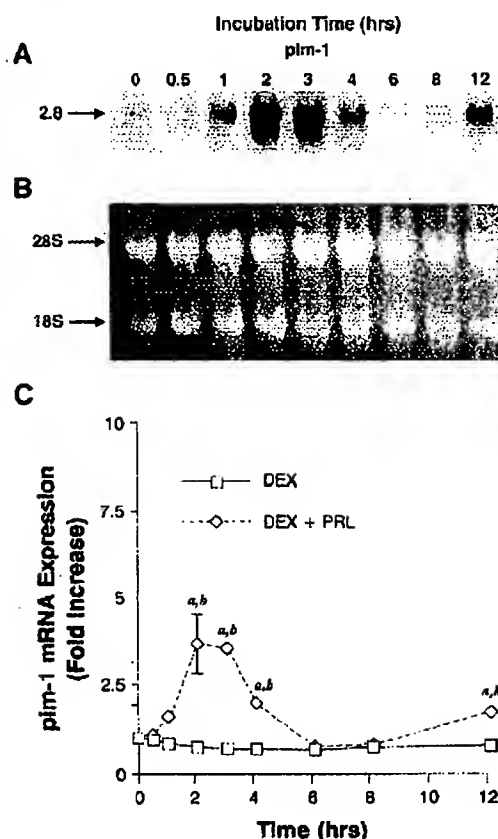


As shown in Figure 4, addition of PRL during the first 6 h of DEX exposure significantly ($p < 0.01$) inhibited glucocorticoid-activated apoptosis. However, addition 9 h after DEX did not completely protect the cells. Thus PRL-responsive mechanisms, which suppress the actions of DEX, most likely require activation within 6 h of glucocorticoid exposure.

Effect of DEX and DEX plus PRL on the expression of *Pim-1*, *Bcl-2* and *Bax* in NaBT-pretreated Nb2-SFJCD1 cells

We have previously demonstrated that expression of *pim-1* is dependent upon PRL stimulation in hormone-dependent Nb2 cells.⁵ In Nb2-SFJCD1 cells, its expression is constitutive, but enhanced by PRL.⁵ More recently, we showed that *pim-1* expression in Nb2-SFJCD1 cells was significantly reduced by pretreatment with NaBT and reverted

Figure 5. Time course of *pim-1* gene expression in NaBT-pretreated Nb2-SFJCD1 cells following addition of DEX or DEX+PRL. (A) NaBT-pretreated (2 mM for 72 h) cells (2×10^7 cells/time point) were incubated with DEX (100 nM) plus PRL (20 ng/ml). At the time points indicated, total RNA was isolated for evaluation of *pim-1* expression by Northern blotting as described in Materials and methods. (B) Equal loading of total RNA was verified by ethidium bromide staining of the gels. (C) Comparison of DEX and DEX+PRL-treated cultures by densitometric evaluation of autoradiographs from an experiment conducted four times. Data are presented as means \pm SEM (when not visible, bars are obscured by the symbols). a: $p < 0.01$ vs. control (time 0); b: $p < 0.01$ vs. DEX.



to a state of PRL-dependency for its enhanced expression.⁸ Since *pim-1* is a protooncogene linked to suppression of apoptosis,¹⁸ we investigated the effect of adding DEX and DEX+PRL on the level of the *pim-1* transcript in NaBT-pretreated Nb2-SFJCD1 cultures. As shown in Figure 5C, DEX did not alter steady state *pim-1* mRNA levels. However, addition of PRL to DEX-containing cultures resulted in substantial, time-dependent changes.

A. R. Buckley et al.

Figure 6. Time courses of *bcl-2* and *bax* gene expressions in NaBT-pretreated Nb2-SFJCD1 cells following addition of DEX or DEX+PRL. NaBT-pretreated (2 mM, 72 h) cells (2×10^7 cells/time point) were incubated with DEX (100 nM) or DEX+PRL (20 ng/ml). At the time points indicated total RNA was isolated from cells treated with DEX+PRL for evaluation of *bcl-2* (A) and *bax* (B) mRNAs by Northern blotting as described in Materials and Methods. (C and D) Comparison of DEX and DEX+PRL-stimulated cultures by densitometric evaluation of *bcl-2* (7.3 kb) and *bax* mRNA bands, respectively. In autoradiographs from experiments repeated more than four times. a: $p < 0.01$ vs. control (time 0); b: $p < 0.01$ vs. DEX.

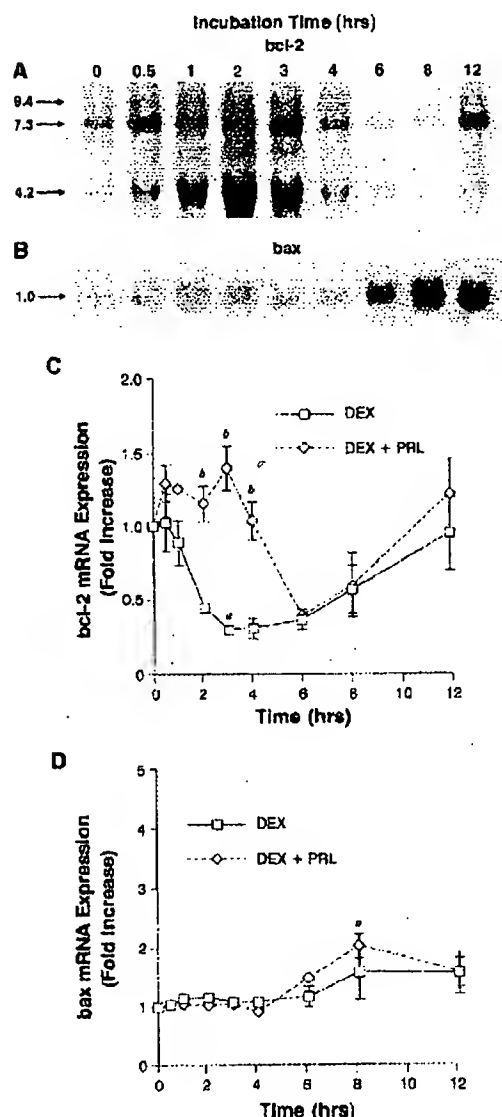
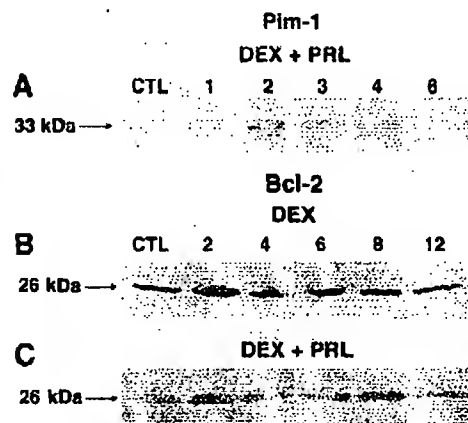


Figure 7. Levels of Pim-1 and Bcl-2 protein in NaBT-pretreated Nb2-SFJCD1 cells following incubation with DEX or DEX+PRL. NaBT-pretreated (2 mM for 72 h) Nb2-SFJCD1 cells (2.5×10^7 cells/time point) were incubated with DEX+PRL or DEX only. (A) At the times indicated (h) cells were harvested for analysis of Pim-1 using immunoprecipitation of [35 S]-MET-labelled Pim-1, as described in Materials and methods. (B and C) For evaluation of Bcl-2, immunoblot analysis of total cell lysates (100 μ g/lane) was conducted, using a monoclonal anti-Bcl-2 antibody. The data presented are representative of results from four experiments.



Within 2–3 h, the levels of *pim-1* mRNA increased to maximal levels, after which they declined to control levels by 6 h, to again increase at 12 h (Figure 5A and C). Thus, addition of PRL to DEX-containing, NaBT-pretreated Nb2-SFJCD1 cultures leads to a rapid and biphasic increase in the *pim-1* transcript, similar to that found following hormone stimulation in quiescent, lactogen-dependent Nb2 cells.⁹

The protooncogene *bcl-2* encodes a 26 kDa, membrane-associated protein which is well-characterized as a suppressor of apoptosis in hematopoietic and other systems.^{15–17} Similar to *pim-1*, expression of *bcl-2* is rapidly induced by PRL in lactogen-dependent Nb2 cells and enhanced in Nb2-SFJCD1 cells.⁷ The effects of DEX and DEX+PRL on expression of 9.4, 7.3 and 4.2 kb *bcl-2* transcripts in NaBT-pretreated Nb2-SFJCD1 cells are shown in Figures 6A and C. Addition of DEX significantly reduced the level of the 7.3 kb transcript within 2–4 h (Figure 6C). In contrast, DEX+PRL slightly augmented and sustained the level of *bcl-2* mRNA through 4 h. The results show that addition of PRL to the DEX-treated cells inhibited the decrease in the *bcl-2* transcripts resulting in a level of expression

Reversal of apoptosis resistance

that was more than threefold greater than that detected in DEX-treated cultures.

The effects of DEX and DEX+PRL on the expression of *bax*, a *bcl-2* homolog believed to facilitate apoptosis,^{15,22,23} were also assessed in NaBT-pretreated Nb2-SFJCD1 cultures. Addition of PRL+DEX, in comparison to DEX only, led to a minor, significant increase in *bax* mRNA levels at 8 h (Figure 6B and D). Thus, while the anti-apoptotic effect of PRL appears to involve a change in the transcript levels of the *bcl-2* gene (Figure 6A and C), it apparently does not depend on a major contribution by its homolog, *bax*.

Levels of Pim-1, Bcl-2 and Bax proteins were assessed to determine whether the observed alterations in the gene transcripts were coupled to parallel changes in protein expression. For determination of the Pim-1 protein, NaBT-pretreated, [³⁵S]-MET-labelled Nb2-SFJCD1 cells were incubated with DEX+PRL followed by immunoprecipitation of [³⁵S]-Pim-1. As shown in Figure 7A, addition of PRL to the DEX-treated cultures transiently increased the level of [³⁵S]-Pim-1. Expression of the protein increased within 1 h, reached maximal levels by 2–3 h, then declined to undetectable levels. This pattern of [³⁵S]-Pim-1 protein expression is essentially identical to that determined for its mRNA expression (Figure 5). As demonstrated in Figures 7B and C, Bcl-2 protein expression at any of the time points evaluated was not significantly altered by treatment with either DEX or DEX+PRL, respectively. Similarly, PRL did not enhance the levels in the cultures of Bax protein (data not shown). Taken together, the results indicate that PRL-induced enhancement of *pim-1* mRNA levels in the DEX-treated cultures (Figure 5) was coupled to a similar augmentation of its protein. However, the changes observed in the levels of *bcl-2* mRNA (Figure 6) were not reflected in its protein level.

Discussion

The original, PRL-dependent rat Nb2 lymphoma line and its hormone-dependent and autonomous sublines represent a novel model for studying mechanisms that underlie malignant progression of cancers of T cell origin.¹ Differential analysis of the genetically-related, but phenotypically distinct, cell

lines can be used to identify chromosomal and molecular alterations that underlie malignant progression, including development of resistance to glucocorticoid-activated apoptosis.¹⁰ The latter is expressed in the autonomous Nb2-SFJCD1 subline which, in contrast to PRL-dependent Nb2 cells⁹ or normal thymocytes,²⁴ is resistant to DEX-activated apoptosis.¹⁰

The previous finding¹ that PRL independence of the Nb2-SFJCD1 line could be reversed to hormone-dependency by treatment with NaBT has allowed a comparison of non-treated cells with NaBT-treated cultures of the same cell line, aimed at identifying changes in gene expression associated with the development of growth factor independence in Nb2 cells.⁸ In the present study it was found that a 72 h treatment of Nb2-SFJCD1 cells with 2 mM NaBT also led to partial reversal of their resistance to DEX-activated apoptosis. Thus, DEX treatment of NaBT-pretreated Nb2-SFJCD1 cells led to DNA fragmentation which was abrogated by PRL in a time- and concentration-dependent manner (Figures 1–4).

It is notable that PRL deprivation of both hormone-dependent and NaBT-pretreated, autonomous Nb2 cells arrests growth in the G₁ phase of cell cycle. In this setting, DEX activated apoptosis and the addition of PRL abrogated the cytolytic response initiated by the steroid. Thus, it appears that staging of cells in the G₁ phase may be an important prerequisite for sensitivity to DEX-activated apoptosis and subsequent mitogen rescue in Nb2 cells. This is consistent with observations made in other DEX-sensitive hematopoietic cell lines in which this steroid is thought to activate apoptosis *via* a mechanism that involves at least two-steps (reviewed in ²⁵). In cultured murine,²⁶ rat²⁷ and human²⁸ T cell lines, DEX also exerted an antiproliferative effect, characterized by accumulation of cells in the G₁ phase of cell cycle, as well as induced apoptosis. Moreover, stimulation with cytokines²⁷ or activation of the T cell receptor^{26,28} inhibited the apoptotic response provoked by the glucocorticoid. These observations led us to investigate whether expression of apoptosis-regulatory genes is altered by DEX or DEX+PRL in NaBT-treated Nb2-SFJCD1 cells.

Previous studies have shown that lactogen-starved Nb2 cells have very low expression of *bcl-2* and *pim-1* which, however, is rapidly augmented by

A. R. Buckley et al.

PRL at mitogenic concentrations. In contrast, both genes are constitutively expressed at elevated levels in autonomous Nb2-SFJCD1 cells^{3,7,8} which are DEX-resistant.¹² Whereas NaBT pretreatment of Nb2-SFJCD1 cells leads to a partial reversal of resistance to DEX-activated apoptosis, as shown in this study (Figures 2 and 3), the NaBT treatment does not appreciably affect their level of *bcl-2* expression (Buckley et al., unpublished observations). This suggests that constitutive *bcl-2* expression in untreated Nb2-SFJCD1 cells⁷ is probably not responsible for their resistance to DEX-activated cell death,¹⁰ and is consistent with the lack of effect of DEX+PRL on Bcl-2 protein levels in NaBT-treated Nb2-SFJCD1 cultures (Figure 7). In contrast, NaBT treatment significantly reduced the constitutive expression of *pim-1* in Nb2-SFJCD1 cells and transiently reverted it to PRL dependency for enhanced expression.⁸ In the present study, it was found that addition of PRL to NaBT-pretreated Nb2-SFJCD1 cultures not only reversed resistance to DEX-activated apoptosis (Figures 1, 3 and 4), but also increased levels of the *pim-1* transcript (Figure 5) and protein (Figure 7). Together, these observations show that there is a strong correlation between the resistance to glucocorticoid actions in Nb2 cells and their enhanced expression of the *pim-1* gene. The results, although correlative, indicate a central role for *pim-1* as a suppressor of apoptosis in the Nb2 pre-T cell lines and as a mediator of the anti-glucocorticoid action of PRL. Support for this suggestion comes from studies which report that overexpression of *pim-1* in thymocytes, obtained from Eu-Pim-1 transgenic *lpr/lpr* mice, confers resistance to DEX-induced apoptosis.¹⁸

The mechanism that affords resistance to DEX-activated apoptosis in Nb2-SFJCD1 cells is presently unclear. Karyotypic analysis has revealed that this subline arose by clonal evolution from the parental line, as indicated by several additional alterations in chromosomal structure.² For example, the Nb2-SFJCD1 cells contain an inversion in one of its chromosomes 1, i.e., inv(1)(q31q41), which is adjacent to the locus reported for the *c-H-ras* gene.¹⁹ Alterations in *H-ras* expression have been reported to enhance tumour invasiveness in mouse lymphomas²⁰ and may participate in advanced tumour progression.²¹ In this context, it is notable that p21^{ras} and its down-stream regulator, mitogen-activated protein kinase (MAPK) are each

constitutively active in Nb2-SFJCD1 cultures.¹² Since PRL-stimulation in hormone-dependent Nb2 cell cultures appears to require activation of this signalling pathway^{32,34} in conjunction with the JAK2-STAT cascade,^{34,35} this observation suggests that enhanced Ras and MAPK may collaborate to confer apoptosis resistance to Nb2-SFJCD1 cells by upregulating expression of genes which suppress apoptosis. Consistent with this hypothesis is our recent observation that protooncogenes, *pim-1* and *c-myc*, which have been linked to regulation of proliferation as well as to apoptosis, are each over-expressed in the Nb2-SFJCD1 subline compared to PRL-dependent Nb2 cells.⁸

Butyrate is a four carbon fatty acid produced in the body by bacterial fermentation of dietary fibre. At concentrations present within the intestinal lumen, it inhibits proliferation and induces differentiation in epithelial cells present within the colon.³⁶⁻³⁸ In addition, prolonged exposure to NaBT activates apoptosis in colonic adenoma and carcinoma, and in human breast cancer cells,³⁹ as well as in the human promyelocytic cell line, HL-60.⁴⁰ However, despite considerable investigation, a clear delineation of the molecular basis for the cellular effects of butyrate has remained elusive. It is clear that butyrate inhibits histone deacetylase which leads to hyperacetylation of histones resulting in altered chromatin structure.⁴¹⁻⁴³ However, it is unlikely that the selective actions on gene transcription provoked by NaBT can be attributed to the nonspecific changes that would occur in chromatin as a result of NaBT-induced inhibition of histone deacetylase. Other proposed mechanisms for the actions of NaBT include alterations in transcription factor activation,⁴⁴⁻⁴⁶ post-transcriptional mRNA processing,⁴⁷ β -oxidation,⁴⁸ tRNA modification⁴⁹ as well as phospholipid⁵⁰ and purine metabolism.⁵¹ Most recently, NaBT has been reported to rapidly induce tyrosyl phosphorylation of a number of cellular proteins, most notably, MAPK, in human K562 erythroleukemia cells.⁵² In that study, increased tyrosyl phosphorylation and enzymatic activity of MAPK was demonstrated within minutes after addition of NaBT to the cultures. Therefore, it is possible that in Nb2-SFJCD1 cells, NaBT may further enhance MAPK activity which may, as a consequence, down-regulate *pim-1* transcription through phosphorylation of transacting factors. Whether MAPK or other signalling path-

ways underlie the observed alterations in *pim-1* transcription and whether this protooncogene mediates an apoptotic response in Nb2 cells warrants further investigation.

References

- Gout PW. Transient requirement for prolactin as a growth initiator following treatment of autonomous Nb2 node rat lymphoma cell cultures with butyrate. *Cancer Res* 1987; 47: 1751-1755.
- Horsman DE, Masui S, Gout PW. Karyotypic changes associated with loss of prolactin dependency of rat Nb2 node lymphoma cell cultures. *Cancer Res* 1991; 51: 282-287.
- Gout PW, Horsman DE, Fux K, de Jong G, Ma S, Bruchovsky N. The rat Nb2 lymphoma: a novel model for tumor progression. *Anticancer Res* 1994; 14: 2485-2492.
- Buckley AR, Buckley DJ, Gout PW, Liang H, Rao Y-P, Blake MJ. Inhibition by genistein of prolactin-induced Nb2 lymphoma cell mitogenesis. *Mol Cell Endocrinol* 1993; 98: 17-25.
- Buckley AR, Buckley DJ, Leff MA, Hoover DS, Magnuson NS. Rapid induction of *pim-1* expression by prolactin and interleukin-2 in rat Nb2 lymphoma cells. *Endocrinology* 1995; 136: 5252-5259.
- Gilks CB, Purter SD, Barker C, Tschlis PN, Gout PW. Prolactin (PRL)-dependent expression of a zinc finger protein-encoding gene, *Gfi-1*, in Nb2 lymphoma cells: constitutive expression in autonomous sublines. *Endocrinology* 1995; 136: 1805-1808.
- Leff MA, Buckley DJ, Krumenacker JS, Reed JC, Miyashita T, Buckley AR. Rapid modulation of the apoptosis regulatory genes, *bcl-2* and *bax* by prolactin in rat Nb2 lymphoma cells. *Endocrinology* 1996; 137: 5456-5462.
- Buckley AR, Leff MA, Buckley DJ, Magnuson NS, de Jong G, Gout PW. Alterations in *pim-1* and *c-myc* expression associated with sodium butyrate-induced growth factor-dependency in autonomous rat Nb2 lymphoma cells. *Cell Growth Diff* 1996; 7: 1713-1721.
- Fletcher-Chiappini SR, Conlxon MM, La Voie HA, Day EB, Witorsch RJ. Glucocorticoid-prolactin interactions in Nb2 lymphoma cells: antiproliferative versus anticytolytic effects. *Proc Soc Exp Biol Med* 1993; 202: 345-352.
- Witorsch RJ, Day EB, LaVoie HA, Hashemi N, Taylor JK. Comparison of glucocorticoid-induced effects in prolactin-dependent and autonomous rat Nb2 lymphoma cells. *Proc Soc Exp Biol Med* 1993; 203: 454-460.
- Gout PW, Beer CT, Noble RL. Prolactin-stimulated growth of cell cultures established from malignant Nb rat lymphomas. *Cancer Res* 1980; 40: 2433-2436.
- Cox JH, Lamb JR, Bal V, et al. The phenotypic and molecular characterization of Nb2 lymphoma cells activated with IL-2 and human growth hormone. *Immunology* 1989; 66: 83-89.
- Richards JF, Beer CT, Bourgeault C, Chen K, Gout PW. Biochemical response of lymphoma cells to mitogenic stimulation by prolactin. *Mol Cell Endocrinol* 1982; 26: 41-49.
- Horsman ND. Prolactin, proliferation, and protooncogenes. *Endocrinology* 1995; 136: 5249-5251.
- Oltvai ZN, Millman CL, Korsmeyer SJ. Bcl-2 heterodimerizes *in vivo* with a conserved homolog, Bax, that accelerates programmed cell death. *Cell* 1993; 74: 609-619.
- Ohtu K, Iwai K, Kasahara Y, et al. Immunoblot analysis of cellular expression of Bcl-2 family proteins, Bcl-2, Bax, Bcl-x and Mcl-1, in peripheral blood and lymphoid tissues. *Int Immunol* 1995; 7: 1817-1825.
- McDonnell TJ, Deane N, Platt FM, et al. *bcl-2*-immunoglobulin transgenic mice demonstrate extended B cell survival and follicular lymphoproliferation. *Cell* 1989; 57: 79-88.
- Moroy T, Grzeschitzek A, Perzold S, Hartmann K-U. Expression of a *Pim-1* transgene accelerates lymphoproliferation and inhibits apoptosis in *lyt11pr* mice. *Proc Natl Acad Sci USA* 1993; 90: 10734-10738.
- Nicoletti I, Migliorati G, Pagliacci MC, Grignani F, Riccardi C. A rapid and simple method for measuring thymocyte apoptosis by propidium iodide staining and flow cytometry. *J Immunol Meth* 1991; 139: 271-279.
- Feinberg AP, Vogelstein B. A technique for radiolabeling DNA restriction endonuclease fragments to high specific activity. *Anal Biochem* 1983; 132: 6-13.
- Church GM, Gilbert W. Genomic sequencing. *Proc Natl Acad Sci USA* 1984; 81: 1991-1995.
- Yin X-M, Oltvai ZN, Korsmeyer SJ. BH1 and BH2 domains of Bcl-2 are required for inhibition of apoptosis and heterodimerization with Bax. *Nature* 1994; 369: 321-323.
- Zhu H, Aime-Sempe C, Satu T, Reed JC. Proapoptotic protein Bax heterodimerizes with Bcl-2 and homodimerizes with Bax via a novel domain (BH3) distinct from BH1 and BH2. *J Biol Chem* 1996; 271: 7440-7444.
- Wyllie AH. Glucocorticoid-induced thymocyte apoptosis is associated with endogenous endonuclease activation. *Nature* 1980; 284: 555-556.
- Smers LA, Van den Berg JD. Bcl-2 expression and glucocorticoid-induced apoptosis of leukemic and lymphoma cells. *Leukemia Lymphoma* 1996; 20: 199-205.
- Zacharchuk CM, Mercep M, Chakraborti PK, Simons SS, Ashwell JD. Programmed T lymphocyte death. Cell activation- and steroid-induced pathways are mutually antagonistic. *J Immunol* 1990; 145: 4037-4045.
- Fernandez-Ruiz E, Rebullu A, Nieto MA, et al. IL-2 protects T cell hybrids from the cytolytic effect of glucocorticoids. Synergistic effect of IL-2 and dexamethasone in the induction of high-affinity IL-2 receptors. *J Immunol* 1989; 143: 4146-4151.
- Tuosto L, Cundari E, Montani MSC, Piccolella E. Analy-

A. R. Buckley et al.

- sis of susceptibility of mature human T lymphocytes to dexamethasone-induced apoptosis. *Eur J Immunol* 1994; 24: 1061-1065.
29. Gollahon LS, Aldaz CM. Chromosomal localization of the rat Harvey-ras-1 gene (HRAS) by in situ hybridization. *Cytogenet Cell Genet* 1992; 61: 123-124.
30. Callard JG, Schijven JF, Roos E. Invasive and metastatic potential induced by ras-transfection into mouse BW5147 T-lymphoma cells. *Cancer Res* 1987; 47: 754-759.
31. Aldaz CM, Chen A, Gollahon LS, Russo J, Zappler K. Nonrandom abnormalities involving chromosome 1 and Harvey-ras-1 alleles in rat mammary tumor progression. *Cancer Res* 1992; 52: 4791-4798.
32. Rao Y-P, Buckley DJ, Buckley AR. Rapid activation of mitogen-activated protein kinase and p21ras by prolactin and interleukin-2 in rat Nb2 node lymphoma cells. *Cell Growth Diff* 1995; 6: 1235-1244.
33. Erwin RA, Kirken RA, Malabarba MG, Farrar WL, Rui H. Prolactin activates ras via signalling proteins SHC, growth factor receptor bound 2, and son of sevenless. *Endocrinology* 1995; 136: 3512-3518.
34. Rui H, Kirken RA, Farrar WL. Activation of receptor-associated tyrosine kinase JAK2 by prolactin. *J Biol Chem* 1994; 269: 5364-5368.
35. Lebron JJ, Ali S, Sofer L, Ullrich A, Kelly PA. Prolactin-induced proliferation of Nb2 cells involves tyrosine phosphorylation of the receptor and its associated tyrosine kinase JAK2. *J Biol Chem* 1994; 269: 14021-14026.
36. Tsao D, Mnriia A, Bella, Luu P, Kim YS. Differential effects of sodium butyrate, dimethyl sulfoxide, and retinoic acid on membrane-associated antigen, enzymes, and glycoproteins on human rectal adenocarcinoma cells. *Cancer Res* 1982; 42: 1052-1058.
37. Hague A, Manning AM, Hanlon KA, Huschtscha LI, Hart D, Paraskeva C. Sodium butyrate induces apoptosis in human colonic tumor cell lines in a p53-independent pathway: implications for the possible role of dietary fibre in the prevention of large-bowel cancer. *Int J Cancer* 1993; 55: 498-505.
38. Herold DP, Zirnstein GW, Bradley JF, Rothberg PG. Sodium butyrate causes an increase in the block in transcriptional elongation in the c-myc gene in SW637 rectal carcinoma cells. *J Biol Chem* 1993; 268: 20466-20472.
39. Souleimani A, Asselin C. Regulation of c-myc expression by sodium butyrate in the colon carcinoma cell line Caco-2. *FEBS Lett* 1993; 326: 45-50.
40. Chang ST, Yong BYM. Potentiation of sodium butyrate-induced apoptosis by vanadate in human promyelocytic leukemia cell line HL-60. *Biochem Biophys Res Commun* 1996; 221: 594-601.
41. Sealy L, Chalkley R. The effect of sodium butyrate on histone modification. *Cell* 1978; 14: 115-121.
42. Buffa LC, Vidali G, Mann RS, Allfrey VG. Suppression of histone deacetylase *in vivo* and *in vitro* by sodium butyrate. *J Biol Chem* 1978; 253: 3364-3366.
43. Kruh J. Effects of sodium butyrate, a new pharmacological agent, on cells in culture. *Mol Cell Biochem* 1982; 42: 65-82.
44. Johnson LA, Tapscott SJ, Eisen H. Sodium butyrate inhibits myogenesis by interfering with the transcriptional activation function of myoD and myogenin. *Mol Cell Biol* 1992; 12: 5123-5130.
45. Mollinedo F, Gajate C, Tagores A, Flores I, Naranjo JR. Differences in expression of transcription factor AP-1 in human promyelocytic HL-60 cells during differentiation towards macrophages versus granulocytes. *Biochem J* 1993; 294: 137-144.
46. Tang SJ, Huang YM, Wang FF. Analysis of c-fos expression in the butyrate-induced P-98 glioma cell differentiation. *Biochem J* 1995; 306: 47-56.
47. Dang J, Wang Y, Doe WF. Sodium butyrate inhibits expression of urokinase and its receptor mRNAs at both transcription and post-transcription levels in colon cancer cells. *FEBS Lett* 1995; 359: 147-150.
48. Finnie IA, Dwarakanath AD, Taylor BA, Rhodes JM. Colonic mucin synthesis is increased by sodium butyrate. *Gut* 1995; 36: 93-99.
49. Chen YL, Wu RT. Altered quinine modification of transfer RNA involved in the differentiation of human K562 erythroleukemia cells in the presence of distinct differentiation inducers. *Cancer Res* 1994; 54: 2192-2198.
50. Sun SH, Chen KC, Chen YW. Effects of sodium butyrate on the transfer of arachidonic acid to phosphatidylcholine in a clonal oligodendrocyte cell line (CB-11). *Lipids* 1994; 29: 467-474.
51. Zoref-Shani E, Lavie R, Bromberg Y, et al. Effects of differentiation-inducing agents on purine nucleotide metabolism in an ovarian cancer cell line. *J Cancer Res Clin Oncol* 1994; 120: 717-722.
52. Rivero JA, Adunyah SE. Sodium butyrate induces tyrosine phosphorylation and activation of MAP kinase (ERK-1) in human K562 cells. *Biochem Biophys Res Commun* 1996; 224: 796-801.



Neuroscience Letters 265 (1999) 191-194

**Neuroscience
Letters**

Alterations in neuropeptide Y levels and Y1 binding sites in the Flinders Sensitive Line rats, a genetic animal model of depression**Laura Caberlotto^{a,b}, Patricia Jimenez^c, David H. Overstreet^d, Yasmin L. Hurd^{b,*}, Aleksander A. Mathé^c, Kjell Fuxe^a**^a*Department of Neuroscience, Division of Cellular and Molecular Neurochemistry, Karolinska Institute, S-171 75, Stockholm, Sweden*^b*Department of Clinical Neuroscience, Psychiatry Section, Karolinska Hospital, S-171 76, Stockholm, Sweden*^c*Department of Clinical Neuroscience, Psychiatry Section, Karolinska Institute, St. Göran Hospital, 112 81 Stockholm, Sweden*^d*Department of Psychiatry, University of North Carolina at Chapel Hill, NC 27599-7175, USA*

Received 11 September 1998; received in revised form 3 March 1999; accepted 3 March 1999

Abstract

Previously, we observed specific alterations of neuropeptide Y (NPY) and Y1 receptor mRNA expression in discrete regions of the Flinders Sensitive Line rats (FSL), an animal model of depression. In order to clarify the correlation between mRNA expression and protein content, radioimmunoassay and receptor autoradiography were currently performed. In the FSL rats, NPY-like immunoreactivity (NPY-LI) was decreased in the hippocampal CA region, while Y1 binding sites were increased; NPY-LI was increased in the arcuate nucleus. Fluoxetine treatment elevated NPY-LI in the arcuate and anterior cingulate cortex and increased Y1 binding sites in the medial amygdala and occipital cortex in both strains. No differences were found regarding the Y2 binding sites. The results demonstrate a good correlation between NPY peptide and mRNA expression, and sustain the possible involvement of NPY and Y1 receptors in depression. © 1999 Elsevier Science Ireland Ltd. All rights reserved.

Keywords: Neuropeptide Y; NPY receptors; Depression; Flinders sensitive line rats; Fluoxetine; Hippocampus

Dysfunction of the neuropeptide Y (NPY) system has been hypothesized in the pathophysiology of depression. Despite some discrepant findings, a number of clinical investigations have demonstrated a decrease of NPY-like immunoreactivity (NPY-LI) in the cerebrospinal fluid of depressed subjects and in the post-mortem frontal cortex of suicide victims [4,17,18]. A potential link between NPY and depression emerged also from experimental animal studies which demonstrated that chronic exposure to antidepressant drugs and repeated electroconvulsive stimuli increases NPY-LI in the neocortex and hippocampus [7,14,15]. In our previous report [1], we found an alteration of the NPY and the Y1, but not the Y2, receptor mRNA expression in specific brain regions of the Flinders Sensitive Line (FSL) rats in comparison with the control Flinders Resistant Line (FRL) rats. These findings supported the possible involvement of NPY and the Y1 receptor subtype in depressive disorders. The FSL rats are considered a

genetic animal model of depression which presents behaviors similar to that seen in depressed patients: alterations in REM sleep, reduced body weight and increased immobility in the forced swim test [12]. In order to clarify the correlation between alterations in mRNA expression and protein content in these animals, we analyzed NPY-LI, and Y1 and Y2 receptor binding sites in the FSL rats compared with the control FRL rats. In addition, the effects of the antidepressant drug fluoxetine were also studied.

Twenty-six FSL and 26 FRL male rats (Sprague-Dawley derived) were kept under standardized lighting conditions at a constant temperature of 23°C with free access to food pellets and tap water. Half of the animals in each strain were injected i.p. every morning for 14 days with 10 µmol/kg (≈3 mg/kg) of the selective serotonin uptake inhibitor fluoxetine hydrochloride (dissolved in 0.9% saline). The other animals were injected similarly with 0.9% saline. The rats were sacrificed 24 h after the last injection of fluoxetine or saline. Sixteen FSL and 16 FRL were sacrificed using focused high energy microwave irradiation [11], the brain removed, and the different regions dissected and frozen in dry ice. NPY-LI were analyzed by competitive

* Corresponding author. Tel: +46-8-5177-2379; fax: +46-8-346-563.

E-mail address: yasmin.hurd@neuro.ks.se (Y.L. Hurd)

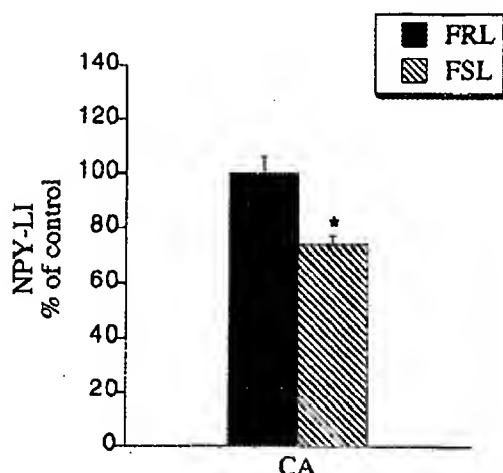


Fig. 1. NPY-LI levels in the hippocampal CA region of the FSL and FRL (control) rats as determined by radioimmunoassay. The bar graph represents the mean \pm SEM ($n = 16$) given as a percentage of the pmol/mg values measured in the FRL rats (set to 100%; CA = 357 ± 2.2 pmol/mg wet weight; * $P \leq 0.01$).

radioimmunoassay as previously described [14], but using a different NPY antiserum obtained from Dr. M. Brown [6]. The other animals, 10 FSL and 10 FRL, were decapitated, the brains quickly removed and treated as previously reported for whole section analysis [1]. In order to visualize NPY Y1- and Y2-like receptor binding sites, *in vitro* receptor autoradiography was performed as described previously by Dumont et al. [3] using 25 pM [125 I] [Leu31Pro34]-PYY or [125 I]PYY3-36, respectively (non-saturating conditions). Non-specific binding was determined by including 1 μ M unlabeled NPY in the incubation solution. The slides were exposed to Amersham Hyperfilm for 3-6 days in the

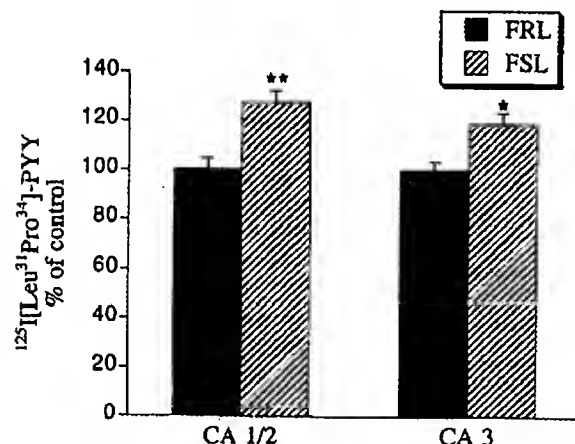


Fig. 2. Levels of NPY Y1 receptor binding in the hippocampal CA1/2 and CA3 regions of the FSL and FRL rats using [125 I] [Leu31Pro34]-PYY. The bar graph represents the mean \pm SEM ($n = 10$) given as a percentage of the fmol/mg values measured in the FRL rats (set to 100%; CA1/2 = 1.01 ± 0.05 fmol/mg; CA3 = 0.91 ± 0.03 fmol/mg; * $P \leq 0.01$, ** $P \leq 0.001$).

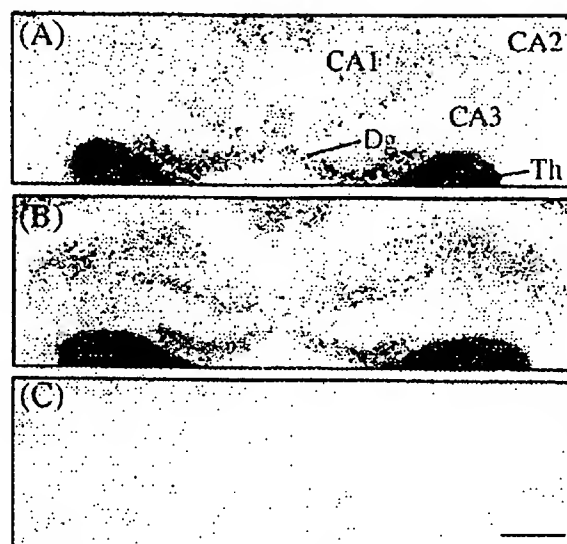


Fig. 3. Computer-generated images of the autoradiographic localization of [125 I] [Leu31Pro34]-PYY in the hippocampal formation (approximately -2.56 mm from Bregma) of a representative FRL (A) and FSL (B) rat, showing the increased levels of Y1 binding sites in the CA regions, but not in the dentate gyrus (Dg), in the FSL rats. (C) Shows the unspecific binding in the same region. Th, thalamus. Scale bar, 1 mm.

presence of [125 I] microscissors (Amersham International, UK) as reference standards. Autoradiograms were used for semi-quantitative analysis as previously described [1]. In order to assess if the fluoxetine treatment was behaviorally efficacious in reversing the exaggerated immobility which is a characteristic of the FSL rats, a modified forced swim test protocol was carried out, as previously described [13]. The swim test was conducted on day 12 of the fluoxetine treatment paradigm in separate groups of animals (eight FSL and eight FRL rats) from those used for the post-mortem analyses. Statistical evaluations of strain differences were assessed by analysis of variance (three-way ANOVA: strain, treatment, and region as a repeated measure). Two-way ANOVA (full factorial strain and treatment) with Tukey-Kramer post-comparison test was subsequently performed using the JMP (3.0v) statistical software package. Using Bonferroni correction, $P < 0.01$ was considered significant for the NPY and Y1 measurements because eight brain regions were studied, and $P \leq 0.02$ for the Y2 measurements because three brain regions were examined.

Regional differences in NPY-LI were found between the Flinders strains; the FSL showed a decrease (26%) in the hippocampal CA region (FRL = 35.7 ± 2.2 pmol/g, FSL = 26.3 ± 1.3 pmol/g; $P \leq 0.005$; Fig. 1) and an increase (16%) in the hypothalamic arcuate nucleus (FRL = 366.6 ± 17 pmol/g, FSL = 424.9 ± 12.4 pmol/g; $P \leq 0.0005$) as compared with the FRL rats.

The fluoxetine treatment caused a significant (14%) increase in NPY-LI in the arcuate nucleus (saline = 369.7 ± 16.8 pmol/g, fluoxetine = 421.77 ± 13.6 pmol/g; $P \leq 0.01$)

and the anterior cingulate cortex (saline = 51.4 ± 1.9 pmol/g, fluoxetine = 58.9 ± 1.9 pmol/g; $P \leq 0.01$) in both strains. In other regions, such as the dentate gyrus, nucleus accumbens, medial amygdala, retrosplenial and occipital cortices, no differences in strain, treatment, or strain \times treatment interaction were observed.

The distribution of Y1 binding sites, detected using [125 I][Leu31Pro34]-PYY, a Y1 agonist, was consistent with that previously described [3], with abundant binding sites in the superficial layers of the cerebral cortex, olfactory tubercle, islands of Calleja, dentate gyrus (Fig. 2) and thalamus. In the FSL rats, higher levels of Y1 binding sites were found in the CA1/2 (27%; FRL = 1.01 ± 0.05 fmol/mg, FSL = 1.29 ± 0.04 fmol/mg; $P \leq 0.0004$) and in the CA3 (19%; FRL = 0.91 ± 0.03 fmol/mg, FSL = 1.08 ± 0.04 fmol/mg; $P \leq 0.003$) regions of the hippocampus (Figs. 2 and 3). Following fluoxetine administration, a significant increase was detected in the medial amygdaloid nucleus (19%; saline = 0.82 ± 0.03 fmol/mg, fluoxetine = 0.99 ± 0.04 fmol/mg; $P \leq 0.01$) and occipital cortex (11%; saline = 294 ± 0.04 fmol/mg, fluoxetine = 3.26 ± 0.04 fmol/mg; $P < 0.0001$). A similar trend ($P \leq 0.017$) was found in the dentate gyrus. No differences in strain, treatment or strain \times treatment interaction were found in other regions: entorhinal, retrosplenial, and anterior cingulate cortices.

The localization of Y2 binding sites was in line with previous findings with high amounts of Y2 binding sites in the hippocampal CA region, lateral septum, ventral tegmental area, substantia nigra and dorsal raphe nucleus. No difference in strain, treatment or strain \times treatment interaction was found in the CA1/2, CA3, or medial amygdala.

In the forced swim test, the FSL rats displayed the typical enhanced immobility as compared with the FRL rats (FSL = 154.6 ± 8.1 s, FRL = 49.5 ± 4.4 s; $P < 0.0001$). Following fluoxetine treatment, a significant reduction in immobility was observed in both strains (saline = 114.5 ± 16.7 s; fluoxetine = 89.6 ± 12.4 s; $P \leq 0.004$), but the fluoxetine-induced effect was slightly more pronounced in the FSL rats.

Our findings showing alteration of NPY-LI and Y1-like binding sites in the FSL rats support the proposed involvement of central NPY mechanisms in depression. The alteration in NPY-LI correlated well with the NPY mRNA expression; both NPY-LI and NPY mRNA expression were decreased in the CA region and increased in the arcuate nucleus of the FSL as compared with the control FRL rats [1].

Another major finding of this study was the strong increase in Y1 binding sites in the CA region of the FSL rats. This could reflect a compensatory mechanism for the reduced levels of NPY in the hippocampus of these animals. Such an inverse relationship has been previously reported. For example, in rats treated with electroconvulsive stimuli, NPY-LI was increased, but NPY binding sites decreased in the hippocampus [5]. In our previous study, we had

observed a decrease in Y1 mRNA expression in the dentate gyrus of the FSL rats [1]. Since the cells of the dentate gyrus project (mossy fibers) mainly within the hippocampus, we expected a decrease in the Y1 binding sites in this area, predominantly in the CA3 region. Nevertheless, it is possible that a change in affinity, and not in the amount of the Y1 receptor, may be responsible for the increased Y1 binding sites. It should be noted, however, that [Leu31Pro34]-PYY binds also, although to a lower extent, to the Y5 receptor subtype and, since the Y5 receptor is abundant in the CA3 region [2], it is possible that the increase in Y1 binding observed in this region could be due in part to an alteration of the Y5 receptor.

The findings that NPY-LI and its Y1 receptor are altered in the CA region of the FSL rats again suggest a dysfunction of the NPY hippocampal system in depressive disorders. Other animal models of depression such as the Fawn Hooded rats also show a decrease in NPY-LI in this architectural structure [9], while no changes are apparent in the learned helpless rats [8], a stress induced experimental model of depressive disorders. Moreover, several treatment paradigms for depression have been shown to augment hippocampal levels of NPY-LI [14] and NPY mRNA [16,19]. Other neurotransmitter systems implicated in affective disorders and in the action of antidepressant drugs are also altered in the hippocampus of the FSL rats. Increased levels of serotonin and 5-hydroxyindoleacetic acid have been observed in the hippocampal formation of the FSL rats, alterations that could be normalized by chronic desipramine treatment [20].

The low dose treatment of fluoxetine used in the present study was shown to be efficacious in reversing the behavioral immobility in the forced swim test which is one of the characteristics of the FSL rats [12]. In line with our previous mRNA results [1], fluoxetine treatment also caused an increase in NPY-LI in the arcuate nucleus and in the anterior cingulate cortex. This is consistent with other studies showing an increase in NPY-LI in the neocortex and in limbic-related structures after lithium [10] or electroconvulsive stimuli [14,15].

In conclusion, this study provides further support for a possible role of the NPY system and, in particular, of the Y1 receptor mediated NPY transmission in the pathophysiology of mood disorders and demonstrates the utility of the FSL rats as an experimental model to study the neurochemical and functional alterations in depression.

We thank Beth Andbjør for technical assistance. This work was supported by funds from the Karolinska Institute and from the Swedish Medical Research Council (grant No. 10414, A.A.M.).

- [1] Caberlotto, L., Fuxe, K., Overstreet, D.H., Gerrard, P. and Hurd, Y.L., Alterations in neuropeptide Y and Y1 receptor mRNA expression in brains from an animal model of

- depression: region specific adaptation after fluoxetine treatment. *Mol. Brain Res.*, 59 (1998) 58-65.
- [2] Dumont, Y., Fournier, A. and Quirion, R., Expression and characterization of the neuropeptide Y Y5 receptor subtype in the rat brain. *J. Neurosci.*, 18 (1998) 5565-5574.
 - [3] Dumont, Y., Fournier, A., St-Pierre, S. and Quirion, R., Autoradiographic distribution of [¹²⁵I] Leu31Pro34] PYY and [¹²⁵I]PYY3-36 binding sites in the rat brain evaluated with two newly developed Y1 and Y2 receptor radioligands. *Synapse*, 22 (1996) 139-158.
 - [4] Gjerris, A., Widerlogy, E., Werdelin, L. and Ekman, R., Cerebrospinal fluid concentrations of neuropeptide Y in depressed patients and in controls. *J. Psychiatr. Neurosci.*, 17 (1992) 23-27.
 - [5] Greisen, M.H., Sheikh, S.P., Bolwig, T.G. and Mikkelsen, J.D., Reduction of neuropeptide Y binding sites in the rat hippocampus after electroconvulsive stimulations. *Brain Res.*, 776 (1997) 105-110.
 - [6] Hellig, M. and Ekman, R., Chronic parenteral antidepressant treatment in rats: unaltered levels and processing of neuropeptide Y (NPY) and corticotropin-releasing hormone (CRH). *Neurochem. Int.*, 26 (1995) 351-355.
 - [7] Hellig, M., Wahlestedt, C., Ekman, R. and Widerlogy, E., Antidepressant drugs increase the concentration of neuropeptide Y (NPY)-like immunoreactivity in the rat brain. *Eur. J. Pharmacol.*, 147 (1988) 465-467.
 - [8] Lachman, H.M., Papolos, D.F., Welner, E.D., Ramazankhena, R., Hartnick, C., Edwards, E. and Henn, F.A., Hippocampal neuropeptide Y mRNA is reduced in a strain of learned helpless resistant rats. *Mol. Brain Res.*, 14 (1992) 94-100.
 - [9] Mathé, A.A., Jimenez, P.A., Theodorsson, E. and Stenfors, C., Neuropeptide Y, neurokinin A and neurotensin in brain regions of Fawn Hooded depressed, Wistar, and Sprague Dawley rats - effect of electroconvulsive stimulation. *Prog. Neuro-Psychopharmacol. Biol. Psychiat.*, 22 (1998) 529-546.
 - [10] Mathé, A.A., Jousisto-Hanson, J., Stenfors, C. and Theodorsson, E., Effect of lithium on tachykinins, calcitonin gene-related peptide, and neuropeptide Y in rat brain. *J. Neurosci. Res.*, 26 (1990) 233-237.
 - [11] Mathé, A.A., Stenfors, C., Brodin, E. and Theodorsson, E., Neuropeptides in brain: effects of microwave irradiation and decapitation. *Life Sci.*, 46 (1989) 287-293.
 - [12] Overstreet, D.H., The Flinders sensitive line rats: an animal model of depression. *Neurosci. Biobehav. Rev.*, 17 (1993) 51-68.
 - [13] Pucilowski, O. and Overstreet, D.H., Effect of chronic antidepressants on responses to epomorphine in selectively bred rat strains. *Behav. Brain Res.*, 32 (1993) 471-475.
 - [14] Stenfors, C., Theodorsson, E. and Mathé, A.A., Effect of repeated electroconvulsive treatment on regional concentrations of tachykinins, neurotensin, vasoactive intestinal polypeptide, neuropeptide Y and galanin in rat brain. *J. Neurosci. Res.*, 24 (1989) 445-450.
 - [15] Wahlestedt, C., Blendy, J.A., Keller, K.J., Hellig, M., Widerlogy, E. and Ekman, R., Electroconvulsive shocks increase the concentration of neocortical and hippocampal neuropeptide Y (NPY)-like immunoreactivity in the rat. *Brain Res.*, 507 (1990) 65-68.
 - [16] Welner, E.D., Mallat, A., Papolos, D.F. and Lachman, H.M., Acute lithium treatment enhances neuropeptide Y gene expression in rat hippocampus. *Mol. Brain Res.*, 12 (1992) 209-214.
 - [17] Widdowson, P.S., Ordway, G.A. and Halaris, A.E., Reduced neuropeptide Y concentrations in suicide brain. *J. Neurochem.*, 59 (1992) 73-80.
 - [18] Widerlogy, E., Lindström, L.H., Wahlestedt, C. and Ekman, R., Neuropeptide Y and peptide YY as possible cerebrospinal markers for major depression and schizophrenia, respectively. *J. Psychiatr. Res.*, 22 (1988) 69-79.
 - [19] Zachrisson, O., Mathé, A.A., Stenfors, C. and Lindefors, N., Region-specific effects of chronic lithium administration on neuropeptide Y and somatostatin mRNA expression in the rat brain. *Neurosci. Lett.*, 194 (1995) 89-92.
 - [20] Zangen, A., Overstreet, D.H. and Yadid, G., High serotonin and 5-hydroxyindoleacetic acid levels in limbic brain regions in a rat model of depression: normalization by chronic antidepressant treatment. *J. Neurochem.*, 69 (1997) 2477-2483.

Neurokinin 1 receptor and relative abundance of the short and long isoforms in the human brain

Laura Caberlotto,¹ Yasmin L. Hurd,² Paul Murdock,³ Jean Philippe Wahlin,³ Sergio Melotto,¹ Mauro Corsi¹ and Renzo Carletti¹

¹Department of Biology, Psychiatry CEDD, GlaxoSmithKline Medicine Research Centre, Verona, Italy

²Karolinska Institute, Department of Clinical Neuroscience, Stockholm, Sweden

³Department of Cellular Genomics, GlaxoSmithKline Medicine Research Centre, Stevenage, UK

Keywords: autoradiography, *in situ* hybridization, substance P, tachykinin, TaqMan

Abstract

Substance P exerts its various biochemical effects mainly via interactions through neurokinin-1 receptors (NK1). Recently, the NK1 receptor has attracted considerable interest for its possible role in a variety of psychiatric disorders including depression and anxiety. However, little is known regarding the anatomical distribution of NK1 in the human central nervous system (CNS). Riboprobe *in situ* hybridization, quantitative PCR and *in vitro* autoradiography were performed. Highest NK1 mRNA levels were localized in the locus coeruleus and ventral striatum, while moderate hybridization signals were observed in the cerebral cortex (most abundant in the visual cortex), hippocampus and different amygdaloid nuclei. Very low levels of the NK1 mRNA were detected in the cerebellum and thalamus. In view of the existence of a long and short isoform of the NK1 receptor, it was of interest to assess whether there was a differential distribution of the two splice variants in the human CNS and peripheral tissues. A quantitative TaqMan PCR analysis showed that the long NK1 isoform was the most prevalent throughout the human brain, while in peripheral tissues the truncated form was the most represented. ³H-Substance P autoradiography revealed a good correlation between receptor binding sites and NK1 mRNA expression throughout the brain, with the highest levels of binding in the locus coeruleus. These results provide the anatomical evidence that the NK1 receptors have a strong association with neuronal systems relevant to mood regulation and stress in the human brain, but do not suggest a region-specific role of the two isoforms in the CNS.

Introduction

Substance P (SP), a member of the tachykinin family of neuropeptides, is widely distributed in the mammalian brain, spinal cord and peripheral tissue. In the CNS, its distribution has been studied in detail in various species and it is mainly found in striatal regions, substantia nigra, and hypothalamus (Kanazawa & Jessell, 1976; Cooper *et al.*, 1981). SP plays a role in a variety of functions through preferential, but not exclusive, activation of NK1 receptors while the other members of the tachykinins family, neurokinin A and neurokinin B, act mainly via NK2 and NK3, respectively.

The NK1 receptor has been cloned from several species, including man (Yokota *et al.*, 1989; Hershey & Krause, 1990), and pharmacological studies have suggested the existence of two receptor isoforms that differ in the length of the carboxyl-terminus (Fong *et al.*, 1992). The anatomical localization of mammalian NK1 has been studied by different techniques and demonstrated the abundance of the receptors in the dorsal striatum, nucleus accumbens, hippocampus, raphe nuclei, and medulla oblongata (Otsuka & Yoshioka, 1993). In the basal ganglia, NK1-like immunoreactivity is localized on large and medium-sized aspiny cholinergic neuronal cells (Aubry *et al.*, 1994) and in midbrain dopaminergic neurons (Whitty *et al.*, 1997).

Clinical and experimental animal studies suggest the involvement of NK1 in numerous central functions such as nociceptive transmission, cognition and basal ganglia functions (Quartara & Maggi, 1998). In

addition, the possible involvement of this receptor in psychiatric and neurological disorders has been investigated and in particular its role in the pathophysiology of depression and anxiety has been demonstrated by Kramer *et al.* (Kramer *et al.*, 1998) showing antidepressant properties of SP antagonists.

Although a few studies have focused on the localization of NK1 receptors in specific regions of the human brain, in particular the striatum (Aubry *et al.*, 1994) and cerebral cortex (Kus *et al.*, 1998; Tooney *et al.*, 2000), a detailed knowledge of its distribution in the human CNS is still lacking. Thus, the anatomical organization of NK1 receptor mRNA expression and binding sites was studied in the postmortem human brain. In addition, as the physiological importance of the short isoform has not been clarified, it was of interest to assess whether there was a differential distribution of the long and short splice variants in different brain regions that could provide the theoretical basis for tissue specific pharmacological targeting of NK1 receptors.

Materials and methods

Preparation of human brain tissue

Brain specimens were obtained at autopsy under approved ethical guidelines at the Karolinska Institute, Stockholm, Sweden. The whole hemisphere of four brains were frozen (-85 °C) and cryosectioned in coronal and horizontal sections using a heavy-duty microtome (PMV400 LKB 2250, Leica, Heidelberg, Germany) as previously described (Brene *et al.*, 1989; Hall *et al.*, 1994). The sections, 100 µm-thick, were thawed onto poly L-lysine-treated glass plates (15 × 20 cm) and stored frozen at -30 °C. The subjects (three females

Correspondence: Dr Laura Caberlotto, as above.

E-mail: Laura.L.Caberlotto@gsk.com

Received 30 October 2002, revised 29 January 2003, accepted 19 February 2003

TABLE 1. Demographic information related to the brain specimens examined

	Gender	Age (hours)	PMI (hours)	Cause of death
1	Female	40	24	Heart failure
2	Male	61	15	Heart failure
3	Female	54	24	Heart failure
4	Female	61	6	Heart failure
5	Male	39	12	Heart failure
6	Female	65	6	Heart failure
7	Male	50	24	Heart failure
8	Male	44	12	Heart failure
9	Male	32	24	Suicide

and one male) had an average age of 54 years (range 40–61) with an average postmortem interval (PMI) of 17 h (range 6–24). Four additional brain specimens (one female and four males; average age 46 ± 6 ; PMI 16 ± 4) obtained at autopsy were immediately blocked into 1.5–2.0 cm-thick coronal slabs, frozen in dry ice-cooled 2-methylbutane, and stored at -70°C . Demographic information on all subjects is provided in Table 1. No macroscopic pathology was found in any of the brain specimens and toxicological screening indicated no presence of neuroactive drugs. Coronal sections (20 μm -thick) were cut from the blocks of tissue using a Jung-Frigocut 2800E cryostat (Leica) and thaw-mounted onto poly L-lysine glass slides.

In situ hybridization

Riboprobe preparation

The NK1 probe was generated by PCR corresponding to nucleotides 127–498 of the patent sequence (M84425). The fragment was subcloned into a pCRII-TOPO vector. Prior to transcription, these plasmids were linearized with the appropriate restriction enzymes for generating the antisense and sense riboprobes. RNA probes complementary to the coding sequences were transcribed from the linearized plasmid template with 150 μCi α - ^{32}P UTP (Amersham). SP6 and T7 RNA polymerase was used for generating the antisense and sense probes, respectively. Transcription occurred in the presence of 10 mM diithiothreitol, 0.5 mM each of ATP, GTP, CTP, and 1 μg linearized plasmid template in a 1 \times transcription buffer for 60 min at 37°C . The labelled probes were then separated from unincorporated nucleotides using spin columns (Pharmacia Biotech, Stockholm, Sweden).

In situ hybridization

In situ hybridization was carried out as previously described (Caberlotto *et al.*, 1997). Briefly, the brain sections were fixed in 4% paraformaldehyde/1 \times phosphate buffered saline for 10 min, rinsed twice in 1 \times PBS and treated with 0.25% acetic anhydride/0.1 M triethanolamine/0.9% sodium chloride for 5 min. The sections were then rinsed in 2 \times SSC, dehydrated in graded series of ethanol (70%, 80%, 95%, 100%) and delipidated with chloroform. They were allowed to air dry before being used or were frozen at -70°C until use. All aqueous solutions were pretreated with 0.1% diethylpyrocarbonate before use. The hybridization buffer consisted of 0.5 mg/mL sheared single stranded DNA, 250 μg /mL Yeast tRNA, 1 \times Denhardt's solution, 10% dextran sulphate, 4 \times SSC, and 50% formamide. Before hybridization, the labelled probe was added to the hybridization cocktail in a concentration of 20×10^3 cpm per μL . A volume of 0.15 mL or 2 mL of this hybridization mixture was applied to the small and big sections, respectively. The sections were coverslipped to prevent evaporation and the hybridization was carried out in a humidified chamber overnight at 55°C . Incubation was followed by washing in graded series of SSC (2 \times , 1 \times , 0.5 \times , 0.1 \times) containing 1 mM diithiothreitol all at room temperature except for the 0.1 \times SSC (53°C) and dehydration was carried out with graded ethanol solutions contain-

ing 300 mM ammonium acetate. The slides were then air dried and exposed to imaging plates (Fuji, Tokyo) along with ^{14}C standards for a period of 3–7 days. The sections were then dipped in Kodak emulsion, exposed for 2 months at 4°C , developed, and counterstained with cresyl violet to facilitate morphological analysis.

Autoradiography

Binding experiments were performed essentially as described by Mantyh *et al.* (Mantyh *et al.*, 1984). Briefly, brain sections were air dried and preincubated for 15 min at room temperature in Tris-HCl (50 mM, pH 7.4) containing 0.02% bovine serum albumin (BSA). Sections were then incubated for 90 min at room temperature in the same buffer containing MnCl_2 (3 mM), bacitracin (0.04 mg/mL), leupeptin (0.004 mg/mL), chymostatin (0.002 mg/mL), and 2 nM ^3H -SP (53 Ci/mmol, Amersham). Non-specific binding was determined in the presence of 1 μM unlabelled SP in the incubation buffer. At the end of the incubation, sections were washed four times (30 s each) in ice cold Tris-HCl (50 mM pH 7.4) containing 0.02% BSA, briefly dipped in ice cold distilled water, dried under a stream of cool air, and exposed to imaging plates for two weeks.

Quantification

The film autoradiograms from the *in situ* hybridization and autoradiography experiments were scanned using a BAS-5000 Bio-Imaging Analyzer (Fuji, Tokyo) and quantified using an image analysis software system (AIS, Imaging Research Inc., Canada). Regions of interest were defined by anatomical landmarks in conjunction with De Armond (DeArmond *et al.*, 1989) human brain atlas. Based on the known radioactivity in the ^{14}C -standards (*in situ* hybridization) or ^3H -standards (autoradiography) relative to their transmittance levels, the optical density values were converted to nCi/g or fmol/ μg protein, respectively. Each specific brain region was selected by individually tracing the structures on the TV monitor with a cursor.

Real time quantitative PCR (TaqMan)

Generation of samples

Human tissue or RNA was purchased (Biochain, San Leandro, CA; Invitrogen, Leek, The Netherlands; Clontech, Palo Alto, CA) or donated (Netherlands Brain Bank, Amsterdam, The Netherlands) and poly A+ RNA was prepared by the PolyATract method according to manufacturers instructions (Promega, USA). The poly A+ RNA samples from 20 body tissues and 19 brain-regions from four individuals per tissue (two males/two females) were quantified using absorbance at 260 nm measurements or the RiboGreen fluorescent method (Molecular Probes, Oregon, USA) and 1 μg of each RNA was reverse transcribed using random nonomers and Superscript II reverse transcriptase according to manufacturers instructions (Life Technologies). The cDNA prepared was diluted to produce up to 1000 replicate 96-well plates using Biomek robotics (Beckman Coulter, High Wycombe, UK), so that each of the wells contained the cDNA produced from 1 ng RNA for the appropriate tissue. The 96-well plates were stored at -80°C prior to use.

TaqMan PCR

TaqMan quantitative PCR was conducted to measure either the gene of interest or housekeeping genes using replicate 96-well plates. A 20- μL volume of a PCR master mix (containing 2.5 μL TaqMan buffer, 6 μL of 25 mM MgCl_2 , 0.5 μL of 10 mM dATP, 0.5 μL of 20 mM dUTP, 0.5 μL of 10 mM dCTP, 0.5 μL of 10 mM dGTP, 0.25 μL uracil-N-glycosylase, 1 μL of 10 μM forward primer, 1 μL of 10 μM reverse primer, 0.5 μL 5 μM TaqMan probe, 0.125 μL TaqGold (PE Biosystems), and water was added to each well using Biomek robotics

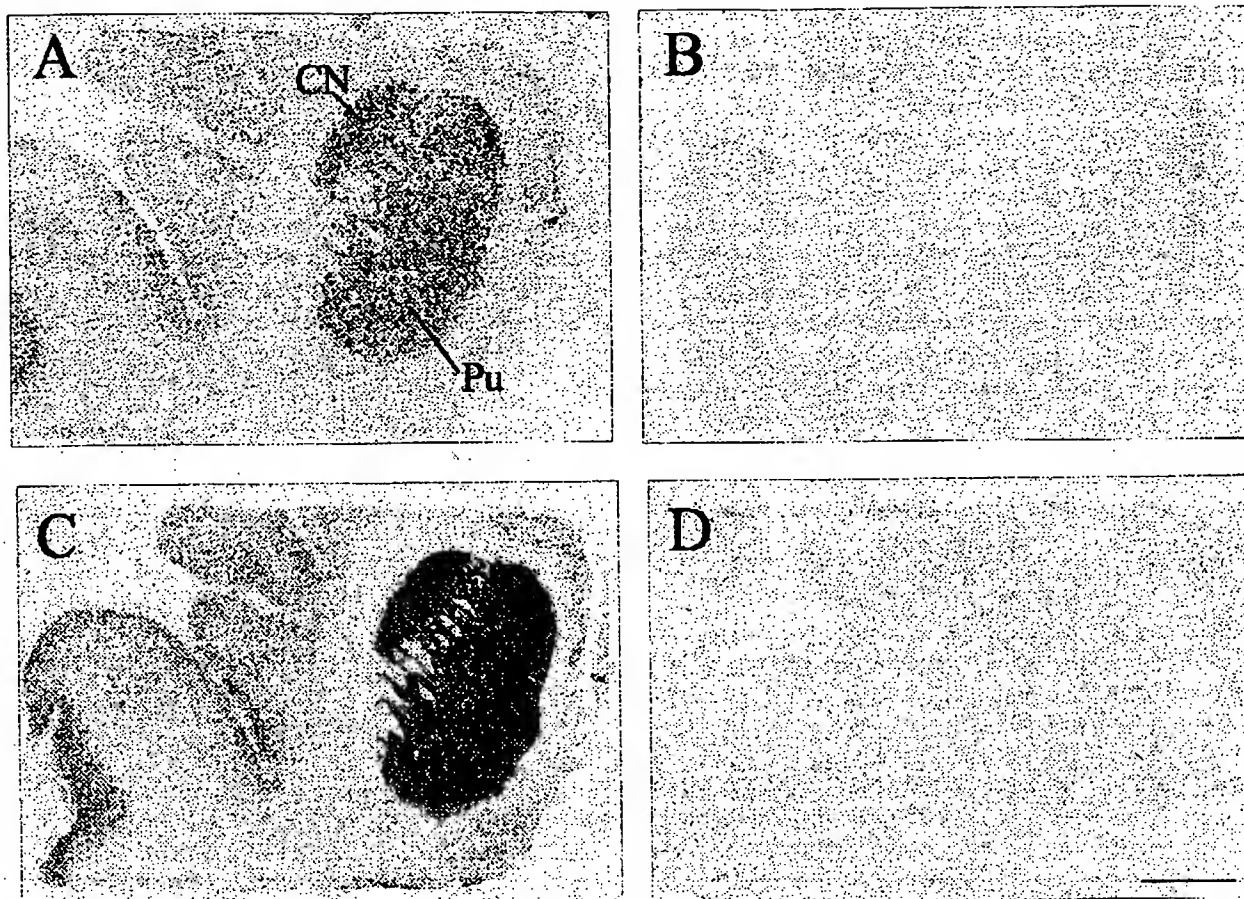


FIG. 1. Autoradiograms showing the distribution of NK1 mRNA using the antisense (A) and sense (B) riboprobe with *in situ* hybridization and the ^3H -SP total (C) and non-specific (D) binding with *in vitro* autoradiography in the human striatum. CN, caudate nucleus; Pu, putamen. Scale bar, 0.5 cm.

(Beckman Coulter, High Wycombe, UK), and the plate capped using optical caps (PE Biosystems). The PCR reaction was carried out on an ABI7700 Sequence Detector (PE Biosystems) using the PCR parameters: 50 °C for 2 min, 95 °C for 10 min and 45 cycles of 94 °C for 15 s, 60 °C for 1 minute, and the level of mRNA-derived cDNA in each sample was calculated from the TaqMan signal using plasmid/genomic DNA calibration standards included in each run. The level of genomic DNA contaminating the original RNA samples was shown to be negligible (< 10 copies genomic DNA/ng RNA) by TaqMan measurement of genomic sequence for 10 genes in replicate samples taken through the reverse transcription procedure described with the omission of reverse transcriptase. Parallel assays were carried out using primers and probes for the housekeeping gene *glyceraldehyde-3-phosphate dehydrogenase* (*GADPH*) for normalization. Gene-specific reagents for *NK1* short: forward primer 5'-tcttctctctctgcctacatc-3', reverse primer 5'-gggtgacatcaccgtgcat-3', TaqMan probe 5'-acccagatctctaccgaagattatccagca-3'; *NK1* long, forward primer 5'-tcttctctctctgcctacatc-3', reverse primer 5'-gccagacggaaacctgcat-3'; housekeeper *GADPH*, forward primer 5'-caaggatccatgacaaacttg-3', reverse primer 5'-gggccatccacagtctctg-3', TaqMan probe 5'-accacagtcacatgccactgccca-3'.

Results

The whole hemisphere horizontal sections revealed a scattered pattern of expression of the NK1 mRNA throughout the brain. The distribution

pattern and the levels of expression were similar in all the subjects tested with some variability typical of human studies. *In situ* hybridization experiments carried out with the sense riboprobe produced no positive hybridization signal (Fig. 1B). Overall, the NK1 mRNA expression was higher in the striatum, moderate in the cerebral cortex, hippocampus and amygdala, and low in the thalamus and cerebellum (Figs 2 and 3).

The distribution of ^3H -SP binding sites was in line with the previously reported localization of ^{125}I -BH-SP (Dietl & Palacios, 1991; Burnet & Harrison, 2000) with strong labelling in the striatum and moderate in the cerebral cortex. The levels of expression of ^3H -SP binding sites were also similar in all the subjects tested. ^3H -SP bound with high specificity to SP binding sites as demonstrated by the reduction of labelling in the presence of 1 μM unlabelled SP (Fig. 1C and D).

A good match between the NK1 mRNA expression and ^3H -SP binding sites was detected with a positive correlation ($r = 0.96$; $P = 0.002$) in the six regions studied with both *in situ* hybridization and receptor autoradiography.

Telencephalon

Low to high levels of the NK1 mRNA were demonstrated in different cortical areas (Figs 2 and 3). In the visual cortex, the expression levels were high as compared to the cingulate and insula cortices. The hybridization signal was present throughout all cortical layers, with the highest expression in the superficial laminae. A different

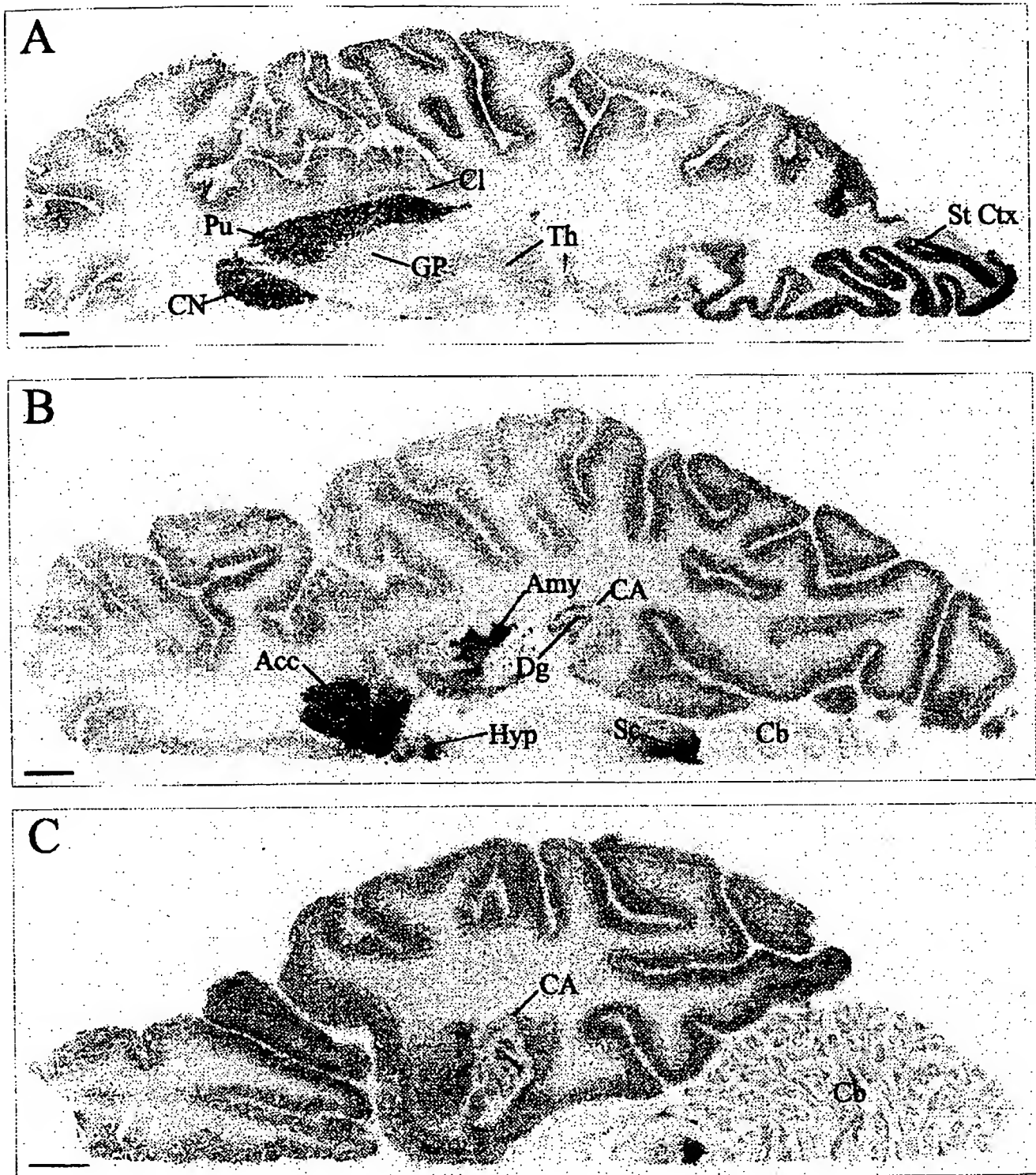


FIG. 2. Autoradiographs showing the distribution of NK1 receptor mRNA expression at different levels of the human brain. The whole human hemisphere horizontal sections are approximately 81.1 mm above (A), 91.8 mm (B) and 101 mm (C) below anterior commissure. Acc, accumbens; Amy, amygdala; CA, cornu ammonis hippocampi; Cb, cerebellum; Cl, claustrum; CN, caudate nucleus; Dg, dentate gyrus; GP, globus pallidus; Hyp, hypothalamus; Pu, putamen; Sc, superior colliculus; ST Ctx, striate cortex; Th, thalamus. Scale bar, 1 cm.

hybridization pattern was detected in the striate cortex (Brodmann area 17) with a strong signal present in both the superficial and deep layers (Fig. 2A). Moderate levels of binding of ^3H -SP were observed in cortical regions, with generally higher density of binding sites in

the superficial as compared to the deeper layers. In the temporal cortex, the level of specific binding in the superficial layers (4.75 ± 0.38 fmol/mg) was twice the level measured in the deep layers (2.47 ± 0.14 fmol/mg).

1740 I. Caberlotto *et al.*

TABLE 2. Levels of NK1 short and long isoforms expressed as copies of the gene mRNA detected per ng mRNA pool

	Expression of NK1 (per ng mRNA pool)		
	Short isoforms	Long isoforms	Short (%)
Cingulate cortex	186 ± 42	584 ± 169	24
Medial frontal gyrus	92 ± 19	456 ± 85	17
Superior frontal gyrus	248 ± 55	377 ± 58	40
Hippocampus	157 ± 60	344 ± 63	31
Parahippocampal gyrus	336 ± 52	316 ± 83	51
Striatum	473 ± 97	3723 ± 881	11
Caudate nucleus	498 ± 179	1789 ± 240	22
Putamen	374 ± 104	1997 ± 448	16
Globus pallidus	112 ± 33	817 ± 728	12
Nucleus accumbens	349 ± 84	2315 ± 502	13
Amygdala	98 ± 15	346 ± 107	22
Hypothalamus	128 ± 43	734 ± 296	15
Thalamus	104 ± 10	94 ± 39	53
Substantia nigra	131 ± 19	62 ± 11	68
Locus coeruleus	172 ± 11	632 ± 149	21
Medulla oblongata	99 ± 17	238 ± 42	29
Cerebellum	153 ± 57	53 ± 41	74
Spinal cord	33 ± 6	135 ± 22	20
CNS	87 ± 12	105 ± 31	45
Pituitary	96 ± 22	12 ± 4	89
Heart	64 ± 23	8 ± 3	88
Lung	97 ± 54	26 ± 17	79
Liver	5 ± 5	1 ± 1	79
Fetal liver	9 ± 1	2 ± 1	82
Pancreas	26 ± 4	14 ± 4	66
Kidney	19 ± 4	42 ± 17	32
Skeletal muscle	59 ± 12	101 ± 15	37
Stomach	30 ± 9	34 ± 10	47
Intestine	43 ± 9	52 ± 18	45
Spleen	56 ± 27	3 ± 1	96
Prostate	119 ± 94	75 ± 39	61
Placenta	21 ± 5	32 ± 13	39
Cartilage	0	1 ± 0	0
Bone	88 ± 27	1 ± 1	99
Bone marrow	2 ± 2	3 ± 2	40
Lymphocytes	28 ± 4	0	100
Macrophages	2 ± 1	0	98
Adipose	188 ± 7	661 ± 156	22

Results are expressed as mean ± SEM measured in four subjects. The last column shows the Short/Total percentage.

In the hippocampus, a moderate NK1 mRNA expression level was seen in the CA region and dentate gyrus (Figs 2, 3 and 4C). Within the CA region, the CA3 division had the strongest hybridization signal. In the dentate gyrus, the hybridization signal was found in the polymorphic layer. ³H-SP autoradiography showed a distinctive distribution pattern, with a substantial amount of binding sites in the dentate gyrus (12.3 ± 3.08 fmol/mg) and a much lower level in the CA regions (2.21 ± 0.85 fmol/mg; Fig. 4D).

The dorsal striatum displayed abundant NK1 mRNA expression with similar high levels in the caudate nucleus and in the putamen (Fig. 4A). A stronger signal was apparent in the ventral striatum (nucleus accumbens) due primarily to intense labelling in the island of Calleja (Figs 1A, 2A and 4A). In addition to the island of Calleja, very strong labelling was seen in the ventral diagonal band of Broca. The globus pallidus instead presented a very weak signal (Fig. 2A). The bed nucleus stria terminalis was only weakly labelled (Fig. 4A). High levels of the ³H-SP binding sites were observed in the same basal ganglia regions (caudate nucleus 20.25 ± 0.57 fmol/mg; putamen 19.22 ± 1.20 fmol/mg; Figs 1C and 4B), with a very low amount of binding sites in the globus pallidus (data not shown). As for the NK1

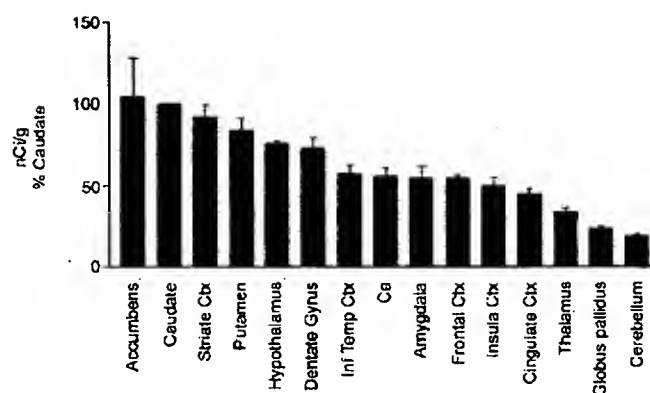


FIG. 3. The average NK1 mRNA expression in the total area of selected human brain regions given as percentage of the nCi/g values measured in the caudate nucleus (set 100%). The caudate nucleus values were 247 ± 28 nCi/g. Percentage values represent mean ± SEM measured in four subjects.

mRNA expression, abundant ³H-SP binding sites were seen in the island of Calleja and ventral diagonal band of Broca and low in the bed nucleus stria terminalis (Fig. 4B).

Positive NK1 hybridization signal was detected in the amygdaloid complex (Figs 2 and 3), with moderate levels in the lateral and accessory basal nuclei and low in the basal nucleus. Stronger hybridization signal was seen in the paralamina nucleus. Moderate levels of binding sites were observed in various amygdaloid nuclei with similar abundance in the lateral (4.2 ± 0.46 fmol/mg), basal (5.1 ± 0.32 fmol/mg) and accessory basal nuclei (6.5 ± 0.34 fmol/mg).

Diencephalon

In the main body of the thalamus, the NK1 mRNA expression was found to be only just above background level (Figs 2A and 3) with no labelling in the central medial thalamic nucleus or in the mammillary body (Fig. 2A). A moderate-to-high signal was seen in the hypothalamus, in particular in the ventral medial hypothalamic nucleus (Fig. 2B).

Mesencephalon and metencephalon

The dorsal raphe nucleus exhibited a low NK1 mRNA expression and binding sites (data not shown). The locus coeruleus displayed a very high level of the NK1 mRNA expression (Figs 4E and 5B) and was also highly enriched in ³H-SP binding sites (130.6 ± 15 fmol/mg; Fig. 4F), representing the area with the strongest NK1 binding signal. Very low NK1 mRNA expression was seen in the cerebellum (Figs 2C and 3).

NK1 isoforms

TaqMan real time PCR demonstrated the relative abundance of NK1 mRNA (short and long isoforms) to be similar to that described with *in situ* hybridization, with the highest abundance in striatum and lowest in thalamus and cerebellum (Fig. 6A). In the CNS, both the long and short isoforms were present in all the regions studied although in different proportions, with the NK1 long isoform being more abundant than the short with the exception of the substantia nigra and cerebellum (Table 2). In the periphery, the NK1 mRNA was found to be highly expressed in the adipose tissue, prostate, and pituitary, while very low to undetectable signal was seen in the cartilage, bone marrow, macrophages, and liver (Fig. 6B). The short isoform seemed to be overall the most prevalent in the periphery (Table 2). In regions such as bone, spleen and in lymphocytes very low to undetectable levels of the long splice variant were found.

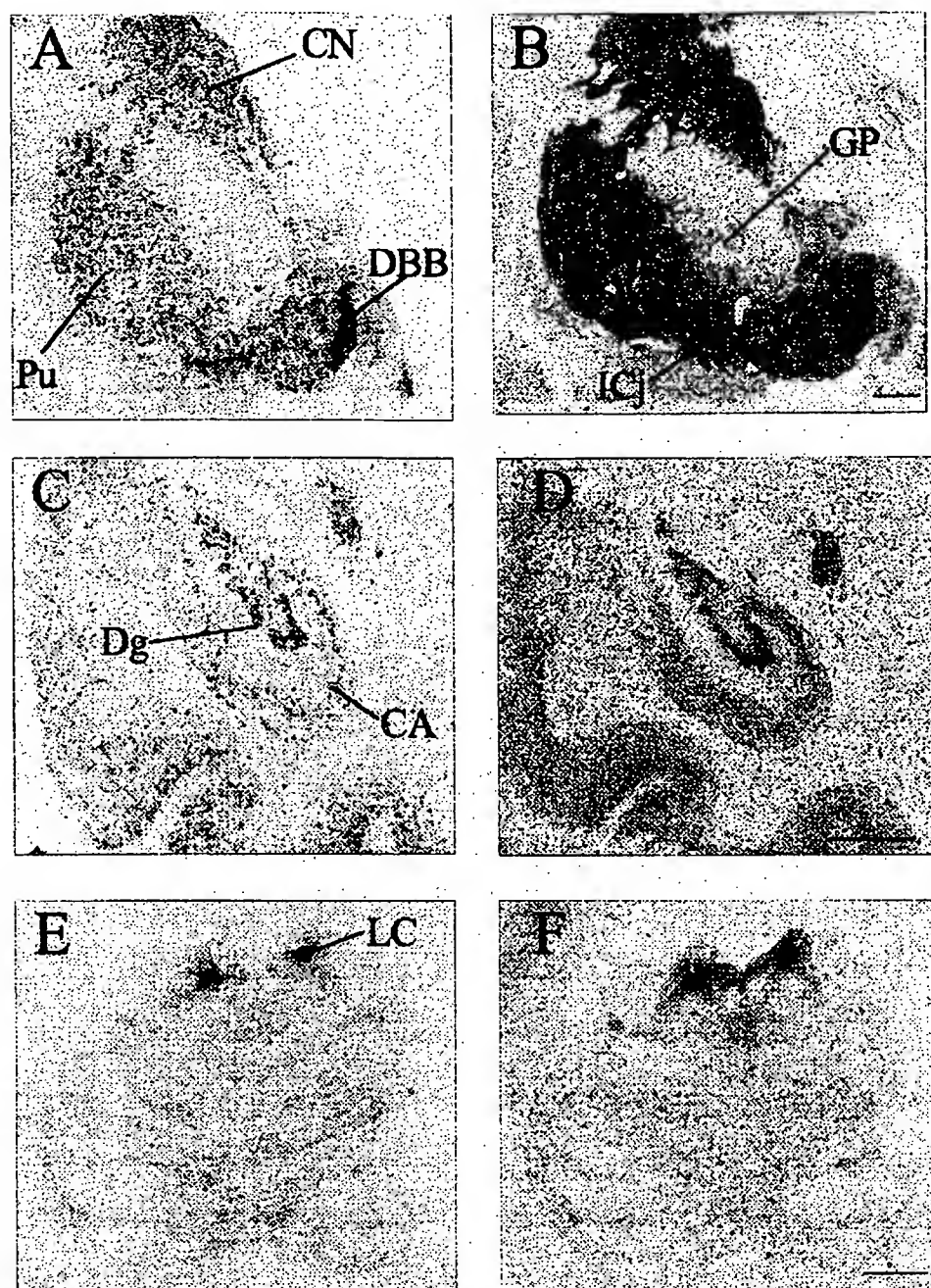


FIG. 4. Distribution of NK1 mRNA (A, C, and E) and ^3H -SP binding sites (B, D and F) in different regions of the human brain: striatum (A and B), hippocampus (C and D), and locus coeruleus (E and F). CA, cornu ammonis hippocampi; CN, caudate nucleus; DBB, diagonal band of Broca; Dg, dentate gyrus; GP, globus pallidus; ICj, Island of Calleja; LC, locus coeruleus; Pu, putamen. Scale bar, 0.5 cm.

Discussion

The present study provides the first detailed distribution of the NK1 mRNA and binding sites in the postmortem human brain with focus on the distribution of the long and short isoforms. The present data demonstrate a strong correlation between NK1 mRNA-expressing cells and ^3H -SP binding sites, suggesting that the NK1 receptors are more likely situated in close proximity to cell bodies rather than in the terminal projections. The anatomical organization also implies a strong association of the NK1/SP system with limbic-related neural networks in the human brain.

Overall, the present data confirmed the abundance of NK1 mRNA expressing cells and binding sites in the striatum. NK1-like immunoreactivity has been previously found in striatal aspiny interneurons (Gerfen, 1991; Parent *et al.*, 1995) which also contain choline acetyltransferase, nitric oxide, and/or somatostatin (Kowall *et al.*, 1993; Li *et al.*, 2000). In the striatum, SP is also very abundant and is present in local collaterals of spiny projection neurons (Gerfen & Young, 1988; Lee *et al.*, 1997) which form synapses with cholinergic interneurons (Marlone *et al.*, 1992) often containing NK1 receptors (Gerfen, 1991; Pickel *et al.*, 2000). Many studies have focused on the possible role of SP in basal ganglia functions and it has been suggested that alterations

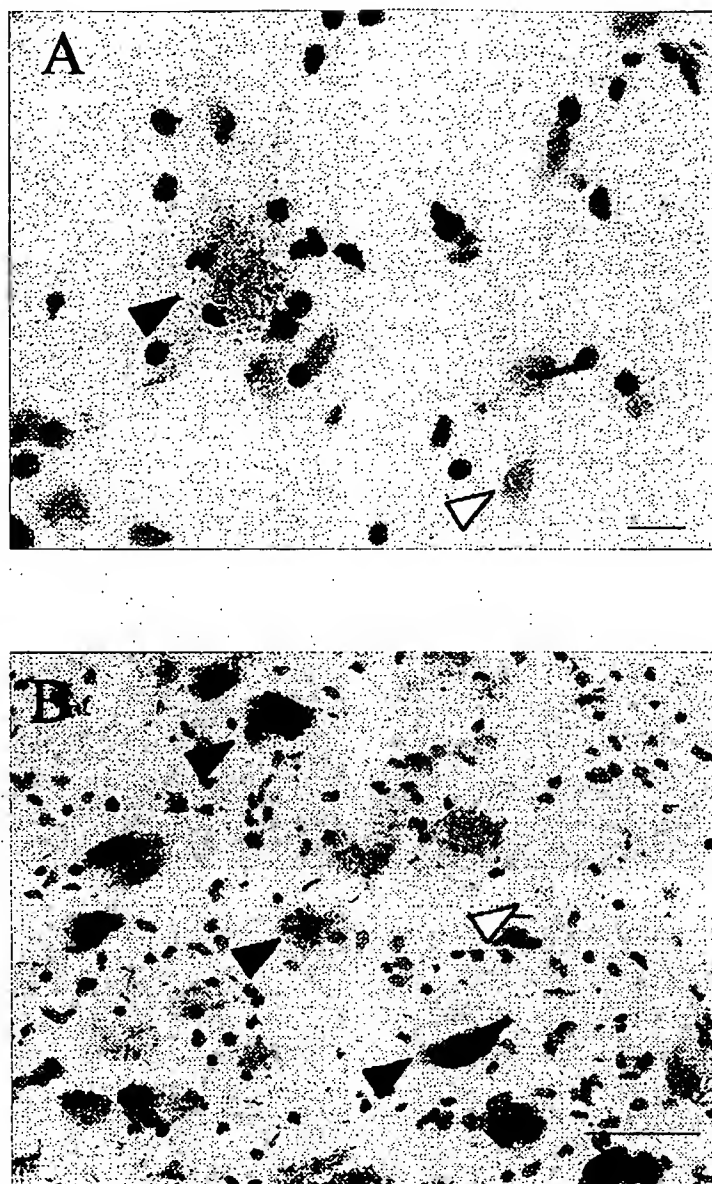


FIG. 5. High magnification bright field photomicrograph showing the localization of NK1 mRNA expression in the caudate nucleus (A) and locus coeruleus (B). Black arrowheads identify the intensely labelled cells and the white point to NK1 mRNA-negative cells. Scale bar, A, 20 μ m; B, 60 μ m.

of tachykinins gene expression could reflect the extrapyramidal motor effect of neuroleptic drugs. In fact, antipsychotic drugs with extrapyramidal side-effects alter tachykinins and NK1 mRNA (Bannon *et al.*, 1986; Humpel *et al.*, 1990), while clozapine, which lacks these side-effects, does not affect the tachykinins (Angulo *et al.*, 1990; Humpel *et al.*, 1990). An involvement of tachykinins in the pathophysiology of Parkinsons disease has also been proposed (Barker, 1991), but no final conclusions have as yet been made.

The NK1 mRNA and binding sites were found in different cortical regions throughout the human brain. Of the cortical regions studied, the striate cortex appeared to be a main NK1 area being enriched in both NK1 mRNA expressing cells and binding sites (Kus *et al.*, 1998), suggesting a possible role of NK1 in mediating SP regulation of visual functions. Previous studies in primates suggest a regulation of the tachykinin system in the visual cortex as tachykinins are reduced after visual deprivation (Hendry *et al.*, 1988; Benson *et al.*, 1994), although the exact role in visual functions is still unclear. In the visual cortex,

NK1 binding sites were highest in layer IV (Kus *et al.*, 1998) and NK1 mRNA was also expressed in deeper layers (present data). The laminar pattern of distribution of NK1 mRNA and binding sites and the localization of NK1-LI in small non-pyramidal cells (Tooney *et al.*, 2000), would imply that the NK1 neuronal cells in the human cortex are mainly interneurons that ramify within layer IV and/or send projection to layers I and II. In the rat and monkey cortex, NK1 positive neurons are also found to be immunoreactive for GABA (Kaneko *et al.*, 1994; Echevarria *et al.*, 1997), neuropeptide Y and somatostatin (Kaneko *et al.*, 1994) and, thus, to be inhibitory interneurons.

In the hippocampal formation, NK1 mRNA and binding sites are found mainly in association with the polymorphic layer of the dentate gyrus consistent with the distribution of NK1-like immunoreactivity (Magloczky *et al.*, 2000). Abundant SP-expressing cells have been documented in the hippocampal region (Dei Fiacco *et al.*, 1987; Hurd *et al.*, 1999). Although very little is known about the functional properties of the NK1 receptor in the hippocampus, a number of

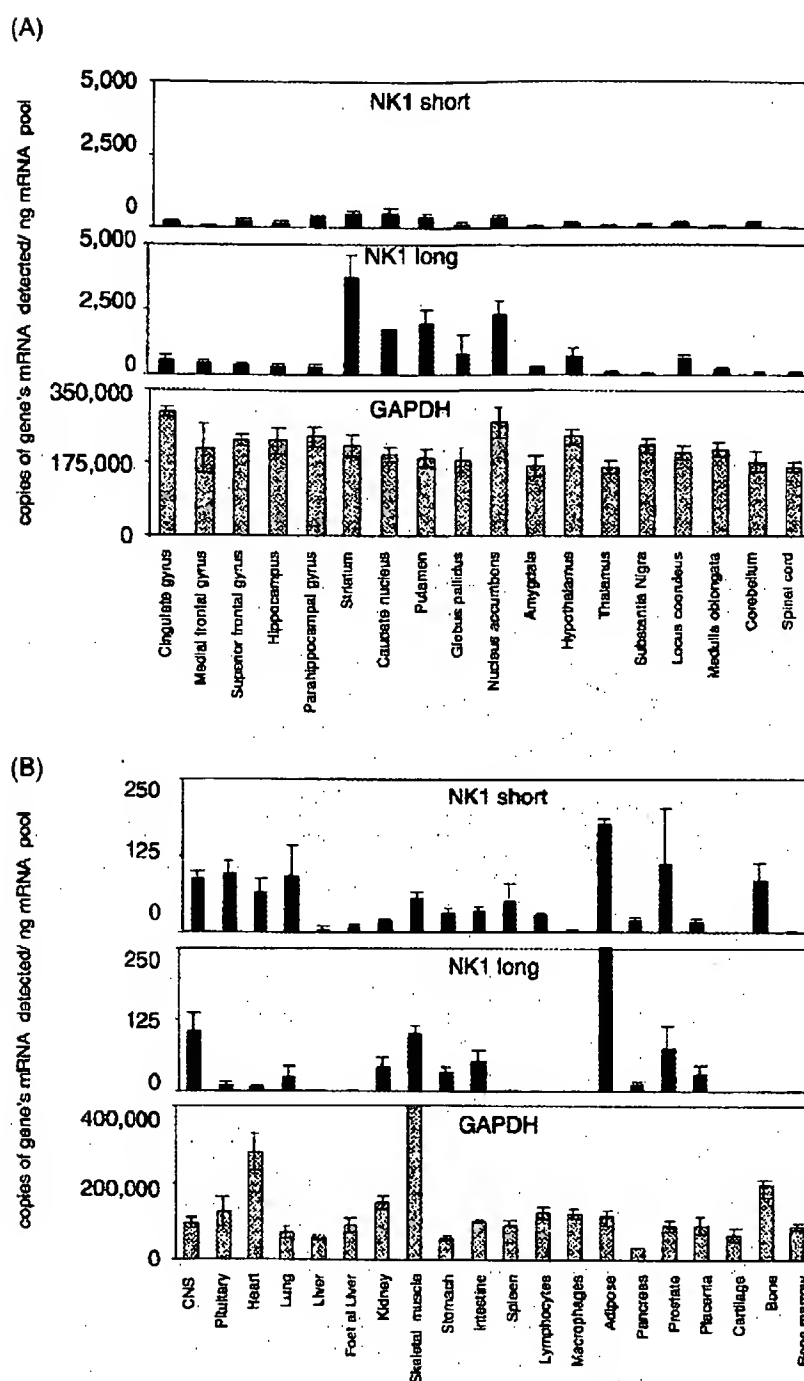


FIG. 6. TaqMan PCR of NK1 mRNA long and short isoforms in human central nervous system (A) and peripheral tissues (B). Data are expressed as copies of gene's mRNA detected per ng mRNA pool normalized to GAPDH to correct for RNA quantity and integrity.

studies have related SP to the modulation of learning and memory processing. Intracerebroventricular injections of SP have been shown to facilitate learning (Flood *et al.*, 1990) and to be effective in counteracting age-related learning deficits (Hasenohr *et al.*, 1990; Hasenohr *et al.*, 1994). In addition to learning and memory, the hippocampus has been strongly implicated in the neurobiology of stress and multiple clinical studies have documented abnormalities in the hippocampus of subjects with major depression disorders (Sheline *et al.*, 1999; Bremner *et al.*, 2000; Frodl *et al.*, 2002; Lee *et al.*, 2002). SP has also been related to the pathophysiology of epilepsy and kainic-

acid induced seizures were found to alter preprotachykinin-A mRNA in the hippocampus (Brene *et al.*, 1992; Zachrisson *et al.*, 1998). Animal and human studies have related NK1 to seizure activity: CP-122721-1, an NK1 antagonist, attenuates kainic-acid induced seizures (Zachrisson *et al.*, 1998) and an induction of changes in the number and distribution of NK1-positive neurons has been reported in the dentate gyrus of epileptic subjects (Magloczky *et al.*, 2000).

The strong expression of NK1 mRNA and binding sites that was apparent in the locus coeruleus, a region also enriched in SP-containing axon terminals (Ribeiro-da-Silva *et al.*, 2000) is intriguing and

supports the hypothesis for a role of SP in depression. A regulation of noradrenergic neurons by tachykinins has also been suggested (Guyenet & Aghajanian, 1977; Cheeseman *et al.*, 1983) and double labelling immunohistochemical studies have demonstrated that NK1 receptors are expressed in the locus coeruleus noradrenergic neurons (Chen *et al.*, 2000). Electrophysiological and pharmacological studies have shown that SP or NK1 agonists and antagonists can affect the activity of locus coeruleus (LC) neurons both *in vitro* and *in vivo* (Guyenet & Aghajanian, 1977; Maubach *et al.*, 2002). Selective NK1 receptor antagonists can attenuate the expression of c-fos-like protein, used as an index of neuronal activation, which is increased in LC following stressful stimulation (Hahn & Bannon, 1999). Recent findings show that both NK1 receptor antagonists and drugs acting on the noradrenergic system, such as imipramine, increase the firing activity of LC neurons, suggesting that this mechanism of action may contribute to their proposed antidepressant effect (Maubach *et al.*, 2002).

The presence of NK1 mRNA and binding sites in the amygdala and other limbic-related regions, such as the nucleus accumbens and diagonal band of Broca, also supports a role for NK1 receptors on the neural pathways involved in emotional responses. Consistent with this hypothesis, focal injection of a selective NK1 receptor antagonist into the basolateral amygdala, was able to inhibit guinea pig neonatal vocalization, which is an index for the efficacy of anxiolytic and antidepressant drugs (Boyce *et al.*, 2001). In addition, in the guinea pig basolateral amygdala, NK1 receptor activation stimulates inhibitory synaptic activity (Maubach *et al.*, 2001). Therefore it has been suggested that SP directly activates NK1 receptors colocalized on a population of GABA interneurons within this amygdaloid nucleus. The SP-induced increase in inhibitory tone is likely to influence also the activity of connected nuclei and pathways involved in emotional behaviour.

In the human dorsal raphe, only low levels of the NK1 mRNA and binding sites were found. Despite the low abundance of the NK1 neurons in this region, previous studies have demonstrated co-expression of SP and 5-HT in a substantial number of neurons of the human dorsal raphe, mainly localized in the larger rostral portion (Baker *et al.*, 1991; Sergeyev *et al.*, 1999). Although this evidence is lacking in the rat dorsal raphe, functional interactions between SP-containing neurons and 5-HT system have been demonstrated in the rodent brain (Shirayama *et al.*, 1996). In mice, both genetic disruption (knock out) and pharmacological blockade of NK1 receptors result in an increase in the firing rate of 5-HT dorsal raphe neurons and in a marked reduction of anxiety and stress-related responses (Frøger *et al.*, 2001; Santarelli *et al.*, 2001).

Long and short isoforms

A differential expression of the two NK1 splice variants in the rat had previously been identified using immunohistochemistry and *in vitro* autoradiography (Mantyh *et al.*, 1996). In the present study, real time quantitative PCR revealed the differential expression profile and the relative abundance of the two splice variants in the human central and peripheral tissues. In the majority of the regions analysed throughout the human brain, there was the overall prevalence of the long variant over the short, although both isoforms were found in all the regions studied. A recent study failed to detect the truncated form in the human brain, but this discrepancy could be due to the low levels of expression of the short form and to the sensitivity of the method used (Page & Bell, 2002). In fact, *in situ* hybridization experiments with riboprobes specific for the long and short splice variants also failed to detect any short isoform hybridization signal in the striatum (data not shown). The two isoforms differ in the carboxy-terminal region and for the

resistance to desensitization, with the short splice variant being more responsive to SP stimulation (Li *et al.*, 1997). This could suggest a possible distinct role in discrete populations, although, in view of the present findings, we cannot relate the two isoforms to region-specific SP-mediated functions in the CNS. The C-terminal region could possibly be of importance for the coupling to different second messengers systems or for the different targeting pathways of the receptor on the neuron, as it has been shown for the metabotropic glutamate receptor mGluR1 (Chan *et al.*, 2001). In support of this last hypothesis, there is evidence of a differential cellular localization of NK1-LI in bone, where NK1-LI is found in the cytoplasm, as compared to neuronal cells that are characterized by cellular membrane localization (Goto & Tanaka, 2002). Further studies are needed to address whether coupling or other functional consequences do differ between the short and the long isoforms.

Opposite to what was seen in the CNS, in the human peripheral tissues, the short isoform was the most represented, with regions such as bone and spleen showing exclusive expression of this transcript. This shorter form does not undergo a rapid desensitization (Li *et al.*, 1997), suggesting a need of a longer responsiveness in these regions. Although the physiological implication of the prevalence of the short isoform in peripheral tissues is not presently known, it could be of importance for the pharmacological targeting of specific tissues.

Species differences

Several studies have examined the anatomical distribution of NK1 receptor in the rodent brain (Dam & Quirion, 1986; Saffroy *et al.*, 1988; Yip & Chahl, 2000). Phylogenetic studies have reported differences in the distribution of NK1 binding sites between rat and guinea pig, showing a good similarity in the basal ganglia, but some differences have been documented in other brain regions such as the cerebral cortex, hippocampus, and cerebellum (Petitet *et al.*, 1993; Saffroy *et al.*, 1994). The present results also provide evidence of species differences between the rodent and the human brains. Overall, the striatal localization seems to be preserved in the different species, but the NK1 distribution in the human cerebral cortex, hippocampus and dorsal raphe bears a closer similarity to the rat as compared to the guinea pig. In the amygdala, NK1 nuclear distribution in humans appears to be distinct from the rodents which show a similar amygdala organization (Saffroy *et al.*, 1994). In addition to anatomical differences, discrepancies in the pharmacological properties of NK1 receptors have also complicated the preclinical evaluations of NK1 receptor ligands (Beresford *et al.*, 1991). The functional relevance of these differences is not clear as in some, although not in all cases, animal studies were highly predictive for the therapeutic effect of a NK1 ligand. In fact, despite the differences in NK1 pharmacology and limbic distribution between the species, NK1 antagonists have been shown to have an anxiolytic-like activity in both guinea pig and rat (File, 1997; Boyce *et al.*, 2001), and clinical trial with the NK1 antagonist MK-869 (Kramer *et al.*, 1998) show improved clinical symptoms in patients with major depression and anxiety. Although in this case the final effect of NK1 blockade seems to be conserved among species, in another therapeutic area such as chronic pain, data from animal studies do not predict the effects of the NK1 ligand in humans (Hill, 2000). Such inconsistencies between the species suggests that some caution should be taken when extrapolating results directly from preclinical to clinical human studies.

Conclusion

In conclusion, the presence of NK1 gene and binding sites in limbic-related areas such as the amygdala and locus coeruleus gives support to

NK1 as a potential target for antidepressant treatment intervention. In addition, the predominance of the long isoform emphasizes a greater contribution of the long splice variant to CNS functions.

Acknowledgements

The authors would like to thank Federico Faggioni for the technical assistance.

Abbreviations

CA, cornu ammonis hippocampi; GADPH, glyceraldehyde-3-phosphate dehydrogenase; LC, locus coeruleus; NK1, neurokinin 1 receptor; SP, substance P.

References

- Angulo, J.A., Cadet, J.L. & McEwen, B.S. (1990) Effect of typical and atypical neuroleptic treatment on protachykinin mRNA levels in the striatum of the rat. *Neurosci. Lett.*, **113**, 217–221.
- Aubry, J.M., Lundstrom, K., Kawashima, E., Ayala, G., Schulz, P., Bartanusz, V. & Kiss, J.Z. (1994) NK1 receptor expression by cholinergic interneurons in human striatum. *Neuroreport*, **5**, 1597–1600.
- Baker, K.G., Halliday, G.M., Hornung, J.P., Geffen, L.B., Cotton, R.G. & Turk, I. (1991) Distribution, morphology and number of monoamine-synthesizing and substance P-containing neurons in the human dorsal raphe nucleus. *Neuroscience*, **42**, 757–775.
- Bannon, M.J., Lee, J.M., Giraud, P., Yung, A., Affolter, H.J. & Bonner, T.I. (1986) Dopamine antagonist haloperidol decreases substance P, substance K, and preprotachykinin mRNAs in rat striatonigral neurons. *J. Biol. Chem.*, **261**, 6640–6642.
- Barker, R. (1991) Substance P and neurodegenerative disorders. A speculative review. *Neuropeptides*, **20**, 73–78.
- Beason-Held, D.L., Huntsman, M.M. & Jones, E.G. (1994) Activity-dependent changes in GAD and preprotachykinin mRNAs in visual cortex of adult monkeys. *Cerebral Cortex*, **4**, 40–51.
- Beresford, I.J., Birch, P.J., Hagan, R.M. & Ireland, S.J. (1991) Investigation into species variants in tachykinin NK1 receptors by use of the non-peptide antagonist, CP-96,345. *Br. J. Pharmacol.*, **104**, 292–293.
- Boyce, S., Smith, D., Carlson, E., Hewson, L., Rigby, M., O'Donnell, R., Harrison, T. & Rupniak, N.M. (2001) Intra-amygdala injection of the substance P (NK1) receptor antagonist L-760735 inhibits neonatal vocalizations in guinea-pigs. *Neuropharmacology*, **41**, 130–137.
- Bremner, J.D., Narayan, M., Anderson, E.R., Staib, L.H., Miller, H.L. & Charney, D.S. (2000) Hippocampal volume reduction in major depression. *Am. J. Psychiatry*, **157**, 115–118.
- Brone, S., Lindfors, N., Ballarin, M. & Persson, H. (1992) Kainic acid-mediated increase of preprotachykinin-A messenger RNA expression in the rat hippocampus and a region-selective attenuation by dexamethasone. *Neuroscience*, **50**, 611–618.
- Brone, S., Lindfors, N., Kopp, J., Sedvall, G. & Persson, H. (1989) Regional distribution of neuropeptide Y mRNA in postmortem human brain. *Brain Res. Mol. Brain Res.*, **6**, 241–249.
- Burnet, P.W. & Harrison, P.J. (2000) Substance P (NK1) receptors in the cingulate cortex in unipolar and bipolar mood disorder and schizophrenia. *Biol. Psychiatry*, **47**, 80–83.
- Caberlotto, L., Fuxe, K., Sedvall, G. & Hurd, Y.L. (1997) Localization of neuropeptide Y Y1 mRNA in the human brain: abundant expression in cerebral cortex and striatum. *Eur. J. Neurosci.*, **9**, 1212–1225.
- Chan, W.Y., Soloviev, M.M., Ciruela, F. & McIlhinney, R.A. (2001) Molecular determinants of metabotropic glutamate receptor 1B trafficking. *Mol. Cell. Neurosci.*, **17**, 577–588.
- Cheesman, H.J., Pincock, R.D. & Henderson, G. (1983) Substance P excitation of rat locus coeruleus neurones. *Eur. J. Pharmacol.*, **94**, 93–99.
- Chen, L.W., Wei, L.C., Lin, H.L. & Rao, Z.R. (2000) Noradrenergic neurons expressing substance P receptor (NK1) in the locus coeruleus complex: a double immunofluorescence study in the rat. *Brain Res.*, **873**, 155–159.
- Cooper, P.E., Fernstrom, M.H., Rorsiad, O.P., Leeman, S.E. & Martin, J.B. (1981) The regional distribution of somatostatin, substance P and neurotensin in human brain. *Brain Res.*, **218**, 219–232.
- Dam, T.V. & Quirion, R. (1986) Pharmacological characterization and autoradiographic localization of substance P receptors in guinea pig brain. *Peptides*, **7**, 855–864.
- DeArmond, S.J., Fusch, M.M. & Dewey, M.M. (1989) *A Photographic Atlas: Structure of the Human Brain*. Oxford University Press, New York.
- Del Fiacco, M., Levanti, M.C., Dessi, M.L. & Zucca, G. (1987) The human hippocampal formation and parahippocampal gyrus: localization of substance P-like immunoreactivity in newborn and adult post-mortem tissue. *Neuroscience*, **21**, 141–150.
- Dietl, M.M. & Palacios, J.M. (1991) Phylogeny of tachykinin receptor localization in the vertebrate central nervous system: apparent absence of neurokinin-2 and neurokinin-3 binding sites in the human brain. *Brain Res.*, **539**, 211–222.
- Echevarria, D., Matur, C. & Albus, K. (1997) Neurons in the rat occipital cortex co-expressing the substance P-receptor and GABA: a comparison between *in vivo* and organotypic cultures. *Eur. J. Neurosci.*, **9**, 1530–1535.
- File, S.E. (1997) Anxiolytic action of a neurokinin receptor antagonist in the social interaction test. *Pharmacol. Biochem. Behav.*, **58**, 747–752.
- Flood, J.F., Baker, M.L., Hernandez, E.N. & Morley, J.E. (1990) Modulation of memory retention by neurokinin B. *Brain Res.*, **520**, 284–290.
- Fong, T.M., Anderson, S.A., Yu, H., Huang, R.R. & Strader, C.D. (1992) Differential activation of intracellular effector by two isoforms of human neurokinin-1 receptor. *Mol. Pharmacol.*, **41**, 24–30.
- Frodl, T., Meisenzahl, E.M., Zetzsch, T., Born, C., Groll, C., Jager, M., Leinsinger, G., Rottler, R., Hahn, K. & Moller, H.J. (2002) Hippocampal changes in patients with a first episode of major depression. *Am. J. Psychiatry*, **159**, 1112–1118.
- Friger, N., Gardier, A.M., Moratalla, R., Alberti, I., Lena, I., Boni, C., De Felipe, C., Rupniak, N.M., Hunt, S.P., Jacquot, C., Hamon, M. & Lanfumey, L. (2001) 5-Hydroxytryptamine (5-HT) 1A autoreceptor adaptive changes in substance P (neurokinin 1) receptor knock-out mice mimic antidepressant-induced desensitization. *J. Neurosci.*, **21**, 8188–8197.
- Gerfen, C.R. (1991) Substance P (neurokinin-1) receptor mRNA is selectively expressed in cholinergic neurons in the striatum and basal forebrain. *Brain Res.*, **556**, 165–170.
- Gerfen, C.R. & Young, W.S. III (1988) Distribution of striatonigral and striatopallidal peptidergic neurons in both patch and matrix compartments: an *in situ* hybridization histochemistry and fluorescent retrograde tracing study. *Brain Res.*, **460**, 161–167.
- Goto, T. & Tanaka, T. (2002) Tachykinins and tachykinin receptors in bone. *Microscopy Res. Technique*, **58**, 91–97.
- Guyenet, P.G. & Aghajanian, G.K. (1977) Excitation of neurons in the nucleus locus coeruleus by substance P and related peptides. *Brain Res.*, **136**, 178–184.
- Hahn, M.K. & Bannon, M.J. (1999) Stress-induced c-fos expression in the rat locus coeruleus is dependent on neurokinin 1 receptor activation. *Neuroscience*, **94**, 1183–1188.
- Hall, H., Sedvall, G., Magnusson, O., Kopp, J., Halldin, C. & Farde, L. (1994) Distribution of D1- and D2-dopamine receptors, and dopamine and its metabolites in the human brain. *Neuropsychopharmacology*, **11**, 245–256.
- Hasenohr, R.U., Frisch, C., Nikolaus, S. & Huston, J.P. (1994) Chronic administration of neurokinin SP improves maze performance in aged *Rattus norvegicus*. *Behav. Neural. Biol.*, **62**, 110–120.
- Hasenohr, R.U., Huston, J.P. & Schuurman, T. (1990) Neuropeptide substance P improves water maze performance in aged rats. *Psychopharmacology*, **101**, 23–26.
- Hendry, S.H., Jones, E.G. & Burstein, N. (1988) Activity-dependent regulation of tachykinin-like immunoreactivity in neurons of monkey visual cortex. *J. Neurosci.*, **8**, 1225–1238.
- Hershey, A.D. & Krause, J.E. (1990) Molecular characterization of a functional cDNA encoding the rat substance P receptor. *Science*, **247**, 958–962.
- Hill, R. (2000) NK1 (substance P) receptor antagonists – why are they not analgesic in humans? *Trends Pharmacol. Sci.*, **21**, 244–246.
- Humpel, C., Knaus, G.A., Auer, B., Knaus, H.G., Haring, C., Theodorsson, E. & Suria, A. (1990) Effects of haloperidol and clozapine on preprotachykinin-A messenger RNA, tachykinin tissue levels, release and neurokinin-1 receptors in the striato-nigral system. *Synapse*, **6**, 1–9.
- Hurd, Y.L., Keller, E., Sotonyi, P. & Sedvall, G. (1999) Preprotachykinin-A mRNA expression in the human and monkey brain: An *in situ* hybridization study. *J. Comp. Neurol.*, **411**, 56–72.
- Kanazawa, I. & Jessell, T. (1976) Post mortem changes and regional distribution of substance P in the rat and mouse nervous system. *Brain Res.*, **117**, 362–367.
- Kaneko, T., Shigemoto, R., Nakanishi, S. & Mizuno, N. (1994) Morphological and chemical characteristics of substance P receptor-immunoreactive neurons in the rat neocortex. *Neuroscience*, **60**, 199–211.
- Kowall, N.W., Quigley, B.J. Jr., Krause, J.E., Lu, F., Knosfsky, B.E. & Ferrante, R.J. (1993) Substance P and substance P receptor histochemistry in human neurodegenerative diseases. *Regulatory Peptides*, **46**, 174–185.
- Kramer, M.S., Cutler, N., Feighner, J., Shrivastava, R., Carman, J., Sramek, J.J., Reines, S.A., Liu, G., Snavely, D., Wyatt-Knowles, F., Halc, J.J., Mills, S.G.,

- MacCoss, M., Swait, C.J., Harrison, T., Hill, R.G., Hefti, F., Scolnick, E.M., Cascieri, M.A., Chicchi, G.G., Sadowski, S., Williams, A.R., Hewson, L., Smith, D. & Rupniak, N.M. (1998) Distinct mechanism for antidepressant activity by blockade of central substance P receptors. *Science*, **281**, 1640-1645.
- Kus, L., Mazzone, S.B., Paxinos, G. & Geraghty, D.P. (1998) Autoradiographic localisation of substance P (NK1) receptors in human primary visual cortex. *Brain Res.*, **794**, 309-312.
- Lee, T., Kanckn, T., Shigemoto, R., Nomura, S. & Mizuno, N. (1997) Collateral projections from striatonigral neurons to substance P receptor-expressing intrinsic neurons in the striatum of the rat. *J. Comp. Neurol.*, **388**, 250-264.
- Lee, A.L., Ogle, W.O. & Sapolsky, R.M. (2002) Stress and depression: possible links to neuron death in the hippocampus. *Bipolar Disorders*, **4**, 117-128.
- Li, H., Leeman, S.E., Slack, B.E., Hauser, G., Saltsman, W.S., Krause, J.E., Blusztajn, J.K. & Boyd, N.D. (1997) A substance P (neurokinin-1) receptor mutant carboxyl-terminally truncated to resemble a naturally occurring receptor isoform displays enhanced responsiveness and resistance to desensitization. *Proc. Natl Acad. Sci. USA*, **94**, 9475-9480.
- Li, J.L., Wang, D., Kancko, T., Shigemoto, R., Nomura, S. & Mizuno, N. (2000) Relationship between neurokinin-1 receptor and substance P in the striatum: light and electron microscopic immunohistochemical study in the rat. *J. Comp. Neurol.*, **418**, 156-163.
- Magloczky, Z., Wittner, L., Borhegyi, Z., Halasz, P., Vajda, J., Czirjak, S. & Freund, T.F. (2000) Changes in the distribution and connectivity of interneurons in the epileptic human dentate gyrus. *Neuroscience*, **96**, 7-25.
- Mantyh, P.W., Hunt, S.P. & Maggio, J.E. (1984) Substance P receptors: localization by light microscopic autoradiography in rat brain using [³H]SP as the radioligand. *Brain Res.*, **307**, 147-165.
- Mantyh, P.W., Rogers, S.D., Ghilardi, J.R., Maggin, J.E., Mantyh, C.R. & Vigna, S.R. (1996) Differential expression of two isoforms of the neurokinin-1 (substance P) receptor *in vivo*. *Brain Res.*, **719**, 8-13.
- Martone, M.E., Armstrong, D.M., Young, S.J. & Groves, P.M. (1992) Ultrastructural examination of enkephalin and substance P input to cholinergic neurons within the rat neostriatum. *Brain Res.*, **594**, 253-262.
- Maubach, K.A., Martin, K., Chicchi, G., Harrison, T., Wheelodon, A., Swain, C.J., Cumberbatch, M.J., Rupniak, N.M. & Seabrook, G.R. (2002) Chronic substance P (NK1) receptor antagonist and conventional antidepressant treatment increases burst firing of monoamine neurons in the locus coeruleus. *Neuroscience*, **109**, 609-617.
- Maubach, K.A., Martin, K., Smith, D.W., Hewson, L., Frankshun, R.A., Harrison, T. & Seabrook, G.R. (2001) Substance P stimulates inhibitory synaptic transmission in the guinea pig basolateral amygdala *in vitro*. *Neuropharmacology*, **40**, 806-817.
- Otsuka, M. & Yoshino, K. (1993) Neurotransmitter functions of mammalian tachykinins. *Physiol. Rev.*, **73**, 229-308.
- Pace, N.M. & Bell, N.J. (2002) The human tachykinin NK1 (short form) and tachykinin NK4 receptor: a reappraisal. *Eur. J. Pharmacol.*, **437**, 27-30.
- Parent, A., Cicchetti, F. & Beach, T.G. (1995) Striatal neurones displaying substance P (NK1) receptor immunoreactivity in human and non-human primates. *Neuroreport*, **6**, 721-724.
- Petit, F., Beaujourn, J.C., Saffroy, M., Torrens, Y., Fardin, V. & Glowinski, J. (1993) NK-1 tachykinin receptor in rat and guinea pig brains: pharmacological and autoradiographical evidence for a species difference. *Peptides*, **14**, 551-559.
- Pickel, V.M., Douglas, J., Chun, J., Gamp, P.D. & Bunnert, N.W. (2000) Neurokinin 1 receptor distribution in cholinergic neurons and targets of substance P terminals in the rat nucleus accumbens. *J. Comp. Neurol.*, **423**, 500-511.
- Quartara, L. & Maggi, C.A. (1998) The tachykinin NK1 receptor. Part II: Distribution and pathophysiological roles. *Neuropeptides*, **32**, 1-49.
- Ribeiro-da-Silva, A. & Hokfelt, T. (2000) Neuroanatomical localisation of Substance P in the CNS and sensory neurons. *Neuropeptides*, **34**, 256-271.
- Saffroy, M., Beaujourn, J.C., Petit, F., Torrens, Y. & Glowinski, J. (1994) Differential localization of ³H-[Pro⁹]SP binding sites in the guinea pig and rat brain. *Brain Res.*, **633**, 317-325.
- Saffroy, M., Beaujourn, J.C., Torrens, Y., Bessy, J., Bergstrom, L. & Glowinski, J. (1988) Localization of tachykinin binding sites (NK1, NK2, NK3 ligands) in the rat brain. *Peptides*, **9**, 227-241.
- Santarelli, L., Gnani, G., Debs, R.C., Sibille, E.T., Blier, P., Hen, R. & Heath, M.J. (2001) Genetic and pharmacological disruption of neurokinin 1 receptor function decreases anxiety-related behaviors and increases serotonergic function. *Proc. Natl Acad. Sci. USA*, **98**, 1912-1917.
- Sergeyev, V., Hokfelt, T. & Hurd, Y. (1999) Serotonin and substance P co-exist in dorsal raphe neurons of the human brain. *Neuroreport*, **10**, 3967-3970.
- Sheline, Y.I., Sanghavi, M., Mintun, M.A. & Gado, M.H. (1999) Depression duration but not age predicts hippocampal volume loss in medically healthy women with recurrent major depression. *J. Neurosci.*, **19**, 5034-5043.
- Shirayama, Y., Mitsushio, H., Takashima, M., Ichikawa, H. & Takahashi, K. (1996) Reduction of substance P after chronic antidepressant treatment in the striatum, substantia nigra and amygdala of the rat. *Brain Res.*, **739**, 70-78.
- Tooney, P.A., Au, G.G. & Chahl, L.A. (2000) Localisation of tachykinin NK1 and NK3 receptors in the human prefrontal and visual cortex. *Neurosci. Lett.*, **283**, 185-188.
- Whitty, C.J., Paul, M.A. & Bannon, M.J. (1997) Neurokinin receptor mRNA localization in human midbrain dopamine neurons. *J. Comp. Neurol.*, **382**, 394-400.
- Yip, J. & Chahl, L.A. (2000) Localization of tachykinin receptors and Fos-like immunoreactivity induced by substance P in guinea-pig brain. *Clin. Exp. Pharmacol. Physiol.*, **27**, 943-946.
- Yokota, Y., Sasai, Y., Tanaka, K., Fujiwara, T., Tsuchida, K., Shigemoto, R., Kakizuka, A., Ohkubo, H. & Nakanishi, S. (1989) Molecular characterization of a functional cDNA for rat substance P receptor. *J. Biol. Chem.*, **264**, 17649-17652.
- Zachrisson, O., Lindfors, N. & Brenc, S. (1998) A tachykinin NK1 receptor antagonist, CP-122,721-1, attenuates kainic acid-induced seizure activity. *Brain Res. Mol. Brain Res.*, **60**, 291-295.

Characterization of Cyclin D2 Expression in Human Endometrium

DooSeok Choi, MD, PhD, Sarah Yoon, MS, EunYoung Lee, MS, SeongSoo Hwang, MS, SangYong Song, MD, JiYoung Kim, MD, Byung-Koo Yoon, MD, PhD, and Je-Ho Lee, MD, PhD

OBJECTIVE: This study was undertaken to investigate cyclin D2 mRNA and protein expression in human endometrium during the menstrual cycle.

METHODS: Endometrial samples were obtained from 15 premenopausal nonpregnant women who had hysterectomies for benign gynecologic reasons. They were divided into the following five groups according to histologic dating: early proliferative ($n = 3$), mid to late proliferative ($n = 3$), early secretory ($n = 3$), mid secretory ($n = 3$), and late secretory ($n = 3$). Cyclin D2 mRNA and protein expression were analyzed using reverse transcriptase-polymerase chain reaction, Western blotting, and immunohistochemistry.

RESULTS: Cyclin D2 mRNA and protein were expressed in human endometrial tissue throughout the menstrual cycle. Cyclin D2 mRNA and protein expression of proliferative phase endometrium were significantly higher than those of secretory phase endometrium ($P < .05$). The staining intensity of cyclin D2 in proliferative phase endometrium was higher than that in secretory phase ($P < .05$). Cyclin D2 mRNA level showed good correlation with cyclin D2 protein level ($R = 0.579$, $P < .03$), and cyclin D2 protein also showed good correlation with immunohistochemical staining intensity ($R = 0.562$, $P < .03$).

CONCLUSION: Cyclin D2 was expressed in human endometrium throughout the menstrual cycle. Cyclin D2 mRNA and protein were expressed at high levels in proliferative phase endometrium, especially in the early proliferative phase, and then decreased in the secretory phase. (*J Soc Gynecol Invest* 2002;9:41-6)
Copyright © 2002 by the Society for Gynecologic Investigation.

KEY WORDS: Cyclin D2, human endometrium, menstrual cycle.

Regulation of the cell cycle within any cell type is complex, involves the balance of many regulatory molecules, and can be altered by numerous external signals acting at multiple steps in the cycle. Cyclins are a group of proteins that are expressed periodically during the progression of the cell cycle.¹ The D-type cyclins (D1, D2, and D3) have been known to be cell cycle activators. Among these cyclins, cyclin D2 is known as a rate-limiting positive cell cycle regulator that has a pivotal role in granulosa cell proliferation in the mouse, rat,² and human ovary.³ Cyclin D2 might be associated with endometrial cell cycle regulation. However, the expression pattern of cyclin D2 during the menstrual cycle in human endometrium has not been described.

To prepare for implantation, the endometrium undergoes a precise developmental progression. The first half of the menstrual cycle, the proliferative phase, is estradiol (E_2) dominated and is characterized by intense mitotic activity of endometrial

glandular epithelium, stromal cells, and vascular endometrium. The second half of the cycle, the secretory phase, is progesterone (P_4) dominated and is characterized by differentiation of endometrial components.⁴

We hypothesized that cyclin D2 participates in the endometrial cell cycle regulation, and so research was undertaken to identify the cyclic expression pattern of cyclin D2 mRNA and protein in human endometrium during the menstrual cycle.

MATERIALS AND METHODS

Patients

Endometrial samples were collected after obtaining informed consent from 15 premenopausal nonpregnant women (age range 36-47 years) who had hysterectomies for benign gynecologic reasons. This study was approved by the Ethical Committee of the Samsung Medical Center. All women who participated in this study had taken neither contraceptives nor hormonal agents for at least 3 months before surgery. The endometrial specimens were obtained from the corpora of the uteri and were divided into the following five categories by histologic dating: early proliferative phase ($n = 3$), mid to late proliferative phase ($n = 3$), early secretory phase ($n = 3$), mid secretory phase ($n = 3$), and late secretory phase ($n = 3$).

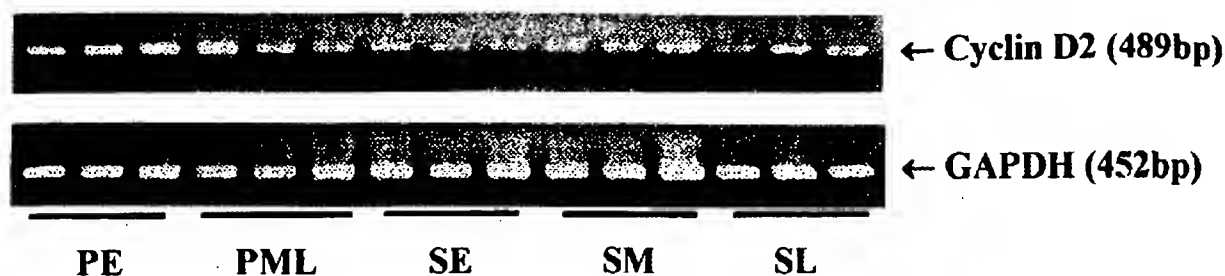
From the Department of Obstetrics and Gynecology, Samsung Medical Center, Sungkyunkwan University School of Medicine, Center for Clinical Research, Samsung Biomedical Research Institute, and Department of Diagnostic Pathology, Samsung Medical Center, Sungkyunkwan University School of Medicine, Seoul, Korea.

Address correspondence and reprint requests to: DooSeok Choi, MD, Department of Obstetrics and Gynecology, Samsung Medical Center, Sungkyunkwan University School of Medicine, 50 Ilwon-Dong Kangnam-Ku, 135-710. E-mail: dschoi@smc.samsung.co.kr

Copyright © 2002 by the Society for Gynecologic Investigation.
Published by Elsevier Science Inc.

1071-5576/02/\$22.00
PII S1071-5576(01)00148-4

A



B

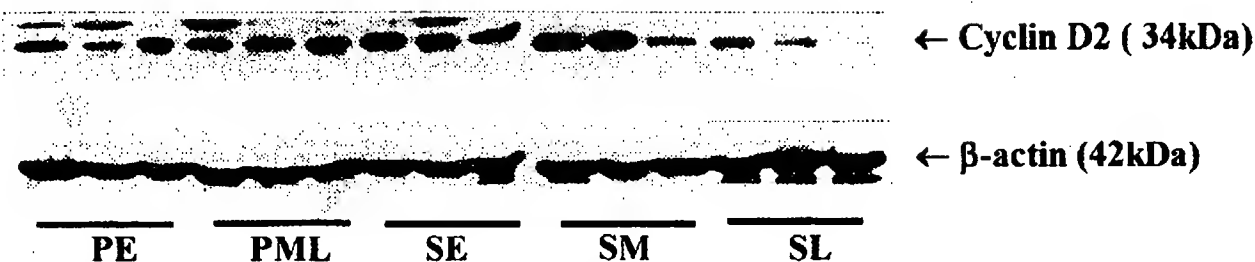


Figure 1. Expression of cyclin D2 mRNA (A) and protein (B) in human endometrium during the menstrual cycle using reverse transcriptase-polymerase chain reaction and Western blotting. PE = early proliferative phase ($n = 3$); PML = mid to late proliferative phase ($n = 3$); SE = early secretory phase ($n = 3$); SM = mid secretory phase ($n = 3$); and SL = late secretory phase ($n = 3$).

Reverse Transcriptase-Polymerase Chain Reaction

Total RNA was extracted from endometrial tissues by TRIzol reagent (Gibco-BRL, Grand Island, NY) according to the manufacturer's instructions. Total RNA (2 μ g) was reverse transcribed in final 25 μ L of Tris buffer (50 mmol/L, pH 8.3) supplemented with potassium chloride (75 mmol/L), magnesium chloride (3 mmol/L), dithiothreitol (5 mmol/L), deoxynucleotide triphosphate (0.5 mmol/L each), oligo dT (1.5 mol/L), and moloney murine leukemia virus (M-MLV) reverse transcriptase (200 U, Promega, Madison, WI) at 42°C for 60 minutes. Polymerase chain reaction (PCR) amplification was performed in a final 50- μ L reaction volume containing 2 μ L of reverse transcribed cDNA, 0.4 mol/L of each primer, 1 U of Taq DNA polymerase (Promega), 1 \times Taq DNA polymerase buffer, magnesium chloride (2.5 mmol/L for cyclin D2 and glyceraldehyde-3-phosphate dehydrogenase [GAPDH]), and deoxynucleotide triphosphate (0.2 mmol/L each). The PCR reaction was conducted in a Progene Thermal Cycler with the following program: denaturing for 1 minute at 95°C, annealing for 45 seconds at 56°C (for cyclin D2) and at 60°C (for GAPDH), and elongation for 2 minutes at 74°C for a total of 30 cycles (for cyclin D2) and 28 cycles (for GAPDH), except for

the last cycle, for which the elongation step was prolonged to 10 minutes at 74°C. The amount of template cDNA used in each reaction was normalized to the amount of GAPDH mRNA. Amplification of template cDNA was in the linear range for the number of PCR cycles, and reverse transcriptase (RT)-PCR of GAPDH transcript was performed using the same amount of cDNA from each sample. The PCR products were visualized by electrophoresis on 1.5% (w/v) agarose gels.

Oligonucleotide Primers

Based on the cDNA sequences available through GenBank, oligonucleotide PCR primers were selected with the assistance of a computer program (DNA STAR) designed to optimize GC content and melting temperature, and to minimize hairpin and dimer formation. The PCR primers were: cyclin D2 forward, 5'-TAC TTC AAG TGC GTG CAG AAG GAC-3'; cyclin D2 reverse, 5'-TCC CAC ACT TCC AGT TCC GAT CAT-3'; GAPDH forward, 5'-ACC ACA GTC CAT GCC ATC AC-3'; and GAPDH reverse, 5'-TCC ACC ACC CTG TTG CTG TA-3', which resulted in products of 489 bp and 452 bp, respectively. The PCR products were sequenced to verify their identity and homology to corresponding cDNA sequences in GenBank.

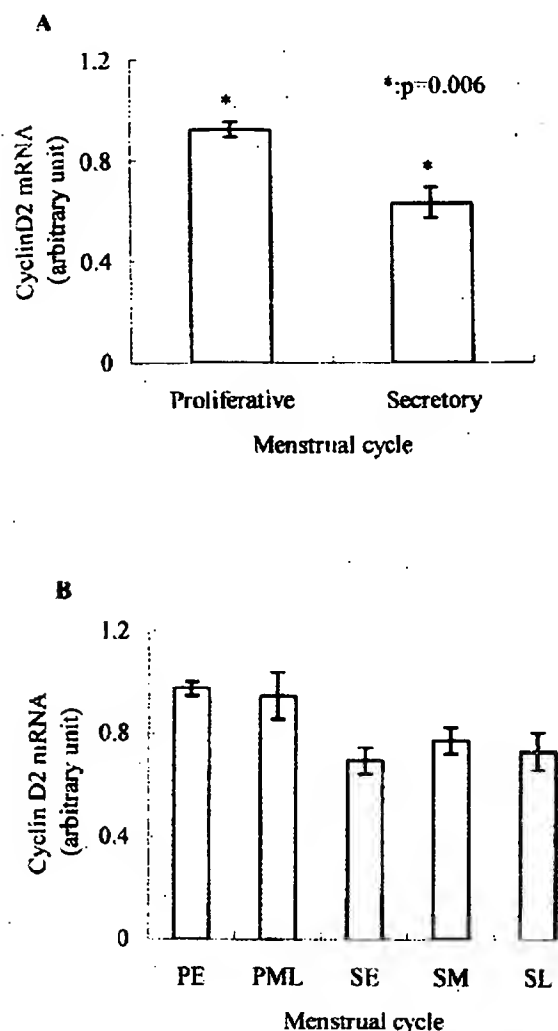


Figure 2. Comparisons of endometrial cyclin D2 mRNA expression during the menstrual cycle. A) Proliferative phase ($n = 6$) compared with secretory phase ($n = 9$). B) Comparison of subgroups. Data are expressed as mean \pm standard error. Abbreviations as in Figure 1.

Immunohistochemistry

Immunohistochemistry was performed on 5- μ m sections of formalin-fixed, paraffin-embedded normal endometrium according to the manufacturer's recommended procedure for the LSAB kit (Dako A/S, Glostrup, Denmark). The sections were baked at 60°C for 1 hour, deparaffinized, and microwaved at 560 MW in citric acid before incubation with appropriate suppressor serum. The cyclin D2 antibody (c-17; Santa Cruz Biotechnology, Santa Cruz, CA) diluted at 1:50 was incubated overnight at 4°C. Sections were lightly counterstained with autohematoxylin (Dako), dehydrated, cleaned, and mounted. Nuclear staining of suprabasal squamous cells of the uterine cervix was used as a positive control. Negative controls were made by replacing the antibody with phosphate-buffered saline (PBS). Positively stained slides were classified into five categories according to the intensity and localization, as follows: 1 = equivocal, 2 = weak cytoplasmic stain of glands, 3 = moderate cytoplasmic stain of glands, 4 = strong cytoplasmic

stain of glands, and 5 = strong cytoplasmic stain of both glands and stromal cells. Scoring of staining intensity was done by two pathologists who were blinded to clinical information.

Western Blot Analysis

Endometrial tissues were homogenized and lysed in 0.5 mL of radioimmunoprecipitation assay buffer (150 mM sodium chloride, 1% ethylphenylpolysthyleneglycol [NP40], 0.5% sodium deoxycholate, 0.1% sodium dodecyl sulfate [SDS], 50 mM Tris pH 8.0) with freshly added 1 mM phenylmethylsulfonylfluoride (PMSF, Sigma, St. Louis, MO) for 30 minutes on ice. The lysates were centrifuged at 13,000 g for 15 minutes at 4°C, and the supernatants were stored at -70°C. Equal amounts of total protein (30 μ g) were separated by SDS-polyacrylamide gel electrophoresis and then transferred to supported westran polyvinylidene fluoride (Schleicher & Schuell, Keene, NH) by applying 100 V for 2 hours with a plate electrode apparatus (Mini Trans-Blot Cell; Bio-Rad, Hercules, CA). The blots were blocked for 2 hours in Tris-buffered saline (TBS) (0.2 M sodium chloride, 0.1% Tween-20, 10 mM Tris pH 7.4) containing 5% nonfat dry milk. Subsequently, the blots were incubated with antibody against cyclin D2 (c-17, 1:1000; Santa Cruz Biotechnology) in TBS, and then the blots were also incubated in anti-rabbit immunoglobulin (Ig) G (1:2000; Amersham Pharmacia Biotech, Freiburg, Germany) in TBS. The blots were washed several times with TBS after each step. The bound antibody was detected with an enhanced chemiluminescence (ECL) system (Amersham Pharmacia Biotech). The blots were stripped with stripping buffer (100 mM β -mercaptoethanol, 2% [w/v] SDS, 62.5 mM Tris-HCl pH 6.7) before application of β -actin antibody. The stripped blots were incubated with antibody against β -actin (1:2000; for the internal standard, Sigma AC-15, St. Louis, MO) in the TBS followed by anti-mouse IgG (1:2000; Amersham Pharmacia Biotech) in TBS.

Densitometry

Gel images were scanned with the Gel Documentation System (Gel Doc 1000, Bio-Rad, Hercules, CA), and relative densities were analyzed using the Multi-analyst fingerprinting program (version 1.1). The relative densities of the bands were expressed as arbitrary absorbance units per area.

Statistical Analysis

The statistical analysis for the differences in cyclin D2 staining intensity and cyclin D2 mRNA expression among endometria of the different menstrual phases was performed using the Kruskal-Wallis test and Mann-Whitney test. The correlation between cyclin D2 protein and mRNA expression was expressed by arbitrary units, and the correlation between cyclin D2 protein and staining intensity was tested by Spearman's correlation analysis. Statistical significance was set at P less than .05.

RESULTS

Cyclin D2 mRNA and protein were detected in all endometrium samples. Using specific oligonucleotide primers and an-

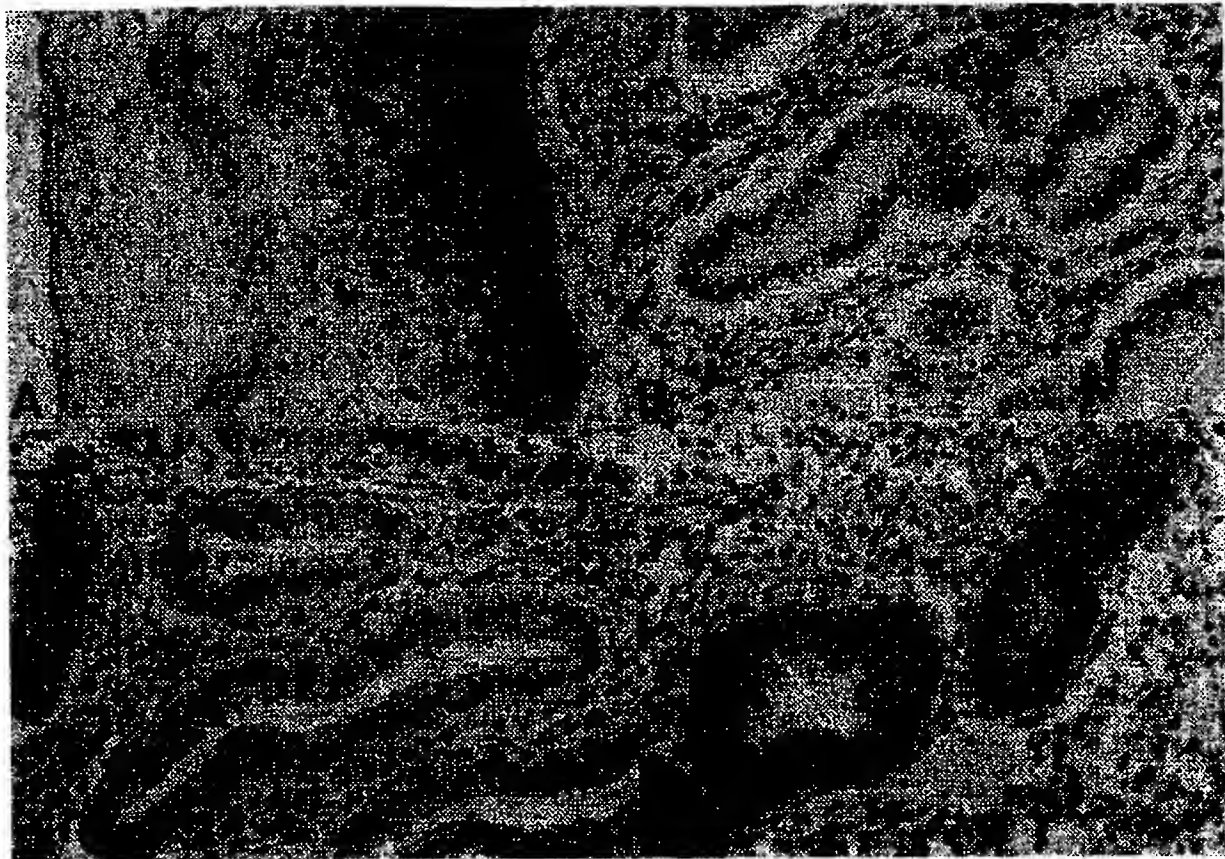


Figure 3. Immunohistochemical localization of cyclin D2 in human endometrium. A) Positive control, nuclear stain of suprabasal squamous cells (*arrows*) in uterine cervix; B) negative control; C) weak cytoplasmic stain of glands (*arrows*) in secretory phase endometrium; D) strong cytoplasmic stain of both glands and stromal cells (*arrows*) in proliferative phase endometrium.

tibody, cyclin D2 mRNA (489 bp) and protein (34 kDa) bands were obtained by RT-PCR and Western blot analysis. We used GAPDH mRNA (452 bp) and β -actin protein (42 kDa) for normalization of the band intensity, respectively (Figure 1).

The cyclin D2 expression was weaker in the endometrium during the secretory phase compared with the proliferative phase (Figure 2A, $P < .05$). In comparisons among subgroups, there were no significant differences in cyclin D2 mRNA expression (Figure 2B). The expression pattern of cyclin D2 protein during the menstrual cycle was similar to that of cyclin D2 mRNA; however, the differences were not statistically significant (data not shown).

Immunohistochemically, the most intense staining of cyclin D2 was noted in the cytoplasm of early proliferative phase endometrial glands. Differences in immunohistochemical pattern between early and mid to late proliferative phase were found in the immunoreactivity of stromal cells. Stromal immunoreactivity was lower in the mid to late proliferative phase. The cytoplasm of early and late secretory phase endometrial glands showed variable immunoreactivity from equivocal to moderate intensities. The mid secretory phase glands showed equivocal cytoplasmic staining pattern. In this study, suprabasal squamous cells of the uterine cervix were included

as a positive internal control and showed moderate nuclear staining intensity (Figure 3).

The staining intensity of cyclin D2 in proliferative phase endometrium was higher than that in secretory phase (Figure 4A, $P < .05$). When compared among subgroups, there were no significant differences except between early proliferative phase and mid secretory phase. Cyclin D2 staining intensity from early proliferative phase was significantly higher than that of mid secretory phase (Figure 4B, $P < .05$).

To correct for possible subjective discrepancies in immunohistochemistry reading, we performed Western blotting as a supportive method. In Western blot analysis, cyclin D2 protein level showed good correlation with immunohistochemical staining intensity ($R = 0.562$, $P < .03$, Figure 5A). Cyclin D2 mRNA level also showed good correlation with cyclin D2 protein level ($R = 0.579$, $P < .03$, Figure 5B).

DISCUSSION

The best known regulators of G1 progression in mammalian cells are the three D-type cyclins (D1–3), of which cell concentrations fluctuate characteristically during progression through G1 in response to mitogenic stimuli.^{2,5,6} D-type G1 cyclins assemble with two major catalytic partners, cdk4 and

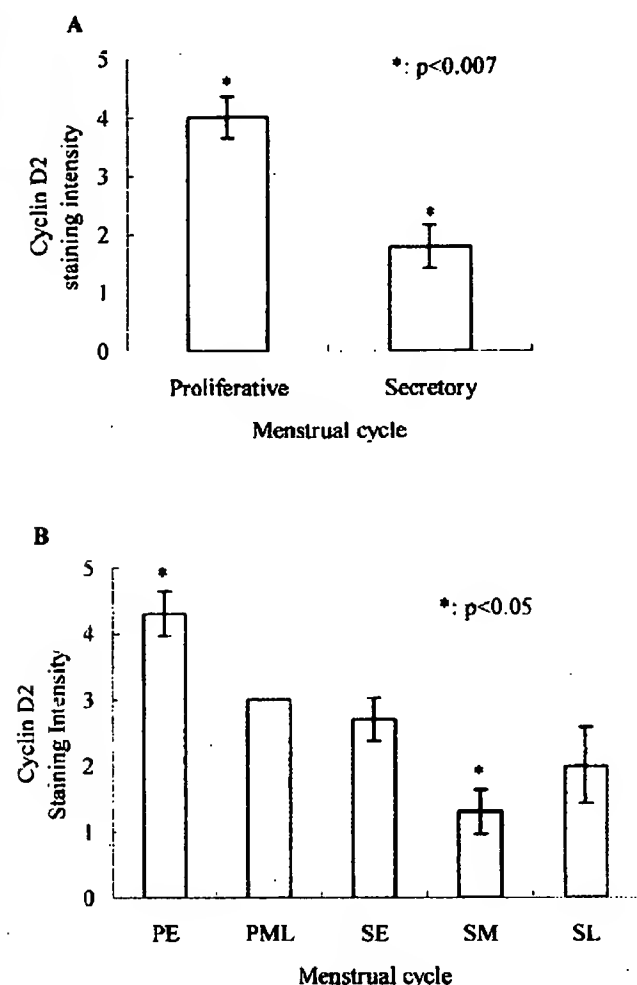


Figure 4. Comparisons of endometrial cyclin D2 staining intensity during the menstrual cycle. A) Proliferative phase ($n = 6$) compared with secretory phase ($n = 9$). B) Comparison of subgroups. Data are expressed as mean \pm standard error. Abbreviations as in Figures 1 and 2.

cdk6, to form functional holoenzymes that are differentially expressed in proliferating cells. Mitogens activate the transcription of cyclin D genes, inducing the assembly of enzymatically active cyclin D-cdk complexes that execute a rate-limiting function later in G1 phases.⁷ Ectopic overexpression of D-type cyclins bypasses the inductive effects of mitogens on cyclin D gene expression, shortening the G1 phase and reducing the growth factor dependency of cells.⁸

We found that cyclin D2 mRNA and protein were expressed in the human endometrium at high levels in the proliferative phase and at significantly lower levels in the secretory phase. In ovary, cyclin D2 mRNA and protein were expressed at high levels in granulosa cells of preovulatory follicles of hypophysectomized rats treated with estradiol and FSH. When hypophysectomized rats treated with estradiol and FSH were injected with hCG, cyclin D2 expression was downregulated within 4 hours and remained low throughout luteinization.⁹⁻¹¹ More recently, we showed that the cyclin

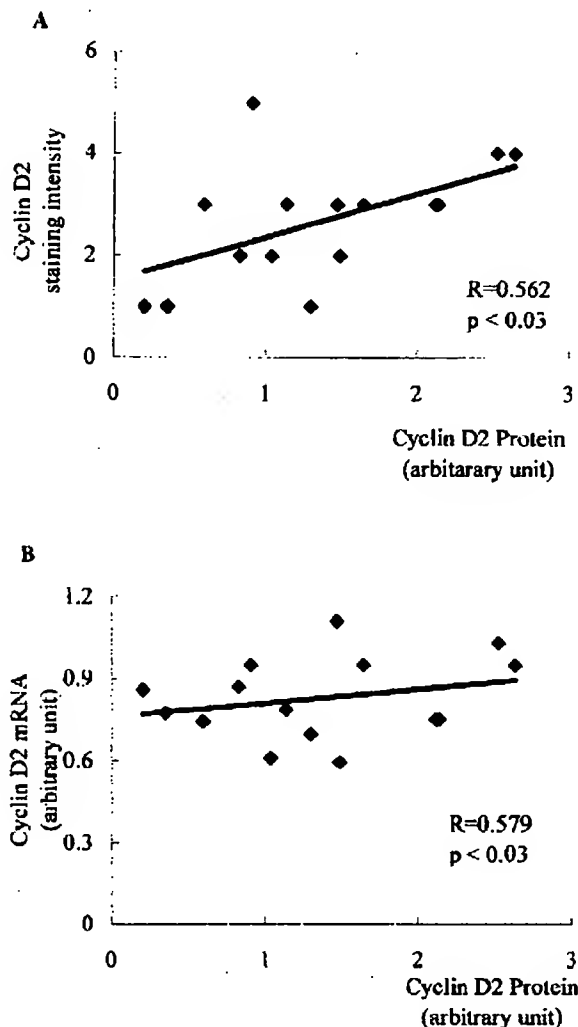


Figure 5. Correlation analysis. A) Cyclin D2 protein and staining intensity. B) Cyclin D2 mRNA and protein. R = Spearman correlation coefficient.

D2 mRNA expression pattern in human luteinized granulosa cells was positively correlated with serum estradiol levels.⁴ But in that study, unexpectedly, the greatest cyclin D2 activity was detected in the early proliferative phase as opposed to the mid to late proliferative phase, in which estrogen was dominant.

According to the nucleotide sequence of the upstream region of the human cyclin D2 gene, the promoter of the cyclin D2 gene lacks the estrogen response element (ERE) and other steroid hormone response elements, but it has an activator protein (AP)-1 transcription factor.¹² Therefore, there might be a modification of sex steroid hormone action through the AP-1 transcription factor according to tissue type. Although we could not completely explain this unexpected result because of small number of samples and possible individual variation, there might have been tissue-specific cyclin D2 regulation through AP-1 which might differ from that of the ERE.

In immunohistochemical staining, the cyclin D2 antibody used in this study (c-17) might cross react with cyclin D1.

Although, according to Shiozawa et al.¹³ only a few nuclei showed positive staining for cyclin D1 in the proliferative phase endometrium, the cross reactivity and high concentration of cyclin D2 antibody did not seem to affect the results of this study. Western blot analysis also supported the immunohistochemical results.

In summary, our preliminary data showed that cyclin D2 is expressed in human endometrium throughout the menstrual cycle. And cyclin D2 mRNA and protein are expressed in the human endometrium at high levels in proliferative phase and decreased significantly in secretory phase.

REFERENCES

1. Sherr CJ. G1 progression: Cycling on cue. *Cell* 1994;79:551-5.
2. Robker RL, Richards JS. Hormone-induced proliferation and differentiation of granulosa cells: A coordinated balance of the cell cyclin regulators cyclin D2 and p27^{Kip1}. *Mol Endocrinol* 1998;12:924-40.
3. Choi DS, Lee EY, Yoon SR, Hwang SS, Yoon BK, Lee JH. Clinical correlation of cyclin D2 mRNA expression in human luteinized granulosa cells. *J Assist Reprod Gener* 2000;17:574-9.
4. Noyes RW, Hertig AT, Rock J. Dating the endometrial biopsy. *Fertil Steril* 1950;1:3-25.
5. Grana X, Reddy EP. Cell cycle control in mammalian cells: Role of cyclins, cyclin-dependent kinases, growth suppressor genes and cyclin-dependent kinase inhibitors. *Oncogene* 1995;11:211-9.
6. Hunter T, Pines F. Cyclins and cancer II: Cyclin D and cdk inhibitors come of age. *Cell* 1994;79:573-82.
7. Baldin V, Lukas J, Marcote MJ, Pagano M, Draetta G. Cyclin D1 is a nuclear protein required for cell cycle progression in G1. *Genes Dev* 1993;7:812-21.
8. Quelle DE, Ashmun RA, Shurtleff SA, Kato JY, Bar-Sagi D, Roussel MF, Sherr CJ. Overexpression of mouse D-type cyclins accelerates G1 phase in rodent fibroblasts. *Genes Dev* 1993;7:1559-71.
9. Richards JS. Hormonal control of follicular growth and maturation in mammals. In: Jones RE, ed. *The vertebrate ovary: Comparative biology and evolution*. New York: Plenum Press, 1978: 331-60.
10. Richards JS. Maturation of ovarian follicles: Action and interactions of pituitary and ovarian hormones on follicular cell differentiation. *Physiol Rev* 1980;60:51-89.
11. Uilenbroek JT, Richards JS. Ovarian follicular development during the rat oestrous cycle: Gonadotropin receptors and follicular responsiveness. *Biol Reprod* 1979;20:1159-65.
12. Brooks AR, Shiffman D, Chan CS, Brooks EE, Milner PG. Functional analysis of the human cyclin D2 and cyclin D3 promoters. *J Biol Chem* 1996;271:9090-9.
13. Shiozawa T, Li SF, Nakayama K, Nikaido T, Fujii S. Relationship between the expression of cyclins/cyclin-dependent kinases and sex-steroid receptors/Ki67 in normal human endometrial glands and stroma during the menstrual cycle. *Mol Hum Reprod* 1996;2:745-52.

Virchows Arch (2004) 445:279–284
DOI 10.1007/s00428-004-1078-1

ORIGINAL ARTICLE

Anne Couvelard · François Paraf ·
Dominique Vidaud · Sylvie Dubois · Michel Vidaud ·
Jean-François Fléjou · Claude Degott

Human chorionic gonadotrophin beta expression in malignant Barrett's oesophagus

Received: 22 April 2004 / Accepted: 14 June 2004 / Published online: 10 August 2004
© Springer-Verlag 2004

Abstract Background: Human chorionic gonadotrophin beta (hCG β) is expressed in several non-trophoblastic tumours, and this is usually associated with aggressive behaviour. Little is known about hCG β expression in Barrett's adenocarcinoma. **Materials and methods:** We determined the hCG β profile in a large series of surgically resected Barrett's adenocarcinoma (a) at mRNA level using real-time quantitative reverse-transcription polymerase chain reaction analysis and (b) at protein level using immunohistochemistry with a polyclonal antibody and with a monoclonal antibody specific for free hCG β . We then sought links between the hCG β protein expression pattern and clinical and pathological parameters, including patient outcome as well as vascular endothelial growth factor (VEGF) expression. **Results:** hCG β protein expression was observed in 43 of 76 (57%) Barrett's adenocarcinomas. We showed a strong correlation between hCG β protein abundance and CG β mRNA level. We observed a statistical link between hCG β protein expression and infiltrative tumour type ($P=0.023$), perineural neoplastic invasion ($P=0.007$) and VEGF protein expression ($P=0.016$). hCG β

expression tended to be associated with a poor outcome (16% versus 36% survival 8 years after resection). **Conclusion:** Expression of hCG β correlates with specific infiltrative characteristics and is associated with higher VEGF expression. Both molecules may play a co-ordinated role in the development of Barrett's adenocarcinomas.

Keywords Barrett's adenocarcinoma · hCG β · Immunohistochemistry · Real-time quantitative RT-PCR · VEGF

Introduction

In the last decade, the incidence of oesophageal adenocarcinoma, developing almost exclusively in columnar-lined Barrett's oesophagus, has been steadily increasing [13]. These adenocarcinomas, most frequently diagnosed in elderly white men, have a poor prognosis, since metastases are often present at the time of diagnosis. Treatment is based on radical surgery, and tumour node metastasis (TNM) stage is the most important prognostic factor [8, 34]. However, the outcome is variable within a given stage, and response to therapy cannot be predicted on that base.

Human chorionic gonadotrophin β subunit (hCG β) is a significant indicator of malignant transformation [1, 2]. It is not only detected in trophoblastic neoplasms [3], but also in carcinomas of breast [7], bladder [24], gynaecological [17], prostatic [36] and gastrointestinal origin [11, 12, 25, 42]. Its expression has been demonstrated to correlate with a more aggressive behaviour and a higher rate of metastasis in such tumours [7, 18, 36]. Factors that regulate hCG β expression during malignancy are poorly known. However, it has been shown, mainly in the ovary, that vascular endothelial growth factor (VEGF) expression increases following gonadotrophin stimulation in vivo and in vitro [22, 31]. To date, no study concerning the expression of hCG β has been reported in Barrett's adenocarcinomas.

The aims of our study were to examine the expression of hCG β using immunohistochemistry and reverse-transcription

A. Couvelard (✉) · S. Dubois · C. Degott
Service d'Anatomie Pathologique,
Hôpital Beaujon,
92118 Clichy cedex, France
e-mail: anne.couvelard@bjn.ap-hop-paris.fr
Tel.: +33-1-40875462
Fax: +33-1-40870077

F. Paraf
Service d'Anatomie Pathologique,
Centre Hospitalier Universitaire Dupuytren,
Limoges, France

D. Vidaud · M. Vidaud
Laboratoire de Génétique Moléculaire—UPRES EA 3618,
Faculté des Sciences Pharmaceutiques et Biologiques,
Université Paris V,
Paris, France

J.-F. Fléjou
Service d'Anatomie Pathologique,
Hôpital Saint-Antoine,
Paris, France

scription polymerase chain reaction (RT-PCR) analysis in a large surgical series of Barrett's adenocarcinoma, to compare hCGB and VEGF expression and to correlate these results with clinico-pathological data and prognosis.

Materials and methods

Patients

A total of 76 patients with Barrett's adenocarcinoma underwent potentially curative surgical resection at Beaujon Hospital between 1976 and 1997. The patients were 73 men and 3 women, with a mean age of 62.2 ± 12.9 years (range 19–84 years). None of the patients had neoadjuvant chemotherapy or radiation therapy before surgery. The medical history of each patient was collected.

Tumour samples

Surgical specimens were received fresh, fixed in 10% neutral formalin and embedded in paraffin wax. Samples for real-time RT-PCR analysis were, immediately after surgery, snap-frozen in liquid nitrogen and stored at -70°C until RNA extraction.

In all patients, the tumour was classified as an adenocarcinoma developed in Barrett's oesophagus by preoperative endoscopy and macroscopic examination of the surgical specimen: the tumour was regarded as having developed in Barrett's oesophagus when specialised metaplastic mucosa was observed between the tumour and the squamous oesophageal mucosa or the gastric mucosa. Samples of adenocarcinoma (76 cases) and Barrett's mucosa around the tumour (negative for dysplasia in 15 cases or with high-grade dysplasia in 15 cases) were selected for immunohistochemistry. For each tumour, the following features were recorded: tumour differentiation, depth of infiltration, perineural neoplastic invasion, vascular invasion, regional lymph-node metastasis, distant metastasis, pTNM (pathological TNM) stage according to the Union Internationale de Lutte Contre le Cancer, stage according to the Rosenberg's classification and tumour type in Lauren's and Ming's classifications of gastric adenocarcinoma [23, 29, 35, 40].

Immunohistochemistry

Immunohistochemistry was performed on formalin-fixed, paraffin-wax-embedded sections using a three-step indirect method for the monoclonal antibody free hCGB (clone FBT11, kind gift from J-M Bidart, Institut Gustave Roussy, Villejuif, France) and a peroxidase anti-peroxidase method for polyclonal antibody [27] (hCGB, polyclonal, Dako, Glostrup, Denmark). The VEGF staining had been previously reported in this series [14]. Sections 3 μm thick were cut from paraffin-embedded tissue, dried at 37°C , deparaffinised, heated in a microwave oven (3 \times 5 min) in buffered citrate (citric acid and sodium citrate, pH 6.2) and treated with 0.1% hydrogen peroxide in methanol for 30 min. After staining with the three-step indirect or peroxidase anti-peroxidase method, the colour reaction was developed by adding 3',3'-diaminobenzidine (Sigma, Saint Quentin Fallavier, France) in Tris-buffered saline (TBS) containing 0.05% hydrogen peroxide for 10 min. Sections were then counterstained with haematoxylin, dehydrated and mounted with permount. Negative control slides were obtained by omitting the primary antibody, replaced by TBS. Normal placental tissue was used as an external positive control for hCGB.

hCGB staining was scored semi-quantitatively for monoclonal and polyclonal antibodies. It was reported from 0 to 4 as follows: 0 negative (no cell positivity), 1 occasional (some isolated positive cells are identified), 2 focal (rare clusters of positive cells are detected), 3 moderate (some clusters of positive cells are detected) and 4 diffuse (isolated and clusters of positive cells found in most areas of the tumour).

hCGB mRNA expression by real-time RT-PCR

Frozen tissue samples of 15 of the 76 Barrett's adenocarcinomas tested using immunohistochemistry were used for real-time RT-PCR analysis. Real-time quantitative RT-PCR using the ABI Prism 7700 Sequence Detection System (Perkin-Elmer Applied Biosystems) was performed according to a previously described method [7]. Briefly, total RNA extracted from frozen Barrett's adenocarcinoma tissues was reverse-transcribed before real-time PCR amplification. Quantitative values were obtained from the threshold cycle (Ct) number at which the increase in the signal associated with exponential growth of PCR products begins to be detected using PE Biosystems analysis software, according to the manufacturer's manuals. The precise amount of total RNA added to each reaction mix (based on optical density) and its quality (i.e. lack of extensive degradation) are both difficult to assess. We therefore also quantified transcripts of the *TBP* gene coding for the TATA box-binding protein (a component of the DNA-binding protein complex TFIID) as the endogenous RNA control, and each sample was normalised on the basis of its TBP content.

Results, expressed as N-fold differences in *CGB* gene expression relative to the *TBP* gene, termed "N_{CGB}", were determined by the formula: $N_{CGB} = 2^{\Delta C_{\text{sample}}}$, where ΔC_{t} value of the sample was determined by subtracting the average Ct value of the *CGB* gene from the average Ct value of the *TBP* gene.

The N_{CGB} values of the samples were subsequently normalised such that the N_{CGB} value to the tumour sample among our tested series that contained the smallest amount of *CGB* mRNA would equal a value of 1.

The nucleotide sequences of the primers used for PCR amplification were the following: CGB-U (5'-GCTACTGCCCCAC-CATGACC-3'), CGB-L (5'-ATGGACTCGAAGCGCACATC-3') and TaqMan fluorogenic probe CGB-P (5'-CCTGCCTCAGGT-GGTGTGCAACTACC-3'), with a CGB-specific product size of 94 bp, and TBP-U (5'-CACGAACCCACGGCACTGATT-3'), TBP-L (5'-TTTCTTGCTGCCAGTCTGGAC-3') and TaqMan fluorogenic probe TBP-P (5'-TGTGCACAGGAGCCAAGAAGTGAAGA-3'), with a TBP-specific product size of 89 bp.

PCR was performed using the TaqMan PCR Core Reagents kit (Perkin-Elmer Applied Biosystems). The thermal cycling conditions comprised an initial denaturation step at 95°C for 10 min and 50 cycles at 95°C for 15 s and 65°C for 1 min. Experiments were performed with duplicates for each data point.

Statistical analysis

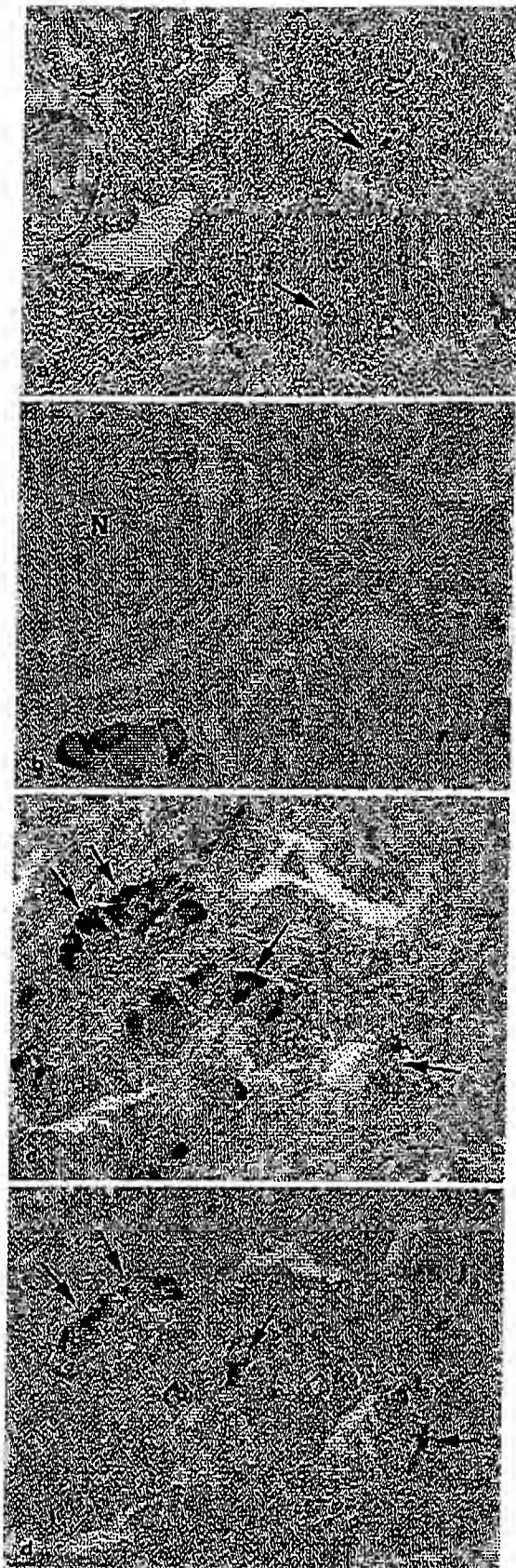
Qualitative data were compared using the chi square test with Yates correction when appropriate. Quantitative data were expressed as mean \pm SEM and compared by the non-parametric Mann-Whitney or Kruskal-Wallis tests. Survival rates were calculated by the Kaplan Meier method using the date of surgery as the starting point and compared by the log-rank test [20, 33]. All deaths were considered, including the postoperative deaths. The follow-up period ranged from 0.9 months to 189 months, with a mean of 36.7 months. At the time of analysis, 17 patients (22%) were alive, with a mean follow up of 93.5 months (range 41.1 months to 189.4 months). A two-tailed *P* value < 0.05 was considered to indicate statistical significance.

Results

Immunohistochemistry

hCGB expression

Staining pattern. hCGB expression was detected in 57% (43/76) of the tumour samples and ranged from score 0 to score 4. No positivity was demonstrated in the normal or



metaplastic mucosa. All positive cases showed the same cytoplasmic staining pattern. The pattern of expression of the monoclonal antibody recognising the free beta subunit of hCG was similar to that observed with the polyclonal antibody. The two antibodies detected the same group of cells in the same areas of tumours; however, the monoclonal antibody stained less cells than the polyclonal one. hCG β -positive cells were, for both antibodies, predominantly observed in deep infiltrative areas and in perineural neoplastic invasion (Fig. 1a, b). Often, hCG β expression was detected in the same cells that showed immunoreactivity for VEGF, as shown in serial sections (Fig. 1c, d).

Correlation with pathological findings. The 76 patients were dichotomised into two subgroups: 43 patients with hCG β expression (score >0) and 33 patients without hCG β expression (score 0). A statistically significant relationship was observed between hCG β expression and perineural neoplastic invasion ($P=0.007$) and infiltrative carcinomas according to Ming's classification ($P=0.023$). There was also a tendency between hCG β immunoreactivity and tumour extension, with a higher rate of pT4 tumours ($P=0.062$), and pTNM stage-III and -IV cancers ($P=0.086$). There was no significant difference between the hCG β -positive and -negative tumours regarding the other pathological features: tumour differentiation, vascular invasion, Lauren's classification, lymph-node status, distant metastasis, TNM and Rosenberg classifications (Table 1). Univariate analysis did not show a significant relationship between hCG β expression and survival, although patients with hCG β -positive tumours tended to have a worse prognosis, with 5-year and 8-year survival rates of 20% and 16% versus 39% and 36% (Fig. 2).

Relationship between hCG β expression status and VEGF expression status

The 76 tumours studied for hCG β expression had previously been tested for VEGF expression. The VEGF staining had been scored semi-quantitatively, and scores ranged from 1 to 11 [14]. The 76 patients were dichotomised into two groups: 64 patients with high VEGF expression (score greater than 3) and 12 patients with low VEGF expression (score 1-3). We found a significant

Fig. 1 Expression of vascular endothelial growth factor (VEGF) and human chorionic gonadotrophin beta (hCG β) using immunohistochemistry. **a** hCG β is strongly detected in invasive tumoral cells situated in the most infiltrating and deeper areas (arrows). Immunoperoxidase with nuclear counterstain using Mayer's haematoxylin. **b** hCG β expression in a Barrett's adenocarcinoma with neoplastic perineural invasion showing a strong cytoplasmic staining pattern. *N* nerve section. Immunoperoxidase with nuclear counterstain using Mayer's haematoxylin. **c** and **d** VEGF (**a**) and hCG β (**b**) expression in serial sections demonstrating a strong cytoplasmic staining in the same glandular territories (arrows) of this well-differentiated Barrett's adenocarcinoma. Immunoperoxidase with nuclear counterstain by Mayer's haematoxylin

282

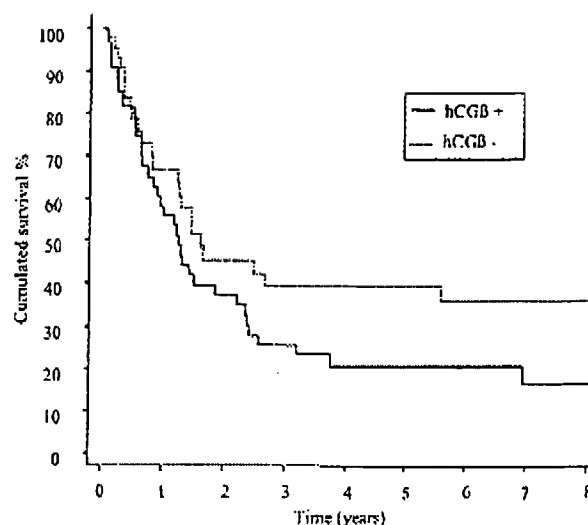
Table 1 Relationship between human chorionic gonadotrophin beta (hCG β) expression and clinico-pathological data. All results are expressed as percentages except for age (years)

	hCG β positive (n=43)	hCG β negative (n=33)	P value
Age (years)	61.5 \pm 14.6	65.4 \pm 9.9	0.191
Tumour differentiation			0.225
Well and moderate	79	67	
Poor	21	33	
Vascular invasion	84	73	0.246
Perineural invasion	67	36	0.007
Ming classification			0.023
Expanding	47	75	
Infiltrative	53	25	
Lauren classification			0.374
Intestinal	79	83	
Diffuse	21	27	
Tumour infiltration			0.062
pT1, pT2, pT3	56	76	
pT4	44	24	
Regional lymph node invasion (N1)	65	55	0.350
Distant metastasis (M1)	12	12	0.947
TNM stage			0.086
Stage I-IIA-III	35	55	
Stage III-IV	65	45	
Rosenberg classification			0.311
Stage I-II	26	36	
Stage III-IV	74	64	
VEGF expression	95	75	0.016
Survival			0.252
2 years	37.2 \pm 7.4	45.5 \pm 8.7	
5 years	20.3 \pm 6.3	39.4 \pm 8.5	
8 years	16.3 \pm 6.2	36.1 \pm 8.4	

positive relationship between hCG β and VEGF expression ($P=0.016$; Table 1).

RT-PCR analysis

CGB mRNA levels were analysed in 15 cases of the 78 Barrett's adenocarcinomas. Large differences in the amount of CGB mRNA were observed (NCGB from 1 to 118) in the 15 Barrett's adenocarcinomas. To better study the link between CGB mRNA level and hCG β immunohistochemistry status, the 15 tumours were subdivided into three groups (6, 6 and 3 tumours, respectively), with tumours with negative (score 0), occasional or focal (score 1 to 3) and diffuse (scored 4) hCG β immunoreactivity status. We observed a significant link between CGB mRNA level and hCG β immunohistochemistry status (Table 2; Kruskal-Wallis test, $P=0.023$). Surprisingly, one tumour (T6) with high CGB mRNA level was hCG β immunoreactive negative. However, tumour sampling was different in frozen and formalin-fixed tissue. This could be explained by the heterogeneous hCG β immunostaining in most tumours.

**Fig. 2** Kaplan Meier survival curves according to human chorionic gonadotrophin beta expression for positive cases ($n=43$) and negative cases ($n=33$)**Table 2** Correlation between human chorionic gonadotrophin beta (hCG β) subunit protein and CGB mRNA levels in Barrett's adenocarcinomas

Samples	Immunohistochemistry* (staining score)	RT-PCR (NCGB value)
Negative hCG β immunoreactivity (score=0)		
T1	0	1
T2	0	1.2
T3	0	1.3
T4	0	2.2
T5	0	4.3
T6	0	9.2
Median		1.7
Occasional or focal hCG β immunoreactivity (score=1 or 2)		
T7	1	2.1
T8	1	4.0
T9	2	4.0
T10	1	5.1
T11	1	6.6
T12	2	14.9
Median		4.5
Diffuse hCG β immunoreactivity (score=4)		
T13	4	10.1
T14	4	11.4
T15	4	118.0
Median		11.4

* The staining score values (determined as described in Materials and methods) indicated in this column were obtained with the polyclonal antibody; identical staining scores were obtained by using the monoclonal antibody (FBT11)

Discussion

We demonstrated, in this series of Barrett's adenocarcinomas, that hCG β expression was related to infiltrative tumours, high VEGF expression and tended to be associated with a poor outcome. hCG β is a significant indicator of malignant transformation. It is not only detected in trophoblastic neoplasms for which it represents a

valuable tumour marker [3], but also in non-trophoblastic tumours, including carcinomas of breast, urinary bladder, gynaecological, prostatic and colonic origin [5, 7, 11, 12, 17, 24, 36, 42]. The role of hCG β in the development of oesophageal adenocarcinoma has never been studied. In this work, we first evaluated the expression of hCG β in Barrett's-related adenocarcinomas using immunohistochemistry with a polyclonal antibody that recognised antigenic regions of the hCG β protein normally present in trophoblastic cells, as previously used in several studies [5, 26, 42]. However, this polyclonal antibody is not specific and cross-reacts with the beta subunit of human luteinizing hormone (LH). In addition, we therefore comparatively studied the expression of the monoclonal antibody specific for the free beta subunit of hCG specifically expressed by tumour tissues [6]. The immunostaining obtained by both antibodies showed similar cellular distribution in all 76 Barrett's adenocarcinomas tested. The two antibodies recognised the same group of cells in the same areas of tumours. We detected with the two antibodies the presence of hCG β in 57% of Barrett's adenocarcinomas. The incidence of expression of hCG β is similar to that reported in other immunohistochemical studies, in colonic and prostatic adenocarcinomas [11, 12, 36, 42]. Moreover, we showed that hCG β expression was associated with an infiltrative tumour pattern ($P=0.023$) and with perineural neoplastic invasion ($P=0.007$). Our results also showed a tendency for a poor outcome associated with hCG β expression in Barrett's adenocarcinoma, although it was not significant. Despite the absence of a significant association with standard prognostic parameters (such as tumour size, pTNM stage or presence of metastasis), expression of hCG β probably reflects aggressive behaviour of Barrett's adenocarcinomas. These results are in accordance with previous studies in some other malignancies showing that hCG β production, evaluated both at the RNA [7] and at the protein levels [15, 36, 42], is correlated with an unfavourable prognosis. Some recent studies also pointed out the interest of the hCG β serum level as an independent prognostic variable in renal carcinoma [18] and gastrointestinal malignancies [25]. We interestingly found that hCG β immunoreactivity was preferentially localised into the deeper invasive areas and around infiltrated nerves. This supports some previous studies suggesting that hCG β may act as a growth factor with characteristics similar to nerve, platelet-derived and β -transforming growth factors [28].

We demonstrated a significant positive correlation between hCG β and VEGF expression. Tumour cells that expressed hCG β often showed immunoreactivity for VEGF, and the two markers were often co-localised in the same tumours. Our results show a positive link between hCG β and VEGF expression in Barrett's adenocarcinoma, in agreement with previous studies in other cancers. VEGF is one of the most potent known tumour angiogenic factors [9, 10, 19, 21, 30, 32, 37, 38].

In vitro and in vivo experiments have shown that in the ovary, VEGF is chorionic gonadotrophin dependent [22, 31, 41]. hCG β may play a significant role in tumour

progression through upregulation of VEGF. Another possible pathway could involve the regulation of VEGF and hCG β by the same factors. It is noteworthy that hypoxia influences the secretion of both of these molecules in trophoblastic-derived cell lines [39]. The above correlates well with the fact that placental cells have angiogenic and invasive properties, which are also characteristic features of malignant cells.

The significance of hCG β production by non-trophoblastic tumours is still under investigation. Whereas the α subunit of hCG is encoded by a single gene (CGA) present on chromosome 6, the β subunit is potentially encoded by at least four genes (CGB 7, 3, 5 and 8), located in a cluster on chromosome 19q13.3 and physically linked to the LHB gene. Bellet et al. have shown that malignant transformation of non-trophoblastic cells was associated with the emergence of the three hCG β genes normally transcribed at a high level in the placenta ("trophoblastic" CGB 3, 5 and 8) [4]. In breast cancer, the detection of these "trophoblastic" CGB genes is of prognostic significance [7]. Moreover, the emergence of these "trophoblastic" CGB genes in breast cancer is accompanied by an increase of the total CGB steady-state mRNA level [16]. In the present study, we report a strong correlation between CGB mRNA copy numbers and hCG β protein abundance, suggesting that this gene is mainly dysregulated at the transcriptional level and points out a role of hCG β in Barrett's adenocarcinoma tumorigenesis.

In conclusion, hCG β and VEGF play a co-ordinated role in the tumorigenesis of Barrett's adenocarcinomas through their angiogenic and invasive properties. Our results may give new insights into the mechanisms of hCG β regulation.

Acknowledgements We thank Jean-Michel Bidart (Institut Gustave Roussy, Villejuif) for generously providing the monoclonal antibody directed against free hCG β , clone FTB11. This work was supported by a Grant for Clinical Research (Association pour la Recherche contre le Cancer).

References

1. Acevedo HF, Krichevsky A, Campbell-Acevedo EA, Galyon JC, Buffo MJ, Hartsock RJ (1992) Expression of membrane associated human chorionic gonadotropin, its subunits, and fragments by cultured human cancer cells. *Cancer* 69:1829-1842
2. Acevedo HF, Tong JY, Hartsock RJ (1995) Human chorionic gonadotropin β subunit gene expression in cultured human fetal and cancer cells of different types and origins. *Cancer* 76:1306-1311
3. Bagshawe KD (1992) Choriocarcinoma: a model for tumor markers. *Acta Oncol* 31:99-106
4. Bellet D, Lazar V, Bieche I, Paradis V, Giovannardi Y, Paterlini P, Lidereau R, Bedossa P, Bidart JM, Vidaud M (1997) Malignant transformation of nontrophoblastic cells is associated with the expression of chorionic gonadotropin beta genes normally transcribed in trophoblastic cells. *Cancer Res* 57:516-523
5. Bhalang K, Kafrawy AH, Miles DA (1999) Immunohistochemical study of the expression of human chorionic gonado-

- tripin-beta in oral squamous cell carcinoma. *Cancer* 85:757-762
6. Bidart JM, Troalen F, Lazar V, Berger P, Marcillac I, Lhomme C, Droz JP, Bellet D (1992) Monoclonal antibodies to the free beta-subunit of human chorionic gonadotropin define three distinct antigenic domains and distinguish between intact and nicked molecules. *Endocrinology* 131:1832-1840
 7. Biccicci I, Lazar V, Nogues C, Poynard T, Giovannardi Y, Bellet D, Lidereau R, Vidaud M (1998) Prognostic value of chorionic gonadotropin beta gene transcripts in human breast carcinoma. *Clin Cancer Res* 4:671-676
 8. Bonavina L, Via A, Incarbone R, Saino G, Peracchia A (2003) Results of surgical therapy in patients with Barrett's adenocarcinoma. *World J Surgery* 27:1062-1066
 9. Brown LF, Berse B, Jackman RW, Tognazzi K, Mancuso EJ, Senger DR, Dvorak HF (1993) Expression of vascular permeability factor (vascular endothelial growth factor) and its receptors in adenocarcinomas of the gastrointestinal tract. *Cancer Res* 53:4727-4735
 10. Brown LF, Berse B, Jackman RW, Tognazzi K, Guidi AJ, Dvorak HF, Senger DR, Connolly JL, Schnitt SJ (1995) Expression of vascular permeability factor (vascular endothelial growth factor) and its receptors in breast cancer. *Hum Pathol* 26:86-91
 11. Buckley CH, Fox H (1979) An immunohistochemical study of the significance of HCG secretion by large bowel adenocarcinoma. *J Clin Pathol* 32:368-372
 12. Campo E, Palacin A, Benasco C, Quesada E, Cardesa A (1987) A human chorionic gonadotropin in colorectal carcinoma. An immunohistochemical study. *Cancer* 59:1611-1616
 13. Cossentino MJ, Wong RK (2003) Barrett's esophagus and risk of esophageal adenocarcinoma. *Semin Gastrointest Dis* 14:128-135
 14. Couvelard A, Paraf F, Gratio V, Scoazec J-Y, Henin D, Degott C, Flejou J-F (2000) Angiogenesis in the neoplastic sequence of Barrett's esophagus. Correlation with VEGF expression. *J Pathol* 192:14-18
 15. Dirnhöfer S, Koessler P, Ensinger C, Feichtinger H, Madersbacher S, Berger P (1998) Production of trophoblastic hormones by transitional cell carcinoma of the bladder: association to tumor stage and grade. *Hum Pathol* 29:377-382
 16. Giovannardi Y, Parfait B, Askeur M, Olivi M, Lidereau R, Vidaud M, Bieche I (2001) Analysis of the human CGB/LHB gene cluster in breast tumors by real-time quantitative RT-PCR assays. *Cancer Lett* 168:93-100
 17. Higashida T, Koizumi T, Yamaguchi S, Ichimura T, Hasegawa K, Nishimura R (2001) Ovarian malignant mixed mesodermal tumor producing the free form of the beta-subunit of human chorionic gonadotropin. *Int J Clin Oncol* 6:97-100
 18. Hatakainen K, Ljungberg B, Paju A, Rasmussen T, Alfthan H, Stenman UH (2002) The free beta-subunit of human chorionic gonadotropin as a prognostic factor in renal cell carcinoma. *Br J Cancer* 86:185-189
 19. Inoue K, Ozeki Y, Suganuma T, Sugiyama Y, Tanaka S (1997) Vascular endothelial growth factor expression in primary esophageal squamous cell carcinoma. Association with angiogenesis and tumor progression. *Cancer* 79:206-213
 20. Kaplan EL, Meier P (1958) Nonparametric estimation from incomplete observations. *J Am Stat Assoc* 53:457-481
 21. Kitadai Y, Haruma K, Tokutomi T, Tanaka S, Sumii K, Carvalho M, Kuwabara M, Yoshida K, Hirai T, Kajiyama G, Tahara E (1998) Significance of vessel count and vascular endothelial growth factor in human esophageal carcinomas. *Clin Cancer Res* 4:2195-2200
 22. Koos RD (1995) Increased expression of vascular endothelial growth/permeability factor in the rat ovary following an ovulatory gonadotropin stimulus: potential roles in follicle rupture. *Biol Reprod* 52:1426-1435
 23. Lauren P (1965) The two histological main types of gastric carcinoma diffuse and so-called intestinal type carcinoma. An attempt at a histo-clinical classification. *Acta Pathol Microbiol Scand* 64:31-49
 24. Lazar V, Diez SG, Laurent A, Giovannardi Y, Radvanyi F, Chopin D, Bidart JM, Bellet D, Vidaud M (1995) Expression of human chorionic gonadotropin beta subunit genes in superficial and invasive bladder carcinomas. *Cancer Res* 55:3735-3738
 25. Luohima J, Finne P, Alfthan H, Stenman UH, Haglund C (2002) Combination of HCGbeta, CA 1-9 and CEA with logistic regression improves accuracy in gastrointestinal malignancies. *Anticancer Res* 22:1759-1764
 26. Marcillac I, Troalen F, Bidart JM, Ghillani P, Ribrag V, Escudier B, Malassagne B, Droz JP, Lhomme C, Rougier P (1992) Free human chorionic gonadotropin beta subunit in gonadal and nongonadal neoplasms. *Cancer Res* 52:3901-3907
 27. Mason DY, Summons RE (1979) The labeled antigen method of immunoperoxidase staining. *J Histochem Cytochem* 27:832-840
 28. Melnied S, Braunstein GD (1983) Human chorionic gonadotropin stimulates proliferation of Nb 2 rat lymphoma cells. *J Clin Endocrinol Metab* 56:1068-1070
 29. Ming S-C (1977) Gastric carcinoma: a pathobiological classification. *Cancer* 39:2475-2485
 30. Misc M, Arii S, Higashitani H, Furutani M, Niwano M, Harada T, Ishigami S, Toda Y, Nakayama H, Fukumoto M, Fujita J, Imamura M (1996) Clinical significance of vascular endothelial growth factor and basic fibroblast growth factor gene expression in liver tumor. *Hepatology* 23:455-464
 31. Neulen J, Raczek S, Pogorzelski M, Grunwald K, Yeo TK, Dvorak HF, Weich HA, Breckwoldt M (1998) Secretion of vascular endothelial growth factor/vascular permeability factor from human luteinized granulosa cells is human chorionic gonadotropin dependent. *Mol Hum Reprod* 4:203-206
 32. Niedergethmann M, Hildenbrand R, Wusthrock B, Hartel M, Sturm JW, Richter A, Post S (2002) High expression of vascular endothelial growth factor predicts early recurrence and poor prognosis after curative resection for ductal adenocarcinoma of the pancreas. *Pancreas* 25:122-129
 33. Peto R, Pike MC, Armitage P (1977) Design and analysis of randomized clinical trials requiring prolonged observation of each patient. II. Analysis and examples. *Br J Cancer* 35:1-39
 34. Reynolds JC, Rahimi P, Hirsch D (2002) Barrett's esophagus: clinical characteristics. *Gastroenterol Clin North Am* 31:441-60
 35. Rosenberg JC, Budev H, Edwards RC, Singal S, Steiger Z, Sundareson AS (1985) Analysis of adenocarcinoma in Barrett's esophagus utilizing a staging system. *Cancer* 55:1353-1360
 36. Sheaff MT, Martin JE, Badenoch DF, Baithun SI (1996) beta hCG as a prognostic marker in adenocarcinoma of the prostate. *J Clin Pathol* 49:329-332
 37. Takahashi Y, Kitadai Y, Bucana CD, Cleary KR, Ellis LM (1995) Expression of vascular endothelial growth factor and its receptor, KDR, correlates with vascularity, metastasis, and proliferation of human colon cancer. *Cancer Res* 55:3964-3968
 38. Takahashi Y, Cleary KR, Mai M, Kitadai Y, Bucana CD, Ellis LM (1996) Significance of vessel count and vascular endothelial growth factor and its receptor (KDR) in intestinal-type gastric cancer. *Clin Cancer Res* 2:1679-1684
 39. Taylor CM, Stevens H, Anthony FW, Wheeler T (1997) Influence of hypoxia on vascular endothelial growth factor and chorionic gonadotropin production in the trophoblast-derived cell lines: JEG, JAR and BeWo. *Placenta* 18:451-458
 40. UICC (1987) TNM Classification of malignant tumors, 4th edition. Hermanek P, Sobin LH (eds) Springer, Berlin Heidelberg New York, pp 40-42
 41. Wang TH, Horng SG, Chang CL, Wu HM, Tsai YJ, Wang HS, Soong YK (2002) Human chorionic gonadotropin-induced ovarian hyperstimulation syndrome is associated with up-regulation of vascular endothelial growth factor. *J Clin Endocrinol Metab* 87:3300-3308
 42. Webb A, Scott-Mackie P, Cunningham D, Norman A, Andreyev J, O'Brien M, Bensted J (1995) The prognostic value of CEA, beta HCG, AFP, CA125, CA19-9 and C-erbB-2, beta HCG immunohistochemistry in advanced colorectal cancer. *Ann Oncol* 6:581-587

Downregulation of ENaC activity and expression by TNF- α in alveolar epithelial cells

André Dagenais, Rosalie Fréchette, Yuko Yamagata, Toshiyuki Yamagata, Jean-François Carmel, Marie-Eve Clermont, Emmanuelle Brochiero, Chantal Massé, and Yves Berthiaume

Centre de recherche, Centre hospitalier de l'Université de Montréal-Hôtel-Dieu, and
Département de médecine, Université de Montréal, Montreal, Quebec, Canada H2W 1T7

Submitted 25 September 2002; accepted in final form 20 September 2003

Dagenais, André, Rosalie Fréchette, Yuko Yamagata, Toshiyuki Yamagata, Jean-François Carmel, Marie-Eve Clermont, Emmanuelle Brochiero, Chantal Massé, and Yves Berthiaume. Downregulation of ENaC activity and expression by TNF- α in alveolar epithelial cells. *Am J Physiol Lung Cell Mol Physiol* 286: L301-L311, 2004. First published September 26, 2003; 10.1152/ajplung.00326.2002.—Sodium absorption by an amiloride-sensitive channel is the main driving force of lung liquid clearance at birth and lung edema clearance in adulthood. In this study, we tested whether tumor necrosis factor- α (TNF- α), a proinflammatory cytokine involved in several lung pathologies, could modulate sodium absorption in cultured alveolar epithelial cells. We found that TNF- α decreased the expression of the α -, β -, and γ -subunits of epithelial sodium channel (ENaC) mRNA to 36, 43, and 16% of the controls after 24-h treatment and reduced to 50% the amount of α -ENaC protein in these cells. There was no impact, however, on α_1 and β_1 Na⁺-K⁺-ATPase mRNA expression. Amiloride-sensitive current and ouabain-sensitive Rb⁺ uptake were reduced, respectively, to 28 and 39% of the controls. A strong correlation was found at different TNF- α concentrations between the decrease of amiloride-sensitive current and α -ENaC mRNA expression. All these data show that TNF- α , a proinflammatory cytokine present during lung infection, has a profound influence on the capacity of alveolar epithelial cells to transport sodium.

sodium ion channel; transepithelial current; cytokine; inflammation

SODIUM ABSORPTION by an amiloride-sensitive channel is the main driving force of lung liquid clearance at birth and lung edema clearance in adulthood. Vectorial diffusion of Na⁺ from the epithelial sodium channel (ENaC) at the apical surface of lung epithelial cells and its extrusion by Na⁺-K⁺-ATPase located at the basolateral side create osmotic pressure that drives water from the alveoli to the interstitium (48). Although several Na⁺ channels and Na⁺ cotransporters are expressed in alveolar epithelial cells (46), ENaC is probably the main channel involved in lung liquid clearance. It is a multimeric channel composed of three related subunits (α , β , and γ) (10, 11) that are expressed in the lung from alveoli to the nasal epithelium (9, 26, 47). The importance of ENaC in lung liquid clearance has been demonstrated in the mouse, where inactivation of the α -subunit by transgene targeting produces a lethal phenotype. These knockout mice die shortly after birth, unable to clear liquid from their lungs (35). In humans, dysregulation of ENaC activity has been associated with lung infection. This is the case in pseudohypoaldosteronism, a rare, recessive genetic disease caused by mutations that inactivate ENaC (13).

Although the disease rarely leads to lung edema (45), liquid volume is increased in the airways (38), and frequent lung infections in early childhood have been reported among these patients (1, 33, 38). In cystic fibrosis, the absence of ENaC downregulation by CFTR is believed to be involved in chronic lung infection with *Pseudomonas*, a hallmark of the disease (20). Several lines of evidence suggest that bacterial (25, 41) and viral infections (40) modulate the amiloride-sensitive Na⁺ transport in lung epithelial cells. In vitro, conditioned medium from LPS-activated macrophages leads to a decrease in amiloride-sensitive current in fetal distal lung epithelial cells (15, 22, 23) via a nitric oxide-dependent mechanism (15, 23).

Tumor necrosis factor- α (TNF- α) is a proinflammatory cytokine that plays an important role in the activation of host defense by promoting the production of a wide spectrum of cytokines (IL-1, IL-6, granulocyte-monocyte colony-stimulating factor, IL-8) in the inflammatory process (27, 63). Although the main sources of TNF- α in the lungs are the monocytes and macrophages, alveolar epithelial cells have been found recently to release TNF- α upon stimulation with LPS (50). TNF- α exerts a vital function in protecting the lung against *Pseudomonas* infection in the mouse (31). High or chronic TNF- α expression can be associated, however, with pulmonary dysfunction. An elevated TNF- α level has been detected in bronchoalveolar lavage (BAL) of patients with acute respiratory distress syndrome (ARDS) (62), and TNF- α injection can lead to septic shock symptoms with respiratory distress and lung edema (66).

By stimulating the ubiquitous receptors TNFR1 or TNFR2, TNF- α can elicit a wide spectrum of cellular responses, ranging from apoptosis to activation of gene expression by nuclear mobilization of transcription factors, such as NF- κ B or c-jun (42, 63). In the lung, TNFR1 mediates signaling between the alveolar space and the endothelium upon TNF- α infusion in alveoli (39). Several studies suggest that TNF- α modulates liquid transport in the alveolus. It has been found to alter alveolar liquid clearance in bacterial pneumonia (58) and in septic peritonitis (6). Direct instillation of TNF- α in the lung also affects lung liquid clearance (28). Although TNF- α has been shown to downregulate the steady-state mRNA level of some ionic channels such as the CFTR (52), nothing is known about its impact on sodium transport expression and activity in alveolar epithelial cells.

Because TNF- α is a major cytokine produced during lung infection, we tested the hypothesis that it could modulate Na⁺

Address for reprint requests and other correspondence: A. Dagenais, Centre de recherche, CHUM-Hôtel-Dieu, 3850 St-Urbain, Montreal, Quebec, Canada, H2W 1T7 (E-mail: andre.dagenais.chum@ssss.gouv.qc.ca).

http://www.ajplung.org

1040-0605/04 \$5.00 Copyright © 2004 the American Physiological Society

L301

transport in alveolar epithelial cells isolated from the rat lung. We found that TNF- α decreases amiloride-sensitive current as well as the steady-state mRNA and protein levels of ENaC in adult alveolar epithelial cells.

MATERIALS AND METHODS

Alveolar epithelial cell isolation and experimental conditions. Alveolar epithelial cells were isolated from male Sprague-Dawley rats as described previously and according to a procedure approved by the animal care and use committee of the institution (18). Perfused lungs were digested with elastase, and the cells purified by a differential adherence technique on bacteriologic plastic plates coated with rat IgG (18). The cells were maintained in minimum essential medium (Invitrogen, Burlington, Ontario, Canada) containing 10% fetal bovine serum (GIBCO, Invitrogen), 0.08 mg/l gentamicin, 0.2% NaHCO₃, 0.01 M HEPES, and 2 mM L-glutamine. For the first 3 days, the medium was also supplemented with 3 μ g/ml trimethoprim and 17 μ g/ml sulfamethoxazole. The cells were plated at 4×10^5 cells/cm² density in 25-cm² plastic flasks or at 1×10^6 cells/cm² on polycarbonate filters and cultured at 37°C with 5% CO₂ in a humidified incubator. The medium was replaced every 2–3 days.

Northern blotting. To study the influence of TNF- α on the steady-state mRNA level for ENaC and Na⁺-K⁺-ATPase subunits, we treated alveolar epithelial cells cultured for 3 days with 100 ng/ml of recombinant mouse TNF- α (Calbiochem, La Jolla, CA) for 4, 6, 8, or 24 h. Total RNA was isolated and quantified by Northern blotting. Total RNA from alveolar epithelial cells was extracted by a modification of the guanidinium-phenol technique (19). For Northern blotting, 10 μ g of total RNA were electrophoresed on 1% agarose-formaldehyde gel and transferred to GeneScreen nylon membranes (NEN, Boston, MA) after overnight blotting with 10 \times SSC. Hybridization was performed, as reported previously, in Church buffer [0.5 M sodium phosphate, pH 7.2, 7% SDS (wt/vol), 1 mM EDTA, pH 8] (19). The nylon membranes were hybridized successively with different cDNA probes (α -, β -, and γ -ENaC; α_1 and β_1 Na⁺-K⁺-ATPase; 18S rRNA). α -ENaC mRNA was detected with a 764-bp mouse α -ENaC cDNA probe (His445 to the stop codon), which has high homology with rat α -ENaC cDNA (19). β - and γ -ENaC mRNAs were detected with the complete cDNA clone, a gift from Dr. B. C. Rossier (Institut de pharmacologie et de toxicologie, Université de Lausanne, Switzerland). The α_1 and β_1 Na⁺-K⁺-ATPase probes were gifts from Dr. J. Orlowski (Physiology Department, McGill University, Montreal, Quebec, Canada). The α_1 Na⁺-K⁺-ATPase probe consisted of a *NarI*-*SnaI* 332-bp cDNA fragment coding from nt 89 to 421 (from the 5'-untranslated region to Arg61). The β_1 Na⁺-K⁺-ATPase probe consisted of a *NcoI*-*SspI* 750-bp cDNA fragment, which encompasses the entire coding region (70). The RNA loaded on each lane was normalized to 18S rRNA and detected by fluorescence scanning of the gels after staining with SYBR green II (Molecular Probes, Eugene, OR) and before blotting RNA on nylon membrane. The SYBR green-stained gels as well as the Northern blots were scanned and analyzed with a Typhoon PhosphorImager (Molecular Dynamics, Sunnyvale, CA). For the actinomycin D series, the blots were hybridized with an 18S rRNA probe as reported previously (18). mRNA expression was always compared with matched, untreated cells for each time period of the study. For reproducibility and statistical reasons, Northern blotting was repeated several times with RNA extracted from cells isolated from different rats. At least three animals ($n = 3$) were used for each time point.

Actinomycin D treatment and α -ENaC mRNA stability. To investigate the importance of transcription in the modulation of α -ENaC mRNA by TNF- α , we cultured alveolar epithelial cells for 3 days and treated them for 6 h with 5 μ g/ml actinomycin D, an inhibitor of transcription, in the presence or absence of 100 ng/ml TNF- α . α -ENaC mRNA expression was studied by Northern blotting as stated

above. The experiment was repeated three times with cells purified from different rats.

To assess α -ENaC mRNA stability after TNF- α treatments, alveolar epithelial cells cultured for 3 days were treated or not for 16 h with 100 ng/ml TNF- α and incubated thereafter with 5 μ g/ml actinomycin D for 0, 4, 6, 8, 10, or 12 h. Total RNA was extracted, and the amount of α -ENaC was quantified by Northern blotting as above.

Western blotting. Alveolar epithelial cells were cultured in 25-cm² flasks for 3 days and treated for 24 h with 100 ng/ml TNF- α . We harvested them by scraping the monolayer with a rubber policeman, followed by 15-min centrifugation at 2,800 g in PBS. The cell pellet was solubilized in 60 μ l of lysis solution (250 mM sucrose, 10 mM Tris-HCl, pH 7.4, 1 mM EGTA, 0.5% vol/vol Triton X-100, 1 mM PMSF, and 25 μ g/ml leupeptin) for 30 min on ice. Protein concentration was evaluated by the Bradford method (8) (Pierce, Rockford, IL). Total proteins (50 μ g) were subjected to SDS-polyacrylamide gel electrophoresis and transferred electrophoretically onto Bio-Rad polyvinylidene difluoride membranes (Hercules, CA). The membranes were blocked for 16 h at 4°C with 5% wt/vol skim milk in PBST buffer (137 mM NaCl, 2.7 mM KCl, 1.5 mM KH₂PO₄, 8.1 mM Na₂HPO₄, 0.05% vol/vol Tween 20, and 0.02% Thimerosal) before incubation in the same buffer for 16 h at 4°C with a 1:1,000 dilution of the PA1-920 antibody (Affinity Bioreagent, Golden, CO), an affinity-purified antibody directed against the L20-C42 NH₂-terminal portion of the rat α -ENaC subunit. After 2 h of incubation at room temperature with a 1:4,000 dilution of horseradish peroxidase-linked secondary antibody (Cell Signaling Technology, Beverly, MA) in 5% skim milk-PBST, the bands were detected by enhanced chemiluminescence (Amersham Biosciences, Piscataway, NJ) on Kodak X-KI films. For quantification, the X-ray films were scanned on a Hewlett-Packard ScanJet, and the bands were quantified by NIH ImageJ software. ENaC antibody specificity was tested on 10- μ g cell lysates of Madin-Darby canine kidney cells transfected with rat α -ENaC tagged with the influenza hemagglutinin (HA) epitope, a gift from Dr. D. Rotin (Sick Children's Hospital, Toronto, Ontario, Canada). For the detection of the HA-rat α -ENaC construct, the cell lysate was tested with an anti-HA mouse monoclonal antibody (clone HA-7) at a 1:10,000 dilution (Sigma, Oakville, Ontario, Canada) followed by an incubation with a 1:4,000 dilution of an anti-mouse IgG antibody (Santa Cruz Biotechnology, Santa Cruz, CA) linked to peroxidase. The HA and α -ENaC antibodies detected the same broad band of 82–96 kDa, the molecular mass expected for glycosylated ENaC (Fig. 4) (59). The α -ENaC antibody detected a band at the same molecular mass in alveolar epithelial cells. Western blots were repeated seven times ($n = 7$) with lysates extracted from cells purified from different rats.

Electrophysiology. The impact of TNF- α on the electrophysiology of alveolar epithelial cells was studied, as reported previously (18), by successively recording potential differences (Pd, mV) and transepithelial resistance (R_{te} , Ω -cm²) across the cell monolayers with an epithelial voltammeter (EVOM; World Precision Instruments, Sarasota, FL). Alveolar cells plated at 1×10^6 cells/cm² density on polycarbonate membranes (catalog no. 3401, 1.0 cm²; Costar Transwell, Toronto, Ontario, Canada) were cultured for 3 days until they formed a tight epithelium. The monolayers were then treated for 24 h at the apical and basolateral sides with 100 ng/ml TNF- α . Transepithelial current across the monolayers was calculated according to the following formula: $I_{te} = Pd/R_{te}$, where I_{te} is transepithelial current generated by the cell monolayer, and R_{te} is its transepithelial resistance. To quantify the amount of amiloride-sensitive current generated by alveolar cells treated for 24 h with TNF- α , I_{te} was measured successively before and after 5-min incubation with 1 μ M amiloride at 37°C. At this concentration, amiloride is a specific inhibitor of ENaC. At least 18 filters ($n = 18$), all coming from different rats, were used for these experiments.

Apical membrane permeabilization by amphotericin B. The apical surface of alveolar cells was permeabilized to determine if the de-

DOWNREGULATION OF ENaC BY TNF- α IN ALVEOLAR EPITHELIAL CELLS

L303

crease in I_{sc} evoked by TNF- α also involved a reduction in Na^+ - K^+ -ATPase activity at the basolateral surface. Cells grown on 24-mm Costar filters (catalog no. 3412, 4.5 cm²; Costar Transwell) were cultivated for 3 days and treated for 24 h with 100 ng/ml TNF as above. For short-circuit current (I_{sc}) measurements, filters were mounted in the Ussing chamber and bathed on the apical and basolateral sides with warm physiological buffer (140 mM NaCl, 5 mM KCl, 1 mM MgCl₂, 1 mM CaCl₂, 10 mM glucose, and 10 mM TES, pH 7.4). I_{sc} was determined with a VCC MC2 voltage clamp amplifier (Physiological Instruments, San Diego, CA) linked to a 4sp PowerLab data acquisition and analysis system (ADInstruments, Grand Junction, CO). When the I_{sc} was stabilized, the cell monolayers were treated with 10 μM amiloride on the apical side, to quantify the amiloride-sensitive current in control and TNF- α -treated cells. The cells were then treated with 10 μM amphotericin B added on the apical side of the monolayers. This treatment gradually raised the I_{sc} to reach a plateau after ~5 min. At that time, the basolateral membrane was bathed with 2 mM ouabain in warm physiological solution to inhibit Na^+ - K^+ -ATPase activity. Amphotericin B and ouabain solution were freshly prepared before the experiment. Amphotericin B was diluted as a concentrated 20 mM solution in DMSO, whereas ouabain was dissolved directly as a 2 mM solution in physiological solution. For each condition tested, five filters ($n = 5$) seeded with cells coming from different animals were analyzed in these experiments.

Dose-dependent modulation of amiloride-sensitive current and α -ENaC mRNA expression by TNF- α in cells cultured on filters. Amiloride-sensitive current and α -ENaC mRNA expression were measured in alveolar epithelial cells treated with different TNF- α concentrations. The cells were cultured on 4-cm² Transwell membranes for RNA extraction. After 3 days of culture, they were treated for 24 h with 0, 5, 10, 20, 50, or 100 ng/ml TNF- α added to the apical and basolateral medium bathing the cell monolayers. The transepithelial amiloride-sensitive current generated by the monolayers was assessed as described above with the EVOM. After these measurements, we isolated total RNA by directly lysing the cells on filters with Trizol reagent according to the manufacturer's protocol (Invitro-

gen). α -ENaC mRNA expression was examined by semiquantitative reverse transcription-polymerase chain reaction. Total RNA (5 μg) was reverse-transcribed with Moloney murine leukemia virus reverse transcriptase (Invitrogen) as reported previously (19). Of the cDNA reaction, 1.5 μl out of 20 μl was subjected to PCR amplification with Taq polymerase as described elsewhere (19). For α -ENaC amplification, 50 pmol (1 μM) of the sense primer 5'-GAG CCT GCC TTT ATG GAT GA-3' located in exon 5 and 50 pmol (1 μM) of the antisense primer 5'-gag ctt tgc aac tcc gtt tc-3' present in exon 11 were used for PCR. For β -actin cDNA amplification, 12.5 pmol (250 nM) of the sense primer 5'-CTA AGG CCA ACC GTG AAA AG located in exon 3 and 12.5 pmol (250 nM) of the antisense primer 5'-GCC ATC TCT TGC TCG AAG TC-3' present in exon 4 were used. The amplification conditions were: 1 min at 94°C for denaturation of DNA, 2 min at 58°C for annealing of the primers, and 2-min incubation at 72°C for elongation. PCR amplifications for α -ENaC and β -actin were done side by side. The reactions were stopped after 21 and 20 cycles, respectively, when amplification was still in the exponential phase. Fifteen microliters of the reactions were run on 1% agarose gel. After electrophoresis, the gels were stained by ethidium bromide, and the amplified products were quantified by scanning with a Typhoon fluorescence scanner (Molecular Dynamics). The results were reported as percentages of control expression after normalization with the β -actin signal. The experiments were repeated four times ($n = 4$) on alveolar epithelial cells purified from different rats.

Rubidium uptake assays. Alveolar epithelial cells were cultured for 3 days in 24-well plates seeded with 3×10^5 cells/cm². Rubidium (Rb^+) uptake was studied as shown previously with some modifications (60). Control cells or cells treated for 24 h with 100 ng/ml TNF- α were incubated for 30 min at 37°C in medium A (140 mM NaCl, 1 mM CaCl₂, 5 mM KCl, 1 mM MgCl₂, 5 mM glucose, 20 mM HEPES). The medium was replaced by medium A in the presence or absence of 2 mM ouabain, and the cells were incubated for 5 min at 37°C. An equivalent volume of medium A containing Rb^{86} at 0.5 $\mu\text{Ci}/\text{ml}$ final concentration was then added to the wells. After 15-min incubation at 37°C, the Rb^+ uptake was stopped by four volumes of

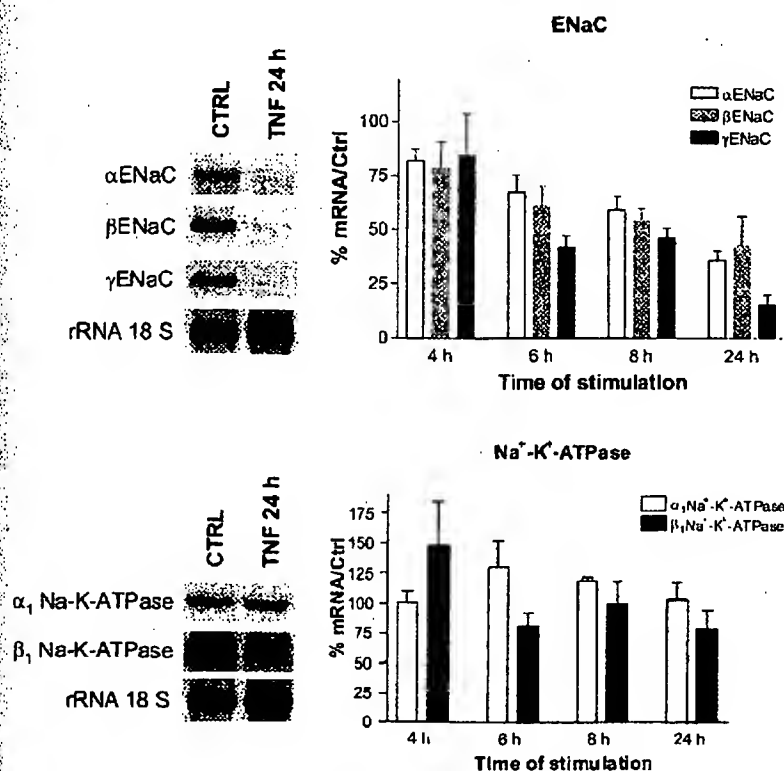


Fig. 1. Modulation of α -, β -, and γ -epithelial sodium channel (ENaC) subunits as well as α_1 and β_1 Na^+ - K^+ -ATPase mRNA expression by TNF- α in alveolar epithelial cells. Alveolar epithelial cells were cultured for 3 days and treated for 4, 6, 8, or 24 h with 100 ng/ml TNF- α . A representative Northern blot is shown for the 24-h time point at left, and densitometric analyses are presented on the right. There is a gradual downregulation of the 3 ENaC subunits compared with time-matched, untreated controls, but no significant modulation of α_1 and β_1 Na^+ - K^+ -ATPase mRNA. The data are presented as percentages of expression \pm SE relative to time-matched, untreated controls. mRNA expression was corrected to 18S rRNA detected by SYBR green fluorescence (see MATERIALS AND METHODS). There was a statistically significant decrease in the level of α -ENaC transcript in TNF-treated cells at all time points studied ($P < 0.05$). For β - and γ -ENaC transcripts, the decrease was significant at the 6-, 8-, and 24-h time points ($P < 0.05$). Cells from at least 3 different rats ($n = 3$) were used for each time point. CTRL/CTRL, control.

L304

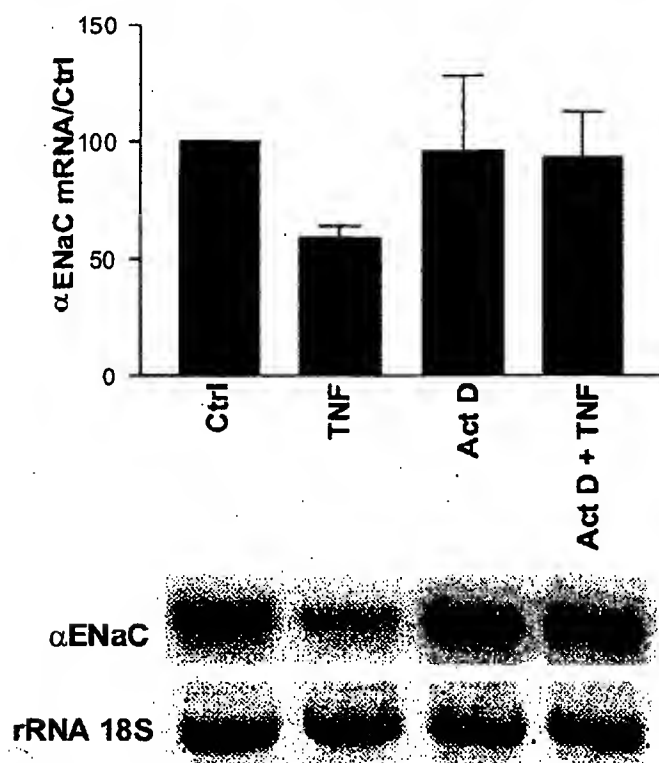
DOWNREGULATION OF ENaC BY TNF- α IN ALVEOLAR EPITHELIAL CELLS

Fig. 2. Northern blot and densitometric analysis of the effect of actinomycin D (Act D) on the downregulation of α -ENaC mRNA by TNF in alveolar epithelial cells. Act D abrogates the downregulation of α -ENaC mRNA by TNF- α . Alveolar epithelial cells were cultured for 3 days and treated for 6 h with 100 ng/ml TNF- α in the presence or absence of 5 μ g/ml Act D, an inhibitor of transcription. The amount of RNA on each lane was corrected for the level of 18S rRNA. Ctrl, $n = 13$; TNF, 100 ng/ml TNF- α 6 h, $n = 17$; Act D, 5 μ g/ml Act D, $n = 3$; Act D + TNF, 100 ng/ml TNF- α + 5 μ g/ml Act D 6 h, $n = 4$.

medium B (10 mM HEPES, pH 7.4, 100 mM MgCl₂) chilled at 0°C and three successive washings with the same medium. The cells were lysed in 1 ml of lysate solution [1% SDS (wt/vol), 4 mM EDTA], and radioactivity was measured with 3 ml of scintillation fluid in a β -counter (TriCarb 1600; Packard Instrument, Downers Grove, IL). Protein concentration was estimated by the Lowry method. Rb⁺ uptake was calculated by the following formula: $Rb \text{ uptake} = Ax/Alp$, where Ax is the cpm of the sample, a is the Rb cpm added (total), and p is the amount of protein (mg). The experiments were performed seven times ($n = 7$) on alveolar epithelial cells purified from different animals.

Statistics. The data are presented as means \pm SE. Comparisons between groups were made by the unpaired t -test, one group t -test, analysis of variance, and post hoc analysis (Fisher paired least significant difference) with Statsview software (SAS Institute, Cary, NC). A probability of $P < 0.05$ was considered to be significant. The α -ENaC mRNA decay curves, amiloride-sensitive current, and α -ENaC mRNA expression after TNF- α treatment were compared by multiple regression analysis.

RESULTS

Modulation of ENaC mRNA expression by TNF- α . The α -, β -, and γ -ENaC subunits of ENaC as well as the α_1 and β_1 subunits of Na⁺-K⁺-ATPase are highly expressed in alveolar epithelial cells cultured from the rat lung (18). After 3 days of culture, the cells reach confluence and are capable of vectorial

sodium transport, resulting in the formation of domes when cultured on plastic. To test the hypothesis that TNF- α could modulate ENaC mRNA expression in alveolar epithelial cells, we treated them for 4, 6, 8, or 24 h with 100 ng/ml TNF- α . Treatment progressively decreased the steady-state mRNA level of the α -, β -, and γ -ENaC subunits to 36, 43, and 16%, respectively, after 24 h, compared with time-matched controls ($P < 0.05$, Fig. 1). However, TNF- α had no effect on expression of the α_1 and β_1 Na⁺-K⁺-ATPase subunits (Fig. 1). Because mRNAs for the three ENaC subunits behave similarly, we decided to focus our investigation on the α -ENaC subunit.

Actinomycin D inhibits TNF- α downregulation of α -ENaC mRNA. TNF- α has been shown to exert its action by activating a wide range of genes. Therefore, we investigated the role of transcription in the downregulation of α -ENaC mRNA expression. Alveolar epithelial cells were treated for 6 h with TNF- α in the presence of 5 μ g/ml actinomycin D, a transcription inhibitor. Treatment abolished the downregulation of ENaC mRNA by TNF- α , suggesting that transcription is involved in this process (Fig. 2).

α -ENaC mRNA stability in TNF- α -treated cells. The cellular pool of a given mRNA is modulated by the regulated balance between gene transcription and mRNA degradation. Because actinomycin D as cotreatment for 6 h abolished the decrease elicited by TNF- α on α -ENaC mRNA, we investigated the impact of TNF- α on α -ENaC mRNA stability after 16 h of treatment, at a time where ENaC mRNA expression has reached its lower steady-state equilibrium. There was a significant difference ($P < 0.05$) in α -ENaC mRNA stability in TNF- α -treated cells (half-life 10.4 h) compared with the controls (half-life 15.1 h) (Fig. 3).

Modulation of α -ENaC protein expression by TNF- α . We investigated whether TNF- α has an impact on the total cellular pool of α -ENaC protein in alveolar epithelial cells treated with 100 ng/ml TNF- α for 24 h. Immunodetection by Western blotting revealed a broad band of 82–96 kDa at the molecular mass expected for native and glycosylated α -ENaC (59).

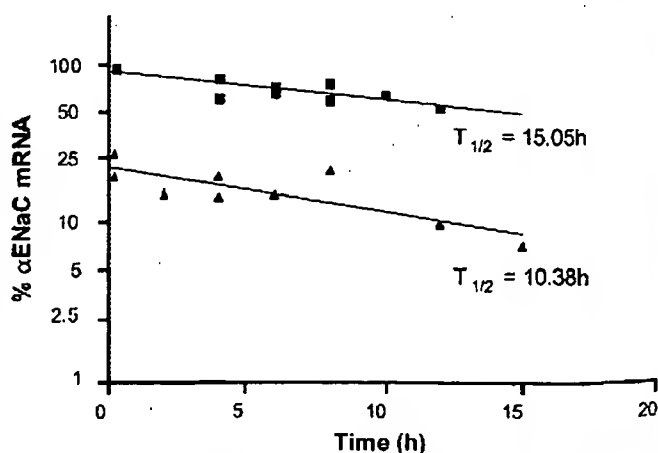


Fig. 3. α -ENaC mRNA stability was determined in control cells and cells treated with 100 ng/ml TNF- α . Alveolar epithelial cells were cultured for 3 days and treated or not for 16 h with 100 ng/ml TNF- α . The cells were incubated thereafter with 5 μ g/ml Act D for 0, 4, 6, 8, 10, or 12 h. 18S rRNA was used to normalize the amount of RNA loaded on each well. The calculated half-life ($T_{1/2}$) is shown. ■, Act D; ▲, Act D + TNF- α . Multiple regression analysis revealed a statistically significant difference in α -ENaC mRNA stability in cells treated with TNF compared with untreated cells ($P < 0.05$).

DOWNREGULATION OF ENaC BY TNF- α IN ALVEOLAR EPITHELIAL CELLS

L305

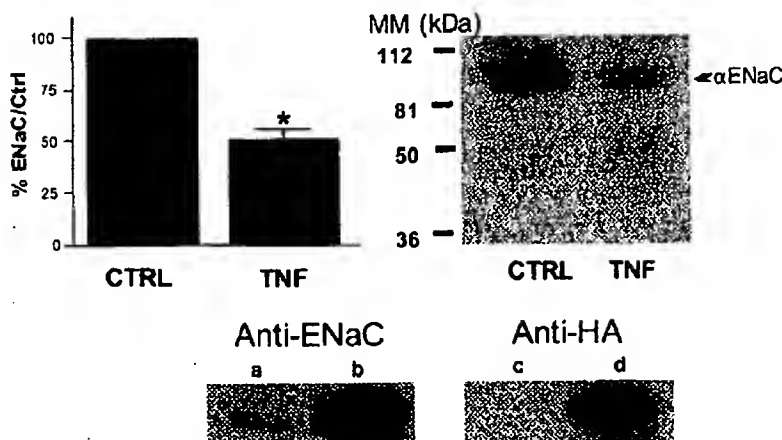


Fig. 4. Immunodetection of α -ENaC in alveolar epithelial cells treated with TNF- α for 24 h. Alveolar epithelial cells were cultured for 3 days and treated or not for 24 h with 100 ng/ml TNF- α . The relative amount of α -ENaC protein was detected by Western blotting with an antibody directed against the NH₂-terminal portion of the protein. *By the 1-sample *t*-test, there is a significant decrease ($P < 0.05$) in the amount of α -ENaC detected in TNF- α -treated cells. A representative chemiluminescent reaction is presented at right. The arrow shows the 82- to 96-kDa band detected by the α -ENaC antibody. At bottom, the specificity of the anti-ENaC antibody (PA1-920) was compared in alveolar type II cells (a) and in a cell lysate of Madin-Darby canine kidney (MDCK) cells transfected with hemagglutinin (HA)-tagged rat α -ENaC (b). Although α -ENaC is much less expressed in alveolar cells (a) than in MDCK transfected cells, the antibody detects a band in the same molecular mass range. As a control, the anti-HA antibody detects a single 97-kDa band in MDCK transfected cells (d) but not in alveolar epithelial cells (c); $n = 7$ for each condition studied. CTRL, control, untreated cells; TNF, TNF- α -treated cells; MM, molecular mass.

TNF- α significantly decreased to $50.0 \pm 4.8\%$ the amount of α -ENaC protein in treated cells compared with untreated controls (Fig. 4).

Influence of TNF- α on I_{te} . The bioelectric properties of alveolar epithelial cells were tested under control conditions and TNF- α treatment. In unstimulated cells, an I_{te} of $6.02 \mu A/cm^2$ was detected across the monolayer (Table 1). This current was inhibited by 65% with $1 \mu M$ amiloride (Table 1), indicating that the cells were actively involved in Na⁺ transport. Treatment for 24 h with 100 ng/ml TNF- α decreased the I_{te} to $2.23 \mu A/cm^2$, a 63% drop compared with untreated cells (Table 1). TNF- α had a major impact on the amiloride-sensitive portion of the current, which dropped from $3.93 \mu A/cm^2$ in control cells to $1.09 \mu A/cm^2$ after treatment. This represents a 72% difference between control and TNF- α -treated cells for the amiloride-sensitive portion of the current. The same results were obtained with a higher amiloride concentration ($10 \mu M$) or with benzamil, a specific ENaC inhibitor (data not shown). TNF- α also affected the proportions of amiloride-sensitive and -insensitive current detected. After treatment, there was a decline in the amiloride-sensitive portion of the current, which fell to 49% of the total current.

Table 1. Bioelectric properties of alveolar type II cells treated for 24 h with TNF- α

	Unstimulated ($n = 23$)	TNF ($n = 18$)
PD, mV	10.4 ± 0.8	4.3 ± 0.19
R_{te} , $\Omega \cdot cm^2$	1700 ± 104	1980 ± 130
I_{te} , $\mu A/cm^2$	6.02 ± 0.12	2.23 ± 0.06
I_{te} amiloride sensitive	3.93 ± 0.10 (65%)	1.09 ± 0.10 (49%)
I_{te} amiloride insensitive	2.09 ± 0.09 (35%)	1.14 ± 0.09 (51%)

Values are means \pm SE. Percentages in parentheses: proportion of amiloride-sensitive and -insensitive current expressed as % of I_{te} ; n , number of filters from different rats; PD, potential difference; R_{te} , transepithelial resistance; I_{te} , transepithelial current.

TNF- α also evoked a 45% decrease in the amiloride-insensitive portion of the current that went from $2.09 \mu A/cm^2$ in control cells to $1.14 \mu A/cm^2$ after treatment. There were no significant differences, however, in R_{te} between control and TNF- α -treated cells (Table 1).

Dose-dependent modulation of amiloride-sensitive current and α -ENaC mRNA expression by TNF- α . To establish whether there was a possible correlation between α -ENaC mRNA expression and amiloride-sensitive current, we seeded alveolar epithelial cells on Costar filters and tested them successively for amiloride-sensitive current and α -ENaC mRNA expression after treatment for 24 h with different concentrations of TNF- α (5–100 ng/ml). TNF- α at 5 ng/ml reduced by 54% the amiloride-sensitive current generated by alveolar epithelial cells (Fig. 5). TNF- α concentration >10 ng/ml did not further decrease the current, which stabilized $\sim 30\%$ of control values. TNF- α also significantly downregulated α -ENaC mRNA expression in alveolar epithelial cells grown on filter. As for amiloride-sensitive current, TNF- α concentration >10 ng/ml did not further reduce mRNA expression of the subunit, which stabilized $\sim 30\%$ (Fig. 5). There was a good correlation ($r = 99$) between α -ENaC mRNA expression and amiloride-sensitive current for the different TNF- α concentrations (Fig. 5).

Ouabain-sensitive Rb⁺ uptake after TNF- α treatment. TNF- α could act through different pathways to reduce the I_{te} of alveolar epithelial cells. Although there was no modulation of α_1 and β_1 Na⁺-K⁺-ATPase mRNA expression by TNF- α , we tested whether the cytokine could affect the activity of the pump after treatment for 24 h with 100 ng/ml TNF- α . Sodium pump activity decreased by 61% in cells treated for 24 h with TNF- α compared with the controls (Fig. 6) ($P < 0.05$).

I_{te} after apical surface permeabilization. The diminution of ouabain-sensitive Rb⁺ uptake after 24-h TNF- α treatment could be secondary to a reduced ability of the apical membrane

L306

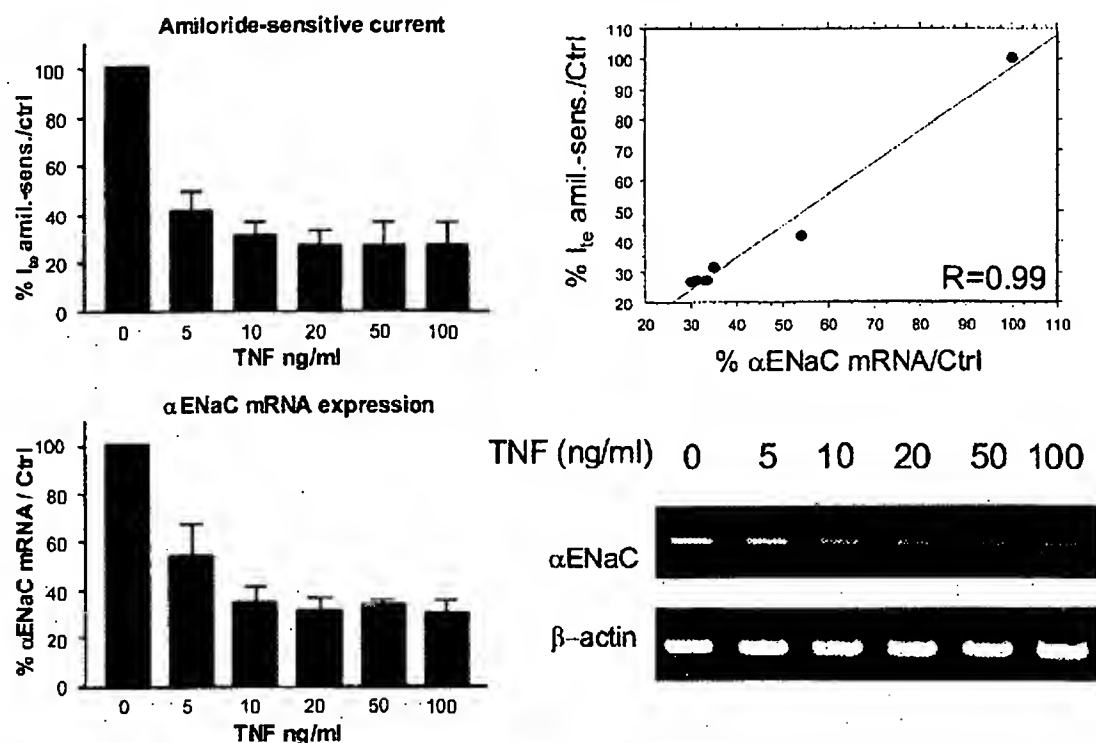
DOWNREGULATION OF ENaC BY TNF- α IN ALVEOLAR EPITHELIAL CELLS

Fig. 5. Amiloride-sensitive current and α -ENaC mRNA expression of alveolar epithelial cells treated with different TNF- α concentrations. Alveolar epithelial cells were cultured for 3 days on 4-cm² Transwell membranes and treated for 24 h with 5, 10, 20, 50, or 100 ng/ml TNF- α . Amiloride-sensitive current and α -ENaC mRNA level were determined successively by epithelial voltinometer and semi-quantitative RT-PCR. The current (*top left*) and mRNA expression (*bottom left*) are reported in the graphs as percentages of control cells. A 5-ng/ml TNF- α concentration was sufficient to significantly decrease amiloride-sensitive current and α -ENaC mRNA expression. $P < 0.05$ ($n = 4$). There is a good correlation between mean calculated values for the percentage of α -ENaC mRNA expression and amiloride-sensitive current ($r = 0.99$) in the regression plot shown at *top right*. A representative gel of the RT-PCR is presented at *bottom right*. I_{sc} , transepithelial current.

to transport Na⁺ or could be the result of a direct inhibiting effect of TNF- α on sodium pump activity. To test the latter hypothesis, we measured the ouabain-sensitive I_{sc} of control and TNF- α -treated cells in the Ussing chamber following amphotericin B permeabilization of the apical membrane. In such conditions, there is no restriction in Na⁺ entry in the cytoplasm by the apical membrane, which allows an estimation of the activity of Na⁺-K⁺-ATPase. Typical traces, presented in Fig. 7, show that 10 μ M apical amiloride treatment decreased

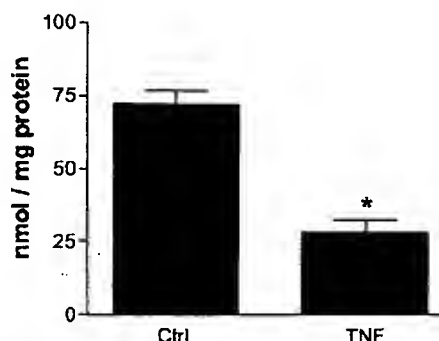


Fig. 6. Ouabain-sensitive Rb⁺ uptake of alveolar epithelial cells treated for 24 h with TNF- α . Uptake is expressed in nmol/mg protein. A 2 mM ouabain concentration was used to inhibit Na⁺-K⁺-ATPase. *There is a significant decrease ($P < 0.05$), by the unpaired *t*-test, in Rb⁺ uptake by TNF- α -treated cells ($n = 7$).

the basal I_{sc} of control and TNF-treated cells. Apical addition of amphotericin B led to a progressive increase in the current, in control and TNF-treated cells, that was inhibited by 2 mM basolateral application of ouabain. The different I_{sc} for control and TNF-treated cells are compared in Fig. 8. As shown previously by EVOM measurement, TNF- α significantly decreased ($P < 0.05$) basal transepithelial current (basal I_{sc}) from 7.01 ± 0.71 to 2.27 ± 0.24 μ A/cm² (Fig. 8A) and amiloride-sensitive I_{sc} from 5.63 ± 0.71 to 1.08 ± 0.16 μ A/cm² (Fig. 8B). After amiloride treatment, apical membrane permeabilization with amphotericin B (see MATERIALS AND METHODS and Fig. 7) increases current of control cells (6.06 ± 0.44 μ A/cm²). There was also a significant increase in current of TNF-treated cells (4.21 ± 0.46 μ A/cm²), but it did not reach the level of control cells ($P < 0.05$) (Fig. 8C). Subsequent addition of ouabain led to the determination of ouabain-sensitive current (ouabain-sensitive I_{sc}) corresponding to the current driven by Na⁺-K⁺-ATPase activity (Fig. 8D) after apical membrane permeabilization. Although ouabain-sensitive current was weaker in TNF-treated cells (2.45 ± 0.29 μ A/cm²) than in the controls (3.15 ± 0.28 μ A/cm²), there were no significant differences between control and TNF-treated cells.

DISCUSSION

In this study, we tested the influence of TNF- α on ENaC expression and activity in cultured alveolar epithelial cells. We

DOWNREGULATION OF ENaC BY TNF- α IN ALVEOLAR EPITHELIAL CELLS

L307

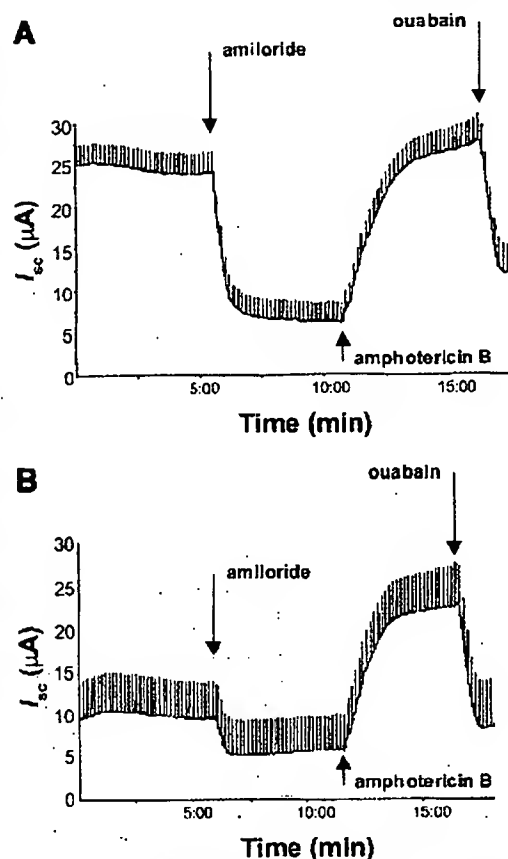


Fig. 7. Typical short-circuit current (I_{sc}) recording of alveolar epithelial cells treated or not with TNF for 24 h following sequential treatment with 10 μ M apical amiloride, 10 μ M apical amphotericin B, and 2 mM basolateral ouabain. Apical administration of amphotericin B allowed apical membrane permeabilization and induced a gradual increase of short-circuit current (I_{sc}) that reached a plateau after 5 min. I_{sc} is expressed in μ A as recorded by the amplifier and not corrected for filter area.

found that 24-h treatment with the cytokine decreased the steady-state mRNA level of the three ENaC subunits and evoked a significant reduction in amiloride-sensitive current generated by the cells.

The treatment of alveolar epithelial cells with 100 ng/ml TNF- α over a 24-h period produced a marked reduction in the expression level of α -, β -, and γ -ENaC mRNA. However, expression of the α_1 and β_1 Na⁺-K⁺-ATPase subunits was not affected, suggesting that sodium channel but not sodium pump mRNAs were affected by TNF- α action. Several studies have revealed that hormones, such as steroids (12, 18) or vasopressin (24, 53); oxygen tension (54, 56, 69, 71); and growth factors, such as keratinocyte growth factor (7, 73), transforming growth factor- β (36), and epithelial growth factor (37) can modulate ENaC mRNA expression. Few data are available concerning the effect of proinflammatory cytokines on ENaC mRNA expression. IL-4, a cytokine involved in asthma pathogenesis, has been shown to decrease γ -ENaC mRNA expression in human bronchial epithelial cells (30). To the best of our knowledge, our results are the first to establish that TNF- α can downregulate ENaC mRNA expression in alveolar epithelial cells.

To study further how TNF- α affects the steady-state mRNA level of ENaC expression, we decided to focus on the α -ENaC

subunit. First, we tested the importance of transcription in the downregulation of α -ENaC mRNA expression by TNF- α . We found that actinomycin D, a drug that blocks the transcription of new RNA, abolished the reduction of α -ENaC mRNA in cells treated for 6 h with TNF- α . These results suggest that α -ENaC mRNA downregulation by TNF- α is a complex process that could require the transcription of one or several genes to decrease α -ENaC mRNA expression. This is similar to what has been reported in vascular smooth muscle cells where actinomycin D blocks the TNF- α downregulation of insulin-like growth factor-1 mRNA (2). In addition to actinomycin D, several inhibitors of putative TNF-activated pathways were tested (data not shown). Inhibitors to P38, inducible nitric oxide synthase, and NF- κ B, as well as γ -glutathione reduced ethyl ester, a membrane-soluble form of glutathione, all failed to inhibit α -ENaC mRNA downregulation by TNF. The pathway by which TNF modulates ENaC expression is therefore not elucidated yet and could involve a complex process.

TNF- α has been demonstrated to downregulate the transcript level of several genes by affecting mRNA stability (52, 57, 68). For this reason, we tested its influence on the stability of α -ENaC transcripts. As shown above, actinomycin D used in cotreatment abolishes the downregulation of α -ENaC mRNA by TNF- α . Therefore, we chose to study the effect of TNF- α on α -ENaC mRNA stability by adding actinomycin D after 16-h TNF- α incubation, since, at this time, the α -ENaC mRNA level has already reached its low steady-state mRNA level. We found that TNF- α significantly decreases α -ENaC mRNA stability. This result suggests that TNF- α could act in part through a posttranscriptional mechanism to downregulate α -ENaC mRNA in alveolar epithelial cells.

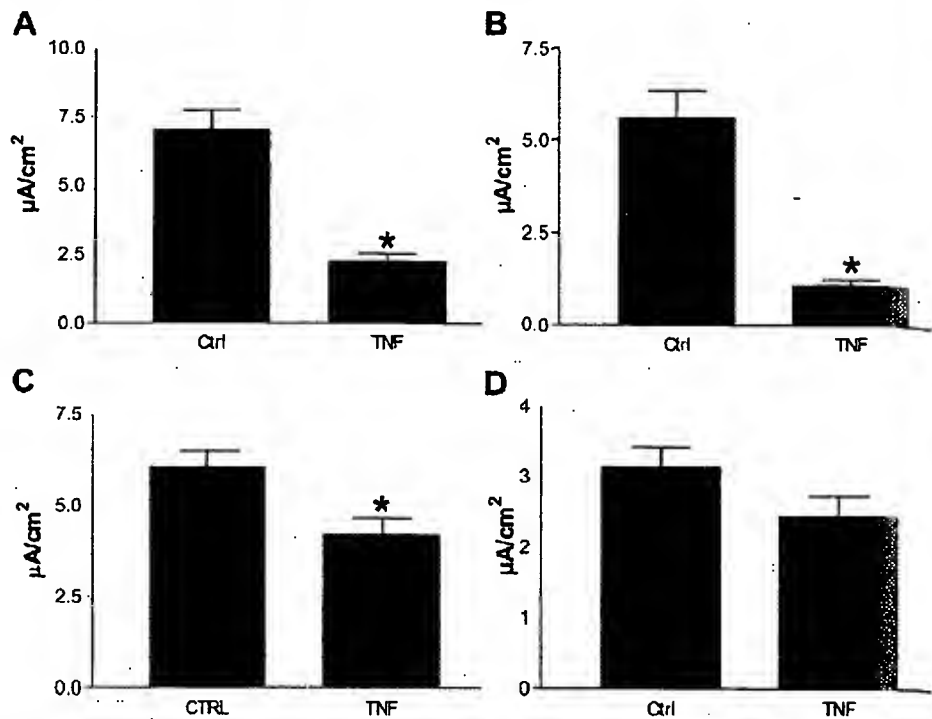
Thereafter, we tested the impact of TNF- α on the amount of α -ENaC protein in the cells and found that it significantly decreased the protein pool in treated cells. The reduction of α -ENaC protein by TNF- α is in the same range as that observed for α -ENaC mRNA. Although no data are available concerning the stability of α -ENaC protein in alveolar epithelial cells, several studies have reported its short half-life (1–2 h) in cultured cells (34, 49, 61, 67). The results presented here suggest that the half-life of α -ENaC protein could be in the same range in alveolar epithelial cells, since a reduction in α -ENaC mRNA brings down the amount of α -ENaC protein.

The bioelectric properties of alveolar epithelial cells were also affected by TNF- α treatment. Amiloride-sensitive current is the main current detected when unstimulated alveolar epithelial cells are cultured on a permeable membrane. This is similar to what has been reported elsewhere for these cells (14, 16). Upon TNF- α treatment, there was a pronounced reduction of amiloride-sensitive and -insensitive current. The effect was more marked for amiloride-sensitive current, which declined by 72% compared with untreated cells. In the experimental conditions used for this study, TNF- α had no toxicity in alveolar epithelial cells since it had no influence on R_{te} . Furthermore, we could not detect significant necrosis or apoptosis induced in the cells by the cytokine (unpublished results). Very few studies have been reported on the effect of TNF- α on ionic transport in alveolar epithelial cells. Our results confirm the work of Zhang et al. (72), who showed that 48 or 72 h treatment with TNF- α decreases the I_{te} across alveolar epithelial cells. The data reported here further reveal that TNF- α can decrease the I_{te} after 24-h treatment and that amiloride-sensi-

L308

DOWNREGULATION OF ENAC BY TNF- α IN ALVEOLAR EPITHELIAL CELLS

Fig. 8. Comparison between I_{sc} of control and TNF-treated cells following sequential treatment with 10 μ M apical amiloride, 10 μ M apical amphotericin B, and 2 mM basolateral ouabain. *TNF- α significantly decreased ($P < 0.05$). A: transepithelial current (basal I_{sc}); B: amiloride-sensitive current (amiloride-sensitive I_{sc}); C: amphotericin B current (amphotericin B I_{sc}) compared with the untreated controls. Significant differences could not be detected (D) for ouabain-sensitive current (ouabain-sensitive I_{sc}) of control and TNF-treated cells, suggesting that TNF does not affect Na^+ - K^+ -ATPase activity. The I_{sc} is expressed as $\mu\text{A}/\text{cm}^2$ of filter. Control, untreated cells, $n = 7$; TNF-treated cells, $n = 6$.



tive current is the main current affected by this agent. We did not, however, find a decline in R_{te} as reported by them (72). The difference could be explained by the diversity of experimental protocols in the two studies, especially the TNF- α concentration administered and the length of treatment, since the authors followed a 48-h treatment protocol. In support of this, Coyne et al. (17) reported that in human primary airway cells, TNF- α has no impact on R_{te} at 24 h but decreases it by 40% after 48 h of treatment.

In A549 cells, an alveolar epithelial cell line, TNF- α has been shown to increase the amiloride-sensitive current within minutes (28). In this model, however, no study was performed after 24-h treatment. It is possible that acute and chronic treatments with TNF- α have different effects on alveolar epithelial cell bioelectric properties.

There was a good correlation ($r = 0.99$) between α -ENaC mRNA expression and the amiloride-sensitive current of alveolar epithelial cells exposed to different TNF- α concentrations. The amiloride-sensitive current depends on several factors, including gene transcription, translation, membrane insertion, and channel activation. The short half-life of ENaC protein in mammalian cells (34, 49, 61, 67) and the relatively long half-life of ENaC mRNA suggest that the pool of α -ENaC mRNA could be very important in modulating the amount of active ENaC at the membrane. These results indicate that downregulation of α -ENaC mRNA expression is probably one of the mechanisms involved in the decrease of sodium transport in alveolar epithelial cells. The 100 ng/ml TNF- α concentration chosen for our study, although used by other investigators, is fairly high. Our data show, however, that 5 ng/ml TNF- α is sufficient to induce significant declines in ENaC activity and expression. This concentration is in the order of magnitude detected in the BAL of patients with cystic fibrosis (5), pneumonia (21), and ARDS (51, 62), as well as in the BAL

of mice infected with *Streptococcus pneumoniae* (4). Our findings indicate that, at the TNF- α concentration found in several lung pathologies, there could be a significant decrease of ENaC expression and activity in the distal lung.

The ability of alveolar epithelial cells to transport sodium depends on ENaC expression and activity at the apical membrane as well as Na^+ - K^+ -ATPase expression and activity at the basolateral membrane. Although TNF- α did not decrease α_1 and β_1 Na^+ - K^+ -ATPase expression, we tested whether 24-h TNF- α treatment affected the activity of the pump. There was a significant reduction of ouabain-sensitive Rb^+ uptake, indicating that the activity of the pump was reduced after 24-h treatment with TNF- α . Two distinct mechanisms could explain such reduction. TNF- α could somehow affect the pump's ability to extrude Na^+ at the basolateral membrane, or the reduced pump activity could be secondary to a restriction of Na^+ entry at the apical membrane. In several Na^+ -reabsorbing epithelia, ENaC is a limiting factor for transepithelial sodium transport (3). Therefore, to evaluate the possibility that the decrease in the ouabain-sensitive Rb^+ uptake observed (Fig. 6) could be related to a decrease in Na^+ entry at the apical membrane, we measured sodium pump activity in control and TNF-treated cells following amphotericin B permeabilization of the apical membrane. Using chamber measurements of control and TNF-treated cells gave I_{sc} in the range of what has been reported in the literature (32, 44, 55). Apical membrane permeabilization with amphotericin B following amiloride treatment increased the I_{sc} in control and TNF-treated cells similarly to what has been described elsewhere (44). In TNF-treated cells, the I_{sc} doubles after apical membrane permeabilization, compared with basal I_{sc} , showing that TNF seems to decrease apical membrane permeability to ion. Although ouabain-sensitive I_{sc} , the portion of the current driven by Na^+ - K^+ -ATPase, was slightly smaller in TNF-treated cells

DOWNREGULATION OF ENAC BY TNF- α IN ALVEOLAR EPITHELIAL CELLS

L309

compared with the controls, a statistically significant difference could not be found. Although it is not possible at this point to exclude any effect of TNF on Na⁺-K⁺-ATPase activity at the basolateral membrane, the permeabilization experiments revealed that, in regard to the effect of TNF on I_{sc} , the apical membrane of the alveolar epithelial cells seems to be the major target of TNF- α action.

There are discrepancies in the literature on the role of TNF- α in the modulation of Na⁺ and water transport in the lung. TNF- α has been demonstrated to increase lung liquid clearance, a process involving amiloride-sensitive transport, during acute bacterial pneumonia (58), intestinal ischemia-reperfusion (6), and direct instillation into the air space (28). However, several reports, including the work presented here, indicate that TNF- α decreases the current and permeability of alveolar epithelial cells (72) and human bronchial epithelial cells (29) but elevates lung permeability in a rat model of acute lung inflammation (43). TNF- α also reduces the expression of aquaporin-5, a water channel involved in transepithelial water transport, in a lung epithelial cell line (65), and in adenovirus-infected lungs (64). As stated above, TNF- α concentration and length of treatment could be important factors in the ability of TNF- α to decrease Na⁺ transport in alveolar epithelial cells. Rezaiguia et al. (58) have reported that in a model of *Pseudomonas* lung infection, TNF- α is produced very rapidly with a sharp peak at 4 h. At 12 h, the TNF- α level practically returns to baseline, and at 24 h, they found an increase in lung liquid clearance (58). Towne et al. (64) report, however, that lung infection with adenovirus leads to lung edema with sustained TNF- α expression still detectable after 14 days. In such a model, aquaporin-1 expression and aquaporin-5 and α -ENaC mRNA levels are reduced on days 7 and 14 postinfection (64). In vitro, the infection of alveolar epithelial cells with *Mycobacterium tuberculosis* also leads to sustained TNF- α expression, still detectable after 4 days, with a decline in I_{sc} generated by the cells (72). Altogether, these results suggest that the nature of sodium transport modulation by TNF- α on the distal lung could vary greatly with the length of treatment.

The data presented in this paper show that sustained TNF- α treatment can downregulate ENaC expression and decrease amiloride-sensitive current in alveolar epithelial cells. These observations suggest that a proinflammatory cytokine, by influencing ENaC expression in the lung, could play an important role during sustained lung inflammation.

ACKNOWLEDGMENTS

The authors acknowledge the editorial work done on this manuscript by Ovid Da Silva, éditeur/rédacteur of the Research Support Office of the Centre de recherche, Centre Hospitalier Universitaire de Montréal.

GRANTS

This work was supported in part by the Canadian Cystic Fibrosis Foundation and the Canadian Institutes of Health Research. Y. Berthiaume is a "Chercheur national" of the Fonds de la recherche en santé du Québec. F. Brochiero is a scholar from the Fonds de la relève of the Université de Montréal.

REFERENCES

- Adams CM, Snyder PM, and Welsh MJ. Interactions between subunits of the human epithelial sodium channel. *J Biol Chem* 272: 27295-27300, 1997.
- Anwar A, Zahid AA, Scheidegger KJ, Brink M, and Delafontaine P. Tumor necrosis factor- α regulates insulin-like growth factor-I and insulin-like growth factor binding protein-3 expression in vascular smooth muscle. *Circulation* 105: 1220-1225, 2002.
- Barbry P and Hofman P. Molecular biology of Na⁺ absorption. *Am J Physiol Gastrointest Liver Physiol* 273: G571-G585, 1997.
- Bergeron Y, Ouellet N, Deslauriers AM, Simard M, Olivier M, and Bergeron MG. Cytokine kinetics and other host factors in response to pneumococcal pulmonary infection in mice. *Infect Immun* 66: 912-922, 1998.
- Boufield TL, Panuska JR, Konstan MW, Hillard KA, Hillard JB, Ghannam H, and Berger M. Inflammatory cytokines in cystic fibrosis lungs. *Am J Respir Crit Care Med* 152: 2111-2118, 1995.
- Borjesson A, Norlin A, Wang X, Andersson R, and Folkesson HG. TNF- α stimulates alveolar liquid clearance during intestinal ischemia-reperfusion in rats. *Am J Physiol Lung Cell Mol Physiol* 278: L3-L12, 2000.
- Borok Z, Danto SI, Dimen LL, Zhang XL, and Lubman RL. Na⁺-K⁺-ATPase expression in alveolar epithelial cells: upregulation of active ion transport by KGF. *Am J Physiol Lung Cell Mol Physiol* 274: L149-L158, 1998.
- Bradford MM. A rapid and sensitive method for the quantitation of microgram quantities of protein utilizing the principle of protein-dye binding. *Anal Biochem* 72: 248-254, 1976.
- Burch LH, Talbot CR, Knowles MR, Canessa CM, Rossier BC, and Boucher RC. Relative expression of the human epithelial Na⁺ channel subunits in normal and cystic fibrosis airways. *Am J Physiol Cell Physiol* 269: C511-C518, 1995.
- Canessa CM, Horisberger JD, and Rossier BC. Epithelial sodium channel related to proteins involved in neurodegeneration. *Nature* 361: 467-470, 1993.
- Canessa CM, Schild L, Buell G, Thorens B, Gautschi I, Horisberger JD, and Rossier BC. Amiloride-sensitive epithelial Na⁺ channel is made of three homologous subunits. *Nature* 367: 463-467, 1994.
- Champigny G, Voilley N, Lingueglia E, Fréland V, Barbry P, and Lazdunski M. Regulation of expression of the lung amiloride-sensitive Na⁺ channel by steroid hormones. *EMBO J* 13: 2177-2181, 1994.
- Chang SS, Grunder S, Hanukoglu A, Rösler A, Mathew PM, Hanukoglu I, Schild L, Lu Y, Shmukets RA, Nelson-Williams C, Rossier BC, and Lifton RP. Mutations in subunits of the epithelial sodium channel cause salt wasting with hyperkalaemic acidosis, pseudohypoaldosteronism type 1. *Nat Genet* 12: 248-253, 1996.
- Cheek JM, Kim KJ, and Crandall ED. Tight monolayers of rat alveolar epithelial cells: bioclectric properties and active sodium transport. *Am J Physiol Cell Physiol* 256: C688-C693, 1989.
- Compeau CG, Rotstein OD, Tohda H, Marunaka Y, Rafi B, Slutsky AS, and O'Brodovich H. Endotoxin-stimulated alveolar macrophages impair lung epithelial Na⁺ transport by an L-Arg-dependent mechanism. *Am J Physiol Cell Physiol* 266: C1330-C1341, 1994.
- Cott GR, Sugahara K, and Mason RJ. Stimulation of net active ion transport across alveolar type II cell monolayers. *Am J Physiol Cell Physiol* 250: C222-C227, 1986.
- Coyne CB, Vanhank MK, Gambrell TM, Carson JL, Boucher RC, and Johnson LG. Regulation of airway tight junctions by proinflammatory cytokines. *Mol Biol Cell* 13: 3218-3234, 2002.
- Dagenals A, Denis C, Vives MF, Girouard S, Masse C, Nguyen T, Yamagata T, Grygorczyk C, Kothary R, and Berthiaume Y. Modulation of α -ENaC and α_1 -Na⁺-K⁺-ATPase by cAMP and dexamethasone in alveolar epithelial cells. *Am J Physiol Lung Cell Mol Physiol* 281: L217-L230, 2001.
- Dagenals A, Kothary R, and Berthiaume Y. The α subunit of the epithelial sodium channel in the mouse: developmental regulation of its expression. *Pediatr Res* 42: 327-334, 1997.
- Davis PB, Drumm M, and Konstan MW. Cystic fibrosis. *Am J Respir Crit Care Med* 154: 1229-1256, 1996.
- Dehoux MS, Routten A, Ostinelli J, Seta N, Dombret MC, Crestani B, Deschenes M, Trouillet JL, and Aubier M. Compartmentalized cytokine production within the human lung in unilateral pneumonia. *Am J Respir Crit Care Med* 150: 710-716, 1994.
- Dickle AJ, Rafi B, Piovesan J, Davreux C, Ding J, Tanswell AK, Rotstein O, and O'Brodovich H. Preventing endotoxin-stimulated alveolar macrophages from decreasing epithelium Na⁺ channel (ENaC) mRNA levels and activity. *Pediatr Res* 48: 304-310, 2000.
- Ding JW, Dickie J, O'Brodovich H, Shluntani Y, Rafi B, Hackam D, Marunaka Y, and Rotstein OD. Inhibition of amiloride-sensitive sodium

- um-channel activity in distal lung epithelial cells by nitric oxide. *Am J Physiol Lung Cell Mol Physiol* 274: L378-L387, 1998.
24. Djeldi S, Fay M, Cluzeaud F, Escoubet B, Eugene E, Capurro C, Bonvalet JP, Farman N, and Blot-Chaubaud M. Transcriptional regulation of sodium transport by vasopressin in renal cells. *J Biol Chem* 272: 32919-32924, 1997.
 25. Evans DJ, Matsumoto PS, Widdicombe JH, Li-Yun C, Mamlnshkis AA, and Miller SS. *Pseudomonas aeruginosa* induces changes in fluid transport across airway surface epithelia. *Am J Physiol Cell Physiol* 275: C1284-C1290, 1998.
 26. Farman N, Talbot CR, Boucher R, Fay M, Canessa C, Rossier B, and Bonvalet JP. Noncoordinated expression of α -, β -, and γ -subunit mRNAs of epithelial Na⁺ channel along rat respiratory tract. *Am J Physiol Cell Physiol* 272: C131-C141, 1997.
 27. Fiers W. Tumor necrosis factor: Characterization at the molecular, cellular and in vivo level. *FEBS Lett* 285: 199-212, 1991.
 28. Fukuda N, Jayr C, Lazrak A, Wang Y, Lucas R, Matalon S, and Matthay MA. Mechanisms of TNF- α stimulation of amiloride-sensitive sodium transport across alveolar epithelium. *Am J Physiol Lung Cell Mol Physiol* 280: L1258-L1265, 2001.
 29. Galletta LJ, Folli C, Marchetti C, Romano L, Carpani D, Chinese M, and Zegarra-Moran O. Modification of transepithelial ion transport in human cultured bronchial epithelial cells by interferon- γ . *Am J Physiol Lung Cell Mol Physiol* 278: L1186-L1194, 2000.
 30. Galletta LJ, Pagesy P, Folli C, Caci E, Romio L, Costes B, Nicolis E, Cabrini G, Goussens M, Ravazzolo R, and Zegarra-Moran O. IL-4 is a potent modulator of ion transport in the human bronchial epithelium in vitro. *J Immunol* 168: 839-845, 2002.
 31. Gosselin D, DeSanctis J, Boulé M, Skamene E, Matouk C, and Radzloch D. Role of tumor necrosis factor α in innate resistance to mouse pulmonary infection with *Pseudomonas aeruginosa*. *Infect Immun* 63: 3272-3278, 1995.
 32. Guo Y, DuVall MD, Crow JP, and Matalon S. Nitric oxide inhibits Na⁺ absorption across cultured alveolar type II monolayers. *Am J Physiol Lung Cell Mol Physiol* 274: L369-L377, 1998.
 33. Hanukoglu A, Bistrizter T, Rakover Y, and Mandelberg A. Pseudohypodosteronism with increased sweat and saliva electrolyte values and frequent lower respiratory tract infections mimicking cystic fibrosis. *J Pediatr* 125: 752-755, 1994.
 34. Hanwell D, Ishikawa T, Saleki R, and Rotin D. Trafficking and cell surface stability of the epithelial Na⁺ channel expressed in epithelial Madin-Darby canine kidney cells. *J Biol Chem* 277: 9772-9779, 2002.
 35. Hummler E, Barker P, Gatzky J, Beermann F, Verdumo C, Schmidt A, Boucher R, and Rossier BC. Early death due to defective neonatal lung liquid clearance in α ENaC-deficient mice. *Nat Genet* 12: 325-328, 1996.
 36. Husted RF, Sigmund RD, and Stokes JB. Mechanisms of inactivation of the action of aldosterone on collecting duct by TGF- β . *Am J Physiol Renal Physiol* 278: F425-F433, 2000.
 37. Kemp PJ, Burak Z, Kim KJ, Lubman RL, Danto SI, and Crandall ED. Epidermal growth factor regulation in adult rat alveolar type II cells of amiloride-sensitive cation channels. *Am J Physiol Cell Physiol* 277: C1058-C1065, 1999.
 38. Kerem E, Bistrizter T, Hanukoglu A, Hufmann T, Zhou Z, Bennett W, MacLaughlin E, Barker P, Nash M, Quittell L, Boucher R, and Knowles MR. Pulmonary epithelial sodium-channel dysfunction and excess airway liquid in pseudohypodosteronism. *N Engl J Med* 341: 156-162, 1999.
 39. Kuebler WM, Parthasarathi K, Wang PM, and Bhattacharya J. A novel signaling mechanism between gas and blood compartments of the lung. *J Clin Invest* 105: 905-913, 2000.
 40. Kunzelmann K, Beesley AH, King NJ, Karupiah G, Young JA, and Cook DI. Influenza virus inhibits amiloride-sensitive Na⁺ channels in respiratory epithelia. *Proc Natl Acad Sci USA* 97: 10282-10287, 2000.
 41. Lambert LC, Trummell HQ, Singh A, Cassell GH, and Bridges RJ. Mycoplasma pulmonis inhibits electrogenic ion transport across murine tracheal epithelial cell monolayers. *Infect Immun* 66: 272-279, 1998.
 42. Leiferwood EC, Poher JS, and Bradley JR. Recent advances in the molecular basis of TNF signal transduction. *Lab Invest* 79: 1041-1050, 1999.
 43. Li XY, Donaldson K, Brown D, and MacNee W. The role of tumor necrosis factor in increased airspace epithelial permeability in acute lung inflammation. *Am J Respir Cell Mol Biol* 13: 185-195, 1995.
 44. Mairbaurl H, Mayer K, Kim KI, Borok Z, Bartsch P, and Crandall ED. Hypoxia decreases active Na transport across primary rat alveolar epithelial cell monolayers. *Am J Physiol Lung Cell Mol Physiol* 282: L659-L665, 2002.
 45. Malagon-Rogers M. A patient with pseudohypodosteronism type I and respiratory distress syndrome. *Pediatr Nephrol* 13: 484-486, 1999.
 46. Matalon S, Benos DJ, and Jackson RM. Biophysical and molecular properties of amiloride-inhibitable Na⁺ channels in alveolar epithelial cells. *Am J Physiol Lung Cell Mol Physiol* 271: L1-L22, 1996.
 47. Matsushita K, McCray PB Jr, Sigmund RD, Welsh MJ, and Stokes JB. Localization of epithelial sodium channel subunit mRNAs in adult rat lungs by in situ hybridization. *Am J Physiol Lung Cell Mol Physiol* 271: L332-L339, 1996.
 48. Matthay MA, Folkesson HG, and Verkman AS. Salt and water transport across alveolar and distal airway epithelia in the adult lung. *Am J Physiol Lung Cell Mol Physiol* 270: L487-L503, 1996.
 49. May A, Puoti A, Gaeggeler HP, Horisberger JD, and Ruckert HC. Early effect of aldosterone on the rate of synthesis of the epithelial sodium channel α subunit in A6 renal cells. *J Am Soc Nephrol* 8: 1813-1822, 1997.
 50. McRitchie DI, Isowa N, Edelson JD, Xavier AM, Cai L, Man HY, Wang YT, Keshavjee SH, Slutsky AS, and Lin M. Production of tumor necrosis factor α by primary cultured rat alveolar epithelial cells. *Cytokine* 12: 644-654, 2000.
 51. Meduri GU, Kohler G, Headley S, Tolley E, Stentz F, and Postlethwaite A. Inflammatory cytokines in the BAL of patients with ARDS. Persistent elevation over time predicts poor outcome. *Chest* 108: 1303-1314, 1995.
 52. Nakamura H, Yoshimura K, Bajocchi G, Trapnell BC, Pavirani A, and Crystal RG. Tumor necrosis factor modulation of expression of the cystic fibrosis transmembrane conductance regulator gene. *FEBS Lett* 314: 366-370, 1992.
 53. Nicco C, Wittner M, DiStefano A, Jounier S, Bankir L, and Bouby N. Chronic exposure to vasopressin upregulates ENaC and sodium transport in the rat renal collecting duct and lung. *Hypertension* 38: 1143-1149, 2001.
 54. Pitkänen O, Tanswell AK, Downey G, and O'Brodovich H. Increased P_{O2} alters the bioelectric properties of fetal distal lung epithelium. *Am J Physiol Lung Cell Mol Physiol* 270: L1060-L1066, 1996.
 55. Planès C, Blot-Chaubaud M, Matthay MA, Couette S, Uchida T, and Clerici C. Hypoxia and β_2 -agonists regulate cell surface expression of the epithelial sodium channel in native alveolar epithelial cells. *J Biol Chem* 277: 47318-47324, 2002.
 56. Planès C, Escoubet B, Blot-Chaubaud M, Friedlander G, Farman N, and Clerici C. Hypoxia downregulates expression and activity of epithelial sodium channels in rat alveolar epithelial cells. *Am J Respir Cell Mol Biol* 17: 508-518, 1997.
 57. Pryhuber GS, Church SL, Kroft T, Panchal A, and Whitsett JA. 3'-Untranslated region of SP-B mRNA mediates inhibitory effects of TPA and TNF- α on SP-B expression. *Am J Physiol Lung Cell Mol Physiol* 267: L16-L24, 1994.
 58. Rezaiguia S, Garat C, Delclaux C, Melgnan M, Fleury J, Legrand P, Matthay MA, and Jayr C. Acute bacterial pneumonia in rats increases alveolar epithelial fluid clearance by a tumor necrosis factor- α -dependent mechanism. *J Clin Invest* 99: 325-335, 1997.
 59. Rotin D, Bar-Sagi D, O'Brodovich H, Meriläinen J, Lehto VP, Causessa CM, Rossier BC, and Downey GP. An SH3 binding region in the epithelial Na⁺ channel (α ENaC) mediates its localization at the apical membrane. *EMBO J* 13: 4440-4450, 1995.
 60. Skriabin G, Orlov S, Massé C, and Berthiaume Y. Phloretin inhibits Na⁺ and K⁺ uptake in cultured alveolar type II cells by reduction of cellular ATP content. *Exp Lung Res* 26: 319-333, 2000.
 61. Strub O, Gantshl I, Ishikawa T, Bretschopf K, Ciechanover A, Schild L, and Rotin D. Regulation of stability and function of the epithelial Na⁺ channel (ENaC) by ubiquitination. *EMBO J* 16: 6325-6336, 1997.
 62. Suter PM, Suter S, Glardin E, Roux-Lombard P, Grau GE, and Dayer JM. High bronchoalveolar levels of tumor necrosis factor and its inhibitors, interleukin-1, interferon, and elastase, in patients with adult respiratory distress syndrome after trauma, shock, or sepsis. *Am Rev Respir Dis* 145: 1016-1022, 1992.
 63. Szatmari Z. Tumor necrosis factor- α : molecular-biological aspects minireview. *Neoplasma* 46: 257-266, 1999.
 64. Towne JE, Harrod KS, Krane CM, and Menon AG. Decreased expression of aquaporin (AQP)1 and AQP5 in mouse lung after acute viral infection. *Am J Respir Cell Mol Biol* 22: 34-44, 2000.

DOWNREGULATION OF ENAC BY TNF- α IN ALVEOLAR EPITHELIAL CELLS

L311

65. Towne JF, Krane CM, Bachurski CJ, and Menon AG. Tumor necrosis factor- α inhibits aquaporin 5 expression in mouse lung epithelial cells. *J Biol Chem* 18657-18664, 2001.
66. Tracey KJ and Cerami A. Tumor necrosis factor: an updated review of its biology. *Crit Care Med* 21: S415-S422, 1993.
67. Weisz OA, Wang JM, Edinger RS, and Johnson JP. Non-coordinate regulation of endogenous epithelial sodium channel (ENaC) subunit expression at the apical membrane of A6 cells in response to various transporting conditions. *J Biol Chem* 275: 39886-39893, 2000.
68. Whitsett JA, Clark JC, Wispe JR, and Pryhuber GS. Effects of TNF- α and phorbol ester on human surfactant protein and MnSOD gene transcription in vitro. *Am J Physiol Lung Cell Mol Physiol* 262: L688-L693, 1992.
69. Wodopia R, Ko HS, Billian J, Wiesner R, Bartsch P, and Mairbaurl H. Hypoxia decreases proteins involved in epithelial electrolyte transport in A549 cells and rat lung. *Am J Physiol Lung Cell Mol Physiol* 279: L1110-L1119, 2000.
70. Young RM, Shull GE, and Lingrel JB. Multiple mRNAs from rat kidney and brain encode single Na⁺,K⁺-ATPase beta subunit protein. *J Biol Chem* 262: 4905-4910, 1987.
71. Yue G, Russel WJ, Benos DJ, Jackson RM, Olman MA, and Matalon S. Increased expression and activity of sodium channels in alveolar type II cells of hyperoxic rats. *Proc Natl Acad Sci USA* 92: 8418-8422, 1995.
72. Zhang M, Kim KJ, Iyer D, Lin Y, Belisle J, McEnery K, Crundall ED, and Barnes PF. Effects of *Mycobacterium tuberculosis* on the bioelectric properties of the alveolar epithelium. *Infect Immun* 65: 692-698, 1997.
73. Zhou L, Graeff RW, McCray PB Jr, Simonet WS, and Whitsett JA. Keratinocyte growth factor stimulates CFTR-independent fluid secretion in the fetal lung in vitro. *Am J Physiol Lung Cell Mol Physiol* 271: L987-L994, 1996.



Original article

Involvement of the CCND1 gene in hairy cell leukemia

C. J. de Boer,¹ J. C. Kluin-Nelemans,² E. Dreef,¹ M. G. D. Kester,² P. M. Kluin,¹
E. Schuurin¹ & J. H. J. M. van Krieken¹

Departments of ¹Pathology and ²Hematology, University of Leiden, Leiden, The Netherlands

Summary

Background: Previous results suggested increased mRNA expression of CCND1 in hairy cell leukemia (HCL). The CCND1 gene is involved in the t(11;14)(q13;q32) chromosomal rearrangement, a characteristic abnormality in mantle cell lymphoma (MCL). We and others reported that, in contrast to other B-cell lymphomas, almost all MCL have overexpression of the CCND1 gene with a good correlation between RNA and protein analysis. Recent studies showed that overexpression of the cyclin D1 protein can be easily detected by immunohistochemistry (IHC) on formalin-fixed, paraffin embedded tissues.

Patients and methods: To investigate whether the CCND1 gene is involved in HCL, we performed IHC on a series of 22 cases using formalin-fixed paraffin embedded splenectomy specimens. For IHC the sections were boiled in citrate buffer. The presence of rearrangements within the BCL-1 locus and the CCND1 gene was analyzed in 13 of 22 cases by Southern blot analysis using all available breakpoint probes. Expression of CCND1 was analyzed at the

mRNA level (Northern blot) and protein level (IHC).

Results: Overexpression of the cyclin D1 protein using IHC was observed in all cases, with strong expression in 5 cases. Pre-existing B- and T-cell areas of the spleen did not express significant levels of the cyclin D1 protein. Seven of 9 cases analyzed by both IHC and Northern blotting showed overexpression of the CCND1 gene with both methods. No genomic abnormalities were observed in any of the 13 cases studied by Southern blot analysis. Additionally, no 11q13 abnormalities were detected by banding analysis of 19 of 22 cases.

Conclusions: The elevated levels of CCND1 mRNA and protein in conjunction with the absence of overt rearrangements within the BCL-1 locus distinguish HCL from MCL and other B-cell malignancies. This suggests that activation of the CCND1 gene in HCL is due to mechanisms other than chromosomal rearrangement.

Key words: BCL-1, CCND1, cyclin D1, HCL, immunohistochemistry, RNA, t(11;14)

Introduction

There have been only a few reports on chromosome abnormalities in hairy cell leukemia (HCL) over the years. Various methods, such as the CD40 *in vitro* proliferation system or B-cell mitogen stimulated cells, have been described for obtaining good metaphase chromosomes which can be used for cytogenetics. Different anomalies have been described, including clonal aberrations and numeric and structural changes in the chromosomes. However, no specific recurrent chromosomal aberrations were observed [1-9]. This paucity of data is explained by the fact that HCL is a rare entity; it is often difficult to obtain good material, and above all, the cells show a very low proliferative capacity. As an alternative, interphase fluorescent *in situ* hybridization using alphoid and satellite probes specific for 16 human chromosomes (chromosomes 2, 4, 5, 13, 14, 19 and 21 not included) showed that HCL appeared to be diploid with non-random gain and loss of chromosomes without any specificity regarding the disease [3]. Involvement of chromosomes 5, 7 and 14q has often been observed, but the presence of 11q13 rearrange-

ments or even t(11;14) are rare [4, 7, 8, 10]. We previously reported mRNA overexpression of CCND1 in some cases of HCL [11], and therefore we analyzed the involvement of the chromosome 11q13 region and in particular the CCND1 gene in HCL.

The chromosome 11q13/BCL-1 region is found in approximately 50% and 70% of mantle cell lymphomas (MCL) at the genomic and cytogenetic level, respectively, translocated to the immunoglobulin heavy chain joining gene complex (Jh) located at chromosome 14q32 (see references [12-14]). The gene involved in this translocation is CCND1. The CCND1 gene is overexpressed in almost all cases of MCL, irrespective of the presence of a t(11;14)(q13;q32) rearrangement, at both the RNA and protein levels [11, 15]. In contrast, the CCND1 gene is not, or only weakly, expressed in normal lymphoid cells and most types of non-Hodgkin's lymphoma. Sporadically, the 11q13 region is rearranged in several other types of B-cell lymphoproliferative disorders such as follicular lymphoma, B-cell prolymphocytic leukemia, chronic lymphocytic leukemia, multiple myeloma (see reference [12]) and hairy cell leukemia [4, 7, 10].

In this study we describe the analysis of rearrangements within the 11q13/BCL-1 region and expression of the CCND1 gene at the protein level using immunohistochemistry in HCL. This study includes 22 cases analyzed by IHC, but also a compilation of previously published banding analyses of HCL using the CD40 culturing system [7], Southern blot analysis for rearrangements within the BCL-1 locus and previously reported Northern blot data [11]. Methods for detecting overexpression of cyclin D1 protein by IHC on routinely processed biopsies of MCL and other B-cell neoplasias, including HCL, have been recently published [15-18]. In our series of HCL, all 22 cases studied by IHC showed overexpression of the cyclin D1 protein, but no breakpoints within the BCL-1 locus could be detected by any of the above-mentioned techniques. This strongly suggests that mechanisms other than translocations are implicated in the deregulation of the CCND1 gene in HCL.

Patients and methods

Patient materials

As a referral hospital, the Department of Hematology received during the late 1970s and the early 1980s many spleen samples from Dutch HCL patients. The diagnosis of HCL was established on the basis of the clinical picture, cytomorphology of neoplastic cells, histology of the spleen and bone marrow, cytochemical staining (tartrate-resistant acid phosphatase positive), and immunophenotyping (reactivity with monoclonal antibodies against CD11c, CD19, CD25, CD103 and expression of monotypic immunoglobulin). Single-cell suspensions were obtained from blood and HCL spleens by gentle mechanical disruption and isolation by Ficoll-Isopaque density gradient centrifugation and frozen in liquid nitrogen. Immunophenotypically, all of the suspensions contained more than 80% hairy cells. The samples analyzed in this study are derived from untreated patients.

For Southern and Northern blot analyses, viable frozen cells were used as described, derived either from spleen samples (18 samples) or peripheral blood samples (2 samples) [11]. For IHC of the cyclin D1 protein, formalin-fixed, paraffin embedded spleen tissue was used as described [15]. In this study 13, 15, and 22 cases were analyzed with Southern blot, Northern blot and immunohistochemistry, respectively, as summarized in Table 1. Of the total of 29 different HCL patients analyzed in this study, 26 were described previously for cytogenetic analysis [7]. In brief, viably frozen cells were cultured by stimulation of the CD40 antigen using anti-CD40

monoclonal antibodies and analyzed by cytogenetics. By this technique, three cases showed clonal aberrations, four showed non-clonal aberrations, and normal karyotypes were observed in 20 cases.

Nucleic acid analysis

Southern blot analysis was performed as described [12]. Briefly, high molecular weight DNA was isolated by proteinase K treatment and phenol-chloroform extraction. 10 µg of DNA was digested with at least three different restriction enzymes (BamHI, EcoRI, HindIII or PstI; Boehringer Mannheim Germany) according to the recommendations of the supplier, blotted onto nylon filters (Hybond NT, Amersham, U.K.) and serially hybridized with various probes (see below). Cases were included only when a rearrangement was observed with the immunoglobulin heavy chain joining gene complex (IgH) probe Jh, indicating a clonal tumor population. The following probes were used for analysis of rearrangements within the 11q13 region: BCL-1b/MTC, p94PS, p11EH, PRAD1-pDY1 (representing the 5' region of CCND1), U21B31 (representing the 3' non-translated region of CCND1), 3128-cDNA (representing the cDNA of CCND1) [11]. Comigration with chromosome 14q32 was assessed by hybridization with a Jh probe. A total of 13 patients were analyzed.

Northern blot analysis was performed as described [11]. In brief, the single cell suspension was washed with phosphate buffered saline (PBS) and RNA was subsequently isolated using ureum/lithiumchloride and phenol-chloroform extraction. 10 µg of RNA was size fractionated on a 1% formaldehyde agarose gel, blotted onto nitrocellulose filters (Schleicher & Schull, Keene, NH; U.S.A.) and serially hybridized with U21B31 and 3128-CCND1. The amount of RNA loaded on the gel was analyzed with probes for GAPDH or 28S (obtained from Dr. M. Quax-Jouken and Dr. J. Schalken, respectively, University of Nijmegen). The cell lines UMSCC-1 and Jurkat were used as positive and negative controls, respectively. A total of 15 cases were analyzed. Three categories were used: -, no detectable expression, +, expression equal to UMSCC-1 and normal lymphoid tissues, ++, expression stronger than UMSCC-1 and normal lymphoid tissues.

Hybridization conditions were as described [11]. Briefly, filters were pre-hybridized for 2 hours at 65 °C in hybridization mix (6 × SSC, 5 × Denhardt's solution, 0.5% SDS, 50 µg/ml salmon sperm DNA and 10% polyethylene glycol (DNA filters) or 10% dextran sulphate (RNA filters)). Purified DNA probes were radiolabeled with 20 µCi of [α^{32} P]dCTP using a random-primed labeling kit (Pharmacia, Uppsala, Sweden). Filters were washed for 30 minutes in 1 × SSC/0.1% SDS and 30 minutes 0.1 × SSC/0.1% SDS at 65 °C after 16 hours of hybridization. Filters were exposed to Kodak X-Omat AR films with intensifying screens at -70 °C.

Immunohistochemical analysis

IHC for the cyclin D1 protein was performed on formalin-fixed, paraffin embedded tissue from splenectomy specimens as recently described [15]. In brief, tissue sections were adhered to 3-aminopropyltriethoxysilane (APES) coated slides and boiled for 25 minutes in 10 mM citrate buffer pH 6.0 and subsequently incubated with the primary antibody. We used the cyclin D1 monoclonal antibody DCS-6 culture supernatant in two dilutions (1:500 and 1:2500). Staining was assessed according to staining of endothelial cells and fibroblasts in the same tissue section. Hence, four categories were used: -; weaker than endothelial cells and fibroblasts; =; equally strong as endothelial cells and fibroblasts; + and ++; stronger and much stronger than endothelial cells and fibroblasts. A total of 22 cases were analyzed.

Table 1. Summary of the analysis of chromosome 11q13 and CCND1 involvement in HCL.

	No. analyzed		
Southern blot	13	11q13 rearrangement	0
Northern blot	15	strong expression (++)	5
		moderate expression (+)	7
		undetectable (-)	3
IHC	22	strong expression (++)	5
		moderate expression (+)	17
		undetectable (-)	0

Results

Our previously published Northern blot results [11] suggested overexpression of the CCND1 gene in at least one-third of HCL. In 12 of 15 cases expression was observed, with high expression in 5 cases and moderate levels of expression in 7 cases (Figure 1). Expression of the CCND1 gene was unlikely to be due to an admixture of accessory cells in the HCL samples since all samples contained more than 80% hairy cells.

Based on these observations and previous reports that IHC on formalin-fixed, paraffin embedded tissues is a reliable and sensitive method for detecting (over)-expression of the cyclin D1 protein in B-cell neoplasia [15-18], we analyzed a large series of HCL spleens by IHC (Table 1 and 2). Using the well-defined cyclin D1-specific monoclonal antibody DCS-6 [19], we observed overexpression in tumor cell nuclei in all cases of HCL ($n=22$). Five cases showed a very strong staining, and the remaining 17 cases showed a moderate level of overexpression. Overexpression was defined by a stronger staining in tumor cells than in fibroblasts and endothelial cells within the same section. Variation in staining intensity among individual tumor cells within the same section was observed in all cases (Figure 2a). In general, the staining intensity was weaker than in

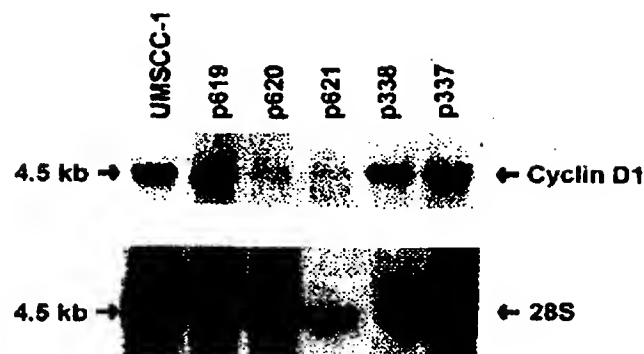


Figure 1. RNA analysis of CCND1 expression in HCL. 10 µg of RNA was size fractionated on a 1% agarose, formaldehyde gel, transferred to a filter and serially hybridized with both CCND1 probes and a 28S probe as control for the amount of RNA loaded. RNA of the cell line UMSCC-1 was used as a reference for CCND1 expression. Cases of HCL indicated at the top, the molecular weight marker at the left, the transcripts on the right.

MCL (Figure 2b), but stronger than in all other B-cell lymphomas and leukemias ($n=48$) and normal lymphoid tissues ($n=10$) tested previously [15]. In some HCL, residual foci of the splenic white pulp were detected. These areas did not stain for cyclin D1 (Figure 2a).

Table 2. Immunohistochemistry for cyclin D1 in hairy cell leukemia.

No.	Case ^a	Sex/ age ^a	Cytogenetics ^a	Southern blot analysis							RNA ^c	IHC	
				Jh ^b	MTC	p94PS	p11EH	5'DI	3'DI	cDNA D1		1:500	1:2500
Cases analyzed for mRNA and IHC													
p336	Gy-W	F/63	normal	RR	-	-	-	-	-	-	++	+	+
p337	Ra	M/49	normal	RR	-	-	-	-	-	-	++	+	+
p338	S-J	F/42	normal	RR	-	-	-	-	-	-	++ ^d	+	+
p339	Rie	M/76	abnormal, nonclonal 46, XY, add (14) (q32), del (6) (p21) [1]/46, XY [24]	RR	-	-	-	-	-	-	+	++	++
p342	Jo	M/57	normal	RR	-	-	-	-	-	-	+	+	+
p343	Ka	M/42	abnormal, nonclonal 46, XY, del (7) (q32) [1]/46, XY [29]	RR	-	-	-	-	-	-	+	++	+
p620	Hof	M/39	normal	na	na	na	na	na	na	na	+	++	+
p627	Mey	M/46	normal	na	na	na	na	na	na	na	-	+	+
p628	Ly	M/35	normal	na	na	na	na	na	na	na	-	+	+
Cases analyzed with IHC only													
p258	Mu	M/47	normal	RR	-	na	na	na	na	na	na	+	+
p331	Mu	M/62	normal	RR	-	-	-	-	-	-	na	++	+
p333	W-J	F/75	abnormal, clonal 46, XX [21]/45, X, -X, add (4) (p15), del (10) (q24) [1] 46, XX, der (18) t(5;18)(q11;q23) [29]/46, XX [17]	RR	-	-	-	-	-	-	na	+	+
p334	Grue	M/46	abnormal, clonal 47, XY, +5 [18]/46, XY [1]	RR	-	-	-	-	-	-	nb	+	+
p804	Wo	M/38	na	na	na	na	na	na	na	na	na	+	+
p805	J-B	F/78	na	na	na	na	na	na	na	na	na	+	+
p806	Be	M/69	na	na	na	na	na	na	na	na	na	+	+
p807	Gra	M/34	normal	na	na	na	na	na	na	na	na	+	+
p808	Za	M/47	normal	na	na	na	na	na	na	na	na	+	+
p809	Ko	F/45	normal	na	na	na	na	na	na	na	na	+	+
p810	Hou	M/39	normal	na	na	na	na	na	na	na	na	++	+
p811	Wou	F/43	normal	na	na	na	na	na	na	na	na	+	+
p812	vDu	M/47	normal	na	na	na	na	na	na	na	na	+	+

^a Adapted from [7]; ^b RR: Jh rearrangement present; ^c adapted from [11]; ^d sample left overnight in culture medium at 37 °C.

na = not analyzed; nb = sample could not be scored.

Scoring: - = negative; + = moderate expression; ++ = strong expression.

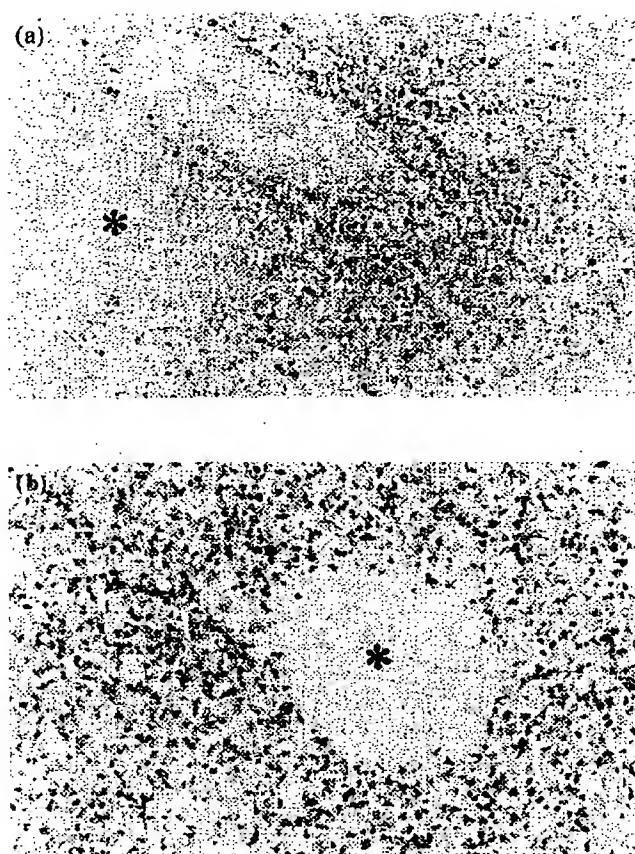


Figure 2. Immunohistochemistry of cyclin D1 in HCL and normal spleen. Sections were stained for cyclin D1 with the DCS-6 antibody (1:2500 dilution of culture supernatant; original magnification 200 \times). A: HCL, showing infiltration of the red pulp by HCL with variable nuclear staining for cyclin D1. Note the absence of staining within the pre-existing lymphoid cells of the white pulp (asterisk). B: MCL, showing a mantle zone growth pattern. Note the very strong expression in the neoplastic mantle zone cells and its absence in the pre-existing follicle center cells (asterisk).

Nine of 22 HCL were tested by both IHC and Northern blot analysis (Table 2). In 7/9 cases increased expression was observed with both Northern blot and immunohistochemistry, although no clear correlation was found in the level of overexpression. In 2/9 cases no overexpression was detected by Northern blot analysis, whereas immunohistochemistry showed moderate expression. All cases of HCL showed the major transcript of 4.5 kb, and no abnormally sized transcripts were detected.

Nine of 22 cases analyzed by IHC were also studied by Southern blot for translocations within the BCL-1 locus. By none of the 6 available breakpoint probes did any of these cases show rearrangements indicative of a t(11;14)(q13;q32). The probes included a 3' probe for CCND1 by which translocations and deletions within the 3' untranslated region of CCND1 can be detected [11]. The overall results of our analysis are shown in Tables 1 and 2. Nineteen of 22 cases analyzed by IHC had been studied before by banding analysis after cul-

turing in the CD40 system [7]. Two cases showed clonal and two non-clonal chromosomal abnormalities, and 15 cases showed a normal karyotype. None of these cases had a t(11;14)(q13;q32) or other abnormalities involving 11q13.

Discussion

Recent reports from our group and others show that IHC is a reliable method to detect (over-) expression of the CCND1 gene in B-cell neoplasia [15–18]. Using this method, we observed that in a series of 22 HCL, all cases showed overexpression of the cyclin D1 protein. Five cases showed very strong expression and the remaining 17 showed moderate levels. These results corroborate the Northern blot results indicating that the majority of HCL have a relatively high expression of the cyclin D1 protein. The high variability observed in expression levels, and even the lack of expression in 2 of 9 cases with Northern blot analysis is perhaps attributable to the use of different materials used for the two methods. For IHC freshly fixed tissues were used but for mRNA analysis splenic cell suspensions were used. CCND1 mRNA has a short half-life (around 30 minutes [20, 21]). We speculate that during the time-consuming procedure of isolation of the HCL cells using FACS-sorting, and subsequent freezing and thawing of the cells, the CCND1 gene product might be partially degraded in some cases. Another possibility could be the presence of an alternatively spliced CCND1 transcript, as has recently been described [22]. Alternative splicing is, however, not likely to have happened in our HCL samples, since in our study CCND1 mRNA levels were analyzed with two different CCND1 probes, a cDNA probe (3128-CCND1) which also hybridizes with the alternatively spliced transcript, and a probe in the 3'-nontranslated region (U21B31), and both probes showed identical results. Therefore, detection of cyclin D1 protein overexpression using IHC seems to be a more reliable method than Northern blotting. In contrast to the present results, Zuckerberg et al. [17] detected overexpression of the cyclin D1 protein in only 1/15 cases of HCL. This could be due to the use of another less-sensitive cyclin D1 antibody, unable to detect the moderate levels of overexpression.

In MCL cyclin D1 overexpression is observed in almost all cases [11, 15]. Depending on the method used, a t(11;14)(q13;q32) can be detected in 50%–75% of the cases [12–14]. In the 22 HCL cases with cyclin D1 overexpression using IHC, we did not detect chromosomal or genomic 11q13 rearrangements by any of the used methods. Clonal and non-clonal 11q13 abnormalities, especially del(11)(q13q21), have been described by Haglund et al. in 8 cases of 36 mitogen-stimulated HCL [4]. Terminal deletions at 11q are frequent in chronic lymphocytic leukemia (CLL) as well, and may occur in tumor subclones. In our recent study, Coignet et al. analyzed 5 cases of CLL with simi-

lar terminal deletions seeking BCL-1 rearrangements using interphase and metaphase FISH with cosmid spanning a 750 kb region around the MTC of the BCL-1 locus [23]. In none of these cases could a BCL-1 breakpoint be detected. Recently, we used the same method in 2 cases of HCL with cytogenetically documented 11q13 abnormalities [7]. No BCL-1 breakpoints were detected (unpublished data). Unfortunately, both the 5 CLL cases with terminal deletions [23] and the present 2 HCL cases with 11q13 translocations could not be studied for cyclin D1 expression since no paraffin embedded material was available.

Our compiled data on expression of the CCND1 gene and 11q13 rearrangements in HCL suggest that either HCL harbor relevant 11q13 breakpoints undetectable by the current methods, or, more likely, that HCL cells have other mechanisms leading to deregulation of the CCND1 gene. Of note, our study made deletions and translocations immediately 3' of the CCND1 gene very unlikely. Such events have been described in a number of cell lines and tumors [11, 24-27] [own unpublished data], and cause the accumulation of mainly the 1.5 kb or abnormally sized CCND1 transcripts by removing mRNA destabilizing sequences. No gross abnormalities were detected in HCL. Furthermore, genomic alterations of the CCND1 gene itself are unlikely to be involved in HCL because we did not observe genomic aberrations with either the 5' CCND1 probe or a CCND1 cDNA probe.

Overexpression of the CCND1 gene is suggested to play a subtle role in tumor development. CCND1 has an essential function in the cell cycle, especially in the G1-S phase transition (reviewed in [28, 29]). Overexpression induced by transfected CCND1 constructs resulted in a shorter G1 phase and total time required for one cell cycle in cell lines. Transgenic mice with an Eμ-CCND1 construct show subtle changes in B- and T-cell composition and only develop B-cell lymphomas after deregulation of other genes such as *myc* [30, 31]. The role of the CCND1 gene in HCL is remarkable, especially since the tumor cells have a very low growth fraction.

Blocking of CCND1 expression by antisense or antibody treatment of cell lines results in a cell cycle block and G1 phase-arrest. The cyclin D1 protein has, furthermore, been shown to be associated with other cell cycle-related proteins such as cyclin-dependent kinase 4 (CDK4), CDK6, p16 and the retinoblastoma gene product pRb. Cyclin D1-CDK complexes can phosphorylate pRb which thereby releases transcription factors. Cyclin D1-CDK complexes are inactive when complexed with p16, an inhibitor of CDK. p16 is therefore believed to be a tumor suppressor gene: absence of p16 could result in the constant activation of cyclin D1-CDK4 complexes. In two reports on p16 in HCL, no obvious deletions or point mutations were found [32, 33]. Constant activation of CCND1 due to loss of p16 is therefore not likely to occur in HCL.

To our knowledge this is the first report on the in-

volvement of the CCND1 gene in HCL. Our results show that CCND1 is indeed involved in HCL. At present, we do not know whether this high expression reflects a structural oncogenic event in the genome of the tumor cells undetectable by current methods, deregulation at the posttranscriptional level, or whether in hairy cells it is physiologic. The latter hypothesis can not be totally excluded, since the normal counterpart of hairy cells is not known and since very few cells in normal lymphoid tissues show a considerable level of expression of the cyclin D1 protein [15].

Acknowledgements

We thank Dr. J. Bartek of the Danish Cancer Society (Copenhagen, Denmark) for providing us with the DCS-6 cyclin D1 specific monoclonal antibody, and Dr. A. Arnold, Dr. T. Carey, Prof. Dr. D. Catovsky, Dr. T. Meeker, Dr. G. Peters, Dr. M. Quax-Jeuken, Prof. Dr. T. Rabbits, Dr. J. Schalken, Prof. Dr. Y. Tsujimoto and Dr. M. Williams for providing probes, and Karin Kleiverda for performing the FISH analysis.

References

1. Chang KL, Stroup R, Weiss LM. Hairy cell leukemia. Current status. *Anatomic Pathol* 1992; 97: 719-38.
2. Ueshima Y, Alimena G, Rowley JD et al. Cytogenetic studies in patients with hairy cell leukemia. *Hematol Oncol* 1983; 1: 215-26.
3. Lewis JP, Tanke HJ, Raap AK et al. Hairy cell leukemia: An interphase cytogenetic study. *Leukemia* 1993; 7: 1334-8.
4. Haglund U, Juliusson G, Stellan B et al. Hairy cell leukemia is characterized by clonal chromosome abnormalities clustered in specific regions. *Blood* 1994; 83: 2637-45.
5. Han T, Sadamori N, Block AMW et al. Cytogenetic studies in chronic lymphocytic leukemia, prolymphocytic leukemia and hairy cell leukemia: A progress report. *Nouvelle Revue Française d'Hématologie* 1988; 30: 393-5.
6. Golomb HM, Lindgren V, Rowley JD. Hairy cell leukemia: An analysis of the chromosomes of 26 patients. *Virchows Archives* 1978; 29: 113-20.
7. Kluin-Nelemans JC, Beverstock GC, Mollevanger P et al. Proliferation and cytogenetic analysis of hairy cell leukemia upon stimulation via the CD40 antigen. *Blood* 1994; 84: 3134-41.
8. Brito-Babapulle V, Pittman S, Melo JV et al. The 14q+ marker in hairy cell leukemia. A cytogenetic study of 15 cases. *Leuk Res* 1986; 10: 131-8.
9. Ohyashiki K, Ohyashiki JH, Takeuchi J et al. Cytogenetic studies in hairy cell leukemia. *Cancer Genet Cytogenet* 1987; 24: 109-17.
10. Nacheva E, Fischer P, O'Connor S et al. Complex chromosomal rearrangements in and unusual variant of hairy cell leukemia. *Cancer Genet Cytogenet* 1992; 62: 186-90.
11. De Boer CJ, Van Krieken JHJM, Kluin-Nelemans JC et al. Cyclin D1 messenger RNA overexpression as a marker for mantle cell lymphoma. *Oncogene* 1995; 10: 1833-40.
12. De Boer CJ, Loyson S, Kluin PM et al. Multiple breakpoints within the BCL-1 locus in B-cell lymphoma: Rearrangement of the cyclin D1 gene. *Cancer Res* 1993; 53: 4148-52.
13. Raffeld M, Jaffe ES. BCL-1, t(11;14), and mantle cell-derived lymphomas. *Blood* 1991; 78: 259-63.

14. Raffeld M, Sander CA, Yano T et al. Mantle cell lymphoma: An update. *Leuk Lymphoma* 1992; 8: 161-6.
15. De Boer CJ, Schuurin E, Dreef E et al. Cyclin D1 protein analysis in the diagnosis of mantle cell lymphoma. *Blood* 1995; 86: 2715-23.
16. Yang W, Zukerberg LR, Motokura T et al. Cyclin D1 (BCL-1, PRAD1) protein expression in low-grade B-cell lymphomas and reactive hyperplasia. *Am J Pathol* 1994; 145: 86-96.
17. Zukerberg LR, Yang W, Arnold A et al. Cyclin D1 expression in non-Hodgkin's lymphoma. *Am J Clin Pathol* 1995; 103: 756-60.
18. Ott MM, Helbing A, Ott G et al. BCL-1 rearrangement and cyclin D1 protein expression in mantle cell lymphoma. *J Pathol* 1996; in press.
19. Lukas J, Pagano M, Staskova Z et al. Cyclin D1 protein oscillates and is essential for cell cycle progression in human tumour cell lines. *Oncogene* 1994; 9: 707-18.
20. Bates S, Parry D, Bonetta L et al. Absence of cyclin D/CDK complexes in cells lacking functional retinoblastoma protein. *Oncogene* 1994; 9: 1633-40.
21. Matsushima H, Ewen ME, Strom DK et al. Identification and properties of an atypical catalytic subunit (p34^{PSK-13}/cdk4) for mammalian D-type G1 cyclins. *Cell* 1992; 71: 323-34.
22. Betticher DC, Thatcher N, Altermatt HJ et al. Alternate splicing produces a novel cyclin D1 transcript. *Oncogene* 1995; 11: 1005-11.
23. Coignet LJA, Schuurin E, Kibbelaar RE et al. Detection of 11q13 rearrangements in hematologic neoplasias by double color fluorescence *in situ* hybridization. *Blood* 1996; in press.
24. Komatsu H, Iida S, Yamamoto K et al. A variant chromosome translocation at 11q13 identifying PRAD1/cyclin D1 as the BCL-1 gene. *Blood* 1994; 84: 1226-31.
25. Withers DA, Harvey RC, Faust JB et al. Characterization of a candidate BCL-1 gene. *Mol Cell Biol* 1991; 11: 4846-53.
26. Rimokh R, Berger F, Bastard C et al. Rearrangement of CCND1 (BCL1/PRAD1) 3' untranslated region in mantle cell lymphomas and t(11q13)-associated leukemias. *Blood* 1994; 84: 3689-96.
27. Seto M, Yamamoto K, Iida S et al. Gene rearrangement and overexpression of PRAD1 in lymphoid malignancy with t(11;14)(q13;q32) translocation. *Oncogene* 1992; 7: 1401-6.
28. Pecper DS, Van der Eb AJ, Zantema A. The G1/S cell-cycle checkpoint in eukaryotic cells. *Biochim Biophys Acta* 1994; 1198: 215-30.
29. Motokura T, Arnold A. Cyclins and oncogenes. *Biochim Biophys Acta* 1993; 1155: 63-78.
30. Bodrug SE, Warner BJ, Bath ML et al. Cyclin D1 transgene impedes lymphocyte maturation and collaborates in lymphomagenesis with the myc gene. *EMBO* 1994; 13: 2124-30.
31. Lovcc H, Grzeschiczek A, Kowalski M et al. Cyclin D1/BCL-1 cooperates with MYC genes in the generation of B-cell lymphoma in transgenic mice. *EMBO J* 1994; 13: 3487-95.
32. Stranks G, Height SE, Mitchell P et al. Deletions and rearrangements of CDKN2 in lymphoid malignancy. *Blood* 1995; 85: 893-901.
33. Otsuki T, Clark HM, Wellmann A et al. Involvement of CDKN2 (p16^{INK4A}/MTS1) and p15^{INK4B}/MTS2 in human leukemias and lymphomas. *Cancer Res* 1995; 55: 1436-40.

Received 20 November 1995; accepted 23 January 1996.

Correspondence to:
Johan H. J. M. van Krieken
Department of Pathology
University of Leiden
P.O. Box 9600
2300 RC Leiden
The Netherlands

Inhibin and activin production and subunit expression in human placental cells cultured *in vitro*

F.Debieve¹, S.Pampfer and K.Thomas

Department of Obstetrics and Gynecological Endocrinology, Université Catholique de Louvain, 1200 Brussels, Belgium

¹To whom correspondence should be addressed: Physiology of Human Reproduction Research Unit, Department of Obstetrics and Gynecological Endocrinology, Faculty of Medicine, OBST 5330, Avenue Em. Mounier 53, B-1200 Brussels, Belgium. E-mail: debieve@obst.ucl.ac.be

Inhibins and activins are dimeric proteins, with each subunit being one of three related protein subunits (α , β A or β B). The mRNA levels of these subunits were studied quantitatively during *in-vitro* differentiation of human cytotrophoblast cells into syncytium, using Northern blot analysis and semi-quantitative reverse transcription-polymerase chain reaction (RT-PCR) analysis. The corresponding protein concentrations were determined by specific enzyme-linked immunosorbent assays for inhibin A, B, pro α C and activin A in cellular protein extracts and culture medium ($n = 5$). Immunofluorescence studies showed syncytium formation after 48 h. The α subunit was present before plating and increased at 48 h ($P < 0.001$) while the β A subunit was weak before plating and increased at 24 h. The β B subunit was not detected. With respect to corresponding protein synthesis, inhibin A ($\alpha + \beta$ A) had risen after 48 h in cellular protein extract and after 72 h in culture medium, while activin A (β A + β B) was detected after 24 h, with no significant variations in culture medium. There was a good correlation between inhibin A and α subunit expression ($r = 0.736$, $P < 0.001$), as well as between activin A and β A subunit expression ($r = 0.755$, $P < 0.001$). This study showed that mRNA expression parallels protein synthesis of inhibin and activin in trophoblast cells. Inhibin A synthesis appears to be dependent on α subunit mRNA expression, rather than on the β A subunit which controls activin A synthesis. This study has also shown that isolated cytotrophoblast cells do not produce dimeric inhibin. However, during the transformation of cytotrophoblast cells into syncytium, β A subunit mRNA expression may be an indicator of cell aggregation, while α subunit mRNA expression may be an indicator of cell fusion.

Key words: activin/inhibin/mRNA/placenta/trophoblast

Introduction

Inhibins and activins are dimeric proteins of the transforming growth factor (TGF) β superfamily (Massagué, 1990; Roberts *et al.*, 1990). They are a combination of three related protein subunits (α , β A and β B), encoded by separate genes (Vale *et al.*, 1988). Inhibin A and B are composed of one α subunit and one of two β subunits while activins are the combinatorial assembly of the β subunits (β A- β A, β B- β B, β A- β B). Initially, they were described as modulators of FSH production by the anterior pituitary (Ying, 1988). Although their function is uncertain, precursor forms of the α subunit of inhibin, containing both the pro- and α C regions of the α subunit, have also been described in human follicular fluid and plasma (Groome *et al.*, 1995).

Molecular biology studies show the presence of α and β subunit mRNA in various tissues (Petraglia, 1997). During pregnancy, the placenta is now recognized as the main source of inhibin A and activin A production (Petraglia *et al.*, 1987; Keelan *et al.*, 1999; Riley *et al.*, 2000). The concentrations in maternal serum increase mainly during the third trimester, reaching maximal values at week 36 (Petraglia *et al.*, 1987; Fowler *et al.*, 1998). Inhibin B in maternal serum during pregnancy is very low, but detectable, but activin AB is not

detected (Fowler *et al.*, 1998). Inhibin pro α C has also been detected during pregnancy (Illingworth *et al.*, 1996; Fowler *et al.*, 1998). Although the role of inhibin and activin in the endocrinology of pregnancy is not understood, the increase of these proteins is expected to have physiological relevance in human pregnancy. Activin A may also play a role during fetal development (Jenkin *et al.*, 1995).

It is now well established that maternal serum inhibin A concentrations are higher in pregnancies associated with Down's syndrome (Aitken *et al.*, 1996). Increased concentrations of maternal serum activin A have also been reported in pregnancies complicated by pre-eclampsia (Muttukrishna *et al.*, 1997). The mechanisms leading to these increased concentrations in pathological states are unknown.

Previous studies on the regulation of inhibin and activin production by trophoblast cells have used non-specific inhibin immunoreactivity or Western blotting as quantitative analysis (Petraglia *et al.*, 1987; Keelan *et al.*, 1994). In-situ hybridization and immunostaining studies show conflicting results concerning the cellular localization of inhibin subunits in placental tissue (Petraglia *et al.*, 1987, 1991; Minami *et al.*, 1992; McCluggage *et al.*, 1998). Moreover, the mechanisms regulating the expression of the mRNAs encoding the different subunits in trophoblast cells has not been elucidated and it

F. Debieve, S. Pampfer and K. Thomas

remains unknown whether the production of these proteins parallels the level of their mRNA.

The in-vitro transformation of isolated cytotrophoblast cells into an endocrine active syncytiotrophoblast has been well-described (Kliman *et al.*, 1986) and is widely used to study hormone synthesis and secretion from trophoblast cells. The aims of this study on human placental cells cultured *in vitro* were (i) to determine the relation between mRNA expression and inhibin and activin synthesis *in vitro*; (ii) to determine which cell population (cytotrophoblast or syncytiotrophoblast) produces these proteins; and (iii) to explore a possible relationship between syncytium transformation and the mRNA expression level of inhibin and activin subunits.

Materials and methods

Cell culture

Term placentae (37–40 weeks pregnant) were collected immediately after elective Caesarean section, from five uncomplicated pregnancies. Cytotrophoblast cells were isolated using a modification of Kliman's method (Kliman *et al.*, 1986). Villous tissue was dissected free of membranes and main vessels, washed with ice-cold 0.9% NaCl and minced into small pieces. The tissue (~60 g) was then digested in 250 ml of 0.25% dispase II (Boehringer Mannheim, Mannheim, Germany) solution in Ca^{2+} , Mg^{2+} -free Hank's balanced salt solution (HBSS-CMF; GibcoBRL Life Technologies, Paisley, UK) for 45 min at 37°C in an oscillating water bath; 10 mg deoxyribonuclease I (Boehringer Mannheim) were then added and digestion allowed to proceed for a further 15 min. The tissue fragments were allowed to settle down for 1 min. The supernatant containing dispersed cells was decanted, filtered through a 100 µm nylon filter and centrifuged for 10 min at 300 g in four 50 ml tubes. The pelleted cells were resuspended in 8 ml of Iscove's modified Dulbecco's medium (IMDM; Gibco BRL Life Technologies) containing 2 mmol/l L-glutamine, 25 mmol/l HEPES (pH 7.4), 50 IU/ml penicillin and 50 µg/ml streptomycin, pooled, filtered through a 40 µm nylon filter and resuspended in 6 ml of the same medium. The isolated cells were then subjected to a further purification by density centrifugation with a discontinuous 5–70% Percoll (Pharmacia Biotech, Buckinghamshire, UK) gradient, made of 5% steps of 3 ml each by dilution of 90% Percoll in HBSS-CMF, in a 50 ml centrifuge tube. The digested cells were layered over this pre-formed Percoll gradient and centrifuged at 1200 g at room temperature for 20 min. The purified cytotrophoblasts were collected in the region corresponding to a density of 1.048–1.062 g/l (estimated by the position of density marker beads run in a parallel Percoll gradient tube), washed with supplemented IMDM, and resuspended in 10 ml of 37°C trypsin solution (0.5 g/l porcine trypsin and 0.5 mmol/l EDTA, 4Na of HBSS; Sigma, St. Louis, MO, USA) for 1 min. The reaction was stopped with 5 ml of fetal calf serum (FCS; GibcoBRL Life Technologies) and placed on ice; another 5 ml FCS was layered in the bottom of the tube before centrifuging for 5 min at 1000 g at room temperature. The pelleted cells were washed and filtered through a 40 µm nylon filter. Finally they were resuspended in supplemented IMDM enriched with 15% FCS and antibiotics and counted by an haemocytometer. Cell viability was assessed by Trypan Blue exclusion.

The purified cytotrophoblasts were plated on 60 mm Primaria Petri dishes (Becton Dickinson, Bedford, MA, USA) at a density of 0.4×10^6 viable cells/cm² in 4 ml supplemented IMDM enriched with 15% FCS and cultured at 37°C in a humid atmosphere of 5% CO₂. The medium was changed daily and cells cultured for 5 days after

plating. On each day, culture medium was recovered and kept frozen at –20°C until the assays were performed. Cells were lysed with TriReagent (Molecular Research Center, Cincinnati, Ohio, USA) and kept frozen at –80°C to further extract total RNA and protein. For immunofluorescence study, the cells were plated in Sonic Seal Slide wells (Nunc A/S, Roskilde, Denmark) at the same density in 1 ml supplemented IMDM. All experiments were repeated five times, each time on independently isolated trophoblast cell cultures.

Immunofluorescence

Trophoblast cultures were analysed at 24, 48 or 72 h after plating. Cells were rinsed with phosphate buffered saline (PBS) at 4°C and fixed for 10 min at 4°C in 100% methanol, rinsed again with PBS and stored at 4°C in PBS for no longer than 4 days. Preparations were preincubated in PBS containing 0.5% bovine serum albumin (BSA), 2.5% normal goat serum and 0.1% saponin for 15 min at 4°C, then incubated with primary monoclonal antibody diluted in the same solution overnight at 4°C. The following mouse primary antibodies (all from Sigma) were used: monoclonal anti-vimentin (1:200), monoclonal anti-desmosomal protein (1:400) and monoclonal anti-alkaline phosphatase (1:4000). The primary antibody was omitted in control slides. Cells were rinsed for 5 min six times in PBS containing 0.1% saponin, followed by a 1 h incubation at room temperature with fluorescein-conjugated goat anti-mouse immunoglobulin G F(ab')₂ fragments (Boehringer Mannheim, 1:500 in the same solution). Cell nuclei were counterstained with 5 µg/ml propidium iodide in washing solution for 5 min at room temperature, followed by six rinses. Slides were mounted using VectaShield mounting medium (Vector Laboratories, Burlingame, CA, USA) and fluorescence was examined using confocal microscopy.

RNA and protein extractions

Total RNA was extracted from frozen samples using the acid guanidine thiocyanate–phenol–chloroform method (Chomczynski *et al.*, 1987), quantified by absorbance at 260 nm, and divided into aliquots as ethanol/sodium acetate precipitate. Proteins were isolated by the same method, resuspended in PBS 1% sodium dodecyl sulphate (SDS), and quantified with the Bradford method using BSA as standard (BioRad Protein Assay; Biorad, Hercules, CA, USA).

Reverse transcriptase–polymerase chain reaction

We used the Superscript One-step reverse transcription–polymerase chain reaction (RT-PCR) system (GibcoBRL) to amplify target sequences of inhibin/activin β A and β B, inhibin α subunits and glyceraldehyde-3-phosphate dehydrogenase (GAPDH) as reference mRNA (Dveksler *et al.*, 1992; Licht *et al.*, 1993). Both cDNA synthesis and PCR were performed consecutively in a single tube using gene-specific primers from 1 µg total RNA in the presence of recombinant ribonuclease inhibitor (RNase Out; GibcoBRL). The 5' sense and 3' antisense oligonucleotides used as primers are listed in Table I (Voutilainen *et al.*, 1991; Dveksler *et al.*, 1992). RT-PCR was carried out using a DNA Thermal Cycler 9700 (Perkin-Elmer, Foster City, CA, USA) to obtain a single band after agarose electrophoresis. Specificity of the PCR products was checked by digestion with restriction enzymes. The cycle number necessary for an exponential phase of the PCR reaction was determined for each cDNA. For the α , β A subunits and GAPDH, reverse transcription was performed at 50°C for 30 min and cDNA amplification at respectively 25, 18, and 19 thermal cycle steps (94°C for 15 s; 56°C for 30 s; 72°C for 90 s). For the β B subunit, reverse transcription was performed at 54°C for 30 min and cDNA amplification was achieved with 30 thermal cycle steps (94°C for 15 s; 66°C for 30 s; 72°C for 90 s).

Inhibin and activin in human placental cells

Table 1. Sequences of oligonucleotides used for reverse transcription-polymerase chain reaction (RT-PCR). The length of the expected PCR products are given (L)

Gene	5' Sense	3' Antisense	L
α	5'-CAGCCACAGATGCCAGCTGT-3'	5'-CTCCGGAGGGCTCTGCAGCAGGCGCAG-3'	502
βA	5'-GTTTCCCGAGTCAGGAACAG-3'	5'-GAGGTTCGCAAAGGGCTATGGCCCCGAT-3'	786
βB	5'-TTCGCCGAGACAGATGGCT-3'	5'-GTGCAAGGAGGAGGCAGACCGGGGACCCC-3'	617
GAPDH	5'-CCATGGAGAAGGCTGGGG-3'	5'-CAAAGTTGTCATGGATGACCTTGGCCA-3'	195

PCR products were quantified by ion-exchange high performance liquid chromatography (HPLC). Each PCR product was diluted in 25 mmol/l Tris-Cl, pH 8 and 25 mmol/l Tris-Cl, 1 mol/l NaCl, pH 8 was used as elution gradient. Chromatograms showed a single peak for each PCR product and the product level was estimated by peak surface measurement. Each inhibin subunit peak surface value was expressed as a ratio to their corresponding GAPDH peak surface value.

Northern blot analysis

For each sample, 15 μ g of total RNA were size-fractionated by electrophoresis on 1% agarose/2.2 mol/l formaldehyde gel and transferred to Hybond-N nylon membranes (Amersham, Buckinghamshire, UK). The same 3'-antisense oligonucleotides used as primers in PCR reactions were used as probes. Those oligonucleotides were 3' end-labelled with [α^{32} P]-dATP (\pm 6000 Ci/mmol; Amersham) using terminal deoxynucleotidyl transferase and purified with Sephadex G50 columns (PharmaciaBiotech). Blots were prehybridized in 10% dextran sulphate, 1% SDS, 1 mol/l NaCl and 25 μ g/ml Torula yeast RNA (Voutilainen *et al.*, 1991), 1 ml/10 cm² membrane, at 60°C for 4 h. Hybridization was performed in the same solution after addition of the probe at 10⁶ cpm/ml for ~18 h. Membranes were washed four times for 20 min in 1× sodium chloride/sodium citrate (SSC), 0.1% SDS. Kodak BioMax Transcreen intensifying screen and Kodak BioMax MS film were used for autoradiography at -70°C for 10 days for inhibin subunits and 3 days for GAPDH.

Autoradiograms were scanned and hybridization signals were estimated by densitometric analysis (Scan Analysis, Biosoft, UK) after background subtraction. Each inhibin subunit mRNA was expressed as the ratio of the corresponding GAPDH density in the same sample.

Inhibin A, B, pro αC and activin A assays

Activin A, inhibin A, B and pro αC were tested with a two-monoclonal antibody solid-phase sandwich microtitre plate enzyme-linked immunosorbent assay (Scotect, Oxford, UK) as described (Fowler *et al.*, 1998). The assay sensitivity was 100 pg/ml for activin A, 2 pg/ml for inhibin A, 15 pg/ml for inhibin B and 2 pg/ml for inhibin pro αC . Inter-plate and intra-plate coefficients of variation were all <10%. Each value was normalized to the protein content of the corresponding cell lysate.

HCG, oestradiol, oestriol and progesterone assays

HCG was tested using a chemiluminescent immunometric assay (DPC, Belgium) according to the manufacturer's protocol. The assay has a sensitivity of 1.1 mIU/ml. Intra- and inter-assay variation coefficients were <10%. Oestradiol (BioMérieux, France), oestriol and progesterone (Amersham, Amersham, UK) were tested using radioimmunoassay, according to the manufacturer's protocol. The sensitivities were 7 pg/ml, 0.08 ng/ml and 0.1 nmole/l respectively. The intra- and inter-assay coefficients of variation were: 6.3 and 8.8% for oestradiol, 2.7 and 6.7% for oestriol, 3.6 and 5.4% for progesterone. Each value was normalized to the protein content of the corresponding cell lysate.

Statistical analysis

Results are presented as mean \pm SEM. Comparisons between days of culture were made using a one-way analysis of variance (Statview, Abacus concepts). In case of heterogeneous distributions (P < 0.05; analysis of variance), post-hoc tests (Fisher's Protected Least Significant Difference) were used to compare subgroups. Correlation studies were performed with a correlation coefficient (Z-score).

Results

Isolation and purification of cytotrophoblast cells from term placenta yielded 1–2 \times 10⁶ cells/g wet weight of tissue. This represented ~1–3% (by DNA content) of the placental tissue. The viability of these cells was >90% when assessed by Trypan Blue exclusion. By phase contrast microscopy, the cells appeared round (mean diameter 10–20 μ m) with a large nucleus and a poorly developed cytoplasm. The protein content of the culture remained constant throughout the 5 day culture period (711 \pm 19 μ g per culture dish after 24 h, and 806 \pm 55 μ g per culture dish after 120 h, F = 2.157, P = 0.12).

Immunofluorescence study (Figure 1) showed that only 5.6 \pm 0.6% of cells were labelled for vimentin (specific for cells of mesenchymal origin; Osborn *et al.*, 1983), at 24 h. Most cells were positive for the desmosomal protein, but remained mononucleated at 24 h, showing a pavement-like pattern. At 48 h, immunofluorescence staining of desmosomal protein disappeared between some cell nuclei, as the cells became multinucleated. There was no difference between 48 and 72 h in syncytium formation. Although most cells were multinucleated, a limited number of mononucleated cells connected to syncytial cells by desmosomes were still present. Immunoreactivity of placental alkaline phosphatase antigen (specific for syncytiotrophoblast cells; Bulmer *et al.*, 1985), increased with days in culture but not all syncytial cells expressed this antigen.

The mRNA expression level of the α , βA and βB subunits were first studied in isolated cytotrophoblast cells before plating and over the 5 days of cell culture. Northern blot analysis of the α subunit showed a major 1.54 kb mRNA and two minor mRNAs (3.15 and 5.51 kb). The reference GAPDH gene probe revealed a major 1.60 kb mRNA and a minor 3.24 kb mRNA. Significant variations of the mRNA expression level of the α subunit (F = 77.135, P < 0.001) were observed during the in-vitro transformation of cytotrophoblast cells into syncytium (Figure 2A and B). The expression was present before plating, with a slight increase after 24 h (P < 0.05). A marked increase was observed after 48 h (P < 0.001) with a maximum level after 72 h (P = 0.01) and a decrease was only observed at 120 h (P < 0.001). RT-PCR analysis showed similar results (F = 5.374, P = 0.003).

F. Debieve, S. Pampfer and K. Thomas

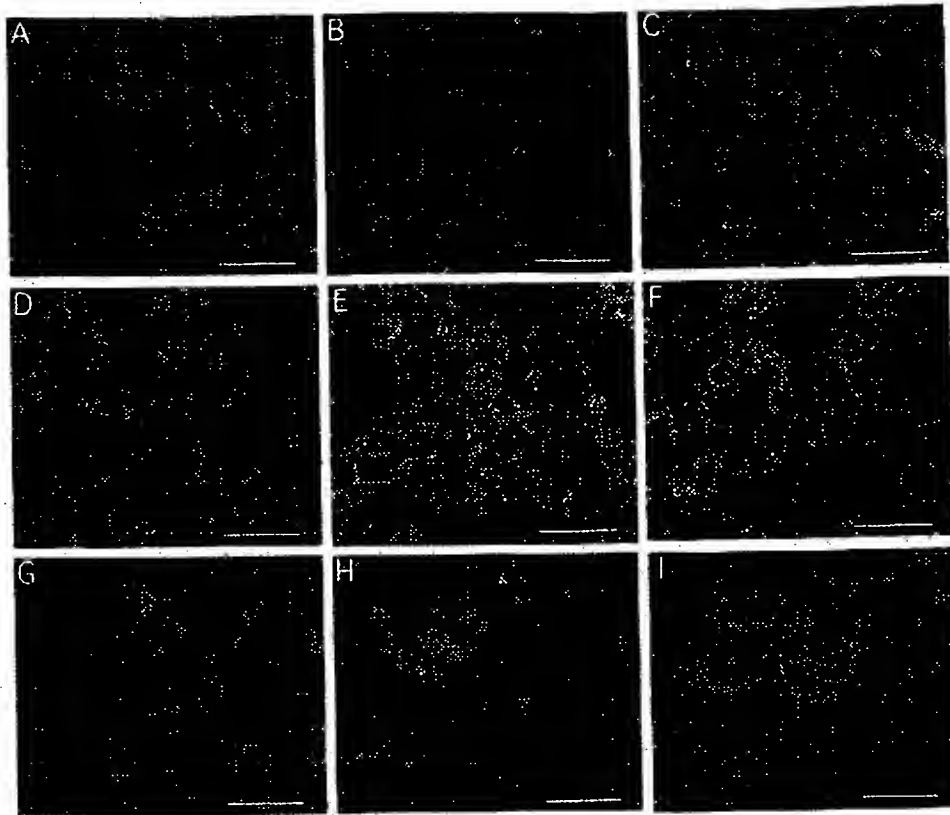


Figure 1. Immunofluorescence study of human cytotrophoblast cells differentiated into syncytium *in vitro*. The nuclei are stained with propidium iodide. Scale bars = 50 μ m. (A) Negative control: Vimentin immunolabelling (B) 24 and (C) 72 h after plating. Desmosomal protein immunolabelling (D) 24, (E) 48 and (F) 72 h after plating. Alkaline phosphatase immunolabelling (G) 24, (H) 48 and (I) 72 h after plating.

Northern blot analysis with the β A subunit probe showed a major 2.83 kb mRNA and five minor mRNAs (1.71, 3.6, 6.3, 7.2 and 11.6 kb). Significant variations of their expression over the culture period were also observed ($F = 20.263$, $P < 0.001$) (Figure 2A and B). β A subunit expression was almost undetectable before plating, but showed a marked increase after only 24 h ($P < 0.001$). Another slight increase could also be observed after 72 h ($P = 0.016$), followed by a decrease after 120 h ($P < 0.05$). RT-PCR analysis showed the same variations (data not shown). No β B subunit expression could be found either by Northern blotting, or by RT-PCR (data not shown).

The secretory function of cultured cells was then evaluated by HCG, oestradiol, oestriol and progesterone release in the medium (Figure 3). Different secretion profiles were observed. HCG (Figure 3A) showed large variations with days of cell culture ($F = 13.252$, $P < 0.001$): the secretion had started to rise after 48 h (not significant), increased after 72 h ($P < 0.001$), then declined ($P = 0.05$). Variations of oestradiol secretion (Figure 3B) were also highly significant ($F = 50.096$, $P < 0.001$) but the secretion increased after only 48 h ($P < 0.05$) with a maximum concentration after 72 h ($P < 0.001$) followed by a plateau. Oestriol was never detected in culture media. There were no significant variations in progesterone secretion (Figure 3C).

The capability of cytotrophoblast cells to produce and secrete inhibin A, B, pro α C and activin A during their syncytial

transformation *in vitro* were then studied by measurement in culture media and cell protein extracts (Figure 3). Significant variations with days of culture were observed for inhibin A (Figure 3D; $F = 17.571$, $P < 0.001$) and inhibin pro α C (Figure 3E; $F = 10.524$, $P < 0.001$) in culture medium. Inhibin A was almost undetected after 24 h but had risen significantly after 72 h ($P < 0.001$) followed by a decrease observed after 120 h ($P < 0.05$). A similar profile was observed in cell protein extracts, with a significant rise after 48 h ($P < 0.001$) and a maximum concentration after 72 h ($P < 0.001$). Inhibin pro α C was detected from the first day of cell culture. After a small decrease after 48 h in cell culture medium (not significant), inhibin pro α C showed a significant peak after 72 h in both culture medium ($P = 0.005$) and cell protein extract ($P < 0.001$). Activin A was detected from the first culture day, showed significant variations over days of culture only in cell protein extracts ($F = 4.932$, $P < 0.005$) with a peak after 72 h ($P < 0.001$) and a decrease at the end of the culture ($P < 0.05$). No inhibin B was detected in either culture medium and cell protein extract over the 5 day culture period.

A relationship between gene expression and protein secretion was investigated using correlation analysis. With respect to inhibin A, there was a better correlation with the α subunit mRNA ($r = 0.736$, $P < 0.001$) compared to the β A subunit mRNA ($r = 0.420$, $P < 0.05$). Similarly, activin A showed a better correlation with the β A subunit mRNA ($r = 0.755$, $P < 0.001$) compared with the α subunit mRNA ($r = 0.494$,

inhibin and activin in human placental cells

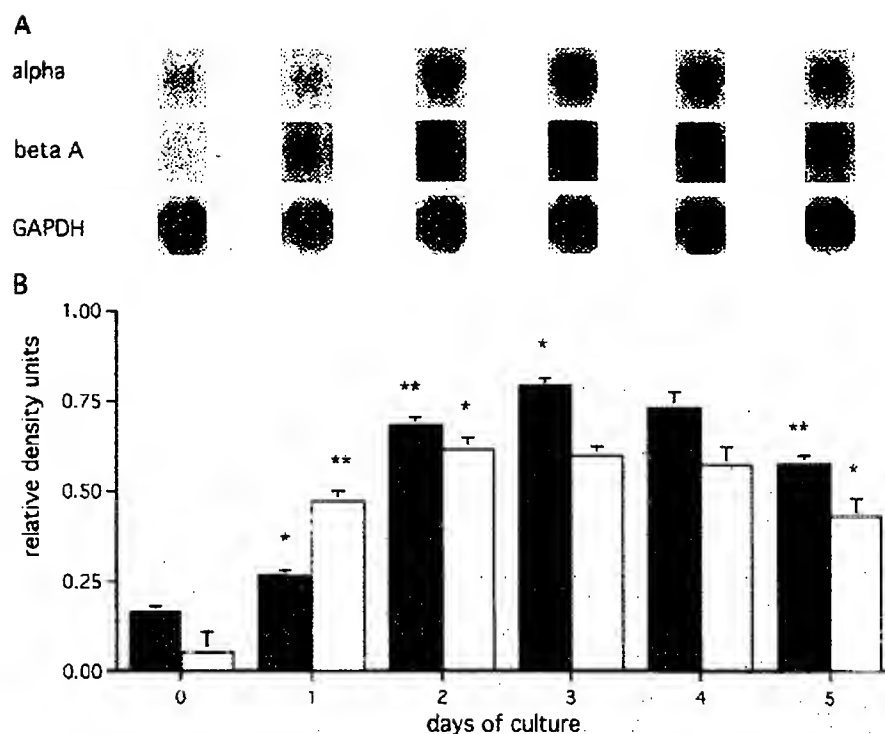


Figure 2. (A) Northern blot analysis. The main mRNA revealed with oligonucleotide probes for α , β A and GAPDH before plating (day 0) and over the 5 day culture period (days 1–5) are presented. (B) Expression levels of inhibin and activin subunits mRNAs before plating and over the 5 day culture period. Results are presented as density ratio to GAPDH mRNA hybridization after scan densitometry of Northern blot analysis (solid bars for α subunit mRNA and open bars for β A subunit mRNA). Values are presented as mean \pm SEM, $n = 5$. Statistically significant differences compared with the mean value on the previous day, * $P < 0.05$ and ** $P < 0.001$ respectively.

$P < 0.05$). Inhibin pro α C was correlated with the α subunit mRNA ($r = 0.475$, $P < 0.05$) but not with the β A mRNA.

Comparison between hormones tested in culture medium over the 5 days culture period showed highly significant correlation ($P < 0.001$) between HCG and oestradiol ($r = 0.761$), inhibin A and HCG ($r = 0.879$), inhibin A and oestradiol ($r = 0.779$), inhibin A and inhibin pro α C ($r = 0.903$) and activin A and progesterone ($r = 0.796$).

Discussion

To the best of our knowledge, this is the first quantitative report of inhibins and activin A expression in human trophoblast cells cultured *in vitro*, at both mRNA and protein levels. The method used to isolate and purify cytotrophoblast cells from term placenta derives from a well-established method (Kliman *et al.*, 1986). We used dispase II rather than trypsin for tissue dissociation because it is less harmful to cell membranes (Green *et al.*, 1979; Keelan *et al.*, 1994). Membrane integrity is known to be essential for cell attachment and subsequent cell fusion, and this was confirmed in the present study.

Cell clumping was avoided by minimizing exposure time in trypsin (Karl *et al.*, 1992), combined with filtration. As reported by others (Richards *et al.*, 1994; Henson *et al.*, 1996), isolated cells were also plated at high density to favour syncytium formation (Ringler and Strauss, 1990). The protein content in our cell culture conditions is comparable with other reports (Henson *et al.*, 1996).

By vimentin immunolabelling, only 5% of cells in these

cultures are of mesenchymal origin (fibroblasts, endothelial cells, macrophages, lymphoid cells; see Osborn and Weber, 1983). By 24 h after plating, most of the cells contain desmosomal protein, demonstrating epithelial origin (this antibody does not stain hemi-desmosomes). Syncytial transformation, suggested by the disappearance of desmosomal protein staining between adjacent cells, had occurred after 48 h of cell culture (Douglas and King, 1990). The increasing number of trophoblast cells expressing alkaline phosphatase antigen, specific for syncytiotrophoblast microvillous membrane (Bulmer and Johnson, 1985), parallels syncytium formation.

However, the 72 h delay before significant increase in HCG or oestradiol suggests step-wise differentiation of trophoblast cells *in vitro*: aggregation, syncytium formation and functional maturation, in agreement with other reports (Bax *et al.*, 1989; Ringler and Strauss, 1990).

No expression of the β B subunit mRNA was found in placental cells cultured *in vitro*. This confirms that inhibin B during pregnancy is mainly produced by decidual cells (Petraglia *et al.*, 1990) or by fetal membranes (Wallace *et al.*, 1997; Riley *et al.*, 2000). Previous studies yielded conflicting results about the cellular localization of inhibin products in placental tissue: syncytiotrophoblast for some (Minami *et al.*, 1992; McCluggage *et al.*, 1998), cytotrophoblast for others (Petraglia *et al.*, 1987, 1991). According to the mRNA expression of inhibin subunits in isolated cytotrophoblast cells before plating, only a significant α subunit expression with almost no β A subunit mRNA expression can be detected. Cytotrophoblast

F. Debieve, S. Pampfer and K. Thomas

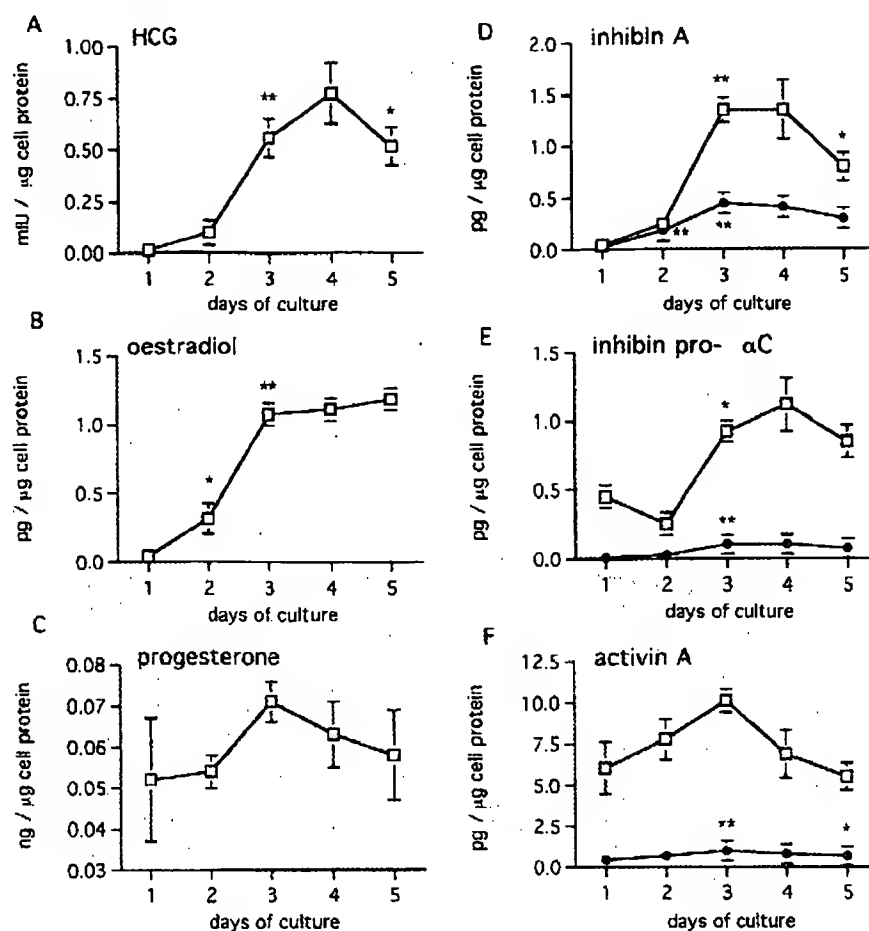


Figure 3. Hormone secretion by trophoblast cells in culture. (A) HCG, (B) oestradiol, (C) progesterone, (D) inhibin A, (E) inhibin pro α C and (F) activin A in culture medium (open squares) and in cell protein extract (filled circles) were followed over the 5 day culture period (medium changed daily). Values are normalized to the protein content of cell lysates, and are means \pm SEM, $n = 5$. Statistically significant differences compared with mean values on the previous day, * $P < 0.05$ and ** $P < 0.001$ respectively.

cells are thus able to produce monomeric inhibin pro α C protein, but not dimeric inhibin A. The use of an antibody to α subunit explains the results shown in other studies.

Correlation studies between gene expression and protein secretion lead us to suspect that inhibin A synthesis is mainly dependent on the expression of the α subunit mRNA and not on the expression of the β A subunit mRNA, which determines activin A synthesis. There is a parallelism between protein production and mRNA expression during transformation *in vitro* of cytotrophoblast cells into syncytium.

In this model, the rise in mRNA expression of inhibin α subunit observed at 48 h coincides with syncytium formation and the rise of inhibin A in cell extracts. Inhibin A released in culture medium showed a significant increase only after 72 h. Therefore, the *in-vitro* differentiation of cytotrophoblast cells into syncytium shows multiple steps: cell aggregation, fusion into syncytium and production of a syncytial specific protein, followed by secretion of this protein in culture medium. We propose that α subunit mRNA expression is an early indicator of syncytium formation *in vitro*.

Activin A secretion and β A subunit mRNA expression are different. Indeed, activin A secretion is present after only 24 h when most of the cells are aggregated. Cell protein extract

and β A subunit mRNA expression show only a slight increase with syncytium formation. Activin A mRNA could therefore be an indicator of cytotrophoblast cell aggregation. This process requires cell movement and the presence of serum in the culture medium is thought to provide motility factors (Bloxam *et al.*, 1997), although differentiation also occurs in serum-free medium when cells are cultured on extracellular matrix-coated surfaces (Ringler and Straws, 1990). The presence of activin receptors on cytotrophoblast cells have been demonstrated (Peng *et al.*, 1993) and Caniggia *et al.* have shown that activin A stimulates the outgrowth of cytotrophoblast cells (Caniggia *et al.*, 1997). Moreover, activin A activity is not counterbalanced by inhibin A at this time of the culture. Therefore, activin A could also be implicated in the syncytium formation process, particularly in the aggregation step.

The strong correlations between inhibin A and HCG or oestradiol, and between activin A and progesterone, suggest possible mutual interactions in their synthesis and secretion, as previously suggested for HCG and immunoreactive inhibin (Petraglia *et al.*, 1987). Another possible explanation is the simultaneous synthesis of those hormones as the cells transform into syncytium.

In conclusion, this study shows that the mRNA expression

Inhibin and activin in human placental cells

of the α and β A subunits parallels inhibin and activin production in trophoblast cells. Inhibin A synthesis seems to be dependent on α subunit mRNA expression and not on β A subunit mRNA expression, the latter controlling activin A synthesis. Isolated cytotrophoblast cells from human term placenta are not able to secrete dimeric forms of inhibin or activin. During transformation of cytotrophoblast cells into syncytium, β A subunit mRNA expression may be an indicator of cell aggregation, while α subunit mRNA expression may be an indicator of cell fusion.

Acknowledgements

Frédéric Debiève is Aspirant from the 'Fonds National de la Recherche Scientifique' (FNRS, Belgium) and research is supported by a grant from FNRS (grant 3.4501.97, FRSM). The authors are grateful to Professor P. Courtoy for providing access to confocal microscopy (grant 9.4531.94, FNRS), scientific advice and critical reading of the manuscript. We are also grateful to H. Kliman for his advice in trophoblast cells cultures. HPLC analysis was performed with the kind help of J.L. Vaerman and P. Moureau from the haematological molecular biology laboratory. We also thank C. Brulet for her excellent technical assistance.

References

- Aitken, D.A., Wallace, E.M., Crossley, J.A. *et al.* (1996) Dimeric inhibin A as a marker for Down's syndrome in early pregnancy. *N. Engl. J. Med.*, **334**, 1321-1326.
- Bax, C.M.R., Ryder, T.A., Mobberley, M.A. *et al.* (1989) Ultrastructural changes and immunocytochemical analysis of human placental trophoblast during short-term culture. *Placenta*, **10**, 179-194.
- Bloxant, D.L., Bax, B.E. and Bax, C.M.R. (197) Culture of syncytiotrophoblast for the study of human placental transfer. Part II: production, culture and use of syncytiotrophoblast. *Placenta*, **18**, 99-108.
- Bulmer, J.N. and Johnson, P.M. (1985) Antigen expression by trophoblast populations in the human placenta and their possible immunobiological relevance. *Placenta*, **6**, 127-140.
- Caniggia, L., Lye, S.J. and Cross, J.C. (1997) Activin is a local regulator of human cytotrophoblast cell differentiation. *Endocrinology*, **138**, 3976-3986.
- Chomczynski, P. and Sacchi, N. (1987) Single step method of RNA isolation by acid guanidinium thiocyanate-phenol-chloroform extraction. *Ann. Biochem.*, **162**, 156-158.
- Douglas, G.C. and King, B.F. (1990) Differentiation of human trophoblast cells *in vitro* as revealed by immunocytochemical staining of desmoplakin and nuclei. *J. Cell. Sci.*, **96**, 131-141.
- Dveksler, G.S., Basile, A.A. and Dierfenbach, C.W. (1992) Analysis of gene expression: use of oligonucleotide primers for glyceraldehyde-3-phosphate dehydrogenase. *PCR Methods Appl.*, **1**, 283-285.
- Fowler, P.A., Evans, L.W., Groome, N.P. *et al.* (1998) A longitudinal study of maternal serum inhibin-A, inhibin-B, activin-A, activin-AB, pro- α C and follistatin during pregnancy. *Hum. Reprod.*, **13**, 3530-3536.
- Greeu, H., Kehinde, O. and Thomas, J. (1979) Growth of cultured human epidermal cells into multiple epithelia suitable for grafting. *Proc. Natl. Acad. Sci. USA*, **76**, 5665-5668.
- Groome, N.P., Illingworth, P.J., O'Brien, M. *et al.* (1995) Quantification of inhibin pro- α C-containing forms in human serum by a new ultrasensitive two-site enzyme-linked immunosorbent assay. *J. Clin. Endocrinol. Metab.*, **80**, 2926-2932.
- Henson, M.C., Shi, W., Greene, S.J. *et al.* (1996) Effects of pregnant human, nonpregnant human, and fetal bovine sera on human chorionic gonadotropin, estradiol, and progesterone release by cultured human trophoblast cells. *Endocrinology*, **137**, 2067-2074.
- Illingworth, P.J., Groome, N.P., Çölin Duncan, W. *et al.* (1996) Measurement of circulating inhibin forms during the establishment of pregnancy. *J. Clin. Endocrinol. Metab.*, **81**, 1471-1475.
- Jenkin, G., McFarlane, J.R. and de Kreiser, D.M. (1995) Implication of inhibin and related proteins in fetal development. *Reprod. Fertil. Dev.*, **7**, 323-331.
- Karl, P.I., Alpy, K.L. and Fisher, S.E. (1992) Serial enzymatic digestion method for isolation of human trophoblasts. [Letter to the Editor.] *Placenta*, **13**, 385-387.
- Keelan, J., Marvin, K.W., Sato, T.A. *et al.* (1999) Concentrations of activin A, inhibin A and follistatin in human amniotic, chorionic and placental tissues at term and preterm. *J. Endocrinol.*, **163**, 99-106.
- Keelan, J., Song, Y. and France, J.T. (1994) Comparative regulation of inhibin, activin and human chorionic gonadotropin production by placental trophoblast cells in culture. *Placenta*, **15**, 803-818.
- Kliman, H.J., Nestler, J.E., Sermasi, E. *et al.* (1986) Purification, characterization, and *in vitro* differentiation of cytotrophoblasts from human term placenta. *Endocrinology*, **118**, 1567-1582.
- Licht, P., Cao, H., Lei, Z.M. *et al.* (1993) Novel self-regulation of human chorionic gonadotropin biosynthesis in term pregnancy human placenta. *Endocrinology*, **133**, 3014-3025.
- Massague, J. (1990) The transforming growth factor beta family. *Ann. Rev. Cell. Biol.*, **6**, 597-641.
- McCluggage, W.G., Ashe, P., Mc Bride, H. *et al.* (1998) Localization of cellular expression of inhibin in trophoblastic tissue. *Histopathology*, **32**, 252-256.
- Minami, S., Yamoto, M. and Nakano, R. (1992) Immunohistochemical localization of inhibin/activin subunits in human placenta. *Obstet. Gynecol.*, **80**, 410-414.
- Munukrishna, S., Knight, P.G., Groome, N.P. *et al.* (1997) Activin A and inhibin A as possible endocrine markers for pre-eclampsia. *Lancet*, **349**, 1285-1288.
- Osborn, M. and Weher, K. (1983) Tumor diagnosis by intermediate filament typing: a novel tool for surgical pathology. *Lab. Invest.*, **48**, 372-394.
- Peng, C., Huang, T.H.J., Jung, E.B. *et al.* (1993) Expression of the type II activin receptor gene in the human placenta. *Endocrinology*, **133**, 3046-3049.
- Petraglia, F. (1997) Inhibin, activin and follistatin in the human placenta - a new family of regulatory proteins. *Placenta*, **18**, 3-8.
- Petraglia, F., Calza, L., Garuti, G.C. *et al.* (1990) Presence and synthesis of inhibin subunits in human decidua. *J. Clin. Endocrinol. Metab.*, **71**, 487-492.
- Petraglia, F., Garuti, G.C., Calza, L. *et al.* (1991) Inhibin subunits in human placenta: localization and messenger ribonucleic acid levels during pregnancy. *Am. J. Obstet. Gynecol.*, **165**, 750-758.
- Petraglia, F., Sawchenko, P., Linn, A.T. *et al.* (1987) Localization, secretion and action of inhibin in human placenta. *Science*, **237**, 187-189.
- Richards, R.G., Hartman, S.M. and Handwerker, S. (1994) Human cytotrophoblast cells cultured in maternal serum progress to a differentiated syncytial phenotype expressing both human chorionic gonadotropin and human placental lactogen. *Endocrinology*, **135**, 321-329.
- Riley, S.C., Leask, R., Balfour, C. *et al.* (2000) Production of inhibin forms by the fetal membranes, decidua, placenta and fetus at parturition. *Hum. Reprod.*, **15**, 578-583.
- Ringler, G.E. and Strauss III, J.F. (1990) *In vitro* systems for the study of human placental endocrine function. *Endocr. Rev.*, **11**, 105-123.
- Roberts, A.B., Flanders, K.C., Kondiah, P. *et al.* (1990) Transforming growth factor beta: biochemistry and roles in embryogenesis, tissue repair and remodeling and carcinogenesis. *Recent Prog. Horm. Res.*, **44**, 157-197.
- Vale, W., Rivier, C. and Hsueh, A. (1988) Chemical and biological characterization of the inhibin family of protein hormones. *Recent Prog. Horm. Res.*, **44**, 1-34.
- Voutilainen, R., Erämaa, M. and Ritvos, O. (1991) Hormonally regulated inhibin gene expression in human fetal and adult adrenals. *J. Clin. Endocrinol. Metab.*, **73**, 1026-1030.
- Wallace, E.M., Riley, S.C., Crossley, J.A. *et al.* (1997) Dimeric inhibins in amniotic fluid, maternal serum, and fetal serum in human pregnancy. *J. Clin. Endocrinol. Metab.*, **82**, 218-222.
- Ying, S.Y. (1988) Inhibins, activins and follistatins: gonadal proteins modulating the secretion of follicle-stimulating hormone. *Endocr. Rev.*, **9**, 267-293.

Received on February 16, 2000; accepted on May 16, 2000

Expression of Membrane-Type Matrix Metalloproteinases 4, 5, and 6 in Mouse Corneas Infected with *P. aeruginosa*

Zhong Dong,¹ Malkhan Katar,¹ Sarah Alousi,² and Richard S. Berk¹

PURPOSE. To investigate the expression and regulation of membrane-type matrix metalloproteinases (MT-MMPs) 4, 5, and 6 in the mouse corneas infected with *Pseudomonas aeruginosa*.

METHODS. C57BL/6J mice were intracorneally infected with *P. aeruginosa*. The expression of MT4, MT5, and MT6-MMP was detected at both the mRNA and protein levels by RT-PCR and immunoblot analysis. Immunohistochemical staining was performed to localize the expression of MT4 and MT5-MMP in the mouse corneas.

RESULTS. Expression of MT4 and MT5-MMP was detected in the normal (uninfected) cornea by RT-PCR and immunoblot analysis. When infected with *P. aeruginosa*, the corneas showed significant induction of each MT-MMP. Localization of MT4 and MT5-MMP revealed that the expression of MT5-MMP was restricted to the epithelial tissue in the normal cornea, whereas the induced expression of MT4 and MT5-MMP was predominantly in the substantia propria, which contained most of the infiltrating cells. MT6-MMP expression was not detected in the uninfected cornea but was upregulated in the infected corneas.

CONCLUSIONS. Expression of MT4, MT5, and MT6-MMP was induced in corneas infected with *P. aeruginosa*. Immunohistochemistry showed predominant immunoreactivity of MT4 and MT5-MMP in the substantia propria. Previous histologic studies have revealed different patterns of inflammatory cell infiltration with an increased number of polymorphonuclear neutrophils (PMNs) during the early stage of inflammation and increased macrophages during the late stage. These results indicate a good correlation between the overexpression of the MT-MMPs in the infected corneas and the inflammatory response—that is, leukocyte infiltration—indicating that inflammatory cells such as macrophages and PMNs may play a role in the upregulation of MT-MMPs during corneal infection, which in turn can cause the destruction of corneal tissue. (*Invest Ophthalmol Vis Sci.* 2001;42:3223-3227)

Recently, studies in our laboratory showed that membrane-type matrix metalloproteinases (MT-MMPs) 1, 2, and 3 were all upregulated in mouse corneas infected with *P. aeruginosa* and the peak of the induction correlated to the inflam-

matory events, suggesting the important role of MT-MMPs in corneal infection and destruction.¹

MMPs are a group of structurally related and zinc-dependent enzymes that play a crucial role in physiologic and pathologic processes, such as embryonic development, endometrial cycling, wound healing, rheumatoid arthritis, tumor invasion, and metastasis.² MMPs have been classified into five broad categories based on their substrate specificity and domain organization. They include collagenases (MMP-1, -8, -13, and -18), stromelysins (MMP-3, -10, and -11), gelatinases (MMP-2 and -9), MT-MMPs (MMP-14, -15, -16, -17, -24, and -25), and other MMPs (MMP-7, -12, -19, -20, -21/22, and -26).³⁻⁷ Since the first member was identified by Sato et al. in 1994,⁸ the MT-MMP subgroup has grown rapidly and now has six members named after the transmembrane domains that anchor the molecules on the plasma membrane.^{3,5,6} MT-MMPs are important in turnover of the extracellular matrix (ECM), because of their dual functions. Similar to other MMPs, they directly cleave ECM proteins, including type I and III collagens, fibronectin, and laminin. In addition, they activate other MMPs such as pro-MMP-2 (gelatinase A) and pro-MMP-13 (collagenase 3) and form an enzymatic cascade for regulation of ECM degradation.^{9,10}

Although classified in the same subgroup, MT4, MT5, and MT6-MMP are different from the other three MT-MMPs in some respects. For example, MT4-MMP has the least sequence identity with other MT-MMPs, except for MT6-MMP.^{11,12} Both MT4-MMP and MT6-MMP are predominantly expressed in leukocytes, and both are glycosylphosphatidylinositol-anchored MMPs.¹²⁻¹⁵ In addition, MT4-MMP also shows TNF- α convertase activity and can potentially process pro-TNF- α to the 17-kDa form.¹¹ These characteristics of MT4-MMP and MT6-MMP suggest that they play a role in inflammation. However, the normal functions of MT4, MT5, and MT6-MMP remain unknown. Their expression and regulation in the cornea have not been reported.

In the present study, we explored expression of newly identified MT4, MT5, and MT6-MMP in the corneas of naive C57BL/6J mice infected with *P. aeruginosa*. RT-PCR, immunoblot analysis, and immunohistochemical staining revealed the significant induction of MT4 and MT5-MMP expression at both the mRNA and protein levels in naive mice over an 8-day period. Similar results were obtained for MT6-MMP gene expression using only RT-PCR due to the absence of available antibody to mouse MT6-MMP.

METHODS

Bacteria

Stock cultures of *P. aeruginosa* 19660 (ATCC, Rockville, MD) were stored at 4°C on tryptone agar slants (Difco Laboratories, Detroit, MI) and were used for the inoculation of 50 to 75 ml of broth medium containing 5% peptone (Difco Laboratories) and 0.25% trypticase soy broth (BBL Microbiology Systems, Cockeysville, MD). Strain 19660 is hemolytic and lecithinolytic and produces exotoxin A, alkaline protease, and elastase under appropriate culture conditions. Cultures were grown on a rotary shaker at 37°C for 16 to 18 hours, centrifuged at

From the ¹Department of Immunology and Microbiology and the ²Cytology Research Core Facility, Wayne State University School of Medicine, Detroit, Michigan.

Supported by National Eye Institute Grant EY-11757 and Grant P30 EY-04068 from the National Institutes of Health, Bethesda, Maryland.

Submitted for publication January 26, 2001; revised August 10, 2001; accepted August 13, 2001.

Commercial relationships policy: N.

The publication costs of this article were defrayed in part by page charge payment. This article must therefore be marked "advertisement" in accordance with 18 U.S.C. §1734 solely to indicate this fact.

Corresponding author: Richard S. Berk, Department of Immunology and Microbiology, Wayne State University School of Medicine, 540 P. Canfield, Detroit, MI 48201. rberk@med.wayne.edu

Investigative Ophthalmology & Visual Science, December 2001, Vol. 42, No. 13
Copyright © Association for Research in Vision and Ophthalmology

3223

8000 rpm at 4°C for 10 minutes, washed with normal saline (Travenol Laboratories, Cambridge, MA), and diluted to a concentration of 2×10^{10} colony-forming units per milliliter. A standard curve was developed to relate viable counts to optical density at 440 nm.

Infection of Animals and Corneal Sample Collection

All animals were treated in accordance with the ARVO Statement for the Use of Animals in Ophthalmic and Vision Research. Age-matched C57BL/6J mice (Jackson Laboratories, Bar Harbor, ME), each weighing 18 to 22 g, were infected at 14 weeks of age. Before infection, they were lightly anesthetized with ether and placed beneath a stereoscopic microscope. The corneal surface was then gently incised with three 1-mm incisions using a sterile 26-gauge needle, taking care not to penetrate the anterior chamber or to damage the sclera. A bacterial suspension (5 μ l) containing 10^6 colony-forming units was topically delivered onto the wounded cornea using a micropipette with a sterile disposable tip. Mice were examined 24 hours later to verify infection. Controls consisted of scratched and unscratched mice that were uninfected.

At selected time points after infection, mice were killed and corneas were excised. Individual samples consisted of 12 pooled corneas per time point for RT-PCR and immunoblot analysis. Single corneas from different time points were used for immunohistochemical staining and histologic study. Immediately after isolation, corneas were rinsed in sterile saline and then processed for the purpose of the different assays. Control mice were treated similarly.

Semiquantitative RT-PCR

Total RNA was extracted from the harvested corneas with extraction reagent (TRIzol, Gibco, Grand Island, NY) according to the manufacturer's instruction. The total RNA was dissolved in water treated with diethylpyrocarbonate (DEPC), and the concentration was measured by a spectrophotometer (UV-1601; Shimadzu, Kyoto, Japan). The samples were treated with DNase I (0.2 U/ μ l; Ambion, Austin, TX) to remove possible DNA contamination. All the reagents needed for RT-PCR were purchased from Perkin Elmer (Norwalk, CT) except *Taq* DNA polymerase and the dNTP mixture, which were purchased from Gibco.

RT-PCR was performed as previously described.¹ Briefly, RT was performed in 0.65-ml RNase-free tubes under optimized conditions in a DNA thermal cycler (model 480; Perkin Elmer). Equal amounts of total RNA (500 ng) from each sample were used for this reaction. The whole product of RT in each tube was amplified by PCR. Cycle parameters were generally a 1-minute melting step at 95°C, a 1-minute annealing step at 55°C, and a 2-minute extension step at 72°C. Thirty cycles were selected for amplification of all target genes, based on results of the experiments that tested the linear range of amplification with different cycles. The following specific primers for MT4-, MT5-, and MT6-MMP were designed and prepared according to the available information for these specific genes (GenBank, provided in the public domain by the National Center for Biotechnology Information, Bethesda, MD, and available at <http://www.ncbi.nlm.nih.gov/genbank>). Because the mRNA sequence for mouse MT6-MMP has not been reported, the primers for human MT6-MMP were prepared and used, assuming there is high homology between human and mouse MT6-MMP. The primers of mouse MT4-MMP (5'-TGG TCT GAT GGT GCA TCC TA-3' and 5'-TGC AGG AAC ATA CTG CCA GA-3') amplified a 205-bp product (gene sequence 1550-1754); the primers of mouse MT5-MMP (5'-GTG ACA GCT CCC CAT TTG AT-3' and 5'-TAG AGT GCT CCA AGC CCA GT-3') amplified a 192-bp product (682-873); and the primers of human MT6-MMP (5'-ATG GCC TGC ATC AAC TCT AT-3' and 5'-AGG GGC CTT TGA AGA AGA AA-3') amplified a ~200-bp product. There were two negative controls: one without reverse transcriptase and the other one without specific primers. The housekeeping gene 18S RNA (Ambion) was also amplified and used as an internal control for the comparison of all time point target genes. Finally, the amplified genes were resolved by 1% agarose gels and revealed by

ethidium bromide staining. RT-PCR for each MT-MMP was repeated at least twice.

To confirm the specificity of the primers, the amplified DNA sequences were subjected to restriction enzyme digestion. The 205-bp PCR product was treated with *Sma*I (Gibco), which recognizes the sequence CCCAAGG. The 192-bp product was treated with *Mbo*I (Gibco), which recognizes the sequence AATTC. Each of them was incubated with respective enzyme (5 U) for 90 minutes, with different reaction buffer and at different temperature, according to the manufacturer's instruction. The results were revealed by 3% agarose gel electrophoresis.

The ~200-bp PCR product was purified with a kit (MinElute; Qiagen, Valencia, CA) according to the manufacturer's instruction. The concentration of the purified DNA was measured by the spectrophotometer at 260 nm. The purified DNA at a concentration of 10 ng/ μ l and human MT6-MMP primers at a concentration of 1 pM/ μ l were then prepared. The DNA samples were analyzed in the DNA Sequencing Facility at the Center for Molecular Medicine and Genetics (Wayne State University, Detroit, MI).

Immunoblot Analysis

Cornea samples were immediately frozen with liquid nitrogen after isolation from mice. To enrich the extracts with membrane-bound proteins, TBS-CM buffer (50 mM Tris [pH 7.5], 150 mM NaCl, 1 mM CaCl_2 , and 1.5% Triton X-114) was used. Samples were homogenized with TBS-CM buffer on ice and then centrifuged at 12,000 rpm at 4°C for 2 minutes. The supernatants were collected and incubated at 37°C for 3 minutes, followed by centrifugation at 12,000 rpm for 2 minutes. The detergent phase, which contained enriched membrane-bound proteins, was saved for immunoblot analysis. The concentrations of the total protein were measured with a bicinchoninic acid (BCA) protein assay. Equal amounts of individual samples (5 μ g) were mixed with 5 μ l of 4 \times sample loading buffer (0.125 M Tris-HCl [pH 6.8], 4% SDS, 40% glycerol, and 0.02% bromophenol blue) containing β -mercaptoethanol and boiled for 5 minutes. The samples and a prestained molecular weight marker (Bio-Rad, Cambridge, MA) were electrophoresed on 12% SDS gels and subsequently transferred to nitrocellulose membranes. The membranes were blocked for 30 minutes in blocking reagent (Blotto; Santa Cruz Biotechnology, Santa Cruz, CA; TBS, containing 0.5% Tween 20, 3% nonfat milk, and 2% bovine serum albumin) and then incubated with a polyclonal anti-human MT4-MMP (AB854, 1 μ g/ml; Chemicon, Temecula, CA) and a polyclonal anti-human MT5-MMP antibody (AB924, 0.2 μ g/ml; R&D, Minneapolis, MN), respectively, on a rocker at room temperature for 2 hours. The species reactivity for MT5-MMP is positive to both human and mouse according to the information from R&D. In addition, alignment of mouse MT4- and MT5-MMP protein sequences with that of human revealed 82.0% and 92.6% of homology, respectively. Samples treated with nonimmune (normal) rabbit IgG or without primary antibody treatment were processed as the negative control. Afterward, the blot was incubated with anti-rabbit secondary antibody conjugated with horseradish peroxidase (0.5 μ g/ml; Roche Molecular Biochemicals, Indianapolis, IN) at room temperature for 1 hour. Finally, the blot was developed by a chemiluminescence kit (Amersham, Arlington Heights, IL), and MT4- and MT5-MMP were visualized as dark bands with corresponding molecular weights. Immunoblot analysis of each MT-MMP was repeated at least twice.

Immunohistochemical Staining

The corneas, harvested on days 0 (uninfected) and 6 after infection (peak inflammatory response), were fixed with 10% buffered formalin overnight, dehydrated with increased concentrations of ethanol and 100% xylene, infiltrated with paraffin overnight, and embedded in fresh paraffin. The tissues were sectioned (4 μ m) to prepare slides, and the slides were deparaffinized, rehydrated, and treated with proteinase K (Sigma, St. Louis, MO). Normal horse serum and 3% hydrogen peroxide were applied separately to reduce nonspecific staining and to

remove endogenous peroxidase. The slides were treated with specific primary antibodies recognizing mouse MT4- and MT5-MMP (the same as used for immunoblot analysis) in a humidified chamber at room temperature for 2 hours, followed by subsequent treatment with a biotinylated anti-rabbit secondary antibody and the ABC reagents (Vectastain; Vector Laboratories, Burlingame, CA). Positive staining was exhibited by diaminobenzidine (DAB; Vector) treatment appearing as brown granules.

RESULTS

Expression of MT4-, MT5-, and MT6-MMP in Mouse Cornea

Semiquantitative RT-PCR was performed to determine whether normal mouse corneas contain mRNA for MT4-, MT5-, and MT6-MMP and whether the MT-MMP expression is modulated by corneal infection. The corneas were harvested on days 0 (control), 1 through 5, and 8 after infection and total RNA was prepared. As shown in Figure 1, the gene expression for MT4- and MT5-MMP was found in normal (uninfected) mouse corneas, whereas MT6-MMP was not detectable by human MT6-MMP primers in uninfected corneas. When mice were infected with *P. aeruginosa*, the MT4-MMP mRNA expression in the cornea remained the same on the first 4 days and was then induced on day 5, remaining high through day 8. The MT5-MMP mRNA expression in the cornea infected with *P. aeruginosa* did not change for the first few days and then showed slight reduction until day 8, when significant induction of the MT5-MMP mRNA expression was observed. In contrast, RT-PCR results showed a ~200-bp mRNA segment that was amplified by human MT6-MMP primers and peaked at day 4. DNA sequencing and alignment with human MT6-MMP revealed 46.6% of gene homology of this DNA segment when compared with human MT6-MMP (data not shown). In addition, there was no significant similarity between the amplified DNA and other known genes.

To verify the amplified MT-MMPs, the amplified DNA sequences were subjected to restriction enzyme digestion. The amplified MT4-MMP product was cleaved by *Sma*I at the site between base pairs 78 and 79, which generated two smaller pieces (78-bp and 127-bp bands). The amplified MT5-MMP product was hydrolyzed by *Mbo*I at the site between bp 64 and 65, which generated two bands of 64 bp and 128 bp (data not shown).

There was no difference in any MT-MMP mRNA expression between the scratched corneas and the unscratched corneas on day 0, indicating that corneal abrasion did not affect the

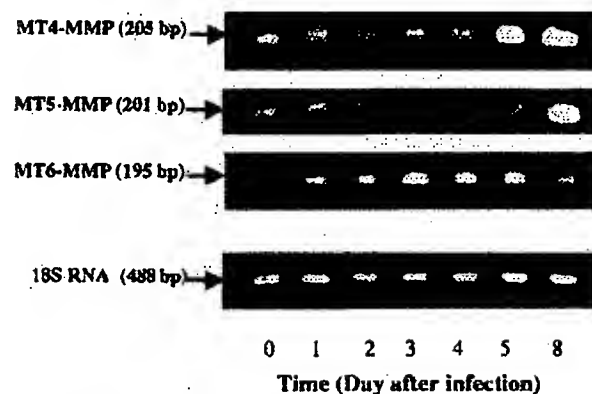


FIGURE 1. mRNA expression of MT4-, MT5-, and MT6-MMP in mouse corneas infected with *P. aeruginosa*.

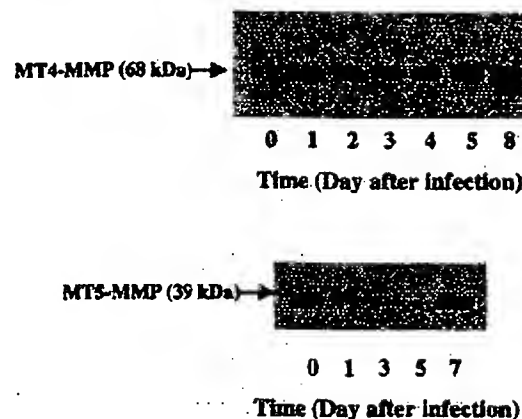


FIGURE 2. Protein expression of MT4- and MT5-MMP in mouse corneas infected with *P. aeruginosa*.

mRNA expression (data not shown). In addition, negative control samples (those not treated with reverse transcriptase or amplified without specific primers) did not exhibit any MT-MMP expression (data not shown).

To confirm MT-MMP expression at the protein level and to compare MT-MMP expression in the corneas at different time points during the infection, immunoblot analysis of corneal extracts was performed. As shown in Figure 2, MT4-MMP with a molecular weight of ~68 kDa was detected in the uninfected mouse corneas (day 0 sample), which had a molecular weight similar to human MT4-MMP identified in brain extracts.¹³ In corneas infected with *P. aeruginosa*, the expression of MT4-MMP was gradually induced and remained at a high level on day 8. MT5-MMP expression in corneas was different from that of MT4-MMP. MT5-MMP with a molecular weight of ~39 kDa, probably the soluble species, was found in normal corneas.⁹ The expression was reduced from day 1 through day 5 after infection. There was a significant induction of MT5-MMP expression on day 7 after infection. These results were consistent with the gene expression of MT5-MMP during the infection.

MT-MMP expression at the protein level in the scratched corneas was comparable to that of the unscratched corneas on day 0. No signals were detected in any negative control samples (data not shown).

Localization of MT4- and MT5-MMPs in Mouse Corneas

To localize MT-MMP expression in the mouse corneas, immunohistochemical staining was performed using the corneal samples of normal and infected mice. As shown in Figure 3, no

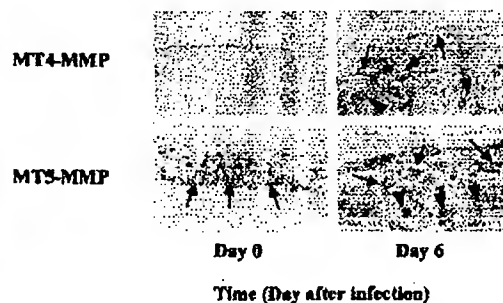


FIGURE 3. Localization (arrows) of MT4- and MT5-MMP expression in mouse corneas infected with *P. aeruginosa*.

positive staining of MT4-MMP was found in the normal cornea, although immunoblot analysis showed a weak band of MT4-MMP on day 0 (normal cornea), perhaps because there is much less sensitivity in immunohistochemical staining than in immunoblot analysis. On day 6, MT4-MMP expression was localized in both epithelial tissue (weak positive staining) and substantia propria (strong positive staining). MT5-MMP expression was observed in corneas of normal mice, mainly localized in the epithelium. On the sixth day after infection, the distribution of MT5-MMP was not restricted to the epithelium but was also detected in the substantia propria.

DISCUSSION

Corneal damage caused by *P. aeruginosa* infection starts with inflammatory reactions such as edema, leukocyte infiltration, and angiogenesis. With continuation of the inflammation, corneal ulceration may occur, and corneal perforation may eventually take place because of the stromal dissolution.¹⁶⁻¹⁸ One of the possible mechanisms responsible for corneal destruction is that both host and bacterial proteases contribute to the degradation of Bowman's membrane and the ECM, which leads to severe corneal damage. Evidence for this hypothesis is based on the observations that purified proteases are able to cleave ECM proteins and that bacterial proteases can cause keratitis by activating host proteases.^{19,20} In addition, the two gelatinases MMP-2 and -9 have been identified in corneal tissues and shown to play a role in corneal ulceration and tissue remodeling in a noninfectious disease model.²¹⁻²³

Although a number of studies have begun to reveal the effects of some MMPs on corneal tissues under physiological and pathologic conditions, little is known about the expression and regulation of MT-MMPs in the cornea. Our recent work on MT1-, MT2-, and MT3-MMP showed that these three MT-MMPs are all present in the normal mouse cornea and that there is a significant induction of each of them in the corneas of naïve (unimmunized) mice intracorneally infected with *P. aeruginosa*, whereas the induction in the infected corneas of immunized mice reaches a much lower level and has a shorter duration.¹

In the present study, we further investigated the expression and regulation of another three recently identified MT-MMPs—MT4-, MT5-, and MT6-MMP, in the mouse corneas infected with *P. aeruginosa*. MT4- and MT5-MMP were identified in the normal (uninfected) mouse cornea at both the mRNA and protein levels, whereas MT6-MMP was not detectable by RT-PCR. Similar to MT1-, MT2-, and MT3-MMP, expression of MT4-, MT5-, and MT6-MMP also showed a significant induction in corneas when mice were intracorneally infected with *P. aeruginosa*. However, the induction pattern was different from that previously observed (MT1-, MT2-, and MT3-MMP). MT4-MMP expression in the infected corneas did not change dramatically until day 5 after infection. It was reported that MT4-MMP was mainly expressed by leukocytes, especially by monocytes and macrophages.¹¹ Indeed, our data showed strong positive staining of MT4-MMP in the cornea on day 6 after infection. Moreover, our previous histologic study also showed increased macrophage infiltration of the corneas during days 6 and 9 after infection.¹ Therefore, the infiltrating macrophages seemed responsible for the induction of MT4-MMP expression in the cornea during the late stage of the inflammation. Although MT5-MMP was primarily identified in human brain tumor,²⁴ basal expression of MT5-MMP was also found in our corneal studies, primarily localized in the epithelial tissue.

Downregulation of MT5-MMP during the early stage of the infection (days 2-4) possibly resulted from injury of epithelial

cells, because they seem to be the only source of MT5-MMP in the normal cornea, according to our studies of immunohistochemical staining. Later induction of MT5-MMP was probably also due to the infiltration of macrophages into the infected cornea. MT6-MMP, also called leukolysin,¹² was not detected in the normal cornea by RT-PCR, but with infection, there was a significant induction of MT6-MMP expression in corneas. It was reported that MT6-MMP was predominantly expressed in leukocytes.^{6,12} Our data regarding MT6-MMP induction correlate well with our previous findings on corneal inflammation as quantified by bacterial numbers, PMNs measured by myeloperoxidase, arachidonic acid metabolites, and cytokines.²⁵⁻²⁷ In addition, previous histologic studies showed that PMNs peak at day 6 after infection and then diminish gradually, which has good correlation with the MT6-MMP induction pattern.¹ Thus, induced expression of MT6-MMP in the cornea may be produced by PMNs.

As members of the MMP family, MT4- and MT5-MMP hydrolyze a variety of ECM components, such as fibronectin, gelatin, fibrinogen, fibrin, and proteoglycans.^{11,28} The induced enzymatic activity during the inflammation may cause degradation of the Bowman membranes and ECM components, leading to severe corneal damage. Similar to other MT-MMPs, MT4-, MT5-, and MT6-MMP are also capable of activating pro-MMP-2.^{5,6,29} Therefore, the induction of these MT-MMPs in the mouse corneas infected with *P. aeruginosa* may also be responsible for corneal damage caused by other proteases that are activated by these MT-MMPs.

Acknowledgments

The authors thank Julianna M. Berk for technical assistance.

References

- Dong Z, Ghabrial M, Katar M, Fridman R, Berk RS. Membrane-type matrix metalloproteinases in mice intracorneally infected with *Pseudomonas aeruginosa*. *Invest Ophthalmol Vis Sci*. 2000;41:4189-4194.
- Woessner JF. The matrix metalloproteinase family. In: Parks WG, Mecham RP, eds. *Matrix Metalloproteinases*. San Diego, CA: Academic Press; 1998:1-14.
- Kahari VM, Saarialho-Kere U. Matrix metalloproteinases and their inhibitors in tumour growth and invasion (review). *Ann Med*. 1999;31:34-45.
- Gururajan R, Grenci J, Lalini JM, Kidd VJ. Isolation and characterization of two novel metalloproteinase genes linked to the Cdc2L locus on human chromosome 1p36.3. *Genomics*. 1998;52:101-106.
- Pei D. Identification and characterization of the fifth membrane-type matrix metalloproteinase MT5-MMP. *J Biol Chem*. 1999;274:8925-8932.
- Velasco G, Cal S, Merlos-Suarez A, et al. Human MT6-matrix metalloproteinase: identification, progelatinase A activation, and expression in brain tumors. *Cancer Res*. 2000;60:877-882.
- de Coignac AB, Elson G, Delneste Y, et al. Cloning of MMP-26. A novel matrixlysin-like proteinase. *Eur J Biochem*. 2000;267:3323-3329.
- Sato H, Takino T, Okada Y, et al. A matrix metalloproteinase expressed on the surface of invasive tumour cells. *Nature*. 1994;370:61-65.
- Strongin AY, Collier I, Bannikov G, Marmer HL, Grant GA, Goldberg GI. Mechanism of cell surface activation of 72-kDa type IV collagenase. Isolation of the activated form of the membrane metalloproteinase. *J Biol Chem*. 1995;270:5331-5338.
- Will H, Atkinson SJ, Butler GS, Smith B, Murphy G. The soluble catalytic domain of membrane type 1 matrix metalloproteinase cleaves the propeptide of procollagenase A and initiates autoproteolytic activation: regulation by TIMP-2 and TIMP-3. *J Biol Chem*. 1996;271:17119-17123.

11. English WR, Puente XS, Freije JM, et al. Membrane type 4 matrix metalloproteinase (MMP17) has tumor necrosis factor- α convertase activity but does not activate pro-MMP2. *J Biol Chem*. 2000;275:14046-14055.
12. Pei D. Leukolysin/MMP25/MT6-MMP: a novel matrix metalloproteinase specifically expressed in the leukocyte lineage. *Cell Res*. 1999;9:291-303.
13. Puente XS, Pendas AM, Llano E, Velasco G, Lopez-Otin C. Molecular cloning of a novel membrane-type matrix metalloproteinase from a human breast carcinoma. *Cancer Res*. 1996;56:944-949.
14. Itoh Y, Kajita M, Kinoh H, Mori H, Okada A, Sciki M. Membrane type 4 matrix metalloproteinase (MT4-MMP, MMP-17) is a glycosylphosphatidylinositol-anchored proteinase. *J Biol Chem*. 1999;274:34260-34266.
15. Kojima S, Itoh Y, Matsumoto S, Masuko Y, Sciki M. Membrane-type 6 matrix metalloproteinase (MT6-MMP, MMP-25) is the second glycosyl-phosphatidyl inositol (GPI)-anchored MMP. *FEBS Lett*. 2000;480:142-146.
16. Wilson LA. In: Duane TD, ed. *Ophthalmology*. New York: Harper & Row; 1978:1-16.
17. Van Horn DJ, Davis SD, Hyndink RA, Pederson HJ. Experimental *Pseudomonas* keratitis in the rabbit: bacteriologic, clinical, and microscopic observations. *Invest Ophthalmol Vis Sci*. 1981;20:213-221.
18. Twining SS, Lohr KM, Moulder JE. The immune system in experimental *Pseudomonas* keratitis: model and early effects. *Invest Ophthalmol Vis Sci*. 1986;27:507-515.
19. Fini ME, Girard MT, Matsubara M. Collagenolytic/gelatinolytic enzymes in corneal wound healing (review). *Acta Ophthalmol Suppl*. 1992;70:26-33.
20. Twining SS, Kirschner SE, Mahnke LA, Frank DW. Effect of *Pseudomonas aeruginosa* elastase, alkaline protease, and exotoxin A on corneal proteinases and proteins. *Invest Ophthalmol Vis Sci*. 1993;34:2699-2712.
21. Fini ME, Girard MT. Expression of collagenolytic/gelatinolytic metalloproteinases by normal cornea. *Invest Ophthalmol Vis Sci*. 1990;31:1779-1788.
22. Azar DT, Hahn TW, Jain S, Yeh YC, Stettin-Stevensen WG. Matrix metalloproteinases are expressed during wound healing after excimer laser keratectomy. *Cornea*. 1996;15:18-24.
23. Matsubara M, Girard MT, Kublin CL, Cinton C, Fini ME. Differential roles for two gelatinolytic enzymes of the matrix metalloproteinase family in the remodelling cornea. *Dev Biol*. 1991;147:425-439.
24. Llano E, Pendas AM, Freije JP, et al. Identification and characterization of human MT5-MMP, a new membrane-bound activator of progelatinase A overexpressed in brain tumors. *Cancer Res*. 1999;59:2570-2676.
25. Hazlett LD, Zucker M, Berk RS. Distribution and kinetics of the inflammatory cell response to ocular challenge with *Pseudomonas aeruginosa* in susceptible versus resistant mice. *Ophthalmic Res*. 1992;24:32-39.
26. Kernacki KA, Berk RS. Characterization of arachidonic acid metabolism and the polymorphonuclear leukocyte response in mice infected intracorneally with *Pseudomonas aeruginosa*. *Invest Ophthalmol Vis Sci*. 1995;36:16-23.
27. Kernacki KA, Berk RS. Characterization of the inflammatory response induced by corneal infection with *Pseudomonas aeruginosa*. *J Ocul Pharmacol*. 1994;10:281-288.
28. Wang X, Yi J, Lei J, Pei D. Expression, purification and characterization of recombinant mouse MT5-MMP protein products. *FEBS Lett*. 1999;462:261-266.
29. Wang Y, Johnson AR, Ye QZ, Dyer RD. Catalytic activities and substrate specificity of the human membrane type 4 matrix metalloproteinase catalytic domain. *J Biol Chem*. 1999;274:33043-33049.

ORIGINAL ARTICLE

Assessment of Proliferative Activity in Colorectal Carcinomas by Quantitative Reverse Transcriptase-Polymerase Chain Reaction (RT-PCR)

Michael Duchrow, Ph.D.,^{1,*} Stefan Häsemeyer, M.D.,¹
Rainer Bröll, M.D.,¹ Hans-Peter Bruch, M.D.,² and
Ute Windhövel, Ph.D.¹

¹Surgical Research Laboratory and ²Surgical Clinic, Medical University
of Lübeck, Lübeck, Germany

ABSTRACT

The monoclonal antibody Ki-67 and the isospecific monoclonal antibody MIB-1 are routinely used in oncology to assess the proliferation index of tumor cells. A more objective and sensitive method is the determination of the of Ki-67 protein-specific mRNA by quantitative reverse transcriptase-polymerase chain reaction (RT-PCR). In 25 resected colorectal adenocarcinomas of different stages and grades we determined between 0.2 and 4.4 amol (10^{-18} mol) Ki-67 protein-specific mRNA per microgram total RNA (median = 0.88 amol). The corresponding Ki-67 indices (expressing the percentage of Ki-67/MIB-1 positive tumor cells) ranged from 41 to 81% (median = 61%). We found a good correlation between Ki-67 index and mRNA expression ($r = 0.75$), a significant correlation between both data and tumor stage (primary tumor, regional nodes, metastasis [pTNM] staging classification) ($p < 0.001$), but not between both data and tumor grade. Both Ki-67 indices ($p = 0.05$) and mRNA levels ($p = 0.014$) correlated significantly to the patients' survival. These results demonstrate that the Ki-67 protein-specific quantitative RT-PCR is a useful method for the characterization of tumor cell proliferation.

KEY WORDS: Colorectal carcinoma; Immunohistochemistry; Ki-67 antigen; MIB-1; Proliferation index; Quantitative RT-PCR.

* Corresponding author. Michael Duchrow, Ph.D., Surgical Research Laboratory, Surgical Clinic, Medical University of Lübeck, Ratzeburger Allee 160, D-23538 Lübeck, Germany. Fax: 49-0451-500-2069.

INTRODUCTION

The monoclonal antibodies Ki-67 (1) and MIB-1 (2) are widely used for the immunohistochemical assessment of the growth fraction of tumor cells. Both antibodies recognize overlapping epitopes of a human nuclear protein that is exclusively expressed in proliferating cells (3). Cell cycle analyses revealed that cells in all active cycle phases (G_1 , S, G_2 , and mitosis) react with Ki-67 and MIB-1, whereas G_0 cells are consistently negative (4). Thus, with antibodies against the Ki-67 protein, a fast and reproducible determination of the growth fraction of a given human cell population became possible with immunohistochemical methods well within the scope of a routine pathology laboratory (5,6). The importance of Ki-67 for measuring the growth fraction in clinical samples of human neoplasms is particularly well illustrated by retrospective studies of, e.g., non-Hodgkin's lymphomas (7-10), human breast carcinomas (11-13), lung carcinomas (14), soft-tissue sarcomas (15), and bladder tumors (16). For example, Gerdes et al. (7) found a significant correlation between the Ki-67 index and high- and low-grade non-Hodgkin's lymphomas. A similar correlation could be observed in soft-tissue sarcomas, for which the Ki-67 index proved to be of great additional prognostic value (15).

Despite these well-documented diagnostic and prognostic applications, the Ki-67 protein has not been identified in molecular terms for a decade. Recently, however, it has been shown that Ki-67 detects two polypeptides of 345 and 395 kDa in immunoblots of proliferating cells (17,18). Successful cloning and sequencing of the full-length Ki-67 protein cDNA (19) and gene locus (20) made it possible to examine the expression of the Ki-67 protein gene. In our study we aimed to quantify the Ki-67 protein mRNA expression in fresh frozen tumor tissues of colorectal carcinomas and to determine the Ki-67 indices (expressing the percentage of Ki-67/MIB-1 positive tumor cells) in formalin-fixed and paraffin-embedded tissue sections immunohistochemically with MIB-1 of the same patients. The results of both methods were compared, and we correlated them to the primary tumor, regional nodes, metastasis (pTNM) staging classification, tumor stage, tumor grade, and patients' prognosis.

MATERIALS AND METHODS

Clinical Data

Our retrospective study included 25 patients (13 females and 12 males) with a median age of 68 years (47-

80 years). All patients had undergone surgery for a colorectal adenocarcinoma between 1994 and 1995 in the Surgical Clinic of the Medical University of Lübeck, Germany. Postoperative tumor staging was determined according to the pTNM classification system of the International Union Against Cancer (UICC) (21). The distribution of the extent of disease according to the pTNM classification was as follows: stage I, 5 (20%); stage II, 6 (24%); stage III, 7 (28%); and stage IV, 7 (28%). Sixteen patients had a moderately differentiated tumor (G2), whereas nine had poorly differentiated carcinomas (G3). Curative tumor resection (R0 resection), defined as the removal of all gross tumors and the demonstration of tumor-negative surgical margins by microscopic examination of the total circumference of the resection line, was possible in 16 patients (65%). Patients' data were documented at the time of surgical treatment between June 1994 and November 1995 and evaluated in 1999 after a maximum of 54 months and a minimum of 45 months. All patients had primary tumors. The follow-up period ranged from 1 to 54 months with a median of 49 months. None of the patients died within 30 days after surgery from postoperative complications.

Immunohistochemistry

Tumor tissues had been fixed in 4.5% formalin and embedded into paraffin in a routine manner as surgical pathology specimens. The paraffin blocks were stored at ambient temperature before analysis. Immunohistochemistry was performed as described by Cattoretti et al. (22) with modifications. Four-micrometer sections of the paraffin blocks were dewaxed in xylene, rehydrated in graded alcohol, and pretreated for antigen retrieval in citrate buffer (pH 6) in a microwave oven (800 W) for four cycles of 10 min. Sections were immunostained with MIB-1 (a mouse immunoglobulin of the IgG1 subclass; kindly provided by Prof. Dr. J. Gerdes, Molecular Immunology, Research-Centre Borstel, Germany) using the avidin biotin complex method (hrp) with 3-amino-9-ethyl-carbazole as chromogen according to the manufacturer's recommendations (DAKO, Glostrup, Denmark) and counterstained with hematoxylin before mounting.

Determination of the Ki-67 Index

A minimum of two MIB-1 immunostained sections per patient were microscopically evaluated using a total magnification of 400 \times and a 10 \times 10 square grid placed in the microscope's eyepiece. Avoiding margins of sections and areas of poorly presented morphology, areas

with the highest number of positive nuclei were chosen to evaluate the Ki-67 index (MIB-1 labeling index), ensuring that the whole section was scanned. Any nuclear staining of tumor cells was considered to be positive. The Ki-67 index was determined in a minimum of five high-power fields per specimen by counting more than 500 of the total number of tumor cells per section. All specimens were examined independently by two experienced investigators without knowledge of clinical or pathohistological data. Cases with discordant results were reanalyzed to obtain a consensus. The Ki-67 index was calculated as the percentage of MIB-1-positive nuclei in relation to all tumor cell nuclei. Intratumoral variations of the Ki-67 indices remained unconsidered. The Ki-67 indices were correlated to the results of the quantitative reverse transcriptase-polymerase chain reaction (RT-PCR), as well as to pTNM category, tumor stage, tumor grade, and patients' survival.

Isolation of Total RNA and RT Reaction

Total RNA from fresh frozen tumor tissues, adjacent mucosa, or HeLa S3 cells (as positive control) was recovered by a modification of methods described by Chomczynski and Sacchi (23) using Trizol[®] according to the manufacturer's instructions (Gibco BRL, Eggenstein, Germany). A routinely hematoxylin/eosin (HE)-stained frozen section of the tumor was used to ensure that the tumor portion of the tissue was >90%. As negative control we used tumor-free adjacent tissues from the same patient. The concentration and purity of RNA were determined spectrophotometrically by measuring its absorption at 260 and 280 nm. The RT reaction was performed with the Superscript kit according to the manufacturer's recommendations (Gibco BRL). Three micrograms total RNA and 0.5 µg poly(dT)₁₂₋₁₈-primer (Pharmacia Biotech, Freiburg, Germany) were used for each reaction. The resultant cDNA (100 µl) was stored at -20°C until needed.

PCR

To determine the integrity of the RNA and the quality of the RT-reaction, a 296-bp fragment of the housekeeping gene β 2-microglobulin (EMBL accession no. J00105; exon one to exon three) was amplified by RT-PCR. To exclude amplification of contaminating genomic DNA, the primer binding sites spanned intron number one or intron number two, respectively. The sequences of the primers were: 5'-ATCCAGCGTACTCCAAAGATT-3' (sense) and 5'-CATGTCTCGATCCCACTTAAGTAT-

3' (antisense). PCR was performed in 100 µl standard reaction volume containing 10 µl of tricine buffer [300 mM tricine; 20 mM MgCl₂; 50 mM β -mercaptoethanol; 0.1% (v/v) gelatin; 1% (w/v) povidone; pH 8.4]; 1 µl of 20 mM dNTP (Pharmacia Biotech), 5 µl each of sense and antisense primer (20 µM), 0.5 µl *Taq* polymerase (5 U/µl, Gibco BRL, Eggenstein, Germany), and finally 10 µl of the cDNA. The reaction mixture was overlaid with mineral oil and subjected to 35 cycles PCR in a TC1 Thermocycler (Perkin-Elmer, Weiterstadt, Germany). The conditions were 2 min denaturation at 94°C, 2 min annealing at 55°C, and 3 min extension at 72°C, with an additional 7 min of incubation at 72°C after the final extension. As a negative control for all PCR experiments, cDNA was replaced by water. The cDNA transcribed from mRNA of HeLa cells was used as positive control. PCR products (10 µl) were electrophoresed through 1% agarose gels prepared with 50 mM Tris-acetic acid, 2 mM ethylenediaminetetraacetic acid (EDTA), pH 7.9 (TAE buffer) and visualized by ethidium bromide and UV light. Only samples with a constant visible 296 bp band of the amplified β 2microglobulin-cDNA were used for further evaluation in quantitative PCR of the *Ki-67* protein gene.

The sequences of the primers for the amplification of the *Ki-67* protein cDNA (EMBL accession no. X65550) were (first round) sense 5'-GATGGAAGCTTCACGGG AAC-3' (exon 13) and antisense 5'-GAAGATAAAGGCATCAAAGC-3' (exon 14) with an expected 1037-bp product; (second round) nested antisense primer with a 5' overhang of the GCN4-protein binding consensus sequence 5'-GGATGACTCATTCAAAGCAAACACCT GAC-3' (exon 13) and biotinylated nested antisense 5'-AGGGACCGAGTCTTGTAAT-3' (exon 14). A 416-bp product spanning intron 13 was expected. The components and conditions for the nested PCR were the same as described above with the exception that a 10 µl aliquot of the first-round product was used as template for the second round and that two rounds of amplification with 30 cycles each were used. The competitive homologous standard (see below) was applied to the reaction mixture of the first round in a known amount (0.88 fg of the plasmid corresponding to 0.27 amol [10^{-18} mol]).

Construction of a Competitive Homologous Standard for the *Ki-67* Protein Gene

The standard (a fragment of the same size and sequence as the native cDNA, but with an artificial *HindIII*-site) was constructed by site-directed mutagenesis using nested PCR with three primers and 1 ng of a cloned *Ki-67* protein cDNA fragment from HeLa cells as template.

The sequences of the primers were (first round) sense 5'-GATGGAAGCTTCACGGGAAC-3' (exon 13) and antisense 5'-TGCTGTTCTGCCTCAGTC-3' (exon 13), (second round) solely antisense 5'-GAAGATAAAGGCATCAAAGC-3' (exon 14). The components and conditions for the PCR were the same as described for nested PCR above, except that 15 cycles were used. The resulting 1037-bp fragment was cloned in *Escherichia coli* using the 3.9-kb PCR^{II}TM-vector (TA cloning kit, Invitrogen, Heidelberg, Germany). The plasmid containing the standard was purified with QIAprep (Qiagen, Hilden, Germany).

Quantification of PCR Products

The PCR products were subjected to spin column purification (QIAquick PCR Purification Kit, Qiagen) and divided into two aliquots—one was incubated with the restriction endonuclease *Hind*III to complete digestion, while the other remained undigested. All digested and undigested products were subjected to the CAPTA-GENETM-GCN4 enzyme-linked immunosorbent immunoassay (ELISA) (Pharmacia Biotech) according to the manufacturer's recommendations. In brief, the 5' overhang of the GCN4-protein binding consensus sequence was specifically bound to the bottom of a 96-well ELISA plate. After extensive washings, the approximate 5' biotin residue of the antisense strand was used as target for a streptavidine alkaline phosphatase-mediated color reaction. The absorbency at 450 nm and the background correction at 620 nm were measured in doublets using an appropriate reader (SLT, Grödig, Austria). The absorbency resulting from the digested aliquot corresponds to the amount of native cDNA, whereas the difference of the absorbency of digested and undigested aliquots corresponds to the amount of the standard. The result of the standard was then used to normalize the data of the native cDNA.

To confirm the PCR products as *Ki-67* protein gene specific, nucleotide sequences of PCR products from five randomly chosen patients with a colorectal tumor were examined by automatic fluorescent dideoxy cycle-sequencing using a Li-Cor 4000L automatic fluorescence DNA sequencer (Li-Cor, Lincoln, NE) according to the manufacturer's recommendations. The sequences obtained were aligned with the published sequence (20).

Statistical Analysis

For quantification of the PCR products, all samples were measured twice and the mean data were calculated.

If the SD of the determined data exceeded 20%, an additional measurement was necessary. The results of the quantitative RT-PCR were correlated to the *Ki-67* indices, as well as to pTNM category, tumor stage, tumor grade, and patients' survival. Survival data were obtained from the tumor surveillance program of our clinic. Statistical evaluation was carried out with the SPSS program package (SPSS GmbH Software, Munich, Germany). The Wilcoxon matched-pairs signed-rank test was used to evaluate significant differences of the *Ki-67* index and the *Ki-67* protein mRNA level versus pTNM categories, tumor stage, and tumor grade. Survival rates of patients were calculated by the method of Kaplan and Meier (24). Patients who were alive at the last follow-up evaluation were censored at that time. Differences in survival between groups of patients with low data (less than median) and high data (greater than or equal to median) were estimated using the log-rank test. A *p* value ≤ 0.05 was considered significant.

RESULTS

In this study we investigated tumor tissues from 25 patients with a colorectal adenocarcinoma. MIB-1-positive tumor cells showed a clear red staining of their nuclei, whereas staining of the cytoplasm was not observed. In normal and adjacent mucosa we found MIB-1-stained nuclei in cells of the proliferation-active zone at the bottom of the crypts. In contrast to the normal or adjacent mucosa, tumor specimens revealed a different pattern of MIB-1 staining. A great intratumoral heterogeneity of stained tumor cell nuclei was observed. Areas showing a high proliferative activity and areas of low occurrence of stained tumor cells could be found. A clear morphological distinction between tumor cells and other cells was always possible.

The *Ki-67* indices of the investigated tumors ranged from 42 to 84% with a mean *Ki-67* index of 60% (median = 61%). We found a correlation between the *Ki-67* index and the tumor stage ($p < 0.001$), between the *Ki-67* index and the depth of tumor invasion ($p = 0.032$), and between the *Ki-67* index and tumors with and without lymph node metastases ($p < 0.001$) (Table 1). Patients having distant metastases had a higher median *Ki-67* index (72%) than patients without metastases (53%) ($p = 0.001$). We found no correlation of the *Ki-67* index to tumor grade.

Forty percent (10 of 25) of the patients died during the median follow up time of 49 months. To find a possible correlation between the *Ki-67* index and patient's prog-

Table 1
Statistics of the Ki-67 Indices and Ki-67 mRNA Levels

Tumor Characteristic	Patients (n)	Median Ki-67 Index	p Value	Median Ki-67 mRNA ^a	p Value
Total	25	61%		0.88 amol	
Stage I and II	11	47%	<0.001	0.31	<0.001
Stage III and IV	14	67%	<0.001	1.06	<0.001
Grade 2	16	63%	^b	0.87 amol	^b
Grade 3	9	59%	^b	0.97 amol	^b
pTNM categories					
T1/T2	7	47%	0.032	0.26 amol	0.014
T3/T4	19	65%			0.014
N0	11	47%	<0.001	0.31 amol	<0.001
N1/N2/N3	14	67%	<0.001	1.06 amol	<0.001
M0	18	53%	0.001	0.62 amol	0.004
M1	7	72%	0.001	1.08 amol	0.004

^a Data equivalent to 1 µg total RNA.

^b Not significant.

nosis, we compared patients with a median index (61%) or less to patients with an index higher than the median. The overall survival rates [Fig. 1(a)] indicated a significantly better prognosis for the group with the lower Ki-67 index ($p = 0.05$).

For the quantification of the RT-PCR products we chose an ELISA, which has the advantages of low cost, easy processing, and fast handling. As a positive control for all PCRs and as a template for evaluation of the sensitivity of the ELISA, we used cDNA from HeLa cells (data not shown). Serial dilutions of this template resulted in a linear absorption range for the ELISA from about

$A_{450} = 0.1$ to $A_{450} = 2.0$. The usable dynamic range for the quantification of PCR products was about one decade. This made it necessary to dilute the cDNA of those samples with Ki-67 protein mRNA content of more than 1.5 amol in a ratio of at least 1:5. For the investigation of tissue material, we found the optimal amount for the added competitive standard plasmid to be 0.8–1.0 fg. All cDNA samples used for quantitative PCR showed a constant visible 296-bp band when amplified with the $\beta 2$ -microglobulin primer, indicating that the procedures of RNA isolation and RT-reaction had no influence on the quantification.

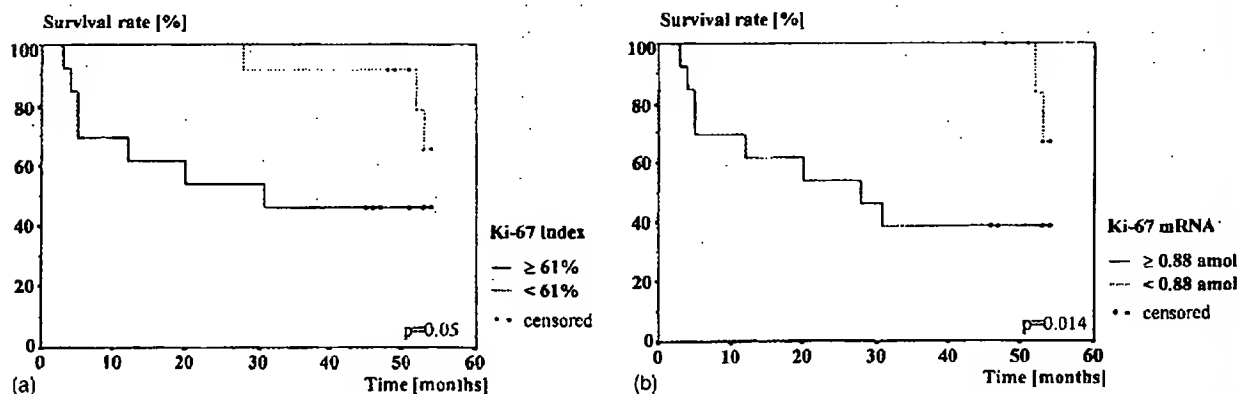


Figure 1. Survival curves of 25 patients with a colorectal carcinoma. (a) Significant difference in survival rates between patients with a Ki-67 index $< 61\%$ and $\geq 61\%$ ($p = 0.05$). (b) Significant difference in survival rates between patients with a Ki-67 protein mRNA level < 0.88 amol per microgram total RNA and ≥ 0.88 amol per microgram total RNA ($p = 0.014$).

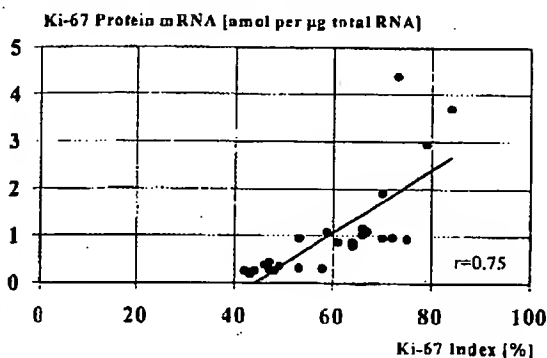


Figure 2. Correlation of Ki-67 protein mRNA expression to Ki-67 indices ($r = 0.75$).

For all investigated tumors the mean total content of the Ki-67 protein mRNA was 1.09 amol in 1 µg of isolated total RNA (median = 0.88 amol). The content varied in a wide range from 0.2 to 4.38 amol. Similar to the Ki-67 index, we found significant correlation between the Ki-67 protein mRNA level and the tumor stage ($p < 0.001$), between the Ki-67 protein mRNA level and the depth of tumor invasion ($p = 0.014$), between the Ki-67 protein mRNA level and tumors with and without lymph node metastases ($p < 0.001$), and between the Ki-67 protein mRNA level and tumors of patients with and without distant metastases ($p = 0.004$) (Table 1). We found no correlation between the Ki-67 protein mRNA level and tumor grade. The correlation between the Ki-67 protein mRNA level and patients' prognosis is shown in Fig. 1(b). The overall survival rates exhibited a significantly better prognosis for the group with lower Ki-67 protein mRNA level than the median ($p = 0.014$). The Ki-67 indices correlated well to the Ki-67 protein mRNA levels (correlation coefficient $r = 0.75$) (Fig. 2).

As a control we investigated 10 randomly chosen samples of tumor-free adjacent tissues from the patients. In these adjacent tissues we measured <0.1 – 0.6 amol (median = 0.1 amol) of Ki-67 protein mRNA per microgram total RNA. However, the content was always lower (0.1–45%) in comparison to the corresponding tumor. Five randomly chosen tumor samples were sequenced to confirm the RT-PCR products as Ki-67 protein specific. The nucleotide sequences of all RT-PCR products examined were identical to the published cDNA sequence (20) (data not shown).

DISCUSSION

Therapeutic decisions for cancer patients are often made on the basis of prognostic factors. In addition to the

traditional pTNM classification, other factors have been validated for routine clinical use, e.g., expression of tumor suppressor genes and oncogenes. The influence of the proliferation rate of tumor cells on patients' survival has been discussed for a long time and this rate is considered to reflect the course of tumor disease. Proliferative activity of tumors can be determined by various methods, e.g., by measuring the doubling time, by calculating the labeling index after ^3H -thymidine or bromodeoxyuridine incorporation, by calculating the mitotic index, or by using cytometry. Flow cytometric determination of S-phase cells is expensive and technically difficult. The other techniques are time consuming and generally impractical for most clinicians.

Currently, pathologists are evaluating proliferation indices almost exclusively by immunohistochemical means. The monoclonal antibody Ki-67 has been shown to be a reliable marker for proliferation, but its use was limited to frozen specimens (5) and previous studies with Ki-67 were often performed on a small number of cases. Recently, this disadvantage was overcome, because the monoclonal antibody MIB-1 is able to recognize the same antigen on formalin-fixed and paraffin-embedded sections (2).

In colorectal carcinomas the proliferative activity of tumor cells was determined in several investigations with different methods. With the help of monoclonal antibodies against the Ki-67 protein, a wide range of proliferative indices for colorectal carcinomas was published: Porschen et al. (25) investigated 52 colorectal carcinomas of patients who had not been treated before operation by radiotherapy or chemotherapy and determined a mean Ki-67 index of $38 \pm 18.4\%$ (7.7–75.3%). Kubota et al. (26) assessed 100 colorectal carcinomas and found a median of $34.6 \pm 22\%$ with Ki-67, whereas Diebold et al. (27) measured $52.8 \pm 8.7\%$ ($n = 6$) with MIB-1. Jansson and Sun (28) investigated 255 colorectal adenocarcinomas immunohistochemically with MIB-1 and found that 62% of the cases had more than 50% positive tumor cells. They did not find a significant relationship between Ki-67 expression and sex, age, tumor location, Dukes' stage, growth pattern, differentiation, DNA content, S-phase fraction, or survival ($p > 0.05$). Ofner et al. (29) determined MIB-1 labeling indices in a series of 106 colorectal carcinomas with three different evaluation methods: semiquantitative estimation (19.2% of the cases had more than 50% positive tumor cells), image analysis (0–59%; mean = 23.8%), and cell count (0–73%; mean = 31.9%). They stressed that determination of growth rates by MIB-1 labeling indices offers neither reproducible results nor clinical relevance in colorectal adenocarcinomas. Although for many tumor entities it has been shown

that high proliferative activity correlates with poor clinical outcome. For colorectal adenocarcinoma this has been reported in only a few publications (e.g., references 30 and 31).

In our study we immunohistochemically determined a median Ki-67 index of 61% (42–84%) with MIB-1, which seems to be in the upper range of previously published data. In contrast to many publications mentioned above, we could demonstrate a correlation between proliferative activity and clinical outcome ($p < 0.05$), but our results have to be interpreted carefully, because of the small number of the patients included in this study.

The studies mentioned above cannot be well compared, because the patient selection and the methods of data interpretation were quite different. Moreover, for predictive purposes patients are included in studies, regardless of whether they received preoperative or postoperative chemotherapy or radiotherapy, and the death of a patient was recorded without any information on the cause. In addition, the mean age of patients with a colorectal carcinoma is usually higher than for those with other tumor entities. These reasons may explain why the rate of survival was independent from the Ki-67 protein expression in most of the examinations. However, some authors believe that a true proliferation rate in neoplasia cannot be measured immunohistochemically because it is a function of both growth fraction and the time required for completion of the cell cycle (28,32).

We hypothesize that some of the problems related to the use of antibodies as proliferation markers may be solved by quantifying gene expression by quantitative RT-PCR: (i) Most tumors consist of heterogeneous cell populations, and therefore tumor cell proliferation may greatly vary intratumorally (5,33,34). The assessment of Ki-67 protein mRNA levels by quantitative RT-PCR may overcome the drawback of intratumoral heterogeneity, because a complete segment (>20 mg tissue) of the tumor is used for isolation of mRNA. The reliability will be improved if more than one sample from different non-necrotic intratumoral regions is assessed by an experienced pathologist. (ii) The Ki-67 protein is expressed during all active cell phases (G_1 , S, G_2 , and M) and, consequently, may be expressed in cells arrested in G_1 /S or G_2 /M as demonstrated with cell cultures by using synchronizing inhibitors (32). During anaphase and telophase the Ki-67 protein rapidly decreases (35), but from G_1 /S to G_2 /M phases it seems to be stabilized, e.g., by post-translational modifications and/or prohibition of degradation. In conclusion, not all cells containing the antigen must be actively proliferating. G_1 /S or G_2 /M cell

cycle arrested tumor cells do not need to express mRNA for the Ki-67 protein. Therefore, assessment of mRNA levels may also eliminate the problem of detectable Ki-67 protein in nonactively proliferating cells. (iii) The use of immunohistochemical markers often depends on a subjective assessment of specimens. Depending on the quality of fixation and labeling, even experienced pathologists will find different results on the same sections. Determination of mRNA levels is a more objective method, and will give reproducible results independent from the investigator's experience.

This is the first report on the assessment of tumor cell proliferation by quantitative RT-PCR. Since the introduction of the PCR, the number of reports using quantitative RT-PCR for mRNA analysis has increased substantially and it has become a routine procedure in many laboratories. One major drawback of the quantitative RT-PCR method is that it is impossible to localize the cellular source of the signal. If the investigated gene is also expressed in nontarget cells, results are indistinguishably influenced by a background signal. In adjacent colon tissue we measured relatively low amounts of Ki-67 protein mRNA, despite the fact that mucosa and submucosa normally contain proliferating cells. We assume that proliferating nontumor cells express the Ki-67 protein and its mRNA on a much lower level than tumor cells. Therefore, unavoidable contamination of tumor samples with adjacent tissue would have only insignificant influence on the quantification of the Ki-67 protein mRNA expression of tumors. Actively proliferating cells of the immune system localized in the tumor stroma or the adjacent colon can also contribute to the signal, but we speculate that the influence is also low.

In our pilot study, in which we investigated 25 colorectal adenocarcinomas by Ki-67 protein RT-PCR and immunohistological staining with MIB-1, we could clearly demonstrate that quantitative RT-PCR is an objective alternative method to determine the proliferative activity of tumor cells in contrast to immunohistochemistry. The performance of RT-PCR combined with ELISA for the quantification of the expression of cDNA encoding for the Ki-67 antigen provides several advantages over previous methods used for quantification in clinical tumor research. The application of ELISA decreases the time and costs of quantification in many cases. The time needed from surgical tumor resection to the quantification of the cDNA was less than 48 hr.

However, future investigations have to show whether the Ki-67 index is an independent prognostic marker for colorectal adenocarcinoma and whether the quantitative RT-PCR is useful to clinical investigations.

ACKNOWLEDGMENTS

We are grateful to Prof. J. Gerdes (Research Centre, Borstel, Germany) and his group for kindly supplying us with MIB-1; Mrs. G. Grosser-Pape, A. Aumüller, E. Gheribi, R. Kaatz, and V. Grobleben for technical assistance in the Surgical Research Laboratory; Mrs. C. Kilaitis, Surgical Clinic, and PD Dr. H.J. Friedrich, Institute for Biometry and Statistics, Medical University of Lübeck for provision and statistical evaluation of the data. Last but not least, we thank all colleagues of our clinic for helping to collect surgical material, and our colleagues in the laboratory, Dr. A. Stofa, M. Schmidt, and T. Ihmann for kind support.

REFERENCES

- Gerdes, J.; Schwab, U.; Lemke, H.; Stein, H. Production of a Mouse Monoclonal Antibody Reactive with a Human Nuclear Antigen Associated with Cell Proliferation. *Int. J. Cancer* **1983**, *31*, 13-20.
- Key, G.; Becker, M.H.; Baron, B.; Duchrow, M.; Schlüter, C.; Flad, H.D.; Gerdes, J. New Ki-67-Equivalent Murine Monoclonal Antibodies (MIB 1-3) Generated Against Bacterially Expressed Parts of the Ki-67 cDNA Containing Three 62 Base Pair Repetitive Elements Encoding for the Ki-67 Epitope. *Lab. Invest.* **1993**, *68*, 629-636.
- Kubbutat, M.H.; Key, G.; Duchrow, M.; Schlüter, C.; Flad, H.D.; Gerdes, J. Epitope Analysis of Antibodies Recognising the Cell Proliferation Associated Nuclear Antigen Previously Defined by the Antibody Ki-67 (Ki-67 Protein). *J. Clin. Pathol.* **1994**, *47*, 524-528.
- Gerdes, J.; Lemke, H.; Baisch, H.; Wacker, H.H.; Schwab, U.; Stein, H. Cell Cycle Analysis of a Cell Proliferation-Associated Human Nuclear Antigen Defined by the Monoclonal Antibody Ki-67. *J. Immunol.* **1984**, *133*, 1710-1715.
- Brown, D.C.; Gatter, K.C. Monoclonal Antibody Ki-67: Its Use in Histopathology. *Histopathology* **1990**, *17*, 489-503.
- Gerdes, J. Ki-67 and Other Proliferation Markers Useful for Immunohistological Diagnostic and Prognostic Evaluations in Human Malignancies. *Semin. Cancer Biol.* **1990**, *1*, 199-206.
- Gerdes, J.; Stein, H.; Pileri, S.; Rivano, M.T.; Gobbi, M.; Ralfkiaer, E.; Nielsen, K.M.; Pallesen, G.; Bartels, H.; Palestro, G.; Delsol, G. Prognostic Relevance of Tumour-Cell Growth Fraction in Malignant Non-Hodgkin's Lymphomas. *Lancet* **1987**, *2* (8556), 448-449.
- Hall, P.A.; Richards, M.A.; Gregory, W.M.; d'Ardenne, A.J.; Lister, T.A.; Stansfeld, A.G. The Prognostic Value of Ki67 Immunostaining in Non-Hodgkin's Lymphoma. *J. Pathol.* **1988**, *154*, 223-235.
- Grogan, T.M.; Spier, C.M.; Richter, L.C.; Rangel, C.S. Immunologic Approaches to the Classification of Non-Hodgkin's Lymphomas. *Cancer Treat. Res.* **1988**, *38*, 31-148.
- Holte, H.; de Lange Davies, C.; Beiske, K.; Stokke, T.; Marton, P.F.; Smeland, E.B.; Hoie, J.; Kvaloy, S. Ki67 and 4F2 Antigen Expression as Well as DNA synthesis Predict Survival at Relapse/Tumour Progression in Low-Grade B-Cell Lymphoma. *Int. J. Cancer* **1989**, *44*, 975-980.
- Nicholson, R.I.; Bouzubar, N.; Walker, K.J.; McClelland, R.; Dixon, A.R.; Robertson, J.F.; Ellis, I.O.; Blamey, R.W. Hormone Sensitivity in Breast Cancer: Influence of Heterogeneity of Oestrogen Receptor Expression and Cell Proliferation. *Eur. J. Cancer* **1991**, *27*, 908-913.
- Wintzer, H.O.; Zipfel, I.; Schulte Monting, J.; Hellerich, U.; von Kleist, S. Ki-67 Immunostaining in Human Breast Tumors and Its Relationship to Prognosis. *Cancer* **1991**, *67*, 421-428.
- Locker, A.P.; Birrell, K.; Bell, J.A.; Nicholson, R.I.; Elston, C.W.; Blamey, R.W.; Ellis, I.O. Ki67 Immunoreactivity in Breast Carcinoma: Relationships to Prognostic Variables and Short Term Survival. *Eur. J. Surg. Oncol.* **1992**, *18*, 224-229.
- Tungekar, M.F.; Gatter, K.C.; Dunnill, M.S.; Mason, D.Y. Ki-67 Immunostaining and Survival in Operable Lung Cancer. *Histopathology* **1991**, *19*, 545-550.
- Ueda, T.; Aozasa, K.; Tsujimoto, M.; Ohsawa, M.; Uchida, A.; Anki, Y.; Ono, K.; Matsumoto, K. Prognostic Significance of Ki-67 Reactivity in Soft Tissue Sarcomas. *Cancer* **1989**, *63*, 1607-1611.
- Fontana, D.; Bellina, M.; Gubetta, L.; Fasolis, G.; Rollic, L.; Scoffone, C.; Propiglia, F.; Colombo, M.; Tarabuzzi, R.; Leonardo, E. Monoclonal Antibody Ki-67 in the Study of the Proliferative Activity of Bladder Carcinoma. *J. Urol.* **1992**, *148*, 1149-1151.
- Gerdes, J.; Li, L.; Schlüter, C.; Duchrow, M.; Wohlenberg, C.; Gerlach, C.; Stahmer, I.; Kloth, S.; Brandt, E.; Flad, H.D. Immunobiochemical and Molecular Biologic Characterization of the Cell Proliferation-Associated Nuclear Antigen That Is Defined by Monoclonal Antibody Ki-67. *Am. J. Pathol.* **1991**, *138*, 867-873.
- Duchrow, M.; Gerdes, J.; Schlüter, C. The Proliferation-Associated Ki-67 Protein: Definition in Molecular Terms. *Cell Prolif.* **1994**, *27*, 235-242.
- Schlüter, C.; Duchrow, M.; Wohlenberg, C.; Becker, M.H.; Key, G.; Flad, H.D.; Gerdes, J. The Cell Proliferation-Associated Antigen of Antibody Ki-67: A Very Large, Ubiquitous Nuclear Protein with Numerous Repeated Elements, Representing a New Kind of Cell Cycle-Maintaining Proteins. *J. Cell Biol.* **1993**, *123*, 513-522.
- Duchrow, M.; Schlüter, C.; Wohlenberg, C.; Flad, H.D.; Gerdes, J. Molecular Characterization of the Gene Locus of the Human Cell Proliferation-Associated Nuclear Protein Defined by Monoclonal Antibody Ki-67. *Cell Prolif.* **1996**, *29*, 1-12.

21. Hernanek, P. [1992 Tumor Classification/Developments]. *Langenbecks Arch. Chir. Suppl. Kongressbd.* **1992**, 40-45.
22. Cattoretti, G.; Becker, M.H.; Key, G.; Duchrow, M.; Schlüter, C.; Galle, J.; Gerdes, J. Monoclonal Antibodies Against Recombinant Parts of the Ki-67 Antigen (MIB 1 and MIB 3) Detect Proliferating Cells in Microwave-Processed Formalin-Fixed Paraffin Sections. *J. Pathol.* **1992**, 168, 357-363.
23. Chomczynski, P.; Sacchi, N. Single-Step Method of RNA Isolation by Acid Guanidinium Thiocyanate-Phenol-Chloroform Extraction. *Anal. Biochem.* **1987**, 162, 156-159.
24. Kaplan, K.P.; Meier, P. Nonparametric Estimation from Incomplete Observations. *J. Am. Stat. Assoc.* **1958**, 53, 457-481.
25. Porschen, R.; Lohe, B.; Hengels, K.J.; Borchard, F. Assessment of Cell Proliferation in Colorectal Carcinomas Using the Monoclonal Antibody Ki-67. Correlation with Pathohistologic Criteria and Influence of Irradiation. *Cancer* **1989**, 64, 2501-2505.
26. Kubota, Y.; Petras, R.E.; Eastcy, K.A.; Bauer, T.W.; Tubbs, R.R.; Fazio, V.W. Ki-67-Determined Growth Fraction Versus Standard Staging and Grading Parameters in Colorectal Carcinoma. A Multivariate Analysis. *Cancer* **1992**, 70, 2602-2609.
27. Diebold, J.; Dopfer, K.; Lai, M.; Lohrs, U. Comparison of Different Monoclonal Antibodies for the Immunohistochemical Assessment of Cell Proliferation in Routine Colorectal Biopsy Specimens. *Scand. J. Gastroenterol.* **1994**, 29, 47-53.
28. Jansson, A.; Sun, X.F. Ki-67 Expression in Relation to Clinicopathological Variables and Prognosis in Colorectal Adenocarcinomas. *Acta Pathol. Microbiol. Immunol. Scand.* **1997**, 105, 730-734.
29. Ofner, D.; Grothaus, A.; Riedmann, B.; Larcher, P.; Maier, H.; Bankfalvi, A.; Schmid, K.W. MIB1 in Colorectal Carcinomas: Its Evaluation by Three Different Methods Reveals Lack of Prognostic Significance. *Anal. Cell Pathol.* **1996**, 12, 61-70.
30. al.Sheneber, I.F.; Shibata, H.R.; Sampalis, J.; Jothy, S. Prognostic Significance of Proliferating Cell Nuclear Antigen Expression in Colorectal Cancer. *Cancer* **1993**, 71, 1954-1959.
31. Mayer, A.; Takimoto, M.; Fritz, E.; Schellander, G.; Kofler, K.; Ludwig, H. The Prognostic Significance of Proliferating Cell Nuclear Antigen, Epidermal Growth Factor Receptor, and *mlr* Gene Expression in Colorectal Cancer. *Cancer* **1993**, 71, 2454-2460.
32. van Oijen, M.G.; Medema, R.H.; Slootweg, P.J.; Rijksen, G. Positivity of the Proliferation Marker Ki-67 in Noncycling Cells. *Am. J. Clin. Pathol.* **1998**, 110, 24-31.
33. Hemming, A.W.; Davis, N.L.; Klufftinger, A.; Robinson, B.; Quenville, N.F.; Liseman, B.; LeRiche, J. Prognostic Markers of Colorectal Cancer: An Evaluation of DNA Content, Epidermal Growth Factor Receptor, and Ki-67. *J. Surg. Oncol.* **1992**, 51, 147-152.
34. Mori, M.; Kakeji, Y.; Adachi, Y.; Moriguchi, S.; Machihara, Y.; Sugimachi, K.; Jessup, J.M.; Chen, L.B.; Steele, G.D.J. The Prognostic Significance of Proliferating Cell Nuclear Antigen in Clinical Gastric Cancer. *Surgery* **1993**, 113, 683-690.
35. Bruno, S.; Darzynkiewicz, Z. Cell Cycle Dependent Expression and Stability of the Nuclear Protein Detected by Ki-67 Antibody in HL-60 Cells. *Cell Prolif.* **1992**, 25, 31-40.

Molecular characterisation of carbohydrate digestion and absorption in equine small intestine

J. DYER, E. FERNANDEZ-CASTAÑO MEREDIZ, K. S. H. SALMON, C. J. PROUDMAN[†], G. B. EDWARDS[†] and S. P. SHIRAZI-BEECHY*

Epithelial Function and Development Group, Department of Veterinary Preclinical Sciences, University of Liverpool, Brownlow Hill and Crown Street, Liverpool L69 7ZJ and [†]Equine Division, The Philip Leverhulme Large Animal Hospital, The University of Liverpool, Leahurst, Neston, Wirral CH64 7TE, UK.

Keywords: horse; small intestine; dietary carbohydrate; SGLT1; disaccharidases

Summary

Dietary carbohydrates, when digested and absorbed in the small intestine of the horse, provide a substantial fraction of metabolisable energy. However, if levels in diets exceed the capacity of the equine small intestine to digest and absorb them, they reach the hindgut, cause alterations in microbial populations and the metabolite products and predispose the horse to gastrointestinal diseases. We set out to determine, at the molecular level, the mechanisms, properties and the site of expression of carbohydrate digestive and absorptive functions of the equine small intestinal brush-border membrane. We have demonstrated that the disaccharidases sucrase, lactase and maltase are expressed diversely along the length of the intestine and D-glucose is transported across the equine intestinal brush-border membrane by a high affinity, low capacity, Na⁺/glucose cotransporter *type 1* isoform (SGLT1). The highest rate of transport is in duodenum > jejunum > ileum. We have cloned and sequenced the cDNA encoding equine SGLT1 and alignment with SGLT1 of other species indicates 85–89% homology at the nucleotide and 84–87% identity at the amino acid levels. We have shown that there is a good correlation between levels of functional SGLT1 protein and SGLT1 mRNA abundance along the length of the small intestine. This indicates that the major site of glucose absorption in horses maintained on conventional grass-based diets is in the proximal intestine, and the expression of equine intestinal SGLT1 along the proximal to distal axis of the intestine is regulated at the level of mRNA abundance. The data presented in this paper are the first to provide information on the capacity of the equine intestine to digest and absorb soluble carbohydrates and has implications for a better feed management, pharmaceutical intervention and for dietary supplementation in horses following intestinal resection.

Introduction

The horse is a nonruminant herbivore and fermentation of plant fibre in the equine large bowel, by resident microflora, results in the formation of short chain fatty acids, which provide a large part

of the horse's energy requirement. Today's horse, however, is subjected to an increasingly artificial diet that contains high levels of concentrates (grain) which, when digested and absorbed in the small intestine, can provide a substantial fraction of metabolisable energy (Alexander 1955; Argenzio and Hintz 1972). However, if levels and components of these diets exceed the ability and capacity of equine small intestine to digest and absorb them, they reach the large bowel, cause alterations in microflora and the fermentation products, and predispose the horse to gastrointestinal disturbances. Any gut dysfunction in horse is threatening, because it can precede colic, the main cause of equine mortality (Hintz and Cymbaluk 1994).

In nonruminant species, digestible dietary carbohydrates are hydrolysed in the intestinal lumen by pancreatic α -amylase and brush-border membrane disaccharidases, sucrase, maltase and lactase, to the monosaccharides, D-glucose, D-fructose and D-galactose. These monosaccharides are absorbed across the enterocyte brush-border membrane by specific monosaccharide transporters (Shirazi-Beechey 1995).

Very little information is available on the mechanisms and intestinal sites of carbohydrate digestion and absorption in the equine intestinal tract. This knowledge is critical for assessing the ability and capacity of the equine intestine to digest and absorb carbohydrates, in order to better understand the pathogenesis of intestinal disease and improve feed management.

The majority of studies relating to carbohydrate digestion and absorption to date have been based on whole animal feed experiments (Argenzio and Hintz 1972; Roberts 1975). While these studies have improved our understanding of carbohydrate metabolism in the horse, the complexity of whole body balance studies would not reveal the processes operative at the molecular level. In this study, we have set out, for the first time, to determine the digestive and absorptive capabilities of equine small intestine at the cellular and molecular levels.

Materials and methods

Collection of tissue

Intestinal tissue, from 23 mature horses (age >4 years) maintained on a grass-based diet, was collected from the local abattoir within 15 min of slaughter; none were geriatric. Sections of small

*Author to whom correspondence should be addressed.

intestine, approximately 20 cm in length, were removed from the proximal (30 cm distal to the pylorus), mid (halfway along the small intestine) and distal (30 cm proximal to the ileocaecal junction) intestine. Sections were opened longitudinally, rinsed in ice-cold 0.9% (w/v) NaCl, pH 7.4, and blotted with paper towels to remove excess mucus. A fresh sample of intestine was fixed in 4% (w/v) phosphate buffered paraformaldehyde, for histology, and the mucosa of the remainder of the same tissue was then removed by scraping. The mucosal scrapings were wrapped in aluminium foil and frozen immediately in liquid nitrogen. Following transportation to the laboratory, frozen tissue samples were stored at -80°C until use. Mucosal scrapings from tissues that were shown to be intact, i.e. with epithelial cells attached to the *muscularis mucosa*, as revealed by histology, were used.

Isolation of brush-border membrane vesicles

Brush-border membrane vesicles (BBMV) were prepared from equine small intestinal mucosal scrapings using a method based on that of Shirazi-Beechey *et al.* (1988, 1990). Briefly, mucosal scrapings were thawed in a solution (100 mmol/l mannitol, 2 mmol/l HEPES/Tris, pH 7.1), containing a cocktail of protease inhibitors (Complete protease inhibitor cocktail tablets; D-glucose UV test kit)¹ (Rowell *et al.* 1997). The mucosal scrapings were homogenised for 2 x 1 min in a Waring blender at the highest setting. The volume was made up to 100 ml with the same buffer, MgCl₂ was added to a final concentration of 10 mmol/l and the homogenate was stirred for 20 min, on ice. The homogenate was centrifuged at 5000 g (3000 rpm, Sorvall SS 34 rotor) for 10 min in a Sorvall RC 5C+ centrifuge (Sorvall RC 5C+ centrifuge)². The pellet was discarded and the supernatant centrifuged at 30,000 g (16,000 rpm, Sorvall SS 34 rotor) for 30 min. The resulting pellet was resuspended in 35 ml solution containing 100 mmol/l mannitol, 2 mmol/l HEPES/Tris, pH 7.4, 0.1 mmol/l MgSO₄, using a Potter/Elvehjem hand-held homogeniser and centrifuged at 30,000 g (16,000 rpm, Sorvall SS 34 rotor) for 45 min. The final pellet, containing purified brush-border membranes, was resuspended in a small volume of isotonic buffer (300 mmol/l mannitol, 20 mmol/l HEPES/Tris, pH 7.4, 0.1 mmol/l MgSO₄, 0.02% [w/v] NaN₃) by passing through a 27 gauge needle several times. The BBMV were divided into aliquots and stored in liquid nitrogen, until use. All steps in the procedure were carried out at 4°C.

Estimation of protein

Protein concentration was determined by its ability to bind Coomassie Blue, according to the Bio-Rad assay technique (Tarpey *et al.* 1995). Bovine γ -globulin (1–100 μ g protein) was used as the standard.

Enzyme assays

Sucrase, maltase and lactase activities were measured at 38°C (equine body temperature) in the original cell homogenates and final brush-border membrane fractions, as described previously (Dahlqvist 1964; Shirazi-Beechey *et al.* 1989, 1990). D-glucose, released as a result of the hydrolysis of disaccharide substrates (sucrose, lactose and maltose, 28 mmol/l final concentration), was measured using a commercially available kit¹ according to the manufacturer's instructions. *p*-chloromercuri-benzoate (pCMB) was included in the lactase assay to inhibit any potential

contamination from lysosomal β -galactosidase.

Alkaline phosphatase was measured at pH 10 in the presence of 5 mmol/l MgCl₂ and 0.25 mmol/l CaCl₂ using *p*-nitrophenyl phosphate as the substrate (Shirazi *et al.* 1981).

The potential presence of any basolateral and organelle membranes was determined by assessing the activities of the following marker enzymes; K⁺-activated phosphatase (basolateral membrane), α -mannosidase (Golgi), Tris-resistant α -glucosidase (endoplasmic reticulum), acid phosphatase (lysosomes) and succinate dehydrogenase (mitochondria), as described previously (Shirazi-Beechey *et al.* 1989, 1990).

Assay of Na⁺-dependent D-glucose transport

Na⁺-dependent D-glucose transport into BBMV was measured at 38°C in a solution containing either 100 mmol/l NaSCN or 100 mmol/l KSCN and 100 mmol/l mannitol, 20 mmol/l HEPES/Tris, pH 7.4, 0.1 mmol/l MgSO₄ and 0.02% (w/v) NaN₃. Incubation was stopped at specific time points (3 s for the initial rate and 3 s, 10 s, 1, 10 and 30 min for the time-course measurements) by the addition of 1 ml ice-cold buffer containing 0.1 mmol/l phlorizin (Shirazi-Beechey *et al.* 1989). Aliquots of this solution were then filtered rapidly through 0.2 μ m cellulose acetate/nitrate filters (0.2 μ m cellulose acetate/nitrate filters)³, using the filtration stop technique, as described previously (Shirazi-Beechey *et al.* 1990). All initial rate measurements were taken after 3 s incubation period as transport was determined to be linear up to 4 s (data not shown). Uptakes were measured in duplicate or triplicate. For the kinetic studies D-glucose concentration was 0.01–2.5 mmol/l. Na⁺-dependent uptake was calculated as the difference in rates measured in the presence and absence of Na⁺.

Competition studies were carried out by determining the initial (3 s) rate of uptake of 0.1 mmol/l D-glucose in the presence of 1 mmol/l competitor (Hediger and Rhoads 1994).

Cloning and sequencing of equine SGLT1

Oligonucleotide primers, derived initially from the consensus nucleotide sequences of ovine and human SGLT1 cDNA and subsequently from the equine SGLT1 sequence, were used in reverse transcription-polymerase chain reaction (RT-PCR) against total RNA isolated from equine jejunal mucosal scrapings. RNA samples were prepared using a commercially available kit (RNeasy Mini Kit)⁴ according to the manufacturer's instructions. First strand synthesis was performed using 200 u Superscript II⁵ RNase H- reverse transcriptase and random primers (pGEM-T)⁶ at 42°C for 60 min. cDNA was purified on a nucleospin column (Machery-Nagel Nucleospin Extract)⁷ and amplified by PCR with 2.5 u Pfu DNA polymerase⁸ and the following primer pairs:

- (1) Sense Ls20, nt 484 (5'-AGATCTCGGCAGACATCTTT-3'), antisense Has2, nt 952 (5'-GCAGCCACCCCTTCACGTGAGA-3')
- (2) Sense s891, nt 891 (5'-ACAGACCAGGTCATCGTGACG-3'), antisense as1599, nt 1599 (5'-GGCAAAGAGGATGATGGCAAAG-3')
- (3) sense s1406, nt 1406 (5'-ACCACCAATTGCAGCTGTCTTC-3'), antisense as2025, nt 2025 (5'-CAGCAGAAAGCAGGACTCAGGC-3')

The reaction conditions were as follows: 1 x reaction buffer (10 mmol/l KCl, 10 mmol/l (NH₄)₂SO₄, 20 mmol/l Tris-HCl, pH 8.75, 0.1% (v/v) Triton X-100, 1 mg/ml BSA), 200 μ mol/l

each dNTP, 50 pmol each primer, 3 mmol/l MgCl₂, 1 µg cDNA. PCR amplification was performed at 94°C, 20 s; 57°C, 20 s; 72°C, 150 s for 30 cycles. A final extension of 7 min at 72°C was included. The RT-PCR products were tailed with adenosine using Thermoprime plus DNA polymerase (AB gene), cloned into pGEM-T⁶ and custom sequenced. Equine specific SGLT1 sense and anti-sense primers were synthesised based on these sequences and used in subsequent reactions to clone the 5'- and 3'-ends of equine SGLT1 (eSGLT1).

The 5'-UTR was cloned using rapid amplification of cDNA ends (RACE) using a commercially available kit⁵ and the following nested gene-specific anti-sense primers; Las18, nt 681 (5'-AAGCAAACCCAGTCAGGATG-3') and Has7, nt 482 (5'-CTTGGTGAAAATGTAGAGCA-3').

The 3'-UTR was cloned by 3' RACE. First strand synthesis was as described for RT-PCR, using the 3' RACE primer (5'-GGCCACGCGTCGACTAGTACT₁₇-3'). A 400 bp product was amplified from the cDNA using Pfu DNA polymerase with the eSGLT1 specific sense primer s1767, nt 1767 (5'-ACACCTTGGAGGAGAGCATTGA-3') and the 3' RACE primer. The product was tailed, cloned into pGEM-T as described and custom sequenced. The GenBank accession number for the equine SGLT1 mRNA sequence is AJ292081.

Western blot analysis

The abundance of SGLT1 protein in the equine intestinal BBMV was determined by western blotting, as described previously (Dyer *et al.* 1997a). The protein contents of BBMV were separated on 8% polyacrylamide gels containing 0.1% (w/v) SDS and were electrotransferred to nitrocellulose membrane (Trans-Blot nitrocellulose)⁹. Samples were blotted with an antibody raised to a synthetic nonodecapeptide (STLFMTDIYTKIRKKASEK) corresponding to a highly conserved region of the SGLT1 amino acid sequence in other species (Hirayama and Wright 1992; Shirazi-Beechey 1995; Dyer *et al.* 1997a; Wood *et al.* 2000), including eSGLT1 (Fig 7). The 75 kDa immunoreactive band was blocked when antibodies were pre-incubated with the immunising peptide indicating the specificity of the immunoreaction. The membranes were developed using the ECL system¹⁰ and exposed to film (BioMax MR film)¹¹. The intensities of the immunoreactive bands, detected in the BBMV, were quantified using scanning densitometry (Phoretix 1D Quantifier)¹² and reported as arbitrary units.

Lactase abundance was determined using a monoclonal antibody (mlac6) to human lactase as described previously (Dyer *et al.* 1997b).

Northern blot analysis

Total RNA was isolated from duodenal, jejunal and ileal mucosal scrapings of equine small intestine using a commercially available kit⁴. RNA samples, 3 µg per lane, were separated on 1% agarose gels containing 0.66 mol/l formaldehyde and transferred to nylon membrane (Hybond N)¹⁰. RNA integrity and equality of loading were determined by methylene blue staining. The nylon membrane was prehybridised for 3 h at 42°C in a buffer containing 50% (v/v) deionised formamide, 5 x SSC, 6 x Denhardt's reagent, 0.2% (w/v) SDS, 10% (w/v) dextran sulphate, 2.5 mmol/l sodium pyrophosphate, 25 mmol/l MES, pH 6.5 and 0.01% (v/v) antifoam B¹³. Equine SGLT1 cDNA (25 ng)

TABLE 1: Disaccharidase activity in BBMV isolated from the intestine of grass-fed horses (mean ± s.e.)

	Specific activity (µmol/min/mg protein)		
	Duodenum	Jejunum	Ileum
Sucrase	0.353 ± 0.088 (n = 7)	0.424 ± 0.075 (n = 7)	0.221 ± 0.037 (n = 7)
Maltase	0.880 ± 0.118 (n = 8)	0.998 ± 0.155 (n = 7)	0.742 ± 0.108 (n = 8)
Lactase	0.068 ± 0.025 (n = 7)	0.101 ± 0.041 (n = 7)	0.029 ± 0.011 (n = 7)

corresponding to nucleotides 1406–2025, was labelled with [³²P]-dCTP by random priming and hybridised with the membrane for 16 h at 42°C. Washes were performed at 55°C for 15 min once with 5 x SSC, 0.5% (w/v) SDS, 0.25% (w/v) sarkosyl and 3 times with 0.1 x SSC, 0.1% (w/v) SDS. The membrane was apposed to x-ray film (BioMax MS)¹¹, with a single intensifying screen, at -80°C for 6 h. The intensity of the transcripts was quantified using scanning densitometry (Phoretix 1D Quantifier)¹².

Statistics

Data are expressed as mean ± s.e. and statistical comparisons are made using one-way analysis of variance, $\alpha = 0.01$.

Results

The intestinal tissue used was obtained from grass-fed horses, slaughtered by conventional methods at the local abattoir. On occasion, histology of the tissue revealed that there had been shedding of the epithelium, as has been reported previously in intestinal tissue of other species obtained from animals slaughtered by conventional methods (Fell 1961; Shirazi-Beechey *et al.* 1989). Therefore, care was taken to use only tissues shown to be intact by histology. Furthermore, a cocktail of protease inhibitors was included in the buffers used to prepare BBMV and this appeared to be essential for maintaining intact equine intestinal brush-border membrane proteins. The specific activities of the brush-border marker enzymes alkaline phosphatase and disaccharidases were 20–25-fold enriched in BBMV over the original cellular homogenate. The activities/abundances of marker proteins characteristic of organelle/basolateral membranes were negligible in BBMV, indicating that the membrane vesicles were derived from the brush-border membrane and were purified.

Equine small intestinal disaccharidases

In order to determine the ability of the equine small intestine to hydrolyse disaccharides, the activities of sucrase, maltase and lactase were determined. The results are presented in Table 1.

Sucrase, maltase and lactase are expressed in equine small intestine. Sucrase specific activities were highest proximally (duodenum = jejunum > ileum), while maltase activity was similar in all 3 regions. The horse appeared to express lactase postweaning (see Table 1). This was confirmed by western blot analysis using a monoclonal antibody specific to the brush-border membrane lactase. The antibody cross-reacts with a single protein with an apparent molecular mass of 150 kDa in equine intestinal BBMV, a similar size to lactase reported in other species

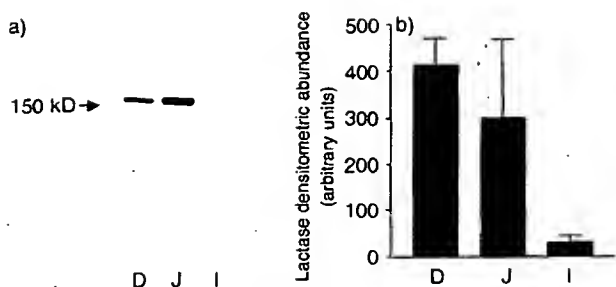


Fig 1: Lactase expression in equine small intestinal brush-border membrane vesicles (BBMV). BBMV (15 µg protein/lane) prepared from equine duodenum (D), jejunum (J) and ileum (I) were separated on 8% polyacrylamide gels, electrotransferred to nitrocellulose membrane and western blotted using an anti-lactase monoclonal antibody (mlac6), as described in Materials and methods. a) The results of a typical western blot indicating the presence of the 150 kDa lactase protein. b) Densitometric analysis of western blots carried out using Phoretix 1D¹². Data are expressed as mean ± s.e. (n = 6) in arbitrary units.

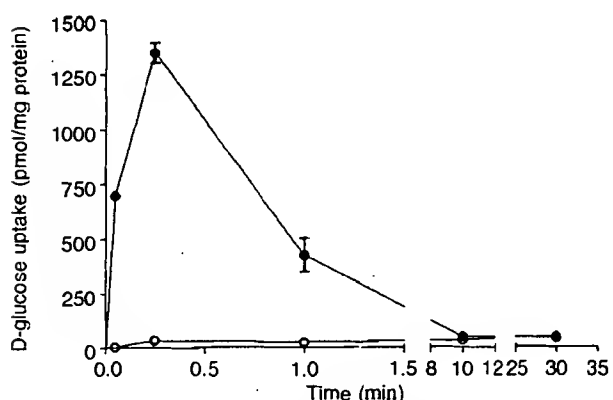


Fig 2: Time course of Na⁺-dependent D-glucose transport by equine duodenal brush-border membrane vesicles. The uptake of 0.1 mmol/l D-glucose into equine duodenal BBMV was measured at 38°C in the presence of an inwardly directed (out>in) concentration gradient of either 100 mmol/l NaSCN (●) or KSCN (○), under zero trans conditions as described in Materials and methods. All uptakes were measured in duplicate and values are presented as mean ± s.e. (n = 3).

(Schlegel-Haueter *et al.* 1972; Mantei *et al.* 1988; Dyer *et al.* 1997b). The results are presented in Figure 1. Densitometric analyses of western blots for lactase in the intestinal brush-border membranes of several horses are shown in Figure 1b. As can be seen, lactase expression was highest in the duodenal and jejunal BBMV, with a marked reduction in levels detected in BBMV from the distal small intestine, $P = 0.065$. The large s.e. seen for jejunal lactase activity and abundance reflect the fact that some horses showed the highest levels of lactase expression in jejunum, whereas others had little lactase expressed in this region. However, all horses expressed higher levels of lactase in the duodenum than the ileum. A similar distribution pattern was seen for lactase activity reported in Table 1, with higher levels of activity in the duodenum and jejunum than in the ileum.

Monosaccharide transport in equine small intestine

Time-course and initial rates of D-glucose transport: The ability of equine small intestine to transport D-glucose was measured in BBMV and results are presented in Figure 2. D-glucose was

TABLE 2: Comparison of sequence data for SGLT1 from various species

Species	No. amino acids	cDNA homology (%)	Amino acid identity (%)	Amino acid similarity (%)
Horse	662	100	100	100
Man	664	88.8	87.0	91.4
Mouse	665	84.7	86.8	91.8
Rabbit	662	85.4	84.6	90.6
Rat	665	84.6	86.5	92.0
Sheep	664	88.6	86.2	89.7

The sequence comparisons are relative to the horse sequence.

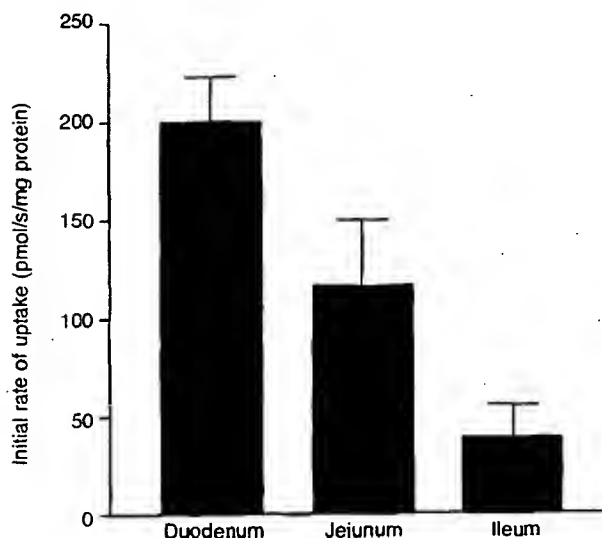


Fig 3: Initial rate of Na⁺-dependent D-glucose transport in equine small intestinal brush-border membrane vesicles. The initial (3 s) rate of 0.1 mmol/l D-glucose uptake into BBMV (0.1 mg protein) was measured at 38°C in the presence of 100 mmol/l NaSCN, as described in Materials and methods. Results are presented as mean ± s.e. (n = 7).

transported into the membrane vesicles in a Na⁺-dependent manner. The uptake exhibited a classical 'overshoot', i.e. a transient increase in intravesicular glucose concentration above that of the incubation medium. When Na⁺ in the incubation medium was replaced by K⁺ the overshoot was abolished and glucose uptake rates were negligible. Na⁺-dependent glucose transport was inhibited when 0.1 mmol/l phlorizin was included in the incubation medium. Phlorizin is a specific inhibitor of Na⁺-dependent D-glucose transport (Wright *et al.* 1994; Shirazi-Beechey 1995). The initial rates of the Na⁺-dependent transport of D-glucose in BBMV isolated from the duodenal, jejunal and ileal mucosa of grazing horses are presented in Figure 3. Transport rates were highest in the duodenum (200 ± 22 pmol/s/mg protein), lower in the jejunum (116 ± 33 pmol/s/mg protein) and lowest in the ileum (38 ± 16 pmol/s/mg protein), ($P = 0.0014$).

Kinetics and substrate specificity of Na⁺-dependent D-glucose transport: The effect of substrate concentration on D-glucose transport in BBMV was investigated and the results, using duodenal BBMV, are presented in Figure 4. Initial rate (3 s) of D-glucose uptake was measured at glucose concentrations of

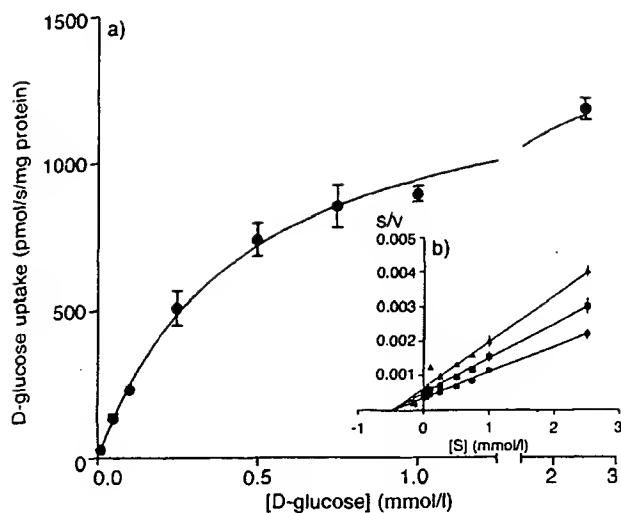


Fig 4. Effect of substrate concentration on the initial rate of D-glucose uptake by equine small intestinal brush-border membrane vesicles. The initial rate of D-glucose transport by equine intestinal BBMVs was measured as a function of D-glucose concentration under zero trans conditions as described in Materials and methods. Results are expressed as (a) Michaelis-Menten plot of D-glucose concentration vs. initial (3 s) rate of D-glucose uptake for duodenal BBMVs and (b) a Hanes plot of linear regression analysis for duodenal (●), jejunal (■) and ileal (▲) BBMVs. Uptakes were carried out in duplicate and are expressed as mean \pm s.e. ($n = 2$).

0.01–2.5 mmol/l D-glucose. Uptake conformed to Michaelis-Menten kinetics (Fig 4a) and linear-regression analysis (Fig 4b) indicated the presence of a single transport system for D-glucose, with a K_m of 0.49 ± 0.06 mmol/l and a V_{max} of 1312 ± 141.9 pmol/s/mg protein. K_m values obtained using jejunal and ileal BBMVs were not significantly different. V_{max} values, however, were 918 ± 73.3 and 698 ± 61 pmol/s/mg protein in the jejunal and the ileal BBMVs, respectively. Kinetic studies indicate that the aboral decline in Na^+ -dependent D-glucose transport is due to decrease in the protein abundance (V_{max}) rather than the affinity of the transporter for glucose. The K_m of 0.49 mmol/l for D-glucose suggests that the Na^+ /glucose cotransporter in equine small intestine is the high affinity isoform SGLT1. SGLT1 has an affinity for D-glucose in the range 0.05–0.8 mmol/l in other species (Malo and Berteloot 1991; Shirazi-Beechey *et al.* 1991a; Hediger and Rhoads 1994; Hirayama *et al.* 1996).

The sugar substrate selectivity of the transporter was investigated by measuring the initial rate of 0.1 mmol/l D-glucose uptake in the presence of 1 mmol/l known substrates of SGLT1 (Hopfer 1987; Shirazi-Beechey 1995). Results are shown in Figure 5. These monosaccharides inhibited D-glucose uptake into equine BBMVs in the order of D-glucose (82.6%) > α -methyl-D-glucose (75.2%) = D-galactose (72.3%) >> 3-O-methyl-D-glucose (29.5%) > D-xylose (16.6%). This pattern of substrate selectivity is similar to that shown for SGLT1 in other species (Wright 1993; Hediger and Rhoads 1994; Diez-Sampedro *et al.* 2001) and further suggests that the equine intestinal Na^+ /glucose cotransporter is the SGLT isoform 1 (see also eSGLT1 sequence).

Cloning and sequencing of equine intestinal SGLT1 cDNA

Using the techniques of reverse transcription-polymerase chain reaction (RT-PCR) and rapid amplification of cDNA ends (RACE),

initially with homologous primers designed against consensus sequences of SGLT1 in other species and subsequently with specific equine SGLT1 primers, 2.17 kb equine SGLT1 cDNA was cloned and sequenced. Translation of the overlapping contiguous sequences indicates that the equine SGLT1 cDNA encodes for a 662 amino acid protein. Hydropathy analysis of the peptide sequence (Vector NTi Suite)¹⁴ suggests a secondary structure with 12 putative membrane-spanning regions and both the N- and C-termini located intracellularly, which is in agreement with models based on hydropathy analysis for SGLT1 in other species (Hediger and Rhoads 1994). Alignment of the eSGLT1 amino acid sequence with those of SGLT1 in other species is shown in Figure 6 with conserved areas shaded grey. Sequence homology data is presented in Table 2. Equine SGLT1 has between 89–85% homology with SGLT1 from other species at the nucleotide level and between 90–92% similarity and 84–87% identity at the amino acid level. SGLT1 has been shown to be N-glycosylated in rabbit, human and sheep at Asn248 (Wright 1993; Shirazi-Beechey 1995). This residue, indicated by an asterisk in Figure 6, is conserved in eSGLT1. Polyclonal antibodies have been raised against a nonodecapeptide (STLFTMDIYTKIRKASEK) corresponding to amino acids 402–420, a conserved intracellular loop region of SGLT1 in other species. This region is boxed in Figure 6. As can be seen, equine SGLT1 shares a high degree of homology with other species over this region, with 17/19 amino acid identity with SGLT1 from human, mouse, rat, rabbit and sheep. Equine SGLT1 shares the same hypervariable regions as SGLT1 in other species. These are most notably amino acids 6–22 at the N-terminus and amino acids 576–600 at the C-terminus. As can be seen in Figure 6, eSGLT1 does not have an extra amino acid at position 579 as do rat and mouse; however, cSGLT1 has the 2 amino acid deletion at positions 592–593, seen previously only in rabbit SGLT1. How these changes may influence the function of equine SGLT1 awaits analysis by expression in heterologous systems.

SGLT1 protein abundance in equine small intestinal BBMVs

In the equine intestinal BBMVs samples, the antibody to SGLT1 cross-reacted with a single band of 75 kDa in all 3 regions of the

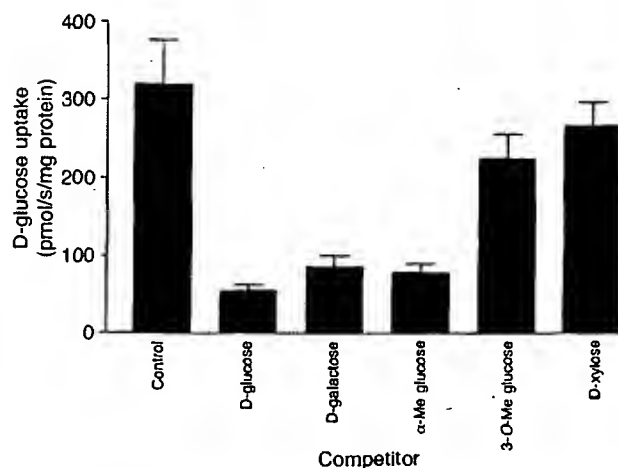


Fig 5. Sugar specificity of equine SGLT1. The initial rate of the Na^+ -dependent uptake of 0.1 mmol/l D-glucose into equine duodenal BBMVs was measured at 38°C in the presence of 1 mmol/l of the indicated competitor. Results are expressed as mean \pm s.e. ($n = 3$).

Horse SGLT1	(1)	1	50
Human SGLT1	(1)	MDSSTWSPGTATTAAPLAS YERIRNAADISVIVIFYFVVMAVGLWAMFST	
Mouse SGLT1	(1)	MDSSTLSPAVTATDAPIPSYERIRNAADISVIVIFYFVVMAVGLWAMFST	
Rabbit SGLT1	(1)	MDSSTLSPLTSTTAAPLESYERIRNAADISVIVIFYFVVMAVGLWAMFST	
Rat SGLT1	(1)	MDSSTLSPAVTATDAPIQSYERIRNAADISVIVIFYFVVMAVGLWAMFST	
Sheep SGLT1	(1)	MDSSTWSPPATATAEPLQAYERIRNAADISVIVIFYFVVMAVGLWAMFST	
Consensus	(1)	MDSSTWSPPATATAAPL SYERIRNAADISVIVIFYFVVMAVGLWAMFST	
1			
Horse SGLT1	(51)	51	100
Human SGLT1	(51)	NRGTVGFFLAGRNMVWPIGASLFASNIGSGHFVGLAGSGAASGIAMGG	
Mouse SGLT1	(51)	NRGTVGFFLAGRSMVWPIGASLFASNIGSGHFVGLAGTGAASGIALGG	
Rabbit SGLT1	(51)	NRGTVGFFLAGRSMVWPIGASLFASNIGSGHFVGLAGTGAASGIATGG	
Rat SGLT1	(51)	NRGTVGFFLAGRSMVWPIGASLFASNIGSGHFVGLAGTGAASGIAMGG	
Sheep SGLT1	(51)	NRGTVGFFLAGRSMVWPIGASLFASNIGSGHFVGLAGTGAASGIATGG	
Consensus	(51)	NRGTVGFFLAGRSMVWPIGASLFASNIGSGHFVGLAGTGAASGIAMGG	
2			
Horse SGLT1	(101)	101	150
Human SGLT1	(101)	FEWNALILVVVLGWVFPVIYIKAGVVTMPEYLKRFGGQRIQVYLSLSL	
Mouse SGLT1	(101)	FEWNALVLVVVLGWLFVPIYIKAGVVTMPEYLKRFGGQRIQVYLSLSL	
Rabbit SGLT1	(101)	FEWNALIMVVVLGWVFPVIYIRAGVVTMPEYLQKRFGGKRIQIYLSLSL	
Rat SGLT1	(101)	FEWNALVFVVVLGWLFVPIYIKAGVVTMPEYLKRFGGKRIQIYLSLSL	
Sheep SGLT1	(101)	FEWNALILVVVLGWVFPVIYIKAGVVTMPEYLKRFGGQRIQVYLSLSL	
Consensus	(101)	FEWNALILVVVLGWVFPVIYIKAGVVTMPEYLKRFGGQRIQIYLSLSL	
3			
Horse SGLT1	(151)	151	200
Human SGLT1	(151)	LLYIFTKISADIFSGAIFINMALGLDLYLAIILLAVTGIYITITGGLAAV	
Mouse SGLT1	(151)	LLYIFTKISADIFSGAIFINLALGLMLYLAIFFLLAITALYITITGGLAAV	
Rabbit SGLT1	(151)	LLYIFTKISADIFSGAIFINLALGLDIYLAIFILLAITALYITITGGLAAV	
Rat SGLT1	(151)	LLYIFTKISADIFSGAIFINLALGLDIYLAIFILLAITALYITITGGLAAV	
Sheep SGLT1	(151)	VLYIFTKISADIFSGAIFINLALGLDLYLAIFILLAITALYITITGGLAAV	
Consensus	(151)	LLYIFTKISADIFSGAIFINLALGLDIYLAIFILLAITALYITITGGLAAV	
4			
Horse SGLT1	(201)	201	250
Human SGLT1	(201)	IYTDTLQTAIMLVGSAILTGFAFNEVGGYEAFFMEKYMKAIPTMISDGNIT	
Mouse SGLT1	(201)	IYTDTLQTVIMLVGSLITLGFAFHEVGGYDAFMEKYMKAIPITVSDGNTT	
Rabbit SGLT1	(201)	IYTDTLQTAIMLVGSFILTGFAPNEVGGYEAFFMDKYMKAIPTKVSNGNFT	
Rat SGLT1	(201)	IYTDTLQTAIMLVGSFILTGFAPNEVGGYEAFFMEKYMKAIPITVSDGNIT	
Sheep SGLT1	(201)	IYTDTLQTVIMLVGSLITLGFAFHEVGGYSAFVTKYMKAIPITVSYGNNT	
Consensus	(201)	IYTDTLQTAIMLVGSFILTGFAPNEVGGYEAFFMEKYMKAIPITVSDGNTT	
5			
Horse SGLT1	(251)	251	300
Human SGLT1	(251)	IKKECYTPRADS FHI FRDPLKGDLPWPGLIFGLFILT LWYWCTDQVIVQR	
Mouse SGLT1	(251)	FQEKCYTPRADS FHI FRDPLTGDLPWPGLIFGMSILT LWYWCTDQVIVQR	
Rabbit SGLT1	(251)	AKKECYTPRADS FHI FRDPI TGDMPPWPGLIFGLAILALWYWCTDQVIVQR	
Rat SGLT1	(251)	IPQKCYTPREDA FHI FRDAITGDIPWPGLVFGMSILT LWYWCTDQVIVQR	
Sheep SGLT1	(251)	VKEECYTPRADS FHI FRDPI TGDMPPWPGLIFGLSILALWYWCTDQVIVQR	
Consensus	(251)	VKKECYTPRADS FHI FRDPLKGDLPWPGLIFGLTII SLWYWCTDQVIVQR	
6			
Horse SGLT1	(301)	301	350
Human SGLT1	(301)	CLSAKNMSHVKGCCIMCGYLKLLPMFLMVMGMVSRI LYTERVACVLPSE	
Mouse SGLT1	(301)	CLSAKNMSHVKGCCILCGYLKLLPMFLMVMGMISRI LYTEKIACVLPSE	
Rabbit SGLT1	(301)	CLSAKNLSHVKGACILCGYLKVMMPFLIVMMGMVSRI LYTDKIVACVLPSE	
Rat SGLT1	(301)	CLSAKNMSHVKGACILCGYLKLLPMFLMVMGMISRI LYTDKIACVLPSE	
Sheep SGLT1	(301)	CLSAKNMSHVKGACIMCGYMKLLPMFLMVMGMISRI LPTKEKIVACVLPSE	
Consensus	(301)	CLSAKNMSHVKGACILCGYLKLLPMFLMVMGMISRI LYTEKIACVLPSE	
7			

Fig 6: Alignment of the deduced amino acid sequence of eSGLT1 with SGLT1 from various species. Sequence alignment was carried out by Clustal W analysis using the alignment programme of Vector NTI¹⁴. Homologous regions are shaded. The boxed area indicates the region to which the anti-peptide antibody was raised. The conserved glycosylation site at Asn248 is indicated (*). Putative membrane spanning regions (Hediger and Rhoads 1994) are indicated by lines below the sequence and are numbered 1 to 12.

Horse SGLT1	(351)	351	400
Human SGLT1	(351)	CEKYCGIKVGCSTNIAYPTLVIELMPDGLRGLMLSVMLASLMSSLTSTIFNS	
Mouse SGLT1	(351)	CEKYCGTKVGCSTNIAYPTLVVELMPNGLRGLMLSVMLASLMSSLTSTIFNS	
Rabbit SGLT1	(351)	CQKYCGTPVGCSTNIAYPTLVVELMPNGLRGLMLSVMMASLMSSLTSTIFNS	
Rat SGLT1	(351)	CERYCGTRVGCSTNIAYPTLVVELMPNGLRGLMLSVMMASLMSSLTSTIFNS	
Sheep SGLT1	(351)	CKKYCGTPVGCSTNIAYPTLVVELMPNGLRGLMLSVMMASLMSSLTSTIFNS	
Consensus	(351)	CEKYCGTKVGCSTNIAYPTLVVELMPNGLRGLMLSVMLASLMSSLTSTIFNS	
8			
Horse SGLT1	(401)	401	450
Human SGLT1	(401)	ASTLFTMDIYTKIRKRASEKELMLVGRFLFILVLIGVSIWVPIVQSAQSG	
Mouse SGLT1	(401)	ASTLFTMDIYAKVRKRASEKELMIAGRLFILVLIGISIAWVPIVQSAQSG	
Rabbit SGLT1	(401)	ASTLFTMDIYTKIRKKASEKELMIAGRLFILVLIGISIAWVPIVQSAQSG	
Rat SGLT1	(401)	ASTLFTMDIYTKIRKASEKELMIAGRLFILVLIGISIAWVPIVQSAQSG	
Sheep SGLT1	(401)	ASTLFTMDIYTKIRKASEKELMIAGRLFILVLIGISIAWVPIVQSAQSG	
Consensus	(401)	ASTLFTMDIYTKIRKKASEKELMIAGRLFILVLIGISIAWVPIVQSAQSG	
9			
Horse SGLT1	(451)	451	500
Human SGLT1	(451)	QLFDYIQSITSYLGPPIAAVFLLAIFWKRTTESGAFWGLILGFLVGLARM	
Mouse SGLT1	(451)	QLFDYIQSITSYLGPPIAAVFLLAIFWKRVNEPGAFWGLILGLLIGISRM	
Rabbit SGLT1	(451)	QLFDYIQSITSYLGPPIAAVFLLAIFCKRVNEPGAFWGLILGFLIGISRM	
Rat SGLT1	(451)	QLFDYIQSITSYLGPPIAAVFLLAIFCKRVNEPGAFWGLILGFLIGISRM	
Sheep SGLT1	(451)	QLFDYIQSITSYLGPPIAAVFLLAIFCKRVNEPGAFWGLIIGFLIGVSRM	
Consensus	(451)	QLFDYIQSITSYLGPPIAAVFLLAIFWKRVNEPGAFWGLILGFLIGISRM	
10			
11			
Horse SGLT1	(501)	501	550
Human SGLT1	(501)	ITEFAYGTGSCTEPSNCPTIICGVHYLYFAIILFAISVITIVVSLFTKP	
Mouse SGLT1	(501)	ITEFAYGTGSCMEPSNCPTIICGVHYLYFAIILFAISFITIVVISLLTKP	
Rabbit SGLT1	(501)	ITEFAYGTGSCMEPSNCPKIICGVHYLYFAIILFVIVITILISFLTKP	
Rat SGLT1	(501)	ITEFAYGTGSCMEPSNCPTIICGVHYLYFAIILFVIVISITVIVVSLFTKP	
Sheep SGLT1	(501)	ITEFAYGTGSCMEPSNCPKIICGVHYLYFAIILFAISVTVIVVISLLTKP	
Consensus	(501)	ITEFAYGTGSCMEPSNCPTIICGVHYLYFAIILFVIVITILVISLLTKP	
12			
Horse SGLT1	(551)	551	600
Human SGLT1	(551)	IPDVHLYRLCWSLRNSKEERIDLDAGEE-NIQDTLEESIEI--EVPEKK	
Mouse SGLT1	(551)	IPDVHLYRLCWSLRNSKEERIDLDAEEE-NIQEGPKETIEIETQVPEKKK	
Rabbit SGLT1	(551)	IPDVHLYRLCWSLRNSKEERIDLDAGEEEDIPEDSKDTIEIDTEAPQKKK	
Rat SGLT1	(551)	IPDVHLYRLCWSLRNSKEERIDLDAGEE-DIQEAPPEATDT--EVPKKKK	
Sheep SGLT1	(551)	IPDVHLYRLCWSLRNSTEERIDLDAGEEEPVEEDPKDTIEIDAEAPQKEK	
Consensus	(551)	IADVHLYRLCWSLRNSKEERIDLDAEDE-DIQDAREDALEIDTEASEKKK	
IPDVHLYRLCWSLRNSKEERIDLDAGEE DIQEAPKDTIEIDTEVPEKKK			
Horse SGLT1	(598)	601	650
Human SGLT1	(600)	GCFFRAYDLFCGLDQKGPKMTKEEEEAMKLKMTDTFEKPLWRTIMNING	
Mouse SGLT1	(601)	GIFRRAYDLFCGLEQHGAPKMTKEEEEAMKMKMTDTSEKPLWRTVLNNG	
Rabbit SGLT1	(600)	GCFFRAYDLFCGLDQKGPKMTKEEEEAMKMKMTDTSEKPLWRTVVNING	
Rat SGLT1	(598)	GFFRAYDLFCGLDQKGPKMTKEEEEAMKLKMTDTSEHPLWRTVVNING	
Sheep SGLT1	(600)	GCFRQAYDMFCGLDQKGPKMTKEEEEAMKLKMTDTSEKRLWRMVVNING	
Consensus	(601)	GCFRRAYDLFCGLDQKGPKMTKEEEEAMKLKMTDTSEKPLWRTVVNING	
Horse SGLT1	(648)	651	665
Human SGLT1	(650)	IILLTVAVFCHAYFA	
Mouse SGLT1	(651)	IILLTVAVFCHAYFA	
Rabbit SGLT1	(648)	IILLAVAVFCHAYFA	
Rat SGLT1	(651)	VILLAVAVFCYAYFA	
Sheep SGLT1	(650)	IILLAVAVFCHAYFA	
Consensus	(651)	IILLAVAVFCHAYFA	

Fig 6 continued: For details see previous page.

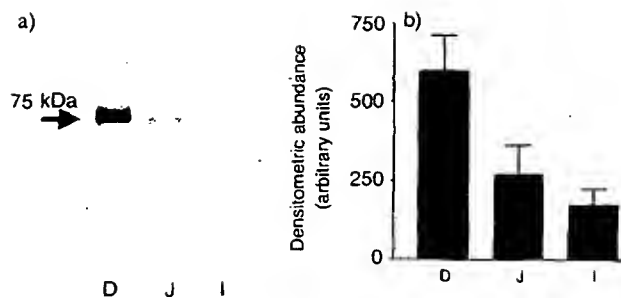


Fig 7: SGLT1 protein abundance in BBMVs isolated from equine small intestine. BBMVs (15 µg protein/lane) prepared from equine duodenum (D), jejunum (J) and ileum (I) were separated on 8% polyacrylamide gels, electrotransferred to nitrocellulose membrane and western blotted using an anti-SGLT1 polyclonal antibody, as described in Materials and methods. a) The results of a typical western blot indicating the presence of the 75 kDa SGLT1 protein. b) Densitometric analysis of western blots carried out using Phoretix 1D¹². Data are expressed as mean \pm s.e. (n = 7) in arbitrary units.

small intestine (Fig 7a), a molecular mass consistent with the size of SGLT1 in other species (Lescale-Matys *et al.* 1993; Shirazi-Beechey 1996; Dyer *et al.* 1997b; Wood *et al.* 2000). Densitometric analyses of immunoreactive bands measured in BBMVs from the duodenum, jejunum and ileum of several grazing horses are shown in Figure 7b. The profile of SGLT1 protein expression along the length of equine small intestine correlated with Na⁺-dependent D-glucose transport rates, with highest levels in the duodenum decreasing distally. These data further support that the proximal to distal decline is due to decrease in the level of functional Na⁺/glucose cotransporter protein in the brush-border membrane.

Northern blot analysis of SGLT1 mRNA in equine intestine

³²P-labelled equine SGLT1 cDNA (nucleotides 1406–2025) hybridised to 3 transcripts of 7, 4.4 and 2.4 kb in equine intestinal RNA samples (Fig 8a), with the 7 and 2.4 kb transcripts being the most abundant. Densitometric analyses of the total area of all transcripts indicate that SGLT1 mRNA levels were highest in the duodenum and decreased distally. This pattern of expression correlates with the SGLT1 activity and protein abundance. The presence of multiple transcripts for SGLT1 is usual, with many species having more than one and some ruminant species having up to 5 (Wood *et al.* 2000). This difference in size appears to be due to variation in the length of the 3' untranslated region (Peng and Lever 1995; Tarpey *et al.* 1995; Wood *et al.* 2000).

The results of these studies indicate collectively that SGLT1 is expressed in the equine small intestine and that SGLT1 expression is highest in the proximal intestine and decreases distally. The high degree of correlation between SGLT1 protein function and abundance with SGLT1 mRNA level suggests that, in mature grazing horses, SGLT1 expression is regulated at the level of mRNA abundance.

Discussion

Little information has been available on the mechanisms and membrane proteins involved in the digestion and absorption of dietary carbohydrates in equine small intestine. Equally, little is known about the sites of carbohydrate digestion and absorption

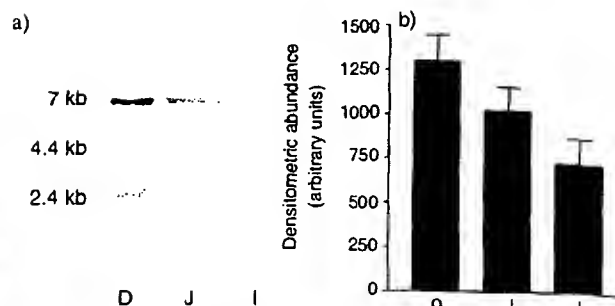


Fig 8: SGLT1 mRNA expression in equine small intestinal mucosa. Total RNA (3 µg per lane) prepared from equine duodenal (D), jejunal (J) and ileal (I) mucosal scrapings was separated on 1% agarose denaturing gels, transferred to nylon membrane and northern blotted using α^{32} P-labelled eSGLT1 cDNA probe, as described in Materials and methods. a) The results of a typical northern blot indicating the presence of 3 SGLT1 transcripts. b) Densitometric analysis of northern blots carried out using Phoretix 1D¹². Data are expressed as mean \pm s.e. (n = 7) in arbitrary units.

along the equine intestinal tract. Alexander (1955) showed that the absorption of glucose takes place in the small intestine of the horse and that this nutrient can fulfil some basal energy requirements. Alexander and Chowdhury (1958) detected the activity of lactase, maltase and amylase in the ileal juice sampled from one pony with an ileal cannula. In the present study, we have determined the level of activity and the abundance of disaccharidases measured in the intestinal brush-border membranes of a large number of mature horses. We have shown that sucrase, maltase and lactase are expressed in the equine intestinal brush-border membrane. Sucrase activity is highest in the proximal small intestine of the horse and levels are similar to those reported in the intestine of other nonruminant species (Kessler *et al.* 1978; Shirazi *et al.* 1981; Shirazi-Beechey *et al.* 1989; Dyer *et al.* 1997b). Maltase is expressed all along the equine small intestine. Maltase activity is similar in proximal, mid and distal regions and is extremely high compared with other species; 1 µmol/min/mg protein in the horse (this study) vs. 0.013–0.054 µmol/min/mg wet weight tissue in man (Dahlqvist 1964; Dyer *et al.* 1997b) and 0.014 µmol/min/mg protein in sheep (Shirazi-Beechey *et al.* 1989, 1991b). The brush-border membrane lactase is the enzyme responsible for the breakdown of the milk sugar, lactose. While the majority of animals and human subjects can digest lactose in suckling life, large populations of non-Caucasians and some animals become lactase deficient in adulthood (Henning *et al.* 1994). Consumption of lactose by these populations leads to intestinal disturbances and diarrhoea. The expression of lactase is preprogrammed (genetically controlled) and is not diet-induced (Duluc *et al.* 1991; Shirazi-Beechey *et al.* 1991b; Henning *et al.* 1994; Dyer *et al.* 1997b). In the studies carried out by Roberts (1975), it was reported that, in horses older than age 3 years, lactose feeding did not produce an increase in plasma glucose levels and induced passing of loose faeces. Based on these studies, he concluded that mature horses do not tolerate lactose. In spite of Roberts' conclusions, some horse-owners feed milk pellets to mature horses, particularly in an attempt to improve the weight and condition of show animals. Our studies indicate clearly that functional lactase is expressed in the intestinal tissue obtained from mature horses. This has been shown by direct measurements of the activity and abundance of lactase in the

purified brush-border membranes isolated from proximal, mid and distal regions of the intestine, indicating that these horses would have the ability to digest lactose. Our data support the conclusion made by Argenzio (1975) that the incidence of disaccharidase deficiency in horses is rare. Analysis of brush-border membrane vesicles prepared from the intestine of weaned, immature (age <4 years), horses demonstrated the presence of much higher lactase levels (data not shown) indicating that, although lactase expression in equine small intestine does decrease in maturity, it is not lost altogether. Further work is underway in our laboratory to investigate the developmental changes in equine small intestinal digestive and absorptive function.

We have shown that glucose and galactose are transported in the equine intestine by a Na⁺/glucose cotransporter isoform 1 (SGLT1). cDNA encoding SGLT1 has been cloned from the intestinal tissue of various species (Hediger *et al.* 1987; Hediger and Rhoads 1994; Shirazi-Beechey 1995; Tarpey *et al.* 1995; Turk and Wright 1997) and the amino acid sequences have been deduced. The comparison of SGLT1 sequences in various species indicates that this protein is conserved throughout evolution (Wright 1993; Shirazi-Beechey 1996). Despite the high percentage of identity in the amino acid sequences, there are some minor differences. These differences in the amino acid sequence have been shown to have a profound effect on the kinetic properties of the transporters. The differences in the amino acid sequence of SGLT1 in various species not only provide information on the relationship between structure and function, but also an insight into the differences in physiological environment encountered by SGLT1 in diverse species.

We have shown that SGLT1 in the intestine of horses consuming grass-based diets is expressed with highest abundance in the proximal intestine and the protein has a high affinity and a low capacity for the sugar substrates. This has physiological significance in the functioning of SGLT1 in the small intestine.

The identification of the regions of the gut involved in the digestion and absorption of dietary sugars will be important, particularly to animals having undergone gastrointestinal surgery when they are maintained subsequently on diets containing soluble digestible carbohydrates. Small intestinal resection (SIR) is commonly performed in the surgical treatment of equine colic (Tate *et al.* 1983), but little is known about the long-term effects of SIR on horse and ponies. Knowledge of the regional functional characteristics of the equine intestine will allow a more accurate prediction of the potential dietary complications the animal may experience during recovery and ways in which the diet can be supplemented during this critical period.

The data presented in this paper provide baseline information for a better understanding of the pathogenesis of dietary-induced intestinal disease and improved feed management in the horse.

Acknowledgements

The financial support of the Home of Rest for Horses and the Horserace Betting Levy Board is gratefully acknowledged. We thank Dr S. Wood for his constructive comments. We are grateful to Professor D. Swallow for the gift of the antibody to lactase. A preliminary report of this work was presented as an oral communication at the British Equine Veterinary Association Congress 2000, Birmingham, UK.

Manufacturers' addresses

- ¹Boehringer-Mannheim, Lewes, East Sussex, UK.
- ²Kendro Laboratory Products Ltd., Bishop's Stortford, Hertfordshire, UK.
- ³Millipore UK Ltd., Watford, Hertfordshire, UK.
- ⁴Qiagen Ltd., Crawley, West Sussex, UK.
- ⁵Invitrogen Life Technologies Ltd., Paisley, UK.
- ⁶Promega UK Ltd., Southampton, UK.
- ⁷Helena Biosciences, Sunderland, Tyne and Wear, UK.
- ⁸Stratagene (Europe) Ltd., Amsterdam, The Netherlands.
- ⁹BioRad Laboratories Ltd., Hemel Hempstead, Hertfordshire, UK.
- ¹⁰Amersham-Pharmacia Biotechnology Ltd., Little Chalfont, Buckinghamshire, UK.
- ¹¹Kodak Ltd., Hemel Hempstead, Hertfordshire, UK.
- ¹²Non-linear Dynamics Ltd., Newcastle Upon Tyne, Tyne and Wear, UK.
- ¹³Sigma-Aldrich Co. Ltd., Poole, Dorset, UK.
- ¹⁴Informax Inc., Oxford, Oxfordshire, UK.

References

- Alexander, F. (1955) Factors affecting the blood sugar concentration in horses. *Quart. J. exp. Physiol.* **40**, 24-31.
- Alexander, F. and Chowdhury, A.K. (1958) Enzymes in the ileal juice of the horse. *Nature* **181**, 190.
- Argenzio, R.A. (1975) Functions of the equine large intestine and their interrelationships in disease. *Cornell Vet.* **65**, 303-330.
- Argenzio, R.A. and Hintz, H.F. (1972) Effect of diet on glucose entry and oxidation rates in ponies. *J. Nutr.* **102**, 879-892.
- Dahlqvist, A. (1964) Method for assay of intestinal disaccharidases. *Analyt. Biochem.* **7**, 18-25.
- Diez-Sampedro, A., Eskandari, S., Wright, E.M. and Hirayama, B.A. (2001) Na⁺-to-sugar stoichiometry of SGLT3. *Am. J. Physiol. Renal Physiol.* **49**, F278-F282.
- Duluc, I., Boukamel, R., Mantei, N., Semenza, G., Raul, F. and Freund, J.N. (1991) Sequence of the precursor of intestinal lactase-phlorizin hydrolase from fetal rat. *Gene* **103**, 275-276.
- Dyer, J., Barker, P.J. and Shirazi-Beechey, S.P. (1997a) Nutrient regulation of the intestinal Na⁺/glucose co-transporter (SGLT1) gene expression. *Biochem. Biophys. res. Comm.* **230**, 624-629.
- Dyer, J., Hosie, K.B. and Shirazi-Beechey, S.P. (1997b) Nutrient regulation of human intestinal sugar transporter (SGLT1) expression. *Gut* **41**, 56-59.
- Fell, B. (1961) Cell shedding in the epithelium of the intestinal mucosa-fact and artifact. *J. path. Bact.* **81**, 251-254.
- Hediger, M.A. and Rhoads, D.B. (1994) Molecular physiology of sodium-glucose cotransporters. *Physiol. Rev.* **74**, 993-1026.
- Hediger, M.A., Coady, M.J., Ikeda, T.S. and Wright, E.M. (1987) Expression cloning and cDNA sequencing of the Na⁺/glucose co-transporter. *Nature* **330**, 379-381.
- Henning, S., Rubin, D. and Shulman, R. (1994) Ontogeny of the intestinal mucosa. In: *Physiology of the Gastrointestinal Tract*, Ed: L. Johnson, Raven Press, New York. pp 571-610.
- Hintz, H.F. and Cymbaluk, N.F. (1994) Nutrition of the horse. *Ann. rev. Nutr.* **14**, 243-267.
- Hirayama, B.A. and Wright, E.M. (1992) Glycosylation of the rabbit intestinal brush border Na⁺/glucose cotransporter. *Biochim. Biophys. Acta* **1103**, 37-44.
- Hirayama, B.A., Lostao, M.P., Panayotova-Heiermann, M., Loo, D.D., Turk, E. and Wright, E.M. (1996) Kinetic and specificity differences between rat, human and rabbit Na⁺-glucose cotransporters (SGLT-1). *Am. J. Physiol.* **270**, G919-G926.
- Hopfer, U. (1987) Membrane transport mechanisms for hexose and amino acids in the small intestine. In: *Physiology of the Gastrointestinal Tract*, Ed: L. Johnson, Raven Press, New York. pp 499-1526.
- Kessler, M., Acuto, O., Storelli, C., Murer, H., Muller, M. and Semenza, G. (1978) A modified procedure for the rapid preparation of efficiently transporting vesicles from small intestinal brush border membranes. Their use in investigating some properties of D-glucose and choline transport systems. *Biochim. Biophys. Acta* **506**, 136-154.
- Lescale-Matys, L., Dyer, J., Scott, D., Freeman, T.C., Wright, E.M. and Shirazi-Beechey, S.P. (1993) Regulation of the ovine intestinal Na⁺/glucose co-transporter (SGLT1) is dissociated from mRNA abundance. *Biochem. J.* **291**, 435-440.
- Malo, C. and Berteloot, A. (1991) Analysis of kinetic data in transport studies: new insights from kinetic studies of Na⁺-D-glucose cotransport in human intestinal brush-border membrane vesicles using a fast sampling, rapid filtration apparatus. *J. membr. Biol.* **122**, 127-141.
- Mantci, N., Villa, M., Enzler, T., Wacker, H., Boll, W., James, P., Hunzicker, W. and

- Semenza, G. (1988) Complete primary structure of human and rabbit lactase-phlorizin hydrolase: implications for biosynthesis, membrane anchoring and evolution of the enzyme. *Embo. J.* 7, 2705-2713.
- Peng, H. and Lever, J.E. (1995) Regulation of Na⁺-coupled glucose transport in LLC-PK1 cells. Message stabilization induced by cyclic AMP elevation is accompanied by binding of a M(r) = 48,000 protein to a uridine-rich domain in the 3'-untranslated region. *J. biol. Chem.* 270, 23996-24003.
- Roberts, M.C. (1975) Carbohydrate digestion and absorption studies in the horse. *Res. vet. Sci.* 18, 64-69.
- Rowell, A., Dyer, J., Hofmann, R.R. and Shirazi-Beechey, S.P. (1997) Expression of Na⁺/glucose cotransporter in the intestinal brush-border membrane of ruminants with different feeding habits. *Biochem. Soc. Trans.* 25, 482S.
- Schlegel-Haueuer, S., Hore, P., Kerry, K.R. and Semenza, G. (1972) The preparation of lactase and glucoamylase of rat small intestine. *Biochim. Biophys. Acta* 258, 506-519.
- Shirazi, S.P., Beechey, R.B. and Bunerworth, P.J. (1981) Potent inhibition of membrane-bound rat intestinal alkaline phosphatase by a new series of phosphate analogues. *Biochem. J.* 194, 797-802.
- Shirazi-Beechey, S.P. (1995) Molecular biology of intestinal glucose transport. *Nutr. res. Rev.* 8, 27-41.
- Shirazi-Beechey, S.P. (1996) Intestinal sodium-dependent D-glucose co-transporter: dietary regulation. *Proc. Nutr. Soc.* 55, 167-178.
- Shirazi-Beechey, S.P., Gorvel, J.-P. and Beechey, R.B. (1988) Phosphate transport in intestinal brush-border membrane. *J. Bioenerg. Biomembr.* 20, 273-288.
- Shirazi-Beechey, S.P., Kemp, R.B., Dyer, J. and Beechey, R.B. (1989) Changes in the functions of the intestinal brush border membrane during the development of the ruminant habit in lambs. *Comp. Biochem. Physiol. [B]* 94, 801-806.
- Shirazi-Beechey, S.P., Hirayama, B.A., Wang, Y., Scott, D., Smith, M.W. and Wright, E.M. (1991a) Ontogenic development of lamb intestinal sodium-glucose co-transporter is regulated by diet. *J. Physiol. (Lond.)* 437, 699-708.
- Shirazi-Beechey, S.P., Smith, M.W., Wang, Y. and James, P.S. (1991b) Postnatal development of lamb intestinal digestive enzymes is not regulated by diet. *J. Physiol. (Lond.)* 437, 691-698.
- Shirazi-Beechey, S.P., Davies, A.G., Tebbutt, K., Dyer, J., Ellis, A., Taylor, C.J., Fairclough, P. and Beechey, R.B. (1990) Preparation and properties of brush-border membrane vesicles from human small intestine. *Gastroenterol.* 98, 676-685.
- Tarpey, P.S., Wood, I.S., Shirazi-Beechey, S.P. and Beechey, R.B. (1995) Amino acid sequence and the cellular location of the Na⁺-dependent D-glucose symporters (SGLT1) in the ovine enterocyte and the parotid acinar cell. *Biochem. J.* 312, 293-300.
- Tate Jr., L.P., Ralston, S.L., Koch, C.M. and Everitt, J.I. (1983) Effects of resection of the small intestine in the pony. *Am. J. vet. Res.* 44, 1187-1191.
- Turk, E. and Wright, E.M. (1997) Membrane topology motifs in the SGLT cotransporter family. *J. membr. Biol.* 159, 1-20.
- Wood, I.S., Dyer, J., Hofmann, R.R. and Shirazi-Beechey, S.P. (2000) Expression of the Na⁺/glucose co-transporter (SGLT1) in the intestine of domestic and wild ruminants. *Pflugers Archiv. European J. Physiol.* 441, 155-162.
- Wright, E.M. (1993) The intestinal Na⁺/glucose cotransporter. *Ann. rev. Physiol.* 55, 575-589.
- Wright, E.M., Hirayama, B.A., Loo, D.D., Turk, E. and Hager, K. (1994) Intestinal sugar transport. In: *Physiology of the Gastrointestinal Tract*, 3rd edn. Ed: L.R. Johnson. Raven Press, New York. pp 1751-1772.

Received for publication: 8.1.01

Accepted: 26.6.01

SEVENTH COLIC RESEARCH SYMPOSIUM

14th-16th July 2002

at The Manchester Conference Centre, Manchester, UK.

Proffered reports on all aspects of recent research in equine gastroenterology from leading groups around the world.



The promotion and publicity of the Seventh Colic Symposium have been generously sponsored by Fort Dodge Animal Health UK.
Further details available from the BEVA office: colic@beva.org.uk

FORT DODGE

EQUINE EMERGENCIES AND CRITICAL CARE - CPD COURSE

12th-13th July 2002

at Leahurst, University of Liverpool, UK.

This is a continuing education course aimed at veterinary surgeons in practice. Presented by internationally renowned speakers.
Further details are available from: CPD Office, Leahurst, Neston, Wirral CH64 7TE • Tel: 0151 794 6016 • Email: cpdvets@liv.ac.uk



Both meetings are hosted by the British Equine Veterinary Association
BEVA 5 Finlay Street, London SW6 6HE Tel: 020 7610 6080 Fax: 020 7610 6823 Website: www.beva.org.uk



Suppressors of Cytokine Signaling Proteins Are Differentially Expressed in Th1 and Th2 Cells: Implications for Th Cell Lineage Commitment and Maintenance

Charles E. Egwuagu,¹ Cheng-Rong Yu, Meifen Zhang, Rashid M. Mahdi, Stephen J. Kim, and Igal Gery

Positive regulatory factors induced by IL-12/STAT4 and IL-4/STAT6 signaling during T cell development contribute to polarized patterns of cytokine expression manifested by differentiated Th cells. These two critical and antagonistic signaling pathways are under negative feedback regulation by a multimember family of intracellular proteins called suppressor of cytokine signaling (SOCS). However, it is not known whether these negative regulatory factors also modulate Th1/Th2 lineage commitment and maintenance. We show here that CD4⁺ naive T cells constitutively express low levels of SOCS1, SOCS2, and SOCS3 mRNAs. These mRNAs and their proteins increase significantly in nonpolarized Th cells after activation by TCR signaling. We further show that differentiation into Th1 or Th2 phenotype is accompanied by preferential expression of distinct SOCS mRNA transcripts and proteins. SOCS1 expression is 5-fold higher in Th1 than in Th2 cells, whereas Th2 cells contain 23-fold higher levels of SOCS3. We also demonstrate that IL-12-induced STAT4 activation is inhibited in Th2 cells that express high levels of SOCS3 whereas IL-4/STAT6 signaling is constitutively activated in Th2 cells, but not Th1 cells, with high SOCS1 expression. These results suggest that mutually exclusive use of STAT4 and STAT6 signaling pathways by differentiated Th cells may derive in part, from SOCS3- or SOCS1-mediated repression of IL-12/STAT4- or IL-4/STAT6 signaling in Th2 and Th1 cells, respectively. Given the strong correlation between distinct patterns of SOCS expression and differentiation into the Th1 or Th2 phenotype, SOCS1 and SOCS3 proteins are therefore Th lineage markers that can serve as therapeutic targets for immune modulation therapy. *The Journal of Immunology*, 2002, 168: 3181–3187.

Differentiation of naive, uncommitted Th precursor cells into Th1 or Th2 cells is a complex developmental process, and understanding the underlying molecular mechanisms may provide a conceptual framework in developing immune modulation therapies against allograft rejection, autoimmune diseases, and allergic diseases. The dominant factors that control the differentiation program are now recognized to be cytokines (1). Th cells activated in the presence of IL-12 differentiate into Th1 cells, predominantly secrete IFN- γ and TNF- β and promote delayed-type hypersensitivity responses (2). In contrast, Th cells that are activated in the presence of IL-4 differentiate into Th2 cells, produce mainly IL-4 and IL-5, and promote humoral and allergic responses (2).

Mutually exclusive use of the IL-12 or IL-4 signal transduction pathway by Th1 and Th2 cells, respectively, has spurred significant interest in understanding how regulation of these pathways are coupled to the differentiation process. IL-12 or IL-4 signaling is mediated by STAT4 and STAT6, respectively (3). Because transduction of cytokine signals through STAT proteins generally results in transcriptional activation of STAT-inducible genes, it is tacitly assumed that Th cells differentiate into Th1 or Th2 pheno-

type because of differential activation of genes that drives them to their respective developmental state. However, recent studies showing that cytokine signaling is under negative feedback regulation by a multimember family of proteins called suppressors of cytokine signaling (SOCS)² have raised the possibility that differentiation toward the Th1 or Th2 pathway may be mediated in part by the selective repression of IL-12/STAT4 or IL-4/STAT6-signaling pathways, respectively (4).

The SOCS family of proteins is at present composed of eight members characterized by the presence of a Src homology 2 domain and a C-terminal conserved domain called the SOCS box (5, 6). Evidence to date suggests that mRNA transcripts encoding SOCS are selectively up-regulated in response to several cytokines including IFN- γ , IL-2, IL-3, IL-4, IL-6, IL-12, IL-13, leukemia-inhibitory factor, stem cell factor, GM-CSF, growth factor, leptin, and erythropoietin (7). The SOCS proteins translated from the corresponding mRNA transcripts inhibit requisite cytokine-induced signaling pathways by classical feedback circuits (5–7). The inhibitory effects derive from direct interaction of SOCS Src homology 2 domains with cytokine receptors and/or Janus kinases (JAK) leading to the recruitment of SOCS proteins to the signaling complex, their inhibition of the binding of STATs to tyrosine-phosphorylated cytokine receptors, and suppression of the catalytic activities of JAKs (8–11). Gene targeting has been used to generate SOCS1^{-/-}, SOCS2^{-/-}, and SOCS3^{-/-} mice (12–16). Deletion of SOCS1 or SOCS3 is lethal in mice; SOCS3 null mice die in utero and mice lacking SOCS1 die within 3 wk after birth. Analysis of

Laboratory of Immunology, National Eye Institute, National Institutes of Health, Bethesda, MD 20892

Received for publication December 12, 2001. Accepted for publication January 24, 2002.

The costs of publication of this article were defrayed in part by the payment of page charges. This article must therefore be hereby marked advertisement in accordance with 18 U.S.C. Section 1734 solely to indicate this fact.

¹ Address correspondence and reprint requests to Dr. Charles E. Egwuagu, Molecular Immunology Section, Laboratory of Immunology, National Institutes of Health, Building 10, Room 10N116, 10 Center Drive, Bethesda, MD 20892-1857. E-mail address: emeku@helix.nih.gov

² Abbreviations used in this paper: SOCS, suppressor of cytokine signaling; HHL, hen egg lysozyme; Tg, transgenic; JAK, Janus kinase; TAMRA, 6-carboxytetramethylrhodamine; CD62L, CD62 ligand; 6FAM, 6-carboxyfluorescein.

the physiological functions of these SOCS proteins reveals requirement of SOCS3 in fetal liver erythropoiesis and placental development, whereas SOCS2 is important in postnatal growth. In contrast, SOCS1 is crucial in regulation of IFN- γ pathways. SOCS1^{-/-} mice have defective thymocyte development, and overexpression of SOCS1 impairs pre-TCR-induced thymocyte proliferation, suggesting that inhibition of cytokine signaling has important influence on T cell differentiation (17, 18).

In this study, we have characterized the repertoires of SOCS mRNAs and proteins expressed in naive and differentiated Th cells to examine the possibility that mutually exclusive patterns of cytokine expression by Th1 and Th2 cells derive from differential expression of SOCS proteins. We show here that Th1 and Th2 cells preferentially express distinct SOCS proteins that may play a role in the selective inhibition of STAT4/IL-12- and STAT6/IL-4-signaling pathways of Th cells. We discuss the implications of our findings on Th cell lineage commitment and/or maintenance.

Materials and Methods

Preparation of hen egg lysozyme (HEL)-specific Th1 and Th2 cells

T lymphocytes expressing HEL-specific TCR were isolated from spleens and lymph nodes of HEL-specific TCR-transgenic (Tg) mice designated "3A9" (a generous gift from M. Davis, Stanford University, Stanford, CA) as described (19). Briefly, CD4⁺ cells were isolated and purified (>97%) Th cells were cultured at 2.5×10^5 /ml in RPMI 1640 supplemented with 50 μ M 2-ME, antibiotics, and 10% FCS (complete medium) with $10 \times$ irradiated syngeneic splenocytes (as APC) in the presence of 2 μ g/ml HEL (Sigma-Aldrich, St. Louis, MO), 10 ng/ml IL-12 (Sigma-Aldrich), and 10 μ g/ml anti-IL-4 Ab (BD Pharmingen, San Diego, CA) for Th1 or 0.2 μ g/ml HEL, 10 ng/ml IL-4 (BD Pharmingen), 10 μ g/ml anti-IFN- γ Ab (BD Pharmingen), and 10 μ g/ml anti-IL-12 Ab (BD Pharmingen) for Th2. After 4 days, cultured cells were expanded with 40 IU/ml IL-2 (Chiron, Emeryville, CA) for 4 days, and these cells are designated as resting Th1 or Th2 cells. Some cells were restimulated at 2.5×10^5 /ml with $10 \times$ irradiated syngeneic APC in the presence of either 2 μ g/ml HEL, 40 IU/ml IL-2, and 10 ng/ml IL-12 for Th1 or 0.2 μ g/ml HEL, 40 IU/ml IL-2, and 10 ng/ml IL-4 for Th2. Three days later, cells were harvested, washed, resuspended in RPMI 1640, and designated as activated Th1 or Th2 cells. The cells designated as "Th" were obtained by incubating purified CD4⁺ cells, with HEL in the absence of the polarizing cytokines or their Abs.

For signal transduction studies, Th1 and Th2 cell lines were established and maintained in IL-2 (40 IU/ml) under polarization conditions described above. However, the HEL protein and APC were substituted by anti-CD3 (0.1 μ g/ml) and anti-CD28 (0.5 μ g/ml) Abs (BD Pharmingen). Activation of the STAT4 or STAT6 signal transduction pathway was analyzed in Th1 and Th2 cells cultured for 2 h under starvation conditions (1% BSA, RPMI 1640). The cells were then treated with IL-12 (10 ng/ml) or IL-4 (10 ng/ml) for 15 or 30 min.

Isolation of naive CD4⁺ T cells and FACS analysis

CD4⁺ T lymphocytes from spleens and lymph nodes of 3A9 mice were purified as described above. The cells were stained with PE-Cy5-CD4 or FITC-CD62 ligand (CD62L) Abs (BD Pharmingen), gated, and sorted out in FACStar Plus-SE cell sorter (BD Biosciences, San Jose, CA). For FACS analysis, purified CD4⁺ T cells (3×10^5) in FACS buffer (1 \times HBSS, 1% FCS, 10 mM HEPES, 0.2% NaN₃) were mixed with staining Ab and incubated at room temperature for 15 min. The cells were then washed twice with FACS buffer, fixed in 1% formaldehyde, and analyzed. mAbs used for staining are anti-CD4, CD62L, CD25, and their corresponding isotype control Abs (BD Pharmingen). Analysis was performed on the BD Biosciences FACSCalibur.

Cytokine measurements

For measurement of cytokines produced by the polarized cells, Th1 or Th2 cells were cultured as described above. Supernatants were collected after the second cycle of activation and assayed for cytokine secretion by ELISA, using kits obtained from Endogen (Woburn, MA).

RNAse protection assay

RNA (10 μ g) was hybridized overnight with (α -³²P)UTP-radiolabeled RNA probes transcribed *in vitro* from cDNA templates indicated in Fig.

1A. Overlapping ssRNA on hybridized dsRNAs was digested, and protected dsRNA duplexes were fractionated on denaturing-urea gels and processed for autoradiography.

Northern blot analysis

Northern blot analysis was performed with 20 μ g RNA as described (20). The integrity and comparability of RNA preparations used for analysis were verified by agarose-formaldehyde gel electrophoresis; comparable amounts of 18S and 28S rRNAs were detected for all RNA preparations. Mouse β -actin, SOCS1, SOCS2, and SOCS3 cDNAs were used as hybridization probes. SOCS-specific cDNAs were kindly provided by D. Hilton (Walter and Eliza Hall Institute, Melbourne, Australia) and H. Young (National Institutes of Health, Bethesda, MD).

Western blotting and immunoprecipitation analyses

Preparation of whole cell lysates, immunoprecipitation, and immunodepletion were performed as described (21). Briefly, samples (40 μ g/lane) were fractionated on 4–20% gradient SDS-PAGE, and SOCS1, SOCS2, SOCS3, or β -actin-specific (Santa Cruz Biotechnology, Santa Cruz, CA) or anti-pSTAT4- or anti-pSTAT6-specific (Zymed Laboratories, San Francisco, CA) polyclonal Abs were used as probes. For immunoprecipitation, 0.2 mg whole cell extract was incubated with protein G-agarose (Pharmacia Biotech, Piscataway, NJ), and anti-SOCS2 Ab for 1 h at 4°C and immunoprecipitates were washed four times in lysis buffer before electrophoresis. Preimmune serum was used in parallel as controls and signals were detected with HRP-conjugated secondary F(ab')₂ Ab (Zymed Laboratories) using the ECL system (Amersham, Arlington Heights, IL).

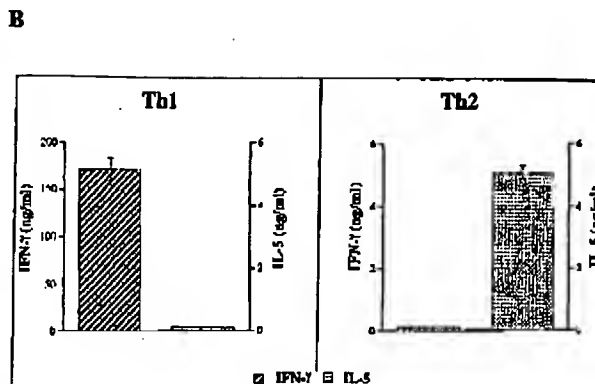
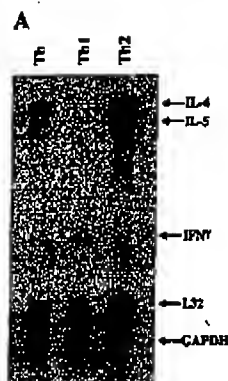
RT-PCR analysis

RNA (5 μ g), SuperScript II Reverse Transcriptase (Life Technologies, Gaithersburg, MD), and oligo(dT)_{12–16} were used for first-strand synthesis as previously described (21). Samples were subjected to hot-start PCR in a reagent mix containing digoxigenin-11-dUTP (Roche, Indianapolis, IN) and AmpliTaq Gold DNA polymerase (Applied Biosystems, Foster City, CA). Primers used for PCR amplification are as follows. For SOCS1, 5'-CTCGAGTAGGATGGTAGCAGCGAA-3' and 5'-CATCTTCAGCTGAGCGCGAAGAA-3'; SOCS2, 5'-GACCAGCTGTCTGGGACGTTGTA-3' and 5'-GAGAGAGAAATACCTTATACCTGGAAT-3'; SOCS3, 5'-TGCGCCATGGTCAACACAGCAAGTTT-3' and 5'-GCTCCTTAAGTGGAGCATTCATACCTGA-3'. For T-bet, 5'-TGCTGTGACGTCTCTAACA-3' and 5'-TGCCCCGCTTCTCTCAACCAA-3'. For c-maf, 5'-GTGCAGCAGACACGCTCT-3' and 5'-CAACTAGCAAGCCACATC-3'. For GATA-3, GAAGGCATCCAGACCCGAAAC-3' and 5'-ACCCATGCGCGGTGACCATGC-3'. For β -actin, 5'-GTGGCCGCTCTAGGCACAA-3' and 5'-TCTTTGCCAATAGTGATGACTTGGC-3'. Amplification was conducted for 35 cycles of 30 s each at 95°C, 60°C, and 72°C, followed by a final 10-min extension at 72°C. Under this condition, amplification was within the linear portion of the Taq amplification curve. First-strand synthesis containing each mRNA sample but no reverse transcriptase was performed to control for possible DNA contamination of mRNAs used as target for PCR amplification; failure to obtain RT-PCR products with any of the PCR amplimers confirmed the absence of contaminating DNA templates. PCR-amplified fragments were fractionated on 1.5% agarose gels. PCR products from naive cells were transferred onto nylon membranes, and signal detection was by the nonradioactive method as recommended for the ECL detection system (Amersham).

Quantitative RT-PCR analysis

First-strand synthesis was performed as described above. A negative control reaction without reverse transcriptase was performed for each RNA sample. RNA samples were normalized to 18S rRNA using the Taqman Ribosomal RNA Control Reagents kit (Applied Biosystems). Real-time PCR was performed on an ABI 7700 (Applied Biosystems) or ICycler iQ Real Time PCR (Bio-Rad, Hercules, CA) Sequence Detection System with the following primers: for SOCS1, 5'-ACCTCTCTGGTGCGGAC-3' and 5'-AAGCCATCTTACGCTGAGC-3'; for SOCS2, 5'-GGTTGCGCGAGGAACAGTC-3' and 5'-GAGCCTCTTTAATTTCTCTTGGC-3'; for SOCS3, 5'-CCCTCAGCTCCAAAAGCGAG-3' and 5'-GCTCTCTCTGCAGCTTGCG-3'. Hybridization probes used are: for SOCS1 (6-carboxyfluorescein (6FAM)-TCGCCAACGGAAGTCTTCTTCG-6-carboxyfluoromethylrhodamine (TAMRA)); for SOCS2 (6FAM-CGCGTCTGCCGAAAGCCCTG-TAMRA); for SOCS3 (6FAM-CCAGCTGGTGGTGAACCGCGT-TAMRA). PCR primers and probes for GAPDH are described in the TaqMan Rodent GAPDH Control Reagents kit (Applied Biosystems). PCR parameters are as recommended for the TaqMan Universal PCR master mix kit (Applied Biosystems). Triplicate samples of 10-fold serial dilutions of

FIGURE 1. Patterns of cytokine gene expression of the polarized Th cells. **A**, RNA protection assay using a mouse cytokine multiprobe template set and RNA samples from Th, Th1, and Th2 cells; L32, 112-bp protected fragment of L32-3A mouse ribosomal protein. **B**, detection of IFN- γ and IL-5 in supernatants from polarized Th1 or Th2 cells by ELISA.



SOCS1, SOCS2, or SOCS3 plasmid cDNA were assayed and used to construct the standard curves.

Results

Generation of Ag-specific Th1 or Th2 cell lineage

Recent studies have shown that SOCS proteins inhibit IL-4 signaling and the cross-talk between IFN- γ and IL-4 signaling pathways in hemopoietic cells (22, 23). Because these pathways have been implicated in Th cell differentiation and lineage commitment, we hypothesized that SOCS genes might be differentially expressed in Th cells and may contribute to establishment of stable Th1 or Th2 phenotype. To examine these possibilities, we generated HEL-specific Th1 and Th2 cells from the spleen and lymph nodes of HEL-specific TCR Tg mice and characterized them by RPA and ELISA cytokine assays. As shown in Fig. 1, the Th1 cells express relatively high levels of IFN- γ but undetectable amounts of IL-4 or IL-5 mRNAs, whereas the Th2 cells contain relatively high levels of IL-4 and IL-5 mRNAs. Nonpolarized Th cells produced lower levels of all three cytokines. Adoptive transfer of the Th1 cells into Tg mice expressing the HEL protein in the ocular lens produced delayed-type hypersensitivity-like ocular inflammatory disease, whereas large numbers of the Th2 cells induced eosinophilic inflammation only in immunodeficient recipients (19), further underscoring the fact that polarized T cells used in this study have the requisite phenotype expected of Th1 or Th2 lineage.

SOCS1, SOCS2, and SOCS3 genes are differentially expressed in Th1 and Th2 cells

We then examined the repertoire of SOCS family members expressed in HEL-stimulated nonpolarized (Th), Th1, and Th2 cells by Northern blot analysis. We found significantly higher levels of SOCS1 and SOCS2 mRNA transcripts in Th1 cells than in Th2 cells (Fig. 2A). In contrast, we detected a considerably higher level of the SOCS3 mRNA transcript in Th2 cells, with very little SOCS3 expression in Th1 cells. Nonpolarized Th cells, consisting of both Th1 and Th2 cells, produced low levels of all three SOCS transcripts. These results were obtained in three separate experiments that used independently derived Th, Th1, and Th2 cells.

In concert with results of our mRNA analyses, the level of SOCS1 protein detected in Th1 cells by Western blot analysis is significantly higher than in Th2 cells (Fig. 2B). Conversely, we detected SOCS3 protein in Th2 but not in Th1 cells. Although we could not detect SOCS2 protein in either Th1 or Th2 cells by Western blot analysis (not shown), it was detected in both cell types by immunoprecipitation, albeit with higher amounts in Th1 cells (Fig. 2B). The low SOCS2 protein level is surprising considering that Th1 cells express high levels of SOCS2 mRNA transcripts. This may suggest that the SOCS2 protein is either unstable

in Th1 cells or that its steady-state concentration is regulated at the level of translation. Together, our protein and mRNA data provide the first evidence that SOCS are differentially expressed in Th1 and Th2 cells.

Quantitative PCR analysis of SOCS1, SOCS2, and SOCS3 expression in Th1 and Th2 cells

We determined the abundance of SOCS1, SOCS2, and SOCS3 in Th1 and Th2 cells by real-time quantitative PCR assay. In Fig. 3, we show real-time PCR amplification profiles of mouse SOCS1, SOCS2, and SOCS3 cDNAs from resting Th, Th1, or Th2 cells. Standard curves generated from the SOCS cDNA dilution series showed excellent linearity indicating precise, quantitative relationship between cDNA copy number, and fluorescence signal intensity within the dynamic range of the assay (data not shown). Assuming that a typical mammalian cell contains 10 pg RNA, our real-time PCR data indicate that Th1 cells contain ~1276 copies of SOCS1 transcripts per cell, as compared with only 246 copies in a Th2 cell. A similar analysis revealed a value of 1225 and 320 copies of SOCS2 transcripts in the Th1 and Th2 cell, respectively. In contrast, 1297 copies of SOCS3 transcripts are detected per Th2 cell and only 56 copies in Th1 cell. The relatively high levels of SOCS expression in Th1 and Th2 cells may be sufficient to influence phenotype-specific cytokine signaling and maintenance of the corresponding differentiated state.

Effects of SOCS expression on IL-12 and IL-4 signaling in Th1 and Th2 cells

Given the differential patterns of SOCS expression in Th1 and Th2 cells, we predicted that IL-4 signaling would be inhibited in Th1

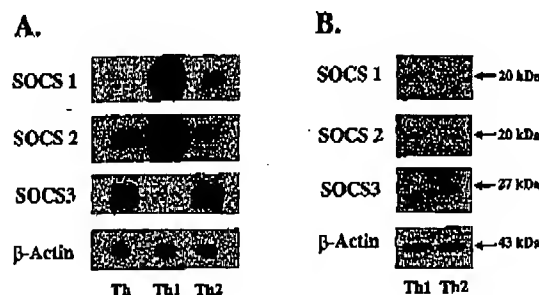


FIGURE 2. SOCS1, SOCS2, and SOCS3 genes are differentially expressed in Th1 and Th2 lymphocytes. **A**, Northern blot analysis (20 μ g RNA/lane) using 32 P-labeled SOCS cDNAs as probes; **B**, Western blot analysis using SOCS1 or SOCS3 polyclonal Ab and 25 μ g whole cell extracts from Th1 or Th2 cells. For SOCS2 protein, 200 μ g extracts were immunoprecipitated and detected using SOCS2-specific Ab. β -Actin expression was determined by Western blotting.

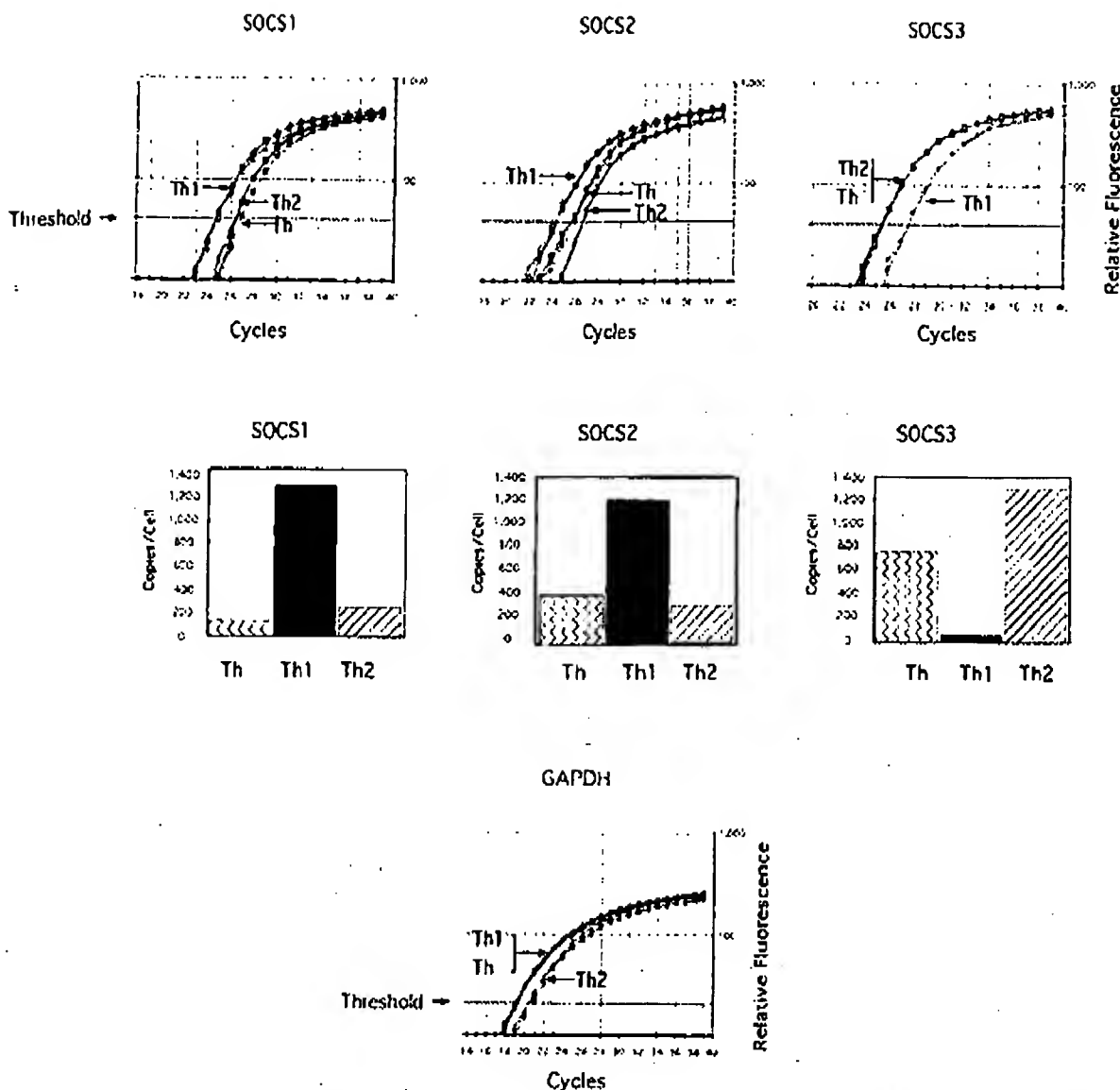


FIGURE 3. Quantitative detection of SOCS mRNA transcripts in Th cell types by real-time PCR. Amplification plots of the relative fluorescence intensity vs cycle number are shown for GAPDH, SOCS1, SOCS2 and SOCS3 target cDNAs. The dynamic range of each assay covers 1–10,000 cDNA copies. Bars show the number of copies (per cell) of SOCS1, SOCS2, and SOCS3 as calculated in the text.

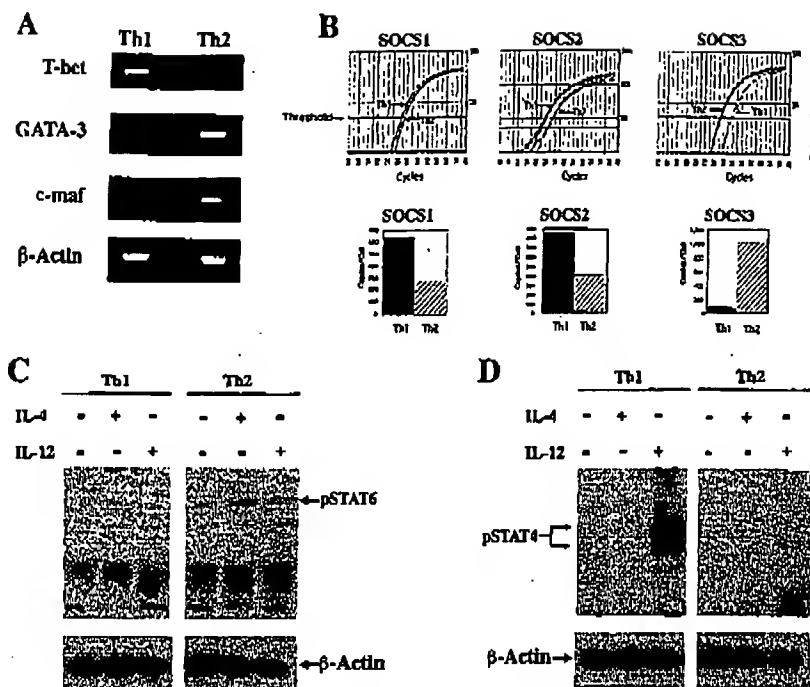
cells by the relatively high levels of SOCS1 and SOCS2 expression in these cells. Conversely, we expected marked inhibition of IL-12 signaling in Th2 cells by high constitutive expression of SOCS3. To test this hypothesis, we established long term Th1 and Th2 cell lines as described above. Before use in our signaling studies, we verified that these cells do indeed retain their respective phenotypes by examining expression patterns of transcription factors that characterize Th1 or Th2 lineage. Consistent with published reports (2, 3), Th1 cells expressed high levels of T-bet, whereas Th2 cells expressed relatively higher levels of GATA-3 and c-maf than did Th1 cells (Fig. 4A). Analysis of these cells by real-time PCR verified that they retain their expected patterns of SOCS expression, with Th1 cells expressing relatively higher levels of SOCS1 and SOCS2, whereas Th2 cells contain higher levels of SOCS3 (Fig. 4B). We then examined activation of STAT6 and STAT4 after treatment of the cells with either IL-4 or IL-12 by Western blotting. In Th2 cells, IL-4 induced strong tyrosine phosphorylation of STAT6, whereas activation of STAT6 in Th1 cells is barely detected (Fig. 4C). We also detected activated STAT6 in

untreated Th2 but not in Th1 cells, suggesting that constitutive and inducible IL-4/STAT6 signals in Th1 cells may be inhibited in part by high SOCS1 and SOCS2 expression. In contrast, IL-12 induced high levels of tyrosine-phosphorylated STAT4 in Th1 but not Th2 cells, suggesting that the high constitutive SOCS3 expression may inhibit IL-12/STAT4 pathway in these cells (Fig. 4D). Although these results clearly show that expression of specific SOCS correlates with activation of specific STAT signaling pathways, this does not necessarily constitute proof that the specific SOCS members mediate the relevant pathways *in vivo*.

SOCS genes are constitutively expressed in naive nonpolarized CD4⁺ lymphocytes

To determine whether differential regulation of the SOCS is intrinsic to Th cells or derives from effects of cytokines that polarize Th cells to the Th1 or Th2 phenotype, we analyzed SOCS expression in naive nonpolarized CD4⁺ T cells. Fresh CD4⁺ cells from the spleen and lymph nodes were isolated on a cell sorter as described

FIGURE 4. Analysis of transcriptional activators and repressors in Th1 and Th2 cell lines. *A*, Detection of lineage-specific transcription factors T-bet, GATA-3, *c-maf* by RT-PCR. *B*, quantitative detection of SOCS mRNA transcripts in activated Th1 or Th2 cell lines by real-time PCR. Amplification plots of the relative fluorescence intensity vs cycle number for GAPDH, SOCS1, SOCS2, and SOCS3 target cDNAs. Bars show the number of copies of each SOCS per cell. Shown are detection by Western blotting of pSTAT6 (*C*) and pSTAT4 (*D*) proteins in Th1 and Th2 whole cell extracts (25 μ g) before and after treatment of the cells with either IL-4 or IL-12.



in *Materials and Methods*. More than 99% of the sorted cells express cell surface CD4. FACS analysis of the cells further reveal that they express high levels of CD62L and low levels of CD25, features associated with a naive phenotype (Fig. 5). Analysis of cDNAs from these cells for the expression of *SOCS1*, *SOCS2*, or *SOCS3* gene by quantitative RT-PCR reveals constitutive expression of *SOCS1*, *SOCS2*, and *SOCS3* mRNA transcripts (Fig. 6).

However, in contrast to significant amounts of mRNAs expressed in Th, Th1, and Th2 cells that allow their detection by the relatively insensitive Northern blot assay, the levels of SOCS transcripts in naive Th cells are very low; their detection required at least 35 cycles of PCR amplification (Fig. 6A). Of particular note is the relatively low abundance of *SOCS1* transcripts detected by real-time PCR in the naive nonpolarized cells (Fig. 6B).

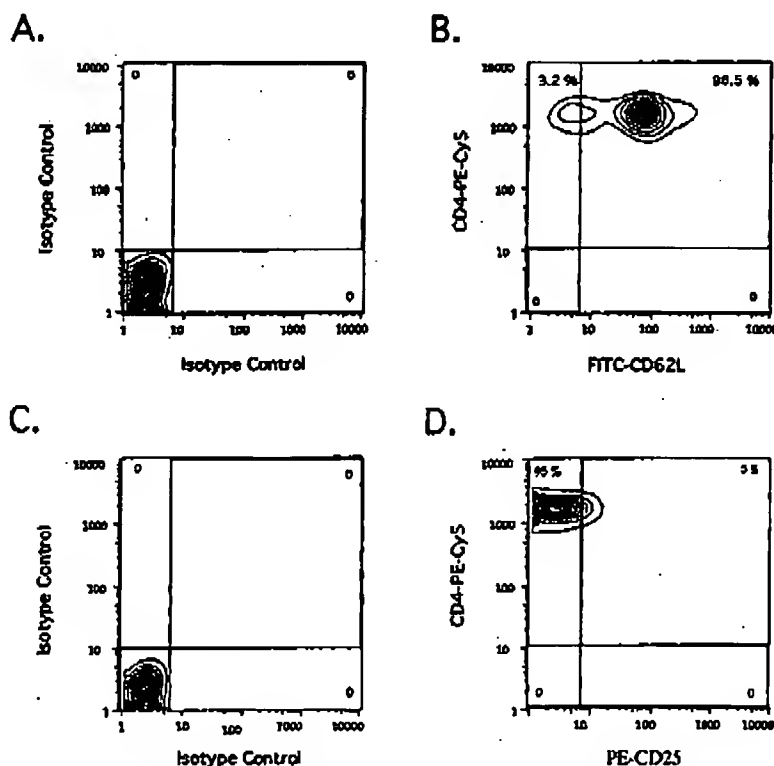


FIGURE 5. Three-color flow cytometric analysis of sorted $CD4^+ CD62L^{high} CD25^-$ naive T cells. $CD4^+$ cells were stained with PE-Cy5-CD4, FITC-CD62L, or PE-CD25 Ab. *A* and *C*, Isotype controls.

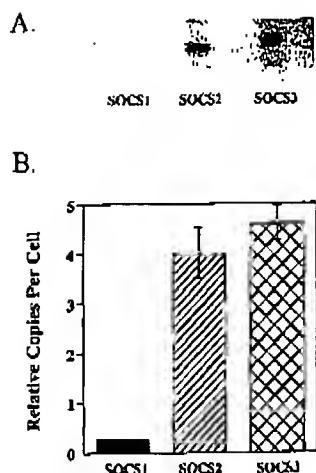


FIGURE 6. RT-PCR analysis of SOCS1, SOCS2, and SOCS3 expression in naive CD4⁺ T cells. *A*, cDNAs from sorted CD4⁺ naive T cells were subjected to 35 cycles of PCR amplification and detected as described in *Materials and Methods*; *B*, real-time PCRs on cDNAs from the sorted CD4⁺ naive T cells were performed as described above.

Discussion

Positive regulatory transcription factors such as T-bet, GATA-3, STAT4, and STAT6 play critical roles in initiating primary immune responses and skewing the response toward the Th1 or Th2 pathway (2, 3, 10). However, the amplitude and duration of the response depend on precise fine-tuning and coordination of lymphocyte responses, and these aspects of the adaptive immune response are regulated by endogenous feedback regulators of cytokine activities (11, 12). Prominent among this class of intracellular regulators are members of the SOCS family of proteins that modulate cytokine signaling in hemopoietic cells by inhibiting kinases and activated STATs or cytokine receptors (11, 12). Significant interest in the SOCS family stems from the belief that SOCS proteins may integrate multiple cytokine signals and mediate cross-communication between antagonistic cytokines elaborated by differentiating Th cells through their inhibitory effects on cytokine receptors (IL-4, IL-6, IL-10, IFN- γ) and signaling molecules (JAKs, STATs, Tec, p95^{cas}).

In this study, we found that three members of the SOCS family are differentially expressed in differentiated Th cells. Th1 cells predominantly express SOCS1 and SOCS2 but synthesize minute amounts of SOCS3 mRNAs or protein. Conversely, Th2 cells express very high levels of SOCS3 but low levels of SOCS1 protein and mRNA. The relatively high levels of SOCS mRNAs and proteins and their restricted patterns of expression in Th1 and Th2 cells underscore the importance of particular SOCS members in Th cell subtypes.

Furthermore, our data suggest that IL-4/STAT6 signaling is repressed in Th1 cells that constitutively express high levels of SOCS1 but not in Th2 cells that contain relatively low amounts of SOCS1. This observation is consistent with another report showing that SOCS1 inhibits IL-4 signaling in M12 B cell line (22). Constitutive expression of SOCS1 in Th1 cells is therefore consistent with a Th cell differentiation model in which SOCS1 promotes differentiation toward the Th1 lineage by stably inhibiting IL-4 signaling, thereby repressing Th2 differentiation. Because IFN- γ signaling is dependent on activated STAT1 and tyrosine phosphorylation of STAT1 is under feedback-inhibition by SOCS1 (5, 6, 24), constitutive expression of SOCS1 may also lead to abrogation of IFN- γ signaling and autocrine stimulation of Th1 cells by

IFN- γ . In fact, the inability to respond to IFN- γ is a hallmark feature of Th1 cells as Th2 cells do respond to IFN- γ signaling, and this has been attributed to the absence of IFN- γ R2 receptors in Th1 cells (25). We suggest that in addition to this explanation, it may well be that constitutive expression of SOCS1 provides a fail-safe mechanism that ensures absence of IFN- γ signaling in Th1 cells. Thus, similar to T-bet, SOCS1 is a Th1 lineage marker and presumably promotes commitment to the Th1 phenotype.

Although the roles of either SOCS2 or SOCS3 in lymphoid cell development have not been established, the preferential use of SOCS3 in Th2 but not Th1 cells is suggestive of its role in the maintenance of the Th2 cell lineage. Therefore IL-12/STAT4 signaling is repressed in Th2 cells with high constitutive expression of SOCS3 but not in Th1 cells that contain relatively low amounts of this SOCS member (Fig. 4). Although there is no direct evidence implicating SOCS3 in the regulation of IL-12, the very high endogenous levels of SOCS3 in Th2 but not in Th1 cells suggest that SOCS3 may constitutively repress IL-12/STAT4 signaling in Th2 cells. Furthermore, in contrast to the low levels of SOCS1 mRNA, SOCS3 mRNA is expressed at relatively high levels in nonpolarized Th cells, suggesting that this SOCS member may also contribute to the initial phase of the differentiation process. Constitutive expression of SOCS2 in naive and differentiated Th cells is particularly intriguing in that this SOCS member functions primarily to regulate growth through its inhibitory effects on growth hormone-induced STAT5-dependent gene transcription. Given that IL-2 effects on Th cells are mediated by STAT5-dependent signaling pathways, overriding the negative regulation of these pathways by SOCS2 and possibly other SOCS proteins may be a necessary requirement for Ag-dependent proliferation and activation of Th cells. Ongoing studies are examining the levels of other SOCS family members such as SOCS4–7, cytokine-induced Src homology 2-containing protein (CIS), proteins containing SOCS box and WD-40 repeats (WSB), proteins containing SOCS box and ankyrin repeats (ASB), proteins containing SOCS box and SPRY domains (SSB), and proteins containing SOCS box and a GTPase domain (RAR) in Th cells and investigating their possible involvement in Th differentiation process and/or maintenance of the polarized patterns of cytokine expression in Th1 and Th2 cells.

A major issue that must be resolved relates to the relative contributions of cytokine and TCR signaling in differential regulation of SOCS expression in Th1 and Th2. The fact that SOCS expression is relatively low in naive Th cells and is up-regulated in response to activation or cytokine signaling suggests that the Th cell differentiation process and expression of SOCS proteins are coordinately regulated. On one hand, the up-regulation of SOCS expression by stimulation with the HEL protein in nonpolarized Th cells suggests that TCR signaling contributes to SOCS induction. In contrast, the preferential up-regulation of SOCS1 expression in Th1 but not Th2 cells after IL-12 stimulation argues for a role of cytokine signaling in SOCS regulation. Our data further suggest that high constitutive SOCS3 expression may be the default pattern of SOCS expression in CD4⁺ cells as naive Th cells, nonpolarized activated Th cells, and Th2 cells express relatively high levels of SOCS3 and very low levels of SOCS1. The functional consequences of elevated expression of SOCS3 may be to drive the majority of CD4⁺ toward a Th2 pattern of cytokine expression. In view of the significant increase of SOCS3 expression in response to Ag stimulation, it is tempting to speculate that a major impact of TCR signaling is transcriptional activation of the *SOCS3* gene of naive CD4⁺. However, cytokines can override the effects of *SOCS3* during Th differentiation. In fact, a major effect of IL-12 signaling in nonpolarized Th cells is to down-regulate *SOCS3* expression in cells committed to the Th1 lineage. In contrast to Th2,

Th₁ and naive CD4⁺ cells, Th₁ differentiation requires IL-12/STAT4 signaling and induction of *SOCS1*. Selective induction of *SOCS1* in differentiating Th₁ cells may inhibit IFN- γ -induced phosphorylation of STAT1, thereby preventing autoregulation of Th₁ cells by IFN- γ . Thus, on activation in a target tissue during the course of an inflammatory response, Th₁ cells produce copious amounts of IFN- γ that act on cells in their microenvironment, but they are refractile to the effects of this cytokine on gene transcription and cell cycle regulation.

In summary, our data show that SOCS mRNAs and proteins are differentially expressed in Th₁ and Th₂ cells. The polarized expression of SOCS proteins in differentiated Th lymphocytes suggests that IL-12/STAT4- and IL-4/STAT6-signaling pathways may be repressed, at least in part, by a SOCS3- or SOCS1-mediated mechanism, respectively. Thus, Th cells that constitutively repress STAT6 signals become Th₁ cells, and those that inhibit STAT4 activities develop into the Th₂ phenotype. Our findings provide impetus for further investigations into the roles of negative regulatory factors in Th cell differentiation and, given the critical roles that SOCS proteins play in the termination of immune or cytokine responses, it is likely that other members of the SOCS family may also regulate Th cell lineage commitment and maintenance. These findings are of interest not merely in the context of Th differentiation but also because SOCS1 and SOCS3 proteins can serve as potential therapeutic targets for immune modulation therapy to skew the immune response toward a desirable outcome.

Acknowledgments

We thank Drs. Howard Young and Chandra Nagineni for critical reading of the manuscript.

References

- O'Garra, A. 1998. Cytokines induce the development of functionally heterogeneous T helper cell subsets. *Immunology* 8:275.
- Glimcher, L. F., and K. M. Murphy. 2000. Lineage commitment in the immune system: the T helper lymphocyte grows up. *Genes Dev.* 14:1693.
- Murphy, K. M., W. Ouyang, J. D. Farrar, J. Yang, S. Ranganath, H. Asnagli, M. Afkarian, and T. L. Murphy. 2000. Signaling and transcription in T helper development. *Annu. Rev. Immunol.* 18:451.
- Wurstler, A. L., T. Tanaka, and M. J. Grusby. 2000. The biology of STAT4 and STAT6. *Oncogene* 19:2577.
- Nicola, N. A., S. E. Nicholson, D. Metcalf, J. G. Zhang, M. Baca, A. Farley, T. A. Willson, R. Starr, W. Alexander, and D. J. Hilton. 1999. Negative regulation of cytokine signaling by the SOCS proteins. *Cold Spring Harbor Symp. Quant. Biol.* 64:397.
- Naka, T., M. Fujimoto, and T. Kishimoto. 1999. Negative regulation of cytokine signaling: STAT-induced STAT inhibitor. *Trends Biochem. Sci.* 24:394.
- Krebs, D. L., and D. J. Hilton. 2001. Socs proteins: negative regulators of cytokine signaling. *Stem Cells* 19:378.
- Nicholson, S. E., T. A. Willson, A. Farley, R. Starr, J. G. Zhang, M. Baca, W. S. Alexander, D. Metcalf, D. J. Hilton, and N. A. Nicola. 1999. Mutational analyses of the SOCS proteins suggest a dual domain requirement but distinct mechanisms for inhibition of LIF and IL-6 signal transduction. *EMBO J.* 18:375.
- Yasukawa, H., H. Misawa, H. Sakamoto, M. Masuhara, A. Sasaki, T. Wakioka, S. Ohtsuka, T. Imaizumi, T. Matsuda, J. N. Ihle, and A. Yoshimura. 1999. The JAK-binding protein JAB inhibits Janus tyrosine kinase activity through binding in the activation loop. *EMBO J.* 18:1309.
- Sasaki, A., H. Yasukawa, T. Shouda, T. Kitamura, I. Dikic, and A. Yoshimura. 2000. CIS/3/SOCS-3 suppresses erythropoietin (EPO) signaling by binding the EPO receptor and JAK2. *J. Biol. Chem.* 275:29338.
- Narazaki, M., M. Fujimoto, T. Motomoto, Y. Morita, H. Saito, T. Kajita, K. Yoshizaki, T. Naka, and T. Kishimoto. 1998. Three distinct domains of SS1-1/SOCS-1/JAB protein are required for its suppression of interleukin 6 signaling. *Proc. Natl. Acad. Sci. USA* 95:13130.
- Alexander, W. S., R. Starr, J. G. Fenner, C. L. Scott, E. Handman, N. S. Sprigg, J. E. Corbin, A. L. Cornish, R. Dorwiche, C. M. Owczarek, et al. 1999. SOCS1 is a critical inhibitor of interferon γ signaling and prevents the potentially fatal neonatal actions of this cytokine. *Cell* 98:597.
- Marine, J. C., D. J. Topham, C. McKay, D. Wang, F. Parganas, D. Stravopodis, A. Yoshimura, and J. N. Ihle. 1999. SOCS1 deficiency causes a lymphocyte-dependent perinatal lethality. *Cell* 98:609.
- Metcalf, D., C. J. Greenhalgh, E. Viney, T. A. Willson, R. Starr, N. A. Nicola, D. J. Hilton, and W. S. Alexander. 2000. Gigantism in mice lacking suppressor of cytokine signalling-2. *Nature* 405:1069.
- Marine, J. C., C. McKay, D. Wang, D. J. Topham, E. Parganas, H. Nakajima, H. Pendeville, H. Yasukawa, A. Sasaki, A. Yoshimura, and J. N. Ihle. 1999. SOCS3 is essential in the regulation of fetal liver erythropoiesis. *Cell* 98:617.
- Roberts, A. W., I. Rohb, S. Rakar, L. Hartley, L. Cluse, N. A. Nicola, D. Metcalf, D. J. Hilton, and W. S. Alexander. 2001. Placental defects and embryonic lethality in mice lacking suppressor of cytokine signaling 3. *Proc. Natl. Acad. Sci. USA* 98:9324.
- Fujimoto, M., T. Naka, R. Nakagawa, Y. Kawazoe, Y. Morita, A. Toteishi, K. Okumura, M. Narazaki, and T. Kishimoto. 2000. Defective thymocyte development and perturbed homeostasis of T cells in STAT-induced STAT inhibitor-1/suppressors of cytokine signaling-1 transgenic mice. *J. Immunol.* 165:1799.
- Trop, S., P. De Sepulveda, J. C. Zuniga-Pflucker, and R. Rottapel. 2001. Overexpression of suppressor of cytokine signaling-1 impairs pre-T-cell receptor-induced proliferation but not differentiation of immature thymocytes. *Blood* 97:2269.
- Kim, S. J., M. Zhang, B. P. Vistica, C. C. Chan, D. F. Shen, E. P. Wawrousek, and I. Gery. Ocular inflammation induced by T-helper lymphocytes type 2. *Invest. Ophthalmol. Vis. Sci.* In press.
- Li, W., C. N. Nagineni, C. Ohtsuka-Maruyama, B. Ebnik, A. B. Chelensky, and C. E. Egwuagu. 1999. Interferon consensus sequence binding protein is constitutively expressed and differentially regulated in the ocular lens. *J. Biol. Chem.* 274:9686.
- Egwuagu, C. E., P. Charukamnoetkanok, and I. Gery. 1997. Cutting edge: Thymic expression of autoantigens correlates with resistance to autoimmune disease. *J. Immunol.* 159:3109.
- Losman, J. A., X. P. Chen, D. Hilton, and P. Rothman. 1999. Cutting edge: SOCS1 is a potent inhibitor of IL-4 signal transduction. *J. Immunol.* 162:3770.
- Dickensheets, H. L., C. Venkataruman, U. Schindler, and R. P. Donnelly. 1999. Interferons inhibit activation of STAT6 by interleukin 4 in human monocytes by inducing SOCS1 gene expression. *Proc. Natl. Acad. Sci. USA* 96:10300.
- Diehl, S., J. Anguita, A. Hoffmeyer, T. Zupion, J. N. Ihle, E. Fikrig, and M. Rincon. 2000. Inhibition of Th1 differentiation by IL-6 is mediated by SOCS1. *Immunity* 13:805.
- Tsu, G. Z., T. von der Weid, B. Lu, S. Cowan, M. Kvatnyuk, A. Pernis, G. Cantoretti, N. S. Braunstein, R. L. Coffman, and P. B. Rothman. 2000. Interferon γ signaling alters the function of T helper type 1 cells. *J. Exp. Med.* 192:977.

Intravitreal invading cells contribute to vitreal cytokine milieu in proliferative vitreoretinopathy

I A El-Ghrably, Harinder S Dua, Gavin M Orr, David Fischer, Patrick J Tighe

Abstract

Aim—To examine the contribution of infiltrating cells in the local production of cytokines within the vitreous of patients with proliferative vitreoretinopathy (PVR). **Methods**—The presence of mRNA coding for IL-6, IL-8, IL-1 β , IL-1 α , TNF α , IFN γ , IL-12, and HPRT was investigated in 25 vitreous samples from patients with PVR, 11 vitreous samples from patients with retinal detachment (RD) not complicated by PVR, and 10 vitreous samples from patients with macular hole (MH). A quantitative reverse transcriptase polymerase chain reaction (RT-PCR) using an internal competitor was used to investigate these samples. From these samples, 15 PVR, 8 RD, and 8 MH were analysed for the protein levels of the same cytokines using enzyme linked immunosorbent assay (ELISA). Spearman correlation was used to test any association between mRNA and cytokine protein levels, as an indicator of the contribution these cells make to the intravitreal cytokine milieu.

Results—A strong correlation was found between mRNA and their respective cytokine levels (protein products) for IL-6, IL-8, IL-1 β , IL-1 α , TNF α , IFN γ (Spearman $r = 0.83, 0.73, 0.67, 0.91, 0.73, \text{ and } 0.73$ respectively), but not for IL-12. The median levels of IL-6, IL-8, IL-1 β , and IFN γ mRNA and their respective cytokines were significantly higher ($p < 0.05$) in patients with PVR than in those with macular hole. There was no statistically significant difference in the median levels of IL-1 α mRNA between PVR and MH but the cytokine IL-1 α was detected at a significantly higher level in PVR compared with MH patients. Between PVR and RD patients, there was no statistically significant difference in mRNA levels for all the investigated cytokines ($p > 0.05$) except for IL-6 where there was a statistical significance ($p = 0.038$). In contrast, the median levels of IL-6, IL-8, and IL-1 β cytokines were significantly higher ($p < 0.05$) in patients with PVR than in those with RD, whereas for IL-1 α and IFN γ no significant statistical difference was detected between PVR and RD patients ($p > 0.05$). When results of RD and MH patients were compared, a statistical difference was only detected in mRNA levels of IFN γ ($p = 0.008$). However, no difference

was detected for IFN γ (protein product) or for any of the other cytokines between RD and MH patients.

Conclusion—Levels of both protein and mRNA encoding IL-6, IL-8, IL-1 β , and IFN γ is significantly increased in vitreous samples from patients with PVR. The strong correlation between ELISA detectable cytokines (protein products) and their respective mRNA levels suggest that intravitreal, invasive cells are the major source of these cytokines, with the exception of IL-12. Cells invading the vitreous do not appear to locally produce IL-12 mRNA. This would appear to implicate cells peripheral to the vitreal mass as the major source of this cytokine.

(Br J Ophthalmol 2001;85:461-470)

Proliferative vitreoretinopathy (PVR) is still the most common cause of failure of surgery for rhegmatogenous retinal detachment (RRD) despite the substantial effort that has been devoted to better understanding and management of this condition during the past 25 years.^{1,2} It is characterised by the formation of membranes extending along both surfaces of the detached retina and within the vitreous.³

The PVR process can be considered as a modified wound healing process, which is initiated by injury (retinal break) that causes a retinal detachment. The most important factor is probably the excessive inflammatory reaction that occurs in some clinical situations that predispose to PVR. The exact pathogenic mechanisms involved in the formation of PVR are not completely understood. However, five distinct stages appear to be important in its development including breakdown of the blood-retinal barrier (BRB), chemotaxis, and cellular migration, cellular proliferation, membrane formation with remodelling of the extracellular matrix, and contraction.⁴⁻⁶

Cytokines are polypeptides produced principally by activated inflammatory and immune cells that regulate immune response and inflammatory reactions.⁷ They act as chemical mediators between different cell types and, either by themselves or by interacting with each other, the cytokine networks may mediate cellular mechanisms of migration, proliferation, and differentiation, which are involved in PVR membrane formation.⁸ Interleukin 1 (IL-1) and IL-6 are functionally related cytokines that have broad spectrum of activity in inflammation and wound healing. In wound healing, IL-6 stimulates the proliferation of fibroblast and glial cells and the synthesis of

Larry A Donoso
Laboratory for Eye
Research, Department
of Ophthalmology,
University of
Nottingham, UK
I A El-Ghrably
H S Dua
G M Orr
P J Tighe

Department of
Immunology
P J Tighe

Wills Eye Hospital,
Philadelphia, USA
D Fischer

Correspondence to:
I A El-Ghrably or H S Dua,
Department of
Ophthalmology, B Floor,
South Block, University
Hospital, Queens Medical
Centre, Nottingham
NG7 2UH, UK
harinder.dua@
nottingham.ac.uk

Accepted for publication
31 October 2000

Table 1 Primer sequences, deletion, and target information: all PCR targets and deletion sites are given as nucleotide positions from the cited Genbank sequence. The α primer in each case was synthesised with a 5' fluorophore attached (fluorophores are those marketed by ABI Applied Biosystems Ltd)

Target	Accession No	PCR product	Deletion site	Primer sequence (5' 3')	Fluorophore
HPRT	M31642	407-566	537-541	(a) GACCAGTCAACAGGGGACAT (b) CGACCTTGACCATCTTTGGA	Hex
IL-1 α	M28983	496-670	521-525	(a) GCTGCTGCATTACATAATCTGG (b) TGGGTATCTCAGGCATCTCC	Fam
IL-1 β	M15330	83-182	153-157	(a) AGCCATGGCAGAGTACCTG (b) CATCTGTTTATGGCCATCAG	Hex
IL-6	M14584	188-332	212-216	(a) AGGTTGTTTTCTGCCAGTGC (b) CACACAGACAGCCACTCACC	Fam
IL-8	M26383	36-253	222-226	(a) AAGAAACCACCGGAAGGAAC (b) TGTGGTCCACTCTCAATCACTC	Fam
IL-12	M65272	835-963	862-866	(a) CCACATTCCTACTTCTGCTGA (b) GGTAAATGCTGGCATTTTTGC	Tet
TNF α	X01394	284-512	306-310	(a) CACCACGCTCTTCTGCCT (b) TCTCAGCTCCAGCCCAAT	Fam
IFN γ	M29383	501-642	524-528	(a) TGACTTGAATGTCCAACGCAAAG (b) GCAGGACAACCATTACTGGGATG	Tet

collagen,⁹ whereas IL-1 stimulates the migration of retinal pigment epithelial (RPE) cells.¹⁰

Tumour necrosis factor alpha (TNF α) is known to be chemotactic for monocytes and fibroblasts,¹¹ and it acts synergistically with interferon gamma (IFN γ) and IL-1 in the induction of ICAM-1 by RPE cells. This may contribute to the immunopathological processes in this disease.¹²

Macrophages, monocytes, T lymphocytes, neutrophils, RPE cells, and glial cells are found in the vitreous of patients with PVR.¹³⁻¹⁶ In RD the presence of these cellular components is variable and the vitreous in MH patients is largely devoid of inflammatory cells. Neutrophils and monocytes, which play an important part in PVR development,¹³ are attracted to inflammatory sites by chemokines such as IL-8. Most cellular components of PVR membranes, including the RPE cells and macrophages, are capable of secreting these cytokines.¹⁴⁻¹⁶

Many studies have been conducted to ascertain the expression of the various cytokines in the vitreous and PVR membranes and their relation to the development of PVR.¹⁷⁻²⁴ These studies have examined either the proteins present within the vitreous, or a limited number of cytokine mRNAs from intravitreal cells, but not both together. Thus, while the proteins have been shown to be present and the potential of cells to express some cytokine mRNAs locally has been reported, there has been no correlation between cytokine levels within the vitreous and the potential for production by the invasive cells. This is essential to establish the impact of cytokine production by the invasive cells on the overall environment.

In previous work from this laboratory²⁵ we reported the detection of IL1 β , IL6, IL8, and TNF α mRNA in vitreous samples from patients with PVR, RD, and MH; however, the methodology used was not quantitative and thus the significance of the production of mRNA in relation to the secreted proteins could not be determined.

In this study we have significantly expanded our investigations by using quantitative techniques for both mRNA and protein detection,

and have expanded the range of studied cytokines to include IFN γ , IL1 α , and IL12 as well as those previously mentioned. To our knowledge this is the first quantitative measurement of both mRNA and protein expression in these conditions. This has allowed us to correlate mRNA and secreted cytokine protein levels to determine whether the cells invading the vitreous play a major part in the production of the detected cytokine milieu. In addition, we have addressed, for the first time, the contribution of IL-12 in the pathogenesis of PVR.

Materials and methods

PATIENTS

A total of 46 consecutive patients (25 with PVR, 11 with RD not complicated by PVR, and 10 patients with macular hole (MH)) in whom vitrectomy was considered necessary, were investigated in the ophthalmology department, QMC, Nottingham, UK. Of the 46 patients, 31 were men and 15 were women. The mean age was 49 years (range 30-87 years). Indications for vitrectomy in eyes with RD were failure of retinal reattachment by conventional methods (buckling and cryo), giant breaks, very posterior breaks, and multiple breaks not suitable for buckle. Patients with a history of recent trauma (3 months), concurrent eye conditions such as infection, vitreous haemorrhage or uveitis, and current topical or systemic steroids were excluded. The severity of PVR was graded according to the criteria of Retina Society Terminology committee.¹ The same observer followed up patients for a period ranging between 4 and 18 months (average 9 months). Data concerning the number of surgeries before PVR development, duration of retinal disease, and severity and recurrence of PVR were documented for the purpose of this study. Patients admitted into the study gave their informed consent and the study complied with the Declaration of Helsinki.

VITREOUS SPECIMENS

Samples were obtained through the conventional three port closed vitrectomy technique. They were collected undiluted by manual suction into a syringe through the aspiration line

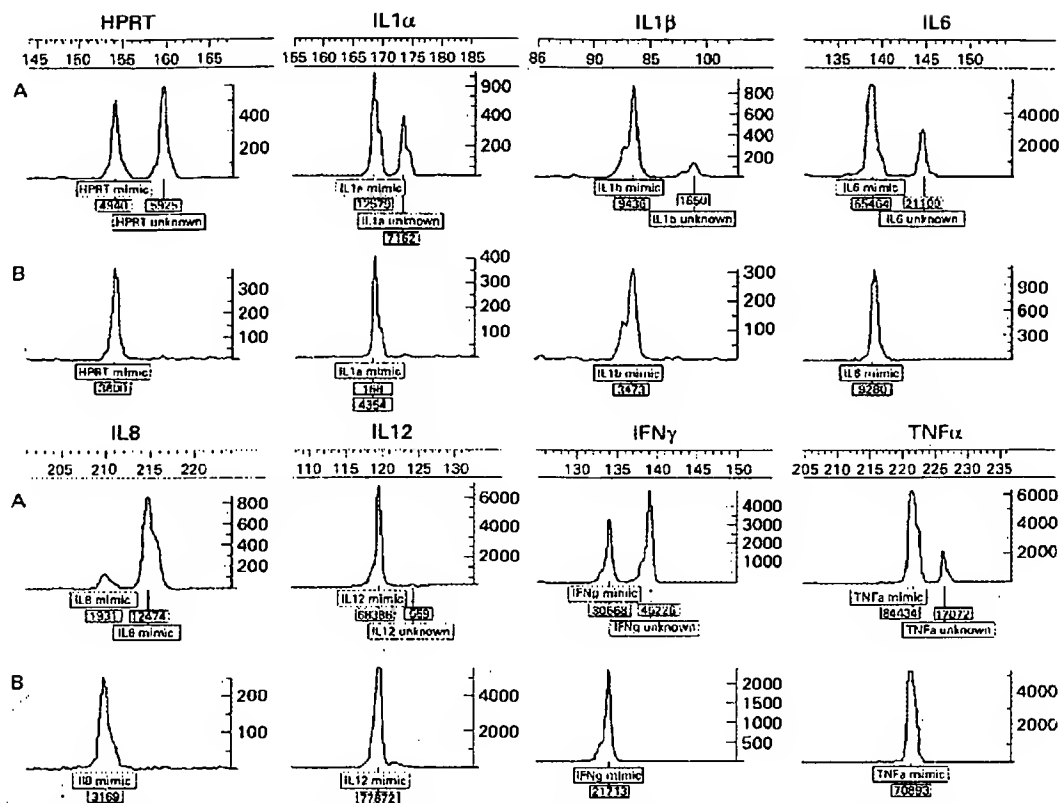


Figure 1 A typical electropherogram plot showing the size and area peaks for mimic and unknown (sample) of investigated cytokines. (A) Positive samples, (B) negative samples. Unknown concentration = (area of unknown/area of mimic) \times mimic concentration.

of vitrectome before opening the infusion line. Intraocular pressure was maintained by indentation. When a sample of approximately 0.75–1 ml was obtained the ocutome was withdrawn and infusion commenced to restore ocular volume. Samples were then transferred to 1.8 ml polypropylene tubes and prepared immediately following surgery. Cells were pelleted by centrifugation at 2500 rpm for 10–15 minutes. Supernatants were divided into aliquots and stored at -70°C until used for enzyme linked immunosorbent assays (ELISA). Cellular pellets were processed rapidly to prevent RNA degradation. Total RNA was extracted using the RNeasy method (Qiagen, UK) following manufacturer's procedure. RNA was stored at -70°C until cDNA synthesis and PCR reaction were carried out. cDNA was prepared from all the RNA extracted from each sample using oligo-(dT) priming in ready to go cDNA synthesis tubes (Pharmacia Biotech, UK) following the manufacturer's procedure.

QUANTITATIVE RT-PCR REACTIONS

Primers

Primer pairs, one of which was fluorescent dye labelled, were synthesised by MWG Biotech (MWG, Germany). All primer pairs were validated by sequencing of PCR products generated under the conditions stated. For primer sequences see Table 1.

To correct for variation in amplification efficiency between individual reactions, target

cDNA was co-amplified with an internal competitor (mimic) of known concentration using the same fluorescent labelled primers. Quantitative PCR was performed using a variation of the method of Pannetier,²⁶ which provides quantitative data even when the PCR is cycled into saturation. This is only possible if the competitor sequence is essentially identical to the true target sequence.²⁷ Highly homologous competitor DNA (mimics) were generated by PCR mutagenesis of the true PCR products for each target sequence. Five base pair deletions were produced in each mimic, 25 bases from the 5' end of either the a or b primer site (depending on most suitable primer design). The location of the PCR targets and deletions are given in Table 1. This method gives mimics which, when co-amplified with cDNA, remain proportional across the detectable range of fluorescent detection (approximately 4 logs) (data not shown). The mimic PCR products were cloned into pT7 blue (Novagen, UK) and verified by sequencing.

PCR amplification was performed by adding 1 μl of each cDNA sample to a final reaction mixture of 25 μl containing 60 mM TRIS.Cl (pH 8.0), 15 mM $(\text{NH}_4)_2\text{SO}_4$, 2 mM Mg Cl_2 , 0.2 mM each dNTP, 0.01% Tween 20, 0.5 units Amplitaq Gold (Perkin Elmer, Warrington, UK), 0.2 μM each primer; 10^3 single strands per reaction of appropriate mimic was added. In negative controls no sample was added to the reaction mix although mimic was still included. Amplification cycles (performed

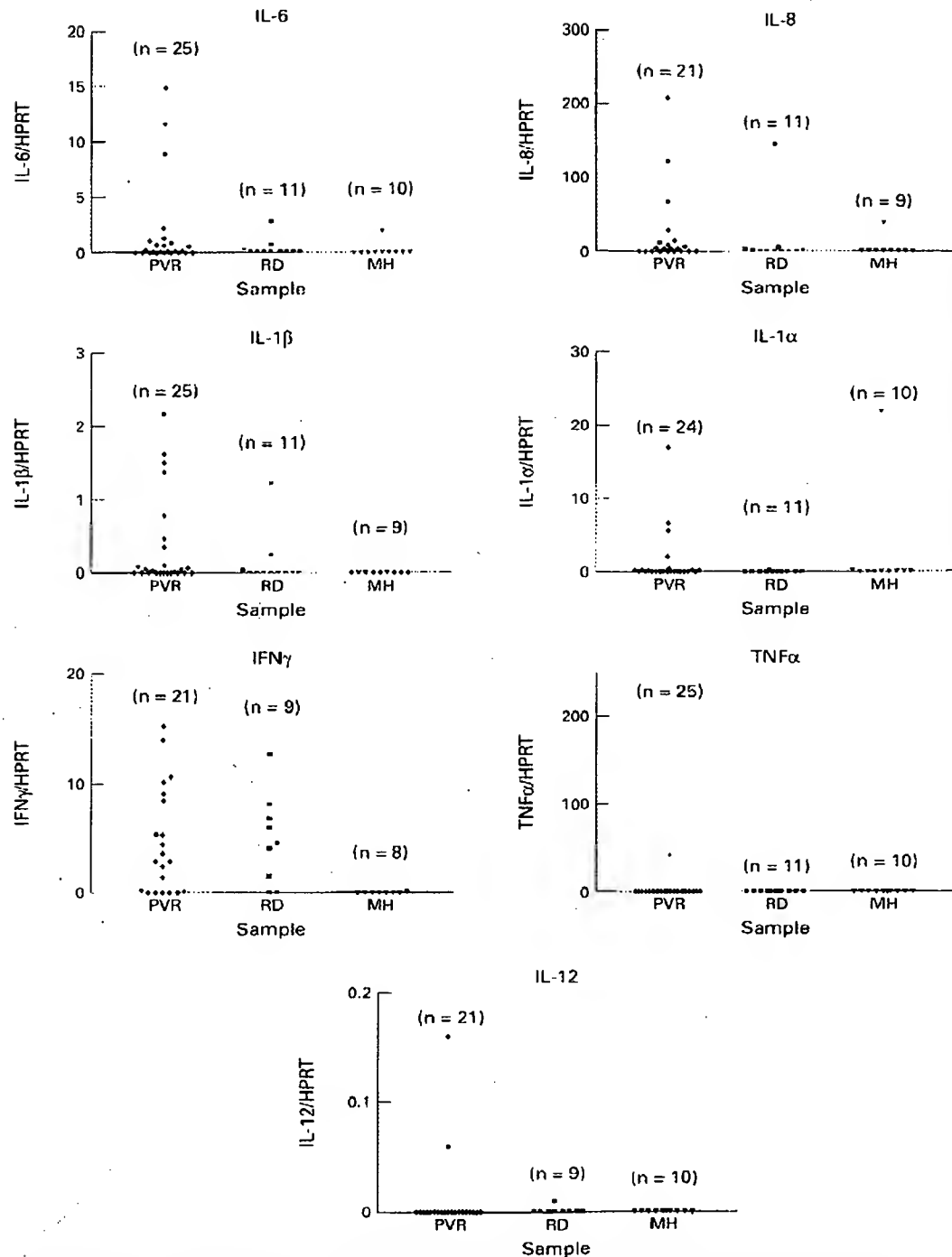


Figure 2 mRNA levels of different cytokines normalised to HPRT in vitreous aspirates obtained from patients with proliferative vitreoretinopathy (PVR), retinal detachment (RD), and macular hole (MH) (control). n = number of investigated samples.

on a Progene instrument from Techne, UK) were; 94°C, 10 minutes, then 37 cycles of 94°C, 1 minute; 54°C, 1 minute; 72°C, 1 minute 30 seconds; followed by 72°C for 15 minutes. Fluorophore labelled PCR products (0.5 µl) were separated and analysed by capillary electrophoresis under denaturing conditions (POP4 polymer) on a Prism310 genetic analyser, (Applied Biosystems). Run conditions were 5 seconds injection, 15 kV, run

24 minutes at 15 kV, 60°C, 36 cm capillary (length to detection). Size and area of DNA peaks were obtained using standard software (Genescan version 2.0 and Genotyper v1.1.1, Perkin Elmer ABI). The amount of each cytokine mRNA in the samples was calibrated by the known concentration of mimic using the following formula:

$$\text{Unknown concentration} = (\text{area of unknown} / \text{area of mimic}) \times \text{mimic concentration}$$

Table 2 Cytokine mRNA levels normalised to HPRT in vitreous samples with summary of statistical data analysis

Cytokine mRNA	No	N (%)	Median	IQR	p Value	
					v MH	v RD
PVR:						
IL-6/HPRT	25	19 (76)	0.16	0.02-1.03	0.005	0.038
IL-8/HPRT	25	23 (92)	4.43	0.81-13.87	0.006	0.081
IL-1 β /HPRT	25	16 (64)	0.04	0.0-0.42	0.004	0.086
TNF α /HPRT	25	5 (20)	0.0	0.0-0.0	†	†
IL-1 α /HPRT	25	14 (56)	0.03	0.0-0.24	0.200	0.072
IFN γ /HPRT	21	18 (85)	2.91	0.10-8.79	<0.001	0.838
IL-12/HPRT	21	2 (10)	0.0	0.0-0.0	†	†
RD:						
IL-6/HPRT	11	3 (27)	0.0	0.0-0.50	0.531	
IL-8/HPRT	11	7 (64)	0.35	0.0-4.82	0.143	
IL-1 β /HPRT	11	3 (27)	0.0	0.0-0.13	0.331	
TNF α /HPRT	11	0 (0)	0.0	0.0-0.0	†	
IL-1 α /HPRT	11	2 (18)	0.0	0.0-0.02	0.912	
IFN γ /HPRT	9	7 (78)	4.4	0.75-7.37	0.008	
IL-12/HPRT	9	1 (11)	0.0	0.0-0.0	†	
MH:						
IL-6/HPRT	10	1 (10)	0.0	0.0-0.0		
IL-8/HPRT	10	3 (30)	0.0	0.0-0.570		
IL-1 β /HPRT	10	1 (10)	0.0	0.0-0.0		
TNF α /HPRT	10	0 (0)	0.0	0.0-0.0		
IL-1 α /HPRT	10	2 (20)	0.0	0.0-0.12		
IFN γ /HPRT	10	3 (30)	0.0	0.0-0.0		
IL-12/HPRT	10	0 (0)	0.0	0.0-0.0		

No = number of samples examined; N = number of positive samples; IQR = interquartile range.

*Significant difference $p < 0.05$ between the two groups (Mann-Whitney).

†No statistical difference was found between groups (Kruskal-Wallis).

HPRT (hypoxanthine phosphoribosyl transferase), a constitutively expressed housekeeping gene was used to normalise the amount of mRNA present in each sample. Peak detection by the analysis software is set to detect appropriately shaped peaks, in the designated size range for each PCR product, with a height of more than 30 arbitrary fluorescence units (AFU) over baseline. Baseline fluorescence for the detection system is, on average, 20 AFU, with some digital noise from the CCD, which is automatically filtered out. Typical electropherogram plots showing the size and area of peaks for mimic and unknown are shown in Figure 1.

Enzyme linked immunosorbent assays (ELISA)

From previously examined vitreous samples, 15 PVR, eight RD, and eight MH were examined for their levels of IL-6, IL-8, IL-1 β , IL-1 α , TNF α , IFN γ , and IL-12 using sandwich enzyme immunoassay kits (R&D systems, Oxon, UK). Different types of kits were used according to sensitivity and expected levels of different cytokines. A calibration run was made on a few vitreous samples before each assay, to determine the appropriate sample dilution. A dilution of 1:3 was found to be appropriate for all cytokines with the exception of IL-1 β where a dilution of 1:2 was used. These preliminary assays ensured that the levels of factors in the samples were within the detectable range of the assay kits.

The vitreous sample volumes used were 150 μ l for IL-6, IL-8, and IL-1 β and 200 μ l for TNF α , IL-1 α , IFN γ , and IL-12. Sonication (on ice) was performed to completely disrupt formed vitreous and yield homogeneous sample for assay and prevent loss of antigenic activity. All samples were examined in duplicates and the average reading was analysed.

The minimum detectable concentrations (sensitivity) for the assay kits were 0.3, 1.6, 0.125, 3.9, 0.7, 15.6, and 0.7 pg/ml for IL-6, IL-8, IL-1 β , IL-1 α , TNF α , IFN γ , and IL-12 respectively. Elisa assays were carried out according to the manufacturer's instructions.

STATISTICAL ANALYSIS

Non-parametric tests were used for statistical analysis of our data, which is not normally distributed. Samples were divided into three groups—PVR, RD, and MH. Vitreous cytokine levels between groups were analysed using the Kruskal-Wallis test, and the levels between two groups were compared using a Mann-Whitney test. The Spearman correlation test was used to test any association between mRNA and cytokine protein levels. Groups in different clinical variables were compared using Kruskal-Wallis and Mann-Whitney tests whenever appropriate. Statistical calculations were performed using commercial software (Prism version 2.01).

Results

CYTOKINE mRNA

mRNA levels of different cytokines in vitreous samples from patients with PVR, RD, and MH were normalised to the level of HPRT mRNA detected in the sample. The HPRT mRNA level would reflect the cellularity of the sample. Uniformly low levels of HPRT were detected indicating the low number of cells present in the vitrectomy samples. By normalising the cytokine mRNA against HPRT mRNA for each sample, spurious differences in cytokine mRNA levels between samples, were avoided. These results are shown in Figure 2.

The median levels of IL-6, IL-8, IL-1 β , and IFN γ mRNA were significantly higher ($p < 0.05$) in patients with PVR than those with macular hole. There was no statistically significant difference between the median levels of the two groups for IL-1 α .

Comparing PVR with RD patients, there was no statistically significant difference in mRNA levels between the two groups in all the investigated cytokines ($p > 0.05$) except for IL-6 where, there was statistical significance ($p = 0.038$). The median level of IFN γ mRNA was significantly higher ($p = 0.008$) in patients with RD than those with MH, otherwise there was no significant difference between the two groups.

There were very few samples with detectable mRNA levels for TNF α and IL-12, (no significant difference between groups was found by Kruskal-Wallis test). Number and percentage of samples with detectable levels of mRNA for different cytokines and the results of statistical analysis between different groups are summarised in Table 2.

CYTOKINE PROTEIN ASSAY

Levels of different cytokines in vitreous samples from patients with PVR, RD, and MH expressed in pg/ml are shown in Figure 3. A summary of the available data and statistical analysis is shown in Table 3. The median levels

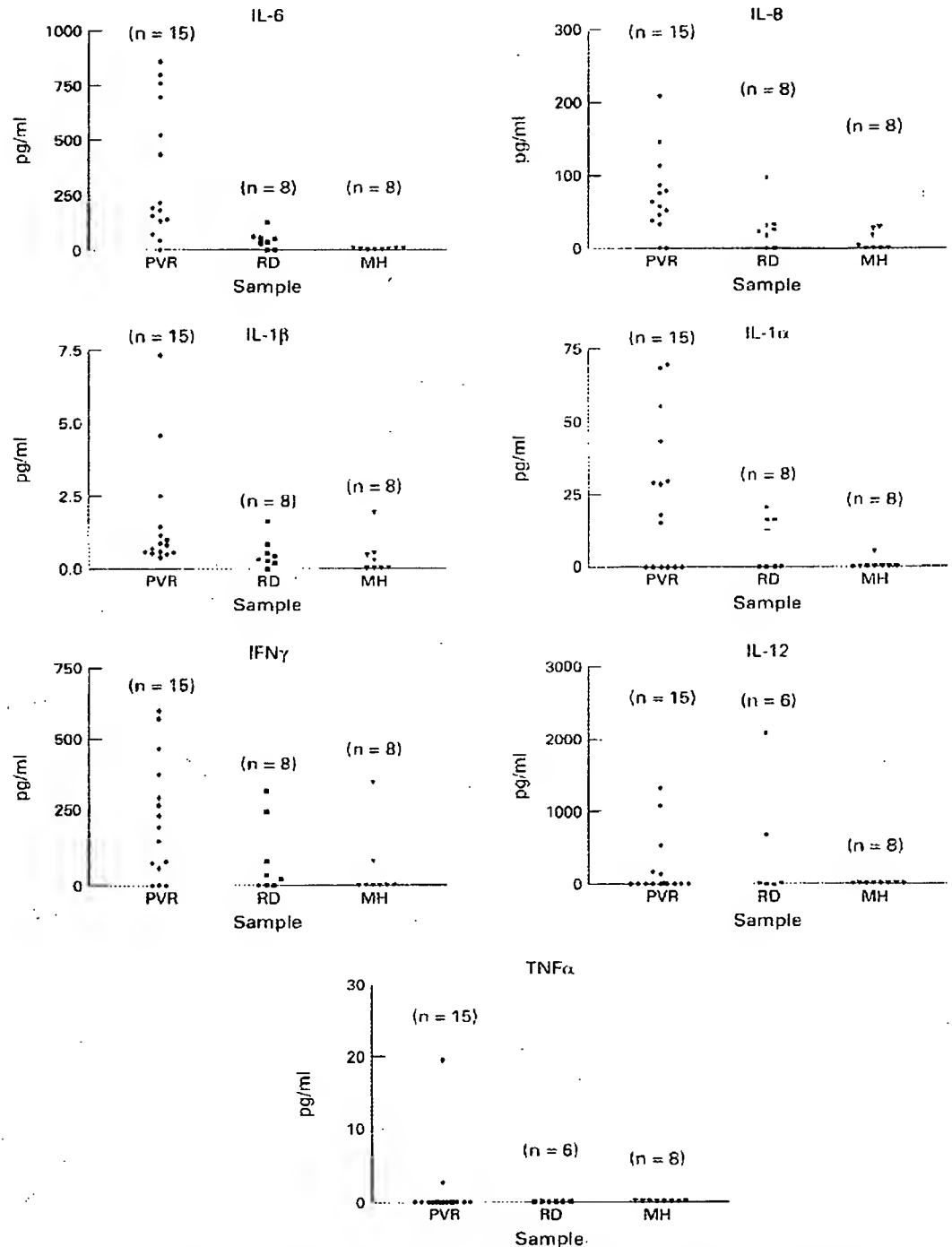


Figure 3. Levels of different cytokines in vitreous aspirates obtained from patients with proliferative vitreoretinopathy (PVR), retinal detachment (RD), and macular hole (MH) (control). n = number of investigated samples. Detection levels were (0.3, 1.6, 0.125, 3.9, 0.7, 15.6, and 0.7 pg/ml for IL-6, IL-8, IL-1β, IL-1α, TNFα, IFNγ, and IL-12 respectively).

of IL-6, IL-8, and IL-1β were significantly higher ($p < 0.05$) in patients with PVR than those with MH and RD. For IL-1α and IFNγ, a significant statistical difference was detected between PVR and MH groups ($p < 0.05$) but not between PVR and RD patients ($p > 0.05$). No significant difference was found between RD and MH groups in all the tested cytokines. According to Kruskal-Wallis test no significant difference between groups was found for TNFα and IL-12 ($p > 0.05$).

CORRELATION BETWEEN mRNA AND CYTOKINE PROTEIN LEVELS

A total of 31 pairs of samples were analysed (29 for IFNγ and IL-12) for their mRNA and protein correlation levels. Statistically significant correlation was found between mRNA and cytokine levels for IL-6, IL-8, IL-1β, IL-1α, TNFα, IFNγ, Spearman $r = 0.83, 0.73, 0.67, 0.91, 0.73$, and 0.73 respectively. No significant correlation was found between mRNA and cytokine levels for IL-12 ($r = 0.18$).

Table 3 Cytokine levels expressed in pg/ml in vitreous samples with summary of statistical data analysis

	Patients		p Value*			
Cytokine	No	N (%)	Median	IQR	v MH	v RD
PVR:						
IL-6	15	14 (93)	190.6	136.4-725.6	<0.001	0.002
IL-8	15	13 (86)	63.56	41.37-128.6	0.003	0.018
IL-1 β	15	15 (100)	0.82	0.57-1.99	0.004	0.014
IL-1 α	15	9 (60)	18.1	ND-49.60	0.033	0.205
TNF α	15	2 (13)	ND	ND	†	†
IFN γ	15	12 (80)	200.8	68.37-426.3	0.030	0.129
IL-12	15	10 (67)	1.457	ND-349.8	†	†
RD:						
IL-6	8	6 (75)	42	14-50.92	0.065	
IL-8	8	6 (75)	22.93	9.08-30.95	0.195	
IL-1 β	8	7 (88)	0.34	0.22-0.66	0.382	
IL-1 α	8	4 (50)	6.25	ND-16.05	0.160	
TNF α	6	0 (0)	ND	ND	†	
IFN γ	8	5 (63)	27.15	ND-165.4	0.382	
IL-12	6	4 (67)	14.51	ND-1365	†	
MH:						
IL-6	8	6 (75)	4.34	0.83-7.05		
IL-8	8	5 (63)	2.50	ND-22.35		
IL-1 β	8	4 (50)	0.14	ND-0.49		
IL-1 α	8	1 (13)	ND	ND		
TNF α	8	0 (0)	ND	ND		
IFN γ	8	2 (25)	ND	ND-40.22		
IL-12	8	3 (38)	ND	ND-0.87		

No = number of samples examined; N = number of positive samples; IQR = interquartile range; ND = below detection level (0.3, 1.6, 0.125, 3.9, 0.7, 15.6, and 0.7 pg/ml for IL-6, IL-8, IL-1 β , IL-1 α , TNF α , IFN γ , and IL-12 respectively).

*Significant difference $p < 0.05$ between the two groups. (Mann-Whitney).

†No statistical difference was found between groups (Kruskal-Wallis).

mRNA LEVELS AND RELATION TO CLINICAL DATA

Table 4 shows summary of clinical variables investigated and their relation to mRNA levels for different cytokines. No significant difference was found between different clinical groups in their mRNA cytokine levels ($p > 0.05$).

Discussion

The precise role of individual cytokines in the pathogenesis of PVR is not obviously clear, but their involvement in regulating immune and inflammatory responses has been well described.⁷

mRNA quantitation can provide information on gene expression and its control, and help in understanding the regulatory systems governing it and the physiological role it performs.²⁸ However, mRNA level is a reflection of gene expression and not protein production, and there is not always a correlation between mRNA and secreted protein levels and this depends upon the regulatory mechanisms for any particular expressed gene.

By studying both mRNA and secreted protein the usefulness of RT-PCR assays was substantially enhanced. The good correlation demonstrated between mRNA and the respective cytokines suggests that, in PVR, mRNA estimation can be an indicator of the respective cytokines secreted. Competitive polymerase chain reaction (PCR) is considered the method of choice for gene expression studies in small clinical samples. The accurate quantitation of PCR products relies on the use of an internal standard, which is designed to contain primer binding and flanking sequences identical to the target gene fragment.^{29,30} In this study the internal standard (mimic) was sufficiently different in size from the target gene fragment (five bases shorter) for unambiguous detection, but is close enough in size to ensure minimal differences in amplification efficiency. The final ratio of amplified target to the amplified competitor is dependent on the initial ratio of the target to the competitor, rendering the reaction independent of the number of amplification cycles.³⁰ Previous work to detect mRNA coding for IL-6, IL-1 β , and TNF α in epiretinal membranes from patients with PVR was carried out by Limb *et al* in 1994.¹¹ They used an *in situ* hybridisation technique which, although sensitive, is technically very demanding for obtaining data on quantitation. We recently reported the use of RT-PCR technique to detect mRNA for IL-6, IL-1 β , IL-8, and TNF α in vitreous samples from patients with PVR.²³ However, no data on the measurement of the protein product (cytokines), in the samples studied, were presented.

Unlike other inflammatory conditions such as coeliac disease,³² and rheumatoid arthritis,³³ in which large amounts of cytokine mRNAs may be expressed in the heavily infiltrated affected tissues, the present results showed that vitreous samples in PVR possessed relatively little cytokine mRNA reflecting the relatively lower number of cells. Although direct estimation of total mRNA in each sample was not carried out, the levels of HPRT mRNA detected were low, indicating that the overall cellularity of the vitreous samples was low. In our study, there was a general trend towards higher levels of IL-6, IL-8, IL-1 β , and IFN γ mRNA in retinal detachment (whether or not complicated by PVR) than MH

Table 4 Relation between clinical variables and cytokine mRNA level normalised to HPRT

Clinical variable		No	Number of patients with detectable cytokine mRNA levels (%)				
			IL-6/HPRT	IL-8/HPRT	IL-1 β /HPRT	IFN γ /HPRT [†]	IL-1 α /HPRT
Severity	C1-C2	19	13 (68)	17 (89)	12 (63)	14 (87)	10 (52)
	C3-D2	6	6 (100)	6 (100)	4 (66)	4 (80)	4 (66)
Duration	2-8 weeks	14	10 (71)	14 (100)	8 (57)	11 (84)	9 (64)
	8-14 weeks	5	4 (80)	4 (80)	3 (60)	3 (75)	3 (60)
	> 14 weeks	6	5 (83)	5 (83)	5 (83)	4 (100)	2 (33)
Recurrence	No	14	9 (64)	12 (86)	7 (50)	10 (83)	6 (43)
	Yes	11	10 (91)	11 (100)	9 (82)	8 (89)	8 (72)
No of previous surgeries	0	7	5 (71)	6 (86)	4 (57)	5 (100)	3 (43)
	1	11	7 (63)	10 (91)	6 (54)	8 (80)	6 (55)
	2-4	7	7 (100)	7 (100)	6 (86)	5 (83)	5 (71)

No = number of samples examined.

[†]Number of samples investigated in each clinical group was slightly less than the examined number for other cytokines, due to insufficient sample.

samples. However, statistically significant higher levels were found only in PVR samples. Similarly, cytokine protein levels were significantly higher for IL-6, IL-8, IL-1 β in PVR than RD and MH. Apart from IL-12, a significant correlation was found ($r > 0.4$) between mRNA and protein levels in all the investigated cytokines. The substantial variation in values within each group of patients, and the number of samples available limit the conclusions that can be drawn from this initial study.

The presence of cytokine protein without detection of its mRNA was apparent in some samples (eight samples for IL-6, seven for IL-8, 10 for IL-1 β , one for IL-1 α , and two for IFN γ). Since translation of mRNA occurs rapidly, this observation does not preclude that these cytokines are produced within the ocular microenvironment. Cytokines may also be produced outside the vitreal microenvironment and permeate the vitreous during breakdown of the blood retinal barrier. Alternatively, cytokines may be expressed by the retina, which is known to be a source of many cytokines and growth factors.³⁴ Retinal tissue is a potential contaminant for vitreous samples and dissected epiretinal membranes. Scleral wounds created during vitreoretinal surgery can act as an important source for growth factors and cytokines.³⁴

In contrast, several samples were found to have mRNA for a cytokine in the absence of detectable protein (four samples for IL-8, one for IL-1 β , four for IL-1 α , three for TNF α , and four for IFN γ). Cytokine proteins may be present below the detection levels of the ELISA kits used. Another possibility is that some of these cytokines are bound to extracellular matrix in epiretinal membranes and not present free in the vitreous (as has been previously shown for TNF α for example).¹⁶ In addition, regulation of secretion of these cytokines at translational and post translational levels may occur.

It was not possible to identify any relation between cytokine mRNA levels and different clinical groups, perhaps because of the small number of samples available in each group. In a recent study,²⁴ in which large numbers of patients were investigated for fewer cytokines by ELISA, IL-6 levels in vitreous were found to be predictive for the development of postoperative PVR. The presence of these cytokines in some macular hole and retinal detachment vitreous samples suggests that any role that these cytokines have in promoting the development of the epiretinal membranes might result from an altered balance in their activities, difference in their microdistribution, or change in receptor expression or activity rather than the absolute presence or absence of the factor.

In the present study, the types of cells expressing each cytokine were not identified. However, the majority of cells present in the vitreous samples of patients with PVR are capable of producing cytokines in vitro. Cultured RPE cells, upon activation, release IL-8, IL-6, and granulocyte-macrophage

colony stimulating factor.^{15, 35} Activated monocytes secrete a heterogeneous mixture of products that together strongly induce expression of many cytokines in human RPE cells.¹⁶ Most if not all of the inducing effect can be accounted for by IL-1 β and TNF α . Glial cells can produce IL-1.¹⁴ Macrophages and T lymphocytes can produce many different cytokines, including IL-1, IL-6, TNF α , and IFN γ .³⁶ In situ hybridisation technique combined with immunohistochemical staining for the vitreous samples or epiretinal membranes from patients with PVR might resolve which cell produce which cytokine.

The cells present in the vitreous at the time of sampling would determine the profile of the mRNA and cytokines detected. The number and type of cells present in the vitreous at different stages of the disease are likely to vary and consequently affect the types of cytokines expressed.³⁶ This may in part explain why, in the present study, only a small number of samples revealed all the cytokines tested.

A novel observation in this current study concerns the cytokine IL-12. IL-12 mRNA was not detected in most of the samples investigated, being present in only two from 21 PVR, one from nine RD, and not in any MH samples. However, IL-12 protein was detected in considerable amounts in examined samples (Table 3). A likely source of this IL-12 may be the iris, ciliary body, and choroid which normally contain dendritic cells.³⁷ Activated dendritic cells are known to be a major source of IL-12. IL-12 is also produced by macrophages and B lymphocytes, which are known to infiltrate PVR membranes. It is also possible that this cytokine is primarily produced in the PVR membranes from where it accesses the vitreous gel. As PVR membranes were not analysed in this study, it not possible to comment on the correlation between IL-12 mRNA and the cytokine, in PVR membranes. IL-12 has multiple effects on T cells and natural killer (NK) cells. These include inducing production of IFN γ and TNF either directly or in synergy with other inducers and acting as a co-mitogen to stimulate proliferation these cells.^{38, 39} The involvement of activated T and B lymphocytes is well documented in the pathogenesis of the disease.^{10, 41}

The synergistic and pleiotropic effects of cytokines may be of particular importance in PVR. For example, IL-1 β and TNF α both present within vitreous and epiretinal membranes, promote the synthesis of IL-6,⁴² and may also stimulate further IL-1 or TNF α production.³⁶ Moreover, IL-6 may induce further production of IL-1 and TNF α .⁴³ IL-1 β is known to enhance the contraction collagen gel⁴⁴ and may have a role PVR membrane contraction. In previous studies, IL-6 was detected at higher levels in PVR than in uncomplicated RD, although the same was not true for IL-1.^{17, 19} In contrast, Kon *et al*⁴⁴ found significantly elevated levels of IL-1 β but not of IL-6 in patients with PVR compared with uncomplicated RD. We detected significantly elevated levels of both IL-6 mRNA and

protein in patients with PVR versus MH and RD. The same was true for IL-1 β protein. IL-1 β has been shown to enhance IL-6 mRNA and protein synthesis in human RPE cells, and at lower concentrations, this effect was enhanced by TGF β to induce IL-8 mRNA but not IL-8 cytokine secretion.⁴⁵ A definitive role for IL-8 in the pathogenesis of PVR is not clear. However, it has been postulated that TNF α and IL-1 β , which were not directly chemotactic for leucocytes, exert their chemotactic effect through induction and release of secondary cytokines including IL-8 and MCP-1.²⁰

IFN γ is known to upregulate MHC class II molecule expression on RPE cells, and enhance presentation of foreign antigens to T cells.⁴⁶ Experimental studies show that epiretinal membrane formation can be accompanied by infiltration of blood borne lymphocytes and monocytes, which persist until the late stages of experimental PVR and are likely to be a source of IFN γ .⁴⁷

In conclusion, our data indicate that levels of mRNA encoding IL-6, IL-8, IL-1 β , and IFN γ is significantly increased in vitreous samples from patients with PVR, indicating local production of these cytokines by vitreous cells and the significant contribution of the invading cells in PVR pathogenesis. Cells invading the vitreous do not appear to locally produce IL-12, and apart from this cytokine there was a good correlation between mRNA and protein levels suggesting that mRNA measurements can provide useful information about cytokine synthesis within the invading cells. Monitoring of mRNA levels may aid in our understanding of this disease process and provide insights into progression, response to treatment, and development of strategies for alternative therapy.

The authors wish to acknowledge the help of Ms Sue Stevens for her excellent technical assistance. We also thank Mr Adrian Rubins and Mr Richard McIntosh for help with the manuscript. Supported by a grant from the Uveitis Foundation, Wills Eye Hospital, Philadelphia, and the government of Egypt (IA El-Ghrably).

- 1 The Retina Society Terminology Committee. The classification of retinal detachment with proliferative vitreoretinopathy. *Ophthalmology* 1983;90:121-5.
- 2 Pastor JC. Proliferative vitreoretinopathy: an overview. *Surv Ophthalmol* 1998;43:3-18.
- 3 Wiedemann P, Weller M. The pathophysiology of proliferative vitreoretinopathy. *Acta Ophthalmol* 1988;189 (Suppl) 7-15.
- 4 Glaser BM, Cardin A, Biscoe B. Proliferative vitreoretinopathy. The mechanism of development of vitreoretinal traction. *Ophthalmology* 1987;94:327-32.
- 5 Charteris DG. Proliferative vitreoretinopathy: pathobiology, surgical management, and adjunctive treatment. *Br J Ophthalmol* 1995;79:953-60.
- 6 Campichino PA. Pathogenic mechanisms in proliferative vitreoretinopathy. *Arch Ophthalmol* 1997;115:237-41.
- 7 Cavillon JM, Huetfner-Cavillon N. Cytokines and inflammation. *Rev Prat* 1993;5:547-52.
- 8 Nagasaki H, Kouichi S. Risk factors for proliferative vitreoretinopathy. *Curr Opin Ophthalmol* 1995;6:70-5.
- 9 Roitt I, Brostoff J, Male D. Cell-mediated immune reactions. In: *Immunology*. 5th ed. London: Mosby, 1998;chapter 10:121-38.
- 10 Abbas AK, Lichtman AH, Pober JS. *Cytokines in cellular and molecular immunology*. 4th ed. Philadelphia: WB Saunders, 2000;chapter 11:235-69.
- 11 Camussi G, Albano E, Tetta C, et al. The molecular action of tumour necrosis factor- α . *Eur J Biochem* 1991;202:3-14.
- 12 Chaum B. Proliferative vitreoretinopathy. *Int Ophthalmol Clin* 1995;35:163-73.
- 13 Elner VM, Burnstine MA, Strieter RM, et al. Cell associated human retinal pigment epithelium interleukin-8 and monocyte chemoattractant protein-1: immunochemical and in situ hybridisation analysis. *Exp Eye Res* 1997;65: 781-9.
- 14 Rnberge FG, Caspi RR, Nussenblatt RB. Glial retinal Muller cells produce IL-1 activity and have a dual effect on autoimmune T helper lymphocytes. *J Immunol* 1988;140: 2193-6.
- 15 Planck SR, Huang X-N, Robertson JE, et al. Retinal pigment epithelial cells produces IL-1 β and granulocyte-macrophage colony stimulating factor in response to IL-1 α . *Curr Eye Res* 1993;12:205-12.
- 16 Jaffe GJ, Roberts WL, Wong HL, et al. Monocyte induced cytokine expression in cultured human retinal pigment epithelial cells. *Exp Eye Res* 1995;60:533-43.
- 17 Limb GA, Little BC, Meager A, et al. Cytokines in proliferative vitreoretinopathy. *Eye* 1991;5:686-93.
- 18 Limb GA, Alam A, Early O, et al. Distribution of cytokine proteins within epiretinal membranes in proliferative vitreoretinopathy. *Curr Eye Res* 1994;13:791-8.
- 19 Kauffmann DJ, Meurs JC, Mertens DA, et al. Cytokine in vitreous humor: interleukin-6 is elevated in proliferative vitreoretinopathy. *Invest Ophthalmol Vis Sci* 1994;35: 900-6.
- 20 Elner SG, Elner VM, Jaffe GJ, et al. Cytokines in proliferative diabetic retinopathy and proliferative vitreoretinopathy. *Curr Eye Res* 1995;10:45-53.
- 21 Abu El-Asrar AM, Damme JV, Put W, et al. Monocyte chemoattractant protein-1 in proliferative vitreoretinal disorders. *Am J Ophthalmol* 1997;123:599-606.
- 22 Aksunger A, Or M, Okur H, et al. Role of interleukin 8 in the pathogenesis of proliferative vitreoretinopathy. *Ophthalmologica* 1997;211:223-5.
- 23 Kenarova B, Voinov L, Apostolov C, et al. Levels of some cytokines in subretinal fluid in proliferative vitreoretinopathy and rhegmatogenous retinal detachment. *Eur J Ophthalmol* 1997;7:64-7.
- 24 Kon CH, Occlleston NI, Aylward GW, et al. Expression of vitreous cytokines in proliferative vitreoretinopathy: a prospective study. *Invest Ophthalmol Vis Sci* 1999;40:705-12.
- 25 El-Ghrably IA, Doo HS, Orr GM, et al. Detection of cytokine mRNA production in infiltrating cells in proliferative vitreoretinopathy using reverse transcription polymerase chain reaction. *Br J Ophthalmol* 1999;83: 1296-9.
- 26 Pannetier C, Delassus S, Darche S, et al. Quantitative titration of nucleic acids by enzymatic amplification reactions run to saturation. *Nucleic Acids Res* 1993;21:577-83.
- 27 Dean GA, Higgins J, LaVoy A, et al. Measurement of feline cytokine gene expression by quantitative-competitive RT-PCR. *Int Immunol Immunopathol* 1998;63:73-82.
- 28 Ferre F, Marchese D, Pezzoli P, et al. Quantitative PCR. An overview. In: Mullis KB, Fierce F, Gibbs RA, eds. *The polymerase chain reaction*. Boston: Birkhauser, 1994:67-88.
- 29 Clementi M, Menzo S, Baguarelli P, et al. Quantitative PCR and RT-PCR in virology. *PCR Methods Appl* 1993;3: 191-6.
- 30 Diviacco S, Norio P, Zentilin L, et al. A novel procedure for quantitative polymerase chain reaction by coamplification of competitive templates. *Gene* 1992;12:313-20.
- 31 Limb GA, Early O, Jones SE, et al. Expression of mRNA encoding for TNF α , IL-1 β , and IL-6 by cells infiltrating retinal membranes. *Graefes Arch Clin Exp Ophthalmol* 1994; 32:646-52.
- 32 Kontakou M, Proczemioslo RT, Sturgess RP, et al. Expression of TNF α , IL-6 and IL-2 mRNA in the jejunum of patients with coeliac disease. *Scand J Gastroenterol* 1995;30:456-63.
- 33 Feldmann M, Brennan FM, Chantry D, et al. Cytokine production in the rheumatoid joint: implications for treatment. *Ann Rheum Dis* 1990;49:480-6.
- 34 Planck SR, Andresevic J, Chen JC, et al. Expression of growth factor mRNA in rabbit PVR model systems. 1992; 11:1031-9.
- 35 Elner VM, Strieter RM, Elner SG, et al. Neutrophil chemotactic factor (IL-8) gene expression by cytokine treated retinal pigment epithelial cells. *Am J Pathol* 1990;136:745-50.
- 36 Balkwill FR, Burke F. The cytokine network. *Immunol Today* 1989;10:299-303.
- 37 McMenamin PG. The distribution of immune cells in the uveal tract of the normal eye. *Eye* 1997;11:183-93.
- 38 D'Andrea A, Rengaraju M, Villante NM, et al. Production of natural killer cell stimulatory factor (interleukin 12) by peripheral blood mononuclear cells. *J Exp Med* 1992;176: 1387-98.
- 39 Sutterwala FS, Mosser DM. The taming of IL-12: suppressing the production of proinflammatory cytokines. *J Leukocyte Biol* 1999;65:543-51.
- 40 Baudouin C, Fredj-Reygrobellet D, Gordon WC, et al. Immunohistochemical study of epiretinal membranes in proliferative vitreoretinopathy. *Am J Ophthalmol* 1990;110: 593-8.
- 41 Charteris DG, Hiscott P, Grierson I, et al. Proliferative vitreoretinopathy. Lymphocytes in epiretinal membranes. *Ophthalmology* 1992;99:1364-67.

- 42 Akira S, Hirano T, Taga T, et al. Biology of multifunctional cytokines: IL-6 and related molecules (IL-1 and TNF α). *FASEB J* 1990;4:2860-7.
- 43 Van Snick J. Interleukin-6. An overview. *Annu Rev Immunol* 1990;8:253-78.
- 44 Choudhury P, Chen W, Hunt RC. Production of platelet-derived growth factor by interleukin-1 β and transforming growth factor- β -stimulated retinal pigment epithelial cells leads to contraction of collagen gels. *Invest Ophthalmol Vis Sci* 1997;38:824-33.
- 45 Kuppner MC, McKillop-Smith S, Correster JV. TGF- β and IL-1 β act in synergy to enhance IL-6 and IL-8 mRNA levels and IL-6 production by human retinal pigment epithelial cells. *Immunology* 1995;84:265-71.
- 46 Jordan JA, Pepose JS, Michels RG, et al. Proliferative vitreoretinopathy membranes. An immunocytochemical study. *Ophthalmology* 1989;96:801-10.
- 47 Hichins CA, Grierson J. Intravitreal injection of fibroblasts: the pathological effects on ocular tissues of the rabbit following an intravitreal injection of autologous skin fibroblasts. *Br J Ophthalmol* 1988;72:498-510.

Reference linking to full text
of more than 200 journals

Toll free links

You can access the FULL TEXT of articles cited in the *British Journal of Ophthalmology* online if the citation is to one of the more than 200 journals hosted by HighWire (<http://highwire.stanford.edu>) without a subscription to that journal.

There are also direct links from references to the Medline abstract for other titles.

www.bjophthalmol.com

Neuroscience 136 (2005) 147-160

MODULATION OF THE GLUTAMATERGIC RECEPTORS (AMPA AND NMDA) AND OF GLUTAMATE VESICULAR TRANSPORTER 2 IN THE RAT FACIAL NUCLEUS AFTER AXOTOMY

L. ELEORE, I. VASSIAS, P.-P. VIDAL AND
C. DE WAELE*

LNRS (CNRS-Paris V), ESA 7060, Centre Universitaire des Saints-Pères, 45 rue des Saints-Pères, 75270 Paris Cedex 06, France

Abstract—Facial nerve axotomy is a good model for studying neuronal plasticity and regeneration in the peripheral nervous system. We investigated in the rat the effect of axotomy on the different subunits of excitatory glutamatergic AMPA (GLuR1-4), NMDA (NR1, NR2A-D) receptors, post-synaptic density 95, vesicular glutamate transporter 2, β catenin and cadherin. mRNA levels and/or protein production were analyzed 1, 3, 8, 30 and 60 days after facial nerve axotomy by *in situ* hybridization and immunohistochemistry.

mRNAs coding for the GLuR2-4, NR1, NR2A, B, D subunits of glutamatergic receptors and for post-synaptic density 95, were less abundant after axotomy. The decrease began as early as 1 or 3 days after axotomy; the mRNAs levels were lowest 8 days post-lesion, and returned to normal or near normal 60 days after the lesion. The NR2C subunit mRNAs were not detected in either lesioned or intact facial nuclei. Immunohistochemistry using specific antibodies against GLuR2-3 subunits and against NR1 confirmed this down-regulation. There was also a large decrease in vesicular glutamate transporter 2 immunostaining in the axotomized facial nuclei at early stages following facial nerve section. In contrast, no decrease of NR2A subunit and of post-synaptic density 95 could be detected at any time following the lesion. β Catenin and cadherin immunoreactivity pattern changed around the cell body of facial motoneuron by day 3 after axotomy, and then, tends to recover at day post-lesion 60 days. Therefore, our results suggest a high correlation between restoration of nerve/muscle synaptic contact, synaptic structure and function in facial nuclei.

To investigate the mechanisms involved in the change of expression of these proteins following axotomy, the facial nerve was perfused with tetrodotoxin for 8 days. The blockade of action potential significantly decreased GLuR2-3, NR1 and NR2A mRNAs in the ipsilateral facial nuclei. Thus, axotomy-induced changes in mRNA abundance seemed to depend partly on disruption of activity. © 2005 Published by Elsevier Ltd on behalf of IBRO.

Key words: excitatory amino acids, motor neuron section, PSD95, beta catenin, cadherin, tetrodotoxin

*Corresponding author. Tel: +01-42-86-33-90; fax: +01-42-86-33-99. E-mail address: catherine.de-waele@univ-paris5.fr (C. de Waele).

Abbreviations: AF, arithmetic fluorescence; AMPAR, α -amino-3-hydroxy-5-methylisoxazole-4-propionic acid receptor; Cy3, cyanine 3; MVN, medial vestibular nucleus; NMDAR, N-methyl-D-aspartate receptor; PBS, phosphate-buffered saline; PFA, paraformaldehyde; PSD95, post-synaptic density; rAF, relative arithmetic fluorescence ratio; rOD, relative optical density; SD, standard deviation; TBS, Tris buffer saline; TBST, Tris buffer saline supplemented with 0.3% Triton X-100; TTX, tetrodotoxin; VGLUT2, vesicular glutamate transporter 2; VIAAT, vesicular inhibitory amino acid transporter

0306-4522/05/\$30.00 + 0.00 © 2005 Published by Elsevier Ltd on behalf of IBRO.
doi:10.1016/j.neuroscience.2005.06.026

Regeneration of the facial nerve after axotomy is an excellent model for studying adult peripheral nervous system plasticity (see for review Moran and Graeber, 2004). Following injury, animals display a characteristic ipsilateral facial nerve palsy including loss of eyelid movements, absence of spontaneous movements of the vibrissae and drooping of the ipsilateral hemicomer of the mouth. These impairments progressively recover with time usually after 30 days with the regeneration of the facial nerve. Regeneration includes the formation of axonal sprouts, their outgrowth as regenerative axons and reinnervation of facial muscle targets (Kreutzberg, 1996).

Facial motoneurons receive numerous glutamatergic nerve terminals from premotor neurons from the trigeminal, the hypoglossal nuclei and from the reticular formation and carry numerous AMPA and NMDA receptors (Border and Mihailoff, 1991; Sato et al., 1993; Wenzel et al., 1995). Several studies have been previously done to study the modulation of excitatory synaptic transmission after axotomy (Garcia Del Cano et al., 2000; Alvarez et al., 2000; Anneser et al., 2000; Linda et al., 2000; Tang and Sim, 1997). However, most of them focused either on one or two subunits of these receptors and were not conducted both at a transcriptional and translational level.

By DNA sequence homology and pharmacological character, AMPA receptors have been demonstrated to be hetero-oligomers made up of four subunits of different combinations of GLuR1–GLuR4 (Wenthold et al., 1992). The major difference between the GLuR1–4 subunits is their ion channel properties: receptor complexes containing the GLuR2 subunit are not permeable to calcium whereas those without the GLuR2 subunit do pass calcium (Mishina et al., 1991). N-methyl-D-aspartate receptors (NMDAR) are heteromeric complexes composed of NR1 and NR2 subunits. Eight variants of NR1 subunit (from NR1-1a to NR1-4b) and of four NR2 subunits isoforms (NR2A–D) have been described due alternative splicing. The NR1 is the ligand binding subunit and seems to be constitutive whereas the different NR2 subunits define the pharmacological properties. In addition, activated NMDAR exhibit voltage dependent inhibition by Mg^{2+} and is highly calcium permeable: the NR1 subunit seems to be responsible for the Ca^{2+} permeability and NMDAR blockage by intracellular Mg^{2+} whereas the NR2A subunit would be responsible for Ca^{2+} sensitivity and NMDAR blockage by extracellular Mg^{2+} (see for review Yamakura and Shimoji, 1999). NMDA induced Ca^{2+} entry is known to be involved in learning, synaptic plasticity and neuronal cell death (Sakimura et al., 1995). Post-synaptic density (PSD95) is

the major component of PSD95, which interacts with the NR2 subunits and some splice variants of NR1 subunit (Kornau et al., 1995). It was supposed to be involved in NMDAR aggregation and signaling pathway (see for review Hata and Takai, 1999). Recently, a glutamate vesicular transporter named VGLUT2, considered as a specific marker of excitatory synapse, has been showed to be expressed in facial nuclei (Kaneko et al., 2002).

Thus, we decided to use this model to investigate how excitatory neurotransmission at the pre- and post-synaptic level is modulated after facial axotomy. We used *in situ* hybridization and immunohistochemistry to study modulation of α -amino-3-hydroxy-5-methylisoxazole-4-propionic acid receptor (AMPA), NMDAR, PSD95 and of the vesicular glutamate transporter VGLUT2, in axotomized facial nucleus motoneurons at different times following the lesion. Furthermore, we examined expression of two adhesion proteins that mediate cell–cell adhesion, the beta catenin and the cadherin, because of they were supposed to be implicated in synaptic plasticity and function in adult CNS (Huntley, 2002). A previous study (Eleore et al., 2005; Vassias et al., 2005) showed a strong down-regulation of the different subunits of the glycinergic and GABAergic receptors following axotomy. However, we failed to detect any changes at the pre-synaptic level by using VIAAT (a vesicular inhibitory amino acid transporter involved in the accumulation and release of glycine into synaptic vesicles) antibody (Eleore et al., 2005).

Our aim was four-fold: 1. To detect the potential changes of excitatory synaptic transmission at pre- and post-synaptic level, in axotomized facial motoneurons; 2. to try to determine a correlation between synaptic stripping and receptor expression modulation; 3. To better determine the effect of electrical activity blockade of the facial nerve in this regulation. 4. To compare the effects of axotomy on lesioned motoneurons between the excitatory and inhibitory synaptic transmission.

EXPERIMENTAL PROCEDURES

Surgical procedures

Animals. Adult male pigmented Long Evans rats (CERJ, Le Genest Saint Isle, France) weighing approximately 250 g were used. They were divided into three groups: animals undergoing

unilateral facial nerve section; those receiving tetrodotoxin (TTX) nerve perfusions, and controls. All studies were carried out in accordance with the European Community Council directive of November 24th, 1986, and following the procedures issued by the French Ministry of Agriculture. All efforts were made to minimize animal suffering and to reduce the number of animals used.

Section of the facial nerve. Under halothane anesthesia, the animals ($n=25$ for *in situ* hybridization and $n=30$ for immunohistochemical study) were subjected to a unilateral section of the left facial nerve near its exit from the stylomastoid foramen. After surgery, the wound was closed with sutures and animals were allowed to recover for 1, 3, 8, 30 or 60 days. Control animals ($n=5$ for *in situ* hybridization and $n=6$ for immunohistochemical study) consisted of non-operated rats or sham-operated animals. Following surgery, the animals displayed unilateral facial palsy with return of some of eyelid and whiskerpad movements after 60 days.

Facial nerve TTX application. TTX (Latoxan, Valence, France) diluted at 250 $\mu\text{g}/\mu\text{l}$ in phosphate buffered saline (0.1 M, pH 7.4, 9 g/l NaCl; PBS) was applied for 8 days to the facial nerve of three rats using a Silastic silicone rubber tubing cuff assembly positioned around the facial nerve and implanted s.c. in the neck (Seburn and Cope, 1997; see also Eleore et al., 2005). Within 24 h of TTX application, animals displayed facial palsy on the injected side, which persisted. Control animals ($n=4$) received a daily infusion of PBS and were not paralyzed. Within 24 h treated animals displayed facial palsy on the injected side, and there was no recovery for the eight days following perfusion. Facial palsy was verified daily. The animals were killed by decapitation 8 days post-lesion and processed for *in situ* hybridization.

In situ hybridization study

Tissue preparation and hybridization procedures were as described previously (de Waele et al., 1994). We used antisense nucleotide oligoprobes (see Table 1) to detect the mRNAs for AMPA receptor subunits (Sato et al., 1993), NMDA receptor subunits (Wenzel et al., 1995) and the PSD95 protein (Fukaya et al., 1999).

After *in situ* hybridization, sections were placed against Biomax MR X-ray film (Kodak, Integra Bioscience, Cergy Pontoise, France) for 15 days for NMDA (NR2A-D) receptor subunit and PSD95 mRNAs, 10 days for AMPA (GLuR1-4) receptor subunit mRNAs, and 5 days for NR1 mRNAs. Then, the sections were exposed to NTB2 photographic emulsion at 4 °C for four weeks. Finally, they were counterstained with Toluidine Blue and coverslipped in Eukitt medium. Slides were scored visually with an Eclipse Nikon microscope under dark- and bright-field illumination. The specificity of oligonucleotide probes was checked by hybridizing sections with the corre-

Table 1. 5'-3' Sequences of AMPAR (GLuR1-4) and NMDA (NR1, NR2A-D) receptor subunit oligonucleotide probes

Name	Sequence 5'-3'
GLuR1	5'-GTC ACT GGT TGT CTG GTC TCG TCC CTC TTC AAA CTC TTC GCT GTG-3'
GLuR2	5'-TTC ACT ACT TTG TGT TTC TCT TCC ATC TTC AAA TTC CTC AGT GTG-3'
GLuR3	5'-AGG GCT TTG TGG GTC ACG AGG TTC TTC ATT GTT GTC TTC CAA GTG-3'
GLuR4	5'-CTG GTC ACT GGG TCC TTC CTT CCC ATC CTC AGG TTC TTC CTG GTG-3'
NR1	5'-CAT CCT GTG AGG GTT CCA GGT GAC TGA ATT GGC CCT TTC TAT GCC GCT GAG TTT GTG GCG-3'
NR1pan	5'-TTC CTC CTC CTC CTC ACT GTT CAC CTT GAA TCG GCC AAA GGG ACT-3'
NR2A	5'-AGA AGG CCC GTG GGA GCT TTC CCT TTG GCT AAG TTT C-3'
NR2B	5'-GGG CCT CCT GGC TCT CTG CCA TCG GCT AGG CAC CTG TTG TAA CCC-3'
NR2C	5'-TGG TCC ACC AGG TTT CTT GCC CTT GGT GAG GTT CTG GTT GAT GCT-3'
NR2D	5'-CTG TGG CTC GA TGG GG CCG TAG TAT CG GTG GAA GCC GTC GGC TAT-3'
PSD95	5'-AGG GGG CGT GTC TTC ATC TTG GTA GCG GTA TTT CTT GGT TGT CAC-3'

sponding AMPA (GLuR1-4) and NMDA (NR1, NR2A-D) sense oligonucleotide probes in the same conditions.

Film autoradiographs (corresponding to eight or 10 sections per animal) were scanned with a CDD video camera and the hybridization signals quantified. The images were digitized with a computerized image analysis system (Visiob 2000, Biocom, France). Relative optical density (rOD) in rat facial nuclei was measured using the Biocom densitometry analysis program (Visiob 2000) and was divided by the rOD of the white matter of the same section to obtain a rOD ratio. rOD was measured on an average of 10 sections for each animal and the mean rOD \pm SD (standard deviation) was calculated for each animal. The results for the NR2C oligonucleotide probe in the facial nuclei were not quantified because no signal was detected.

Immunohistochemical study

AMPA. Tissue preparation and immunohistochemical procedures were as described previously for detection of GLuR2-3 subunits (Fritschy et al., 1998). Antibodies from Chemicon (by Euromedex, Souffelweisham, France) diluted 1/50 were used.

NMDAR. For NMDAR immunohistochemical analysis, rats were killed by perfusion with 4% paraformaldehyde (PFA) supplemented with 15% picric acid in 0.1 M phosphate buffer, pH 7.4. The brain was removed, post-fixed in same solution for one hour at room temperature, and then stored in 30% sucrose in phosphate buffer for cryoprotection. Coronal sections 25 μ m thick were cut with a cryostat and conserved, briefly, in Tris buffer saline (TBS) until use. After several washes in TBS, sections were free-floated in 5% normal goat serum and then primary antibody was applied overnight at 4 °C. Antibodies for NR1 (Chemicon, ref. AB 1516; 1/100) and NR2A (Upstate by Euromedex, ref. 06313; 1/1000) diluted in TBS supplemented with 0.3% Triton X-100 (TBST) were used for recognizing the NMDA receptor subunit. After rinsing in TBS, bound antibodies were labeled by incubation for 1 h at room temperature with Alexa 488-conjugated goat anti-rabbit (Molecular Probes by Interchim, Montluçon, France) diluted 1/400 in TBST supplemented with 5% normal goat serum. Finally, the sections were washed and coverslipped with Vectashield (Vector Laboratories by Biovalley, Conches, France).

PSD95, VGLUT2, β catenin and pan cadherin. Coronal slices 14 μ m thick were post-fixed either in PFA 2% in PBS for 90 s for immunodetection of VGLUT2 and β catenin, and 5 min for immunodetection of pan cadherin, or in PFA 4% in PBS for 5 min for immunodetection of PSD95. After thorough rinsing, sections were directly dipped into PBS containing 0.5% Triton X-100, 20% bovine serum albumin and the primary antibody, either anti-VGLUT2 (Chemicon) diluted 1/2500, anti PSD95 (Alexis Biochemicals by Cogem, France) diluted 1/100, anti β catenin (ref. 610154; Transduction Laboratories) diluted 1/200, anti pan cadherin (ref. c1821; Sigma Aldrich) 1/200. Incubation with the primary antibody was continued in a wet chamber at 4 °C overnight. Sections were then rinsed in PBS, and bound antibodies were labeled by incubation for 1 h at room temperature with cyanine-3 (Cy3)-conjugated goat anti-guinea-pig, anti-rabbit or anti-mouse antibodies (Jackson Laboratories by Interchim, Montluçon, France) diluted 1/400 in PBS supplemented with 2% normal goat serum. Finally, the sections were washed and coverslipped with Vectashield. The reaction was stopped by three rinses in PBS. The stained sections were mounted in Vectashield medium (Vector Laboratories) and stored at -20 °C. Controls consisted of sections that had not been incubated in the primary antiserum.

Data analysis. Data from normal rats and from unilaterally facial-sectioned rats 1, 3, 8, 30 and 60 days post-lesion were used. The stained sections were analyzed for changes in the density of immunoreactive facial nuclei as assessed under a

microscope (Eclipse E800, Nikon). For each animal, an average of 10 sections was analyzed. Sections were mapped on video images (Coolsnap camera) and digitized with a computerized image analysis system (Metaview, Rupper Scientific, France). For each section, the boundary of the facial nucleus was determined at low magnification from the adjacent Cresyl Violet-counterstained sections. The intensity of the Cy3 signal was automatically quantified using the same conditions of exposure time and illumination. Arithmetic fluorescence (AF) was measured in whole images of facial nuclei on a linear scale from 0 to 255 relative intensity units per pixel. For PSD95, β catenin and pan cadherin, the intensity of the signal was determined in individual sections for five rectangular areas of about 19,322 μ m². For GLuR2/3, NR1 and NR2A receptor subunits, the intensity of the signal was measured in each cell whose soma was clearly defined and was in a rectangular field of the same dimensions. The mean AF \pm SD was then calculated from the measurements of six sections for each animal.

Finally, the relative arithmetic fluorescence ratio (rAF) was calculated by dividing the AF obtained for the axotomized facial nucleus by that for the intact one of the same section. The rAF in the medial vestibular nuclei was also determined as the AF for the ipsilateral medial vestibular nucleus (MVN) divided by the AF for the contralateral MVN of the same section. As the NVM were not directly affected by the lesion, these nuclei serve as internal controls for immunohistochemistry and data validity.

Statistical analysis. The mean values from the *in situ* hybridization and immunochemistry studies were tested for statistical significance using non-parametric tests (Statistica, Statsoft Inc.). The Kruskal-Wellis one-way analysis of variance for independent variables was used to search for differences between labeling in control animals and that on each side of operated rats. The Wilcoxon matched pairs test was used to test for differences between the deafferented and the intact side in each experimental group. The Mann-Whitney test was used to test the statistical significance of the differences between the mean values for vestibular and facial nuclei in each group. A value of $P < 0.05$ was considered to be statistically significant.

RESULTS

Labeling of AMPAR (GLuR1-4) subunit mRNAs in rat facial nuclei

GLuR1. *In situ* hybridization failed to show any differences in the intensity of GLuR1 mRNA labeling between the axotomized and intact facial nuclei (Fig. 1 for day post-lesion 8). There was no significant difference in the mean rOD between the axotomized and intact facial nuclei of lesioned animals and those of the controls at any times following surgery. No differences could be detected at the cellular level on emulsified slides (data not shown).

GLuR2–GLuR3. Axotomy resulted in pronounced down-regulation of GLuR2 and GLuR3 mRNAs in facial nuclei on the lesioned side (Fig. 1). The abundance of these mRNAs started to decline as early as the first day post-lesion ($P \leq 0.01$), reached a minimum 8 days post-lesion (the mean rOD was decreased by about 45% for GLuR2 and 64% for GLuR3; $P \leq 0.01$), and remained at low level for at least 30 days post-lesion ($P \leq 0.01$). A return to normal values was observed on day 60 post-lesion (Fig. 2A). The signals for GLuR2 and GLuR3 mRNAs in the contralateral facial nuclei were indistinguishable from controls at all post-operative times studied (1–60 days).

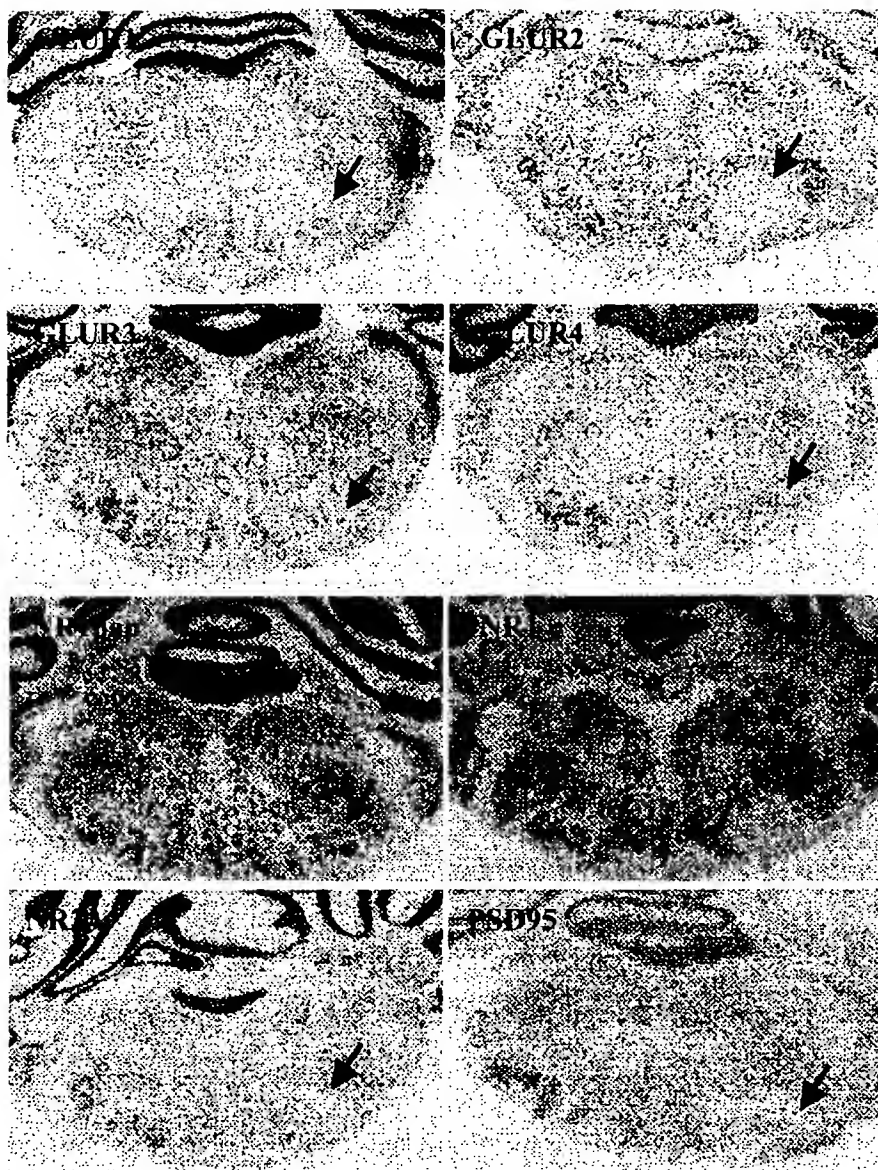


Fig. 1. Autoradiographs of *in situ* hybridization data obtained in axotomized animals with oligonucleotide probes for GLuR1-4, NR1pan, NR1, NR2A and PSD95 mRNAs. The ^{35}S -labeled antisense probes for GLuR1-4, NR1pan, NR1, NR2A and PSD95 mRNAs were hybridized with brainstem sections containing the facial nuclei from rats with unilateral facial axotomy 8 days following the lesion. The black arrows indicate the lesioned side. Note the decrease of mRNAs coding for GLuR2, GLuR3 and GLuR4 subunits of AMPAR receptors, NR1, NR2A subunits of NMDA receptors and the NMDAR anchoring protein, PSD95, in the deafferented facial nuclei. Notice that GLuR1 labeling was similar in intact and axotomized facial nuclei (black arrow) at this stage.

GLuR4. GLuR4 mRNA was also affected by the lesion but the decrease began later—3 days after axotomy. The abundance was lowest after 8 days (decrease of about 33%) and then progressively returned to normal values by day 60 (Figs. 1 and 2A). Facial nuclei of control rat and contralateral facial nuclei of operated rat were indistinguishable at all stages following the lesion. This decrease on the ipsilateral side was significant compared with values for the intact facial nucleus of lesioned animals and to that for the facial nucleus of control rats (Fig. 2A), on

days post-lesion three ($P \leq 0.01$), eight ($P \leq 0.01$), 30 ($P \leq 0.05$) and 60 ($P \leq 0.05$).

In summary, GLuR2-3 mRNAs were substantially reduced after facial nerve lesion, GLuR4 mRNAs were down-regulated less strongly and GLuR1 mRNAs were unaffected. All these findings were confirmed at the cellular level (Fig. 3).

We used immunohistochemistry to determine whether the changes in mRNA abundance were associated with similar effects on AMPA receptor subunit pro-

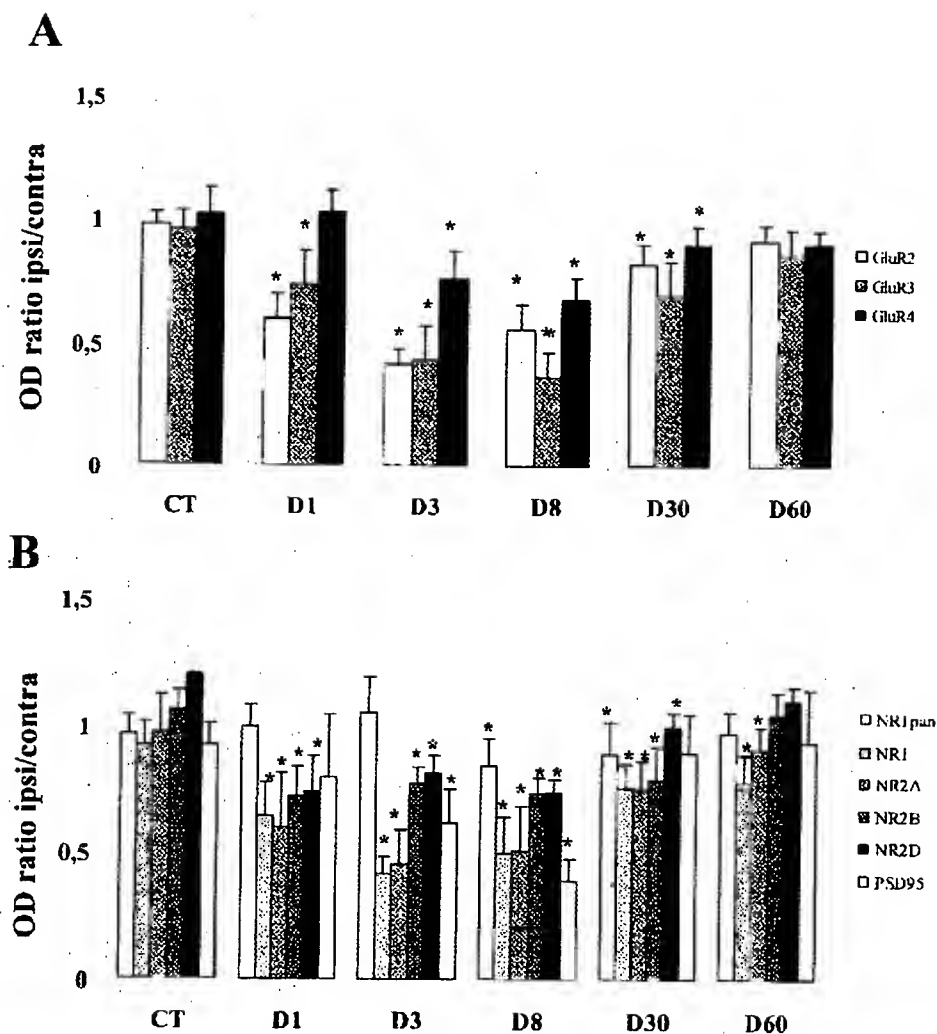


Fig. 2. Graphs of *in situ* hybridization data obtained in lesioned rats with the oligonucleotide probes for AMPAR, NMDAR subunits and PSD95 mRNAs. (A) Graphs showing the mean rOD ratio measured from autoradiographs with the GLuR2-4 oligonucleotide probes in the facial nuclei of control rats and of axotomized rats 1 day, 3 days, 8 days, 30 days and 60 days following surgery. (B) Graphs showing the mean rOD ratio measured from autoradiographs with the NR1pan, NR1, NR2A, B and D oligonucleotide probes in the facial nuclei of control rats and of axotomized rats 1 day, 3 days, 8 days, 30 days and 60 days following surgery. The error bars represent the standard deviation. Contra, facial nucleus contralateral to the lesion; Ipsi: facial nucleus ipsilateral to the lesion. * Significant difference between sides ipsilateral and contralateral to the lesion.

duction. Due to the absence of changes for GLuR1 mRNA and the small decrease for GLuR4 mRNA in axotomized facial nuclei, only GLuR2-3 proteins were analyzed.

GLuR2/3 subunit Immunolabeling in rat facial nuclei

In the facial nuclei, the neuropil showed a relatively low level of GLuR2/3 immunoreactivity whereas neuronal cell bodies of the facial motoneurons gave an intense signal. No positive labeling was detected in sections where the primary antibody was omitted. Facial nerve axotomy-induced down-regulation of GLuR2/3 protein production in the facial nuclei ipsilateral to the lesion (Fig. 4 illustrates the asymmetrical facial nuclei labeling on 8 day post-lesion). The decrease was greatest in cells bodies. There was also a difference in AF ratio between the intact and

axotomized facial nuclei (Fig. 5). GLuR2/3 expression began to decline at 3 days post-lesion ($P < 0.01$), was lowest 8 days post-lesion (corresponding to a decrease of 69%; $P \leq 0.01$) and returned to normal values after 60 days.

Labeling of NMDAR (NR1, NR2A-D) subunits and PSD 95 mRNAs in rat facial nuclei

NR1. We used two probes for NR1: the first named NR1 is specific for the exon 5 of NR1, and the second, NR1pan, recognizes all NR1 variants. The intensity of labeling with NR1 in the axotomized and intact facial nuclei was asymmetrical (Fig. 1, black arrow) at 8 days post-lesion. The mRNA signal started to decrease 1 day post-lesion ($P \leq 0.001$) and reached its lowest value—50% ($P \leq 0.001$)—on day 8. It then increased progressively to 30 days post-lesion and remained lower than normal 60

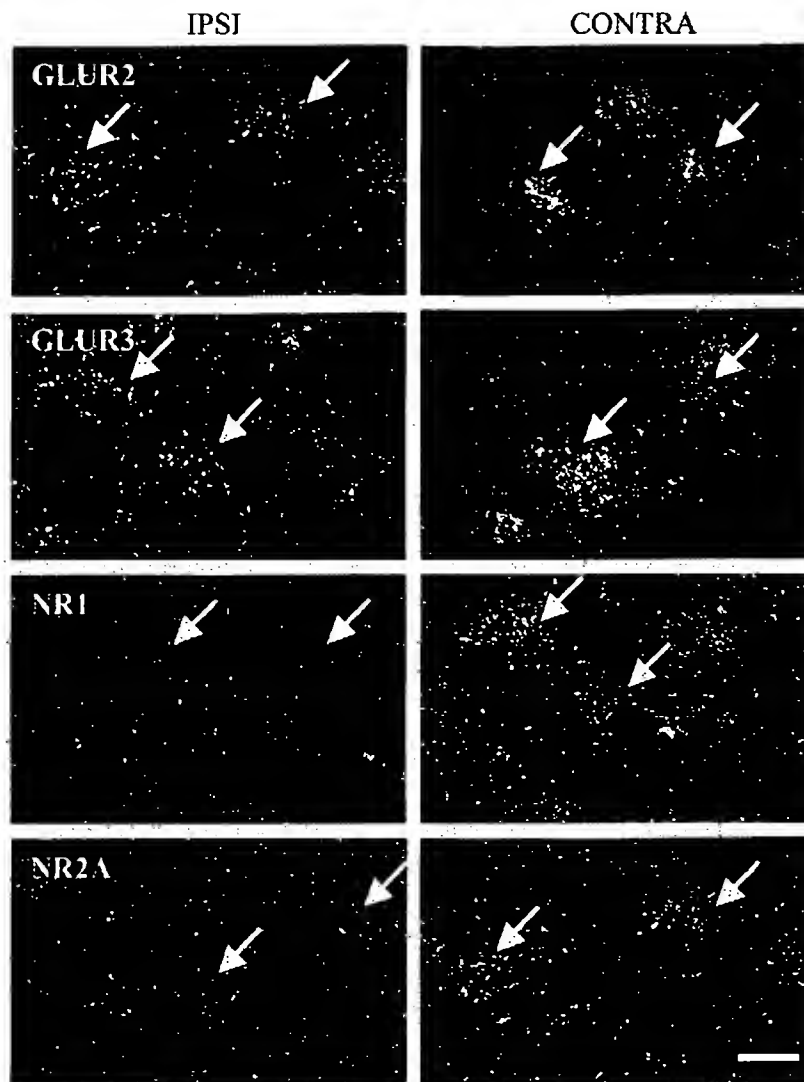


Fig. 3. Photomicrographs of *in situ* hybridization in the facial nucleus with the GLuR2, GLuR3, GLuR4, NR1 and NR2A oligonucleotide probes. Dark-field photomicrographs showing labeling of the mRNAs for the GLuR2, GLuR3, GLuR4 subunits of AMPAR, NR1 and NR2A subunits of NMDAR in the ipsilateral and contralateral facial nucleus 8 days post-lesion. Note the lower density of silver grains over ipsilateral axotomized facial nuclei than over the contralateral intact facial nuclei (white arrows). Scale bar = 20 μ m.

days post-lesion ($P \leq 0.01$) (Fig. 2). Changes in the NR1 signal observed on autoradiographs were confirmed at the cellular level (Fig. 3). Labeling with the NR1pan oligo-probe, which recognized all NR1 variants, decreased less (about 15%, $P \leq 0.001$) than that with NR1 8 days after facial nerve axotomy (Figs. 1 and 2B).

NR2A. Unilateral section of the facial nerve also affects NR2A subunit gene expression in the ipsilateral facial nuclei. There was less NR2A mRNA labeling in the axotomized facial nuclei than on the intact side on day post-lesion 8 (Fig. 1). The labeling began to decrease 1 day post-lesion, was lowest on day 8 corresponding to a decrease of 49% ($P < 0.01$), and then progressively re-increased (Fig. 2B). Labeling in contralateral facial nuclei was indistinguishable from that in facial nuclei of control rat, at all stages following the lesion.

NR2B-D. *In situ* hybridization demonstrated a moderate reduction of NR2B and NR2D mRNAs in the axotomized facial nuclei. The amount of mRNA started to decrease by day post-lesion 1 and reached its lowest value on day 8, when the decrease amounted to 27% for NR2B ($P < 0.001$) and to 26% for NR2D. It increased by day 30 and returned to normal levels by day 60 (Fig. 2B). mRNAs coding for the NR2C subunit were not detected at any time following the lesion or in intact animals.

PSD 95. PSD95 mRNA abundance was also altered by facial axotomy (Fig. 1). Within one day of facial nerve section, a decrease in PSD95 mRNA labeling was observed in facial nuclei ipsilateral to the lesion, the signal was lowest at 8 days post-lesion (decrease of about 55%.

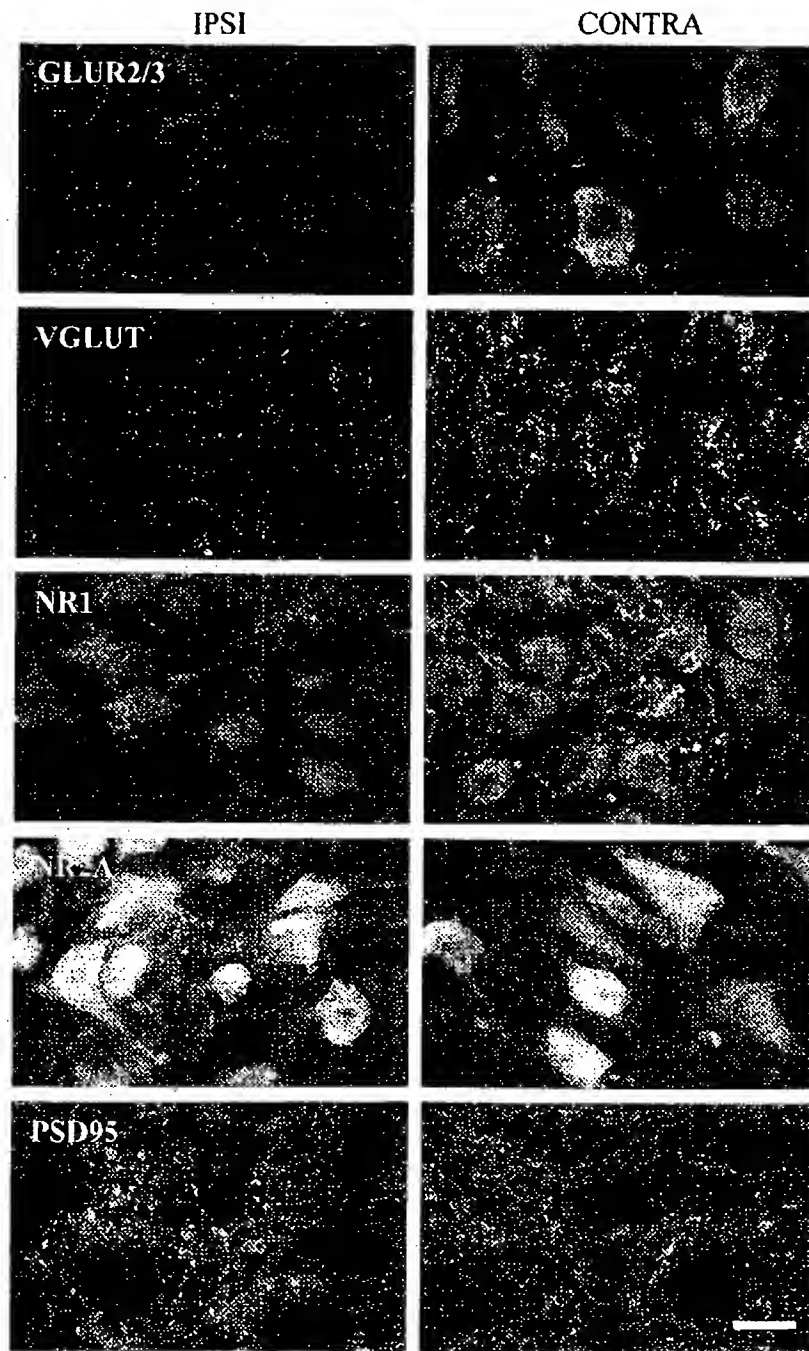


Fig. 4. GLuR2/3, VGLUT2, NR1, NR2A and PSD95 fluorescence photomicrographs of coronal sections through the facial nuclei of control and unilaterally axotomized adult rat on day post-lesion 8. Note the clear asymmetry of signal intensity between the intact and deafferented facial nuclei for GLuR2/3 subunits and VGLUT2, and the similarity of the signal intensity in the axotomized and intact nuclei for NR2A and PSD95. Scale bar=20 μ m.

$P < 0.001$) and was still lower than baseline 30 days post-lesion. A return to normal values was observed at day post-lesion 60 (Fig. 2B).

All autoradiograph observations were confirmed at the cellular level. Thus, silver grain density was substantially lower in the axotomized facial nucleus than in the con-

tralateral facial nucleus for NR1, NR2A, NR2B and D, and PSD95 (Fig. 3).

In summary, mRNAs for NR1 and NR2A, B and D subunits were lost from motoneurons following axotomy. No expression of NR2C could be detected. As NR1 and NR2A subunit mRNAs were the most abundant in the

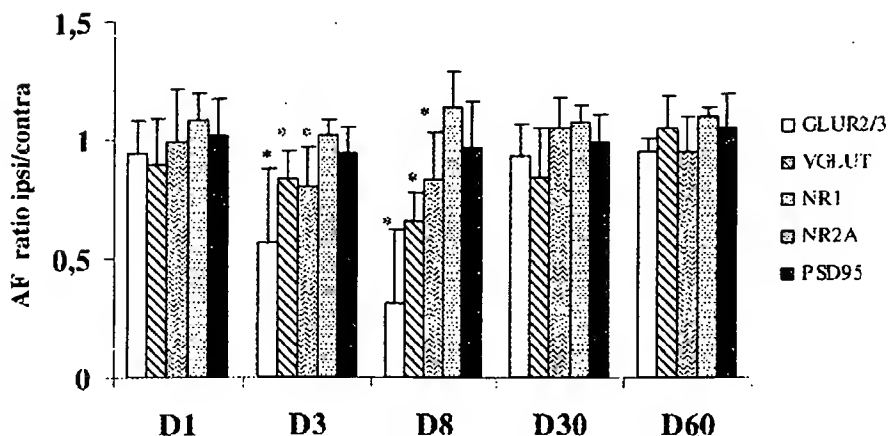


Fig. 5. Changes in AMPAR subunit, NMDAR subunit, VGLUT2 and PSD95 immunoreactivity in facial nuclei of axotomized rats. Graphs showing the arithmetic mean rAF (ipsi/contra) in the facial nuclei for the GLUR2/3, VGLUT2, NR1, NR2A and PSD95 antibodies in rats with unilateral facial axotomy 1, 3, 8, 30 and 60 days following the lesion. The error bars represent the standard deviation. * Significant difference between sides ipsilateral and contralateral to the lesion.

facial nuclei, we also studied the corresponding proteins after axotomy in parallel with the PSD95 protein by means of immunohistochemistry. We also studied the VGLUT2 protein, implicated in glutamate accumulation in presynaptic vesicle.

Immunolabeling of NR1 and NR2A subunits and PSD95 in rat facial nuclei

NMDAR subunits. In facial neurons, strong NR1 and NR2A signals were visible in neuronal somata and proximal dendrites and some staining was also present in the neuropil (Fig. 4). Facial nerve axotomy resulted in a decrease of NR1 subunit immunostaining in the facial nuclei ipsilateral to the lesion. The decrease was greater in the neuropil than in cell bodies (Fig. 4). The decrease in AF, although small, was significant ($P < 0.001$, Fig. 5) 3 and 8 days post-lesion (16%). In contrast, NR2A immunoreactivity appeared to be unaffected by axotomy at all time points and the pattern of NR2A immunolabeling in the ipsilateral side was similar to that of the contralateral side (Fig. 4). AF quantification confirmed these results (Fig. 5).

PSD95. A strong PSD95 labeling was observed in the neuropil of the facial nuclei. PSD95 immunostaining on the ipsilateral side was similar to that in the intact facial nuclei of axotomized rats and those of control rats at all times following the lesion (Fig. 4). Fluorescence intensity quantification confirmed that axotomy did not significantly affect AF: there was no difference ($P > 0.05$) for PSD95 between the two facial nuclei (Fig. 5).

VGLUT2 immunolabeling in facial nuclei of normal and lesioned rats

VGLUT2 labeling was confined to the neuropil in the facial nuclei where it appeared as punctuated staining, believed to correspond to axonal varicosities. Following

facial nerve section, there was a large decrease in VGLUT2 staining of the axotomized facial nuclei (Fig. 4). VGLUT2 immunoreactivity in injured nuclei was lower 3 and 8 days post-lesion (corresponding to a decrease of about 35%; $P < 0.001$), started to recover at 30 days post-lesion and returned to the control level by 60 days post-lesion (Fig. 5).

β Catenin and pan cadherin immunolabeling in facial nuclei of normal and lesioned rats

In normal facial nuclei, β catenin and pan cadherin immunolabeling showed a homogeneous and strong fibrous pattern confined to the neuropil and a staining closely related to the periphery of neuronal cell body. Between one and three days after axotomy, change in distribution of β catenin and pan cadherin immunostaining pattern became obvious: immunostaining remained conspicuous in neuropil, but it was markedly decreased at the periphery of cell soma. The loss of the strings labeling surrounding the facial motoneuron somata was most pronounced on day 8 (Fig. 6). Staining with both antibodies began to reappear at 30 days post-operatively, but concerned a small number of neuron. At day post-lesion 60, the labeling pattern was almost identical to/uninjured side. Absence of changes in β catenin and pan cadherin expression level observed on slices was confirmed by quantification of immunofluorescence intensity (Fig. 6).

TTX-treated rats

TTX caused facial palsy similar to that observed after facial nerve axotomy. It reduced GLUR2, GLUR3, NR1, and NR2A transcripts in the facial nuclei ipsilateral to the perfused side (Table 2). In PBS-treated animals, labeling for AMPAR and NMDAR subunits mRNAs was indistinguishable from those of control animals. We did not test either NMDAR subunits or PSD95 after TTX

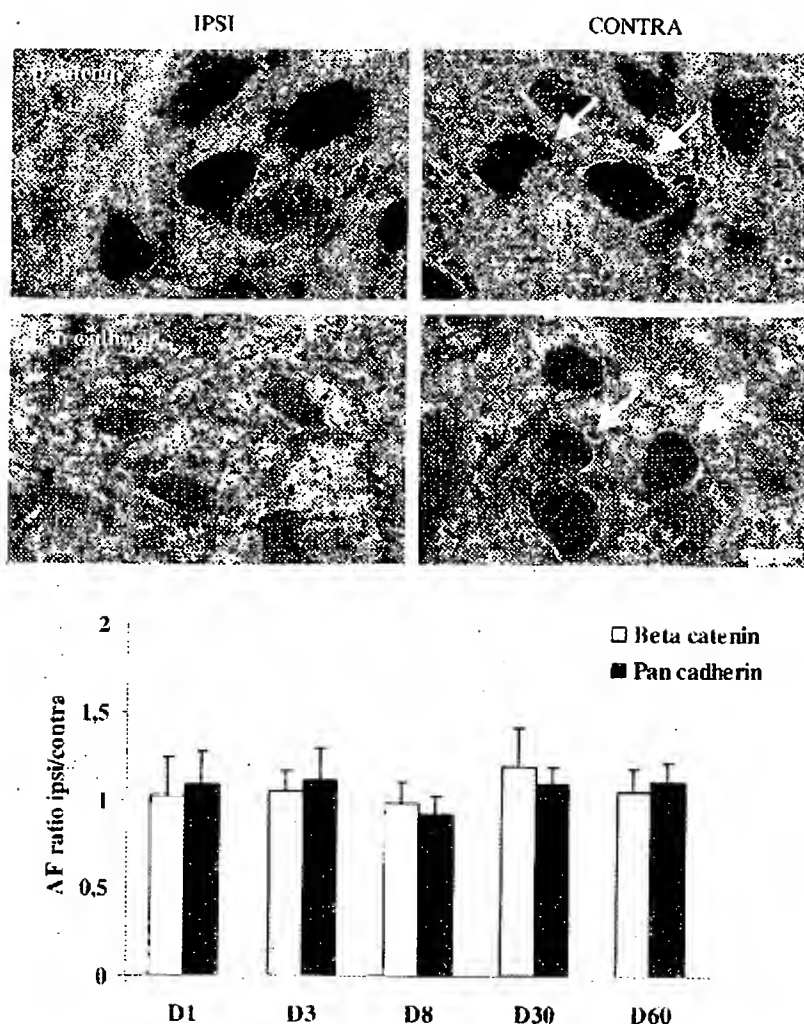


Fig. 6. Changes in β catenin and cadherin immunoreactivity in facial nuclei of axotomized rats. In the top panels, β catenin and cadherin immunofluorescence photomicrographs of coronal sections through the facial nuclei of control and unilaterally axotomized adult rat on day post-lesion 8. Note the thin rim of immunoreactivity which surrounds neuronal perikarya in contralateral facial nuclei and the loss of this staining on the ipsilateral side. Scale bar = 20 μ m. Below, graph showing the arithmetic mean rAF (ipsi/contra) in the facial nuclei for β catenin and cadherin antibodies in rats with unilateral facial axotomy 8 days following the lesion. The error bars represent the standard deviation. Note the similarity of the signal intensity in the axotomized and intact facial nuclei.

because the expression level of these proteins was not or little affected by sectioning of the facial nerve. There was a significantly lower optical density decrease in TTX-treated than axotomized facial nerves (36% compared with 69% respectively after facial axotomy).

Table 2. Mean optical density ratio ipsi/contra decrease in facial nuclei after axotomy or TTX injection for mRNAs coding for GLuR2, GLuR3, NR1 and NR2A subunits

	GLuR2	GLuR3	NR1	NR2A
SF	45%	64%	50%	49%
TTX	28% (*)	27% (***)	37% (*)	31% (*)

(*) $P < 0.05$; (***) $P < 0.001$.

DISCUSSION

AMPA and NMDAR expression in the facial nuclei of axotomized rats

Facial axotomy reduces excitatory neurotransmission mediated through AMPA receptors in lesioned motoneurons. In particular, the glutamate receptor subunits GLuR2 and GLuR3 are strongly decreased. Our findings are in accordance with previous data in axotomized sciatic (Kenniss and Holstege, 1997; Alvarez et al., 2000) and hypoglossal motoneurons (Tang and Sim, 1997; Alvarez et al., 1997; Garcia Del Cano et al., 2000). This decrease may induce an increase in intracellular calcium concentration, which may be excitotoxic for facial motoneurons. Indeed, Ca^{2+} permeability of AMPAR has been shown to vary with the relative abundance of GLuR2 mRNAs (Jonas et al., 1994).

As most of these neurons did not die, at least three types of mechanism may be suggested as protecting the facial motoneurons from excitotoxic effects: 1. The decrease of VGLUT2 following axotomy; 2. an up-regulation of the glutamate transporter (GLT-1) in activated microglia of axotomized facial nuclei (Lopez-Redondo et al., 2000) 3. The influence of Iba-1, a calcium binding protein, which was increased in microglial cells (Ito et al., 1998) and which could decrease the intracellular Ca^{2+} motoneuron concentration.

For the NMDA receptors, the data described in the literature were more heterogeneous: mRNAs encoding the NR1 subunits were reported to be unaffected by axotomy in rat ipsilateral facial, spinal (Sanner et al., 1994a,b) and hypoglossal motoneurons (Garcia Del Cano et al., 2000). Only one electrophysiological study found that NMDAR of the dorsal motor vagus motoneurons became less sensitive *in vitro* to extracellular Mg^{2+} after axonal crush injuries (Furukawa et al., 2000). Finally, Western blotting showed that NR2A subunit expression was decreased in axotomized vagal motoneurons whereas expression of NR1, NR2B, NR2C and NR2D subunits did not change significantly (Nabekura et al., 2002). Unlike these previous works, we found a large transcriptional decrease of all the NR1 and NR2A subunits although these changes were not always associated with any large reduction of the respective proteins, especially NR2A. The discrepancy between our study and previous *in situ* hybridization studies may result from the probe used. Indeed, in accordance with Sanner et al. (1994a), no NR1 mRNA change could be detected with a probe that recognized all NR1 variants (NR1pan). We only observed a significant decrease of mRNAs coding for the NR1 subunit by using a probe specific for the exon 5 of NR1 mRNA. Exon 5 splicing results in the absence of NR1-1a variants (Zukin and Bennett, 1995). These NR1 variants were also shown to be decreased in the rat superior olivary complex after unilateral cochlear ablation (Nakagawa et al., 2000). Treatment with NR1 antisense oligonucleotide probes decreased NR1 mRNA synthesis and prevented neurotoxicity induced by NMDA *in vivo* and *in vitro* in ischemic rats (Sun and Faden, 1995; Wahlestedt et al., 1993). In addition, treatment of the facial nerve with MK-801, a specific non-competitive antagonist of NMDAR, enhanced NR1 mRNA transcription and cell death (Sanner et al., 1994a). These data suggest that the differential regulation of NR1 variants may have a neuroprotective effect on axotomized facial motoneurons.

Finally, NR2A seemed to be regulated at a transcriptional but not at a translational level. This discrepancy with data published by Nabekura et al. (2002) is unlikely to be due to differences in the commercialized antibodies used as they all recognize the C-terminal portion of NR2A subunit. It could result from the different methods used (Western blotting versus immunohistochemical methods) or from differences between the models used (facial axotomy versus vagal axotomy).

VGLUT2 in intact and facially axotomized rats

We showed for the first time, a strong decrease of VGLUT2-immunoreactivity in facial motoneurons, which occurred as early as day post-lesion three and which tends to return to the control level by 60 days post-lesion. These data are in agreement with previous morphological findings. Unilateral enucleation results in a decrease in the VGLUT2-immunoreactivity in the dorsal lateral geniculate nucleus and in the superior colliculus within four days, whereas VGLUT1 expression is unaffected (Fujiyama et al., 2003). VGLUT1 immunostaining was decreased in fibers in the ipsilateral ventral horn one week after dorsal root rhizotomy (Oliveira et al., 2003). Finally, transection of the sciatic nerve produced a reduction of VGLUT1 immunoreactivity in the spinal cord (Hughes et al., 2004). We previously failed to detect any modulation of a vesicular transporter named VIAAT, involved in inhibitory amino acid (GABA and glycine) accumulation into synaptic vesicle (Eleore et al., 2005). This allows us to suggest that excitatory and inhibitory inputs of facial nuclei are differentially modulated after the lesion, with a preference for maintaining an inhibitory influence. A preferential loss of glutamatergic synaptic terminals compared with inhibitory ones was previously reported after intramedullary axotomy (Linda et al., 2000). Loss of VGLUT2 immunoreactivity may partly result from the glial synaptic stripping, which occurred on the lesioned facial motoneurons (Neiss et al., 1992). Similar temporal time courses were found between VGLUT2, a selective marker of glutamatergic afferents and synaptic markers such as synapsin (Eleore et al., 2005) pan-cadherins and betacatenine.

PSD95 in intact and facially axotomized rats

Che et al. (2000) showed that in rats PSD95 mRNAs were down-regulated within 1 day of facial nerve axotomy and returned to normal levels when target reconnection was reestablished, i.e. at 35 days post-lesion. The authors suggested that PSD95 may be involved in synaptogenesis and recovery of synaptic function after lesion. However, we found no evidence of a change in the amount of PSD95 protein at any time following the facial nerve injury. A transient global ischemia in the rat hippocampus induced changes in the composition of post-synaptic densities, inducing an alteration of PSD95 and NR2A interaction without changing their abundance (Takagi et al., 2000; Hou et al., 2002). A similar event may occur after facial nerve axotomy. The central role of PSD95 in NMDAR signaling pathways and not in receptor distribution regulation has been extensively documented (Kennedy, 2000; Sattler et al., 1999; Tezuka et al., 1999; Migaud et al., 1998) and PSD95 preferentially binds to the NR2A subunit in the NMDA receptor. Thus, a complex containing NR2A, PSD95 and other PSD proteins at the synapse may be involved in the synaptic (NMDAR-mediated synaptic plasticity) response to axotomy and promotion of neuronal survival.

β catenin and pan cadherin in intact and facially axotomized rats

Axotomy of facial nerve motor neuron led to a variety of cellular and molecular response of both glial and neuronal cells. Numerous studies have shown that microglial cells proliferate around injured neuronal perikarya (Aldskogius and Kozlova, 1998) and are supposed to be responsible for the synaptic stripping events (Neiss et al., 1992; Ulenkate et al., 1993). Astrocytes cells became hypertrophic, increased the glial fibrillary acidic protein expression and then surrounded injured neuron (Graeber, 1994). However, the regulation and the role of protein physically associated with the synapse during this event are not known in detail. In this study, we have chosen β catenin and cadherin protein, as reliable markers to observe synaptic stripping phenomenon. These proteins are known to border the transmitter release zones containing synaptic vesicles, which were associated with protein like synaptophysin and synapsin (Uchida et al., 1996).

Facial axotomy produced a fragmentation of the continuous rim of β catenin and pan cadherin immunoreactivity around neuronal cell body, evident at 3 days post-lesion. These change in facial motor neuron immunolabeling for both adhesion protein, coincided with massive detachment of the presynaptic bouton from cell body of facial motor neurons. Recovery began to occur at day post-lesion 30 and was almost complete at day post-lesion at 60, i.e. when facial nerve and peripheral muscles were reconnected (Che et al., 2000). Guntinas-Lichius et al. (1994) and our previous study (Eleore et al., 2005) showed a similar synaptophysin and synapsin immunolabeling expression pattern, change with similar temporal time course in axotomized facial nuclei. In contrast, synaptophysin and synapsin labeling modulations seemed to occur later (at 14 days post-lesion) in rat spinal cord after sciatic nerve axotomy. This may be due to the site (proximal versus distal) between the site of nerve section and neuronal cell body, in both the facial and sciatic axotomy model. Although the mechanism by which β catenin and cadherin are modulated after facial axotomy was unknown, their expression appears to be correlated with changes in synaptic efficacy, remodeling, and with NMDAR activity: β catenin redistribution induced by depolarization could be completely blocked by NMDAR antagonists (Murase et al., 2002).

Comparison of excitatory and inhibitory synaptic transmission after facial axotomy

At least four conclusions could be drawn from our present study and from the two previous ones we performed in the axotomy facial model on the modulation of inhibitory amino acid receptors (glycinergic and GABAergic receptors; Eleore et al., 2005; Vassias et al., 2005) following facial axotomy (Table 3):

1. The axotomy-induced down-regulation in receptor expression seems to be more severe for inhibitory ones (glycinergic and GABA) in comparison to excitatory receptors as NMDAR subunits (NR1, NR2A) which appeared to be less affected at the protein level. To confirm this as-

Table 3. Regulated expression of amino acid receptors, related vesicular transporters and anchoring protein, and of synaptic-associated protein, following facial nerve lesion

	mRNA	Protein
Excitatory amino acid receptors		
AMPA		
GLuR1	↔	nd
GLuR2	↓↓	↓
GLuR3	↓↓	↓
GLuR4	↓	nd
NMDAR		
NR1	↓↓	↓
NR2A	↓↓	↔
NR2B	↓↓	nd
NR2C	↔	nd
NR2D	↓↓	nd
Anchoring protein		
PSD95	↓	↔
Vesicular transporter		
VGLUT2	nd	↓↓
Inhibitory amino acid receptors		
GABA_AR		
α1	↓↓	↓↓
α2	↔	nd
β1	↔	nd
β2	↓↓	↔
β3	↔	↔
γ2	↓↓	↓↓
GABA_BR		
B1A	↔	↔
B1B	↓↓	↔
B2	↓↓	↓↓
GLYR		
α1	↓↓	↓↓
α2	↔	nd
α3	↔	nd
β1	↓↓	↓↓
Anchoring protein		
Gephyrin	↓↓	↓↓
Vesicular transporter		
VIAAT	nd	↔
Synaptic protein		
Synapsin	nd	↔
β Catenin	nd	↔
Cadherin	nd	↔

(nd) not determined, (↔) no change, (↓) weak decrease, (↓↓) strong decrease.

sumption it was necessary to complete our study with the other NMDAR subunits like NR3A/B, and the other glutamate receptor (kainate and metabotropic glutamate receptor).

2. At the presynaptic level, we were unable to detect any modulation of VIAAT protein at any stages (1-60 days) following the lesion. It was not the case for glutamatergic afferents: VGLUT2 was drastically reduced and the decrease began as soon as day post-lesion 3.

3. The scaffold proteins, gephyrin and PSD95, were differentially regulated: gephyrin expression level fell sharply after facial nerve lesion, whereas PSD95 protein was not altered.

4. Recovery of the most subunits involved in AMPA and NMDA receptors was almost complete (between 80 and 100%) at day post-lesion 30, which was not the case for the different subunits of glycinergic and GABAergic receptors (between 30% and 80%).

Therefore, in the facial axotomy model, the effect of axotomy seems to occur both at a pre- and post-synaptic level whereas it was mainly post-synaptic for inhibitory receptors. These differences could be due to the different ways the receptors were addressed and anchored to the cytoplasmic membrane and to the role of inhibitory and excitatory inputs on facial nuclei. Further studies using electron microscopy are necessary to elucidate that point.

Influence of electrical activity

Here, we showed that TTX, a toxin which blocks voltage sensitive sodium channels, reduced the amounts of AMPAR (GLuR2, GLuR3) subunits and NMDAR (NR1, NR2A) subunit mRNAs in facial nuclei, although less strongly than that following axotomy. This indicates that ongoing neuronal activity was required, but only for decrease in the subunits gene transcription. Most of the studies on NMDAR showed modulation of their subunits after TTX treatment, and thus were in line with our results. Indeed, NMDAR subunits increased in ventral motoneurons into the spinal cord (Grossman and Wrathall, 2000), whereas their expression decreased in visual cortical neuron following TTX injection (Wong-Riley et al., 1998; Zhang and Wong-Riley, 1999; Catalano et al., 1997). On the opposite side, there are controversial results on change of AMPAR in response to TTX infusion. Alvarez et al. (2000) and Grossman and Wrathall (2000) reported that AMPA GLuR2/3 subunit abundance was not affected by TTX nerve blockade in sciatic motoneurons and ventral spinal cord, respectively. Down-regulation of GLuR2 subunits was detected in visual cortical neurons treated by TTX (Bai and Wong-Riley, 2003; Wong-Riley and Jacobs, 2002). Difference in methodological experiments can explain this variability: cell culture versus *in vitro* studies. However, it is not the case, between Alvarez experiments and our study. To understand this apparent contradictory result, we can propose at least two hypotheses:

1. First, TTX effects were mainly studied at the protein level and not at messenger level. We can suppose that whereas protein density was not affected, signalization mechanism of AMPAR was altered by TTX.

2. Second, in the Alvarez et al. (2000) experiments, the osmotic minipumps were located at the level of the tibial branch of the sciatic nerve, thus far to the neuronal cell body and after nerve division into two branches including the tibial nerve and the peroneal nerve. In comparison, the facial nerve was smaller and it still forms a single tract at the level of stylomastoid foramen. These anatomical differences and the length between the place of application of the TTX and the soma of the concerned neurons, may explain the results obtained in both cases.

CONCLUSIONS

Our data suggest that glutamatergic synaptic transmission of facial motoneurons is severely altered by axotomy. Furthermore, the reduction occurred not only at post-synaptic level, but also at pre-synaptic level. This contrasts with modulation of inhibitory synaptic transition on lesioned facial nuclei, and suggests the existence of two different regulatory pathways for both types of neurotransmission. Finally, the loss of the AMPAR and NMDAR subunits was partly induced by activity disruption.

Acknowledgments—We would like to thank Dr. Mohamed Reza Ardehali for his counsel and Martine Pouradier for her excellent technical assistance. This work was supported by grants from the "conseil general of Guadeloupe," France.

REFERENCES

- Aldskogius H, Kozlova EN (1998) Central neuron-glial and glial-glial interactions following axon injury. *Prog Neurobiol* 55:1–26.
- Alvarez FJ, Dewey DE, Carr PA, Cope TC, Fyffe RE (1997) Down-regulation of metabotropic glutamate receptor 1a in motoneurons after axotomy. *Neuroreport* 8:1711–1716.
- Alvarez FJ, Fyffe RE, Dewey DE, Haftel VK, Cope TC (2000) Factors regulating AMPA-type glutamate receptor subunit changes induced by sciatic nerve injury in rat. *J Comp Neurol* 426:229–242.
- Anneser JM, Berthele A, Borasio GD, Castro-Lopes JM, Zieglanger W, Tolle TR (2000) Axotomy of the sciatic nerve differentially affects expression of metabotropic glutamate receptor mRNA in adult rat motoneurons. *Brain Res* 868:215–221.
- Bai X, Wong-Riley MT (2003) Neuronal activity regulates protein and gene expressions of GLuR2 in postnatal rat visual cortical neurons in culture. *J Neurocytol* 32:71–78.
- Border BG, Mihailoff GA (1991) Glutamate immunoreactivity in the rat basilar pons: light and electron microscopy reveals labeled boutons and cells of origin of afferent projections. *Neuroscience* 45:47–61.
- Catalano SM, Chang CK, Shatz CJ (1997) Activity-dependent regulation of NMDAR1 immunoreactivity in the developing visual cortex. *J Neurosci* 17:8376–8390.
- Che YH, Tamatani M, Tohyama M (2000) Changes in mRNA for post-synaptic density-95 (PSD-95) and carboxy-terminal PDZ ligand of neuronal nitric oxide synthase following facial nerve transection. *Mol Brain Res* 76:325–335.
- de Waele C, Abilbol M, Chat M, Menini C, Mallet J, Vidal PP (1994) Distribution of glutamatergic receptors and GAD mRNA-containing neurons in the vestibular nuclei of normal and hemilabyrinthectomized rats. *Eur J Neurosci* 6:565–576.
- Eleore L, Vassias I, Vidal PP, Triller A, de Waele C (2005) Modulation of Glycine receptors subunits and gephyrin expression into the rat facial nucleus after axotomy. *Eur J Neurosci*, 21:669–678.
- Fritschy JM, Weinmann O, Wenzel A, Benke D (1998) Synapse-specific localization of NMDA and GABA(A) receptor subunits revealed by antigen-retrieval immunohistochemistry. *J Comp Neurol* 390:94–210.
- Fujiyama F, Hioki H, Tomloka R, Taki K, Tamamaki N, Nomura S, Okamoto K, Kaneko T (2003) Changes of immunocytochemical localization of vesicular glutamate transporters in the rat visual system after the retinofugal denervation. *J Comp Neurol* 465:234–249.
- Fukaya M, Ueda H, Yamauchi K, Inoue Y, Watanabe M (1999) Distinct spatiotemporal expression of mRNAs for the PSD-95/SAP90 protein family in the mouse brain. *Neurosci Res* 33:11–18.
- Furukawa Y, Okada M, Akaike N, Hayashi T, Nabekura J (2000) Reduction of voltage dependent magnesium block of N-methyl-D-

- aspartate receptor-mediated current by in vivo axonal injury. *Neuroscience* 96:385–392.
- Garcia Del Cano G, Gerrikagoitia I, Sarasa M, Matute C, Martinez-Millan L (2000) Ionotropic glutamate receptor subunits are differentially regulated in the motoneuronal pools of the rat hypoglossal nucleus in response to axotomy. *J Neurocytol* 29:509–523.
- Graeber MB (1994) The role of astrocytes in facial nerve regeneration. *Eur Arch Otorhinolaryngol* S75–S77.
- Grossman SD, Wrathall JR (2000) The role of activity blockade on glutamate receptor subunit expression in the spinal cord. *Brain Res* 880:183–186.
- Guntinas-Lichius O, Neiss WF, Gunkel A, Stennert E (1994) Differences in glial, synaptic and motoneuron responses in the facial nucleus of the rat brainstem following facial, nerve resection and nerve suture reanastomosis. *Eur Arch Otorhinolaryngol* 51:410–417.
- Hata Y, Takai Y (1999) Roles of postsynaptic density-95/synapse-associated protein 90 and its interacting proteins in the organization of synapses. *Review. Cell Mol Life Sci* 56:461–472.
- Hou XY, Zhang GY, Yan JZ, Chen M, Liu Y (2002) Activation of NMDA receptors and L-type voltage-gated calcium channels mediates enhanced formation of Fyn-PSD95-NR2A complex after transient brain ischemia. *Brain Res* 955:123–132.
- Hughes DI, Polgar E, Shehab SA, Todd AJ (2004) Peripheral axotomy induces depletion of the vesicular glutamate transporter VGLUT1 in central terminals of myelinated afferent fibres in the rat spinal cord. *Brain Res* 1017:69–76.
- Huntley GW (2002) Dynamic aspects of cadherin-mediated adhesion in synapse development and plasticity. *Review. Biol Cell* 94(6):335–344.
- Ito D, Imai Y, Ohsawa K, Nakajima K, Fukuchi Y, Kohsaka S (1998) Microglia-specific localisation of a novel calcium binding protein, Iba1. *Mol Brain Res* 57:1–9.
- Jonas P, Racca C, Sakmann B, Seeburg PH, Monyer H (1994) Differences in Ca²⁺ permeability of AMPA-type glutamate receptor channels in neocortical neurons caused by differential GluR-B subunit expression. *Neuron* 12:1281–1289.
- Kaneko T, Fujiyama F, Hioki H (2002) Immunohistochemical localization of candidates for vesicular glutamate transporters in the rat brain. *J Comp Neurol* 444:39–62.
- Kennedy MB (2000) Signal-processing machines at the postsynaptic density. *Review. Science* 290:750–754.
- Kennis JH, Holstege JC (1997) A differential and time-dependent decrease in AMPA-type glutamate receptor subunits in spinal motoneurons after sciatic nerve injury. *Exp Neurol* 147:18–27.
- Kornau HC, Schenker LT, Kennedy MB, Seeburg PH (1995) Domain interaction between NMDA receptor subunits and the postsynaptic density protein PSD-95. *Science* 269:1737–1740.
- Krutzberg GW (1996) Principles of neuronal regeneration. *Review. Acta Neurochir Suppl (Wien)* 66:103–106.
- Linda H, Shupliakov O, Omung G, Ottersen OP, Storm-Mathisen J, Risling M, Cullheim S (2000) Ultrastructural evidence for a preferential elimination of glutamate immunoreactive synaptic terminals from spinal motoneurons after intramedullary axotomy. *J Comp Neurol* 425:10–23.
- Lopez-Redondo F, Nakejima K, Honda S, Kohsaka S (2000) Glutamate transporter GLT-1 is highly expressed in activated microglia following facial nerve axotomy. *Mol Brain Res* 76:429–435.
- Migaud M, Charlesworth P, Dempster M, Webster LC, Walabe AM, Mekhinson M, He Y, Ramsay MF, Morris RG, Morrison JH, O'Dell TJ, Grant SG (1998) Enhanced long-term potentiation and impaired learning in mice with mutant postsynaptic density-95 protein. *Nature* 396:433–439.
- Mishina M, Sakimura K, Mori H, Kushiya E, Harabayashi M, Uchino S, Nagahara K (1991) A single amino acid residue determines the Ca²⁺ permeability of AMPA-selective glutamate receptor channels. *Biochem Biophys Res Commun* 180:813–821.
- Moran LB, Graeber MB (2004) The facial nerve axotomy model. *Review. Brain Res Rev* 44:154–178.
- Murase S, Mosser E, Schuman EM (2002) Depolarization drives beta-Catenin into neuronal spines promoting changes in synaptic structure and function. *Neuron* 35:91–105.
- Nabekura J, Ueno T, Katsurabayashi S, Furuta A, Akaike N, Okada M (2002) Reduced NR2A expression and prolonged decay of NMDA receptor-mediated synaptic current in rat vagal motoneurons following axotomy. *J Physiol* 539:735–741.
- Nakagawa H, Sato K, Shiraishi Y, Kuriyama H, Altschuler RA (2000) NMDAR1 isoforms in the rat superior olivary complex and changes after unilateral cochlear ablation. *Mol Brain Res* 77:246–257.
- Neiss WF, Lichius OG, Angelov DN, Gunkel A, Stennert E (1992) The hypoglossal-facial anastomosis as model of neuronal plasticity in the rat. *Ann Anat* 174:419–433.
- Oliveira AL, Hydling F, Olsson E, Shi T, Edwards RH, Fujlyama F, Kaneko T, Hokfelt T, Cullheim S, Meister B (2003) Cellular localization of three vesicular glutamate transporter mRNAs and proteins in rat spinal cord and dorsal root ganglia. *Synapse* 50:117–129.
- Sakimura K, Kutsuwada T, Ito I, Manabe T, Takayama C, Kushiya E, Yagi T, Aizawa S, Inoue Y, Sugiyama H, Mishina M (1995) Reduced hippocampal LTP and spatial learning in mice lacking NMDA receptor epsilon 1 subunit. *Nature* 373:151–155.
- Sanner C, Elliott JL, Snider WD (1994a) Upregulation of NMDAR1 mRNA induced by MK-801 is associated with massive death of axotomized motor neurones in adult rats. *Neurobiol Dis* 1:121–129.
- Sanner CA, Cunningham TJ, Goldberger ME (1994b) NMDA receptor blockade rescues Clarke's and red nucleus neurons after spinal hemisection. *J Neurosci* 14:6472–6480.
- Sato K, Kiyama H, Tohyama M (1993) The differential expression patterns of messenger RNAs encoding non-N-methyl-D-aspartate glutamate receptor subunits (GluR1–4) in the rat brain. *Neuroscience* 52:515–539.
- Sattler R, Xiong Z, Lu WY, Hafner M, MacDonald JF, Tymianski M (1999) Specific coupling of NMDA receptor activation to nitric oxide neurotoxicity by PSD-95 protein. *Science* 284:1845–1848.
- Seburn KL, Cope TC (1997) Low-frequency depression of the monosynaptic reflex is not altered by tetrodotoxin-induced nerve conduction blockade. *J Neurophysiol* 78:19–23.
- Sun FY, Faden AI (1995) Pretreatment with antisense oligodeoxynucleotides directed against the NMDA-R1 receptor enhances survival and behavioral recovery following traumatic brain injury in rat. *Brain Res* 693:163–168.
- Takagi N, Logan R, Teves L, Wallace MC, Gurd JW (2000) Altered interaction between PSD-95 and the NMDA receptor following transient global ischemia. *J Neurochem* 74:169–178.
- Tang FR, Sim MK (1997) Expression of glutamate receptor subunits 2/3 and 4 in the hypoglossal nucleus of the rat after neurectomy. *Exp Brain Res* 117:453–456.
- Tezuka T, Umemori H, Akiyama T, Nakanishi S, Yamamoto T (1999) PSD-95 promotes Fyn-mediated tyrosine phosphorylation of the N-methyl-D-aspartate receptor subunit NR2A. *Proc Natl Acad Sci U S A* 96:435–440.
- Uchida N, Honjo Y, Johnson KR, Wheelock MJ, Takeichi M (1996) The catenin/cadherin adhesion system is localized in synaptic junctions bordering transmitter release zones. *J Cell Biol* 135:767–779.
- Ulenkate HJ, Verhagen MA, Gispen WH, Jonnekens FG (1993) The neurotrophic analogue of ACTH(4–9) reduces the perineuronal microglial reaction after rat facial nerve crush. *Glia* 9:219–226.
- Vassias I, Lecolle S, Vidal PP, de Weele C (2005) Modulation of GABA receptor subunits in rat facial nuclei after axotomy. *Mol Brain Res* 135:260–275.
- Wahlestedt C, Golanov E, Yamamoto S, Yee F, Ericson H, Yoo H, Inturrisi CE, Reis DJ (1993) Antisense oligodeoxynucleotides to NMDA-R1 receptor channel protect cortical neurons from excitotoxicity and reduce focal ischaemic infarctions. *Nature* 363:260–263.

- Wenthold RJ, Yokotani N, Doi K, Wada K (1992) Immunochemical characterization of the non-NMDA glutamate receptor using subunit-specific antibodies. Evidence for a hetero-oligomeric structure in rat brain. *J Biol Chem* 267:501-507.
- Wenzel A, Scheurer L, Kunzi R, Fritschy JM, Mohler H, Benke D (1995) Distribution of NMDA receptor subunit proteins NR2A, 2B, 2C and 2D in rat brain. *Neuroreport* 7:45-48.
- Wong-Riley MT, Huang Z, Liebl W, Nie F, Xu H, Zhang C (1998) Neurochemical organization of the macaque retina: effect of TTX on levels and gene expression of cytochrome oxidase and nitric oxide synthase and on the immunoreactivity of Na⁺ K⁺ ATPase and NMDA receptor subunit 1. *Vision Res* 38:1455-1477.
- Wong-Riley MT, Jacobs P (2002) AMPA glutamate receptor subunit 2 in normal and visually deprived macaque visual cortex. *Vis Neurosci* 19:563-573.
- Yamakura T, Shimoji K (1999) Subunit- and site-specific pharmacology of the NMDA receptor channel. *Rev Prog Neurobiol* 59:279-298.
- Zhang C, Wong-Riley M (1999) Expression and regulation of NMDA receptor subunit R1 and neuronal nitric oxide synthase in cortical neuronal cultures: correlation with cytochrome oxidase. *J Neurocytol* 28:525-539.
- Zukin RS, Bennett MV (1995) Alternatively spliced isoforms of the NMDAR1 receptor subunit. Review. *Trends Neurosci* 18:306-313.

(Accepted 15 June 2005)
(Available online 21 September 2005)

FGH52352

CI-06859669-0

FGH52352

CISTI ICIST

CI-06859669-0

Document Delivery Service
in partnership with the Canadian Agriculture LibraryService de fourniture de Documents
en collaboration avec la Bibliothèque canadienne de l'agriculture**THIS IS NOT AN INVOICE / CECI N'EST PAS UNE FACTURE**LYNN BRAZIL
LIBRARIANHELLER EHRMAN WHITE & MCAULIFFE
275 MIDDLEFIELD RD
MENLO PARK, CA 94025
UNITED STATES

ORDER NUMBER:	CI-06859669-0
Account Number:	FGH52352
Delivery Mode:	F31
Delivery Address:	650/324-6034
Submitted:	2007/05/11 18:24:37
Received:	2007/05/11 18:24:37
Printed:	2007/05/11 22:01:20

Direct	Periodical	OPENURLOPAC	UNITED STATES
--------	------------	-------------	---------------

Client Number: 3978

Title: **HEPATOLOGY : OFFICIAL JOURNAL OF THE AMERICAN ASSOCIATION FOR THE
STUDY OF LIVER DISEASES.**

DB Ref. No.: IRN10274315

ISSN: ISSN02709139

Vol./Issue: 35/5

Date: 2002

Pages: 1063-71

Article Title: **THE P21(CIP1) PROTEIN, A CYCLIN INHIBITOR, REGULATES THE LEVELS AND THE
INTRACELLULAR LOCALIZATION OF CDC25A IN MICE REGENERATING LIVERS.**

Article Author: JAIME, M., ET AL.,

Report Number: IRN10274315

Publisher: WILLIAMS & WILKINS,

**Estimated cost for this 9 page document: \$12.5 document supply fee +
\$32 copyright = \$44.5**

The attached document has been copied under license from Access Copyright/COPIBEC or other rights holders through direct agreements. Further reproduction, electronic storage or electronic transmission, even for internal purposes, is prohibited unless you are independently licensed to do so by the rights holder.

Phone/Téléphone: 1-800-668-1222 (Canada - U.S./E.-U.) (613) 998-8544 (International)

www.nrc.ca/cisti

Fax/Télécopieur: (613) 993-7619

www.cnrc.ca/icist

info.cisti@nrc.ca

info.icist@nrc.ca

National Research
Council CanadaConseil national
de recherches Canada

Page

1 / 1

The p21^{Cip1} Protein, a Cyclin Inhibitor, Regulates the Levels and the Intracellular Localization of CDC25A in Mice Regenerating Livers

Maribel Jaime,^{1,2} Maria Jesús Pujol,¹ Joan Serratos,² Cristina Pantoja,³ Núria Canela,¹ Oriol Casanovas,¹ Manuel Serrano,³ Neus Agell,¹ and Oriol Bachs¹

Liver cells from p21^{Cip1}^{-/-} mice subjected to partial hepatectomy (PH) progress into DNA synthesis faster than those from wild-type mice. These cells also show a premature induction of cyclin E/cyclin-dependent kinase (CDK) 2 activity. We studied the mechanisms whereby cells lacking p21^{Cip1} showed a premature induction of this activity. Whereas the levels of CDK2, cyclin E, and p27^{Kip1} were similar in both wild-type and p21^{Cip1}^{-/-} mice, those of the activator CDC25A were much higher in p21^{Cip1}^{-/-} quiescent and regenerating livers than in wild-type animals. Moreover, p21^{Cip1}^{-/-} cells also showed a premature translocation of CDC25A from cytoplasm into the nucleus. The ectopic expression of p21^{Cip1} into mice embryo fibroblasts from p21^{Cip1}^{-/-} mice decreased the levels of CDC25A and delayed its nuclear translocation. The levels of CDC25A messenger RNA in p21^{Cip1}^{-/-} cells were higher than in wild-type cells, suggesting that this increase might be responsible, at least in part, for the high levels of CDC25A protein in these cells. Thus, the results reported here indicate that p21^{Cip1} regulates the levels and the intracellular localization of CDC25A. We also found a good correlation between CDC25A nuclear translocation and cyclin E/CDK2 activation. In conclusion, premature translocation of CDC25A to the nucleus might be involved in the advanced induction of cyclin E/CDK2 activity and DNA replication in cells from animals lacking p21^{Cip1}. (HEPATOLOGY 2002;35:1063-1071.)

Cell-cycle progression is orchestrated by a family of serine-threonine kinases named cyclin-dependent kinases (CDKs). CDK activity is regulated by the association with cyclins, phosphorylation of posi-

tive and negative regulatory sites, and binding to proteins called CDK inhibitors.¹ Specific cyclin/CDK complexes are activated at different intervals during the cell cycle. Thus, cyclin D/CDK4 is activated at mid-G₁, and cyclin E/CDK2 complexes are necessary for G₁/S transition, cyclin A/CDK2 for progression of DNA synthesis, and cyclin A-B/CDC2 for mitosis.^{2,3} The activation of cyclin D/CDK4 complexes at mid-G₁ is responsible for the phosphorylation of pRB and the other members of the pocket family (p107 and p130).⁴⁻⁶ Pocket proteins form complexes with transcription factors of the E2F family. This interaction with pocket proteins blocks the transcriptional activity of E2Fs but also forms active transcriptional repressor complexes at the promoter of some cell-cycle genes. Phosphorylation of pocket proteins disrupts the transcriptional blockade and permits the expression of genes necessary for cell-cycle progression (cyclin A, proliferating cell nuclear antigen [PCNA], and so on).⁷⁻⁹ The expression of cyclins E and A at mid-late G₁ permits the formation of cyclin E/CDK2 and cyclin A/CDK2 complexes, which need to be activated by the CDK activating kinase and the phosphatase CDC25A. Active cyclin E/CDK2 complexes further phosphorylate the

Abbreviations: CDK, cyclin-dependent kinase; PCNA, proliferating cell nuclear antigen; PH, partial hepatectomy; MEF, mice embryonic fibroblast; FCS, fetal calf serum.

From the ¹Department of Cell Biology and Pathology, Faculty of Medicine, Institut d'Investigacions Biomèdiques August Pi Sunyer (IDIBAPS), University of Barcelona, Barcelona, Spain; ²Department of Pharmacology and Toxicology, Institut d'Investigacions Biomèdiques de Barcelona (IIBB-CSIC), IDIBAPS, Barcelona, Spain; and ³Department of Immunology and Oncology, Centro Nacional de Biotecnología, CSIC, Campus de Cantoblanco, Madrid, Spain.

Received June 27, 2001; accepted February 3, 2002.

Supported by the Comisión Interministerial de Ciencia y Tecnología (Spain) grants SAF-98-0067, SAF-99-0028, SAF2000-0052, and SAF 2001-2240. The Department of Immunology and Oncology at the National Center of Biotechnology is supported by the Pharmacia Corporation and the Spanish Research Council. M.J. is a recipient of a fellowship from the programa de formación de personal investigador of the Spanish government.

Address reprint requests to: Oriol Bachs, Ph.D., Departament de Biologia Cel·lular, Facultat de Medicina, Universitat de Barcelona, Casanova 143, 08036 Barcelona, Spain. E-mail: bachs@medicina.ub.es; fax: (34) 93-402-19-07.

Copyright © 2002 by the American Association for the Study of Liver Diseases.

0270-9139/02/3505-0009\$35.00/0

doi:10.1053/jhep.2002.32678

pocket proteins¹⁰ and are involved in the "firing" of DNA replication, possibly by phosphorylating proteins associated with replication origins.^{10,11} Cyclin A/CDK2 complexes are necessary for S-phase progression, although the putative substrates for these complexes are still unknown.

Two families of CDK inhibitors have been described, namely the Ink4 family and the Cip/Kip family.¹² The Ink4 members include p16^{ink4a}, p15^{ink4b}, p18^{ink4c}, and p19^{ink4d}, which bind specifically to CDK4 and its homologue CDK6. The Cip/Kip proteins, which include p21^{Cip1}, p27^{Kip1}, and p57^{Kip2}, bind to a wide range of cyclin/CDK complexes. Recent reports indicate that whereas p21^{Cip1} behaves as an inhibitor of cyclin E-A/CDK2 complexes, it plays a role as a cyclin D1/CDK4 activator.^{13,14} The protein p21^{Cip1} participates in the assembly of cyclin D1/CDK4 complexes and is necessary for the translocation of these complexes from the cytoplasm into the nucleus. Moreover, p21^{Cip1} binds to PCNA and as a consequence inhibits PCNA-mediated DNA polymerase activity.¹⁵ Recent reports indicate that a growing number of proteins (calmodulin, SET, HPV-16 E7, E2F1, c-Myc, TOK-1, CARB, and so on) bind to p21^{Cip1}, indicating that it might have additional functions in the cells.¹⁶⁻²¹ Studies performed in regenerating livers from p21^{Cip1}^{-/-} mice indicate that the absence of p21^{Cip1} leads to more rapid progression through G₁ phase.²² These results suggest that p21^{Cip1} acts as a brake of CDK2 activity during mid-G₁. However, a recent report indicates that the binding of p21^{Cip1} to cyclin E/CDK2 and cyclin A/CDK2 is similar in active and inactive complexes during rat liver regeneration.²³ Thus, the premature activation of cyclin E/CDK2 complexes in p21^{Cip1}^{-/-} mice might not only be explained by the lack of the association of p21^{Cip1} with these complexes, but other mechanisms likely might be involved. Here we have analyzed the possible mechanisms whereby p21^{Cip1} modulates CDK2 activity *in vivo* using p21^{Cip1}^{-/-} mice subjected to partial hepatectomy (PH). Our results indicate that p21^{Cip1} regulates the levels and the intracellular location of CDC25A in mice liver cells. This new function of p21^{Cip1} might be crucial for the regulation of cyclin E/CDK2 activity *in vivo*.

Materials and Methods

Animals and PHs. Male (2-3 months old) C57Bl/6 wild-type or p21^{Cip1}^{-/-} mice²⁴ were used for all experiments. Animals were treated according to the European Community laws for animal care. PHs were performed according to Higgins and Anderson, in which 66% of liver mass was removed.²⁵

Cell Cultures. Mice embryonic fibroblasts (MEFs) were derived from day-13.5 embryos obtained from the corresponding colonies of wild-type or p21^{Cip1}^{-/-} mice. MEFs were prepared as described.²⁶ MEFs were grown in Dulbecco's modified Eagle medium (Biological Industries, Kibbutz beit Haemek, Israel) supplemented with 10% fetal calf serum (FCS) (Biological Industries). For synchronization, MEFs were cultured in serum-depleted medium (0.1% FCS) for 48 hours. Quiescent cells were trypsinized, replated at low density, and stimulated with medium containing 10% FCS.

Retroviral Transduction. Retroviral gene transfer was performed using high-titer retroviral stocks generated by transient transfection of an ecotropic packaging cell line (Phoenix) as described.²⁷ Briefly, Phoenix cells (5 × 10⁶) were plated in 10-cm-diameter dishes, incubated for 24 hours, and then transfected by calcium-phosphate precipitation with 20 µg of retroviral plasmid (pLPC or pLPC containing the complementary DNA of human p21^{Cip1}) (15 hours at 37°C). After 48 hours, the virus-containing medium was filtered (0.45-µm filter; Millipore, Bedford, MA) and supplemented with 4 µg/mL polybrene (Sigma Chemical Co., St. Louis, MO). Viral supernatants were used to infect early-passage MEFs (less than 4 population doublings). For infections, the culture medium was replaced by the appropriate viral supernatant, and then the culture plates were centrifuged (1 hour at 1,500 rpm) and incubated at 37°C overnight. Infected cell populations were selected for 3 days in selection medium that contained 2.5 µg/mL puromycin (Gibco, Paisley, Scotland).

Determination of DNA Synthetic Activity. DNA synthesis in mice livers was evaluated as described²⁸ by measuring the radioactivity incorporated into DNA following an intraperitoneal injection (0.5 µCi/g of body weight) of methyl-[³H]-thymidine (Amersham, Buckinghamshire, UK) 1 hour before the mice were killed. DNA synthesis in MEFs was determined by measuring the incorporation of methyl-[³H]-thymidine (4 µCi/mL; Amersham) into DNA as described.²⁹

Generation of CDC25A Antibodies. The CDC25A antibodies used in the Western blot experiments were generated by injecting rabbits with a peptide coupled to keyhole limpet hemocyanin following standard protocols. This peptide corresponds to the NH₂-terminal sequence of human CDC25A protein (MELGPEPPHRRRLI). This sequence does not exist in either CDC25B or CDC25C. The antibodies were checked by Western blotting on purified recombinant CDC25A and cell extracts and showed a specific reaction with a single band comigrating with recombinant CDC25A (data not shown).

Gel Electrophoresis and Western Blotting. Livers were homogenized with a Potter-Elvehjem Teflon glass homogenizer in 10 vol of STM buffer (250 mmol/L sucrose, 50 mmol/L Tris-HCl, pH 7.4, and 5 mmol/L MgSO_4) containing 1 mmol/L phenylmethylsulfonyl fluoride and 1 $\mu\text{g}/\text{mL}$ aprotinin at 4°C. Homogenates were subjected to Western blotting as described.³⁰ Briefly, the proteins were separated electrophoretically in sodium dodecyl sulfate/polyacrylamide gels and then transferred onto Immobilon-P membranes (Millipore) at 60 V for 2 hours at 4°C. Membranes were preincubated in phosphate-buffered saline containing 5% skim milk powder for 1 hour at room temperature, and then they were incubated for 1 hour in Tris-buffered saline, 0.5% skim milk powder, and 1% bovine serum albumin containing antibodies against the following: CDK2 (UBI 06-505; Upstate Biotechnology, Lake Placid, NY), cyclin E (UBI 06-459; Upstate Biotechnology), cyclin A (SC-596; Santa Cruz Biotechnology, Santa Cruz, CA), p21^{Cip1} (SC-397G; Santa Cruz Biotechnology), p27^{Kip1} (SC-528G; Santa Cruz), PCNA (1170406; Boehringer, Ottweila, Germany), CDK7 (SC-857; Santa Cruz Biotechnology), or CDC25A. Alkaline phosphatase-labeled (Promega, Madison, WI) or horseradish peroxidase-labeled (Bio-Rad, Hercules, CA) antibodies were used as secondary antibodies. To check the equal loading of the gels, Western blots using anti-actin antibodies (ICN Biochemicals, Costa Mesa, CA) were performed.

Immunoprecipitation, Kinase Assays, and Western Blotting. To determine the activity of cyclin E/CDK2 and cyclin A/CDK2 complexes, liver samples were lysed for 30 minutes on ice in buffer L (50 mmol/L Tris-HCl, pH 7.4, 0.1% Triton X-100, 5 mmol/L ethylenediaminetetraacetic acid, and 250 mmol/L NaCl) containing 50 mmol/L NaF, 0.1 mmol/L Na_3VO_4 , 1 mmol/L phenylmethylsulfonyl fluoride, 10 $\mu\text{g}/\text{mL}$ leupeptin, and 0.5 $\mu\text{g}/\text{mL}$ aprotinin. Samples were then clarified by centrifugation at 10,000g for 10 minutes at 4°C. Supernatants were incubated overnight at 4°C with antibodies against cyclin E (UBI 06-459; Upstate Biotechnology) or cyclin A (SC-596; Santa Cruz Biotechnology), followed by incubation with protein A beads (Pierce, Rockford, IL) for 1 hour at 4°C. After centrifugation, the immunoprecipitates were washed 3 times with buffer L and once with kinase buffer (20 mmol/L HEPES, pH 7.4, 10 mmol/L magnesium acetate, 1 mmol/L dithiothreitol, 50 mmol/L NaF, 0.1 mmol/L Na_3VO_4 , 1 mmol/L phenylmethylsulfonyl fluoride, 10 $\mu\text{g}/\text{mL}$ leupeptin, and 0.5 $\mu\text{g}/\text{mL}$ aprotinin). The samples were then incubated for 30 minutes at 30°C in kinase buffer containing 3 μg histone H1 (Boehringer Mannheim), 20 $\mu\text{mol}/\text{L}$ adenosine triphosphate, and 5 μCi (γ -³²P)-adenosine triphosphate (Amer-

sham) in a total volume of 20 μL . Reactions were stopped by adding Laemmli sample buffer. The proteins were separated electrophoretically in 12% sodium dodecyl sulfate/polyacrylamide gels. The gels were dried, and phosphorylated histone H1 was detected by autoradiography. To determine the amount of CDK2 associated with cyclin E or cyclin A, the immunoprecipitates were subjected to Western blotting using anti-CDK2 antibodies instead of kinase assays.

Immunohistochemistry. Fresh liver tissue from non-operated and regenerating mice were subjected to immunohistochemistry analysis as previously described.²³ Slides were incubated overnight at 4°C with anti-CDC25A antibodies (SC-7157; Santa Cruz Biotechnology). The ABC detection system (ABC kit for rabbit polyclonal antibodies; Vector) was used. The slides were subsequently incubated for 45 minutes, first with the biotinylated second antibodies and then with the labeled ABC. Diaminobenzidine was then applied as a chromogen and incubated for 10 minutes. Finally, the slides were rinsed in phosphate-buffered saline and mounted for examination. The negative control slides were treated in an identical manner except that the primary antibodies were omitted. To determine CDC25A nuclear expression in synchronized MEFs, cells at different times after addition of FCS were fixed in 4% paraformaldehyde in 0.1 mol/L phosphate buffer for 20 minutes at room temperature. After rinsing in phosphate-buffered saline, cells were incubated with anti-CDC25A antibodies as in the case of liver tissue (both anti-CDC25A antibodies, SC-7157 and those generated in our laboratory, gave similar results). To quantify MEFs with nuclear staining, a minimum of 5 random microscopic fields containing 100 cells each were measured at different times after addition of FCS. The fraction of positive nuclei with respect to total nuclei was expressed as a percentage. For each selected time point, the mean and SD were determined ($n = 3$). Each time point was compared with the appropriate control (0 hours) and analyzed using an unpaired Student's *t* test.

To detect PCNA expression in synchronized MEFs, cells were fixed at different times after addition of FCS with 100% methanol at -20°C for 8 minutes and incubated with monoclonal anti-PCNA antibodies (Onco-gene NA03) overnight at 4°C. After rinsing in phosphate-buffered saline, cells were incubated with an anti-mouse fluorescein isothiocyanate-conjugated secondary antibody for 1 hour at room temperature. MEFs with PCNA-positive immunostaining were counted per mm^2 microscopic area in at least 10 random fields in each sample.

Northern Blot Analysis. For Northern blots, 10 μg of total RNA was electrophoresed in denaturing agarose

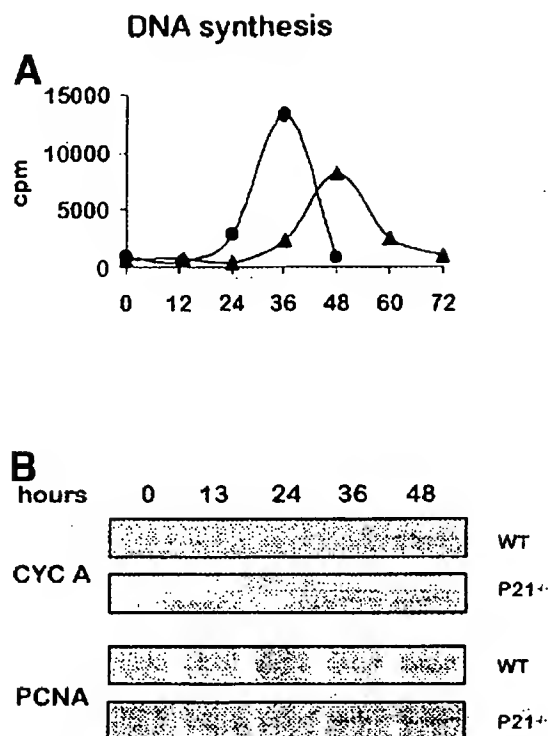


Fig. 1. DNA synthesis, cyclin A, and PCNA expression in regenerating livers from wild-type (WT) and p21^{Cip1-/-} mice. (A) DNA synthesis was measured as described in Materials and Methods section in liver samples from wild-type (▲) or p21^{Cip1-/-} (●) mice obtained at the indicated time points after PH. (B) Levels of cyclin A (CYC A) and PCNA were determined by Western blot analysis in livers obtained at the indicated time points after PH.

gels, transferred to Hybond-N+ membranes, and probed according to standard procedures. The CDC25A probe consisted of a fragment of 1.5 kilobases containing the coding region of murine CDC25A and labeled by random priming. Hybridization was performed at high-stringency conditions. Membranes were reused after complete stripping of the probes. Quantification was performed using a phosphorimager and corrected for the total RNA input using the signal for G-actin as reference.

Results

Cell-Cycle Entry Occurs Earlier in Regenerating Livers From p21^{Cip1-/-} Mice Than in Wild-Type Mice. Wild-type mice subjected to PH started DNA synthesis at 36 hours and showed a maximum at 48 hours after PH. In contrast, DNA synthesis was advanced in p21^{Cip1-/-} mice, starting at 24 hours and showing a peak at 36 hours after PH (Fig. 1A). We also measured the levels of 2 proteins (PCNA and cyclin A) whose expression depends on E2F transcription factors.^{31,32} Figure 1B shows that both PCNA and cyclin A were detected at 36

hours after PH in p21^{Cip1-/-} mice, whereas both proteins appeared at 48 hours after PH in wild-type animals. These results are in agreement with a previous report indicating that DNA synthesis and cyclin A and PCNA expression occurs earlier in regenerating p21^{Cip1-/-} mice than in wild-type animals.²²

Cyclin/CDK Complexes and Activities in Regenerating Livers From Wild-Type and p21^{Cip1-/-} Mice.

Because the onset of DNA replication and the expression of E2F-dependent genes depends on the activity of cyclin/CDK complexes and the subsequent phosphorylation of pocket proteins, we further measured the activity of cyclins E/A/CDK2 in both wild-type and p21^{Cip1-/-} mice. In wild-type livers, cyclin E/CDK2 activity was undetectable in nonoperated animals and until 24 hours after PH. At 36 hours, slight activity was observed; the activity was maximal at 40 hours and then subsequently decreased (Fig. 2). In contrast, in p21^{Cip1-/-} liver cells, cyclin E/CDK2 activity was prematurely induced. It was significantly detected at 24 hours and maximal at 36 to 48 hours after PH (Fig. 2). Likewise, the amount of CDK2 associated with cyclin E was determined at different times after PH. As shown in Fig. 2, in wild-type animals, significant amounts of CDK2 were associated with cyclin E at 24 hours and 36 hours after PH, when the activity was absent or low. At 40 to 48 hours, when the activity was high, the levels of CDK2 associated with cyclin E were similar or lower than at 24 to 36 hours. Thus, the induction of CDK2 activity was not associated with a significant increase in the formation of cyclin E/CDK2 complexes. In p21^{Cip1-/-} mice, some complexes were

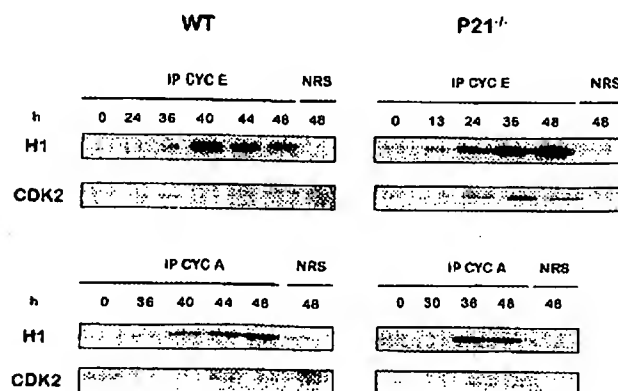


Fig. 2. Cyclin E/CDK2 and cyclin A/CDK2 complexes and activities in regenerating livers from wild-type (WT) and p21^{Cip1-/-} mice. Samples from livers at time points from 0 to 48 hours after PH were subjected to immunoprecipitation with antibodies against cyclin E (CYC E) or cyclin A (CYC A). Immunoprecipitation with a normal rabbit serum (NRS) was used as a control. The immunoprecipitates were subjected to kinase assays as described in Materials and Methods using histone H1 (H1) as substrate. The immunoprecipitates were also subjected to Western blotting to determine the amount of CDK2 present in these complexes.

seen at 0 and 13 hours after PH when the activity was absent or very low. At later times, cyclin E/CDK2 complexes and high activity were detected (Fig. 2). As expected for the advanced expression of cyclin A in $p21^{Cip1-/-}$ mice, cyclin A/CDK2 complexes appeared at 36 hours after PH, in parallel with cyclin A/CDK2 activity (Fig. 2). In wild-type animals, complexes were detected between 40 and 48 hours, also in parallel with cyclin A/CDK2 activity (Fig. 2).

Expression of Cell-Cycle Regulatory Proteins in Regenerating Livers From $p21^{Cip1-/-}$ Mice. To study the mechanism involved in the premature activation of cyclin E/CDK2 complexes in $p21^{Cip1-/-}$ mice, the expression of cyclin E, CDK2, $p27^{Kip1}$, and $p21^{Cip1}$ was measured at different times after PH. No significant differences in the expression of these proteins between the 2 types of mice were found, with the obvious exception of $p21^{Cip1}$ that was not expressed in $p21^{Cip1-/-}$ mice (Fig. 3). The levels of CDK4, CDK6, cyclin D1, and cyclin D3 were also studied, but no differences were observed between the 2 types of animals (data not shown). Thus, we decided to further analyze the expression of the activators CDK7 and

CDC25A (Fig. 3). Interestingly, we found that the levels of CDC25A were much more elevated in $p21^{Cip1-/-}$ mice than in wild-type animals at any time after PH but also in quiescent livers. In contrast, the expression of CDK7 was similar in both cases. These results suggest that $p21^{Cip1}$ regulates the expression of CDC25A and that the high levels of CDC25A could play a role in the faster cell-cycle progression in cells lacking $p21^{Cip1}$.

Intracellular Localization of CDC25A During Liver Regeneration in Wild-Type and $p21^{Cip1-/-}$ Mice. Despite the high constitutive levels of CDC25A in $p21^{Cip1-/-}$ quiescent liver cells, the activity of cyclin E/CDK2 was not induced until 24 hours after PH. This suggests the existence of additional regulatory mechanisms for CDK2 activity. We have considered whether the intracellular localization of CDC25A could play a role in defining the timing of cyclin E/CDK2 activation. Thus, we analyzed the subcellular distribution of CDC25A during liver regeneration in wild-type and $p21^{Cip1-/-}$ liver cells. Immunohistochemical experiments showed that, in wild-type animals, CDC25A was located in the cytoplasm until 24 hours after PH. At 36 hours, it was already nuclear and remained in this compartment until at least 48 hours after PH (Fig. 4). Interestingly, in $p21^{Cip1-/-}$ livers, CDC25A translocated to the nucleus at 24 hours and then remained nuclear until at least 48 hours after PH (Fig. 4). These results indicate that $p21^{Cip1}$ also regulates the nuclear location of CDC25A. On comparison of Figs. 2 and 4, it can be seen that a good correlation exists between cyclin E/CDK2 activation and CDC25A nuclear localization. Thus, these results suggest that CDC25A might be involved in the advanced activation of cyclin E/CDK2 in $p21^{Cip1-/-}$ animals.

Ectopic Expression of $p21^{Cip1}$ in MEFs From $p21^{Cip1-/-}$ Mice Decreased the Levels of CDC25A and Delayed Its Translocation Into the Nucleus. To further show that the absence of $p21^{Cip1}$ is responsible for the increased levels of CDC25A, we analyzed the effect of introducing $p21^{Cip1}$ into $p21^{Cip1-/-}$ cells. To perform this analysis, we used MEFs from $p21^{Cip1-/-}$ mice. Similar to that observed in regenerating liver, serum-stimulated MEFs from $p21^{Cip1-/-}$ mice showed an advanced peak of DNA synthesis and PCNA expression (Fig. 5). As observed in liver cells, the levels of CDC25A in asynchronously growing MEFs were higher in $p21^{Cip1-/-}$ than in wild-type mice (Fig. 6A). The infection of $p21^{Cip1-/-}$ MEFs with retroviral vectors carrying human wild-type/ $p21^{Cip1}$ generated a moderated expression of $p21^{Cip1}$ protein comparable to the endogenous levels of $p21^{Cip1}$ in wild-type MEFs (Fig. 6A). Interestingly, in these cells, CDC25A decreased to levels similar to those of wild-type MEFs (Fig. 6A). The expression of $p21^{Cip1}$ did not induce

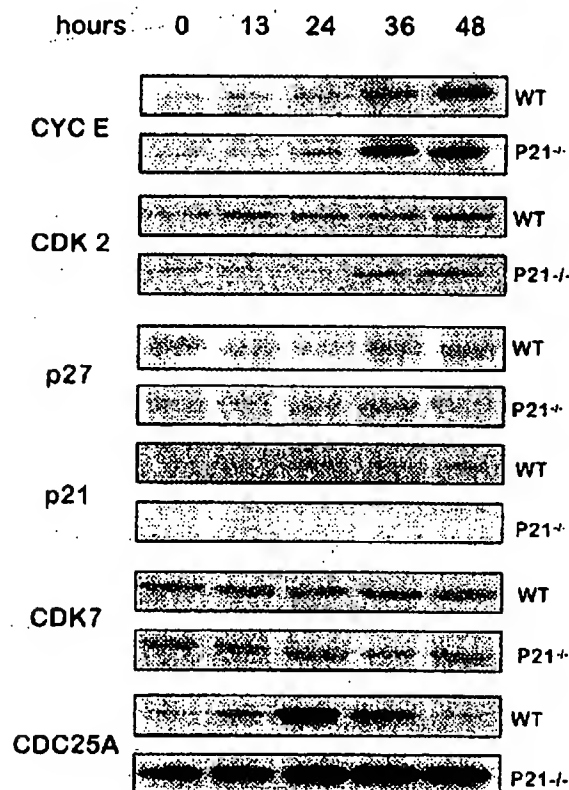


Fig. 3. Levels of cyclin E (CYC E), CDK2, $p27^{Kip1}$, $p21^{Cip1}$, CDK7, and CDC25A in regenerating livers from wild-type (WT) and $p21^{Cip1-/-}$ mice. The levels of cyclin E, CDK2, $p27^{Kip1}$, $p21^{Cip1}$, CDK7, and CDC25A were measured by Western blotting in liver homogenates obtained at different times after PH.

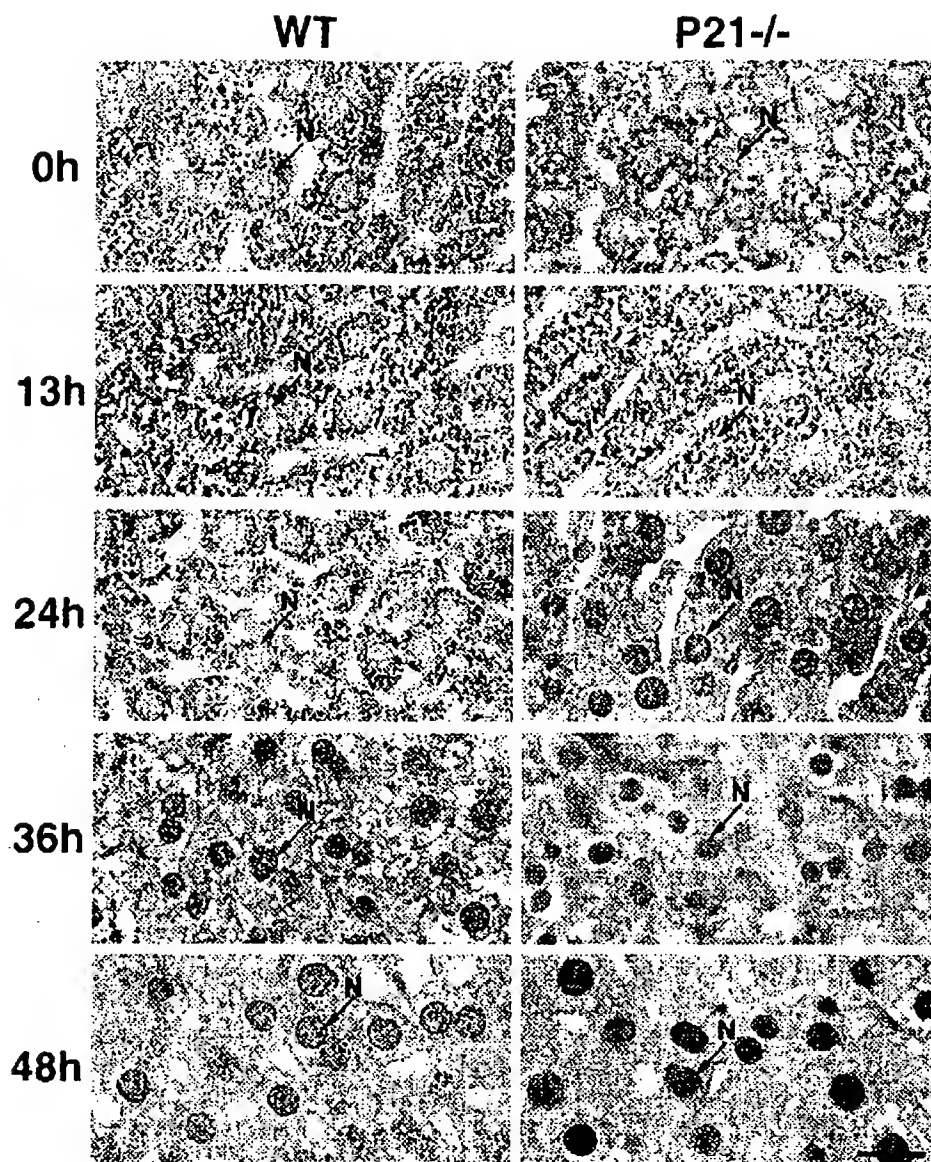


Fig. 4. Immunohistochemical detection of CDC25A in regenerating livers from wild-type (WT) and $p21^{Cip1-/-}$ mice. Liver sections from nonoperated (0) and hepatectomized rats at the indicated time points after PH were immunostained with anti-CDC25A. Arrows indicate the position of nuclei (N). (Bar = 20 μ m.)

cell-cycle arrest (Fig. 6B), indicating that the reduction of CDC25A levels was not due to a block of cell proliferation. In $p21^{Cip1-/-}$ MEFs, the nuclear transport of CDC25A occurred earlier than in wild-type MEFs (Fig. 7A). Interestingly, the ectopic expression of $p21^{Cip1}$ in $p21^{Cip1-/-}$ MEFs delayed CDC25A transport into the nucleus (Fig. 7B), confirming that $p21^{Cip1}$ regulates the nuclear transport of CDC25A.

Levels of CDC25A Messenger RNA in Wild-Type and $p21^{Cip1-/-}$ MEFs. To analyze whether the increased levels of CDC25A protein observed in $p21^{Cip1-/-}$ cells might be mediated by an elevation in the amount of CDC25A messenger RNA, we performed a Northern blot analysis in wild-type and $p21^{Cip1-/-}$ MEFs. Results indicate that CDC25A messenger RNA levels were slightly but significantly higher (33% increase) in

$p21^{Cip1-/-}$ MEFs than in wild-type MEFs. These results indicate that $p21^{Cip1}$ might at least partially regulate the expression of CDC25A at the transcriptional level (Fig. 7C).

Discussion

In the past few years, a number of reports have shown that $p21^{Cip1}$ is a multifunctional protein that might regulate cell-cycle progression at several different levels.¹²⁻²¹ Quiescent cells from young animals have low levels of $p21^{Cip1}$. After mitogenic stimulation, the expression of $p21^{Cip1}$ is induced, showing a peak at mid-late G₁. The levels of this protein then subsequently decrease. This peak of $p21^{Cip1}$ is probably first involved in the translocation of cyclin D1/CDK4 from cytoplasm to the nucleus

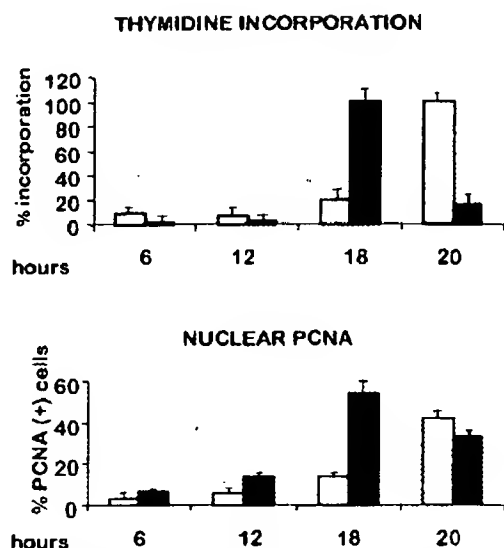


Fig. 5. DNA synthesis and PCNA expression in MEFs from wild-type and p21^{Cip1}^{-/-} mice. MEFs from wild-type (□) and p21^{Cip1}^{-/-} (■) mice were synchronized by 48 hours of serum starvation and then stimulated to proliferate by addition of FCS. Cells were harvested at different times after activation, and DNA synthesis was measured by [³H]-thymidine incorporation as described in Materials and Methods. PCNA expression was determined by immunocytochemical analysis. Results are represented as the percentage of positive cells. In both cases, the values are the mean \pm SD from 3 independent experiments.

because the amount of nuclear cyclin D1/CDK4 complexes is reduced in cells lacking p21^{Cip1}.^{13,14} The mitogen-induced peak of p21^{Cip1} might later be involved in modulating CDK2 activity. This is based on the fact that the induction of CDK2 activity after mitogenic stimulation is advanced in p21^{Cip1}^{-/-} cells and consequently cells move faster to S phase.²² However, the mechanism whereby p21^{Cip1} modulates the timing of CDK2 activity is still controversial.²³ The results reported here indicate that p21^{Cip1} regulates the levels of CDC25A and its intracellular localization. Our observations also showed a very good correlation between CDC25A nuclear localization and cyclin E/CDK2 activation in both wild-type cells and p21^{Cip1}^{-/-} cells. Thus, p21^{Cip1} down-regulates CDC25A and temporally blocks the translocation of CDC25A from cytoplasm to the nucleus at mid-G₁, avoiding the premature activation of cyclin E/CDK2. CDC25A specifically dephosphorylates tyr15 residue of CDK2, which is critical for CDK2 activation at late G₁.³³ Ectopic overexpression of CDC25A in human cell lines leads to premature activation of cyclin E- and cyclin A-dependent kinases and to advanced entry on S phase.^{33,34} These data are in agreement with our results showing high levels of CDC25A and premature induction of cyclin E-A/CDK2 activities and DNA synthesis in p21^{Cip1}^{-/-} liver cells.

p21^{Cip1} and CDC25A compete for the binding to the same cyclin domain in cyclin/CDK complexes; as a con-

sequence, cyclin/CDK complexes containing p21^{Cip1} are more resistant to the action of CDC25A.³⁵ Thus, in cells lacking p21^{Cip1}, the capability of CDC25A to activate cyclin E/CDK2 complexes might be higher than in wild-type cells. However, this fact does not explain why the levels of CDC25A are higher in p21^{Cip1}^{-/-} cells than in wild-type cells and why CDC25A translocates prematurely to the nucleus in p21^{Cip1}^{-/-} cells.

Our results showed a slight but significant increase of CDC25A messenger RNA in p21^{Cip1}^{-/-} cells (33%) that might be responsible, at least in part, for the high levels of CDC25A protein observed in these cells. It has been shown that p21^{Cip1} binds directly to E2F-1/DP-1 and STAT3, inhibiting their transcriptional activities.^{16,36} The ability of p21^{Cip1} to act as a transcriptional modulator is supported by another report describing that p21^{Cip1}, when overexpressed in a human cell line, selectively in-

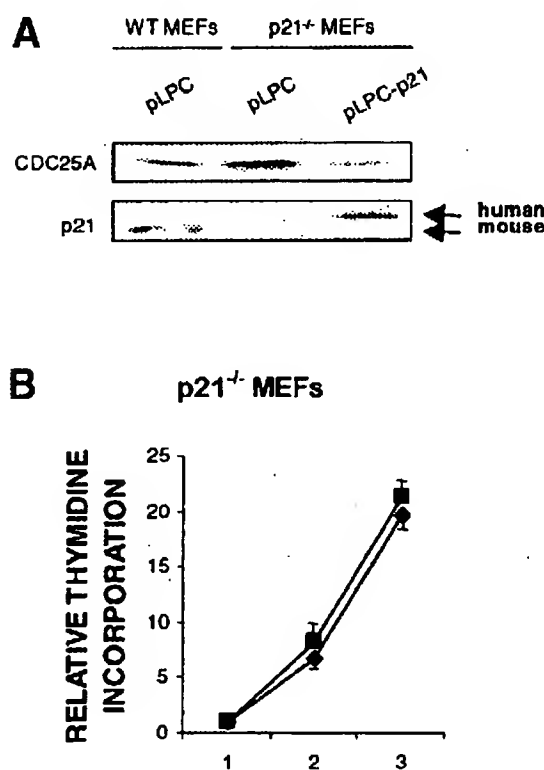


Fig. 6. Effect of ectopic expression of p21^{Cip1} on the levels of CDC25A. (A) Western blot of CDC25A and p21^{Cip1} in asynchronously growing wild-type (WT) or p21^{Cip1}^{-/-} MEFs infected with retroviruses containing an empty vector (pLPC) or a vector carrying the complementary DNA of human p21^{Cip1} (pLPC-p21) as indicated. After 16 hours of infection, cells were selected during 4 days as described in Materials and Methods. Cells were then harvested and the levels of CDC25A and p21^{Cip1} measured by Western blotting. (B) [³H]-Thymidine incorporation was measured in p21^{Cip1}^{-/-} cells infected with an empty vector (■) or a vector carrying the complementary DNA of human p21^{Cip1} (●). Infected cells were collected at 2 or 4 days after selection, and [³H]-thymidine incorporation was measured as described in Materials and Methods. Results are expressed as the mean \pm SD.

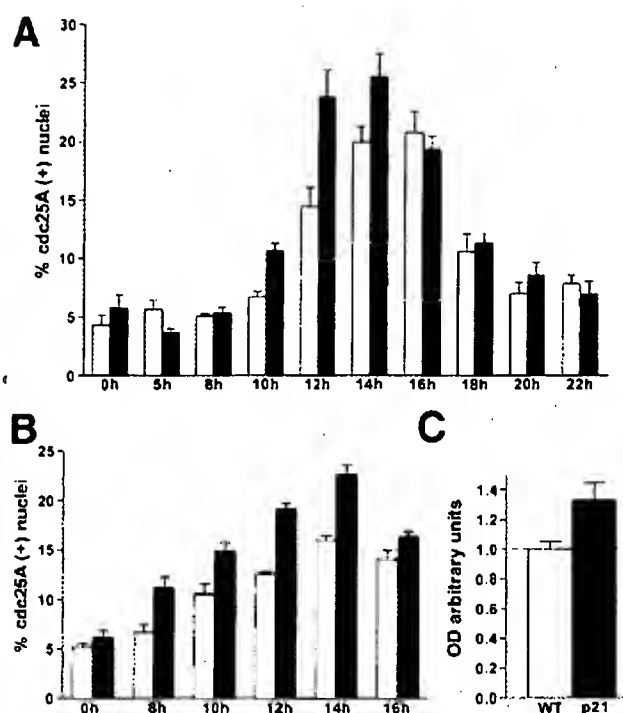


Fig. 7. Effect of ectopic expression of p21^{Cip1} on nuclear translocation of CDC25A. (A) Percentage of CDC25A-positive nuclei in wild-type (□) and p21^{Cip1}^{-/-} MEFs (■) at different times after addition of FCS. CDC25A translocation in p21^{Cip1}^{-/-} MEFs was significantly higher ($P \leq .05$) at 10 hours than at 0 hours. In wild-type MEFs, a significant increase was not observed until 12 hours. (B) Percentage of CDC25A-positive nuclei in p21^{Cip1}^{-/-} MEFs infected with retroviruses containing an empty vector (pLPC) (□) or a vector carrying the complementary DNA of human p21^{Cip1} (pLPC-p21) (■). CDC25A translocation in pLPC cells was significantly higher ($P \leq .05$) at 8 hours than at 0 hours. In pLPC-p21 cells, a significant increase was not observed until 10 hours. In all cases, MEFs were synchronized by serum starvation by 48 hours and then stimulated to proliferate with addition of FCS. Values are the mean \pm SD from 3 independent experiments. (C) Levels of CDC25A messenger RNA in wild-type (□) and in p21^{Cip1}^{-/-} MEFs (■). Results were quantified and expressed as arbitrary units, giving a value of 1 to results of wild-type MEFs. Results are the mean \pm SD from 3 independent experiments.

hibits a set of genes involved in mitosis, DNA replication, segregation, and repair.³⁷ The recent finding that CDC25A is an E2F target gene with expression directly regulated by E2F-1 opens the possibility that, in wild-type cells, p21^{Cip1} might down-regulate the levels of CDC25A through binding to E2F-1.³⁸ This could explain why cells lacking p21^{Cip1} might contain higher levels of CDC25A.

The mechanism by which p21^{Cip1} modulates the translocation of CDC25A from cytoplasm to the nucleus is still far to be established. It has been shown that p21^{Cip1} positively regulates the nuclear translocation of cyclin D1/CDK4 complexes^{13,14} and that this translocation is dependent on calmodulin, which directly associates with the carboxy-terminus of p21^{Cip1}, a region containing several nuclear localization signals.^{18,39} In addition to cal-

modulin, other proteins associate with this region of p21^{Cip1}.¹⁹⁻²¹ In most cases, the function of these interactions still remains to be established. Thus, the participation of these p21^{Cip1}-binding proteins in the regulation of CDC25A nuclear transport may not be excluded.

In summary, the results reported here show for the first time a new function for p21^{Cip1} as a regulator of the levels and the nuclear translocation of the phosphatase CDC25A, an activator of cyclin E-A/CDK2 complexes. This new function of p21^{Cip1} might be involved in defining the timing of the induction of cyclin E/CDK2 activity and the onset of DNA replication in regenerating mice liver cells.

Acknowledgment: The authors thank Sonia Alcázar for technical assistance.

References

- Morgan DO. Cyclin-dependent kinases: engines, clocks, and microprocessors. *Annu Rev Cell Dev Biol* 1997;13:261-291.
- Sherr CJ. G1 phase progression: cycling on cue. *Cell* 1994;79:551-555.
- Pines J. Cyclins and cyclin-dependent kinases: a biochemical view. *Biochem J* 1995;308:697-711.
- Weinberg RA. The retinoblastoma protein and cell cycle control. *Cell* 1995;81:323-330.
- Xiao ZX, Ginsberg D, Ewen M, Livingston DM. Regulation of the retinoblastoma protein-related protein p107 by G1 cyclin-associated kinases. *Proc Natl Acad Sci U S A* 1996;93:4633-4637.
- Mayol X, Garriga J, Grana X. Cell cycle-dependent phosphorylation of the retinoblastoma-related protein p130. *Oncogene* 1995;11:801-808.
- Lam EW, La Thangue NB. DP and E2F proteins: coordinating transcription with cell cycle progression. *Curr Opin Cell Biol* 1994;6:859-866.
- Helin K. Regulation of cell proliferation by the E2F transcription factors. *Curr Opin Genet Dev* 1998;8:28-35.
- Harbour JW, Dean DC. The Rb/E2F pathway: expanding roles and emerging paradigms. *Genes Dev* 2000;14:2393-2409.
- Lundberg AS, Weinberg RA. Functional inactivation of the retinoblastoma protein requires sequential modification by at least two distinct cyclin-cdk complexes. *Mol Cell Biol* 1998;18:753-761.
- Krude T, Jackman M, Pines J, Lasky RA. Cyclin/Cdk-dependent initiation of DNA replication in a human cell-free system. *Cell* 1997;88:109-119.
- Sherr CJ, Roberts JM. Inhibitors of mammalian G1 cyclin-dependent kinases. *Genes Dev* 1995;9:1149-1163.
- LaBaer J, Garrett MD, Stevenson LF, Slingerland JM, Sandhu C, Chou HS, Fattaey A, et al. New functional activities for the p21 family of CDK inhibitors. *Genes Dev* 1997;11:847-862.
- Cheng M, Olivier P, Diehl JA, Fero M, Roussel MF, Roberts JM, Sherr CJ. The p21(Cip1) and p27(Kip1) CDK inhibitors are essential activators of cyclin D-dependent kinases in murine fibroblasts. *EMBO J* 1999;18:1571-1583.
- Waga S, Hannon GJ, Beach D, Stillman B. The p21 inhibitor of cyclin-dependent kinases controls DNA replication by interaction with PCNA. *Nature* 1994;369:574-578.

16. Delavaine L, La Thangue NB. Control of E2F activity by p21^{Waf1/Cip1}. *Oncogene* 1999;18:5381-5392.
17. Estanyol JM, Jaumot M, Casanovas O, Rodriguez-Vilarrupla A, Agell N, Bachs O. The protein SET regulates the inhibitory effect of p21^(Cip1) on cyclin E-cyclin-dependent kinase 2 activity. *J Biol Chem* 1999;274:33161-33165.
18. Taules M, Rodriguez-Vilarrupla A, Rius E, Estanyol JM, Casanovas O, Sacks DB, Perez-Paya E, et al. Calmodulin binds to p21^(Cip1) and is involved in the regulation of its nuclear localization. *J Biol Chem* 1999;274:24445-24448.
19. Dotto GP. p21^(WAF1/Cip1): more than a break to the cell cycle? *Biochim Biophys Acta* 2000;1471:M43-M56.
20. Ono T, Kitaura H, Ugai H, Murata T, Yokoyama KK, Iguchi-Ariga SM, Ariga H. TOK-1, a novel p21^{cip1}-binding protein that cooperatively enhances p21-dependent inhibitory activity toward CDK2 kinase. *J Biol Chem* 2000;275:31145-31154.
21. McShea A, Samuel T, Eppel JT, Galloway DA, Funk JO. Identification of CIP-1-associated regulator of cyclin B (CARB), a novel p21-binding protein acting in the G2 phase of the cell cycle. *J Biol Chem* 2000;275:23181-23186.
22. Albrecht JH, Poon RY, Ahonen CL, Ricland BM, Deng C, Crary GS. Involvement of p21 and p27 in the regulation of CDK activity and cell cycle progression in the regenerating liver. *Oncogene* 1998;16:2141-2150.
23. Pujol MJ, Jaime M, Serratos J, Jaumot M, Agell N, Bachs O. Differential association of p21^{CIP1} and p27^{KIP1} with cyclin E-CDK2 during rat liver regeneration. *J Hepatol* 2000;33:266-274.
24. Brugarolas J, Chandrasekaran C, Gordon JI, Beach D, Jacks T, Hannon GJ. Radiation-induced cell cycle arrest compromised by p21 deficiency. *Nature* 1995;377:552-557.
25. Higgins GM, Anderson RM. Experimental pathology of the liver: restoration of liver of the white rat following partial surgical removal. *Arch Pathol* 1931;12:186-202.
26. Serrano M, Lee H, Chin L, Cordon-Cardo C, Beach D, DePinho RA. Role of the INK4a locus in tumor suppression and cell mortality. *Cell* 1996;85:27-37.
27. Serrano M, Liu AW, McCurrach ME, Beach D, Lowe SW. Oncogenic ras provokes premature cell senescence associated with accumulation of p53 and p16^{INK4a}. *Cell* 1997;88:593-602.
28. Blazsek I, Gaal D. Endogenous thymic factors regulating cell proliferation and analysis of their mechanism of action. *Cell Tissue Kinet* 1978;11:265-277.
29. Cripps-Wolfman J, Henshaw EC, Bambara RA. Alterations in the phosphorylation and activity of DNA polymerase alpha correlate with the change in replicative DNA synthesis as quiescent cells re-enter the cell cycle. *J Biol Chem* 1989;264:19478-19486.
30. Bosser R, Faura M, Serratos J, Renau-Piqueras J, Pruschy M, Bachs O. Phosphorylation of rat liver heterogeneous nuclear ribonucleoproteins A2 and C can be modulated by calmodulin. *Mol Cell Biol* 1995;15:661-670.
31. Lee HH, Chiang WH, Chiang SH, Liu YC, Hwang J, Ng SY. Regulation of cyclin D1, DNA topoisomerase I, and proliferating cell nuclear antigen promoters during the cell cycle. *Gene Exp* 1995;4:95-109.
32. Schulze A, Zerfass K, Spitkovsky D, Middendorp S, Berges J, Helin K, Jansen-Durr P, et al. Cell cycle regulation of the cyclin A gene promoter is mediated by a variant E2F site. *Proc Natl Acad Sci U S A* 1995;92:11264-11268.
33. Blomberg I, Hoffmann I. Ectopic expression of Cdc25A accelerates the G(1)/S transition and leads to premature activation of cyclin E- and cyclin A-dependent kinases. *Mol Cell Biol* 1999;19:6183-6194.
34. Sexl V, Diehl JA, Sherr CJ, Ashmun R, Beach D, Roussel MF. A rate limiting function of cdc25A for S phase entry inversely correlates with tyrosine dephosphorylation of Cdk2. *Oncogene* 1999;18:573-582.
35. Saha P, Eichbaum Q, Silberman ED, Mayer BJ, Dutta A. p21^{CIP1} and Cdc25A: competition between an inhibitor and an activator of cyclin-dependent kinases. *Mol Cell Biol* 1997;17:4338-4345.
36. Coqueret O, Gascan H. Functional interaction of STAT3 transcription factor with the cell cycle inhibitor p21^{WAF1/CIP1}/SDI1. *J Biol Chem* 2000;275:18794-18800.
37. Chang BD, Watanabe K, Broude EV, Fang J, Poole JC, Kalinichenko TV, Roninson IB. Effects of p21^{Waf1/Cip1}/SDI1 on cellular gene expression: implications for carcinogenesis, senescence, and age-related diseases. *Proc Natl Acad Sci U S A* 2000;97:4291-4296.
38. Vigo E, Muller H, Prosperini E, Hateboer G, Cartwright P, Moroni MC, Helin K. CDC25A phosphatase is a target of E2F and is required for efficient E2F-induced S phase. *Mol Cell Biol* 1999;19:6379-6395.
39. Taules M, Rius E, Talaya D, Lopez-Girona A, Bachs O, Agell N. Calmodulin is essential for cyclin-dependent kinase 4 (Cdk4) activity and nuclear accumulation of cyclin D1-Cdk4 during G1. *J Biol Chem* 1998;273:33279-33286.

Free Rad. Res., Vol. 24, No. 6, pp. 451-459
Reprints available directly from the publisher
Photocopying permitted by license only

© 1996 OPA (Overseas Publishers Association)
Amsterdam B.V. Published in the Netherlands by
Harwood Academic Publishers GmbH
Printed in Malaysia

Altered Levels of Scavenging Enzymes in Embryos Subjected to a Diabetic Environment

HENRIK FORSBERG¹, L. A. HÅKAN BORG¹, ENRICO CAGLIERO² and ULF J. ERIKSSON¹

¹Department of Medical Cell Biology, University of Uppsala, Biomedicum, P. O. Box 571, S-751 23 Uppsala, Sweden, ²Schepens Eye Research Institute, Department of Ophthalmology, Harvard Medical School, Boston, MA, USA

Accepted by Professor S. Orrenius

(Received October 7th, 1995; in revised form, November 23rd, 1995)

Maternal diabetes during pregnancy is associated with an increased rate of congenital malformations in the offspring. The exact molecular etiology of the disturbed embryogenesis is unknown, but an involvement of radical oxygen species in the teratological process has been suggested. Oxidative damage presupposes an imbalance between the activity of the free oxygen radicals and the antioxidant defence mechanisms on the cellular level. The aim of the present study was to investigate if maternal diabetes *in vivo*, or high glucose *in vitro* alters the expression of the free oxygen radical scavenging enzymes superoxide dismutase (CuZnSOD and MnSOD), catalase and glutathione peroxidase in rat embryos during late organogenesis. We studied offspring of normal and diabetic rats on gestational days 11 and 12, and also evaluated day-11 embryos after a 48 hour culture period in 10 mM or 50 mM glucose concentration. Both maternal diabetes and high glucose culture caused growth retardation and increased rate of congenital malformations in the embryos. The CuZnSOD and MnSOD enzymes were expressed on gestational day 11 and both CuZnSOD, MnSOD and catalase were expressed on day 12 with increased concentrations of MnSOD transcripts when challenged by a diabetic milieu. There was a good correlation between mRNA, protein, and activity levels, suggesting that the regulation of these enzymes occurs primarily at the pre-translational level. Maternal diabetes *in vivo* and high

glucose concentration *in vitro* induced increased MnSOD expression, concomitant with increased total SOD activity, and a tentative decrease in catalase expression and activity in the embryos. These findings support the notion of enhanced oxidative stress in the embryo as an etiologic agent in diabetic teratogenesis.

Key words: scavenging enzyme, free oxygen radical, rat embryo, diabetes, malformation, gene expression

Abbreviations: MnSOD, superoxide dismutase localized to the mitochondria containing manganese; CuZnSOD, superoxide dismutase localized to the cytoplasm containing copper and zinc; N, and MD, normal, and (manifestly) diabetic rats; N11, N12, offspring of N rats on gestational day 11, and 12; MD11, MD12, offspring of MD rats on gestational day 11, and 12.

INTRODUCTION

Diabetic pregnancy is despite major improvements in medical and obstetrical care, still associated with a 2-3 fold increased incidence of major malformations in the offspring.^{1,2} The exact cellular and molecular mechanisms are largely unknown. A diabetes-like environment *in vitro* or

Corresponding author: Ulf J. Eriksson, Department of Medical Cell Biology, University of Uppsala, Biomedicum, P. O. Box 571, S-751 23 Uppsala, Sweden, Telephone: (46) 18 17 41 29, Fax: (46) 18 55 07 20

maternal diabetes *in vivo* have been shown to produce both growth retardation and congenital malformations in experimental animals.³ The search for teratological agents in various experimental models of diabetic pregnancy, both *in vivo* and *in vitro*, has identified a handful of possible compounds and mechanisms. Thus, metabolites which are elevated in a diabetic milieu, such as glucose, β -hydroxybutyrate, triglycerides, and branched chain amino acids have shown an association with compromised embryonic development *in vivo*.⁴ Furthermore, addition of excess glucose,⁵ β -hydroxybutyrate,⁶ and a metabolite of leucine, α -ketoisocaproate,⁷ to rodent embryo culture *in vitro* have demonstrated that these agents have strong teratogenic activity. Notably, these compounds are all oxidizable substrates and are likely to be metabolized by the embryo.

Recently it has been suggested that the embryonic oxidative metabolism is directly coupled to the teratogenic process via excess of free oxygen radicals in the embryo.^{7,8} Free oxygen radicals are known to generate disturbed *in vitro* development *per se*,⁹ and exogenous supplementation of the free oxygen radical scavenging enzyme superoxide dismutase to embryo culture with high concentration of glucose, β -hydroxybutyrate and α -ketoisocaproate protects against malformations.^{7,8} Therefore, it seems plausible that oxidative stress constitutes a link between the diabetes-like environment *in vitro* and embryonic dysmorphogenesis.

The scavenging enzymes – catalase, glutathione peroxidase and superoxide dismutase – are prominent members of the cellular antioxidant defence which metabolizes the reactive oxygen derivatives such as hydrogen peroxide (catalase and glutathione peroxidase) and the superoxide ion (superoxide dismutase). In addition, there are two intracellular isoenzymes of superoxide dismutase – CuZnSOD and MnSOD. The former enzyme is localized in the cytoplasm and the latter in the mitochondria of the cell.¹⁰

The possibility that a diabetic environment induces congenital malformations in the offspring via increased oxygen radical activity prompted us

to investigate whether maternal diabetes and high glucose *in vitro* may alter the expression and/or activity of CuZnSOD, MnSOD, catalase and glutathione peroxidase in rat embryos during the critical period of organogenesis. In a previous study we found marked changes in gene expression of the two extracellular matrix proteins laminin and fibronectin in embryos subjected to a diabetic or hyperglycemic environment.¹¹ The aim of this study was to identify effects on the cellular antioxidant defence mechanisms exerted by a diabetes-like milieu.

MATERIALS AND METHODS

Animals and Embryo Culture

Female Sprague-Dawley rats from a malformation prone U substrain were made diabetic by a single *i.v.* injection of streptozotocin at a dose of 40 mg/kg body weight. Two to three weeks after the injection diabetic females (>20 mM serum glucose) were caged overnight with non-diabetic male Sprague-Dawley rats. The following morning was denoted gestational day 0 if a positive vaginal smear was found. Rat embryos from normal and diabetic mothers were excised on day 11 and 12, examined under a stereo microscope and stored at -80°C for subsequent RNA and protein studies. Day-9 embryos from normal mothers were explanted and cultured for 48 hours in 10 or 50 mM glucose as outlined in earlier reports.^{7,8} After culture, morphological analysis was performed as previously described.^{7,8}

RNA Studies

Total RNA was extracted with the guanidine isothiocyanate method¹² and poly (A)⁺ RNA isolated by oligo-dT affinity chromatography (Fast Track mRNA Isolation Kit; Invitrogen, San Diego, CA, USA). The RNA samples, either total or poly-A⁺ RNA fraction, were subjected to electrophoresis on 1% agarose gel containing 2.2 M formaldehyde, transferred to a nylon membrane and

EMBRYONIC SUPEROXIDE DISMUTASE IN DIABETES

453

hybridized to ^{32}P -labelled cDNA probes coding for human CuZnSOD,¹³ human MnSOD,¹⁴ rat catalase,¹⁵ mouse glutathione peroxidase,¹⁶ and human γ -actin.¹⁷ Hybridization was performed at 42°C in a solution containing 50% formamide, 5X SSPE, 2.5X Denhart's solution, 0.1% SDS and 100 mg/ml denatured salmon sperm DNA. The membranes were washed in 0.1X SSPE, 0.1% SDS at 55°C and incubated with Kodak X-Omat AR film at -80°C. Densitometric analysis of the autoradiograms was performed after non-saturating exposures with a Quick Scan Jr densitometer (Helena Laboratories, Beaumont, TX, USA). Hybridization to γ -actin, a transcript not altered by maternal diabetes, was used as an internal control to correct for loading inequalities.

Immunoblot Analysis

Embryos were sonicated and about 30 μg protein per well were resolved by 14% SDS-polyacrylamide gel electrophoresis. The polypeptide bands were transferred to a nitrocellulose membrane using electroblotting (Bio-Rad Laboratories, Richmond, CA, USA) and incubated with polyclonal rabbit antibody to rat CuZnSOD and rat MnSOD.¹⁸ Secondary horseradish peroxidase-labelled sheep anti-rabbit antibodies were subsequently applied and the antigen-antibody complex was visualized by chemiluminescence (ECL western blotting analysis system, Amersham

International, Little Chalfont, Buckinghamshire, UK), detected by a Kodak X-Omat AR film. The bands were quantitated densitometrically and data were expressed as arbitrary densitometric units per μg protein loaded in each well. The protein content of the sonicated embryos was determined by the method of Lowry *et al.*¹⁹ using bovine serum albumin as a standard.

Enzymatic Activity Studies

Activity measurements was performed as previously described.⁸ Briefly, superoxide dismutase activity was measured as inhibition of xanthine oxidase-generated luminol chemiluminescence.²⁰ Peroxidative activity of catalase was utilized for spectrophotometric determination by the production of formaldehyde from methanol.²¹ Glutathione peroxidase activity was established by estimating absorbance changes due to the hydroperoxide-specific oxidation of NADPH in an enzymatic cycling assay.²² The DNA content of the embryos was measured fluorometrically as described by Kissane and Robins²³ and Hinegardner.²⁴

Statistical Analysis

Differences between means were evaluated with the aid of Student's two-tailed unpaired *t*-test, or with χ^2 -statistics with Yates' correction, whichever method was applicable.²⁵

TABLE 1 Embryo morphology

	number of observations	crown-rump length (mm)	number of somites	malformation score (0-10)
10 G	20	4.1 \pm 0.3	29.3 \pm 0.5	0.2
50 G	31	2.7 \pm 0.2*	22.3 \pm 0.4*	8.9*
N 11	42	4.5 \pm 0.1	29.1 \pm 0.3	0.2
MD 11	55	2.9 \pm 0.1*	25.1 \pm 0.2*	4.5*
N 12	16	6.6 \pm 0.1	35.2 \pm 0.3	0.2
MD 12	30	4.7 \pm 0.2*	29.7 \pm 0.3*	2.1

Crown rump length, somite number and malformation score in embryos cultured in 10 mM or 50 mM glucose concentration (10 G, 50 G), and in day-11 and day-12 embryos of normal (N) and diabetic rats (MD).

Significance: * = $p < 0.05$ versus either 10 G embryos *in vitro*, or N 11 or N 12 embryos *in vivo*. Student's two-tailed unpaired *t*-test, or χ^2 -statistics (with Yates' correction) (25).

TABLE 2 Enzymatic activity

	superoxide dismutase	catalase	glutathione peroxidase
10 G	12.0 ± 0.9 (12)	3.2 ± 0.4 (8)	12.2 ± 1.8 (9)
50 G	16.5 ± 1.5* (12)	3.6 ± 0.3 (8)	10.9 ± 1.3 (9)
N 11	14.4 ± 1.1 (4)	1.1 ± 0.1 (6)	7.9 ± 2.7 (3)
MD 11	18.5 ± 1.1* (3)	0.8 ± 0.1 (6)	7.2 ± 1.4 (5)
N 12	10.7 ± 0.6 (4)	0.9 ± 0.1 (3)	5.7 ± 0.4 (4)
MD 12	15.3 ± 1.6* (3)	1.0 ± 0.2 (2)	6.0 ± 0.5 (2)

Activities of superoxide dismutase, catalase, and glutathione peroxidase in embryos cultured in 10 mM or 50 mM glucose concentration (10 G, 50 G), and in day-11 and day-12 embryos of normal (N) and diabetic rats (MD). Superoxide dismutase activity is expressed as mU/μg DNA, catalase and glutathione peroxidase are expressed as pKat/μg DNA. Number of observations in parentheses.

Significance: * = $p < 0.05$ versus either 10 G embryos *in vitro*, or N 11 or N 12 embryos *in vivo*. Student's two-tailed unpaired *t*-test (25).

RESULTS

The morphological analysis of the embryos were in agreement with previously published data^{4,7,8,26}. Embryos from diabetic rats were smaller than offspring from normal rats, culture in 10 mM glucose produced embryos with a morphology closely corresponding to that occurring *in vivo*, while culture in 50 mM glucose had a profound growth retarding and teratogenic effect, yielding decreased crown rump length, decreased somite number and increased malformation score (Table 1).

We found a 30–40% increase in the activity of superoxide dismutase in embryos cultured in 50 mM glucose compared with 10 mM glucose culture, as well as in embryos from diabetic rats compared with embryos of normal rats (Table 2). Exposure to a diabetic environment did not appear to affect the activity of glutathione peroxidase, whereas catalase tended to be decreased by about 30% in the MD 11 embryos compared to the N 11 embryos ($0.05 < p < 0.1$, Table 2).

To determine the relative contribution of CuZnSOD and MnSOD to the increase in total SOD activity, and to dissect the mechanisms

TABLE 3 Superoxide dismutase expression

	mRNA		Protein	
	CuZnSOD	MnSOD	CuZnSOD	MnSOD
50 G	94 ± 20 (6)	134 (2)	109 ± 67 (13)	124 ± 64 (13)
MD 11	95 ± 39 (7)	164 (2)	ND	ND
MD 12	112 ± 37 (6)	121 (3)	93 ± 51 (12)	138 ± 82* (20)

Superoxide dismutase mRNA and protein levels in embryos cultured in 50 mM glucose concentration (50 G), and in day-11 and day-12 embryos of diabetic rats (MD 11 and MD 12). Data are expressed as percent of either embryos cultured in 10 mM glucose *in vitro*, or day-11 or day-12 embryos from normal rats *in vivo*. (mean ± SD), "ND" denotes not determined value.

Significance: * = $p < 0.05$ versus either 10 G embryos *in vitro*, or N 11 or N 12 embryos *in vivo*. Student's two-tailed unpaired *t*-test (25).

underlying this effect of the diabetic milieu we measured both mRNA and protein levels of the CuZnSOD and MnSOD. Both CuZnSOD mRNA and protein levels were unchanged in the diabetic compared to the control conditions, both *in vivo* and *in vitro* (Table 3). In order to detect the rare message of MnSOD we had to use polyA selected mRNA from pooled RNA of 10–20 embryos. This diminished the number of determinations, thereby precluding statistical comparison. However, since the results were reproducible in 2–3 Northern blots, each representing 10–20 embryos, the reported mean values should be regarded as highly representative of the expression of this gene (Table 3, Figures 1 and 2). Both MnSOD mRNA and protein levels were thus increased in embryos from diabetic rats and in high glucose culture. The increase in MnSOD mRNA and protein levels were compatible with the increased superoxide dismutase activity in the embryos exposed to a diabetic environment. Thus, the MnSOD protein was significantly increased in day-12 embryos of diabetic rats, although in the high-glucose cultured embryos the numerical difference failed to reach statistical significance ($0.05 < p < 0.1$, Table 3).

In accordance with the activity data, maternal diabetes or high glucose culture had no significant effect on the expression of catalase and glutathione

EMBRYONIC SUPEROXIDE DISMUTASE IN DIABETES

455

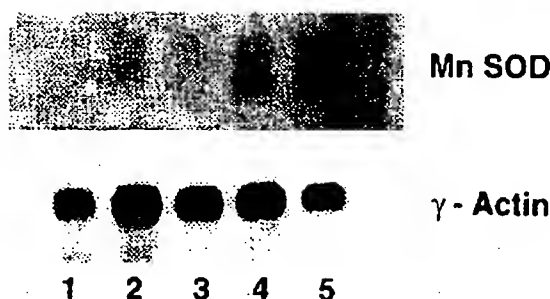


FIGURE 1 Northern blot analysis of poly-A⁺ RNA from day-11 rat embryos cultured *in vitro* for 48 h in 10 and 50 mM glucose. Hybridization was to cDNAs coding for MnSOD and γ -actin. Lane 1: 50 mM glucose - 0.5 mg RNA, Lane 2: 10 mM glucose - 1 mg RNA, Lane 3: 50 mM glucose - 1 mg RNA, Lane 4: 10 mM glucose - 2 mg RNA, Lane 5: 50 mM glucose - 2 mg RNA. The steady state levels of MnSOD transcripts is elevated in high glucose-cultured embryos when normalized with the mRNA levels of γ -actin, the latter indicating the total amount of RNA.

peroxidase in the embryos (Table 4). The catalase activity level of 70% seen in MD 11 embryos corresponded to a catalase mRNA level of 76% in these embryos, however, without statistically significance versus the N 11 embryos (Table 4).

DISCUSSION

In this study we observed that a diabetic environment *in vivo* and *in vitro* increases the total superoxide dismutase activity by increasing the expression of the MnSOD gene. Since generation of reactive oxygen species has been found to enhance the expression of MnSOD,²⁷ this finding supports the notion of enhanced oxidative stress in diabetic pregnancy. We found also, however, a trend towards decreased catalase mRNA concentration and decreased catalase activity in MD 11 embryos. This tentative change may surpass the increase in SOD activity, and makes it difficult to predict the net effect of a diabetic environment on the total activity of radical scavenging enzymes in the embryo. Since the antioxidative status in the cell is dependent on the equilibrium of different anti-oxidant compounds, a rise in SOD activity in com-

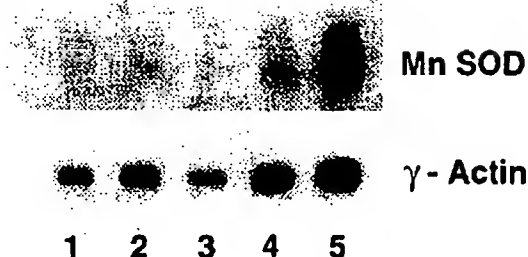


FIGURE 2 Northern blot analysis of poly-A⁺ RNA from day-12 rat embryos from normal (N) and diabetic (D) rats. Hybridization was to cDNAs coding for MnSOD and γ -actin. Lane 1: N - 1.25 mg RNA, Lane 2: D - 1.25 mg RNA, Lane 3: D - 1.25 mg RNA, Lane 4: N - 2.5 mg RNA, Lane 5: D - 2.5 mg RNA. Increased MnSOD mRNA concentrations are evident in embryos from diabetic rats.

bination with impaired catalase activity may cause an increased steady state concentration of hydrogen peroxide in the embryo, leading to increased production of hydroxyl radicals via the Fenton reaction. In high-glucose cultured embryos there was no decrease in catalase activity despite a tentative diminution of catalase mRNA. The superoxide dismutase activity was, however, increased in analogy to the MD 11 embryos.

In previous studies, exogenous supplementation of the free oxygen radical scavenging enzymes superoxide dismutase, catalase and glutathione peroxidase protected against malformations in 50 mM glucose culture.⁸ Superoxide dismutase also repressed the teratogenic effects of

TABLE 4 Catalase and glutathione peroxidase mRNA

	catalase	glutathione peroxidase
50 G	84 \pm 39 (6)	ND
MD 11	76 \pm 44 (7)	ND
MD 12	119 \pm 42 (6)	134 \pm 63 (15)

mRNA levels of catalase and glutathione peroxidase in embryos cultured in 50 mM glucose concentration (50 G), and in day-11 and day-12 embryos of diabetic rats (MD). Data is either expressed as percent of embryos cultured in 10 mM glucose *in vitro*, or day-11 or day-12 embryos from normal rats *in vivo* (mean \pm SD). "ND" denotes not determined value. Number of observations in parentheses.

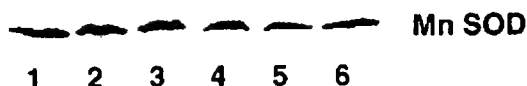


FIGURE 3 Western blot of protein from day-12 rat embryos from normal (N) and diabetic (D) rats. The antibody used was a polyclonal rabbit-anti mouse MnSOD and 30 mg protein from each homogenized embryo was applied to the wells. Lane 1-3: D embryos, lane 4-6: N embryos. Note the slight upregulation of MnSOD protein in the D embryos.

excessive concentrations *in vitro* of the intermediate metabolites, pyruvate, β -hydroxybutyrate, and α -ketoisocaproate, all of which are elevated in diabetes.⁷ It was thus hypothesized that embryonic excess of oxidizable metabolites followed by intramitochondrial overload might result in increased free oxygen radical leakage from the electron transport chain.³

In a recent series of morphological studies, high amplitude swelling, reduced number of cristae and ruptured membranes of mitochondria in neural epithelial cells in embryos from diabetic rats or exposed to high glucose during culture *in vitro* have been demonstrated.²⁸

A transgenic mouse strain containing an increased gene dosage and activity of CuZnSOD²⁹ has recently been shown to be more resistant to the teratogenic effects of high glucose concentrations *in vitro*,³⁰ as well as to the negative influence of a diabetic intrauterine milieu *in vivo*.³¹ These findings suggest that the embryonic antioxidant capacity is of prime importance for modulation of the teratogenic effect of a diabetic environment.

In view of these studies suggesting an involvement of embryonic free oxygen radicals in the teratogenic process, we decided to investigate if the embryonic enzymatic antioxidant defence would be affected by maternal diabetes at the mRNA and/or protein levels.

The CuZnSOD in the cytoplasm and the mitochondrial MnSOD³² catalyze the same reaction converting the superoxide ion ($O_2^{\cdot -}$) to hydrogen peroxide (H_2O_2). Glutathione peroxidase and catalase metabolize the breakdown of hydrogen

peroxide to water. MnSOD is the main inducible scavenging enzyme, since MnSOD expression in adult tissues has been shown to be augmented by oxidative stress by hydrogen peroxide and superoxide ion,³³ X-ray irradiation,²⁷ cytokines,^{34,35} and phorbol esters.³⁶

In experimental animals the CuZnSOD mRNA levels correlated well with the enzymatic activity, indicating that regulation of the enzyme was exerted mainly at the transcriptional level.³⁷ CuZnSOD mRNA and glutathione peroxidase mRNA levels were not linked to oxygen consumption or oxygen tension in fetal or neonatal rats.³⁸ In neonatal lungs, though, the activities of total SOD, catalase and glutathione peroxidase were increased after exposure to normobaric hyperoxia.³⁹

The diabetic state has been shown to affect the antioxidant status in several tissues. Diabetic children exhibited lower serum antioxidant activity, expressed as lowered capacity to trap peroxy radicals.⁴⁰ In streptozotocin-diabetic rats, the urinary excretion of thiobarbituric acid positive material was increased, indicating a high level of oxidative stress in these animals.⁴¹ Activities of catalase, glutathione reductase and CuZnSOD were elevated in the pancreas of streptozotocin-induced diabetic rats while hepatic enzymatic activities were downregulated in the same animals. Interestingly, 4 weeks of insulin treatment reversed all the alterations in enzymatic activities.⁴² Dobashi and coworkers reported that in hypertrophied kidneys from diabetic rats the total CuZnSOD content was normal, but CuZnSOD was increased in degenerating tubules. MnSOD levels were elevated in thick ascending limbs of Henle's loops, indicating that the cells might adapt to oxidative stress.⁴³ Another possible mechanism of diabetes to increase the effect of the oxidative stress was suggested by Arai and collaborators who reported that glycosylated erythrocyte CuZnSOD has lower activity than non-glycosylated enzyme.⁴⁴ Of interest are also the findings that connective tissue stiffening in diabetic patients was shown to be related to serum lipid peroxide concentration,⁴⁵

and that antioxidant treatment of diabetic animals can diminish the neurological complications of the disease.^{46,47} If the embryonic dysmorphogenesis is an analogous process to the induction of complications, it follows that antioxidant treatment should block also the teratogenic effect of diabetic pregnancy, and, indeed, there are results indicating the validity of such an approach.⁴⁸

Little is known about the antioxidant capacity of the developing embryo. El-Hage and co-workers first detected scavenging enzyme mRNA in gestational day-8 mouse embryos. The *in utero* mRNA concentrations were higher than in adult tissue while the specific enzymatic activities increased with age.⁴⁹ It was speculated that the mRNAs accumulated *in utero* and were not translated until after birth when the fetus adapts to aerobic respiration, at which time the activities of the antioxidant enzymes increase considerably.^{49,50} CuZnSOD and MnSOD protein have previously been found in day-12 rats embryos, but only in cardiomyocytes and later in hepatocytes.¹⁸ Recent attempts to determine antioxidant capacity in the offspring have indicated decreased embryonic α -tocopherol/MDA ratio in day-11 embryos of manifestly diabetic rats, the effect of a combined decrease in vitamin E levels, and an increase of MDA concentration in these embryos.⁵¹

Our data in the present investigation show that the CuZnSOD and MnSOD enzymes are expressed on gestational day 11 and both CuZnSOD, MnSOD and catalase are expressed on day 12 with increased concentrations of MnSOD transcripts when challenged by a diabetic milieu. Moreover, there was a good correlation between mRNA, protein, and activity levels, suggesting that the regulation of these enzymes occurs primarily at the pretranslational level.

The embryos are apparently not able to protect themselves against the reactive oxygen species at the levels present in our systems, perhaps due to the fact that embryos normally are exposed to a anaerobic milieu, in line with the findings of El-Hage and coworkers.⁴⁹ The imbalance in activity

levels of superoxide dismutase and catalase in the embryo observed in the present study could be interpreted as an indirect evidence of embryonic oxidant stress exerted by abnormal maternal metabolism leading to anomalous embryonic development.

In conclusion, this study has shown a diabetes-induced increase in MnSOD expression, concomitant with increased total SOD activity, and a tentative decrease in catalase expression and activity. These findings support the notion of enhanced oxidative stress in the embryo as an etiologic agent in diabetic teratogenesis.

Acknowledgements

The authors wish to express their gratitude to Ms. Parri Wentzel for excellent technical assistance. The study was supported by The Swedish Diabetes Association, The Bank of Sweden Tercentenary Foundation, The Juvenile Diabetes Foundation International, The Novo Nordisk Foundation, The Family Ernfrors Fund, and The Swedish Medical Research Council (Grant No. 12X-7475).

References

1. J.L. Mills (1982) Malformations in infants of diabetic mothers. *Teratology*, 25, 385-394.
2. U. Hanson, B. Persson and S. Thunell (1990) Relationship between hemoglobin A_{1c} in early type 1 (insulin-dependent) diabetic pregnancy and the occurrence of spontaneous abortion and fetal malformation in Sweden. *Diabetologia*, 33, 100-104.
3. U.J. Eriksson, L.A.H. Borg, H. Forsberg and J. Styrud (1991) Diabetic embryopathy. Studies with animal and *in vitro* models. *Diabetes*, 40, (Suppl 2), 94-98.
4. J. Styrud, L. Thunberg, O. Nybacka and U.J. Eriksson (1995) Correlations between maternal metabolism and deranged development in the offspring of normal and diabetic rats. *Pediatric Research*, 37, 343-353.
5. D.L. Cockcroft and P.T. Coppola (1977) Teratogenic effects of excess glucose on head-fold rat embryos in culture. *Teratology*, 16, 141-146, 1977.
6. W.E. Horton Jr. and T.W. Sadler (1983) Effects of maternal diabetes on early embryogenesis. Alterations in morphogenesis produced by the ketone body, B-hydroxybutyrate. *Diabetes*, 32, 610-616.
7. U.J. Eriksson and L.A.H. Borg (1993) Diabetes and embryonic malformations. Role of substrate-induced free-oxygen radical production for dysmorphogenesis in cultured rat embryos. *Diabetes*, 42, 411-419.
8. U.J. Eriksson and L.A.H. Borg (1991) Protection by free oxygen radical scavenging enzymes against glucose-induced embryonic malformations *in vitro*. *Diabetologia*, 34, 325-331.
9. P.C. Jenkinson, D. Anderson and S.D. Gangolli (1986) Malformations induced in cultured rat embryos by

- enzymatically generated active oxygen species. *Teratogenesis, Carcinogenesis and Mutagenesis*, 6, 547-554.
10. Y. Sun (1990) Free radicals, antioxidant enzymes and carcinogenesis. *Free Radical Biology and Medicine*, 8, 583-599.
 11. E. Cagliero, H. Forsberg, R. Sala, M. Lorenzi and U.J. Eriksson (1993) Maternal diabetes induces increased expression of extracellular matrix components in rat embryos. *Diabetes*, 42, 975-980.
 12. J.M. Chirgwin, A.E. Przybyla, R.J. MacDonald and W.J. Rutter (1979) Isolation of biologically active ribonucleic acid from sources enriched in ribonuclease. *Biochemistry*, 18, 5294-5299.
 13. J. Lleman-Hurwitz, N. Dafni, V. Lavie and Y. Groner (1982) Human cytoplasmic superoxide dismutase cDNA clone: A probe for studying the molecular biology of Down's syndrome. *Proceedings of the National Academy of Sciences*, 79, 2808-2811.
 14. K. Xiang, N.J. Cox, R.A. Halliwell and G.I. Bell (1987) Multiple Taq I RFLPs at the human manganese superoxide dismutase (SOD 2) locus on chromosome 6. *Nucleic Acids Research*, 15, 7654.
 15. H. Nakashima, M. Yamamoto, K. Goto, T. Osumi, T. Hashimoto and H. Endo (1989) Isolation and characterization of the rat catalase-encoding gene. *Gene*, 79, 279-288.
 16. G.T. Mullenbach, A. Tabrizi, B.D. Irvine, G.I. Bell, J.A. Tainer and R.A. Halliwell (1988) Selenocysteine's mechanism of incorporation and evolution revealed in cDNAs of three glutathione peroxidases. *Protein*, 2, 239-246.
 17. P. Gunning, P. Ponte, H. Okayama, J. Engel, H. Blau and L. Kedes (1983) Isolation and characterization of full-length cDNA clones for human α -, β - and γ -Actin mRNAs: Skeletal but not cytoplasmic actins have an amino-terminal cysteine that is subsequently removed. *Molecular and Cellular Biology*, 3, 787-795.
 18. A. Murim, K. Asayama, K. Dobashi, K. Suzuki, A. Kawaoi and K. Kato (1992) Immunohistochemical localization of superoxide dismutases in fetal and neonatal rat tissues. *Journal of Histochemistry and Cytochemistry*, 40, 1705-1713.
 19. O.H. Lowry, N.J. Rosebrough, A.L. Farr, R.J. Randall (1951) Protein measurement with the folin phenol reagent. *Journal of Biological Chemistry*, 193, 265-275.
 20. K. Puget and A.M. Michelson (1974) Iron containing superoxide dismutases from luminous bacteria. *Biochimie*, 56, 1255-1267.
 21. L.H. Johansson and L.A.H. Borg (1988) A spectrophotometric method for determination of catalase activity in small tissue samples. *Analytical Biochemistry*, 174, 331-336.
 22. D.E. Paglia and W.N. Valentine (1967) Studies on the quantitative and qualitative characterisation of erythrocyte glutathione peroxidase. *Journal of Laboratory and Clinical Medicine*, 70, 158-169.
 23. J.M. Kissane and B. Robins (1958) The fluorometric measurement of deoxyribonucleic acid in animal tissues with special reference to the central nervous system. *Journal of Biological Chemistry*, 233, 184-188.
 24. R.T. Hinegardner (1971) An improved fluorometric assay for DNA. *Analytical Biochemistry*, 39, 197-201.
 25. B. Ostle (1963) *Statistics in research*, (2nd Ed) Ames, IA, Iowa State University Press.
 26. U.J. Eriksson, E. Dahlström, K.S. Larsson and C. Hellerström (1982) Increased incidence of congenital malformations in the offspring of diabetic rats and their prevention by maternal insulin therapy. *Diabetes*, 31, 1-6.
 27. L.W. Oberley, D.K. St. Clair, A.P. Autor and T.D. Oberley (1987) Increase in manganese superoxide dismutase activity in the mouse heart after X-irradiation. *Archives of Biochemistry and Biophysics*, 254, 69-80.
 28. X. Yang, L.A.H. Borg and U.J. Eriksson (1995) Altered mitochondrial morphology of rat embryos in diabetic pregnancy. *Anatomical Record*, 241, 255-267.
 29. C.J. Epstein, K.V. Avraham, M. Lovett, S. Smith, O. Elroy-Stein, G. Rotman, C. Bry and Y. Groner (1987) Transgenic mice with increased Cu/Zn-superoxide activity: Animal model of dosage effects in Down's syndrome. *Proceedings of the National Academy of Sciences*, 84, 8044-8048.
 30. U.J. Eriksson, L.A.H. Borg, A. Sjöberg, P. Wentzel, Z. Hagay and Y. Groner (1993) Embryos transgenic for superoxide dismutase (SOD) show resistance to a teratogenic diabetic environment in vitro. *Diabetologia*, 36, (Suppl 1): A41.
 31. Z.J. Hagay, Y. Weiss, I. Zusman, M. Peled-Kamar, U.J. Eriksson and Y. Groner (1995) Prevention of hyperglycemia-associated embryopathy by embryonic overexpression of the free radical scavenger copper zinc superoxide dismutase gene. *American Journal of Obstetrics and Gynecology*, 173, 1036-1041.
 32. R.A. Weisiger and I. Fridovich (1973) Superoxide dismutase. Organelle specificity. *Journal of Biological Chemistry*, 248, 3582-3592.
 33. S. Shull, N.H. Heintz, M. Periasamy, M. Manohar, Y.M.W. Janssen, J.P. Marsh and B.T. Mossman (1991) Differential regulation of antioxidant enzymes in response to oxidants. *Journal of Biological Chemistry*, 266, 24398-24403.
 34. C.A. Harris (1991) Manganese superoxide dismutase is induced by IFN- γ in multiple cell types. Synergistic induction by IFN- γ and tumor necrosis factor or IL-1. *Journal of Immunology*, 147, 149-154.
 35. G.A. Visner, S.E. Chesrown, J. Monnier, U.S. Ryan and H.S. Nick (1992) Regulation of manganese superoxide dismutase: IL-1 and TNF induction in pulmonary artery and microvascular endothelial cells. *Biochemical and Biophysical Research Communications*, 188, 453-462.
 36. J. Fujii and N. Taniguchi (1991) Phorbol ester induces manganese-superoxide dismutase in tumor necrosis factor-resistant cells. *Journal of Biological Chemistry*, 266, 23142-23146.
 37. J.-M. Delabar, A. Nicole, L. d'Auriol, Y. Jacob, M. Meunier-Rotival, F. Galibert, P.-M. Sinet, and H. Jérôme (1987) Cloning and sequencing of a rat CuZn superoxide dismutase cDNA. *European Journal of Biochemistry*, 166, 181-187.
 38. J.B. de Haan, M.J. Tymms, F. Cristiano and I. Kola, (1994) Expression of Copper/Zinc superoxide dismutase and glutathione peroxidase in organs of developing mouse embryos, fetuses and neonates. *Pediatric Research*, 35, 188-196.
 39. J.B. Hoffman, M. Stevens and A.P. Autor (1980) Adaptation to hyperoxia in the neonatal rat: Kinetic parameters of the oxygen-mediated induction of lung superoxide dismutases, catalase and glutathione peroxidase. *Toxicology*, 16, 215-225.
 40. K. Asayama, N. Uchida, T. Nakane, H. Hayashibe, K. Dobashi, S. Amemiya, K. Kato and S. Nakazawa (1993) Anti-oxidants in serum of children with insulin-dependent diabetes mellitus. *Free Radical Biology and Medicine*, 15, 597-602.
 41. D.D. Gallaher, A.S. Csalany, D.W. Shoeman and J.M. Olson (1993) Diabetes increases excretion of urinary malondialdehyde conjugates in rats. *Lipids*, 28, 663-666.

EMBRYONIC SUPEROXIDE DISMUTASE IN DIABETES

459

42. S.A. Wohaieb and D.V. Godin (1987) Alterations in free radical tissue-defence mechanisms in streptozotocin-induced diabetes in rat. Effects of insulin treatment. *Diabetes*, 36, 1014-1018.
43. K. Dobashi, K. Asayama, H. Hayashibe, N. Uchida, M. Kobayashi, A. Kawaoi and K. Kato (1991) Effects of diabetes mellitus induced by streptozotocin on renal superoxide dismutases in the rat. *Virchows Archiv B Cell Pathology*, 60, 67-72.
44. K. Arai, S. Iizuka, Y. Tada, K. Oikawa and N. Taniguchi (1987) Increase in the glycosylated form of erythrocyte CuZn-superoxide dismutase in diabetes and close association of the nonenzymatic glycosylation with the enzyme. *Biochimica et Biophysica Acta*, 924, 292-296.
45. Y. Aoki, K. Yazaki, K. Shirotori, Y. Yanagisawa, H. Oguchi, K. Kiyosawa and S. Furuta (1993) Stiffening of connective tissue in elderly diabetic patients: Relevance to diabetic nephropathy and oxidative stress. *Diabetologia*, 36, 79-83.
46. B. Bravenboer, A.C. Kappelle, F.P.T. Hamers, T. van Buren, D.W. Erkelens and W.H. Gispen (1992) Potential use of glutathione for the prevention and treatment of diabetic neuropathy in the streptozotocin-induced diabetic rat. *Diabetologia*, 35, 813-817.
47. N.E. Cotter, N.A. Cameron, V. Archibald, K.C. Dines and E.K. Maxfield (1994) Anti-oxidant and pro-oxidant effects on nerve conduction velocity, endoneurial blood flow and oxygen tension in non-diabetic and streptozotocin-diabetic rats. *Diabetologia*, 37, 449-459.
48. U.J. Eriksson (1994) Antioxidants protect rat embryos from diabetes-induced dysmorphogenesis. *15th International Diabetes Federation Congress Abstracts*, 410.
49. S. El-Hage and S.M. Singh (1990) Temporal expression of genes encoding free radical-metabolizing enzymes is associated with higher mRNA levels during in utero development in mice. *Developmental Genetics*, 11, 149-159.
50. E. Gerdin, O. Tydén and U.J. Eriksson (1985) The development of antioxidant enzyme defence in the perinatal rat lung: Activities of superoxide dismutase, glutathione peroxidase and catalase. *Pediatric Research*, 19, 687-691.
51. C.M. Simán, L.A.H. Borg and U.J. Eriksson (1994) Disturbed development, low vitamin E concentration, and increased lipid peroxidation in embryos of diabetic rats. *Diabetologia*, 37, (Suppl 1): A171.

0012-7227/99/1334-1548\$08.00/0
 Endocrinology
 Copyright © 1999 by The Endocrine Society

Vol. 133, No. 4
 Printed in U.S.A.

Induction of the Estrogen Receptor by Growth Hormone and Glucocorticoid Substitution in Primary Cultures of Rat Hepatocytes*

BO FREYSCHUSS, ANNELI STAVREUS-EVERS, LENA SAHLIN, AND HÅKAN ERIKSSON

Department of Reproductive Endocrinology, Karolinska Hospital, 104 01 Stockholm, Sweden

ABSTRACT

Hepatic estrogen receptors (ER) mediate estrogenic effects on mammalian liver metabolism and are thereby involved in the regulation of important physiological/pathological processes, such as coagulation, atherosclerosis, and hypertension. The regulation of the formation of the ER in primary cultures of rat hepatocytes was studied by assaying ER and ER mRNA under different endocrine conditions. The ER concentration was measured using two different methods, a ligand-binding technique and an ER enzyme immunoassay. The results obtained by the two methods showed good correlation, and linear regression analysis gave a correlation coefficient of 0.95. ER concentrations fell to low steady state levels within 16 h after establishing the cell

culture and remained low in the absence of hormonal substitution. Upon medium supplementation with pituitary GH and the glucocorticoid dexamethasone (DEX) in combination, the ER concentration increased 6-fold from 4.2 ± 1.0 to 25.8 ± 7.0 fmol/mg cytosolic protein. ER mRNA was measured by solution hybridization. Substitution with GH and DEX in combination increased ER mRNA to $210 \pm 14\%$ of control levels. No effect on ER mRNA stability was seen after hormone treatment. It is concluded that the regulatory effects of GH and DEX on the hepatic ER in this *in vitro* system are very similar to the effects of these hormones under *in vivo* conditions. The inducible expression of the ER has never before, to our knowledge, been demonstrated in any mammalian liver cell culture system. (*Endocrinology* 133: 1548-1554, 1993)

ESTROGEN receptors (ER) have been detected in a number of tissues from different animal species. The biological effects promoted by the ER-ligand complex vary in different target organs. In reproductive tissues, estrogens primarily stimulate growth, whereas in the mammalian liver, the synthesis of specific proteins, such as angiotensinogen (1, 2) apoproteins (3), low density lipoprotein receptors (4, 5), and coagulation factors (6, 7), is stimulated.

The receptor concentration is critical for the biological response of a hormone. For example, when rat liver ER are reduced to 10% of control levels by hypophysectomy (Hx), no response to estrogen treatment is seen (8-10). Endocrine regulation of the hepatic ER has been extensively studied *in vivo*. Due to the complexity of the *in vivo* situation, further studies require the establishment of a well functioning *in vitro* system. The inducible expression of the rat ER has never been demonstrated in any mammalian liver cell culture system.

It has been virtually impossible to maintain detectable ER levels in primary hepatocyte cultures grown on collagen, fibronectin, or other standard coating materials, regardless of the type of hormonal substitution (11). After 18 h of culture on standard coating materials, the ER level is 10% of the initial level, and after 42 h, no estrogen receptors are detectable (12). Recent insights concerning the importance of cellular adherence to extracellular matrix have led to the

development of new techniques to maintain cellular differentiation *in vitro*. Hepatocytes cultured on extracellular matrix prepared from the Engelberth-Holm-Swarm mouse sarcoma (13) maintain an adult liver cell phenotype and respond to hormone treatment, including GH (14-17). GH in combination with glucocorticoids has been shown to be the most potent inducer of hepatic ER *in vivo* (18). Therefore, we investigated the potential of this primary cell culture system for studies on the induction of hepatic ER.

Materials and Methods

Animals

Intact adult female Sprague-Dawley rats (220 ± 20 g) were purchased from Eklunds (Stockholm, Sweden). The animals were housed in a controlled environment at 20°C on a regular illumination schedule of 12 h of light and 12 h of darkness each day. Standard pellet food and water were provided *ad libitum*.

Cell culture medium and hormonal substitution

Cells were cultured in phenol red containing Williams' medium B from Gibco (Grand Island, NY). The medium was supplemented with penicillin (100 IU/ml), streptomycin (100 µg/ml), and L-glutamine (2 mM) from Gibco; and sodium selenite (0.1 µM), ascorbic acid (0.3 mM), and insulin (26 IU/liter) from Sigma (St. Louis, MO). Where indicated, dexamethasone (DEX; Decadron), purchased from Merck, Sharp, and Dome Research Laboratories (West Point, PA), and/or human GH (Genotropin), generously provided by Kabi Pharmacia AB (Stockholm, Sweden), were added to the culture medium in concentrations of 100 nM and 500 ng/ml, respectively. Where indicated 17β-estradiol (Sigma) was added to the medium in a concentration of 10 nM. Actinomycin-D (Sigma) was used in a concentration of 10 µg/ml.

Received January 13, 1993.

Address requests for reprints to: Dr. Håkan Eriksson, Department of Reproductive Endocrinology, Karolinska Hospital, Box 60500, 104 01 Stockholm, Sweden.

*This work was supported by grants from the Swedish Medical Research Council (03X-3972) and the Karolinska Institutets fonden.

REGULATION OF EXPRESSION OF HEPATIC ER

1549

Preparation of primary hepatocytes

The livers were perfused *in situ* through the portal vein with 0.25 mM EGTA in Krebs-Ringer solution (flow rate, 32 ml/min). After 300 ml EGTA solution, the liver was perfused with 400 ml culture medium containing collagenase type IV from Sigma (0.2 mg/ml) and supplemented as described above (flow rate, 16 ml/min). After the perfusion, the livers were transferred to a bowl with 40 ml culture medium containing collagenase (24 µg/ml) and carefully minced with blunt forceps. The cells were filtered through a nylon mesh (200 µm) into a round-bottom 50-ml centrifuge tube and centrifuged at $50 \times g$ for 2 min. The cells were washed twice with 30 ml and thereafter diluted in 20 ml culture medium. Cell viability (85–95%) and recovery were estimated in 0.2% trypan blue using a Bürker counting chamber. The cells were plated at medium density (70,000 cells/cm²) on plastic 60-mm dishes (Costar, Cambridge, MA) precoated with 270 µl Matrigel (Serva, Heidelberg, Germany)/dish. The culture medium was changed after 2 and 16 h, and every 24 h thereafter. Substitution with GH and DEX was initiated after 64 h of culture (day 3). Cells were harvested for measurement of ER mRNA on day 4 and for ER protein on day 5, after having been exposed to hormonal substitution for 24 and 48 h, respectively. Cell viability at the time of harvesting was 98–100%. The cells remained fully viable for at least 7 days in culture, at which time the initial cell number had been reduced by half.

Preparation of high speed cytosol and nuclei

All procedures were performed at 0–4 °C. The cells were washed twice with PBS (pH 7.8), after which 2 ml PBS were added. The cells were then scraped off [for ER enzyme immunoassay (EIA), 10 cell dishes; for ligand binding, 50 cell dishes] and centrifuged at $500 \times g$ in a Beckman GPR centrifuge (Palo Alto, CA) for 5 min. The supernatant was discarded, and TE buffer (10 mM Tris and 1.5 mM EDTA, pH 7.4) was added. The tubes were kept on ice for 15–30 min, homogenized in a Dounce B homogenizer (30 strokes; Kontes Co., Vineland, NJ), and centrifuged in a Beckman JA20 rotor at $1,200 \times g$ for 20 min. The lipid layer was removed, the pellet was saved for nuclei preparation (see below), and the supernatant was recentrifuged in a Beckman J170 rotor at $184,000 \times g$ for 65 min. A small portion of the supernatant was removed for protein determination according to the method of Lowry *et al.* (19). The remainder of the high speed cytosol was transferred to a beaker. Pulverized ammonium sulfate was added to 35% saturation, and the solution was stirred for 60 min. The precipitate was collected after centrifugation in a Beckman JS13 rotor at $10,000 \times g$ for 10 min. The precipitate was dissolved in TE buffer and used in ligand binding and ER EIA analyses. The nuclear pellet saved after the JA20 rotor centrifugation was rehomogenized using a Dounce B homogenizer and recentrifuged in a Beckman JA20 rotor at $5,000 \times g$ for 20 min. The pellet was diluted with TE buffer to a volume of 7 ml, of which 6 ml were used in a nuclear exchange assay. The remaining 1 ml was centrifuged in a Beckman JA20 rotor at $1,200 \times g$ for 15 min, and thereafter washed and recentrifuged three times with 1 ml TE buffer. The pellet was extracted twice with 0.5 ml 0.4 M KCl in TEM-SH buffer (10 mM Tris-HCl, 1.5 mM EDTA, 10 mM sodium molybdate, and 1 mM monothioglycerol, pH 7.4).

Detection of high speed cytosol ER

The ligand binding assays of high speed cytosol receptors were performed in the presence of a wide range of [2,4,6,7-³H]estradiol (New England Nuclear, Boston, MA) concentrations (0.4–8 nM) and a 100-fold excess of cold diethylstilbestrol (Sigma). After incubation for 16 h at 4 °C, the measurement of specific estrogen binding was performed using the dextran-coated charcoal method (20). Radioactivity was determined in a liquid scintillation counter. Data were plotted according to the method of Scatchard (21). The ER concentration and K_d were calculated by linear regression analysis. The ER EIA, an enzyme immunoassay purchased from Abbot Laboratories (Chicago, IL), was performed according to the manual. Data are expressed as the mean \pm 1 SEM.

Nuclear exchange assay

Binding studies of the nuclei were performed using the same [³H] estradiol and diethylstilbestrol concentrations as those mentioned above. After the 16-h incubation, the nuclei were centrifuged in a Beckman GPR centrifuge at $1000 \times g$ for 15 min. The pellets were washed (1 ml TE buffer) and recentrifuged three times, then extracted with 1 ml ethanol at 37 °C for 30 min, chilled on ice for 15 min, and centrifuged in a Beckman GPR centrifuge at $1000 \times g$ for 15 min. The radioactivity of the supernatants was monitored in a liquid scintillation counter. Data were plotted according to the Scatchard method (21), as described above.

Solution hybridization analysis of mRNA

Five petri dishes of cells per group were harvested as described above. After centrifugation of the cells for 5 min at $500 \times g$ in ice-cold PBS, total nucleic acids were prepared by digestion with proteinase-K (0.2 mg/ml) in $1 \times$ SET [1% sodium dodecyl sulfate, 20 mM Tris-HCl (pH 7.5), and 10 mM EDTA], followed by subsequent extraction with phenol-chloroform, as described by Durnham and Palmiter (22). The DNA concentration was measured fluorometrically. The probe used for ER mRNA determinations was derived from pMOR101, a SP64 plasmid containing the whole open reading frame of the mouse ER (23). Restriction of this plasmid with *Eg*II allows the synthesis of a probe corresponding to nucleotides 1470–2062, which encode the C-terminal half of the steroid-binding domain (E) and all of domain F. Levels of ER mRNA were analyzed using [³²S]UTP-labeled cRNA probes transcribed *in vitro* from a cDNA vector construct according to the method of Melton *et al.* (24), using reagents from Promega Biotech (Madison, WI) and [³²S] UTP from Amersham (Aylesbury, Buckinghamshire, United Kingdom). [³²S]UTP-labeled cRNA was hybridized (20,000 cpm/incubation) at 70 °C to total nucleic acid samples, as described previously (25). Incubations were performed in hexaplets in microcentrifuge vials in a total volume of 40 µl containing 0.6 M NaCl, 20 mM Tris-HCl (pH 7.5), 4 mM EDTA, 0.1% sodium dodecyl sulfate, 10 mM dithiothreitol, and 25% formamide. After overnight incubation, each sample was treated for 45 min at 37 °C in 1 ml of a solution containing 40 µg RNase-A, 2 µg RNase-T1 (Boehringer Mannheim, Mannheim, Germany), and 100 µg calf thymus DNA. Labeled hybrids protected from RNase digestion were precipitated by the addition of 100 µl 6 M trichloroacetic acid and collected on filters (GF/C, Whatman, Clifton, NJ). Radioactivity was determined in a liquid scintillation counter. Data are presented as the mean \pm 1 SEM.

Results

Cytosolic and nuclear ER were measured in female rat hepatocytes cultured on dishes precoated with Matrigel in the presence or absence of GH and DEX. ER were analyzed using two different techniques, ER EIA and a ligand binding assay, followed by Scatchard analysis. The results of the two methods showed good correlation, and linear regression gave a correlation coefficient of 0.95 and a slope of 0.94 (Fig. 1). ER concentrations, expressed either as femtomoles of ER per mg cytosolic protein or femtomoles of ER per µg DNA, showed good correlation. Linear regression analysis gave a correlation coefficient of 0.92. ER synthesis could not be stimulated in hepatocytes cultured on collagen type I or fibronectin. In these cases, ER levels remained undetectable during 5 days of culture regardless of substitution with GH and DEX (data not shown).

Ligand binding assay

Due to its very low abundance, the concentration of nuclear ER in the control groups could not be estimated using the ligand binding assay. To enable comparison of the effects

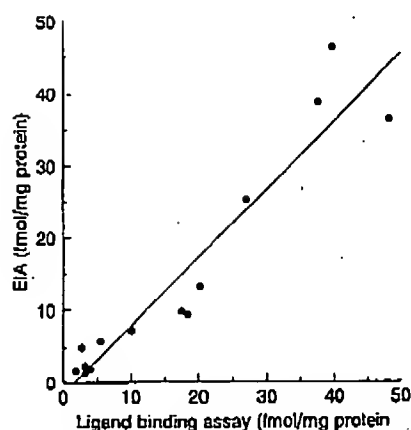


FIG. 1. Comparison of ligand binding assay and ER EIA for measuring ER concentrations in primary cultures of rat hepatocytes. The methods showed good correlation, and linear regression gave a correlation coefficient of 0.95 and a slope of 0.94.

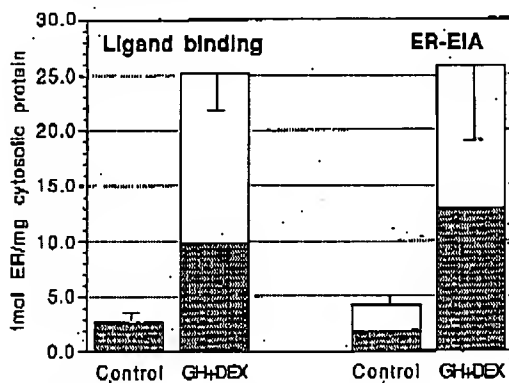


FIG. 2. Effects of substitution with GH and DEX in combination on ER concentrations in primary cultures of female rat hepatocytes. The cells were cultured in insulin-containing medium. Hormonal substitution was initiated after 64 h of culture, and the cells were harvested after 112 h. Cytosolic (□) and nuclear (■) ER concentrations were measured using ER EIA or the ligand binding assay, followed by Scatchard analysis. The nuclear receptor concentration for the control group could not be estimated using the ligand binding assay. Data are presented as the mean \pm 1 SEM ($n = 3$).

of hormonal substitution on total ER concentration, the data for the nuclear ER concentrations of the control groups were replaced by data from the ER EIA analysis. Total ER concentrations were 5.0 ± 0.8 fmol/mg in the control groups ($n = 3$) and 25.3 ± 3.1 fmol/mg cytosolic protein in the GH- and DEX-treated groups ($n = 3$). Thus, a 5.1-fold induction after hormone stimulation was observed (Fig. 2). The K_d of the ER-ligand complex for the GH- plus DEX-treated groups was 1.75 ± 0.9 nM for the cytosolic receptor and 1.94 ± 0.8 nM for the nuclear receptor. The nuclear fraction averaged 61% of the total receptor pool in the GH- plus DEX-treated groups. The ER concentrations of the nuclear fractions in the control groups could not be estimated using the ligand-binding technique.

ER EIA

The results of the comparative measurements of ER concentrations using the ER EIA are presented in Fig. 2. The

total ER concentrations were 4.2 ± 1.0 fmol/mg cytosolic protein in the control groups ($n = 3$) and 25.8 ± 7.0 fmol/mg in the GH- plus DEX-treated groups ($n = 3$). Thus, substitution with GH and DEX increased the ER concentration by a factor of 6.1. The nuclear ER population averaged 56% of the total ER levels in the control groups and 50% in the GH plus DEX groups. ER levels were more than doubled after substitution with GH alone, but were reduced by half ($P = NS$) after treatment with DEX alone (Fig. 3). Substitution with estradiol did not affect ER levels. The ER remained equally divided between the two intracellular compartments regardless of type of hormonal substitution.

ER mRNA

ER mRNA concentrations, measured as counts per min/ μ g DNA, were increased to $210 \pm 14\%$ ($n = 10$) of the control levels after substitution with GH and DEX in combination. Substitution with GH or DEX alone did not affect ER mRNA levels. Substitution with estradiol caused a 47% ($P = NS$) increase in ER mRNA levels (Fig. 3).

Time studies of ER and ER mRNA concentrations

A time study showed a rapid and substantial decrease in ER levels. Receptor concentrations fell to low control steady state levels within 16 h after establishing the culture and remained low until a combination of GH and DEX was added to the medium (Fig. 4). Immediately after perfusion, 90–95% of all ER were recovered in the cytosolic fraction. After 2 h of culture, 95% of the ER were recovered in the nuclear fraction. After 16 h, ER were evenly divided between the two compartments and remained so throughout the experiment.

A time study of the increase in ER mRNA (Fig. 5) was performed as follows. Culture medium was changed at 62 h. GH and DEX substitution was initiated at 64 h, and the cells were harvested at different time points. Maximal ER mRNA

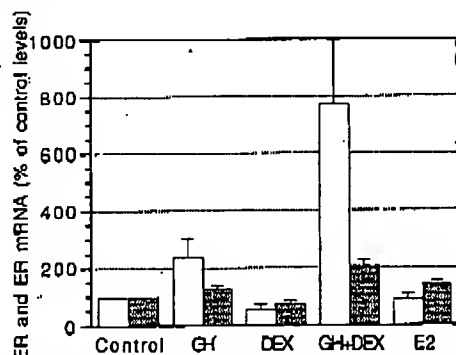


FIG. 3. Effects of substitution with GH, DEX, or a combination of GH and DEX or estradiol (E2) on ER and ER mRNA levels in primary cultures of female rat hepatocytes. The cells were cultured in insulin-containing medium. Hormonal substitution was initiated after 64 h of culture, and the cells were harvested after 112 h. Total ER concentrations (□) were measured as femtomoles per mg cytosolic protein using ER EIA. ER mRNA levels (■) were measured as counts per min/ μ g DNA using solution hybridization. Data are presented as the mean \pm 1 SEM ($n = 3$).

REGULATION OF EXPRESSION OF HEPATIC ER

1551

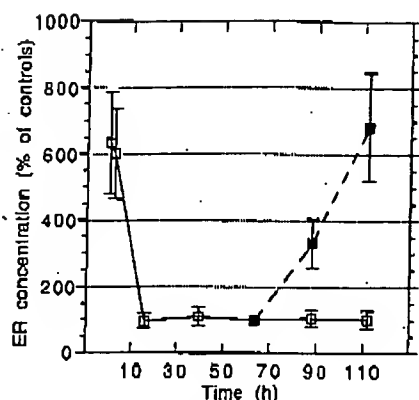


FIG. 4. Time study of ER concentrations in primary cultures of female rat hepatocytes. The cells were cultured in insulin-containing medium. GH and DEX substitution in combination (■) or no hormonal treatment (□) was initiated at 64 h. ER were measured as femtomoles per mg cytosolic protein using ER EIA. Data are presented as the mean \pm 1 SEM (n = 3).

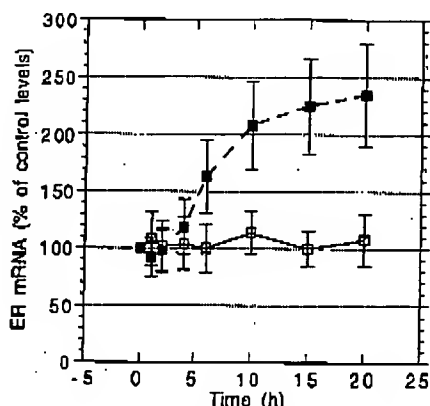


FIG. 5. Time study of ER mRNA concentrations in primary cultures of female rat hepatocytes. The hepatocytes were cultured in insulin-containing medium. The cells received no hormonal substitution (□) or GH and DEX in combination (■) after 64 h of culture (0 h). ER mRNA levels were measured as counts per min/ μ g DNA using solution hybridization. Data are presented as the mean \pm 1 SEM (n = 3).

levels were reached 24 h after the initiation of hormonal substitution and remained steady for at least another 24 h.

Effects of phenol red dye

The potential estrogenic effects of phenol red dye in the culture medium were evaluated by the use of phenol-free Williams' medium E from Gibco. This did not affect the cellular response to GH and DEX with respect to ER regulation, ER mRNA regulation, or intracellular localization of the ER (Fig. 6).

mRNA stability

To address the question of whether the increase in ER mRNA observed after substitution with GH and DEX was caused by an altered ER mRNA stability, cells were cultured with actinomycin-D in the presence or absence of hormones. One group received actinomycin-D at 88 h of culture. The

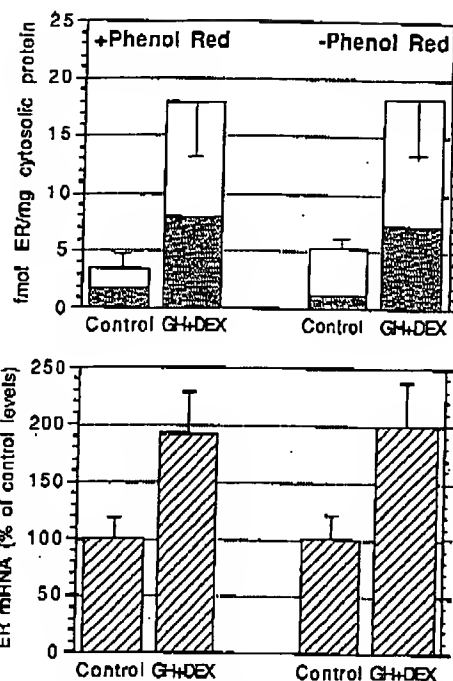


FIG. 6. Effects of phenol red on the concentration and intracellular localization of ER in primary female rat hepatocytes. The hepatocytes were cultured in insulin-containing medium in the presence or absence of phenol red. Substitution with GH and DEX (D) was initiated at 64 h of culture, and the cells were harvested at 112 h. Cytosolic (□) and nuclear (■) ER concentrations were measured using ER EIA. ER mRNA levels (■) were measured as counts per min/ μ g DNA using solution hybridization. Data are presented as the mean \pm 1 SEM (n = 3).

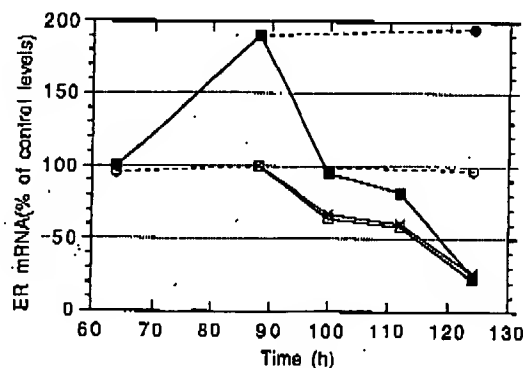


FIG. 7. Effects of GH and DEX substitution on ER mRNA stability in primary cultures of rat hepatocytes. The hepatocytes were cultured in insulin-containing medium. The cells received actinomycin-D at 88 h (□); GH, DEX, and actinomycin-D at 88 h (X); GH and DEX at 64 h and actinomycin-D at 88 h (■); no hormonal substitution (○); or GH and DEX at 64 h (●). ER mRNA concentrations were measured as counts per min/ μ g DNA using solution hybridization (n = 3).

second group received actinomycin-D plus GH and DEX at 88 h of culture. The third group received GH and DEX at 64 h, then actinomycin-D was added at 88 h of culture. Group 4 received no hormonal substitution and group 5 received GH plus DEX at 64 h of culture. ER mRNA stability was not affected by substitution with GH and DEX (Fig. 7).

Discussion

Hepatocyte culture: loss of differentiation

Primary cultures of hepatocytes are vitiated by loss of differentiation after liver tissue disaggregation in the rat (26) and other species (27). The synthesis of liver-specific proteins, such as albumin, is decreased, and the expression of cytoskeleton components is increased (28, 29). The use of cell dishes coated with individual components of extracellular matrix, such as collagen, fibronectin, or laminin, does not preserve differentiated hepatocyte functions, although laminin seems to be more supportive of normal function than the others (30). Type I collagen in hydrated gel form may temporarily delay loss of differentiation (29, 31). The effect of type I collagen is improved by growing the hepatocytes between two layers (32). Hepatocytes cultured in thin liver slices retain tissue-specific transcription in simple culture medium (33). These observations suggest that organ architecture is important for liver function. The best results, however, have been achieved by using an extracellular matrix derived from the Engelberth-Holm-Swarm sarcoma, called Matrigel. Cells cultured on Matrigel maintain a cuboidal shape and aggregate in clusters (34). Many liver functions, such as the synthesis of albumin, transferrin, haptoglobin, and hemopexin, are completely or partly preserved, whereas cell proliferation is suppressed. The massive induction of actin and tubulin and the appearance of α -fetoprotein observed in cultures on single matrix components are suppressed by Matrigel (29, 34). We found that ER synthesis could not be stimulated by GH and DEX in hepatocytes cultured on collagen type I or fibronectin, whereas Matrigel served as an excellent medium in this respect.

Comparison of the ER EIA and ligand binding assays

The comparative study of the measurement of ER concentrations in 1665 human breast cancer cytosols in 9 laboratories suggests that the ER EIA is an excellent alternative to the ligand-binding technique followed by Scatchard plot analysis (35). The ER EIA also functions well in measuring the ER concentrations in primary cultures of rat hepatocytes. The ER EIA detects ER at very low levels. Compared with the ligand binding assay, the ER EIA reduces the number of required cell dishes per experiment by a factor of 5. The ER EIA measures the receptor by recognition of a specific protein epitope and does not establish whether the receptor is capable of ligand binding. By recognizing partly degraded receptors, the ER EIA might give results with slightly higher ER concentrations than the ligand binding assay. The 2 methods were compared in order to confirm whether the ER concentration value obtained by ER EIA was in agreement with the concentration of specific estrogen-binding sites assayed by ligand binding. The results showed good correlation between the 2 methods, and linear regression gave a correlation coefficient of 0.95 and a slope of 0.94. The ligand binding assay is not very accurate when measuring low ER concentrations. The use of the ligand binding assay requires large numbers of cells, which makes the method impractical. Even when using 50 cell dishes/group, the ER concentrations

of the nuclear fractions in the control groups were too low to allow estimation of a value using the ligand binding assay. Because of these practical considerations and the high concordance between the 2 methods, we conclude that the ER EIA is the preferable method of ER analysis in this cell system.

Endocrine regulation of hepatic ER in vivo

The hepatic ER is mainly regulated by GH and thyroid hormones (18, 36), as opposed to the uterine ER, which is mainly regulated by estrogens and progestins (37, 38). Hepatic ER levels are not affected by endogenous serum estradiol fluctuations (39). Hx drastically reduces the hepatic ER to 15% of control levels, but barely affects the uterine ER concentration. Continuous infusion of GH to hypophysectomized (Hx) female rats triples hepatic ER concentrations, whereas daily injections of the same doses of GH have no effect (40). This indicates that not only the hormone, but also the female-type secretion pattern, are important in ER regulation. This has also been shown for other types of female hepatic metabolism, for example in the regulation of cytochrome P450 (41) and alcohol dehydrogenase (42). Substitution with GH and DEX in combination further increases ER concentrations to around 50% of the original ER levels, but substitution with glucocorticoids alone does not increase receptor concentrations (18). The actions of DEX seem to be permissive and not direct. The effects of DEX on GH action may partly be due to the increase in rat hepatic GH receptors observed after DEX treatment *in vivo* and *in vitro* (43).

The results of these *in vitro* experiments are very encouraging, because the effects of hormonal substitution are similar to those observed *in vivo*. Addition of GH and DEX to the serum-free medium caused a 6-fold induction of ER levels in the hepatocytes. This is of the same magnitude as the 5-fold increase observed after GH and DEX substitution *in vivo* (18). The effects on ER levels after treatment with either GH or DEX *in vitro* are similar to those observed after substitution of Hx animals with the same hormones (18). The effects of either DEX or the combination of DEX and GH on ER mRNA levels were similar to the *in vivo* situation. Substitution with GH, however, doubled the levels of hepatic ER mRNA in Hx animals (44). This effect was not observed in the primary culture system, in which ER mRNA levels basically remained unchanged after GH treatment. The effects of estradiol treatment *in vitro* were identical to *in vivo* results obtained in our laboratory (data not shown).

Receptor localization

Immediately after perfusion, 90–95% of all ER were recovered in the cytosolic fraction. This is equal to the percentage observed after the use of standard homogenization procedures on whole livers *in vivo* (45). After 2 h of culture, 95% of the ER were located in the nuclear fraction. After 16 h of culture, the ER were equally divided between the two compartments and remained so throughout the experiment. The use of phenol-free medium did not affect the intracellular localization of ER. This indicates that the nuclear trans-

REGULATION OF EXPRESSION OF HEPATIC ER

1553

location of unoccupied ER in this cell system was not due to any possible estrogenic effects of phenol red dye (46-49). We cannot explain this interesting phenomenon.

Conclusion

GH is a major stimulator of ER synthesis, and DEX has an important permissive effect on its action. This is clearly displayed by the effects on ER and ER mRNA. Receptor levels were increased 6-fold, whereas mRNA levels were increased by a factor of 2 after treatment with GH and DEX in combination. This indicates that posttranscriptional processes are involved. No effect on ER mRNA stability was observed after treatment with GH and DEX in combination. This suggests that the increase in ER mRNA levels observed after hormonal substitution was due to increased transcription. However, other mechanisms, such as alteration of nuclear RNA splicing or RNA transport to the cytoplasm, might be the regulated steps as well. Primary culture on Matrigel is an excellent model system for studies of the endocrine regulation of hepatic ER. The effects of hormonal substitution *in vitro* closely resemble those observed *in vivo*. The system might also be suitable for studies of the effects of estrogens on hepatic metabolism.

Acknowledgments

We are very grateful to Agneta Mode of the Department of Medical Nutrition, NOVUM, for help in setting up the primary hepatocyte culture system and for critical review of the manuscript. Technical advice on primary cultures of hepatocytes from Eva Floby is gratefully acknowledged. The pMOR101 gene fragment was kindly supplied by Dr. M. G. Parker, Imperial Cancer Research Fund (London, United Kingdom). Gonotropin was generously provided by Kabi Pharmacia AB.

References

- Krakoff LR, Eisenfeldt AJ 1977 Hormonal control of plasma renin substrate (angiotensinogen). *Circ Res* 41:43-46
- Klett C, Ganten D, Hellmann W, Kaling M, Ryffel GH, Weimar-Ehl T, Hackenthal E 1992 Regulation of hepatic angiotensinogen synthesis and secretion by steroid hormones. *Endocrinology* 130:3660-3668
- Moorjani S, Dupont A, Labrie F, De Lignieres B, Cusan L, Dupont P, Mailloux J, Lupien P-J 1991 Changes in plasma lipoprotein and apoprotein composition in relation to oral versus percutaneous administration of estrogen alone or in cyclic association with uterogest in menopausal women. *J Clin Endocrinol Metab* 73:373-379
- Rudling MJ 1987 Role of the liver for receptor-mediated catabolism of low-density lipoprotein in the 17 α -ethinyl estradiol-treated rat. *Biochim Biophys Acta* 919:175-180
- Brindley DN, Salter AM 1991 Hormonal regulation of the hepatic low density lipoprotein receptor and the catabolism of low density lipoproteins: relationship with the secretion of very low density lipoproteins. *Prog Lipid Res* 30:1991
- Meade TW 1981 Oral contraceptives, clotting factors and thrombosis. *J Am Obstet Gynecol* 142:758-761
- von Schoultz B, Carlström K, Collste L, Eriksson A, Henriksson P, Pousette A, Stege R 1989 Estrogen therapy and liver function-metabolic effects of oral and parenteral administration. *Prostate* 14:389-395
- Thompson C, Pearlie M, Hudson P, Lucier W 1983 Correlation of estrogen receptor concentrations and estrogen-mediated elevation of very low density lipoproteins. *Endocrinology* 112:1389-1397
- Steinberg M, Tolkdorf S, Gordon AS 1967 Relation of the adrenal and pituitary to the hypocholesterolemic effect of estrogen in rats. *Endocrinology* 81:340-344
- Rudling M, Norstedt G, Olivecrona H, Reihner E, Gustavsson JA, Angelin B 1992 Importance of growth hormone for the induction of hepatic low density lipoprotein receptors. *Proc Natl Acad Sci USA* 89:6983-6987
- Roepke J, Crabb DW 1987 Loss of sexual differentiation of rat hepatocytes in short term culture. *Alcohol Alcoholism* 263-264
- Crabb DW, Roepke J 1987 Loss of growth hormone-dependent characteristics of rat hepatocytes in culture. *In Vitro Cell Dev Biol* 23:303-307
- Orkin RW, Gehron P, McGoodwin EB, Martin GR, Valentine T, Swann J 1977 A murine tumor producing a matrix of basement membrane. *J Exp Med* 145:204-220
- Guzelian PS, Li D, Schuetz EG, Thomas P, Levin W, Mode A, Gustafsson J-Å 1988 Sex change in cytochrome P-450 phenotype by growth hormone treatment of rat hepatocytes maintained in a culture system on matrigel. *Proc Natl Acad Sci USA* 85:9783-9787
- Schuetz EG, Schuetz JD, May B, Guzelian PS 1990 Regulation of cytochrome P-450b/e and P-450 gene expression by growth hormone in adult rat hepatocytes cultured on a reconstituted basement membrane. *J Biol Chem* 265:1188-1192
- Tollet P, Enberg E, Mode A 1990 Growth hormone (GH) regulation of cytochrome P-450C12, insulin-like growth factor-1 (IGF-1) and GH receptor mRNA expression in primary rat hepatocytes: a hormonal interplay with insulin, IGF-1 and thyroid hormone. *Mol Endocrinol* 4:1934-1942
- Tollet P, Legraverend C, Gustafsson J-Å, Mode A 1991 A role for protein kinases in the regulation of cytochrome P-450C12 and messenger RNA expression in primary adult rat hepatocytes. *Mol Endocrinol* 5:1351-1358
- Norstedt G, Wrangé Ö, Gustafsson J-Å 1981 Multihormonal regulation of the estrogen receptor in rat liver. *Endocrinology* 108:1190-1196
- Lowry OH, Rosebrough NJ, Farr AL, Randall RJ 1951 Protein measurement with the Folin phenol reagent. *J Biol Chem* 193:265-275
- Clark JH, Peck EJJ 1979 Methods of steroid receptor assay. In: Gross F, Grumbach MM, Labhart A, Lipsett MB, Mann T, Samuels LT, Zander J (eds) *Female Sex Steroids. Receptors and Function*. Springer-Verlag, Berlin, pp 29-31
- Scatchard G 1949 The attractions of proteins for small molecules and ions. *Ann NY Acad Sci* 51:660-672
- Durnham DM, Palmiter RD 1983 A practical approach for quantitating specific mRNA by solution hybridization. *Anal Biochem* 131:385-393
- Hillier SG, Saunders PTK, White R, Parker MG 1989 Oestrogen receptor mRNA and a related RNA transcript in mouse ovaries. *Mol Endocrinol* 2:39-45
- Melton DA, Krieg PA, Rebagliati MR, Maniatis R, Zinn K, Green MR 1984 Efficient synthesis of biologically active RNA and RNA hybridization probes from plasmids containing bacteriophage SP6 promoter. *Nucleic Acids Res* 12:7035-7056
- Mathews LS, Norstedt G, Palmiter RD 1986 Regulation of insulin-like growth factor I gene expression by growth hormone. *Proc Natl Acad Sci USA* 83:9343-9347
- Berry MN, Edwards AM, Barritt GJ 1991 Isolated hepatocytes preparation, properties and applications. In: Burdon RH, van Knippenberg PH (eds) *Laboratory Techniques in Biochemistry and Molecular Biology*. Elsevier, Amsterdam, pp 265-278
- Wolffe AP, Tata R 1984 Primary culture, cellular stress and differentiated function. *FEBS Lett* 176:8-15
- Sawada N, Tomomura A, Sattler CA, Sattler GL, Kleinman HK, Pitot HC 1987 Effects of extracellular matrix components on the growth and differentiation of cultured hepatocytes. *In Vitro Cell Dev Biol* 23:267
- Ben-Zeev A, Robinson GS, Bucher NLR, Farmer SR 1988 Cell-cell and cell-matrix interactions differentially regulate the expression of hepatic and cytoskeletal genes in primary cultures of rat hepatocytes. *Proc Natl Acad Sci USA* 85:2161
- Bisell DM, Arenson DM, Maher JJ, Roll FJ 1987 Support of cultured hepatocytes by a laminin-rich gel. Evidence for a function-

- ally significant subendothelial matrix in normal rat liver. *J Clin Invest* 79:801
31. Sirica AE, Richards W, Tsukada Y, Sattler CA, Pitot HC 1979 Fetal phenotypic expression by adult hepatocytes on collagen gel/nylon meshes. *Proc Natl Acad Sci USA* 76:283
 32. Dunn JCY, Yarmush ML, Koebe HG, Tompkins RG 1989 Hepatocyte function and extracellular matrix geometry: long term culture in a sandwich configuration. *FASEB J* 3:174
 33. Clayton DF, Harrelson A, Darnell JEJ 1985 Dependence of liver-specific transcription on tissue organization. *Mol Cell Biol* 5:2623
 34. Schuetz EG, Li D, Omiecinski CJ, Muller-Eberhard U, Kleinman HK, Elswick B, Guzelian PS 1988 Regulation of gene expression in adult rat hepatocytes cultured on a basement membrane matrix. *J Cell Physiol* 134:309-323
 35. Blankenstein MA 1990 Comparison of ligand binding assay and enzyme immunoassay of estrogen receptor in human breast cancer cytosols. *Breast Cancer Res Treat* 17:91-98
 36. Eriksson HA, Freyschuss B 1988 Effects of thyroid hormones on the receptor level in estrogen target organs. *J Steroid Biochem* 29:401-405
 37. Eriksson HA 1982 Different regulation of the concentration of estrogen receptors in the rat liver and uterus following ovariectomy. *FEBS Lett* 149:91-95
 38. Clark JH, Peck EJJ 1979 Female sex steroids. Receptors and function. In: Gross F, Grumbach MM, Labhart A, Lipsett MB, Mann T, Samuels LT, Zander J (eds) *Monographs on Endocrinology*. Springer-Verlag, Berlin, pp 99-109
 39. Eriksson HA 1989 Regulation of estrogen receptor concentration in target organs of the rat. In: Eriksson H, Gustavsson JA (eds) *Steroid Hormone Receptors: Structure and Function*. Elsevier, Amsterdam, pp 389-404
 40. Norstedt G 1982 A comparison between the effects of growth hormone on prolactin receptors and estrogen receptors in rat liver. *Endocrinology* 110:2107-2112
 41. Mode A, Wiersma-Larsson E, Ström A, Zaphiropoulos PG, Gustafsson J-A 1988 A dual role of growth hormone as a feminizing and a masculinizing factor in the control of sex specific cytochrome P-450 isozymes in rat liver. *J Endocrinol* 120:311-317
 42. Crabb DW, Morzorati S, Simon J 1985 Central nervous system control of liver alcohol dehydrogenase activity in rats. *Life Sci* 37:2381-2387
 43. Nilmi S, Hayakawa T, Tanaka A 1991 Effect of cell density on induction of growth hormone receptors by dexamethasone in primary cultured rat hepatocytes. *Biochem Biophys Res Commun* 174:928-933
 44. Freyschuss B, Sahlin L, Eriksson HA 1991 Regulatory effects of growth hormone, glucocorticoids and thyroid hormone on the estrogen receptor level in the rat liver. *J Steroid Biochem* 56:367-374
 45. Eisenfeld AJ, Aten RF 1980 Estrogen receptors in the mammalian liver: developmental and metabolic aspects. In: Kaye AM, Kaye M (eds) *The Development of Responsiveness to Steroid Hormones*. Pergamon Press, Exeter, pp 107-124
 46. Rajendran KG, Lopez T, Farikh I 1987 Estrogenic effect of phenol red in MCF-7 cells is achieved through activation of estrogen receptor by interaction distinct from the steroid binding site. *Biochem Biophys Res Commun* 142:724-731
 47. Wakeling AE 1989 Comparative effects on the effects of steroidal and nonsteroidal oestrogen antagonists on the proliferation of human breast cancer cells. *J Steroid Biochem* 34:183-188
 48. Ortmann O, Sturm R, Knuppen R, Emons G 1990 Weak estrogenic activity of phenol red in the pituitary gonadotroph: re-evaluation of estrogen and antiestrogen effects. *J Steroid Biochem* 35:17-22
 49. Welshons WV 1988 Estrogenic activity of phenol red. *Mol Cell Endocrinol* 57:169-178

NEOPLASIA

Cyclin D1-negative mantle cell lymphoma: a clinicopathologic study based on gene expression profiling

Kai Fu, Dennis D. Weisenburger, Timothy C. Greiner, Sandeep Dave, George Wright, Andreas Rosenwald, Michael Chiorazzi, Javeed Iqbal, Stefan Gess, Reiner Siebert, Daphne De Jong, Elaine S. Jaffe, Wyndham H. Wilson, Jan Delabie, German Ott, Bhavana J. Dave, Warren G. Sanger, Lynette M. Smith, Lisa Rimsza, Rita M. Brazier, H. Konrad Müller-Hermelink, Elias Campo, Randy D. Gascoyne, Louis M. Staudt, and Wing C. Chan, for the Lymphoma/Leukemia Molecular Profiling Project

Cyclin D1 overexpression is believed to be essential in the pathogenesis of mantle cell lymphoma (MCL). Hence, the existence of cyclin D1-negative MCL has been controversial and difficult to substantiate. Our previous gene expression profiling study identified several cases that lacked cyclin D1 expression, but had a gene expression signature typical of MCL. Herein, we report the clinical, pathologic, and genetic features of 6 cases of cyclin D1-negative MCL. All 6 cases exhibited

the characteristic morphologic features and the unique gene expression signature of MCL but lacked the t(11;14)(q13;q32) by fluorescence in situ hybridization (FISH) analysis. The tumor cells also failed to express cyclin D1 protein, but instead expressed either cyclin D2 (2 cases) or cyclin D3 (4 cases). There was good correlation between cyclin D protein expression and the corresponding mRNA expression levels by gene expression analysis. Using interphase FISH, we did not detect

chromosomal translocations or amplifications involving *CCND2* and *CCND3* loci in these cases. Patients with cyclin D1-negative MCL were similar clinically to those with cyclin D1-positive MCL. In conclusion, cases of cyclin D1-negative MCL do exist and are part of the spectrum of MCL. Up-regulation of cyclin D2 or D3 may substitute for cyclin D1 in the pathogenesis of MCL. (Blood. 2005;106:4315-4321)

© 2005 by The American Society of Hematology

Introduction

Mantle cell lymphoma (MCL) is now recognized as an aggressive B-cell lymphoma with various growth patterns (mantle zone, nodular, or diffuse) and a broad range of cytologic features.¹⁻⁵ Most cases of MCL exhibit a characteristic phenotype (CD20⁺, CD5⁺, CD43⁺, CD3⁻, CD10⁻, CD23⁻) and have the t(11;14)(q13;q32) with overexpression of the cyclin D1 (*CCND1*) gene on chromosome 11q13.^{6,7} Cyclin D1, a D-type cyclin that is not expressed in normal B lymphocytes, plays a key role in cell cycle regulation during the G₁ to S phase transition by binding to cyclin-dependent kinase 4 (CDK4) and CDK6, resulting in phosphorylation and inactivation of the retinoblastoma protein (RB).⁸⁻¹⁰ The current World Health Organization guidelines for the diagnosis of MCL rely on morphologic examination and immunophenotyping, with demonstration of cyclin D1 protein overexpression and/or the t(11;14)(q13;q32) for confirmation.¹¹

The existence of cyclin D1-negative MCL has been controversial and difficult to substantiate since cyclin D1 overexpression is believed to be essential in the pathogenesis of MCL. Most reported cases of cyclin D1-negative MCL have been attributed to suboptimal immunostaining,

inadequate genetic or molecular analyses, or misdiagnosis. Nevertheless, in a recent study of 99 lymphomas that were morphologically consistent with MCL, we identified a small group of cases that lacked cyclin D1 mRNA expression by both quantitative reverse transcriptase-polymerase chain reaction (RT-PCR) and Lymphochip cDNA microarray analyses.¹² However, these cases had the characteristic MCL gene expression signature by cDNA microarray analysis and, therefore, were considered to be cases of cyclin D1-negative MCL. We have further refined the algorithm for diagnosing MCL using gene expression profiling and, herein, we report the clinical, pathologic, and genetic features of 6 cases of cyclin D1-negative MCL.

Patients, materials, and methods

Case selection

The lymph node biopsies from 6 patients without a previous history of malignancy are included in this study. All 6 cases were reviewed by a panel

From the Departments of Pathology and Microbiology, Preventive and Societal Medicine, and the Human Genetics Laboratory, University of Nebraska Medical Center, Omaha, NE; the Metabolism Branch, and Sections of Hematopathology and Lymphoma Clinical Research, Center for Cancer Research, and the Biometric Research Branch, Division of Cancer Treatment and Diagnosis, National Cancer Institute, National Institutes of Health, Bethesda, MD; the Department of Pathology, University of Würzburg, Würzburg, Germany; the Institute of Human Genetics, University Hospital Schleswig-Holstein, Kiel, Germany; the Department of Pathology, The Netherlands Cancer Institute/Antoni van Leeuwenhoek Hospital, Amsterdam, the Netherlands; the Department of Pathology, Norwegian Radium Hospital, Oslo, Norway; the Department of Pathology, University of Arizona Health Sciences Center, Tucson, AZ; the Department of Pathology, University of Oregon Health Sciences Center, Portland, OR; the Department of Pathology, Hospital Clinic, University of Barcelona, Barcelona, Spain; and the Department of Pathology, British Columbia Cancer Agency, Vancouver, BC.

Submitted April 29, 2005; accepted August 12, 2005. Prepublished online as Blood First Edition Paper, August 25, 2005; DOI 10.1182/blood-2005-04-1753.

Supported in part by the United States Public Health Service grants CA36727 and CA84967 awarded by the National Cancer Institute, the Department of Health and Human Services (W.C.C.), the Lymphoma Research Foundation (mantle cell lymphoma grantee: T.C.G.), and Deutsche Krebshilfe (A.R., R.S., G.O., H.K.M.-H.).

The Lymphoma/Leukemia Molecular Profiling Project's full membership is listed in Appendix.

The online version of the article contains a data supplement.

Reprints: Kai Fu, Department of Pathology and Microbiology, University of Nebraska Medical Center, 983135 Nebraska Medical Center, Omaha, NE 68198-3135; e-mail: kfu@unmc.edu.

The publication costs of this article were defrayed in part by page charge payment. Therefore, and solely to indicate this fact, this article is hereby marked "advertisement" in accordance with 18 U.S.C. section 1734.

© 2005 by The American Society of Hematology

of expert hematopathologists to confirm the diagnosis. Two of these cases were identified in our previous report.¹² This study was approved by the institutional review board at the University of Nebraska Medical Center. Informed consent was provided according to the Declaration of Helsinki.

Quantitative reverse transcriptase–polymerase chain reaction (RT-PCR)

To measure cyclin D1 mRNA expression, 2.5-ng aliquots of mRNA were analyzed by quantitative RT-PCR using TaqMan reagents and a thermal cycler (Applied Biosystems, Foster City, CA).¹² The samples were run in triplicate and the β 2-microglobulin transcript was used as a reference. Primers and probes for β 2-microglobulin and the coding region of cyclin D1 have been previously described.¹³

Microarray gene expression profiling

Lymphochip cDNA microarrays containing 12 196 cDNA elements¹⁴ were used to profile mRNA expression in the lymphoma samples. A set of MCL signature genes that can be used to distinguish MCL from other lymphoma subtypes has been described previously.¹² These cases were further analyzed for gene expression using Affymetrix Human U133 A/B microarrays (Affymetrix, Santa Clara, CA). The gene expression profiles of these cases were compared with those of other B-cell non-Hodgkin lymphomas, including the various subtypes of diffuse large B-cell lymphoma, follicular lymphoma, chronic lymphocytic leukemia/small lymphocytic lymphoma, extranodal marginal zone lymphoma, mucosa-associated lymphoid tissue (MALT) type, and splenic marginal zone lymphoma. The distributions of the Bayesian predictor for each category were used to estimate the probability that any particular case belonged to that category by applying Bayes rule.^{12,15} Specifically, for each lymphoma category we generated a Bayesian predictor between that category and cyclin D1–positive MCL samples, based on the 50 genes with the largest *t*-statistics between them. Only those cases for which all pair-wise predictors agreed that there was a more than 90% estimated probability of the case being MCL were considered to be cyclin D1–negative MCL samples. This set of models was applied to our data set in a leave-one-out, cross-validated fashion so that the models tested on a given case were based on a data set that excluded that case. Cases for which there was a less than 90% likelihood of being in any category were termed unclassified.

Histologic and Immunologic studies

The lymph node specimens were fixed in 10% neutral buffered formalin and embedded in paraffin, and 4- μ m sections were cut and stained with hematoxylin and eosin (H&E) for histologic evaluation. Immunohistochemical stains for cyclin D1 protein were performed on formalin-fixed, paraffin-embedded tissue sections. Briefly, after depurification in xylene and rehydration in graded alcohols, endogenous peroxidase was blocked with hydrogen peroxide. Heat-induced antigen retrieval was performed using citrate buffer, pH 6.0.¹⁶ After rinsing in phosphate-buffered saline,

mouse anti-cyclin D1 antibody was applied at a dilution of 1:200. The rabbit monoclonal antibody SP4 against cyclin D1 (Neomarkers, Fremont, CA) was also used, using the suggested procedure for antigen retrieval with minor modification (Table 1).¹⁷ Antibodies against CD3, CD5, CD20, CD23, CD43, cyclin D2, cyclin D3, cyclin E, RB, and p27^{kip1} were also used for immunohistochemical stains (Table 1). These stains were performed on a Ventana ES automated immunostainer (Ventana Biotech, Tucson, AZ) with a streptavidin-biotin peroxidase detection system. Positivity for the cyclins, RB and p27^{kip1} was defined as a strong nuclear staining in more than 50% of the neoplastic cells.

Fluorescence in situ hybridization (FISH) analysis

Interphase FISH analysis was performed on cells left over from prior cytogenetic analyses or on formalin-fixed, paraffin-embedded tissue sections. For detection of the t(11;14)(q13;q32), a commercially available LSI IGH/CCND1 double-color, double-fusion probe was used (Vysis, Downers Grove, IL). For break-apart FISH assays for the *CCND1* (11q13), *CCND2* (12p13), and *CDKN1B/p27KIP1* (12p13) loci, appropriate bacterial artificial chromosome (BAC) clones flanking the respective genes were selected using bioinformatic resources available at the University of California at Santa Cruz (<http://genome.ucsc.edu>). All BAC clones were derived from the RPC111 library and were obtained from Invitrogen/Research Genetics (Carlsbad, CA) or the Sanger Center (Hinxton, United Kingdom). The following clones were used: *CCND1* (pooled RP11-211G23/RP11-378E8 and pooled RP11-30016/RP11-626H12), *CCND2* (RP11-578L13 and RP11-388F6), and *CDKN1B/p27KIP1* (RP11-180M15 and RP11-59H1). For each locus, centromeric and telomeric BAC clones were differentially labeled with Spectrum Orange or Spectrum Green (Vysis) and pooled for break-apart assays. Bacterial culture, BAC DNA isolation and labeling, probe preparation, and FISH on cytogenetic suspensions were performed as previously described.^{18,19} The *CCND3* locus was investigated using a recently described break-apart assay.²⁰ Locus-specific interphase FISH was performed on paraffin-embedded tissue sections according to the manufacturer's instructions (Vysis) or recently described protocols²¹ with minor modifications. Whenever possible, at least 100 cells were analyzed.

INK4a/ARF locus deletion analysis

To detect genomic loss of *INK4a/ARF* tumor suppressor locus in the specimens, we performed quantitative real-time PCR assays using genomic DNA as previously described.¹² The *REL* locus on chromosome 2p was chosen as the reference gene, and a cutoff ratio of *INK4a/ARF* locus copy number relative to *REL* locus copy number was used to assess tumor DNA for genomic deletions. A tumor DNA sample that yielded an *INK4a/ARF*-to-*REL* ratio below the cutoff ratio was considered to have a genomic deletion of the *INK4a/ARF* locus. The primers and probe sets for the *INK4a/ARF* and the *REL* loci have been described previously.^{22,23}

Table 1. Antibodies and methods for immunohistochemical stains

Antibody	Clone	Source	Dilution	Retrieval
CD3	PS1	Ventana Medical Systems, Tucson, AZ	Neat	A
CD5	4C7	Novocastra, Newcastle upon Tyne, United Kingdom	1:20	A
CD20	L26	DAKO, Carpinteria, CA	1:200	A
CD23	BU38	The Binding Site, San Diego, CA	1:5	B
CD43	LSO	Ventana Medical Systems	Neat	None
Cyclin D1	DCS-6	DAKO	1:200	A
Cyclin D1	SP4	Neomarkers	1:100	C
Cyclin D2	Polyclonal	Santa Cruz Biotech, Santa Cruz, CA	1:500	D
Cyclin D3	DCS-22	Neomarkers	1:100	E
Cyclin E	13A3	Novocastra	1:10	E
RB	RbY	DAKO	1:10	A
p27 ^{kip1}	SX53G8	DAKO	1:20	A

A indicates 10 mM citrate buffer, pH 6.0, 30 minutes, water bath (95°C); B, protease I enzymatic digestion, 0 minutes; C, 1 mM EDTA (ethylenediaminetetraacetic acid, pH 8.0), 30 minutes, water bath (95°C); D, 1 mM EDTA, pH 8.0, 60 minutes, water bath (95°C); and E, 10 mM citrate buffer, pH 6.0, 10 minutes, pressure cooker (115°C).

Statistical analysis

The clinical characteristics of the cyclin D1-negative and cyclin D1-positive cases were compared using Fisher exact test. Overall survival was calculated as the time from initial diagnosis to the date of death or last follow-up, and those alive at last follow-up were treated as censored. The Kaplan-Meier method was used to estimate the overall survival distributions of the 2 groups, and the log-rank test was used to compare the distributions.

Results

Case selection

In our previous study,¹² we identified 7 cyclin D1-negative cases by quantitative RT-PCR and cDNA microarray analysis among 99 cases of lymphoma with MCL morphology. Subsequent studies revealed that 1 of these 7 cases had the characteristic t(11;14)(q13;q32) by FISH analysis and expressed cyclin D1 protein by immunohistochemical staining (data not shown). Thus, this case was thought to be a false-negative case and was reclassified as a cyclin D1-positive MCL. During the interim, we performed additional gene expression profiling analysis using Affymetrix U133A/B microarrays and refined the algorithm for diagnosing MCL. Using the refined algorithm, 4 of the other 6 original cases were regarded as unclassifiable B-cell lymphomas and, thus, were excluded from the current study. Recently, we identified 4 additional cases of MCL that were negative for cyclin D1 by both immunohistochemistry and quantitative RT-PCR analysis. All 6 cases in the current study (2 from the previous study and 4 newly identified) exhibited the characteristic gene expression signature of MCL, which is distinct from the other common types of B-cell non-Hodgkin lymphoma including the various subtypes of diffuse large B-cell lymphoma, follicular lymphoma, small lymphocytic lymphoma/chronic lymphocytic leukemia, extranodal marginal zone lymphoma, MALT type, and splenic marginal zone lymphoma (Figure 1 and Table S1, which is available on the Blood website; see the Supplemental Materials link at the top of the online article). By applying Bayesian analysis, all 6 cases were predicted as MCL in all pair-wise models with 99.99% confidence. On the other hand, none of the cases from the other categories were predicted as MCL with more than 20% confidence in their respective cross-validated, pair-wise comparisons. Therefore, these 6 cases are considered to be bona fide cases of cyclin D1-negative MCL.

Histologic and immunologic features

All 6 cases exhibited a nodular or diffuse growth pattern and consisted of tumor cells with typical mantle cell cytology (Table 2, Figure 2A, and Figure S1). Immunophenotypic analysis of the tumor cells demonstrated a B-cell phenotype in all cases. Expression of CD5 antigen was noted in all 6 cases. The tumor cells in 1 of the 6 cases were weakly positive for CD23 antigen. Expression of CD43 antigen was noted in 5 of the 6 cases (Table 2).

Detection of cell cycle regulatory proteins

Immunostains for cyclin D1 and p27^{Kip1} were performed on all 6 cases, and stains for cyclins D2, D3, E, and RB were performed on 5 cases with available formalin-fixed, paraffin-embedded tissue (Table 2). All 6 cases were negative for cyclin D1 by using the mouse monoclonal antibody DCS-6 (Figure 2B). Four of the 6 cases were also studied using the newly available rabbit monoclonal antibody SP4, and all 4 cases were negative for cyclin D1 (data

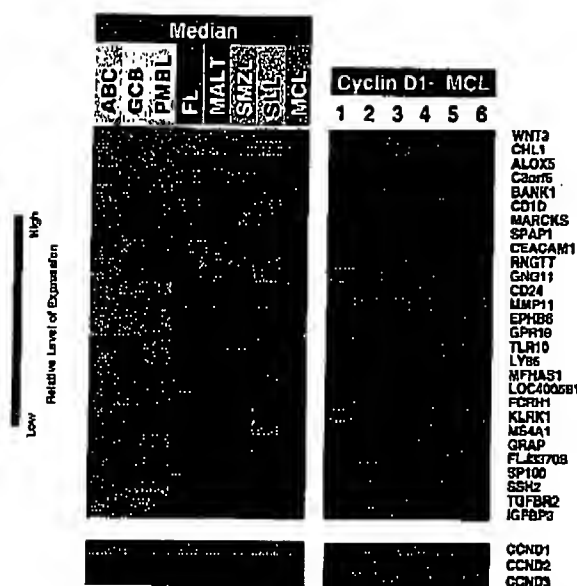


Figure 1. Expression profiles of mantle cell lymphoma (MCL) signature genes in 6 cases of cyclin D1-negative MCL using Affymetrix U133 A/B arrays. These expression profiles are compared with 22 cases of cyclin D1-positive MCL: 78 cases of activated B-cell-like (ABC), 85 cases of germinal center B-cell-like (GCB), and 33 cases of primary mediastinal (PMBL) variants of diffuse large B-cell lymphoma, 193 cases of follicular lymphoma (FL), 14 cases of extranodal marginal zone lymphoma, MALT type (MALT), 6 cases of splenic marginal zone lymphoma (SMZL), and 14 cases of small lymphocytic lymphoma (SLL) (median expression levels of the MCL signature genes in these entities are shown). In the 6 cases of cyclin D1-negative MCL, each column represents a single lymphoma specimen and each row represents the level of expression of a single gene in the MCL signature. Red squares indicate increased expression and green squares indicate decreased expression relative to the median expression level, according to the color scale shown over a 4-fold range. In the bottom panel, the gene expression levels of the D-type cyclins in the various entities and the 6 cases of cyclin D1-negative MCL are shown according to the color scale over a 16-fold range. For microarray data of all cases, refer to Table S1.

not shown). Two cases (cases 1 and 2) demonstrated overexpression of cyclin D2 by immunostaining (Figure 2C), which correlated well with the increased cyclin D2 mRNA levels detected by microarray analysis (Figure 1, lower panel). Both of these cases were negative for cyclin D3. Three cases (cases 3-5) exhibited overexpression of cyclin D3 by immunostaining (Figure 2D), which correlated well with the increased cyclin D3 mRNA levels detected by microarray analysis (Figure 1, lower panel), and these cases were negative for cyclin D2. Case 6 also showed up-regulation of cyclin D3 mRNA by microarray analysis (Figure 1, lower panel), but the tissue block from this case was not available for immunostains.

All of the cases studied were negative for cyclin E, but showed positive immunostaining for RB (Table 2). The expression levels of RB protein were similar in all of the cases and were comparable with that seen in cases of cyclin D1-positive MCL (data not shown). Down-regulation of p27^{Kip1} protein expression was observed in all 6 cases with the intensity of nuclear staining much weaker than that seen in reactive T lymphocytes (Table 2).

Genetic features

FISH analysis for the t(11;14)(q13;q32) was performed on all 6 cases and none displayed the *IGH/CCND1* fusion. FISH studies with a locus-specific probe were also negative for variant translocations or amplifications involving the *CCND1* locus at band 11q13 in all of the 6 cases (Table 2). Conventional cytogenetic analysis was also performed on case 6 and did not reveal a chromosomal alteration affecting band 11q13. FISH analysis using break-apart

Table 2. Pathologic and genetic features of 6 patients with cyclin D1-negative MCL

	Case no. 1	Case no. 2	Case no. 3	Case no. 4	Case no. 5	Case no. 6
Pathologic features						
Growth pattern	Nodular	Diffuse	Nodular	Diffuse	Nodular	Nodular
Cytology	Typical	Typical	Typical	Typical	Typical	Typical
CD20	+	+	+	+	+	+
CD3	-	-	-	-	-	-
CD5	+	+	+	+	+	+
CD23	-	-	-	+	-	-
CD43	+	+	-	+	+	+
Cyclin D1	-	-	-	-	-	-
Cyclin D2	+	+	-	-	-	NA
Cyclin D3	-	-	+	+	+	NA
Cyclin E	-	-	-	-	-	NA
FB	+	+	+	+	+	NA
p27 ^{Kip1}	-	-	-	-	-	-
Genetic features						
t(11;14)(q13;q32)	-	-	-	-	-	-
11q13 (cyclin D1)	Normal*	Normal	Normal	Normal	Normal	Normal
12p13 (cyclin D2)	Normal	Normal	Normal	Normal	Normal	Normal
6p21 (cyclin D3)	Normal	Normal	Normal	Normal	Normal	Normal
12p13 (p27 ^{Kip1})	Normal	Normal	Normal	Normal	Normal	Normal

+ indicates positive; -, negative; + (w), weakly positive; and NA, not available.

*Normal indicates no split or amplification.

probes for the *CCND2* (12p13), *CCND3* (6p21), and *CDKN1B/p27KIP1* (12p13) loci did not reveal any evidence of chromosomal translocation or amplification in these cases (Table 2). We also used a quantitative PCR assay to evaluate the genomic loss of one or both alleles of the *INK4a/ARF* locus, which encodes the tumor suppressor proteins p16^{INK4a} and p14^{ARF}. No *INK4a/ARF* locus deletions were detected in any of the 6 cases of cyclin D1-negative MCL.

Clinical features

The clinical features of the 6 patients are summarized in Table 3. The patients consisted of 5 males and 1 female, with a median age of 61 years (range, 54-77 years). All patients presented with stage IV disease. Lymphadenopathy was the most common presentation

and extranodal sites were involved by lymphoma in all 6 patients. Five patients received combination chemotherapy initially, but none of these patients achieved a complete clinical response. One patient (case 1) was not treated initially and developed gastrointestinal involvement 26 months after the initial diagnosis. At the time of last follow-up, one of the patients had died and the other 5 were alive with disease.

Ninety-three cases (92 cases in the original study plus the false-negative case) of cyclin D1-positive MCL¹² were used for comparison. The median follow-up for these patients was 26 months (range, 7-166 months). The clinical features including age and sex distribution, stage, presence of B symptoms, serum lactate dehydrogenase (LDH) levels, extranodal sites, International Prognostic Index (IPI) scores, types of treatment, and clinical responses were similar between the cyclin D1-positive and cyclin D1-negative groups (data not shown). At the time of last follow-up, 65 of 93 patients with cyclin D1-positive MCL had died, with a median overall survival of 31 months. No significant difference in overall survival between the cyclin D1-positive and cyclin D1-negative groups was identified.

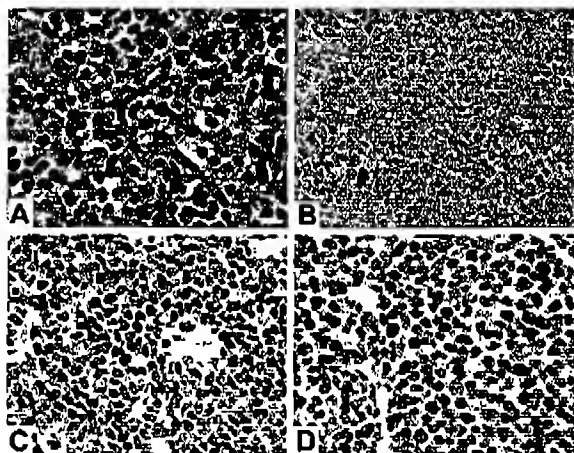


Figure 2. Cytologic features and expression of D-type cyclins in cyclin D1-negative MCL. (A) Typical MCL cytology (case 1) (hematoxylin and eosin stain; original magnification, × 500); (B) cyclin D1 protein, showing only a rare nontumor cell with nuclear staining (case 1); (C) cyclin D2 protein, showing strong nuclear staining of the tumor cells (case 2); (D) cyclin D3 protein, showing strong nuclear staining of the tumor cells (case 4). Panels B-D are immunoperoxidase stains; original magnification, × 400. Figure S1 provides high-power photos of cytomorphology of other 5 cases.

Discussion

In the current study, we have confirmed and extended our previous findings in which we identified a new variant of MCL, which we designated cyclin D1-negative MCL.¹² All 6 cases in this study were negative for cyclin D1 mRNA expression by both quantitative RT-PCR and gene expression analysis. These cases also lacked the characteristic *IGH/CCND1* fusion by FISH analysis and were negative for cyclin D1 protein expression by immunostains. Nevertheless, all of the cases exhibited the characteristic pathologic features of MCL and, more importantly, shared the characteristic MCL gene expression profile by microarray analysis. Therefore, these cases are regarded as bona fide cases of cyclin D1-negative MCL. The existence of such cases sheds new light on the pathobiology of MCL and challenges the idea that cyclin D1 overexpression is essential in the pathogenesis of MCL. We have

Table 3. Clinical features of 6 patients with cyclin D1-negative MCL

	Case no. 1	Case no. 2	Case no. 3	Case no. 4	Case no. 5	Case no. 6
Age, y/sex	54/F	61/M	61/M	60/M	54/M	77/M
B symptoms	—	+	—	+	—	—
Serum LDH level	Normal	High	Normal	High	Normal	Normal
Extranodal sites	BM, PB	BM	BM	BM, spleen	GM	BM, lung, GI
IPI score	2	3	2	3	2	3
Initial therapy	None	R-CHOP	CHOP	COP	CHOP	COP
Response	NA	PR	PR	PR	PR	PR
Progression	+	—	+	+	—	+
Follow-up, mo	38	5	88	19	70	30
Status	AWD	AWD	DOD	AWD	AWD	AWD

All patients were at Ann Arbor stage IV.

LDH indicates lactate dehydrogenase; IPI, International Prognostic Index; BM, bone marrow; PB, peripheral blood; GI, gastrointestinal tract; R, Rituxan; CHOP, cyclophosphamide, doxorubicin, vincristine, and prednisone; COP, cyclophosphamide, vincristine, and prednisone; NA, nonapplicable; PR, partial response; AWD, alive with disease; and DOD, dead of disease.

also demonstrated that patients with cyclin D1-negative MCL have clinical and pathologic features similar to those with cyclin D1-positive MCL. In particular, tumors in both groups had the similar growth patterns and common cytologic and immunohistochemical features. Similar age and sex distribution, stage, serum LDH levels, extranodal sites, IPI scores, response to initial treatment, and overall survival were seen in the cyclin D1-positive and -negative groups.

Yatabe et al²⁴ previously reported 151 cases of lymphoma with the morphologic features of MCL. Among these, they identified 23 cases (15%) that were negative for cyclin D1 protein expression by immunohistochemical staining performed on formalin-fixed, paraffin-embedded tissue. Conventional cytogenetics was performed on only 3 of these 23 cases, and all 3 were negative for the t(11;14)(q13;q32). However, FISH or quantitative RT-PCR analysis was not performed on any of these cases. Compared with their group of cyclin D1-positive MCL ($n = 128$), the cyclin D1-negative cases had a significantly better overall survival. In another report, Hashimoto et al²⁵ identified 3 cases of apparent cyclin D1-negative MCL by immunostains and compared them with 14 cases of typical cyclin D1-positive MCL. They also suggested that cyclin D1-negative MCL is a more indolent form of MCL. However, both of these studies failed to provide convincing evidence that their cases of cyclin D1-negative MCL were actually true cases of MCL. In fact, Yatabe et al²⁴ noted in their paper that some of their cyclin D1-negative cases might have been marginal zone B-cell lymphomas or atypical small lymphocytic lymphomas. In contrast, we have clearly demonstrated the characteristic MCL gene expression signature in all of our cases of cyclin D1-negative MCL, and we did not find any significant differences in the clinical features between our 2 groups of MCL. However, since there are only 6 patients in our cyclin D1-negative group, with some having relatively short clinical follow-up, additional studies are warranted to confirm our findings.

The pathogenic mechanisms involved in the development of the cyclin D1-negative MCL are currently unknown. Since the oncogenic effect of overexpressed cyclin D1 is considered to be cell cycle dysregulation, we examined other proteins involved in cell cycle control, especially during the G₁ to S phase transition. The D-type cyclins, D1, D2, and D3, are all positive promoters of cell cycle progression from the G₁ to S phase. The D-type cyclins are similar in structure and biochemical function,²⁶ but are expressed in a lineage-specific manner.²⁷ There is considerable redundancy in the growth-promoting function of the D-type cyclins, since only limited phenotypic consequences due to the absence of either cyclin D1, D2, or D3 are seen in gene knock-out mice.²⁸⁻³¹ In

nonneoplastic lymph nodes and tonsils, cyclin D2 is found mainly in interfollicular T cells, whereas cyclin D3 is found in centroblasts in lymphoid follicles and in scattered B cells and T cells of the interfollicular areas.³² However, cyclin D1 is not expressed in nonneoplastic T cells or B cells.^{6,33} In low-grade B-cell malignancies, overexpression of cyclin D2 mRNA was observed by Northern blot analysis in 29 of 34 cases of chronic lymphocytic leukemia and in all 7 cases of lymphoplasmacytic lymphoma, but not in 2 cases of MCL.³⁴ Cyclin D3 appears to be expressed more ubiquitously in B-cell malignancies, including follicular lymphoma, marginal zone lymphoma, and diffuse large B-cell lymphoma,³⁰ but is usually not expressed in lymphoid malignancies with either cyclin D1 or D2 overexpression.³⁵⁻³⁷ In the current study, overexpression of either cyclin D2 or D3 was observed in all 6 cases of cyclin D1-negative MCL, indicating an important substitutive role for these cyclins in the pathogenesis of cyclin D1-negative MCL. However, the mechanism of cyclin D2 or D3 up-regulation in our cases remains unclear. We did not find any chromosomal translocations or gene amplifications involving the cyclin D2 or D3 gene loci by FISH analysis in these cases. Our findings are consistent with several previous studies that suggested that deregulation of cyclin D2 or D3 expression is often due to epigenetic mechanisms.³⁸⁻⁴⁰

Dysregulation of other genes or factors important in cell cycle control could also play a role in the pathogenesis of such cases. These may include dysregulation of p27^{Kip1}, up-regulation of cyclin E, inactivation of the RB gene, and deletion of the p16^{INK4a}/p14^{ARF} locus, as well as involvement of other genes. The p27^{Kip1} protein regulates cellular progression from G₁ into S phase by inhibiting the cyclin E/CDK2 complex.⁴¹ Regulation of p27^{Kip1} occurs primarily through posttranscriptional mechanisms, including sequestration by cyclin D1 or cyclin D3,^{42,43} or proteasomal degradation.⁴⁴ In a prior study, the expression of p27^{Kip1}, as assessed by immunostains, was noted in only 5 of 40 cases of typical MCL, but was found in 8 of 10 cases of blastic MCL.⁴⁵ In the current study, down-regulation of p27^{Kip1} protein expression was seen in all 6 cases, similar to that seen in typical cyclin D1-positive MCL.

The E-type cyclins, including cyclin E1 and E2, are also important in the G₁ phase of the cell cycle. When combined with CDK2, cyclin E promotes the hyperphosphorylation of RB protein and, thereby, facilitates the entry of cells into S phase.⁴⁶ None of our cases, however, was positive for cyclin E expression, arguing against a role for cyclin E in the pathogenesis of cyclin D1-negative MCL. Inactivation of the RB tumor suppressor gene has been implicated in the development of various types of human malignancy. However, RB protein expression was identified in all

of our cases and the expression levels were similar to those seen in cyclin D1-positive MCL. Our findings are consistent with a previous study in which the authors concluded that RB protein appears to be normally regulated in MCL.⁴⁷ We also investigated whether deletions of the tumor suppressor genes p16^{INK4a} and p14^{ARF} play a role in cyclin D1-negative MCL. p16^{INK4a} regulates the G₁/S phase transition by forming binary complexes with CDK4 and CDK6, thereby preventing these subunits from association with D-type cyclins.⁴⁸ Deletion of p16^{INK4a} or cyclin D1 overexpression may therefore promote the G₁/S phase transition by the same mechanism. An important function of p14^{ARF} is to augment p53 function by antagonizing murine double minute 2 (MDM2), and loss of p14^{ARF} function may contribute to the enhanced proliferation in tumor cells.⁴⁹ As we have shown previously, INK4a/ARF locus deletions occur in up to 21% (18/85) of cases of MCL and are preferentially observed among the more proliferative cases.¹² However, deletion of the INK4a/ARF locus was not identified in any of the 6 cases, arguing against a role for p16^{INK4a}/p14^{ARF} in the pathogenesis of cyclin D1-negative MCL.

Careful morphologic examination, with knowledge of the full spectrum of pathology in MCL, is critical in order to suspect a diagnosis of cyclin D1-negative MCL. This diagnosis may be challenging, particularly since some cases are weakly positive for CD23 or fail to express CD43. However, all 6 cases in our study were positive for CD5, which should suggest the diagnosis of MCL. In such cases, positive immunostains for cyclin D2 or D3 are supportive of this diagnosis. Nevertheless, careful examination to

rule out other types of low-grade B-cell lymphoma, which may also be positive for cyclin D2 or D3, is essential. In the near future, gene expression profiling, or a panel of immunostains based on the MCL signature, will provide the means to confirm this diagnosis. Gene expression studies may also shed further light on the pathogenesis and biology of cyclin D1-negative MCL.

Acknowledgments

The authors wish to thank Gregory Cochran for performing the immunostains, Diane L. Pickering and Adrian Wiestner for technical assistance, James C. Lynch for advice regarding statistical analysis, and other members of the Lymphoma/Leukemia Molecular Profiling Project.

Appendix

The Lymphoma/Leukemia Molecular Profiling Project is an international consortium of the following institutions: the University of Nebraska Medical Center, the National Cancer Institute, the University of Arizona Health Sciences Center, the University of Oregon Health Sciences Center, the University of Rochester Medical Center, Cleveland Clinic, the British Columbia Cancer Agency, University of Würzburg in Germany, University of Barcelona in Spain, Norwegian Radium Hospital in Oslo, and St Bartholomew's Hospital in London.

References

- Weisenburger DD, Armitage JO. Mantle cell lymphoma: an entity comes of age. *Blood*. 1996;87:4483-4494.
- Swerdlow SH, Zukerberg LR, Yang W, Harris NL, Williams ME. The morphologic spectrum of non-Hodgkin's lymphomas with BCL1/cyclin D1 gene rearrangements. *Am J Surg Pathol*. 1996;20:627-640.
- Campo E, Raffeld M, Jaffe ES. Mantle-cell lymphoma. *Semin Hematol*. 1999;36:115-127.
- Ott G, Kalla J, Ott MM, et al. Blastoid variants of mantle cell lymphoma: frequent bcl-1 rearrangements at the major translocation cluster region and tetraploid chromosome clones. *Blood*. 1997;89:1421-1428.
- Weisenburger DD, Vose JM, Greiner TC, et al. Mantle cell lymphoma: a clinicopathologic study of 68 cases from the Nebraska Lymphoma Study Group. *Am J Hematol*. 2000;64:190-199.
- Rosenberg CL, Wong E, Pahty EM, et al. PRAD1, a candidate BCL1 oncogene: mapping and expression in centrocytic lymphoma. *Proc Natl Acad Sci U S A*. 1991;88:9533-9542.
- Banks PM, Chan J, Cleary ML, et al. Mantle cell lymphoma: a proposal for unification of morphologic, immunologic, and molecular data. *Am J Surg Pathol*. 1992;16:637-640.
- Matsushime H, Quelle DE, Shurtleff SA, Shibuya M, Sherr CJ, Kato JY. D-type cyclin-dependent kinase activity in mammalian cells. *Mol Cell Biol*. 1994;14:2066-2076.
- Meyerson M, Harlow E. Identification of G1 kinase activity for cdk6, a novel cyclin D partner. *Mol Cell Biol*. 1994;14:2077-2086.
- Millnacht S, Lees JA, Desai D, Harlow E, Morgan DO, Weinberg RA. Distinct sub-populations of the retinoblastoma protein show a distinct pattern of phosphorylation. *EMBO J*. 1994;13:118-127.
- Jaffe ES, Harris NL, Stein H, Vardiman JW, eds. *World Health Organization Classification of Tumors: Pathology and Genetics of Tumors of Hematopoietic and Lymphoid Tissues*. Lyon, France: IARC Press; 2001.
- Rosenwald A, Wright G, Wiestner A, et al. The proliferation gene expression signature is a quantitative integrator of oncogenic events that predicts survival in mantle cell lymphoma. *Cancer Cell*. 2003;3:185-197.
- Bljward KE, Aguilera NS, Monczak Y, Trudel M, Taubenberger JK, Uchey JH. Quantitative real-time reverse transcription-PCR assay for cyclin D1 expression: utility in the diagnosis of mantle cell lymphoma. *Clin Chem*. 2001;47:195-201.
- Alizadeh A, Eisen M, Davis RE, et al. The lymphochip: a specialized cDNA microarray for the genomic-scale analysis of gene expression in normal and malignant lymphocytes. *Cold Spring Harb Symp Quant Biol*. 1998;64:71-78.
- Wright G, Tan B, Rosenwald A, Hunt EH, Wiestner A, Staudt LM. A gene expression-based method to diagnose clinically distinct subgroups of diffuse large B cell lymphoma. *Proc Natl Acad Sci U S A*. 2003;100:9991-9998.
- Brynes RK, McCourt A, Tamayo R, Jenkins K, Ballifora H. Demonstration of cyclin D1 (bcl-1) in mantle cell lymphoma: enhanced staining using heat and ultrasound epitope retrieval. *Appl Immunohistochem*. 1997;5:45-48.
- Cheuk W, Wong KO, Wong CS, Chan JK. Consistent immunostaining for cyclin D1 can be achieved on a routine basis using a newly available rabbit monoclonal antibody. *Am J Surg Pathol*. 2004;28:801-807.
- Schlegelberger B, Harder S, Zühlke-Jenisch R, Zhang Y, Siebert R. Classical and molecular cytogenetics of tumor cells. In: Wagner RD, ed. *Diagnostic Cytogenetics*. Berlin, Germany: Springer-Verlag; 1999:151-185.
- Martin-Suero JI, Chudoba I, Harder L, et al. Multicolor-FISH: expanding the possibilities of combined morphologic, immunophenotypic, and genetic single cell analyses. *Am J Pathol*. 2002;161:413-420.
- Sonoki T, Harder L, Horsman DE, et al. Cyclin D3 is a target gene of t(6;14)(p21.1;q32.3) of mature B-cell malignancies. *Blood*. 2001;98:2837-2844.
- Ye H, Liu H, Attygalle A, et al. Variable frequencies of t(11;18)(q21;q21) in MALT lymphomas of different sites: significant association with *CagA* strains of *H pylori* in gastric MALT lymphoma. *Blood*. 2003;102:1012-1018.
- Labuhn M, Jones G, Spelz EJ, et al. Quantitative real-time PCR does not show selective targeting of p14(ARF) but concomitant inactivation of both p16(INK4A) and p14(ARF) in 105 human primary gliomas. *Oncogene*. 2001;20:1103-1109.
- Goff LK, Neat MJ, Crawley CR, et al. The use of real-time quantitative polymerase chain reaction and comparative genomic hybridization to identify amplification of the *FEL* gene in follicular lymphoma. *Br J Haematol*. 2000;111:618-625.
- Yataba Y, Suzuki R, Tobinai K, et al. Significance of cyclin D1 overexpression for the diagnosis of mantle cell lymphoma: a clinicopathologic comparison of cyclin D1-positive MCL and cyclin D1-negative MCL-like B-cell lymphoma. *Blood*. 2000;95:2253-2261.
- Hashimoto Y, Nakamura N, Kuze T, Abe M. The evaluation of the biological behavior and grade among cases with mantle cell lymphoma. *Louk Lymphoma*. 2002;43:523-530.
- Inaba T, Matsushime H, Valentine M, Rousset MF, Sherr CJ, Look AT. Genomic organization, chromosomal localization, and independent expression of human cyclin D genes. *Genomics*. 1992;13:565-574.
- Sherr CJ, Kato J, Quelle DE, Matsushime M, Rousset MF. D-type cyclins and their cyclin-dependent kinases: G1 phase integrators of the mitogenic response. *Cold Spring Harb Symp Quant Biol*. 1994;59:11-19.
- Sicinski P, Donaher JL, Parker SB, et al. Cyclin D1 provides a link between development and oncogenesis in the retina and breast. *Cell*. 1995;82:621-630.

29. Sicinski P, Donaher JL, Geng Y, et al. Cyclin D2 is an FSH-responsive gene involved in gonadal cell proliferation and oncogenesis. *Nature*. 1996;381:470-474.
30. Ciernyeh MA, Kenney AM, Sicinska E, et al. Development of mice expressing a single D-type cyclin. *Genes Dev*. 2002;16:3277-3288.
31. Sicinska E, Allantia I, Le Cam L, et al. Requirement for cyclin D3 in lymphocyte development and T cell leukemias. *Cancer Cell*. 2003;4:451-461.
32. Teramoto N, Pokrovskaja K, Szekely L, et al. Expression of cyclin D2 and D3 in lymphoid lesions. *Int J Cancer*. 1999;81:543-550.
33. Yang W, Zukerberg LR, Motokura T, Arnold A, Harris NL. Cyclin D1 (Bcl-1, PRAD1) protein expression in low-grade B-cell lymphomas and reactive hyperplasia. *Am J Pathol*. 1994;145:86-96.
34. Delmer A, Aichenbaum-Cymbalista F, Tang R, et al. Overexpression of cyclin D2 in chronic B-cell malignancies. *Blood*. 1995;85:2870-2876.
35. Ott MM, Bartkova J, Bartek J, et al. Cyclin D1 expression in mantle cell lymphoma is accompanied by downregulation of cyclin D3 and is not related to the proliferative activity. *Blood*. 1997;90:3154-3158.
36. Doglioni C, Chiarelli C, Maci E, et al. Cyclin D3 expression in normal, reactive and neoplastic tissues. *J Pathol*. 1998;185:159-166.
37. Suzuki R, Kuroda H, Komatsu H, et al. Selective usage of D-type cyclins in lymphoid malignancies. *Leukemia*. 1999;13:1395-1342.
38. Andreasson P, Johansson B, Arheden K, et al. Genomic amplification of CCND2 is rare in non-Hodgkin lymphomas. *Cancer Genet Cytogenet*. 1998;102:81-82.
39. Pruneri G, Fabris S, Fasani R, et al. Immunoreactivity for cyclin D3 is frequently detectable in high-grade primary gastric lymphomas in the absence of the t(6;14)(p21.1;q32.3) chromosomal translocation. *J Pathol*. 2003;200:596-601.
40. Bergsagel PL, Kuehl WM. Critical roles for immunoglobulin translocations and cyclin D dysregulation in multiple myeloma. *Immunol Rev*. 2003;194:96-104.
41. Polyak K, Kato JY, Solomon MJ, et al. p27Kip1, a cyclin-Cdk inhibitor, links transforming growth factor-beta and contact inhibition to cell cycle arrest. *Genes Dev*. 1994;8:9-22.
42. Quintanilla-Martinez L, Davies-Hill T, Fend F, et al. Sequestration of p27Kip1 protein by cyclin D1 in typical and blastic variants of mantle cell lymphoma (MCL): implications for pathogenesis. *Blood*. 2003;101:3181-3187.
43. Lin Z, Lin S, Lin MS. Growth regulation by p27Kip1 is abrogated by multiple mechanisms in aggressive malignant lymphomas. *Br J Haematol*. 2003;121:739-748.
44. Chiarelli R, Budel LM, Skotnik J, et al. Increased proteasome degradation of cyclin-dependent kinase inhibitor p27 is associated with a decreased overall survival in mantle cell lymphoma. *Blood*. 2000;95:618-626.
45. Quintanilla-Martinez L, Thieblemont C, Fond F, et al. Mantle cell lymphomas lack expression of p27Kip1, a cyclin-dependent kinase inhibitor. *Am J Pathol*. 1998;153:175-182.
46. Sherr CJ. Cancer cell cycles. *Science*. 1996;274:1872-1877.
47. Jares P, Campo E, Pinyol M, et al. Expression of retinoblastoma gene product (pRb) in mantle cell lymphomas: correlation with cyclin D1 (PRAD1/CCND1) mRNA levels and proliferative activity. *Am J Pathol*. 1996;148:1591-1600.
48. Sherr CJ, McCormick F. The Rb and p53 pathways in cancer. *Cancer Cell*. 2002;2:103-112.

BIOLOGY OF REPRODUCTION 54, 700-708 (1996)

Oxytocin Receptors in Bovine Cervix: Distribution and Gene Expression during the Estrous Cycle¹

A-R. Fuchs,^{2,4,5} R. Ivell,⁵ P.A. Fields,⁶ S-M.T. Chang,⁷ and M.J. Fields^{3,7}

*Department of Obstetrics and Gynecology,⁴ Cornell University Medical College, New York, New York 10021
Institute for Hormone and Fertility Research,⁵ Hamburg, Germany*

*Department of Structural and Cellular Biology,⁶ University of South Alabama, Mobile, Alabama 36688
Animal Science Department,⁷ University of Florida, Gainesville, Florida 32611*

ABSTRACT

Oxytocin (OT) receptor (OTR) concentrations were determined in the cervix of nonpregnant cows on cycle Days 0, 3, 7-8, 17, and 19 ($n = 3-4$ cows each day); [³H]OT was used as the labeled ligand. Mucosal and muscle layers of the cervix were also analyzed separately for both ligand binding and expression of the OTR gene using a newly developed RNase protection assay (RAP). Cellular localization of OTR protein was determined by immunohistochemistry. All regions of cervix from cows at estrus had high concentrations of OTR; in the luteal phase, all were sharply down-regulated. At estrus the mucosal layer had about 30-fold higher concentrations than the muscle layer. OTR mRNA was readily detected by RAP in the mucosa from estrous cows, while much weaker signals were found in the muscle. On Days 7-17, the OTR mRNA signals in both mucosa and muscle were very faint or nondetectable. Thus, there was a good correlation between ligand binding and mRNA expression, which suggests that OTR concentrations are mainly regulated at the transcriptional level. The epithelial cells at the luminal surface of the mucosa were the principal site of immunoreactive OTR; muscle cells showed significantly weaker signals. Previously, OT was found to stimulate prostaglandin (PG) E₂ output in vitro in bovine cervical tissues. Since PGE₂ is capable of softening the cervix, our findings suggest that OT may have a novel physiological function to cause softening of the bovine cervix mediated by the release of PGE₂.

INTRODUCTION

Oxytocin (OT) has in recent years been shown to have other actions on the tissues of the female reproductive tract than the stimulation of myometrial contractions. These include, among others, the stimulation of prostaglandin (PG) F_{2a} release from endometrium and decidua [1-3] and PGE₂ from amnion [2, 4]. The OT receptors (OTR) that mediate these actions are similar to myometrial OTR with respect to the shared affinities for the neurohypophyseal peptides and their analogues [5, 6]. Preliminary results of our research indicated that the bovine cervix may also be a target for OT [7]. We have now expanded these studies, and we have determined the topographic distribution of OTR within the nonpregnant bovine cervix at various stages of the estrous cycle and analyzed the expression of the OTR gene in these tissues. The cellular localization of the OTR in the cervical tissues was also determined by immunohistochemical methods. The expression of the gene for the OT peptide has recently been demonstrated in some nonendocrine tis-

sues of the reproductive tract [8, 9]. We therefore analyzed the cervical tissues also for the expression of the OT gene.

MATERIALS AND METHODS

Animals and Tissues

Tissues were obtained from purebred Hereford or Angus cows belonging to the herd of the USDA Subtropical Agriculture Research Station, Brooksville, FL. The day of estrus (Day 0) was assigned when the cow was observed to stand for mounting by a penis-deflected bull. Tissues were obtained at the University of Florida Meat Laboratory from cows (2 or 3 per day) slaughtered on Days 0, 3, 7, 8, 17, or 19. The cervix was removed immediately after exsanguination, dissected into suitable pieces, and snap-frozen in liquid nitrogen. Vagina was taken from a few of the cows (Days 0 and 7).

In experiment 1, three cross-sectional slices were taken from each cervix as shown in Figure 1. One segment was from the region of the cranial end, one from the region of the caudal end, and one from the mid-portion. The slices were divided into pieces consisting of both muscle and mucosa layers, which were snap-frozen in liquid N₂ and kept at -80°C until receptor assay.

In experiment 2, the cervical tissues were divided into mucosal and muscle layers for separate analysis. One aliquot of each frozen tissue was used for measurement of ligand binding and another for RNA extraction and immunohistochemistry. All tissues were kept at -80°C until shipped in dry ice for further processing.

Accepted November 16, 1995.

Received September 12, 1995.

¹This work was supported by a grant from the USA-Israel Binational Agricultural Research and Development Fund (BARD #US-2333-93), the Fogarty Foundation Grant #FO6 TW02093-01, the Warner-Lambert Foundation, and Grant Iv7-1 from the Deutsche Forschungsgemeinschaft. Florida Agricultural Experiment Station Journal Series No. R-04858.

²Correspondence: Anna-Rita Fuchs, Department of Obstetrics and Gynecology, Cornell University Medical College, 515 E. 71 Street, Room S-412, New York, NY 10021. FAX: (212) 746-8996.

³Reprint requests: MJ Fields, Animal Science Dept., University of Florida, 459 Shealy, Room 125, Gainesville, FL 32611-1288.

OXYTOCIN RECEPTORS IN BOVINE CERVIX

701

Additionally, cross sections of the cervix from all three regions were collected for histological analysis. Tissues were collected from cows at estrus and Day 7 of the estrous cycle.

Receptor Assays

Crude microsomal preparations were used for receptor assay as previously described [10]. Frozen tissues were quickly pulverized and then homogenized in a 10 mM Tris buffer containing 1.5 mM EDTA, 0.5 mM dithiothreitol, and 0.002% PMSF, pH 7.4. The pellets were obtained by centrifugation of 1000 g supernatants at $160\,000 \times g$ for 30 min. After washing with the same buffer, the pellets were resuspended in Ca^{2+} -free Hanks' solution, pH 7.0, and stored at -80°C . Protein concentrations were determined according to the methods of Lowry et al. [11] with BSA as standard.

Ligand binding assays were performed as previously described [10]. Tritiated OT ($[\text{H}]\text{OT}$; sp. act. 36.6 Ci/mmol, one lot 48.5 Ci/mmol; New England Nuclear, Boston, MA) was used as the labeled ligand. Assay buffer consisted of 50 mM Tris maleate, 5 mM MnCl_2 , 0.002% PMSF and 0.1% BSA, pH 7.4; incubation temperature was 22°C and duration was 60 min. Separation of bound and free ligands was achieved by rapid filtration through Whatman (Clifton, NJ) GF/F filters using a Brandel Cell Harvester (Gaithersburg, MD). Binding was initially characterized in saturation assays using 8–10 different concentrations of $[\text{H}]\text{OT}$ (5×10^{-11} to 5×10^{-8} molar), and by displacement assays with the following: unlabeled OT; an OT antagonist (1- β -mercapto- β , β -cyclopenta-methylene-propionic acid-2-tyrosine [O-methyl]-4-threonine-8-ornithine-9-Tyrosine NH₂) vasotocin (OVTA); arginine vasopressin (AVP); a V_1 subtype agonist (2-phenyl-alanine-8-ornithine) vasopressin (PAVP); and V_1 antagonist (1- β -mercapto- β , β -cyclopenta-methylene-propionic acid-2-tyrosine[O-methyl]-8-arginine)-vasopressin, the "Manning Compound" (MC). OVTA was a gift from Prof. M. Manning, Department of Biochemistry, Medical College of Ohio (Toledo, OH); PAVP was obtained from Peninsula (Belmont, CA), and the other peptides were obtained from Bachem (Torrance, CA). Chemicals other than peptides were from Sigma Chemical Co. (St. Louis, MO). The data were analyzed by a computerized curve fitting program, LIGAND (Biosoft, Elsevier, NJ), which identifies the parameters K_m , K_d , K_p , and B_{max} (the binding capacity). B_{max} values for the individual samples were determined using four different concentrations of $[\text{H}]\text{OT}$ (10^{-10} to 10^{-8} M); the data were analyzed with the LIGAND program. Protein concentrations used for each assay ranged from 50 to 200 $\mu\text{g}/\text{ml}$. Within this range, ligand binding was linearly correlated to protein concentration. Nonspecific binding (NSB) was determined at each concentration of $[\text{H}]\text{OT}$ in the presence of 1.1 μM unlabeled OT. NSB was lowest in mucosal and muscle preparations, about 1% of total counts; in cross-sectional prepa-

rations it was 2–4% of total cpm. All assays were run in duplicate, and results were expressed in fmol/mg microsomal protein.

Histology of Cervical Tissue

Cross-sectional pieces from each region of the cervix were placed in Carson's modified Millonig's phosphate-buffered formalin [12], embedded in paraffin, and sectioned (5- μm thick) onto glass slides. The sections were stained for collagen using Gomori's trichrome stain [12] and for elastin using orcein stain and hematoxylin as a counter stain [12].

Immunohistochemical Localization of Bovine OTR

A monoclonal antibody was used to identify the cellular localization of the receptor protein in cervical mucosa and cervical muscle of the cervix obtained from a parturient cow. The antibody (courtesy of Dr. T. Kimura, Osaka, Japan) was developed by Takemura et al. [13] in mice against a 21-amino-acid-long peptide sequence comprising the extracellular, amino-terminal region of the OT receptor gene that shows high homology between the human, rat, and bovine genes. Frozen cryostat sections of pieces of cervical mucosa and muscle tissue were mounted on gelatin-coated slides. Sections were fixed in cold methanol (-20°C) and then air-dried before immunostaining. Antibodies were applied at different dilutions (1:100, 1:500, 1:1000, 1:2000). Immunoenzymatic labeling was carried out using the alkaline phosphatase technique (APAAP-complex; Dianova, Hamburg, Germany). The specificity of staining was monitored in control sections where the hormone-specific antibody was replaced by pure mouse IgM. After counterstaining with hematoxylin, all sections were mounted in glycerine jelly and examined through a Nikon Epiphot (Melville, NJ) microscope. Muscle tissue from the jaw was used as a negative control tissue.

RNA Preparation

Total RNA was prepared by guanidinium isothiocyanate extraction from UltraTurrax (Janke and Kandal, Staufen, Germany) homogenates followed by ultracentrifugation through cesium chloride cushion. All RNA samples were subjected to phenol/chloroform purification steps, as previously described [14]. The quality of the RNA samples was assessed by measuring optical densities and by gel-electrophoresis on 1.2% agarose gels. All preparations had a ratio of optical densities at 260 nm and 280 nm between 1.6 and 1.8. The samples were stored in diethylpyrocarbonate-treated water at -20°C .

Detection of Specific OTR Gene Transcripts

RNase protection assays (RPA) were established as previously described [13, 16] to detect gene transcripts for bovine OTR and for bovine glyceraldehyde phosphate dehy-

TABLE 1. Avidity of unlabeled OT and various analogs to cervical [3 H] OT binding sites. The cervical membrane preparations were from a cow at estrus.

Compound	K _i , nmol/L
OT	1.0
OVTA	0.5
AVP	2.3
PAVP	6.4
MC	14.9

drogenase (GAPDH) as control. The sequence of the bovine OTR gene [15] had not yet been determined when these studies began. Oligonucleotides suitable for use in a polymerase chain reaction assay were based on the human OTR sequence [13]. The upstream and downstream primers were derived from regions corresponding to the third extracellular loop (5' primer: CCTGGGGACCCAAGGCCTAC) and the sixth transmembrane domain (3' primer: AAGAAGAAAGGCGTCCAGCACACGA), respectively. Using a standard reverse transcriptase-polymerase chain reaction (RT-PCR) protocol, bovine myometrium from term uteri was used to program the synthesis of the single-stranded cDNA, and the resulting product was cloned into plasmid vector pCRII (Invitrogen, San Diego, CA). The sequence of this fragment of bovine OTR cDNA, determined by double-stranded sequencing, showed 85% homology to the corresponding region of human OTR cDNA. For OTR mRNA, the cRNA probe was produced as described previously by *in vitro* transcription of the plasmid pCRII containing a cloned RT-PCR fragment, using T7 RNA polymerase following linearization of the plasmid with *Hind*III. The probe length is 425 b, which includes 123 b of the multiple cloning site, and protects an mRNA sequence of 302 b. The bovine GAPDH assay was similarly designed with a probe size of 321 b, including 123

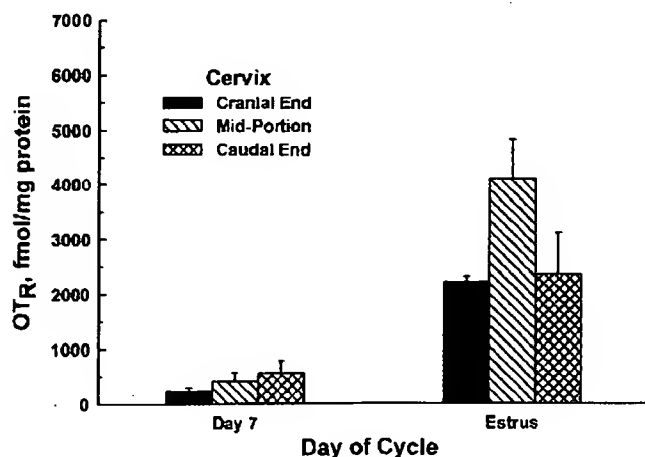


FIG. 1. OTR concentrations in three different cross-sectional segments of the bovine cervix (cranial, midportion, and caudal) at estrus ($n = 4$ cows) and Day 7 ($n = 3$ cows). Data (fmol/mg protein) represent mean \pm SE. OTR concentrations in all three segments were higher at estrus than at Day 7 ($p < 0.05$). At estrus, the midportion had the greatest concentration of OTR.

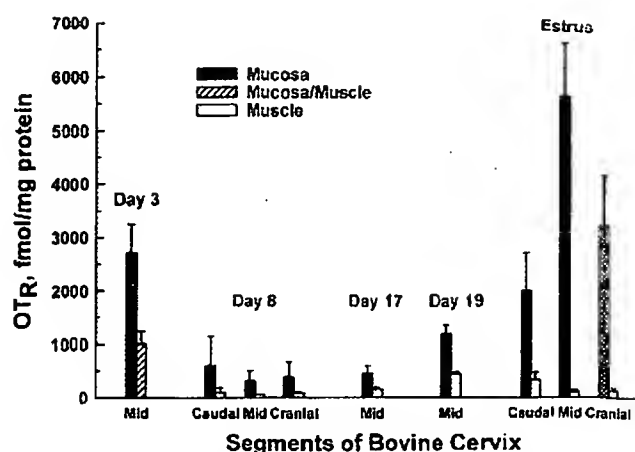


FIG. 2. OTR concentration in mucosa and muscle layers from three regions of the cervix (cranial, midportion, and caudal) collected from cows at estrus and Days 3, 8, 17, and 19 ($n = 3-4$ cows each day). Data (fmol/mg protein) represent mean \pm SE. OTR concentration in mucosa was higher than in muscle regardless of day of estrous cycle or region of cervix ($p < 0.005$). The highest concentration of OTR was found in the mucosal layer of the midportion at estrus ($p < 0.01$).

b of the multiple cloning site, and it protects an mRNA sequence of 198 b. The GAPDH antisense cRNA was transcribed *in vitro* from the plasmid pCRII, containing a bovine GAPDH PCR fragment, using T3 RNA polymerase, after linearization of the plasmid with *Eco*RI. All cRNA probes were prepared in the presence of [32 P]CTP as described in the instructions to the commercial RPA kit used (Ambion, Austin, TX); the probes were subsequently purified by polyacrylamide gel-electrophoresis on 6% gels. For the actual RPA, 10 μ g of total RNA from each tissue was hybridized with the OTR- and GAPDH-specific cRNA probes in the same reaction vial. Due to the difference in size of the protected fragments for the two cRNAs, they can be readily separated on the polyacrylamide gel.

Detection of OT Gene Transcripts

Reverse transcriptase PCR assay for OT mRNA has been described in detail elsewhere [16]. It yields a 300-b PCR fragment that can be specifically detected after Southern blotting by use of an internal radioactively labeled oligonucleotide probe.

Statistical Analysis

One-way analysis of variance (ANOVA) was used to distinguish differences among the three topographic regions of the cervix. Differences among the days of estrous cycle were also analyzed by one-way ANOVA for each type of tissue separately, followed by Newman-Keul's test. Differences between mucosa and muscle were assessed by paired *t*-test. Differences were considered significant when $p < 0.05$.

OXYTOCIN RECEPTORS IN BOVINE CERVIX

703

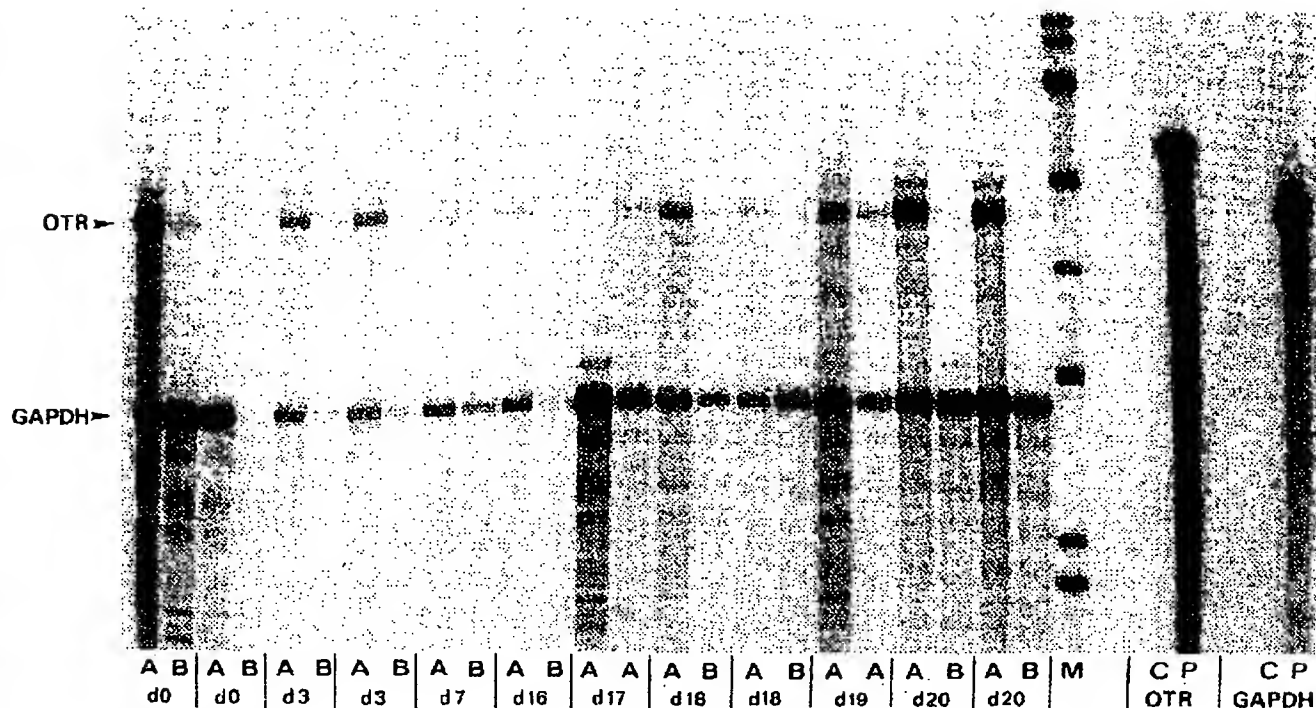


FIG. 3. RNase protection assays specific for mRNA encoding for OTR (length of protected fragment 302 b) and GAPDH as control (length of protected fragment 198 b). Lanes marked A represent cervical mucosa and those marked B represent muscle from cows at different days of the estrous cycle. Lane M: *Hinf*I digested PhiX174 DNA size marker, end-labeled with [32 P]dCTP. The probes were loaded on lanes marked OTR and GAPDH; C, RNase digested probes; P, undigested probes. Whereas signals for GAPDH were similar at all days, signals for OTR were markedly lower in the luteal phase than at estrus, particularly in the mucosal tissues. At Day 19 signals for OTR had increased from Days 7 and 17 levels and were similar to estrous levels.

RESULTS

OT Ligand Binding in Cervical Tissues

Saturation analysis of cross-sectional cervical tissue from estrous cows with 8–10 point assays indicated that high affinity, saturable binding sites were present that fitted a one-site model ($K_d = 5.9 \pm 0.4 \times 10^8$ L/mol; Hill coefficient = 0.986 ± 0.006). Unlabeled OT displaced the labeled ligand with similar affinity (K_i : 1.0 nmol/L) and similar B_{max} as [3 H]OT. The inhibition constants of the specific OT antagonist (OVTA), arginine vasopressin (AVP), the V_1 subtype agonist (PAVP), and the V_1 subtype antagonist (MC) are shown in Table 1. All exhibited a similar B_{max} as unlabeled OT, and the individual Hill coefficients did not differ significantly from unity (range 0.92–1.004).

The OTR concentration in the cervix, when averaged for the three regions (cranial end, mid-portion and caudal end), was 2730 ± 435 fmol/mg at estrus (3 cows). In luteal phase, on Days 7 and 8, receptor concentrations were markedly lower (400 ± 96 fmol/mg, 4 cows, $p < 0.005$). OTR concentrations in the vagina (average of single samples) were similar to those in the cervix, however, the difference in receptor density between estrus and Day 7 was not significant in vaginal tissues (1460 ± 781 fmol/mg, $n = 4$ and

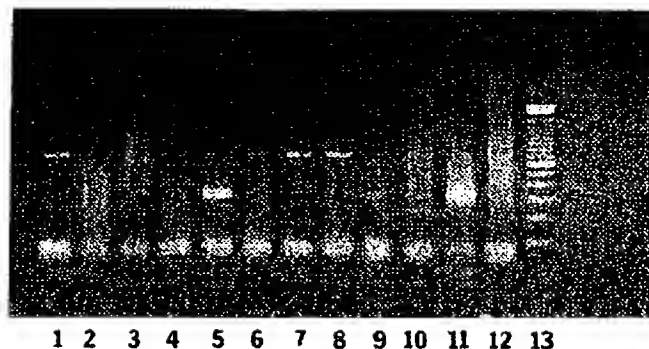


FIG. 4. RT-PCR assay for detection of OT encoding transcripts in seven samples of cervical mucosa (lanes 1–7). For comparison, samples from corpora lutea of three term pregnant cows were included (lanes 8–10). cDNA template from Day 3 corpus luteum served as positive control (lane 11), and H_2O as negative control (lane 12). Lane 13, 1 Kb marker. The PCR products were prepared from equivalent amounts of total RNA and were separated on 1.2% agarose gel. The assay yields a 310 b PCR fragment (arrow), which was present in the Day 3 corpus luteum (lane 11) and cervical mucosa from a Day 17 cow (lane 5) but was absent in the other six cervical samples, two from Day 0 and one each from Days 3, 7, 16, and 19 of estrous cycle. The three term corpora lutea showed weak signals for the 310 b fragment.

753 ± 204 fmol/mg, $n = 2$, respectively). The receptor affinity for [3 H]OT did not differ with respect to regional origin of the tissue or stage of the estrous cycle.

The distribution of OTR along the cranio-caudal axis of

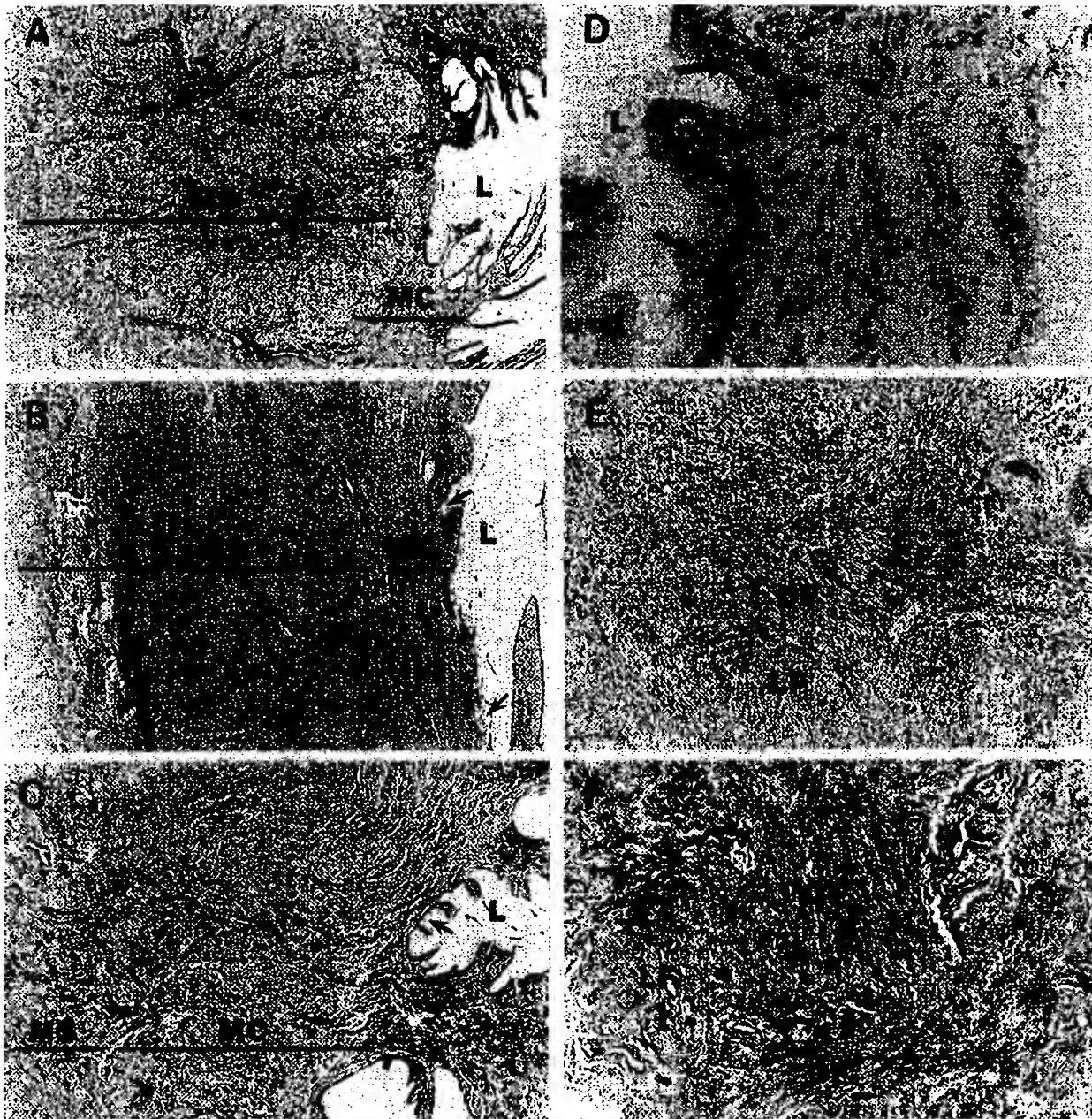


FIG. 5. Light microscopic photographs from different regions of the bovine cervix at Day 7 of the estrous cycle. A,D) Cranial end. B,E) Mid-portion. C,F) Caudal end. A,B,C,E,F) Gomori's trichrome was used for staining the connective tissue. The connective tissue collagen stains blue-green and the smooth muscle and epithelial cells stain red. D) Orcein staining was used for elastin with hematoxylin counterstain in a cranial region of the cervix. The elastin fibers stain brown (small arrows) while the basal nuclei of mucosa epithelial cells stain bluish purple (large arrows). Note the clear apical cytoplasm of the luminal epithelial cells, which is distended with secretory material (arrows) into the lumen (L) of the cervix. A,B,C) The cervical mucosa consists of mucin-filled columnar epithelial cells (arrows) and underlying stromal cells. The underlying tissue layer consists of two distinct regions, mucosa (MC) and muscle (MS). The mucosa layer contains bundles of longitudinal smooth muscle dispersed in the connective tissue. The muscle layer contains abundant smooth muscle dispersed in connective tissue in a complex arrangement. The arrowhead in C represents the area of magnification shown in F. E,F) The muscle fibers are arranged in longitudinal (LF), circular (CF), and oblique transverse (OF) configurations dispersed throughout the different regions of the cervix end throughout the muscle layers. A-C, $\times 40$; D, $\times 400$; E and F, $\times 100$.

the cervix varied significantly in tissues from estrous cows ($p < 0.05$), but in the luteal phase the differences were not significant. At estrus the mid-portion of the cervix had the highest OTR concentration (Fig. 1).

Cervical mucosa had significantly higher OTR concentrations than the muscle layer in all three regions and at all stages of the estrous cycle ($p < 0.005$) (Fig. 2). The greatest difference between the two layers was observed at the time

OXYTOCIN RECEPTORS IN BOVINE CERVIX

705

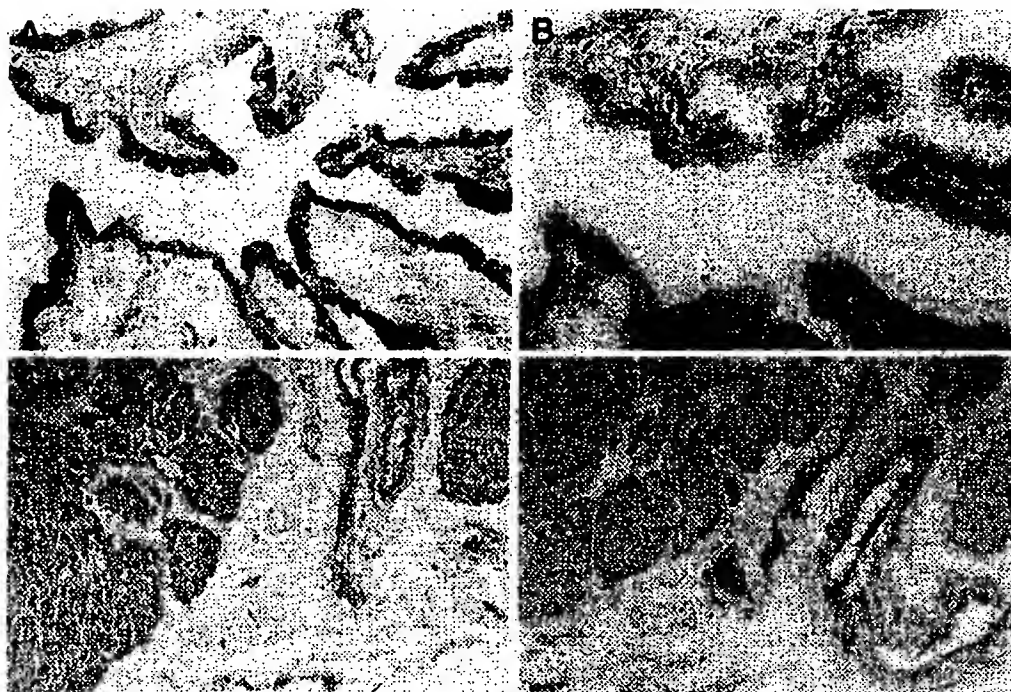


FIG. 6. Localization of immunoreactive OTR (OTR-ir) in cervical tissues of an estrous cow using the alkaline phosphatase method. A,B) Cervical mucosa. C,D) Cervical muscle. The monoclonal antibody was used at a dilution of 1:2000; adjacent sections were used as controls (B,D) and were treated with pure mouse IgM. Intense staining for OTR-ir (red) was detected in the epithelial cells of the mucosa; staining of other cells in the mucosal layer was not detected. In the muscular part of the cervix, staining for OTR-ir was restricted to the muscle cells and was less intense than in the epithelial cells. A and C, $\times 233$; C and D, $\times 93$.

of estrus. On Day 3, OTR concentrations in the mucosal layer had declined significantly ($p < 0.05$) from estrous values, and a further decline was observed on Days 8 and 17 ($p < 0.01$). The drop in cervical OTR density during the luteal phase affected mainly the mucosal layer ($p < 0.01$); the variations in the muscle layer were not significant. OTR concentrations in mucosa on Days 8 and 17 were on the average reduced to 8% of estrous values, whereas in the muscle layer they were reduced to about 60% of values at estrus (not significant). Return towards Day 0 values was evident on Day 19 when mucosal OTR concentrations had increased in two of the three cows to a mean 1638 ± 137 fmol/mg, whereas in the third cow, OTR concentrations were similar to those in the midluteal phase, 291 fmol/mg. Receptor affinity was similar in the two tissues at all days of the estrous cycle; the mean K_D for mucosa was 1.31 ± 0.18 nmol/L and for muscle, 1.04 ± 0.08 nmol/L.

Some regional variation in the mucosal OTR density was evident in the cervix of estrous cows but not in the cervix of luteal-phase cows. The highest concentration of OTR in the mucosal layer was found in the mid-portion; the regional differences among the muscle layers were not significant on any day of the cycle.

Detection of OTR mRNA in Bovine Cervical Tissues

With use of the RPA, mRNA for the OTR gene could be readily detected in cervical tissues obtained from estrous

cows (Fig. 3). In mucosa obtained at the time of behavioral estrus (Day 0), the signal for OTR mRNA was strong in all three regions of the cervix. The signals were markedly weaker on Day 3 than on Day 0, and on Day 7 they were further reduced to almost nondetectable levels. Weak bands of OTR mRNA were again visible in mucosal tissue on Day 17, and strong bands were seen on Day 19 in two of three cows. In the muscular layer, OTR mRNA levels were lower than in the mucosal layer at all stages of estrous cycle (Fig. 3).

Detection of OT Peptide Gene Transcripts in Cervical Tissue

Using the RT-PCR assay, which is an extremely sensitive though only semiquantitative assay system, positive signal for OT cDNA was detected in only one of several samples of cervical mucosa (Day 17), whereas strong positive signals were readily obtained from bovine corpora lutea from Day 3 and weak signals from corpora lutea from three term pregnant cows (Fig. 4).

Histology of Bovine Cervix

A light microscopic evaluation of the cervix from a non-pregnant cow on Day 7 is represented in Figure 5. Sections from the cranial region are shown in panels A and D, from the midportion in panels B and E, and from the caudal re-

gion in panels C and F. Gomori's trichrome stain for connective tissue was used in all sections except D, in which orcein staining for elastin and hematoxylin counterstain were used. Collagen stains blue-green, smooth muscle and epithelial cells stain red, elastin fibers stain brown (small arrows in panel D), and the nuclei of the epithelial cells stain bluish purple (large arrows, panel D). The cervix comprises two distinct layers, mucosa (MC) and muscle (MS), shown in A, B, and C. Mucosa consists of mucin-filled, columnar epithelial cells lining the luminal surface (small arrows; L = lumen) and an immediately adjacent area of dense connective tissue. This area is narrow in the cranial region (A) and increases in width towards the caudal region (C). Muscle layer (MS) is beneath the mucosal layer and can be divided into two distinct regions: inner, shown in panels A, B, C, E, and F; and outer (not shown). The inner muscle layer contains collagen bundles and elastin fibers interspersed among an abundance of smooth muscle, which comprises longitudinal (LF), circular (CF), and oblique transverse running fibers (OF) arranged in a complex manner, as shown in greater magnification in panels E and F. The arrowhead in panel C represents the area of magnification shown in panel F. The outer muscular layer is characterized by collagen bundles, elastin fibers and numerous, primarily longitudinally oriented smooth muscle fibers. The epithelial cells of the mucosa are present in a single layer as shown in greater magnification in panel D (large arrows). They are distended and have clear cytoplasm in the apical area, indicative of active secretion of mucin into the cervical lumen (L). The underlying stromal cells are dispersed in the dense connective tissue containing elastin fibers (small arrows) and a small amount of smooth muscle arranged predominantly in circular manner. No distinct differences were seen in bovine cervix at estrus and Day 7 using the staining procedures of this study.

Immunohistochemistry for Localization of OTR Protein

In cervical mucosa from cows at estrus, staining for the OTR protein was localized exclusively in the epithelial cell layer (Fig. 6A). All epithelial cells appeared to be strongly stained, and no significant differences were noted among the different regions of the cervix (not shown). The collagenous submucosa showed no staining, and in the muscle layer only muscle cells were positively stained (Fig. 6C).

DISCUSSION

The present results confirm and expand our preliminary observations on the presence of high concentrations of OTR in the bovine cervix at estrus [7]. The ligand binding in bovine cervical tissues had characteristics similar to those for bovine endometrial and myometrial OT receptors [10]. In all these tissues, the OTR have a relatively high affinity for arginine vasopressin and V_1 subtype agonists and antago-

nists. The concentrations in cervical mucosa of estrous cows were similar or even higher than those found to be present in the endometrium of cows of the same breeds and at the same stage of the cycle [10]. As in endometrium, OTR concentrations in cervical mucosa declined dramatically in the luteal phase, indicating similar regulation by gonadal hormones of OTR gene expression in these two tissues. OTR concentrations in cervical muscle and myometrium also varied in a similar manner: OTR density in both tissues showed only minor variations during the cycle, although a trend toward lower values on Days 7–8 was evident in both tissues [10].

Changes in ligand binding and OTR mRNA level in cervical tissues during the estrous cycle were well correlated, suggesting that OTR protein concentrations are regulated mainly at the transcriptional level. Similar relationships between ligand binding and OTR mRNA levels were also observed in bovine endometrium and myometrium [14, 17].

No physiological function has previously been assigned to OT in cervical tissues. Contractions of the nonpregnant bovine cervix in response to OT injections *in vivo* have, however, been observed; the responses were stronger in the early luteal than in the midluteal phase [18]. We have reported elsewhere that OT caused a selective stimulation of PGE_2 output from cervical tissues of estrous cows *in vitro*; PGE_{20} output was minimal and was not affected by OT [17]. OT had a smaller effect on PGE_2 output in cervical tissues obtained 3–4 days after estrus and no effect in tissues from cows in the luteal phase [17]. Thus the responses corresponded to OTR concentrations at these stages of the cycle and are presumably OTR mediated. The presence of OTR mainly in the mucosal layer is in agreement with this notion, since epithelial and stromal cells have been shown to produce PGE_2 and PGE_{20} [19], whereas muscle cells produce mostly PGI_2 . PGE_2 has been shown to produce cervical softening in pregnant humans and sheep [19–23]. One of the functions of OT *in vivo* may therefore be to soften the cervix around the time of ovulation. Indeed, injections of OT at the time of ovulation were found to produce significant cervical dilation in nonpregnant sheep, which facilitated artificial insemination [24]. The presence of OTR in ovine nonpregnant cervix has recently been reported [25]. These findings, taken together, support the concept that OT can cause the release of PGE_2 from cervical epithelium. Besides the epithelial cells covering the luminal surface of the mucosa, as shown in Figure 6, the submucosa contains other PGE_2 producing cells such as mast cells, blood vessels, and lymphatics [26, 27]. Some of these cell types could possibly be the origin of the OT stimulated prostaglandin E_2 release seen in the *in vitro* experiments reported previously [17]. However, no staining for the immunoreactive OTR protein was detected in any of these cells, so the epithelial cells must be the source of OT-induced PGE_2 release. PGE_2 could then act in a paracrine manner on the underlying submu-

OXYTOCIN RECEPTORS IN BOVINE CERVIX

707

cosa and muscle to cause remodeling and loosening of the tight collagen bundles.

Endogenous OT for the stimulation of cervical OTR can originate in both the ovary and/or the posterior pituitary. Bovine corpus luteum and hypothalamus possess considerable OT synthesizing capacity [15]. Nonendocrine organs, such as uterus or the cervix, are not likely to supply OT for cervical stimulation, since the OT gene is only sporadically, if at all, expressed in tissues of the bovine reproductive tract [15], including the cervical mucosa, as shown in the present study.

The contribution of ovarian OT to the circulating OT pool is greatest in the mid- and late luteal phase, and minimal around estrus [28], as determined from the concentration gradient between vena cava and vena jugularis. Peripheral plasma concentrations of OT, measured in daily samples in cyclic cows, are low, and the cyclic variations range only from about 1 pg/ml around estrus to 3–5 pg/ml in late luteal phase (Days 17–19) [10, 28]. However, OT is secreted in pulses from both the ovary and the pituitary [28, 29], and during such pulses circulating concentrations increase many-fold. Moreover, it has been established that pulsatile OT is much more effective per unit OT than OT infused at a steady rate [30, 31]. Measurement of circulating OT levels is therefore not a reliable indicator of activation of tissue OTR by endogenous ligand, unless very frequent sampling is employed. Bovine theca and granulosa cells also express the OT gene, the expression of which is initiated at the time of the LH surge, and ovarian OT mRNA reaches maximum levels by Day 3 [15]. Therefore, it is possible that some OT could be released from the ovary upon appropriate stimulus also at the time of estrus. Pituitary is, nevertheless, the main source of circulating OT at this stage of the cycle. Mating may stimulate OT release since milk ejection has been observed in cows during mating [32, 33]. Importantly, the marked increase in receptor concentrations is by itself sufficient to initiate responses to low endogenous concentrations of OT also without an increase in plasma OT, since the response is related to the concentration of receptors even at concentrations of free ligand, which are much below the dissociation constant of the receptor [34].

Whether the findings in cows apply to other species remains to be seen. We have previously reported that in pregnant and nonpregnant women, cervical OTR concentrations are very low; however, in these studies only the muscular part was analyzed [35, 36]. Kobuto et al. [37] have recently reported the presence of OTR-containing cells in the endocervical scrapings from pregnant women at term. The cells were not characterized, but they probably originated in the cervical epithelium, suggesting that human cervical mucosa may also be a target organ for OT.

We conclude that cervical mucosa of nonpregnant cows is an important target organ for OT, whereas effects of OT on cervical muscle appear to be of minor significance, due

to the sparse receptor population in the muscular tissue. The cervical OTR concentrations are modulated in a striking fashion during the estrous cycle, and the regulation appears to be mainly at the transcriptional level. Since OT stimulates PGE₂ output in cervical tissue in vitro, we propose that the cellular response to systemic OT in cervical mucosa consists of PGE₂ release from the epithelial cells; the free PGE₂ may in turn act in a paracrine manner on the adjacent connective and muscle tissues to promote cervical dilatation and facilitate sperm transport at the time of ovulation.

ACKNOWLEDGMENTS

The authors want to thank Marga Balvers at the Institute for Hormone and Fertility Research for performing the immunohistochemistry; Dr. Tadeshi Kimura at the Department of OB/GYN, Osaka University Medical College, Japan, for the antibody; Dr. Chad C. Chase at U.S. Department of Agriculture Subtropical Agriculture Research Station and Professor Donald L. Wakeman at the University of Florida for providing the cows; Mr. Larry Eubanks at the University of Florida Meats Laboratory for the processing of animals, and Florence Ndikum-Moffur for assistance in tissue collection.

REFERENCES

- Roberts JS, McCracken JA, Gavagan JE, Soloff MS. Oxytocin stimulated release of prostaglandin F_{2α} from ovine endometrium in vitro: correlation with estrous cycle and oxytocin receptor binding. *Endocrinology* 1976; 99:1107–1114.
- Fuchs A-R, Fuchs F, Husslein P, Soloff MS, Fernstrom MJ. Oxytocin receptors and human parturition: dual role for oxytocin in the initiation of labor. *Science* 1982; 215:1396–1398.
- McCracken JA, Schramm W, Barcikowski B, Wilson L. The identification of PGF_{2α} as a luteolytic hormone and the hormonal control of its synthesis. *Acta Vet Scand Suppl* 1984; 77:71–88.
- Fuchs A-R, Husslein P, Fuchs F. Oxytocin and the initiation of human parturition. II. Stimulation of prostaglandin production in human decidua by oxytocin. *Am J Obstet Gynecol* 1981; 141:688–697.
- Moore JJ, Moore RM, Vanderkooy D. Protein kinase-C activation is required for oxytocin induced prostaglandin production in human amnion cells. *J Clin Endocrinol & Metab* 1991; 72:1073–1080.
- Ivanisevic M, Behrens O, Helmer H, Fuchs A-R. Vasopressin receptors in human pregnant myometrium and decidua: interactions with oxytocin and vasopressin agonists and antagonists. *Am J Obstet Gynecol* 1989; 161:1637–1643.
- Fuchs A-R, Ivanisevic M, Vangsted A, Demarez K. Oxytocin antagonist (dTrp) and oxytocin receptors in myometrium and decidua. *Am J Perinatol* 1989; 6:205–206.
- Fuchs A-R, Fields PA, Chang S-M, Ndikum-Moffur F, Rollyson MK, Fields MJ. Bovine cervix: target organ for oxytocin. In: *Int Union Physiol Scientists (IUPS) Congress*, Glasgow, U.K.; Aug. 1–8, 1993; 22 (Abstract 215).
- Lefebvre DL, Gaid H, Bennett R, Lariviere R, Zingg HH. Oxytocin gene expression in rat uterus. *Science* 1992; 256:1553–1555.
- Chibbar R, Miller FD, Mitchell RE. Synthesis of oxytocin in amnion, chorion and decidua may influence the timing of human parturition. *J Clin Invest* 1993; 91:185–192.
- Fuchs A-R, Behrens O, Helmer H, Liu CH, Barros CM, Fields MJ. Oxytocin and vasopressin receptors in bovine endometrium and myometrium during the estrous cycle and early pregnancy. *Endocrinology* 1990; 127:629–636.
- Lowry OH, Rosebrough NI, Farr AF, Randall RJ. Protein measurements with the Folin phenol reagent. *J Biochem* 1951; 193:265–275.
- Sheehan DC, Hrapchak BB. *Theory and Practice of Histochemistry*. Columbus, OH: Battelle Press; 1987: 46, 170, 198.
- Takemura M, Kimura T, Nomura S, Makino Y, Inoue T, Kichuchi T, Kubota Y, Tokugawa Y, Nobunaga T, Kamiura S, Onoue H, Azuma C, Saji F, Kitamura Y, Tanizawa O. Expression and localization of human oxytocin receptor mRNA and its protein in chorion and decidua during parturition. *J Clin Invest* 1994; 93:2319–2324.
- Ivell R, Rust W, Einspanier A, Hartung S, Fields MJ, Fuchs A-R. Oxytocin and oxytocin gene expression in the reproductive tract of the pregnant cow: rescue of luteal oxytocin production at term. *Biol Reprod* 1995; 53:553–560.
- Bathgate R, Rust W, Balvers M, Hartung S, Ivell R. Structure and expression of the bovine oxytocin receptor gene. *DNA Cell Biol* 1995; 14:1037–1048.
- Ivell R, Furuya K, Brackmann B, Dawood Y, Khan-Dawood F. Expression of oxytocin and vasopressin genes in human and bovine gonadal tissues. *Endocrinology* 1990; 127:2990–2996.

17. Fuchs A-R, Fields MJ, Chang S-M, Friedman S, Shemesh M, Ivell R. Oxytocin and the timing of parturition. In: Ivell R, Russell J (eds.), *Oxytocin: Cellular and Molecular Approaches in Medicine and Research*. Oxford: Plenum Publ.; 1996 (in press).
18. Fitzpatrick RJ. On oxytocin and uterine function. In: Heller H (ed.), *The Neurohypophysis*. London: Butterworths Science Publ.; 1957: 203-217.
19. Fortier MA, Guilbault LA, Grasso F. Specific properties of epithelial and stromal cells from the endometrium of cows. *J Reprod Fertil* 1988; 83:239-248.
20. Srys SJ, Dresser BL, Ott TE, Clark KE. Effects of prostaglandin E2 on cervical compliance in pregnant ewes. *Am J Obstet Gynecol* 1981; 140:415-419.
21. Ulldberg N, Ekman G, Malinström A, Spnrrong B. Biochemical and morphological changes of the human cervix after local application of PGE₂ in pregnancy. *Lancet* 1981; 1:268.
22. Fuchs A-R, Goeschen K, Rasnussen AB, Rehnström JV. Cervical ripening by endocervical and extra-amniotic PGE₂. *Prostaglandins* 1984; 28:217-227.
23. Rajhi MR, Solomon S, Poole AR. Biochemical evidence of collagenase mediated collagenolysis as a mechanism of cervical dilatation at parturition in the guinea pig. *Biol Reprod* 1991; 45:764-772.
24. Khalifa RME, Sayre DL, Lewis GS. Exogenous oxytocin dilates the cervix in ewes. *J Anim Sci* 1992; 70:38-42.
25. Matthews EL, Ayad VJ. Characterization and localization of a putative oxytocin receptor in the cervix of the oestrous ewe. *J Endocrinol* 1994; 142:397-405.
26. Herrick JB. The cytologic changes in cervical mucosa of the cow (*Bos taurus*) throughout the estrous cycle. *Am J Vet Res* 1951; 12:276-283.
27. Heydon RA, Adams NR. Comparative morphology and mucus histochemistry of the ruminant cervix: differences between crypt and surface epithelium. *Biol Reprod* 1979; 21:557-562.
28. Schams D, Schallenberger E, Meyer HHD, Bullermann B, Breiting H-J, Enzenhofer G, Koll R, Kruip TAM, Walters DL, Karg H. Ovarian oxytocin during the estrous cycle in cattle. In: Amico JA, Robinson AG (eds.), *Oxytocin: Laboratory and Clinical Studies*. (Int Congr Series 666). Amsterdam: Elsevier Science Publ. (Biomed Div); 1985: 315-334.
29. Fuchs A-R. Oxytocin and animal parturition. In: Amico JA, Robinson AG (eds.), *Oxytocin: Clinical and Laboratory Studies*. (Int Congr Series 666). Amsterdam: Elsevier Science Publ. (Biomed Div); 1985: 207-235.
30. Randolph GW, Fuchs A-R. Pulsatile administration enhances the effect and reduces the dose of oxytocin required for induction of labor. *Am J Perinatol* 1989; 6:176-180.
31. Dawood MY. Uterine stimulation with oxytocin. In: Garfield RE (ed.), *Uterine Contractility: Mechanisms of Control*. Norwell, MA: Serono Symposia, USA; 1990: 255-369.
32. Hays RL, Vandemark NL. Effect of stimulation of the reproductive organs of cow on release of oxytocin-like substance. *Endocrinology* 1953; 52:634-637.
33. Campbell B, Petersen WE. Milk "let-down" and the orgasm in the human female. *Hum Biol* 1953; 25:165-168.
34. Levitzki A. Quantitative aspects of ligand binding to receptors. In: Schulster D, Levitzki A (eds.), *Cellular Receptors for Hormones and Neurotransmitters*. New York: John Wiley & Sons; 1980: 2-28.
35. Fuchs A-R, Fuchs F, Husslein P, Soloff MS. Oxytocin receptors in nonpregnant human uterus. *J Clin Endocrinol & Metab* 1985; 60:37-41.
36. Fuchs A-R, Fuchs F, Husslein P, Soloff MS. Oxytocin receptors in human uterus. *Am J Obstet Gynecol* 1983; 150:734-741.
37. Kubota Y, Kimura T, Takenura M, Inoue T, Kikuchi T, Ono M, Kanai T, Azuma C, Saji F, Tanizawa O. A novel method for detection of uterine oxytocin receptor in preparation for delivery using scraped endocervical cells. *Horm Metab Res* 1994; 26:442-443.

Silencing of the *thrombomodulin* gene in human malignant melanoma

Junichi Furuta^{a,b}, Atsushi Kaneda^a, Yoshihiro Umebayashi^b, Fujio Otsuka^b, Takashi Sugimura^a and Toshikazu Ushijima^a

The loss of *thrombomodulin* (*TM*) expression is associated with tumour growth, infiltration and lymph node metastasis in human tumours. In melanoma cell lines, *TM* is reported to mediate cell adhesion, and its introduction into *TM*-negative melanoma cell lines suppresses their growth. In this study, we analysed *TM* expression in surgical melanoma specimens and the role of its promoter methylation in the loss of its expression. In 15 (75%) of the 20 specimens (five from a primary site and 15 from metastatic sites), melanoma cells lacked *TM* immunoreactivity. Methylation of the *TM* promoter region was detected in 10 (67%) of the 15 *TM*-negative specimens by methylation-specific polymerase chain reaction, whereas methylation was detected in two (40%) of the five *TM*-positive specimens. In cell lines, complete methylation of the *TM* promoter CpG island was detected in six (46%) of 13 melanoma cell lines, whereas no methylation was detected in two cultured normal melanocytes. There was a good correlation between the methylated status of the CpG island and the loss of *TM* messenger RNA (mRNA) expression. Treatment of melanoma cell lines with a demethylating agent, 5-aza-2'-deoxycytidine, induced

demethylation of the promoter CpG island and the restoration of mRNA and protein expression. These findings suggest that most human melanomas lack *TM* expression, and that methylation of the promoter CpG island is one of the mechanisms responsible. *Melanoma Res* 15:15–20 © 2005 Lippincott Williams & Wilkins.

Melanoma Research 2005, 15:15–20

Keywords: Melanoma, methylation, silencing, thrombomodulin

^aCarcinogenesis Division, National Cancer Center Research Institute, Tokyo, Japan and ^bDepartment of Dermatology, Institute of Clinical Medicine, University of Tsukuba, Ibaraki, Japan.

Sponsorship: This work was supported in part by a Grant-in-Aid for Cancer Research from the Ministry of Health, Labor and Welfare, J.F. is a recipient of Research Resident Fellowships from the Foundation of Cancer Research.

Correspondence and requests for reprints to Dr Toshikazu Ushijima, Carcinogenesis Division, National Cancer Center Research Institute, 5-1-1 Tsukiji, Chuo-ku, Tokyo 104-0045, Japan.
Tel: +81 3 3547 5240; fax: +81 3 5565 1753;
e-mail: tushijim@ncc.go.jp

Received 13 January 2004 Accepted (after revision) 8 October 2004

Introduction

Thrombomodulin (*TM*) not only plays a critical role in anticoagulant activity, but is also involved in various biological and pathological processes, including thrombosis, arteriosclerosis, stroke, inflammation and cancer [1]. *TM* is a glycosylated transmembrane protein with a large extracellular domain that comprises a C-type lectin-like domain, six epidermal growth factor (EGF) modules and a serine/threonine-rich region [1]. *TM* is expressed mainly in endothelial cells, but is also found in a wide range of other cells, including platelets, monocytes, synovial lining cells, transitional epithelium in the urter and squamous epithelium in the skin, oral mucosa, larynx, oesophagus and vagina [2–6].

With regard to the role of *TM* in tumours, an association between a high expression of *TM* and a low-malignancy phenotype has been reported for oesophageal squamous cell carcinomas, lung squamous cell carcinomas and hepatocellular carcinomas [7–10]. When cell proliferation was compared between melanoma cell lines subcloned from four patients, a negative correlation between *TM* expression and cell proliferation was observed *in vitro*

[11]. When wild-type *TM* was introduced into B16 melanoma cells, a *TM*-negative mouse melanoma cell line, cell proliferation *in vitro* and tumour growth *in vivo* were decreased [11]. The introduction of green fluorescent protein (GFP)-tagged *TM* into A2058, a *TM*-negative human melanoma cell line, resulted in the accumulation of *TM* in cell-to-cell adhesion sites, established a morphology with compact clustering and produced a decreased cell proliferation rate *in vitro* and decreased tumour growth *in vivo* [12]. The addition of soluble *TM* in a reconstituted basement membrane (Matrigel[®]) inhibited the invasive activity of B16F10 melanoma cells into the Matrigel [13].

All of these studies strongly indicate that *TM* expression status is an important factor determining the malignant potential of many tumours, including human melanomas. However, *TM* expression has not been analysed in surgical specimens of human melanomas. Therefore, in this study, we analysed *TM* expression in surgical specimens of human melanomas. Furthermore, we analysed the involvement of DNA methylation-associated gene silencing in *TM* inactivation, as we have recently

found that the *T1/* gene is silenced in human gastric cancers by methylation of a CpG island (CGI) in its 5' upstream region [14].

Materials and methods

Surgical melanoma specimens, cultured normal melanocytes and melanoma cell lines

Twenty melanoma specimens, five from primary sites and 15 from metastatic sites, were obtained from patients undergoing tumour resections at Tsukuba University Hospital with informed consent. All samples were embedded in paraffin and fixed in formalin. Two cultured neonatal normal epidermal melanocytes (HEM1, HEM2) were purchased from Cascade Biologics (Portland, OR, USA). MeWo, VMRC-MELG, A2058, C32TG and GAK were obtained from the Health Science Research Resources Bank, Japan Health Sciences Foundation (Sennan, Japan); G361, SK-MEL-28 and HMV-1 were obtained from the Cell Resource Center for Biomedical Research, Institute of Development, Aging and Cancer, Tohoku University (Sendai, Japan); COLO 679 and MMAc were obtained from RIKEN BioResource Center (Tsukuba, Japan); and WM-266-4 and WM-115 were obtained from the American Type Culture Collection (Rockville, MD, USA). TK-Mel-1 was established by J.F. from a skin metastasis of a melanoma obtained at Tsukuba University Hospital.

From surgical specimens, melanoma tissue was dissected from 50 µm thick tissue sections by a fine needle, deparaffinized and incubated in lysis buffer [50 mM Tris-HCl, pH 8.5, 1 mM ethylenediaminetetraacetic acid (EDTA), 0.5% Tween-20, 200 mg/ml of proteinase K] at 55°C for 3 days with fresh proteinase K every 24 h. DNA was purified by phenol/chloroform extraction and ethanol precipitation. From cell lines, DNA was extracted by standard phenol/chloroform procedures. RNA was isolated with ISOGEN (NIPPON GENE, Tokyo, Japan).

Immunohistochemistry

TM antibody, TM (D-3), a mouse monoclonal antibody against amino acids 22–321 of TM protein, was purchased from Santa Cruz Biotechnology (Santa Cruz, CA, USA). Formalin-fixed and paraffin-embedded sections were sliced at 5 µm thickness, deparaffinized and heated in 10 mM citrate buffer (pH 6.0) for 15 min at 121°C. After blocking, the sections were incubated with the antibody at a dilution of 200-fold at 4°C overnight. The binding of the first antibody was detected by a specific second antibody and the Vectastain Elite ABC kit (Vector Laboratories, Burlingame, CA, USA). Slides were counterstained with Mayer's haematoxylin. As a negative control, the absence of staining without the primary antibody was confirmed. As an internal positive control, staining of vascular endothelium was confirmed.

5-Aza-2'-deoxycytidine (5-Aza-dC) treatment

Cells were seeded at a density of 6×10^5 cells per 10 cm dish on day 0, and exposed to freshly prepared 1 µM 5-Aza-dC (Sigma, St. Louis, MO, USA) for 24 h on days 1 and 3. The cells were harvested on day 4.

Sodium bisulphite modification, methylation-specific polymerase chain reaction (MSP) and bisulphite sequencing

Five hundred nanograms of digested DNA were denatured in 0.3 N NaOH at 37°C for 15 min [15]. To the denatured DNA, 3.6 N sodium bisulphite (pH 5.0) and 0.6 mM hydroquinone were added, and the sample underwent 15 cycles of denaturation at 95°C for 30 s and incubation at 50°C for 15 min. The sample was desalted with the Wizard DNA Clean-Up system (Promega, Madison, WI, USA), and desulphonated by treatment with 0.3 N NaOH. The DNA sample was ethanol precipitated and dissolved in 20 µl of Tris-EDTA buffer.

With a set of primers specific to the methylated or unmethylated sequence (M or U set, respectively), MSP [16] was performed using 0.5 µl of the sodium bisulphite-treated DNA. MSP primers were designed within the promoter region as reported previously [17]. DNA methylated with *Sss*I methylase and DNA from HEM1 were used to determine specific annealing temperatures for M and U sets, respectively. Minimal polymerase chain reaction (PCR) cycles to produce visible bands for these control samples were determined for M and U sets, respectively. For samples from cultured normal melanocytes and melanoma cell lines, four cycles were added. For samples from surgical melanoma specimens, four more cycles were added because their DNA had been degraded. The primer sequences were 5'-GGT GAT TTTATG TGT GAG GGT-3' (sense) and 5'-CTC CCT CCC TAA ACA TTC A-3' (antisense) for the U set (120 bp), and 5'-TGA TTT TAT GCG CGA GGG C-3' (sense) and 5'-CCT CCC TCC CTA AAC GTT CG-3' (antisense) for the M set (119 bp). The annealing temperature and amplification cycles were 59°C and 34 cycles for the U set and 65°C and 34 cycles for the M set.

For bisulphite sequencing, a set of primers common to the methylated and unmethylated sequences was used. The PCR product was cloned into the pGEM-T Easy vector (Promega), and ten clones were sequenced. The primer sequences were 5'-AGG AGG ATT AAG AGA TGA AAG AG-3' (sense) and 5'-CAA CCC AAA CAC TTC TTA CC-3' (antisense) (375 bp). The annealing temperature and amplification cycles were 59°C and 35 cycles, respectively.

Quantitative real-time reverse transcriptase-polymerase chain reaction (RT-PCR)

After treatment with DNase I (Invitrogen, Carlsbad, CA, USA), complementary DNA (cDNA) was synthesized

from 3 µg of total RNA using Superscript II (Invitrogen). Real-time PCR was performed using SYBR Green PCR Core Reagents (PE Applied Biosystems, Foster City, CA, USA) and an iCycler Thermal Cycler (Bio-Rad Laboratories, Hercules, CA, USA). The number of molecules of a specific cDNA in a sample was measured by comparing its amplification with that of standard samples containing 10^1 to 10^6 molecules. The expression level of *TM* in each sample was obtained by normalizing the number of its cDNA molecules with that of the *GAPDH* gene. The primer sequences were 5'-GGT GAT TAG AGG GAG GAG AA-3' (sense) and 5'-CGC AGT CTG TGT CTT CGT TA-3' (antisense) (97 bp) for *TM*, and 5'-AGG TGA AGC TCG GAG TCA ACG-3' (sense) and 5'-AGG GGT CAT TGA TGG CAA CA-3' (antisense) (102 bp) for *GAPDH*.

Immunoblotting

Total protein lysate (20 µg per lane) was separated by 10% sodium dodecylsulphate (SDS)-polyacrylamide gel electrophoresis and transferred to a polyvinylidene difluoride membrane (Immobilon, Millipore, Bedford, MA, USA). TM protein was detected by a primary antibody (1:500 dilution), TM (D-3), and by a second goat anti-mouse IgG antibody conjugated with peroxidase (1:10,000 dilution; KPL, Gaithersburg, MD, USA). The specific complex was visualized by enhanced chemiluminescence (Amersham Biosciences, Piscataway, NJ, USA). A rabbit anti-Actin antibody (1:500 dilution; Biomedical Technologies, Stoughton, MA, USA) and a second donkey anti-rabbit IgG antibody conjugated with peroxidase

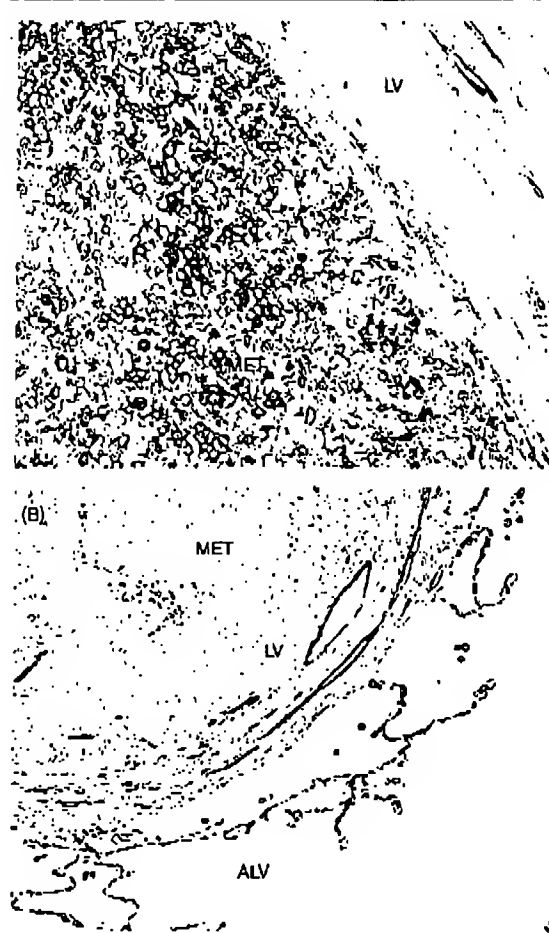
(1:5000 dilution; Chemicon International, Temecula, CA, USA) were used as a control.

Results

Immunohistochemistry of TM

In 15 (75%) of 20 surgical specimens, melanoma cells lacked TM immunoreactivity (Table 1, representative results in Fig. 1). In the five TM-positive specimens, strong cell membrane staining was evident in melanoma cells, and positive staining was observed in the majority of melanoma cells (Fig. 1A). In contrast, in TM-negative specimens, all melanoma cells lacked positive staining,

Fig. 1



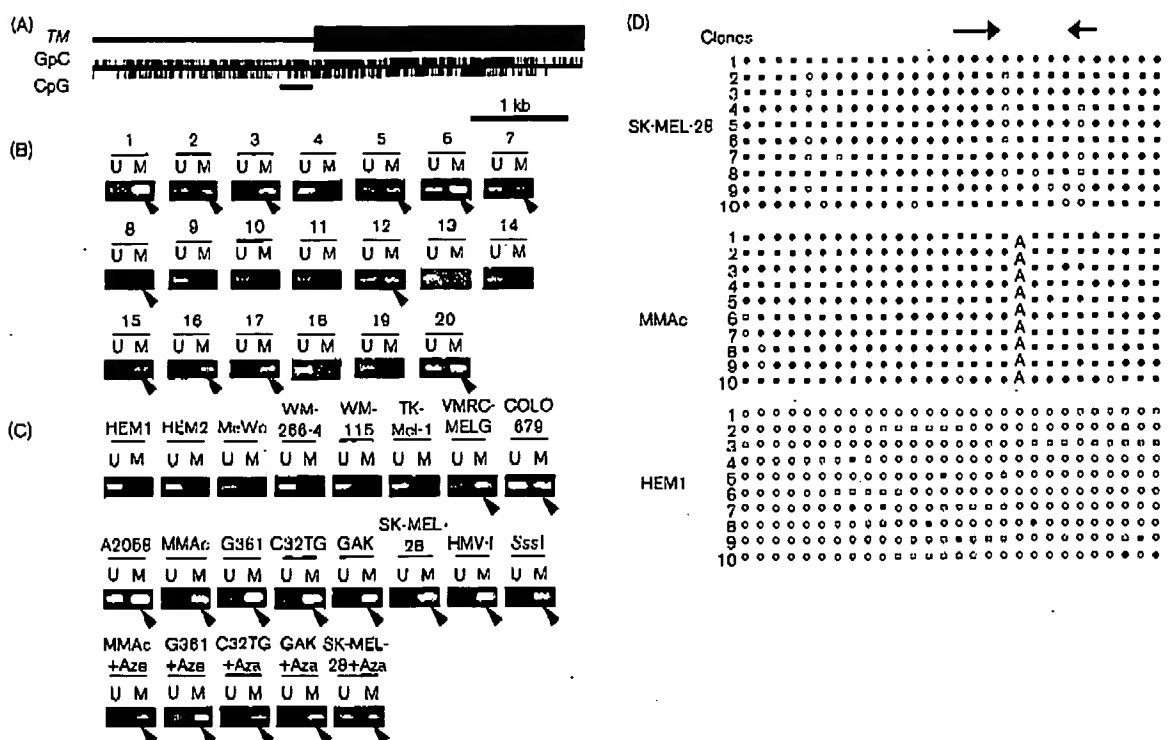
Representative immunohistochemical analysis of thrombomodulin (TM) expression in surgical specimens of melanoma metastatic foci. Sections from melanomas were stained with anti-TM (D-3) antibody. Fifteen (75%) of 20 melanoma specimens lacked TM immunoreactivity. (A) Lymph node metastasis of a melanoma (case 11) without promoter methylation. Strong immunoreactivity was observed in the cell membrane. LV, endothelial cells of lymph vessels; MET, metastatic region of melanoma. (B) Lung metastasis of a melanoma (case 6) with promoter methylation. ALV, vascular endothelial cells of the alveolar cavity. Original magnifications, $\times 100$.

Table 1 Thrombomodulin (TM) expression and methylation status in surgical specimens

Sample	Origin	TM immunoreactivity	Methylation status
1	Primary site	+	U+M
2	Primary site	-	U+M
3	Primary site	-	M
4	Primary site	+	U
5	Primary site	+	U+M
6	Lung metastasis	-	U+M
7	Lung metastasis	-	U+M
8	Lung metastasis	-	U+M
9	Lymph node metastasis	-	U
10	Lymph node metastasis	-	U
11	Lymph node metastasis	+	U
12	Lymph node metastasis	+	U+M
13	Lymph node metastasis	+	U
14	Skin metastasis	-	U
15	Skin metastasis	-	U+M
16	Skin metastasis	-	M
17	Skin metastasis	-	U+M
18	Skin metastasis	-	U
19	Intestinal metastasis	-	U
20	Liver metastasis	-	U+M

TM immunoreactivity is shown by '+' (positive) and '-' (negative). Methylation status determined by methylation-specific polymerase chain reaction (MSP) is shown by 'M' (only methylated DNA molecules detected), 'U' (only unmethylated DNA molecules detected) and 'U+M' (both unmethylated and methylated DNA molecules detected). There was no clear correlation between the loss of TM immunoreactivity and the original sites of the samples.

Fig. 2



Genomic structure of the thrombomodulin (TM) promoter region and its methylation analysis. (A) Structure of a 4-kb CpG island spanning from exon 1 to the 5' upstream region. Each vertical mark, an individual GpC or CpG site; bar, region analysed by bisulphite sequencing. (B) Methylation analysis of the promoter region by methylation-specific polymerase chain reaction (MSP) in the surgical melanoma specimens. U and M, primer sets for unmethylated and methylated DNA sequences, respectively. The presence of methylated DNA molecules is shown by arrow heads. (C) Methylation analysis of the promoter regions by MSP in cultured normal melanocytes (HEM1 and HEM2) and melanoma cell lines. MeWo, WM-266-4, WM-115, TK-Mel-1, VMRC-MELG, COLO 679, A2058, MMac, G361, C32TG, GAK, SK-MEL-28 and HMV-1, melanoma cell lines; +Aza, melanoma cell lines after treatment with 5-aza-2'-deoxycytidine (5-Aza-dC); Sssl, genomic DNA of HEM1 treated with Sssl methylase. (D) Methylation analysis of the promoter regions by bisulphite sequencing in two melanoma cell lines (SK-MEL-28 and MMac) and HEM1. For each sample, 10 clones were sequenced. Filled circle, methylated CpG site; open circle, unmethylated CpG site. Arrows show the positions of CpG sites recognized by MSP primers. The cytosine at the 19th CpG site had a C to A polymorphism in MMac.

whereas endothelial cells of lymph vessels and vascular vessels were clearly stained, as reported previously (Fig. 1B) [2,18]. Three of the five (60%) specimens from primary sites lacked positive staining, whereas 12 of the 15 (80%) specimens from metastatic sites lacked positive staining. This showed that the majority of surgical melanoma specimens lacked TM expression, whereas the remaining melanomas showed TM expression.

Methylation status of TM promoter region CGI

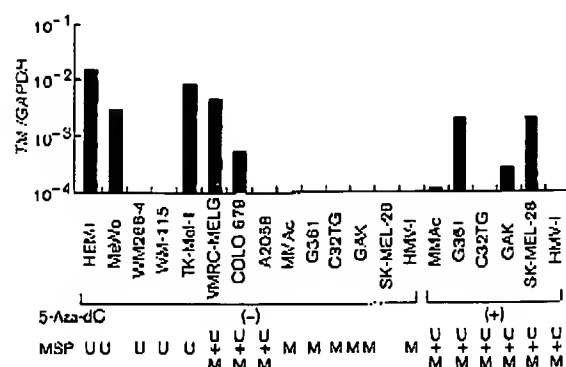
A 4-kb CGI that met a criterion described by Takai and Jones [19] spanned from exon 1 to the 5' upstream region of the TM gene, and the methylation status of a region overlapping the promoter region was analysed by MSP (Fig. 2A). Methylation was detected in 12 (60%) of the 20 specimens, but the region was not methylated in HEMs. Methylation was detected in 10 (67%) of the 15 TM-

negative specimens and in two (40%) of the five TM-positive specimens (Table 1, Fig. 2B).

In surgical specimens, contamination of normal cells in melanoma samples was present, and it was difficult to determine the allelic status of methylation. Therefore, the methylation status was further analysed in melanoma cell lines (Fig. 2C). Methylation was detected in nine (69%) of 13 melanoma cell lines, whereas no methylation was detected in the two cultured normal melanocytes, HEM1 and HEM2. In six of the nine melanoma cell lines, MMac, G361, C32TG, GAK, SK-MEL-28 and HMV-1, only methylated DNA molecules were detected by MSP.

Bisulphite sequencing was performed in SK-MEL-1 and MMac, in which only methylated DNA molecules were detected by MSP, and in HEM1. The methylation status

Fig. 3



Expression levels of thrombomodulin (TM) in cultured normal melanocytes and melanoma cell lines analysed by quantitative reverse transcriptase-polymerase chain reaction (RT-PCR). Expression levels were normalized to that of GAPDH, and are shown on a logarithmic scale. The methylation status of each sample in the promoter region is shown below the names of the samples. With or without 5-aza-2'-deoxycytidine (5-Aza-dC) treatment is indicated as '+' or '-'; respectively. Expression status correlates with methylation status in the promoter region. M, only methylated DNA molecules detected; U, only unmethylated DNA molecules detected; U+M, both unmethylated and methylated DNA molecules detected.

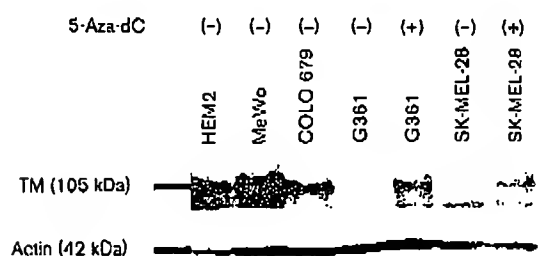
of the 120-bp region between the primers of MSP was in complete accordance with the results by MSP (Fig. 2D). It was also observed that the methylation status detected by MSP was in good accordance with the methylation status of a broader region (331 bp).

Messenger RNA (mRNA) expression of TM and restoration by 5-Aza-dC in melanoma cell lines

The expression levels of TM were analysed in a cultured normal melanocyte, HEM1, and in 13 melanoma cell lines by quantitative real-time RT-PCR (Fig. 3). TM was abundantly expressed in the normal cultured melanocyte, HEM1. Of the melanoma cell lines, TM expression was lost in all six cell lines that showed only methylated DNA molecules, whereas some expression was detected in four of the six cell lines that showed both unmethylated and methylated DNA molecules or only unmethylated DNA molecules.

To examine the role of the methylation of CGI in the promoter region in the loss of TM expression, six melanoma cell lines, MMAC, G361, C32TG, GAK, SK-MEL-28 and HMV-1, which showed only methylated DNA molecules, were treated with 5-Aza-dC, a demethylating agent. In four (MMAC, G361, GAK and SK-MEL-28), CGI in the TM promoter region was demethylated (Fig. 2C), and TM was re-expressed (Fig. 3). This showed that methylation of CGI in the promoter region was critically involved in the loss of TM expression.

Fig. 4



Western blot analysis of thrombomodulin (TM) protein expression. HEM2, four melanoma cell lines before the addition of 5-aza-2'-deoxycytidine (5-Aza-dC) and two melanoma cell lines after the addition of 5-Aza-dC were analysed. TM protein expression was observed in melanoma cell lines without methylation, but not in those with complete methylation. The expression in cell lines with complete methylation was restored by the addition of 5-Aza-dC.

Immunoblot analysis of TM protein

To confirm the results obtained by RT-PCR, immunoblot analysis was performed using cell lines with abundant re-expression of TM: G361 and SK-MEL-28 (Fig. 4). Before treatment with 5-Aza-dC, TM protein was detected in HEM2 and in two melanoma cell lines (MeWo and COLO 679) that showed only unmethylated DNA molecules and mRNA expression. In contrast, TM protein was not detected in two cell lines (G361 and SK-MEL-28) that showed only methylated DNA molecules and no mRNA expression. After treatment of G361 and SK-MEL-28 with 5-Aza-dC, TM protein was detected. These results confirmed that TM mRNA detected by RT-PCR, especially that re-expressed after 5-Aza-dC treatment, was translated into TM protein.

Discussion

In this report, TM expression was found to be absent in most of the surgical melanoma specimens, although we mainly used metastatic samples to isolate DNA mostly from melanoma cells. It has been reported that low TM expression is associated with high-malignancy phenotypes in oesophageal, lung and liver cancers [7-10], and that TM has a growth suppressive effect on melanoma cell lines [11-13]. However, this study is the first to show that some human melanomas lack TM expression. To determine the mechanisms, we further analysed the methylation status of CGI in the TM promoter region. It was shown that CGI was methylated, and played a critical role in the loss of TM expression, as known for CGIs in promoter regions of tumour suppressor genes, such as *p16* [20], *E-cadherin* [21] and *hMLH1* [22]. Although gene silencing can be analysed only in melanoma cell lines, the presence of the aberrant methylation of the promoter CGI strongly suggests that its silencing is also present *in vivo*.

in exon
lation
for sets
M-266-
za,

r each
G sites

TM-

ills in
ult to
efore,
noma
nine
lation
cytes,
lines,
MV-1,
MSP

l and
were
ratus

Five of the 15 TM-negative surgical specimens showed no TM methylation. It was therefore indicated that other mechanisms, such as chromosomal deletions, mutations and a lack of upstream signals, were involved. Although the loss of the TM locus (20p12-ccn) is infrequent in melanomas [23], its loss has been reported in melanoma cells with high invasive capacity [24]. With regard to mutations, no information is available in melanomas, and an analysis is necessary. Three cell lines, WM-266-4, WM-115 and A2058, retained unmethylated DNA molecules, but did not express TM mRNA. The loss of expression of a tumour suppressor gene that can be potentially silenced by promoter methylation has been observed even without methylation for several tumour suppressor genes, such as *CDH1*, *RAR β* and *hMLH1* [25-27].

In human normal skin specimens, epidermal melanocytes lacked TM immunoreactivity in our study (data not shown) and in a previous report [6], whereas TM expression was evident in cultured normal melanocytes. One possibility is that TM expression is necessary only on limited occasions, such as cell proliferation. Indeed, epidermal melanocytes are known not to proliferate *in situ* unless specifically stimulated, e.g. by ultraviolet light [28], whereas cultured normal melanocytes keep proliferating. TM may be expressed only when cells are proliferating, and may maintain cell proliferation within an appropriate range. To support this hypothesis, normal hepatocytes showed no TM immunoreactivity, but TM-positive hepatocellular carcinomas showed better prognosis [10].

In conclusion, our findings show that TM is not expressed in most human melanomas, and that methylation of the promoter CGI is one of the mechanisms for the loss of expression.

References

1. Weiler H, Isenmann BH. Thrombomodulin. *J Thromb Haemost* 2003; 1:1515-1524.
2. Maruyama I, Bell CE, Mejerus PW. Thrombomodulin is found on endothelium of arteries, veins, capillaries, and lymphatics, and on syncytiotrophoblast of human placenta. *J Cell Biol* 1985; 101:363-371.
3. Suzuki K, Nishio K, Hayashi T, Kosaka Y. Functionally active thrombomodulin is present in human platelets. *J Biochem (Tokyo)* 1989; 104:628-632.
4. McCachren SS, Diggs J, Weinberg JB, Dillman WA. Thrombomodulin expression by human blood monocytes and by human synovial tissue lining macrophages. *Blood* 1991; 78:3128-3132.
5. Obama H, Obama K, Takemoto M, Soejima Y, Shirahama T, Ohi Y, et al. Expression of thrombomodulin in the epithelium of the urinary bladder: a possible source of urinary thrombomodulin. *Anticancer Res* 1999; 19:1143-1147.
6. Lager DJ, Collington EJ, Worth SF, Rafo TJ, Lentz SR. Cellular localization of thrombomodulin in human epithelium and squamous malignancies. *Am J Pathol* 1995; 146:933-943.
7. Tazuka Y, Yonazawa S, Maruyama I, Matsushita Y, Shimizu T, Obama H, et al. Expression of thrombomodulin in esophageal squamous cell carcinoma and its relationship to lymph node metastasis. *Cancer Res* 1995; 55:4196-4200.
8. Matsushita Y, Yoshie K, Imamura Y, Ogawa H, Imamura H, Takao S, et al. A subcloned human esophageal squamous cell carcinoma cell line with low thrombomodulin expression showed increased invasiveness compared with a high thrombomodulin-expressing clone - thrombomodulin as a possible candidate for an adhesion molecule of squamous cell carcinoma. *Cancer Lett* 1998; 127:195-201.
9. Ogawa H, Yonazawa S, Maruyama I, Matsushita Y, Tazuka Y, Toyoyama H, et al. Expression of thrombomodulin in squamous cell carcinoma of the lung: its relationship to lymph node metastasis and prognosis of the patients. *Cancer Lett* 2000; 148:95-103.
10. Suehiro T, Shimada M, Matsuura T, Takatori A, Yumamoto K, Sugimachi K. Thrombomodulin inhibits intrahepatic spread in human hepatocellular carcinoma. *Hepatology* 1995; 21:1285-1290.
11. Zhang Y, Weller-Gueller H, Chen J, Wilhelm O, Deng Y, Qiu F, et al. Thrombomodulin modulates growth of tumor cells independent of its anticoagulant activity. *J Clin Invest* 1998; 101:1301-1309.
12. Huang HC, Shi GY, Jiang SJ, Shi CS, Wu CM, Yang HY, et al. Thrombomodulin-mediated cell adhesion: involvement of its lectin-like domain. *J Biol Chem* 2003; 278:46750-46759.
13. Hosaka Y, Higuchi T, Tsumagari M, Ishii H. Inhibition of invasion and experimental metastasis of murine melanoma cells by human soluble thrombomodulin. *Cancer Lett* 2000; 161:231-240.
14. Kanada A, Kaminishi M, Yanagihara K, Sugimura T, Ushijima T. Identification of silencing of nine genes in human gastric cancers. *Cancer Res* 2002; 62:6645-6650.
15. Clark SJ, Harrison J, Paul CL, Frommer M. High sensitivity mapping of methylated cytosines. *Nucleic Acids Res* 1994; 22:2890-2897.
16. Herman JG, Graff JR, Myohanen S, Nelkin BD, Baylin SB. Methylation-specific PCR: a novel PCR assay for methylation status of CpG islands. *Proc Natl Acad Sci USA* 1996; 93:9821-9826.
17. Tazawa R, Hirogawa S, Suzuki K, Hirokawa K, Aoki N. Functional characterization of the 5'-regulatory region of the human thrombomodulin gene. *J Biochem (Tokyo)* 1993; 113:600-606.
18. Tamura A, Matsubara O, Hirokawa K, Aoki N. Detection of thrombomodulin in human lung cancer cells. *Am J Pathol* 1993; 142:79-85.
19. Takai D, Jones PA. Comprehensive analysis of CpG islands in human chromosomes 21 and 22. *Proc Natl Acad Sci USA* 2002; 99:3740-3745.
20. Morio A, Herman JG, Mao L, Lee OJ, Gabrielson E, Burger PC, et al. 5' CpG island methylation is associated with transcriptional silencing of the tumour suppressor p16/CDKN2/MTS1 in human cancers. *Nat Med* 1995; 1:686-692.
21. Yoshiura K, Kanai Y, Ochiai A, Shimoyama Y, Sugimura T, Hirohashi S. Silencing of the E-cadherin invasion-suppressor gene by CpG methylation in human carcinomas. *Proc Natl Acad Sci USA* 1995; 92:7416-7419.
22. Kane MF, Loda M, Gaida GM, Lipman J, Mishra R, Goldman H, et al. Methylation of the hMLH1 promoter correlates with lack of expression of hMLH1 in sporadic colon tumors and mismatch repair-defective human tumor cell lines. *Cancer Res* 1997; 57:808-811.
23. Bastian BC, LeBoit PE, Hamm H, Brooker EB, Pinkel D. Chromosomal gains and losses in primary cutaneous melanomas detected by comparative genomic hybridization. *Cancer Res* 1998; 58:2170-2175.
24. Gunther K, Fischer A, Buettner R, Bosserhoff AK. Detection of invasion-related chromosomal changes in highly and weakly invasive melanoma cell clones by a modified comparative genomic hybridization approach. *Melanoma Res* 2001; 11:105-115.
25. Poser I, Dominguez D, de Herreros AG, Varnai A, Buettner R, Bosserhoff AK. Loss of E-cadherin expression in melanoma cells involves up-regulation of the transcriptional repressor Snail. *J Biol Chem* 2001; 276:24661-24666.
26. Suh YA, Lee HY, Virmani A, Wong J, Mann KK, Miller WH, Jr, et al. Loss of retinoic acid receptor beta gene expression is linked to aberrant histone H3 acetylation in lung cancer cell lines. *Cancer Res* 2002; 62:3945-3949.
27. Deng G, Peng E, Gum J, Terdiman J, Steisner M, Kim YS. Methylation of hMLH1 promoter correlates with the gene silencing with a region-specific manner in colorectal cancer. *Br J Cancer* 2002; 86:574-579.
28. Herlyn M, Shih IM. Interactions of melanocytes and melanoma cells with the microenvironment. *Pigment Cell Res* 1994; 7:81-88.

A Sampling of the Yeast Proteome

B. FUTCHER,^{1*} G. I. LATTER,¹ P. MONARDO,¹ C. S. MCLAUGHLIN,² AND J. I. GARRELS³

Cold Spring Harbor Laboratory, Cold Spring Harbor, New York 11724¹; Department of Biological Chemistry, University of California, Irvine, California 92717²; and Proteome, Inc., Beverly, Massachusetts 01915³

Received 15 June 1999/Returned for modification 16 July 1999/Accepted 28 July 1999

In this study, we examined yeast proteins by two-dimensional (2D) gel electrophoresis and gathered quantitative information from about 1,400 spots. We found that there is an enormous range of protein abundance and, for identified spots, a good correlation between protein abundance, mRNA abundance, and codon bias. For each molecule of well-translated mRNA, there were about 4,000 molecules of protein. The relative abundance of proteins was measured in glucose and ethanol media. Protein turnover was examined and found to be insignificant for abundant proteins. Some phosphoproteins were identified. The behavior of proteins in differential centrifugation experiments was examined. Such experiments with 2D gels can give a global view of the yeast proteome.

The sequence of the yeast genome has been determined (9). More recently, the number of mRNA molecules for each expressed gene has been measured (27, 30). The next logical level of analysis is that of the expressed set of proteins. We have begun to analyze the yeast proteome by using two-dimensional (2D) gels.

2D gel electrophoresis separates proteins according to isoelectric point in one dimension and molecular weight in the other dimension (21), allowing resolution of thousands of proteins on a single gel. Although modern imaging and computing techniques can extract quantitative data for each of the spots in a 2D gel, there are only a few cases in which quantitative data have been gathered from 2D gels. 2D gel electrophoresis is almost unique in its ability to examine biological responses over thousands of proteins simultaneously and should therefore allow us a relatively comprehensive view of cellular metabolism.

We and others have worked toward assembling a yeast protein database consisting of a collection of identified spots in 2D gels and of data on each of these spots under various conditions (2, 7, 8, 10, 23, 25). These data could then be used in analyzing a protein or a metabolic process. *Saccharomyces cerevisiae* is a good organism for this approach since it has a well-understood physiology as well as a large number of mutants, and its genome has been sequenced. Given the sequence and the relative lack of introns in *S. cerevisiae*, it is easy to predict the sequence of the primary protein product of most genes. This aids tremendously in identifying these proteins on 2D gels.

There are three pillars on which such a database rests: (i) visualization of many protein spots simultaneously, (ii) quantification of the protein in each spot, and (iii) identification of the gene product for each spot. Our first efforts at visualization and identification for *S. cerevisiae* have been described elsewhere (7, 8). Here we describe quantitative data for these proteins under a variety of experimental conditions.

MATERIALS AND METHODS

Strains and media. *S. cerevisiae* W303 (MATa *ade2-1 his3-11,15 leu2-3, 112 trp1-1 ura3-1 can1-100*) was used (26). –Met YNB (yeast nitrogen base) medium was 1.7 g of YNB (Difco) per liter, 5 g of ammonium sulfate per liter, and

adenine, uracil, and all amino acids except methionine; –Met.–Cys YNB medium was the same but without methionine or cysteine. Medium was supplemented with 2% glucose (for most experiments) or with 2% ethanol (for ethanol experiments). Low-phosphate YEPD was described by Warner (28).

Isotopic labeling of yeast and preparation of cell extracts. Yeast strains were labeled and proteins were extracted as described by Garrels et al. (7, 8). Briefly, cells were grown to 5×10^6 cells per ml at 30°C; 1 ml of culture was transferred to a fresh tube, and 0.3 mCi of [³⁵S]methionine (e.g., Express protein labeling mix; New England Nuclear) was added to this 1-ml culture. The cells were incubated for a further 10 to 15 min and then transferred to a 1.5-ml microfuge tube, chilled on ice, and harvested by centrifugation. The supernatant was removed, and the cell pellet was resuspended in 100 µl of lysis buffer (20 mM Tris-HCl [pH 7.6], 10 mM NaF, 10 mM sodium pyrophosphate, 0.5 mM EDTA, 0.1% deoxycholate; just before use, phenylmethylsulfonyl fluoride was added to 1 mM, leupeptin was added to 1 µg/ml, pepstatin was added to 1 µg/ml, tosyl-sulfonyl phenylalanyl chloromethyl ketone was added to 10 µg/ml, and soybean trypsin inhibitor was added to 10 µg/ml).

The resuspended cells were transferred to a screw-cap 1.5-ml polypropylene tube containing 0.28 g of glass beads (0.5-mm diameter; Biospec Products) or 0.40 g of zirconia beads (0.5-mm diameter; Biospec Products). After the cap was secured, the tube was inserted into a MiniBeadbeater 8 (Biospec Products) and shaken at medium high speed at 4°C for 1 min. Breakage was typically 75%. Tubes were then spun in a microfuge for 10 s at 5,000 × g at 4°C.

With a very fine pipette tip, liquid was withdrawn from the beads and transferred to a prechilled 1.5-ml tube containing 7 µl of DNase I (0.5 mg/ml; Cooper product no. 6330)–RNase A (0.25 mg/ml; Cooper product no. 5679)–Mg (50 mM MgCl₂) mix. Typically 70 µl of liquid was recovered. The mixture was incubated on ice for 10 min to allow the RNase and DNase to work.

Next, 75 µl of 2× SDS (2× SDS is 0.6% sodium dodecyl sulfate [SDS], 2% mercaptoethanol, and 0.1 M Tris-HCl [pH 8]) was added. The tube was plunged into boiling water, incubated for 1 min, and then plunged into ice. After cooling, the tube was centrifuged at 4°C for 3 min at 14,000 × g. The supernatant was transferred to a fresh tube and frozen at –70°C. About 5 µl of this supernatant was used for each 2D gel.

2D polyacrylamide gels. 2D gels were made and run as described elsewhere (6–8).

Image analysis of the gels. The Quest II software system was used for quantitative image analysis (20, 22). Two techniques were used to collect quantitative data for analysis by Quest II software. First, before the advent of phosphorimagers, gels were dried and fluorographed. Each gel was exposed to film for three different times (typically 1 day, 2 weeks, and 6 weeks) to increase the dynamic range of the data. The films were scanned along with calibration strips to relate film optical density to disintegrations per minute in the gels and analyzed by the software to obtain a linear relationship between disintegrations per minute in the spots and optical densities of the film images. The quantitative data are expressed as parts per million of the total cellular protein. This value is calculated from the disintegrations per minute of the sample loaded onto the gel and by comparing the film density of each data spot with density of the film over the calibration strips of known radioactivity exposed to the same film. This yields the disintegrations per minute per millimeter for each spot on the gel and thence its parts-per-million value.

After the advent of phosphorimaging, gels bearing ³⁵S-labeled proteins were exposed to phosphorimager screens and scanned by a Fuji phosphorimager, typically for two exposures per gel. Calibration strips of known radioactivity were exposed simultaneously. Scan data from the phosphorimager was assimilated by Quest II software, and quantitative data were recorded for the spots on the gels.

* Corresponding author. Mailing address: Cold Spring Harbor Laboratory, Cold Spring Harbor, NY 11724. Phone: (516) 367-8828. Fax: (516) 367-8369. E-mail: fletcher@cshl.org.

Measurements of protein turnover. Cells in exponential phase were pulse-labeled with [35 S]methionine, excess cold Met and Cys were added, and samples of equal volume were taken from the culture at intervals up to 90 min (in one experiment) or up to 160 min (in a second experiment). Incorporation of 35 S into protein was essentially 100% by the first sample (10 min). Extracts were made, and equal fractions of the samples were loaded on 2D gels (i.e., the different samples had different amounts of protein but equal amounts of 35 S). Spots were quantitated with a phosphorimaging and Quest software.

The software was queried for spots whose radioactivity decreased through the time course. The algorithm examined all data points for all spots, drew a best-fit line through the data points, and looked for spots where this line had a statistically significant negative slope. In one of the experiments, there was one such spot. To the eye, this was a minor, unidentified spot seen only in the first two samples (10 and 20 min). In the other experiment, the Quest software found no spots meeting the criteria. Therefore, we concluded that none of the identified spots (and all but one of the visible spots) represented proteins with long half-lives.

Centrifugal fractionation. Cells were labeled, harvested, and broken with glass beads by the standard method described above except that no detergent (i.e., no deoxycholate) was present in the lysis buffer. The crude lysate was cleared of unbroken cells and large debris by centrifugation at $300 \times g$ for 30 s. The supernatant of this centrifugation was then spun at $16,000 \times g$ for 10 min to give the pellet used for Fig. 6B. The supernatant of the $16,000 \times g$, 10-min spin was then spun at $100,000 \times g$ for 30 min to give the supernatant used for Fig. 6A.

Protein abundance calculations. A haploid yeast cell contains about 4×10^{-12} g of protein (1, 15). Assuming a mean protein mass of 50 kDa, there are about 50×10^6 molecules of protein per cell. There are about 1.8 methionines per 10 kDa of protein mass, which implies 4.5×10^8 molecules of methionine per cell (neglecting the small pool of free Met). We measured (i) the counts per minute in each spot on the 2D gels, (ii) the total number of counts on each gel (by integrating counts over the entire gel), and (iii) the total number of counts loaded on the gel (by scintillation counting of the original sample). Thus, we know what fraction of the total incorporated radioactivity is present in each spot. After correcting for the methionine (and cysteine [see below]) content of each protein, we calculated an absolute number of protein molecules based on the fraction of radioactivity in each spot and on 50×10^6 total molecules per cell.

The labeling mixture used contained about one-fifth as much radioactive cysteine as radioactive methionine. Therefore, the number of cysteine molecules per protein was also taken into account in calculating the number of molecules of protein, but Cys molecules were weighted one-fifth as heavily as Met molecules.

mRNA abundance calculations. For estimation of mRNA abundance, we used SAGE (serial analysis of gene expression) data (27) and Affymetrix chip hybridization data (29a, 30). The mRNA column in Table 1 shows mRNA abundance calculated from SAGE data alone. However, the SAGE data came from cells growing in YEPD medium, whereas our protein measurements were from cells growing in YNB medium. In addition, SAGE data for low-abundance mRNAs suffers from statistical variation. Therefore, we also used chip hybridization data (29a, 30) for mRNA from cells grown in YNB. These hybridization data also had disadvantages. First, the amounts of high-abundance mRNAs were systematically underestimated, probably because of saturation in the hybridizations, which used 10 μ g of cRNA. For example, the abundance of *ADH1* mRNA was 197 copies per cell by SAGE but only 32 copies per cell by hybridization, and the abundance of *ENO2* mRNA was 248 copies per cell by SAGE but only 41 by hybridization. When the amount of cRNA used in the hybridization was reduced to 1 μ g, the apparent amounts of mRNA were similar to the amounts determined by SAGE (29a, 29b). However, experiments using 1 μ g of cRNA have been done for only some genes (29a). Because amounts of mRNA were normalized to 15,000 per cell, and because the amounts of abundant mRNAs were underestimated, there is a 2.2-fold overestimate of the abundance of nonabundant mRNAs. We calculated this factor of 2.2 by adding together the number of mRNA molecules from a large number of genes expressed at a low level for both SAGE data and hybridization data. The sum for the same genes from hybridization data is 2.2-fold greater than that from SAGE data.

To take into account these difficulties, we compiled a list of "adjusted" mRNA abundance as follows. For all high-abundance mRNAs of our identified proteins, we used SAGE data. For all of these particular mRNAs, chip hybridization suggested that mRNA abundance was the same in YEPD and YNB media. For medium-abundance mRNAs, SAGE data were used, but when hybridization data showed a significant difference between YEPD and YNB, then the SAGE data were adjusted by the appropriate factor. Finally, for low-abundance mRNAs, we used data from chip hybridizations from YNB medium but divided by 2.2 to normalize to the SAGE results. These calculations were completed without reference to protein abundance.

CAI. The codon adaptation index (CAI) was taken from the yeast proteome database (YPD) (13), for which calculations were made according to Sharp and Li (24). Briefly, the index uses a reference set of highly expressed genes to assign a value to each codon, and then a score for a gene is calculated from the frequency of use of the various codons in that gene (24).

Statistical analysis. The JMP program was used with the aid of T. Tully. The JMP program showed that neither mRNA nor protein abundances were normally distributed; therefore, Spearman rank correlation coefficients (r_s) were

calculated. The mRNA (adjusted and unadjusted) and protein data were also transformed so that Pearson product-moment correlation coefficients (r_p) could be calculated. First, this was done by a Box-Cox transformation of log-transformed data. This transformation produced normal distributions, and an r_p of 0.76 was achieved. However, because the Box-Cox transformation is complex, we also did a simpler logarithmic transformation. This produced a normal distribution for the protein data. However, the distribution for the mRNA and adjusted mRNA data was close to, but not quite, normal. Nevertheless, we calculated the r_p and found that it was 0.76, identical to the coefficient from the Box-Cox transformed data. We therefore believe that this correlation coefficient is not misleading, despite the fact that the log(mRNA) distribution is not quite normal.

RESULTS

Visualization of 1,400 spots on three gel systems. Yeast proteins have isoelectric points ranging from 3.1 to 12.8, and masses ranging from less than 10 kDa to 470 kDa. It is difficult to examine all proteins on a single kind of gel, because a gel with the needed range in pI and mass would give poor resolution of the thousands of spots in the central region of the gel. Therefore, we have used three gel systems: (i) pH "4 to 8" with 10% polyacrylamide; (ii) pH "3 to 10" with 10% polyacrylamide; and (iii) nonequilibrium with 15% polyacrylamide (7, 8). Each gel system allows good resolution of a subset of yeast proteins.

Figure 1 shows a pH 4–8, 10% polyacrylamide gel. The pH at the basic end of the isoelectric focusing gel cannot be maintained throughout focusing, and so the proteins resolved on such gels have isoelectric points between pH 4 and pH 6.7. For these pH 4–8 gels, we see 600 to 900 spots on the best gels after multiple exposures.

The pH 3–10 gels (not shown) extend the pI range somewhat beyond pH 7.5, allowing detection of several hundred additional spots. Finally, we use nonequilibrium gels with 15% acrylamide in the second dimension. These allow visualization of about 100 very basic proteins and about 170 small proteins (less than 20 kDa). In total, using all three gel systems, about 1,400 spots can be seen. These represent about 1,200 different proteins, which is about one-quarter to one-third of the proteins expressed under these conditions (27, 30). Here, we focus on the proteins seen on the pH 4–8 gels.

Although nearly all expressed proteins are present on these gels, the number seen is limited by a problem we call coverage. Since there are thousands of proteins on each gel, many proteins comigrate or nearly comigrate. When two proteins are resolved, but are close together, and one protein spot is much more intense than the other, a problem arises in visualizing the weaker spot: at long exposures when the weak signal is strong enough for detection, the signal from the strong spot spreads and covers the signal from the weaker spot. Thus, weak spots can be seen only when they are well separated from strong spots.

For a given gel, the number of detectable spots initially rises with exposure time. However, beyond an optimal exposure, the number of distinguishable spots begins to decrease, because signals from strong spots cover signals from nearby weak spots. At long exposures, the whole autoradiogram turns black. Thus, there is an optimum exposure yielding the maximum number of spots, and at this exposure the weakest spots are not seen.

Largely because of the problem of coverage, the proteins seen are strongly biased toward abundant proteins. All identified proteins have a CAI of 0.18 or more, and we have identified no transcription factors or protein kinases, which are nonabundant proteins. Thus, this technology is useful for examining protein synthesis, amino acid metabolism, and glycolysis but not for examining transcription, DNA replication, or the cell cycle.

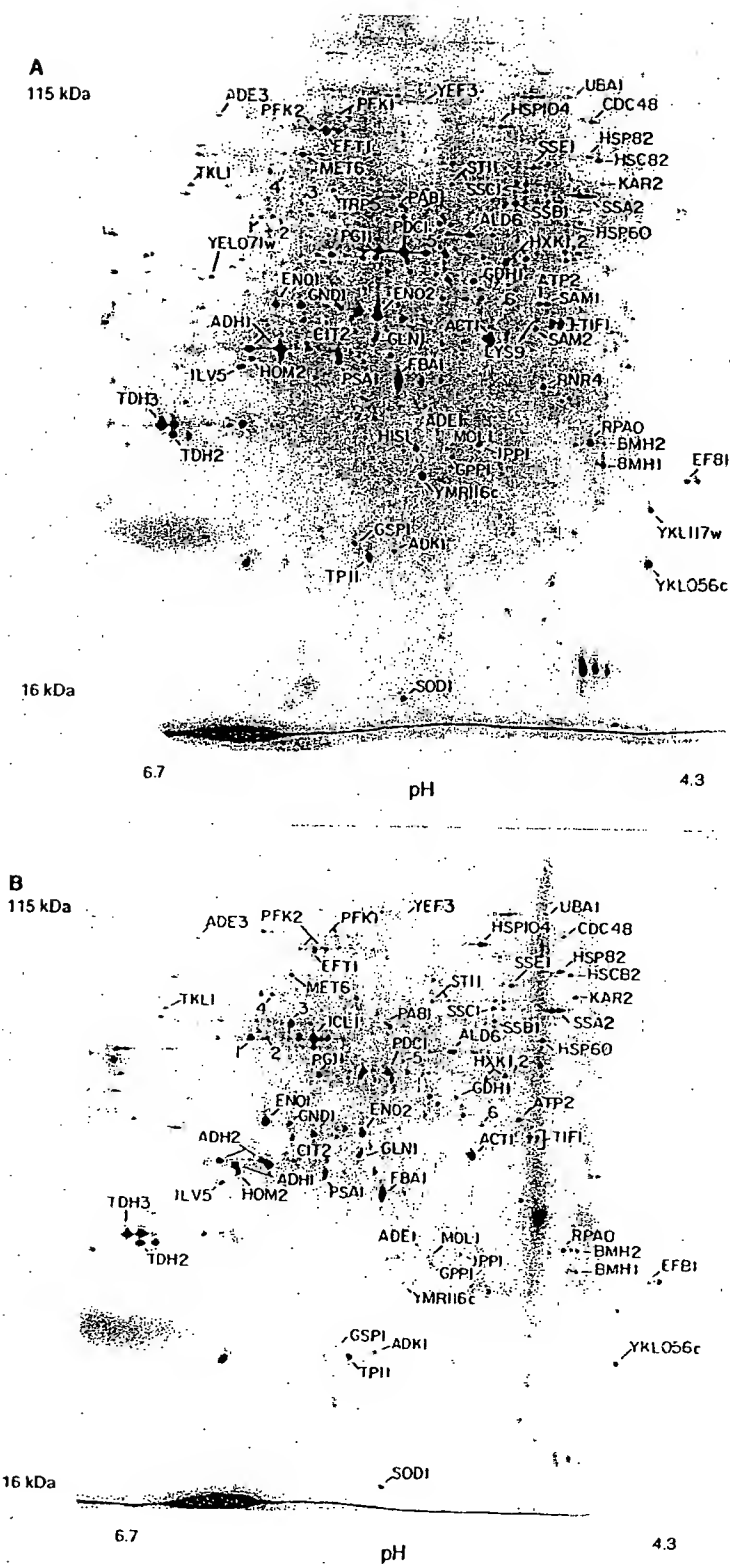


FIG. 1. 2D gels. The horizontal axis is the isoelectric focusing dimension, which stretches from pI 6.7 (left) to pI 4.3 (right). The vertical axis is the polyacrylamide gel dimension, which stretches from about 15 kDa (bottom) to at least 130 kDa (top). For panel A, extract was made from cells in log phase in glucose; for panel B, cells were grown in ethanol. The spots labeled 1 through 6 are unidentified proteins highly induced in ethanol.

Spot identification. The identification of various spots has been described elsewhere (7, 8). At present, 169 different spots representing 148 proteins have been identified. Many of these spots have been independently identified (2, 10, 23, 25). The main methods used in spot identification have been analysis of amino acid composition, gene overexpression, peptide sequencing, and mass spectrometry.

Pulse-chase experiments and protein turnover. Pulse-chase experiments were done to measure protein half-lives (Materials and Methods). Cells were labeled with [35 S]methionine for 10 min, and then an excess of unlabeled methionine was added. Samples were taken at 0, 10, 20, 30, 60, and 90 min after the beginning of the chase. Equal amounts of 35 S were loaded from each sample; 2D gels were run, and spots were quantitated. Surprisingly, almost every spot was nearly constant in amount of radioactivity over the entire time course (not shown). A few spots shifted from one position to another because of post-translational modifications (e.g., phosphorylation of Rpa0 and Efb1). Thus, the proteins being visualized are all or nearly all very stable proteins, with half-lives of more than 90 min. Gygi et al. (10) have come to a similar conclusion by using the N-end rule to predict protein half-lives. This result does not imply that all yeast proteins are stable. The proteins being visualized are abundant proteins; this is partly because they are stable proteins.

Protein quantitation. Because all of the proteins seen had effectively the same half-life, the abundance of each protein was directly proportional to the amount of radioactivity incorporated during labeling. Thus, after taking into account the total number of protein molecules per cell, the average content of methionine and cysteine, and the methionine and cysteine content of each identified protein, we could calculate the abundance of each identified protein (Tables 1 and 2; Materials and Methods). About 1,000 unidentified proteins were also quantified, assuming an average content of Met and Cys.

Many proteins give multiple spots (7, 8). The contribution from each spot was summed to give the total protein amount. However, many proteins probably have minor spots that we are not aware of, causing the amount of protein to be underestimated.

When the proteins on a pH 4–8 gel were ordered by abundance, the most abundant protein had 8,904 ppm, the 10th most abundant had 2,842 ppm, the 100th most abundant had 314 ppm, the 500th most abundant had 57 ppm, and the 1,000th most abundant (visualized at greater than optimum exposure) had 23 ppm. Thus, there is more than a 300-fold range in abundance among the visualized proteins. The most abundant 10 proteins account for about 25% of the total protein on the pH 4–8 gel, the most abundant 60 proteins account for 50%, and the most abundant 500 proteins account for 80%. Since it seems likely that the pH 4–8 gels give a representative sampling of all proteins, we estimate that half of the total cellular protein is accounted for by fewer than 100 different gene products, principally glycolytic enzymes and proteins involved in protein synthesis.

Correlation of protein abundance with mRNA abundance. Estimates of mRNA abundance for each gene have been made by SAGE (27) and by hybridization of cRNA to oligonucleotide arrays (30). These two methods give broadly similar results, yet each method has strengths and weaknesses (Materials and Methods). Table 1 lists the number of molecules of mRNA per cell for each gene studied. One measurement (mRNA) uses data from SAGE analysis alone (27); a second incorporates data from both SAGE and hybridization (30) (adjusted mRNA) (Table 1; Materials and Methods). We correlated protein abundance with mRNA abundance (Fig. 2). For ad-

justed mRNA versus protein, the Spearman rank correlation coefficient, r_s , was 0.74 ($P < 0.0001$), and the Pearson correlation coefficient, r_p , on log transformed data (Materials and Methods) was 0.76 ($P < 0.00001$). We obtained similar correlations for mRNA versus protein and also for other data transformations (Materials and Methods). Thus, several statistical methods show a strong and significant correlation between mRNA abundance and protein abundance. Of course, the correlation is far from perfect; for mRNAs of a given abundance, there is at least a 10-fold range of protein abundance (Fig. 2). Some of this scatter is probably due to posttranscriptional regulation, and some is due to errors in the mRNA or protein data. For example, the protein Yef3 runs poorly on our gels, giving multiple smeared spots. Its abundance has probably been underestimated, partly explaining the low protein/mRNA ratio of Yef3. It is the most extreme outlier in Fig. 2.

These data on mRNA (27, 30) and protein abundance (Table 1) suggest that for each mRNA molecule, there are on average 4,000 molecules of the cognate protein. For instance, for Act1 (actin) there are about 54 molecules of mRNA per cell and about 205,000 molecules of protein. Assuming an mRNA half-life of 30 min (12) and a cell doubling time of 120 min, this suggests that an individual molecule of mRNA might be translated roughly 1,000 times. These calculations are limited to mRNAs for abundant proteins, which are likely to be the mRNAs that are translated best.

A full complement of cell protein is synthesized in about 120 min under these conditions. Thus, 4,000 molecules of protein per molecule of mRNA implies that translation initiates on an mRNA about once every 2 s. This is a remarkably high rate; it implies that if an average mRNA bears 10 ribosomes engaged in translation, then each ribosome completes translation in 20 s; if an average protein has 450 residues; this in turn implies translation of over 20 amino acids per s, a rate considerably higher than estimated for mammals (3 to 8 amino acids per s) (18). These estimates depend on the amount of mRNA per cell (11, 27).

The large number of protein molecules that can be made from a single mRNA raises the issue of how abundance is controlled for less abundant proteins. Many nonabundant proteins may be unstable, and this would reduce the protein/mRNA ratio. In addition, many nonabundant proteins may be translated at suboptimal rates. We have found that mRNAs for nonabundant proteins usually have suboptimal contexts for translational initiation. For example, there are over 600 yeast genes which probably have short open reading frames in the mRNA upstream of the main open reading frame (17a). These may be devices for reducing the amount of protein made from a molecule of mRNA.

Correlation of codon bias with protein abundance. The mRNAs for highly expressed proteins preferentially use some codons rather than others specifying the same amino acid (14). This preference is called codon bias. The codons preferred are those for which the tRNAs are present in the greatest amounts. Use of these codons may make translation faster or more efficient and may decrease misincorporation. These effects are most important for the cell for abundant proteins, and so codon bias is most extreme for abundant proteins. The effect can be dramatic—highly biased mRNAs may use only 25 of the 61 codons.

We asked whether the correlation of codon bias with abundance continues for medium-abundance proteins. There are various mathematical expressions quantifying codon bias; here, we have used the CAI (24) (Materials and Methods) because it gives a result between 0 and 1. The r_s for CAI versus protein abundance is 0.80 ($P < 0.0001$), similar to the mRNA-protein

TABLE 1. Quantitative data*

Function	Name	CAI	mRNA	Adjusted mRNA	Protein (Glu) (10 ³)	Protein (Eth) (10 ³)	E/G ratio
Carbohydrate metabolism	Adh1	0.810	197	197	1,230	972	0.79
	Adh2	0.504	0		0	963	>20
	Cit2	0.185	1	2.8	23	288	12
	Eno1	0.870	No <i>Nla</i>		410	974	2.4
	Eno2	0.892	248	248	650	215	0.33
	Fba1	0.868	179	179	640	608	0.95
	Hxk1,2	0.500	13	10.5	62	46	
	Idl1	0.251	0		0	671	>20
	Pdb1	0.342	5	5	41	33	
	Pdc1	0.903	226	226	280	205	0.73
	Pfk1	0.465	5	5	75	53	0.71
	Pgi1	0.681	14	14	160	120	0.75
	Pyc1	0.260	1	0.7	37	34	
	Tal1	0.579	5	5	110	35	
	Tdh2	0.904	63	63	430	876	NR
	Tdh3	0.924	460	460	1,670	1,927	NR
	Tpi1	0.817	No <i>Nla</i>		No Met	No Met	
Protein synthesis	Efb1	0.762	33	16.5	358	362	
	Eft1,2	0.801	26	26	99	54	0.55
	Prt1	0.303	4	0.7	12	6	
	Rpa0	0.793	246	246	277	100	0.36
	Tif1,2	0.752	29	29	233	106	0.46
	Yef3	0.777	36	36	14	ND	
Heat shock	Hsc82	0.581	2	2.9	112	75	0.67
	Hsp60	0.381	9	2.3	35	82	2.3
	Hsp82	0.517	2	1.3	52	135	2.6
	Hsp104	0.304	7	7	70	161	2.3
	Kar2	0.439	5	10.1	43	102	2.4
	Ssa1	0.709	2	4.3	303	421	1.4
	Ssa2	0.802	10	5	213	324	1.5
	Ssb1,2	0.850	50	50	270	85	
	Ssc1	0.521	2	2.6	68	80	1.2
	Sse1	0.521	8	8	96	48	
	Sti1	0.247	1	1.1	25	44	1.7
Amino acid synthesis	Ade1	0.229	4	4	14	27	
	Ade3	0.276	2	1.7	12	9	
	Ade5,7	0.257	2	1.4	14	4	
	Arg4	0.229	1	8.1	41	41	
	Gdh1	0.585	10	27	148	55	
	Gln1	0.524	11	11	77	104	1.3
	His4	0.267	3	3	15	23	1.5
	Ilv5	0.801	6	6	152	109	0.7
	Lys9	0.332	4	4	32	17	0.52
	Met6	0.657	No <i>Nla</i>	22	190	80	0.42
	Pro2	0.248	3	3	30	12	
	Ser1	0.258	2	1.2	15	8	
	Trp5	0.319	5	5	28	12	
Miscellaneous	Act1	0.710	54	54	205	164	0.78
	Adk1	0.531	No <i>Nla</i>		47	43	
	Ald6	0.520	3	3	181	159	
	Aip2	0.424	1	4.1	76	109	1.4
	Bmh1	0.322	46	46	191	137	0.72
	Bmh2	0.384	1	1.4	134	147	
	Cdc48	0.306	2	2.4	32	26	
	Cdc60	0.299	2	0.86	6	2	
	Erg20	0.373	5	5	92	39	
	Gpp1	0.603	16	5	234	158	
	Gsp1	0.621	3	3	115	39	
	Ipp1	0.620	4	4	254	147	0.34
	Lcb1	0.173	0.3	0.8	19	40	0.58
	Mol1	0.423	0	0.45	20	16	
	Pab1	0.488	3	3	41	19	
	Psa1	0.600	15	15	148	56	0.47
	Rnr4	0.497	6	6	44	37	
	Sam1	0.494	5	5	59	21	
	Sam2	0.497	3	15	63	20	
	Sod1	0.376	36	36	631	618	
	Uba1	0.212	2	2	14	20	
	YKL056	0.731	62	62	253	112	0.44
	YLR109	0.549	21	21	930		
	YMR116	0.777	41	41	184	40	0.20

* CAI, a measure of codon bias, is taken from the YPD. mRNA, number of mRNA molecules per cell from SAGE data (27); adjusted mRNA, number of mRNA molecules per cell based on both SAGE and chip hybridization (30) (see Materials and Methods); Protein (Glu), number of molecules of protein per cell in YNB-glucose; Protein (Eth), number of molecules of protein per cell in YNB-ethanol; E/G ratio, ratio of protein abundance in ethanol to glucose. The E/G ratio is not given if it was close to 1 or if it was not repeatable (NR) in multiple gels. Some gene products (e.g., Tif1 and Tif2 [Tif1,2]) were difficult to distinguish on either a protein or an mRNA basis; these are pooled. No *Nla*, there was no suitable *Nla*III site in the 3' region of the gene, and so there are no SAGE mRNA data; No Met, the mature gene product contains no methionines; and so there are no reliable protein data.

TABLE 2. Functions of proteins listed in Table 1

Name ^a	YPD title lines ^b
Adh1	Alcohol dehydrogenase I; cytoplasmic isozyme reducing acetaldehyde to ethanol, regenerating NAD ⁺
Adh2	Alcohol dehydrogenase II; oxidizes ethanol to acetaldehyde, glucose repressed
Cit2	Citrate synthase, peroxisomal (nonmitochondrial); converts acetyl-CoA and oxaloacetate to citrate plus CoA
Eno1	Enolase 1 (2-phosphoglycerate dehydratase); converts 2-phospho-D-glycerate to phosphoenolpyruvate in glycolysis
Eno2	Enolase 2 (2-phosphoglycerate dehydratase); converts 2-phospho-D-glycerate to phosphoenolpyruvate in glycolysis
Fba1	Fructose biphosphate aldolase II; sixth step in glycolysis
Hxk1	Hexokinase I; converts hexoses to hexose phosphates in glycolysis; repressed by glucose
Hxk2	Hexokinase II; converts hexoses to hexose phosphates in glycolysis and plays a regulatory role in glucose repression
Icl1	Isocitrate lyase, peroxisomal; carries out part of the glyoxylate cycle; required for gluconeogenesis
Pdb1	Pyruvate dehydrogenase complex, E1 beta subunit
Pdc1	Pyruvate decarboxylase isozyme 1
Pfk1	Phosphofructokinase alpha subunit; part of a complex with Pfk2p which carries out a key regulatory step in glycolysis
Pgi1	Glucose-6-phosphate isomerase, converts glucose-6-phosphate to fructose-6-phosphate
Pyc1	Pyruvate carboxylase 1; converts pyruvate to oxaloacetate for gluconeogenesis
Tal1	Transaldolase; component of nonoxidative part of pentose phosphate pathway
Tdh2	Glyceraldehyde-3-phosphate dehydrogenase 2; converts D-glyceraldehyde 3-phosphate to 1,3-dephosphoglycerate
Tdh3	Glyceraldehyde-3-phosphate dehydrogenase 3; converts D-glyceraldehyde 3-phosphate to 1,3-dephosphoglycerate
Tpi1	Triosephosphate isomerase; interconverts glyceraldehyde-3-phosphate and dihydroxyacetone phosphate
Efb1	Translation elongation factor EF-1B; GDP/GTP exchange factor for Tef1p/Tef2p
Eft1	Translation elongation factor EF-2; contains diphthamide which is not essential for activity; identical to Eft2p
Eft2	Translation elongation factor EF-2; contains diphthamide which is not essential for activity; identical to Eft1p
Pti1	Translation initiation factor eIF3 beta subunit (p90); has an RNA recognition domain
Rpa0 (RPPO)	Acidic ribosomal protein A0
Tif1	Translation initiation factor 4A (eIF4A) of the DEAD box family
Tif2	Translation initiation factor 4A (eIF4A) of the DEAD box family
Yef3	Translation elongation factor EF-3A; member of ATP-binding cassette superfamily
Hsc82	Chaperonin homologous to <i>E. coli</i> HtpG and mammalian HSP90
Hsp60	Mitochondrial chaperonin that cooperates with Hsp10p; homolog of <i>E. coli</i> GroEL
Hsp82	Heat-inducible chaperonin homologous to <i>E. coli</i> HtpG and mammalian HSP90
Hsp104	Heat shock protein required for induced thermotolerance and for resolubilizing aggregates of denatured proteins; important for [psi ⁺]-to-[PSI ⁺] prion conversion
Kar2	Heat shock protein of the endoplasmic reticulum lumen required for protein translocation across the endoplasmic reticulum membrane and for nuclear fusion; member of the HSP70 family
Ssa1	Cytoplasmic chaperone; heat shock protein of the HSP70 family
Ssa2	Cytoplasmic chaperone; member of the HSP70 family
Ssb1	Heat shock protein of HSP70 family involved in the translational apparatus
Ssb2	Heat shock protein of HSP70 family, cytoplasmic
Ssc1	Mitochondrial protein that acts as an import motor with Tim44p and plays a chaperonin role in receiving and folding of protein chains during import; heat shock protein of HSP70 family
Sse1	Heat shock protein of the HSP70 family; multicopy suppressor of mutants with hyperactivated Ras/cyclic AMP pathway
Ssi1	Stress-induced protein required for optimal growth at high and low temperature; has tetratricopeptide repeats
Adc1	Phosphoribosylamidoimidazole-succinocarboxamide synthase; catalyzes the seventh step in de novo purine biosynthesis pathway
Adc3	C, tetrahydrofolate synthase (trifunctional enzyme), cytoplasmic
Adc5,7	Phosphoribosylamine-glycine ligase plus phosphoribosylformylglycinamide cyclo-ligase; bifunctional protein
Arg4	Argininosuccinate lyase; catalyzes the final step in arginine biosynthesis
Gdh1	Glutamate dehydrogenase (NADP ⁺); combines ammonia and α -ketoglutarate to form glutamate
Glu1	Glutamine synthetase; combines ammonia to glutamate in ATP-driven reaction
His4	Phosphoribosyl-AMP cyclohydrolase/phosphoribosyl-ATP pyrophosphohydrolase/histidinol dehydrogenase; 2nd, 3rd, and 10th steps of his biosynthesis pathway
Ils5	Ketol-acid reductoisomerase (acetohydroxy, acid reductoisomerase) (alpha-keto- β -hydroxyacyl) reductoisomerase; second step in Val and Ile biosynthesis pathway
Lys9	Saccharopine dehydrogenase (NADP ⁺ , L-glutamate forming) (saccharopine reductase), seventh step in lysine biosynthesis pathway
Met6	Homocysteine methyltransferase; (S-methyltetrahydropteroyl triglutamate-homocysteine methyltransferase), methionine synthase, cobalamin independent
Pro2	γ -Glutamyl phosphate reductase (phosphoglutamate dehydrogenase), proline biosynthetic enzyme
Sei1	Phosphoserine transaminase; involved in synthesis of serine from 3-phosphoglycerate
Trp5	Tryptophan synthase, last (5th) step in tryptophan biosynthesis pathway
Act1	Actin; involved in cell polarization, endocytosis, and other cytoskeletal functions
Adk1	Adenylate kinase (GTP:AMP phosphotransferase), cytoplasmic
Ald6	Cytosolic acetaldehyde dehydrogenase
Atp2	Beta subunit of F1-ATP synthase; 3 copies are found in each F1 oligomer
Bmh1	Homolog of mammalian 14-3-3 protein; has strong similarity to Bmh2p
Bmh2	Homolog of mammalian 14-3-3 protein; has strong similarity to Bmh1p
Cdc48	Protein of the AAA family of ATPases; required for cell division and homotypic membrane fusion
Cdc60	Leucyl-tRNA synthetase, cytoplasmic
Erg20	Farnesyl pyrophosphate synthetase; may be rate-limiting step in sterol biosynthesis pathway
Gpp1 (Rhr2)	DL-Glycerol phosphate phosphatase
Gsp1	Ran, a GTP-binding protein of the Ras superfamily involved in trafficking through nuclear pores
Ipp1	Inorganic pyrophosphatase, cytoplasmic
Lcb1	Component of serine C-palmitoyltransferase; first step in biosynthesis of long-chain base component of sphingolipids
Mol1 (Thi4)	Thiamine-repressed protein essential for growth in the absence of thiamine
Pab1	Poly(A)-binding protein of cytoplasm and nucleus; part of the 3'-end RNA-processing complex (cleavage factor I); has 4 RNA recognition domains
Psa1	Mannose-1-phosphate guanyltansferase; GDP-mannose pyrophosphorylase
Rnr4	Ribonucleotide reductase small subunit
Sam1	S-Adenosylmethionine synthetase 1
Sam2	S-Adenosylmethionine synthetase 2
Sod1	Copper-zinc superoxide dismutase
Uba1	Ubiquitin-activating (E1) enzyme
YKL056	Resembles translationally controlled tumor protein of animal cells and higher plants
YLR109 (Ahp1)	Alkyl hydroperoxide reductase
YMR116 (Asc1)	Abundant protein with effects on translational efficiency and cell size, has two WD (WD:40) repeats

^a Accepted name from the *Saccharomyces* genome database and YPD. Names in parentheses represent recent changes.

^b Courtesy of Protocom, Inc., reprinted with permission.

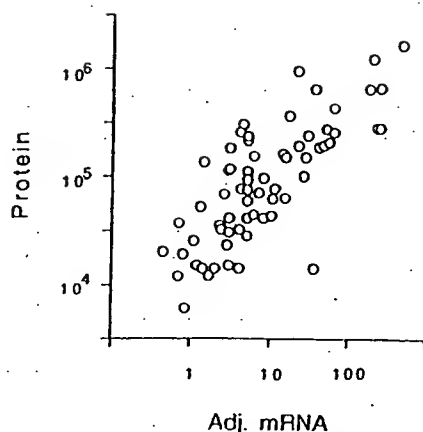


FIG. 2. Correlation of protein abundance with adjusted mRNA abundance. The number of molecules per cell of each protein is plotted against the number of molecules per cell of the cognate mRNA, with an r_p of 0.76. Note the logarithmic axes. Data for mRNA were taken from references 27 and 30 and combined as described in Materials and Methods.

correlation, confirming a strong correlation between CAI and protein abundance (Fig. 3). The relationship between CAI and protein abundance is log linear from about 1,000,000 to about 10,000 molecules per cell. We have no data for rarer proteins.

It is not clear whether CAI reflects maximum or average levels of protein expression. The proteins used for the CAI-protein correlation included some proteins which were not expressed at maximum levels under the condition of the experiment (Hsc82, Hsp104, Ssa1, Ade1, Arg4, His4, and others). When these proteins were removed from consideration and the correlation between CAI and the remaining (presumably constitutive) proteins was recalculated, the r_s was essentially unchanged (not shown).

The equation describing the graph in Fig. 3 is $\log(\text{protein molecules/cell}) = (2.3 \times \text{CAI}) + 3.7$. Thus, under certain conditions (a CAI of 0.3 or greater; a constitutively expressed gene), a very rough estimate of protein abundance can be made by raising 10 to the power of $[(2.3 \times \text{CAI}) + 3.7]$.

The distribution of CAI over the genome (Fig. 4) consists of a lower, bell-shaped distribution, possibly indicating a region where there is no selection for codon bias, and an upper, flat distribution, starting at a CAI of about 0.3, possibly indicating a region where there is selection for codon bias. Almost all of the proteins whose abundance we have measured are in the upper, flat portion of the distribution. In the lower, bell-shaped region, we do not know whether there is a correlation between CAI and protein abundance.

Changes in protein abundance in glucose and ethanol. A comparison of cells grown in glucose (Fig. 1A) with cells grown in ethanol (Fig. 1B) is shown in Table 1. As is well known, some proteins are induced tremendously during growth on ethanol. Two striking examples are the peroxisomal enzymes Icl1 (isocitrate lyase) and Cit2 (citrate synthase), which are induced in ethanol by more than 100- and 12-fold, respectively (Fig. 1; Table 1). These enzymes are key components of the glyoxylate shunt, which diverts some acetyl coenzyme A (acetyl-CoA) from the tricarboxylic acid cycle to gluconeogenesis. *S. cerevisiae* requires large amounts of carbohydrate for its cell wall; in ethanol medium, this carbohydrate comes from gluconeogenesis, which depends on the glyoxylate shunt and on the glycolytic pathway running in reverse. The need for

gluconeogenesis also explains why glycolytic enzymes are abundant even in ethanol medium. Thus, 2D gel analysis shows the prominence of the glycolytic and glyoxylate shunt enzymes in cells grown on ethanol, emphasizing that gluconeogenesis, presumably largely for production of the cell wall, is a major metabolic activity under these conditions.

During gluconeogenesis, substrate-product relationships are reversed for the glycolytic enzymes. One might expect that not all glycolytic enzymes would be well adapted to the reverse reaction. Indeed, 2D gels show that in ethanol, Adh2 (alcohol dehydrogenase 2) is strongly induced (16), while its isozyme Adh1 is not greatly affected. Adh1 and Adh2 each interconvert acetaldehyde and ethanol. Adh1 has a relatively high K_m for ethanol (17 mM), while Adh2 has a lower K_m (0.8 mM) (5). Thus, it is thought that Adh1 is specialized for glycolysis (acetaldehyde to ethanol), while Adh2 is specialized for respiration (ethanol to acetaldehyde) (5, 29). Similarly, Eno1 (enolase 1) is induced in ethanol, while its isozyme Eno2 (enolase 2) decreases in abundance (Table 1) (4, 19). Eno1 is inhibited by 2-phosphoglycerate (the glycolytic substrate), while Eno2 is inhibited by phosphoenolpyruvate (the gluconeogenic substrate) (4). Perhaps Eno1 has a lower K_m for phosphoenolpyruvate than does Eno2, though to our knowledge this has not been tested. Thus, the 2D gels distinguish isozymes specialized for growth on glucose (Adh1 and Eno2) from isozymes specialized for ethanol (Adh2 and Eno1).

Many heat shock proteins (e.g., Hsp60, Hsp82, Hsp104, and Kar2) were about twofold more abundant in ethanol medium than in glucose medium. This is consistent with the increased heat resistance of cells grown in ethanol (3).

Enzymes involved in protein synthesis (Efl1, Rpa0, and Tif1) were about twice as abundant in glucose medium as in ethanol medium. This may reflect the higher growth rate of the cells in glucose.

Phosphorylation of proteins. To examine protein phosphorylation, we labeled cells with ^{32}P and ran 2D gels to examine phosphoproteins. About 300 distinct spots, probably representing 150 to 200 proteins, could be seen on pH 4–8 gels (Fig. 5B). We then aligned autoradiograms of three gels, each with a different kind of labeled protein (^{32}P only [Fig. 5B], ^{32}P plus ^{35}S [Fig. 5A], and ^{35}S only [not shown, but see Fig. 1 for example]). In this way, we made provisional identification of

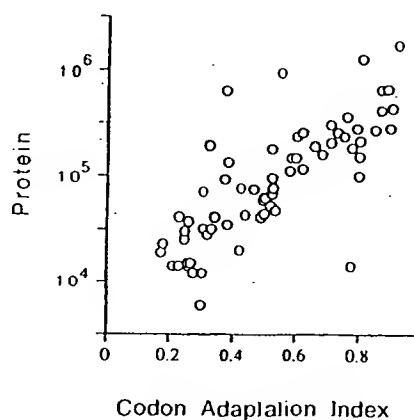


FIG. 3. Correlation of protein abundance with CAI. The number of molecules per cell of each protein is plotted against the CAI for that protein. Note the logarithmic scale on the protein axis. Data for the CAI are from the YPD database (13).

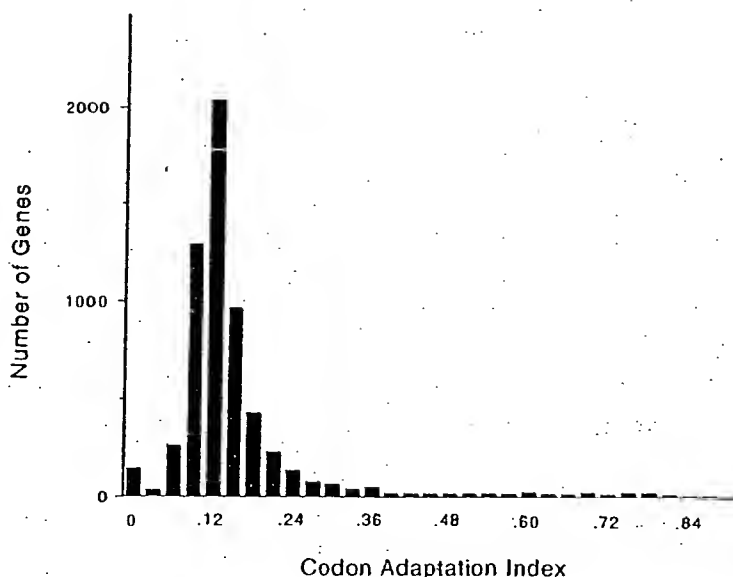


FIG. 4. Distribution of CAI over the whole genome, shown in intervals of 0.030 (i.e., there are 150 genes with a CAI between 0.000 and 0.030, inclusive; 31 genes with a CAI between 0.031 and 0.060; 269 genes with a CAI between 0.061 and 0.090; 1,296 genes with a CAI between 0.091 and 0.120; etc.). The distribution peaks with 2,028 genes with a CAI between 0.121 and 0.150.

some of the ^{32}P -labeled spots as particular ^{35}S -labeled spots. All such identifications are somewhat uncertain, since precise alignments are difficult, and of course multiple spots may exactly comigrate. Nevertheless, we believe that most of the provisional identifications are probably correct. Among the major ^{32}P -labeled proteins are the hexokinases Hxk1 and Hxk2, the acidic ribosome-associated protein Rpa0, the translation factors Yef3 and Efb1, and probably Hsp70 heat shock proteins of the Ssa and Ssb families. Rpa0 and Efb1 are quantitatively monophosphorylated.

Many yeast proteins resolve into multiple spots on these 2D gels (7). Yef3 has five or more spots, at least four of which comigrate with ^{32}P . Tif1 has a major spot showing no ^{32}P labeling and a minor, more acidic spot which overlaps with some ^{32}P label. Tif1 has at least seven spots (7); two of these overlap with some ^{32}P label, but five do not (Fig. 5). Efb1 has at least three spots (7), and none of these overlap with ^{32}P , although there are three nearby, unidentified ^{32}P -labeled spots (a, c, and d in Fig. 5). Spots that seem to be extra forms of Met6, Pdc1, Eno2, and Fba1 can be seen in Fig. 6A, but there is little ^{32}P at these positions in Fig. 5. Thus, phosphorylation explains some but not all of the different protein isoforms seen.

The cell cycle is regulated in part by phosphorylation. We compared ^{32}P -labeled proteins from cells synchronized in G₁ with α -factor, in cells synchronized in G₁ by depletion of G₁ cyclins, and in cells synchronized in M phase with nocodazole. Only very minor differences were seen, and these were difficult to reproduce. The cell cycle proteins regulated by phosphorylation may not be abundant enough for this technique to be applied easily.

Centrifugal fractionation. We fractionated ^{35}S -labeled extracts by centrifugation (Materials and Methods). Figure 6A shows the proteins in the supernatant of a high-speed ($100,000 \times g$, 30 min) centrifugation, while Fig. 6B shows the proteins in the pellet of a low-speed ($16,000 \times g$, 10 min) centrifugation. Many proteins are tremendously enriched in one fraction or the other, while others are present in both.

Most glycolytic enzymes (e.g., Tdh2, Tdh3, Eno2, Pdc1, Adh1, and Fba1) are enriched in the supernatant fraction. The only exception is Pfk1 (not indicated), which is found in both pellet and supernatant fractions. Many proteins involved in protein synthesis (Efb1, Yef3, Prt1, Tif1, and Rpa0) are in the pellet, possibly because of the association of ribosomes with the endoplasmic reticulum. However, Efb1 is in the supernatant, as is a substantial portion of the Efb1. Perhaps surprisingly, several mitochondrial proteins (Atp2 [not shown] and Ily5) are largely in the supernatant. Perhaps glass bead breakage of cells releases mitochondrial proteins. The nuclear protein Gsp1 is in the pellet fraction. The enrichment produced by centrifugation makes it possible to see minor spots which are otherwise poorly resolved from surrounding proteins. Figure 6B shows that the previously identified Tif1 spot is surrounded by as many as six other spots that cofractionate. We observed six identical or very similar additional spots when we overexpressed Tif1 from a high-copy-number plasmid (not shown). Signal overlaps only one or two of these spots in ^{32}P -labeling experiments (Fig. 5), and so the different forms are not mainly due to different phosphorylation states.

DISCUSSION

Our experience with developing a 2D gel protein database for *S. cerevisiae* is summarized here. With current technology, we can see the most abundant 1,200 proteins, which is about one-third to one-quarter of the proteins expressed. The remaining proteins will be difficult to see and study with the methods that we have used, not because of a lack of sensitivity but because weak spots are covered by nearby strong spots.

Of the 1,200 proteins seen, we have identified 148, with a bias toward the most abundant proteins. Steady application of the methods already used would allow identification of most of the remaining proteins. Gene overexpression will be particularly useful, since it is not affected by the lower abundance of the remaining visible proteins.

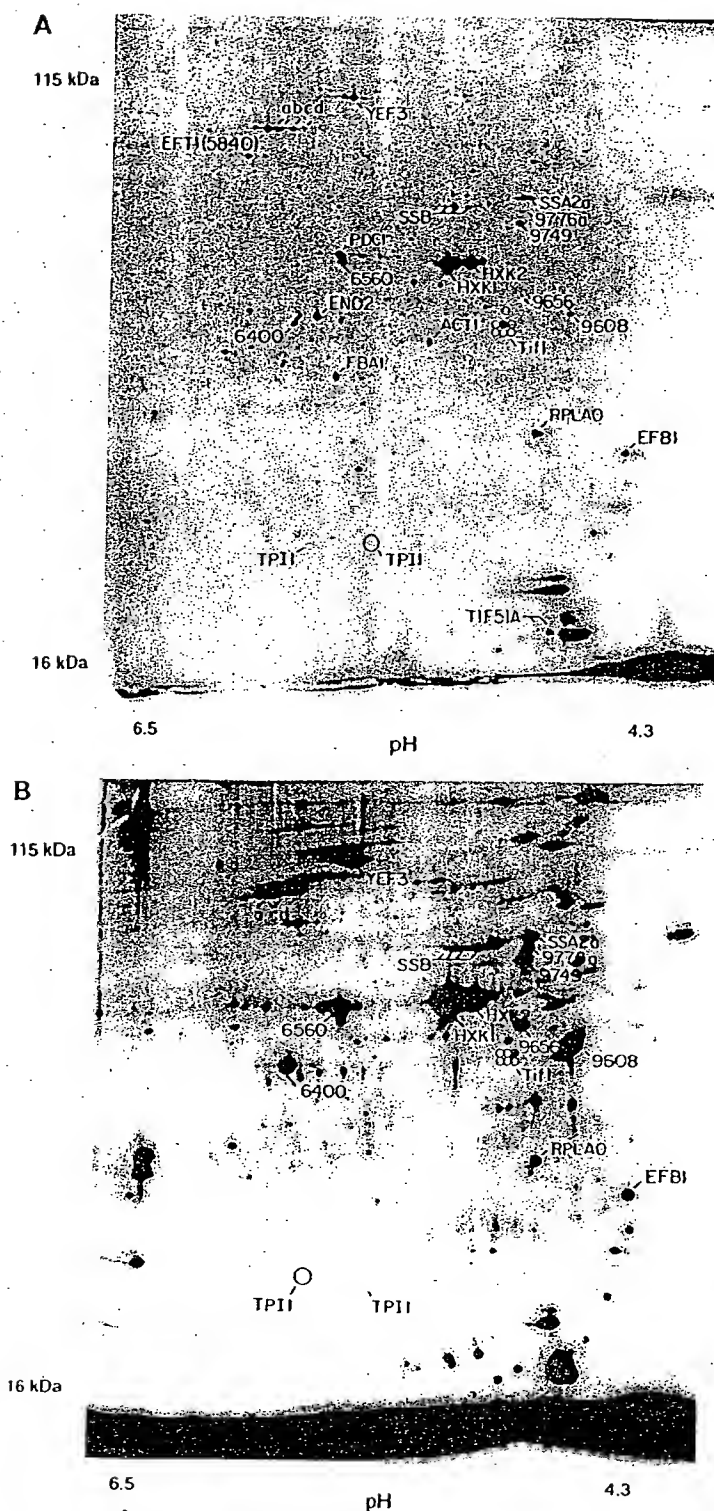


FIG. 5. Phosphorylated proteins. (A) Mixture of ^{32}P -labeled proteins and ^{35}S -labeled proteins. Two separate labeling reactions were done, one with ^{32}P and one with ^{35}S , and extracts were mixed and run on a 2D gel. Spots marked with numbers rather than gene names represent spots noted on ^{35}S gels but unidentified. Spots labeling with ^{32}P were identified by (i) increased labeling compared to the ^{35}S -only gel (not shown); (ii) the characteristic fuzziness of a ^{32}P -labeled spot; and (iii) the decay of signal intensity seen on exposures made 4 weeks later (not shown). A minor form of Tpi1 and at least six minor forms of Tif1 have been noted in overexpression experiments (see also Fig. 6B); positions of the minor forms are indicated by circles. (B) ^{32}P -only labeling. The major form of Tpi1, which is not labeled with ^{32}P , is indicated by a large circle; positions of seven forms of Tif1 are indicated by smaller circles.

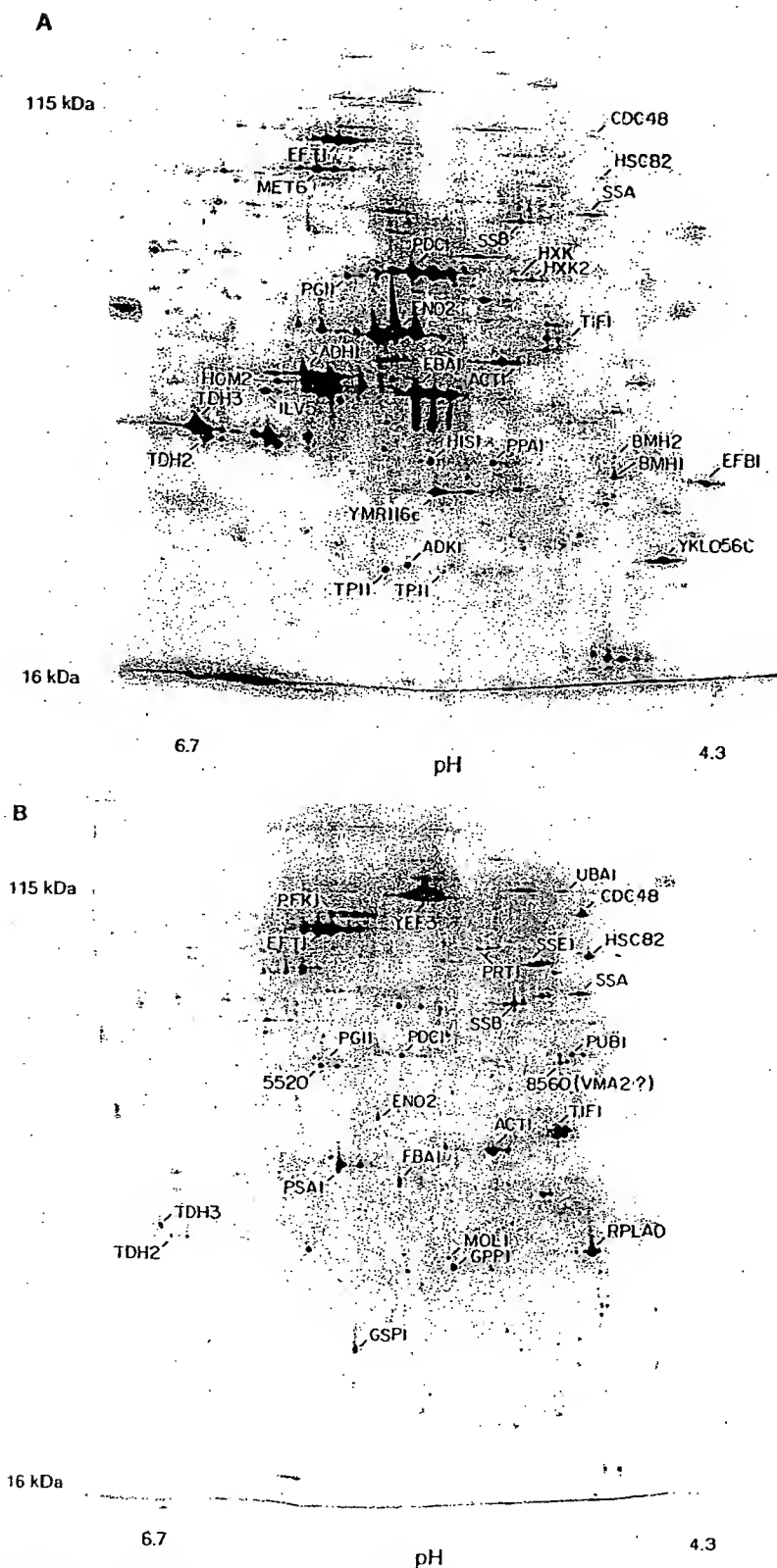


FIG. 6. Fractionation by centrifugation. (A) Proteins in the supernatant of a $100,000 \times g$, 30-min spin; proteins in the pellet of a $16,000 \times g$, 10-min spin. Supernatant fractions examined in multiple experiments done over a wide range of g forces looked similar to each other, as did the pellet fractions.

2D gels of the kind that we have used are not suitable for visualization of rare proteins. However it will be possible to study on a global basis metabolic processes involving relatively abundant proteins, such as protein synthesis, glycolysis, gluconeogenesis, amino acid synthesis, cell wall synthesis, nucleotide synthesis, lipid metabolism, and the heat shock response.

Gygi et al. (10) have recently completed a study similar to ours. Despite generating broadly similar data, Gygi et al. reached markedly different conclusions. We believe that both mRNA abundance and codon bias are useful predictors of protein abundance. However, Gygi et al. feel that mRNA abundance is a poor predictor of protein abundance and that "codon bias is not a predictor of either protein or mRNA levels" (10). These different conclusions are partly a matter of viewpoint. Gygi et al. focus on the fact that the correlations of mRNA and codon bias with protein abundance are far from perfect, while we focus on the fact that, considering the wide range of mRNA and protein abundance and the undoubted presence of other mechanisms affecting protein abundance, the correlations are quite good.

However, the different conclusions are also partly due to different methods of statistical analysis and to real differences in data. With respect to statistics, Gygi et al. used the Pearson product-moment correlation coefficient (r_p) to measure the covariance of mRNA and protein abundance. Depending on the subset of data included, their r_p values ranged from 0.1 to 0.94. Because of the low r_p values with some subsets of the data, Gygi et al. concluded that the correlation of mRNA to protein was poor. However, the r_p correlation is a parametric statistic and so requires variates following a bivariate normal distribution; that is, it would be valid only if both mRNA and protein abundances were normally distributed. In fact, both distributions are very far from normal (data not shown), and so a calculation of r_p is inappropriate. There was no statistical backing for the assertion that codon bias fails to predict protein abundance.

We have taken two statistical approaches. First, we have used the Spearman rank correlation coefficient (r_s). Since this statistic is nonparametric, there is no requirement for the data to be normally distributed. Using the r_s , we find that mRNA abundance is well correlated with protein abundance ($r_s = 0.74$), and the CAI is also well correlated with protein abundance ($r_s = 0.80$) (and also with mRNA abundance [data not shown]). For the data of Gygi et al. (10), we obtained similar results, though with their data the correlation is not as good; $r_s = 0.59$ for the mRNA-to-protein correlation, and $r_s = 0.59$ for the codon bias-to-protein correlation.

In a second approach, we transformed the mRNA and protein data to forms where they were normally distributed, to allow calculation of an r_p (Materials and Methods). Two transformations, Box-Cox and logarithmic, were used; both gave good correlations with our data [e.g., $r_p = 0.76$ for $\log(\text{adjusted RNA})$ to $\log(\text{protein})$]. We were not able to transform the data of Gygi et al. to a normal distribution.

Finally, there are also some differences in data between the two studies. These may be partly due to the different measurement techniques used: Gygi et al. measured protein abundance by cutting spots out of gels and measuring the radioactivity in each spot by scintillation counting, whereas we used phosphorimaging of intact gels coupled to image analysis. We compared our data to theirs for the proteins common between the studies (but excluding proteins whose mRNAs are known to differ between rich and minimal media, and excluding Tif1, which was anomalous in differing by 100-fold between the two data sets). The r_s between the two protein data sets was 0.88 ($P < 0.0001$). Although this is a strong correlation, the fact that

it is less than 1.0 suggests that there may have been errors in measuring protein abundance in one or both studies. After normalizing the two data sets to assume the same amount of protein per cell, we found a systematic tendency for the protein abundance data of Gygi et al. to be slightly higher than ours for the highest-abundance proteins and also for the lowest-abundance proteins but slightly lower than ours for the middle-abundance proteins. These systematic differences suggest some systematic errors in protein measurement. Although we do not know what the errors are, we suggest the following as a reasonable speculation. For the highest-abundance proteins, we may have underestimated the amount of protein because of a slightly nonlinear response of the phosphorimager screens. For the lowest-abundance proteins, Gygi et al. may have overestimated the amount of protein because of difficulties in accurately cutting very small spots out of the gel and because of difficulties in background subtraction for these small, weak spots. The difference in the middle abundance proteins may be a consequence of normalization, given the two errors above.

The low-abundance proteins in the data set of Gygi et al. have a poor correlation with mRNA abundance. We calculate that the r_s is 0.74 for the top 54 proteins of Gygi et al. but only 0.22 for the bottom 53 proteins, a statistically significant difference. However, with our data set, the r_s is 0.62 for the top 33 proteins and 0.56 (not significantly different) for the bottom 33 proteins (which are comparable in abundance to the bottom 53 proteins of Gygi et al.). Thus, our data set maintains a good correlation between mRNA and protein abundance even at low protein abundance. This is consistent with our speculation that protein quantification by phosphorimaging and image analysis may be more accurate for small, weak spots than is cutting out spots followed by scintillation counting. Our relatively good correlations even for nonabundant proteins may also reflect the fact that we used both SAGE data and RNA hybridization data, which is most helpful for the least abundant mRNAs. In summary, we feel that the poor correlation of protein to mRNA for the nonabundant proteins of Gygi et al. may reflect difficulty in accurately measuring these nonabundant proteins and mRNAs, rather than indicating a truly poor correlation *in vivo*. It is not surprising that observed correlations would be poorer with less-abundant proteins and mRNAs, simply because the accuracy of measurement would be worse.

How well can mRNA abundance predict protein abundance? With $r_p = 0.76$ for logarithmically transformed mRNA and protein data, the coefficient of determination, $(r_p)^2$, is 0.58. This means that more than half (in log space) of the variation in protein abundance is explained by variation in mRNA abundance. When converted back to arithmetic values, protein abundances vary over about 200-fold (Table 1), and $(r_p)^2 = 0.58$ for the log data means that of this 200-fold variation, about 20-fold is explained by variation in the abundance of mRNA and about 10-fold is unexplained (but could be due partly to measurement errors). For proteins much less abundant than those considered here, we imagine the *in vivo* correlation between mRNA and protein abundance will be worse, and other regulatory mechanisms such as protein turnover will be more important.

Some important conclusions can be drawn from this sampling of the proteome. First, there is an enormous range of protein abundance, from nearly 2,000,000 molecules per cell for some glycolytic enzymes to about 100 per cell for some cell cycle proteins (26a). Second, about half of all cellular protein is found in fewer than 100 different gene products, which are mostly involved in carbohydrate metabolism or protein synthe-

sis. Third, the correlation between protein abundance and CAI is log linear as far as we can see, which is from about 10,000 protein molecules per cell to about 1,000,000. This is somewhat surprising, because it implies that selective forces for codon bias are significant even at moderate expression levels. It also means that codon bias is a useful predictor of protein abundance even for moderately low bias proteins. Fourth, there is a good correlation between protein abundance and mRNA abundance for the proteins that we have studied. This validates the use of mRNA abundance as a rough predictor of protein abundance, at least for relatively abundant proteins. Fifth, for these abundant proteins, there are about 4,000 molecules of protein for each molecule of mRNA. This last conclusion raises questions as to how the levels of nonabundant proteins are regulated and suggests that protein instability, regulated translation, suboptimal rates of translation, and other mechanisms in addition to transcriptional control may be very important for these proteins.

ACKNOWLEDGMENTS

We thank Neena Sareen and Nick Bizios (CSHL 2D gel laboratory) for production of 2D gels, Tom Volpe for help with some experiments, Corine Driessens for help with calculations and statistics, and Herman Wijnen and Nick Edgington for comments on the manuscript. We especially thank Tim Tully for in-depth statistical analysis and for insightful discussions on statistical interpretations.

This work was supported by grant P41-RR02188 from the NIH Biomedical Research Technology Program, Division of Research Resources, to J.J.G., by Small Business Innovation Research grant R44 GM54110 to Proteome, Inc., by grant DAMD17-94-J4050 from the Army Breast Cancer Program to B.F., and by NIH grant RO1 GM45410 to B.F.

REFERENCES

- Baroni, M. D., E. Martegani, P. Muntli, and L. Alberghina. 1989. Cell size modulation by *CDC25* and *RAS2* genes in *Saccharomyces cerevisiae*. *Mol. Cell. Biol.* 9:2715-2723.
- Boucherie, H., F. Sagliocco, R. Joubert, J. Maillet, J. Labarre, and M. Perrot. 1996. Two-dimensional gel protein database of *Saccharomyces cerevisiae*. *Electrophoresis* 17:1683-1699.
- Elliott, B., and B. Futcher. 1993. Stress resistance of yeast cells is largely independent of cell cycle phase. *Yeast* 9:33-42.
- Entian, K. D., B. Meurer, H. Kohler, K. H. Mann, and D. Mecke. 1987. Studies on the regulation of enolases and compartmentation of cytosolic enzymes in *Saccharomyces cerevisiae*. *Biochim. Biophys. Acta* 923:214-221.
- Ganzhorn, A. J., D. W. Green, A. D. Hershey, R. M. Gould, and B. V. Plapp. 1987. Kinetic characterization of yeast alcohol dehydrogenases. Amino acid residue 294 and substrate specificity. *J. Biol. Chem.* 262:3754-3761.
- Garrels, J. I. 1989. The Quest system for quantitative analysis of two-dimensional gels. *J. Biol. Chem.* 264:5269-5282.
- Garrels, J. I., B. Futcher, R. Kobayashi, G. J. Latter, H. Schwender, T. Volpe, J. R. Warner, and C. S. McLaughlin. 1994. Protein identifications for a *Saccharomyces cerevisiae* protein database. *Electrophoresis* 15:1466-1486.
- Garrels, J. I., C. S. McLaughlin, J. R. Warner, B. Futcher, G. J. Latter, R. Kobayashi, H. Schwender, T. Volpe, D. S. Anderson, R. Mesquita-Fuentes, and W. E. Payne. 1997. Proteome studies of *S. cerevisiae*: identification and characterization of abundant proteins. *Electrophoresis* 18:1347-1360.
- Goffeau, A., B. G. Barrell, H. Bussey, R. W. Davis, H. Dujon, H. Feldmann, F. Galibert, J. D. Hoheisel, C. Jacq, M. Johnston, E. J. Louis, H. W. Mewes, Y. Murakami, P. Philippsen, H. Tettelin, and S. G. Oliver. 1996. Life with 6000 genes. *Science* 274:563-567.
- Gygi, S. P., Y. Rochon, B. R. Franza, and R. Aebersold. 1999. Correlation between protein and mRNA abundance in yeast. *Mol. Cell. Biol.* 19:1720-1730.
- Hersford, L. M., and M. Rosbash. 1977. Number and distribution of polyadenylated RNA sequences in yeast. *Cell* 10:453-462.
- Herrick, D., R. Parker, and A. Jacobson. 1990. Identification and comparison of stable and unstable mRNAs in *Saccharomyces cerevisiae*. *Mol. Cell. Biol.* 10:2269-2284.
- Hodges, P. E., A. H. McKee, B. P. Davis, W. E. Payne, and J. I. Garrels. 1999. The Yeast Proteome Database (YPD): a model for the organization of genome-wide functional data. *Nucleic Acids Res.* 27:69-73.
- Ikemura, T. 1985. Codon usage and tRNA content in unicellular and multicellular organisms. *Mol. Biol. Evol.* 2:13-34.
- Johnston, G. C., F. R. Pringle, and L. H. Hartwell. 1977. Coordination of growth with cell division in the yeast *S. cerevisiae*. *Exp. Cell Res.* 105:79-98.
- Johnston, M., and M. Carlson. 1992. Regulation of carbon and phosphate utilization, p. 193-281. In E. Jones, J. Pringle, and J. Broach (ed.), *The molecular and cellular biology of the yeast Saccharomyces*. Cold Spring Harbor Laboratory Press, Cold Spring Harbor, N.Y.
- Kornblatt, M. J., and A. Klugerman. 1989. Characterization of the enolase isozymes of rabbit brain: kinetic differences between mammalian and yeast enolases. *Biochem. Cell. Biol.* 67:103-107.
- Latter, G., and B. Futcher. Unpublished data.
- Mathews, B., N. Sonenberg, and J. W. B. Hershey. 1996. Origins and targets of translational control, p. 1-29. In J. W. B. Hershey, M. B. Mathews, and N. Sonenberg (ed.), *Translational control*. Cold Spring Harbor Laboratory Press, Cold Spring Harbor, N.Y.
- McAlister, L., and M. J. Holland. 1982. Targeted deletion of a yeast enolase structural gene. Identification and isolation of yeast enolase isozymes. *J. Biol. Chem.* 257:7181-7188.
- Monardo, P. J., T. Boutell, J. I. Garrels, and G. J. Latter. 1994. A distributed system for two-dimensional gel analysis. *Comput. Appl. Biosci.* 10:137-143.
- O'Farrell, P. H. 1975. High resolution two-dimensional electrophoresis of proteins. *J. Biol. Chem.* 250:4007-4021.
- Patterson, S. D., and G. J. Latter. 1993. Evaluation of storage phosphor imaging for quantitative analysis of 2-D gels using the Quest II system. *BioTechniques* 15:1076-1083.
- Sagliocco, F., J. C. Guillemot, C. Monribot, J. Capdevielle, M. Perrot, E. Ferran, P. Ferrara, and H. Boucherie. 1996. Identification of proteins of the yeast protein map using genetically manipulated strains and peptide-mass fingerprinting. *Yeast* 12:1519-1533.
- Sharp, P. M., and W. H. Li. 1987. The Codon Adaptation Index—a measure of directional synonymous codon usage bias, and its potential applications. *Nucleic Acids Res.* 15:1281-1295.
- Shevchenko, A., O. N. Jensen, A. V. Podilejnikov, F. Sagliocco, M. Wilm, O. Vurm, P. Mortensen, A. Shevchenko, H. Boucherie, and M. Mann. 1996. Linking genome and proteome by mass spectrometry: large-scale identification of yeast proteins from two dimensional gels. *Proc. Natl. Acad. Sci. USA* 93:14440-14445.
- Thomas, B. J., and R. Rothstein. 1989. Elevated recombination rates in transcriptionally active DNA. *Cell* 56:619-630.
- Tyres, M., and B. Futcher. Unpublished data.
- Velculescu, V. E., L. Zhang, W. Zhou, J. Vogelstein, M. A. Basrai, D. E. Bassett, Jr., P. Hieter, B. Vogelstein, and K. W. Kinzler. 1997. Characterization of the yeast transcriptome. *Cell* 88:243-251.
- Warner, J. 1991. Labeling of RNA and phosphoproteins in *S. cerevisiae*. *Methods Enzymol.* 194:423-428.
- Wills, C. 1976. Production of yeast alcohol dehydrogenase isoenzymes by selection. *Nature* 261:26-29.
- Wodicka, L. Personal communication.
- Wodicka, L. Unpublished data.
- Wodicka, L., H. Dong, M. Mittmann, M.-H. Ho, and D. J. Lockhart. 1997. Genome-wide expression monitoring in *Saccharomyces cerevisiae*. *Nat. Biotechnol.* 15:1359-1367.



Pergamon

Biochemical Pharmacology, Vol. 49, No. 7, pp. 873-881, 1995.
Copyright © 1995 Elsevier Science Ltd
Printed in Great Britain. All rights reserved.
0006-2952/95 \$9.50 + 0.00

0006-2952(94)00515-X

PRE-TRANSLATIONAL REGULATION OF CYTOCHROME P450 GENES IS RESPONSIBLE FOR DISEASE-SPECIFIC CHANGES OF INDIVIDUAL P450 ENZYMES AMONG PATIENTS WITH CIRRHOSIS

JACOB GEORGE, CHRISTOPHER LIDDLE, MICHAEL MURRAY,
KAREN BYTH and GEOFFREY C. FARRELL*

Storr Liver Unit, Department of Gastroenterology and Hepatology, University of Sydney at
Westmead Hospital, Westmead, NSW 2145, Australia

(Received 7 April 1994; accepted 8 November 1994)

Abstract—We have recently reported that disease-specific differential alterations in the hepatic expression of xenobiotic-metabolizing cytochrome P450 (CYP P450) enzymes occur in patients with advanced liver disease. In order to determine whether the observed changes in CYP proteins are modulated at pre- or post-translational levels, we have now examined the hepatic levels of mRNA for CYPs 1A2, 2C9, 2E1 and 3A4 by solution hybridization in the same livers of 20 controls (surgical waste from histologically normal livers), 32 cases of hepatocellular and 18 of cholestatic severe chronic liver disease. CYP1A2 mRNA and CYP1A immunoreactive protein were both reduced in livers with hepatocellular and cholestatic types of cirrhosis. In contrast, CYP3A4 mRNA and protein were reduced only in livers from patients with hepatocellular diseases. For 1A2 and 3A4 there were significant correlations between mRNA species and the respective protein contents ($r_{S1A2} = 0.74$, $r_{S3A4} = 0.64$, $P < 0.0001$). CYP2C9 mRNA was reduced in patients with both cholestatic and hepatocellular types of liver disease, but 2C protein was reduced only in patients with cholestatic dysfunction. The correlation between CYP2C9 mRNA and protein, was also significant ($r_s = 0.36$, $P < 0.005$) but mRNA levels accounted for only 13% of the variability in protein rankings. This is probably a consequence of other CYP2C proteins apart from 2C9 being detected by the anti-2C antibody. CYP2E1 mRNA and protein were reduced in patients with cholestatic liver disease, but in hepatocellular disease the expression of only CYP2E1 mRNA was decreased. CYP2E1 mRNA was significantly correlated with CYP2E1 protein but accounted for only 18% of the variability in protein rankings ($r_s = 0.43$, $P < 0.0005$). Taken collectively these data indicate that the disease-specific alterations of xenobiotic-metabolizing CYP enzymes among patients with cirrhosis is due, at least in part, to pre-translational mechanisms. The lack of a strong correlation between CYP2E1 mRNA and protein suggests that this gene, like its rat ortholog, may be subject to pre-translational as well as translational and/or post-translational regulation.

Key words: cytochrome P450; CYP; CYP regulation; CYP1A2; CYP2E1; CYP2C9; CYP3A4; human cirrhosis; liver disease

The cytochrome P450s comprise a superfamily of enzymes that play a major role in the detoxification of foreign compounds (xenobiotics) and in the metabolism of endogenous lipids. To date, 221 CYP genes and 12 putative pseudogenes have been described in 31 eukaryotic and 11 prokaryotic species. Twelve gene families and 22 subfamilies have been described in man; 17 have been mapped to the genome [1]. The recommended nomenclature has been adopted in the present work; in some cases the CYP term has been dropped, e.g. 2E1 instead of CYP2E1 [1].

In man, members of the CYP1, 2 and 3 families are predominantly involved in the hepatic metabolism of xenobiotics including drugs and environmental pollutants. Induction by these substances at the gene, mRNA or protein level may alter CYP

expression and catalytic function. The expression of CYP enzymes is subject to large inter-individual variation; in man, genetically determined polymorphisms in drug oxidation, and developmental and tissue-specific regulation of some CYP isoforms have been described [2-4]. CYP expression may also be modulated by hormones, cytokines and disease states.

The regulation of CYP expression is complex involving transcriptional, post-transcriptional and post-translational events. Neonatal imprinting, sex-specific and sex-independent developmental expression, and tissue-specific regulation have been described in animals [5]. Although liver disease appears to decrease pathways of hepatic drug metabolism, the expression and regulation of individual CYPs is uncertain. *In vivo* studies have shown that drug metabolism is significantly altered in severe liver disease [6-9]. However, the contribution of confounding variables such as hepatic blood flow, hepatocyte number and interference by co-administered drugs cannot be estimated or eliminated by this approach. We have recently shown

* Corresponding author: FAX (612) 635 7582.

† Abbreviations: cDNA, complementary DNA; cRNA, complementary RNA; CYP P450, cytochrome P450; IgG, immunoglobulin G; tNA, total nucleic acid; UTP, uridine triphosphate.

in vitro, using isoform-specific catalytic activities and protein immunoquantitation, that 1A2, 2C, 2E1 and 3A proteins are differentially altered in patients with different types of end stage chronic liver disease [10]. In order to determine whether the observed changes in CYP protein content could be due to impaired gene-specific protein synthesis, we now report the results of a systematic determination of hepatic mRNA levels for key protein representatives of the above CYP subfamilies.

MATERIALS AND METHODS

Materials. All chemicals were of analytical grade or similar purity and unless otherwise stated were from either Sigma (Sydney, Australia), Boehringer Mannheim (Sydney, Australia), or Merck (Darmstadt, Germany).

Human tissue. The protocols for experiments on human tissue were approved by the Human Ethics Committees of the Western Sydney Area Health Service and the Royal Prince Alfred Hospital, Sydney. Informed consent was obtained from the subjects.

The study population comprised 70 patients whose clinical characteristics have been reported elsewhere [10]. Briefly, morphologically normal liver was obtained from 20 patients undergoing hepatobiliary surgery for the resection of benign ($N = 4$) or malignant tumors ($N = 14$), or other conditions ($N = 2$). Cirrhotic liver was obtained at the time of orthotopic liver transplantation from 50 patients with advanced hepatic disease. Diagnoses were according to conventional criteria as recognized by the International Hepatology Informatics Group [11]. Tissue from the superior surface of the right lobe of the liver was obtained from patients with cirrhosis, and where possible (subjects undergoing right hepatic lobectomy) from this same region in controls.

Within 15 min of surgical removal, blocks of liver tissue (weight 30–50 g) from control and diseased patients were snap frozen in liquid nitrogen and stored at -70° . Aliquots of liver (weight 250–500 mg) were stored separately under the same conditions for the extraction of nucleic acids.

Data obtained from perusal of patient records included: age, sex, diagnosis, liver histology, presence and nature of non-hepatic disease, previous surgery (including portosystemic shunts), concomitant infection, a semiquantitative assessment of nutritional status, and immediate (previous week) and past history of cigarette smoking or alcohol consumption. The results of liver tests; the serum albumin concentration, prothrombin time, and investigations performed to confirm the clinical diagnosis were noted. Using the criteria of Child, as modified by Pugh, a functional assessment of the severity of liver disease was obtained [12].

All medications consumed in the 2 weeks prior to surgery were recorded. Drugs were classified according to their ability to induce or inhibit CYPs; this information for individual drugs was ascertained by searching the Medline database.

Preparation and storage of microsomes. Microsomes were prepared from liver tissue within 3 weeks

of collection, using differential ultracentrifugation as previously described [13]. The resulting microsomal pellets were resuspended in 50 mM potassium phosphate buffer (pH 7.4) containing 1 mM EDTA and 20% glycerol. Microsomes were snap frozen in liquid nitrogen and stored at -70° . CYP proteins were immunoquantitated within 8 weeks. Storage for this duration did not alter the protein content of microsomes.

Immunoquantitation of microsomal proteins. Reagents for electrophoresis and immunoblotting were from BioRad (Richmond, CA, U.S.A.). The microsomal content of CYP1A2, 2C, 2E1 and 3A was quantitated by immunoblotting [15] after electrophoresis on 7.5% polyacrylamide gels in SDS and transfer to nitrocellulose membranes [16], as described previously [10]. Immunoblotting reactions were performed following incubation with primary antibody, and then incubation with a combination of 125 I-labelled and peroxidase-labelled anti-sheep (1A2) or anti-rabbit IgG (2C, 2E1, 3A). Immunoreactive proteins were visualized with 4-chloro-1-naphthol/hydrogen peroxide, excised and radioactivity determined by gamma counting. Because authentic standards of the human CYPs of interest were not available, a single microsomal preparation was selected as a "control" with which to compare other samples. Patient samples were electrophoresed in duplicate and results expressed as a percentage of that in the "control".

The following polyclonal anti-CYP IgGs were used in immunochemical studies. Anti-rabbit CYP1A2 IgG raised in sheep was a gift from Dr P. Mauri (INSERM U 128, Montpellier, France). This antibody apparently recognized two proteins in rat microsomes (1A1 and 1A2), but only a single protein in human liver tissue (1A2). Anti-human CYP2C IgG generated in rabbit was a gift from Dr P. H. Beaune (Chu Necker, INSERM U 75, Paris, France). The extent of sequence similarity between members of the 2C gene subfamily in man suggests that this antibody would detect other 2C proteins in liver. Anti-human CYP2E1 IgG raised in rabbit was a gift from Dr M. Ingelman-Sundberg (Karolinska Institute, Stockholm, Sweden) and recognized a single protein in human liver. Rabbit anti-human CYP3A4 IgG was a gift from Dr F. P. Guengerich (Vanderbilt University, Nashville, Tennessee, U.S.A.). Given the amino acid sequence similarity between the various human 3A subfamily proteins, this antibody probably also recognizes 3A3, 3A5 and 3A7.

Isolation of total nucleic acid. Total nucleic acids (tNA) were isolated from liver tissue by proteinase K digestion followed by phenol-chloroform extraction as previously described [17]. tNA content was determined spectrophotometrically from the absorbance at 260 nm. The concentration of DNA was quantified using the method of Labarca and Paigen [18].

Solution hybridization analysis of CYP mRNAs. The relative abundances of the mRNAs for CYP1A2, 2C9, 2E1 and 3A4 were determined by the method of Melton *et al.* [19], using [32 S]UTP (1000 Ci/mmol, Amersham, Sydney, Australia) labelled cRNA probes transcribed *in vitro* using a commercial kit.

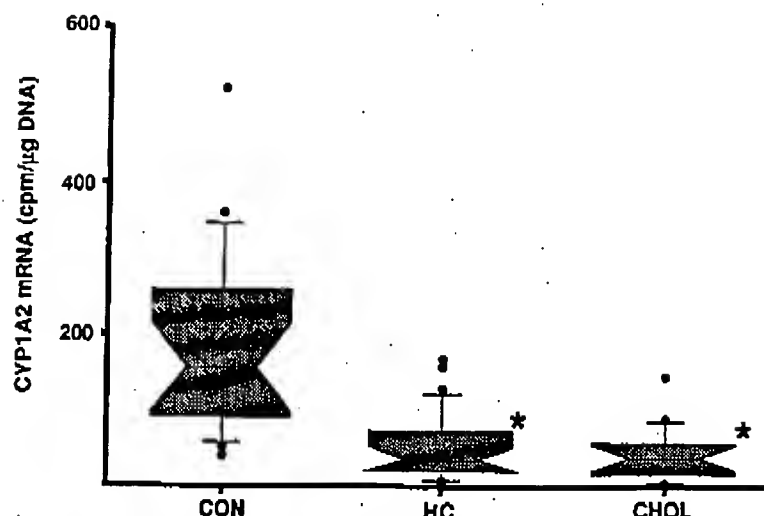


Fig. 1. CYP1A2 mRNA levels in control (CON) patients (N = 20) and in those with hepatocellular (HC, N = 32) and cholestatic (CHOL, N = 18) liver disease. Data are presented as box plots; the median values are indicated by the bar within the shaded areas, which in turn comprise the 25th to 75th percentiles. Error bars denote 10th and 90th percentiles. *P<0.0005 relative to controls.

(Riboprobe, Promega Inc, Sydney, Australia). Extensive computer assisted sequence comparisons for all known human cDNAs, particularly human CYP sequences, were carried out in order to minimize cross-hybridization with other genes. Probe sequences were as follows: CYP1A2, bases 686-735 of the published sequence [20]; CYP2C9, bases 1543-1625 [21]; CYP2E1, bases 525-574 [22]; and CYP3A4, bases 1716-1765 [23]. Probe sequences were obtained by synthesis of both DNA strands followed by annealing and ligation as previously described [24]. The 2C9 sequence was obtained by reverse transcriptase polymerase chain reaction using RNA extracted from human liver and primers whose sequences were derived from the published cDNA sequence. All probe sequences were ligated into the polylinker region of the pGEM 3Z plasmid vector. Maximum sequence similarities of the probes to CYPs within the same family or subfamily were: CYP1A2, <50%; CYP2C9, 80%; CYP2E1, <50%; CYP3A4, 82%. The greatest similarity between the CYP3A4 probe and other CYP3A sequences was with the fetal form CYP3A7, which is expressed in <50% of adults and accounts for <5% of total CYP content in adult liver microsomes [4]. It has been demonstrated previously that, under conditions of high stringency, this degree of similarity does not result in cross-reactivity between probes [24].

Optimal assay conditions with regard to temperature were determined for each probe, being set at 5-10° below the melting point of the labelled RNA-RNA hybrid. The following hybridization temperatures were used: CYP1A2, 75°; CYP2C9, 65°; CYP2E1, 75° and CYP3A4, 70°. Hybridization of aliquots of tRNA were performed in triplicate. The hybridization mix (40 μL), consisted of tRNA sample (5, 7.5 and 10 μL), 0.6 M NaCl, 22 mM Tris HCl (pH 7.5), 5 mM EDTA, 0.1% SDS, 1 mM

dithiothreitol, 20% deionized formamide, transfer RNA (1.23 μg), and approximately 30,000 cpm of probe. After overnight incubation at the appropriate temperature, samples were exposed to RNase in a 1 mL reaction mixture containing 0.3 M NaCl, 10 mM Tris HCl (pH 7.5), 2 mM EDTA, salmon sperm DNA (0.1 mg), RNase A (40 μg) and RNase T1 (500 U) for 45 min at 37°. Undigested hybrids were precipitated by the addition of 100 μL of 6 M trichloroacetic acid, and collected by vacuum filtration onto glass-fiber filters. Specific activity was determined by liquid scintillation spectrometry.

Standard curves were constructed for each assay using tRNA extracted from a control liver. This confirmed linearity of probe hybridization and allowed for comparisons of results between assays. mRNA determinations from patient samples were within the linear region of the standard curve. Samples run without the addition of nucleic acid were used to determine background radioactivity. The adequacy of probe input was checked using probe solution that was not exposed to RNase. Results were expressed in cpm/μg DNA.

Statistical analyses. Results were analysed by non-parametric methods because examination of the data for frequency distributions of mRNA and protein content revealed that these were not normally distributed. The Mann-Whitney U test was used for two group comparisons and the Kruskal-Wallis test if more than two groups. The Bonferroni correction was used to adjust for multiple comparisons. Correlations between mRNA and protein content were expressed as Spearman rank correlations (r_s). Data were analysed on a digital computer (Macintosh SE, Apple Computer, Cupertino, CA, U.S.A.) and a commercial statistical package (Statview 512+, Brain Power Inc, Calabasas, CA, U.S.A.). The significance level for all tests was P<0.05.

mRNAs.
CYP1A2,
a method
2 μmol,
1 cRNA
ercial kit

RESULTS

Characteristics of patients studied

The clinical and other characteristics of the patients have been described elsewhere [10]; there were no important differences between groups in relation to age, gender or the severity of liver disease. The 20 control subjects had normal biochemical and hematological indices, and histology of hepatic tissue used for subsequent analysis was normal. Patients with liver disease had cirrhosis confirmed on biopsy.

Five control subjects consumed alcohol (≥ 10 g/day) and 5 patients (3 controls, 2 cirrhotics) were current smokers (> 5 cigarettes/day). Because alcohol induces 2E1 [22], and cigarette smoking increases levels of 1A2 [25], these patients were excluded from statistical analysis of the 2E1 and 1A2 data, respectively. Eight controls were currently consuming prescribed drugs, but none were taking compounds known to induce or inhibit the CYPs of interest. Patients with liver disease were usually taking multiple medications. The majority of drugs were either without effect (based on literature information) or were reversible inhibitors of CYP mediated metabolism (including the fluoroquinolones, acetaminophen, cimetidine and anti-hypertensives). The latter compounds are likely to be removed in the wash steps performed during the preparation of microsomes. None of the patients received drugs that have been associated with mechanism-based inhibition of CYP enzymes [26]. Compounds known to induce CYPs included rifampicin (received by 3 patients), omeprazole (2 patients) and the glucocorticoids prednisone, hydrocortisone or dexamethasone (13 patients with hepatocellular and 1 patient with cholestatic liver disease).

Microsomal CYP protein content in control and diseased liver

These results have been reported previously [10], but are summarized here in order to permit comparison with the mRNA data. Microsomal 3A protein was decreased only in hepatocellular disease, while 1A2 protein was reduced in microsomes from patients with hepatocellular and cholestatic types of hepatic dysfunction. In contrast, immunoreactive levels of 2E1 were maintained in hepatocellular disease but were decreased in livers from patients with cholestatic forms of cirrhosis. 2C protein was decreased in patients with cholestatic disease. There was a trend that suggested decreased 2C protein in hepatic microsomes from patients with hepatocellular disease, but this did not attain statistical significance.

CYP-specific mRNA levels in control and diseased liver

Large inter-individual variations (up to three orders of magnitude) were noted in the CYP-specific mRNA content of hepatic tissue from controls and patients with advanced hepatic disease. This variability in mRNA expression was greatest for CYP3A4. Thus CYP1A2, CYP2C9, CYP2E1 and CYP3A4 mRNA levels varied 14-, 9-, 11- and 136-fold in control subjects. In cirrhotic liver, this variability was even more striking being 56-, 17-, 44-

and 1200-fold with regard to CYP1A2, CYP2C9, CYP2E1 and CYP3A4, respectively (Figs 1-4).

CYP1A2 mRNA levels were decreased in patients with both hepatocellular ($P < 0.0005$) and cholestatic ($P < 0.0005$) forms of cirrhosis (Fig. 1). In contrast, CYP3A4 mRNA was reduced in patients with hepatocellular disease ($P < 0.001$) but was maintained in those with chronic cholestatic conditions (Fig. 4). CYP2C9 and CYP2E1 mRNA concentrations were significantly lower in patients that had either type of liver disease compared to controls ($P < 0.05$) (Figs 2 and 3).

Correlations between CYP mRNA and content of corresponding CYP proteins

Significant correlations were noted between mRNA levels and protein content for CYP1A2 ($r_s = 0.74$, $P < 0.0001$) and CYP3A4 ($r_s = 0.64$, $P < 0.0001$) (Table 1, Fig. 5). For these two proteins, mRNA levels accounted for 55% (CYP1A2) and 41% (CYP3A4) of the data variance in protein rankings. The relationship between CYP2C9 and CYP2E1 mRNA concentrations and their corresponding protein concentrations, were statistically significant ($r_{s2C9} = 0.36$, $P < 0.005$, $r_{s2E1} = 0.43$, $P < 0.0005$), but mRNA levels accounted for a much smaller proportion of the variability in protein rankings (13% and 18%, respectively) (Table 1).

DISCUSSION

To our knowledge, no previous studies have examined the influence of advanced hepatic disease on CYP mRNA expression. Studies on normal tissue attest to the difficulty of interpreting such data. Using RNase protection assays, Palmer *et al.* [27], noted large inter-individual variations in the expression of four CYP mRNA species in normal liver tissue. CYP1A2 and CYP2C mRNA concentrations displayed a 30-fold inter-subject variation, while 10- and 1000-fold differences were noted for the mRNAs encoding CYP2B and CYP2A, respectively. Using cDNA probes and Northern hybridization, Forrester *et al.* [28], examined the expression of CYP1A1, CYP2A6, CYP2B6, CYP2C8, CYP2D6, CYP2E1 and CYP3A3 in 12 livers from renal transplant donors. Again extremely large variations were noted in mRNA levels from samples. Moreover correlations between mRNA values and the content of the respective CYP proteins were poor. This discrepancy did not appear to be related to the integrity of the mRNA because, in samples where the mRNA levels encoding a particular CYP were low, other CYP isoform-specific mRNAs were highly expressed. Ratanasavanh *et al.* [29], correlated the levels of CYP2C and CYP3A mRNA in nine histologically normal livers (two fetal, two newborns, three children and two adults) with immunochemically determined 2C and 3A protein content. The cDNAs used recognized all mRNA species from the corresponding subfamily. CYP3A mRNA levels roughly paralleled those of 3A protein ($r = 0.71$, $P < 0.05$). While there was a correlation between 2C mRNA and protein ($r = 0.66$), this was not significant ($P = 0.07$) perhaps as a consequence of the small sample size. Thus, the few studies exploring

2, CYP2C9, Figs 1-4).
ed in patients
nd cholestatic.
In contrast,
patients with
as maintained
ions (Fig. 4).
trations were
either type of
(0.05) (Figs 2

nd content of

ed between
YP1A2 ($r_s =$
4, $P < 0.0001$)
cins, mRNA
) and 41%
ein rankings.
nd CYP2E1
rresponding
ly significant
(0.0005), but
uch smaller
in rankings
).

studies have
patic disease
ormal tissue
; such data
r *et al.* [27],
ons in the
(normal liver
ncentrations
on, while 10-
the mRNAs
ively. Using
on, Forrester
of CYP1A1,
6, CYP2E1
d transplant
s were noted
correlations
tent of the,
discrepancy
egrity of the
RNA levels
other CYP
expressed.
he levels of
istologically
orns, three
ochemically
The cDNAs
from the
RNA levels
a ($r = 0.71$,
between 2C
t significant
of the small
exploring

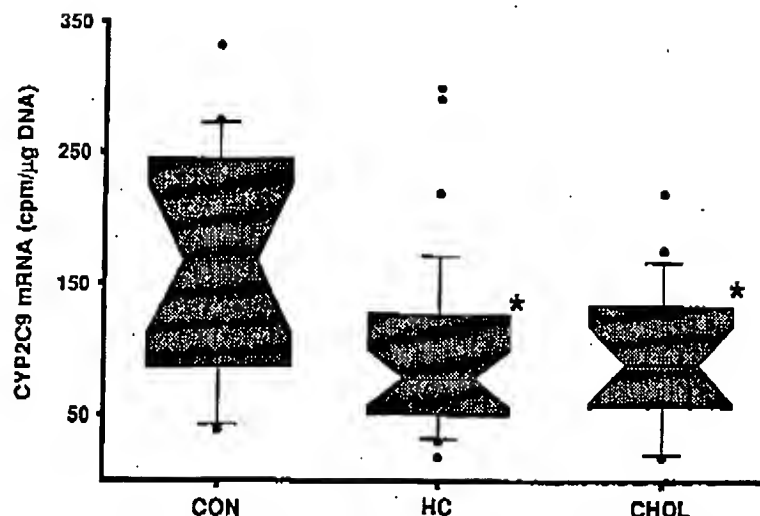


Fig. 2. CYP2C9 mRNA levels in control (CON) patients (N = 20) and in those with hepatocellular (HC, N = 32) and cholestatic (CHOL, N = 18) liver disease. Method of data presentation is the same as for Fig. 1. * $P < 0.05$ relative to controls.

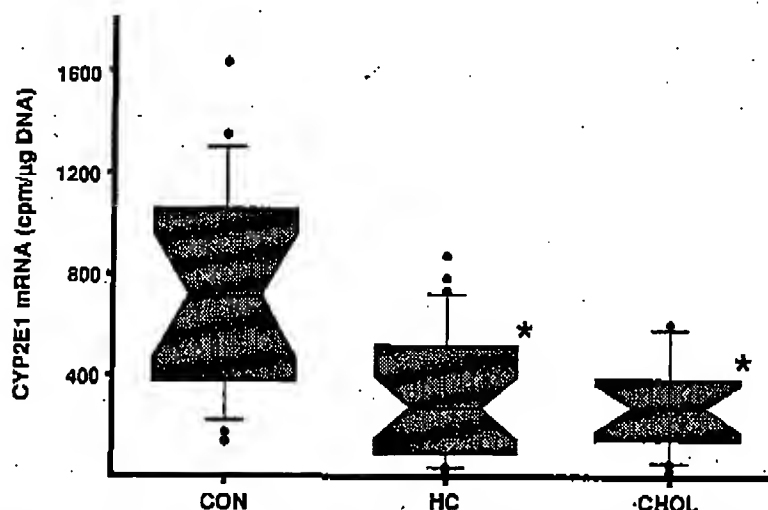


Fig. 3. CYP2E1 mRNA levels in control (CON) patients (N = 20) and in those with hepatocellular (HC, N = 32) and cholestatic (CHOL, N = 18) liver disease. Method of data presentation is the same as for Fig. 1. * $P < 0.005$ relative to controls.

relationships between CYP mRNA and the immunoreactive protein products in healthy liver tissue have failed to find striking correlations.

It has been reported, by *in situ* hybridization, that the apparent concentrations of CYP2A and CYP2B mRNAs were increased in two cirrhotic patients compared to controls. Signals were particularly intense in isolated hepatocytes at the junctions between fibrous septa and hepatic nodules. Hybridization using CYP3A and CYP2C probes gave weak signals compared to controls [30]. Using immunohistochemical techniques, Ratanasavanh *et*

al. [29] examined the intralobular distribution of 1A2, 2C and 3A proteins in four patients with cirrhosis. Striking variability in immunoreactivity for all three proteins was noted between hepatocyte nodules in cirrhotic liver.

We have shown previously that there are disease-specific alterations in CYP protein expression and catalytic activities in patients with advanced liver disease [10]. The current study extends this work, demonstrating disease-specific alterations in CYP1A2 and CYP3A4 mRNA. CYP1A2 mRNA, in tandem with changes in 1A2 protein, was reduced

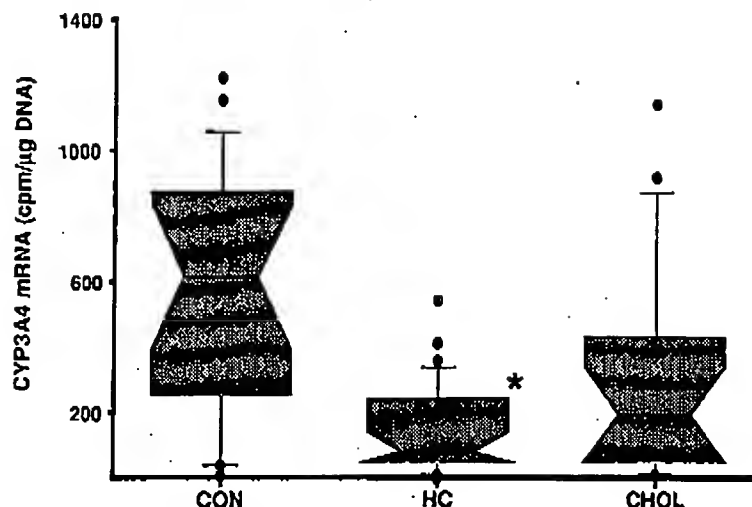


Fig. 4. CYP3A4 mRNA levels in control (CON) patients (N = 20) and in those with hepatocellular (HC, N = 32) and cholestatic (CHOL, N = 18) liver disease. Method of data presentation is the same as for Fig. 1. A single extreme value (2438 cpm/μg DNA) has not been drawn in the CHOL group to facilitate preparation of the figure. *P < 0.001 relative to controls.

Table 1. Correlations between hepatic content of CYP-specific mRNA and related microsomal protein

CYP	r_s	P value
1A2	0.74	P < 0.0001
2C	0.36	P < 0.005
2E1	0.43	P < 0.0005
3A	0.64	P < 0.0001

r_s is the Spearman rank correlation. The data were derived from 20 control and 50 cirrhotic livers (see Materials and Methods).

in patients with either hepatocellular or cholestatic types of liver disease. In contrast, CYP3A4 mRNA (and 3A protein) was reduced in patients with hepatocellular disorders but appeared to be maintained in those with chronic cholestatic disease. Close correlations were evident between mRNA and protein levels for these two isoforms. These data indicate that the disease-specific alterations observed in 3A and 1A2 protein can be partly accounted for by altered pre-translational regulation of the CYP genes for these isoforms. Further, such pre-translational regulation accounts for at least 40–55% of the variability of these protein rankings. It is acknowledged that there are several reasons why levels of mRNA may be reduced, such as decreased CYP transcription and/or enhanced mRNA turnover. Which of these are operative in chronic liver disease requires further study.

CYP2C9 and CYP2E1 mRNA species were diminished in all cirrhotic livers, including those with hepatocellular and cholestatic disease. This observation is consistent with the suggestion that the

mRNAs corresponding to these enzymes are at least partly subject to regulation at the pre-translational level. In contrast, protein quantitation revealed that 2C and 2E1 proteins were significantly reduced only in patients with cholestatic liver disorders, the median values compared to controls being reduced by 66% for 2C and 51% for 2E. There was a tendency towards a reduction in the median values of 2C (43%) but not of 2E1 (19%) protein in hepatocellular disease.

The polyclonal anti-human 2C9 antibody used in our studies recognized one protein in immunoblotting analyses of human microsomes. Given the high degree of sequence similarity between the various proteins in this subfamily, this signal most likely represents a summation of the changes in the levels of all members of the CYP2C subfamily. Immunoreactive 2C protein in the present study was decreased in microsomes from patients with cholestatic disease. There was also a trend suggesting a decrease in microsomes from patients with hepatocellular disease, a finding broadly reflecting those obtained by CYP2C9 mRNA quantitation. According to the selected sequences for the solution hybridization assay, it is likely that the CYP2C9 mRNA probe used recognizes CYP2C9 but not CYP2C8, CYP2C10, CYP2C17, CYP2C18 or CYP2C19. The correlation between 2C protein and mRNA levels, while significant (P < 0.005), was not as close (r_s = 0.36) as that observed for CYP1A2 and CYP3A4. The complexity of the genes within the CYP2C subfamily and the lack of specificity of the polyclonal antibody used in the present study are factors that probably account for this finding.

While the regulation of CYP2E1 in man has not been elucidated, its expression in rat liver appears to be modulated at several points. Transcriptional

CYP gene regulation in human cirrhosis

879

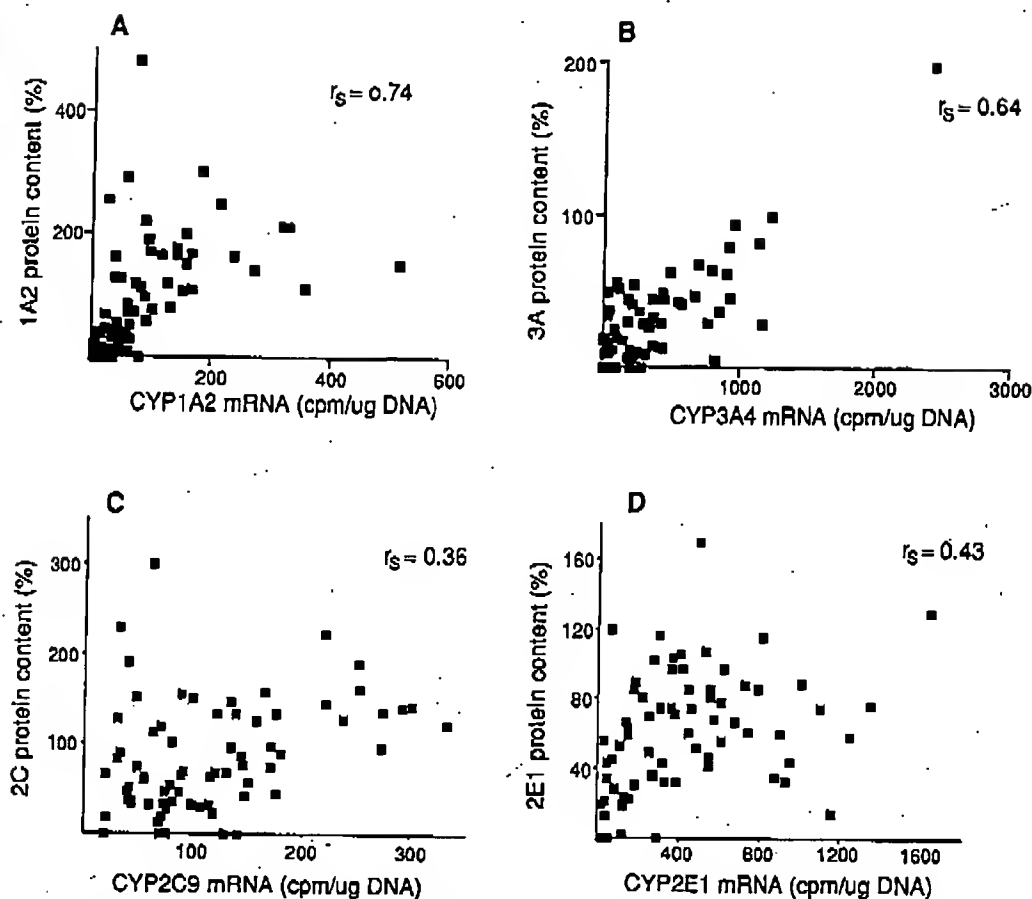


Fig. 5. Scatter plots of CYP mRNA content versus relative microsomal protein in 70 patients for CYP1A2 (A), CYP3A4 (B), CYP2C9 (C) and CYP2E1 (D). Values are Spearman rank correlation coefficients (r_s). Correlations were highly significant ($P_{1A2 \text{ and } 3A4} < 0.0001$, $P_{2C9} < 0.005$, $P_{2E1} < 0.0005$).

activation during development [22] and pre-translational activation with increases in mRNA levels have been observed in experimental diabetes, fasting, ethanol feeding and during ketosis induced by a high fat diet [31–34]. Translational regulation and post-translational modulation by protein stabilization without elevation of CYP2E1 mRNA occur after exposure to substrates such as acetone, ethanol and pyridine [35–37]. Growth hormone and carbon tetrachloride may decrease the expression of this protein [38, 39]. In man, enhanced expression of 2E1 protein has been noted in alcoholics and in patients treated with the inducing agent isoniazid [40, 41]. Pre-translational control may be important in such regulation [42], though other studies have not confirmed this [43].

While we have demonstrated decreased levels of hepatic CYP2E1 mRNA in patients with liver disease, the lack of close correlation ($r_s = 0.43$) between protein and mRNA would suggest that differential protein stabilization or post-transcriptional regulation may also occur in man. In a study of nine healthy human liver samples, Wrighton *et al.* [43] found a similar lack of correlation between the amount of CYP2E1 mRNA and 2E1 protein.

There are several factors that could account for the findings on 2E1 protein expression which have been noted in the present study as well as by others [44]. Increased stability of 2E1 protein and/or increased translation of 2E1 mRNA could occur in patients with hepatocellular disease; it is possible that opposite influences may occur in those with chronic cholestasis. Whether post-transcriptional changes contribute to the observed differential expression of 2E1 proteins in patients with advanced hepatocellular and cholestatic disease has not been addressed by the present studies. Patients with chronic cholestasis have high circulating levels of bile acids and cholesterol. These factors, as well as hormones and cytokines, are putative agents that may alter the expression of 2E1 protein by post-transcriptional processes and such potential effects warrant further study.

In summary, the present results clearly demonstrate that disease-specific changes in the expression of three xenobiotic-metabolizing CYP enzymes (1A2, 2C and 3A) can be attributed, in part, to pre-translational regulation of the respective CYP genes. In contrast, pre- and post-translational (or translational) regulation may account for the

at least
slational
d that
ed only
rs, the
reduced
was a
values
tein in

used in
blotting
re high
various
it likely
in the
family.
dy was
s with
gesting
s with
flecting
itation.
olution
YP2C9
ut not
18 or
ein and
was not
YP1A2
within
icity of
t study
ding.
as not
ppears
ptional

observed differential effect of hepatocellular and cholestatic diseases on 2E1 protein expression. It is now important to identify the factors which modulate these changes in the diseased liver. *In vitro* studies using cultured human hepatocytes may be helpful in identifying potential humoral regulators and the molecular mechanisms involved.

Acknowledgements—We gratefully acknowledge the help of Professors G. McCaughan and R. Sheil from the Australian National Liver Transplant Center, Royal Prince Alfred Hospital, and Professor J. M. Little, Westmead Hospital, Sydney for the supply of surgical tissue. Grateful thanks are due to Professor P. H. Beaune, P. Maurel, M. Ingelman-Sundberg and F. P. Guengerich for their generous gifts of CYP antibodies and other helpful advice. This research was supported in part by a project grant from the Australian National Health and Medical Research Council (NH&MRC). J. G. is an NH&MRC Medical Postgraduate Research Scholar.

These results have been presented in part at the American Association for the Study of Liver Diseases Meeting, Chicago, November 1993, and have been published in abstract form in *Hepatology* 18: 129A, 315A, 1993.

REFERENCES

1. Nelson DR, Kamataki T, Waxman DJ, Guengerich FP, Estabrook RW, Feyereisen R, Gonzales FJ, Coon MJ, Gunsalus IC, Gotoh O, Okuda K and Nebert DW, The P450 superfamily: update on new sequences, gene mapping, accession numbers, early trivial names of enzymes, and nomenclature. *DNA Cell Biol* 12: 1–51, 1993.
2. Mahgoub A, Dring LG, Idle JR, Lancaster R and Smith RL, Polymorphic hydroxylation of debrisoquine in man. *Lancet* 2: 584–586, 1977.
3. Song BJ, Friedman FK, Park SS, Tsokos GC and Gelboin HV, Monoclonal antibody-directed radioimmunoassay detects cytochrome P-450 in human placenta and lymphocytes. *Science* 228: 490–492, 1985.
4. Kitada M, Kamataki T, Itahashi K, Rikihisa T, Kato R and Kanakubo Y, Purification and properties of cytochrome P-450 from homogenates of human fetal livers. *Arch Biochem Biophys* 241: 275–280, 1985.
5. Gonzales FJ, The molecular biology of cytochrome P450s. *Pharmacol Rev* 40: 243–288, 1988.
6. Thomson PD, McIlmou KL, Richardson JA, Cohn K, Steinbrunn W, Cuddeback R and Rowland M, Lidocaine pharmacokinetics in advanced heart failure, liver disease, and renal failure in humans. *Ann Intern Med* 78: 499–508, 1973.
7. Zilly W, Breimer DD and Richter E, Hexobarbital disposition in compensated and decompensated cirrhosis of the liver. *Clin Pharmacol Ther* 23: 525–534, 1978.
8. Farrell GC, Cooksley WGE and Powell LW, Drug metabolism in liver disease: activity of hepatic microsomal metabolizing enzymes. *Clin Pharmacol Ther* 26: 483–492, 1979.
9. Ene MD and Roberts CJC, Pharmacokinetics of nifedipine after oral administration in chronic liver disease. *J Clin Pharmacol* 27: 1001–1004, 1987.
10. George J, Murray M, Byth K and Farrell GC, Differential alterations of cytochrome P450 proteins in livers from patients with severe chronic liver disease. *Hepatology* (in press).
11. International Hepatology Informatics Group, *Diseases of the Liver and Biliary Tract. Standardization of Nomenclature, Diagnostic Criteria and Prognosis*. Raven Press, New York, 1994.
12. Pugh RNH, Murray-Lyon IM, Dawson JL, Pietroni MC and Williams R, Transection of the oesophagus for bleeding oesophageal varices. *Br J Surg* 60: 646–649, 1973.
13. Murray M, Zaluzny L and Farrell GC, Drug metabolism in cirrhosis. Selective changes in cytochrome P-450 isozymes in the choline deficient rat model. *Biochem Pharmacol* 35: 1817–1824, 1986.
14. McConahcy PJ and Dixon FJ, Radioiodination of proteins by the use of the chloramine-T method. *Methods Enzymol* 70: 210–213, 1980.
15. Laemmli UK, Cleavage of structural proteins during the assembly of the head of bacteriophage T4. *Nature* 227: 680–685, 1970.
16. Towbin H, Staehelin T and Gordon J, Electrophoretic transfer of proteins from polyacrylamide gels to nitrocellulose sheets: procedure and some applications. *Proc Natl Acad Sci USA* 76: 4350–4354, 1979.
17. Duram DM and Palmiter RD, A practical approach for quantitating specific mRNAs by solution hybridization. *Anal Biochem* 131: 385–393, 1983.
18. Labarca C and Paigen K, A simple, rapid and sensitive DNA assay procedure. *Anal Biochem* 102: 344–352, 1980.
19. Melton DA, Krieg PA, Rebagliati MR, Maniatis T, Zinn K and Green MR, Efficient *in vitro* synthesis of biologically active RNA and RNA hybridization probes from plasmids containing a bacteriophage SP6 promoter. *Nucleic Acids Res* 12: 7035–7056, 1984.
20. Quattrocchi LC, Peadarthur UR, Okino ST, Potenza C and Tukey RH, Human cytochrome P-450 mRNA and gene: part of a multigene family that contains *Alu* sequences in its mRNA. *Proc Natl Acad Sci USA* 83: 6731–6735, 1986.
21. Romkes M, Faletto MB, Blaisdell JA, Raucy JL and Goldstein JA, Cloning and expression of complementary DNAs for multiple members of the human cytochrome P450C subfamily. *Biochemistry* 30: 3247–3255, 1991.
22. Song BJ, Gelboin HV, Park SS, Yang CS and Gonzalez FJ, Complementary DNA and protein sequences of ethanol-inducible rat and human P450s: transcriptional and post-transcriptional regulation of the rat enzyme. *J Biol Chem* 261: 16689–16697, 1986.
23. Gonzalez FJ, Schmid BJ, Umeno M, McBride OW, Hardwick JP, Meyer UA, Gelboin HV and Idle JR, Human p450PCN1: sequence, chromosomal localization, and direct evidence through cDNA expression that P450PCN1 is nifedipine oxidase. *DNA Cell Biol* 7: 79–86, 1988.
24. Liddle C, Mode A, Legravend C and Gustafsson J-A, Constitutive expression and hormonal regulation of male sexually differentiated cytochromes P450 in primary cultured rat hepatocytes. *Arch Biochem Biophys* 298: 159–166, 1992.
25. Szwarc D, Boobis AR, Edwards RJ and Davies DS, A form of cytochrome P450 in man, orthologous to form d in the rat, catalyses the O-de-ethylation of phenacetin and is inducible by cigarette smoking. *Br J Clin Pharmacol* 26: 363–372, 1988.
26. Murray M, P450 enzymes: inhibition mechanisms, genetic regulation and effects of liver disease. *Clin Pharmacokinet* 23: 132–146, 1992.
27. Palmer CNA, Shephard EA and Phillips IR, Quantification of cytochrome P-450 gene expression in human tissues. *Biochem Soc Trans* 18: 615–616, 1990.
28. Forrester LM, Henderson CJ, Glancey MJ, Back DJ, Park BK, Ball SE, Kitteringham NR, McLaren AW, Miles JS, Skett P and Wolf CR, Relative expression of cytochrome P450 isoenzymes in human liver and association with the metabolism of drugs and xenobiotics. *Biochem J* 281: 359–368, 1992.
29. Ratanasavanh D, Beaune P, Morel F, Flinois J-P, Guengerich FP and Guillouzo A, Intralobular distribution and quantitation of cytochrome P-450

c oesophagus
Surg 60: 646-

ig metabolism
hrome P-450
del. *Biochem*

iodination of
e-T method.

oteins during
gc 14. *Nature*

ectrophoretic
aide gels to
applications.
1979.

lapproach for
ybridization.

and sensitive
02: 344-352,

Maniatis T,
ynthesis of
zation probes
ophage SP6
56, 1984.
I, Potenza C
0 mRNA and
contains *Alu*
Sci USA 83:

laucy JL and
implimentary
cytochrome
2:3255, 1991.
and Gonzalez
sequences of
anscriptional
rat enzyme.

McBride OW,
IV and Idle
chromosomal
ugh cDNA
xidase. *DNA*

Justafsson J-
regulation of
ics P450 in
ch *Biochem*

l Davies DS,
thologous to
thylation of
noking. *Br J*

mechanisms,
hesease. *Clin*

Phillips IR.
expression in
5-616, 1990.
IJ, Back DJ,
cLaren AW,
c expression
an liver and
drugs and
2.

, Flinois J-
Intralobular
rome P-450

enzymes in human liver as a function of age. *Hepatology* 13: 1142-1151, 1991.

30. Palmer CNA, Coates PJ, Davies SE, Shephard EA and Phillips IR, Localization of cytochrome P-450 gene expression in normal and diseased human liver by *in situ* hybridization of wax-embedded archival material. *Hepatology* 16: 682-687, 1992.
31. Song BJ, Matsunaga T, Hardwick JP, Park SS, Veech RL, Gelboin HV and Gonzalez FJ, Stabilization of cytochrome P450j messenger ribonucleic acid in the diabetic rat. *Mol Endocrinol* 1: 542-547, 1987.
32. Hong J, Pau J, Gonzalez FJ, Gelboin HV and Yang CS, The induction of a specific form of cytochrome P-450 (P-450j) by fasting. *Biochem Biophys Res Commun* 142: 1077-1083, 1987.
33. Diehl AM, Bisgaard HC, Kren BT and Steer CJ, Ethanol interferes with regeneration-associated changes in biotransforming enzymes: a potential mechanism underlying ethanol's carcinogenicity? *Hepatology* 13: 722-727, 1991.
34. Yun Y-P, Casazza JP, Sohn DH, Veech RL and Song BJ, Pretranslational activation of cytochrome P450IIE during ketosis induced by a high fat diet. *Mol Pharmacol* 41: 474-479, 1992.
35. Song BJ, Veech RL, Park SS, Gelboin HV and Gonzalez FJ, Induction of rat hepatic N-nitrosodimethylamine demethylase by acetone is due to protein stabilization. *J Biol Chem* 264: 3568-3572, 1989.
36. Eliasson E, Johansson I and Ingelman-Sundberg M, Ligand-dependent maintenance of ethanol-inducible cytochrome P-450 in primary rat hepatocyte cell cultures. *Biochem Biophys Res Commun* 150: 436-443, 1988.
37. Kim SJ and Novak RF, Induction of rat hepatic P450IIE1 (CYP2E1) by pyridine: evidence of a role of protein synthesis in the absence of transcriptional activation. *Biochem Biophys Res Commun* 166: 1072-1079, 1990.
38. Yamazoe Y, Murayama N, Shimada M, Imaoka S, Funae Y and Kato R, Suppression of hepatic levels of ethanol-inducible P-450DM/j by growth hormone: relationship between the increased level of P450-DM/j and depletion of growth hormone in diabetes. *Mol Pharmacol* 36: 716-722, 1989.
39. Sohn DH, Yun YP, Park KS, Veech RL and Song BJ, Posttranslational reduction of cytochrome P450IIE by CCl₄, its substrate. *Biochem Biophys Res Commun* 179: 449-454, 1991.
40. Wrighton SA, Thomas PE, Ryan DE and Levin W, Purification and characterization of ethanol-inducible human hepatic cytochrome P-450HLj. *Arch Biochem Biophys* 258: 292-297, 1987.
41. Zand R, Nelson SD, Slattery JT, Thummel KE, Kalhorn TF, Adams SP and Wright JM, Inhibition and induction of cytochrome P4502E1-catalyzed oxidation by isoniazid in humans. *Clin Pharmacol Ther* 54: 142-149, 1993.
42. Takahashi T, Lasker JM, Rosman AS and Lieber CS, Induction of cytochrome P-450 2E1 in the human liver by ethanol is caused by a corresponding increase in encoding messenger RNA. *Hepatology* 17: 236-245, 1993.
43. Wrighton SA, Thomas PE, Molowa DT, Haniu M, Shively JE, Maines SL, Watkins PB, Parker G, Mendez-Picon G, Levin W and Guzelian PS, Characterization of ethanol-inducible human liver N-nitrosodimethylamine demethylase. *Biochemistry* 25: 6731-6735, 1986.
44. Guengerich FP and Turvy CG, Comparison of levels of several human microsomal cytochrome P-450 enzymes and epoxide hydrolase in normal and disease states using immunochemical analysis of surgical liver samples. *J Pharmacol Exp Ther* 256: 1189-1194, 1991.

Cyclooxygenase-2 Expression in Macrophages: Modulation by Protein Kinase C- α ¹

Mélanie Giroux and Albert Descoteaux²

Cyclooxygenase-2 (COX-2) is an inducible enzyme responsible for high levels of PG production during inflammation and immune responses. Previous studies with pharmacological inhibitors suggested a role for protein kinase C (PKC) in PG production possibly by regulating COX-2 expression. In this study, we addressed the role of PKC- α in the modulation of COX-2 expression and PGE₂ synthesis by the overexpressing of a dominant-negative (DN) mutant of this isoenzyme in the mouse macrophage cell line RAW 264.7. We investigated the effect of various stimuli on COX-2 expression, namely, LPS, IFN- γ , and the intracellular parasite *Leishmania donovani*. Whereas LPS-induced COX-2 mRNA and protein expression were down-regulated in DN PKC- α -overexpressing clones, IFN- γ -induced COX-2 expression was up-regulated in DN PKC- α -overexpressing clones with respect to normal RAW 264.7 cells. Measurements of PGE₂ levels revealed a strong correlation between PGE₂ secretion and IFN- γ -induced COX-2 mRNA and protein levels in DN PKC- α -overexpressing clones. Taken together, these results suggest a role for PKC- α in the modulation of LPS- and IFN- γ -induced COX-2 expression, as well as in IFN- γ -induced PGE₂ secretion. *The Journal of Immunology*, 2000, 165: 3985-3991.

Prostaglandins are important mediators of inflammatory and immune responses. Their secretion is induced by various stimuli including LPS, phorbol esters, cytokines, and phagocytosis (1). PGE₂ is one of the main PGs secreted in large quantities by macrophages and acts as an autocrine regulator of their activity (2, 3). Cyclooxygenases (COX),³ the key enzymes responsible for the conversion of arachidonic acid to PGs, exist in two isoforms with different physiological functions. Whereas COX-1 is constitutively expressed in most cell types and is responsible for regulating normal physiological functions (3, 4), COX-2 is inducible in cells playing a role in inflammation such as macrophages, fibroblasts, and endothelial cells (5, 6). In human and murine macrophages, COX-2 expression is induced by LPS, IL-1, and phorbol esters (6-9). Studies with the murine macrophage cell line RAW 264.7 indicated that accumulation of COX-2 mRNA can be induced by a combination of IFN- γ and LPS but not by IFN- γ alone (10). In addition to soluble mediators, pathogens such as the intracellular parasite *Leishmania donovani* can increase synthesis of PGE₂, possibly by inducing alterations in the COX pathway (11, 12).

Previous studies using protein kinase C (PKC) inhibitors and activators suggested that PGE₂ synthesis requires the activation of PKC in the mouse macrophage cell line RAW 264.7, as well as in

peritoneal macrophages (1, 13). Twelve isoenzymes of PKC, a family of protein serine/threonine kinases, have been identified so far. Differences in their structure, requirement for activity, subcellular localization, and substrate specificity suggest that in a given cell, the various PKC isoenzymes may exert specific functions. Six of them are expressed in macrophages but their respective roles in the regulation of macrophage functions are poorly understood (14, 15). Using clones of the RAW 264.7 macrophage cell line overexpressing a dominant-negative (DN) mutant of PKC- α (DN PKC- α), we recently reported that PKC- α regulates selective LPS-induced responses, including inducible NO synthase (iNOS) and IL-1 α expression (16). This study led us to propose a role for PKC- α in the regulation of inflammatory responses. Previous studies based on selective depletion of PKC isoenzymes and their differential sensitivities to pharmacological inhibitors led to the suggestion that PKC- α regulates zymosan-stimulated arachidonic acid metabolism and eicosanoid synthesis in peritoneal macrophages (17). To further investigate the role of PKC- α in the regulation of COX-2 expression and PGE₂ secretion, we used DN PKC- α -overexpressing clones of the RAW 264.7 macrophage line (16). We obtained evidence that PKC- α modulates COX-2 expression in macrophages exposed to both LPS and IFN- γ , thereby providing additional evidence that PKC- α is involved in the regulation of macrophage inflammatory responses.

Materials and Methods

Cell lines

The murine macrophage cell line RAW 264.7 transfected with the expression vector pCIN-4, and the DN PKC- α -overexpressing clones B1 and C2 (16) were cultured in a 37°C incubator with 5% CO₂ in DMEM with glutamine (Life Technologies, Ontario, Canada), containing 10% heat-inactivated FBS (HyClone, Logan, UT), 10 mM HEPES pH 7.3, and antibiotics supplemented with 200 μ g/ml G418 (Life Technologies).

Bone marrow-derived macrophages (BMM)

BMM were obtained as previously described (18). Briefly, bone marrow cells obtained from femurs of 6- to 8-wk-old female BALB/c mice (Charles River, St-Constant, Québec, Canada), were freed of RBC by osmotic shock and resuspended in complete medium with 15% (v/v) L929 cell-conditioned medium. After 1 day in culture (37°C, 5% CO₂), nonadherent cells were transferred into new culture dishes and then allowed to differentiate

Institut National de la Recherche Scientifique-Institut Armand-Frappier, Université du Québec, Laval, Québec, Canada

Received for publication November 17, 1999. Accepted for publication July 14, 2000.

The costs of publication of this article were defrayed in part by the payment of page charges. This article must therefore be hereby marked *advertisement* in accordance with 18 U.S.C. Section 1734 solely to indicate this fact.

¹ This work was supported by Grant MT-12933 from the Medical Research Council of Canada and from an establishment grant from the Fonds pour la Formation de Chercheurs et l'Aide à la Recherche du Québec. A.D. is a Medical Research Council Scholar.

² Address correspondence and reprint requests to Dr. Albert Descoteaux, Institut Armand-Frappier, Université du Québec, 531 Boulevard des Prairies, Laval, Québec, Canada H7V 1B7. E-mail address: albert.descoteaux@iaf.quebec.ca

³ Abbreviations used in this paper: COX, cyclooxygenase; PKC, protein kinase C; BMM, bone marrow derived-macrophage(s); DN, dominant-negative; iNOS, inducible NO synthase; ICSPB, IFN consensus sequence binding protein; L-NMMA, N^G-monomethyl-L-arginine monoacetate.

3986

PKC- α AND COX-2 EXPRESSION IN MACROPHAGES

and adhere for 6 days. BMM were made quiescent by culturing them in CSF-1-free medium for 18 h before being used.

L. donovani

Promastigotes of *L. donovani* (Ethiopian strain LV9, obtained from G. Matlashewski, McGill University, Montreal, QC, Canada) were freshly derived from amastigotes isolated from the spleen of an infected hamster and were grown in at 26°C in RPMI 1640 supplemented with 20% heat-inactivated FBS, 100 μ M adenine, 5 μ M hemin, 1 μ M biotin, 20 mM 2-[N-morpholino]ethanesulfonic acid, pH 5.5, and antibiotics. For infections with *L. donovani*, 2.5×10^6 adherent macrophages were incubated with 2.5×10^7 parasites for 8 h.

Northern blot analyses

Total RNA preparation and Northern blot analyses were performed essentially as described previously (16, 19). The probe for murine COX-2 consisted of the 1.2-kb *EcoRI*/*Apal* fragment from COX-2 cDNA amplified by PCR using oligodeoxynucleotides AD-24 (5'-CCCCTTCCTGCGAAGTTTAATC-3') and AD-25 (5'-GCATCTGGACGAGGTTTTC-3').

Plasmids

The luciferase reporter vector (pTIS10L) containing the promoter region of the mouse COX-2 gene (20) (-963/+70 from the transcription initiation site) was provided by Harvey Herschman (University of California, Los Angeles, CA) and was used for transient transfections studies. The PKC- α expression vector (pCMV-PKC- α) was constructed by insertion of the human wild-type PKC- α cDNA (21) into the *HindIII* site of the expression vector pRCMV (Invitrogen, San Diego, CA) and was used for overexpression analyses. The pRL-TK plasmid encoding the *Renilla* luciferase was obtained from Promega (Madison, WI).

Transient transfections

Adherent cells (2.5×10^5 /well) were transfected using GenePorter (Gene Therapy Systems, San Diego, CA) with 0.25 μ g of COX-2 luciferase reporter plasmid, and either 0.65 μ g of pRCMV (Invitrogen) or pCMV-PKC- α expression vector. All transfections included 0.1 μ g of pRL-TK (Promega) as transfection efficiency control. Cells were transfected with 250 μ l DNA/GenePorter mix for 5 h, and 1 ml of serum-free medium was added. Cells were treated 7 h later with 100 ng/ml LPS and harvested at 12 h in Reporter lysis buffer (Promega). Firefly and *Renilla* luciferase values were obtained by analyzing 20 μ l of cell extracts according to standard instructions provided in the Dual Luciferase kit (Promega) using a Lumat LB 9507 luminometer (EG & G Berthold, Nashua, NH). Statistically significant differences were identified using the unpaired Student's *t* test. Values of *p* = 0.01 were considered statistically significant.

Western blot analyses

Western blot analyses were performed as described previously (16). Anti-COX-2 mAbs were obtained from Transduction Laboratories (Lexington, KY).

PGE₂ production

PGE₂ levels in the supernatants of macrophage were measured by competitive immunoassay (EIA; Cayman Chemicals, Ann Arbor, MI) after 8 h of incubation with different stimuli as recommended by the manufacturer. When indicated, the COX inhibitors NS398 (5 μ M) and valeryl salicylate (1 mM) (Cayman Chemicals) or the iNOS inhibitor *N*^G-monomethyl-L-arginine monooacetate (L-NMMA; 500 μ M) (Alexis, San Diego, CA) were used. Statistically significant differences were identified using the unpaired Student's *t* test. Values of *p* = 0.01 were considered statistically significant.

Results

Effect of DN PKC- α overexpression on LPS-induced COX-2 expression

In macrophages, COX-2 expression is strongly induced by LPS, phorbol-ester, and several cytokines (22). To investigate the role of PKC- α in this process, we measured COX-2 mRNA accumulation and protein level expression in normal RAW 264.7 cells (containing the empty vector) and in DN PKC- α -overexpressing clones (B1 and C2; Ref. 16) after stimulation with LPS (10 and 100 ng/ml) for 8 h. In normal RAW 264.7 cells, LPS induced the expres-

sion of COX-2 mRNA accumulation and protein synthesis in a dose-dependent manner (Fig. 1, A and B, lanes 1-3). In DN PKC- α -overexpressing clones, LPS-induced COX-2 mRNA accumulation, and protein levels were significantly inhibited. Densitometric analyses revealed that in clone B1, COX-2 mRNA levels were reduced by 10- to 20-fold (Fig. 1A, lanes 4-6), and protein levels were reduced by ~4-fold (Fig. 1B, lanes 4-6) with respect to the levels observed in control cells. In clone C2, LPS-induced COX-2 mRNA levels were barely detectable (Fig. 1A, lanes 7-9), whereas COX-2 protein levels were reduced by ~3- to 5-fold with respect to control cells (Fig. 1B, lanes 7-9). Thus, similar to LPS-induced IL-1 α and iNOS expression (16), DN PKC- α overexpression strongly inhibited LPS-induced COX-2 expression in RAW 264.7 macrophages.

Overexpression of PKC- α increases LPS-induced COX-2 promoter activity

The inhibition of LPS-induced COX-2 expression in DN PKC- α -overexpressing macrophages indicated that PKC- α plays a role in modulating COX-2 expression. To further demonstrate the involvement of PKC- α in the induction of COX-2 by LPS, we transiently transfected RAW 264.7 cells with a COX-2-luciferase reporter and a wild-type PKC- α expression vector. Overexpression of wild-type PKC- α had no effect on basal COX-2 promoter activity in untreated RAW 264.7 cells (Fig. 2). In contrast, PKC- α overexpression significantly increased LPS-stimulated COX-2 promoter activity by ~2-fold with respect to controls (Fig. 2, *p* = 0.0001, *n* = 3). These data are consistent with PKC- α playing a role in modulating COX-2 expression in LPS-stimulated macrophages.

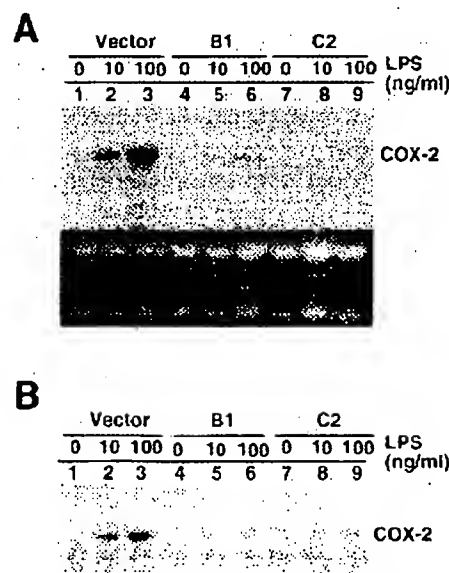


FIGURE 1. Effect of DN PKC- α overexpression on LPS-induced COX-2 expression. Adherent cells (vector alone, clone B1, and clone C2) were incubated in the absence (lanes 1, 4, and 7) or in the presence of either 10 ng/ml (lanes 2, 5, and 8) or 100 ng/ml (lanes 3, 6, and 9) LPS for 8 h. Total RNA was extracted and Northern blot analyses was performed (A), and cell extracts were prepared for Western blot analyses (B) as described in *Materials and Methods*. RNA integrity and loading were assessed by ethidium bromide staining. Similar results were obtained in at least three separate experiments.

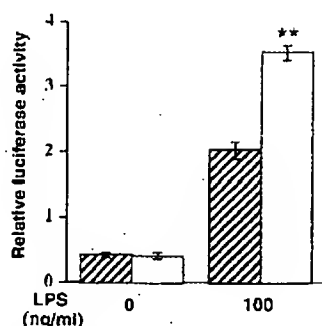


FIGURE 2. Overexpression of PKC- α increases LPS-induced COX-2 promoter activity in RAW 264.7 macrophages. Adherent RAW 264.7 cells were transiently transfected with the COX-2/Luc reporter construct and pRL-TK for 5 h along with either the control vector (▨) or the wild-type PKC- α expression vector (□). Cells were incubated for 7 h and then stimulated with 100 ng/ml LPS for 12 h. Firefly and *Renilla* luciferase activities were determined in cell extracts. Data are expressed as a ratio of firefly luciferase value/*Renilla* luciferase value. Experiments were performed in triplicate and are representative of results obtained in two separate experiments. **, $p = 0.0001$ as compared with LPS-stimulated cells transfected with control vector.

Effect of DN PKC- α overexpression on COX-2 expression following a stimulation with IFN- γ

IFN- γ is a potent regulator of macrophage function (23). In addition to inducing the expression of several genes, incubation of macrophages with IFN- γ enhances their responsiveness to LPS (10, 24). To determine whether PKC- α plays a role in the regulation of IFN- γ -induced responses, we have measured the induction of COX-2 mRNA accumulation and protein synthesis in control RAW 264.7 cells and in the DN PKC- α -overexpressing clones B1 and C2 in response to 100 U/ml IFN- γ alone or in combination with 100 ng/ml LPS. Macrophages were primed with 100 U/ml IFN- γ for 18 h before the addition of either 100 U/ml IFN- γ or the combination of 100 U/ml IFN- γ and 100 ng/ml LPS. IFN- γ induced an important increase of COX-2 mRNA accumulation in DN PKC- α -overexpressing cells (20-fold for clone B1 and 60-fold for clone C2) (Fig. 3A, lanes 6 and 10) compared with control cells (Fig. 3A, lane 2). Similar results were obtained with the levels of COX-2 protein expression, as in clone B1 (Fig. 3B, lane 6) and in clone C2 (Fig. 3B, lane 10). COX-2 levels were increased by 2- and 4-fold, respectively, compared with the levels observed in control cells (Fig. 3B, lane 2). This significant increase in IFN- γ -induced COX-2 expression in DN PKC- α -overexpressing RAW 264.7 cells suggested that PKC- α negatively modulates IFN- γ -induced COX-2 expression. When macrophages were exposed to a combination of both IFN- γ and LPS, high levels of COX-2 mRNA and protein were induced independently of DN PKC- α overexpression (Fig. 3, A and B, lanes 4, 8, and 12). Thus, DN PKC- α overexpression had little effect on the synergistic effect of LPS and IFN- γ on the induction of COX-2 mRNA accumulation and protein synthesis.

COX-2 expression following a phagocytic stimulation with *L. donovani* promastigotes

Infection with the intracellular protozoan *L. donovani* stimulates macrophages to secrete PGE₂, possibly by inducing COX-2 expression (11, 12). Thus we determined whether PKC- α was involved in this process by comparing the induction of COX-2 mRNA accumulation and protein synthesis in normal RAW 264.7 cells and in DN PKC- α -overexpressing clones following phagocytosis of *L. donovani* promastigotes. For priming experiments,

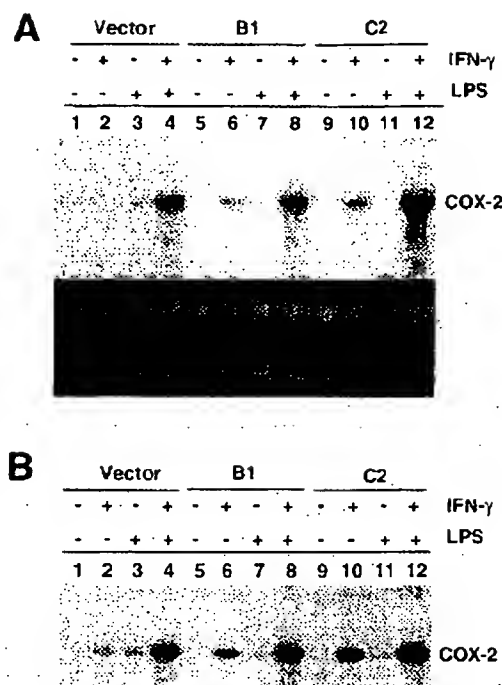


FIGURE 3. Effect of DN PKC- α overexpression on COX-2 expression induced by LPS and IFN- γ . Adherent cells (vector alone, clone B1, and clone C2) were incubated in the absence (lanes 1, 5, and 9) or in the presence of either 100 U/ml IFN- γ (lanes 2, 6, and 10), 100 ng/ml LPS (lanes 3, 7, and 11), or a combination of both (lanes 4, 8, and 12) for 8 h. For priming experiments, cells were first incubated with 100 U/ml IFN- γ for 18 h followed by additional stimulation with IFN- γ , or IFN- γ and LPS. Total RNA was extracted, Northern blot analysis was performed (A), and cell extracts were prepared for Western blot analyses (B) as described in *Materials and Methods*. RNA integrity and loading were assessed by ethidium bromide staining. Similar results were obtained in at least three separate experiments.

cells were incubated for 18 h with 100 U/ml IFN- γ before the addition of either 100 U/ml IFN- γ alone or in combination with *L. donovani* promastigotes for an additional 8 h. Phagocytic stimulation with *L. donovani* promastigotes failed to induce COX-2 mRNA accumulation as well as protein synthesis in control RAW 264.7 macrophages (Fig. 4, A and B, lane 3) and in the two DN PKC- α -overexpressing clones (Fig. 4, A and B, lane 7 for clone B1 and lane 11 for clone C2). Priming with IFN- γ had no effect on the induction of COX-2 expression following phagocytosis of *L. donovani*, as COX-2 mRNA and protein levels induced by IFN- γ alone (Fig. 4, A and B, lane 2 for control cells, lane 6 for clone B1, and lane 10 for clone C2) were similar to those induced by the combination of IFN- γ and *L. donovani* (Fig. 4, A and B, lane 4 for control cells, lane 8 for clone B1, and lane 12 for clone C2). In naive BMM, *L. donovani* evaded the induction of COX-2 expression (Fig. 5, A and B, lane 5), whereas priming with IFN- γ led to the induction of COX-2 mRNA and protein synthesis by *L. donovani* promastigotes in BMM (Fig. 5, A and B, lane 6).

Effect of DN PKC- α overexpression on PGE₂ secretion

We compared the ability of control RAW 264.7 cells and clones B1 and C2 to secrete PGE₂ in response to either LPS (10 or 100 ng/ml), 100 U/ml IFN- γ , or *L. donovani*. As shown in Fig. 6A, in the presence of 10 ng/ml (▨) and 100 ng/ml (■) LPS, control RAW 264.7 cells as well as DN PKC- α -overexpressing clones B1 and C2 secreted PGE₂ in a dose-dependent manner. In contrast to

3988

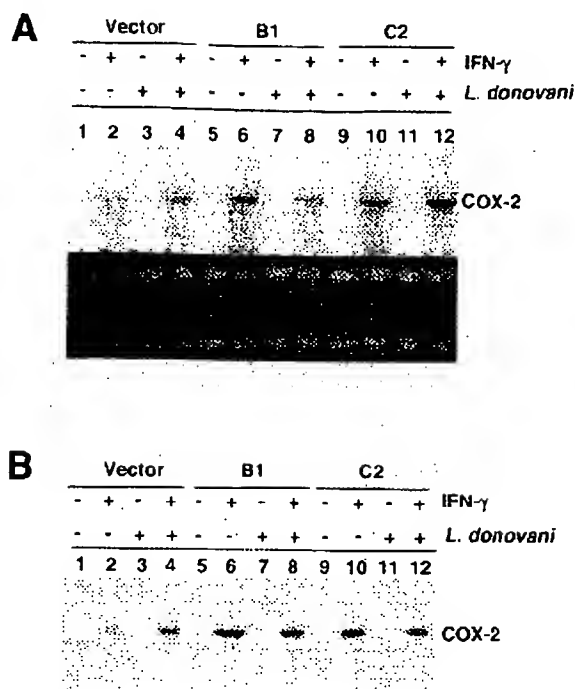
PKC- α AND COX-2 EXPRESSION IN MACROPHAGES

FIGURE 4. Effect of DN PKC- α overexpression on COX-2 expression induced by *L. donovani* promastigotes. Adherent cells (vector alone, clone B1, and clone C2) were incubated in the absence (lanes 1, 5, and 9) or in the presence of different stimuli, namely, 100 U/ml IFN- γ (lanes 2, 6, and 10), *L. donovani* promastigotes (lanes 3, 7, and 11), or a combination of both (lanes 4, 8, and 12) for 8 h. For priming experiments, cells were first incubated with 100 U/ml IFN- γ for 18 h followed by additional stimulation with *L. donovani* and IFN- γ , or IFN- γ alone. Total RNA was extracted, Northern blot analysis was performed (A), and cell extracts were prepared for Western blot analyses (B) as described in *Materials and Methods*. RNA integrity and loading were assessed by ethidium bromide staining. Similar results were obtained in at least three separate experiments.

COX-2 mRNA and protein levels, overexpression of DN PKC- α did not affect LPS-induced PGE₂ secretion by RAW 264.7 cells. (For 10 ng/ml LPS, $p = 0.15$ for B1 vs control cells, and $p = 0.02$ for C2 vs control cells, $n = 3$. For 100 ng/ml LPS, $p = 0.103$ for B1 vs control cells, and $p = 0.07$ for C2 vs control cells, $n = 3$.) Data obtained with the specific COX-2 inhibitor NS-398 (5 μ M) (25) confirmed that COX-2 activation is the major pathway responsible for LPS-stimulated PGE₂ secretion (Table 1). The observation that valeryl salicylate, a COX-1 inhibitor (26), reduced LPS-induced PGE₂ production by 50% suggested a role for COX-1, although it is possible that COX-2 activity was also inhibited at the concentration used (1 mM) (Table 1). As shown in Fig. 6B, IFN- γ induced the secretion of minimal PGE₂ levels in control RAW 264.7 cells, whereas DN PKC- α -overexpression increased IFN- γ -induced PGE₂ secretion by 35-fold by clone B1 ($p = 0.005$, $n = 3$) and 70-fold by clone C2 ($p = 0.01$, $n = 3$). Collectively, these results indicated that DN PKC- α overexpression had no effect on LPS-induced PGE₂ secretion but strongly up-regulated IFN- γ -induced PGE₂ secretion. When macrophages were exposed to a combination of IFN- γ and LPS, control RAW 264.7 cells and the DN PKC- α -overexpressing clones B1 and C2 secreted similar PGE₂ levels ($p = 0.04$ for B1 vs control cells, and $p = 0.795$ for C2 vs control cells, $n = 3$) (Fig. 6C). As observed for COX-2 mRNA and protein synthesis, *L. donovani* promastigotes failed to induce PGE₂ secretion in control RAW 264.7 cells as well as in DN PKC- α -overexpressing clones B1 and C2 (data not shown).

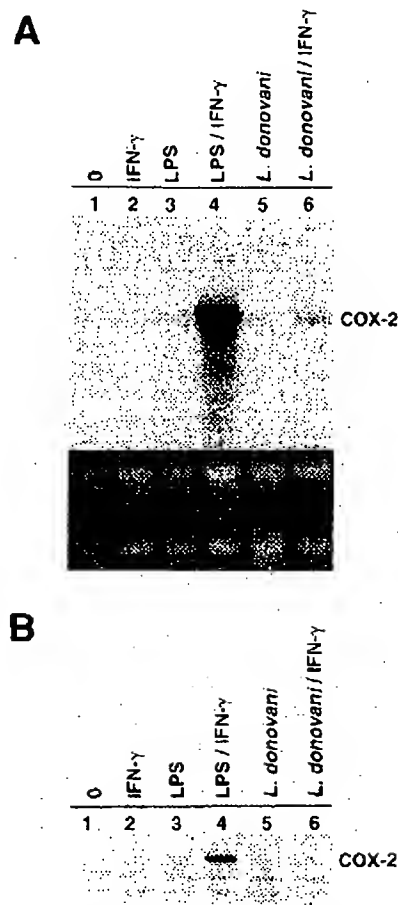


FIGURE 5. COX-2 expression in BMM. BMM were incubated in the absence (lane 1) or in the presence of different stimuli (lanes 2–6) for 8 h. For priming experiments, cells were first incubated with 100 U/ml IFN- γ for 18 h followed by 100 ng/ml LPS, *L. donovani* promastigotes, or 100 U/ml IFN- γ . Total RNA was extracted, Northern blot analysis was performed (A), and cell extracts were prepared for Western blot analyses (B) as described in *Materials and Methods*. RNA integrity and loading were assessed by ethidium bromide staining. Similar results were obtained in at least three separate experiments.

Discussion

PGs are important regulatory mediators for the maintenance of numerous physiological functions and are synthesized by most mammalian tissues (3, 27). In inflammatory reactions, macrophages are the main producers of large quantities of PGE₂ (10, 28). COX-2, the inducible COX isoform, has been identified in activated macrophages and constitutes the key enzyme responsible for the high production of inflammatory PGs such as PGE₂ (3, 5, 29). A role for PKC in the regulation of PG production (possibly by regulating COX-2 expression) has been suggested after treatment of macrophages with PKC inhibitors or activators (1, 13). In this study, we investigated the role of PKC- α in the regulation of COX-2 expression in macrophages. To this end, we have stably overexpressed a DN mutant of this isoenzyme in the murine macrophage cell line RAW 264.7 (16). We obtained evidence suggesting that PKC- α activity is important for the modulation of COX-2 expression in macrophages exposed to either LPS or IFN- γ .

Previous studies suggested that PKC is involved in the regulation of COX-2 expression. A role for PKC- α in the regulation of

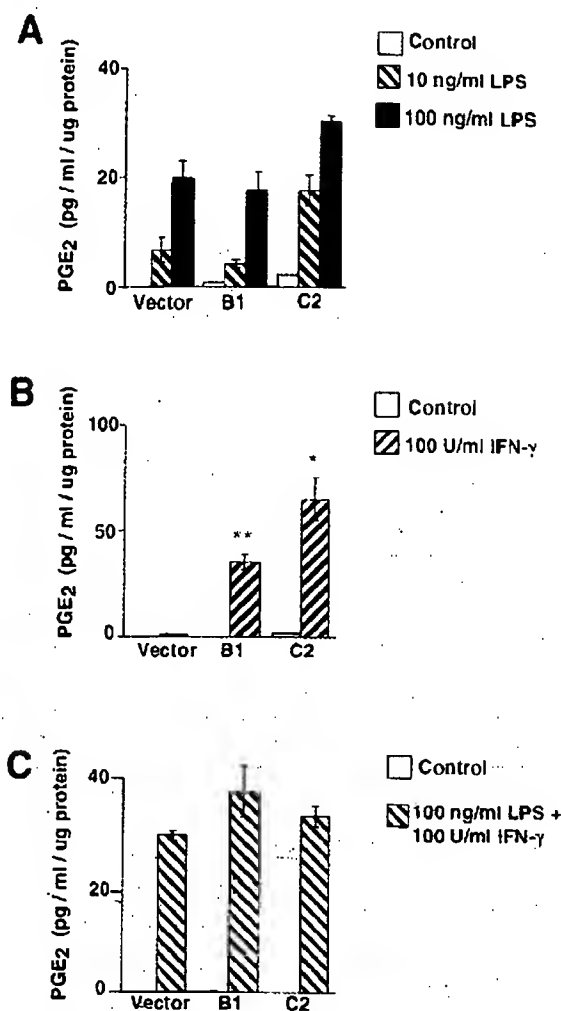


FIGURE 6. Effect of DN PKC- α on PGE₂ secretion. Adherent cells (vector alone, clone B1, and clone C2) were incubated in the absence or presence of either 10 ng/ml or 100 ng/ml LPS (A), 100 U/ml IFN- γ (B), or a combination of 100 U/ml IFN- γ and 100 ng/ml LPS (C) for 8 h. Cells stimulated with IFN- γ were first incubated for 18 h with 100 U/ml IFN- γ . Levels of PGE₂ in cell supernatants were determined by ELISA as described in *Materials and Methods*. Experiments were performed in triplicate and are representative of results obtained in three separate experiments. *, $p < 0.05$; **, $p < 0.01$ as compared with IFN- γ -treated control cells.

zymosan-induced PGE₂ secretion in mouse peritoneal macrophages has been previously proposed based on the selective down-regulation of PKC isoenzymes and on their differential sensitivities to pharmacological inhibitors (17). Recently, it has been reported that overexpression of wild-type PKC- α in mouse epidermis increases phorbol esters-induced expression of specific proinflammatory mediators, including COX-2, suggesting that PKC- α plays a role in cutaneous inflammation (30). Our data obtained with DN PKC- α -overexpressing clones suggest that this isoenzyme is required for COX-2 expression in the RAW 264.7 macrophage cell line. However, the possibility exists that stable overexpression of the DN PKC- α might have affected basal PKC- α activity levels, thereby altering the maintenance of normal cellular functions. A possible consequence of such alterations could be the loss of regulator(s), which could potentially affect signal transduction pathways leading to COX-2 expression. Accordingly, PKC- α would play a secondary role in LPS-induced COX-2 expression. In con-

trast, our observation that overexpression of wild-type PKC- α increases LPS-induced COX-2 promoter activity is not consistent with this possibility and argues in favor of a direct role for PKC- α (Fig. 2). Thus, our observations further support a role for PKC- α in the modulation of COX-2 expression in macrophages, and hence in the regulation of inflammatory responses.

The mechanism by which PKC- α modulates COX-2 expression remains obscure. One possibility is that PKC- α is required for the activation of specific transcription factors. In this regard, few studies have addressed the identity of the transcription factor(s) regulating COX-2 expression (31–33). The ubiquitous transcription factor NF- κ B, one of the main mediators of LPS responses (34), binds to regulatory sequences within the promoter region (–403 to –395 bp) of both the human and mouse COX-2 genes to regulate COX-2 expression (35). Because LPS-induced NF- κ B activation takes place normally in DN PKC- α -overexpressing macrophages (16), it is likely that transcription factor(s) other than NF- κ B and required for LPS-induced COX-2 expression may be defective in our DN PKC- α overexpressing clones. Consensus binding sites for NF-IL6 have been identified within the COX-2 promoter region, and recent evidence indicated that this regulatory sequence is responsible for the induction of human COX-2 by LPS, through NF-IL6 β (C/EBP δ) (33). More recently, it has been established that although that NF- κ B is not required, NF-IL6 is essential for LPS-induced COX-2 gene expression in RAW 264.7 cells (36). Further studies will be required to examine whether a defective activation of NF-IL6 could account for the inhibition of LPS-induced COX-2 expression in the DN PKC- α overexpressing RAW 264.7 macrophages. In this regard, preliminary evidence indicated that DN PKC- α overexpression inhibited LPS-induced NF-IL6 activation in RAW 264.7 cells (F. Chano and A. Descoteaux, unpublished data).

IFN- γ is a pleiotropic cytokine that plays a key role in modulating immune and inflammatory responses (37) and regulates several macrophage functions (38). Previous studies in human macrophages demonstrated that IFN- γ priming is required for the induction of COX-2 expression following stimulation with either IFN- γ or TNF- α . Moreover, IFN- γ , in combination with either LPS or TNF- α , induced a synergistic increase in the accumulation of COX-2 mRNA (24). However, this synergistic effect is not universal, as IFN- γ priming down-regulated COX-2 gene transcription in response to IL-1 β but not to LPS in human macrophages (6). Despite these observations, no data exist on the regulation of COX-2 expression by PKC following stimulation with IFN- γ . In contrast to LPS-induced COX-2 expression, we found that levels of COX-2 mRNA were significantly enhanced in DN PKC- α -overexpressing macrophages following a stimulation with IFN- γ . These data suggest that PKC- α negatively modulates COX-2 expression in response to IFN- γ . Two possible mechanisms may account for these results. First, overexpression of DN PKC- α influences the transcriptional activity of the COX-2 promoter, possibly by regulating the activation of IFN- γ -induced transcription factor(s). IFN consensus sequence binding protein (ICSBP), which is primarily expressed in cells of the macrophage and lymphocytic lineages, is a member of the IFN regulatory factor family that binds to a DNA sequence, known as the IFN-stimulated response element (ISRE), which mediates IFN- γ responsiveness for several genes (39, 40). ICSBP mRNA levels become elevated in response to IFN- γ , but not IFN- α/β , in macrophage cell lines and in thioglycollate-elicited peritoneal macrophages (41). Thus, the selectivity of ICSBP for macrophages and other cells of the immune system, coupled with its strong inducibility and long half-life in macrophages, suggests that it could play a critical role in the down-regulation of macrophage activity after activation by IFN- γ (42).

Table 1. Effect of COX and iNOS inhibitors on LPS-induced PGE₂ secretion in RAW 264.7 macrophages^a

Inhibitors	PGE ₂ (pg/ml/ μ g protein) ^b			
	Vector		Clone C2	
	Control	LPS	Control	LPS
None	0.07 \pm 0.00	12.89 \pm 0.91	0.09 \pm 0.04	13.58 \pm 3.20
NS-398	0.13 \pm 0.06	0.08 \pm 0.04	0.07 \pm 0.01	0.08 \pm 0.04
Valeryl salicylate	0.12 \pm 0.01	7.61 \pm 1.63	0.16 \pm 0.07	6.12 \pm 0.83
L-NMMA	0.12 \pm 0.05	13.20 \pm 1.34	0.15 \pm 0.05	14.19 \pm 2.12

^a Macrophages (2.5×10^5 per well) were incubated for 15 min in the absence or presence of either NS-398 (5 μ M), valeryl salicylate (1 mM), or L-NMMA (500 μ M) prior to the addition of 100 ng/ml LPS. PGE₂ levels in the supernatants were measured after 8 h as described in *Materials and Methods*.

^b Results are expressed in picograms per milliliter PGE₂ produced per microgram total protein. The values represent the mean \pm SD of one experiment performed in triplicate samples. Similar results were obtained in a separate experiment.

Recent studies provided evidence that ICSBP can selectively suppress the expression of IFN-responsive genes (40). Furthermore, induction of ICSBP mRNA by IFN- γ was found previously to be inhibited by PKC inhibitors (41). Considering these observations, it will be of interest to verify the role of ICSBP in IFN- γ -induced COX-2 expression in DN PKC- α overexpressing RAW 264.7 cells in response to IFN- γ . Second, the steady-state levels of COX-2 transcripts are the result of a balance between the rate of gene transcription and the rate of degradation of the mRNA produced. The 3' untranslated region of COX-2 mRNA contains conserved AUUA repeats also found in other short-lived mRNA species, such as GM-CSF mRNA (20, 43), that are important in determining mRNA stability and translation (44, 45). Whether PKC- α activity negatively regulates the binding of putative cytosolic factors to the 3' untranslated region of the COX-2 transcripts, and hence influences COX-2 mRNA stability in IFN- γ -stimulated macrophages, is an hypothesis that will deserve further attention.

L. donovani is an obligate intracellular protozoan that resides within mononuclear phagocytes of infected mammals (46). A previous study demonstrated that infection of murine peritoneal macrophages with *L. donovani* induced specific alterations in COX and lipoxygenase pathways. This response involved selective increase of some metabolites, such as PGE₂ (11). Another study in spleen cells indicated an *ex vivo* evidence for increased COX activity (12). Because LPS- and IFN- γ -induced COX-2 expression are modulated by PKC- α it was of interest to determine whether DN PKC- α overexpression would influence COX-2 expression during phagocytosis of *L. donovani* promastigotes. However, we failed to detect COX-2 expression in RAW 264.7 cells exposed to *L. donovani* promastigotes. In contrast to RAW 264.7 cells, IFN- γ treatment of BMM before infection with *L. donovani* promastigotes allowed the induction of COX-2 expression.

Whereas COX-2 mRNA and protein synthesis were inhibited, LPS-induced PGE₂ secretion was normal in DN PKC- α -overexpressing macrophages. A recent study reported that secretion of NO attenuates PGE₂ production in response to LPS in RAW 264.7 macrophages (47). Moreover, it was shown that NO suppresses the activity and expression of COX-2 mRNA in LPS-stimulated rat peritoneal macrophages (48). However, data obtained with the iNOS inhibitor L-NMMA (Table I) ruled out the possibility that our data are related to the low levels of NO secreted by LPS-stimulated DN PKC- α -overexpressing clones (16). In contrast, PGE₂ secretion was increased in DN PKC- α -overexpressing clones compared with control RAW 264.7 cells in response to IFN- γ .

In summary, we have provided evidence suggesting a role for PKC- α in the modulation of COX-2 expression in macrophages. Further knowledge of the mechanism that regulates COX-2 ex-

pression may potentially lead to the development of novel anti-inflammatory therapies.

Acknowledgments

We thank K. Chadec for critical comments and helpful discussions, J. Giroux for helping with calculations, and H. R. Herschman for the COX-2-luciferase reporter construct pTIS10L.

References

- Burch, R. M. 1987. Protein kinase C mediates endotoxin and zymosan-induced prostaglandin synthesis. *Eur. J. Pharmacol.* 142:431.
- Russell, S. W., and J. L. Pace. 1984. Both the kind and magnitude of stimulus are important in overcoming the negative regulation of macrophage activation by PGE₂. *J. Leukocyte Biol.* 35:291.
- Dubois, R. N., S. B. Abramson, L. Crofford, R. A. Gupta, L. S. Simon, L. B. Van De Pille, and P. E. Lipsky. 1998. Cyclooxygenase in biology and disease. *FASEB J.* 12:1063.
- Langenbach, R., S. G. Morham, H. F. Tian, C. D. Loftin, B. I. Ghanayem, P. C. Chulada, J. F. Mahler, C. A. Lee, E. H. Goulding, and K. D. Kluckman. 1995. Prostaglandin synthase 1 gene disruption in mice reduces arachidonic acid-induced inflammation and indomethacin-induced gastric ulceration. *Cell* 83:483.
- Morham, S. G., R. Langenbach, C. D. Loftin, H. F. Tian, N. Vouloumanos, J. C. Jenette, J. F. Mahler, K. D. Kluckman, A. Ledford, and C. A. Lee. 1995. Prostaglandin synthase 2 gene disruption causes severe renal pathology in the mouse. *Cell* 83:473.
- Baños-Rodiles, M., and K. Chadec. 1998. Novel regulation of cyclooxygenase-2 expression and prostaglandin E₂ production by IFN- γ in human macrophages. *J. Immunol.* 161:2441.
- Lee, S. H., E. Soyoola, P. Chanmugam, S. Hart, W. Sun, H. Zhong, S. Liou, D. Simons, and D. Hwang. 1992. Selective expression of mitogen-inducible cyclooxygenase in macrophages stimulated with lipopolysaccharide. *J. Biol. Chem.* 267:25934.
- Bachwich, P. R., S. W. Chensue, J. W. Larrick, and S. L. Kunkel. 1986. Tumor necrosis factor stimulates interleukin-1 and prostaglandin E₂ production in resting macrophages. *Biochem. Biophys. Res. Commun.* 136:94.
- Hla, T., and K. Neilson. 1992. Human cyclooxygenase-2 cDNA. *Proc. Natl. Acad. Sci. USA* 89:7384.
- Riese, J., T. Hoff, A. Nordhoff, D. L. DeWitt, K. Resch, and V. Kaever. 1994. Transient expression of prostaglandin endoperoxide synthase-2 during mouse macrophage activation. *J. Leukocyte Biol.* 55:476.
- Reiner, N. E., and C. J. Malemud. 1985. Arachidonic acid metabolism by murine peritoneal macrophages infected with *Leishmania donovani*: in vitro evidence for parasite-induced alterations in cyclooxygenase and lipoxygenase pathways. *J. Immunol.* 134:556.
- Reiner, N. E., and C. J. Malemud. 1984. Arachidonic acid metabolism in murine leishmaniasis (*Donovani*): *ex vivo* evidence for increased cyclooxygenase and 5-lipoxygenase activity in spleen cells. *Cell. Immunol.* 88:501.
- Pfannkuche, H. J., V. Kaever, and K. Resch. 1986. A possible role of protein kinase C in regulating prostaglandin synthesis of mouse peritoneal macrophages. *Biochem. Biophys. Res. Commun.* 139:604.
- Newton, A. C. 1995. Protein kinase C: structure, function, and regulation. *J. Biol. Chem.* 270:28495.
- Blohe, G. C., S. Stribling, L. M. Obeid, and Y. A. Hannun. 1996. Protein kinase C isoenzymes: regulation and function. *Cancer Surv.* 27:213.
- St-Denis, A., F. Chano, P. Tremblay, Y. St-Pierre, and A. Descoteaux. 1998. Protein kinase C- α modulates lipopolysaccharide-induced functions in a murine macrophage cell line. *J. Biol. Chem.* 273:32787.
- Huwiler, A., and J. Pfeilschifter. 1993. A role for protein kinase C- α in zymosan-stimulated eicosanoid synthesis in mouse peritoneal macrophages. *Eur. J. Biochem.* 217:69.
- Descoteaux, A., and G. Matlashewski. 1989. *c-fos* and tumor necrosis factor gene expression in *Leishmania donovani*-infected macrophages. *Mol. Cell. Biol.* 9:5223.

19. Descoteaux, A., and G. Matlaszewski. 1990. Regulation of tumor necrosis factor gene expression and protein synthesis in murine macrophages treated with recombinant tumor necrosis factor. *J. Immunol.* 145:846.
20. Fletcher, B. S., D. A. Kujubu, D. M. Percin, and H. R. Herschman. 1992. Structure of the mitogen-inducible TIS10 gene and demonstration that the TIS10-encoded protein is a functional prostaglandin G/H synthase. *J. Biol. Chem.* 267:4338.
21. Finkenzeller, G., D. Marmé, and H. Ilug. 1990. Sequence of human protein kinase C α . *Nucleic Acids Res.* 18:2183.
22. Smith, W. L., R. M. Garavito, and D. L. DeWitt. 1996. Prostaglandin endoperoxide H synthases (cyclooxygenases)-1 and -2. *J. Biol. Chem.* 271:33157.
23. Stark, G. R., I. M. Kerr, B. R. Williams, R. H. Silverman, and R. D. Schreiber. 1998. How cells respond to interferons. *Annu. Rev. Biochem.* 67:227.
24. Arias-Negrete, S., K. Keller, and K. Chadee. 1995. Proinflammatory cytokines regulate cyclooxygenase-2 mRNA expression in human macrophages. *Biochem. Biophys. Res. Commun.* 208:582.
25. Futaki, N., I. Arai, Y. Hamasaka, S. Takahashi, S. Higuchi, and S. Otomo. 1993. Selective inhibition of NS-398 on prostinoid production in inflamed tissue in rat carrageenan-air-pouch inflammation. *J. Pharm. Pharmacol.* 45:753.
26. Davidson, M. E., and R. J. Lang. 2000. Effects of selective inhibitors of cyclooxygenase-1 (COX-1) and cyclooxygenase-2 (COX-2) on the spontaneous myogenic contractions in the upper urinary tract of the guinea-pig and rat. *Br. J. Pharmacol.* 129:661.
27. Williams, J. A., and E. Shacter. 1997. Regulation of macrophage cytokine production by prostaglandin E_2 : distinct roles of cyclooxygenase-1 and -2. *J. Biol. Chem.* 272:25693.
28. Phipps, R. P., S. H. Stein, and R. L. Roper. 1991. A new view of prostaglandin E regulation of the immune response. *Immunol. Today* 12:349.
29. Pennisi, E. 1998. Building a better aspirin. *Science* 280:1191.
30. Wang, H. Q., and R. C. Smart. 1999. Overexpression of protein kinase C- α in the epidermis of transgenic mice results in striking alterations in phorbol ester-induced inflammation and COX-2, MIP-2 and TNF- α expression but not tumor promotion. *J. Cell Sci.* 112:3497.
31. Bauer, M. K., K. Lieb, K. Schulze-Osthoff, M. Berger, P. J. Gehicke-Haerter, J. Bauer, and B. L. Fichich. 1997. Expression and regulation of cyclooxygenase-2 in rat microglia. *Eur. J. Biochem.* 243:726.
32. D'Acquisto, F., T. Iuvone, L. Rombola, L. Sautebin, M. Di Rosa, and R. Carnuccio. 1997. Involvement of NF- κ B in the regulation of cyclooxygenase-2 protein expression in LPS-stimulated J774 macrophages. *FEBS Lett.* 418:175.
33. Kim, Y., and S. M. Fischer. 1998. Transcriptional regulation of cyclooxygenase-2 in mouse skin carcinoma cells: regulatory role of CCAAT/enhancer-binding proteins in the differential expression of cyclooxygenase-2 in normal and neoplastic tissues. *J. Biol. Chem.* 273:27686.
34. Sweet, M. J., and D. A. Hume. 1996. Endotoxin signal transduction in macrophages. *J. Leukocyte Biol.* 60:8.
35. Yamamoto, K., T. Arakawa, N. Ueda, and S. Yanamoto. 1995. Transcriptional roles of nuclear factor κ B and nuclear factor-interleukin-6 in the tumor necrosis factor α -dependent induction of cyclooxygenase-2 in MC3T3-E1 cells. *J. Biol. Chem.* 270:31315.
36. Wadleigh D. J., S. T. Reddy, E. Knpp, S. Ghosh, and H. R. Herschman. 2000. Transcriptional activation of the cyclooxygenase-2 gene in endotoxin-treated RAW 264.7 macrophages. *J. Biol. Chem.* 275:6259.
37. Young, H. A., and K. J. Hardy. 1995. Role of interferon- γ in immune cell regulation. *J. Leukocyte Biol.* 58:373.
38. Adams, D. O., and T. A. Hamilton. 1987. Molecular transductional mechanisms by which IFN γ and other signals regulate macrophage development. *Immunol. Rev.* 97:5.
39. Friedman, R. L., and G. R. Stark. 1985. α -Interferon-induced transcription of H1A and metallothionein genes containing homologous upstream sequences. *Nature* 314:637.
40. Kantakamalakul, W., A. D. Politis, S. Marecki, T. Sullivan, K. Ozato, M. J. Fentoo, and S. N. Vogel. 1999. Regulation of IFN consensus sequence binding protein expression in murine macrophages. *J. Immunol.* 162:7417.
41. Politis, A. D., J. Sivo, P. H. Driggers, K. Ozato, and S. N. Vogel. 1992. Modulation of interferon consensus sequence binding protein mRNA in murine peritoneal macrophages. Induction by IFN- γ and down-regulation by IFN- α , dexamethasone, and protein kinase inhibitors. *J. Immunol.* 148:801.
42. Politis, A. D., K. Ozato, J. E. Coligan, and S. N. Vogel. 1994. Regulation of IFN- γ -induced nuclear expression of IFN consensus sequence binding protein in murine peritoneal macrophages. *J. Immunol.* 152:2270.
43. Shaw, G., and R. Kamen. 1986. A conserved AU sequence from the 3' untranslated region of GM-CSF mRNA mediates selective mRNA degradation. *Cell* 46:659.
44. Hel, Z., S. Di Marco, and D. Radzioch. 1998. Characterization of the RNA binding proteins forming complexes with a novel putative regulatory region in the 3' UTR of TNF- α mRNA. *Nucleic Acids Res.* 26:2803.
45. Gueydan, C., L. Houzel, A. Marchant, A. Sels, G. Huez, and V. Kruys. 1996. Engagement of tumor necrosis factor mRNA by an endotoxin-inducible cytoplasmic protein. *Mol. Med.* 2:479.
46. Liew, P. Y., and C. A. O'Donnell. 1993. Immunology of leishmaniasis. *Adv. Parasitol.* 32:161.
47. Patel, R., M. G. Altur, M. Dave, S. B. Abramson, and A. R. Amin. 1999. Regulation of cytosolic COX-2 and prostaglandin E_2 production by nitric oxide in activated murine macrophages. *J. Immunol.* 162:4191.
48. Habib, A., C. Bernard, M. Lehet, C. Creminon, B. Esposito, A. Tedgui, and J. Maclof. 1997. Regulation of the expression of cyclooxygenase-2 by nitric oxide in rat peritoneal macrophages. *J. Immunol.* 158:3845.

Transcript profiling of human platelets using microarray and serial analysis of gene expression

Dmitri V. Gnatlenko, John J. Dunn, Sean R. McCorkle, David Weissmann, Peter L. Perrotta, and Wadie F. Bahou

Human platelets are anucleate blood cells that retain cytoplasmic mRNA and maintain functionally intact protein translational capabilities. We have adapted complementary techniques of microarray and serial analysis of gene expression (SAGE) for genetic profiling of highly purified human blood platelets. Microarray analysis using the Affymetrix HG-U95Av2 approximately 12 600-probe set maximally identified the expression of 2147 (range, 13%-17%) platelet-expressed transcripts, with approximately 22% collectively involved in metabolism and receptor/signaling, and an overrepresentation of genes with unassigned function (32%). In contrast, a modified SAGE protocol using the Type IIS restriction enzyme

MmeI (generating 21-base pair [bp] or 22-bp tags) demonstrated that 89% of tags represented mitochondrial (mt) transcripts (enriched in 16S and 12S ribosomal RNAs), presumably related to persistent mt-transcription in the absence of nuclear-derived transcripts. The frequency of non-mt SAGE tags paralleled average difference values (relative expression) for the most "abundant" transcripts as determined by microarray analysis, establishing the concordance of both techniques for platelet profiling. Quantitative reverse transcription-polymerase chain reaction (PCR) confirmed the highest frequency of mt-derived transcripts, along with the mRNAs for neurogranin (NGN, a protein kinase C substrate) and

the complement lysis inhibitor clusterin among the top 5 most abundant transcripts. For confirmatory characterization, immunoblots and flow cytometric analyses were performed, establishing abundant cell-surface expression of clusterin and intracellular expression of NGN. These observations demonstrate a strong correlation between high transcript abundance and protein expression, and they establish the validity of transcript analysis as a tool for identifying novel platelet proteins that may regulate normal and pathologic platelet (and/or megakaryocyte) functions. (Blood. 2003;101:2285-2293)

© 2003 by The American Society of Hematology

Introduction

Human blood platelets play critical roles in normal hemostatic processes and pathologic conditions such as thrombosis, vascular remodeling, inflammation, and wound repair. Generated as cytoplasmic buds from precursor bone marrow megakaryocytes, platelets are anucleate and lack nuclear DNA, although they retain megakaryocyte-derived mRNAs.^{1,2} Platelets contain rough endoplasmic reticulum and polyribosomes, and they retain the ability for protein biosynthesis from cytoplasmic mRNA.³ Quiescent platelets generally display minimal translational activity, although newly formed platelets such as those found in patients with immune thrombocytopenic purpura (ITP) synthesize various α -granule and membrane glycoproteins (GPs), including GPIb and GPIIb/IIIa ($\alpha_{IIb}\beta_3$). Furthermore, stimulation of quiescent platelets by agonists such as α -thrombin increases protein synthesis of various platelet proteins, including Bcl-3.⁴ Like nucleated cells, the rapid translation of preexisting mRNAs may be regulated by integrin ligation to extracellular matrices.⁵ In the case of platelets, the primary integrin involved in this process appears to be $\alpha_{IIb}\beta_3$ with cooperative signals mediated by the collagen receptor $\alpha_2\beta_1$.^{6,7}

Integrin-mediated platelet protein synthesis appears to be regulated at the level of translation initiation involving the eukaryotic initiation factor 4E (eIF4E). Instead of directly influencing eIF4E activity via posttranslational modifications (ie, phosphorylation), platelet eIF4E activity best correlates with its spatial redistribution to the mRNA-enriched cytoskeleton.⁸ Furthermore, because protein translation is partially inhibited by the immunosuppressant rapamycin, it suggests that adhesion- and/or aggregation-induced outside-in signaling function to regulate protein synthesis through the mTOR (mammalian target of rapamycin) pathway.^{6,8,9}

Despite the biologic importance of platelets and their intact protein synthetic capabilities, remarkably little is known about platelet mRNAs. Younger platelets contain larger amounts of mRNA with a greater capacity for protein synthesis, as determined by using fluorescent nucleic acid dyes such as thiazole orange.¹⁰ This assay has been used as a quantitative determinant of younger or "reticulated" platelets (RPs). Indeed increased reticulated platelets are typically found in patients with conditions associated with rapid platelet turnover such as ITP; typically RP percentages in

From the Department of Medicine, Department of Pathology, and Program in Genetics, State University of New York, Stony Brook; Biology Department, Brookhaven National Laboratory, Upton, NY; and Department of Pathology, Robert Wood Johnson Medical Center, New Brunswick, NJ.

Submitted September 16, 2002; accepted November 3, 2002. Prepublished online as Blood First Edition Paper, November 14, 2002; DOI 10.1182/blood-2002-09-2797.

Supported by grants HL49141 and HL53665, by a Veteran's Administration REAP award (W.F.B.), and by National Institutes of Health Center grant MO1 10710-5 to the University Hospital General Clinical Research Center. W.B. is an Established Investigator of the American Heart Association. Studies at

Brookhaven National Laboratory were supported by a Laboratory Directed Research and Development award (J.J.D.) and by the Offices of Biological and Environmental Research, and of Basic Energy Sciences (Division of Energy Biosciences) of the US Department of Energy.

Reprints: Wadie F. Bahou, Division of Hematology, HSCT15-040, State University of New York at Stony Brook, Stony Brook, NY 11794-8151; e-mail: wbahou@notes.cc.sunysb.edu.

The publication costs of this article were delayed in part by page charge payment. Therefore, and solely to indicate this fact, this article is hereby marked "advertisement" in accordance with 18 U.S.C. section 1734.

© 2003 by The American Society of Hematology

such patients approach 10% to 20% of all platelets, considerably higher than in healthy control subjects.¹¹ Interestingly, high RPs have been associated with enhanced thrombotic risk when identified in patients with thrombocytosis,¹⁰ suggesting that quantitatively increased mRNA levels may be associated with the prothrombotic phenotype. Whether this is related to globally altered gene expression profiles or to select changes more evident during situations of rapid platelet turnover remains unknown. Certainly, technical limitations of this assay limit its utility in defining prothrombotic genotypes,¹⁰⁻¹² and it cannot identify differentially expressed genes that may be causally implicated in disordered platelet phenotypes.

Toward the goal of defining the molecular anatomy of the platelet genome, we have adapted complementary techniques of microarray and serial analysis of gene expression (SAGE) for genetic profiling of highly purified human blood platelets. Microarray technology represents a "closed" profiling strategy limited by the target genes imprinted onto gene chips. In contrast, SAGE is an "open" architectural system that can be used to identify novel genes and to quantify differentially expressed mRNAs.¹³⁻¹⁵ The sequence of each tag along with its positional location uniquely identifies the gene from which it is derived, and differentially expressed genes can be identified in a quantitative manner because the tag frequency reflects the mRNA level at the time of cellular harvest and analysis. By using both technologies, we have identified a number of previously uncharacterized genes that appear to be expressed in human platelets, while simultaneously establishing the dominant frequency of mitochondrial-expressed genomes comprising the platelet mRNA pool. These observations provide a panoramic overview of the platelet transcriptome, while additionally providing insights into the molecular pathways regulating platelet (and/or megakaryocyte) function in normal and pathologic conditions.

Materials and methods

Reagents and supplies

Thermus aquaticus (Taq) polymerase was purchased from (Roche, Indianapolis, IN). T4 DNA ligase was purchased from Invitrogen (Carlsbad, CA), and restriction enzymes were from New England Biolabs (Beverly, MA), except for *MmeI*, which was obtained from the Center for Technology Transfer (Gdansk, Poland). All oligonucleotides were synthesized on an Applied Biosystems (Foster City, CA) 3-channel synthesizer and are listed in Table 1. Monoclonal antibodies used for flow cytometric analysis included the FITC (fluorescein isothiocyanate)-conjugated anti-CD41 (α_{IIb}β₃) immunoglobulin G1 (IgG1; Immunotech, Miami, FL); phycoerythrin (PE)-conjugated anti-glycophorin (IgG2; Becton Dickinson Pharmingen, San Diego, CA); and peridinin chlorophyll protein (PERCP)-conjugated anti-CD45 (IgG1; Becton Dickinson Pharmingen).

Platelet isolation, purification, and immunodetection

All human subjects provided informed consent for an IRB (Institutional Review Board)-approved protocol completed in conjunction with the General Clinical Research Center at Stony Brook University Hospital. Peripheral blood (20 mL) from healthy volunteers drawn into 2 mL of 4% sodium citrate (0.4% vol/vol final concentration) was used to isolate erythrocytes by differential centrifugation (1500g) or to isolate pure leukocytes by density-gradient centrifugation as previously described.¹⁶ Platelets collected from healthy volunteers by apheresis were used within 24 hours of collection. After addition of 2 mM EDTA (ethylenediaminetetraacetic acid), apheresis-derived platelets from a single donor were centrifuged at 140g for 15 minutes at 25°C. To minimize leukocyte contamination, only the upper 9/10 of the platelet-rich plasma (PRP) was

used for gel filtration over a BioGel A50M column (1000 mL total volume) equilibrated with HBMT (HEPES-buffered modified Tyrodes buffer: 10 mM HEPES (N-2-hydroxyethylpiperazine-N'-2-ethanesulfonic acid) pH 7.4, 150 mM NaCl, 2.5 mM KCl, 0.3 mM NaH₂PO₄, 12 mM NaHCO₃, 0.2% bovine serum albumen [BSA], 0.1% glucose, 2 mM EDTA). Gel-filtered platelets (GFPs) were subsequently filtered through a 5-μm nonwetting nylon filament filter (BioDesign, Carmel, NY) at 25°C and harvested by centrifugation at 1500g for 10 minutes at 25°C. Platelets were gently and thoroughly resuspended in 10 mL HBMT buffer and incubated with 120 μL murine monoclonal anti-CD45 antibody conjugated to magnetic microbeads (Miltenyi Biotec, Bergisch Gladbach, Germany) on a rotating platform for 45 minutes at 25°C. Magnetic separation columns were used to capture CD45⁺ cells (leukocyte fraction) by positive selection (MACS II; Miltenyi Biotec). Purified platelets were concentrated by centrifugation at 1500g and immediately used for total RNA isolation.

The efficiency of platelet purification was documented at each step by flow cytometry.¹⁷ Briefly, aliquots containing 2 × 10⁶ platelets were incubated with saturating concentrations of FITC-conjugated anti-CD41, PE-conjugated anti-glycophorin, and PERCP-conjugated anti-CD45 for 15 minutes in the dark at 25°C, washed with phosphate-buffered saline (PBS), and fixed in PBS/1% formalin. Samples were analyzed using a FACScan (fluorescence-activated cell sorter scan) flow cytometer (Becton Dickinson) using CELLQuest software designed to quantify the number of CD45⁺ and glycophorin-positive events in the sample (expressed as the number of events per 100 000 CD41⁺ events). For some experiments, fixed platelets were permeabilized with 0.1% Triton-X/PBS for 30 minutes at 25°C prior to the addition of primary antibodies, all as previously described.¹⁷

Platelet protein detection was completed by sodium dodecyl sulfate (SDS)-polyacrylamide gel electrophoresis (PAGE) and immunoblot analysis as previously described, using the species-specific horseradish peroxidase-conjugated secondary antibody and enhanced chemiluminescence.¹⁸ Antibodies included the anticlusarin monoclonal antibody (Quidel, Santa Clara, CA; 1:1000 primary and 1:10 000 secondary) and the antineurogranin rabbit polyclonal antibody (Chemicon International, Temecula, CA; 1:1000 primary and 1:10 000 secondary).

Molecular analyses and microarray profiling

Purified, individual cell fractions were resuspended in 10 mL Trizol reagent (Invitrogen), transferred into diethylpyrocarbonate (DEPC)-treated Corex (Springfield, MA) tubes, and serially purified and precipitated by using isopropanol essentially as previously described.¹⁶ Total cellular RNA was harvested by centrifugation at 12 500g for 20 minutes at 4°C, washed 2 times with 75% ethanol (10 mL/tube), and resuspended in 100 μL DEPC-treated water. Platelet mRNA quantitation was performed by using fluorescence-based real-time PCR (polymerase chain reaction) technology (TaqMan Real-Time PCR; Applied Biosystems, Foster City, CA). Oligonucleotide primer pairs were generated by using Primer3 software (www.genome.wi.mit.edu), designed to generate approximately 200-base pair (bp) PCR products at the same annealing temperature, and are outlined in Table 1. Purified platelet mRNA (4 μg) was used for first-strand cDNA synthesis using oligo(dT) and SuperScript II reverse transcriptase (Invitrogen). For real-time reverse transcription (RT)-PCR analysis, the RT reaction was equally divided among primer pairs and used in a 40-cycle PCR reaction for each target gene by using the following cycle: 94°C for 30 seconds, 55°C for 30 seconds, 72°C for 1 minute, and 71°C for 10 seconds (40 cycles total). mRNA levels were quantified by monitoring real-time fluorometric intensity of SYBR green I. Relative mRNA abundance was determined from triplicate assays performed in parallel for each primer pair and was calculated by using the comparative threshold cycle number (Δ-Ct method) as previously described.¹⁸

Gene expression profiles were completed by using the approximately 17 600-probe set HG-U95Av2 gene chip (Affymetrix, Santa Clara, CA). Total cellular RNA (5 μg) was used for cDNA synthesis by using SuperScript Choice system (Life Technologies, Rockville, MD) and an oligo(dT) primer containing the T7 polymerase recognition sequence (Primer S1; Table 1), followed by cDNA purification using GFX spin columns. In vitro transcription was completed in the presence of biotinylated ribonucleotides by using a BioArray HighYield RNA Transcript

Table 1. Oligonucleotide primers

Primer	Gene and primer direction	Sequence (5' - 3')	Nucleotide Position
S1	Oligo (dT)	5'-Bn-GGCCAGTGAATGTGAATACGACTCACTATAGGAGGCGG- (dT) ₂₄ -3'	—
Cassette A	SAGE	5'-TTTGGATTTCGTGGTGGAGTACAACTAGGCTTAATCCGACATG-3' 3'-*CCTAAAGACCACTCATGTTGATCCGAATANGCTP-5'	—
Cassette B	SAGE	5'-pTTTCATGGCGGAGACGTCCGCCACTAGTGTGCACTGACTA*-3' 3'-NNAAGTACGCCCTCTGCAGGCGGTGATCAGCGTTGACTGAT-5'	—
S2	SAGE	5'-Bn-GGATTTCGTGGTGGAGTACA-3'	—
S3	SAGE	5'-Bn-TAGTCAGGTGCGACACTAGTGGC-3'	—
GP4	Glycoprotein IIb [F]	5'-AGGGCTTTGAGAGACTCATCTGTA-3'	2094-2117
GP5	Glycoprotein IIb [R]	5'-ACAATCTTCTGCTTTGGATTCTG-3'	2301-2279
GP6	Glycoprotein IIIa [F]	5'-TATAAAGAGGCCAGCTCTACCTTC-3'	2335-2358
GP7	Glycoprotein IIIa [R]	5'-CACTTCCACATACATGACATTCTCC-3'	2532-2509
PAR18	PAR1 [F]	5'-AATGTCAGTTCTGATATGGAAGCA-3'	2585-2608
PAR19	PAR1 [R]	5'-CCCAATGTTCAAATCTCTTACG-3'	2776-2753
SR8	16S rRNA [F]	5'-TGCAAGGTAGCATTAATCACTTGT-3'	2586-2609
SR9	16S rRNA [R]	5'-GTTAGGACCTGTGGTCTTGTAG-3'	2785-2762
NADH10	NADH2 [F]	5'-CTAGCCCCCATCTCAAATCATATAC-3'	4875-4898
NADH11	NADH2 [R]	5'-AATGGTTATGTTAGGCTTGTACGG-3'	5075-5052
THYM12	Thymosin β4 [F]	5'-AAGACAGAGACGACAGAGAAAAAT-3'	135-158
THYM13	Thymosin β4 [R]	5'-GCAGCAGATCATTTAACTTGAT-3'	336-313
CLUS14	Clusterin [F]	5'-CCAACAGAAATTCATACGAGAAGG-3'	1006-1028
CLUS15	Clusterin [R]	5'-CGTTATATTCTCTGGTCAACCTCT-3'	1222-1199
NRG16	Neurogranin [F]	5'-GCCCTTTTATGTTAGTTCTGCAGTC-3'	1351-1374
NRG17	Neurogranin [R]	5'-TTTCTTTAAGTGAGTGTGCTTGG-3'	1567-1544
TCR18	T-cell receptor β-chain [F]	5'-CCCAACTATGTTTGGTATCGT-3'	131-153
TCR19	T-cell receptor β-chain [R]	5'-CTAGCACTGCAGATGAGAAGCT-3'	332-310
CD4520	CD45 [F]	5'-GCTCAGAAATGGACAAGTA-3'	3771-3788
CD4521	CD45 [R]	5'-CACACCACATACACATACA-3'	4280-4261

[F] indicates forward (sense) strand; [R], reverse (antisense) strand; Bn, biotin; p, a phosphorylated 5' end (cassettes A and B); underlining, *Nla*III sites in cassettes A and B; arrows, corresponding sequence for S2 and S3 within cassettes A and B, respectively; bold, the *Mme*I site; and N, A, C, T, or G, nucleotide position based on the following accession numbers: glycoprotein IIb (J02764), glycoprotein IIIa (M35999), PAR1 (M62424), 16S rRNA and NADH2 (NC_001807), thymosin β4 (M17733), clusterin (M25915), neurogranin (X99076), TCR β-chain (AF043182), CD45 (Y00638).

*Indicates an amino-modified 3' end in both cassettes; —, not applicable.

Labeling Kit (Enzo Diagnostics, Farmingdale, NY), and, after metal-induced fragmentation, 15 μg biotinylated cRNA was hybridized to the JIG-U95Av2 oligonucleotide probe array for 16 hours at 45°C. After washing, the cRNA was detected with streptavidin-phycoerythrin (Molecular Probes, Eugene, OR) and analysis was completed by using a Hewlett-Packard Gene Array Scanner (Affymetrix). The average difference value (AD) for each probe set was quantified using MAS 4.01 software (Affymetrix), calculated as an average of fluorescence differences for perfectly matched versus single-nucleotide mismatched 25-mer oligonucleotides (16 to 20 oligonucleotide pairs per probe set). The software is designed to exclude "positive calls" in the presence of high average differences with associated high mismatch intensities.

SAGE profiles

Platelet SAGE libraries were generated essentially as previously described,¹⁵ modified as outlined in Figure 1 for the use of *Mme*I as the tagging enzyme.¹⁹ This type IIS restriction enzyme cleaves 20 of 18 bp past its nonpalindromic (TCCRAC) recognition sequence, thereby generating longer tags (21- or 22-mer) than those obtained using *Bsm*FI as the standard tagging enzyme (13-14 bp tags). These longer *Mme*I-generated tags potentially provide for more definitive "tag-to-gene" identification and are particularly useful in characterizing expression patterns in the absence of complete genomic sequence data (comprehensive methods detailed in Dunn et al¹⁸). Briefly, poly(A) mRNA was isolated from 10 μg total platelet RNA using the oligo-dT S1 primer conjugated to magnetic beads (Dyna Bead, Lake Success, NY), followed by cDNA synthesis using Super-Script II reverse transcriptase (Invitrogen). The cDNA was then digested

with the restriction enzyme *Nla*III (anchoring enzyme), ligated to cassette A using T4 DNA ligase, and, after the beads were extensively washed, the cDNA was digested with *Mme*I to release the tags from the beads. After purification, tags were ligated to degenerate cassette B linkers (specifically

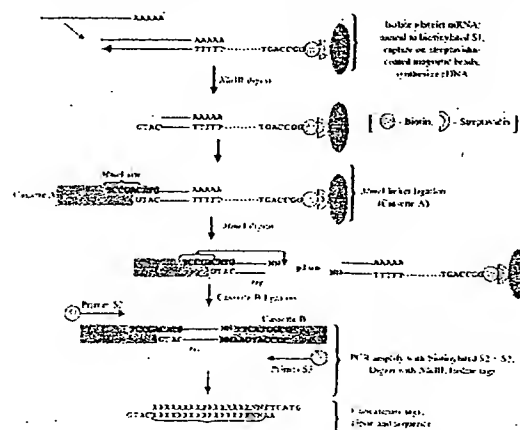


Figure 1. Schema outlining the modified SAGE protocol used in platelet analyses. The final tags are flanked by the *Nla*III (anchoring enzyme) CATG sequence, thereby providing tag-to-gene identification when exported to a relational database (refer to "Bioinformatic analyses" and Table 1 for details).

designed to anneal to the nonuniform *MmeI* overhangs), and PCR-amplified using biotinylated primers S2 and S3 for 30 cycles (95°C for 30 seconds; 58°C for 30 seconds; 72°C for 30 seconds) using Platinum Taq DNA polymerase (Gibco BRL). A fraction (20%) of the pooled PCR products were then subjected to one round of linear amplification using primer pair S2/S3, followed by a second round of 25 amplifications using primer S2 alone (95°C for 30 seconds, 58°C for 30 seconds, 72°C for 30 seconds). Primer S3 was subsequently added for one cycle (95°C for 2.5 minutes, 58°C for 30 seconds, 72°C for 5 minutes); the latter steps were collectively adapted to exclude heteroduplex formation.¹⁸ Unincorporated primers were removed by incubation with 200 U *Escherichia coli* exonuclease I for 60 minutes at 37°C. PCR products were then pooled and digested with *NlaIII* to release tags, and biotinylated linker arms were cleared using streptavidin-coated immunoaffinity magnetic beads (DynaL Biotech). Tags were concatamerized using 5 U/μL T4 DNA ligase, and products more than 100 bp were isolated by size-fractionation in low-melting agarose gels. The DNA was purified by GFX spin columns, and the concatamers were cloned into the *SphI* site of pZero (Invitrogen). After transformation into *E. coli* TOP10 cells, recombinant clones were isolated and sequenced in 96-well microtiter plates using an ABI 377 sequencer and ABI Prism BigDye terminator chemistry (Perkin-Elmer Applied Biosystems, Branchburg, NJ).

Bioinformatic analyses

Functional grouping of genes determined to be present by Affymetrix MAS 4.01 software was performed using a dChip program linked to the National Center for Biotechnology LocusLink, which is an annotated reference database for genes and their postulated functions.²⁰ Of the approximately 12 600-probe sets represented on the Affymetrix HG-U95Av2 Gene chip, functional annotations exist for approximately 8100 with the remainder categorized as unknown. Microarray data were visualized and analyzed using BRB-ArrayTools software (Version 2.1), kindly developed and provided by Dr Richard Simon and Amy Peng (linus.nci.nih.gov/BRB-ArrayTools.html). A logarithmic (base 2) transformation was applied to the average difference values for individual data sets for determination of microarray concordancies. Discordancy was defined as a 2-log difference in the maximum log intensities between individual experiments.

SAGE tags were extracted by using in-house SAGE software uniquely modified to identify *MmeI* tags. The software ensures that only unambiguous 21- to 22-bp tag sequences are extracted for transcript profiling. Tags with ambiguities (Ns), lengths other than 21 or 22 bp, or with ambiguous orientations were extracted to separate files for manual editing or further examination. Finalized data were exported to a relational database for tag quantification and genetic identification.²⁰

Results

Platelet purification

To ensure that the RNA profiles accurately represented those of circulating blood platelets, a number of complementary methods were implemented to remove contaminating nucleated leukocytes. Purification methods incorporating gel filtration, a 5-μm leukocyte reduction filter, and magnetic CD45 immunodepletion allowed for the cumulative enrichment of highly purified platelets. The efficacy of this purification method was initially established by using peripheral blood platelet-rich plasma as the starting material. The final product contained no more than 3 to 5 leukocytes per 1×10^5 platelets as determined by parallel flow cytometric analysis, representing an approximate 450-fold reduction of nucleated leukocytes. These results correlated well with molecular evidence for leukocyte depletion as determined by RT-PCR using both CD45 and T-cell receptor β -chain (TCR β) primers (see Figure 2). Because the total RNA yield from peripheral blood platelets was insufficient for microarray studies, we adapted the protocol to platelet apheresis donors with nearly identical final purity (Figure

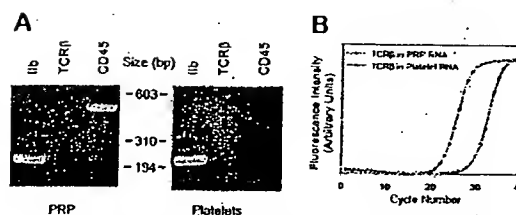


Figure 2. Determination of platelet purity. (A) Total cellular RNA (1.8 μg) from platelet-rich plasma (PRP) or purified platelets from a single apheresis donor were analyzed by RT-PCR (35 cycles) using oligonucleotide primers specific for glycoprotein IIb (GPIIb), T-cell receptor β -chain (TCR β), or CD45. 10 μL of the 50 μL reactions were analyzed by ethidium-stained agarose gel electrophoresis. Minimal to no TCR β gene product was visually evident only in PRP. Size markers corresponding to *HaeIII*-restricted ϕ X174 DNA are shown. (B) Real-time RT-PCR was completed by using 1.8 μg total RNA and TCR β -specific oligonucleotide primers optimized for quantitative analysis by real-time PCR.¹⁸ On the basis of parallel determinations using RNA isolated from known amounts of purified leukocyte standards, the leukocyte-depletion protocol represents an approximate 2.5-log purification from the starting PRP. Results are representative of one complete set of experiments repeated on 2 separate occasions, and data points represent the mean from triplicate wells, with standard errors of the mean (SEM) less than 1% (not shown).

2). The platelet recovery was nearly 65% of the starting material, yielding approximately 2.3×10^{11} platelets from an initial apheresis pack containing approximately 3.6×10^{11} platelets. The bulk of the losses occurred during the initial centrifugation and filtration steps. The purification protocol was less effective at removing erythrocytes, although there were less than 50 glycophorin-positive cells per 1×10^5 platelets after the final purification step. Nonetheless, these cells represent unlikely sources for contaminating cellular RNA (see "Cellular microarray analysis" below).

Cellular microarray analysis

The purified platelet RNA was sufficient for microarray studies and was used for cRNA generation and hybridization to the Affymetrix HG-U95Av2 GeneChip. The anatomic profile of platelet RNAs from 3 healthy male donors was determined by using Affymetrix software. Of the 12 599 probe sets imprinted onto the chip, a maximum of 2147 (17%) transcripts were computationally identified as "present" by the Affymetrix software, 152 (1.2%) were equivocal, and nearly 82% were absent. As a fraction of the total genes present on the chip, the percentage of platelet-expressed genes (15%-17%) was generally lower than that obtained from other human cell types in which 30% to 50% of genes are present as determined by Affymetrix software (J. Schwedes, personal communication, May 2002). The "limited number" of platelet-expressed transcripts presumably reflects the lack of ongoing gene transcription in the anucleate platelet. Because less than 1% of circulating red blood cells contain residual RNA, it is unlikely that any of these transcripts are erythrocyte derived, although this was formally addressed by isolating total cellular RNA from 20 mL of whole blood (corresponding to an ~3-log fold excess of erythrocytes than that identified in our final sample). The total cellular yield of RNA from this starting material was approximately 250 ng, suggesting that less than 1 ng erythrocyte-derived RNA was present in the purified platelet preparations. Despite this, however, both α - and β -globin transcripts—along with both the ferritin heavy and light chains—were identified as abundant transcripts (Table 2). Although the most parsimonious explanation would be residual contaminating erythrocytes, this is not supported by our erythrocyte contamination estimates, and their significance remains unresolved.

As a means of better dissecting the molecular anatomy of the platelet, expressed genes were grouped on the basis of assigned

Table 2. Top 50 human platelet-expressed genes

Accession no.	Gene symbol	AD values, range*	Gene transcript†	Leukocyte expression‡
M17733	TMSB4X	140 142-307 852	Thymosin β 4 mRNA, complete cds	+
X99076	NRGN	101 510-148 279	Neurogranin gene	+
M25079	HBB	40 839-229 556	β -globin mRNA, complete cds	+
M25915	CLU	84 720-140 246	Complement cytotoxicity inhibitor (clusterin) complete cds	—
J04755	FTHP1	82 980-148 621	Feritin H processed pseudogene, complete cds	—
D78361	OAZ1	73 098-118 140	mRNA for ornithine decarboxylase antizyme	—
X04409	GNAS	77 761-94 781	mRNA for coupling protein G(s) α -subunit (alpha-S1)	—
M25897	PF4	62 811-126 908	Platelet factor 4 mRNA, complete cds	—
AB021288	B2M	61 689-108 921	β 2-microglobulin	+
X00351	ACTB	25 143-73 775	mRNA for β -actin	—
D21261	TAGLN2	76 687-101 931	mRNA for KIAA0120 gene	+
AL031670	FTLL1	69 865-99 966	Feritin, light polypeptide 1	+
U59632	GPIIB	41 404-110 328	Platelet glycoprotein IIb chain mRNA	—
M21121	CCL5	47 308-106 399	T-cell-specific protein (RANTES) mRNA, complete cds	—
X13710	GPX1	41 318-96 878	Unspliced mRNA for glutathione peroxidase	—
J00153	HBA1	21 326-144 201	Alpha globin gene cluster on chromosome 16	+
M22919	MYL6	46 337-106 833	Nonmuscle/smooth muscle alkali myosin light chain gene	+
L20941	FTH1	52 787-74 763	Feritin heavy chain mRNA, complete cds	—
J03040	SPARC	51 156-74 261	SPARC/osonectin mRNA, complete cds	—
X56009	GNAS	45 543-72 096	GSA mRNA for α subunit of GsGTP binding protein	—
X58536	HLA	31 183-82 613	mRNA for major HLA class I locus C heavy chain	+
M54995	PPBP	46 571-67 169	Connective tissue activation peptide III mRNA	—
U34995	GAPD	35 095-70 250	Normal keratinocyte subtraction library mRNA, clone H22a	+
L40399	MLM3	32 107-73 364	Clone zap112 (mult. protein homolog 3) mRNA	—
X77548	NCOA4	31 452-61 036	cDNA for RFG (RET proto-oncogene RET/PTC3)	—
U90551	H2AFL	35 086-51 892	Histone 2A-like protein (H2A/I) mRNA	—
M11353	H3F3A	31 614-55 813	H3.3 histone class C mRNA	—
Z12962	RPL41	36 003-54 853	mRNA for homologue to yeast ribosomal protein L41	+
X06956	TUBA1	20 988-61 798	HALPH1A 44 gene for α -tubulin	—
AB028950	TLN1	24 571-58 611	mRNA for KIAA 1027 protein	—
Y12711	PGRMC1	33 680-43 174	mRNA for putative progesterone binding protein	—
M16279	MIC2	30 894-48 166	Integrated membrane protein (MIC2) mRNA	—
D78577	YWHAH	24 785-50 437	Brain 14-3-3 protein β -chain	—
AF070585	TOP3B	20 027-67 945	Clone 24675, unknown cDNA	—
AA524802	Unknown	23 846-39 481	CDNA, IMAGE clone 954213	—
AB009010	UBC	28 745-38 389	mRNA for polyubiquitin UbC	+
X57985	H2AFQ	21 678-52 108	Genes for histones H2B.1 and H2A	—
X54304	MLCB	25 733-34 109	mRNA for myosin regulatory light chain	—
M14539	F13A1	23 691-48 474	Factor XIII subunit α -polypeptide mRNA, 3' end	—
AI540958	Unknown	24 872-41 118	cDNA, PEC 1.2_15_HOI.r 5' end/clone	—
AL050396	FLNA	13 634-55 235	cDNA DKF2p586K1720	—
X56841	HLA-E	12 890-49 327	Nonclassical MHC class I antigen gene	—
M26252	PKM2	15 450-47 786	TCB (cytosolic thyroid hormone-binding protein)	—
M14630	PTMA	19 314-45 088	Prothymosin alpha mRNA	—
AF045229	RGS10	19 156-34 243	Regulator of G protein signaling 10 mRNA	—
AA477898	Unknown	16 863-44 756	cDNA, Z834108.r15' end	—
X95404	FL1	15 216-37 456	mRNA for nonmuscle type cofilin	—
M34480	ITGA2B	8 627-45 495	Platelet glycoprotein IIb (GPIIb) mRNA	—
Z83738	H2BFE	18 001-31 306	H1 H2B/e gene	—
L19779	H2AFO	17 319-38 951	Histone H2A.2 mRNA, complete cds	—

*Gene expression quantifications were calculated as the average difference (AD) value (matched versus mismatched oligonucleotides) for each probe set using Affymetrix GeneChip software, version 4.01. The range of values from 3 distinct platelet microarrays is shown; the normalization value for all microarray analyses was 250.

†Transcripts are rank-ordered (highest to lowest) using BRB-ArrayTools software by log-intensities of AD values obtained from 3 different healthy donors; 33 of the top 40 transcripts were listed among the top 50 in all 3 microarray sets.

‡Leukocyte expression was determined by microarray analysis using purified peripheral blood leukocytes, followed by construction of rank-intensity plots for comparison to platelet top 50 transcripts.²⁹ Top leukocyte-derived transcripts identified within the ranked top 50 platelet transcripts are depicted by a (+) present, or (–) absent. cds indicates coding sequence.

gene annotations, and this analysis was used to provide a panoramic definition of the platelet transcriptome. Of the genes that could be cataloged within assigned "clusters," those involved in metabolism (11%) and receptor/signaling (11%) represented the largest groups. Also evident in these analyses is the relatively large percentage of genes involved in functions unrelated to these key groups (ie, miscellaneous, 25%), and the overrepresentation of genes with unknown function (32%) as annotated by Affymetrix

and RefSeq databases.²¹ These results identify a vast array (nearly one half) of platelet genes (and gene products) that presumably have important, but poorly characterized functions, in platelet and/or megakaryocyte biology.

Although microarray analysis is not truly quantitative, rank-ordering using the mean log-intensities from 3 independent microarray analyses allowed for the categorization of the top platelet transcripts (Table 2). Computational analyses demonstrated that

only 10 of the top 100 genes were discordant among the 3 platelet microarrays, although 71 of 100 genes were discordant between platelet and leukocyte arrays. An inventory of the top 50 platelet genes is listed in Table 2, which also delineates those found to be highly expressed in peripheral blood leukocytes by parallel microarray experiments with this purified cellular fraction (data not shown). Further analysis of these cell subsets demonstrated that approximately 25% ($n = 547$) of the total platelet transcripts were platelet restricted. Furthermore, only 10 of the 50 most highly expressed genes were found to overlap, confirming the distinct cellular profiles of each transcriptome. Of the 12 overlap genes, 3 corresponded to globin or ferritin chains (again suggesting the presence of contaminating reticulocytes in both purified fractions), and another 4 were involved in actin cytoskeletal reorganization and human leukocyte antigen (HLA) expression, gene products that regulate critical functions in both cell types. Given the importance of cytoskeletal reorganization in downstream platelet activation events, it is not unexpected that components of the actin machinery system would demonstrate prominent transcript expression. Previous estimates suggest that 20% to 30% of the total platelet proteome is comprised of actin with other components such as actin-binding protein, myosin, and talin accounting for an additional 2% to 5% of the total protein.^{1,22} The mRNAs encoding the actin-related machinery are overrepresented in our microarray analysis, with 8 such transcripts found among the 50 highest platelet-expressed genes. Interestingly thymosin β 4 demonstrated the highest expression pattern. In unstimulated platelets, 30% to 40% of actin is polymerized as F-actin,²² whereas the balance of actin monomers (G-actin) are polymerization inhibited by sequestering proteins such as profilin (100 μ M) and thymosin β 4 (600 μ M).²³ The high thymosin β 4 transcript expression not only correlates with its known abundance in platelets but also supports the importance of actin inhibitory proteins in maintaining the nonstimulated state of circulating platelets.

Platelet SAGE analyses

Although these initial studies identified the distribution and relative expression patterns of the genes within the Affymetrix data set, they do not allow for analyses of genes that are unrepresented by these oligonucleotide chips. Unlike closed microarray profiling strategies, SAGE is an open architectural system that is ideally suited for novel gene and pathway identification. Accordingly, the platelet RNA used for microarray studies was used for platelet SAGE. A total of 2033 tags were initially cataloged, of which 1800 (89%) corresponded to mitochondrial-derived genes. These results were quite different from those obtained by microarray analyses, but the discrepancy can be resolved by the nonrepresentation of the mitochondrial genome on the gene chip. The mitochondrial genome is a compact approximately 16.6-kilobase (kb) sequence encoding 13 genes and 2 ribosomal subunits.²⁴ Primary mitochondrial transcripts are polycistronic and typically contain premature termination or unpredictable splice sites, resulting in multiple polyadenylated transcripts from individual genes.^{24,25} Indeed, the overall distribution of platelet-derived mitochondrial SAGE tags is quite similar to that found in muscle.²² All 13 genes containing *Nla*III sites were detected, whereas neither of the non-*Nla*III-containing genes were identified (nicotinamide adenine dinucleotide [NADH] dehydrogenase subunit 4L and adenosine triphosphatase [ATPase] 8). Most of the tags were from the 16S and 12S ribosomal RNAs—which collectively accounted for 68% of the total mitochondrial tags—with the fewest tags represented by NADH dehydrogenase subunits 3, 5, 6, and cytochrome c oxidase I

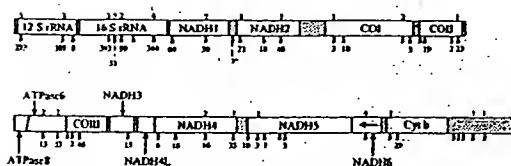


Figure 3. Schema of the mitochondrial genome with SAGE tag distributions (only tags with identical matches are displayed). The abundance of the SAGE tags ($n = 1800$) at individual *Nla*III sites (arrows) within the mitochondrial heavy strand is shown on the bottom, whereas those tags corresponding to the mitochondrial light strand are delineated above the arrows (the presence of an unaccompanied arrow implies no SAGE tags at that *Nla*III site). The gene products of mt-DNA (RefSeq accession no. NC_001807) are delineated by the open rectangles, whereas stippled boxes represent tRNA genes and control regions (the single tag represented by the ['] refers to mitochondrial transfer RNA-serine). Note that NADH6 is encoded by the light strand and that there are no *Nla*III sites within the ATPase8 gene segment. COI, cytochrome c oxidase subunit; Cyt b, cytochrome b.

(Figure 3). The NADH dehydrogenase subunit 6 RNA is the only mRNA encoded by the light (L) strand of mitochondrial DNA and was the least abundantly detected transcript.

The unusually high preponderance of mitochondrial-derived genes is not inconsistent with the known enrichment of these genomes in human platelets,^{1,24} and presumably reflects persistent transcription from the mitochondrial (mt) genome in the absence of nuclear-derived transcripts. This overrepresentation of mtDNA in platelets is considerably greater than that of its closest cell type (skeletal muscle), in which mt genomes represent approximately 20% to 25% of all SAGE tags.²⁵ Interestingly, the energy metabolism of platelets is not dissimilar from that of skeletal muscle, both cell types actively using glycolysis and large amounts of glycogen for ATP generation.²⁶ Like muscle, platelets are metabolically adapted to rapidly expend large amounts of energy required for aggregation, granule release, and clot retraction. Similar to the situation in all eukaryotic cells, platelet mitochondria represent the primary source of ATP, which is generated from oxidative phosphorylation reactions occurring within these organelles. Mitochondria are also responsible for most of the toxic reactive oxygen species generated as by-products of oxidative phosphorylation and are central regulators of the apoptotic process in other cellular types. The mtDNA encodes polypeptides found within 4 of the 5 multifunctional complexes that regulate oxidative phosphorylation within the platelet mitochondria.²⁷ Whether the continued generation of these polypeptides has a role in platelet energy metabolism and/or the apoptotic mechanisms regulating platelet survival remains speculative, although not inconsistent with our observations.

Comparative analysis of SAGE and microarray transcript abundance

Complete SAGE libraries require the sequencing of up to 30 000 tags for an exhaustive cataloging of individual mRNAs, especially those with limited copy numbers.^{13,28} Given the preponderance of mt-derived transcripts, comparable sampling would have required sequence analysis of nearly 300 000 SAGE tags, an inordinate number for comprehensive analysis of the platelet transcriptome. For platelets, alternative methodologies incorporating subtractive SAGE will be required for more comprehensive transcript profiling.²⁹ Our initial sampling of nonmitochondrial genes remains informative, however, and entirely consistent with the results of platelet microarray studies. As shown in Table 3, SAGE tags for the genes encoding thymosin β 4, β 2-microglobulin, neurogranin, and the platelet glycoprotein 1b β polypeptide were among the most frequently identified platelet genes, similar to the rank-ordered results determined by microarray analysis. To formally confirm the

Table 3. SAGE-identified nonmitochondrial tags

Frequency	CATG + SAGE tags*	Accession no.†	Gene	Microarray‡
26	GTTGTGGTTAATCTGGT	NM_004048.1	β 2-microglobulin (B2M), mRNA	PPP
21	TTGGTGAAGGAAGAGT	NM_021109.1	Thymosin β 4; X chromosome (TMSB4X), mRNA	P
8	AGCTCCGAGCCAGGTC	NM_002620.1	Platelet factor 4 variant 1 (PF4V1), mRNA	p
8	AGCTCCGAGCCGGGTT	NM_002619.1	Platelet factor 4 (PF4), mRNA	P
7	TGTATAAGACAACCTC	NM_002704.1	Proplatelet basic protein (β -thromboglobulin)	Pp
5	GGGCACAATGCGGTCCA	NM_000407.1	Glycoprotein Ibb polypeptide, mRNA	P
3	AGGTAATAAAGGTAAT	NM_003512.1	H2A histone family, member L (H2AFL), mRNA	P
3	AGTGGCAAGTAAATGGC	NM_021914.2	Cofilin 2 (muscle) (CFL2), mRNA	N/A
3	TGACTGTGCTGGGTGG	NM_006176.1	Neurogranin (protein kinase C substrate, RC3) mRNA	P
3	TTGGGGTTTCCTTTACC	NM_002032.1	Ferritin, heavy polypeptide 1 (FTH1), mRNA	P
2	CCCTTGTGACTACCTAT	NM_025158.1	Hypothetical protein FLJ22251 (FLJ22251), mRNA	N/A
2	CTGTGAACCCAGCTAC	NM_032779.1	Hypothetical protein FLJ14397 (FLJ14397), mRNA	N/A
2	CTGTAGTCCAGCTAC	NM_017962.1	Hypothetical protein FLJ20825 (FLJ20825), mRNA	N/A

*Unique tags identified more than once.

†Refers to the RefSeq accession no.²¹ Note that this number does not necessarily correspond to the accession no. provided by Affymetrix software annotations (Table 1).

‡Presence (P) or absence (A) is based on results from 3 distinct platelet microarray experiments. Capitalized "P" designates a gene that is in the top 50 on all 3 microarray experiments, whereas small "p" designates those transcripts not in the top 50. Two of the genes (β 2-microglobulin and β -thromboglobulin) are represented by 3 and 2 probe sets, respectively, on the HG-U95Av2 gene chip; for β 2-M, all 3 probe sets were in the top 50 genes, whereas for thymosin β 4 1 of 2 was in the top 50 for all experiments (the other probe set was in the top 75 for all experiments). N/A indicates oligonucleotide not present on Affymetrix HG-U95Av2 gene chip.

results independently obtained by SAGE and microarray analysis, quantitative RT-PCR was completed by using oligonucleotide primers specific for 2 abundant mitochondrial transcripts, 16S rRNA and NADH2 thymosin β 4 (high-abundance by microarray and SAGE), 2 incompletely characterized high-abundance transcripts (neurogranin and clusterin; see "Protein immunoanalysis of platelet clusterin and neurogranin"), a low-abundant transcript (T-cell receptor β -polypeptide), and the genes encoding proteins with well-established quantitative determinations (ie, glycoprotein α _{IIb} β 3 [\sim 50 000 receptors/platelet]; protease-activated receptor-1 (PAR1) [\sim 1800 receptors/platelet]).¹ As shown in Figure 4, these analyses reveal excellent concordance between SAGE and microarray studies, demonstrating the predominant frequency of the mitochondrial-derived 16S rRNA/NADH2 transcripts, with incrementally lower expression of other transcripts as initially demonstrated by microarray (16S > NADH2 > thymosin β 4 > neurogranin > clusterin > α _{IIb} β 3 > PAR1 > TCR β).

Given the small number of nonmitochondrial SAGE tags available for analysis ($n = 233$), limited conclusions can be drawn using traditional (nonsubtraction) platelet SAGE libraries as pre-

sented here. Overall, a total of 126 unique tags were identified, the majority of which (94) were represented only once. Of the total unique tags, nearly one half represented novel genes not present on the Affymetrix U95Av2 GeneChip. Of the genes with unique tags identified more than once, there was excellent concordance with microarray expression analysis, with nearly all of the SAGE tags in Table 3 corresponding to platelet top 75 microarray transcripts. The platelet factor (PF) 4 variant represents a single aberration because this was rank-ordered approximately 350 by microarray, although its SAGE tag frequency was identical to that of the predominant PF4 transcript. The lack of extensive nonmitochondrial SAGE sampling precludes any further extrapolations from this apparent aberration. Of note, a subset of these tags had long poly(A) tracts; although they all corresponded to genes identified in the RefSeq database.²¹ We cannot exclude the possibility of a SAGE artifact for this small subset of tags (\sim 2%, representing 46 of 2033 tags), although the authenticity of the vast majority of tags (\sim 98%) clearly validates the methodology. These tags are most likely explained by the unique biology of the platelet (ie, mRNA decay in the absence of de novo transcription) or to mRNA degradation occurring during the extensive purification methods. In summary, even with a remarkably limited sampling, the power of this approach in gene identification of relatively abundant and less abundant transcripts is evident. It is clear, however, given the unique molecular anatomy of the platelet (ie, abundance of mitochondrial transcripts), that SAGE adaptations will be required for more comprehensive genetic profiling.²⁹

Protein immunoanalysis of platelet clusterin and neurogranin

Although most of the "most abundant" transcripts would conform to a priori predictions for platelet-expressed mRNAs, a number of transcripts were identified that had been poorly characterized in human platelets. To further establish the authenticity of highly expressed transcripts such as clusterin and neurogranin, confirmatory protein analyses were completed. As shown in Figure 5, both proteins were clearly detected in purified platelet lysates; furthermore, their cellular platelet distributions conformed to those predicted based on previously proposed functions. Note for example that clusterin—functionally characterized as a complement lysis inhibitor able to block the terminal complement reaction—is primarily expressed on the extracellular platelet membrane.³⁰

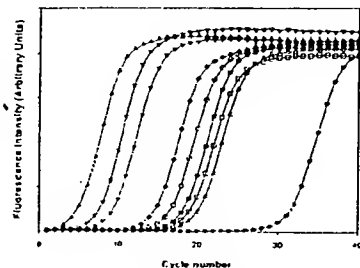


Figure 4. Quantitative real-time RT-PCR analysis of platelet transcripts. Real-time RT-PCR was completed by using purified platelet RNA and oligonucleotide primer pairs specifically designed using Primer3 software to generate similarly-sized (\sim 200-bp) PCR products, optimized to the same annealing temperature. In graph, (□) represents Ibb, (■) represents Iiba, (△) represents PAR1, (▲) represents 16S rRNA, (▽) represents NADH2, (▼) represents thymosin, (○) represents clusterin, (●) represents neurogranin, and (●) represents TCR β . Curves are representative of one complete set of experiments (repeated twice), and line plots reflect average determinations from 3 wells performed in parallel with SEM less than 1% for all data points.

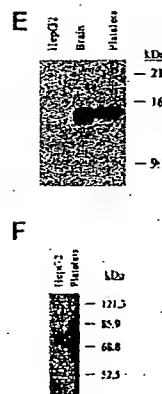
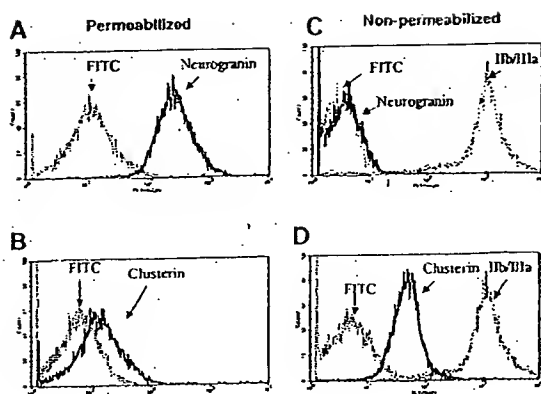


Figure 5. Immunocytometric analysis of platelet neurogranin and clusterin. (A-D) Gel-filtered platelets were either fixed in 3.7% formaldehyde (nonpermeabilized) or fixed with permeabilization in the presence of 0.1% Triton-X, followed by flow cytometric analysis using anti-clusterin, anti- α IIb β 3, or anti-neurogranin antibodies and the FITC-conjugated species-specific secondary antibody (in C, the FITC-conjugated anti-rabbit and anti-mouse controls are essentially superimposed). (E-F) Ten micrograms of solubilized HepG2 cells (hepatocyte cell line), human brain, or purified platelet lysates were analyzed by SDS-PAGE,¹⁷ and immunoblot analysis were completed by using 1:1000 dilutions of either anti-neurogranin (18% SDS-PAGE) or anti-clusterin (8% SDS-PAGE) antibodies. The anti-clusterin antibody recognized 2 platelet immunoreactive species under shorter exposure. Although the relative neurogranin and clusterin protein abundances are suboptimally quantified by these analyses, platelet clusterin appears to demonstrate considerable expression when compared with that previously identified in hepatocytes.³¹

Given the importance of complement activation in platelet destruction, the prominent expression of cell-surface clusterin might suggest a role for this protein in normal and pathologic events regulating platelet survival. Interestingly, a clusterin-deficient knockout mouse has been generated that demonstrates enhanced cardiac dysfunction in a model of autoimmune myocarditis.³¹ Although these mice apparently have normal baseline hemograms (B. Aronow, personal communication, October 2002), it remains unestablished if they would be predisposed to immune-type thrombocytopenia in systemic models of autoimmunity.

Similarly, the gene encoding an intracellular effector protein that may have key roles in downstream platelet activation events has now been demonstrated to have abundant transcript expression in human platelets. Neurogranin is a highly expressed platelet transcript with its gene product demonstrating a primarily intracellular pattern of distribution. Neurogranin is generally described as a brain-specific, Ca^{2+} -sensitive calmodulin-binding phosphoprotein that is preferentially expressed in neuronal cell bodies and dendrites.^{32,33} It is a specific protein kinase C (PKC) substrate that can also be modified by nitric oxide and other oxidants to form intramolecular disulfide bonds. Both its phosphorylation and oxidation state attenuate its binding affinity for calmodulin.³³ In stimulated platelets, PKC generation is linked to various activation pathways such as calcium-regulated kinases, mitogen-activated protein (MAP) kinases, and receptor tyrosine kinases.³ Thus, these observations suggest that platelet neurogranin may function as a previously unidentified component of a PKC-dependent activation pathway coupled to one (or more) of these effector proteins.

Discussion

These data provide documentation for a unique platelet mRNA profile that may provide a tool for analyzing platelet molecular networks. Nonetheless, the molecular analysis of the platelet transcriptome may be confounded by the constant decay of mRNAs in the absence of new gene transcription, a situation that may, for example, limit the identification of low-abundance transcripts. Similarly, because the circulating platelet pool contains

a mixed population of variably aged platelets, a "static" mRNA profile represents an average of this heterogeneous blood pool. Despite these potential limitations, the combination of genomic and proteomic technologies are likely to provide powerful tools for the global analysis of platelet function. Current strategies for cataloging "whole cellular proteomes" are generally accomplished by using 2 developing methodologies: (1) high resolution 2-dimensional polyacrylamide gel electrophoresis (2-DE) with mass spectrometric sequence identification,³⁴ and (2) microcapillary liquid chromatography with tandem mass spectrometry (μ LC-MC/MC).³⁵ Further modifications of both procedures have been devised for direct comparative studies between 2 cellular proteomes. The introduction of 2-DE differential gel electrophoresis has now made it possible to detect and quantify differences between experimental sample pairs resolved on the same 2-dimensional gel.³⁶ Likewise, the application of isotope-coded affinity tags to μ LC-MC/MC represent a novel means of quantitative analyses between cellular proteomes.³⁷ The success of both approaches relies on the availability of comprehensive genomic databases and mathematical algorithms for optimal protein identification. Indeed, mathematical modeling studies have demonstrated the need to delineate both protein and mRNA expression levels for optimal definition of intracellular networks.³⁸ Our data present an initial framework for delineating platelet function by defining the molecular anatomy of human platelets, information that is likely to provide important clues into the dynamic protein interactions regulating normal and pathologic platelet functions. Furthermore, because the platelet transcriptome mirrors the mRNAs derived from precursor megakaryocytes, these analyses may provide insights into the biochemical and molecular events regulating megakaryocytopoiesis and/or proplatelet formation.

Acknowledgments

We thank Dr Maurcen Krause, Jean Wainer, and Lesley Scudder for assistance with some of the experiments; John Schwedes (University DNA microarray facility) with the microarray analysis; and Ms Shirley Murray for manuscript preparation.

References

- Steinberg P, Hill R. Platelets and megakaryocytes. In: Le R, et al, eds. *Wintrobe's Clinical Hematology*. Baltimore, MD: Williams & Wilkins; 1999.
- Newman P, Gorski J, White G, Gidwitz S, Cretnay C, Aster R. Enzymatic amplification of platelet-specific messenger RNA using the polymerase chain reaction. *J Clin Invest*. 1988;82:739-743.
- Kieffer N, Guichard J, Faivel J, Vainchenko W, Breton-Gorius J. Biosynthesis of major platelet proteins in human blood platelets. *Eur J Biochem*. 1987;164:189-195.
- Weyrich A, Dixon D, Palla R, et al. Signal-dependent translation of a regulatory protein, Bcl-2, in activated human platelets. *Proc Natl Acad Sci U S A*. 1998;95:5556-5561.
- Benecke BJ, Ben Zeev A, Penman S. The control of mRNA production, translation and turnover in

- suspended and reattached anchorage-dependent fibroblasts. *Cell*. 1978;14:931-939.
6. Pablo R, Weyrich AS, Dixon DA, et al. Integrin-dependent control of translation: engagement of integrin α IIb β 3 regulates synthesis of proteins in activated human platelets. *J Cell Biol*. 1999;144:175-184.
 7. Chicurel ME, Singer RH, Meyer CJ, Ingber DE. Integrin binding and mechanical tension induce movement of mRNA and ribosomes to focal adhesions. *Nature*. 1998;392:730-733.
 8. Lindemann S, Tolley N, Eyre J, Kraiss L, Mahoney T, Weyrich A. Integrins regulate the intracellular distribution of eukaryotic initiation factor 4E in platelets. *J Biol Chem*. 2001;276:33947-33951.
 9. Brown EJ, Schreiber SL. A signaling pathway to translational control. *Cell*. 1996;86:517-520.
 10. Rinder H, Schuster J, Rinder C, Wang C, Schwesdter H, Smith B. Correlation of thrombosis with increased platelet turnover in thrombocytosis. *Blood*. 1998;91:1288-1294.
 11. Richards E, Bogdan T. Quantitation of reticulated platelets: methodology and clinical application. *Br J Haematol*. 1995;91:445-451.
 12. Robinson M, Mackie I, Khair K, et al. Flow cytometric analysis of reticulated platelets: evidence for a large proportion of non-specific labelling of dense granules by fluorescent dyes. *Br J Haematol*. 1998;100:351-357.
 13. Velculescu V, Zhang L, Vogelstein B, Kinzler K. Serial analysis of gene expression. *Science*. 1995;270:484-487.
 14. Zhang L, Zhou W, Velculescu V, et al. Gene expression profiles in normal and cancer cells. *Science*. 1997;276:1268-1272.
 15. Morin PJ, Sparks AB, Korinek V, et al. Activation of beta-catenin-Tcf signaling in colon cancer by mutations in beta-catenin or APC. *Science*. 1997;275:1787-1790.
 16. Bahou W, Campbell A, Wicha M. cDNA cloning and molecular characterization of MSE55: a novel human serum constituent protein that displays bone marrow stromal endothelial cell-specific expression. *J Biol Chem*. 1992;267:13986-13992.
 17. Bahou W, Collier B, Potter C, Norton K, Kutok J, Gofigorsky M. The thrombin receptor extracellular domain contains sites crucial for peptide ligand-induced activation. *J Clin Invest*. 1993;91:1405-1413.
 18. Heid C, Stevens J, Livak K, Williams P. Real-time quantitative PCR. *Genome Res*. 1996;6:986-994.
 19. Dunn J, McCorkle S, Praissman L, et al. Genome signature tags (GSTs): a system for profiling genomic DNA. *Nucleic Acid Res*. 2001;29:137-140.
 20. Kroll T, Wolf S. Ranking: a closer look on globalization methods for normalization of gene expression arrays. *Nucleic Acids Res*. 2002;30:e50.
 21. Pruitt KD, Maglott DR. RefSeq and LocusLink: NCBI gene-centered resources. *Nucleic Acids Res*. 2001;29:137-140.
 22. Fox JE, Boyles JK, Reynolds CC, Phillips DR. Actin filament content and organization in unstimulated platelets. *J Cell Biol*. 1984;98:1985-1991.
 23. Safer D, Elzinga M, Nachmias VT. Thymosin beta 4 and Fx, an actin-sequestering peptide, are indistinguishable. *J Biol Chem*. 1991;266:4029-4032.
 24. Wallace DC. Mouse models for mitochondrial disease. *Am J Med Genet*. 2001;106:71-93.
 25. Welle S, Bhatt K, Thornton C. Inventory of high-abundance mRNAs in skeletal muscle of normal men. *Genome Res*. 1999;9:506-513.
 26. Karparkin S, Charnatz A, Langer RM. Glycogenesis and glycconeogenesis in human platelets. Incorporation of glucose, pyruvate, and citrate into platelet glycogen; glycogen synthetase and fructose-1,6-diphosphatase activity. *J Clin Invest*. 1970;49:140-149.
 27. Roha S, Robinson BH. Mitochondria, oxygen free radicals, and apoptosis. *Am J Med Genet*. 2001;106:62-70.
 28. Yu J, Zhang L, Hwang P, Rago C, Kinzler K, Vogelstein B. Identification and classification of p53-regulated genes. *Proc Natl Acad Sci U S A*. 1999;96:14517-14522.
 29. Wang E, Miller L, Ohnmacht G, Liu E, Marincola F. High-fidelity mRNA amplification for gene profiling. *Nat Biotechnol*. 2000;18:157-159.
 30. Kirschbaum L, Sharpe JA, Murphy B, et al. Molecular cloning and characterization of the novel, human complement-associated protein, SP-40.40: a link between the complement and reproductive systems. *EMBO J*. 1989;8:711-718.
 31. McLaughlin L, Zhu G, Mistry M, et al. Apolipoprotein J clusterin limits the severity of murine autoimmune myocarditis. *J Clin Invest*. 2000;105:1105-1113.
 32. Martinez DA, Perez JL, Bernal J, Coloma A. Structure, organization, and chromosomal mapping of the human neurogranin gene (NRGN). *Genomics*. 1997;41:243-249.
 33. Wu J, Li J, Huang K, Huang F. Attenuation of PKC and PKA signal transduction in the neurogranin knockout mouse. *J Biol Chem*. 2002;277:19498-19505.
 34. Gygi S, Rochon Y, Franza B, Aebersold R. Correlation between protein and mRNA abundance in yeast. *Mol Cell Biol*. 1999;19:1720-1730.
 35. Link A, Eng J, Schieltz DM, et al. Direct analysis of protein complexes using mass spectrometry. *Nat Biotechnol*. 1999;17:676-682.
 36. Untch M, Morgan M, Minden J. Difference gel electrophoresis: a single gel method for detecting changes in protein extracts. *Electrophoresis*. 1997;18:2071-2077.
 37. Gygi S, Rist B, Gerber SA, Turecek F, Gelb MH, Aebersold R. Quantitative analysis of complex protein mixtures using isotope-coded affinity tags. *Nat Biotechnol*. 1999;17:994-999.
 38. Hatizmanikatis V, Lee K. Dynamical analysis of gene networks requires both mRNA and protein expression information. *Metabol Eng*. 1999;1:275-281.

Overexpression of a DEAD Box Protein (DDX1) in Neuroblastoma and Retinoblastoma Cell Lines*

(Received for publication, November 17, 1997, and in revised form, June 2, 1998)

Roseline Godbout‡, Mary Packer, and Wenjun Bie

From the Department of Oncology, Cross Cancer Institute and University of Alberta, 11560 University Ave., Edmonton, Alberta T6G1Z2, Canada

The DEAD box gene, *DDX1*, is a putative RNA helicase that is co-amplified with *MYCN* in a subset of retinoblastoma (RB) and neuroblastoma (NB) tumors and cell lines. Although gene amplification usually involves hundreds to thousands of kilobase pairs of DNA, a number of studies suggest that co-amplified genes are only overexpressed if they provide a selective advantage to the cells in which they are amplified. Here, we further characterize *DDX1* by identifying its putative transcription and translation initiation sites. We analyze *DDX1* protein levels in *MYCN/DDX1*-amplified NB and RB cell lines using polyclonal antibodies specific to *DDX1* and show that there is a good correlation with *DDX1* gene copy number, *DDX1* transcript levels, and *DDX1* protein levels in all cell lines studied. *DDX1* protein is found in both the nucleus and cytoplasm of *DDX1*-amplified lines but is localized primarily to the nucleus of nonamplified cells. Our results indicate that *DDX1* may be involved in either the formation or progression of a subset of NB and RB tumors and suggest that *DDX1* normally plays a role in the metabolism of RNAs located in the nucleus of the cell.

DEAD box proteins are a family of putative RNA helicases that are characterized by eight conserved amino acid motifs, one of which is the ATP hydrolysis motif containing the core amino acid sequence DEAD (Asp-Glu-Ala-Asp) (1–3). Over 40 members of the DEAD box family have been isolated from a variety of organisms including bacteria, yeast, insects, amphibians, mammals, and plants. The prototypic DEAD box protein is the translation initiation factor, eukaryotic initiation factor 4A, which, when combined with eukaryotic initiation factor 4B, unwinds double-stranded RNA (4). Other DEAD box proteins, such as p68, Vasa, and An3, can effectively and independently destabilize/unwind short RNA duplexes *in vitro* (5–7). Although some DEAD box proteins play general roles in cellular processes such as translation initiation (eukaryotic initiation factor 4A (4)), RNA splicing (PRP5, PRP28, and SPP81 in yeast (8–10)), and ribosomal assembly (SrmB in *Escherichia coli* (11)), the function of most DEAD box proteins remains unknown. Many of the DEAD box proteins found in higher eukaryotes are tissue- or stage-specific. For example, *PL10* mRNA is expressed only in the male germ line, and its product

has been proposed to have a specific role in translational regulation during spermatogenesis (12). Vasa and ME31B are maternal proteins that may be involved in embryogenesis (13, 14). p68, found in dividing cells (15), is believed to be required for the formation of nucleoli and may also have a function in the regulation of cell growth and division (16, 17). Other DEAD box proteins are implicated in RNA degradation, mRNA stability, and RNA editing (18–20).

The human DEAD box protein gene *DDX1*¹ was identified by differential screening of a cDNA library enriched in transcripts present in the two RB cell lines Y79 and RB522A (21). The longest *DDX1* cDNA insert isolated from this library was 2.4 kb with an open reading frame from position 1 to 2201. All eight conserved motifs characteristic of DEAD box proteins are found in the predicted amino acid sequence of *DDX1* as well as a region with homology to the heterogeneous nuclear ribonucleoprotein U, a protein believed to participate in the processing of heterogeneous nuclear RNA to mRNA (22, 23). The region of homology to heterogeneous nuclear ribonucleoprotein U spans 128 amino acids and is located between the first two conserved DEAD box protein motifs, 1a and 1b.

The proto-oncogene *MYCN* encodes a member of the MYC family of transcription factors that bind to an E box element (CACGTG) when dimerized with the MAX protein (24, 25). The *MYCN* gene is amplified and overexpressed in approximately one-third of all NB tumors (26, 27). Amplification of *MYCN* is associated with rapid tumor progression and a poor clinical prognosis (26, 27). *MYCN* overexpression is usually achieved by increasing gene copy number rather than by up-regulating basal expression of *MYCN* (27, 28). Because gene amplification involves hundreds to thousands of kilobase pairs of contiguous DNA (29–32), it is possible that co-amplification of a gene located in proximity to *MYCN* may contribute to the poor clinical prognosis of *MYCN*-amplified tumors. The *DDX1* gene maps to the same chromosomal band as *MYCN*, 2p24, and is located ~400 kb telomeric to the *MYCN* gene (33–36). All four *MYCN*-amplified RB tumor cell lines tested to date are amplified for *DDX1* (21),² while approximately two-thirds of NB cell lines and 38–68% of NB tumors are co-amplified for both genes (37–39). George *et al.* (39) found a significant decrease in the mean disease-free survival of patients with *DDX1/MYCN*-amplified NB tumors compared with *MYCN*-amplified tumors. Similarly, Squire *et al.* (38) observed a trend toward a worse clinical prognosis when both genes were amplified in the tumors of NB patients. To date, there have been no reports of a

* This work was supported by the National Cancer Institute of Canada with funds from the Canadian Cancer Society. The costs of publication of this article were defrayed in part by the payment of page charges. This article must therefore be hereby marked "advertisement" in accordance with 18 U.S.C. Section 1734 solely to indicate this fact.

The nucleotide sequence(s) reported in this paper has been submitted to the GenBank™/EBI Data Bank with accession number(s) X70649.

‡ To whom correspondence should be addressed: Dept. of Oncology, Cross Cancer Institute, 11560 University Ave., Edmonton, Alberta T6G 1Z2, Canada. Tel.: 403-432-8901; Fax: 403-432-8892.

¹ The abbreviations used are: *DDX1*, DEAD box 1; NB, neuroblastoma; RB, retinoblastoma; RACE, rapid amplification of cDNA ends; PAGE, polyacrylamide gel electrophoresis; nt, nucleotide(s); MOPS, 4-morpholinepropanesulfonic acid; bp, base pair(s); kb, kilobase(s) or kilobase pair(s).

² R. Godbout, unpublished results.

tumor amplified only for *DDX1*, and the role that this gene plays in cancer formation and progression is not known.

Because of the high rate of rearrangements in amplified DNA (31, 40), it is unlikely that a gene located ~400 kb from the *MYCN* gene will be consistently amplified as an intact unit unless its product provides a growth advantage to the cell. Based on Southern blot analysis, the *DDX1* gene extends over more than 30 kb, and there are no gross rearrangements of this gene in *DDX1*-amplified tumors (21, 38). Furthermore, there is a good correlation between *DDX1* transcript levels and gene copy number in the tumors analyzed to date. However, we need to show that *DDX1* protein is overexpressed in *DDX1*-amplified tumors if we are to entertain the possibility that this protein plays a role in the tumorigenic process. Here, we isolate and characterize the 5'-end of *DDX1* mRNA and extend the *DDX1* cDNA sequence by ~300 nt. We identify the predicted initiation codon of *DDX1* and generate antisera that specifically recognize *DDX1* protein. We analyze levels of *DDX1* protein in both *DDX1*-amplified and nonamplified RB and NB tumors and study the subcellular location of this protein in the cell.

MATERIALS AND METHODS

Library Screening—A human fetal brain cDNA library (Stratagene) was screened using a 320-bp DNA fragment from the 5'-end of the 2.4-kb *DDX1* cDNA previously described (23). Phagemids containing positive inserts were excised from λ ZAP II following the supplier's directions. The ends of the cDNA inserts were sequenced using the dideoxynucleotide chain termination method with T7 DNA polymerase (Amersham Pharmacia Biotech).

A human placenta genomic library (CLONTECH) was screened with the 5'-end of *DDX1* cDNA. Positive plaques were purified, and the genomic DNA was analyzed using restriction enzymes and Southern blotting. *EcoRI*-digested DNA fragments from these clones were subcloned into pBluescript and digested with exonuclease III and mung bean nuclease to obtain sequentially deleted clones. The exon/intron map of the 5' portion of the *DDX1* gene was obtained by comparing the sequence of *DDX1* cDNA with that of the genomic DNA.

Rapid Amplification of cDNA Ends (RACE)—We used the AmpliFINDER RACE kit (CLONTECH) to extend the 5'-end of *DDX1* cDNA. Briefly, two μ g of poly(A)⁺ RNA isolated from RB522A was reverse transcribed at 52 °C using either primer P1 or P3 (Fig. 1A). The RNA template was hydrolyzed, and excess primer was removed. A single-stranded AmpliFINDER anchor containing an *EcoRI* site was ligated to the 3'-end of the cDNA using T4 RNA ligase. The cDNA was amplified using either primer P2 or P4 (Fig. 1A) and AmpliFINDER anchor primer. RACE products were cloned into pBluescript.

Primer Extension—Poly(A)⁺ RNAs were isolated from RB and NB cell lines as described previously (21, 38). The 21-nt primers 5'-TTCGT-TCTGGGCACCATGTGT-3' (primer P4 in Fig. 1A) and 5'-TGGGAC-CTAGGGCTTCTGGAC-3' (primer P3 in Fig. 1A) were end-labeled with [γ -³²P]ATP (3000 Ci/mmol; Mandel Scientific) and T4 polynucleotide kinase. Each of the labeled primers was annealed to 2 μ g of poly(A)⁺ RNA at 45 °C for 90 min, and the cDNA was extended at 42 °C for 60 min using avian myeloblastosis virus reverse transcriptase (Promega). The primer extension products were heat-denatured and run on a 8% polyacrylamide gel containing 7 M urea in 1× TBE buffer. A G + A sequencing ladder served as the size standard.

S1 Nuclease Protection Assay—The S1 nuclease protection assay to map the transcription initiation site of *DDX1* was performed as described by Favaloro *et al.* (41). The DNA probe was prepared by digesting genomic DNA spanning the upstream region of *DDX1* and exon 1 with *AvaI*, labeling the ends with [γ -³²P]ATP (3000 Ci/mmol) and polynucleotide kinase, and removing the label from one of the ends by digesting the DNA with *SphI* (Fig. 4). The RNA samples were resuspended in a hybridization mixture containing 80% formamide, 40 mM PIPES, 400 mM NaCl, 1 mM EDTA, and the heat-denatured *SphI*-*AvaI* probe labeled at the *AvaI* site. The samples were incubated at 45 °C for 16 h and digested with 3000 units/ml S1 nuclease (Boehringer Mannheim) for 60 min at 37 °C. The samples were precipitated with ethanol; resuspended in 80% formaldehyde, TBE buffer, 0.1% bromophenol blue, xylene cyanol; denatured at 90 °C for 2 min; and electrophoresed in a 7 M urea, 8% polyacrylamide gel in TBE buffer.

Northern and Southern Blot Analysis—Poly(A)⁺ RNAs were isolated from RB and NB cell lines as described previously (21, 38). Two μ g of

poly(A)⁺ RNA/lane were electrophoresed in a 6% formaldehyde, 1.5% agarose gel in MOPS buffer (20 mM MOPS, 5 mM sodium acetate, 1 mM EDTA, pH 7.0) and transferred to nitrocellulose filter in 3 M sodium chloride, 0.3 M sodium citrate. The filters were hybridized to the following DNA probes, ³²P-labeled by nick translation: (i) a 1.6-kb *EcoRI* insert from *DDX1* cDNA clone 1042 (21), (ii) a 260-bp cDNA fragment spanning the 3'-end of *DDX1* exon 1 as well as exons 2 and 3, (iii) a 160-bp fragment derived from the 5'-end of *DDX1* exon 1, and (iv) α -actin cDNA to control for lane to lane variation in RNA levels. Filters were hybridized and washed under high stringency. Southern blot analysis was as described previously (21).

Preparation of Anti-DDX1 Antiserum—To prepare antiserum to the C terminus of the *DDX1* protein, we inserted a 1.8-kb *EcoRI* fragment from bp 848 to 2668 of *DDX1* cDNA (Fig. 1B) into *EcoRI*-digested pMAL-c2 expression vector (New England Biolabs). DH5 α cells transformed with this vector were grown to mid-log phase and induced with 0.1 mM isopropyl-1-thio- β -D-thiogalactoside. The cells were harvested 3–4 h postinduction and lysed by sonication. Soluble maltose binding protein-DDX1 fusion protein was affinity-purified using amylose resin, and the maltose-binding protein was cleaved with factor Xa. The *DDX1* protein was purified on a SDS-PAGE gel, electroeluted, and concentrated. Approximately 100 μ g of protein was injected into rabbits at 4–6-week intervals. For the initial injection, the protein was dispersed in complete Freund's adjuvant (Sigma), while subsequent injections were prepared in Freund's incomplete adjuvant. Blood was collected from each rabbit 10 days after injection, and the specificity of the antiserum was tested using cell extracts from RB522A. To prepare antiserum to the N terminus of *DDX1* protein, a *DDX1* cDNA fragment from bp 268 to 851 (Fig. 1B) was inserted into pGEX-4T2 (Amersham Pharmacia Biotech). The recombinant protein produced from this construct contains the first 186 amino acids of the predicted *DDX1* sequence. Soluble glutathione S-transferase-DDX1 fusion protein was purified with glutathione-Sepharose 4B (Amersham Pharmacia Biotech). The glutathione S-transferase component of the fusion protein was cleaved with thrombin.

Subcellular Fractionations and Western Blot Analysis—We used two different procedures for subcellular fractionations. First, we isolated nuclear and S100 (soluble cytoplasmic) fractions from RB522A, IMR-32, Y79, RB(E)-2, HeLa, and HL60 using the procedure of Dignam (42). On average, we obtained 5–6 times more protein in the cytosolic fractions than in the nuclear fractions. Second, 10⁸ RB522A cells were lysed and fractionated into S4 (soluble cytoplasmic components), P2 (heavy mitochondria, plasma membrane fragments), P3 (mitochondria, lysosomes, peroxisomes, and Golgi membranes), and P4 fractions (membrane vesicles from rough and smooth endoplasmic reticulum, Golgi, and plasma membrane) by differential centrifugation (43). We obtained 8 mg of protein in the S4 fraction, 1 mg in P2, 0.5 mg in P3, and 2 mg in P4 fraction. The procedures related to the immunoelectron microscopy have been previously described (44).

For Western blot analysis, proteins were electrophoresed in polyacrylamide-SDS gels and electroblotted onto nitrocellulose using the standard protocol for protein transfer described by Schleicher and Schuell. The filters were incubated with a 1:5000 dilution of *DDX1* antiserum, a 1:200 dilution of anti-MYCYN monoclonal antibody (Boehringer Mannheim), or a 1:200 dilution of anti-actin (Santa Cruz Biotechnology, Inc., Santa Cruz, CA). For the colorimetric analysis, antigen-antibody interactions were visualized using either alkaline phosphatase-linked goat anti-rabbit IgG (for *DDX1*) or goat anti-mouse IgG (for MYCYN) at a 1:3000 dilution. For the ECL Western blotting analysis (Amersham Pharmacia Biotech), we used a 1:100,000 dilution of peroxidase-linked secondary anti-rabbit IgG antibody (for *DDX1*) or secondary anti-goat IgG antibody (Jackson ImmunoResearch Laboratories).

RESULTS

Identification of the 5'-End of the *DDX1* Transcript—We have previously reported the sequence of *DDX1* cDNA isolated from an RB cDNA library (21, 23). This 2.4-kb *DDX1* cDNA contains an open reading frame spanning positions 1–2201 with a methionine encoded by the first three nucleotides (Fig. 1A). There is a polyadenylation signal and poly(A) tail in the 3'-untranslated region, indicating that the sequence is complete at the 3'-end. Manohar *et al.* (37) have also isolated *DDX1* cDNA from the NB cell line LA-N-5. Their cDNA extended the 5'-end of our sequence by 42 bp and included an additional in frame methionine (double underlined in Fig. 1A). The possi-



ity of additional in frame methionines located further upstream could not be excluded, because there were no predicted stop codons in the upstream region of the cDNA.

We next used the RACE procedure in an attempt to isolate additional 5' sequence. The nested primers used to amplify the 5'-end of the *DDX1* transcript are labeled as primers P1 and P2 in Fig. 1A and are located downstream of the three in frame methionines (*double underlined* in Fig. 1A). Poly(A)⁺ RNA from RB522A was reverse transcribed at 52 °C using primer P1, and the reverse transcribed cDNA was amplified using the nested primer P2 and the 5'-RACE primer. Using this approach, we generated a product that was 230 bp longer than any of the cDNAs obtained by screening libraries (Fig. 1A). Sequencing of this 230-bp cDNA revealed an in frame stop codon (*boldface double underline* in Fig. 1A) located 123 bp



upstream of the predicted translation initiation site. We then prepared primers P3 and P4, located near the 5'-end of the RACE cDNA (Fig. 1A) and repeated the RACE procedure to see if additional 5' sequences could be obtained. The resulting RACE products did not extend the *DDX1* cDNA sequence further.

The location of the *DDX1* transcription initiation site was verified by primer extension. Poly(A)⁺ RNA was prepared from the following two cell lines: *DDX1*-amplified RB cell line RB522A and a nonamplified RB cell line RB(E)-2. RB522A has elevated levels of *DDX1* mRNA, while RB(E)-2 has at least 20-fold lower levels of this transcript. Three products of 40, 43, and 46 nt (with a weak signal at 45 nt) were detected in RB522A using primer P4 (Figs. 1A and 2). The 40-nt product corresponded exactly with the 5'-end of the RACE-derived cDNA while the 43- and 46-nt products extended the predicted size of the *DDX1* transcript by 3 and 6 nt, respectively. None of these products were observed in RB(E)-2. Bands of identical sizes to those obtained with RB522A mRNA were also observed in the *DDX1*-amplified NB cell line BE(2)-C but not in the *DDX1*-amplified NB cell line IMR-32 (data not shown). The same predicted *DDX1* transcription initiation site was identified with primer P3 except that the bands were of weaker

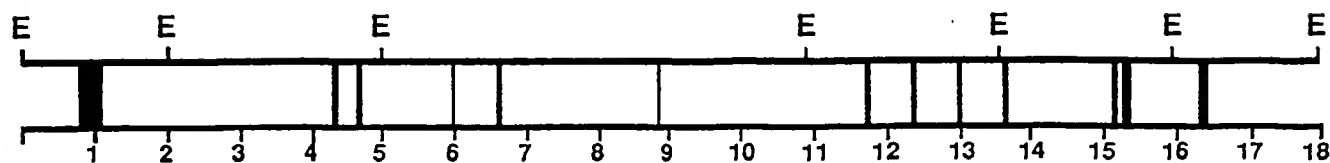


FIG. 3. Genomic map of the 5'-end of *DDX1*. The exons are represented by the black boxes, and distances are in kilobase pairs. The locations of *EcoRI* (E) sites are indicated.

intensity (data not shown). We have designated the transcription start site identified by primer extension as +1 (Fig. 1A).

The sequence of the 6 nt extending beyond the RACE cDNA was obtained by comparison of the cDNA sequence with that of *DDX1* genomic DNA. Bacteriophages containing *DDX1* genomic DNA were isolated by screening a human placenta library with 5' *DDX1* cDNA. Eighteen kb of DNA were sequenced from two bacteriophages with overlapping *DDX1* genomic DNA. Thirteen exons were identified within this 18-kb region (Fig. 3) corresponding to cDNA sequences from position 1 to 1249. The 310-bp exon 1 was by far the longest of the 13 exons sequenced, corresponding to the entire 5'-untranslated region of *DDX1* as well as the first in frame methionine. The sequences transcribed from exons 1, 2, and 3 are indicated in Fig. 1A.

Knowledge of the genomic structure of *DDX1* allowed us to use the S1 protection assay, a technique that is independent of reverse transcriptase, to further define the 5'-end of the *DDX1* transcript. Poly(A)⁺ RNAs from six *DDX1*-amplified lines (RB lines: Y79 and RB522A; NB lines: BE(2)-C, IMR-32, LA-N-1, and LA-N-5) and six nonamplified lines (RB lines: RB(E)-2 and RB412; NB lines: GOTO, NB-1, NUB-7, and SK-N-MC) were hybridized to a DNA probe that extended from position -745 in the 5'-flanking *DDX1* DNA to position +164 in exon 1. This DNA probe was labeled at position +164 as indicated in Fig. 4. Nonhybridized DNA was digested with S1 nuclease, and the sizes of the protected fragments were analyzed on a denaturing polyacrylamide gel. Bands of 150–153 nt were observed in lane 2 (RB522A), lane 5 (BE(2)-C), and lane 8 (LA-N-1) with bands of much weaker intensity in lane 7 (IMR-32) (Fig. 4). Specific bands were not detected in either *DDX1*-amplified Y79 and LA-N-5 or the nonamplified lines. Although the sizes of the S1 protected bands in RB522A, BE(2)-C, and LA-N-1 were 5 and 11 nt shorter than predicted based on RACE and primer extensions, respectively, there was general agreement with all three techniques regarding the location of the *DDX1* transcription initiation site (Fig. 1A). The smaller S1 nuclease protected products could have arisen as the result of S1 digestion of the 5'-end of the RNA:DNA heteroduplex because of its relatively high rU:dA content (45).

Identification of the same transcription initiation site in three *DDX1*-amplified lines suggests that this represents the bona fide start site of *DDX1* transcription. However, it was not clear why this start site was either very weak or not detected in three other amplified lines. To determine whether the 5'-end of exon 1 is transcribed in all *DDX1*-amplified lines, we carried out a direct analysis of the 5'-end of the *DDX1* transcript by Northern blotting. Two probes were used for this analysis: the 5' probe contained a 160-bp fragment from bp 1 to 160 (5'-half of exon 1), and the 3' probe contained a 260-bp fragment from bp 160 to 420 (3'-half of exon 1 as well as exons 2 and 3) (Fig. 1A). With the 3' probe, we obtained bands of similar size and intensity in four *DDX1*-amplified lines (RB522A, BE(2)-C, IMR-32, and LA-N-5). Band intensity was somewhat weaker in Y79 and stronger in LA-N-1 in comparison with the other lines (Fig. 5). No signal was detected in the non-*DDX1*-amplified line RB412. With the 5' probe, a relatively strong signal was observed in RB522A, BE(2)-C, and LA-N-1, while a considerably weaker

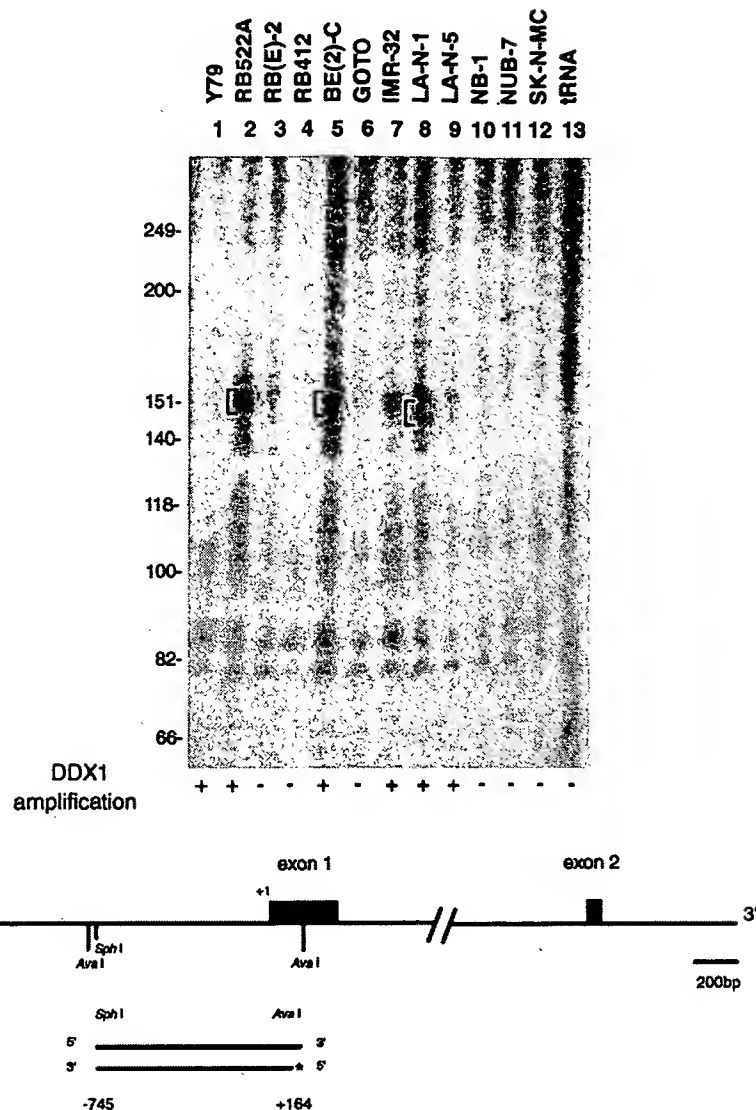
but readily apparent signal was detected in Y79, IMR-32, and LA-N-5. The signal obtained with actin indicates that, with the exception of LA-N-1, similar amounts of RNA were loaded in each lane and that the RNA was not degraded. These results indicate that at least a portion of the 160-bp 5'-end of exon 1 is transcribed in all *DDX1*-amplified lines.

Based on primer extension, S1 nuclease protection assay, Northern blot analysis and the sequencing of the RACE products, we conclude that the *DDX1* transcript is 2.7 kb with an open reading frame spanning nucleotides 295–2515 encoding a predicted protein of 740 amino acids with an estimated molecular weight of 82.4 (Fig. 1B). An in frame stop codon is located 123 nt upstream of the predicted translation initiation site, at positions 172–174. The first in frame methionine following the stop codon is in agreement with the Kozak consensus sequence (46). Furthermore, the predicted start methionine codon for human *DDX1* corresponds perfectly with that of *Drosophila* *DDX1* (47). A stop codon is located 15 nt upstream of the initiation codon in *Drosophila* *DDX1*.

Analysis of *DDX1* Protein Levels in Neuroblastoma and Retinoblastoma—We and others have previously shown that there is a good correlation between gene copy number and RNA levels in *DDX1*-amplified RB and NB cell lines (37, 38). To determine whether the correlation extends to *DDX1* protein levels, we prepared antiserum to two nonoverlapping recombinant *DDX1* proteins. First, we prepared a C terminus recombinant protein construct by inserting a 1.8-kb *EcoRI* fragment from bp 848 to 2668 (amino acids 185–740) (Fig. 1B) into the pMAL-c2 expression vector. Recombinant protein expression was induced with isopropyl-1-thio- β -D-thiogalactoside, and the 110-kDa maltose-binding protein-*DDX1* fusion product was purified by affinity chromatography using amylose resin, followed by electrophoresis on a SDS-PAGE gel after cleaving the maltose-binding protein fusion partner with factor Xa. Second, we prepared an N terminus construct by ligating a DNA fragment from bp 268 to 851 (amino acids 1–186) into pGEX-4T2. The 50-kDa glutathione S-transferase-*DDX1* fusion protein was purified by affinity chromatography on a glutathione column. This N terminus fusion protein contains only the first of the eight conserved motifs found in all DEAD box proteins, while the C terminus fusion protein includes the remaining seven motifs.

We measured *DDX1* protein levels in total cell extracts of three RB and 10 NB cell lines. Using antiserum to the N terminus fusion protein, we observed a strong signal in all *DDX1*-amplified cell lines: the RB cell lines Y79 (lane 1) and RB522A (lane 2) and the NB cell lines BE(2)-C (lane 4), IMR-32 (lane 6), LA-N-1 (lane 8), and LA-N-5 (lane 9) (Fig. 6). Two bands were observed in the majority of extracts. Of the amplified lines, Y79 produced the weakest signal, with the most intense signal observed in LA-N-1. There was an excellent correlation with *DDX1* protein and mRNA levels in these cell lines, with lower levels of *DDX1* mRNA observed in Y79 and higher levels in LA-N-1 (Fig. 7A). As shown in Fig. 7B, this correlation extended to *DDX1* gene copy number. No gross DNA rearrangements were seen in the *DDX1*-amplified lines; however, three small bands of altered size were observed in the RB412 lane. Although the nature of the DNA alteration is not known, it is noteworthy that *DDX1* transcript levels in RB412

FIG. 4. S1 nuclease mapping of the 5'-end of the *DDX1* transcript. Two μg of poly(A)⁺ RNA from four RB lines (*DDX1*-amplified Y79 and RB522A and nonamplified RB(E)-2 and RB412), eight NB lines (*DDX1*-amplified BE(2)-C, IMR-32, LA-N-1, and LA-N-5 and nonamplified GOTO, NB-1, NUB-7, and SK-N-MC), and tRNA as a negative control were hybridized to a *Sph*I–*Ava*I fragment labeled at the *Ava*I site with [γ -³²P]ATP and polynucleotide kinase. Bands of 150–153 nt are shown in lanes 2 (RB522A), 5 (BE(2)-C), and 8 (LA-N-1) with much weaker bands in lane 7 (IMR-32). A map of the probe indicating the transcription initiation site identified by primer extension (+), the labeling site (*), and exons 1 and 2, is shown at the bottom.



are extremely low (Fig. 7A) and that the top *DDX1* protein band in RB412 cell extracts is smaller in size than the top band from the other cell extracts (Fig. 6).

Two *DDX1* protein bands were present in most of the lanes in Fig. 6. The same two bands were detected with antiserum to the C terminus of the *DDX1* protein, as well as a third band at ~60 kDa (data not shown). There was no variation in the intensity of the 60-kDa band in *DDX1*-amplified and nonamplified cell extracts. The 60-kDa band probably represents another member of the DEAD box protein family, because the C terminus *DDX1* protein used to prepare this antiserum contained seven of the eight conserved motifs found in all DEAD box proteins. To obtain an estimate of the size of the two *DDX1* bands, we ran cellular extracts from RB522A on a 7% SDS-PAGE gel with the BenchMark protein ladder (Life Technologies, Inc.). The size of the *DDX1* protein was determined using the Alpha Imager 2000 documentation and analysis system for molecular weight calculation. Based on this analysis, the estimated molecular mass of the top band is 89.5 kDa, while that of the bottom band is 83.5 kDa. The 84-kDa band may represent the unmodified product encoded by the *DDX1* transcript (capable of encoding a protein with a predicted molecular mass of 82.4 kDa), while the top band may represent post-translational modification of *DDX1* protein (e.g. phosphorylation). Another possibility is that the top band represents intact *DDX1*

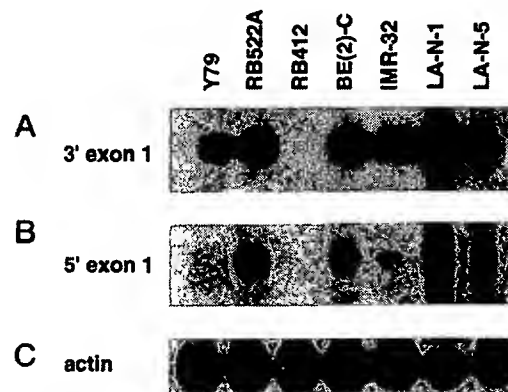


FIG. 5. Northern blot analysis of the 5'-end of the *DDX1* transcript. Two μg of poly(A)⁺ RNA isolated from *DDX1*-amplified Y79, RB522A, BE(2)-C, IMR-32, LA-N-1, and LA-N-5 and nonamplified RB412 were electrophoresed in a 1.5% agarose-formaldehyde gel. The RNA was transferred to a nitrocellulose filter and sequentially hybridized with a 260-bp fragment from *DDX1* cDNA from bp +160 to +420 (3'-end of exon 1 as well as exons 2 and 3) (A), a 160-bp fragment from *DDX1* cDNA from bp +1 to +160 (5'-end of exon 1) (B), and actin cDNA (C). The DNA was labeled with [³²P]dCTP by nick translation. The blots were hybridized and washed under high stringency.

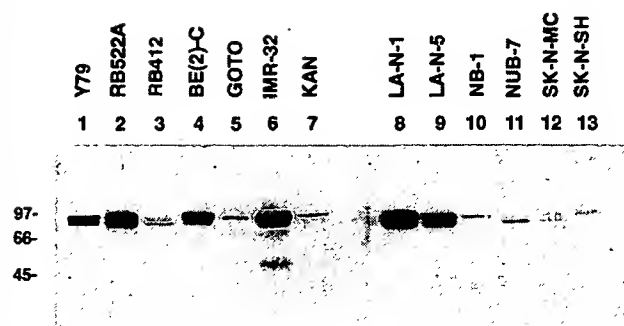


Fig. 6. DDX1 protein expression in RB and NB cell lines. Western blots were prepared using total cellular extracts from three RB (Y79, RB522A, and RB412) and 10 NB cell lines (BE(2)-C, GOTO, IMR-32, KAN, LA-N-1, LA-N-5, NB-1, NUB-7, SK-N-MC, and SK-N-SH). The lines that are amplified for the *DDX1* gene are Y79, RB522A, BE(2)-C, IMR-32, LA-N-1, and LA-N-5. Twenty μ g of protein were loaded in each lane and electrophoresed in a 10% SDS-PAGE gel. DDX1 was detected using a 1:5000 dilution of the antiserum to the amino terminus of DDX1 protein. Size markers in kilodaltons are indicated on the side.

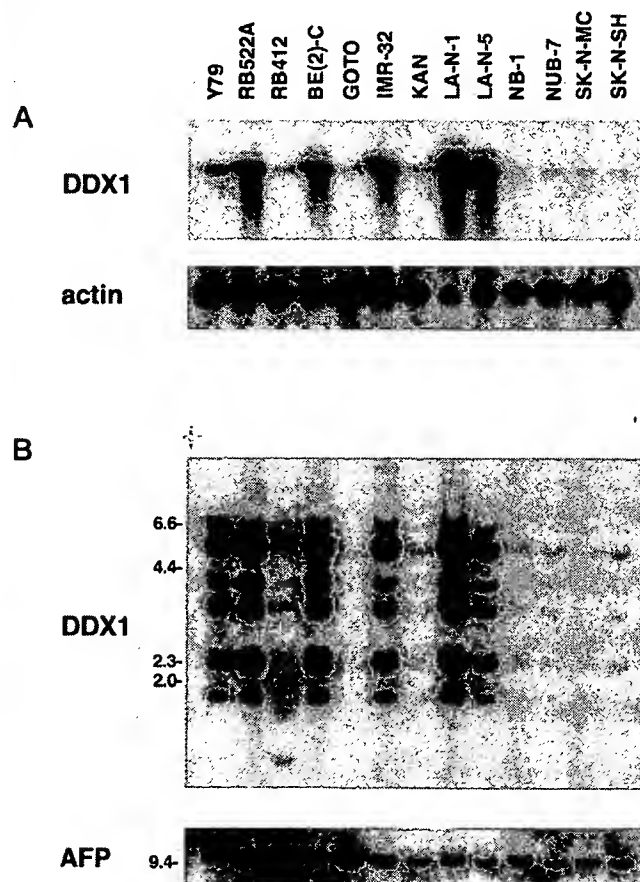


Fig. 7. Northern and Southern blot analyses of *DDX1* in RB and NB cell lines. A, 2 μ g of poly(A)⁺ RNA were loaded in each lane, electrophoresed in a 1.5% agarose-formaldehyde gel, and transferred to a nitrocellulose filter. The filter was first hybridized to a ³²P-labeled 1.6-kb *DDX1* cDNA (clone 1042) (21), stripped, and rehybridized to actin DNA. B, 10 μ g of genomic DNA from each of the indicated cell lines were digested with *Eco*RI, electrophoresed in a 1% agarose gel, and transferred to a nitrocellulose filter. The filter was hybridized to ³²P-labeled clone 1042 *DDX1* cDNA, stripped, and reprobed with labeled α -fetoprotein cDNA. Markers (in kilobase pairs) are indicated on the side.

and the lower band is a specific truncated or degradation product of DDX1. Yet a third possibility is that the two bands represent the products of differentially spliced transcripts or

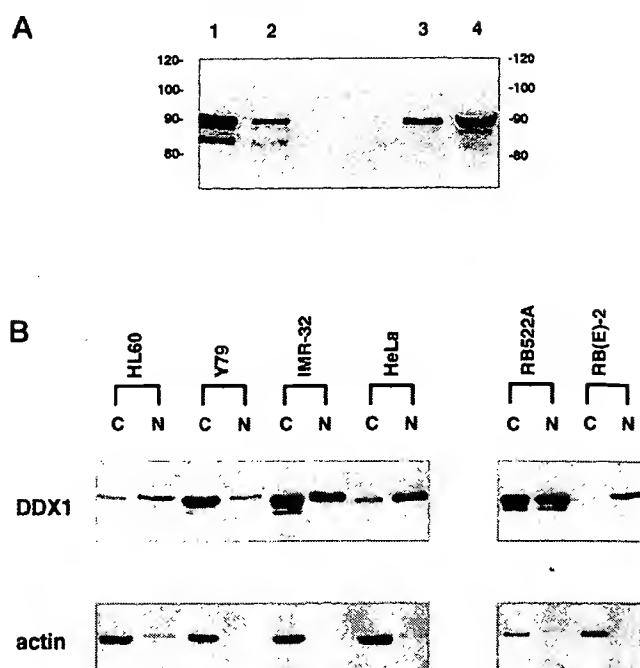


Fig. 8. Distribution of DDX1 in the nucleus and cytoplasm. A, cytosolic and nuclear extracts were prepared from RB522A and electrophoresed in a 7% SDS-PAGE gel. Cytosolic extracts were loaded in lanes 1 (20 μ g of protein) and 2 (10 μ g), while nuclear extracts were loaded in lanes 3 (10 μ g) and 4 (20 μ g). DDX1 was visualized using a 1:5000 dilution of the antiserum to the N terminus. The BenchMark protein ladder size markers (kilodaltons) are indicated on the left. B, cytosolic and nuclear extracts were prepared from HL60, Y79, IMR-32, HeLa, RB522A, and RB(E)-2 and electrophoresed in an 8% SDS-PAGE gel. Twenty μ g of proteins were loaded in each lane marked C (cytosolic) and N (nuclear). DDX1 was visualized using a 1:5000 dilution of the antiserum to the N terminus. Actin levels were analyzed using a 1:200 dilution of anti-actin antibody (Santa Cruz Biotechnology).

different translation initiation sites. However, the lack of any obvious differences in *DDX1* transcript sizes in the three RB and 10 NB lines analyzed in Fig. 7A does not support the latter possibility (e.g. compare the *DDX1* transcript size in NUB-7 (which produces the lower DDX1 protein band) and in NB-1 (which produces the higher DDX1 protein band)).

Subcellular Localization of DDX1 Protein—DEAD box proteins have been implicated in a variety of cellular functions including RNA splicing in the nucleus, translation initiation in the cytoplasm, and ribosome assembly in the nucleolus. To obtain an indication of the possible role of DDX1, we studied its subcellular location. Nuclear and cytosolic extracts were prepared from *DDX1*-amplified RB522A and run on a 7% SDS-PAGE gel. Although there was more DDX1 protein in the cytosol than in the nucleus on a per cell basis, the proportion of DDX1 protein relative to total protein was similar in both cellular compartments (Fig. 8A). Both the 90- and 84-kDa bands were present in cytosol and nuclear extracts, although the bottom band was more readily apparent in the cytosol. By running the gel for an extended period of time (twice as long as usual), we were able to detect an additional weak band at ~88 kDa in both nuclear and cytosolic extracts.

To determine whether DDX1 consistently localizes to both the cytoplasm and nucleus, we prepared cytosol and nuclear extracts from two additional *DDX1*-amplified lines, Y79 and IMR-32, as well as from nonamplified RB(E)-2, HL60, and HeLa. DDX1 protein was found in both the nucleus and cytoplasm of IMR-32, primarily in the cytoplasm of Y79, and mainly in the nucleus of the three nonamplified lines (Fig. 8B). In addition, DDX1 was almost exclusively found in nuclear

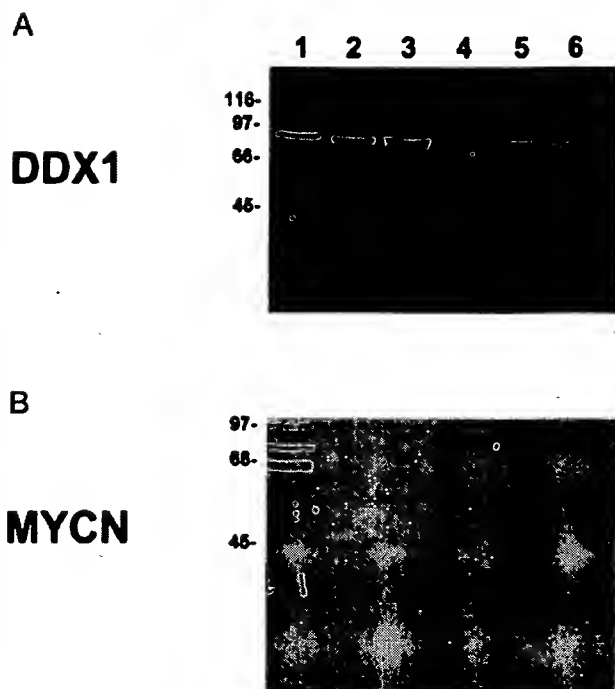


FIG. 9. Subcellular location of DDX1 protein. RB522A cells were fractionated into nuclear (lane 1), S100 and S4 cytosol (lanes 2 and 3), P2 membrane (lane 4), P3 membrane (lane 5), and P4 membrane (lane 6) fractions. Twenty μ g of protein were loaded in each lane and run on a 10% SDS-PAGE gel. A, DDX1 protein was detected using a 1:5000 dilution of the antiserum to the N terminus of DDX1. B, MYCN protein was detected using a commercially available antibody at a 1:200 dilution. Size markers (kilodaltons) are indicated on the side.

extracts prepared from normal GM38 fibroblasts (data not shown). We used anti-actin antibody to ensure that our nuclear and cytosolic extracts were not cross-contaminated (Fig. 8B).

We next carried out a more detailed analysis of DDX1 subcellular location using two different approaches: (i) fractionation of cellular components into nuclei; S100 or S4 cytosol (containing soluble cytoplasmic components, including 40 S ribosomes); P2 (heavy mitochondria, plasma membrane fragments plus material trapped by these membranes); P3 (mitochondria, lysosomes, peroxisomes, Golgi membranes, some rough endoplasmic reticulum); and P4 (microsomes from smooth and rough endoplasmic reticulum, Golgi and plasma membranes) (43); and (ii) immunogold electron microscopy. The DDX1-amplified RB522A cell line was used for both experiments. The fractionation procedures indicate that DDX1 is mainly in the nucleus and in the cytosol (S4 and S100 fractions) of RB522A cells (Fig. 9A). As a control, we used anti-human MYCN antibody to determine the location of MYCN (also amplified in RB522A) in our subcellular fractions. As shown in Fig. 9B, MYCN was primarily found in the nucleus, as one would expect of a transcription factor.

For the electron microscopy analysis, antiserum to the N terminus of DDX1 was coupled to protein A gold particles, and the distribution of DDX1 was examined in RB522A cells fixed in paraformaldehyde and glutaraldehyde. DDX1 was present in both the cytoplasm and nucleus (data not shown). There was no association with either cell organelles or with nuclear or plasma membranes.

DISCUSSION

There are presently few clues as to the function of DDX1 in normal and cancer cells. Our earlier data indicate that DDX1 mRNA is present at higher levels in fetal tissues of neural origin (retina and brain) compared with other fetal tissues (21).

There may therefore be a requirement for elevated levels of this putative RNA helicase for the efficient production or processing of neural specific transcripts. A role in cancer formation or progression is an intriguing possibility, because overexpression of an RNA unwinding protein could affect the secondary structure of RNAs in such a way as to alter the expression of specific proteins in tumor cells. DDX1 is co-amplified with MYCN in a subset of RB and NB cell lines and tumors (37–39). MYCN amplification is common in stage IV NB tumors and is a well documented indicator of poor prognosis. A general trend toward a poorer clinical prognosis is observed when both the MYCN and DDX1 genes are amplified compared with when only MYCN is amplified (38, 39), suggesting a possible role for DDX1 in NB tumor formation or progression.

It is generally accepted that co-amplified genes are not overexpressed unless they provide a selective growth advantage to the cell (48, 49). For example, although ERBB2 is closely linked to ERBB2 in breast cancer and both genes are commonly amplified in these tumors, ERBB2 is not overexpressed (48). Similarly, three genes mapping to 12q13–14 (CDK4, SAS, and MDM2) are overexpressed in a high percentage of malignant gliomas showing amplification of this chromosomal region, while other genes mapping to this region (GADD153, GLI, and A2MR) are rarely overexpressed in gene-amplified malignant gliomas (50, 51). The first three genes are probably the main targets of the amplification process, while the latter three genes are probably incidentally included in the amplicons. The data shown here indicate that DDX1 is overexpressed at both the protein and RNA levels in DDX1-amplified RB and NB cell lines and that there is a strong correlation between DDX1 gene copy number, DDX1 RNA levels, and DDX1 protein levels in these lines. Our results are therefore consistent with DDX1 overexpression playing a positive role in some aspect of NB and RB tumor formation or progression. Recently, Weiss *et al.* (52) have shown that transgenic mice that overexpress MYCN develop NB tumors several months after birth. They conclude that MYCN overexpression can contribute to the initiation of tumorigenesis but that additional events are required for tumor formation. Amplification of DDX1 may represent one of many alternative pathways by which a normal precursor “neuroblast” or “retinoblast” cell gains malignant properties.

The function of the majority of tissue-specific or developmentally regulated DEAD box genes remains unknown. However, some members of this protein family have been either directly or indirectly implicated in tumorigenesis. For example, the p68 gene has been found to be mutated in the ultraviolet light-induced murine tumor 8101 (53), while DDX6 (also known as RCK or p54) is encoded by a gene located at the breakpoint of the translocation involving chromosomes 11 and 14 in a cell line derived from a B-cell lymphoma (54, 55). Similarly, the production of a chimeric protein between DDX10 and the nucleoporin gene NUP98 has been proposed to be involved in the pathogenesis of a subset of myeloid malignancies with inv(11)(p15q22) (56). Interestingly, Grandori *et al.* (57) have shown that MYCC interacts with a DEAD box gene called MrDb, suggesting that the transcription of some DEAD box genes could be regulated through interaction with members of the MYC family. Future work will involve determining whether DDX1 represents another member of the DEAD box family with a role in the tumorigenic process.

DEAD box proteins have been implicated in translation initiation, RNA splicing, RNA degradation, and RNA stability (3, 18, 19). We carried out subcellular localization studies in an attempt to obtain a general indication of the function of DDX1. We found DDX1 protein in both the cytoplasm and nucleus of DDX1-amplified NB and RB lines. In contrast, DDX1 was

mainly located in the nucleus of nonamplified cell lines and normal fibroblast cultures. DDX1 was not associated with cellular organelles or with membranes based on immunoelectron microscopy. We therefore propose that the primary role of DDX1 is in the nucleus. The presence of DDX1 in the cytoplasm of DDX1-amplified cells may indicate that the amount of DDX1 protein that is allowed in the nucleus is tightly regulated. Alternatively, DDX1 may play a dual role in the nucleus and cytoplasm of DDX1-amplified cells.

An important component of our analysis was to identify the translation and transcription initiation sites of DDX1. We used a combination of techniques to identify the transcription start site: screening of RB and fetal brain libraries, RACE, primer extension, genomic DNA sequencing, S1 nuclease mapping, and Northern blot analysis using probes to the predicted 5'-end of the transcript. The transcription start site identified using these techniques is located ~300 nt upstream of the predicted translation initiation codon and was readily detected in three DDX1-amplified lines and barely detectable in a fourth amplified line. The 5'-untranslated region as well as the first in frame methionine are encoded within the first exon of DDX1. An in frame stop codon is located 123 nt upstream of the predicted initiation codon. We were unable to identify the transcription initiation site of DDX1 in two of the six amplified lines tested as well as in nonamplified lines. Although it remains possible that there are different transcription start sites in different cell lines, detection of lower levels (rather than the absence) of the 5'-most 160 nt of the DDX1 transcript in IMR-32, Y79, and LA-N-5 compared with RB522A, BE(2)-C, and LA-N-1 supports a quantitative rather than a qualitative difference in the 5'-end of this transcript in these cells. Our results suggest that the 5'-end of DDX1 mRNA is rarely intact, even in mRNA preparations that otherwise appear to be of high quality based on analysis of control transcripts. The 5'-end of DDX1 mRNA may therefore be especially susceptible to degradation, perhaps because of its sequence and/or secondary structure.

In conclusion, we have mapped the 5'-end of the 2.7-kb DDX1 transcript and have identified the predicted translation initiation site of DDX1 protein. We have found that DDX1-amplified RB and NB tumor lines overexpress DDX1 protein and that there is a good correlation between gene copy number and both transcript and protein levels in these cells. We have shown that DDX1 protein is primarily located in the nucleus of cells that are not DDX1-amplified. In contrast, DDX1 is present in both the nucleus and cytoplasm of DDX1-amplified NB and RB lines. A cytoplasmic location in DDX1-amplified lines may indicate that the amount of nuclear DDX1 is tightly regulated or that DDX1 plays a dual role in the cytoplasm and nucleus of these cells.

Acknowledgments—We thank Walter Dixon, Brenda Gallie, Ajay Pandita, Jeremy Squire, and Herman Yeger for the neuroblastoma and retinoblastoma cell lines. We thank Halyna Marusyk for carrying out the electron microscopy analyses. We are grateful to Randy Anderson for expert help in the preparation of the manuscript and to Stacey Hume for helpful discussions.

REFERENCES

- Linder, P., Lasko, P. F., Ashburner, M., Leroy, P., Nielsen, P. J., Nishi, K., Schnier, J., and Slonimski, P. P. (1989) *Nature* 337, 121–122.
- Wassarman, D. A., and Steitz, J. A. (1991) *Nature* 349, 463–464.
- Schmid, S. R., and Linder, P. (1992) *Mol. Microbiol.* 6, 283–292.
- Rozen, F., Edery, I., Meerovitch, K., Dever, T. E., Merrick, W. C., and Sonenberg, N. (1990) *Mol. Cell. Biol.* 10, 1134–1144.
- Hirling, H., Scheffner, M., Restle, T., and Stahl, H. (1989) *Nature* 339, 562–564.
- Liang, L., Diehl-Jones, W., and Lasko, P. (1994) *Development* 120, 1201–1211.
- Gururajan R., Mathews, L., Longo, F., and Weeks, D. L. (1994) *Proc. Natl. Acad. Sci. U. S. A.* 91, 2056–2060.
- Dalbadie-McFarland, G., and Abelson, J. (1990) *Proc. Natl. Acad. Sci. U. S. A.* 87, 4236–4240.
- Jamieson, D. J., Rahe, B., Pringle, J., and Beggs, J. D. (1991) *Nature* 349, 715–717.
- Strauss, E. J., and Guthrie, C. (1994) *Nucleic Acids Res.* 22, 3187–3193.
- Nishi, K., Morel-Deville, F., Hershey, J. W. B., Leighton, T., and Schnier, J. (1988) *Nature* 336, 496–498.
- Leroy, P., Alzari, P., Sassoon, D., Wolgemuth, D., and Fellous, M. (1989) *Cell* 57, 549–559.
- Hay, B., Jan, L. Y., and Jan, Y. N. (1988) *Cell* 55, 577–587.
- De Valoir, T., Tucker, M., Belikoff, E. J., Camp, L. A. Bolduc, C., and Beckingham, K. (1991) *Proc. Natl. Acad. Sci. U. S. A.* 88, 2113–2117.
- Ford, M. J., Anton, I. A., and Lane, D. P. (1988) *Nature* 332, 736–738.
- Iggo, R. D., and Lane, D. P. (1989) *EMBO J.* 8, 1827–1831.
- Buelt, M. K., Glidden, B. J., and Storm, D. R. (1994) *J. Biol. Chem.* 269, 29367–29370.
- lost, I., and Dreyfuss, M. (1994) *Nature* 372, 193–196.
- Py, B., Higgins, C. F., Krisch, H. M., and Carpousis, A. J. (1996) *Nature* 381, 169–172.
- Missel, A., Souza, A. E., Nörskau, G., and Göringer, H. U. (1997) *Mol. Cell. Biol.* 17, 4895–4903.
- Godbout, R., and Squire, J. (1993) *Proc. Natl. Acad. Sci. U. S. A.* 90, 7578–7582.
- Kiledjian, M., and Dreyfuss, G. (1992) *EMBO J.* 11, 2655–2664.
- Godbout, R., Hale, M., and Bisgrove, D. (1994) *Gene (Amst.)* 138, 243–245.
- Blackwood, E. M., and Eisenman, R. N. (1991) *Science* 251, 1211–1217.
- Amati, B., Dalton, S., Brooks, M. W., Littlewood, T. D., Evan, G. I., and Land, H. (1992) *Nature* 359, 423–426.
- Brodeur, G. M., Seeger, R. C., Schwab, M., Varmus, H. E., and Bishop, J. M. (1984) *Science* 224, 1121–1124.
- Seeger, R. C., Brodeur, G. M., Sather, H., Dalton, A., Siegel, S. E., Wong, K. Y., and Hammond, D. (1985) *N. Engl. J. Med.* 313, 1111–1116.
- Cohn, S. L., Salwen, H., Quasney, M. W., Ikegaki, N., Cowan, J. M., Herst, C. V., Sharon, B., Kennett, R. H., and Rosen, S. T. (1991) *Prog. Clin. Biol. Res.* 366, 21–27.
- Cowell, J. K. (1982) *Annu. Rev. Genet.* 16, 21–59.
- Zehnbaue, B. A., Small, D., Brodeur, G. M., Seeger, R., and Vogelstein, B. (1988) *Mol. Cell. Biol.* 8, 522–530.
- Akiyama, K., and Nishi, Y. (1991) *Nucleic Acids Res.* 19, 6887–6894.
- Schneider, S. S., Hiemstra, J. L., Zehnbaue, B. A., Taillon-Miller, P., Le Paslier, D., Vogelstein, B., and Brodeur, G. M. (1992) *Mol. Cell. Biol.* 12, 5563–5570.
- Amler, L. C., Schürmann, J., and Schwab, M. (1996) *Genes Chromosomes Cancer* 15, 134–137.
- Kuroda, H., White, P. S., Sulman, E. P., Manohar, C., Reiter, J. L., Cohn, S. L., and Brodeur, G. M. (1996) *Oncogene* 13, 1561–1565.
- Noguchi, Y., Akiyama, K., Yokoyama, M., Kanda, N., Matsunaga, T., and Nishi, Y. (1996) *Genes Chromosomes Cancer* 15, 129–133.
- Pandita, A., Godbout, R., Zielenska, M., Thorner, P., Bayani, J., and Squire, J. A. (1997) *Genes Chromosomes Cancer* 20, 243–252.
- Manohar, C. F., Salwen, H. R., Brodeur, G. M., and Cohn, S. L. (1995) *Genes Chromosomes Cancer* 14, 196–203.
- Squire, J. A., Thorner, P. S., Weitzman, S., Maggi, J. D., Dirks, P., Doyle, J., Hale, M., and Godbout, R. (1995) *Oncogene* 10, 1417–1422.
- George, R. E., Kenyon, R. M., McGuckin, A. G., Malcolm, A. J., Pearson, A. D. J., and Lunec, J. (1996) *Oncogene* 12, 1583–1587.
- Reiter, J. L., and Brodeur, G. M. (1996) *Genomics* 32, 97–103.
- Favaloro, J., Treisman, R., and Kamen, R. (1980) *Methods Enzymol.* 65, 718–745.
- Dignam, J. D. (1990) *Methods Enzymol.* 182, 194–203.
- Graham, J. (1984) in *Centrifugation: A Practical Approach* (Rickwood, D. ed.) 2nd Ed., pp. 161–182, IRL Press, Oxford.
- Godbout, R., Marusyk, H., Bisgrove, D., Dabbagh, L., and Poppema, S. (1995) *Exp. Eye Res.* 60, 645–657.
- Miller, K. G., and Sollner-Webb, B. (1981) *Cell* 27, 165–174.
- Kozak, M. (1988) *Nucleic Acids Res.* 15, 8125–8132.
- Rafti, F., Scarvelis, D., and Lasko, P. F. (1996) *Gene (Amst.)* 171, 225–229.
- Van de Vijver, M., van de Bersselaar, R., Devilee, P., Cornelisse, C., Peterse, J., and Nusse, R. (1987) *Mol. Cell. Biol.* 7, 2019–2023.
- Gaudray, P., Szegetowski, P., Escot, C., Birnbaum, D., and Theillet, C. (1992) *Mutat. Res.* 276, 317–328.
- Forus, A., Florence, V. A., Maelandsmo, G. M., Meltzer, P. S., Fodstad, O., and Myklebost, O. (1993) *Cell Growth Differ.* 4, 1065–1070.
- Reifenberger, G., Reifenberger, J., Ichimura, K., Meltzer, P. S., and Collins, V. P. (1994) *Cancer Res.* 54, 4299–4303.
- Weiss, W. A., Aldape, K., Mohapatra, G., Feuerstein, B. G., and Bishop, J. M. (1997) *EMBO J.* 16, 2985–2995.
- Dubey, B. P., Hendrickson, R. C., Meredith, S. C., Siegel, C. T., Shabanowitz, J., Skipper, J. C. A., Engelhard, V. H., Hunt, D. F., and Schreiber, H. (1997) *J. Exp. Med.* 185, 695–705.
- Akao, Y., Seto, M., Yamamoto, K., Iida, S., Nakazawa, S., Inazawa, J., Abe, T., Takahashi, T., and Ueda, R. (1992) *Cancer Res.* 52, 6083–6087.
- Lu, D., and Yunis, J. J. (1992) *Nucleic Acids Res.* 20, 1967–1972.
- Arai, Y., Hosoda, F., Kobayashi, H., Arai, K., Hayashi, Y., Kamada, N., Kaneko, Y., and Ohki, M. (1997) *Blood* 89, 3936–3944.
- Grandori, C., Mac, J., Siebelt, F., Ayer, D. E., and Eisenman, R. N. (1996) *EMBO J.* 15, 4344–4357.

Modulation of gap junction mediated intercellular communication in TM3 Leydig cells

R C S Goldenberg¹, F S A Fortes¹, J M Cristancho^{1,3},
M M Morales¹, C R Franci², W A Varanda²
and A C Campos de Carvalho¹

¹Institute of Biophysics Carlos Chagas Filho, UFRJ, Brazil

²Department of Physiology, Faculty of Medicine of Ribeirão Preto, USP, Av. Bandeirantes, 3900 14049-900 Ribeirão Preto, Brazil

³Surcolombian University, Neiva, Colombia

(Requests for offprints should be addressed to A C C de Carvalho, Instituto de Biofísica Carlos Chagas Filho, Universidade Federal do Rio de Janeiro, Av. Brigadeiro Trompowsky s/n, Cidade Universitária, Ilha do Fundão, Rio de Janeiro RJ 21941-900, Brasil; Email: acarlos@biof.ufrj.br)

Abstract

Long-term modulation of intercellular communication via gap junctions was investigated in TM3 Leydig cells, under low and high confluence states, and upon treatment of the cells for different times with activators of protein kinase A (PKA) and protein kinase C (PKC). Cells in low confluence were readily coupled, as determined by transfer of the dye Lucifer Yellow; on reaching confluence, the cells uncoupled. Western blots and RT-PCR revealed that connexin 43 (Cx43) was abundantly expressed in TM3 Leydig cells and its expression was decreased after the cells achieved confluence. Stimulation of PKA or PKC induced a decrease in cell-cell communication. Staurosporin, an inhibitor of protein kinases, increased coupling and was able to prevent and reverse the uncoupling actions of dibutyryl cAMP and 12-O-tetradecanoyl-phorbol-13-

acetate (TPA). Under modulation by confluence, Cx43 was localized to the appositional membranes when cells were coupled and was mainly in the cytoplasm when they were uncoupled. In addition, cAMP and TPA reduced the surface membrane labeling for Cx43, whereas staurosporin increased it. These data show a strong correlation between functional coupling and the membrane distribution of Cx43, implying that this connexin has an important role in intercellular communication between TM3 cells. Furthermore, increased testosterone secretion in response to luteinizing hormone was accompanied by a decrease in intercellular communication, suggesting that gap junction mediated coupling may be a modulator of hormone secretion in TM3 cells.

Journal of Endocrinology (2003) 177, 327–335

Introduction

Gap junctions are plasma membrane specializations responsible for the transfer of small molecules (up to ~1 kDa) and ions between adjoining cells (Bennett *et al.* 1991). Gap junction mediated intercellular communication has been implicated in fundamental cellular processes such as embryonic development, cell differentiation, proliferation and growth control. The proteins forming gap junctions, named connexins, are phosphoproteins (with the exception of connexin 26 (Cx26)) that can be phosphorylated by protein kinases activated by neurotransmitters, growth factors, hormones, oncogenes and exogenous chemicals. In particular, activation of protein kinases A and C is known to modulate junctional communication between cells. PKC has been shown to phosphorylate Cx43 in serine and threonine residues of the carboxyl tail of the protein (Moreno *et al.* 1994, Oh *et al.* 1991), but to date the phosphorylation of Cx43 by PKA has not been

unequivocally shown. Nevertheless, 12-O-tetradecanoyl-phorbol-13-acetate (TPA) and cAMP have been found to induce a variety of effects in cells expressing Cx43, leading both to inhibition and to enhancement of gap junction communication, depending on cell type and developmental stage (Oh *et al.* 1991, Risley *et al.* 1992, Xie & Hu 1992, Hünster & Weingant 1993, Lampe 1994).

In the testis, cellular interactions are essential for adequate functioning of many different cell types (Skinner 1982) and, to date, 11 types of connexin have been identified in its constituent cells (Kadle *et al.* 1991, Haefliger *et al.* 1992, Risley *et al.* 1992, Risley 2000). Freshly dissociated Leydig cells show both electrical and metabolic coupling, and Cx43 has been reported as the main functional component of their gap junctions (Pérez-Armendariz *et al.* 1994, Varanda & Campos de Carvalho 1994). Although electrical characteristics of the gap junction in these cells have been well characterized, modulation processes have not yet been extensively

studied. Given that gap junction communication has been shown to modulate secretion in endocrine and exocrine organs (Rüegg & Burgess 1989, Granot & Dekel 1994, You *et al.* 2000), it is important to study the regulation of junctional communication in TM3 Leydig cells. The main purpose of the present study was to examine the extent to which coupling between these cells can be influenced by PKA and PKC, and to correlate this modulation of coupling to the expression of Cx43 and the secretion of testosterone.

Materials and Methods

Cell culture

TM3 Leydig cells, a non-tumorigenic cell line derived from mouse testis, were obtained from the American Type Culture Collection. We decided to use this cell line in our studies because they respond to luteinizing hormone (LH) by increasing testosterone production and secretion, through mechanisms similar to those encountered in freshly isolated cells. The cells were grown in a mixture of Ham's F-12 medium plus Dulbecco's Modified Eagle Medium (1:1 v:v), supplemented with 5 mM NaHCO₃, 15 mM *N*-[2-hydroxyethyl] piperazine-*N'*-[2-ethane sulfonic acid], 7.5–10% fetal bovine serum and 1% penicillin/streptomycin, pH 7.4. Serum concentration (7.5 or 10%) did not affect cell properties. Cells were plated at either low or high density, depending on the type of experiment intended, for at least 12 h before the experiment, and then treated with a specific drug for times ranging from 15 min to 12 h. For subconfluent cultures, the cells were plated at approximately 200 cells/mm². For confluent cultures, the cells were plated at 400 cells/mm². At the time of the experiments, the low-density cultures had 320 cells/mm² and high-density cultures had 650 cells/mm². The cells were always cultured in the presence of fetal bovine serum and kept in an atmosphere of 5% CO₂ and 95% O₂ at 37 °C in an incubator (Forma Scientific).

Dye transfer

TM3 cells in low- or high-confluence cultures were plated in plastic dishes and injected with Lucifer Yellow CH (5% in 150 mM LiCl without pH adjustment), with the aid of glass microelectrodes (resistance between 40 and 70 MΩ) by application of short hyperpolarizing current pulses (0.1 nA, 100 ms), using a WPI amplifier model 7060. Dye transfer was observed in a Nikon Diaphot inverted microscope, equipped with xenon arc illumination, and photographs were taken using Kodak TMAX400 film, 2 min after injection of dye into one cell (Srivinas *et al.* 1999). For measurement of modulation of coupling by pharmacological agents, a minimum of 90 cells were injected for

every time point in each of at least three independent experiments; values were plotted as a function of time after drug application. The percent of coupled cells was evaluated as the number of injections that resulted in the transfer of Lucifer Yellow to neighboring cell(s), in relation to the total number of injections in a given assay. Results are presented as means ± S.E.M.

Immunofluorescence and Western blots

Cultured TM3 cells were plated in high or low confluence on 25 cm² plastic culture flasks or glass coverslips, previously treated with poly-L-lysine, for Western blot and immunofluorescence respectively. Cells were kept in culture for at least 12 h before experimental maneuvers. For western blots, the TM3 cells were treated with dibutyryl (db)-cAMP or TPA for 12 h. Staurosporin was used in TM3 cells after the 12 h treatment with PKA and PKC activators, and cells were incubated for 1 h with staurosporin. Homogenates from sister cultures (control and treated) were obtained by scraping 25 cm² flasks in 1 mM NaHCO₃ (pH 8.3) containing 1 mM of the protease inhibitor phenylmethylsulfonyl fluoride (PMSF), and were centrifuged at 10 000 r.p.m. for 10 min. Total protein content was determined by the Bradford method (Bradford 1976) and 100 µg samples were loaded in each lane of a 10% SDS-PAGE system. Protein was then transferred to nitrocellulose and the membrane was incubated with polyclonal antibody to residues 346–360 of the Cx43 sequence (kindly provided by Dr E L Hertzberg, Albert Einstein College of Medicine, New York, USA), as previously described (Varanda & Campos de Carvalho 1994). Heart homogenate was used as positive control and densitometry was performed using the gel analysis software Sigma Gel (v1.1, Jandel Scientific, Chicago, IL, USA). Results are presented as means ± S.E.M.

For immunofluorescence, the cells were treated with db-cAMP, TPA or staurosporin for the same time intervals described above and then fixed in ethanol (70%) at –20 °C for 20 min. Cx43 was detected as described previously for other cell types (Dermietzel *et al.* 1991). In short, cells were incubated, for 30 min at room temperature, with 0.1% IgG-free bovine serum albumin (BSA) to reduce non-specific binding. This was followed by incubation with the polyclonal antibody for Cx43, described above, diluted 1/500, for 1 h at room temperature. Then the cells were washed four times, for 10 min each time, with phosphate-buffered saline (PBS) and incubated with the secondary antibody (goat anti-rabbit IgG conjugated with fluorescein isothiocyanate diluted 1/150), for 1 h at room temperature. The coverslips were then washed with PBS four times, for 10 min each time, and mounted with 10 µl of a solution containing *P*-phenylenediamine + glycerol + PBS in the proportions 29:9:1. Fluorescence was observed on a Zeiss Axiovert 100 microscope. Because of the repeated washes and poor adherence of TM3

cells to the coverslips, it was common to lose cells during processing for immunofluorescence.

Radioimmunoassay

Leydig cells were cultured in 75 cm² flasks and subjected to treatment with LH (LH-RP3 No. AFP7187B; National Institute of Diabetes, Digestive and Kidney Diseases, USA) for the indicated times. Testosterone concentration was assayed in the incubation media by radioimmunoassay. Cells in five different incubation bottles were treated with either 1 or 10 ng/ml LH. The results are normalized for 10⁶ cells (number of cells determined by counting in Neubauer chamber) and the initial value (zero time) was taken as the concentration of testosterone detected in the incubation medium (DMEM+10% FCS) without cells. ³H-Testosterone was obtained from NEN Life Science Products and the specific antibody was a generous gift from Dr José Antunes Rodrigues (Department of Physiology, Faculty of Medicine of Ribeirão Preto, University of São Paulo, Brazil). The lower limit of detection of the assay was 0.3 ng/ml sample and the intra-assay coefficient of variation was 5.4%.

Isolation of total RNA

Total RNA from all subconfluent or confluent cells and rat heart tissue was extracted by Trizol reagent (Gibco BRL, Grand Island, NY, USA). RNase-free DNase I (1 U/μl) was used to treat the isolated RNA for 1 h, to eliminate contamination with genomic DNA. The treatment was terminated by extraction with phenol–chloroform–isoamyl alcohol (PCI) in the proportions 25:24:1 (vol/vol) and precipitation with ethanol.

Reverse transcriptase-polymerase chain reaction

In order to prepare first-strand DNA, total RNA isolated from TM3 Leydig cells (*n* = 3–4) and rat heart cells was reverse-transcribed with SuperScript (Gibco BRL) at 37 °C for 60 min, extracted with PCI and precipitated with ethanol. The cDNA synthesis was primed with oligo-dT primer. A PCR technique was used to amplify the synthesized cDNA. The following solution was used: 0.2 μmol/l primers, 0.2 mmol/l each dNTP, 50 mmol/l KCl, 10 mmol/l Tris HCl (pH 8.3) and 1.5 mmol/l MgCl₂ plus 2.5 U AmpliTaq (Perkin Elmer, New Jersey, NJ, USA). The primers synthesized for Cx43 (sense: 5'-ATGAGCAGTCTGCCTTTCGT-3'; antisense: 5'-CACCACCAGCATGAAGATGA-3') correspond to nucleotides 346–366 and 2076–2093 respectively of the rat Cx43 sequence (GeneBank accession number: XM 027460) and are predicted to amplify a 459 bp PCR product. PCR was performed with 34 cycles of denaturation (94 °C, 1 min), annealing (55 °C, 1 min) and extension (72 °C, 1 min). Rat glyceraldehyde-3-phosphate

dehydrogenase (GAPDH) primers predicted to amplify a 221 bp PCR product (sense: 5'-GTCTTCACCACCAT GGAG-3'; antisense: 5'-CGATGCCAAAGTTGTCA TG-3') corresponding respectively to nucleotides 326–343 and 518–536 of the rat *GAPDH* gene were added into the same RT-PCR reaction tubes and their products were used as internal controls (GeneBank accession number: M17701). PCR products were size-fractionated by agarose gel electrophoresis. The expected Cx43 and GAPDH bands from the same sample were submitted to a densitometry analysis using the gel analysis software Sigma Gel (v1.1, Jandel Scientific) and normalized by dividing the Cx43 values by the corresponding GAPDH values.

The semi-quantitative method of RT-PCR used for studies of expression of Cx43 mRNA in TM3 Leydig cells was validated in preliminary experiments. Firstly, the optimal PCR conditions that yielded a single band on agarose gel electrophoresis were determined for Cx43 and *GAPDH* genes in the same reaction tube. Secondly, to determine whether the method was semi-quantitative, serial quantities of total RNA (62.5, 125, 250, 500, 1000 and 2000 ng) extracted from TM3 cells were used for RT-PCR amplification for Cx43 and *GAPDH* genes in the same reaction tube. Thirdly, experiments were performed to determine the optimal number of PCR cycles that yielded PCR products in the linear phase of amplification of both genes in the same reaction. Finally, to ensure that the reactions were consistent, PCR reactions were performed at least twice. Only one of these reactions was included for final densitometry analysis, and the selection was arbitrary. For the semi-quantitative PCR comparing the confluent and subconfluent cells and the drug treatments, the optimal total amount of RNA was 500 ng and the optimal number of PCR cycles was 34. All reactions included a negative control RT(–). The identity of the amplification was confirmed by determination of the molecular size on agarose gel electrophoresis with a 100 bp DNA molecular marker (Gibco BRL). Results are presented as means ± S.E.M.

Statistical analysis

One-way analysis of variance followed by the Newman–Keuls multiple comparison test was used for data presented in Figs 2, 3 and 6. For data given in Fig. 1 we used the χ^2 test, and for those in Figs 4, 5, 8 and 9 we performed Student's non-paired *t*-test. In all cases, statistical significance was considered to be present at *P* < 0.05.

Results

When examined at high density in confluent cultures, TM3 Leydig cells showed a poor degree of dye coupling (Fig. 1A, B) demonstrated by the low proportion of injections that resulted in the spread of Lucifer Yellow

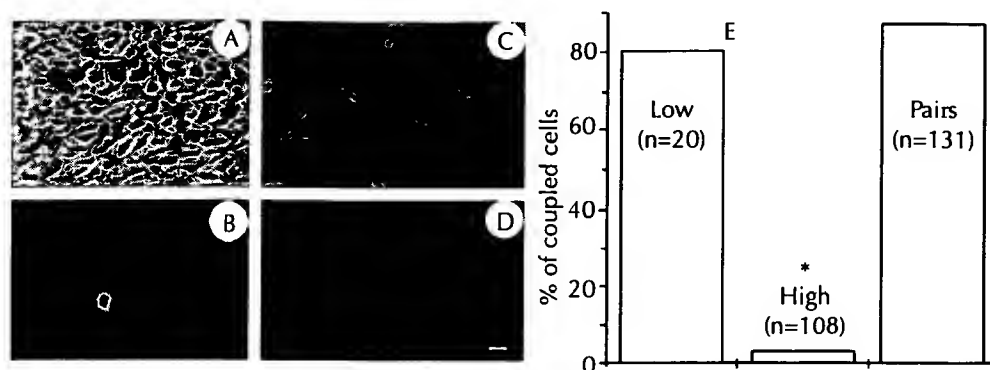


Figure 1 Gap junction coupling between TM3 Leydig cells. (A) Phase and (B) fluorescence pictures of cells cultured under high confluence; (C) phase and (D) fluorescence pictures of cells forming pairs in a low-confluence culture. In (B) and (D) Lucifer Yellow was injected in one cell and pictures taken 2 min later. (E) Histogram of the percentage of coupled cells in each condition. Low, low-confluence cultures; High, high-confluence cultures; Pairs, cells in low confluence forming pairs; n, number of cells that were injected with Lucifer Yellow in each condition. Calibration bar in (D) represents 20 μ m.

between the cells (3% ($n=108$), histogram in Fig. 1). In contrast, when cultured at low density as subconfluent cultures, the cells showed a high degree of coupling, with 80% of the injected cells ($n=20$) showing transfer of the dye. This number is very similar to that observed in cell pairs (Fig. 1C, D) in which 87% of the pairs were coupled ($n=131$, histogram in Fig. 1), and is in agreement with previous reports based on electrophysiological measurements (Pérez-Armendariz *et al.* 1994, Varanda & Campos de Carvalho 1994, Cristancho *et al.* 2000).

Western blots revealed the presence of Cx43 in TM3 cells. Figure 2 illustrates an experiment in which Cx43 was detected in subconfluent and confluent sister cultures. Densitometry shows that the labeling was more intense for subconfluent (lane 1) than for confluent (lane 2) cultures, indicating that the expression of this protein is modulated by contact between the cells.

The results of semi-quantitative RT-PCR using Cx43-specific oligonucleotides and RNA extracted from Leydig cells in confluent and subconfluent cultures are shown in Fig. 3. Expression of Cx43 mRNA was reduced in confluent cultures (to 47.5% of subconfluent culture values, $P<0.05$), in agreement with the diminished expression of protein.

It is widely accepted that db-cAMP and TPA activate PKA and PKC respectively (Berridge 1984). PKA activation generally leads to increased intercellular communication, but PKC activation usually has the opposite effect. Figure 4A shows the effect of PKA activation on gap junction intercellular communication 1, 6 and 12 h after a single addition of db-cAMP (0.5 mM) to the culture medium. Figure 4B illustrates similar experiments using TPA (50 nM) to activate PKC. Both cAMP and TPA greatly reduced gap junction intercellular communication in subconfluent TM3 cell cultures. A significant reduction was already apparent in the first 1 h after addition of the

drugs to the medium (>80% of the cells uncoupled), and this was maintained after 12 h of a single drug application.

Staurosporin, an inhibitor of protein kinases, is able to couple TM3 cells in confluent cultures and to reverse the uncoupling effects of both TPA and c-AMP in subconfluent cultures. Figure 5 illustrates a typical experiment in which cells in a subconfluent culture were injected with

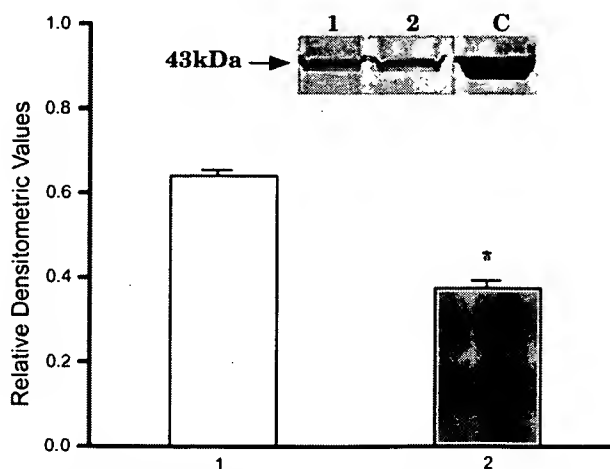


Figure 2 Western blot for Cx43. Lanes 1 and 2: homogenates of TM3 Leydig cells cultured under low and high confluence, respectively. Lane C: a rat heart homogenate used as positive control for Cx43. Each lane of the gel was loaded with 100 μ g total protein before transfer to nitrocellulose. The band for cells in low confluence was more intensely marked than that for high-confluence cells. As the amount of protein loaded in the gel was the same, this difference can be used as a semi-quantitative estimate of Cx43 expression. The histogram represents the mean \pm S.E.M. ($n=3$) of the relative densitometry values for Cx43 labeling, taking the rat heart homogenate as control. *Protein expression in confluent cultures was significantly different from that in subconfluent ones ($P<0.05$).

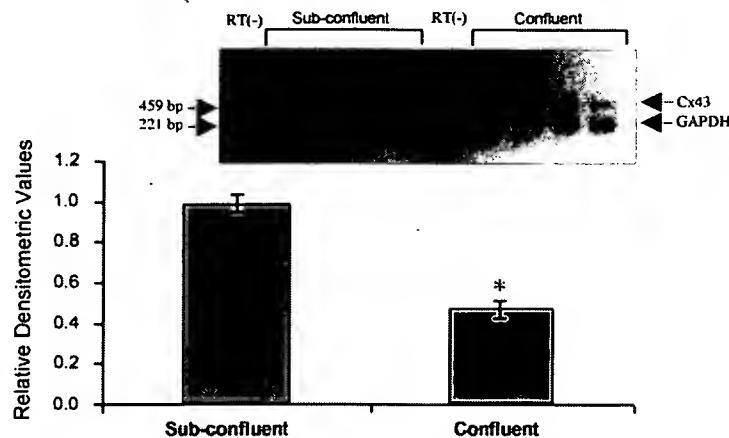


Figure 3 Relative expression of Cx43 in total RNA isolated from subconfluent and confluent TM3 Leydig cells: results obtained by amplifying Cx43 and GAPDH-RT-PCR products. The histogram represents the mean \pm S.E.M. for the ratio between the Cx43 and GAPDH bands ($n=4$). The insert shows the agarose gel of a semi-quantitative RT-PCR experiment. RT(-), negative control, performed with 500 ng total RNA derived from subconfluent cells in the absence of reverse transcriptase. *Expression of mRNA in confluent cultures was significantly different from that in subconfluent cultures ($P<0.05$).

Lucifer Yellow, db-cAMP (500 μ M) was added for 1 h and dye coupling was again measured, and then 1 mM staurosporin was added, in the presence of db-cAMP, for 30 min and coupling was assayed once more. The histogram shows that staurosporin restored gap junction intercellular communication to the control condition even in the presence of db-cAMP. Similar results were obtained when cells were treated first with TPA and then with staurosporin (not shown).

Interestingly, total expression of the Cx43 protein in TM3 Leydig cells treated with cAMP, TPA and staurosporin was not altered in relation to control (Fig. 6A). Accordingly, semi-quantitative RT-PCR using total RNA from the same treated cells showed that Cx43 mRNA was not altered in relation to that in control cultures (Fig. 6B).

Indirect immunofluorescence was used to evaluate whether the cellular localization of Cx43 was directly

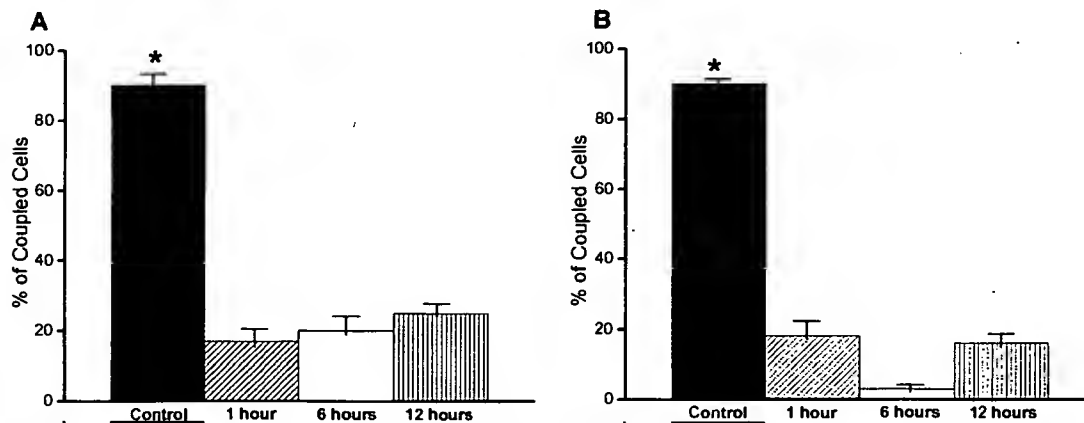


Figure 4 Junctional coupling in TM3 Leydig cells was decreased by cAMP (A) or TPA (B). The drugs were added to subconfluent cultures at a concentration of 500 μ M for cAMP or 50 nM for TPA, for 1, 6 and 12 h. Control, no drug added. The degree of coupling was assessed by injecting Lucifer Yellow in one cell of a group and counting the number of cells labeled after 2 min. A total of 720 cells was injected in three different culture dishes for each group (control, 1 h, 6 h and 12 h). For each experiment, the percentage of coupled cells (number of injected cells that passed dye to neighbors/total number of injected cells) was determined and means \pm S.D. were plotted for each experimental condition. *Coupling in the control was significantly greater than that in any of the treated cultures ($P<0.05$).

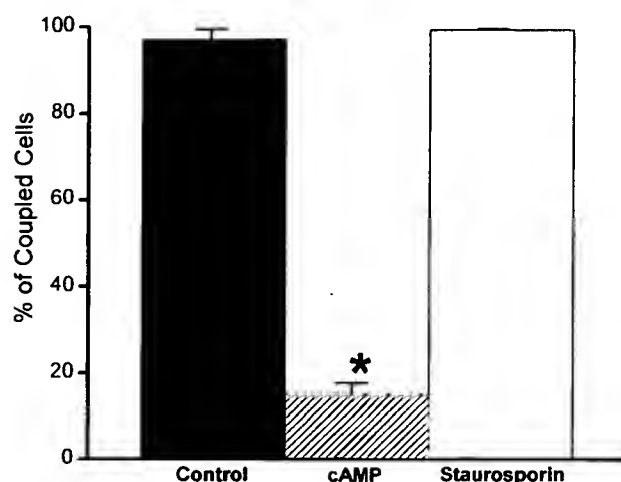


Figure 5 Staurosporin reversed the uncoupling effect of cAMP. At least 30 cells were injected with Lucifer Yellow in each of these subconfluent-culture dishes. The percentage of coupled cells in each dish was determined and means \pm s.d. were plotted (number of cells injected in each condition was 90). Control coupling was determined 12 h after plating (black bar); cAMP (500 μ M) was applied to the same cultures for 1 h and coupling was again determined (cross-hatched bar). Staurosporin (1 mM) was then added in the presence of cAMP, restoring the degree of coupling to control values (open bar). *Coupling during cAMP treatment was significantly lower than that in the two other groups ($P < 0.05$).

related to coupling in cells at low and high confluence. In low-confluence cultures and in pairs of TM3 Leydig cells, immunoreactivity for Cx43 was detected at appositional membranes, in addition to diffusely in the cytoplasm (Fig. 7A). In high-confluence cultures, TM3 Leydig cell immunoreactivity was detected mainly as points dispersed in the cytosol, with no detectable labeling in appositional membrane regions (not shown). In agreement with the findings of the dye-coupling experiments, when subconfluent cultures or cell pairs were treated with 500 μ M db-cAMP (Fig. 7B) or 50 nM TPA (Fig. 7C) for 1 h, they showed labeling over the cytosol and the perinuclear region, with disappearance of the appositional labeling (compare Figs 7A, 7B and 7C). In contrast, confluent cells treated with 1 mM staurosporin for 1 h showed intense reactivity at the appositional membranes (Fig. 7D). Incubation with secondary antibody alone did not label the cells (not shown).

To investigate the effects of a physiological modulator of Leydig cells, we exposed TM3 subconfluent cultures to LH and measured hormone secretion and gap junction intercellular communication in the cultures. When testosterone secretion by the TM3 cells in subconfluent cultures was determined during a 12 h period, control values were within the ranges reported in the literature (Pérez-Armendariz *et al.* 1996). Upon exposure of the cells to LH (1 or 10 ng/ml), testosterone secretion increased during the first hour and then was maintained at high levels

during the 12 h period (Fig. 8). Figure 9 shows that, 15 min and 1 h after application to TM3 Leydig cells, LH in concentrations of 1 and 10 ng/ml significantly reduced gap junction intercellular communication and that, 3 h after exposure of the cells to LH, coupling was totally abolished. These results were to be expected, because LH acts by increasing adenyl cyclase activity in these cells, resulting in activation of PKA.

Discussion

In this study we have shown that TM3 Leydig cells are coupled through intercellular gap junctions in a manner similar to that described for freshly dissociated Leydig cells from mouse testis (Pérez-Armendariz *et al.* 1994, 1996, Varanda & Campos de Carvalho 1994). We have also shown that the junctional communication between TM3 cells is modulated by cell density, as coupling in cells under high confluence was lower than that observed under low confluence or in cell pairs.

Cx43 has an important role in gap junction communication in TM3 Leydig cells, based on the correlation between modulation of cell-cell coupling and the expression of Cx43 at appositional membranes shown in this study. Previous experiments in which we showed that junctional conductance properties in TM3 cells were similar to those obtained in communication-deficient cell lines transfected with Cx43 cDNA reinforce this idea. To date, 11 different connexins have been reported to be present in the testis, communicating between the different cell types that constitute this organ (Kadle *et al.* 1991, Haefliger *et al.* 1992, Risley *et al.* 1992, Risley 2000). Preliminary experiments using RT-PCR in TM3 Leydig cells have identified six connexin transcripts, of which connexins 31, 37, 40, 43, 45 and 50 have been described in testis (Risley 2000). Whether or not all these connexins contribute to functional coupling between TM3 cells remains to be investigated.

Our experiments show that, in TM3 Leydig cells, db-cAMP and TPA drastically reduce junctional coupling 1 h after application. A rapid decrease (in minutes) in electrical coupling has been reported (Cristancho *et al.* 2000) after activation of PKA and PKC, indicating that these protein kinases act to reduce intercellular communication by both short- and long-term mechanisms in TM3 cells. These findings are consistent with the hypothesis that their activation may induce effects directly on the channel – with respect to the fast reduction in junctional conductance – and may also interfere with the assembly, degradation, or both, of channel protein. In agreement with that, a 12 h exposure to cAMP or TPA induced disappearance of Cx43 membrane reactivity, restricting it to the cytoplasm of cells in subconfluent cultures, whereas total Cx43 protein concentrations and message levels were unaltered by these treatments.

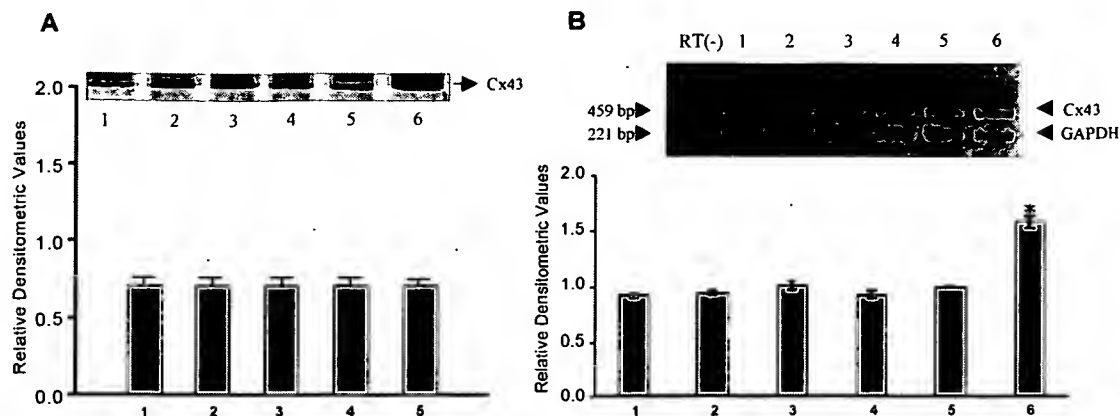


Figure 6 cAMP, TPA and staurosporin did not affect the expression of Cx43 protein (A) or mRNA (B). (A and B) Lanes 1–4: homogenates of TM3 subconfluent Leydig cell cultures treated with TPA+staurosporin, cAMP+staurosporin, TPA, and cAMP respectively; lane 5: control TM3 subconfluent culture (not treated); lane 6: a rat heart homogenate used as a positive control for Cx43. (A) Each lane of the gel was loaded with 100 µg total protein before transfer to nitrocellulose. The histogram represents relative densitometry values for Cx43 labeling, taking the rat heart homogenate as control ($n=3$). Expression of Cx43 was not altered by any of the treatments. (B) Relative expression of Cx43 mRNA in subconfluent TM3 Leydig cells, obtained by amplified Cx43 and GAPDH RT-PCR products. The histogram represents the mean \pm S.E.M. values for the ratio between the Cx43 and GAPDH bands ($n=3$). The insert shows the agarose gel of a semi-quantitative RT-PCR experiment. RT(–), negative control, performed with 500 µg total RNA derived from subconfluent cells in the absence of reverse transcriptase. *Expression of mRNA in rat heart tissue was significantly different from treated and un-treated subconfluent TM3 cells ($P<0.05$). There were no significant differences between all groups of TM3 cells.

The results reported here for db-cAMP are the opposite of what has been found in the majority of other cell types, in which cAMP enhances coupling in spite of the fact that it decreases single channel conductance (Kwak *et al.* 1995, Moreno *et al.* 1994). Nonetheless, Sacai *et al.* (1992) and Cole & Garfield (1986) reported cAMP-dependent reduction of coupling in myometrial cells and argued that their results were dependent on the stage of maturation of the cell. In addition, in immature rat prefrontal cortex, both cAMP and β -adrenoceptor activation reduced gap junctional coupling, as demonstrated by a decline in transfer of dye between cells (Rorig *et al.* 1995).

In contrast, our results with TPA are in agreement with most of those reported in the literature, in which a reduction in junctional conductance has been clearly seen in preparations in which Cx43 seems to be the main gap junction forming protein (Yada *et al.* 1985, De Mello 1991, Giaume *et al.* 1991, Spray *et al.* 1991). Nonetheless, exceptions have been observed: an increase in coupling after treatment with TPA has been reported in Sertoli cells (Grassi *et al.* 1986) and in corpus cavernosum smooth muscle cells (Moreno *et al.* 1993).

It should be pointed out that the data obtained with dye coupling, western blot, immunofluorescence and semi-quantitative RT-PCR in the TM3 cells were consistent. Immunofluorescence showed that the TM3 cells displayed Cx43 reactivity localized to the appositional membranes when in pairs or in low confluence, compatible with the high degree of dye coupling measured under these

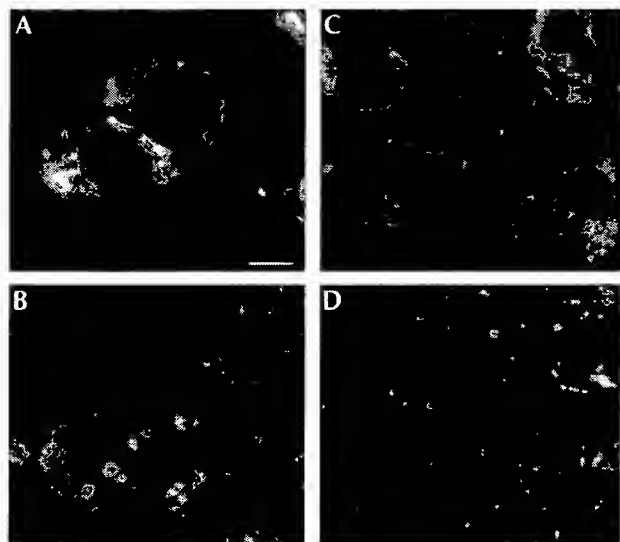


Figure 7 Indirect immunofluorescence for Cx43. (A) Cells forming pairs showed immunoreactivity mainly localized to the appositional membranes, where the gap junction plaques are localized. (B) Treatment of cells in low confluence with 500 µM db-cAMP displaced the immunoreactivity from the appositional membranes and dispersed it in the cytoplasm. (C) Immunoreactivity of cells in low confluence treated with 50 nM TPA. Labeling was diffuse in the cytoplasm, but there was no appositional membrane labeling. (D) Intense membrane labeling in high-confluence cultures treated with 1 mM staurosporin for 1 h. Calibration bar represents 5 µm for (A), (B) and (C), and 10 µm for (D).

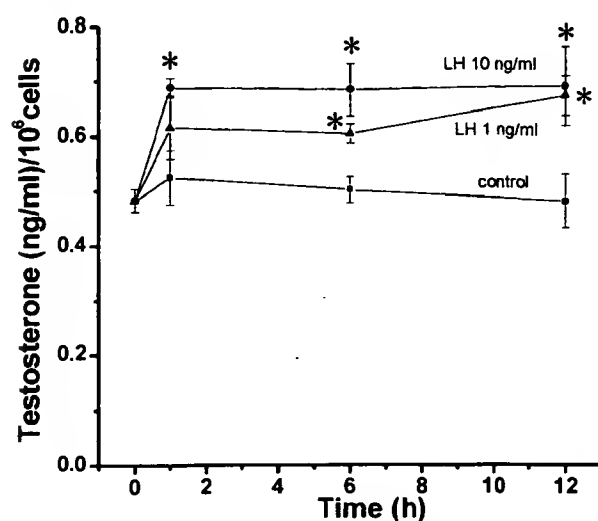


Figure 8 LH-induced testosterone secretion in TM3 Leydig cells. Cells were incubated in the absence of LH (control) and in the presence of 1 ng/ml or 10 ng/ml of the hormone. Values are means \pm S.E.M. ($n=5$). *Statistically different from control (Student's non-paired *t*-test, $P<0.05$).

conditions. In contrast, confluent cultures not only showed poor dye coupling, but also displayed immunoreactivity to Cx43 localized in the cytoplasm, and not in appositional membranes. Accordingly, western blots and the semi-quantitative RT-PCR of confluent cultures showed a lower expression of Cx43 protein and mRNA respectively, when compared with subconfluent cultures. However, Cx43 mRNA and Cx43 protein concentrations differed by approximately twofold, whereas the percentage of coupling varied by almost 30-fold when we compared subconfluent and confluent cultures, suggesting that other connexins may form gap junction channels between TM3 cells, or that the localization of Cx43 at membrane appositional areas is the relevant variable.

Granot & Dekkel (1994) and You *et al.* (2000) have reported that the expression of gap junctions between rat ovarian cells and between rat Leydig cells respectively can be modulated by PKA and LH – known to induce an increase in the intracellular concentration of cAMP (Duffau *et al.* 1980, Rüegg & Burgess 1989). Both groups showed that LH induced a significant decrease in Cx43 mRNA levels after incubation for 24 h, and in the ovarian cells staurosporin blocked these effects.

Many authors have shown that secretion is accompanied by uncoupling in endocrine and exocrine organs. You *et al.* (2000) have directly measured the production of testosterone and levels of Cx43 mRNA during stimulation of rat Leydig cells by human chorionic gonadotrophin (hCG), both in culture and *in vivo*. As expected, hCG treatment led to an increase in testosterone formation and a decrease in Cx43 mRNA levels – an effect that was also mimicked by cAMP. These results are consistent with

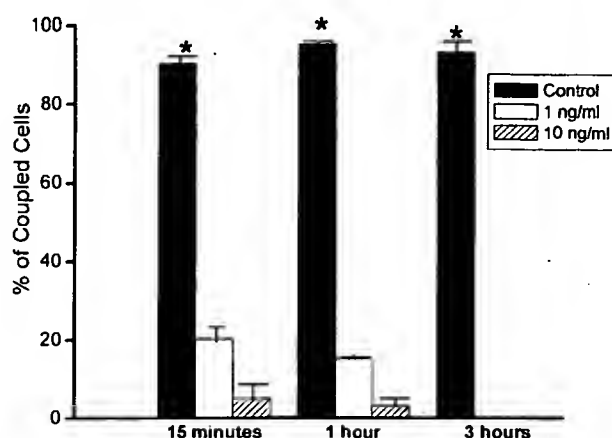


Figure 9 Junctional coupling in TM3 Leydig cells was decreased by LH. Treatment of the cells with 1 ng/ml and 10 ng/ml LH decreased the degree of coupling in subconfluent cultures exposed to the hormone for 15 min, 1 h and 3 h compared with control (no drug added). The number of cells injected in each condition was 90. *The degree of coupling in the non-treated cells was significantly different from that in treated cells ($P<0.05$).

experiments in which we found that LH at concentrations ranging from 1 to 10 ng/ml induced a marked uncoupling of the TM3 cells and a sustained increase in production of testosterone by the TM3 cells. Taken together, these data imply that gap junction mediated intercellular communication may have an important role in modulating hormone production in Leydig cells.

Acknowledgements

We thank Ms Sonia A Zanon and Mr José Fernando Aguiar for excellent technical assistance. We acknowledge Programa Nacional de Excelência (PRONEX), Conselho Nacional de Desenvolvimento Científico e Tecnológico (CNPq), Fundação de Amparo a Pesquisa do Estado do Rio de Janeiro (FAPERJ), Fundação de Amparo a Pesquisa do Estado de São Paulo (FAPESP), Financiadora de Estudos e Projetos (FINEP), Fundação Universitária José Bonifácio (FUEB) and Surcolombian University, for financial support.

References

- Bennett MVL, Barrio LC, Bargiello TA, Spray DC, Hertzberg E & Sáez JC 1991 Gap junctions: new tools, new answers, new questions. *Neuron* 6 305–320.
- Berridge M 1984 Inositol triphosphate and diacylglycerol as second messengers. *Biochemical Journal* 240 345–360.
- Bradford MM 1976 Rapid and sensitive method for the quantitation of microgram quantities of protein utilizing the principle of protein–dye binding. *Analytical Biochemistry* 72 248–254.
- Cole WC & Garfield RE 1986 Evidence for physiological regulation of myometrial junction permeability. *American Journal of Physiology* 251 C422–C420.

- Cristancho JM, Campos de Carvalho AC & Varanda WA 2000 Short term regulation of cell-cell communication in TM3 Leydig cells – a perforated patch study. *Biochimica et Biophysica Acta* **1496** 325–332.
- De Mello W 1991 Effect of vasopressin and protein kinase c inhibitors on junctional conductance in isolated heart cell pairs. *Cell Biology International* **15** 467–478.
- Dermietzel R, Leibstein A, Frixen V, Janssen-Timmen V, Traub O & Willecke K 1991 Gap junctions in several systems share antigenic determinants with liver gap junctions. *EMBO Journal* **3** 2261–2270.
- Duffau ML, Baukal AJ & Catt KJ 1980 Hormone-induced guanyl nucleotide binding and activation of adenylate cyclase in the Leydig cell. *PNAS* **77** 5837–5841.
- Giaume C, Fromaget C, El Aoumari A, Cordier J, Glowinsky J & Gross D 1991 Gap junction in cultured astrocytes: single-channel currents and characterization of channel forming protein. *Neuron* **6** 133–143.
- Granot I & Dekel N 1994 Phosphorylation and expression of connexin-43 ovarian gap junction protein are regulated by luteinizing hormone. *Journal of Biological Chemistry* **269** 30502–30509.
- Grassi F, Monaco L, Fraticchio G, Dolci S, Ianni E, Conti M, Eubesi F & Stefanini M 1986 Putative second messengers affect cell coupling in the seminiferous tubules. *Cell Biology International Reports* **10** 631–639.
- Haefliger JA, Bruzzone BR, Jenkins NA, Gilbert DJ, Copland NG & Paul LD 1992 Four novel members of the connexin family of gap junction proteins. *Journal of Biological Chemistry* **267** 2057–2064.
- Hünster PN & Weingant R 1993 Effects of phorbol ester on gap junctions of neonatal rat heart cells. *Pflügers Archiv European Journal of Physiology* **423** 181–188.
- Kadle R, Zhang JT & Nicholson BJ 1991 Tissue specific distribution of differentially phosphorylated forms of connexin 43. *Molecular and Cellular Biology* **11** 363–369.
- Kwak BR, Van Veen TAB, Analbers LJS & Jongsma HJ 1995 TPA increases conductance but decreases permeability in neonatal rat cardiomyocyte gap junction channels. *Experimental Cell Research* **220** 456–463.
- Lampe PD 1994 Analyzing phorbol esters on gap junctional communication: a dramatic inhibition of assembly. *Journal of Cell Biology* **127** 1895–1900.
- Moreno AP, Campos de Carvalho AC, Christ G, Melman A & Spray DC 1993 Gap junctions between human corpus cavernosum smooth muscle cells: gating properties and unitary conductance. *American Journal of Physiology* **264** C80–C92.
- Moreno AP, Sáez JC, Fishman GI & Spray DC 1994 Human connexin43 gap junction channels. Regulation of unitary conductances by phosphorylation. *Circulation Research* **74** 1050–1057.
- Oh SY, Gruper CG & Murray AW 1991 Phorbol ester induces phosphorylation and down regulation of connexin 43 in WB cells. *Biochimica et Biophysica Acta* **1094** 243–245.
- Pérez-Armendariz EM, Romano MC, Luna J, Miranda C, Bennett MVL & Moreno AP 1994 Characterization of gap junctions between pairs of Leydig cells from mouse testis. *American Journal of Physiology* **267** C570–C580.
- Pérez-Armendariz EM, Luna J, Miranda C, Talavera ID & Romano MC 1996 Luteinizing and human chorionic gonadotropin hormones increase intercellular communication and gap junctions in cultured mouse Leydig cells. *Endocrine* **4** 141–150.
- Risley MS 2000 Connexin gene expression in seminiferous tubules of the Sprague-Dawley Rat. *Biology of Reproduction* **62** 748–754.
- Risley MS, Tan IP, Roy C & Sáez JC 1992 Cell-cell stage dependent distribution of connexin gap junctions in testes. *Journal of Cell Science* **103** 81–96.
- Rorig B, Klaus G & Sutor B 1995 Dye coupling between pyramidal neurons in developing rat prefrontal and frontal-cortex is reduced by protein-kinase-A activation and dopamine. *Journal of Neuroscience* **15** 7386–7400.
- Rüegg B, Burgess GM 1989 Staurosporin, K-252 and UCN-01: potent but nonspecific inhibitors of protein kinases. *Trends in Pharmacological Sciences* **10** 218–220.
- Sacai N, Blennerhasset MG & Garfield RE 1992 Intracellular cyclic AMP concentration modulates gap junction permeability in parturient rat myometrium. *Canadian Journal of Physiology and Pharmacology* **70** 358–364.
- Skinner MK 1982 Cell-cell interactions in the testis. *Annals of the New York Academy of Sciences* **513** 158–171.
- Spray DC, Moreno AP, Kessler JA & Dermietzel R 1991 Characterization of gap junctions between cultured leptomeningeal cells. *Cells Brain Research* **568** 1–14.
- Srinivas M, Costa M, Gao Y, Fort A, Fishman GI & Spray DC 1999 Voltage dependence of macroscopic and unitary currents of gap junction channels formed by mouse connexin 50 expressed in rat neuroblastoma cells. *Journal of Physiology* **517** 673–689.
- Varanda WA & Campos de Carvalho AC 1994 Intercellular communication between mouse Leydig cells. *American Journal of Physiology* **267** C563–C569.
- Xie H-Q & Hu VW 1992 Intercellular communication through gap junctions is reduced in senescent cells. *Biophysical Journal* **62** 45–47.
- Yada T, Rose B & Loewenstein WR 1985 Diacylglycerol down regulates junctional permeability. TMB-8 blocks this effect. *Journal of Membrane Biology* **88** 217–232.
- You S, Li W & Lin T 2000 Expression and regulation of connexin43 in rat Leydig cells. *Journal of Endocrinology* **166** 447–453.

Received in final form 29 January 2003

Accepted 4 February 2003

Expression level of Ubc9 protein in rat tissues[Ⓢ]

Filip Gołębiowski¹, Aneta Szulc¹, Monika Sakowicz¹, Andrzej Szutowicz²
and Tadeusz Pawełczyk^{1✉}

¹*Department of Molecular Medicine, and* ²*Department of Laboratory Medicine,
Medical University of Gdańsk, 80-211 Gdańsk, Poland*

Received: 27 September, 2003; revised: 28 November, 2003; accepted: 09 December, 2003

Key words: recombinant protein, Ubc9, tissue distribution, rat

Ubc9 is a homologue of the E2 ubiquitin conjugating enzyme and participates in the covalent linking of SUMO-1 molecule to the target protein. In this report we describe a simple and efficient method for obtaining pure human recombinant Ubc9 protein. The purified Ubc9 retained its native structure and was fully active in an *in vitro* sumoylation assay with the promyelocytic leukaemia (PML) peptide as a substrate. In order to better understand the physiology of Ubc9 protein we examined its levels in several rat tissues. Immunoblot analyses performed on tissue extracts revealed quantitative and qualitative differences in the expression pattern of Ubc9. The Ubc9 protein was present at a high level in spleen and lung. Moderate level of Ubc9 was detected in kidney and liver. Low amount of Ubc9 was observed in brain, whereas the 18 kDa band of Ubc9 was barely visible or absent in heart and skeletal muscle. In heart and muscle extracts the Ubc9 antibodies recognized a 38 kDa protein band. This band was not visible in extracts of other rat tissues. A comparison of the relative levels of Ubc9 mRNA and protein indicated that the overall expression level of Ubc9 was the highest in spleen and lung. In spleen, lung, kidney, brain, liver and heart there was a good correlation between the 18 kDa protein and Ubc9 mRNA levels. In skeletal muscle the Ubc9 mRNA level was unproportionally high comparing to the level of the 18 kDa protein.

The presented data indicate that in the rat the expression of the Ubc9 protein appears to have some degree of tissue specificity.

Sumoylation is a post-translational modification of proteins involving formation of an isopeptide bond between the carboxyl terminus of SUMO-1 (also known as UBL1, sentrin,

[Ⓢ]This work was supported by the State Committee for Scientific Research (KBN, Poland) grant No. 6 P05A 037 20 to T.P.

✉To whom correspondence should be addressed; tel.: (48 58) 349 2750; fax: (48 58) 349 2759; e-mail: tkpaw@amg.gda.pl

Abbreviations: GST, glutathione-S-transferase; PBS, phosphate-buffered saline; TBS, Tris-buffered saline.

PIC1, SMTP3 or GMP1) and a lysine side chain of the target protein (Müller *et al.*, 2001; Tatham *et al.*, 2003). The SUMO-1 pathway involves ATP-dependent SUMO-1 activation catalyzed by the heterodimeric SUMO-1 activating enzyme (SAE1/SAE2), transfer of SUMO-1 to the SUMO-1-conjugating enzyme Ubc9 in a transesterification reaction and the final transfer of SUMO-1 from the SUMO-1-Ubc9 complex to the target protein. Covalent attachment of SUMO-1, unlike ubiquitination, does not result in degradation of the modified proteins, but enhances their stability or affects their subcellular compartmentalization (Matunis *et al.*, 1996; Desterro *et al.*, 1998; Kang *et al.*, 2003). Modification of proteins by SUMO-1 has been shown to be involved in multiple vital cellular processes, including DNA repair and replication, nuclear transport, oncogenesis, response to viral infection and the inflammation (Mao *et al.*, 2000; Mahajan *et al.*, 1997; Rodriguez *et al.*, 1999; Hofmann *et al.*, 2000; Baier *et al.*, 2003).

The Ubc9 protein has been reported to associate with a large variety of cellular proteins including the putative tumor suppressor protein Fhit (Shi *et al.*, 2000). Ubc9 may modulate the activity of the interacting protein directly or by catalyzing the covalent attachment of SUMO-1. Direct activation of androgen receptor (Poukka *et al.*, 1999) and abrogation of TEL (product of an E-26 transforming specific (ETS)-related gene) repressor activity (Chakrabarti *et al.*, 1999) by interacting Ubc9 protein have been reported.

To date little is known about the physiology of the Ubc9 protein in spite of the intense research being conducted on the sumoylation process. As the first step toward understanding of the physiological role of Ubc9 we have examined the expression levels of Ubc9 in several rat tissues. In order to study the interaction of Ubc9 with other proteins we also developed a simple and efficient method for obtaining pure human recombinant Ubc9 protein.

MATERIALS AND METHODS

4-(2-Aminoethyl)-benzenesulfonyl fluoride hydrochloride (Pefabloc SC) was from Roche Applied Science (Mannheim, Germany). *Escherichia coli* BL21(DE3), and DH5 α , oligo(dT), and dNTPs were from Invitrogen (Garlsbad, CA, U.S.A.). All primers were from Integrated DNA Technologies, Inc. (Coralville, IA, U.S.A.). Total RNA Prep Plus Kit, Plasmid Miniprep Plus and DNA Clean-Up Kit were from A&A Biotechnology (Gdańsk, Poland). Moloney murine leukemia virus reverse transcriptase (MMLV-RT), and Tfi DNA polymerase were from Epicentre Technologies (Madison, WI, U.S.A.). RNasin was from Promega (Madison, WI, U.S.A.). *Bam*HI and *Eco*RI were from Fermentas AB (Vilnius, Lithuania). Leupeptin, isopropyl β -D-thiogalactopyranoside, ampicillin, alkaline phosphatase-conjugated goat anti-rabbit IgG, 5-bromo-4-chloro-3-indoyl phosphate, and Nitro Blue Tetrazolium were from Sigma-Aldrich Sp. z o.o. (Poznań, Poland). Transfer Membrane was from Millipore Corp. (Bedford, MA, U.S.A.). Recombinant SUMO-1, GST-PML fusion peptide and SAE1/SAE2 activating proteins were obtained from Dr. Ronald T. Hay from the Institute of Biomolecular Sciences at University of St. Andrews in Scotland.

RNA extraction and reverse transcription. Total RNA was extracted from human blood cells or from rat tissues with the use of Total RNA Prep Plus Kit and stored at -40°C . Reverse transcription was performed in 20 μl final volume of 50 mM Tris/HCl, pH 8.3, 75 mM KCl, 10 mM MgCl_2 , 10 mM DTT, 1 mM dNTPs, 500 ng oligo(dT), 12.5 U of reverse transcriptase (MMLV-RT), 10 U of RNasin, and 1–3 μg of RNA. The reactions were incubated for 10 min at 22°C , 90 min at 37°C and 5 min at 95°C .

Multiplex PCR. In order to assess the level of the *UBC9* gene transcript, we performed multiplex PCR with β -actin mRNA as a reference template. For *UBC9* amplification the primers UBC24, CACCCATTTGGATCCGTG-

GC (forward) and UBC119, GGAGTACG-GGGAATTCTAA ATGAACC (reverse) were used. This defines a DNA fragment of 310 base pairs. The primers were based on the rat cDNA sequence (Gen Bank, Accession No. NW 047334). Primers for β -actin amplification were as described (Sakowicz *et al.*, 2001), and the product was 511 base pairs long. The reaction mixture contained 50 mM Tris/HCl, pH 9.0, 20 mM ammonium sulfate, 300 ng of template, 0.40 μ M each of the 5' and 3' primers, 0.375 mM of each dNTP, 3.75 mM $MgCl_2$ and 0.75 U of Tth DNA polymerase. The PCR for β -actin and Ubc9 consisted of an initial denaturation at 95°C for 3 min and 34 cycles of 30 s at 95°C, 30 s at 57°C, 30 s at 72°C, and a final extension of 10 min at 72°C amplification.

The PCR reactions were performed in an Eppendorf-Mastercycler. The PCR products were separated by agarose gel electrophoresis and assessed by quantitation of ethidium bromide-stained bands with the use of the Gel Doc 2000 system (Bio-Rad). The relative amounts (OD/mm²) of both amplified transcripts were compared using the computer program Quantity One (Bio-Rad).

Cloning of the UBC9 gene. Unless otherwise indicated, the recombinant DNA methods used were those of Sambrook *et al.* (1989). In order to obtain cDNA for hUbc9 we run a PCR reaction with the primers PCU-1 GGATCCTTGAACATGGCGGGGATC (forward) and PCU-3, AGCAGTCTTCCTTCCTTAAGCAA (reverse), which introduced restriction enzyme cleavage sites (underlined) for *Bam*HI and *Eco*RI, respectively. The primers were based on the human cDNA sequence (National Center for Biotechnology Information, accession No. U31933). The PCR reaction was performed in 20 μ l final volume in 50 mM Tris/HCl, pH 7.5, 20 mM ammonium sulfate, 2.5 mM $MgCl_2$, 0.25 mM dNTPs, 1 U of Tfi DNA polymerase, 0.5 μ M primers and 1–2 μ g of human blood cell cDNA. The PCR consisted of an initial denaturation at 94°C for 3 min and 35 cycles of 30 s at 94°C, 30 s at

59°C, 45 s at 72°C, and a final extension of 10 min at 72°C. The PCR product (529 bp) was then cut with appropriate enzymes and ligated into the unique *Bam*HI and *Eco*RI sites in pGEX-TKG vector (Kowara *et al.*, 1999). The pGEX-TKG/*UBC9* plasmid was produced in *E. coli* DH5 α cells. The cloned cDNA was sequenced and was confirmed to be complete hUbc9 coding cDNA.

Cell growth and expression of hUbc9. pGEX-TKG/*UBC9* was used for the expression of hUbc9 as a fusion protein with *Schistosoma japonicum* glutathione-S-transferase (GST) at the amino-terminus. *E. coli* BL21(DE3) cells were transformed with the above-mentioned plasmid and colonies were grown on agar plates containing 100 μ g/ml ampicillin. Picked colonies were grown overnight at 37°C in ampicillin-containing Luria-Bertani (LB) medium and 1 ml of this culture was inoculated into 1 l of fresh medium, and incubated at 37°C to an absorbance of 0.7–0.8 (measured at 600 nm). Expression of the GST-hUbc9 protein was induced by the addition of 1 mM isopropyl β -D-thiogalactopyranoside (IPTG). Following induction, the cells were grown for 3 h and harvested by centrifugation.

Purification of hUbc9. All steps were done at 4°C. Cell pellet from 1 l culture was suspended in 40 ml of potassium phosphate-buffered saline (PBS), pH 7.4, 1 mM EDTA, 5 mM β -mercaptoethanol, 10 μ g/ml leupeptin, 0.2 mM Pefablock SC, 1 mM benzamidine (buffer A), placed on powdered dry ice and sonicated. The crude cell extract was clarified by centrifugation at 50 000 $\times g$ for 30 min. The obtained supernatant was supplemented with Triton X-100 to a final concentration of 1% and passed through a 7 ml agarose-glutathione column preequilibrated with buffer A containing 1% Triton X-100 (buffer A1). The column was washed successively with 200 ml of buffer A1 containing 1 mM ATP, 10 mM $MgCl_2$, and then with 1 l of Tris-buffered saline (TBS), pH 8.0, 1 mM EDTA, 1 mM DTT, 10 μ g/ml leupeptin, 0.2 mM Pefablock SC,

1 mM benzamidine. Finally, the GST-hUbc9 protein was eluted from the column with 10 ml of buffer TBS, pH 8.0, containing 5 mM glutathione. Fractions containing high protein concentration were combined, desalted on Sephadex G-25 M (Pharmacia columns PD-10) previously equilibrated with PBS, pH 7.4, 2.5 mM CaCl_2 . The desalted solution of GST-hUbc9 (4–6 mg) was incubated with thrombin (100 U) at 4°C for 6–8 h. Then the solution was passed successively through a 3 ml agarose-glutathione column, and agarose-benzamidine column. Cleaved hUbc9 protein was dialyzed to PBS, pH 7.4.

SUMO-1 conjugation assay. The conjugation assay was performed using the PML peptide (PRKVIKMESEE) fused to GST (GST-PML) as a substrate. The reaction mixture (10 μl) contained 120 ng SAE1/SAE2, 2 μg [^{125}I]-SUMO-1($\Delta 98-101$), 200 ng Ubc9, 600 ng GST-PML, 50 mM Tris/HCl, pH 7.5 and an ATP-regenerating system (5 mM MgCl_2 , 2 mM ATP, 10 mM creatine phosphate, 3.5 U/ml of creatine kinase, 0.6 U/ml of inorganic pyrophosphatase). Reactions were incubated at 37°C for 3 h. The reactions were terminated by addition of SDS-sample buffer containing β -mercaptoethanol and the reaction products were fractionated by SDS/PAGE (15%). The dried gels were analysed by phosphor imaging (Fujifilm FLA-3000). Radiolabelling of SUMO-1($\Delta 98-101$) with [^{125}I] (Amersham) was performed by the chloramine T method as described by Ciechanover *et al.* (1980).

Preparation of tissues homogenates. Wistar rats weighing approx. 200 g were killed by decapitation. The tissue of interest was removed and homogenized in 3 vol. of PBS, pH 7.4, 1 mM Pefabloc SC, using a power-driven pestle. The resulting homogenate was supplemented with 2% SDS, 75 mM DTT, 10% glycerol, 0.1% bromophenol blue and boiled at 100°C for 3 min. After centrifugation the supernatant was stored at 4°C.

Antibodies. Polyclonal antibodies against the hUbc9 protein were generated in rabbits.

Rabbits were subcutaneously injected in the back of the neck with 500 μg of purified recombinant hUbc9 protein in Freund's adjuvant followed by three boosts with 300 μg of antigen each every 3 weeks. The antibodies were purified by chromatography on a protein A-agarose column.

SDS/PAGE and immunoblotting. Samples (100 μg of protein) were separated by polyacrylamide gel electrophoresis (15% acrylamide) in the presence of sodium dodecyl sulfate (SDS/PAGE) (Laemmli, 1970) and the protein bands were developed by Coomassie Brilliant Blue staining or electrophoretically transferred to Immobilon poly(vinylidenedifluoride) transfer membrane (Millipore). The membrane was blocked with 3% bovine albumin (fraction V) in phosphate buffered saline (PBS) with 0.02% NaN_3 and then washed with PBS. The blocked membrane strips were incubated with rabbit anti hUbc9 polyclonal antibodies (dilution 1:10 000). Immunostaining was done using alkaline phosphatase-conjugated goat anti-rabbit IgG (dilution 1:20 000), the chromogenic substrate 5-bromo-4-chloro-3-indoyl phosphate and Nitro Blue Tetrazolium. The developed bands were quantified by use of the Gel Doc 2000 system (Bio-Rad) and relative amounts were compared using the computer program Quantity One (Bio-Rad).

Analytical. Protein concentration was determined by the method of Bradford (1976) with bovine serum albumin as a standard. In solutions containing SDS or Triton X-100 protein concentrations were determined by the method of Lowry (1951). DNA and RNA concentrations were determined by measuring the absorbance at 260 nm.

RESULTS

Expression of GST-hUbc9

In order to optimize the expression conditions of GST-hUbc9, we cultured the bacterial

cells at different temperatures and for various periods of time. Expression of GST-hUbc9 at 37°C for 3 h after induction produced 15–20 mg of GST-hUbc9 from 1 l of culture as assessed by densitometric analysis of SDS/PAGE (Fig. 1). Prolongation of the ex-

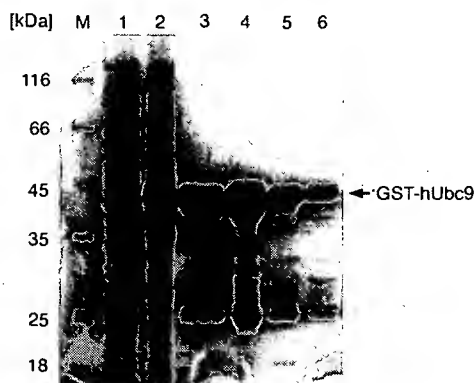


Figure 1. Expression in *E. coli* and purification of GST-hUbc9 protein on agarose-glutathione.

On individual lanes of 12% SDS/PAGE were loaded: (1), 50 μ g of *E. coli* lysate (non-induced); (2), 50 μ g of lysate of *E. coli* cells induced for 3 h; (3–6) 20 μ g of protein eluted by 5 mM glutathione from glutathione-agarose column (fractions containing the protein peak). On lane M molecular mass markers were loaded.

pression time at 37 °C did not increase the total yield of the protein, whereas the amount of soluble protein (protein recovered in the high-speed supernatant) decreased (not shown). Expression of GST-hUbc9 in *E. coli* strain BL21(DE3) cultured at 24°C for 16 h or at 18°C for 48 h did not produce a higher amount of this protein. There were no losses in the yield of GST-hUbc9 from bacterial cultures stored on agar plates for up to 30–40 days at 4°C. Cells stored on agar plates longer than 40 days produced cultures with a lower yield of GST-hUbc9.

Purification of hUbc9

Usually the process of protein purification started with 4–6 g of *E. coli* cells obtained from 1 l of culture. The purification of GST-hUbc9 on the glutathione-agarose yielded

essentially pure protein contaminated mainly by a protein of 27 kDa on SDS/PAGE (Fig. 1). Immunoblot analysis showed that this protein band is recognized by anti-GST polyclonal antibodies (not shown). GST was removed from the GST-hUbc9 fusion protein by incubation with thrombin. Incubation of GST-hUbc9 with thrombin at 4°C for 6–8 h resulted in complete cleavage of the GST tag (Fig. 2). There were no unspecific cleavage

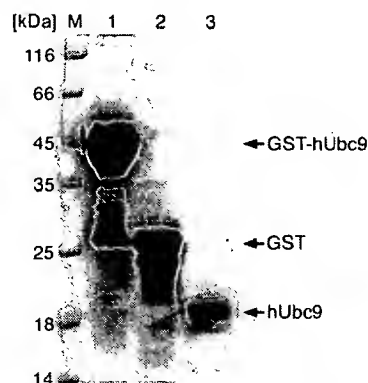


Figure 2. Thrombin cleavage of the GST-hUbc9 protein.

The GST-hUbc9 protein purified on glutathione agarose column (lane 1) was cleaved with thrombin as described under Materials and Methods. Lane 2, GST-hUbc9 protein after 7 h incubation at 4°C with thrombin. Lane 3, recombinant hUbc9 protein purified from thrombin and the cleaved GST. On each lane of 15% SDS/PAGE (1–3) 20 μ g of protein was loaded. Lane M, the molecular mass markers.

products. The observed shift in mobility of hUbc9 after the removal of the GST tag was of the order expected from the removal of 27 kDa protein. Thrombin and the cleaved GST tag were removed by passing successively through an agarose-glutathione column (GST retained), and an agarose-benzamidine column (thrombin retained). The purification yielded 5–10 mg of electrophoretically pure hUbc9 (Fig. 2).

Catalytic properties of recombinant hUbc9

In order to characterize the apparent size of native recombinant hUbc9, the purified pro-

tein was subjected to a gel filtration on Sephacryl S-100 column calibrated with globular monomeric proteins. Ubc9 eluted slightly faster than the 14.4 kDa lysozyme (not shown). Therefore it may be assumed that the purified Ubc9 protein was present in monomeric form.

Human Ubc9 is a homologue of the ubiquitin-conjugating enzyme E2. In the SUMO-1 pathway Ubc9 transfers activated SUMO-1 to the target protein. In order to examine the enzymatic activity of purified recombinant hUbc9 we performed *in vitro* SUMO-1 conjugation assay with the promyelocytic leukaemia (PML) peptide as a substrate. The PML peptide (PRKVIKMESEE) contains the consensus sequence ψ KxE (where ψ is a hydrophobic amino acid and x is any amino acid) essential for SUMO-1 modification. Analysis of the reaction products separated on SDS/PAGE indicated that the 39 kDa protein band corresponding to GST-PML-SUMO-1 was only visible when the reaction was run in the presence of recombinant hUbc9 (Fig. 3). This indicates that the obtained hUbc9 protein preserved its native SUMO-1 conjugating activity.

Expression of Ubc9 in rat tissues

In order to examine Ubc9 expression in various rat tissues we assessed its protein and mRNA level. A comparison of the amino-acid sequences of human (AAC50603) and rat (NP037182) Ubc9 proteins reveals that they are identical in 97%. Therefore, in our experiments we could use polyclonal antibodies against hUbc9. Densitometry analysis of Western blot presented in Fig. 4 indicated that the Ubc9 protein was present at a high level in spleen and was slightly less abundant in lung. A moderate level of Ubc9 was detected in kidney and liver. Low amount of Ubc9 was observed in brain, whereas the 18 kDa band of Ubc9 was barely visible or absent in heart and skeletal muscle. In contrast, in heart and muscle extracts the anti-Ubc9

polyclonal antibodies recognized a 38 kDa protein band (Fig. 4). This band was not visible in extracts of other rat tissues.

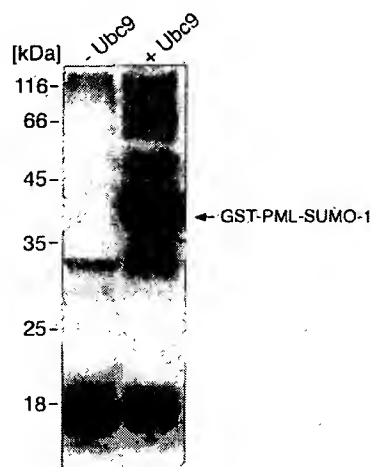


Figure 3. Sumoylation of GST-PML.

Sumoylation of PML peptide (PRKVIKMESEE) fused to GST was performed in the absence (-Ubc9) and in the presence (+Ubc9) of purified recombinant human Ubc9 as described in Materials and Methods. The reaction products were fractionated by SDS/PAGE (15%) and the dried gels were analyzed by phosphor imaging (Fujifilm FLA-3000).

In the rat tissues examined we also evaluated the level of Ubc9 mRNA by multiplex RT-PCR. As a reference transcript we amplified a fragment (511 bp) of β -actin. The data presented in Fig. 5 indicate that spleen and lung contained similar and the highest level of Ubc9 mRNA. Kidney, liver, brain, and skeletal muscle contained similar levels (about 40% of that found in the spleen) of Ubc9 mRNA. The lowest level of Ubc9 mRNA was found in the heart. A comparison of the relative level of Ubc9 mRNA and protein indicated that the overall expression level of Ubc9 was the highest in spleen and lung. In spleen, lung, kidney, brain, liver and heart there was a good correlation between the 18 kDa protein and Ubc9 mRNA levels. In skeletal muscle the Ubc9 mRNA level was unproportionally high relative to the level of the 18 kDa protein.

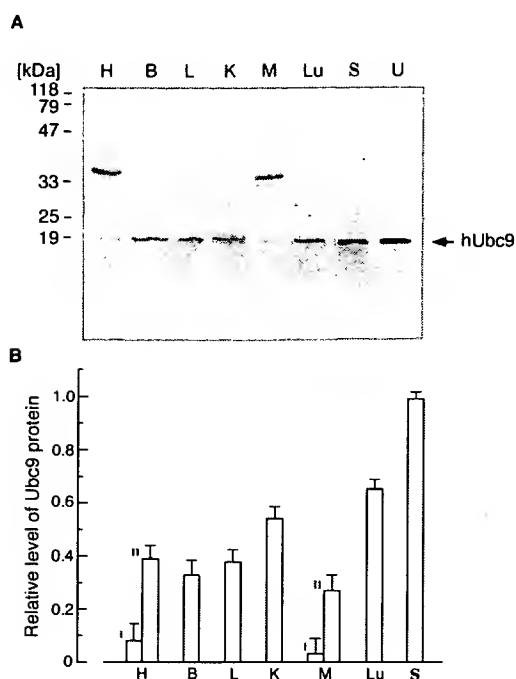


Figure 4. Ubc9 protein levels in rat tissues.

A. Extracts (100 μ g) of the tissues examined were subjected to 15% SDS/PAGE and transferred to an Immobilon membrane as described under Materials and Methods. The membranes were immunoblotted with anti-Ubc9 IgG. Lanes H, B, L, K, M, Lu, S refer to extracts of heart, brain, liver, kidney, skeletal muscle, lung, and spleen, respectively. On lane U purified recombinant hUbc9 protein (25 ng) was loaded. The presented blot is representative of those performed on tissue extracts obtained from four different animals. **B.** The blot shown in part A was scanned and the bands were quantitated. The data are presented as a ratio of the intensity of each protein band to the most intensive band visible in the spleen extract \pm S.D. ($n = 4$). In the case of heart and skeletal muscle the I and II bars represent the protein bands of 18 and 38 kDa, respectively.

DISCUSSION

The expression and purification system described in this contribution allowed the production of large quantities of soluble hUbc9 protein. The obtained GST fusion protein was efficiently cleaved by thrombin owing to the presence of a glycine spacer prior to the

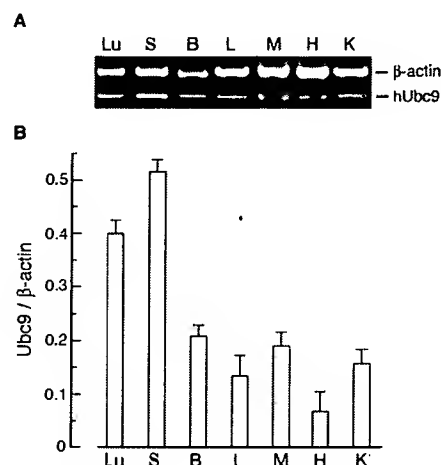


Figure 5. UBC9 gene transcript levels in rat tissues.

The Ubc9 mRNA level was assessed by quantitation of multiplex RT-PCR products as described under Materials and Methods. **A.** Multiplex RT-PCR products were separated by 2% agarose gel electrophoresis. Lanes K, H, L, Lu, M, S, and B refer to the PCR products obtained for kidney, heart, liver, lung, muscle, spleen and brain, respectively. The gel shown is representative of those obtained for three rats. **B.** Multiplex RT-PCR products were assessed by quantitation of ethidium bromide-stained bands. The ratio of the Ubc9 PCR product (OD/mm^2) to the β -actin PCR product was calculated ($\text{Ubc9}/\beta\text{-actin}$). The data are mean \pm S.D. ($n = 4$).

thrombin cleavage site (Hakes & Dixon, 1992). Digestion of the GST-hUbc9 protein with thrombin leaves only three unrelated amino acids at the N-terminus of hUbc9. These three additional amino acids should not cause any significant disturbances in the structure of the recombinant hUbc9 protein nor affect its function. Functionality of the protein produced was confirmed in an *in vitro* sumoylation assay (Fig. 5). The assumed physiological role of Ubc9 protein is to transfer the SUMO-1 protein from the SUMO-1- SAE1/SAE2 thioester complex to the target protein substrate. The Ubc9 region that is involved in target protein recognition and interaction has been found to be located in the C-terminal part of the protein (Donghai *et al.*, 2002). It was demonstrated that mutations of Q126, Q130, A131, E132, Y134 and T135 residues significantly affect the Ubc9 interaction with target proteins lead-

ing to diminished SUMO-1 conjugation. The N-terminal part of Ubc9 forms an α -helical structure that is not involved in the binding to the target protein (Donghai *et al.*, 2002), but the interaction of Ubc9 with heterodimeric SAE1/SAE2 was reported to involve the C-terminal part of the N-terminal α -helix of Ubc9 (Bencsath *et al.*, 2002).

The data presented in this study show for the first time the distribution of Ubc9 protein and mRNA in rat tissues. Analysis of the immunoblots of the seven rat tissues studied revealed that there are quantitative and qualitative differences among them. The highest content of Ubc9 protein was observed in spleen whereas heart and skeletal muscle exhibited very low levels of Ubc9 (Fig. 4). In the examined tissues the level of the Ubc9 protein correlated well with its mRNA level except for skeletal muscle, where the Ubc9 transcript level was unproportionally high. Such a pattern of Ubc9 expression is different from that obtained for human tissues. The Ubc9 mRNA level was reported to be the highest in human heart and smooth muscle (Wang *et al.*, 1996). In human tissues Northern blot analyses identified *UBC9* transcripts of 4.4, 2.4, and 1.3 kb length. The 1.3 kb transcript was the main transcript present in all analyzed human tissues, whereas the 2.4 and 4.4 kb transcripts were mainly expressed in heart and smooth muscle (Wang *et al.*, 1996). Thus, the about 38 kDa protein bands recognized by anti Ubc9 antibodies observed in our studies, could be the products of alternatively spliced transcripts. The Ubc9 protein, beside its enzymatic activity involved in the sumoylation pathway, also displays other activities that are not related to sumoylation. Therefore, changes in Ubc9 expression may affect many cellular processes that are independent of sumoylation including enhancement of the activity of transcription factors and promotion of nuclear translocation (Hahn *et al.*, 1997; Poukka *et al.*, 1999; Chakrabarti *et al.*, 1999; Kurtzman & Schechter, 2001; Kaul *et al.*, 2002).

Concluding, the presented results indicate that Ubc9 is ubiquitously expressed in rat but at different levels in different tissues. Moreover, our data indicate that the pattern of Ubc9 expression observed in the rat differs significantly from that observed in the human. In order to find out the identity of the 38 kDa protein recognized by Ubc9 antibodies further experiments are required.

REFERENCES

- Baier A, Meineckel I, Gay S, Pap T. (2003) Apoptosis in rheumatoid arthritis. *Curr Opin Rheumatol.*; **15**: 274-9.
- Bencsath KP, Podgorski MS, Pagala VR, Slaughter CA, Schulman BA. (2002) Identification of multifunctional binding site on Ubc9p required for Smpt3p conjugation. *J Biol Chem.*; **277**: 47938-45.
- Bradford MM. (1976) A rapid and sensitive method for the quantitation of microgram quantities of protein utilizing the principle of protein-dye binding. *Anal Biochem.*; **72**: 248-54.
- Chakrabarti SR, Sood R, Ganguly S, Bohlander S, Shen Z, Nucifora G. (1999) Modulation of TEL transcription activity by interaction with the ubiquitin-conjugating enzyme UBC9. *Proc Natl Acad Sci U S A.*; **96**: 7467-72.
- Ciechanover A, Heller H, Elias S, Haas AL, Hershko A. (1980) ATP-dependent conjugation of reticulocyte proteins with the polypeptide required for protein degradation. *Proc Natl Acad Sci U S A.*; **77**: 1365-8.
- Desterro JM, Rodriguez MS, Hay RT. (1998) SUMO-1 modification of I κ B α inhibits NF- κ B activation. *Mol Cell.*; **2**: 233-9.
- Donghai L, Tatham MH, Yu B, Kim S, Hay RT, Chen Y. (2002) Identification of a substrate recognition site on Ubc9. *J Biol Chem.*; **277**: 21740-8.
- Golebiowski F, Kowara R, Pawelczyk T. (2001) Distribution of Fhit protein in rat tissues and its intracellular localization. *Mol Cell Biochem.*; **226**: 49-55.

- Hahn SL, Wasylyk B, Criqui-Filipe P, Criqui P. (1997) Modulation of ETS-1 transcriptional activity by huUBC9, a ubiquitin-conjugating enzyme. *Oncogene*; **15**: 1489-95.
- Hakes DJ, Dixon JE. (1992) New vectors for high level expression of recombinant proteins in bacteria. *Anal Biochem*; **202**: 293-8.
- Hofmann H, Floss S, Stamminger T. (2000) Covalent modification of the transactivator protein IE2-p86 of human cytomegalovirus by conjugation to the ubiquitin-homologous proteins SUMO-1 and hSMT3b. *J Virol*; **74**: 2510-24.
- Kang SI, Chang W-J, Cho S-G, Kim IY. (2003) Modification of promyelocytic leukemia zinc finger protein (PLZF) by SUMO-1 conjugation regulates its transcriptional repressor activity. *J Biol Chem*. (in press).
- Kaul S, Blackford JA, Cho S, Simons SS Jr. (2002) Ubc9 is a novel modulator of the induction properties of glucocorticoid receptors. *J Biol Chem*; **277**: 12541-9.
- Kowara R, Gryckiewicz E, Matecki A, Pawelczyk T. (1999) The ultraviolet studies on protein-lipid interaction of a protein kinase C- γ phorbol-binding domain. *Acta Biochim Polon*; **46**: 405-17.
- Kurtzman AL, Schechter N. (2001) Ubc9 interacts with a nuclear localization signal and mediates nuclear localization of the paired-like homeobox protein Vsx-1 independent of SUMO-1 modification. *Proc Natl Acad Sci U S A*; **98**: 5602-7.
- Laemmli UK. (1970) Cleavage of structural proteins during the assembly of the head of bacteriophage T4. *Nature*; **227**: 680-5.
- Lowry OH, Rosebrough NJ, Farr AL, Randall RJ. (1951) Protein measurements with the Folin phenol reagent. *J Biol Chem*; **193**: 263-73.
- Mahajan R, Delphin C, Guan T, Gerace L, Melchior F. (1997) A small ubiquitin-related polypeptide involved in targeting RanGAP1 to nuclear pore complex protein RanBP2. *Cell*; **88**: 97-107.
- Mao Y, Sun M, Desai SD, Liu LF. (2000) SUMO-1 conjugation to topoisomerase I: a possible repair response to topoisomerase-mediated DNA damage. *Proc Natl Acad Sci U S A*; **97**: 4046-51.
- Matunis MJ, Coutavas E, Blobel G. ((1996) A novel ubiquitin-like modification modulates the partitioning of the Ran-GTPase-activating protein RanGAP1 between the cytosol and the nuclear pore complex. *J Cell Biol*; **135**: 1457-70.
- Müller S, Hoege C, Pyrowolakis G, Jentsch S. (2001) SUMO, ubiquitin's mysterious cousin. *Mol Cell Biol*; **2**: 202-10.
- Poukka H, Aarnisalo P, Karvonen U, Palvimo JJ, Janne OA. (1999) Ubc9 interacts with the androgen receptor and activates receptor-dependent transcription. *J Biol Chem*; **274**: 19441-6.
- Rodriguez MS, Desterro JM, Lain S, Midgley CA, Lane DP, Hay RT. (1999) SUMO-1 modification activates the transcriptional response of p53. *EMBO J*; **18**: 6455-61.
- Sakowicz M, Grdeń M, Pawelczyk T. (2001) Expression level of adenosine kinase in rat tissues. Lack of phosphate effect on the enzyme activity. *Acta Biochim Polon*; **48**: 745-54.
- Sambrook J, Fritsch EF, Maniatis F. (1989) In *Molecular cloning: a laboratory manual*. 2nd ed. Cold Spring Harbor Laboratory Press, Cold Spring Harbor, NY.
- Shi Y, Zou M, Farid NR, Paterson MC. (2000) Association of FHIT (fragile histidine triad), a candidate tumor suppressor gene, with the ubiquitin-conjugating enzyme hUBC9. *Biochem J*; **352**: 443-8.
- Tatham MH, Kim S, Yu B, Jaffray E, Song J, Zheng J, Rodriguez MS, Hay RT, Chen Y. (2003) Role of an N-terminal site of Ubc9 in SUMO-1, -2, and -3 binding and conjugation. *Biochemistry*; **42**: 9959-69.
- Wang ZY, Qiu QQ, Seufert W, Taguchi T, Testa JR, Whitmore SA, Callen DF, Welsh D, Shenk T, Deuel TF. (1996) Molecular cloning of the cDNA and chromosome localization of the gene for human ubiquitin-conjugating enzyme 9. *J Biol Chem*; **271**: 24811-6.



Analysis of mRNA expression and protein abundance data: an approach for the comparison of the enrichment of features in the cellular population of proteins and transcripts

Dov Greenbaum^{3,†}, Ronald Jansen^{1,†} and Mark Gerstein^{1,2,*}

¹Departments of Molecular Biophysics & Biochemistry, ²Computer Science and
³Genetics, 266 Whitney Avenue, Yale University, PO Box 208114, New Haven,
CT 06520, USA

Received on July 2, 2001; revised on October 5, 2001; accepted on October 22, 2001

ABSTRACT

Motivation: Protein abundance is related to mRNA expression through many different cellular processes. Up to now, there have been conflicting results on how correlated the levels of these two quantities are. Given that expression and abundance data are significantly more complex and noisy than the underlying genomic sequence information, it is reasonable to simplify and average them in terms of broad proteomic categories and features (e.g. functions or secondary structures), for understanding their relationship. Furthermore, it will be essential to integrate, within a common framework, the results of many varied experiments by different investigators. This will allow one to survey the characteristics of highly expressed genes and proteins.

Results: To this end, we outline a formalism for merging and scaling many different gene expression and protein abundance data sets into a comprehensive reference set, and we develop an approach for analyzing this in terms of broad categories, such as composition, function, structure and localization. As the various experiments are not always done using the same set of genes, sampling bias becomes a central issue, and our formalism is designed to explicitly show this and correct for it. We apply our formalism to the currently available gene expression and protein abundance data for yeast. Overall, we found substantial agreement between gene expression and protein abundance, in terms of the enrichment of structural and functional categories. This agreement, which was considerably greater than the simple correlation between these quantities for individual genes, reflects the way broad categories collect many individual measurements into simple, robust averages. In particular, we found

that in comparison to the population of genes in the yeast genome, the cellular populations of transcripts and proteins (weighted by their respective abundances, the transcriptome and what we dub the translome) were both enriched in: (i) the small amino acids Val, Gly, and Ala; (ii) low molecular weight proteins; (iii) helices and sheets relative to coils; (iv) cytoplasmic proteins relative to nuclear ones; and (v) proteins involved in 'protein synthesis,' 'cell structure,' and 'energy production.'

Supplementary information: <http://genecensus.org/expression/translatome>

Contact: mark.gerstein@yale.edu

INTRODUCTION

High throughput experimentation, measuring mRNA (Schena *et al.*, 1995; Eisen and Brown, 1999; Ferea and Brown, 1999; Lipshutz *et al.*, 1999) and protein expression (Anderson and Seilhamer, 1997; Futcher *et al.*, 1999; Gygi *et al.*, 1999a; Ross-Macdonald *et al.*, 1999; Lopez, 2000; MacBeath and Schreiber, 2000; Nelson *et al.*, 2000; Zhu *et al.*, 2000) are currently the single richest source of genomic information. However, how to best interpret this data is still an open question (Bassett *et al.*, 1996; Wittes and Friedman, 1999; Zhang, 1999; Gerstein and Jansen, 2000; Searls, 2000; Sherlock, 2000; Claverie, 1999; Einarson and Golemis, 2000; Epstein and Butow, 2000; Shapiro and Harris, 2000). Understanding how protein abundance is related to mRNA transcript levels is essential for interpreting gene expression, protein interactions, structures and functions in a cellular system (Hatzimanikatis *et al.*, 1999). Moreover, as protein concentration is the more relevant variable with respect to enzyme activity, it connects genomics to the physical chemistry of the cell (Kidd *et al.*, 2001). Protein abundance may also be invaluable for diagnostics and for determining drug targets (Corrals *et al.*, 2000).

*To whom correspondence should be addressed.

†These authors contributed equally to this work.

Previously, we surveyed the population of protein features—such as folds, amino acid composition, and functions—in yeast, and other recently sequenced genomes (Gerstein, 1997, 1998a,b; Gerstein and Hegyi, 1998; Hegyi and Gerstein, 1999; Das and Gerstein, 2000; Lin and Gerstein, 2000), and we extended this concept to compare the population of features in the yeast transcriptome to that in the genome (Drawid *et al.*, 2000; Jansen and Gerstein, 2000). Others have also done related work (Frishman and Mewes, 1997; Tatusov *et al.*, 1997; Jones, 1998; Wallin and von Heijne, 1998; Frishman and Mewes, 1999; Wolf *et al.*, 1999). Here, we present a new methodology to compare the features of the mRNA expression population with the protein abundance population.

Precise terminology is essential for this comparison. Unfortunately, 'proteome' is used inconsistently. Proteome can logically be used to describe all the distinct proteins in the genome (Qi *et al.*, 1996; Cavalcoli *et al.*, 1997; Fey *et al.*, 1997; Garrels *et al.*, 1997; Gaasterland, 1999; Jones, 1999; Sali, 1999; Tekaiia *et al.*, 1999; Bairoch, 2000; Cambillau and Claverie, 2000; Doolittle, 2000; Pandey and Mann, 2000; Rubin *et al.*, 2000) and, in this context, it is equivalent to what others may refer to as the coding part of the genome. However, in papers on two-dimensional (2D) electrophoresis, it is often used to describe the sum total of proteins in a cell, taking into account the different levels of protein abundance (Shevchenko *et al.*, 1996; Gygi *et al.*, 2000a; Lopez, 2000; Washburn and Yates, 2000). In an effort to be clear, we propose the term 'translatome' for this second usage of proteome.

With this definition, we are able to refer compactly to three different cellular populations. These are illustrated in Figure 1.

- (i) We use the term *genome* when we refer to the population of open reading frames, where each ORF counts once.
- (ii) We use the term *transcriptome* when we refer to the population of mRNA transcripts. This term was originally coined by Velculescu *et al.* (1997). Note that each ORF may give rise to different numbers of transcripts. Consequently, the transcriptome is essentially the same as the genome but with each ORF weighted by its expression level.
- (iii) The next level is the cellular population of proteins. As each protein represents a translated transcript, we make an analogy with the term transcriptome and use the term *translatome* as described above to describe this third population. Thus, the translatome is a subset of the genome where each ORF is weighted by its associated level of protein abundance.

Note that one could also, less compactly call the translatome a 'weighted proteome.' However, doing so assumes one of the two aforementioned definitions of proteome. To avoid ambiguity, we studiously avoid the use of proteome altogether in the paper.

Differences between the translatome and the transcriptome exist given that transcripts from different genes can give rise to different numbers of proteins, due to different rates of translation and protein degradation. Post-transcriptional modifications further affect the translatome.

In our analysis of the transcriptome and translatome, we focus on global protein features rather than the comparison of individual genes. Previous analyses have shown that differences between mRNA expression and protein abundance levels can be quite dramatic for individual genes. This may either be due to the noise in the data or to fundamental biological processes. However, our analyses show that the variation between transcriptome and translatome is much smaller for global properties that are computed by averaging over the properties of many individual genes.

METHODS

Data sources used

For our analysis we culled many divergent data sets, representing protein abundance and mRNA expression experiments and also other sources of genome annotation. These are all summarized in Table 1.

Biases in the data

The databases that annotate the specific genes may not always be accurate (Ishii *et al.*, 2000). Gene Chip experiments suffer with regard to cross hybridization and the saturation of probes. SAGE data degrades for lowly expressed mRNAs. 2D gels are unable to resolve membrane proteins (approximately 30% of the genome) and basic proteins (Gerstein, 1998c; Krogh *et al.*, 2001). In addition, the procedures for identification and quantification of the protein spots are subject to uncertainties (Haynes and Yates, 2000). Human biases include the lack of low abundance proteins (Fey and Larsen, 2001; Gygi *et al.*, 2000b; Harry *et al.*, 2000) and the differences between laboratories in sample preparation. Our reference expression data set attempts to resolve these problems.

Data set scaling

A reference set for mRNA expression. With many different mRNA expression data sets available, it is worthwhile to integrate them into a single unified reference set, with the intention of reducing the noise and errors contained in the individual data sets and to obtain a unified estimate of the normal expression state in a cell.

We adopt an iterative scaling and merging formalism,

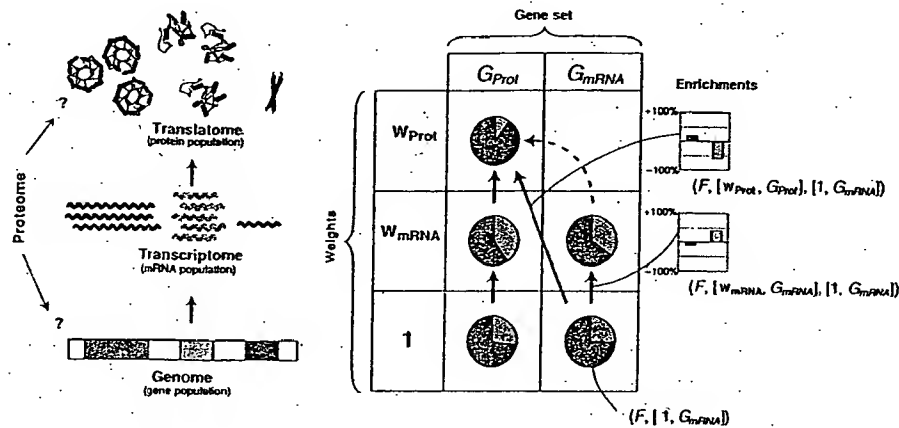


Fig. 1. Schematic overview of the analysis. On the left-side we outline the terms we use to describe the process of gene expression. The coding section of the genome is transcribed into a population of mRNA transcripts called the 'transcriptome.' The transcripts in turn are translated to a population of proteins; we use the term 'translatome' for this protein population rather than the alternative 'proteome' because the latter term may be confounded with the protein complement of the genome (which is not necessarily associated with a quantitative abundance level).

The matrix in the middle schematically shows an analysis of the three stages of expression. In general, we define a protein 'population' as a set of genes associated with a corresponding number of expression or abundance levels ('weights'): In the matrix each row represents a weight and each column a gene set. In particular, we differentiate between the mRNA reference expression set ($G_{mRNA} = G_{Gen}$), which essentially covers the complete genome, and the reference protein abundance set (G_{Prot}) which contains the proteins in data sets 2-DE #1 and 2-DE #2 (see Table 1) because the protein abundance set is a significantly smaller subset of the genome. By definition, this subset contains only proteins that can be identified by 2-D gel electrophoresis and is therefore biased in this sense. The enrichment figures throughout this paper, through a comparison of the right- and left-sides of this figure, show the results of the experimental biases of 2D gels on the data set. Each pie chart represents a composition of a particular protein feature F (for instance, an amino acid composition) in a population (represented by the symbol μ). We can further look at the 'enrichment' of this feature in one population relative to another (represented by the symbol Δ , see Section 'Methods' for an explanation of the formalism).

which we summarize below. We present a more detailed review of the methods on our web site.

We start with the values of one gene chip data set U_i where i is used throughout as a subscript to denote gene number. We then transform the values of the next Gene Chip data set X_i to Y_i with the following non-linear regression: $\min \sum_i (Y_i - U_i)^2$ with $Y_i = A X_i^B$ where A and B are the parameters of the regression. Note that two Gene Chip sets may not be defined for the same set of genes, so we have to perform the fit only over the genes common to both sets. The motivation for scaling is that the dynamic range of observed expression levels varies somewhat between different data sets, although cell types and growth conditions are very similar. Reasons for disparity may include different calibration procedures for relating fluorescence intensity to a cellular concentration (measured in copies of transcripts per cell) or different protocols for harvesting and reverse-transcribing the cellular mRNA.

We then merge and average the data to create a new

reference set V as follows:

$$\text{If } U_i \text{ and } Y_i \text{ are both defined for gene } i \text{ and } \frac{|Y_i - U_i|}{Y_i + U_i} < \alpha$$

$$\text{Then } V_i = \frac{1}{2}(Y_i + U_i)$$

$$\text{Else if only } Y_i \text{ exists, } V_i = Y_i$$

$$\text{Else } V_i = U_i.$$

As presented above, where only one data set has a value for the corresponding ORF, we incorporated that value and did not exclude it. When both data sets have values for an ORF, we averaged the values if they were within 15% of each other; otherwise, we just stayed with the original chip data set U_i . We used $\alpha = 15\%$ in order to prevent outliers from skewing the result. This 15% value is a reasonable threshold for excluding outliers though other values (e.g. 10 or 20%) would give similar results (data not shown). Other data sets are subsequently included in the same procedure, continuing the iteration from the new

expression values V_i . The initial iteration starts with the Young Expression Set, as U_i , since we have the highest confidence in its accuracy.

The SAGE data (Velculescu *et al.*, 1997) was not included in the above procedure since it is of a fundamentally different nature. An advantage of the SAGE technology over Gene Chips is that there is no possible signal saturation for high expression levels, as is possible for chips (Futcher *et al.*, 1999). Conversely, SAGE values are less reliable for lowly expressed genes since there is a chance that one might not sequence a SAGE tag corresponding to such a gene altogether. Therefore, if after the last iteration, the average Gene Chip expression level V_i was both above a certain threshold β and below the SAGE expression level S_i for the same gene, it was replaced with the SAGE value; otherwise the average Gene Chip value was kept. This gave us our final expression set w_{mRNA} . Our treatment of the SAGE data is modeled after that in Futcher *et al.* (1999), and like them, we used $\beta = 16$.

This incorporation of the SAGE data into the reference data set ensures that the highly expressed outliers are as accurate as possible.

Rather than plain arithmetic averaging, this overall scaling procedure with the α cutoff avoids 'artificial averages' that combine very different values for a particular gene. Some expression values might be statistical outliers. In addition, it may be possible that the expression levels of a variety of genes can only be within mutually exclusive ranges or modes, such as when two alternative pathways are switched on or off. Simply averaging these would give values that are less representative of the particular mode values. This situation is analogous to that in averaging together an ensemble of protein structures (i.e. from NMR structure determination). Each structure could be stereochemically correct, with all side-chain atoms in predefined rotamer configurations. However, an average of all structures could yield one that is stereochemically incorrect if this involved averaging over particular side-chains in different rotameric states.

With regard to our regression analysis, we have investigated both non-linear and linear fits but found a non-linear procedure to be more advantageous. The non-linear relationship between different expression data sets perhaps reflects saturation in one or more of the Gene Chips—not an uncommon phenomenon. This non-linearity is immediately evident on scatter plots of two data sets against one another (see website). Accordingly, the non-linear fit produces a smaller residual than the linear fit: 98 297 (non-linear) versus 122 182 (linear) for the scaling of the Church data set and 59 828 (non-linear) versus 67 462 (linear) for the Samson data set.

A reference set for protein abundance. We followed a similar procedure to calculate a reference protein abundance set from the two gel electrophoresis data sets. We first scaled the two data sets against the mRNA expression reference data set, getting regression parameters C_j and D_j :

$$\min \sum_i (P_{i,j} - C_j w_{\text{mRNA},i}^{D_j})^2$$

where the subscript j indicates the data set 2-DE #1 or 2-DE #2 respectively; $P_{i,j}$ is the protein abundance value in data set j , and $w_{\text{mRNA},i}$ the corresponding reference expression value, and C_j and D_j are the parameters of the non-linear regression.

Using these parameters, we transformed the values of set 2-DE #2 onto 2-DE #1. Then we combined both sets into the reference protein set w_{Prot} by averaging them, if both values existed. Otherwise, by using the existing value, viz:

$$Q_{i,2} \equiv C_1 \left(\frac{P_{i,2}}{C_2} \right)^{D_1/D_2}$$

$w_{\text{Prot},i} = (P_{i,1} + Q_{i,2})/2$ if both $P_{i,1}$ and $Q_{i,2}$ exist.

Else if only $P_{i,1}$ exists, $w_{\text{Prot},i} = P_{i,1}$

Else if $Q_{i,2}$ exists, $w_{\text{Prot},i} = Q_{i,2}$.

Enrichment of features

Formalism. In the next part of our analysis, we want to group a number of proteins together into various categories based on common features and characterize those features that are enriched in one population relative to another, i.e. the translome population of proteins as measured by 2D gels relative to the transcriptome population of transcripts or the genome population of genes. To this end, we set up a formalism that could be applied universally to all the attributes that we were interested in. Due to the limitations of the experiments, the translome, transcriptome, and genome populations are defined on different sets of genes, and sometimes we want to remove this 'selection bias' by forcing them to be compared on exactly the same set of genes. This is a key aspect of our formalism as presented in Figure 1.

We call an entity like $[w, G]$ a 'population,' where G is a set describing a particular selection of genes from the genome and w is vector of weights associated with each element of this population. In particular, we focus on three main populations here:

- (i) $[1, G_{\text{Gen}}]$ is the population of genes in the genome, all 6280 genes weighed once ($w = 1$);
- (ii) $[w_{\text{mRNA}}, G_{\text{mRNA}}]$ is the observed population of the transcripts in the transcriptome, i.e. the 6249 genes in the reference expression set weighed by their reference expression value;

- (iii) $[w_{\text{Prot}}, G_{\text{Prot}}]$ is the observed cellular population of the proteins in the translome, i.e. the 181 genes in the reference abundance set weighted by their reference abundance value.

(The set of genes in the genome G_{Gen} is approximately equal to the genes in set G_{mRNA} , such that we can use both symbols interchangeably.) We can also use this notation to describe specific experiments—e.g. $[w_{\text{lacZ}}, G_{\text{lacZ}}]$ describes the gene set and weights relating to the transposon abundance set.

Furthermore, we define F_j as the value of a feature F in ORF j . For example, F could be the composition of leucine (a real number) or a binary value (0 or 1) indicating whether an ORF contains a trans-membrane segment. Given these definitions, the weighted average of feature F in population $[w, G]$ is:

$$\mu(F, [w, G]) \equiv \frac{\sum_{j \in G} w_j F_j}{\sum_{j \in G} w_j}$$

The weighted averages of two populations $[w, G]$ and $[v, S]$ can be compared by simply looking at their relative difference Δ :

$$\Delta(F, [v, S], [w, G]) = \frac{\mu(F, [v, S]) - \mu(F, [w, G])}{\mu(F, [w, G])}$$

where v and w are weights for the sets of ORFs S and G respectively. We call Δ the 'enrichment' of feature F because it indicates whether F is enriched (if Δ is positive) or depleted (if Δ is negative) in population $[v, S]$ relative to $[w, G]$.

Usually, the gene set G is defined by the particular experiment, for which the weight w was measured. However, it is also possible to combine the gene set associated with one experiment with expression levels from another set. One may want to do this to compute the enrichment only on the genes common to both populations, for which there are defined values for both w and v , viz: $\Delta(F, [v, S \cap G], [w, S \cap G])$. In practice, this is most relevant for comparing G_{Prot} and G_{mRNA} . Since G_{Prot} is completely a subset of G_{mRNA} , we need not explicitly deal with intersections if we calculate all statistics directly over G_{Prot} .

One can adjust the weight vectors to take into account different types of averaging. For instance, when computing the amino acid composition ($F = aa$) from the amino acid compositions of individual ORFs $F_j = aa_j$ ($\forall j \in G$), we weight by ORF length. In the case of expression weights, we have:

$$w_j = N_j w_{\text{mRNA}, j} \quad \forall j \in G$$

where N_j is a measure of the length of ORF j (such as the number of amino acids).

On the other hand, when computing the average molecular weight per amino acid, we need to normalize by the number of amino acids per ORF, which is equivalent to choosing the following weights:

$$w_j = \frac{w_{\text{mRNA}, j}}{N_j} \quad \forall j \in G$$

Application of methodology to quantitative abundance sets

Having defined our formalism, we applied it to a diverse set of protein features in yeast.

Amino acid enrichment. As shown in Figure 2a, we used our methodology to measure the enrichment of individual amino acids in both the translome and the transcriptome relative to the genome. We found that three amino acids—valine, glycine and alanine—were consistently enriched in both transcriptome and translome populations.

In Figure 2a we compare different gene sets. In Figure 2b we focus mainly on the variation in enrichments when all the comparisons are restricted to the set of 181 genes ($G_{\text{Prot}} \cap G_{\text{mRNA}} = G_{\text{Prot}}$) common to all data sets. Thus, the differences between the populations now only reflect the effects of differential transcription of certain genes and differential translation of certain transcripts. We find here an enrichment specifically of cysteine in the translome in relation to the transcriptome.

To measure the statistical significance of the results on amino acid enrichment, we have performed a control analysis on a randomized data set (Figure 2d). We randomly permuted the expression values of the ORFs 1000 times and then recomputed the enrichments. This allowed us to compute distributions for the amino acid enrichments and, from integrating these, one-sided p -values indicating the significance of the observed enrichments.

Amino acid enrichment in Transposon data set. We also tried to extend our methodology, ineffectively, to cope with the semi-quantitative Transposon set. We used only those 450 ORFs that consistently yielded either no expression or high expression, as binary data, on or off. We show the enrichments of amino acids computed from this filtered Transposon abundance set in Figure 2a. Overall, the enrichments from this set seemed to be attenuated in comparison to other data.

Biomass enrichment. A corollary to amino acid enrichments is the determination of the average biomass of the transcriptome and translome populations (shown in Figure 2c). We found that the average molecular weight of a protein in both populations was, on average, lower than in the genome population. These preliminary observations suggest a cell preference to use less energetically expensive proteins for those that are highly transcribed or trans-

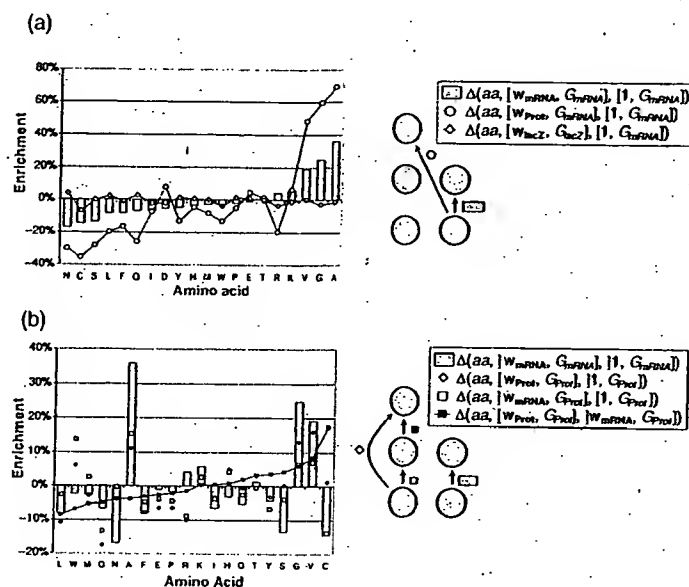


Fig. 2. Amino acid and biomass enrichment. (a) Shows the amino acid enrichments between different populations as indicated by the legend to the right of the plot (the legend is ordered in the same way as the schematic illustration in Figure 1). The bars indicate the enrichment of the transcriptome relative to the genome, whereas the circles indicate the enrichment of the translome relative to the genome. In addition, we also show the enrichment for protein abundance from the Transposon abundance set, represented by the circles with the line through them. (b) Shows a different view of amino acid enrichment from that contained in (a), now focusing on changes, and thus restricting the comparison to the genes common to all the data sets. The graph is ordered according to the enrichment from transcriptome to translome (black squares). We focus here only on the changes for the abundance gene set (G_{Pro}) to exclude the effects that arise from looking at different subsets. In this view the enrichments from genome to transcriptome (white squares) and from genome to translome (white diamonds) look more similar than do the analogous sets in (a). To make comparison with (a) easier we again show the enrichment from genome to the transcriptome for the complete gene set (G_{Gen} , shown in bars). (c) Shows biomass enrichment. The left panel depicts the average molecular weight per ORF (in units of kDa) and the right panel, the average molecular weight per amino acid (in units of Daltons) in each of the three stages of gene expression. The numbers inside the circles indicate the average molecular weights. The values next to the arrows indicate the enrichments in biomass between different populations. Both the circle diameters and the arrow widths are functions of the corresponding values (the hollow arrow indicates a positive value). It is very clear that the average molecular weight per ORF is much lower in the translome (by 20 or 15%) and transcriptome (by 29%) than in the genome. This relative depletion of biomass mainly takes place as a result of transcription; the effect of translation is less clear, depending on the populations compared. On the other hand, the depletion in the average molecular weight per amino acid (-3.3% from genome to translome) is an order of magnitude smaller than in the average weight per ORF. This shows that the yeast cell favors the expression of shorter ORFs over longer ones, and agrees with our earlier observation that there is a negative correlation between maximum ORF length and mRNA expression (Jansen and Gerstein, 2000); it seems that this effect mainly takes place during transcription rather than translation. (d) This plot shows that the amino acid enrichments are statistically significant. We have assessed significance by randomly permuting the expression levels among the genes and then recomputing the amino acid enrichments. This procedure can be repeated and used to generate distributions of random enrichments that can then be compared against the observed enrichments. In the plot the gray bars represent the observed enrichments already shown in Figure 3a. On top of the gray bars we show standard boxplots of enrichment distributions based on 1000 random permutations. (The middle line represents the distribution median. The upper and lower sides of the box coincide with the upper and lower quartiles. Outliers are shown as dots and defined as data points that are outside the range of the whiskers, the length of which is 1.5 the interquartile distance.) Based on the random distributions, we can compute one-sided p -values for the observed enrichments. Amino acids for which the p -values are less than 10^{-3} are shown in bold font.

lated. However, we also found that the average molecular weight *per amino acid* differed much less between the transcriptome and the translome on the one hand, and the

genome on the other hand (though it was still slightly less). This finding indicates that lower molecular weights in the translome and transcriptome relative to the genome are

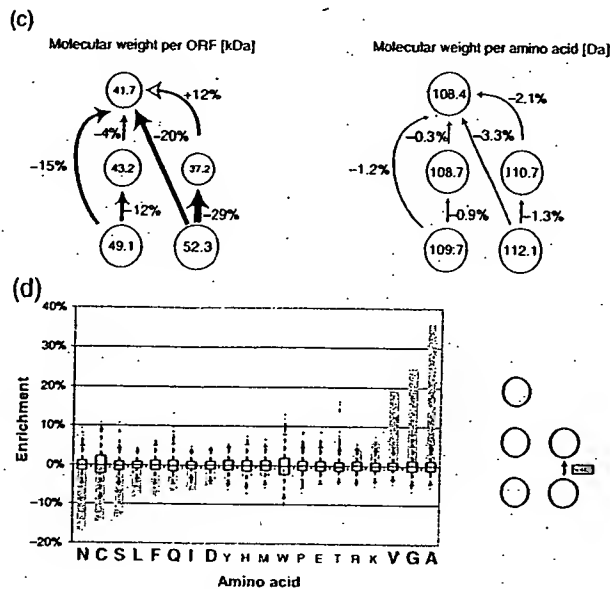


Fig. 2. Cont.

predominantly due to greater expression of shorter proteins rather than the incorporation of smaller amino acids.

Secondary structure composition. We also used our methodology to study the enrichment of secondary-structural features. Secondary structural annotation was derived from structure prediction applied uniformly to all the ORFs in the yeast genome as described in Table 1. As shown in Figure 3a, all three populations—genome, transcriptome, and translatome—had a fairly similar composition of secondary structures—sheets, helices, and coils. The differences between populations were marginal and based only on the small subset of genes.

We also found that Transmembrane (TM) proteins were significantly depleted in the transcriptome (see website and caption). These results are consistent with our previous analyses (Jansen and Gerstein, 2000). The protein abundance data does not have any membrane proteins.

Subcellular localization. Figure 3c shows the enrichment of proteins associated with the various subcellular compartments. For clarity, we divided the cell into five distinct subcellular compartments, (see Table 1). We found that, in comparison to the genome, both the transcriptome and translatome are enriched in cytoplasmic proteins. This is true whether we make our comparisons in

relation to the relatively large reference mRNA expression set or the smaller reference protein abundance set. As Figure 3c shows, the 2D gel experiments are clearly biased towards proteins from the cytoplasm. However, in the biased subset G_{Prot} transcription and translation lead to an even higher fraction of cytoplasmic proteins in the translatome.

Functional categories. Finally, we compared the enrichment of various functional categories in both the translatome and the transcriptome (see Figure 3b). This gives us a broad yet informative view of the cell as a whole. As described in Table 1, we used the top-level of the MIPS scheme for the functional category definitions. We found broad differences between the various populations, with some of the functional categories showing strikingly high enrichments.

DISCUSSION AND CONCLUSION

We developed: (i) a methodology for integrating many different types of gene expression and protein abundance into a common framework and applied this to a preliminary analysis; (ii) a procedure for scaling and merging different mRNA and protein sets together; and (iii) an approach for computing the enrichment of various proteomic features in the population of transcripts and proteins. We showed that by analyzing broad categories instead of individual noisy

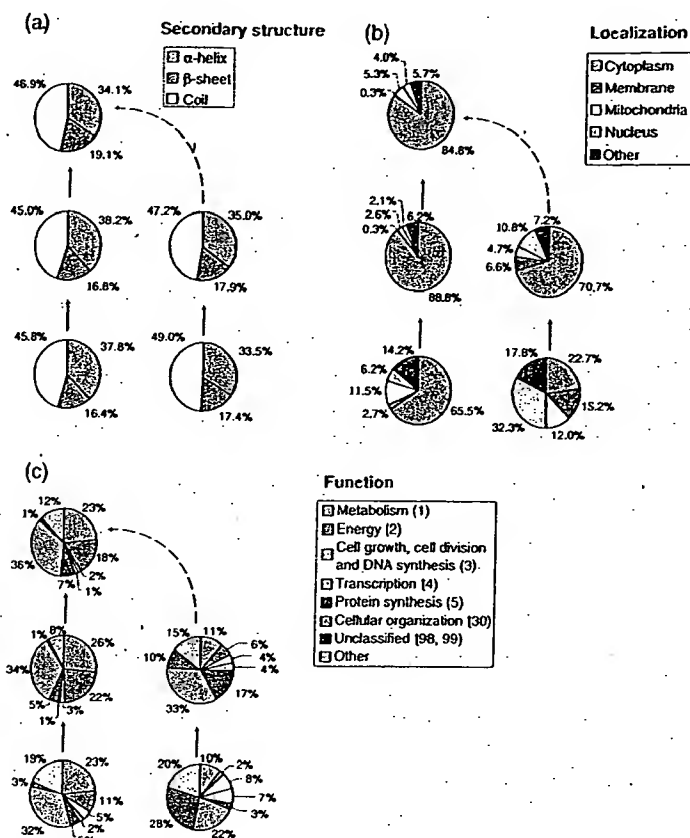


Fig. 3. Breakdown of the transcriptome and translome in terms of broad categories relating to structure, localization, and function. All of the subfigures are analogous to the schematic illustration in Figure 1. (a) Represents the composition of secondary structure in the different populations. (b) Represents the distribution of subcellular localizations associated with proteins in the various populations. We used standardized localizations developed earlier (Drawid and Gerstein, 2000), which, in turn, were derived from the MIPS, YPD, and SwissProt databases (Bairoch and Apweiler, 2000; Costanzo *et al.*, 2000; Mewes *et al.*, 2000). The subcellular localization has been experimentally determined for less than half of the yeast proteins, so our analysis applies only to this subset. (c) Shows the division of ORFs into different functional categories (according to the MIPS classification) in the various populations. Only the largest functional categories of the top level of the MIPS classification are shown. The group 'other' contains the smaller top-level categories lumped together. This 'other' group is different from the group 'unclassified,' which contains genes without any functional description.

data points, we could find logical trends in the underlying data. For example, individual transcription factors might have higher or lower protein abundance than one expects from their mRNA expression, but the category 'transcription factors' as a whole has a similar representation in the transcriptome and translome.

We found, as previously described (Futcher *et al.*, 1999; Gygi *et al.*, 1999b; Greenbaum *et al.*, 2001), a weak correlation between individual measurements of mRNA

and protein abundance. The outliers of this correlation tend to be associated with cellular organization. One might conceive of using these outliers (i.e. those with significantly different transcriptional and translational behavior) to find consensus regulatory sequences. One possible method would involve using predicted mRNA structures (Jaeger *et al.*, 1990; Zuker, 2000) to find and investigate consensus structural elements in these outliers to which the yeast translational machinery is known to be

Table 1. Data sets

Data set	Description	Size (ORFs)	Reference
mRNA expression			
Young	Gene chip profiles yeast cells with mutations that affect transcription	5455	Holstege <i>et al.</i> (1998)
Church	Gene chip profiles of yeast cells under four different conditions	6263	Roth <i>et al.</i> (1998)
Samson	Comparing gene chip profiles for yeast cells subjected to alkylating agent	6090	Jelinsky and Samson (1999)
SAGE	Yeast cells during vegetative growth	3778	Velculescu <i>et al.</i> (1997)
Reference expression	Scaling and integrating the mRNA expression set into one data source	6249	—
Protein abundance			
2-DE #1	Measurement of yeast protein abundance by 2D gel electrophoresis and mass spectrometry	156	Gygi <i>et al.</i> (1999a,b)
2-DE #2	Similar to 2-DE set #1	71	Futcher <i>et al.</i> (1999)
Transposon	Large-scale fusions of yeast genes with <i>lacZ</i> by transposon insertion	1410	Ross-Macdonald <i>et al.</i> (1999)
Reference abundance	Scaling and integrating the 2-DE data sets into one data source	181	—
Annotation			
Annotated localization	Subcellular localizations of yeast proteins	2133 (6280)	Drawid and Gerstein (2000)
TM segments	Predicted TM and soluble proteins in yeast	2710 (6280)	Gerstein (1998a,b,c)
MIPS functions	Functional categories for yeast ORFs	3519 (6194)	Mewes <i>et al.</i> (2000)
GOR secondary structure	Predicted secondary structure yeast ORFs	6280	Gerstein (1998a,b,c)

This table provides an overview of the data sets used in our analysis. The table is divided into three sections. The top section lists different mRNA expression sets. The middle section shows the protein abundance data sets used. The bottom section contains different annotations of protein features. The column 'Data set' lists a shorthand reference to each data set used throughout this paper. The next columns contain a brief description of the data sets, the number of ORFs contained in each of them, and the literature reference. In contrast to the other data we investigated, the reference expression and abundance data sets have been calculated for the purpose of our analysis (see text). An expanded version of the table is available on our web site.

Some further information on the genome annotations:

Localization. Protein localization information from YPD, MIPS and SwissProt were merged, filtered and standardized (Bairoch and Apweiler, 2000; Costanzo *et al.*, 2000; Mewes *et al.*, 2000) into five simplified compartments—cytoplasm, nucleus, membrane, extracellular (including proteins in ER and golgi), and mitochondrial—according to the protocol in Drawid *et al.* (2000). This yielded a standardized annotation of protein subcellular localization for 2133 out of 6280 ORFs.

TM segments. In 2710 out of 6280 yeast ORFs TM segments are predicted to occur, ranging from low to high confidence (732 ORFs). The TM prediction was performed as follows: the values from the scale for amino acids in a window of size 20 (the typical size of a TM helix) were averaged and then compared against a cutoff of -1 kcal mol^{-1} . A value under this cutoff was taken to indicate the existence of a TM helix. Initial hydrophobic stretches corresponding to signal sequences for membrane insertion were excluded. (These have the pattern of a charged residue within the first seven, followed by a stretch of 14 with an average hydrophobicity under the cutoff.) These parameters have been used, tested, and refined on surveys of membrane protein in genomes. 'Sure' membrane proteins had at least two TM-segments with an average hydrophobicity less than -2 kcal mol^{-1} (Rost *et al.*, 1995; Gerstein *et al.*, 2000; Sanjoni *et al.*, 2000; Senes *et al.*, 2000).

Functions. MIPS functional categories have been assigned to 3519 out of 6194 ORFs. (The remainder are assigned to category '98' or '99,' which corresponds to unclassified function.)

sensitive (McCarthy, 1998).

In relation to functional categories, we found three trends that were particularly notable: (i) the 'cellular

organization,' 'protein synthesis,' and 'energy production' categories were increasingly enriched as we moved from genome to transcriptome to translome. In the transcrip-

tome and translome population relative to the genome; (ii) proteins with 'unclassified function' are significantly depleted, perhaps reflecting a bias against studying them; (iii) proteins in the 'transcription' and 'cell growth, cell division, and DNA synthesis' categories were consistently depleted. This reflects the fact that many of these proteins, such as transcription factors, act as 'switches' such that only small quantities of the protein are necessary to activate or deactivate a process. These results concur with previous calculations (Jansen and Gerstein, 2000) wherein we found the transcriptome is enriched specifically with proteins involved in protein synthesis and energy.

Limitations given the small size of the protein abundance data

Even with the extended coverage made possible by merging many data sets together into reference sets, the analysis is still limited by the minimal data. This was most applicable to the protein abundance measurements, potentially biasing our statistical results towards certain protein families. Moreover, the 181 proteins in G_{ProI} do not represent a random sample. They are skewed towards highly expressed, well-studied proteins. Our methodology attempts to control for this gene-selection bias through our enrichment formalism, which allows one to rather precisely gauge various aspects of the bias. Conversely, many protein features in both the translome and the transcriptome are dominated by highly expressed proteins. Under these circumstances, it is often sufficient to look at this smaller number of dominating proteins to characterize the whole population. This is similar to the development of the codon adaptation index for yeast (Sharp and Li, 1987). While based on only 24 highly expressed proteins, it has proven to be robust in predicting expression levels for the entire genome.

We believe that the essential formalism and approach that we develop will remain quite relevant for future data sets (Smith, 2000).

ACKNOWLEDGEMENT

M.G. thanks the Keck foundation for support.

REFERENCES

- An, H., Scopes, R.K. et al. (1991) Gel electrophoretic analysis of *Zymomonas mobilis* glycolytic and fermentative enzymes: identification of alcohol dehydrogenase 11 as a stress protein. *J. Bacteriol.*, 173, 5975–5982.
- Anderson, L. and Seilhamer, J. (1997) A comparison of selected mRNA and protein abundances in human liver. *Electrophoresis*, 18, 533–537.
- Bairoch, A. (2000) Serendipity in bioinformatics, the tribulations of a Swiss bioinformatician through exciting times! *Bioinformatics*, 16, 48–64.
- Bairoch, A. and Apweiler, R. (2000) The SWISS-PROT protein sequence database and its supplement TrEMBL in 2000. *Nucleic Acids Res.*, 28, 45–48.
- Bassett, D.E. Jr., Basrai, M.A. et al. (1996) Exploiting the complete yeast genome sequence. *Curr. Opin. Genet. Dev.*, 6, 763–766.
- Batke, J., Benito, V.A. et al. (1992) A possible in vivo mechanism of intermediate transfer by glycolytic enzyme complexes: steady state fluorescence anisotropy analysis of an enzyme complex formation. *Arch. Biochem. Biophys.*, 296, 654–659.
- Cambillau, C. and Claverie, J.M. (2000) Structural and genomic correlates of hyperthermostability. *J. Biol. Chem.*, 275, 32383–32386.
- Cavalcoli, J.D., VanBogelen, R.A. et al. (1997) Unique identification of proteins from small genome organisms: theoretical feasibility of high throughput proteome analysis. *Electrophoresis*, 18, 2703–2708.
- Claverie, J.M. (1999) Computational methods for the identification of differential and coordinated gene expression [in process citation]. *Hum. Mol. Genet.*, 8, 1821–1832.
- Corthals, G., Wasinger, V.C., Hochstrasser, D.F. and Sanchez, J.C. (2000) The dynamic range of protein expression: a challenge for proteomic research. *Electrophoresis*, 21, 1104–1115.
- Costanzo, M.C., Hogan, J.D. et al. (2000) The Yeast Proteome Database (YPD) and *Caenorhabditis elegans* Proteome Database (WormPD): comprehensive resources for the organization and comparison of model organism protein information. *Nucleic Acids Res.*, 28, 73–76.
- Das, R. and Gerstein, M. (2000) The stability of thermophilic proteins: a study based on comprehensive genome comparison. *Funct. Int. Genom.*, 1, 33–45.
- Doolittle, W.F. (2000) The nature of the universal ancestor and the evolution of the proteome. *Curr. Opin. Struct. Biol.*, 10, 355–358.
- Drawid, A. and Gerstein, M. (2000) A Bayesian system integrating expression data with sequence patterns for localizing proteins: comprehensive application to the yeast genome. *J. Mol. Biol.*, 301, 1059–1075.
- Drawid, A., Jansen, R. et al. (2000) Gene expression levels are correlated with protein subcellular localization. *Trends Genet.*, 10, 426–430.
- Einarson, M. and Golemis, E. (2000) Encroaching genomics: adapting large-scale science to small academic laboratories. *Physiol. Genom.*, 2, 85–92.
- Eisen, M.B. and Brown, P.O. (1999) DNA arrays for analysis of gene expression. *Meth. Enzymol.*, 303, 179–205.
- Epstein, C. and Butow, R. (2000) Microarray technology—enhanced versatility, persistent challenge. *Curr. Opin. Biotechnol.*, 11, 36–41.
- Ferea, T. and Brown, P. (1999) Observing the living genome. *Curr. Opin. Genet. Dev.*, 9, 715–722.
- Fey, S.J., Nawrocki, A. et al. (1997) Proteome analysis of *Saccharomyces cerevisiae*: a methodological outline. *Electrophoresis*, 18, 1361–72.
- Fey, S.J. and Larsen, P.M. (2001) 2D or not 2D. Two-dimensional gel electrophoresis. *Curr. Opin. Chem. Biol.*, 5, 26–33.
- Frishman, D. and Mewes, H.W. (1997) Protein structural classes in five complete genomes [letter]. *Nat. Struct. Biol.*, 4, 626–628.
- Frishman, D. and Mewes, H.W. (1999) Genome-based structural biology. *Prog. Biophys. Mol. Biol.*, 72, 1–17.

- Futcher, B., Laiter, G. *et al.* (1999) A sampling of the yeast proteome. *Mol. Cell Biol.*, **19**, 7357–7368.
- Gaasterland, T. (1999) Archaeal genomics. *Curr. Opin. Microbiol.*, **2**, 542–547.
- Garrels, J.I., McLaughlin, C.S. *et al.* (1997) Proteome studies of *Saccharomyces cerevisiae*: identification and characterization of abundant proteins. *Electrophoresis*, **18**, 1347–1360.
- Gerstein, M. (1997) A structural census of genomes: comparing bacterial, eukaryotic, and archaeal genomes in terms of protein structure. *J. Mol. Biol.*, **274**, 562–576.
- Gerstein, M. (1998a) How representative are the known structures of the proteins in a complete genome? A comprehensive structural census. *Fold. Des.*, **3**, 497–512.
- Gerstein, M. (1998b) Patterns of protein-fold usage in eight microbial genomes: a comprehensive structural census. *Proteins*, **33**, 518–534.
- Gerstein, M. (1998c) Patterns of protein-fold usage in eight microbial genomes: a comprehensive structural census. *Proteins*, **33**, 518–534.
- Gerstein, M. and Hegyi, H. (1998) Comparing genomes in terms of protein structure: surveys of a finite parts list. *FEMS Microbiol. Rev.*, **22**, 277–304.
- Gerstein, M. and Jansen, R. (2000) The current excitement in bioinformatics, analysis of whole-genome expression data: how does it relate to protein structure and function. *Curr. Opin. Struct. Biol.*, **10**, 574–584.
- Gerstein, M., Lin, J. *et al.* (2000) Protein folds in the worm genome. *Pac. Symp. Biocomput.*, 30–41.
- Greenbaum, D., Luscombe, N. *et al.* (2001) Interrelating different types of genomic data, from proteome to secretome: 'oming in on function. *Genome Res.*, **11**, 1463–1468.
- Gygi, S.P., Rist, B. *et al.* (1999a) Quantitative analysis of complex protein mixtures using isotope-coded affinity tags. *Nature Biotechnol.*, **17**, 994–999.
- Gygi, S.P., Rochon, Y. *et al.* (1999b) Correlation between protein and mRNA abundance in yeast. *Mol. Cell Biol.*, **19**, 1720–1730.
- Gygi, S.P., Corhals, G.L. *et al.* (2000a) Evaluation of two-dimensional gel electrophoresis-based proteome analysis technology. *Proc. Natl Acad. Sci. USA*, **97**, 9390–9395.
- Gygi, S.P., Rist, B. *et al.* (2000b) Measuring gene expression by quantitative proteome analysis. *Curr. Opin. Biotechnol.*, **11**, 396–401.
- Harry, J.L., Wilkins, M.R. *et al.* (2000) Proteomics: capacity versus utility. *Electrophoresis*, **21**, 1071–1081.
- Hatzimanikatis, V., Choe, L.H. *et al.* (1999) Proteomics: theoretical and experimental considerations. *Biotechnol. Prog.*, **15**, 312–318.
- Haynes, P.A. and Yates, J.R. (2000) Proteome profiling: pitfalls and progress. *Yeast*, **17**, 81–87.
- Hegyi, H. and Gerstein, M. (1999) The relationship between protein structure and function: a comprehensive survey with application to the yeast genome. *J. Mol. Biol.*, **288**, 147–164.
- Holstege, F.C., Jennings, E.G. *et al.* (1998) Dissecting the regulatory circuitry of a eukaryotic genome. *Cell*, **95**, 717–728.
- Ishii, M., Hashimoto, S. *et al.* (2000) Direct comparison of genechip and SAGE on the quantitative accuracy in transcript profiling analysis. *Genomics*, **68**, 136–143.
- Ito, T., Tashiro, K. *et al.* (2000) Toward a protein–protein interaction map of the budding yeast: a comprehensive system to examine two-hybrid interactions in all possible combinations between the yeast proteins. *Proc. Natl Acad. Sci. USA*, **97**, 1143–1147.
- Jaeger, J.A., Turner, D.H. *et al.* (1990) Predicting optimal and suboptimal secondary structure for RNA. *Meth. Enzymol.*, **183**, 281–306.
- Jansen, R. and Gerstein, M. (2000) Analysis of the yeast transcriptome with structural and functional categories: characterizing highly expressed proteins. *Nucleic Acids Res.*, **28**, 1481–1488.
- Jelinsky, S.A. and Samson, L.D. (1999) Global response of *Saccharomyces cerevisiae* to an alkylating agent. *Proc. Natl Acad. Sci. USA*, **96**, 1486–1491.
- Jones, D.T. (1998) Do transmembrane protein superfolds exist? *FEBS Lett.*, **423**, 281–285.
- Jones, D.T. (1999) GenTHREADER: an efficient and reliable protein fold recognition method for genomic sequences. *J. Mol. Biol.*, **287**, 797–815.
- Kidd, D. *et al.* (2001) Profiling serine hydrolase activities in complex proteomes. *Biochemistry*, **40**, 4005–4015.
- Klose, J. (1975) Protein mapping by combined isoelectric focusing and electrophoresis of mouse tissues. A novel approach to testing for induced point mutations in mammals. *Humangenetik*, **26**, 231–243.
- Krogh, A. *et al.* (2001) Predicting transmembrane protein topology with a hidden Markov model: application to complete genomes. *J. Mol. Biol.*, **305**, 567–580.
- Lin, J. and Gerstein, M. (2000) Whole-genome trees based on the occurrence of folds and orthologs: implications for comparing genomes on different levels. *Genome Res.*, **10**, 808–818.
- Lipshutz, R.F. S., Gingeras, T.R. and Lockhart, D.J. (1999) High density synthetic oligonucleotide arrays. *Nature Genet.*, **21**, 20–24.
- Lopez, M.F. (2000) Better approaches to finding the needle in a haystack: optimizing proteome analysis through automation. *Electrophoresis*, **21**, 1082–1093.
- MacBeath, G. and Schreiber, S.L. (2000) Printing proteins as microarrays for high-throughput function determination. *Science*, **289**, 1760–1763.
- Matton, D.P., Constabel, P. *et al.* (1990) Alcohol dehydrogenase gene expression in potato following elicitor and stress treatment. *Plant Mol. Biol.*, **14**, 775–783.
- McCarthy, J.E. (1998) Posttranscriptional control of gene expression in yeast. *Microbiol. Mol. Biol. Rev.*, **62**, 1492–1553.
- Mewes, H.W., Frishman, D. *et al.* (2000) MIPS: a database for genomes and protein sequences. *Nucleic Acids Res.*, **28**, 27–40.
- Millar, A.A., Olive, M.R. *et al.* (1994) The expression and anaerobic induction of alcohol dehydrogenase in cotton. *Biochem. Genet.*, **32**, 279–300.
- Molloy, M.P. (2000) Two-dimensional electrophoresis of membrane proteins using immobilized pH gradients. *Anal. Biochem.*, **280**, 1–10.
- Nauchitel, V.V. and Somorjai, R.L. (1994) Spatial and free energy distribution patterns of amino acid residues in water soluble proteins. *Biophys. Chem.*, **51**, 327–336.
- Nelson, R.W., Nedelkov, D. *et al.* (2000) Biosensor chip mass spectrometry: a chip-based proteomics approach. *Electrophoresis*, **21**, 1155–1163.
- O'Farrell, P.H. (1975) High resolution two-dimensional elec-

- trophoresis of proteins. *J. Biol. Chem.*, 250, 4007-4021.
- Pandey,A. and Mann,M. (2000) Proteomics to study genes and genomes. *Nature*, 405, 837-846.
- Qi,S.Y., Moir,A. et al. (1996) Proteome of *Salmonella typhimurium* SL1344: identification of novel abundant cell envelope proteins and assignment to a two-dimensional reference map. *J. Bacteriol.*, 178, 5032-5038.
- Ross-Macdonald,P., Coelho,P.S. et al. (1999) Large-scale analysis of the yeast genome by transposon tagging and gene disruption. *Nature*, 402, 413-418.
- Rost,B., Casadio,R. et al. (1995) Transmembrane helices predicted at 95% accuracy. *Protein Sci.*, 4, 521-533.
- Roth,F.P., Hughes,J.D. et al. (1998) Finding DNA regulatory motifs within unaligned noncoding sequences clustered by whole-genome mRNA quantitation. *Nature Biotechnol.*, 16, 939-945.
- Rubin,G.M., Yandell,M.D. et al. (2000) Comparative genomics of the eukaryotes. *Science*, 287, 2204-2215.
- Sali,A. (1999) Functional links between proteins. *Nature*, 402, 25-26.
- Santoni,V., Molloy,M. et al. (2000) Membrane proteins and proteomics: an amour impossible? *Electrophoresis*, 21, 1054-1070.
- Schena,M., Shalon,D. et al. (1995) Quantitative monitoring of gene expression patterns with a complementary DNA microarray. *Science*, 270, 467-470.
- Searls,D.B. (2000) Using bioinformatics in gene and drug discovery. *Drug Discov. Today*, 5, 135-143.
- Senes,A., Gerstein,M. et al. (2000) Statistical analysis of amino acid patterns in transmembrane helices: the GxxxG motif occurs frequently and in association with beta-branched residues at neighboring positions. *J. Mol. Biol.*, 296, 921-936.
- Shapiro,L. and Harris,T. (2000) Finding function through structural genomics. *Curr. Opin. Biotechnol.*, 11, 31-35.
- Sharp,P.M. and Li,W.H. (1987) The codon adaptation index—a measure of directional synonymous codon usage bias, and its potential applications. *Nucleic Acids Res.*, 15, 1281-1295.
- Sherlock,G. (2000) Analysis of large-scale gene expression data. *Curr. Opin. Immunol.*, 12, 201-205.
- Shevchenko,A., Jensen,O.N. et al. (1996) Linking genome and proteome by mass spectrometry: large-scale identification of yeast proteins from two dimensional gels. *Proc. Natl Acad. Sci. USA*, 93, 14 440-14 445.
- Smith,R.D. (2000) Probing proteomes-seeing the whole picture? *Nature Biotechnol.*, 18, 1041-1042.
- Tatusov,R.L., Koonin,E.V. et al. (1997) A genomic perspective on protein families. *Science*, 278, 631-637.
- Tekaia,F., Lazzano,A. et al. (1999) The genomic tree as revealed from whole proteome comparisons. *Genome Res.*, 9, 550-557.
- Velculescu,V.E., Zhang,L. et al. (1997) Characterization of the yeast transcriptome. *Cell*, 88, 243-251.
- Wallin,E. and von Heijne,G. (1998) Genome-wide analysis of integral membrane proteins from eubacterial, archaean, and eukaryotic organisms. *Protein Sci.*, 7, 1029-1038.
- Washburn,M.P., Wolters,D. et al. (2001) Large-scale analysis of the yeast proteome by multidimensional protein identification technology. *Nature Biotechnol.*, 19, 242-247.
- Washburn,M.P. and Yates,J.R. 3rd (2000) Analysis of the microbial proteome. *Curr. Opin. Microbiol.*, 3, 292-297.
- Wittes,J. and Friedman,H.P. (1999) Searching for evidence of altered gene expression: a comment on statistical analysis of microarray data [editorial; comment]. *J. Natl Cancer Inst.*, 91, 400-401.
- Wolf,Y.I., Brenner,S.E. et al. (1999) Distribution of protein folds in the three superkingdoms of life. *Genome Res.*, 9, 17-26.
- Young,K.H. (1998) Yeast two-hybrid: so many interactions, (in) so little time *Biol. Reprod.*, 58, 302-311.
- Zhang,M.Q. (1999) Large-scale gene expression data analysis: a new challenge to computational biologists (published erratum appears in *Genome Res.*, 1999, 9, 1156). *Genome Res.*, 9, 681-688.
- Zhu,H., Klemic,J.F. et al. (2000) Analysis of yeast protein kinases using protein chips. *Nature Genet.*, 26, 283-289.
- Zuker,M. (2000) Calculating nucleic acid secondary structure. *Curr. Opin. Struct. Biol.*, 10, 303-310.

Thymidine Kinase, Thymidylate Synthase, and Dihydropyrimidine Dehydrogenase Profiles of Cell Lines of the National Cancer Institute's Anticancer Drug Screen

Jean L. Grem,¹ Kathleen D. Danenberg, Katherine Behan, Allyson Parr, Lauren Young, Peter V. Danenberg, Diana Nguyen, James Drake, Anne Monks, and Carmen J. Allegra

Developmental Therapeutics Department, Medicine Branch, Division of Clinical Sciences, National Cancer Institute at the National Naval Medical Center, Bethesda, Maryland 20889 [J. L. G., K. B., A. P., L. Y., D. N., C. J. A.]; Norris Cancer Center, University of Southern California, Los Angeles, California 90033 [K. D. D., P. V. D.]; Developmental Therapeutics Program, Division of Cancer Treatment and Diagnosis, National Cancer Institute, Bethesda, Maryland 20852 [J. D.]; and Science Applications International Corporation-Frederick, National Cancer Institute-Frederick Cancer Research and Development Center, Frederick, Maryland 21702 [A. M.]

ABSTRACT

Purpose: To determine the expression of three targets of 5-fluorouracil (5-FU) and 5-fluoro-2'-deoxyuridine (FdUrd) in human tumor cell lines and to compare these with the 50% growth inhibition concentrations (GI₅₀) from the National Cancer Institute database.

Experimental Design: Thymidine kinase (TK) activity was assessed by conversion of [³H]thymidine to [³H]TMP. Thymidylate synthase (TS) protein expression was determined by Western analysis. TS and dihydropyrimidine dehydrogenase (DPD) mRNA expression were measured by quantitative reverse transcription-PCR.

Results: The median (range) for the targets were as follows: 5-FU GI₅₀, 20.8 μM (0.8–536); FdUrd GI₅₀, 0.75 μM (0.25–237); TK, 0.93 nmol/min/mg (0.16–5.7); in arbitrary units: TS protein, 0.41 (0.05–2.95); TS mRNA, 1.05 (0.12–6.41); and DPD mRNA, 1.09 (0.00–24.4). A moderately strong correlation was noted between 5-FU and FdUrd GI₅₀s ($r = 0.60$), whereas a weak-moderate correlation was seen between TS mRNA and protein expression ($r = 0.45$). Neither TS expression nor TK activity correlated with 5-FU or FdUrd GI₅₀s, whereas lines with lower DPD expression tended to be more sensitive to 5-FU. Cell lines with faster doubling times and wild-type p53 were significantly more sensitive to 5-FU and FdUrd.

Conclusions: The lack of correlation may in part be attributable to the influence of downstream factors such as p53, the observation that the more sensitive cell lines with faster doubling times also had higher TS levels, and the standard procedure of the screen that uses a relatively short (48-h) drug exposure.

INTRODUCTION

The NCI² has established a panel consisting of 60 human cancer cell lines to serve as a screen for drug discovery (1–5). The panel represents nine histologies including leukemia, melanoma, and carcinomas arising in the lung, colon, CNS, ovary, kidney, prostate, and breast. Growth inhibition for a particular compound is summarized by the 50% growth inhibition concentration for the cell line panel. A mean graph can be generated both with and without log transformation; the relative sensitivity of each cell line is then compared with the mean for the entire cell panel (6–7). The COMPARE algorithm analyzes these activity patterns by searching among the database of tested compounds for similar profiles for activity, whereas the DISCOVERY software program uses additional analytical tools. Comparison of the “fingerprint” for drug sensitivity among investigational agents with those of drugs with established mechanisms of action can provide insight into potential cross-resistance between analogues and to assign unknown compounds into classes of anticancer agents with different mechanisms of action (8–11). These cell lines are currently undergoing biochemical and molecular characterization to elucidate the basis for differential chemosensitivity responses. It is hoped that matching the pattern of mRNA or protein expression with sensitivity to investigational agents may also assist in identifying novel agents that selectively target a particular phenotype (12, 13).

The antimetabolite 5-FU has clinically useful activity against a variety of human epithelial malignancies, and its deoxyribonucleoside metabolite, FdUrd, is primarily used for regional delivery to treat hepatic metastasis (14). The objectives of this study were to measure several key determinants of sensitivity to fluoropyrimidines and to compare either protein or mRNA expression with the growth-inhibitory activity of 5-FU and FdUrd in the NCI database. The targets selected included TS, TK, and DPD. TS governs the *de novo* synthesis of TMP

Received 6/28/00; revised 12/28/00; accepted 1/8/01.

The costs of publication of this article were defrayed in part by the payment of page charges. This article must therefore be hereby marked advertisement in accordance with 18 U.S.C. Section 1734 solely to indicate this fact.

¹ To whom requests for reprints should be addressed, at NCI-Medicine Branch, National Naval Medical Center, Building 8, Room 5101, 8901 Wisconsin Avenue, Bethesda, MD 20889-5105; Phone: (301) 435-5382; Fax: (301) 480-1683.

² The abbreviations used are: NCI, National Cancer Institute; 5-FU, 5-fluorouracil; FdUrd, 5-fluoro-2'-deoxyuridine; FdUMP, 5-fluoro-2'-deoxyuridine 5'-monophosphate; TS, thymidylate synthase; TK, thymidine kinase; DPD, dihydropyrimidine dehydrogenase; FBS, fetal bovine serum; GI₅₀, concentration of drug that produces 50% growth inhibition; HPLC, high performance liquid chromatography; CNS, central nervous system.

Table 1 Summary of target expression

Histology/Cell line	5-FU GI ₅₀ (μ M)	FdUrd GI ₅₀ (μ M)	TK activity (nmol/min/mg)	Relative TS protein	Relative TS mRNA	Relative DPD mRNA
Leukemia						
CCRF	29.79	0.41	1.71	1.77	3.01	2.06
HL-60	15.49	0.49	0.76	2.95		
K 562	16.87	0.77	5.70	0.49	3.07	0.00
MOLT 4	13.74	0.36	0.19	2.76	6.41	8.03
RPMI 8226	5.74	1.95	4.90	0.42	1.13	0.42
SR	8.99	0.37	2.76	1.40	0.44	3.44
NSCL						
A549	2.09	0.33	1.56	0.47		
EKVX	535.80	236.59	0.32	0.27	0.90	1.77
HOP 62	11.99	0.34	0.35	0.41	1.07	2.33
HOP 92	49.66	0.95	0.28	0.10	0.15	1.94
NCI H226	272.27	13.65	0.66	0.88		
NCI H23	11.27	0.33	0.49	0.43	2.73	0.04
H322 M	31.92	1.54			1.05	1.31
NCI 460	1.05	0.30	0.28	0.41	0.88	0.18
NCI H522	36.22	0.64	1.05		1.20	6.83
Colon						
COLO 205	6.89	1.19	1.20	0.11	1.00	0.003
HCC 2998	1.21	0.29	0.16	0.31	1.04	0.006
HCT116	3.99	0.29	2.79	1.65	2.21	0.42
HCT 15	6.32	3.46	1.44	1.18	1.46	0.65
HT 29	6.01	0.75	0.89	0.17	1.43	0.25
KM 12	11.64	17.14	2.73	0.28	0.53	0.27
SW 620	22.54	23.39	1.24	1.17	0.85	0.007
CNS						
SF 268	52.24	0.36	1.49		0.70	24.37
SF 295	51.40	0.31	1.12	0.85	0.76	0.46
SF 539	0.82	0.31	0.55	0.10	0.43	1.82
SNB 19	121.90	1.08	0.50	0.19	0.12	8.58
SNB 75	163.31	0.99		0.75	0.38	0.37
U 251	42.66	0.45	0.81	0.71	1.04	3.38
Melanoma						
LOX IMV1	5.83	0.29	0.42	0.27	1.08	4.21
MALME 3M	20.75	35.00	0.62	0.36	1.86	0.008
M14	31.84	0.35	1.61	0.83	1.74	0.72
SK MEL-2	359.75	115.35	0.72	0.40	2.90	1.72
SK MEL-28	27.29	3.18	0.31	0.40	1.37	0.04
SK MEL-5	10.81	0.30	1.31	0.28	1.79	0.01
UACC257	98.17	1.79	0.81	0.79	0.47	0.000
UACC 62	10.47	0.28	0.56	0.74	4.94	1.55
Ovary						
IGROV 1	16.75	19.23	0.55	0.92	1.18	0.63
OVCAR 3	28.91	1.27	1.00	0.17	0.79	0.28
OVCAR 4	62.52	28.71	1.53	0.33	0.81	0.17
OVCAR 5	118.30	103.04	0.70	0.16	1.37	2.54
OVCAR 8	16.98	0.30	1.41	0.54	1.01	1.03
SK OV-3	125.31	20.84	0.37	0.29	2.02	7.61
Renal						
786-O	12.88	0.37	0.97	2.11	0.77	0.32
A 498	6.18	0.72	0.32	0.05	0.23	0.32
ACHN	10.02	0.33	0.40	0.09	1.14	0.90
CAKI 1	5.20	0.53	4.94	0.84	1.13	1.63
RXF 393	54.95	2.16	1.53	0.30	1.49	2.68
SN12 C	24.10	0.30	1.27	0.41	0.59	1.55
TK-10	244.91	5.05	1.40	1.55	0.65	1.21
UO-31	6.68	0.58	0.57	0.29	0.60	1.62
Prostate						
PC 3	39.63	0.58	1.70	0.29	1.79	1.15
DU145	5.82	0.42		0.35		
Breast						
MCF7	1.67	0.29				
MCF7/ADR-RES	50.23	0.76			0.84	1.61
MDA-MB-231	322.11	22.39		0.42		
HS 578T	207.97	4.12	0.42	0.21		
MDA MB-435	9.91	2.12	2.45	1.32	1.64	1.25
MDA-N	7.76	1.29	2.39	1.23		
BT-549	84.33	1.81	0.34	0.44		

Table 1 Continued

Histology/Cell line	5-FU GI ₅₀ (μ M)	FdUrd GI ₅₀ (μ M)	TK activity (nmol/min/mg)	Relative TS protein	Relative TS mRNA	Relative DPD mRNA
T-47D	46.24	25.12	2.86	0.25		
SK-BR3	1.74	1.74				
MDA-MB-468	30.34	0.25				
MAX401	77.98	11.09				
Median	20.75	0.75	0.93	0.41	1.05	4.65
Minimum	0.82	0.25	0.16	0.05	0.12	0.00
Maximum	535.80	236.59	5.95	2.95	6.41	101.76

(thymidylate) from dUMP. In the presence of 5,10-methylenetetrahydrofolate, FdUMP forms a slowly reversible covalent complex with TS. TS inhibition leads to both depletion of TTP, which is necessary for DNA synthesis and repair, and accumulation of dUMP. Both FdUMP and dUMP can be anabolized to the triphosphate forms and then become incorporated into DNA. These "incorrect" residues are recognized and removed from DNA through the action of the uracil base excision repair complex. Uracil DNA glycosylase removes the fraudulent nucleobase, followed by excision of the base-free sugar phosphate residue by an AP endonuclease, thus creating a single strand break. TS inhibition is accompanied by elevation of dATP pools, thus accentuating the deoxynucleotide imbalance. Depending on the severity of the genotoxic stress, apoptosis pathways may be induced. TK converts FdUrd to FdUMP. DPD inactivates 5-FU by catalyzing its conversion to dihydrofluorouracil. The rationale for selecting these particular molecular targets is based on evidence that increased expression of TS and DPD is associated with insensitivity to 5-FU in both preclinical and clinical studies, whereas decreased expression of TK leads to insensitivity to FdUrd (15–30).

MATERIALS AND METHODS

Frozen cell pellets were provided by the cell culture facility at the Frederick Cancer Research Facility, Division of Cancer Treatment and Diagnosis, NCI for the current studies. Separate batches were supplied for the protein assays and the mRNA assays. [³H]Thymidine (25 Ci/mmol) was obtained from Moravsek Biochemicals (Brea, CA). Unless otherwise stated, chemicals were obtained from Sigma Chemical Co. (St. Louis, MO).

Drug Sensitivity Testing. The standard operating procedures used for drug sensitivity testing in the NCI cell line screen have been described previously (1). The cell culture medium is prepared by adding 25 ml of FBS and 5 ml of 100 mM glutamine to 500 ml of RPMI 1640. The cells are grown at 37°C in a humidified atmosphere with 5% CO₂. Cell lines are dispersed into a series of 96-well microtiter plates; the inoculation densities vary, depending on the growth characteristics of each particular cell line. The cells are incubated for 24 h in the absence of drug, and then serial 10-fold dilutions of drug are added. After a 48-h incubation, the protein content is determined by sulforhodamine B staining. The percentage growth inhibition is determined by the following equation: $100 \times (T - T_0/C - T_0)$, where T_0 is the absorbance of the wells at time zero prior to adding drugs, T is absorbance of the test wells after 48 h of drug

exposure, and C is the absorbance of control wells after 48 h incubation. The GI₅₀s in the Developmental Therapeutics Program database represent a median of 656 separate experiments (range, 7–687) for 5-FU and a median of 109 separate experiments (range, 1–123) for FdUrd.

Measurement of TK Activity. TK activity was determined by measuring the rate of conversion of radiolabeled thymidine to thymidine nucleotides (31). The frozen cell pellets were brought up in a solution containing 50 mM Tris (pH 7.4), 1 mM EDTA (pH 7.4), 10% glycerol, and 5 mM β -mercaptoethanol, and a cellular lysate was prepared by sonication on ice. An aliquot of the lysate containing 200–300 μ g of protein was incubated in a 1.5-ml microcentrifuge tube that contained the following (final concentrations): 0.1 mM thymidine, 220,000 dpm [³H]thymidine, 10 mM ATP, 50 mM Tris-HCl (pH 8.0), 5 mM MgCl₂, and 10 mM sodium fluoride. The samples were incubated in a shaking water bath at 37°C for 15 min. The reaction was stopped by placing the tubes in boiling water for 1 min. A aliquot of the sample (50 μ l) was spotted on each of two 25-mm Whatman DE81 filters labeled in pencil with a sample identifier. After drying, the discs were washed three times with distilled water, and then each was then placed in a scintillation vial, following which 1 ml 0.2 N HCl/0.4 M KCl was added. The vials were gently agitated for 15 min on an orbital shaker, and then scintillation fluid was added; radioactivity was determined in a liquid scintillation counter. The activity was calculated by the following equation: $[(\text{dpm in sample} - \text{background dpm}) \div \text{total dpm}] \times (20 \text{ nmol}) \div (\text{mg protein} \times \text{min incubated})$. The amount of protein in the cellular lysate was determined by the Bio-Rad protein dye (Hercules, CA) using a standard curve of BSA, fraction V.

Determination of TS Protein Content. TS protein content was determined by semiquantitative Western blot analysis as described previously (32). Equal amounts of protein from a cellular lysate were loaded onto a 12.5% polyacrylamide gel. TS106 monoclonal antibody was the primary antibody, and horseradish peroxidase goat antimouse IgG was the secondary antibody. The antigen/antibody complexes were visualized using the Enhanced Chemiluminescence kit (ECL Amersham, Evanston, IL). Each gel included a reference cell line (NCI-H630 colon cancer cells) to permit assessment of relative protein content across gels. The blots were stripped and reprobed with antibody to α -tubulin to correct for possible differences in protein loading.

mRNA Extraction, cDNA Synthesis, and PCR Quantitation of TS and DPD mRNA. mRNA was isolated using the QuickPrep micro-mRNA isolation kit (Amersham Pharmacia Biotech, Inc., Piscataway, NJ) according to the manufacturer's instructions. The mRNA was immediately reverse transcribed using random hexamers as described previously (33). Real-time quantitative PCR amplification was performed using specific target, doubly labeled fluorogenic probes with the ABI Prism 7700 Sequence Detection System (PE Applied Biosystems, Foster City, CA). Primers and probes were selected with Primer Express software version 1.0 (PE Applied Biosystems). The specificity of the chosen sequences was confirmed by conducting BlastN searches (GenBank). The expression of the β -actin gene was used as an internal standard. The TaqMan probes were labeled with 6-carboxy-fluorescein (5'-end) and 6-carboxy-tetramethylrhodamine (3'-end). The sequences were as follows: TS, forward primer (p763) = GGCCTCGGTGTGCCTTT, reverse primer (p 825) = GATGTGCGCAATCATGTACGT, and TaqMan probe (p 781), AACATCGCCAGCTACGCCCTGC; DPD, forward primer (p 70) = TCACTGGCAGACTCGAGACTGT, reverse primer (p 201) = TGGCCGAAGTGGAACACA, and TaqMan Probe (p 108) = CCGCCGAGTCCTTACTGAGCACAGG; and β -actin, forward primer (p 592) = TGAGCGCGGTACAGCTT, reverse primer (p 651) = TCCTTAATGTCACGCACGATTT, and TaqMan probe (p 611) = ACCACCACGGCCGAGCGG.

Serial dilutions of the cDNA were prepared. During the PCR reaction, the reporter signal is normalized to an internal passive reference dye (ROX) to correct for any non-PCR-related fluctuations in fluorescence signal. The cycle number at which the normalized fluorescent signal exceeds the threshold (C_T) is inversely proportional to the log of the quantity of input cDNA (set at 10 times the background fluorescence). Each 96-well plate contained a control cDNA sample to allow correction for plate-to-plate variability. By assigning relative mRNA values to wells containing the calibrator, the C_T for each well is converted to a quantity of mRNA. A graph was constructed with input cDNA on the X axis and mRNA quantity on the Y axis. Relative mRNA expression was determined by dividing the slope of the regression line for the target of interest by the slope of the regression line for β -actin. TS mRNA was normalized to NCI-H630 cells, and DPD mRNA was normalized to SK-1, a human hepatocellular line.

Measurement of Thymidine Levels in FBS. Because the standard operating procedure of the NCI cell line screen uses 5% FBS that is nondialyzed, the thymidine concentration was measured. The cell line screen currently is using FBS from BioWhittaker (Lot 0S083F); prior to that, FBS from Life Technologies, Inc. (Lot 100863) was used. A standard curve was constructed using dialyzed FBS; 1-ml aliquots of dialyzed FBS were spiked with thymidine ranging from 0.2 to 50 nmol, and each sample was spiked with 50 nmol FdUrd (the internal standard). Four 1-ml aliquots of the current lot of FBS from BioWhittaker and from a random lot of FBS from Life Technologies, Inc. were spiked with 50 nmol of FdUrd only. Glacial acetic acid, 50 μ l, was added to decrease protein binding of the nucleosides. The samples were vortex mixed and then deproteinized with 2 ml of acetonitrile. After centrifugation (2000 $\times g$ for 20 min at 4°C), the supernatant was collected and concentrated to dry-

ness under a stream of filtered, compressed air. The samples were resuspended in 500 μ l of water and filtered through a 0.2 μ m syringe filter; 200 μ l from each sample were placed in a autosampler vial. The samples were analyzed by reversed-phase HPLC using a 4.6 \times 250 mm Aqua column (Phenomenex, Torres, CA). The mobile phase was 1% glacial acetic acid/1.4% acetonitrile run at 1 ml/min for 40 min; the column was washed with 70% acetonitrile for 2 min and equilibrated at initial conditions for 6 min prior to the next run. FdUrd and thymidine were monitored at 268 nm, and the retention times were 16.17 ± 0.43 min and 28.53 ± 0.72 min (mean \pm SD), respectively. A standard curve was constructed by plotting the total nmol thymidine per ml versus the ratio of the areas of thymidine/FdUrd. The recovery of the nucleosides was determined by comparison with a standard curve prepared in water that was not subjected to the extraction procedure. The recovery of FdUrd and thymidine were $88.5 \pm 4.1\%$ and $88.0 \pm 10.6\%$, respectively. The within-run coefficients of variation averaged $12.8 \pm 0.92\%$, and the between-run coefficients of variation were $2.22 \pm 1.25\%$. Quality control samples included with each HPLC run were within 1.3% of the predicted value.

Statistical and Graphical Analysis. Graphical analysis was performed with SigmaPlot 2000 for Windows (SPSS, Inc., Chicago, IL), and statistical analysis was performed with SigmaStat for Windows version 2.03 (SPSS, Inc.). The strength of linear association between pairs of variables was determined by the Pearson product moment correlation coefficient: $r = 0.70$, strong correlation; $0.5 < r < 0.7$, moderately strong correlation; and $r = 0.3-0.5$, weak to moderate correlation. The Wilcoxon rank sum test was used to test whether values of continuous variables differed between groups separated into two subsets with respect to values falling above or below the median for the group.

RESULTS

Sensitivity to 5-FU and FdUrd by Histological Groups.

The parameters of interest by individual cell line are shown in Table 1, whereas the median values for each histological group are presented in Table 2. Mean graph representations for log-transformed target data and GI_{50} s are shown in Fig. 1. A striking degree of variability was seen for the GI_{50} s for a 48-h drug exposure to 5-FU (653-fold) and FdUrd (946-fold). Overall, the colon cancer panel was the most sensitive to 5-FU, whereas the CNS, ovary, and breast cancer panels had median GI_{50} s > 45 μ M. Five of the nine histological panels had a median FdUrd $GI_{50} < 1$ μ M, whereas the ovarian panel was the least sensitive.

FdUrd is predominantly metabolized to FdUMP and is a more selective inhibitor of TS. 5-FU can be metabolized to both FdUMP and to FUTP; the subsequent incorporation of the latter into RNA interferes with normal RNA processing and function. Because the mechanism of action with 5-FU is broader than that of FdUrd, we compared the cytotoxicity of these two drugs. The GI_{50} s for FdUrd were 34-fold lower than those of 5-FU (median, 0.82 versus 20.75 μ M; $P < 0.001$, paired rank sum test). Because of the wide range of GI_{50} s, a comparison between 5-FU and FdUrd values was performed after log transformation. A

Table 2 Median values for each histological group

Histology	GI ₅₀ 5-FU (μM)	GI ₅₀ FdUrd (μM)	TK activity (nmol/min/mg)	TS protein vs. H630 (arbitrary units)	TS mRNA vs. H630 (arbitrary units)	DPD mRNA vs. SK1 (arbitrary units)
Leukemia	14.61	0.45	2.24	1.58	1.13	2.06
NSCL	31.92	0.64	0.42	0.42	1.05	1.77
Colon	6.32	1.19	1.24	0.31	1.05	0.25
CNS	51.82	0.41	0.80	0.71	0.57	2.60
Melanoma	24.02	1.07	0.67	0.40	1.77	0.38
Ovary	45.71	20.04	0.85	0.31	1.10	0.83
Renal	11.45	0.56	1.34	0.36	0.71	1.38
Prostate	22.72	0.50	0.57	0.32	1.79	1.15
Breast	46.24	1.81	2.39	0.43	1.24	1.43

moderately strong correlation was seen among 63 cell lines (Fig. 2).

TK Activity. TK activity, determined in 54 cell lines, varied by 37-fold. The median values were highest in the breast cancer and leukemia panels. Although a correlation between TK activity and sensitivity to FdUrd was expected, no such relation was seen with either FdUrd or 5-FU (data not shown).

TS Protein Content and mRNA Expression. TS protein content varied 59-fold among the 55 cell lines tested. The leukemia panel had the highest median TS protein level, whereas the median values for the other histologies were similar. TS mRNA expression varied by a similar magnitude (53-fold). Because TS expression is regulated at both the transcriptional and translational level, an important question is how closely the TS mRNA and protein levels match. A weak to moderate correlation was noted (Fig. 3).

Although we expected that TS expression would influence sensitivity to 5-FU and FdUrd, no such correlation was seen (data not shown). If the data were sorted by TS protein content, no appreciable differences in the 5-FU GI₅₀s were evident among the cell lines with TS protein below the median *versus* those with higher values (22.4 and 16.8 μM), or for FdUrd (1.02 and 0.54 μM). Similarly, the distribution of 5-FU and FdUrd GI₅₀s overlapped in cell lines with lower *versus* higher TS mRNA expression: 5-FU, 24.1 *versus* 13.7 μM; FdUrd, 0.58 *versus* 0.75 μM, respectively.

DPD mRNA Expression. DPD expression showed a tremendous degree of variability. Two of the 50 cell lines tested (melanoma line UACC257 and leukemia line K562) had no detectable DPD mRNA expression. Five other lines (colon lines COLO 205, HCC 2998, SW620, and melanoma lines MALME 3M and SK MEL-5) had extremely low levels. Thus, the colon cancer and melanoma panels had the lowest median DPD values, whereas the CNS panel had the highest value. When TS and DPD were normalized to β-actin, on average, DPD mRNA expression was 42-fold lower than TS mRNA expression (data not shown). The cell lines with DPD values below the median tended to be more sensitive to 5-FU than the lines with higher DPD expression (12.9 *versus* 36.2 μM), whereas sensitivity to FdUrd was not affected by DPD expression (0.77 *versus* 0.58 μM, respectively; Fig. 4).

Correlations with Cell Line Doubling Times. Because cytotoxicity is determined at hour 48 of drug exposure under the standard protocol for the NCI cell line screen, cellular doubling time is a potentially important variable in drug sensitivity. The

doubling times of the cell line panel have been published previously (34). The median time is 34 h and ranges from 18 to 88 h. As might have been predicted, cell lines with faster doubling times (<median) were significantly more sensitive to both 5-FU (median GI₅₀, 5.0-fold lower; Fig. 5A) and FdUrd (median GI₅₀, 4.9-fold lower; Fig. 5B). The rate of cellular proliferation is thought to influence expression of TS and TK. Cell lines with faster doubling times tended to have higher TK activities (median, 1.9-fold higher; Fig. 5C) and TS protein content (median, 1.5-fold higher; Fig. 5D).

Correlations with p53 Gene Mutation. Mutations in p53 tend to render cells less sensitive to the effects of DNA-damaging agents. Because TS inhibition is associated with induction of DNA strand breaks and interference with DNA repair, we evaluated whether p53 gene status influenced sensitivity to fluoropyrimidines. The p53 gene status is known in 59 of the lines tested in the current study, and 68% have a mutation (34). Cell lines with wild-type p53 were significantly more sensitive to 5-FU (median GI₅₀, 9.0 *versus* 29.4 μM; Fig. 6, *top panel*) and to FdUrd (median GI₅₀, 0.36 *versus* 1.04 μM; Fig. 6, *bottom panel*).

Determination of Thymidine Levels in FBS. To estimate the extracellular thymidine concentrations under the standard operating conditions of the NCI cell line screen, thymidine levels in two different lots of FBS from different suppliers used by the NCI cell line screen were determined. The concentrations in four replicate samples from each lot were 4.57 ± 0.28 μM and 4.65 ± 0.17 μM (mean ± SD). Because the amount of FBS was diluted to 4.7% of the total volume of the cell culture medium, the final thymidine concentration would therefore be ~0.22 μM. In contrast, 10–20 μM thymidine is typically required in *in vitro* models to protect against the toxicity of 5-fluoropyrimidines (35–37).

DISCUSSION

The present study was undertaken as part of an ongoing effort to characterize the molecular and biochemical profile of the cancer cell lines that comprise the NCI's drug screening panel. There was a surprising degree of variability in the GI₅₀s for a 48-h exposure to both 5-FU and FdUrd in this model. The tolerated 5-FU dose when given by weekly 48-h continuous infusion is 1750 mg/m²/24 h (38). When 5-FU is given as a 48-h infusion every 2 weeks with two consecutive daily doses of 500 mg/m² leucovorin, the recommended 5-FU dose is 1500–2000

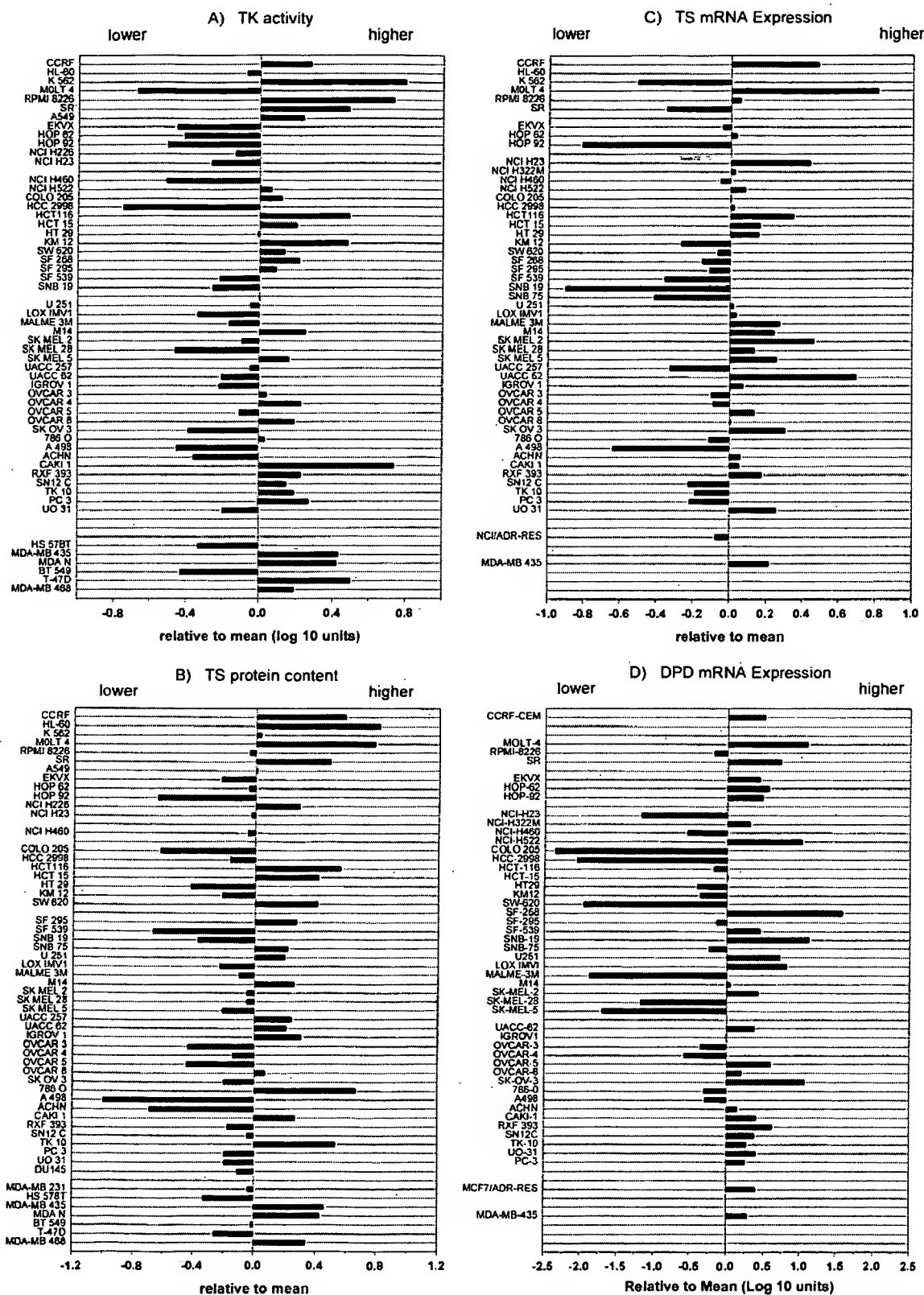


Fig. 1 Mean plot representations of the targets, 5-FU and FdUrd. The expression of each target was log transformed, and the mean was then calculated. To generate the mean plot, the mean value was subtracted from that of each individual cell line. A, TK activity. B, TS protein content. C, TS mRNA expression. D, DPD mRNA expression. E, 5-FU. F, FdUrd.

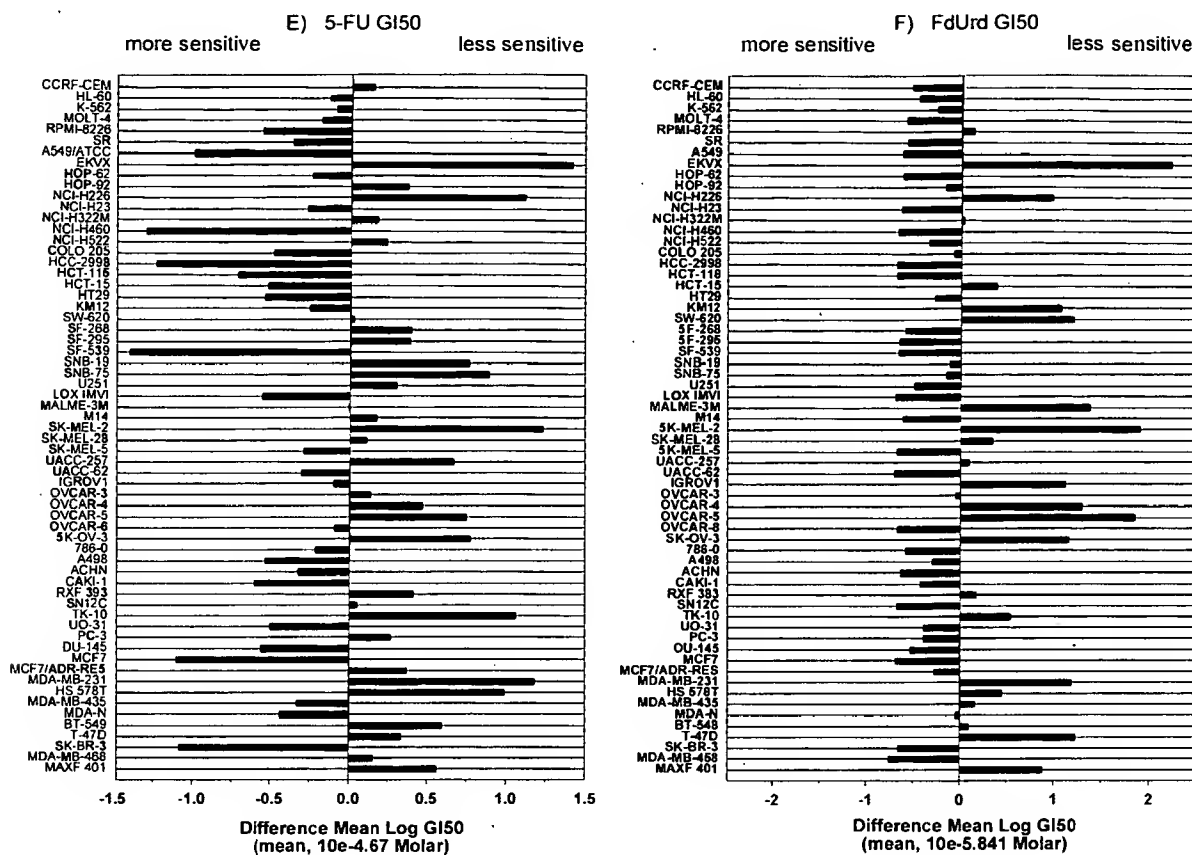


Fig. 1 Continued.

mg/m²/24 h (39). The achievable 5-FU plasma levels with such doses is in the range of 5–7 μ M (40–42). The 5-FU GI₅₀ was <10 μ M in only 30% of the cell lines. The cell lines were significantly more sensitive to FdUrd, and the GI₅₀ was <1 μ M in 57%. There is no published clinical experience with a 48-h continuous infusion of FdUrd to provide a reference for achievable plasma levels.

No correlation was noted between TK activity and sensitivity to either FdUrd or 5-FU. Previous investigators have reported that the basis for insensitivity of cancer cell lines selected *in vitro* for resistance to FdUrd has been either deletion of TK, which would prevent activation of the drug, or deficiency in facilitated nucleoside transport, which would limit cellular permeation (26–30, 43–44). None of the cell lines in the panel have been subjected to such selection pressure, and TK activity was detectable in every cell line. The membrane-based facilitated nucleoside transport system is complex and composed of at least eight distinct members. This latter target has not yet been characterized in the NCI cell line panel. However, cell lines deficient in nucleoside transport retain sensitivity to 5-FU, which uses a different facilitated transport system for pyrimidine and purine bases (43–45).

TS protein and mRNA expression each varied by ~50-fold among the cell lines; there was a weak-moderate correlation between increasing TS mRNA expression and higher TS protein

content. The correlation coefficient reflects the tightness of fit of the data points around the regression line, whereas the highly significant *P* indicates that the trend for TS mRNA and TS protein to increase in concert is not random.

On the basis of prior studies suggesting that high TS expression is associated with insensitivity to 5-FU, we anticipated seeing a correlation between either TS protein content and/or TS mRNA expression and GI₅₀s in the present study. However, no such relationship was evident by either linear regression or when the values were stratified into two categories relative to the median values for the population. This lack of correlation may be attributable to a number of factors. The duration of drug exposure was only 48 h, whereas the median doubling time has been reported to be 34 h (34). Indeed, the cell lines with faster doubling times were five times more sensitive to 5-FU and FdUrd than lines with slower doubling times. Duration of exposure to these two 5-fluoropyrimidines is known to be a critical factor influencing cytotoxicity (14). The observation that the cancer lines with the fastest doubling times had significantly higher TS protein content may account for why TS protein content did not correlate with sensitivity to 5-FU and FdUrd.

The standard operating procedure of the NCI cell line screen specifies the use of nondialyzed FBS, which contains thymidine. The vendor of the FBS used by the NCI drug screen

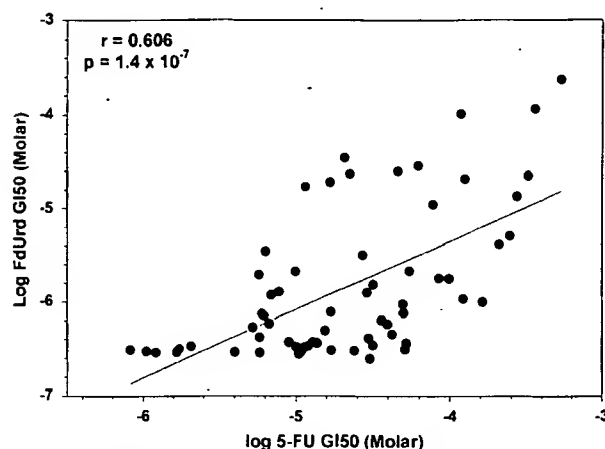


Fig. 2 Correlation between GI_{50} s for 5-FU and fluorodeoxyuridine. The 50% growth inhibitory concentrations (log transformation of the GI_{50} in molar units) after a 48-h drug exposure for 5-FU and FdUrd for 63 cell lines are shown. The Pearson correlation coefficient and P are shown. The tendency for both GI_{50} s to increase in concert was highly significant.

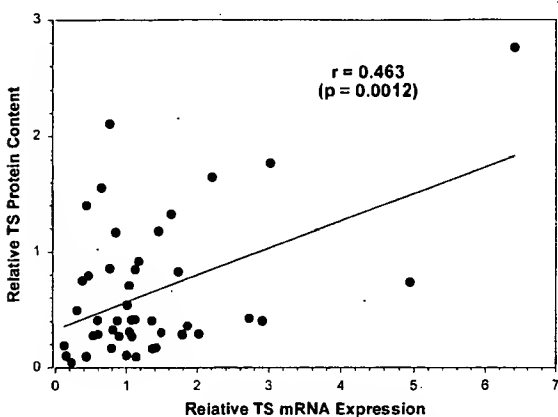


Fig. 3 Relationship between TS mRNA expression and protein content. Both TS protein content and TS mRNA expression were normalized versus NCI-H630 cells and thus have arbitrary units. The Pearson correlation coefficient and P are shown. TS protein content tended to increase in parallel with TS mRNA expression ($n = 46$), and P indicates that the slope was significantly different from zero.

does not define the thymidine concentrations in their serum. Therefore, we measured the thymidine levels by an HPLC method. The concentration in two separate lots of FBS from two different suppliers used by the NCI cell line screening facility were about $4.6 \mu\text{M}$. These results are consistent with the thymidine concentration in FBS in the component database of HyClone Laboratories (Logan, UT): $5.3 \pm 2.9 \mu\text{M}$.³ However, because the contribution of FBS to the total volume of the cell culture medium is $<5\%$, the final concentration in the medium

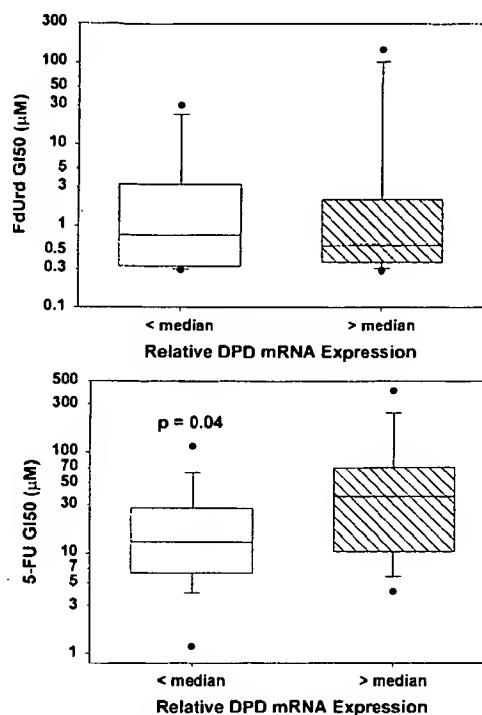


Fig. 4 GI_{50} values stratified according to lower versus higher DPD mRNA expression. The 50 cell lines in which DPD mRNA expression was available were stratified into two groups relative to the median; the distribution of 5-FU or FdUrd GI_{50} s according to DPD mRNA expression is presented in box plot format; the median value is displayed. The top and bottom of the rectangles are the 75th and 25th percentiles; the top and bottom whiskers are the 90th and 10th percentiles. ●, 95th and 5th percentiles.

is about $0.22 \mu\text{M}$, which is at least 40-fold lower than the thymidine concentrations typically required for *in vitro* protection against 5-FU. Furthermore, the final thymidine concentration is in the range reported for thymidine in human plasma (46), which is considered to be insufficient to protect against the cytotoxicity of TS inhibitors (47). In addition, all of the cell lines were significantly more sensitive to FdUrd than to 5-FU (average GI_{50} , 34-fold lower), a finding that would not be expected if the concentration of thymidine was sufficient to rescue the cells from FdUMP-mediated TS inhibition.

Lethality associated with 5-fluoropyrimidines may in some cases be attributed to "post-replicative" cell death mechanisms, in which programmed cell death occurs in the cell cycle(s) subsequent to the one in which the cells were initially exposed to the damaging agent. Although the precise basis for delayed apoptosis is not clear, a possible explanation is that initial sublethal damage to genes that are essential for cell survival may ultimately lead to cell death with subsequent rounds of DNA replication (48). The observation that the estimated 50% lethal concentration (LC_{50}) for 5-FU was $>1000 \mu\text{M}$ in 100% of the cell lines (data not shown) supports the premise that the culture methods used do not allow 5-FU-mediated lethality to become manifest. Similarly, FdUrd was not associated with lethality in this 48-h assay; only 2 of 63 lines had a $LC_{50} < 10 \mu\text{M}$, and the LC_{50} was $>1000 \mu\text{M}$ in 94% of the lines. Factors

³ Internet address: http://www.hyclone.com/comp_request/index.htm.

Fig. 5 Correlations with doubling times. The doubling times of the cell lines have been published previously (34). For each pair of variables, the data were stratified into two groups (above and below median) according to the published doubling times for the cell line panel. The data are presented in box plot format, as described in the legend to Fig. 4. *P* for the rank sum test is shown.

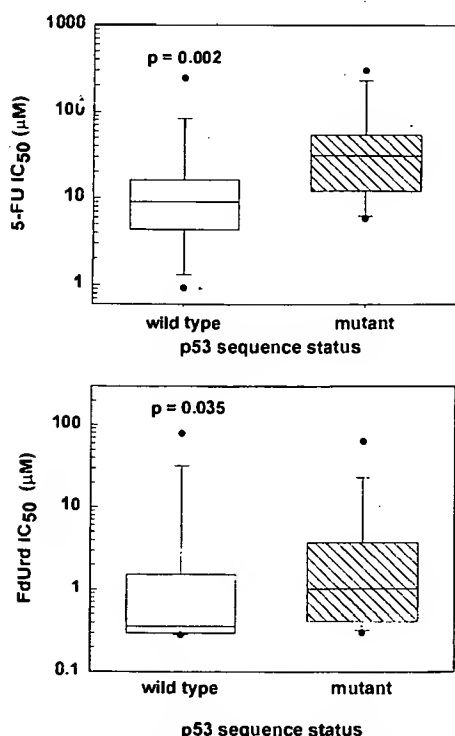
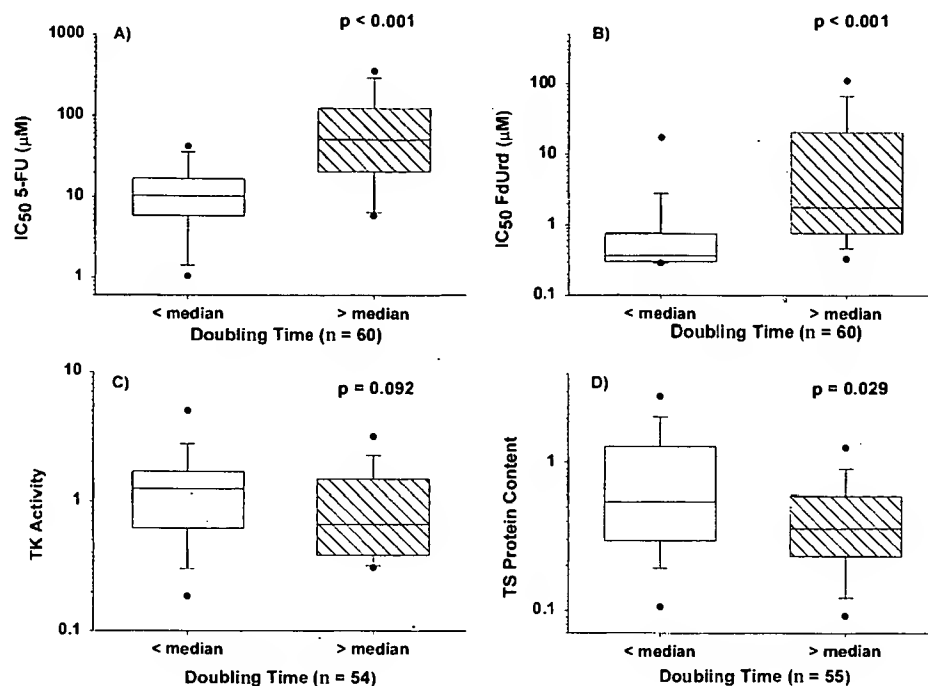


Fig. 6 Influence of *p53* gene status on sensitivity to 5-FU and FdUrd. The *p53* status of the cell lines in the NCI drug screening panel have been published previously (34). Information was available in 59 cell lines that included GI₅₀s for 5-FU and FdUrd as well as the *p53* mutational status. Cells with wild-type *p53* were significantly more sensitive to 5-FU (top), and to a lesser extent, to FdUrd.

operating downstream from the targets analyzed also play a pivotal role in 5-FU sensitivity. The pattern and extent of DNA damage induced by 5-fluoropyrimidines in human cancer cell lines varies and may be affected not only by the activity of enzymes involved in DNA repair but also by downstream pathways that are required to implement cellular destruction (49–51). There was a striking association between wild-type *p53* gene status and sensitivity to 5-FU; although there was greater variability, *p53* gene status also influenced sensitivity to FdUrd. This observation is consistent with the literature indicating that although TS inhibition is necessary for induction of apoptosis, downstream factors such as *p53*, *Bcl-2*, and *dUTPase* influence whether TS inhibition is sufficient for cell death (49–51).

DPD mRNA expression showed the greatest degree of variability. Two cell lines had no detectable DPD mRNA expression using a primer/probe set that evaluated the 5' portion of the message. In addition, five other lines had extremely low levels of DPD mRNA expression. Although there was no linear correlation between DPD mRNA expression and GI₅₀s, cell lines with lower DPD values tended to be more sensitive to 5-FU, whereas no such relationship was noted between DPD expression and FdUrd sensitivity.

In summary, we found no correlation between either TS mRNA expression, TS protein content, or TK activity and sensitivity to either 5-FU or FdUrd when cytotoxicity was assessed by the standard operating procedures of the NCI drug screen. Wild-type *p53* status was a strong predictor of sensitivity to 5-FU and to a lesser extent, to FdUrd, suggesting that factors operating downstream from the targets measured may be more important determinants of sensitivity to 5-fluoropyrimidines under these experimental conditions. In view of the known relevance of TS as a determinant of response to 5-FU-based therapy

in the clinical arena, the lack of correlation between TS expression and sensitivity to 5-FU/FdUrd raises a cautionary note regarding interpretation of correlative data using the standard protocol of the cell line screen. Future compounds with unknown or novel mechanisms of action will be tested under a similar, specific protocol. Our results raise the concern that this protocol may fail to detect potentially useful activity of compounds with unknown or novel mechanisms of action, particularly when the agents are not associated with early induction of programmed cell death.

REFERENCES

- Monks, A., Scudiero, D., Skehan, P., Shoemaker, R., Paull, K., Vistica, D., Hose, C., Langley, J., Cronise, P., Vaigro-Wolff, A., *et al.* Feasibility of a high-flux anticancer drug screen using a diverse panel of cultured human tumor cell lines. *J. Natl. Cancer Inst.*, **83**: 757-766, 1991.
- Stinson, S. F., Alley, M. C., Kopp, W. C., Fiebig, H. H., Mullendore, L. A., Pittman, A. F., Kenney, S., Keller, J., and Boyd, M. R. Morphological and immunocytochemical characteristics of human tumor cell lines for use in a disease-oriented anticancer drug screen. *Anticancer Res.*, **12**: 1035-1053, 1992.
- Grever, M. R., Schepartz, S. A., and Chabner, B. A. The National Cancer Institute: cancer drug discovery and development program. *Semin. Oncol.*, **19**: 622-638, 1992.
- Boyd, M. R., and Paull, K. D. Some practical considerations and applications of the National Cancer Institute *in vitro* anticancer drug discovery screen. *Drug Dev. Res.*, **34**: 91-109, 1995.
- Monks, A., Scudiero, D. A., Johnson, G. S., Paull, K. D., and Sausville, E. A. The NCI anti-cancer drug screen: a smart screen to identify effectors of novel targets. *Anticancer Drug Des.*, **12**: 533-541, 1997.
- Paull, K. D., Shoemaker, R. H., Hodes, L., Monks, A., Scudiero, D. A., Rubinstein, L., Plowman, J., and Boyd, M. R. Display and analysis of patterns of differential activity of drugs against human tumor cell lines: development of mean graph and compare algorithm. *J. Natl. Cancer Inst.*, **81**: 1088-1092, 1989.
- Hodes, L., Paull, K., Koutsoukos, A., and Rubinstein, L. Exploratory data analytic techniques to evaluate anticancer agents screened in a cell culture panel. *J. Biopharm. Stat.*, **2**: 31-48, 1992.
- Weinstein, J. N., Kohn, K. W., Grever, M. R., Viswanadhan, V. N., Rubinstein, L. V., Monks, A. P., Scudiero, D. A., Welch, L., Koutsoukos, A. D., Chiausa, A. J., and Paull, K. D. Neural computing in cancer drug development: predicting mechanism of action. *Science (Washington DC)*, **258**: 447-451, 1992.
- Koutsoukos, A. D., Rubinstein, L. V., Faraggi, D., Simon, R. M., Kalyandrug, S., Weinstein, J. N., Kohn, K. W., and Paull, K. D. Discrimination techniques applied to the NCI *in vitro* anti-tumor drug screen: predicting biochemical mechanism of action. *Stat. Med.*, **13**: 719-730, 1994.
- Weinstein, J. N., Myers, T. G., O'Connor, P. M., Friend, S. H., Fornace, A. J., Jr., Kohn, K. W., Fojo, T., Bates, S. E., Rubinstein, L. V., Anderson, N. L., Buolamwini, J. K., van Osdol, W. W., Monks, A. P., Scudiero, D. A., Sausville, E. A., Zaharevitz, D. W., Bunow, B., Viswanadhan, V. N., Johnson, G. S., Wittes, R. E., and Paull, K. D. An information-intensive approach to the molecular pharmacology of cancer. *Science (Washington DC)*, **275**: 343-349, 1997.
- Bates, S. E., Fojo, A. T., Weinstein, J. N., Myers, T. G., Alvarez, M., Paull, K. D., and Chabner, B. A. Molecular targets in the National Cancer Institute drug screen. *J. Cancer Res. Clin. Oncol.*, **121**: 495-500, 1995.
- Leteurtre, F., Kohlhaagen, G., Paull, K. D., and Pommier, Y. Topoisomerase II inhibition and cytotoxicity of the anthrapyrazoles DuP 937 and DuP 941 (Losoxantrone) in the National Cancer Institute preclinical antitumor drug discovery screen. *J. Natl. Cancer Inst.*, **86**: 1239-1244, 1994.
- Cholody, W. M., Hernandez, L., Hassner, L., Scudiero, D. A., Djurickovic, D. B., and Michejda, C. J. Bisimidazoacridones and related compounds: new antineoplastic agents with high selectivity against colon tumors. *J. Med. Chem.*, **38**: 3043-3052, 1995.
- Grem, J. L. Fluoropyrimidines. In: B. A. Chabner and D. L. Longo (eds.), *Cancer Chemotherapy and Biotherapy: Principles and Practice*, Ed. 2, pp. 149-211. Philadelphia: Lippincott-Raven Publishers, 1996.
- Alexander, H. R., Grem, J. L., Hamilton, J. M., Pass, H. I., Hong, M., Fraker, D. L., Steinberg, S. M., McAtee, N., Allegra, C. J., and Johnston, P. G. Thymidylate synthase protein expression association with response to neoadjuvant chemotherapy and resection for locally advanced gastric and gastroesophageal adenocarcinoma. *Cancer (Phila.)*, **1**: 49-54, 1995.
- Johnston, P. G., Lenz, H. J., Leichman, C. G., Danenberg, K. D., Allegra, C. J., Danenberg, P. V., and Leichman, L. Thymidylate synthase gene and protein expression correlate and are associated with response to 5-fluorouracil in human colorectal and gastric tumors. *Cancer Res.*, **55**: 1407-1412, 1995.
- Lenz, H. J., Leichman, C. G., Danenberg, K. D., Danenberg, P. V., Groshen, S., Cohen, H., Laine, L., Crookes, P., Silberman, H., Baranda, J., Garcia, Y., Li, J., and Leichman, L. Thymidylate synthase mRNA level in adenocarcinoma of the stomach: a predictor for primary tumor response and overall survival. *J. Clin. Oncol.*, **14**: 176-182, 1996.
- Leichman, C. G., Lenz, H. J., Leichman, L., Danenberg, K., Baranda, J., Groshen, S., Boswell, W., Metzger, R., Tan, M., and Danenberg, P. V. Quantitation of intratumoral thymidylate synthase expression predicts for disseminated colorectal cancer response and resistance to protracted-infusion fluorouracil and weekly leucovorin. *J. Clin. Oncol.*, **15**: 3223-3229, 1997.
- Kornmann, M., Link, K. H., Lenz, H. J., Pillasch, J., Metzger, R., Butzer, U., Leder, G. H., Weindel, M., Safi, F., Danenberg, K. D., Beger, H. G., and Danenberg, P. V. Thymidylate synthase is a predictor for response and resistance in hepatic artery infusion chemotherapy. *Cancer Lett.*, **118**: 29-35, 1997.
- Lenz, H. J., Hayashi, K., Salonga, D., Danenberg, K. D., Danenberg, P. V., Metzger, R., Banerjee, D., Bertino, J. R., Groshen, S., Leichman, L. P., and Leichman, C. G. p53 point mutations and thymidylate synthase messenger RNA levels in disseminated colorectal cancer: an analysis of response and survival. *Clin. Cancer Res.*, **4**: 1243-1250, 1998.
- Lenz, H. J., Danenberg, K. D., Leichman, C. G., Florentine, B., Johnston, P. G., Groshen, S., Zhou, L., Xiong, Y. P., Danenberg, P. V., and Leichman, L. P. p53 and thymidylate synthase expression in untreated stage II colon cancer: associations with recurrence, survival, and site. *Clin. Cancer Res.*, **4**: 1227-1234, 1998.
- Ishikawa, Y., Kubota, T., Otani, Y., Watanabe, M., Teramoto, T., Kumai, K., Kitajima, M., Takechi, T., Okabe, H., and Fukushima, M. Dihydropyrimidine dehydrogenase activity and messenger RNA level may be related to the antitumor effect of 5-fluorouracil on human tumor xenografts in nude mice. *Clin. Cancer Res.*, **5**: 883-889, 1999.
- Fischel, J. L., Etienne, M. C., Spector, T., Formento, P., Renee, N., and Milano, G. Dihydropyrimidine dehydrogenase: a tumoral target for fluorouracil modulation. *Clin. Cancer Res.*, **1**: 991-996, 1995.
- Etienne, M. C., Cheradame, S., Fischel, J. L., Formento, P., Dassonville, O., Renee, N., Schneider, M., Thyss, A., Demard, F., and Milano, G. Response to fluorouracil therapy in cancer patients: the role of tumoral dihydropyrimidine dehydrogenase activity. *J. Clin. Oncol.*, **13**: 1663-1670, 1995.
- Salonga, D., Danenberg, K. D., Johnson, M., Metzger, R., Groshen, S., Tsao-Wei, D. D., Lenz, H. J., Leichman, C. G., Leichman, L., Diasio, R. B., and Danenberg, P. V. Colorectal tumors responding to 5-fluorouracil have low gene expression levels of dihydropyrimidine dehydrogenase, thymidylate synthase, and thymidine phosphorylase. *Clin. Cancer Res.*, **6**: 1322-1327, 2000.
- Mulkins, M. A., and Heidelberger, C. Isolation of fluoropyrimidine-resistant murine leukemic cell lines by one-step mutation and selection. *Cancer Res.*, **42**: 956-964, 1982.

27. Mulkins, M. A., and Heidelberger, C. Biochemical characterization of fluoropyrimidine-resistant murine leukemic cell lines. *Cancer Res.*, 42: 965-973, 1982.
28. Inaba, M., Naoe, Y., and Mitsuhashi, J. Mechanisms for 5-fluorouracil resistance in human colon cancer DLD-1 cells. *Biol. Pharm. Bull.*, 21: 569-573, 1998.
29. van der Wilt, C. L., Smid, K., Veerman, G., and Peters, G. J. The role of thymidine kinase activity in murine colon tumours treated with 5-fluorouracil. *Adv. Exp. Med. Biol.*, 431: 653-656, 1998.
30. Agarwal, R. P., Han, T., and Fernandez, M. Collateral resistance of a dideoxycytidine-resistant cell line to 5-fluoro-2'-deoxyuridine. *Biochem. Biophys. Res. Commun.*, 262: 657-660, 1999.
31. Munch-Petersen, B. Differences in the kinetic properties of thymidine kinase isoenzymes in unstimulated and phytohemagglutinin-stimulated human lymphocytes. *Mol. Cell. Biochem.*, 64: 173-185, 1984.
32. Johnston, P. G., Drake, J. C., Trepel, J., and Allegra, C. J. Immunological quantitation of thymidylate synthase using the monoclonal antibody TS106 in 5-fluorouracil-sensitive and -resistant human cancer cell lines. *Cancer Res.*, 52: 4306-4312, 1992.
33. Horikoshi, T., Danenberg, K., Stadbauer, T. H. W., Volkenandt, M., Shea, L. C. C., Aigner, K., Gustavsson, B., Leichman, L., Frösing, R., Ray, M., Gibson, N., Spears, C. P., and Danenberg, P. V. Quantitation of thymidylate synthase, dihydrofolate reductase, and DT-diaphorase gene expression in human tumors using the polymerase chain reaction. *Cancer Res.*, 52: 108-116, 1992.
34. O'Connor, P. M., Jackman, J., Bae, I., Myers, T. G., Fan, S., Mutoh, M., Scudiero, D. A., Monks, A., Sausville, E. A., Weinstein, J. N., Friend, S., Fornace, A. J., Jr., and Kohn, K. W. Characterization of the p53 tumor suppressor pathway in cell lines of the National Cancer Institute anticancer drug screen and correlations with the growth-inhibitory potency of 123 anticancer agents. *Cancer Res.*, 57: 4285-4300, 1997.
35. Grem, J. L., and Fischer, P. H. Augmentation of 5-fluorouracil cytotoxicity in human colon cancer cells by dipyrindamole. *Cancer Res.*, 45: 2967-2972, 1985.
36. Johnston, P. G., Geoffrey, F., Drake, J., Voeller, D., Grem, J. L., and Allegra, C. J. The cellular interaction of 5-fluorouracil and cisplatin in a human colon carcinoma cell line. *Eur. J. Cancer*, 32A: 2148-2154, 1996.
37. Ren, Q., Van Groeningen, C. J., Hardcastle, A., Aherne, G. W., Geoffroy, F., Allegra, C. J., Johnston, P. G., and Grem, J. L. Determinants of cytotoxicity with prolonged exposure to fluorouracil in human colon cancer cells. *Oncol. Res.*, 9: 77-88, 1997.
38. Aranda, E., Diaz-Rubio, E., Cervantes, A., Anton-Torres, A., Carrato, A., Massuti, T., Tabernero, J. M., Sastre, J., Tres, A., Aparicio, J., Lopez-Vega, J. M., Barneto, I., and Garcia-Conde, J. Randomized trial comparing monthly low-dose leucovorin and fluorouracil bolus with weekly high-dose 48-hour continuous-infusion fluorouracil for advanced colorectal cancer: a Spanish Cooperative Group for Gastrointestinal Tumor Therapy (TTD) study. *Ann. Oncol.*, 9: 727-731, 1998.
39. Beerblock, K., Rinaldi, Y., Andre, T., Louvet, C., Raymond, E., Tournigand, C., Carola, E., Favre, R., de Gramont, A., and Krulik, M. Bimonthly high dose leucovorin and 5-fluorouracil 48-hour continuous infusion in patients with advanced colorectal carcinoma. Groupe d'Etude et de Recherche sur les Cancers de l'Ovaire et Digestifs (GER-COD). *Cancer (Phila.)*, 79: 1100-1105, 1997.
40. Erlichman, C., Fine, S., and Elhakim, T. Plasma pharmacokinetics of 5-FU given by continuous infusion with allopurinol. *Cancer Treat. Rep.*, 70: 903-904, 1986.
41. Remick, S. C., Grem, J. L., Fischer, P. H., Tutsch, K. D., Alberti, D. B., Nieting, L. M., Tombes, M. B., Bruggink, J., Willson, J. K., and Trump, D. L. Phase I trial of 5-fluorouracil and dipyrindamole administered by 72-hour concurrent continuous infusion. *Cancer Res.*, 50: 2667-2672, 1990.
42. Grem, J. L., McAtee, N., Steinberg, S. M., Hamilton, J. M., Murphy, R. F., Drake, J., Chisena, T., Balis, F., Cysyk, R., Arbuck, S. G., Balis, F., Cysyk, R., Goldstein, L., Sorensen, J. M., Chen, A., Setser, A., Jordan, E., Goldspiel, B., Carvalho, M., and Allegra, C. J. A Phase I study of continuous infusion 5-fluorouracil plus calcium leucovorin in combination with *n*-(phosphonacetyl)-L-aspartate in metastatic gastrointestinal adenocarcinoma. *Cancer Res.*, 53: 4828-4836, 1993.
43. Sobrero, A. F., Moir, R. D., Bertino, J. R., and Handschumacher, R. E. Defective facilitated diffusion of nucleosides, a primary mechanism of resistance to 5-fluoro-2'-deoxyuridine in the HCT-8 human carcinoma. *Cancer Res.*, 45: 3155-3160, 1985.
44. Sobrero, A. F., Handschumacher, R. E., and Bertino, J. R. Highly selective drug combinations for human colon cancer cells resistant *in vitro* to 5-fluoro-2'-deoxyuridine. *Cancer Res.*, 45: 3161-3163, 1985.
45. Domin, B. A., Mahony, W. B., and Zimmerman, T. P. Transport of 5-fluorouracil and uracil into human erythrocytes. *Biochem. Pharmacol.*, 46: 503-510, 1993.
46. Howell, S. B., Mansfield, S. J., and Taetle, R. Significance of variation in serum thymidine concentration for the marrow toxicity of methotrexate. *Cancer Chemother. Pharmacol.*, 5: 221-226, 1981.
47. Takemura, Y., and Jackman, A. L. Folate-based thymidylate synthase inhibitors in cancer chemotherapy. *Anticancer Drugs*, 8: 3-16, 1997.
48. Darzynkiewicz, Z. Methods in analysis of apoptosis and cell necrosis. In: J. Parker and C. Stewart (eds.), *The Purdue Cytometry CD-ROM Volume 3*. Purdue University, West Lafayette: J. Paul Robinson, Publisher, 1997.
49. Lowe, S. W., Ruley, H. E., Jacks, T., and Housman, D. E. p53-dependent apoptosis modulates the cytotoxicity of anticancer agents. *Cell*, 74: 957-967, 1993.
50. Fisher, T. C., Milner, A. E., Gregory, C. D., Jackman, A. L., Aherne, G. W., Hartley, J. A., Dive, C., and Hickman, J. A. Bcl-2 modulation of apoptosis induced by anticancer drugs: resistance to thymidylate stress is independent of classical resistance pathways. *Cancer Res.*, 53: 3321-3326, 1993.
51. Canman, C. E., Lawrence, T. S., Shewach, D. S., Tang, H. Y., and Maybaum, J. Resistance to fluorodeoxyuridine-induced DNA damage and cytotoxicity correlates with an elevation of deoxyuridine triphosphatase activity and failure to accumulate deoxyuridine triphosphate. *Cancer Res.*, 53: 5219-5224, 1993.

Available online at www.sciencedirect.com

SCIENCE @ DIRECT®

Regulatory Peptides 117 (2004) 127–139

REGULATORY
PEPTIDESwww.elsevier.com/locate/regpep

Galanin in pituitary adenomas

Eva Grenbäck^{a,*}, Per Bjellerup^b, Ella Wallerman^a, Lars Lundblad^c,
Anders Änggård^c, Kaj Ericson^d, Katarina Åman^c, Marc Landry^f,
Wolfgang E. Schmidt^g, Tomas Hökfelt^e, Anna-Lena Hulting^a

^aDepartment of Molecular Medicine, Endocrine and Diabetes Unit, Karolinska Hospital, Stockholm S-17176, Sweden^bDepartment of Clinical Chemistry, Stockholm, Sweden^cDepartment of Otorhinolaryngology, Stockholm, Sweden^dDepartment of Neuroradiology, Karolinska Hospital, Stockholm, Sweden^eDepartment of Neuroscience, Karolinska Institutet, Stockholm, Sweden^fLaboratoire de Biologie Cellulaire, Université de Bordeaux II, Bordeaux, France^gDepartment of Medicine I, St. Josef Hospital, Ruhr-University Bochum, Bochum, Germany

Received 25 March 2003; received in revised form 23 September 2003; accepted 1 October 2003

Abstract

Tumor galanin content was measured in extracts from human pituitary adenomas using a specific RIA method for monitoring human galanin. Twenty-two out of twenty-four tumors contained galanin with notably high levels in corticotroph adenomas, varying levels in clinically inactive tumors, and low levels in GH secreting adenomas. Tumor galanin and ACTH contents were closely correlated in all tumors. In four young patients with microadenomas and highly active Mb Cushing tumor galanin was inversely related to tumor volume. The molecular form of tumor galanin, studied with reverse-phase HPLC, was homogenous with the majority of tumor galanin coeluting with standard human galanin. In the tumors analysed with *in situ* hybridization there was a good correlation between galanin peptide levels and galanin mRNA expression. In some tumors galanin mRNA and POMC levels coexisted, in others they were essentially in different cell populations. Levels of plasma galanin-LI were not related to tumor galanin concentration, and galanin levels were in the same range in sinus petrosus close to the pituitary venous drainage as in peripheral blood. Corticotrophin releasing hormone injections in two patients caused ACTH, but no detectable galanin release into sinus petrosus. Our results demonstrate that corticotroph, but not GH adenomas, express high levels of galanin, in addition to ACTH, and that in some tumors both polypeptides are synthesised in the same cell population. However, galanin levels in plasma were not influenced by the tumor galanin content.

© 2003 Elsevier B.V. All rights reserved.

Keywords: Acromegaly; ACTH; Cushing's disease; GH; Pituitary tumor; Prolactinoma; Pro-opiomelanocortin

1. Introduction

Galanin was first isolated from porcine intestine in 1983 by Tatemoto et al. [1]. In most species galanin is a 29 amino acid, C-terminally amidated peptide, whereas the human form contains 30 amino acids with a non-amidated C-terminal [2–5]. A major breakthrough was the cloning of the rat galanin gene from the rat anterior pituitary and hypothalamus, and the demonstration of its estrogen sensi-

tivity [6,7]. Galanin has been shown to have multiple biological effects. Thus, it seems to be involved in, for example, regulation of feeding (see Refs. [8–10]), in learning (see Refs. [11,12]), and in responses to nerve injury and pain (see Ref. [13]). The first galanin receptor was cloned by Habert-Ortholi et al. [14] and subsequently two further galanin receptor subtypes were identified [15,16]. The creation of a galanin knock-out mouse [17] and of galanin overexpressing mice [18–20] have provided new insights into the physiological roles of galanin.

Galanin-like immunoreactivity (LI) is spread throughout the central nervous system, including the hypothalamus, with the most intense immunoreactivity in the median eminence [21–24], suggesting participation in neuroendocrine processes controlling anterior pituitary hormone se-

Abbreviations: I.I., like immunoreactivity; PAD, pathological anatomical diagnosis; TdT, terminal deoxynucleotidyl transferase.

* Corresponding author. Tel.: +46-8-517-73065; fax: +46-8-517-73096.

E-mail address: Eva.Grenback@ks.se (E. Grenbäck).

cretion (see Refs. [9,25–27]). For example, galanin increases GH secretion not only in animal models but also in humans. Thus, given intravenously (i.v.) to man galanin gives rise to a GH peak, delayed in time but equal to and additive to that produced by GHRH [28,29]. On the other hand, galanin has been shown to inhibit the hypothalamo–pituitary–adrenal (HPA) axis [30–33]. Galanin has been proposed to act as a mitogen in estrogen-induced prolactinomas in the rat [34,35]. Galanin gene expression also shows a direct correlation to somatotroph hyperplasia in GHRH transgenic mice [36].

In the rat pituitary galanin is mainly present in the lactotrophs [7], whereas in the human pituitary galanin is coexpressed with ACTH. Thus, several groups [37–44] have studied galanin-LI in pituitary adenomas establishing its presence in ACTH-producing adenomas, but with varying results as to its presence in somatotroph, lactotroph and clinically inactive adenomas.

The aim of this study was to investigate the presence, concentration and molecular form(s) of galanin in different types of pituitary adenomas using an extraction procedure and a newly developed radioimmunoassay (RIA), as well as reverse-phase (RP)-HPLC. In addition, we wished to compare tumor and serum levels of galanin to some other pituitary hormones, with special reference to the ACTH–cortisol axis. Finally, some tumors were analysed with *in situ* hybridisation for expression of galanin and POMC. The results of these analyses were correlated to clinical data. Preliminary data from this investigation have previously been reported [45].

2. Material and methods

2.1. Patients

Samples for tumor extraction were obtained from 24 patients with pituitary adenomas (Table 1), 15 women (26–78 years, mean 49.7 years) and 9 men (31–74 years, mean 53.3 years) who underwent transsphenoidal surgery at the Department of Otorhinolaryngology, Karolinska Hospital. Seven patients had hypersecretion of ACTH, six of GH, and one of prolactin (PRL). Ten tumors were clinically inactive (Table 1). The tumors were identified by clinical symptoms and signs as well as magnetic resonance imaging scans. The size of the seven ACTH-producing tumors was measured on contrast-enhanced T1-weighted coronal and sagittal images after correction for scaling. The standard formula for volume measurement of a rotational ellipsoid was used for volume calculations [46]. The size of the remaining tumors was assessed with stage and grade according to Hardy and Wilson (see Ref. [47]). Separate tumor samples were also analysed in the Department of Pathology of the Karolinska Hospital.

The patients with Cushing's disease had clinical symptoms and signs of hypercortisolism. The diagnosis was

confirmed by elevated ACTH and cortisol levels, absent diurnal rhythm, pathological CRH-test ($n=6$) with sinus petrosus sampling ($n=4$) or low and high dose dexamethasone ($n=1$). All had pituitary microadenomas visible on MRI scans. They were all cured clinically and biochemically after surgery. Separate pathological anatomical examination confirmed a pituitary adenoma in six cases. In one case (#6) there was insufficient material for analysis.

Galanin was monitored in two patients during sinus petrosus sampling. Samples were not available for galanin analysis from a further two patients who underwent sinus petrosus sampling, confirming in both cases ACTH producing pituitary adenoma. For control, plasma samples were collected from 22 healthy individuals (12 men, 28–55 years old; 10 women 25–62 years old).

The study was approved by the Ethics Committee of Karolinska Institutet (nos. 96-145 and 99-326).

2.2. Samples

Tumor samples for extraction and *in situ* hybridisation were collected at surgery, placed on dry ice and kept frozen at -70°C .

Blood samples for galanin measurement were collected in EDTA plasma tubes in the morning fasting state prior to surgery and during sinus petrosus sampling. Samples were placed on ice and centrifuged at 4°C (2400 rpm) for 10 min. Plasma was withdrawn and stored at -70°C until analysis.

2.3. Extraction procedure

For extraction, frozen tumor tissues were weighed, cut, still in frozen state, boiled for 10 min in acetic acid (1 mol/l), cooled on ice, homogenized and centrifuged for 10 min (2000 rpm) at 4°C . After collection of the supernatant, the pellet was resuspended in water, followed by a second boiling, homogenization and centrifugation as above. The supernatants from these two extraction procedures were pooled, lyophilised and stored at 4°C . Samples were reconstituted in phosphate buffer (0.05 mol/l; pH 7.4) before assay.

2.4. Gel permeation chromatography

Gel permeation chromatography was performed on one tumor rich in galanin (#5; Table 1). A Sephadex G-50 Superfine (Pharmacia, Uppsala, Sweden) column (2.6×97 cm) was equilibrated and eluted at room temperature with formic acid (0.1 mol/l) with 0.02% sodium azide. Void volume (V_0) was determined with Dextran blue and total volume (V_t) with ^{22}Na . Human synthetic galanin (Peninsula, Belmont, CA) in RIA buffer was used for column calibration. Tumor extract (50 μl in 1 ml water) was eluted at a flow rate of 15 ml/h, and the eluate was collected in fractions (2 ml), which were lyophilised and stored at 4°C until

Table 1
Twenty-four patients with pituitary tumors operated between 1994 and 1996

Pat. id. #	Tumor type	Age	Sex	T-gal, pmol/mg protein	P-gal, pmol/l	T-ACTH/mg prot	T-ACTH/T-gal
1	ACTH	26	f	620	55	2737.4	4.42
2	ACTH	29	f	587	52	1302.24	2.22
3	ACTH	31	m	111	130	657.27	5.92
4	ACTH	35	m	851	32	72666.67	85.39
5	ACTH	66	m	82.2	–	18860	229.4
6	ACTH	67	f	247	37	4065.04	16.46
7	ACTH	78	f	43.5	38	551.05	12.67
8	GH	29	f	0.04*	60	0.67	16.75
9	GH	40	f	1.87	80	20.39	10.9
10	GH	45	m	0.18	–	7.88	43.7
11	GH	49	f	0.12	54	5.06	42.17
12	GH	51	m	0.22	–	3.07	13.95
13	GH	64	m	0.08	<20	0.37	4.63
14	PRL	44	f	0.13	58	13.03	100.2
15	Inactive	34	f	10.2	116	975.4	95.6
16	Inactive	46	f	199	<20	4261.9	21.4
17	Inactive	52	f	0.16	53	1.23	7.69
18	Inactive	53	m	17.1	44	37.67	2.2
19	Inactive	55	f	99.9	<20	5092.78	50.98
20	Inactive	56	f	0.20	–	0.49	2.45
21	Inactive	62	m	0.21	–	3.48	16.57
22	Inactive	69	f	0.13*	40	6.45	49.61
23	Inactive	72	f	1.85	82	20.16	10.9
24	Inactive	74	m	5.67	38	553.6	97.6

Inactive: clinically inactive adenoma.

Patients are arranged according to tumor type, and age. Sex, tumor galanin content (T-GAL) and plasma galanin (P-GAL) are listed.

* Below detection limit in the RIA. For the purpose of calculation, they were assigned values of 20 pmol/l, i.e. the limit of detection.

assay. For RIA, each fraction was dissolved in 100 µl RIA buffer.

2.5. Reverse-phase-HPLC

Extracts from the nine adenomas containing the largest amounts of galanin, i.e. seven ACTH-secreting adenomas (#1–7; Table 1) and two clinically inactive adenomas (#16, #19; Table 1) were analysed with RP-HPLC. A 218TP C₁₈-Column (5 µm, 4.6 × 250 mm) from Vydac (Hesperia, CA) was used to separate the galanin-LI. The samples were eluted (1 ml/min) with a linear gradient of

water/acetonitrile (HPLC-grade, Merck, Darmstadt, Germany) with 0.1% trifluoroacetic acid (Merck) increasing from 20% to 70% by 1%/min. Aliquots of 0.5 ml were sampled. The fractions were lyophilized and redissolved in 100 µl RIA buffer before analysis. One sample with very high galanin content (#1; Table 2) was diluted 1:10 before chromatography.

2.6. Radioimmunoassay

Antiserum to human galanin(1–30) was produced as described before [48]. Briefly, human galanin(1–30) was

Table 2
Seven patients with ACTH producing pituitary adenomas

Pat. id. #	T-gal, pmol/mg protein	T-ACTH, pmol/mg protein	P-ACTH, pmol/l	S-Cortisol, nmol/l	U-Cortisol, nmol/24 h
1	620.16	2737.4	60	1190	2360
2	587.31	1302.24	7.3	576	1985
3	111.19	657.27	30	476	3192
4	850.67	72666.67	17	639	3394
5	82.15	18860	36	794	794
6	247.38	4065.04	15	579	1056
7	43.51	551.05	5.2	558	846

The table shows tumor tissue content of galanin (T-GAL) and ACTH (T-ACTH) in pmol/mg protein, morning fasting blood levels of ACTH and cortisol and 24 h urinary cortisol excretion.

Reference ranges: P-ACTH, 2–11 pmol/l.

S-Cortisol, 170–600 nmol/l.

U-Cortisol, 70–500 nmol/24 h.

synthesized by Fmoc-solid phase synthesis and purified to apparent homogeneity by RP-HPLC. Five mg galanin were coupled to 30 mg keyhole limpet hemocyanine with 0.25 mg carbodiimide. New Zealand white rabbits were immunized with 0.25 mg peptide equivalent dissolved in 1 ml saline emulsified in 1.5 ml complete Freund's adjuvant (Sigma, St. Louis, MO). Booster injections at 4–6 weeks intervals were done with 0.08–0.1 mg peptide equivalent mixed with 1.5 ml incomplete Freund's adjuvant. The antiserum used was obtained 10 days after the third booster injection.

Final antibody concentration in the assay was 1:750,000 yielding a 30% binding. Synthetic human galanin (Peninsula) was used as standard and 125 I-labelled human galanin (New England Nuclear, NEN, Boston, MA) as tracer. The RIA buffer was a phosphate buffer (0.05 mol/l; pH 7.4) containing 0.1% BSA, 0.02% NaN_3 , 0.01% Triton X, and 10 ml Trisylol/l buffer.

In the assay, 100 μ l of standard or samples in duplicates (or in single samples from chromatography) were preincubated with 100 μ l antibody for 24 h at 4 °C. After the addition of 100 μ l tracer (approx. 8000 cpm) incubation continued for another 24 h. Free and bound radioligand were separated by adding 500 μ l sheep anti-rabbit antibodies (Pharmacia decanting suspension; Pharmacia, Uppsala, Sweden). After 30 min incubation and addition of 500 μ l water, the samples were centrifuged at 4 °C (3000 rpm) for 15 min and decanted, and the radioactivity in the bound fraction was counted in a gamma counter.

Serial dilutions of tumor extracts showed good parallelism with the standard curve. Non-specific binding in the RIA was 2%. Detection limit was 20 pmol/L and IC_{50} 312 pmol/L. Intraassay variation was 5% and interassay variation 14%.

Crossreactivity was measured at 50% binding, or at the highest binding for those peptides not attaining a 50% binding. In this assay, there was 62% cross-reactivity with rat galanin, 36% with galanin(1–16), and 0.8% with pancreastatin, whereas less than 0.1% was found for galanin(20–30), galanin message-associated peptide(1–41) or –(44–49), CRH, GHRH, somatostatin, vasoactive intestinal polypeptide, peptide histidine-isoleucine, calcitonin gene-related peptide or oxytocin.

ACTH in tumor tissue was analysed by an immunoradiometric assay (IRMA) from Brahms Diagnostica (Berlin, Germany) using two monoclonal antibodies recognizing different binding sites on the antigen. The assay was carried out in two steps to prevent antigen excess resulting in falsely low values. The tumor samples were diluted stepwise with the zero-standard.

Protein content was analysed with the Bio Rad Protein Assay (BioRad, Munich, Germany).

2.7. Preparation of probes

Altogether three oligonucleotides (Scandinavian Gene Synthesis, Köping, Sweden) were used in this study for in

situ detection of POMC mRNA ($n=1$) and human galanin mRNA ($n=2$). Oligonucleotides were designed as below from published gene sequences.

(A) Oligonucleotide complementary to POMC mRNA [49]:

(i) 5'GCCCTCCCGTGGACTTGGCTCCGGACGGC-CATCTCCCCCGCCGTCTCTTCCTC3'

(B) Oligonucleotides complementary to human galanin mRNA [3]:

(i) 5'CTGTGGTTGCCAACGGCATGTGGGCCCA-GCAGGTAGCCCGCGCTGTTC3'

(ii) 5'GTCAAAGCTTCTGGTTTCATGTCATC-TTCGGGCCGACGACCCGCTT3'

All oligonucleotides were chosen in regions presenting few homologies with sequences of related mRNAs, and they were checked against the Genbank database.

The oligonucleotides complementary to human galanin mRNA were labelled as previously described [50] at the 3'-end using terminal deoxynucleotidyl transferase (TdT) (Amersham, Amersham, UK) in a cobalt-containing buffer with 35 S-dATP (New England Nuclear, Boston, MA, USA) to a specific activity of $1-4 \times 10^9$ cpm/ μ g and purified in Nensorb-20 columns (New England Nuclear). The oligonucleotide complementary to POMC mRNA was labelled by tailing at the 3'-end with digoxigenin-11-dUTP (Boehringer Mannheim, Mannheim, Germany) according to published protocols [51]. Briefly, 100 pmol of each probe were incubated in a final volume of 20 μ l with 1 nmol of digoxigenin-11-dUTP, 9 nmol of dATP (Sigma), 50 units of TdT and 4.2 μ l of cobalt-containing buffer. After 45 min at 37 °C the reaction was stopped before purification by ethanol precipitation, and probes were then stored at –20 °C.

2.8. In situ hybridization procedures

The frozen pituitary tumors were cut at 14 μ m thickness in a cryostat (Microm, Heidelberg, Germany) and thaw-mounted onto Probe On slides (Fisher Scientific, Pittsburgh, PA). The sections were then processed as described earlier [50]. In brief, tissue sections were air-dried and incubated for 16 h at 42 °C with 0.5 μ g of each of the two radioactively labelled human galanin probes and 10 nmol/l of the digoxigenin-labelled POMC probe. The probes were diluted in a hybridization solution containing 50% deionized formamide (Baker, Deventer, The Netherlands), $4 \times$ standard saline citrate (SSC, $1 \times \text{SSC} = 0.15 \text{ M NaCl}$ and $0.015 \text{ M NaCitrate}$), $1 \times$ Denhardt's solution (0.02% bovine serum albumin, 0.02% Ficoll (Pharmacia), 0.02% polyvinylpyrrolidone), 0.02 M NaPO_4 (pH 7.0), 1% *N*-lauroyl-sarcosine, 10% dextran sulphate (Pharmacia), 500 mg/l denatured salmon testis DNA (Sigma) and 200 mM dithiothreitol (Sigma). After hybridization, the sections were rinsed in $1 \times \text{SSC}$, 4×15 min at 55 °C followed by 30 min

at room temperature. The sections were then immersed for 30 min in buffer A (0.1 M Tris, pH 7.5, 1 M NaCl, 2 mM $MgCl_2$) containing 0.5% bovine serum albumin (Sigma) and incubated overnight at 4 °C in the same solution with alkaline-phosphatase conjugated anti-digoxigenin F(ab) fragment (1:5000; Boehringer Mannheim). Afterwards, they were rinsed 3×10 min in buffer A and twice in buffer B (0.1 M Tris, pH 9.5, 0.1 M NaCl, 5 mM $MgCl_2$). Alkaline-phosphatase activity was developed by incubating the sections with 44 μ l NBT and 33 μ l BCIP (Gibco, Gaithersburg, MD) diluted in 10 ml buffer B. The enzymatic reaction was stopped by extensive rinsings in distilled water and in buffer B.

The sections were air dried and coated twice with 3% collodion dissolved in amyl acetate (LKB, Stockholm, Sweden) [52]. They were then dipped into Ilford K5 nuclear emulsion (Ilford, Mobberly, Cheshire, UK) diluted 1:1 with distilled water, exposed for 3 weeks, developed in Kodak D19 for 3 min and fixed in Kodak 3000 for 8 min. After mounting in glycerol, the sections were analysed in a Nikon Microphot-FX microscope equipped with a dark field condenser.

2.9. Statistical analysis

Results are presented as mean \pm SEM, unless otherwise stated. Comparisons between groups were assessed by Mann–Whitney Rank Sum test or by one-way ANOVA, followed by Duncan's Multiple Comparison procedure. When applicable, non-normally distributed variables were log transformed before analysis, in order to get a more closely approximated Gaussian distribution. Correlations were performed using least square linear regression analysis. For the purpose of calculation, undetectable levels of galanin (#8, 22) were assigned values of 20 pmol/l. Statistical significance was set at $p < 0.05$. Statistical analyses

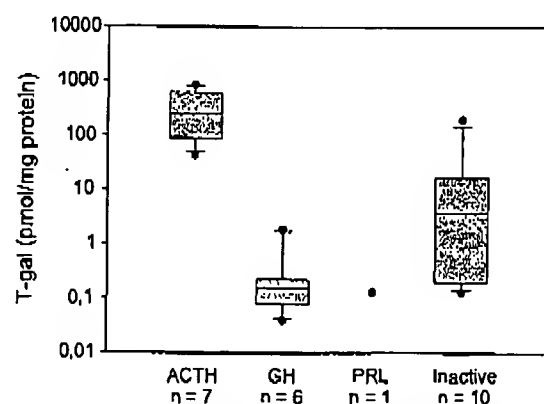


Fig. 1. Galanin concentration in 24 pituitary adenomas arranged according to tumor type. Box plots indicate the median and the lower and upper quartiles, the whiskers the 10th and 90th percentiles, and the outliers are shown as circles.

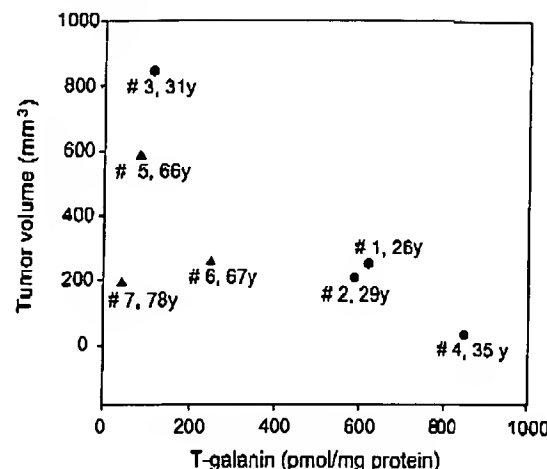


Fig. 2. Tumor galanin content related to tumor volume in seven patients with ACTH secreting adenomas. Patients number and age are given in the figure. Dots indicate young patients, triangles old ones.

were performed using SigmaStat for Windows (Jandel Scientific, Erkrath, Germany).

3. Results

3.1. Tumor samples

Galanin-LI was present in extracts from 22 of the 24 pituitary adenomas examined in this study (Table 1; Fig. 1). High levels of galanin-LI ranging between 43.5 and 851 pmol/mg protein (mean 363 pmol/mg) were found in the seven adenomas from patients with Cushing's disease (#1–7, Table 2). The six GH-producing adenomas contained low

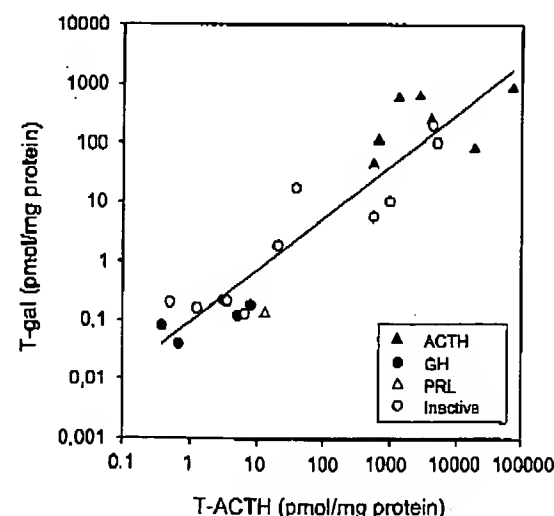


Fig. 3. Tumor galanin content related to tumor ACTH content in 24 pituitary adenomas specified to tumor type. There is a good correlation between galanin and ACTH tumor concentration ($r = 0.932$; $p < 0.001$).

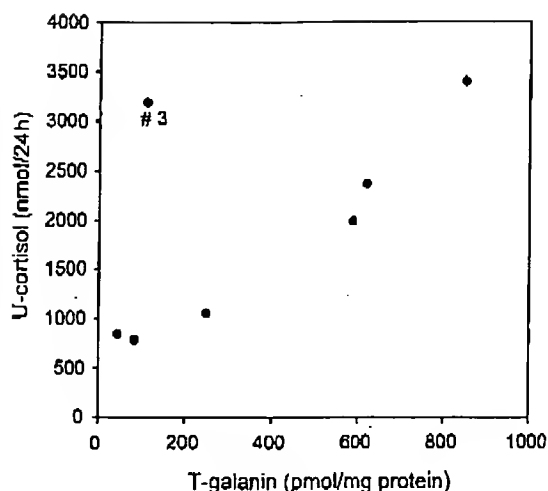


Fig. 4. Tumor galanin content related to 24 h urinary cortisol excretion in seven patients with ACTH secreting pituitary adenomas. Exclusion of patient #3 results in $r=0.974$; $p<0.001$. If included $r=0.614$; $p<0.142$.

amounts of galanin-LI, from 0.04 to 1.87 pmol/mg protein (mean 0.41 pmol/mg) (#8–13, Table 1). Also, the single prolactinoma had very low galanin-LI (#14, Table 1).

The 10 clinically inactive adenomas contained varying amounts of galanin-LI (#15–24, Table 1). Five of these adenomas had low galanin content, ranging from 0.13 to 1.85 pmol/mg (#17, 20–23, Table 1), three had levels in the

intermediate range (5.67–17.1 pmol/mg; #15, 18, 24), whereas two adenomas were rich in galanin-LI (99.9 and 199 pmol/mg; #16, 19, respectively). There was no correlation between galanin levels, or patients age, or sex, irrespective of tumor type. Tumor volume did not correlate to tumor galanin or ACTH-content in the seven patients with Mb Cushing (Fig. 2) ($r=0.638$; $p=0.123$). However, the four youngest patients, who also exhibited the highest cortisol per 24 h (#1–4, Table 2) had an inverse relation between tumor-galanin and volume (Fig. 2).

ACTH was detectable in all adenomas studied, and there was a close correlation between galanin-LI and ACTH levels in the adenomas as a group ($r=0.932$, $p<0.001$; Fig. 3), as well as in the clinically inactive adenomas ($r=0.919$, $p<0.001$), but a less strong correlation among the GH adenomas ($r=0.8429$; $p<0.05$). The seven corticotroph adenomas did not show any correlation between galanin and ACTH content ($r=0.434$). In this group of patients 24-h urinary cortisol excretion correlated strongly to tumor galanin-LI in six out of seven patients (Fig. 4). In the seventh patient (#3) comparatively low tumor galanin-LI and ACTH values were associated with high urinary cortisol. This patient had the largest tumor in the Mb Cushing group. No correlation was found between urinary cortisol excretion and tumor ACTH levels, nor did plasma ACTH or serum cortisol relate to tumor galanin-LI or ACTH content (Table 2). After surgery, all these patients had subnormal cortisol levels. One patient (#2) had recurrent disease a few years later.

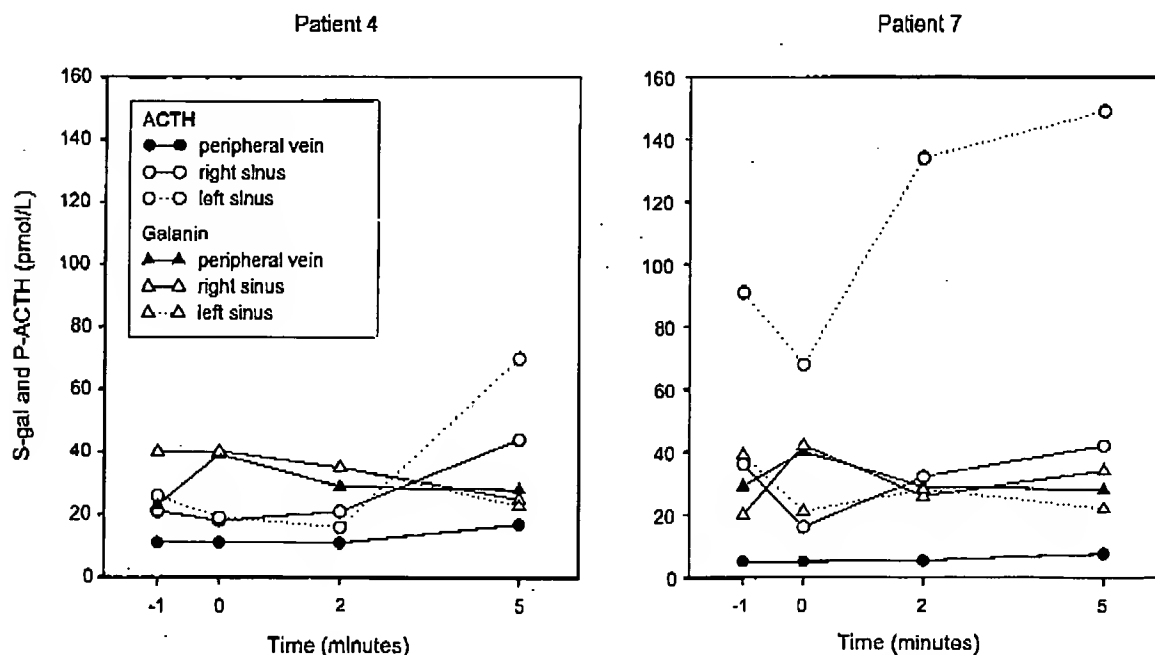


Fig. 5. Sinus petrosus sampling during CRH stimulation test in two patients with ACTH-producing tumors (#4 and 7; Table 1). After injection of 100 µg human CRH (Corticobias®, Bissendorf, The Netherlands), samples were drawn from right and left cavernous sinus and peripheral vein at -1, 0, 2, and 5 min and analyzed for ACTH and galanin.

3.2. Plasma samples

Galanin-LI in peripheral blood was measured in all but five patients (Table 1). The levels ranged from undetectable to 130 pmol/l (mean 54.2 ± 30 pmol/l). There was, however, no correlation to tumor type, nor to tumor size, galanin-LI content, patient age or sex (not shown).

Galanin-LI in plasma from healthy controls was 93.7 ± 44 pmol/l (101.9 – 48.7 pmol/l in the men and 83.9 – 37.6 pmol/l in the women), i.e. it was higher in controls than in the patient group. These control samples were collected 5 years after the patient samples and analysed with a slightly modified RIA including Trasylol to further prevent peptide degradation. Galanin-LI and ACTH were measured in sinus petrosus blood samples from two patients with Cushing's disease (#4, 7) after CRH stimulation (Fig. 5). A rise in plasma ACTH was noted in the left sinus of both patients, with no change in peripheral ACTH levels. No effect was observed on levels of galanin-LI in sinus petrosus or in the periphery, nor did basal plasma concentrations of galanin-LI in sinus petrosus differ from those in the periphery. Thus, there was no correspondence to the high levels of galanin-LI detected in tumor extracts from these two patients.

3.3. Chromatography

Gel permeation chromatography of onc tumor (#5, Table 1) revealed one major peak of galanin-LI with the same retention as synthetic human galanin. RP-HPLC of nine adenoma extracts (Fig. 6) showed that in eight of these tumors the majority of galanin-LI had the same retention as synthetic human galanin (16 min) (Fig. 6A). The main peak with galanin-like material was preceded by a smaller one with an elution time of 9–11 min in six extracts and of 13 min in two tissue extracts. Onc adenoma (#6, Table 1) differed from the rest, in that there was only one major chromatographic peak with galanin-like material with a longer retention time (20 min) coinciding with synthetic galanin(1–16) (Fig. 6B).

3.4. In situ hybridization

The in situ hybridization analysis showed that the pieces of the various tumors processed with this technique could be divided into at least three groups with regard to galanin expression. (i) A galanin signal was found in a large number of cells, sometimes apparently all cells of the tissue piece;

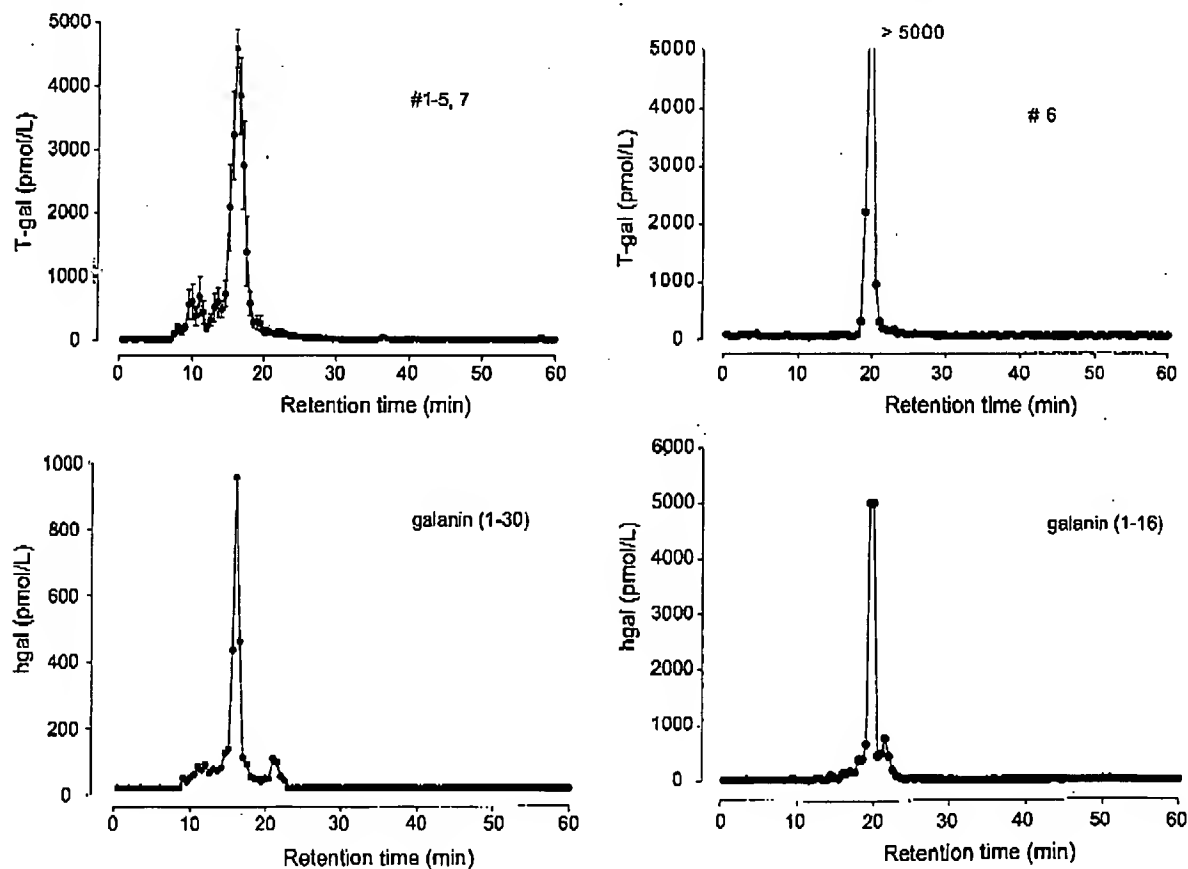


Fig. 6. (A, B) Reverse-phase high performance liquid chromatography of galanin immunoreactivity in pituitary extracts. (A) Results are mean \pm SEM of eight pituitary adenomas. (B) Results of one pituitary adenoma. (C) Elution of human galanin (1–30). (D) Elution of galanin 1–16. Please note different scale in (C).

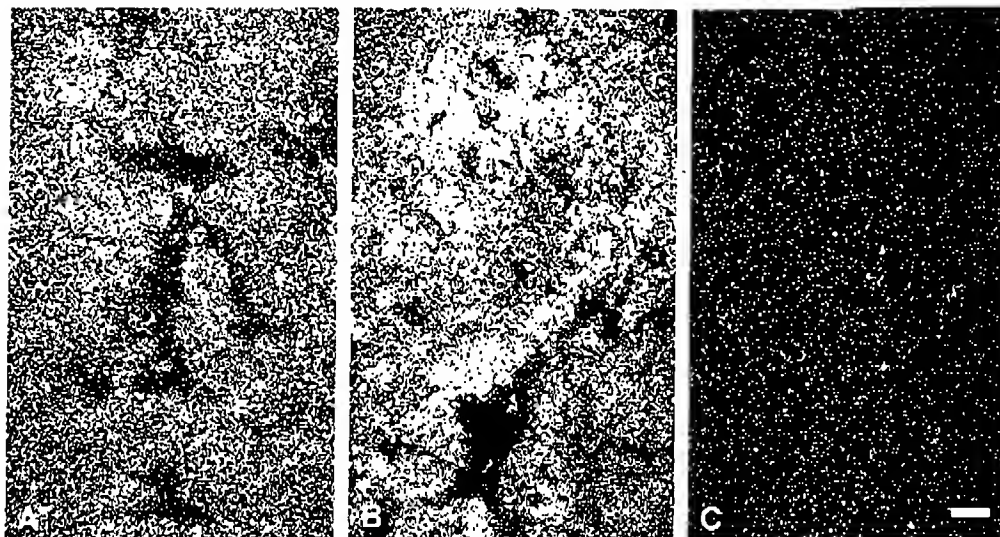


Fig. 7. (A–C). Darkfield micrographs of ACTH-producing adenomas (A, C, #1; B, #2) after hybridization with probes complementary to prepro-galanin mRNA (A, B) and after addition of excess of cold probe (C). A very strong signal is seen evenly distributed over both tumors (A, B) but only few grains in the controls (C). Scale bar indicates 50 μ m for all micrographs.

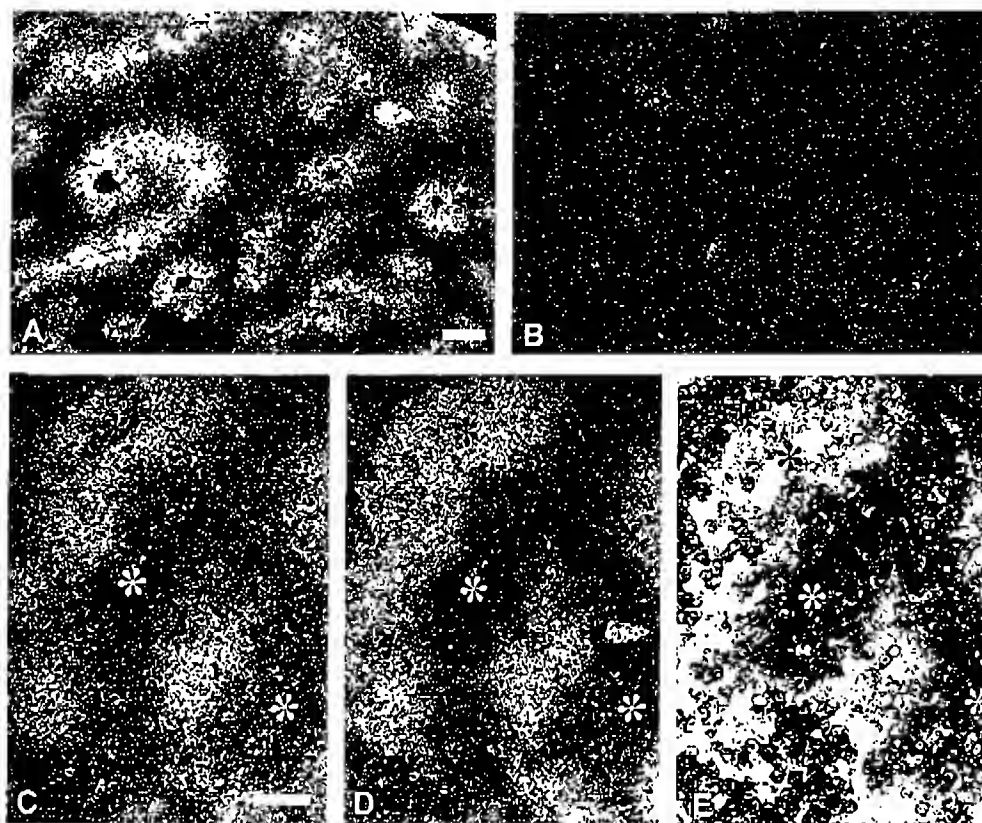


Fig. 8. (A–F). Darkfield (A–C), brightfield (E) and combined dark and brightfield (D) micrographs of ACTH-producing adenoma (#4) after double-hybridization with radioactive probes complementary to prepro galanin mRNA (A, C, D) and non-radioactive probe complementary to POMC mRNA (D, E) or after hybridization with an excess of galanin cold probe (B). A strong galanin signal (bright grains) is seen in strands within the tumor tissue (A, C), and they are complementary to the POMC mRNA (dark labelling) distribution (C–E). No signal is seen in the control section (B). Scale bars indicate 50 μ m (A–B; C–D–E).

(ii) a limited number of cells expressed galanin mRNA; and (iii) no galanin mRNA expression could be detected. Two tumors showed an extremely strong signal that could not be blocked by an excess of cold probe, that is the signal was considered to be unspecific.

To group (i), i.e. strongly galanin mRNA expressing tumors, belonged patients #1 (Fig. 7A), #2 (Fig. 7B) and #4 (Fig. 8A, C), whereby one of the two pieces analysed of tumor #2 showed a less compact distribution (data not shown) and #4 showed a markedly uneven distribution with

distinct bands of positive cell groups separated by areas with a low signal (Fig. 8A, C). Tumor #5 showed a signal all over the sections but of a comparatively low intensity (data not shown). To the second group (ii) with a limited number of cells expressing galanin mRNA belonged tumors #3 (Fig. 9A) and #19 (Fig. 9D); in the latter galanin-positive cells often formed small groups (Fig. 9E). In fact, in general the tissue piece of this tumor processed for *in situ* hybridization appeared to have a normal pituitary morphology at the cellular level (Fig. 9E). In group (iii) no detectable signal

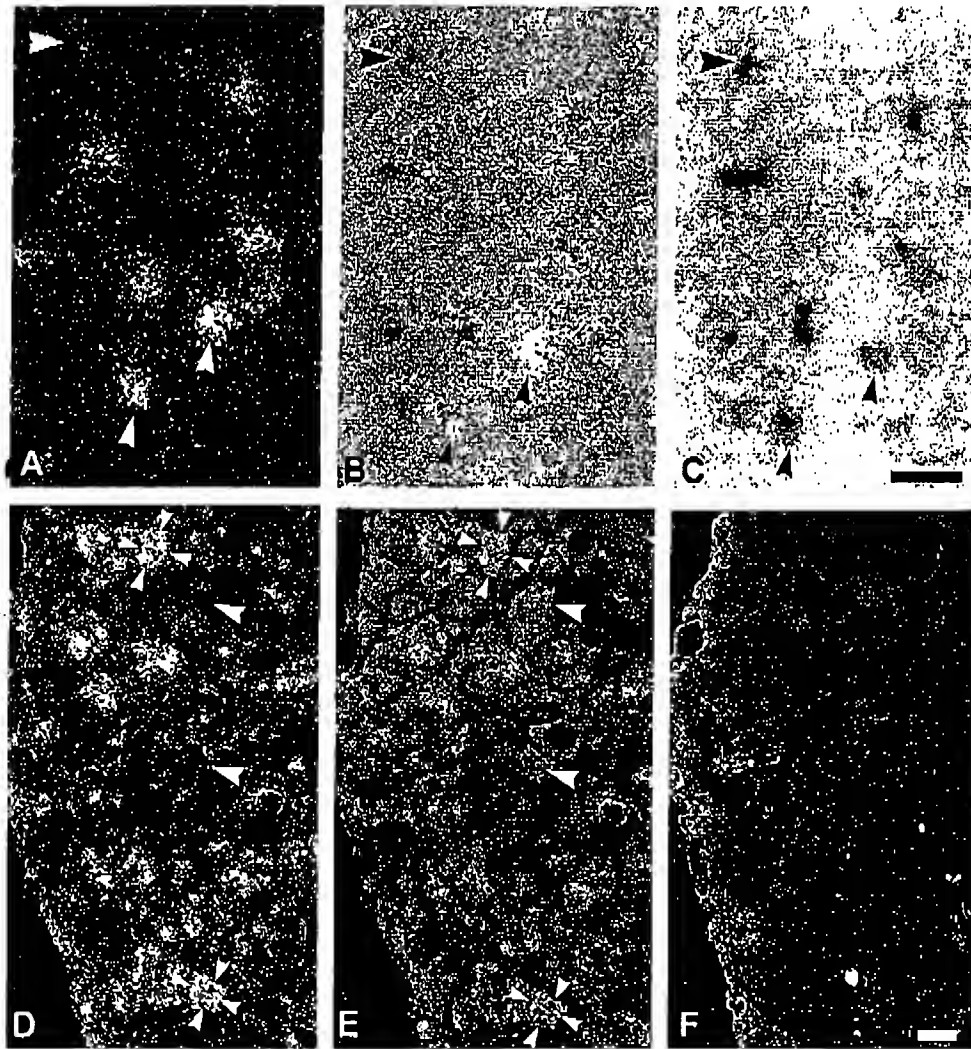


Fig. 9. (A–F) Darkfield (A, D–F), brightfield (C) and combined dark- and brightfield (B) micrographs of ACTH-producing adenoma (#3) (A–C) and of a clinically inactive tumor (#19) (D–F) after double-hybridization with radioactive probe complementary to prepro-galanin mRNA and non-radioactive probe complementary to POMC mRNA (A–C) or after hybridization with probe complementary to prepro-galanin mRNA without (D) or with (E) hisbenzimidazole contrast staining, or after hybridization with an excess of cold probe added to the hybridization cocktail (F). (A–C) Double *in situ* hybridization reveals several cells expressing both prepro-galanin mRNA (bright grains) and POMC mRNA (dark labelling) (small arrowheads) as well as POMC mRNA-positive and prepro-galanin mRNA-negative cells (big arrowheads). (D–F) Note strong signals in restricted areas of the tissue (A) which in D can often be seen to consist of small groups of cells (small arrowheads). Big arrowheads point to negative cell groups. Note low signal in the control experiment (F). Scale bars indicate 50 μ m (A–B–C; D–E–F).

was observed in tumors #10, #16, #17, or #21 (data not shown).

Some tumors were processed for double *in situ* hybridization with a non-radioactive POMC mRNA probe. A high degree of coexistence was observed in tumors #1 and #3, whereby this was observed in the majority of cells in tumor #3, but POMC mRNA-positive, galanin mRNA-negative cells were also observed (Fig. 9A–C). In tumor #1 all galanin mRNA positive cells had a POMC mRNA signal. Tumor #4 showed a clear separation between the non-radioactive POMC mRNA signal and the radioactive galanin signal (cf. Fig. 8E with C and D), suggesting synthesis in separate cells. However, POMC mRNA-galanin mRNA coexistence situations could not be excluded. Finally, in some tumors (eg. #10 and #21) a very strong signal was observed after incubation with the galanin mRNA probes. In all other tumors described above (Figs. 7C, 8B and 9F), the signal could be blocked by addition of an excess ($100\times$) of cold probe, except in tumors #10 and #21. They had a very strong signal which was observed to the same extent after addition of cold probe (data not shown). In agreement, both tumors (#10, 21) had very low galanin levels as monitored with RIA.

4. Discussion

In this study, using a RIA for human galanin, we demonstrate high levels of this peptide in extracts from ACTH-producing pituitary adenomas, moderate and varying galanin levels in clinically non-functioning adenomas and low or not detectable levels in GH- and PRL-producing adenomas, with a good correlation to ACTH levels in the adenomas. Moreover, the RIA data were supported by the *in situ* hybridization results; a significant galanin signal was only found in the corticotroph adenomas. Double *in situ* hybridization revealed coexistence of galanin mRNA and POMC mRNA in most tumors, although a clear cellular dissociation of the two transcripts was seen in some other tumours.

When discussing these results, one should keep in mind that different parts of the tumor tissue sample were analyzed in each of the various assays. Thus, differences in distribution of various markers within the tumor should be considered. Such differences were, in fact, encountered in the *in situ* hybridization analysis.

4.1. Galanin in corticotroph adenomas

A number of studies, using mainly immunostaining and *in situ* hybridization, have demonstrated presence of galanin in pituitary adenomas, especially in ACTH-producing tumors (see Table 3 for overview). Here we show that galanin levels in pituitary adenoma extracts vary with tumor type and correlate strongly with ACTH levels, supporting previous studies showing co-production of the two peptides. Indeed, the present *in situ* hybridization results using

Table 3

Galanin in human pituitary adenomas and in normal pituitaries

Reference	Pituitary adenomas				Normal pituitaries
	ACTH	GH	PRL	Inactive	
Hulting et al. [37]	–	1/1	–	–	–
Vrontakis et al. [38]	13/18	0/4	0/8	0/5	23/23
Hsu et al. [40]	16/19	5/11	2/14	9/18	7/7
Polak et al. [41]	6/6	3/8	2/2	0/7	–
Sano et al. [42]	9/14	0/10	0/9	0/9	–
Bennet et al. [39]	–	2/4	0/1	3/13	30/30
Invitti et al. [43]	5/5	–	–	–	–
Leung et al. [44]	10/16	1/26	1/19	25/89	6/6

Review of data published 1989–2002.

double-labeling on single sections show conclusively that individual cells can synthesize both ACTH and galanin. However, whereas coexistence of galanin and POMC mRNA was found in apparently all cells of one corticotroph adenoma (#1, 2, Table 1; Fig. 7A, B), another tumor of this type showed a clear separation of the two signals (#4, Table 1; Fig. 8A, C–E). Moreover, co-expression of galanin and POMC mRNA in the ACTH adenomas was reflected in a close correspondence between tumor content of galanin and ACTH, whereas when the peptides were expressed in separate cells RIA tumor content of ACTH vastly exceeded that of galanin. Thus, absence of a correlation between these two peptides in extracts from corticotroph adenomas may reflect an expression of ACTH and galanin in different cell populations.

A clinical significance of this differential expression could not be related to age, sex, tumor size or pituitary function. However, as shown by Invitti et al. [43], the *in vivo* release of galanin in response to CRH varies among patients with Cushing's disease. We found no elevation of plasma galanin in sinus petrosus from two patients with Cushing's disease. Thus, although both patients showed a marked unilateral response to CRH, there was no similar effect on galanin levels. One of these patients (#4) was analyzed with double-labeling *in situ* hybridization, and in this patient galanin and ACTH were synthesized in distinctly separate cell populations (Fig. 8). Perhaps the variability in the response to CRH can be explained by the extent of colocalization of ACTH and galanin. Thus, when the peptides are produced in different cells, CRH may only cause release of ACTH. It would therefore be interesting to know whether or not type-1 CRH receptors [53] are present in ACTH-negative, galanin-positive cells. It should here be mentioned that in the normal state, stimulation of ACTH secretion with CRH, desmopressin or physical exercise does not affect plasma galanin levels [43,54,55].

The clinical significance of the presence of galanin in ACTH adenomas was also investigated by Leung et al. [44], showing that galanin-positive adenomas were smaller and had better prognosis than those not expressing galanin. The present study supports this finding; we have found that all seven corticotroph adenomas were galanin-positive, and

they were small and were successfully removed. Interestingly, in the four young patients with microadenomas and highly active Mb Cushing (#1–4) tumor galanin was inversely related to tumor volume. In contrast to Leung et al. [44] we found a correlation in six of seven corticotroph adenomas between galanin content and 24 h urinary cortisol excretion, representing integrated ACTH-cortisol production. To what extent galanin can serve as a marker for tumor activity as well as act as a growth inhibitory factor in this type of tumor requires analysis of a larger material.

4.2. Galanin in clinically inactive GH and PRL adenomas

The capacity of non-ACTH tumors to synthesize galanin has been controversial. Vrontakis et al. [38] and Sano et al. [42] found galanin-LI exclusively coexpressed with ACTH and not present in any other type of pituitary adenoma. We have previously demonstrated the presence of galanin in a GH adenoma [37], and Polak et al. [41] in GH and PRL adenomas. Hsu et al. [40], in addition, found galanin-LI in half of the non-functioning adenomas, including a few which were negative for ACTH. In the largest and most recent study, Leung et al. [44] demonstrated galanin-LI in one third of the clinically inactive adenomas but rarely in GH- or PRL-producing adenomas.

In the only previous study based on extraction, Bennet et al. [39], using an antiserum against porcine galanin and a porcine tracer, found detectable galanin in two of four GH adenomas and in three of thirteen clinically active adenomas. With the present extraction method we find galanin-LI in all but two of the non-ACTH adenomas studied. However, galanin levels above 5 pmol/mg protein were only seen in 5 of the 10 clinically inactive adenomas and in none of the GH- or PRL-producing adenomas.

The presence of galanin was shown in all normal pituitaries examined in previous studies [38–40,44]. In fact, extraction yielded markedly higher galanin concentrations in normal pituitaries than in non-ACTH pituitary adenomas [39]. Since the present study is based on tissue obtained at pituitary surgery, it does not include a control group of normal pituitaries. However, in a previous study of extracts from 280 postmortem pituitaries Schmidt et al. [5] reported 410 pmol galanin per gram frozen tissue. In our material the mean galanin content was 13,950 pmol/g frozen tissue in ACTH adenomas, 3.6 pmol in GH adenomas and 1.4–4170 pmol in clinically inactive adenomas.

The highly variable galanin content found in the clinically inactive adenomas correlated well with ACTH content in the same adenomas, and presence of normal corticotrophs in the samples containing high galanin and ACTH cannot be excluded. In one case (#19) this was verified by PAD showing normal pituitary tissue in 9 of 10 samples (cf. Fig. 9D–F). This patient also incurred a postoperative panhypopituitarism. Indeed, the three patients who became ACTH deficient after surgery (#18, 19, 24) had elevated tumor galanin-LI (mean 40.9 pmol/mg protein), whereas those with

preoperative ACTH failure (#10, 20, 21, 23) had low levels (mean 0.61 pmol/mg protein).

The patient (#16) with the highest tumor galanin content among the clinically inactive adenomas had shown clinical signs of Mb Cushing. However, laboratory investigation, performed after a tumor apoplexy, revealed normal ACTH and cortisol secretion. This patient had a recurrence of Cushing's disease a few years after surgery. Our sample may have contained ACTH adenomatous tissue or normal pituitary as indicated by immunocytochemistry.

4.3. Identity of galanin in pituitary tumors

The molecular form of galanin was studied with RP-HPLC in the seven corticotroph adenomas and the two clinically inactive adenomas with high galanin content (#1–7) (#16, 19). The elution pattern was shown to be remarkably homogenous with a small peak preceding the main form eluting with synthetic human galanin (Fig. 5A). It agrees with the pattern found in non-ACTH pituitary adenomas by Bennet et al. [39] and corresponds to the structure determined by Schmidt et al. [5] who isolated and sequenced galanin from purified extracts of postmortem pituitaries. Our finding indicates that the molecular form of galanin in corticotroph adenomas is identical to that found in clinically inactive tumors and in the normal pituitary. The small polar peak eluting earlier than galanin(1–30) probably represents degradation products which have been shown to elute prior to the main form [56]. In one case (#6) we found that galanin eluted later than human standard with a peak coinciding with galanin(1–16) (Fig. 5B). This fragment has not been found *in vivo* in the rat [56,57] or in man [2,5,28,58], and our finding suggests a different processing of tumor galanin in this patient.

4.4. Concluding remarks

We found that galanin is present in human corticotroph adenomas and provide conclusive evidence at the transcript level for cellular colocalization with POMC in some, but not all tumors. Our results also indicate that galanin present in other types of pituitary adenomas is associated with normal pituitary tissue. The molecular form of tumorous pituitary galanin is homogenous representing genuine human galanin (1–30), but in one adenoma a form of galanin coeluting with galanin(1–16) was identified. No evidence of galanin secretion from these adenomas into local or peripheral circulation was obtained, pointing to a mainly auto- and/or paracrine role for galanin produced in corticotroph adenomas.

Acknowledgements

The study was supported by grants from Stockholm County Council, Seidey and Rolf Fredriksson's Research

Foundation, the Swedish MRC (04X-2887), Marianne and Marcus Wallenberg's Foundation and an Unrestricted Bristol-Myers Squibb Neuroscience Grant. We are grateful to Agneta Hilding, Department of Molecular Medicine, Endocrine and Diabetes Unit, Karolinska Institutet for assistance with the statistical evaluation, and to Dr. Anders Höög for pathological anatomical diagnosis.

References

- [1] Tatemoto K, Rökacsek Á, Jörnvall H, McDonald TJ, Mutt V. Galanin—a novel biologically active peptide from porcine intestine. *FEBS Lett* 1983;164:124–8.
- [2] Bersani M, Johnson AH, Højrup P, Dunning BE, Andreasen JJ, Holst JJ. Human galanin: primary structure and identification of two molecular forms. *FEBS Lett* 1991;283:189–94.
- [3] Evans H, Shine J. Human galanin: molecular cloning reveals a unique structure. *Endocrinology* 1991;129:1682–4.
- [4] McKnight GL, Karlén AE, Kowalyk S, Mathewes SL, Sheppard PO, O'Hara PJ, et al. Sequence of human galanin and its inhibition of glucose-stimulated insulin secretion from RIN cells. *Diabetes* 1991;41:82–7.
- [5] Schmidt WE, Kratzin II, Eckert K, Dreves D, Mundkowski G, Clemens A, et al. Isolation and primary structure of pituitary human galanin, a 30-residue nonamidated neuropeptide. *Proc Natl Acad Sci U S A* 1991;88:11435–9.
- [6] Vrontakis ME, Peden LM, Duckworth ML, Friesen HG. Isolation and characterization of a complementary DNA (galanin) clone from estrogen-induced pituitary tumor messenger RNA. *J Biol Chem* 1987;262:16755–8.
- [7] Kaplan LM, Gabriel SM, Koenig JL, Sunday ME, Spindel ER, Martin JB, et al. Galanin is an estrogen-inducible secretory product of the rat anterior pituitary. *Proc Natl Acad Sci U S A* 1988;85:7408–12.
- [8] Crawley JN. The role of galanin in feeding behaviour. *Neuropeptides* 1999;33:369–75.
- [9] Kalra SP, Horvath TL. Neuroendocrine interactions between galanin, opioids, and neuropeptide Y in the control of reproduction and appetite. *Ann N Y Acad Sci* 1998;863:236–40.
- [10] Leibowitz S. Differential functions of hypothalamic galanin cell groups in the regulation of eating and body weight. *Ann N Y Acad Sci* 1998;863:206–20.
- [11] McDonald MP, Gleuscu TC, Robinson JK, Crawley J. Galanin inhibits performance on rodent memory tasks. In: Hökfelt T, Bartfai T, Crawley J, editors. *Galanin basic research discoveries and therapeutic implications*. New York: NY Acad. Sci.; 1998. p. 206–20.
- [12] Ögren S-O, Schödt PA, Kehr J, Yoshitake T, Misane I, Mannström P, et al. Modulation of acetylcholine and serotonin transmission by galanin. *Ann N Y Acad Sci U S A* 1998;863:342–63.
- [13] Xu XJ, Hökfelt T, Bartfai T, Wiesenfeld-Hallin Z. Galanin and spinal nociceptive mechanisms: recent advances and therapeutic implications. *Neuropeptides* 2000;34:137–47.
- [14] Habert-Ortoli E, Amirano F, Loquet L, Laburthe M, Maysaux JF. Molecular cloning of a functional human galanin receptor. *Proc Natl Acad Sci U S A* 1994;91:9780–3.
- [15] Brunchek TA, Smith KE, Gerald C, Walker MW. Galanin receptor subtypes. *Trends Pharmacol Sci* 2000;21:109–16.
- [16] Lissaa TP, Shine J. Galanin and galanin receptors. *Results Probl Cell Differ* 1999;26:257–91.
- [17] Wynick D, Small CJ, Bacon A, Holmes FE, Norman M, Ormandy CJ, et al. Galanin regulates prolactin release and lactotroph proliferation. *Proc Natl Acad Sci U S A* 1998;95:12671–6.
- [18] Cai A, Hayes JD, Patel N, Hyde JF. Targeted overexpression of galanin in lactotrophs of transgenic mice induces hyperprolactinemia and pituitary hyperplasia. *Endocrinology* 1999;140:4955–64.
- [19] Kokaia M, Holmberg K, Nanohashvili A, Xu Z-QD, Kokaia Z, Lendahl U, et al. Suppressed kindling epileptogenesis in mice with ectopic overexpression of galanin. *Proc Natl Acad Sci U S A* 2001;98:14006–11.
- [20] Steiner RA, Hohmann JG, Hollos A, Wrenn CC, Cadd G, Jureus A, et al. Galanin transgenic mice display cognitive and neurochemical deficits characteristic of Alzheimer's disease. *Proc Natl Acad Sci U S A* 2001;98:4184–9.
- [21] Rökacsek Á, Melander T, Hökfelt T, Lundberg JM, Totemoto K, Carlquist M, et al. A galanin-like peptide in the central nervous system and intestine of the rat. *Neurosci Lett* 1984;47:161–6.
- [22] Skofitsch G, Jacobowitz DM. Immunohistochemical mapping of galanin-like neurons in the rat central nervous system. *Peptides* 1985;6:509–46.
- [23] Skofitsch G, Jacobowitz DM. Quantitative distribution of galanin-like immunoreactivity in the rat central nervous system. *Peptides* 1986;7:609–13.
- [24] Melander T, Hökfelt T, Rökacsek Á. Distribution of galanin-like immunoreactivity in the rat central nervous system. *J Comp Neurol* 1986;248:475–517.
- [25] Bloch GJ, Butler PC, Eckersell CB, Mills RH. Gonadal steroid-dependent GAL-IR cells within the medial preoptic nucleus (MPN) and the stimulatory effects of GAL within the MPN on sexual behaviors. *Ann N Y Acad Sci U S A* 1998;863:188–205.
- [26] Hohmann JG, Clifton DK, Steiner RA. Galanin: Analysis of its coexpression in gonadotropin-releasing hormone and growth hormone-releasing hormone neurons. *Ann N Y Acad Sci U S A* 1998;863:221–35.
- [27] Merchenthaler I. LHRH and sexual dimorphism. *Ann N Y Acad Sci U S A* 1998;863:175–87.
- [28] Bauer FE, Ginsberg L, Venetiko M, MacKay DJ, Burin JM, Bloom SR. Growth hormone release in man induced by galanin, a new hypothalamic peptide. *Lancet* 1986;26:192–5.
- [29] Davis TME, Burin JM, Bloom SR. Growth hormone release in response to GH-releasing hormone in man is 3-fold enhanced by galanin. *J Clin Endocrinol Metab* 1987;65:1248–52.
- [30] Cimini V. Galanin inhibits ACTH release in vitro and can be demonstrated immunocytochemically in dispersed corticotrophs. *Exp Cell Res* 1996;228:212–5.
- [31] Giustina A, Licini M, Schettino M, Dogu M, Pizzucolo G, Negro-Villar A. Physiological role of galanin in the regulation of anterior pituitary function in humans. *Am J Physiol* 1994;266:E57–61.
- [32] Hooi SC, Muir DM, Martin JB, Koenig JL. Galanergic mechanisms are involved in the regulation of corticotropin and thyrotropin secretion in the rat. *Endocrinology* 1990;127:2281–9.
- [33] Hooi SC, Koenig JL, Gabriel SM, Muir D, Martin JB. Influence of thyroid hormone on the concentration of galanin in the rat brain and pituitary. *Neuroendocrinology* 1990;51:351–6.
- [34] Wynick D, Smith DM, Ghatei M, Akinsanya K, Bhogal R, Purkiss P, et al. Characterization of a high-affinity galanin receptor in the rat anterior pituitary: Absence of biological effect and reduced membrane binding of the antagonist M15 differentiate it from the brain/gut receptor. *Proc Natl Acad Sci U S A* 1993;90:4231–5.
- [35] Wynick D, Hammond PJ, Akinsanya KO, Bloom SR. Galanin regulates basal and oestrogen-stimulated lactotroph function. *Nature* 1993;364:529–32.
- [36] Moore JPI, Morrison DG, Hyde JF. Galanin gene expression is increased in the anterior pituitary gland of the human growth hormone-releasing hormone transgenic mice. *Endocrinology* 1994;134:2005–10.
- [37] Hulting A-L, Meister B, Grimelius L, Wersäll J, Ånggård A, Hökfelt T. Production of a galanin-like peptide by a human pituitary adenoma: immunohistochemical evidence. *Acta Physiol Scand* 1989;137:561–2.
- [38] Vrontakis ME, Samu T, Kovacs K, Friesen HG. Presence of galanin-like immunoreactivity in non-tumorous corticotrophs and corticotroph adenomas of the human pituitary. *J Clin Endocrinol Metab* 1990;70:747–51.

- [39] Bennet WM, Hill SF, Glatte MA, Bloom SR. Galanin in the normal pituitary and brain and in pituitary adenomas. *J Endocrinol* 1991; 130:453–7.
- [40] Hsu DW, Hooi SC, Hedley-Whyte T, Strauss RM, Kaplan LM. Coexpression of galanin and adrenocorticotrophic hormone in human pituitary and pituitary adenomas. *Am J Pathol* 1991;138:997–909.
- [41] Polak JM, Gibson S, Gentleman S, Steel J, Van Noorden S. Galanin: distribution, ontogeny and expression following manipulation of the endocrine and nervous system. In: Hökfelt T, Bartfai T, Jacobowitz P, Ottoson D., editors. *Galanin a new multifunctional peptide in the neuro-endocrine system*. London: Macmillan; 1991. p. 117–34.
- [42] Sano T, Vrontakis ME, Kovacs K, Asu SL, Friesen HG. Galanin immunoreactivity in neuroendocrine tumors. *Arch Pathol Lab Med* 1991;115:926–9.
- [43] Invitti C, Pecori F, Girakli P, Dubini A, Moroni P, Losa M, et al. Galanin is released by adrenocorticotropin-secreting pituitary adenomas in vivo and in vitro. *J Clin Endocrinol Metab* 1999;4:1351–6.
- [44] Leung B, Iismaa TP, Leung K-C, Hort VJ, Turner J, Sheehy JP, et al. Galanin in human pituitary adenomas: frequency and clinical significance. *Clin Endocrinol* 2002;56:397–403.
- [45] Grenbäck E, Bjellrup P, Hulting A-L, Lundblad L, Ånggård A. Galanin in hypophysadenoma. *Proc Ann Meeting Swedish Med Soc* 1997;29P:162.
- [46] P. Lundin, *Magnetic resonance imaging of pituitary macroadenomas*. Thesis, Uppsala ISBN 91-628-0511-8 1992.
- [47] Wilson CB. A decade of pituitary microsurgery. The Herbert Olivecrona lecture. *J Neurosurg* 1984;61:814–33.
- [48] Schmidt WE, Siegel EG, Lamberts R, Galtwitz B, Creutzfeldt W. Pancreastatin: molecular and immunocytochemical characterization of a novel peptide in porcine and human tissues. *Endocrinology* 1988;123:1395–404.
- [49] Drouin J, Goodman HM. Most of the ending region of rat ACTH beta-LPH precursor gene lacks intervening sequences. *Nature* 1980; 288:610–3.
- [50] Dagerlind Å, Friberg K, Dean A, Hökfelt T. Sensitive mRNA detection using unfixed tissue: combined radioactive and non-radioactive in situ hybridization histochemistry. *Histochemistry* 1992; 98:39–49.
- [51] Schmitz GG, Walter T, Seibl R, Kessler C. Nonradioactive labeling of oligonucleotides in vitro with the haptan digoxigenin by tailing with terminal transferase. *Ann Biochem* 1991;192:222–31.
- [52] Broberger C, Landry M, Wong H, Walsh J, Hökfelt T. Subtypes Y1 and Y2 of the neuropeptide Y receptor are respectively expressed in proopiomelanocortin and neuropeptide Y-containing neurons of the rat hypothalamic arcuate nucleus. *Neuroendocrinology* 1997;66: 393–408.
- [53] Aguilera G, Rabaden-Diehl C, Nikodemova M. Regulation of pituitary corticotropin releasing hormone receptors. *Peptides* 2001;22: 769–74.
- [54] Ceresini G, Freddi M, Paccotti P, Valentini G, Merchenthaler I. Effects of ovine corticotropin-releasing hormone injection and desmopressin coadministration on galanin and adrenotropin plasma levels in normal women. *J Clin Endocrinol Metab* 1997;82:607–10.
- [55] Ceresini G, Marchini L, Fobbo A, Freddi M, Pasolini G, Reali N, et al. Evaluation of circulating galanin levels after exercise-induced pituitary hormone secretion in man. *Metabolism* 1997;82:282–6.
- [56] Land T, Langel U, Bartfai T. Hypothalamic degradation of galanin (1–29) and galanin (1–16): identification and characterization of the peptidolytic products. *Brain Res* 1991;558:245–50.
- [57] Redecs K, Langel Ü, Xu X-J, Wiesenfeld-Hallin Z, Bartfai T. Biological activities of two endogenously occurring N-terminally extended forms of galanin in the rat spinal cord. *Eur J Pharmacol* 1994;259: 151–6.
- [58] Bauer FE, Hacker GW, Terenghi G, Adrian TE, Polak JM, Bloom SR. Localization and molecular forms of galanin in human adrenals: elevated levels in pheochromocytomas. *J Clin Endocrinol Metab* 1986; 63:1372.

10010
01
01
13
01
1998

1019-6439
Received on: 07-23-98
International Journal of
Oncology.

International Journal of Oncology



ISSN 1019-6439

An international journal devoted to Oncology Research and Cancer Treatment

VOLUME 13, NUMBER 2, AUGUST 1998



Protein abundance and mRNA levels of the adipocyte-type fatty acid binding protein correlate in non-invasive and invasive bladder transitional cell carcinomas

IRINA GROMOVA¹, PAVEL GROMOV¹, HANS WOLF² and JULIO E. CELIS¹

¹Department of Medical Biochemistry and Danish Centre for Human Genome Research, The University of Aarhus, DK-8000, Aarhus C; ²Department of Urology, Skejby Hospital, Aarhus, Denmark

Received April 30, 1998; Accepted June 3, 1998

Abstract. The adipocyte type fatty acid-binding protein (A-FABP) is a small molecular weight fatty acid-binding protein whose expression correlates both with the grade of atypia and the stage of bladder transitional cell carcinomas (TCCs). To determine if the protein abundance correlates with the mRNA levels in non-invasive and invasive lesions, we have analysed fresh TCCs (grade II, Ta; grade III, T₂) by two-dimensional polyacrylamide gel electrophoresis (2D-PAGE) and measured the mRNA levels using the reverse transcription linked polymerase chain reaction (RT-PCR). Overall, the results showed a good correlation between protein abundance and mRNA levels, indicating that the lack of expression of the protein observed in some lesions reflects low levels of transcription of the A-FABP gene rather than translational regulation. In addition, our studies showed that the loss of A-FABP protein observed in some tumors is not compensated by an increase in the skin fatty acid-binding protein PA-FABP, as is the case in the A-FABP knockout mice.

Introduction

Bladder cancer accounts for 4.7% of all human cancers diagnosed. The spectrum of bladder tumors is broad with various histological types that include transitional cell carcinomas (TCCs), squamous cell carcinomas (SCCs), and adenocarcinomas (1-3). TCCs are by far the most prevalent tumors as they represent nearly 95% of all bladder cancers in

the Western Hemisphere. At first presentation, about 70% of the urinary bladder TCCs are diagnosed as differentiated superficial lesions that are confined either to the mucosa (Ta), or to the underlying connective tissue (T₁). The rest correspond to highly invasive, poorly differentiated tumors.

Non-invasive TCCs occur as two distinct growth patterns, papillary and non-papillary (flat) lesions (1,2); that display significant differences in their malignant potential and that are believed to originate from different genetic alterations (4-6). Papillary carcinomas usually correspond to low-grade lesions which frequently recur multiple times. These tumors begin as areas of hyperplasia that later undergo a process of dedifferentiation (grades I-IV). Invasive tumors may arise from these lesions, but often are derived from non-papillary carcinoma *in situ* that usually is of high grade at presentation and tend to invade and progress to muscle invasion and metastatic disease.

To date, many attempts have been made to pinpoint genetic changes that underly progression of bladder cancer as well as to identify molecular markers that correlate with tumor progression. Cytogenetic studies and molecular genetic data have shown that chromosomes 3p, 4p, 4q, 5q, 8p, 9p, 9q, 11p, 13q, 14q, 17p and 18q are frequently altered in bladder urothelial tumors (4,5 and refs. therein), and as a whole they have supported the notion that bladder cancer is a multistep process. Recently, Spruck *et al* (6) showed that chromosome 9 alterations occur early during development, while p53 mutations appear later in the process and confer invasive properties. The situation however is reverse in the case of Cis, as a large fraction of these lesions contain p53 mutations (5,6,8,9). Besides pointing towards two divergent pathways of bladder tumor progression, these studies implied that the order in which the genetic changes occur is important in determining the outcome of the lesion.

Assessment of bladder cancer is based on a thorough pathological examination of biopsy material which establishes the histological type of the tumor, its degree of differentiation (grade), and depth of invasion of the bladder wall (staging) (10-12). In spite of strict criteria for the pathological assessment of these lesions, there exist a significant inter-pathologist variation, a fact that emphasises the need for objective markers that may aid their classification. With this in mind, we are exploring the possibility of using proteome (13)

Correspondence to: Dr Irina Gromova, Department of Medical Biochemistry and Danish Centre for Human Genome Research, The University of Aarhus, DK-8000, Aarhus C, Denmark

Abbreviations: A-FABP, adipocyte type fatty acid-binding protein; PA-FABP, psoriasis associated fatty acid-binding protein; RT-PCR, reverse transcription linked polymerase chain reaction; 2D PAGE, two-dimensional polyacrylamide gel electrophoresis

Key words: progression, proteome, protein profiling, A-FABP protein and mRNA levels

expression profiles of these lesions as fingerprints to define their grade of atypia and eventually their stage (3,14). So far, more than 400 tumors of various grades and stages have been analysed by two-dimensional polyacrylamide gel electrophoresis (2D PAGE), and preliminary experiments have shown that even though the overall protein expression profiles of tumors of the same grade and stage are very similar, there are important differences suggesting that morphologically 'identical' TCCs may be further subdivided (1). Of the biomarkers of TCC progression identified so far, the adipocyte-type fatty acid binding protein (A-FABP) is perhaps one of the most interesting as the levels of this polypeptide have been shown to correlate both with the grade of atypia as well as with the stage of the disease (3). Given the putative importance of A-FABP as a progression marker, and since Anderson and Seilheimer (15) recently showed that post-transcriptional regulation of gene expression is a frequent phenomena in higher organisms, we have compared the levels of A-FABP mRNA and protein in non-invasive and invasive bladder TCCs expressing and lacking this protein.

Materials and methods

Tumors. Fresh bladder tumors were obtained immediately after transurethral resection. The grade and clinical stage of the tumors were determined by the pathologist at the Aarhus Municipal hospital. Clean tumors devoid of blood clots were divided into small pieces for 2D PAGE and DNA, and RNA preparation. The latter were immediately frozen in liquid nitrogen and store at -80°C until use.

[³⁵S]-methionine labeling and 2D-PAGE. In a few cases, small tumor pieces were labeled with [³⁵S]-methionine as previously described (3). 2D-PAGE was performed according to published procedures (16; see also <http://biobase.dk/cgi-bin/celis>).

RT-PCR. Frozen tumor samples were ground to powder in liquid nitrogen and total RNA was isolated using the acid guanidium isothiocyanate/phenol chloroform extraction procedure (17). The samples were treated with RNase-free DNases I (Pharmacia) to eliminate contaminating genomic DNA using the protocols recommended by the supplier. Poly(A)⁺ RNA was prepared using Poly (A)⁺ Quick columns according to the manufacturer's instructions (Stratagene). The synthesis of cDNA for RT-PCR reactions were carried out using the Gibco BRL SuperScript Kit. Two µg of total RNAs was mixed with oligo -dT11 primer, PCR buffer, MgCl₂ (25 mM), 0.1 M DDT and 10 mM dNTP. The mixture was incubated at 42°C for 5 min followed by the addition of SuperScript II reverse transcriptase and further incubation at 42°C for 50 min. The reaction was terminated by raising the temperature to 70°C for 15 min, followed by additional incubation at 37°C for 20 min in the presence of RNase H to deplete the RNA. Primers for known and cloned genes were purchase from Pharmacia as follows: A-FABP, Upper (from 186-208 bp) 5'-GATCATCAGTGTGAATGGGGAT-3'/lower (from 374-397 bp) 5'-CATCCTCTCGTTTCTCTTTATG-3'; β-actin upper 5'-GAGGTTGGCTCTGACTGTACCAC-3'/lower 5'-CTCATTCAGCTCTCGAACATCTCG-3'.

Table 1. Expression of A-FABP in non-invasive and invasive bladder TCCs:

TCC	Grade/ stage	Level of A-FABP protein ^a	Level of A-FABP mRNA ^b
154	GrlI/Ta	+	++
166-5	GrlI/Ta	-	+
532-1	GrlI/Ta	++++	++++
533-1	GrlI/Ta	+	+
607-1	GrlI/Ta	-	-
692-1	GrlI/Ta	+++	+++
709-1	GrlI/Ta	-	-
763-1	GrlI/Ta	++	++
581-1	GrlI/Ta	+	+
616-1	GrlI/Ta	+	++
428-5	GrlI/T ₂ -T ₄	-	-
570-2	GrlI/T ₂ -T ₄	-	-
612-3	GrlI/T ₂ -T ₄	-	-
711-1	GrlI/T ₂ -T ₄	-	-
712-1	GrlI/T ₂ -T ₄	-	-
727-1	GrlI/T ₂ -T ₄	-	-

^aThe levels of A-FABP protein were determined based on the visual analysis of Coomassie Brilliant Blue stained gels and represent the average estimate of at least two different runs. Tumors scored as positive differed significantly with respect to the levels of the protein, and therefore are indicated with either four (very high), three (high), two (medium) and one (low) cross (see also Fig. 1);

^bThe mRNA levels were determined based on the intensity of Ethidium Bromide stained cDNA bands separated on agarose gel using the Bio-Rad Gel Doc 1000 system and represent the average estimate of at least three independent experiments. Corresponding mRNA levels are represented by crosses as described above.

PCR reactions were performed in a Progene thermal cycler using the Advantage Klen Tag Polymerase (Clontech). The cycling parameters consisted of 30 sec of denaturation at 94°C, with annealing of 30 sec at 60°C for β-actin or at 64°C for A-FABP. The extension time was for 2 min at 68°C for 29-40 cycles with the final extension of 7 min at 68°C. The PCR products were separated on 1.5% agarose gel electrophoresis followed by ethidium bromide staining and photography under UV light.

Results

A-FABP protein levels in non-invasive and invasive TCCs. One hundred suspected TCCs removed at the Department of Urology, Skejby Hospital, were analysed by high resolution 2D PAGE and Coomassie Brilliant Blue staining. Of these, 10 grade II, Ta TCCs (Table 1) were chosen to correlate A-FABP protein and mRNA levels as these lesions yielded acceptable protein profiles both in terms of their purity as

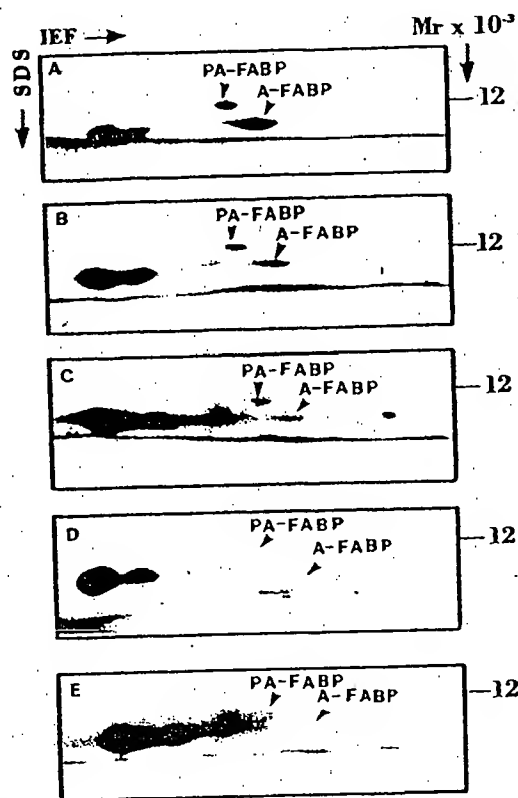


Figure 1. IEF 2D gels of whole cellular extracts from non-invasive and invasive TCCs. A, TCC 532-1; B, TCC 692-1; C, TCC 763-1; D, TCC 709-1 and E, TCC 711-1. Only the relevant area of the gels are shown.

assessed by monitoring for the absence of vimentin (contamination with connective tissue) and desmin (contamination with smooth muscle cells), as well as polypeptide resolution. In addition, reasonable amounts of these tumors were available for mRNA preparation.

Table I shows the levels of A-FABP protein expression in the 10 tumors analysed by 2D PAGE. The data were scored entirely based on the visual analysis of Coomassie Brilliant Blue stained gels and represent an average estimate of at least two different runs. Tumors scored as positive differed significantly with respect to the levels of this protein, and therefore are indicated with either four (very high), three (high), two (medium) and one cross (low). Representative examples of Coomassie stained 2D gels of tumors exhibiting very high (TCC 532-1, Fig. 1A), high (TCC 692-1; Fig. 1B), medium (TCC 763-1, Fig. 1C) and undetectable levels (TCC 709-1 and TCC 711-1 Fig. 1D-E) of A-FABP are shown in Fig. 1 (only the relevant area of the gels are shown).

A-FABP mRNA levels in non-invasive grade II, Ta TCCs. Since in many instances only a limited amount of fresh tumor was available, we used RT-PCR to determine the levels of A-FABP mRNA in the ten TCCs analysed by 2D PAGE (Fig. 1). Following amplification, the PCR products were analysed by conventional 1.5% agarose gel electrophoresis and visualised by ethidium bromide staining as shown in Fig. 2. The amount

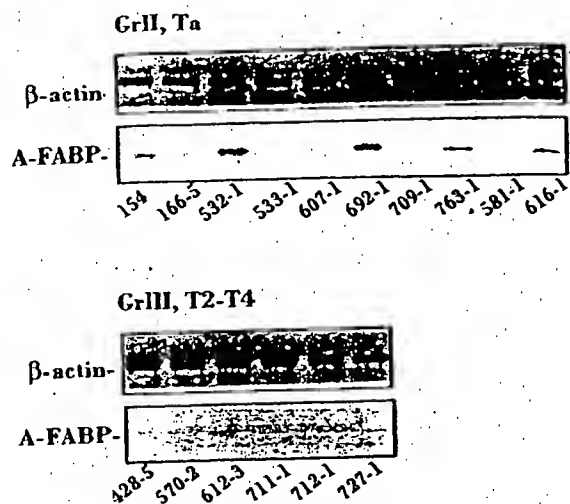


Figure 2. RT-PCR analysis of A-FABP mRNA expression in non-invasive (Gr II, Ta) and invasive TCCs (Gr III, T₂-T₄). For RT-PCR analysis, the ss c-DNA was synthesized by Reverse Transcriptase using total RNA, and used for RT-PCR amplification. The PCR products were resolved on 1.5% agarose gels and visualised under UV light following ethidium bromide staining. The A-FABP panels show the results of amplifications where the pair of gene specific primers was used to generate the 220 bp DNA fragment. Amplification of A-FABP was obtained after 30 cycles of PCR. The β -actin panels represent the amplification of the β -actin gene, which was used as an internal control to confirm that equal amounts of c-DNA were used in each reaction.

of cDNA in each lane was normalised using several house-keeping genes so as to achieve a more accurate assessment of the expression of the A-FABP mRNA. As shown in Fig. 2, TCC 532-1 exhibited the highest amount of A-FABP mRNA, followed by TCCs 692-1, 763-1, 616-1, 581-1, 154-1, 166-5 and 533-1. Undetectable levels of A-FABP mRNA were observed in the case of TCCs 607-1 and 709-1 (Fig. 2). Relative mRNA levels for the ten TCCs are given in Table I.

A-FABP protein and mRNA levels in invasive grade III, T₂-T₄ TCCs. Of the invasive TCCs (grade III, T₂-T₄) analysed by 2D PAGE only six yielded reasonable protein profiles for further study. As shown in Table I, none of these lesions expressed detectable levels of A-FABP as determined by Coomassie Brilliant Blue staining (Fig. 1E, TCC 711-1). In line with these results, the RT-PCR analysis of these tumors also revealed undetectable level of A-FABP mRNA (Fig. 2, Gr III T₂-T₄; Table I).

Loss of A-FABP protein is not compensated by an increase in PA-FABP. Recent studies of A-FABP knockout mice have shown that the loss of A-FABP in fat tissue is compensated by an increase in the skin fatty acid-binding protein mall (18). Our studies, however, indicated that the human homologue of mall, PA-FABP (19), did not compensate for the loss of A-FABP either in the non-invasive or the invasive tumors analysed in this study (Fig. 1D and E). In addition, Fig. 3 shows 2D gels of [³⁵S]-methionine labeled proteins from two grade II, Ta TCCs (192-4, T₁; Fig. 3A and 192-4, T₁; Fig. 3B).

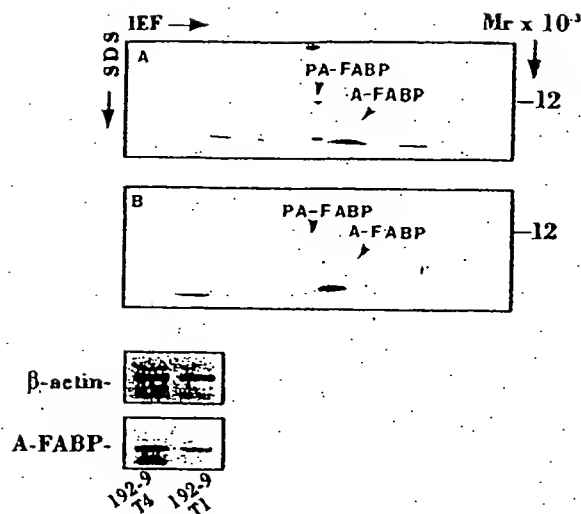


Figure 3. Levels of A-FABP and PA-FABP protein in grade II, Ta tumors resected from the same patient. The two upper panels show the 2D gel autoradiograms of [35 S]-methionine labeled proteins from TCCs (grade II, Ta) resected from the same patient. A, TCC 192-9 tumor 4 and B, TCC 192-9 tumor 1. Only the relevant area of the autoradiograms are shown. The low panel shows the RT-PCR analysis of A-FABP mRNA expression in the same tumors (see also legend to Fig. 2).

which differ significantly in their levels of A-FABP protein and mRNA (Fig. 3, low panel). As shown in Fig. 3, the decrease in A-FABP observed in TCC 129-4, T₁ is not accompanied by an increase in the PA-FABP protein (Fig. 1E).

Discussion

Of the TCC progression markers identified to date, A-FABP is perhaps one of the most interesting as its presence correlates both with the grade of atypia ($p=0.0006$) and the stage of the disease ($p=0.0269$) (3). A-FABP is a low molecular weight protein belonging to a cytosolic multigene family of lipid-binding proteins that include heart, liver, intestinal, muscle, brain, skin and epithelial isoforms (20). Members of the FABP family are highly expressed in differentiated cells and show narrow tissue distribution. Their precise function is at present unknown, although there is evidence suggesting that they may play roles in intracellular lipid transport and metabolism, signal transduction (21,22) as well as growth control and differentiation (23). The role in signal transduction has been inferred from the fact that long-chain fatty acids and their metabolites can act as primary and second messengers in specific signalling pathways (24). Recently, it has been shown that A-FABP may play a central role in the pathway that links obesity with insulin resistance, most likely by connecting the fatty acid metabolism with the expression of TNF- α (18). Furthermore, there is evidence indicating that the A-FABP gene contains sequence information necessary for differentiation-dependent expression in adipocytes (25). Our own data derived from the study of TCCs and normal urothelium suggest that A-FABP may be required for normal urothelium differentiation (1), as may be the case for PA-FABP in the skin (19).

Considering the potential prognostic value of A-FABP protein and/or mRNA in TCC progression it was important to determine if the levels of both type of macromolecules correlated both in the non-invasive and the invasive lesions expressing and lacking A-FABP. The need for such correlation was underlined by recent studies of Anderson and Scilhamer (15), who reported a lack of overall correlation between the mRNA and protein levels of 45 rat proteins analysed by 2D PAGE in combination with cDNA arrays. Their data yielded a correlation coefficient of 0.45 which is half way between weak and perfect correlation. Clearly, our data showed a very good correlation between the protein and mRNA levels of A-FABP in all tumors analysed indicating that the loss of A-FABP protein observed in some tumors is not due to post-transcriptional regulation.

Recently, knockout mice carrying a null mutation in the *aP2* gene encoding for A-FABP was produced (18). These animals do not show an obvious morphological or metabolic phenotype, but exhibit a 20-fold increase in the levels of the keratinocyte type FABP (*malI*), which may compensate for the loss of the deleted gene (18). The human homologue of the *malI* gene, PA-FABP, was cloned in our laboratory and has been shown to be highly upregulated in psoriatic skin as well as in abnormally differentiated primary keratinocytes (19). PA-FABP is expressed in normal urothelium together with A-FABP (3), and ongoing studies in the laboratory have shown that its level decreases significantly as tumors progress. Interestingly, the studies reported in this article did not reveal a compensatory up- or down-regulation of PA-FABP in the TCCs analysed, supporting the contention that PA-FABP may also play a role in cell growth and differentiation (19).

Acknowledgements

We would like to thank Lotte Quist, Gitte Ratz, Jette B. Lauridsen, Bodil Basse, Ariana Celis, Bent Hein and Pamela Celis for expert technical assistance. We also thank Torben Ørntoft for helpful discussion. I. Gromova was supported by a senior fellowship from the Danish Cancer Society. The work was supported by grants from the Danish Cancer Society and the Danish Biotechnology Programme.

References

1. Friedell GH, Nagy GK and Cohen SM: The pathology of human bladder cancer and related lesions. In: *The Pathology of Bladder Cancer*. I. Bryan GT and Cohen SM (eds). CRC Press Inc., Boca Raton FL, pp11-42, 1983.
2. Pauli BU, Alroy J and Weinstein RS: The ultrastructure and pathology of urinary bladder cancer. In: *The Pathology of Bladder Cancer*. II. Bryan GT and Cohen SM (eds). CRC Press Inc., Boca Raton FL, pp41-140, 1983.
3. Celis JE, Østergaard M, Basse B, Celis A, Lauridsen JB, Ratz GP, Andersen J, Hein B, Wolf H, Ørntoft TF and Rasmussen HH: Loss of adipocyte-type fatty acid binding protein and other protein biomarkers is associated with progression of human bladder transitional cell carcinomas. *Cancer Res* 56: 4782-4790, 1996.
4. Heney NM, Ahmed S, Flanagan MJ, Frable W, Corder MP, Hafermann MD and Hawkins IR: Superficial bladder cancer: progression and recurrence. *J Urol* 130: 1083-1086, 1983.
5. Simoneau AR and Jones PA: Bladder cancer: the molecular progression to invasive disease (Review). *World J Urol* 12: 89-95, 1994.
6. Spruck CH, Ohnishi PF, Gonzalez-Zulueta M, Esrig D, Miyao N, Tsai YC, Lerner SP, Schmutte C, Yang AS and Cote R: Two molecular pathways to transitional cell carcinoma of the bladder. *Cancer Res* 54: 784-788, 1994.

7. Rosin MP, Cairns P, Epstein JI, Schoenberg MP and Sidransky D: Partial allelotype of carcinoma *in situ* of the human bladder. *Cancer Res* 55: 5213-5216, 1995.
8. Birchmeier W and Birchmeier C: Epithelial-mesenchymal transitions in development and tumour progression. In: *Epithelial-Mesenchymal Interactions in Cancer*. Goldberg ID and Rosen EM (eds). Birkhäuser, Basel, pp1-15, 1995.
9. Sidransky D, von Eschenbach A, Tsai YC, Jones P, Summerhayes I, Marshall F, Paul M, Green P, Hamilton SR, Frost P, *et al*: Identification of p53 gene mutations in bladder cancers and urine samples. *Science* 252: 706-709, 1991.
10. Lopez-Beltran A, Croghan GA, Croghan I, Huben RP, Mettlin C and Gaeta JF: Prognostic factors in survival of bladder cancer. *Cancer* 70: 799-807, 1992.
11. Kern WH: The grade and pathologic stage of bladder cancer. *Cancer* 53: 1185-1189, 1984.
12. Jordan AM, Weingarten J and Murphy WM: Transitional cell neoplasms of the urinary bladder. Can biologic potential be predicted from histologic grading? *Cancer* 60: 2766-2774, 1987.
13. Wilkins MR, Sanchez JC, Gooley AA, Appel RD, Humphery-Smith I, Hochstrasser DF and Williams KL: Progress with proteome projects: why all proteins expressed by a genome should be identified and how to do it. *Biotechnol Genet Eng Rev* 13: 19-50, 1996.
14. Ostergaard M, Rasmussen HH, Nielsen HV, Vorum H, Ørntoft TF, Wolf H and Celis JE: Proteome profiling of bladder squamous cell carcinomas: identification of markers that define their degree of differentiation. *Cancer Res* 57: 4111-4117, 1997.
15. Anderson L and Seilhamer J: A comparison of selected mRNA and protein abundances in human liver. *Electrophoresis* 18: 533-537, 1997.
16. Celis JE, Ratz G, Basse B, Lauridsen JB and Celis A: High resolution two-dimensional gel electrophoresis of proteins: isoelectric focusing and non-equilibrium pH gradient electrophoresis (NEPHGE). In: *Cell Biology: A Laboratory Handbook*. III. Celis JE (ed). Academic Press, pp222-230, 1994.
17. Chomczynski P and Sacchi N: Single-step method of RNA isolation by acid guanidinium thiocyanate-phenol-chloroform extraction. *Anal Biochem* 162: 156-159, 1987.
18. Hotamisligil GS, Johnson RS, Distel RJ, Ellis R, Papaioannou VE and Spiegelman BM: Uncoupling of obesity from insulin resistance through a targeted mutation in aP2, the adipocyte fatty acid binding protein. *Science* 274: 1377-1379, 1996.
19. Madsen P, Rasmussen HH, Leffers H, Honore B and Celis JE: Molecular cloning and expression of a novel keratinocyte protein psoriasis-associated fatty acid-binding protein (PA-FABP) that is highly up-regulated in psoriatic skin and that shares similarity to fatty acid-binding proteins. *J Invest Dermatol* 99: 299-305, 1992.
20. Veerkamp JH, Paulussen RJ, Peeters RA, Maatman RG, van Moerkerk HT and van Kuppevelt TH: Detection, tissue distribution and (sub)cellular localization of fatty acid-binding protein types. *Mol Cell Biochem* 98: 11-18, 1990.
21. Glatz JF, Vork MM, Cistola DP and van der Vusse GJ: Cytoplasmic fatty acid binding protein: significance for intracellular transport of fatty acids and putative role on signal transduction pathways. *Prostaglandins Leukot Essent Fatty Acids* 48: 33-41, 1993.
22. Spitsberg VL, Matlashvili E and Gorewit RC: Association and coexpression of fatty-acid-binding protein and glycoprotein CD36 in the bovine mammary gland. *Eur J Biochem* 230: 872-878, 1995.
23. Yang Y, Spitzer E, Kenney N, Zschiesche W, Li M, Kromminga A, Muller T, Spener F, Lezius A, Veerkamp JH, *et al*: Members of the fatty acid binding protein family are differentiation factors for the mammary gland. *J Cell Biol* 127: 1097-1109, 1994.
24. Glatz JF, Borchers T, Spener F and van der Vusse GJ: Fatty acids in cell signalling: modulation by lipid binding proteins. *Prostaglandins Leukot Essent Fatty Acids* 52: 121-127, 1995.
25. Hunt CR, Ro JH, Dobson DE, Min HY and Spiegelman BM: Adipocyte P2 gene: developmental expression and homology of 5'-flanking sequences among fat cell-specific genes. *Proc Natl Acad Sci USA* 83: 3786-3790, 1986.

· 论著 ·

巨噬细胞移动抑制因子在急性呼吸窘迫综合征发病中的作用

郭禹标 谢灿茂

【摘要】 目的 探讨巨噬细胞移动抑制因子(MIF)在急性呼吸窘迫综合征(ARDS)中的表达和作用。方法 ARDS 组 12 例,对照组 20 例,用 ELISA 法测定患者血清 MIF 水平,采用流式细胞仪检测外周血单个核细胞(PBMC)MIF 的表达,用免疫组织化学双重染色和原位杂交技术观察肺组织中 MIF mRNA 和蛋白表达水平。结果 ARDS 患者外周血清 MIF 水平和 PBMC MIF 表达率明显高于正常人 ($P < 0.01$)。原位杂交和免疫组化染色结果显示,正常肺组织中未见 MIF mRNA 和蛋白表达,而在 ARDS 肺组织中 MIF 表达水平明显增高,肺间质、肺泡腔内可见巨噬细胞浸润并见有 MIF 表达,病理损伤较严重处 MIF 表达更强且与巨噬细胞浸润数量明显相关。结论 ARDS 患者血清 MIF 水平和外周血单个核细胞表达 MIF 增多,肺组织存在 MIF 表达增多及巨噬细胞浸润情况,提示 MIF 在 ARDS 发病中起重要作用。

【关键词】 急性呼吸窘迫综合征; 巨噬细胞; 细胞因子; 巨噬细胞移动抑制因子

The pathogenic role of macrophage migration inhibitory factor in acute respiratory distress syndrome
GUO Yubiao, XIE Canmao. Department of Respiratory Medicine, First Affiliated Hospital of Zhongshan University, Guangzhou 510080, China

【Abstract】 Objective To investigate the expression and pathogenic role of macrophage migration inhibitory factor(MIF) in human acute respiratory distress syndrome(ARDS). Methods The serum level of MIF in ARDS patients and normal persons were measured by ELISA method. Peripheral blood mononuclear cell (PBMC) MIF expression was determined by flow-cytometry. The expression of MIF mRNA and protein in the lung tissues were detected by using double immuno histochemistry labeling and in situ hybridization. Results The serum level of MIF increased significantly in ARDS patients as compared with normal persons ($P < 0.01$); The percentage of PBMC MIF expression was higher in ARDS patients than in normal controls ($P < 0.01$). In situ hybridization and immunohistochemistry showed undetectable or weak MIF mRNA and protein expression in normal lungs. In contrast, there was marked upregulation of MIF mRNA and protein expression in the ARDS lungs. In ARDS, macrophages infiltrated the alveolar space and interstitium, most of which also expressed MIF. Infiltrating macrophages were almost restricted to the areas of severe tissue damage. The MIF expression level showed a strong correlation with the number of infiltrating macrophages. Conclusions The serum level of MIF and PBMC MIF expression increased in ARDS patients with enhanced pulmonary MIF expression and macrophage infiltration, which suggests that MIF plays a pivotal role in the pathogenesis of ARDS.

【Key words】 Acute respiratory distress syndrome; Macrophage; Cytokine; Macrophage migration inhibitory factor

急性肺损伤(ALI)和急性呼吸窘迫综合征(ARDS)的病理基础是由多种炎症细胞(中性粒细胞、巨噬细胞和淋巴细胞)参与的肺脏局部炎症反应和炎症反应失控所致的肺毛细血管膜损伤。近年来对 ALI/ARDS 研究的一个重要趋势是认为仅仅根据临床指标定义 ALI/ARDS 是不够的,如能结合肺泡局部与嗜中性粒细胞等炎症细胞聚集和激活有关的

化学免疫指标才更有利于该综合征的诊断和治疗^[1,2]。在油酸致 ALI 动物模型中我们发现巨噬细胞移动抑制因子(MIF)和巨噬细胞浸润在介导急性肺损伤中可能起重要作用,其表达强弱可反映肺组织损害及病变严重程度^[3]。那么 MIF 表达及巨噬细胞浸润在临床上 ALI/ARDS 患者中有无类似作用呢?本部分临床研究通过测定 ARDS 患者血中 MIF 和肺组织中 MIF 表达的水平,探讨 MIF 在 ARDS 发病机制中的作用。

对象与方法

一、临床资料

1. ARDS 组: 选择 1999 年 10 月 ~ 2001 年 1 月在我院外科重症监护病房(SICU)和内科重症监护病房(MICU)收治的 ARDS 患者 12 例, 其中男 8 例, 女 4 例, 年龄 22 ~ 62 岁, 发病原因中败血症并 ARDS 5 例, 肾移植术后并巨细胞病毒感染 3 例, 重症胰腺炎 1 例, 弥漫性血管内凝血(DIC)1 例, 肺挫伤 1 例, 羊水栓塞 1 例。所有病例均符合 ARDS 诊断标准^[1]。

2. 正常对照组: 20 名正常对照为健康献血者, 男性 10 人, 女性 10 人, 年龄 20 ~ 60 岁。

二、实验材料

抗人 MIF 单克隆抗体(monoclonal anti-human MIF antibody)为 R & D 公司产品; 小鼠抗人 MIF 抗体, 由香港大学医学院蓝辉耀教授惠赠; KP₁ 为小鼠抗人 CD68 抗体, 可识别单核细胞和巨噬细胞, 由香港大学医学院提供。链霉菌抗生素蛋白-过氧化物酶免疫组化染色试剂盒, 从福州迈新生物技术公司购买; LSAB + 免疫组化染色试剂盒, 从 DAKO 公司购买。地高辛标记的 MIF cDNA 探针(人 MIF 质粒由香港大学医学院蓝辉耀教授惠赠)。

三、方法

1. 血清 MIF 水平测定: 采用酶联免疫法(ELISA)测定正常人及 ARDS 患者血清 MIF 水平(每例患者在确诊 ARDS 的第一个 24 h 内抽血), 具体参照 R & D 公司试剂盒提供方法稍加改进。

2. 流式细胞仪检测外周血单个核细胞(PBMC) MIF 表达: 取空腹肝素抗凝血 5 ml, PBS 稀释 1 倍, 沿管壁加入有 3 ml 淋巴细胞分离液的离心管中。离心 2 000 r/min, 25 min, 用毛细吸管轻轻插到呈白膜的 PBMC 层, 吸入另一离心管中, 用 PBS 洗 2 次。4℃中性甲醛固定 0.5 h, 用含 0.4% Triton X-100 PBS 洗 3 次, 于 37℃孵育 0.5 h。PBS 洗 3 次, 加入抗人 MIF 抗体。PBS 洗 3 次, 再加异硫氰酸荧光素(FITC)标记的抗体(小鼠抗人 IgG1)于 37℃孵育 0.5 h。流式细胞仪检测 PBMC MIF 蛋白表达率。

3. 肺组织活检标本作 MIF 和 KP₁ 免疫组织化学双重染色: (1)肺活检和标本处理: 上述 ARDS 组 8 例患者经抢救无效死亡, 即行尸体肺活检。另 10 例在光镜下没有明显异常的肺标本为来源于气胸/肺大疱肺叶切除手术, 但远离肺大疱的正常肺组织。组织置于中性甲醛液固定, 石蜡包埋后用切片机制

成 4 μm 厚的石蜡切片, 常规 Bioclear 脱蜡 20 min, 经梯队酒精(100%、95%、70%)脱水。(2)具体方法: 肺组织标本参考 Lan 等^[4]微波免疫组化双重染色法操作。每一重染色均采用不加第一抗体的方法作为阴性对照。第一重染色用 PAP 法, 第一抗体为 KP₁, DBA 显色, 阳性物呈棕色。第二重染色用 APAAP 法, 第二抗体为 MIF 抗体, fast blue 显色, 阳性物呈蓝色。切片水洗后用 PAS 套染, 利用装于目镜上的显微方格尺, 在 100× 高倍视野连续随机计算肺泡内区 10 个, 外区 10 个方格标尺中染色阳性细胞数, 以细胞数/mm² 表示。计算平均每 mm² 肺间质和肺实质中 KP₁⁺、MIF⁺ 染色阳性及 KP₁⁺/MIF⁺ 同时染色阳性细胞数, 以均数 ± 标准差表示。

4. 肺组织 MIF 原位杂交: 地高辛标记的 MIF cDNA 探针(按地高辛标记试剂盒标记 MIF 探针, 浓度 200 ng/ml)。具体方法参照试剂盒说明并作稍微改动。

四、统计学处理

结果中所有数据以 $\bar{x} \pm s$ 表达, 正常人和 ARDS 患者血清 MIF 水平、PBMC MIF 蛋白表达率及肺组织中 MIF 表达水平的比较用方差分析, MIF 表达水平与巨噬细胞浸润的相关性用直线相关分析法, 采用 SPSS 10.0 FOR WIN 统计软件, 以 $P < 0.05$ 为统计学有差异的标准。

结 果

一、ARDS 患者外周血 MIF 水平

ELISA 方法测定结果显示, ARDS 患者外周血清 MIF 水平和 PBMC MIF 表达率明显高于正常对照组 ($P < 0.01$)(表 1)。

表 1 ARDS 患者和正常人外周血清 MIF 水平和 PBMC MIF 表达率($\bar{x} \pm s$)

组别	例数	血清 MIF(ng/L)	PBMC MIF(%)
正常对照组	20	41 ± 30	0.93 ± 0.26
ARDS 组	12	2 230 ± 40*	5.61 ± 1.93*

注: 与正常对照组比较, * $P < 0.01$

二、ARDS 患者 PBMC MIF 蛋白表达

流式细胞仪检查结果显示, ARDS 患者 PBMC MIF 蛋白表达明显高于正常对照组 ($P < 0.05$)(表 1)。ARDS 患者 PBMC 细胞涂片经免疫组化双重染色后 KP₁ 和 MIF 均阳性。

三、MIF 在肺组织中表达

原位杂交和免疫组化染色结果显示,正常肺组织未见 MIF mRNA 和蛋白表达(图 1,2)。而在 ARDS 患者肺间质、肺实质中 MIF 蛋白表达增加,肺间质、肺泡腔内部分巨噬细胞见有 MIF 表达(图 3,4,表 2)。

四、MIF 表达与巨噬细胞在 ARDS 组织中浸润

免疫组化染色结果显示,正常肺组织可见极少数巨噬细胞,在 ARDS 肺间质及肺泡腔中巨噬细胞的浸润数量明显增多,且大多数巨噬细胞聚集在 MIF 强表达的部位,病理损害较重处巨噬细胞浸润较多,肺泡间质 MIF 表达(阳性肺泡数)与间质浸润的巨噬细胞数,两者呈明显的相关关系($r=0.896$, $P<0.01$)(图 3,表 2,图 5)。

表 2 ARDS 患者肺组织 MIF 表达与巨噬细胞浸润($\bar{x} \pm s$)

组别	例数	肺间质		
		KP ⁺ 细胞数(/mm ²)	MIF ⁺ (%)	MIF ⁺ mRNA (%)
正常组	10	10 \pm 8	1.3 \pm 0.9	1.05 \pm 0.12
ARDS 组	8	276 \pm 122 [*]	35.8 \pm 8.5 [*]	40.13 \pm 11.08 [*]

注:与正常组比较,^{*} $P<0.01$

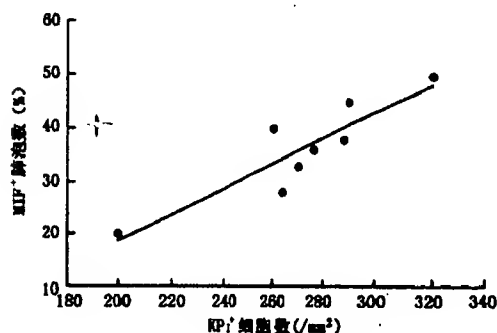


图 5 KP⁺ 细胞数与 MIF⁺ 肺泡数的相关关系

讨 论

ARDS 的发病机制复杂,至今仍未阐明。现已知可能参与 ALI 和 ARDS 发病的细胞有多形核白细胞(PMN)、血小板、红细胞和巨噬细胞(M ϕ)等;炎症介质主要有氧自由基、补体系统、蛋白溶解酶、溶酶体、纤维蛋白及其降解产物、花生四烯酸代谢产物、凝血和纤溶系统、血小板活化因子、细胞因子如肿瘤坏死因子和白细胞介素-8 等。这些物质在 ALI 和 ARDS 的病程中,可能是多种细胞、多种介质、多种途径的反应^[5]。既往对 ARDS 的研究着重于中性粒细胞及其相关细胞因子,而对巨噬细胞浸润引起的肺损伤及其介导机制则研究较少。研究表明,在

ALI 或 ARDS 早期,M ϕ 可能在有关 PMN 应答方面起了启动器样作用,即当机体遭受创伤或感染等多种刺激下,M ϕ 持续、过度激活,分泌大量的炎症介质并进一步趋化、激活 PMN,促使 PMN 在肺泡腔-肺毛细血管内大量聚集并最终引起肺泡损伤和毛细血管通透性增加^[6]。本实验证明在人 ARDS 肺组织中除 PMN 外同时存在着巨噬细胞的局部浸润,这与油酸致 ALI 动物模型的发现相仿^[3],提示 M ϕ 亦是参与 ALI/ARDS 早期炎症的效应细胞之一。

虽然已知巨噬细胞在组织损害中起重要作用,但其具体发挥作用机制则尚未明了。MIF 是一种含 115 个氨基酸的蛋白质,相对分子质量约 12 500。MIF 可作为垂体激素和 M ϕ /T 细胞的细胞因子控制宿主应激应答和炎症性应答^[7,8]。MIF 能抑制巨噬细胞游走,促进巨噬细胞在炎症局部浸润、增生、激活及分泌一些细胞因子,在内毒素休克中起重要作用^[8,9]。垂体前叶及外周的单核巨噬细胞是产生 MIF 的主要来源^[9,10]。本实验中 PBMC 上表达 MIF 增多,表明外周血单核/巨噬细胞是产生 MIF 的主要来源。Hironi 等^[11]报道脂多糖(LPS)诱发的急性肺损伤动物模型中,MIF 的抗体可抑制、减少白细胞在肺泡腔的聚集。我们^[3]在油酸致 ALI 动物模型中发现 MIF 抗体通过下调 MIF 表达,可减少巨噬细胞浸润而起保护作用。Donnelly 等^[12]报道在 ARDS 患者,支气管肺泡灌洗液(BALF)中 MIF 表达增多,MIF 的抗体可逆转、减少 IL-8、TNF 的分泌和作用。本临床研究通过免疫组化和原位杂交证实在 ARDS 患者肺组织中 MIF 表达增多且伴有巨噬细胞浸润(部分巨噬细胞上表达 MIF),且病理损伤明显处 MIF 表达尤其明显。这些结果与油酸致急性肺损伤动物模型相似,与国外 Donnelly 等^[12]研究一致,提示 MIF 介导了巨噬细胞浸润和 ARDS 患者的肺损伤。本实验发现 ARDS 患者血清 MIF 水平明显升高,结合动物模型结果,提示 MIF 可能作为 ALI/ARDS 诊断的较敏感的化学免疫指标。综合我们的动物模型、临床研究和国外学者的报道,MIF 在脂多糖、内毒素败血症、或非感染性诱导的肺损伤发病机制中起一定的作用,这些结果和发现为细胞因子、炎症介质拮抗剂如抗 MIF 单抗进一步的临床应用研究提供了依据。但值得注意的是,MIF 亦可作为垂体激素,当下丘脑-垂体-肾上腺(HPA)轴受刺激后,垂体前叶以“激素样”方式分泌 MIF,故 MIF 水平升高不排除 ALI/ARDS 时各种直接或间接因素所致的机体应激状态

及相关的中枢性释放。肺脏局部和血中 MIF 升高与 HPA 轴及应激的关系尚有待深入研究。

ARDS 病理改变分成 3 期^[13]: 早期为渗出期, 中期为增生期, 晚期为纤维化期。本部分临床研究由于入选病例数少, ARDS 的基础病因不一, ARDS 病程早晚难以推测, 且肺组织病理大部分为尸体肺, 故研究结果难免以偏盖全。那么究竟在 ALI/ARDS 不同病因、不同时期, MIF 表达及巨噬细胞浸润与疾病发生发展关系如何, 特别是巨噬细胞浸润与其后的肺纤维化改变、预后转归的关系还有待大宗的、客观的临床试验设计进一步研究探讨。

致谢 本实验方法得到香港大学医学院蓝辉耀教授和陈永雄博士的指导及大力协助

(本文图 1~4 见插图 6-1)

参考文献

- 1 中华医学会呼吸病学分会. 急性肺损伤和急性呼吸窘迫综合征的诊断标准(草案). 中华结核和呼吸杂志, 2000, 23: 203.
- 2 刘又宁. 对成人呼吸窘迫综合征诊断问题的几点认识. 中华结核和呼吸杂志, 2000, 23: 199-200.
- 3 郭禹标, 陈永雄, 谢灿茂, 等. 巨噬细胞移动抑制因子在油酸致急性肺损伤动物模型肺组织中的表达. 中国病理生理杂志, 2001, 17: 40-42.
- 4 Lan HY, Ma W, Nikolic-Paterson D, et al. A novel, simple, reliable and sensitive method for multiple immunoenzyme staining: use of microwave oven heating to block antibody cross-reactivity and retrieve antigens. J Histochem Cytochem, 1995, 43: 97-102.
- 5 Baughman RP, Gunther KL, Rashkin MC, et al. Changes in the inflammatory response of the lung during acute respiratory distress syndrome: prognostic indicators. Am J Respir Crit Care Med, 1996, 154: 76-81.
- 6 金敏顺, 陈正堂. 单核/巨噬细胞释放的趋化性细胞因子与急性肺损伤. 国外医学呼吸系统分册, 1997, 17: 133-136.
- 7 Bernhagen J, Calandra T, Bucala R, et al. Regulation of the immune response by macrophage migration inhibitory factor: biological and structure features. J Mol Med, 1998, 76: 151-161.
- 8 黄仕和, 许四宏. 巨噬细胞移动抑制因子的研究进展. 微生物学免疫学进展, 1999, 27(4): 78-80.
- 9 Bucala R. MIF, a previously unrecognized pituitary hormone and macrophage cytokine, is a pivotal mediator in endotoxic shock. Circulation Shock, 1994, 44: 35-39.
- 10 Calandra T, Bernhagen J, Mitchell RA, et al. The macrophage is an important and previously unrecognized source of macrophage migration inhibitory factor. J Exp Med, 1994, 179: 1895-1902.
- 11 Hironi M, Maasharu N, Kenji M, et al. Effect of anti-macrophage migration factor antibody on lipopolysaccharide-induced pulmonary neutrophil accumulation. Am Respir Crit Care Med, 1998, 158: 573-579.
- 12 Donnelly SC, Haslett C, Reid PT, et al. Regulatory role for macrophage migration factor in acute respiratory distress syndrome. Nat Med, 1997, 3: 320-323.
- 13 Tomaszefski JF Jr. Pulmonary pathology of acute respiratory distress syndrome. Clin Chest Med, 2000, 21: 435-466.

(收稿日期: 2001-10-09)

(本文编辑: 王娟)

第二次全国抗栓溶栓学术研讨会征文通知

由中华血液学分会血栓与止血学组、中华医学会、中华医学杂志、中华神经学分会共同举办的全国抗栓溶栓学术研讨会, 定于 2003 年在乌鲁木齐召开, 现将会议有关事项通知如下。

1. 征文内容: 血栓形成的机制; 血栓疾病相对因素的临床监测; 血栓性疾病实验室检测; 影像学诊断; 血栓性疾病的抗凝溶栓疗法; 心脑血管疾病的抗栓溶栓; 介入治疗的抗栓溶栓; 血管性疾病与外科手术病人的抗凝溶栓; 妊娠期凝血及纤溶系统改变; 产科 DIC 的病因; 血栓性疾病在临床诊治中存在的问题及防治对策等。

2. 征文要求: (1) 请寄全文及 1 000 字摘要各一份, 摘要中不要图但结果部分, 一定要用数据来说明问题; (2) 来稿请加盖公章, 附单位介绍信; (3) 稿件请一律提供打印件, 自留底稿, 恕不退还; 可通过电子信箱投稿(地址: nmjc@263.net); (4) 截稿日期: 2002 年 12 月 10 日; (5) 稿件请寄北京东四西大街 42 号中华医学杂志编辑部纪莉莹收, 注明“抗栓会议”字样, 电话: 010-65273362。本次会议为国家继续教育项目, 将授予国家级继续教育学分。希望心血管、血液、神经、呼吸、外科、检验、妇产科医师能够参加会议共同研讨, 以进一步提高临床诊治水平。

《机械通气波形分析与临床应用》一书出版

上海市第一人民医院呼吸科主任兼内科教研室主任周新教授、陈宇清主治医师编著, 全国麻醉学教育分会主任委员、中华医学会麻醉学分会副主任委员曾因明教授作序的《机械通气波形分析与临床应用》一书, 已由世界图书出版公司于 2002 年 3 月正式出版发行。该书以呼吸科、ICU、麻醉科等临床医师为主要对象, 详细介绍了机械通气各种模式的波形特点及临床应用, 可作为各级临床医师的案头参考书和继续教育教材, 也可供研究人员和大学生阅读。该书已由各地新华书店经销。欲购书者也可与陈宇清医师联系。地址: 上海市武进路 85 号, 邮编 200080。电话: 021-63071428。

Available online at www.sciencedirect.com

SCIENCE @ DIRECT®

Biochemical Pharmacology 69 (2005) 993–999

www.elsevier.com/locate/biochempharm**Biochemical
Pharmacology**

Restored expression and activity of organic ion transporters rOAT1, rOAT3 and rOCT2 after hyperuricemia in the rat kidney

Yasushi Habu^a, Ikuko Yano^a, Masahiro Okuda^a, Atsushi Fukatsu^b, Ken-ichi Inui^{a,*}^a Department of Pharmacy, Kyoto University Hospital, Faculty of Medicine, Kyoto University, Sakyo-ku, Kyoto 606-8507, Japan^b Division of Artificial Kidneys, Kyoto University Hospital, Faculty of Medicine, Kyoto University, Sakyo-ku, Kyoto 606-8507, Japan

Received 22 October 2004; accepted 13 December 2004

Abstract

We previously reported that in hyperuricemic rats, renal impairment occurred and organic ion transport activity decreased, accompanied with a specific decrease in the expression of rat organic anion transporters, rOAT1 and rOAT3, and organic cation transporter, rOCT2. In the present study, we investigated the reversibility of the organic ion transport activity and expression of organic ion transporters (slc22a) during recovery from hyperuricemia. Hyperuricemia was induced by the administration of a chow containing uric acid and oxonic acid, an inhibitor of uric acid metabolism. Four days after discontinuance of the chow, the plasma uric acid concentration returned to the normal level, and renal functions such as creatinine clearance and BUN levels were restored, although the recovery of tubulointerstitial injury was varied in sites of the kidney. Basolateral uptake of *p*-aminohippurate (PAH) and tetraethylammonium (TEA), and both protein and mRNA levels of rOAT1, rOAT3 and rOCT2 in the kidney gradually improved during 14 days of recovery from hyperuricemia. Basolateral PAH transport showed a higher correlation with the protein level of rOAT1 ($r^2 = 0.80$) than rOAT3 ($r^2 = 0.34$), whereas basolateral TEA transport showed a strong correlation with rOCT2 protein ($r^2 = 0.91$). The plasma testosterone concentration, which is a dominant factor in the regulation of rOCT2, was gradually restored during the recovery from hyperuricemia, but the correlation between the plasma testosterone level and rOCT2 protein expression in the kidney was not significant. These results suggest that the regulation of organic ion transporters, rOAT1, rOAT3 and rOCT2, by hyperuricemia is reversible, and the organic ion transport activity restores according to the expression levels of these transporters.

© 2005 Elsevier Inc. All rights reserved.

Keywords: Renal transport; Organic anion transporter; Organic cation transporter; slc22a; Rats; Hyperuricemia

1. Introduction

Urinary excretion of various compounds including endogenous metabolites, drugs and xenobiotics is an important physiological function of the renal proximal tubules. In renal tubules, membrane transport systems mediate the tubular secretion, and several isoforms of organic anion and cation transporters have been characterized [1,2]. Two organic anion transporters, OAT1 and OAT3, at the renal basolateral membrane mediated the renal tubular secretion of several anionic drugs including *p*-aminohippurate (PAH), nonsteroidal anti-inflammatory drugs, methotrexate and cephalosporins [3–8]. On the other hand, organic cation transporters, OCT1 and OCT2, were localized to basolateral membranes of renal

tubular cells, and contributed to the transport of many cationic compounds including tetraethylammonium (TEA), cimetidine, monoamines and procainamide [8–12].

We previously reported that renal organic anion and cation transport activity across the basolateral membrane was decreased in hyperuricemic rats, accompanied with decreased expression of some organic ion transporters, rOAT1, rOAT3 and rOCT2 [13]. In contrast, the renal expression levels of rOCT1, OAT-K1 and OAT-K2, kidney-specific organic anion transporters, and organic anion transporting polypeptide 1 (oatp1) were unchanged in hyperuricemic rat kidney [13]. Renal clearances of methotrexate and cimetidine were also decreased in hyperuricemic rats, suggesting that the down-regulation of rOAT1, rOAT3 and rOCT2 partly accounts for the decreased renal disposition of these drugs [13].

Altered expression of renal organic ion transporters has been reported using several animal models with renal impairment induced by cisplatin and by subtotal nephrect-

Abbreviations: PAH, *p*-aminohippurate; TEA, tetraethylammonium

* Corresponding author. Tel.: +81 75 751 3577; fax: +81 75 751 4207.

E-mail address: inui@kuhp.kyoto-u.ac.jp (K.-i. Inui).

0006-2952/\$ – see front matter © 2005 Elsevier Inc. All rights reserved.
doi:10.1016/j.bcp.2004.12.004

omy [14-17]. However, little information is available on the alterations in the expression of renal organic ion transporters during the recovery from renal impairment. On one hand, renal functions were decreased in hyperuricemic rats induced by the administration of a chow containing uric acid and oxonic acid, an inhibitor of uric acid metabolism [18]. After administration of the chow was discontinued, renal functions such as the fractional reabsorption of sodium and phosphate were improved, although the urine concentrating ability, calcium reabsorption and the capacity to excrete ammonium remained impaired [18]. Therefore, renal functions including renal organic ion transport might change at different rates during recovery from hyperuricemia in rats.

In the present study, we examined the alteration of organic ion transport activity and the expression of organic ion transporters including rOAT1, rOAT3 and rOCT2 in the kidney during recovery from hyperuricemia in rats.

2. Materials and methods

2.1. Materials

D-[1-³H(N)]-mannitol (973 GBq/mmol) and *p*-[glycyl-1-¹⁴C]-aminohippuric acid (1.9 GBq/mmol) were obtained from Perkin-ElmerTM Life Sciences. [1-¹⁴C] Tetraethylammonium bromide (2.04 GBq/mmol) was obtained from American Radiolabeled Chemicals. Oxonic acid and uric acid were purchased from Aldrich and Wako Pure Chemical Industries, respectively. All other chemicals used were of the highest purity available.

2.2. Animals

The animal experiments were performed in accordance with the Guidelines for Animal Experiments of Kyoto University. The experimental protocol was approved by the Animal Research Committee, Graduate School of Medicine, Kyoto University. Male Wistar rats weighing 190-235 g were fed ground rat chow and water freely for 10-24 days. Hyperuricemia was induced with ground standard rat chow containing 2.5% uric acid and 5% oxonic acid for 10 days as described in our previous report (0-day recovery group) [13]. During recovery from hyperuricemia, the rats were fed standard rat chow for 4, 7 or 14 days (4, 7 or 14-day recovery group).

2.3. Biochemical tests

The concentration of blood urea nitrogen (BUN) and creatinine in plasma and urine were measured by the urease-indophenol method and Jaffé method using kits obtained from Wako Pure Chemical Industries, respectively. Plasma uric acid concentration was determined by high performance liquid chromatography as described in

the previous report [13]. Plasma concentration of testosterone was measured with an enzyme immunoassay kit (Cayman Chemical Company).

2.4. Histological analyses

Kidneys of rats during recovery from hyperuricemia were removed and immediately fixed for 1 day at room temperature in carnoy fixative (ethanol:chloroform:acetic acid = 6:3:1) and preserved in 70% ethanol. Conventional histological sections were stained with periodic acid-Schiff reagent [8].

2.5. Uptake of PAH and TEA into renal slices

Renal slices were prepared with a Stadie-Riggs microtome and the uptake of [¹⁴C]PAH (5 μ M, 0.93 kBq/mL) or [¹⁴C]TEA (5 μ M, 1.03 kBq/mL) were measured as previously described [13]. [³H]Mannitol (5 μ M, 22.8 kBq/mL) was used to calculate the extracellular trapping and nonspecific uptake of [¹⁴C]PAH and [¹⁴C]TEA as well as to evaluate the viability of slices.

2.6. Western blot analyses

Preparation of crude membrane fractions and Western blot analyses were performed as previously reported [13].

2.7. Northern blot analyses

Total RNA was extracted from the kidney using TRI-ZOLTM reagent (Invitrogen Co.). Then, Northern blot analyses were performed as previously described [13].

2.8. Statistical analyses

The statistical significance of differences between mean values was calculated using the non-paired *t*-test, or by the one-way analysis of variance with the Scheffé test for post hoc analysis. *P*-values of <0.05 were considered significant.

3. Results

Several physiological and biochemical parameters were measured during the recovery period of hyperuricemia in rats (Fig. 1). The body weight gradually increased during recovery for 14 days. Plasma uric acid returned to the normal level during the initial 4 days of recovery. Improvement of BUN, plasma creatinine and creatinine clearance during the initial 4 days suggested that renal functions have been recovered quickly. In contrast, urine volume returned to normal more slowly than the above parameters.

Histological analyses of the kidney were performed and shown in Fig. 2. The tubular lumen was dilated in a diffuse

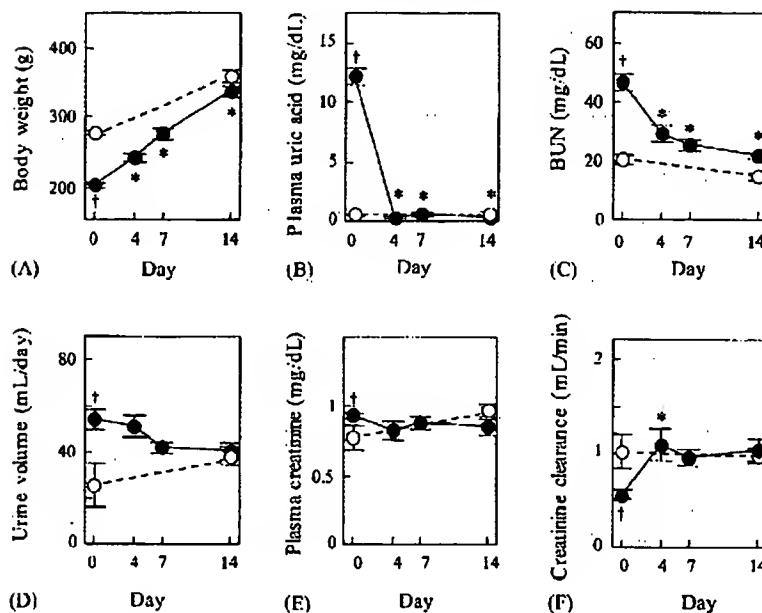


Fig. 1. Physiological and biochemical parameters during recovery from hyperuricemia. At 4, 7 and 14 days recovery from hyperuricemia, body weight (A), plasma uric acid (B), BUN (C), urine volume (D), plasma creatinine (E) and creatinine clearance (F) were measured (●). Open circles represent the values of normal rats. Each point represents the mean \pm S.E. of 5-13 rats. * $P < 0.05$, vs. normal rats. * $P < 0.05$, vs. hyperuricemic rats on day 0.

area filled with detached tubular epithelial cells and was infiltrated by mono- and poly-nuclear cells in hyperuricemic rat kidney (0-day recovery group) as previously reported [13]. Moreover, inflammatory cells also infiltrated into the interstitium and in tubules [13]. This tubulointerstitial pathology was observed in the diffuse area on day 4, and visible in the focal area on day 7, which was almost disappeared on day 14 (Fig. 2).

We then evaluated basolateral organic anion and cation transport activity by the uptake of PAH and TEA into renal slices (Fig. 3). The PAH and TEA uptake into renal slices in the 0-day recovery group were much lower than those in normal rats. In the 4-days recovery group, PAH and TEA uptake were significantly increased compared with those in 0-day recovery group. The PAH and TEA uptake in the 14-days recovery groups achieved similar uptake activity to those in control group at 30 or 60 min.

The expression of rOAT1, rOAT3 and rOCT2 protein during the recovery period of hyperuricemic rats was examined by Western blot analyses (Fig. 4). The expression of these transporters of 0-day recovery group was significantly decreased in hyperuricemic rats compared with normal rats, and the expression levels of rOAT1 and rOAT3 in 7- and 14-days recovery group significantly increased compared with those in 0-day recovery group. The expression of rOCT2 protein gradually increased until 14-days of recovery.

The mRNA expression of rOAT1 and rOCT2 during recovery from hyperuricemia was analyzed by Northern blot analyses (Fig. 5). The mRNA expression of both transporters in the 0-day recovery group was much lower than that in normal rats, and the rOAT1 mRNA expression

significantly increased in the 7- and 14-days recovery group compared with 0-day recovery group. Recovery of rOCT2 mRNA expression was significant on day 14. Moreover, the expression of rOAT1 and rOCT2 protein was significantly correlated with that of mRNA, respectively (rOAT1, $r^2 = 0.66$, $P < 0.05$; rOCT2, $r^2 = 0.45$, $P < 0.05$).

We investigated the correlation between basolateral PAH and TEA transport and the protein level of rOAT1, rOAT3 and rOCT2 (Fig. 6). Initial PAH transport at 15 min across basolateral membrane showed a high correlation with the protein level of rOAT1 ($r^2 = 0.80$, $P < 0.05$), but not with that of rOAT3 ($r^2 = 0.34$, $P = 0.35$). On one hand, basolateral TEA transport showed a high correlation with the protein level of rOCT2 ($r^2 = 0.91$, $P < 0.05$).

Finally, we measured plasma concentration of testosterone, which was the dominant factor mediating sex-related difference in the expression of rOCT2 [19]. Plasma testosterone concentration was decreased in the 0-day recovery group (control, 3.23 ± 0.59 ng/mL; 0 day, 1.08 ± 0.10 ng/mL; mean \pm S.E., $n = 6$) and was gradually increased during the recovery period of hyperuricemia (4 days, 1.68 ± 0.45 ng/mL; 7 days, 3.61 ± 0.24 ng/mL; 14 days, 4.51 ± 1.26 ng/mL; mean \pm S.E., $n = 6$). However, plasma testosterone levels and the expression of rOCT2 protein did not show a significant linear correlation (Fig. 7, $r^2 = 0.14$, $P = 0.14$).

4. Discussion

Hyperuricemia is often the first clinical manifestation of gout and accompanies renal failure. Recently, serum uric

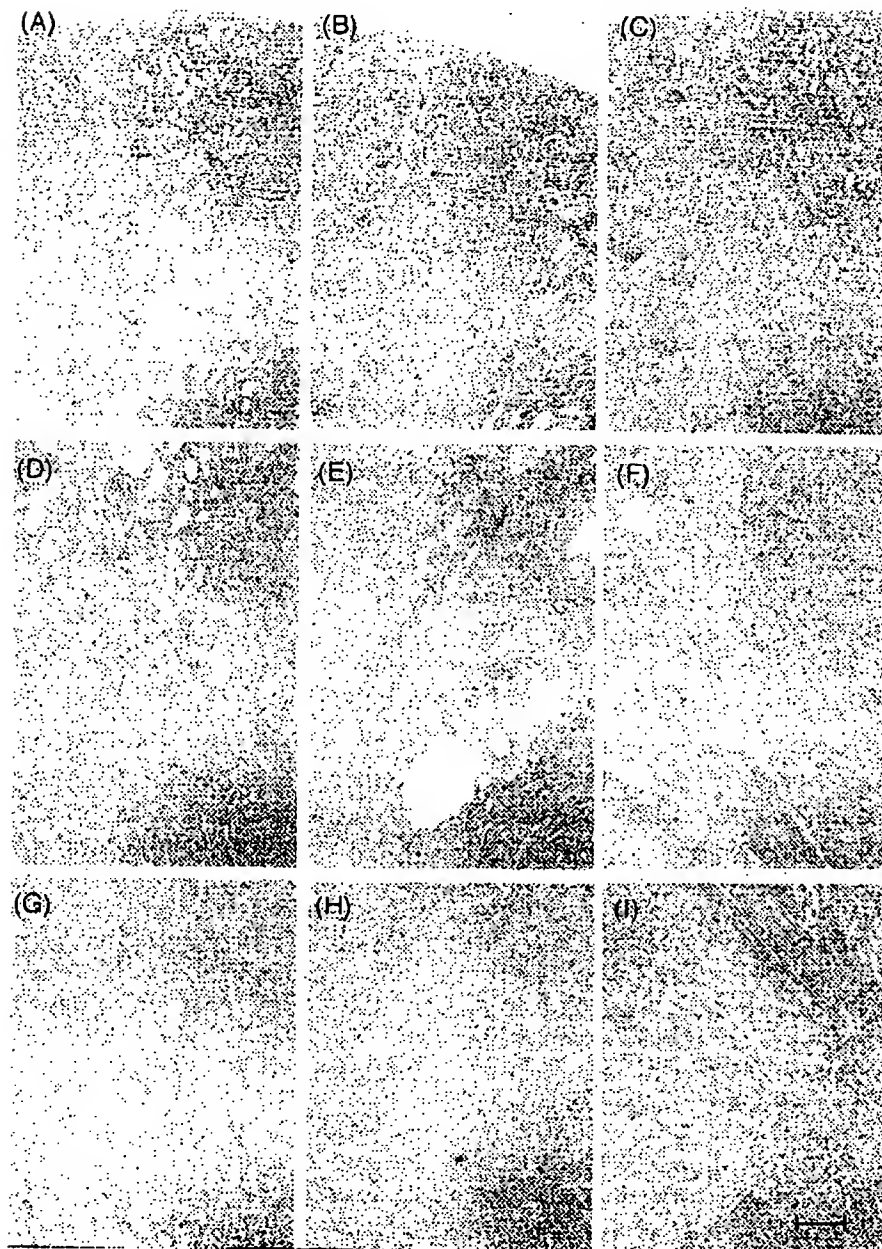


Fig. 2. Periodic acid-Schiff staining of cortex (A–C), outer medulla (D–F) and inner medulla (G–I) in the serial picture from each typical rat kidney at 4—(A, D and G), 7—(B, E and H) and 14—(C, F and I) days recovery from hyperuricemia; bar = 100 μ m.

acid was found to be an independent risk factor for development of renal insufficiency in a study of 6403 subjects [20]. Mazaali et al. reported that crystal-independent mechanism, mediated in part by activation of the renin-angiotensin system and downregulation of NO synthase expression, contributed to renal injury in hyperuricemia [21]. Actually, we did not observe urate crystals in any part of kidneys in our experiments (Fig. 2). We previously reported that plasma creatinine and BUN levels increased, and that basolateral organic ion transport activity decreased, accompanied with specifically decreased expression of rOAT1, rOAT3 and rOCT2 in the kidney of hyperuricemic rats [13]. In this study, we investigated

renal organic ion transport activity and the expression of rOAT1, rOAT3 and rOCT2 in kidney during recovery from hyperuricemia.

During the initial 4 days, BUN, plasma creatinine and creatinine clearance were restored significantly (Fig. 1), suggesting that renal functions recovered quickly. On the other hand, the recovery of tubulointerstitial injury was varied in sites of the kidney, probably because of the different severity of damage as shown in Fig. 2. Organic anion and cation transport activity across basolateral membranes and the expression of organic ion transporters, rOAT1, rOAT3 and rOCT2 in the kidney also gradually improved (Figs. 3 and 4). Interestingly, basolateral PAH

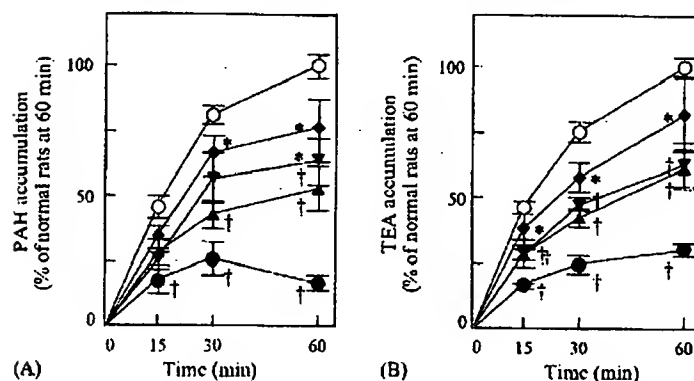


Fig. 3. Accumulation of PAH (A) and TEA (B) into renal slices during the recovery from hyperuricemia. Renal slices from normal (○) and hyperuricemic rats at 0: ●, 4: ▲, 7: ▼ and 14: ◆ days of recovery were incubated at 25 °C in incubation buffer containing 5 μ M [14 C]PAH or 5 μ M [14 C]TEA for the periods indicated. n-[3 H]Mannitol was used to estimate the extracellular trapping and non-specific uptake of [14 C]PAH and [14 C]TEA. Each point represents the mean \pm S.E. for 5–8 slices from different rats. * P < 0.05, vs. normal rats. † P < 0.05, vs. hyperuricemic rats on day 0.

transport showed a higher correlation with the protein level of rOAT1 than that of rOAT3 (Fig. 6), demonstrating that rOAT1 was a dominant transporter mediating the basolateral uptake of PAH. Basolateral TEA transport showed a high correlation with the protein level of rOCT2 (Fig. 6). As far as we know, this is the first report demonstrating the restoration of renal organic ion transporters (slc22a) during recovery from renal impairment, accompanying the change of basolateral uptake of PAH and TEA in the kidney.

The expression of rOCT2 is regulated by testosterone [19]. In contrast to rOCT2, renal expression of rOAT1 and rOCT1 was not changed between male and female, suggesting little or no contribution of testosterone in the regulation of renal rOAT1 and rOCT1 [22]. In addition,

both plasma testosterone levels and the expression levels of rOCT2 decreased in 5/6 nephrectomized rats, where the expression levels of rOCT2 were restored by the administration of physiological concentrations of testosterone [17]. In clinical cases, a lower serum testosterone level was reported to be associated with chronic renal failure [23,24]. In the present study, both rOCT2 expression and plasma testosterone concentration decreased in hyperuricemia, and were restored to normal during recovery from hyperuricemia. However, the correlation between rOCT2 expression and plasma testosterone concentration was not significant. These results suggested that the decreased plasma testosterone level was one of the determinants of rOCT2 expression in hyperuricemic rats.

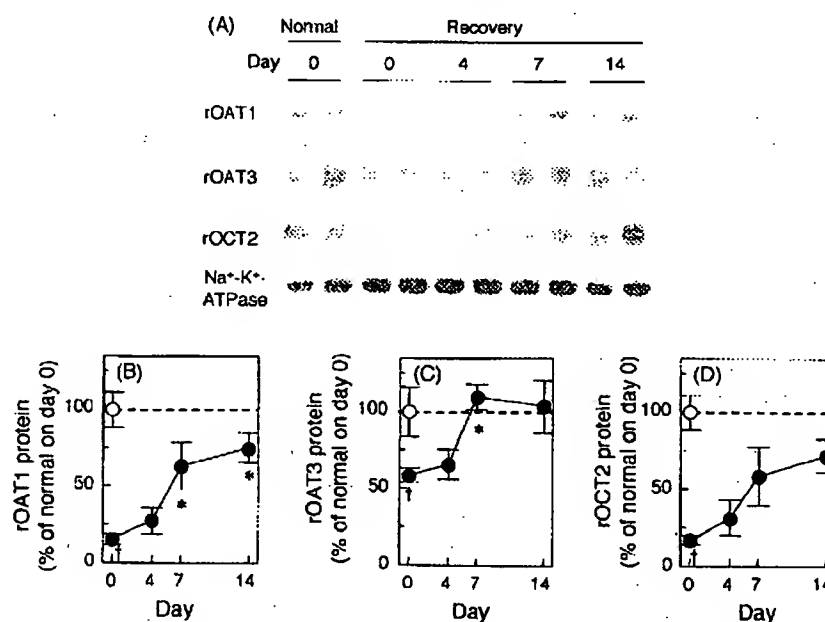


Fig. 4. Western blot analyses of rOAT1, rOAT3 and rOCT2 in crude membrane fractions from the kidneys during recovery from hyperuricemia. Crude membrane fractions from the kidneys of normal and hyperuricemic rats at 0, 4, 7 and 14 days of recovery were separated by SDS-PAGE. rOAT1, rOAT3, rOCT2 and Na⁺-K⁺-ATPase α -1 subunit were identified with each antibody. The results in a typical experiment are shown in panel (A). The ratio of rOAT1 (B), rOAT3 (C) and rOCT2 (D) density to Na⁺-K⁺-ATPase α -1 subunit density. Each point represents the mean \pm S.E. for three normal (○) and four hyperuricemic (●) rats from two experiments. * P < 0.05, vs. normal rats. † P < 0.05, vs. hyperuricemic rats on day 0.

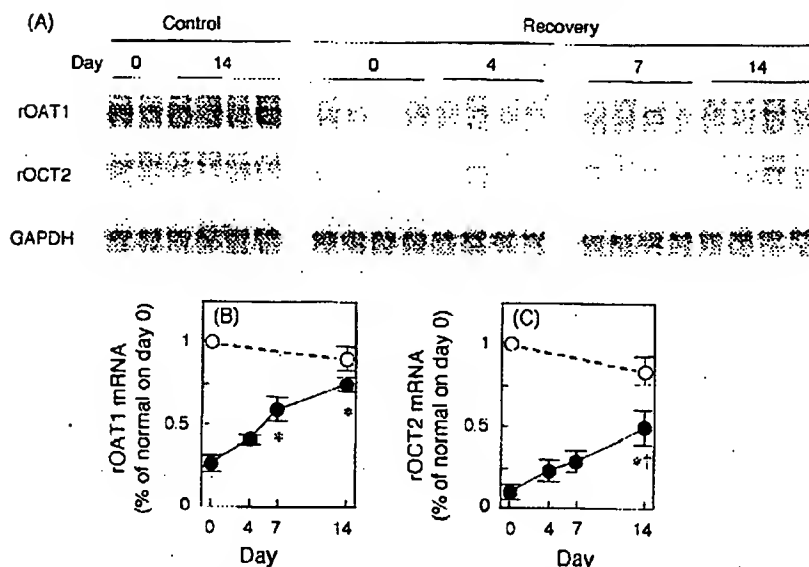


Fig. 5. Northern blot analyses of rOAT1 and rOCT2 during recovery from hyperuricemia. Total RNA (5 μ g) from the kidneys of normal and hyperuricemic rats at 0, 4, 7 and 14 days of recovery was hybridized with rOAT1, rOCT2 and GAPDH cDNA probes under high stringency. The results in a typical experiment are shown in panel (A). Densitometry of rOAT1 (B) and rOCT2 (C) mRNAs was corrected for loading with GAPDH mRNA. Each point represents the mean \pm S.E. for two to four normal (○) and four hyperuricemic (●) rats. * $P < 0.05$, vs. normal rats. * $P < 0.05$, vs. hyperuricemic rats on day 0.

The dosage regimen of various drugs for patients with renal insufficiency is generally determined according to the value of creatinine clearance. However, renal excretion of ionic drugs into urine is mediated not only by glomerular filtration but also by tubular secretion via organic anion and cation transporters. Actually, the dosage schedule based on creatinine clearance was demonstrated to be inadequate for

ampicillin and cephalexin dosing in some patients with renal insufficiency [25]. Recently, we reported that the elimination rate of cefazolin, which is a substrate of hOAT3, was significantly correlated with the levels of hOAT3 mRNA in humans [26]. In the present study, basolateral uptake of PAH and TEA in the kidney was significantly correlated with the expression of rOAT1 and

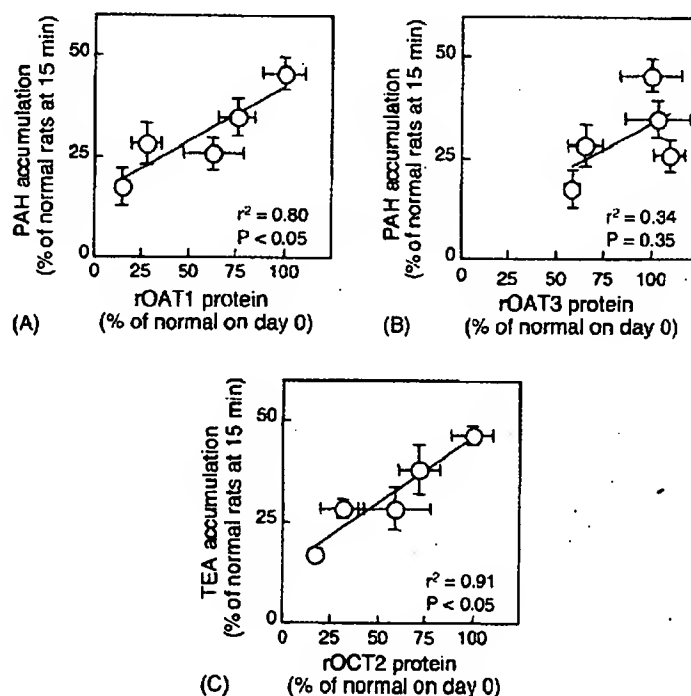


Fig. 6. Correlation between protein levels of rOAT1 (A), rOAT3 (B) and rOCT2 (C) and initial uptake activity of PAH (A and B) and TEA (C) by the renal slices during recovery from hyperuricemia. The linear regression was obtained with the mean values of rOAT1, rOAT3 and rOCT2 at protein levels and initial uptake activity of PAH and TEA. Each point represents the mean \pm S.E. obtained in Figs. 3 and 4.

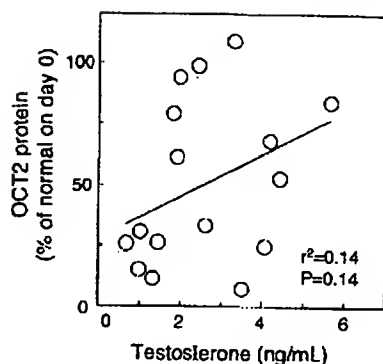


Fig. 7. Correlation between plasma testosterone and rOCT2 protein levels in the kidney during recovery from hyperuricemia. The linear regression was obtained with the plasma concentration of testosterone and rOCT2 protein levels of 17 rats during recovery from hyperuricemia.

rOCT2, respectively. Moreover, the recovery rate of rOAT1, rOAT3 and rOCT2 expression was slower than that of creatinine clearance. Based on these findings, dosage regimens according to the activity of organic anion and cation transport in addition to creatinine clearance should be helpful for precise dosage regimen in the patients with renal dysfunctions.

In conclusion, renal expression of organic ion transporters, rOAT1, rOAT3 and rOCT2, was reversibly regulated by hyperuricemia, accompanying the change of organic ion transport. Although further clinical investigations on the expression levels of drug transporters in several disease states are needed, the expression profiles of drug transporters may be useful information for understanding the alteration of renal drug secretion.

Acknowledgments

This work was supported in part by a Grant-in-Aid for Scientific Research from the Ministry of Education, Culture, Sports, Science and Technology of Japan.

References

- [1] Pritchard JB, Miller DS. Mechanisms mediating renal secretion of organic anions and cations. *Physiol Rev* 1993;73:765-96.
- [2] Inui K, Masuda S, Saito H. Cellular and molecular aspects of drug transport in the kidney. *Kidney Int* 2000;58:944-58.
- [3] Sekine T, Watanabe N, Hosoyamada M, Kanai Y, Endou H. Expression cloning and characterization of a novel multispecific organic anion transporter. *J Biol Chem* 1997;272:18526-9.
- [4] Sweet DH, Wolff NA, Pritchard JB. Expression cloning and characterization of ROAT1. The basolateral organic anion transporter in rat kidney. *J Biol Chem* 1997;272:30088-95.
- [5] Cha SH, Sekine T, Fukushima J, Kanai Y, Kobayashi Y, Goya T, et al. Identification and characterization of human organic anion transporter 3 expressing predominantly in the kidney. *Mol Pharmacol* 2001;59:1277-86.
- [6] Sekine T, Cha SH, Endou H. The multispecific organic anion transporter (OAT) family. *Pflügers Arch* 2000;440:337-50.
- [7] Uwai Y, Okuda M, Takami K, Hashimoto Y, Inui K. Functional characterization of the rat multispecific organic anion transporter OAT1 mediating basolateral uptake of anionic drugs in the kidney. *FEBS Lett* 1998;438:321-4.
- [8] Motohashi H, Sakurai Y, Saito H, Masuda S, Urakami Y, Goto M, et al. Gene expression levels and immunolocalization of organic ion transporters in the human kidney. *J Am Soc Nephrol* 2003;13:866-74.
- [9] Gründemann D, Gorboulev V, Gamharyan S, Veyhl M, Koepsell H. Drug excretion mediated by a new prototype of polyspecific transporter. *Nature* 1994;372:549-52.
- [10] Okuda M, Saito H, Urakami Y, Takano M, Inui K. cDNA cloning and functional expression of a novel rat kidney organic cation transporter, OCT2. *Biochem Biophys Res Commun* 1996;224:500-7.
- [11] Koepsell H, Gorboulev V, Arndt P. Molecular pharmacology of organic cation transporters in kidney. *J Membr Biol* 1999;167:103-17.
- [12] Urakami Y, Okuda M, Masuda S, Akazawa M, Saito H, Inui K. Distinct characteristics of organic cation transporters, OCT1 and OCT2, in the basolateral membrane of renal tubules. *Pharm Res* 2001;18:1528-34.
- [13] Habu Y, Yano I, Takeuchi A, Saito H, Okuda M, Fukatsu A, et al. Decreased activity of basolateral organic ion transports in hyperuricemic rat kidney: roles of organic ion transporters, rOAT1, rOAT3 and rOCT2. *Biochem Pharmacol* 2003;66:1107-14.
- [14] Huang Q, Dunn II RT, Jayadev S, DiSorbo O, Pack FD, Farr SB, et al. Assessment of cisplatin-induced nephrotoxicity by microarray technology. *Toxicol Sci* 2001;63:196-207.
- [15] Demeule M, Brasseur M, Béliveau R. Cisplatin induces renal expression of P-glycoprotein and canalicular multispecific organic anion transporter. *Am J Physiol Renal Physiol* 1999;277:F832-40.
- [16] Laouari D, Yang R, Veau C, Blanke I, Friedlander G. Two apical multidrug transporters, P-gp and MRP2, are differently altered in chronic renal failure. *Am J Physiol Renal Physiol* 2001;280:F636-45.
- [17] Ji L, Masuda S, Saito H, Inui K. Down-regulation of rat organic cation transporter rOCT2 by 5/6 nephrectomy. *Kidney Int* 2002;62:514-24.
- [18] Brown EA, Kliger AS, Hayslett JP, Finkelstein FO. Renal function in rats with acute medullary injury. *Nephron* 1980;26:64-8.
- [19] Urakami Y, Okuda M, Saito H, Inui K. Hormonal regulation of organic cation transporter OCT2 expression in rat kidney. *FEBS Lett* 2000;473:173-6.
- [20] Iseki K, Oshiro S, Tozawa M, Iseki C, Ikemiya Y, Takishita S. Significance of hyperuricemia on the early detection of renal failure in a cohort of screened subjects. *Hypertens Res* 2001;24:691-7.
- [21] Mazzaoli M, Hughes J, Kim Y-G, Jefferson JA, Kang D-H, Godon KL, et al. Elevated uric acid increases blood pressure in the rat by a novel crystal-independent mechanism. *Hypertension* 2001;38:1101-1106.
- [22] Urakami Y, Nakamura N, Takahashi K, Okuda M, Saito H, Hashimoto Y, et al. Gender differences in expression of organic cation transporter OCT2 in rat kidney. *FEBS Lett* 1999;461:339-42.
- [23] Joven J, Villabona C, Rubies-Prat J, Espinel E, Galard R. Hormonal profile and serum zinc levels in uraemic men with gonadal dysfunction undergoing haemodialysis. *Clin Chim Acta* 1985;148:239-45.
- [24] Mitchell R, Bauerfeld C, Schaefer F, Scharer K, Robertson WR. Less acidic forms of luteinizing hormone are associated with lower testosterone secretion in men on haemodialysis treatment. *Clin Endocrinol* 1994;41:65-73.
- [25] Hori R, Okumura K, Kamiya A, Nihira H, Nakano H. Ampicillin and cephalixin in renal insufficiency. *Clin Pharmacol Ther* 1983;34:792-8.
- [26] Sakurai Y, Motohashi H, Ueo H, Masuda S, Saito H, Okuda M, et al. Expression levels of renal organic anion transporters (OATs) and their correlation with anionic drug excretion in patients with renal diseases. *Pharm Res* 2004;21:61-7.

FGH52352

CI-06859634-9

FGH52352

CISTI ICIST

CI-06859634-9

Document Delivery Service
in partnership with the Canadian Agriculture LibraryService de fourniture de Documents
en collaboration avec la Bibliothèque canadienne de l'agriculture**THIS IS NOT AN INVOICE / CECI N'EST PAS UNE FACTURE**LYNN BRAZIL
LIBRARIANHELLER EHRMAN WHITE & MCAULIFFE
275 MIDDLEFIELD RD
MENLO PARK, CA 94025
UNITED STATES

ORDER NUMBER:	CI-06859634-9
Account Number:	FGH52352
Delivery Mode:	F31
Delivery Address:	650/324-6034
Submitted:	2007/05/11 17:31:30
Received:	2007/05/11 17:31:30
Printed:	2007/05/11 22:31:28

Direct	Periodical	OPENURLOPAC	UNITED STATES
--------	------------	-------------	---------------

Client Number:	39780-7000 CD
Title:	REGULATORY PEPTIDES
DB Ref. No.:	IRN1018966X
ISSN:	ISSN01670115
Vol./Issue:	117/2
Date:	2004
Pages:	127-39
Article Title:	GALANIN PITUITARY ADENOMAS
Article Author:	GRENBACK, E., ET AL.
Report Number:	IRN1018966X
Publisher:	ELSEVIER/NORTH-HOLLAND,

Estimated cost for this 13 page document: \$12.5 document supply fee +
\$32 copyright = \$44.5

The attached document has been copied under license from Access Copyright/COPIBEC or other rights holders through direct agreements. Further reproduction, electronic storage or electronic transmission, even for internal purposes, is prohibited unless you are independently licensed to do so by the rights holder.

Phone/Téléphone: 1-800-668-1222 (Canada - U.S./E.-U.) (613) 998-8544 (International)
www.nrc.ca/cisti Fax/Télécopieur: (613) 993-7619 www.cnrc.ca/icist
info.cisti@nrc.ca info.icist@nrc.ca



National Research Council Canada
Conseil national de recherches Canada

Page

1 / 1

Available online at www.sciencedirect.com

SCIENCE @ DIRECT®

Regulatory Peptides 117 (2004) 127–139

REGULATORY
PEPTIDESwww.elsevier.com/locate/regpep

Galanin in pituitary adenomas

Eva Grenbäck^{a,*}, Per Bjellerup^b, Ella Wallerman^a, Lars Lundblad^c,
Anders Änggård^c, Kaj Ericson^d, Katarina Åman^c, Marc Landry^f,
Wolfgang E. Schmidt^g, Tomas Hökfelt^e, Anna-Lena Hulting^a

^aDepartment of Molecular Medicine, Endocrine and Diabetes Unit, Karolinska Hospital, Stockholm S-17176, Sweden^bDepartment of Clinical Chemistry, Stockholm, Sweden^cDepartment of Otorhinolaryngology, Stockholm, Sweden^dDepartment of Neuroradiology, Karolinska Hospital, Stockholm, Sweden^eDepartment of Neuroscience, Karolinska Institutet, Stockholm, Sweden^fLaboratoire de Biologie Cellulaire, Université de Bordeaux II, Bordeaux, France^gDepartment of Medicine I, St. Josef Hospital, Ruhr-University Bochum, Bochum, Germany

Received 25 March 2003; received in revised form 23 September 2003; accepted 1 October 2003

Abstract

Tumor galanin content was measured in extracts from human pituitary adenomas using a specific RIA method for monitoring human galanin. Twenty-two out of twenty-four tumors contained galanin with notably high levels in corticotroph adenomas, varying levels in clinically inactive tumors, and low levels in GH secreting adenomas. Tumor galanin and ACTH contents were closely correlated in all tumors. In four young patients with microadenomas and highly active Mb Cushing tumor galanin was inversely related to tumor volume. The molecular form of tumor galanin, studied with reverse-phase HPLC, was homogenous with the majority of tumor galanin coeluting with standard human galanin. In the tumors analysed with *in situ* hybridization there was a good correlation between galanin peptide levels and galanin mRNA expression. In some tumors galanin mRNA and POMC levels coexisted, in others they were essentially in different cell populations. Levels of plasma galanin-LI were not related to tumor galanin concentration, and galanin levels were in the same range in sinus petrosus close to the pituitary venous drainage as in peripheral blood. Corticotrophin releasing hormone injections in two patients caused ACTH, but no detectable galanin release into sinus petrosus. Our results demonstrate that corticotroph, but not GH adenomas, express high levels of galanin, in addition to ACTH, and that in some tumors both polypeptides are synthesised in the same cell population. However, galanin levels in plasma were not influenced by the tumor galanin content.

© 2003 Elsevier B.V. All rights reserved.

Keywords: Acromegaly; ACTH; Cushing's disease; GH; Pituitary tumor; Prolactinoma; Pro-opiomelanocortin

1. Introduction

Galanin was first isolated from porcine intestine in 1983 by Tatemoto et al. [1]. In most species galanin is a 29 amino acid, C-terminally amidated peptide, whereas the human form contains 30 amino acids with a non-amidated C-terminal [2–5]. A major breakthrough was the cloning of the rat galanin gene from the rat anterior pituitary and hypothalamus, and the demonstration of its estrogen sensi-

tivity [6,7]. Galanin has been shown to have multiple biological effects. Thus, it seems to be involved in, for example, regulation of feeding (see Refs. [8–10]), in learning (see Refs. [11,12]), and in responses to nerve injury and pain (see Ref. [13]). The first galanin receptor was cloned by Habert-Ortholi et al. [14] and subsequently two further galanin receptor subtypes were identified [15,16]. The creation of a galanin knock-out mouse [17] and of galanin overexpressing mice [18–20] have provided new insights into the physiological roles of galanin.

Galanin-like immunoreactivity (LI) is spread throughout the central nervous system, including the hypothalamus, with the most intense immunoreactivity in the median eminence [21–24], suggesting participation in neuroendocrine processes controlling anterior pituitary hormone se-

Abbreviations: LI, like immunoreactivity; PAD, pathological anatomical diagnosis; TdT, terminal deoxynucleotidyl transferase.

* Corresponding author. Tel.: +46-8-517-73065; fax: +46-8-517-73096.

E-mail address: Eva.Grenback@ks.se (E. Grenbäck).

0167-0115/\$ - see front matter © 2003 Elsevier B.V. All rights reserved.
doi:10.1016/j.regpep.2003.10.022

cretion (see Refs. [9,25–27]). For example, galanin increases GH secretion not only in animal models but also in humans. Thus, given intravenously (i.v.) to man galanin gives rise to a GH peak, delayed in time but equal to and additive to that produced by GHRH [28,29]. On the other hand, galanin has been shown to inhibit the hypothalamo–pituitary–adrenal (HPA) axis [30–33]. Galanin has been proposed to act as a mitogen in estrogen-induced prolactinomas in the rat [34,35]. Galanin gene expression also shows a direct correlation to somatotroph hyperplasia in GHRH transgenic mice [36].

In the rat pituitary galanin is mainly present in the lactotrophs [7], whereas in the human pituitary galanin is coexpressed with ACTH. Thus, several groups [37–44] have studied galanin-LI in pituitary adenomas establishing its presence in ACTH-producing adenomas, but with varying results as to its presence in somatotroph, lactotroph and clinically inactive adenomas.

The aim of this study was to investigate the presence, concentration and molecular form(s) of galanin in different types of pituitary adenomas using an extraction procedure and a newly developed radioimmunoassay (RIA), as well as reverse-phase (RP)-HPLC. In addition, we wished to compare tumor and serum levels of galanin to some other pituitary hormones, with special reference to the ACTH–cortisol axis. Finally, some tumors were analysed with *in situ* hybridisation for expression of galanin and POMC. The results of these analyses were correlated to clinical data. Preliminary data from this investigation have previously been reported [45].

2. Material and methods

2.1. Patients

Samples for tumor extraction were obtained from 24 patients with pituitary adenomas (Table 1), 15 women (26–78 years, mean 49.7 years) and 9 men (31–74 years, mean 53.3 years) who underwent transsphenoidal surgery at the Department of Otorhinolaryngology, Karolinska Hospital. Seven patients had hypersecretion of ACTH, six of GH, and one of prolactin (PRL). Ten tumors were clinically inactive (Table 1). The tumors were identified by clinical symptoms and signs as well as magnetic resonance imaging scans. The size of the seven ACTH-producing tumors was measured on contrast-enhanced T1-weighted coronal and sagittal images after correction for scaling. The standard formula for volume measurement of a rotational ellipsoid was used for volume calculations [46]. The size of the remaining tumors was assessed with stage and grade according to Hardy and Wilson (see Ref. [47]). Separate tumor samples were also analysed in the Department of Pathology of the Karolinska Hospital.

The patients with Cushing's disease had clinical symptoms and signs of hypercortisolism. The diagnosis was

confirmed by elevated ACTH and cortisol levels, absent diurnal rhythm, pathological CRH-test ($n=6$) with sinus petrosus sampling ($n=4$) or low and high dose dexamethasone ($n=1$). All had pituitary microadenomas visible on MRI scans. They were all cured clinically and biochemically after surgery. Separate pathological anatomical examination confirmed a pituitary adenoma in six cases. In one case (#6) there was insufficient material for analysis.

Galanin was monitored in two patients during sinus petrosus sampling. Samples were not available for galanin analysis from a further two patients who underwent sinus petrosus sampling, confirming in both cases ACTH producing pituitary adenoma. For control, plasma samples were collected from 22 healthy individuals (12 men, 28–55 years old; 10 women 25–62 years old).

The study was approved by the Ethics Committee of Karolinska Institutet (nos. 96-145 and 99-326).

2.2. Samples

Tumor samples for extraction and *in situ* hybridisation were collected at surgery, placed on dry ice and kept frozen at -70°C .

Blood samples for galanin measurement were collected in EDTA plasma tubes in the morning fasting state prior to surgery and during sinus petrosus sampling. Samples were placed on ice and centrifuged at 4°C (2400 rpm) for 10 min. Plasma was withdrawn and stored at -70°C until analysis.

2.3. Extraction procedure

For extraction, frozen tumor tissues were weighed, cut, still in frozen state, boiled for 10 min in acetic acid (1 mol/l), cooled on ice, homogenized and centrifuged for 10 min (2000 rpm) at 4°C . After collection of the supernatant, the pellet was resuspended in water, followed by a second boiling, homogenization and centrifugation as above. The supernatants from these two extraction procedures were pooled, lyophilised and stored at 4°C . Samples were reconstituted in phosphate buffer (0.05 mol/l; pH 7.4) before assay.

2.4. Gel permeation chromatography

Gel permeation chromatography was performed on one tumor rich in galanin (#5; Table 1). A Sephadex G-50 Superfine (Pharmacia, Uppsala, Sweden) column (2.6 × 97 cm) was equilibrated and eluted at room temperature with formic acid (0.1 mol/l) with 0.02% sodium azide. Void volume (V_0) was determined with Dextran blue and total volume (V_t) with ^{22}Na . Human synthetic galanin (Peninsula, Belmont, CA) in RIA buffer was used for column calibration. Tumor extract (50 μl in 1 ml water) was eluted at a flow rate of 15 ml/h, and the eluate was collected in fractions (2 ml), which were lyophilised and stored at 4°C until

Table 1

Twenty-four patients with pituitary tumors operated between 1994 and 1996

Pat. id. #	Tumor type	Age	Sex	T-gal, pmol/mg protein	P-gal, pmol/l	T-ACTH, ng prot	T-ACTH/T-gal
1	ACTH	26	f	620	55	2737.4	4.42
2	ACTH	29	f	587	52	1302.24	2.22
3	ACTH	31	m	111	130	657.27	5.92
4	ACTH	35	m	851	32	72666.67	85.39
5	ACTH	66	m	82.2	—	18860	229.4
6	ACTH	67	f	247	37	4065.04	16.46
7	ACTH	78	f	43.5	38	551.05	12.67
8	GH	29	f	0.04*	60	0.67	16.75
9	GH	40	f	1.87	80	20.39	10.9
10	GH	45	m	0.18	—	7.88	43.7
11	GH	49	f	0.12	54	5.06	42.17
12	GH	51	m	0.22	—	3.07	13.95
13	GII	64	m	0.08	<20	0.37	4.63
14	PR1	44	f	0.13	58	13.03	100.2
15	Inactive	34	f	10.2	116	975.4	95.6
16	Inactive	46	f	199	<20	4261.9	21.4
17	Inactive	52	f	0.16	53	1.23	7.69
18	Inactive	53	m	17.1	44	37.67	2.2
19	Inactive	55	f	99.9	<20	5092.78	50.98
20	Inactive	56	f	0.20	—	0.49	2.45
21	Inactive	62	m	0.21	—	3.48	16.57
22	Inactive	69	f	0.13*	40	6.45	49.61
23	Inactive	72	f	1.85	82	20.16	10.9
24	Inactive	74	m	5.67	38	553.6	97.6

Inactive: clinically inactive adenoma.

Patients are arranged according to tumor type, and age. Sex, tumor galanin content (T-GAL) and plasma galanin (P-GAL) are listed.

* Below detection limit in the RIA. For the purpose of calculation, they were assigned values of 20 pmol/l, i.e. the limit of detection.

assay. For RIA, each fraction was dissolved in 100 μ l RIA buffer.

2.5. Reverse-phase-HPLC

Extracts from the nine adenomas containing the largest amounts of galanin, i.e. seven ACTH-secreting adenomas (#1–7; Table 1) and two clinically inactive adenomas (#16, #19; Table 1) were analysed with RP-HPLC. A 218TP C₁₈-Column (5 μ m, 4.6 \times 250 mm) from Vydac (Hesperia, CA) was used to separate the galanin-LI. The samples were eluted (1 ml/min) with a linear gradient of

water/acetonitrile (HPLC-grade, Merck, Darmstadt, Germany) with 0.1% trifluoroacetic acid (Merck) increasing from 20% to 70% by 1%/min. Aliquots of 0.5 ml were sampled. The fractions were lyophilized and redissolved in 100 μ l RIA buffer before analysis. One sample with very high galanin content (#1; Table 2) was diluted 1:10 before chromatography.

2.6. Radioimmunoassay

Antiserum to human galanin(1–30) was produced as described before [48]. Briefly, human galanin(1–30) was

Table 2

Seven patients with ACTH producing pituitary adenomas

Pat. id. #	T-gal, pmol/mg protein	T-ACTH, pmol/mg protein	P-ACTH, pmol/l	S-Cortisol, nmol/l	U-Cortisol, nmol/24 h
1	620.16	2737.4	60	1190	2360
2	587.31	1302.24	7.3	576	1985
3	111.19	657.27	30	476	3192
4	850.67	72666.67	17	639	3394
5	82.15	18860	36	794	794
6	247.38	4065.04	15	579	1056
7	43.51	551.05	5.2	558	846

The table shows tumor tissue content of galanin (T-GAL) and ACTH (T-ACTH) in pmol/mg protein, morning fasting blood levels of ACTH and cortisol and 24 h urinary cortisol excretion.

Reference ranges: P-ACTH, 2–11 pmol/l.

S-Cortisol, 170–600 nmol/l.

U-Cortisol, 70–500 nmol/24 h.

synthesized by Fmoc-solid phase synthesis and purified to apparent homogeneity by RP-HPLC. Five mg galanin were coupled to 30 mg keyhole limpet hemocyanine with 0.25 mg carbodiimide. New Zealand white rabbits were immunized with 0.25 mg peptide equivalent dissolved in 1 ml saline emulsified in 1.5 ml complete Freund's adjuvant (Sigma, St. Louis, MO). Booster injections at 4–6 weeks intervals were done with 0.08–0.1 mg peptide equivalent mixed with 1.5 ml incomplete Freund's adjuvant. The antiserum used was obtained 10 days after the third booster injection.

Final antibody concentration in the assay was 1:750,000 yielding a 30% binding. Synthetic human galanin (Peninsula) was used as standard and ^{125}I -labelled human galanin (New England Nuclear, NEN, Boston, MA) as tracer. The RIA buffer was a phosphate buffer (0.05 mol/l; pH 7.4) containing 0.1% BSA, 0.02% NaN_3 , 0.01% Triton X, and 10 ml Trasylol/l buffer.

In the assay, 100 μl of standard or samples in duplicates (or in single samples from chromatography) were preincubated with 100 μl antibody for 24 h at 4 °C. After the addition of 100 μl tracer (approx. 8000 cpm) incubation continued for another 24 h. Free and bound radioligand were separated by adding 500 μl sheep anti-rabbit antibodies (Pharmacia decanting suspension; Pharmacia, Uppsala, Sweden). After 30 min incubation and addition of 500 μl water, the samples were centrifuged at 4 °C (3000 rpm) for 15 min and decanted, and the radioactivity in the bound fraction was counted in a gamma counter.

Serial dilutions of tumor extracts showed good parallelism with the standard curve. Non-specific binding in the RIA was 2%. Detection limit was 20 pmol/L and IC_{50} 312 pmol/l. Intraassay variation was 5% and interassay variation 14%.

Crossreactivity was measured at 50% binding, or at the highest binding for those peptides not attaining a 50% binding. In this assay, there was 62% cross-reactivity with rat galanin, 36% with galanin(1–16), and 0.8% with pancreastatin, whereas less than 0.1% was found for galanin(20–30), galanin message-associated peptide(1–41) or –(44–49), CRH, GHRH, somatostatin, vasoactive intestinal polypeptide, peptide histidine-isoleucine, calcitonin gene-related peptide or oxytocin.

ACTH in tumor tissue was analysed by an immunoradiometric assay (IRMA) from Brahms Diagnostica (Berlin, Germany) using two monoclonal antibodies recognizing different binding sites on the antigen. The assay was carried out in two steps to prevent antigen excess resulting in falsely low values. The tumor samples were diluted stepwise with the zero-standard.

Protein content was analysed with the Bio Rad Protein Assay (BioRad, Munich, Germany).

2.7. Preparation of probes

Altogether three oligonucleotides (Scandinavian Gene Synthesis, Köping, Sweden) were used in this study for in

situ detection of POMC mRNA ($n=1$) and human galanin mRNA ($n=2$). Oligonucleotides were designed as below from published gene sequences.

- (A) Oligonucleotide complementary to POMC mRNA [49]:
 - (i) 5'GCCCTCCCGTGGACTTGGCTCCGGACGGC-CATCTCCCCCGCCGTCTCTTCTC3'
- (B) Oligonucleotides complementary to human galanin mRNA [3]:
 - (i) 5'CTGTGGTTGCCAACGGCATGTGGGCCCA-GCAGGTAGCCCGCGCTGTTTC3'
 - (ii) 5'GTCAAAGCTTCCTGGTTTCATGTCATC-TTCGGGCCGCAGCACCCGCTT3'

All oligonucleotides were chosen in regions presenting few homologies with sequences of related mRNAs, and they were checked against the Genbank database.

The oligonucleotides complementary to human galanin mRNA were labelled as previously described [50] at the 3'-end using terminal deoxynucleotidyl transferase (TdT) (Amersham, Amersham, UK) in a cobalt-containing buffer with ^{35}S -dATP (New England Nuclear, Boston, MA, USA) to a specific activity of $1\text{--}4 \times 10^9$ cpm/ μg and purified in Nensorb-20 columns (New England Nuclear). The oligonucleotide complementary to POMC mRNA was labelled by tailing at the 3'-end with digoxigenin-11-dUTP (Boehringer Mannheim, Mannheim, Germany) according to published protocols [51]. Briefly, 100 pmol of each probe were incubated in a final volume of 20 μl with 1 nmol of digoxigenin-11-dUTP, 9 nmol of dATP (Sigma), 50 units of TdT and 4.2 μl of cobalt-containing buffer. After 45 min at 37 °C the reaction was stopped before purification by ethanol precipitation, and probes were then stored at –20 °C.

2.8. In situ hybridization procedures

The frozen pituitary tumors were cut at 14 μm thickness in a cryostat (Microm, Heidelberg, Germany) and thaw-mounted onto Probe On slides (Fisher Scientific, Pittsburgh, PA). The sections were then processed as described earlier [50]. In brief, tissue sections were air-dried and incubated for 16 h at 42 °C with 0.5 ng of each of the two radioactively labelled human galanin probes and 10 nmol/l of the digoxigenin-labelled POMC probe. The probes were diluted in a hybridization solution containing 50% deionized formamide (Baker, Deventer, The Netherlands), $4 \times$ standard saline citrate (SSC, $1 \times \text{SSC} = 0.15 \text{ M NaCl}$ and $0.015 \text{ M NaCitrate}$), $1 \times$ Denhardt's solution (0.02% bovine serum albumin, 0.02% Ficoll (Pharmacia), 0.02% polyvinylpyrrolidone), 0.02 M NaPO_4 (pH 7.0), 1% *N*-lauroyl-sarcosine, 10% dextran sulphate (Pharmacia), 500 mg/l denatured salmon testis DNA (Sigma) and 200 mM dithiothreitol (Sigma). After hybridization, the sections were rinsed in $1 \times \text{SSC}$, $4 \times 15 \text{ min}$ at 55 °C followed by 30 min

at room temperature. The sections were then immersed for 30 min in buffer A (0.1 M Tris, pH 7.5, 1 M NaCl, 2 mM $MgCl_2$) containing 0.5% bovine serum albumin (Sigma) and incubated overnight at 4 °C in the same solution with alkaline-phosphatase conjugated anti-digoxigenin F(ab) fragment (1:5000; Boehringer Mannheim). Afterwards, they were rinsed 3×10 min in buffer A and twice in buffer B (0.1 M Tris, pH 9.5, 0.1 M NaCl, 5 mM $MgCl_2$). Alkaline-phosphatase activity was developed by incubating the sections with 44 μ l NBT and 33 μ l BCIP (Gibco, Gaithersburg, MD) diluted in 10 ml buffer B. The enzymatic reaction was stopped by extensive rinsings in distilled water and in buffer B.

The sections were air dried and coated twice with 3% collodion dissolved in amyl acetate (LKB, Stockholm, Sweden) [52]. They were then dipped into Ilford K5 nuclear emulsion (Ilford, Mobberly, Cheshire, UK) diluted 1:1 with distilled water, exposed for 3 weeks, developed in Kodak D19 for 3 min and fixed in Kodak 3000 for 8 min. After mounting in glycerol, the sections were analysed in a Nikon Microphot-FX microscope equipped with a dark field condenser.

2.9. Statistical analysis

Results are presented as mean \pm SEM, unless otherwise stated. Comparisons between groups were assessed by Mann–Whitney Rank Sum test or by one-way ANOVA, followed by Duncan's Multiple Comparison procedure. When applicable, non-normally distributed variables were log transformed before analysis, in order to get a more closely approximated Gaussian distribution. Correlations were performed using least square linear regression analysis. For the purpose of calculation, undetectable levels of galanin (#8, 22) were assigned values of 20 pmol/l. Statistical significance was set at $p < 0.05$. Statistical analyses

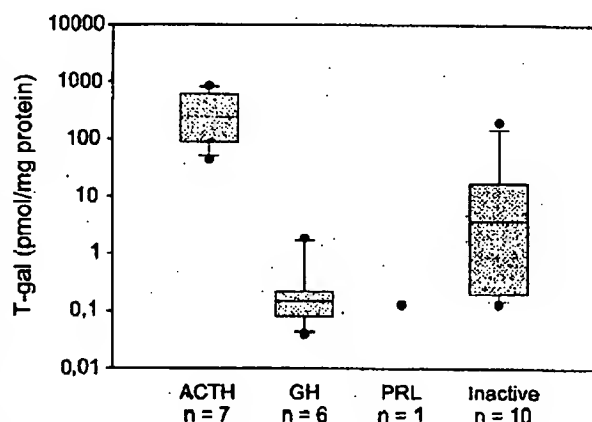


Fig. 1. Galanin concentration in 24 pituitary adenomas arranged according to tumor type. Box plots indicate the median and the lower and upper quartiles, the whiskers the 10th and 90th percentiles, and the outliers are shown as circles.

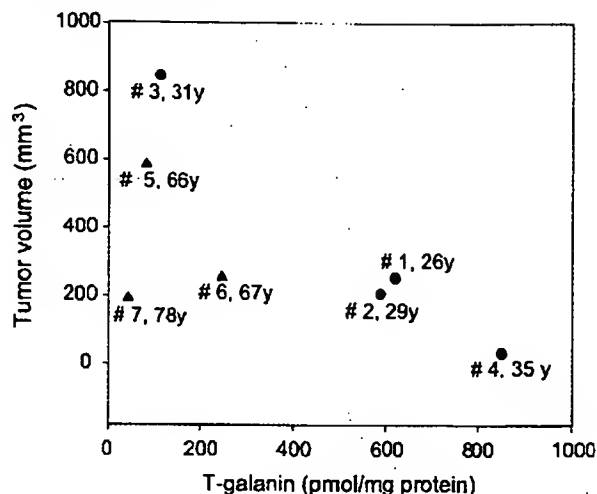


Fig. 2. Tumor galanin content related to tumor volume in seven patients with ACTH secreting adenomas. Patients number and age are given in the figure. Dots indicate young patients, triangles old ones.

were performed using SigmaStat for Windows (Jandel Scientific, Erkrath, Germany).

3. Results

3.1. Tumor samples

Galanin-LI was present in extracts from 22 of the 24 pituitary adenomas examined in this study (Table 1; Fig. 1). High levels of galanin-LI ranging between 43.5 and 851 pmol/mg protein (mean 363 pmol/mg) were found in the seven adenomas from patients with Cushing's disease (#1–7, Table 2). The six GH-producing adenomas contained low

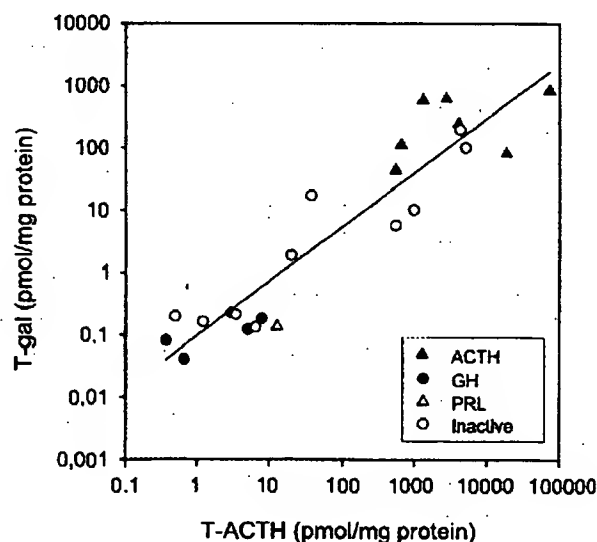


Fig. 3. Tumor galanin content related to tumor ACTH content in 24 pituitary adenomas specified to tumor type. There is a good correlation between galanin and ACTH tumor concentration ($r = 0.932$, $p < 0.001$).

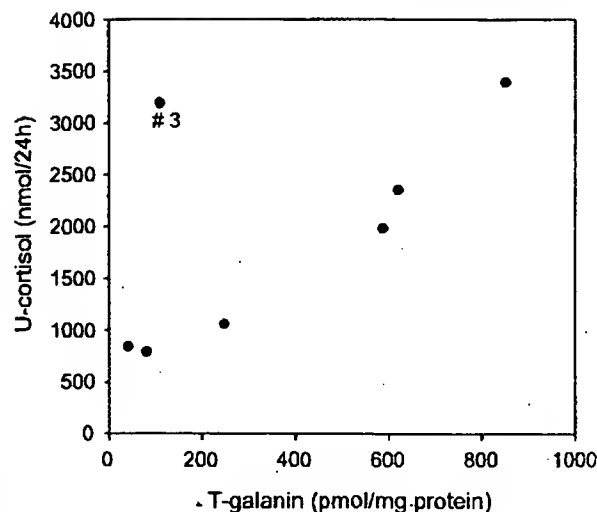


Fig. 4. Tumor galanin content related to 24 h urinary cortisol excretion in seven patients with ACTH secreting pituitary adenomas. Exclusion of patient #3 results in $r=0.974$; $p<0.001$. If included $r=0.614$; $p=0.142$.

amounts of galanin-LI, from 0.04 to 1.87 pmol/mg protein (mean 0.41 pmol/mg) (#8-13, Table 1). Also, the single prolactinoma had very low galanin-LI (#14, Table 1).

The 10 clinically inactive adenomas contained varying amounts of galanin-LI (#15-24, Table 1). Five of these adenomas had low galanin content, ranging from 0.13 to 1.85 pmol/mg (#17, 20-23, Table 1), three had levels in the

intermediate range (5.67-17.1 pmol/mg; #15, 18, 24), whereas two adenomas were rich in galanin-LI (99.9 and 199 pmol/mg; #16, 19, respectively). There was no correlation between galanin levels, or patients age, or sex, irrespective of tumor type. Tumor volume did not correlate to tumor galanin or ACTH-content in the seven patients with Mb Cushing (Fig. 2) ($r=0.638$; $p=0.123$). However, the four youngest patients, who also exhibited the highest cortisol per 24 h (#1-4, Table 2) had an inverse relation between tumor-galanin and volume (Fig. 2).

ACTH was detectable in all adenomas studied, and there was a close correlation between galanin-LI and ACTH levels in the adenomas as a group ($r=0.932$, $p<0.001$; Fig. 3), as well as in the clinically inactive adenomas ($r=0.919$, $p<0.001$), but a less strong correlation among the GII adenomas ($r=0.8429$, $p<0.05$). The seven corticotroph adenomas did not show any correlation between galanin and ACTH content ($r=0.434$). In this group of patients 24-h urinary cortisol excretion correlated strongly to tumor galanin-LI in six out of seven patients (Fig. 4). In the seventh patient (#3) comparatively low tumor galanin-LI and ACTH values were associated with high urinary cortisol. This patient had the largest tumor in the Mb Cushing group. No correlation was found between urinary cortisol excretion and tumor ACTH levels, nor did plasma ACTH or serum cortisol relate to tumor galanin-LI or ACTH content (Table 2). After surgery, all these patients had subnormal cortisol levels. One patient (#2) had recurrent disease a few years later.

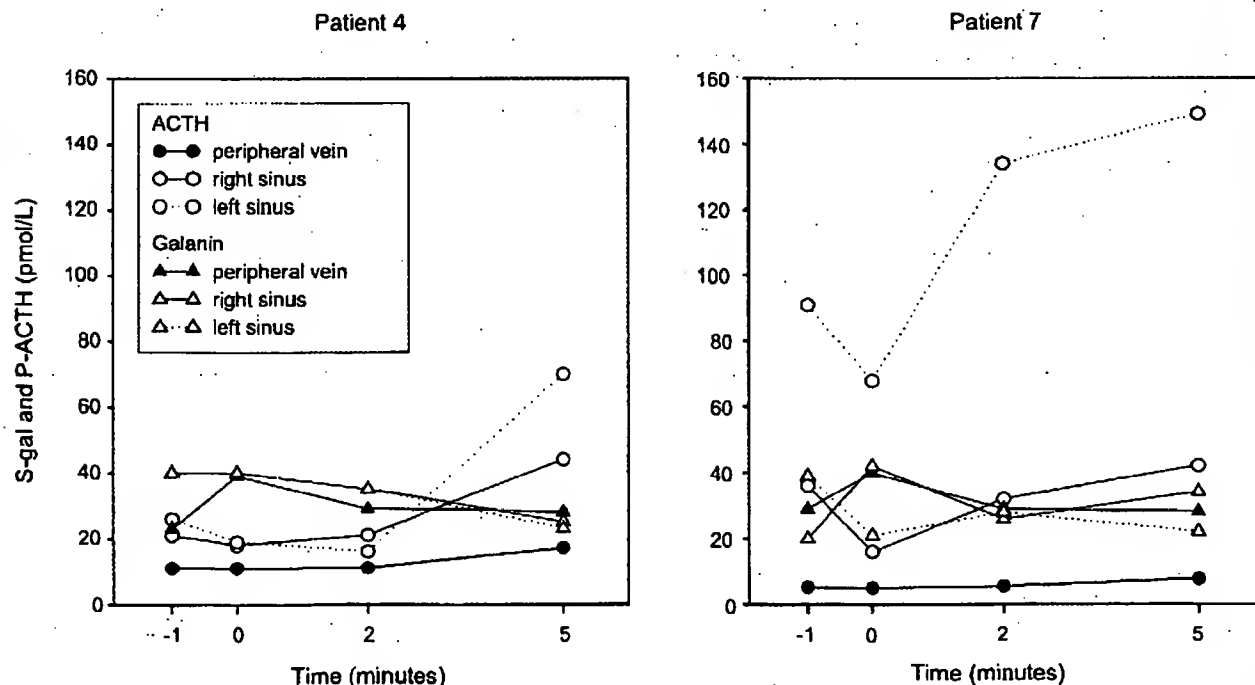


Fig. 5. Sinus petrosus sampling during CRH stimulation test in two patients with ACTH-producing tumors (#4 and 7; Table 1). After injection of 100 µg human CRH (Corticobiss®, Bissendorf, The Netherlands), samples were drawn from right and left cavernous sinus and peripheral vein at -1, 0, 2, and 5 min and analyzed for ACTH and galanin.

3.2. Plasma samples

Galanin-LI in peripheral blood was measured in all but five patients (Table 1). The levels ranged from undetectable to 130 pmol/l (mean 54.2 ± 30 pmol/l). There was, however, no correlation to tumor type, nor to tumor size, galanin-LI content, patient age or sex (not shown).

Galanin-LI in plasma from healthy controls was 93.7 ± 44 pmol/l (101.9–48.7 pmol/l in the men and 83.9–37.6 pmol/l in the women), i.e. it was higher in controls than in the patient group. These control samples were collected 5 years after the patient samples and analysed with a slightly modified RIA including Trasylol to further prevent peptide degradation. Galanin-LI and ACTH were measured in sinus petrosus blood samples from two patients with Cushing's disease (#4, 7) after CRH stimulation (Fig. 5). A rise in plasma ACTH was noted in the left sinus of both patients, with no change in peripheral ACTH levels. No effect was observed on levels of galanin-LI in sinus petrosus or in the periphery, nor did basal plasma concentrations of galanin-LI in sinus petrosus differ from those in the periphery. Thus, there was no correspondence to the high levels of galanin-LI detected in tumor extracts from these two patients.

3.3. Chromatography

Gel permeation chromatography of one tumor (#5, Table 1) revealed one major peak of galanin-LI with the same retention as synthetic human galanin. RP-HPLC of nine adenoma extracts (Fig. 6) showed that in eight of these tumors the majority of galanin-LI had the same retention as synthetic human galanin (16 min) (Fig. 6A). The main peak with galanin-like material was preceded by a smaller one with an elution time of 9–11 min in six extracts and of 13 min in two tissue extracts. One adenoma (#6, Table 1) differed from the rest, in that there was only one major chromatographic peak with galanin-like material with a longer retention time (20 min) coinciding with synthetic galanin(1–16) (Fig. 6B).

3.4. In situ hybridization

The in situ hybridization analysis showed that the pieces of the various tumors processed with this technique could be divided into at least three groups with regard to galanin expression. (i) A galanin signal was found in a large number of cells, sometimes apparently all cells of the tissue piece;

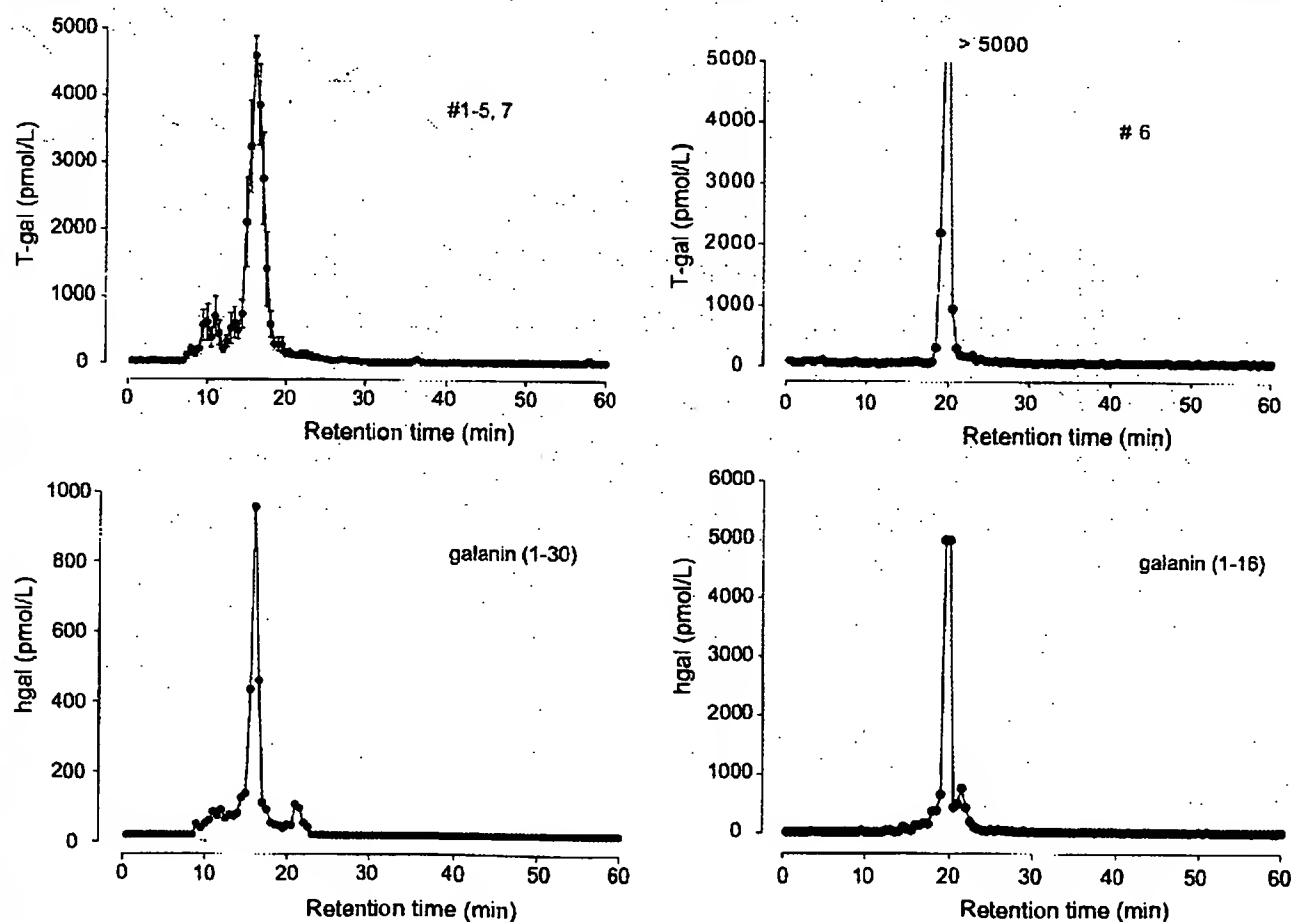


Fig. 6. (A, B) Reverse-phase high performance liquid chromatography of galanin immunoreactivity in pituitary extracts. (A) Results are mean \pm SEM of eight pituitary adenomas. (B) Results of one pituitary adenoma. (C) Elution of human galanin (1–30). (D) Elution of galanin 1–16. Please note different scale in (C).

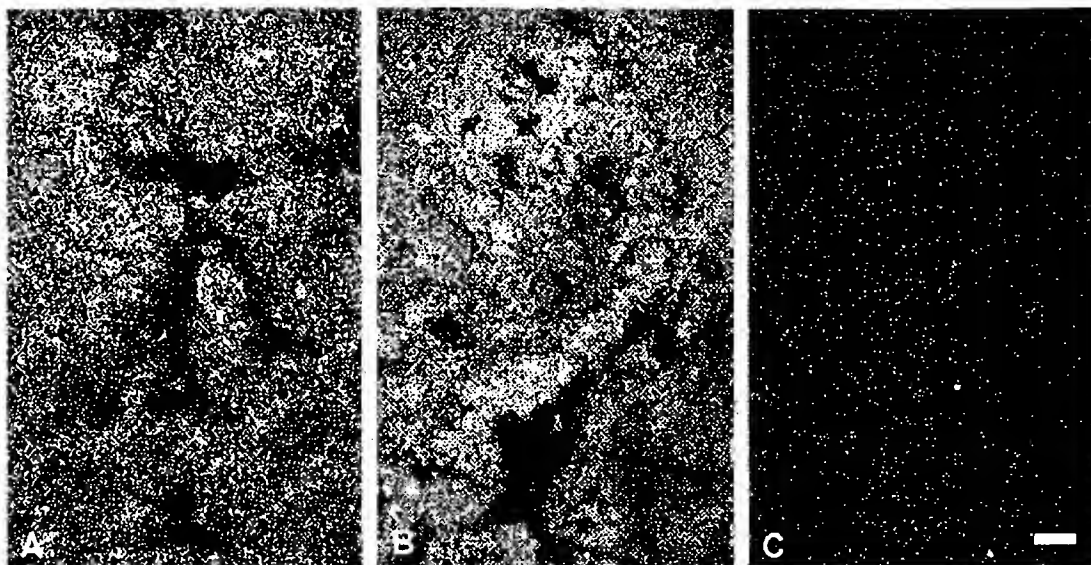


Fig. 7. (A-C). Darkfield micrographs of ACTH-producing adenomas (A, C, #1; B, #2) after hybridization with probes complementary to prepro-galanin mRNA (A, B) and after addition of excess of cold probe (C). A very strong signal is seen evenly distributed over both tumors (A, B) but only few grains in the controls (C). Scale bar indicates 50 μ m for all micrographs.

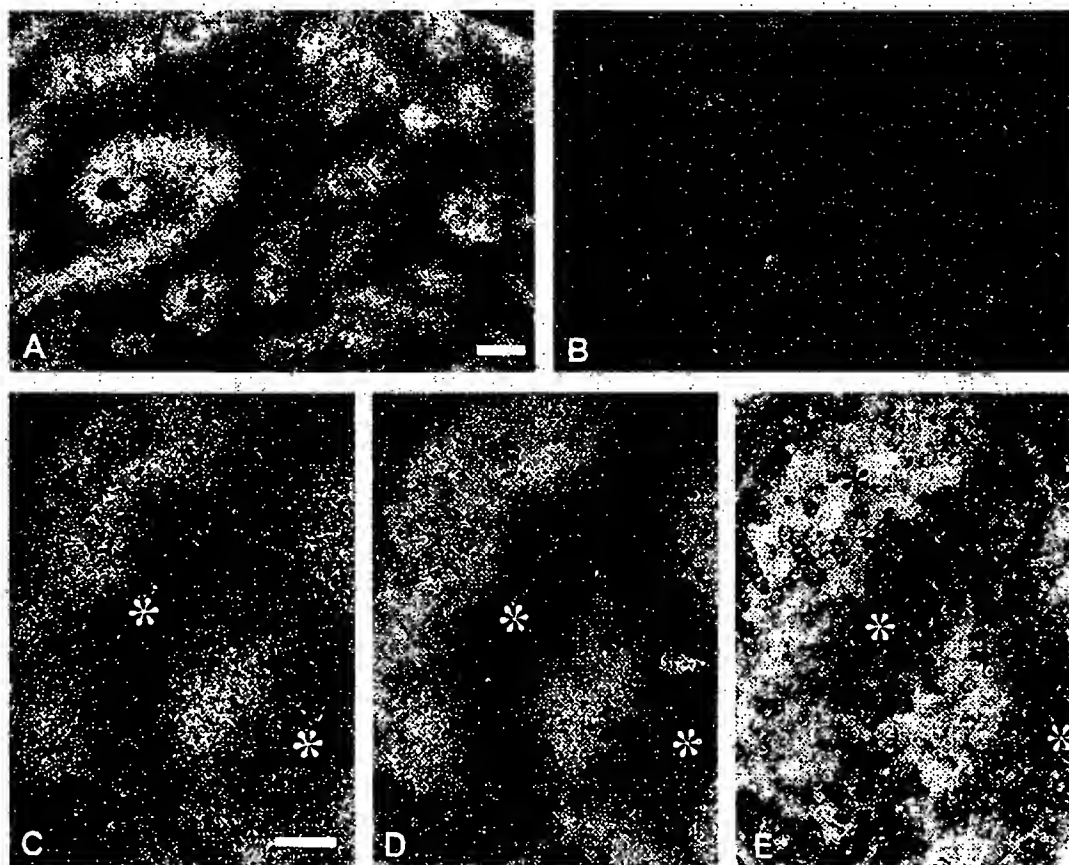


Fig. 8. (A-E) Darkfield (A-C), brightfield (E) and combined dark- and brightfield (D) micrographs of ACTH-producing adenoma (#4) after double-hybridization with radioactive probes complementary to prepro-galanin mRNA (A, C, D) and non-radioactive probe complementary to POMC mRNA (D, E) or after hybridization with an excess of galanin cold probe (B). A strong galanin signal (bright grains) is seen in strands within the tumor tissue (A, C), and they are complementary to the POMC mRNA (dark labelling) distribution (C-E). No signal is seen in the control section (B). Scale bars indicate 50 μ m (A=B; C=D=E).

(ii) a limited number of cells expressed galanin mRNA; and (iii) no galanin mRNA expression could be detected. Two tumors showed an extremely strong signal that could not be blocked by an excess of cold probe, that is the signal was considered to be unspecific.

To group (i), i.e. strongly galanin mRNA expressing tumors, belonged patients #1 (Fig. 7A), #2 (Fig. 7B) and #4 (Fig. 8A, C), whereby one of the two pieces analysed of tumor #2 showed a less compact distribution (data not shown) and #4 showed a markedly uneven distribution with

distinct bands of positive cell groups separated by areas with a low signal (Fig. 8A, C). Tumor #5 showed a signal all over the sections but of a comparatively low intensity (data not shown). To the second group (ii) with a limited number of cells expressing galanin mRNA belonged tumors #3 (Fig. 9A) and #19 (Fig. 9D); in the latter galanin-positive cells often formed small groups (Fig. 9E). In fact, in general the tissue piece of this tumor processed for *in situ* hybridization appeared to have a normal pituitary morphology at the cellular level (Fig. 9E). In group (iii) no detectable signal

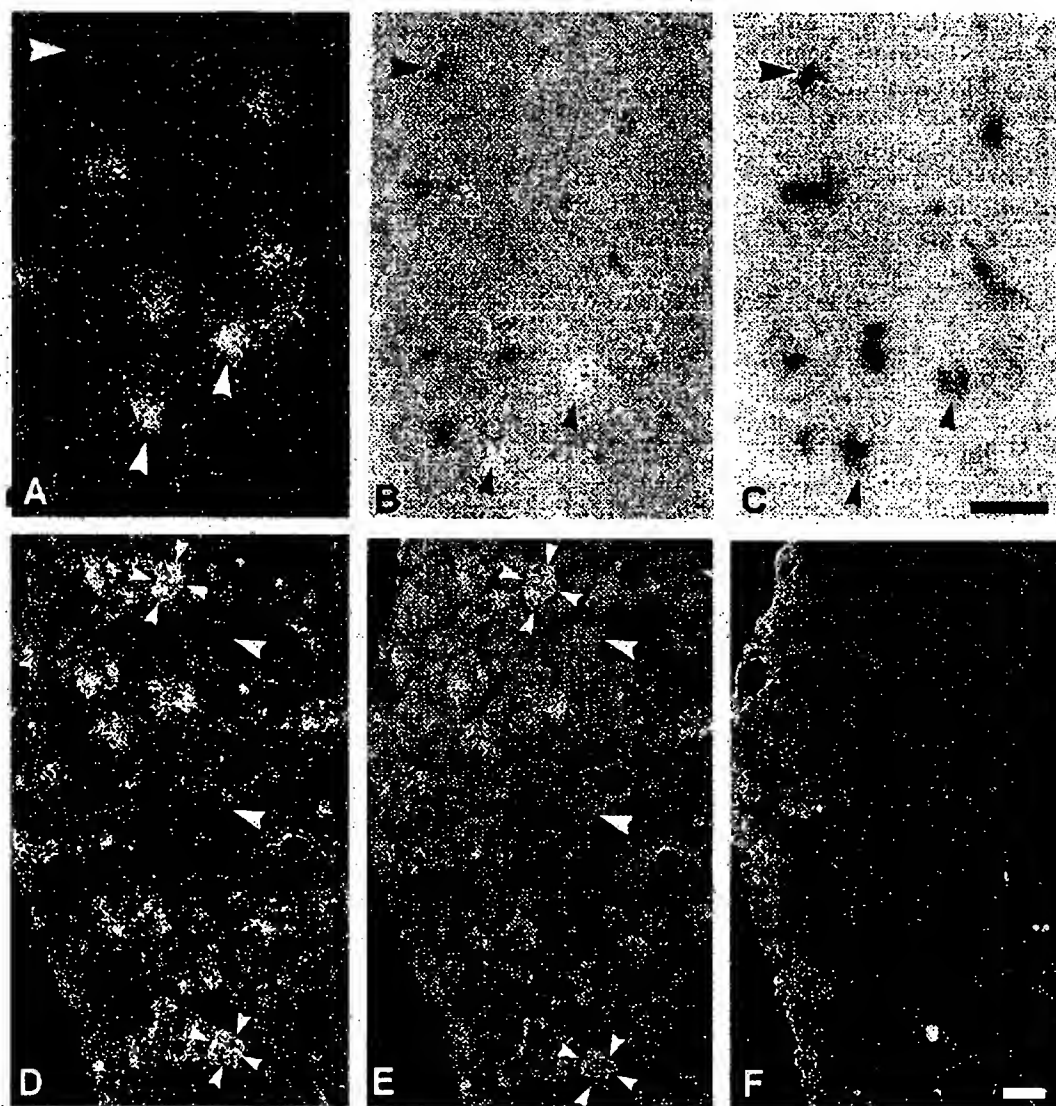


Fig. 9. (A–F) Darkfield (A, D–F), brightfield (C) and combined dark and brightfield (B) micrographs of ACTH-producing adenoma (#3) (A–C) and of a clinically inactive tumor (#19) (D–F) after double-hybridization with radioactive probe complementary to prepro-galanin mRNA and non-radioactive probe complementary to POMC mRNA (A–C) or after hybridization with probe complementary to prepro-galanin mRNA without (D) or with (E) bisbenzimidazole contrast staining, or after hybridization with an excess of cold probe added to the hybridization cocktail (F). (A–C) Double *in situ* hybridization reveals several cells expressing both prepro-galanin mRNA (bright grains) and POMC mRNA (dark labelling) (small arrowheads) as well as POMC mRNA-positive and prepro-galanin mRNA-negative cells (big arrowheads). (D–F) Note strong signals in restricted areas of the tissue (A) which in B can often be seen to consist of small groups of cells (small arrowheads). Big arrowheads point to negative cell groups. Note low signal in the control experiment (F). Scale bars indicate 50 μ m (A = B = C; D = E = F).

was observed in tumors #10, #16, #17, or #21 (data not shown).

Some tumors were processed for double in situ hybridization with a non-radioactive POMC mRNA probe. A high degree of coexistence was observed in tumors #1 and #3, whereby this was observed in the majority of cells in tumor #3, but POMC mRNA-positive, galanin mRNA-negative cells were also observed (Fig. 9A-C). In tumor #1 all galanin mRNA positive cells had a POMC mRNA signal. Tumor #4 showed a clear separation between the non-radioactive POMC mRNA signal and the radioactive galanin signal (cf. Fig. 8E with C and D), suggesting synthesis in separate cells. However, POMC mRNA-galanin mRNA coexistence situations could not be excluded. Finally, in some tumors (eg. #10 and #21) a very strong signal was observed after incubation with the galanin mRNA probes. In all other tumors described above (Figs. 7C, 8B and 9F), the signal could be blocked by addition of an excess ($100 \times$) of cold probe, except in tumors #10 and #21. They had a very strong signal which was observed to the same extent after addition of cold probe (data not shown). In agreement, both tumors (#10, 21) had very low galanin levels as monitored with RIA.

4. Discussion

In this study, using a RIA for human galanin, we demonstrate high levels of this peptide in extracts from ACTH-producing pituitary adenomas, moderate and varying galanin levels in clinically non-functioning adenomas and low or not detectable levels in GH and PRL-producing adenomas, with a good correlation to ACTH levels in the adenomas. Moreover, the RIA data were supported by the in situ hybridization results; a significant galanin signal was only found in the corticotroph adenomas. Double in situ hybridization revealed coexistence of galanin mRNA and POMC mRNA in most tumors, although a clear cellular dissociation of the two transcripts was seen in some other tumours.

When discussing these results, one should keep in mind that different parts of the tumor tissue sample were analyzed in each of the various assays. Thus, differences in distribution of various markers within the tumor should be considered. Such differences were, in fact, encountered in the in situ hybridization analysis.

4.1. Galanin in corticotroph adenomas

A number of studies, using mainly immunostaining and in situ hybridization, have demonstrated presence of galanin in pituitary adenomas, especially in ACTH-producing tumors (see Table 3 for overview). Here we show that galanin levels in pituitary adenoma extracts vary with tumor type and correlate strongly with ACTH levels, supporting previous studies showing co-production of the two peptides. Indeed, the present in situ hybridization results using

Table 3

Galanin in human pituitary adenomas and in normal pituitaries

Reference	Pituitary adenomas				Normal pituitaries
	ACTH	GH	PRL	Inactive	
Hulting et al. [37]	-	1/1	-	-	-
Vrontakis et al. [38]	13/18	0/4	0/8	0/5	23/23
Hsu et al. [40]	16/19	5/11	2/14	9/18	7/7
Polak et al. [41]	6/6	3/8	2/2	0/7	-
Sano et al. [42]	9/14	0/10	0/9	0/9	-
Bennet et al. [39]	-	2/4	0/1	3/13	30/30
Invitti et al. [43]	5/5	-	-	-	-
Leung et al. [44]	10/16	1/26	1/19	25/89	6/6

Review of data published 1989-2002.

double-labeling on single sections show conclusively that individual cells can synthesize both ACTH and galanin. However, whereas coexistence of galanin and POMC mRNA was found in apparently all cells of one corticotroph adenoma (#1, 2, Table 1; Fig. 7A, B), another tumor of this type showed a clear separation of the two signals (#4, Table 1; Fig. 8A, C-E). Moreover, co-expression of galanin and POMC mRNA in the ACTH adenomas was reflected in a close correspondence between tumor content of galanin and ACTH, whereas when the peptides were expressed in separate cells RIA tumor content of ACTH vastly exceeded that of galanin. Thus, absence of a correlation between these two peptides in extracts from corticotroph adenomas may reflect an expression of ACTH and galanin in different cell populations.

A clinical significance of this differential expression could not be related to age, sex, tumor size or pituitary function. However, as shown by Invitti et al. [43], the in vivo release of galanin in response to CRH varies among patients with Cushing's disease. We found no elevation of plasma galanin in sinus petrosus from two patients with Cushing's disease. Thus, although both patients showed a marked unilateral response to CRH, there was no similar effect on galanin levels. One of these patients (#4) was analyzed with double-labeling in situ hybridization, and in this patient galanin and ACTH were synthesized in distinctly separate cell populations (Fig. 8). Perhaps the variability in the response to CRH can be explained by the extent of colocalization of ACTH and galanin. Thus, when the peptides are produced in different cells, CRH may only cause release of ACTH. It would therefore be interesting to know whether or not type-1 CRH receptors [53] are present in ACTH-negative, galanin-positive cells. It should here be mentioned that in the normal state, stimulation of ACTH secretion with CRH, desmopressin or physical exercise does not affect plasma galanin levels [43,54,55].

The clinical significance of the presence of galanin in ACTH adenomas was also investigated by Leung et al. [44], showing that galanin-positive adenomas were smaller and had better prognosis than those not expressing galanin. The present study supports this finding; we have found that all seven corticotroph adenomas were galanin-positive, and

they were small and were successfully removed. Interestingly, in the four young patients with microadenomas and highly active Mb Cushing (#1–4) tumor galanin was inversely related to tumor volume. In contrast to Leung et al. [44] we found a correlation in six of seven corticotroph adenomas between galanin content and 24 h urinary cortisol excretion, representing integrated ACTH-cortisol production. To what extent galanin can serve as a marker for tumor activity as well as act as a growth inhibitory factor in this type of tumor requires analysis of a larger material.

4.2. Galanin in clinically inactive GH and PRL adenomas

The capacity of non-ACTH tumors to synthesize galanin has been controversial. Vrontakis et al. [38] and Sano et al. [42] found galanin-LI exclusively coexpressed with ACTH and not present in any other type of pituitary adenoma. We have previously demonstrated the presence of galanin in a GH adenoma [37], and Polak et al. [41] in GH and PRL adenomas. Hsu et al. [40], in addition, found galanin-LI in half of the non-functioning adenomas, including a few which were negative for ACTH. In the largest and most recent study, Leung et al. [44] demonstrated galanin-LI in one third of the clinically inactive adenomas but rarely in GH- or PRL-producing adenomas.

In the only previous study based on extraction, Bennet et al. [39], using an antiserum against porcine galanin and a porcine tracer, found detectable galanin in two of four GH adenomas and in three of thirteen clinically active adenomas. With the present extraction method we find galanin-LI in all but two of the non-ACTH adenomas studied. However, galanin levels above 5 pmol/mg protein were only seen in 5 of the 10 clinically inactive adenomas and in none of the GH- or PRL-producing adenomas.

The presence of galanin was shown in all normal pituitaries examined in previous studies [38–40,44]. In fact, extraction yielded markedly higher galanin concentrations in normal pituitaries than in non-ACTH pituitary adenomas [39]. Since the present study is based on tissue obtained at pituitary surgery, it does not include a control group of normal pituitaries. However, in a previous study of extracts from 280 postmortem pituitaries Schmidt et al. [5] reported 410 pmol galanin per gram frozen tissue. In our material the mean galanin content was 13,950 pmol/g frozen tissue in ACTH adenomas, 3.6 pmol in GH adenomas and 1.4–4170 pmol in clinically inactive adenomas.

The highly variable galanin content found in the clinically inactive adenomas correlated well with ACTH content in the same adenomas, and presence of normal corticotrophs in the samples containing high galanin and ACTH cannot be excluded. In one case (#19) this was verified by PAD showing normal pituitary tissue in 9 of 10 samples (cf. Fig. 9D–F). This patient also incurred a postoperative panhypopituitarism. Indeed, the three patients who became ACTH deficient after surgery (#18, 19, 24) had elevated tumor galanin-LI (mean 40.9 pmol/mg protein), whereas those with

preoperative ACTH failure (#10, 20, 21, 23) had low levels (mean 0.61 pmol/mg protein).

The patient (#16) with the highest tumor galanin content among the clinically inactive adenomas had shown clinical signs of Mb Cushing. However, laboratory investigation, performed after a tumor apoplexy, revealed normal ACTH and cortisol secretion. This patient had a recurrence of Cushing's disease a few years after surgery. Our sample may have contained ACTH adenomatous tissue or normal pituitary as indicated by immunocytochemistry.

4.3. Identity of galanin in pituitary tumors

The molecular form of galanin was studied with RP-HPLC in the seven corticotroph adenomas and the two clinically inactive adenomas with high galanin content (#1–7) (#16, 19). The elution pattern was shown to be remarkably homogenous, with a small peak preceding the main form eluting with synthetic human galanin (Fig. 5A). It agrees with the pattern found in non-ACTH pituitary adenomas by Bennet et al. [39] and corresponds to the structure determined by Schmidt et al. [5] who isolated and sequenced galanin from purified extracts of postmortem pituitaries. Our finding indicates that the molecular form of galanin in corticotroph adenomas is identical to that found in clinically inactive tumors and in the normal pituitary. The small polar peak eluting earlier than galanin(1–30) probably represents degradation products which have been shown to elute prior to the main form [56]. In one case (#6) we found that galanin eluted later than human standard with a peak coinciding with galanin(1–16) (Fig. 5B). This fragment has not been found *in vivo* in the rat [56,57] or in man [2,5,28,58], and our finding suggests a different processing of tumor galanin in this patient.

4.4. Concluding remarks

We found that galanin is present in human corticotroph adenomas and provide conclusive evidence at the transcript level for cellular colocalization with POMC in some, but not all tumors. Our results also indicate that galanin present in other types of pituitary adenomas is associated with normal pituitary tissue. The molecular form of tumorous pituitary galanin is homogenous representing genuine human galanin (1–30), but in one adenoma a form of galanin coeluting with galanin(1–16) was identified. No evidence of galanin secretion from these adenomas into local or peripheral circulation was obtained, pointing to a mainly auto- and/or paracrine role for galanin produced in corticotroph adenomas.

Acknowledgements

The study was supported by grants from Stockholm County Council, Seidey and Rolf Fredriksson's Research

Foundation, the Swedish MRC (04X-2887), Marianne and Marcus Wallenberg's Foundation and an Unrestricted Bristol-Myers Squibb Neuroscience Grant. We are grateful to Agneta Hilding, Department of Molecular Medicine, Endocrine and Diabetes Unit, Karolinska Institutet for assistance with the statistical evaluation, and to Dr. Anders Höög for pathological anatomical diagnosis.

References

- [1] Tatemoto K, Rökaeus Å, Jömvall H, McDonald TJ, Mutt V. Galanin—a novel biologically active peptide from porcine intestine. *FEBS Lett* 1983;164:124–8.
- [2] Bersani M, Johnsen AH, Højrup P, Dunning BE, Andreassen JJ, Holst JJ. Human galanin: primary structure and identification of two molecular forms. *FEBS Lett* 1991;283:189–94.
- [3] Evans H, Shine J. Human galanin: molecular cloning reveals a unique structure. *Endocrinology* 1991;129:1682–4.
- [4] McKnight GL, Karlén AF, Kowalyk S, Mathewes SL, Sheppard PO, O'Hara PJ, et al. Sequence of human galanin and its inhibition of glucose-stimulated insulin secretion from RIN cells. *Diabetes* 1991;41:82–7.
- [5] Schmidt WE, Kratzin II, Eckart K, Dreys D, Mundkowski G, Clemens A, et al. Isolation and primary structure of pituitary human galanin, a 30-residue nonamidated neuropeptide. *Proc Natl Acad Sci U S A* 1991;88:11435–9.
- [6] Vrontakis MF, Peden LM, Duckworth ML, Friesen HG. Isolation and characterization of a complementary DNA (galanin) clone from estrogen-induced pituitary tumor messenger RNA. *J Biol Chem* 1987;262:16755–8.
- [7] Kaplan LM, Gabriel SM, Koenig JL, Sunday ME, Spindel ER, Martin JB, et al. Galanin is an estrogen-inducible secretory product of the rat anterior pituitary. *Proc Natl Acad Sci U S A* 1988;85:7408–12.
- [8] Crawley JN. The role of galanin in feeding behaviour. *Neuropeptides* 1999;33:369–75.
- [9] Kalra SP, Horvath TL. Neuroendocrine interactions between galanin, opioids, and neuropeptide Y in the control of reproduction and appetite. *Ann N Y Acad Sci* 1998;863:236–40.
- [10] Leibowitz S. Differential functions of hypothalamic galanin cell groups in the regulation of eating and body weight. *Ann N Y Acad Sci* 1998;863:206–20.
- [11] McDonald MP, Gleason TC, Robinson JK, Crawley J. Galanin inhibits performance on rodent memory tasks. In: Hökfelt T, Bartfai T, Crawley J, editors. *Galanin basic research discoveries and therapeutic implications*. New York: NY Acad. Sci.; 1998. p. 206–20.
- [12] Ögren S-O, Schödt PA, Kehr J, Yoshitake T, Misane I, Mannström P, et al. Modulation of acetylcholine and serotonin transmission by galanin. *Ann N Y Acad Sci U S A* 1998;863:342–63.
- [13] Xu XJ, Hökfelt T, Bartfai T, Wiesenfeld-Hallin Z. Galanin and spinal nociceptive mechanisms: recent advances and therapeutic implications. *Neuropeptides* 2000;34:137–47.
- [14] Habert-Ortoli E, Amiranoff B, Loquet I, Laburthe M, Mayaux JF. Molecular cloning of a functional human galanin receptor. *Proc Natl Acad Sci U S A* 1994;91:9780–3.
- [15] Brancsek TA, Smith KE, Gerald C, Walker MW. Galanin receptor subtypes. *Trends Pharmacol Sci* 2000;21:109–16.
- [16] Lissma TP, Shine J. Galanin and galanin receptors. *Results Probl Cell Differ* 1999;26:257–91.
- [17] Wynick D, Small CJ, Bacon A, Holmes FE, Norman M, Ormandy CJ, et al. Galanin regulates prolactin release and lactotroph proliferation. *Proc Natl Acad Sci U S A* 1998;95:12671–6.
- [18] Cai A, Hayes JD, Patel N, Hyde JF. Targeted overexpression of galanin in lactotrophs of transgenic mice induces hyperprolactinemia and pituitary hyperplasia. *Endocrinology* 1999;140:4955–64.
- [19] Kokaia M, Holmberg K, Nanobashvili A, Xu Z-QD, Kokaia Z, Lendahl U, et al. Suppressed kindling epileptogenesis in mice with ectopic overexpression of galanin. *Proc Natl Acad Sci U S A* 2001;98:14006–11.
- [20] Steiner RA, Holman JG, Holmes A, Wrenn CC, Cadd G, Jureus A, et al. Galanin transgenic mice display cognitive and neurochemical deficits characteristic of Alzheimer's disease. *Proc Natl Acad Sci U S A* 2001;98:4184–9.
- [21] Rökaeus Å, Melander T, Hökfelt T, Lundberg JM, Tatemoto K, Carlquist M, et al. A galanin-like peptide in the central nervous system and intestine of the rat. *Neurosci Lett* 1984;47:161–6.
- [22] Skofitsch G, Jacobowitz DM. Immunohistochemical mapping of galanin-like neurons in the rat central nervous system. *Peptides* 1985;6:509–46.
- [23] Skofitsch G, Jacobowitz DM. Quantitative distribution of galanin-like immunoreactivity in the rat central nervous system. *Peptides* 1986;7:609–13.
- [24] Melander T, Hökfelt T, Rökaeus Å. Distribution of galanin-like immunoreactivity in the rat central nervous system. *J Comp Neurol* 1986;248:475–517.
- [25] Bloch GJ, Butler PC, Eckersell CB, Mills RH. Gonadal steroid-dependent GAL-IR cells within the medial preoptic nucleus (MPN) and the stimulatory effects of GAL within the MPN on sexual behaviors. *Ann N Y Acad Sci U S A* 1998;863:188–205.
- [26] Hohmann JG, Clifton DK, Steiner RA. Galanin: Analysis of its coexpression in gonadotrophin-releasing hormone and growth hormone-releasing hormone neurons. *Ann N Y Acad Sci U S A* 1998;863:221–35.
- [27] Merchenthaler I. LHRH and sexual dimorphism. *Ann N Y Acad Sci U S A* 1998;863:175–87.
- [28] Bauer FF, Ginsberg L, Venetikonu M, MacKay DJ, Birn JM, Bloom SR. Growth hormone release in man induced by galanin, a new hypothalamic peptide. *Lancet* 1986;2:192–5.
- [29] Davis TME, Burrin JM, Bloom SR. Growth hormone release in response to GHRH-releasing hormone in man is 3-fold enhanced by galanin. *J Clin Endocrinol Metab* 1987;65:1248–52.
- [30] Cimino V. Galanin inhibits ACTH release in vitro and can be demonstrated immunocytochemically in dispersed corticotrophs. *Exp Cell Res* 1996;228:212–5.
- [31] Giustina A, Licini M, Schettino M, Dogli M, Pizzoccolo G, Negro-Villar A. Physiological role of galanin in the regulation of anterior pituitary function in humans. *Am J Physiol* 1994;266:F57–61.
- [32] Hooi SC, Maiter DM, Martin JB, Koenig JL. Galaninergic mechanisms are involved in the regulation of corticotropin and thyrotropin secretion in the rat. *Endocrinology* 1990;127:2281–9.
- [33] Hooi SC, Koenig JL, Gabriel SM, Maiter D, Martin JB. Influence of thyroid hormone on the concentration of galanin in the rat brain and pituitary. *Neuroendocrinology* 1990;51:351–6.
- [34] Wynick D, Smith DM, Gliatei M, Akinsanya K, Bhogal R, Purkiss P, et al. Characterization of a high-affinity galanin receptor in the rat anterior pituitary: Absence of biological effect and reduced membrane binding of the antagonist M15 differentiate it from the brain/gut receptor. *Proc Natl Acad Sci U S A* 1993;90:4231–5.
- [35] Wynick D, Hammond PJ, Akinsanya KO, Bloom SR. Galanin regulates basal and oestrogen-stimulated lactotroph function. *Nature* 1993;364:529–32.
- [36] Moore PJ, Morrison DG, Hyde JF. Galanin gene expression is increased in the anterior pituitary gland of the human growth hormone-releasing hormone transgenic mice. *Endocrinology* 1994;134:2005–10.
- [37] Halling A-L, Meister B, Grimelius L, Wersäll J, Ånggård A, Hökfelt T. Production of a galanin-like peptide by a human pituitary adenoma: immunohistochemical evidence. *Acta Physiol Scand* 1989;137:561–2.
- [38] Vrontakis MF, Sano T, Kovacs K, Friesen HG. Presence of galanin-like immunoreactivity in non-tumorous corticotrophs and corticotroph adenomas of the human pituitary. *J Clin Endocrinol Metab* 1990;70:747–51.

- [39] Bennet WM, Hill SF, Ghatei MA, Bloom SR. Galanin in the normal pituitary and brain and in pituitary adenomas. *J Endocrinol* 1991; 130:463-7.
- [40] Hsu DW, Hori SC, Hedley-Whyte T, Strauss RM, Kaplan LM. Coexpression of galanin and adrenocorticotrophic hormone in human pituitary and pituitary adenomas. *Am J Pathol* 1991;138:897-909.
- [41] Polak JM, Gibson S, Gentleman S, Steel J, Van Noorden S. Galanin: distribution, ontogeny and expression following manipulation of the endocrine and nervous system. In: Hökfelt T, Bartfai T, Jacobowitz D., Ottoson D., editors. Galanin a new multifunctional peptide in the neuro-endocrine system. London: Macmillan; 1991. p. 117-34.
- [42] Sano T, Vrontakis MF, Kovacs K, Asa SL, Friesen HG. Galanin immunoreactivity in neuroendocrine tumors. *Arch Pathol Lab Med* 1991;115:926-9.
- [43] Invitti C, Pecori F, Girakli P, Dubini A, Moroni P, Losa M, et al. Galanin is released by adrenocorticotrophin-secreting pituitary adenomas in vivo and in vitro. *J Clin Endocrinol Metab* 1999;4:1351-6.
- [44] Leung B, Lisina TP, Leung K-C, Hori YJ, Turner J, Sheehy JP, et al. Galanin in human pituitary adenomas: frequency and clinical significance. *Clin Endocrinol* 2002;56:397-403.
- [45] Grenbäck E, Bjellerup P, Holting A-I, Lundblad L, Ånggård A. Galanin in hypophysadenoma. *Proc Ann Meeting Swedish Med Soc* 1997;29P:162.
- [46] P. Lundin, Magnetic resonance imaging of pituitary macroadenomas. Thesis, Uppsala ISBN 91-628-0511-8 1992.
- [47] Wilson CB. A decade of pituitary microsurgery. The Herbert Olivecrona lecture. *J Neurosurg* 1984;61:314-33.
- [48] Schmidt WE, Siegel EG, Lamberts R, Gullwitz B, Creutzfeldt W. Puncrustatin: molecular and immunocytochemical characterization of a novel peptide in porcine and human tissues. *Endocrinology* 1988;123:1395-404.
- [49] Drouin J, Goodman HM. Most of the coding region of rat ACTH beta-LPH precursor gene lacks intervening sequences. *Nature* 1980; 288:610-3.
- [50] Dagerlind Å, Friberg K, Beun A, Hökfelt T. Sensitive mRNA detection using unfixed tissue: combined radioactive and non-radioactive in situ hybridization histochemistry. *Histochemistry* 1992; 98:39-49.
- [51] Schmitz GG, Walter T, Seibl R, Kessler C. Nonradioactive labeling of oligonucleotides in vitro with the hapten digoxigenin by tailing with terminal transferase. *Ann Biochem* 1991;192:222-31.
- [52] Broberger C, Landry M, Wong H, Walsh J, Hökfelt T. Subtypes Y1 and Y2 of the neuropeptide Y receptor are respectively expressed in proopiomelanocortin and neuropeptide Y-containing neurons of the rat hypothalamic arcuate nucleus. *Neuroendocrinology* 1997;66: 393-408.
- [53] Aguilera G, Rabadan-Diehl C, Nikodemova M. Regulation of pituitary corticotropin releasing hormone receptors. *Peptides* 2001;22: 769-74.
- [54] Ceresini G, Freddi M, Paccotti P, Valenti G, Merchenthaler I. Effects of ovine corticotropin-releasing hormone injection and desmopressin coadministration on galanin and adrenotropin plasma levels in normal women. *J Clin Endocrinol Metab* 1997;82:607-10.
- [55] Ceresini G, Marchini L, Fabbro A, Freddi M, Pasolini G, Reali N, et al. Evaluation of circulating galanin levels after exercise-induced pituitary hormone secretion in man. *Metabolism* 1997;82:282-6.
- [56] Land T, Langel U, Bartfai T. Hypothalamic degradation of galanin (1-29) and galanin (1-16): identification and characterization of the peptidolytic products. *Brain Res* 1991;558:245-50.
- [57] Hedecs K, Langel U, Xu X.-J., Wiesenfeld-Hallin Z, Bartfai T. Biological activities of two endogenously occurring N-terminally extended forms of galanin in the rat spinal cord. *Eur J Pharmacol* 1994;259: 151-6.
- [58] Bauer FE, Hacker GW, Terenghi G, Adrian TE, Polak JM, Bloom SR. Localization and molecular forms of galanin in human adrenals: elevated levels in pheochromocytomas. *J Clin Endocrinol Metab* 1986; 63:1372.

Regulation of Cytochrome P4501A1 in Teleosts: Sustained Induction of CYP1A1 mRNA, Protein, and Catalytic Activity by 2,3,7,8-Tetrachlorodibenzofuran in the Marine Fish *Stenotomus chrysops*¹

MARK E. HAHN² AND JOHN J. STEGEMAN

Biology Department, Woods Hole Oceanographic Institution, Woods Hole, Massachusetts 02543

Received December 28, 1993; accepted March 29, 1994

Regulation of Cytochrome P4501A1 in Teleosts: Sustained Induction of CYP1A1 mRNA, Protein, and Catalytic Activity by 2,3,7,8-Tetrachlorodibenzofuran in the Marine Fish *Stenotomus chrysops*. HAHN, M. E., AND STEGEMAN, J. J. (1994). *Toxicol. Appl. Pharmacol.* 127, 187-198.

Cytochrome P4501A1 (CYP1A1) is known to play important roles in the activation and detoxification of carcinogens and other toxicants in vertebrate animals, including fish. Although extensively studied in mammalian systems, the regulation of CYP1A forms in other vertebrates is less well understood. We examined the time course and dose-response relationships for induction of CYP1A1 mRNA, protein, and catalytic activity by 2,3,7,8-tetrachlorodibenzofuran (TCDF) in the marine fish *Stenotomus chrysops* (scup). The time course of CYP1A1 induction was determined following a single ip dose (10 nmol/kg) of 2,3,7,8-TCDF. Hepatic ethoxyresorufin *O*-deethylase activity was increased after 1 day, reached a maximum by 8 days, and was still elevated 14 days after treatment. The content of immunodetectable CYP1A1 protein in liver was elevated on Day 1 and continued to increase through 14 days. CYP1A1 protein content was also strongly induced in heart and gill beginning at 2 days after treatment and extending through Day 14. Hepatic CYP1A1 mRNA was strongly induced by 1 day after dosing and remained elevated through 14 days. The sustained induction of CYP1A1 mRNA by 2,3,7,8-TCDF contrasts with the transient induction seen previously in fish treated with nonhalogenated inducers and most likely reflects differences in persistence of the inducers. Dose-response studies indicated that induction of CYP1A1 mRNA, protein, and catalytic activity occurred following doses of 2,3,7,8-TCDF as low as 0.4 nmol/kg (120 ng/kg), within the range of whole-body contents of this congener measured in fish from contaminated environments. The estimated dose producing half-maximal CYP1A1 induction in scup was approximately 2-10 nmol/kg, suggesting that the sensitivity of these fish to induction may be as great as or greater than that of

rats. In contrast to previous results obtained with 3,3',4,4'-tetrachlorobiphenyl (TCB) and β -naphthoflavone, which appear to inhibit or inactivate CYP1A1 in fish and other vertebrates, there was a good correlation among levels of CYP1A1 mRNA, protein, and catalytic activity in individual fish following various doses of 2,3,7,8-TCDF. The difference in response to 2,3,7,8-TCDF versus 3,3',4,4'-TCB may reflect differences in the inducing potencies of the two compounds relative to their similar potencies as inhibitors of CYP1A1 catalytic activity. In additional studies to evaluate structure-activity relationships for CYP1A1 induction by chlorinated dibenzofurans in fish, scup were treated with 2,3,6,8-tetrachlorodibenzofuran (2,3,6,8-TCDF). At 10 or 50 nmol/kg, 2,3,6,8-TCDF was inactive as an inducer of CYP1A1 mRNA, protein, or catalytic activity. Overall, these results illustrate temporal and dose-dependent aspects of CYP1A1 induction in fish that are highly inducer-specific; the results also indicate that fundamental features of CYP1A1 regulation appear to be conserved in fish and mammals, two widely divergent groups of vertebrates.

© 1994 Academic Press, Inc.

Multiple forms of cytochrome P450 (P450) occur in diverse groups of organisms, where they play important roles in the oxidative metabolism of a wide variety of endogenous and xenobiotic compounds (Gonzalez, 1989; Nelson *et al.*, 1993; Stegeman and Hahn, 1993). The properties and regulation of P450 forms in animals of various taxa could determine the susceptibility of those animals to toxic effects, including chemical carcinogenesis, resulting from pollutant exposure. Information on the comparative structure, function, and regulation of P450 forms is essential for a more complete understanding of mechanisms of toxicity and for predicting chemical effects in diverse groups of animals. Of special interest in this regard are fish, a group that includes species of ecological, commercial, and aesthetic importance, many of which are exposed to a variety of pollutants in both marine and freshwater environments.

The P450 gene superfamily is composed of multiple families and subfamilies (Nelson *et al.*, 1993). P450 forms in the 1A subfamily are of toxicological significance due to their

¹ Presented in part at the 29th annual meeting of the Society of Toxicology, Miami Beach, FL, February 1990 (*Toxicologist* 10, 28) and at the 11th annual meeting of the Society of Environmental Toxicology and Chemistry, Arlington, VA, November 1990.

² To whom correspondence and reprint requests should be addressed.

involvement in the activation and detoxification of procarcinogens and other toxicants (Nebert, 1989) and in the metabolism of endogenous compounds such as estradiol and arachidonic acid (Rifkind *et al.*, 1990; Spink *et al.*, 1990). Whereas two 1A forms (CYP1A1 and CYP1A2) are known in mammals, the 1A subfamily in most fish consists of a single form (CYP1A1)³. In both mammals and fish, CYP1A forms are highly inducible by polynuclear aromatic hydrocarbons (PAH) and halogenated aromatic hydrocarbons (HAH); the latter group includes the chlorinated dibenzo-*p*-dioxins, dibenzofurans, and biphenyls, some of which are ubiquitous and extremely toxic environmental contaminants (Poland and Knutson, 1982). In addition to the important roles of induced 1A forms in the metabolism of environmental contaminants, induction of CYP1A1 has been used as a model system for examining mechanisms of xenobiotic-altered gene expression (Whitlock, 1990).

In mammals, CYP1A genes are regulated mainly by transcriptional mechanisms (Okino *et al.*, 1992; Pasco *et al.*, 1993). Induction is controlled by the Ah receptor, a ligand-activated transcription factor that binds certain PAH and HAH inducers with high affinity. Following ligand binding, the Ah receptor is activated to a form that interacts with enhancer sequences in the CYP1A1 promoter to initiate transcription of the CYP1A1 gene and the subsequent accumulation of CYP1A1 mRNA (Whitlock, 1990). Much less is known about the regulation of CYP1A forms in non-mammalian species (reviewed in Andersson and Forlin, 1992; Stegeman and Hahn, 1993). The Ah receptor has been identified in fish (Heilmann *et al.*, 1988; Lorenzen and Okey, 1990; Swanson and Percow, 1991; Hahn *et al.*, 1992, 1994), but its involvement in CYP1A1 regulation, though expected, has not yet been defined. However, studies in trout (*Oncorhynchus mykiss*) (Haasch *et al.*, 1988; Heilmann *et al.*, 1988) and killifish (*Fundulus heteroclitus*) (Klopper-Sams and Stegeman, 1989) have shown that induction of CYP1A protein and catalytic activity by the model nonhalogenated inducers β -naphthoflavone (BNF) and 3-methylcholanthrene is preceded by elevated levels of CYP1A mRNA. Others have shown induction of CYP1A mRNA in fish or fish cells following exposure to halogenated inducers such as 3,3',4,4'-tetrachlorobiphenyl (TCB) and 2,3,7,8-tetrachlorodibenzo-*p*-dioxin (Gooch *et al.*, 1989; Pesonen *et al.*, 1992).

These reports notwithstanding, there are critical deficiencies in our understanding of the regulation of CYP1A expression in fish. Knowledge of structure-induction relationships in fish is limited (Gooch *et al.*, 1989; Janz and Metcalfe, 1991; Skaare *et al.*, 1991; van der Weiden, 1993), and dose-response relationships have been established for few compounds (James and Bend, 1980; Melancon and

Lech, 1983; Gooch *et al.*, 1989; Stegeman *et al.*, 1990; Janz and Metcalfe, 1991; van der Weiden *et al.*, 1992). In most cases these are known only at the level of catalytic activity. In addition, the time course of induction following single or continuous exposure to different types of inducers is not completely understood (Klopper-Sams and Stegeman, 1989; Pesonen *et al.*, 1992; Haasch *et al.*, 1993b; Celander *et al.*, 1993). Such information is important for interpreting studies of environmental induction and the decline of induced CYP1A during depuration of environmental chemicals after removal of fish from contaminated environments (Kreamer *et al.*, 1991; Stegeman *et al.*, 1991; Wirgin *et al.*, 1992; Haasch *et al.*, 1993a). Recent studies showing that prior exposure history affects CYP1A inducibility (Monosson and Stegeman, 1991; Wirgin *et al.*, 1992) highlight this need. Other questions concern the temporal and dose-dependent control of induction in extrahepatic organs compared to liver. Finally, discrepancies between CYP1A induction measured at the level of mRNA, protein, or catalytic activity have been described and appear to occur in an inducer-specific manner (Gooch *et al.*, 1989; Klopper-Sams and Stegeman, 1992; Haasch *et al.*, 1993b; van der Weiden *et al.*, 1993). Thus, it is important to define the relationships among these three parameters following treatment with various classes of inducing compounds. In the present study, we used 2,3,7,8- and 2,3,6,8-tetrachlorodibenzofuran (TCDF) to examine the temporal, dose-dependent, and structure-dependent expression of CYP1A1 mRNA, protein, and catalytic activity in the marine teleost *Stenotomus chrysops* (scup).

MATERIALS AND METHODS

Chemicals. Solutions of 2,3,7,8-TCDF (98% pure; 50 μ g/ml in toluene) and 2,3,6,8-TCDF (98% pure; 48 μ g/ml in isooctane) were purchased from ChemSyn/Wellington Laboratories (Lenexa, KS). Dosing solutions were prepared by adding an appropriate volume of these to corn oil and removing the toluene or isooctane under a stream of nitrogen. The rainbow trout CYP1A1 cDNA probe (pF450-3') was obtained from Dr. Daniel Nebert (University of Cincinnati). Nitro blue tetrazolium, 5-bromo-4-chloro-3-indolylphosphate, and bovine serum albumin were purchased from Sigma (St. Louis, MO). Other chemicals were obtained as described previously (Klopper-Sams *et al.*, 1987; Gooch *et al.*, 1989).

Animals and treatment. Scup were obtained by angling in local waters, held in flowing Nantucket Sound seawater at 16–20°C, and fed alternate rations of Purina Trout Chow and frozen squid for >9 months prior to use. The sex of individual scup cannot be determined from external morphology, so the fish used in these experiments included both males and females. The initial body weights and gonadosomatic indices (GSI) of fish used in the three experiments are shown in Table 1. The GSI is an index of sexual maturity in seasonally reproducing fish. Certain monooxygenase functions are known to be sexually differentiated in gonadally mature scup but not in gonadally regressed scup (Gray *et al.*, 1991). The GSI values of 1% or less shown in Table 1 indicate that the scup used here were gonadally regressed; this was confirmed by histological analysis (Smolowitz *et al.*, 1991). Such fish would not be expected to show sex-related differences in monooxygenase function; therefore, data from males and females have been combined in this report.

³ P450 nomenclature is as described by Nelson *et al.* (1993) and Stegeman (1992). The trivial name for the CYP1A1 representative from scup is P450E.

SUSTAINED INDUCTION OF CYP1A1 BY TCDF IN FISH

189

TABLE 1
Body Weights, Sexes, and Gonadosomatic Indices (GSI) of Scup Used for the Three Experiments

Experiment	Fish weight ^a	Males		Females	
		Number	GSI ^b	Number	GSI ^b
2378 Time course	291 ± 69	8	0.165 ± 0.115	13	0.624 ± 0.213
2378 Dose-response	247 ± 46	10	0.345 ± 0.252	14	1.11 ± 0.73
2368 Dose-response	160 ± 22	8	0.078 ± 0.026	4	0.405 ± 0.057

^a Approximate fish weight (grams) on day of dosing.

^b (Gonad weight/body weight) × 100, measured on day of sampling.

Fish were treated with a single intraperitoneal injection of TCDF in corn oil, or corn oil alone (1 ml/kg). The time course experiment took place in October, 1988, and utilized scup weighing between 160 and 430 g (mean: 291 g); the fish were held in flowing seawater that varied from 15 to 20°C during the 2-week experiment. Scup were killed by cervical transection at 1, 2, 4, 8, and 14 days following treatment; tissues were removed immediately for fixation (Smolowitz *et al.*, 1991) or preparation of RNA (liver) or microsomes (liver, heart, gill). The dose-response experiments took place in May and June of 1989. For 2,3,7,8-TCDF, mean fish weight was 247 ± 46 g at the time of treatment, and water temperature was approximately 17°C during the experiment. For 2,3,6,8-TCDF, mean fish weight was 160 ± 22 g and water temperature was 21–22°C. Scup were killed 4 days after dosing, and tissues were obtained and prepared as described above. For all experiments, effluent water from tanks containing TCDF-treated fish was filtered through a bed of activated charcoal prior to release.

Preparation of microsomes. Individual livers were homogenized in 4 vol of TK buffer (50 mM Tris, 0.15 M KCl, pH 7.4), and centrifuged at 750g (10 min) and 12,000g (10 min). The supernate was centrifuged at 100,000g for 70 min to pellet the microsomes. Microsomal pellets were resuspended in 1–2 ml of TEDG buffer (0.1 M Tris, pH 7.6, with 1 mM EDTA, 1 mM dithiothreitol, and 20% glycerol) per gram of original tissue wet weight. Pooled hearts (minus the bulbus arteriosus) and gill filaments from two or three fish per group (time course experiment only) were homogenized and microsomes were prepared as described above, except that a second set of low speed spins was conducted on heart homogenates prior to high-speed centrifugation.

Microsomal assays and immunoblotting. Ethoxyresorufin O-deethylase (EROD) activity was measured at 30°C as described by Klotz *et al.* (1984). Total cytochrome P450 content was determined spectrally as described previously (Stegeman *et al.*, 1979). Microsomal NADPH-cytochrome c reductase activity was assayed at 30°C as described by Stegeman *et al.* (1979), with cytochrome c at 1.1 mg/ml and KCN at 1 mM. Denaturing polyacrylamide gel electrophoresis and immunoblotting of microsomal protein was performed as described earlier (Klopper-Sams *et al.*, 1987; Hahn *et al.*, 1993). The primary antibody was MAb 1-12-3 (Park *et al.*, 1986) raised against scup CYP1A1 (trivial name: P450E); this antibody is specific for CYP1A forms in vertebrates (Stegeman, 1989). CYP1A1 protein levels were quantitated by video imaging densitometry (Master Scan, Scanalytics/CSPI, Billerica, MA), using purified scup CYP1A1 as the standard. The optical densities of the standard bands were linearly related to the amount of standard protein loaded on the gel. Each microsomal sample was analyzed by immunoblotting at least twice.

RNA isolation and hybridizations. Total hepatic RNA was isolated by the method of Chirgwin *et al.* (1979) as described previously (Klopper-Sams and Stegeman, 1989). RNA concentrations and purity were assessed spectrophotometrically; A260/A280 ratios were consistently in the range of 2.14–2.17. For Northern blots, 15 µg of hepatic total RNA was electrophoresed in 1% agarose gels containing 2.2 M formaldehyde and trans-

ferred to nitrocellulose (Schleicher & Schuell, 0.45 µm). Uniform loading of lanes was assessed visually on the ethidium bromide-stained gels; complete transfer of the RNA to nitrocellulose was confirmed by staining of the gel after transfer. The nitrocellulose was baked for 2 hr at 78°C and the blots were hybridized to a ³²P-labeled (by nick translation) trout CYP1A1 cDNA probe (pP,450-3') (Heilmann *et al.*, 1988). Blots were prehybridized overnight at 42°C in 50% deionized formamide, 5× Denhardt's, 0.5% SDS, 5× SSC (20× SSC = 3 M NaCl/0.3 M Na citrate, pH 7.0), and 100 µg/ml sheared *Escherichia coli* DNA. Hybridization was performed in an identical solution containing labeled probe (0.4 µg, 1 × 10⁶ dpm) for 24 hr. The blots were washed in 2× SSC, 0.5% SDS (room temperature, 5 min); 2× SSC, 0.1% SDS (room temperature, 15 min); 2× SSC, 0.1% SDS (50°C, 15 min); 1× SSC, 0.1% SDS (50°C, 15 min); and 0.5× SSC, 0.1% SDS (50°C, 20 min). Fluorography was performed using Kodak XAR-5 film and an intensifying screen at -70°C. The pP,450-3' probe hybridizes to a single band on Northern blots of hepatic total RNA from scup treated with CYP1A1 inducers (see Results); this permitted quantitation of CYP1A1 mRNA using a slot blotting technique. Individual or pooled samples (1–20 µg) of total RNA in 6× SSC and 7.4% formaldehyde were heated to 60°C for 15 min and applied to nitrocellulose using a Millipore slot blot apparatus. The nitrocellulose was then baked, prehybridized, hybridized, and washed as described above. Relative amounts of CYP1A1 mRNA were determined by densitometry of autoradiographs of the slot blots. For samples of RNA from both untreated and TCDF-treated scup, autoradiographic intensity was linearly related to the amount of RNA loaded over a range of 1–20 µg. The exposure times used for quantitation of mRNA levels were within the linear range of film response, as determined by multiple loadings and exposures of each blot. Results are expressed relative to the mean signal intensity of samples from control scup for each experiment.

Statistical analysis. Data are reported as means ± SD. Prior to group comparisons, Bartlett's test was used to determine if variances were homogeneous (Gad and Weil, 1982). Data sets with homogeneous variances were analyzed by one-way analysis of variance and, if significant ($p < 0.05$) differences were indicated, by Scheffé's *F* test. Data with nonhomogeneous variances were transformed by taking logarithms (base 10) and the transformed data were analyzed as described above. When the log transformation did not result in homogeneous variances, the untransformed data were analyzed using a Kruskal-Wallis nonparametric one-way analysis of variance; if significant ($p < 0.05$) differences were indicated, groups were compared using Dunn's distribution-free method for comparing multiple treatments with a control, with experiment-wise error rate controlled at $\alpha = 0.10$ (Hollander and Wolfe, 1973).

RESULTS

Time Course of Induction

In a preliminary experiment, 2,3,7,8-TCDF (10 nmol/kg) was found to induce EROD activity and immunoreac-

tive CYP1A1 protein approximately 20- and 40-fold, respectively, in scup (Hahn *et al.*, 1989). In that experiment, CYP1A1 induction was measured at only a single time point (5 days). Subsequently, we determined a more complete time course of induction by this compound. A single dose of 2,3,7,8-TCDF (10 nmol/kg; 3.06 µg/kg) was administered by intraperitoneal injection, and fish were sampled at various times up to 14 days after treatment. No deaths occurred during this period, and gross signs of toxicity were not observed in any of the fish.

Total cytochrome P450 was increased by 2 days after dosing and continued to increase throughout the 2-week period (Fig. 1A). Elevated levels of immunodetectable CYP1A1 protein were evident on the first day of sampling (Day 1) and continued to rise through 14 days, when CYP1A1 protein content of treated fish was more than 23-fold greater than that of control fish (Fig. 1B). The absolute levels of induced CYP1A1 protein closely matched the increase in total P450 at each time point, suggesting that the elevated amounts of P450 detected spectrally consisted mainly, if not entirely, of CYP1A1 holoenzyme.

CYP1A1 is known to be the major catalyst of EROD activity in scup (Stegeman *et al.*, 1985). EROD activity in 2,3,7,8-TCDF-treated fish was significantly increased by Day 1 and continued to increase in a pattern similar to that of CYP1A1 protein (Fig. 1C). Maximal induction (51-fold) occurred on Day 8; after 14 days, EROD activity remained highly induced. NADPH-cytochrome *c* reductase activities did not differ among any groups of treated or control fish in this experiment (data not shown).

The trout CYP1A1 cDNA probe pSP_{450-3'} (Heilmann *et al.*, 1988) hybridized to a single band (approximately 2.4 kb) in Northern blots of total hepatic RNA from 2,3,7,8-TCDF-treated scup (see below), as seen previously for some teleosts treated with other PAH-type inducers (Heilmann *et al.*, 1988; Kloepper-Sams and Stegeman, 1989). Hybridization of this probe to hepatic total RNA applied to slot blots was performed to quantitate the changes in CYP1A1 mRNA produced by 2,3,7,8-TCDF (Fig. 1D). CYP1A1 mRNA levels were increased 56-fold after 1 day of treatment, with maximal levels achieved after 4 to 8 days (87- to 89-fold). By 14 days, mean levels of CYP1A1 mRNA were still elevated (49-fold), but were 55% of those achieved at Day 4, and appeared to be declining.

Induction of CYP1A1 by 2,3,7,8-TCDF also occurred in several extrahepatic tissues. Immunohistochemical detection of induced CYP1A1 protein in extrahepatic organs of scup from this experiment (sampled at Days 4 or 8) has been described elsewhere (Smolowitz *et al.*, 1991). In addition, the time course of CYP1A1 protein content was determined on pooled samples of microsomes prepared from hearts and gills of corn oil- and TCDF-treated fish. In both tissues, a clear elevation in amounts of CYP1A1 protein was evident on Day 2 after TCDF treatment and was main-

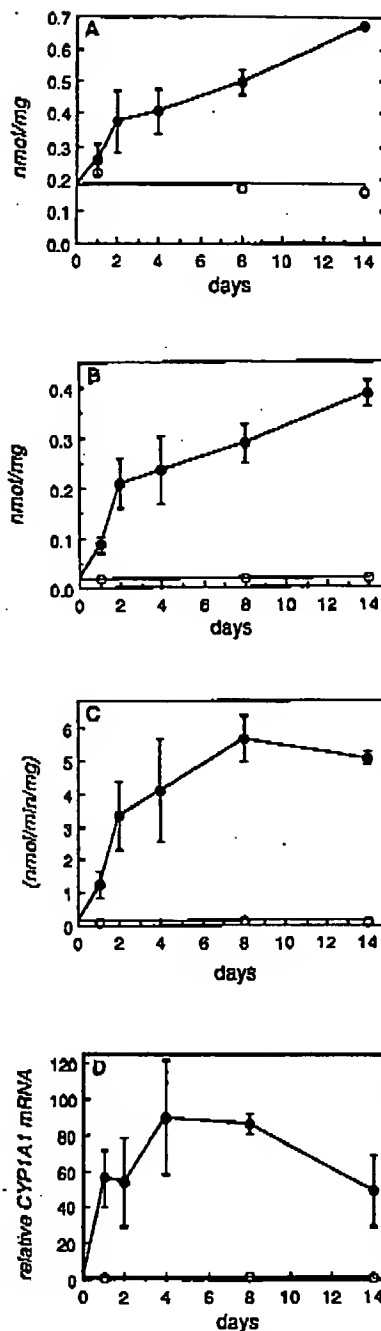


FIG. 1. Time course of induction of hepatic total cytochrome P450, CYP1A1 protein, CYP1A1 catalytic activity, and CYP1A1 mRNA by 2,3,7,8-TCDF. Scup were injected with corn oil (open symbols) or 2,3,7,8-TCDF (10 nmol/kg; filled symbols) and killed at the specified times. Points are the means (\pm SD) of three (TCDF) or two (corn oil) fish per time point. (A) Total cytochrome P450. (B) CYP1A1 protein. (C) EROD activity. (D) CYP1A1 mRNA, from slot blots of 10 or 20 µg total hepatic RNA from individual animals, normalized to the mean control value. Statistical analysis of the untransformed data (A) or \log_{10} -transformed data (B-D) by one-way analysis of variance and Scheffé's *F* test indicated significant differences ($p < .05$) for all TCDF-treated groups versus the mean of all six controls, except for total P450 (A) on Day 1, which was not significantly different from the control value.

SUSTAINED INDUCTION OF CYP1A1 BY TCDF IN FISH

191

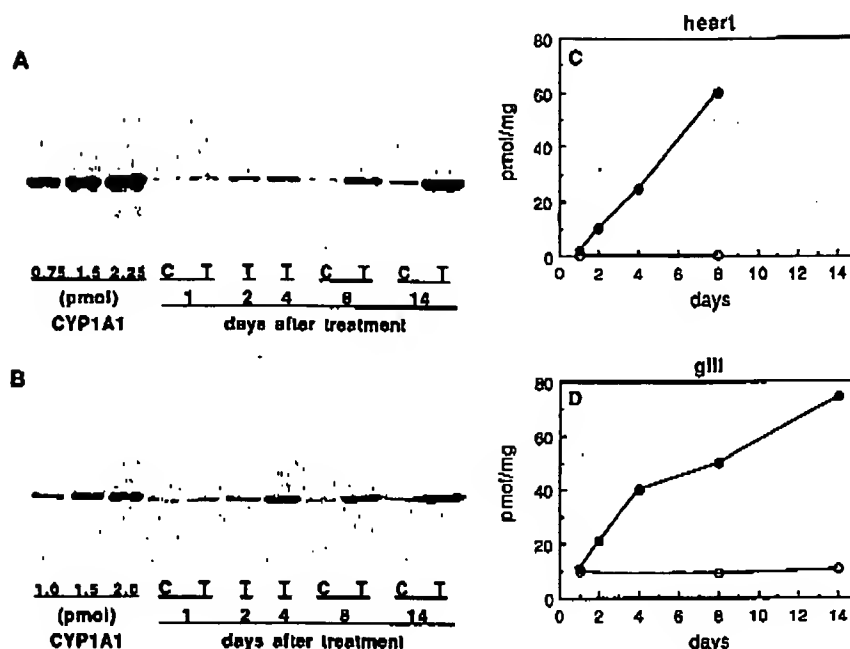


FIG. 2. Time course of CYP1A1 protein induction by 2,3,7,8-TCDF in scup heart and gill. Scup were treated with corn oil or 2,3,7,8-TCDF (10 nmol/kg) and microsomes were prepared at the specified times from pooled hearts or gills as described under Materials and Methods. (A and B) Immunoblots of heart (A) and gill (B) microsomes. Immunoblots were performed using 10 μ g (heart) or 40 μ g (gill) of microsomal protein. Left lanes contained the indicated amounts of purified scup CYP1A1 protein. Additional standards were also run, but are not shown. The different intensities of the CYP1A1 standards in the two blots reflect different development times. Gill samples were analyzed twice, with similar results. (C and D) Data from densitometric analysis of heart (C) and gill (D) immunoblots shown in A and B. Open symbols, corn oil-treated fish; Filled symbols, TCDF-treated fish. Data from 14-day control and TCDF-treated scup hearts were omitted from (C). The 14-day data indicate that strong induction is maintained at this time point, but electrophoretic patterns of total microsomal protein for these two samples were different from those obtained with samples from the other time points, precluding quantitative comparisons between 14-day samples and those from other times.

tained through 14 days (Fig. 2). The pattern of time-dependent expression of CYP1A1 protein in these two tissues was similar to that seen in liver (compare Fig. 2 to Fig. 1B).

Dose-Response

The sensitivity of the CYP1A1 induction response in scup was evaluated by treating groups of fish with single doses of 0, 0.08, 0.4, 2.0, or 10 nmol 2,3,7,8-TCDF per kilogram (equivalent to 0, 0.024, 0.12, 0.61, or 3.06 μ g/kg). Based on results of the time course experiment, Day 4 was chosen as the time of sampling. No statistically significant ($p < .05$) differences in relative liver weight, yield of microsomal protein, total cytochrome P450, or NADPH-cytochrome *c* reductase were found at any dose (Table 2). However, there was an apparent shift in the absorption maxima of the dithionite-reduced difference spectra of CO-treated microsomes, from approximately 450 nm in control fish to 447–448 nm in fish treated with the highest dose of 2,3,7,8-TCDF.

The dose-dependent patterns of response of CYP1A1 mRNA, protein, and catalytic activity following 2,3,7,8-TCDF treatment were qualitatively similar. No changes

were evident at 0.08 nmol/kg, the lowest dose tested, but an increase in the mean values of all three parameters was seen at higher doses (Table 2). Figures 3 and 4 illustrate the dose-dependent induction of CYP1A1 protein and mRNA, respectively. There were significant interanimal differences at the 0.4 nmol/kg dose, with only 2 of 5 animals responding. However, in these 2 animals induction was evident at all three levels: mRNA, protein, and catalytic activity. At the two highest doses, the frequency of response and degree of induction increased, with 4/5 and 3/4 animals showing a strong response in the 2 and 10 nmol/kg groups, respectively. The maximal level of induced CYP1A1 observed in this experiment was lower and more variable than that seen in fish treated with an equivalent dose (10 nmol/kg) and killed at the same time (4 days) in the time course experiment. Nevertheless, it is clear that the fish were highly induced in both experiments.

Using mean values of CYP1A1 mRNA, protein, or activity, and if the levels achieved at 10 nmol/kg represent maximal induction, the ED_{50} for CYP1A1 induction in scup is approximately 2–3 nmol/kg. While it is not certain that maximal induction was achieved by the 10 nmol/kg dose in this experiment, the levels of CYP1A1 protein and EROD

TABLE 2
CYP1A1 Expression in Livers of Scup Treated with Various Doses of 2,3,7,8-TCDF

Dose (nmol/kg)	(n)	Body weight (g)	Relative liver weight (% BW)	Microsomal yield (mg protein/ g liver)	Total P450 (pmol/mg)	CYP1A1 mRNA (relative units)	CYP1A1 protein (pmol/mg)	EROD activity (nmol·min ⁻¹ ·mg ⁻¹)	NADPH-cytochrome c reductase (nmol·min ⁻¹ ·mg ⁻¹)
0	(5)	237 ± 55	1.25 ± 0.22	15.0 ± 2.1	176 ± 40	1.00 ± 0.61	1.7 ± 1.4	0.170 ± 0.075	111 ± 11
0.08	(5)	236 ± 21	1.09 ± 0.20	13.4 ± 1.8	182 ± 39	0.94 ± 0.21	2.2 ± 1.3	0.215 ± 0.092	100 ± 3
0.4	(5)	240 ± 57	1.12 ± 0.42	13.9 ± 1.2	214 ± 80	1.60 ± 1.32	12.1 ± 18.3	0.481 ± 0.445	102 ± 22
2	(5)	235 ± 39	1.23 ± 0.18	12.3 ± 3.5	210 ± 43	4.16 ± 1.88*	25.7 ± 12.6*	1.13 ± 0.54*	101 ± 13
10	(4)	225 ± 54	1.29 ± 0.07	16.3 ± 3.3	257 ± 127	9.31 ± 5.05*	83.1 ± 63.5*	2.54 ± 1.94*	81 ± 22

Note. Scup were treated ip with the indicated doses of 2,3,7,8-TCDF, killed 4 days later, and analyzed as described under Materials and Methods. Data are reported as means ± SD. Statistical analyses were by parametric (body weight, liver weight, microsomal yield, total P450) or nonparametric (CYP1A1 mRNA, CYP1A1 protein, EROD, NADPH-cytochrome c reductase) methods as described in the text.

* Significantly different from controls (Kruskal-Wallis test significant at $p < 0.05$; this treatment significantly different from control as determined by Dunn's multiple comparison method with experiment-wise error rate controlled at $\alpha = 0.10$). One-way analysis of variance and Scheffe's F test on log-transformed data for CYP1A1 mRNA, CYP1A1 protein, and EROD gave identical results.

activity in fish treated with 10 nmol/kg in the time course experiment are among the highest we have seen in scup treated with any inducer. Thus, we consider the true ED₅₀ value for 2,3,7,8-TCDF to be in the range of 2–10 nmol/kg.

Structure-Activity Relationship

Induction of CYP1A1 by chlorinated biphenyls, dibenzo-*p*-dioxins, and dibenzofurans shows a marked structure-activity relationship in mammals (Goldstein and Safe, 1989), but evidence for such a relationship in fish is more limited (Gooch *et al.*, 1989; van der Weiden, 1993). Of the chlorinated dibenzo-*p*-dioxin and dibenzofuran congeners that have been examined, all have been 2,3,7,8-substituted (Hahn *et al.*, 1989; Muir *et al.*, 1990, 1992; van der Weiden, 1993). We therefore evaluated the ability of 2,3,6,8-TCDF to induce CYP1A1 in scup. This congener was shown previ-

ously to be a poor inducer of CYP1A1 catalytic activities (AHH and EROD) in rats or rat cells (Bandiera *et al.*, 1984; Doyle and Fries, 1986). 2,3,6,8-TCDF was administered at 10 and 50 nmol/kg (3.06 and 15.3 µg/kg); fish were killed 4 days later and responses were measured as in the previous experiments. The fish used in this study were slightly smaller than those used in the other two experiments, but earlier studies have shown that scup in this size range are highly responsive to PAH and HAH inducers of CYP1A1 (Stegeman *et al.*, 1981).

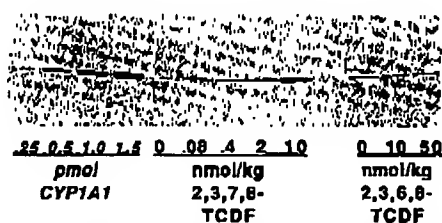


FIG. 3. Immunoblot illustrating the hepatic content of CYP1A1 protein in scup treated with various doses 2,3,7,8-TCDF or 2,3,6,8-TCDF. Scup were injected with corn oil, 2,3,7,8-TCDF, or 2,3,6,8-TCDF (doses indicated in the figure) and killed after 4 days. Hepatic microsomes were prepared from individual fish and analyzed by immunoblotting, the results of which are shown in Tables 2 and 3. Aliquots of the microsomal samples were then pooled within each group and analyzed by immunoblotting to obtain the blot presented here. Each sample lane represents 50 µg of microsomal protein. Left lanes contained the indicated amounts of purified scup CYP1A1 protein.

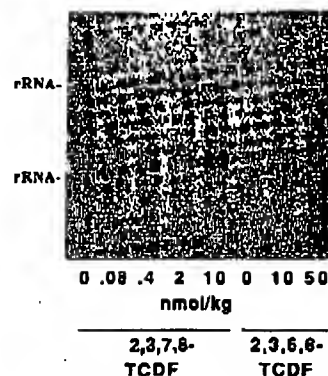


FIG. 4. Northern blot of hepatic total RNA from 2,3,7,8- and 2,3,6,8-TCDF-treated scup. Scup were injected with corn oil, 2,3,7,8-TCDF, or 2,3,6,8-TCDF and killed after 4 days. Total hepatic RNA (15 µg per lane) from one fish per treatment group was used for Northern blots with hybridization to the trout CYP1A1 cDNA probe as described under Materials and Methods. Migration of the ribosomal RNA bands is indicated on the left side of the figure. Migration was from top to bottom. Lane 1: corn oil; lane 2: 2,3,7,8-TCDF (0.08 nmol/kg); lane 3: 2,3,7,8-TCDF (0.4 nmol/kg); lane 4: 2,3,7,8-TCDF (2 nmol/kg); lane 5: 2,3,7,8-TCDF (10 nmol/kg); lane 6: corn oil; lane 7: 2,3,6,8-TCDF (10 nmol/kg); lane 8: 2,3,6,8-TCDF (50 nmol/kg). For comparison, hepatic EROD activities of the fish used for this blot were: 0.166, 0.219, 0.351, 1.149, 2.685, 0.173, 0.147, and 0.193 nmol·min⁻¹·mg⁻¹ for lanes 1 through 8, respectively.

SUSTAINED INDUCTION OF CYP1A1 BY TCDF IN FISH

193

TABLE 3
CYP1A1 Expression in Livers of Scup Treated with Two Doses of 2,3,6,8-TCDF

Dose (nmol/kg)	(n)	Body weight (g)	Relative liver weight (% BW)	Microsomal yield (mg protein/ g liver)	Total P450 (pmol/mg)	CYP1A1 protein (pmol/mg)	EROD activity (nmol · min ⁻¹ · mg ⁻¹)
0	(4)	138 ± 19	1.02 ± 0.14	14.6 ± 1.9	188 ± 50	3.9 ± 3.5	0.324 ± 0.284
10	(4)	149 ± 19	0.95 ± 0.11	13.9 ± 1.8	167 ± 43	2.1 ± 1.0	0.216 ± 0.082
50	(4)	146 ± 26	0.98 ± 0.15	15.0 ± 2.5	219 ± 58	2.6 ± 0.9	0.270 ± 0.112

Note. Scup were treated ip with the indicated doses of 2,3,6,8-TCDF, killed 4 days later, and analyzed as described under Materials and Methods. Data are reported as means ± SD. Statistical analyses were by nonparametric (CYP1A1 protein) or parametric (all others) methods as described in the text. No significant differences were present.

Relative liver weights and microsomal yield were similar to those found in the time course and 2,3,7,8-TCDF dose-response experiments and did not differ between groups treated with 0, 10, or 50 nmol 2,3,6,8-TCDF/kg (Table 3). Total P450, CYP1A1 protein, and EROD activity also did not differ among the treatment groups (Table 3), nor was there evidence of CYP1A1 induction (protein or activity) in any individual animal. Hepatic total RNA from one animal from each group was analyzed on a Northern blot hybridized to pF-P₄₅₀-3'. The intensity of bands hybridizing to the CYP1A1 probe was somewhat greater in the two 2,3,6,8-TCDF-treated fish than in the corn oil-treated fish, but these bands were much less intense than those seen at the two highest doses of 2,3,7,8-TCDF (Fig. 4). Insufficient tissue was available for preparation and analysis of RNA from other 2,3,6,8-TCDF-treated fish.

DISCUSSION

In this study, induction of scup CYP1A1 by 2,3,7,8-TCDF was measured at the level of mRNA, protein, and catalytic activity. To our knowledge, this is the first report to examine all three of these parameters simultaneously in animals treated with a polychlorinated dibenzofuran, and the first comparison of dose-response and temporal aspects of induction at these three levels, for any halogenated inducer. As discussed below, there are important differences, as well as similarities, between our findings and those of earlier studies examining CYP1A1 induction in fish and mammals.

Temporal Aspects

A single dose of 2,3,7,8-TCDF produced a sustained elevation of CYP1A1 mRNA through 14 days in the present study (Fig. 1D). In previous studies examining the time course of CYP1A1 induction in killifish (*F. heteroclitus*) and rainbow trout (*O. mykiss*) treated with the nonhalogenated inducer BNF, induced CYP1A mRNA peaked at 18–

40 hr and returned to control levels by 2–6 days after treatment (Haasch *et al.*, 1988; Kloepper-Sams and Stegeman, 1989). A similar temporal pattern is seen in BNF-treated scup (Kloepper-Sams and Stegeman, unpublished results; Gooch *et al.*, 1989).

A distinction between halogenated and nonhalogenated inducers in the duration of CYP1A1 mRNA induction has also been reported for *in vitro* systems examined over shorter time intervals (1–4 days). For example, CYP1A1 mRNA levels were elevated for 96 hr in rainbow trout hepatocytes treated with 2,3,7,8-TCDD, whereas induction following BNF was not maintained (Pesonen *et al.*, 1992). Studies in human keratinocytes (Berghard *et al.*, 1992) and rat hepatoma cells (Xu and Bresnick, 1990) treated with 2,3,7,8-TCDF versus BNF or benzo[a]pyrene, respectively, also showed a similar distinction. All of these findings most likely reflect differences in the persistence of inducer. In fish, BNF is known to be rapidly metabolized by hepatic microsomes (Stegeman *et al.*, 1984). Although similar *in vitro* metabolism experiments have not been done with 2,3,7,8-TCDF, whole-body half-lives for this compound in some fish are relatively long (e.g., 14 days (Maslanka *et al.*, 1992) and 40–77 days (Muir *et al.*, 1992)). Consistent with the hypothesis that persistence of inducer is an important factor influencing the time course of induction, Haasch *et al.* (1993b) have shown that continuous exposure to BNF, unlike a single exposure, produces sustained induction of CYP1A1 mRNA like that seen here for 2,3,7,8-TCDF.

Understanding the temporal aspects of induction and their inducer dependence is important for interpreting studies of CYP1A1 induction in fish sampled from contaminated environments (Kreamer *et al.*, 1991; Wirgin *et al.*, 1991, 1992; Haasch *et al.*, 1993a; Courtenay *et al.*, 1993). Our results and the others cited above suggest that fish inhabiting environments where PAH contaminants predominate would require constant exposure to maintain elevated CYP1A1, measured as mRNA. Where planar, halogenated compounds are prevalent, CYP1A1 levels would be expected to remain elevated for some time after removal from

the contaminated site (e.g., by migration or capture). Thus, rates of decline in CYP1A1 mRNA levels in fish removed from such environments could provide clues to the identity of inducers acting in those fish.

Most of the studies investigating the regulation of CYP1A1 expression in fish have focused on liver. However, this enzyme is also induced in extrahepatic tissues of fish (Payne *et al.*, 1984; Van Veld *et al.*, 1988; Miller *et al.*, 1989; Stegeman *et al.*, 1989) as well as mammals (Goldstein and Linko, 1984). In an earlier report (Smolowitz *et al.*, 1991), we described the immunohistochemical localization of induced CYP1A1 protein in extrahepatic tissues of scup sampled 4 or 8 days following TCDF treatment. Induction occurred in epithelial cells of kidney, gill, gut, spleen, testis, and ovary and in endothelial cells of those organs and heart, brain, and red muscle. Here we report the time course of that induction for two extrahepatic organs, gill and heart, as determined by immunoblotting. The temporal patterns of induced CYP1A1 protein levels in gill and heart of these fish were similar to the pattern of expression seen in liver, with the extent of induction increasing throughout the 14-day period (compare Figs. 1 and 2). A possible difference was the apparent delay in induction seen in the extrahepatic tissues: while elevated levels of hepatic CYP1A1 protein were clearly evident on the first day of sampling, CYP1A1 levels in gill and heart were not increased until Day 2. We have no data on the tissue distribution or kinetics of the inducer (TCDF) in these fish, but given the route of exposure used (ip), we might expect liver to be an initial site of accumulation, followed by redistribution to other organs. This would be consistent with the patterns of induction seen here. Studies comparing the temporal patterns of induction in different tissues to the pattern and time course of TCDF tissue distribution are needed to properly address this question. Nevertheless, these results show that generally similar temporal patterns of CYP1A1 induction are seen in organs in which the response occurs in multiple cell types (liver, gill) compared to an organ with only a single induced cell type (endothelium of heart) (Smolowitz *et al.*, 1991).

Sensitivity of Fish to CYP1A1 Induction

The lowest dose producing CYP1A1 induction in this study was 0.4 nmol 2,3,7,8-TCDF/kg (120 ng/kg); heterogeneity in the response of fish to TCDF was especially evident at this dose. Kreamer *et al.* (1991) have also reported heterogeneity in the CYP1A induction response, in tomcod exposed to Hudson River sediment. A range of induction sensitivities is to be expected in highly outbred populations such as fish obtained from the wild. Interestingly, we have observed differences between individual scup in the amount of Ah receptor detected by photoaffinity labeling

(Hahn *et al.*, 1994), but whether such apparent differences in Ah receptor expression underlie the heterogeneity in response to TCDF reported here is not known. In any case, our results indicate that some fish are capable of responding to doses of 2,3,7,8-TCDF as low as 120 ng/kg. Muir *et al.* (1992) recently examined induction of EROD activity following prolonged exposure to dietary TCDF; they obtained a threshold for induction, expressed as the whole-body concentration of accumulated inducer, of 1 $\mu\text{g/kg}$. That some of the fish in our study appeared to be two- to eight-fold more sensitive may reflect actual species differences in sensitivity or differences in the route of exposure and dose rate used in each study.

It is interesting to compare the CYP1A1 induction sensitivity of fish to that of mammals. Bandiera *et al.* (1984) reported an ED₅₀ value for AHH induction by 2,3,7,8-TCDF in the rat of 650 nmol/kg, measured 14 days after treatment. Since the time course of induction has not been evaluated in rats and TCDF is cleared relatively rapidly in this species (Birnbaum *et al.*, 1980), this could represent an overestimate of the true ED₅₀. Estimated ED₅₀ values from other reports include 32 nmol/kg (Yoshihara *et al.*, 1981) and 3×1.6 nmol/kg (Goldstein *et al.*, 1978). The estimated ED₅₀ for induction of scup CYP1A1 by 2,3,7,8-TCDF (2–10 nmol/kg; see Results) suggests that the sensitivity of scup may be as great as or greater than that of rats.

Determining the sensitivity of fish to different inducing compounds is important with respect to the use of CYP1A1 induction in environmental monitoring. 2,3,7,8-TCDF and other polychlorinated dibenzofurans, derived from a number of sources, are present at several coastal sites (e.g., Pruell *et al.*, 1990), and 2,3,7,8-TCDF is the most prominent polychlorinated dibenzofuran found in fish (DeVault *et al.*, 1989; Rappé *et al.*, 1991). The lowest dose producing induction in our study (120 ng/kg) is within the range of whole-body contents of 2,3,7,8-TCDF that have been measured in fish (42–1185 ng/kg (DeVault *et al.*, 1989; Mah *et al.*, 1989; Rogers *et al.*, 1989; EPA, 1992; Hodson *et al.*, 1992)). These data suggest that 2,3,7,8-TCDF could be an important contributor to the CYP1A1 induction seen in fish from sites contaminated by chlorinated dibenzofurans (Stegeman *et al.*, 1991; Hodson *et al.*, 1992; Haasch *et al.*, 1993a).

Relationship among Changes in CYP1A1 mRNA, Protein, and Catalytic Activity

Increases in CYP1A1 mRNA and protein observed previously in fish treated with PAH and HAH are consistent with a mechanism of induction involving transcriptional enhancement leading to new synthesis of these CYP1A1 gene products (Haasch *et al.*, 1988; Kloepper-Sams and Stegeman, 1989). However, several recent studies have found a lack of concordance between patterns of induced

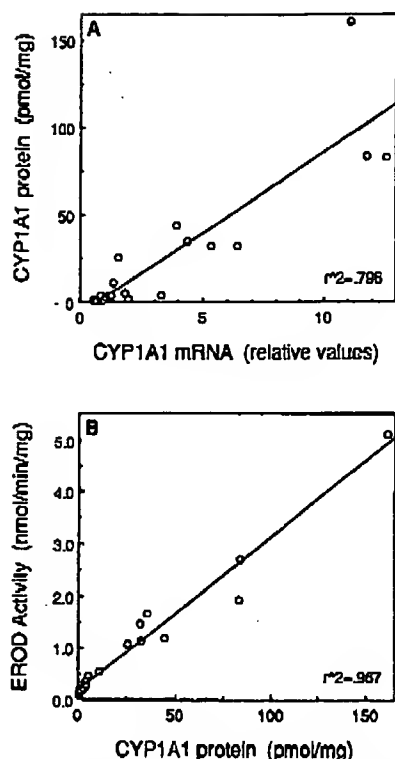


FIG. 5. Relationship between CYP1A1 mRNA and protein (A) and CYP1A1 protein and EROD activity (B) in individual scup treated with various doses of 2,3,7,8-TCDF. See text for details.

CYP1A1 mRNA, protein, and catalytic activity following treatment of fish with some inducers, suggesting that post-transcriptional events may affect the manifestation of the induction response. In the studies of Gooch *et al.* (1989), CYP1A1 activity and protein were not highly correlated in scup given various doses of 3,3',4,4'-TCB; moreover, reduced amounts of both CYP1A1 protein and activity were observed at high doses relative to lower doses, despite strongly elevated levels of CYP1A1 mRNA in all cases. Haasch *et al.* (1993b) reported similar discrepancies in rainbow trout exposed continuously to high concentrations of BNF.

Such discrepancies between CYP1A1 mRNA, protein, and catalytic activity were not seen in this study. In the 2,3,7,8-TCDF dose-response experiment, there were statistically significant, linear relationships between CYP1A1 mRNA and protein ($r^2 = 0.796$) and CYP1A1 protein and catalytic activity ($r^2 = 0.967$) in paired comparisons of individual fish (Fig. 5). In contrast, such high correlations were not observed when 3,3',4,4'-TCB was the inducer ($r^2 = 0.299$ for CYP1A1 protein versus EROD activity, calculated from the data of Gooch *et al.* (1989)). We note that although the experimental protocols used in the two studies were almost identical, the doses of inducer were quite different: 0.08–10 nmol/kg for TCDF versus 345–34,500

nmol/kg for 3,3',4,4'-TCB. 2,3,7,8-TCDF is much more potent than 3,3',4,4'-TCB as an inducer of CYP1A1 in fish (this study; Gooch *et al.*, 1989) as well as in fish hepatoma cells (M. Hahn, unpublished studies). However, *in vitro* experiments indicate that the EROD-inhibitory potencies of these two compounds are similar ($K_i = 22$ and 41 nM for 3,3',4,4'-TCB and 2,3,7,8-TCDF, respectively, using scup hepatic microsomes) (M. Hahn, unpublished data). Thus, the different results of our study compared to those of Gooch *et al.* (1989) may reflect the different inducing potencies of TCDF and TCB, relative to their similar potencies as inhibitors of CYP1A1 catalytic function.

Mechanism of CYP1A1 Induction in Fish

The data presented here, together with results of previous work, allow generalizations concerning the regulation of CYP1A1 gene expression in fish. A major conclusion is that the fundamental features of the CYP1A1 induction mechanism appear to be conserved in fish and mammals, two widely divergent groups of vertebrates. Several lines of evidence support this conclusion: (1) The structure-activity relationships for CYP1A induction in fish—to the extent they are known—are similar to those found in mammals, as illustrated by the lack of response to 2,3,6,8-TCDF in this study and by the inability or reduced ability of high doses of nonplanar PCB congeners to induce CYP1A in other studies (Gooch *et al.*, 1989; Skaare *et al.*, 1991). (2) The sensitivity of fish to CYP1A induction by PAH and planar HAH is at least equal to that of other vertebrates (discussed above; see also James and Bend, 1980; Hahn *et al.*, 1989). (3) Induced levels of CYP1A1 mRNA that precede increases in protein and catalytic activity in fish (Haasch *et al.*, 1988; Kloepper-Sams and Stegeman, 1989) are consistent with transcriptional activation like that seen in rats and mice, although such a mechanism has not yet been formally demonstrated in fish. (4) The evidence cited in 1 through 3 above suggests that induction is controlled by a specific and sensitive recognition mechanism, such as a ligand-receptor interaction. The presence of a protein with properties of the Ah receptor has now been demonstrated in several species of fish, including scup (Hahn *et al.*, 1992, 1994); future studies will be aimed at characterizing that protein and its role in the induction process in fish. However, despite the fundamental similarities in CYP1A1 induction mechanisms in mammals and fish, there may be important differences as well (e.g., Kloepper-Sams and Stegeman, 1992). Further examination of the expression of CYP1A1 and other P450 genes from a comparative perspective may provide fundamental insights into the mechanisms of gene regulation and the evolution of gene regulatory systems.

ACKNOWLEDGMENTS

This work was supported in part by a Surdna Foundation Postdoctoral Fellowship and National Research Service Award ES05479 to M.E.H. and

by US PHS Grant ES04220 (J.J.S.) and EPA Grant R817988. The authors thank Bruce R. Woodin for expert technical assistance and Drs. Pamela J. Kloepper-Sams and Roxanna M. Smolowitz for advice. This paper is dedicated to Edward J. and Rosemary L. Hahn on the occasion of their 41st wedding anniversary. Contribution No. 8569 from the Woods Hole Oceanographic Institution.

REFERENCES

- Andersson, T., and Forlin, L. (1992). Regulation of the cytochrome P-450 enzyme system in fish. *Aquat. Toxicol.* 24, 1-20.
- Bandiera, S., Sawyer, T., Ronkes, M., Zmudzka, B., Safe, L., Mason, G., Keys, B., and Safe, S. (1984). Polychlorinated dibenzofurans (PCDFs): Effects of structure on binding to the 2,3,7,8-TCDD cytosolic receptor protein, AHH induction and toxicity. *Toxicology* 32, 131-144.
- Berghard, A., Gradin, K., and Toftgård, R. (1992). The stability of dioxin-receptor ligands influences cytochrome P4501A1 expression in human keratinocytes. *Carcinogenesis* 13, 651-655.
- Birnbaum, L. S., Decad, G. M., and Matthews, H. B. (1980). Disposition and excretion of 2,3,7,8-tetrachlorodibenzofuran in the rat. *Toxicol. Appl. Pharmacol.* 55, 342-352.
- Celander, M., Leaver, M. J., George, S. G., and Forlin, L. (1993). Induction of cytochrome P4501A1 and conjugating enzymes in rainbow trout (*Oncorhynchus mykiss*) liver: A time course study. *Comp. Biochem. Physiol.* 106C, 343-349.
- Chirgwin, J. M., Przybyla, A. E., MacDonald, R. J., and Rutter, W. J. (1979). Isolation of biologically active ribonucleic acid from sources enriched in ribonuclease. *Biochemistry* 18, 5294-5299.
- Courtenay, S., Grunwald, C., Kremer, G.-L., Alexander, R., and Wirgin, I. (1993). Induction and clearance of cytochrome P4501A mRNA in Atlantic tomcod caged in bleached kraft mill effluent in the Miramichi River. *Aquat. Toxicol.* 27, 225-244.
- DeVault, D., Dunn, W., Bergqvist, P.-A., Wiberg, K., and Rappe, C. (1989). Polychlorinated dibenzofurans and polychlorinated dibenzodioxins in Great Lakes fish: A baseline and interlake comparison. *Environ. Toxicol. Chem.* 8, 1013-1022.
- Doyle, E. A., and Fries, G. F. (1986). Induction of aryl hydrocarbon hydroxylase by chlorinated dibenzofurans in rats. *Chemosphere* 15, 1745-1748.
- EPA (1992). National Study of Chemical Residues in Fish. U.S. Environmental Protection Agency, September, 1992, EPA 823-R-92-008a.
- Gad, S. C., and Weil, C. S. (1982). Statistics for toxicologists. In *Principles and Methods of Toxicology* (A. W. Hayes, Ed.), pp. 273-320. Raven Press, New York.
- Goldstein, J. A., Hass, J. R., Linko, P., and Harvan, D. J. (1978). 2,3,7,8-Tetrachlorodibenzofuran in a commercially available 99% pure polychlorinated biphenyl isomer identified as the inducer of hepatic cytochrome P448 and aryl hydrocarbon hydroxylase in the rat. *Drug Metab. Dispos.* 6, 258-264.
- Goldstein, J. A., and Linko, P. (1984). Differential induction of two 2,3,7,8-tetrachlorodibenzo-p-dioxin-inducible forms of cytochrome P-450 in extrahepatic versus hepatic tissues. *Mol. Pharmacol.* 25, 185-191.
- Goldstein, J. A., and Safe, S. (1989). Mechanism of action and structure-activity relationships for the chlorinated dibenzo-p-dioxins and related compounds. In *Halogenated Biphenyls, Terphenyls, Naphthalenes, Dibenzodioxins and Related Products* (R. D. Kimbrough and A. A. Jensen, Eds.), pp. 239-293. Elsevier Science, Amsterdam.
- Gonzalez, F. J. (1989). The molecular biology of cytochrome P-450s. *Pharmacol. Rev.* 40, 243-287.
- Gooch, J. W., Elskus, A. A., Kloepper-Sams, P. J., Hahn, M. E., and Stegeman, J. J. (1989). Effects of ortho and non-ortho substituted polychlorinated biphenyl congeners on the hepatic monooxygenase system in scup (*Stenotomus chrysops*). *Toxicol. Appl. Pharmacol.* 98, 422-433.
- Gray, E. S., Woodin, B. R., and Stegeman, J. J. (1991). Sex differences in hepatic monooxygenases in winter flounder (*Pseudopleuronectes americanus*) and scup (*Stenotomus chrysops*) and regulation of P450 forms by estradiol. *J. Exper. Zool.* 259, 330-342.
- Haasch, M. L., Kleinow, K. M., and Lech, J. J. (1988). Induction of cytochrome P-450 mRNA in rainbow trout: *In vitro* translation and immunoprecipitation. *Toxicol. Appl. Pharmacol.* 94, 246-253.
- Haasch, M. L., Prince, R., Wejksnora, P. J., Cooper, K. R., and Lech, J. J. (1993a). Caged and wild fish: Induction of hepatic cytochrome P-450 (CYP1A1) as an environmental monitor. *Environ. Toxicol. Chem.* 12, 885-895.
- Haasch, M. L., Quardokus, E. M., Sutherland, L. A., Goodrich, M. S., and Lech, J. J. (1993b). Hepatic CYP1A1 induction in rainbow trout by continuous flowthrough exposure to β -naphthoflavone. *Fundam. Appl. Toxicol.* 20, 72-82.
- Hahn, M. E., Lamb, T. M., Schultz, M. E., Smolowitz, R. M., and Stegeman, J. J. (1993). Cytochrome P4501A induction and inhibition by 3,3',4,4'-tetrachlorobiphenyl in an Ah receptor-containing fish hepatoma cell line (PLHC-1). *Aquat. Toxicol.* 26, 185-208.
- Hahn, M. E., Poland, A., Glover, E., and Stegeman, J. J. (1992). The Ah receptor in marine animals: Phylogenetic distribution and relationship to P4501A inducibility. *Mar. Environ. Res.* 34, 87-92.
- Hahn, M. E., Poland, A., Glover, E., and Stegeman, J. J. (1994). Photoaffinity labeling of the Ah receptor: Phylogenetic survey of diverse vertebrate and invertebrate species. *Arch. Biochem. Biophys.* 310, 218-228.
- Hahn, M. E., Woodin, B. R., and Stegeman, J. J. (1989). Induction of cytochrome P450E (P4501A1) by 2,3,7,8-tetrachlorodibenzofuran (2,3,7,8-TCDF) in the marine fish scup (*Stenotomus chrysops*). *Mar. Environ. Res.* 28, 61-65.
- Heilmann, L. J., Sheen, Y. Y., Bigelow, S. W., and Nebert, D. W. (1988). The trout P4501A1: cDNA and deduced protein sequence, expression in liver, and evolutionary significance. *DNA* 7, 379-387.
- Hodson, P. V., McWhirter, M., Ralph, K., Gray, B., Thivierge, D., Carey, J. H., van der Kraak, G., Whittle, D. M., and Levcsque, M.-C. (1992). Effects of bleached Kraft mill effluent on fish in the St. Maurice River, Quebec. *Environ. Toxicol. Chem.* 11, 1635-1651.
- Hollander, M., and Wolfe, D. A. (1973). *Nonparametric Statistical Methods*. 1973. Wiley, New York.
- James, M. O., and Bend, J. R. (1980). Polycyclic aromatic hydrocarbon induction of cytochrome P-450-dependent mixed-function oxidases in marine fish. *Toxicol. Appl. Pharmacol.* 54, 117-133.
- Janz, D. M., and Metcalfe, C. D. (1991). Relative induction of aryl hydrocarbon hydroxylase by 2,3,7,8-TCDD and two coplanar PCBs in rainbow trout (*Oncorhynchus mykiss*). *Environ. Toxicol. Chem.* 10, 917-923.
- Kloepper-Sams, P. J., Park, S. S., Gelboin, H. V., and Stegeman, J. J. (1987). Specificity and cross-reactivity of monoclonal and polyclonal antibodies against cytochrome P450E of the marine fish scup. *Arch. Biochem. Biophys.* 253, 268-278.
- Kloepper-Sams, P. J., and Stegeman, J. J. (1989). The temporal relationships between cytochrome P-450E protein content, catalytic activity and mRNA levels in the teleost *Fundulus heteroclitus* following treatment with β -naphthoflavone. *Arch. Biochem. Biophys.* 268, 525-535.
- Kloepper-Sams, P. J., and Stegeman, J. J. (1992). Effects of temperature acclimation on the expression of hepatic cytochrome P4501A mRNA and protein in the fish *Fundulus heteroclitus*. *Arch. Biochem. Biophys.* 299, 38-46.
- Klotz, A. V., Stegeman, J. J., and Walsh, C. (1984). An alternative 7-eth-

SUSTAINED INDUCTION OF CYP1A1 BY TCDF IN FISH

197

- oxyresorufin O-deethylase activity assay: A continuous visible spectrophotometric method for measurement of cytochrome P-450 monooxygenase activity. *Anal. Biochem.* 140, 138-145.
- Kreamer, G. L., Squibb, K., Gioeli, D., Garte, S. J., and Wirgin, I. (1991). Cytochrome P450IA mRNA expression in feral Hudson River tomcod. *Environ. Res.* 55, 64-78.
- Lorenzen, A., and Okey, A. B. (1990). Detection and characterization of [³H]2,3,7,8-tetrachlorodibenzo-p-dioxin binding to Ah receptor in a rainbow trout hepatoma cell line. *Toxicol. Appl. Pharmacol.* 106, 53-62.
- Mah, F. T. S., MacDonald, D. D., Sheehan, S. W., Tuominen, T. M., and Valiela, D. (1989). Dioxins and furans in sediment and fish from the vicinity of ten inland pulp mills in British Columbia. *Environ. Can. Inland Waters, Pacific Yukon Reg. May*, 1989.
- Maslanka, R., Steward, A. R., Pangrekar, J., Kumar, S., and Sikka, H. C. (1992). Disposition and metabolism of 2,3,7,8-tetrachlorodibenzofuran (TCDF) in rainbow trout. *Mar. Environ. Res.* 34, 255-259.
- Melancon, M. J., and Lech, J. J. (1983). Dose-effect relationship for induction of hepatic monooxygenase activity in rainbow trout and carp by Aroclor 1254. *Aquat. Toxicol.* 4, 51-61.
- Miller, M. R., Hinton, D. E., and Stegeman, J. J. (1989). Cytochrome P-450E induction and localization in gill pillar (endothelial) cells of scup and rainbow trout. *Aquat. Toxicol.* 14, 307-322.
- Monosson, E., and Stegeman, J. J. (1991). Cytochrome P450E (P450IA) induction and inhibition in winter flounder by 3,3',4,4'-tetrachlorobiphenyl: Comparison of response in fish from Georges Bank and Narragansett Bay. *Environ. Toxicol. Chem.* 10, 765-774.
- Muir, D. C. G., Yarechewski, A. L., Metner, D. A., and Lockhart, W. L. (1992). Dietary 2,3,7,8-tetrachlorodibenzofuran in rainbow trout: Accumulation, disposition, and hepatic mixed-function oxidase enzyme induction. *Toxicol. Appl. Pharmacol.* 117, 65-74.
- Muir, D. C. G., Yarechewski, A. L., Metner, D. A., Lockhart, W. L., Webster, G. R. B., and Friesen, K. J. (1990). Dietary accumulation and sustained hepatic mixed function oxidase induction by 2,3,4,7,8-pentachlorodibenzofuran in rainbow trout. *Environ. Toxicol. Chem.* 9, 1463-1472.
- Nebert, D. W. (1989). The Ah locus: Genetic differences in toxicity, cancer, mutation, and birth defects. *CRC Crit. Rev. Toxicol.* 20, 137-152.
- Nelson, D. R., Kamataki, T., Waxman, D. J., Guengerich, F. P., Estabrook, R. W., Feyereisen, R., Gonzalez, F. J., Coon, M. J., Gunsalus, I. C., Gotoh, O., Okuda, K., and Nebert, D. W. (1993). The P450 superfamily—Update on new sequences, gene mapping, Accession Numbers, early trivial names of enzymes, and nomenclature. *DNA Cell Biol.* 12, 1-51.
- Okino, S. T., Pendurthi, U. R., and Tukey, R. H. (1992). Phorbol esters inhibit the dioxin receptor-mediated transcriptional activation of the mouse cyp1a-1 and cyp1a-2 genes by 2,3,7,8-tetrachlorodibenzo-p-dioxin. *J. Biol. Chem.* 267, 6991-6998.
- Park, S. S., Miller, H., Klotz, A. V., Kloepper-Sams, P. J., Stegeman, J. J., and Gelboin, H. V. (1986). Monoclonal antibodies to liver microsomal cytochrome P-450E of the marine fish *Stenotomus chrysops* (scup): Cross-reactivity with 3-methylcholanthrene induced rat cytochrome P-450. *Arch. Biochem. Biophys.* 249, 339-350.
- Pasco, D. S., Boyum, K. W., Elbi, C., Siu, C. S., and Fagan, J. B. (1993). Inducer-dependent transcriptional activation of the P450IA2 gene in vivo and in isolated hepatocytes. *J. Biol. Chem.* 268, 1053-1057.
- Payne, J. F., Bauld, C., Dey, A. C., Kiceniuk, J. W., and Williams, U. (1984). Selectivity of mixed-function oxygenase enzyme induction in flounder (*Pseudopleuronectes americanus*) collected at the site of the Baie Verte, Newfoundland oil spill. *Comp. Biochem. Physiol.* 79C, 15-19.
- Pesonen, M., Goksøyr, A., and Andersson, T. (1992). Expression of P450IA1 in a primary culture of rainbow trout hepatocytes exposed to β -naphthoflavone or 2,3,7,8-tetrachlorodibenzo-p-dioxin. *Arch. Biochem. Biophys.* 292, 228-233.
- Poland, A., and Knutson, J. C. (1982). 2,3,7,8-Tetrachlorodibenzo-p-dioxin and related halogenated aromatic hydrocarbons: examination of the mechanism of toxicity. *Annu. Rev. Pharmacol. Toxicol.* 22, 517-554.
- Pruell, R. J., Norwood, C. B., Bowen, R. D., Boothman, W. S., Rogerson, P. F., Hackert, M., and Butterworth, B. C. (1990). Geochemical study of sediment contamination in New Bedford Harbor, Massachusetts. *Mar. Environ. Res.* 29, 77-102.
- Rapp, C., Bergqvist, P.-A., Kjeller, L.-O., Swanson, S., Belton, T., Ruppel, B., Lockwood, K., and Kahn, P. C. (1991). Levels and patterns of PCDD and PCDF contamination in fish, crabs, and lobsters from Newark bay and the New York Bight. *Chemosphere* 22, 239-266.
- Rifkind, A. B., Gannon, M., and Gross, S. S. (1990). Arachidonic acid metabolism by dioxin-induced cytochrome P-450: A new hypothesis on the role of P-450 in dioxin toxicity. *Biochem. Biophys. Res. Commun.* 172, 1180-1188.
- Rogers, I. H., Levings, C. D., Lockhart, W. L., and Norstrom, R. J. (1989). Observations on overwintering juvenile chinook salmon (*Oncorhynchus tshawytscha*) exposed to bleached kraft mill effluent in the upper Fraser River, British Columbia. *Chemosphere* 19, 1853-1868.
- Skaare, J. U., Jensen, E. G., Goksøyr, A., and Egeas, E. (1991). Response of xenobiotic metabolizing enzymes of rainbow trout (*Oncorhynchus mykiss*) to the mono-ortho substituted polychlorinated PCB congener 2,3',4,4',5-pentachlorobiphenyl, PCB-118, detected by enzyme activities and immunochemical methods. *Arch. Environ. Contam. Toxicol.* 20, 349-352.
- Smolowitz, R. M., Hahn, M. E., and Stegeman, J. J. (1991). Immunohistochemical localization of cytochrome P450IA1 induced by 3,3',4,4'-tetrachlorobiphenyl and by 2,3,7,8-tetrachlorodibenzofuran in liver and extrahepatic tissues of the teleost *Stenotomus chrysops* (scup). *Drug Metab. Dispos.* 19, 113-123.
- Spink, D. C., Lincoln, D. W., Dickerman, H. W., and Gierthy, J. F. (1990). 2,3,7,8-tetrachlorodibenzo-p-dioxin causes an extensive alteration of 17 β -estradiol metabolism in MCF-7 breast tumor cells. *Proc. Natl. Acad. Sci. USA* 87, 6917-6921.
- Stegeman, J. J. (1989). Cytochrome P450 forms in fish: Catalytic, immunological and sequence similarities. *Xenobiotica* 19, 1093-1110.
- Stegeman, J. J. (1992). Nomenclature for hydrocarbon inducible cytochrome P450 in fish. *Mar. Environ. Res.* 34, 133-138.
- Stegeman, J. J., Binder, R. L., and Orren, A. (1979). Hepatic and extrahepatic microsomal electron-transport components and mixed-function oxygenases in the marine fish *Stenotomus versicolor*. *Biochem. Pharmacol.* 28, 3431-3439.
- Stegeman, J. J., and Hahn, M. E. (1993). Biochemistry and molecular biology of monooxygenases: Current perspectives on forms, functions, and regulation of cytochrome P450 in aquatic species. In *Aquatic Toxicology: Molecular, Biochemical and Cellular Perspectives* (D. C. Malins and G. K. Ostrander, Eds.), pp. 87-206. CRC/Lewis, Boca Raton.
- Stegeman, J. J., Klotz, A. V., Woodin, B. R., and Pajor, A. M. (1981). Induction of hepatic cytochrome P-450 in fish and the indication of environmental induction in scup. *Aquat. Toxicol.* 1, 197-212.
- Stegeman, J. J., Melancon, M. J., and Woodin, B. R. (1984). in vitro and in vivo metabolism of α -naphthoflavone (ANF) and β -naphthoflavone (BNF) in fish. *Pharmacologist* 26, 172.
- Stegeman, J. J., Miller, M. R., and Hinton, D. E. (1989). Cytochrome P450IA1 induction and localization in endothelium of vertebrate (teleost) heart. *Mol. Pharmacol.* 36, 723-729.

- Stegeman, J. J., Renton, K. W., Woodin, B. R., Zhang, Y.-S., and Addison, R. F. (1990). Experimental and environmental induction of cytochrome P450E in fish from Bermuda waters. *J. Exp. Mar. Biol. Ecol.* 138, 49-67.
- Stegeman, J. J., Smolowitz, R. M., and Hahn, M. E. (1991). Immunohistochemical localization of environmentally induced cytochrome P450IA1 in multiple organs of the marine teleost *Stenotomus chrysops* (scup). *Toxicol. Appl. Pharmacol.* 110, 486-504.
- Stegeman, J. J., Woodin, B. R., Park, S. S., Kloepper-Sams, P. J., and Gelboin, H. V. (1985). Microsomal cytochrome P-450 function in fish evaluated with polyclonal and monoclonal antibodies to cytochrome P-450E from scup (*Stenotomus chrysops*). *Mar. Environ. Res.* 17, 83-86.
- Swanson, H. I., and Perdew, G. H. (1991). Detection of the Ah receptor in rainbow trout. Use of 2-azido-3-^[125I]jodo-7,8-dibromodibenzo-p-dioxin in cell culture. *Toxicol. Lett.* 58, 85-95.
- van der Weiden, M. E. J. (1993). Cytochrome P450 1A induction in carp as a biological indicator for the aquatic contamination of chlorinated polyaromatics. Ph.D. thesis, Research Institute of Toxicology, University of Utrecht.
- van der Weiden, M. E. J., Celander, M., Seinen, W., van den Berg, M., Goksoyr, A., and Forlin, L. (1993). Induction of cytochrome P450 1A in fish treated with 2,3,7,8-tetrachlorodibenzo-p-dioxin or chemically contaminated sediment. *Environ. Toxicol. Chem.* 12, 989-999.
- van der Weiden, M. E. J., Kolk, J. v. d., Bleumink, R., Seinen, W., and van den Berg, M. (1992). Concurrence of P450 1A1 induction and toxic effects after administration of a low dose of 2,3,7,8-tetrachlorodibenzo-p-dioxin (TCDD) in the rainbow trout (*Oncorhynchus mykiss*). *Aquat. Toxicol.* 24, 123-142.
- Van Veld, P. A., Stegeman, J. J., Woodin, B. R., Pauon, J. S., and Lee, R. F. (1988). Induction of monooxygenase activity in the intestine of spot (*Leiostomus xanthurus*), a marine teleost, by dietary polycyclic aromatic hydrocarbons. *Drug Metab. Dispos.* 16, 659-665.
- Whitlock, J. P. (1990). Genetic and molecular aspects of 2,3,7,8-tetrachlorodibenzo-p-dioxin action. *Annu. Rev. Pharmacol. Toxicol.* 30, 251-277.
- Wirgin, I., Kreamer, G.-L., and Garte, S. J. (1991). Genetic polymorphism of cytochrome P-450IA in cancer-prone Hudson River tomcod. *Aquat. Toxicol.* 19, 205-214.
- Wirgin, I., Kreamer, G. L., Grunwald, C., Squibb, K., Garte, S. J., and Courtenay, S. (1992). Effects of prior exposure history on cytochrome P450IA mRNA induction by PCB congener 77 in Atlantic tomcod. *Mar. Environ. Res.* 34, 103-108.
- Xu, L.-C., and Bresnick, E. (1990). Induction of cytochrome P450IA1 in rat hepatoma cell by polycyclic hydrocarbons and a dioxin. *Biochem. Pharmacol.* 40, 1399-1403.
- Yoshihara, S., Nagata, K., Yoshimura, H., Kuroki, H., and Masuda, Y. (1981). Inductive effect on hepatic enzymes and acute toxicity of individual polychlorinated dibenzofuran congeners in rats. *Toxicol. Appl. Pharmacol.* 59, 580-588.

Breast Cancer Research and Treatment

Marc E. Lippman, MD, editor-in-chief

UNIVERSITY OF WISCONSIN
University of Wisconsin

DEC 17 1992

1305 Linden Drive
Madison, WI 53706

Kluwer Academic Publishers

Breast Cancer Research and Treatment

Marc E. Lippman, M.D. ¹ (Editor-in-Chief), Gary C. Chamness, Ph.D. ² / Robert L. Dickson, Ph.D. ¹ (Editors),
C. Kent Osborne, M.D. ² / Gary M. Clark, Ph.D. ² (Associate Editors)

¹ Vincent T. Lombardi Cancer Research Center, Georgetown University, Washington DC, USA

² University of Texas Health Science Center at San Antonio, San Antonio, TX, USA

Editorial office address:

Karen S. Cullen, BREA Editorial Office, Kluwer Academic Publishers, 101 Philip Drive, Assinippi Park,
Norwell, MA 02061, USA; Tel: 617-871-6300; Fax: 617-871-6528; E-mail: Karen@world.std.com.

EDITORIAL ADVISORY BOARD

George Blumenschein (Arlington,
Texas)

Gianni Bonadonna (Milan, Italy)

Paul P. Carbone (Madison,
Wisconsin)

Dean P. Edwards (Denver,
Colorado)

Evert Engelsman (Amsterdam, The
Netherlands)

Bernard Fisher (Pittsburgh,
Pennsylvania)

Edwin Fisher (Pittsburgh,
Pennsylvania)

Jan-Åke Gustafsson (Stockholm,
Sweden)

Kathryn Horwitz (Denver,
Colorado)

Elwood V. Jensen (Hamburg,
Germany)

V. Craig Jordan (Madison, Wisconsin)

Roger King (London, United Kingdom)

Heinrich Maass (Hamburg, Germany)

Kenneth S. McCarty, Jr. (Durham,
North Carolina)

Daniel Medina (Houston, Texas)

Henri Rochefort (Montpellier, France)

Richard Santen (Hershey,
Pennsylvania)

Jeffrey Schlom (Bethesda, Maryland)

Haruo Sugano (Tokyo, Japan)

Jeffrey M. Trent (Tucson, Arizona)

ISSN 0167-6806

All Rights Reserved

© 1992 by Kluwer Academic Publishers

No part of the material protected by this copyright notice may be reproduced or utilised in any form or by any means, electronic or mechanical, including photocopying, recording or by any information storage and retrieval system, without written permission from the copyright owner.

Printed in The Netherlands

Brief communication

Expression of the pS2 gene in breast tissues assessed by pS2-mRNA analysis and pS2-protein radioimmunoassay

Erika Hähnel, Peter Robbins, Jennet Harvey, Gregory Sterrett and Roland Hähnel
Department of Pathology, University of Western Australia, Queen Elizabeth II Medical Centre, Nedlands, 6009, Western Australia

Key words: breast tissue, pS2-mRNA, pS2 protein, radioimmunoassay

Summary

The expression of the pS2 gene in breast tissues was assessed by measuring pS2-protein using a radioimmunoassay, and by determining pS2-mRNA using Northern blotting. There was a good correlation between the two measurements, indicating that expression of the pS2 gene in breast tissues may be assessed by either method. Since radioimmunoassay is technically easier and more efficient than Northern blotting, radioimmunoassay will be the method of choice in routine applications.

Introduction

Expression of the pS2 gene is controlled by estrogen. This was first described in the MCF-7 breast cancer cell line [1]. pS2 expression has since been reported to be useful as a prognostic indicator [2, 3], although this was not confirmed in another series [4].

pS2 expression may be assessed in tissue homogenates by analysis of pS2-mRNA [5], by radioimmunoassay of the pS2-protein [2], or by immunocytochemical detection of the pS2 protein in tissue sections [5]. It was the aim of this study to establish the correlation between pS2-mRNA and pS2-protein by radioimmunoassay in a series of tissues obtained from mastectomy specimens performed for carcinoma of the breast. Primary breast carcinoma tissue, metastatic carcinoma within axillary nodes, and macroscopically benign breast tissue were examined.

Materials and methods

Breast tissues

Tissue specimens from mastectomies performed for carcinoma of the breast were examined. 32 primary breast carcinomas, 10 axillary lymph nodes containing metastatic breast carcinoma, and 20 samples of uninvolved breast tissue were analyzed for pS2 expression.

The primary breast carcinomas were histologically classified using a conventional subclassification. The presence or absence of primary tumour was assessed. The presence of metastatic carcinoma within lymph nodes studied was verified by histological examination of the node remnant after sampling.

'Uninvolved' breast tissue was sampled from sites well removed from the primary breast tumour (usually in another quadrant of the breast), and was selected only if the tissue appeared macroscopically unremarkable. Tissue sampling occurred imme-

diately upon arrival of the mastectomy specimen in the laboratory, with minimal delays between removal and sampling.

Tissues for pS2 analysis were snap frozen in liquid nitrogen and stored at -70°C until processed.

Extraction of RNA and determination of pS2-mRNA

Details of the procedure have been described in our previous paper [6]. Briefly, the deep-frozen tissue was homogenized in a micro-dismembrator. The homogeneous powder was extracted with guanidiniumisothiocyanatephenolchloroformisoamylalcohol, and RNA was precipitated with isopropanol. The washed RNA pellet was dissolved in SDS and glyoxylated, and the RNA preparation loaded onto agarose gel. After electrophoresis the gel was capillary blotted onto Zeta-probe membranes. Membranes were hybridized overnight with cDNA probes pS2 and 36B4, which were labeled with [$\alpha^{32}\text{P}$] dCTP by nick translations. Washed membranes were exposed to Kodak X-omat AR film. Relative intensities of the mRNA bands were assessed visually as not detectable, very weak, weak, medium, strong, and very strong, taking the intensities of the ubiquitous 36B4 bands into account.

Radioimmunoassay of pS2-protein

Deep frozen specimens were pulverized with a microdismembrator. The tissue powder was suspended in 10 volumes of pH 7.5 phosphate buffer. The homogenate was centrifuged in a refrigerated centrifuge at 4°C for 60 minutes at 2600xg. The supernatant was removed with a Pasteur pipette, carefully avoiding the fat layer on the top. The protein concentration in the supernatant was estimated by use of the Coomassie dye-binding method [7]. An aliquot of the supernatant was diluted to a protein concentration between 1 and 2 mg/ml before assay of the pS2-protein. In one case the protein concentration of the supernatant was well below 1 mg/ml.

The estimation of the pS2-protein was performed using a solid phase, two-site radioimmunoassay. The kits were bought from CIS Biointernational, Gif-sur-Yvette, France (ELSA-PS2). In this method the molecules of pS2 are sandwiched between two monoclonal antibodies; the first one is coated on the ELSA solid phase, the second one is radiolabeled with 125-iodine. The radioactivity bound to the ELSA is proportional to the concentration of pS2-protein. Details of the procedure are supplied with the kit [8].

Results and discussion

32 primary breast carcinomas, metastatic breast carcinoma in 10 lymph nodes, and 20 samples of benign breast tissue from mastectomies were investigated. Two of the carcinomas were of the infiltrating lobular type, two were ductal carcinomas *in situ*, one was a multicentric invasive ductal carcinoma, all others were invasive ductal carcinomas.

Examples of pS2 Northern blots have been shown in our previous paper [6] which demonstrate that undegraded pS2-mRNA can be isolated by the method used.

The results of the pS2-protein and pS2-mRNA assays are shown on Fig. 1. There was a good correlation between the two types of results. When pS2-mRNA could not be detected by Northern blot, pS2-protein results were usually below 1 ng/mg protein (22 of 30), or between 1 and 3.7 ng/mg (6 of 30). Two were exceptions (7.7 and 14.6); one of them could have been due to the very low protein content in the cytosol which would lead to a large pS2 value and an associated error. There was no explanation for the other high result. Very weak pS2-mRNA signals on Northern blots corresponded to pS2-protein values between 1.1 and 19.2 with an average of 6.6 ng/mg protein (median 5.7). The mean and median pS2-protein concentration in the tissue with weak pS2-mRNA signals were 14.3 and 10.7 ng/mg protein, respectively. The average pS2-protein concentration increased to 32.7 (median 31.5) ng/mg protein for tissues assessed as medium pS2-mRNA intensity, and to 43.3 (median 53.8) ng/mg protein for tissues with strong or very strong

pS2-mRNA signals. These values should be used as an approximate guide only, since the number of samples in the various groups was fairly small. One-way analysis of variance confirmed that the means of the pS2-protein values in the groups made up according to their pS2-mRNA signal intensity, were significantly different ($p < 10^{-6}$).

If the pS2 gene is expressed, its expression is on average greater in breast carcinomas than in uninvolved breast tissue. If one takes pS2-protein values above 4 ng/mg protein as cut-off, the average pS2-protein in 14 breast cancers was 34.3 (median 35.2), while it was only 18.1 (median 13.8) in 12 uninvolved breast tissue samples. If the cut-off is taken at 10 ng/mg protein, average pS2-protein in breast carcinoma is also about twice the level of uninvolved tissue. There were not enough lymph node metastases which expressed the pS2 gene to allow a comparison with carcinoma or uninvolved breast tissue.

Recent preliminary results of pS2 by radioimmunoassay [9] are similar to ours for breast cancer but considerably lower than our results for normal breast tissue.

The values of the pS2-protein measured obviously depend on the protein used for calibration. We used the pS2-protein standards supplied with the CIS kit, which according to the supplier gave values from 0 to 740 ng/mg protein in a series of 205 breast cancer cytosols. Previously, a different standard had been used for presumably the same series of breast carcinomas [2], and a conversion factor to current standards is given as 2.8 [8].

It was noticed that the correlation between pS2-protein and pS2-mRNA was better in breast carcinoma specimens than in uninvolved breast tissue. This is unexplained, though it could be due to the variable content of cell or tissue types in adjoining parts of a specimen, a variation more likely to occur in our sampling of non-malignant breast tissue compared to sampling of carcinomas. A similar variability in breast carcinoma specimens will probably have a smaller influence on the pS2 results, since the malignant cells – if they do express the pS2 gene – contain more pS2-protein than normal breast.

CORRELATION OF pS2 - mRNA AND pS2 - PROTEIN

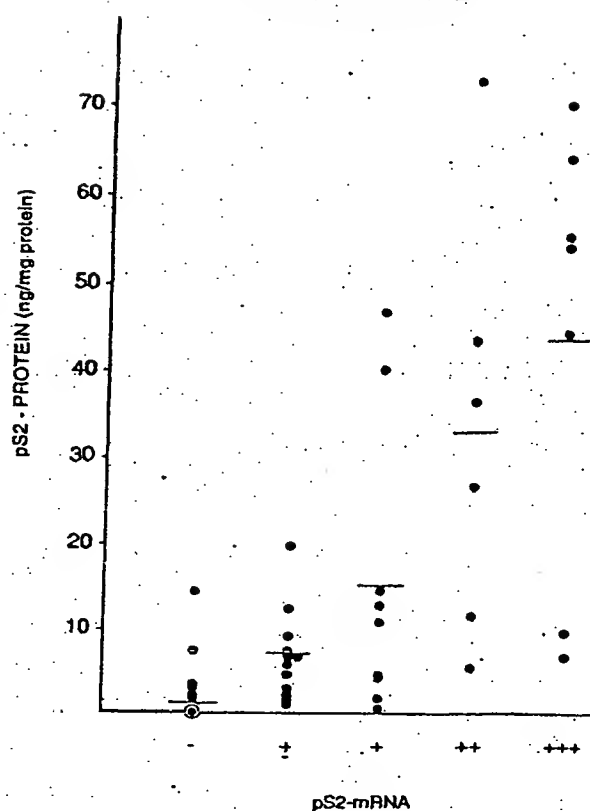


Fig. 1. Correlation between pS2-protein by radioimmunoassay and pS2-mRNA by Northern blot. ⊙ = 22 results below 1. The horizontal lines indicate the mean values.

Acknowledgements

This investigation was supported in part by a grant from the Sir Charles Gairdner Hospital Research Foundation. The authors wish to thank Professor P. Chambon, Strasbourg, France, for the gift of pS2 and 36B4 cDNAs. A preliminary account of our results was presented at the First Joint Conference of the American Association for Cancer Research and the European Association for Cancer Research, held at Santa Margherita, Italy, 6–9 November, 1991.

References

1. Masiakowski P, Breathnach R, Bloch J, Gannon F, Krust A, Cham-

- bon P: Cloning of cDNA sequences of hormone-regulated genes from the MCF-7 human breast cancer cell lines. *Nucleic Acids Res* 10: 7895-7903, 1982
2. Foekens JA, Rio MC, Seguin P, Van Putten WLJ, Fauque J, Nap M, Klijn JGM, Chambon P: Predication of relapse and survival in breast cancer patients by pS2 protein status. *Cancer Res* 50: 3832-3837, 1990
3. Foekens JA, Van Putten WLJ, Portengen H, Rodenburg CJ, Reubi JC, Berns PMJJ, Henzen-Logmans SC, Van Der Burg MEL, Alexieva-Figusch J, Klijn JGM: Prognostic value of pS2 protein and receptors for epidermal growth factor, insulin-like growth factor, and somatostatin in patients with breast and ovarian cancer. *J Steroid Biochem Molec Biol* 37: 815-821, 1990
4. Henry JA, Piggott NH, Mallick UK, Nicholson S, Farndon JR, Westley BR, May FEB: pNR-2/pS2 immunohistochemical staining in breast cancer: Correlation with prognostic factors and endocrine response. *Br J Cancer* 63: 615-622, 1991
5. Rio MC, Bellocq JP, Gairard B, Rasmussen UB, Krust A, Kochl C, Calderoli H, Schiff V, Renaud R, Chambon P: Specific expression of the pS2 gene in subclasses of breast cancer in comparison with expression of the estrogen and progesterone receptors and the oncogene ERBB2. *Proc Natl Acad Sci USA* 84: 9243-9247, 1987
6. Hähnel E, Joyce R, Sierren GF, Harvey JM, Hähnel R: Detection of estradiol-induced messenger RNA (pS2) in uninvolved breast tissue from mastectomies for breast cancer. *Breast Cancer Res Treat* 20: 167-176, 1991
7. Bradford M: A rapid and sensitive method for the quantitation of microgram quantities of protein utilizing the principle of protein-dye binding. *Anal Biochem* 72: 248-254, 1976
8. CIS ELSA-pS2: Immunoradiometric assay of pS2 protein. Package insert, December, 1990
9. Kouyoumdjian JC, Boissier B, Rymer JC, Bagnard G, Rotten D, Levailani JP, Constancis B, Philippon C, Floury C, Thirion B: Determination of several prognostic parameters in human normal breast, benign mastopathies, and adenocarcinomas. *J Tumour Marker Oncol* 6: 111, 1991

The role of the epidermal growth factor receptor in sustaining neutrophil inflammation in severe asthma

L. M. Hamilton^{*1}, C. Torres-Lozano^{†1}, S. M. Puddicombe^{*}, A. Richter^{*}, I. Kimber[‡], R. J. Dearman[‡], B. Vrugt[§], R. Aalbers[§], S. T. Holgate^{*}, R. Djukanović^{*}, S. J. Wilson^{*} and D. E. Davies^{*}

^{*}Division of Infection, Inflammation & Repair, School of Medicine, University of Southampton, UK, [†]CMNO-IMSS, CUCS-UdeG, Mexico, [‡]Syngenta, Central Toxicology Laboratory, Macclesfield, UK and [§]Pathology Department, Martini Hospital, Groningen, The Netherlands

Summary

Background The extent of epithelial injury in asthma is reflected by expression of the epidermal growth factor receptor (EGFR), which is increased in proportion to disease severity and is corticosteroid refractory. Although the EGFR is involved in epithelial growth and differentiation, it is unknown whether it also contributes to the inflammatory response in asthma.

Objectives Because severe asthma is characterized by neutrophilic inflammation, we investigated the relationship between EGFR activation and production of IL-8 and macrophage inhibitory protein-1 alpha (MIP-1α) using *in vitro* culture models and examined the association between epithelial expression of IL-8 and EGFR in bronchial biopsies from asthmatic subjects.

Methods H292 or primary bronchial epithelial cells were exposed to EGF or H₂O₂ to achieve ligand-dependent and ligand-independent EGFR activation; IL-8 mRNA was measured by real-time PCR and IL-8 and MIP-1α protein measured by enzyme-linked immunosorbent assay (ELISA). Epithelial IL-8 and EGFR expression in bronchial biopsies from asthmatic subjects was examined by immunohistochemistry and quantified by image analysis.

Results Using H292 cells, EGF and H₂O₂ increased IL-8 gene expression and release and this was completely suppressed by the EGFR-selective tyrosine kinase inhibitor, AG1478, but only partially by dexamethasone. MIP-1α release was not stimulated by EGF, whereas H₂O₂ caused a 1.8-fold increase and this was insensitive to AG1478. EGF also significantly stimulated IL-8 release from asthmatic or normal primary epithelial cell cultures established from bronchial brushings. In bronchial biopsies, epithelial IL-8, MIP-1α, EGFR and submucosal neutrophils were all significantly increased in severe compared to mild disease and there was a strong correlation between EGFR and IL-8 expression ($r = 0.70$, $P < 0.001$).

Conclusions These results suggest that in severe asthma, epithelial damage has the potential to contribute to neutrophilic inflammation through enhanced production of IL-8 via EGFR-dependent mechanisms.

Keywords asthma, chemokine, epidermal growth factor, inflammation, neutrophils, tyrosine kinase

Submitted 23 July 2002; revised 3 October 2002; accepted 1 November 2002

Introduction

The extent of epithelial injury in asthma is reflected by expression of the epidermal growth factor receptor (EGFR, HER1, ErbB1) whose levels are increased in proportion to asthma severity and are refractory to corticosteroid therapy [1]. Activation of the EGFR can elicit a range of phenotypic responses in the target cell including growth promotion, growth inhibition, protection against apoptosis, induction of differentiation, reorganization of the cytoskeleton and cell migration [2]. These

pleiotropic responses are brought about by transmission of specific intracellular signals in response to ligand-induced EGFR homo- or heterodimerization and activation of the intrinsic tyrosine kinase activity of the receptor [3].

Although the EGF ligand family are best known as mitogens, proliferating cell nuclear antigen (PCNA), a marker of proliferation, is not increased in asthmatic bronchial epithelium, even where epithelial damage is apparent [4]. This appears to be due to expression of the cyclin-dependent kinase inhibitor, p21^{waf}, which prevents cell cycle progression from G1 into S phase [5]. Animal studies have also demonstrated that the EGFR plays a role in goblet cell differentiation in the airways [6, 7]. A close correlation between EGFR activation and induction of MUC5AC mRNA expression has also been demonstrated in normal and asthmatic bronchial epithelium [8].

Correspondence: D. E. Davies, Division of Infection, Inflammation & Repair Mailpoint 810, Level D Centre Block, Southampton General Hospital, Southampton SO16 6YD, UK. E-mail: donnad@soton.ac.uk

¹These authors contributed equally to work described in this manuscript.

Many phenotypic responses downstream of the EGFR require temporal regulation of the expression of multiple genes. Recognizing that the EGFR plays a major role in the wound-healing response, we considered the possibility that, in addition to regulating the phenotypic behaviour of the responding cell, EGFR activation may also directly co-ordinate responses of inflammatory cells within the wound environment by secretion of soluble mediators involved in cell-cell communication. Although there is little information about such a proinflammatory role for the EGFR, it has been shown that treatment of a colonic adenocarcinoma cell line with EGF caused increased IL-8 synthesis [9] and that an EGFR antibody inhibited IL-8 expression by human transitional cell carcinomas grown orthotopically in nude mice [10]. More recently, EGF has been shown to cause IL-8 release from BEAS-2B cells [11], consistent with a role for the EGFR in the pathogenesis of airway inflammation. In view of the fact that severe asthma is characterized by neutrophilic inflammation and increased production of IL-8 [12, 13], the purpose of this study was to characterize the relationship between EGFR activation and production of the neutrophil chemoattractants IL-8 and macrophage inhibitory protein 1 alpha (MIP-1 α) using bronchial epithelial cells cultured *in vitro* and to establish whether there was a relationship between the high levels of EGFR expression in asthma and epithelial IL-8 or MIP-1 α expression *in vivo*.

Materials and methods

Bronchoscopy

Bronchial biopsies and bronchial epithelial cell brushings were obtained by fiberoptic bronchoscopy, in accordance with standard guidelines [14]. Surface epithelial cells were obtained by gentle bronchial brushing and bronchial biopsies were taken from the subcarinae of the lower and middle lobes using alligator forceps. Written informed consent was obtained from all volunteers and ethical approval was obtained from the Joint Ethics Committee of Southampton University and General Hospital.

Primary cell culture

Primary bronchial epithelial cells were established from bronchial brushings obtained by fiberoptic bronchoscopy from five asthmatic volunteers (two males, three females), mean age 33.4 years (range 20–58) and mean forced expiratory volume of 1 s (FEV₁) 73.9% (range 63–83%) predicted. Subjects were receiving regular treatment with salbutamol ($n = 1$) alone or together with inhaled corticosteroids ($n = 4$). Primary cultures were also established from seven non-asthmatic control subjects (two males, five females), mean age 34.7 years (range 21–53) and mean FEV₁ 106.7% (range 95–120%) predicted. Primary cultures were grown in bronchial epithelial growth medium (BEGM; Clonetics, San Diego, CA, USA) as previously described [15].

Effects of oxidants, cytokines and growth factors on cytokine production

Serum-starved NCI-H292 cells (24 h in serum-free medium; Ultraculture, Biowhittaker, Wokingham, UK) were treated with H₂O₂ or EGF at the doses stated for 24 h in the absence

or presence of dexamethasone (1 μ M) or tyrphostin AG1478 (1 μ M). Both inhibitors were dissolved in dimethyl sulphoxide (DMSO); control incubations showed that this vehicle was without effect at the doses used. Primary bronchial epithelial cells were used at passage two and were rendered quiescent in bronchial epithelial cell basal medium (BEBM; Clonetics) supplemented with 1% bovine serum albumin, and insulin, transferrin and sodium selenite supplement (Sigma, Poole, UK) prior to use. Cells were then stimulated in the same medium with EGF (10 ng/mL) or TNF- α (10 ng/mL) in the absence or presence of AG1478 (1 μ M) for 24 h.

Following exposures, culture supernatants were harvested by centrifugation and stored at -80°C prior to assay for IL-8 and MIP-1 α by enzyme-linked immunosorbent assay (ELISA) according to the manufacturer's instructions (Biosource Europe, Nivelles, Belgium). The cell monolayer was fixed in formal saline and cell number determined by the method of Oliver et al. [16]. Cytokine levels were corrected for cell number.

Analysis of EGFR phosphorylation using SDS-PAGE and western blotting

Serum-starved H292 cells were treated in serum-free medium in the absence or presence of 10 ng/mL EGF or 300 μ M H₂O₂ alone or in combination with AG1478 (1 μ M) for 0–60 min. At the end of each time point, cells were lysed and tyrosine phosphorylated proteins analysed by sodium dodecyl sulphate polyacrylamide gel electrophoresis (SDS-PAGE) and western blotting. To confirm phosphorylation of the EGFR in the presence of EGF and H₂O₂, tyrosine phosphorylated proteins were immunoprecipitated using PY-20 agarose and EGFR detected by SDS-PAGE and western blotting with an anti-EGFR antibody, using previously described protocols [1].

Analysis of IL-8 gene expression

Serum-starved H292 cells were treated with Ultraculture \pm EGF (10 ng/mL) or H₂O₂ (300 μ M) in the presence or absence of AG1478 (1 μ M) and left for 8 h. RNA was extracted using TRIzol reagent (Invitrogen, Paisley, UK), DNase-treated and reverse transcribed using random hexamers. IL-8 primer and probe sequences labelled with 5'-reporter dye FAM (6-carboxy-fluorescein) and 3'-quencher dye TAMRA (6-carboxy-N',N',N',N'-tetramethyl-rhodamine) were: forward primer, 5'-AAG-GAACCATCTCACCTGTGTGTAAC-3'; reverse primer, 5'-TTAGCACTCCCTGGCAAACTG-3'; and probe, FAM-5'-CTGCCAAGAGAGCCACGGCCAG-3'-TAMARA. Primers directed against ribosomal RNA (18S rRNA) were used as the endogenous control (Applied Biosystems, Warrington, UK). Real-time detection of the multiplex PCR reaction was followed on an ABI Prism 7700 sequence detection system (Applied Biosystems, Warrington, UK). Standard curves were generated using serial dilutions of cDNA obtained from pooled samples; the relative primer efficiencies of both systems, as indicated by the gradient of the standard curves, were within $\pm 2\%$ of each other. Data were normalized relative to the 18S rRNA.

Immunohistochemistry

For immunohistochemistry, glycol methacrylate-embedded bronchial biopsies were collected from 15 non-asthmatic subjects, 14 atopic mild asthmatics and 10 severe asthmatics. The

healthy control group (nine males, six females) had a mean age of 22.0 years (range 20–46) and a mean FEV₁ 106% (range 78–147%) predicted. The asthma groups were as defined by the GINA guidelines [17]. The mild asthmatics (12 males, two females) had a mean age of 26.4 years (range 19–54) and a mean FEV₁ 93.6% predicted (range 82–107%). The severe group (one male, nine females) with a matched mean age of 28.6 years (range 13–53) had a significantly lower ($P=0.001$) mean FEV₁ of 74.9% predicted (range 53–95%). The mild asthmatics were receiving salbutamol only and the severe group was on a mean inhaled steroid dose of 3060 µg/day (range 2000–4000) and oral corticosteroid dose of 37.5 mg/day (range 2.5–100).

Two-micron sections were cut from glycol methacrylate (GMA)-embedded biopsies and stained immunohistochemically [18]. Mouse monoclonal antibodies (mAbs) against IL-8 (Alexis, Nottingham, UK), MIP-1α (R&D Systems, Abingdon, UK) and neutrophil elastase (Dako, Cambridge, UK) were used together with a sheep polyclonal antibody against the EGFR (University of Southampton) [1]. For controls, the primary antibodies were replaced with isotype-matched immunoglobulin or buffer alone.

All slides were randomly coded and assessed by an observer blinded to the code. Positive epithelial staining was measured based on red/blue/green colour composition using computerized image analysis (Colourvision, Improvision, UK), as previously described [1]. The number of neutrophils and eosinophils were counted within the submucosa, the area measured by image analysis and number of cells/mm² submucosa calculated.

Statistical analysis

Immunohistochemistry data was analysed by the Mann-Whitney *U*-test. H292 epithelial cell culture data was analysed using Student's *t*-test, whereas primary epithelial cell data, which were not normally distributed, were analysed by Wilcoxon rank sum test. A probability value, $P < 0.05$ was considered significant.

Results

Stimulation of IL-8 expression and release from bronchial epithelial cells

To determine whether the EGFR could contribute to ongoing inflammation in asthma, we measured the ability of EGF and H₂O₂ to stimulate the expression and release of IL-8 from monolayers of H292 bronchial epithelial cells. Under the conditions tested, both EGF and H₂O₂ stimulated a rapid increase in tyrosine phosphorylation of the EGFR (Fig. 1) via ligand-dependent and ligand-independent mechanisms, respectively; this increase could be blocked by the EGFR-selective [1] tyrosine kinase inhibitor, tyrphostin AG1478. Following treatment with either EGF or H₂O₂, analysis of IL-8 gene transcription using real-time PCR showed that either treatment caused a significant increase in IL-8 mRNA and this response was also completely blocked by AG1478 (Fig. 2).

Consistent with the increased gene transcription, EGF was found to cause a dose-dependent increase in IL-8 release from the H292 cells and this was also blocked by AG1478 (Fig. 3a). As severe asthma is corticosteroid refractory, we also examined the effect of dexamethasone on EGF-induced IL-8 release. In this case, inhibition was observed but the extent of inhibition

decreased as the dose of EGF increased; at the three highest concentrations of EGF, IL-8 release in the presence of dexamethasone was significantly increased above baseline (Fig. 3a). Increased IL-8 production was also observed when cells were treated with H₂O₂, but in this case all doses were maximally stimulating (Fig. 3b). As for EGF, AG1478 completely blocked IL-8 release in response to H₂O₂ whereas dexamethasone caused 39% inhibition irrespective of H₂O₂ dose.

To investigate whether EGF might also affect release of other neutrophilic chemokines, we also examined release of MIP-1α. However, in this case no increase was observed upon treatment with either EGF or AG1478 alone, although some suppression was observed when the cells were cultured in the presence of EGF together with AG1478 (Fig. 4a); the reasons for this are unclear. In contrast, treatment with either 500 or 600 µM H₂O₂ caused a significant ($P < 0.004$) increase in MIP-1α release and this was partially suppressed by dexamethasone ($P < 0.04$, 500 µM H₂O₂; $P < 0.01$, 600 µM H₂O₂), but not by AG1478 ($P > 0.05$; Fig. 4b). The failure of AG1478 to affect MIP-1α release induced by H₂O₂ indicates that it is acting to

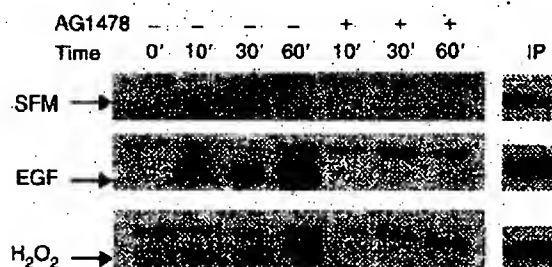


Fig. 1. Induction of EGFR phosphorylation by EGF and H₂O₂. H292 bronchial epithelial cells were treated in serum-free medium in the absence or presence of EGF (10 ng/mL) or H₂O₂ (300 µM) without or with AG1478 (1 µM) for 0–60 min. Phosphotyrosine-containing proteins in cell lysates were detected by western blotting (left panel). The 170 kDa phosphoprotein indicated by the arrow was confirmed as the EGFR by immunoprecipitation using PY-20 agarose followed by western blotting for the presence of the EGFR (right panel). The blots shown are representative of 3 individual experiments.

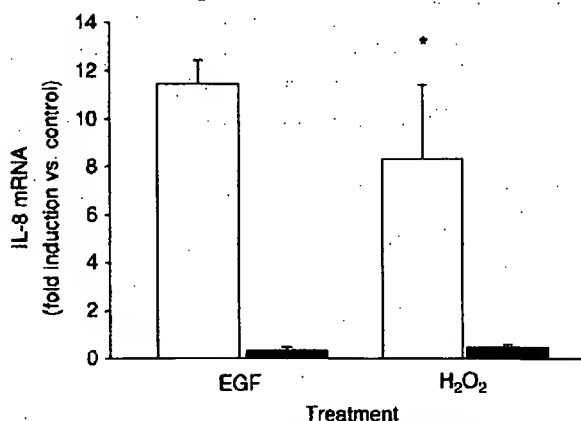


Fig. 2. Induction of IL-8 gene expression by EGF and H₂O₂. Quiescent H292 bronchial epithelial cells were treated in the presence of EGF (10 ng/mL) or H₂O₂ (300 µM) without (□) or with 1 µM AG1478 (■) for 8 h and then IL-8 mRNA analysed by real-time PCR. Data are mean ± SEM ($n=3$ for EGF-treated cells; $n=5$ for H₂O₂-treated cells) and are normalized relative to IL-8 gene expression in untreated cells. * $P < 0.05$ versus untreated control cells.

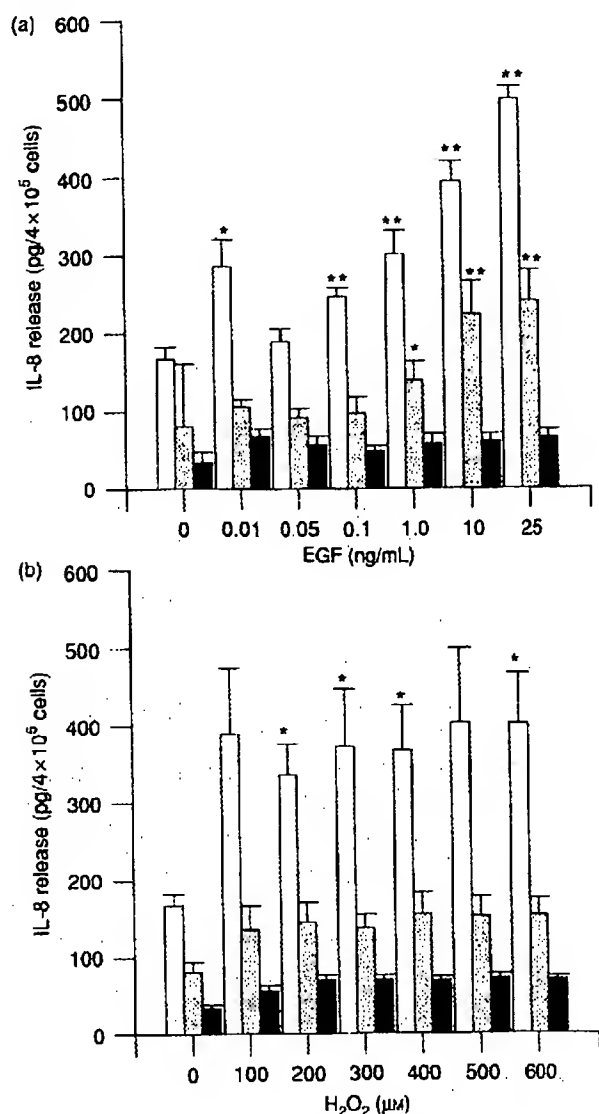


Fig. 3. IL-8 release from H292 bronchial epithelial cells. Quiescent cells were treated with increasing doses of EGF (a) or H₂O₂ (b) in the absence (open bar) or presence of 1 μM dexamethasone (grey bar) or 1 μM AG1478 (black bar) for 24 h. The graphs show IL-8 release into the culture supernatant after correcting for cell number. Data are mean ± SEM ($n = 6$); * $P < 0.05$, ** $P < 0.001$ versus appropriate baseline controls (i.e. SFM alone for comparison of EGF- or H₂O₂-treated cells; SFM + dex for comparisons in the presence of dex; or SFM + AG1478 for comparisons in the presence of AG1478).

selectively to inhibit aspects of H292 cell function mediated via the EGFR.

As the responses of cell lines are sometimes atypical, we further investigated the effect of EGF using primary asthmatic bronchial epithelial cell cultures established from bronchial brushings. As observed with the H292 cell line, EGF caused a 3 ± 1.07 -fold increase ($P < 0.05$) in IL-8 release from these asthmatic cell cultures and this was completely blocked by AG1478 (Fig. 5a); although H₂O₂ caused a 2 ± 1.0 -fold increase in IL-8 release, this failed to reach statistical significance. In the same experiments, TNF-α (10 ng/mL) caused a 3.9 ± 1.0 -fold increase ($P < 0.05$) in IL-8 release. It was also noted that AG1478 suppressed basal IL-8 release, suggesting autocrine

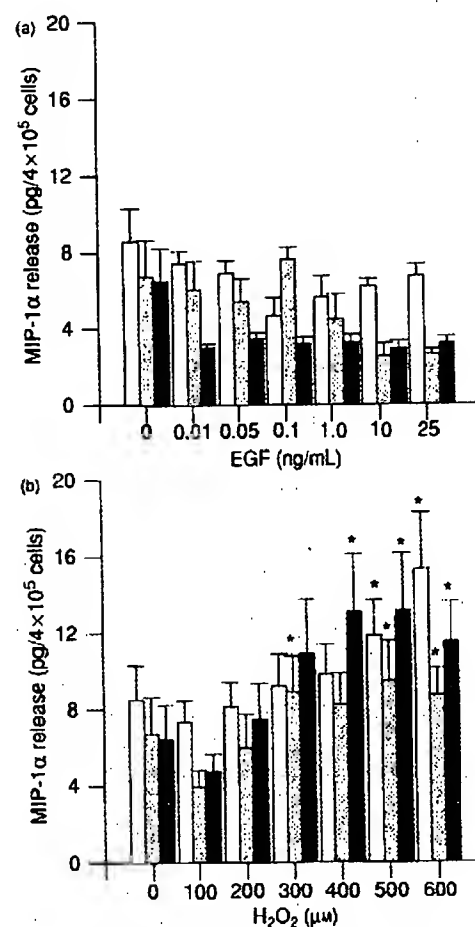


Fig. 4. MIP-1α release from H292 bronchial epithelial cells. Quiescent cells were treated with increasing doses of EGF (a) or H₂O₂ (b) in the absence (open bar) or presence of 1 μM dexamethasone (grey bar) or 1 μM AG1478 (black bar) for 24 h. The graphs show MIP-1α release into the culture supernatant after correcting for cell number. Data are mean ± SEM ($n = 5$ or 6); * $P < 0.05$ versus appropriate controls (i.e. SFM alone for comparison of EGF- or H₂O₂-treated cells; SFM + dex for comparisons in the presence of dex; or SFM + AG1478 for comparisons in the presence of AG1478).

stimulation of the cells. Measurement of EGF or oxidant-stimulated IL-8 release from primary cultures derived from seven normal subjects revealed responses comparable to those of the asthmatic cultures (Fig. 5b) with EGF causing a 3.3 ± 0.6 -fold increase ($P < 0.05$) but H₂O₂ failing to significantly stimulate above baseline. For comparison, there was a 7.5 ± 1.5 -fold increase ($P < 0.05$) in response to TNF-α. The slightly lower response of the asthmatic cells to EGF or TNF-α was not statistically significant ($P > 0.1$) and did not show any correlation with steroid use.

Immunohistochemical analysis of chemokine expression in bronchial biopsies from mild and severe asthmatic subjects

To assess whether there was any relationship between EGFR expression and epithelial IL-8 in asthma, we undertook immunohistochemical analysis of bronchial biopsies from asthmatic subjects with varying degrees of disease severity. As we have demonstrated previously [1], expression of the EGFR was

significantly higher in subjects with severe asthma compared to those with mild asthma or normal controls (% epithelial staining) median 18.6 (range 0.9–38.6) in severe asthma compared to median 6.4 (range 0.5–18.3; $P = 0.04$) in mild asthma; or median 6.0 (range 0.0–14.3; $P = 0.02$) in the non-asthmatic controls. Significantly higher levels of IL-8 and MIP-1 α were also observed in the bronchial epithelium of the severe asthmatics compared to the mild asthmatics or normal controls (Fig. 6a). Expression of IL-8 (% epithelial staining) in severe asthma was found to be median 8.5 (range 2.5–14.3) versus median 1.4 (range 0–5.5) in mild asthma ($P = 0.001$) or median 0.6 (range 0.0–1.9) in normal controls ($P < 0.001$); whereas that for MIP-1 α was median 17.3 (range 2.8–31.0) versus median 7.6 (range 1.1–15.7; $P = 0.04$) in mild asthma and median 0.4 (range 0.0–6.2; $P = 0.001$) in the non-asthmatic bronchial epithelium. There was no significant difference in either epithelial EGFR or IL-8 expression between the non-asthmatic controls and the mild asthmatic group; this may reflect the relatively mild degree of disease within this asthmatic group [mean FEV₁ 93.6% predicted (range 82–107%)]. Consistent with the higher levels of neutrophil chemoattractants detected at the severe end of the disease spectrum, significantly more neutrophils were observed in the submucosa of the severe asthmatics (24 neutrophils/mm², range 11–174) compared to the mild asthmatics (12 neutrophils/

mm², range 1–24; $P = 0.007$). The expression of EGFR in the asthmatic biopsies strongly correlated with IL-8 expression ($r = 0.70$, $P < 0.001$; Fig. 6b), and there was a trend for a significant correlation between both EGFR and IL-8 with the number of neutrophils in the submucosa ($r = 0.43$, $P = 0.06$; and $r = 0.41$, $P = 0.08$, respectively). In those patients using corticosteroids, there was no significant correlation between any of the measured parameters and steroid dose.

Discussion

Chronic severe asthmatic patients have a greatly impaired quality of life and account for up to 50% of the health costs of this disease [19]. Although treatment with corticosteroids significantly reduces airway inflammation in mild asthma [20], this is not the case at the severe end of the spectrum where neutrophilic inflammation and high IL-8 levels persist despite high doses of both oral and inhaled corticosteroids [12, 13]. While corticosteroids may contribute to inflammation by reducing neutrophil apoptosis [21], this does not fully explain the underlying reason(s) for neutrophil influx into the airways in severe disease.

As we have previously reported [1], expression of EGFR is increased in the bronchial epithelium of severe asthmatic

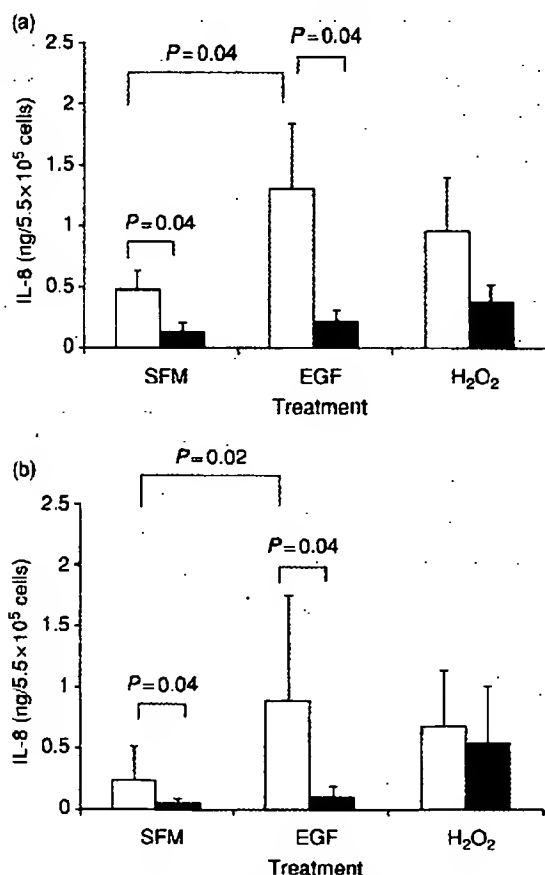


Fig. 5. IL-8 release from primary asthmatic (a) or normal (b) bronchial epithelial cells. Quiescent cells were treated with EGF (10 ng/mL) or H₂O₂ (300 μ M) in the absence (□) or presence of 1 μ M AG1478 (■) for 24 h. The graphs show IL-8 release into the culture supernatant after correcting for cell number. Data are mean \pm SEM ($n = 5$ (asthma) or 7 (normal)); significance values were determined using Wilcoxon's rank sum test.

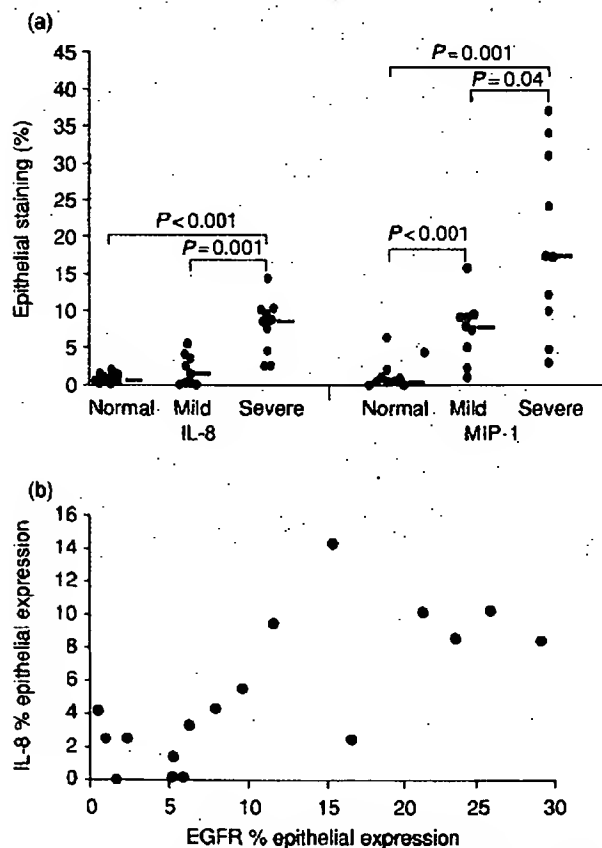


Fig. 6. (a) Comparative analysis of the epithelial expression of IL-8 and MIP-1 α in bronchial epithelium of non-asthmatic control subjects or those with mild or severe asthma. Data are expressed as percentage epithelial staining which was determined by computer-aided image analysis. (b) Correlation between IL-8 and EGFR expression in asthmatic bronchial epithelium.

subjects. This increase is steroid refractory and it is not a consequence of corticosteroid treatment [1]. As EGFR levels increase in the skin [22], gastrointestinal tract [23] and lungs [24, 25] in response to tissue injury, the high levels observed throughout the epithelium of severe asthmatic subjects would suggest that there is widespread, ongoing stress and damage in the airways. In normal epithelium, EGFRs are expressed on the basolateral surface [1] and are spatially separate from their activating ligands contained in the apical lining fluid [26]. In contrast, in severe asthma EGFR immunostaining is also evident on the apical surface suggesting the potential for cognate ligand receptor interactions [1]. Thus, our finding that EGF stimulates IL-8 mRNA synthesis and release from bronchial epithelial cells provides a link between EGFR up-regulation in response to tissue injury and induction of a neutrophilic inflammatory response mediated by the resident cells. Our finding that EGFR expression in the bronchial epithelium closely correlated with the expression of IL-8, and that both EGFR and IL-8 showed a trend for correlation with neutrophil numbers further supports this cause-effect relationship. Such a response may explain the increase in epithelial IL-8 expression after exposure of volunteers to agents such as ozone, DEPs or NO₂ which also have the capacity to cause epithelial damage [27-29]. The demonstration of increased epithelial IL-8 expression in the present study, is consistent with previous studies which have shown increased levels of IL-8 in lavage fluid of severe asthmatics [12, 13]. Because EGFRs are increased in the bronchial epithelium of smokers [30], a similar mechanism may also contribute to IL-8 expression and neutrophilia in smokers and COPD patients. As the barrier to the external environment, the bronchial epithelium may have a critical role as a sensor of environmental stress, with exaggerated responses having pathological consequences.

Studies using the human epithelial cell lines, A549 and BEAS-2B, have shown that H₂O₂ induces expression of IL-8 [31, 32]; however, our studies using H292 and primary bronchial epithelial cells extend these observations by showing that IL-8 gene transcription and release stimulated by either H₂O₂ or EGF is mediated by EGFR-dependent pathways. The present study confirms the previous study with BEAS-2B cells [11] and extends it by demonstrating that EGF can overcome the inhibitory effects of corticosteroids. Corticosteroids suppress IL-8 production in mild asthma, but in the severe asthmatic epithelium increased expression of both IL-8 and MIP-1 α was evident, even though the subjects were on a mean inhaled steroid dose of 3.1 mg/day and a mean oral dose of 37.5 mg/day. As EGFR levels are elevated in severe asthma independent of therapy, these receptors offer increased signalling capacity that might contribute to the insensitivity of IL-8 release to corticosteroid therapy. The selectivity of the EGF-induced response was further demonstrated with the observation that MIP-1 α release was only provoked by H₂O₂ and this did not involve the EGFR. These differences may be due to differential activation of transcription factors. EGF has been demonstrated to activate NF- κ B [33], consistent with the known involvement of NF- κ B for IL-8 transcription and the partial suppression of IL-8 release by dexamethasone. However, the inability of dexamethasone to fully block EGF-stimulated IL-8 release suggests the activation of other transcription factors by EGF. Likely candidates are the *lef*/*tcf* transcription factors that are activated by EGF or Wnt signalling and are known to activate IL-8 gene transcription [34]. In contrast, MIP-1 α transcription does not

appear to involve nuclear factor kappa B (NF- κ B), but may involve other transcription factors such as activator protein (AP)-1 which is known to be activated by oxidants [31, 32].

Based on the results presented, we postulate that several self-perpetuating cycles are established in the airways in severe asthma with neutrophils occupying a central role (Fig. 7). In the first, tissue injury leads to increased surface EGFR expression with ligand-dependent EGFR activation causing IL-8 release and neutrophil influx. As neutrophil numbers and EGFR expression in severe asthma are both refractory to corticosteroid treatment [1, 21], these observations are consistent with a link between persistent neutrophil-mediated inflammation and epithelial damage. As a consequence of neutrophil influx, endogenous oxidants act directly on the epithelium to stimulate release of MIP-1 α , which attracts more neutrophils into the airways, leading to further tissue activation and injury. Superimposed on these two cycles is a third cycle in which the responses to tissue injury are amplified by TNF- α released by neutrophils and other inflammatory cells, including macrophages and mast cells. The importance of oxidants is further emphasized by the antioxidant status of the epithelium and its ability to resist oxidative stress. It has been shown that antioxidants levels are lower in the epithelium [35, 36] and bronchoalveolar lavage (BAL) [37] of asthmatic when compared to normal subjects. These decreases will be accompanied by increases in oxidant levels from the polluting stimuli and infiltrating neutrophils. Another interaction between neutrophils and EGFR activation has recently been identified where neutrophil-derived oxidants cause mucus hypersecretion [38], another feature of severe asthma.

While these self-perpetuating cycles of inflammation and tissue injury explain the chronic nature of airway inflammation in severe asthma, they do not explain how the appropriate microenvironment is created in the airway that establishes this inflammation. Nor do they account for the increased sensitivity of asthmatic subjects to innocuous components of the inhaled environment. One possible explanation can be provided by our recent studies where we have demonstrated that asthmatic epithelial cells are more susceptible to oxidant-induced apoptosis than are those from healthy controls [15]. Susceptibility to environmental oxidants may be triggering a mechanism that facilitates the initial inflammatory responses that enable the

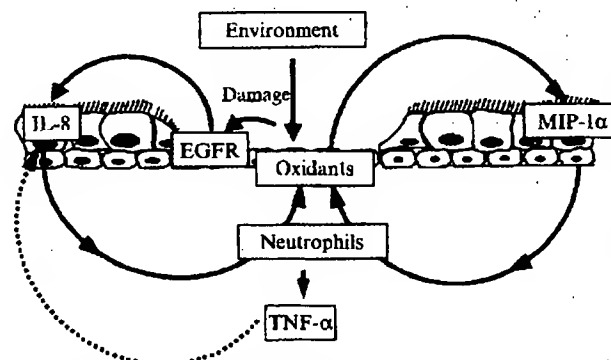


Fig. 7. Schematic representation showing how self-perpetuating cycles of chronic inflammation, tissue injury and sustained neutrophilic inflammation are established in the bronchial mucosa of severe asthmatics.

chronic cycles to become established. Together, these observations would readily account for the involvement of environmental pollutants in asthma exacerbations and the rising trends in asthma over the last 30 years.

In conclusion, our data highlight the importance of the bronchial epithelium in the regulation and modulation of inflammation, particularly in chronic severe asthma that is refractory to corticosteroid therapy. As the barrier to the external environment, we postulate that the epithelium plays a key role in translating gene by environment interactions in asthma and other inflammatory airway diseases and that it may represent a new target for therapeutic intervention.

Acknowledgements

This work was supported by Programme Grant number G8604034 from the Medical Research Council UK, the Sir Jules Thorn Charitable Trust, by the Instituto Mexicano del Seguro Social and CONACYT.

References

- Puddicombe SM, Polosa R, Richter A et al. The involvement of the epidermal growth factor receptor in epithelial repair in asthma. *FASEB J* 2000; 14:1362-74.
- Davies DE, Polosa R, Puddicombe SM, Richter A, Holgate ST. The epidermal growth factor receptor and its ligand family: their potential role in repair and remodelling in asthma. *Allergy* 1999; 54:771-83.
- Olayioye MA, Neve RM, Lane HA, Hynes NE. The ErbB signaling network: receptor heterodimerization in development and cancer. *EMBO J* 2000; 19:3159-67.
- Demoly P, Simony-Lafontaine J, Chanez P et al. Cell proliferation in the bronchial mucosa of asthmatics and chronic bronchitics. *Am J Respir Crit Care Med* 1994; 150:214-7.
- Puddicombe SM, Torres-Lozano C, Richter A et al. Impaired epithelial proliferation and expression of the cyclin dependent kinase inhibitor, p21^{waf}, in asthmatic bronchial epithelium. *Am J Respir Cell Mol Biol* 2003; 28:61-8.
- Takeyama K, Dabbagh K, Lee HM et al. Epidermal growth factor system regulates mucin production in airways. *Proc Natl Acad Sci USA* 1999; 96:3081-6.
- Shim JJ, Dabbagh K, Ueki IF et al. IL-13 induces mucin production by stimulating epidermal growth factor receptors and by activating neutrophils. *Am J Physiol Lung Cell Mol Physiol* 2001; 280: L134-40.
- Takeyama K, Fahy JV, Nadel JA. Relationship of epidermal growth factor receptors to goblet cell production in human bronchi. *Am J Respir Crit Care Med* 2001; 163:511-6.
- Schuerer-Maly CC, Eckmann L, Kagnoff MF, Falco MT, Maly FE. Colonic epithelial cell lines as a source of interleukin-8: stimulation by inflammatory cytokines and bacterial lipopolysaccharide. *Immunology* 1994; 81:85-91.
- Perrotte P, Matsumoto T, Inoue K et al. Anti-epidermal growth factor receptor antibody C225 inhibits angiogenesis in human transitional cell carcinoma growing orthotopically in nude mice. *Clin Cancer Res* 1999; 5:257-65.
- Subauste MC, Proud D. Effects of tumor necrosis factor- α , epidermal growth factor and transforming growth factor- α on interleukin-8 production by, and human rhinovirus replication in, bronchial epithelial cells. *Int Immunopharmacol* 2001; 1:1229-34.
- Jatakanon A, Uasuf C, Maziak W, Lim S, Chung KF, Barnes PJ. Neutrophilic inflammation in severe persistent asthma. *Am J Respir Crit Care Med* 1999; 160:1532-9.
- Ordóñez CL, Shaughnessy TE, Matthay MA, Fahy JV. Increased neutrophil numbers and IL-8 levels in airway secretions in acute severe asthma: clinical and biologic significance. *Am J Respir Crit Care Med* 2000; 161:1185-90.
- NIH Workshop Summary and Guidelines. Investigative use of bronchoscopy, lavage and bronchial biopsies in asthma and other airways diseases. *Eur Respir J* 1992; 5:115-21.
- Bucchieri F, Puddicombe SM, Jordan JL et al. Asthmatic bronchial epithelium is more susceptible to oxidant-induced apoptosis. *Am J Respir Cell Mol Biol* 2002; 27:179-85.
- Oliver MH, Harrison NK, Bishop JE, Cole PJ, Laurent GJ. A rapid and convenient assay for counting cells cultured in microwell plates: application for assessment of growth factors. *J Cell Sci* 1989; 92:513-8.
- WHO/NHLBI Workshop Report. Global Strategy for Asthma Management and Prevention. NIH Publication number 96-3659A. Bethesda, MD: National Institute of Health, National Heart, Lung and Blood Institute, 1995.
- Britten KM, Howarth PH, Roche WR. Immunohistochemistry on resin sections: a comparison of resin embedding techniques for small mucosal biopsies. *Biotech Histochem* 1993; 68:271-80.
- Serra-Batlles J, Plaza V, Morejon E, Comella A, Brugués J. Costs of asthma according to the degree of severity. *Eur Respir J* 1998; 12:1322-6.
- Djukanovic R, Wilson JW, Britten KM et al. Effect of an inhaled corticosteroid on airway inflammation and symptoms in asthma. *Am Rev Respir Dis* 1992; 145:669-74.
- Cox G. Glucocorticoid treatment inhibits apoptosis in human neutrophils: separation of survival and activation outcomes. *J Immunol* 1995; 154:4719-25.
- Antoniades HN, Galanopoulos T, Neville-Golden J, Kiritsy CP, Lynch SE. Expression of growth factor and receptor mRNAs in skin epithelial cells following acute cutaneous injury. *Am J Pathol* 1993; 142:1099-110.
- Hoffmann P, Reinshagen M, Zeeh JM et al. Increased expression of epidermal growth factor-receptor in an experimental model of colitis in rats. *Scand J Gastroenterol* 2000; 35:1174-80.
- Mudtes DK, Busby HK, Strandjord TP, Clark JG. Expression of transforming growth factor- α and epidermal growth factor receptor is increased following bleomycin-induced lung injury in rats. *Am J Respir Cell Mol Biol* 1994; 11:540-51.
- Tesfaigzi J, Johnson NF, Lechner JF. Induction of EGF receptor and ErbB-2 during endotoxin-induced alveolar type II cell proliferation in the rat lung. *Int J Exp Pathol* 1996; 77:143-54.
- Kumar RK, O'Grady R, Di Girolamo N. Epidermal growth factor-like molecular species in normal bronchoalveolar lavage fluid. *Lung* 1996; 174:171-9.
- Krishna MT, Madden J, Teran LM et al. Effects of 0.2 ppm ozone on biomarkers of inflammation in bronchoalveolar lavage fluid and bronchial mucosa of healthy subjects. *Eur Respir J* 1998; 11:1294-300.
- Salvi S, Nordcnhall C, Blomberg A et al. Acute exposure to diesel exhaust increases IL-8 and GRO- α production in healthy human airways. *Am J Respir Crit Care Med* 2000; 161:550-7.
- Blomberg A, Krishna MT, Bocchino V et al. The inflammatory effects of 2 ppm NO₂ on the airways of healthy subjects [published erratum appears in *Am J Respir Crit Care Med* 1997; 156:2028]. *Am J Respir Crit Care Med* 1997; 156:418-24.
- Barsky SH, Roth MD, Kleerup EC, Simmons M, Tashkin DP. Histopathologic and molecular alterations in bronchial epithelium in habitual smokers of marijuana, cocaine, and/or tobacco. *J Natl Cancer Inst* 1998; 90:1198-205.
- Lakshminarayanan V, Drab-Weiss EA, Roebuck KA. H₂O₂ and tumor necrosis factor- α induce differential binding of

- the redox-responsive transcription factors AP-1 and NF-kappaB to the interleukin-8 promoter in endothelial and epithelial cells. *J Biol Chem* 1998; 273:32670-8.
- 32 Lakshminarayanan V, Beno DW, Costa RH, Roebuck KA. Differential regulation of interleukin-8 and intercellular adhesion molecule-1 by H₂O₂ and tumor necrosis factor-alpha in endothelial and epithelial cells. *J Biol Chem* 1997; 272:32910-8.
- 33 Biswas DK, Cruz AP, Gansberger E, Pardee AB. Epidermal growth factor-induced nuclear factor kappa B activation. A major pathway of cell-cycle progression in estrogen-receptor negative breast cancer cells. *Proc Natl Acad Sci USA* 2000; 97:8542-7.
- 34 Levy L, Neuveut C, Renard CA et al. Transcriptional activation of interleukin-8 by beta-catenin-TCF4. *J Biol Chem* 2002; 277:42386-93.
- 35 de Raeye HR, Thunnissen FB, Kaneko FT et al. Decreased Cu, Zn-SOD activity in asthmatic airway epithelium: correction by inhaled corticosteroid *in vivo*. *Am J Physiol* 1997; 272: L148-54.
- 36 Smith LJ, Shamsuddin M, Sporn PH, Denenberg M, Anderson J. Reduced superoxide dismutase in lung cells of patients with asthma. *Free Radic Biol Med* 1997; 22:1301-7.
- 37 Kelly FJ, Mudway I, Blomberg A, Frew A, Sandstrom T. Altered lung antioxidant status in patients with mild asthma. *Lancet* 1999; 354:482-3.
- 38 Takeyama K, Dahbagh K, Jeong SJ, Dao-Pick T, Ueki IF, Nadel JA. Oxidative stress causes mucin synthesis via transactivation of epidermal growth factor receptor: role of neutrophils. *J Immunol* 2000; 164:1546-52.

P-Cadherin Overexpression Is an Indicator of Clinical Outcome in Invasive Breast Carcinomas and Is Associated with *CDH3* Promoter Hypomethylation

Joana Paredes,¹ André Albergaria,¹ João T. Oliveira,¹ Carmen Jerónimo,^{2,3} Fernanda Milanezi,^{1,5} and Fernando C. Schmitt^{1,4}

Abstract **Purpose:** P-cadherin overexpression has been reported in breast carcinomas, where it was associated with proliferative high-grade histological tumors. This study aimed to analyze P-cadherin expression in invasive breast cancer and to correlate it with tumor markers, pathologic features, and patient survival. Another purpose was to evaluate the P-cadherin promoter methylation pattern as the molecular mechanism underlying this gene regulation.

Experimental Design: Using a series of invasive breast carcinomas, P-cadherin expression was evaluated and correlated with histologic grade, estrogen receptor, MIB-1, and p53 and c-erbB-2 expression. In order to assess whether P-cadherin expression was associated with changes in *CDH3* promoter methylation, we studied the methylation status of a gene 5'-flanking region in these same carcinomas. This analysis was also done for normal tissue and for a breast cancer cell line treated with a demethylating agent.

Results: P-cadherin expression showed a strong correlation with high histologic grade, increased proliferation, c-erbB-2 and p53 expression, lack of estrogen receptor, and poor patient survival. This overexpression can be regulated by gene promoter methylation because the 5-Aza-2'-deoxycytidine treatment of MCF-7/AZ cells increased P-cadherin mRNA and protein levels. Additionally, we found that 71% of P-cadherin-negative cases showed promoter methylation, whereas 65% of positive ones were unmethylated ($P = 0.005$). The normal P-cadherin-negative breast epithelial cells showed consistent *CDH3* promoter methylation.

Conclusions: P-cadherin expression was strongly associated with tumor aggressiveness, being a good indicator of clinical outcome. Moreover, the aberrant expression of P-cadherin in breast cancer might be regulated by gene promoter hypomethylation.

Cadherins are cell-cell adhesion glycoproteins that form calcium-dependent intercellular junctions and play an essential role in morphogenesis and in the development and maintenance of adult tissues and organs (1). During embryogenesis, the cell expression of specific cadherins results in homophilic interactions that are critical in the

process of cell sorting and tissue stratification (2-4). Alterations in these cellular attachments play an important role in cell destabilization and may modify the carefully regulated differentiation process of the epithelial structures (5, 6). For this reason, the functional loss or overexpression of cadherins and the molecular mechanisms underlying the control of the genes codifying these proteins have been implicated in carcinogenesis (7).

The cadherin family is subdivided into various subfamilies, including the classical E-, P-, and N-cadherins, each demonstrating a specific tissue distribution (8). Although E-cadherin is expressed in all epithelial tissues, the expression of P-cadherin is only restricted to the basal or lower layers of stratified epithelia, including prostate and skin, and also to the breast myoepithelial cells (6, 9). This unique distribution of P-cadherin suggests that, in addition to maintaining cellular adhesion, this molecule may also have other unknown functions, which can be important in cell differentiation and proliferation (5, 6).

Up-regulation of P-cadherin has been shown in several lesions, including breast cancer, in which there is usually down-regulation of E-cadherin (10). Breast carcinomas show aberrant P-cadherin expression in ~30% of the cases and has been reported as a prognostic marker of poor outcome in patients (11, 12). The differential pattern of P-cadherin expression in

Authors' Affiliations: ¹Institute of Pathology and Molecular Immunology of Porto University (IPATIMUP); ²Department of Genetics, Portuguese Oncology Institute of Porto; ³School of Health Sciences - Fernando Pessoa University, Porto; ⁴Medical Faculty, Porto University, Porto; and ⁵School of Health Sciences, University of Minho, Braga, Portugal

Received 1/10/05; revised 5/16/05; accepted 5/24/05.

Grant support: Portuguese Science and Technology Foundation (Joana Paredes: SFRH/BD/1450/2000) and from the Azorean Science and Technology Foundation (André Albergaria: DRCT-76/2004).

The costs of publication of this article were defrayed in part by the payment of page charges. This article must therefore be hereby marked *advertisement* in accordance with 18 U.S.C. Section 1734 solely to indicate this fact.

Note: J. Paredes and A. Albergaria contributed equally to this paper and should both be considered as first authors.

Requests for reprints: Joana Paredes, Institute of Pathology and Molecular Immunology of Porto University, Rua Dr. Roberto Frias s/n 4200-465 Oporto, Portugal. Phone: 351-22557-0700; Fax: 351-22557-0799; E-mail: jp@ipatimup.pt.

© 2005 American Association for Cancer Research.
doi:10.1158/1078-0432.CCR-05-0059

breast cancer development, coupled with its possible prognostic value, prompted us to investigate its expression in a series of invasive breast carcinomas.

Furthermore, we have previously found that P-cadherin aberrant expression results from a lack of estrogen receptor- α (ER- α) signaling and induces *in vitro* cell invasion in a juxtamembrane domain-dependent manner (13). Additionally, based on the fact that the 5'-flanking region (Genbank no. X95824) of the P-cadherin gene (*CDH3*) has been characterized as a CpG island (14), we thought that promoter methylation could be a putative molecular mechanism responsible for its transcriptional regulation.

This hypothesis is also supported by the fact that the same mechanism of regulation was shown for the E-cadherin gene. Aberrant methylation across the promoter region of this gene results in a selective inactivation of its transcription (15, 16). E- and P-cadherin genes exhibit a similar genomic organization, both containing 16 exons and a similar promoter region (17). The localization of the human P-cadherin gene is at 32 kb upstream of the human E-cadherin gene, also mapping to chromosome 16q22.1, showing the evolutionary conservation of the tandem arrangement of two genes encoding cell adhesion molecules, suggesting that the close proximity of these genes may be important for their regulation (18).

The 5'-flanking region of the E-cadherin gene has been sequenced and found to be extremely CG-enriched, meeting the criteria for a "CpG island" (19, 20). Methylation of E-cadherin has been shown in breast cancer and in some other cancers and cell lines (16, 21–24), although this functional block of E-cadherin expression can be removed with exposure of cell lines to demethylating agents *in vitro* (25–27). Additional factors regarding the E-cadherin gene, which seem important to transcriptional regulation, include a palindromic sequence E-pal (where transcriptional repressors as Snail and Slug bind) and a Sp-1 binding site (19).

In contrast, the comparison of the 5'-flanking sequence of the human P-cadherin gene with the one for E-cadherin shows no homology for this palindromic sequence E-pal (17). In the P-cadherin promoter, there is conservation of a CAAT box, with no TATA box, and three E boxes (helix-loop-helix binding motif). A putative Sp-1 binding site is also conserved (14). An *Alu* repeat is present ~700 bp upstream from the translation start site, and analogous to the human E-cadherin sequence, shows a CG-rich region characteristic of a CpG island (14).

Genes that show a CpG island within their promoter region are normally regulated by methylation. Few studies describing P-cadherin promoter methylation status have been published thus far and, to the best of our knowledge, none have been done in human breast cancer specimens. However, cytosine methylation of this region was described in P-cadherin-nonexpressing prostate cancer cell lines (LNCaP, TSU-PR1, and DuPRO) but not in cell lines expressing this gene (PC3, DU145, and PPC1; refs. 14, 19). Simultaneously, a recent study describing epigenetic silencing of E- and P-cadherin gene expression in human melanoma cell lines was reported, in which methylation-specific PCR analysis revealed that P-cadherin seems to be silenced by methylation events (28).

Although these studies point to cytosine methylation as a possible mechanism of P-cadherin expression regulation, Jarrard et al. claim that other mechanisms should be able to regulate the consistent loss of P-cadherin expression in *in vivo*

prostate cancer specimens. In contrast with breast cancer models, these authors found that P-cadherin is restricted to basal epithelial cells in normal prostate samples, but is down-regulated in prostatic intraepithelial neoplasia and is absent in all prostate cancer specimens analyzed. Additionally, the lack of expression was not associated with methylation of the P-cadherin promoter (14).

Based on all these results, we decided to evaluate if the promoter methylation could be the molecular mechanism responsible for the transcription regulation of the *CDH3* gene, using a series of invasive breast carcinomas. These results were compared with normal breast tissue, and confirmed in a breast cancer cell line treated with a demethylating agent.

Materials and Methods

Breast tumor samples

Formalin-fixed paraffin-embedded blocks of 150 invasive breast carcinomas were retrieved from the histopathology files at the Department of Pathology, Hospital Xeral Cies, Vigo, Spain, selected from a cohort of patients with follow-up information. From all cases, we analyzed the available relevant data, including age, tumor size, mitotic index, axillary metastasis, tumor grade, ER- α status, MIB-1, c-erbB-2, and p53 expression. The mean age of the patients at diagnosis was 56 years (range, 28–82 years old). The size of the tumors ranged from 1 to 10 cm (mean, 2.8 ± 1.5 cm). ER- α was evaluated in 150 tumors, where 100 cases were positive. MIB-1 expression was assessed in 147 cases, 70 with <15% of positive cells and 77 with >15% of positive cells. C-erbB-2 expression was analyzed in 139 cases and p53 expression in 145 cases, 34 cases were positive for c-erbB-2 and 66 were positive for p53. As a measure of prognosis, we analyzed the clinical data concerning disease-free survival, defined as the time from diagnosis to first recurrence or last contact, and the overall survival, defined as the time from diagnosis to death by breast cancer or last contact.

Immunohistochemistry

Immunohistochemical studies of representative sections were carried out using standard methods. Sections cut 2 μ m thick were mounted on gelatin (Merck, Merck KGaA, Darmstadt, Germany) and chromium (III) potassium sulfate 12-hydrate-coated slides (Merck), dried overnight at 37°C, deparaffinized with xylene and hydrated. An antigen retrieval method was carried out by microwave treatment, in a 0.05% detergent solution for E- and N-cadherin antibodies (10 minutes), and with a 10 mmol/L citrate buffer, pH 6.0 (DAKO Corporation, Carpinteria, CA) for P-cadherin antibody (30 minutes). Endogenous peroxidase was blocked with 3% hydrogen peroxide in methanol for 10 minutes. Sections were submitted to protein blockage with a specific serum (Ultravision block, LabVision Corporation, Fremont, CA) and incubated with the monoclonal primary antibody for 30 minutes at room temperature (E-cadherin, HECD-1, 1:200, Zymed Laboratory, San Francisco, CA; P-cadherin, clone 56, 1:50, Transduction Laboratories, Lexington, KY; and N-cadherin, clone 3B9, 1:400, Zymed Laboratory). The other steps of immunohistochemical staining were done using standard protocols on an automated LabVision Autostainer (LabVision Corporation), with a specific kit based on streptavidin-biotin-peroxidase method. Subsequently, the sections were counterstained with Mayer's hematoxylin, dehydrated, cleared, and mounted.

Positive and negative controls were included with each batch of staining to ensure consistency between consecutive runs. Paraffin sections of normal skin tissue were used as positive controls for E-cadherin, normal breast tissue was used for P-cadherin, and cardiac muscle was used for N-cadherin. Immunohistochemical results were not assessed in some cases (49 for E-cadherin, 3 for P-cadherin, and 8 for N-cadherin) because there was no more tumor material available.

Quantification of immunostaining

All tumors presenting an unequivocal membranous staining for cadherin in at least 10% of the neoplastic cells were scored as positive. Cells with cytoplasmic expression alone were not considered. The assessment of immunohistochemical results was based on a semiquantitative evaluation, which did not include staining intensity, as previously reported (29).

Cell culture and treatments

The human MCF-7/AZ breast cancer cell line was obtained from Prof. Marc Mareel (Laboratory of Experimental Cancerology, Chent University, Belgium) and routinely maintained at 37°C and 10% CO₂, in 50% DMEM/50% Ham's F12 media (Invitrogen, Merelbeke, Belgium), supplemented with 10% heat-inactivated fetal bovine serum (Invitrogen), 100 IU/mL penicillin, and 100 g/mL streptomycin (Invitrogen).

These cells were incubated during 5 days with 2.5 µmol/L of 5-Aza-2'-deoxycytidine (Sigma Chemical Co., St. Louis, MO), which reduces the level of 5-methylcytosine in DNA, or just with DMSO (which was the vehicle of this drug) for use as a control. After 5 days, RNA and protein cell lysates were isolated from these cells.

Reverse transcription-PCR analysis

Reverse transcription-PCR experiments were done using total RNA, which was extracted from $\sim 5 \times 10^6$ cells using the Qiagen RNeasy kit (Qiagen, Chatsworth, CA). One microgram of total RNA was reverse-transcribed with oligo(dT) primers using the Qiagen RT kit (Qiagen) according to the manufacturer's instructions. P-cadherin cDNA was amplified using the sense primer 5'-ACCAACACACAACACATTC and the antisense primer 5'-CCATCATCCACATCTTCATCC, in order to generate a 287-bp product. PCRs were done in 250 ng template cDNA using the Qiagen Taq PCR kit (Qiagen) according to the manufacturer's instructions. Reactions were done in a Minicycler (Biozym, Landgraaf, the Netherlands) with an initial denaturation at 94°C for 3 minutes; 20, 30, or 35 cycles of 94°C for 50 seconds (denaturation), 55°C for 50 seconds (annealing), and 72°C for 1 minute (elongation), followed by a final extension at 72°C for 10 minutes.

Western blot analysis

All lysates were made of cells $\sim 90\%$ confluence, which were washed thrice with PBS. Cells were lysed with PBS containing 1% Triton X-100, 1% Nonidet P-40 (Sigma), and the following protease inhibitors: aprotinin (10 µg/mL), leupeptin (10 µg/mL; ICN Biomedicals, Costa Mesa, CA), phenylmethylsulfonyl fluoride (1.72 mmol/L), NaF (100 µmol/L), NaVO₃ (500 µmol/L), and Na₄P₂O₇ (500 µg/mL; Sigma). After clearing the lysates, protein concentration was determined using the R_c Dc protein assay (BioRad, Richmond, CA), and samples were prepared such that equal amounts of protein were to be loaded. Sample buffer (Laemmli) with 5% 2-mercaptoethanol and 0.012% bromophenol blue was added, followed by boiling for 5 minutes and separation of proteins by gel electrophoresis on an 8% polyacrylamide gel and transfer onto a nitrocellulose membrane (Amersham Pharmacia Biotech, Piscataway, NJ). Quenching and immunostaining of the blots were done in 5% nonfat dry milk in PBS containing 0.5% Tween 20. The membranes were

quenched for 1 hour, incubated with primary antibody for P-cadherin (clone 56, 1:500, Transduction Laboratories) for 1 hour, washed four times for 10 minutes, incubated with horseradish peroxidase-conjugated secondary antibody for 45 minutes, and washed six times for 10 minutes. Detection was done using enhanced chemiluminescence reagent (Amersham Pharmacia Biotech) as a substrate.

Laser-assisted tissue microdissection

To analyze the methylation pattern in normal epithelia, five frozen normal breast tissues were selected from the archive of the Department of Pathology, Hospital São João, Porto, Portugal. These frozen samples were included in ornithine carbamyl transferase solution (Bright, Huntingdon, England) and sections 10 µm thick were placed in specific slides for laser microdissection. The slides were stained with H&E and visualized in a Laser Microdissector Microscope (PALM, Bernried, Germany). Breast normal glandular epithelia were identified in the sections and only prominent epithelial cells were selected for microdissection (Fig. 1A). In all cases, $>10,000$ epithelial cells were cautiously laser-cut and laser pressure-catapulted for a specific vial (Fig. 1B), from which DNA extraction was done according to Qiagen protocols for DNA extraction from laser tissue microdissection.

Methylation-specific PCR analysis

In order to optimize the methylation-specific PCR technique, we used genomic DNA extracted from nine frozen breast tumor tissues retrieved from the Portuguese Oncology Institute of Coimbra (IPOFC-CROC, Portugal). The tumor tissues were macerated and genomic DNA extraction was done according to the standard protocol for human tissues—Genomic DNA from Tissue Kit (NucleoSpin Tissue, Macherey-Nagel, CmbH & Co., KC, Düren, Germany). Genomic DNA (200 ng/µL) was converted by bisulfite treatment as described below. Because we studied P-cadherin protein expression in these frozen tumor cases, these methylation-specific PCR results were also considered for statistical analysis, together with 55 cases from the series of paraffin-embedded samples, where tumor material was still available to perform DNA extraction.

DNA extraction

Fifty-five paraffin-embedded samples were cut to 10-µm-thick sections and, after identification of the tumor areas of interest, these were carefully microdissected. The samples were then placed into microcentrifuge tubes with a freshly prepared lysis buffer/proteinase K mixture, and incubated overnight at 56°C until complete lysis of the fragments. The DNA extraction was done according to the same standard protocol for human tissues previously referred to. DNA from all 64 samples (55 paraffin-embedded and 9 frozen cases) was quantified, and wild-type DNA from each case was amplified using P-cadherin-specific primers. Genomic blood DNA was used as wild-type positive control (Fig. 2A).

Methylation analysis

Bisulfite treatment. Sodium bisulfite conversion of P-cadherin 5' CpC island was done in 3 µg of genomic DNA from the total 64 tumor cases. This same treatment was applied to DNA extracted from the five normal breast tissues that were laser-microdissected. Briefly, and based on the standard protocol described elsewhere (30), DNA was denatured by incubation with NaOH (final concentration, 0.2 mol/L), for 20 minutes at 50°C. To function as a carrier, 1 µg of salmon sperm DNA (Stratagene, La Jolla, CA) was mixed with the initial human DNA. A freshly made sodium bisulfite solution [2.5 mol/L sodium bisulfite (Sigma), 125 mmol/L hydroquinone (Sigma), and NaOH 2 mol/L (pH 5.0)] was added to the DNA sample, in order to convert the unmethylated cytosines to uracils. This conversion allows the distinction between methylated and unmethylated DNA. After 3 hours of incubation in the dark at 70°C, converted DNA was purified, using a commercial Wizard DNA purification resin, as described by the manufacturer (Promega Corporation, Madison, WI). Finally, the purified DNA was eluted into 45 µL of preheated (80°C) water.

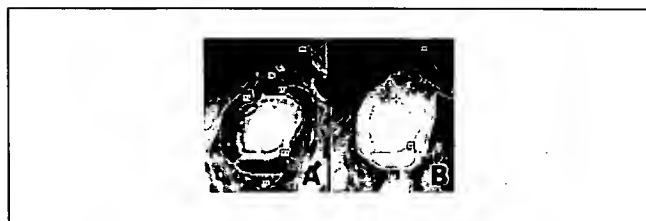


Fig. 1. Illustration of a normal mammary duct selected for laser tissue microdissection: A, only clearly identifiable epithelial cells layer were cautiously selected; B, the epithelial cell clusters were laser-cut and catapulted for a special vial for DNA extraction.

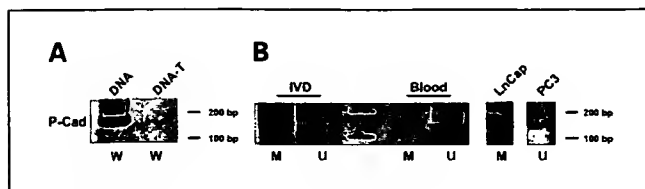


Fig. 2. Wild-type and methylation control patterns of the analyzed P-cadherin promoter region (W, wild-type; M, methylated; U, unmethylated): **A**, wild-type pattern of genomic DNA untreated and treated with bisulfite (DNA-T). As expected, P-cadherin wild-type primers do not recognize the promoter site of bisulfite-transformed DNA. **B**, on the left, the blood DNA treated with CpG methylase M.SssI (*in vitro* DNA) was only amplified with P-cadherin primers specifically designed for methylated promoter region after the bisulfite treatment. Bisulfite-treated DNA from blood was used as a positive control for the unmethylated promoter region. On the right, bisulfite-treated DNA from LNCaP and PC3 cell lines were also used as P-cadherin methylation and unmethylation positive controls, respectively.

Modification was completed by NaOH treatment (final concentration, 0.3 mol/L) for 10 minutes at room temperature, followed by neutralization reaction with 75 μ L of ammonium acetate 6 mol/L. DNA precipitation was done by adding 2 μ L of glycogen (5 mg/mL; MBI Fermentas), and after pellet washing with 70% ethanol, DNA was dried, resuspended in 40 μ L of water and stored at -20°C .

Methylation-specific PCR analysis. After the bisulfite treatment, all samples were amplified by PCR. For a final volume of 25 μ L of PCR reaction mix, 400 ng of bisulfite-modified DNA was added to the PCR mix containing 1 \times PCR buffer [16.6 mmol/L ammonium sulfate, 67 mmol/L Tris (pH 8.8), 6.7 mmol/L MgCl_2 , and 10 mmol/L 2-mercaptoethanol], deoxynucleotide triphosphates (each at 1 mmol/L), 0.6 μ mol/L primers, 2% DMSO and 1 unit Platinum Taq DNA polymerase (Life Technologies, Inc., Rockville, MD). The gene-specific primer sequences for both methylated and unmethylated P-cadherin promoter were, respectively: P-cad-M (sense 5'-CCCCCATTTCTCTCCCT; antisense 5'-ATAAAACAAC-TACCCACACC); P-cad-U (sense 5'-CCTCCCATTTCTCTCTTC; antisense 5'-ATAAAACAAC-TACCACAACAACA). The annealing temperature was 55°C , generating a 140-bp product. Reactions were hot-started at 95°C for 5 minutes and PCR amplification was carried out in a thermocycler for 38 cycles (30 seconds at 95°C ; 30 seconds at 55°C , the annealing temperature, and 45 seconds at 72°C). A final extension was done at 72°C for 10 minutes. Negative controls, without DNA, were done for all sets of PCRs. Each PCR

product was directly loaded into a nondenaturing 6% polyacrylamide gel, and stained with silver nitrate. As a positive methylation control, we used blood DNA treated with CpC methylase M.SssI (BioLabs Inc., New England; *in vitro* DNA), and blood bisulfite-treated DNA was used as a positive unmethylated control (Fig. 2B). Genomic DNA was also obtained from human prostate cancer cell lines, for use as additional positive methylation controls: LNCaP, which present methylation within the *CDH3* promoter, and PC3, which express detectable P-cadherin and are unmethylated at *CDH3* promoter (ref. 14; Fig. 2B).

As already mentioned, we also did PCR amplification for P-cadherin promoter wild-type sequence, and the primers used were: P-cad-W (sense 5'-CCCCCCCCACCTCCTCCCCC; antisense 5'-CTCAACCAC-CTCCCCCACC). The annealing temperature was 67°C , generating a 142-bp product. Human DNA extracted from blood leukocytes was used as positive controls. For a final volume of 30 μ L of PCR reaction mix, 200 ng of DNA was added to 1 \times PCR buffer [500 mmol/L KCl, 100 mmol/L Tris (pH 8.8), and 0.8% NP40], deoxynucleotide triphosphates (each at 0.2 mmol/L), 0.3 μ mol/L primers, and 1 unit of Taq DNA polymerase (Amersham Pharmacia Biotech). The PCR amplification was carried out using the following conditions: 1 cycle at 95°C for 5 minutes, and 35 cycles at 95°C for 30 seconds, followed by 67°C (specific annealing temperature) for 30 seconds and 72°C for 45 seconds. Additionally, a final extension at 72°C for 10 minutes was done. Negative controls without DNA were used for all sets of PCRs. As expected, P-cadherin wild-type primers did not recognize the promoter site of bisulfite-transformed DNA (Fig. 2A). All the amplified products were directly loaded and stained as described above.

In order to classify the methylation status of the cases that were studied, the ones showing only methylated alleles were considered *methylated* (M; or with complete methylation), and the ones with only unmethylated alleles were considered *unmethylated* (U; or with complete demethylation). The cases that showed partial methylation, which means the presence of both methylated and unmethylated alleles, were also considered methylated (M), based on previous reports describing methylation-specific PCR analysis (24, 31, 32).

Statistical analysis

For statistical analysis, contingency tables and χ^2 test were done to estimate the relationship between staining patterns of the different cadherins and several of the factors analyzed, such as tumor grade, lymph node metastasis, vascular invasion, ER- α , MIB-1, c-erbB-2 and

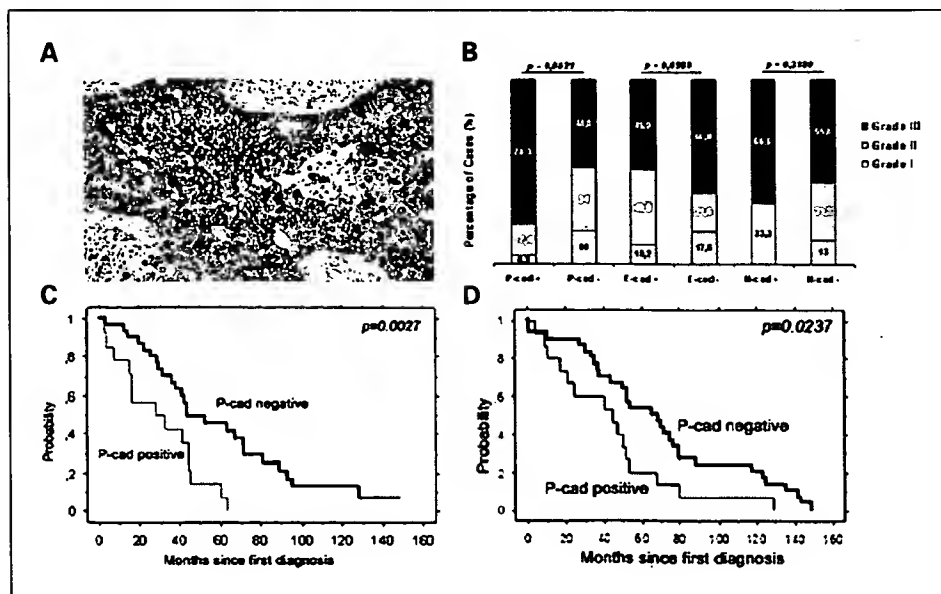


Fig. 3. **A**, strong membranous and cytoplasmic expression of P-cadherin in a high-grade invasive breast carcinoma. H&E, $\times 400$. **B**, correlation between P-, E-, and N-cadherin expression and tumor histologic grade. **C** and **D**, Kaplan-Meier curves showing probability of disease-free survival and overall survival, respectively, for patients with P-cadherin-positive tumors versus patients with P-cadherin-negative tumors (log-rank test).

Table 1. Correlation between P-, E-, and N-cadherin expression and ER- α , MIB-1, c-erbB-2, and p53-positive expression

	P-cad +	P-cad -	P	E-cad +	E-cad -	P	N-cad +	N-cad -	P
ER- α	34.8% (16 of 46)	80.2% (81 of 101)	<0.0001	75.5% (37 of 49)	61.53% (32 of 52)	0.1315	100% (3 of 3)	68.3% (95 of 139)	0.2408
MIB-1	76% (35 of 46)	42.9% (42 of 98)	0.0002	46.8% (22 of 47)	54.9% (28 of 51)	0.4233	33.3% (1 of 3)	52.2% (71 of 136)	0.5176
c-erbB-2	41.5% (17 of 41)	17.9% (17 of 95)	0.0036	32.56% (14 of 43)	20% (10 of 50)	0.1676	33.3% (1 of 3)	23.4% (30 of 128)	0.6902
p53	62.2% (28 of 45)	37.8% (37 of 98)	0.0064	39.6% (19 of 48)	50% (25 of 50)	0.3000	50% (1 of 2)	46.6% (63 of 135)	0.9253
Total	46	101		49	52		3	139	

p53 expression, and *CDH3* methylation status. ANOVA was used to investigate differences in tumor size and mitotic index. Two values were considered significantly different when $P < 0.05$. Univariate survival curves were estimated using the method of Kaplan-Meier and compared using the log-rank test. Statistical analyses were carried out using StatView 5.0 Software (SAS Institute Inc., Cary, NC).

Results

Cadherin expression and correlation with biological markers

From the 150 cases of the studied series, 149 were graded in accordance with the modified criteria of Bloom and Richardson (14, 33): 21 were classified as grade I (14.1%), 44 as grade II (29.5%), and 84 as grade III (56.4%) tumors.

P-cadherin immunoreactivity was absent in 101 (68.7%) primary breast cancers analyzed and aberrantly expressed in 46 cases (31.3%). Distribution of P-cadherin in tumor cells showed membranous staining frequently associated with cytoplasmic expression (Fig. 3A). P-cadherin expression was always found in myoepithelial cells from normal ducts/acini and from ducts containing *in situ* carcinoma, but not in acinar or ductal normal epithelial cells.

P-cadherin expression showed a statistically significant correlation with histologic grade, because this protein was essentially present in high-grade tumors (36 of 46; 78.3%), whereas grade I cases were almost all negative ($P = 0.0021$; Fig. 3B).

Statistical analysis revealed an inverse correlation between P-cadherin expression and ER- α status: 80.2% of P-cadherin-negative cases were ER- α -positive. The χ^2 test showed that this difference was statistically significant ($P < 0.0001$; Table 1). The correlation between P-cadherin and MIB-1, and c-erbB-2 and p53 expressions, was also evaluated: the majority of P-cadherin-positive cases were highly proliferative ($P = 0.0002$), and significantly related to c-erbB-2 ($P = 0.0036$) and p53 expression ($P = 0.0064$; Table 1). Additionally, an important association was observed with high mitotic index ($P = 0.0003$, data not shown). No significant correlation was found between P-cadherin expression and tumor size, axillary lymph node metastasis, and angiogenesis. Although invasive ductal carcinomas and medullary carcinomas were frequently P-cadherin-positive, a statistically significant difference with the tumor histologic type was not reached.

Concerning E-cadherin, half of the studied cases were negative (52 of 101; 51.5%), showing a clear decrease of membranous staining in the neoplastic epithelial cells. N-cadherin was only found in 2.11% (3 of 142) of the tumors, and its expression was restricted to a small population of cells with a faint membranous staining, and with cytoplasmic expression. No correlation was found between the expression

of these two cadherins and any of other tumor parameters studied here (Table 1; Fig. 3B), and there were also no significant associations between the expression of cadherins.

Cadherin expression and survival analysis

The mean follow-up time was 113 ± 53 months (range, 1-176 months). There were 12 local recurrences after diagnosis,

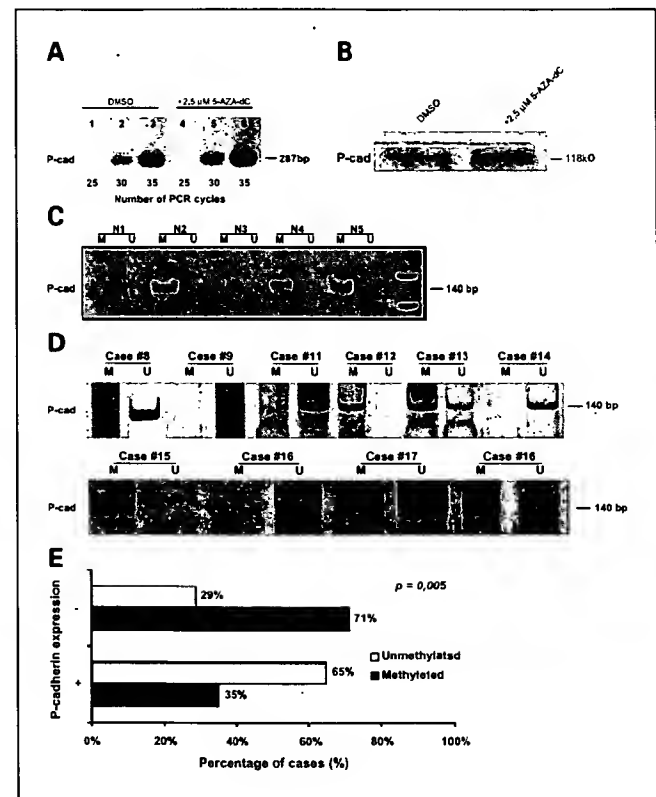


Fig. 4. A, reverse transcription-PCR analysis of P-cadherin mRNA levels after 5-Aza-2'-deoxycytidine treatment of MCF-7/AZ cells for 5 days. The analysis was done after the indicated number of cycles of PCR amplification. In the presence of the demethylating agent, the increased P-cad mRNA was more evident at the 30-cycle point, during the exponential phase of the PCR reaction. B, immunoblotting, for P-cadherin analysis, of cell lysates from MCF-7/AZ cells that had been treated with 5-Aza-2'-deoxycytidine. In comparison with the control cells, there was an increased P-cadherin expression in the MCF-7/AZ cells that were incubated with the demethylating agent. C, methylation-specific PCR results from the five normal breast tissues, where epithelial cell layers were laser microdissected from the ducts. All the cases showed complete *CDH3* promoter methylation. D, examples of complete or partial methylation and unmethylation patterns: complete methylation pattern (cases 12 and 15), partial methylation pattern (cases 13 and 18), and complete unmethylation pattern (cases 8, 9, 11, 14, 16, and 17). E, correlation between P-cadherin expression and the methylation status of the analyzed gene promoter region. The majority of P-cadherin-negative cases were unmethylated on this promoter region ($P = 0.005$).

Table 2. *CDH3* promoter methylation status and P-cadherin expression in the 64 breast tumor samples studied by methylation-specific PCR analysis

Patient no.	<i>CDH3</i> promoter methylation		P-cadherin expression	Patient no.	<i>CDH3</i> promoter methylation		P-cadherin expression
	Alleles	Status			Alleles	Status	
#1	U/U	U	positive	#72	U/U	U	negative
#2	U/U	U	negative	#73	M/M	M	positive
#3	U/U	U	positive	#74	M/M	M	negative
#4	U/U	U	negative	#75	M/M	M	negative
#5	U/U	U	negative	#76	M/M	M	positive
#6	M/U	M	negative	#77	M/M	M	negative
#7	M/U	M	negative	#78	M/M	M	negative
#8	U/U	U	positive	#79	M/M	M	negative
#9	U/U	U	positive	#80	M/M	M	negative
#11	U/U	U	positive	#81	M/M	M	positive
#12	M/M	M	negative	#85	M/M	M	negative
#13	M/U	M	negative	#86	M/M	M	negative
#14	U/U	U	positive	#111	M/M	M	negative
#15	M/M	M	negative	#113	M/M	M	negative
#16	U/U	U	positive	#119	M/M	M	negative
#17	U/U	U	positive	#125	M/M	M	positive
#18	M/U	M	negative	#126	M/M	M	negative
#19	M/U	M	negative	#127	M/M	M	positive
#20	U/U	U	positive	#132	M/M	M	negative
#21	M/U	M	positive	#133	M/M	M	positive
#22	U/U	U	positive	#134	M/M	M	negative
#24	M/U	M	negative	#135	M/M	M	negative
#25	U/U	U	positive	#138	M/M	M	negative
#41	M/M	M	negative	#148	M/M	M	negative
#42	M/M	M	positive	#151	U/U	U	positive
#51	U/U	U	negative	#153	U/U	U	negative
#59	U/U	U	negative	#154	U/U	U	positive
#60	U/U	U	negative	#155	U/U	U	negative
#61	U/U	U	negative	#157	M/M	M	negative
#65	M/M	M	negative	#159	U/U	U	negative
#66	U/U	U	positive	#160	U/U	U	negative
#67	M/M	M	negative	#161	U/U	U	positive

45 cases with distant metastasis, and 45 deaths because of breast cancer in the cohort. Disease-free survival and overall survival differed significantly between classes of P-cadherin expression, as revealed in Kaplan-Meier plots. The probabilities of disease-free and overall survival were significantly lower for patients with P-cadherin-positive tumors ($P = 0.0027$ and $P = 0.0237$, respectively; Fig. 3C and D). The interval between diagnosis and local recurrence also showed a slight correlation with P-cadherin expression: a mean of 35 ± 20.15 months for positive and 73.6 ± 32 months for negative tumors ($P = 0.0545$). No correlation was found between E- or N-cadherin expression and disease-free and overall survival.

P-cadherin promoter methylation

MCF-7/AZ cells treated with 5-Aza-2'-deoxycytidine. To evaluate whether it would be reasonable to test our hypothesis in a breast cancer series, we treated MCF-7/AZ cells, which present lower levels of P-cadherin, with the demethylating agent 5-Aza-2'-deoxycytidine ($2.5 \mu\text{mol/L}$). After 5 days, we harvested the cells, and we analyzed P-cadherin mRNA and protein levels,

by reverse transcription-PCR and Western blot, respectively. We observed an increase of both levels, suggesting that hypomethylation of the promoter accompanies transcriptional activation of the *CDH3* gene in this breast cancer cell line (Fig. 4A and B).

Normal breast epithelial cells. P-cadherin promoter methylation was analyzed in five cases of normal breast tissue, from which only epithelial cells were microdissected. Methylation of P-cadherin gene was found in all the cases analyzed, because none of the samples showed the presence of unmethylated alleles (Fig. 4C). Indeed, these results are highly correlated with P-cadherin expression because normal breast epithelial cells are negative for this protein. This evidence supported the hypothesis that the transcriptional inactivation of P-cadherin in such cells could be regulated by *CDH3* promoter methylation.

Invasive breast carcinomas. P-cadherin promoter methylation was analyzed in 64 cases of invasive carcinomas (Table 2). Methylation of P-cadherin gene was found in 58% (37 of 64) of invasive carcinomas, whereas P-cadherin unmethylation was found in 42% (27 of 64; Fig. 4D; Table 2). When these results

were correlated with P-cadherin expression, a statistically significant association was found between these variables: 71% of P-cadherin-negative cases were methylated, whereas 65% of positive cases were unmethylated ($P = 0.005$; Fig. 4E; Table 2). Interestingly, six out of seven cases showing partial methylation (with both methylated and unmethylated alleles) were negative for P-cadherin expression, reinforcing the correlation that was observed. Thus, the transcriptional control of P-cadherin in human breast cancer might be associated with changes of *CDH3* CpG island promoter methylation.

Discussion

Over the last 5 years, research on breast cancer has suggested the use of many new prognostic markers. Some of these markers could raise questions, not only about divergent phenotypes, but also about different histogenesis. One of these examples is P-cadherin, which has been identified as a possible valuable indicator of poor prognosis in breast cancer patients (12). In this study, confirming the results obtained by others (11, 12, 29, 34), P-cadherin was indeed significantly expressed in high-grade, ER- α -negative, and highly proliferative invasive breast tumors. Furthermore, a shorter patient disease-free and overall survival in P-cadherin-positive invasive carcinomas was found using the statistical univariate analysis done.

The phenotype acquired by this specific subset of tumors is actually classified as myoepithelial/basal-like, which means the acquisition of molecules frequently restricted to the myoepithelia of normal breast tissue and loss of the ones expressed by epithelial cells (35). These characteristics have indeed been already associated with poor patient survival (35), confirming that P-cadherin is one of the proteins related to biological aggressiveness in breast carcinomas. In a recent report from our group regarding the involvement of P-cadherin in cell invasion, we have shown that this molecule has an effective proinvasive activity in the MCF-7/AZ breast cancer cell line, through its interaction with signaling proteins bound to the juxtamembrane domain (13). In a way, these results give an explanation as to why P-cadherin is correlated with poor prognosis in breast cancer patients. Accordingly, Taniuchi et al. also showed that overexpressed P-cadherin/*CDH3* promotes the motility of pancreatic cancer cells by its interaction with p120ctn and consequent activation of Rho-family GTPases (36). Based on these results, the blocking of P-cadherin activity, or its associated signaling, could probably be a novel therapeutic approach for treatment of aggressive breast carcinomas.

We have already found a direct link between P-cadherin expression and the lack of ER- α signaling in breast cancer cells, showing that P-cadherin expression depends on an estrogen-independent cell environment (13). Additionally, genetic or epigenetic alterations in the P-cadherin gene is likely to regulate the behavior of neoplastic cells as compared with that of normal epithelial cells: cell-cell interactions may be changed, leading to modified intercellular communication and, consequently, altered intracellular signaling (37).

DNA methylation of promoter CpG islands has been recognized as an important mechanism for regulation of gene expression and transcriptional modification in mammals. Although considerable work has been done on the epigenetic control of tumor suppressor genes, little is known about the

potential role of promoter CpG demethylation in the activation of oncogenes (32).

The present study showed a statistically significant correlation between the methylation patterns of the *CDH3* promoter region of P-cadherin and its aberrant protein expression levels in breast carcinomas. This methylation status of the DNA chromatin in P-cadherin promoter region might play a role in the ability of transcription factors to bind to the transcription start site, thus regulating mRNA transcription, and consequently its protein expression. Our results are supported by Jarrard and collaborators' data in prostate cancer cell lines (14). They showed that *CDH3* promoter methylation occurs in P-cadherin-negative cell lines, but not in cell lines expressing this gene, and showed a complete ablation of P-cadherin transcriptional activity when methylation was present to any extent within the GC-rich promoter region. This was also described in a recent study done in melanoma cell lines (28), and is in keeping with reports on the role of promoter methylation for transcriptional regulation of tissue-specific genes (38). Moreover, the treatment of an extensive culture of MCF-7/AZ breast cancer cell line with 5-Aza-2'-deoxycytidine demethylating agent induced the expression levels of P-cadherin mRNA and protein. These results provided clear evidence that the observed correlation *in vivo* is backed up by experimental *in vitro* data.

In contrast with our results, these same authors have reported the absence of a correlation between *in vivo* P-cadherin expression in prostate adenocarcinomas and the methylation status of the *CDH3* promoter (14). In prostate tissue, P-cadherin is strongly expressed on basal epithelial cells and is completely negative in luminal epithelial cells. However, in contrast with breast cancer, this protein was absent in the prostate cancers analyzed in this study. Additionally, the methylation status of a P-cadherin CpG island was examined in 12 normal and matched primary prostate cancers, using methylation-sensitive enzymes. Although all the restriction sites analyzed were found to be unmethylated in P-cadherin-positive normal tissues, no detectable methylation was shown in any tumor sample, showing no correlation with the absence of P-cadherin expression (14). In our opinion, the conflicting results obtained by these authors can be explained by two reasons: (a) the number of cases that were studied and (b) the distinct methodology that was used. Also in our series, we obtained cases that did not show correlation between the promoter methylation status and the protein expression: 29% of the P-cadherin-negative cases showed unmethylation pattern, and 35% of the positive cases were methylated. However, using statistical analysis in a large tumor series, we were able to find a significant correlation between P-cadherin expression and gene hypomethylation. Statistics using only 12 cases cannot be representative of the methylation process as a regulator mechanism occurring in cancer cells. Besides, these authors claim that the normal prostate tissue is completely unmethylated for the P-cadherin gene in all the restriction sites analyzed. Because normal tissue includes basal P-cadherin-positive cells as well as luminal P-cadherin-negative cells, it was expected to find both methylated and unmethylated alleles in these samples. Therefore, we used methylation-specific PCR assays in order to analyze larger DNA fragments, and also microdissected our samples to get more homogenous cell populations.

Furthermore, supporting our hypothesis, the laser-microdissected normal breast epithelia showed complete methylation

of the *CDH3* promoter region in the five cases studied, suggesting that P-cadherin protein expression is repressed in normal epithelial cells by this specific molecular mechanism. Based on these results, we can suggest that, during breast carcinogenesis, progressive hypomethylation of *CDH3* alleles occurs, which induces its expression in some mammary carcinomas, where its functional activity induces cancer cell invasion and motility (13, 36). This progressive *CDH3* promoter hypomethylation is clearly seen in cases presenting partial methylation, which were still negative for P-cadherin expression like the normal epithelial cells.

Cancer-associated DNA hypomethylation is as prevalent as cancer-linked hypermethylation, although its biological significance in carcinogenesis is less understood. There are several examples of other tumor-overexpressed genes, which become promoter-hypomethylated during carcinogenesis, supporting the data observed within *CDH3*. The cyclin D2 gene is overexpressed in a subset of gastric carcinomas, and Oshimo et al. have shown that DNA hypomethylation is a mechanism underlying the increased expression of cyclin D2 in cancer cells and that its progressive demethylation may be involved in the development and progression of gastric carcinoma (32). Also, the melanoma antigen (*MAGE*)-encoding genes are expressed in various tumor types via demethylation of their promoter CpG islands (39), which are silent in all nonneoplastic tissues except for the testis and placenta. Honda et al. have found that *MAGE-A1* and *-A3* demethylation occurs during progressive stages of gastric

cancer, and tended to be associated with a worse patient prognosis (40). Also in breast cancer, urokinase-type plasminogen activator, which is only expressed by highly invasive cancer cells and has been implicated in tumor motility, invasion, and angiogenesis, was also found to be the result of hypomethylation of its coding gene (41–43).

In conclusion, although there is just a small number of genes that have been shown to be transcriptionally activated by DNA demethylation, in comparison with the list of tumor suppressor genes that are silenced by hypermethylation in cancer cells, all these studies are consistent with the hypothesis that hypomethylation of critical genes plays a role in cancer invasion and metastasis. Based on this, the methylation inhibition of these genes, like urokinase-type plasminogen activator and P-cadherin in breast cancer, can be used as a novel therapeutic approach to silence their expression and, consequently, to block tumor progression into the aggressive and metastatic stages of the disease.

Acknowledgments

We thank Drs. Jorge Cameselle (from Hospital Xeral Cies, Vigo, Spain), Isabel Amendeira (from the S. João Hospital, Porto, Portugal), and Manuela Lacerda (from Portuguese Institute of Oncology of Coimbra, Portugal) for the biological material used in this study. We also would like to thank Dina Leitão and Vasco Serra for the immunohistochemical assay for P- and E-cadherin, respectively, Sara Ricardo for the slide preparations used for tumor microdissection, and Paula Silva and Cátia Moutinho for the normal breast tissue laser microdissection (Project SIFEC No. 15-02-01-FDR-00235).

References

- Conacci-Sorrell M, Zhurinsky J, Ben Ze'ev A. The cadherin-catenin adhesion system in signaling and cancer. *J Clin Invest* 2002;109:987–91.
- Nose A, Nagafuchi A, Takeichi M. Expressed recombinant cadherins mediate cell sorting in model systems. *Cell* 1988;54:993–1001.
- Steinberg MS, Takeichi M. Experimental specification of cell sorting, tissue spreading, and specific spatial patterning by quantitative differences in cadherin expression. *Proc Natl Acad Sci U S A* 1994;91:206–9.
- Takeichi M. Cadherin cell adhesion receptors as a morphogenetic regulator. *Science* 1991;251:1451–5.
- Daniel CW, Strickland P, Friedmann Y. Expression and functional role of E- and P-cadherins in mouse mammary ductal morphogenesis and growth. *Dev Biol* 1995;169:511–9.
- Nose A, Takeichi M. A novel cadherin cell adhesion molecule: its expression patterns associated with implantation and organogenesis of mouse embryos. *J Cell Biol* 1986;103:2649–58.
- Behrens J. Cadherins and catenins: role in signal transduction and tumor progression. *Cancer Metastasis Rev* 1999;18:15–30.
- Takeichi M. The cadherins: cell-cell adhesion molecules controlling animal morphogenesis. *Development* 1988;102:639–55.
- Shimoyama Y, Hirohashi S, Hirano S, et al. Cadherin cell-adhesion molecules in human epithelial tissues and carcinomas. *Cancer Res* 1989;49:2128–33.
- Palacios J, Benito N, Pizarro A, et al. Anomalous expression of P-cadherin in breast carcinoma. Correlation with E-cadherin expression and pathological features. *Am J Pathol* 1995;146:605–12.
- Gamallo C, Moreno-Bueno G, Sarrio D, Calero F, Hardisson D, Palacios J. The prognostic significance of P-cadherin in infiltrating ductal breast carcinoma. *Mod Pathol* 2001;14:650–4.
- Peralta SA, Knudsen KA, Salazar H, Han AC, Keshgegian AA. P-cadherin expression in breast carcinoma indicates poor survival. *Cancer* 1999;86:1263–72.
- Paredes J, Stove C, Stove V, et al. P-cadherin is up-regulated by the antiestrogen ICI 162,780 and promotes invasion of human breast cancer cells. *Cancer Res* 2004;64:8309–17.
- Jarrard DF, Paul R, van Bokhoven A, et al. P-cadherin is a basal cell-specific epithelial marker that is not expressed in prostate cancer. *Clin Cancer Res* 1997;3:2121–8.
- Baylin SB, Makos M, Wu JJ, et al. Abnormal patterns of DNA methylation in human neoplasia: potential consequences for tumor progression. *Cancer Cell* 1991;3:383–90.
- Graff JR, Herman JG, Lapidus RG, et al. E-cadherin expression is silenced by DNA hypermethylation in human breast and prostate carcinomas. *Cancer Res* 1995;55:5195–9.
- Faraldo ML, Cano A. The 5' flanking sequences of the mouse P-cadherin gene. Homologies to 5' sequences of the E-cadherin gene and identification of a first 215 base pair intron. *J Mol Biol* 1993;231:935–41.
- Bussemakers MJ, van Bokhoven A, Voller M, Smit FP, Schalken JA. The genes for the calcium-dependent cell adhesion molecules P- and E-cadherin are tandemly arranged in the human genome. *Biochem Biophys Res Commun* 1994;203:1291–4.
- Bussemakers MJ, van Bokhoven A, Mees SG, Kemler R, Schalken JA. Molecular cloning and characterization of the human E-cadherin cDNA. *Mol Biol Rep* 1993;17:123–8.
- Bussemakers MJ, Girolodi LA, van Bokhoven A, Schalken JA. Transcriptional regulation of the human E-cadherin gene in human prostate cancer cell lines: characterization of the human E-cadherin gene promoter. *Biochem Biophys Res Commun* 1994;203:1284–90.
- Chang HW, Chow V, Lam KY, Wei W, Yuen A. Loss of E-cadherin expression resulting from promoter hypermethylation in oral tongue carcinoma and its prognostic significance. *Cancer* 2002;94:386–92.
- Droufakou S, Deshmane V, Roylance R, Hanby A, Tomlinson I, Hart IR. Multiple ways of silencing E-cadherin gene expression in lobular carcinoma of the breast. *Int J Cancer* 2001;92:404–8.
- Nakayama S, Sasaki A, Mese H, Alcalde RE, Tsuji T, Matsumura T. The E-cadherin gene is silenced by CpG methylation in human oral squamous cell carcinomas. *Int J Cancer* 2001;93:667–73.
- Nass SJ, Herman JG, Gabrielson E, et al. Aberrant methylation of the estrogen receptor and E-cadherin 5' CpG islands increases with malignant progression in human breast cancer. *Cancer Res* 2000;60:4346–8.
- Gagnon J, Shaker S, Primeau M, Hurtubise A, Mompalmer RL. Interaction of 5-aza-2'-deoxycytidine and desipeptide on antineoplastic activity and activation of 14–3-3 σ . E-cadherin and tissue inhibitor of metalloproteinase 3 expression in human breast carcinoma cells. *Anticancer Drugs* 2003;14:193–202.
- Hurtubise A, Mompalmer RL. Evaluation of antineoplastic action of 5-aza-2'-deoxycytidine (Dacogen) and docetaxel (Taxotere) on human breast, lung and prostate carcinoma cell lines. *Anticancer Drugs* 2004;15:161–7.
- Nam JS, Ino Y, Kanai Y, Sakamoto M, Hirohashi S. 5-aza-2'-deoxycytidine restores the E-cadherin system in E-cadherin-silenced cancer cells and reduces cancer metastasis. *Clin Exp Metastasis* 2004;21:49–56.
- Tsutsunuma A, Hamada J, Tada M, et al. Epigenetic silencing of E- and P-cadherin gene expression in human melanoma cell lines. *Int J Oncol* 2004;25:1415–21.
- Paredes J, Milanezi F, Viegas L, Amendeira I, Schmitt F. P-cadherin expression is associated with high-grade ductal carcinoma *in situ* of the breast. *Virchows Arch* 2002;440:16–21.

30. Herman JG, Graff JR, Myohanen S, Nelkin BD, Baylin SB. Methylation-specific PCR: a novel PCR assay for methylation status of CpG islands. *Proc Natl Acad Sci U S A* 1996;93:9821–6.
31. Graff JR, Gabrielson E, Fujii H, Baylin SB, Herman JG. Methylation patterns of the E-cadherin 5' CpG island are unstable and reflect the dynamic, heterogeneous loss of E-cadherin expression during metastatic progression. *J Biol Chem* 2000;275:2727–32.
32. Oshimo Y, Nakayama H, Ito R, et al. Promoter methylation of cyclin D2 gene in gastric carcinoma. *Int J Oncol* 2003;23:1663–70.
33. Bloom HJ, Richardson WW. Histological grading and prognosis in breast cancer. *Br J Cancer* 1957;11:359–77.
34. Paredes J, Milanezi F, Reis-Filho JS, Leitao D, Athanazio D, Schmitt F. Aberrant P-cadherin expression: is it associated with estrogen-independent growth in breast cancer? *Pathol Res Pract* 2002;198:795–801.
35. Perou CM, Sortie T, Eisen MB, et al. Molecular portraits of human breast tumours. *Nature* 2000;406:747–52.
36. Taniuchi K, Nakagawa H, Hosokawa M, et al. Over-expressed P-cadherin/CDH3 promotes motility of pancreatic cancer cells by interacting with p120ctn and activating rho-family GTPases. *Cancer Res* 2005;65:3092–9.
37. Wheelock MJ, Soler AP, Knudsen KA. Cadherin junctions in mammary tumors. *J Mammary Gland Biol Neoplasia* 2001;6:275–85.
38. Mesquita P, Peixoto AJ, Seruca R, et al. Role of site-specific promoter hypomethylation in aberrant MUC2 mucin expression in mucinous gastric carcinomas. *Cancer Lett* 2003;189:129–36.
39. De Smet C, Lorient A, Boon T. Promoter-dependent mechanism leading to selective hypomethylation within the 5' region of gene MAGE-A1 in tumor cells. *Mol Cell Biol* 2004;24:47B1–90.
40. Honda T, Tamura G, Waki T, et al. Demethylation of MAGE promoters during gastric cancer progression. *Br J Cancer* 2004;90:83B–43.
41. Pakneshan P, Szyf M, Farias-Eisner R, Rabbani SA. Reversal of the hypomethylation status of urokinase (uPA) promoter blocks breast cancer growth and metastasis. *J Biol Chem* 2004;279:31735–44.
42. Guo Y, Pakneshan P, Gladu J, Slack A, Szyf M, Rabbani SA. Regulation of DNA methylation in human breast cancer. Effect on the urokinase-type plasminogen activator gene production and tumor invasion. *J Biol Chem* 2002;277:41571–9.
43. Pakneshan P, Tetu B, Rabbani SA. Demethylation of urokinase promoter as a prognostic marker in patients with breast carcinoma. *Clin Cancer Res* 2004;10:3035–41.

PHYSIOLOGY AND MANAGEMENT

Mammary-Derived Growth Inhibitor Protein and Messenger Ribonucleic Acid Concentrations in Different Physiological States of the Gland

I. POLITIS and R. C. GOREWIT
Department of Animal Science
Cornell University
Ithaca 14853

T. MULLER and R. GROSSE
Department of Cellular Biochemistry
Academy of Sciences
Berlin-Buch, Germany 1115

ABSTRACT

Expression of mammary-derived growth inhibitor in tissue from lactating and involuting bovine mammary glands was investigated. Seventeen lactating, pregnant (220 to 272 d in gestation) cows were divided in two groups of 8 and 9 cows each. Cows of the first group were slaughtered while in lactation. Cows of the second group (9 involuting cows) were slaughtered at 13 to 52 d following sudden cessation of milking. High concentrations of mammary-derived growth inhibitor (63% of the total protein) were detected in mammary tissue of lactating cows. Mammary-derived growth inhibitor (<10% of the total protein) was dramatically reduced during most of the involution period (13 to 45 d following cessation of milking). Mammary-derived growth inhibitor was again detected (.28% of the total protein) during the last stage of the involution (46 to 53 d after cessation of milking), which coincided with colostrum formation. When steady state concentrations of mammary-derived growth inhibitor mRNA were examined, the results obtained mirrored those obtained at the protein concentration. These data suggest that regulation of mammary-derived growth inhibitor occurs via modulation of the steady state concentration of its mRNA. Furthermore, there is a strong

correlation between mammary-derived growth inhibitor expression and lactation in dairy cows.

(Key words: mammary-derived growth inhibitor, lactation, involution)

Abbreviation key: MDGI = mammary-derived growth inhibitor.

INTRODUCTION

Mammary-derived growth inhibitor (MDGI) is a 13-kDa protein purified from the lactating bovine mammary gland (2, 9, 10). In situ hybridization and immunohistochemical analysis showed that MDGI is actually produced by mammary epithelial cells (9). Mammary-derived growth inhibitor inhibits proliferation of several normal and transformed mammary epithelial cell lines in a dose-dependent and reversible manner (6). The MDGI protein and mRNA are higher in fully differentiated lactating glands than in rapidly developing glands of pregnant animals (9, 10). Mammary-derived growth inhibitor may fulfill a role in the onset of differentiation coupled with inhibition of mammary epithelial cell proliferation (6).

Dairy cows require a nonlactating period of approximately 60 d prior to lactation to achieve maximal milk production in the subsequent lactation (8, 11, 15). The nonlactating period of the dairy cow is divided into three distinct stages: 1) an initial period of active involution, which begins just after the cessation of milking and is completed by approximately 30 d in the dry period; 2) a period of steady state involution (31 to 45 d after cessation of milking); and 3) a period of colostrum formation prior to the initiation of lactation (46

Received December 12, 1991.
Accepted February 10, 1992.

to 60 d following cessation of milking) (8, 14, 15). Politis et al. (12, 13) detected very low concentrations of MDGI in the mammary glands of dairy cows during the first two stages of mammary involution. It is not known whether MDGI is expressed in the bovine mammary gland during the last stage of involution, which coincides with colostrum formation. Furthermore, there is no published information on changes of MDGI mRNA between lactating and involuting animals.

The objective of the present study was to investigate changes in MDGI mRNA and protein concentrations between lactating and involuting animals. Emphasis was placed on the last stage of involution, which coincided with colostrum formation. Our work provides more basic knowledge toward understanding the molecular events affecting MDGI expression during mammary growth and development.

MATERIALS AND METHODS

Animals

Seventeen lactating, pregnant (220 to 272 d in gestation) Holstein cows were used throughout this investigation. Eight cows were slaughtered while in lactation. The remaining 9 cows were slaughtered during the dry period according to the following schedule: 3 cows at 12 to 30 d, another set of 3 cows at 31 to 45 d, and the remaining 3 cows at 46 to 53 d following sudden cessation of milking. These days were chosen to correspond with the three distinct stages of the involution process: active involution, steady state involution, and colostrum formation (8, 14, 15). Cessation of milking occurred at approximately 300 DIM. At slaughter, the udder was removed quickly, and approximately 15 to 20 g of mammary tissue parenchyma were dissected, frozen in liquid nitrogen, and transported immediately to our laboratory.

Tissue Preparation for MDGI Protein Determination

Mammary tissue (10 g), obtained at the local slaughter house, was minced with scissors and homogenized using a Brinkman homogenizer (Kinematica GmbH, Steinhofhalde, Switzerland) in 25 ml of homogenization buffer (50 mM Tris-HCl, pH 7.5, 25 mM KCl,

5 mM $MgCl_2$) supplemented with .25 M sucrose and protease inhibitors: pepstatin A (.5 μ g/ml) and phenylmethylsulfonylsulfate (.5 mM). The homogenate was centrifuged at $1000 \times g$ for 10 min. The supernatant was recovered and centrifuged at $100,000 \times g$ for 30 min to obtain a pellet containing microsomes and mitochondria and a supernatant denoted as the cytoplasmic fraction.

Detection of MDGI Antigen

Western blot analysis using anti-MDGI rabbit serum was employed to examine the presence or absence of MDGI in the cytoplasmic fraction of bovine mammary tissue (12, 13). The cytoplasmic fraction contains the majority of MDGI present in the mammary cells (10, 12, 13). Anti-MDGI rabbit IgG was produced by R. Grosse in the Central Institute of Molecular Biology, Academy of Sciences, Berlin-Buch, Germany. All details regarding preparation and the specificity of this antibody have been described earlier (2, 10, 12, 13).

The SDS-PAGE was carried out using 15% acrylamide-resolving gels and 4% acrylamide-stacking gels as described by Bohmer et al. (2). Samples were electrophoresed in .02 M Tris, .15 M glycine buffer (pH 8.3) at 30 mA for 5 h along with standards from 2.5 to 116 kDa (Sigma Chemical Co., St. Louis, MO) in adjacent lanes. Gel portions containing standards were cut, stained for 30 min in 1% (wt/vol) Coomassie brilliant blue dye and 50% (wt/vol) trichloroacetic acid, and destained in 20% (vol/vol) acetic acid. Portions of the gels containing fractionated proteins present in the cytoplasmic fraction of mammary tissue were further processed for Western blots.

Western blots were prepared using immobilon membranes (Millipore, Bedford, MA). Electrostatic transfer of samples previously fractionated by SDS-PAGE (30 V, 12 h, 4°C; Bio-Rad Transblot apparatus, Bio-Rad, Richmond, CA) was carried out in .02 M Tris, .15 M glycine (pH 8.3) containing 20% methanol. Initially, membranes were incubated at room temperature for 30 min in Tris-buffered saline (50 mM Tris, .9% NaCl, pH 7.5) containing 3% gelatin. Subsequently, all washes and incubations were carried out with Tris-buffered saline containing 1% gelatin. After washing, the membranes were incubated for 12 h with

anti-MDGI rabbit IgG (2 µg/ml); they were then washed and incubated for 2 h with the secondary antibody, peroxidase-conjugated anti-rabbit IgG (1:1000 dilution; Sigma Chemical Co.). To ensure antibody specificity, a control lane was loaded with 1 µg of purified MDGI. The MDGI antigen was purified by R. Grosse in the Central Institute of Molecular Biology. All details of this purification procedure have been described earlier (6). All membranes were washed and stained with .003% hydrogen peroxide and 4-chloro-1-naphthol (.6 mg/ml; Bio-Rad).

Determination of MDGI Protein Content

An ELISA methodology was developed to measure MDGI concentration in the cytoplasmic fraction of bovine mammary cells obtained from lactating and involuting glands. Briefly, test samples were initially incubated in .1% SDS at 37°C for 30 min. This step is necessary because MDGI has the tendency to precipitate. Samples were then diluted in .1 M sodium bicarbonate buffer (pH 9.6), incubated overnight at 4°C in a 96-well polystyrene microtiter plate, and then equilibrated for 1 h at 37°C with 100 µl of anti-MDGI rabbit IgG (.8 µg/ml). Wells were washed six times with PBS (.14 M NaCl, .01 M NaH₂PO₄, pH 7.2) containing .05% Tween 80, incubated for 1 h at 37°C with 100 µl of anti-rabbit IgG-peroxidase conjugate (1:2000 dilution), and washed again six times with PBS. One hundred microliters of .182 mM 2',2'-azineo-diethylbenzothiazoline sulfonate (Sigma Chemical Co.) in .1 M citrate buffer (pH 5.2) containing .003% hydrogen peroxide were then added to each well. Absorbance was measured at 405 nm after 10 min. Controls included in the assays were 1) wells coated with bovine serum albumin without sample and 2) wells with the first antibody layer substituted by nonimmune serum. The sensitivity of this assay system was 1 ng/ml, and absorbance was linear with MDGI concentration up to 10 ng/ml. Recovery of an added mass of MDGI was 91.8%, and intraassay and interassay coefficients of variation were less than 10%.

The MDGI protein concentration was expressed as micrograms of MDGI per milligram of total protein. Total protein in cytoplasmic and microsomal fractions of mammary tissue

was determined by the method of Bradford (3) using bovine serum albumin as a standard.

Isolation of Total RNA from Mammary Tissue

Total cellular RNA from mammary tissue was isolated by the method of Chomczynski and Sacchi (4). Mammary tissue (1 g) was cut into small pieces, while frozen, with a sterile razor blade in a petri dish. Mammary gland pieces were lysed by the addition of 10 ml of RNazol (CINNA/BIOTECH, Frienswood, TX). The larger pieces of the tissue were homogenized by drawing the lysis buffer and tissue through a syringe fitted with an 18-gauge needle and subsequently were transferred to a fresh polypropylene tube. One milliliter of chloroform was then added, and the final suspension was mixed vigorously and then placed on ice for 15 min. Samples were centrifuged at 10,000 × g for 20 min at 4°C. After centrifugation, the upper aqueous phase containing RNA was transferred to a new tube, mixed with an equal volume of isopropanol, and then placed at -70°C for 1 h to precipitate RNA. Sedimentation at 10,000 × g for 20 min was then performed, the supernatant was discarded, and the RNA pellet was washed twice with 95% ethanol, sedimented, vacuum dried (15 min), and dissolved in .2 ml of H₂O.

Northern Blot Analysis

Hybridization of immobilized RNA to radiolabeled cDNA probes was performed as described previously (1). Briefly, 8 µg of total RNA were separated by electrophoresis on a 1.2% agarose gel containing 6% formaldehyde. The gel was rinsed twice in 10 × SSC (.15 M NaCl, .015 M sodium citrate, pH 7.0) for 10 min at room temperature, and the RNA was transferred to zeta probe membranes (Bio-Rad) by capillary blotting with 20 × SSC for 20 h. Following transfer, the membrane was placed in a plastic bag containing 8 ml of prehybridization buffer [50% formamide, 4 × (.15 M NaCl, .01 M NaH₂PO₄, 1 mM EDTA, pH 7.4), 1% SDS, 200 µg/ml of salmon sperm DNA, and 5 mg/ml of skim milk powder] for 20 h at 42°C. Membranes were hybridized in the same solution containing 4 × 10⁵ cpm/ml of ³²P-labeled MDGI cDNA, labeled using nick-translation (1). The membranes were washed at 42°C for 20 min in approximately 300 ml of 2

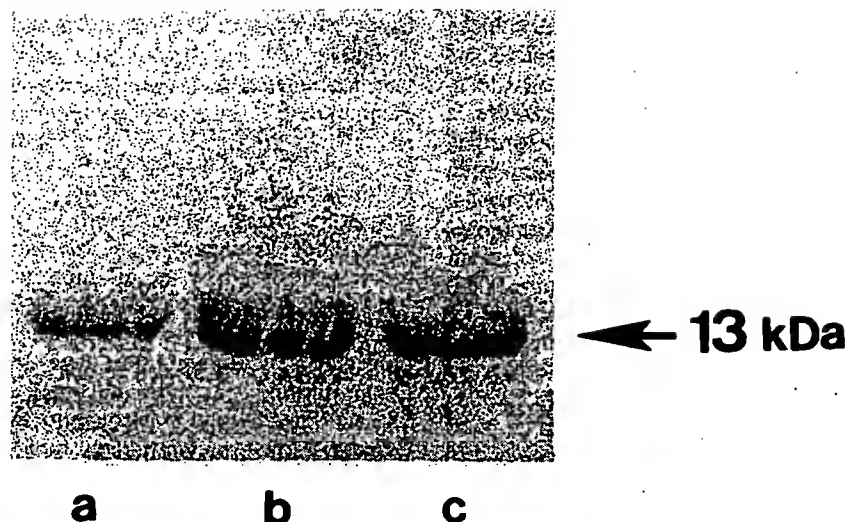


Figure 1. Western blot analysis of mammary tissue mammary-derived growth inhibitor (MDGI). Proteins from cytoplasmic fraction of mammary cells were separated by SDS-PAGE, blotted onto nitrocellulose, and detected with anti-MDGI rabbit serum and anti-rabbit IgG-peroxidase conjugate. Lane a, 15 μ g of cytoplasmic mammary cell extract obtained from involuting cows (4 to 53 d following cessation of milking); lane b, 5 μ g of cytoplasmic mammary cell extract obtained from lactating cows; lane c, .35 μ g of purified MDGI.

\times SSC-.1% SDS, then with .5 \times SSC-.1% SDS, and then .1 \times SSC-.1% SDS. The membranes were then exposed to Kodak XAR-S X-ray film (Eastman Kodak Co., Rochester, NY) at -72°C for 24 h using two intensifying screens. Relative radioactivity was estimated from the autoradiograms by densitometry.

Membranes were stripped with 50 mM NaOH at room temperature for 30 min and were probed for a second time with a mouse 18-S rRNA probe to estimate the amount of total RNA in each lane and, therefore, to normalize for variability in RNA loaded to each well and transfer efficiency.

Statistical Analysis

All data were expressed as means and standard deviations. Differences between means were evaluated using the Student's *t* test ($P < .05$).

RESULTS

Western blot analysis was performed to establish the presence of MDGI antigen in mammary tissue obtained from glands at different

physiological stages. Figure 1 shows the presence of a 13-kDa immunoreactive MDGI antigen in mammary tissue obtained from involuting cows at 46 to 53 d after cessation of milking (lane a) and from lactating cows (lane b), which comigrated with purified MDGI (lane c).

To gain more insight into the pattern of MDGI production, ELISA methodology was employed to measure MDGI protein concentrations in mammary tissue. Table 1 shows the presence of high concentrations of MDGI (6.3 $\mu\text{g}/\text{mg}$ of total protein) in mammary tissue obtained from lactating cows. However, MDGI was present at very low concentrations ($<.8$ $\mu\text{g}/\text{mg}$ of total protein) in mammary tissue obtained from mammary glands at the first stage (less than 30 d after cessation of milking) or second stage (31 to 45 d after cessation of milking) of involution. The MDGI was again detected (2.8 $\mu\text{g}/\text{mg}$ of total protein) during the last stage of involution (46 to 53 d after cessation of milking), which coincided with colostrum formation.

To investigate the level at which the expression of MDGI is regulated, the steady state concentrations of MDGI mRNA concentra-

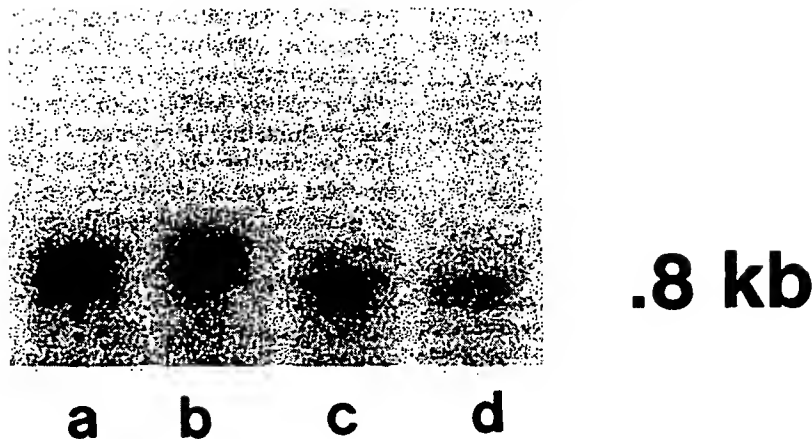


Figure 2. Mammary-derived growth inhibitor (MDGI) mRNA isolated from mammary tissue obtained from lactating and involuting glands. Total RNA (8 μ g) was electrophoresed on agarose gel and transferred to membrane, and the filter was probed with a nick-translated MDGI cDNA probe. Lanes a and b, total RNA isolated from lactating mammary glands; Lanes c and d, total RNA isolated from involuting mammary glands (46 to 53 d following cessation of milking).

tions were explored. Total RNA from bovine mammary tissue was hybridized with a bovine MDGI cDNA, and the results are presented in Figure 2. As shown, bovine MDGI was encoded by a single RNA species of approximately 800 nucleotides long, a size in agreement with that previously reported (6). Relative amounts of MDGI mRNA were initially determined by scanning the autoradiogram. Then, the blot was stripped, hybridized with a 18-S rRNA probe, and scanned for a second time to estimate the amount of total RNA in each lane. Values obtained for MDGI mRNA from the first scanning were then divided by the corresponding 18-S rRNA values from the second scanning, therefore accounting for variability in the amount of RNA loaded to each lane and transfer efficiency. The normalized values were then expressed as percentage of the maximal stimulation; the maximally stimulated sample was arbitrarily assigned a value of 100%. The results are presented in Table 2. As shown, maximal stimulation of MDGI mRNA occurred in mammary tissue obtained from lactating animals. Lower (threefold) MDGI mRNA were detected in mammary tissue obtained from involuting animals at the last stage of involution (46 to 53 d following cessation of milking). This coincided with colostrum formation. We were unable to detect appreciable mRNA in mammary

glands of involuting cows (first and second stages).

DISCUSSION

The first novel finding emerging from this study is the presence of MDGI in mammary tissue obtained from glands during the last stage of the involution, which coincided with colostrum formation. Western blot analysis, however, reflects the presence or absence of MDGI antigen. It does not address the possibility of quantitative differences in concentra-

TABLE 1. Mammary-derived growth inhibitor (MDGI)¹ antigen in mammary tissue obtained from lactating and involuting Holstein cows.

Source	MDGI Antigen	
	(μ g/mg of proteins)	
	\bar{X}	SD
Lactating	6.3	1.2
Involution stage ²		
First	.08	.06
Second	.04	.03
Third	.28	.12

¹The MDGI expression was determined by ELISA.

²First stage corresponds to 12 to 30 d, second stage to 31 to 45 d, and third stage to 46 to 53 d following sudden cessation of milking.

TABLE 2. Mammary-derived growth inhibitor (MDGI) mRNA in mammary tissue obtained from lactating and involuting Holstein cows.

Source	Relative amounts of MDGI mRNA (%)
Lactating	100
Involution stage ²	
First	ND ²
Second	ND
Third	36

¹First stage corresponds to 12 to 30 d, second stage to 31 to 45 d, and third stage to 46 to 53 d following sudden cessation of milking.

²Not detected.

tions of MDGI expression. To address this question, an ELISA used to measure MDGI protein concentrations showed much higher MDGI in mammary tissue obtained from glands of lactating than from glands of involuting cows (first and second stages). Again MDGI was detected at lower, but still appreciable, concentrations than those in lactating glands during the last stage of involution (46 to 53 d after cessation of milking), which coincided with colostrum formation.

Relatively little is known about the specific mechanism or mechanisms, including the role of growth factors or growth inhibitors in triggering or initiating the process of active milk (colostrum) secretion prior to parturition. Two weeks prior to parturition, mammary glands undergo several functional changes characterized by colostrum formation (5, 7, 9). Colostrogenesis is favored by the hormonal environment at the end of pregnancy and occurs in two stages: 1) the first stage, which comprises the prepartum period, is characterized by the appearance of precolostral fluid; 2) the second stage, which begins immediately prior to parturition, is characterized by the onset of active milk secretion (5, 7). What is the physiological significance of the presence of high concentrations of MDGI during this period? In considering a reasonable explanation, we recall that two roles have been proposed for MDGI: epithelial cell differentiation and inhibition of cell proliferation (6). Near parturition, two key phenomena occur: intense growth and differen-

tiation of the secretory epithelium (9). The presence of high concentrations of MDGI during the prepartum period likely is consistent with a role for MDGI in differentiation rather than proliferation of mammary epithelial cells. The question of whether MDGI production in the third stage of involution is a consequence of initiation of colostrum production, or involvement of MDGI in the regulation of these phenomena, or both cannot be answered at the moment.

The second major finding of the present study was that the regulatory mechanism for control of MDGI expression in mammary cells *in vivo* is via modulation of the steady state concentration of its mRNA. This is because changes in MDGI mRNA concentrations were almost identical to those observed at the protein level. The MDGI mRNA was highest in lactating glands; MDGI mRNA in involuting glands (third stage) was still approximately 36% of the fully induced concentrations observed in lactating glands. The MDGI mRNA was not detected in involuting glands obtained during the first and second periods.

Two mechanisms for MDGI mRNA regulation are consistent with these observations: 1) modulation of MDGI mRNA through changes in transcriptional activity of the MDGI gene and 2) modulation through stabilization of MDGI mRNA. Further experiments involving measurements of transcription rates will more clearly define how the message levels are being modulated.

Based on the results obtained at the protein level, one should expect some, even though limited, MDGI mRNA in involuting cows (first and second stages). These are two possible explanations for this inconsistency. First, the MDGI protein may have been actually produced at an earlier stage of lactation and remained within the mammary gland in association with milk fat. This explanation is consistent with earlier findings (6), suggesting that MDGI is found in milk in strong association with milk fat globule membrane. Second, MDGI mRNA was present at concentrations lower than the detection limit of our system. It is generally more difficult to detect mRNA species in tissues from cells in culture, especially when the particular mRNA species is scarce.

Considering the limited MDGI expression in mammary glands of involuting cows (first and second stages), two major possibilities can be envisaged: limited secretion from substantial loss of mammary epithelial cells or reduced synthetic activity per cell, alone or in combination. It is unlikely that the lack of MDGI mRNA is due to cell loss, because loss of mammary epithelial cells does not occur to a significant extent during involution in the bovine species (8, 15). We favor the second hypothesis, that the limited secretion is due to reduced synthetic ability per cell, based on several studies showing that inactive mammary epithelial cells prevail during the first and second stages of mammary involution (8, 11, 13). The question of whether lack of MDGI production is a consequence of these cellular events, or whether it is involved in the regulation of these events, or both cannot be answered at the moment.

The presence of MDGI in lactating and involuting glands 2 wk prior to parturition, at the stage of colostrum formation, suggests that a relationship exists between the presence of MDGI and the functional state of the gland. These results and recent results of others (6) that MDGI can substitute for prolactin in inducing β -casein expression led us to hypothesize a role for MDGI in differentiation of epithelial cells along with inhibition of cell proliferation.

In summary, the present observations document the presence of high concentrations of MDGI in lactating and involuting mammary glands at the time of colostrum formation. Our initial investigation of the molecular events that occur in mammary glands has led to the realization that regulation of MDGI production occurs at the level of the steady-state concentration of MDGI mRNA. Additional experiments should lead to a further clarification of the mechanism or mechanisms affecting MDGI expression and ultimately to a better understanding of the physiological significance of these events.

ACKNOWLEDGMENTS

The research reported herein was supported by funds from the New York State Agriculture Research Station.

REFERENCES

- 1 Ausubel, F. M., R. Brent, R. E. Kingston, D. P. Moore, J. E. Seidman, J. A. Smith, and K. Strahl. 1991. Current protocols in molecular biology. Vol. I. (Suppl. 8). Massachusetts General Hospital, Harvard Med. School, Cambridge, MA.
- 2 Bohmer, F.-D., W. Lehmann, F. Noll, R. Samtleben, P. Langen, and R. Grosse. 1985. Specific neutralizing antiserum against a polypeptide growth inhibitor for mammary cells purified from bovine mammary gland. *Biochim. Biophys. Acta* 846:145.
- 3 Bradford, M. M. 1976. A rapid and sensitive method for the quantitation of microgram quantities of protein utilizing the principle of protein dye-binding. *Anal. Biochem.* 72:248.
- 4 Chomczynski, P., and N. Sacchi. 1987. Single step method of RNA isolation by added guanidinium thiocyanate-phenol chloroform extraction. *Anal. Biochem.* 162:56.
- 5 Fleet, I. R., J. H. Goode, M. H. Hamon, M. S. Laurie, J. L. Linzell, and M. Peaker. 1975. Secretory activity of the goat mammary glands during pregnancy and the onset of lactation. *J. Physiol.* 251:763.
- 6 Grosse, R., and P. Langen. 1990. Mammary-derived growth inhibitor. Page 249 in *Handbook of experimental pharmacology*. Vol. 95/II. Peptide growth factors and their receptors II. M. B. Sporn and A. B. Roberts, ed. Springer-Verlag, New York, NY.
- 7 Hartmann, P. E. 1973. Changes in the composition and yield of mammary secretion of cows during the initiation of lactation. *J. Endocrinol.* 59:231.
- 8 Hurley, W. L. 1989. Mammary gland function during involution. *J. Dairy Sci.* 72:1637.
- 9 Kurtz, A., F. Vogel, K. Funa, C. H. Heldin, and R. Grosse. 1989. Developmental regulation of mammary-derived growth inhibitor expression in bovine mammary tissue. *J. Cell Biol.* 110:1779.
- 10 Muller, T., A. Kurtz, F. Vogel, H. Breter, F. Schneider, U. Angstrom, M. Mieth, F.-D. Bohmer, and R. Grosse. 1989. A mammary-derived growth inhibitor (MDGI) related to 70 kDa antigen identified in nuclei of mammary epithelial cells. *J. Cell Physiol.* 138:415.
- 11 Oliver, S. P., and L. M. Sordillo. 1989. Approaches to the manipulation of mammary involution. *J. Dairy Sci.* 72:1647.
- 12 Politis, I., R. C. Gorewit, T. Muller, and R. Grosse. 1991. Mammary-derived growth inhibitor in lactation and involution. *Domest. Anim. Endocrinol.* 9:89.
- 13 Politis, I., R. C. Gorewit, T. Muller, and R. Grosse. 1992. Comparison of mammary-derived growth inhibitor production in mammary tissue of lactating, pregnant versus nonlactating, pregnant Holstein cows. *Can. J. Anim. Sci.* 72(June).
- 14 Smith, K. L., and D. A. Todhunter. 1982. The physiology of mammary glands during the dry period and the relationship to infection. Page 87 in *Proc. 21st Annu. Mtg. Natl. Mastitis Council, Inc.*, Arlington, VA.
- 15 Sordillo, L. M., and S. C. Nickerson. 1988. Morphologic changes in the bovine mammary gland during involution and lactogenesis. *Am. J. Vet. Res.* 49:1112.

T-Cell Receptor V β -Family Usage in Primary Cutaneous and Primary Nodal T-Cell Non-Hodgkin's Lymphomas

Abraham H. Preesman, Huai-Zhong Hu, Marcel G. J. Tilanus, Bernard de Geus, Henk-Jan Schuurman, Roelie Reitsma, Dick F. van Wichen, Willem A. van Vloten, Roel A. de Weger

Departments of Pathology (AHP, H-ZH, H-JS, RR, DFvW, RAdW) (division of Histo- and Cytochemistry & Electron Microscopy), Dermatology (AHP, WAvV), and Molecular Genetics (MGJT, RAdW), University Hospital Utrecht, Utrecht, The Netherlands; Department of Clinical Immunology (H-ZH), The First Affiliated Hospital, West China University of Medical Sciences, Chengdu, Sichuan, People's Republic of China; and Department of Immunology (BdG), TNO-Institute for Aging and Vascular Research, Zernikedreef, Leiden, The Netherlands

To evaluate whether the expression of T-cell receptor (TCR) V β families in eight cases of malignant T-cell lymphomas took place in a preferential manner, we analyzed four cases of mycosis fungoides (MF), the most common form of primary cutaneous T-cell non-Hodgkin's lymphomas (NHL), and four cases of primary nodal T-cell NHL.

The usage of V β families in T-cell populations was investigated on mRNA that was transcribed to cDNA using a C β primer and reverse transcriptase. Subsequently, the specific usage of the families was analyzed by polymerase chain reaction (PCR) using combinations of the selected C β -oligonucleotide primer and one of the family-specific V β primers.

Peripheral blood lymphocytes from four healthy volunteers and 1 "reactive" lymph node served as a control and expressed all 20 V β families tested for. In T-cell lines, with restricted V β expression, and in three patients with advanced MF, only one or two V β families were expressed at the

mRNA level. In an early MF lesion this monoclonal expression was absent: several V β families were expressed with a weak intensity. This may indicate either a polyclonal origin of MF, or that too few monoclonal neoplastic cells were present in the tissue specimen.

In the four nodal T-cell NHL, only one family could be clearly distinguished, whereas some of the other V β families showed only a weak expression. These latter families represent the reactive T-cell component in the nodal T-cell NHL. Both in nodal T-cell NHL and in MF there was no preferential expression of a particular V β family. There was a good correlation between PCR data and the expression of V β -family protein products observed by immunohistochemistry on tissue sections of the T-cell lymphomas.

All T-cell lines, three cases of MF, and three cases of nodal T-cell NHL showed a rearrangement of the TCR β chain on DNA level. *J Invest Dermatol* 99:587-593, 1992

The $\alpha\beta$ T-cell receptor (TCR) heterodimer is used by 95% of human T cells to recognize antigen in combination with MHC molecules [1,2]. Both α and β chains have variable (V), junction (J), and constant (C) regions. In addition the β chain has a diversity (D)

region [3]. The gene segments encoding these regions are physically separated in the germline, but are combined together during T-cell development by somatic rearrangement [4]. The human V β gene segments are organized in at least 20 families, each consisting of one to seven homologous members [3,5]. Each T-cell that expresses TCR β chains on its cell surface, whether normal or malignant, has rearranged at least one of the available V β genes to generate an antigen receptor [5]. The RNA transcripts for TCR β chain are then spliced to yield a continuous V-D-J-C template for translation [2,4].

DNA from polyclonal lymphocytes do not contain detectable specific gene rearrangements because the structure of the rearranged gene(s) varies from cell to cell [6]. Analysis of rearrangement of TCR β chain genes is important for establishing the clonality of malignant cells in leukemia or lymphoma patients at the time of presentation or at relapse [7]. In nodal T-cell non-Hodgkin's lymphomas (NHL) [6-8], and in advanced cases of mycosis fungoides (MF) [8-10], clonality has been established. However, in the early plaque-like lesions of MF in no [9] or only a few cases [10] have clonal gene-rearrangements been observed.

The expression of the TCR V β genes at the protein level has been investigated in cutaneous and nodal T-cell lymphomas using monoclonal antibodies against V-region framework determinants [5,11-14]. These immunohistochemical studies confirmed the usefulness of these monoclonal antibodies, but the data were controversial. In one study [11] a preferential usage of V β 8 in cutaneous lymphomas was described, but in others the V β family usages was at random

Manuscript received November 21, 1991; accepted for publication May 13, 1992.

Reprint requests to: Dr. A. H. Preesman, Department of Dermatology, University Hospital Utrecht, P. O. Box 85500, 3508 GA Utrecht, The Netherlands.

Abbreviations:

cDNA: copy DNA
DEPC: diethyl pyrocarbonate
DNA: deoxyribonucleic acid
dNTP: deoxynucleosidetriphosphate
DTT: dithiothreitol
MF: mycosis fungoides
MHC: major histocompatibility complex
mRNA: messenger RNA
NHL: non-Hodgkin's lymphoma
OD: optical density
PBL: peripheral blood lymphocytes
PCR: polymerase chain reaction
RNA: ribonucleic acid
SDS: sodium dodecylsulfate
TCR: T-cell receptor

Table 1. Primer Sequences of T-Cell Receptor β Chain

Primer	Sequence	Family Member
V β 5'		3'
1	GCAAAAGGAAACATTCTTGAACG	
2	AGAGTCTCATGCTGATGGC	
3	AGGACGGGAGAGAAAGTTTTC	
4	GGCCACATATGAGAGTGGATTGTC	
5a	CAGTGAGACACAGAGAAAC	5.1; 5.4
5b	CCCTAACTATAGCTCTGAGCTG	5.2; 5.3
6	GGGGCAGGGCCAGAGTTTCTAAT	
7	CTTAAACCTTCACCTACACGC	
8	CTTTAAACAACAGTTTCCG	
9	CAGTTCCAAATCGCTTCTCAC	
10	GGATTGTGTTCTCTATAAAAGC	
11	CCACTATTCCTATGGAGTTAATTCC	
12a	GTCACCAGACTGAGAACACCGCTA	12.1; 12.2
12b	GATTCATTACTCAGTTGGTG	12.3; 12.4
13	GCATGACACTGCAGTGTGCC	
14	ACCCAAGATACCTCATCACAG	
15	TCTCAGACTAAGGGTCATGATAGA	
16	CTGTTACATTTTGTGAAAGAGTC	
17	CTCACAGATAGTAAATGACTTTC	
18	AGCCCAATGAAAGGACACAGTCAT	
19	ACCCCGAAGAAAGGACATACTTTT	
20	GAGGGAACATCAAACCCCAACCTA	
C β	GGCCTTTTGGGTGTGGGAGATCTCTGCTTCTGATGGC	

[5,12-14]. However, only a limited number of family-specific monoclonal antibodies is available. We used the polymerase chain reaction (PCR) to detect the expression of 20 different TCR V β families at the mRNA level in T-cell lymphomas. These data were compared with immunohistology using available V β -family specific monoclonal antibodies on tissue sections of the same lymphoma. Our results showed the clonality of the malignant cells, and did not indicate a preferential usage of a particular V β -family in the different lymphomas studied.

MATERIALS AND METHODS

Tissues and Cells Skin biopsies (4 mm) were analyzed from four patients with MF, three in an advanced stage of MF, and one in an early stage. The diagnosis of MF was made according to clinical and histopathologic criteria [15]. Surgically removed tissue specimen of four patients with nodal T-cell NHL and one reactive lymph node were also analyzed. Part of the tissue was used for the immunohistologic analysis. The T-cell lines Jurkat, HSB (obtained from Dr. R. H. L. Bolhuis, Rotterdam, The Netherlands) and Molt3, that served as a control, were cultured in RPMI 1640 medium supplemented with 5% fetal calf serum. Cells were counted and pelleted, and the supernatant was removed. Control peripheral blood lymphocytes from four healthy volunteers were harvested by Ficoll-Hypaque method, and the mononuclear cell fraction was analyzed. All material was snap frozen and stored in liquid nitrogen.

Immunohistology Tumor cells in all tissues were immunohistochemically phenotyped on frozen tissue sections using the indirect immunoperoxidase method [16]. Primary monoclonal antibodies used were against CD2, CD3, CD4, CD8, CD22 (Becton Dickinson, Mountain View, CA), $\alpha\beta$ -TCR, $\gamma\delta$ -TCR, and the V families V β 5a, V β 5b, V β 6, V β 8, and V β 12 (T-cell Sciences Inc, Cambridge, MA).

Gene-Rearrangements High molecular weight DNA was isolated from parts of the frozen tissues and from frozen cells. Ten micrograms of DNA was completely digested with EcoRI or BamHI (Boehringer Mannheim, Mannheim, West Germany), separated on 0.8% agarose gel, and subsequently transferred to nylon membrane filters (Hybond N⁺; Amersham, UK) for hybridization. Hybridization was performed using ³²P-labeled DNA probes at 65°C in a buffer containing 7% sodium dodecylsulfate (SDS),

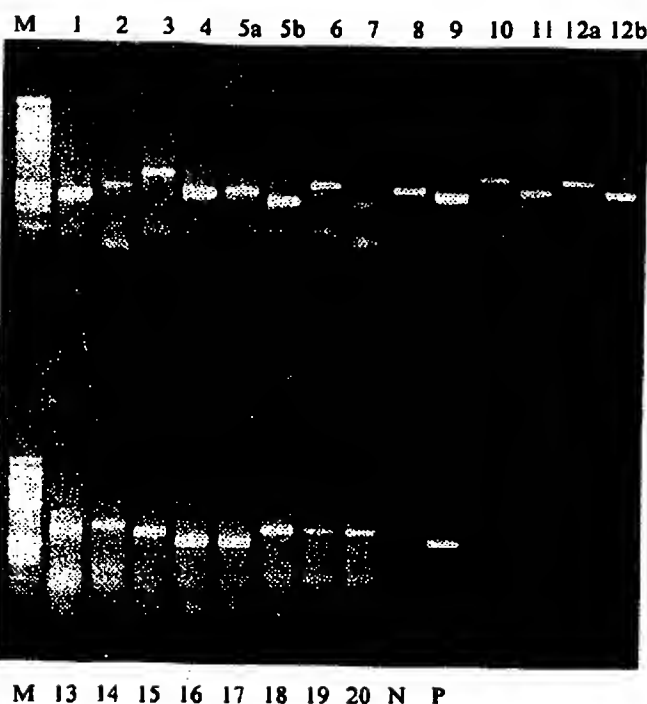


Figure 1. V β -gene family expression in normal peripheral blood lymphocytes. The mRNA isolated from the cells was transcribed to cDNA using a specific C β primer. This cDNA was amplified by PCR using C β and V β primers. The PCR products were electrophoresed on a 2% agarose gel. The ethidium bromide stained gel showed the expression of all 20 tested V β families (lane numbers indicate V β -family number) in PBL2. M, marker lane (Phi-X digested with HaeIII); N, negative control; and P, positive control (Jurkat cDNA amplified with C β and V β 8 primer).

0.5 M phosphate buffer (pH 7.2), and 0.1 μ g/ml herring sperm DNA. The probes were labeled using a primer gene labeling system (Promega, Madison, WI). DNA fragments hybridized with labeled probes were detected by autoradiography with X-OMAT AR film (Kodak, Rochester, NY). The probes used were C β , a 0.7-kb fragment, and J β , a 4.4-kb fragment (both a kind gift from Dr. H. van Oostveen, Department of Pathology, Free University, Amsterdam, The Netherlands).

RNA Isolation RNA was prepared using a single-step method of RNA isolation by acid guanidinium thiocyanate-phenol-chloroform extraction [17]. Briefly, 0.3 g biopsied tissue was homogenized using a homogenizer (Janke & Kunkel IKA, Staufen, West Germany) or 3×10^7 frozen cells were dissolved in 3 ml of the solution D (4 M guanidinium thiocyanate, 25 mM sodium citrate [pH 7], 0.5% sarcosyl, and 0.1 M 2-mercaptoethanol). The suspension was vortexed for about 20 seconds. Subsequently, 0.3 ml 2 M sodium acetate (pH 4), 3 ml phenol (water saturated), and 0.6 ml chloroform-isoamylalcohol mixture (49:1) was added, with thorough mixing after addition of each reagent. The final suspension was shaken vigorously and cooled on ice for at least 15 min. Then the suspension was centrifuged at 5,000 rpm at 4°C for 15 min. The aqueous phase that contained RNA was transferred into 1.5 ml Eppendorf tubes (0.5 ml in each tube) and 1 ml 100% ethanol was added. The tubes were kept at -20°C for at least 1 h to precipitate the RNA, and then centrifuged at 14,000 rpm at 4°C for 15 min, and the supernants were discarded carefully. The pellet in each tube was dissolved in 0.15 ml solution D, and 0.375 ml cold 100% ethanol was added. The tubes were kept at -70°C for 30 min and subsequently centrifuged (14,000 rpm at 4°C, for 15 min). The supernants were discarded carefully, and the pellets were washed in 1 ml 70% ethanol and dried in a speedvac (Savant, New York, NY) concentrator. The dried pellets were dissolved in DEPC (diethyl

Table II. Expression of T-Cell Receptor V β Genes on mRNA Level

V β	1	2	3	4	5a	5b	6	7	8	9	10	11	12a	12b	13	14	15	16	17	18	19	20
RL	+	+	+	+	+	+	+	+	+	+	+	+	+	+	+	+	+	+	+	+	+	+
PBL 1	+	+	+	+	+	+	+	+	+	+	+	+	+	+	+	+	+	+	+	+	+	+
PBL 2	+	+	+	+	+	+	+	+	+	+	+	+	+	+	+	+	+	+	+	+	+	+
PBL 3	+	+	+	+	+	+	+	+	+	+	+	+	+	+	+	+	+	+	+	+	+	+
PBL 4	+	+	+	+	+	+	+	+	+	+	+	+	+	+	+	+	+	+	+	+	+	+
HSB	+	+	+	+	+	+	+	+	+	+	+	+	+	+	+	+	+	+	+	+	+	+
Jurkat	+	+	+	+	+	+	+	+	+	+	+	+	+	+	+	+	+	+	+	+	+	+
Molt 3	+	+	+	+	+	+	+	+	+	+	+	+	+	+	+	+	+	+	+	+	+	+
MF 1	+	+	+	+	+	+	+	+	+	+	+	+	+	+	+	+	+	+	+	+	+	+
MF 2	+	+	+	+	+	+	+	+	+	+	+	+	+	+	+	+	+	+	+	+	+	+
MF 3	+	+	+	+	+	+	+	+	+	+	+	+	+	+	+	+	+	+	+	+	+	+
MF 4	+	+	+	+	+	+	+	+	+	+	+	+	+	+	+	+	+	+	+	+	+	+
NNHL 1	+	+	+	+	+	+	+	+	+	+	+	+	+	+	+	+	+	+	+	+	+	+
NNHL 2	+	+	+	+	+	+	+	+	+	+	+	+	+	+	+	+	+	+	+	+	+	+
NNHL 3	+	+	+	+	+	+	+	+	+	+	+	+	+	+	+	+	+	+	+	+	+	+
NNHL 4	+	+	+	+	+	+	+	+	+	+	+	+	+	+	+	+	+	+	+	+	+	+

* RL, reactive lymph node; PBL, peripheral blood lymphocytes from normal individuals; cDNA, synthesized from mRNA of T-cell line Jurkat was always used as positive control, +++ when the positivity was as strong as the positive control, + when the PCR product was easily recognized, ++ when it was between the upper two conditions, ± when PCR product was just recognized, -- when there was no PCR product present; MF, mycosis fungoides; NNHL, nodal non-Hodgkin's lymphoma.

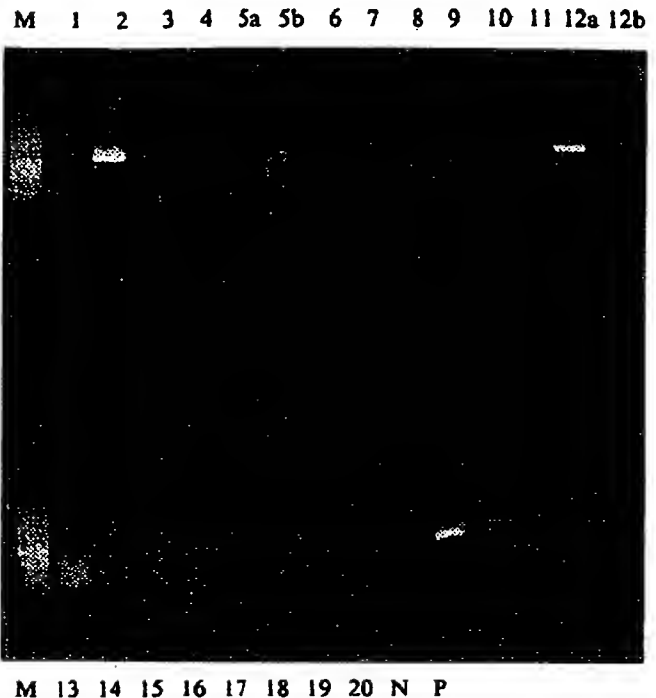


Figure 2. V β -gene family expression in T-cell line Molt3 cells. For explanation see Fig 1. The ethidium bromide stained gel showed the expression of two V β families in this cell line (V β 2 and V β 12a).

pyrocarbonate)-treated water, and the RNA concentration was measured using a spectrophotometer (U-2000, Hitachi, Tokyo, Japan).

Primers One C β and 22 V β primers that are specific for 20 different V β families have been designed using the program DNASIS (created by LKB-Pharmacia; Table I). For the V β families 5 and 12, two primers were selected, because no primer sequences common to all family members were found. The primer oligonucleotides were synthesized by using a DNA autosynthesizer (ABI 381A, Foster City, CA) using the β -cyanoethylphosphoramidite chemistry, based upon 1 OD = 30 μ g/ml. The primers were purified according to the method described in the ABI user's bulletin and diluted to a concentration of 0.5 μ g/ μ l.

cDNA Synthesis cDNA was synthesized on a template of total RNA sample at 42°C for 1 h in a 30- μ l cDNA-reaction buffer containing 2.5 μ g C β primer, dNTP (1 mM final concentration), DTT (dithiothreitol, 10 mM final concentration), and 25 U avian myeloblastosis virus reverse transcriptase (Promega, Madison, WI). Upon incubation, 3 μ l 0.2 M EDTA was added to the mixture to

Table III. Immunohistologic Phenotyping of the Tested T-Cell Lymphoma

Case ^a	CD2	CD3	CD4	CD5	CD8	CD22
MF 1	+	+	+	+	-	±
MF 2	+	+	+	+	-	-
MF 3	+	+	+	-	-	±
MF 4	+	+	-	-	-	-
NNHL 1	+	+	+	+	-	-
NNHL 2	+	+	+	+	+	-
NNHL 3	+	+	+	-	-	-
NNHL 4	+	+	+	+	-	-

^a MF, mycosis fungoides; NNHL, nodal non-Hodgkin's lymphoma.

+ , >75% of the cells positive; ±, weak expression; -, absent or occasional.

Table IV. T-Cell Receptor Expression on T-Cell Lymphoma Cells

Case	TCR Expression (immunohistology)							Gene-Rearrangement*	
	$\alpha\beta$	$\gamma\delta$	V β 5a	V β 5b	V β 6	V β 8	V β 12	C β	J β
MF 1	+	—	—	—	—	—	—	R	R
MF 2	+	—	—	—	—	—	—	ND	ND
MF 3	+	—	—	—	—	—	—	R	R
MF 4	+	—	—	—	—	—	—	R	R
NNHL 1	+	—	—	—	+	—	—	GL	GL
NNHL 2	+	—	—	—	—	—	—	R	R
NNHL 3	+	—	—	—	—	—	—	R	R
NNHL 4	+	—	—	—	—	—	—	R	R

* Isolated DNA was digested with EcoRI and BamHI, electrophoresed, blotted, and tested for rearrangement with C β and J β probes (see Materials and Methods). R, one or more rearrangements fragments present. GL, germline configuration. ND, not done. MF, mycosis fungoides. NNHL, nodal non-Hodgkin's lymphoma. +, > 75% of the tumor cells positive. —, absent, expression on reactive lymphocytes may be present.

stop the reaction. Purification was performed adding 70 μ l MilliQ water and 100 μ l phenol/chloroform mixture (1:1). After thorough mixing the tubes were centrifuged at 14,000 rpm. Then the water phase was transferred to another fresh Eppendorf tube. This step was repeated twice, and the second time 100 μ l chloroform/isoamylalcohol mixture (49:1) was used instead of phenol/chloroform. Ten microliters 3 M sodium acetate and 200 μ l 100% ethanol were added to the tube and kept at -70°C for 30 min. The tube was centrifuged for 15 min, and the supernatant was discarded carefully. The pellet was washed with 70% ethanol and dried in the speedvac concentrator. Finally, the pellet was dissolved in MilliQ water to obtain a concentration of 1.0 $\mu\text{g}/\mu\text{l}$ cDNA.

Polymerase Chain Reaction The PCR cocktail was 50 μ l PCR buffer containing dNTP (0.8 mM as final concentration), 1.0 μg cDNA, 0.25 μg C β primer, 0.25 μg of one of the 22 V β primers, and 0.5 U Taq polymerase (Perkin Elmer Cetus, Norwalk, CT). The cDNA reversely transcribed from the mRNA of Jurkat cells and the V β 8 primer were always used as positive control. The negative control was the same as the positive control except using 1 μ l MilliQ water instead of cDNA. To prevent evaporation, the cocktails were covered with three droplets of mineral oil, and then amplified by an automated DNA thermal cycler (Perkin Elmer Cetus, Norwalk, CT) for 35 cycles. The amplification cycle profile included denaturation for 1 min at 95°C , annealing for 1 min at 60°C , and extension for 2 min at 72°C . Twenty microliters of PCR reaction product from each tube was electrophoresed in 2% agarose gel. The gel was stained with 1% ethidium bromide and visualized

under ultraviolet light. Markers used were Phi-X digested with HaeIII and λ DNA digested with HindIII.

RESULTS

Control Experiments for V β Gene Family Analysis at the mRNA Level

Controls: In peripheral blood lymphocytes of four healthy volunteers, all 20 TCR V β families tested for were expressed. The intensities of the product bands, which represent the different V β gene family PCR products in the electrophoresed gels, varied among the V β genes and individuals (Fig 1, Table II). These experiments showed that the primer set selected was suitable to detect the 20 families. Despite the fact that no effort was made to quantify the differences in intensity of the different V β families within one individual, the differences between the four individuals were clear. In PBL1 most families were expressed with a similar intensity, whereas in PBL 4 differences among the families were large (Table II).

The reactive lymph node was also positive for all the 20 V β families. In this lymph node the differences in individual V β family expression was compared to the PBL large, e.g., families 4, 5.b, 9, and 18 are strong, whereas family 10 is only weakly expressed (Table II).

Cell Lines: The T-cell lines Jurkat and HSB only expressed one V β gene (V β 8 for Jurkat and V β 5.a for HSB), but Molt3 expressed 2 V β families at the mRNA level (Fig 2, Table II). These experiments showed that there was no cross-reactivity of the various V β -specific primers in the PCR reaction, that T-cell clones expressed one TCR V β family, as expected, and T-cell lines revealed a limited number of V β families.

Lymphomas

Immunophenotyping and Gene Rearrangements: The immunophenotypes of the four cutaneous and four nodal T-cell NHL are summarized in Tables III and IV. All T-cell lymphomas were $\alpha\beta$ -TCR-bearing cells. One of the MF patients showed loss of CD5, another of both CD4 and CD5. Two revealed the complete helper/inducer immunophenotype; there were no CD8⁺ MF cases. In MF 1, 3, and 4 most cells were tumor cells, whereas in MF2 (early lesion) few tumor cells were present in the dermal infiltrate and in the epidermis. The nodal T-cell NHL expressed either CD4 and/or CD8; one case showed loss of CD5. The amount of pre-existing non-tumor tissue in the various tissues was variable. Tissue of nodal NHL 1 and 2 were mainly composed of tumor cells with scattered reactive T lymphocytes. In nodal NHL3 the major non-tumor components were macrophages and plasma cells. In nodal NHL4 areas of pre-existing lymphoid tissue were present.

All T-cell lines, 3 cases of advanced MF and 3 cases of nodal NHL

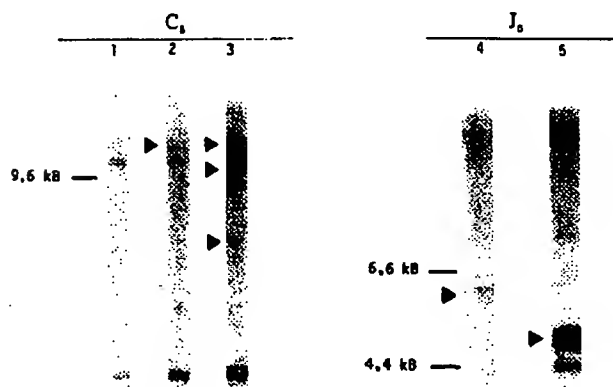


Figure 3. T-cell receptor gene rearrangements in tested T-cell NHL. Lanes 1-3 represent DNA isolated from nodal NHL 1, 2, and 4, respectively, digested with EcoRI and hybridized with a C β probe. Lanes 4 and 5 represent DNA isolated from MF 4 and 3, respectively, digested with EcoRI and hybridized with J β probe. Arrows, rearranged bands.

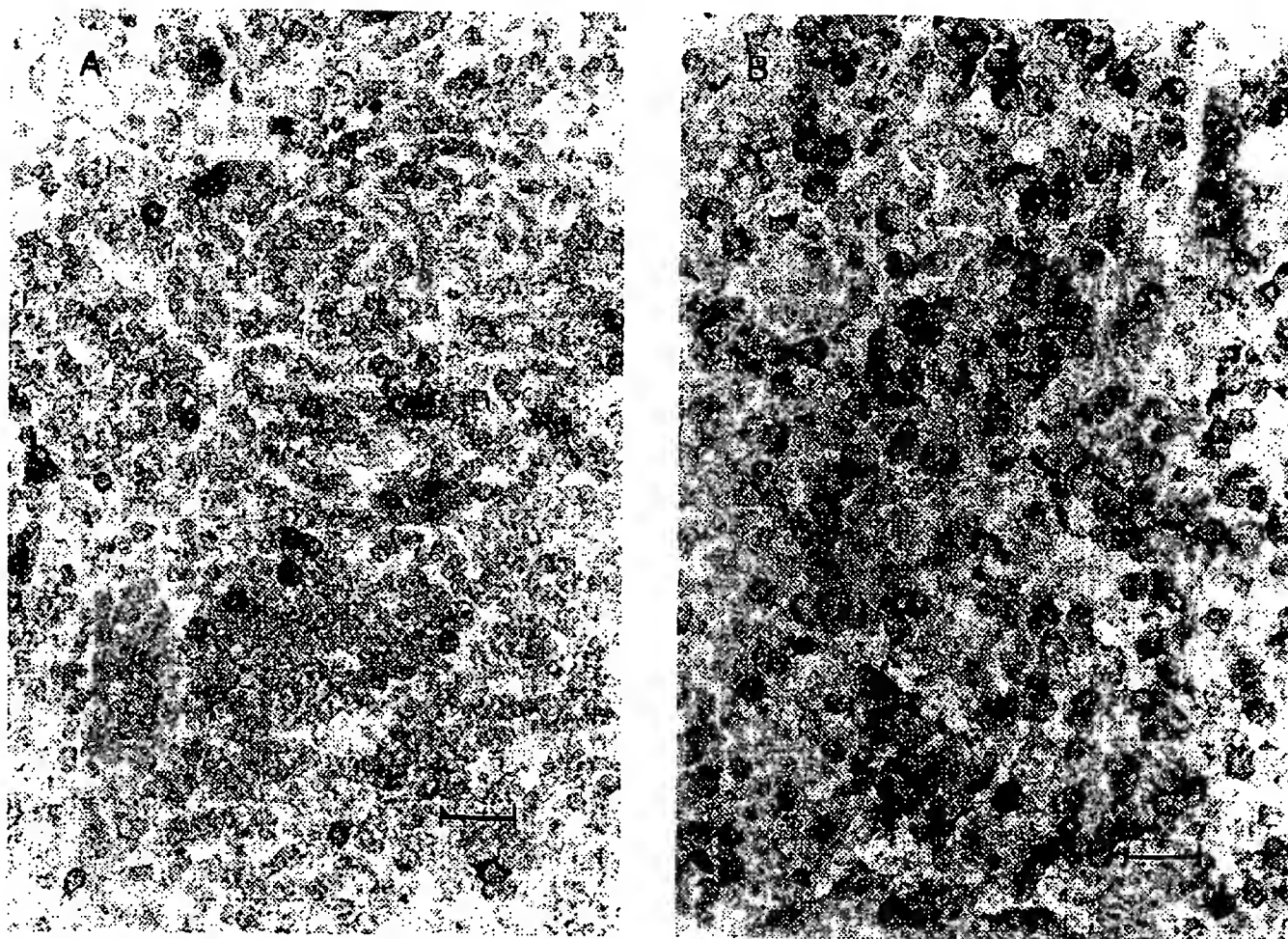


Figure 4. Immunohistochemical localization of V β 6 expressing lymphocytes. *A:* V β 6 expressing T lymphocytes in the paracortical area of a reactive lymph node (case RL in Table II). Bar, 33 μ m. *B:* V β 6-expressing tumor cells in a nodal T-cell NHL (case NNHL 1). Bar, 33 μ m.

showed a clonal gene-rearrangement with the C β and the J β probes (Fig 3, Table IV).

Immunohistology of TCR V Gene Families: All T-cell lymphomas were analyzed with the available monoclonal antibodies for the presence of V β 5a, V β 5b, V β 6, V β 8, and V β 12 TCR gene families (Table IV). In all nodal T-cell NHL and MF cases small numbers of reactive small T lymphocytes were detected expressing either one of the V families. Only one of the nodal T-cell NHL lymphomas (case NNHL 1) could be typed for its V β family, V β 6 (Fig 4B). All others were negative and expressed V β families to which no antibodies were available (compare Tables II and IV).

V β Gene Family Analysis at the mRNA Level: The three MF cases at the advanced stage strongly expressed one to two V β families; the rest of the V β families were weakly expressed or absent (Fig 5A, Table II). The patient at the early stage of MF (case MF2 in Table II) expressed 11 different V β families with a weak intensity. The other V β families were absent.

In each of the four nodal T-cell NHL only one V β family could be clearly distinguished in each case. The other V β families showed a weak expression or were missing (Fig 5B, Table II). In nodal NHL 1, 2, and 4 with either reactive lymphocytes within the tumor or pre-existing normal lymphoid tissue, many other families were weakly expressed. These latter families represented the reactive T-cell component with a polyclonal V β expression. In the nodal

NHL3, with few reactive T cells, no additional V β families were detected.

DISCUSSION

The TCR V β usage can be examined at the levels of rearranged DNA, mRNA, and proteins [5,10-13,18,19]. As the available monoclonal antibodies can only detect a limited number of V β families, we established a PCR method to detect the TCR V β usage at the mRNA level. For this aim lymphocytes from peripheral blood, lymph node tissue, but especially also small skin biopsies were used. By this method it is possible to evaluate preferential expressed V β families in a heterogeneous population of T cells that each expresses a different V β . This method used a C β primer to specifically select the mRNA or TCR β chains when the cDNA was synthesized. Then TCR V β primers specific for each V β family were used in the PCR. The control experiments showed that we were able to detect all 20 V β families screened for.

In PCR experiments using serial dilutions of cDNA, the intensity of PCR product bands decreased with decreasing cDNA amounts (data not shown). Obviously, the intensities of PCR product bands were positively related to the original amounts of the templates, although other methods should be applied to quantify the results. For our goal the PCR had a powerful capacity in amplifying specific fragments of cDNA from a mixture of templates [20] and 1 μ g template cDNA for each reaction tube was sufficient to show the TCR V β families in our PCR method. In PBL and the reactive lymph node, all the TCR V β families were present, and the intensi-

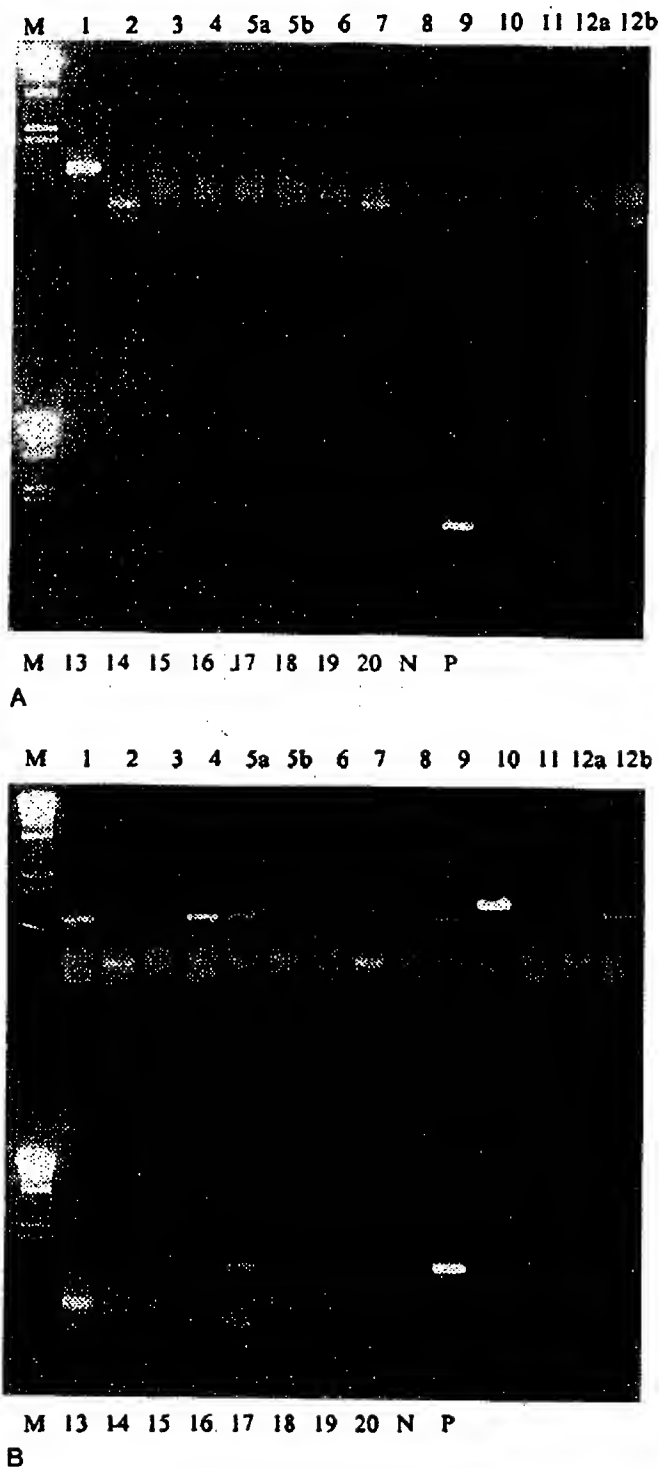


Figure 5. V β -gene family expression in T-cell NHL. A: expression of only V β 1 in MF 1. B: strong expression of only V β 10 in nodal NHL 2, weak expression of various other V β families is detected as well (see Table II). For explanation see Fig 1. Marker λ DNA was digested with HindIII.

ties of many bands were high (++ to +++), Table II). This indicated that the T-cell populations of PBL and the benign lymph node were polyclonal, the distribution of TCR V β families in the non-malignant cases is relatively equal, and all V β families were present in these lymphocyte populations.

In contrast, the T-cell lines Jurkat and HSB expressed monoclonal V β family usage, and the T-cell line Molt3 expressed TCR V β 2 and V β 12a families. Sangster et al [21] studied DNA rearrangements in Molt3 cells using probes for TCR C β and J β . When C β

probe was used, there were 2 rearranged bands and when J β probe was used three rearranged bands were found. This was confirmed by our gene-rearrangement studies (data not shown). In general, T cells express only one TCR, due to allelic exclusion. Molecular analysis of TCR β genes in a number of clonal T-cell populations has revealed that in most cases there is only a single productive VDJ β rearrangement [22]. But apparent violations of allelic exclusions of the TCR β genes were reported. In a human diphtheria toxoid-specific T-cell clone two different TCR β transcripts were identified [23]. Both these transcripts contained an open reading frame, suggesting that they were capable of encoding functional β chains. Cell-surface expression, however, was not examined. A cytochrome C-specific T-cell clone was also shown to display two different TCR β chains [24]. We suggest that the expression of the two TCR V β genes at the mRNA level of Molt3 cell line can be explained either by the violation of allelic exclusion of TCR β genes, or the Molt3 cell line is composed of two different clones.

Of the eight T-cell lymphoproliferative malignancies, six had overexpression of one of the V β families. One of the MF cases expressed two V β families and the early MF case weakly expressed 10 V β families. In nodal T-cell NHL and advanced MF cases, the tumor cells predominated, but small numbers of non-malignant lymphocytes could be identified microscopically. This correlated with our PCR results, showing one (or 2) strong-product band, and in some cases weak bands of other V β families. It can be inferred that the single or double strong PCR product bands in each T-cell neoplasia case represented the V β expression of the malignant cells, and the weak bands were from the remaining non-malignant cells as supported by immunohistology. In nodal NHL case 1, the malignant cells were positive with a monoclonal antibody against TCR V β 6 (Table 4). The tumorous infiltrate was sufficient for immunohistochemical and mRNA analysis. However, the amount of malignant cells in the tissue specimen left, was too low to detect the clonal cell proliferation on DNA level (Tables II and IV). Monoclonal antibodies against other V families showed lymphocytes distributed evenly and sparsely in the lymph node. Similarly, the PCR gave a strong TCR V β 6 band and weak bands of several other V β families. Immunohistologic examination of the other malignancies showed an even and sparse distribution of small reactive lymphocytes, but the malignant lymphocytes were negative. This correlated with the PCR data as these results showed a V β expression of the malignant cells to which no monoclonal antibodies were available. Our data are in agreement with the basic concept that (almost) all cancers are clonal [25].

To these observations there was one apparent exception, the MF case that failed to give a clonal usage of a TCR V β gene. This MF was at the early stage of the disease. This may suggest that the tumor cells were not predominant in the biopsied tissue, or that MF is polyclonal in the origin.

Studies of the TCR V β gene usages in cutaneous and nodal T-cell lymphomas using monoclonal antibodies have been done by several groups [5,11-14]. Due to the lack of monoclonal antibodies to all V β families, only 2-7 different antibodies were used. The positive rates of detections of TCR V β gene usages by tumor cells were low. We had a similar experience, using five different monoclonal antibodies against four TCR V β families in the study of 8 T-cell NHL; only one gave a positive result. At present, the PCR is the method of choice in the study of TCR V β -family usage in T-cell neoplasia, as all different families can be analyzed. Jack and co-workers [11] examined frozen skin biopsies from 16 cutaneous T-cell lymphomas using two monoclonal antibodies against TCR V β 8 and V β 5. Ten reacted with one monoclonal antibody, MX11, likely to have V β 8 specificity. Even more striking was their finding that all 10 of the plaque and tumor lesions were reacting with MX11. They suggested that the cutaneous T-cell lymphoma cells employ a restricted range of TCR variable region gene expression. Charley et al [5] investigated blood lymphocytes from three patients with Sezary syndrome, a leukemic form of cutaneous T-cell lymphoma. In one patient, more than 99% of the cells reacted with the monoclonal antibody against V β 5. Cells from the other two patients were non-reactive with the antibodies against TCR V β 5.2, 5.3, 6, 8, and 12.

Another study by Clark et al [12] did not show restricted usage of TCR V β genes either. A recent study by Poppema et al [14] with seven V β monoclonal antibodies recognizing four distinct V β families on 44 T-cell lymphomas showed a restricted V β gene usage in 29% of the cases studied, without preference for a specific V β family. Our study at the mRNA level had a higher positive rate, but the results failed to give any evidence of preferential usage of particular V β families.

The detection of V β families of T-cell NHL may be clinically useful for 1) prospective followup of patients during treatment (monitoring relapse of disease, or detecting extranodal or extra-cutaneous localization of T-cell NHL), 2) retrospective analysis of T-cell NHL, and 3) therapeutic approaches with monoclonal anti-V β antibodies. For these reasons we preferred to use specific V β -family primers, instead of V β -general primers, as these latter primers may not detect all families with the same sensitivity [26]. This approach can easily be adapted by addition of new primers when new V β families are discovered [27], that will be missed with the present primer set. However, with our panel of primers we could determine the V β family in all T-cell NHL studied, except the early-stage MF, indicating that the most regular expressed V β families were incorporated in the panel.

Although, the number of samples were limited, the results indicated two applications for TCR V β family detection by PCR method. First, it might be used to differentiate malignant and non-malignant T-cell proliferations. As in the reactive lymph node, all 22 TCR V β families were expressed at the mRNA level. In the malignant cases, however, it was shown that only 1-2 TCR V β genes were used by the T-cell lymphomas. Second, it might give insight in the selection process(es) leading to a oligo- or monoclonal cell population. For example, in this study we showed that at the early stage of MF, as in case MF2, polyclonal TCR V β family expression were detected, all with a relatively weak intensity. But in the advanced-stage MF patients, 1-2 TCR V β genes were strongly expressed, suggesting a homologous tumor cell population in the biopsied tissues. The expression of two V β families can indicate either a biclonal origin of the tumor or a loss of allelic exclusion with two reproductively rearranged TCR β chains. The gene-rearrangement studies were not informative on this aspect.

In conclusion, the investigation of TCR V β gene usage of T-cell neoplasia at the mRNA and protein levels can give additional information on the stage of disease. A limited expression of certain V β families in nodal and/or cutaneous T-cell NHL might give a clue on the etiology of these lymphomas [11]. However, our study, both in nodal T-cell NHL and MF, did not show such a preferential expression of a particular V β family.

We wish to thank Dr. J. Razing for his advice during the course of this study. Dr. L. Selleri is gratefully acknowledged for his precise primer searches and Mrs. Th. Lots, Mrs. K. Bosboom-Kalsbeek, and Mrs. W. T. M. van Blokland for their excellent technical assistance.

This work was supported in part by grants from the University Hospital and the University of Utrecht. Dr. H. Z. Hu is supported by a World Health Organization fellowship.

REFERENCES

- Berger MS: Prognostic factors in lymphomas: the contribution of immunophenotyping and molecular studies. *Curr Opin Immunol* 2:719-723, 1990
- Hochstenbach F, Brenner MB: Newly identified $\gamma\delta$ and $\beta\delta$ T-cell receptors. *J Clin Immunol* 10:1-18, 1990
- Wilson RK, Lai E, Concannon P, Barth RK, Hood LR: Structure, organization and polymorphism of murine and human T-cell receptor α and β chain gene families. *Immunol Rev* 101:149-172, 1988
- Caccia N, Toyonaga B, Kimura N, Mak TW: The α and β chains of the T-cell receptor. In: Mak TW (ed.). *The T-Cell Receptor*. Plenum Press, New York, 1988, pp 9-51
- Charley M, McCoy JP, Deng JS, Jegasothy B: Anti-V region antibodies as "almost clonotypic" reagents for the study of cutaneous T cell lymphomas and leukemias. *J Invest Dermatol* 95:614-617, 1990
- Williams ME, Innes DJ, Borowitz MJ, Lovell MA, Swerdlow SH, Hurtubise PE, Brynes RK, Chan WC, Byrne GE, Whitcomb CC, Thomas CY: Immunoglobulin and T cell receptor gene rearrangements in human lymphoma and leukemia. *Blood* 69:79-86, 1987
- Minden MD, Mak TW: The structure of the T cell antigen receptors genes in normal and malignant T cells. *Blood* 68:327-336, 1986
- Bertness V, Kirsch I, Hollis G, Johnson B, Bunn PA: T-cell receptor gene rearrangements as clinical markers of human T-cell lymphomas. *N Engl J Med* 313:534-538, 1985
- Ralfkiaer E, O'Connor NTJ, Crick J, Wantzin GL, Mason DY: Genotypic analysis of cutaneous T-cell lymphomas. *J Invest Dermatol* 88:762-765, 1987
- Dosaka N, Tanaka T, Fujita M, Miyachi Y, Horio T, Imamura S: Southern blot analysis of clonal rearrangements of T-cell receptor gene in plaque lesion of Mycosis Fungoides. *J Invest Dermatol* 93:626-629, 1989
- Jack AC, Boylston AW, Carrel S, Grigor I: Cutaneous T-cell lymphoma cells employ a restricted range of T-cell antigen receptor variable region genes. *Am J Pathol* 136:17-21, 1990
- Clark DM, Boylston AW, Hall PA, Carrel S: Antibodies to T cell antigen receptor beta chain families detect monoclonal T cell proliferation. *Lancet* II:835-837, 1986
- Salter DM, Krajewski AS, Dewar AE, Clark D, Boylston AW, Carrel S: The use of anti-clonotypic T cell receptor antibodies in the diagnosis of T cell lymphoma (abstr). *J Pathol* 155:344A, 1988
- Poppema S, Herperle B: Restricted V gene usage in T-cell lymphomas as detected by anti-T-cell receptor variable region reagents. *Am J Pathol* 138:1479-1484, 1991
- Edelson RL: Cutaneous T-cell lymphoma: mycosis fungoides, Sezary syndrome and other variants. *J Am Acad Derm* 2:89-106, 1980
- Schuurman HJ, Huppes W, Verdonk LF, van Baarlen J, van Unnik JAM: Immunophenotyping of non-Hodgkin's lymphoma. Correlation with relapse free survival. *Am J Pathol* 131:102-111, 1988
- Chomczynski P, Sacchi N: Single-step method of RNA isolation by acid guanidinium thiocyanate-phenol-chloroform extraction. *Analyt Biochem* 162:156-159, 1987
- Concannon P, Pickering LA, Kung P, Hood L: Diversity and structure of human T-cell receptor β -chain variable region genes. *Proc Natl Acad Sci* 83:6598-6602, 1986
- Bragado R, Lauzurica P, Lopez D, Castro JAL: T cell receptor V β gene usage in a human alloreactive response. *J Exp Med* 171:1189-1204, 1990
- Erlach HA: Polymerase chain reaction. *J Clin Immunol* 9:437-447, 1989
- Sangster RN, Minowada J, Suciu-Foca N, Minden M, Mak TW: Rearrangement and expression of the α , β , and γ chain T cell receptor genes in human thymic leukemia cells and functional T cells. *J Exp Med* 163:1491-1508, 1986
- Kronenberg M, Siu G, Hood L, Shastri N: The molecular genetics of the T-cell antigen receptor and T-cell antigen recognition. *Annu Rev Immunol* 4:529-591, 1986
- Triebel F, Breathnach R, Graziani M, Hercend T, Debre P: Evidence for expression of two distinct T cell receptor β -chain transcripts in a human diphtheria toxoid-specific T cell clone. *J Immunol* 140:300-304, 1988
- Matis LA, Ezquerro A, Coligan JE: Expression of two distinct T cell receptor α/β heterodimers by an antigen-specific T cell clone. *J Exp Med* 168:2379-2384, 1988
- Butturini A, Gale RP: Relationship between clonality and transformation in acute leukemia. *Leukemia Res* 15:1-7, 1991
- Lessin SR, Rook AH, Rovera G: Molecular diagnosis of cutaneous T-cell lymphoma: polymerase chain reaction amplification of T-cell antigen receptor β -chain gene rearrangements. *J Invest Dermatol* 96:299-302, 1991
- Ferradini L, Roman-Roman S, Azocar J, Michalaki H, Triebel F, Hercend T: Studies on the human T-cell receptor α/β variable region genes. II Identification of four additional V β subfamilies. *Eur J Immunol* 21:935-942, 1991

Osteoarthritis and Cartilage (2002) 10, 253-263

© 2002 Osteoarthritis Research Society International

doi:10.1053/joca.2001.0508, available online at <http://www.idealibrary.com> on IDEAL®

1063-4584/02/040253+11 \$22.00/0

Osteoarthritis and Cartilage

Journal of the Osteoarthritis Research Society International



Matrilin-3 in human articular cartilage: increased expression in osteoarthritis

O. Pullig*, G. Weseloh*, A. R. Klatt†, R. Wagnert and B. Swoboda*

*Division of Orthopaedic Rheumatology, Department of Orthopaedics, University of Erlangen-Nuremberg, Rathsberger Str. 57, D-91054 Erlangen, Germany

†Institute for Biochemistry, Medical Faculty, University of Cologne, Joseph-Stelzmann-Str. 52, D-50931 Köln, Germany

Summary

Objective: Matrilin-3 is a member of the recently described matrilin family of extracellular matrix proteins containing von Willebrand factor A-like domains. The matrilin-3 subunit can form homo-tetramers as well as hetero-oligomers together with subunits of matrilin-1 (cartilage matrix protein). It has a restricted tissue distribution and is strongly expressed in growing skeletal tissues. Detailed information on expression and distribution of extracellular matrix proteins is important to understand cartilage function in health and in disease like osteoarthritis (OA).

Methods: Normal and osteoarthritic cartilage were systematically analysed for matrilin-3 expression, using immunohistochemistry, Western blot analysis, *in situ* hybridization, and quantitative PCR.

Results: Our results indicate that matrilin-3 is a mandatory component of mature articular cartilage with its expression being restricted to chondrocytes from the tangential zone and the upper middle cartilage zone. Osteoarthritic cartilage samples with only moderate morphological osteoarthritic degenerations have elevated levels of matrilin-3 mRNA. In parallel, we found an increased deposition of matrilin-3 protein in the cartilage matrix. Matrilin-3 staining was diffusely distributed in the cartilage matrix, with no cellular staining being detectable. In cartilage samples with minor osteoarthritic lesions, matrilin-3 deposition was restricted to the middle zone and to the upper deep zone. A strong correlation was found between enhanced matrilin-3 gene and protein expression and the extent of tissue damage. Sections with severe osteoarthritic degeneration showed the highest amount of matrilin-3 mRNA, strong signals in *in situ* hybridization, and prominent protein deposition in the middle and deep cartilage zone.

Conclusion: We conclude that matrilin-3 is an integral component of human articular cartilage matrix and that the enhanced expression of matrilin-3 in OA may be a cellular response to the modified microenvironment in the disease. © 2002 Osteoarthritis Research Society International

Key words: Chondrocyte differentiation, Matrilin, Matrilin-3, Osteoarthritis.

Introduction

Osteoarthritis (OA) is a degenerative joint disease, involving mechanical, biochemical, hormonal, and genetic factors. The relative importance of these factors varies in the disease process and cannot be defined easily in patients with OA. The continuous loss of the articular cartilage matrix is the prominent feature of the progressive osteoarthritic process. The cartilage of articular joints is an extremely specialized tissue which enables a stable and smooth movement of the joint surfaces and, equally important, the dissipation of mechanical load under physiological conditions. Type II collagen and aggrecan, the two most abundant components of the cartilage extracellular matrix, are major contributors to these properties and have, therefore, been analysed extensively^{1,2}. Cartilage collagen fibrils form highly organized three-dimensional structures

responsible for the tissue stiffness. Under-hydrated proteoglycans within this meshwork contribute to the compensation of the load stress and are mainly responsible for the visco-elastic properties of the articular cartilage matrix. Additional components of the extracellular matrix such as type VI collagen, are implicated as being important in the mechano-protective filament structures that surround the chondrocytes³. Other cartilage proteins and proteoglycans such as COMP, CILP, fibronectin, and decorin have putative functions in cell-matrix and matrix-matrix interactions (reviewed in Neame *et al.*⁴).

Matrilin-3 belongs to a family of extracellular matrix proteins with members that share similarities in their modular compositions (reviewed in Deák *et al.*⁵). Matrilin-1 (earlier called cartilage matrix protein or CMP), -2, -3, and -4 share an N-terminal signal peptide domain, often followed by a short stretch of positively charged amino acids and a von Willebrand factor A (vWFA)-like domain. Close to the vWFA-like domain, one or several epidermal growth factor (EGF)-like domains are found. The number of EGF-like domains varies among the matrilins, with four EGF-like domains found in matrilin-3⁶⁻⁸. A second vWFA-like domain occurs in matrilin-1, -2, and -4, however in matrilin-3 this domain is absent^{7,9}. At the C-terminal end of the molecule, all matrilins carry a coil-coiled α -helical

Received 23 July; accepted 19 October 2001.

Funds were received from the DFG (PU114/4-1, WA1338/2-1).

Address correspondence to: Oliver Pullig, Ph.D., Division of Orthopaedic Rheumatology, Department of Orthopaedic Surgery, University of Erlangen-Nuremberg, Rathsbergerstraße 57, D-91054 Erlangen, Germany. Tel: +49/9131/822276; Fax: +49/9131/8523657; E-mail: oliver.pullig@med.uni-erlangen.de

Table I
Primers used for matrilin-3 riboprobe preparation (#1 and #2) and for quantitative competitive PCR (#3 and #3')

Primer pair	Primer sequence	PCR products (bp)
#1 (forward)	5'cat gtt cag cca ctg agg aa	785
#1 (reverse)	5'cag aat gaa tta aaa atg gca atg	
#2 (forward)	5'cag gtg ttt gca aga gca ga	529
#2 (reverse)	5'acc cca tag gtc tcc acg ta	
#3 (forward)	5'cat gtt cag cca ctg agg aa	525
#3 (reverse)	5'aac agg tgt gca aaa gaa tgc	
#3' (reverse)	5'aac agg tgt gca aaa gaa lgc gca att taa cga tgt att tgt cca	202

domain, responsible for the assembly into oligomeric aggregates (for refs see Deák *et al.*⁵).

Matrilin-3 is a recently discovered matrilin with a putative function in the assembly of the cartilage extracellular matrix^{6,7}. It is expressed in growing skeletal tissues of man, mouse and chicken^{7,8,10,11}. In 6-week-old mice, matrilin-3 mRNA is mainly found in the epiphyseal growth plate and in the bone forming cells¹⁰. The expression pattern of matrilin-3 in the growth plate is similar to that of matrilin-1¹². Therefore, expression of matrilin-3 indicates a role in the development of skeletal tissues. However, in normal adult articular cartilage, matrilin-1 expression is very limited or absent^{13,14}.

The expression of matrilin-3 in osteoarthritic cartilage has not been previously studied. In the progress of OA, articular cartilage chondrocytes behave similarly to those in the epiphyseal growth plate in that they differentiate, undergo hypertrophy, and, in a further differentiation step, express a posthypertrophic phenotype^{15,16}. We have systematically analysed the expression of matrilin-3 mRNA and protein in normal and osteoarthritic cartilage to define its role in the physiology and pathophysiology of osteoarthritic cartilage. Our results contribute to a better understanding of the complex matrix interactions in OA.

Material and methods

CARTILAGE/BONE SAMPLES

Thirty osteoarthritic cartilage/bone samples were obtained from 17 patients with primary OA (54- to 75 year-old donors) undergoing total knee replacement. Clinical data were carefully reviewed to exclude any forms of secondary OA and inflammatory joint diseases like rheumatoid arthritis. Normal cartilage was collected from five human knees at the time of autopsy within 18 h after death (34- to 56-year-old donors). In these five knees, the femorotibial and patellafemoral joint faces were completely free from any signs of OA. Video printouts were used to document the region where samples were taken. Osteoarthritic changes were classified histomorphologically, using the grading system of Mankin². Mankin score 0: normal cartilage with a smooth surface and a regular zonal distribution of the chondrocytes. Mankin score 1-4: cartilage surface shows fibrillations and a superficial loss of proteoglycans (safranin-O staining); the zonal structure is intact. Mankin score 5-8: Cartilage samples have clefts reaching down to the middle cartilage zone; clusters of proliferating chondrocytes are present. Mankin score ≥9: cartilage samples are severely affected; clefts are reaching down to the deep zone; the tangential zone is lost and chondrocyte clusters are present. Five samples (Mankin

score 0), eight samples (Mankin score 1-4), 12 samples (Mankin score 5-8), and 10 samples (Mankin score ≥9) were included in the study. This investigation has been approved by the local ethics commission (application No. 2078).

Cartilage/bone samples of 1 cm thickness with a cartilage surface of about 2.0×0.5 cm were incubated in freshly prepared paraformaldehyde, 4% (w/v), buffered with 0.01 M sodium phosphate, pH 7.4, containing 0.14 M NaCl (PBS) for 12 h at 4°C. The tissue samples were decalcified in diethyl-pyrocabonate (DEPC)-treated 0.2 M EDTA, pH 8.0, for several weeks at 4°C. The buffer was changed twice a week. Tissue specimens were then dehydrated through graded concentrations of ethanol and xylene and finally embedded in paraffin. Cartilage/bone and cartilage sections (5 µm) were mounted on glass slides, precoated with 1% (v/v) 3-aminopropyl triethoxysilane, and heated for 90 min at 65°C.

PREPARATION OF THE MATRILIN-3 RNA PROBE

Total RNA was extracted from human knee cartilage. 0.5 g of cartilage was frozen in liquid nitrogen and pulverized using a stainless steel mortar and pestle. Extraction was performed using cold guanidine Isothiocyanate buffer and a subsequent extraction with phenol¹⁷. 0.5 µg of total RNA was transcribed into single-stranded cDNA using AMV reverse transcriptase (Roche, Mannheim, Germany) and Oligo-p(dT)15 as a primer according to the manufacturer's protocol (Roche). Two double-stranded cDNA fragments were generated by PCR using primer pair 1 and 2 (Table I). The primer pair 1 spans 785 bases (position 1103-2087) of the coding region of the human matrilin-3 cDNA (Accession No. AJ224741)⁸. The primer pair 2 spans 529 bases (position 238-766) of the coding region of the human matrilin-3 cDNA. After standard PCR (annealing temperature: 60°C, 35 cycles), a T7 promoter-adaptor (Ambion, Austin, TX, U.S.A.) was ligated non-directionally. The transcription template was performed using a second PCR with the gene-specific forward primer and a T7 promoter-adaptor primer (Ambion). The amplified PCR products were checked by sequencing (MWG, Ebersberg, Germany).

For *in vitro* transcription and labeling, 100 ng of the template was transcribed in 1 mM ATP, 1 mM CTP, 1 mM GTP, 0.65 mM UTP and 0.35 mM digoxigenin-11-UTP in 40 mM Tris-HCl, pH 8.0, 6 mM MgCl₂, 10 mM dithiothreitol, 2 mM spermidine and 40 U T7 RNA-Polymerase (Roche). The components were incubated for 2 h at 37°C. Template DNA was removed with 20 U DNase I (Roche). The reaction was stopped by adding 2 µl 0.2 M EDTA pH 8.0. RNA was further purified by ethanol precipitation and resuspended in 100 µl DEPC-treated H₂O. Transcripts

were checked for integrity, length, and labeling efficiency by denaturing gel electrophoresis followed by Northern blotting and digoxigenin detection using the DIG-nucleic-acid-detection-kit (Roche). For *in situ* hybridization, approximately 100 ng of matrilin-3 antisense or sense riboprobe were used for each tissue section. Immediately before use, riboprobes were incubated for 10 min at 96°C followed by 2 min at 4°C.

IN SITU HYBRIDIZATION

Tissue sections were deparaffinized in xylene and rehydrated through graded concentrations of ethanol (100% to 50%). Sections were incubated with proteinase K, 50 µg/ml in 100 mM Tris, pH 7.5, with 50 mM EDTA, for 15 min at 37°C and postfixed in 4% (w/v) paraformaldehyde/PBS for 1 min. Sections were briefly washed in DEPC-treated double distilled water and acetylated twice for 5 min in 0.1 M triethanolamine by adding 0.3% (v/v) acetic acid anhydride. Sections were briefly incubated in PBS, dehydrated using increasing concentrations of ethanol (50% to 100%), and air-dried under dust-free conditions. Sections were prehybridized with hybridization buffer containing 50% formamide (v/v), 10% dextran (w/v), 0.026% Denhardt's solution (v/v), 0.5 mg/ml fish sperm DNA (Roche), 0.8 M NaCl, 0.6 mM DTT, 0.6 mM EDTA, 7 mM Tris, pH 7.5. They were carefully covered with Parafilm (Sigma, Munich, Germany) and prehybridization carried out for 1 h at 55°C. 50 µl of the hybridization solution containing 100 ng of the matrilin-3 probe was applied to each section. The sections were then covered with Parafilm and incubated in a humidified chamber overnight at 55°C. Sense strand *in situ* hybridization was also performed with the matrilin-3 probes using similar conditions as for the anti-sense hybridization. After hybridization, the sections were washed with 2× sodium chloride, sodium citrate (SSC), 50% formamide for 30 min at 52°C and with TNE buffer (10 mM Tris, pH 7.5, 0.5 M NaCl, 1 mM EDTA) at 37°C for 10 min. Non-specific binding was abolished by RNase treatment (RNase A, 5 µg/ml, in 5 mM Tris, 0.5 M NaCl, pH 7.5, 5 mM EDTA) for 1 h at 37°C. Sections were briefly washed in TNE at 37°C, and then washed in 2×SSC for 20 min at 52°C, and two times in 0.2×SSC for 20 min at 52°C. Detection of bound probes was performed using a commercially available nucleic-acid-detection-kit (Roche). Briefly, sections were incubated in blocking solution containing 10% (v/v) fetal calf serum. After blocking, an anti-digoxigenin alkaline phosphatase-labeled antibody was added and bound antibodies were detected after incubation with the substrate solution (X-phosphate/NBT) overnight. Sections were counterstained with 0.5% (w/v) light green (Merck, Darmstadt, Germany) in 5% (v/v) ethanol and mounted in Entellan (Merck).

Nucleic acid sequence homologies were tested using the FASTA program of the EMBL, Heidelberg, Germany. Homologies to listed RNA sequences were less than 55% within an overlapping region of maximal 500 base pairs for the 785 bp probe and less than 60% within an overlapping region of maximal 504 base pairs for the 529 bp probe. The specificity of the probes was controlled by using two different matrilin-3 mRNA probes, which were directed against different portions of the same transcript. Further controls for both matrilin-3 mRNA probes were performed by blocking the signal using unlabeled riboprobes prior the labeled probe. Integrity of the mRNA in cartilage and bone was assessed using a 115 base pair antisense

riboprobe for the human 28S RNA (nucleotide 4400–4415, Accession No. M11167, Ambion, Austin, U.S.A.). The hybridization protocol was similar to those used for the matrilin-3 probes, however probe concentration and hybridization temperature was reduced (10 ng per section at 43°C).

IMMUNOLocalIZATION OF MATRILIN-3

Tissue sections were deparaffinized in xylene and rehydrated. Human cartilage/bone sections were digested with 2 mg/ml hyaluronidase (Merck) in PBS, pH 5.5, for 15 min at 37°C and with 1 mg/ml pronase (Roche) in PBS, pH 7.4, for 30 min at 37°C. After two washes in PBS, sections were incubated in PBS containing 5% (w/v) bovine serum albumin (BSA). The sections were incubated with affinity purified polyclonal antibodies against matrilin-3 in 1% (w/v) BSA/PBS and incubated overnight at 4°C. The specificity of these antibodies has been demonstrated elsewhere¹⁰. After three washes in tris-buffered saline (TBS), a biotin-labeled donkey anti-rabbit IgG antibody (Dianova, Hamburg, Germany) diluted 1:200 in 1% (w/v) BSA/TBS was added and incubated for 30 min at room temperature. After that, alkaline-phosphatase-labeled streptavidin was added according to the protocol of the manufacturer (Dako, Hamburg, Germany). After three short washes in TBS, bound antibodies were visualized using Fast Red (Sigma) as a color substrate. To exclude non-specific background staining, sections were incubated with affinity purified rabbit IgG (Dako), 1:20 000 in 1% (w/v) BSA/PBS and immunohistochemical detection was performed as described above.

WESTERN BLOT ANALYSIS

Cartilage extracts were obtained from normal (N=4) and osteoarthritic samples (N=6), taken from the femoral condyles of human knee joints. Hyaline cartilage was peeled off from the underlying bone and homogenized at 4°C with an Ultraturax homogenizer (Jahnke and Kunkel, Germany) in 4 M guanidinium chloride, 50 mM sodium acetate, pH 5.8, containing proteinase inhibitors (10 mM N-ethylmaleimide, 10 mM phenyl methane sulfonyl fluoride, 10 mM benzamide hydrochloride). After 48 h of stirring at 4°C the insoluble material was removed by centrifugation at 13,000 g, 4°C, for 1 h. Proteins were separated from proteoglycans using an equilibrium centrifugation in a self-forming cesium chloride gradient. The extract was adjusted to a density of 1.35 mg/ml by the addition of solid cesium chloride. A Kontron swing-out rotor (TST 28.38) equipped with polyallomer thick wall tubes (38.5 ml) was used and centrifugation was done for 70 h (105,000×g; r_{av} = 23.89 cm) at 18°C. The gradient was divided into four equal portions from which the two top fractions were pooled and dialysed twice against 50 mM sodium acetate, pH 5.8, containing proteinase inhibitors (see above) and then against distilled water at 4°C for 12 h. Samples corresponding to 15 µg protein were lyophilized and redissolved in 1% SDS/sample buffer without dithiothreitol, denatured at 95°C for 5 min and analysed in a vertical SDS gel electrophoresis unit (Pharmacia, Freiburg, Germany) using a 4–22% gradient polyacrylamide gel in a discontinuous buffer system (0.8 mA/cm²). Proteins were blotted onto a nitrocellulose membrane for 2 h by using a constant current of 100 mA. Blotting efficiency and protein loading were controlled by reversible staining with Ponceau S-Red.

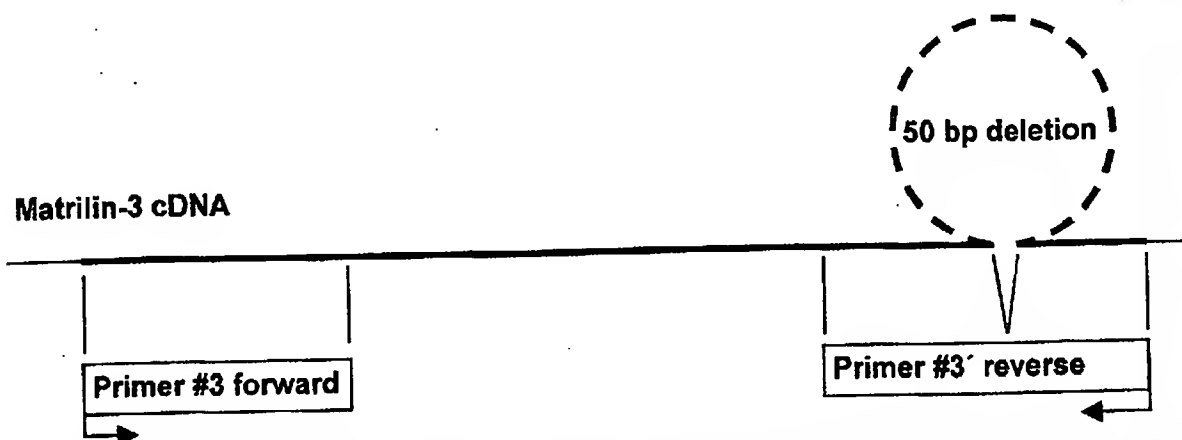


Fig. 1. Preparation of the internal standard (competitor) for quantitative determination of matrilin-3 mRNA. The first 21 bases (reading from the 5' end) of primer #3' and the following 24 bases are complementary to two different regions within the matrilin-3 cDNA. Binding results in a loop formation, leading to a 50 bp deletion in the PCR fragment. The mutated competitor was purified by electrophoretic size fractioning after gel electrophoresis.

For immunodetection of matrilin-3, the nitrocellulose membrane was destained with distilled water and incubated in TBS containing 1% non-fat dry milk blocking solution (Roche) for 1 h at room temperature. The polyclonal matrilin-3 antibody was diluted in 0.5% blocking solution and incubated for 2 h at room temperature. The membrane was extensively washed in TBS containing 0.1% Tween (TBST) followed by washing in 0.1% blocking solution. A horseradish peroxidase-conjugated goat anti-rabbit antibody (Dianova) was used at 1:1000 dilution in 0.5% blocking solution after 30 min of incubation at room temperature and appropriate washing in TBST. Chemiluminescence detection was carried out according to the manufacturer's protocol (Roche). Light emissions were visualized on a light sensitive X-ray film (Roche) after 5 to 10 min exposure time.

QUANTITATIVE DETERMINATION OF MATRILIN-3 mRNA USING COMPETITIVE PCR

Total RNA was extracted from human knee cartilage and 100 ng transcribed into cDNA as described above. Competitive quantitative PCR (cq-PCR) was carried out using a modification of the protocol of Riedy *et al.*¹⁸ and Köhler *et al.*¹⁹ Quantification of the matrilin-3 mRNA was based on the competitive amplification of matrilin-3 cDNA and an internal cDNA standard (=competitor) with identical primer binding sites. The competitor was generated by PCR, using final concentrations of 0.2 μ M of primer #3 and 0.2 μ M of primer #3' (Table I), 1.5 mM $MgCl_2$, 10 mM Tris pH 8.3, 50 mM KCl pH 8.3, and 2.5U/100 μ l Taq DNA Polymerase (Roche). Temperature cycling profile was 94°C for 1 min, 55°C annealing for 1 min and 72°C extension for 2 min. Binding of primer #3' causes the formation of a loop on the sense strand (Fig. 1). In the following PCR reaction, the Taq polymerase elongates primer #3' resulting in a cDNA having a 50 bp deletion within the PCR fragment. 30 μ l of the PCR reaction mixture was size fractionated on a 2% agarose gel, following staining with ethidium bromide. The 202 bp competitor was excised from the gel and purified (gel extraction kit, Qiagen, Hilden, Germany). The concentration of the competitor was determined by measuring the absorbance of aliquots at 260 nm. For cq-PCR the PCR reaction mixture (25 μ l) contained 1 μ l of

each patient's cartilage cDNA (equivalent to 5 ng total RNA), 1 mM deoxynucleotide mix (Roche), 0.2 μ M primer #3 forward, 0.2 μ M primer #3 reverse, 1.5 mM $MgCl_2$, 10 mM Tris pH 8.3, 50 mM KCl, pH 8.3. One cycle with 94°C, 30 s and 60°C, 30 s was performed. After that, defined amounts of competitor were added to each tube at room temperature (0.6, 2.4, 9.8, 39, 156, 625, and 2500 fg), tubes were replaced into the thermal cycler at 72°C and 0.625 U Taq DNA Polymerase (Roche) was added. Incubation was continued for 1 min at 72°C to synthesize a double stranded cDNA. PCR was then performed by 28 cycles of denaturation at 94°C for 30 s, annealing at 60°C for 30 s and elongation at 72°C for 60 s, ending with a final incubation at 72°C for 10 min to complete polymerization. 10 μ l of the PCR product was size fractionated on a 2% agarose gel and visualized using ethidium bromide staining. The gel was recorded by video camera and the intensities of the amplified fragments were calculated using the Scion image software tool (Scion Corporation, Frederick, U.S.A.). To correct for differences in molecular weight, competitor values and matrilin-3 cDNA values were divided by their base pair numbers²⁰.

The ratio of competitor intensity to matrilin-3 intensity vs the known amount of competitor cDNA was plotted in a log-log scale. At the point where competitor intensity and matrilin-3 intensity are in equivalence [$\log(\text{ratio})=1$], the amount of matrilin-3 cDNA is equal to the known amount of competitor template. Results are expressed in femtogram of matrilin-3 cDNA/ng RNA. For control, amplification was performed using 5 ng of the RNA preparation instead of reversed transcribed cDNA to exclude unspecific amplification of DNA. The grading of the cartilage samples from which mRNA was extracted was done by histomorphological validation of the adjacent areas using the Mankin score.

The specificity of the PCR reaction without competitor was checked by sequencing analyses of the amplified PCR product (results not shown). The number of cycles used in cq-PCR was restricted to the exponential phase of the amplification (28 cycles). The linearity of the cq-PCR was controlled by using increasing amounts of cDNA (0–1000 ng). We compared the matrilin-3 mRNA values obtained from normal cartilage and from cartilage with minor and severe lesions, using a non-parametric statistic test (Mann-Whitney U-test). All data are presented as

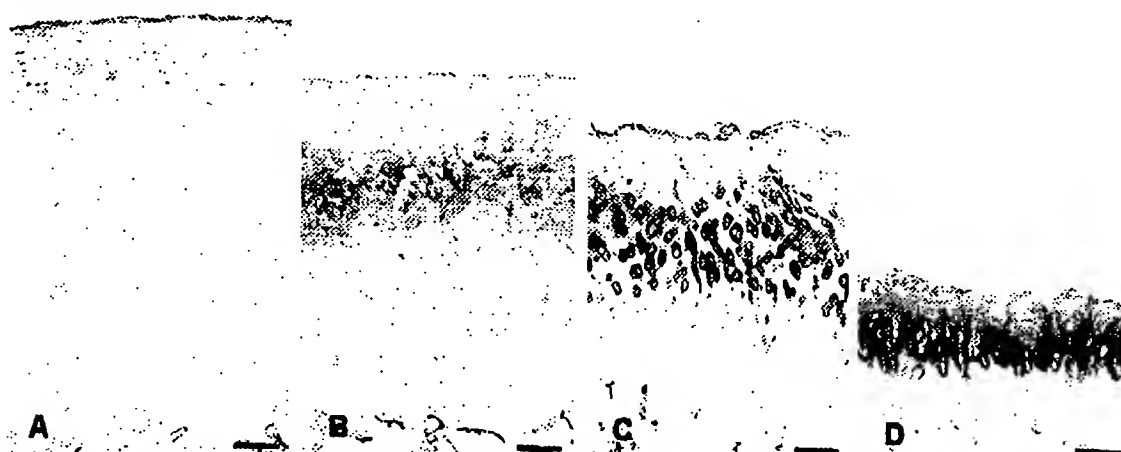


Fig. 2. Distribution of matrilin-3 in normal cartilage/bone sections (A) and sections with mild (B), moderate (C), and severe (D) osteoarthritic lesions. Sections were obtained from femoral load-bearing area and incubated with an affinity purified polyclonal antibody against matrilin-3. Note that the zonal matrilin-3 expression varies from normal to osteoarthritic stages. The territorial deposition of matrilin-3 increases in moderate and severe OA (bar=250 μ m).

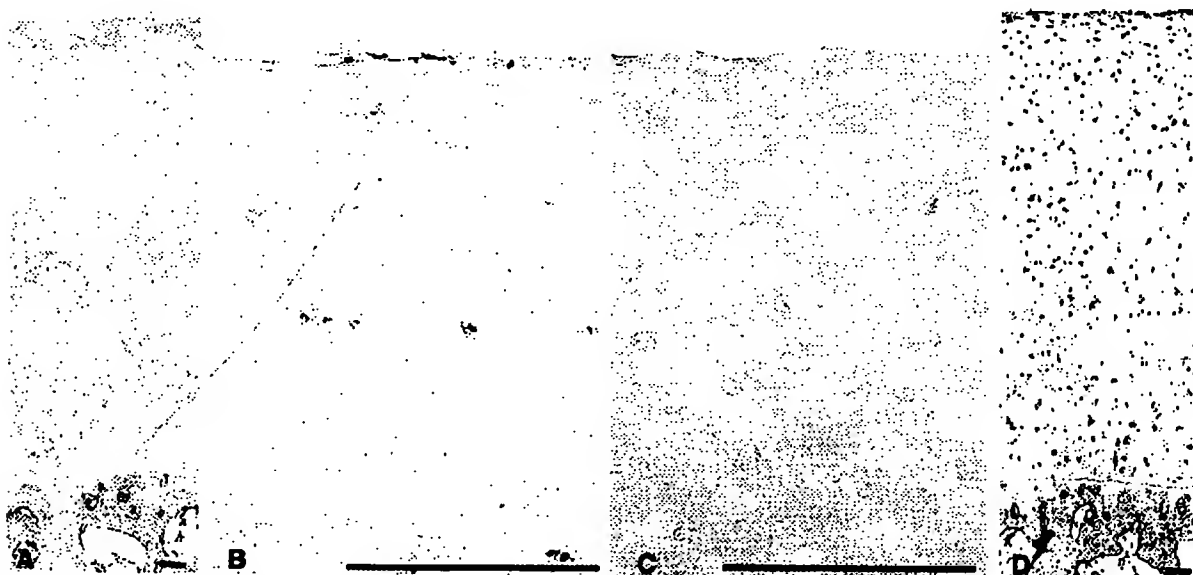


Fig. 3. Localization of matrilin-3 in normal cartilage (bar=100 μ m). (A) Immunostaining using a polyclonal antibody against matrilin-3. Matrilin-3 deposition is visible in the tangential zone and subchondral bone. (B) Focal expression of matrilin-3 mRNA is visible in chondrocytes of the tangential zone and the upper middle zone. (C) *In situ* hybridization using the matrilin-3 sense probe as a negative control. (D) Positive control *in situ* hybridization using the digoxigenin-labeled 28S mRNA probe.

means. Each quantification by PCR was carried out in duplicates. Significant differences were defined as $P < 0.05$.

Results

PROTEIN AND mRNA LOCALIZATION OF MATRILIN-3 IN NORMAL AND OSTEOARTHRITIC CARTILAGE/BONE

Normal and osteoarthritic cartilage samples were taken from the load bearing area of femoral condyles. Enzymatic pretreatment of the paraffin embedded tissue with hyaluronidase/pronase enhanced staining intensity for matrilin-3 and was therefore used on all tissue sections processed for immunohistochemistry. In all specimens from both normal and osteoarthritic tissue, matrilin-3 depositions

were observed (Fig. 2). In normal cartilage, several layers can be separated by morphological criteria. The lamina splendens, a thin layer directly facing the articular joint space is followed by the tangential, middle, deep, and calcified cartilage zone. Below, the subchondral bone with the bone trabeculae is found. In sections of normal cartilage [Figs 2(A) and 3(A)] the lamina splendens, the tangential and the upper middle zones were stained. Matrilin-3 staining was diffusely distributed in the cartilage matrix, no cellular staining was detectable. In general, staining intensity was faint. In the lower middle zone, the deep zone, and the calcified zone no matrilin-3 deposition was detectable. In subchondral bone trabeculae and in the osteocytes within newly formed osteoid, matrilin-3 staining was present.

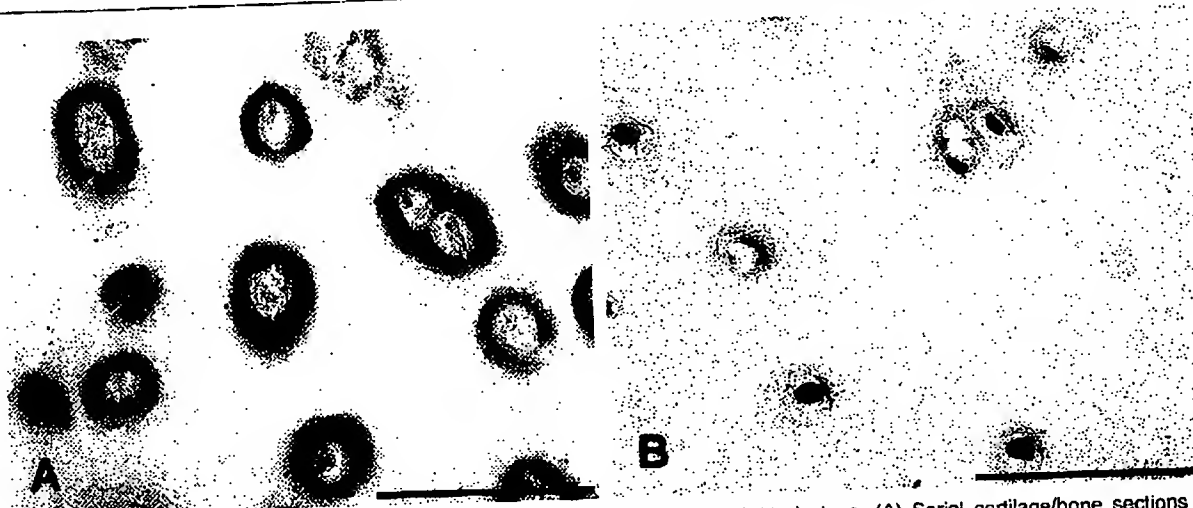


Fig. 4. Matrilin-3 in cartilage/bone sections from patients with moderate osteoarthritic lesions. (A) Serial cartilage/bone sections were incubated with a polyclonal antibody against matrilin-3. Chondrocytes from the middle cartilage zone show a prominent deposition of matrilin-3 within the territorial matrix (bar=100 μ m). (B) Corresponding *in situ* hybridization for detection of matrilin-3 mRNA. Incubation with a digoxigenin-labeled matrilin-3 riboprobe followed by immunological detection and substrate staining gives signals in the chondrocytes of the middle cartilage zone.

In cartilage samples with minor osteoarthritic lesions (Mankin score 1–4) the zonal organization is intact, however, the articular surface is fibrillated, with small clefts reaching down to the tangential zone. In these samples ($N=10$), matrilin-3 deposition was concentrated in the middle zone with some staining seen also in the upper deep zone [Fig. 2(B)]. In bone, cells lining the subchondral bone trabeculae and osteocytes stained positive [Fig. 6(A)]. Staining for matrilin-3 in cartilage increased in correlation with the severity of the osteoarthritic lesions. In samples with moderate OA (Mankin score 5–8), the tangential zone is absent. Again, matrilin-3 was most prominent in the middle zone and in the upper deep zone [Fig. 2(C)]. In comparison to samples with mild osteoarthritic lesions, the staining intensity increased. In addition to a diffuse interterritorial staining, a strong territorial staining was visible in the middle and upper deep zone [Fig. 4(A)]. In stages with severe matrix degeneration (Mankin score >8), the upper middle zone was mostly absent and clefts reached down to the deep zone [Figs 2(D) and 5(A)]. Matrilin-3 deposition was detectable in the upper deep zone, again no staining was visible in the lower deep and calcified zone [Figs 2(D) and 5(A)]. The extracellular matrix stained in a diffuse pattern and focally a cellular staining was observed. In general, matrilin-3 deposition within the extracellular cartilage matrix was diminished or absent in the cartilage zone adjacent to the articular joint space, independent of the osteoarthritic defects.

To complement the immunohistochemical results the distribution of matrilin-3 mRNA was determined. Chondrocytes expressing matrilin-3 could be detected in all cartilage samples. In normal cartilage, matrilin-3 mRNA was restricted to chondrocytes of the articular surface and of the upper middle zone [Fig. 3(B)] and the signal intensity was low. To exclude degradation and loss of mRNA during decalcification and fixation, samples were incubated with the 28S RNA probe as a positive control [Fig. 3(D)]. A negative control with the matrilin-3 sense probe in comparable labeling efficiency as the anti-sense probe failed to detect any hybridization signal [Fig. 3(C)]. In normal cartilage/bone sections a signal was detected in all nucleated cells. In cartilage samples showing mild,

moderate, or severe osteoarthritic lesions, matrilin-3 mRNA expression correlated with the observed protein deposition and the signal intensity was increased as compared to normal samples. Cartilage with mild or moderate osteoarthritic lesions showed a preferred matrilin-3 mRNA synthesis in the middle cartilage zone. In serial sections of the same region, a distinct matrilin-3 mRNA expression is visible [Fig. 4(B)].

In addition to the correlated expression of mRNA and protein, proliferating chondrocytes near the articular joint space showed mRNA expression with no or weak protein deposition [Fig. 5(B), arrows].

In bone, matrilin-3 protein deposition was correlated with matrilin-3 gene expression. Bone cells lining the bone trabeculae as well as osteocytes within the new-formed osteoid contained matrilin-3 mRNA [Figs 6(A), (B)]. In bone cells, the signal intensity was unchanged between normal and osteoarthritic samples. Tibia samples were also analysed and demonstrated no significant differences in the staining pattern compared to the femoral samples (results not shown). When using a second mRNA probe directed against a different portion of the matrilin-3 transcript, an identical distribution pattern was detected (results not shown). Hybridization of osteoarthritic samples with the sense probe showed no hybridization signal (data not shown).

QUANTITATIVE DETERMINATION OF MATRILIN-3 mRNA IN NORMAL AND OSTEOARTHRITIC CARTILAGE

Quantification of matrilin-3 mRNA in normal and osteoarthritic cartilage was carried out using defined serial dilutions of competitor (0.6 fg to 156 fg). The linearity of the assay was controlled using a constant amount of competitor (156 fg) and increasing amounts of cDNA (10–1000 ng). A linear correlation was obtained between 50 and 500 ng for cDNA from normal cartilage and between 50 and 750 ng for cDNA from osteoarthritic cartilage (results not shown). In five normal samples, a mean value of 0.85 fg/ng mRNA was determined by qc-PCR [Fig. 7(B)], while the mean value in chondrocytes from tissue with minor osteoarthritic

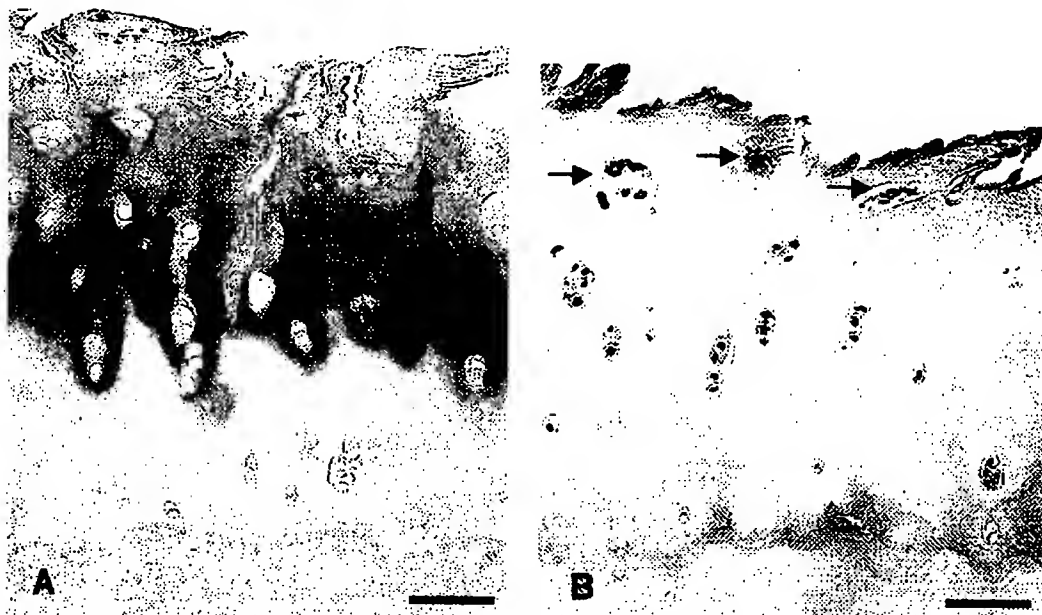


Fig. 5. Distribution of matrilin-3 in cartilage/bone section from end stage osteoarthritis with severe lesions of the articular surface. (A) Immunohistochemical localization, using a polyclonal antibody against matrilin-3. Protein deposition is concentrated to the upper deep cartilage zone. (B) *In situ* hybridization using a 785 bp digoxigenin labeled riboprobe for matrilin-3. Matrilin-3 mRNA expression correlates with the protein pattern. Proliferating chondrocytes, near the articular joint space show mRNA expression without pronounced protein deposition in the surrounding extracellular matrix (arrows).

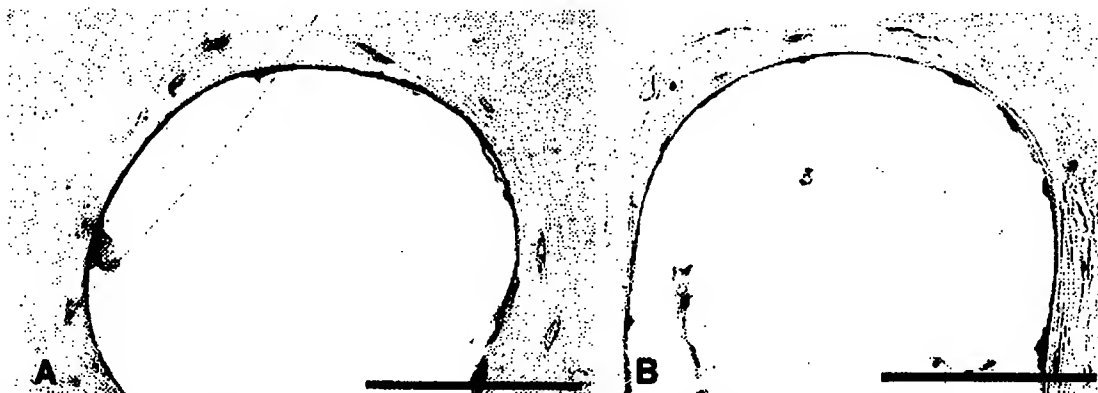


Fig. 6. Matrilin-3 expression in subchondral bone (bar=100 μ m). (A) Decalcified cartilage/bone paraffin sections (minor osteoarthritic lesions) were incubated with a polyclonal antibody against matrilin-3. Matrilin-3 deposition is visible in osteogenic cells lining the subchondral bone trabeculae and in the adjacent osteocytes. (B) Corresponding *in situ* hybridization. A serial section was incubated with a digoxigenin-labeled riboprobe for matrilin-3 mRNA. Matrilin-3 mRNA expression correlates with protein deposition.

lesions was 12.9 fg/ng mRNA. In samples with severe osteoarthritic lesions the mean level of matrilin-3 mRNA was 32 fg/ng mRNA. Thus, matrilin-3 mRNA amounts were significantly increased in severely osteoarthritic samples as compared to samples with minor lesions ($P=0.0095$, Mann-Whitney U-test).

ANALYSIS OF MATRILIN-3 IN NORMAL AND OSTEOARTHRITIC CARTILAGE EXTRACTS BY IMMUNOBLOTS

Purified cartilage extracts were analysed under reducing and non-reducing conditions on a 4–22% SDS-PAGE gel, followed by Western blotting using an affinity purified polyclonal antibody against matrilin-3. Under non-reducing conditions, a complex band pattern was seen in samples from

healthy donors as well as in osteoarthritic cartilages [Fig. 8(C)]. Higher oligomeric forms migrated above 200 kDa, presumably representing tetrameric and trimeric molecules that in part also contain subunits of matrilin-1^{10,21–23}. Further, two bands around 60 kDa represent intact and slightly degraded matrilin-3 subunits. Indeed, in matrilin-4 a cleavage site was recently located in the linker between the second vWFA-like domain and the coiled-coil domain²⁴. A sequence with homology to that at which matrilin-4 is cleaved is present in matrilin-3 between the fourth EGF-like domain and the coiled coil domain. Under reducing conditions, a single band at around 70 kDa appears that presumably represents both the processed and the unprocessed monomers, which are not resolved under reducing conditions [Fig. 8(D)]. The degraded forms of matrilin-3 are

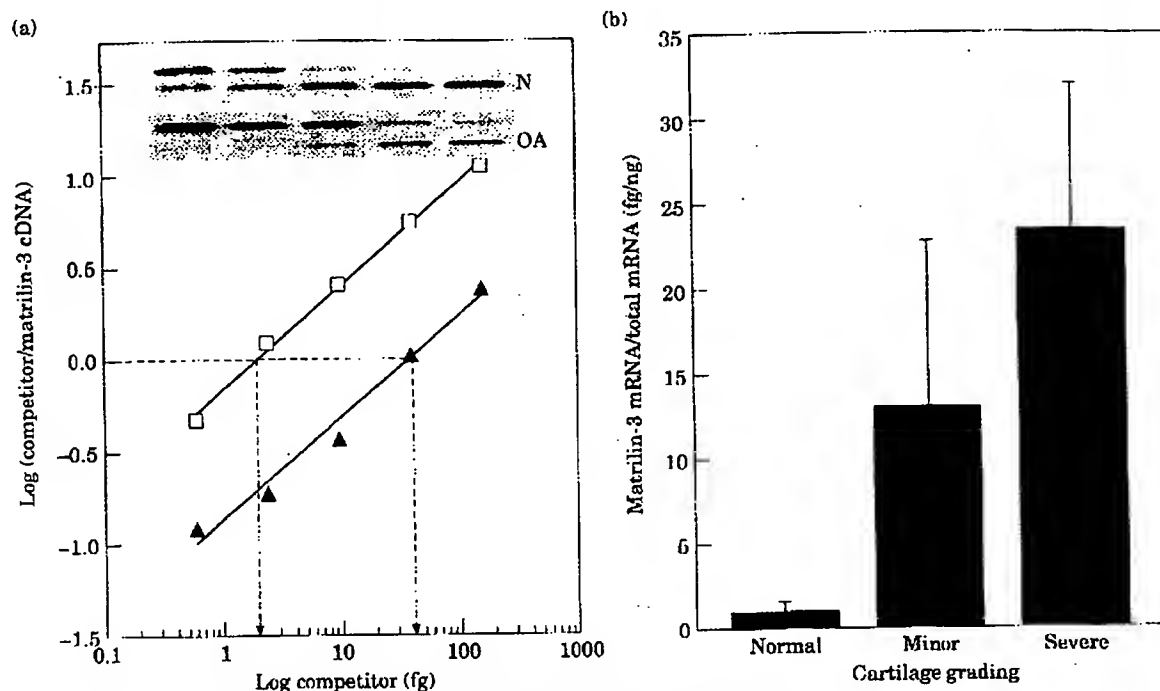


Fig. 7. Competitive quantitative PCR analysis of the matrilin-3 mRNA. (a) Representative results of the competitive quantitative PCR. cDNA of normal (N) and osteoarthritic (OA) cartilage was amplified in the presence of defined amounts of competitor DNA (0.6 fg to 156 fg). 10 μ l of the PCR products were size fractionated in an agarose gel containing ethidium bromide. The amounts of matrilin-3 fragment (upper band) and the competitor fragment (lower band) were quantified by video densitometry, set in relation, and plotted versus the amount of competitor. The amounts of matrilin-3 cDNA in the normal samples (\square) and in the osteoarthritic samples (\blacktriangle) were calculated from the equivalence point (log 0). (b) Quantification of matrilin-3 mRNA in normal cartilages (N=4) and in cartilages with moderate osteoarthritic lesions (N=6) and severe osteoarthritic lesions (N=6). Matrilin-3 mRNA is significantly increased in osteoarthritic cartilage samples as compared to normal and in samples with moderate lesions as compared to such with severe lesions ($P=0.0095$, Mann-Whitney-U Test).

more prominent in osteoarthritic than in healthy cartilage. The comparable loading of individual lanes was checked by reversible staining of blotted proteins with Ponceau red [Fig. 8(A),(B)].

Discussion

Only limited information has been available on the localization and expression of matrilin-3 in adult human cartilage. Expression has been demonstrated in chondrocytes of the mouse epiphyseal growth plate and a function in the skeletal development has been proposed¹⁰. Proteins with a restricted expression in the growing cartilage of the epiphyseal growth plate characterize certain chondrocyte differentiation stages with a defined phenotype. Interestingly, it has been shown that matrix components of the growth plate are often re-expressed under the pathological conditions in osteoarthritis. This applies not only to type X collagen, alkaline phosphatase, osteocalcin, and osteopontin^{15,16,25,26}, but, as we report here, also to matrilin-3. However, matrilin-3 is expressed at low levels also in normal human articular cartilage.

In normal cartilage, matrilin-3 has a restricted deposition within the transition of the superficial layer and the middle cartilage zone. Matrilin-3 expression, as shown by quantitative RT-PCR, *in situ* hybridization, immunohistochemistry and immunoblots, correlates with the progression of cartilage degeneration. Interestingly, matrilin-3 deposition is not

limited to a certain zone in cartilage, but it is restricted within a defined distance of about 100 to 200 μ m from the articular joint space (Fig. 2). The staining pattern we observe is pericellular, indicating a function of matrilin-3 in preserving the pericellular environment. Also, type VI collagen is preferentially deposited in the pericellular capsule and the pericellular matrix and is therefore thought to be involved in protective structures serving to withstand the mechanical forces of the extracellular cartilage matrix²⁷. On the structural level, both, matrilin-3 and type VI collagen contain vWFA-like domains. Members of the vWFA-domain superfamily have different functions in cell differentiation, cell migration, cell adhesion, hemostasis, and immune response, but share common characteristics in their participation in cell-cell and cell-matrix interactions (reviewed in Colombatti and Bonaldo²⁸). In analogy to type VI collagen, matrilin-3 has been shown to be deposited in pericellular meshworks around rat chondrosarcoma cells and in mouse sternal and tracheal cartilages¹⁰. Matrilin-3 or matrilin-3 containing filaments may be anchored via interactions with cells or with extracellular components. The interactions of matrilin-3 have not yet been studied, but the structurally related matrilin-1 has been shown to bind to $\alpha 1 \beta 1$ integrin²⁹ as well as to cartilage proteoglycans^{30,31}, type II collagen³², and itself²².

Our results show a low but significant expression of matrilin-3 mRNA in normal human cartilage, which is highly upregulated in osteoarthritic cartilage. For matrilin-1, a low or minimal expression has been observed in normal

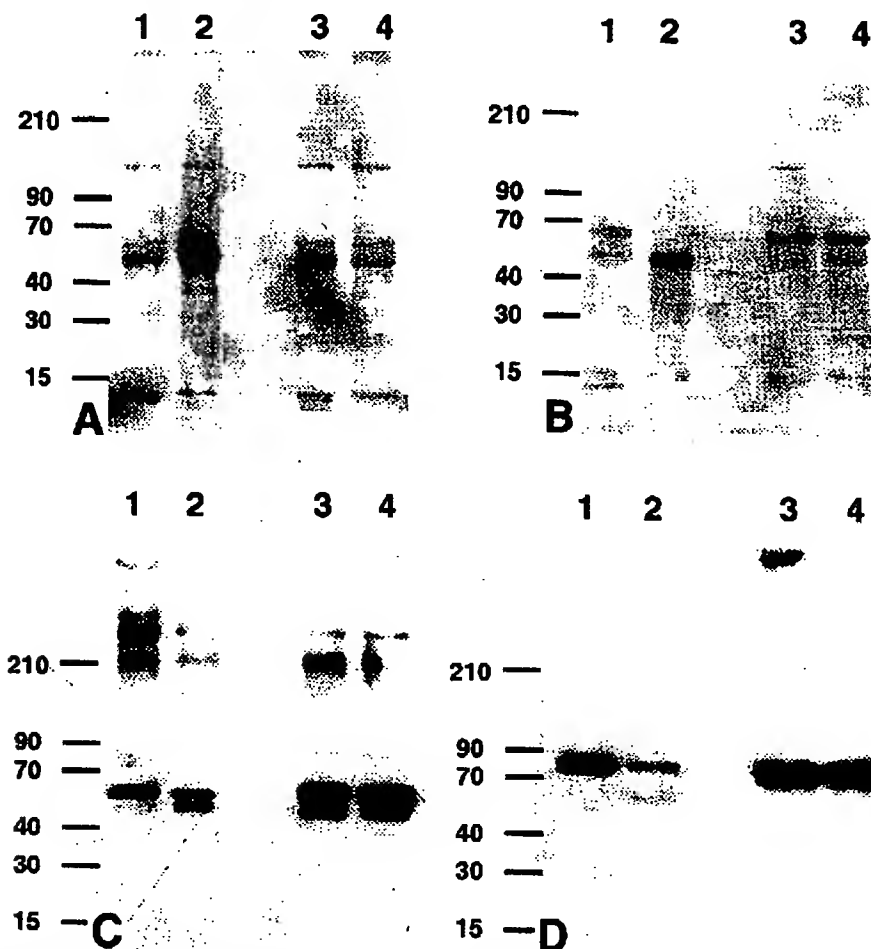


Fig. 8. SDS-PAGE and immunoblot for matrilin-3 of extracts of normal and osteoarthritic cartilage. 15 μ g of partially purified extracts of normal (lane 1, 2) and osteoarthritic (lane 3, 4) cartilage were separated by SDS-PAGE in a 4–22% polyacrylamide gel under non-reducing (A), (C) or reducing (B), (D) conditions. Proteins were visualized by Ponceau red staining (A), (B) to show equal loading or with Immunoblot with an affinity purified antibody against matrilin-3.

human articular cartilage using immunohistochemical methods^{13,14}. In OA, matrilin-1 deposition increases and the immunohistological staining is more pronouncedly cellular and pericellular, with low or absent staining of the interterritorial matrix¹⁴. Together with our data on matrilin-3 deposition and synthesis, a coexpression of matrilin-1 and matrilin-3 in hetero-oligomers in the cellular environment is likely and may indeed be due to the two types of matrilin subunits occurring in hybrid oligomers^{10,21–23} or in hybrid filaments.

Data on the functional role of matrilin-3 in cartilage are limited but from deletion analysis in cell culture, there is evidence that vWFA-like domains enables interactions with cellular or extracellular components^{10,21,22}. So far, no binding partners for matrilin-3 have been identified *in vivo* except the formation of matrilin-3 homomers and heteromers with matrilin-1^{10,21,22}. Through expression analysis in developing mouse joints, matrilin-3 was shown to be an integral component of developing cartilage. In the growth plate, expression was observed in the resting cartilage zone as well as in the proliferating and hypertrophic zones, implicating that matrilin-3 participates in cartilage development. In contrast, in mouse articular cartilage matrilin-3 is present in lower amounts and deposit only at

the periphery of the joints. This is in agreement with our results showing low expression in the superficial cartilage zone of normal human articular cartilage. In OA, along with an enhanced disintegration of the cellular microenvironment matrilin-3 is gradually lost from the territorial matrix. This indicates that the structural organization is destroyed and a pericellular anchoring of matrilin-3 is reduced. This may in part be due to an increased proteolysis of matrilin-3 in osteoarthritic cartilage. In parallel, there is an increase in matrilin-3 synthesis. Chondrocyte maturation and hypertrophy during development is regulated by factors such as Indian hedgehog protein, PTH-related peptide, the group of bone morphogenic proteins and members of the fibroblast growth factor family. There is evidence, that these proteins influence the differentiation and hypertrophy of chondrocytes also in osteoarthritis and therefore may contribute to matrilin-3 up-regulation. In comparison to the strict regulation of cellular differentiation and activation during embryonal development, the chondrocyte biosynthetic activity in OA is unbalanced, resulting in a matrix which is unable to withstand the physiological mechanical forces.

The low expression of matrilin-3 in normal cartilage and the correlation of tissue damage with the induction of matrilin-3 expression shows that matrilin-3 may be used as

a marker for the progression of OA. Studies on the function of matrilin-3 in cartilage as well as the determination of matrilin-3 in body fluids would be helpful in understanding and monitoring the disease process of OA.

Acknowledgments

The authors thank Mats Paulsson for his helpful discussion and for critical reading of the manuscript. Furthermore, we thank Katrin Seifert and Herbert Rohrmüller for their skillful technical assistance.

References

- Lippiello L, Hall D, Mankin HJ. Collagen synthesis in normal and osteoarthritic human cartilage. *J Clin Invest* 1977;59:593-600.
- Mankin HJ, Dorfman H, Lippiello L, Zarins A. Biochemical and metabolic abnormalities in articular cartilage from osteoarthritic human hips. II. Correlation of morphology with biochemical and metabolic data. *J Bone Joint Surg* 1971;53:523-37.
- Poole CA. Articular cartilage chondrons: form, function and failure. *J Anat* 1997;191:1-13.
- Neame PJ, Tapp H, Azizan A. Noncollagenous, non-proteoglycan macromolecules of cartilage. *Cell Mol Life Sci* 1999;55:1327-40.
- Deák F, Wagener R, Kiss I, Paulsson M. The matrilins: a novel family of oligomeric extracellular matrix proteins. *Matrix Biol* 1999;18:55-64.
- Belluoccio D, Trueb B. Matrilin-3 from chicken cartilage. *FEBS Lett* 1997;415:212-6.
- Wagener R, Kobbe B, Paulsson M. Primary structure of matrilin-3, a new member of a family of extracellular matrix proteins related to cartilage matrix protein (matrilin-1) and von Willebrand factor. *FEBS Lett* 1997;413:129-34.
- Belluoccio D, Schenker T, Baici A, Trueb B. Characterization of human matrilin-3 (MATN3). *Genomics* 1998;53:391-4.
- Wagener R, Kobbe B, Aszódi A, Liu Z, Beier DR, Paulsson M. Structure and mapping of the mouse matrilin-3 gene (Matn3), a member of a gene family containing a U12-type AT-AC intron. *Mamm Genome* 2000;11:85-90.
- Klatt AR, Nitsche DP, Kobbe B, Mörgelin M, Paulsson M, Wagener R. Molecular structure and tissue distribution of matrilin-3, a filament-forming extracellular matrix protein expressed during skeletal development. *J Biol Chem* 2000;275:3999-4006.
- Segat D, Frie C, Nitsche PD, Klatt AR, Piecha D, Korpos E, Deák F, Wagener R, Paulsson M, Smyth N. Expression of matrilin-1, -2 and -3 in developing mouse limbs and heart. *Matrix Biol* 2000;19:649-55.
- Chen Q, Johnson DM, Haudenschild DR, Goetinck PF. Progression and recapitulation of the chondrocyte differentiation program: cartilage matrix protein is a marker for cartilage maturation. *Dev Biol* 1995;172:293-306.
- Mundlos S, Zabel B. Developmental expression of human cartilage matrix protein. *Dev Dyn* 1994;199:241-52.
- Okimura A, Okada Y, Makihira S, Pan H, Yu L, Tanne K, Imai K, Yamada H, Kawamoto T, Noshiro M, Yan W, Kato Y. Enhancement of cartilage matrix protein synthesis in arthritic cartilage. *Arthritis Rheum* 1997;40:1029-36.
- Pullig O, Weseloh G, Ronneberger D, Käkönen S-M, Swoboda B. Chondrocyte differentiation in human osteoarthritis: expression of osteocalcin in normal and osteoarthritic cartilage and bone. *Calcif Tissue Int* 2000;67:230-40.
- Pullig O, Weseloh G, Gauer S, Swoboda B. Osteopontin is expressed by adult human osteoarthritic chondrocytes: protein and mRNA analysis of normal and osteoarthritic cartilage. *Matrix Biol* 2000;19:245-55.
- Chomczynski P, Sacchi N. Single-step method of RNA isolation by acid guanidinium thiocyanate-phenol-chloroform extraction. *Anal Biochem* 1987;162:156-59.
- Riedy MC, Timm EA, Stewart CC. Quantitative RT-PCR for measuring gene expression. *Bio-Techniques* 1995;18:70-4.
- Köhler T. Quantitative RT-PCR: Amplification of synthesized mdr-1 cDNA. In: Köhler T, Ed. Quantification of mRNA by Polymerase Chain Reaction. Berlin: Springer-Verlag 1995:71-80.
- Menzo S, Bagnarelli P, Giacca M, Manzin A, Varaldo PE, Clementi M. Absolute quantitation of viremia in human immunodeficiency virus infection by competitive reverse transcription and polymerase chain reaction. *J Clin Microbiol* 1992;30:1752-7.
- Wu JJ, Eyre DR. Matrilin-3 forms disulfide-linked oligomers with matrilin-1 in bovine epiphyseal cartilage. *J Biol Chem* 1998;273:17433-8.
- Chen Q, Zhang Y, Johnson DM, Goetinck PF. Assembly of a novel cartilage matrix protein filamentous network: molecular basis of differential requirement of von Willebrand factor A domains. *Mol Biol Cell* 1999;10:2149-62.
- Kleemann-Fischer D, Kleemann GR, Engel D, Yates JR, 3rd, Wu JJ, Eyre DR. Molecular properties of matrilin-3 isolated from human growth cartilage. *Arch Biochem Biophys* 2001;387:209-15.
- Klatt AR, Nitsche DP, Kobbe B, Macht M, Paulsson M, Wagener R. Molecular structure, processing and tissue distribution of matrilin-4. *J Biol Chem* 2001;276:17267-75.
- Rees JA, Ali SY. Ultrastructural localisation of alkaline phosphatase activity in osteoarthritic human articular cartilage. *Ann Rheum Dis* 1988;47:747-53.
- von der Mark K, Kirsch T, Nerlich A, Kuss A, Weseloh G, Glücker K, *et al.* Type X collagen synthesis in human osteoarthritic cartilage. Indication of chondrocyte hypertrophy. *Arthritis Rheum* 1992;35:806-11.
- Poole CA, Ayad S, Schofield JR. Chondrons from articular cartilage: I. Immunolocalization of type VI collagen in the pericellular capsule of isolated canine tibial chondrons. *J Cell Sci* 1988;90:635-43.
- Colombatti A, Bonaldi P. The superfamily of proteins with von Willebrand factor type A-like domains: one theme common to components of extracellular matrix, hemostasis, cellular adhesion, and defense mechanisms. *Blood* 1991;77:2305-15.

29. Makihira S, Yan W, Ohno S, Kawamoto T, Fujimoto K, Okimura A, *et al*. Enhancement of cell adhesion and spreading by a cartilage-specific noncollagenous protein, cartilage matrix protein (CMP/Matrilin-1), via integrin $\alpha 1 \beta 1$. *J Biol Chem* 1999;274:11417-23.
30. Paulsson M, Heinegård D. Matrix proteins bound to associatively prepared proteoglycans from bovine cartilage. *Biochem J* 1979;183:539-45.
31. Hauser N, Paulsson M, Heinegård D, Mörgelin M. Interaction of cartilage matrix protein with aggrecan. Increased covalent cross-linking with tissue maturation. *J Biol Chem* 1996;271:32247-52.
32. Winterbottom N, Tondravi MM, Harrington TL, Klier FG, Vertel BM, Goetinck PF. Cartilage matrix protein is a component of the collagen fibril of cartilage. *Dev Dyn* 1992;193:266-76.

Biochemical Pharmacology, Vol. 60, pp. 1639-1646, 2000.
© 2000 Elsevier Science Inc. All rights reserved.



ISSN 0006-2952/00/\$-see front matter
PII S0006-2952(00)00500-1

Up-regulation of Mitochondrial Peripheral Benzodiazepine Receptor Expression by Tumor Necrosis Factor alpha in Testicular Leydig Cells

POSSIBLE INVOLVEMENT IN CELL SURVIVAL

Catherine Rey,* Claire Mauduit,† Olivier Naureils,* Mohamed Benahmed,†
Pierre Louisot* and Françoise Gasnier*‡

*INSERM U. 189 AND †INSERM U. 407, FACULTÉ DE MÉDECINE LYON-SUD, BP12,
69921 OULLINS CEDEX, FRANCE

ABSTRACT. Porcine Leydig cells in primary cultures are resistant to tumor necrosis factor alpha (TNF α) cytotoxicity. Here we report that these cells can be rendered sensitive to TNF α killing by treatment with the translational inhibitor cycloheximide, suggesting the existence of proteins that can suppress the death stimulus induced by the cytokine. In search of these cytoprotective proteins, we focused on the constituents of the mitochondrial permeability transition pore (PT pore), whose opening has been shown to play a critical role in the TNF α -mediated death pathway. We found that TNF α up-regulated mRNA and protein expression of the mitochondrial peripheral benzodiazepine receptor (PBR), an outer membrane-derived constituent of the pore. A strong correlation was established between the resistance of the cells to TNF α killing and the density of PBR-binding sites. Concomitantly, TNF α down-regulated Bcl-2 mRNA and protein expression. As Bcl-2 has been shown to be an endogenous inhibitor of the PT pore, we hypothesize that the TNF α -induced up-regulation of PBR expression may compensate for the decrease in Bcl-2 levels to prevent the opening of the PT pore. *BIOCHEM PHARMACOL* 60;11:1639-1646, 2000. © 2000 Elsevier Science Inc.

KEY WORDS. testis; Leydig cells; mitochondria; peripheral benzodiazepine receptor; Bcl-2; TNF

TNF α is a multifunctional cytokine that elicits numerous cellular reactions depending on the cellular context. Beside its tumoricidal activity by which it was originally defined [1], TNF α has been shown to play a major role in inflammation, septic shock, and viral replication. The biochemical basis by which TNF α mediates such a wide array of effects is not fully understood [2].

Considerable attention has recently been paid to the TNF α -mediated death pathway where production of reactive oxygen intermediates [3], caspase activation [4], loss of mitochondrial membrane potential [5, 6], and cytochrome c release from mitochondria [6] seem to play a critical role in activation of the signaling. All these biochemical perturbations that converge on mitochondria may be mediated by opening of the mitochondrial PT pore, a Bcl-2-regulated, large, non-specific pore also called megachannel or multiple conductance channel [7-10]. Although the molecular constituents of the pore have not been definitively

established, it appears to consist of several proteins located at the mitochondrial contact sites, membrane microdomains where the outer and inner membranes come into close apposition [11, 12]. Thus, the outer membrane porin (also called voltage-dependent anion channel or VDAC) and PBR, as well as the inner membrane adenine nucleotide translocator (ANT, also called ATP/ADP carrier), have been implicated in PT pore formation [13].

While TNF α induces death of tumor cells and virally infected cells, normal cells are generally insensitive to its toxic effects. However, as many normal cells can be rendered sensitive to TNF α by treatment with RNA or protein synthesis inhibitors, a postulate has emerged that TNF α also activates a cell survival pathway that protects against its cytotoxic effects. Several cytoprotective TNF-inducible genes have been described, including the Bcl-2 family member A1 [14], manganous superoxide dismutase [15, 16], the A20 zinc-finger protein [17], plasminogen activator inhibitor type-2 [18], and γ -glutamylcysteine synthetase [19]. Nuclear factor- κ B activation has been shown to play a key role in the regulation of these genes [20].

Porcine Leydig cells in primary cultures are resistant to TNF α cytotoxicity [21]. However, TNF α strongly affects their metabolism. Indeed, we have previously shown that TNF α exerts an inhibitory action on Leydig cell steroido-

‡ Corresponding author: Dr. Françoise Gasnier, Physiopathologie Subcellulaire, INSERM U 189, Faculté de Médecine Lyon-Sud, B.P. 12, F-69921 Oullins cedex, France. Tel. +33 478 86 31 58; FAX +33 478 50 71 52; E-mail: fgasnier@lyon-sud.univ-lyon.fr

§ Abbreviations: TNF α , tumor necrosis factor alpha; PT pore, permeability transition pore; PBR, peripheral benzodiazepine receptor; and RT-PCR, reverse transcription-polymerase chain reaction.

Received 20 January 2000; accepted 12 May 2000.

genesis through a decrease in steroidogenic acute regulatory protein expression and that such an inhibitory action is probably mediated by TNF α receptor p55 expressed in the testicular cells [22]. We report here that these cells can be rendered sensitive to TNF α killing by treatment with the translational inhibitor cycloheximide. In search of the mechanism by which Leydig cells resist TNF α challenge, we focused on the PT pore constituents. We show that TNF α up-regulates PBR expression and concomitantly down-regulates Bcl-2 expression in these cells. As the resistance of the cells to TNF α killing was correlated with the density of PBR-binding sites, it is suggested that the increase in PBR expression may compensate for the decrease in Bcl-2 levels to prevent the opening of the PT pore and rescue cells from TNF α -induced death.

MATERIALS AND METHODS

Materials

[³H]PK11195 (1-(2-chlorophenyl))-N-methyl-N-(1-methylpropyl)-3-isoquinoline-carboxamide, specific activity 75 Ci/mmol, was purchased from NEN. Unlabeled PK11195 was a gift from Dr C. Caillard of Rhône-Poulenc Rorer Co. Human recombinant TNF α was obtained from Prepro Tech. Dulbecco's modified Eagle's/Ham's F-12 medium, Moloney murine leukemia virus reverse transcriptase, and TRIzol were obtained from Life Technologies. Collagenase/dispase was obtained from Boehringer. Insulin, transferrin, vitamin E, HEPES, and deoxyribonuclease type I (DNase) were purchased from Sigma Chemical Co. [α -³²P]dCTP was purchased from Amersham. Taq polymerase was obtained from Appligene-Oncor and oligonucleotide primers from Genset.

Leydig Cell Preparation and Culture

Leydig cells were prepared from immature porcine testes (2–3 weeks old) by collagenase treatment as described in [23]. They were cultured in 10-cm Petri dishes (20 \times 10⁶ cells/dish) at 32° in a humidified atmosphere of 5% CO₂, 95% air in Dulbecco's modified Eagle's/Ham's F-12 medium (1:1) containing sodium bicarbonate (1.2 mg/mL), 15 mM HEPES and gentamicin (20 μ g/mL). This medium was supplemented with insulin (2 μ g/mL), transferrin (5 μ g/mL), and α -tocopherol (10 μ g/mL).

Preparation of Purified Mitochondria

Mitochondria were isolated by differential centrifugation as described in [22].

Viability Assay

Cell viability was determined by the release of lactate dehydrogenase into the culture medium, using the detection kit from Boehringer. Cells were seeded at 10⁶ cells/well in triplicate in 6-well plates. They were pretreated with

TNF α (20 ng/mL) for 50 hr and then challenged for an additional 15 hr with TNF α (20 ng/mL) and different doses of cycloheximide (0–5 μ g/mL). Control cells were treated with cycloheximide alone (0–5 μ g/mL) for 15 hr. Cycloheximide was not cytotoxic at the concentrations used within the time frame of the experiments.

Radioligand-Binding Assays

Cultures were washed with medium, scraped from the dishes, and collected by centrifugation at 180 \times g for 10 min. [³H]PK11195 binding studies on 20 μ g protein from cell suspensions in Tris-buffered saline (TBS) or on 5 μ g protein from mitochondria were performed at 0° in a final incubation volume of 0.25 mL, using 0.9 nM of the radiolabeled ligand. Non-specific binding was determined in the presence of 10⁻⁵ M unlabeled ligand. After a 30-min incubation, the assays were stopped by filtration through Whatman GF/C filters pretreated with 10 μ M unlabeled ligand and washed with 15 mL ice-cold TBS. Radioactivity trapped on the filters was determined by liquid scintillation counting. Total binding was approximately 10% of the total free radioligand included in the assay and specific binding was 90% of the total binding.

Western Blot Analysis

Proteins from whole Leydig cells were resolved on 12% SDS/polyacrylamide gels and electrophoretically transferred to nitrocellulose membranes using 10 mM CAPS (3-[cyclohexylamino]-1-propanesulfonic acid) pH 11, containing 10% methanol. The transfer was performed at a constant voltage of 100 V for 30 min. Following transfer, the membrane was incubated in a blocking buffer (TBS buffer containing 5% non-fat dry milk) for 2 hr at room temperature. The membrane was rinsed three times with TBS/Tween 0.1% (3 \times 10 min), then incubated with an anti-Bcl-2 monoclonal antibody from Santa Cruz Biotechnology (1/1000 dilution in TBS containing 2% non-fat dry milk) for 2 hr at room temperature. The membrane was rinsed with TBS/Tween 0.1% (3 \times 10 min) and then incubated with horseradish peroxidase-labeled rabbit anti-mouse immunoglobulin G. Bound antibodies were detected by chemiluminescence using a Pierce detection kit and Biomax MR film from Kodak. Band intensities were estimated by densitometric scanning using the BioImage scanner. Protein concentration was determined by the Bradford assay [24].

RNA Extraction

Total RNAs were extracted from porcine Leydig cells with TRIzol reagent. The amount of RNA was estimated by spectrophotometry at 260 nm.

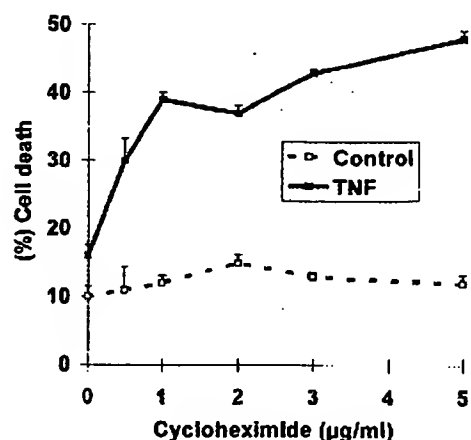


FIG. 1. Sensitization of Leydig cells to the cytotoxicity of TNF α by cycloheximide. Cells were pretreated with TNF α (20 ng/mL) for 50 hr and then challenged for an additional 15 hr with TNF α (20 ng/mL) in combination with increasing concentrations of cycloheximide (0–5 μ g/mL) for 15 hr. Viability was determined by the release of lactate dehydrogenase into the culture medium. The results represent the means \pm SD of three experiments.

RT-PCR Analysis

Single-stranded complementary DNAs (cDNAs) were obtained from reverse transcription of 2 μ g of total RNAs using random hexanucleotides as primers (5 μ M) in the presence of dNTP (0.2 mM), dithiothreitol (10 μ M), and Moloney murine leukemia virus reverse transcriptase (10 U/ μ L), 1 hr at 37°. cDNAs (1 μ L of RT mixture) were amplified by PCR with Taq polymerase (0.01 U/ μ L), dNTP (100 μ M), [α -³²P]dATP (0.045 μ Ci), and specific primers (2 μ M). The mixture was first heated at 92° for 5 min. Amplification was carried out for 28 cycles (PBR and Bcl-2) or 18 cycles (β -actin) at 92° for 30 sec, 50° (PBR), 57° (Bcl-2), and 61° (β -actin) for 30 sec, and 70° for 30 sec using a Perkin Elmer 9700 thermocycler. At the end of the cycles, the reaction mixture was heated at 70° for 10 min. PCR products were analyzed on 8% polyacrylamide gels and visualized by autoradiography. The oligonucleotide primers for PBR were: 5'TGGAAAGAGCTGGGAGGCTTC 3' (forward), 5'CGCCATACGCAGTAGTTGAG 3' (reverse). PBR-amplified products were 266 bp. The oligonucleotide primers for Bcl-2 were: 5'AGCGTCAACGGGAGATGTC 3' (forward), 5'GTGATGCAAGCTCCACCAAG 3' (reverse). Bcl-2-amplified products were 212 bp. The oligonucleotide primers for β -actin were: 5'TTGCTGATCCACATCTGCTG 3' (forward), 5'GACAGGATGCAGAAGGAGAT 3' (reverse). β -Actin-amplified products were 146 bp. PCR analysis for PBR, Bcl-2, and β -actin were carried out from the logarithmic phase of amplification. PCR-amplified products were checked by restriction enzymes. RT-PCR primers were designed inside separate exons to avoid any bias due to residual genomic contamination. Moreover, for all primers,

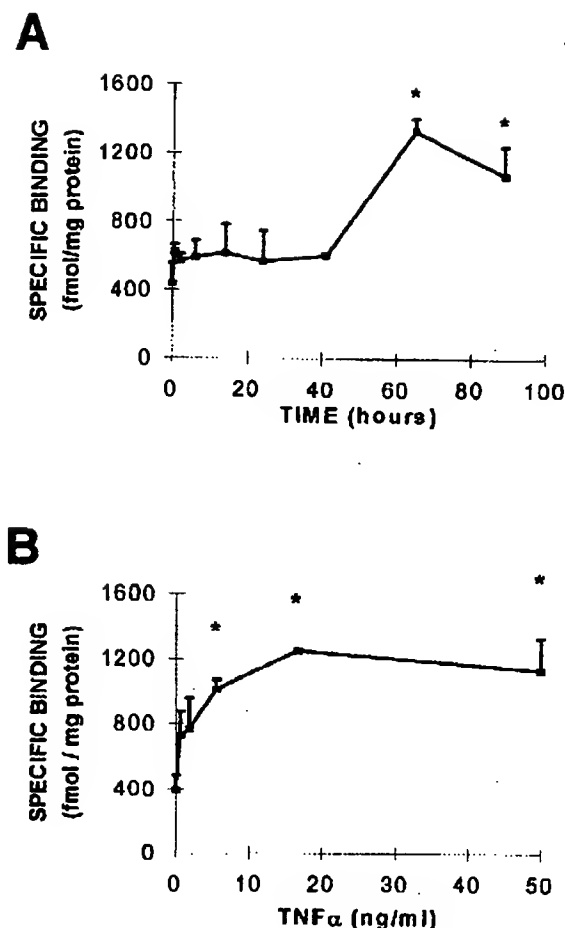


FIG. 2. (A) Effect of the duration of TNF α treatment on [³H]PK11195 binding in Leydig cells. Leydig cells were treated with 20 ng/mL of TNF α for various time periods. [³H]PK11195 binding studies were performed on 20 μ g protein from cell suspensions as described in Materials and Methods. Data shown represent mean values \pm SD from three different experiments. * indicates that the values were significantly different from control values (time 0) as determined by one-way analysis of variance followed by Tukey-Kramer's post hoc test ($P < 0.001$). (B) Dose-response relationship of TNF α on [³H]PK11195 binding in Leydig cells. Porcine Leydig cells were exposed for 65 hr to various concentrations of TNF α . Cultures were then processed for binding as described in Fig. 2A. Data shown represent mean values \pm SD from three independent experiments. * indicates that the values were significantly different from control values (no TNF α treatment) as determined by one-way analysis of variance followed by Tukey-Kramer's post hoc test ($P < 0.01$).

no amplification was observed when PCR was performed on RNA preparations.

Data Analysis

All experiments reported here were repeated three times with independent cell preparations. Significant differences among groups were examined by one-way analysis of variance followed by Tukey-Kramer's post hoc test. Statistical analysis was performed using the GraphPad Instat tm program.

TABLE 1. Binding characteristics of PBR in control and TNF α -treated Leydig cells

	Cell homogenate		Mitochondria	
	K_d (nM)	B_{max} (pmol/mg prot)	K_d (nM)	B_{max} (pmol/mg prot)
Control	7.2 ± 1.4	4.1 ± 0.3	4.1 ± 1.7	18.1 ± 0.5
TNF α	5.0 ± 0.6	$8.5 \pm 1.0^*$	7.6 ± 4.2	$40.0 \pm 7.8^\dagger$

Leydig cells were treated with 20 ng/mL of TNF α for 65 hr or kept untreated. [3 H]PK11195 (0.9 nM)-binding studies were performed on 20 μ g of protein from the cell homogenate in the presence of increasing concentrations of unlabeled ligand (1 nM to 0.1 μ M). Binding characteristics of PBR were also measured on isolated mitochondria. Curve fitting was performed by computer-assisted non-linear regression analysis (CurveExpert 1.3 program). Values of dissociation constant (K_d) and maximal number of binding sites (B_{max}) are expressed as the means \pm SEM of three independent experiments.

* $P < 0.03$ versus homogenate from control cells (paired *t*-test).

$^\dagger P < 0.05$ versus mitochondria from control cells (paired *t*-test).

RESULTS

Sensitization of Leydig Cells to the Cytotoxicity of TNF α by Cycloheximide

Porcine Leydig cells in primary cultures are resistant to TNF α killing [21]. However, these cells can be rendered sensitive to TNF α cytotoxicity by treatment with the translational inhibitor cycloheximide. As shown in Fig. 1, as little as 0.5 μ g/mL of cycloheximide was effective in eliciting cellular death in TNF α -treated cells (30% dead cells versus 15% dead cells in TNF α -alone-treated cells). With 5 μ g/mL of cycloheximide, almost 50% of the TNF α -treated cells died within 15 hr. Data from cycloheximide-alone-treated cells indicated that cycloheximide was not cytotoxic at the concentrations used in the experiments. It appears likely, from these results, that Leydig cells are protected from TNF α -mediated cytolysis by proteins that need to be continuously synthesized.

Effect of TNF α on [3 H]PK11195 Binding

In search of the cytoprotective proteins, we focused on one of the putative constituents of the mitochondrial PT pore, namely PBR. PK11195 was used as a prototypic ligand of this receptor. Primary cultures of porcine Leydig cells were treated with TNF α for various time periods. The cells were then harvested and assayed for [3 H]PK11195 binding. As shown in Fig. 2A, the addition of 20 ng/mL of TNF α to Leydig cells resulted in a significant increase in [3 H]PK11195 binding to these cells. A maximal effect to 2.5- to 3-fold of control occurred after long-term treatments \geq 65 hr. When cells were exposed to various concentrations of TNF α for 65 hr, a significant dose-dependent increase in [3 H]PK11195 binding was observed (Fig. 2B). The maximal response was achieved with concentrations close to 20 ng/mL, after which a plateau was reached. In the concentration of 16–50 ng/mL, an increase of ~175–200% in ligand binding above the level in untreated cells was observed.

In non-treated cells, non-linear regression analysis revealed binding sites for PK11195 having K_d and B_{max} values of 7.2 ± 1.4 nM and 4.1 ± 0.3 pmol/mg, respectively (Table 1). Treatment of Leydig cells with 20 ng/mL of TNF α for 65 hr resulted in a 2-fold increase in the density

of the binding sites ($B_{max} = 8.5 \pm 1.0$ pmol/mg), whereas the equilibrium dissociation constant was unaffected ($K_d = 5.0 \pm 0.6$ nM).

As a subset of PBR at the plasma membrane has also been demonstrated in some cells [25], studies were performed to verify that TNF α elicited an increase in the density of the mitochondrial PBR sites. As seen in Table 1, purified mitochondria from TNF α -treated cells exhibited a 2-fold increase in the maximal number of PK11195-binding sites when compared with mitochondria from control cells (40.0 ± 7.8 pmol/mg of protein versus 18.1 ± 0.5 pmol/mg). No significant alteration in the equilibrium dissociation constant was observed in the mitochondria from TNF α -treated cells.

Effect of TNF α on PBR mRNA

As TNF α up-regulated the number of PBR-binding sites in Leydig cells, we investigated whether the cytokine also affected PBR mRNA levels through the RT-PCR approach. The expression of β -actin was also determined for each sample and used as an internal control for the efficiency of each RT-PCR reaction. Although this method is only semiquantitative, Fig. 3A indicates that short-term treatments of Leydig cells with TNF α (20 ng/mL) did not significantly affect PBR mRNA levels. However, periods of treatment longer than 40 hr elicited an increase in PBR mRNA levels, a maximal response being achieved with 65 hr of treatment. TNF α increased PBR mRNA levels in a dose-dependent manner as shown in Fig. 3B. The concentration of TNF α required to achieve a maximal response was in the range of 16–50 ng/mL.

Correlation between the Density of PBR-Binding Sites and Cell Viability

Because Leydig cells can be rendered sensitive to TNF α cytotoxicity by treatment with cycloheximide, studies were done to determine whether PBR levels were correlated with cell survival. Leydig cells were treated with different doses of cycloheximide in combination with 20 ng/mL of TNF α . PBR levels were evaluated by measuring the binding of [3 H]PK11195 in whole Leydig cells, while cell death was

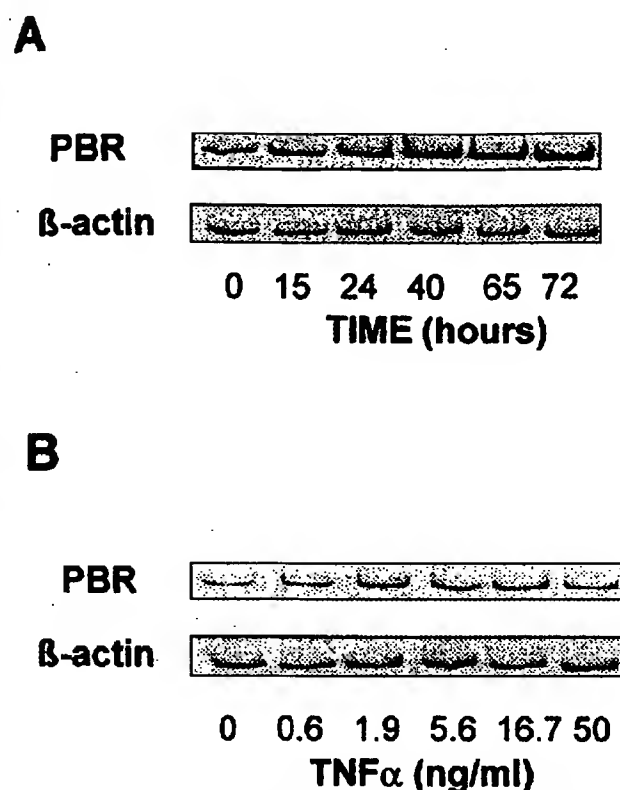


FIG. 3. (A) Effect of the duration of TNF α treatment on PBR mRNA levels. Leydig cells were treated with 20 ng/mL of TNF α for various time periods (0–72 hr). RT-PCR experiments were conducted as described in Materials and Methods. A representative PCR is shown. (B) Dose effect of TNF α on PBR mRNA levels. Leydig cells were cultured for 65 hr in the presence of various concentrations of TNF α (0–50 ng/mL). RT-PCR experiments were conducted as described in Materials and Methods. A representative PCR is shown.

determined by the release of lactate dehydrogenase into the culture medium. As stated in Fig. 4, increasing concentrations of cycloheximide strongly antagonized the increase in PBR ligation induced by TNF α . While TNF α alone increased [3 H]PK11195 binding to 176% of the binding observed in untreated control cells, the combination of TNF α with 3 μ g/mL of cycloheximide decreased [3 H]PK11195 binding to 70% of the control. Under these conditions, the B_{\max} value was decreased to 3.1 pmol/mg (B_{\max} value with 3 μ g/mL of cycloheximide in the absence of TNF α treatment was 3.3 pmol/mg), while the K_d value was unchanged. When cell viability was concomitantly analyzed, a correlation was found between the decrease in PBR levels and enhanced cell death (Fig. 4, inset).

Effect of TNF α on Bcl-2 Protein and mRNA Expression

As PBR is known to be associated with the voltage-dependent anion channel and the adenine nucleotide translocator in a complex that participates in the mitochondrial permeability transition, we were interested in

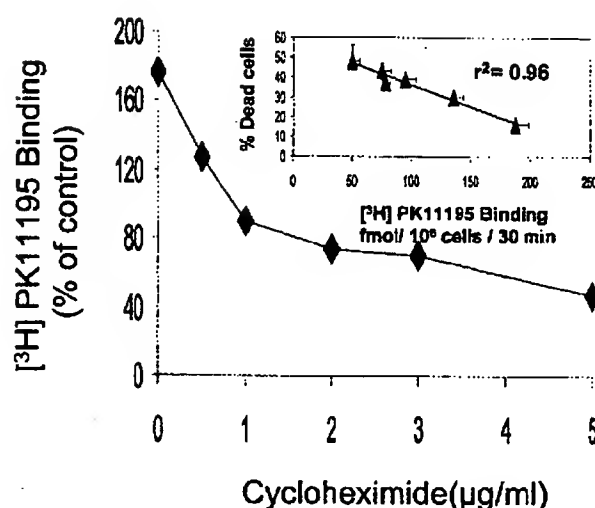


FIG. 4. Effect of cycloheximide on [3 H]PK11195 binding in TNF α -treated cells. Cells were pretreated with TNF α (20 ng/mL) for 50 hr and then challenged for an additional 15 hr with TNF α (20 ng/mL) and different doses of cycloheximide (0–5 μ g/mL). Cells were then assayed for [3 H]PK11195 binding as described in Materials and Methods. The results represent the means \pm SD of three experiments. The average [3 H]PK11195 binding from untreated cells (100%) was 106 ± 12 fmol/ 10^6 cells/30 min. Inset shows the correlation between the density of PBR sites and the resistance to TNF α cytotoxicity. Cell viability, determined by the release of lactate dehydrogenase into the culture medium, was plotted against PBR levels evaluated by measuring the binding of [3 H]PK11195 in Leydig cells. The line represents the best fit to the data points with a correlation coefficient $r^2 = 0.96$.

studying the effect of TNF α on the expression of Bcl-2, a protein known to regulate the opening of the PT pore. As shown by anti-Bcl-2 Western blotting (Fig. 5A), long-term treatments of Leydig cells with TNF α (20 ng/mL) down-regulated Bcl-2 expression, a 65-hr treatment resulting in a 3-fold decrease in the expression of the protein. RT-PCR for Bcl-2 demonstrated that TNF α also affected Bcl-2 mRNA expression. Indeed, while short-term treatments did not significantly reduce Bcl-2 mRNA levels, a decrease in the levels of Bcl-2 mRNA was observed for periods of treatment longer than 65 hr (Fig. 5B).

DISCUSSION

Porcine Leydig cells in primary cultures are resistant to TNF α killing, although this cytokine dramatically but reversibly disturbs the steroidogenic function of the cells [21, 22]. Yet, we have shown that those cells that express the TNF α receptor 55 [22] can be rendered sensitive to the cytotoxic effects of the cytokine by treatment with the protein synthesis inhibitor cycloheximide. These results are consistent with the existence of proteins that can suppress the death stimulus generated by TNF α in Leydig cells.

In search of the mechanism by which Leydig cells resist TNF α challenge, we focused on the mitochondrial permeability transition pore. Indeed, the opening of this pore,

1644

C. Rey et al.

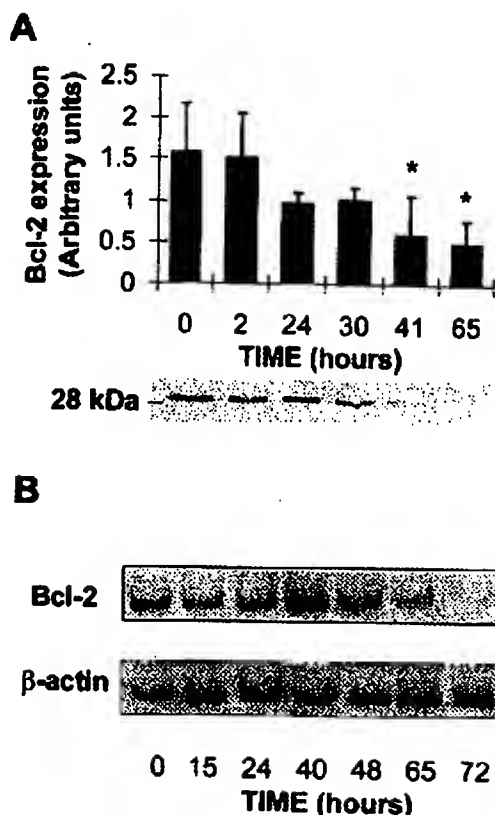


FIG. 5. (A) Long-term time-course study of TNF α on Bcl-2 protein expression. Leydig cells were treated with 20 ng/mL of TNF α for various time periods (0–65 hr). Western blot analyses were performed as described in Materials and Methods. Upper panel, Integrated intensities of Bcl-2 protein (from whole Leydig cells, 30 μ g in each sample) Western blotted from three independent experiments. * indicates that the values were significantly different from control values (time 0) as determined by one-way analysis of variance followed by Tukey-Kramer's post hoc test ($P < 0.01$). Lower panel, a representative autoradiograph showing the immunodetected protein. (B) Effect of duration of TNF α treatment on Bcl-2 mRNA level. Porcine Leydig cells were incubated with TNF α (20 ng/mL) for various time periods (between 0–72 hr). Total cellular mRNAs were then extracted and RT-PCR was performed as described in Materials and Methods. A representative PCR is shown.

which is regulated by Bcl-2, has been shown to be a critical event in the process of lethal cell injury induced by TNF α [7]. While the molecular constituents of the pore remain only partially defined, a speculative model includes the inner membrane adenine nucleotide translocator and outer membrane proteins such as the voltage-dependent anion channel and the mitochondrial benzodiazepine receptor. Although PBR are found in virtually all mammalian tissues, they are particularly abundant in steroid-producing tissues such as adrenal, testis, and ovary [26]. Various functions have been ascribed to the PBR, including control of cell proliferation and differentiation [27, 28], modulation of monocyte functions [29], intracellular transport of anion [30] porphyrin and heme [31], as well as intramitochondrial cholesterol translocation [26]. However, the failure to

generate PBR-negative gene knockout mouse because of the early death of animals during embryogenesis [32] suggests that PBR are also involved in critical functions. Of particular interest when considering this context are experiments investigating PBR ligation in various cultured cells that have shown either a facilitation of the induction of the mitochondrial permeability transition by a number of stimuli including chemotherapeutic drugs and irradiation [33, 34] or a protection against apoptosis induced by TNF α [35].

Recently, PBR have been reported to participate in the protection of hematopoietic cells against oxygen radical damage [36]. Indeed, Carayon et al. established a strong correlation between the ability of hematopoietic cell lines to resist H₂O₂ cytotoxicity and the level of PBR expression. Moreover, the transfection of Jurkat cells that do not express PBR with the human PBR cDNA increased their resistance to oxygen radical damage. Noteworthy are the findings of Yeliseev et al., who showed numerous parallels between PBR and a bacterial "oxygen" sensor, the tryptophan-rich sensory protein (TspO) of *Rhodospirillum rubrum* [37]. The striking similarity between the proteins even led the authors to propose TspO as a model for the structure and function of the mammalian PBR [38].

In the present work, we found that TNF α up-regulated PBR expression in porcine Leydig cells. As an overproduction of intracellular reactive oxygen intermediates (ROI) generated from mitochondria seems to be a critical event in mediating the cytotoxic effects of TNF α [3, 16], it appears likely that this up-regulation could be involved in the resistance of Leydig cells to the oxidative stress induced by the cytokine.

Of particular interest was the finding that the increase in PBR sites occurred concomitantly with a down-regulation of Bcl-2 expression. The Bcl-2 oncoprotein resides mainly on the cytoplasmic face of the mitochondrial outer membrane, where it is located at the contact sites between the outer and inner membranes [39]. As PBR shares properties with Bcl-2, it has been suggested that the proteins could have some common functions [36]. Indeed, recent findings of Schendel et al. [40] provided biophysical evidence that Bcl-2 forms channels in lipid membranes, while three-dimensional modeling of PBR revealed that the receptor could function as a channel [41]. As Bcl-2 has been shown to be an endogenous inhibitor of mitochondrial PT, our data support the hypothesis that the up-regulation of PBR expression observed in TNF α -treated Leydig cells could compensate for the decrease in Bcl-2 levels to prevent the opening of the PT pore. Moreover, this hypothesis is consistent with the observation that a large number of PBR sites associate with low Bcl-2 expression in phagocytic cells known to produce high levels of reactive oxygen species [36].

The fact that TNF α induced similar effects (up-regulation of PBR expression and down-regulation of Bcl-2 expression) in Seroli cells (data not shown) may indicate that gonadal cells have developed common mechanisms to

protect against TNF α killing. Indeed, the long half-lives of these terminally differentiated cells suggest that they are very efficiently protected from cell death. It appears, therefore, that PBR could act as an antidote to TNF α cytotoxicity in cells that require an extended life span, such as Leydig and Sertoli cells. Worth mentioning in this context are the findings that higher PBR levels are present in various tumor tissues when compared to normal ones [42-44] and that patients with tumors expressing high PBR levels have a shorter life expectancy than patients with tumors having lower PBR contents [44].

An increase in PBR sites has also been observed in brain after experimental injuries as well as in certain neuropathological states [45-47]. *In vitro* studies suggest that this up-regulation of PBR expression may be mediated by cytokines such as interleukin-1 and TNF α , which are released by cells of the monocytic lineage found in the injured brain [48]. In our models of gonadal cells, the TNF α could originate from the intersitial macrophages that might be activated during an immune challenge or chronic inflammatory diseases.

In conclusion, PBR was known to mediate the intramitochondrial cholesterol transport in steroidogenic cells [26]. However, considering the recent work of Papadopoulos et al., which provides evidence that PBR is a component of the mitochondrial apoptosis cascade in corpus luteum cells [49], as well as the data presented here, it appears likely that PBR may also fulfill other functions in these cells related to the protection from cell death.

This work was supported by the Institut National de la Santé et de la Recherche Médicale (INSERM), the Centre National de la Recherche Scientifique (CNRS), and the University of Lyon (Lyon-Sud Medical School). We thank Dr. C. Caillard (Rhône-Poulenc Rorer) for kindly providing unlabeled PK1195. We are grateful to Dr. P. Fonlupt (INSERM U.280) for help with the statistical procedures. We are indebted to Dr. G. Quash (INSERM U.329) for careful reading of the manuscript and helpful comments and discussions.

References

1. Carswell EA, Old LJ, Kassel RL, Green S, Fiore N and Williamson B, An endotoxin-induced serum factor that causes necrosis of tumors. *Proc Natl Acad Sci USA* 72: 3666-3670, 1975.
2. Bazzoni F and Beutler B, The tumor necrosis factor ligand and receptor families. *N Engl J Med* 334: 1717-1725, 1996.
3. Goossens V, Grooten J, De Vos K and Fiers W, Direct evidence for tumor necrosis factor-induced mitochondrial reactive oxygen intermediates and their involvement in cytotoxicity. *Proc Natl Acad Sci USA* 92: 8115-8119, 1995.
4. Ashkenasi A and Dixit VM, Death receptors: Signalling and modulation. *Science* 281: 1305-1308, 1998.
5. Zamzami N, Marchetti P, Castedo M, Zanin C, Vayssière JL, Petit PX and Kroemer G, Reduction in mitochondrial potential constitutes an early irreversible step of programmed lymphocyte death *in vivo*. *J Exp Med* 181: 1661-1672, 1995.
6. Reed JC, Cytochrome c: Can't live with it—Can't live without it. *Cell* 91: 559-562, 1997.
7. Pastorino JG, Simbula G, Yamamoto K, Glascott PA, Rothman RJ and Farber JL, The cytotoxicity of tumor necrosis factor depends on induction of the mitochondrial permeability transition. *J Biol Chem* 271: 29792-29798, 1996.
8. Marchetti P, Castedo M, Susin SA, Zamzami N, Hirsch T, Haefliger A, Hirsch F, Geuskens M and Kroemer G, Mitochondrial permeability transition is a central coordinating event of apoptosis. *J Exp Med* 184: 1155-1160, 1996.
9. Kroemer G, Zamzami N and Susin SA, Mitochondrial control of apoptosis. *Immunol Today* 18: 44-51, 1997.
10. Kroemer G, The proto-oncogene Bcl-2 and its role in regulating apoptosis. *Nat Med* 3: 614-620, 1997.
11. Ardail D, Privat JP, Egret-Charlier M, Levrat C, Lermé F and Louisot P, Mitochondrial contact sites. Lipid composition and dynamics. *J Biol Chem* 265: 18797-18802, 1990.
12. Ardail D, Gasnier F, Lermé F, Simonot C, Louisot P and Gateau-Roesch O, Involvement of mitochondrial contact sites in the subcellular compartmentalization of phospholipid biosynthetic enzymes. *J Biol Chem* 268: 25985-25992, 1993.
13. Zoratti M and Szabo I, The mitochondrial permeability transition. *Biochim Biophys Acta* 1241: 139-176, 1995.
14. Karsan A, Yee E and Harlan JM, Endothelial cell death induced by tumor necrosis factor α is inhibited by the Bcl-2 family member A1. *J Biol Chem* 271: 27201-27204, 1996.
15. Wong GH, Elwell JH, Oberley LW and Goeddel DV, Manganese superoxide dismutase is essential for cellular resistance to cytotoxicity of tumor necrosis factor. *Cell* 58: 923-931, 1989.
16. Manna SK, Zhang HJ, Yan T, Oberley LW and Aggarwal BB, Overexpression of manganese superoxide dismutase suppresses tumor necrosis factor-induced apoptosis and activation of nuclear transcription factor-kappa B and activated protein-1. *J Biol Chem* 273: 13245-13254, 1998.
17. Opipari AW, Hu HM, Yabkowitz R and Dixit VM, The A20 zinc finger protein protects cells from tumor necrosis factor cytotoxicity. *J Biol Chem* 267: 12424-12427, 1992.
18. Kumar S and Baglioni C, Protection from tumor necrosis factor-mediated cytolysis by overexpression of plasminogen activator inhibitor type-2. *J Biol Chem* 266: 20960-20964, 1991.
19. Morales A, Garcia-Ruiz C, Miranda M, Mari M, Colclll A, Atdite E and Fernandez-Checa JC, Tumor necrosis factor increases hepatocellular glutathione by transcriptional regulation of the heavy subunit chain of gamma-glutamylcysteine synthetase. *J Biol Chem* 272: 30371-30379, 1997.
20. Giri DK and Aggarwal BB, Constitutive activation of NF- κ B causes resistance to apoptosis in human cutaneous T cell lymphoma HuT-78 cells. *J Biol Chem* 273: 14008-14014, 1998.
21. Mauduit C, Hartmann DJ, Chauvin MA, Revul A, Morera AM and Benahmed M, Tumor necrosis factor- α inhibits gonadotropin action in cultured porcine Leydig cells: Site(s) of action. *Endocrinology* 129: 2933-2940, 1991.
22. Mauduit C, Gasnier F, Rey C, Chauvin MA, Stocco DM, Louisot P and Benahmed M, Tumor necrosis factor- α inhibits Leydig cell steroidogenesis through a decrease in steroidogenic acute regulatory protein expression. *Endocrinology* 139: 2863-2868, 1998.
23. Benahmed M, Morera AM, Chauvin MA and de Peretti E, Somatomedin C/insulin-like growth factor I as a possible intratesticular regulator of Leydig cell activity. *Mol Cell Endocrinol* 50: 69-77, 1987.
24. Bradford MM, A rapid and sensitive method for the quantification of microgram quantities of protein utilizing the principle of protein-dye binding. *Anal Biochem* 72: 248-254, 1976.
25. Olson JM, Ciliax BJ, Mancini WR and Young AB, Presence of peripheral-type benzodiazepine binding sites on human erythrocyte membranes. *Eur J Pharmacol* 152: 47-53, 1988.

26. Papadopoulos V, Peripheral-type benzodiazepine/diazepam binding inhibitor receptor: Biological role in steroidogenic cell function. *Endocr Rev* 14: 222-240, 1993.
27. Camins A, Dicz-Fernandez C, Pujadas E, Camarasa J and Escubedo E, A new aspect of the antiproliferative action of peripheral-type benzodiazepine receptor ligands. *Eur J Pharmacol* 272: 289-292, 1995.
28. Wang JK, Morgan JJ and Spector S, Differentiation of Friend erythroleukemia cells induced by benzodiazepines. *Proc Natl Acad Sci USA* 81: 3770-3772, 1984.
29. Taupin V, Gogusev J, Descamps-Latscha B and Zavala F, Modulation of tumor necrosis factor- α , interleukin-1 β , interleukin-6, interleukin-8 and granulocyte/macrophage colony-stimulating factor expression in human monocytes by an endogenous anxiogenic benzodiazepine ligand, triakontatetraneuropeptide: Evidence for a role of prostaglandins. *Mol Pharmacol* 43: 64-69, 1993.
30. Basile AS, Leuclens HW and Skolnick P, Regulation of renal peripheral benzodiazepine receptors by anion transport inhibitors. *Life Sci* 42: 715-726, 1988.
31. Taketani S, Kohno H, Okuda M, Furukawa T and Tokunaga R, Induction of peripheral-type benzodiazepine receptors during differentiation of mouse erythroleukemia cells. A possible involvement of these receptors in heme biosynthesis. *J Biol Chem* 269: 7527-7531, 1994.
32. Papadopoulos V, Structure and function of the peripheral-type benzodiazepine receptor in steroidogenic cells. *Proc Soc Exp Biol Med* 217: 130-142, 1998.
33. Pastorino JG, Simbula G, Gilfor E, Hoek JB and Farber JL, Protoporphyrin IX, an endogenous ligand of the peripheral benzodiazepine receptor, potentiates induction of the mitochondrial permeability transition and the killing of cultured hepatocytes by rotenone. *J Biol Chem* 269: 31041-31046, 1994.
34. Hirsch T, Decaudin D, Susin SA, Marchetti P, Larochette N, Resche-Rigon M and Kroemer G, PK11195, a ligand of the mitochondrial benzodiazepine receptor, facilitates the induction of apoptosis and reverses Bcl-2-mediated cytoprotection. *Exp Cell Res* 241: 426-434, 1998.
35. Bono F, Lamarche I, Frahonnaud V, Le Fur G and Herbert JM, Peripheral benzodiazepine receptor agonists exhibit potent antiapoptotic activities. *Biochem Biophys Res Commun* 265: 457-461, 1999.
36. Carayon P, Portier M, Dussosoy D, Bord A, Petitprêtre G, Canat X, Le Fur G and Casellas P, Involvement of peripheral benzodiazepine receptors in the protection of hematopoietic cells against oxygen radical damage. *Blood* 87: 3170-3178, 1996.
37. Yeliseev AA, Krueger KE and Kaplan S, A mammalian mitochondrial drug receptor functions as a bacterial "oxygen" sensor. *Proc Natl Acad Sci USA* 94: 5101-5106, 1997.
38. Yeliseev AA and Kaplan S, TspO of *Rhodobacter sphaeroides*. A structural and functional model for the mammalian peripheral benzodiazepine receptor. *J Biol Chem* 275: 5657-5667, 2000.
39. Riparbelli MG, Callaini G, Tripodi SA, Cintorino M, Tosi P and Dallai R, Localization of the Bcl-2 protein to the outer mitochondrial membrane by electron microscopy. *Exp Cell Res* 221: 363-369, 1995.
40. Schendel SL, Xie Z, Monta MO, Matsuyama J, Montal M and Reed JC, Channel formation by antiapoptotic protein Bcl-2. *Proc Natl Acad Sci USA* 94: 5113-5118, 1997.
41. Bemassau JM, Reversat JL, Ferrara P, Caput D and Le Fur G, A 3D model of the peripheral benzodiazepine receptor and its implication in intra mitochondrial cholesterol transport. *J Mol Graph* 11: 236-245, 1993.
42. Katz Y, Eitan A, Amiri Z and Gavish M, Dramatic increase in peripheral benzodiazepine binding sites in human colonic adenocarcinoma as compared to normal colon. *Eur J Pharmacol* 148: 483-484, 1988.
43. Katz Y, Ben-Baruch G, Kloog Y, Menczer J and Gavish M, Increased density of peripheral benzodiazepine-binding sites in ovarian carcinomas as compared with benign ovarian tumours and normal ovaries. *Clin Sci (Colch)* 78: 155-158, 1990.
44. Miettinen H, Kononen J, Haapasalo H, Hclén P, Sallinen P, Harjuntausta T, Helin H and Alho H, Expression of peripheral-type benzodiazepine receptor and diazepam. *Cancer Res* 55: 2691-2695, 1995.
45. Schoemaker H, Morelli M, Deshmukh P and Yamamura HI, [3 H]Ro5-4864 benzodiazepine binding in the kainate lesioned striatum and Huntington's diseased basal ganglia. *Brain Res* 248: 396-401, 1982.
46. Price GW, Ahier SP, Myers HR, Manjil L, Cremer JF, Luthra SK, Pascali C, Pike V and Frackowiak RSJ, In vivo binding to peripheral benzodiazepine binding sites in lesioned rat brain: Comparison between [3 H]PK11195 and [18 F]PK14105 as markers for neuronal damage. *J Neurochem* 55: 175-185, 1990.
47. Benavides J, Cornu P, Dennis T, Dubois A, Hauw JJ, MacKenzie ET, Sazdovitch V and Scatton B, Imaging of human brain lesions with an omega 3 site radioligand. *Ann Neurol* 24: 708-712, 1988.
48. Bourdiol F, Toulmond S, Serrano A, Benavides J and Scatton B, Increase in peripheral type benzodiazepine binding sites in the rat cortex and striatum after local injection of interleukin-1, tumour necrosis factor- α and lipopolysaccharide. *Brain Res* 543: 194-200, 1991.
49. Papadopoulos V, Dharmarajan A, Li H, Culty M, Lemay M and Sridaran R, Mitochondrial peripheral-type benzodiazepine receptor expression. Correlation with gonadotropin-releasing hormone (GnRH) agonist-induced apoptosis in the corpus luteum. *Biochem Pharmacol* 58: 1389-1393, 1999.

FGH52352

CI-06859610-1

FGH52352

CISTI ICIST

CI-06859610-1

Document Delivery Service
in partnership with the Canadian Agriculture LibraryService de fourniture de Documents
en collaboration avec la Bibliothèque canadienne de l'agriculture**THIS IS NOT AN INVOICE / CECI N'EST PAS UNE FACTURE**LYNN BRAZIL
LIBRARIANHELLER EHRMAN WHITE & MCAULIFFE
275 MIDDLEFIELD RD
MENLO PARK, CA 94025
UNITED STATES

ORDER NUMBER: CI-06859610-1
Account Number: FGH52352
Delivery Mode: F31
Delivery Address: 650/324-6034
Submitted: 2007/05/11 17:06:12
Received: 2007/05/11 17:06:12
Printed: 2007/05/11 21:17:37

Direct	Periodical	OPENURLOPAC	UNITED STATES

Client Number: 39780-7000 CD
Title: MELANOMA RESEARCH.
DB Ref. No.: IRN10504928
ISSN: ISSN09608931
Vol./Issue: 15/1
Date: 2005
Pages: 15-20
Article Title: SILENCING OF THE THROMBOMODULIN GENE IN HUMAN MALIGNANT MELANOMA
Article Author: FURUTA, J., ET AL
Report Number: IRN10504928
Publisher: RAPID COMMUNICATIONS OF OXFORD,

Estimated cost for this 6 page document: \$12.5 document supply fee +
\$30 copyright = \$42.5

The attached document has been copied under license from Access Copyright/COPIBEC or other rights holders through direct agreements. Further reproduction, electronic storage or electronic transmission, even for internal purposes, is prohibited unless you are independently licensed to do so by the rights holder.

Phone/Téléphone: 1-800-668-1222 (Canada - U.S./E.-U.) (613) 998-8544 (International)
www.nrc.ca/cisti Fax/Télécopieur: (613) 993-7619 www.cnr.ca/icist
info.cisti@nrc.ca info.icist@nrc.ca



National Research Council Canada
Conseil national de recherches Canada

Page

1 / 1

Silencing of the *thrombomodulin* gene in human malignant melanoma

Junichi Furuta^{a,b}, Atsushi Kaneda^a, Yoshihiro Umebayashi^b, Fujio Otsuka^b, Takashi Sugimura^a and Toshikazu Ushijima^a

The loss of *thrombomodulin* (TM) expression is associated with tumour growth, infiltration and lymph node metastasis in human tumours. In melanoma cell lines, TM is reported to mediate cell adhesion, and its introduction into TM-negative melanoma cell lines suppresses their growth. In this study, we analysed TM expression in surgical melanoma specimens and the role of its promoter methylation in the loss of its expression. In 15 (75%) of the 20 specimens (five from a primary site and 15 from metastatic sites), melanoma cells lacked TM immunoreactivity. Methylation of the TM promoter region was detected in 10 (67%) of the 15 TM-negative specimens by methylation-specific polymerase chain reaction, whereas methylation was detected in two (40%) of the five TM-positive specimens. In cell lines, complete methylation of the TM promoter CpG island was detected in six (46%) of 13 melanoma cell lines, whereas no methylation was detected in two cultured normal melanocytes. There was a good correlation between the methylated status of the CpG island and the loss of TM messenger RNA (mRNA) expression. Treatment of melanoma cell lines with a demethylating agent, 5-aza-2'-deoxycytidine, induced

demethylation of the promoter CpG island and the restoration of mRNA and protein expression. These findings suggest that most human melanomas lack TM expression, and that methylation of the promoter CpG island is one of the mechanisms responsible. *Melanoma Res* 15:15-20 © 2005 Lippincott Williams & Wilkins.

Melanoma Research 2005, 15:15-20

Keywords: Melanoma, methylation, silencing, thrombomodulin

^aCarcinogenesis Division, National Cancer Center Research Institute, Tokyo, Japan and ^bDepartment of Dermatology, Institute of Clinical Medicine, University of Tsukuba, Ibaraki, Japan.

Sponsorship: This work was supported in part by a Grant-in-Aid for Cancer Research from the Ministry of Health, Labor and Welfare. J.F. is a recipient of Research Resident Fellowships from the Foundation of Cancer Research.

Correspondence and requests for reprints to Dr Toshikazu Ushijima, Carcinogenesis Division, National Cancer Center Research Institute, 5-1-1 Tsukiji, Chuo-ku, Tokyo 104-0045, Japan. Tel: +81 3 3647 5240; fax: +81 3 5565 1753; e-mail: tushijim@ncc.go.jp

Received 13 January 2004 Accepted (after revision) 8 October 2004

Introduction

Thrombomodulin (TM) not only plays a critical role in anticoagulant activity, but is also involved in various biological and pathological processes, including thrombosis, arteriosclerosis, stroke, inflammation and cancer [1]. TM is a glycosylated transmembrane protein with a large extracellular domain that comprises a C-type lectin-like domain, six epidermal growth factor (EGF) modules and a serine/threonine-rich region [1]. TM is expressed mainly in endothelial cells, but is also found in a wide range of other cells, including platelets, monocytes, synovial lining cells, transitional epithelium in the ureter and squamous epithelium in the skin, oral mucosa, larynx, oesophagus and vagina [2-6].

With regard to the role of TM in tumours, an association between a high expression of TM and a low-malignancy phenotype has been reported for oesophageal squamous cell carcinomas, lung squamous cell carcinomas and hepatocellular carcinomas [7-10]. When cell proliferation was compared between melanoma cell lines subcloned from four patients, a negative correlation between TM expression and cell proliferation was observed *in vitro*

[11]. When wild-type TM was introduced into B16 melanoma cells, a TM-negative mouse melanoma cell line, cell proliferation *in vitro* and tumour growth *in vivo* were decreased [11]. The introduction of green fluorescent protein (GFP)-tagged TM into A2058, a TM-negative human melanoma cell line, resulted in the accumulation of TM in cell-to-cell adhesion sites, established a morphology with compact clustering and produced a decreased cell proliferation rate *in vitro* and decreased tumour growth *in vivo* [12]. The addition of soluble TM in a reconstituted basement membrane (Matrigel[®]) inhibited the invasive activity of B16F10 melanoma cells into the Matrigel [13].

All of these studies strongly indicate that TM expression status is an important factor determining the malignant potential of many tumours, including human melanomas. However, TM expression has not been analysed in surgical specimens of human melanomas. Therefore, in this study, we analysed TM expression in surgical specimens of human melanomas. Furthermore, we analysed the involvement of DNA methylation-associated gene silencing in TM inactivation, as we have recently

found that the *TM* gene is silenced in human gastric cancers by methylation of a CpG island (CGI) in its 5' upstream region [14].

Materials and methods

Surgical melanoma specimens, cultured normal melanocytes and melanoma cell lines

Twenty melanoma specimens, five from primary sites and 15 from metastatic sites, were obtained from patients undergoing tumour resections at Tsukuba University Hospital with informed consent. All samples were embedded in paraffin and fixed in formalin. Two cultured neonatal normal epidermal melanocytes (HEM1, HEM2) were purchased from Cascade Biologics (Portland, OR, USA). MeWo, VMRC-MELG, A2058, C32TG and GAK were obtained from the Health Science Research Resources Bank, Japan Health Sciences Foundation (Sennan, Japan); G361, SK-MEL-28 and HMV-1 were obtained from the Cell Resource Center for Biomedical Research, Institute of Development, Aging and Cancer, Tohoku University (Sendai, Japan); COLO 679 and MMac were obtained from RIKEN BioResource Center (Tsukuba, Japan); and WM-266-4 and WM-115 were obtained from the American Type Culture Collection (Rockville, MD, USA). TK-Mel-1 was established by J.E. from a skin metastasis of a melanoma obtained at Tsukuba University Hospital.

From surgical specimens, melanoma tissue was dissected from 50 µm thick tissue sections by a fine needle, deparaffinized and incubated in lysis buffer [50 mM Tris-HCl, pH 8.5, 1 mM ethylenediaminetetraacetic acid (EDTA), 0.5% Tween-20, 200 mg/ml of proteinase K] at 55°C for 3 days with fresh proteinase K every 24 h. DNA was purified by phenol/chloroform extraction and ethanol precipitation. From cell lines, DNA was extracted by standard phenol/chloroform procedures. RNA was isolated with ISOGEN (NIPPON GENE, Tokyo, Japan).

Immunohistochemistry

TM antibody, TM (D-3), a mouse monoclonal antibody against amino acids 22-321 of TM protein, was purchased from Santa Cruz Biotechnology (Santa Cruz, CA, USA). Formalin-fixed and paraffin-embedded sections were sliced at 5 µm thickness, deparaffinized and heated in 10 mM citrate buffer (pH 6.0) for 15 min at 121°C. After blocking, the sections were incubated with the antibody at a dilution of 200-fold at 4°C overnight. The binding of the first antibody was detected by a specific second antibody and the Vectastain Elite ABC kit (Vector Laboratories, Burlingame, CA, USA). Slides were counterstained with Mayer's haematoxylin. As a negative control, the absence of staining without the primary antibody was confirmed. As an internal positive control, staining of vascular endothelium was confirmed.

5-Aza-2'-deoxycytidine (5-Aza-dC) treatment

Cells were seeded at a density of 6×10^5 cells per 10 cm dish on day 0, and exposed to freshly prepared 1 µM 5-Aza-dC (Sigma, St. Louis, MO, USA) for 24 h on days 1 and 3. The cells were harvested on day 4.

Sodium bisulphite modification, methylation-specific polymerase chain reaction (MSP) and bisulphite sequencing

Five hundred nanograms of digested DNA were denatured in 0.3 N NaOH at 37°C for 15 min [15]. To the denatured DNA, 3.6 N sodium bisulphite (pH 5.0) and 0.6 mM hydroquinone were added, and the sample underwent 15 cycles of denaturation at 95°C for 30 s and incubation at 50°C for 15 min. The sample was desalted with the Wizard DNA Clean-Up system (Promega, Madison, WI, USA), and desulphonated by treatment with 0.3 N NaOH. The DNA sample was ethanol precipitated and dissolved in 20 µl of Tris-EDTA buffer.

With a set of primers specific to the methylated or unmethylated sequence (M or U set, respectively), MSP [16] was performed using 0.5 µl of the sodium bisulphite-treated DNA. MSP primers were designed within the promoter region as reported previously [17]. DNA methylated with *Sss*I methylase and DNA from HEM1 were used to determine specific annealing temperatures for M and U sets, respectively. Minimal polymerase chain reaction (PCR) cycles to produce visible bands for these control samples were determined for M and U sets, respectively. For samples from cultured normal melanocytes and melanoma cell lines, four cycles were added. For samples from surgical melanoma specimens, four more cycles were added because their DNA had been degraded. The primer sequences were 5'-GGT GAT TTT ATG TGT GAG GGT-3' (sense) and 5'-CTC CCT CCC TAA ACA TTC A-3' (antisense) for the U set (120 bp), and 5'-TGA TTT TAT GCG CGA GGG C-3' (sense) and 5'-CCT CCC TCC CTA AAC GTT CG-3' (antisense) for the M set (119 bp). The annealing temperature and amplification cycles were 59°C and 34 cycles for the U set and 65°C and 34 cycles for the M set.

For bisulphite sequencing, a set of primers common to the methylated and unmethylated sequences was used. The PCR product was cloned into the pGEM-T Easy vector (Promega), and ten clones were sequenced. The primer sequences were 5'-AGG AGG ATT AAG AGA TGA AAG AG-3' (sense) and 5'-CAA CCC AAA CAC TTC TTA CG-3' (antisense) (375 bp). The annealing temperature and amplification cycles were 59°C and 35 cycles, respectively.

Quantitative real-time reverse transcriptase-polymerase chain reaction (RT-PCR)

After treatment with DNase I (Invitrogen, Carlsbad, CA, USA), complementary DNA (cDNA) was synthesized

from 3 µg of total RNA using Superscript II (Invitrogen). Real-time PCR was performed using SYBR Green PCR Core Reagents (PE Applied Biosystems, Foster City, CA, USA) and an iCycler Thermal Cycler (Bio-Rad Laboratories, Hercules, CA, USA). The number of molecules of a specific cDNA in a sample was measured by comparing its amplification with that of standard samples containing 10^1 to 10^6 molecules. The expression level of *TM* in each sample was obtained by normalizing the number of its cDNA molecules with that of the *GAPDH* gene. The primer sequences were 5'-GGT GAT TAG AGG GAG GAG AA-3' (sense) and 5'-GGC AGT CTG TGT CTT CGT TA-3' (antisense) (97 bp) for *TM*, and 5'-AGG TGA AGG TCG GAG TCA ACG-3' (sense) and 5'-AGG GGT CAT TGA TGG CAA CA-3' (antisense) (102 bp) for *GAPDH*.

Immunoblotting

Total protein lysate (20 µg per lane) was separated by 10% sodium dodecylsulphate (SDS)-polyacrylamide gel electrophoresis and transferred to a polyvinylidene difluoride membrane (Immobilon, Millipore, Bedford, MA, USA). TM protein was detected by a primary antibody (1:500 dilution), TM (D-3), and by a second goat anti-mouse IgG antibody conjugated with peroxidase (1:10 000 dilution; KPL, Gaithersburg, MD, USA). The specific complex was visualized by enhanced chemiluminescence (Amersham Biosciences, Piscataway, NJ, USA). A rabbit anti-Actin antibody (1:500 dilution; Biomedical Technologies, Stoughton, MA, USA) and a second donkey anti-rabbit IgG antibody conjugated with peroxidase

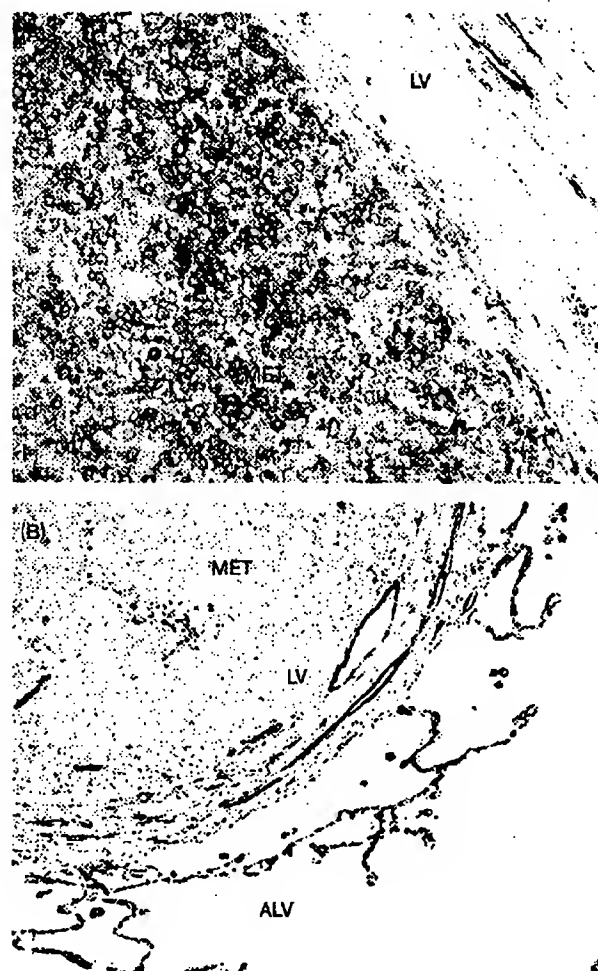
(1:5000 dilution; Chemicon International, Temecula, CA, USA) were used as a control.

Results

Immunohistochemistry of TM

In 15 (75%) of 20 surgical specimens, melanoma cells lacked TM immunoreactivity (Table 1, representative results in Fig. 1). In the five TM-positive specimens, strong cell membrane staining was evident in melanoma cells, and positive staining was observed in the majority of melanoma cells (Fig. 1A). In contrast, in TM-negative specimens, all melanoma cells lacked positive staining,

Fig. 1



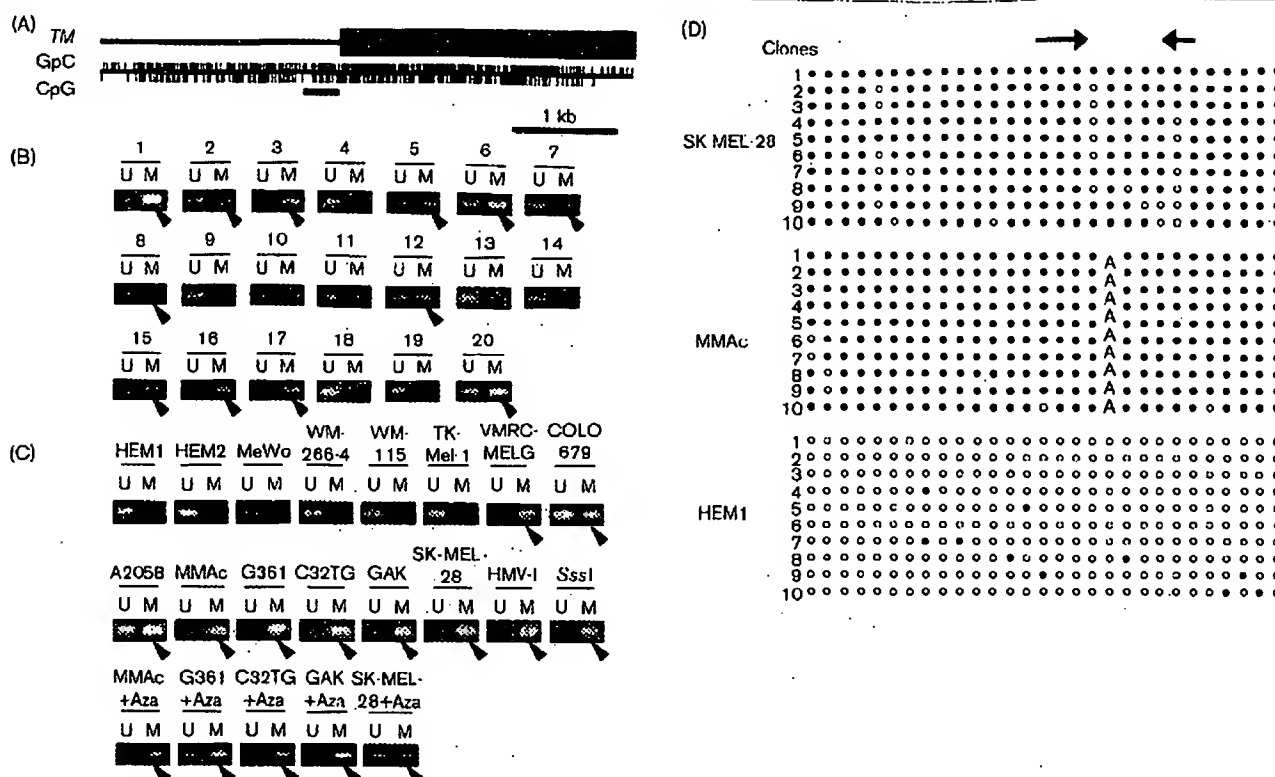
Representative immunohistochemical analysis of thrombomodulin (TM) expression in surgical specimens of melanoma metastatic foci. Sections from melanomas were stained with anti-TM (D-3) antibody. Fifteen (75%) of 20 melanoma specimens lacked TM immunoreactivity. (A) Lymph node metastasis of a melanoma (case 11) without promoter methylation. Strong immunoreactivity was observed in the cell membrane. LV, endothelial cells of lymph vessels; MET, metastatic region of melanoma. (B) Lung metastasis of a melanoma (case 6) with promoter methylation. ALV, vascular endothelial cells of the alveolar cavity. Original magnifications, $\times 100$.

Table 1 Thrombomodulin (TM) expression and methylation status in surgical specimens

Sample	Origin	TM immunoreactivity	Methylation status
1	Primary site	-	U+M
2	Primary site	-	U+M
3	Primary site	-	M
4	Primary site	+	U
5	Primary site	+	U+M
6	Lung metastasis	-	U+M
7	Lung metastasis	-	U+M
8	Lung metastasis	-	U+M
9	Lymph node metastasis	-	U
10	Lymph node metastasis	-	U
11	Lymph node metastasis	+	U
12	Lymph node metastasis	+	U+M
13	Lymph node metastasis	+	U
14	Skin metastasis	-	U
15	Skin metastasis	-	U+M
16	Skin metastasis	-	M
17	Skin metastasis	-	U+M
18	Skin metastasis	-	U
19	Intestinal metastasis	-	U
20	Liver metastasis	-	U+M

TM immunoreactivity is shown by '+' (positive) and '-' (negative). Methylation status determined by methylation-specific polymerase chain reaction (MSP) is shown by 'M' (only methylated DNA molecules detected), U (only unmethylated DNA molecules detected) and U+M (both unmethylated and methylated DNA molecules detected). There was no clear correlation between the loss of TM immunoreactivity and the original sites of the samples.

Fig. 2



Genomic structure of the thrombomodulin (TM) promoter region and its methylation analysis. (A) Structure of a 4-kb CpG island spanning from exon 1 to the 5' upstream region. Each vertical mark, an individual GpC or CpG site; bar, region analysed by bisulphite sequencing. (B) Methylation analysis of the promoter region by methylation-specific polymerase chain reaction (MSP) in the surgical melanoma specimens. U and M, primer sets for unmethylated and methylated DNA sequences, respectively. The presence of methylated DNA molecules is shown by arrow heads. (C) Methylation analysis of the promoter regions by MSP in cultured normal melanocytes (HEM1 and HEM2) and melanoma cell lines. MeWo, WM-266-4, WM-115, TK-Mel-1, VMRC-MELG, COLO 679, A2058, MMAc, G361, C32TG, GAK, SK-MEL-28 and HMV-1, melanoma cell lines; +Aza, melanoma cell lines after treatment with 5-aza-2'-deoxycytidine (5-Aza-dC); Sssl, genomic DNA of HEM1 treated with Sssl methylase. (D) Methylation analysis of the promoter regions by bisulphite sequencing in two melanoma cell lines (SK-MEL-28 and MMAc) and HEM1. For each sample, 10 clones were sequenced. Filled circle, methylated CpG site; open circle, unmethylated CpG site. Arrows show the positions of CpG sites recognized by MSP primers. The cytosine at the 19th CpG site had a C to A polymorphism in MMAc.

whereas endothelial cells of lymph vessels and vascular vessels were clearly stained, as reported previously (Fig. 1B) [2,18]. Three of the five (60%) specimens from primary sites lacked positive staining, whereas 12 of the 15 (80%) specimens from metastatic sites lacked positive staining. This showed that the majority of surgical melanoma specimens lacked TM expression, whereas the remaining melanomas showed TM expression.

Methylation status of TM promoter region CGI

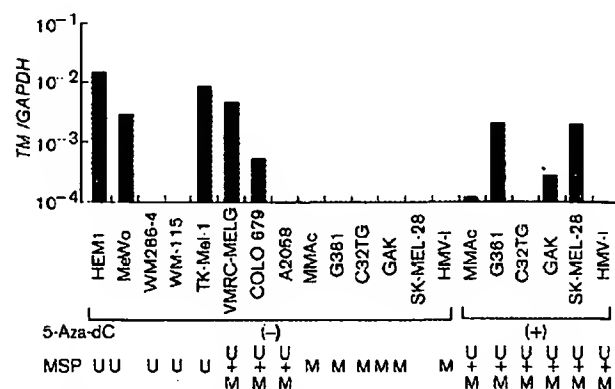
A 4-kb CGI that met a criterion described by Takai and Jones [19] spanned from exon 1 to the 5' upstream region of the TM gene, and the methylation status of a region overlapping the promoter region was analysed by MSP (Fig. 2A). Methylation was detected in 12 (60%) of the 20 specimens, but the region was not methylated in HEMs. Methylation was detected in 10 (67%) of the 15 TM-

negative specimens and in two (40%) of the five TM-positive specimens (Table 1, Fig. 2B).

In surgical specimens, contamination of normal cells in melanoma samples was present, and it was difficult to determine the allelic status of methylation. Therefore, the methylation status was further analysed in melanoma cell lines (Fig. 2C). Methylation was detected in nine (69%) of 13 melanoma cell lines, whereas no methylation was detected in the two cultured normal melanocytes, HEM1 and HEM2. In six of the nine melanoma cell lines, MMAc, G361, C32TG, GAK, SK-MEL-28 and HMV-1, only methylated DNA molecules were detected by MSP.

Bisulphite sequencing was performed in SK-MEL-1 and MMAc, in which only methylated DNA molecules were detected by MSP, and in HEM1. The methylation status

Fig. 3



Expression levels of thrombomodulin (TM) in cultured normal melanocytes and melanoma cell lines analysed by quantitative reverse transcriptase-polymerase chain reaction (RT-PCR). Expression levels were normalized to that of GAPDH, and are shown on a logarithmic scale. The methylation status of each sample in the promoter region is shown below the names of the samples. With or without 5-aza-2'-deoxycytidine (5-Aza-dC) treatment is indicated as '(+)' or '(-)', respectively. Expression status correlates with methylation status in the promoter region. M, only methylated DNA molecules detected; U, only unmethylated DNA molecules detected; U + M, both unmethylated and methylated DNA molecules detected.

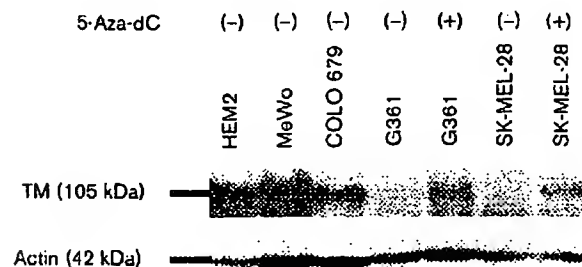
of the 120-bp region between the primers of MSP was in complete accordance with the results by MSP (Fig. 2D). It was also observed that the methylation status detected by MSP was in good accordance with the methylation status of a broader region (331 bp).

Messenger RNA (mRNA) expression of TM and restoration by 5-Aza-dC in melanoma cell lines

The expression levels of *TM* were analysed in a cultured normal melanocyte, HEM1, and in 13 melanoma cell lines by quantitative real-time RT-PCR (Fig. 3). *TM* was abundantly expressed in the normal cultured melanocyte; HEM1. Of the melanoma cell lines, *TM* expression was lost in all six cell lines that showed only methylated DNA molecules, whereas some expression was detected in four of the six cell lines that showed both unmethylated and methylated DNA molecules or only unmethylated DNA molecules.

To examine the role of the methylation of CGI in the promoter region in the loss of *TM* expression, six melanoma cell lines, MMAC, G361, C32TG, GAK, SK-MEL-28 and HMV-1, which showed only methylated DNA molecules, were treated with 5-Aza-dC, a demethylating agent. In four (MMAC, G361, GAK and SK-MEL-28), CGI in the *TM* promoter region was demethylated (Fig. 2C), and *TM* was re-expressed (Fig. 3). This showed that methylation of CGI in the promoter region was critically involved in the loss of *TM* expression.

Fig. 4



Western blot analysis of thrombomodulin (TM) protein expression. HEM2, four melanoma cell lines before the addition of 5-aza-2'-deoxycytidine (5-Aza-dC) and two melanoma cell lines after the addition of 5-Aza-dC were analysed. TM protein expression was observed in melanoma cell lines without methylation, but not in those with complete methylation. The expression in cell lines with complete methylation was restored by the addition of 5-Aza-dC.

Immunoblot analysis of TM protein

To confirm the results obtained by RT-PCR, immunoblot analysis was performed using cell lines with abundant re-expression of TM: G361 and SK-MEL-28 (Fig. 4). Before treatment with 5-Aza-dC, TM protein was detected in HEM2 and in two melanoma cell lines (MeWo and COLO 679) that showed only unmethylated DNA molecules and mRNA expression. In contrast, TM protein was not detected in two cell lines (G361 and SK-MEL-28) that showed only methylated DNA molecules and no mRNA expression. After treatment of G361 and SK-MEL-28 with 5-Aza-dC, TM protein was detected. These results confirmed that *TM* mRNA detected by RT-PCR, especially that re-expressed after 5-Aza-dC treatment, was translated into TM protein.

Discussion

In this report, TM expression was found to be absent in most of the surgical melanoma specimens, although we mainly used metastatic samples to isolate DNA mostly from melanoma cells. It has been reported that low TM expression is associated with high-malignancy phenotypes in oesophageal, lung and liver cancers [7-10], and that TM has a growth suppressive effect on melanoma cell lines [11-13]. However, this study is the first to show that some human melanomas lack TM expression. To determine the mechanisms, we further analysed the methylation status of CGI in the *TM* promoter region. It was shown that CGI was methylated, and played a critical role in the loss of *TM* expression, as known for CGIs in promoter regions of tumour suppressor genes, such as *p16* [20], *E-cadherin* [21] and *hMLH1* [22]. Although gene silencing can be analysed only in melanoma cell lines, the presence of the aberrant methylation of the promoter CGI strongly suggests that its silencing is also present *in vivo*.

Five of the 15 TM-negative surgical specimens showed no TM methylation. It was therefore indicated that other mechanisms, such as chromosomal deletions, mutations and a lack of upstream signals, were involved. Although the loss of the TM locus (20p12-cen) is infrequent in melanomas [23], its loss has been reported in melanoma cells with high invasive capacity [24]. With regard to mutations, no information is available in melanomas, and an analysis is necessary. Three cell lines, WM-266-4, WM-115 and A2058, retained unmethylated DNA molecules, but did not express TM mRNA. The loss of expression of a tumour suppressor gene that can be potentially silenced by promoter methylation has been observed even without methylation for several tumour suppressor genes, such as *CDH1*, *RARB* and *hMLH1* [25-27].

In human normal skin specimens, epidermal melanocytes lacked TM immunoreactivity in our study (data not shown) and in a previous report [6], whereas TM expression was evident in cultured normal melanocytes. One possibility is that TM expression is necessary only on limited occasions, such as cell proliferation. Indeed, epidermal melanocytes are known not to proliferate *in situ* unless specifically stimulated, e.g. by ultraviolet light [28], whereas cultured normal melanocytes keep proliferating. TM may be expressed only when cells are proliferating, and may maintain cell proliferation within an appropriate range. To support this hypothesis, normal hepatocytes showed no TM immunoreactivity, but TM-positive hepatocellular carcinomas showed better prognosis [10].

In conclusion, our findings show that TM is not expressed in most human melanomas, and that methylation of the promoter CGI is one of the mechanisms for the loss of expression.

References

- Weiler H, Isermann BH. Thrombomodulin. *J Thromb Haemost* 2003; 1:1515-1524.
- Maruyama I, Bell CE, Majerus PW. Thrombomodulin is found on endothelium of arteries, veins, capillaries, and lymphatics, and on syncytiotrophoblast of human placenta. *J Cell Biol* 1985; 101:363-371.
- Suzuki K, Nishiohara J, Hayashi T, Kosaka Y. Functionally active thrombomodulin is present in human platelets. *J Biochem (Tokyo)* 1988; 104:628-632.
- McCachran SS, Diggs J, Weinberg JB, Dittman WA. Thrombomodulin expression by human blood monocytes and by human synovial tissue lining macrophages. *Blood* 1991; 78:3128-3132.
- Obama H, Obama K, Takemoto M, Soejima Y, Shirahama T, Ohi Y, et al. Expression of thrombomodulin in the epithelium of the urinary bladder: a possible source of urinary thrombomodulin. *Anticancer Res* 1999; 19:1143-1147.
- Lager DJ, Callaghan EJ, Worth SF, Raife TJ, Lentz SR. Cellular localization of thrombomodulin in human epithelium and squamous malignancies. *Am J Pathol* 1995; 146:933-943.
- Tezuka Y, Yonezawa S, Maruyama I, Matsushita Y, Shimizu T, Obama H, et al. Expression of thrombomodulin in esophageal squamous cell carcinoma and its relationship to lymph node metastasis. *Cancer Res* 1995; 55:4196-4200.
- Matsushita Y, Yoshiie K, Imamura Y, Ogawa H, Imamura H, Takao S, et al. A subcloned human esophageal squamous cell carcinoma cell line with low thrombomodulin expression showed increased invasiveness compared with a high thrombomodulin-expressing clone - thrombomodulin as a possible candidate for an adhesion molecule of squamous cell carcinoma. *Cancer Lett* 1998; 127:195-201.
- Ogawa H, Yonezawa S, Maruyama I, Matsushita Y, Tezuka Y, Toyoyama H, et al. Expression of thrombomodulin in squamous cell carcinoma of the lung: its relationship to lymph node metastasis and prognosis of the patients. *Cancer Lett* 2000; 149:95-103.
- Suehiro T, Shimada M, Matsumata T, Taketomi A, Yamamoto K, Sugimachi K. Thrombomodulin inhibits intrahepatic spread in human hepatocellular carcinoma. *Hepatology* 1995; 21:1285-1290.
- Zhang Y, Weiler-Guetter H, Chen J, Wilhelm O, Deng Y, Qiu F, et al. Thrombomodulin modulates growth of tumor cells independent of its anticoagulant activity. *J Clin Invest* 1998; 101:1301-1309.
- Huang HC, Shi GY, Jiang SJ, Shi CS, Wu CM, Yang HY, et al. Thrombomodulin-mediated cell adhesion: involvement of its lectin-like domain. *J Biol Chem* 2003; 278:46750-46759.
- Hosaka Y, Higuchi T, Tsunagami M, Ishii H. Inhibition of invasion and experimental metastasis of murine melanoma cells by human soluble thrombomodulin. *Cancer Lett* 2000; 161:231-240.
- Kaneda A, Kaminishi M, Yanagihara K, Sugimura T, Ushijima T. Identification of silencing of nine genes in human gastric cancers. *Cancer Res* 2002; 62:6645-6650.
- Clark SJ, Harrison J, Paul CL, Frommer M. High sensitivity mapping of methylated cytosines. *Nucleic Acids Res* 1994; 22:2990-2997.
- Herman JG, Graff JR, Myohanen S, Nelkin BD, Baylin SB. Methylation-specific PCR: a novel PCR assay for methylation status of CpG islands. *Proc Natl Acad Sci USA* 1996; 93:9821-9826.
- Tazawa R, Hirosewa S, Suzuki K, Hirokawa K, Aoki N. Functional characterization of the 5'-regulatory region of the human thrombomodulin gene. *J Biochem (Tokyo)* 1993; 113:600-606.
- Tamura A, Matsubara O, Hirokawa K, Aoki N. Detection of thrombomodulin in human lung cancer cells. *Am J Pathol* 1993; 142:79-85.
- Takai D, Jones PA. Comprehensive analysis of CpG islands in human chromosomes 21 and 22. *Proc Natl Acad Sci USA* 2002; 99:3740-3745.
- Merlo A, Herman JG, Mao L, Lee DJ, Gabrielson E, Burger PC, et al. 5' CpG island methylation is associated with transcriptional silencing of the tumour suppressor p16/CDKN2/MTS1 in human cancers. *Nat Med* 1995; 1:686-692.
- Yoshiura K, Kanai Y, Ochiai A, Shimoyama Y, Sugimura T, Hirohashi S. Silencing of the E-cadherin invasion-suppressor gene by CpG methylation in human carcinomas. *Proc Natl Acad Sci USA* 1995; 92:7416-7419.
- Kane MF, Loda M, Gaida GM, Lipman J, Mishra R, Goldman H, et al. Methylation of the hMLH1 promoter correlates with lack of expression of hMLH1 in sporadic colon tumors and mismatch repair-defective human tumor cell lines. *Cancer Res* 1997; 57:808-811.
- Bastian BC, LeBoit PE, Hamm H, Brckner EB, Pinkel D. Chromosomal gains and losses in primary cutaneous melanomas detected by comparative genomic hybridization. *Cancer Res* 1998; 58:2170-2175.
- Gunthor K, Fleischer A, Buettner R, Bosserhoff AK. Detection of invasion-related chromosomal changes in highly and weakly invasive melanoma cell clones by a modified comparative genomic hybridization approach. *Melanoma Res* 2001; 11:105-115.
- Poser I, Dominguez D, de Hairs AG, Varnai A, Buettner R, Bosserhoff AK. Loss of E-cadherin expression in melanoma cells involves up-regulation of the transcriptional repressor Snail. *J Biol Chem* 2001; 276:24661-24666.
- Suh YA, Lee HY, Virmani A, Wong J, Mann KK, Miller WH, Jr., et al. Loss of retinoic acid receptor beta gene expression is linked to aberrant histone H3 acetylation in lung cancer cell lines. *Cancer Res* 2002; 62:3945-3949.
- Deng G, Peng E, Gum-J, Terdiman J, Slesenger M, Kim YS. Methylation of hMLH1 promoter correlates with the gene silencing with a region-specific manner in colorectal cancer. *Br J Cancer* 2002; 86:574-579.
- Harlyn M, Shih IM. Interactions of melanocytes and melanoma cells with the microenvironment. *Pigment Cell Res* 1994; 7:81-88.

GLUT1 Messenger RNA and Protein Induction Relates to the Malignant Transformation of Cervical Cancer

Christian Rudlowski, MD,¹ Albert J. Becker, MD,² Willibald Schroder, MD,³ Werner Rath, MD,¹ Reinhard Büttner, MD,⁴ and Markus Moser, PhD⁵

Key Words: GLUT1; HPV; Human papillomavirus; Cervical neoplasm; Glucose metabolism

DOI: 10.13094/KYNOM5862JW2GD7

Abstract

We studied whether induction of glucose transporters (GLUTs) 1 to 4 correlates with human papillomavirus (HPV)-dependent malignant transformation of cervical epithelium. Tissue samples of cervical intraepithelial neoplasia (CIN; grades 1 to 3), invasive carcinomas, and lymph node metastasis were examined. HPV typing was performed. Tissue sections were immunostained with GLUT1 to GLUT4 antibodies. Messenger RNA (mRNA) *in situ* hybridization confirmed GLUT1 protein expression.

Weak expression of GLUT1 was found in nondysplastic HPV-positive and HPV-negative epithelium; significant expression was observed in preneoplastic lesions, correlating with the degree of dysplasia. In CIN 3 high-risk HPV lesions, cervical cancer, and metastasis, GLUT1 was expressed at highest levels with a strong correlation of GLUT1 mRNA and protein expression. Immunostains for GLUT2 to GLUT4 were negative.

Cervical tumor cells respond to enhanced glucose utilization by up-regulation of GLUT1. The strong induction of GLUT1 mRNA and protein in HPV-positive CIN 3 lesions suggests GLUT1 overexpression as an early event in cervical neoplasia. GLUT1 is potentially relevant as a diagnostic tool and glucose metabolism as a therapeutic target in cervical cancer.

It has been known for several decades that tumor cells show enhanced glucose metabolism compared with benign tissues.¹ A continuous supply of glucose is the predominant source of adenosine triphosphate generation and substrate storage in mammalian cells. Molecular cloning of the glucose transporter protein 1 (GLUT1) that catalyzes the uptake of glucose in erythrocytes² and the subsequent identification of homologous genes (GLUT2, GLUT3, GLUT4, and GLUT5) revealed a family of genes to facilitate diffusion of hexoses into mammalian cells.³ On the basis of sequence similarities and functional characteristics, GLUTs can be divided into 3 subfamilies, referred to as class I (GLUTs 1-4), class II (GLUTs 5, 7, 9, and 11), and class III (GLUTs 6, 8, 10, and 12 and the myo-inositol transporter HMIT1).⁴

Altered expression of glucose transporter proteins has been described in different tissues under various conditions such as transformation by oncogenes, hypoxia, and exposure to insulin.⁵ *In vivo*, the storage of glycogen has been related to the differentiation status of squamous cell epithelia.^{6,7} In glucose-deprived 3T3-L1 adipocytes, GLUT1 activation by glucosylation relates to increased storage of glycogen.⁸ Cell culture experiments showed that the expression of GLUT1 transporter protein is induced by certain oncogenes such as *ras* and *src*^{9,10} and regulated by the growth factors such as platelet-derived growth factor and epidermal growth factor.^{11,12}

Furthermore, members of the class I family of glucose transporter proteins were expressed strongly in various solid tumors such as breast cancer,^{13,14} renal cell carcinomas,^{15,16} brain tumors,¹⁷ and gastrointestinal malignomas.¹⁸ So far, class II and III GLUT members have not been observed to be relevant for tumorigenesis or tumor progression.¹⁹

Little is known about the expression pattern of GLUTs in cervical neoplasms. Increased glucose uptake demonstrated by positron emission tomography (PET)²⁰ suggests a potential pathophysiologic role of glucose metabolism in cervical cancer. The malignant progression of cervical carcinomas from preinvasive lesions may serve as a paradigm for tumorigenesis along well-defined pathologic stages and pathogenesis. The development of cervical neoplasia is associated with the human papillomavirus (HPV). Viral integration guarantees perpetual expression of HPV-related viral oncogenes. These molecular changes are produced most consistently by the prototypic high-risk HPV types (eg, 16, 18, 31, and 33), but many others (low-risk types, eg, 6, 11, and 40) may be associated with invasive cancer.

We studied the relationship of HPV-related cervical tumor transformation, cellular glycogen storage and expression, and distribution of GLUT1, GLUT2, GLUT3, and GLUT4.

Materials and Methods

Tissue sections were prepared from formalin-fixed, paraffin-embedded archival specimens of cervical neoplasms obtained by surgery. Of 90 available tissue samples from cone biopsies performed for precancerous cervical lesions, 18 were mild cervical intraepithelial neoplasia (CIN 1), 24 were moderate (CIN 2), and 48 were severe dysplastic lesions (CIN 3). The cervical carcinoma specimens and the cervical lymph node metastasis specimens were obtained from 94 patients who underwent radical surgical resections at the Department of Gynecology and Obstetrics, University Hospital, Aachen, Germany, between August 1995 and September 1997. Tissue specimens from 22 pelvic lymph node metastases were studied. The histologic diagnosis and grade of dysplasia were confirmed by 2 pathologists (R.B. and M.M.) according to the criteria of the International Federation of Gynecology and Obstetrics (FIGO classification) and the World Health Organization.²¹ The tissue specimens were examined histologically and contained predominantly neoplastic cells, and the population of tumor cells was no less than 50% of all cells in the specimens. Paraffin-fixed tissue sections from 34 unselected benign cervical lesions were used as control samples and contained changes such as inflammatory or squamous atypia, immature metaplasia, or basal cell hyperplasia.

For immunohistochemical analysis, 3- μ m sections were deparaffinized and rehydrated. After rinsing with phosphate-buffered saline, endogenous peroxidase activity was inhibited by incubation in 3% hydrogen peroxide solution for 30 minutes, and the slides were incubated in a 1:10 solution of equine normal serum to block nonspecific staining.

After antigen retrieval by microwave treatment (600 W) for 5 minutes (3 times) in a 10-mmol/L concentration of sodium citrate, slides were incubated for 60 minutes with

polyclonal rabbit antihuman GLUT1 (DAKO, Hamburg, Germany) and polyclonal rabbit GLUT2, GLUT3, and GLUT4 antibodies (Biogenesis, New Field, England). The antibodies were diluted with bovine serum albumin according to the manufacturer's instructions. As a negative control, slides were reacted with equal amounts of nonspecific IgG instead of the specific primary antibody. After rinsing in phosphate-buffered saline, slides were incubated with a 1:50 dilution of biotinylated secondary antibody (DAKO) for 30 minutes and developed using the ABC technique (Vectastain ABC Systems, Vector Laboratories, Peterborough, England) according to the manufacturer's instructions. Immunocomplexes were visualized with the chromogen diaminobenzidine. Staining for glycogen was performed by the periodic acid-Schiff (PAS) reaction and counterstaining with toluidine blue.

The specificity of GLUT1 staining was confirmed routinely in all cases by staining of parallel tissue sections with GLUT1 antiserum that had been preincubated with the immunizing peptide (25 μ g/mL for 1 hour at 25°C). GLUT1 immunostaining was blocked by this peptide competition in all cases. The sections were evaluated semiquantitatively for immunoreactivity and PAS staining, based on a scoring system that was defined by the product of the intensity of the staining and the percentage of the stained cells. The specimens were subdivided into strong (50% or more marked cells), moderate (25%-49%), weak (10%-24%), and not marked for GLUT1 and glycogen (<10%). Grading was performed by consensus of 2 observers (R.B. and M.M.) in a blinded manner without previous knowledge of the histopathologic and clinical data for each case.

In situ hybridization was performed on paraffin-embedded tissue samples from different cervical biopsies as described previously²² using phosphorus 33 (³³P)-labeled sense and antisense complementary RNA riboprobes for rat GLUT1. Briefly, Proteinase K-pretreated slides (10 μ g/mL) were acetylated in acetic anhydride diluted 1:400 in a 0.1-mol/L concentration of triethanolamine (pH 8.0) and hybridized overnight in 50% formamide, 10% dextran sulfate, a 10-mmol/L concentration of tris(hydroxymethyl) aminomethane (pH 8.0), a 10-mmol/L concentration of sodium phosphate (pH 7.0), 2 \times standard saline citrate, a 5-mmol/L concentration of EDTA (pH 8.0), 150- μ g/mL concentration of transfer RNA, a 10-mmol/L concentration of dithiothreitol, and a 10-mmol/L concentration of β -mercaptoethanol supplemented with 5×10^4 cpm/ μ L of ³³P-labeled sense or antisense riboprobes at 50°C. Finally, slides were washed twice in 50% formamide-2 \times standard saline citrate-20-mmol/L concentration of β -mercaptoethanol, digested with RNase A (20 μ g/mL) for 30 minutes at 37°C, and washed again 3 times with the same washing buffer for 30 minutes each at 50°C. After dehydrating, slides were

coated with Kodak NTB2 emulsion (Kodak, Rochester, NY) and exposed for 8 to 10 days. The intensity of the silver staining was examined by darkfield microscopy, and digitalized images were examined using ImageJ 1.27z software (National Institutes of Health, Bethesda, MD). The Student *t* test was used for statistical analysis.

For detection and typing of HPV, tissue sections were digested by Proteinase K, and DNA was extracted using the DNA Mini Kit (Qiagen, Hilden, Germany) according to the manufacturer's instructions. To detect HPV DNA, a 2-tiered polymerase chain reaction (PCR)-direct sequencing method was performed according to Focli-Fonseca et al²¹ with slight modifications. We used the general consensus primers GP5+/GP6+ and the MY09/MY11 primers for amplification of HPV DNA. Forty cycles of amplification were run with an initial denaturation at 95°C for 5 minutes and for 30 seconds in each cycle. Temperatures of 37°C and 58°C were set for 30 seconds for annealing of the primer pairs GP5+/GP6+ and MY09/MY11, respectively. An extension step was done at 72°C for 5 minutes. The integrity of human genomic DNA was verified by PCR amplification of the β -globin gene. This reaction served as a positive control. The amplification products of the 2 consensus primer pairs and the β -globin PCR were run on a 2% agarose gel and stained with ethidium bromide.

PCR products were purified using the High Pure PCR product purification kit (Roche Diagnostics, Mannheim, Germany) according to the manufacturer's instructions. The sequence of 1 strand of the purified PCR fragments was determined with the Big-Dye Terminator sequencing kit (Applied Biosystems, Foster City, CA) using 3 to 5 pmol of GP5+ or MY09 as the sequencing primers. The results of the sequencing reactions were analyzed on an ABI Prism 310 automated sequencer (Applied Biosystems). The obtained sequences were compared with documented virus sequences available in the GenBank databank using the BLAST program (Blast, Pittsboro, NC). The high-risk group comprised HPV types 16, 18, 31, 33, 35, 39, 45, 51, 52, 56, 58, 59, 66, and 68, and the low-risk group included HPV types 6, 11, 40, 42, 43, and 44. The Student *t* test was used for statistical analysis.

Results

GLUT1-expressing epithelial cells were observed in squamous epithelial cells of normal and dysplastic cervical tissue probes. However, GLUT1 expression in normal epithelial cells was limited to the basal cell layers (Image 1A). Staining intensity was weak and varied in the basal compartment from a focal to homogeneous pattern distribution. All 34 specimens obtained from benign cervical tissue were classified as weak or not marked. Compared with GLUT1 expression in the proliferative cell compartment in the basal cell layer, changes such as inflammatory atypia,

metaplasia, and hyperplasia showed similar GLUT1 expression patterns and also were classified as weakly marked.

The intensity of GLUT1 expression was unaltered from the HPV status. Of 14 HPV-positive specimens, 6 showed high-risk positivity and 8 showed low-risk positivity (Table 1).

Erythrocytes and vascular endothelium served as internal positive controls and demonstrated strong GLUT1 positivity. Simultaneous PAS staining of the epithelium revealed the glycogen content to be correlated inversely to the expression of GLUT1 (Figure 1). The glycogen staining was limited predominantly to the upper cell compartments, which contain the functional epithelium. In good agreement with these immunostaining results, *in situ* hybridization showed GLUT1 messenger RNA (mRNA) expression to be present specifically in the basal epithelium (Image 1B).

In mildly dysplastic epithelium (*n* = 18), weak GLUT1 expression was limited to the basal cell layers (Image 1C) and (Image 1D), and in moderate dysplasia (*n* = 24), enhanced expression was extended to the basal and parabasal compartments. The GLUT1 expression pattern was independent of HPV status. In CIN 1 lesions, 4 cases were in the high-risk HPV group, 6 were in the low-risk HPV group, and 8 were HPV-negative cases. Compared with benign cervical changes, significantly increased GLUT1 expression was observed in CIN 1 lesions (Image 2).

Strong GLUT1 mRNA and protein expression was observed in all 48 CIN 3 lesions of the cervix uteri (Image 1E) and (Image 1F). GLUT1 expression was continuously strong throughout the entire dysplastic epithelium, including the basal, suprabasal, and apical parts of the cervical epithelium. Of 48 CIN 3 lesions, 46 were HPV positive; 34 cases belong to the high-risk group and 12 to the low-risk group. No differences between the HPV type or status and GLUT1 expression were observed. Only weak glycogen storage was observed in CIN 3 lesional tissue samples.

Tumors with moderate dysplasia showed a high percentage of HPV positivity (high-risk HPV, 16 cases; low-risk HPV, 3 cases; HPV type not assignable, 2 cases; HPV-negative, 3 cases). The intensity of GLUT1 protein expression depended on the extent of dysplasia and was accompanied by inversely correlated glycogen content in the nondysplastic areas of the epithelium (Figure 1).

GLUT1 overexpression was demonstrated in all 94 cases of invasive cervical carcinoma and all 22 cervical metastases (Image 1G) and (Image 1H). The intensity of GLUT1 protein expression did not vary significantly between different tumor stages, the degree of tumor differentiation, or HPV status. A high-risk HPV type was detectable in 84 cases and a low-risk type in 8 cases. In 2 specimens, no HPV was detectable.

GLUT1 expression was observed predominantly at the tumor periphery compared with the center of well-differentiated

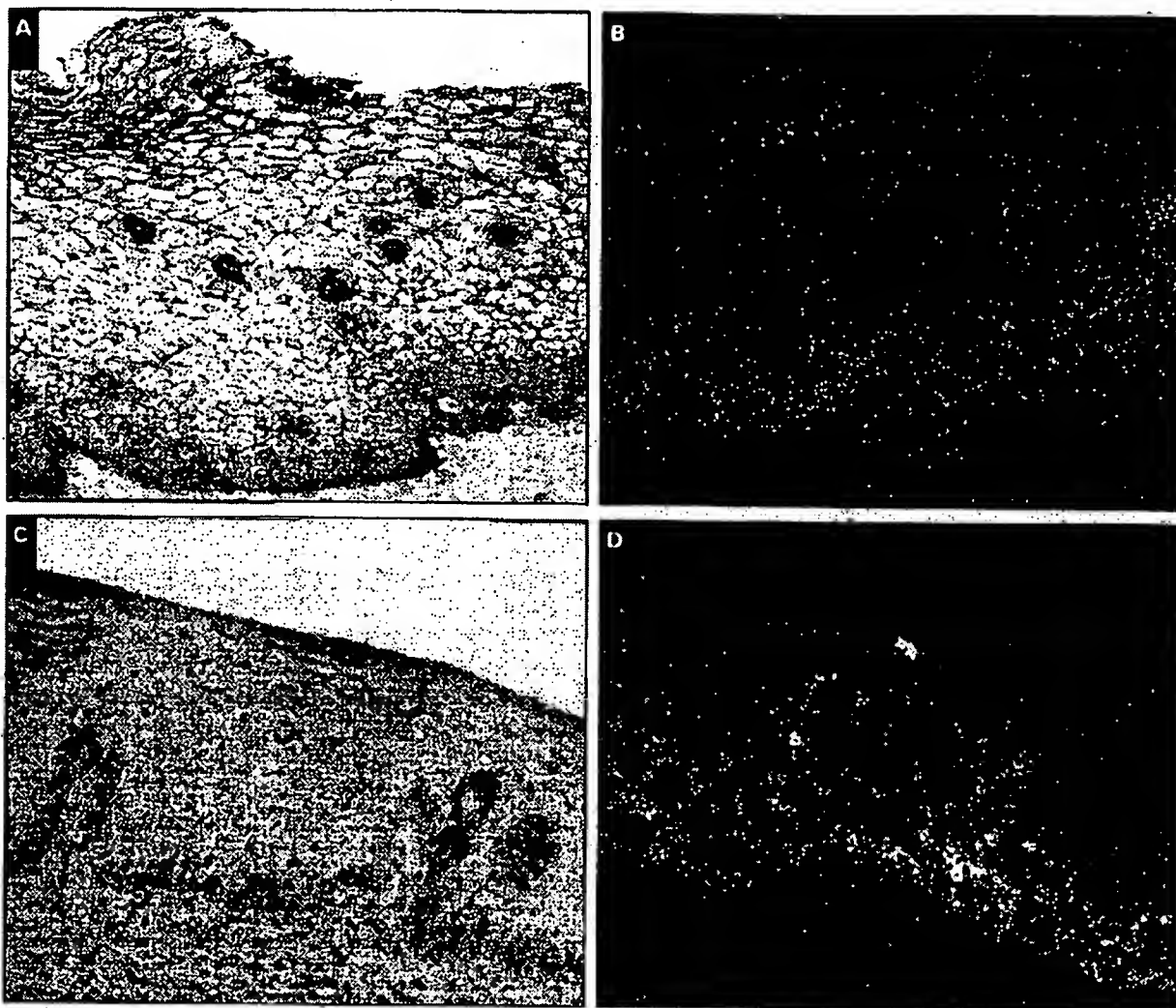


Figure 1 Glucose transporter (GLUT) 1 immunoreactivity with simultaneous periodic acid-Schiff (PAS) staining and GLUT1 messenger RNA (mRNA) silver staining in normal cervical epithelium (**A**, GLUT1 and PAS, x200; **B**, GLUT1 mRNA and silver staining, x200), cervical intraepithelial neoplasia (CIN) 1 lesions (**C**, GLUT1 and PAS, x200; **D**, GLUT1 mRNA and silver staining,

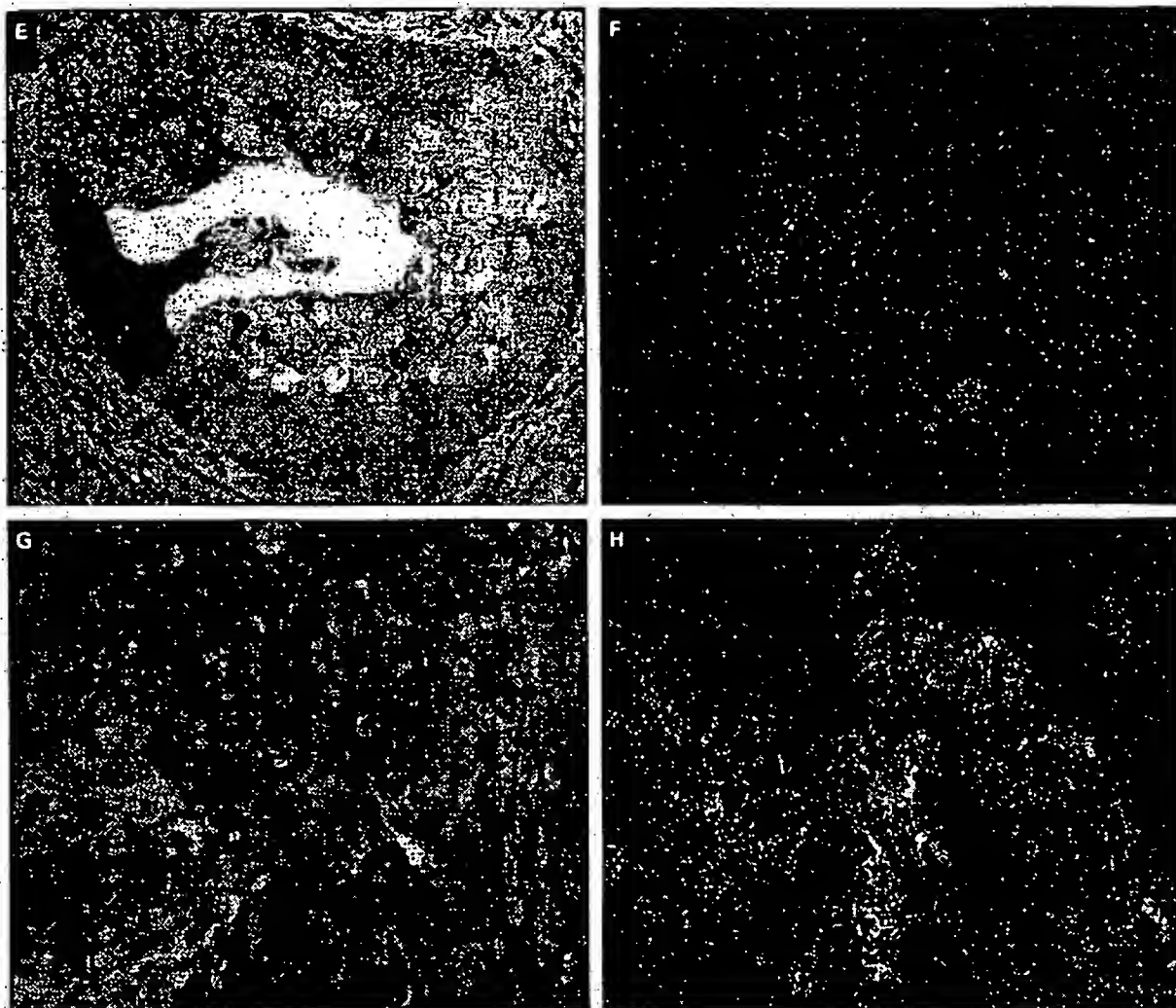
tumor areas. By PAS staining, we found an accumulation of glycogen in well-differentiated tumor areas, which was correlated inversely with GLUT1 expression. A similar distribution pattern was found in the lymph node metastases. **Figure 2** illustrates the results of GLUT1 mRNA in situ hybridization. The intensity of the specific silver staining correlated significantly with the extent of cervical dysplasia and showed similar levels in CIN 3 lesions and cervical carcinoma. Overexpression of mRNA was limited to dysplastic cells and matched the patterns of GLUT1 protein distribution revealed by immunohistochemical analysis.

Immunostains for GLUT2, GLUT3, and GLUT4 were negative in epithelial cells of both benign and dysplastic

lesions. Only inflammatory cells reacted with the antibodies and served as an internal positive control. In the advanced and poorly differentiated tumors, there was a pattern of expression similar to that in the dysplastic precursor lesions.

Discussion

Based on numerous molecular and epidemiologic studies, it has been demonstrated that specific types of HPV (high-risk HPVs, but also to a lower extent low-risk HPVs) can be detected in a transcriptionally active form in about 95% of cervical cancer biopsy specimens.²⁴ Although the high-risk HPV-encoded oncogenes E6 and E7 induce



×200), CIN 3 lesions (E, GLUT1 and PAS, ×200; F, GLUT1 mRNA and silver staining, ×200), and cervical cancer (G, GLUT1 and PAS, ×200; H, GLUT1 mRNA and silver staining, ×200). Expression of GLUT1 mRNA and protein in normal epithelial cells was limited to the basal proliferative cell layers, whereas PAS staining was restricted to the upper cell compartments. In the CIN 3 lesions and cervical carcinoma, strong expression of GLUT1 mRNA and protein was observed.

Table 1
HPV Status, GLUT1 Expression, and PAS Staining in the Study Group*

	Benign Cervical Tissue (n = 34)	CIN 1 (n = 18)	CIN 2 (n = 24)	CIN 3 (n = 48)	Cervical Cancer (n = 94)
HPV positive	14 (41)	10 (56)	21 (88) [†]	46 (96)	92 (98)
High risk	6 (18)	4 (22)	16 (67)	34 (71)	84 (89)
Low risk	8 (24)	6 (33)	3 (13)	12 (25)	8 (9)
GLUT1 expression	+	+	++	+++	+++
PAS staining	+++	+++	++	+	-

CIN, cervical intraepithelial neoplasia; GLUT, glucose transporter; HPV, human papillomavirus; PAS, periodic acid-Schiff; -, negative; +, weak; ++, moderate; +++, strong.
* Data for HPV are given as number (percentage). High-risk HPV infection was related closely to the degree of dysplasia and coincided with increasing GLUT1 expression.

[†] In 2 cases (8%), the HPV type was not assignable.

Rudlowaki et al / GLUT1 EXPRESSION IN CERVICAL NEOPLASMS

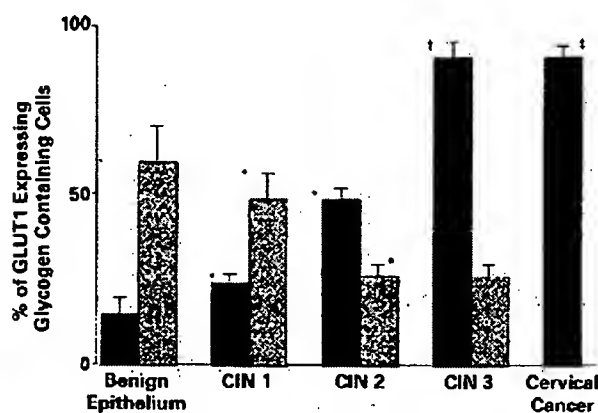


Figure 1 Glucose transporter (GLUT) 1 protein expression (black bars) and cellular glycogen content (gray bars) in benign and dysplastic cervical epithelium. The immunoreactivity of GLUT1 was associated strongly with the degree of dysplasia and correlated inversely with the cellular glycogen content. However, cervical intraepithelial neoplasia (CIN) 3 and cervical cancer showed equivalent levels of strong GLUT1 overexpression. * $P < .01$. † $P < .001$. ‡ In the center of well-differentiated cervical cancer, mild periodic acid-Schiff-positive staining was observed.

cellular immortalization,²⁵ their expression alone is not sufficient to cause malignant transformation.²⁶ Additional events must accumulate to convert a cell toward malignancy and to induce cervical cancer. It has been shown that the course of malignant disease not only is the result of failing intracellular

and immunologic surveillance mechanisms²⁷ but also is determined by efficient blood vessel formation to support the outgrowing tumor with nutrients, hormones, and oxygen.²⁸ Many tumorigenic cells are characterized not only by increased mitotic rates but also by high catabolic utilization of glucose and an increased number of specific glucose transporters.^{1,29} A sufficient intracellular glucose supply mediated by glucose transporters seems to be a prerequisite for enhanced HPV transcription and the expression of the E6 and E7 oncoproteins. In cell culture experiments using cervical cancer cells, specific suppression of the HPV 18 transcription was found by adding the glycolytic pathway inhibitor 2-deoxyglucose.³⁰

Our results demonstrate that human cervical carcinomas and their metastases selectively overexpress GLUT1. In benign cervical epithelium, moderate GLUT1 expression was restricted to the proliferating basal cell layers of the mucosa and changes such as inflammatory or squamous atypia, immature metaplasia, or basal cell hyperplasia. These findings are in line with the differentiation-related expression pattern of GLUT1 in normal human epidermis, in which GLUT1 is expressed in the basal layer and, to a lesser extent, in the immediate suprabasal layer of the epidermis.³¹ GLUT1 mRNA expression precisely coincided with protein overexpression in normal epithelium, cervical dysplasia, and invasive cancers. These findings strongly suggest that the increased GLUT1 expression in cervical neoplasms is mediated by transcriptional mechanisms.

In vitro studies on fibroblasts transfected with *ras* and *src* oncogenes revealed elevated levels of GLUT1 expression and an increase of transmembranous glucose transport.¹⁰ These

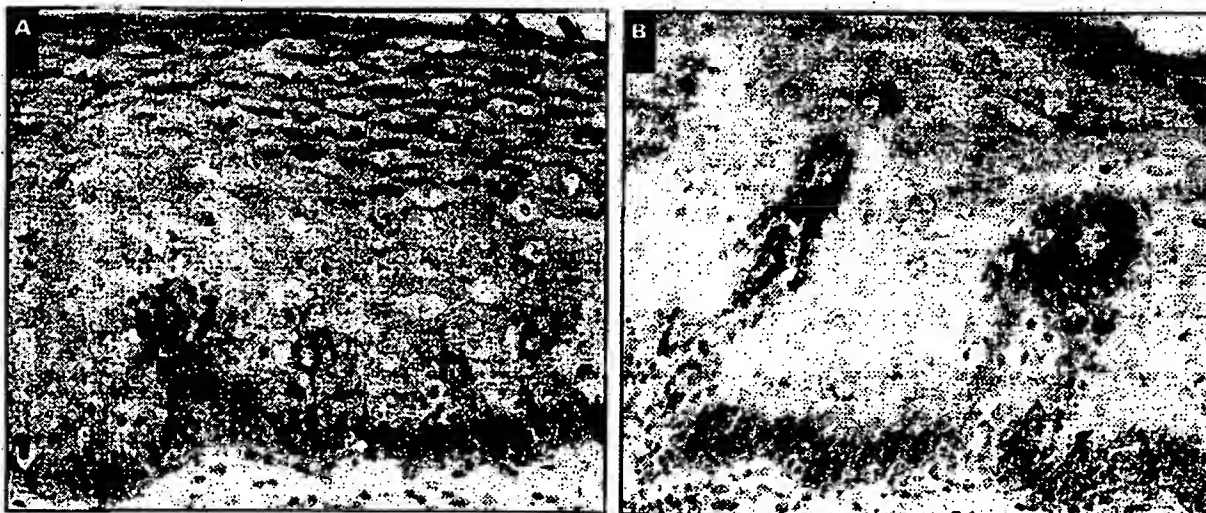


Image 2 Glucose transporter (GLUT) 1 protein immunoreactivity in cervical intraepithelial neoplasia 1 dysplasia (A, $\times 200$) vs reparative cervical changes (B, $\times 200$). The staining intensity of GLUT1 in low-grade dysplasia was increased markedly compared with the benign specimen. B, The arrow shows GLUT1 staining of erythrocytes, which serve as an internal control for GLUT1 positivity.

results support our present findings indicating that GLUT1 overexpression parallels malignant transformation of cervical epithelial cells. However, the regulatory mechanisms of GLUT1 induction are, so far, poorly understood. Tumor hypoxia might be a key step for up-regulation of GLUT1 transcripts.³²

However, we have observed overexpression in preneoplastic lesions. This might suggest direct oncogene-triggered mechanisms as potential factors for GLUT1 up-regulation. GLUT1 expression was not correlated with the HPV status or type in either benign or dysplastic cervical epithelium. High-risk HPV types were detectable predominantly in CIN 2 and 3 lesions and invasive cervical cancer and had good correlation with the dysplastic stage. All high-risk HPV-infected CIN 2 and 3 lesions and carcinoma showed enhanced GLUT1 expression. There is certain evidence that these cases are associated with virus transcription and the expression of E6 and E7 oncogenes.²⁴ An enhanced cellular glucose supply mediated by an increasing number of GLUT1 transporters could be a requirement for successful HPV-dependent malignant transformation.

Our results indicate that the clinical observation of an increased glucose uptake of cervical cancer cells was related to an exclusive transmembranous overexpression of GLUT1. These data strongly suggest that the observed relationship between increased GLUT1 expression and the intracellular accumulation of 2-fluoro-deoxy-D-glucose (FDG) in tumor cells represents the biologic basis for diagnosis using fluorine 18-labeled FDG PET.^{20,33} Enhanced expression of GLUT1 was detected already in moderate cervical dysplasia and much more in carcinoma in situ. In these preneoplastic lesions, the staining pattern of GLUT1 expression was stronger than in normal or mildly dysplastic mucosa and extended into the superficial cell layers depending on the degree of dysplasia. The observation that the preneoplastic lesions with increased GLUT1 expression were not detected by PET analysis may be explained by the small dimension of the epithelial dysplasia and the limited resolution of PET.

We also analyzed the cellular glycogen content to determine whether alterations in glucose uptake are linked to tumor-associated changes in the storage of this polysaccharide. The glycogen content was of special interest because the presence of glycogen is known to be related to cellular maturation of squamous epithelium and disappears with loss of differentiation during neoplastic transformation.⁶ In the present study, glycogen was found only in nondividing cells of the superficial layers of the benign cervical epithelium, whereas the basal layers did not contain glycogen (Image 1A). The glycogen content in normal and preneoplastic lesions generally correlated inversely with GLUT1 expression, exhibiting intense glycogen storage in normal and reduced or absent storage in dysplastic epithelium. Thus, reduction of glycogen content was related closely to the

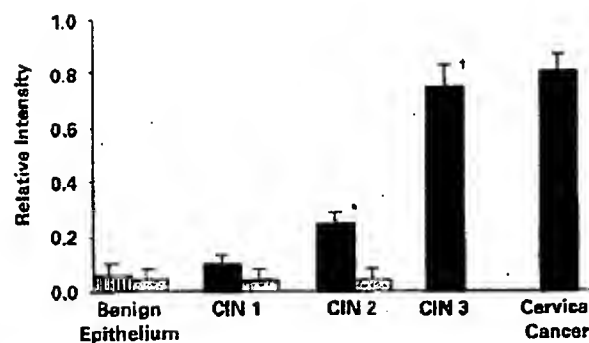


Figure 2 Glucose transporter (GLUT) 1 messenger RNA (mRNA) expression in the proliferative compartment of the benign cervical epithelium (hatched bar) and in dysplastic epithelium (black bars). The gray bars represent the relative intensity in the functional cell compartments. GLUT1 mRNA expression in cervical epithelium correlated significantly with the degree of dysplasia. * $P < .01$. † $P < .001$. CIN, cervical intraepithelial neoplasia.

degree of dysplasia and was associated strongly with increased GLUT1 expression.

The observed storage pattern of glycogen was correlated inversely with the extension of the proliferation compartment and is in line with previous observations showing an association between glycogen content and tumor cell development, as well as differentiation in squamous cell carcinoma tumorigenesis.³⁴ This cellular feature reflects the growing and metastasizing potency of cervical carcinomas, as increased utilization of glucose is a necessary condition of growing tumors and may be the pathophysiologic basis for induction of glucose transporter protein expression in the cell membrane. The lack of expression in benign cervical tissue and in the well-differentiated center of some cervical tumors gives rise to the assumption that GLUT1 expression might be regarded as a characteristic feature of tumor cell clones with an increased energy requirement.

In contrast with data from colon³⁵ and non-small cell pulmonary carcinoma,³⁶ no correlation between GLUT1 expression and prognostic clinicopathologic features was found in the present study. This difference can be explained easily, since significant overexpression of GLUT1 is observed in premalignant cervical lesions and well-differentiated carcinomas. We, therefore, believe that GLUT1 overexpression is an early event in the development of cervical carcinomas. Our findings also may have substantial implications for the potential therapeutic application of cytotoxic agents conjugated to glucose in the treatment of premalignant or malignant cervical lesions. Further studies are required to explore whether this strategy will lead to more specific drug delivery to the neoplastic cell compartment.

Rudlowski et al / GLUT1 EXPRESSION IN CERVICAL NEOPLASMS

From the ¹Department of Gynecology and Obstetrics, University Hospital Heidelberg, Heidelberg; ²Department of Neuropathology and ³Institute of Pathology, University of Bonn Medical Center, Bonn; ⁴Central Hospital, Bremen, University of Bonn Medical Center; and ⁵Department for Molecular Medicine, Max-Planck-Institut für Biochemie, Martinsried, Germany.

Address reprint requests to Dr Rudlowski: Dept of Gynecology and Obstetrics, University Hospital Heidelberg, Vossstr 7-9, D-69115 Heidelberg, Germany.

References

1. Warburg O. On the origin of cancer cells. *Science*. 1956;123:309-314.
2. Mueckler M, Canuso C, Baldwin SA, et al. Sequence and structure of a human glucose transporter. *Science*. 1985;229:941-945.
3. Gould GW, Bell GI. Facilitative glucose transporters: an expanding family. *Trends Biochem Sci*. 1990;15:18-23.
4. Joost HG, Bell GI, Best JD, et al. Nomenclature of the GLUT/SLC2A family of sugar/polyol transport facilitators. *Am J Physiol Endocrinol Metab*. 2002;282:E974-E976.
5. Olson AL, Pessin JE. Structure, function, and regulation of the mammalian facilitative glucose transporter gene family. *Annu Rev Nutr*. 1996;16:235-256.
6. Das DK, Chowdury JR. The use of glycogen studies in the evaluation of treatment for carcinoma of the cervix uteri. *Acta Cytol*. 1981;25:566-571.
7. Reisser C, Eichhorn K, Herold-Mende C, et al. Expression of facilitative glucose transport proteins during development of squamous cell carcinomas of the head and neck. *Int J Cancer*. 1999;80:194-198.
8. McMahon RJ, Frost SC. Glycogen: a carbohydrate source for GLUT-1 glycosylation during glucose deprivation of 3T3-L1 adipocytes. *Am J Physiol*. 1996;270:E640-E645.
9. Birnbaum MJ, Haspel HC, Rosen OM. Transformation of rat fibroblasts by FSV rapidly increases glucose transporter gene transcription. *Science*. 1987;235:1495-1498.
10. Flier JS, Mueckler MM, Usher P, et al. Elevated levels of glucose transport and transporter messenger RNA are induced by *ras* or *src* oncogenes. *Science*. 1987;235:1492-1495.
11. Rollins BJ, Morrison ED, Usher P, et al. Platelet-derived growth factor regulates glucose transporter expression. *J Biol Chem*. 1988;263:16523-16526.
12. Hiraki Y, Rosen OM, Birnbaum MJ. Growth factors rapidly induce expression of the glucose transporter gene. *J Biol Chem*. 1988;263:13655-13662.
13. Alo PL, Visca P, Botti C, et al. Immunohistochemical expression of human erythrocyte glucose transporter and fatty acid synthase in infiltrating breast carcinomas and adjacent typical/atypical hyperplastic or normal breast tissue. *Am J Clin Pathol*. 2001;116:129-134.
14. Brown RS, Wahl RL. Overexpression of Glut-1 glucose transporter in human breast cancer: an immunohistochemical study. *Cancer*. 1993;72:2979-2985.
15. Ahn YS, Zerban H, Grobholz R, et al. Sequential changes in glycogen content, expression of glucose transporters and enzymic patterns during development of clear/acidophilic cell tumors in rat kidney. *Carcinogenesis*. 1992;13:2329-2334.
16. Nagase Y, Takata K, Moriyama N, et al. Immunohistochemical localization of glucose transporters in human renal cell carcinoma. *J Urol*. 1995;153:798-801.
17. Tsukamoto H, Hamada Y, Wu D, et al. GLUT1 glucose transporter: differential gene transcription and mRNA binding to cytosolic and polysome proteins in brain and peripheral tissues. *Brain Res Mol Brain Res*. 1998;58:170-177.
18. Noguchi Y, Marat D, Saito A, et al. Expression of facilitative glucose transporters in gastric tumors. *Hepato-gastroenterology*. 1999;46:2683-2689.
19. Joost HG, Thorens B. The extended GLUT-family of sugar/polyol transport facilitators: nomenclature, sequence characteristics, and potential function of its novel members (review). *Mol Membr Biol*. 2001;18:247-256.
20. Sugawara Y, Eishrich A, Kosuda S, et al. Evaluation of FDG PET in patients with cervical cancer. *J Nucl Med*. 1999;40:1125-1131.
21. Cervix uteri. In: *American Joint Committee on Cancer: AJCC Cancer Staging Manual*. 5th ed. Philadelphia, PA: Lippincott; 1997:189-194.
22. Moser M, Imhof A, Pscherer A, et al. Cloning and characterization of a second AP-2 transcription factor: AP-2 beta. *Development*. 1995;121:2779-2788.
23. Feoli-Fonseca JC, Oligny LL, Brochu P, et al. Human papillomavirus (HPV) study of 691 pathological specimens from Quebec by PCR-direct sequencing approach. *J Med Virol*. 2001;63:284-292.
24. zur Hausen H. Papillomavirus infections: a major cause of human cancers. *Biochim Biophys Acta*. 1996;1288:F55-F78.
25. Munger K, Phelps WC, Bubbi V, et al. The E6 and E7 genes of the human papillomavirus type 16 together are necessary and sufficient for transformation of primary human keratinocytes. *J Virol*. 1989;63:4417-4421.
26. Durst M, Dzarlieva-Petrusevska RT, Boukamp P, et al. Molecular and cytogenetic analysis of immortalized human primary keratinocytes obtained after transfection with human papillomavirus type 16 DNA. *Oncogene*. 1987;1:251-256.
27. Altmann A, Jochims I, Rosl F. Intra- and extracellular control mechanisms of human papillomavirus infection. *Intervirology*. 1994;37:180-188.
28. Risau W. Mechanisms of angiogenesis. *Nature*. 1997;386:671-674.
29. Younes M, Lechago LV, Sornuano JR, et al. Wide expression of the human erythrocyte glucose transporter Glut1 in human cancers. *Cancer Res*. 1996;56:1164-1167.
30. Maehama T, Patzelt A, Lengert M, et al. Selective down-regulation of human papillomavirus transcription by 2-deoxyglucose. *Int J Cancer*. 1998;76:639-646.
31. Cherzi R, Melioli G, de Luca M, et al. "HepG2/erythroid/brain" type glucose transporter (GLUT1) is highly expressed in human epidermis: keratinocyte differentiation affects GLUT1 levels in reconstituted epidermis. *J Cell Physiol*. 1992;150:463-474.
32. Airley R, Lancaster J, Davidson S, et al. Glucose transporter glut-1 expression correlates with tumor hypoxia and predicts metastasis-free survival in advanced carcinoma of the cervix. *Clin Cancer Res*. 2001;7:928-934.
33. Umesaki N, Tanaka T, Miyama M, et al. The role of ¹⁸F-fluoro-2-deoxy-D-glucose positron emission tomography (¹⁸F-FDG-PET) in the diagnosis of recurrence and lymph node metastasis of cervical cancer. *Oncol Rep*. 2000;7:1261-1264.
34. Voldstedlund M, Dabelsteen E. Expression of GLUT1 in stratified squamous epithelia and oral carcinoma from humans and rats. *APMIS*. 1997;105:537-545.
35. Haber RS, Rathana A, Weiser KR, et al. GLUT1 glucose transporter expression in colorectal carcinoma: a marker for poor prognosis. *Cancer*. 1998;83:34-40.
36. Younes M, Brown RW, Stephenson M, et al. Overexpression of Glut1 and Glut3 in stage I non-small cell lung carcinoma is associated with poor survival. *Cancer*. 1997;80:1046-1051.

Experimental Cell Research 275, 185–199 (2002)

doi:10.1006/excr.2002.5499, available online at <http://www.idealibrary.com> on IDEAL®

Expression and Distribution of Laminin $\alpha 1$ and $\alpha 2$ Chains in Embryonic and Adult Mouse Tissues: An Immunochemical Approach

Takako Sasaki,* Richard Giltay,* Ulrika Talts,† Rupert Timpl,* and Jan F. Talts*†¹

*Max-Planck-Institute for Biochemistry, D-82152 Martinsried, Germany; and †Department of Cell and Molecular Biology, Lund University, S-22184 Lund, Sweden

Protein levels, mRNA expression, and localization of laminin $\alpha 1$ and $\alpha 2$ chains in development and in adult mice were examined. Recombinant fragments were used to obtain high-titer-specific polyclonal antibodies for establishing quantitative radioimmuno-inhibition assays. This often demonstrated an abundance of $\alpha 2$ chain, but also distinct amounts of $\alpha 1$ chain for adult tissues. The highest amounts of $\alpha 1$ were found in placenta, kidney, testis, and liver and exceeded those of $\alpha 2$. All other tissue extracts showed a higher content of $\alpha 2$, which was particularly high in heart and muscle when compared to $\alpha 1$. Content of $\gamma 1$ chain, shared by most laminins, was also analyzed. This demonstrated $\gamma 1$ chain levels being equal to or moderately exceeding the sum of $\alpha 1$ and $\alpha 2$ chains, indicating that these isoforms represent the major known laminin isoforms in most adult mouse tissues so far examined. Moreover, we found good correlation between radioimmuno-inhibition data and mRNA levels of adult tissues as measured by quantitative real-time reverse transcriptase-PCR. Embryonic tissues were also analyzed by radioimmuno-inhibition assays. This demonstrated for day 11 embryos comparable amounts of $\alpha 1$ and $\gamma 1$ and a more than 25-fold lower content of $\alpha 2$. This content increased to about 10% of $\alpha 1$ in day 13 embryos. The day 18 embryo showed in heart, kidney, and liver, but not yet in brain and lung, $\alpha 1/\alpha 2$ chain ratios comparable to those in adult tissues. Immunostaining demonstrated $\alpha 1$ in Reichert's membrane (day 7.5), while $\alpha 2$ could not be detected before day 11.5. These data were compared with immunohistochemical localization results on several more embryonic and adult tissue sections. Our results regarding localization are consistent with those of earlier work with some notable exceptions. This was in part due to epitope masking for monoclonal antibodies commonly used in previous studies in esophagus, intestine, stomach, liver, kidney, and spleen.

© 2002 Elsevier Science (USA)

¹To whom correspondence and reprint requests should be addressed at Department of Cell and Molecular Biology, Section for Cell and Developmental Biology, B 12, BMC, S-221 84 Lund, Sweden. Fax: +46 46 2220855. E-mail: Jan.Talts@medkem.lu.se.

Key Words: laminin; immunofluorescence; RT-PCR; radioimmuno-inhibition assay; monoclonal antibody; epitope; masking.

INTRODUCTION

Basement membranes separate dissimilar cell types and thus compartmentalize almost all tissues. They are thin sheets of extracellular matrix whose main components are type IV collagen, nidogen, sulfated proteoglycans, and laminins [1, 2]. Laminins are found in all basement membranes, but also in embryonic mesenchyme and loose connective tissue. Laminin-1, with the chain composition $\alpha 1\beta 1\gamma 1$, was initially discovered and purified from the Engelbreth-Holm Swarm tumor [3] and from cultures of teratocarcinoma cells [4]. Another protein initially named merosin was found in tissue extracts from placenta [5] and was subsequently shown to be a second laminin α chain, named $\alpha 2$ [6]. Subsequently it was realized that the laminins are a family of proteins. All native laminins identified so far are composed of one α , one β , and one γ chain and 12 different heterotrimers have been proposed based on five α , three β , and three γ chains [1, 7].

In vitro studies have indicated that laminins mediate a variety of biological functions. First they form a self-assembling structural network to which other components of the basement membrane attach [8]. Second, they attach cells to the extracellular matrix via α -dystroglycan [9, 10] and integrin receptors [11]. Third, they convey information to the cell interior via these receptors, as exemplified by mesenchymal to epithelial transitions in kidney [12], myogenesis in skeletal muscle [13, 14], and outgrowth of neurites [15]. Studies of mutated genes as well as gene targeting experiments have indicated different functional roles for the different laminins [7].

Laminin $\alpha 1$ and $\alpha 2$, with lengths of about 3000 residues, have an identical modular structure when compared to all other known α chains [7, 16]. They share in their N-terminal LN modules (domain VI) binding sites for $\alpha 1\beta 1/\alpha 2\beta 1$ integrins, heparin, and self-assembly



sites [17–20]. Different C-terminal LG modules of both chains, however, participate in binding of other β 1 integrins, α -dystroglycan, heparin, and sulfatides [7, 21, 22]. A unique property of the α 2 chain includes binding of a phenolic glycolipid at the surface of *Mycobacterium leprae* through α 2LG5, which promotes entry of the pathogen into Schwann cells [23]. A further difference is proteolytic processing of the α 2 chain module LG3, which modulates α -dystroglycan binding [24], while the α 1 chain is not processed.

Other potential differences may exist in the function of both α chains, as suggested from light microscopy tissue localization studies based on several monoclonal and polyclonal antibodies and from mRNA analyses. The α 1 chain is apparently the first laminin α chain produced at early preimplantation stages during development [25] and becomes deposited in many epithelial tissues during organogenesis [26]. This changes to a more restricted distribution in adult mouse and human tissues [27, 28]. The α 2 chain presumably does not appear before day 11 of mouse development, but then becomes prominently expressed in skeletal and heart muscle, several epithelial tissues, peripheral nerves, and various blood vessels [29–31]. In addition, a few immunogold stainings have shown that laminins containing α 1 [32] and α 2 chains [33] are deposited in basement membranes of kidney and muscle and of capillary walls and thus in a proper position for binding to cellular receptors.

In the present study we have used several recombinant fragments of mouse laminin α 1 and α 2 chains in order to obtain specific polyclonal antibodies for establishing quantitative radioimmuno-inhibition assays. This often demonstrated an abundance of α 2 chain, but also distinct amounts of α 1 chain for adult tissues and good correlation to mRNA levels measured. However, some different patterns were observed for embryonic tissues and cultured cells. These data were compared with immunohistochemical localization on tissue sections and provided a comprehensive overview of the deposition of both chains during development and adult stages.

MATERIALS AND METHODS

Recombinant proteins and antibodies. The recombinant mouse laminin fragments α 1VI/V [20], α 1LG4 [21], α 2LG1-3 and α 2LG4-5 [34], and α 4LG1-3 and α 4LG4-5 [33] were previously described. Novel mouse laminin fragments included α 2VI/V (positions 1–513 [16]), α 3BVI/V (positions 1–468), and α 5VI/V (positions 1–480), the latter two including a complete N-terminal sequence recently deposited in the data bank (AJ293592, AJ293593). The coding sequences were amplified by RT-PCR using mouse RNA from heart (α 2), epidermal Pam 212 cells (α 3B), and embryonic endothelial cells (α 5) and inserted into the episomal expression vector pCEP-Pu by using appropriate restriction sites in front of the signal peptides and after the stop codon [35]. Transfected human 293-EBNA cells were then used to obtain serum-free conditioned medium for purification. This was

accomplished by a combination of heparin affinity and molecular sieve chromatography (α 2) or by DEAE-cellulose and molecular sieve chromatography (α 3B, α 5) following standard protocols [20, 36]. The purified recombinant fragments showed a single N-terminal sequence and the expected shapes after rotary shadowing electron microscopy [37].

Rabbit antisera against α 1VI/V [20] and against α 2LG1-3 and α 2LG4-5 [34] have been previously described. Rat monoclonal antibodies (Mab 198 and 200) against mouse laminin-1 fragment E3 [38] were recently shown to bind to the α 1LG4 module [21]. A rabbit antiserum against mouse α 2VI/V was generated following standard protocols.

Tissue extracts and cell cultures. Tissues from adult and embryonic mice and mouse EHS tumor [39] were extracted with Tris buffer, pH 7.4, containing 10 mM EDTA (16 h, 4°C) followed by the same buffer containing in addition 1% Nonidet P-40, 0.5% deoxycholate, 1% SDS (4 h, 4°C) [40]. This was followed for a few tissues by a stepwise treatment with heparitinase and chondroitinase ABC under conditions optimal for removal of glycosaminoglycans from the basement membrane proteoglycan perlecan [36]. Final digestions were performed with bacterial collagenase (0.5 mg/ml) in neutral buffer containing 1 mM CaCl₂ and Pefabloc [40] followed by pepsin (0.1 mg/ml) in 0.1 M acetic acid at 16°C (22 h).

Serum-free conditioned medium (24 h) was collected from cells grown to near confluency and cell lysates were prepared by extraction with 1 ml of detergent. Mouse epidermal Pam 212 and embryonic PYS-2 cells and rat Schwannoma RN22 and Rugli glioma cells were those used previously [41, 42]. The mouse embryonic carcinoma cell line F9 was used prior to and after stimulation with dibutyl cAMP and retinoic acid [43]. The mouse endothelioma cell line cEnd.2 was kindly supplied by Dr. E. Wagner [44]. Endothelial progenitor cells from day 7.5 mouse embryos [45] and the endothelial IBE cell line derived from mouse brain [46] were provided by Drs. A. Hatzopoulos and L. Claesson-Welsh, respectively. Fibroblasts and myoblasts from adult mice were a gift of Dr. U. Mayer.

Immunohistochemical assays. Specific radioimmuno-inhibition assays for recombinant laminin fragments α 1VI/V [20], α 1LG4 [21], and γ IIIb3-5, here using an antiserum against laminin fragment P1 [47], have previously been described. The same procedure was used to establish assays for fragments α 2VI/V, α 2LG1-3, and α 2LG4-5 [48]. ELISA assays [21] and immunoblotting of reduced antigens [49] followed standard protocols.

Quantitative real-time reverse transcriptase-PCR. Total RNA was isolated as described [50]. To analyze mRNA levels of laminin α 1 and α 2, quantitative reverse transcriptase (RT)-PCR with sequence-specific hybridization probes (TIB Molbiol, Berlin, Germany) was performed on a LightCycler (Roche). Total RNA was transcribed into cDNA using oligo(dT)₁₂₋₁₈ primers and Superscript II Reverse Transcriptase (Gibco) according to the manufacturer's instructions. In order to ensure that equal amounts of starting material were used, analyses with GAPDH primers were run in parallel. The primer pairs (TIB Molbiol) used were the following: for laminin α 1, TGTAAGATGGCAAGGTCTTATTCA and CTCAGGCAGTTCTGTTTGATGT; for laminin α 2, TGTCGTGGGGATCTGTATGTC and CAAGAAGGTCCAATCCAACTTT; for GAPDH, TTGTCAGCAATGCATCCTGC and CCGTTCAGCTCTGGGATGAC. The probes used were the following: for laminin α 1, the fluorescein-labeled probe CTGAAAGC-CCCCACACCCATTCCA and the LightCycler-Red-640-labeled probe TCGGCAGACACCAACGATCCCATTTA; for laminin α 2, the fluorescein-labeled probe ACCTCCAGCTTTCACGTTGGGACAT and the LightCycler-Red-640-labeled probe CTTTCCGAATGCAGAGAGTGGGACTT; for GAPDH, the fluorescein-labeled probe CACCCA-GAAGACTGTGGATGGCCCT and the LightCycler-Red-640-labeled probe TGGAAAGCTGTGGCGTGATGGCCG. Standard curves were obtained for each set of probes with serial dilutions of DNA. LightCycler software was used to generate amplification curves. The number of cycles (*n*) corresponding to where the fluorescence signal

LAMININ $\alpha 1$ AND $\alpha 2$ CHAINS IN TISSUES

187

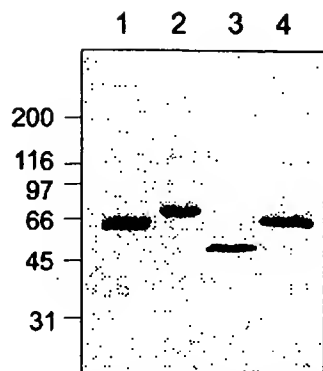


FIG. 1. SDS-gel electrophoresis of purified recombinant fragments from the N-terminal region of mouse laminin α chains. The lanes were loaded with fragments $\alpha 1\text{VI/V}$ (1), $\alpha 2\text{VI/V}$ (2), $\alpha 3\text{VI/V}$ (3), and $\alpha 5\text{VI/V}$ (4). The run was calibrated with marker proteins denoted at the left margin in kDa.

(amplification of DNA) becomes logarithmic was used to calculate relative amounts of mRNA by the formula $2^{\Delta n}$, where $\Delta n = n_{\text{GAPDH}} - n_{\text{laminin}}$. Each increase in Δn by 1 equals a twofold increase in specifically amplified mRNA.

Immunohistochemistry. Staining of cryosections with antibodies was performed as follows. Sections were washed in phosphate-buffered saline (PBS) and blocked with 1% BSA in PBS for 30 min at room temperature. Antibody solutions were applied followed by a 1-h incubation at RT. Slides were washed in PBS/BSA and secondary antibodies coupled to a fluorochrome (Cy2/Cy3; Jackson ImmunoResearch Lab. Inc., West Grove, PA) were used for detection. Paraffin-embedded sections were dewaxed with xylene and rehydrated through a downgraded ethanol series. Sections were treated with Protease XXIV (Sigma) (20 $\mu\text{g}/\text{ml}$) at RT for 20 min, incubated with primary antibodies as above, and subsequently stained using the Vectastain ABC elite kit (Vector Laboratories Inc., Burlingame, CA) following the manufacturer's instructions, rinsed again, stained with hematoxylin, and counterstained with eosin. Affinity-purified rabbit antibodies were used at 5 $\mu\text{g}/\text{ml}$ and monoclonal antibodies at 10 $\mu\text{g}/\text{ml}$ throughout these studies. To rule out unspecific binding of antibodies to tissue sections, antibodies were preincubated (24 h, 4°C) at a 1:4 ratio with the recombinant proteins against which they were made. After such preincubations no staining was evident, also indicating the specificity of the antibodies in immunohistology.

RESULTS

Specificity and Versatility of Antibodies against Recombinant Fragments of Laminin $\alpha 1$ and $\alpha 2$ Chains

Recombinant production in human 293 or 293-EBNA cells was used for several fragments of mouse laminin α chain in order to assure their proper folding and secretion into serum-free culture medium as demonstrated in several previous studies [20, 21, 34]. They included the N-terminal fragments $\alpha 1\text{VI/V}$ and $\alpha 2\text{VI/V}$ from the $\alpha 1$ and $\alpha 2$ chains, respectively, consisting of one LN module (domain VI) and four LE modules from domain V and of one LN and three LE modules in fragments $\alpha 3\text{VI/V}$ and $\alpha 5\text{VI/V}$. They were all ob-

tained in a highly purified form after conventional chromatography, as demonstrated by SDS-gel electrophoresis (Fig. 1). Further fragments studied included $\alpha 1\text{LG4}$, $\alpha 2\text{LG1-3}$, and $\alpha 2\text{LG4-5}$ derived from the C-terminal region of the $\alpha 1$ and $\alpha 2$ chains [21, 34].

These $\alpha 1$ and $\alpha 2$ chain fragments were used to produce rabbit antisera of high titers in ELISA and radioimmunoassays (1:5000 to 1:20,000) against the antigens used for immunization and insignificant cross-reactions (titer $< 1:100$) for homologous fragments from the other chain isoform. In addition we used rat monoclonal antibodies against mouse $\alpha 1\text{LG4-5}$ [38], which did not cross-react with $\alpha 2\text{LG4-5}$ and $\alpha 4\text{LG4-5}$ (Fig. 2). Furthermore, it was possible to establish specific and sensitive radioimmuno-inhibition assays useful for quantitative analyses, as shown for fragments $\alpha 2\text{VI/V}$ and $\alpha 2\text{LG1-3}$ (Fig. 3). The $\alpha 2\text{VI/V}$ assay could be inhibited by 50% at low concentrations of $\alpha 2\text{VI/V}$ ($\text{IC}_{50} =$

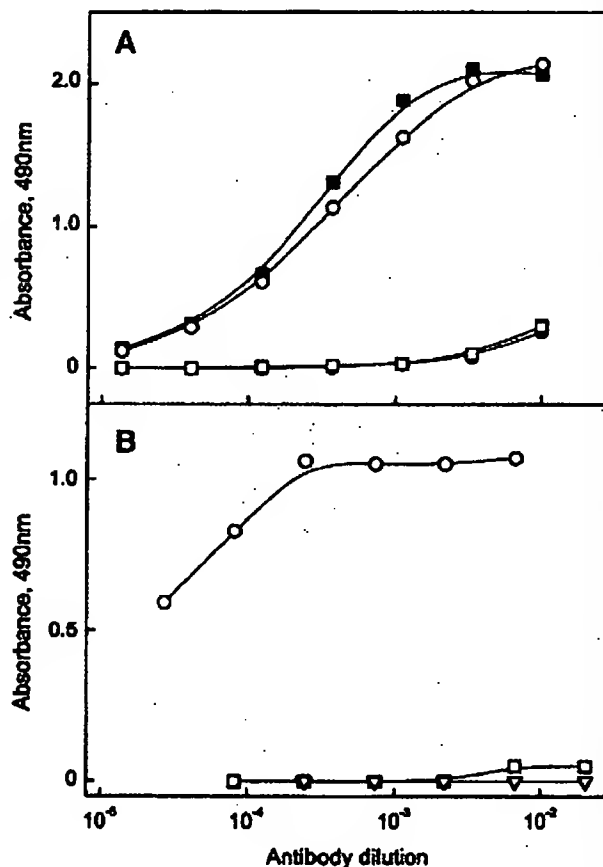


FIG. 2. ELISA titration of affinity-purified antibodies (A) and a rat monoclonal antibody (B) against laminin $\alpha 1$ and $\alpha 2$ chain fragments. The antibodies used were against $\alpha 1\text{VI/V}$ (open symbols) and $\alpha 2\text{VI/V}$ (closed symbols) in (A) and mAb 200 in (B). Antigens used in (A) were recombinant $\alpha 1\text{VI/V}$ (○, ●) and $\alpha 2\text{VI/V}$ (□, ■) and in (B) $\alpha 1\text{LG4-5}$ (○), $\alpha 2\text{LG1-3}$ (□), and $\alpha 4\text{LG4-5}$ (▽). No binding was observed with $\alpha 3\text{VI/V}$, $\alpha 5\text{VI/V}$, and $\alpha 3\text{LG4-5}$. The antibody concentrations were in the range 0.6–1.0 mg/ml .

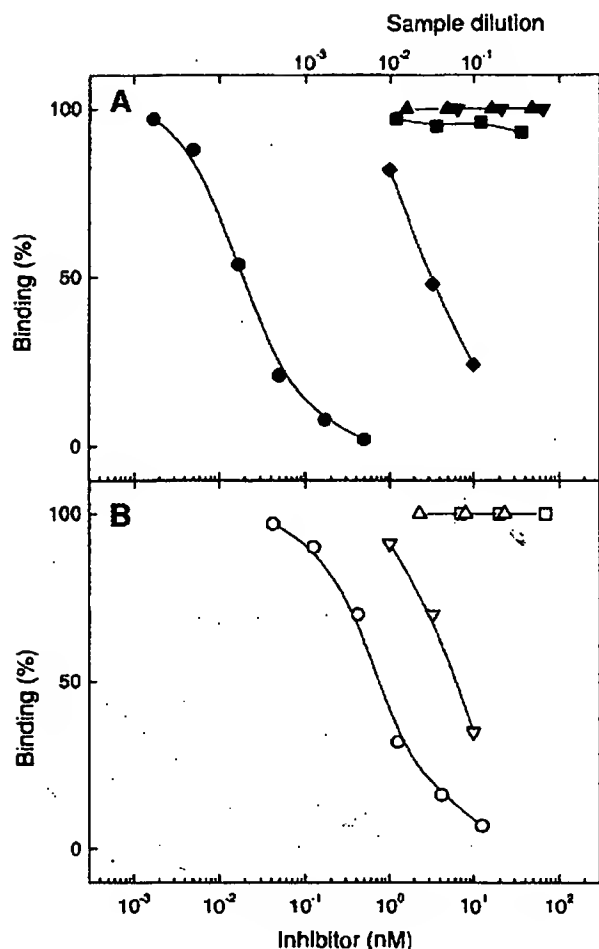


FIG. 3. Radioimmuno-inhibition assays specific for N-terminal (A) and C-terminal (B) fragments of laminin $\alpha 2$ chains. The assays consisted of a 125 I-labeled (1 ng/0.4 ml) fragment $\alpha 2$ VI/V (A) or $\alpha 2$ LG1-3 (B) and a fixed dilution of the corresponding rabbit antisera. Inhibitors of the binding in (A) were fragments $\alpha 2$ VI/V (●), $\alpha 1$ VI/V (■), $\alpha 3$ VI/V (▲), and $\alpha 5$ VI/V (▼) at the concentrations indicated and a mouse kidney EDTA extract (●) used at the dilutions shown on top. Inhibitors in (B) were $\alpha 2$ LG1-3 (○), $\alpha 2$ LG4-5 (□), laminin fragment E8 containing $\alpha 1$ LG1-3 (△), and mouse testis EDTA extract (▽).

0.01 nM), while 10,000-fold higher concentrations of $\alpha 1$ VI/V, $\alpha 2$ VI/V, and $\alpha 5$ VI/V had no effects (Fig. 3A). A similar assay for $\alpha 2$ LG1-3 had a lower sensitivity ($IC_{50} = 0.5$ nM) but was not inhibited by 200-fold higher concentrations of $\alpha 2$ LG4-5 and $\alpha 1$ LG1-3 (Fig. 3B). However, both assays could be clearly inhibited by mouse tissue extracts showing the same dose-response profiles as the reference inhibitors (Fig. 3), indicating that $\alpha 2$ -chain-containing laminins in these extracts have the same affinity for the antibodies as the recombinant fragments [48]. A similar specific assay was established for fragment $\alpha 2$ LG4-5 with $IC_{50} = 0.2$ nM, which could not be inhibited by a 100-fold excess of $\alpha 2$ LG1-3 or $\alpha 1$ LG4-5 (data not shown). Further radio-

immuno-inhibition assays used were described previously [20, 21], including fragments $\alpha 1$ VI/V ($IC_{50} = 0.2$ nM) and $\alpha 1$ LG4 ($IC_{50} = 0.1$ nM), which could be inhibited in an equivalent manner by laminin-1 ($\alpha 1\beta 1\gamma 1$) and as demonstrated now by mouse tissue extracts, while the corresponding $\alpha 2$ chain fragments were inactive ($IC_{50} > 20$ nM). The various antibodies were also useful in analyzing reduced tissue extracts and demonstrated characteristic 300- and 80-kDa bands in adult mouse heart and skeletal muscle by anti- $\alpha 2$ LG1-3 (Fig. 4), consistent with previous observations of an internal proteolytic cleavage within the $\alpha 2$ LG3 module [34]. The $\alpha 1$ -chain-specific antibodies blotted only a 400-kDa band, indicating lack of proteolytic modification. However, antibodies against $\alpha 1$ VI/V and $\alpha 2$ VI/V did not react with $\alpha 1$ and $\alpha 2$ chains after reduction. They were therefore examined by immunoprecipitation followed by immunoblot analysis with antibodies against $\alpha 1$ LG4 and $\alpha 2$ LG1-3 (Fig. 5). This demonstrated in kidney extracts a single 400-kDa $\alpha 1$ chain and two $\alpha 2$ chain bands of about 300 and 70–80 kDa, as shown for muscle (Fig. 4). Only the $\alpha 2$ chain bands could be detected in lung extracts, reflecting the low content of $\alpha 1$ chain as determined by radioimmunoassay (Table 2).

Contents of Protein and mRNA Expression of $\alpha 1$ and $\alpha 2$ Chains in Adult Mouse Tissues

In order to exploit the quantitative analysis of tissue extracts as indicated from radioimmuno-inhibition assays, it was initially important to identify appropriate solubilization conditions. Previous studies with the EHS tumor have shown that almost all of laminin-1 could be solubilized by EDTA-containing neutral buffer followed by a denaturing solvent [51]. We have now used the EHS tumor and adult muscle and kidney, which, after extraction with EDTA and detergent, were subsequently digested to remove glycosaminoglycans followed by treatments with bacterial collagenase and pepsin, which essentially solubilized all of the tissues. Analyses of these extracts by radioimmuno-inhibition assays (Table 1) demonstrated that 71–92% of $\alpha 1$ and $\alpha 2$ chains were already dissolved in the first two extracts. Similar distribution and total yields were also observed for laminin $\gamma 1$ chain based on a recombinant fragment that is stable against pepsin digestion [47].

A larger number of tissues was then analyzed by $\alpha 1$ VI/V and $\alpha 2$ VI/V assays after extraction with EDTA/detergent or EDTA alone (Table 2). The highest amounts of $\alpha 1$ chain were found in placenta, kidney, testis, and liver and exceeded those of the $\alpha 2$ chain. All other tissue extracts showed a higher content of $\alpha 2$ chains, which was particularly high in heart and muscle when compared to that of $\alpha 1$. Extracts of the EHS tumor, which produces only basement membranes and

LAMININ $\alpha 1$ AND $\alpha 2$ CHAINS IN TISSUES

189

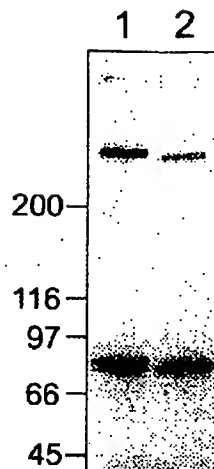


FIG. 4. Immunoblot of mouse tissue extracts with affinity-purified rabbit antibody against $\alpha 2$ LG1-3. Reduced EDTA extracts from heart (lane 1) and skeletal muscle (lane 2) were separated by SDS-gel electrophoresis and the run was calibrated with marker proteins denoted in kDa at the left margin. The prominent band of 70–80 kDa consists of $\alpha 2$ LG4-5 with some part of the $\alpha 2$ LG3 module [34] and is completely released from the $\alpha 2$ chain, which then migrates as a 300-kDa component.

no other extracellular tissue [39], yielded as expected the highest amounts of $\alpha 1$ chain (7620 pmol/g, in good agreement with previous biochemical data (6720 pmol/g; [51])). For a further validation of these data we used in addition several more radioimmuno-inhibition assays specific for LG fragments from the C-terminal region of the laminin $\alpha 1$ and $\alpha 2$ chains (Table 2). This demonstrated a good agreement between $\alpha 1$ VI/V and $\alpha 1$ LG4 assays for heart, muscle, kidney, testis, and brain. A reasonable agreement within the usual variability of such assays (20–30%; [48]) was also found,

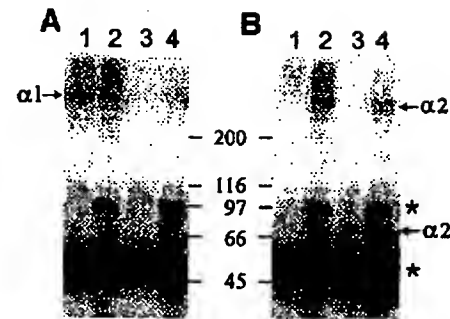


FIG. 5. Immunoblot detection of laminin $\alpha 1$ and $\alpha 2$ chains after immunoprecipitation of mouse kidney and lung extracts. Detergent extracts of adult kidney (lanes 1, 2) and lung (lanes 3, 4) were immunoprecipitated with purified antibodies against $\alpha 1$ VI/V (lanes 1, 3) or $\alpha 2$ VI/V (lanes 2, 4) and after SDS-gel electrophoresis of the precipitates under reducing conditions blotted with purified antibodies against $\alpha 1$ LG4 (A) or $\alpha 2$ LG1-3 (B). The asterisks denote the immunoglobulin heavy chain 50- and 100-kDa bands reacting with the secondary anti-IgG antibodies. Only these bands are seen if the blotting antibodies are omitted (not shown).

except for kidney between $\alpha 2$ VI/V and $\alpha 2$ LG1-3 assays. With an assay specific for $\alpha 2$ LG4-5 some twofold higher amounts were detected in muscle and heart compared to the $\alpha 2$ LG1-3 assay. This apparently reflects some higher solubility of the C-terminal $\alpha 2$ LG4-5 structure, which in these tissues is already completely released by proteolysis (Fig. 4). All these tissue extracts were also analyzed by the $\gamma 1$ chain assay (Table 1 and data not shown) which is shared by most laminins, including those containing $\alpha 1$ and $\alpha 2$ chains [7]. This demonstrated $\gamma 1$ chain levels being equal to or moderately exceeding the sum of $\alpha 1$ and $\alpha 2$ chains, indicating that these isoforms represent the major laminins in adult mouse tissues so far examined.

Previous studies by RNase protection assay demon-

TABLE 1

Amounts of Laminin $\gamma 1$, $\alpha 1$, and $\alpha 2$ Chain Solubilized by Successive Extractions from Mouse Tissues

Extraction step	Percentage of total extractable					
	EHS tumor		Skeletal muscle		Kidney*	
	$\gamma 1$ III	$\alpha 1$ VI/V	$\gamma 1$ III	$\alpha 2$ VI/V	$\alpha 1$ VI/V	$\alpha 2$ VI/V
EDTA	68	79	65	67	58	54
Detergent	21	13	14	19	13	22
HS/CS	3	3	10	7	11	8
Collagenase	7	5	11	6	18	16
Pepsin	1	n.d.	<1	n.d.	n.d.	n.d.
Total (pmol/g)	7821	8250	153	110	87	24

Note. The extracts were obtained by neutral buffer containing EDTA, followed by detergent and digestions with heparitinase/chondroitinase (HS/CS), bacterial collagenase, and pepsin. Contents were determined by radioimmuno-inhibition assays specific for recombinant fragments of the three laminin chains. n.d., not determined.

* The total content in the $\gamma 1$ III assay was 167 pmol/g.

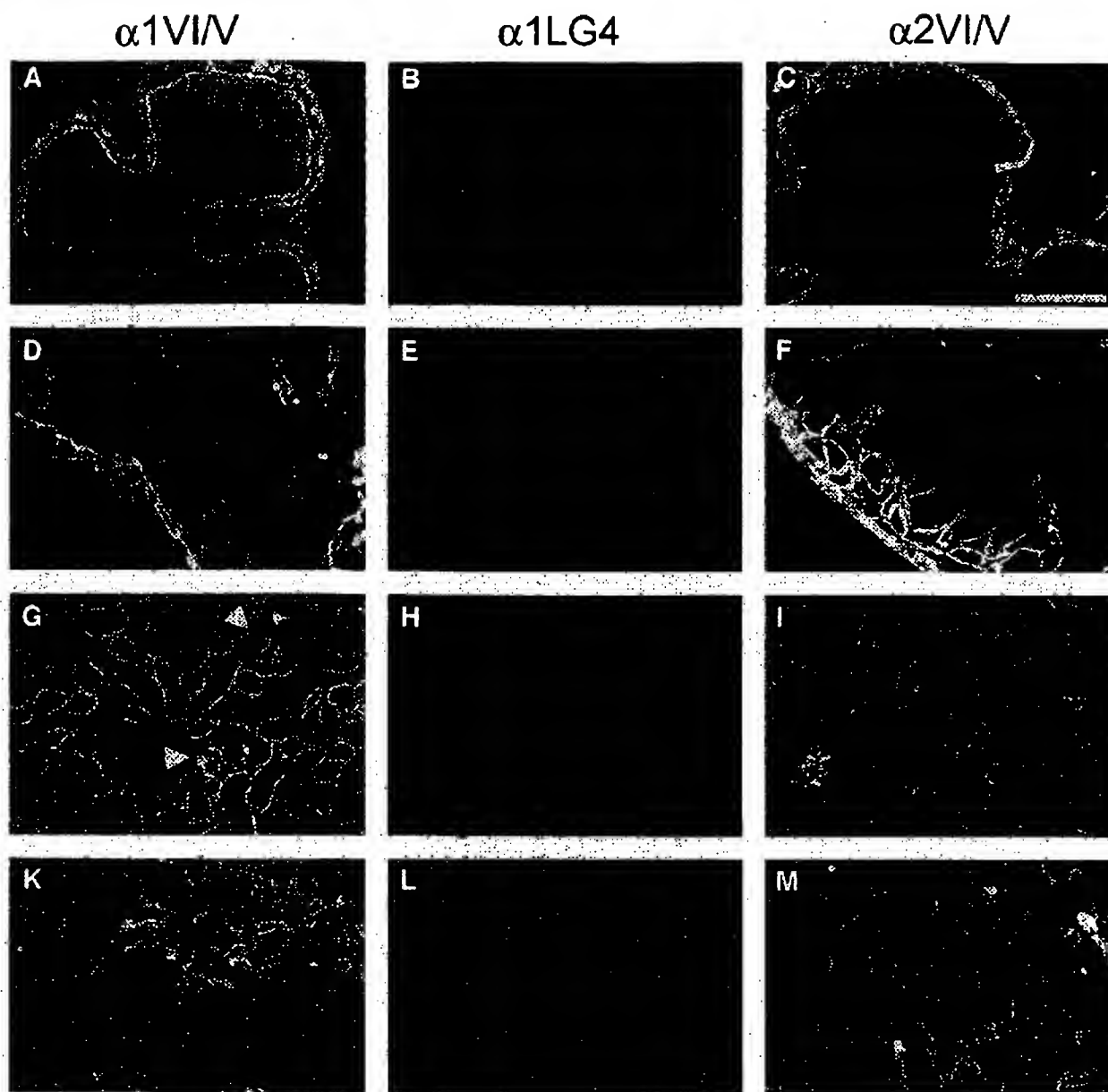


FIG. 8. Immunofluorescence staining of cryosections from adult mouse tissues and evidence for epitope masking in (A–C) lower esophagus, (D–F) intestine, (G–I) kidney, (K–M) spleen. Double stainings were done with mAb 200 (B, E, H, L) reacting with laminin $\alpha 1\text{LG4}$ and polyclonal rabbit antibody against laminin $\alpha 2\text{VI/V}$ (C, F, I, M) and staining of consecutive sections with polyclonal rabbit antibody against laminin $\alpha 1\text{VI/V}$ (A, D, G, K). In these tissues no staining for laminin $\alpha 1$ could be detected with mAb 200 or in kidney only in a subset of tubuli (H). With a polyclonal antibody against $\alpha 1\text{VI/V}$ staining of laminin $\alpha 1$ could be detected in the epithelial basement membrane of lower esophagus (A), the crypt of intestine (D), in glomerular basement membranes (arrowheads indicate glomeruli) and along tubuli of kidney (G), and in spleen (K). Laminin $\alpha 2$ was readily detected in the smooth muscle layer of lower esophagus (C) and intestine (F), the crypt basement membrane, blood vessels surrounding the digestive tract and blood vessels of villi (F), and kidney (I). Laminin $\alpha 2$ was also detected in kidney glomeruli (I) and in spleen (M). Bar, 100 μm .

rected against domain VI/V of $\alpha 1$ chain (not shown), whereas $\alpha 2$ chain was seen only in maternal tissue surrounding the placenta (Fig. 6B). Later in embryonic development both isoforms could be detected around neural tissue. At 11.5 days of development both $\alpha 1$ and

$\alpha 2$ chains were expressed in basement membranes surrounding spinal cord (Figs. 6C and 6D) and in the meninges. At higher magnification it was possible to see how blood vessels growing into the brain stained positive for $\alpha 2$, whereas no staining for $\alpha 1$ could be

LAMININ $\alpha 1$ AND $\alpha 2$ CHAINS IN TISSUES

193

TABLE 4

Amounts of Laminin $\alpha 1$ and $\alpha 2$ Chain Determined by Radioimmuno-inhibition Assays in Embryonic Tissues

Tissue extract (day)	Content (pmol/g wet tissue) in assay for		
	$\alpha 1$ VI/V	$\alpha 2$ VI/V	$\gamma 1$ III
Embryo (11)	25	<1	16
Embryo (13)	28	3	21
Body (18)*	<0.3	25	36
Brain (18)	6	2	2
Heart (18)	<0.5	17	30
Kidney (18)	127	20	144
Liver (18)	6	2	15
Lung (18)	13	12	66

Note. All tissues were extracted by EDTA followed by detergent.
* Remaining tissues after removal of the organs listed below.

detected in these blood vessels (Figs. 6E and 6F). Apart from meninges, the only other area in day 11.5 embryos where expression of both isoforms could be detected was skin. Endocardial cushion tissue and primordial heart were negative for both laminin isoforms (not shown), whereas dorsal aorta stained positive for $\alpha 2$ chain, but negative for $\alpha 1$ chain (Figs. 6G and 6H). In the digestive system, exemplified by stomach, $\alpha 1$ was detected in basement membranes underlying epithelial cells, as was a very faint expression of $\alpha 2$ (Figs. 6I and 6K). In mesonephros $\alpha 1$ chain staining could be seen, but only very weak staining for $\alpha 2$ was detected (Figs. 6L and 6M). Overall, epithelial structures expressed laminin $\alpha 1$ at an early stage, whereas laminin $\alpha 2$ was expressed in the vicinity of blood vessels at this stage.

Adult mouse tissues were double stained with mAbs against laminin $\alpha 1$ chain (198, 200) and polyclonal antibodies against laminin $\alpha 2$ chain (domains VI/V or LG1-3). In some organs, here exemplified by liver, the monoclonals directed against $\alpha 1$ LG4 did not stain under immunofluorescence (Fig. 7A), but when tissues were pretreated with protease for immunohistochemistry we saw staining (Fig. 7D). Single staining with polyclonal antibodies directed against domain VI/V of $\alpha 1$ chain (Fig. 7B) as well as immunofluorescence staining using monoclonals directed against $\alpha 1$ LG4 after protease pretreatment (Fig. 7C) were made to ascertain if epitope masking occurred. Both staining patterns were in agreement with immunohistochemistry data. We therefore conclude that epitope masking of laminin $\alpha 1$ LG4 occurs.

In liver, $\alpha 1$ chain was seen along sinusoids in the space of Disse (Figs. 7B-7D). This is interesting since the sinusoidal lining cells are an endothelium continuous with the endothelium of the central vein. This would be one of the few endothelia where laminin $\alpha 1$ is

expressed. Laminin $\alpha 2$, on the other hand, was seen only along blood vessels in liver (Figs. 7E and 7F). Organs other than liver where we found evidence for epitope masking were esophagus, intestine, kidney, spleen (Figs. 8A-8M), and stomach (not shown). In those organs we could detect $\alpha 1$ chain in immunofluorescence with a polyclonal antibody directed against $\alpha 1$ VI/V. In the digestive system no laminin $\alpha 1$ could be detected with monoclonal antibodies directed against the G domain (Figs. 8B and 8E). However, when using antisera directed against domain $\alpha 1$ VI/V, epithelial basement membranes of lower esophagus (Fig. 8A), stomach (not shown), and small intestine (Fig. 8D) were positive. Laminin $\alpha 2$ was readily detected in the smooth muscle layer surrounding lower esophagus (Fig. 8C), stomach (not shown), and small intestine (Fig. 8F). Laminin $\alpha 2$ was also detected in basement membrane of the crypt, blood vessels surrounding the digestive tract, and blood vessels of intestinal villi (Fig. 8F). In kidney, $\alpha 2$ chain was detected in glomeruli and around blood vessels (Fig. 8I). Using an antibody specific for domain VI/V we saw $\alpha 1$ chain staining in basement membranes surrounding glomeruli as well as in tubuli (Fig. 8G). Organs of the immune system were also examined. Lymph nodes and thymus stained only weakly for $\alpha 1$ chains, with a little more staining for $\alpha 2$ chains (not shown). Spleen stained strongly for laminin $\alpha 2$ chain (Fig. 8M), not at all with antibody against $\alpha 1$ LG4 (Fig. 8L) and moderately with antibody against $\alpha 1$ VI/V (Fig. 8K).

In order to give visibility to the tissue, some organs were selected for immunohistochemistry. They were

TABLE 5

Production of Laminin $\alpha 1$ and $\alpha 2$ Chains by Cultured Mouse and Rat (R) Cell Lines

Tissue (extract)		Assay specific for	
		$\alpha 1$ VI/V	$\alpha 2$ VI/V
Myoblast	M	<0.1	2.0
	C	0.27	0.28
Fibroblast	M	1.8	0.4
Pam 212	M + C	<0.1	<0.1
Day 7.5 EC	M	12	<0.1
	C	9.6	<0.05
IBE EC	M	<0.06	0.8
eEnd.2 EC	M	0.7	0.2
PYS-2	M	93	<0.1
F9	M	1.2	<0.03
F9 stimulated	M	25	<0.03
RN 22 Schwannoma (R)	M	<0.06	2.0
Rugli glioma (R)	M	1.1	<0.3

Note. The amounts were determined by radioimmuno-inhibition assays specific for domains VI/V and are expressed as pmoles present in the medium (M) and cell lysate (C) of a 6-cm culture plate. EC, endothelial cells.

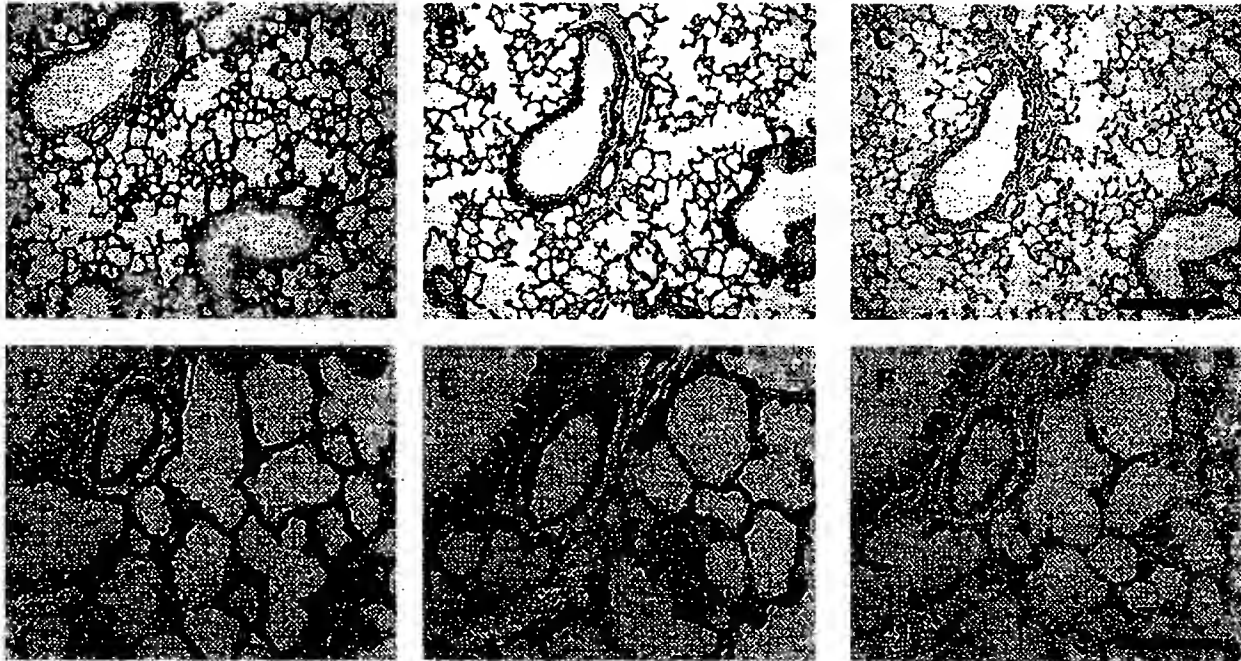


FIG. 9. Immunoperoxidase staining of paraffin-embedded sections from adult mouse lung. Stainings were done with mAb 198 (A, D) against laminin α 1LG4, polyclonal rabbit antibody against laminin α 2LG1-3 (B, E), and control rat IgG (C, F). Laminin α 1 was seen beneath epithelial cells of terminal and respiratory bronchioles, alveolar ducts, and alveoli (A, D). Laminin α 2 was present in the layer of smooth muscle lining terminal bronchioles, smooth muscle controlling opening of alveoli, veins, and arteries (B, E). Basement membranes of the blood-air barrier contain both laminin α 1 and α 2 (D, E). Sections were stained with hematoxylin and counterstained with eosin. Bar, for A-C, 200 μ m and 50 μ m for D-F.

stained with antibodies against α 2LG1-3 and α 1LG4 after protease treatment. In lung, α 1 chain was seen beneath epithelial cells of bronchioles and along epithelial cells of respiratory bronchioles, alveolar ducts, and alveoli (Figs. 9A and 9D). Laminin α 2 was present in the layer of smooth muscle lining terminal bronchioles, smooth muscle controlling opening of alveoli, and in veins and arteries (Figs. 9B and 9E). The basement membrane between epithelial and endothelial cells of the blood-air barrier appeared to contain both α 1 and α 2 chains. No unspecific staining was seen when sections were incubated with control rat IgG (Figs. 9C and 9F). Adrenal gland showed positive staining for both α 1 and α 2 chains in the capsule. The cortex was weakly positive for both laminin isoforms, with the most staining around cells of zona glomerulosa and zona fasciculata. The medulla was heavily stained for α 2 chain (not shown).

In some tissues the staining patterns for α 1 chain agreed better with those of previous studies and no evidence for epitope masking were obtained allowing double staining with the mAbs 198 and 200. In adult mouse brain, meninges were positive for both α 1 and α 2 chain (Figs. 10A and 10B) as in brain of early embryo. Blood vessels were positive for laminin α 2 (Fig. 10B) and interestingly some medium-sized blood vessels stained positive for both α 1 and α 2 (Figs. 10A

and 10B). In embryonic brain, we could see that blood vessels growing into the brain stained positive for α 2 chain, whereas no staining for α 1 chain could be detected in these blood vessels. Since expression of α 1 in the adult was seen only in larger vessels, a likely explanation is that invaginated epithelial cells located here are the source of detected α 1 chain. In testis both α 1 and α 2 chains were expressed in basement membranes surrounding seminiferous tubules (Figs. 10C and 10D). Laminin α 2 could also be detected around blood vessels in fibromuscular walls between seminiferous tubules (Fig. 10D). In heart and skeletal muscle no α 1 chain could be detected, whereas strong staining for α 2 chain was seen (Figs. 10E-10I). Thyroid gland stained strongly for both laminin α 1 (Fig. 10K) and α 2 (Fig. 10L). In pancreas connective tissue septa surrounding each acinus and along ducts were heavily stained for α 2 chain (Fig. 10N), whereas no staining could be detected for α 1 chain (Fig. 10M).

DISCUSSION

Since the discovery of the laminin α 2 chain in the form of a fragment derived from human placenta [5] a comparison of its expression and deposition with that of the α 1 chain has been an attractive way to approach the understanding of potential differences in their

LAMININ $\alpha 1$ AND $\alpha 2$ CHAINS IN TISSUES

195

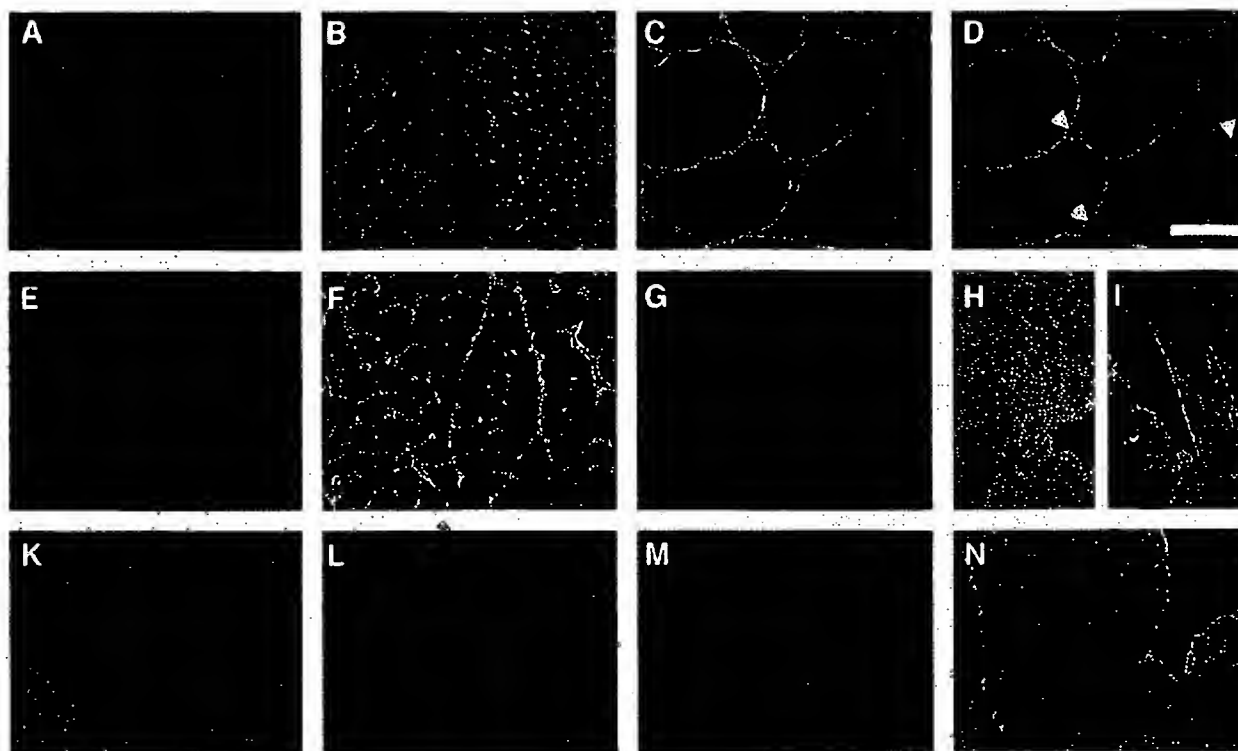


FIG. 10. Immunofluorescence staining of cryosections from adult mouse tissues from (A, B) brain, (C, D) testis, (E, F) muscle, (G, H) heart, (I, J) heart sagittal sections, (K, L) thyroid gland, and (M, N) pancreas. Double stainings were done with mAb 198 (A, C, E, G, M) or with mAb 200 (K) both reacting with laminin $\alpha 1$ LG4 and polyclonal rabbit antibody against laminin $\alpha 2$ LG1-3 (B, D, F, H, N) or laminin $\alpha 2$ VI/V (L). Polyclonal rabbit antibody against $\alpha 2$ LG1-3 was also used to stain heart sagittal sections (I). In brain, meninges were positive for both laminin $\alpha 1$ and $\alpha 2$ (A, B) as in the early embryo brain. Blood vessels of the brain were positive for laminin $\alpha 2$ (B) and interestingly some blood vessels stained positive for both $\alpha 1$ and $\alpha 2$ (A, B). In testis both laminins $\alpha 1$ and $\alpha 2$ were expressed in basement membranes surrounding seminiferous tubules (C, D). Laminin $\alpha 2$ could also be detected around blood vessels (arrowheads) in fibromuscular walls between seminiferous tubules (D). In skeletal muscle and heart no laminin $\alpha 1$ could be detected (E, G), whereas strong staining for $\alpha 2$ was seen (F, H, I). Thyroid gland stained strongly for both laminins $\alpha 1$ (Fig. 6K) and $\alpha 2$ (Fig. 6L). In pancreas the connective tissue septa surrounding each acinus and along ducts were heavily stained for laminin $\alpha 2$ (N), whereas no staining could be detected for laminin $\alpha 1$ (M). Bar: 200 μ m for A, B, E-I and 100 μ m for C, D, K-N.

functions. All previous studies were based on immunostaining at the light microscopy level, *in situ* hybridization, and some analyses of mRNA levels [reviewed in 7, 29]. We have now added more quantitative aspects to these studies by using polyclonal antibodies against recombinant laminin fragments, highly specific for the $\alpha 1$ or $\alpha 2$ chains, respectively, as shown by various immunochemical assays. There were also no cross-reactions with laminin $\alpha 3$ B, $\alpha 4$, and $\alpha 5$ chain fragments so far examined. It was further shown that extraction of tissues with EDTA-containing neutral buffer, which should solubilize noncovalently linked networks of laminins [19, 51], followed by detergent is already sufficient to solubilize a large portion of the laminins containing $\alpha 1$ and $\alpha 2$ chains. However, this may not be the case for all tissues and might need further examinations.

Using radioimmuno-inhibition assays specific for different domains of both α chains, the amounts determined in several adult tissue extracts were comparable

within a factor of 2. Furthermore, the sum of both α chains did not, in most cases, exceed the content of $\gamma 1$ chain shared by all $\alpha 1/\alpha 2$ -containing laminins and serving as an internal control. Together, our data indicate that these radioimmunoassays allow reliable quantitations of laminins in tissue extracts. The content of extractable $\alpha 2$ chain was highest in heart and muscle (150–300 pmol/g), while the content of $\alpha 1$ chain was more than 100-fold lower, in agreement with several previous and our immunostaining results. All other tissues showed lower contents of $\alpha 2$ chain accompanied by variable amounts of $\alpha 1$ chain, exceeding or equivalent to those of $\alpha 2$ chain levels only in liver, testis, and kidney. In most cases similar relationships were also found for $\alpha 1$ and $\alpha 2$ mRNA by quantitative RT-PCR, demonstrating continuous synthesis of $\alpha 1$ chain, although at relatively low levels, not detected in previous studies [30]. The extractable amount of $\alpha 1$ chain was below 10% of the level of extractable $\alpha 2$ chain only in heart, muscle, lung, and stomach. Con-

sidering that both chains share quite a few similar functions it suggests that the concentration of $\alpha 1$ chain in most adult tissues is still high enough to compensate for $\alpha 2$ chain deficiency or mutations in mice which show normal development and subsequently only a restricted phenotype after birth [52, 53].

The $\alpha 1$ chain is apparently the first laminin α chain produced during early mouse embryogenesis and also seems to be a prominent component in most tissues at some later developmental stages [26], in agreement with relatively high tissue contents in embryos determined by quantitative assays (Table 4). The $\alpha 2$ chain, however, was barely detectable in day 11 embryos but increased steadily during subsequent embryonic stages, even though not approaching the amounts found in adult organs. Consistent with these observations is the high and exclusive production of $\alpha 1$ chains in early embryonic cell lines (F9, PYS-2, endothelial progenitor cells). The F9 teratocarcinoma cells were previously shown to synthesize mainly laminin-1 and considerably increased production upon stimulation to differentiate into parietal endoderm [43, 54]. However, this was not accompanied by a significant production of $\alpha 2$ chain, as shown here by radioimmunoassays. Another interesting aspect relates to laminin synthesis by endothelial cells which, as shown for two other cell lines, produce either $\alpha 2$ exclusively or both α chains simultaneously. Together with some immunostaining data (see below) it emphasizes a role of $\alpha 1$ chain laminins during early stages of angiogenesis, which deserve a closer examination. In this context it is also of interest that mouse placenta showed a high content of $\alpha 1$ chain (480 pmol/g) but only little $\alpha 2$ chain. This was also indicated by similar differences in mRNA [30] and placenta would thus be an ideal substrate for comparing maternal and embryo-derived capillaries. However, such patterns may be different in other species, as indicated by the high yields of $\alpha 2$ chain laminins obtained from human placenta [5, 55].

Laminin $\alpha 2$ was mainly found in the vicinity of mesoderm-derived cells. Knockout experiments and naturally occurring mutations have shown that development progress without the $\alpha 2$ chain [52, 53]. Myogenesis occurs in two waves in the mouse, one at approximately 10–14 days of embryonic development and another between day 16 of embryonic development and day 3 of postnatal life [56]. We found expression of laminin $\alpha 2$ in blood vessels at 11.5 days of development, whereas expression in muscle tissue appeared later. One previous study found weak expression of $\alpha 1$ at myotendinous junctions and $\alpha 2$ in a patchy basement membrane coating myotubes at this early stage [31], whereas other studies find no $\alpha 1$ chain expression and no or weak $\alpha 2$ chain expression [57, 58]. In humans, laminin $\alpha 1$ chain is expressed at myotendinous junctions at 8 weeks of gestation [59]. Here, we found

no expression of either laminin $\alpha 1$ or $\alpha 2$ chains. However, primary myoblasts in culture expressed small amounts of $\alpha 2$ chain. As the shift from $\alpha 1$ -chain-positive somite basement membranes [29] to $\alpha 2$ -chain-positive sarcolemmal basement membranes occurs around this time, exact developmental stage could lead to different results. Another possibility is that we failed to detect the very faint expression detected by others [31, 59]. In various human congenital muscle dystrophies there is an absence or reduced levels of laminin $\alpha 2$. In *dy/dy* mice, laminin $\alpha 2$ chain is also absent [60]. In spite of this, development occurs normally, indicating that laminin $\alpha 2$ is not crucial for myogenesis during development. Rather, this molecule appears to be required for maintenance of the differentiated phenotype, since gross symptoms of muscular dystrophy in laminin $\alpha 2$ knockout mice [53] and *dy/dy* mice [52] appear only after myogenic events are complete. Similarly, early endothelial cells *in vivo* or in culture did not express laminin $\alpha 2$ before formation of the vasculature.

In the digestive system $\alpha 2$ chain was detected in smooth muscle and in vasculature. No $\alpha 1$ chain could be detected in the epithelial basement membrane of the crypt using mAbs directed against the C-terminal globular domain. However, we showed the presence of laminin $\alpha 1$ mRNA by real-time PCR and protein by radioimmuno-inhibition assay and using antibodies directed toward the N-terminal part of $\alpha 1$ chain. Earlier studies have shown the absence [27] of laminin $\alpha 1$ in this location. A distinct possibility is that the epitopes recognized by mAbs 198 and 200 located on $\alpha 1$ LG4 are masked in intestine. Both antibodies were previously shown to bind only weakly to some $\alpha 1$ LG4 mutants which showed a strong reduction of heparin/ α -dystroglycan interaction, suggesting a considerable overlap with the antibody binding epitope [21]. In fact, mAb 200 inhibits the binding of $\alpha 1$ LG4–5 to α -dystroglycan [61]. Together with the ability of such antibodies to block the binding of heparin and cell adhesion [38] it indicates that occupation of $\alpha 1$ LG4 by proteoglycans or cellular receptors could be responsible for masking the antigenic epitope, particularly in tissues of the digestive system. As shown for liver, a brief proteolytic treatment causes exposure of this epitope. In kidney, $\alpha 2$ chain was detected in glomeruli, in agreement with an earlier comprehensive study of the differential expression of laminin α chains in kidney [62]. Laminin $\alpha 2$ was also found around blood vessels. This is not in agreement with results from the same study. Using an antibody specific for domain VI/V we saw $\alpha 1$ chain staining in glomerular basement membranes as well as in tubuli, also not in complete agreement with earlier results [62]. Moreover, the data from quantitative PCR and radioimmuno-inhibition assays support the strong basement membrane staining of $\alpha 1$ chain in adult kid-

ney seen here. Both of these differences could be due to the fact that our antibodies reacted with the N-terminal parts of the α chains.

Other organs where we detected $\alpha 1$ chain expression with antibodies against the N-terminal domains VI/V and not with antibodies against $\alpha 1$ LG4 were liver and spleen. The expression pattern of laminins in mouse liver has until now received only cursory examination [27]. In liver, $\alpha 1$ chain was deposited along sinusoids in the space of Disse. Investigations in rat have shown that laminins are expressed during gestation and disappear from this region by 6 to 8 weeks of postnatal life, to reappear only during hepatic regeneration [63]. However, others have found laminin to be localized on sinusoidal surfaces in both normal and regenerating hepatic parenchyma [64]. This controversy could perhaps in some part be explained by epitope masking, as shown for laminin $\alpha 1$ here.

High or very high expression of laminin $\alpha 2$ was found in some organs previously not reported for mouse, notably pancreas and adrenal and thyroid glands. An earlier study showing $\alpha 2$ chain expression in pancreas was done on the mRNA level on human fetal tissues [65] and porcine thyroid glands have also been shown to express $\alpha 2$ chains [66]. Laminin $\alpha 1$ chain expression was recently found in adrenal gland cortex [27], but expression of $\alpha 2$ chain was not examined before.

Laminin $\alpha 1$ deposited at epithelial-mesenchymal boundaries has been shown to be important for lung development [67]. However, earlier studies have only detected $\alpha 1$ chain expression in fetal [67, 68] and not in adult [27, 30] tissues. Here, we show that $\alpha 1$ chain is expressed in adult lung by both quantitative RT-PCR and immunohistochemistry. However, only small amounts are deposited as detected by radioimmuno-inhibition assay and immunoblotting. More recently, $\alpha 2$ chain was identified in developing human [65, 69] and adult mouse [16] lung. We found $\alpha 2$ chain in the layer of smooth muscle lining terminal bronchioles, in smooth muscle controlling the opening of alveoli, and in veins and arteries. Colocalization of $\alpha 1$ and $\alpha 2$ chains was seen only in the basement membrane between epithelial and endothelial cells of the blood-air barrier. In several muscular dystrophies in which respiratory problems lead to early death the underlying cause is laminin-2 deficiency [70]. However, it is still unclear whether this is due to poor ventilation with a skeletal muscle defect as the cause or a primary defect in lung smooth muscle.

Taken together, our results would suggest that laminin $\alpha 2$ chain is expressed by differentiated mature cells of mesodermal origin, while laminin $\alpha 1$ chain is highly expressed by developing epithelial cells, with some residual expression in mature epithelial cells. They would also suggest that this hitherto undetected $\alpha 1$

chain expression is high enough that it perhaps could, to some degree, compensate for deficiencies in other α chains [7] if it is produced in the right tissue compartment. The quantitative analysis of the production of other laminin α chains relative to $\alpha 1$ and $\alpha 2$ chains remains an open issue. By using similar experimental approaches we have now developed specific radioimmunoassays for the $\alpha 3$, $\alpha 4$, and $\alpha 5$ chains and used them to determine contents in adult mouse tissue extracts [71, 72]. The data indicated that in most tissues analyzed here (Table 2) laminins containing $\alpha 1$ or $\alpha 2$ chains are the major products. Exceptions were skin and intestine, which contained the $\alpha 3$ chain as major component, while only a few more tissues (lung, stomach, placenta) had a relatively high proportion of $\alpha 4$ and $\alpha 5$ chains. However, further studies are required to outline the significance of such differences with regard to the biological functions of these laminins.

We are grateful for the expert technical assistance of Mischa Reiter and Sabine Sass and thank Peter Ekblom for discussions. We also thank Lydia Sorokin for monoclonal antibodies against laminin $\alpha 1$ chain. This work was supported by grants from Kungliga Fysiografiska Sällskapet i Lund and The Swedish Natural Science Research Council (both to J.F.T.), from Alice och Knut Wallenbergs stiftelse (to U.T.), and by the Deutsche Forschungsgemeinschaft (Ti 95/8-1) and EC Project QLK3-CT2000-00084 (both to R.T.).

REFERENCES

1. Timpl, R. (1996). Macromolecular organization of basement membranes. *Curr. Opin. Cell Biol.* 8, 618-624.
2. Timpl, R., and Brown, J. C. (1996). Supramolecular assembly of basement membranes. *Bioessays* 18, 123-132.
3. Timpl, R., Rohde, H., Robey, P. G., Rennard, S. I., Foidart, J. M., and Martin, G. R. (1979). Laminin—A glycoprotein from basement membranes. *J. Biol. Chem.* 254, 9933-9937.
4. Chung, A. E., Jaffe, R., Freeman, I. L., Veignes, J.-P., Bragin-ski, J. E., and Carlin, B. (1979). Properties of a basement membrane-related glycoprotein synthesized in culture by a mouse embryonal carcinoma-derived cell line. *Cell* 16, 277-287.
5. Leivo, I., and Engvall, E. (1988). Merosin, a protein specific for basement membranes of Schwann cells, striated muscle, and trophoblast, is expressed late in nerve and muscle development. *Proc. Natl. Acad. Sci. USA* 85, 1544-1548.
6. Ehrig, K., Leivo, I., Argraves, W. S., Ruoslahti, E., and Engvall, E. (1990). Merosin, a tissue-specific basement membrane protein, is a laminin-like protein. *Proc. Natl. Acad. Sci. USA* 87, 3264-3268.
7. Colognato, H., and Yurchenco, P. D. (2000). Form and function: The laminin family of heterotrimers. *Dev. Dyn.* 218, 213-234.
8. Yurchenco, P. D. (1994). Assembly of laminin and type IV collagen into basement membrane networks. In "Extracellular Matrix Assembly and Structure" (P. D. Yurchenco, D. E. Birk, and R. P. Mecham, Eds.), pp. 351-388, Academic Press, San Diego.
9. Smalheiser, N. R. (1993). Cranin interacts specifically with the sulfatide binding domain of laminin. *J. Neurosci. Res.* 36, 528-538.
10. Yamada, Y., Shimizu, T., Tanaka, T., Campbell, K. P., and Matsumura, K. (1994). Dystroglycan is a binding protein of

- laminin and merosin in peripheral nerve. *FEBS Lett.* **352**, 49-53.
11. Aumailley, M., Gimond, C., and Rousselle, P. (1996). Integrin-mediated cellular interactions with laminin. In "The Laminins" (P. Ekblom and R. Timpl, Eds.), pp. 127-158. Harwood Academic, Reading.
 12. Klein, G., Langegger, M., Timpl, R., and Ekblom, P. (1988). Role of laminin A chain in the development of epithelial cell polarity. *Cell* **55**, 331-341.
 13. Foster, R. F., Thompson, J. M., and Kaufman, S. J. (1987). A laminin substrate promotes myogenesis in rat skeletal muscle cultures: Analysis of replication and development using anti-desmin and anti-BrdUrd monoclonal antibodies. *Dev. Biol.* **122**, 11-20.
 14. Vochon, P. H., Loechel, F., Xu, H., Wewer, U. M., and Engvall, E. (1996). Merosin and laminin in myogenesis: Specific requirements for merosin in myotube stability and survival. *J. Cell Biol.* **134**, 1483-1497.
 15. Reichardt, L. F., and Tomaselli, K. J. (1991). Extracellular matrix molecules and their receptors: functions in neural development. *Annu. Rev. Neurosci.* **14**, 531-570.
 16. Bernier, S. M., Utani, A., Sugiyama, S., Dori, T., Polistina, C., and Yamada, Y. (1994). Cloning and expression of laminin $\alpha 2$ chain (M-chain) in the mouse. *Matrix Biol.* **14**, 447-455.
 17. Colognato-Pyke, J., O'Rear, J. J., Yamada, Y., Carbonetto, S., Cheng, Y.-S., and Yurchenco, P. D. (1995). Mapping of network-forming, heparin-binding, and $\alpha 1 \beta 1$ integrin-recognition sites within the α -chain short arm of laminin-1. *J. Biol. Chem.* **270**, 9398-9406.
 18. Colognato, H., MacCarrick, M., O'Rear, J. J., and Yurchenco, P. D. (1997). The laminin $\alpha 2$ -chain short arm mediates cell adhesion through both the $\alpha 1 \beta 1$ and $\alpha 2 \beta 1$ integrins. *J. Biol. Chem.* **272**, 29330-29336.
 19. Cheng, Y.-S., Champliand, M.-F., Burgesson, R. E., Marinkovich, M. P., and Yurchenco, P. D. (1997). Self-assembly of laminin isoforms. *J. Biol. Chem.* **272**, 31525-31532.
 20. Eitner, N., Göhring, W., Sasaki, T., Mann, K., and Timpl, R. (1998). The N-terminal globular domain of the laminin $\alpha 1$ chain binds to $\alpha 1 \beta 1$ and $\alpha 2 \beta 1$ integrins and the heparan sulfate-containing domains of perlecan. *FEBS Lett.* **430**, 217-221.
 21. Andac, Z., Sasaki, T., Mann, K., Brancaccio, A., Deutzmann, R., and Timpl, R. (1999). Analysis of heparin, α -dystroglycan and sulfate binding to the G domain of laminin $\alpha 1$ chain by site-directed mutagenesis. *J. Mol. Biol.* **287**, 253-264.
 22. Talts, J. F., Andac, Z., Göhring, W., Brancaccio, A., and Timpl, R. (1999). Binding of the G domains of laminin $\alpha 1$ and $\alpha 2$ chains and perlecan to heparin, sulfates, α -dystroglycan and several extracellular matrix proteins. *EMBO J.* **18**, 863-870.
 23. Ng, V., Zanazzi, G., Timpl, R., Talts, J. F., Salzer, J. L., Brennan, P. J., and Rambukkana, A. (2000). Role of the cell wall phenolic glycolipid-1 in the peripheral nerve predilection of *Mycobacterium leprae*. *Cell* **103**, 511-524.
 24. Talts, J. F., and Timpl, R. (1999). Mutation of a basic sequence in the laminin $\alpha 2$ LG3 module leads to lack of proteolytic processing and has different effects on $\beta 1$ integrin-mediated cell adhesion and α -dystroglycan binding. *FEBS Lett.* **458**, 319-323.
 25. Dziadek, M., and Timpl, R. (1985). Expression of nidogen and laminin in basement membranes during mouse embryogenesis and in teratocarcinoma cells. *Dev. Biol.* **111**, 372-382.
 26. Ekblom, P., Durbeej, M., and Ekblom, M. (1996). Laminin isoforms in development. In "The Laminins" (P. Ekblom and R. Timpl, Eds.), pp. 185-216. Harwood Academic, Reading.
 27. Falk, M., Ferletta, M., Forsberg, E., and Ekblom, P. (1999). Restricted distribution of laminin $\alpha 1$ chain in normal adult mouse tissues. *Matrix Biol.* **18**, 557-568.
 28. Virtanen, I., Gullberg, D., Rissanen, J., Kivilaakso, E., Kiviluoto, T., Laitinen, L. A., Lehto, V.-P., and Ekblom, P. (2000). Laminin $\alpha 1$ -chain shows a restricted distribution in epithelial basement membranes of fetal and adult human tissues. *Exp. Cell Res.* **257**, 298-309.
 29. Gullberg, D., Tiger, C. F., and Velling, T. (1999). Laminins during muscle development and in muscular dystrophies. *Cell. Mol. Life Sci.* **56**, 442-460.
 30. Miner, J. H., Patton, B. L., Lentz, S. I., Gilbert, D. J., Snider, W. D., Jenkins, N. A., Copeland, N. G., and Sanes, J. R. (1997). The laminin alpha chains: Expression, developmental transitions, and chromosomal locations of alpha1-5, identification of heterotrimeric laminins 8-11, and cloning of a novel alpha3 isoform. *J. Cell Biol.* **137**, 685-701.
 31. Patton, B. L., Miner, J. H., Chiu, A. Y., and Sanes, J. R. (1997). Distribution and function of laminins in the neuromuscular system of developing, adult and mutant mice. *J. Cell Biol.* **139**, 1507-1521.
 32. Miosge, N., Günther, E., Heyder, E., Manshausen, B., and Horken, R. (1995). Light and electron microscopic localization of the $\alpha 1$ -chain and the E1 and E8 domains of laminin-1 in mouse kidney using monoclonal antibodies to establish the orientation of laminin-1 within basement membranes. *J. Histochem. Cytochem.* **43**, 675-680.
 33. Talts, J. F., Sasaki, T., Miosge, N., Göhring, W., Mann, K., Mayne, R., and Timpl, R. (2000). Structural and functional analysis of the recombinant G domain of the laminin $\alpha 4$ chain and its proteolytic processing in tissues. *J. Biol. Chem.* **275**, 35192-35199.
 34. Talts, J. F., Mann, K., Yamada, Y., and Timpl, R. (1998). Structural analysis and proteolytic processing of recombinant G domain of mouse laminin $\alpha 2$ chain. *FEBS Lett.* **426**, 71-76.
 35. Kohfeldt, E., Maurer, P., Vannahme, C., and Timpl, R. (1997). Properties of the extracellular calcium binding module of the proteoglycan testican. *FEBS Lett.* **414**, 557-561.
 36. Costell, M., Mann, K., Yamada, Y., and Timpl, R. (1997). Characterization of recombinant perlecan domain I and its substitution by glycosaminoglycans and oligosaccharides. *Eur. J. Biochem.* **243**, 115-121.
 37. Garbe, J. H., Göhring, W., Mann, K., Timpl, R., and Sasaki, T. (2002). Complete sequence, recombinant analysis and binding to laminins and sulphated ligands of the N-terminal domains of laminin $\alpha 3 \beta$ and $\alpha 5$ chains. *Biochem. J.* **362**, 213-221.
 38. Sorokin, I., Conzelmann, S., Ekblom, P., Battaglia, C., Aumailley, M., and Timpl, R. (1992). Monoclonal antibodies against laminin A chain fragment E3 and their effects on binding to cells and proteoglycan and on kidney development. *Exp. Cell Res.* **201**, 137-144.
 39. Orkin, R. W., Gehron, P., McGoodwin, E. B., Martin, G. R., Valentine, T., and Swann, R. (1977). A murine tumor producing a matrix of basement membrane. *J. Exp. Med.* **145**, 204-220.
 40. Miosge, N., Sasaki, T., and Timpl, R. (1999). Angiogenesis inhibitor endostatin is a distinct component of elastic fibers in vessel walls. *FASEB J.* **13**, 1743-1750.
 41. Aumailley, M., Mann, K., von der Mark, H., and Timpl, R. (1989). Cell attachment properties of collagen type VI and Arg-Gly-Asp dependent binding to its $\alpha 2(VI)$ and $\alpha 3(VI)$ chains. *Exp. Cell Res.* **181**, 463-474.
 42. Battaglia, C., Aumailley, M., Mann, K., Mayer, U., and Timpl, R. (1993). Structural basis of $\beta 1$ integrin-mediated cell adhe-

LAMININ $\alpha 1$ AND $\alpha 2$ CHAINS IN TISSUES

199

- sion to a large heparan sulphate proteoglycan from basement membranes. *Eur. J. Cell Biol.* **61**, 92-99.
43. Prehm, P., Dessau, W., and Timpl, R. (1982). Rates of synthesis of basement membrane proteins by differentiating teratocarcinoma stem cells and their modulation by hormones. *Connective Tissue Res.* **10**, 275-285.
 44. Williams, R. L., Risau, W., Zerwes, H. G., Drexler, H., Aguzzi, A., and Wagner, E. F. (1989). Endothelial cells expressing the polyoma middle oncogene induce hemangiomas by host cell recruitment. *Cell* **57**, 1053-10663.
 45. Hatzopoulos, A. K., Folkman, J., Vasile, E., Eiselen, G. K., and Rosenberg, R. D. (1998). Isolation and characterization of endothelial progenitor cells from mouse embryos. *Development* **125**, 1457-1468.
 46. Kanda, S., Tomasini-Johansson, B., Klingt, P., Dixelius, J., Rubin, K., and Claesson-Welsh, L. (1999). Signaling via fibroblast growth factor receptor-1 is dependent on extracellular matrix in capillary endothelial cell differentiation. *Exp. Cell Res.* **248**, 203-213.
 47. Mayer, U., Nischt, R., Pöschl, E., Mann, K., Fukuda, K., Gerl, M., Yamada, Y., and Timpl, R. (1993). A single EGF-like motif of laminin is responsible for high affinity nidogen binding. *EMBO J.* **12**, 1879-1885.
 48. Timpl, R., and Risteli, L. (1982). Radioimmunoassays in studies of connective tissue proteins. In "Immunochemistry of the Extracellular Matrix" (H. Furthmayr, Ed.), Vol. 1, pp. 199-235. CRC Press, Boca Raton.
 49. Sasaki, T., Wiedemann, H., Matzner, M., Chu, M.-L., and Timpl, R. (1996). Expression of fibulin-2 by fibroblasts and deposition with fibronectin into a fibrillar matrix. *J. Cell Sci.* **109**, 2895-2904.
 50. Chomczynski, P., and Sacchi, N. (1987). Single-step method of RNA isolation by acid-guanidiniumthiocyanate-phenol chloroform extraction. *Anal. Biochem.* **162**, 156-159.
 51. Paulsson, M., Aumailley, M., Deutzmann, R., Timpl, R., Beck, K., and Engel, J. (1987). Laminin-nidogen complex: Extraction with chelating agents and structural characterization. *Eur. J. Biochem.* **166**, 11-19.
 52. Michelson, A. M., Russell, E., and Harman, P. J. (1955). Dystrophin Muscularis: A hereditary primary myopathy in the house mouse. *Proc. Natl. Acad. Sci. USA* **41**, 1079-1084.
 53. Miyagoe, Y., Hanaoka, K., Nonaka, I., Hayasaka, M., Nabeshima, Y., Arahata, K., Nabeshima, Y., and Takeda, S. (1997). Laminin alpha2 chain-null mutant mice by targeted disruption of the Lama2 gene: A new model of merosin (laminin 2)-deficient congenital muscular dystrophy. *FEBS Lett.* **415**, 33-9.
 54. Strickland, S., Smith, K. K., and Marotti, K. R. (1980). Hormonal induction of differentiation in teratocarcinoma stem cells: Generation of parietal endoderm by retinoic acid and dibutyryl cyclic AMP. *Cell* **21**, 347-355.
 55. Brown, J. C., Wiedemann, H., and Timpl, R. (1994). Protein binding and cell adhesion properties of two laminin isoforms (AmB1eB2e, AmB1sB2e) from human placenta. *J. Cell Sci.* **107**, 329-338.
 56. Stockdale, F. E. (1992). Myogenic cell lineages. *Dev. Biol.* **154**, 284-298.
 57. Tiger, C., and Gullberg, D. (1997). Absence of laminin $\alpha 1$ chain in the skeletal muscle of dysrophic dy/dy mice. *Muscle Nerve* **20**, 1515-1524.
 58. Schuler, F., and Sorokin, J. (1995). Expression of laminin isoforms in mouse myogenic cells in vitro and in vivo. *J. Cell Sci.* **108**, 3795-805.
 59. Pedrosa-Domellöf, F., Tiger, C.-F., Virtanen, I., Thornell, L.-E., and Gullberg, D. (2000). Laminin chains in developing and adult human myotendinous junctions. *J. Histochem. Cytochem.* **48**, 201-209.
 60. Xu, H., Wu, X.-R., Wewer, U. N., and Engvall, E. (1994). Murine muscular dystrophy caused by a mutation in the laminin alpha 2 (Lama2) gene. *Nature Genet.* **8**, 297-302.
 61. Durbeej, M., Talts, J. F., Henry, M. D., Yurchenco, P. D., Campbell, K. P., and Ekblom, P. (2001). Dystroglycan binding to laminin $\alpha 1$ LG4 module influences epithelial morphogenesis of salivary gland and lung in vitro. *Differentiation* **68**, 121-134.
 62. Sorokin, L. M., Pausch, F., Durbeej, M., and Ekblom, P. (1997). Differential expression of five laminin α chains in developing and adult mouse kidney. *Dev. Dyn.* **210**, 446-462.
 63. Amenta, P. S., and Harrison, D. (1997). Expression and potential role of the extracellular matrix in hepatic ontogenesis: A review. *Microsc. Res. Tech.* **39**, 372-386.
 64. Gimenez, A., Hostench, J., Stamatoglou, S. C., and Enrich, C. (1995). Differential expression of A and B laminin chains during rat liver regeneration. *Hepatology* **22**, 1259-1262.
 65. Vuolteenaho, R., Nissinen, M., Sainio, K., Byers, M., Eddy, R., Hirvonen, H., Shows, T. B., Sariola, H., Engvall, E., and Trygvason, K. (1994). Human laminin M chain (merosin): Complete primary structure, chromosomal assignment, and expression of the M and A chain in human fetal tissues. *J. Cell Biol.* **124**, 381-394.
 66. Andre, F., Filippi, P., and Feracci, H. (1994). Merosin is synthesized by thyroid cells in primary culture irrespective of cellular organization. *J. Cell Sci.* **107**, 183-193.
 67. Schuger, L., Skubitz, A. P. N., Zhang, J., Sorokin, L., and He, L. (1997). Laminin $\alpha 1$ chain synthesis in the mouse developing lung: requirement for epithelial-mesenchymal contact and possible role in bronchial smooth muscle development. *J. Cell Biol.* **139**, 553-562.
 68. Klein, G., Ekblom, M., Fecker, L., Timpl, R., and Ekblom, P. (1990). Differential expression of laminin-A and B chains during development of embryonic mouse organs. *Development* **11**, 823-837.
 69. Virtanen, I., Laitinen, A., Taneli, T., Pääkkö, P., Laitinen, L. A., Burgeson, R. E., and Letho, V.-P. (1996). Differential expression of laminins and their integrin receptors in developing and adult human lung. *Am. J. Respir. Cell Mol. Biol.* **15**, 184-196.
 70. Mendell, J. R., Sahenk, Z., and Prior, T. W. (1995). The childhood muscular dystrophies: Diseases sharing a common pathogenesis of membrane instability. *J. Child Neurol.* **10**, 150-159.
 71. Sasaki, T., Mann, K., and Timpl, R. (2001). Modification of the laminin $\alpha 4$ chain by chondroitin sulfate attachment to its N-terminal domain. *FEBS Lett.* **505**, 173-178.
 72. Sasaki, T., and Timpl, R. (2001). Domain IVa of laminin $\alpha 5$ chain is cell-adhesive and binds $\beta 1$ and $\alpha \beta 3$ integrins through Arg-Gly-Asp. *FEBS Lett.* **509**, 181-185.

Received November 14, 2001

Revised version received January 17, 2001

Published online March 26, 2002

Discordant Regulation of Granzyme H and Granzyme B Expression in Human Lymphocytes*

Received for publication, November 14, 2003, and in revised form, April 5, 2004
Published, JBC Papers in Press, April 6, 2004, DOI 10.1074/jbc.M312481200

Karin A. Sedelies^{‡§}, Thomas J. Sayers[¶], Kirsten M. Edwards^{‡||}, Weisan Chen^{**},
Daniel G. Pellicci^{‡§§}, Dale I. Godfrey^{‡§§}, and Joseph A. Trapani^{‡¶¶}

From the [‡]Cancer Immunology Laboratory, Peter MacCallum Cancer Centre, Locked Bag 1, A'Beckett Street, East Melbourne, 8006, Australia, the [¶]Basic Research program, SAIC-Frederick Inc., NCI, National Institutes of Health, Frederick, MD, 21702, the ^{**}Ludwig Institute for Cancer Research, Austin and Repatriation Medical Center, Studley Road, Heidelberg, 3084, Australia, and the ^{‡§}Department of Pathology and Immunology, Monash University Medical School, Melbourne, Victoria 3181, Australia

We analyzed the expression of granzyme H in human blood leukocytes, using a novel monoclonal antibody raised against recombinant granzyme H. 33-kDa granzyme H was easily detected in unfractionated peripheral blood mononuclear cells, due to its high constitutive expression in CD3⁺CD56⁺ natural killer (NK) cells, whereas granzyme B was less abundant. The NK lymphoma cell lines, YT and Lopez, also expressed high granzyme H levels. Unstimulated CD4⁺ and particularly CD8⁺ T cells expressed far lower levels of granzyme H than NK cells, and various agents that classically induce T cell activation, proliferation, and enhanced granzyme B expression failed to induce granzyme H expression in T cells. Also, granzyme H was not detected in NK T cells, monocytes, or neutrophils. There was a good correlation between mRNA and protein expression in cells that synthesize both granzymes B and H, suggesting that *gzmH* gene transcription is regulated similarly to *gzmB*. Overall, our data indicate that although the *gzmB* and *gzmH* genes are tightly linked, expression of the proteins is quite discordant in T and NK cells. The finding that granzyme H is frequently more abundant than granzyme B in NK cells is consistent with a role for granzyme H in complementing the pro-apoptotic function of granzyme B in human NK cells.

Cytotoxic T lymphocytes and natural killer (NK)¹ cells are cytotoxic lymphocytes that are responsible for inducing rapid apoptosis of virus-infected or transformed cells (1, 2). Cytotoxic

lymphocytes utilize two pathways for killing target cells, both of which require direct cell contact. The first pathway involves exocytosis of potent toxins from secretory granules stored in the effector cell cytoplasm, whereas the second is triggered by clustering of death receptors on the target cell membrane following interaction with their respective ligands (tumor necrosis factor superfamily members) expressed on the killer cell (1, 2). Cytotoxic granules contain two major types of toxin that co-operatively induce target cell apoptosis: granzymes (gzms), a family of serine proteases, and a pore-forming protein, perforin. The precise mechanism of gzm/perforin synergy has not been clarified; however, it is likely that gzms enter the target cell by endocytosis (3, 4), whereas perforin enables pro-apoptotic gzms access to their substrates in the target cell cytosol by destabilizing endosomes (5, 6). The more traditionally held notion of perforin permitting access to the cytosol through plasma membrane pores may also apply in some circumstances (6).

Gzms are closely related to one another structurally, and their genes are clustered in several loci on distinct chromosomes (7). In both humans and rodents, each locus encodes proteases with a single broad type of substrate cleavage. Gzms A and K are trypsin-like proteases ("tryptases") that cleave proteins at basic residues, and their genes are linked on human chromosome 5 (8). Gzm M preferentially cleaves at residues with long, uncharged side chains (Met, Leu), and its gene is closely linked to the neutrophil elastase gene on human chromosome 19 (9). The genes for gzms B and H are located on chromosome 14, tightly linked with the gene encoding cathepsin G, another chymotrypsin-like protease ("chymase") that, unlike the gzms, is expressed in cells of the myeloid lineage but not in lymphocytes (7, 10). These three genes all map to within 60 kb of one another. Gzm B cleaves its substrates adjacent to acidic residues, particularly Asp (11), and plays a central role in eliciting death of the target cell by perturbing mitochondria and activating caspases (12, 13). Its absence from the granules of lymphocytes from gene knockout mice slows the rate of target cell DNA damage (14).

In the mouse, the gene for gzm B is tightly linked to at least four other granzyme genes predicted to code for functional chymases (gzms C-F); however, only one such chymase, gzm H, performs this function in humans (15). Gzm C is now known to possess an unusual type of pro-apoptotic activity characterized by mitochondrial swelling and disruption that does not require prior caspase activity (16). However, no such evidence has yet come forward for human gzm H. We recently showed that

* This work was supported in part by federal funds from the NCI, National Institutes of Health, under Contract N01-CO-56000. The costs of publication of this article were defrayed in part by the payment of page charges. This article must therefore be hereby marked "advertisement" in accordance with 18 U.S.C. Section 1734 solely to indicate this fact.

The content of this publication does not necessarily reflect the views or policies of the Department of Health and Human Services, nor does mention of trade names, commercial products or organizations imply endorsement by the U. S. government.

§ Supported by project grants and a research fellowship from the National Health and Medical Research Council of Australia.

¶ Present address: Dept. of Pathology and Harvard Center for Cancer Biology, Harvard Medical School, Boston, MA 02115.

§§ Present address: Dept. of Microbiology and Immunology, University of Melbourne, Parkville, 3052, Australia.

|| Supported by a research fellowship from the National Health and Medical Research Council of Australia. To whom correspondence should be addressed. Tel.: 61-3-9656-3726; Fax: 61-3-9656-1411; E-mail: joe.trapani@petermac.org.

¹ The abbreviations used are: NK, natural killer; NKT, NK T; gzm, granzyme; PBMC, peripheral blood mononuclear cell; mAb, monoclonal

antibody; PBS, phosphate-buffered saline; ELISA, enzyme-linked immunosorbent assay; PHA, phytohemagglutinin.

recombinant gzm H expressed in baculovirus-infected insect cells preferentially cleaves substrates with Phe or Tyr at the P1 position (15). Despite sharing this substrate specificity with mouse gzms C–F, gzm H has no direct structural equivalent in the mouse and appears to be a uniquely human protein. Gzm H has a very high amino acid identity (>90%) with many portions of the gzm B sequence, particularly near the amino terminus of the molecule (10) despite performing a distinct enzymic function. It has been inferred from the high degree of sequence similarity that the *gzmH* gene arose by duplication of part of the 5' end of the *gzmB* gene (particularly exons 3 and 4) and fusion with the 3' end of another primordial serine protease gene (10).

The function of gzm H is unknown, and its study has been greatly hindered by a lack of reagents able to distinguish it from gzm B at the protein or mRNA levels. The cellular expression of gzm H has been reported in just one study that assessed gzm H mRNA expression in human T cells (10). This study concluded that like gzm B, gzm H is expressed at high levels in activated T cells. However, in another study, a portion of the *gzmH* promoter was used to preferentially direct the transgenic expression of SV-40 T antigen to the mouse lymphoid compartment. The transgene was not activated in allo-stimulated cytotoxic T lymphocytes that expressed high levels of gzm B but was highly expressed in activated NK cells and in NK and NK/T cell tumors that arose in these animals (17). Although the genes encoding cathepsin G and gzms B and H are very tightly linked, cathepsin G and gzm B have markedly different cellular expression profiles, as cathepsin G is expressed exclusively by cells of the myeloid lineage, particularly neutrophils and monocytes (18). It is therefore quite feasible that gzms B and H may be differentially expressed and regulated among leukocyte subsets. The availability of correctly folded, proteolytically active gzm H enabled us to attempt raising monospecific reagents for this protease. Having produced a novel gzm H-specific mAb, we now demonstrate that gzm H is expressed solely in lymphocytes, but its constitutive expression pattern is quite distinct from that of gzm B, as is its expression in response to a variety of stimuli that strongly induce gzm B expression.

EXPERIMENTAL PROCEDURES

Antibodies—Antibodies used in Western blotting and immunohistochemistry included several mAbs made by our laboratory: 2C5 (anti-gzm B) (19), 4H10 (anti-gzm M) (20), PB2 (anti-perforin) (21), and 7D8 (anti-PI-9) (22). In addition, mAb GB7 (anti-gzm B) was purchased from Serotec.

Cell lines, Tissue Samples, and Immunohistochemistry—The human tumor cell lines used in this study were all cultured in RPMI medium supplemented with 10% fetal bovine serum, 2 mM L-glutamine, penicillin, and streptomycin in a CO₂ incubator at 37 °C. These included YT (human NK), HL-60 and U937 (human myeloid), Daudi and Raji (human B cell), Jurkat and CEM (human T cell), HeLa (cervical carcinoma), Lovo and COLO205 (colon adenocarcinoma), and MDA-MB-435 (human breast adenocarcinoma) tumor cell lines. Lysates of homogeneous populations of human T cell lymphoma samples of two unrelated individuals (derived from lymph node biopsies) were also analyzed. Immunohistochemical studies were performed as described previously (23).

Recombinant gzm Expression—Recombinant human gzm B and gzm H were purified from the culture supernatants of baculovirus-infected Sf9 cells, 3–5 days after infection, as described (15). The poly-histidine-tagged gzm proteins were purified by nickel affinity chromatography and dialyzed against PBS. The gzms were tested for their proteolytic activity by assaying the cleavage of tripeptide substrates Ala-Ala-Asp-S-benzyl (for gzm B, a kind gift from Drs. Chih-Min Kam and Jim Powers, Georgia Institute of Technology, Atlanta, GA) or Phe-Leu-Phe-S-benzyl (for gzm H, purchased from Sigma).

mAb Production and Screening—Five- to seven-week-old female BALB/c mice were immunized into the peritoneal cavity with purified, recombinant gzm H (50 µg) mixed with Freund's complete adjuvant.

Two to four weeks later, the mice were boosted with the same antigen mixed with incomplete adjuvant. Three days following a further similar immunization, a mouse was sacrificed, and its spleen cells were fused with NS-1 mouse myeloma cells, using polyethylene glycol. Ten days later, hybridomas were screened for secretion of anti-gzm H mAbs using a solid phase ELISA assay in which gzm H (or gzm B as a control) was coated onto the wells of a 96-well polyvinyl chloride plate. Positive hybridomas were cloned by limiting dilution, and the clones were expanded and cryopreserved in liquid nitrogen.

Production of a Rabbit Polyclonal Antiserum—Polyclonal antiserum was raised in New Zealand White rabbits by immunization with purified recombinant human gzm B (200 µg) mixed with Freund's complete adjuvant and injected into multiple sites subcutaneously in volumes of <0.1 ml. Three booster immunizations were given intramuscularly with incomplete adjuvant at 3–4-week intervals.

Isolation of Leukocyte Subsets—For isolation of neutrophils, cell pellets collected after Ficoll-Hypaque centrifugation were dispersed in PBS containing 3% dextran and left to stand at ambient temperature for 30 min to rouleau the red cells. Neutrophils were then pelleted from the supernatants and resuspended in hypotonic buffer containing 0.2% NaCl for 1.5–2.0 min to lyse the remaining red cells. The tonicity was then adjusted to 0.9% NaCl, and the cells were again pelleted and washed. Cells were >95% neutrophils, by Giemsa staining. Monocytes were sorted from peripheral blood mononuclear cells (PBMC) with anti-CD14 fluorescein isothiocyanate and were at least 82% pure. CD3⁺CD56⁺ T cells and CD3⁺CD56⁺ NK cells were purified from PBMC by fluorescence-activated cell sorter sorting and were reproducibly >96% pure. For isolation of NKT cells, PBMC were cultured in medium containing IL-2, IL-7, and α -galactosylceramide (generously provided by Kirin Breweries, Gunma, Japan) for 7 days. Cells that stained positive with phytohemagglutinin-conjugated CD1d/ α -galactosylceramide tetramer (generously provided by Drs. Stephané Sidobre and Mitchell Kronenberg, La Jolla Institute for Allergy and Immunology, La Jolla, CA) and CD3-fluorescein isothiocyanate were collected by fluorescence-activated cell sorter sorting, and purity was found to be 95%.

T and NK Cell Stimulation—Human PBMC and purified populations of T and NK cells were incubated in medium supplemented with recombinant human interleukin-2 (IL-2, 100–500 units/ml; Chiron Corp.) and/or phytohemagglutinin (PHA) (2 µg/ml) or anti-CD3 mAb HIT3A (10 ng/ml; Pharmingen) for up to 10 days prior to harvest and analysis for gzm expression.

Protein Immunoblotting—Cell lysates were fractionated on 12.5% SDS-polyacrylamide gels, and the proteins were electroblotted onto polyvinylidene difluoride membranes. Nonspecific protein binding was blocked by preincubation with 5% nonfat skim milk in PBS at 4 °C for 2 h. Membranes were incubated with mAb (hybridoma culture supernatant, typically diluted 1/5 to 1/20 in PBS) at 4 °C overnight and washed, and then bound Ig was detected with goat anti-mouse Ig conjugated to horseradish peroxidase.

Generation of gzm-specific cDNA Probes Northern Blotting, and Real-time PCR Analysis—cDNA probes specific for the 3'-untranslated regions of gzm B and H mRNA/cDNA were produced by PCR amplification of each respective cDNA clone, using synthetic oligonucleotide primers. The gzm B probe was amplified using the oligonucleotides 5'-GAAACGCTACTAACTACAGG-3' and 5'-CCACTCAGCTAAGAGGT-3' and was 129 nucleotides in length. The gzm H probe was similarly amplified using the oligonucleotides 5'-AGAACAAATGAAGCGCTC-3' and 5'-ACACGCGGCCGCGATCCATTATTACAGTCC-3' and was 138 nucleotides in length. Each probe was purified from 2% agarose gels and labeled with [α -³²P]dATP by nick translation or random priming with synthetic hexanucleotides. The radiolabeled probes were used to identify gzm-specific mRNA in Northern blot experiments. Total cellular RNA was isolated from various populations of human cells and cell lines (10 µg/lane) and separated by electrophoresis on 1% formaldehyde/agarose gels, and then transferred to nylon membranes by capillary transfer. The membrane was allowed to dry at room temperature and then baked at 80 °C for 2 h. Prehybridization was in buffer containing 50% formamide, 1% SDS, and 5× SSC (pH 6.8) solution at 42 °C. Following hybridization with preboiled radiolabeled cDNA probe for 16 h, the filters were washed at low stringency and then under high stringency conditions (0.1× SSC, 1% SDS, 60 °C for 2 × 20 min), air-dried, and exposed to x-ray film (Kodak) for 1–3 days at –80 °C. In some experiments, plasmid DNA was spotted onto nylon membranes (50 ng/spot) and then denatured in NaOH. The membranes were baked at 80 °C for 2 h and then prehybridized and hybridized as described above. For real-time-PCR, 2 µg of DNase-treated RNA was reverse transcribed using M-MLV reverse transcriptase Rnase H minus, point

mutant (Promega). PCR primers for each gene were designed using Primer Express software (Applied Biosystems, Foster City, CA) with a melting temperature at 58–60 °C and a resulting product of 75–150 bp. Triplicate 20- μ l PCR reactions were carried out using SYBR green master mix (Applied Biosystems), initially for 15 min at 95 °C followed by 39 cycles of 95 °C for 15 s and 60 °C for 60 s in the ABI Prism 7700 sequence detection system. The levels of gzm H and B mRNA were normalized to that of ribosomal protein L32. Primer pairs were as follows: L32, forward, 5'-TTCTGGTCCACAACGTCAAG-3' and reverse, 5'-TGTGAGCGATCTCGGCAC-3'; gzm B, forward, 5'-GCGGTG-GCTTCCTGATACAAG-3', and reverse, 5'-CCCCCAAGGTGACATTT-ATGG-3'; gzm H, forward, 5'-TGGCGGCATCCTAGTGAGAA-3', and reverse 5'-GCCCCAAGGTGACATTTATG-3'. Primer efficiency for gzm B and H was demonstrated by the overlapping amplification profiles of equal quantities of gzm B and H cDNA.

Granule Fractionation.—For cell fractionation experiments, YT human NK tumor cells (3×10^6) were harvested, washed several times in PBS, and lysed by nitrogen cavitation, as described (24). The cell lysate was fractionated on a continuous Percoll density gradient as described, and 1-ml fractions were collected, starting with the dense (bottom) end of the gradient. Following the removal of Percoll by ultracentrifugation, aliquots of each fraction were analyzed by SDS-PAGE and Western blot.

RESULTS

To determine the cellular and subcellular expression of gzm H, it was first necessary to produce an antiserum that could distinguish it from other granzymes, particularly its closest structural relative gzm B, with which it shares ~75% amino acid identity (25). We have previously expressed and purified catalytically active gzm H secreted by baculovirus-infected insect cells (15), so this protein was used as an immunogen for mAb production in BALB/c mice. Of 800 hybridoma culture supernatants screened for mAb secretion in a solid phase ELISA assay, 48 were found to secrete an Ig that bound to gzm H. All but one of these mAbs produced an equivalent signal when tested on purified gzm B, indicating they detected an epitope common to both granzymes (data not shown). However, the mAb produced by hybridoma 4G5 specifically recognized gzm H and failed to react with gzm B in the ELISA assay (Fig. 1A). Conversely, mAb 2C5, which we have used extensively in studies on gzm B (12, 13, 19, 26, 27), was specific for gzm B and failed to recognize gzm H. MAb 4G5 detected as little as 3 ng of gzm H but did not react at all with gzm B in Western blots (Fig. 1B). In the reciprocal experiment, mAb 2C5 reacted strongly with gzm B in Western blots but did not react with gzm H (data not shown). By contrast with both mAbs, a polyclonal rabbit antiserum raised against gzm B showed strong cross-reactivity with gzm H, once again demonstrating the close structural similarity of the two granzymes (Fig. 1B). Interestingly, mAb GB7, a commercially available reagent purported to specifically detect gzmB, produced an equivalent signal with gzm B and H (Fig. 1C). Similar analyses using other recombinant granzymes also demonstrated that both 4G5 and 2C5 did not react with recombinant human gzm M, a more distant relative of gzm B and H (~35% amino acid identity; data not shown) (7).

Having shown that 4G5 specifically detects gzm H, we next used the mAb in Western blotting on whole cell lysates made from a series of hemopoietic and non-hemopoietic cells lines. The human NK leukemia cell lines YT (Fig. 2) and Lopez (data not shown) both demonstrated a 33-kDa protein that co-migrated with recombinant gzmH. The predicted molecular mass on reduced SDS-PAGE was consistent with a gzm H polypeptide backbone of 26 kDa (deduced from the cDNA sequence) and ~7 kDa of added carbohydrate. Gzm H was not expressed by the acute T cell leukemia lines Jurkat and CEM, the B lymphoma cell lines Daudi and Raji, the myeloid cell lines HL-60 and U937, or cells from two lymph node biopsies excised from patients with disseminated T cell lymphoma. Similarly, no signal was detectable in the human carcinoma cell lines 293

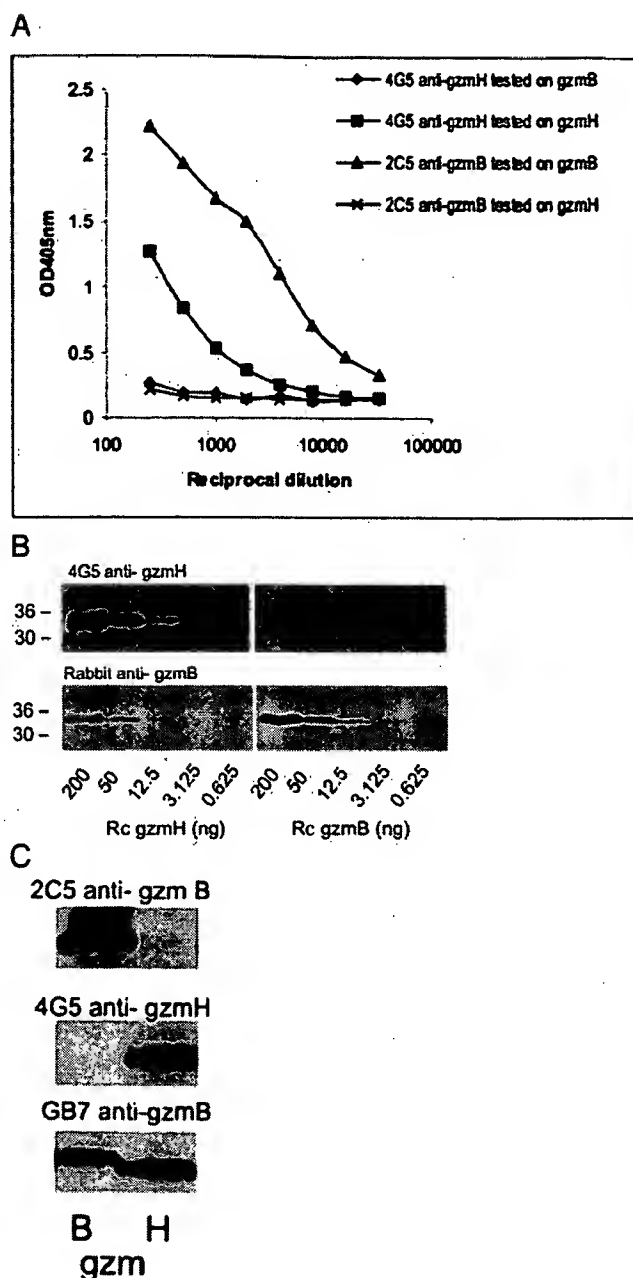


FIG. 1. Specificity of anti-gzm B and H mAbs. A, solid-phase ELISA assay in which serially diluted mAbs raised against human gzm B peptide (2C5, Ref. 19) and recombinant gzm H (4G5, this study) were tested on both recombinant purified gzm B and H. B, Western blot showing reactivity of 4G5 (tissue culture supernatant, diluted 1/10) and a polyclonal rabbit antiserum raised against recombinant (Rc) human gzmB (1/1000) with various quantities of each recombinant gzm protein. C, Western blot showing reactivity of mAbs 4G5, 2C5, and GB7, which has been considered to react specifically with gzmB, with recombinant gzm B and H (indicated by B and H).

(embryonal kidney), HeLa (cervical), or the adenocarcinomas Lovo, COLO 205, and MDA-MB435. As Lopez and YT cells both contain large numbers of cytolytic granules and also express perforin and gzm B and M (24), the co-expression of gzm H by these cell lines was consistent with a possible role for gzm H in cytotoxic granule-mediated cell death.

To determine the subcellular localization of gzm H, we initially performed immunohistochemistry on pelleted YT cells, using mAbs 2C5 (anti-gzmB) and 4H10 (anti-gzmM) as controls (Fig. 3A). As was shown previously, gzm B and M were localized to granules in the cytoplasm of YT cells (20, 26). Cytoplas-

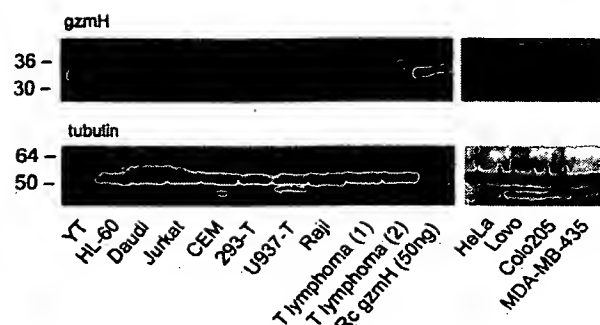


FIG. 2. Expression of gzmH in human tumor cell lines. A Western blot analysis of whole cell lysates derived from a variety of hemopoietic and non-hemopoietic tumor cell lines and two primary T cell lymphomas, as described under "Experimental Procedures," is shown. The same panel of lysates was also probed with a mAb detecting tubulin, as a loading control. Rc gzmH = recombinant gzmH, which was run as a positive control. The numerals at the left indicate the migration of molecular size markers in kDa.

mic staining in YT cells was also observed with the gzmH mAb; however, the strength of the staining varied considerably from cell to cell: some YT cells (about 50%) stained strongly, a minority stained weakly, and the remainder (about 25%) showed no staining. The heterogeneity of staining was not due to limiting Ig, as similar numbers of strongly and weakly staining cells were observed over a range of antiserum concentrations (data not shown). None of the granzyme mAbs bound to Jurkat cells, which were used as a negative control in this experiment (Fig. 2). To definitively demonstrate gzmH localization to cytotoxic granules, a lysate of mechanically disrupted YT cells was fractionated on a Percoll density gradient (Fig. 3B). The fractions were analyzed by Western blotting with antibodies specific for gzms B and H, perforin, and the serpin, PI-9, which is localized to the cytosol of cytotoxic lymphocytes rather than granules (26). Gzm H was co-localized with the granule proteins perforin and gzmB in fractions 6–8 at the dense end of the gradient (specific gravity 1.10–1.13 g/ml, data not shown). Fractions 6–8 were free of PI-9, which is abundant in the cytosol of YT cells (represented by the least dense fractions, 14–18) but is not a significant constituent of the granules (26).

Almost all of the human and rodent granzymes described to date are expressed constitutively by NK cells and in an inducible manner by CD8+ (and some CD4+) T cells, when they become activated and adopt an effector phenotype (28). The two granzymes known to play a pivotal role in target cell apoptosis, gzm B, which is encoded by a gene that is very tightly linked to that of gzm H, and gzm A, encoded on a different chromosome, Chr 5 (8) are both regulated in this way. One exception to this general "rule" is gzm M, which is constitutively expressed by NK cells but not by human or rodent T cells when they become activated (20, 23). We therefore wished to determine which leukocyte subsets (if any) in normal human peripheral blood express gzmH, both in their quiescent state or following exposure to activating stimuli. Initially, we subjected unfractionated PBMC from normal individuals to Western blotting, either prior to or after exposure to agents that cause T cell activation and proliferation *in vitro* (Fig. 4A). Surprisingly, freshly isolated, unstimulated PBMC from unrelated donors showed strong constitutive gzm H expression, whereas the expression of gzm B by the same cells was very low or absent (Fig. 4A). From past studies, gzmB is known to be expressed at low levels in unstimulated NK cells (23) and is induced from very low levels in stimulated CD4+ and CD8+ T cells (10, 29–31). Consistent with this pattern of expression, exposure of PBMC to the T cell stimuli IL-2 and anti-CD3 mAb (Fig. 4A) over

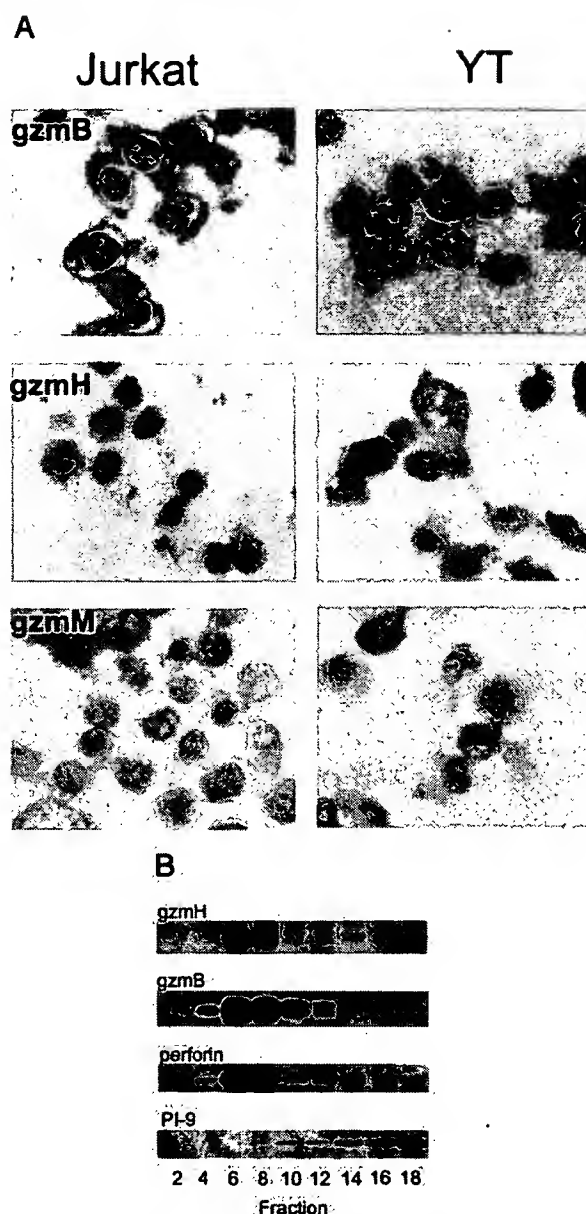


FIG. 3. Expression of gzms B, H and M in YT NK leukemia cells. A, immunohistochemical analysis of YT and Jurkat (human T cell leukemia) cells, probed with mAbs specifically detecting gzms B, H and M (see "Experimental Procedures"). B, Western blot analysis of alternate Percoll density gradient fractions of a cytoplasmic lysate of YT cells. The numerals indicate fraction numbers, collected from the bottom (dense) end of the gradient (see "Experimental Procedures"). The fractions were probed with mAbs specific for gzmH (4G5), the known granule proteins gzmB (2C5) and perforin (PB2), and PI-9 (7D8), which is absent from granules but located in the cytosol.

4-day time course experiments caused a strong induction of gzmB protein. The response to IL-2/anti-CD3 had peaked within 24 h and then declined slightly from days 2–4. Next, we sorted fresh PBMC into CD3+CD56⁺ T cells and CD3-CD56⁺ NK cells (Fig. 4B). The T cells constitutively expressed no gzm B and low levels of gzm H, whereas the NK cells gave a strong signal for gzm H and a substantially weaker signal for gzm B. As NK cells make up only 2–5% of PBMC, it is likely that gzm B would be undetectable in Western analysis of unfractionated PBMC in most instances (Fig. 4A). Exposure of the T cells to IL-2/PHA caused a strong and continual up-regulation of gzm B levels up until day 4. By stark contrast, the level of gzm H expression did not increase above constitutive levels but re-

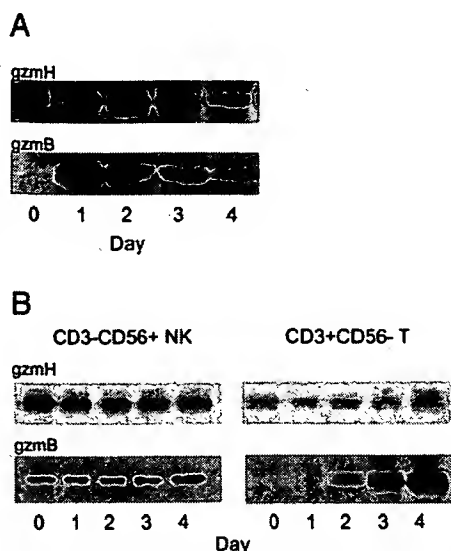


FIG. 4. Expression of granzymes B and H in activated human PBMC. A, Western blot analysis with mAbs 4G5 (anti-gzmH) and 2C5 (anti-gzm B) of whole cell lysates of unstimulated PBMC (day 0; 5×10^6 cells/lane) and of similar numbers of cells cultured in medium supplemented with IL-2 and anti-CD3 mAb for the number of days indicated. B, Western blot analysis of whole cell lysates of unstimulated CD3+CD56⁻ T and CD3-CD56⁺ NK cells (day 0; 5×10^6 cells/lane) and of similar numbers of cells cultured in medium supplemented with PHA/IL-2 (T cells) or 100 units/ml IL-2 (NK cells) for the number of days indicated.

mained constant (Fig. 4B). In purified NK cells exposed to IL-2, the levels of gzm H remained unchanged, whereas gzm B levels increased somewhat (Fig. 4B).

To further define which cell types were responsible for gzm H expression, we next examined more highly purified PBMC subsets (Fig. 5). As shown previously, gzm H was expressed at very high levels in unstimulated CD3⁺CD56⁺ NK cells and at far lower levels in unstimulated CD4⁺/CD8⁺ T cells (Fig. 5A). Consistent with previous observations, the unstimulated NK cells also expressed small amounts of gzm B and far larger quantities of gzm M (23). Purified CD4⁺ and CD8⁺ T cells were also examined separately for granzyme expression upon *in vitro* stimulation with PHA and IL-2. Again consistent with previous findings, both T cell subsets expressed large amounts of gzm B, whereas gzm M was undetectable. Gzm H was expressed in activated CD4⁺ cells, but contrary to previous reports (10), the level of expression was not increased in comparison with unstimulated CD4⁺ cells. Despite expressing large quantities of gzm B, the stimulated CD8⁺ T cells expressed no detectable gzmH (Fig. 5A). As NK cells expressed large quantities of gzm H, we were also interested in whether NKT cells also expressed gzm H. As the number of NKT cells in PBMC is typically only 0.1%, unfractionated PBMC from a healthy donor were stimulated *in vitro* with IL-2, IL-7, and α -galactosylceramide for 7 days. This resulted in the proportion of cells staining with phosphatidylethanolamine-labeled CD1d/ α -galactosylceramide tetramer increasing to ~1.5% (data not shown). When these NKT cells were sorted to homogeneity and analyzed by protein immunoblotting (Fig. 5B), they were found to lack expression of gzm H, whereas small amounts of gzm B were expressed. Neither polymorphonuclear leukocytes nor monocytes expressed detectable gzmH (Fig. 5B). It was therefore concluded that gzm H is expressed predominantly by NK cells and weakly by CD4⁺ T cells but not by CD8⁺ T cells in unstimulated human peripheral blood. A number of stimuli that strongly induce gzm B expression had no effect on gzm H protein levels. The absence of 4G5 reactivity with myeloid cells

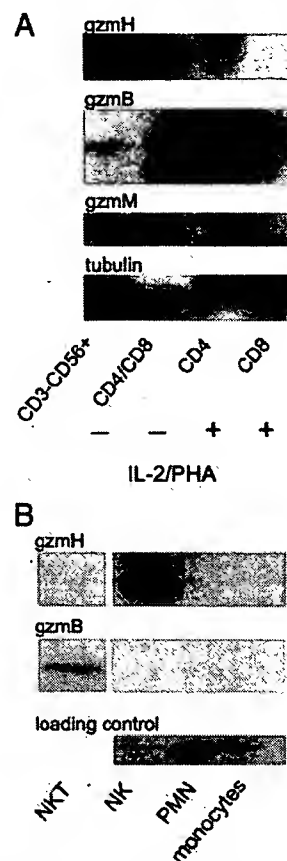


FIG. 5. Expression of granzymes B, H and M in human lymphocyte subsets. A, Western blot analysis of whole cell lysates of unstimulated human CD3-CD56⁺ NK cells, unstimulated CD4⁺ and CD8⁺ T cells (CD4/CD8), and CD4⁺ or CD8⁺ T cells cultured with PHA and IL-2 for 5 days. The expression of tubulin was used as a loading control. B, Western blot analysis of whole cell lysates of peripheral blood NKT cells expanded in culture medium supplemented with IL-2 and IL-7 for 7 days, unstimulated CD3-CD56⁺ NK cells, and freshly isolated polymorphonuclear leukocytes (PMN) and monocytes. Staining with an anti-serpin antibody that detects the serpin PAI-2 was used as a loading control.

indicated that this mAb does not cross-react with cathepsin G, a closely related serine protease expressed at high levels in myeloid cells but not at all in lymphocytes (18).

Our results were not in agreement with a previous report that indicated that gzm H is inducible upon T cell activation (10). This study was performed without the benefit of a specific gzm H antiserum and relied on mRNA expression studies performed with cDNA probes. To determine whether the previous findings may have resulted from cross-reactivity of the gzm H cDNA probe with gzm B mRNA, we generated probes specific for gzm B and gzm H mRNAs based on unique, gzm-specific sequences located in the 3'-untranslated regions of both genes. Unlike the respective full-length gzmB and gzm H cDNAs, which cross-reacted strongly, even under highly stringent hybridization and washing conditions (Fig. 6), the 3'-untranslated region probes were highly specific for granzymes B and H (Fig. 6, bottom panel). Neither set of probes reacted with gzm A, which has a far lower degree of sequence similarity with both gzm H and gzm B. This result shows the importance of checking for possible cross-reactivity of all reagents purported to specifically detect either gzm B or H. The *gzmH* and *gzmB* genes are tightly linked to that encoding cathepsin G, and all three proteases share considerable structural and sequence similarity. Our demonstration that gzmH protein is not expressed in myeloid cells clearly indicates that gene sequences

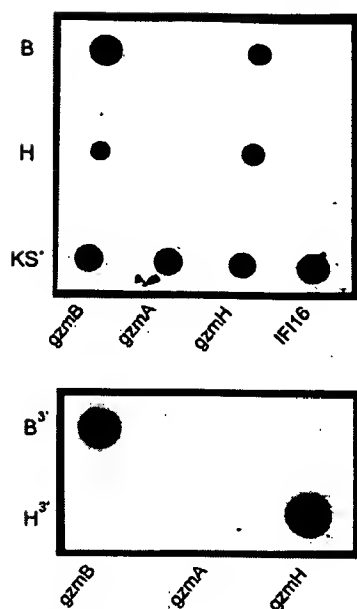


FIG. 6. Expression of gzm B and H mRNA in YT cells and human PBMC. DNA dot blot analysis in which full-length cDNAs encoding human gzms A, B, and H cloned into the plasmid vector, pBLUESCRIPT KS+, were spotted onto nylon filters (50 ng/spot). cDNA encoding the human non-granzyme protein IFI 16 was used as negative control. Replicate filters were probed and washed under high stringency conditions with [α - 32 P]dATP-labeled, full-length, purified cDNA inserts encoding gzm B (B) or gzmH (H) or with plasmid DNA (KS+). Lower panel, similar filters spotted with cDNAs encoding gzms A, B, or H were probed and washed under high stringency conditions with [α - 32 P]dATP-labeled, purified PCR-generated DNA probes specific for the 3'-untranslated sequences of human gzmB (3'B) or gzmH (3'H) cDNA (see "Experimental Procedures").

regulating cell-specific expression of gzm H and cathepsin G have not been conserved. It is also known that myeloid cells store large quantities of cathepsin G in their cytoplasmic granules but produce mRNA only during the promyelocyte stage of development, switching off gene transcription during cell maturation (32). To determine whether mature NK cells store gzm H protein in the absence of its mRNA, we used gzm B- and gzm H-specific primers to perform quantitative real-time PCR analysis of sorted CD3⁺CD56⁺ peripheral blood NK cells. We were able to detect mRNA encoding both gzms B and H (Fig. 7). Although gzm H protein was considerably more abundant than gzm B in NK cells (see above), gzm B and gzm H mRNAs were about equally abundant in freshly isolated NK cells when compared with a control mRNA, L32. Therefore, *gzmH* gene transcripts are still present in mature NK cells, unlike the case with *CatG* transcripts in myeloid cells (see Ref. 34).

DISCUSSION

We have produced a new mAb, 4G5, which specifically detects gzm H, and used it to compare the expression of gzms B and H in a variety of cell lines and human primary cells. The two gzms have very similar amino acid sequences (~75% sequence identity) and are predicted to have similar three-dimensional structures, as both are chymotrypsin-like serine proteases. It was therefore essential to first show that 4G5 and the anti-gzm B mAb used in this study, 2C5, react specifically with their respective target antigens. This was demonstrated in several ways. Firstly, the mAb produced by hybridoma 4G5 was unique among 48 mAbs produced that recognized recombinant gzm H in that it failed to recognize gzm B in a solid phase ELISA assay. As we were specifically attempting to produce a gzm H-specific mAb, screening for cross-reactivity with gzm B was included in the initial screen of hybridoma

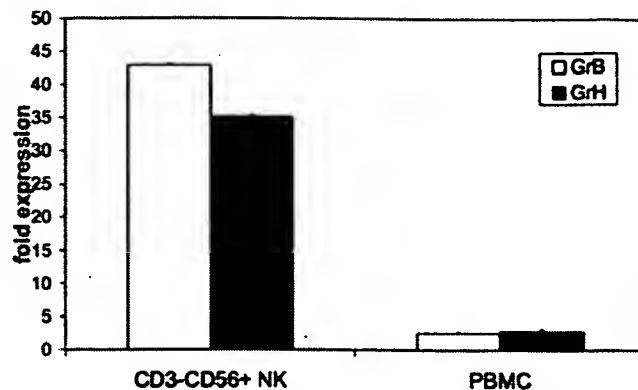


FIG. 7. mRNAs encoding gzms B and H are both expressed in unstimulated CD3⁺CD56⁺ NK cells. Real-time PCR amplification of RNA extracted from freshly isolated, purified CD3⁺CD56⁺ peripheral blood NK cells and unfractionated PBMC of a normal donor is shown. The result is expressed as the mean expression level \pm standard deviation of triplicate assays, relative to L32 mRNA. The data shown are representative of four experiments carried out with RNA from two unrelated donors.

supernatants, enabling the other 47 mAbs to be eliminated. Secondly, the specificity of 4G5 for gzm H was shown in Western blot analysis using purified proteins as targets. As recombinant proteins were used, there was no possibility that either mAb was actually detecting small amounts of an alternative gzm present as a contaminant. Thirdly, immunohistochemical staining of the human NK tumor cell line YT demonstrated markedly different patterns of staining for gzms B and H. Although gzm B staining was uniform and strong across all cells, gzm H staining was identified only in a subset of cells, and the strength of staining varied considerably from cell to cell. We are currently attempting to ascertain the factors that govern gzmH expression in individual YT cells.

This study has raised a number of unexpected results. The major finding is that the expression of gzms B and H is quite discordant in human lymphocyte subsets, both in unstimulated T and NK cells and when the cells were stimulated with a variety of agents that induce activation and proliferation. For example, gzm H is constitutively expressed at high levels in peripheral blood NK cells, whereas gzm B is expressed at much lower levels by the same cells. Stimuli that typically induce strong gzm B expression also had little effect on gzm H levels in either T or NK cells exposed to various cytokines and mitogens. Previously, Heusel *et al.* (33) also used sensitive nuclease protection assays to show a likely discrepancy in gzm B and H regulation in human lymphocytes, with the highest levels of gzm H mRNA identified in stimulated NK cells but virtually none in T cells. Human NK cell (large granular lymphocyte) tumors have also been shown to express mRNA for both gzms B and H in microarray studies that are said to have used nucleic acid probes that can distinguish between the two gzms (34). Thus, contrary to previous belief, the principal gzms expressed by resting NK cells are gzms H (this report) and gzms A and M (23) but not gzm B. By contrast, the expression of all gzms is elevated in both of the NK tumor cell lines (YT and Lopez) that have been examined to date (23, 31). The findings in primary NK cells raise the important question of how NK cells achieve target cell apoptosis when they express low levels of gzm B, which is thought to have the strongest pro-apoptotic activity of any of the gzms. In the absence of gzm B, gzms A, M, and H would all be candidates to fulfil a pro-apoptotic function, individually or jointly. Although CD3⁺CD56⁺ circulating NK cells expressed large amounts of gzmH, the very low numbers of circulating NKT cells in peripheral blood meant that it was not possible to determine whether unstimulated NKT cells also

express gzm H. To recover enough cells for analysis, we expanded the NKT cells in IL-2 and IL-7, raising the possibility that these stimuli may have down-regulated gzmH expression during *in vitro* culture.

The pattern of expression of gzm H protein was again quite distinct from that of gzm B in peripheral blood T lymphocytes that were stimulated in various ways in relatively short term cultures *in vitro*. All of the stimuli examined in this study led to very marked induction of gzmB protein, both in CD4+ and CD8+ PBMC. However, gzm H protein was expressed at low levels in CD4+ T cells but was not detected in CD8+ T cells and was not induced by mitogens and mediators of T cell activation including IL-2, PHA, concanavalin A, and anti-CD3 used alone or in various combinations. Collectively our data clearly indicate that gzmB and H, the products of very tightly linked genes, are nevertheless regulated in very distinct ways. Despite this, the real-time PCR data presented in this study also indicate that regulation of the *gzmH* gene is dissimilar to *CatG* as *CatG* mRNA is not found once myeloid cell maturation occurs. That is, the regulation of all three closely linked genes is unique.

By contrast with the monoclonal reagents used in this study, polyclonal antisera raised against gzm B (Fig. 1B) or gzm H (data not shown) were strongly reactive with both gzmB, as were 47/48 of the mAbs raised against recombinant gzmH. This indicates that at least one epitope shared between the two closely related gzmB is commonly recognized by mice and other species. Given the close structural similarities between human granzymes, we anticipated that it might be problematic to produce monospecific mouse antisera when we started to produce anti-gzm mAbs some years ago. Initially, our strategy was to identify stretches of the gzm amino acid sequence that were hydrophilic (suggesting orientation to the exterior of the protease) and polymorphic among the gzmB of that species. When we used synthetic polypeptides corresponding to such portions of gzm sequences to immunize mice, we identified an apparent immunodominant epitope mapping between residues 139 and 158 (using the amino-terminal isoleucine residue of processed gzm B as residue 1) (35). These peptides proved useful for producing monospecific mAbs for gzmB (2C5, used in the present study) (19) and gzmM (20). However, peptides from the corresponding region of gzm H largely produced mAbs (in many independent fusions) that were able to detect the immunizing peptide but not native gzmH (data not shown). The availability of recombinant, correctly folded gzmH produced in baculovirus-infected cells has allowed us to successfully revisit this difficult endeavor.

As with serological reagents, the current study also shows that full-length cDNA probes used in Northern blot analysis do not specifically detect either gzm B or H. Rather, we propose that shorter cDNAs spanning the unique 3'-untranslated regions of both genes are far more suitable for Northern blotting and related assays such as *in situ* hybridization. For other purposes, the use of gzm-specific primers for PCR amplification may be a suitable alternative. As the reagents purporting to detect gzm B are increasingly coming into use for diagnostic purposes both in inflammatory and neoplastic diseases (36–38), we urge extreme caution when interpreting results obtained with mAbs or DNA probes, the reactivity of which with other gzm family members and cathepsin G has not been adequately excluded.

REFERENCES

- Barry, M., and Bleackley, R. C. (2002) *Nat. Rev. Immunol.* 2, 401–409
- Trapani, J. A., and Smyth, M. J. (2002) *Nat. Rev. Immunol.* 2, 735–747
- Motyka, B., Korbitt, G., Pinkoski, M. J., Heibin, J. A., Caputo, A., Hobman, M., Barry, M., Shostak, I., Sawchuk, T., Holmes, C. F., Gaudie, J., and Bleackley, R. C. (2000) *Cell* 103, 491–500
- Trapani, J. A., Sutton, V. R., Thia, K. Y., Li, Y. Q., Froelich, C. J., Jans, D. A., Sandrin, M. S., and Browne, K. A. (2003) *J. Cell Biol.* 160, 223–233
- Froelich, C. J., Orth, K., Turbov, J., Seth, P., Gottlieb, R., Babior, B., Shah, G. M., Bleackley, R. C., Dixit, V. M., and Hanna, W. (1996) *J. Biol. Chem.* 271, 29073–29079
- Browne, K. A., Blink, E., Sutton, V. R., Froelich, C. J., Jans, D. A., and Trapani, J. A. (1999) *Mol. Cell Biol.* 19, 8604–8615
- Smyth, M. J., O'Connor, M. D., and Trapani, J. A. (1996) *J. Leukocyte Biol.* 60, 555–562
- Baker, E., Sayers, T. J., Sutherland, G. R., and Smyth, M. J. (1994) *Immunogenetics* 40, 235–237
- Smyth, M. J., Sayers, T. J., Wiltout, T., Powers, J. C., and Trapani, J. A. (1993) *J. Immunol.* 151, 6195–6205
- Haddad, P., Jenne, D., Tschopp, J., Clement, M. V., Mathieu-Mahul, D., and Sasportes, M. (1991) *Int. Immunol.* 3, 57–66
- Odake, S., Kam, C. M., Narasimhan, L., Poe, M., Blake, J. T., Krahenbuhl, O., Tschopp, J., and Powers, J. C. (1991) *Biochemistry* 30, 2217–2227
- Sutton, V. R., Davis, J. E., Cancilla, M., Johnstone, R. W., Ruefli, A. A., Sedelies, K., Browne, K. A., and Trapani, J. A. (2000) *J. Exp. Med.* 192, 1403–1414
- Sutton, V. R., Wolk, M. E., Cancilla, M., and Trapani, J. A. (2003) *Immunity* 18, 319–329
- Heusel, J. W., Wesselschmidt, R. L., Shresta, S., Russell, J. H., and Ley, T. J. (1994) *Cell* 76, 977–987
- Edwarda, K. M., Kam, C. M., Powers, J. C., and Trapani, J. A. (1999) *J. Biol. Chem.* 274, 30468–30473
- Johnson, H., Scorrano, L., Korsmeyer, S. J., and Ley, T. J. (2003) *Blood* 101, 3093–3101
- MacIvor, D. M., Phom, C. T., and Ley, T. J. (1999) *Blood* 93, 963–973
- Hohn, P. A., Popescu, N. C., Hanson, R. D., Salvesen, G., and Ley, T. J. (1989) *J. Biol. Chem.* 264, 13412–13419
- Trapani, J. A., Browne, K. A., Dawson, M., and Smyth, M. J. (1993) *Biochem. Biophys. Res. Commun.* 195, 910–920
- Smyth, M. J., O'Connor, M. D., Kelly, J. M., Ganesvaran, P., Thia, K. Y., and Trapani, J. A. (1995) *Biochem. Biophys. Res. Commun.* 217, 675–683
- Geisberg, M., Trapani, J. A., and Dupont, B. (1990) *Tissue Antigens* 35, 229–233
- Hirst, C. E., Buzza, M. S., Sutton, V. R., Trapani, J. A., Loveland, K. L., and Bird, P. I. (2001) *Mol. Hum. Reprod.* 7, 1133–1142
- Sayers, T. J., Brooks, A. D., Ward, J. M., Hoshino, T., Bere, W. E., Wiegand, G. W., Kelly, J. M., Smyth, M. J., and Kelley, J. M. (2001) *J. Immunol.* 166, 765–771
- Davis, J. E., S. V., Browne, K. A., and Trapani, J. A. (2003) *J. Immunol. Methods*
- Klein, J. L., Selvakumar, A., Trapani, J. A., and Dupont, B. (1990) *Tissue Antigens* 35, 220–228
- Sun, J., Bird, C. H., Sutton, V., McDonald, L., Coughlin, P. B., De Jong, T. A., Trapani, J. A., and Bird, P. I. (1996) *J. Biol. Chem.* 271, 27802–27809
- Sutton, V. R., Vaux, D. L., and Trapani, J. A. (1997) *J. Immunol.* 158, 5783–5790
- Trapani, J. A. (1998) *Int. Rev. Cytol.* 182, 111–192
- Liu, C. C., Rafii, S., Granelli-Piperno, A., Trapani, J. A., and Young, J. D. (1989) *J. Exp. Med.* 170, 2105–2118
- Smyth, M. J., Ortaldo, J. R., Shinkai, Y., Yagita, H., Nakata, M., Okumura, K., and Young, H. A. (1990) *J. Exp. Med.* 171, 1269–1281
- Trapani, J. A., Klein, J. L., White, P. C., and Dupont, B. (1988) *Proc. Natl. Acad. Sci. U. S. A.* 85, 6924–6928
- Hanson, R. D., C. N., Burnett, D., Campbell, E. J., Senior, R. M., and Ley, T. J. (1990) *J. Biol. Chem.* 265, 1524–1530
- Heusel, J. W., Hanson, R. D., Silverman, G. A., and Ley, T. J. (1991) *J. Biol. Chem.* 266, 6152–6158
- Kothapalli, R., Bailey, R. D., Kusmartseva, I., Mane, S., Epling-Burnette, P. K., and Loughran, T. P., Jr. (2003) *Int. J. Oncol.* 22, 33–39
- Apostolidia, V. A., Browne, K. A., Smyth, M. J., and Trapani, J. A. (1995) *Mol. Immunol.* 32, 909–917
- Tak, P. P., Spaeny-Dekking, L., Kraan, M. C., Breedveld, F. C., Froelich, C. J., and Hack, C. E. (1999) *Clin. Exp. Immunol.* 116, 366–370
- Medema, J. P., de Jong, J., Peltenburg, L. T., Verdegaa, E. M., Gorter, A., Bres, S. A., Franken, K. L., Hahne, M., Albar, J. P., Melief, C. J., and Offringa, R. (2001) *Proc. Natl. Acad. Sci. U. S. A.* 98, 11515–11520
- Netto, M. V., Fonseca, B. A., Dantas, M., Saber, L. T., Castro, M. C., and Ferraz, A. S. (2002) *Transplant Proc.* 34, 476–478

NEOPLASIA

Brief report

BCL2 protein expression parallels its mRNA level in normal and malignant B cells

Yulei Shen, Javeed Iqbal, James Z. Huang, Guimei Zhou, and Wing C. Chan

The regulation of B-cell lymphoma 2 (BCL2) protein expression in germinal center (GC) B cells has been controversial. Previous reports have indicated post-transcriptional regulation plays a dominant role. However, a number of recent studies contradicted these reports. Using real-time polymerase chain reaction (PCR) and Standardized Reverse Transcriptase-PCR (StaRT-PCR), we measured the level of mRNA expression in GC, mantle zone

(MNZ), and marginal zone (MGZ) cells from laser capture microdissection. Both quantitative RT-PCR measurements of microdissected GC cells from tonsils showed that GC cells had low expression of *BCL2* transcripts commensurate with the low protein expression level. These results are in agreement with microarray studies on fluorescence-activated cell sorter (FACS)-sorted cells and microdissected GC cells. We also examined *BCL2*

mRNA and protein expression on a series of 30 cases of diffuse large B-cell lymphoma (DLBCL) and found, in general, a good correlation. The results suggested that BCL2 protein expression is regulated at the transcriptional level in normal B cells and in the neoplastic cells in most B-cell lymphoproliferative disorders. (Blood. 2004;104:2936-2939)

© 2004 by The American Society of Hematology

Introduction

BCL2 was identified in follicular lymphoma (FL) cells, the neoplastic counterpart of normal germinal center (GC) B cells, with the t(14;18)(q32;q21) chromosomal translocation.^{1,2} Translocation of *BCL2* at 18q21 to the proximity of the immunoglobulin heavy chain (IgH) enhancer at 14q32 up-regulates *BCL2* gene expression and confers resistance to apoptosis. B-cell lymphoma 2 (*BCL2*) protein is expressed in 89% of FLs with t(14;18), in contrast to 25% of those without t(14;18).³ Normal GC B cells have a very low level of *BCL2* protein expression (Figure 1A). However, there were reports of high expression of *BCL2* mRNA in GC B cells,⁴⁻⁶ leading to the conclusion that *BCL2* protein expression is regulated at the posttranscriptional level. However, a number of recent studies contradicted the previous reports of high *BCL2* mRNA expression in GC B cells, including several microarray gene expression profiling studies (Figure 1B).⁷⁻¹¹

Microarrays do not provide a very precise measurement of mRNA level and the experiments were performed on fluorescence-activated cell sorter (FACS)-isolated cells. To obtain more precise measurements and to directly measure *BCL2* mRNA expression in GC B cells, we used real-time polymerase chain reaction (PCR) and Standardized Reverse Transcriptase-PCR (StaRT-PCR) studies to determine the level of *BCL2* transcripts in laser capture microdissected normal lymphoid tissues. We also compared the *BCL2* protein expression in 30 cases of diffuse large B-cell lymphoma (DLBCL) with microarray-determined *BCL2* mRNA expression levels. Our results clearly showed that GC B cells have low expression of *BCL2* transcripts paralleling the low protein expression level. There is also a good correlation between mRNA and protein expression in DLBCL.

Study design

Laser capture microdissection (LCM)

To detect mRNA expression of *BCL2* in normal GC, mantle zone (MNZ), and marginal zone (MGZ) cells, we dissected these 3 compartments from snap-frozen reactive tonsils or spleens using LCM (Arcturus PixCell II System, Mountain View, CA). DNA-free RNA was extracted using Absolutely RNA MicroRNA Isolation Kit (Stratagene, La Jolla, CA) and was reverse transcribed into cDNA for analysis. Informed consent was obtained, and the Institutional Review Board of the University of Nebraska approved this study.

Quantitative RT-PCR assay

The expression of *BCL2*, relative to the housekeeping gene β -actin (ACTB), was measured by real-time PCR as described previously.¹² StaRT-PCR is a competitive quantitative RT-PCR assay performed by Gene Express Inc (Toledo, OH).

Immunohistochemistry for BCL2

Formalin-fixed, paraffin-embedded 5- μ m tissue sections were stained with BCL2 (clone 24) antibody (Dako, Carpinteria, CA) as described previously.¹⁴ BCL2 immunostaining was scored semiquantitatively combining the intensity of staining with the proportion of cells positive for the stain (intensity of staining graded as 1+, 2+, and 3+; and the % of cells positive graded as 1+ [10%-25%], 2+ [25%-75%], 3+ [> 75%]; BCL2 protein index = intensity score \times numeric positive score).

Analysis of cDNA microarray data

We correlated BCL2 protein expression and *BCL2* mRNA level measured by cDNA microarray in a series of previously reported DLBCL cases.⁹ Of

From the Department of Pathology and Microbiology, University of Nebraska Medical Center, Omaha, NE; and Department of Pathology, Oregon University Health & Science Center, Portland, OR.

Submitted January 21, 2004; accepted June 10, 2004. Prepublished online as Blood First Edition Paper, July 8, 2004; DOI 10.1182/blood-2004-01-0243.

Supported in part by a National Cancer Institute (NCI) grant (CA84967), Department of Health and Human Services.

Reprints: Wing C. Chan, Department of Pathology and Microbiology, 983135 Nebraska Medical Center, Omaha, NE; e-mail: jchan@unmc.edu.

The publication costs of this article were delayed in part by page charge payment. Therefore, and solely to indicate this fact, this article is hereby marked "advertisement" in accordance with 18 U.S.C. section 1734.

© 2004 by The American Society of Hematology

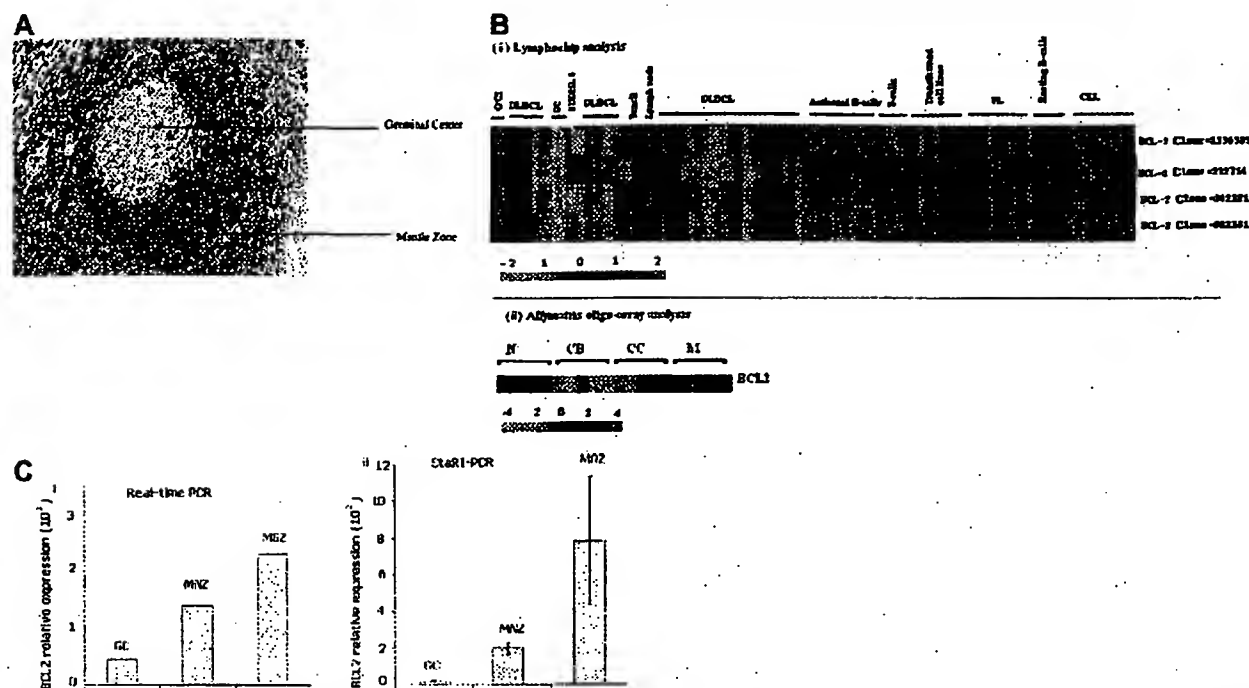


Figure 1. BCL2 expression in GC B cells. (A) BCL2 in paraffin-embedded reactive tonsil. The tissue section was stained with the avidin-biotin-peroxidase complex (ABC) method. GC B cells are negative for BCL2, whereas MNZ B cells show strong positive staining. Scattered BCL2-positive T cells are seen in the GC. The image was acquired using an Arcurus PixCell II microscope (Mountain View, CA); the image is 200× original magnification (20× objective) and was captured using the PixCell II Image Archiving workstation. (B) BCL2 mRNA expression on Lymphochip and oligonucleotide array. Previously published data revealed low expression of mRNA in GC B cells. (i) Lymphochip analysis.⁹ (ii) Affymetrix chip analysis.¹⁰ CB indicates centroblast; CC, centrocyte; N, naive B cell; and M, memory B cell. Also note the high expression of BCL2 message in CLL and FL. Only clone 232714 measures truncated transcripts resulting from translocation of the BCL2 gene at the major breakpoint region. (C) BCL2 expression in microdissected germinal center (GC), mantle zone (MNZ), and marginal zone (MGZ) cells measured by real-time PCR (i) and StaRT-PCR (ii). Standard deviation from 3 independent experiments is shown.

the 3 different BCL2 clones (232714, 342181, 1336385) on the Lymphochip microarray, only clone 232714 with a more 5' sequence could measure message with a truncated 3' end due to translocation at the major breakpoint region.¹⁴ However, clone 232714 is located far from the 3' end of the transcript and may fail to accurately measure the normal BCL2 transcripts. We used the mean values measured by the BCL2 clones that are located close to the 3' end (342181, 1336385) of the transcript to represent the gene expression level in cases where this mean value was greater than the measurement by clone 232714.

Results and discussion

BCL2 is an antiapoptosis factor important in normal B-cell development and differentiation.¹⁵ Previous reports showed that both naive and memory B cells have detectable BCL2 protein expression, whereas both centroblasts and centrocytes in normal GCs express very low levels of BCL2.⁷ There were a number of studies reporting that GC B cells contained abundant BCL2 mRNA and hence suggested that BCL2 protein expression may be regulated at a posttranscriptional level.⁴⁻⁶ We and others have observed low mRNA expression in gene expression profiling studies of purified GC B cells,⁹⁻¹² which contradict previous reports. In 2 previous studies using in situ hybridization, the oligonucleotide probe used was complementary to 105 to 134 of the translated region of BCL2 containing 100% G and C sequence. A basic local alignment search tool (BLAST) search of this sequence showed 18- to 19-bp stretches that are identical to known human transcripts (eg, HRY, HSVRG1) and might lead to nonspecific binding.

We used the more accurate quantitative PCR assays on microdissected whole GC, MNZ, and MGZ cells to provide independent confirmation of the microarray data. Real-time PCR showed that

naive and memory B cells expressed 4- to 10-fold more BCL2 mRNA than GC B cells, even though more T cells that expressed BCL2 mRNA were present in the GC than in the MNZ and MGZ compartments (Figure 1Ci). StaRT-PCR, a competitive quantitative PCR assay using BCL2 primers (F1 and R1) about 900 bp upstream of our real-time PCR primer pairs (F2 and R2; Table 1), confirmed the real-time PCR results (Figure 1Cii). BCL2 mRNA level in GC B cells (1.6×10^3 BCL2 molecules/ 10^6 ACTB molecules) was markedly lower than in MNZ cells (1.8×10^3 BCL2 molecules/ 10^6 ACTB molecules) and MGZ cells (7.8×10^3 BCL2 molecules/ 10^6 ACTB molecules; Figure 1C). These results on tissue compartments were in agreement with previous reports where FACS-sorted GC B cells had much lower expression of BCL2 than in activated and resting blood B cells and naive and memory B cells⁹ (Figure 1B). Microarray experiments showed an increased expression of

Table 1. BCL2 primers and probe sequences used in quantitative RT-PCR

Primers*	Sequence (5'-3')	Length of the product
F1	TTTATGAGAGACCGAGTCCG	392 bp (BCL2, exon 3)
R1	AGCCAAAGTGCATGTGCTA	StaRT-PCR
F2	TTGCTTTACGTGGCTGTTC	94 bp (BCL2, exon 3)
R2	GAGACCTTGAAGGACAGCCAT	Real-time PCR
BCL2 probe	FAM-CCGACCCAGAGCCCTCTGCC-TAMRA	

F indicates forward; and R, reverse.

*F1 and R1 were applied in StaRT-PCR and F2 and R2 were used in real-time PCR.

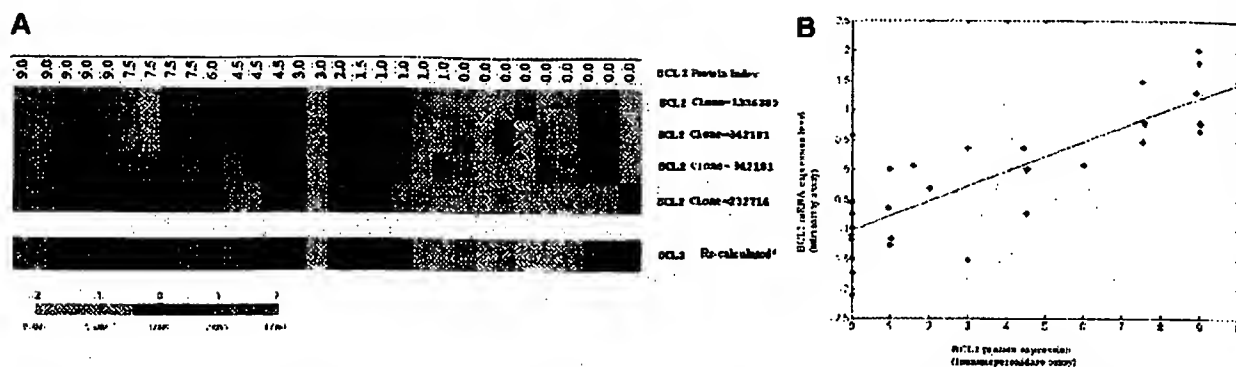


Figure 2. The correlation between *BCL2* protein and mRNA expression level. (A) Correlation of *BCL2* protein index with *BCL2* mRNA measured by cDNA microarray in 30 cases of DLBCL. Protein index was generated based on the scores of staining intensity and the percentage of positive cells with immunohistochemistry. RNA was measured with the Lymphochip microarray.⁹ Each row represents measurements by a separate cDNA clone on the microarray. Gene expression is represented by the ratio between each experimental mRNA sample to the reference mRNA standard and is depicted according to the color scale shown at the bottom. Gray indicates missing or excluded data. (B) Scatter plot between *BCL2* mRNA expression on cDNA microarray and *BCL2* protein index measured by immunohistochemistry. *BCL2* mRNA expression was calculated as detailed in "Study design" to more accurately reflect the true expression levels (*). The least squares fit line indicates good correlation ($r = 0.81$) of *BCL2* protein level with *BCL2* mRNA level.

BCL2 mRNA in follicular lymphoma (FL) and chronic lymphocytic leukemia (CLL), neoplastic conditions that are known to be very frequently *BCL2* protein positive. In DLBCL, *BCL2* mRNA expression was more variable. However, there is good correlation between *BCL2* protein expression level measured by immunohistochemistry and mRNA level measured from microarray analysis. (Figure 2B; $r = 0.81$).

Experiments using FACS-sorted and microdissected cell populations indicated that *BCL2* protein expression paralleled *BCL2* mRNA expression and *BCL2* transcript is not present at a high level in GC B cells as previously reported. Hence, *BCL2* protein expression in GCs is likely regulated at the transcriptional level. There is also a good correlation between *BCL2* mRNA and protein expression in B-cell neoplasias, suggesting that *BCL2* protein expression is similarly regulated in most B-cell malignancies (Figures 1B and 2A-B). However, our study does not exclude the presence of modified *BCL2* transcripts that may fine-tune the level of protein expression in certain situations.¹⁶

Recent studies have provided some insight on the transcriptional control of the *BCL2*. Two promoters, P1 (5') and P2 (3'), can regulate *BCL2* transcription,¹⁷ and P1 is the active one in normal B cells. Depending on the cell type and differentiation stage, various transcription factors and regulatory elements have been demon-

strated to regulate the expression of the *BCL2* gene. *BCL2* expression has been found to be regulated by transcription factors such as Aiolos and/or c-Myb in T cells,^{18,19} cyclic adenosine monophosphate (cAMP)-responsive element-binding proteins in B cells,²⁰ and the Brn-3a pou family proteins in neuronal cells.²¹ Transcription factors of the nuclear factor κ B (NF- κ B) family, such as p50 homodimers, may contribute to the enhancement of *BCL2* transcription.²² Negative regulatory elements that may interact with p53,²³ the Fts family proteins in pre-B cells,²⁴ and Rel/NF- κ B in pro-B cells have also been described.²⁵ In addition, Wilms tumor-1 (WT1) protein has been shown to repress *BCL2* activity in HeLa cells and B cells.²⁶ Further experiments on the transcriptional regulation of *BCL2* in the GC will lead to a better understanding of the mechanism controlling *BCL2* protein expression in B lymphocytes.

Acknowledgments

The authors wish to thank Robert S Wicker for his assistance in the real-time PCR assay and James C Lynch, Li Xiao and Lynette Smith for statistical analysis.

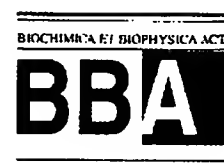
References

- Cleary ML, Smith SD, Sklar J. Cloning and structural analysis of cDNAs for bcl-2 and a hybrid bcl-2/immunoglobulin transcript resulting from the t(14;18) translocation. *Cell*. 1986;47:19-28.
- Tsujimoto Y, Finger LR, Yunis J, Nowell PC, Croce CM. Cloning of the chromosome breakpoint of neoplastic B cells with the t(14;18) chromosome translocation. *Science*. 1984;226:1097-1099.
- Skininder BF, Horsman DE, Dupuis B, Gascoyne RD. Bcl-6 and Bcl-2 protein expression in diffuse large B-cell lymphoma and follicular lymphoma: correlation with 3q27 and 18q21 chromosomal abnormalities. *Hum Pathol*. 1999;30:803-808.
- Akagi T, Kondo E, Yoshino T. Expression of Bcl-2 protein and Bcl-2 mRNA in normal and neoplastic lymphoid tissues. *Leuk Lymphoma*. 1994;13:81-87.
- Chleq-Deschamps CM, LeBrun DP, Huie P, et al. Topographical dissociation of BCL-2 messenger RNA and protein expression in human lymphoid tissues. *Blood*. 1993;81:293-298.
- Kondo E, Nakamura S, Onoue H, et al. Detection of bcl-2 protein and bcl-2 messenger RNA in normal and neoplastic lymphoid tissues by immunohistochemistry and in situ hybridization. *Blood*. 1992;80:2044-2051.
- Martinez-Velazquez H, Gurel C, de Bouteiller O, Fugier I, Banchereau J, Liu YJ. Human germinal center B cells express the apoptosis-inducing genes Fas, c-myc, P53, and Bax but not the survival gene bcl-2. *J Exp Med*. 1996;183:971-977.
- Lebecque S, de Bouteiller O, Arpin C, Banchereau J, Liu YJ. Germinal center founder cells display propensity for apoptosis before onset of somatic mutation. *J Exp Med*. 1997;185:563-571.
- Alizadeh AA, Eisen MB, Davis RE, et al. Distinct types of diffuse large B-cell lymphoma identified by gene expression profiling. *Nature*. 2000;403:503-511.
- Klein U, Tu Y, Stolovitzky GA, et al. Transcriptional analysis of the B cell germinal center reaction. *Proc Natl Acad Sci U S A*. 2003;100:2639-2644.
- Husson H, Ceridec EG, Neuberg D, et al. Gene expression profiling of follicular lymphoma and normal germinal center B cells using cDNA arrays. *Blood*. 2002;99:282-289.
- Klein U, Tu Y, Stolovitzky GA, et al. Gene expression profiling of B cell chronic lymphocytic leukemia reveals a homogeneous phenotype related to memory B cells. *J Exp Med*. 2001;194:1625-1638.
- Pan Z, Shen Y, Du C, et al. Two newly characterized germinal center B-cell-associated genes, GCET1 and GCET2, have differential expression in normal and neoplastic B cells. *Am J Pathol*. 2003;163:135-144.
- Huang JZ, Sanger WG, Greiner TC, et al. The t(14;18) defines a unique subset of diffuse large

- B-cell lymphoma with a germinal center B-cell gene expression profile. *Blood*. 2002;99:2285-2290.
15. Rajewsky K. Clonal selection and learning in the antibody system. *Nature*. 1986;381:751-758.
 16. Uhlmann EJ, Subramanian T, Vater CA, Lutz R, Chinnadurai G. A potent cell death activity associated with transient high level expression of BCL-2. *J Biol Chem*. 1998;273:17926-17932.
 17. Seto M, Jaeger U, Hockett RD, et al. Alternative promoters and exons, somatic mutation and down-regulation of the Bcl-2 Ig fusion gene in lymphoma. *EMBO J*. 1988;7:123-131.
 18. Salomoni P, Perrotti D, Martinez R, Franceschi C, Calabretta B. Resistance to apoptosis in CTLL-2 cells constitutively expressing c-Myb is associated with induction of BCL-2 expression and Myb-dependent regulation of bcl-2 promoter activity. *Proc Natl Acad Sci U S A*. 1997;94:3296-3301.
 19. Romero F, Martinez AC, Camonis J, Rebollo A. Aiolos transcription factor controls cell death in T cells by regulating Bcl-2 expression and its cellular localization. *EMBO J*. 1998;18:3419-3430.
 20. Wilson BE, Mochon E, Boxer LM. Induction of bcl-2 expression by phosphorylated CREB proteins during B-cell activation and rescue from apoptosis. *Mol Cell Biol*. 1996;16:5546-5556.
 21. Smith MD, Ensor EA, Coffin RS, Boxer LM, Latchman DS. Bcl-2 transcription from the proximal P2 promoter is activated in neuronal cells by the Brn-3a POU family transcription factor. *J Biol Chem*. 1998;273:16715-16722.
 22. Kurland JF, Kodym R, Story MD, Spurgers KB, McDonnell TJ, Meyn RE. NF-kappaB1 (p50) homodimers contribute to transcription of the bcl-2 oncogene. *J Biol Chem*. 2001;276:45380-45386.
 23. Miyashita T, Harigai M, Hanada M, Reed JC. Identification of a p53-dependent negative response element in the bcl-2 gene. *Cancer Res*. 1994;54:3131-3135.
 24. Chen HM, Boxer LM. Pi 1 binding sites are negative regulators of bcl-2 expression in pre-B cells. *Mol Cell Biol*. 1995;15:3840-3847.
 25. Sahur US, Dixit MN, Chen CL, Byrom MW, Kerr LA. Rel/NF-kappaB represses bcl-2 transcription in pro-B lymphocytes. *Gene Expr*. 1999;6:219-229.
 26. Heckman C, Mochon E, Arcinas M, Boxer LM. The WT1 protein is a negative regulator of the normal bcl-2 allele in t(14;18) lymphomas. *J Biol Chem*. 1997;272:19609-19614.



Biochimica et Biophysica Acta 1368 (1998) 129–136



Quantitative determinations of the steady state transcript levels of hexokinase isozymes and glucose transporter isoforms in normal rat tissues and the malignant tumor cell line AH130

Yasuo Shinohara^{*}, Kenji Yamamoto, Katsuyuki Inoo, Naoshi Yamazaki, Hiroshi Terada

Faculty of Pharmaceutical Sciences, University of Tokushima, Shomachi-1, Tokushima 770, Japan

Received 19 March 1997; revised 29 July 1997; accepted 31 July 1997

Abstract

The steady state transcript levels of the four hexokinase (HK) isozymes and four glucose transporter (GLUT) isoforms were determined quantitatively by Northern analysis of RNA samples from rat tissues using synthetic fragments of the RNAs encoding the HK isozymes and GLUT isoforms. Results showed that the levels of HK isozyme transcripts were low in rat tissues, the level of that most highly expressed, the type I isozyme (HKI), in the brain being 0.025% of the total poly(A)⁺ RNA. A good correlation was found between the reported HK activities and the total amounts of transcripts encoding all HK isozymes in various tissues, showing that the HK activities in tissues can be estimated from the total amount of transcripts encoding HK isozymes. The proposed associated expressions of HK isozymes and GLUT isoforms in particular tissues were confirmed at their transcript levels. The steady state transcript levels of type II HK and the type I GLUT isoform in the malignant tumor cell line AH130 were also determined quantitatively. © 1998 Elsevier Science B.V.

Keywords: Hexokinase; Glucose transporter; Energy metabolism; Northern blotting; Quantitative evaluation of transcript levels

1. Introduction

The uptake of glucose and its phosphorylation are major processes in cellular glucose metabolism. In mammalian cells, four isoforms of the transporter (GLUT1 to GLUT4) are known to facilitate the uptake of glucose through the plasma membrane (for recent reviews, see [1–5]). GLUT1 is expressed in a variety of tissues, and so is thought to be responsible

for “basal” glucose uptake in various cells. On the other hand, the expressions of the other isoforms are tissue specific: GLUT2 is predominantly expressed in the liver, pancreatic β -cells, small intestine and kidney, GLUT3 in the brain, and GLUT4 in muscles and adipose tissue [1–5].

The first step in the sequential reactions in glucose metabolism is catalyzed by the four (type I to IV) isozymes of hexokinase (HK) (for reviews, see [6,7]). As type I HK (HKI) is expressed predominantly in all tissues except skeletal muscle and liver, it is considered as the “basic” HK, like GLUT1 of the GLUT isoforms. Expression of the type II isozyme (HKII) is highest in skeletal muscle and adipose tissue, that of the type III isozyme (HKIII) at very low levels in all tissues, and that of the type IV isozyme (HKIV),

Abbreviations: GLUT, glucose transporter; HK, hexokinase; SSC, saline sodium citrate; RT-PCR, reverse transcription followed by the polymerase chain reaction; BAT, brown adipose tissue; WAT, white adipose tissue

^{*} Corresponding author. Fax: +81 886 33 5196; E-mail: yasuo@ph.tokushima-u.ac.jp

0005-2736/98/\$19.00 © 1998 Elsevier Science B.V. All rights reserved.
PII S0005-2736(97)00189-2

usually known as glucokinase (GK), at high levels in the liver and pancreatic β -cells (for reviews, see [8–10]).

Based on these tissue specific distributions of the GLUT isoforms and HK isozymes, their associated expressions have been postulated [9,10]: GLUT1 with HKI, GLUT4 with HKII, and GLUT2 with HKIV. However, these combinations were mainly concluded from the qualitative transcript levels of the GLUT isoforms and enzymic activities of the HK isozymes. For understanding the mechanisms controlling energy metabolism in various tissues, quantitative comparison of their transcript levels in various tissues is of importance. Therefore, in this study, we analyzed the steady state transcript levels of GLUT isoforms and HK isozymes quantitatively using synthesized RNA fragments. We also determined the transcript levels of HKII and GLUT1 in the malignant tumor cell line AH130.

2. Materials and methods

2.1. Materials

Isogen, used in purification of RNA, and an in vitro RNA synthesis kit were purchased from Nippon Gène (Tokyo). *Taq* DNA polymerase, a *BcaBEST* DNA labeling kit and Oligotex dT <super> were from TaKaRa Shuzo (Kyoto). [α - 32 P]dCTP (specific radioactivity, 111 TBq/mmol) was from Amersham (Bucks., U.K.). The multifunctional phagemids pTZ18R and pTZ19R were obtained from Toyobo (Osaka) and from Riken DNA Bank (Wako), respectively.

2.2. Construction of plasmids and preparation of cDNA probes

All cDNA fragments except that of HKI were prepared by RT-PCR as described previously [11,12] using first strand cDNAs prepared by reverse transcription of mRNA as templates. The cDNA fragments of GLUT isoforms with nucleotide sequences 414–929 for GLUT1 [13], 507–951 for GLUT2 [14], 278–771 for GLUT3 [15] and 242–799 for GLUT4 [16] and those of HK isozymes with nucleotide sequences of 1615–2133 for type II [17], 2250–2677 for type III [18] and 116–696 for type IV [19] were

amplified. A cDNA clone of rat HKI was obtained from a cDNA library of rat heart (Clontech, code RL1006b). The inserted cDNA fragment of HKI was subcloned into pUC19 vector using restriction sites of *EcoRI* that were added artificially during preparation of the library. From this plasmid, a cDNA fragment of about 510bp corresponding to nucleotides 937–1452 [20], prepared by digestion with *EcoRI* and *NcoI*, was used for construction of the expression vector. These cDNA fragments were subcloned into the multifunctional phagemid pTZ18R or pTZ19R, and after confirmation of their nucleotide sequences, the plasmids obtained were digested with the restriction endonucleases at the multicloning sites. The inserted cDNA fragments were gel-purified and used as probes in Northern blotting. As we used different regions of the entire cDNAs encoding GLUT isoforms and HK isozymes as probes, the cross-hybridizations between probes and RNA samples could not be examined by Northern blot analysis. However, on use of high stringency hybridization conditions, the degrees of cross-hybridizations of all probes used in this study were estimated to be less than 5% by Southern blot analysis (data not shown).

2.3. Preparations poly(A)⁺ RNA samples from rat various tissues

RNA samples of various tissues were obtained from 4-week old male Wistar rats fed on standard laboratory chow with water ad libitum at 24°C. Tissues from five rats were pooled and total RNAs were purified with Isogen by the method recommended by the supplier, which was essentially based on the report of Chomczynski and Sacchi [21]. Poly(A)⁺ RNA was purified from total RNA using oligotex dT <super>.

2.4. Preparation of synthetic RNA fragments

Fragments of the RNAs encoding GLUT isoforms and HK isozymes were prepared as follows. First, for obtaining double stranded linear DNA, the expression vectors prepared as described above were digested at the 3'-terminus of the inserted cDNA fragment and digested plasmids were precipitated with ethanol. With 1.0 μ g samples of these linearized DNAs as templates, the RNA fragments encoding GLUT iso-

forms and HK isozymes were transcribed using T7 RNA polymerase. After complete digestion of template DNA with DNaseI, synthesized RNA fragments were purified by phenol/chloroform extraction and then repeated ethanol precipitation. The concentrations of RNA samples were determined spectrophotometrically in a Shimadzu spectrophotometer, model UV-160.

2.5. Northern blotting and quantitative determination of transcript levels

Northern blotting was carried out essentially as described previously [22,23]. Briefly, RNA was subjected to electrophoresis in 1.0% agarose containing formaldehyde, transferred to a nitrocellulose membrane, and hybridized by the standard procedure. Unless otherwise noted, samples of 1.0 μ g of poly(A)⁺ RNA obtained from various normal tissues of Wistar rats and 10–100 pg of synthesized RNA fragments were used for analyses. After hybridization with probes, the membranes were washed three times with 2 \times saline sodium citrate (SSC) containing 0.1% SDS at room temperature for 10 min and twice with 1 \times SSC containing 0.1% SDS at 60°C for 30 min each time and exposed to X-ray film with an intensifying screen at –80°C. The amount of each transcript was determined from its intensity in the autoradiogram with an ATTO image analyzer model AE-6900 connected to a Macintosh model Quadra 650. The amount of each transcript was normalized based on the intensity of the hybridization signal observed with the corresponding synthesized RNA fragment.

For staining of the transferred RNA, the membrane was first soaked in 5% acetic acid for 15 min, then immersed in solution containing 0.04% methylene blue and 500 mM sodium acetate (pH 5.2) for 10 min and washed with water for 10 min.

3. Results

3.1. Purity of synthesized RNA samples

For quantitative evaluation of transcript levels, it is important to determine the exact concentrations of synthesized RNA samples and their high purities. Contaminating free nucleotides in the RNA samples

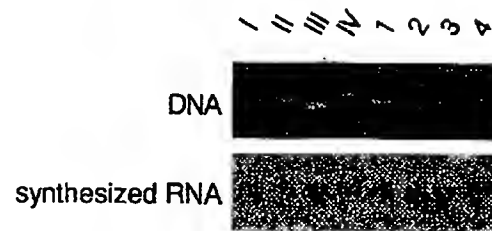


Fig. 1. Denaturation agarose gel electrophoresis of synthesized RNA samples of HK isozymes and GLUT1 isoforms. After synthesis of RNAs, template DNAs were completely digested with DNaseI. Then after elimination of the DNaseI by phenol/chloroform extraction, RNA samples were purified by repeated ethanol precipitation. For confirmation of their purities and concentrations, a fixed amount of each RNA sample (2.5 μ g) was subjected to electrophoresis in denaturing agarose gel. The RNA samples were transferred to a nitrocellulose membrane and stained by methylene blue. 1 to IV and 1–4 represent RNA samples of HKI to HKIV and GLUT1 to GLUT4, respectively. The panel labeled “DNA” shows results on electrophoresis of the cDNA fragments used as probes in non-denaturing agarose gel.

used as substrates in RNA synthesis would increase the “apparent” concentration of RNA samples. Thus, we first purified synthesized RNA samples by repeated ethanol precipitation to eliminate contaminating free nucleotides completely. The extent of elimination of free nucleotides from the synthesized RNA samples was examined by measuring the optical absorbance of the filtrate obtained by centrifugation of RNA samples in Ultrafree C3-LGS (Millipore, cut-off M.W. = 10000) at 4500 $\times g$ for 20 min and was concluded to be negligible in all RNA samples (data not shown). Then, after determination of the concentrations of synthesized RNA samples from their absorbances, we further examined the purities and amounts of RNA by denaturing agarose gel electrophoresis. As shown in Fig. 1, results showed that all the synthesized RNA samples gave a single band of the same intensity at the expected site of migration. Therefore, their purities were concluded to be high enough for further quantitative analyses.

3.2. Steady state transcript levels of HK isozymes in rat tissues

Next, we analyzed the steady state transcript levels of the four HK isozymes in rat normal tissues. For this, samples of 1.0 μ g of poly(A)⁺ RNA obtained from rat brain, heart, kidney, liver, skeletal muscle,

and white and brown adipose tissues (WAT and BAT) were subjected to electrophoresis and transferred on nitrocellulose membranes. Four membranes with each of these samples prepared in this way were used for hybridization with probes. As shown in Fig. 2, the transcript of HKI was observed in all tissues except liver; the signal was strongest in the brain, and the intensities in the heart, kidney and WAT were almost the same, while those in skeletal muscle and BAT were very weak. The signal of HKII was weak in heart, skeletal muscle and adipose tissues. HKIII gave no significant signal except a weak one in brain. Expression of HKIV was only observed in the liver.

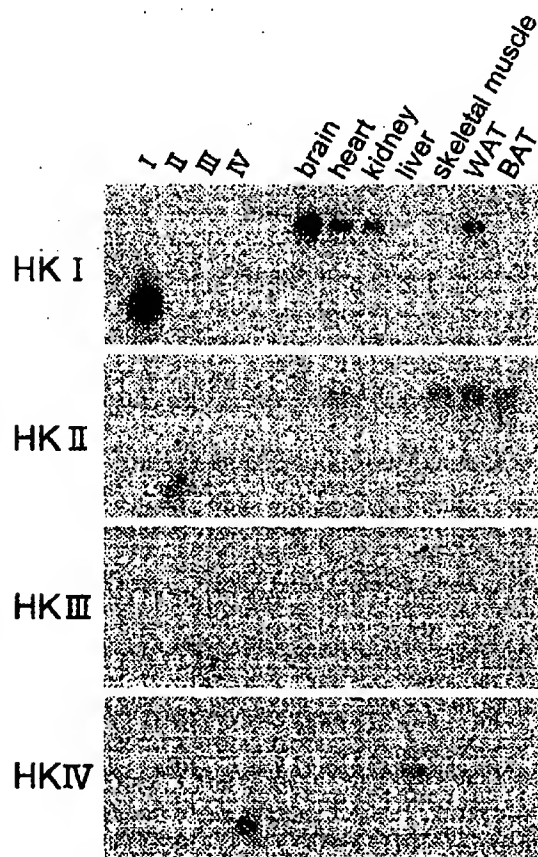


Fig. 2. Steady state transcript levels of the four HK isozymes in various rat tissues. Samples of 1 μ g of poly(A)⁺ RNA obtained from various tissues were subjected to denaturing agarose gel electrophoresis, transferred to nitrocellulose membranes and hybridized with probes. I to IV show results for synthesized RNA samples encoding HKI to HKIV, respectively.

3.3. Quantitative determinations of the steady state transcript levels of HK isozymes

In general, the steady state transcript levels of particular proteins in various tissues can be compared by the intensities of their hybridization bands, as described above. However, it is difficult to compare the amounts of the transcripts of different isoforms or isozymes exactly due to the different specific radioactivities and the affinities of the probes with transcripts. Therefore, we measured the intensities of hybridization bands with known amounts of synthesized RNA fragments used as standards. As the steady state transcript levels of these four HK isozymes were markedly different in various tissues, we used various amounts of RNA fragments of the four isozymes to determine the amount of each transcript exactly; 100 pg for HKI, 20 pg for HKII, 10 pg for HKIII, and 20 pg for HKIV. As the hybridization intensity of the synthesized RNA fragment of HKII used as external standard was not different from that in the presence of poly(A)⁺ RNAs of WAT, it was concluded that presence of irrelevant RNAs did not cause any changes in the hybridization intensities of synthesized RNA fragments. In addition, we examined the purity of poly(A)⁺ RNA from the steady state transcript levels of β -actin in these RNA samples. Results showed that the transcript levels of β -actin were not markedly different in RNA samples from various tissues (data not shown). Therefore, the transcript levels of these HK isozymes in different tissues could be determined quantitatively based on the assumption that the probes hybridize with the synthesized RNA fragments and transcripts in various tissues equally and gave the same signal intensity.

Table 1 shows normalized values for the steady state transcript levels of HK isozymes in various tissues. HKI, the most abundantly expressed HK isozyme, was found in the brain at a level of 0.382 fmol/ μ g of poly(A)⁺ RNA. Of the four isozymes, the level of HKIII was the lowest, its highest level being only 0.006 fmol/ μ g of poly(A)⁺ in the brain. Assuming that the average length of transcripts was 2.0 kb, the total amount of transcripts in 1.0 μ g of poly(A)⁺ RNA was calculated to be 1.52 pmol. Therefore, even in the brain, the amount of transcripts encoding HKI was estimated to be only 0.025% of the total poly(A)⁺ RNA, indicating a very

Table 1
Amounts of transcripts encoding the four isozymes of hexokinase in normal rat tissues

Tissue	HKI	HKII	HKIII	HKIV	Total (relative amount in %)
Brain	0.382	0.010	0.006	ND	0.398 (100)
Heart	0.130	0.074	ND	ND	0.204 (51.3)
Kidney	0.079	ND	ND	ND	0.079 (19.8)
Liver	ND	ND	ND	0.058	0.058 (14.6)
Muscle	0.009	0.112	ND	ND	0.121 (30.4)
WAT	0.101	0.170	ND	ND	0.271 (68.1)
BAT	0.007	0.156	ND	ND	0.163 (41.0)

Values are shown in fmol/ μ g poly(A)⁺ RNA. Numbers in parentheses in the column labeled "total" represent the sum of each transcript relative to that in brain. WAT and BAT: white adipose tissue and brown adipose tissue, respectively. ND: no hybridized band, or too low signal intensity to be analyzed.

low level of transcripts of HK isozymes. The total amounts of the transcripts encoding these HK isozymes in various tissues were determined from the sum of amounts of the transcripts of all the HK isozymes. Results indicated that HKI and HKII are the major determinants of the steady state transcript level of the HK isozymes.

3.4. Quantitative analysis of steady state transcript levels of GLUT isoforms in various tissues

Next, we determined the amounts of the transcripts encoding the four GLUT isoforms in RNA samples obtained from various rat tissues in the same way as for HK isozymes. As shown in Fig. 3, the tissue distributions of these four GLUT isoforms were essentially the same as those reported previously [13–16,24–26]. For quantification of the transcript levels, Northern blot analysis was performed with fixed amounts of synthesized RNA fragments; 50 pg for GLUT1, 100 pg for GLUT2, 20 pg for GLUT3 and 100 pg for GLUT4. From the hybridization intensities of these RNA fragments, the amounts of transcripts were determined quantitatively as summarized in Table 2.

The transcribed levels of HK isozymes in various tissues were markedly different, but those of the GLUT isoforms were less, the maximum difference being about 5-fold between the highest level of GLUT4 in muscle (0.699 fmol/ μ g of poly(A)⁺) and the lowest level of GLUT3 in the brain (0.139 fmol/ μ g of poly(A)⁺ RNA). In addition, the results in Tables 1 and 2 showed the specific association of the expressions of certain HK isozymes and

GLUT isoforms, as suggested previously [9,10]: HKI with GLUT1, HKII with GLUT4 and HKIV with GLUT2.

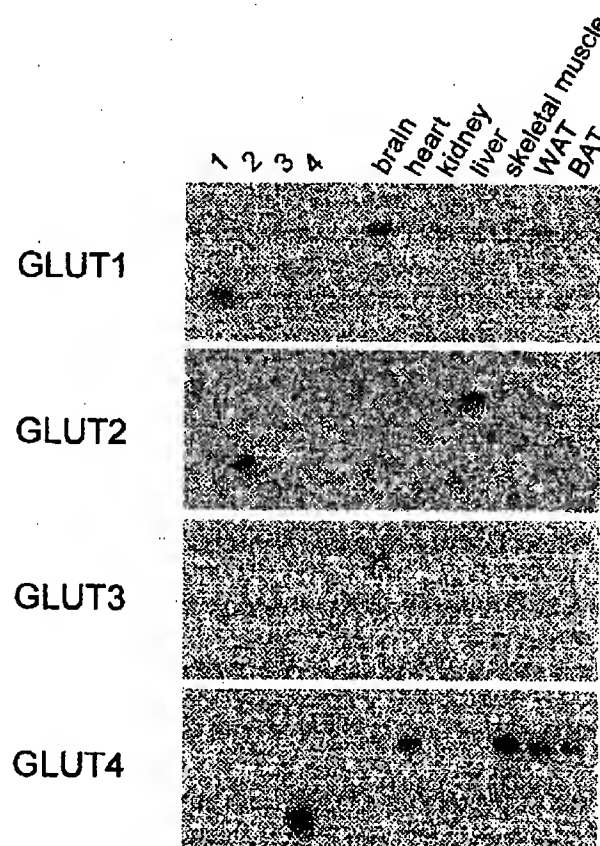


Fig. 3. Steady state transcript levels of the four GLUT isoforms in various rat tissues. Samples of 1 μ g of poly(A)⁺ RNA from the indicated tissues were analyzed as described in the legend of Fig. 2. Results for synthetic RNA samples encoding GLUT1 to GLUT4 are shown in columns 1–4.

Table 2

Amounts of transcripts encoding the four GLUT isoforms in normal rat tissues

Tissue	GLUT1	GLUT2	GLUT3	GLUT4	Total (relative amount in %)
Brain	0.297	ND	0.139	ND	0.436 (100)
Heart	0.019	ND	ND	0.288	0.307 (70.4)
Kidney	0.076	ND	ND	0.018	0.094 (21.6)
Liver	ND	0.616	ND	ND	0.616 (141.3)
Muscle	0.011	ND	ND	0.699	0.710 (162.8)
WAT	0.090	ND	0.045	0.464	0.599 (137.4)
BAT	ND	ND	ND	0.239	0.239 (54.8)

Values are shown in fmol/ μ g poly(A)⁺ RNA. For details, see legend to Table 1.

3.5. Quantitative analysis of steady state transcript levels of GLUT1 and HKII in the malignant tumor cell line AH130

We found previously that the steady state transcript level of HKII was specifically and remarkably elevated in a synchronized manner with that of GLUT1, in rapidly growing poorly differentiated malignant tumor cell lines such as rat AH130 [12,23]. Therefore, we next determined their absolute amounts in AH130 cells by the method described above. The amounts of the transcripts encoding HKII and GLUT1 expressed in AH130 cells were determined to be 2.5 and 18.5 fmol/ μ g of poly(A)⁺ RNA, respectively. These values are significantly greater than those observed in normal tissues. As described above, the highest transcript level of HKII was observed in white adipose tissue (0.170 fmol/ μ g of poly(A)⁺ RNA) and that of GLUT1 in the brain (0.297 fmol/ μ g of poly(A)⁺ RNA). Namely, the transcript levels of HKII and GLUT1 in AH130 cells were approximately 15 and 62 times those in normal tissues, respectively, corresponding to about 0.16% and 1.22% of the total poly(A)⁺ RNA species, respectively.

4. Discussion

The transcript levels of particular proteins have usually been compared by northern blot analysis using the same amounts of mRNAs. However, this is not possible for quantitative determination of the transcript levels of different mRNA species due to the differences in the specific radio activities and affinities of the probes. For quantitative determina-

tion of the transcript levels of proteins in various tissues by Northern analysis, the intensities of hybridization bands of mRNA samples with probes must be normalized by the hybridization intensities with exact amounts of synthesized RNA fragments. By this procedure, the amount of a steady state transcript encoding certain protein can be determined exactly and compared with those of other proteins. To our knowledge, this method was first carried out by Stepien et al. [27] for determination of the transcript levels of three isoforms of the human mitochondrial adenine nucleotide translocator (ANT1-3) in various tissues.

In this study, based on the method of Stepien et al. [27], we determined the "absolute" amounts of the HK isozymes and GLUT isoforms transcribed. For this, we first synthesized RNAs of HK isozymes and GLUT isoforms and determined their concentrations exactly. Then, we determined their steady state transcript levels quantitatively in normal rat tissues and the transcript levels of HKII and GLUT1 in the malignant tumor cell line AH130. Results showed that the transcript level of HKI in the kidney was as low as 0.0052% of the total poly(A)⁺ RNA (Table 1, 0.079 fmol/ μ g of poly(A)⁺ RNA (= 1.52 pmol)). This value was in accordance with the results of cDNA screening. Namely, Nishi et al. [29] reported that on molecular cloning of cDNA clones encoding HKI from a cDNA library of human kidney, 79 clones of 1×10^6 phages gave positive signal in the first screening. This finding indicates that the amount of HKI mRNA is 0.0079% of the total mRNA. Similarly, from the yield of glucokinase from the liver, the content of glucokinase in total liver proteins was estimated to be as low as 0.005% by Andreone et al. [19]. The present study indicated a similar value of

0.0038% (Table 1). Thus, the results of the present study are in accord with reported results. In this study, we expressed the amount of a particular mRNA relative to total poly(A)⁺ RNAs in the tissue cells. When the total amount of poly(A)⁺ RNAs in cells changes markedly, description of the amount of transcript relative to the total amount of cellular DNA might be useful.

The total amounts of transcripts encoding the four HK isozymes in various tissues were determined from the sums of the amounts of each transcript as shown in Table 1. The relative transcript levels in various tissues were in the order, brain (100), white adipose tissue (68), heart (51), brown adipose tissue (41), skeletal muscle (30), kidney (20) and liver (15). It is interesting that the same order was observed in the HK activity in various tissues except skeletal muscle, although the specific enzyme activities of HK isozymes were different, being in the order: brain (100), heart (62), kidney (49), liver (15) and skeletal muscle (10) [30]. Therefore, the sum of the amounts of transcripts could be a useful parameter of the total HK activities in various tissues. The exceptional low HK activity in skeletal muscle from that expected by the steady state transcript level could be because expression of the most abundant type II HK in skeletal muscle is known to depend greatly on the contractile activity (more than 30-fold) [31]. Therefore, the activity and transcript level of HKII in skeletal muscle may vary remarkably in different samples.

We confirmed in this study that a certain HK isozyme is expressed in association with a particular GLUT isoform in various tissues: HKI with GLUT1, HKII with GLUT4, and HKIV(GK) with GLUT2 [9,10]. Therefore, the expressions of these HK isozymes and GLUT isoforms could be regulated by the same mechanisms. The molecular mechanisms of the transcriptional regulations of GLUT isoforms and HK isozymes in various tissues has been studied extensively [8–10,32,33], but it is still unknown whether the expressions of HK isozymes in a particular tissue are regulated by the same mechanism as those of the GLUT isoforms. To understand the mechanisms regulating energy metabolism in various tissues, it is important to examine how the associated expressions of HK isozymes and GLUT isoforms in tissues are regulated.

According to the "general association" concept

[9,10], expression of HKI is associated with that of GLUT1 in normal tissues. Recently, we found a novel association of HKII with GLUT1 in various malignant tumor cells (submitted for publication and also Ref. [12]). This finding was confirmed by quantitative determinations of the transcript levels of HKII and GLUT1 in AH130 cells, which showed that the transcriptional regulations of HKII and GLUT1 in malignant tumor cells are different from those in normal tissues. Recently, two enhancer elements that are responsive to serum, growth factor and oncogenes were found in the gene encoding the GLUT1 isoform [33]. The gene encoding HKII has been studied extensively [11,12,28,34–40], but the mechanism of its transcriptional regulation during carcinogenesis is not yet understood. Studies on the molecular mechanism of its transcriptional regulation in relation to that of the GLUT1 gene in tumor cells are in progress.

References

- [1] C.F. Bruant, W.I. Sivitz, H. Fukumoto, T. Kayano, S. Nagamatsu, S. Seino, J.E. Pessin, G.I. Bell, *Recent Prog. Horm. Res.* 47 (1991) 349–387.
- [2] J.E. Pessin, G.I. Bell, *Annu. Rev. Physiol.* 54 (1992) 911–930.
- [3] G.I. Bell, C.F. Bruant, J. Takeda, G.W. Gould, *J. Biol. Chem.* 268 (1993) 19161–19164.
- [4] G.W. Gould, G.D. Holman, *Biochem. J.* 295 (1993) 329–341.
- [5] S.A. Baldwin, *Biochim. Biophys. Acta* 1154 (1993) 17–49.
- [6] J.E. Wilson, in: R. Beitner (Ed.), *Regulation of Carbohydrate Metabolism*, vol. I, CRC Press, Boca Raton, 1985, pp. 45–85.
- [7] J.E. Wilson, *Rev. Physiol. Biochem. Pharmacol.* 126 (1995) 65–198.
- [8] P.B. Iynedjian, *Biochem. J.* 293 (1993) 1–13.
- [9] R.L. Printz, M.A. Magnuson, D.K. Granner, *Annu. Rev. Nutr.* 13 (1993) 463–496.
- [10] S.J. Pilkis, I.T. Weber, R.W. Harrison, G.I. Bell, *J. Biol. Chem.* 269 (1994) 21925–21928.
- [11] K. Kogure, Y. Shinohara, H. Terada, *J. Biol. Chem.* 268 (1993) 8422–8424.
- [12] Y. Shinohara, K. Yamamoto, K. Kogure, J. Ichihara, H. Terada, *Cancer Lett.* 82 (1994) 27–32.
- [13] M.J. Birnbaum, H.C. Haspel, O.M. Rosen, *Proc. Natl. Acad. Sci. U.S.A.* 83 (1986) 5784–5788.
- [14] B. Thorens, H.K. Sarkar, H.R. Kaback, H.F. Lodish, *Cell* 55 (1988) 281–290.
- [15] S. Magamatsu, H. Sawa, K. Kamada, Y. Nakamichi, K. Yoshimoto, T. Hoshino, *FEBS Lett.* 334 (1993) 289–295.

- [16] M.J. Birnbaum, *Cell* 57 (1989) 305-315.
- [17] A.P. Thelen, J.E. Wilson, *Arch. Biochem. Biophys.* 286 (1991) 645-651.
- [18] D.A. Schwab, J.E. Wilson, *Arch. Biochem. Biophys.* 285 (1991) 365-370.
- [19] T.L. Andreone, R.L. Printz, S.J. Pilgis, M.A. Magnuson, D.K. Granner, *J. Biol. Chem.* 264 (1989) 363-369.
- [20] D.A. Schwab, J.E. Wilson, *Proc. Natl. Acad. Sci. U.S.A.* 86 (1989) 2563-2567.
- [21] P. Chomczynski, N. Sacchi, *Anal. Biochem.* 162 (1987) 156-159.
- [22] A. Shima, Y. Shinohara, K. Doi, H. Terada, *Biochim. Biophys. Acta* 1223 (1994) 1-8.
- [23] Y. Shinohara, J. Ichihara, H. Terada, *FEBS Lett.* 291 (1991) 55-57.
- [24] J.S. Flier, M. Mueckler, A.L. McCall, H.F. Lodish, *J. Clin. Invest.* 79 (1987) 657-661.
- [25] D.E. James, M. Strube, M. Mueckler, *Nature* 38 (1989) 883-887.
- [26] M.J. Charron, F.C. Brosius III, S.L. Alper, H.F. Lodish, *Proc. Natl. Acad. Sci. U.S.A.* 86 (1989) 2535-2539.
- [27] G. Stjepien, A. Torroni, A.B. Chung, J.A. Hodge, D.C. Wallace, *J. Biol. Chem.* 267 (1992) 14592-14597.
- [28] R.L. Printz, S. Koch, L.R. Potter, R.M. O'Doherty, J.J. Ticsinga, S. Moritz, D.K. Granner, *J. Biol. Chem.* 268 (1993) 5209-5219.
- [29] S. Nishi, S. Seino, G.I. Bell, *Biochem. Biophys. Res. Commun.* 157 (1988) 937-948.
- [30] M. Dixon, E.C. Webb, *Enzymes*, 3rd edition, Longman, London, 1979, pp. 634-636.
- [31] F.E. Weber, D. Pette, *FEBS Lett.* 238 (1988) 71-73.
- [32] K.H. Kaestner, R.J. Christy, J.C. McLennan, L.T. Braiterman, P. Cornelius, P.H. Pekala, M.D. Lane, *Proc. Natl. Acad. Sci. U.S.A.* 86 (1989) 3150-3154.
- [33] T. Murakami, T. Nishiyama, T. Shirotani, Y. Shinohara, M. Kan, K. Ishii, F. Kanai, S. Nakazuru, Y. Ebina, *J. Biol. Chem.* 267 (1992) 9300-9306.
- [34] M. Malkki, M. Laakso, S.S. Deeb, *Biochem. Biophys. Res. Commun.* 205 (1994) 490-496.
- [35] J. Ichihara, Y. Shinohara, K. Kogure, H. Terada, *Biochim. Biophys. Acta* 1260 (1995) 365-368.
- [36] S.P. Mathupala, A. Rempel, P.L. Pedersen, *J. Biol. Chem.* 270 (1995) 16918-16925.
- [37] A. Rempel, S.P. Mathupala, C.A. Griffin, A.L. Hawkins, P.L. Pedersen, *Cancer Res.* 56 (1996) 2468-2471.
- [38] A. Rempel, S.P. Mathupala, P.L. Pedersen, *FEBS Lett.* 385 (1996) 233-237.
- [39] H. Osawa, C. Sutherland, R.B. Robey, R.L. Printz, D.K. Granner, *J. Biol. Chem.* 271 (1996) 16690-16694.
- [40] H. Osawa, R.B. Robey, R.L. Printz, D.K. Granner, *J. Biol. Chem.* 271 (1996) 17296-17303.

Photochemistry and Photobiology, 2002, 75(3): 302-310

UVA Irradiation-induced Activation of Activator Protein-1 is Correlated with Induced Expression of AP-1 Family Members in the Human Keratinocyte Cell Line HaCaT¹

Amy L. Silvers and G. Timothy Bowden*

Department of Radiation Oncology, Arizona Cancer Center, The University of Arizona, Tucson, AZ

Received 17 October 2001; accepted 7 December 2001

ABSTRACT

To determine whether the transcription factor activator protein-1 (AP-1) could be modulated by ultraviolet A (UVA) exposure, we examined AP-1 DNA-binding activity and transactivation after exposure to UVA in the human immortalized keratinocyte cell line HaCaT. Maximal AP-1 transactivation was observed with 250 kJ/m² UVA between 3 and 4 h after irradiation. DNA binding of AP-1 to the target 12-O-tetradecanoylphorbol-13-acetate response element sequence was maximally induced 1-3 h after irradiation. Both *de novo* transcription and translation contributed to the UVA-induced AP-1 DNA binding. c-Fos was implicated as a primary component of the AP-1 DNA-binding complex. Other components of the complex included Fra-2, c-Jun, JunB and JunD. UVA irradiation induced protein expression of c-Fos, c-Jun, Fra-1 and Fra-2. Phosphorylated forms of these induced proteins were determined at specific time points. A strong correlation existed between UVA-induced AP-1 activity and accumulation of c-Fos, c-Jun and Fra-1 proteins. UVA irradiation also induced *c-fos* and *c-jun* mRNA expression and transcriptional activation of the *c-fos* gene promoter. These results demonstrate that UVA irradiation activates AP-1 and that *c-fos* induction may

play a critical role in the response of these human keratinocytes to UVA irradiation.

INTRODUCTION

The major risk factor for the development of nonmelanoma skin cancer is exposure to sunlight (1). The UV spectrum of solar radiation is subdivided into three regions: short wavelength ultraviolet C (UVC) (<280 nm), midwavelength ultraviolet B (UVB) (280-320 nm) and long wavelength ultraviolet A (UVA) (320-400 nm). Because stratospheric ozone completely absorbs UVC and a large portion of UVB, 90-99% of the solar radiation at the earth's surface is UVA radiation (2). UVA radiation accounts for approximately 10-20% of the carcinogenic dose of sunlight (3). Although UVB is approximately 1000-10000 times more carcinogenic per J/m² than UVA (4,5), chronic UVA exposure alone has been shown to induce photoaging (6) and skin tumors (papillomas and squamous cell carcinomas) (3,5,7) in experimental animals. Much higher doses of UVA are required to induce gene transcription, but these doses are environmentally attainable (8).

Because UVA radiation is only weakly absorbed by biomolecules such as DNA and proteins, its deleterious effects are manifested through the induction of oxidative damage. UVA-induced gene expression has been shown to involve the generation of singlet O₂ after UVA absorption by cellular chromophores (9,10).

Although a more prominent role of UVA in skin tumorigenesis has recently emerged, the precise signaling pathway(s) that are activated in response to UVA have not been fully elucidated. Solar UVA radiation has been found to non-enzymatically trigger the ceramide signaling cascade through singlet O₂, resulting in activator protein-2 (AP-2) activation and induction of intercellular adhesion molecule-1 expression in cultured normal human keratinocytes (9,11). UVA and singlet O₂ activated c-Jun NH₂-terminal kinase (JNK) and p38 but not extracellular signal-regulated kinase (ERK) mitogen-activated protein kinases (MAPK) in human skin fibroblasts (12,13). However, in human keratinocytes, UVA irradiation induced oxidative stress, ceramide production and activation of JNK, p38 and ERK MAPK (14). In normal human lymphoblast cell lines, Zhang *et al.* (15) found that UVA irradiation induced apoptosis through the

¹Posted on the website on January 8, 2002

*To whom correspondence should be addressed at: Department of Radiation Oncology, Arizona Cancer Center, Room 4999, 1515 N. Campbell Avenue, Tucson, AZ 85724, USA. Fax: 520-626-4979; e-mail: tbowden@azcc.arizona.edu

Abbreviations: AP-1, activator protein-1; AP-2, activator protein-2; DMEM, Dulbecco modified Eagle medium; DTT, dithiothreitol; EGTA, ethylene glycol-bis(β-aminocaprylate)-N,N,N',N'-tetraacetic acid; ERK, extracellular signal-regulated kinase; GAPDH, glyceraldehyde-3-phosphate dehydrogenase; GSK-3, glycogen synthase kinase-3; HRP, horseradish peroxidase; JNK, c-Jun NH₂-terminal kinase; MAPK, mitogen-activated protein kinase; NEB, New England Biolabs Inc.; NF-κB, nuclear factor kappa B; PBS, phosphate-buffered saline; PKA, protein kinase A; PKC, protein kinase C; PPI, protein phosphatase 1; PP2A, protein phosphatase 2A; SC, Santa Cruz Biotechnology; SD, standard deviation; SDS, sodium dodecyl sulfate; SSC, sodium chloride-sodium citrate solution; STAT, signal transducer and activator of transcription; TBP, TATA-binding protein; TBST, Tris-buffered saline with 0.05% Tween 20; TPA, 12-O-tetradecanoylphorbol-13-acetate; TRE, TPA response element; UVA, ultraviolet A; UVB, ultraviolet B; UVC, ultraviolet C.

© 2002 American Society for Photobiology 0031-8655/02 \$5.00+0.00

activation of JNK via the sphingomyelinase-ceramide pathway. UVA radiation has also been found to induce the expression or activation of heme-oxygenase 1, protein phosphatase CL100, matrix metalloproteinases, phospholipases such as phospholipase A₂, nuclear factor kappa B (NF- κ B), protein kinase C (PKC), signal transducers and activators of transcription (STAT)-1 and -3, the ribosomal S6 kinases p70^{S6K} and p90^{RSK} and activator protein-1 (AP-1) (16-23).

AP-1 is an important regulatory protein involved in cell growth, differentiation, cellular stress and apoptosis that can be induced by growth factors, cytokines, 12-*O*-tetradecanoylphorbol-13-acetate (TPA) and transforming oncoproteins (24). The AP-1 complex consists of heterodimers of Fos (c-Fos, Fra-1, Fra-2, FosB) and Jun (c-Jun, JunB, JunD) family members or homodimers and heterodimers of Jun family members that bind to the TPA response element (TRE) in the promoters of AP-1-inducible genes, contributing to their transcriptional activation (24).

Deregulated expression of the AP-1 complex has been shown to play a prominent role in the promotion of skin tumors. Loss of AP-1 DNA-binding activity was correlated with loss of proliferation and induction of differentiation in human keratinocytes (25). Similarly, the tumorigenic phenotype of malignant mouse epidermal cells was suppressed by the stable expression of a mutant c-Jun protein that inhibited AP-1-mediated transcriptional transactivation (26). Also, induction of AP-1 was detected in mouse epidermal JB6 cells that were susceptible to tumor promotion by TPA but not in resistant variants (27). Lastly, transduction of mouse keratinocytes with retroviruses encoding v-*ras*^{Ha} and v-*fos* caused the malignant conversion of these cells (28), whereas mice lacking the c-*fos* gene failed to develop malignant skin tumors upon *ras* gene activation and tumor promotion (29).

Increased AP-1 activity in response to UV irradiation has been reported previously. UVC irradiation of the transformed cervix-derived carcinoma cell line, HcLa, initiated the Ras-Raf-MAPK signaling cascade and resulted in AP-1 activation (30). UVB-induced AP-1 transactivation and induction of c-Fos were detected in JB6 murine epidermal cells (31,32). Recently, AP-1 activation was observed in cultured fibroblasts using the natural sunlight spectrum-emitting UVA-340 energy source (33). Experiments using *in vivo* mouse models (SKH-1 hairless mice and AP-1-luciferase transgenic mice) also detected UV-induced AP-1 activation (34,35).

Our laboratory has previously shown that UVB irradiation induces AP-1 activation in the human immortalized keratinocyte cell line HaCaT (36). This cell line contains two mutant p53 alleles but does not induce tumors upon subcutaneous injection into athymic nude mice. The cells form normal epidermis when transplanted to graft sites on these immune-compromised mice. Therefore, these cells are representative of initiated human skin cells and allow examination of the promoting effects of UVA irradiation. In light of the apparent role of AP-1 in skin tumorigenesis and its involvement in UVB-induced signal transduction, we have begun to examine its potential role in UVA-induced signaling pathways leading to skin tumor promotion. The purpose of this study was to determine if UVA irradiation induced AP-1 activation, to characterize the UVA-induced

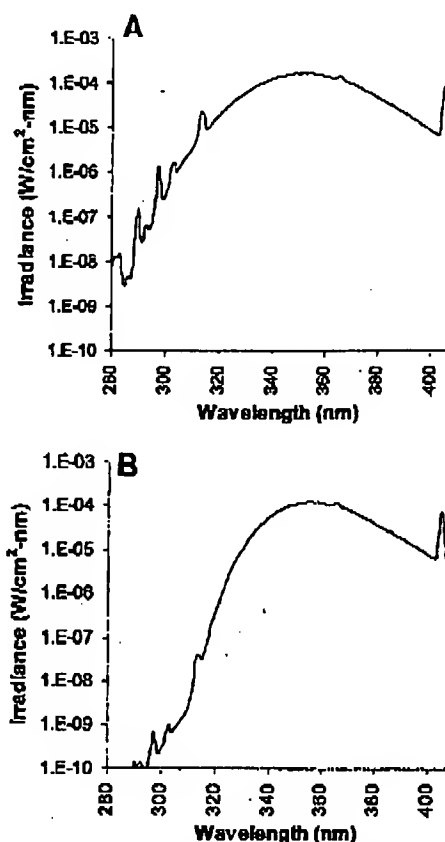


Figure 1. Spectral irradiance of the F20T12/BL/HO UVA bulbs. (a) Irradiance at 5.6 cm from the surface of interest; (b) Irradiance at 5.6 cm from the surface of interest through a 4 mm plate glass to filter wavelengths <320 nm.

AP-1 complex and to determine the expression patterns of the AP-1 family members in these HaCaT cells.

MATERIALS AND METHODS

Cell culture. The human keratinocyte cell line HaCaT was stably transfected with a sequence from the human collagenase-1 gene promoter (-73 to +63), which contained one endogenous AP-1 binding site driving a luciferase reporter gene (HCL14 cells), as reported previously (36). HaCaT cells were also stably transfected with a sequence from the human c-*fos* gene promoter (-404 to +41) driving a luciferase reporter gene (FL30 cells), as reported previously (36). These cells were cultured in Dulbecco modified Eagle medium (DMEM) supplemented with 10% fetal bovine serum, 100 units/mL penicillin-streptomycin at 37°C under 5% CO₂. Cells were grown to 90-100% confluence and then serum-starved for 24-28 h before treatment.

UVA irradiation. Cells were irradiated with a bank of four F20T12/BL/HO fluorescent UVA bulbs (National Biological Corp., Twinsburg, OH) with a peak emission at 365 nm. The bulbs were powered by an Advance electronic ballast REL-AP32-RH-TP (120 V, 60 Hz, 90 A) (Advance Transformer Co., Chicago, IL). Four-millimeter plate glass was used to filter wavelengths below 320 nm (Fig. 1). Irradiation doses were measured using a UVX radiometer equipped with a UVX-36 sensor (UVP, Inc., Upland, CA). Irradiation was performed in a sterile, well-ventilated laminar flow hood to eliminate the possibility of thermal stimulation. Cells were irradiated in phosphate-buffered saline (PBS) supplemented with 0.01% MgCl₂ and 0.01% CaCl₂. Control cells were mock-irradiated under similar conditions. To determine the potential effects of maintaining

cells in supplemented PBS for extended periods of time, a second set of control cells, which was kept in serum-free medium at 37°C under 5% CO₂ for the treatment duration, was also used (s.d.). Cultures were continued in serum-free DMEM until harvest.

Luciferase assay for AP-1 and *c-fos* transactivation. Total cellular protein was extracted in lysis buffer (15 mM MgSO₄, 25 mM glycylglycine, 4 mM ethylene glycol-bis(β-aminoethyl ether)-N,N,N',N'-tetraacetic acid [EGTA], 1% vol/vol Triton X-100, 1 mM dithiothreitol [DTT]). Luciferase activity of 30 µg total cellular protein was measured using the TD-20/20 luminometer (Turner Designs, Sunnydale, CA).

Electrophoretic mobility shift assays. Nuclear protein lysates were isolated using the method of Dignani *et al.* (37). Gel shift assays were performed using 2.5 µg nuclear protein, 1 ng/µl [³²P]-dCTP-labeled double-stranded 22-mer TRE probe containing the AP-1 binding site (TGAGTCA) in the context of the human collagenase-1 promoter and 1 µg/µl poly dIdC to ensure minimal nonspecific binding. After a 10 min preincubation of nuclear protein and poly dIdC at room temperature, the labeled probe was added and incubated for an additional 20 min. DNA complexes were then electrophoresed in 4.8% polyacrylamide gels and exposed to Phosphor screens for analysis (Molecular Dynamics Inc., Sunnyvale, CA). Gel supershift assays entailed a preincubation of 2.5 µg nuclear protein with increasing concentrations of antibodies against AP-1 family members at 4°C for 2 h, addition of poly dIdC and incubation for 10 min at room temperature and, finally, addition of the [³²P]-dCTP-labeled TRE probe and incubation at room temperature for an additional 20 min.

Western analysis. Total cellular protein was extracted in NPB buffer (150 mM NaCl, 20 mM Tris pH 7.5, 1 mM ethylenediaminetetraacetic acid, 1 mM EGTA, 2.5 mM Na₂P₂O₇, 1 mM β-glycerol phosphate, 1 mM Na₂VO₄, 1 µg/mL leupeptin and 1% Triton X-100). Forty micrograms of total cell lysate was boiled in 4× sample buffer (0.2 M Tris pH 7, 8% sodium dodecyl sulfate [SDS], 20% β-mercaptoethanol and 12% sucrose), resolved on 12.5% SDS-polyacrylamide gels and transferred to Immobilon-P nylon membranes (Millipore Corp., Bedford, MA). Membranes were blocked with 5% evaporated milk-1× Tris-buffered saline with 0.05% Tween 20 (TBST) for 2 h at room temperature or overnight at 4°C, incubated with primary antibodies against AP-1 family members for 2 h at room temperature and then incubated with horseradish-peroxidase (HRP)-conjugated secondary antibodies for 1 h at room temperature. Membranes were washed three times for 10 min each in 1× TBST between antibody incubations. All primary antibodies were obtained from Santa Cruz Biotechnology (SC), Santa Cruz, CA, except where indicated. All HRP-conjugated secondary antibodies were obtained from New England Biolabs Inc. (NEB), Beverly, MA, except where indicated. Antibody concentrations were as follows: c-Fos sc-8047 at 1:1000 and anti-mouse secondary antibody (SC) at 1:5000; Fra-2 sc-604 at 1:1000 and anti-rabbit secondary antibody (SC) at 1:40000; Fra-1 sc-605 at 1:1000 and anti-rabbit secondary antibody at 1:10000; FosB sc-8013 at 1:200 and anti-mouse secondary antibody (SC) at 1:3500; c-Jun sc-1694 at 1:500 and anti-rabbit secondary antibody at 1:2000; JunB sc-046 at 1:1000 and anti-rabbit secondary antibody at 1:2000; JunD sc-74 at 1:1000 and anti-rabbit secondary antibody at 1:2000; and Phospho-c-Jun (Ser 73) (NEB) at 1:800 and anti-rabbit secondary antibody at 1:2000. Antigen-antibody complexes were detected using the ECL kit (Amersham Pharmacia Biotech, Piscataway, NJ).

Protein phosphatase treatment. Protein phosphatase 1 (PPI) (NEB) treatment entailed the incubation of 40 µg concentrated total cellular protein with 5 units PPI in 1× MnCl₂ and 1× PPI buffer for 10 min at 30°C. Protein phosphatase 2A (PP2A) (Upstate Biotechnology, Lake Placid, NY) treatment involved the incubation of 40 µg of concentrated total cellular protein with 0.5 units PP2A in PP2A buffer (50 mM Tris-Cl, pH 7.5, 1 mM MnCl₂, 1 mM DTT) for 20 min at 30°C. Both treatments were followed by electrophoresis in 12.5% SDS-polyacrylamide gels, transfer to Immobilon-P membranes and immunodetection.

Northern analysis. Total RNA was extracted using the RNeasy Mini Kit (Qiagen Inc., Valencia, CA). Twenty micrograms of total RNA was diluted in 10 µL sample buffer (50% formamide, 0.02% formaldehyde, 1× 3-(N-morpholino)propanesulfonic acid, 0.1 mg/mL ethidium bromide), electrophoresed on 1% agarose-formaldehyde

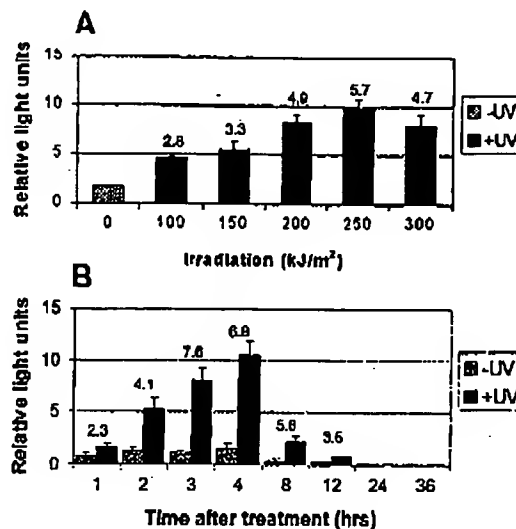


Figure 2. UVA induction of AP-1 transactivation. (a) Dose response of UVA-irradiated HCL14 cells at 4 h after irradiation. Cells were either mock-treated or UVA-irradiated for distinct periods of time corresponding to UVA doses between 100 and 300 kJ/m² and then harvested 4 h after irradiation. (b) Time course of HCL14 cells irradiated with 250 kJ/m² UVA. Cells were either mock-treated or irradiated with 250 kJ/m² UVA and then incubated in serum-free medium until each desired time point. Thirty micrograms of total cell lysate was analyzed for each luciferase activity assay. Fold inductions with respect to mock-treated controls are listed above their respective bar(s) for each data set. Each bar represents the mean \pm standard deviation (SD) of triplicate samples. The data are representative of duplicate experiments.

hyde gels at constant voltage and transferred to GeneScreen nylon membranes (NEN Life Science Products, Boston, MA), using the Pressure Control Station (Stratagene, La Jolla, CA). RNA was then cross-linked to the membrane using the GS Gene Linker (Biodad Laboratories, Hercules, CA). Northern probes were labeled with [³²P]-α-dCTP using the DECAPrime II kit (Ambion Inc., Austin, TX). The *c-fos* probe was a 2.2 kb *Eco*R1 fragment of mouse *c-fos* cDNA generated from the plasmid *pfos-ks*. The *c-jun* probe was a 0.65 kb *Eco*R1 fragment of human *c-jun* cDNA generated from the plasmid *pcDNA3.1/His*. The glyceraldehyde-3'-phosphate dehydrogenase (GAPDH) control probe was a 0.75 kb *Pst*I-*Xba*I fragment of human GAPDH cDNA generated from the plasmid *PT2-GAP*. After hybridization, membranes were washed in 2× sodium chloride-sodium citrate solution (SSC), 0.1% SDS and 0.1× SSC, 0.1% SDS and exposed to Phosphor screens for analysis.

RESULTS

UVA induction of AP-1 transactivation

The immortalized, human keratinocyte cell line HaCaT was stably transfected with an AP-1 luciferase reporter plasmid containing a 136 bp fragment of the human collagenase-1 gene promoter (-73 to +63) with one endogenous AP-1 binding site (HCL14 cells), as reported previously (36). Transactivation through AP-1 was detected with 100 kJ/m² UVA, but maximal AP-1 transactivation was observed with 250 kJ/m² UVA (Fig. 2a). The time course comparing unirradiated and 250 kJ/m² UVA-irradiated HCL14 cells revealed a transient induction of AP-1 transactivation between 2 and 8 h after irradiation, with maximal induction between the 3 and 4 h time points (Fig. 2b). Although the cultured cells were serum-starved for at least 24 h before treatment

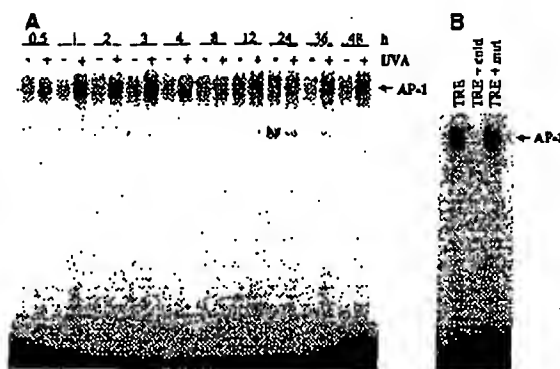


Figure 3. Electrophoretic mobility shifts of the AP-1 DNA-binding complex. Nuclear protein lysates (2.5 μ g) from HCL14 cells were incubated with [32 P] α - 32 P-labeled TRE probes and electrophoresed on 4.8% polyacrylamide gels. (a) AP-1 DNA-binding time course using 250 kJ/m² UVA irradiation. (b) Competition assays using post-1 h UVA-irradiated nuclear protein lysates with 50X unlabeled wild-type TRE (cold) and 50X mutated TRE (mut) probes. Gel shift assays were performed in duplicate.

to reduce basal levels of AP-1 activity, unirradiated cells still showed detectable levels of AP-1 transactivation at most time points.

UVA induction of AP-1 DNA binding

Gel shift assays were performed on nuclear proteins that were extracted from unirradiated and 250 kJ/m² UVA-irradiated HCL14 cells, using a radiolabeled, double-stranded 22-mer oligonucleotide containing the human collagenase-1 TRE AP-1 DNA-binding site. AP-1 DNA complexes were detected in both irradiated and unirradiated cells. However, enhanced DNA binding to the target TRE sequence was detected as early as 0.5 h after irradiation and was maximal between 1 and 3 h after irradiation (Fig. 3a). Competition assays were performed to verify the specificity of the AP-1 DNA-binding complex, using 50X unlabeled wild-type TRE probes to decrease detectable complexes and 50X mutated TRE probes that did not compete with labeled probes and recovered complex detection (Fig. 3b).

Characterization of the AP-1 DNA-binding complex

Gel supershift assays, using increasing concentrations of antibodies to AP-1 family member antigens, were performed to determine which AP-1 proteins were bound to the radiolabeled double-stranded TRE oligonucleotide. Before AP-1 DNA annealing, nuclear proteins were incubated with 1–4 μ g antibodies against AP-1 Jun and Fos family members. Gel shift assays were then performed as usual. The 1 h time point in the range of maximal induction of AP-1 DNA binding was used in these experiments. The TATA-binding protein (TBP), which has not been shown to directly bind to the TRE site, was used as a negative control. c-Fos was implicated as a primary component in this AP-1 DNA-binding complex. The c-Fos antibody caused significant reduction of the AP-1 DNA complex shift and produced two slower migrating forms of the complex (Fig. 4). Other AP-1 family members that also produced slower migrating forms included Fra-2, c-Jun, JunB and JunD (Fig. 4). However, the lack

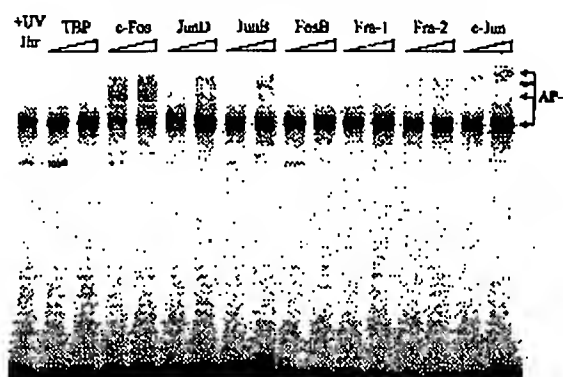


Figure 4. Characterization of the AP-1 DNA-binding complex. Post-1 h UVA-irradiated nuclear protein lysates from HCL14 cells were used to characterize the complex components. TBP, which has not been shown to bind to the TRE binding site, served as a negative control. Concentrations of 1 and 4 μ g primary antibodies are shown to demonstrate AP-1 gel shift band clearing, AP-1 supershift ability or both. Gel shift assays were performed in duplicate.

of AP-1 DNA complex clearing suggests that they are minor components of the AP-1 DNA complexes formed in these UVA-irradiated HaCaT cells.

Contribution of both RNA and protein synthesis to UVA-induced AP-1 DNA binding

To determine whether RNA synthesis or protein synthesis (or both) was required to achieve UVA-induced enhancement of DNA binding detected at 1 h after irradiation, HCL14 cells were treated with the RNA synthesis inhibitor actinomycin D or the protein synthesis inhibitor cycloheximide. UVA induction of AP-1 DNA binding was significantly reduced in both treatment groups, suggesting that transcription and translation of AP-1 complex family members does occur and contributes to the UVA-induced complex formation in HaCaT cells (Fig. 5). However, mRNA and protein stabilization cannot be ruled out and may account for the residual complexes detected using the inhibitor-treated nuclear protein lysates. Increased levels of AP-1 DNA binding complexes were occasionally detected in unirradiated; cycloheximide-treated HCL14 cells (data not shown). Protein synthesis inhibitors have been shown to activate or stabilize the expression of immediate early genes, including Fos and Jun family members (38,39).

Effects of UVA on Fos and Jun family member protein levels

Western blot analyses were performed on AP-1 family members to determine if protein expression levels correlated with UVA-induced AP-1 DNA binding and AP-1 transactivation. Expression of c-Fos, the primary component in the AP-1 DNA binding complex, was dramatically induced with 250 kJ/m² UVA irradiation. Increased expression was initially detected at 0.5 h after irradiation and continued up to 4 h after irradiation (Fig. 6a). Slower migrating forms predominated at 2, 3 and 4 h after irradiation, suggesting a post-translationally modified form of c-Fos at these time points. Increased c-Jun in irradiated cells was detected between 1

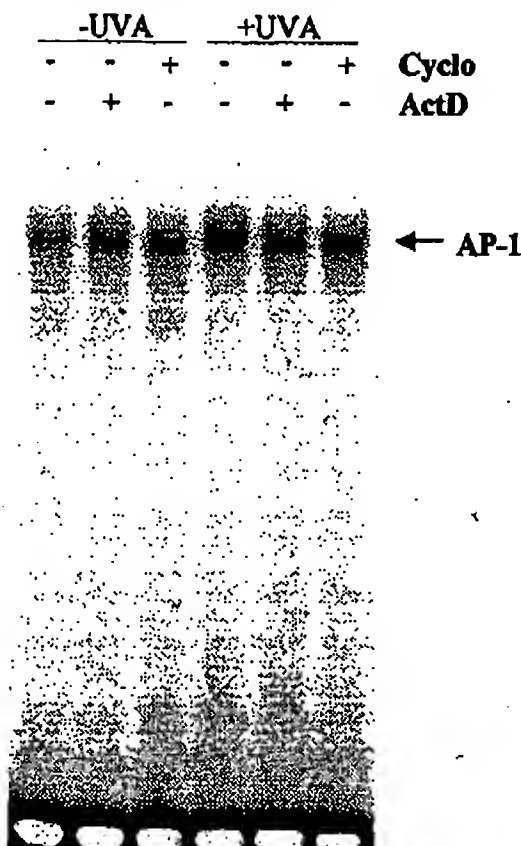


Figure 5. Effects of transcription and translation inhibition on AP-1 DNA-binding. HCL14 cells were pretreated with 1 μ g/mL actinomycin D (ActD) or 10 μ g/mL cycloheximide (Cyclo) in serum-free medium for 30 min, irradiated with 250 kJ/m² UVA and then continued in serum-free medium supplemented with the respective inhibitors for 1 h after irradiation. Nuclear protein lysates (2.5 μ g) were then incubated with [³²P] α -dCTP-labeled TRE probes and electrophoresed on 4.8% polyacrylamide gels. Gel shift assays were performed in triplicate.

and 8 h after irradiation (Fig. 6a). Basal levels of c-Jun were observed at every time point examined. Interestingly, a slightly slower migrating form of c-Jun was observed at 15 and 30 min after UVA irradiation, also suggesting posttranslational modification of c-Jun. Phosphorylation at serine 63 and serine 73 of c-Jun leads to increased stability and enhanced transcriptional activity of the protein (40). To determine the phosphorylation status of c-Jun at serine 73, Western blot analysis was performed using a phospho-specific antibody. Although phosphorylated forms could not be detected in unirradiated HCL14 cells, c-Jun appeared to be phosphorylated at amino acid 73 in irradiated cells up to 4 h after irradiation, and its detection revealed banding patterns similar to those seen for total c-Jun expression (Fig. 6b). Induction of an approximately 35 kDa Fra-1 protein was observed at 2 to 4 h after irradiation. However, an approximately 40 kDa uninduced protein product was also apparent at every time point examined (Fig. 6a). Immunodetection of Fra-2 revealed induction of a slower migrating form at 15 and 30 min after irradiation and induction of a faster mi-

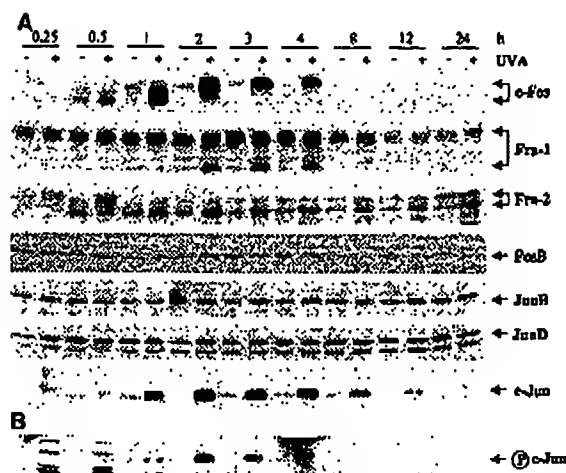


Figure 6. Western blot time course of AP-1 family member expression using 250 kJ/m² UVA irradiation. Forty micrograms of total cellular protein was electrophoresed on 12.5% SDS-polyacrylamide gels, transferred to Immobilon-P membranes and immunodetected using optimal primary and secondary antibody concentrations for (a) each AP-1 family member, and (b) the phosphorylated form of c-Jun at amino acid 73. Western blot data are representative of two independent experiments.

grating form from 2 to 24 h after irradiation (Fig. 6a). These results suggest the initial induction of a posttranslationally modified form of Fra-2, followed by the induction of a less modified form. The remaining AP-1 family members (FosB, JunB, JunD) did not show significant changes in protein expression after UVA irradiation (Fig. 6a).

Protein phosphatase treatment of UVA irradiation-induced AP-1 complex components

In an attempt to determine if the slower migrating species of the UVA-induced proteins were phosphorylated forms, total cell lysates from selected postirradiation time points were treated with PP1 or PP2A, enzymes that can recognize and cleave phosphates at serine and threonine residues. PP1 treatment shifted the uninduced 40 kDa Fra-1 band to a faster migrating form in both UVA-irradiated and unirradiated HCL14 cells but had little effect on the UVA-induced faster migrating 35 kDa species (Fig. 7a). PP1 treatment also shifted the slower migrating band of Fra-2 to a faster migrating form in both treated and untreated cells (Fig. 7a). Because PP1 treatment did not significantly change the UVA-induced banding patterns of c-Fos and c-Jun, total protein lysates were incubated with PP2A and immunodetected with c-Fos and c-Jun antibodies. The slower migrating forms of c-Jun at 15 and 30 min in the UVA-irradiated samples were shifted to faster migrating forms, but the UVA-induced protein bands were not affected (Fig. 7b). c-Fos banding patterns were dramatically changed upon PP2A treatment. Slower migrating forms that were detected in both irradiated and unirradiated lysates were significantly shifted to faster migrating forms, with the predominant band migrating at approximately 40 kDa (Fig. 7b).

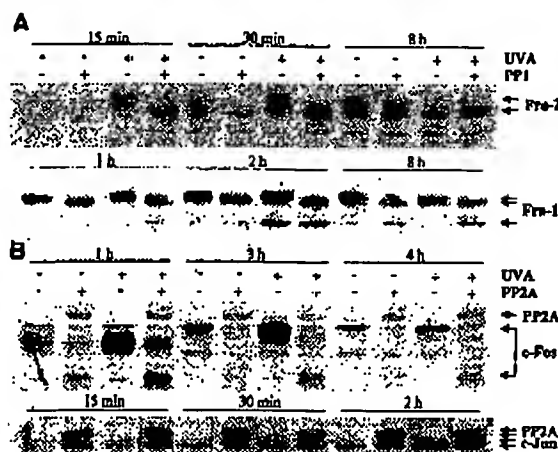


Figure 7. Protein phosphatase treatment of UVA irradiation-induced AP-1 family members. Concentrated total cellular protein was isolated from mock-treated or 250 kJ/m² UVA-irradiated HCL14 cells. (a) Forty micrograms protein from selected time points was treated with 5 units PP1 for 10 min at 30°C, electrophoresed on 12.5% SDS-polyacrylamide gels, transferred to Immobilon-P membranes and immunodetected with antibodies against Fra-1 and Fra-2 antigens. (b) Forty micrograms protein from selected time points was treated with 0.5 units PP2A for 20 min at 30°C, electrophoresed on 12.5% SDS-polyacrylamide gels, transferred to Immobilon-P membranes and immunodetected with antibodies against c-Fos and c-Jun antigens. Western blot data are representative of two independent experiments.

UVA induction of *c-fos* and *c-jun* mRNA levels and *c-fos* transcriptional activation

c-Fos can be regulated at the level of transcription, RNA stability, protein degradation and posttranslational modification (41). Because *c-Fos* was implicated as a primary component of the AP-1 DNA binding complex and its protein expression was induced in response to UVA irradiation, *c-fos* mRNA levels and the transcriptional activation of the *c-fos* gene were additionally examined to further delineate the mechanism of its activation. Transcripts of *c-fos* were detectable immediately after irradiation and continued to be detected up to 1.5 h after irradiation (Fig. 8). Although transcripts were also detected in unirradiated samples up to 45 min after irradiation, differential expression between irradiated and unirradiated samples was observed between 15 and 90 min after irradiation. Initially elevated *c-fos* transcripts in both irradiated and unirradiated HaCaT cells may be a stress response to the long irradiation period in supplemented PBS that was necessary to achieve 250 kJ/m² UVA irradiation.

c-Jun mRNA levels were also examined in an attempt to correlate *c-jun* transcription with translation of the c-Jun protein. *c-Jun* transcripts were observed at every time point in both irradiated and unirradiated HCL14 cells. Induction of *c-jun* transcripts with 250 kJ/m² UVA was detected between 15 min and 4 h after irradiation, with maximal induction at approximately 90 min after irradiation (Fig. 8). UVA-induced increases in *c-jun* mRNA levels were slightly delayed and, although transient, sustained for a longer period of time than UVA-induced *c-fos* mRNA levels.

The HaCaT cell line was also stably transfected with a *c-fos* luciferase reporter plasmid containing a 445 bp fragment

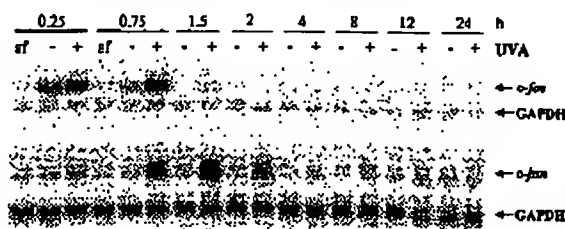


Figure 8. Northern blot time course of *c-fos* and *c-jun* expression using 250 kJ/m² UVA. Twenty micrograms total RNA from mock-treated and UVA-irradiated HCL14 cells was electrophoresed in 1% agarose-formaldehyde gels, transferred to nylon membranes under 75 lb pressure and hybridized with 25 ng [³²P]α-dCTP-labeled *c-fos* and *c-jun* cDNA probes. [³²P]α-dCTP-labeled GAPDH cDNA served as a loading control. mRNA levels of control cells held in serum-free medium at 37°C and under 5% CO₂ (sf) are shown at 15 and 45 min time points to demonstrate expression changes that may be related to extensive irradiation periods. Northern blot data are representative of two independent experiments.

of the human *c-fos* gene promoter, as reported previously (36). This FL30 cell line was irradiated with 250 kJ/m² UVA, and total protein lysates were examined for luciferase activity. Significant UVA induction of *c-fos* transactivation was detected between 2 and 8 h after irradiation, with maximal *c-fos* transactivation between 3 and 4 h after irradiation (Fig. 9). These results suggest that transcriptional activation of the *c-fos* gene contributes to the detectable increase in UVA-induced *c-fos* mRNA expression.

DISCUSSION

UVA radiation is the most abundant and most penetrating component of solar radiation that reaches the earth's surface (2). Chronic exposure to UVA plays an important role in dermal and epidermal photodamage and is a contributing factor in the development of skin cancer (3,5-7). UV radiation exposure leads to increased gene expression in mammalian cells (11,32). The mechanisms by which UVA irradiation leads to increased transcriptional expression and activation of human genes are currently under investigation. Deregulated expression of the AP-1 complex has been shown to play a prominent role in the promotion of skin tumors and may be required to maintain the tumorigenic phenotype (25-29).

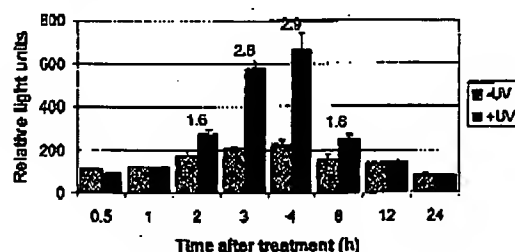


Figure 9. UVA induction of *c-fos* transactivation. Time course experiments analyzing the luciferase activity of 30 µg total cell lysate from mock-treated and 250 kJ/m² UVA-irradiated FL30 cells were performed. Fold inductions with respect to mock-treated controls are listed above the set of bars for each time point. Each bar represents the mean ± SD of triplicate samples. The data are representative of duplicate experiments.

In this study, 250 kJ/m² UVA irradiation enhanced AP-1 DNA binding to a TRE oligonucleotide and caused increased AP-1 transactivation in a dose-dependent manner in the immortalized, human keratinocyte cell line HaCaT. As expected, maximal AP-1 DNA binding slightly preceded, in time, the AP-1 transactivation detected upon UVA irradiation. Transcription and translation of AP-1 complex components contributed to the UVA-induced enhanced AP-1 DNA binding. However, mRNA or protein stabilization (or both) cannot be excluded and may account for the residual AP-1 DNA complexes that were detected in inhibitor-treated nuclear protein extracts. This is in contrast to the report of Djavaheri-Mergny *et al.* (19), who found that UVA activation of AP-1 DNA binding was maintained after treatment with cycloheximide before, during and after irradiation. The rapid induction of the AP-1 DNA binding complex within the first hour and the lack of effective cycloheximide inhibition suggested a posttranslational effect of UVA on AP-1 activity in NCTC 2544 cells (19).

The occasional increase in DNA binding, which we observed in the cycloheximide-treated, unirradiated cells (data not shown), may have been caused by a cycloheximide-induced ribotoxic stress response that led to heightened activation of preexisting AP-1 complex proteins. Because cycloheximide was not added to the cells during mock or UVA irradiation treatment, translation of mRNA transcripts may have occurred at that time. Because UV radiation has also been found to inhibit protein synthesis (42), we did not observe this phenomenon in UVA- and cycloheximide-treated cells.

c-Fos was implicated as a primary component in the AP-1 DNA binding complex, and its expression was induced at both the transcriptional and translational levels upon UVA stimulation. Other minor complex components included c-Jun, JunB, JunD and Fra-2. Djavaheri-Mergny *et al.* (19) reported the presence of c-Jun and c-Fos in the AP-1 DNA complexes induced with 190 kJ/m² UVA irradiation in NCTC 2544 human keratinocytes. However, other Fos and Jun family member antibodies were not tested for their ability to supershift the AP-1 DNA-binding complex.

UVA induction of AP-1 complex proteins, AP-1 DNA binding and AP-1 transactivation occurred more rapidly than induction by UVB in HaCaT cells. Whereas UVA-induced AP-1 transactivation and protein level changes in c-Fos, c-Jun and Fra-1 occurred between 2 and 4 h after irradiation, UVB induction of AP-1 activation occurred maximally between 12 and 24 h after irradiation (36). Time kinetic differences for UVA- and UVB-induced apoptosis (43), cell cycle arrest (44) and DNA damage repair (45) have also been reported. Therefore, the signaling pathways that are activated in response to UVA and UVB insult leading to AP-1 transactivation may differ as well.

c-Fos, c-Jun and Fra-1 protein accumulation paralleled the induction of AP-1 transactivation by UVA irradiation. Additionally, the unaltered expression of JunB, JunD and FosB implicated these proteins as possible contributors to the detectable basal levels of AP-1 activity. The actual protein complexes formed in these irradiated and unirradiated human keratinocytes have not been fully elucidated. Although Fra-2 protein expression was detected in both irradiated and unirradiated cells, the slight induction of the faster migrating

form at later time points suggests a possible role for this protein in UVA-induced AP-1 activity as well.

Induction of c-fos mRNA levels and transcriptional activation of the c-fos gene promoter by UVA suggest that *de novo* transcription of c-fos occurs in these keratinocytes. Interestingly, c-jun mRNA levels were also induced upon UVA irradiation but peaked at a later time point, appeared to be less sensitive to the stress of treatment conditions and remained upregulated for an extended period of time when compared with UVA-induced c-fos expression. The sustained induction of c-jun RNA levels may be a consequence of c-Jun's ability to positively autoregulate its own transcription through an AP-1 binding site in its promoter region (46,47). This autoactivation of c-jun mRNA may first require the posttranslational modification of existing c-Jun proteins that we observed at 15 and 30 min after UVA irradiation (47).

Immediate early gene products are frequently posttranslationally modified to induce their transcriptional activator potential in response to extracellular stimuli (30). The apparent Fra-1 and Fra-2 protein shifts detected after PP1 treatment are testament to the posttranslational phosphorylation of these proteins. In fact, Gruda *et al.* (48) reported that Fra-1 and Fra-2 proteins were highly phosphorylated in serum-stimulated, asynchronously growing 3T3 cells and that their phosphorylation caused dramatic shifts in the electrophoretic mobility of the proteins. The inability of PP1 treatment to produce significant shifts for c-Fos and c-Jun suggested that these proteins may not be suitable substrates for PP1 activity. PP1 is a serine-threonine phosphatase that may not be able to recognize the phosphorylation sites of these proteins. Recognition and cleavage of only a few key sites may not change the mobility of the proteins dramatically enough to be detected by Western blot analysis.

c-Fos can be phosphorylated by protein kinase A (PKA), PKC, MAPK, p34^{cdc2}, DNA protein kinase, glycogen synthase kinase-3 (GSK-3) and rsk at multiple sites in the regulatory regions of the protein (49,50). We detected a distinct reduction in c-Fos mobility upon induction of the protein by UVA irradiation. Distinct conformational alterations and charge effects that change the electrophoretic mobility of c-Fos have been reported previously in *in vitro* phosphorylation assays with p34^{cdc2}, PKA and PKC (50). Because c-Fos is known to be extensively phosphorylated on serine and threonine residues in the nucleus (50), we attempted phosphate cleavage with another serine-threonine phosphatase, PP2A, which appears to be the major kinase phosphatase responsible for the downregulation of activated protein kinases (51). Although protein bands for the PP2A enzyme itself were also detected with the c-Fos antibody, dramatic shifts in c-Fos protein migration were detected with this phosphatase. The predominant shifted band migrated at approximately 40 kDa and was more pronounced in the UVA-irradiated lysates. Barber and Verma (52) demonstrated that most, if not all, c-Fos phosphate groups were in the form of phosphoesters. Hydrolysis of these phosphoesters caused a dramatic increase in the electrophoretic mobility of c-Fos, with extreme shifts resulting in a 15 kDa molecular mass difference.

c-Jun is preferentially dephosphorylated by purified preparations of PP2A in okadaic acid-treated cells, and its activ-

ity can be regulated by this phosphatase. The site of PP2A-catalyzed dephosphorylation of c-Jun has been mapped to the amino acid serine at position 63 (53,54). PP2A treatment shifted the slower migrating form of c-Jun in the UVA-irradiated cells at 15 and 30 min after irradiation to a faster migrating form. The phospho-form of c-Jun serine 73 was detected between 2 and 4 h after irradiation, but there was a concomitant lack of PP1- or PP2A-induced band shifting at these time points. Serine 73 may not be a target for PP1 or PP2A dephosphorylation. Additionally, c-Jun contains repressive serine-threonine phosphorylation sites near the basic region that holds c-Jun in an inactive state (24,55). GSK-3 has been shown to phosphorylate these sites and modulate the DNA-binding activity of c-Jun (41). Therefore, c-Jun requires a delicate balance of phosphorylation-dephosphorylation events to achieve maximal transactivation potential.

Although most studies of UV-induced signal transduction pathways leading to altered gene expression have focused on UVB and UVC radiations, UVA effects on signal transduction and activation of stress response genes are current topics of great interest. The oxidative stress induced by UVA irradiation is primarily mediated through reactive oxygen intermediates and has been found to induce the expression or activation of several key signal transduction genes, such as JNK, p38 and c-Fos in human skin fibroblasts (12,13,56). Intracellular glutathione depletion reduced the intracellular redox equivalents and significantly increased the expression of c-Fos and c-Jun in UVA-irradiated human skin fibroblasts (57). UVA-induced NF- κ B activation in human skin fibroblasts was correlated with membrane damage (20). In human keratinocytes, UVA radiation activated STAT1 (18), AP-1 (19), AP-2 (11), PKC (17) and the MAPK (ERK, JNK and p38) (14) but decreased NF- κ B DNA-binding activity (58). In mouse epidermal cells, phosphorylation and activation of STAT3, p70^{STAT3} and p90^{STAT3} after UVA exposure have also been reported (21-23).

This study further characterized the role of AP-1 activation in UVA-irradiated human keratinocytes and implicated key components that are activated in response to this oxidative stress. Taken together, these results demonstrated that UVA irradiation induces AP-1 DNA binding and AP-1 activation in the human keratinocyte cell line HaCaT. Accumulation of c-fos mRNA and protein may play a critical role in the response of these cells to UVA irradiation. c-Fos has poor affinity to DNA and cannot transactivate without a jun family member (24,41). Therefore, the combined effects of other AP-1 family members whose expression is induced (c-Jun, Fra-1, Fra-2) or that bind to the AP-1 site in response to UVA irradiation (c-Jun, JunB, JunD, Fra-2) are also important to ultimately achieve AP-1 induction in these keratinocytes.

Acknowledgements—We thank Barbara G. Grant of UVR Research Institute for measuring the spectral irradiance of our UVA irradiation system. This work was supported, in part, by the National Cancer Institute-funded grant R25CA78447 through the Cancer Prevention and Control Program at the Arizona Cancer Center, Tucson, AZ. This work was also supported by the National Institutes of Health grants CA27502 and CA23074.

REFERENCES

- Urbach, P. (1997) Ultraviolet radiation and skin cancer of humans. *J. Photochem. Photobiol. B: Biol.* 40, 3-7.
- Madronich, S. (1993) The atmosphere and UV-B radiation at ground level. In *Environmental UV Photobiology* (Edited by A. R. Young, L. O. Björn, J. Moan and W. Nultsch), pp. 1-39. Plenum Press, New York.
- de Laat, A., J. C. van der Leun and F. R. de Gruijl (1997) Carcinogenesis induced by UVA (365-nm) radiation: the dose-time dependence of tumor formation in hairless mice. *Carcinogenesis* 18, 1013-1020.
- Berg, R. J., F. R. de Gruijl and J. C. van der Leun (1993) Interaction between ultraviolet A and ultraviolet B radiations in skin cancer induction in hairless mice. *Cancer Res.* 53, 4212-4217.
- Steenborg, H. J. and J. C. van der Leun (1990) Tumorigenesis by a long wavelength UV-A source. *Photochem. Photobiol.* 51, 325-330.
- Kligman, L. H. (1991) The hairless mouse and photoaging. *Photochem. Photobiol.* 54, 1109-1118.
- Kelchens, G., F. R. de Gruijl and J. C. van der Leun (1991) Tumorigenesis by short-wave ultraviolet A: papillomas versus squamous cell carcinomas. *Carcinogenesis* 12, 1377-1382.
- Reider, K., C. Blautner, A. Knebel, M. Jordanov, P. Herrlich and H. J. Rahmsdorf (1997) UV-induced signal transduction. *J. Photochem. Photobiol. B: Biol.* 37, 1-17.
- Grether-Beck, S., G. Bonizzi, H. Schmitt-Rendlen, I. Felsner, A. Timmer, H. Sies, J. P. Johnson, J. Pielle and J. Krutmann (2000) Non-enzymatic triggering of the ceramide signalling cascade by solar UVA radiation. *EMBO J.* 19, 5793-5800.
- Tyrell, R. M. (1991) UVA (320-380 nm) as an oxidative stress. In *Oxidative Stress: Oxidants and Antioxidants* (Edited by H. Sies), pp. 57-83. Academic Press, London.
- Grether-Beck, S., S. Olazola-Horn, H. Schmitt, M. Grewe, A. Jahnke, J. P. Johnson, K. Briviba, H. Sies and J. Krutmann (1996) Activation of transcription factor AP-2 mediates UVA radiation- and singlet oxygen-induced expression of the human intercellular adhesion molecule 1 gene. *Proc. Natl. Acad. Sci. USA* 93, 14586-14591.
- Klotz, L. O., K. Briviba and H. Sies (1997) Singlet oxygen mediates the activation of JNK by UVA radiation in human skin fibroblasts. *FEBS Lett.* 408, 289-291.
- Klotz, L. O., C. Pellicoux, K. Briviba, C. Pierlot, J. M. Aubry and H. Sies (1999) Mitogen-activated protein kinase (p38-, JNK-, ERK-) activation pattern induced by extracellular and intracellular singlet oxygen and UVA. *Eur. J. Biochem.* 260, 917-922.
- Maziere, C., M. A. Conte, L. Leborgne, T. Levaie, W. Hornebeck, R. Santus and J. C. Maziere (2001) UVA radiation stimulates ceramide production: relationship to oxidative stress and potential role in ERK, JNK, and p38 activation. *Biochem. Biophys. Res. Commun.* 281, 289-294.
- Zhang, Y., P. Majumdar, P. C. Schmid, Z. Dong, S. Zhong, W. Y. Ma, R. E. Brown, A. M. Bole and H. H. Schmid (2001) Involvement of the acid sphingomyelinase pathway in UVA-induced apoptosis. *J. Biol. Chem.* 276, 11775-11782.
- Tyrell, R. M. (1996) UV activation of mammalian stress proteins. In *Stress-Inducible Cellular Responses* (Edited by U. Feige, R. I. Morimoto, I. Yahara and B. S. Polla), pp. 255-271. Birkhäuser Verlag, Boston.
- Matsui, M. S., N. Wang, D. MacFarlane and V. A. DeLeo (1994) Long-wave ultraviolet radiation induces protein kinase C in normal human keratinocytes. *Photochem. Photobiol.* 59, 53-57.
- Maziere, C., F. Dantin, P. Dubois, R. Santus and J. Maziere (2000) Biphasic effect of UVA radiation on STAT1 activity and tyrosine phosphorylation in cultured human keratinocytes. *Free Radic. Biol. Med.* 28, 1430-1437.
- Djavaheri-Mergny, M., J. L. Mergny, F. Bertrand, R. Santus, C. Maziere, L. Dubertret and J. C. Maziere (1996) Ultraviolet-A induces activation of AP-1 in cultured human keratinocytes. *FEBS Lett.* 384, 92-96.
- Vile, G. F., A. Tanow-Ilischew and R. M. Tyrell (1995) Activation of NF-kappa B in human skin fibroblasts by the oxidative stress generated by UVA radiation. *Photochem. Photobiol.* 62, 463-468.
- Zhang, Y., S. Zhong, Z. Dong, N. Chen, A. M. Bole and W.

- Ma (2001) UVA induces Scr381 phosphorylation of p90RSK/MAPKAP-K1 via ERK and JNK pathways. *J. Biol. Chem.* 276, 14572-14580.
22. Zhang, Y., Z. Dong, M. Nomura, S. Zhong, N. Chen and A. M. Dode (2001) Signal transduction pathways involved in phosphorylation and activation of p70S6K following exposure to UVA irradiation. *J. Biol. Chem.* 276, 20913-20923.
 23. Zhang, Y., G. Liu and Z. Dong (2001) MSK1 and JNKs mediate phosphorylation of STAT3 in UVA-irradiated mouse epidermal JB6 cells. *J. Biol. Chem.* 276, 42534-42542.
 24. Angel, P. and M. Karin (1991) The role of Jun, Fos and the AP-1 complex in cell-proliferation and transformation. *Biochim. Biophys. Acta* 1072, 129-157.
 25. Brista, P., F. D'Anna, A. T. Franzi and R. Gherzi (1993) AP-1 activity during normal human keratinocyte differentiation: evidence for a cytosolic modulator of AP-1/DNA binding. *Exp. Cell Res.* 204, 136-146.
 26. Domann, F. E., J. P. Levy, M. J. Birner and G. T. Bowden (1994) Stable expression of a c-JUN deletion mutant in two malignant mouse epidermal cell lines blocks tumor formation in nude mice. *Cell Growth Differ.* 5, 9-16.
 27. Bernstein, L. R. and N. H. Colburn (1989) AP1/jun function is differentially induced in promotion-sensitive and resistant JB6 cells. *Science* 244, 566-569.
 28. Greenhalgh, D. A., D. J. Welty, A. Player and S. H. Yuspa (1990) Two oncogenes, v-fos and v-ras, cooperate to convert normal keratinocytes to squamous cell carcinoma. *Proc. Natl. Acad. Sci. USA* 87, 643-647.
 29. Sney, E., S. E. Rutberg, E. Mueller, H. Oppenheim, J. Smulak, S. H. Yuspa and B. M. Spiegelman (1995) c-fos is required for malignant progression of skin tumors. *Cell* 82, 721-732.
 30. Sachsenmaier, C., A. Rüdler-Pohl, R. Zinck, A. Nordheim, P. Horrich and H. J. Rahmsdorf (1994) Involvement of growth factor receptors in the mammalian UVC response. *Cell* 78, 963-972.
 31. Huang, C., W. Ma, G. T. Bowden and Z. Dong (1996) Ultraviolet B-induced activated protein-1 activation does not require epidermal growth factor receptor but is blocked by a dominant negative PKC λ delta. *J. Biol. Chem.* 271, 31262-31268.
 32. Shah, G., R. Ghosh, P. A. Amstad and P. A. Cerutti (1993) Mechanism of induction of c-fos by ultraviolet B (290-320 nm) in mouse JB6 epidermal cells. *Cancer Res.* 53, 38-45.
 33. Nakano, H., F. P. Gasparro and J. Uitto (2001) UVA-340 as energy source, mimicking natural sunlight, activates the transcription factor AP-1 in cultured fibroblasts: evidence for involvement of protein kinase-C. *Photochem. Photobiol.* 74, 274-282.
 34. Hong, J. T., E. J. Kim, K. S. Ahn, K. M. Jung, Y. P. Yun, Y. K. Park and S. H. Lee (2001) Inhibitory effect of glycolic acid on ultraviolet-induced skin tumorigenesis in SKH-1 hairless mice and its mechanism of action. *Mol. Carcinog.* 31, 152-160.
 35. Huang, C., W. Y. Ma, D. Hanenberger, M. P. Cleary, G. T. Bowden and Z. Dong (1997) Inhibition of ultraviolet B-induced activator protein-1 (AP-1) activity by aspirin in AP-1-luciferase transgenic mice. *J. Biol. Chem.* 272, 26325-26331.
 36. Chen, W., A. H. Borchers, Z. Dong, M. B. Powell and G. T. Bowden (1998) UVB irradiation-induced activator protein-1 activation correlates with increased c-fos gene expression in a human keratinocyte cell line. *J. Biol. Chem.* 273, 32176-32181.
 37. Dignam, J. D., R. M. Lebovitz and R. G. Roeder (1983) Accurate transcription initiation by RNA polymerase II in a soluble extract from isolated mammalian nuclei. *Nucleic Acids Res.* 11, 1475-1489.
 38. Rittling, S. R., C. W. Gibson, S. Ferrari and R. Baserga (1985) The effect of cycloheximide on the expression of cell cycle dependent genes. *Biochem. Biophys. Res. Commun.* 132, 327-335.
 39. Cochran, B. H., J. Zullo, I. M. Verma and C. D. Siles (1984) Expression of the c-fos gene and of an fos-related gene is stimulated by platelet-derived growth factor. *Science* 226, 1080-1082.
 40. Karin, M., Z. Liu and E. Zandi (1997) AP-1 function and regulation. *Curr. Opin. Cell Biol.* 9, 240-246.
 41. Woodgett, J. R. (1990) Fos and jun: two into one will go. *Semin. Cancer Biol.* 1, 389-397.
 42. Jordanov, M. S., D. Pribnow, J. L. Magu, T. H. Dinh, J. A. Pearsons and B. E. Magu (1998) Ultraviolet radiation triggers the ribotoxic stress response in mammalian cells. *J. Biol. Chem.* 273, 15794-15803.
 43. Qadar, D. E. and A. D. Lucas (1995) Spectral dependence of UV-induced immediate and delayed apoptosis: the role of membrane and DNA damage. *Photochem. Photobiol.* 62, 108-113.
 44. de Laat, A., M. van Tilburg, J. C. van der Leun, W. A. van Vloten and F. R. de Gruijl (1996) Cell cycle kinetics following UVA irradiation in comparison to UVB and UVC irradiation. *Photochem. Photobiol.* 63, 492-497.
 45. Lehmann, J., D. Pollet, S. Peker, V. Steinkraus and U. Hoppe (1998) Kinetics of DNA strand breaks and protection by antioxidants in UVA- or UVB-irradiated HaCaT keratinocytes using the single cell gel electrophoresis assay. *Mutat. Res.* 407, 97-108.
 46. Angel, P., K. Hattori, T. Smol and M. Karin (1988) The jun proto-oncogene is positively autoregulated by its product, Jun/AP-1. *Cell* 55, 875-885.
 47. Trejo, J., J. C. Chambard, M. Karin and J. H. Brown (1992) Biphasic increase in c-jun mRNA is required for induction of AP-1-mediated gene transcription: differential effects of muscarinic and thrombin receptor activation. *Mol. Cell Biol.* 12, 4742-4750.
 48. Gruda, M. C., K. Kovary, R. Metz and R. Bravo (1994) Regulation of Fra-1 and Fra-2 phosphorylation differs during the cell cycle of fibroblasts and phosphorylation in vitro by MAP kinase affects DNA binding activity. *Oncogene* 9, 2537-2547.
 49. Curran, T., C. Abate, S. Baker, T. Kerppola and S. Xanthopoulos (1993) The regulation of c-fos: too much is never enough. *Adv. Second Messenger Phosphoprotein Res.* 28, 271-277.
 50. Abate, C., D. R. Marshak and T. Curran (1991) Fos is phosphorylated by p34cdc2, cAMP-dependent protein kinase and protein kinase C at multiple sites clustered within regulatory regions. *Oncogene* 6, 2179-2185.
 51. Millward, T. A., S. Zolnierowicz and B. A. Hemmings (1999) Regulation of protein kinase cascades by protein phosphatase 2A. *Trends Biochem. Sci.* 24, 186-191.
 52. Barber, J. R. and I. M. Verma (1987) Modification of fos proteins: phosphorylation of c-fos, but not v-fos, is stimulated by 12-tetradecanoyl-phorbol-13-acetate and serum. *Mol. Cell Biol.* 7, 2201-2211.
 53. Zolnierowicz, S. (2000) Type 2A protein phosphatase, the complex regulator of numerous signaling pathways. *Biochem. Pharmacol.* 60, 1225-1235.
 54. Al-Murrani, S. W., J. R. Woodgett and Z. Damuni (1999) Expression of I2PP2A, an inhibitor of protein phosphatase 2A, induces c-Jun and AP-1 activity. *Biochem. J.* 341, 293-298.
 55. Boyle, W. J., T. Smol, L. H. Defize, P. Angel, J. R. Woodgett, M. Karin and T. Hunter (1991) Activation of protein kinase C decreases phosphorylation of c-Jun at sites that negatively regulate its DNA-binding activity. *Cell* 64, 573-584.
 56. Bose, B., M. Soriani and R. M. Tyrrell (1999) Activation of expression of the c-fos oncogene by UVA irradiation in cultured human skin fibroblasts. *Photochem. Photobiol.* 69, 489-493.
 57. Soriani, M., V. Hejnadi and R. M. Tyrrell (2000) Modulation of c-jun and c-fos transcription by UVB and UVA radiations in human dermal fibroblasts and KB cells. *Photochem. Photobiol.* 71, 551-558.
 58. Djavaheri-Mergny, M., M. P. Gras, J. L. Mergny and L. Dubertret (1999) UV-A-induced decrease in nuclear factor-kappaB activity in human keratinocytes. *Biochem. J.* 338, 607-613.

Rat kidney glutamyl aminopeptidase (aminopeptidase A): molecular identity and cellular localization

LIJUN SONG, MINGQI YE, MARTA TROYANOVSKAYA,
ELIZABETH WILK, SHERWIN WILK, AND DENNIS P. HEALY

Department of Pharmacology, Mount Sinai School of Medicine, City University of New York,
New York, New York 10029

Song, Lijun, Mingqi Ye, Marta Troyanovskaya, Elizabeth Wilk, Sherwin Wilk, and Dennis P. Healy. Rat kidney glutamyl aminopeptidase (aminopeptidase A): molecular identity and cellular localization. *Am. J. Physiol.* 267 (Renal Fluid Electrolyte Physiol. 36): F546-F557, 1994. — Glutamyl aminopeptidase [aminopeptidase A (EAP), EC 3.4.11.7] is an ectoenzyme that selectively hydrolyzes acidic amino acid residues from the amino terminus of oligopeptides. EAP activity is highest within the kidney and small intestine. The murine pre-B cell BP-1/6C3 and the human kidney glycoprotein gp160 differentiation antigens have been reported to have biochemical properties indistinguishable from EAP. It is not known, however, if rat kidney EAP is a homologue of these antigens or molecularly distinct. Using the reverse transcription-polymerase chain reaction method with oligonucleotide primers based on the BP-1/6C3 nucleotide sequence, we isolated a 450-bp partial cDNA from rat kidney poly(A)⁺ RNA. The partial cDNA encoded a predicted protein that was 92% and 86% identical to the murine BP-1/6C3 and human gp160 antigens, respectively; the amino acid sequence within the zinc-binding domain was completely conserved. Purification of EAP from rat kidney and microsequence analysis of a tryptic digest peptide fragment (18-mer) indicated that the fragment was highly similar to a region within the BP-1/6C3 and gp160 proteins. Northern blot hybridization and immunoblot analyses were also consistent with labeling of products the same size as reported for the BP-1/6C3 and gp160 antigens. There was a good correlation between the cellular distribution of EAP mRNA and EAP immunoreactivity, with proximal tubules and glomerular mesangial cells having the highest densities. These results indicate that rat kidney EAP is a species homologue of the murine BP-1/6C3 and human gp160 antigens. Furthermore, on the basis of its cellular localization, rat kidney EAP is likely to be involved in degradation of oligopeptides within the glomerulus and the glomerular filtrate. Since cells that express EAP also express receptors for angiotensin II, an intrarenal vasoactive hormone that is a substrate for EAP, these results further suggest that EAP may play a role in modulating the activity of intrarenal angiotensin II.

aminopeptidase A; angiotensinase; angiotensin II; proximal tubules; mesangial cells

GLUTAMYL AMINOPEPTIDASE [aminopeptidase A (EAP), EC 3.4.11.7] is an ectoenzyme that selectively hydrolyzes amino-terminal glutamyl and aspartyl residues from oligopeptides (11). EAP levels are highest within the brush border of kidney proximal tubules and enterocytes of the small intestine, areas that are enriched with peptidases (10, 20). At these sites EAP is believed to participate in the degradation of oligopeptides for nutritive purposes. EAP has also been shown to be an "angiotensinase," hydrolyzing the biologically active

peptide [Asp¹]angiotensin II (ANG II) to [des-Asp¹]ANG II (ANG III) in the circulation (1, 21). In the kidney, ANG II decreases renal blood flow and increases proximal tubule reabsorption of sodium (15, 19). In addition, all the components of the renin-angiotensin system have been localized within the kidney (32), suggesting that an intrarenal renin-angiotensin system may play an important role in kidney function (3, 22). The importance of EAP in modulating ANG II activity within the kidney has not been determined.

Recent cloning and functional expression studies indicate that two previously characterized differentiation antigens have biochemical and enzymological properties indistinguishable from EAP. The murine pre-B cell differentiation antigen BP-1/6C3 has sequence homology with members of the zinc-dependent metalloenzyme family (36, 37) and EAP-like activity when expressed in vitro (33). More recently, the human kidney differentiation antigen glycoprotein gp160 was purified and cloned and found to be 78% identical to BP-1/6C3 (26). Renal cell carcinomas expressing gp160 have EAP activity, and immunoprecipitation of gp160 depletes cells of EAP activity. Moreover, isolation of cDNA clones from human kidney cDNA libraries indicates that the differentiation antigens and the kidney transcripts are identical (23, 26). Thus these lines of evidence indicate that the BP-1/6C3 and gp160 antigens represent a form of kidney EAP.

Purification studies indicate that EAP exists as a homodimer with molecular mass ranging from 247 to 300 kDa, with the monomeric form having a molecular mass ranging from 120 to 140 kDa under dissociating conditions (34). Some heterogeneity in the size of the monomeric forms has been reported (6, 13, 17). Herzig et al. (17) have reported that purification of bromelain-solubilized EAP from human kidney yielded two isoforms, a 127-kDa form that was localized to glomeruli and tubules and a 117-kDa form that was localized primarily to tubules. The relationship between the EAP isoforms and the gp160 antigen in human kidney has not been determined. We have reported that immunoblots with purified rat EAP yield only a single band, whereas immunoblots with kidney homogenates yielded two bands of 136 and 101 kDa on sodium dodecyl sulfate-polyacrylamide gel electrophoresis (SDS-PAGE) (31). It is not clear whether the smaller forms of EAP seen in immunoblots represent multiple isoforms of EAP, partial proteolytic digestion of the native enzyme, or cross-reactivity with a closely related enzyme(s).

In an effort to characterize the rat kidney form of EAP, we used the reverse transcription-polymerase chain reaction (RT-PCR) procedure with oligonucleotide

RAT KIDNEY GLUTAMYL AMINOPEPTIDASE

F547

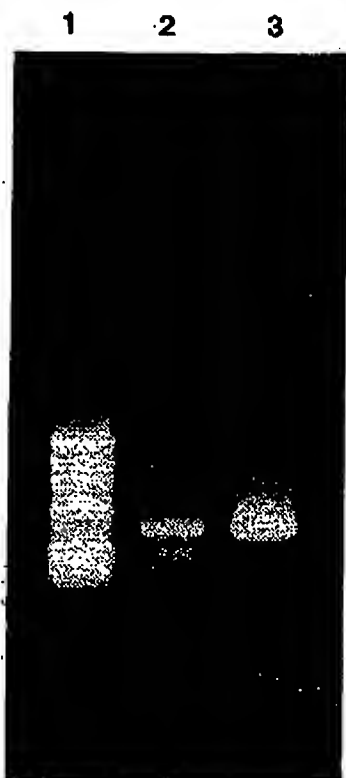


Fig. 1: Agarose gel electrophoresis of polymerase chain reaction (PCR) products from amplification of rat kidney cortex cDNA with mouse BP-1/6C3 primers. Lane 1, DNA markers (1,353; 1,078; 872; 603; and 310 bp, top to bottom); lane 2, 25 cycles; lane 3, second round of 25 cycles. Note that an intense reaction product of the expected size (arrowhead, 450 bp) was seen after 25 cycles (lane 2), which was then reamplified an additional 25 cycles (lane 3).

primers based on the murine BP-1/6C3 sequence to isolate a partial cDNA for rat kidney EAP. The partial cDNA was then used to synthesize radiolabeled synthetic antisense RNA (riboprobes) that could be used to localize EAP mRNA by in situ hybridization. The distribution of the EAP mRNA was then correlated with the distribution of EAP immunoreactivity.

METHODS

PCR analysis. Poly(A)⁺ RNA was isolated from the kidney by first isolating total RNA (5), followed by passage over an oligo(dT) cellulose column (28). First-strand cDNA synthesis was performed with poly(A)⁺ RNA as template in the presence of reverse transcriptase and an oligo(dT) primer (Superscript RNA reverse transcriptase; BRL, Gaithersburg, MD). The PCR primers were designed to amplify an ~450-bp region of the BP-1/6C3 cDNA that includes the zinc-binding domain of the processed protein; sense primer (EAP-1) corresponding to nucleotides 1228–1250 of the murine BP-1/6C3 antigen, 5' GAGATGGTGGATGACAACCTGGAA 3'; antisense primer (EAP-2) corresponding to nucleotides 1651–1674 of BP-1/6C3, 5' CCACAAGTCGTCCACCACTCCAT 3'. Each primer contained an additional 10 nucleotides encoding an *Xho* I restriction site at the 5' end that was used for subcloning of the amplified cDNA into a plasmid vector. Kidney cDNA was submitted to 25 cycles of PCR amplification with PCR primers

in the presence of *Taq* DNA polymerase in the following sequence: first cycle 5 min at 94°C, 2 min at 55°C, 3 min at 72°C; subsequent cycles 1 min at 94°C, 2 min at 50°C, and 3 min at 72°C; last cycle 1 min at 94°C, 2 min at 50°C, and 10 min at 72°C. The PCR products were then separated on a 1% agarose gel, and the bands were examined under ultraviolet illumination. PCR controls included 1) amplification with template but without primers, 2) amplification with mRNA without the RT step, and 3) amplification without template.

The PCR-amplified product was then subcloned into a plasmid (TA cloning vector, Invitrogen, San Diego, CA) and used for transformation of INVαF competent *Escherichia coli*. Positive transformants containing plasmids with inserts were selected by growing bacteria on Luria-Bertani plates containing kanamycin, isopropyl-β-D-thiogalactopyranoside and Blue-Gal. Plasmids were isolated from minicultures and digested with *Xho* I. Plasmids containing the PCR product were then sequenced directly by the dideoxynucleotide chain-termination method with [α -³²P]dATP and sequence-specific oligonucleotide primers (Sequenase, United States Biochemical, Cleveland, OH).

Northern blot analysis. Total RNA (10 μ g) from rat kidney and jejunum were size fractionated by electrophoresis on a 1% agarose-formaldehyde gel and transferred to Micron Separation (Westboro, MA) nitrocellulose membrane and fixed by baking for 2 h at 80°C. Membranes were prehybridized 4 h at 39°C in hybridization buffer [25 mM potassium phosphate (pH 7.4), 5 \times SSC (1 \times SSC is 0.15 M NaCl and 0.015 M sodium citrate, pH 7.0), 5 \times Denhardt's solution, 50 μ g/ml denatured salmon sperm DNA, and 50% formamide]. The membranes were transferred to fresh hybridization buffer containing ³²P-labeled probe and 10% dextran sulfate and incubated overnight at 39°C. The filters were then washed two times each in 2 \times SSC and 1 \times SSC at room temperature, followed by a single wash in 0.1 \times SSC at 55°C.

The radiolabeled probe was prepared by excision of the partial cDNA PCR product (50–80 ng) from the plasmid with *Xho* I, random priming with hexanucleotides and 50 μ Ci of [α -³²P]dCTP (New England Biolab kit), and extension with DNA polymerase I. Specific activity of the probe was $\sim 5 \times 10^8$ counts \cdot min⁻¹ \cdot μ g⁻¹.

Isolation of glomeruli. Rat kidney glomeruli were isolated according to the procedure of Fujiwara et al. (8) with some modifications. Briefly, eight Sprague-Dawley rats (200 g) were killed, and the kidneys were removed and placed in ice-cold Dulbecco's phosphate-buffered saline (PBS), pH 7.4, containing (in mM) 137 NaCl, 2.7 KCl, 8.1 Na₂HPO₄, 1.5 KH₂PO₄, 0.9 CaCl₂, 0.49 MgCl₂, and 5.6 glucose. The cortex was dissected and minced to paste-like consistency and then suspended in cold Dulbecco's PBS. The suspension was passed through a 25-gauge needle repeatedly and pushed successively through 200- μ m and 150- μ m sieves. The glomeruli were collected on a 50- μ m sieve that was washed with Dulbecco's PBS. The purity of the isolated glomeruli was confirmed by light microscopy.

Enzyme activity. EAP activity was assayed with α -glutamyl-2-naphthylamide and α -aspartyl-2-naphthylamide as substrates. Specific activities were expressed as units per milligram protein, where one unit equals the hydrolysis of 1 nmol substrate/min.

Immunoblotting. Immunoblotting was conducted as described previously (31). Briefly, 35 μ g of protein were separated on a 10% SDS-PAGE gel run at 250 V for 2 h. The protein was transferred to an Immobilon membrane (Millipore, Bedford, MA) in a transfer apparatus containing transfer buffer of 25 mM Tris(hydroxymethyl)aminomethane (Tris) base, 192 mM glycine, and 15% methanol at 70 V for 1 h. After transfer, the membrane was washed with PBS 2 \times 5 min and

P548

RAT KIDNEY GLUTAMYL AMINOPEPTIDASE

A

1 GAGATGGTGGATGACAACCTGGAAGAAAACCACTTTTCATGAAGTCCGTCCGATGAGCACT
 61 TACCTGGTGTGCTTTGCTGTACATCAGTTCACTCGATACAGAGAACATCCAGGAGTGGC
 121 AAACCACTCACTGTTTACGTCCAGCCCAACCAAAAGCAAACAGCAGAGTATGCGGCAAAAC
 181 ATAACCAAAGCTGTGTTTGACTTCTTTGAAGACTACTTCGCTATGGAGTATTCTCTTCCG
 241 AAACTGGATAAAATTGCTATTCCAGATTTGGCACCGGCGCCATGGAAACTGGGGACTT
 301 GTCACCTACCGAGAAACAAACCTGCTTTATGACCCCTGCTATCGGCCTCATCCAACCAG
 361 CAGAGAGTAGCCAGCGTGGTTGCCACGAGCTCGTGACCAGTGGTTTGGAAATATCGTG
 401 ACCATGGACTGGTGGGACGACTTGTGG

B

Rat		KTTFMKSVPMSTYLVCFVHQFTSIQRTSRSGKPLTVYVQPNQKQ
Mouse	265V.....R..A.E.K.....K.....E
Human	273	R...E.....D.VK.I.N.....I....E..H
Rat		TAEYAANITKAVDFDFEDYFAMEYSLPKLDKIAIPDFGTGAMENW
Mouse	310Q....Y.....A.....
Human	318S...Y..E....N.....
Rat		GLVTYRETNLLYDPLLSASSNQQRVASVVAHELVBQWFGNIVT
Mouse	355T..
Human	363	..I.....KE.....T.....

Fig. 2. A: nucleotide sequence of the partial cDNA obtained from rat kidney using oligonucleotide primers (underlined) based on the BP-1/6C3 sequence. B: deduced amino acid sequence of the partial cDNA from rat kidney compared with mouse BP-1/6C3 and human glycoprotein gp160. Amino acids that are not identical in all 3 sequences are noted. (Numbers refer to published amino acid sequence of BP-1/6C3 and gp160.) The putative zinc-binding domain (bold letters) was completely conserved.

incubated with a blocking buffer containing 5% nonfat dry milk and 0.02% sodium azide and agitated for 1 h. Blots were incubated with primary antiserum diluted 1:1,000 in PBS containing 3% bovine serum albumin (BSA) for 12–18 h at 4°C. The membranes were washed with PBS and incubated with peroxidase-labeled goat secondary antibody at 37°C for 2 h. The membrane was washed with PBS and incubated with 0.6 mg/ml diaminobenzidine (Sigma, St. Louis, MO) in 50 mM Tris-HCl (pH 7.6) and containing 0.03% hydrogen peroxide for 5–10 min. The membrane was washed with PBS and then dried.

Specificity of the immunoblot staining was tested by preabsorbing the antiserum with purified EAP (1 µg/ml), membrane alanyl aminopeptidase (mAAP; aminopeptidase M, aminopeptidase N, EC 3.4.11.2) (1 µg/ml), and dipeptidyl peptidase IV (DPP IV; EC 3.4.14.5) (1 µg/ml) and comparing the staining pattern to antiserum that was not preabsorbed.

Enzyme purification and sequence determination. EAP was purified to apparent homogeneity from rat kidney using affinity chromatography as described (31). DPP IV, mAAP, and EAP copurify up to the phenyl Sepharose step. DPP IV is resolved from the other two enzymes by phenyl Sepharose chromatography (34). mAAP is resolved from EAP by affinity

chromatography (31). DPP IV and mAAP were apparently homogeneous as judged by SDS-PAGE.

An aliquot of EAP was subjected to SDS-PAGE on a 12.5% gel. The protein was stained with Coomassie blue and transferred to an Immobilon polyvinylidene fluoride membrane (Millipore). The band was excised and sent to the Yale Protein and Nucleic Acid Chemistry facility for trypsinization, high-performance liquid chromatography (HPLC) separation, and microsequencing.

In situ hybridization. Four male Sprague-Dawley rats (175–200 g) were decapitated, and the kidneys were removed and frozen to microtome chucks. Ten-micrometer cryostat sections were collected onto clean microscope slides subbed with 2% 3-aminopropyltriethoxysilane (Sigma). The sections were dried under vacuum for 10 min and then fixed with 8% paraformaldehyde in phosphate buffer for 5 min, dehydrated, and vacuum dried. A ³⁵S-labeled riboprobe complementary to the EAP mRNA was transcribed in vitro using the cDNA as template. Radiolabeled sense strand RNA was synthesized in a similar manner and used as a control. Probes were synthesized by incubating 1 µg of linearized cDNA in a total reaction volume of 12 µl containing 100 mM dithiothreitol, RNasin, 1 mM unlabeled nucleotide triphosphates (ATP, GTP, and UTP),

RAT KIDNEY GLUTAMYL AMINOPEPTIDASE

F549

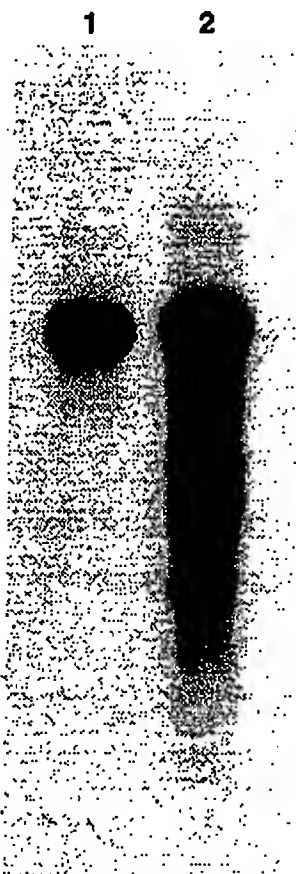


Fig. 3. Northern blot analyses of rat total RNA from kidney (lane 1) and small intestine (lane 2) probed with the kidney partial cDNA. Ten micrograms of total RNA was size fractionated on an agarose-formaldehyde gel and transferred to nitrocellulose sheets. The blots were hybridized with 32 P-labeled probes from the aminopeptidase A (EAP) partial cDNA clone. Blots were then washed under high-stringency conditions and exposed overnight to X-ray film.

100 μ M CTP, 10 pmol of [32 S]CTP (New England Nuclear, sp act 1,220 Ci/mmol), and T7 or T3 polymerase for 1 h at 37°C. The template DNA was then digested with DNase and the labeled probe precipitated and resuspended in hybridization buffer. The activity of the labeled riboprobe was $\sim 8 \times 10^5$ counts \cdot min $^{-1}$ \cdot μ l $^{-1}$.

Slide-mounted sections were prehybridized for 2 h at 50°C in a 1:1 mixture of formamide and prehybridization buffer containing 0.6 M NaCl, 20 mM piperazine-*N,N'*-bis(2-ethanesulfonic acid) buffer (pH 6.7), 1 \times Denhardt's solution, 1 mM EDTA, 500 μ g/ml yeast total RNA, 50 μ g/ml yeast tRNA, 1 mg/ml salmon sperm DNA, and 500 μ g/ml sodium pyrophosphate. Hybridization buffer was identical to prehybridization buffer, except that it contained 2.5 μ M α -thiol-nucleotide triphosphates and 200 mM dithiothreitol (Sigma). The slides were then transferred to hybridization solution comprised of a mixture of hybridization buffer, dextran sulfate, and formamide (4:1:5) and containing the 32 S-labeled riboprobe at a final concentration of 5×10^6 counts \cdot min $^{-1}$ \cdot ml $^{-1}$. Slides were incubated overnight at 50°C. The next day the sections were washed twice for 10 min at room temperature in 10 mM Tris-HCl (pH 8), 0.3 M NaCl, 0.1% sodium pyrophosphate, and 10 mM dithiothreitol and then treated with RNase (30 μ g/ml) for 30 min at room temperature in 0.3 M NaCl, 10 mM

Tris-HCl, and 1 mM EDTA. The RNase solution was then blotted off and the sections washed for 10 min at room temperature in 0.3 M NaCl, 2 mM Tris-HCl, 1 mM EDTA, 0.05% sodium pyrophosphate, and 1 mM dithiothreitol followed by a 3-h wash at 50°C in 0.075 M NaCl, 2 mM Tris-HCl, 1 mM EDTA, and 1 mM dithiothreitol. The slides were then transferred to fresh buffer and washed overnight at room temperature. The next day the sections were dehydrated for 2 min each in 70% alcohol containing 300 mM ammonium acetate, 90% alcohol containing 300 mM ammonium acetate, and finally 100% alcohol. The sections were vacuum dried and exposed to Kodak XAR film for 1–20 days. After the film was developed, the slides were then dipped in liquid emulsion (Kodak NTB3, diluted 1:1) for high-resolution autoradiography. After exposure for 1–2 mo, the emulsion was developed, and the sections were counterstained lightly with cresyl violet, dehydrated, and coverslipped.

Immunocytochemistry. Six male Sprague-Dawley rats (175–200 g, Charles River Breeding Laboratories, Wilmington, MA) were housed on a 12:12-h light-dark schedule and allowed free access to food and water. Rats not operated on were processed for immunocytochemistry as described previously (16). Briefly, animals were anesthetized with pentobarbital (50 mg/kg ip) and perfused transcardially with ~ 100 ml of PBS (pH 7.4) followed by 1 ml/g body wt of 5% paraformaldehyde in 0.3 M sodium phosphate buffer, pH 7.4, over a period of 10 min. The kidneys were removed and postfixed in the same fixative for 1 h and then transferred through increasing concentrations of sucrose in PBS (2 h overnight) up to 18%. The kidneys were frozen to microtome chucks with powdered dry ice, and 20- μ m transverse sections were cut in the cryostat (-20° C) and mounted on subbed microscope slides. Sections were washed three times in PBS and preincubated for 30 min with 2% normal goat serum in PBS containing 0.1% Triton X-100. The goat serum was then removed and replaced by diluted immune sera (1:5,000 to 1:10,000) in PBS containing 0.1% Triton X-100 and 0.1% BSA. The sections were then stored overnight at 4°C. The sections were rinsed with PBS and incubated with biotinylated goat anti-rabbit immunoglobulin G (Vector Laboratories) in a 1:222 dilution with PBS-Triton X-100-BSA. The sections were washed three times in PBS and incubated for 45 min with streptavidin-horseradish peroxidase conjugate. Unbound conjugate was removed by washing with PBS. The peroxidase reaction was developed by treating the sections with a freshly prepared 0.05% solution of 3,3'-diaminobenzidine (Sigma) containing 0.003% hydrogen peroxide in 50 mM phosphate buffer, pH 7.4, for 5–10 min. One-half of the slides were counterstained lightly with cresyl violet. All slides were dried, dehydrated in alcohol and xylene, coverslipped with Permount (Fisher Scientific, Pittsburgh, PA), and viewed under a Zeiss microscope.

Additional immunocytochemical staining was conducted on kidney sections from nonperfused animals. The sections were prepared identically as described above for *in situ* hybridization, i.e., unfixed cryostat kidney sections were mounted on slides and fixed in 3% paraformaldehyde for 5 min. Sections were also processed identically for immunohistochemistry through the biotinylated secondary antibody step. After washing, the slides were incubated with fluorescein isothiocyanate-labeled avidin (Vector Labs) at a dilution of 1:100 for 1 h at room temperature, washed, dried, and coverslipped with mineral oil. Sections were viewed under a Zeiss microscope equipped with a mercury/xenon lamp and epifluorescence.

Immunocytochemical controls consisted of staining in the presence of preimmune serum or immune serum preabsorbed with purified EAP, mAAP, and DPP IV at a concentration of 1 μ g/ml.

F550

RAT KIDNEY GLUTAMYL AMINOPEPTIDASE

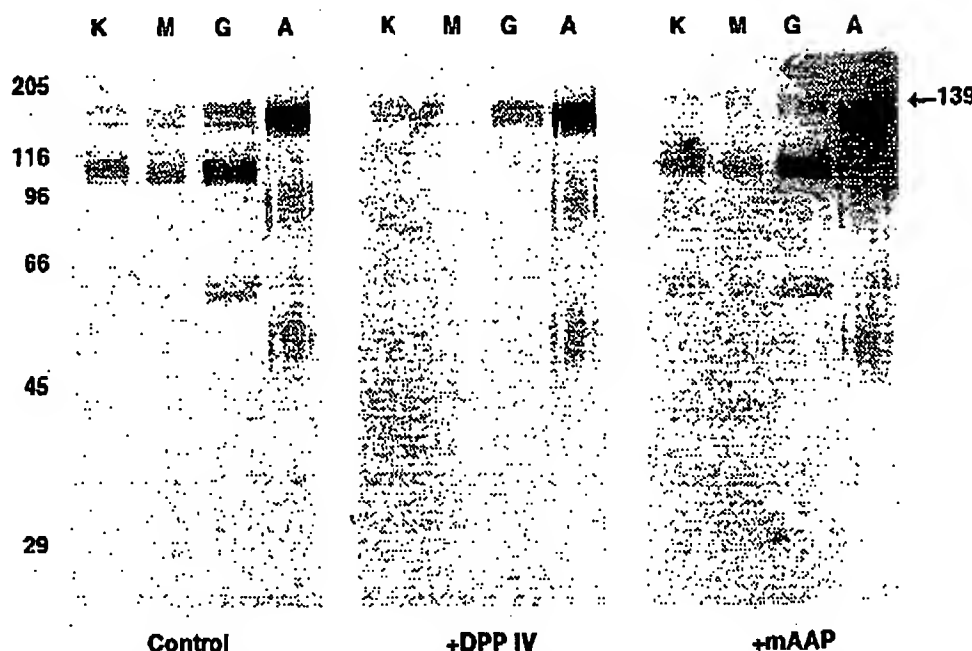


Fig. 4. Immunoblots of rat kidney EAP. Purified EAP (A) and homogenate protein (35 μ g/lane) from total kidney (K), outer medulla (M), and isolated glomeruli (G) were separated by SDS-polyacrylamide gel electrophoresis under reducing conditions, transferred to nitrocellulose sheets, and immunostained with EAP antiserum (1:1,000 dilution). Size of labeled bands was determined by comparison to molecular mass markers (29–205 kDa). The staining pattern with control immune serum was compared with that with immune serum preabsorbed with either 1 μ g/ml dipeptidyl peptidase IV (+DPP IV) or with 1 μ g/ml membrane alanyl aminopeptidase (+mAAP). The size of the putative EAP protein from this typical experiment (arrow) was 139 kDa.

RESULTS

Amplification of rat kidney cDNA with PCR primers based on the murine BP-1/6C3 sequence resulted in generation of a PCR product of the predicted size (Fig. 1). Four clones were sequenced, and each contained identical cDNA inserts (Fig. 2). The 450-bp cDNAs were 90% and 82% identical at the nucleotide level and 92% and 86% identical at the amino acid level to the BP-1/6C3 and gp160 differentiation antigen sequences, respectively (Fig. 2). Examination of the partial cDNA in the area encoding the zinc-binding domain indicated that the predicted amino acid sequence was identical to the zinc-binding domain of the BP-1/6C3 and gp160 antigens (Fig. 2).

Northern blot hybridization studies of rat kidney or jejunum total RNA with the rat partial cDNA resulted in strong hybridization of a band at 4.1 kb (Fig. 3). A less intense band was seen at 6.3 kb.

Studies by Herzig et al. (17) suggested that one form of EAP was distributed on both tubules and glomeruli and a second isoform was expressed on tubules only. We therefore compared the SDS-PAGE immunoblot staining for EAP from isolated glomeruli to that seen with total kidney homogenates and outer medulla (enriched with tubular segments) homogenate. Immunoblots with EAP antiserum (1:1,000 dilution) typically resulted in labeling of three bands: 136 ± 0.9 , 128 ± 0.9 , and 106 ± 1.2 kDa ($n = 5$) (Fig. 4). A fourth lightly stained band was seen at ~ 50 kDa and was most prominent in the protein from the isolated glomeruli. The immunoblot pattern of staining was similar to that reported previously for kidney homogenates (31) except that the diffuse upper band seen previously could now be separated into two distinct bands of 137 and 129 kDa. The outer medulla and the isolated glomeruli yielded a similar pattern of staining except that the staining was

Rat EAP	Gln-Val-Lys-Pro-Ile-Ala- <u>xxx</u> -Ser-Leu-Gly- <u>xxx</u> -Gln- <u>xxx</u> -Thr-Gly-Ser- <u>xxx</u> -Ile
Murine BP-1/6C3	...Gln-Val-Lys-Pro- <u>Val</u> -Ala-Asp- <u>Leu</u> -Leu-Gly-Trp-Gln-Asp-Thr-Gly-Ser-His-Ile...
Human gp160	...Gln-Val-Lys-Pro-Ile-Ala-Asp-Ser-Leu-Gly-Trp- <u>Asn</u> -Asp- <u>Ala</u> -Gly- <u>Asp</u> -His- <u>Val</u> ...

Fig. 5. Amino acid sequence of a partial tryptic peptide of EAP purified from rat kidney. XXX, amino acids that could not be identified with certainty. Amino acids from corresponding regions of BP-1/6C3 or gp160 that were not identical to the rat sequence are underlined.

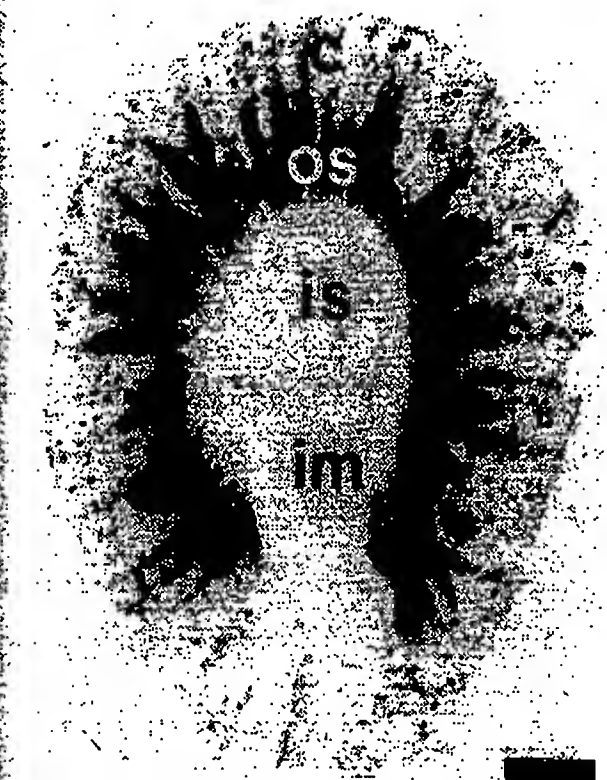


Fig. 6. In situ hybridization of rat kidney EAP mRNA. Shown is an autoradiogram of a transverse section of rat kidney incubated with an EAP antisense ^{35}S -labeled riboprobe and exposed to Kodak XAR film for 3 days. The heaviest labeling was in the outer stripe (os) of the outer medulla, extending into the cortex (c) as the medullary rays. Cortical labeling was punctate, with the size and distribution suggestive of glomeruli. The inner stripe (is) of the outer medulla and the inner medulla (im) were not labeled. Scale bar, 3 mm.

more intense with the isolated glomeruli. This is consistent with the EAP-specific activity being elevated in the isolated glomeruli compared with either the total kidney homogenate or the outer medulla homogenate: kidney 13.3 ± 2.3 , outer medulla 13.5 ± 1.1 , and glomeruli $45.2 \pm 4.7 \mu\text{mol} \cdot \text{h}^{-1} \cdot \text{mg protein}^{-1}$ ($n = 5$). Interestingly, only a single band of $132 \pm 1.9 \text{ kDa}$ was seen with EAP purified from rat kidney (Fig. 4). To determine if the smaller bands were proteolytic products of the 137-kDa band, we isolated kidney protein in the presence of a battery of protease inhibitors (18). Immunostaining of kidney protein under these conditions did not alter the pattern of the immunostaining (data not shown). Previous studies indicated that preabsorption of the EAP antiserum with purified kidney EAP completely blocked the immunoblot staining (31), results that were confirmed in this study by preabsorption with $1 \mu\text{g/ml}$ of purified EAP (data not shown). We then determined if the antiserum cross-reacted with other aminopeptidases, namely mAAP and DPP IV. Preabsorption of the EAP antiserum with DPP IV blocked the staining of the 106- and 50-kDa bands (Fig. 4). The immunostaining of the higher-molecular-weight doublet was not affected. Likewise, preabsorption of the

antiserum with purified mAAP blocked the staining of the 129-kDa band but not the 137-kDa or the 106-kDa band. Preabsorption of the antiserum with mAAP and DPP IV simultaneously resulted in staining of only the 137-kDa band (data not shown). Preabsorption with mAAP or DPP IV, separately or together, did not affect the staining of the purified EAP. The slightly smaller form of the purified EAP compared with the EAP from kidney homogenates can be accounted for by the use of autolysis as the first step in the purification to solubilize EAP from the kidney membranes (31). These results indicate that kidney EAP is 137 kDa, mAAP is 128 kDa, and DPP IV is 106 kDa on SDS-PAGE.

Purified kidney EAP was subjected to tryptic digestion, and the fragments were separated by HPLC. A single fragment was selected for microsequencing. Four amino acids within this 18-mer fragment could not be identified with certainty (Fig. 5). Comparison of the 14 remaining amino acids to the BP-1/6C3 and gp160 amino acid sequences indicated that the peptide fragment corresponded to amino acids 714–731 of BP-1/6C3 and 723–740 of gp160. Twelve of the 14 amino acids were identical in the rat and mouse, with both substitutions being conservative (isoleucine for valine and serine for leucine). Four amino acids were different in rat and human, with only one (serine for aspartic acid) being nonconservative.

The distribution of EAP mRNA localized by in situ hybridization was compared with the distribution of the enzyme localized by immunocytochemistry. In situ hybridization of rat kidney EAP with ^{35}S -labeled antisense single-stranded riboprobes indicated that EAP mRNA was highest in the outer stripe of the outer medulla, corresponding to the S3 segment of the proximal tubule, and to both superficial and juxtamedullary glomeruli in the cortex (Fig. 6). The low-power in situ hybridization suggested that there was minimal tubular labeling in the cortex. This was confirmed by higher resolution in situ hybridization, which indicated that the cortical labeling was primarily within glomeruli (Fig. 7). There was a notable absence of labeling of the proximal convoluted tubules (e.g., surrounding the glomerulus in Fig. 7A). Other cortical tubules, including distal convoluted tubules and cortical collecting ducts, were also unlabeled. High-resolution in situ hybridization indicated that the glomerular labeling was not distributed uniformly but that, depending on the plane of section, labeling was concentrated in bands and patches (Fig. 7, B–E). The majority of the cells within the glomeruli were not labeled. This pattern of labeling is most consistent with labeling of mesangial cells and not epithelial or endothelial cells, but the identity of the labeled cells could not be determined unequivocally. Labeling was also seen within the terminal portion of the afferent arteriole corresponding to juxtaglomerular (JG) cells (Fig. 8A). There was no detectable labeling elsewhere within the vasculature. In larger caliber vessels it was possible to determine that neither the endothelial cells nor the tunica media smooth muscle cells were labeled (Fig. 8B). In the medulla, positive hybridization was detected primarily within descending

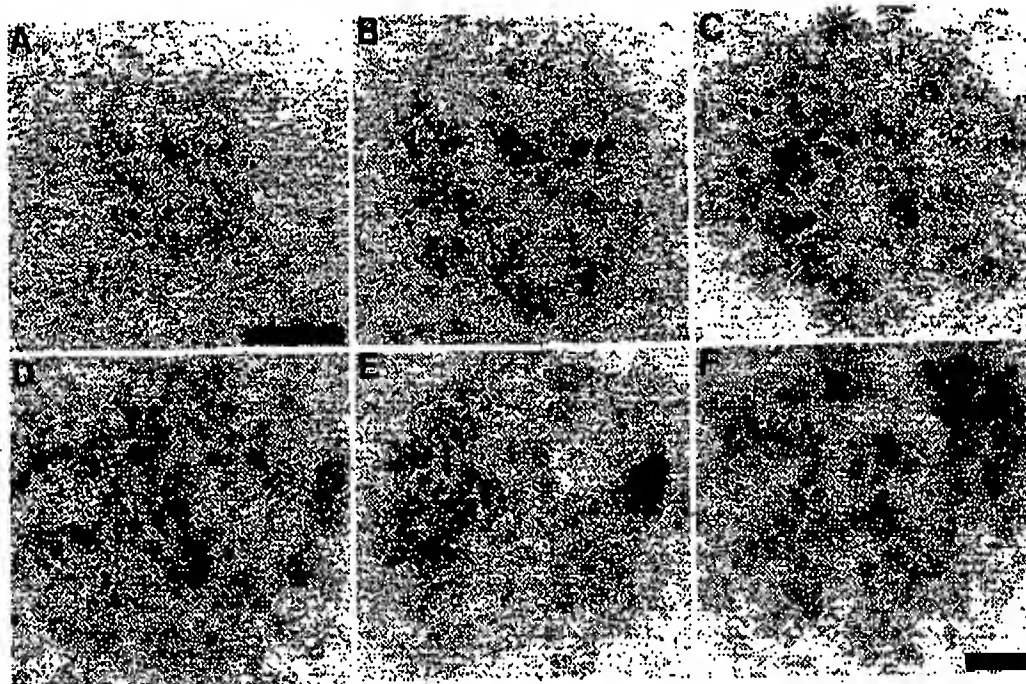


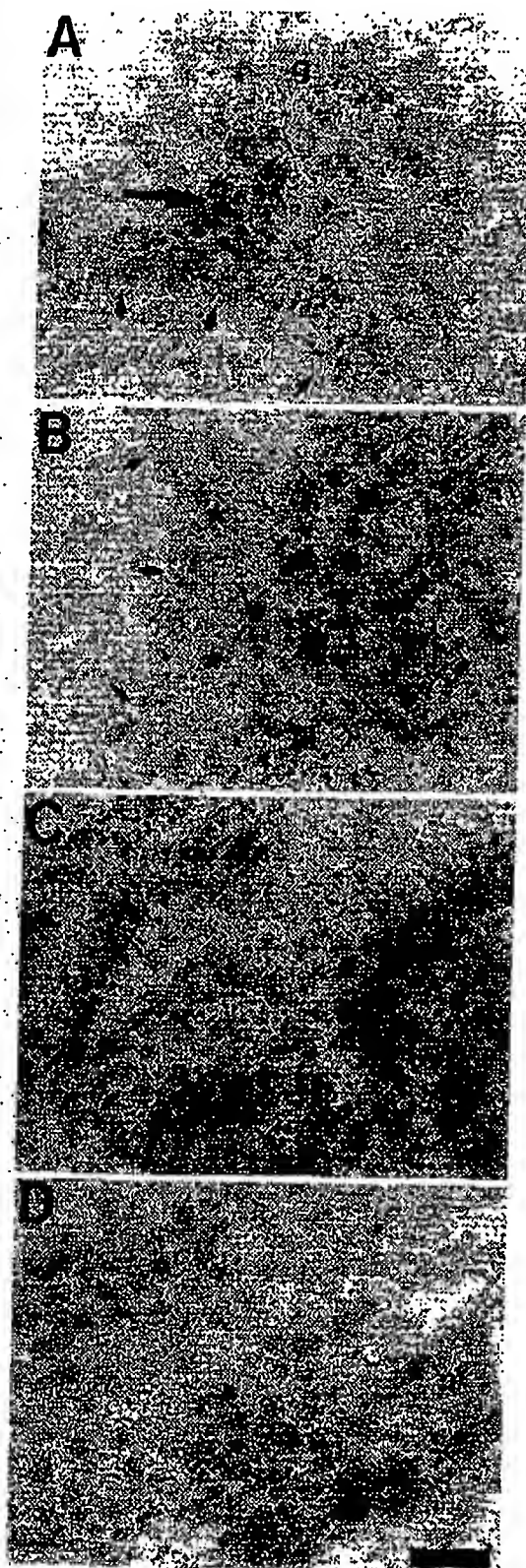
Fig. 7. In situ hybridization of EAP mRNA within glomeruli. Sections of rat kidney similar to that shown in Fig. 1 were dipped in liquid emulsion and exposed for a period of 1 mo. Sections were counterstained lightly with cresyl violet. A: intermediate magnification of a labeled glomerulus surrounded by unlabeled tubules. Scale bar, 40 μ m. B: higher power magnification of the glomerulus in A. Note that the pattern of labeling within the glomerulus is seen as clusters of silver grains and that not all cells are labeled. C-E: additional representative glomeruli showing typical labeling within glomeruli, including patches (C), cord-like patches (D), and clusters of grains situated on the extreme edge of the glomerulus, generally near the vascular pole (E). F: labeling of a glomerulus from a section incubated with an EAP 32 S-labeled sense riboprobe. Scale bar, 25 μ m.

proximal tubule segments in medullary rays in the outer stripe of the outer medulla (Figs. 6 and 8C). Tubules within the inner stripe of the outer medulla (including thick ascending limb cells) and inner medulla were also unlabeled. Control hybridization with sense riboprobes yielded only diffuse background labeling (Figs. 7F and 8D).

Previous studies characterizing the antiserum against rat kidney EAP for use in immunocytochemistry indicated that there was no cross-reactivity with the closely related enzyme mAAP (16, 31). However, under the conditions used for immunoblotting, the EAP antiserum cross-reacted with both mAAP and DPP IV (Fig. 4). The degree of cross-reactivity seen with antiserum is related to the concentration of antiserum and antigen. In the immunoblot studies the antiserum was used at a dilution of 1:1,000. For immunocytochemistry, dilutions of 1:5,000 or 1:10,000 were typically used (16). To determine the specificity of the antiserum under the conditions used for immunocytochemistry, we repeated the preabsorption studies in the absence or presence of 1 μ g/ml mAAP, 1 μ g/ml DPP IV, or 1 μ g/ml EAP (Fig. 9). Low-power magnification of EAP staining in the kidney cortex indicated that heavy staining was present within tubules and less intense staining within glomeruli (Fig. 9A). Preabsorption of the antiserum with either mAAP (Fig. 9B) or DPP IV (Fig. 9C) had no effect on the immunocytochemical staining pattern, whereas preab-

sorption of the antiserum with EAP (Fig. 9D) almost completely abolished the immunostaining. Therefore, under the conditions that were used here for immunocytochemistry, we concluded that the antiserum was specific for EAP.

Low-power magnification of immunostained sections of kidney cortex indicated that cortical immunostaining was primarily within proximal convoluted tubules (Fig. 9). Immunostaining within glomeruli was apparently less intense and more diffuse (Fig. 9). The weak immunostaining did not appear to correlate with the higher EAP activity seen in isolated glomerular preparations (above). We then tested if the discrepancy between EAP activity and immunoreactivity within glomeruli was sensitive to the type of fixation. Indeed, cryostat sections that were lightly fixed directly on the slide exhibited intense EAP immunostaining within the glomeruli (Fig. 10). The absence of EAP immunostaining within perfusion-fixed kidneys suggests that EAP immunoreactivity was diminished within vascular elements, such as glomeruli, due to the relatively higher concentration of fixative within the vasculature during perfusion than in the surrounding nonvascular tissues, such as tubules. Close examination of the glomerular staining with EAP antiserum indicated that the immunoreactivity was concentrated primarily within mesangial cells. The stellate appearance of mesangial cells with multiple processes terminating on glomerular capillaries was readily seen (Fig.



10B). EAP immunofluorescence appeared to be concentrated at sites where mesangial cell processes contacted the capillary walls. Endothelial cells lining the capillaries were not labeled. Although the compromised preservation of the tissue made precise localization difficult, there was no clear demonstration of epithelial cell staining. Immunostaining within proximal tubules was concentrated solely within the apical brush border (Fig. 11).

DISCUSSION

As noted above, various lines of evidence indicate that the murine BP-1/6C3 and human gp160 antigens are identical to EAP (23, 26, 33, 36, 37). To isolate a partial cDNA for rat kidney EAP, we designed oligonucleotide primers based on the murine BP-1/6C3 nucleotide sequence and used RT-PCR. The PCR product was highly similar to the BP-1/6C3 and gp160 sequences: 90% and 82% identical at the nucleotide level and 92% and 86% identical at the amino acid level, respectively. The amplified cDNA included the region of the zinc-binding domain, an area that is essential for EAP enzymatic activity (33). The predicted amino acid sequence of the partial cDNA within the zinc-binding domain was completely conserved compared with the murine BP-1/6C3 and human gp160 sequences. Northern blot analysis of rat kidney and small intestine total RNA resulted in labeling of a major band of 4.1 kb, identical in size to the BP-1/6C3 and gp160 transcripts (23, 26, 36). Examination of the predicted amino acid sequence of the rat EAP with the murine EAP indicated that, of the 11 amino acid substitutions, six were nonconservative, i.e., a charged amino acid for an uncharged amino acid. However, of the six nonconservative substitutions between mouse BP-1/6C3 and rat EAP, five are either identical or conservative relative to the human gp160 sequence. In addition, the amino acid sequence of a tryptic digest peptide of EAP purified from rat kidney indicated that it was highly similar to a region of the BP-1/6C3 and gp160 antigens. It is interesting to note that the two amino acids in the partial peptide fragment of kidney EAP that did not match the predicted sequence of murine BP-1/6C3 were conserved between the rat EAP and human gp160 sequences. Thus, on the basis of the sequence analysis of the partial cDNA, the hybridization analysis, and the partial amino

Fig. 8. In situ hybridization of tubular and vascular elements labeled with an EAP antisense 32 S-labeled riboprobe. A: shown is the terminal portion of an afferent arteriole (small arrows) as it gives off a short branch to a glomerulus (g) and then continues out of frame. The segment of the afferent arteriole that enters the glomerulus corresponds to the juxtaglomerular cell region. Note the moderate density of silver grains over the juxtaglomerular cells (large arrow). B: cross section through a portion of an interlobular artery showing unlabeled endothelial cells (small arrows) and the smooth muscle cells of the tunica media (stars). Note the heavy labeling of the tubule immediately adjacent to the artery. C: high-power view of a longitudinal section through a medullary ray showing heavily labeled straight descending proximal tubules adjacent to an unlabeled cortical collecting duct. D: hybridization of an EAP 32 S-labeled sense riboprobe with a section through a medullary ray similar to that shown in C. Note the complete absence of labeled tubules. Scale bar, 25 μ m.

acid sequence, we conclude that the rat kidney EAP is homologous to the murine BP-1/6C3 and human gp160 proteins.

With antiserum raised against EAP purified from rat kidney, we noted previously that immunoblots with purified EAP yielded only a single band, whereas immunoblots with kidney homogenates yielded two bands on SDS-PAGE (31). Here we showed similar results except that the broad upper band could now be distinguished as two distinct bands of 137 and 129 kDa. A lower band of 106 kDa was also seen. It was not clear whether the multiple bands represented partial proteolytic digestion of the native enzyme, EAP isozymes, or cross-reactivity with a closely related enzyme(s). We ruled out that the smaller bands were proteolytic products of EAP, because the immunoblot pattern was unchanged when kidney tissue samples were isolated in the presence of a spectrum of protease inhibitors. As noted previously, some variation has been reported on the size of EAP monomers isolated from the kidney of various species (6, 13, 17). However, we determined that the multiple bands actually represented cross-reactivity of the EAP antiserum with other kidney peptidases. Preabsorption of the EAP antiserum with purified mAAP blocked staining of the 129-kDa band, and preabsorption with purified DPP IV blocked staining of the 106-kDa band. The 129- and 106-kDa bands are in good agreement with previous reports on the size of purified mAAP and DPP IV, respectively (2, 20). These results indicate that rat kidney expresses only a single sized EAP monomeric form of 137 kDa on SDS-PAGE and that the additional bands seen on immunoblots of rat kidney represented cross-reactivity of the antiserum with mAAP and DPP IV. The cross-reactivity of the antiserum to other peptidases was somewhat surprising, since the purified EAP material had no detectable mAAP or DPP IV activity. Since EAP and mAAP are related enzymes and are 34% identical (36), it is possible that these two enzymes share common epitopes. On the other hand, DPP IV and EAP are unrelated enzymes (serine proteinase vs. a metalloproteinase). Moreover, comparison of the sequences of EAP and DPP IV revealed no significant homology. Since kidney DPP IV levels are high, the possibility that the purified EAP material contained trace contaminants of enzymatically inactive DPP IV fragments cannot be ruled out. A repeat of the purification procedure while monitoring EAP-containing fractions by immunoblotting confirmed that the 106-kDa band was separated from the upper bands by phenyl Sepharose chromatography, the step at which DPP IV activity is separated from EAP/mAAP activity (unpublished observations). The

Fig. 9. Effects of preabsorption of the EAP antiserum (1:5,000 dilution) with purified mAAP and DPP IV on the immunocytochemical staining pattern in rat kidney. A: immunostaining with control antiserum. Note the typical staining pattern in the outer cortex, with heavily labeled proximal convoluted tubules and lighter stained glomeruli. B: immunostaining with antiserum preabsorbed with mAAP (1 μ g/ml). Note there is no reduction in staining. C: immunostaining with antiserum preabsorbed with DPP IV (1 μ g/ml). Note there is no reduction in staining. D: immunostaining with antiserum preabsorbed with EAP (1 μ g/ml). Note the almost complete absence of immunostaining. Scale bar, 100 μ m.

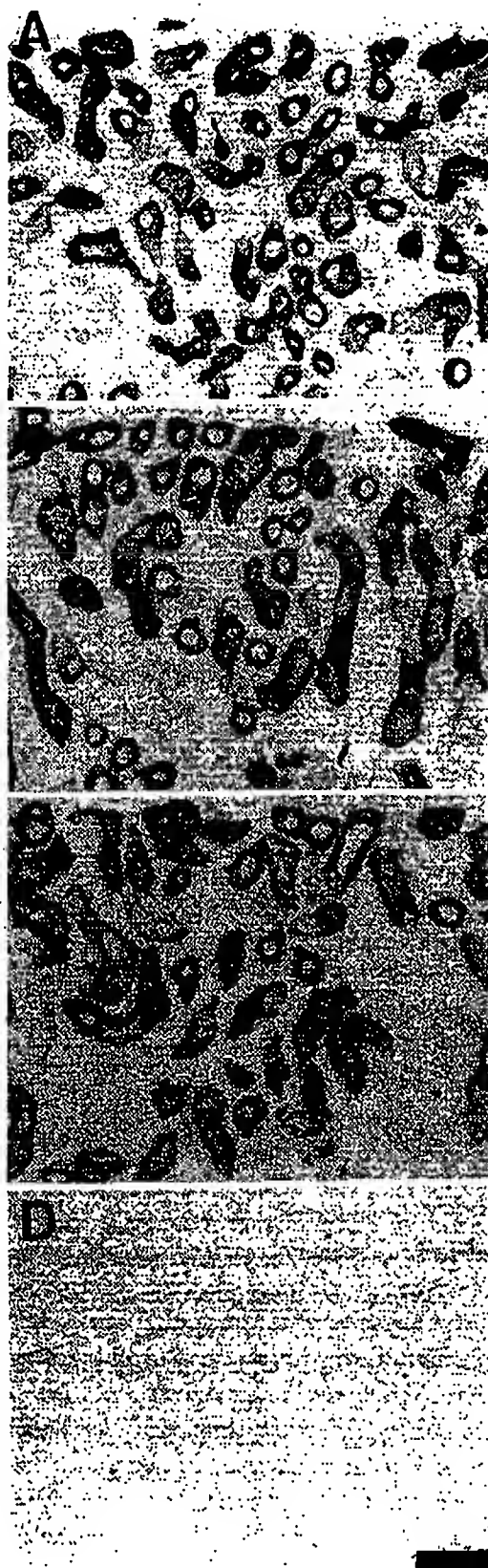


Fig. 9. non and met glom with mes deva grap conc cyto capil cont Scale groa istr lern wer with resu seen rum sult repr non

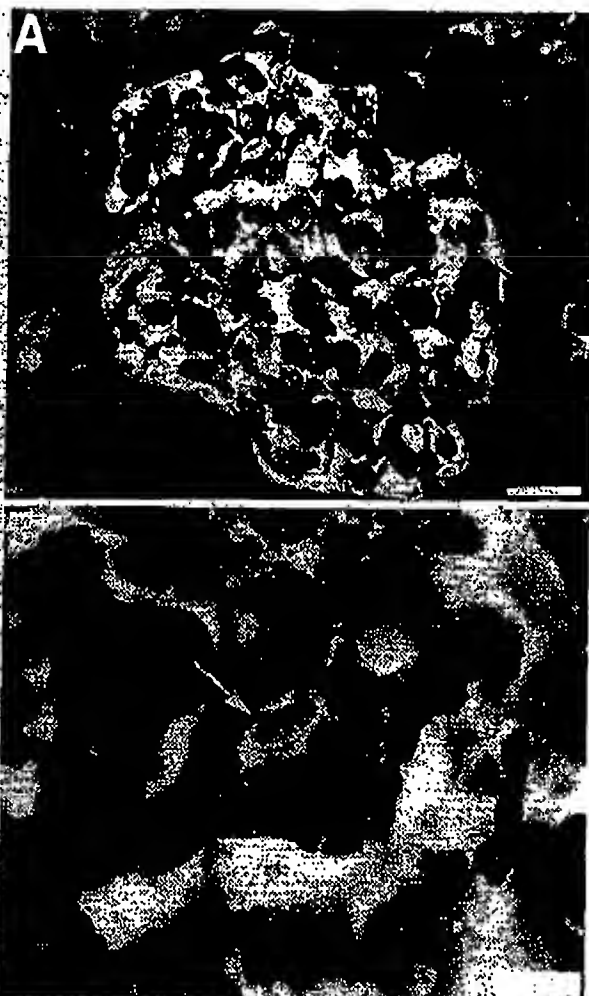


Fig. 10. EAP immunofluorescent staining within a glomerulus. A: nonperfused kidney was cryostat sectioned, fixed directly on the slide, and immunostained with EAP antiserum using an immunofluorescent method. A: photomicrograph of EAP immunoreactivity within a glomerulus. Note that EAP immunofluorescence was concentrated within the mesangium, specifically within mesangial cells (arrow) and mesangial cell processes. The endothelial cell linings of capillaries were devoid of staining (*). Scale bar, 25 μ m. B: higher power photomicrograph of the labeled mesangial cell in A, shown by arrow. Note again concentration of EAP immunofluorescence within the mesangial cell cytoplasm and the processes (small arrowheads) that terminate on the capillary walls. Areas of the capillary wall that mesangial cell processes contact appear to have a greater density of EAP immunoreactivity. Scale bar, 10 μ m.

greater dilution of the antiserum for immunocytochemistry apparently minimizes the cross-reactivity problems, since the immunocytochemical staining patterns were not affected by preabsorption of the antiserum with either mAAP or DPP IV. Furthermore, these results raise doubts as to whether the multiple bands seen in previous immunoblot studies with EAP antiserum actually represent EAP isoforms. Rather, our results would suggest that the multiple bands either represent degradation of EAP or cross-reactivity to a non-EAP protein.

With only one exception, the distributions of EAP mRNA and EAP immunoreactivity within rat kidney were very similar. The highest levels of EAP mRNA were detected within the outer stripe of the outer medulla. High-resolution *in situ* hybridization indicated that the labeling in the outer stripe was restricted to the straight descending (S3) segment of the proximal tubules. The S3 segment of the proximal tubule also contained high levels of EAP immunoreactivity, confirming previous histochemical studies (21, 25). No EAP mRNA was detected, however, within proximal convoluted tubules, an area that contains high levels of EAP immunoreactivity. The reason for the apparent discrepancy between hybridization and immunoreactivity patterns in the proximal convoluted tubule is unlikely to be due to the existence of different EAP isoforms, since the probe used for *in situ* hybridization would be expected to recognize transcripts from all EAP isoforms; the probe contained the region of the zinc-binding domain, an area absolutely essential for EAP activity (33). Another possible explanation for the high level of EAP immunoreactivity and the low level of EAP mRNA in the



Fig. 11. High-power photomicrograph of EAP immunoreactivity within proximal tubules. A: immunostaining within a proximal tubule cut in cross section. Note that the staining is restricted to the apical membrane (arrow). B: staining in presence of preimmune serum. Note absence of apical membrane immunostaining (arrow). Scale bar, 10 μ m.

proximal convoluted tubules could be that there is low turnover of the EAP protein within convoluted tubules (and thus low mRNA). Likewise, the absence of detectable EAP mRNA in proximal convoluted tubules might simply reflect the lower sensitivity of the in situ hybridization method.

EAP immunoreactivity and mRNA were not detected in large blood vessels. Relatively low concentrations of EAP mRNA could be detected within some, but not all, afferent arteriole JG cells. EAP immunoreactivity was not consistently seen within JG cells. Whether this indicates that expression of EAP in the JG cells is near the level of detection for both techniques or whether there is only a subset of afferent arterioles that express EAP is not clear at this time. Higher levels of EAP mRNA and immunoreactivity were detected in glomeruli. The presence of EAP immunoreactivity and EAP mRNA within glomeruli confirmed the results that indicated that EAP enzymatic activity was enriched in isolated glomeruli compared with kidney homogenates. High-resolution in situ hybridization indicated that EAP mRNA was not uniformly distributed within the glomeruli. Rather, the hybridization pattern was cord-like patches, suggestive of labeling within the mesangium, possibly mesangial cells. Immunocytochemical staining of EAP within glomeruli from perfusion-fixed kidneys was diffuse and could not be localized to distinct cell bodies. However, in nonperfused kidneys where sections were fixed directly on the slides, EAP immunofluorescence was concentrated within mesangial cells, and in particular in areas where mesangial cell processes contacted capillary walls. The presence of EAP immunoreactivity within mesangial cell bodies is consistent with the in situ hybridization pattern of EAP mRNA in glomeruli. EAP immunoreactivity within mesangial cells is also consistent with a previous report from our laboratory that showed that EAP immunoreactivity in rat brain is associated with cerebral microvessel pericytes (16). Pericytes and mesangial cells are both perivascular adventitial cells that are known to have extensive cell processes that entwine small blood vessels. Both cell types are thought to be derived from the same progenitor cells (29).

Although EAP is not specific for a single substrate, some degree of functional specificity would occur if EAP was localized to cells that were exposed to extracellular fluids enriched with a particular substrate. EAP has been shown to hydrolyze [Asp¹]ANG II to ANG III ([des-Asp¹]ANG II) (1, 21, 34). In most tissues ANG III is less potent than ANG II, so the hydrolysis of ANG II by EAP is viewed as a degradation step (34). However, some studies indicate that the lower potency of ANG III is attributed to the greater susceptibility of this peptide to enzymatic degradation (34). In some tissues, including brain and adrenal, ANG III has significant bioactivity (12, 35), suggesting that the hydrolysis of ANG II to ANG III is a conversion step rather than degradation. It is interesting then to consider that the distribution of EAP within the kidney coincides with cells known to express ANG II receptors, principally the type 1 receptor subtype (4, 7, 9, 14, 27, 30, 38). ANG II receptors are

known to be present on juxtaglomerular cells, mesangial cells, afferent and efferent arterioles, and proximal tubules. In addition, all the components of the renin-angiotensin system are localized within the kidney (3, 32). Thus the colocalization of EAP and ANG II receptors within the kidney suggests that EAP could play an important role in modulating the activity of both circulating and locally formed ANG II.

In summary, the results presented here indicate that 1) rat kidney EAP is homologous to the murine BP-1/6C3 and human kidney gp160 differentiation antigens; 2) the monomeric form of EAP in rat kidney is a single-sized protein of 137 kDa; 3) rat kidney EAP gene expression is highest within the proximal tubules and glomerular mesangial cells; and 4) the localization of EAP within the kidney correlates with the cellular distribution of ANG II receptors. EAP may therefore have multiple physiological functions within the kidney, depending on its localization, i.e., metabolism of oligopeptides in the glomerular filtrate and degradation/conversion of circulating or intrarenally synthesized bioactive peptides, including ANG II.

This work was supported by National Institutes of Health Grants HL-42585 (to D. P. Healy) and NS-17392 (to S. Wilk) and by the American Heart Association, New York City Affiliate (D. P. Healy). D. P. Healy is an Established Investigator of the American Heart Association. S. Wilk is supported by National Institute of Mental Health Research Scientist Award MH-00350, and M. Troyanovskaya is supported by National Institute on Drug Abuse Postdoctoral Training Grant DA-07135.

Address for reprint requests: D. P. Healy, Dept. of Pharmacology, Box 1215, Mount Sinai School of Medicine, One Gustave L. Levy Place, New York, NY 10029.

Received 17 December 1993; accepted in final form 26 April 1994.

REFERENCES

1. Ahmad, S., and P. E. Ward. Role of aminopeptidase activity in the regulation of the pressor activity of circulating angiotensin. *J. Pharmacol. Exp. Ther.* 252: 643-650, 1990.
2. Brownlee, J., C. H. Williams, G. P. Brennan, and D. W. Halton. Purification and immunochemical studies of dipeptidyl peptidase IV from bovine kidney. *Biol. Chem. Hoppe-Seyler* 373: 911-914, 1992.
3. Burns, K. D., T. Homma, and R. C. Harris. The intrarenal renin-angiotensin system. *Semin. Nephrol.* 13: 13-30, 1993.
4. Chansel, D., S. Czekalski, P. Pham, and R. Ardailon. Characterization of angiotensin II receptor subtypes in human glomeruli and mesangial cells. *Am. J. Physiol.* 262 (Renal Fluid Electrolyte Physiol. 31): F432-F441, 1992.
5. Chomczynski, P., and N. Sacchi. Single-step method of RNA isolation by acid guanidinium thiocyanate-phenol-chloroform extraction. *Anal. Biochem.* 162: 156-159, 1987.
6. Danielson, E. M., O. Noren, H. Sjöström, J. Ingram, and A. J. Kenny. Proteins and the kidney microvillar membrane. Aspartate aminopeptidase: purification by immunoabsorbent chromatography and properties of the detergent- and proteinase-solubilized forms. *Biochem. J.* 189: 591-603, 1980.
7. Edwards, R., E. J. Stock, E. F. Weidley, N. Aiyar, R. M. Keenan, D. T. Hill, and J. Weinstein. Characterization of renal angiotensin II receptors using subtype selective antagonists. *J. Pharmacol. Exp. Ther.* 260: 933-938, 1992.
8. Fujiwara, Y., E. Kitamura, N. Ueda, M. Fukunaga, Y. Orita, and T. Kamada. Mechanism of action of angiotensin II on isolated rat glomeruli. *Kidney Int.* 36: 985-991, 1989.
9. Gasc, J. M., C. Monnot, E. Clauser, and P. Corvol. Co-expression of type 1 angiotensin II receptor (AT₁R) and renin mRNAs in juxtaglomerular cells of the rat kidney. *Endocrinology* 132: 2723-2725, 1993.

RAT KIDNEY GLUTAMYL AMINOPEPTIDASE

F557

10. George, S. G., and A. J. Kenny. Studies on the enzymology of purified preparations of brush border from rabbit kidney. *Biochem. J.* 134: 43-57, 1973.
11. Gleaner, G. G., P. J. McMillan, and J. E. Folk. A mammalian peptidase specific for the hydrolysis of N-terminal α -L-glutamyl and aspartyl residues. *Nature Lond.* 194: 867-868, 1962.
12. Goodfriend, T. L., and M. J. Peach. Angiotensin III: (des-aspartic acid¹) angiotensin II. Evidence and speculation for its role as an important agonist in the renin-angiotensin system. *Circ. Res.* 37, Suppl. 1: 183-148, 1975.
13. Gorvel, J. P., A. Benajiba, and S. Maroux. Purification and characterization of the rabbit intestinal brush-border aminopeptidase A. *Biochim. Biophys. Acta* 615: 271-274, 1980.
14. Grone, H. J., M. Simon, and E. Fuchs. Autoradiographic characterization of angiotensin receptor subtypes in fetal and adult human kidney. *Am. J. Physiol.* 262 (Renal Fluid Electrolyte Physiol. 31): F328-F331, 1992.
15. Hall, J. E. Control of sodium excretion by angiotensin II: intrarenal mechanisms and blood pressure regulation. *Am. J. Physiol.* 250 (Regulatory Integrative Comp. Physiol. 19): R980-R972, 1986.
16. Healy, D. P., and S. Wilk. Localization of immunoreactive glutamyl aminopeptidase in rat brain. II: Distribution and correlation with angiotensin II. *Brain Res.* 606: 295-303, 1993.
17. Herzog, C. M., W. Schoeppe, and J. E. Scherberich. Angiotensinase A (aminopeptidase A): properties of chromatographically purified isoforms from human kidney. *J. Chromatogr.* 625: 73-82, 1992.
18. Huo, T., M. Q. Ye, and D. P. Healy. Characterization of a dopamine receptor (DA_{2A}) in the kidney inner medulla. *Proc. Natl. Acad. Sci. USA* 88: 3170-3174, 1991.
19. Ichikawa, I., and R. C. Harris. Angiotensin actions in the kidney: renewed interest into the old hormone. *Kidney Int.* 40: 583-596, 1991.
20. Kenny, A. J., and S. Maroux. Topology of microvillar membrane hydrolases of kidney and intestine. *Physiol. Rev.* 62: 91-128, 1983.
21. Kugler, P. Aminopeptidase A is angiotensinase A. I. Quantitative histochemical studies in kidney glomerulus. *Histochemistry* 74: 229-245, 1982.
22. Levens, N. R., M. J. Peach, and R. M. Carey. Role of the intrarenal renin-angiotensin system in the control of renal function. *Circ. Res.* 48: 157-167, 1981.
23. Li, L., J. Wang, and M. D. Cooper. cDNA cloning and expression of human glutamyl aminopeptidase (aminopeptidase A). *Genomics* 17: 657-664, 1993.
24. Lajda, Z., and R. Gossrau. Study on aminopeptidase A. *Histochemistry* 67: 267-290, 1980.
25. Nanus, D. M., D. Engelstein, G. A. Gastl, L. Gluck, M. J. Vidal, M. Morrison, C. L. Finstad, N. H. Bander, and A. P. Albino. Molecular cloning of the human kidney differentiation antigen gp160: human aminopeptidase A. *Proc. Natl. Acad. Sci. USA* 90: 7069-7073, 1993.
26. Paxton, W. G., M. Runge, C. Horvath, C. Cohen, R. W. Alexander, and K. E. Bernstein. Immunohistochemical localization of rat angiotensin AT₁ receptor. *Am. J. Physiol.* 264 (Renal Fluid Electrolyte Physiol. 33): F989-F995, 1993.
27. Sambrook, J., E. F. Fritsch, and T. Maniatis. *Molecular Cloning*, Cold Spring Harbor Laboratory Press, 1989.
28. Sims, D. E. The pericyte—a review. *Tissue Cell* 18: 153-174, 1986.
29. Smith, R. D., A. T. Chiu, P. C. Wong, W. F. Herblin, and P. B. M. W. M. Timmermans. Pharmacology of nonpeptide angiotensin II receptor antagonists. *Annu. Rev. Pharmacol. Toxicol.* 32: 135-166, 1992.
30. Song, L. J., E. Wilk, S. Wilk, and D. P. Healy. Localization of immunoreactive glutamyl aminopeptidase in rat brain. I. Association with cerebral microvessels. *Brain Res.* 606: 286-294, 1993.
31. Taugner, R., E. Hackenthal, E. Rix, R. Nobiling, and K. Poulsen. Immunocytochemistry of the renin-angiotensin system: renin, angiotensinogen, angiotensin I, angiotensin II, and converting enzyme in the kidneys of mice, rats, and tree shrews. *Kidney Int.* 22 (Suppl. 12): S33-S43, 1982.
32. Wang, J., and M. D. Cooper. Histidine residue in the zinc-binding motif of aminopeptidase A is critical for enzymatic activity. *Proc. Natl. Acad. Sci. USA* 90: 1222-1226, 1993.
33. Wilk, S., and D. P. Healy. Glutamyl aminopeptidase (aminopeptidase A), the BP-1/6C3 antigen. *Adv. Neuroimmunol.* 3: 195-207, 1993.
34. Wright, J. W., S. L. Morseth, R. H. Abhold, and J. W. Harding. Pressor action and dipsogenicity induced by angiotensin II and III in rats. *Am. J. Physiol.* 249 (Regulatory Integrative Comp. Physiol. 18): R514-R521, 1985.
35. Wu, Q., J. M. Lahti, G. M. Air, P. D. Burrows, and M. D. Cooper. Molecular cloning of the murine BP-1/6C3 antigen: a member of the zinc-dependent metalloproteinase family. *Proc. Natl. Acad. Sci. USA* 87: 993-997, 1990.
36. Wu, Q., L. Li, M. D. Cooper, M. Piorres, and J. P. Gorvel. Aminopeptidase A activity of the murine B-lymphocyte differentiation antigen BP-1/6C3. *Proc. Natl. Acad. Sci. USA* 88: 676-680, 1991.
37. Zhou, J., K. Song, P. J. Harris, F. A. O. Mendelsohn. In vitro autoradiography reveals predominantly AT₁ angiotensin II receptors in rat kidney. *Renal Physiol. Biochem.* 15: 291-299, 1992.

JOURNAL OF INTERFERON AND CYTOKINE RESEARCH 18:1039-1044 (1998)
Mary Ann Liebert, Inc.

Tumor Necrosis Factor- α Upregulates the Prostaglandin E₂ EP1 Receptor Subtype and the Cyclooxygenase-2 Isoform in Cultured Amnion WISH Cells

ERIC P. SPAZIANI, RAYMOND R. BENOIT, JOHN C.M. TSIBRIS, STANLEY F. GOULD, and
WILLIAM F. O'BRIEN

ABSTRACT

Recent studies have demonstrated a strong correlation between infection and preterm labor. Preterm delivery is also associated with high levels of cytokines and prostaglandins in amniotic fluid. The purpose of this study was to investigate the effect of tumor necrosis factor- α (TNF- α) on the levels of cyclooxygenase, prostaglandin E₂ production (PGE₂), and expression of the PGE₂ receptor subtype EP1 in amnion WISH cell culture. Amnion WISH cell cultures were incubated in increasing concentrations of TNF- α (0–50 ng/ml). Changes in cyclooxygenase and EP1 receptor proteins were evaluated by Western blot analysis. Changes in EP1 mRNA were evaluated by Northern blot, and culture fluid concentrations of PGE₂ were estimated by enzyme immunoassay (EIA). EP1 protein ($p < 0.01$), EP1 mRNA ($p < 0.05$), cyclooxygenase-2 (COX-2) protein ($p < 0.001$), and PGE₂ concentrations ($p < 0.01$) all increased with increasing concentrations of TNF- α . Changes in COX-1 protein were not observed following TNF- α -incubation. The results suggest that TNF- α may play a role in infection-induced preterm labor by its pleiotropic ability to simultaneously stimulate COX-2 activity, PGE₂ concentrations, and PGE₂ EP1 receptor levels in human amnion.

INTRODUCTION

PRETERM DELIVERIES ARE A LEADING CAUSE of infant morbidity and mortality⁽¹⁾ and often are associated with preterm labor (PTL) and premature rupture of the membranes (PROM). The underlying causes of PTL and PROM have not been fully defined. Among a number of factors associated with PTL and PROM is a strong correlation with infection.⁽²⁾ Intraamniotic infection is a common finding in women with PTL and PROM.⁽³⁾ In addition, cytokines are often found in amniotic fluid of patients experiencing preterm labor,⁽⁴⁾ along with increases in amniotic fluid prostaglandins, including prostaglandin E₂ (PGE₂).⁽⁵⁾ Prostaglandins are known to increase during term and preterm labor,⁽⁶⁾ are believed to be a major component of the biochemical processes associated with labor,⁽⁷⁾ and are clinically used as both abortifacents (prostaglandin F_{2 α} , PGF_{2 α}) and as inducers of cervical ripening.⁽⁸⁾ Several cytokines, including interleukin-1 β (IL-1 β) and tumor necrosis factor- α (TNF- α), have been identified as stimulators of prostaglandin production and increased cyclooxygenase activity in a variety of reproductive tissues.^(9,10) Cyclooxy-

genase, the enzyme that converts arachidonic acid to prostaglandins, is present in two forms, a constitutive form (COX-1) and an inducible form (COX-2).⁽¹¹⁾ Changes in COX-2 levels and activity have been well documented in maternal and fetal tissues during labor.⁽¹²⁾

The actions of PGE₂ are mediated by its binding to specific membrane receptors, which in turn activate second messenger systems and initiate cellular function.⁽¹³⁾ PGE receptors are classified into four subtypes, EP1, EP2, EP3, and EP4, on the basis of their response to various agonists and antagonists.⁽¹⁴⁾ The binding affinity of the EP1 receptor for PGE₂ is highly specific, with a poor affinity for other prostaglandins, including PGF_{2 α} .⁽¹⁵⁾ In general, EP1 and EP3 receptors are associated with stimulatory functions. The EP1 receptor has been associated with changes in intracellular calcium and smooth muscle contraction, including myometrium.⁽¹⁶⁾

Despite the abundance of evidence demonstrating an association between term and preterm labor with increased prostaglandins and cytokines in amniotic fluid, the mechanisms for production and regulation of these agents during infection-induced preterm labor are still unclear. In addition, the regula-

tion of PGE₂ receptors in maternal-fetal tissues has not been extensively explored. If infection-induced cytokine production leads to increased prostaglandin production, the most likely initial target for infection-produced cytokines would be the fetal amnion, as it would be the first tissue exposed to elevated cytokine concentrations. Therefore, in view of the possible role of PGE₂ in the mechanism of cytokine-induced preterm labor, we sought to investigate the effect of TNF- α on the levels of cyclooxygenase, PGE₂ production, and the expression of the PGE receptor subtype EP1 in amnion WISH cells in culture.

MATERIALS AND METHODS

Cell cultures

The human amnion cell line WISH (Wistar Institute Susan Hayflick) was used to conduct these experiments. Amnion WISH cells (American Type Culture Collection, Washington, DC) were seeded into sterile vented 25 cm² polyethylene tissue culture flasks at a concentration of approximately 5×10^6 cells per flask. The culture medium consisted of Dulbecco's modified Eagle's medium (DMEM) F-12 Ham mixture (1:1) containing 15% heat-inactivated fetal bovine serum (FBS) supplemented with 15 mM HEPES, 2 mM L-glutamine, 100 g/ml gentamicin, and 25 μ g/ml amphotericin B. Cultures were grown to 80% confluence in a humidified incubator at 37°C and 5% CO₂.

After the cells reached 80% confluence, the culture medium was removed, and the cells were washed in phosphate-buffered saline (PBS) and incubated for 18 h in concentrations of TNF- α (2, 10, 25, and 50 ng/ml). To verify that changes in EP1 receptor protein were not a function of a feedback loop involving PGE₂, cultures were also incubated with a high concentration TNF- α (50 ng/ml) and indomethacin (10 mg/ml) in combination. Indomethacin is a class II nonsteroidal anti-inflammatory drug (NSAID) that prevents the overall production of prostaglandins by competitive inhibition of the enzyme cyclooxygenase.⁽¹¹⁾ Cultures incubated in medium alone served as controls.

After incubation in TNF- α , cells were scraped and homogenized on ice in a glass-Teflon homogenizer in 50 mM Tris, pH 7.5, containing 2 mM EDTA, 0.25 M sucrose, 10 μ g/ml leupeptin, 50 μ g/ml pepstatin A, 1 mM PMSF, 1 mM DTT, with 1% Triton-X 100. After 30 min, the crude homogenate was spun at 1000g for 15 min. Crude homogenates were assayed for protein content using a micro-bicinchoninic acid method (BCA) with BSA as standard.⁽¹⁷⁾ An aliquot of culture fluid was collected for PGE₂ measurement by enzyme immunoassay (EIA) (Caymen Chemical Co, Ann Arbor, MI).

Western blot analysis

Changes in EP1 receptor and cyclooxygenase protein levels were evaluated by Western blot analysis. Total protein lysate (25 μ g) was separated on a 7.5% Tris-glycine gel by electrophoresis (SDS-PAGE). Molecular weights were estimated using prestained molecular weight markers (Bio-Rad Labs., Hercules, CA). Following SDS-PAGE, proteins were transferred to nitrocellulose membranes for 2 h at 200 mA in 25 mM Tris and 192 mM glycine buffer, pH 8.3, containing 20%

methanol. EP1 receptor bands were detected using EP1 polyclonal antibodies, prepared as previously described.⁽¹⁸⁾ Equal protein loading was verified by staining the nitrocellulose membranes with 0.1% Ponceau S solution.

Changes in COX-1 and COX-2 enzymes were evaluated using polyclonal antibodies (Caymen Chemical Co.) The COX-2 primary antibody did not cross-react with the COX-1 primary antibody. Prestained molecular weight markers (BioRad) were used to identify molecular weights for cyclooxygenase enzyme proteins. Purified COX-1 and COX-2 isolated from ovine placenta (Caymen Chemical Co.) were used as standards.

Blots were developed with an enhanced chemiluminescence detection system (Amersham, Arlington Heights, IL), and band intensity was measured after scanning the gels with image analysis software (Jandel Scientific, San Rafael, CA).

Northern blot analysis

Changes in EP1 mRNA synthesis were evaluated by Northern blot analysis. After incubation of cultured cells in TNF- α , total RNA was extracted using the Tri-Reagent procedure (Molecular Research, Inc., Cincinnati, OH). Absorbance at 260 nm was used to estimate total RNA. The A260:A280 ratio was used to estimate the purity of the preparation.

Total RNA (15 μ g) was separated on a 1% denaturing agarose gel at 90 V. RNA was transferred to nylon membrane overnight in 20 \times sodium citrate buffer (SSC) (3 M NaCl, 0.3 M C₆H₅Na₃O₇·2H₂O using a downward transfer system (Schleicher & Schull, Keene, NH) and cross-linked with UV light (0.29 J/cm²). Nucleic acid size was determined using RNA molecular weight markers (BioRad). Equal loading was verified by ethidium bromide staining.

Membranes were hybridized with a denatured [³²P]-labeled EP1 cDNA probe (Merck Frosst, Quebec, Canada) in High Efficiency Hybridization Buffer (Molecular Research, Inc.) overnight at 60°C. Blots were washed three times in 1 \times SSC/0.1% SDS buffer for 7 min at 55°C and developed by autoradiography. Bands were quantified using image analysis software (Jandel Scientific).

Statistical analysis

Statistical analysis of EP1 receptor and cyclooxygenase protein density, mRNA density, and culture fluid PGE₂ levels was performed using a one-way analysis of variance (ANOVA). Differences between groups were determined using a Student-Newman-Keuls multiple *t*-test. *p* < 0.05 was considered significant.

RESULTS

PGE₂ production

Incubation of amnion WISH cell cultures in TNF- α resulted in a significant increase in culture fluid PGE₂ levels (pg/ μ g protein/18 h) (*p* < 0.001, *n* = 6) for all concentrations of TNF- α elevated when compared with controls (Fig. 1). Incubation of WISH cells with high TNF- α (50 ng/ml) and indomethacin (10 μ g/ml) in combination resulted in inhibition of PGE₂ to near control levels.

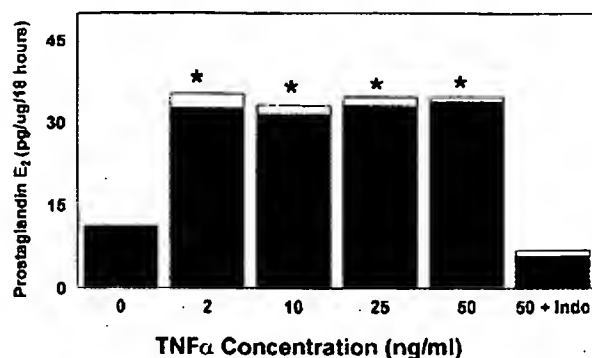
PGE RECEPTORS AND TNF- α 

FIG. 1. The effect of TNF- α on amnion WISH cell culture fluid PGE₂ concentrations and PGE₂ levels after coincubation of cells in TNF- α and indomethacin (Indo). Data are expressed as mean \pm SEM, $n = 6$ replicates per each TNF- α concentration. *Significant difference from control, $p < 0.01$. Above a concentration of 2 ng/ml there is a significant increase in PGE₂ production that is not dose dependent and is inhibited by indomethacin.

Western blot analysis

Cyclooxygenase. Incubation of amnion cell cultures in increasing concentrations of TNF- α resulted in a dose-dependent increase in the 74 kDa COX-2 isoform protein ($r = 0.783$) (Fig. 2). A significant difference ($p < 0.001$, $n = 6$) in protein density was observed for all concentrations of TNF- α evaluated. No change in the 72 kDa COX-1 protein ($n = 4$) was observed over the range of TNF- α concentrations evaluated when compared with controls (Fig. 2). Coincubation of amnion cultures in TNF- α and indomethacin had no effect on COX-1 or COX-2 protein production.

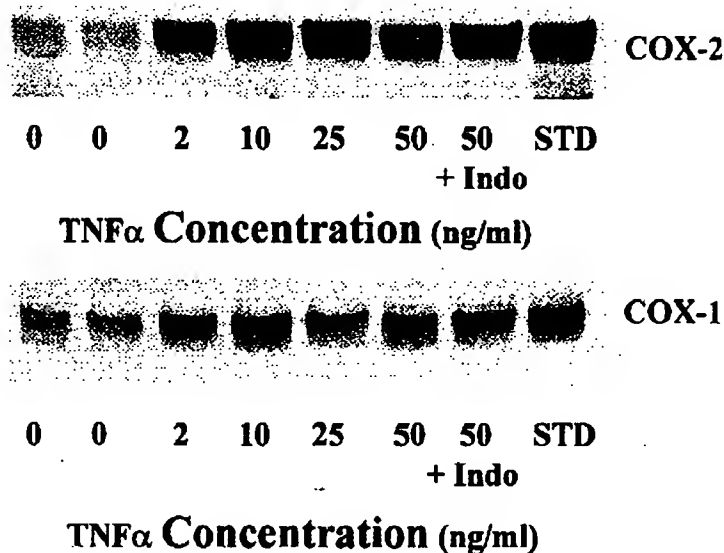


FIG. 2. Representative Western blots demonstrating the effect of increasing concentrations of TNF- α on the 72 kDa COX-1 and the 74 kDa COX-2 protein concentrations in amnion WISH cells. COX-2 protein levels are increased in the presence of TNF- α . The increase is dose-dependent ($r = 0.783$) and is not inhibited by indomethacin. COX-1 proteins were unaffected.

1041

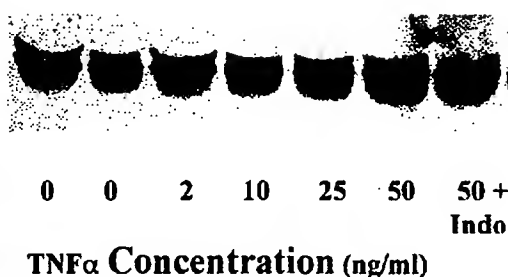
kDa
75
42
31.5

FIG. 3. Representative Western blot for EP1 proteins incubated in increasing concentrations of TNF- α alone and in combination with indomethacin (Indo). EP1 receptor proteins were increased with increasing TNF- α concentrations of 10 ng/ml or greater. Indomethacin did not inhibit production of the EP1 protein.

PGE₂ EP1 Receptor Subtype. Western blot analysis of cell homogenates for the EP1 receptor protein demonstrated the presence of a single band that migrated at a molecular weight of approximately 42 kDa. Incubation of amnion cells in TNF- α resulted in the increased synthesis of EP1 receptor proteins for concentrations > 10 ng/ml ($p < 0.01$, $n = 6$) (Fig. 3). The production of EP1 receptor proteins was unaffected by the indomethacin inhibition of PGE₂ synthesis.

Northern blot analysis

Northern blot analysis demonstrated a dose-dependent increase in EP1 mRNA (4.6 kb) with increasing concentrations of TNF- α ($r = 0.85$, $p < 0.05$, $n = 3$) (Fig. 4). Coincubation of amnion cells with indomethacin and TNF- α had no effect on EP1 mRNA synthesis.

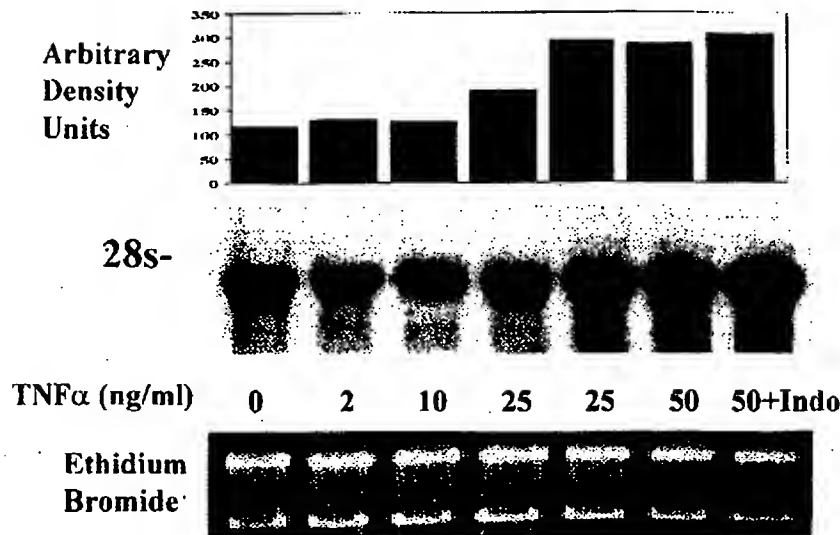


FIG. 4. Representative Northern blot of EP1 mRNA for cells incubated in increasing concentrations of TNF- α alone and in combination with indomethacin (Indo). (Top) Graphic representation of arbitrary density. The migration of the 28S ribosomal RNA band is indicated. Equal loading was verified by ethidium bromide staining of the 28S and 18S RNA bands. EP1 mRNA increased with increasing concentrations of TNF- α ($r = 0.850$).

DISCUSSION

We investigated the effects of the cytokine TNF- α on a human amnion cell line originally established in 1958. The cell line was established from a primary monolayer of human amnion, which was subsequently submitted to the American Type Culture Collection in the 163rd passage in June 1963.⁽¹⁹⁾ This cell line has served as a model system for studies of amnion cell prostaglandin regulation by a number of investigators, and it has been shown previously that proinflammatory cytokines, such as IL-1 β and TNF- α , when added to amnion WISH cell cultures, will cause enhanced production of PGE₂.⁽²⁰⁾ Furthermore, the concentration of TNF- α required to stimulate PGE production in human amnion appears to be similar to the concentrations of TNF- α found in the amniotic fluid of women with preterm labor and chorioamnionitis.⁽²¹⁾

Cytokines, including TNF- α , have been demonstrated to affect PGE₂ production in a number of other tissue types.⁽²²⁾ In this study, we have demonstrated that exposure of amnion WISH cells to TNF- α causes a significant increase in PGE₂ production and has a striking effect on the amount and activity of the inducible form of cyclooxygenase, COX-2. TNF- α has been demonstrated previously to induce COX-2 activity and concentrations in amnion that parallel prostaglandin production,⁽¹⁰⁾ and the concentrations of TNF- α used in the present study were similar to those used by previous investigators to study COX-2 in primary amnion cultures.⁽²¹⁾ It is clinically significant that the concentrations of TNF- α used in this and other studies are similar to concentrations of TNF- α found in human amniotic fluid *in vivo*. Importantly, we observed that despite high levels of TNF- α -induced PGE₂, the amount of both the EP1 receptor protein and mRNA increased. Previous studies in

our laboratory have demonstrated that PE1 receptors, in the absence of cytokine stimulation, are effectively downregulated by increasing concentrations of the agonist GPE₂. The mechanism for this reduction is probably the sequestration and degradation of the receptor because decreased protein levels are not accompanied by a similar decrease in EP1 mRNA. EP1 receptor levels also continue to increase in the presence of TNF- α despite inhibition of cyclooxygenase activity by indomethacin, further supporting a direct effect of TNF- α on EP1 receptor production independent of PGE₂ levels.

TNF- α appears to shortcircuit the normal pathways for receptor downregulation in the presence of increasing agonist. This may play an important role in the mediation of infection-induced preterm labor. In contrast to the physiologic downregulation associated with PGE₂ exposure, continuing stimulation by infection-induced cytokine release would not only produce a sustained release of PGE₂ but would also cause a synergistic decrease in the stimulatory threshold required to effect PGE₂ production by the amnion cells. Thus, stimulation of PGE₂ associated with infection-related cytokines would fail to respond to normal cellular control mechanisms and would then lead to irreversible stimulation of the myometrium.

There is little evidence for a direct effect of cytokines on myometrial contractility, and it is likely that they act through one or more mediators. A probable candidate for this role is PGE₂. Unlike oxytocin, which has minimal effect on uterine smooth muscle until close to term, PGE₂ stimulates myometrial activity in nonpregnant women as well as throughout gestation. Because the amnion is a well-established source of PGE₂ and is in direct contact with both amniotic fluid and the uterine decidua, it is a good candidate for the production of sufficient quantities of PGE₂ to both induce and sustain continued and

PGE RECEPTORS AND TNF- α

1043

coordinated uterine muscle contractions. Stimulation of the EP1 receptor is associated with smooth muscle contractions in a number of tissues, including the uterus.⁽¹⁶⁾

The actions of all known cytokines are pleiotropic in their biologic effects because of their ability to elicit a number of effects in a number of different tissues.⁽²³⁾ The actions of TNF- α in amnion WISH cells are consistent in this regard through its ability to simultaneously stimulate COX-2 activity and subsequent PGE₂ production, as well as EP1 receptor levels. Amnion cells producing high levels of PGE₂ in the presence of TNF- α , a condition that might be similar in pregnant patients with chorioamnionitis, also produced increased numbers of PGE₂ EP1 receptors. This highly unusual response would suggest that EP1 receptor production exceeds the rate of internalization of the agonist-bound receptor, as we observed an increase in both EP1 protein and mRNA synthesis. Previous experiments by our laboratory have demonstrated that IL-1 β has the same effect on PGE₂ production and EP1 receptor expression.⁽¹⁸⁾ In addition, the possibility of multiple TNF- α receptor types being stimulated and involved in this response must be considered. Two distinct receptor types for TNF- α have been identified and observed to act both through separate signal pathways and in a synergistic manner.⁽²⁴⁾

In summary, the findings of this investigation suggest that TNF- α may play a decisive role in the initiation of infection-induced preterm labor by its pleiotropic ability to simultaneously stimulate COX-2 activity, PGE₂ concentrations, and EP1 receptor levels in human amnion. Studies are underway to characterize the effects of these cytokines on human myometrial cells:

ACKNOWLEDGMENTS

We thank Dr. Kathleen Metters at the Merck Centre for Therapeutic Research, Quebec, Canada, for the EP1 cDNA probe, Dr. Lois Hunt for her assistance in development of the EP1 antibody, and Dr. Allahyar Jazayeri for his assistance with Northern blot analysis.

REFERENCES

- COOPER, R.L., GOLDBERG, R.L., CREASY, R.K., DUBARD, M.B., DAVIS, R.O., ENTMAN, S.S., IAMS, J.D., and CLIVER, S.P. (1993). A multicenter study of preterm birth weight and gestational age-specific neonatal mortality. *Am. J. Obstet. Gynecol.* 168, 78-84.
- GIBBS, R.S., ROMERO, R., HILLIER, S.L., ESCHENBACH, D.A., and SWEET, R.L. (1992). A review of premature birth and subclinical infection. *Am. J. Obstet. Gynecol.* 166, 1515-1528.
- HILLIER, S.L., MARTIUS, J., and KROHN, M.J. (1988). A case control study of chorioamnionitic infection and histologic chorioamnionitis in prematurity. *N. Engl. J. Med.* 319, 972-978.
- ROMERO, R., BRODY, D.T., OYARZUN, E., MAZOR, M., WU, Y.K., HOBBS, J.C., and DURUM, S.K. (1989). Infection and labor. III. Interleukin-1: a signal for the onset of parturition. *Am. J. Obstet. Gynecol.* 160, 1117-1123.
- ROMERO, R., MUNOZ, H., GOMEZ, H., PARRA, H., POLANCO, M., VALVERDE, V., HASBUN, J., GARRIDO, J., GHEZZI, F., MAZOR, M., TOLOSA, J., and MITCHELL, M.D. (1995). Increase in prostaglandin bioavailability precedes the onset of human parturition. *Prostaglandins Leukotrienes Essential Fatty Acids* 54, 187-193.
- TEIXEIRA, F.J., ZAKAR, T., HIRST, J.J., GUO, F., SADOWSHY, D.W., MACHIN, G., DEMIANCZUK, N., RESCH, B., and OLSON, D. (1994). Prostaglandin endoperoxide-H synthase (PGHS) activity and immunoreactive PGHS-1 and PGHS-2 levels in human amnion throughout gestation, at term, and during labor. *J. Clin. Endocrinol. Metab.* 78, 1396-1402.
- OLSON, D.M., MIJOVIC, J.E., and SADOWSKY, D.W. (1995). Control of human parturition. *Semin. Perinatol.* 9, 52-63.
- O'BRIEN, W.F. (1995). The role of prostaglandins in labor and delivery. *Clin. Perinatol.* 22, 973-974.
- XUE, S., BROCKMAN, D.E., SLATER, D.M., and MYATT, L. (1995). Interleukin-1 β induces the synthesis and activity of cytosolic phospholipase A₂ and the release of prostaglandin E₂ in human amnion-derived WISH cells. *Prostaglandins* 49, 351-369.
- POLLARD, J.K., and MITCHELL, M.D. (1993). Tumor necrosis factor alpha stimulates amnion prostaglandin biosynthesis primarily via an action on fatty acid cyclooxygenase. *Prostaglandins* 46, 499-510.
- SMITH, W.L., and DEWITT, D.L. (1996). Prostaglandin endoperoxide synthases-1 and -2. *Adv. Immunol.* 62, 167-214.
- FUENTES, A., SPAZIANI, E.P., and O'BRIEN, W.F. (1996). The expression of cyclooxygenase-2 (COX-2) in amnion and decidua following spontaneous labor. *Prostaglandins* 52, 261-267.
- NEGISHI, M.Y., SUGIMOTO, Y., and ICHIKAWA, I. (1995). Molecular mechanisms of diverse actions of prostanoïd receptors. *Biochem. Biophys. Acta* 1259, 109-120.
- ICHIKAWA, I., SUGIMOTO, Y., and NEGISHI, M.Y. (1996). Molecular aspects of the structures and functions of prostaglandin E receptors. *J. Lipid Med. Cell Sig.* 14, 83-87.
- WATABE, A., SUGIMOTO, Y., HONDO, H., IRIE, A., NAMBA, T., NEGISHI, M., ITO, S., NARUMIYA, S., and ICHIKAWA, A. (1993). Cloning and expression of cDNA for a mouse EP1 subtype of prostaglandin E receptor. *J. Biol. Chem.* 268, 20175-20178.
- ASBOTH, G., PHANUEF, S., EUROPE-FINNER, N., TOTTH, M., and BERNAL, A. (1996). Prostaglandin E₂ activates phospholipase C and elevates intracellular calcium in cultured myometrial cells: involvement of EP1 and EP3 receptor subtypes. *Endocrinology* 137, 2572-2579.
- SMITH, P.K., KROHN, R.I., HERMANSON, G.T., MALLIA, A.K., GARTNER, F.H., PROVANZANO, M.D., FUGIMOTO, E.K., GOEKE, N.M., OLSON, B.J., and KLENK, D.C. (1985). Measurement of protein using bicinchoninic acid. *Anal. Biochem.* 150, 76-85.
- SPAZIANI, E.P., TSIBRIS, J.C.M., HUNT, L.T., BENOIT, R.R., and O'BRIEN, W.F. (1997). The effect of interleukin-1 β and interleukin-4 on the expression of prostaglandin receptors EP1 and EP3 in amnion WISH cells. *Am. J. Reprod. Immunol.* 38, 279-285.
- HAYFLICK, L. (1961). The establishment of a line (WISH) of human amnion cells in continuous cultivation. *Exp. Cell Res.* 23, 14-20.
- ALBERT, T.J., SU, H.-C., ZIMMERMAN, P.D., IAMS, J.D., and KNISS, D.A. (1994). Interleukin-1 β regulates the inducible cyclooxygenase in amnion-derived WISH cells. *Prostaglandins* 48, 401-416.
- ROMERO, R., MANOGUE, K.R., MITCHELL, M.D., WU, Y.K., OYARZUN, E., HOBBS, J.C., and CERAMI, A. (1989). Infection and labor. IV: Cachectin-tumor necrosis factor in the amniotic

1044

SPAZIANI ET AL.

fluid of women with intraamniotic infection and preterm labor. *Am. J. Obstet. Gynecol.* **161**, 336-341.

22. PEPLOW, P.V. (1996). Actions of cytokines in relation to arachidonic acid metabolism and eicosanoid production. *Prostaglandins Leukotrienes Essential Fatty Acids* **54**, 303-317.
23. TROTTA, P.P. (1991). Cytokines: an overview. *Am. J. Reprod. Immunol.* **25**, 137-141.
24. MUKHERJEE, R., SINGH, S., CHATURVEDI, M.M., and AGGARWAL, B.B. (1998). Evidence for a synergistic role of two types of human tumor necrosis factor receptors for ligand-dependent activation of the nuclear transcription factor NF- κ B. *J. Interferon Cytokine Res.* **18**, 117-123.

Address reprint requests to:

Dr. Eric P. Spaziani

University of South Florida Health Science Center

Department of Obstetrics & Gynecology

Box 18, 12901 Bruce B. Downs Boulevard

Tampa, FL 33612

Tel: (813) 974-7018

Fax: (813) 974-7026

E-mail: espazian@com1.med.usf.edu

Received 24 June 1998/Accepted 12 August 1998

Original Research Article

Skin
Pharmacology
and Applied
Skin
Physiology

Skin Pharmacol Appl Skin Physiol 2003;16:143-150
DOI: 10.1159/000069754

Received:
April 29, 2002
Accepted after revision:
September 27, 2002

Transcriptional Activity of Potent Glucocorticoids: Relevance of Glucocorticoid Receptor Isoforms and Drug Metabolites

I. Spika^a S. Hammer^a B. Kleuser^a H.C. Korting^b
M. Schäfer-Korting^a

^aInstitut für Pharmazie, Abteilung für Pharmakologie und Toxikologie,
Freie Universität Berlin, Berlin, ^bKlinik und Poliklinik für Dermatologie und Allergologie,
Ludwig-Maximilians-Universität, München, Germany

Key Words

Prednicarbate · Glucocorticoids ·
Transactivation · Keratinocytes · Fibroblasts

Abstract

As compared to standard glucocorticoids (GC), prednicarbate (PC) is favorable in the treatment of eczema due to its high benefit/risk ratio. The remarkable anti-inflammatory effects of PC are in strong contrast to its reported low glucocorticoid receptor (GR) binding affinity. In transfected COS-7 cells we related the transcriptional potencies of PC, its metabolites and conventional GC to their receptor binding properties. Moreover, the expression pattern of the human GR isoform hGR α and its mutual dominant negative inhibitor hGR β in skin cells have been investigated as well as the influence of hGR β on receptor binding and transactivation. hGR α

mRNA and protein was largely overexpressed in skin cells. hGR β showed no influence on hGR α binding and transactivation. Concentration response curves indicated the greater transactivation potency of betamethasone 17-valerate followed by dexamethasone and prednisolone 17-ethylcarbonate. Native PC appeared almost as potent as dexamethasone. With both a strong correlation was observed between transactivation and GR binding.

Copyright © 2003 S. Karger AG, Basel

Introduction

Topical glucocorticoids (GC) are the most effective treatment currently available for inflammatory skin diseases. The potent suppression of inflammation, however, is associated with a serious side effect on fibroblast

KARGER

Fax +41 61 306 12 34
E-Mail karger@karger.ch
www.karger.com

© 2003 S. Karger AG, Basel
1422-2468/03/0163-0143\$19.50/0

Accessible online at:
www.karger.com/epb

Monika Schäfer-Korting
Institut für Pharmazie, Abteilung für Pharmakologie und Toxikologie
Freie Universität Berlin, Königin-Luise-Strasse 2 + 4
D-14195 Berlin (Germany), Tel. +49 30 838 53283
Fax +49 30 838 54399, E-Mail msk@zedat.fu-berlin.de

proliferation leading to skin atrophy following prolonged GC application. Prednicarbate (PC) is the first topical GC with an improved benefit/risk ratio combining significant anti-inflammatory activity with minor reduction of skin thickness, as compared to e.g. betamethasone 17-valerate (BMV) [1-3]. The results of clinical studies are confirmed by those of cell culture experiments [4, 5]. In the skin PC is metabolized by ester-cleavage resulting in the formation of prednisolone 17-ethylcarbonate (P17EC), which is converted to prednisolone 21-ethylcarbonate (P21EC) and finally to prednisolone (PD). The hydrolytic rate, however, differs in keratinocytes and fibroblasts, which is not true with BMV [6-8].

GC effects are mediated by the intracellular glucocorticoid receptor (GR) transactivating or repressing target genes (for review see [9]). In man, two isoforms of GR named hGR α and hGR β have been detected which differ only at their C-termini [10]. The isoforms result from an alternative splicing event in exon 9 of the human GR gene and are identical through amino acid 727, but then they diverge. hGR β is unable to bind GC but has been reported to act as a dominant negative inhibitor of glucocorticoid-induced transactivation in some cell types [11-13]. However, it is still not clear whether this effect is specific or only results from non-specific sequestration [14]. Elevated tissue levels of hGR β have been associated with e.g. steroid resistant asthma [15-17] and colitis ulcerosa [18] proposing a role for hGR β in tissue sensitivity to GC.

To further identify the molecular mechanism of action of atrophogenic and less atrophogenic GC, we have compared receptor binding and transactivation of PC and its metabolites to those of conventional GC as BMV and dexamethasone (DEX). Moreover, the expression of hGR β in cutaneous cells and its influence on hGR α binding and transactivation have been determined.

Materials and Methods

Materials

Betamethasone 17-valerate (BMV) was obtained from Glaxo Wellcome (Hamburg, Germany), RU486, PC and its metabolites (P17EC, P21EC, PD) from Aventis Pharma (Frankfurt, Germany), [1,2,4,6,7-³H]dexamethasone (37 MBq/ml) from Amersham (Buckinghamshire, UK). HPLC solvents were from Merck (Darmstadt, Germany). Betamethasone (BM), dexamethasone (DEX), reagents and media except where noted were purchased from Sigma (Deisenhofen, Germany). Glucocorticoid stock solutions (10 mM) were stored at -80 °C and diluted in ethanol to the appropriate concentrations immediately before the experiments.

Cell Culture and Transfection

Keratinocytes and fibroblasts obtained from human juvenile foreskin were cultivated as previously described [7]. For experiments cells of the second and third passage were used. COS-7 cells (ATCC, Rockville, MD) were cultured in Dulbecco's modified Eagle's medium (DMEM) containing 10% fetal calf serum (Biochrom, Berlin, Germany), glutamin (2 mM), 100 U/ml penicillin and 100 µg/ml streptomycin. The plasmids pRShGR α and pRShGR β coding for the human GR α and GR β [10] were kindly donated by Dr. R. Evans (Salk Institute, La Jolla, Calif.). pmGR coding for the murine GR [19] and pMMTV-CAT containing the CAT gene under transcriptional control of the MMTV promoter were kindly provided by Dr. M. Danielsen (Georgetown University, Washington, D.C.). Subconfluent COS-7 cells were transfected with a mixture of 1.25 µg plasmid DNA and 5 µl lipofectamine reagent per ml of serum-free DMEM (GIBCO BRL, Life Technologies, Karlsruhe, Germany) according to the manufacturer's instructions.

RT-PCR

mRNA from keratinocytes and fibroblasts was extracted using the QuickPrep™ Micro mRNA purification kit (Amersham, Buckinghamshire, UK) and quantified by UV-absorption (260 nm). 500 ng RNA was reverse transcribed by 200 U of Superscript™ II reverse transcriptase in the presence of oligo dT primers (both GIBCO BRL, Gaithersburg, Md.) according to the manufacturer's instructions. For amplification of hGR α and hGR β cDNA a common 3' primer was used: 5' CTT AAG GAC GGT CTG AAG AGC 3' corresponding to nucleotides 2158-2178. Downstream primers were specific to hGR α and hGR β mRNA respectively: hGR α nucleotide 2616-2635 (5' GCC

AAG TCT TGG CCC TCT AT 3') and hGR β nucleotide 2503–2523 (5' CCT AAG GAC GGT CTG AAG AGC 3'). The mixture was incubated with 1.25 U *Thermus islandicus* polymerase (Advanced Biotechnologies, Epsom, UK) for 2 min at 94 °C, then 10 cycles at 94 °C for 1 min, at 60 °C for 30 s, at 72 °C for 30 s, followed by 40 cycles at 92 °C for 1 min, at 60 °C for 30 s, at 72 °C for 30 s. 5 μ l of the reaction mixture were removed at 2-cycle intervals, amplified fragments were separated in 2% agarose gels and stained with ethidium bromide. Plotting the intensity of the ethidium bromide fluorescence as a function of cycle number for keratinocyte and fibroblast cDNA generated amplification curves. These were also obtained for external standards of linearized pRShGR α and pRShGR β plasmids at ratios of 1:1 to 1,000:1. Plotting the plasmid ratio against the difference in cycle number required to amplify the same amount of cDNA resulted in a standard curve which allowed to calculate the cellular hGR α /hGR β cDNA (and hence mRNA) ratio.

Immunoblotting

Cytosolic extracts from keratinocytes and fibroblasts were prepared in a buffer containing 20 mM Tris-HCl pH 7.5; 2 mM EDTA; 150 mM NaCl; 0.5% Triton X-100 and a mixture of protease inhibitors (0.1 mM phenylmethylsulfonyl fluoride, 1 μ g/ml aprotinin, 1 μ M pepstatin, 1 μ M leupeptin). After determination of the protein concentrations 150 μ g protein were resolved on 7.5% SDS-polyacrylamide gels, transferred to polyvinylidene difluoride membranes and blotted with hGR α and hGR β specific antibodies (Affinity Bioreagents/Dianova, Hamburg, Germany).

Hormone Binding

Subconfluent COS-7 cells were transfected with pRShGR α +/- a 5-fold molar excess of pRShGR β . For whole-cell binding assays cells splitted into 24-well plates were incubated with GC (0.01–10,000 nM) and [³H]dexamethasone at 37 °C for 2 h. For competition experiments 10 nM [³H]dexamethasone were used. Cells washed twice with phosphate-buffered saline (PBS) were lysed in buffer containing 2% SDS, 10% glycerol and 10 mM Tris-HCl (pH 6.8). Bound [³H]dexamethasone was quantified by liquid scintillation counting. Nonspecific binding was determined by adding a 500-fold excess of nonlabeled dexamethasone. For cytosolic binding experiments transfected COS-7 cells were harvested 48 h after transfection and lysed by sonication (Bandelin, Berlin, Germany) in a buffer containing 20 mM Tris-HCl (pH 7.5), 1 mM EDTA, 10 mM NaMoO₄, 10% glycerol and 2 mM DTT. Separated from cellular debris by centrifugation

the supernatant was incubated for 3 h at 4 °C with [³H]dexamethasone with or without the competing steroids. 1% dextrane-coated charcoal suspension served to separate bound and free steroid.

Transactivation

COS-7 cells were transfected with pmGR or pRShGR α and a twofold molar excess of pMMTV-CAT. Cells splitted into 24-well plates were grown in the presence of GC (0.01–1,000 nM) for 24 h. To study the influences of hGR β pRShGR β was cotransfected at different molar ratios. The total amount of DNA was kept constant by adding salmon sperm DNA. Transfection efficiency was determinable by 0.1 μ g of pSV- β -Gal (Promega, Mannheim, Germany) cotransfection. A modification of the phase separation method served to measure CAT activity [20]. Deacetylases of lysed cells were inactivated by heating to 65 °C. 200 μ l reaction buffer (125 mM Tris-HCl pH 7.8, 0.3 mM chloramphenicol) and 0.01 μ Ci [³H]acetyl-CoA (ICN Biomedicals, Costa Mesa, Calif.) were added and the samples overlaid with 1 ml of a water-immiscible scintillation fluid (Econofluor-2, Packard, Groningen, Netherlands) were incubated at 37 °C for 24 h. Transfection efficiency was measured using a galactosidase assay system (Promega).

HPLC

To follow steroid metabolism COS-7 cells incubated in growth medium with PC were lysed by 3 freeze/thaw cycles. Extraction and HPLC analysis were performed as described [7]. In parallel COS-7 cell viability was controlled by MTT-test [7].

Statistical Analysis

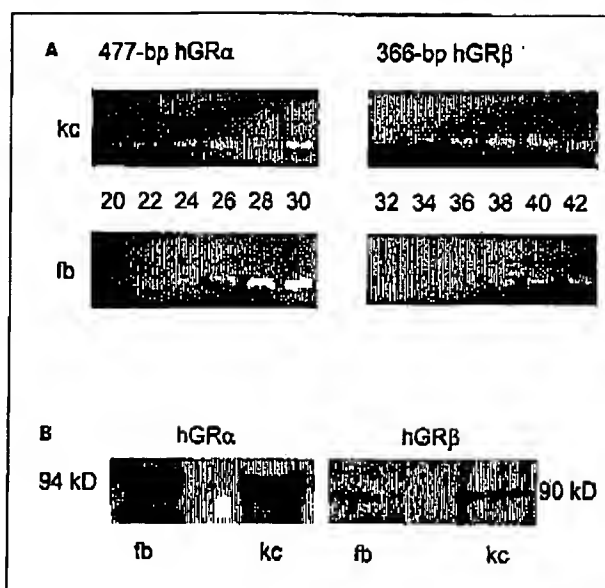
Data obtained from independent experiments performed in triplicate are expressed as mean \pm SD. Receptor binding (RBA) as well as GC induced CAT activation derived from EC₅₀ values of the concentration response curves are related to DEX activity set 100. Statistics were performed using Student's *t* test with *p* \leq 0.05 indicating a difference.

Results

hGR α and hGR β Expression in Keratinocytes and Fibroblasts

RT-PCR was performed on mRNA isolated from primary keratinocytes and fibroblasts using primers that hybridise on either

Fig. 1. hGR α and hGR β expression in keratinocytes (kc) and fibroblasts (fb). **A** Quantitative RT-PCR of mRNA isolated from human keratinocytes and fibroblasts. The representative ethidium bromide-stained agarose gel shows the amplification of hGR α and hGR β fragments using hGR α - or hGR β -specific primers. Aliquots of the PCR reaction were removed at two-cycle intervals. **B** Immunoblotting of cytosolic fractions from keratinocytes and fibroblasts with hGR α and hGR β specific antibodies.



side of the alternatively spliced region of the hGR α or hGR β mRNA. In both keratinocytes and fibroblasts a 477-bp as well as a 366-bp PCR product could be detected suggesting that hGR α and hGR β mRNA was present in both cell types (fig. 1A). When the reverse transcriptase was omitted from the RT-PCR reaction no PCR products were generated demonstrating that only cDNA produced by the RT step served as template.

The relative levels of the hGR α and hGR β transcripts in keratinocytes and fibroblasts obtained from a standard curve generated from samples with defined hGR α /hGR β cDNA ratios were calculated to 328 for keratinocytes and 710 for fibroblasts. These results demonstrate a large overexpression of hGR α mRNA in both cell types with a higher relative extent of hGR β mRNA in keratinocytes. RT-PCR findings were confirmed by immunoblotting with hGR α and hGR β specific antibodies (fig. 1B).

Hormone Binding Studies

The importance of the different amount of the GR subtypes in keratinocytes and fibroblasts for cell sensitivity to different GC has been evaluated, first regarding GC binding. hGR α transfected COS-7 cells bound [3 H]dexamethasone with a K_D of 2.45 nM (fig. 2A), as expected hGR β did not bind dexamethasone. Cotransfection of hGR α and an even 5-fold molar excess of hGR β did not change the hGR α binding affinity of [3 H]dexamethasone (K_D = 2.5 nM; fig. 2A). Studies of different topical GC with overexpressed hGR α demonstrated a high receptor binding affinity of BMV and RU 486 (table 1). DEX, the active PC metabolite P17EC, but also native PC were almost equipotent, while P21EC and PD bound with low affinity. Experiments on cell lysates were in good accordance with data derived from whole-cell assays (table 1) indicating that the high binding affinity of PC is not due to superior cell pene-

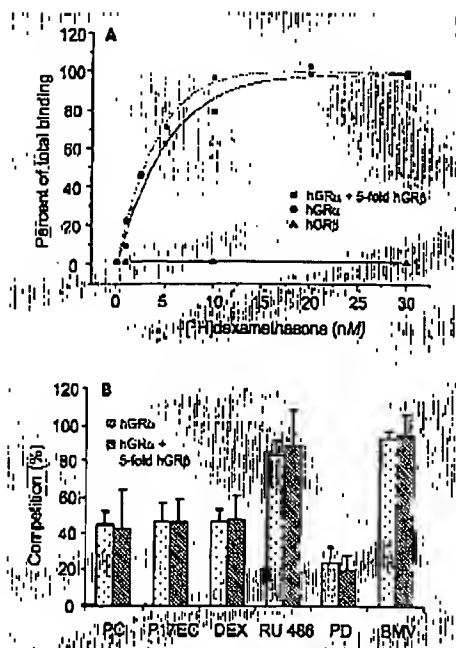


Fig. 2. Influence of hGR β on hGR α GC binding. **A** Specific binding of [3 H]dexamethasone to hGR α , hGR β or hGR α in the presence of a 5-fold molar excess of hGR β . Transfected COS-7 cells were incubated with [3 H]dexamethasone as indicated; the amount of bound [3 H]dexamethasone was determined by liquid scintillation counting. **B** Competition of various GC 10 nM with [3 H]dexamethasone for hGR α binding in the presence or absence of hGR β . COS-7 cells were transfected with either hGR α or hGR α plus a 5-fold molar excess of hGR β .

tration. hGR β had no influence on hGR α binding capacity and specificity in vitro as binding of GC was not changed by a 5-fold excess of hGR β (fig. 2B).

Transcriptional Activation by Different GC

To investigate the relation between receptor binding affinity and GR-mediated transactivation of gene expression, CAT reporter gene assays were performed. Optimal transac-

tivation occurred 24 h after stimulation with GC. Once more BMV induced the highest CAT activity, P17EC and native PC turned out equipotent to DEX, while PD and P21EC were less effective (table 1). As expected RU486 as a GC antagonist did not influence CAT activity but inhibited CAT activity induced by other GC completely. Equivalent results were obtained investigating mGR or hGR α (data not shown). To exclude that the high transcriptional activity of PC is a result of formation of active P17EC, CAT assays were also performed after 2 h incubation, whereas almost equal transcriptional activity of DEX and PC was detected. Moreover, with PC 2.5 μ M incubation for 2 h metabolites (P17EC, P21EC and PD) were not detected by HPLC analysis and even after 24 h PC was degraded only to a minor extent. P17EC was 9.5 ± 0.7 and P21EC was 9.6 ± 0.5 % of total drug. PD appeared by 3.5 ± 0.3 %. To exclude artificially low metabolism rates due to enzyme saturation metabolism studies were repeated increasing the PC amount 10-fold (25 μ M). The results (P17EC 8.3 ± 0.1 %, P21EC 10.9 ± 0.04 %, PD 1.8 ± 0.03 % of total GC) resembled those seen with PC at a concentration of 2.5 μ M. Toxic effects of PC and its metabolites on COS-7 cells were excluded by MTT tests showing an unchanged formazan reduction. Finally, studies focused on the influence of hGR β on hGR α mediated transactivation in our CAT reporter system. No significant decrease of hGR α transactivation could be detected when hGR β was co-transfected up to a 10-fold molar excess (fig. 3).

Discussion

It has been well established that topical GC differ in their benefit/risk ratio [2, 3]. However, the molecular reasons for these differ-

Table 1. Receptor binding (RBA) and relative transactivation activities

	Whole-cell binding assay	Cytosolic binding assay	Trans-activation
Dexamethasone	100	100	100
Prednicarbate	74	82	76
P17EC	110	144	103
P21EC	15	8	15
Prednisolone	9	29	20
BMV	1,370	774	776
RU486	4,670		

RBA values were derived from EC_{50} values of the competition curves to replace 50% of bound [3H]dexamethasone, relative transactivation from EC_{50} values of the concentration response curves. EC_{50} values are related to DEX activity set 100.

ences are still unknown. Therefore it was of interest to compare receptor binding and transactivation properties of PC and its metabolites to those of standard GC as DEX and BMV.

Transfection of GR-deficient COS-7 cells with plasmids coding for human GR and cotransfection with a GC responsive CAT reporter gene (pMMTV-CAT) allowed to study receptor binding as well as transactivation processes [19]. Since PC is rapidly metabolized in keratinocytes [7] biodegradation of the double ester in COS-7 cells was assessed by HPLC/UV absorption to exclude that transactivation activity results from active PC metabolites. COS-7 cells induced only low PC metabolism indicating that COS-7 cells represent an ideal system for studying GC-ester effects.

Here we show the high substance-specific receptor binding and transactivation potency of native PC. Whole-cell and cytosolic binding assays revealed that in contrast to many other GC esters [21] the 21-ester group of PC does not impair GC activity (table 1). Controversially in synovial tissue PC has been identified to bind with low affinity to the GR [22].

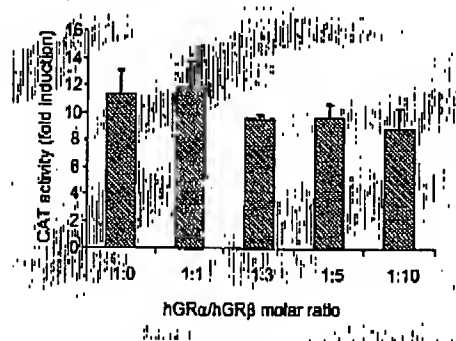


Fig. 3. Influence of hGRβ on hGRα transcriptional activity regarding different molar ratios. COS-7 cells were cotransfected with hGRα and hGRβ as indicated. Salmon sperm DNA was added to keep the total amount of DNA constant. Data are expressed as fold induction over the noninduced control.

Clinical studies in atopic dermatitis and healthy volunteers confirmed an equipotent efficiency of PC compared to BMV. In receptor binding and transactivation experiments, however, BMV was clearly more potent than PC. This discrepancy may result from an improved skin penetration of PC, which plays an essential role in GC efficacy.

In humans two GR subtypes have been discovered, termed hGR α and hGR β [10]. As elevated levels of hGR β occur in cells of patients with steroid resistant inflammatory diseases [15–18] it has been suggested that expression of GR subtypes regulate cell responsiveness to GC treatment. Our data show that the epithelial derived keratinocytes form hGR β mRNA to a higher relative extent than fibroblasts from endothelial origin. Furthermore, we demonstrate a large overexpression of hGR α mRNA as compared to hGR β mRNA in keratinocytes (328-fold) and fibroblasts (710-fold; fig. 1A). These results were confirmed by immunoblotting indicating a strong overexpression of hGR α protein in both cell types and a higher relative level of hGR β in keratinocytes compared to fibroblasts (fig. 1B). Bamberger et al. [11] have suggested that hGR β could act as dominant negative inhibitor of GC action on GC-responsive promoters, an effect that was not seen by others [14]. In COS-7 cells cotransfection experiments exclude relevant influences of hGR β ; hGR α binding affinity for different GC has not changed even in the presence of a 5-fold molar excess of hGR β (fig. 2) and also CAT activity is not influenced by hGR β cotransfection at an equimolar ratio (fig. 3). Therefore the function of hGR β remains unidentified.

GC act via the GR by binding to glucocorticoid response elements in target gene promoters leading to increased transcription of genes coding for anti-inflammatory proteins like interleukin-1 receptor antagonist, interleukin-10 and I κ B. Besides this, protein-protein interactions with AP-1 and NF κ B frequently result in transrepression processes [for review see 23]. Recently, it has been reported that budesonide is favorable for the treatment of bronchial asthma as unwanted effects are less distinct [24]. At the molecular level budesonide revealed a high transrepression but low transactivation activity suggest-

ing that the anti-inflammatory properties are controlled by the transrepression of transcription factors whereas unwanted effects are due to transactivation. Furthermore a novel class of selective ligands of GR has been identified which are potent inducers of transrepression but not of transactivation [25, 26]. These dissociated GC decreased interleukin synthesis as well as NF κ B and AP-1 activity in vitro [27]. Studies in rats, however, did not indicate a reduction of side effects as thymus involution, loss of body weight and bone turnover occurred as well using these ligands. Belvisi et al. suggested that these unwanted effects are not a consequence of transactivation but may be due to transrepression [28]. With topical GC frequently used for inflammatory skin diseases, however, GC receptor binding and transactivation correlate with anti-inflammatory activity.

In conclusion, data presented here show that the strong effect of the double ester PC on transactivation is a result of its high binding affinity. Additional investigations of transrepression potencies will further improve the insight into the molecular reasons for the strong anti-inflammatory but low antiproliferative potential of PC.

Acknowledgments

The authors thank M. Danielsen and R. Evans for providing plasmids. Irina Spika was a recipient of fellowships from the Berliner Graduiertenförderung and from the Berliner Programm zur Förderung der Chancengleichheit von Frauen in Forschung und Lehre. Furthermore, financial support of the Deutsche Forschungsgemeinschaft is gratefully acknowledged.

References

- 1 Korting HC, Unholzer A, Schäfer-Korting M, Tausch L, Gassmüller J, Nietsch KH: Different skin thinning potential of equipotent medium-strength glucocorticoids. *Skin Pharmacol Appl Skin Physiol* 2002;15: 85-91.
- 2 Hanifin J, Abrams B, Cherill R: Management of atopic dermatitis with prednicarbate emollient cream 0.1%, a nonhalogenated prednisolone derivative. *J Geriatr Dermatol* 1994;2:119-127.
- 3 Schäfer-Korting M, Korting HC, Kerschner MJ, Lenhard S: Prednicarbate activity and benefit/risk ratio in relation to other topical glucocorticoids. *Clin Pharmacol Ther* 1993; 54:448-456.
- 4 Lange K, Gysler A, Bader M, Kleuser B, Korting HC, Schäfer-Korting M: Prednicarbate versus conventional topical glucocorticoids: Pharmacodynamic characterization in vitro. *Pharm Res* 1997;14:1744-1749.
- 5 Lange K, Kleuser B, Gysler A, Bader M, Maier C, Scheidereit C, Korting HC, Schäfer-Korting M: Cutaneous inflammation and proliferation in vitro: Differential effects and mode of action of topical glucocorticoids. *Skin Pharmacol Appl Skin Physiol* 2000;13:93-103.
- 6 Barth J, Lehr KH, Derendorf H, Möllmann HW, Hühner T, Hochhaus G: Studies on the pharmacokinetics and metabolism of prednicarbate after cutaneous and oral administration. *Skin Pharmacol* 1993; 6:179-186.
- 7 Gysler A, Lange K, Korting HC, Schäfer-Korting M: Prednicarbate biotransformation in human foreskin keratinocytes and fibroblasts. *Pharm Res* 1997;14:793-797.
- 8 Gysler A, Kleuser B, Sijpe W, Lange K, Korting HC, Hölthje HD, Schäfer-Korting M: Skin penetration and metabolism of topical glucocorticoids in reconstructed epidermis and in excised human skin. *Pharm Res* 1999;16:1386-1391.
- 9 Göllicher M, Heck S, Herrlich P: Transcriptional cross-talk, the second mode of steroid hormone receptor action. *J Mol Med* 1998;76:480-489.
- 10 Hollenberg SM, Weinberger C, Ong ES, Cerelli G, Oro A, Lebo R, Thompson ED, Rosenfeld MG, Evans RM: Primary structure and expression of a functional human glucocorticoid receptor cDNA. *Nature* 1985;318:635-641.
- 11 Bamberger CM, Bamberger AM, de Castro M, Chrousos GP: Glucocorticoid receptor beta: a potential endogenous inhibitor of glucocorticoid action in humans. *J Clin Invest* 1995;95:2435-2441.
- 12 Oakley RL, Sar M, Cidlowski JA: The human glucocorticoid receptor beta isoform. Expression, biochemical properties, and putative function. *J Biol Chem* 1996;271:9550-9559.
- 13 Oakley RL, Jewell CM, Yudit MR, Boferiade DM, Cidlowski JA: The dominant negative activity of the human glucocorticoid receptor beta isoform. Specificity and mechanisms of action. *J Biol Chem* 1999; 274:27857-27866.
- 14 Hecht K, Carlstedt-Duke J, Stierma P, Gustafsson J, Bronnegard M, Wikstrom AC: Evidence that the beta-isoform of the human glucocorticoid receptor does not act as a physiologically significant repressor. *J Biol Chem* 1997;272:26659-26664.
- 15 Hamid QA, Wenzel SE, Hawk PJ, Tsicopoulos A, Wallner B, Lafite JJ, Chrousos GP, Szefer SJ, Leung DY: Increased glucocorticoid receptor beta in airway cells of glucocorticoid-insensitive asthma. *Am J Respir Crit Care Med* 1999;159:1600-1604.
- 16 Leung DY, Hamid Q, Vortem A, Szefer SJ, Voss W, Minshall E, Chrousos GP, Klemm DJ: Association of glucocorticoid insensitivity with increased expression of glucocorticoid receptor beta. *J Exp Med* 1997;186:1567-1574.
- 17 Sousa AR, Lane SJ, Cidlowski JA, Shaynov DZ, Lee TH: Glucocorticoid resistance in asthma is associated with elevated in vivo expression of the glucocorticoid receptor beta-isoform. *J Allergy Clin Immunol* 2000;105:943-950.
- 18 Honda M, Orii F, Ayabe T, Imai S, Ashida T, Obara T, Kohno Y: Expression of glucocorticoid receptor beta in lymphocytes of patients with glucocorticoid-resistant ulcerative colitis. *Gastroenterology* 2000;118: 859-866.
- 19 Danielsen M, Northrop JP, Ringold GM: The mouse glucocorticoid receptor: mapping of functional domains by cloning, sequencing and expression of wild-type and mutant receptor proteins. *EMBO J* 1986;5: 2513-2522.
- 20 Neumann JR, Moroney CA, Russian KO: A novel rapid assay for chloramphenicol acetyltransferase. *Biotechniques* 1987;5:444-447.
- 21 Ponet M, Kempenaar J, Shroot B, Caron JC: Glucocorticoids: binding affinity and lipophilicity. *J Pharm Sci* 1986;75:973-975.
- 22 Förtner M, Möllmann H, Rohdewald P: Glucocorticoid receptors in human synovial tissue and relative receptor affinities of glucocorticoid-21-esters. *Pharm Res* 1988;5:623-627.
- 23 Barnes PJ: Anti-inflammatory actions of glucocorticoids: molecular mechanisms. *Clin Sci* 1998;94:557-572.
- 24 Jaffuel D, Demoly P, Gougat C, Balaguer P, Mautino G, Godard P, Boosquet J, Malhieu M: Transcriptional potencies of inhaled glucocorticoids. *Am J Respir Crit Care Med* 2000;162:57-63.
- 25 Vayssiere BM, Dupont S, Choquart A, Pellé F, Garcia T, Marchandeu C, Gronemeyer H, Resche-Rigon M: Synthetic glucocorticoids that dissociate transactivation and AP-1 transrepression exhibit antiinflammatory activity in vivo. *Mol Endocrinol* 1997;11:1245-1255.
- 26 Bamberger CM, Else T, Bamberger AM, Beil FU, Schulte HM: Dissociative glucocorticoid activity of medroxyprogesterone acetate in normal human lymphocytes. *J Clin Endocrinol Metab* 1999;84:4055-4061.
- 27 Vanden Bergh W, Francesconi E, De Brusscher K, Resche-Rigon M, Haegeman G: Dissociated glucocorticoids with anti-inflammatory potential repress interleukin-6 gene expression by a nuclear factor-kappaB-dependent mechanism. *Mol Pharmacol* 1999;56:797-806.
- 28 Belvisi MG, Wicks SL, Ballman CII, Bottoms SE, Redford JE, Woodman P, Brown TJ, Webber SE, Foster ML: Therapeutic benefit of a dissociated glucocorticoid and the relevance of in vitro separation of transrepression from transactivation activity. *J Immunol* 2001;166:1975-1982.

Specific Inhibition of AQP1 Water Channels in Isolated Rat Intrahepatic Bile Duct Units by Small Interfering RNAs*

Received for publication, November 26, 2002
Published, JBC Papers in Press, December 4, 2002, DOI 10.1074/jbc.M212079200

Patrick L. Splinter, Anatoliy I. Masyuk, and Nicholas F. LaRusso†

From the Center for Basic Research in Digestive Diseases, Division of Gastroenterology and Hepatology, Mayo Medical School, Clinic, and Foundation, Rochester, Minnesota 55905

Cholangiocytes express water channels (*i.e.* aquaporins (AQPs)), proteins that are increasingly recognized as important in water transport by biliary epithelia. However, direct functional studies demonstrating AQP-mediated water transport in cholangiocytes are limited, in part because of the lack of specific AQP inhibitors. To address this issue, we designed, synthesized, and utilized small interfering RNAs (siRNAs) selective for AQP1 and investigated their effectiveness in altering AQP1-mediated water transport in intrahepatic bile duct units (IBDUs) isolated from rat liver. Twenty-four hours after transfection of IBDUs with siRNAs targeting two different regions of the AQP1 transcript, both AQP1 mRNA and protein expression were inhibited by 76.6–92.0 and 57.9–79.4%, respectively. siRNAs containing the same percent of base pairs as the AQP1-siRNAs but in random sequence (*i.e.* scrambled siRNAs) had no effect. Suppression of AQP1 expression in cholangiocytes resulted in a decrease in water transport by IBDUs in response to both an inward osmotic gradient (200 mosm) or a secretory agonist (forskolin), the osmotic water permeability coefficient (P_f) decreasing up to 58.8% and net water secretion (J_w) decreasing up to 87%. A strong correlation between AQP1 protein expression and water transport in IBDUs transfected with AQP1-siRNAs was consistent with the decrease in water transport by IBDUs resulting from AQP1 gene silencing by AQP1-siRNAs. This study is the first to demonstrate the feasibility of utilizing siRNAs to specifically reduce the expression of AQPs in epithelial cells and provides direct evidence of the contribution of AQP1 to water transport by biliary epithelia.

Intrahepatic bile duct epithelial cells (*i.e.* cholangiocytes) play an essential role in bile formation, and by integrated absorptive and secretory processes, they contribute up to 40% of daily bile production in humans (1, 2). Because bile is a complex fluid composed of >98% water, cholangiocytes like other water-transporting epithelial cells are required to rapidly transport large amounts of water in response to osmotic gradients generated by transported ions and solutes, a situation in

which specific water channel proteins (*i.e.* aquaporins (AQPs))¹ are probably involved (3–6). Indeed, our initial observation (7) that isolated rat cholangiocytes are capable of rapid mercury-sensitive, temperature-independent transmembrane water transport in response to osmotic gradients was consistent with transport via water channels rather than by diffusion through the lipid bilayer. Our more recent molecular studies have demonstrated that rat cholangiocytes express six AQPs (*i.e.* AQP 0, 1, 4, 5, 8, and 9) from the known 11 AQPs in mammals (5, 7–11). Moreover, at least two of them (*i.e.* AQP1 and AQP4) contribute to the water permeability of both the apical and basolateral cholangiocyte membrane domains, AQP1 facilitating mainly the apical transport of water and AQP4 modulating its basolateral movement (7–9, 11). Nevertheless, direct studies of the contribution of AQPs to water transport in intrahepatic bile ducts and other tissues have been severely hampered by the lack of specific AQPs inhibitors.

Recently, several groups have described post-transcriptional gene silencing or RNA interference in a wide variety of organisms using double-stranded RNAs of ~200–1000 nucleotides in length that specifically suppress the expression of a target mRNA (reviewed in Refs. 12–18). According to the prevailing model, double-stranded RNA is processed into small interfering double-stranded RNAs (siRNAs) of 19–25 nucleotides in length, which act as guides for the RNA-induced silencing enzymatic complex required for the cleavage of the target mRNAs (15–18). Although the physiological significance of post-transcriptional gene silencing and RNA interference is still under study, powerful new technology for selective inhibition of specific gene expression employing siRNAs is rapidly evolving (19–26).

In this study, we present data demonstrating that AQP1 gene expression in cholangiocytes is specifically suppressed by AQP1-siRNAs, resulting in a significant decrease of water transport by this cell type. These data show the feasibility of utilizing siRNAs to specifically reduce the expression of AQPs in epithelial cells and provide direct evidence of the contribution of AQP1 to water transport in biliary epithelia.

EXPERIMENTAL PROCEDURES

Materials—All of the chemicals were of highest purity commercially available and were purchased from Sigma unless otherwise indicated.

Animals—Male Fisher 344 rats (225–250 g) were obtained from Harlan Sprague-Dawley (Indianapolis, IN), housed in temperature-controlled room (22 °C) with 12-h light-dark cycles, and maintained on a standard diet with free access to water. All of the experimental procedures were approved by the Animal Use and Care Committee of the Mayo Foundation.

* This work was supported by Grant DK24031 (to N. F. L.) from the National Institutes of Health, American Gastroenterological Association/Elsevier Research Initiative Award (to A. I. M.), and by the Mayo Foundation. The costs of publication of this article were defrayed in part by the payment of page charges. This article must therefore be hereby marked “advertisement” in accordance with 18 U.S.C. Section 1734 solely to indicate this fact.

† To whom correspondence should be addressed: Center for Basic Research in Digestive Diseases, Mayo Clinic, 200 First St., S. W., Rochester, MN 55905. Tel.: 507-284-1006; Fax: 507-284-0762; E-mail: larusso.nicholas@mayo.edu.

¹ The abbreviations used are: AQP, aquaporin; siRNA, small interfering RNA; PBS, phosphate-buffered saline; P_f , osmotic water permeability coefficient; J_w , net water secretion; IBDU, intrahepatic bile duct unit; ODN, oligonucleotide.

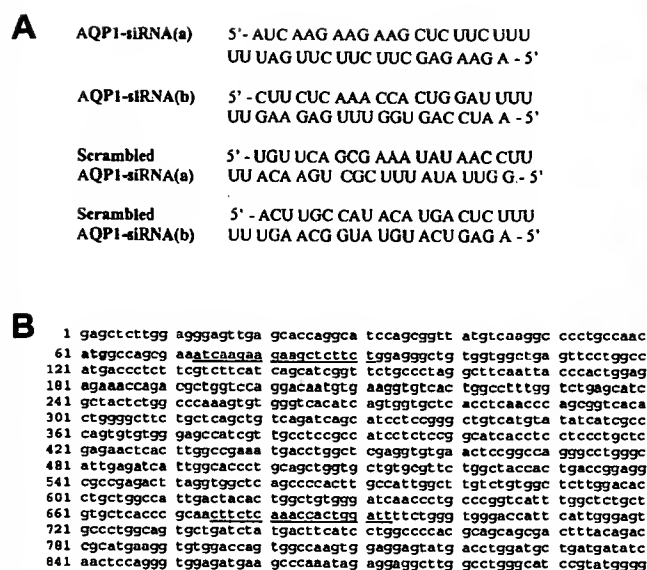


FIG. 1. Sequences and expected duplexes for siRNAs (A) and sites of targeting (B) within AQP1 mRNA. A, the sense (top) and antisense (bottom) strands of siRNAs targeting AQP1 message and the scrambled AQP1-siRNAs are shown. B, the partial mRNA sequence of rat AQP1 (GenBankTM accession number NM_012778). Two potential sites of targeting by siRNAs are underlined. The start codon is in a boldface.

Solutions—The composition of isotonic (290 mosM) Ringer-HCO₃ buffer was (in mM): 120.0 NaCl, 5.9 KCl, 1.2 Na₂HPO₄, 1.0 MgSO₄, 25.0 NaHCO₃, 1.25 CaCl₂, and 5.0 C₆H₁₂O₆, pH 7.4. Hypotonic (90 mosM) solution was prepared by decreasing the concentration of NaCl. The precise osmolality of Ringer-HCO₃ buffer solutions was determined with a freezing point osmometer (The Advanced Micro-Osmometer, Model 3300, Advanced Instruments, Inc., Norwood, MA). For water transport experiments with forskolin, the perfusate contained 140 mM NaCl and 5 mM Na₂HPO₄, pH 7.2. The composition of lysis buffer was 50 mM Tris-HCl, pH 7.5, 150 mM NaCl, 0.1% sodium Nonidet P-40, 0.1% sodium dodecyl sulfate, and 0.1% sodium dodecyl sulfate. The composition of phosphate-buffered saline (PBS) was (in mM): 137 NaCl, 2.7 KCl, 10 NaHPO₄, and 1.8 KH₂PO₄.

AQP1-siRNAs Design, Synthesis, and Labeling—Sequence information regarding mature rat AQP1 mRNA was extracted from the NCBI Entrez nucleotide data base. Two target sites within AQP1 gene were chosen from the rat AQP1 mRNA sequence (GenBankTM accession NM_012778). Following selection, each target site was searched with NCBI BlastN to confirm specificity only to AQP1. Two different siRNAs designated AQP1-siRNA(a) and AQP1-siRNA(b), which target nucleotides 71–91 and 673–693 of the rat AQP1 mRNA sequence, respectively, and two nonspecific siRNA duplexes containing the same nucleotides but in irregular sequence (i.e. scrambled AQP1-siRNA(a) and AQP1-siRNA(b)) were prepared by a transcription-based method using the Silencer siRNA construction kit (Ambion, Austin, TX) according to manufacturer's instructions. The 29-mer sense and antisense DNA oligonucleotide templates (21 nucleotides specific to AQP1 and 8 nucleotides specific to T7 promoter primer sequence 5'-CCTGTCTC-3') were synthesized by the Mayo Molecular Core facility. One of the constructed siRNAs, AQP1-siRNA(b), was labeled with Cy3 following manufacturer's instructions (Ambion). The efficacy of AQP1-siRNA labeling with Cy3 was estimated by acrylamide gel analysis of the Silencer siRNA-labeling positive control experiment (Ambion) and found to be ~20%.

IBDUs Isolation and Transfection with siRNAs—IBDUs, which are portions of intrahepatic bile ducts ranging in luminal diameter from 100 to 125 μ m and in length from 0.6 to 1.2 mm, were isolated from normal rat liver as we described previously (27). IBDUs were cultured from 0 to 24 h in normal rat cholangiocyte medium containing 10 nM AQP1-siRNAs or corresponding scrambled AQP1-siRNAs. Exogenous delivery of siRNAs to cholangiocytes was carried out with or without a lipid carrier (i.e. TransMessengerTM transfection reagent (Qiagen, Valencia, CA)).

Fluorescence Analysis of the siRNAs Uptake by IBDUs—IBDUs were incubated in normal rat cholangiocyte medium with 0, 0.5, 1, 5, 10, and 20 nM Cy3-AQP1-siRNA(b) with or without a lipid carrier for 24 h at 37 °C. AQP1-siRNA(b)-Cy3 then was visualized in IBDUs by fluores-

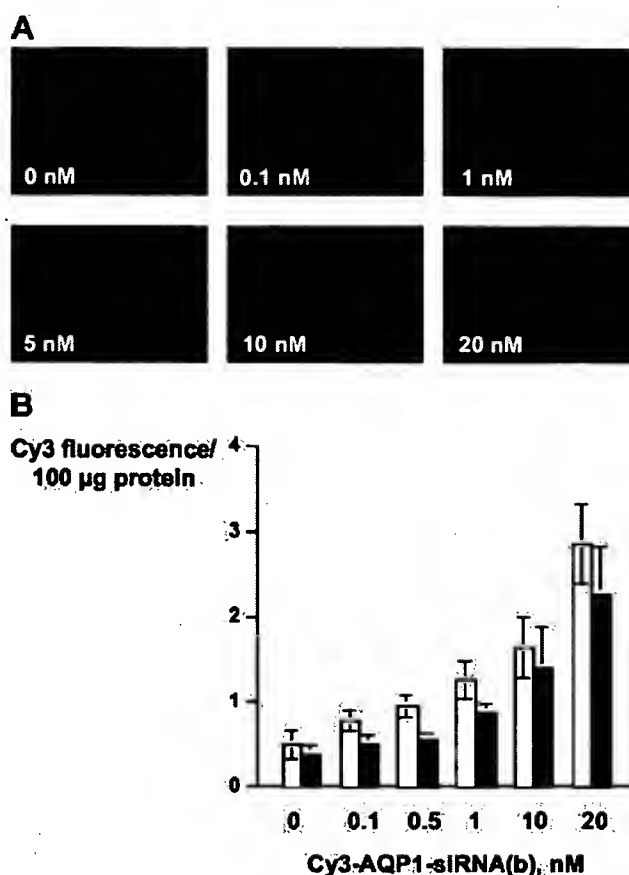


FIG. 2. Uptake of AQP1-siRNAs by IBDUs. A, visualizing of AQP1-siRNA in IBDUs. IBDUs were incubated 24 h in normal rat cholangiocyte medium containing naked Cy3-labeled AQP1-siRNA(b) from 0 to 20 nM. IBDUs analyzed by fluorescent microscopy showed a significant increase in Cy3-AQP1-siRNA(b) fluorescence (red). B, IBDUs take up AQP1-siRNAs in a dose-dependent manner. 24 h after incubation with Cy3 labeled AQP1-siRNA(b) in the absence (white bars) or presence (black bars) of the lipid carrier, the fluorescence intensity of IBDUs was measured and normalized to 100 μ g of protein. The uptake of Cy3-AQP1-siRNA(b) increased with increasing concentrations of siRNA(b) independent of the presence of the lipid carrier. Values are the mean \pm S.E. of three separate experiments with 4–6 IBDUs in each group.

cent microscopy, and Cy3 fluorescence was measured by a method proposed for analysis of fluorescent antisense oligonucleotides (28). After the incubation, IBDUs were washed three times with PBS and then lysed in 200 μ l of a lysis buffer. Total cellular Cy3-AQP1-siRNA(b) fluorescent emission (λ_{ex} = 552; λ_{em} = 568 nm) was measured with a PerkinElmer LS 55 luminescence spectrophotometer. An aliquot of the cell lysate was taken to measure the amount of total protein using the fluorescence assay, and the Cy3 fluorescence was normalized to 100 μ g of total protein. For visualization of AQP1 suppression in IBDUs by AQP1-siRNA, IBDUs were incubated with 10 nM Cy3-AQP1-siRNA(b) for 0, 12, and 24 h at 37 °C on poly-L-lysine-treated chamber slides. Following the incubation, the IBDUs were fixed with cold 100% methanol for 5 min and air-dried. The slides were then washed three times with 1 \times PBS and permeabilized in 0.2% Triton-PBS for 2 min at room temperature. IBDUs were blocked for 20 min in blocking buffer (10% normal sheep serum, 0.05% Tween 20 in PBS) at room temperature and incubated with affinity-purified AQP1 antibody (Alpha Diagnostics, San Antonio, TX) at a 1:50 dilution in blocking buffer overnight at 4 °C. Following the primary antibody incubation, the IBDUs were washed with 1 \times PBS three times and incubated at a 1:100 anti-goat IgG fluorescein isothiocyanate conjugate (Sigma) secondary antibody for 1 h at room temperature. AQP1-siRNA(b)-Cy3 and AQP1 fluorescence in IBDUs was then determined by using scanning laser confocal microscopy keeping the pinhole and detector gain setting identical while analyzing the different IBDUs and quantified using LSM 510 Image Examiner software (Carl Zeiss, Thornwood, NY).

RNA Isolation and Analysis by Real-time Reverse Transcriptase-PCR—IBDUs were lysed in 1 ml of Tri-Reagent with 5 μ l of Glyco-Blue

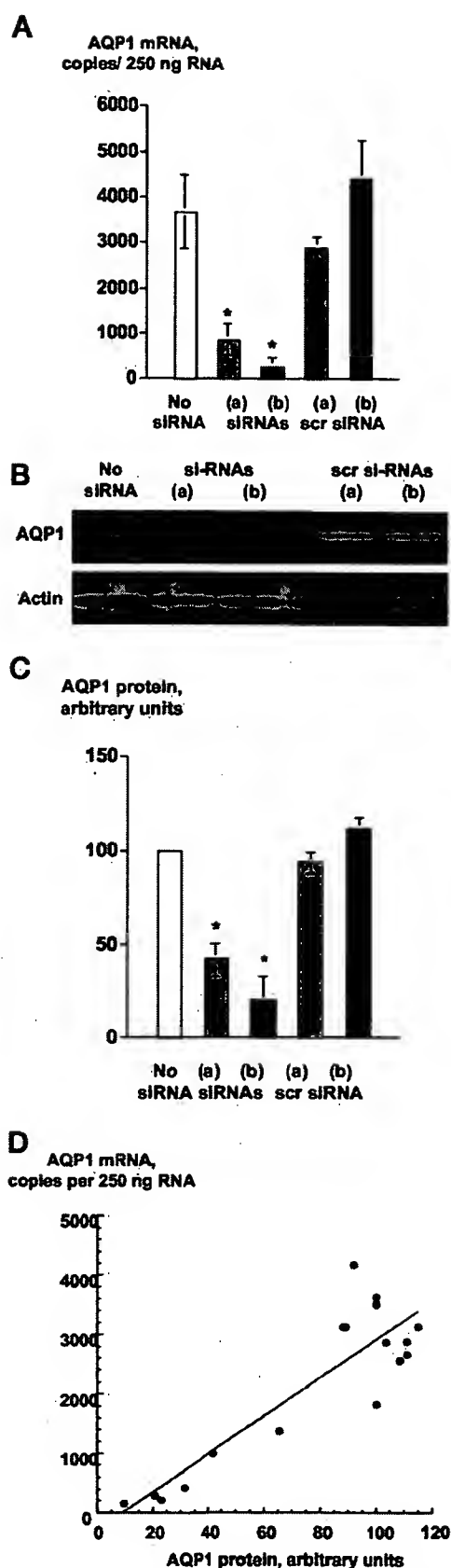


FIG. 3. Suppression of AQP1 gene in IBDUs by AQP1-siRNAs. IBDUs were transfected with 10 nM AQP1-siRNA(a), AQP1-siRNA(b), and corresponding scrambled AQP1-siRNAs for 24 h. A, a significant suppression of AQP1 mRNA level occurred in IBDUs transfected with AQP1-siRNA(a) and AQP1-siRNA(b) but not with scrambled (scr) AQP1-siRNAs. Representative immunoblots (B) and quantitative analysis (C) show a significant suppression of AQP1 protein levels by both

(Ambion) added as a co-precipitant and stored at room temperature for 5 min. After the addition of 0.1 ml of 1-bromo-3-chloro-propane, the samples were vigorously shaken, incubated for 15 min at room temperature, and centrifuged at $12,000 \times g$ for 15 min at 4°C . The aqueous phase was transferred to a new tube, and 0.5 ml of isopropyl alcohol was added. The samples were mixed, stored for 10 min, and centrifuged at $12,000 \times g$ for 15 min at 4°C . After removing the supernatant, the RNA pellet was washed with 75% EtOH and repelleted by centrifugation at $12,000 \times g$ for 15 min at 4°C . RNA was resuspended in RNA Secure solution (Ambion), and the concentration and purity were determined by spectroscopy. Quantitation of AQP1 message was accomplished by real-time PCR. A standard curve to AQP1 was generated by amplifying AQP1 from freshly isolated rat cholangiocyte cDNA using rat AQP1-specific primers (sense, 5'-AGTTGAGCACCAGGCATCC-3', and antisense, 5'-CACTGATGTGACCCACACTTTG-3'). The 259-bp amplicon was electrophoresed on a 1.5% agarose gel, visualized with ethidium bromide, and gel-extracted. The amplicon was subsequently diluted and used as template for the PCR reaction. One-step reverse transcriptase-PCR for AQP1 and 18 S ribosome (Ambion) was performed using the LightCycler RNA Master SYBR Green I kit according to manufacturer's instructions.

Protein Analysis by Western Blotting—Total lysates were obtained by lysing the IBDUs with M-PERTM mammalian protein extraction reagent (Pierce). The lysates were heated to 60°C for 10 min in sample buffer containing 0.8 M dithiothreitol and 10% SDS for protein denaturation and solubilization. The samples were then subjected to electrophoresis through a 12% SDS-polyacrylamide gel and transferred overnight to a nitrocellulose membrane. The blots were blocked with 5% (w/v) nonfat dry milk and 0.2% (v/v) Tween 20. After blocking, the blots were incubated with affinity-purified rabbit anti-rat antibodies to AQP1 (Alpha Diagnostics) at a dilution of 1:1000 overnight at 4°C . The blots were washed and incubated for 1 h with a horseradish peroxidase-conjugated goat anti-rabbit immunoglobulin (1:2000 dilution) at room temperature. Protein bands were detected using an enhanced chemiluminescence detection system (ECL Plus, Amersham Biosciences). After exposing the nitrocellulose membranes to Kodak X-Omat AR film, the autoradiographs were scanned and quantified by densitometry using Molecular Analyst software (Bio-Rad).

Measurement of Water Movement across Intrahepatic Biliary Epithelia—IBDUs were perfused with 1 mM of the impermeable volume marker, fluorescein sulfonate (fluorescein-5(6)-sulfonic acid trisodium salt (Molecular Probes, Eugene, OR)) at a rate of 20–80 nl/min as described previously in detail (3). Net water movement (J_w) and osmotic water permeability coefficient (P_f) in response to established osmotic gradient (200 mosm) or stimulated by forskolin were measured as described previously (3).

Statistical Analysis—All of the values are expressed as the mean \pm S.E. Statistical analysis was performed by the Student's *t* test, and results were considered statistically different at $p < 0.05$.

RESULTS

Design of AQP1-siRNAs—We selected two target regions of rat AQP1 mRNA (i.e. 71–91 and 673–693 sequences) by scanning the length of the AQP1 gene for AA-dinucleotide sequences and downstream 19 nucleotides without significant homology to other genes by using an appropriate genome data base. The antisense strands of synthesized AQP1-siRNAs are the reverse complement of the target sequences (Fig. 1). The sense strands of the AQP1-siRNAs have the same sequences as the target mRNA sequences with the exception that they lack the 5'-AA sequence (Fig. 1). A uridine dimer was incorporated at the 3' end of the sense strands siRNAs (Fig. 1). Thus, the end products are two double-stranded 21-mer siRNAs (i.e. AQP1-siRNA(a) and AQP1-siRNA(b)) that theoretically should reduce the expression of AQP1 mRNA and protein and two siRNAs (i.e. scrambled AQP1-siRNA(a) and AQP1-siRNA(b)) that theoretically should not be effective in AQP1 gene silencing.

Uptake of AQP1-siRNA by IBDUs—IBDUs incubated for 24 h in normal rat cholangiocyte culture medium containing

AQP1-siRNAs but not scrambled siRNAs. D, a correlation between AQP1 mRNA and protein expression levels was seen ($y = -298.34 + 32.079x$; $r = 0.8821$). Values are the mean \pm S.E. of three independent experiments with 4–6 IBDUs in each group (*, $p < 0.05$).

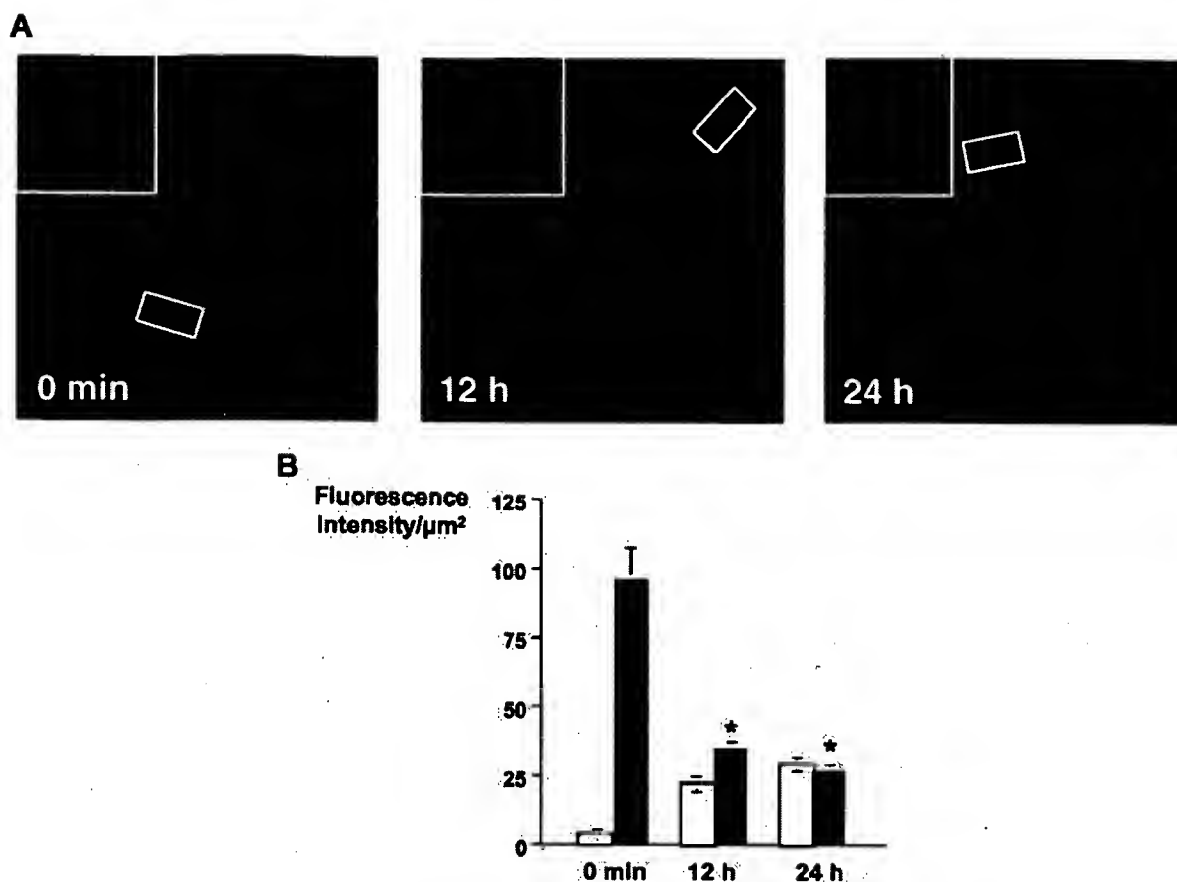


FIG. 4. Visualizing of AQP1 suppression in IBDUs by AQP1-siRNA. A, AQP1-siRNA(b) was labeled with Cy3 and transfected into cholangiocytes of IBDUs. At the times indicated, IBDUs were analyzed using confocal fluorescent microscopy for fluorescence intensity of Cy3-labeled AQP1-siRNA(b) (red) and AQP1 (green). Top left patterns show higher magnification of region in inset. B, in IBDUs treated with AQP1-siRNA, an increase in Cy3 immunofluorescence (white bars) and decrease in AQP1 immunofluorescence (black bars) occurred during 12–24 h, reflecting accumulation of AQP1-siRNA in cholangiocytes and rapid and effective suppression of AQP1 expression in these cells, respectively. Values are the mean \pm S.E. of three separate experiments with 3–4 IBDUs in each group. (*, $p < 0.05$ for AQP1 fluorescence compared with point 0 min).

various amounts (i.e. 0–20 nM) of Cy3-labeled AQP1-siRNA(b) in the absence or presence of the lipid carrier took up AQP1-siRNA in a dose-dependent manner (Fig. 2). However, no lipid carrier-dependent uptake of siRNA by IBDUs was observed. Given that only 20% AQP1-siRNA(b) transfected into cholangiocytes was labeled with Cy3 (see “Materials and Methods” for details), we conclude that the amount of AQP1-siRNA taken up by cholangiocytes was 5 times greater, suggesting that IBDUs could be effectively transfected with siRNAs in the absence of the lipid carrier. Based on this observation and given that a transfection reagent could potentially affect cholangiocytes function, studies of AQP1 gene suppression in IBDUs were performed by using naked AQP1-siRNAs.

AQP1 Gene Suppression in IBDUs by siRNAs—The levels of AQP1 mRNA and protein in IBDUs transfected with 10 nM each of four different naked siRNAs (i.e. two siRNAs to different regions of the AQP1 and two corresponding scrambled AQP1-siRNAs) are shown in Fig. 3. Both siRNAs to different sequences within the AQP1 gene effectively inhibited AQP1 mRNA (Fig. 3A) and protein expression (Fig. 3B). AQP1 mRNA and protein levels were inhibited by AQP1-siRNA(a) by 76.6 and 57.9%, respectively. AQP1-siRNA(b) was more effective, suppressing AQP1 mRNA and protein levels by 92.0 and 79.4%, respectively. In contrast, two scrambled AQP1-siRNAs had no effect on AQP1 gene expression. Moreover, AQP1-siRNAs had no effect on mRNA expression for AQP4 (data not shown), an AQP, which is also expressed in rat cholangiocytes (11), providing evidence that both AQP1-siRNA(a) and AQP1-siRNA(b)

were specific for AQP1. Because there is a strong correlation between AQP1 mRNA and protein suppression by siRNAs (Fig. 3C), these data suggest that AQP1 silencing in cholangiocytes results from a reduction in the amount of AQP1 mRNA available for translation. These data also suggest that AQP1-siRNAs were highly specific and efficient in AQP1 gene silencing in rat IBDUs.

Visualizing of AQP1 Gene Suppression in IBDUs by AQP1-siRNA—IBDUs incubated with 10 nM Cy3-labeled AQP1-siRNA(b) for 12–24 h were analyzed for AQP1 expression using immunofluorescence as described under “Materials and Methods.” The data in Fig. 4 show that fluorescence intensity of AQP1 (green) decreased in transfected IBDUs as the fluorescence intensity of AQP1-siRNA(b) (red) increased. 12 and 24 h after IBDUs transfection with AQP1-siRNA, AQP1 immunofluorescence in cholangiocytes was reduced by 63 and 72%, respectively, suggesting that AQP1 could be silenced in cholangiocytes as quickly as 12 h post-transfection.

Inhibition of AQP1-mediated Water Transport by siRNAs—Water transport characteristics (i.e. P_f and J_w) in AQP1-siRNA-nontransfected IBDUs and in IBDUs transfected with 10 nM AQP1-siRNAs were determined from the volume of water transported into the lumen of IBDUs either in response to a 200 mOsm transepithelial osmotic gradient (lumen osmolality > bath osmolality) (Fig. 5) or in response to 100 μM forskolin (Fig. 6), an agent known to stimulate biliary bicarbonate and water secretion (2–4). The P_f in AQP1-siRNA-nontransfected IBDUs and IBDUs transfected with scrambled AQP1-siRNAs

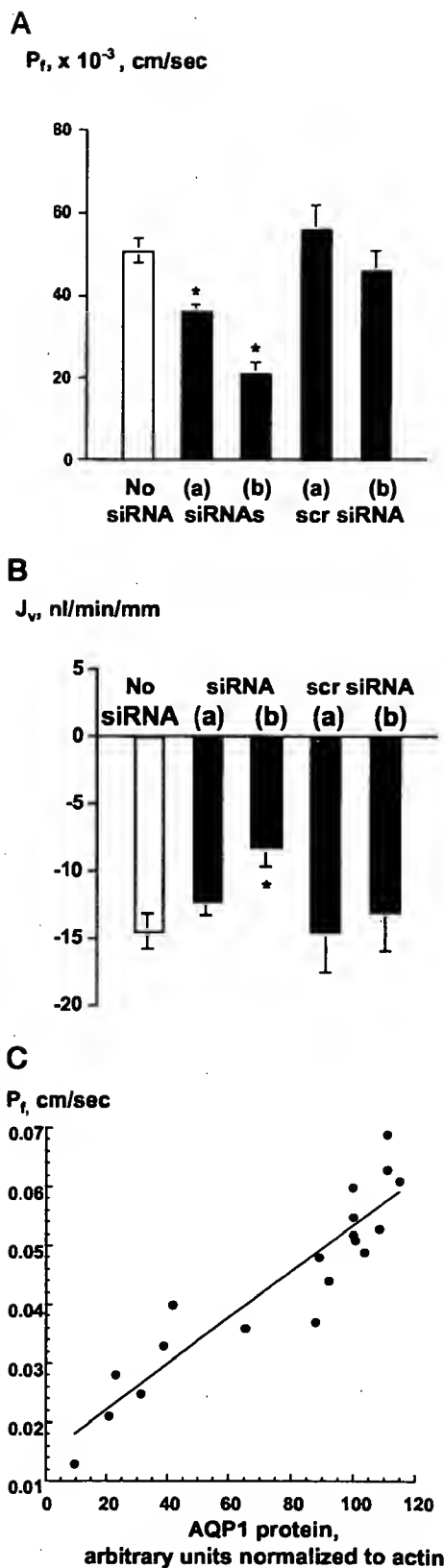


FIG. 5. Water transport in response to transepithelial osmotic gradient in IBDUs transfected with AQP1-siRNAs. **A**, osmotic water permeability coefficients (P_f) reflect rapid water transport across biliary epithelia in response to an inward osmotic gradient (200 mosM) in nontransfected IBDUs and in IBDUs transfected with scrambled (scr) AQP1-siRNAs. P_f values decreased by 29.4 and 58.8% in IBDUs transfected with AQP1-siRNA(a) and AQP1-siRNA(b), respectively. **B**, net water movement (J_v) values in IBDUs transfected with AQP1-siRNAs reflect a decrease of water secretion by 42.8% in IBDUs trans-

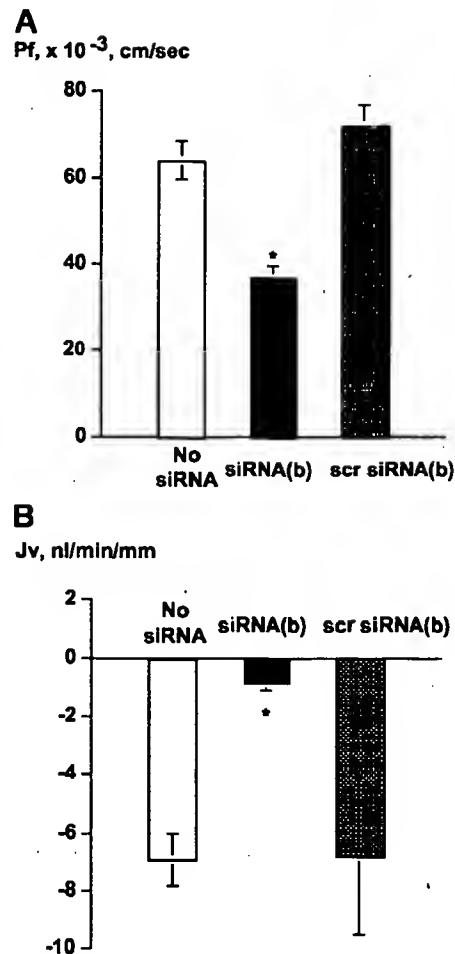


FIG. 6. Water transport in response to forskolin in IBDUs transfected with AQP1-siRNA. **A**, osmotic water permeability coefficient (P_f) in AQP1-siRNA-nontransfected IBDUs (white bar) and in IBDUs transfected with scrambled (scr) AQP1-siRNA(b) (gray bar) stimulated with forskolin (100 μmol) showed rapid water transport across biliary epithelia. In IBDUs transfected with AQP1-siRNA(b) (black bar) for 24 h, osmotic water permeability in response to forskolin decreased by 53.1%. **B**, net water secretion (J_v) in IBDUs transfected with AQP1-siRNA(b) (black bar) in response to forskolin decreased by 87% compared with nontransfected IBDUs (white bar) and IBDUs transfected with scrambled AQP1-siRNA(b) (gray bar). Values are the mean \pm S.E. of three microperfused IBDUs in each group (*, $p < 0.05$).

ranged from 50×10^{-3} to 72×10^{-3} cm/sec (Figs. 5 and 6). When a transepithelial osmotic gradient was established in IBDUs transfected with AQP1-siRNA(a) and AQP1-siRNA(b), P_f was decreased by 29.4 and 58.8%, respectively (Fig. 5A). In IBDUs transfected with AQP1-siRNA(b), P_f was also decreased by 53.1% in response to forskolin (Fig. 6A). In IBDUs transfected with AQP1-siRNA(b), J_v across biliary epithelia in response to an osmotic gradient or forskolin was decreased by 42.8 and 87.6%, respectively (Figs. 5B and 6B). A strong correlation between AQP1 protein expression and water transport in IBDUs transfected with AQP1-siRNAs was shown (Fig. 5C), suggesting that a decrease of cholangiocyte osmotic water permeability is a result of specific AQP1 gene silencing by AQP1-siRNAs.

fectured with AQP1-siRNA(b) compared with nontransfected IBDUs. **C**, a correlation between AQP1 protein expression and P_f was seen ($y = 0.014192 + 0.00039212 \times x$; $r = 0.9254$). Values are the mean \pm S.E. of 4–6 microperfused IBDUs in each group (*, $p < 0.05$).

DISCUSSION

The major objectives of this study were to develop and utilize siRNAs to directly investigate the importance of AQP1 in water transport by biliary epithelia. Although several lines of evidence indicate that AQPs are involved in water transport by cholangiocytes (4–11), the absence of specific AQP inhibitors has impaired direct testing of hypotheses related to this issue. Indeed, until this study, no specific pharmacological inhibitors of AQPs had been reported.

Our results show that AQP1-siRNAs effectively (*i.e.* by 57.9–79.4%), specifically (*i.e.* AQP1-siRNAs but not scrambled AQP1-siRNAs), and rapidly (*i.e.* during 12 h after transfection of IBDUs) down-regulate endogenously expressed AQP1 but not AQP4 in cholangiocytes. Moreover, direct quantitation of water transport in IBDUs transfected with siRNAs to AQP1 demonstrates that P_f and J_v are significantly decreased compared with IBDUs transfected with scrambled siRNAs. The observed decrease of net water secretion in IBDUs transfected with AQP1-siRNA(b) under different experimental conditions (*i.e.* an inward osmotic gradient or a secretory agonist) suggests that as much as 65% of water transported across biliary epithelia may be AQP1-mediated. Taken together, these findings demonstrate for the first time that inhibition of AQP1 expression in mammalian cells by siRNAs results in inhibition of water transport.

We found that cholangiocytes effectively take up siRNA duplexes if IBDUs are incubated with AQP1-siRNAs either in the absence or presence of transfection reagent. This observation is in contrast to published data (29) that siRNAs are taken up by cultured HeLa, COS-1, and 293 cells only in the presence of transfection agent. However, our data are consistent with recently published results that hepatocytes *in vivo* can be effectively transfected with naked siRNAs (30, 31). Although a precise explanation for these differences is not apparent, they emphasize the importance of assessing both forms of siRNAs when employing this gene-silencing approach.

In our study, we utilized two different siRNAs constructed against different regions of AQP1 mRNA. Whereas both constructs inhibited AQP1 expression and function in cholangiocytes, siRNA-designated AQP1-siRNA(b) was more effective. We have no explanation as to why these two siRNAs differed in their inhibitory activity, but this phenomenon has been observed for other genes. For example, several siRNAs synthesized against different sites on the same target mRNA demonstrated striking differences in silencing efficiency (29).

To our knowledge, this study is the first to successfully utilize siRNA gene-silencing technology to achieve AQP gene suppression in epithelial cells. AQP gene silencing has previously been achieved primarily by developing transgenic null mice lacking AQPs and by using dominant negative mutants or antisense oligonucleotides (ODNs). The phenotype analysis of transgenic mice deficient in AQP1, AQP3, AQP4, and AQP5 has provided new insights into their critical role in water transport in the kidney, brain, eye, ear, salivary glands, skin, and gastrointestinal organs (32–40). However, given that cholangiocytes express numerous AQPs, deletion of a single AQP might not significantly affect biliary water transport *in vivo* because other cholangiocyte AQPs could undergo compensatory up-regulation. Dominant negative mutants, which exert their effects in the presence of the wild-type gene product, have also been employed in water-transporting studies, demonstrating dominant negative effects of AQP2 and AQP4 mutants on AQP-mediated water transport in *Xenopus* oocytes (41–43), LLC-PK₁ cells (44), and mouse cholangiocytes (45). This experimental approach also has its limitations being applicable principally to studies utilizing cultured cell systems. Antisense

ODNs have been used to a limited degree to suppress AQP function. For example, the P_f of *Xenopus laevis* oocytes injected with poly(A)⁺ RNA from cultured bovine corneal epithelial cells was inhibited by coinjection with AQP5 ODNs (46). Also, the expression of AQP1 in human trabecular meshwork cells was suppressed by corresponding ODNs (47). Although useful, the specificity of this approach is somewhat limited because non-specific hybridization of ODNs with intracellular protein rather than mRNAs has been reported previously (48). Moreover, the efficiency of gene silencing by ODNs is relatively low (*e.g.* only one of eight antisense oligonucleotides is expected to provide a specific suppression of a targeted gene) (49). Our own experience has been that AQP1 ODNs are not effective in inhibiting AQP1 expression and function in isolated rat IBDUs (data not shown).

The advantages of siRNA technology for effective and specific suppression of selected genes are becoming increasingly apparent. Recent studies (19–26) indicate that siRNAs directed against endogenous genes can inhibit the expression of virtually any protein-coding gene in any mammalian cells. Importantly, RNA and protein analysis indicate that only the targeted gene is affected by the corresponding siRNA (15–26).

In summary, we designed and utilized siRNAs to AQP1 that markedly diminished the expression of this protein in IBDUs. As a result, cholangiocyte osmotic water permeability and net water secretion were significantly reduced, suggesting that at least 65% of water transported across biliary epithelia is AQP1-mediated. These data are the first to demonstrate the feasibility of utilizing siRNAs to specifically reduce the expression of AQPs in epithelial cells. They also provide further evidence of the importance of AQP1 in water transport by biliary epithelia.

Acknowledgment—We thank Deb Hintz for secretarial assistance.

REFERENCES

- Alpini, G., Phillips, J. O., and LaRusso, N. F. (1994) in *The Liver: Biology and Pathobiology* (Arias, I. M., Boyer, J. L., Fausto, N., Jakoby, W. B., Schachter, D. A., and Shafritz, D. A., eds), 3rd Ed., pp. 623–653, Raven Press, Ltd., New York.
- Boyer, J. L. (1996) *Am. J. Physiol.* 270, G1–G5.
- Masyuk, A. I., Gong, A.-Y., Kip, S., Burke, M. J., and LaRusso, N. F. (2000) *Gastroenterology* 119, 1672–1680.
- Cova, E., Gong, A.-Y., Marinelli, R. A., and LaRusso, N. F. (2001) *Hepatology* 34, 456–463.
- Masyuk, A. I., Marinelli, R. A., and LaRusso, N. F. (2002) *Gastroenterology* 122, 545–562.
- Masyuk, A. I., Masyuk, T. V., Tietz, P. S., Splinter, P. L., and LaRusso, N. F. (2002) *Am. J. Physiol.* 283, C785–C791.
- Roberts, S. K., Yano, M., Ueno, Y., Pham, L., Alpini, G., Agre, P., and LaRusso, N. F. (1994) *Proc. Natl. Acad. Sci. U. S. A.* 91, 13009–13013.
- Marinelli, R. A., Pham, L., Agre, P., and LaRusso, N. F. (1997) *J. Biol. Chem.* 272, 12984–12988.
- Marinelli, R. A., Tietz, P. S., Pham, L. D., Rueckert, L., Agre, P., and LaRusso, N. F. (1999) *Am. J. Physiol.* 276, G280–G286.
- Splinter, P. L., Huebert, R. C., Marinelli, R. A., Pham, L. D., and LaRusso, N. F. (2000) *Hepatology* 32, 175A.
- Marinelli, R. A., Pham, L. D., Tietz, P. S., and LaRusso, N. F. (2000) *Hepatology* 31, 1313–1317.
- Fire, A. (1999) *Trends Genet.* 15, 358–363.
- Sharp, P. A. (2001) *Genes Dev.* 15, 485–490.
- Zamore, P. D. (2001) *Nat. Struct. Biol.* 8, 746–750.
- Tuschl, T. (2001) *ChemBiochemistry* 2, 239–245.
- Hutvagner, G., and Zamore, P. D. (2002) *Curr. Opin. Gen. Dev.* 12, 225–232.
- Plasterk, R. H. A. (2002) *Science* 296, 1263–1265.
- Zamore, P. D. (2002) *Science* 296, 1265–1269.
- Caplen, N. J., Parrish, S., Imani, F., Fire, A., and Morgan, R. A. (2001) *Proc. Natl. Acad. Sci. U. S. A.* 98, 9742–9747.
- Harborth, J., Elbashir, S. M., Borchert, K., Tuschl, T., and Weber, K. (2001) *J. Cell Sci.* 114, 4557–4565.
- Elbashir, S. M., Harborth, J., Lendeckel, W., Yalcin, A., Weber, K., and Tuschl, T. (2001) *Nature* 411, 494–498.
- Elbashir, S. M., Harborth, J., Weber, K., and Tuschl, T. (2002) *Methods* 26, 199–213.
- Caplen, N. J. (2002) *Trends Biotechnol.* 20, 49–51.
- Yu, J.-Y., DeRuiter, S. L., and Turner, D. L. (2002) *Proc. Natl. Acad. Sci. U. S. A.* 99, 6047–6052.
- Donze, O., and Ricard, D. (2002) *Nucleic Acids Res.* 30, 1–4.
- Paddison, P. J., Caudy, A. A., Bernstein, E., Hannon, G. J., and Conklin, D. S. (2002) *Genes Dev.* 16, 948–958.
- Roberts, S. K., Kunts, S. M., Gores, G. J., and LaRusso, N. F. (1993) *Proc. Natl.*

- Acad. Sci. U. S. A.* 90, 9080–9084
28. Li, B., Hughes, J. A., and Phillips, M. I. (1997) *Neurochem. Int.* 31, 393–403
 29. Holen, T., Amarzguioui, M., Wiiger, M. T., Babaie, E., and Prydz, H. (2002) *Nucleic Acids Res.* 30, 1757–1766
 30. McCaffrey, A. P., Meuse, L., Pham, T.-T. T., Conclin, D. S., Hammon, G. J., and Kay, M. A. (2002) *Nature* 418, 38–39
 31. Lewis, D. L., Hagstrom, J. E., Loomis, A. G., Wolff, J. A., and Herweijer, H. (2002) *Nat. Genet.*, on line
 32. Ma, T., Song, Y., Gillespie, A., Carlson, E. J., Epstein, C. J., and Verkman, A. S. (1999) *J. Biol. Chem.* 274, 20071–20074
 33. Ma, T., and Verkman, A. S. (1999) *J. Physiol. (London)* 517, 317–326
 34. Verkman, A. S. (2000) *Curr. Opin. Nephrol. Hypertens.* 9, 517–522
 35. Verkman, A. S., Yang, B., Song, Y., Manley, G. T., and Ma, T. (2000) *Exp. Physiol.* 85, S233–S241
 36. Li, J., and Verkman, A. S. (2001) *J. Biol. Chem.* 276, 31233–31237
 37. Ma, T., Jayaraman, S., Wang, K. S., Song, Y., Yang, B., Li, J., Bastidas, J. A., and Verkman, A. S. (2001) *Am. J. Physiol.* 280, C126–C134
 38. Verkman, A. S. (2002) *Exp. Nephrol.* 10, 235–240
 39. Ma, T., Hara, M., Sougrat, R., Verbavatz, J. M., and Verkman, A. S. (2002) *J. Biol. Chem.* 277, 17147–17153
 40. Zhang, D., Vetrivel, L., and Verkman, A. S. (2002) *J. Gen. Physiol.* 119, 561–569
 41. Shi, L., and Verkman, A. S. (1996) *Biochemistry* 35, 538–544
 42. Kamsteeg, E.-J., Wormhoudt, T. A. M., Rijss, J. P. L., van Os, C. H., and Deen, P. M. T. (1999) *EMBO J.* 18, 2394–2400
 43. Marr, N., Kamsteeg, E. J., van Raak, M., van Os, C. H., and Deen, P. M. T. (2001) *Eur. J. Physiol.* 442, 73–77
 44. Yamashita, Y., Hirai, K., Katayama, Y., Fushimi, K., Sasaki, S., and Marumo, F. (2000) *Am. J. Physiol.* 278, F395–F405
 45. Splinter, P. L., Masyuk, A. I., Marinelli, R. A., Urrutia, R. A., Ueno, Y., and LaRusso, N. F. (2002) *Gastroenterology* 123, (suppl.) 63
 46. Kang, F., Kuang, K., Li, J., and Fischbarg, J. (1999) *Invest. Ophthalmol. Vis. Sci.* 40, 253–257
 47. Stamer, W. D., Peppel, K., O'Donnell, M. E., Roberts, B. C., Wu, F., and Epstein, D. L. (2001) *Invest. Ophthalmol. Vis. Sci.* 42, 1803–1811
 48. Krieg, A. M., and Stein, C. A. (1995) *Antisense Res. Dev.* 5, 241
 49. Stein, C. A. (2001) *J. Clin. Invest.* 108, 641–644

[CANCER RESEARCH 53, 878-883, February 15, 1993]

Type IV Collagenase (M_r 72,000) Expression in Human Prostate: Benign and Malignant Tissue¹

Mark E. Stearns² and Min Wang

Department of Pathology, Medical College of Pennsylvania, Philadelphia, Pennsylvania 19129

ABSTRACT

The expression of type IV collagenase (M_r 72,000) has been examined in tissues from patients with benign prostatic hyperplasia (6 patients) and varying Gleason grades of malignant prostate cancer (18 patients). Immunoperoxidase labeling indicated that expression of the type IV collagenase was weak or nonexistent in benign tissue but consistently strong in the glandular and ductal epithelial cells of prostate tumors diagnosed at Gleason grades 1-8. In moderate to advanced cancer (i.e., Gleason grades 2 to 8), invasive tumor foci in the stromal tissue produced relatively modest amounts of type IV collagenase. The normal stromal tissue (i.e., fibroblasts) uniformly failed to produce detectable levels of type IV collagenase in the 24 patients examined. Northern and quantitative slot blot hybridization assays demonstrated that collagenase type IV mRNA levels were low in benign tissue and high in malignant tumors. In contrast, the stromal cells did not express significant amounts of type IV collagenase mRNA. Enzyme-linked immunosorbent assays demonstrated that the amounts of type IV collagenase protein correlated directly with the mRNA levels in the tumor tissue. The studies suggest that type IV collagenase may be selectively overexpressed by malignant, preinvasive prostatic epithelial cells.

INTRODUCTION

Prostate cancer ranks first as the cause of cancer deaths in adult males in the United States. Distant metastases to the lymph nodes and vertebrae bone marrow are the principal reasons for death. In prostate cancer, tumor size is a poor indicator of metastatic behavior, but the degree of cell differentiation, the extent of basement membrane destruction, and localized invasion of the stroma are fair prognostic factors.

Destruction of the basement membrane has been observed in colorectal adenocarcinoma, gastric carcinoma, and prostate adenocarcinoma (1-3). The implication is that type IV collagenase (and other proteases) is overproduced to facilitate penetration of the basement membrane material and invasion of the stroma (4). Thus, type IV collagenase production may serve as a good marker and prognostic factor for tumor progression.

There are a few *in vivo* studies, notably in breast and colon cancer, which have shown an association between increased collagenase production and malignant aggressiveness. One early study revealed that a direct relationship existed between increased levels of collagenase synthesis and the extent of tumor dissemination in explants of mice mammary tumors (5). Recent papers by Stetler-Stevenson and colleagues (6-8) and others have clearly shown that an increased expression of the M_r 72,000 type IV collagenase occurred in malignant breast cancer (7, 8), colon adenocarcinomas (8-10), and gastric cancer (8). The investigators observed that the invasive ductal and lobular tumor cells expressed high levels of type IV collagenase. In general, they found that increased collagenase expression is associated with the progression of tumor cells for each of these cancers. Likewise, Van

Der Stappen *et al.* (11) found that enhanced collagenase activity is associated with increased tumor penetration of the surrounding stroma and poor differentiation of tumors.

In contrast to the above findings, one group reported that they observed no striking differences in the level of collagenase secreted by benign and malignant breast tumors (12). The contradictory nature of these results is puzzling but may arise as a result of the patient makeup, differences in the antibodies used, or masking of antigen sites or the antibody-antigen recognition sites. Further work is required to resolve such differences and to determine if other tumor tissues (i.e., prostate cancer) or the surrounding stroma selectively overexpress specific collagenases.

In our laboratory, we have investigated the role of metalloproteases in prostate cancer invasion and metastasis (13-15). We observed that high levels of a M_r 72,000 type IV collagenase were secreted in highly invasive subclones (i.e., a PC-3 ML subclone) isolated from the PC-3 human prostatic parent line. Conversely, totally noninvasive PC-3 subclones isolated from the same parent line produced very low levels of the protease. The invasive PC-3 subclones were highly metastatic following *i.v.* injection in SCID mice (16) and overexpressed collagenase type IV *in vivo*.³ The noninvasive PC-3 subclones were totally nonmetastatic (16), grew slowly subcutaneously, and failed to express the protease *in vivo*.⁴ Taken together, the data suggested that type IV collagenase expression may be involved with tumor invasion and, perhaps, may be an excellent prognostic marker for metastatic cells in human tumors.

To learn more about the relationship of type IV collagenase (M_r 72,000) expression to tumor phenotype *in vivo*, we have examined BPH⁵ and malignant prostate tissue from transurethral resection of the prostate of 24 patients. Immunoperoxidase labeling has demonstrated that the benign or BPH patients (6 of 6) expressed the enzyme in a variable fashion. In comparison, all the tumors given a Gleason grade greater than 1 uniformly expressed significant amounts of type IV collagenase. Quantitative Northern and slot blotting cDNA hybridization assays of RNA extracted from frozen tumor tissue showed that the amounts of collagenase IV increased with higher Gleason scores. ELISAs of protein extracts of the same tissue consistently indicated that the collagenase IV levels were low in BPH tissue and increased proportionally in tissues with an increased Gleason grade. We suggest, therefore, that collagenase IV levels may be an excellent prognostic indicator of the grade of progression of the disease.

MATERIALS AND METHODS

Prostate tissue was obtained fresh within 5 min of surgery from transurethral resection of the prostate (provided by Dr. Lester Karafin at the Department of Urology at the Medical College of Pennsylvania). For histology, pieces of the tissue samples were immediately fixed in 95% methanol at 4°C for 30 min, postfix in 10% neutral buffered formalin for 18 h, and embedded in paraffin for sectioning and immunostaining. Samples of the above tissue (1 g) also were

Received 7/24/92; accepted 12/4/92.

The costs of publication of this article were defrayed in part by the payment of page charges. This article must therefore be hereby marked advertisement in accordance with 18 U.S.C. Section 1734 solely to indicate this fact.

¹Supported by NIH Grant CA58716 to M. E. S.

²To whom requests for reprints should be addressed, at Department of Pathology, Medical College of Pennsylvania, 3300 Henry Avenue, Philadelphia, PA 19129.

³M. Stearns and M. Wang, unpublished data.

⁴M. Stearns and M. Wang, unpublished data.

⁵The abbreviations used are: BPH, benign prostatic hyperplasia; cDNA, complementary DNA; ELISA, enzyme-linked immunosorbent assay; TC, tumor collagenase; TA, tumor actin; NC, normal tissue collagenase; NA, normal tissue actin; PBS, phosphate-buffered saline; SDS-PAGE, sodium dodecyl sulfate-polyacrylamide gel electrophoresis; PAP, peroxidase anti-peroxidase.

TYPE IV COLLAGENASE EXPRESSION IN HUMAN PROSTATE

frozen by dipping in liquid nitrogen and stored at -70°C . Other pieces were fixed in formalin and sent to pathology for diagnosis. Twenty-four patients were sampled in total (17), including 6 benign, and 18 patients were assigned a Gleason grade of 1 to 8 by the pathologist.

Immunoperoxidase Labeling. The avidin-biotin immunoperoxidase technique was used to label tissue sections according to methods of Hsu *et al.* (18). In brief, the sections were dewaxed, rehydrated, and incubated with 0.5% H_2O_2 at room temperature in absolute ethanol for 60 min (3 times). The sections were incubated with 5% normal goat serum plus 1% bovine serum albumin. The solutions were removed, and the primary antibodies were added at dilutions of 1:200 for 2 h at 37°C in a 5% CO_2 incubator. Biotinylated goat anti-rabbit IgG (1:200 dilution) was added for 1 h. Avidin-biotin-peroxidase (Vectastain Kit; Vector Laboratories, Burlingame, CA) was added for 1 h, and the reaction developed for exactly 15 min with freshly prepared (0.5 mg/ml) 3,3'-diaminobenzidine tetrahydrochloride (Sigma, St. Louis, MO) and 5 μM H_2O_2 in 50 mM Tris (pH 7.6). All the antibodies were diluted with 50 mM Tris-buffered saline (pH 7.6). Ten representative sections from each specimen were selected, and the slides were photographed using a Zeiss microscope and a $\times 40$ planapo lens.

ELISA Assays. For ELISA assays, 2-g pieces of human prostate tissue snap-frozen in liquid nitrogen were ground to a fine powder on dry ice using a mortar and pestle. The powder was resuspended in 1 ml 0.1 M Tris-HCl (pH 7.2) at 4°C with shaking for 1 h. Following centrifugation at $10,000 \times g$ for 30 min, the supernatant (≈ 1 ml) was concentrated to 0.2 ml with an Amicon filter (10,000 molecular weight cut-off). The protein concentrations were determined using a Bio-Rad kit and 40, 30, and 20 μg of each sample added to individual 96-well ELISA plates (Costar, Inc.). Following 1 h of incubation at 37°C , the sample was removed, the wells were washed 3 times with PBS (pH 7.2) and incubated with PBS plus 5% normal goat serum, and then primary antibody was added for 1 h at 37°C . Finally, the wells were washed with PBS and incubated with secondary antibody-rhodamine conjugates (Sigma). Following 3 washes with PBS, the plates were read on an automated ELISA reader. The background fluorescence from secondary antibody binding was presubtracted by the ELISA reader prior to reading the primary antibody signal.

Extraction and Purification of Collagenase. The PC-3 ML cells were cultured, and conditioned medium was prepared according to published procedures (15). The M_r 72,000 type IV collagenase was purified from the conditioned medium of human prostatic PC-3 ML cells (14, 15) according to the method of Collier *et al.* (19). Crude protein extracts were prepared from pieces (0.5 to 1 g) of pulverized prostate tissue. The pulverized powder was resuspended in 0.5 ml Dulbecco's modified Eagle's medium and 0.5 M 4-(2-hydroxyethyl)-1-piperazineethanesulfonic acid buffer (pH 7.2), and centrifuged at $3000 \times g$ for 10 min, and the supernatant was prepared for SDS-PAGE and Western blotting. Collagenase IV was purified using a protein A-linked (New Brunswick Institutes, Trenton, NJ) collagenase IV antibody affinity column (15).

SDS-PAGE (8% gels) was carried out according to the method of Laemmli *et al.* (20). Silver staining was performed according to the method of Merrill *et al.* (21). Western blots were carried out by the method of Towbin *et al.* (22). Protein measurements were made with a Bio-Rad kit (Bio-Rad) using the manufacturer's procedures. Gelatinase assays were conducted according to previously published methods (23).

Extraction of RNA. RNA was extracted from pieces of human prostate tumor tissue and from 2-mm³ pieces of adjacent normal tissue obtained from resections of the 24 patients sampled. To extract RNA the fresh tissue was frozen in liquid nitrogen and stored at -70°C . The frozen tissue was reduced to a powder using a mortar and pestle, and RNA was extracted with guanidine isothiocyanate and isolated by centrifugation on CsCl gradients according to published methods (24). Pieces of the tissue were also prepared by cryosectioning for histopathology and Gleason grading.

Northern Blots. The extracted RNA (5 μg) was eluted on 1% w/v agarose gels cross-linked with 2 M formaldehyde as described by Maniatis *et al.* (25). The fractionated RNA was transferred to GeneScreen Plus membranes (Dupont, Inc.) and the membranes were washed with $2\times$ standard saline citrate and UV-cross-linked with $1.5 \times 10^5 \mu\text{cm}^2$ utilizing a UV Stratalinker 2400 kit (Stratagene, Inc.). Following prehybridization, the membranes were hybridized for 18 h at 42°C with the type IV collagenase cDNA radiolabeled with [α - ^{32}P]dCTP (NEN, Ind.) using the random primer technique. The hybridized

filters were washed in $1\times$ standard saline citrate containing 1% sodium dodecyl sulfate at 65°C for 1 h. Autoradiography was carried out at -70°C with an intensifying screen. The M_r 72,000 type IV collagenase cDNA was a gift of Dr. Gregory Goldberg and colleagues (19, 26).

Slot blots with the collagenase cDNA were carried out utilizing a Bio-Rad apparatus and methods described by Levy *et al.* (6). Three dilutions of each total RNA (1, 2, 3 $\mu\text{g}/\text{ml}$) were prepared and blotted to Zeta-Probe membranes (Bio-Rad), processed, and hybridized with ^{32}P -labeled cDNA as described above for the Northern blots. Signals in individual slots were extracted with Clorox bleach and quantified using a scintillation counter (Beckman 9000S). The data were averages \pm SD of triplicate experiments.

RESULTS

Western Blotting. The polyclonal antibodies raised against type IV collagenase were previously shown to bind crude M_r 72,000 type IV collagenase isolated from either the cytoplasm or the conditioned media of two different human prostatic cell lines (*i.e.*, PC-3 and DU 145) (13–15).

Western blots (Fig. 1, Lane 4) demonstrated that the antibodies recognized the M_r 72,000 protease in crude tissue extracts from a patient with advanced cancer (*i.e.*, Gleason grade 8) (Table 1). Western blots (Fig. 2A) further showed that following protein A antibody affinity purification and activation of the proenzyme (with 10 μM organomercurial chlorate for 30 min at 37°C) the antibodies specifically recognized the M_r 72,000 proenzyme isolated from BPH and Gleason grade 8 tumor tissue. The antibodies did not bind the M_r 64,000 zymogen or the NH_3 -terminal fragment generated by activation (Fig. 2A, *arrow*). The zymograph in Fig. 2B confirmed that both BPH and Gleason grade 8 tissue extracts contained the M_r 72,000 prozymogen and M_r 64,000 activated zymogen gelatinase.



Fig. 1. Western blot of crude tissue extracts from a Gleason grade 8 (Table 1) prostate tumor. The crude extracts (Lanes 1 and 2) were blotted with the M_r 72,000 type IV collagenase antibody (Lanes 3 and 4). In Lane 3 there was a total absence of labeling with antibody, which was preabsorbed with affinity-purified human type IV collagenase (*i.e.*, with 100 $\mu\text{g}/\text{ml}$ for 30 min at 37°C) purified from PC-3 ML cells. In Lane 4 the type IV collagenase antibody specifically binds the M_r 72,000 prozymogen. The lanes were loaded with 10 mg total protein and both first-degree and PAP second-degree antibodies used at a dilution of 1:200.

TYPE IV COLLAGENASE EXPRESSION IN HUMAN PROSTATE

Table 1 Slot blot hybridization assays of total cellular RNA from prostate tumor tissue and adjacent normal stroma

Ten, 7.5, and 5 µg of each RNA sample were eluted on the filters and hybridized with [α - 32 P]dCTP-labeled type IV collagenase cDNA. Duplicate experiments were carried out using 32 P-radiolabeled B-actin cDNA. Filters were extracted with Clorox bleach for scintillation counting. Each data point was the average \pm SD of triplicate measurements of the three RNA dilutions.

Patient sample	Gleason grade	dpm $\times 10^3$				Ratio		
		TC	NC	TA	NA	TC:NC	NC:NA	TC:TA
1	Benign	4.6 \pm 0.1	2.3 \pm 0.1	23 \pm 0.5	20 \pm 0.4	2.0	0.1	0.2
2	Benign	5.0 \pm 0.2	2.1 \pm 0.2	22 \pm 0.1	22 \pm 0.3	2.4	0.1	0.2
3	Benign	6.6 \pm 0.1	2.0 \pm 0.2	20 \pm 0.4	23 \pm 0.2	3.3	0.1	0.3
4	Benign	4.1 \pm 0.3	2.1 \pm 0.1	19 \pm 0.4	20 \pm 0.4	2.0	0.1	0.2
5	Benign	4.5 \pm 0.1	2.2 \pm 0.2	24 \pm 0.4	23 \pm 0.1	2.0	0.1	0.2
6	Benign	4.6 \pm 0.2	2.3 \pm 0.1	21 \pm 0.3	22 \pm 2.0	2.0	0.1	0.2
7	1	12.5 \pm 0.4	2.5 \pm 0.2	25 \pm 0.2	21 \pm 0.4	5.0	0.1	0.5
8	1	2.1 \pm 0.3	4.2 \pm 0.3	21 \pm 0.5	25 \pm 0.4	0.5	0.2	0.1
9	2	24.0 \pm 0.8	4.8 \pm 0.3	24 \pm 0.6	25 \pm 0.3	5.0	0.2	1.0
10	2	22.0 \pm 1.0	2.2 \pm 0.1	22 \pm 0.4	20 \pm 0.2	10.0	0.1	1.0
11	3	24.0 \pm 1.1	6.0 \pm 0.2	20 \pm 0.3	22 \pm 0.1	4.0	0.3	1.2
12	4	107.0 \pm 2.5	4.2 \pm 0.1	21 \pm 0.4	19 \pm 0.2	25.0	0.2	5.1
13	4	116.0 \pm 3.1	1.9 \pm 0.1	19 \pm 0.4	22 \pm 0.3	61.0	0.1	6.1
14	4	97.0 \pm 2.0	9.2 \pm 0.3	23 \pm 0.6	21 \pm 0.4	10.0	0.4	4.2
15	6	156.0 \pm 4.2	6.6 \pm 0.3	20 \pm 0.4	19 \pm 0.3	24.0	0.3	7.8
16	6	154.0 \pm 5.1	2.2 \pm 0.2	22 \pm 0.3	22 \pm 0.4	70.0	0.1	7.0
17	6	120.0 \pm 4.1	1.6 \pm 0.3	16 \pm 0.4	19 \pm 0.4	75.0	0.1	7.5
18	6	195.0 \pm 3.8	3.0 \pm 0.1	30 \pm 0.3	23 \pm 0.4	65.0	0.1	6.5
19	8	232.0 \pm 5.5	2.3 \pm 0.1	23 \pm 0.3	20 \pm 0.4	101.0	0.1	10.1
20	8	240.0 \pm 5.6	7.3 \pm 0.1	22 \pm 0.4	22 \pm 0.6	33.0	0.3	10.9
21	8	228.0 \pm 6.6	9.6 \pm 0.3	24 \pm 0.5	26 \pm 0.5	24.0	0.4	9.5
22	8	265.0 \pm 7.1	2.3 \pm 0.1	23 \pm 0.6	23 \pm 0.4	115.0	0.1	11.5
23	8	231.0 \pm 4.1	2.1 \pm 0.1	21 \pm 0.4	20 \pm 0.4	110.0	0.1	11.0
24	8	187.0 \pm 3.0	2.2 \pm 0.4	22 \pm 0.3	22 \pm 0.2	85.0	0.1	8.5

PAP Immunolabeling. The expression of the *M*, 72,000 collagenase was examined by PAP antibody labeling of benign and malignant human prostate tissue (Table 1). Fig. 3 compares the relative extent of antibody labeling observed in benign (Fig. 3A) and malignant tissue (Fig. 3, B and C). In benign tissue, some of the glandular and ductal epithelial cells express the *M*, 72,000 protease, but always to variable degrees. Many of the cells and glands failed to express any detectable collagenase (Fig. 3A). In comparison, in the tumor tissue, the epithelial cells within the glands and ducts were strongly labeled (Fig. 3B, Gleason grade 6). The tumor cells of invasive foci within the stromal tissue were also labeled in these tissue (Fig. 3C). Fig. 3 shows an example of what was typically observed in the 24 patients examined. In all cases, there was positively no indication that the basement membrane, the extracellular matrix, the surrounding stromal cells, or nearby normal tissue (Fig. 3D) was labeled beyond faint background levels. Labeling with secondary avidin-biotin peroxidase-labeled antibodies also produced background levels of labeling. Finally, labeling with β -actin antibodies (Cappel Laboratories, Inc.) showed uniform labeling of the epithelial and stromal cells in all of the specimens (data not shown).

Northern and Slot Blotting. We have measured the mRNA content of the *M*, 72,000 type IV collagenase in extracts of flash-frozen tumor tissue. These tumor-rich areas and normal tissue were identified by histological examination of cryosections, and the tumor tissue and normal tissue were removed from the block by dissection. These tissues were then pulverized on dry ice for extraction of the RNA.

Fig. 4 shows Northern blots of total cellular RNA extracted from benign tissue (Lane 1) and from malignant tissue which was assigned Gleason grades of 1, 2, or 3 (Fig. 4A) and 4, 6, or 8 (Fig. 4B). The *M*, 72,000 type IV collagenase was expressed in barely detectable amounts in benign tissue (Fig. 4A, Lane 1). In contrast, the protease was expressed in significant amounts in malignant tissue taken from patients with Gleason grades of 1-8 (Fig. 4A, Lanes 2-4; Fig. 4B, Lanes 1-4).

In all of these experiments, we were unable to separate the glandular tissue from the invasive tumor foci. More importantly, variable amounts of stromal tissue were present in the samples. This did not appear to be a problem, however, since the extracts from the normal



Fig. 2. A and B, SDS-PAGE (Lanes 1 and 2) and the corresponding Western blots (Lanes 3 and 4), showing that the type IV collagenase antibodies recognized the affinity-purified *M*, 72,000 proenzyme from both BPH (Lanes 1 and 3) and Gleason grade 8 (Lanes 2 and 4) patients. Lane 5 shows no labeling with 2° antibodies alone of BPH extracts. Following activation with 10 µM organomercurial chlorate only the proenzyme at *M*, 72,000 was recognized by the antibody. The cleaved, COOH-terminal (*M*, 64,000) and NH₂-terminal fragment (arrowhead) were not labeled. B, zymography of the BPH (Lane 1) and Gleason grade 8 (Lane 2) protein extracts. The two bands at *M*, 72,000 and 64,000 demonstrate gelatinase activity of the proenzyme and zymogen form of the enzyme. The lanes were loaded with 30 mg (Lane 1) and 10 mg of total protein from the crude whole cell extracts.

TYPE IV COLLAGENASE EXPRESSION IN HUMAN PROSTATE

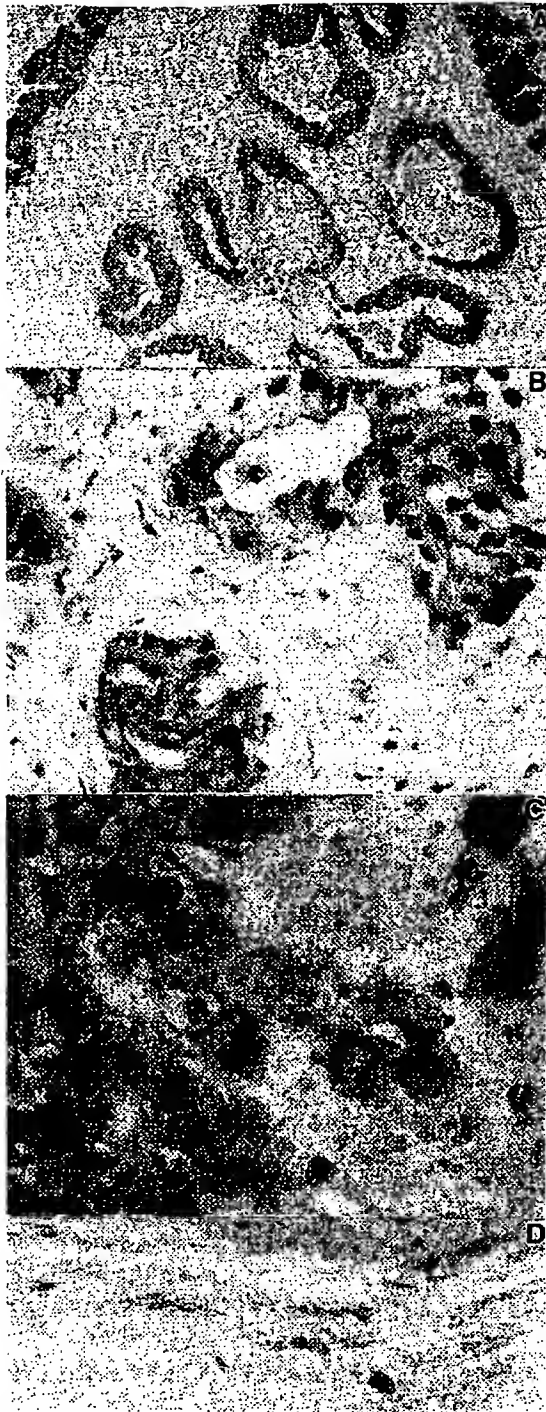


Fig. 3. A-C, immunoperoxidase-labeled human prostate tissue from a benign (A) and malignant tumor (B and C), Gleason grade 6. The glandular and ductal tissue are shown in A and B; an invasive focus is shown in C. D, unlabeled normal tissue from the specimen in B and C. The collagenase IV antibodies were used at dilutions of 1:250. A, $\times 800$; B and C, $\times 1200$; D, 800.

stromal tissue of different patient samples did not contain detectable type IV collagenase mRNA.

Slot blot hybridization assays were carried out on total RNA extracted from the tumor-rich regions and the nearby normal stromal tissue of frozen prostate tissue from 24 patients (Table 1). Scintillation counting revealed that ^{32}P -labeled type IV collagenase cDNA binding to the filters increased with the assigned Gleason grade for the tumor (Table 1). The levels of cDNA binding to RNA extracted from benign

tissue and from normal stromal tissue of each specimen (*i.e.*, taken from each of the respective patients) was low. The ratio of collagenase IV ^{32}P -cDNA binding to tumor tissue (TC) versus normal stromal tissue (NC) increased significantly as a function of the Gleason grade. The ratio was approximately 2–3-fold in benign tissue; 0.5–5-fold at Gleason grade 1; 5–10-fold at Gleason grade 2; 10–61-fold at Gleason grade 4; 24–75-fold at Gleason grade 6; and 24–115-fold at Gleason grade 8.

Control measurements showed that the levels of β -actin ^{32}P -cDNA binding to duplicate samples of both TA and NA remained fairly constant in the 24 patient tissues examined. The TC:TA ratio ranged from 0.2 in benign to 11.5 in grade 8 tumor tissue. In contrast, there was no significant change in the NC:NA ratio in normal stromal tissue extracts.

ELISAs of Collagenase IV Levels. ELISAs (Table 2) of the patient samples in Table 1 demonstrated that the collagenase IV protein levels (TC) directly correlated with the RNA levels in the 24 tumor tissue samples. The ELISA values increased progressively from about 0.01 in BPH to as high as 0.60 in Gleason grade 8 tumor tissue. The TA levels were fairly constant in all the tissue samples and varied from

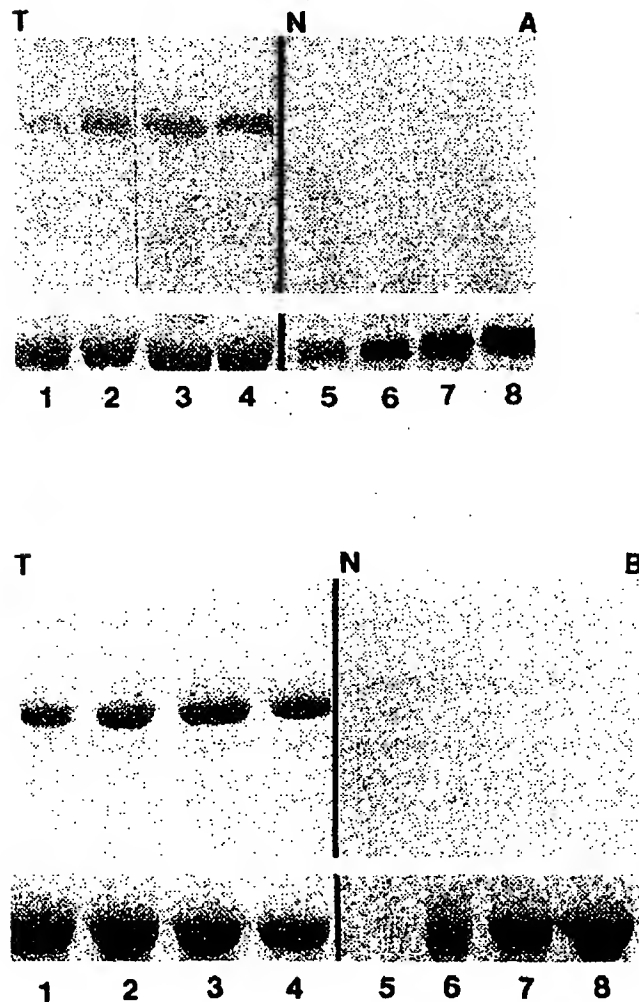


Fig. 4. A and B, Northern blot analysis of total cellular RNA from prostate tumor tissue (T, Lanes 1–4) and adjacent normal stromal tissue (N, Lanes 5–8), respectively. In A, the tissue was from benign tissue (Lanes 1 and 5); and from tissue with a Gleason grade of 1 (Lanes 2 and 6); 2 (Lanes 3 and 7); or 3 (Lanes 4 and 8). In B the Gleason grade was 4 (Lanes 1 and 5); 6 (Lanes 2 and 6); 6 (Lanes 3 and 7); or 8 (Lanes 4 and 8). Each well was loaded with 6 μg total RNA, and the membranes were hybridized with $[\alpha\text{-}^{32}\text{P}]\text{dCTP}$ -labeled cDNA to the M_r 72,000 collagenase (upper band) and β -actin (lower band). Note that in B, lane 5, the β -actin blot was faint.

TYPE IV COLLAGENASE EXPRESSION IN HUMAN PROSTATE

Table 2 ELISA assays

Protein was extracted from 2 g of tissue, and 40, 30, and 20 µg of protein were applied to membrane filters. The first-degree antibodies were used at dilutions of 1:250, and rhodamine-tagged second-degree antibodies were used at 1:200 dilutions. Data are averages \pm SD from duplicate studies and triplicate measurements for each protein concentration of each sample.

Patient sample	TC	TA	NC	NA	TC:TA
1	0.01 \pm 0.01	0.44 \pm 0.11	0.01	0.51 \pm 0.20	0.02
2	0.01 \pm 0.01	0.35 \pm 0.12	0.02	0.48 \pm 0.18	0.03
3	0.02 \pm 0.01	0.50 \pm 0.10	0.03	0.44 \pm 0.15	0.04
4	0.01 \pm 0.01	0.43 \pm 0.08	0.01	0.48 \pm 0.14	0.02
5	0.02 \pm 0.01	0.48 \pm 0.07	0.02	0.46 \pm 0.12	0.04
6	0.03 \pm 0.02	0.33 \pm 0.06	0.01	0.47 \pm 0.11	0.09
7	0.03 \pm 0.01	0.40 \pm 0.05	0.00	0.55 \pm 0.13	0.08
8	0.05 \pm 0.02	0.43 \pm 0.12	0.00	0.54 \pm 0.21	0.12
9	0.06 \pm 0.02	0.49 \pm 0.11	0.00	0.58 \pm 0.22	0.12
10	0.10 \pm 0.03	0.44 \pm 0.10	0.00	0.61 \pm 0.18	0.23
11	0.13 \pm 0.04	0.46 \pm 0.15	0.00	0.40 \pm 0.16	0.28
12	0.18 \pm 0.05	0.38 \pm 0.07	0.01	0.44 \pm 0.12	0.47
13	0.23 \pm 0.04	0.46 \pm 0.06	0.02	0.47 \pm 0.15	0.50
14	0.25 \pm 0.03	0.37 \pm 0.05	0.01	0.49 \pm 0.22	0.68
15	0.20 \pm 0.05	0.47 \pm 0.04	0.01	0.48 \pm 0.21	0.43
16	0.29 \pm 0.10	0.44 \pm 0.20	0.02	0.46 \pm 0.20	0.66
17	0.33 \pm 0.08	0.49 \pm 0.17	0.01	0.41 \pm 0.12	0.67
18	0.25 \pm 0.06	0.35 \pm 0.15	0.01	0.42 \pm 0.08	0.71
19	0.36 \pm 0.04	0.42 \pm 0.11	0.02	0.44 \pm 0.06	0.86
20	0.42 \pm 0.03	0.51 \pm 0.13	0.02	0.48 \pm 0.07	0.82
21	0.30 \pm 0.02	0.53 \pm 0.14	0.01	0.50 \pm 0.11	0.57
22	0.52 \pm 0.08	0.40 \pm 0.09	0.02	0.51 \pm 0.09	1.30
23	0.60 \pm 0.12	0.44 \pm 0.08	0.01	0.52 \pm 0.07	1.36
24	0.45 \pm 0.13	0.52 \pm 0.07	0.01	0.56 \pm 0.06	0.86
25	0.40 \pm 0.11	0.50 \pm 0.06	0.01	0.49 \pm 0.04	0.80

0.35 to 0.52. Accordingly, the TC:TA ratio increased from 0.02 in BPH to 1.36 in Gleason grade 8 (Table 2). The collagenase IV levels in the adjacent normal tissue of the patient samples consistently yielded values below 0.01. The NA levels in these tissue varied from 0.41 to 0.56, and the ratio of collagenase IV to actin was fairly constant at about 0.02.

DISCUSSION

An increased secretion of metalloproteinases (*i.e.*, type IV collagenase and other proteases) has been associated with the invasive and metastatic phenotype of tumors (4–8, 10, 12, 13–15, 19, 27). For example, *in vivo* studies with several human primary colorectal carcinoma cell lines which exhibited high type IV collagenase levels have shown that the cells have a correspondingly high ability to metastasize in nude mice. Following *ras* oncogene transfection, *in vivo* studies have further demonstrated an association of enhanced expression of the *M*_r 72,000 type IV collagenase with an invasive phenotype (19). Likewise, quantitative *in vitro* studies with Boyden chemotactic chambers (13, 28) and animal model studies have indicated that the ability of tumor cells to invade basement membrane material was directly associated with their metastatic aggressiveness *in vivo* (2).

Utilizing collagenase antibodies which recognized the uncleaved *M*_r 72,000 type IV collagenase, we discerned qualitative differences in the levels of cytoplasmic collagenase expressed by benign, malignant, and invasive tumor foci. Immunoperoxidase labeling showed that the epithelial cells in benign tissue were either labeled, poorly labeled, or not labeled at all, indicating that there was variable expression of the protease in the nonmalignant epithelial cells of the glands and ducts. In comparison, the malignant epithelial tumor cells strongly expressed collagenase at consistently high levels. Cells in the invasive tumor foci also expressed the protease but often in comparatively modest amounts.

Levy *et al.* (6) have found that antibodies raised against a *M*_r 72,000 human collagenase preferentially labeled only the invasive carcinoma cells of the colon. The stromal cells were not labeled in their prepa-

rations. Likewise, Hewitt *et al.* (10) recently have reported that type IV collagenase and its inhibitor, tissue inhibitor of metalloproteinase, were both overexpressed in advanced colorectal cancer. The benign and normal tissue produced very little of either the protease or tissue inhibitor of metalloproteinase. Interestingly, their immunolabeling studies indicated that both type IV collagenase and tissue inhibitor of metalloproteinase were also localized in the extracellular matrix immediately adjacent to the tumor tissue. More importantly, increased staining of the matrix was observed at the leading invasive edge of the tumor, indicating a direct involvement of protease secretion in the process of invasion.

We observed only background levels or no staining by type IV collagenase antibodies in the extracellular matrix surrounding prostate tumor tissues. Similar results were obtained with both alcohol/aldehyde fixed sections and cryosections (6-µm thickness). Antibody affinity and titer did not appear to be a problem, since labeling with higher first-degree and second-degree antibody titers (1:100 and 1:20 dilutions, respectively) also failed to produce staining of the basement membrane, the stromal cells, or the extracellular matrix (data not shown). We believe, therefore, that the levels of protease in the extracellular matrix may be below detectable limits. However, antigenic masking could occur, or the protease may be localized on the outer cell surface of the invasive cells and thus appear to be part of the cytoplasmic pool.

The variable nature of the labeling in benign tissue suggested that quantitative measurements of both type IV collagenase mRNA and protease levels were essential for prognostic purposes. To measure the mRNA levels, we utilized the *M*_r 72,000 type IV collagenase cDNA clone of Goldberg *et al.* (26). Northern blots showed that the cDNA detected mRNA in BPH and the malignant tissue at Gleason grade 1 to 8. The slot blot cDNA hybridization results clearly showed that mRNA expression increased dramatically as a function of the malignant status of the human prostate tissue examined. Low and variable levels of mRNA were detected in benign and low-grade tumors (*i.e.*, Gleason grade 1); whereas the more advanced tumors expressed quantitatively significant increases in type IV mRNA in direct proportion to the tumor grade.

ELISA measurements of the *M*_r 72,000 proenzyme present in tissue sample extracts mirrored the cDNA hybridization results and showed that the collagenase IV levels were also increased as a function of the Gleason grade of the tumor tissue. Benign tissue expressed low or background levels of detectable collagenase IV. Thus, although collagenase is detectable in the BPH epithelial cells by immunoperoxidase labeling, the overall levels of protease synthesis (and presumably secretion) are low in benign epithelial cells and surrounding tissue.

In other studies of prostate cancer, Albini *et al.* (28) found by Northern blot analysis that PUMP-1 (*i.e.*, human metalloproteinase 1) was expressed in 27% of normal prostate tissues, in 72% adenocarcinomas, and in 66% of the lymph node metastases examined. *In situ* hybridization with PUMP-1 antisense ³²S-labeled mRNA revealed that the gene was expressed in epithelial cells of the prostate adenocarcinomas. Invasive and metastatic cells also expressed the gene, but the stromal cells did not express PUMP-1.

In addition, Pajouh *et al.* (29) carried out Northern blot studies of type I and type IV collagenase and stromelysin I expression. They reported that 6 of 10 adenocarcinomas and 0 of 4 normal prostate tissues expressed type IV collagenase. All of the 9 adenocarcinomas and 4 of 4 normal prostate specimens examined expressed type I collagenase. Stromelysin I was not expressed in 13 adenocarcinomas. Their data suggested that several metalloproteinases may be produced by malignant tumor cells to facilitate penetration of the basement membrane and stroma.

TYPE IV COLLAGENASE EXPRESSION IN HUMAN PROSTATE

The data in this paper concur with the results in Pajouh's report. Our quantitative assays strongly suggest that increased type IV collagenase production is associated with and, therefore, is a good prognostic marker for malignant epithelial tumor cells in prostate cancer.

ACKNOWLEDGMENTS

The authors would like to thank Dr. Lester Karafin for the supply of prostate tissue and Dr. Miles McFarland for pathological reports on the patients.

REFERENCES

1. Foster, S. J., Talbot, I. C., Claytin, D. G., and Crichtley, D. R. Tumor basement membrane laminin in adenocarcinoma of the rectum: an immunohistochemical study of biologic and clinical significance. *Int. J. Cancer*, 37: 813-817, 1986.
2. Daneker, G. G., Mercurio, A. M., Guerra, L., Wolf, B., Salem, R. R., Bagli, D. J., and Steele, G. D. Laminin expression in colorectal carcinomas with varying degrees of differentiation. *Arch. Surg.*, 122: 1470-1474, 1987.
3. Nakamura, K., Mori, M., and Enjoji, M. Distribution of basement membrane antigens in clinical gastric adenocarcinomas: an immunohistochemical study. *J. Clin. Pathol. (Lond.)*, 40: 1418-1423, 1987.
4. Liotta, L. A., Tryggvason, K., Garbisa, S., Hart, I., Foltz, C. M., and Shafie, S. Metastatic potential correlates with enzymatic degradation of basement membrane collagen. *Nature (Lond.)*, 284: 67-68, 1980.
5. Tarin, D., Hoyt, B. J., and Evans, D. J. Correlation of collagenase secretion with metastatic colonization potential in naturally occurring murine mammary tumors. *Br. J. Cancer*, 46: 266-278, 1982.
6. Levy, A. T., Cioce, V., Sobel, M. E., Garbisa, S., Grigioni, W. F., Liotta, L. A., and Stetler-Stevenson, W. G. Increased expression of the M_r 72,000 type IV collagenase in human colonic adenocarcinoma. *Cancer Res.*, 51: 439-444, 1991.
7. Monteagudo, C., Merino, M. J., San-Juan, J., Liotta, L. A., and Stetler-Stevenson, W. G. Immunohistochemical distribution of type IV collagenase in normal, benign, and malignant breast tissue. *Am. J. Pathol.*, 136: 585-592, 1990.
8. D'Errico, A., Garbisa, S., Liotta, L. A., Casimiro, V., Stetler-Stevenson, W. G., and Grigioni, W. F. Augmentation of type IV collagenase, laminin receptor, and Ki67 proliferation antigen associated with human colon, gastric, and breast carcinoma progression. *Mod. Pathol.*, 4: 239-246, 1991.
9. Irimura, T., Yamori, T., Bennett, S. C., Ota, D. M., and Cleary, K. R. The relationship of collagenolytic activity to stage of human colorectal carcinoma. *Int. J. Cancer*, 40: 24-31, 1987.
10. Hewitt, R. E., Leach, I. H., Powe, D. G., Clark, I. M., Cawston, T. E., and Turner, D. R. Distribution of collagenase and tissue inhibitor of metalloproteinases (TIMP) in colorectal tumours. *Int. J. Cancer*, 49: 666-672, 1991.
11. Van Der Stappen, J. W. J., Hendriks, T., and Wobbes, T. Correlation between collagenolytic activity and grade of histological differentiation in colorectal tumours. *Int. J. Cancer*, 45: 1071-1078, 1990.
12. Ogilvie, S. J., Hailey, J. A., Jucaba, S. F., Lee, E. C. G., and Tarin, D. Collagenase secretion by human breast neoplasms: a clinicopathologic investigation. *J. Nat. Cancer Inst.*, 74: 19-28, 1985.
13. Wang, M., and Stearns, M. E. Blocking of collagenase secretion by estramustine during *in vitro* tumor cell invasion. *Cancer Res.*, 48: 6262-6271, 1988.
14. Stearns, M. E., and Wang, M. Regulation of kinsin expression and type IV collagenase secretion in invasive human prostate PC-3 tumor sublines. *Cancer Res.*, 51: 5866-5875, 1991.
15. Stearns, M. E., Wang, M., and Sousa, O. Evidence that estramustine binds MAP-1A to inhibit type IV collagenase secretion. *J. Cell Sci.*, 98: 55-63, 1991.
16. Wang, M., and Stearns, M. E. Isolation and characterization of PC-3 human prostatic tumor sublines which preferentially metastasize to select organs in SCID mice. *Differentiation*, 48: 115-125, 1991.
17. Gleason, D. F., Mellinger, G. T., and Veterans Administration Cooperative Urological Research Group. Prediction of prognosis for prostatic adenocarcinoma by combined histological grading and clinical staging. *J. Urol.*, 111: 58-64, 1974.
18. Hsu, S. M., Raine, L., and Sanger, H. The use of avidin-biotin-peroxidase complex (ABC) in immunoperoxidase technique: a comparison between ABC and unlabeled antibody (PAP) procedures. *J. Histochem. Cytochem.*, 29: 577-580, 1981.
19. Collier, I. E., Wilhelm, S. M., Fisen, A. Z., Marmer, B. L., Grant, G. A., Seltzer, J. L., Kronberger, A., He, C., Bauer, E. A., and Goldberg, G. I. *H-ras* oncogene-transformed human bronchial epithelial cells (TBE-1) secrete a single metalloproteinase capable of degrading basement membrane collagen. *J. Biol. Chem.*, 263: 6578-6587, 1988.
20. Laemmli, U. K. Cleavage of structural proteins during the assembly of the head of bacteriophage T4. *Nature (Lond.)*, 227: 680-685, 1970.
21. Merrill, C. R., Goldman, D., Sedman, S. A., and Ebert, M. H. Ultrasensitive stain for proteins in polyacrylamide gels shows regional variation in cerebrospinal fluid proteins. *Science (Washington DC)*, 211: 1437-1438, 1981.
22. Towbin, H., Staehelin, T., and Gordon, J. Electrophoretic transfer of proteins from polyacrylamide gels to nitrocellulose sheets: procedures and some applications. *Proc. Natl. Acad. Sci. USA*, 76: 4350-4354, 1979.
23. Stearns, M. E., and Wang, M. Taxol blocks processes essential for prostate tumor cell (PC-3 ML) invasion and metastases. *Cancer Res.*, 52: 3776-3781, 1992.
24. Davis, I. G., Dibner, M. D., and Batty, J. F. *Basic Methods in Molecular Biology*, pp. 130-135. New York: Elsevier Science Publishing Co., Inc., 1986.
25. Maniatis, T., Fritsch, E. F., and Sambrook, J. *Molecular Cloning: A Laboratory Manual*. Cold Spring Harbor, NY: Cold Spring Harbor Laboratory, 1982.
26. Goldberg, G. I., Marmer, B. L., Grant, G. A., Eisen, A. Z., Wilhelm, S., and He, C. Human 72-kilodalton type IV collagenase forms a complex with a tissue inhibitor of metalloproteinase designated TIMP-2. *Proc. Natl. Acad. Sci. USA*, 86: 8207-8211, 1989.
27. Liotta, L. A., Abe, S., Robey, P. G., and Martin, G. R. Preferential digestion of basement membrane collagen by an enzyme derived from a metastatic murine tumor. *Proc. Natl. Acad. Sci. USA*, 76: 2268-2272, 1979.
28. Albini, A., Iwamoto, Y., Kleinman, H. K., Martin, G. R., Aaronson, S. A., Kozlowski, J. M., and McFwan, R. N. A rapid *in vitro* assay for quantitating the invasive potential of tumor cells. *Cancer Res.*, 47: 3239-3245, 1987.
29. Pajouh, M. S., Nagle, R. B., Breathnach, R., Finch, J. S., Brawer, M. K., and Bowden, G. T. Expression of metalloproteinase genes in human prostate cancer. *J. Cancer Res. Clin. Oncol.*, 117: 144-150, 1991.

FGH52352

CI-06859658-7

FGH52352

CISTI ICIST

CI-06859658-7

Document Delivery Service
in partnership with the Canadian Agriculture LibraryService de fourniture de Documents
en collaboration avec la Bibliothèque canadienne de l'agriculture**THIS IS NOT AN INVOICE / CECI N'EST PAS UNE FACTURE**LYNN BRAZIL
LIBRARIANHELLER EHRMAN WHITE & MCAULIFFE
275 MIDDLEFIELD RD
MENLO PARK, CA 94025
UNITED STATES

ORDER NUMBER:	CI-06859658-7
Account Number:	FGH52352
Delivery Mode:	F31
Delivery Address:	650/324-6034
Submitted:	2007/05/11 18:05:35
Received:	2007/05/11 18:05:35
Printed:	2007/05/11 21:35:09

Direct	Periodical	OPENURLOPAC	UNITED STATES
--------	------------	-------------	---------------

Client Number:	39780-7000 CD
Title:	CANCER RESEARCH : THE OFFICIAL ORGAN OF THE AMERICAN ASSOCIATION FOR CANCER RESEARCH, INC.
DB Ref. No.:	IRN10154206
ISSN:	ISSN00085472
Vol./Issue:	54/2
Date:	3500
Article Title:	ELEVATION OF TOPOISOMERASE I MESSENGER RNA, PROTEIN, AND CATALYTIC ACTIVITY IN HUMAN TUMORS: DEMONSTRATION OF TUMOR-TYPE SPECIFICITY AND IMPLICATIONS FOR CANCER
Article Author:	HUSAIN, I., ET AL
Report Number:	IRN10154206
Publisher:	WAVERLY PRESS,

Estimated cost for this 8 page document: \$12.5 document supply fee +
\$15 copyright = \$27.5

The attached document has been copied under license from Access Copyright/COPIBEC or other rights holders through direct agreements. Further reproduction, electronic storage or electronic transmission, even for internal purposes, is prohibited unless you are independently licensed to do so by the rights holder.

Phone/Téléphone: 1-800-668-1222 (Canada - U.S./E.-U.) (613) 998-8544 (International)
www.nrc.ca/cisti Fax/Télécopieur: (613) 993-7619 www.cnr.ca/icist
info.cisti@nrc.ca info.icist@nrc.ca



National Research Council Canada
Conseil national de recherches Canada

Page 1 / 1

[CANCER RESEARCH 54, 539-546, January 15, 1994]

Elevation of Topoisomerase I Messenger RNA, Protein, and Catalytic Activity in Human Tumors: Demonstration of Tumor-type Specificity and Implications for Cancer Chemotherapy

Intisar Husain, James L. Mohler, Hillard F. Seigler, and Jeffrey M. Besterman¹

Department of Cell Biology, Glaxo Inc. Research Institute, Research Triangle Park, North Carolina 27709 [J. H., J. M. B.]; Division of Urology, Department of Surgery, and University of North Carolina-Lineberger Comprehensive Cancer Center, University of North Carolina, Chapel Hill, North Carolina 27599 [J. L. M.]; and the Department of Surgery, Duke University Medical Center, Durham, North Carolina 27710 [H. F. S.]

ABSTRACT

Topoisomerase I has been identified as an intracellular target of camptothecin, a plant alkaloid with anticancer activity. Various lines of evidence suggest that the sensitivity of cells to this drug is directly related to the topoisomerase I content. In humans, the levels of topoisomerase I have been shown to be elevated in colorectal tumors, compared to normal colon mucosa. The aim of our study was to determine whether (a) topoisomerase I levels are elevated in other solid tumors, (b) the elevated enzyme is catalytically active in these tumors, and (c) the increase in topoisomerase I levels in colorectal tumors is a result of increased transcription or translation. Topoisomerase I levels were quantitated in crude extracts from colorectal, prostate, and kidney tumors and their matched normal counterparts by Western blotting and by direct determination of catalytic activity, and mRNA levels were determined by Northern blotting. By Western blotting, colorectal tumors showed 5-35-fold increases in topoisomerase I levels, compared to their normal colon mucosa. In the case of prostate tumors, the increase was 2-10-fold, compared with benign hyperplastic prostate tissue from the same patients. However, no difference was observed in topoisomerase I levels in kidney tumors, compared to their normal counterparts. The catalytic activity of topoisomerase I was determined by a quantitative ³²P-transfer assay in crude homogenates, without isolating nuclei. Colorectal and prostate tumors exhibited 11-40- and 4-26-fold increases, respectively, in catalytic activity. However, kidney tumors did not show any alteration in catalytic activity, compared to their normal matched samples. Thus, for all three tumor types there was a good correlation between enzyme levels and catalytic activity. Finally, colorectal tumors were analyzed for steady state mRNA levels. A 2-33-fold increase in mRNA levels was found in colorectal tumors, compared to normal colon mucosa. These results suggest that alterations in topoisomerase I expression in humans are tumor type specific and that the increase in topoisomerase I levels results from either increased transcription of the topoisomerase I gene or increased mRNA stability.

INTRODUCTION

Topoisomerases are nuclear enzymes that control the topological states of DNA by catalyzing the concerted breaking and rejoining of DNA strands. Two major types of topoisomerases, topoisomerase I and topoisomerase II, have been identified in all eukaryotic cells. Topoisomerase I creates a transient single-strand nick and passes the intact strand through the break before resealing. Topoisomerase II makes a double-strand break and passes an intact double strand through the nick before the nick is sealed. These enzymes have been implicated in many important cellular processes such as replication, transcription, recombination, DNA repair, and chromosome segregation at mitosis (1, 2).

Received 8/5/93; accepted 11/15/93.

The costs of publication of this article were defrayed in part by the payment of page charges. This article must therefore be hereby marked advertisement in accordance with 18 U.S.C. Section 1734 solely to indicate this fact.

¹ To whom requests for reprints should be addressed, at Department of Cell Biology, Glaxo Inc. Research Institute, Five Moore Drive, Research Triangle Park, NC 27709.

Both types of topoisomerases have generated extensive clinical interest after their identification as molecular targets of several anti-tumor drugs (2, 3). Topoisomerase II-directed drugs are diversified in structure and include both DNA intercalators and nonintercalators. Many of these drugs, i.e., Adriamycin, mitoxantrone, and etoposide, are in clinical use.

Recently, topoisomerase I has been identified as a molecular target of camptothecin, a plant alkaloid that shows antitumor activity in various animal tumor models (4, 5). Camptothecin and its derivatives interfere with the DNA breakage-reunion reaction by stabilizing a key covalent intermediate between DNA and the enzyme, resulting in the cleavage of DNA (4, 6).

The sensitivity of cells to the topoisomerase-targeted drugs appears to be related to the level of topoisomerases in the nucleus (7-11). Selective toxicity of topoisomerase II inhibitors toward rapidly proliferating tumor cells might be due to the high levels of topoisomerase II in these cells, compared to low levels of this enzyme in quiescent cells (12, 13). In contrast to topoisomerase II, the levels of topoisomerase I do not change with the cell cycle. However, the recent finding by Giovenella *et al.* (14) that topoisomerase I levels appear elevated in advanced stages of human colorectal adenocarcinoma, compared to normal colonic mucosa, suggests that topoisomerase I may also be an important target of antitumor drugs for tumors showing elevated levels of this enzyme.

Increased expression of topoisomerase I in tumors, compared to normal tissue, could provide selective therapeutic cytotoxicity of drugs directed against topoisomerase I. This prediction is supported by the following observations: (a) baby hamster kidney cells overexpressing topoisomerase I are hypersensitive to camptothecin (9); and (b) camptothecin-resistant tumor cell lines express decreased levels of topoisomerase I (10).

In spite of the clinical importance of topoisomerase I, data concerning the quantitation of this enzyme in human tumor biopsies are very limited (14-16). Furthermore, in these studies topoisomerase I levels have not been correlated with the catalytic activity of the enzyme and its expression at the mRNA level.

In an attempt to understand the regulation of DNA topoisomerase I, we studied the expression of topoisomerase I in human tumor specimens and their normal counterparts. Specifically, we wanted to answer the following questions. (a) Are the levels of topoisomerase I, which are elevated in colorectal adenocarcinoma, also elevated in other solid tumors or is this phenomenon specific to colorectal tumors? (b) Is the elevated topoisomerase I catalytically active in these tumors? (c) Are increased levels of topoisomerase I due to increased transcription or translation? Our results indicate that in tumors of the colon and prostate, but not kidney, topoisomerase I catalytic activity, protein levels, and mRNA content were significantly elevated, compared to matched normal controls. The increase in the topoisomerase I levels results from either increased transcription of the topoisomerase I gene or increased mRNA stability.

TOPOISOMERASE I EXPRESSION IN HUMAN TUMOR BIOPSIES

MATERIALS AND METHODS

PMSF,² leupeptin, pepstatin A, and Sephadex G-50 quick-spin columns were purchased from Boehringer Mannheim. Plasmid pBR322, DNase I, and the random primer labeling kit were supplied by Bethesda Research Laboratories. [³²P]dCTP (3000 and 6000 Ci/mmol) and nick translation kits were from DuPont New England Nuclear Corporation. [¹²⁵I]-labeled Protein A was supplied by Amersham. Klenow fragment, polynucleotide kinase, T₄ ligase, and restriction enzymes were purchased from either BRL or Promega Corporation. The Sequenase kit and cDNA synthesis kit were supplied by United States Biochemical Corporation. Immobilon-P and Nytran membranes were purchased from Millipore (Bedford, MA). Human scleroderma sera containing antitopoisomerase I antibodies (17) were a gift from Dr. Paul Agnis, North Carolina State University. Polyclonal antibodies against purified topoisomerase were a gift from Dr. Leroy F. Liu, The Johns Hopkins University School of Medicine (Baltimore, MD). Peptides for raising antibodies were synthesized at the Department of Microbiology and Immunology, University of North Carolina (Chapel Hill, NC). The IgG purification kit and Sulfolink coupling gel for preparation of the affinity column were obtained from Pierce Chemical Company.

Tissues. Samples of colorectal tumors and normal colon were obtained from patients who underwent surgery at Duke University Medical Center (Tables 1, 2, and 3). When the tumor was dissected, care was taken to ensure that normal components of bowel wall were not included. For normal colon, just the mucosa was dissected away and elements of bowel wall including the muscle layers and serosa were not included. Samples of prostatic adenocarcinoma and grossly normal peripheral zone from the contralateral lobe were obtained at radical retropubic prostatectomy, for clinically localized carcinoma, from nine patients treated at the University of North Carolina (Table 1). Eight patients with clinically organ-confined renal masses had tumor and normal renal cortical tissue sampled at radical nephrectomy at the University of North Carolina (Table 1). All specimens were frozen immediately in liquid nitrogen and stored at -100°C. The identity of all tissues studied was confirmed microscopically and all specimens were free of necrosis and preservation or preparation damage. The clinical and pathological characteristics of patients with colorectal, prostate, and renal malignancies are summarized in Tables 1 and 3.

Plasmid containing GAPDH cDNA was a gift from Dr. Cheryl Walker, Chemical Industry Institute of Toxicology (Research Triangle Park, NC). HeLa cells were obtained from the Linberger Comprehensive Cancer Center, University of North Carolina (Chapel Hill, NC). The HT-29 human colon adenocarcinoma cell line was obtained from the American Type Culture Collection (Rockville, MD). The cells were grown in McCoy's 5A medium containing 10% fetal bovine serum and 2 mM glutamine, in an atmosphere of 5% CO₂ at 37°C.

Preparation of Nick-translated ³²P-Labeled DNA. Nick-translated pBR322 DNA was prepared using [³²P]dCTP (6000 Ci/mmol) and a nick translation kit, according to the manufacturer's instructions. The reaction was stopped by adding EDTA to a final concentration of 20 mM. Unincorporated dCTP was removed with G-50 Sephadex quick-spin columns.

Preparation of Crude Extracts from Human Tissues and HT-29 Cells for Topoisomerase I Activity. All steps during extract preparation were performed at 4°C. Frozen tissues (0.15–0.30 g) were first ground with mortar and pestle in the presence of liquid nitrogen, suspended in buffer A (10 mM Tris-HCl, pH 7.5, 10 mM 2-mercaptoethanol, 10 mM EDTA, 0.25% Triton X-100, 1 mM PMSF, 1 μM leupeptin, 1 μM pepstatin) at 0.19 g tissue/ml, and homogenized with a Potter-Elvehjem Teflon-glass homogenizer. The extract was kept on ice for 30 min, an equal volume of nuclear lysis buffer B (buffer A containing 2 M NaCl) was added slowly, and the mixture was stirred gently on ice for 2 h. The suspension was centrifuged at 10,000 rpm in an SS-34 rotor for 2 h. Polyethylene glycol 8000 was added slowly to the supernatant (final concentration, 5%), the mixture was stirred on ice for 30 min, and the supernatant was cleared by centrifugation in a Beckman ultracentrifuge. The supernatant was dialyzed against buffer containing 20 mM Tris-HCl, pH 7.5, 50 mM NaCl,

Table 1 Topoisomerase I levels in colorectal, prostate, and kidney tumors expressed as the ratio of tumor to normal and the relationship between the topoisomerase I levels and staging of tumors

Topoisomerase I levels were estimated by Western blot analysis using equal protein from tissue homogenates of tumor and matched normal samples from the same patients as described in "Materials and Methods" and Fig. 1. The catalytic activity of topoisomerase I was determined by the ³²P transfer assay using three protein concentrations from tumors and corresponding normal tissue extracts as described in "Materials and Methods" and Fig. 6. Values in the linear range were used to calculate the ratio. ND, not determined. The results of Western blot analysis on the colorectal tumor of patient 7 are shown in Fig. 1, Lanes 1 and 2, on the prostate tumors of patient 12 in Fig. 1, Lanes 3 and 4, on the kidney tumor of patient 18, in Fig. 1, Lanes 5 and 6. The catalytic activity measurements for the colorectal tumor of patient 2, the prostate tumor of patient 12, and kidney tumor of patient 18 are shown in Fig. 6, Lanes 1 and 2, Lanes 3 and 4, and Lanes 5 and 6, respectively.

Tumor	Patient	Catalytic activity	Western blot	Dukes staging	Grade	Stage
Colorectal	1	17.0	8.0	C2		
	2	13.0	5.5	B2		
	3	11.0	5.0	B2		
	4	40.0	20.6	Adenoma		
	5	15.0	6.5	C2		
	6	ND	5.0	B1		
	7	ND	18.5	C2		
	8	ND	35.0	B1		
Prostate ^a	9	4.0	2.4		5 + 4 = 9	P ₃₃ N ₀ M ₀
	10	8.5	5.2		4 + 3 = 7	P ₃₃ N ₀ M ₀
	11	1.0	2.3		4 + 3 = 7	P ₃₃ N ₀ M ₀
	12	26.0	10.6		3 + 3 = 6	P ₃₃ N ₀ M ₀
	13	9.5	6.6		3 + 4 = 7	P ₃₃ N ₀ M ₀
	14	1.0	0.9		5 + 4 = 9	P ₃₃ N ₀ M ₀
	15	ND	6.0		3 + 3 = 6	P ₃₃ N ₀ M ₀
	16	ND	3.3		3 + 4 = 7	P ₂₀ N ₀ M ₀
	17	ND	2.3		4 + 4 = 8	P ₃₃ N ₀ M ₀
	18	1.9	1.5		1	P ₁ N ₀ M ₀
Kidney ^b	19	1.8	1.0		1	P ₃₃ N ₀ M ₀
	20	2.5	1.0		2	P ₃₃ N ₀ M ₀
	21	ND	1.0		2	P ₃₃ N ₀ M ₀
	22	ND	0.9		2	P ₁ N ₀ M ₀
	23	ND	0.7		2	P ₁ N ₀ M ₀
	24	ND	1.6		2	P ₃₃ N ₀ M ₀
	25	ND	1.0		3	P ₃₃ N ₂ M ₀

^a Grade as reported in Ref. 37; stage as reported in Ref. 38.

^b Stage as reported in Ref. 39.

10 mM 2-mercaptoethanol, 1 mM EDTA, 10% glycerol, 1 mM PMSF, 1 μM pepstatin, and 1 μM leupeptin, for 12 h at 4°C. The dialyzed supernatant was centrifuged in a microfuge to remove any suspended material and assayed for topoisomerase I activity. Crude extracts from HT-29 cells were prepared after the cells were washed 3 times with phosphate-buffered saline containing 1 mM PMSF, 1 μM pepstatin, and 1 μM leupeptin, as described for tissue homogenates. Protein was estimated by the bicinchoninic acid protein assay reagent (Pierce), using bovine serum albumin as a standard.

Preparation of Nuclear Extracts from HT-29 Cells. Cells were lysed in lysis buffer (30 mM Tris-HCl, pH 7.5, 0.3 M sucrose, 2 mM MgCl₂, 2 mM dithiothreitol, 15 mM 2-mercaptoethanol, 0.1 mM EDTA, 0.25% Triton X-100, 1 mM PMSF, 1 μM leupeptin, 1 μM pepstatin) by homogenization in a Potter-Elvehjem Teflon-glass homogenizer. The suspension was kept on ice for 15 min and centrifuged at 1500 rpm in an SS-34 rotor for 10 min. The nuclear pellet was washed three times with buffer A and resuspended in the same buffer. The nuclei were lysed by adding an equal volume of buffer B. After this step, the protocol for preparation of crude homogenates was followed.

Antibodies and Immunoblot Analysis. The following peptides from the predicted amino acid sequence for topoisomerase I (18) were used for raising polyclonal antibodies: (a) CNHQAPPKTFEKSMMNLQTK (amino acids 630–650), (b) CERYPEGIKWKFLHKGPFV (amino acids 209–227), and (c) CKSSPPQIKDEPEDDGYFVP (amino acids 110–128). For raising polyclonal antibodies against topoisomerase II, peptide CLNSGVSKPDPAKTKN (amino acids 1446–1461) from the predicted amino acid sequence for topoisomerase II (19) was used. Peptides were coupled to the carrier protein keyhole limpet hemocyanin, via *m*-maleimidobenzoic acid *N*-hydroxysuccinimide ester, through a cysteine residue, injected intradermally into rabbits after mixing with Freund's complete adjuvant, and subsequently injected i.m. at multiple sites in incomplete Freund's adjuvant. IgG was purified from high-titer antisera using an ImmunoPurePlus (A) IgG purification kit. Topoisomerase I-specific antibodies were purified by passing the IgG fraction over an affinity column

² The abbreviations used are: PMSF, phenylmethylsulfonyl fluoride; SDS, sodium dodecyl sulfate; PAGE, polyacrylamide gel electrophoresis; GAPDH, glyceraldehyde-3-phosphate dehydrogenase; SSC, saline-sodium citrate buffer; SSPE, saline-sodium phosphate-EDTA buffer; cDNA, complementary DNA; poly(A)⁺, polyadenylated; TBST, Tris-buffered saline/Tween.

TOPOISOMERASE I EXPRESSION IN HUMAN TUMOR BIOPSIES

Table 2. Topoisomerase I content (ng/mg protein)

Topoisomerase I contents from human surgical specimens were determined by Western blot analysis. Quantitation was done by separating equal amounts of protein from normal and tumor tissue homogenates along with different concentrations of HeLa cell lysates. A value of 0.6 ng topoisomerase I/10⁶ HeLa cells (20) was used to calculate the topoisomerase I contents. Values are means \pm SD.

Tumor type	Normal	Tumor
Colorectal	2.7 \pm 1.8 (n = 7)	24.6 \pm 10.2 (n = 6)
Prostate	3.7 \pm 1.0 (n = 7)	15.5 \pm 10.1 (n = 7)
Kidney	4.9 \pm 0.6 (n = 4)	4.7 \pm 1.0 (n = 4)

Table 3. Topoisomerase I mRNA levels in colorectal tumors expressed as the ratio of tumor to normal and clinical and pathological characteristics of these patients

mRNA from normal colon and colon tumor from each patient (2 μ g) was analyzed as described in Fig. 8. Values represent ratio of tumor to normal. Patients 26–30 in whom mRNA levels were measured were different from patients 1–8 who were used for quantitating topoisomerase I levels and its catalytic activity.

Patient	Age (yr)	Sex	Dukes staging	Topoisomerase I mRNA levels
26	70	Male	B2	17.0
27	53	Female	B1	33.0
28	75	Female	C2	10.0
29	72	Male	B2	2.0
30	63	Male	B1	3.0

prepared by coupling peptide to Sulfolink coupling gel through the cysteine residue of the peptide. Affinity-purified antibodies were dialyzed and stored at -100°C in phosphate-buffered saline containing 0.5 mg/ml bovine serum albumin and 0.02% sodium azide.

For immunoblot analysis, tissues were homogenized in buffer A at 4°C and then extracted with an equal volume of SDS sample buffer (4% SDS, 10% 2-mercaptoethanol, and 0.004% bromophenol blue in 160 mM Tris-HCl, pH 6.8). Proteins were separated electrophoretically by 7.5% SDS-PAGE. SDS-polyacrylamide gels and Immobilon-P membranes were equilibrated in transfer buffer (20 mM Tris, 192 mM glycine, pH 8.2, containing 0.08% SDS and 20% methanol) for 30 min. The proteins were transferred to Immobilon-P membrane at 45 V for 25 min in transfer buffer. The blots were incubated overnight in blocking buffer, 3% powdered nonfat milk, in TBST (10 mM Tris, pH 8.0, 150 mM NaCl, 0.05% Tween 20, 0.02% sodium azide). The blots were then incubated for 6 h with topoisomerase I-specific affinity-purified antibodies diluted 1:200 in blocking buffer; they were washed three times with TBST and incubated with ¹²⁵I-labeled Protein A in blocking buffer (1 μ Ci/ml) for 45–60 min. After the blots were washed three times with TBST, they were subjected to autoradiography and the topoisomerase I-related bands were quantitated by densitometry, or the bands were quantitated directly from the filters by phosphorimaging (Molecular Dynamics).

Preabsorption of Autoimmune Serum or Topoisomerase I Peptide Antibodies with HeLa Cell Extract Topoisomerase I. HeLa cell lysate was fractionated by preparative SDS-PAGE and the proteins were transferred to Immobilon-P. A strip of the membrane was cut away and incubated with the anti-topoisomerase I peptide antibodies or autoimmune serum, and the topoisomerase I-related band was detected with ¹²⁵I-labeled Protein A. This membrane piece was aligned with the remaining untreated membrane. The membrane band corresponding to the topoisomerase I band was cut out. Autoimmune serum or anti-topoisomerase I peptide antibodies were preabsorbed on this membrane containing topoisomerase I.

Assay of Topoisomerase I Activity in Crude Extracts. Topoisomerase I catalytic activity was determined by a specific, sensitive, and quantitative assay based on the formation of a covalent enzyme-DNA intermediate (20, 21). The cycle of strand breakage and religation during topoisomerase I action proceeds through an intermediate in which a covalent linkage is formed between a tyrosine residue on the enzyme and a 3'-phosphoryl residue at the cleavage site in DNA. This assay measures the transfer of ³²P from ³²P-labeled DNA to topoisomerase I. ³²P-labeled topoisomerase I molecules are identified by SDS-PAGE and quantitated by phosphorimaging or by densitometry.

The reaction mixture contained 50 mM Tris-HCl, pH 7.5, 60 mM NaCl, 5 mM MgCl₂, 1 mM dithiothreitol, 0.1 μ g pBR322 nick-translated DNA (specific activity, 4–5 \times 10⁸ cpm/ μ g DNA), 30 μ g/ml nuclease-free bovine serum albumin, and 1–5 μ l of tissue homogenate, in a total volume of 30 μ l. After

incubation at 37°C for 30 min, DNase I was added at a concentration of 125 μ g/ml and the incubation was continued for an additional 15 min. The reaction was stopped by adding an equal volume of buffer containing 0.16 M Tris-HCl, pH 6.8, 4% SDS, 30% glycerol, and 10% 2-mercaptoethanol. The samples were boiled for 5 min and proteins were separated by 7.5% SDS-PAGE at 200 V for 45 min. The gels were dried onto Whatman No. 3MM paper and autoradiographed. The topoisomerase I-related bands were quantitated by use of either a phosphorimager or a densitometer. The addition of protease inhibitors during enzyme incubation did not have any significant effect on either purified topoisomerase I or topoisomerase I catalytic activity from tissue homogenates. The enzyme activity was stable at least for 1 week when tissue extracts were stored at -100°C . At 4°C , about 80% of the topoisomerase I activity was lost in about 2 weeks.

Preparation of a Topoisomerase I-specific cDNA Probe. The cDNA was synthesized from 2 μ g total RNA from HeLa cells using random hexamers and Moloney murine leukemia virus reverse transcriptase. The topoisomerase I-specific cDNA was amplified by polymerase chain reaction using CAGAATTCGACCTCGAGATGAGGATGATGTTG and GCAAGCTTG-TATTTCTGCCAGTCCTTCTCACC forward and backward primers, respectively. These primers were selected from the topoisomerase I cDNA sequence (18) and synthesized with EcoRI and HindIII sites. The 930-base pair amplified cDNA was purified and cloned into EcoRI/HindIII sites of pGEM3Zf⁺ (Promega Corporation). Identity of the topoisomerase I cDNA was confirmed by digesting the DNA with EcoRI and HindIII to confirm its expected size, by sequencing 5' and 3' ends, and by determining the presence of sites for restriction enzymes.

Preparation and Analysis of Poly(A)⁺ RNA. Total RNA from human tissues was prepared by the guanidinium isothiocyanate method as described by Chirgwin *et al.* (22). Polyadenylated RNA was purified by three cycles of oligothymidylate-cellulose chromatography. Poly(A)⁺ RNA was also isolated directly from tissues using the Poly(A) tract 1000 kit from Promega Corporation. RNA was quantitated by its absorbance at 260 nm. Poly(A)⁺ RNA (2 μ g/lane) was denatured at 65°C for 10 min in 50% formamide, 6.5% formaldehyde, 40 mM 3-(N-morpholino)propanesulfonic acid and 1 mM EDTA pH adjusted to 7.0 with acetic acid buffer and separated on a 1% agarose gel containing 0.74% formaldehyde. The RNA was transferred onto a Nytran membrane in 20 \times SSC overnight and immobilized by exposure of the filter to UV in Stratilinker UV cross-linker (Stratagene Inc.). Filters were prehybridized in 5 \times Denhardt's reagent, 5 \times SSPE, 0.5% SDS, 50% formamide, 0.25 mg/ml heat-denatured salmon sperm DNA, at 42°C for 18 h. Hybridization was performed at 42°C for 48 h in 1 \times Denhardt's reagent, 5 \times SSPE, 0.25% SDS, 50% formamide, with 0.25 mg/ml salmon sperm DNA and ³²P-labeled topoisomerase I-specific probe (both heat denatured by boiling for 10 min). The filters were washed in the following sequence: once in 2 \times SSC/0.1% SDS at room temperature for 10 min, twice in 1 \times SSC/0.1% SDS at 42°C for 15 min each time, twice in 0.1 \times SSC/0.1% SDS at 50°C for 15 min, and finally twice in 0.1 \times SSC/0.1% SDS at 60°C for 15 min each time. The filters were partially dried and exposed to X-ray film at -100°C with an intensifying screen. The topoisomerase I-specific probe was removed by washing the filter in 0.01 \times SSPE/0.5% SDS at 85°C for 20 min. To normalize for loading differences, the same filter was hybridized with a GAPDH probe. The topoisomerase I-specific 4.1-kilobase bands were quantitated by scanning autoradiographs with a densitometer.

RESULTS

Detection and Quantitation of Topoisomerase I in Human Tumors by Immunoblotting. Human topoisomerase I is a single polypeptide chain of *M*_r 100,000 and is known to produce smaller degradation products (*M*_r 60,000–70,000) in cell extracts because of proteolysis (23–25). Topoisomerase I has been purified from a variety of human cells (10, 23), including the human colon tumor cell line HT-29 (10). Therefore, throughout this work, HT-29 cells were used as a standard of comparison. Topoisomerase I levels in matched pairs of human tumors and normal tissue counterparts were analyzed using an affinity-purified polyclonal antibody raised against peptide *a* (see "Materials and Methods"). As seen in Fig. 1, this antibody reacted with *M*_r 54,000, 68,000, and 100,000 bands from normal colon and

TOPOISOMERASE I EXPRESSION IN HUMAN TUMOR BIOPSIES

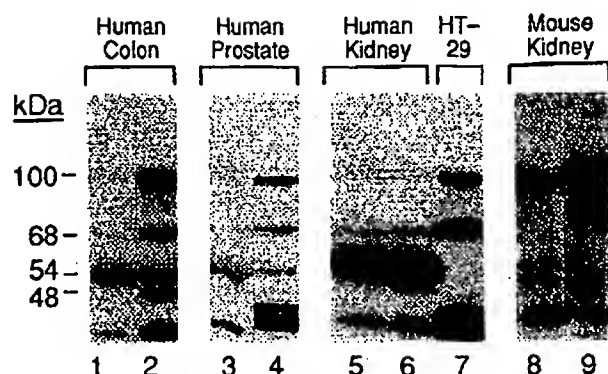


Fig. 1. Analysis of topoisomerase I in human and mouse tissues by Western blot analysis. Protein from tissue homogenates (60–120 μ g) was separated by 7.5% SDS-PAGE and transferred to Immobilon-P transfer membranes. The blots were treated with affinity-purified anti-topoisomerase I peptide antibodies. The bands were detected with 125 I-labeled Protein A. Lanes 1 and 2, normal colon and colon tumor; lanes 3 and 4, benign prostatic hyperplasia and prostate tumor; lanes 5 and 6, normal kidney and kidney tumor; lane 7, HT-29 cell extract; lanes 8 and 9, mouse kidney tissue homogenate and kidney nuclear extract, respectively. Results for colorectal, prostatic, and kidney tumors are for patients 7, 12, and 18, respectively.

colon tumors, benign prostatic tissue and prostatic tumor, and normal kidney and kidney tumors. The M_r 54,000 band appeared specific to human tissues, because the band was almost undetectable in crude or nuclear extracts from mouse liver (data not shown) and mouse kidney (Fig. 1, Lanes 8 and 9). A variety of anti-topoisomerase I antibodies cross-reacted with these three bands, i.e., human autoimmune sera containing autoantibodies against topoisomerase I from four different scleroderma patients, polyclonal antibodies raised against peptides b and c of the topoisomerase I molecule, and polyclonal antibodies raised against purified topoisomerase I from HeLa cells (data not shown). However, preabsorption experiments suggested that the M_r 54,000 band is not derived from topoisomerase I but that the M_r 68,000 band is. As shown in Fig. 2, preabsorption of the polyclonal antibodies raised against peptide a with a molar excess of peptide I inhibited reactivity with purified calf thymus topoisomerase I (Fig. 2, Lane 8 versus Lane 12) and the topoisomerase I-specific M_r 68,000 (Fig. 2, Lanes 1 and 2 versus Lanes 3 and 4 and Lane 6 versus Lane 10) and M_r 100,000 (Fig. 2, Lane 5 versus Lane 9) bands from human tissues and the HT-29 human colon tumor cell line (Fig. 2, Lane 7 versus Lane 11) but did not inhibit reactivity with the M_r 54,000 band in human tissues (Fig. 2, Lanes 1 and 2 versus Lanes 3 and 4 and Lanes 5 and 6 versus Lanes 9 and 10). Similar results were observed when the polyclonal antibodies were preabsorbed with HeLa cell extract topoisomerase I before blotting (data not shown). Preabsorption of the autoimmune sera with HeLa cell extract topoisomerase I also did not inhibit reactivity with the M_r 54,000 protein band (Fig. 2, Lane 13 versus Lane 16), while inhibiting reactivity with purified calf thymus topoisomerase I and topoisomerase I from HeLa cell lysate (compare Fig. 2, Lanes 14 and 15 with Lanes 17 and 18). Preabsorption of antibodies raised with a peptide derived from topoisomerase II had no effect (data not shown). Therefore, these results strongly suggest that the M_r 100,000 and 68,000 bands, but not the M_r 54,000 band, from the human tumors are, indeed, topoisomerase I. These observations are consistent with the M_r 100,000 band being intact topoisomerase I (23–25) and the M_r 68,000 band being a degradation product. Indeed, a M_r 68,000 carboxyl-terminal fragment of topoisomerase I is produced during purification from HeLa cells (23). Therefore, in general, peptide antibodies detected only a M_r 68,000 form of topoisomerase I in human kidney tissues (Fig. 1, Lane 5 and 6; Fig. 2, Lanes 1 and 2) and M_r 68,000 and 100,000 forms in colorectal and prostatic tissues (Fig. 1, Lanes 1–4). However, occasionally only the M_r 68,000 band was observed in both colorectal and

prostatic tissues (Fig. 2, Lane 6, and Fig. 3, Lane 1 for colon; data for prostate not shown).

In all tumor types studied, occasionally an additional M_r 48,000 band was detected which was not present in the normal tissue counterparts (Fig. 1, Lanes 2, 4, and 6; Fig. 2, Lanes 2, 5, and 6). This band was also inhibited by preabsorption of antibodies with peptide I (Fig. 2, Lane 2 versus Lane 4 and Lanes 5 and 6 versus Lanes 9 and 10), suggesting that the M_r 48,000 protein band is also related to topoisomerase I. The M_r 48,000 band was also recognized by autoimmune serum (Fig. 3, compare Lanes 1 and 2 with Lanes 4 and 5). The identity of other lower molecular weight bands observed in human tissues and HT-29 cell extracts has not been reported, although partial inhibition of these bands was observed upon preabsorption of antibodies with peptide (Fig. 2, Lanes 3, 4, and 9–11). However, these other bands were not detected with autoimmune serum (Fig. 3, Lanes 4–6); therefore, we believe it is unlikely that these other lower molecular weight bands represent topoisomerase I.

Having identified the M_r 100,000, 68,000, and 48,000 bands as being topoisomerase I, by Western blotting, we quantitated topoisomerase I levels in human colon, prostate, and kidney tumors using affinity-purified polyclonal antibodies raised against peptide I. As summarized in Tables 1 and 2 and Fig. 4, elevated levels of topoisomerase I were observed in eight colorectal tumors and eight of nine prostate tumors. Colon tumors exhibited 5–35-fold increases in topoisomerase I levels, compared to the normal colon mucosa from the same patient. In prostate tumors, topoisomerase I levels were 2–10-fold higher, compared to benign hyperplastic prostate tissue from the same patients. In one prostate tumor, topoisomerase I levels were the

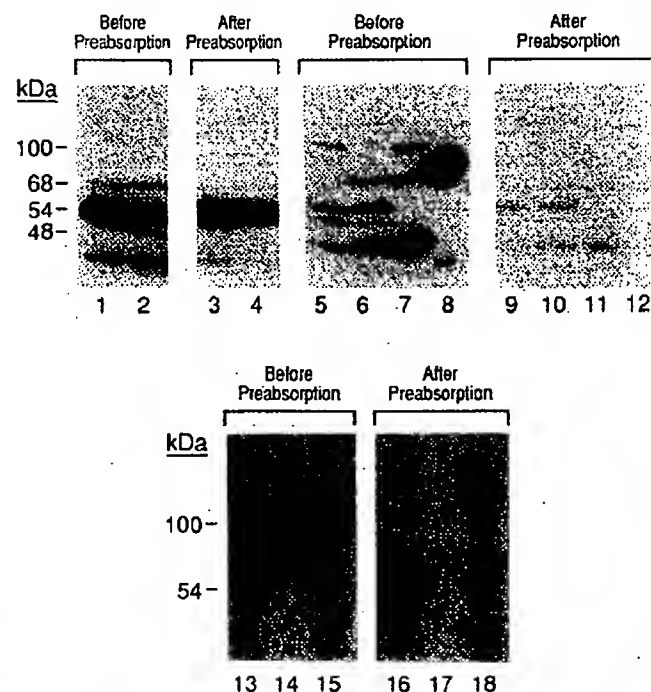


Fig. 2. Identification of topoisomerase I-related bands in human tumors by immunoblotting. Immunoblotting was performed as described in Fig. 1. For preabsorption, peptide antibodies (1:200 dilution) were first incubated with a 50-fold molar excess of peptide I at 4°C for 1 h before incubation with the blots. Autoimmune serum (1:6000 dilution) was preabsorbed with HeLa cell extract as described in "Materials and Methods." Lanes 1 and 2, normal kidney and kidney tumor; lanes 3 and 4, normal kidney and kidney tumor after preabsorption; lane 5, prostatic tumor; lane 6, colon tumor; lane 7, HT-29 cell extract; lane 8, purified calf thymus topoisomerase I; lanes 9–12, same as lanes 5–8 except antibodies were preabsorbed with peptide; lane 13, human kidney tumor; lane 14, purified calf thymus topoisomerase I; lane 15, HeLa cell lysates; lanes 16–18, same as lanes 13–15 except autoimmune serum was preabsorbed with the HeLa cell extract. Occasionally a M_r 100,000 topoisomerase I band was detected in kidney tissues. The kidney homogenates used in lane 2 and lane 13 are from different kidney tumor samples.

TOPOISOMERASE I EXPRESSION IN HUMAN TUMOR BIOPSIES

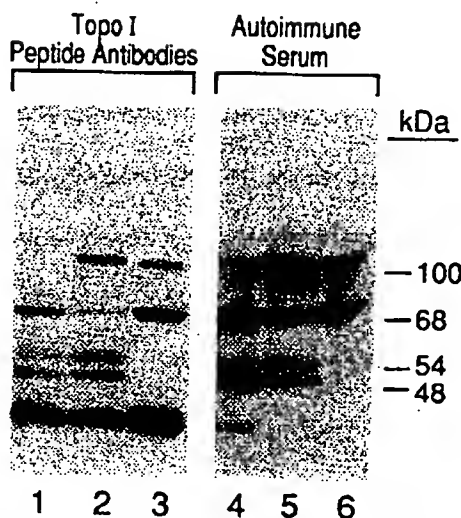


Fig. 3. Detection of topoisomerase I in tissue homogenates by immunoblotting using affinity-purified anti-topoisomerase I peptide antibodies and autoimmune serum from scleroderma patients. Immunoblotting was performed as described in Fig. 1. Lane 1, colon tumor; lane 2, prostate tumor; lane 3, HT-29 extract; lanes 4-6, same as lanes 1-3 except autoimmune serum (1:2000 dilution) was used instead of anti-topoisomerase I peptide antibodies. A weak M_r 100,000 band (lane 1) detected by anti-peptide antibodies, compared to a strong M_r 100,000 band in lane 4 detected by autoimmune serum, is probably due to the high affinity of these autoimmune antibodies.

same as in normal tissue. In contrast, eight kidney tumors did not exhibit any elevation of this enzyme, compared to their corresponding normal matched samples. Normal colorectal, prostate, and kidney tissues showed similar levels of topoisomerase I (Table 2).

Quantitation of Topoisomerase I Catalytic Activity in Crude Extracts from Human Tumors. To determine whether the topoisomerase I which is elevated in human tumor tissues is enzymatically active, we measured the catalytic activity of the enzyme in tumor tissues by a specific, sensitive, and quantitative assay based on the formation of a covalent enzyme-DNA intermediate through a tyrosine residue on the enzyme and a 3'-phosphoryl residue at the cleavage site on DNA (20). This assay has been used previously for quantitating topoisomerase I in nuclear extracts from cultured cells (20, 21) but not in cell or tissue extracts without first preparing nuclei. Here, we have adapted this assay and demonstrate that it is possible to quantitate topoisomerase I catalytic activity in crude extracts from human tumor specimens without preparing nuclei.

We first measured topoisomerase I activity in crude extracts from the HT-29 human colon tumor cell line without isolating nuclei. As shown in Fig. 5, an ATP-independent topoisomerase I-specific band of M_r 84,000 was detected (Fig. 5, Lanes 1 and 2). This single M_r 84,000 band probably results from the degradation of the M_r 100,000 band to the M_r 68,000 form during the extraction procedure, and the M_r 68,000 band then migrates as an M_r 84,000 species due to the attachment of a short oligonucleotide after DNase I digestion (see "Discussion"). Preabsorption of the crude extracts with polyclonal antibodies raised against peptide I of topoisomerase I or with scleroderma serum reduced or prevented the appearance of the topoisomerase I-specific band (Fig. 5, Lanes 3-6), whereas preabsorption with antibodies against topoisomerase II had no effect (Fig. 5, Lanes 7 and 8), suggesting that the assay can measure topoisomerase I activity directly in crude extracts. The total activity of topoisomerase I measured in the crude extract from HT-29 cells was similar to that measured in nuclear extracts from the same number of HT-29 cells (data not shown). Using this approach, we detected a topoisomerase I-specific band in crude extracts from human colon, prostate, and kidney tumors (Fig. 6). Results of topoisomerase I estimation in colon, prostate, and kidney tumors by the ^{32}P transfer assay are summarized in Table 1 and Fig.

4 for comparison with the Western blotting measurements. Compared to paired normal tissue, colon and prostate tumors showed 11-40- and 4-26-fold increases, respectively, in catalytic activity of topoisomerase I. Kidney tumors did not show a significant change in catalytic activity, compared to their normal counterparts. In general, there was a good correlation between catalytic activity of the enzyme and its level in tumor tissue (Fig. 7).

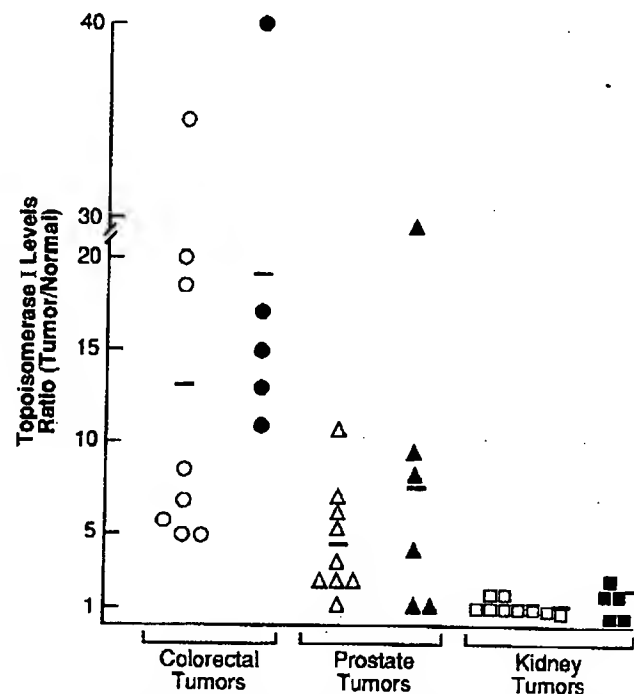


Fig. 4. Topoisomerase I levels in colorectal, prostate, and kidney tumors. Topoisomerase I levels were estimated in human tumor and matched normal samples by Western blotting (O, Δ, □). The catalytic activity of topoisomerase I in the same samples was determined by the ^{32}P -transfer assay (●, ▲, ■). Topoisomerase I levels are expressed as the ratio of tumor to normal values. — denotes mean values for each tumor type. In two kidney samples, the ratio of tumor to normal values for catalytic activity was <1. In these samples the intensity of topoisomerase I-related bands in the tumors was much lower than in their matched normal tissues, making it difficult to quantitate accurately. Therefore, the values for these two kidney tumor samples were not included in determination of a mean value.

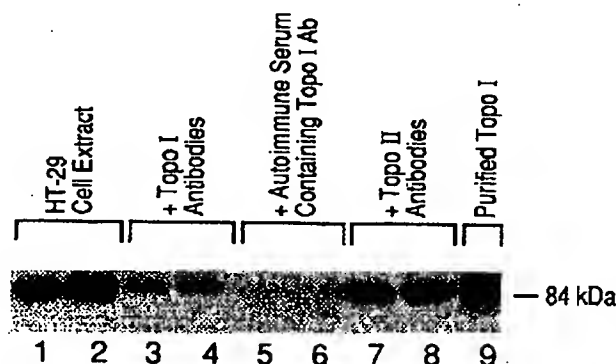


Fig. 5. Determination of topoisomerase I catalytic activity in crude extracts from the HT-29 colon tumor cell line by the ^{32}P -transfer assay. HT-29 cell extracts were incubated with ^{32}P -labeled nick-translated pBR322 DNA. ^{32}P -labeled proteins were analyzed by SDS-PAGE as described in "Materials and Methods." Gels were dried and autoradiographed. Lanes 1 and 2, 2 and 4 μ l of HT-29 extracts; lanes 3 and 4, HT-29 extracts (2 and 4 μ l) preabsorbed with anti-topoisomerase I peptide antibodies before incubation with nick-translated DNA; lanes 5 and 6, HT-29 extracts (2 and 4 μ l) preabsorbed with autoimmune serum containing anti-topoisomerase I antibodies; lanes 7 and 8, 2 and 4 μ l of HT-29 extracts preabsorbed with affinity-purified anti-topoisomerase II peptide polyclonal antibodies; lane 9, purified topoisomerase I from calf thymus.

TOPOISOMERASE I EXPRESSION IN HUMAN TUMOR BIOPSIES

Detection of Topoisomerase I mRNA by Northern Blot Analysis. To measure the steady state levels of mRNA, we isolated poly(A)⁺ RNA from five human colon tumors and corresponding normal colon mucosa (these specimens were not from the patients listed in Tables 1 and 2). A 930-base pair DNA topoisomerase I-specific probe hybridized to a single mRNA species of 4.1 kilobases. This corresponds to the size of the topoisomerase I mRNA which has been described previously (18, 26). Fig. 8 is an autoradiogram of a Northern blot. Quantitative analysis by densitometry showed that levels of topoisomerase I mRNA were elevated in all five colon tumors, compared to the normal colon mucosa (Fig. 8; Table 3). Loading differences were corrected for by hybridizing the filters with a GAPDH cDNA probe (27). In addition, the gel was stained after the transfer step to

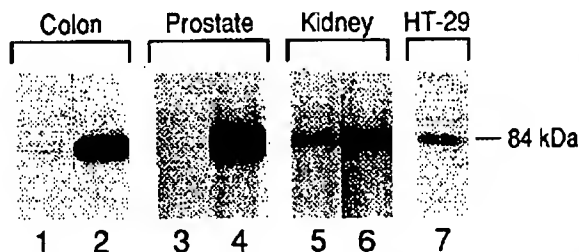


Fig. 6. Estimation of topoisomerase I catalytic activity in human colon, prostate, and kidney tumors and their matched normal counterparts by the ³²P-transfer assay. One to 5 μ l of crude homogenates from tumors and their normal counterparts, containing equal amounts of protein, were used in assays. Activity was determined as described in "Materials and Methods" and Fig. 5. A single M_r 84,000 topoisomerase I band was detected and quantitated by densitometry. Lanes 1 and 2, normal colon and colon tumor homogenate; lanes 3 and 4, benign prostatic hyperplasia and prostate tumor homogenates; lanes 5 and 6, normal kidney and kidney tumor homogenate; lane 7, HT-29 cell extract. The catalytic activity determined in colorectal, prostate, and kidney tumors was for patients 2, 12, and 18, respectively.

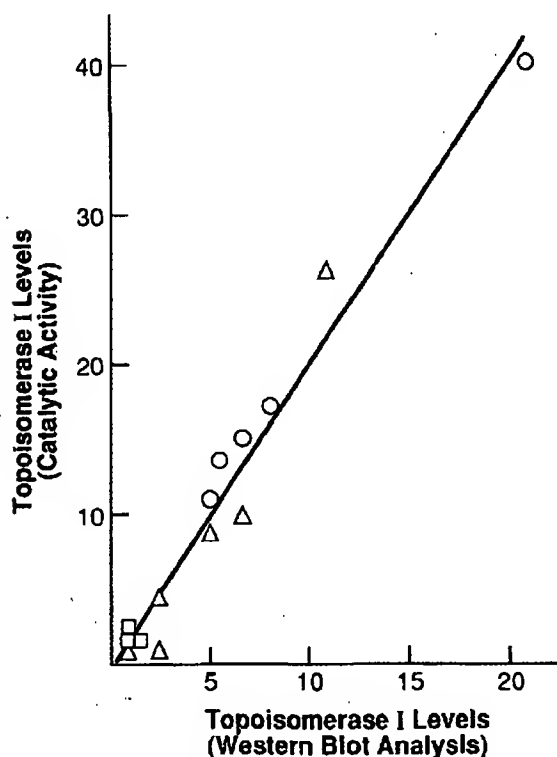


Fig. 7. Relationship between topoisomerase I protein levels and catalytic activity. Topoisomerase I levels determined by Western blotting were plotted against catalytic activity determined by the ³²P-transfer assay. The data are from Table 1. O, colon tumor; Δ , prostate tumor; \square , kidney tumor.

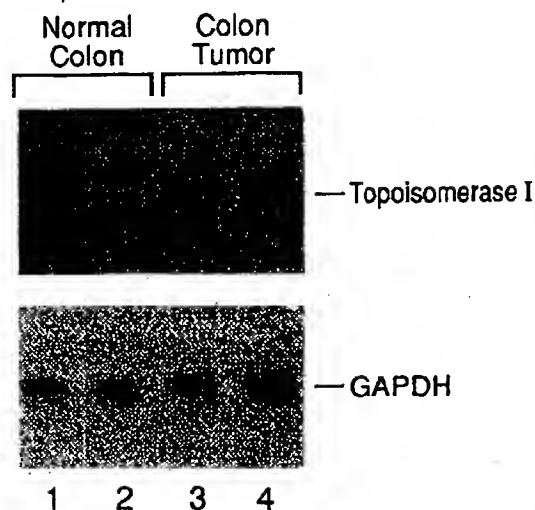


Fig. 8. Northern blot analysis of topoisomerase I mRNA from normal colon and colon tumors. Two μ g poly(A)⁺ RNA from normal colon and colon tumors were fractionated on 1% agarose-formaldehyde gels, transferred to Nytran membranes, and hybridized with the 970-base pair topoisomerase I cDNA fragment as described in "Materials and Methods." The topoisomerase I-specific bands were quantitated by densitometry. The same filter was hybridized with GAPDH probe, to normalize the RNA loading differences, after removing the topoisomerase probe. Lanes 1 and 3, normal colon and colon tumor from one patient; lanes 2 and 4, normal colon and colon tumor from a second patient.

ensure equal transfer of RNA from all lanes. These results suggest that increased levels of topoisomerase I in colon tumors might result from either increased transcription of the topoisomerase I gene or increased stability of mRNA in these tumors.

Relationship between Topoisomerase I Levels in Colorectal, Prostate, and Kidney Tumors and Their Staging. When the patients' tumor samples were stratified according to their staging, there was no correlation between levels of topoisomerase I in tumors and their staging (Table 1). However, a larger number of samples are probably required to establish such a relationship.

DISCUSSION

Topoisomerase I has been identified as an intracellular target of camptothecin, a plant alkaloid with anticancer activity. Various lines of evidence suggest that the sensitivity of cells to camptothecin is directly related to the topoisomerase I content (9-11). Giovanella *et al.* (14) suggested that the topoisomerase I levels were elevated in human colon adenocarcinoma, based on immunoblotting. We have confirmed and significantly extended the findings of those investigators. In this report we have quantitated the expression of topoisomerase I at the level of catalytic activity, protein content, and mRNA content in surgical specimens of human colorectal, prostate, and kidney tumors and in matched normal tissue from the same patients. Results indicate that in tumors of the colon and prostate, but not kidney, topoisomerase I catalytic activity, protein expression, and mRNA content (colon only) were significantly elevated, compared to matched controls. There was a good correlation between mRNA levels, enzyme levels, and catalytic activity. However, no correlation was seen between levels of topoisomerase I in tumor samples and their staging.

To our knowledge this is the first report to utilize crude extracts and the quantitative ³²P-transfer assay for determination of topoisomerase I catalytic activity in human tissues. This is also the first report wherein levels of topoisomerase I protein have been correlated with its catalytic activity in human tumor tissues. In addition to the work reported here, Van der Zee *et al.* (15) measured topoisomerase I catalytic activity in human malignant ovarian tumors by a semiquan-

titative relaxation assay and found the activity to be 8-fold elevated, compared to benign tumors of the ovary.

Human topoisomerase I has a native molecular weight of 100,000 but is known to readily undergo proteolysis during extraction of cells and tissues (23-25). Topoisomerase I levels were quantitated by Western blotting using affinity-purified peptide antibodies. In colon and prostate tissues *M*, 68,000 and 100,000 protein bands were detected, while in kidney only the *M*, 68,000 band was detected by the antibodies. In all tumor types studied an additional *M*, 48,000 band was detected occasionally which was not present in the normal tissue counterparts. Preabsorption of antibodies with the topoisomerase I peptide antigen resulted in inhibition of the *M*, 48,000, 68,000, and 100,000 bands, suggesting that all three protein bands are related to topoisomerase I. Thus, even though samples were prepared in buffer containing proteolytic inhibitors and tissues were solubilized by adding boiling SDS sample buffer, proteolysis of topoisomerase I was only partially preventable. Preabsorption experiments suggest that the *M*, 54,000 band detected in all tumor types is not related to topoisomerase I.

Topoisomerase I catalytic activity was measured in crude extracts from tumor and normal tissues by a ³²P-transfer assay. We used this method because it allowed us to determine topoisomerase I catalytic activity in small surgical specimens without the need to prepare nuclei. This method is sensitive, specific, and quantitative, in contrast to the semiquantitative relaxation assay used by others to estimate topoisomerase I activity. A single topoisomerase I-specific band (*M*, 84,000) was detected in crude extracts from HT-29 cells and from colon, prostate, and kidney tissues. It is possible that during extraction of the enzyme all of the *M*, 100,000 band is cleaved to the *M*, 68,000 form, even in the presence of proteolytic inhibitors. Indeed, a *M*, 68,000 carboxyl-terminal fragment, which retains relaxation activity has been detected during topoisomerase I purification from HeLa cells (23). Furthermore, in a few samples of colon and prostate we detected only the *M*, 68,000 band by Western blotting. Champoux (28) has shown that digestion of DNA by DNase I after covalent intermediate formation leaves an oligonucleotide residue approximately 17 ± 8 nucleotides long attached to topoisomerase I, resulting in reduced mobility of the enzyme. This might explain the mobility shift from the *M*, 68,000 active form of the enzyme in Western blotting to the *M*, 84,000 form in the ³²P-transfer assay (Fig. 6). Indeed, calf thymus topoisomerase I (native molecular weight, 84,000) is degraded mostly to the *M*, 68,000 form (Fig. 2, Lane 14), which then migrates as an *M*, 84,000 band in the activity assay because the oligonucleotide residue is attached to it (Fig. 5, Lane 9). The *M*, 48,000 fragment occasionally observed in tumor tissues by Western blotting might not have catalytic activity, because we never observed a corresponding band in the catalytic activity assay.

Quantitative analysis showed that the catalytic activity of topoisomerase I was elevated in colon and prostate tumors. These results demonstrate that the increase in catalytic activity is due to an increase in the amount of the enzyme. In general, the increase in catalytic activity is slightly more than the increase in enzyme content. We do not have a full explanation for this observation. However, it has been shown that the *M*, 68,000 form of topoisomerase I from chicken RBC shows about 2-fold higher activity than the intact *M*, 100,000 form of the enzyme (25). In addition, it is possible that intracellular factors present in crude homogenates may modulate the topoisomerase I activity.

Increased levels of mRNA detected in colorectal tumor samples, compared to normal specimens from the same patients, suggest that the increased topoisomerase I levels results from either increased transcription of the topoisomerase I gene or increased mRNA stability. The average increase of 13-fold in topoisomerase I mRNA levels in

colorectal tumors is very close to the average 13-fold increase in topoisomerase I protein levels determined by Western blotting. However, increased levels of topoisomerase I in some tumors might also be due to translational regulation or alteration of protein stability, because mRNA and protein levels were determined in different tumor samples and there was a wide range of RNA and protein levels in different samples. The increased transcription of the topoisomerase I gene observed in colorectal tumors might result from transactivation of the topoisomerase I gene by as yet unknown transcription factors through various potential regulatory transcriptional elements present in the promoter region of the topoisomerase I gene (29, 30). One such candidate might be *c-fos*. The *c-fos* gene is one of the earliest known genes activated in response to mitogenic stimuli (31). The 5' regulatory sequences for topoisomerase I contain an AP-1 binding site (29, 30). Therefore, *c-fos* might activate topoisomerase expression through binding to the AP-1 site. This speculation is supported by the recent observation of Scanlon *et al.* (32) that increased expression of *c-fos* in cisplatin-resistant cell lines is accompanied by enhanced topoisomerase I expression.

Increases in topoisomerase I mRNA levels have been observed in response to partial hepatectomy in rats (33), after serum stimulation of resting HeLa 299 cells (34), and after treatment of human fibroblast cells with phorbol 12-myristate 13-acetate (35). Infection of HeLa cells by adenovirus also resulted in increased topoisomerase I-specific mRNA (36). This increase in mRNA was not accompanied by a corresponding increase in topoisomerase I protein, suggesting that topoisomerase I protein synthesis could be regulated at both the transcriptional and translational levels. The latter results are contradictory to the observation of Chow and Pearson (20), who showed that increased topoisomerase activity after adenovirus infection of HeLa cells was due to a corresponding increase in the amount of enzyme.

In conclusion, we have shown that topoisomerase I levels and catalytic activity are elevated in human colorectal and prostate tumors, but not kidney tumors, probably as a result of either increased transcription or increased mRNA stability. These results and the observation that cells overexpressing active topoisomerase I are hypersensitive to camptothecin (9) suggest that estimation of topoisomerase I in tumor biopsies from patients may be useful as a diagnostic tool for predicting the responsiveness and selective cytotoxicity of topoisomerase I-directed drugs. Specifically, these results suggest that colorectal and prostate carcinomas may be more responsive to topoisomerase I-directed chemotherapeutic agents than carcinoma of the kidney.

ACKNOWLEDGMENTS

We thank Renae Crosby for making the cDNA probe for topoisomerase I, John Bisi for Northern blot analysis of normal colon and colon tumor samples, and Mary Ellen Buchbalt for her help in preparing the manuscript.

REFERENCES

1. Wang, J. C. DNA topoisomerases. *Annu. Rev. Biochem.*, 54: 665-697, 1985.
2. Wang, J. C. Recent studies on DNA topoisomerases. *Biochim. Biophys. Acta*, 909: 1-9, 1987.
3. Liu, L. F. DNA topoisomerase poisons as antitumor drugs. *Annu. Rev. Biochem.*, 58: 351-375, 1989.
4. Hsiang, Y.-H., Hertzberg, R., Hecht, S., and Liu, L. F. Camptothecin induces protein-linked DNA breaks via mammalian DNA topoisomerase I. *J. Biol. Chem.*, 260: 14873-14878, 1985.
5. Kunimoto, T., Niita, K., Tanaka, T., Uehara, N., Baha, H., Takuchi, M., Yokokura, T., Sawada, S., Miyasaka, T., and Mutai, M. Antitumor activity of 7-ethyl-10-[4-(1-piperidino)-1-piperidino]carbonyloxy-camptothecin, a novel water soluble derivative of camptothecin, against murine tumors. *Cancer Res.*, 47: 5944-5947, 1987.
6. Schneider, E., Hsiang, Y.-H., and Liu, L. F. DNA topoisomerases as anticancer drug targets. *Adv. Pharmacol.*, 27: 149-183, 1990.
7. Davies, S. M., Robson, C. N., Davies, S. L., and Hickson, I. D. Nuclear topoisomerase II levels correlate with the sensitivity of mammalian cells to intercalating agents and epipodophyllotoxins. *J. Biol. Chem.*, 263: 17724-17729, 1988.
8. Fry, A. M., Chresta, C. M., Davis, S. M., Walker, M. C., Harris, A. L., Hartley, J. A.,

TOPOISOMERASE I EXPRESSION IN HUMAN TUMOR BIOPSIES

- Masters, J. R. W., and Hickson, I. D. Relationship between topoisomerase II levels and chemosensitivity in human tumor cell lines. *Cancer Res.*, 51: 6592-6595, 1991.
9. Madden, K. R., and Champoux, J. J. Over-expression of human topoisomerase I in baby hamster kidney cells: hypersensitivity to clonal isolates in camptothecin. *Cancer Res.*, 52: 525-532, 1992.
 10. Sugimoto, Y., Tsukahara, S., Ohhara, T., Isue, T., and Tsuruo, T. Decreased expression of DNA topoisomerase I in camptothecin resistant tumor cell lines as determined by a monoclonal antibody. *Cancer Res.*, 50: 6925-6930, 1990.
 11. Bjornsti, M.-A., Benedetti, P., Vigilanti, G. A., and Wang, J. C. Expression of human DNA topoisomerase I in yeast cells lacking yeast DNA topoisomerase I: restoration of sensitivity of the cells to the antitumor drug camptothecin. *Cancer Res.*, 49: 6318-6323, 1989.
 12. Heck, M. S., and Earnshaw, W. C. Topoisomerase II: a specific marker for cell proliferation. *J. Cell. Biol.*, 103: 2569-2581, 1986.
 13. D'Arpa, P., and Liu, L. F. Topoisomerase-targeting antitumor drugs. *Biochim. Biophys. Acta*, 939: 163-177, 1989.
 14. Giovannella, B. C., Steblin, J. S., Wall, M. E., Wani, M. C., Nicholas, A. W., Liu, L. F., Silber, R., and Pomesil, M. DNA topoisomerase I targeted chemotherapy of human colon cancer in xenografts. *Science (Washington DC)*, 246: 1046-1048, 1989.
 15. Van der Zee, A. G. J., Hollema, H., Jong, S., Boonstra, H., Gouw, A., Willemse, P. H. B., Zijlstra, J. G., and Varies, E. G. E. P-glycoprotein expression and DNA topoisomerase I and II activity in benign tumors of the ovary and in malignant tumors of the ovary, before and after platinum/cyclophosphamide chemotherapy. *Cancer Res.*, 51: 5915-5920, 1991.
 16. Holden, J. A., Rolfson, D. H., and Wittwer, C. T. Human DNA topoisomerase II: evaluation of enzyme activity in normal and neoplastic tissues. *Biochemistry*, 29: 2127-2134, 1990.
 17. Shcio, J. H., Bordwell, B., Rothfield, N. F., and Earnshaw, W. C. High titers of autoantibodies to topoisomerase I (sc170) in sera from scleroderma patients. *Science (Washington DC)*, 231: 737-740, 1986.
 18. D'Arpa, P., Machlin, P. S., Ratic, H. III, Rothfield, N. F., Cleveland, D. W., and Earnshaw, W. C. cDNA cloning of human DNA topoisomerase I: catalytic activity of a 67.7 kd carboxyl-terminal fragment. *Proc. Natl. Acad. Sci. USA*, 85: 2543-2547, 1988.
 19. Tsni-Pflufelder, M., Liu, L. F., Liu, A. A., Tewey, K. M., Whang-Peng, J., Knutsen, T., Huebner, K., Croce, C. M., and Wang, J. C. Cloning and sequencing of cDNA encoding human DNA topoisomerase II and localization of the gene to chromosome region 17q21-22. *Proc. Natl. Acad. Sci. USA*, 85: 7177-7181, 1988.
 20. Chow, K., and Pearson, G. D. Adenovirus infection elevates levels of cellular topoisomerase I. *Proc. Natl. Acad. Sci. USA*, 82: 2247-2251, 1985.
 21. Crespi, M. D., Meadovan, A. G., and Baldi, A. Increment of DNA topoisomerase I: chemically and virally transformed cells. *Exp. Cell Res.*, 175: 206-215, 1988.
 22. Chirgwin, J. M., Przybyl, A. E., McDonald, R. J., and Rulter, W. J. Isolation of biologically active ribonucleic acid from sources enriched in ribonuclease. *Biochemistry*, 18: 5294-5299, 1979.
 23. Liu, L. F., and Miller, K. G. Eukaryotic DNA topoisomerases: two forms of type I DNA topoisomerases from HeLa cell nuclei. *Proc. Natl. Acad. Sci. USA*, 78: 3487-3491, 1981.
 24. Champoux, J. J. Proteins that affect DNA conformation. *Annu. Rev. Biochem.*, 47: 449-479, 1978.
 25. Tricole, T., and Kowalski, D. Topoisomerase I from chicken erythrocytes: purification, characterization and detection by a deoxyribonucleic acid binding assay. *Biochemistry*, 22: 2025-2031, 1983.
 26. Juan, C.-C., Hwang, J., Liu, A. A., Whang-Peng, J., Knutsen, T., Huebner, K., Croce, C. M., Zhang, H., Wang, J. C., and Liu, L. F. Human DNA topoisomerase I is encoded by a single-copy gene that maps to chromosome region 20q12-13.2. *Proc. Natl. Acad. Sci. USA*, 85: 8910-8913, 1988.
 27. Fort, P., Marty, L., Pischarczyk, M., Elsabrouty, S., Dani, C., Jeancour, P., and Blanchard, J. M. Various rat adult tissues express only one major mRNA species from the glyceraldehyde-3-phosphate-dehydrogenase multigenic family. *Nucleic Acids Res.*, 13: 1431-1442, 1985.
 28. Champoux, J. J. DNA is linked to the rat liver DNA nicking-closing enzyme by a phosphodiester bond to tyrosine. *J. Biol. Chem.*, 256: 4805-4809, 1981.
 29. Kunze, N., Klein, M., Richter, A., and Knippers, R. Structural characterization of the human DNA topoisomerase I gene promoter. *Eur. J. Biochem.*, 194: 323-330, 1990.
 30. Kunze, N., Yang, G., Dolberg, M., Sundarp, R., Knippers, R., and Richter, A. Structure of the human type I DNA topoisomerase gene. *J. Biol. Chem.*, 266: 9610-9616, 1991.
 31. Greenberg, M. E., and Ziff, E. B. Stimulation of 3T3 cells induces transcription of the c-fos proto-oncogene. *Nature (Lond.)*, 311: 433-438, 1984.
 32. Scanlon, K. J., Jiao, L., Funato, T., Wang, W., Tone, T., Rossi, J. J., and Kashami-Sabel, M. Ribozyme mediated cleavage of c-fos mRNA reduces gene expression of DNA synthesis enzyme and metallothionein. *Proc. Natl. Acad. Sci. USA*, 88: 10591-10595, 1991.
 33. Sobczak, J., Tournier, M. F., Lotti, A. M., and Douquet, M. Gene expression in regenerating liver in relation to cell proliferation and stress. *Eur. J. Biochem.*, 180: 49-53, 1989.
 34. Romig, H., and Richter, A. Expression of the topoisomerase I gene in serum stimulated human fibroblasts. *Biochim. Biophys. Acta*, 1048: 274-280, 1990.
 35. Hwang, C. L., Chen, M. S., and Hwang, J. Phorbol ester transiently increases topoisomerase I mRNA in human skin fibroblasts. *J. Biol. Chem.*, 264: 14923-14926, 1989.
 36. Romig, H., and Richter, A. Expression of the type I DNA topoisomerase gene in adenovirus-5 infected human cells. *Nucleic Acids Res.*, 18: 801-808, 1990.
 37. Gleason, D. F., Mellinger, G. T., and the VA Cooperative Urological Research Group. Prediction of prognosis for prostatic adenocarcinoma by combined histological grading and clinical staging. *J. Urol.*, 111: 58, 1974.
 38. Schroder, F. H., Hermanek, P., Denis, L., Gospodarowicz, M. K., and Pavone-Macaluso, M. The TNM classification of prostate cancer. *Prostate*, 4 (Suppl.): 129-138, 1992.
 39. Hermanek, P., Sobin, L. H. (eds.) TNM Classification of Malignant Tumors, Ed. 4, Berlin: Springer Verlag, 1987.

FGH52352

CI-06859209-6

FGH52352

CISTI ICIST

CI-06859209-6

Document Delivery Service
in partnership with the Canadian Agriculture LibraryService de fourniture de Documents
en collaboration avec la Bibliothèque canadienne de l'agriculture**THIS IS NOT AN INVOICE / CECI N'EST PAS UNE FACTURE**LYNN BRAZIL
LIBRARIANHELLER EHRMAN WHITE & MCAULIFFE
275 MIDDLEFIELD RD
MENLO PARK, CA 94025
UNITED STATES

ORDER NUMBER: CI-06859209-6

Account Number: FGH52352

Delivery Mode: F31

Delivery Address: 650/324-6034

Submitted: 2007/05/11 14:24:52

Received: 2007/05/11 14:24:52

Printed: 2007/05/11 21:36:40

Direct	Periodical	OPENURLOPAC	UNITED STATES

Client Number: 39780-7000 CD

Title: THE BRITISH JOURNAL OF CANCER

DB Ref. No.: IRN1006168X

ISSN: ISSN00070920

Vol./Issue: 93/7

Date: 2005

Pages: 774-80

Article Title: A EXPRESSION OF THE UBIQUITIN-PROTEASOME PATHWAY AND MUSCLE LOSS IN
EXPERIMENTAL CANCER CACHEXI"

Article Author: KHAL, J., ET AL

Report Number: IRN1006168X

Publisher: H.K. LEWIS AND CO.,

Estimated cost for this 7 page document: \$12.5 document supply fee +
\$30 copyright = \$42.5

The attached document has been copied under license from Access Copyright/COPIBEC or other
rights holders through direct agreements. Further reproduction, electronic storage or electronic transmission,
even for internal purposes, is prohibited unless you are independently licensed to do so by the rights holder.

Phone/Téléphone: 1-800-668-1222 (Canada - U.S./E.-U.) (613) 998-8544 (International)

www.nrc.ca/cisti

Fax/Télécopieur: (613) 993-7619

www.cnrc.ca/icist

info.cisti@nrc.ca

info.icist@nrc.ca

National Research
Council CanadaConseil national
de recherches Canada

Page

1 / 1



Expression of the ubiquitin-proteasome pathway and muscle loss in experimental cancer cachexia

J Khal¹, SM Wyke¹, ST Russell¹, AV Hine¹ and MJ Tisdale^{*,1}

¹Pharmaceutical Sciences Research Institute, Aston University, Birmingham B4 7ET, UK

Muscle protein degradation is thought to play a major role in muscle atrophy in cancer cachexia. To investigate the importance of the ubiquitin-proteasome pathway, which has been suggested to be the main degradative pathway mediating progressive protein loss in cachexia, the expression of mRNA for proteasome subunits C2 and C5 as well as the ubiquitin-conjugating enzyme, E2_{14k}, has been determined in gastrocnemius and pectoral muscles of mice bearing the MAC16 adenocarcinoma, using competitive quantitative reverse transcriptase polymerase chain reaction. Protein levels of proteasome subunits and E2_{14k} were determined by immunoblotting, to ensure changes in mRNA were reflected in changes in protein expression. Muscle weights correlated linearly with weight loss during the course of the study. There was a good correlation between expression of C2 and E2_{14k} mRNA and protein levels in gastrocnemius muscle with increases of 6–8-fold for C2 and two-fold for E2_{14k} between 12 and 20% weight loss, followed by a decrease in expression at weight losses of 25–27%, although loss of muscle protein continued. In contrast, expression of C5 mRNA only increased two-fold and was elevated similarly at all weight losses between 7.5 and 27%. Both proteasome functional activity, and proteasome-specific tyrosine release as a measure of total protein degradation was also maximal at 18–20% weight loss and decreased at higher weight loss. Proteasome expression in pectoral muscle followed a different pattern with increases in C2 and C5 and E2_{14k} mRNA only being seen at weight losses above 17%, although muscle loss increased progressively with increasing weight loss. These results suggest that activation of the ubiquitin-proteasome pathway plays a major role in protein loss in gastrocnemius muscle, up to 20% weight loss, but that other factors such as depression in protein synthesis may play a more important role at higher weight loss.

British Journal of Cancer (2005) 93, 774–780. doi:10.1038/sj.bjc.6602780 www.bjcancer.com

Published online 6 September 2005

© 2005 Cancer Research UK

Keywords: cachexia; protein degradation; ubiquitin-proteasome proteolysis; gastrocnemius muscle

Loss of skeletal muscle is a prominent feature of cancer cachexia, resulting in weakness, immobility and finally death. Body composition analysis of lung cancer patients who had lost 30% of their body weight revealed a 75% reduction in skeletal muscle mass, while visceral proteins were preserved (Fearon, 1992). Loss of skeletal muscle protein is thought to arise from a suppression of protein synthesis (Emery *et al*, 1984) and/or an increase in protein breakdown and oxidation of amino acids (O'Keefe *et al*, 1990).

A number of experimental animal tumours have been developed to study the mechanism of muscle wasting in cachexia. In the murine MAC16 colon adenocarcinoma model, weight loss occurs with small tumour burden (less than 0.1% of host weight), and without a reduction of food and water intake (Beck and Tisdale, 1987), allowing a study of the metabolic components of cachexia. As in cancer patients, the major components of body weight loss in the MAC16 model are adipose tissue and skeletal muscle mass. Loss of skeletal muscle mass arises from a reduction (by 60%) in protein synthesis and an increase (three-fold) in protein degradation (Beck *et al*, 1991). As was found in a rat model of cancer cachexia (Baracos *et al*, 1995; Llovera *et al*, 1997), the major contribution to the loss of muscle mass in mice bearing the MAC16 tumour appears to arise from an upregulation of the ATP-

ubiquitin-dependent proteolytic pathway (Lorite *et al*, 1998), as reflected by increased levels of ubiquitin-conjugated proteins and increased mRNA levels for the 14kDa ubiquitin carrier protein, E2 and the C9 proteasome subunit in gastrocnemius muscle. However, as with other studies in animals this was only measured after weight loss had developed, and there have been no measurements of the expression of the major components of the ubiquitin-proteasome pathway at different extents of weight loss, or a comparison between different muscle types to understand if this pathway totally explains protein degradation. However, a study in gastric cancer patients showed an increase in expression of ubiquitin mRNA and proteasome activity compared with controls, and proteasome activity correlated both with stage of disease and weight loss (Bossola *et al*, 2003).

The purpose of the present study was to measure changes in expression of the key regulatory components of the ubiquitin-proteasome proteolytic pathway in skeletal muscle with the development of cachexia in the MAC16 model. Protein degradation in this model has been shown to increase progressively with increasing weight loss between 15 and 30%, up to a maximum increase of 240% at a weight loss of 30% (Smith and Tisdale, 1993a). Expression of mRNA for E2, and the proteasome subunits C2 and C5, representing α and β subunits of the proteasome respectively, have been determined in gastrocnemius and pectoral muscle by quantitative RT-PCR as a measure of the ubiquitin-proteasome pathway. These are considered to be representative of

*Correspondence: MJ Tisdale; E-mail: mj.tisdale@aston.ac.uk

Revised 10 August 2005; accepted 10 August 2005; published online 6 September 2005

proteasome structural and catalytic subunits indicative of proteasome expression. Previous studies (Lorite *et al*, 2001; Whitehouse *et al*, 2001) have shown that subunits of the 19S regulator change in concert with the proteasome α -subunit. As a measure of ubiquitin conjugation mRNA levels for E2_{14k} have been determined, which was originally suggested to be rate-limiting for ubiquitin conjugation during starvation (Wing and Banville, 1994), although studies in E2_{14k} knockout mice suggest that it is nonessential (Adegoke *et al*, 2002). However, recent data suggest that the ubiquitin-protein ligases (E3), muscle ring-finger 1 (MURF1); (Bodine *et al*, 2001) and muscle atrophy F box (MAFbx)/atrogin-1 (Gomes *et al*, 2001), may be the rate-limiting step in various conditions of muscle atrophy including cachexia.

In this study, the expression of some components of the ubiquitin-proteasome pathway has been monitored with increasing weight loss in gastrocnemius and pectoral muscle of mice bearing the MAC16 tumour, since some reports (Khal *et al*, 2005) suggest that the expression of this pathway in the skeletal muscle of cancer patients decreases at weight losses greater than 20%. Measurements of protein levels of proteasome α -subunits and E2_{14k} have also been determined by immunoblotting to ensure that changes in mRNA are reflected in changes in protein expression.

MATERIALS AND METHODS

Materials

Mouse monoclonal antibody to 20S proteasome subunits α 1, 2, 3, 5 and 7 (clone MCP231) was purchased from Affinity Research Products (Exeter, UK). Rabbit polyclonal antisera to E2_{14k} was a gift from Dr Simon Wing (McGill University, Montreal, Canada). The antibody detected E2_{14k} as a M_r 17 kDa band (Rajapurohitam *et al*, 1999). Goat polyclonal antiserum to MURF3 (E3) and peroxidase-conjugated rabbit polyclonal antisera to goat IgG were purchased from Abcam Ltd (Cambridge, UK). Mouse monoclonal anti-PIF antibody was prepared as previously (Todorov *et al*, 1996). Peroxidase-conjugated goat anti-rabbit and rabbit anti-mouse secondary antibodies were from Dako Ltd (Cambridge, UK).

WizardTM mini or maxi preps, used to prepare plasmid DNA from overnight cultures of bacterial clones, were obtained from Promega (Southampton, UK), as were the T7 RNA polymerase kit, RNasin inhibitor, reverse transcriptase, reverse transcription buffer and PCR grade magnesium chloride. Taq polymerase and Hybond C were from Amersham Biosciences UK Ltd (Bucks, UK), TRI reagent for RNA isolation was purchased from Sigma-Aldrich Co-Ltd (Dorset, UK), while the oligonucleotide primers were from MWG Biotech (Ebersberg, Germany). RNA storage buffer was purchased from Ambion Ltd (Cambridgeshire, UK) and PCR buffer was from Roche, Switzerland.

Animals

All animal experiments have been carried out with ethical committee approval. The ethical guidelines that were followed met the standards required by the UKCCR guidelines (Workman *et al*, 1998).

Pure strain NMRI mice were obtained from our own inbred colony and were fed a rat and mouse breeding diet (Special Diet Services, Witham, UK). Fragments of the MAC16 colon adenocarcinoma, excised from donor animals with established weight loss, were implanted into the flanks of NMRI mice by means of a trocar, as described (Beck and Tisdale, 1987). Animals started to lose weight approximately 10–12 days after transplantation. Animals were terminated at various extents of weight loss, and both gastrocnemius and pectoral muscles were removed, and

immediately frozen in liquid nitrogen, and stored at -70°C before further analysis.

Measurement of protein degradation *ex vivo*

Gastrocnemius muscles were excised from mice bearing the MAC16 tumour, and with varying extents of weight loss, and preincubated for 45 min in 3 ml oxygenated (95% oxygen/5% carbon dioxide) Krebs–Henseleit bicarbonate buffer, pH 7.4, containing 5 mmol l^{-1} glucose and 0.5 mmol l^{-1} cycloheximide. Protein degradation was determined by the release of tyrosine (Waalkes and Udenfriend, 1957) over a 2 h period in the absence and presence of lactacystin ($10\text{ }\mu\text{M}$). Tyrosine release, which was blocked in the presence of lactacystin, was considered to be proteasome specific.

Measurement of proteasome activity

The 'chymotrypsin-like' enzyme activity of the proteasome was measured fluorometrically as described by Orino *et al* (1991). Muscles were removed from animals with varying degrees of weight loss and homogenized with a teflon glass homogenizer in 20 mM Tris-HCl, pH 7.5, 2 mM ATP, 5 mM MgCl₂ and 1 mM DTT on ice at 4°C . The homogenate was further dissociated by sonication at 4°C , and the sonicate was then centrifuged at 18 000 g for 10 min, and the supernatant was used to measure enzyme activity by the release of aminomethylcoumarin (AMC) from succinyl-LLVY-AMC. The reaction was performed for 1 h at room temperature in 100 mM Tris, HCl, pH 8.0, and was terminated by the addition of 80 mM sodium acetate, pH 4.3. The fluorescence of AMC was determined with an excitation wavelength of 360 nm and an emission wavelength of 460 nm. The reaction was performed in the presence and absence of the specific proteasome inhibitor lactacystin, and only lactacystin suppressible activity was considered to be proteasome specific. The activity was adjusted for the protein concentration of the sample, determined using the Bradford assay (Sigma Aldridge, Dorset, UK).

Quantitative RT-PCR

Total RNA was extracted from muscle using TRI-reagent and the RNA concentration was determined from the absorbance at 260 nm. To quantitate the mRNA of interest, increasing amounts of competitor RNA, which differed from the mRNA of interest by containing a short deletion, were added to 250 ng of total RNA and coamplified using RT-PCR. The amount of specific mRNA was calculated from the amount of competitor, when equal amounts of PCR product were obtained from the competitor and target RNA.

The C2 proteasome subunit mRNA was amplified using the primer pairs: 5'-CGCACGGAGTGTCTGGTTGCAC-3' (forward) and 5'-GTACGAGCTGATTGAGAACGG-3' (reverse) and corresponds to positions 176–187 and 531–552 bp. The competitor primer was designed to produce a DNA fragment containing a 76-bp deletion by producing a loop in the DNA during the PCR amplification process. The sequence of this primer was 5'-GTACGAGCTGATTGAGAACGGCATAACCAGCAATGAGCAGCC-3', which corresponds to the reverse complement of bases 561–552 and 435–455 of the mouse C2 gene. The competitor product was 309 bp. The C5 proteasome mRNA was obtained from the mouse gene using the primer pairs: 5'-TCAACGGAGGTACTGTATTGG-3' and 5'-GCATGGCACTTGCTGAGCC-3' at positions 101–121 and 496–514 bp. The competitor primer was designed 117 bp upstream of the reverse primer producing a product 277 bp long. The sequence of this primer was 5'-GCATGGCACTTGCTGAGCCGATGGCACTTGCTGAGCC-3', which corresponds to the reverse complement of bases 496–514 and 358–377 of the mouse C5 gene. The E2_{14k} competitor was obtained from the rat gene using the primer pairs: 5'-CTCATGCGGGATTCAAGCG-3' and 5'-CTCTTCTCA



TACTCCCCGTTTGCAT-3'. The competitor primer contained a 111 bp deletion and the sequence was 5'-CTCTTCTCATAC'CCC GTTGCATCGCTTCTGCAGGATGTC, which corresponds to the reverse complement of bases 143-168 and 312-321 of the rat gene. The competitor DNAs were blunt ended and then ligated into a pET30a vector, which had been blunt-end cut with *Sma*I restriction enzyme. The ligated vector was used to transform DH5 α competent cells. Plasmid DNA was prepared from PCR positive clones using Wizard-mini-prep. Competitor RNA was produced using T7 RNA polymerase kit, and quantitated using the optical density at 260 nm. Six serial two-fold dilutions were prepared containing known concentrations of competitor. The particular dilutions used were selected to span the selected concentration of C2, C5 and E2_{14k} in the sample.

To synthesise the cDNA template, a mixture consisting of 250 ng target RNA, the particular dilution of the competitor RNA and 0.5 μ g of random hexamer was incubated at 70°C for 5 min in a thermal cycler (Genetic Research, Instrumentation Ltd, Essex, UK) and then chilled on ice before the addition of 2.5 μ l 5 \times reverse transcription buffer, 3 μ l of 10 mM each of dATP, dGTP, dCTP, dTTP, 5 units of RNasin inhibitor and 1 unit reverse transcriptase in a total volume of 12.5 μ l. Incubation was at 37°C for 1 h. For the amplification of the cDNA by PCR, 50 μ l of PCR mix was added to each tube. The PCR mixture contained 1 \times PCR buffer (without magnesium) together with 3 mM MgCl₂ (E2), 3.5 mM MgCl₂ (C5) and 2.5 mM MgCl₂ (C2) together with 1 U *Taq* polymerase. For the E2 gene 10 pmol of each of the primers 5'-CTCATGCGGGATT CAAGCG-3' and 5'-CTCTTCTCATACT'CCCGTTTG-3' were used, while for the C5 gene 10 pmol of each of the primers 5'-TCAACGGAGGTACTGTATTGG-3' and 5'-GCATGGCACITGCT GAGCC-3' were used. For the C2 gene, 20 pmol of each of the primers 5'-CGCACGCAGTGCTGGTTGCAC-3' and 5'-GTACGAG CTGATTGAGAACCG-3' were used. The temperature-cycling profile for amplification was as follows: 95°C for 2 min for one cycle followed by 95°C for 30 s, 58°C annealing for 1 min and 72°C extension for 1 min for 30 cycles. Control reactions containing all components except reverse transcriptase and another without template were carried out alongside each experiment to show that the RNA (both target and competitor) had no DNA contamination, while the second control showed that there was no contamination in the PCR mixture. Coamplification of E2 target and competitor produced DNA fragments of 395 and 284-bp, respectively; C2 target and competitor produced 385 and 309-bp fragments and C5 target and competitor produced 414 and 297-bp fragments, respectively.

For analysis of results, 15 μ l of PCR products were separated on a 2% (w/v) agarose gel containing ethidium bromide. The gel images were visualised on a UV transilluminator and photographed. The intensity of the bands was quantitated using a Phoretix photo-imager programme. The volumes of the competitor and target bands were plotted against the known serial dilutions of the competitor used in the experiment. The amount of the sample RNA corresponds to the amount of competitor when the ratio of competitor to target is 1.0.

Western blot analysis

Cytosolic protein (5 μ g for E2 and 20S proteasome α -subunits) was resolved on 10% sodium dodecylsulphate, polyacrylamide gels. Proteins were then transferred to nitrocellulose membranes (Hybond C), which had been blocked with 5% Marvel in Tris buffered saline (TBS) at 4°C overnight. The primary and secondary antibodies, peroxidase conjugated either rabbit anti-goat, goat anti-rabbit or rabbit anti-mouse IgG, were used at a 1:1500 dilution. Incubation was for 1 h at room temperature and development was by enhanced chemiluminescence (ECL) (Amersham). Blots were scanned by a densitometer to quantitate differences, and a parallel gel was stained by coomassie blue stain to ensure

equal loading. The intensity of bands was quantitated using 'Phoretix 1D Advanced' software as above.

Statistical analysis

Results were expressed as means \pm s.e.m. of three separate determinations on different animals. Differences were determined by one-way analysis of variance (ANOVA) followed by Tukey-Kramer multiple comparison test. *P*-values less than 0.05 were considered to be significant.

RESULTS

The effect of increasing weight loss on expression of C2 and C5 mRNA as well as 20S proteasome α -subunit protein levels, detected by Western blotting, and gastrocnemius muscle weights of mice bearing the MAC16 tumour is shown in Figure 1. Although the monoclonal antibody to the 20S proteasome reacts with six different α -type subunits, only three bands were apparent at approximate *M_r* 29, 32 and 35 kDa (Whitehouse *et al*, 2001) (Figure 1A). There was a good correlation between expression of C2 mRNA (Figure 1C) and proteasome protein (Figure 1B), with a 6-8-fold increase in C2 mRNA with increasing weight loss from 12%, reaching a maximum at 15-20% weight loss. Although C2 mRNA expression at 25-27% weight loss was significantly enhanced above that found in animals without weight loss (Figure 1C), it was significantly decreased (*P* < 0.05) compared with animals exhibiting 20% weight loss. In contrast, expression of C5 mRNA was significantly increased (by two-fold) at all weight losses (Figure 1D), with no significant difference between animals with 7.5% weight loss and those with 27% weight loss. Gastrocnemius muscle weight was directly proportional to total body weight loss, showing progressive loss of skeletal muscle as the cachexia progresses (Figure 1E). Proteasome functional activity in gastrocnemius muscle as determined by the 'chymotrypsin-like' enzyme activity, the dominant catalytic activity of the β -subunits of the proteasome, was found to follow a similar change with weight loss as expression of protein and mRNA of proteasome α -subunits, with an initial increase with weight loss up to 20% followed by a decrease at higher weight loss (Figure 1F).

The effect of progressive weight loss on the expression of the ubiquitin conjugating protein E2 in gastrocnemius muscle followed a similar pattern to that observed with proteasome α -subunits (Figure 2). Thus, expression of E2 mRNA was increased two-fold in gastrocnemius muscle of mice with 12% weight loss and remained elevated up to 20% weight loss (Figure 2C). The expression of E2 mRNA in gastrocnemius muscle of mice with 25 and 27% weight loss was not significantly different from that in mice without weight loss (Figure 2C). The expression of E2_{14k} protein, detected by Western blotting, followed a similar pattern reaching maximal expression at 15-17% weight loss (Figure 2A, B). Proteasome-specific protein degradation in gastrocnemius muscle, determined by the release of tyrosine in the presence of the specific proteasome inhibitor lactacystin (Fenteany and Schreiber, 1998), also peaked between 17 and 20% weight loss and then decreased at higher weight loss (Figure 2D). These results suggest that the ubiquitin-proteasome proteolytic pathway plays a minor role in the degradation of proteins in gastrocnemius muscle at weight loss greater than 20%.

Proteasome functional activity in pectoral muscle followed a similar pattern to that found in gastrocnemius muscle (Figure 3A) peaking at weight loss between 18 and 22%. Expression of mRNA for the catalytic β subunit (C5) also peaked at weight loss between 17 and 25% with a decrease at higher weight loss (Figure 3B). However, expression of mRNA for the proteasome α -subunit C2 (Figure 3C) as well as protein expression of α -subunits (Figure 3D and E) increased with increasing weight loss with no evidence for a

Proteasome expression in skeletal muscle in cachexia

J Khal et al

MPG

777

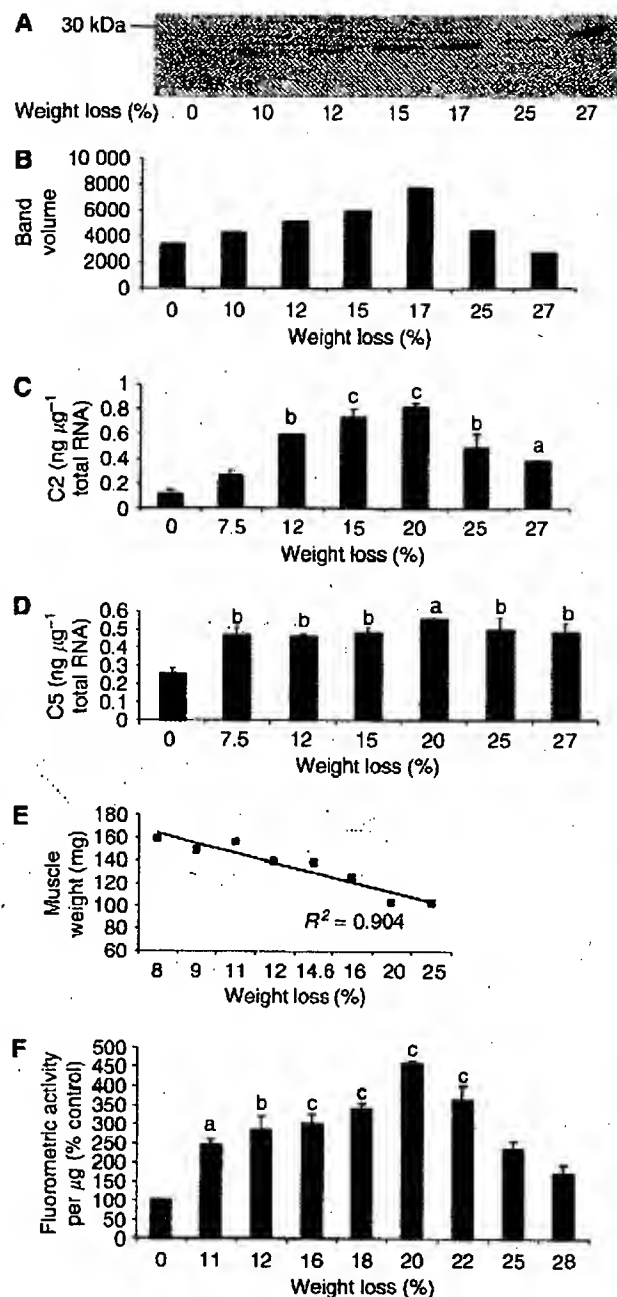


Figure 1 (A) Expression of 20S proteasome α-subunits in soluble fractions of gastrocnemius muscles of mice bearing the MAC16 tumour and with different extents of weight loss, as detected by immunoblotting. (B) Densitometric analysis of band intensities in (A) reported in arbitrary units. (C) Expression of C2 mRNA and (D) expression of C5 mRNA in gastrocnemius muscle from mice with different extents of weight loss. Differences from animals without weight loss are expressed as a, $P < 0.05$, b, $P < 0.01$ and c, $P < 0.001$. (E) Relationship between weight of gastrocnemius muscle and percentage weight loss. (F) Proteasome proteolytic activity, as measured by the 'chymotrypsin-like' enzyme activity, in gastrocnemius muscle of mice with different extents of weight loss. The symbols for significance are the same as in (D).

maximum. As with gastrocnemius muscle there was a linear correlation between pectoral muscle weight and total body weight loss (Figure 3F). Expression of E2 mRNA was little changed with increase in weight loss in pectoral muscle (Figure 4), with a

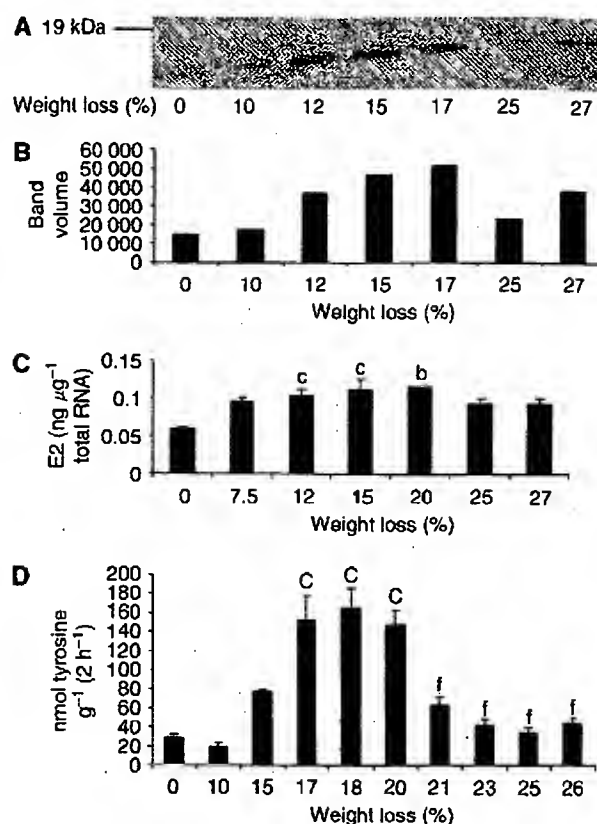


Figure 2 (A) Expression of E2_{4k} in soluble extracts of gastrocnemius muscles from mice bearing the MAC16 tumour and with different extents of weight loss, as detected by immunoblotting. (B) Densitometric analysis of band intensities in (A) reported in arbitrary units. (C) Expression of E2 mRNA in gastrocnemius muscle from mice with different extents of weight loss. (D) Total protein degradation, as measured by tyrosine release, in gastrocnemius muscle of mice with different extents of weight loss. The figures represent protein degradation inhibited by lactacystin (10 μM). Differences from animals without weight loss are expressed as b, $P < 0.01$ or c, $P < 0.001$.

significant increase in expression only being seen in animals with 27% weight loss. This suggests that E2 may not be a rate-limiting step in proteasome proteolysis in this muscle.

DISCUSSION

Skeletal muscle contains multiple proteolytic pathways for intracellular protein catabolism. Of these, the lysosomal system, including cathepsins B, D and H, is mainly concerned with the digestion of extracellular proteins, although some cytosolic proteins are engulfed in autophagic vacuoles that fuse with lysosomes and are degraded (Dice, 1990). The cytosolic calcium-activated pathway (calpains) appears to play an important role in tissue injury, necrosis and autolysis (Lecker et al, 1999). These two processes have been suggested to contribute less than 15–20% towards total protein breakdown in muscle (Attaix et al, 1998; Lecker et al, 1999) and do not breakdown myofibrillar proteins (Lovell et al, 1986). However, the calcium/calpain pathway has been suggested to release myofilaments from the sarcomere in an early and perhaps rate-limiting component of the catabolic response in muscle (Hasselgren and Fischer, 2001). Further catabolism of the actin and myosin released from the myofilaments is considered to occur via the ubiquitin-proteasome proteolytic pathway.

Proteasome expression in skeletal muscle in cachexia

J Khal et al



778

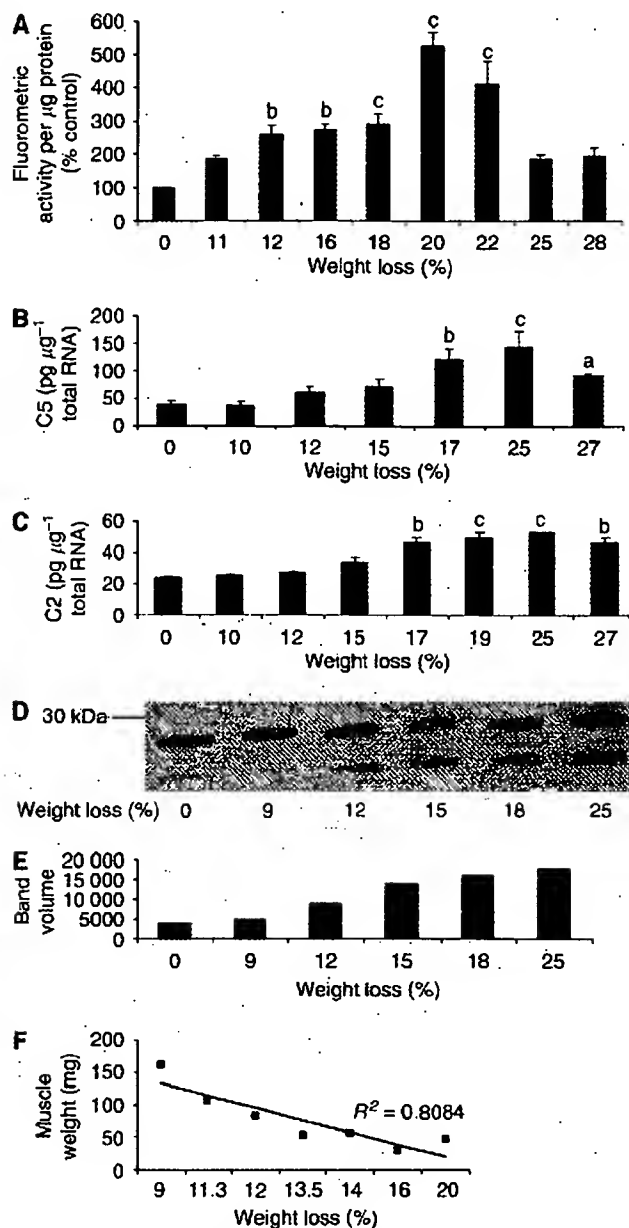


Figure 3 (A) Proteasome proteolytic activity, as measured by the 'chymotrypsin-like' enzyme activity, in pectoral muscle of mice bearing the MAC16 tumour and with different extents of weight loss. (B) Expression of C5 mRNA and (C) expression of C2 mRNA in pectoral muscle from cachectic mice bearing the MAC16 tumour. (D) Expression of 20S proteasome α -subunits, determined by immunoblotting, in soluble extracts of pectoral muscle from mice bearing the MAC16 tumour and different extents of weight loss. (E) Densitometric analysis of band intensities in (D). Differences from animals without weight loss are expressed as a, $P < 0.05$, b, $P < 0.01$ and c, $P < 0.001$. (F) Relationship between weight of pectoral muscle and percentage weight loss.

In this process, substrates are marked for degradation through the attachment of a polyubiquitin chain by a series of enzymatic steps mediated by the ubiquitin-activating enzyme (E1), the ubiquitin-conjugating enzyme (E2) and the ubiquitin-protein ligases (E3) (Lecker *et al*, 1999). The polyubiquitinated substrate then enters the proteolytic chamber of the 26S proteasome, where it is unfolded and cleaved to short oligopeptides having mean lengths of 6–9 residues (Kisselev *et al*, 1999). The proteasome is a

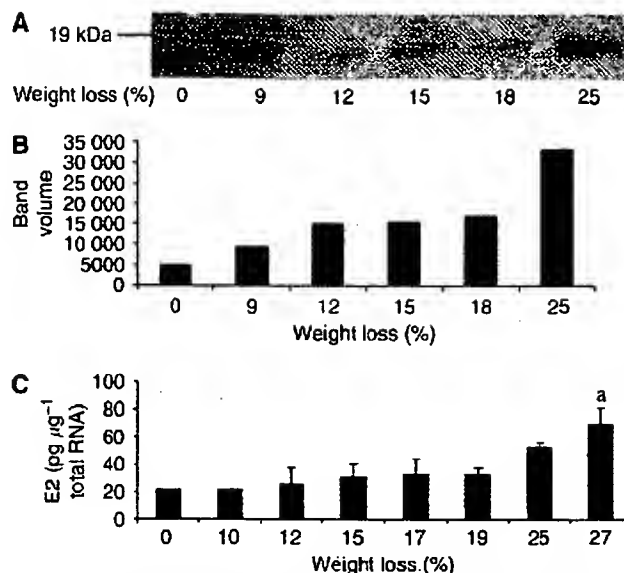


Figure 4 (A) Expression of E2_{14k} in soluble extracts of pectoral muscle from mice bearing the MAC16 tumour and different extents of weight loss, detected by immunoblotting. (B) Densitometric analysis of band intensities in (A) reported in arbitrary units. (C) Expression of E2 mRNA in pectoral muscle of mice with different extents of weight loss. Differences from animals without weight loss are expressed as a, $P < 0.05$.

tube-like structure appearing as a stack of four rings; two outer α -rings and two inner β -rings in order of $\alpha\beta\beta\alpha$ (Lecker *et al*, 1999). Proteolytic activity is found on the β -subunits of the proteasome.

Most studies in cancer patients with weight loss of 10% or higher have suggested that the ubiquitin-proteasome pathway in skeletal muscle shows an increased expression and activity (Williams *et al*, 1999; Bossola *et al*, 2003). However, a study of lung cancer patients referred for curative resection and with a weight loss of only 2.9% showed no increase in expression of components of the ubiquitin-proteasome pathway, while mRNA levels of cathepsin B in skeletal muscle were much higher (Jagoe *et al*, 2002). This suggests that activation of the ubiquitin-proteasome pathway may only occur when weight loss becomes substantial, although Bossola *et al* (2001) reported an increase in ubiquitin mRNA in skeletal muscle of patients when the weight loss was only $5.6 \pm 4.9\%$.

In this study, we have measured the expression of one α (C2) and one β -subunit (C5) of the proteasome during the progression of loss of gastrocnemius and pectoral muscle in the murine MAC16 cachexia model, as a representative of proteasome structure and function. We chose these genes since protein breakdown in cancer cachexia has been suggested to require increased gene expression of proteasome subunits (Temparis *et al*, 1994) and mRNA levels for proteasome subunits C2 and C5 were found to be increased in extensor digitorum longus (EDL) muscles of rats starved for 2 days, as well as in soleus muscles undergoing denervation atrophy (Medina *et al*, 1995). In addition, we have measured expression of mRNA for the ubiquitin-conjugating enzyme (E2_{14k}). Expression of mRNA has been quantitated using RT-competitive PCR, which is based on competitive coamplification of the specific target sequence with an internal standard sharing primer recognition sites in one reaction tube (Auboeuf and Vidal, 1997). Quantitation can then be performed by comparing the PCR signals of the specific template with those obtained with known concentrations of the competitor. Protein expression has also been determined by immunoblotting, since it has been suggested that in various cells elevated concentrations of mRNA of proteasome subunits were not found to be accompanied by increased concentrations of

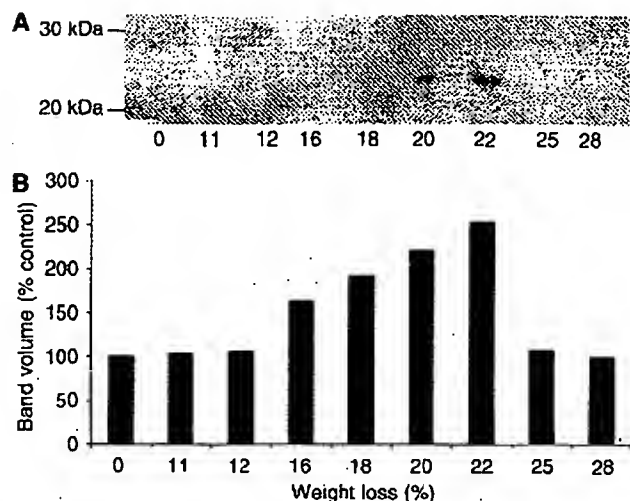


Figure 5 (A) Expression of PIF in urinary extracts of mice bearing the MAC16 tumour. Urine (2 ml) was treated with ammonium sulphate (80% w/v) and stirred overnight at 4°C. The precipitated protein was recovered by centrifugation at 3000 g for 30 min, dialysed against water using an Amicon filtration cell and 15 µg was used for immunoblotting using anti-PIF monoclonal antibody. (B) Densitometric analysis of the band intensities in (A) reported in arbitrary units.

proteasomes (Kanayama *et al*, 1991; Shimbara *et al*, 1992). We have also measured protein expression of E2_{14k}.

Using this approach, we have demonstrated a correlation between increases in mRNA and protein expression of proteasome α subunits in both gastrocnemius and pectoral muscle. We have also demonstrated a correlation between E2 mRNA and protein levels, although this was less strongly correlated with muscle weight, suggesting that it was not rate-limiting for proteasome proteolysis as might be predicted (Adegokc *et al*, 2002). Proteasome expression and activity in both pectoral and gastrocnemius muscles increased progressively with increasing weight loss up to about 20% followed by a decrease at higher weight loss, except for C2 mRNA in pectoralis muscle, which remained elevated. There was also a decrease in E2 expression at weight losses greater than 20%. Proteasome specific total protein degradation in gastrocnemius muscle, as determined by tyrosine release in the presence of lactacystin, also peaked at 18–20% weight loss and then decreased. A similar rise and fall of the ubiquitin-proteasome pathway was observed in psoas muscle of alloxan-induced diabetic rabbits (Galban *et al*, 2001). Thus, the activity increased 3 and 5 days after diabetes induction, but fell down to control values by day 7, and thereafter decreased below control. In pectoral muscle, both mRNA and protein for proteasome α -subunits tended to increase with increasing weight loss, suggesting a lack of coordination between synthesis of α and β subunits. We have previously shown (Smith and Tisdale, 1993a)

that total body nitrogen and the nitrogen content of gastrocnemius muscle decreases with increasing weight loss in mice bearing the MAC16 tumour. The protein content of skeletal muscle is a balance between the rate of protein synthesis and the rate of degradation. Protein synthesis is depressed in muscle of weight-losing mice bearing the MAC16 tumour, and this reduction in protein synthesis may be the major factor contributing to loss of protein at weight losses greater than 20%.

Using the release of tyrosine as a measure of muscle protein degradation breakdown to detect serum factors from the MAC16 tumour that increase protein degradation, activity was found to increase with increasing weight loss up to 20%, and with further weight loss the activity was found to fall to a value not significantly different from that found in animals without weight loss (Smith and Tisdale, 1993b). This circulatory factor has now been isolated and identified (Todorov *et al*, 1996) and shown to be a sulphated glycoprotein of M_r 24 kDa called proteolysis factor (PIF), which induces an increased expression of both proteasome subunits and E2 in gastrocnemius muscle (Lorite *et al*, 2001). Proteolysis factor has been shown to be responsible for the loss of skeletal muscle in cachectic mice (Lorite *et al*, 1998). Using Western blotting to detect urinary PIF in mice bearing the MAC16 tumour, excretion levels were found to be maximal at weight loss between 20 and 22% (Figure 5). This pattern parallels changes in expression of proteasome subunits in both gastrocnemius and pectoral muscle suggesting that PIF is responsible for the upregulation of the ubiquitin-proteasome pathway. Expression of C2 and C5 mRNA in rectus abdominis muscle of cachectic cancer patients was also found to be maximal at a weight loss of 12–19% (Khal *et al*, 2005). The rate of muscle catabolism, as measured by phenylalanine release, in a rat model of cachexia was also highest at small tumour burdens and decreased as the tumour grew larger (de Blaauw *et al*, 1997). This appeared to be caused by the loss of capacity of the tumour to further break down muscle. The reason for this is not known, but it may be that as the tumour grows and becomes necrotic cells capable of synthesizing PIF are lost. Alternatively, the tumour microenvironment may not be conducive to the synthesis of a highly glycosylated peptide.

The mechanism for the loss of protein in gastrocnemius muscle at weight losses greater than 20% requires further investigation, but the lack of bioactivity of serum from mice bearing the MAC16 tumour at weight losses of 20–25% (Smith and Tisdale, 1993b) suggests that a circulatory factor is not responsible for the protein degradation, and the present results suggest that the ubiquitin-proteasome pathway alone cannot account for the high level of protein breakdown. This suggests that depression of protein synthesis may be more important than an increase in protein degradation at high weight loss.

ACKNOWLEDGEMENTS

This work was supported by the Lustgarten Foundation for Pancreatic Cancer Research. We thank Mr M Wynter and Mr W Fleury for tumour transplantation and animal care.

REFERENCES

- Adegokc OA, Bedard N, Roest HP, Wing SS (2002) Ubiquitin-conjugating enzyme E2_{4k}/HR6B is dispensable for increased protein catabolism in muscle of fasted mice. *Am J Physiol* 283: E482–E489
- Attai D, Aourousseau E, Combarret L, Kee A, Larbaud D, Ralliere C, Souweine B, Taillandier D, Tiliganac T (1998) Ubiquitin-proteasome dependent proteolysis in skeletal muscle. *Reprod Nutr Dev* 38: 153–165
- Auboeuf D, Vidal H (1997) The use of the reverse transcriptase competitive polymerase chain reaction to investigate the *in vivo* regulation of gene expression in small tissue samples. *Anal Biochem* 245: 141–148
- Baracos VE, De Vivo C, Hogle DHR, Goldberg AL (1995) Activation of the ATP-ubiquitin-proteasome pathway in skeletal muscle of cachectic rats bearing a hepatoma. *Am J Physiol* 268: E996–E1006
- Beck SA, Smith KL, Tisdale MJ (1991) Anticachectic and antitumour effect of eicosapentaenoic acid and its effect on protein turnover. *Cancer Res* 51: 6089–6093
- Beck SA, Tisdale MJ (1987) Production of lipolytic and proteolytic factors by a murine tumour-producing cachexia in the host. *Cancer Res* 47: 5919–5923



- Rodine SC, Latres E, Baumhueter S, Lai VK M, Nunez L, Clarke BA, Poueymiron WT, Panaro FJ, Na E, Dharmarajan K, Pan AQ, Valenzuela DM, DeChiara TM, Stitt TN, Yancopoulos GD, Glass DJ (2001) Identification of protein ligases required for skeletal muscle atrophy. *Science* 294: 1704-1707
- Bossola M, Muscaritoli M, Costelli P, Bellantone R, Pacelli F, Busquets S, Argiles J, Lopez-Soriano FJ, Civello IM, Baccino FM, Fanelli FR, Doglietto GB (2001) Increased muscle ubiquitin mRNA levels in gastric cancer patients. *Am J Physiol* 280: R1518-R1523
- Bossola M, Muscaritoli M, Costelli P, Grieco G, Bonelli G, Pacelli F, Fanelli FR, Doglietto GB, Baccino FM (2003) Increased muscle proteasome activity correlates with disease severity in gastric cancer patients. *Ann Surg* 237: 384-389
- de Blaauw I, Heineman S, Deutz NEP, von Meyenfeldt MF (1997) Increased whole-body protein and glutamine turnover in advanced cancer is not matched by an increased muscle protein and glutamine turnover. *J Surg Res* 68: 44-55
- Dice JF (1990) Peptide sequences that target cytosolic proteins for lysosomal proteolysis. *TPBS* 15: 305-309
- Emery PW, Edwards RHT, Rennie MJ, Souhami RL, Halliday D (1984) Protein synthesis in muscle measured *in vivo* in cachectic patients with cancer. *BMJ* 289: 584-589
- Fearon KCH (1992) The mechanisms and treatment of weight loss in cancer. *Proc Nutr Soc* 51: 251-265
- Fenteany G, Schreiber SL (1998) Lactacystin, proteasome function, and cell fate. *J Biol Chem* 273: 8545-8548
- Galban VD, Evangelista EA, Migliorini RH, Kettelhut IC (2001) Role of ubiquitin-proteasome-dependent proteolytic process in degradation of muscle protein from diabetic rabbits. *Mol Cell Biochem* 225: 35-41
- Gomes MD, Lecker SH, Jagoe RT, Navon A, Goldberg AL (2001) Atrogin-1, a muscle-specific F-box protein highly expressed during muscle atrophy. *Proc Natl Acad Sci USA* 98: 14440-14445
- Hasselgren PO, Fischer JE (2001) Muscle cachexia: current concepts of intracellular mechanisms and molecular regulation. *Ann Surg* 233: 9-17
- Jagoe RT, Redfern CPE, Roberts RG, Gibson GJ, Goodship THJ (2002) Skeletal muscle mRNA levels for cathepsin B, but not components for the ubiquitin-proteasome pathway, are increased in patients with lung cancer referred for thoracotomy. *Clin Sci* 102: 353-361
- Kanayama H, Tanaka K, Aki M, Kagawa S, Miyaji H, Satoh M, Okada F, Satoh S, Shimbara N, Ichihara A (1991) Changes in expressions of proteasome and ubiquitin genes in human renal cancer cells. *Cancer Res* 51: 6677-6685
- Khal J, Hine AV, Fearon KCH, Dejong CHC, Tisdale MJ (2005) Increased expression of proteasome subunits in skeletal muscle of cancer patients with weight loss. *Int J Biochem Cell Biol* in press. Available online
- Kisselev AF, Akopian TN, Woo KM, Goldberg AL (1999) The size of peptides generated from protein by mammalian 26 and 20S proteasomes. *J Biol Chem* 274: 3363-3371
- Lecker SH, Solomon V, Mitch WE, Goldberg AL (1999) Muscle protein breakdown and the critical role of the ubiquitin-proteasome pathway in normal and disease states. *J Nutr* 129: 227S-237S
- Llovera M, Garcia-Martinez C, Agell N, Lopez-Soriano FJ, Argiles JM (1997) TNF can directly induce the expression of ubiquitin-dependent proteolytic system in rat soleus muscles. *Biochem Biophys Res Commun* 230: 238-241
- Lorite MJ, Smith IJ, Arnold JA, Morris A, Thompson MG, Tisdale MJ (2001) Activation of ATP-ubiquitin-dependent proteolysis in skeletal muscle *in vivo* and murine myoblasts *in vitro* by a proteolysis-inducing factor (PIF). *Br J Cancer* 35: 297-302
- Lorite MJ, Thompson MG, Drake JL, Carling G, Tisdale MJ (1998) Mechanism of muscle protein degradation induced by a cancer cachectic factor. *Br J Cancer* 78: 850-856
- Lovell BB, Ruderman NB, Goodman MN (1986) Evidence that lysosomes are not involved in the degradation of myofibrillar proteins in rat skeletal muscle. *Biochem J* 234: 237-240
- Medina R, Wing SS, Goldberg AL (1995) Increase in levels of polyubiquitin and proteasome mRNA in skeletal muscle during starvation and denervation atrophy. *Biochem J* 307: 631-637
- O'Keefe SJD, Ogden J, Ramjee G, Rund J (1990) Contribution of elevated protein turnover and anorexia to cachexia in patients with hepatocellular carcinoma. *Cancer Res* 50: 1226-1233
- Orino E, Tanaka K, Tamura T, Sone S, Ogura T, Ichihara A (1991) ATP-dependent reversible association of proteasomes with multiple protein components to form 26S complexes that degrade ubiquitinated proteins in human HL-60 cells. *FEBS Lett* 284: 206-210
- Rajapurohitam V, Morales CR, El-Alfy M, Lefrancois S, Bedard N, Wing SS (1999) Activation of a UBC4-dependent pathway of ubiquitin conjugation during postnatal development of the rat testis. *Dev Biol* 212: 217-228
- Shimbara N, Orino E, Sone S, Ogura T, Takashina M, Shono M, Tanura T, Ichihara A (1992) Regulation of gene expression of proteasomes (multi-protease complexes) during growth and differentiation of human haematopoietic cells. *J Biol Chem* 267: 18100-18109
- Smith KL, Tisdale MJ (1993a) Increased protein degradation and decreased protein synthesis in skeletal muscle during cancer cachexia. *Br J Cancer* 67: 680-685
- Smith KL, Tisdale MJ (1993b) Mechanism of muscle protein degradation in cancer cachexia. *Br J Cancer* 68: 314-318
- Temparis S, Asensi M, Taillandier D, Auroousseau E, Larbaud D, Obled A, Bechet D, Ferrara M, Estrella JM, Attaix D (1994) Increased ATP-ubiquitin-dependent proteolysis in skeletal muscles of tumour-bearing rats. *Cancer Res* 54: 5568-5573
- Todorov P, Cariuk P, McDevitt T, Coles B, Fearon K, Tisdale M (1996) Characterization of a cancer cachectic factor. *Nature* 379: 739-742
- Waalkes TP, Udenfriend SA (1957) A fluorimetric method for the estimation of tyrosine in plasma and tissues. *J Lab Clin Med* 50: 733-736
- Whitehouse AS, Smith HJ, Drake JL, Tisdale MJ (2001) Mechanism of attenuation of skeletal muscle protein catabolism in cancer cachexia by eicosapentaenoic acid. *Cancer Res* 61: 3604-3609
- Williams A, Sun X, Fischer JE, Hasselgren P-O (1999) The expression of genes in the ubiquitin-proteasome proteolytic pathway is increased in skeletal muscle from patients with cancer. *Surgery* 126: 744-750
- Wing SS, Banville D (1994) 14-kDa ubiquitin-conjugating enzyme. Structure of the rat gene and regulation upon fasting and by insulin. *Am J Physiol* 267: E39-E48
- Workman P, Twentyman P, Balkwill F, Balmain A, Chaplin D, Double J, Embleton J, Newell D, Raymond R, Stables J, Stephens T, Wallace J (1998) United Kingdom Co-ordinating Committee in Cancer Research (UKCCR) guidelines for the welfare of animals in experimental neoplasia (second Edition). *Br J Cancer* 77: 1-10

FGH52352

CI-06859205-2

FGH52352

CISTI ICIST

CI-06859205-2

Document Delivery Service
in partnership with the Canadian Agriculture LibraryService de fourniture de Documents
en collaboration avec la Bibliothèque canadienne de l'agriculture**THIS IS NOT AN INVOICE / CECI N'EST PAS UNE FACTURE**LYNN BRAZIL
LIBRARIANHELLER EHRMAN WHITE & MCAULIFFE
275 MIDDLEFIELD RD
MENLO PARK, CA 94025
UNITED STATES

ORDER NUMBER: CI-06859205-2
Account Number: FGH52352
Delivery Mode: F31
Delivery Address: 650/324-6034
Submitted: 2007/05/11 14:21:10
Received: 2007/05/11 14:21:10
Printed: 2007/05/11 21:37:06

Direct	Periodical	OPENURLOPAC	UNITED STATES

Client Number: 39780-7000 CD
Title: THE BRITISH JOURNAL OF CANCER
DB Ref. No.: IRN1006168X
ISSN: ISSN00070920
Vol./Issue: 89/11
Date: 2003
Pages: 2104-9
Article Title: A AN INCREASED HIGH-MOBILITY GROUP A2 EXPRESSION LEVEL IS ASSOCIATED WITH MALIGNANT PHENOTYPE IN PANCREATIC EXOCRINE TISSUE
Article Author: ABE, N., ET AL.
Report Number: IRN1006168X
Publisher: H.K. LEWIS AND CO.,

Estimated cost for this 6 page document: \$12.5 document supply fee +
\$30 copyright = \$42.5

The attached document has been copied under license from Access Copyright/COPIBEC or other rights holders through direct agreements. Further reproduction, electronic storage or electronic transmission, even for internal purposes, is prohibited unless you are independently licensed to do so by the rights holder.

Phone/Téléphone: 1-800-668-1222 (Canada - U.S./E.-U.) (613) 998-8544 (International)

www.nrc.ca/cisti
info.cisti@nrc.ca

Fax/Télécopieur: (613) 993-7619

www.cnrc.ca/icist
info.icist@nrc.caNational Research Council Canada
Conseil national de recherches Canada

Page 1 / 1



An increased high-mobility group A2 expression level is associated with malignant phenotype in pancreatic exocrine tissue

N Abe^{*,1}, T Watanabe², Y Suzuki¹, N Matsumoto¹, T Masaki¹, T Mori¹, M Sugiyama¹, G Chiappetta³, A Fusco⁴ and Y Atomi¹

¹First Department of Surgery, Kyorin University School of Medicine, 6-20-2, Shinkawa, Mitaka, Tokyo 181-8611, Japan; ²Department of Clinical Pathology, Kyorin University School of Medicine, 6-20-2, Shinkawa, Mitaka, Tokyo 181-8611, Japan; ³Istituto Nazionale dei Tumori Fondazione Senatore Pascale, via M Semmola, Naples 80131, Italy; ⁴Dipartimento di Biologia e Patologia Cellulare e Molecolare, C/o Centro di Endocrinologia ed Oncologia Sperimentale del CNR, Università di Napoli 'Federico II', via Pansini, 5, Naples 80131, Italy

The altered form of the high-mobility group A2 (HMGA2) gene is somehow related to the generation of human benign and malignant tumours of mesenchymal origin. However, only a few data on the expression of HMGA2 in malignant tumour originating from epithelial tissue are available. In this study, we examined the HMGA2 expression level in pancreatic carcinoma, and investigated whether alterations in the HMGA2 expression level are associated with a malignant phenotype in pancreatic tissue. High-mobility group A2 mRNA and protein expression was determined in eight surgically resected specimens of non-neoplastic tissue (six specimens of normal pancreatic tissue and two of chronic pancreatitis tissue) and 27 pancreatic carcinomas by highly sensitive reverse transcriptase polymerase chain reaction (RT-PCR) techniques and immunohistochemical staining, respectively. Reverse transcriptase polymerase chain reaction analysis revealed the expression of the HMGA2 gene in non-neoplastic pancreatic tissue, although its expression level was significantly lower than that in carcinoma. Immunohistochemical analysis indicated that the presence of the HMGA2 gene in non-neoplastic pancreatic tissue observed in RT-PCR reflects its abundant expression in islet cells, together with its focal expression in duct epithelial cells. Intense and multifocal or diffuse HMGA2 immunoreactivity was noted in all the pancreatic carcinoma examined. A strong correlation between HMGA2 overexpression and the diagnosis of carcinoma was statistically verified. Based on these findings, we propose that an increased expression level of the HMGA2 protein is closely associated with the malignant phenotype in the pancreatic exocrine system, and accordingly, HMGA2 could serve as a potential diagnostic molecular marker for distinguishing pancreatic malignant cells from non-neoplastic pancreatic exocrine cells.

British Journal of Cancer (2003) 89, 2104–2109. doi:10.1038/sj.bjc.6601391 www.bjcancer.com

© 2003 Cancer Research UK

Keywords: HMGA2; pancreatic cancer; RT-PCR; immunostaining

The high-mobility group A (HMGA) family of proteins in mammals is composed of four proteins: HMGA1a, HMGA1b, HMGA1c, and HMGA2. The former three proteins are encoded by a single functional gene, that is, HMGA1 (formerly HMGI(Y)), while the last one is a product of a separate gene, that is, HMGA2 (formerly HMGI-C) (Manfioletti *et al*, 1991; Johnson *et al*, 1998). High-mobility group A2 has an approximately 50% amino-acid sequence homology with HMGA1, and features an internal 11 amino-acid deletion that characterises HMGA1 (Manfioletti *et al*, 1991; Tallini and Dal Cin, 1999). High-mobility group A2 proteins bind to the minor groove of AT-rich DNA sequences, thereby inducing a bend within the DNA (Thanos and Maniatis, 1992). They cannot initiate transcription; but they can enhance promoter binding of transcription factors (Thanos and Maniatis, 1992; Grosschedl *et al*, 1994; Mantovani *et al*, 1998).

High-mobility group A2 has been shown to be expressed abundantly during embryogenesis, but its expression is either

undetectable or remains at low levels in other normal adult tissues (Manfioletti *et al*, 1991; Zhou *et al*, 1995; Rogalla *et al*, 1996; Rommel *et al*, 1997; Hirning-Folz *et al*, 1998), suggesting that HMGA2 plays an important role (or roles) in cell proliferation and/or differentiation. Consistent with this, it has been demonstrated that HMGA proteins are phosphorylated in a cell-cycle-dependent manner (Reeves *et al*, 1991). Functionally, knocking out the HMGA2 gene in mice leads to the pygmy phenotype with characteristic hypoplasia of mesenchymal tissue, thereby confirming the important role(s) of HMGA2 in mammalian growth and development (Zhou *et al*, 1995).

The altered form of the HMGA2 gene, on the other hand, could somehow be related to the generation of human benign and malignant tumours. Rearrangements of the HMGA2 gene, for example, have been frequently observed in benign tumours of mesenchymal origin (Ashar *et al*, 1995; Schoenmakers *et al*, 1995). In such cases, the gene rearrangements were the consequence of chromosomal translocation involving regions 12q13–15, where the HMGA2 gene is located. The HMGA2 modifications consist of the loss of the carboxyl-terminal tail and its fusion with ectopic sequences (Ashar *et al*, 1995; Schoenmakers *et al*, 1995). The truncation of HMGA2, rather than its fusion with other genes, has

*Correspondence: Dr N Abe; E-mail: abentg@kyorin-u.ac.jp

Received 17 February 2003; revised 14 July 2003; accepted 16 September 2003

also been shown to be responsible for cell transformation (Pedeletti *et al*, 1998). This was confirmed in transgenic mice carrying a truncated HMGA2, which developed a giant phenotype together with a marked expansion of the retroperitoneal and subcutaneous white adipose tissues (Battista *et al*, 1999; Arlotta *et al*, 2000). Interestingly, most of these tumours related to the alteration in HMGA2 are of nonepithelial origin. In contrast, only a few data on the expression of HMGA2 in human malignant tumour originating from epithelial tissue are available (Rogalla *et al*, 1997). The overexpression of HMGA2 mRNA has been shown to be closely associated with high histologic grade in breast cancer (Rogalla *et al*, 1997), suggesting that the expression level of the HMGA2 protein/gene could be a potential clinicopathological marker with prognostic implications for a wide range of cancers. To test this possibility, we examined the HMGA2 expression in pancreatic cancers in the present study, and investigated whether alterations in HMGA2 are associated with the malignant phenotype of tumours in pancreatic tissue. To this end, HMGA2 mRNA expression was first analysed by highly sensitive reverse transcriptase-polymerase chain reaction (RT-PCR) techniques. Immunohistochemical detection of HMGA2 protein using a specific antibody was also attempted. Although relatively simple and easy to perform, immunohistochemistry is a potential method of examining whether the expression of a certain protein is specific to tumour cells, because it allows precise correlation of the protein expression with the phenotype of the cells on individual cell basis (Abe *et al*, 2000). In this sense, immunohistochemistry can provide more useful information than other assays by which proteins and/or mRNAs are extracted from tumours; possibly including a mixture of proteins from normal and irrelevant cells such as acinar cells or islet cells of the pancreas in the analysis (Abe *et al*, 2000). Based on the above considerations, we determined HMGA2 protein expression immunohistochemically on surgically resected specimens, normal pancreatic tissue, chronic pancreatitis tissue, and carcinomas of the pancreas.

MATERIALS AND METHODS

Tissue samples

The tissue samples were obtained at the time of surgery at the First Department of Surgery, Kyorin University Hospital, between October 1996 and August 2001. Specimens from 27 pancreatic carcinomas (20 primary carcinomas, four liver metastases, two peritoneal metastases, and one lymph node metastasis) and eight non-neoplastic tissues (six normal pancreatic and two chronic pancreatitis tissues) were obtained. In all, 27 carcinomas were histologically diagnosed as 12 well-differentiated tubular adenocarcinomas, six moderately differentiated tubular adenocarcinomas, seven poorly differentiated tubular adenocarcinomas, and two adenosquamous carcinomas (they were evaluated histologically according to the criteria of the Japan Pancreas Society). Normal pancreatic tissues were obtained from either patients who have undergone pancreatectomy due to pancreatic neoplasms or those with gastric cancer who have undergone pancreatectomy for lymph node dissection. In either case, specimens were obtained from a macroscopically healthy region distinct from the neoplastic lesion. All patients gave their informed consent prior to their inclusion in the study. Among the samples, those from 17 pancreatic carcinomas and six non-neoplastic pancreatic tissues were frozen on dry ice immediately after surgical resection for molecular investigation (RT-PCR), and stored at -80°C until use. All the tissue specimens were fixed for immunohistochemical analysis as soon as possible after surgical resection in 4% paraformaldehyde in phosphate-buffered saline (PBS) at 4°C for 14 h, followed by cryoprotection in a graded concentration series of sucrose in PBS. The specimens were then embedded in the OCT

HMGA2 expression in pancreatic carcinoma

N Abe *et al*



2105

compound, frozen, and stored at -80°C until analysis. All the tissue specimens were histologically examined and pathological diagnoses were confirmed.

RT-PCR analysis

Reverse transcriptase-polymerase chain reaction for the HMGA2 expression was performed using a heminested PCR technique as described previously (Rogalla *et al*, 1996; Rommel *et al*, 1997). Total RNA was extracted by a modified guanidine thiocyanate method as described previously (Miyatani *et al*, 1986). cDNA was synthesised using the adapter primer (AP) AAG GAT CCG TCG ACA TC (T)17 and Superscript II reverse transcriptase (Gibco BRL, Gaithersburg, MD, USA). For the first and second rounds of the heminested PCR, the same lower primer (Rev) 5'-TCC TCC TGA GCA GGC TTC-3' (exon 4/5) was used. The forward primer 5'-CTT CAG CCC AGG GAC AAC-3' (exon 1) and the nested primer 5'-CAT CGC CTC AGA AGA GAG GAC-3' (exon 1) were used as upper primers. The PCR amplifications were both performed for 30 cycles (1 min at 94°C , 1 min at 53°C , and 2 min at 72°C). As a control reaction for intact RNA and cDNA, PCR amplification of the cDNA of the housekeeping gene β -actin was performed for all samples to exclude false-negative PCR results. Only those samples positive for β -actin were used for this study. The resulting PCR products were clearly visualised by gel electrophoresis on a 2% agarose-gel stained with ethidium bromide as bands at 220 base pairs (bp) for HMGA2 and at 154 bp for β -actin (Figure 1). The resulting bands were sequenced and their sequences were found to be identical to that of HMGA2.

Immunohistochemical analysis

Immunohistochemical examinations were performed by the avidin-biotin complex immunoperoxidase technique using an Avidin-Biotinylated Enzyme Complex kit (Vector Laboratories, Inc. CA, USA) as described previously (Abe *et al*, 1999, 2000, 2002). The HMGA2 protein expression was immunohistochemically analysed on surgically resected specimens, together with four pancreatic cancer cell lines (PANC-1, MIA PaCa-2, BxPC-3, and AsPC-1) using HMGA2-specific antibodies, raised in rabbit against the recombinant HMGA2 protein (Berlingieri *et al*, 1995). In brief, frozen sections 5 (5 m thick) were prepared, transferred onto poly-L-lysine-coated slides, air-dried, and then washed in PBS, followed by quenching of endogenous peroxidase activity with 0.3% hydrogen peroxide in methanol. After further rinsing with PBS, the sections were incubated with normal goat serum for 20 min at room temperature to block nonspecific binding, and then incubated with the primary anti-HMGA2 antibody (1:100 dilution) 14 h at 4°C . After another wash in 0.2% Triton X in PBS, the sections were further incubated with biotinylated anti-rabbit IgG for 30 min at room temperature, followed by washes in 0.2% Triton X in PBS. After the addition of streptavidin-biotin-conjugated peroxidase and incubation for 30 min at room temperature, the



Figure 1 Reverse transcriptase-polymerase chain reaction products of HMGA2 after gel electrophoresis and ethidium bromide staining. Results show specific 220-bp bands. (0), DNA molecular weight marker; lane 1, positive control (hepatoma cell line HEP3B, which is known to express high level of HMGA2); lane 2, normal pancreas; lane 3, chronic pancreatitis; lane 4-11, pancreatic carcinomas.



HMGA2 expression in pancreatic carcinoma

N Abe et al

2106

sections were washed in 0.2% Triton X in PBS, and then the localisation of the HMGA2 protein was visualised by incubating the sections with 3,3'-diaminobenzidine. The slides were counterstained with Mayer's haematoxylin, dehydrated in a graded alcohol series, cleared in xylene, and mounted. Negative control staining was carried out by replacing the primary antibody with normal rabbit serum under the same experimental conditions. The immunostained slides were evaluated microscopically by a single investigator (NA) according to the criteria published previously (Abe et al, 1999, 2000) without prior knowledge of the clinical data for each case. The percentage of HMGA2-positive cells was scored by counting approximately 300-1000 tumour cells in three randomly selected fields (Abe et al, 1999, 2000, 2002). The immunohistochemical evaluation was considered positive when the HMGA2 nuclear immunoreactivity was detected in more than 20% of the cells according to the criteria published previously (Abe et al, 1999, 2000).

RESULTS

Expression of HMGA2 mRNA determined by RT-PCR

Among the six non-neoplastic tissue samples, five, including three normal tissues and two chronic pancreatitis tissues, gave rise to detectable HMGA2 bands, while one normal tissue sample showed no detectable HMGA2 band. The signal intensities of the HMGA2 band in chronic pancreatitis tissue samples were almost equivalent to those observed in the normal tissue samples. All the 17 samples of pancreatic carcinomas also showed HMGA2 bands by RT-PCR (Figure 1, Table 1). When the signal intensities of these HMGA2 bands were compared between non-neoplastic and carcinoma samples, the latter showed at least several fold more intense band than the former (Figure 1). Thus, an increased expression level of the HMGA2 mRNA is a distinct feature of pancreatic carcinoma.

Expression of HMGA2 protein determined by immunohistochemistry

To determine whether the altered HMGA2 mRNA expression observed in pancreatic carcinoma is associated with alterations in protein expression, we analysed the expression of the HMGA2 protein by immunohistochemistry. Its expression was first analysed in four pancreatic cancer cell lines. Intense multifocal or diffuse HMGA2 nuclear immunoreactivity was characteristically observed in these cell lines (Figures 2A-D). In both normal pancreas and chronic pancreatitis tissues, acinar cells did not exhibit any detectable HMGA2 immunoreactivity; however, a small proportion of duct epithelial cells showed faint HMGA2 immunoreactivity (Figure 3A). On the other hand, in the endocrine region, islet cells showed intense and diffuse HMGA2 immunoreactivity

(Figures 3B and F). In these cells, although HMGA2 immunoreactivity was localised mainly in the nuclei, faint staining was also observed within the cytoplasm. These results clearly indicated that the presence of the HMGA2 gene in non-neoplastic pancreatic tissue observed in the RT-PCR analysis reflects its expression in islet cells, together with its focal expression in duct epithelial cells. No significant difference in immunohistochemical findings was found between normal tissues and chronic pancreatitis tissues. When the expression of the HMGA2 protein in surgical specimens of carcinomas was then analysed, multifocally or diffusely distributed intense HMGA2 immunoreactivity was noted in all the pancreatic carcinoma specimens examined (Figures 3C-F). Intense nuclear staining was characteristically observed in the carcinoma cells. High-mobility group A2-positive carcinoma cells were observed regardless of the degree of differentiation (well/moderately or poorly differentiated tubular adenocarcinoma), histology type (tubular adenocarcinoma or adenosquamous carcinoma), or tumour site (primary or metastatic site). A strong correlation between HMGA2 overexpression and the diagnosis of carcinoma was noted (Fisher's exact probability, $P < 0.0001$, Table 1).

DISCUSSION

To evaluate the association between HMGA2 expression and the pathological diagnosis of pancreatic carcinoma, we investigated the expression of HMGA2 gene/protein in duct cell carcinoma and non-neoplastic tissue of the pancreas. High-mobility group A2 expression has been shown to be undetectable or to remain at low levels in normal adult tissues (Manfioletti et al, 1991; Zhou et al, 1995; Rogalla et al, 1996; Rommel et al, 1997; Hirning-Folz et al, 1998; Gattas et al, 1999). In the present study, however, a highly sensitive RT-PCR analysis revealed the expression of the HMGA2 gene in non-neoplastic pancreatic tissue, although its expression level was significantly lower than that in carcinoma. Immunohistochemical analysis indicated that the presence of the HMGA2 gene in non-neoplastic pancreatic tissue observed in the RT-PCR analysis reflects its abundant expression in islet cells together with its focal expression in duct epithelial cells. Thus, this study showed that the HMGA2 gene or protein is present even in normal pancreatic tissue. In HMGA2 immunohistochemical analysis, while only a small proportion of duct epithelial cells in the non-neoplastic tissue specimens showed HMGA2 immunoreactivity, a significantly higher proportion of carcinoma cells showed intense staining. In fact, a strong correlation between HMGA2 overexpression and the diagnosis of carcinoma was statistically verified. These findings indicate that an increased expression level of the HMGA2 protein is closely associated with the malignant phenotype in the pancreatic exocrine system, and accordingly, HMGA2 could serve as a potential diagnostic molecular marker for distinguishing pancreatic malignant cells from non-neoplastic pancreatic exocrine cells. A possible application of the results of the present study would be the determination of the HMGA2 gene and/or protein expression level in pancreatic juice collected at the time of endoscopic retrograde pancreatography. Using a sensitive and quantitative method such as competitive RT-PCR or immunoassay, the detection of even a small number of cancer cells could well be expected.

In order to evaluate the biological significance of the present results, it would be essential to understand the mechanisms by which the HMGA2 gene is involved in tumorigenesis, which unfortunately remain largely unclear. A clue to this issue was, however, provided by a recent report that transgenic mice carrying the HMGA2 gene developed pituitary adenomas (Fedele et al, 2002). These findings indicate that the high HMGA2 expression level has a critical role in neoplastic transformation of cells. Another clue was also demonstrated when antisense HMGA2 RNA

Table 1 HMGA2 expression in pancreatic carcinoma

Histological type of specimens	No. of positive specimens/no. of specimens analysed by RT-PCR	No. of positive ^a specimens/no. of specimens analysed by immunohistochemistry
Non-neoplastic tissue		
Normal pancreas	3/4 (75%)	0/6 (0%)
Chronic pancreatitis	2/2 (100%)	3/2 (0%)
Duct cell carcinoma	17/17 (100%)	27/27 (100%)

^aThe immunostained slides were scored as positive for immunohistochemistry when HMGA2 nuclear immunoreactivity was detected in more than 20% of the cells in the exocrine region.

HMGA2 expression in pancreatic carcinoma

N Abe et al



2107

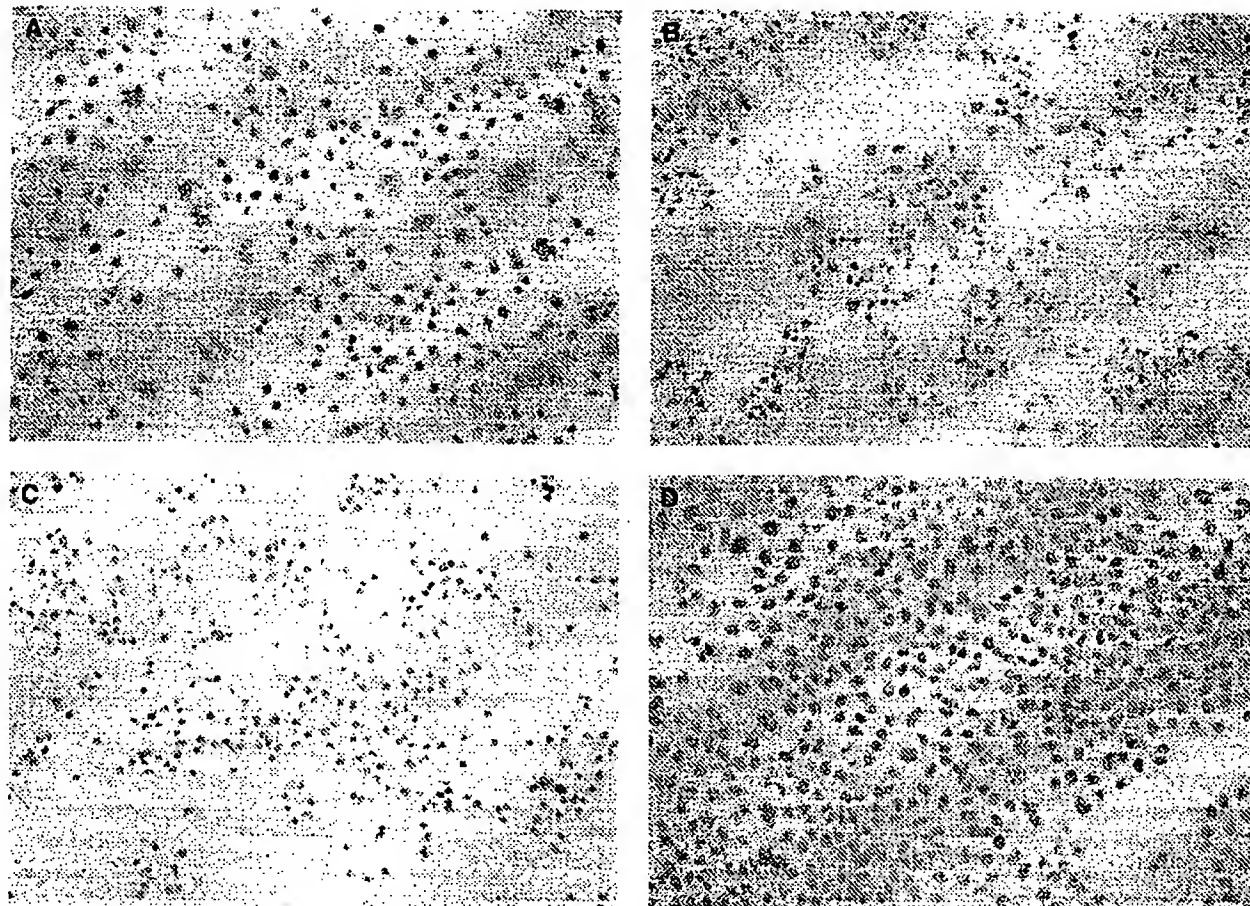


Figure 2 Immunohistochemical demonstration of the HMGA2 protein expression in pancreatic cancer cell lines. (A) AsPC-1 (Mayer's haematoxylin; original magnification $\times 200$). (B) PANC-1 (Mayer's haematoxylin; original magnification $\times 200$). (C) MIA PaCa-2 (Mayer's haematoxylin; original magnification $\times 100$). (D) BxPC-3 (Mayer's haematoxylin; original magnification $\times 200$). Intense multifocal or diffuse HMGA2 nuclear immunoreactivity (brown colour) was characteristically observed in cancer cells.

was shown to prevent retrovirally induced neoplastic transformation of rat thyroid cells *in vitro* (Berlingieri *et al*, 1995). The interaction between HMGA2 and the AP-1 transcriptional complex is considered to be responsible for the activation of genes whose expressions are associated with carcinogenesis (Vallone *et al*, 1997), since thyroid neoplastic transformation is associated with a drastic increase in AP-1 activity. This AP-1 activity is blocked by suppressing HMGA protein synthesis *in vitro* (Battista *et al*, 1998). The absence or decreased AP-1 transcriptional activity, which is directly or indirectly regulated by HMGA proteins, would inhibit the expression of AP-1-dependent genes, such as those of vascular endothelial growth factor (VEGF), collagenase I (matrix metalloproteinase-1; MMP-1), and stromelysin (MMP-3), which are essential for neoplastic transformation of cells (Vallone *et al*, 1997). In fact, significant downregulations of these mRNA expression levels were demonstrated in the retrovirally infected thyroid cell lines expressing the antisense HMGA2 (Vallone *et al*, 1997). Considering that the overexpression of the AP-1 (Tessari *et al*, 1999; Meggiato *et al*, 2003), VEGF (Seo *et al*, 2000), MMP-1 (Ito *et al*, 1999), and MMP-3 (Bramhall *et al*, 1996) has been demonstrated in human pancreatic cancer, together with our results, the interactions among these molecules may play an important role in pancreatic neoplastic transformation *in vivo*. Further studies, including the determination of expression levels of these molecules in tissue samples, have yet to be carried out to further clarify this issue. Conversely, the HMGA2 gene has recently

been shown not to be necessary for the malignant transformation of thyroid cells *in vivo* (Scala *et al*, 2001). This was demonstrated by comparing the frequency of radiation or papilloma virus E7 gene-induced thyroid carcinomas in mice carrying disrupted HMGA2 (pygmy mice) and that in mice carrying wild-type HMGA2 (Scala *et al*, 2001). Pygmy mice developed thyroid carcinomas with the same frequency as wild-type mice and furthermore, these two carcinomas generated in different mice showed no significant macroscopic and microscopic differences, indicating that HMGA2 is not sufficient for *in vivo* malignant transformation of thyroid cells (Scala *et al*, 2001). Several hypotheses could be considered to explain the discrepancy with the previous *in vitro* data, showing that HMGA2 is required for *v-mos*- and *v-ras*-Ki-induced cell transformations. One possible explanation would be that HMGA1, rather than HMGA2, may be required for thyroid cell transformation. This hypothesis is supported by the evidence that adenovirus carrying the HMGA1 gene in an antisense orientation induces programmed cell death in carcinoma cell lines derived from human thyroid, lung, colon, and breast cancers (Scala *et al*, 2000). We previously demonstrated that human pancreatic carcinoma expresses high HMGA1 levels (Abe *et al*, 2000, 2002), indicating that both HMGA2 and HMGA1 are overexpressed in this lesion. The expression of only one of the HMGA genes may be sufficient to lead epithelial cells of the pancreatic duct to exhibit the malignant phenotype. Further studies, such as the generation of HMGA1-knockout mice and



2108

HMGA2 expression in pancreatic carcinoma N Abe et al

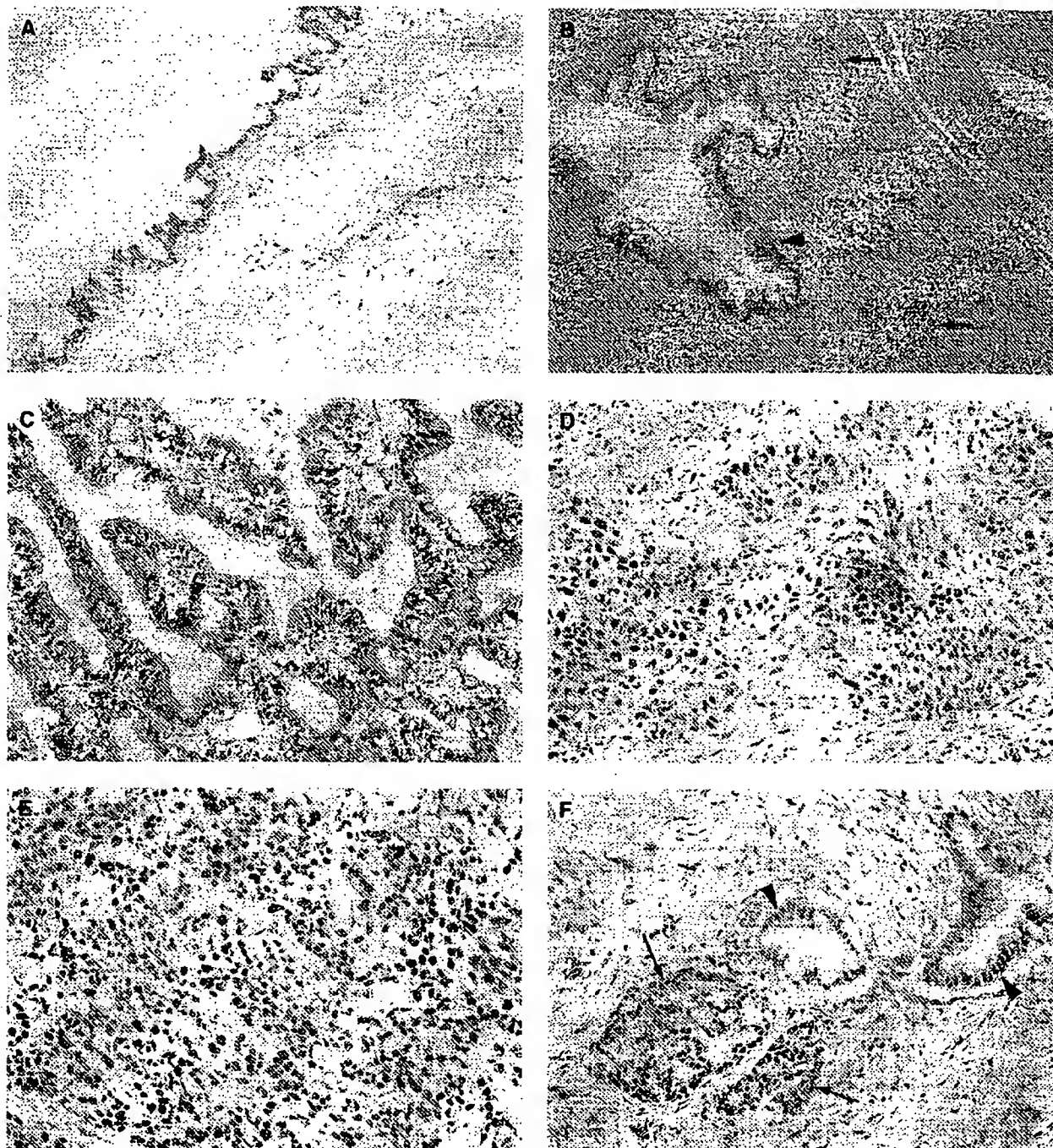


Figure 3 Immunohistochemical demonstration of the HMGA2 protein expression in surgically resected specimens of non-neoplastic pancreatic tissues and pancreatic carcinomas. (A) Non-neoplastic epithelial cells of the main pancreatic duct. A small proportion of duct epithelial cells show HMGA2 immunoreactivity (arrows). (Mayer's haematoxylin; original magnification $\times 200$). (B) Epithelial cells of branch pancreatic duct and islets in chronic pancreatitis tissue. Islet cells showed intense and diffuse HMGA2 immunoreactivity (arrows), while epithelial cells of the branch pancreatic duct did not exhibit any detectable HMGA2 immunoreactivity (arrowhead) (Mayer's haematoxylin; original magnification $\times 100$). (C) Primary pancreatic carcinoma exhibiting well-differentiated tubular adenocarcinoma (Mayer's haematoxylin; original magnification $\times 200$). (D) Primary pancreatic carcinoma exhibiting adenosquamous carcinoma (Mayer's haematoxylin; original magnification $\times 200$). (E) Metastatic lesion in the liver (Mayer's haematoxylin; original magnification $\times 200$). Intense and multifocal or diffuse HMGA2 immunoreactivity was noted in all the pancreatic carcinomas (C–E). (F) Section including both carcinoma cells and islet cells (Mayer's haematoxylin; original magnification $\times 200$). Islet cells showed intense and diffuse HMGA2 immunoreactivity (arrows), which was almost equivalent to that observed in carcinoma cells (arrowheads).

subsequent analysis of their susceptibility to developing malignancies, need to be carried out in order to clarify the role of a single HMGA gene in carcinogenesis in a wide variety of epithelial tissues.

In conclusion, this study has clearly demonstrated that an increased expression level of the HMGA2 gene/protein is closely associated with the malignant phenotype in pancreatic exocrine tissue, suggesting that HMGA2 could play a vital role in

tumorigenesis in the pancreatic exocrine system. The strong correlation between HMGA2 overexpression and the histological diagnosis of carcinoma indicates that the determination of the expression level of HMGA2 can be of great value in the diagnosis of pancreatic neoplasms.

REFERENCES

- Abe N, Watanabe T, Izumisato Y, Masaki T, Mori T, Sugiyama M, Chiappetta G, Fusco A, Fujioka Y, Atomi Y (2002) Diagnostic significance of high mobility group 1(Y) protein expression in intraductal papillary mucinous tumors of the pancreas. *Pancreas* 25: 149-153
- Abe N, Watanabe T, Masaki T, Mori T, Sugiyama M, Uchimura H, Fujioka Y, Chiappetta G, Fusco A, Atomi Y (2000) Pancreatic duct cell carcinomas express high levels of high mobility group 1(Y) (HMGI(Y)) proteins. *Cancer Res* 60: 3117-3122
- Abe N, Watanabe T, Sugiyama M, Uchimura H, Chiappetta G, Fusco A, Atomi Y (1999) Determination of high mobility group 1(Y) expression level in colorectal neoplasias: a potential diagnostic marker. *Cancer Res* 59: 1169-1174
- Arlotta P, Tai AK, Manfioletti G, Clifford C, Jay G, Ono SJ (2000) Transgenic mice expressing a truncated form of the high mobility group 1-C protein develop adiposity and an abnormally high prevalence of lipomas. *J Biol Chem* 275: 14394-14400
- Ashar HR, Fejzo MS, Tkachenko A, Zhou X, Fletcher JA, Weremowicz S, Morton CC, Chada K (1995) Disruption of the architectural factor HMGI-C: DNA-binding AT hook motifs fused in lipomas to distinct transcriptional regulatory domains. *Cell* 82: 57-65
- Battista S, de Nigris F, Fedele M, Chiappetta G, Scala S, Vallone D, Pierantoni GM, Megar T, Satoro M, Viglietto G, Verde P, Fusco A (1998) Increase in AP-1 activity is a general event in thyroid cell transformation *in vitro* and *in vivo*. *Oncogene* 17: 377-385
- Battista S, Fidanza V, Fedele M, Klein-Szanto AJ, Outwater E, Brunner H, Santoro M, Croce CM, Fusco A (1999) The expression of a truncated HMGI-C gene induces gigantism associated with lipomatosis. *Cancer Res* 59: 4793-4797
- Berlingieri MT, Manfioletti G, Santoro M, Bandiera A, Visconti R, Giancotti V, Fusco A (1995) Inhibition of HMGI-C protein synthesis suppresses retrovirally induced neoplastic transformation of rat thyroid cells. *Mol Cell Biol* 15: 1545-1553
- Bramhall SK, Stamp GWH, Dunn J, Lemoine NR, Neoptolemos JP (1996) Expression of collagenase (MMP2), stromelysin (MMP3) and tissue inhibitor of the metalloproteinases (TIMP1) in pancreatic and ampullary disease. *Br J Cancer* 73: 972-978
- Fedele M, Battista S, Kenyon L, Baldassarre G, Fidanza V, Klein-Szanto AJ, Parlow AF, Visone R, Pierantoni GM, Outwater E, Santoro M, Croce CM, Fusco A (2002) Overexpression of the HMGA2 gene in transgenic mice leads to the onset of pituitary adenomas. *Oncogene* 21: 3190-3198
- Fedele M, Berlingieri MT, Scala S, Chiariotti L, Viglietto G, Rippel V, Bullerdick J, Santoro M, Fusco A (1998) Truncated and chimeric HMGI-C genes induce neoplastic transformation of NIH3T3 murine fibroblasts. *Oncogene* 17: 413-418
- Gattas GJF, Quade BJ, Novak RA, Morton CC (1999) HMGI-C expression in human adult and fetal tissues and in uterine leiomyomata. *Genes Chromosomes Cancer* 25: 316-322
- Grosschedl R, Giese K, Pagel J (1994) HMG domain proteins; architectural elements in the assembly of nucleoprotein structures. *Trends Genet* 10: 94-100
- Hirning-Folz U, Wilda M, Rippe V, Bullerdick J, Hameister H (1998) The expression pattern of the Hmgic gene during development. *Genes Chromosomes Cancer* 23: 350-357
- Ito T, Ito M, Shinzawa J, Naito S, Kanematsu T, Sekine I (1999) Expression of the MMP-1 in human pancreatic carcinoma: relationship with prognostic factor. *Mod Pathol* 12: 669-674
- Johnson KR, Lehn DA, Elton TS, Barr PJ, Reeves R (1998) Complete murine cDNA sequence, genomic structure, and tissue expression of the high mobility group protein HMGI(Y). *J Biol Chem* 263: 18338-18342
- Manfioletti G, Giancotti V, Bandiera A, Buratti E, Sauticwre P, Cary P, Crane-Robinson C, Coles B, Goodwin GH (1991) cDNA cloning of the HMGI-C phosphoprotein, a nuclear protein associated with neoplastic and undifferentiated phenotypes. *Nucleic Acids Res* 19: 6793-6797
- Mantovani F, Covaceuszach S, Rustighi A, Sgarra R, Heath C, Goodwin GH, Manfioletti G (1998) NF- κ B mediated transcriptional activation is enhanced by the architectural factor HMGI-C. *Nucleic Acids Res* 26: 1433-1439
- Meggiato T, Calabrese F, De Cesare CM, Baliell N, Valente M, Del Favero G (2003) C-JUN and CPP (CASPASE 3) in human pancreatic cancer: relation to cell proliferation and death. *Pancreas* 26: 65-70
- Miyatani S, Winkles JA, Sargent TD, Dawid IB (1986) Stage-specific keratins in *Xenopus laevis* embryos and tadpoles: the XK81 gene family. *J Cell Biol* 103: 1957-1965
- Reeves R, Langan TA, Nissen MS (1991) Phosphorylation of the DNA-binding domain of nonhistone high-mobility group 1 protein by cdc2 kinase: reduction of binding affinity. *Proc Natl Acad Sci USA* 88: 1671-1675
- Rogalla P, Drechsler K, Frey G, Hennig Y, Helmke B, Bonk U, Bullerdick J (1996) HMGI-C expression patterns in human tissues. Implications for the genesis of frequent mesenchymal tumors. *Am J Pathol* 149: 775-779
- Rogalla P, Drechsler K, Kazmierczak B, Rippe V, Bonk U, Bullerdick J (1997) Expression of HMGI-C, a member of the high mobility group protein family, in a subset of breast cancers: relationship to histological grade. *Mol Carcinog* 19: 153-156
- Romuel B, Rogalla P, Jox A, Kalle CV, Kazmierczak B, Wolf J, Bullerdick J (1997) HMGI-C, a member of the high mobility group family of proteins, is expressed in hematopoietic stem cells and in leukemic cells. *Leukemia Lymphoma* 26: 603-607
- Scala S, Portella G, Fedele M, Chiappetta G, Fusco A (2000) Adenovirus-mediated suppression of HMGI(Y) protein synthesis as potential therapy of human malignant neoplasias. *Proc Natl Acad Sci USA* 97: 4256-4261
- Scala S, Portella G, Vitagliano D, Ledent C, Chiappetta G, Giancotti V, Dumont J, Fusco A (2001) HMGI-C gene expression is not required for *in vivo* thyroid cell transformation. *Carcinogenesis* 22: 251-256
- Schoenmakers EFPM, Wanschura S, Moles R, Bullerdick J, Van den Berghe II, Van de Ven WJM (1995) Recurrent rearrangements in the high mobility group protein gene, HMGI-C, in benign mesenchymal tumours. *Nat Genet* 10: 436-444
- Seo Y, Baba H, Fukuda T, Takashima M, Sugimachi K (2000) High expression of vascular endothelial growth factor is associated with liver metastasis and a poor prognosis for patients with ductal pancreatic adenocarcinoma. *Cancer* 88: 2239-2245
- Tallini G, Dal Cin P (1999) HMGI(Y) and HMGI-C dysregulation: a common occurrence in human tumors. *Adv Anat Pathol* 6: 237-246
- Tessari G, Ferrara C, Poletti A, Giacom C, Meggiato T, Martinez D, Del Favero G, Naccarato R (1999) The expression of proto-oncogene c-jun in human pancreatic cancer. *Anticancer Res* 863-867
- Thanos D, Maniatis T (1992) The high mobility group protein HMGI(Y) is required for NF- κ B dependent virus induction of the human IFN- β gene. *Cell* 71: 777-789
- Vallone D, Battista S, Pierantoni GM, Fedele M, Casalino L, Santoro M, Viglietto G, Fusco A, Verde P (1997) Neoplastic transformation of rat thyroid cells requires the junB and fra-1 gene induction which is dependent on the HMGI-C gene product. *EMBO J* 16: 5310-5321
- Zhou X, Benson KF, Ashar HR, Chada K (1995) Mutation responsible for the mouse pygmy phenotype in the developmentally regulated factor HMGI-C. *Nature* 376: 771-774

THE DECOMPENSATED DETRUSOR III: IMPACT OF BLADDER OUTLET OBSTRUCTION ON SARCOPLASMIC ENDOPLASMIC RETICULUM PROTEIN AND GENE EXPRESSION

RAIMUND STEIN, CHAOLIANG GONG, JOEL C. HUTCHESON, DOUGLAS A. CANNING AND
STEPHEN A. ZDERIC

From the Division of Urology, Children's Hospital of Philadelphia, Philadelphia, Pennsylvania

ABSTRACT

Purpose: Regulation of calcium ion homeostasis has a significant role in smooth muscle contractility. The sarcoplasmic endoplasmic reticulum, calcium, magnesium, adenosine triphosphatase (SERCA) is a regulatory ion pump that may have a role in the functional outcome after outlet obstruction. We investigate what correlation if any existed between SERCA protein and gene expression, and the contractile properties in the same bladder.

Materials and Methods: Standardized partial bladder outlet obstructions were created in adult New Zealand white rabbits, which were divided into control, sham operated and obstructed groups. Muscle strip studies subcategorized the obstructed group into compensated (force greater than 50% of control) and decompensated (force less than 50% of control). Microsomal membrane and total RNA fractions were prepared from the same bladder tissue. Membrane proteins were used for Western blot analysis using a SERCA specific monoclonal antibody, and total RNA was assessed with Northern blot analysis.

Results: The relative intensities of signals for the Western and Northern blots demonstrated a strong correlation between protein and gene expression. Furthermore there was a strong association between the loss of SERCA messenger RNA and protein expression and loss of bladder function.

Conclusions: Bladder contractility after outlet obstruction is influenced in part by smooth muscle cell ability to maintain calcium homeostasis via SERCA. The loss of SERCA protein expression is mediated by down-regulation in gene expression in the same bladder. These data suggest that smooth muscle ion pump gene expression is in part mechanically (pressure work) regulated.

KEY WORDS: bladder, rabbits, Ca^{2+} -transporting atpase

Partial bladder outlet obstruction in human and animal models results in numerous changes in the detrusor. Although in humans the degree, duration and cause of obstruction vary from individual to individual, in animal models we have the advantage of creating the same degree of obstruction in each and studying the bladder at defined time points. In human studies it is known that the detrusor may accommodate to an imposed obstruction and continue to empty, albeit with higher pressures and increased work, which may be considered a compensatory response. Sullivan and Yalla observed in older patients with benign prostate hyperplasia a point when no further compensation occurs and decompensation sets in manifested as a loss of detrusor reserve, which is the difference between maximal isometric pressure and maximal voiding pressure.¹ Clinically this loss of detrusor reserve correlated with increases in residual urine, and exact reasons why some bladders adapt to an equally imposed workload and others do not remain unknown.

Despite standardized approaches to creating experimental partial outlet obstruction, some bladders adapt to the imposed workload and others do not.² Some have advocated primary myogenic failure as the primary reason for this decompensation, and others claim that the muscle itself is unchanged and that large accumulations of extracellular matrix alone account for the less effective bladder emptying.³ Evidence has also accumulated to suggest that bladder wall

hypoxia⁴ may be an etiological factor as well as injury to the nerves in the bladder wall.⁵

The function of the detrusor smooth muscle depends on many factors, including the calcium sequestration and release system.⁶ Detrusor contractility depends on the interaction of the contractile proteins actin and myosin following phosphorylation of myosin light chain. This phosphorylation by myosin light chain kinase is triggered by a phasic increase in intracellular-free calcium concentration. This transient increase in cytosolic free calcium is mediated by extracellular influx via ion channels in the plasma membrane and release from intracellular storage sites. Intracellular calcium storage sites were first described in bladder smooth muscle by Mostwin,⁷ and have been shown to change with normal development⁸ and outlet obstruction.²

The sarcoplasmic endoplasmic reticulum, calcium, magnesium, adenosine triphosphatase (SERCA) is an ion pump, which is responsible for maintaining normal intracellular calcium gradients. SERCA functions by pumping 2 mol. of calcium ions into the sarcoplasmic reticulum storage sites per mol. of adenosine triphosphate expended. SERCA was first characterized by MacLennan in striated muscle.⁹ Monoclonal antibodies were developed against the isoforms.¹⁰ Three isoforms exist that are the products of alternative splicing,¹¹ and the rabbit gastric smooth muscle SERCA2 gene has been cloned.^{12,13}

In patients with congestive heart failure leading to transplantation a loss of SERCA activity was observed,^{14,15} and similar findings were seen in experimental models of aortic

Supported by National Institutes of Health Grants P50DK52620, K12DK12-02196 and DFG931/1-1, and the Leonard and Madlyn Abramson Chair in Pediatric Urology.

DECOMPENSATED DETRUSOR III

1027

stenosis.^{16,17} In addition to initiating muscle contractility, calcium has a pivotal role in other cellular functions, such as exocytosis, endocytosis, and protein synthesis and assembly. It has been established that calcium ion dysregulation is a central feature of the cellular injury process, which may result in fibrosis or apoptosis.¹⁸ We investigated the relationship between SERCA protein and gene expression, and correlated this with the contractile properties in the same bladder.

MATERIAL AND METHODS

Operative procedure. All studies were performed in 4-month-old, male New Zealand white rabbits and were approved by the Children's Hospital of Philadelphia animal use committee. After sedation with 35 mg/kg. ketamine and 5 mg/kg. xylazine intravenous administration of sodium pentobarbital (thiopental sodium) was used to induce deep anesthesia. After inserting an 8Fr catheter into the bladder via the urethra, which were handled as little as possible, the bladder neck was exposed through a small vertical abdominal incision. Once the ureters and vas deferens were identified, a 2-zero silk suture was placed below the bladder neck with a straight Keith needle. Mobilization of the perivesical fat was reduced to a minimum, and no right angle clamps were used during dissection. To maximize standardization of the partial outlet obstruction a second 8Fr catheter was placed outside the urethra, and the silk suture was tied around both catheters, which were then removed. In the sham operated group the silk suture was cut and removed after an identical dissection. All operations were performed by the same investigator (R. S.).

Tissue procurement. After 7, 14 and 28 days deep anesthesia was induced, and the bladders were excised through the same midline incision, blotted dry with paper towels and weighed. The bladder trigone was removed and the mucosa was peeled away leaving the detrusor muscle with the attached serosa.

Smooth muscle physiology and bladder classification. Three $0.2 \times 0.2 \times 1$ cm. muscle strips were prepared and the remaining detrusor muscle was immediately transferred for storage in liquid nitrogen. The muscle strips were attached by a 4-zero silk suture to a post in a 5 ml. tissue organ bath at 1 end and an isometric force transducer at the other end. The transducer was calibrated with known weights, and its output was directed to a polygraph. The tissue organ baths were maintained at 37°C and contained Tyrode's solution (125 mM. sodium chloride, 2.7 mM. potassium chloride, 1.8 mM. calcium chloride, 0.5 mM. magnesium chloride, 23.8 mM. sodium bicarbonate, 0.4 mM. sodium phosphoric acid and 5.6 mM. glucose) perfused by a bubbled mixture of 95% oxygen and 5% carbon dioxide. After equilibration for 30 minutes at slack length the strips were gradually stretched to the length where optimal force is generated. Peak tensions were measured in response to field stimulation (32 Hz. and 80 V.), high potassium chloride containing solution (127 mM. potassium chloride, 1.8 mM., calcium chloride, 0.5 mM. magnesium chloride, 23.8 mM. sodium bicarbonate, 0.4 mM. sodium phosphoric acid and 5.6 mM. glucose) and direct cholinergic stimulation (200 μ mol. bethanechol chloride). After completion of the experiments the muscle between the 2 silk sutures was weighed. All results are expressed in gm. tension per 100 mg. tissue.

Rabbits were divided into control (no operation), sham operated and obstructed groups. Muscle strip studies subcategorized the obstructed group of bladders into compensated (force more than 50% of control developed at cholinergic stimulation) and decompensated (force less than 50% of control). All results are presented using these definitions.

Protein, RNA and DNA probe preparation. Individual detrusor smooth muscle samples were split into 2 fractions, with 1 used for isolation of membrane proteins and the other

used for RNA. This procedure allowed for the correlation of protein and gene expression in the same bladder with known contractile properties. The frozen detrusor muscle was minced by scissors on ice followed by homogenization in a 10 mM. sodium bicarbonate TRIZMA² buffer (15 ml./1 gm. tissue) containing protease inhibitor cocktail (100 μ l./gm. tissue). Homogenization was followed by low speed centrifugation (25 minutes with $1,600 \times$ gravity at 4°C). The resulting supernatant was centrifuged for 35 minutes at $8,600 \times$ gravity at 4°C and was then ultracentrifuged at $93,000 \times$ gravity for 120 minutes at 4°C. Membrane pellets were suspended in the aforementioned buffer and stored at -80°C until use. Determination of the total protein content was done according to a modification of the Lowry method.^{19,20}

For total RNA isolation frozen tissue was ground in a mortar and pestle in liquid nitrogen, 100 mg. frozen powder were added to a prechilled glass tube on dry ice, 2.0 ml. TRIZOL¹ reagent were added and the tissue was homogenized. The sample was then placed at room temperature for 5 minutes to permit complete dissociation of nucleoprotein complexes. The homogenate was aliquoted into 2 equal 1 ml. volumes, 0.2 ml. chloroform was added and centrifugation was performed at $11,000 \times$ gravity for 15 minutes at 4°C. The colorless upper aqueous phase containing RNA was transferred into a fresh tube and an equal volume of isopropyl alcohol was added. After centrifugation at $12,000 \times$ gravity for 15 minutes at 2°C the RNA precipitate formed a gel-like pellet on the bottom of the tube and the supernatant was removed. RNA was washed in 75% alcohol, precipitated, air-dried for 20 minutes and dissolved in 60 to 100 μ l. DEPC water. Isolated RNA was quantified spectrophotometrically and its quality was assessed by loading 2 to 4 μ g. RNA sample containing 0.5 μ g. etidium bromide in a lane of a native 1.0% agarose gel in 0.5 \times tris-borate-edic acid buffer. Strong, high quality ribosomal bands of equal intensity and no degradation were observed for all samples.

An 800 bp SERCA2 probe was cut from the Bluescript plasmid by EcoRI and separated from the vector by agarose gel electrophoresis. The 800 bp probe was electro-eluted from the gel and its size was checked with agarose gel electrophoresis. Then 50 to 80 ng. of the probe were labeled using DNA labeling beads (deoxycytidine triphosphate) and isolated by ProbeQuant G-50 Micro Column.[†]

Western blot. The membrane fraction was dissolved in 6% sodium dodecyl sulfate, 50 mM. dithiothreitol, 10 mM. ethylenediamine tetraacetic acid, 0.83 mM. benzamide, 0.23 mM. phenylmethylsulfonyl fluoride, 1 mM. iodoacetamide, 0.5 M. sucrose and 130 mM. TRIZMA base adjusted to pH 6.8 and heated at 100°C for 5 minutes. A standard gel electrophoresis with 4.0% polyacrylamide stacking gel, 7.5% polyacrylamide separating gel and 20 μ g. membrane protein per lane was performed at 110 V. until the tracking dye reached the bottom. The running buffer was 0.025 M. TRIZMA base, 0.192 M. glycine and 10% sodium dodecyl sulfate (SDS), adjusted to pH 8.3. Gels were removed and proteins were blotted on to nitrocellulose membranes using a transfer system at 60 V. overnight at 4°C. Transfer buffer consisted of 0.025 M. TRIZMA base, 0.192 M. glycine and 20% methanol. The membrane was then immersed in 10% nonfat milk in phosphate buffered saline containing 1.85 mM. sodium biphosphate, 8.39 mM. disodium phosphate and 150 mM. sodium chloride, adjusted to pH 7.4 for 1 hour. The membrane was then washed 4 times at 10 minutes each with phosphate buffered saline and Tween (0.3%).

The mouse SERCA2 monoclonal antibody was diluted 1:1,000 in phosphate buffered saline containing 0.1% 0.77 mM. sodium azide, 0.1% NP-40 and 3% bovine albumin frac-

* Sigma Chemical Co., St. Louis, Missouri.

† Life Technologies, Rockville, Maryland.

‡ Amersham Pharmacia Biotech, Arlington Heights, Illinois.

tion, and was incubated with the membrane overnight at 4°C. The membrane was washed 5 times with phosphate buffered saline with 0.3% Tween, and incubated for 1½ hours at room temperature with horseradish peroxidase labeled goat anti-mouse IgG antibody diluted 1:10,000 in phosphate buffered saline containing 0.1% nitrogen phosphorus-40. After discarding the antibody solution, the membrane was washed 5 times in phosphate buffered saline and Tween buffer, and was incubated for 1 minute in chemiluminescence Western blotting detection reagents. Membranes were placed in a cassette and x-ray film was developed to show the bands. Correlation was made with known molecular weight standards.

Northern blot. We mixed 15 µg. total RNA with 4× volume sample loading buffer, consisting of 62.5% deionized formamide, 1.14 M. formaldehyde, 1.25× MESA buffer, 200 µg./ml. bromophenol blue and 20 µg./ml. EtBr, incubated it in a boiling water bath for 10 minutes and then transferred it to ice for 2 minutes. Equal amounts of 15 µg. × total RNA were loaded into wells in a 1.0% agarose gel containing 0.66 M. formaldehyde and 1× MESA buffer, and subjected to electrophoresis. A 0.24 to 9.5 kb. RNA ladder was used as molecular weight standards. After electrophoresis RNA was transferred by capillary transfer from gel to nylon membrane overnight using 10× saline, sodium, phosphate, ethylenediaminetetraacetic acid buffer as the transfer buffer. RNA was immobilized on the membrane by ultraviolet irradiation. The nylon membrane was placed in a roller bottle, 10 ml. of hybridization solution were added and the bottle was incubated at 68°C for 30 minutes. The labeled probe was added to 100 µl./ml. sonicated salmon sperm DNA solution, mixed with prehybridization solution, and continued to roll and incubate for 90 minutes at 68°C. This process was followed by 3 washes for 20 minutes at room temperature with 150 ml. 2× saline/sodium citrate buffer and 0.1% sodium dodecyl sulfate wash solution. Two washes for 45 minutes at 60°C with 0.1× saline/sodium citrate buffer and 0.1% SDS were performed for high stringency conditions. The membrane was exposed to x-ray film for 36 to 120 hours at -80°C. The results shown are with the RS87 clone, which is directed against the 3-inch end of the messenger (m)RNA.

Densitometry for Western blots was done on each blot using commercial software. On each Western blot 20 µg. from 1 or 2 control bladders were loaded. The intensity of each band at 110 kD. was normalized to the band of the control bladders on the same blot, which was set for 100%. If 2 control bladders were investigated on 1 blot the average intensity was set to 100%. For Northern blots the SERCA band was quantified by densitometry and normalized to the 18S band with the ratio for the control bladders set for 100%. For statistics the 2-sided t test was performed, and $p < 0.05$ was considered significant.

RESULTS

Results (mean plus or minus standard error of mean) of bladder weight and contractile responses to several stimuli, including electrical field stimulation, high potassium chloride and bethanechol are summarized in table 1. When results of outlet obstruction in this rabbit population were

analyzed as a function of time the effects of obstruction on contractile performance were uniform at 1, 2 and 4 weeks. At each time point 1 of 3 bladders had maintained a reasonable degree of contractile performance and 2 of 3 demonstrated poor performance. For this reason we subdivided the obstructed bladders into the 2 categories of compensated (contractile force more than 50% of control) and decompensated (contractile force less than 50% of control).

For the Western blot SERCA protein expression was determined in 10 control, 7 sham operated, 10 compensated and 10 decompensated bladders. Band intensity was normalized to the control group on each blot, and there was a significant decrease in the decompensated group as determined by scanning densitometry. For the Northern blot SERCA gene expression was determined in 3 control, 5 sham operated, 6 compensated and 5 decompensated bladders. In the same bladders the protein expression was also determined, and band intensity was normalized to the control group. A direct comparison between the Western and Northern blots from the same bladders revealed a correlation between the expression of SERCA mRNA and protein expression (see figure). SERCA protein and mRNA expression were significantly lower in the decompensated group (table 2).

DISCUSSION

The fate of the bladder following partial bladder outlet obstruction has been extensively studied and reviewed.²¹⁻²³ There exists a bewildering array of models, species and experimental results not all of which are in agreement. A common theme to all of these studies is that a true bladder obstruction produces an increase in bladder mass.^{6,21,24-26} What remains controversial is how much the physical properties of the bladder change and to which bladder wall fraction these physiological alterations may be attributed. The extent to which bladder contractile performance was affected varied among studies. Some have argued that the muscle fraction in the bladder undergoes minimal hypertrophy and that any changes in contractility are a function of the smooth muscle density in the collagen. Cher et al further bolstered this argument by showing that in a series of obstructions there were no changes in the percentage of myosin light chain phosphorylation.³ They concluded that the muscle itself is unchanged and that the altered contractile performance of the bladder wall may be explained by increased or decreased matrix deposition.

In our prior series² as well as the current series we reported significant alterations in the contractile properties of the bladder wall using a muscle strip analysis. It could be argued that the loss of contractile force in our series of obstructions represents a loss of muscle fraction in the bladder smooth muscle due to an accumulation of the matrix component. However, to account for the full decrease in contractile performance muscle content of the tissue would have to decrease 5-fold. In our histological and immunohistochemical studies of these bladders we have seen no such dramatic changes in the muscle fraction.

The lack of change in myosin light chain phosphorylation is also cited as evidence that the muscle is unaffected by obstruction. However, Gerthoffer reported that in trachealis

TABLE 1. Bladder weights and responses to field stimulation, potassium chloride solution and cholinergic stimulation with bethanechol

	Control	Sham Control	Compensated	Decompensated
No.	10	10	14	23
Bladder wt. (gm.)	2.0 (0.1)	2.3 (0.4)	4.4 (0.4)*	9.8 (0.64)*,†
Mean gm. tension/100 mg. field stimulation (SEM)	23.4 (2.9)	24.2 (3.7)	17.9 (4.5)*	1.1 (0.3)*,†
Mean gm. tension/100 mg. potassium chloride (SEM)	24.8 (2.1)	24.1 (3.6)	16 (2.9)*	2.5 (0.4)*,†
Mean gm. tension/100 mg. bethanechol (SEM)	32.8 (3.6)	35.2 (4.1)	26.9 (3.5)*	5.6 (0.7)*,†

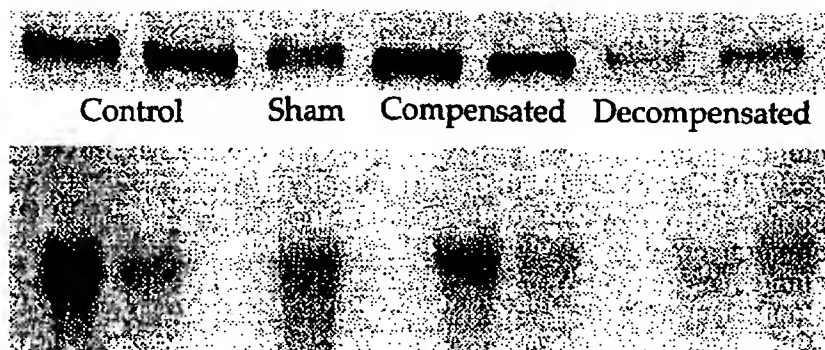
Field stimulation was 32 Hz., 80 V.; potassium chloride 127 mM., and bethanechol 200 µmol.

* $p < 0.05$ versus control and sham groups.

† $p < 0.05$ compensated versus decompensated groups.

DECOMPENSATED DETRUSOR III

1029



Western blot analysis in 2 control, 1 sham, 2 compensated and 2 decompensated bladders using 20 μ g. protein for each line. Band appears at 110 kD. Lower panel shows Northern blot from same bladders using 15 μ g. RNA per line.

TABLE 2. Relative intensity of the Western and Northern blots compared to the control bladders

	Control	Sham Control	Compensated	Decompensated
Western blot:				
No.	10	7	10	10
Mean intensity \pm SEM	100 \pm 2	95 \pm 9	70 \pm 6*	41 \pm 3*,†
Northern blot:				
No.	3	7	10	10
Mean intensity \pm SEM	100 \pm 18	72 \pm 8	65 \pm 11	40 \pm 5*,†

*Control or sham groups versus decompensated group $p < 0.05$.

†Decompensated versus compensated group $p < 0.05$.

smooth muscle the myosin light chain phosphorylation was unchanged at 70% following stimulation, yet the force developed by these same smooth muscle strips was proportional to the calcium concentration in the buffers.²⁷ These data would suggest that in smooth muscle the cytosolic calcium transient can affect force generation despite an identical percentage of myosin light chain phosphorylation. The loss of sarcoplasmic reticulum could lead to alterations in the calcium transients and alter force generation. The experiments of Gerthoffer in trachealis smooth muscle will be repeated in the bladder to help resolve this controversy. However, it is clear that the greatest loss of SERCA expression is seen in bladders with the worst contractile performance in the muscle strip studies. This evidence implies that there is a loss of the sarcoplasmic reticulum and the intracellular calcium regulatory mechanisms are perturbed. The accompanying pattern of gene expression would suggest that the loss of SERCA is mediated by a transcriptional mechanism.

We have also shown that identical outlet obstructions result in bladders that may adapt to the imposed workload (compensated) or lose the ability to maintain force and enter a decompensated state. This decompensated state is characterized by an increased bladder mass, decreased contractility of the bladder wall strips and increased deposition of extracellular matrix. It might be argued that bladders that were compensated were never truly obstructed initially. Our preliminary data from metabolic cage monitoring suggest that these animals are truly obstructed as manifested by increases in urinary frequency and diminished voiding volumes. In addition, video urodynamic studies were performed in awake rabbits demonstrating that voiding pressures were elevated in all animals after obstruction.

Ample evidence exists in the cardiac literature to support the notion that cytosolic calcium handling is a pathway to end stage congestive heart failure. Human and animal models of aortic stenosis have resulted in an end stage cardiomyopathy, which has been well characterized at a physiological level.¹⁵⁻¹⁷ In these situations a diminished ejection fraction correlated well with a loss of SERCA activity by assay and Western blot. This loss of SERCA was associated with diminished gene expression by Northern blot analysis. During normal cardiac development there was an increase in SERCA

expression at the protein and nucleic acid levels.²⁸ We reported similar changes in the developing rabbit bladder after studying the expression of the ryanodine ion channel and SERCA as measures of sarcoplasmic reticulum density.^{29,30} Although one cannot directly compare the responses of the bladder and heart to outflow obstruction,³¹ one cannot help but be struck by the molecular similarities with our data.

Why should it be that despite identically performed outlet obstructions 1 of 3 animals demonstrated compensated bladder function whereas 2 of 3 showed evidence of decompensation? Is the loss of SERCA expression a cause of decompensation or merely an associated finding? We speculate that those animals in whom sarcoplasmic reticulum function is preserved perform better and adapt to the new workload. However, to answer this question fully further work remains to be done, and we are seeking to answer this question via 2 main approaches. 1) We are studying the effects that reversal of outlet obstruction has on bladder function and sarcoplasmic reticulum expression. 2) We have developed the ability to study murine bladder physiology³² and are creating a reproducible model of outlet obstruction in the mouse. This procedure will enable us to study the normal phenotype as well as the response to obstruction in a variety of sarcoplasmic reticulum specific transgenic and knockout mice.

What is the clinical relevance of these observations? Levin et al in a series on human tissues from patients with outlet obstruction have also seen a loss in SERCA expression as measured by the thapsigargin assay.³³ Experimentally they reported that spectrin degradation products are increased after outlet obstruction, which implies that calpain has been activated.³⁴ Their study is significant because calpain is a proteolytic enzyme that becomes activated only in the presence of sustained cytosolic calcium perturbations. Such an understanding of the pathophysiology of bladder smooth muscle cell dysfunction is essential if one is to design novel therapeutic strategies to prevent the onset of end stage bladder.

CONCLUSIONS

Bladder performance after outlet obstruction is influenced by smooth muscle cell ability to maintain calcium homeosta-

sis, and SERCA is an important protein that regulates cytosolic calcium transients. The loss of SERCA protein expression is mediated by down-regulation in gene expression in the decompensated bladder. These data suggest that smooth muscle ion pump gene expression is in part mechanically (pressure work) regulated.

DNA probe was provided by Dr. Ashok Grover.

REFERENCES

1. Sullivan, M. P. and Yalla, S. V.: Detrusor contractility and compliance characteristics in adult male patients with obstructive and nonobstructive voiding dysfunction. *J Urol*, 155: 1995, 1996
2. Zderic, S. A., Rohrmann, D., Gong, C. et al: The decompensated detrusor II: evidence for loss of sarcoplasmic reticulum function after bladder outlet obstruction in the rabbit. *J Urol*, 156: 587, 1996
3. Cher, M. L., Kamm, K. E. and McConnell, J. D.: Stress generation and myosin phosphorylation in the obstructed bladder. *J Urol*, suppl., 143: 355A, abstract 665, 1990
4. Brading, A. F.: Alterations in the physiological properties of urinary bladder smooth muscle caused by bladder emptying against an obstruction. *Scand J Urol Nephrol*, suppl., 184: 51, 1997
5. Levin, R. M., Saito, M., Wein, A. J. et al: Effect of partial outlet obstruction on choline acetyltransferase activity in the rat and rabbit. *Neurourol Urodyn*, 12: 255, 1993
6. Zderic, S. A., Wein, A., Rohrmann, D. et al: Mechanisms of bladder smooth-muscle hypertrophy and decompensation: lessons from normal development and the response to outlet obstruction. *World J Urol*, 16: 350, 1998
7. Mostwin, J. L.: Receptor operated intracellular calcium stores in the smooth muscle of the guinea pig bladder. *J Urol*, 133: 900, 1985
8. Zderic, S. A., Sillen, U., Liu, G. et al: Developmental aspects of bladder contractile function: evidence for an intracellular calcium pool. *J Urol*, 150: 623, 1993
9. MacLennan, D. H.: Purification and properties of an adenosine triphosphatase from sarcoplasmic reticulum. *J Biol Chem*, 245: 4508, 1970
10. Jorgensen, A. O., Arnold, W., Pepper, D. R. et al: A monoclonal antibody to the Ca^{2+} -ATPase of cardiac sarcoplasmic reticulum cross-reacts with slow type I but not with fast type II canine skeletal muscle fibers: an immunocytochemical and immunochemical study. *Cell Motil Cytoskeleton*, 9: 164, 1988
11. MacLennan, D. H., Brandl, C. J., Korezak, B. et al: Amino-acid sequence of a Ca^{2+} + Mg^{2+} -dependent ATPase from rabbit muscle sarcoplasmic reticulum, deduced from its complementary DNA sequence. *Nature*, 316: 696, 1985
12. Mearow, K. M., Thilander, B. G., Khan, I. et al: In situ hybridization and immunocytochemical localization of SERCA2 encoded Ca^{2+} pump in rabbit heart and stomach. *Mol Cell Biochem*, 121: 155, 1993
13. Khan, I. and Grover, A. K.: Cloning of internal Ca pump from rabbit stomach smooth muscle. *Nucleic Acids Res*, 18: 4026, 1990
14. Hasenfuss, G., Reinecke, H., Studer, R. et al: Relation between myocardial function and expression of sarcoplasmic reticulum Ca^{2+} -ATPase in failing and nonfailing human myocardium. *Circ Res*, 75: 434, 1994
15. Meuse, A. J., Perrault, C. L. and Mogan, J. P.: Pathophysiology of cardiac hypertrophy and failure of human myocardium: abnormalities of calcium handling. In: *Cellular and Molecular Alterations in the Failing Human Heart*. Edited by G. Hasenfuss, C. Holubarsch, H. Just et al. New York: Springer Verlag, pp. 223-233, 1992
16. Feldman, A. M., Weinberg, E. O., Ray, P. E. et al: Selective changes in cardiac gene expression during compensated hypertrophy and the transition to cardiac decompensation in rats with chronic aortic banding. *Circ Res*, 73: 184, 1993
17. Komuro, I., Kurabayashi, M., Shibasaki, Y. et al: Molecular cloning and characterization of a Ca^{2+} + Mg^{2+} -dependent adenosine triphosphatase from rat cardiac sarcoplasmic reticulum. Regulation of its expression by pressure overload and developmental stage. *J Clin Invest*, 83: 1102, 1989
18. Trump, B. F. and Berezesky, I. K.: Calcium-mediated cell injury and death. *FASEB J*, 9: 219, 1995
19. Lowry, O. H., Rosenbrough, N. J., Farr, A. L. et al: Protein measurement with the folin phenol reagent. *J Biol Chem*, 193: 265, 1951
20. Peterson, G. L.: Review of the Folin phenol protein quantification method of Lowry, Rosenbrough, Farr and Randall. *Anal Biochem*, 100: 201, 1979
21. Zderic, S. A., Wein, A. J., Monson, F. C. et al: The effects of infravesical obstruction on the bladder. *Probl Urol*, 5: 357, 1991
22. Levin, R. M., Haugaard, N., Levin, S. S. et al: Bladder function in experimental outlet obstruction: pharmacologic responses to alterations in innervation, energetics, calcium mobilization, and genetics. In: *Muscle, Matrix, and Bladder Function*. Edited by S. A. Zderic. New York: Plenum, pp. 7-20, 1995
23. Baskin, L. S. and Hayward, S. W.: *Advances in Bladder Research*. New York: Plenum, 1999
24. Peters, C.: Congenital bladder obstruction: research strategies and directions. In: *Muscle Matrix and Bladder Function*. Edited by S. A. Zderic. New York: Plenum, pp. 117-130, 1995
25. Mostwin, J. L., Karim, O. M., van Koeveeringe, G. et al: The guinea pig as a model of gradual urethral obstruction. *J Urol*, 145: 854, 1991
26. Levin, R. M., Longhurst, P. A., Barasha, B. et al: Studies on experimental bladder outlet obstruction in the cat: long-term functional effects. *J Urol*, 148: 939, 1992
27. Gerthoffer, W. T.: Dissociation of myosin phosphorylation and active tension during muscarinic stimulation of tracheal smooth muscle. *J Pharmacol Exp Ther*, 240: 8, 1987
28. Fisher, D. J., Tate, C. A. and Phillips, S.: Developmental regulation of the sarcoplasmic reticulum calcium pump in the rabbit heart. *Pediatr Res*, 31: 474, 1992
29. Zderic, S. A., Gong, C. and DiSanto, M. et al: Calcium ion homeostasis in urinary bladder smooth muscle. In: *Advances in Bladder-Research*. Edited by L. S. Baskin and S. W. Hayward. New York: Plenum, pp. 15-170, 1999
30. Gong, C., Zderic, S. A. and Levin, R. M.: Ontogeny of the ryanodine receptor in rabbit urinary bladder smooth muscle. *Mol Cell Biochem*, 137: 169, 1994
31. Chien, K. R.: Stress pathways and heart failure. *Cell*, 98: 555, 1999
32. Hutcheson, J. C., Canning, D. A., Wein, A. J. et al: Murine in vitro whole bladder physiology. In: *Advances in Bladder Research*. Edited by A. Atala. New York: Kluwer, in press, 2000
33. Levin, R. M., Haugaard, N., Mogavero, L. et al: Biochemical evaluation of obstructive bladder dysfunction in men secondary to BPH: a preliminary report. *Urology*, 53: 446, 1999
34. Zhao, Y., Levin, S. S., Wein, A. J. et al: Correlation of ischemia/reperfusion or partial outlet obstruction-induced spectrin proteolysis by calpain with contractile dysfunction in rabbit bladder. *Urology*, 49: 293, 1997

TNF- α and IL-8 Are Upregulated in the Epidermis of Normal Human Skin after UVB Exposure: Correlation with Neutrophil Accumulation and E-Selectin Expression

Ian Strickland,*† Lesley E. Rhodes,* Brian F. Flanagan,† and Peter S. Friedmann*

Departments of *Dermatology and †Immunology, University of Liverpool, Liverpool, United Kingdom

The *in vivo* response to ultraviolet B (UVB) radiation in skin is characterized by the accumulation of both mononuclear and polymorphonuclear cells within the dermis and an induction of vascular endothelial adhesion molecules. Epidermal production of cytokines (IL-8 and TNF- α) has been strongly implicated in the development of UVB-induced inflammation. In the current study, we examined the time course of IL-8 and TNF- α mRNA and protein expression in the epidermis over a 24-h period after *in vivo* UVB irradiation. Also, the induction of adhesion molecule expression and the accumulation of neutrophils within the dermis were followed. We found constitutive expression of both cytokines (mRNA and protein) in the epidermis of unirradiated skin. IL-8 was rapidly upregulated after irradiation and mRNA and protein increased at 4 h, reaching a maximum between 8 and 24 h. TNF- α mRNA and protein was minimally in-

creased by 8 h after UVB irradiation and reached a maximum by 24 h. No significant alteration in ICAM-1 or VCAM-1 expression was observed. E-selectin expression, which was absent from control samples, was increased from 4 h onward and also reached a maximum at 24 h, coinciding with peak neutrophil accumulation. A strong correlation ($r = 0.96$) was found between number of E-selectin-positive vessels and numbers of infiltrating neutrophils at this time. Moreover, because E-selectin expression was increased before any apparent increase in TNF- α protein (4 h), TNF- α does not appear to be involved in the early induction of the adhesion molecule, but cytokines such as TNF- α and IL-8 may act subsequently to augment the inflammatory response. **Key words:** adhesion molecules. *J Invest Dermatol* 108:763-768, 1997

The skin is the primary interface between the environment and the body and is an active immunologic microenvironment. It protects against constant microbial and chemical assault and also against the harmful effects of ultraviolet radiation (UVB). The acute effects of UVB radiation (290-320 nm) in human skin result in an inflammatory response, detectable clinically as erythema that can last up to 96 h. The first observable event is a vasodilatory response with increase in blood flow detectable within 1 h of UVB irradiation (Diffey and Oakley, 1987). The vasodilation, mediated by prostaglandin- E_2 and nitric oxide, increases progressively to reach a peak at 24 h. Furthermore, an inflammatory infiltrate occurs that contains mainly neutrophils and is maximal at 24 h (Hawk *et al.*, 1988). The mechanisms involved in neutrophil recruitment are not clearly understood, although their entry will depend upon both a specific chemoattractant stimulus and appropriate microvascular adhesion molecule expression, of which E-selectin and intracellular adhesion molecule (ICAM-1) are the most important. There is

strong evidence for the involvement of cytokines, and after UVB irradiation there is upregulation of cytokine expression such as interleukin (IL)-1, IL-8, IL-10, IL-15, and tumor necrosis factor α (TNF- α) by various cells including keratinocytes (Enk *et al.*, 1995), and dermal fibroblasts (de Kossodo *et al.*, 1995).

IL-8, a member of the C-X-C supergene family of chemokines, is strongly chemotactic for neutrophils, lymphocytes, and basophils and thus could be a likely candidate for neutrophil recruitment in the UVB-induced inflammatory response (Liebler *et al.*, 1994). In humans, the primary source of IL-8 is monocytes (Colditz *et al.*, 1992), although it is now known that a wide variety of other cells including fibroblasts, keratinocytes, and endothelial cells can produce this factor. It has been previously reported that after UVB exposure of cultured human epidermal keratinocytes, IL-8 mRNA is rapidly upregulated (within 1 h; Kondo *et al.*, 1993). Entry of neutrophils into skin sites is dependent upon both a chemotactic signal and the interaction of the cell surface ligand sialyl Lewis-x with the specific endothelial adhesion molecule E-selectin (Springer, 1990). Since E-selectin is not constitutively expressed by the dermal vasculature, it must be induced by inflammatory mediators prior to any cellular infiltration. UVB has been shown to upregulate E-selectin expression on vascular endothelium *in vivo* (Norris *et al.*, 1991). Evidence from mice suggests that the upregulation of E-selectin is likely to be mediated indirectly, through release of TNF- α (Streitclain *et al.*, 1993). TNF- α has also been shown to be

Manuscript received June 12, 1996; revised November 27, 1996; accepted for publication December 13, 1996.

Reprint requests to: Professor P.S. Friedmann, Department of Dermatology, University of Liverpool, Post Office Box 147, Liverpool L69 3BX, U.K.

Abbreviation: VCAM-1, vascular cell adhesion molecule-1.

upregulated in human epidermis after UVB irradiation (Orholm *et al.*, 1988). In the current study, we have examined the development of the cutaneous inflammatory response *in vivo* after UVB irradiation. In particular, we have examined the interrelationship of epidermal cytokine production, vascular adhesion molecule expression, and neutrophil accumulation.

MATERIALS AND METHODS

Patients and UVB Irradiation Normal healthy Caucasian volunteers ($n = 4$, mean age = 41 y, three males) of sun-reactive skin type II or III were recruited for study. Each individual was irradiated with a previously determined dose ($2.5\times$ minimal erythema dose) of UVB (by using a Philips TL20W/12 fluorescent lamp) at three sites on the buttock. The sites were biopsied at 4, 8, and 24 h after irradiation and from an untreated control site to allow construction of a time course. Biopsies were bisected, and one-half was snap-frozen for immunohistochemical analysis and the other was fixed overnight in 4% (wt/vol) paraformaldehyde in phosphate-buffered saline (PBS) and paraffin embedded for *in situ* hybridization and cytokine immunohistochemistry.

Preparation of Digoxigenin-Labeled Riboprobes Riboprobes for IL-8 and TNF- α were synthesized from the respective coding region cDNA fragments subcloned into the vector pCRTM II (Invitrogen, Leek, The Netherlands). This vector contains SP6 and T7 RNA polymerase initiation sites for the synthesis of sense and anti-sense RNA probes. The TNF- α probe was synthesized from a 254-bp fragment corresponding to positions 336–589 of the full-length TNF- α sequence (Wang *et al.*, 1985) and IL-8 probes were synthesized from a fragment corresponding to nucleotides 101–302 of the IL-8 sequence (Matsumura *et al.*, 1988). Transcription reactions containing 1 μ g of linearized plasmid DNA were carried out under standard conditions (Sambrook *et al.*, 1989) in the presence of 0.33 mM digoxigenin-11-UTP (Boehringer Mannheim). Reaction products were analyzed by gel electrophoresis and template DNA was removed by addition of 10 units of RNase-free DNase 1 (Boehringer Mannheim, Germany) for 15 min at 37°C prior to use.

In Situ Hybridization Paraffin-embedded tissue sections (5 μ m) were deparaffinized in xylene and then rehydrated through a series of alcohols to water (RNase free). Sections were incubated for 10 min in 2X sodium saline citrate (SSC) at 60°C and then treated for 30 min with 10 μ g per ml proteinase K (Boehringer Mannheim) in 50 mM Tris(hydroxymethyl)aminomethane buffer (pH 7.6). Proteinase treatment was halted by incubation in ice-cold 0.4% paraformaldehyde (BDH, Leicestershire, UK) in PBS for 20 min, and sections were washed in Tris(hydroxymethyl)aminomethane-buffered saline. Sections were hybridized for 16 h with anti-sense or control sense IL-8 and TNF- α riboprobes at 40 ng per ml in a solution containing 2.5X SSC, 50% formamide (Boehringer Mannheim), and 10% dextran sulfate (Sigma, St. Louis, MO) at 42°C in a moist environment (Hybrid-Omnislide, Hybrid, Middlesex, UK). Slides were then subjected to post-hybridization stringency washes in 2X SSC at room temperature for 30 min and then at 0.1X SSC and 50% formamide (BDH) at 42°C for 60 min (Hybrid-Omnislide). Bound probe was detected by incubation with a mouse anti-digoxigenin alkaline phosphatase-conjugated Fab fragment (Boehringer Mannheim) and 4-nitroblue tetrazolium/5-bromo-4-chloro-3-indolyl phosphate (Boehringer Mannheim). Sections were mounted in an aqueous mountant (Aquamount, BDH).

Immunohistochemical Examination of Tissue

Immunolocalization of Adhesion Molecules and Neutrophils Cryostat sections (5 μ m) were first incubated with 10% (vol/vol) normal nonimmune goat serum (Zymed Histostain-SP, Cambridge Bioscience, Cambridge, UK) to block nonspecific binding of the secondary antibody. Sections were then incubated with monoclonal mouse antibodies against neutrophil elastase (Dakopatts, High Wycombe, UK), E-selectin, ICAM-1, or vascular cell adhesion molecule-1 (VCAM-1; a gift from Dr. D. Haskard, Hammersmith Hospital, London, United Kingdom; Norris *et al.*, 1991) for 60 min. Normal mouse serum served as a negative control (diluted 1:10 in PBS). Antibodies were used at dilutions of 1:100 in PBS containing 0.1% bovine serum albumin (Sigma). Endogenous peroxidase activity was quenched by incubation in 3% (vol/vol) hydrogen peroxide (Sigma) in methanol (BDH). Sections were then incubated with a biotinylated goat anti-mouse immunoglobulin antibody (Zymed Histostain-SP, Cambridge Bioscience) followed by a streptavidin-peroxidase conjugate (Zymed Histostain-SP, Cambridge Bioscience). A substrate chromogen mixture (hydrogen peroxide and aminoethyl carbazole in buffer (Zymed Histostain-SP, Cambridge Bioscience)) was then applied to each section to allow visualization of the resulting complex. Finally, sections were washed thoroughly with distilled

water, counterstained with haemalum (BDH), and mounted in an aqueous slide mountant (Aquamount, BDH) prior to microscopic examination. All incubations were performed at room temperature. Quantification was performed by two blinded observers and a minimum of four high-power fields were assessed per section. E-selectin staining was expressed as intensity of stain (0 = no staining, 1 = weak staining, 2 = moderate staining, 3 = strong staining, and 4 = intense staining) and as mean number of positive vessels per high-power field. Neutrophil numbers were expressed solely as mean number of positive cells per high-power field.

Immunolocalization of IL-8 and TNF- α Paraffin-embedded tissue sections (5 μ m) were rehydrated through a series of alcohols to water. Sections were incubated in a microwave oven (600 W) for 20 min in 10 mM citrate buffer (pH 6.0) and allowed to cool. The staining protocol was then as for frozen sections. The primary antibodies used were mouse monoclonal antibodies against IL-8 (R&D Systems, Oxford, UK) and TNF- α (Nash *et al.*, 1991; gift of Dr. P.J. McLaughlin, Liverpool University, Liverpool, United Kingdom). They were used at a dilution of 1:40; normal mouse serum (diluted 1:10 in PBS) was used as a negative control.

RESULTS

Interleukin-8 and TNF- α Are Upregulated in the Epidermis after UVB Irradiation IL-8 and TNF- α mRNA was constitutively expressed in the epidermis of all unirradiated control biopsies (time 0 h). IL-8 message expression was present at equal levels throughout the whole epidermis (Fig 1A). There was an observable increase in IL-8 mRNA by 4 h after irradiation (Fig 1B) that reached a maximum between 8 (Fig 1C) and 24 h (Fig 1D). All strata of the epidermis showed equal strength of staining. Results from each individual were comparable. Control sense probes gave consistently negative results (Fig 1E).

IL-8 protein was demonstrable in the epidermis of control biopsies at low levels (Fig 1F). Expression of IL-8 protein was slightly upregulated at 4 h and increased progressively thereafter, reaching a maximum by 24 h (Fig 1G–I). At this time, expression was suprabasal with strong focal patches of granular perivascular keratinocyte staining.

Staining for TNF- α mRNA was moderately strong and mainly suprabasal (Fig 2A). An increase in mRNA expression was observable by 8 h after irradiation and reached a maximum by 24 h (Fig 2B–D). At this time, all layers of the epidermis showed strong expression of TNF- α mRNA; control sense probes gave consistently negative results (Fig 2E). An observable increase in TNF- α protein was observed at 8 h but was maximal at 24 h after irradiation; staining was cytosolic and extended through all layers of the epidermis (Fig 2F). As with the IL-8 findings, results from all individuals were comparable.

E-Selectin, but not ICAM-1 or VCAM-1, Is Upregulated on the Dermal Microvasculature after UVB Irradiation In unirradiated control biopsies, E-selectin was only weakly expressed on vascular endothelium in three of four biopsies (Fig 3A,C). By 4 h after irradiation, an increase in E-selectin staining was evident in the superficial and mid dermis. Expression increased progressively, reaching a maximum by 24 h (Fig 3A,B) in terms of intensity of stain (median = 3, data not shown) and number of vessels stained per high-power field (mean = 2.8, Fig 3B). No increase in microvascular expression of ICAM-1 or VCAM-1 was observed over the time course in any of the biopsies, but weak epidermal expression of ICAM-1 was detected at 24 h after UVB irradiation (two of four biopsies; data not shown).

Neutrophils Accumulate in the Dermis of the Skin after UVB Irradiation Neutrophils were identified in frozen sections by staining of neutrophil elastase. In control samples, few positive cells were present (mean = 1.2 per high-power field). After irradiation, however, there was a progressive increase in number of neutrophils, first noticeable by 8 h (mean = 13.7 per high-power field). By 24 h, this increase had reached statistical significance compared to control samples, shown by paired Student's *t* test ($p < 0.05$) (Fig 4). Furthermore, there was a direct correlation between the number of E-selectin-positive vessels per high-power field and

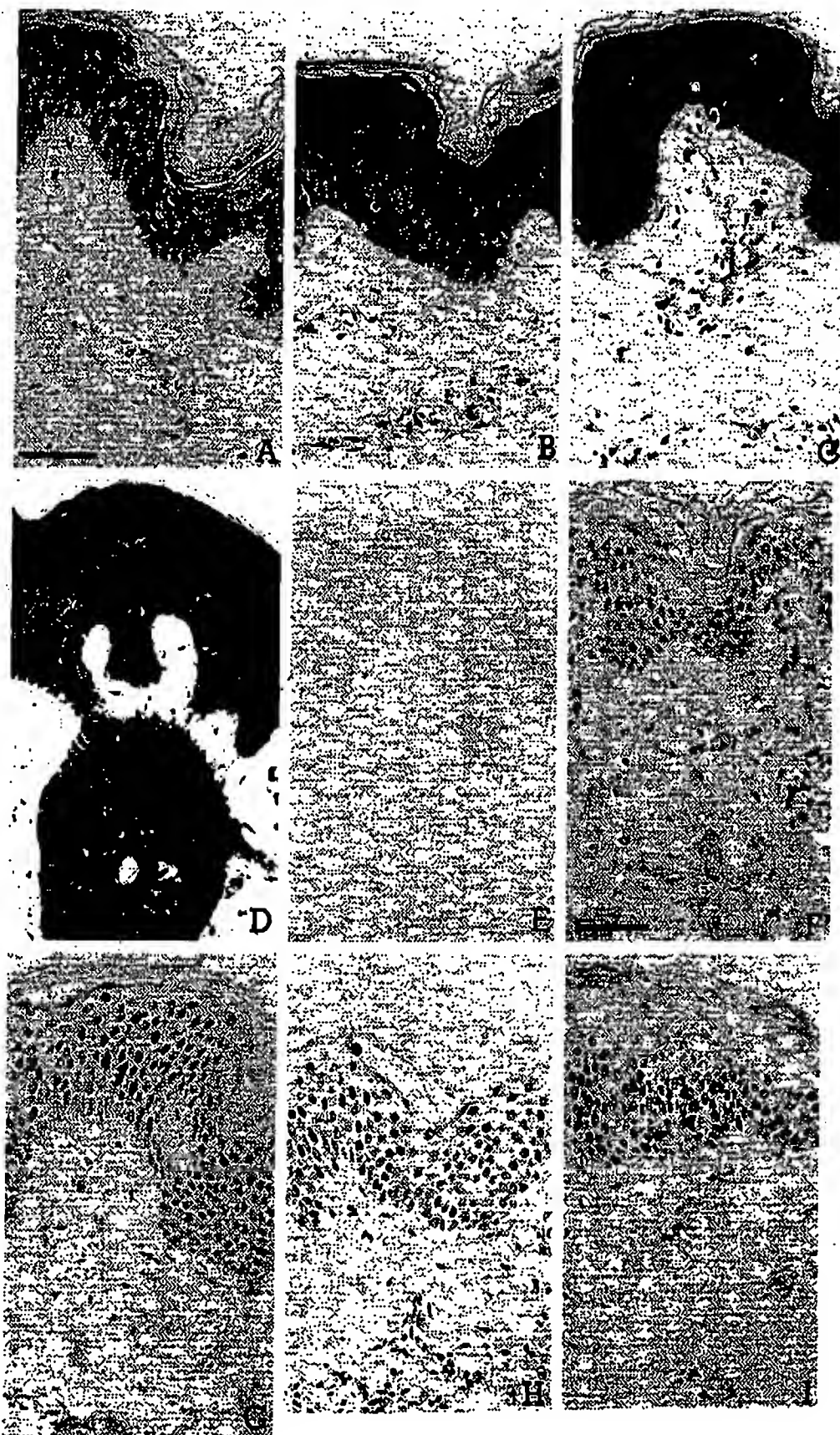
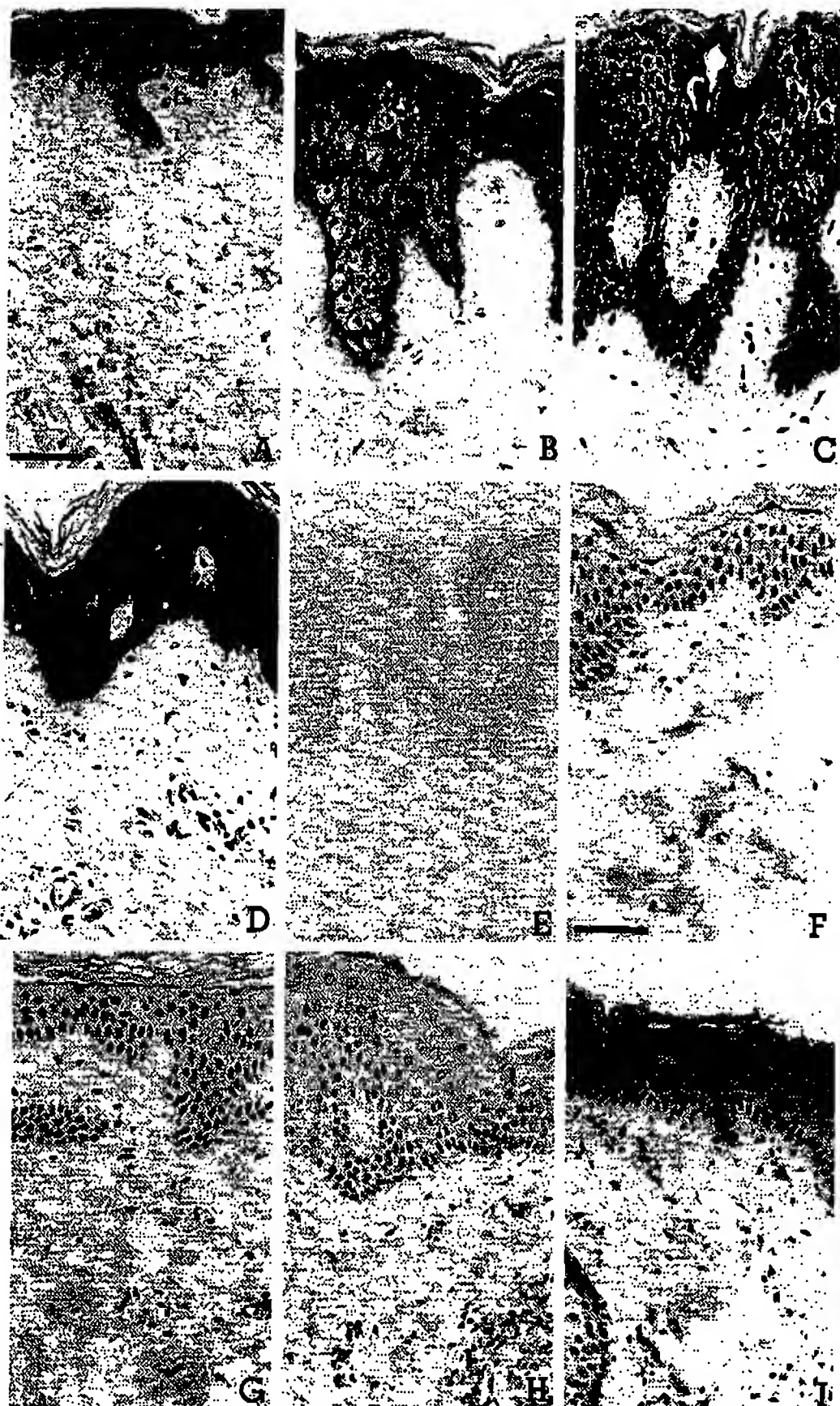


Figure 1. IL-8 mRNA and protein expression increase after UVB-irradiation of normal human skin. Normal healthy Caucasian volunteers ($n = 4$) were irradiated with $2.5\times$ minimal erythema dose of UVB then biopsied at 4, 8, and 24 h and from an unirradiated site. (A–I) Nonradioactive *in situ* hybridization was performed with a digoxigenin-labeled ciprobe to localize the cytokine. (A) Control unirradiated skin. (B) Four hours after UVB. (C) Eight hours after UVB. (D) Twenty-four hours after UVB. (E) Sense probe control used on skin 24 h after UVB irradiation. (F–I) Immunocytochemical techniques were employed to localize IL-8 protein in biopsies from the same volunteers. (F) Control unirradiated skin. (G) Four hours after UVB. (H) Eight hours after UVB. (I) Twenty-four hours after UVB. Normal mouse serum gave consistently negative results. Both mRNA and protein increased progressively, reaching a maximum at 24 h. Scale bar, 50 μ m.

Figure 2. $\text{TNF-}\alpha$ mRNA and protein expression increase after UVB irradiation of normal human skin. For experimental details refer to Fig 1 legend. (A-E) *In situ* hybridization results. (A) Control unirradiated skin. (B) Four hours after UVB. (C) Eight hours after UVB. (D) Twenty-four hours after UVB. (E) Sense probe control used on skin 24 h after irradiation. (F-I) Immunohistochemical localization of $\text{TNF-}\alpha$. (F) Control unirradiated skin. (G) Four hours after UVB. (H) Eight hours after UVB. (I) Twenty-four hours after UVB. Normal mouse serum gave consistently negative results. $\text{TNF-}\alpha$ was present at all time points in the epidermis of the skin, although no increase in expression was observed until 8 h after UVB and reached a maximum at 24 h. Scale bar, 50 μm .



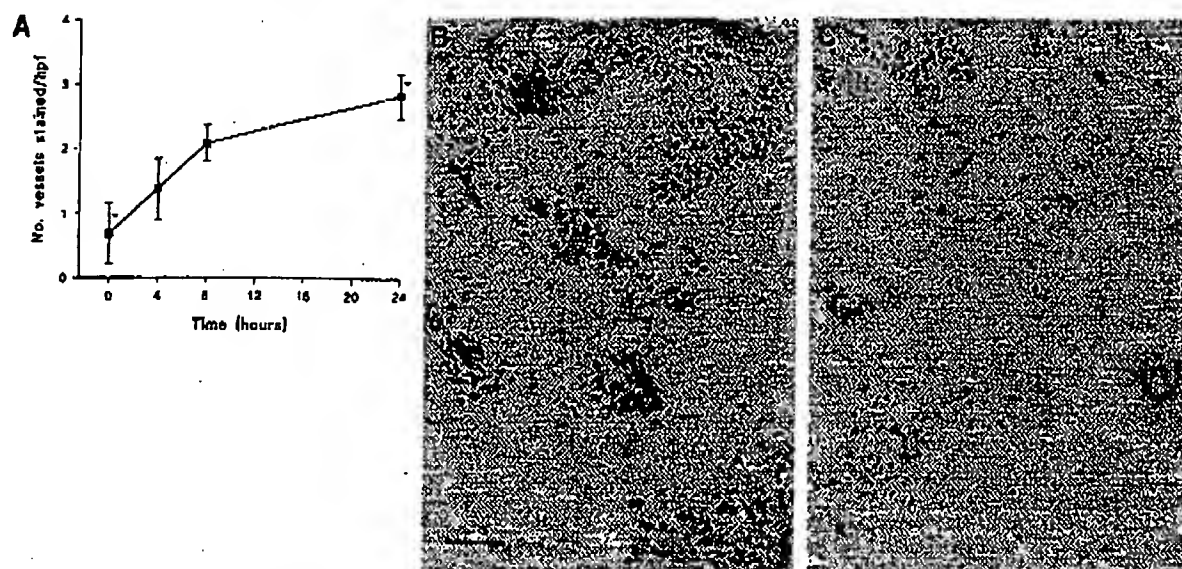


Figure 3. E-selectin is upregulated on the microvasculature after UVB-irradiation of normal human skin. UVB-irradiated skin (see Fig 1 legend) was stained for E-selectin by immunohistochemical techniques. (A) E-selectin staining was expressed as numbers of positive vessels per high-power field. Error bars, SEM (n = 4). *p < 0.05. (B) Strong staining of E-selectin can be observed on the microvasculature at 24 h. (C) Unirradiated control skin. Scale bar, 50 μ m.

numbers of neutrophils per high-power field over the time course ($r = 0.96$).

DISCUSSION

In the current study, we followed the changes of several components of the UVB-induced inflammatory response over a 24-h period. In unirradiated epidermis, TNF- α and IL-8 were constitutively expressed at both mRNA and protein levels. After UVB irradiation, both showed increased expression, IL-8 increasing several hours before TNF- α . Dermal microvasculature showed increased E-selectin expression after 4 h, before an increase in TNF- α protein, and it continued to increase thereafter. Neutrophil infiltration was first detectable at 8 h and reached a maximum by 24 h. The mechanisms underlying these different components of the response to ultraviolet irradiation have been the subject of speculation for some time. It has been suggested that in mice and humans, the inflammatory response induced by UVB is mediated principally by TNF- α (Vincek *et al*, 1993). Furthermore, polymorphic alleles at the TNF- α and Lps loci dictate whether mice are susceptible or resistant to UVB-mediated inhibition of cutaneous

immunity (Yoshicawa *et al*, 1990). The current findings suggest that TNF- α is a rather late mediator in the reaction. The earliest vascular response, in the form of vasodilation, is detectable between 1 and 2 h after UVB exposure (Duffy and Oakley, 1987). Nitric oxide (Warren, 1994) and prostaglandin- E_2 (Black *et al*, 1978a,b) are both known to be involved in this part of the response. We have confirmed the findings of Norris *et al* (1991) that E-selectin expression is increased by 4 h, whereas ICAM-1 and VCAM-1 show little change after *in vivo* irradiation (data not shown). The time of this increase appears to be well before detectable changes in expression of TNF- α , which raises the possibility that it may be due to a direct effect of UVB on endothelial cells or that some other mediator is involved.

Everett *et al* (1966) demonstrated that 10–15% of UVB penetrates to the superficial dermis. Hence it is possible that UVB has a direct effect on microvascular endothelial cells. Indeed, Cornelius *et al* (1994) showed that cultured human dermal microvascular endothelial cells exposed *in vitro* to UVB showed increased expression of ICAM-1, although, interestingly, E-selectin and VCAM-1 were unchanged. This response was not inhibited by antibodies against

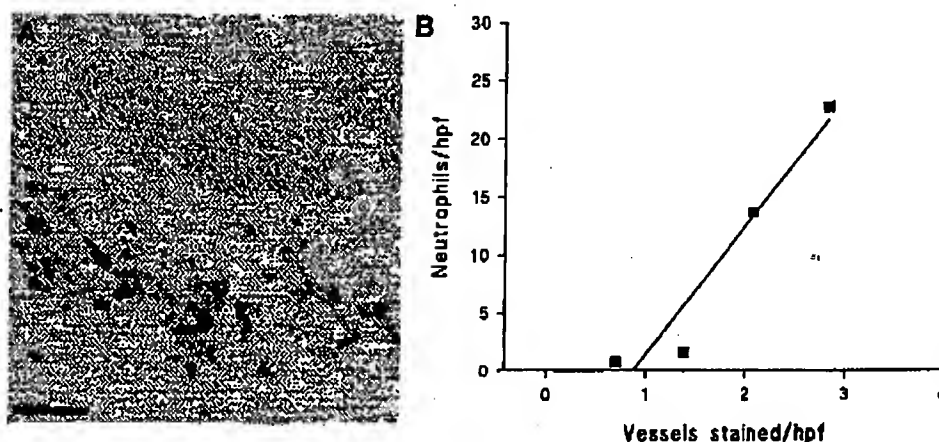


Figure 4. Neutrophils accumulate in the dermis of normal human skin after UVB-irradiation. (A) Normal human skin, 24 h after UVB irradiation (see Fig 1 legend) was stained for neutrophil elastase by immunohistochemical techniques to allow visualization of neutrophils. Normal mouse serum gave consistently negative results. Positive cells can be observed scattered throughout the dermis. Scale bar, 50 μ m. (B) Correlation between numbers of E-selectin stained vessels and numbers of infiltrating neutrophils.

IL-1 or TNF- α . Our observation that E-selectin but not ICAM-1 (data not shown) is increased after UVB *in vivo* may reflect differences between cultured human dermal microvascular endothelial cells and their *in vivo* counterparts, which make up a heterogeneous cell population, differing in structure, function, antigenic composition, metabolic properties, and their responses to growth factors (Kumar *et al*, 1987). Furthermore, endothelial cells can show different levels of response to different stimuli; for example, chemical perturbation of skin with irritant or contact sensitizers results in greater increases in expression of ICAM-1 than of E-selectin (Friedmann *et al* 1992). Thus, our observations suggest that the initial activation of E-selectin expression could be triggered directly by UVB, whereas the subsequent response is augmented via the effects of TNF- α .

Our observations of the activation of IL-8 expression confirms findings by Kondo *et al* (1993) that in UV-irradiated keratinocytes, IL-8 mRNA is increased from 1 h onward. The time course of increase of IL-8 protein expression, rising between 4 and 8 h, is compatible with the possibility that this cytokine is acting as a chemoattractant for neutrophils (Oppenheim *et al* 1991). The neutrophil infiltration was first observed at 8 h and increased progressively thereafter. It is interesting to note the granular staining pattern of IL-8 after UVB irradiation, which may indicate "packaging" of this cytokine prior to secretion. The mechanism by which IL-8 expression is activated is not clear. It may be a direct effect of UVB, because cultured keratinocytes exposed to UVB show increased IL-8 expression (Kondo *et al*, 1993), but its expression may also be subject to modulation by either IL-1 or TNF- α . Indeed, the IL-8 gene contains 5' regulatory elements that confer responsiveness to induction by TNF- α and IL-1. These DNA sequences include putative binding sites for transcription factors including NF- κ B and AP-1 (Mukaida *et al* 1990).

The function of neutrophils in UVB-irradiated sites is unclear, but there is evidence they may be involved in "repair" processes, some of which appear relevant to the changes of photoaging. Thus, Starcher and Conrad (1995) showed that in normal mice, after UVB exposure, the elastin fiber content of skin increased. By contrast, in neutrophil-elastase-deficient mice, there was no increase in elastin fibers even though inflammatory sites in both types of mice contained similar numbers of infiltrating cells.

We have demonstrated that after UVB irradiation of human skin, expression of IL-8 and TNF- α is increased in the epidermis from 4 h. E-selectin, but not ICAM-1 or VCAM-1, is upregulated on dermal microvascular endothelium. Moreover, this change is detectable before the cytokine upregulation has really developed, suggesting that it may be a direct response of endothelial cells to UVB or that some other mediator is involved. The cytokines may contribute by augmenting E-selectin expression and may act as a chemoattractant for neutrophils.

We acknowledge the four volunteers who took part in this study. We also thank Dr. P.J. McLaughlin (Department of Immunology, Liverpool University, Liverpool, United Kingdom) who donated a sample of his TNF- α monoclonal antibody and Dr. D.O. Haskard (Hammersmith Hospital, London, United Kingdom) who donated monoclonal antibodies to ICAM-1, E-selectin, and VCAM-1.

REFERENCES

- Black AK, Greaves MW, Hansby CN, Plummer NA: Increased prostaglandins E_2 and $F_{2\alpha}$ in human skin at 6 and 24 h after ultraviolet B irradiation (290–320nm). *Br J Clin Pharmacol* 5:431–436, 1978a
- Black AK, Greaves MW, Hansby CN, Plummer NA, Warin AP: The effects of indomethacin on arachidonic acid and prostaglandins E_2 and $F_{2\alpha}$ after UVB and UVC irradiation. *Br J Clin Pharmacol* 6:261–266, 1978b
- Colditz IG, Watson DL: The effect of cytokines and chemokine agonists on the migration of T lymphocytes into skin. *Immunology* 76:272–278, 1992
- Cornelius LA, Sepp N, Li LJ, Degize K, Swerfick RA, Lawley TJ, Caughey SW: Selective up-regulation of intercellular adhesion molecule 1 (ICAM-1) by ultraviolet B in human dermal microvascular endothelial cells. *J Invest Dermatol* 103:23–28, 1994
- de Kamodo S, Cruz PD, Drugherty I, Thompson PM, Silva-Valdez M, Beutler B: Expression of the tumor necrosis factor gene by dermal fibroblasts in response to ultraviolet irradiation or lipopolysaccharide. *J Invest Dermatol* 104(3):318–322, 1995
- Difley BL, Oakley AM: The onset of ultraviolet erythema. *Br J Dermatol* 116:183–187, 1987
- Enk CD, Sredni D, Blauvelt A, Katz SI: Induction of IL-10 gene-expression in human keratinocytes by UVB exposure *in-vivo* and *in-vitro*. *J Immunol* 154:4851–4856, 1995
- Everett MA, Yeagers P, Sayre RM, Oton RL: Penetration of epidermis by ultraviolet rays. *Photochem Photobiol* 5:533–542, 1966
- Friedmann PS, Strickland L, Metson AA, Johnson PM: Early time course of recruitment of immune surveillance in human skin after chemical provocation. *Clin Exp Immunol* 91:351–356, 1992
- Hawk JLM, Murphy GM, Holden CA: The presence of neutrophils in human cutaneous ultraviolet-B inflammation. *Br J Dermatol* 188:27–30, 1988
- Kondo S, Kato T, Sauder DN, McKenzie RC: IL-8 gene expression and production in human keratinocytes and their modulation by UVB. *J Invest Dermatol* 110(5):690–694, 1993
- Kumar S, West DC, Ager A: Heterogeneity in endothelial cells from large vessels and microvessels. *Differentiation* 36:57–70, 1987
- Lieber JM, Kunkel SL, Burdick MD, Standiford TJ, Rolfe MW, Strieter RM: Production of IL-8 and monocyte chemoattractant peptide-1 by peripheral blood monocytes. Diverse responses to phytohemagglutinin and lipopolysaccharide. *J Immunol* 152:241–249, 1994
- Morishima K, Morishima K, Yoshinaka T, Lavi S, Kobayashi Y, Lew W, Appella E, Kung HF, Leonard EJ, Oppenheim JJ: Molecular cloning of a human monocyte-derived neutrophil chemoattractant factor (MDNCF) and the induction of MDNCF mRNA by interleukin 1 and tumor necrosis factor. *J Exp Med* 167:1883–1893, 1988
- Mukaida N, Mabe Y, Morishima K: Analysis of the regulation of interleukin 8 (IL-8) gene-expression by proinflammatory cytokines. *Lymphokine Res* 9(4):582–587, 1990
- Nash JRG, McLaughlin PJ, Hoyle C, Roberts D: Immunolocalization of tumor necrosis factor alpha in lung tissue from patients dying with adult respiratory syndrome. *Histopathology* 19:1225–1229, 1991
- Nooris P, Poston RN, Thomas DS, Thornhill M, Hawk J, Haskard DO: The expression of endothelial leukocyte adhesion molecule-1 (ELAM-1), intercellular adhesion molecule-1 (ICAM-1) and vascular adhesion molecule-1 (VCAM-1) in experimental cutaneous inflammation: a comparison of ultraviolet B erythema and delayed hypersensitivity. *J Invest Dermatol* 96:763–770, 1991
- Ozholm A, Ozholm P, Striberg D, Bendtzen K: Immunohistochemical detection of interleukin-1-like molecules and tumour necrosis factor in human-epidermis before and after UVB-irradiation *in-vivo*. *Br J Dermatol* 118:369–376, 1988
- Sambrook S, Fritsch EF, Maniatis T: *Molecular Cloning: A Laboratory Manual*. 2nd ed. Cold Spring Harbor Press, Plainview, NY, 1989
- Springer TA: Adhesion receptors of the immune system. *Nature* 346:425–433, 1990
- Starcher H, Conrad M: A role for neutrophil elastase in the progression of solar elastosis. *Connective Tissue Research* 31:133–140, 1995
- Stetler JW: Sunlight and skin-associated lymphoid tissue (SALT) – if UVB is the trigger and TNF- α is its mediator, what is the message. *J Invest Dermatol* 100:47–52, 1993
- Vinok V, Kurimotu I, Medema JP, Prieto E, Sreelak JW: Tumor necrosis factor alpha polymorphism correlates with deleterious effects of ultraviolet D light on cutaneous immunity. *Cancer Res* 53:728–732, 1993
- Wang AM, Czeisny AA, Lohr MG, Lin LS, Strickler J, Van Arsdale JN, Yamamoto R, Mark DF: Molecular cloning of the complementary DNA for human tumor necrosis factor. *Science* 228:149–154, 1985
- Warren JB: Nitric oxide and human skin blood flow responses to acetylcholine and ultraviolet. *FASEB J* 8:247–251, 1994
- Yoshizawa T, Stetler JW: Genetic basis of the effects of ultraviolet light D on cutaneous immunity—evidence that polymorphism at the TNF- α and LPS loci governs susceptibility. *Immunogenetics* 32:398–405, 1990

Kidney International, Vol. 57 (2000), pp. 1521-1538

Basic fibroblast growth factor expression is increased in human renal fibrogenesis and may mediate autocrine fibroblast proliferation

FRANK STRUTZ, MICHAEL ZEISBERG, BERNHARD HEMMERLEIN, BURKHARD SATTLER, KLAUS HUMMEL, VOLKER BECKER, and GERHARD A. MÜLLER

Department of Nephrology and Rheumatology, and Department of Pathology, Georg-August-University Göttingen, Göttingen, Germany, and Department of Rheumatology, University of Zürich, Zürich, Switzerland

Basic fibroblast growth factor expression is increased in human renal fibrogenesis and may mediate autocrine fibroblast proliferation.

Background. Interstitial fibroblasts play a critical role in renal fibrogenesis, and autocrine proliferation of these cells may account for continuous matrix synthesis. Basic fibroblast growth factor (FGF-2) is mitogenic for most cells and exerts intracrine, autocrine, and paracrine effects on epithelial and mesenchymal cells. The aims of the present studies were to localize and quantitate the expression of FGF-2 in normal and pathologic human kidneys and to study the *in vitro* effects of FGF-2 on proliferation, differentiation, and matrix production of isolated cortical kidney fibroblasts.

Methods. FGF-2 protein expression was localized by immunofluorescence double labelings in normal and fibrotic human kidneys. Subsequently, interstitial FGF-2 labeling was determined semiquantitatively in 8 normal kidneys and 39 kidneys with variable degrees of interstitial fibrosis and was correlated with the morphometrically determined interstitial cortical volume. In addition, FGF-2 expression was quantitated by immunoblot analysis in three normal and six fibrotic kidneys. FGF-2 mRNA was localized by *in situ* hybridizations. Seven primary cortical fibroblast lines were established, and expression of FGF-2 and FGF receptor-1 (FGFR-1) were examined. The effects of FGF-2 on cell proliferation were determined by bromodeoxyuridine incorporation and cell counts, those on differentiation into myofibroblasts by staining for α -smooth muscle actin, and those on matrix synthesis by enzyme-linked immunosorbent assay for collagen type I and fibronectin. Finally, proliferative activity *in vivo* was evaluated by expression of MIB-1 (Ki-67 antigen).

Results. In normal kidneys, FGF-2 expression was confined to glomerular, vascular, and a few tubular as well as interstitial fibroblast-like cells. The expression of FGF-2 protein was increased in human kidneys, with tubulointerstitial scarring correlating with the degree of interstitial fibrosis ($r = 0.84$, $P <$

0.01). Immunoblot analyses confirmed a significant increase in FGF-2 protein expression in kidneys with interstitial scarring. *In situ* hybridization studies demonstrated low-level detection of FGF-2 mRNA in normal kidneys. However, FGF-2 mRNA expression was robustly up-regulated in interstitial and tubular cells in end-stage kidneys, indicating that these cells are the source of excess FGF-2 protein. Primary cortical fibroblasts express FGF-2 and FGFR-1 *in vitro*. FGF-2 induced a robust growth response in these cells that could be blocked specifically by a neutralizing FGF-2 antibody. Interestingly, the addition of the neutralizing antibody alone did reduce basal proliferation up to 31.5%. In addition, FGF-2 induced expression of α -smooth muscle actin up to 1.6-fold, but no significant effect was observed on the synthesis of collagen type I and fibronectin. Finally, staining for MIB-1 revealed a good correlation of interstitial FGF-2 positivity with interstitial and tubular proliferative activity ($r = 0.71$, $P < 0.01$ for interstitial proliferation, $N = 30$).

Conclusions. Interstitial FGF-2 protein and mRNA expression correlate with interstitial scarring. FGF-2 is a strong mitogen for cortical kidney fibroblasts and may promote autocrine fibroblast growth. Expression of FGF-2 correlates with interstitial and tubular proliferation *in vivo*.

Fibrosis is a process that is characterized by excessive deposition of matrix components compromising organ function because of replacement of normal organ tissue. Tissue fibrosis can affect almost any organ but prefers tissues with common inflammations, such as the skin, the lung, the liver, and the kidney [1]. Inflammation is caused by the recruitment of infiltrating inflammatory cells such as lymphocytes and monocytes/macrophages. Inflammatory infiltration is followed by activation and proliferation of matrix-producing cells, mainly fibroblasts, which synthesize excessive amounts of extracellular matrix. Cytokines seem to play a decisive role in the pathogenesis of organ scarring. Human fetuses heal without scar early in gestation and begin to show scarring late in development [2]. The anatomical difference between the scarless fetal wound healing and the adult scar formation lies in the organization of matrix. Whereas

Key words: FGF-2, fibrosis, kidney, interstitial fibroblast, cell proliferation.

Received for publication July 27, 1999

and in revised form October 27, 1999

Accepted for publication November 1, 1999

© 2000 by the International Society of Nephrology

fibroblasts deposit matrix in an organized fashion, similar to normal skin in fetal wounds, adult wounds are characterized by the deposition of disorganized collagen fibers [3]. Studies by Whitby and Ferguson have demonstrated that the differential expression of certain cytokines is one of the key reasons for scar formation. Transforming growth factor- β (TGF- β) immunostaining, for example, was absent in fetal mouse wounds and was abundant in neonatal and adult mouse wounds [4]. Another cytokine that was markedly up-regulated in postnatal wounds with fibrosis was basic fibroblast growth factor (FGF-2). Whitby and Ferguson demonstrated that, similar to TGF- β , FGF-2 is present in neonatal and adult mouse lips but cannot be detected in fetal mouse lip wounds [4]. Thus, similar to TGF- β , FGF-2 may play an important role in the scarring process.

In the kidney, chronic tubulointerstitial fibrosis is the final common pathway of glomerular, vascular, or interstitial inflammations, often resulting in end-stage renal disease [5]. The severity of chronic tubulointerstitial disease is the single best histologic correlate of the decline in renal function and prognosis for organ function [1, 6]. As in other scarring processes, a number of cytokines have been implicated in renal fibrogenesis, including platelet-derived growth factor (PDGF) and TGF- β . PDGF is a strong mitogen for some but not all fibroblasts [7], and PDGF-BB has been shown to cause interstitial cell proliferation, the appearance of myofibroblasts, and kidney fibrosis in rats if given intravenously in high doses [8]. TGF- β affects all phases of wound healing, including the inflammatory response and matrix accumulation [9, 10]. Increased expression of TGF- β 1 has been described in a variety of animal models and human diseases associated with renal fibrosis [reviewed in 1]. However, the role of other cytokines, such as FGF-2, is less well defined. FGF-2 belongs to the family of fibroblast growth and differentiation factors that currently contains nine members [11]. Up-regulated expression of FGF-2 has been linked to fibrogenesis in a number of animal models. Injection of FGF-2 into subcutaneous tissue of newborn mice caused slight fibrotic changes after seven days of injection, whereas simultaneous application with TGF- β resulted in persistent skin fibrosis [12]. Moreover, FGF-2 is a strong mitogen for pulmonary fibroblasts and hepatic stellate cells, and has thus been implicated in the pathogenesis of lung and liver fibrosis, although the exact role remains to be elucidated.

Regarding the kidney, FGF-2 protein was isolated from whole kidney homogenates as early as 1985 [13]. Floege et al, as well as Takeuchi et al, reported strong immunostaining in Bowman's capsule, the glomerular mesangium, blood vessels, and the interstitium, as well as within some tubules in rats [14, 15], although their results could not be confirmed by all investigators [16, 17] and the exact localization of FGF-2 protein in the kidney

remains controversial. Recently, Floege et al analyzed FGF-2 expression in normal human kidneys using four different antibodies, and localized it most consistently to distal tubular epithelial and vascular smooth muscle cells [18]. FGF-2 is mitogenic for mesangial [19], proximal-tubular epithelial [20], glomerular endothelial [21], and glomerular epithelial cells [15]. Floege et al demonstrated that FGF-2 was synthesized by mesangial cells in vitro and in vivo [14]. Furthermore, FGF-2 infusions into rats injected with an antimesangial cell antibody (anti-Thy 1.1) resulted in a fourfold increase in glomerular cell proliferation [22] and led to increased podocyte injury and glomerulosclerosis in rats with membranous nephropathy [23]. Similarly, treatment of rats for 8 and 13 weeks with subcutaneous FGF-2 injections resulted in focal segmental glomerulosclerosis, with an increase of the peritubular interstitium [24]. Finally, Ray et al studied a transgenic mouse model of HIV-associated nephropathy and described increased interstitial staining for FGF-2 colocalized with extracellular matrix [25].

The aims of the present study were the evaluation of FGF-2 expression in normal and fibrotic human kidneys and its potential role in renal fibrogenesis.

METHODS

Materials

Rabbit polyclonal antibody to FGF-2 (Ab-2) and mouse monoclonal antibody to FGF receptor-1 (FGFR-1) were purchased from Calbiochem (La Jolla, CA, USA). Human recombinant FGF-1 and FGF-2 were from R&D Systems (Minneapolis, MN, USA), as was the neutralizing goat polyclonal antibody to FGF-2. Mouse monoclonal antibody to collagen type I was obtained from Southern Biotechnology (Birmingham, AL, USA). Polyclonal rabbit antibody to fibronectin antibody was purchased from Sigma (St. Louis, MO, USA), and mouse monoclonal antibody to heparan sulfate was from Boehringer Mannheim (Mannheim, Germany). For cell characterization, the following additional mouse monoclonal antibodies were used: anticytokeratin (Dako, Carpinteria, CA, USA), antivimentin (Boehringer Mannheim), anti-factor VIII (Dako), anti-human lymphocyte antigen-DR (HLA-DR) (Dako), anti- α -smooth muscle actin (Paesel+Lorei, Wiesbaden, Germany), anticollagen type III (Southern Biotechnology), anti-CD 44 (Pharmingen, San Diego, CA, USA), anti-CD 54, and anti-CD 68 (Dako). The mouse monoclonal antibody to collagen type IV was a generous gift from Steven Gay (University of Zürich, Zürich, Switzerland). Trypsin-ethylenediaminetetraacetic acid (EDTA), Dulbecco's modified Eagle's medium (DMEM), Iscove's modified Dulbecco's medium, and fetal calf serum (FCS) were obtained from GIBCO BRL Ltd. (Paisley, Scotland). Cell culture dishes were from Becton Dickinson (Franklin Lakes, NJ, USA).

Patient material

Kidney tissues from 39 patients with primary and secondary renal diseases and a variable degree of tubulointerstitial fibrosis were used in this study. Tissues included 32 biopsies and 7 nephrectomy specimens. The nephrectomies were performed in patients with end-stage renal disease caused by intractable hypertension or recurrent urinary tract infections. The use of parts of nephrectomy specimens or kidney biopsies for research purposes was approved by the ethics committee of the Georg-August-University, and written consent was obtained from all patients prior to nephrectomy or kidney biopsy. Normal-appearing kidney tissue from kidneys that proved either unsuitable for transplantation or were explanted because of tumor nephrectomies were used as controls ($N = 8$).

Cell culture

Human medullary fibroblast cell lines Tk 173 (obtained from a normal kidney) and Tk 188 (from a kidney with tubulointerstitial fibrosis) have been characterized previously [26] and were cultured in DMEM supplemented with 10% FCS, penicillin (100 U/mL), and streptomycin (100 U/mL). For the isolation of primary human renal fibroblasts, cortical parts of renal biopsy cylinders or nephrectomy specimens were cut and emerged in DMEM medium with 20% FCS and penicillin/streptomycin in the previously mentioned concentrations. When cells had grown to confluence, they were characterized by immunofluorescence for cytokeratin, vimentin, α -smooth muscle actin, collagen types I, III, IV, factor VIII, CD 68, and HLA-DR. Cells that were positive for vimentin and at least collagen types I and III, and negative for cytokeratin, factor VIII and HLA class II were considered to be fibroblasts and were used for induction assays in passages 2 through 8. For detection of heparan sulfate proteoglycane expression, fluorescence activated cell sorting (FACS) analysis was performed as described previously [26].

Specificity of the basic fibroblast growth factor antibody

To determine the specificity of the applied antibody, FGF-2 expression in Tk 173 and Tk 188 fibroblasts (which are easier to culture than primary fibroblasts) was first analyzed by immunocytochemistry as described previously, using the anti-FGF-2 and the secondary FITC-antirabbit antibodies at concentrations of 1:20 [27]. For Northern blot analyses, total cellular RNA was extracted from cultured cells using RNA-clean™ (AGS, Heidelberg, Germany) according to the manufacturer's instructions. Concentration of RNA was determined by absorbance at 260 nm, and samples were stored at -80°C prior to use. Northern blot analysis was performed as described [28]. Briefly, 40 μg of total RNA were electrophoresed on a 1.0% agarose gel containing 2.2 mol/L

formaldehyde using $1 \times$ MOPS, pH 7.0, as the running buffer. Photographs of ethidium-bromide-stained gels were taken under ultraviolet illumination. RNA was subsequently transferred to a nylon membrane (Hybond N; Amersham, Arlington Heights, IL, USA) by capillary transfer for 12 hours with $20 \times$ standard saline citrate (SSC) as the transfer buffer. Blots were baked at 80°C and prehybridized for one hour at 68°C in prehybridization solution containing 0.5 mol/L Na_2HPO_4 buffer (pH 7.2), 0.5 mol/L EDTA (pH 8.0), 25% sodium dodecyl sulfate (SDS), and 1.5% blocking reagent. FGF-2 specific oligonucleotides (R&D Systems) were labeled with digoxigenin using a kit (Boehringer Mannheim) according to the manufacturer's instructions. Hybridizations were performed overnight at 58°C using the prehybridization solution. After washing, anti-DIG alkaline phosphate and disodium 3-(4-methoxy-2-oxo-1,2-dioxetane-3,2'-(5'-chloro)tricyclo[3.3.1.1^{3,7}]decan-4-yl)phenyl phosphate (CSPD) substrate (both Boehringer Mannheim) were added, and autoradiograms were obtained.

Subsequently, immunoblots were performed as described previously [27]. Briefly, lysates from Tk 173 and Tk 188 fibroblasts were obtained by lysis with a detergent-based buffer containing 0.4% sodium deoxycholate, 1% NP-40, 1.9% EGTA, and 10 mmol/L Tris (pH 7.4). One hundred micrograms of total cellular protein and 50 ng FGF-2 control protein were run on an 18% SDS-polyacrylamide electrophoresis gel and transferred to a nitrocellulose membrane (Hybond™ ECL™; Amersham) by electroblotting. Membranes were stained with Ponceau red to control for adequate transfer and equally loaded amounts. After blocking, the membrane was incubated with the respective antibody (anti-FGF-2 in a concentration of 1:40) followed by the secondary antibody (donkey-antirabbit, horseradish peroxidase-linked, concentration 1:3000; Amersham). Positive reaction products were identified by enhanced chemiluminescence (ECL; Amersham) according to the manufacturer's protocol.

Immunohistochemical staining for basic fibroblast growth factor and morphometric evaluation of interstitial volume

Tissue from normal human kidneys, renal biopsies, and end-stage kidneys were snap frozen in liquid nitrogen. Sections of 4 to 6 μm were cut, mounted on microscope slides, and fixed in ice-cold acetone for 10 minutes. Sections were then allowed to dry, and unspecific binding was blocked by incubation with goat serum. Anti-FGF-2 antibody was added in a concentration of 1:20. After incubation for 60 minutes and several washes in phosphate-buffered saline (PBS), FITC-antirabbit was added in a concentration of 1:20. Positivity was evaluated with an Axiophot S100 microscope (Zeiss, Jena, Germany). Interstitial cortical staining for FGF-2 was rated by two

blinded investigators as in normal kidneys (+), increased (++) , robustly increased (+++), or absent (-). Negative controls consisted in substitution of the primary antibody with an irrelevant rabbit polyclonal antibody or PBS.

In selected sections, double labelings were performed to characterize FGF-2-positive interstitial cells. In that case, an addition of the anti-FGF-2 antibody was followed by staining for α -smooth muscle actin, vimentin, cytokeratin, HLA-DR, CD 44, CD 54, and CD 68. FITC-anti-rabbit and the appropriate rhodamin-labeled antibody were added sequentially at a concentration of 1:20. Photographs were taken either by double or by sequential exposure using Zeiss camera and software (MC 200 Chip).

Selected sections from normal and fibrotic kidneys were also paraffin embedded after fixation in formaldehyde using a standard avidin-biotin complex (ABC) method, as described previously [27].

For morphometric evaluation, all tissue specimens were fixed in 4% buffered formalin solution (pH 7.4) and embedded in paraffin. Tissue sections were stained for trichrome or PAS, and point counting was performed as described by Bohle et al [29]. Only those specimens containing at least five glomeruli were evaluated. Five projection fields of the cortex were examined per kidney using a lattice of 1 cm at a magnification of $\times 250$, discriminating between interstitium, tubular epithelia, glomeruli, and vasculature. Big blood vessels were ignored. The value for the interstitium was expressed as a percentage of the analyzed cortex.

Quantitation of basic fibroblast growth factor expression

Expression of FGF-2 protein was quantitated by immunoblot analysis. Briefly, lysates were obtained from six kidneys with considerable interstitial scarring and three control kidneys. Immunoblots were performed as described earlier in this article using 100 μ g of protein and 50 ng of FGF-2 recombinant protein as positive control. After staining for Ponceau red, blots were analyzed densitometrically for later normalization. Positive reaction products were again identified by chemiluminescence using a Fluor-STM Multiimager (Bio-Rad, Hercules, CA, USA), and densitometric analysis was performed with Multi-AnalystTM software (Bio-Rad).

Vector assembly and in situ hybridization for basic fibroblast growth factor

In situ hybridizations were performed on 6 μ m sections of snap-frozen tissue from freshly explanted kidneys using a digoxigenin-labeled cRNA probe. FGF-2 cDNA was purchased from R&D Systems, digested with Hind III and BamHI, and cloned into pBS SK II (Stratagene, La Jolla, CA, USA) as described [30]. The new vector was named FGF-2-pBS. Correct ligation was verified by sequence analysis using Alf-Express (Pharmacia,

Piscataway, NJ, USA). The vector was linearized with the appropriate enzyme, and FGF-2 sense/antisense riboprobes were synthesized and labeled with digoxigenin by in vitro transcription with the DIG RNA labeling kit (Boehringer Mannheim) as described [31]. Tissue sections were mounted on SectionlockTM slides (Polysciences, Eppelheim, Germany), briefly heated to 50°C to ensure fixation, dried for 30 minutes, and fixed in 3% paraformaldehyde for 7 minutes. Washing in PBS and $2 \times$ SSC was followed by prehybridization for 60 minutes at 43°C in hybridization buffer (Amersham) containing 50% formamide (Sigma). Hybridization was then performed in 40 to 60 μ L hybridization buffer per section containing the cRNA probe at a concentration of 200 ng/mL, followed by washing in $2 \times$ SSC for 5 minutes at 37°C and twice for 15 minutes in $0.1 \times$ SSC, SDS at 68°C. After a final wash in 100 mmol/L Tris-HCl and 150 mmol/L NaCl for five minutes at room temperature, 1% blocking buffer and 10% goat serum (Dako) were added, and the sections were incubated with a 1:500 dilution of alkaline-phosphatase conjugated anti-DIG antibody for two hours at room temperature. Detection was performed after several washes in 100 mmol/L Tris-HCl, 150 mmol/L NaCl with detection buffer containing 0.18 mg/mL 5-bromo-4-chloro-3-indolyl-phosphate (BCIP), 0.34 mg/mL nitro blue tetrazolium (NBT), and 240 μ g/mL levanisole. After 12 hours, color reaction was stopped by washing in 10 mmol/L Tris (pH 8) and 1 mmol/L EDTA for five minutes, and coverslips were mounted. Sections from human synovia, which is known to express FGF-2 abundantly, served as positive control.

Proliferation assay

Proliferation studies in primary cortical fibroblasts were performed using nonradioactive bromodeoxyuridine incorporation assays (Amersham) based on the method by Gratzner [32]. Four $\times 10^3$ cells were plated per well in 96-well microtiter plates containing DMEM medium with the usual supplements and incubated overnight to allow cell attachment. Cells were then made quiescent by replacement of DMEM medium with Iscove's medium and subsequent incubation for 24 hours. In preliminary experiments, cytokines were added, and proliferation was measured after 24, 48, 72, and 96 hours. FGF-2 was used in concentrations of 0.1, 1, 10, and 100 ng/mL (equivalent to 5.5×10^{-12} mol/L, 5.5×10^{-11} mol/L, 5.5×10^{-10} mol/L, and 5.5×10^{-9} mol/L, respectively). In a second set of experiments, 1 ng/mL FGF-2 was added, and bromodeoxyuridine incorporation was measured after 72 hours. The specificity of the response to FGF-2 was determined by addition of a neutralizing FGF-2 antibody in a concentration of 10 μ g/mL (which had been determined in titration experiments with Tk 173 fibroblasts) or a nonrelevant IgG. Both antibodies were also added without FGF-2 to study their

intrinsic effects on proliferation. Medium was changed to Iscove's containing BrdU/FdU in a dilution of 1:500 four hours prior to measurements. Cells were then washed three times in PBS and fixed in methanol containing 2% hydrogen peroxide followed by denaturation in 1N HCl for 10 minutes. After a further three times of washing in PBS containing 0.1% Tween and blocking for 30 minutes in PBS (0.1% Tween, 3% BSA), 50 μ L of anti-BrdU antibody were added and incubated for 45 minutes. Cells were again washed three times in PBS/Tween, and peroxidase substrate was added (100 μ L/well). Optical densities were subsequently determined photometrically at 405 nm (Dynatech MR 4000; Dynatech, Denkendorf, Germany). All experiments were performed in triplicate and repeated five times. Results are shown in percentage of negative control (Iscove's medium = 100%).

In a third set of experiments, confluent monolayers of fibroblasts were trypsinized, and cells were seeded at 4×10^4 cells per well in 96-well culture plates. After 12 hours, DMEM medium was replaced by Iscove's medium. After a further 24 hours, cells were incubated with various factors (FGF-2 at concentrations of 0.1, 1, 10, and 100 ng/mL, FGF-2 (1 ng/mL) + FGF-neutralizing antibody (10 μ g/mL), FGF-2 (10 ng/mL) + irrelevant IgG, and FGF-2 (1 ng/mL) + heparin (10 μ g/mL) for 72 hours before cell counts were performed. PDGF-BB at 10 ng/mL and heparin alone (10 μ g/mL) served as controls. Again, all experiments were performed in triplicate and repeated five times.

Immunofluorescence staining of α -smooth muscle actin

The effects of FGF-2 on the differentiation of kidney fibroblasts into myofibroblasts were assessed by immunofluorescent staining of α -smooth muscle actin after continuous exposure to FGF-2 for 48 hours. Cells were seeded in microchamber slides and incubated in regular medium for 12 hours. After 24 hours of incubation in Iscove's medium for quiescence, FGF-2 was added in concentrations of 0.1, 1.0, and 10 ng/mL. At the end of incubation, cells were washed twice with PBS and fixed with ethanol/acetic acid (50:50, vol/vol) for 20 minutes at 4°C. The cells were subsequently washed again and incubated for two hours at room temperature with a 1:200 dilution of a monoclonal mouse antibody to human α -actin isoform of smooth muscle cells. Cells were then washed again with PBS and incubated for 60 minutes at room temperature with the FITC-conjugated rabbit-antimouse antibody. Control cultures were incubated without application of the primary antibody. Incubation with TGF- β 1 (1 ng/mL) served as a positive control. Cells with the typical α -actin structure were considered to be α -actin positive. Additional staining with the Hoechst dye H33258 to identify nuclei was performed to facilitate cell counting. For each group, 500 cells were

determined microscopically using an Axiophot S100 microscope (Zeiss) by a blinded investigator, and the percentage of α -smooth muscle actin-positive cells was calculated. Each experiment was repeated three times independently.

Matrix synthesis

Enzyme-linked immunosorbent assay (ELISA) of supernatants were performed as described [33], with some modifications, including the use of chemiluminescence to enhance sensitivity [34]. Eight $\times 10^3$ cells were plated per well, and cells were again made quiescent by incubation in serum-free medium for 24 hours. Next, FGF-2 was added in concentrations of 0.1, 1.0, and 10 ng/mL followed by incubation for 48 hours. Human recombinant TGF- β 1 (R&D Systems) in a concentration of 1 ng/mL served as a positive control. Fifty μ g/mL ascorbic acid and 50 μ g/mL propionitrile (both from Sigma) were added in experiments evaluating collagen synthesis. Supernatants were transferred to a Maxisorp™ plate and incubated overnight at room temperature. Plates were subsequently dried for two hours and blocked with 3% dried milk. Incubation with 50 μ L of the primary antibody (anticollagen type I was used in a concentration of 1:300 and antifibronectin at 1:5000) was followed by washing two times with PBS/0.1% Tween and incubation with the secondary antibody [antimouse-IgG-AP and antirabbit-IgG-AP (both Boehringer Mannheim, Germany), both used at a concentration of 1:1000]. After two additional wash steps, 100 μ L of CSPD-Ready-to-Use substrate (Boehringer Mannheim) were added, and quantitation was performed in a luminometer (Mikrolumat CB 96P; Berthold, Bad Wildbad, Germany) using MikroWin™ software (Mikrotek, Overath, Germany). Nonspecific binding was determined by incubation with the secondary antibody only. The value was normally less than 5% of the total chemiluminescence and was subtracted from each assay. All assays were performed in triplicate and repeated five times. Standardization was obtained for the collagen type I ELISA using human type I collagen (Becton Dickinson, Bedford, MA, USA). The limit of detection was 1 ng/mL, with a working range of 10 to 1000 ng/mL. Human fibronectin (Sigma) served as standard for the fibronectin ELISA. The working range of that ELISA was 0.1 to 10 μ g/mL, with a limit of detection of 10 ng/mL. All values were corrected for cell counts (10^3 cells), which were performed after transfer of supernatants.

Evaluation of cell proliferation in vivo

Immunostaining with MIB-1 (Dako) was used to evaluate cell proliferation in vivo. Five-micrometer thick sections were cut, dewaxed, and rehydrated according to routine procedures. Sections were pretreated in a microwave oven for 5 minutes and then incubated for 60 min-

utes at room temperature with the MIB-1 antibody, which was used in a concentration of 1:50. The streptavidin-biotin/alkaline phosphatase complex technique (Dako) was performed, and Fast Red™ was used as the chromogen. The sections were counterstained with hematoxylin. All stained nuclei were rated as positive. Proliferative activity within the interstitium and tubular epithelium was quantitated separately by counting MIB-1-positive cells in four fields at $\times 250$ magnification using an integration grid.

Statistical analysis

All values are expressed as mean \pm SEM unless specified. Analysis of variance (ANOVA) was used to determine statistical differences between growth factor-treated groups and controls using Sigma-Stat™ software (Jandel Scientific, San Rafael, CA, USA). Further analysis was carried out using Bonferroni's test to control for multiple testing. For nonnormally distributed data (MIB-1 staining), the Mann-Whitney rank sum test was applied. A correlation between semiquantitative interstitial FGF-2 staining, morphometric volume, and MIB-1 positivity was evaluated by Spearman's rank-order correlation coefficient. *P* values < 0.05 were considered significant.

RESULTS

Specificity of the anti-basic fibroblast growth factor antibody

Since the exact localization of FGF-2 in the kidney is still controversial, we first determined the specificity of the antibody used for our studies. First, immunofluorescence labeling demonstrated that the two fibroblast lines, Tk 173 and Tk 188, were positive for FGF-2 using the Ab-2 antibody. These results were corroborated by Northern and Western blot analyses (Fig. 1). Northern blot analysis confirmed that both fibroblast lines express FGF-2 mRNA, with a main band at 7.0 kb (Fig. 1A). In addition, the immunoblot demonstrated that the antibody detects a specific 18 kD band in the two fibroblast lines corresponding to the size of the recombinant protein (Fig. 1B). The two additional bands found mainly in Tk 173 fibroblasts probably correspond to multiple translation initiation sites [35]. There was no cross-reactivity of the antibody with FGF-1 (acidic fibroblast growth factor; data not shown).

Basic fibroblast growth factor expression is expressed in interstitial fibroblast-like cells and increased in kidneys with tubulointerstitial fibrosis

Basic fibroblast growth factor expression was first analyzed in frozen sections of normal kidneys by indirect immunofluorescence. Immunolabeling of normal kidneys demonstrated FGF-2 protein within glomeruli, tu-

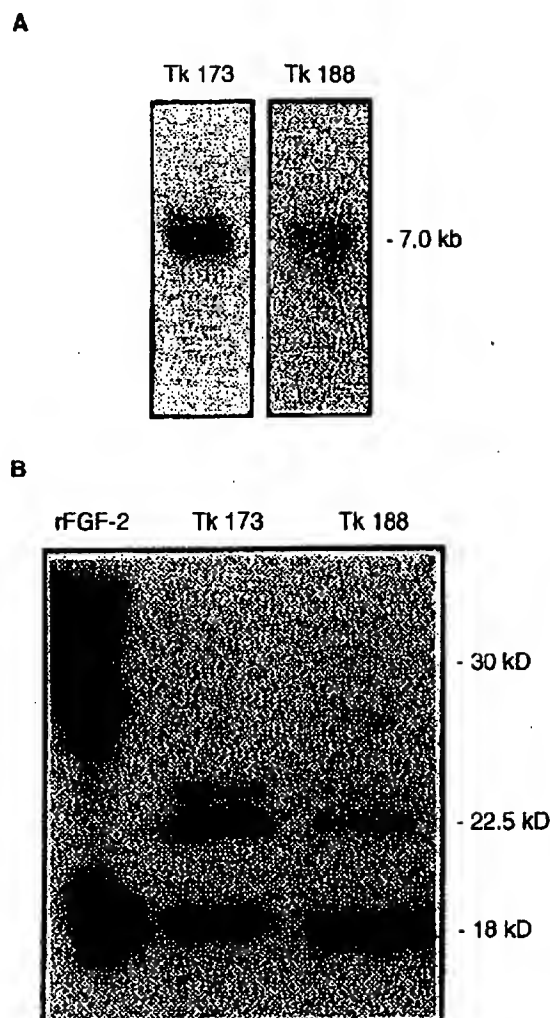


Fig. 1. Specificity of the anti-basic fibroblast growth factor (anti-FGF-2) antibody. The two kidney fibroblast cell lines Tk 173 and Tk 188 express FGF-2 as determined by Northern blot (A) and immunoblot analyses (B). Northern blot gave a main band at 7.0 kb, as expected for FGF-2 (A). Immunoblot analysis demonstrated a main band at 18 kD corresponding to the size of the recombinant protein. Additional bands at 22.5 and 24 kD correspond to multiple translation initiation sites (B). One hundred micrograms of total cellular protein were loaded onto each lane, and 50 ng of recombinant FGF-2 control protein (rFGF-2) served as positive control.

nica media of blood vessels, few tubular (mainly distal by morphology), and many, albeit not all, interstitial cells (Fig. 2). The number of positive interstitial cells was considerably smaller in paraffin sections, probably because of differences in antigen stability (data not shown). To further characterize the FGF-2-positive cells within the interstitium, immunofluorescent double labelings were performed in normal kidneys and biopsies from kidneys with minimal interstitial involvement (interstitium morphometrically $< 25\%$). The results are depicted in Figure 2. Most of the FGF-2-positive cells within the interstitium stained also positive for CD 54 (intercellular

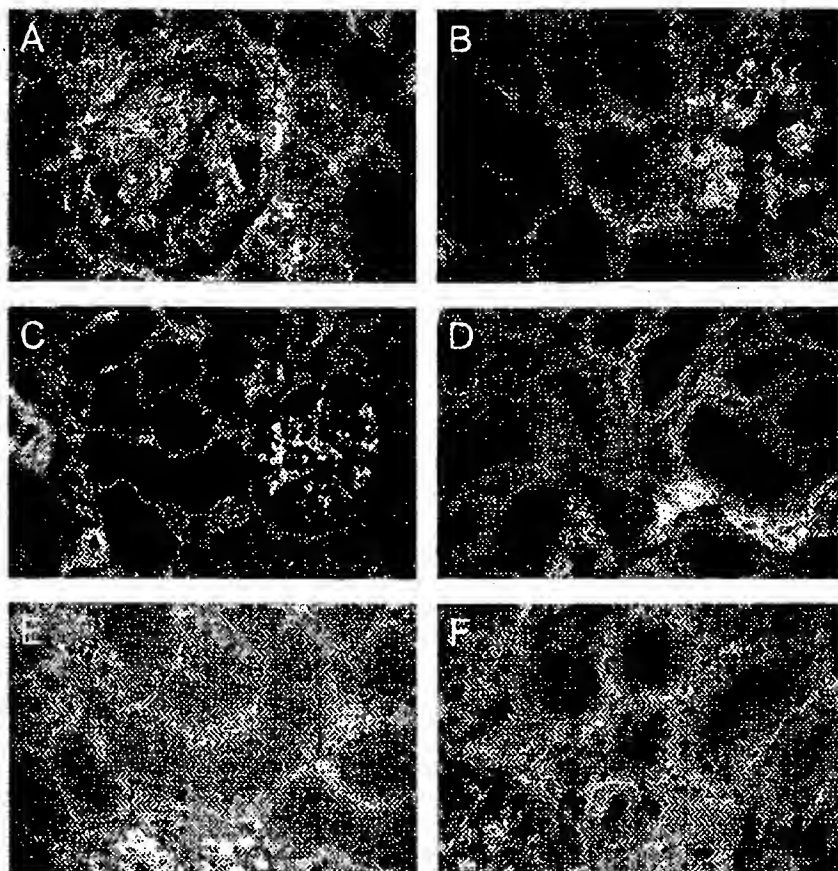


Fig. 2. Localization of FGF-2-positive cells in cortical tissue of a normal kidney by immunofluorescence. Indirect immunofluorescence double labellings for FGF-2 (FITC labeled) and HLA-DR (A), CD 68 (B), α -smooth muscle actin (C), cytokeratin (D), CD 54 (E), and CD 44 (F) (rhodamine labeled) were performed in a human kidney without interstitial scarring. There is a close correlation in staining within the interstitium for FGF-2 and α -smooth muscle actin, CD 54, and CD 44. However, some interstitial cells stain exclusively for α -smooth muscle actin (C), some exclusively for FGF-2 and not for CD 54 (E), or CD 44 (F). A number of cells coexpress FGF-2 and HLA-DR (A), although most interstitial cells stain only for FGF-2. There are very few coexpressions between FGF-2 and CD 68 (B). Interstitial cells do not express cytokeratin; however, some tubular cells display coexpression of FGF-2 and cytokeratin (D). Original magnification $\times 200$.

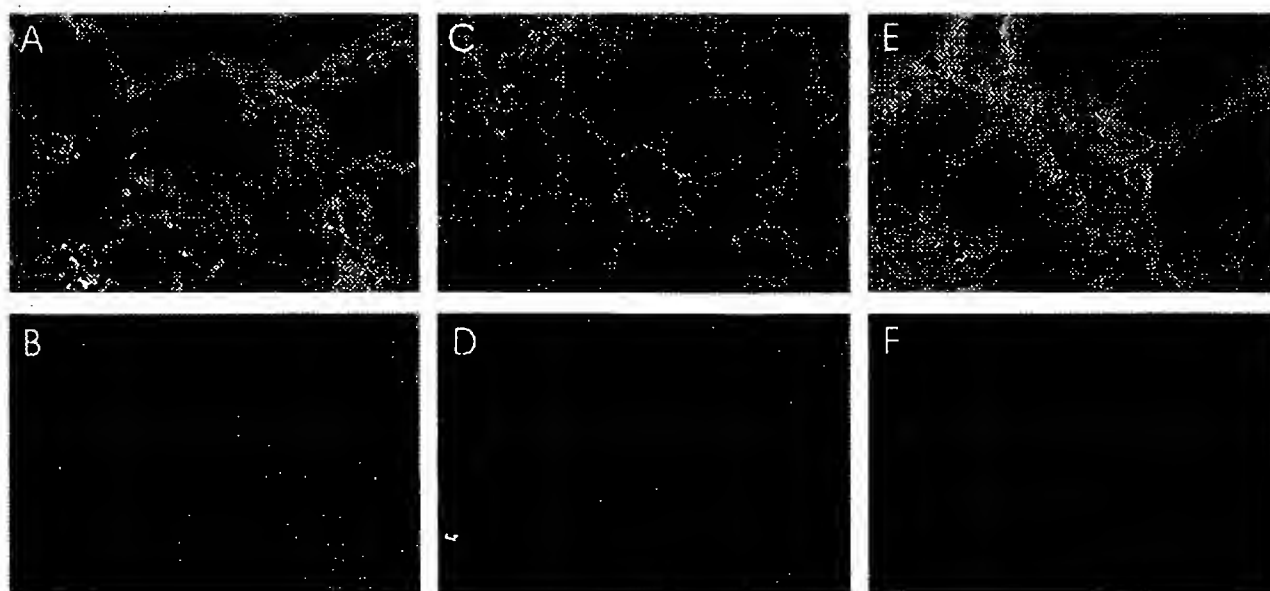


Fig. 3. Staining for FGF-2 in a fibrotic kidney. Indirect immunofluorescence for FGF-2 (A, C, E) and vimentin (B), α -smooth muscle actin (D), and CD 44 (F) in a human kidney with marked interstitial fibrosis. The staining for all four molecules is increased compared with a normal kidney. There is marked coexpression for FGF-2 and all three markers of interstitial fibroblasts; however, again, the overlap in staining is not complete. Some interstitial cells label exclusively for FGF-2 and some exclusively for α -smooth muscle actin (C and D). Original magnification $\times 400$ (A and B) and $\times 200$ (C, D, E and F).

adhesion molecule-1; Fig. 2E) and CD 44 (Fig. 2F), although many FGF-2-positive cells did not label for both. In addition, almost all FGF-2-positive cells did stain for vimentin as well (data not shown). There was a considerable overlap in interstitial staining for FGF-2 and α -smooth muscle actin (Fig. 2C); however, there were some cells that expressed α -smooth muscle actin but not FGF-2. There was some coexpression of FGF-2 and HLA-DR (Fig. 2A), but most FGF-2-positive interstitial cells were negative for the HLA class II molecule, which is expressed on dendritic cells and macrophages. Only occasionally was coexpression of FGF-2 and the macrophage marker CD 68 observed (Fig. 2B), indicating that only very few FGF-2-positive cells are macrophages. Judging by the difference in staining for CD 68 and HLA-DR, some of the cells that stained for FGF-2 may be dendritic cells, but the majority clearly are not. CD 44, CD 54, and α -smooth muscle actin have all been propagated as potential markers of fibroblasts [36, 37]. Thus, it seems reasonable to assume that most FGF-2-positive cells within the interstitium are probably fibroblasts or fibroblast-like cells.

We next compared the sections from eight normal renal tissues (from 3 female and 5 male patients, mean age 56.9 years) and 39 kidneys (from 12 female and 27 male patients, mean age 45.0 years), each with varying degrees of tubulointerstitial fibrosis. Since we were particularly interested in the correlation between FGF-2 expression and the degree of interstitial scarring, a variety of renal diseases was examined. Table 1 displays the characteristics of patients and tissue types. The relative percentage of the cortical interstitium was determined by morphometric analysis. In normal kidneys, the relative percentage of the interstitium varied between 15 and 25%. Conversely, in the nephrectomy specimens from patients with renal disease, the interstitium occupied between 49 and 72%. No change of FGF-2 expression was observed in normal human kidneys. However, robust up-regulation of FGF-2 expression was noted in kidneys with interstitial scarring. Table 1 summarizes the results. Figure 3 depicts the staining results in a kidney with marked interstitial fibrosis. FGF-2-positive cells (Fig. 3A, C, and E) also stained positive for vimentin (Fig. 3B), α -smooth muscle actin (Fig. 3D), and CD 44 (Fig. 3F). Again, there was only little co-staining for the dendritic cell and macrophage marker HLA-DR and only occasional co-staining for the macrophage marker CD 68 (data not shown), excluding prominent expression in these cells. In paraffin-embedded sections, there was an accentuation of extracellular matrix staining, including tubular basement membrane, whereas fewer cellular elements were labeled.

When the expression of FGF-2 was correlated with the cortical interstitial volume, we found a good correlation ($r = 0.64$, $P < 0.01$). However, four of the biopsy specimens displayed an enlargement of the interstitial volume caused exclusively by interstitial infiltration with-

out significant interstitial scarring (numbers 14, 15, 33, and 34). No increase in FGF-2 expression was observed in any of the four specimens. Thus, when FGF-2 protein expression was correlated with the interstitial volume only in those kidneys in which widening of the interstitial space was due to scarring, we found an even better correlation ($r = 0.84$, $P < 0.01$). Figure 4 illustrates the correlation graphically.

When the specimens from patients with glomerulonephritis ($N = 20$) were analyzed exclusively, the correlation was still significant ($r = 0.65$, $r < 0.01$). The number of individual diseases was too small to analyze them separately. However, looking at the specimens with IgA nephritis, there may be a biphasic expression pattern of FGF-2 with a +++ expression at interstitial volumes of 37 to 46% and a ++ expression at volumes of 55 to 71%. There was no correlation between interstitial FGF-2 staining and interstitial volume in the specimens from patients with tubulointerstitial nephritis.

FGF-2 protein expression is increased in cortical tissue from kidneys with interstitial fibrosis

Although our immunofluorescence labeling studies had shown a good correlation between interstitial volume and interstitial FGF-2 labeling, we wanted to confirm this finding by immunoblot analysis. Thus, protein was isolated from cortical tissue from three normal kidneys and six kidneys with marked interstitial scarring [from patients 10 (that is, FK1), 11 (FK2), 13 (FK3), 18 (FK4), 19 (FK5), and 24 (FK6)]. With the exception of FK1, all fibrotic kidneys contained more FGF-2 than their normal counterparts (Fig. 5A). Figure 5B summarizes the result after densitometric analysis ($P = 0.048$).

In situ hybridizations reveal increased FGF-2 mRNA expression within the tubulointerstitium in end-stage kidneys

In situ hybridizations were performed to localize FGF-2-synthesizing cells in three normal and three end-stage kidneys with interstitial fibrosis, tubular atrophy, and dilation. As expected, hybridization with the sense probe gave no signal (Fig. 6A). Conversely, hybridization with the antisense probe demonstrated weak staining within glomeruli and blood vessels, as well as occasional tubular and interstitial cells in normal kidneys (Fig. 6B), indicating that these cells synthesize FGF-2 themselves. Furthermore, similar to what was observed by immunofluorescent staining, in situ hybridizations of fibrotic end-stage kidneys revealed a robust increase in signal for FGF-2 mRNA within interstitial cells (Fig. 6C, D). The majority of interstitial cells displayed FGF-2 mRNA positivity. There was also increased staining in tubular cells, even in some tubules that were dilated and atrophic. Conversely, there was no increased FGF-2 mRNA synthesis within the glomeruli of the analyzed kidneys, indicating that most FGF-2 is, in fact, synthesized in nonglo-

Table 1. Characteristics of the kidney specimens

Patient #	Sex	Age	Tissue	Diagnosis	FGF-2 staining	Interstitial volume
1	M	68	Biopsy	MGN	++	22%
2	M	31	Biopsy	MGN	+	25%
3	F	47	Biopsy	Chronic rejection	+++	55%
4	M	69	Biopsy	IgA nephropathy	+++	46%
5	M	54	Biopsy	Amyloidosis	++	48%
6	M	22	Biopsy	RPGN	++	38%
7	M	27	Biopsy	CRF	+++	65%
8	M	34	Biopsy	Chronic rejection	++	68%
9	M	60	Biopsy	IgA nephropathy	++	55%
10	F	41	Nephrectomy	ESRD	+++	68%
11	M	83	Nephrectomy	ESRD	++	61%
12	M	34	Biopsy	IgA nephropathy	+	36%
13	M	59	Nephrectomy	ESRD	+++	76%
14	M	53	Biopsy	TIN	+	78%
15	F	17	Biopsy	TIN	+	50%
16	M	49	Biopsy	Amyloidosis	++	40%
17	M	22	Biopsy	RPGN	+	22%
18	F	71	Nephrectomy	ESRD	+++	72%
19	M	27	Nephrectomy	ESRD	+++	70%
20	F	28	Biopsy	IgA nephropathy	++	37%
21	M	25	Biopsy	IgA nephropathy	+++	37%
22	M	25	Biopsy	Chronic rejection	+++	50%
23	M	48	Biopsy	Diabetic nephropathy	++	31%
24	F	57	Nephrectomy	ESRD	+++	49%
25	F	43	Biopsy	CRF	++	41%
26	M	27	Biopsy	IgA nephropathy	++	42%
27	M	30	Biopsy	FSGS	++	36%
28	M	42	Biopsy	FSGS	+	18%
29	F	22	Nephrectomy	Diabetic nephropathy	+	20%
30	F	58	Biopsy	RPGN	++	46%
31	M	49	Biopsy	FSGS	+++	74%
32	M	17	Biopsy	FSGS	+	27%
33	F	67	Biopsy	TIN	+	70%
34	M	78	Biopsy	TIN	+	46%
35	M	64	Biopsy	MGN	+	18%
36	F	29	Biopsy	MGN	++	42%
37	M	50	Biopsy	FSGS	+	22%
38	F	67	Biopsy	RPGN	++	25%
39	M	60	Biopsy	IgA nephropathy	++	71%
40	F	64	Nephrectomy	Normal kidney	+	23%
41	M	54	Nephrectomy	Normal kidney	+	19%
42	M	45	Nephrectomy	Normal kidney	+	25%
43	M	71	Nephrectomy	Normal kidney	+	21%
44	F	53	Nephrectomy	Normal kidney	+	15%
45	F	48	Nephrectomy	Normal kidney	+	16%
46	M	61	Nephrectomy	Normal kidney	+	24%
47	M	59	Nephrectomy	Normal kidney	+	20%

There were 6 cases of end-stage renal disease (ESRD), 4 cases of acute tubulointerstitial nephritis (TIN), 4 cases of rapidly progressive glomerulonephritis (RPGN), 7 cases of IgA nephropathy, 4 cases of membranous glomerulonephritis (MGN), 5 cases of focal segmental glomerulosclerosis (FSGS), 3 cases of chronic transplant rejection, 2 cases of amyloidosis, 2 cases of diabetic nephropathy, and 2 cases of chronic renal failure of unknown origin (CRF). Eight normal kidneys served as controls. Interstitial FGF-2 labeling was determined semiquantitatively, and interstitial volume determined morphometrically. Interstitial FGF-2 staining was rated as in normal kidneys (+), increased (++), or robustly increased (+++).

merular cells. Thus, we conclude that the results of the in situ hybridizations parallel the protein stainings, demonstrating that increased FGF-2 mRNA synthesis takes place in interstitial cells within the kidney and that increased protein detection is not due to mere accumulation of extrarenally synthesized FGF-2.

Detection of FGF-2 expression and its low- and high-affinity receptors in human primary cortical fibroblasts

To evaluate the possible role of FGF-2 in human renal fibrogenesis, the expression of FGF-2 and its high- and

low-affinity receptors were examined in seven primary cortical fibroblast lines. All cell lines were characterized as fibroblasts and synthesized extracellular matrix components, including collagen types I and III, as well as fibronectin. Expression of FGFR-1, one of four high-affinity receptors, was analyzed by immunoblot analysis. The immunoblot analysis demonstrated a double band at approximately 120 kD in all seven fibroblast lines (Fig. 7A). The most robust expression of FGFR-1 was observed in fibroblasts isolated from kidneys 25, 31, and 39, with interstitial volumes of 41, 74, and 79%, respec-

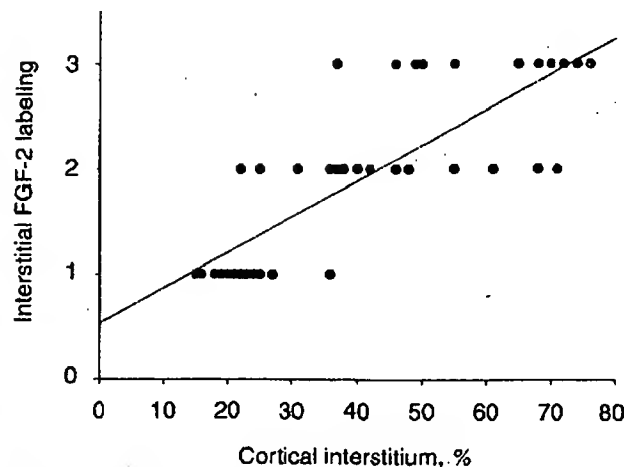


Fig. 4. Correlation of staining for FGF-2 and morphometric volume. There was a positive correlation between semiquantitative FGF-2 labeling and morphometrically determined volume. Four cases of acute tubulointerstitial nephritis have been omitted for this analysis (discussed in the Results section). $P < 0.01$; $r = 0.84$, by Spearman's rank order coefficient.

tively. In addition, FACS analyses confirmed the expression of heparan sulfate proteoglycane, which serves as a low-affinity receptor for FGF-2 in all seven cell lines. There was no difference in the level of expression (data not shown).

Basic fibroblast growth factor protein itself could also be detected in all seven fibroblast lines studied (Fig. 7B). Interestingly, the level of FGF-2 protein expression correlated with the degree of interstitial scarring of the kidney from which the cells were isolated. Whereas F33 and F34, isolated from patients 33 and 34 with tubulointerstitial nephritis and no interstitial scarring, displayed relatively moderate positivity for FGF-2, the level of expression was much higher in the fibroblasts isolated from kidneys with interstitial scarring. In addition, there was a good correlation between the relative level of FGF-2 protein expression in the seven fibroblast lines and the semiquantitative FGF-2 immunofluorescence labeling in the kidneys from which the cells were isolated ($r = 0.76$, $P = 0.038$).

FGF-2 is a strong mitogen for renal fibroblasts, induces differentiation into myofibroblasts, and has no major effect on matrix protein synthesis

To evaluate the function of FGF-2, proliferation, differentiation into myofibroblasts, and matrix protein synthesis of human renal fibroblasts were examined in five different primary cortical fibroblast lines. In a first set of experiments, performed in F25 fibroblasts, FGF-2 caused a robust induction of proliferation, which was time and dose dependent. The increase of bromodeoxyuridine incorporation was significant after 48 hours

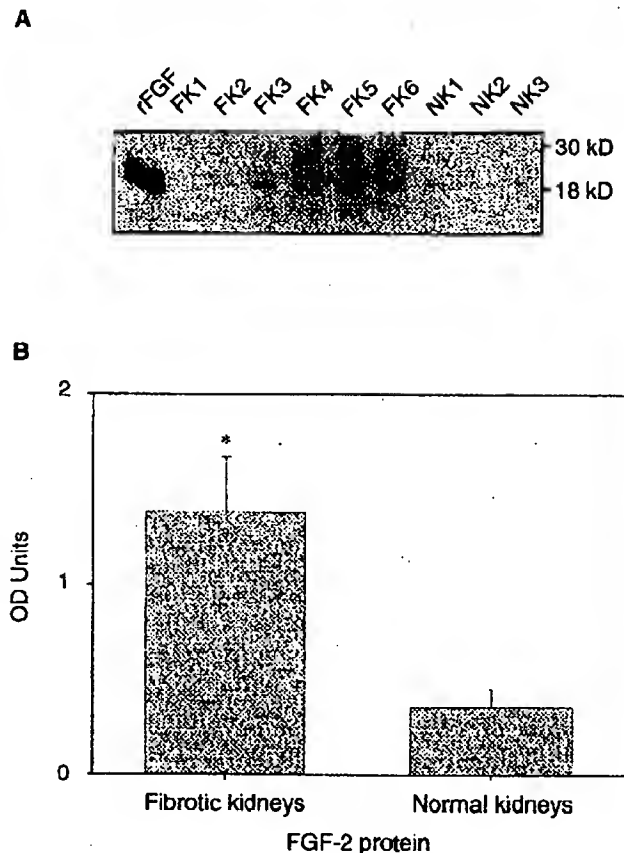


Fig. 5. Expression of FGF-2 protein in kidneys with and without interstitial scarring. FGF-2 protein expression was examined by immunoblot analysis in three normal (NK1 through NK3) and six kidneys with at least 10% interstitial fibrosis (FK1 through FK6). With the exception of FK1, all fibrotic kidneys express more FGF-2 than their nonfibrotic counterparts (A). (B) The densitometric analysis. * $P < 0.05$.

($187.8 \pm 8.9\%$) at a concentration of 1 ng/mL. The maximum increase was seen with a concentration of 10 ng/mL after 72 hours ($267.3 \pm 24.9\%$). Figure 8 summarizes the findings obtained with bromodeoxyuridine incorporation after stimulation with FGF-2 at a concentration of 1 ng/mL for 72 hours in three of the five fibroblast lines. F25 and F26 were isolated from biopsies of patients 25 and 26, displaying increased interstitial volumes because of fibrosis of 41 and 42%, respectively. Conversely, F34 originated from patient 34 with tubulointerstitial nephritis and no interstitial scarring. Bromodeoxyuridine incorporation was increased between $166.3 \pm 3.2\%$ in F34 cells and $247.0 \pm 15.4\%$ in F26 fibroblasts. This increase could be specifically inhibited by addition of a neutralizing antibody to FGF-2, whereas a nonrelevant IgG did not have an effect on FGF-2-induced proliferation. Interestingly, the addition of the FGF-2 neutralizing antibody alone did decrease bromodeoxyuridine incorporation in all five fibroblast lines. However, because of the low level of basal proliferative activity, that decrease was

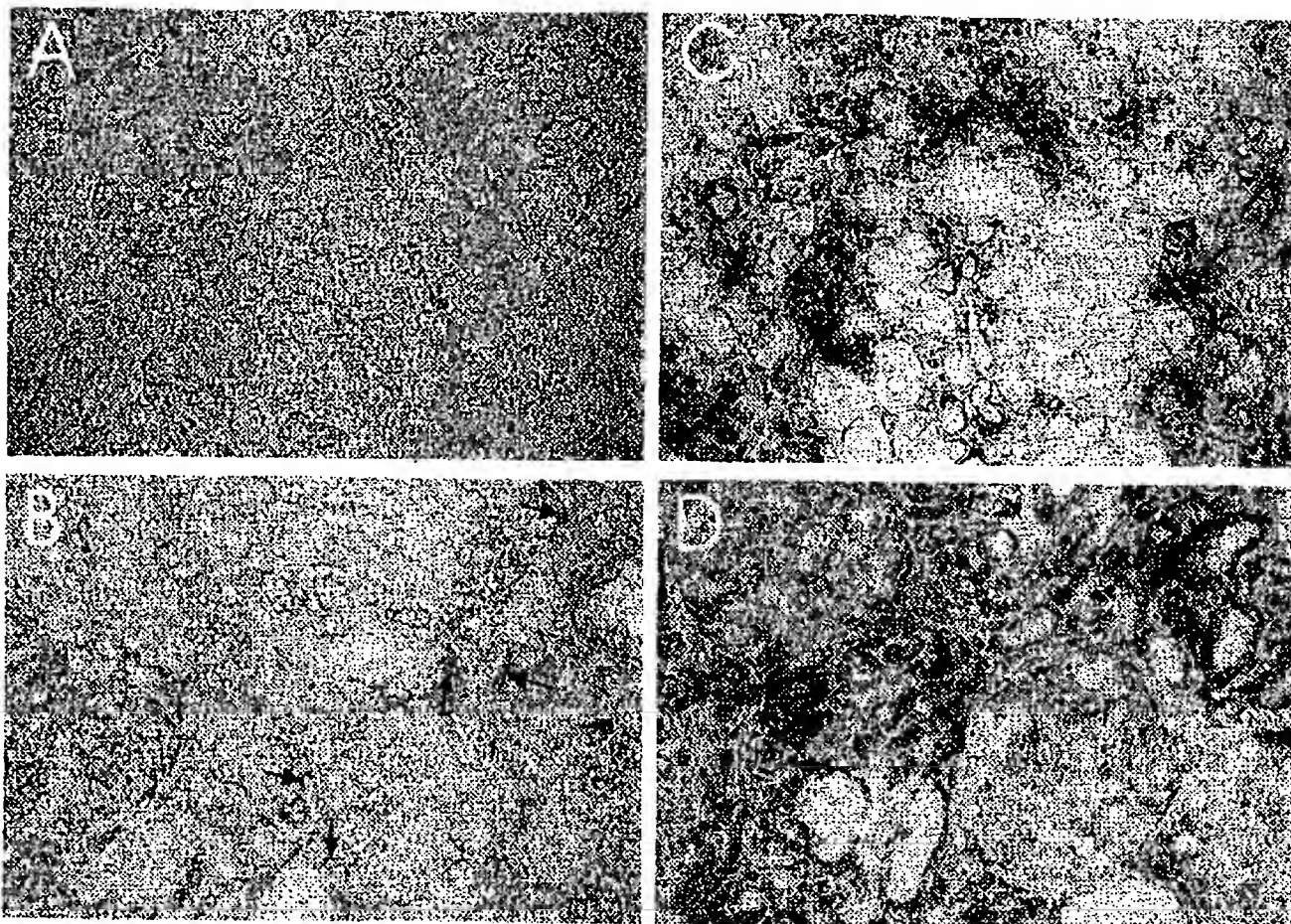


Fig. 6. In situ hybridizations for FGF-2 in normal control kidney and end-stage kidneys. There is no staining in a normal kidney hybridized with the FGF-2 sense riboprobe (A). Hybridization of a normal kidney with the FGF-2 antisense riboprobe revealed faint staining of some glomerular, tubular, vascular, and interstitial (arrows) cells. The hybridization signal was robustly up-regulated in kidneys from patients with end-stage renal disease (C and D). Staining for FGF-2 mRNA was concentrated within the interstitium (C) and in some tubular cells (D), even in some tubules that appear atrophic (C). Conversely, there was no increased staining for FGF-2 mRNA within glomeruli. Original magnification $\times 200$ (A, B, and D) and $\times 100$ (C).

statistically significant in only three cell lines (maximum inhibition 31.5% in F25 cells). Conversely, the addition of the nonrelevant IgG resulted in either no change or an increase in bromodeoxyuridine uptake. In a third set of proliferation experiments, bromodeoxyuridine incorporation assays were confirmed by cell counting. In these experiments, cell numbers increased dose dependently to a maximal $234.3 \pm 15.8\%$ ($P < 0.01$) in F25 and to $197.4 \pm 18.6\%$ ($P < 0.01$) in F34 fibroblasts after 96 hours of incubation at a concentration of 10 ng/mL. Again, the higher concentration (100 ng/mL) did not have any superior effect to the 10 ng/mL concentration. There was no additional effect of heparin, which by itself caused a slight reduction in proliferation (maximum inhibition of $18.9 \pm 4.5\%$; NS).

Activation of fibroblasts into so-called myofibroblasts represents a key step in renal fibrogenesis. We evaluated the effects of FGF-2 on the expression of α -smooth mus-

cle actin, which serves as a marker for myofibroblast formation. In two primary cortical fibroblast lines, F6 isolated from a kidney with mild interstitial scarring (interstitial volume 38%) and F39 from a kidney with an interstitial volume of 71%, FGF-2 resulted in a time- and dose-dependent induction of α -smooth muscle actin expression. Figure 9 summarizes the results observed after 72 hours. The increase was similar to that obtained with TGF- β 1 (increase of α -smooth muscle actin-positive cells from 52.3 ± 3.3 to $82.3 \pm 1.9\%$ after 72 hours of incubation with 1 ng/mL FGF-2; $P < 0.01$). Of course, we do not know if these changes were due to de novo expression of α -smooth muscle actin or due to clonal selection of positive cells caused by cell population heterogeneity.

Finally, the influence of FGF-2 on extracellular matrix synthesis was evaluated by ELISAs for collagen type I and fibronectin in F6 and F39 fibroblasts. Whereas

1532

Strutz et al: FGF-2 in human renal fibrogenesis

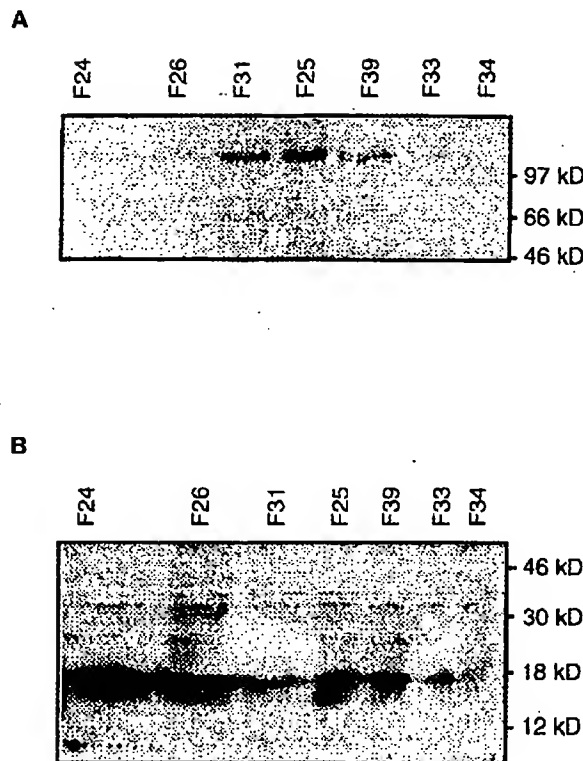


Fig. 7. Expression of FGF-2 and FGFR-1 in seven primary cortical fibroblast lines. (A) The expression of FGFR-1. (B) The expression of FGF-2 by immunoblot analyses. F33 and F34 were isolated from kidney biopsies without interstitial scarring, and the other five fibroblast lines were from kidneys with moderate (F25 and F26) and severe interstitial scarring (F24, F31, and F39). There was a good correlation between the degree of interstitial scarring and the expression of FGF-2, however, no such correlation could be found regarding the expression of FGFR-1 (discussed in the Results section).

TGF- β 1 (at a concentration of 1 ng/mL) increased secretion of collagen type I (from 101.0 ± 9.8 ng/ 10^3 cells to 1018.9 ± 98.5 ng/ 10^3 cells in F39 fibroblasts after stimulation for 48 h) and fibronectin (from 31.8 ± 4.5 μ g/ 10^3 cells to 48.7 ± 3.5 μ g/ 10^3 cells, again after 48 h of stimulation) compared with controls in both cell lines, no significant effect could be observed using three different concentrations of FGF-2, although there was a tendency for a decrease in secretion for collagen type I in both cell lines (data not shown).

Increased FGF-2 expression correlates with increased interstitial and tubular MIB-1 staining

After having established that FGF-2 is a mitogen for human cortical kidney fibroblasts in vitro, we tried to determine whether increased FGF-2 expression was correlated with increased proliferative activity in vivo. Thus, we stained for expression of the Ki-67 antigen, which is associated with cell proliferation using the MIB-1 antibody. We were able to perform stainings for MIB-1 in cortical tissue from 24 patients and 8 normal controls.

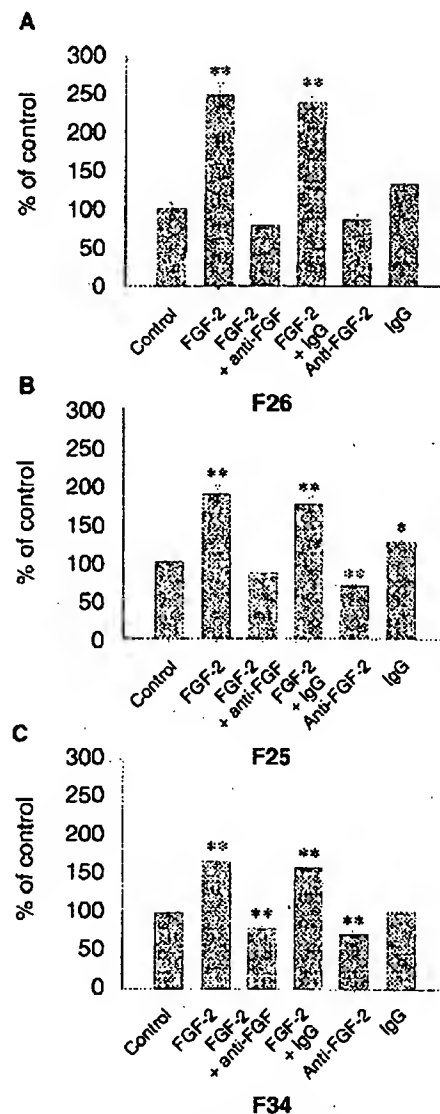


Fig. 8. Effects of FGF-2 on proliferation in primary cortical fibroblasts. FGF-2 was added in a concentration 1.0 ng/mL to F26 (A), F25 (B), and F34 (C) fibroblasts and proliferation was determined after 72 hours by bromodeoxyuridine incorporation. Specificity was determined by the addition of a neutralizing FGF-2 antibody and a nonspecific immunoglobulin (IgG). FGF-2 induced a robust proliferative response in all three fibroblast lines, which could be blocked specifically by the neutralizing FGF-2 antibody. The addition of the neutralizing FGF-2 antibody alone resulted in a significant inhibition of proliferation in two of the three tested cell lines, whereas the nonspecific IgG resulted rather in a promitogenic response. Values are given in percentage of negative control (Isocove's medium) and are a mean of five independent experiments. All experiments were conducted in triplicates. * $P < 0.05$ vs. control; ** $P < 0.01$ vs. control.

Fifteen patient specimens could not be analyzed because of the lack of tissue that had been used up for other purposes (specimens from patients 5, 7, 14 through 17, 21, 23, 27, 29, 30, 32, and 35 through 37). In normal kidneys, only few interstitial and tubular cells displayed MIB-1 positivity (median 1.5 in both; Fig. 10A), whereas

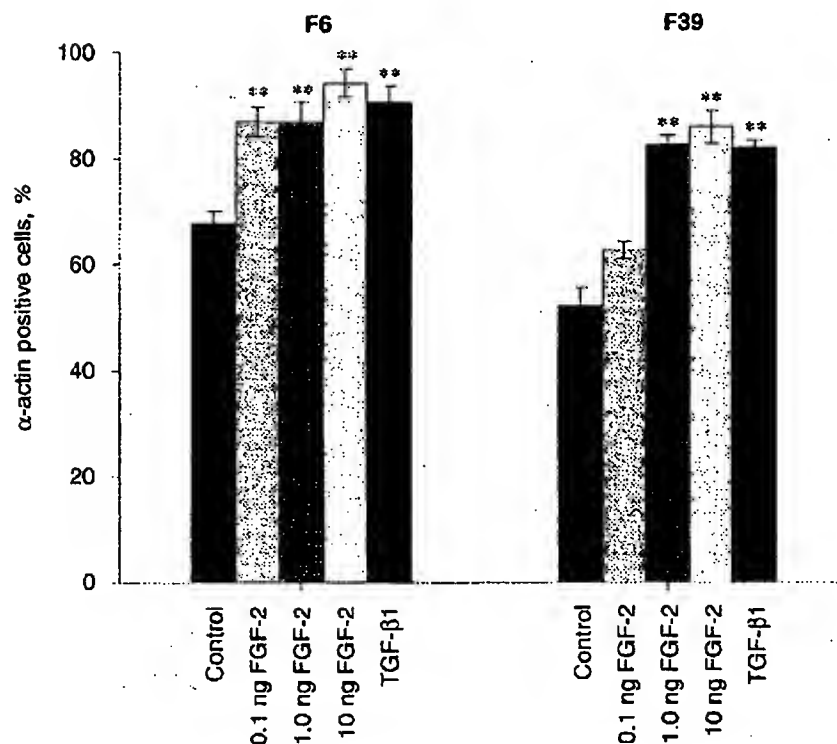


Fig. 9. Expression of α -smooth muscle actin in primary cortical fibroblasts. The number of α -smooth muscle actin-positive cells was determined after incubation with three different concentrations of FGF-2 (0.1, 1.0, or 10 ng/mL) for 48 hours. Iscove's medium served as a negative control, and TGF- β 1 (1 ng/mL) served as a positive control. FGF-2 induced the expression of α -smooth muscle actin in both cell lines significantly. ** $P < 0.01$ vs. control.

the number of MIB-1-positive cells was considerably higher in patient specimens (median 13.5, $P = 0.001$ in interstitial, median 9.0, $P = 0.008$ in tubular cells; Fig. 10 B-D). The highest number of MIB-1-positive cells within the interstitium was observed in the two biopsies from patients with tubulointerstitial nephritis (numbers 33 and 34), which is not surprising given the high proliferative activity of infiltrating monocytes/macrophages and lymphocytes. When the number of MIB-1-positive cells was correlated with the semiquantitative FGF-2 staining, there was a positive correlation with the number of interstitial ($r = 0.48$, $P < 0.01$) and tubular ($r = 0.53$, $P < 0.01$) positive cells. However, the correlation was much more robust when we omitted the two patients with acute interstitial nephritis, who had a high proliferative activity of infiltrating mononuclear cells but a low level interstitial FGF-2 staining. In that case ($N = 30$), correlation of FGF-2 staining with MIB-1-positive interstitial cells ($r = 0.71$, $P < 0.01$) and tubular cells ($r = 0.66$, $P < 0.01$) was much better. The results are displayed in Figure 11. Thus, the results of the MIB-1 staining demonstrate that FGF-2 positivity is correlated positively with the number of MIB-1-positive cells within the interstitium and in tubular epithelia in scarring processes. This was even true when glomerular diseases were analyzed separately with a positive correlation between FGF-2 staining and interstitial MIB-1 positivity ($r = 0.64$, $P < 0.05$), although the number of analyzed tissues was small ($N =$

11). There does not seem to be a correlation of FGF-2 staining with acute inflammatory processes, although the number of tissues studied is too limited in that regard.

DISCUSSION

Virtually all forms of chronic progressive renal disease are accompanied by changes in the tubulointerstitium, irrespective of the primary renal disease [38]. This is not surprising since renal tubules, interstitium, and vasculature comprise more than 80% of the renal cortex [39]. Tubulointerstitial changes consist of interstitial inflammation followed by fibrosis, tubular atrophy, and dilation. Along with glomerular scarring, interstitial fibrosis is an accurate predictor of renal function, even for primary glomerular diseases [29]. One of the most perplexing features of renal fibrogenesis is the fact that fibrosis often progresses despite resolution of the primary inflammatory stimulus [40]. Thus, we and others have propagated the existence of autocrine cytokine loops, which may represent one of the key differences between regular wound healing and scarring [41-43].

The current studies that combined descriptive and functional analyses were undertaken to elucidate the role of FGF-2 in renal fibrogenesis. We have carefully analyzed the usefulness of the antibody used in our study given the controversial information regarding the detection of FGF-2. Different splice variants may be the reason that a variety of studies came to different conclusions

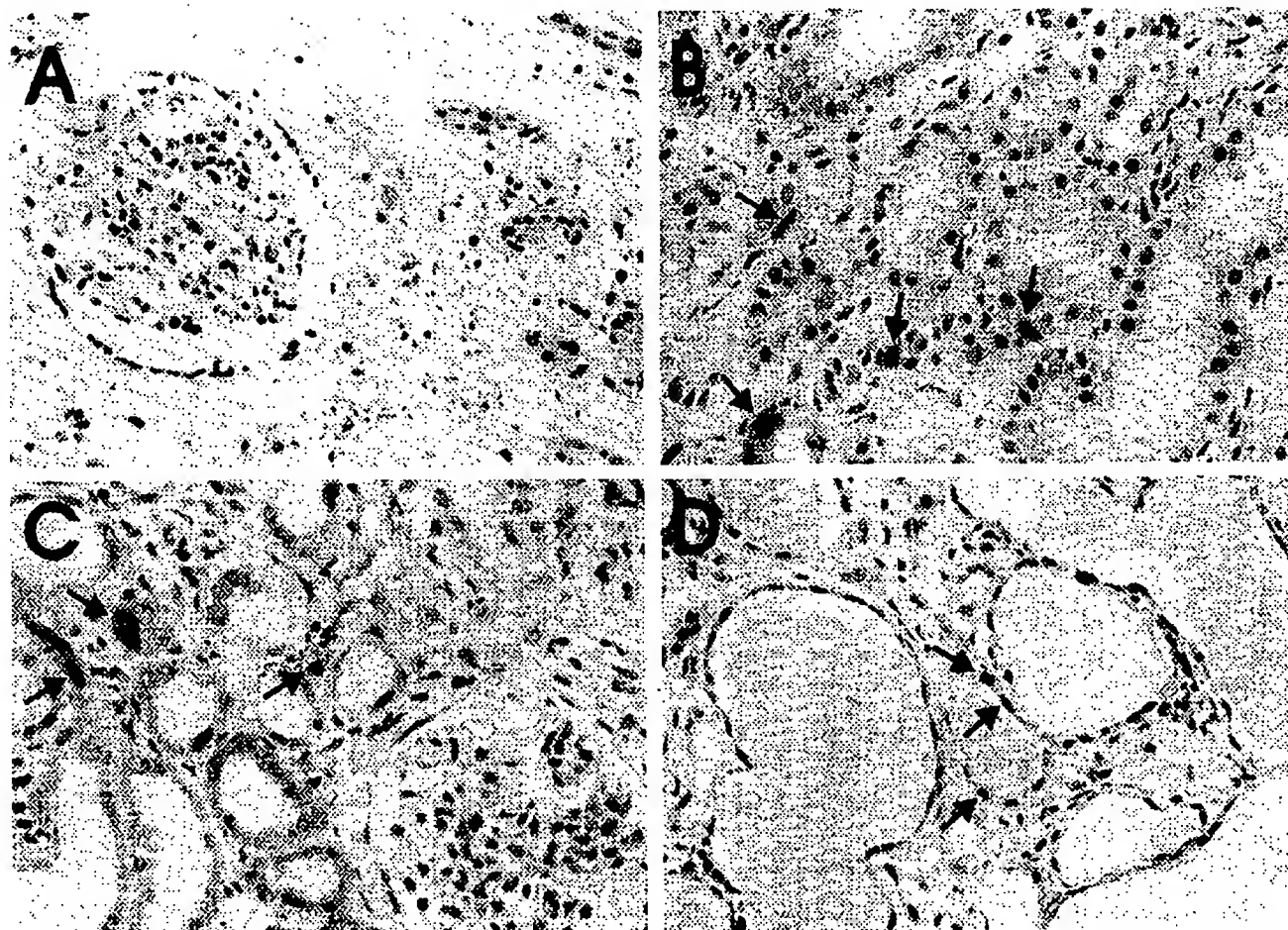


Fig. 10. Immunohistochemical staining for MIB-1-positive cells. Whereas normal kidneys displayed either no or only occasional MIB-1-positive cells (A), staining of kidneys with variable degrees of interstitial scarring demonstrate positive tubular and interstitial cells (highlighted by arrows). (B) Taken from patient 4 (IgA nephritis, interstitial space 46%, FGF-2 +++). (C) Taken from patient 36 (SLE, interstitial space 42%, FGF-2 ++). (D) Taken from patient 10 (end-stage renal disease caused by amyloidosis, interstitial space 68%, FGF-2 +++). Original magnification $\times 400$.

regarding the localization of FGF-2. As was shown in the medullary Tk 173 and Tk 188 fibroblasts, the Ab-2 antibody mainly detects the 18 kD band, but also the 22.5 and 24 kD bands described previously [35]. These higher molecular weight forms may target intracellular FGF-2 to a nuclear localization [44]; however, their exact role is currently unclear. The higher molecular weight forms could not be detected in our primary cortical fibroblasts. Thus, the 18 kD band seems to be the dominating isoform in kidney fibroblasts.

Our study demonstrates that FGF-2 protein can be detected in glomerular, vascular, a few (mainly distal) tubular, as well as interstitial fibroblast-like cells in normal human kidneys. In cryosections, more interstitial cells were labeled than in paraffin-embedded tissue sections, which may explain the differences to the study by Floege et al, who described only occasional interstitial cell positivity [18]. The *in situ* hybridizations confirmed that the same cells that stain positive for FGF-2 in cryo-

sections also synthesize FGF-2 mRNA. In addition, we have demonstrated for the first time that the expression of FGF-2 protein and mRNA is increased in kidneys with tubulointerstitial scarring, irrespective of the primary disease. Furthermore, our study has shown that primary cortical fibroblasts express FGF-2 and one of its high-affinity receptors. FGF-2 causes a robust induction in proliferation in these cells and induces α -smooth muscle actin expression as marker for myofibroblast formation but has no major effect on synthesis of collagen type I and fibronectin. Proliferative activity in tubular epithelial and interstitial cells is increased in diseased human kidneys and correlates with staining for FGF-2. Finally, basal proliferation in cortical fibroblasts can be reduced by the addition of a neutralizing antibody to FGF-2, pointing to a possible autocrine mechanism of fibroblast proliferation. Thus, our study provides evidence for the existence of an autocrine loop in human renal fibrogenesis, which is characterized by constitutive

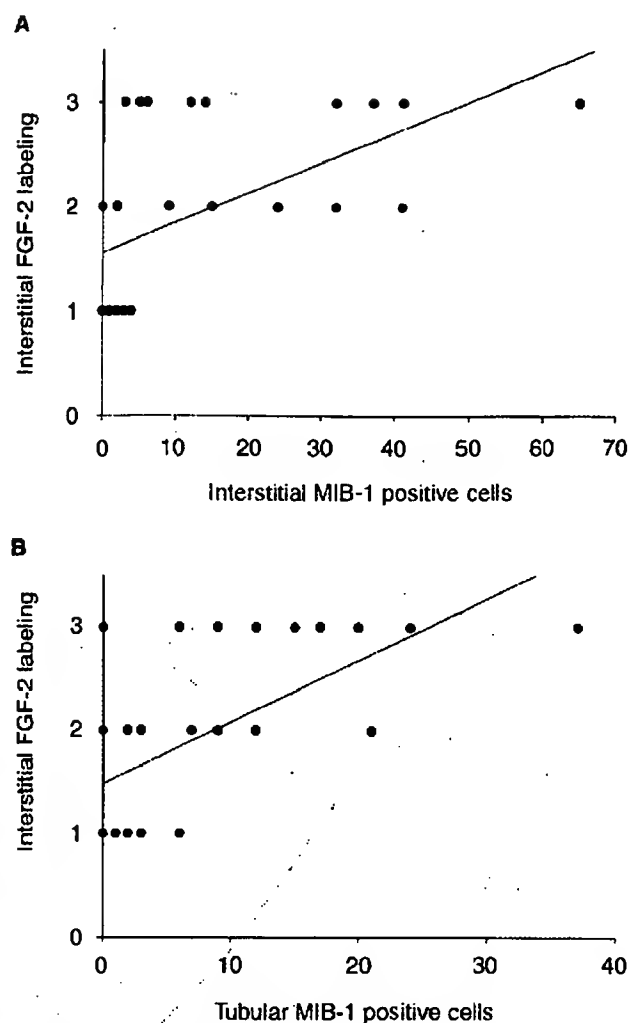


Fig. 11. Correlation of interstitial FGF-2 labeling with MIB-1-positive interstitial (A) and tubular epithelial (B) cells. There was a positive correlation between semiquantitative FGF-2 labeling and the number of proliferating interstitial (A; $P < 0.01$, $r = 0.71$), as well as tubular epithelial (B; $P < 0.01$, $r = 0.66$) cells. Two cases of acute tubulointerstitial nephritis have been omitted for this analysis (see results for details). The r depicts the value for Spearman's rank order coefficient.

expression of FGF-2 and its receptors, up-regulation in disease state, induction of proliferation, and decreased proliferation after neutralization of the cytokine.

The increased expression of FGF-2 in renal fibrogenesis, although demonstrated for the first time, is not surprising. The association of FGF-2 expression with proliferative fibrogenesis was first demonstrated by Gonzalez et al in patients with Dupuytren's contracture [45]. They noted already intense staining for FGF-2 associated with increased synthesis for FGF-2 and FGFR-1 mRNA in fibroblasts. Charlotte et al found increased expression of FGF-2 in the carbon tetrachloride model of rat liver fibrosis [46]. In that study, FGF-2 expression was localized to myofibroblastic liver cells. Interestingly, FGF-2

knockout mice display delayed wound healing [47], further pointing to a critical role for the cytokine in matrix formation. Unlike most other polypeptide growth factors, FGF-2 lacks a conventional leader sequence for secretion, and the mechanisms for its release are still unclear [11]. Chronically injured cells, however, release FGF-2 efficiently, and the mitogenic effect of the cytokine is potentiated by tissue injury [48]. In addition, as was originally shown by Mignatti, Morimoto, and Rifkin, FGF-2 may be secreted by viable cells [49].

What is the role of proliferation in renal fibrogenesis? Proliferation was thought to play only a little role, if at all, in the progression of renal disease. However, as was demonstrated by Nadasdy et al in a study of 28 human end-stage kidneys, even scarred kidneys display high proliferative activity in tubuli and interstitial cells [50]. Similar results were recently described by Thomas et al in the subtotal nephrectomy model of chronic renal failure [51]. These findings are corroborated by our study. It is intriguing to speculate that fibroblasts and tubular epithelial cells stimulate each other in the process of renal fibrogenesis, as indicated by the paralleled proliferation. We and others have recently demonstrated that tubular epithelial cells may acquire certain characteristics of fibroblasts [27, 52]. Although we did not examine this aspect in the current study, FGF-2 may be a candidate cytokine that could play a role in that process. Clearly, the interaction between tubular epithelial cells and fibroblasts plays a role not only in the initiation of interstitial inflammation, but also in progressive renal scarring. In the study by Ray et al in their transgenic mouse model of HIV-associated nephropathy, FGF-2 detection was associated with interstitial areas that contained both cell injury and proliferation [25]. Thus, proliferation does play a critical role in the progression of renal disease, and autocrine/paracrine secretion of FGF-2 may be important in the perpetuation of the process. Autocrine stimulation of cell proliferation caused by FGF-2 has been described in a number of cells, including tubular epithelial [43], endothelial [53], and vascular smooth muscle [54] cells. In these cell types, as in cortical fibroblasts, the efficacy of the neutralizing antibody indicates that the protein does get secreted before binding to its receptors.

Basic fibroblast growth factor exerts its effects via low- and four high-affinity receptors. The high-affinity receptors consist of four transmembrane tyrosine kinases (FGFR-1 to -4) [11]. Our study has demonstrated that primary cortical fibroblasts express FGFR-1, also known as *flg*, and heparan sulfate proteoglycan, which potentiates the binding to the high-affinity receptors [55]. Floege et al noted occasional interstitial staining for *flg* [18]. In our study, only three of the five examined fibroblast lines from kidneys with interstitial fibrosis displayed an up-regulated expression for FGFR-1. One possible explana-

tion is the redundancy of the fibroblast receptor system, including multiple splice variants. In a recent study by Ford et al, all seven receptor isoforms assayed by the group were expressed in whole cortex by reverse transcription-polymerase chain reaction assay [56]. Thus, increased expression of one of the other high-affinity receptors may explain the lack of up-regulation of FGFR-1 in two kidneys with interstitial scarring. Alternatively, down-regulation of FGFR-1 during a late stage of fibrogenesis may protect the kidney from uncontrolled proliferation. The mechanism of overexpression of FGF-2 and FGFR-1 has been described in certain tumor cells, including human hepatoma cells [57].

Heparan sulfate proteoglycan is a low-affinity receptor for FGF-2. Its expression in all seven primary cortical fibroblasts may explain why heparin (which otherwise is known to increase the proliferative effects of FGF-2) did not have any additional effects on proliferation. Conversely, the slight reduction in proliferation caused by heparin itself may be explained by competition with this low-affinity receptor [58].

Our findings of FGF-2 and FGFR-1 detection in human kidney fibroblasts or fibroblast-like cells are in concordance with observations by other groups in dermal [59], mammary gland [60], and human liver [61] fibroblasts. However, we extend those findings, demonstrating that renal fibroblasts (or fibroblast-like cells) do express FGF-2 in vivo as well. The interstitial cells that express FGF-2 are predominantly renal fibroblast-like cells as shown by double labelings. Vimentin, α -smooth muscle actin, CD 44, and CD 54 are all markers for fibroblasts in the kidney [36, 37]. However, though almost all CD 44- and CD 54-positive cells within the interstitium expressed FGF-2, some interstitial cells displayed exclusive FGF-2 positivity. In addition, a number of α -smooth muscle actin-positive cells were negative for FGF-2. Renal interstitial fibroblasts are a heterogeneous population [62], and studies on these cells are still hampered by the lack of a definite fibroblast marker [1]. Most of these cells seem to express FGF-2 in vivo, although some subpopulations may not. Conversely, some nonfibroblast cells such as monocytes/macrophages or dendritic cells express FGF-2, although the majority of these cells do not under normal conditions.

Previous studies suggested that extrarenal sources may contribute to FGF-2 deposition in the kidney [25]. Although we cannot completely exclude that possibility, it seems unlikely given the marked up-regulation of FGF-2 mRNA synthesis in fibrotic kidneys, as demonstrated by the in situ hybridization studies. Increased staining for FGF-2 in renal disease has been described before in various animal models [14, 25] and in patients with focal and segmental glomerulosclerosis and IgA nephropathy [63]. In that latter study, FGF-2 could be detected in glomeruli and in areas of tubulointerstitial damage, cor-

relating with the degree of interstitial injury. Morita et al examined the expression of FGF-2 binding domains in human kidneys. FGF-2 binding heparan sulfate domains are present in the basement membrane proteoglycan perlecan, but are absent from other glycosaminoglycans such as fibroglycan and glypican [64]. Heparan sulfate was detected in sections with glomerular sclerosis and interstitial fibrosis; however, only the fibrotic sections contained FGF-2 binding [65]. Interestingly, a small population of macrophage-like parenchymal cells was identified in that study which expressed the FGF-2-binding domain on the cell surface, which is in concordance with the results of our study.

No significant effect of FGF-2 on synthesis of matrix components was observed in our study, although there was a tendency for decreased synthesis of collagen type I. Decreased synthesis of collagen type I in cells of mesenchymal origin after incubation with FGF-2 has been described before. Tan et al, for example, demonstrated a down-regulation of collagen gene expression in keloid fibroblasts [66]. Thus, unlike TGF- β 1, a role of FGF-2 in the accumulation of extracellular matrix is not supported by our study nor by the literature. However, FGF-2 does induce expression of α -smooth muscle actin as an indicator of myofibroblast formation. In that regard, it is similar to TGF- β 1, which is the prototype of a profibrogenic cytokine in the kidney. Expression of α -smooth muscle actin has been correlated with interstitial matrix formation and even with prognosis in a number of studies in the kidney [67] and other organs [68]. It certainly represents a critical step in fibrogenesis [69].

In summary, we have demonstrated that FGF-2 is expressed in interstitial fibroblast-like cells and that it is robustly up-regulated within these and tubular epithelial cells in human kidney fibrosis. Whereas FGF-2 does not seem to play a role in interstitial matrix production, it may have a critical role in fibroblast proliferation and myofibroblast formation. The continuity of fibroblast proliferation is probably one of the major differences between fibrosis and restitutional healing. Our study points to an important role of FGF-2 in that process. Clearly, further studies are necessary that delineate the differences between regular wound healing with no or minor scar formation and interstitial fibrosis resulting in progressive loss of organ function.

ACKNOWLEDGMENTS

This work was supported in part by grants from the Deutsche Forschungsgemeinschaft (DFG) to F. Strutz (DFG Str 388/3-1) and G.A. Müller (DFG Mü 523/7-1). M. Zeisberg was awarded a graduate grant from the DFG. The authors wish to acknowledge the excellent technical assistance of M. Dietrich and A. Renzhausen. Parts of this work were presented in abstract form at the national meetings of the American Society of Nephrology in November 1996 in New Orleans, LA, USA (*J Am Soc Nephrol* 7:A2596, 1996) and in November 1997 in San Antonio, TX, USA (*J Am Soc Nephrol* 8:A2456, 1997).

Reprint requests to Frank Strutz, M.D., Department of Nephrology and Rheumatology, Georg-August University Göttingen, Robert-Koch-Str. 40, 37075 Göttingen, Germany.
E-mail: fstrutz@gwdg.de

APPENDIX

Abbreviations used in this article are: ABC, avidin-biotin complex; CRF, chronic renal failure; DMEM, Dulbecco's modified Eagle's medium; ED1A, ethylenediaminetetraacetic acid; ELISA, enzyme-linked immunosorbent assay; ESRD, end-stage renal disease; FACS, fluorescence activated cell sorting; FCS, fetal calf serum; FGF-1, acidic fibroblast growth factor; FGF-2, basic fibroblast growth factor; FGFR-1, fibroblast growth factor receptor-1; FSGS, focal segmental glomerulosclerosis; MGN, membranous glomerulonephritis; PBS, phosphate-buffered saline; PDGF, platelet-derived growth factor; RPGN, rapidly progressive glomerulonephritis; SDS, sodium dodecyl sulfate; SSC, standard saline citrate; TGF- β , transforming growth factor- β ; and TIN, acute tubulointerstitial nephritis.

REFERENCES

1. Eddy AA: Molecular insights into renal interstitial fibrosis. *J Am Soc Nephrol* 7:2495-2508, 1996
2. Adzick NS, Lorenz HP: Cells, matrix, growth factors and the surgeon: The biology of scarless fetal wound repair. *Ann Surg* 220:10-18, 1994
3. Whitby DJ, Ferguson MWJ: The extracellular matrix of lip wounds in fetal, neonatal, and adult mice. *Development* 112:651-668, 1991
4. Whitby DJ, Ferguson MWJ: Immunohistochemical localization of growth factors in fetal wound healing. *Dev Biol* 147:207-215, 1991
5. El Nahas AM, Muchaneta-Kubara EC, Essawy M, Soyilemezoglu O: Renal fibrosis: Insights into pathogenesis and treatment. *Int J Biochem Cell Biol* 29:55-62, 1997
6. Bohle A, Müller GA, Wehrmann M, Mackensen-Haen S, Xiao JC: The pathogenesis of chronic renal failure in the primary glomerulopathies, renal vasculopathies, and chronic interstitial nephritides. *Kidney Int* 49(Suppl 54):S2-S9, 1996
7. Knecht A, Fine LG, Kleinman KS, Rodemann HP, Müller GA, Woo DDL, Norman JT: Fibroblasts of rabbit kidney in culture. II. Paracrine stimulation of papillary fibroblasts by PDGF. *Am J Physiol* 261:F292-F299, 1991
8. Tang WW, Ulrich TR, Lacey DL, Hill DC, Qi M, Kaufman SA, Yee J: Platelet derived growth factor-BB induces renal tubulointerstitial myofibroblast formation and tubulointerstitial fibrosis. *Am J Pathol* 148:1169-1180, 1996
9. Sporn MB, Roberts AB: Transforming growth factor- β : Recent progress and new challenges. *J Cell Biol* 119:1017-1021, 1992
10. Border WA, Noble NA: Mechanisms of disease: Transforming growth factor β in tissue fibrosis. *N Engl J Med* 331:1286-1292, 1994
11. Friesel RE, Maciag T: Molecular mechanisms of angiogenesis: Fibroblast growth factor signal transduction. *FASEB J* 9:919-925, 1995
12. Shinozaki M, Kawara S, Hayashi N, Kakimoto T, Igarashi A, Takehara K: Induction of subcutaneous tissue fibrosis in newborn mice by transforming growth factor β : Simultaneous application with basic fibroblast growth factor causes persistent fibrosis. *Biochem Biophys Res Commun* 237:292-296, 1997
13. Baird A, Esch F, Bühlen P, Ling N, Gospodarowicz D: Isolation and partial characterization of an endothelial cell growth factor from the bovine kidney: Homology with basic fibroblast growth factor. *Regul Pept* 12:201-213, 1985
14. Floege J, Eng E, Lindner V, Young BA, Reidy MA, Johnson RJ: Rat glomerular mesangial cells synthesize basic fibroblast growth factor: Release, upregulated synthesis, and mitogenicity in mesangial proliferative glomerulonephritis. *J Clin Invest* 90:2362-2369, 1992
15. Takeuchi A, Yoshizawa N, Yamamoto M, Sawasaki Y, Oda T, Senoo A, Niwa H, Fuse Y: Basic fibroblast growth factor promotes proliferation of rat glomerular visceral epithelial cells in vitro. *Am J Pathol* 141:107-116, 1992
16. Hughes SE, Hall PA: Immunolocalization of fibroblast growth factor receptor 1 and its ligands in human tissues. *Lab Invest* 69:173-182, 1993
17. Caikhi J, Alcorn D, Cancilla B, Key B, Berea JL, Nurmumbe V, Ryan GB, Bertram JF: Light-microscopic immunolocalization of fibroblast growth factor-1 and -2 in adult rat kidney. *Cell Tissue Res* 285:179-187, 1996
18. Floege J, Hudkins KL, Eitner F, Cui Y, Morrison RS, Schelling MA, Alpers CE: Localization of fibroblast growth factor-2 (basic FGF) and FGF receptor-1 in adult human kidney. *Kidney Int* 56:883-897, 1999
19. Silver BJ, Jaffer FF, Abboud HE: Platelet-derived growth factor synthesis in mesangial cells: induction by multiple peptide mitogens. *Proc Natl Acad Sci USA* 86:1056-1060, 1988
20. Kanda S, Nomata K, Saha PK, Nishimura N, Yamada J, Kanatake H, Saito Y: Growth factor regulation of renal cortical tubular cells by epidermal growth factor, insulin-like growth factor-1, acidic and basic fibroblast growth factor, and transforming growth factor- β . *Cell Biol Int Rep* 13:687-699, 1989
21. Ballermann BJ: Regulation of bovine glomerular endothelial cell growth in vitro. *Am J Physiol* 256:C182-C189, 1989
22. Floege J, Eng E, Young CE, Barrett TB, Bowen-Pope DF, Johnson RJ: Infusion of platelet-derived growth factor or basic fibroblast growth factor induces selective glomerular mesangial cell proliferation and matrix accumulation in rats. *J Clin Invest* 92:2952-2962, 1993
23. Floege J, Kriz W, Schulze M, Susani M, Kerjaschki D, Mooney A, Couser WG, Koch KM: Basic fibroblast growth factor augments podocyte injury and induces glomerulosclerosis in rats with experimental membranous nephropathy. *J Clin Invest* 96:2809-2819, 1995
24. Kriz W, Hänel B, Rösener S, Elger M: Long-term treatment of rats with FGF-2 results in focal segmental glomerulosclerosis. *Kidney Int* 48:1435-1450, 1995
25. Ray PE, Bruggeman LA, Weeks BS, Kopp JB, Bryant JL, Owens JW, Notkins AL, Klotman PE: bFGF and its low affinity receptors in the pathogenesis of HIV-associated nephropathy in transgenic mice. *Kidney Int* 46:759-772, 1994
26. Müller GA, Frank J, Rodemann HP, Engler-Blum G: Human renal fibroblast cell lines (FKIF and FNKF) are new tools to investigate pathophysiologic mechanisms of renal interstitial fibrosis. *Exp Nephrol* 3:127-133, 1995
27. Strutz F, Okada H, Lo CW, Danoff T, Carone B, Tomaszewski J, Nelson EG: Identification and characterization of fibroblast-specific protein 1 (FSP1). *J Cell Biol* 130:393-405, 1995
28. Engler-Blum G, Meier M, Frank J, Müller GA: Reduction of background problems in nonradioactive northern and southern blot analyses enables higher sensitivity than 32 P-based hybridizations. *Anal Biochem* 210:235-244, 1993
29. Bohle A, Grund KE, Mackensen S, Tolon M: Correlations between renal interstitium and level of serum creatinine: Morphometric investigations of biopsies in perimembranous glomerulonephritis. *Virchows Arch A Pathol Anat Histol* 373:15-22, 1977
30. Albert SE, Strutz F, Shelton K, Haverly T, Sun MJ, Li S, Denham A, Maki RA, Nelson EG: Characterization of a cis-acting regulatory element which silences expression of the class II-A β gene in epithelium. *J Exp Med* 180:233-240, 1994
31. Dukman HB, Mentzel S, de Jong AS, Assmann KJ: RNA in situ hybridization using digoxigenin labeled cRNA probes. *Biochemica* 2:21-25, 1995
32. Gratzner HG: Monoclonal antibody to 5-bromo- and 5-iododeoxyuridine: A new reagent for detection of DNA replication. *Science* 218:474-475, 1982
33. Jacot TA, Striker GE, Sytler-Stevenson M, Striker LJ: Mesangial cells from transgenic mice with progressive glomerulosclerosis exhibit stable, phenotypic changes including undetectable MMP-9 and increased type IV collagen. *Lab Invest* 75:791-799, 1996
34. Kricka LJ: Labels, labeling, analytical strategies, and applications. in *Nonisotopic Probing, Blotting, and Sequencing*, edited by Kricka LJ. San Diego, New York, Boston, London, Sydney, Tokyo, Toronto, Academic Press, 1995, pp 3-40
35. Florjanczyk RZ, Sommer A: Human basic fibroblast growth factor

- gene encodes four polypeptides: Three initiate translation from non-AUG codons. *Proc Natl Acad Sci USA* 86:3978-3981, 1989
36. CLAYTON A, STEADMAN R, WILLIAMS JD: Cells isolated from the human cortical interstitium resemble myofibroblasts and bind neurotrophins in an ICAM-1-dependent manner. *J Am Soc Nephrol* 8:604-615, 1997
 37. ALPERS CE, HUDKINS KL, FLOEGE J, JOHNSON RJ: Human renal cortical interstitial cells with some features of smooth muscle cells participate in tubulointerstitial and crescentic glomerular injury. *J Am Soc Nephrol* 5:201-210, 1994
 38. NATH KA: Tubulointerstitial changes as a major determinant in the progression of renal damage. *Am J Kidney Dis* 20:1-17, 1992
 39. PALMER BF: The renal tubule in the progression of chronic renal failure. *J Invest Med* 45:346-361, 1997
 40. FOGO AB, KON V: Pathophysiology of progressive renal disease, in *Immunologic Renal Diseases*, edited by NELSON EG, COUSER WG, Philadelphia, Lippincott-Raven, 1997, pp 683-704
 41. LONNEMANN G, SHAPIRO I, ENGLER-BLUM G, MÖLLER GA, KOCI KM, DINARELLO CA: Cytokines in human renal interstitial fibrosis. I. IL-1 is an autocrine growth factor for cultured fibrosis-derived kidney fibroblasts. *Kidney Int* 47:837-844, 1995
 42. PHILLIPS AO, TOPLEY N, MORRISSEY K, WILLIAMS JD, STEADMAN R: Basic fibroblast growth factor β 1 from human proximal tubular cells in the absence of de novo gene transcription or mRNA translation. *Lab Invest* 76:591-600, 1997
 43. ANDERSON RJ, RAY CJ: Potential autocrine and paracrine mechanisms of recovery from mechanical injury of renal tubular epithelial cells. *Am J Physiol* 274:F463-F472, 1998
 44. MASON JJ: The ins and outs of fibroblast growth factors. *Cell* 78:547-552, 1994
 45. GONZALEZ A-M, BUSCAGLIA M, FOX R, ISACCHI A, SARMIENTOS P, FARRIS J, ONG M, MARTINEAU D, LAPPI DA, BAIRD A: Basic fibroblast growth factor in Dupuytren's contracture. *Am J Pathol* 141:661-671, 1992
 46. CHARLOTTE F, WIN KM, PRÉAUX AM, DHUMEAUX D, ZAFRANI ES, MAVIER P: Immunolocalization of heparin-binding growth factors (HBGF) types 1 and 2 in rat liver: Selective hyperexpression of HBGF-2 in carbon tetrachloride-induced fibrosis. *J Pathol* 169:471-476, 1993
 47. ORTEGA S, ITTMANN M, TSANG SH, FHRlich M, BASILICO C: Neuronal defects and delayed wound healing in mice lacking fibroblast growth factor 2. *Proc Natl Acad Sci USA* 95:5672-5677, 1998
 48. MUTHUKRISHNAN L, WARDER E, McNEIL PL: Basic fibroblast growth factor is efficiently released from a cytosolic storage site through plasma membrane disruptions of endothelial cells. *J Cell Physiol* 148:1-16, 1991
 49. MIGNATTI P, MORIMOTO T, RIEKIN DB: Basic fibroblast growth factor released by single, isolated cells stimulates their migration in an autocrine manner. *Proc Natl Acad Sci USA* 88:11007-11011, 1991
 50. NADARDY T, LASZIK Z, BLICK KE, JOHNSON DL, SILVA FG: Tubular atrophy in the end-stage kidney: A lectin and immunohistochemical study. *Hum Pathol* 25:22-28, 1994
 51. THOMAS GL, YANG B, WAGNER BE, SAVILL J, ELNAHAS AM: Cellular apoptosis and proliferation in experimental renal fibrosis. *Nephrol Dial Transplant* 13:2216-2226, 1998
 52. NG YY, HUANG TP, YANG WC, CHEN ZP, YANG AH, MU W, NIKOLIC-PATERSON DJ, ATKINS RC, LAN HY: Tubular epithelial-myofibroblast transdifferentiation in progressive tubulointerstitial fibrosis in 5/6 nephrectomized rats. *Kidney Int* 54:864-876, 1998
 53. SCHWEIGERER L, NEUFELD G, FRIEDMAN J, ABRAHAM JA, FIDDES JC, GOSPODAROWICZ D: Capillary endothelial cells express basic fibroblast growth factor, a mitogen that promotes their own growth. *Nature* 325:257-259, 1987
 54. DAVIS MG, ZHOU M, ALI S, COFFIN JD, DOETSCHMAN T, DORN GW: Intracrine and autocrine effects of basic fibroblast growth factor in vascular smooth muscle cells. *J Mol Cell Cardiol* 29:1061-1072, 1997
 55. YAYON A, KLAGSBRUN M, ESKO JD, LEDER P, ORNITZ DM: Cell surface heparin-like molecules are required for binding of basic fibroblast growth factor to its high affinity receptors. *Cell* 64:841-848, 1991
 56. FORB MD, CAUCHI J, GREFFERATH U, BERTRAM JF: Expression of fibroblast growth factors and their receptors in rat glomeruli. *Kidney Int* 51:1729-1738, 1997
 57. KIN M, SATA M, UENO T, TORIMURA T, INUZUKA S, TSUJI R, SUJAKU K, SAKAMOTO M, SUGAWARA H, TAMAKI S, TANIKAWA K: Basic fibroblast growth factor regulates proliferation and motility of human hepatoma cells by an autocrine mechanism. *J Hepatol* 27:677-687, 1997
 58. RIECK P, OLIVER L, ENGELMANN K, FUHRMANN G, HARTMANN C, COURTUIS Y: The role of exogenous/endogenous basic fibroblast growth factor (FGF2) and transforming growth factor β (TGF β -1) on human corneal endothelial cells proliferation *in vitro*. *Exp Cell Res* 220:36-46, 1995
 59. WANG Y, RAO U, MASCAU R, RICHARDS TJ, PANSON AJ, EDINGTON HD, SHIFF-SPOLOE JM, DONNELLY SS, KIRKWOOD JM, BECKER D: Molecular analysis of melanoma precursor cells. *Cell Growth Differ* 7:1733-1740, 1996
 60. BARRACLOUGH R, FERNIG DG, RUDLAND PS, SMITH JA: Synthesis of basic fibroblast growth factor upon differentiation of rat mammary epithelial to myoepithelial-like cells in culture. *J Cell Physiol* 144:333-344, 1990
 61. ROSENBAUM J, BIAZEJEWSKI S, PREAUX A-M, MALLAT A, DHUMEAUX D, MAVIER P: Fibroblast growth factor 2 and transforming growth factor β 1 interactions in human liver fibroblasts. *Gastroenterology* 109:1986-1996, 1995
 62. MÜLLER GA, STRUTZ F: Renal fibroblast heterogeneity. *Kidney Int* 48(Suppl 50):S33-S36, 1995
 63. STEIN-OAKLEY AN, MAGUIRE JA, DOWLING J, PERRY G, THOMSON NM: Altered expression of fibrogenic growth factors in IgA nephropathy and focal and segmental glomerulosclerosis. *Kidney Int* 51:195-204, 1997
 64. AVIEZER D, HECHT D, SAFRAN M, EISINGER M, DAVID G, YAYON A: Perlecan, basal lamina proteoglycan, promotes basic fibroblast growth factor-receptor binding, mitogenesis and angiogenesis. *Cell* 79:1005-1013, 1994
 65. MORITA H, SHINZATO T, DAVID G, MIZUTANI A, HARUCHI H, FUJITA Y, ITO M, ASAI J, MAEDA K, KIMATA K: Basic fibroblast growth factor-binding domain of heparan sulfate in the human glomerulosclerosis and renal tubulointerstitial fibrosis. *Lab Invest* 71:528-535, 1994
 66. TAN EMI, ROJDA S, GREENBAUM SS, MOORE JH, FOX JW, SOLLBERG S: Acidic and basic fibroblast growth factors down-regulate collagen gene expression in keloid fibroblasts. *Am J Pathol* 142:463-470, 1993
 67. DIAMOND JR, VANGOOR H, DING G, ENGELMYER E: Myofibroblasts in experimental hydronephrosis. *Am J Pathol* 146:121-129, 1995
 68. ZHANG K, REKTER MD, GORUON D, PHAN SH: Myofibroblasts and their role in lung collagen gene expression during pulmonary fibrosis. *Am J Pathol* 145:114-125, 1994
 69. STRUTZ F, MÜLLER GA: Interstitial pathomechanisms underlying progressive tubulointerstitial damage. *Kidney Blood Press Res* 22:67-75, 1999

FGH52352

CI-06861814-4

FGH52352

CISTI ICIST

CI-06861814-4

Document Delivery Service
in partnership with the Canadian Agriculture LibraryService de fourniture de Documents
en collaboration avec la Bibliothèque canadienne de l'agriculture**THIS IS NOT AN INVOICE / CECI N'EST PAS UNE FACTURE**LYNN BRAZIL
LIBRARIANHELLER EHRMAN WHITE & MCAULIFFE
275 MIDDLEFIELD RD
MENLO PARK, CA 94025
UNITED STATES

ORDER NUMBER: CI-06861814-4
Account Number: FGH52352
Delivery Mode: F31
Delivery Address: 650/324-6034
Submitted: 2007/05/14 14:38:48
Received: 2007/05/14 14:38:48
Printed: 2007/05/15 00:12:14

Direct	Periodical	OPENURLOPAC	UNITED STATES

Client Number: 39780-7000 CD
Title: AMERICAN JOURNAL OF PHYSIOLOGY.
DB Ref. No.: IRN10008871
ISSN: ISSN00029513
Vol./Issue: 267/4 PT 2
Date: 1994
Pages: F546-57
Article Title: A RAT KIDNEY GLUTAMYL AMINOPEPTIDASE (AMINOPEPTIDASE A): MOLECULAR IDENTITY AND CELLULAR LOCALIZATION,
Article Author: SONG, L., ET AL.
Report Number: IRN10008871
Publisher: AMERICAN PHYSIOLOGICAL SOCIETY ETC.

Estimated cost for this 12 page document: \$12.5 document supply fee +
\$8 copyright = \$20.5

The attached document has been copied under license from Access Copyright/COPIBEC or other rights holders through direct agreements. Further reproduction, electronic storage or electronic transmission, even for internal purposes, is prohibited unless you are independently licensed to do so by the rights holder.

Phone/Téléphone: 1-800-668-1222 (Canada - U.S./E.-U.) (613) 998-8544 (International)
www.nrc.ca/cisti Fax/Télécopieur: (613) 993-7619 www.nrc.ca/icist
info.cisti@nrc.ca info.icist@nrc.ca



National Research Council Canada
Conseil national de recherches Canada

Page 1 / 1

Rat kidney glutamyl aminopeptidase (aminopeptidase A): molecular identity and cellular localization

LIJUN SONG, MINGQI YE, MARTA TROYANOVSKAYA,
ELIZABETH WILK, SHERWIN WILK, AND DENNIS P. HEALY

Department of Pharmacology, Mount Sinai School of Medicine, City University of New York,
New York, New York 10029

Song, Lijun, Mingqi Ye, Marta Troyanovskaya, Elizabeth Wilk, Sherwin Wilk, and Dennis P. Healy. Rat kidney glutamyl aminopeptidase (aminopeptidase A): molecular identity and cellular localization. *Am. J. Physiol.* 267 (Renal Fluid Electrolyte Physiol. 36): F546-F557, 1994.—Glutamyl aminopeptidase [aminopeptidase A (EAP), EC 3.4.11.7] is an ectoenzyme that selectively hydrolyzes acidic amino acid residues from the amino terminus of oligopeptides. EAP activity is highest within the kidney and small intestine. The murine pre-B cell BP-1/6C3 and the human kidney glycoprotein gp160 differentiation antigens have been reported to have biochemical properties indistinguishable from EAP. It is not known, however, if rat kidney EAP is a homologue of these antigens or molecularly distinct. Using the reverse transcription-polymerase chain reaction method with oligonucleotide primers based on the BP-1/6C3 nucleotide sequence, we isolated a 450-bp partial cDNA from rat kidney poly(A)⁺ RNA. The partial cDNA encoded a predicted protein that was 92% and 86% identical to the murine BP-1/6C3 and human gp160 antigens, respectively; the amino acid sequence within the zinc-binding domain was completely conserved. Purification of EAP from rat kidney and microsequence analysis of a tryptic digest peptide fragment (18-mer) indicated that the fragment was highly similar to a region within the BP-1/6C3 and gp160 proteins. Northern blot hybridization and immunoblot analyses were also consistent with labeling of products the same size as reported for the BP-1/6C3 and gp160 antigens. There was a good correlation between the cellular distribution of EAP mRNA and EAP immunoreactivity, with proximal tubules and glomerular mesangial cells having the highest densities. These results indicate that rat kidney EAP is a species homologue of the murine BP-1/6C3 and human gp160 antigens. Furthermore, on the basis of its cellular localization, rat kidney EAP is likely to be involved in degradation of oligopeptides within the glomerulus and the glomerular filtrate. Since cells that express EAP also express receptors for angiotensin II, an intrarenal vasoactive hormone that is a substrate for EAP, these results further suggest that EAP may play a role in modulating the activity of intrarenal angiotensin II.

aminopeptidase A; angiotensinase; angiotensin II; proximal tubules; mesangial cells

GLUTAMYL AMINOPEPTIDASE [aminopeptidase A (EAP), EC 3.4.11.7] is an ectoenzyme that selectively hydrolyzes amino-terminal glutamyl and aspartyl residues from oligopeptides (11). EAP levels are highest within the brush border of kidney proximal tubules and enterocytes of the small intestine, areas that are enriched with peptidases (10, 20). At these sites EAP is believed to participate in the degradation of oligopeptides for nutritive purposes. EAP has also been shown to be an "angiotensinase," hydrolyzing the biologically active

peptide [Asp¹]angiotensin II (ANG II) to [des-Asp¹]ANG II (ANG III) in the circulation (1, 21). In the kidney, ANG II decreases renal blood flow and increases proximal tubule reabsorption of sodium (15, 19). In addition, all the components of the renin-angiotensin system have been localized within the kidney (32), suggesting that an intrarenal renin-angiotensin system may play an important role in kidney function (3, 22). The importance of EAP in modulating ANG II activity within the kidney has not been determined.

Recent cloning and functional expression studies indicate that two previously characterized differentiation antigens have biochemical and enzymological properties indistinguishable from EAP. The murine pre-B cell differentiation antigen BP-1/6C3 has sequence homology with members of the zinc-dependent metalloenzyme family (36, 37) and EAP-like activity when expressed in vitro (33). More recently, the human kidney differentiation antigen glycoprotein gp160 was purified and cloned and found to be 78% identical to BP-1/6C3 (26). Renal cell carcinomas expressing gp160 have EAP activity, and immunoprecipitation of gp160 depletes cells of EAP activity. Moreover, isolation of cDNA clones from human kidney cDNA libraries indicates that the differentiation antigens and the kidney transcripts are identical (23, 26). Thus these lines of evidence indicate that the BP-1/6C3 and gp160 antigens represent a form of kidney EAP.

Purification studies indicate that EAP exists as a homodimer with molecular mass ranging from 247 to 300 kDa, with the monomeric form having a molecular mass ranging from 120 to 140 kDa under dissociating conditions (34). Some heterogeneity in the size of the monomeric forms has been reported (6, 13, 17). Herzog et al. (17) have reported that purification of bromelain-solubilized EAP from human kidney yielded two isoforms, a 127-kDa form that was localized to glomeruli and tubules and a 117-kDa form that was localized primarily to tubules. The relationship between the EAP isoforms and the gp160 antigen in human kidney has not been determined. We have reported that immunoblots with purified rat EAP yield only a single band, whereas immunoblots with kidney homogenates yielded two bands of 136 and 101 kDa on sodium dodecyl sulfate-polyacrylamide gel electrophoresis (SDS-PAGE) (31). It is not clear whether the smaller forms of EAP seen in immunoblots represent multiple isoforms of EAP, partial proteolytic digestion of the native enzyme, or cross-reactivity with a closely related enzyme(s).

In an effort to characterize the rat kidney form of EAP, we used the reverse transcription-polymerase chain reaction (RT-PCR) procedure with oligonucleotide

RAT KIDNEY GLUTAMYL AMINOPEPTIDASE

F547

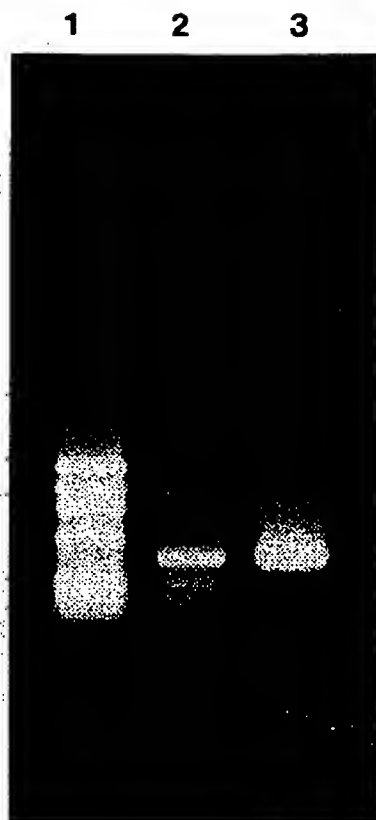


Fig. 1. Agarose gel electrophoresis of polymerase chain reaction (PCR) products from amplification of rat kidney cortex cDNA with mouse BP-1/6C3 primers. Lane 1, DNA markers (1,353; 1,078; 872; 603; and 310 bp, top to bottom); lane 2, 25 cycles; lane 3, second round of 25 cycles. Note that an intense reaction product of the expected size (arrowhead, 450 bp) was seen after 25 cycles (lane 2), which was then reamplified an additional 25 cycles (lane 3).

primers based on the murine BP-1/6C3 sequence to isolate a partial cDNA for rat kidney EAP. The partial cDNA was then used to synthesize radiolabeled synthetic antisense RNA (riboprobes) that could be used to localize EAP mRNA *in situ* hybridization. The distribution of the EAP mRNA was then correlated with the distribution of EAP immunoreactivity.

METHODS

PCR analysis. Poly(A)⁺ RNA was isolated from the kidney by first isolating total RNA (5), followed by passage over an oligo(dT) cellulose column (28). First-strand cDNA synthesis was performed with poly(A)⁺ RNA as template in the presence of reverse transcriptase and an oligo(dT) primer (Superscript RNA reverse transcriptase; BRL, Gaithersburg, MD). The PCR primers were designed to amplify an ~450-bp region of the BP-1/6C3 cDNA that includes the zinc-binding domain of the processed protein; sense primer (EAP-1) corresponding to nucleotides 1228–1250 of the murine BP-1/6C3 antigen, 5' GAGATGGTGGATGACAACCTGGAA 3'; antisense primer (EAP-2) corresponding to nucleotides 1651–1674 of BP-1/6C3, 5' CCACAAGTCGTCACCAAGTCCAT 3'. Each primer contained an additional 10 nucleotides encoding an *Xho* I restriction site at the 5' end that was used for subcloning of the amplified cDNA into a plasmid vector. Kidney cDNA was submitted to 25 cycles of PCR amplification with PCR primers

in the presence of *Taq* DNA polymerase in the following sequence: first cycle 5 min at 94°C, 2 min at 55°C, 3 min at 72°C; subsequent cycles 1 min at 94°C, 2 min at 50°C, and 3 min at 72°C; last cycle 1 min at 94°C, 2 min at 50°C, and 10 min at 72°C. The PCR products were then separated on a 1% agarose gel, and the bands were examined under ultraviolet illumination. PCR controls included 1) amplification with template but without primers, 2) amplification with mRNA without the RT step, and 3) amplification without template.

The PCR-amplified product was then subcloned into a plasmid (TA cloning vector, Invitrogen, San Diego, CA) and used for transformation of INVαF competent *Escherichia coli*. Positive transformants containing plasmids with inserts were selected by growing bacteria on Luria-Bertani plates containing kanamycin, isopropyl-β-D-thiogalactopyranoside and Blue-Gal. Plasmids were isolated from minicultures and digested with *Xho* I. Plasmids containing the PCR product were then sequenced directly by the dideoxynucleotide chain-termination method with [α-³²P]dATP and sequence-specific oligonucleotide primers (Sequenase, United States Biochemical, Cleveland, OH).

Northern blot analysis. Total RNA (10 μg) from rat kidney and jejunum were size fractionated by electrophoresis on a 1% agarose-formaldehyde gel and transferred to Micron Separation (Westboro, MA) nitrocellulose membrane and fixed by baking for 2 h at 80°C. Membranes were prehybridized 4 h at 39°C in hybridization buffer [25 mM potassium phosphate (pH 7.4), 5× SSC (1× SSC is 0.15 M NaCl and 0.015 M sodium citrate, pH 7.0), 5× Denhardt's solution, 50 μg/ml denatured salmon sperm DNA, and 50% formamide]. The membranes were transferred to fresh hybridization buffer containing ³²P-labeled probe and 10% dextran sulfate and incubated overnight at 39°C. The filters were then washed two times each in 2× SSC and 1× SSC at room temperature, followed by a single wash in 0.1× SSC at 55°C.

The radiolabeled probe was prepared by excision of the partial cDNA PCR product (50–80 ng) from the plasmid with *Xho* I, random priming with hexanucleotides and 50 μCi of [α-³²P]dCTP (New England Biolab kit), and extension with DNA polymerase I. Specific activity of the probe was ~5 × 10⁶ counts·min⁻¹·μg⁻¹.

Isolation of glomeruli. Rat kidney glomeruli were isolated according to the procedure of Fujiwara et al. (8) with some modifications. Briefly, eight Sprague-Dawley rats (200 g) were killed, and the kidneys were removed and placed in ice-cold Dulbecco's phosphate-buffered saline (PBS), pH 7.4, containing (in mM) 137 NaCl, 2.7 KCl, 8.1 Na₂HPO₄, 1.5 KH₂PO₄, 0.9 CaCl₂, 0.49 MgCl₂, and 5.6 glucose. The cortex was dissected and minced to paste-like consistency and then suspended in cold Dulbecco's PBS. The suspension was passed through a 25-gauge needle repeatedly and pushed successively through 200-μm and 150-μm sieves. The glomeruli were collected on a 50-μm sieve that was washed with Dulbecco's PBS. The purity of the isolated glomeruli was confirmed by light microscopy.

Enzyme activity. EAP activity was assayed with α-glutamyl-2-naphthylamide and α-aspartyl-2-naphthylamide as substrates. Specific activities were expressed as units per milligram protein, where one unit equals the hydrolysis of 1 nmol substrate/min.

Immunoblotting. Immunoblotting was conducted as described previously (31). Briefly, 35 μg of protein were separated on a 10% SDS-PAGE gel run at 250 V for 2 h. The protein was transferred to an Immobilon membrane (Millipore, Bedford, MA) in a transfer apparatus containing transfer buffer of 25 mM Tris(hydroxymethyl)aminomethane (Tris) base, 192 mM glycine, and 15% methanol at 70 V for 1 h. After transfer, the membrane was washed with PBS 2 × 5 min and

F548

RAT KIDNEY GLUTAMYL AMINOPEPTIDASE

A

1 GAGATGGTGGATGACAACTGGAAGAAAACCACTTTCATGAAGTCCGTCCCGATGAGCACT
 61 TACCTGGTGTGCTTTGCTGTACATCAGTTCACCTCGATACAGAGAACATCCAGGAGTGGC
 121 AAACCACTCACTGTTTACGTCCAGCCCAACCAAAAGCAAACAGCAGAGTATGCGGCAAAC
 181 ATAACCAAAGCTGTGTTTGACTTCTTTGAAGACTACTTCGCTATGGAGTATTCTCTTCCG
 241 AAACCTGGATAAAATTGCTATTCCAGATTTTGGCACCGGCGCCATGGAAAACCTGGGGACTT
 301 GTCACCTACCGAGAAACAAACCTGCTTTATGACCCCTGCTATCGGCCTCATCCAACAG
 361 CAGAGAGTAGCCAGCGTGGTTGCCACGAGCTCGTGCACCACTGGTTTGGAAATATCGTG
 401 ACCATGGACTGGTGGGACGACTTGTGG

B

Rat		KTTFMKSVPMSTYLVCFVHQFTSIQRTSRSGKPLTVYVQPNQKQ
Mouse	265V.....R..A.E.K.....K.....E
Human	273	R...E.....D.VK.I.N.....I....E..H
Rat		TAEYAANITKAVFDFEDYFAMEYSLPKLDKIAIPDFGTGAMENW
Mouse	310Q....Y.....A.....
Human	318S...Y..E....N.....
Rat		GLVTYRETNLLYDPLLSASSNQQRVASVVAHELVBQWFGNIVT
Mouse	355T..
Human	363	..I.....KE.....T.....

Fig. 2. A: nucleotide sequence of the partial cDNA obtained from rat kidney using oligonucleotide primers (underlined) based on the BP-1/6C3 sequence. B: deduced amino acid sequence of the partial cDNA from rat kidney compared with mouse BP-1/6C3 and human glycoprotein gp160. Amino acids that are not identical in all 3 sequences are noted. (Numbers refer to published amino acid sequence of BP-1/6C3 and gp160.) The putative zinc-binding domain (bold letters) was completely conserved.

incubated with a blocking buffer containing 5% nonfat dry milk and 0.02% sodium azide and agitated for 1 h. Blots were incubated with primary antiserum diluted 1:1,000 in PBS containing 3% bovine serum albumin (BSA) for 12–18 h at 4°C. The membranes were washed with PBS and incubated with peroxidase-labeled goat secondary antibody at 37°C for 2 h. The membrane was washed with PBS and incubated with 0.6 mg/ml diaminobenzidine (Sigma, St. Louis, MO) in 50 mM Tris-HCl (pH 7.6) and containing 0.03% hydrogen peroxide for 5–10 min. The membrane was washed with PBS and then dried.

Specificity of the immunoblot staining was tested by preabsorbing the antiserum with purified EAP (1 µg/ml), membrane alanyl aminopeptidase (mAAP; aminopeptidase M, aminopeptidase N; EC 3.4.11.2) (1 µg/ml), and dipeptidyl peptidase IV (DPP IV; EC 3.4.14.5) (1 µg/ml) and comparing the staining pattern to antiserum that was not preabsorbed.

Enzyme purification and sequence determination. EAP was purified to apparent homogeneity from rat kidney using affinity chromatography as described (31). DPP IV, mAAP, and EAP copurify up to the phenyl Sepharose step. DPP IV is resolved from the other two enzymes by phenyl Sepharose chromatography (34). mAAP is resolved from EAP by affinity

chromatography (31). DPP IV and mAAP were apparently homogeneous as judged by SDS-PAGE.

An aliquot of EAP was subjected to SDS-PAGE on a 12.5% gel. The protein was stained with Coomassie blue and transferred to an Immobilon polyvinylidene fluoride membrane (Millipore). The band was excised and sent to the Yale Protein and Nucleic Acid Chemistry facility for trypsinization, high-performance liquid chromatography (HPLC) separation, and microsequencing.

In situ hybridization. Four male Sprague-Dawley rats (175–200 g) were decapitated, and the kidneys were removed and frozen to microtome chucks. Ten-micrometer cryostat sections were collected onto clean microscope slides subbed with 2% 3-aminopropyltriethoxysilane (Sigma). The sections were dried under vacuum for 10 min and then fixed with 3% paraformaldehyde in phosphate buffer for 5 min, dehydrated, and vacuum dried. A ³²S-labeled riboprobe complementary to the EAP mRNA was transcribed in vitro using the cDNA as template. Radiolabeled sense strand RNA was synthesized in a similar manner and used as a control. Probes were synthesized by incubating 1 µg of linearized cDNA in a total reaction volume of 12 µl containing 100 mM dithiothreitol, RNasin, 1 mM unlabeled nucleotide triphosphates (ATP, GTP, and UTP),

RAT KIDNEY GLUTAMYL AMINOPEPTIDASE

F549

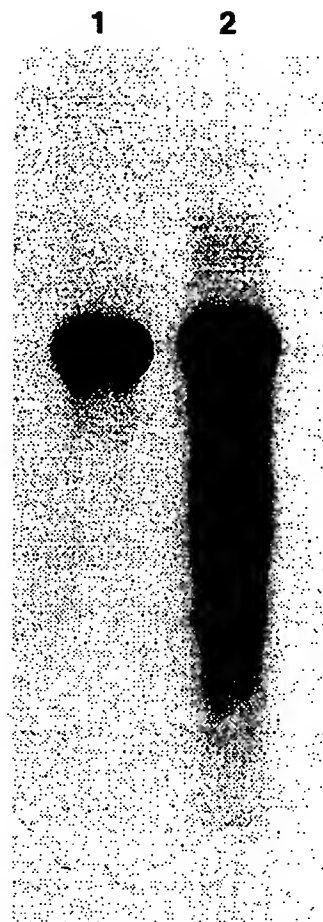


Fig. 3. Northern blot analyses of rat total RNA from kidney (lane 1) and small intestine (lane 2) probed with the kidney partial cDNA. Ten micrograms of total RNA was size fractionated on an agarose-formaldehyde gel and transferred to nitrocellulose sheets. The blots were hybridized with ^{32}P -labeled probes from the aminopeptidase A (EAP) partial cDNA clone. Blots were then washed under high-stringency conditions and exposed overnight to X-ray film.

100 μM CTP, 10 pmol of [^{35}S]CTP (New England Nuclear, sp act 1,220 Ci/mmol), and T7 or T3 polymerase for 1 h at 37°C. The template DNA was then digested with DNase and the labeled probe precipitated and resuspended in hybridization buffer. The activity of the labeled riboprobe was $\sim 8 \times 10^5$ counts $\cdot \text{min}^{-1} \cdot \mu\text{l}^{-1}$.

Slide-mounted sections were prehybridized for 2 h at 50°C in a 1:1 mixture of formamide and prehybridization buffer containing 0.6 M NaCl, 20 mM piperazine- N,N' -bis(2-ethanesulfonic acid) buffer (pH 6.7), 1 \times Denhardt's solution, 1 mM EDTA, 500 $\mu\text{g}/\text{ml}$ yeast total RNA, 50 $\mu\text{g}/\text{ml}$ yeast tRNA, 1 mg/ml salmon sperm DNA, and 500 $\mu\text{g}/\text{ml}$ sodium pyrophosphate. Hybridization buffer was identical to prehybridization buffer, except that it contained 2.5 μM α -thiol-nucleotide triphosphates and 200 mM dithiothreitol (Sigma). The slides were then transferred to hybridization solution comprised of a mixture of hybridization buffer, dextran sulfate, and formamide (4:1:5) and containing the ^{35}S -labeled riboprobe at a final concentration of 5×10^6 – 10^7 counts $\cdot \text{min}^{-1} \cdot \text{ml}^{-1}$. Slides were incubated overnight at 50°C. The next day the sections were washed twice for 10 min at room temperature in 10 mM Tris-HCl (pH 8), 0.3 M NaCl, 0.1% sodium pyrophosphate, and 10 mM dithiothreitol and then treated with RNase (30 $\mu\text{g}/\text{ml}$) for 30 min at room temperature in 0.3 M NaCl, 10 mM

Tris-HCl, and 1 mM EDTA. The RNase solution was then blotted off and the sections washed for 10 min at room temperature in 0.3 M NaCl, 2 mM Tris-HCl, 1 mM EDTA, 0.05% sodium pyrophosphate, and 1 mM dithiothreitol followed by a 3-h wash at 50°C in 0.075 M NaCl, 2 mM Tris-HCl, 1 mM EDTA, and 1 mM dithiothreitol. The slides were then transferred to fresh buffer and washed overnight at room temperature. The next day the sections were dehydrated for 2 min each in 70% alcohol containing 300 mM ammonium acetate, 90% alcohol containing 300 mM ammonium acetate, and finally 100% alcohol. The sections were vacuum dried and exposed to Kodak XAR film for 1–20 days. After the film was developed, the slides were then dipped in liquid emulsion (Kodak NTB3, diluted 1:1) for high-resolution autoradiography. After exposure for 1–2 mo, the emulsion was developed, and the sections were counterstained lightly with cresyl violet, dehydrated, and coverslipped.

Immunocytochemistry. Six male Sprague-Dawley rats (175–200 g, Charles River Breeding Laboratories, Wilmington, MA) were housed on a 12:12-h light-dark schedule and allowed free access to food and water. Rats not operated on were processed for immunocytochemistry as described previously (16). Briefly, animals were anesthetized with pentobarbital (50 mg/kg ip) and perfused transcardially with ~ 100 ml of PBS (pH 7.4) followed by 1 ml/g body wt of 5% paraformaldehyde in 0.3 M sodium phosphate buffer, pH 7.4, over a period of 10 min. The kidneys were removed and postfixed in the same fixative for 1 h and then transferred through increasing concentrations of sucrose in PBS (2 h overnight) up to 18%. The kidneys were frozen to microtome chucks with powdered dry ice, and 20- μm transverse sections were cut in the cryostat (-20°C) and mounted on subbed microscope slides. Sections were washed three times in PBS and preincubated for 30 min with 2% normal goat serum in PBS containing 0.1% Triton X-100. The goat serum was then removed and replaced by diluted immune sera (1:5,000 to 1:10,000) in PBS containing 0.1% Triton X-100 and 0.1% BSA. The sections were then stored overnight at 4°C. The sections were rinsed with PBS and incubated with biotinylated goat anti-rabbit immunoglobulin G (Vector Laboratories) in a 1:222 dilution with PBS-Triton X-100-BSA. The sections were washed three times in PBS and incubated for 45 min with streptavidin-horseradish peroxidase conjugate. Unbound conjugate was removed by washing with PBS. The peroxidase reaction was developed by treating the sections with a freshly prepared 0.05% solution of 3,3'-diaminobenzidine (Sigma) containing 0.003% hydrogen peroxide in 50 mM phosphate buffer, pH 7.4, for 5–10 min. One-half of the slides were counterstained lightly with cresyl violet. All slides were dried, dehydrated in alcohol and xylene, coverslipped with Permount (Fisher Scientific, Pittsburgh, PA), and viewed under a Zeiss microscope.

Additional immunocytochemical staining was conducted on kidney sections from nonperfused animals. The sections were prepared identically as described above for *in situ* hybridization, i.e., unfixed cryostat kidney sections were mounted on slides and fixed in 3% paraformaldehyde for 5 min. Sections were also processed identically for immunohistochemistry through the biotinylated secondary antibody step. After washing, the slides were incubated with fluorescein isothiocyanate-labeled avidin (Vector Labs) at a dilution of 1:100 for 1 h at room temperature, washed, dried, and coverslipped with mineral oil. Sections were viewed under a Zeiss microscope equipped with a mercury/xenon lamp and epifluorescence.

Immunocytochemical controls consisted of staining in the presence of preimmune serum or immune serum preabsorbed with purified EAP, mAAP, and DPP IV at a concentration of 1 $\mu\text{g}/\text{ml}$.

F550

RAT KIDNEY GLUTAMYL AMINOPEPTIDASE

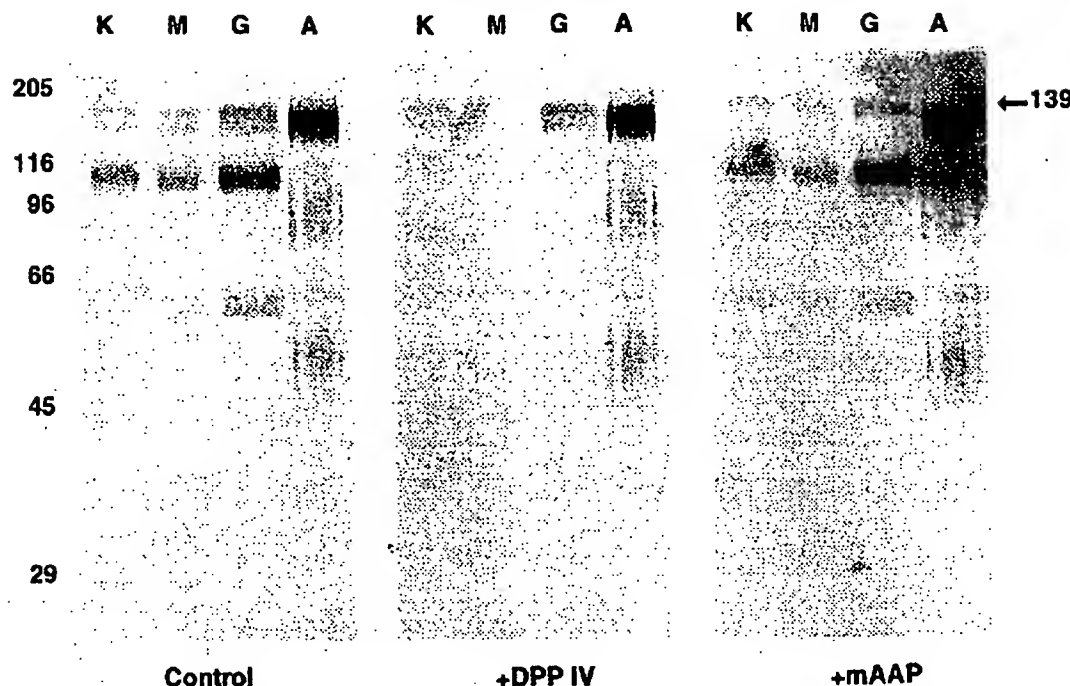


Fig. 4. Immunoblots of rat kidney EAP. Purified EAP (A) and homogenate protein (35 μ g/lane) from total kidney (K), outer medulla (M), and isolated glomeruli (G) were separated by SDS-polyacrylamide gel electrophoresis under reducing conditions, transferred to nitrocellulose sheets, and immunostained with EAP antiserum (1:1,000 dilution). Size of labeled bands was determined by comparison to molecular mass markers (29–205 kDa). The staining pattern with control immune serum was compared with that with immune serum preabsorbed with either 1 μ g/ml dipeptidyl peptidase IV (+DPP IV) or with 1 μ g/ml membrane alanyl aminopeptidase (+mAAP). The size of the putative EAP protein from this typical experiment (arrow) was 139 kDa.

RESULTS

Amplification of rat kidney cDNA with PCR primers based on the murine BP-1/6C3 sequence resulted in generation of a PCR product of the predicted size (Fig. 1). Four clones were sequenced, and each contained identical cDNA inserts (Fig. 2). The 450-bp cDNAs were 90% and 82% identical at the nucleotide level and 92% and 86% identical at the amino acid level to the BP-1/6C3 and gp160 differentiation antigen sequences, respectively (Fig. 2). Examination of the partial cDNA in the area encoding the zinc-binding domain indicated that the predicted amino acid sequence was identical to the zinc-binding domain of the BP-1/6C3 and gp160 antigens (Fig. 2).

Northern blot hybridization studies of rat kidney or jejunum total RNA with the rat partial cDNA resulted in strong hybridization of a band at 4.1 kb (Fig. 3). A less intense band was seen at 6.3 kb.

Studies by Herzig et al. (17) suggested that one form of EAP was distributed on both tubules and glomeruli and a second isoform was expressed on tubules only. We therefore compared the SDS-PAGE immunoblot staining for EAP from isolated glomeruli to that seen with total kidney homogenates and outer medulla (enriched with tubular segments) homogenate. Immunoblots with EAP antiserum (1:1,000 dilution) typically resulted in labeling of three bands: 136 ± 0.9 , 128 ± 0.9 , and 106 ± 1.2 kDa ($n = 5$) (Fig. 4). A fourth lightly stained band was seen at ~ 50 kDa and was most prominent in the protein from the isolated glomeruli. The immunoblot pattern of staining was similar to that reported previously for kidney homogenates (31) except that the diffuse upper band seen previously could now be separated into two distinct bands of 137 and 129 kDa. The outer medulla and the isolated glomeruli yielded a similar pattern of staining except that the staining was

Rat EAP	Gln-Val-Lys-Pro-Ile-Ala-xxx-Ser-Leu-Gly-xxx-Gln-xxx-Thr-Gly-Ser-xxx-Ile
Murine BP-1/6C3	...Gln-Val-Lys-Pro- <u>Val</u> -Ala-Asp- <u>Leu</u> -Leu-Gly-Trp-Gln-Asp-Thr-Gly-Ser-His-Ile...
Human gp160	...Gln-Val-Lys-Pro-Ile-Ala-Asp-Ser-Leu-Gly-Trp- <u>Asn</u> -Asp- <u>Ala</u> -Gly- <u>Asp</u> -His- <u>Val</u> ...

Fig. 5. Amino acid sequence of a partial tryptic peptide of EAP purified from rat kidney. XXX, amino acids that could not be identified with certainty. Amino acids from corresponding regions of BP-1/6C3 or gp160 that were not identical to the rat sequence are underlined.

RAT KIDNEY GLUTAMYL AMINOPEPTIDASE

F551

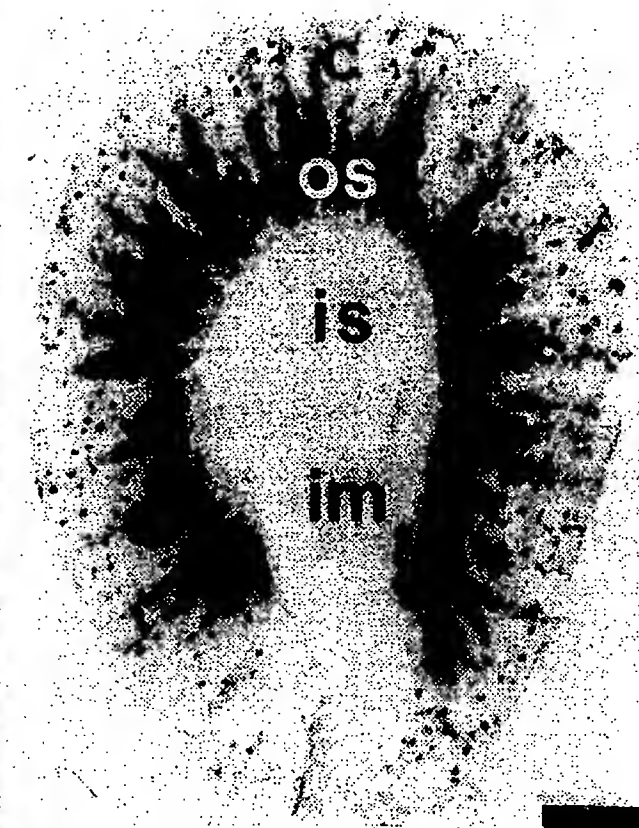


Fig. 6. In situ hybridization of rat kidney EAP mRNA. Shown is an autoradiogram of a transverse section of rat kidney incubated with an EAP antisense ^{35}S -labeled riboprobe and exposed to Kodak XAR film for 3 days. The heaviest labeling was in the outer stripe (os) of the outer medulla, extending into the cortex (c) as the medullary rays. Cortical labeling was punctate, with the size and distribution suggestive of glomeruli. The inner stripe (is) of the outer medulla and the inner medulla (im) were not labeled. Scale bar, 3 mm.

more intense with the isolated glomeruli. This is consistent with the EAP-specific activity being elevated in the isolated glomeruli compared with either the total kidney homogenate or the outer medulla homogenate: kidney 13.3 ± 2.3 , outer medulla 13.5 ± 1.1 , and glomeruli $45.2 \pm 4.7 \mu\text{mol} \cdot \text{h}^{-1} \cdot \text{mg protein}^{-1}$ ($n = 5$). Interestingly, only a single band of $132 \pm 1.9 \text{ kDa}$ was seen with EAP purified from rat kidney (Fig. 4). To determine if the smaller bands were proteolytic products of the 137-kDa band, we isolated kidney protein in the presence of a battery of protease inhibitors (18). Immunostaining of kidney protein under these conditions did not alter the pattern of the immunostaining (data not shown). Previous studies indicated that preabsorption of the EAP antiserum with purified kidney EAP completely blocked the immunoblot staining (31), results that were confirmed in this study by preabsorption with $1 \mu\text{g/ml}$ of purified EAP (data not shown). We then determined if the antiserum cross-reacted with other aminopeptidases, namely mAAP and DPP IV. Preabsorption of the EAP antiserum with DPP IV blocked the staining of the 106- and 50-kDa bands (Fig. 4). The immunostaining of the higher-molecular-weight doublet was not affected. Likewise, preabsorption of the

antiserum with purified mAAP blocked the staining of the 129-kDa band but not the 137-kDa or the 106-kDa band. Preabsorption of the antiserum with mAAP and DPP IV simultaneously resulted in staining of only the 137-kDa band (data not shown). Preabsorption with mAAP or DPP IV, separately or together, did not affect the staining of the purified EAP. The slightly smaller form of the purified EAP compared with the EAP from kidney homogenates can be accounted for by the use of autolysis as the first step in the purification to solubilize EAP from the kidney membranes (31). These results indicate that kidney EAP is 137 kDa, mAAP is 128 kDa, and DPP IV is 106 kDa on SDS-PAGE.

Purified kidney EAP was subjected to tryptic digestion, and the fragments were separated by HPLC. A single fragment was selected for microsequencing. Four amino acids within this 18-mer fragment could not be identified with certainty (Fig. 5). Comparison of the 14 remaining amino acids to the BP-1/6C3 and gp160 amino acid sequences indicated that the peptide fragment corresponded to amino acids 714–731 of BP-1/6C3 and 723–740 of gp160. Twelve of the 14 amino acids were identical in the rat and mouse, with both substitutions being conservative (isoleucine for valine and serine for leucine). Four amino acids were different in rat and human, with only one (serine for aspartic acid) being nonconservative.

The distribution of EAP mRNA localized by in situ hybridization was compared with the distribution of the enzyme localized by immunocytochemistry. In situ hybridization of rat kidney EAP with ^{35}S -labeled antisense single-stranded riboprobes indicated that EAP mRNA was highest in the outer stripe of the outer medulla, corresponding to the S3 segment of the proximal tubule, and to both superficial and juxtamedullary glomeruli in the cortex (Fig. 6). The low-power in situ hybridization suggested that there was minimal tubular labeling in the cortex. This was confirmed by higher resolution in situ hybridization, which indicated that the cortical labeling was primarily within glomeruli (Fig. 7). There was a notable absence of labeling of the proximal convoluted tubules (e.g., surrounding the glomerulus in Fig. 7A). Other cortical tubules, including distal convoluted tubules and cortical collecting ducts, were also unlabeled. High-resolution in situ hybridization indicated that the glomerular labeling was not distributed uniformly but that, depending on the plane of section, labeling was concentrated in bands and patches (Fig. 7, B–E). The majority of the cells within the glomeruli were not labeled. This pattern of labeling is most consistent with labeling of mesangial cells and not epithelial or endothelial cells, but the identity of the labeled cells could not be determined unequivocally. Labeling was also seen within the terminal portion of the afferent arteriole corresponding to juxtaglomerular (JG) cells (Fig. 8A). There was no detectable labeling elsewhere within the vasculature. In larger caliber vessels it was possible to determine that neither the endothelial cells nor the tunica media smooth muscle cells were labeled (Fig. 8B). In the medulla, positive hybridization was detected primarily within descending

F552

RAT KIDNEY GLUTAMYL AMINOPEPTIDASE

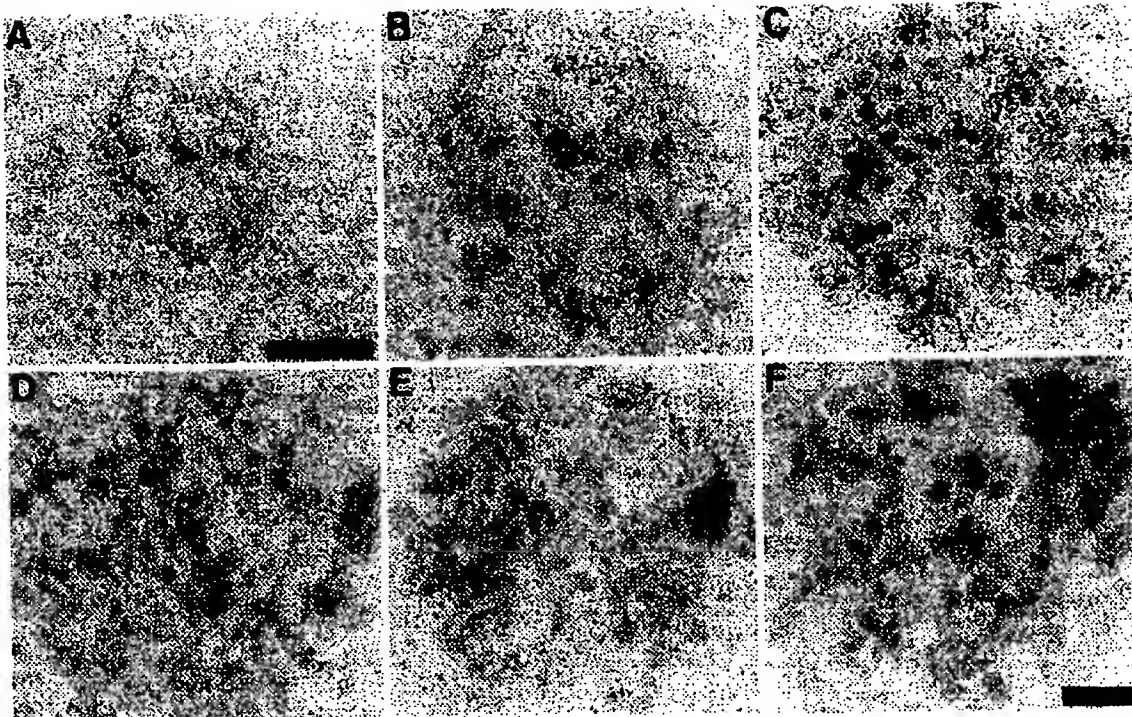


Fig. 7. In situ hybridization of EAP mRNA within glomeruli. Sections of rat kidney similar to that shown in Fig. 1 were dipped in liquid emulsion and exposed for a period of 1 mo. Sections were counterstained lightly with cresyl violet. A: intermediate magnification of a labeled glomerulus surrounded by unlabeled tubules. Scale bar, 40 μ m. B: higher power magnification of the glomerulus in A. Note that the pattern of labeling within the glomerulus is seen as clusters of silver grains and that not all cells are labeled. C-E: additional representative glomeruli showing typical labeling within glomeruli, including patches (C), cord-like patches (D), and clusters of grains situated on the extreme edge of the glomerulus, generally near the vascular pole (E). F: labeling of a glomerulus from a section incubated with an EAP 35 S-labeled sense riboprobe. Scale bar, 25 μ m.

proximal tubule segments in medullary rays in the outer stripe of the outer medulla (Figs. 6 and 8C). Tubules within the inner stripe of the outer medulla (including thick ascending limb cells) and inner medulla were also unlabeled. Control hybridization with sense riboprobes yielded only diffuse background labeling (Figs. 7F and 8D).

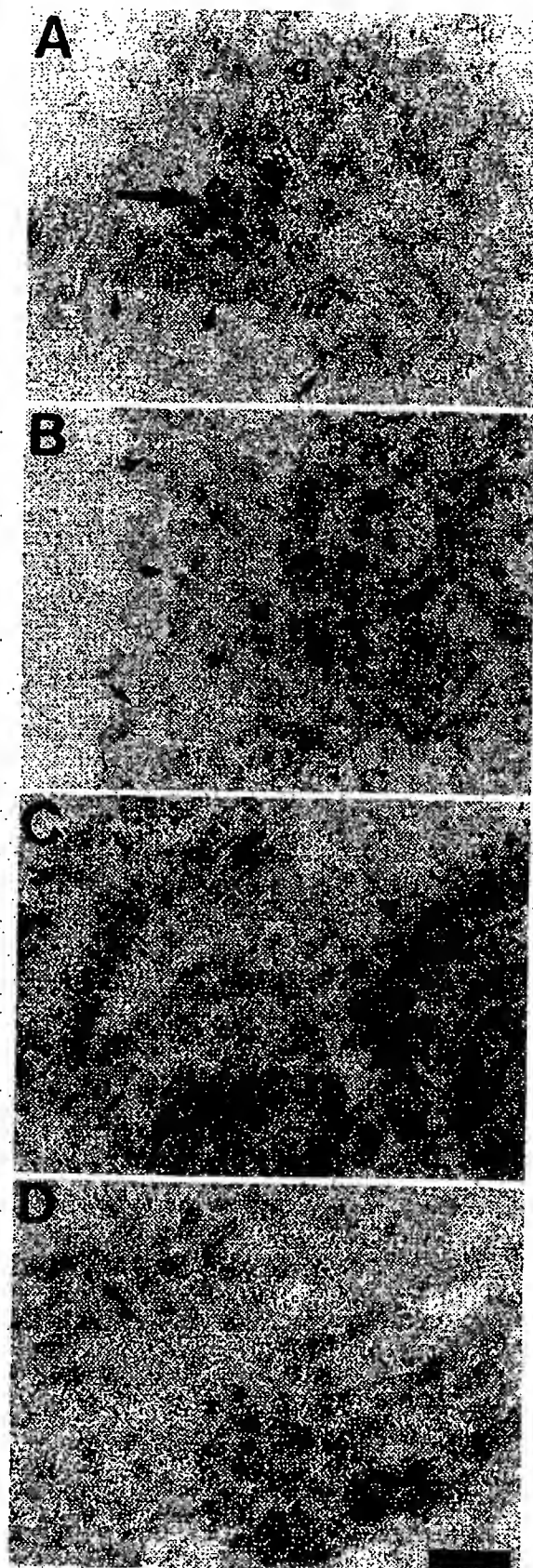
Previous studies characterizing the antiserum against rat kidney EAP for use in immunocytochemistry indicated that there was no cross-reactivity with the closely related enzyme mAAP (16, 31). However, under the conditions used for immunoblotting, the EAP antiserum cross-reacted with both mAAP and DPP IV (Fig. 4). The degree of cross-reactivity seen with antiserum is related to the concentration of antiserum and antigen. In the immunoblot studies the antiserum was used at a dilution of 1:1,000. For immunocytochemistry, dilutions of 1:5,000 or 1:10,000 were typically used (16). To determine the specificity of the antiserum under the conditions used for immunocytochemistry, we repeated the preabsorption studies in the absence or presence of 1 μ g/ml mAAP, 1 μ g/ml DPP IV, or 1 μ g/ml EAP (Fig. 9). Low-power magnification of EAP staining in the kidney cortex indicated that heavy staining was present within tubules and less intense staining within glomeruli (Fig. 9A). Preabsorption of the antiserum with either mAAP (Fig. 9B) or DPP IV (Fig. 9C) had no effect on the immunocytochemical staining pattern, whereas preab-

sorption of the antiserum with EAP (Fig. 9D) almost completely abolished the immunostaining. Therefore, under the conditions that were used here for immunocytochemistry, we concluded that the antiserum was specific for EAP.

Low-power magnification of immunostained sections of kidney cortex indicated that cortical immunostaining was primarily within proximal convoluted tubules (Fig. 9). Immunostaining within glomeruli was apparently less intense and more diffuse (Fig. 9). The weak immunostaining did not appear to correlate with the higher EAP activity seen in isolated glomerular preparations (above). We then tested if the discrepancy between EAP activity and immunoreactivity within glomeruli was sensitive to the type of fixation. Indeed, cryostat sections that were lightly fixed directly on the slide exhibited intense EAP immunostaining within the glomeruli (Fig. 10). The absence of EAP immunostaining within perfusion-fixed kidneys suggests that EAP immunoreactivity was diminished within vascular elements, such as glomeruli, due to the relatively higher concentration of fixative within the vasculature during perfusion than in the surrounding nonvascular tissues, such as tubules. Close examination of the glomerular staining with EAP antiserum indicated that the immunoreactivity was concentrated primarily within mesangial cells. The stellate appearance of mesangial cells with multiple processes terminating on glomerular capillaries was readily seen (Fig.

RAT KIDNEY GLUTAMYL AMINOPEPTIDASE

F553



10B). EAP immunofluorescence appeared to be concentrated at sites where mesangial cell processes contacted the capillary walls. Endothelial cells lining the capillaries were not labeled. Although the compromised preservation of the tissue made precise localization difficult, there was no clear demonstration of epithelial cell staining. Immunostaining within proximal tubules was concentrated solely within the apical brush border (Fig. 11).

DISCUSSION

As noted above, various lines of evidence indicate that the murine BP-1/6C3 and human gp160 antigens are identical to EAP (23, 26, 33, 36, 37). To isolate a partial cDNA for rat kidney EAP, we designed oligonucleotide primers based on the murine BP-1/6C3 nucleotide sequence and used RT-PCR. The PCR product was highly similar to the BP-1/6C3 and gp160 sequences: 90% and 82% identical at the nucleotide level and 92% and 86% identical at the amino acid level, respectively. The amplified cDNA included the region of the zinc-binding domain, an area that is essential for EAP enzymatic activity (33). The predicted amino acid sequence of the partial cDNA within the zinc-binding domain was completely conserved compared with the murine BP-1/6C3 and human gp160 sequences. Northern blot analysis of rat kidney and small intestine total RNA resulted in labeling of a major band of 4.1 kb, identical in size to the BP-1/6C3 and gp160 transcripts (23, 26, 36). Examination of the predicted amino acid sequence of the rat EAP with the murine EAP indicated that, of the 11 amino acid substitutions, six were nonconservative, i.e., a charged amino acid for an uncharged amino acid. However, of the six nonconservative substitutions between mouse BP-1/6C3 and rat EAP, five are either identical or conservative relative to the human gp160 sequence. In addition, the amino acid sequence of a tryptic digest peptide of EAP purified from rat kidney indicated that it was highly similar to a region of the BP-1/6C3 and gp160 antigens. It is interesting to note that the two amino acids in the partial peptide fragment of kidney EAP that did not match the predicted sequence of murine BP-1/6C3 were conserved between the rat EAP and human gp160 sequences. Thus, on the basis of the sequence analysis of the partial cDNA, the hybridization analysis, and the partial amino

Fig. 8. In situ hybridization of tubular and vascular elements labeled with an EAP antisense ^{35}S -labeled riboprobe. A: shown is the terminal portion of an afferent arteriole (small arrows) as it gives off a short branch to 1 glomerulus (g) and then continues out of frame. The segment of the afferent arteriole that enters the glomerulus corresponds to the juxtaglomerular cell region. Note the moderate density of silver grains over the juxtaglomerular cells (large arrow). B: cross section through a portion of an interlobular artery showing unlabeled endothelial cells (small arrows) and the smooth muscle cells of the tunica media (stars). Note the heavy labeling of the tubule immediately adjacent to the artery. C: high-power view of a longitudinal section through a medullary ray showing heavily labeled straight descending proximal tubules adjacent to an unlabeled cortical collecting duct. D: hybridization of an EAP ^{35}S -labeled sense riboprobe with a section through a medullary ray similar to that shown in C. Note the complete absence of labeled tubules. Scale bar, 25 μm .

F554

RAT KIDNEY GLUTAMYL AMINOPEPTIDASE

acid sequence, we conclude that the rat kidney EAP is homologous to the murine BP-1/6C3 and human gp160 proteins.

With antiserum raised against EAP purified from rat kidney, we noted previously that immunoblots with purified EAP yielded only a single band, whereas immunoblots with kidney homogenates yielded two bands on SDS-PAGE (31). Here we showed similar results except that the broad upper band could now be distinguished as two distinct bands of 137 and 129 kDa. A lower band of 106 kDa was also seen. It was not clear whether the multiple bands represented partial proteolytic digestion of the native enzyme, EAP isozymes, or cross-reactivity with a closely related enzyme(s). We ruled out that the smaller bands were proteolytic products of EAP, because the immunoblot pattern was unchanged when kidney tissue samples were isolated in the presence of a spectrum of protease inhibitors. As noted previously, some variation has been reported on the size of EAP monomers isolated from the kidney of various species (6, 13, 17). However, we determined that the multiple bands actually represented cross-reactivity of the EAP antiserum with other kidney peptidases. Preabsorption of the EAP antiserum with purified mAAP blocked staining of the 129-kDa band, and preabsorption with purified DPP IV blocked staining of the 106-kDa band. The 129- and 106-kDa bands are in good agreement with previous reports on the size of purified mAAP and DPP IV, respectively (2, 20). These results indicate that rat kidney expresses only a single sized EAP monomeric form of 137 kDa on SDS-PAGE and that the additional bands seen on immunoblots of rat kidney represented cross-reactivity of the antiserum with mAAP and DPP IV. The cross-reactivity of the antiserum to other peptidases was somewhat surprising, since the purified EAP material had no detectable mAAP or DPP IV activity. Since EAP and mAAP are related enzymes and are 34% identical (36), it is possible that these two enzymes share common epitopes. On the other hand, DPP IV and EAP are unrelated enzymes (serine proteinase vs. a metalloproteinase). Moreover, comparison of the sequences of EAP and DPP IV revealed no significant homology. Since kidney DPP IV levels are high, the possibility that the purified EAP material contained trace contaminants of enzymatically inactive DPP IV fragments cannot be ruled out. A repeat of the purification procedure while monitoring EAP-containing fractions by immunoblotting confirmed that the 106-kDa band was separated from the upper bands by phenyl Sepharose chromatography, the step at which DPP IV activity is separated from EAP/mAAP activity (unpublished observations). The

Fig. 9. Effects of preabsorption of the EAP antiserum (1:5,000 dilution) with purified mAAP and DPP IV on the immunocytochemical staining pattern in rat kidney. A: immunostaining with control antiserum. Note the typical staining pattern in the outer cortex, with heavily labeled proximal convoluted tubules and lighter stained glomeruli. B: immunostaining with antiserum preabsorbed with mAAP (1 μ g/ml). Note there is no reduction in staining. C: immunostaining with antiserum preabsorbed with DPP IV (1 μ g/ml). Note there is no reduction in staining. D: immunostaining with antiserum preabsorbed with EAP (1 μ g/ml). Note the almost complete absence of immunostaining. Scale bar, 100 μ m.

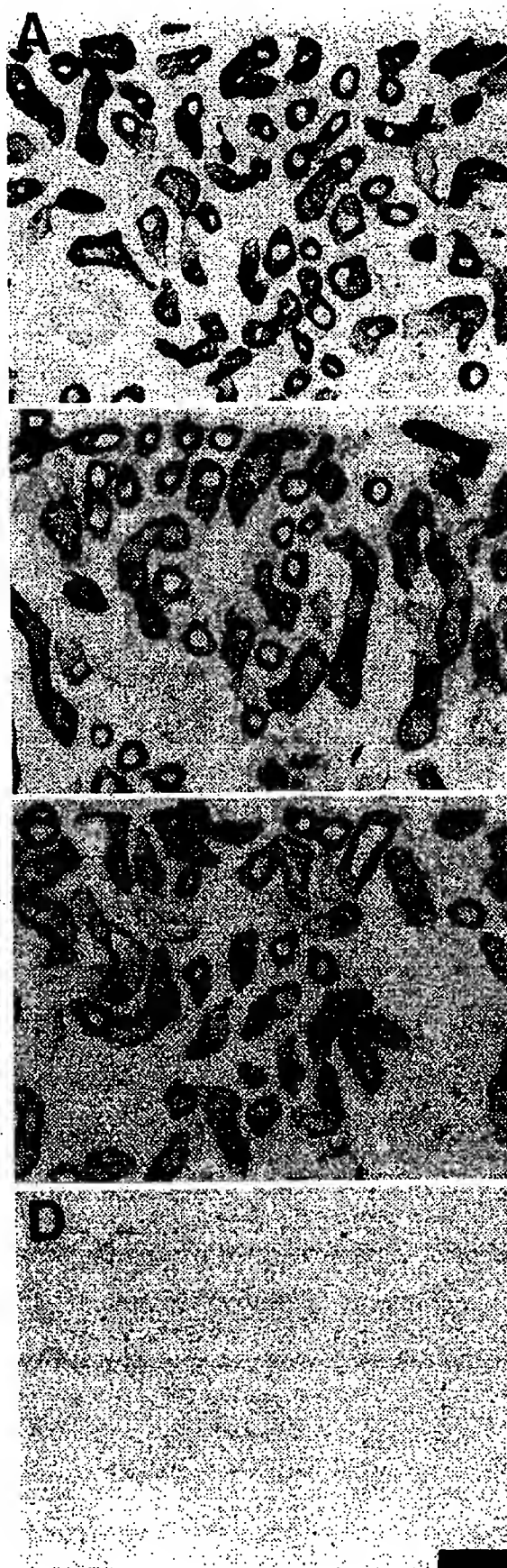


Fig.
non
and
met
glom
with
mes
dev
grap
con
cyto
cap
cont
Scale

gr
istr
lem
wer
with
resu
seer
rum
sult
repr
non

RAT KIDNEY GLUTAMYL AMINOPEPTIDASE

F555

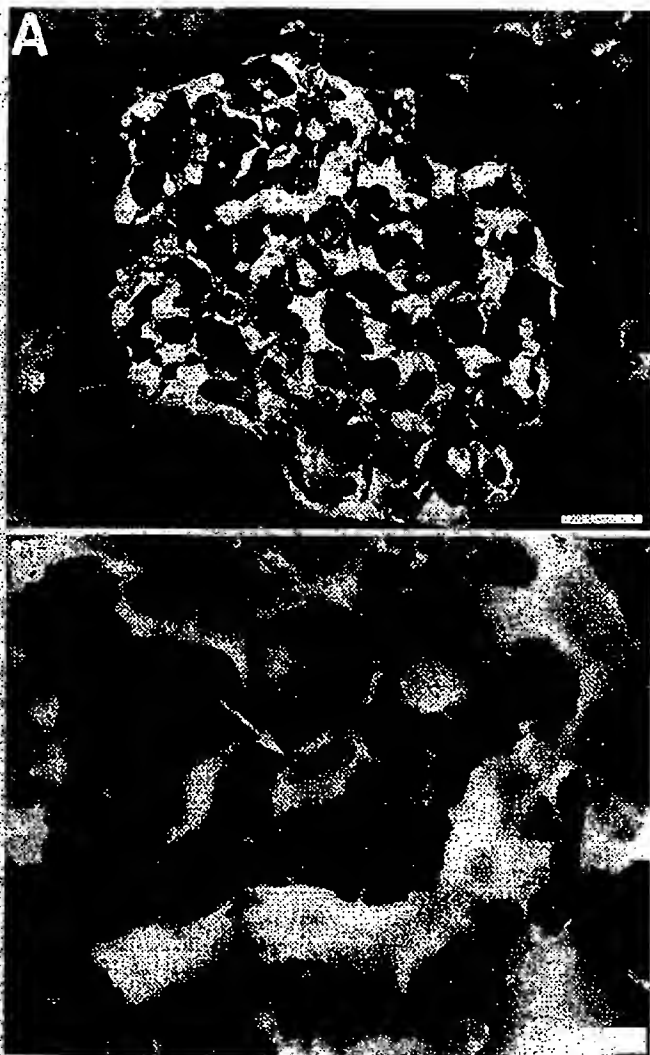


Fig. 10. EAP immunofluorescent staining within a glomerulus. A nonperfused kidney was cryostat sectioned, fixed directly on the slide, and immunostained with EAP antiserum using an immunofluorescent method. A: photomicrograph of EAP immunoreactivity within a glomerulus. Note that EAP immunofluorescence was concentrated within the mesangium, specifically within mesangial cells (arrow) and mesangial cell processes. The endothelial cell linings of capillaries were devoid of staining (*). Scale bar, 25 μ m. B: higher power photomicrograph of the labeled mesangial cell in A, shown by arrow. Note again concentration of EAP immunofluorescence within the mesangial cell cytoplasm and the processes (small arrowheads) that terminate on the capillary walls. Areas of the capillary wall that mesangial cell processes contact appear to have a greater density of EAP immunoreactivity. Scale bar, 10 μ m.

greater dilution of the antiserum for immunocytochemistry apparently minimizes the cross-reactivity problems, since the immunocytochemical staining patterns were not affected by preabsorption of the antiserum with either mAAP or DPP IV. Furthermore, these results raise doubts as to whether the multiple bands seen in previous immunoblot studies with EAP antiserum actually represent EAP isoforms. Rather, our results would suggest that the multiple bands either represent degradation of EAP or cross-reactivity to a non-EAP protein.

With only one exception, the distributions of EAP mRNA and EAP immunoreactivity within rat kidney were very similar. The highest levels of EAP mRNA were detected within the outer stripe of the outer medulla. High-resolution *in situ* hybridization indicated that the labeling in the outer stripe was restricted to the straight descending (S3) segment of the proximal tubules. The S3 segment of the proximal tubule also contained high levels of EAP immunoreactivity, confirming previous histochemical studies (21, 25). No EAP mRNA was detected, however, within proximal convoluted tubules, an area that contains high levels of EAP immunoreactivity. The reason for the apparent discrepancy between hybridization and immunoreactivity patterns in the proximal convoluted tubule is unlikely to be due to the existence of different EAP isoforms, since the probe used for *in situ* hybridization would be expected to recognize transcripts from all EAP isoforms; the probe contained the region of the zinc-binding domain, an area absolutely essential for EAP activity (33). Another possible explanation for the high level of EAP immunoreactivity and the low level of EAP mRNA in the



Fig. 11. High-power photomicrograph of EAP immunoreactivity within proximal tubules. A: immunostaining within a proximal tubule cut in cross section. Note that the staining is restricted to the apical membrane (arrow). B: staining in presence of preimmune serum. Note absence of apical membrane immunostaining (arrow). Scale bar, 10 μ m.

F556

RAT KIDNEY GLUTAMYL AMINOPEPTIDASE

proximal convoluted tubules could be that there is low turnover of the EAP protein within convoluted tubules (and thus low mRNA). Likewise, the absence of detectable EAP mRNA in proximal convoluted tubules might simply reflect the lower sensitivity of the in situ hybridization method.

EAP immunoreactivity and mRNA were not detected in large blood vessels. Relatively low concentrations of EAP mRNA could be detected within some, but not all, afferent arteriole JG cells. EAP immunoreactivity was not consistently seen within JG cells. Whether this indicates that expression of EAP in the JG cells is near the level of detection for both techniques or whether there is only a subset of afferent arterioles that express EAP is not clear at this time. Higher levels of EAP mRNA and immunoreactivity were detected in glomeruli. The presence of EAP immunoreactivity and EAP mRNA within glomeruli confirmed the results that indicated that EAP enzymatic activity was enriched in isolated glomeruli compared with kidney homogenates. High-resolution in situ hybridization indicated that EAP mRNA was not uniformly distributed within the glomeruli. Rather, the hybridization pattern was cord-like patches, suggestive of labeling within the mesangium, possibly mesangial cells. Immunocytochemical staining of EAP within glomeruli from perfusion-fixed kidneys was diffuse and could not be localized to distinct cell bodies. However, in nonperfused kidneys where sections were fixed directly on the slides, EAP immunofluorescence was concentrated within mesangial cells, and in particular in areas where mesangial cell processes contacted capillary walls. The presence of EAP immunoreactivity within mesangial cell bodies is consistent with the in situ hybridization pattern of EAP mRNA in glomeruli. EAP immunoreactivity within mesangial cells is also consistent with a previous report from our laboratory that showed that EAP immunoreactivity in rat brain is associated with cerebral microvessel pericytes (16). Pericytes and mesangial cells are both perivascular adventitial cells that are known to have extensive cell processes that entwine small blood vessels. Both cell types are thought to be derived from the same progenitor cells (29).

Although EAP is not specific for a single substrate, some degree of functional specificity would occur if EAP was localized to cells that were exposed to extracellular fluids enriched with a particular substrate. EAP has been shown to hydrolyze [Asp¹]ANG II to ANG III ([des-Asp¹]ANG II) (1, 21, 34). In most tissues ANG III is less potent than ANG II, so the hydrolysis of ANG II by EAP is viewed as a degradation step (34). However, some studies indicate that the lower potency of ANG III is attributed to the greater susceptibility of this peptide to enzymatic degradation (34). In some tissues, including brain and adrenal, ANG III has significant bioactivity (12, 35), suggesting that the hydrolysis of ANG II to ANG III is a conversion step rather than degradation. It is interesting then to consider that the distribution of EAP within the kidney coincides with cells known to express ANG II receptors, principally the type 1 receptor subtype (4, 7, 9, 14, 27, 30, 38). ANG II receptors are

known to be present on juxtaglomerular cells, mesangial cells, afferent and efferent arterioles, and proximal tubules. In addition, all the components of the renin-angiotensin system are localized within the kidney (3, 32). Thus the colocalization of EAP and ANG II receptors within the kidney suggests that EAP could play an important role in modulating the activity of both circulating and locally formed ANG II.

In summary, the results presented here indicate that: 1) rat kidney EAP is homologous to the murine BP-1/6C3 and human kidney gp160 differentiation antigens; 2) the monomeric form of EAP in rat kidney is a single-sized protein of 137 kDa; 3) rat kidney EAP gene expression is highest within the proximal tubules and glomerular mesangial cells; and 4) the localization of EAP within the kidney correlates with the cellular distribution of ANG II receptors. EAP may therefore have multiple physiological functions within the kidney, depending on its localization, i.e., metabolism of oligopeptides in the glomerular filtrate and degradation/conversion of circulating or intrarenally synthesized bioactive peptides, including ANG II.

This work was supported by National Institutes of Health Grants HL-42585 (to D. P. Healy) and NS-17392 (to S. Wilk) and by the American Heart Association, New York City Affiliate (D. P. Healy). D. P. Healy is an Established Investigator of the American Heart Association. S. Wilk is supported by National Institute of Mental Health Research Scientist Award MH-00350, and M. Troyanovskaya is supported by National Institute on Drug Abuse Postdoctoral Training Grant DA-07135.

Address for reprint requests: D. P. Healy, Dept. of Pharmacology, Box 1215, Mount Sinai School of Medicine, One Gustave L. Levy Place, New York, NY 10029.

Received 17 December 1993; accepted in final form 26 April 1994.

REFERENCES

1. Ahmad, S., and P. E. Ward. Role of aminopeptidase activity in the regulation of the pressor activity of circulating angiotensins. *J. Pharmacol. Exp. Ther.* 252: 643-650, 1990.
2. Brownlee, J., C. H. Williams, G. P. Brennan, and D. W. Halton. Purification and immunochemical studies of dipeptidyl peptidase IV from bovine kidney. *Biol. Chem. Hoppe-Seyler* 373: 911-914, 1992.
3. Burns, K. D., T. Homma, and R. C. Harris. The intrarenal renin-angiotensin system. *Semin. Nephrol.* 13: 13-30, 1993.
4. Chansel, D., S. Czekalski, P. Pham, and R. Ardailou. Characterization of angiotensin II receptor subtypes in human glomeruli and mesangial cells. *Am. J. Physiol.* 262 (Renal Fluid Electrolyte Physiol. 31): F432-F441, 1992.
5. Chomczynski, P., and N. Sacchi. Single-step method of RNA isolation by acid guanidinium thiocyanate-phenol-chloroform extraction. *Anal. Biochem.* 162: 156-159, 1987.
6. Danielson, E. M., O. Noren, H. Sjostrom, J. Ingram, and A. J. Kenny. Proteins and the kidney microvillar membrane. Aspartate aminopeptidase: purification by immunoabsorbent chromatography and properties of the detergent- and proteinase-solubilized forms. *Biochem. J.* 189: 591-603, 1980.
7. Edwards, R., E. J. Stack, E. F. Weidley, N. Altyar, R. M. Keenan, D. T. Hill, and J. Weinstock. Characterization of renal angiotensin II receptors using subtype selective antagonists. *J. Pharmacol. Exp. Ther.* 260: 933-938, 1992.
8. Fujiwara, Y., E. Kitamura, N. Ueda, M. Fukunaga, Y. Orita, and T. Kamada. Mechanism of action of angiotensin II on isolated rat glomeruli. *Kidney Int.* 36: 985-991, 1989.
9. Gasc, J. M., C. Monnot, E. Clauser, and P. Corvol. Co-expression of type 1 angiotensin II receptor (AT₁R) and renin mRNAs in juxtaglomerular cells of the rat kidney. *Endocrinology* 132: 2723-2725, 1993.

RAT KIDNEY GLUTAMYL AMINOPEPTIDASE

F557

10. George, S. G., and A. J. Kenny. Studies on the enzymology of purified preparations of brush border from rabbit kidney. *Biochem. J.* 134: 43-57, 1973.
11. Glenner, G. G., P. J. McMillan, and J. E. Folk. A mammalian peptidase specific for the hydrolysis of N-terminal α -L-glutamyl and aspartyl residues. *Nature Lond.* 194: 867-868, 1962.
12. Goodfriend, T. L., and M. J. Peach. Angiotensin III: (des-aspartic acid¹) angiotensin II. Evidence and speculation for its role as an important agonist in the renin-angiotensin system. *Circ. Res.* 37, Suppl. 1: 183-148, 1975.
13. Gorvel, J. P., A. Benajiba, and S. Maroux. Purification and characterization of the rabbit intestinal brush-border aminopeptidase A. *Biochim. Biophys. Acta* 615: 271-274, 1980.
14. Grone, H. J., M. Simon, and E. Fuchs. Autoradiographic characterization of angiotensin receptor subtypes in fetal and adult human kidney. *Am. J. Physiol.* 262 (Renal Fluid Electrolyte Physiol. 31): F326-F331, 1992.
15. Hall, J. E. Control of sodium excretion by angiotensin II: intrarenal mechanisms and blood pressure regulation. *Am. J. Physiol.* 250 (Regulatory Integrative Comp. Physiol. 19): R960-R972, 1986.
16. Healy, D. P., and S. Wilk. Localization of immunoreactive glutamyl aminopeptidase in rat brain. II. Distribution and correlation with angiotensin II. *Brain Res.* 606: 295-303, 1993.
17. Herzig, C. M., W. Schoeppe, and J. E. Scherberich. Angiotensinase A (aminopeptidase A): properties of chromatographically purified isoforms from human kidney. *J. Chromatogr.* 625: 73-82, 1992.
18. Huo, T., M. Q. Ye, and D. P. Healy. Characterization of a dopamine receptor (DA_{2A}) in the kidney inner medulla. *Proc. Natl. Acad. Sci. USA* 88: 3170-3174, 1991.
19. Ichikawa, I., and R. C. Harris. Angiotensin actions in the kidney: renewed interest into the old hormone. *Kidney Int.* 40: 583-596, 1991.
20. Kenny, A. J., and S. Maroux. Topology of microvillar membrane hydrolases of kidney and intestine. *Physiol. Rev.* 62: 91-128, 1993.
21. Kugler, P. Aminopeptidase A is angiotensinase A. I. Quantitative histochemical studies in kidney glomerulus. *Histochemistry* 74: 229-245, 1982.
22. Levens, N. R., M. J. Peach, and R. M. Carey. Role of the intrarenal renin-angiotensin system in the control of renal function. *Circ. Res.* 48: 157-167, 1981.
23. Li, L., J. Wang, and M. D. Cooper. cDNA cloning and expression of human glutamyl aminopeptidase (aminopeptidase A). *Genomics* 17: 657-664, 1993.
24. Lojda, Z., and R. Gossrau. Study on aminopeptidase A. *Histochemistry* 67: 267-290, 1980.
25. Nanus, D. M., D. Engelstein, G. A. Gastl, L. Gluck, M. J. Vidal, M. Morrison, C. L. Finstad, N. H. Bander, and A. P. Albino. Molecular cloning of the human kidney differentiation antigen gp160: human aminopeptidase A. *Proc. Natl. Acad. Sci. USA* 90: 7069-7073, 1993.
26. Paxton, W. G., M. Runge, C. Horaist, C. Cohen, R. W. Alexander, and K. E. Bernstein. Immunohistochemical localization of rat angiotensin AT₁ receptor. *Am. J. Physiol.* 264 (Renal Fluid Electrolyte Physiol. 33): F989-F995, 1993.
27. Sambrook, J., E. F. Fritsch, and T. Maniatis. Molecular Cloning, Cold Spring Harbor Laboratory Press, 1989.
28. Sims, D. E. The pericyte—a review. *Tissue Cell* 18: 153-174, 1986.
29. Smith, R. D., A. T. Chiu, P. C. Wong, W. F. Herblin, and P. B. M. W. M. Timmermans. Pharmacology of nonpeptide angiotensin II receptor antagonists. *Annu. Rev. Pharmacol. Toxicol.* 32: 135-165, 1992.
30. Song, L. J., E. Wilk, S. Wilk, and D. P. Healy. Localization of immunoreactive glutamyl aminopeptidase in rat brain. I. Association with cerebral microvessels. *Brain Res.* 606: 286-294, 1993.
31. Taugner, R., E. Hackenthal, E. Rix, R. Nobiling, and K. Poulsen. Immunocytochemistry of the renin-angiotensin system: renin, angiotensinogen, angiotensin I, angiotensin II, and converting enzyme in the kidneys of mice, rats, and tree shrews. *Kidney Int.* 22 (Suppl 12): S33-S43, 1982.
32. Wang, J., and M. D. Cooper. Histidine residue in the zinc-binding motif of aminopeptidase A is critical for enzymatic activity. *Proc. Natl. Acad. Sci. USA* 90: 1222-1226, 1993.
33. Wilk, S., and D. P. Healy. Glutamyl aminopeptidase (aminopeptidase A), the BP-1/6C3 antigen. *Adv. Neuroimmunol.* 3: 195-207, 1993.
34. Wright, J. W., S. L. Morseth, R. H. Abhold, and J. W. Harding. Pressor action and dipsogenicity induced by angiotensin II and III in rats. *Am. J. Physiol.* 249 (Regulatory Integrative Comp. Physiol. 18): R514-R521, 1985.
35. Wu, Q., J. M. Lahti, G. M. Air, P. D. Burrows, and M. D. Cooper. Molecular cloning of the murine BP-1/6C3 antigen: a member of the zinc-dependent metallopeptidase family. *Proc. Natl. Acad. Sci. USA* 87: 993-997, 1990.
36. Wu, Q., L. Li, M. D. Cooper, M. Pierres, and J. P. Gorvel. Aminopeptidase A activity of the murine B-lymphocyte differentiation antigen BP-1/6C3. *Proc. Natl. Acad. Sci. USA* 88: 676-680, 1991.
37. Zhou, J., K. Song, P. J. Harris, F. A. O. Mendelsohn. In vitro autoradiography reveals predominantly AT₁ angiotensin II receptors in rat kidney. *Renal Physiol. Biochem.* 15: 231-239, 1992.

FGH52352

CI-06861804-2

FGH52352

CISTI ICIST

CI-06861804-2

Document Delivery Service
in partnership with the Canadian Agriculture LibraryService de fourniture de Documents
en collaboration avec la Bibliothèque canadienne de l'agriculture**THIS IS NOT AN INVOICE / CECI N'EST PAS UNE FACTURE**LYNN BRAZIL
LIBRARIANHELLER EHRMAN WHITE & MCAULIFFE
275 MIDDLEFIELD RD
MENLO PARK, CA 94025
UNITED STATES

ORDER NUMBER: CI-06861804-2
Account Number: FGH52352
Delivery Mode: F31
Delivery Address: 650/324-6034
Submitted: 2007/05/14 14:35:43
Received: 2007/05/14 14:35:43
Printed: 2007/05/15 00:15:49

Direct	Periodical	OPENURLOPAC	UNITED STATES

Client Number: 39780-7000 CD
Title: PHOTOCHEMISTRY AND PHOTOBIOLOGY.
DB Ref. No.: IRN10196298
ISSN: ISSN00318655
Vol./Issue: 75/3
Date: 2002
Pages: 302-10
Article Title: A UVA IRRADIATION-INDUCED ACTIVATION OF ACTIVATOR PROTEIN-1 IS CORRELATED WITH INDUCED EXPRESSION OF AP-1 FAMILY MEMEBERS IN THE HUMAN KER
Article Author: SILVERS, A.L., ET AL.
Report Number: IRN10196298
Publisher: PERGAMON PRESS.

Estimated cost for this 9 page document: \$12.5 document supply fee +
\$39 copyright = \$51.5

The attached document has been copied under license from Access Copyright/COPIBEC or other rights holders through direct agreements. Further reproduction, electronic storage or electronic transmission, even for internal purposes, is prohibited unless you are independently licensed to do so by the rights holder.

Phone/Téléphone: 1-800-668-1222 (Canada - U.S./E.-U.) (613) 998-8544 (International)

www.nrc.ca/cisti
info.cisti@nrc.ca

Fax/Télécopieur: (613) 993-7619

www.cnr.ca/icist
info.icist@nrc.caNational Research
Council CanadaConseil national
de recherches Canada

Page

1 / 1

Photochemistry and Photobiology, 2002, 75(3): 302-310

UVA Irradiation-induced Activation of Activator Protein-1 is Correlated with Induced Expression of AP-1 Family Members in the Human Keratinocyte Cell Line HaCaT¹

Amy L. Silvers and G. Timothy Bowden*

Department of Radiation Oncology, Arizona Cancer Center, The University of Arizona, Tucson, AZ

Received 17 October 2001; accepted 7 December 2001

ABSTRACT

To determine whether the transcription factor activator protein-1 (AP-1) could be modulated by ultraviolet A (UVA) exposure, we examined AP-1 DNA-binding activity and transactivation after exposure to UVA in the human immortalized keratinocyte cell line HaCaT. Maximal AP-1 transactivation was observed with 250 kJ/m² UVA between 3 and 4 h after irradiation. DNA binding of AP-1 to the target 12-*O*-tetradecanoylphorbol-13-acetate response element sequence was maximally induced 1-3 h after irradiation. Both *de novo* transcription and translation contributed to the UVA-induced AP-1 DNA binding. c-Fos was implicated as a primary component of the AP-1 DNA-binding complex. Other components of the complex included Fra-2, c-Jun, JunB and JunD. UVA irradiation induced protein expression of c-Fos, c-Jun, Fra-1 and Fra-2. Phosphorylated forms of these induced proteins were determined at specific time points. A strong correlation existed between UVA-induced AP-1 activity and accumulation of c-Fos, c-Jun and Fra-1 proteins. UVA irradiation also induced c-fos and c-jun mRNA expression and transcriptional activation of the c-fos gene promoter. These results demonstrate that UVA irradiation activates AP-1 and that c-fos induction may

play a critical role in the response of these human keratinocytes to UVA irradiation.

INTRODUCTION

The major risk factor for the development of nonmelanoma skin cancer is exposure to sunlight (1). The UV spectrum of solar radiation is subdivided into three regions: short wavelength ultraviolet C (UVC) (<280 nm), midwavelength ultraviolet B (UVB) (280-320 nm) and long wavelength ultraviolet A (UVA) (320-400 nm). Because stratospheric ozone completely absorbs UVC and a large portion of UVB, 90-99% of the solar radiation at the earth's surface is UVA radiation (2). UVA radiation accounts for approximately 10-20% of the carcinogenic dose of sunlight (3). Although UVB is approximately 1000-10000 times more carcinogenic per J/m² than UVA (4,5), chronic UVA exposure alone has been shown to induce photoaging (6) and skin tumors (papillomas and squamous cell carcinomas) (3,5,7) in experimental animals. Much higher doses of UVA are required to induce gene transcription, but these doses are environmentally attainable (8).

Because UVA radiation is only weakly absorbed by biomolecules such as DNA and proteins, its deleterious effects are manifested through the induction of oxidative damage. UVA-induced gene expression has been shown to involve the generation of singlet O₂ after UVA absorption by cellular chromophores (9,10).

Although a more prominent role of UVA in skin tumorigenesis has recently emerged, the precise signaling pathway(s) that are activated in response to UVA have not been fully elucidated. Solar UVA radiation has been found to non-enzymatically trigger the ceramide signaling cascade through singlet O₂, resulting in activator protein-2 (AP-2) activation and induction of intercellular adhesion molecule-1 expression in cultured normal human keratinocytes (9,11). UVA and singlet O₂ activated c-Jun NH₂-terminal kinase (JNK) and p38 but not extracellular signal-regulated kinase (ERK) mitogen-activated protein kinases (MAPK) in human skin fibroblasts (12,13). However, in human keratinocytes, UVA irradiation induced oxidative stress, ceramide production and activation of JNK, p38 and ERK MAPK (14). In normal human lymphoblast cell lines, Zhang *et al.* (15) found that UVA irradiation induced apoptosis through the

¹Posted on the website on January 8, 2002

*To whom correspondence should be addressed at: Department of Radiation Oncology, Arizona Cancer Center, Room 4999, 1515 N. Campbell Avenue, Tucson, AZ 85724, USA. Fax: 520-626-4979; e-mail: tbowden@azcc.arizona.edu

Abbreviations: AP-1, activator protein-1; AP-2, activator protein-2; DMEM, Dulbecco modified Eagle medium; DTT, dithiothreitol; EGTA, ethylene glycol-bis(β-aminoethyl ether)-N,N,N',N'-tetraacetic acid; ERK, extracellular signal-regulated kinase; GAPDH, glyceraldehyde-3'-phosphate dehydrogenase; GSK-3, glycogen synthase kinase-3; HRP, horseradish-peroxidase; JNK, c-Jun NH₂-terminal kinase; MAPK, mitogen-activated protein kinase; NEB, New England Biolabs Inc.; NF-κB, nuclear factor kappa B; PBS, phosphate-buffered saline; PKA, protein kinase A; PKC, protein kinase C; PPI, protein phosphatase 1; PP2A, protein phosphatase 2A; SC, Santa Cruz Biotechnology; SD, standard deviation; SDS, sodium dodecyl sulfate; SSC, sodium chloride-sodium citrate solution; STAT, signal transducer and activator of transcription; TBP, TATA-binding protein; TBST, Tris-buffered saline with 0.05% Tween 20; TPA, 12-*O*-tetradecanoylphorbol-13-acetate; TRE, TPA response element; UVA, ultraviolet A; UVB, ultraviolet B; UVC, ultraviolet C.

© 2002 American Society for Photobiology 0031-8655/02 \$5.00+0.00

activation of JNK via the sphingomyelinase-ceramide pathway. UVA radiation has also been found to induce the expression or activation of heme-oxygenase 1, protein phosphatase CL100, matrix metalloproteinases, phospholipases such as phospholipase A₂, nuclear factor kappa B (NF- κ B), protein kinase C (PKC), signal transducers and activators of transcription (STAT)-1 and -3, the ribosomal S6 kinases p70^{S6K} and p90^{RSK} and activator protein-1 (AP-1) (16-23).

AP-1 is an important regulatory protein involved in cell growth, differentiation, cellular stress and apoptosis that can be induced by growth factors, cytokines, 12-*O*-tetradecanoylphorbol-13-acetate (TPA) and transforming oncoproteins (24). The AP-1 complex consists of heterodimers of Fos (c-Fos, Fra-1, Fra-2, FosB) and Jun (c-Jun, JunB, JunD) family members or homodimers and heterodimers of Jun family members that bind to the TPA response element (TRE) in the promoters of AP-1-inducible genes, contributing to their transcriptional activation (24).

Deregulated expression of the AP-1 complex has been shown to play a prominent role in the promotion of skin tumors. Loss of AP-1 DNA-binding activity was correlated with loss of proliferation and induction of differentiation in human keratinocytes (25). Similarly, the tumorigenic phenotype of malignant mouse epidermal cells was suppressed by the stable expression of a mutant c-Jun protein that inhibited AP-1-mediated transcriptional transactivation (26). Also, induction of AP-1 was detected in mouse epidermal JB6 cells that were susceptible to tumor promotion by TPA but not in resistant variants (27). Lastly, transduction of mouse keratinocytes with retroviruses encoding *v-ras*^{Hu} and *v-fos* caused the malignant conversion of these cells (28), whereas mice lacking the *c-fos* gene failed to develop malignant skin tumors upon *ras* gene activation and tumor promotion (29).

Increased AP-1 activity in response to UV irradiation has been reported previously. UVC irradiation of the transformed cervix-derived carcinoma cell line, HeLa, initiated the Ras-Raf-MAPK signaling cascade and resulted in AP-1 activation (30). UVB-induced AP-1 transactivation and induction of c-Fos were detected in JB6 murine epidermal cells (31,32). Recently, AP-1 activation was observed in cultured fibroblasts using the natural sunlight spectrum-emitting UVA-340 energy source (33). Experiments using *in vivo* mouse models (SKH-1 hairless mice and AP-1-luciferase transgenic mice) also detected UV-induced AP-1 activation (34,35).

Our laboratory has previously shown that UVB irradiation induces AP-1 activation in the human immortalized keratinocyte cell line HaCaT (36). This cell line contains two mutant p53 alleles but does not induce tumors upon subcutaneous injection into athymic nude mice. The cells form normal epidermis when transplanted to graft sites on these immune-compromised mice. Therefore, these cells are representative of initiated human skin cells and allow examination of the promoting effects of UVA irradiation. In light of the apparent role of AP-1 in skin tumorigenesis and its involvement in UVB-induced signal transduction, we have begun to examine its potential role in UVA-induced signaling pathways leading to skin tumor promotion. The purpose of this study was to determine if UVA irradiation induced AP-1 activation, to characterize the UVA-induced

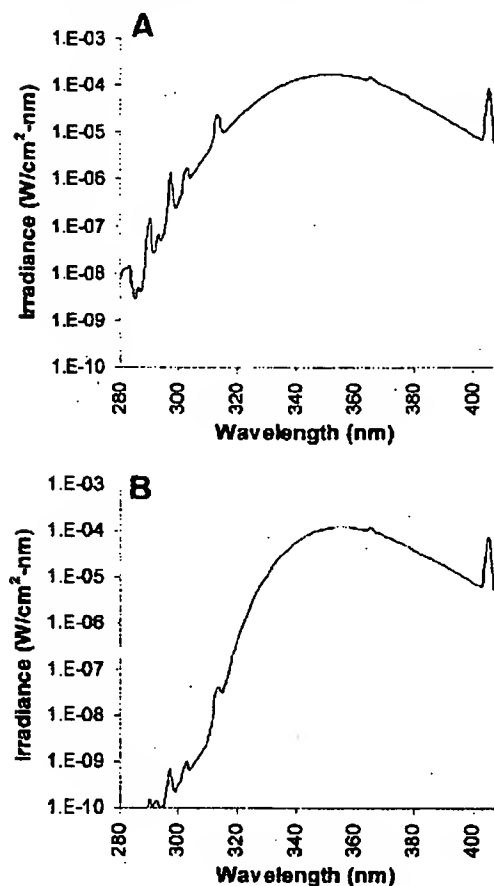


Figure 1. Spectral irradiance of the F20T12/BL/HO UVA bulbs. (a) Irradiance at 5.6 cm from the surface of interest; (b) Irradiance at 5.6 cm from the surface of interest through a 4 mm plate glass to filter wavelengths <320 nm.

AP-1 complex and to determine the expression patterns of the AP-1 family members in these HaCaT cells.

MATERIALS AND METHODS

Cell culture. The human keratinocyte cell line HaCaT was stably transfected with a sequence from the human collagenase-1 gene promoter (-73 to +63), which contained one endogenous AP-1 binding site driving a luciferase reporter gene (HCL14 cells), as reported previously (36). HaCaT cells were also stably transfected with a sequence from the human *c-fos* gene promoter (-404 to +41) driving a luciferase reporter gene (FL30 cells), as reported previously (36). These cells were cultured in Dulbecco modified Eagle medium (DMEM) supplemented with 10% fetal bovine serum, 100 units/mL penicillin-streptomycin at 37°C under 5% CO₂. Cells were grown to 90-100% confluence and then serum-starved for 24-28 h before treatment.

UVA irradiation. Cells were irradiated with a bank of four F20T12/BL/HO fluorescent UVA bulbs (National Biological Corp., Twinsburg, OH) with a peak emission at 365 nm. The bulbs were powered by an Advance electronic ballast REL-4P32-RH-TP (120 V, 60 Hz, 90 A) (Advance Transformer Co., Chicago, IL). Four-millimeter plate glass was used to filter wavelengths below 320 nm (Fig. 1). Irradiation doses were measured using a UVX radiometer equipped with a UVX-36 sensor (UVP, Inc., Upland, CA). Irradiation was performed in a sterile, well-ventilated laminar flow hood to eliminate the possibility of thermal stimulation. Cells were irradiated in phosphate-buffered saline (PBS) supplemented with 0.01% MgCl₂ and 0.01% CaCl₂. Control cells were mock-irradiated under similar conditions. To determine the potential effects of maintaining

304 Amy L. Silvers and G. Timothy Bowden

cells in supplemented PBS for extended periods of time, a second set of control cells, which was kept in serum-free medium at 37°C under 5% CO₂ for the treatment duration, was also used (sf). Cultures were continued in serum-free DMEM until harvest.

Luciferase assay for AP-1 and c-fos transactivation. Total cellular protein was extracted in lysis buffer (15 mM MgSO₄, 25 mM glycylglycine, 4 mM ethylene glycol-bis(β-aminoethyl ether)-N,N,N',N'-tetraacetic acid [EGTA], 1% vol/vol Triton X-100, 1 mM dithiothreitol [DTT]). Luciferase activity of 30 µg total cellular protein was measured using the TD-2020 luminometer (Turner Designs, Sunnydale, CA).

Electrophoretic mobility shift assays. Nuclear protein lysates were isolated using the method of Dignam *et al.* (37). Gel shift assays were performed using 2.5 µg nuclear protein, 1 ng/µL [³²P]-dCTP-labeled double-stranded 22-mer TRE probe containing the AP-1 binding site (TGAGTCA) in the context of the human collagenase-1 promoter and 1 µg/µL poly dIdC to ensure minimal nonspecific binding. After a 10 min preincubation of nuclear protein and poly dIdC at room temperature, the labeled probe was added and incubated for an additional 20 min. DNA complexes were then electrophoresed in 4.8% polyacrylamide gels and exposed to Phosphor screens for analysis (Molecular Dynamics Inc., Sunnyvale, CA). Gel supershift assays entailed a preincubation of 2.5 µg nuclear protein with increasing concentrations of antibodies against AP-1 family members at 4°C for 2 h, addition of poly dIdC and incubation for 10 min at room temperature and, finally, addition of the [³²P]-α-dCTP-labeled TRE probe and incubation at room temperature for an additional 20 min.

Western analysis. Total cellular protein was extracted in NEB buffer (150 mM NaCl, 20 mM Tris pH 7.5, 1 mM ethylenediaminetetraacetic acid, 1 mM EGTA, 2.5 mM Na₂P₂O₇, 1 mM β-glycerol phosphate, 1 mM Na₃VO₄, 1 µg/mL leupeptin and 1% Triton X-100). Forty micrograms of total cell lysate was boiled in 4× sample buffer (0.2 M Tris pH 7, 8% sodium dodecyl sulfate [SDS], 20% β-mercaptoethanol and 12% sucrose), resolved on 12.5% SDS-polyacrylamide gels and transferred to Immobilon-P nylon membranes (Millipore Corp., Bedford, MA). Membranes were blocked with 5% evaporated milk-1× Tris-buffered saline with 0.05% Tween 20 (TBST) for 2 h at room temperature or overnight at 4°C, incubated with primary antibodies against AP-1 family members for 2 h at room temperature and then incubated with horseradish-peroxidase (HRP)-conjugated secondary antibodies for 1 h at room temperature. Membranes were washed three times for 10 min each in 1× TBST between antibody incubations. All primary antibodies were obtained from Santa Cruz Biotechnology (SC), Santa Cruz, CA, except where indicated. All HRP-conjugated secondary antibodies were obtained from New England Biolabs Inc. (NEB), Beverly, MA, except where indicated. Antibody concentrations were as follows: c-Fos sc-8047 at 1:1000 and anti-mouse secondary antibody (SC) at 1:5000; Fra-2 sc-604 at 1:1000 and anti-rabbit secondary antibody (SC) at 1:40000; Fra-1 sc-605 at 1:1000 and anti-rabbit secondary antibody at 1:10000; FosB sc-8013 at 1:200 and anti-mouse secondary antibody (SC) at 1:3500; c-Jun sc-1694 at 1:500 and anti-rabbit secondary antibody at 1:2000; JunB sc-046 at 1:1000 and anti-rabbit secondary antibody at 1:2000; JunD sc-74 at 1:1000 and anti-rabbit secondary antibody at 1:2000; and Phospho-c-Jun (Ser 73) (NEB) at 1:800 and anti-rabbit secondary antibody at 1:2000. Antigen-antibody complexes were detected using the ECL kit (Amersham Pharmacia Biotech, Piscataway, NJ).

Protein phosphatase treatment. Protein phosphatase 1 (PP1) (NEB) treatment entailed the incubation of 40 µg concentrated total cellular protein with 5 units PP1 in 1× MnCl₂ and 1× PP1 buffer for 10 min at 30°C. Protein phosphatase 2A (PP2A) (Upstate Biotechnology, Lake Placid, NY) treatment involved the incubation of 40 µg of concentrated total cellular protein with 0.5 units PP2A in PP2A buffer (50 mM Tris-Cl, pH 7.5, 1 mM MnCl₂, 1 mM DTT) for 20 min at 30°C. Both treatments were followed by electrophoresis in 12.5% SDS-polyacrylamide gels, transfer to Immobilon-P membranes and immunodetection.

Northern analysis. Total RNA was extracted using the RNeasy Mini Kit (Qiagen Inc., Valencia, CA). Twenty micrograms of total RNA was diluted in 10 µL sample buffer (50% formamide, 0.02% formaldehyde, 1× 3-(N-morpholino)propanesulfonic acid, 0.1 mg/mL ethidium bromide), electrophoresed on 1% agarose-formaldehyde

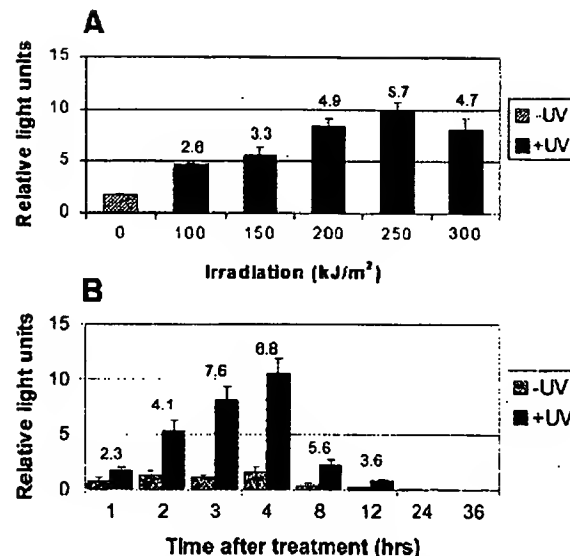


Figure 2. UVA induction of AP-1 transactivation. (a) Dose response of UVA-irradiated HCL14 cells at 4 h after irradiation. Cells were either mock-treated or UVA-irradiated for distinct periods of time corresponding to UVA doses between 100 and 300 kJ/m² and then harvested 4 h after irradiation. (b) Time course of HCL14 cells irradiated with 250 kJ/m² UVA. Cells were either mock-treated or irradiated with 250 kJ/m² UVA and then incubated in serum-free medium until each desired time point. Thirty micrograms of total cell lysate was analyzed for each luciferase activity assay. Fold inductions with respect to mock-treated controls are listed above their respective bars for each data set. Each bar represents the mean \pm standard deviation (SD) of triplicate samples. The data are representative of duplicate experiments.

hyde gels at constant voltage and transferred to GeneScreen nylon membranes (NEN Life Science Products, Boston, MA), using the Pressure Control Station (Stratagene, La Jolla, CA). RNA was then cross-linked to the membrane using the GS Gene Linker (Biorad Laboratories, Hercules, CA). Northern probes were labeled with [³²P]-α-dCTP using the DECAPrime II kit (Amshion Inc., Austin, TX). The c-fos probe was a 2.2 kb EcoRI fragment of mouse c-fos cDNA generated from the plasmid pfos-ks. The c-jun probe was a 0.65 kb EcoRI fragment of human c-jun cDNA generated from the plasmid pcDNA3.1/His. The glyceraldehyde-3'-phosphate dehydrogenase (GAPDH) control probe was a 0.75 kb PstI-XbaI fragment of human GAPDH cDNA generated from the plasmid PTZ-GAP. After hybridization, membranes were washed in 2× sodium chloride-sodium citrate solution (SSC), 0.1% SDS and 0.1× SSC, 0.1% SDS and exposed to Phosphor screens for analysis.

RESULTS

UVA induction of AP-1 transactivation

The immortalized, human keratinocyte cell line HaCaT was stably transfected with an AP-1 luciferase reporter plasmid containing a 136 bp fragment of the human collagenase-1 gene promoter (-73 to +63) with one endogenous AP-1 binding site (HCL14 cells), as reported previously (36). Transactivation through AP-1 was detected with 100 kJ/m² UVA, but maximal AP-1 transactivation was observed with 250 kJ/m² UVA (Fig. 2a). The time course comparing un-irradiated and 250 kJ/m² UVA-irradiated HCL14 cells revealed a transient induction of AP-1 transactivation between 2 and 8 h after irradiation, with maximal induction between the 3 and 4 h time points (Fig. 2b). Although the cultured cells were serum-starved for at least 24 h before treatment

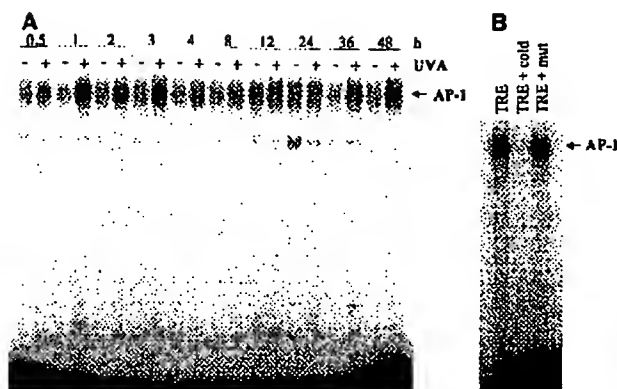


Figure 3. Electrophoretic mobility shifts of the AP-1 DNA-binding complex. Nuclear protein lysates (2.5 μ g) from HCL14 cells were incubated with [32 P] α -dCTP-labeled TRE probes and electrophoresed on 4.8% polyacrylamide gels. (a) AP-1 DNA-binding time course using 250 kJ/m² UVA irradiation. (b) Competition assays using post-1 h UVA-irradiated nuclear protein lysates with 50 \times unlabeled wild-type TRE (cold) and 50 \times mutated TRE (mut) probes. Gel shift assays were performed in duplicate.

to reduce basal levels of AP-1 activity, unirradiated cells still showed detectable levels of AP-1 transactivation at most time points.

UVA Induction of AP-1 DNA binding

Gel shift assays were performed on nuclear proteins that were extracted from unirradiated and 250 kJ/m² UVA-irradiated HCL14 cells using a radiolabeled, double-stranded 22-mer oligonucleotide containing the human collagenase-1 TRE AP-1 DNA-binding site. AP-1 DNA complexes were detected in both irradiated and unirradiated cells. However, enhanced DNA binding to the target TRE sequence was detected as early as 0.5 h after irradiation and was maximal between 1 and 3 h after irradiation (Fig. 3a). Competition assays were performed to verify the specificity of the AP-1 DNA-binding complex, using 50 \times unlabeled wild-type TRE probes to decrease detectable complexes and 50 \times mutated TRE probes that did not compete with labeled probes and recovered complex detection (Fig. 3b).

Characterization of the AP-1 DNA-binding complex

Gel supershift assays, using increasing concentrations of antibodies to AP-1 family member antigens, were performed to determine which AP-1 proteins were bound to the radiolabeled double-stranded TRE oligonucleotide. Before AP-1 DNA annealing, nuclear proteins were incubated with 1–4 μ g antibodies against AP-1 Jun and Fos family members. Gel shift assays were then performed as usual. The 1 h time point in the range of maximal induction of AP-1 DNA binding was used in these experiments. The TATA-binding protein (TBP), which has not been shown to directly bind to the TRE site, was used as a negative control. c-Fos was implicated as a primary component in this AP-1 DNA-binding complex. The c-Fos antibody caused significant reduction of the AP-1 DNA complex shift and produced two slower migrating forms of the complex (Fig. 4). Other AP-1 family members that also produced slower migrating forms included Fra-2, c-Jun, JunB and JunD (Fig. 4). However, the lack

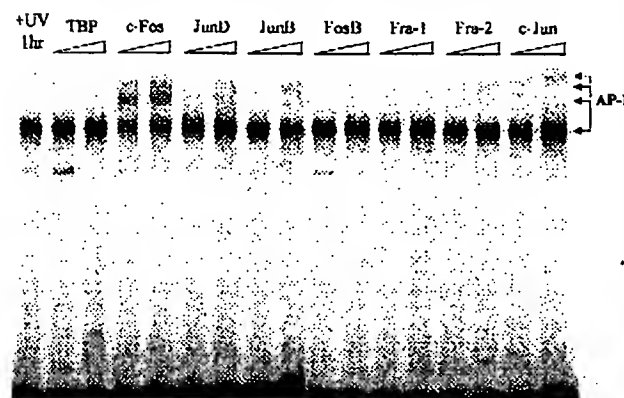


Figure 4. Characterization of the AP-1 DNA-binding complex. Post-1 h UVA-irradiated nuclear protein lysates from HCL14 cells were used to characterize the complex components. TBP, which has not been shown to bind to the TRE binding site, served as a negative control. Concentrations of 1 and 4 μ g primary antibodies are shown to demonstrate AP-1 gel shift band clearing, AP-1 supershift ability or both. Gel shift assays were performed in duplicate.

of AP-1 DNA complex clearing suggests that they are minor components of the AP-1 DNA complexes formed in these UVA-irradiated HaCaT cells.

Contribution of both RNA and protein synthesis to UVA-induced AP-1 DNA binding

To determine whether RNA synthesis or protein synthesis (or both) was required to achieve UVA-induced enhancement of DNA binding detected at 1 h after irradiation, HCL14 cells were treated with the RNA synthesis inhibitor actinomycin D or the protein synthesis inhibitor cycloheximide. UVA induction of AP-1 DNA binding was significantly reduced in both treatment groups, suggesting that transcription and translation of AP-1 complex family members does occur and contributes to the UVA-induced complex formation in HaCaT cells (Fig. 5). However, mRNA and protein stabilization cannot be ruled out and may account for the residual complexes detected using the inhibitor-treated nuclear protein lysates. Increased levels of AP-1 DNA binding complexes were occasionally detected in unirradiated, cycloheximide-treated HCL14 cells (data not shown). Protein synthesis inhibitors have been shown to activate or stabilize the expression of immediate early genes, including Fos and Jun family members (38,39).

Effects of UVA on Fos and Jun family member protein levels

Western blot analyses were performed on AP-1 family members to determine if protein expression levels correlated with UVA-induced AP-1 DNA binding and AP-1 transactivation. Expression of c-Fos, the primary component in the AP-1 DNA binding complex, was dramatically induced with 250 kJ/m² UVA irradiation. Increased expression was initially detected at 0.5 h after irradiation and continued up to 4 h after irradiation (Fig. 6a). Slower migrating forms predominated at 2, 3 and 4 h after irradiation, suggesting a post-translationally modified form of c-Fos at these time points. Increased c-Jun in irradiated cells was detected between 1

306 Amy L. Silvers and G. Timothy Bowden

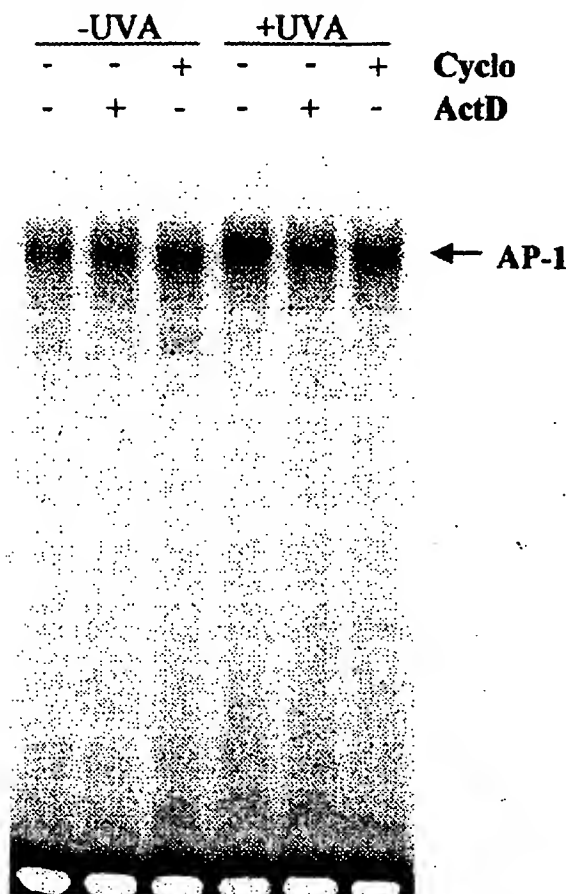


Figure 5. Effects of transcription and translation inhibition on AP-1 DNA-binding. HCL14 cells were pretreated with 1 $\mu\text{g}/\text{mL}$ actinomycin D (ActD) or 10 $\mu\text{g}/\text{mL}$ cycloheximide (Cyclo) in serum-free medium for 30 min, irradiated with 250 kJ/m^2 UVA and then continued in serum-free medium supplemented with the respective inhibitors for 1 h after irradiation. Nuclear protein lysates (2.5 μg) were then incubated with [^{32}P]- α -dCTP-labeled TRE probes and electrophoresed on 4.8% polyacrylamide gels. Gel shift assays were performed in triplicate.

and 8 h after irradiation (Fig. 6a). Basal levels of c-Jun were observed at every time point examined. Interestingly, a slightly slower migrating form of c-Jun was observed at 15 and 30 min after UVA irradiation, also suggesting posttranslational modification of c-Jun. Phosphorylation at serine 63 and serine 73 of c-Jun leads to increased stability and enhanced transcriptional activity of the protein (40). To determine the phosphorylation status of c-Jun at serine 73, Western blot analysis was performed using a phospho-specific antibody. Although phosphorylated forms could not be detected in unirradiated HCL14 cells, c-Jun appeared to be phosphorylated at amino acid 73 in irradiated cells up to 4 h after irradiation, and its detection revealed banding patterns similar to those seen for total c-Jun expression (Fig. 6b). Induction of an approximately 35 kDa Fra-1 protein was observed at 2 to 4 h after irradiation. However, an approximately 40 kDa uninduced protein product was also apparent at every time point examined (Fig. 6a). Immunodetection of Fra-2 revealed induction of a slower migrating form at 15 and 30 min after irradiation and induction of a faster mi-

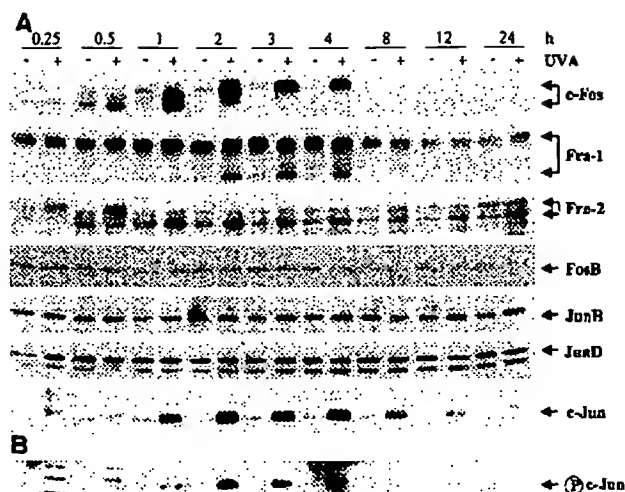


Figure 6. Western blot time course of AP-1 family member expression using 250 kJ/m^2 UVA irradiation. Forty micrograms of total cellular protein was electrophoresed on 12.5% SDS-polyacrylamide gels, transferred to Immobilon-P membranes and immunodetected using optimal primary and secondary antibody concentrations for (a) each AP-1 family member, and (b) the phosphorylated form of c-Jun at amino acid 73. Western blot data are representative of two independent experiments.

grating form from 2 to 24 h after irradiation (Fig. 6a). These results suggest the initial induction of a posttranslationally modified form of Fra-2, followed by the induction of a less modified form. The remaining AP-1 family members (FosB, JunB, JunD) did not show significant changes in protein expression after UVA irradiation (Fig. 6a).

Protein phosphatase treatment of UVA irradiation-induced AP-1 complex components

In an attempt to determine if the slower migrating species of the UVA-induced proteins were phosphorylated forms, total cell lysates from selected postirradiation time points were treated with PP1 or PP2A, enzymes that can recognize and cleave phosphates at serine and threonine residues. PP1 treatment shifted the uninduced 40 kDa Fra-1 band to a faster migrating form in both UVA-irradiated and unirradiated HCL14 cells but had little effect on the UVA-induced faster migrating 35 kDa species (Fig. 7a). PP1 treatment also shifted the slower migrating band of Fra-2 to a faster migrating form in both treated and untreated cells (Fig. 7a). Because PP1 treatment did not significantly change the UVA-induced banding patterns of c-Fos and c-Jun, total protein lysates were incubated with PP2A and immunodetected with c-Fos and c-Jun antibodies. The slower migrating forms of c-Jun at 15 and 30 min in the UVA-irradiated samples were shifted to faster migrating forms, but the UVA-induced protein bands were not affected (Fig. 7b). c-Fos banding patterns were dramatically changed upon PP2A treatment. Slower migrating forms that were detected in both irradiated and unirradiated lysates were significantly shifted to faster migrating forms, with the predominant band migrating at approximately 40 kDa (Fig. 7b).

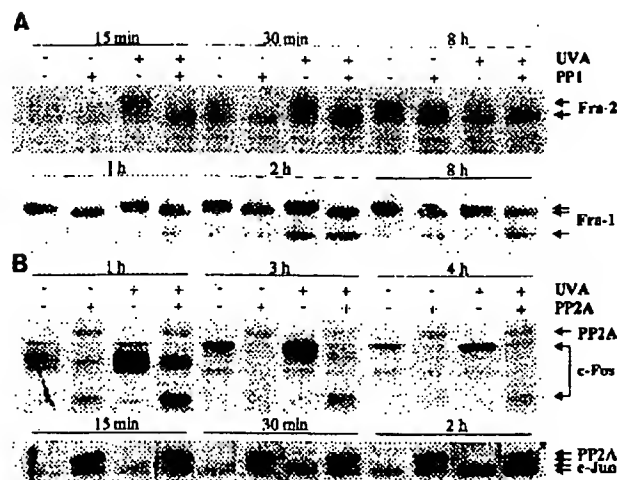


Figure 7. Protein phosphatase treatment of UVA irradiation-induced AP-1 family members. Concentrated total cellular protein was isolated from mock-treated or 250 kJ/m² UVA-irradiated HCL14 cells. (a) Forty micrograms protein from selected time points was treated with 5 units PPI for 10 min at 30°C, electrophoresed on 12.5% SDS-polyacrylamide gels, transferred to Immobilon-P membranes and immunodetected with antibodies against Fra-1 and Fra-2 antigens. (b) Forty micrograms protein from selected time points was treated with 0.5 units PP2A for 20 min at 30°C, electrophoresed on 12.5% SDS-polyacrylamide gels, transferred to Immobilon-P membranes and immunodetected with antibodies against c-Fos and c-Jun antigens. Western blot data are representative of two independent experiments.

UVA induction of *c-fos* and *c-jun* mRNA levels and *c-fos* transcriptional activation

c-Fos can be regulated at the level of transcription, RNA stability, protein degradation and posttranslational modification (41). Because *c-Fos* was implicated as a primary component of the AP-1 DNA binding complex and its protein expression was induced in response to UVA irradiation, *c-fos* mRNA levels and the transcriptional activation of the *c-fos* gene were additionally examined to further delineate the mechanism of its activation. Transcripts of *c-fos* were detectable immediately after irradiation and continued to be detected up to 1.5 h after irradiation (Fig. 8). Although transcripts were also detected in unirradiated samples up to 45 min after irradiation, differential expression between irradiated and unirradiated samples was observed between 15 and 90 min after irradiation. Initially elevated *c-fos* transcripts in both irradiated and unirradiated HaCaT cells may be a stress response to the long irradiation period in supplemented PBS that was necessary to achieve 250 kJ/m² UVA irradiation.

c-Jun mRNA levels were also examined in an attempt to correlate *c-jun* transcription with translation of the *c-Jun* protein. *c-Jun* transcripts were observed at every time point in both irradiated and unirradiated HCL14 cells. Induction of *c-jun* transcripts with 250 kJ/m² UVA was detected between 15 min and 4 h after irradiation, with maximal induction at approximately 90 min after irradiation (Fig. 8). UVA-induced increases in *c-jun* mRNA levels were slightly delayed and, although transient, sustained for a longer period of time than UVA-induced *c-fos* mRNA levels.

The HaCaT cell line was also stably transfected with a *c-fos* luciferase reporter plasmid containing a 445 bp fragment

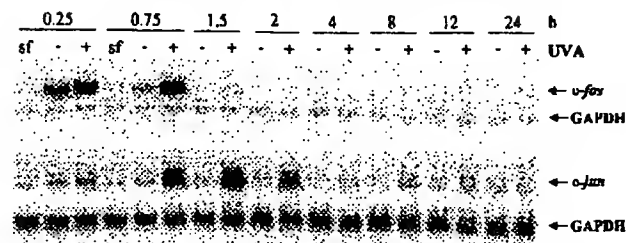


Figure 8. Northern blot time course of *c-fos* and *c-jun* expression using 250 kJ/m² UVA. Twenty micrograms total RNA from mock-treated and UVA-irradiated HCL14 cells was electrophoresed in 1% agarose-formaldehyde gels, transferred to nylon membranes under 75 lb pressure and hybridized with 25 ng [³²P]α-dCTP-labeled *c-fos* and *c-jun* cDNA probes. [³²P]α-dCTP-labeled GAPDH cDNA served as a loading control. mRNA levels of control cells held in serum-free medium at 37°C and under 5% CO₂ (sf) are shown at 15 and 45 min time points to demonstrate expression changes that may be related to extensive irradiation periods. Northern blot data are representative of two independent experiments.

of the human *c-fos* gene promoter, as reported previously (36). This FL30 cell line was irradiated with 250 kJ/m² UVA, and total protein lysates were examined for luciferase activity. Significant UVA induction of *c-fos* transactivation was detected between 2 and 8 h after irradiation, with maximal *c-fos* transactivation between 3 and 4 h after irradiation (Fig. 9). These results suggest that transcriptional activation of the *c-fos* gene contributes to the detectable increase in UVA-induced *c-fos* mRNA expression.

DISCUSSION

UVA radiation is the most abundant and most penetrating component of solar radiation that reaches the earth's surface (2). Chronic exposure to UVA plays an important role in dermal and epidermal photodamage and is a contributing factor in the development of skin cancer (3,5-7). UV radiation exposure leads to increased gene expression in mammalian cells (11,32). The mechanisms by which UVA irradiation leads to increased transcriptional expression and activation of human genes are currently under investigation. Deregulated expression of the AP-1 complex has been shown to play a prominent role in the promotion of skin tumors and may be required to maintain the tumorigenic phenotype (25-29).

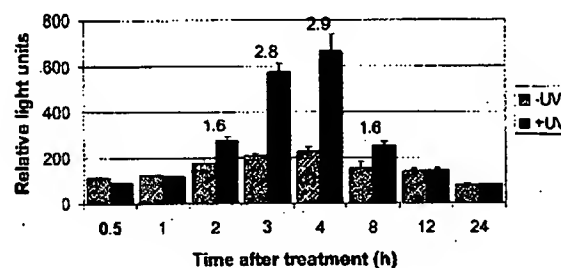


Figure 9. UVA induction of *c-fos* transactivation. Time course experiments analyzing the luciferase activity of 30 μg total cell lysate from mock-treated and 250 kJ/m² UVA-irradiated FL30 cells were performed. Fold inductions with respect to mock-treated controls are listed above the set of bars for each time point. Each bar represents the mean ± SD of triplicate samples. The data are representative of duplicate experiments.

308 Amy L. Silvers and G. Timothy Bowden

In this study, 250 kJ/m² UVA irradiation enhanced AP-1 DNA binding to a TRE oligonucleotide and caused increased AP-1 transactivation in a dose-dependent manner in the immortalized, human keratinocyte cell line HaCaT. As expected, maximal AP-1 DNA binding slightly preceded, in time, the AP-1 transactivation detected upon UVA irradiation. Transcription and translation of AP-1 complex components contributed to the UVA-induced enhanced AP-1 DNA binding. However, mRNA or protein stabilization (or both) cannot be excluded and may account for the residual AP-1 DNA complexes that were detected in inhibitor-treated nuclear protein extracts. This is in contrast to the report of Djavaheri-Mergny *et al.* (19), who found that UVA activation of AP-1 DNA binding was maintained after treatment with cycloheximide before, during and after irradiation. The rapid induction of the AP-1 DNA binding complex within the first hour and the lack of effective cycloheximide inhibition suggested a posttranslational effect of UVA on AP-1 activity in NCTC 2544 cells (19).

The occasional increase in DNA binding, which we observed in the cycloheximide-treated, unirradiated cells (data not shown), may have been caused by a cycloheximide-induced ribotoxic stress response that led to heightened activation of preexisting AP-1 complex proteins. Because cycloheximide was not added to the cells during mock or UVA irradiation treatment, translation of mRNA transcripts may have occurred at that time. Because UV radiation has also been found to inhibit protein synthesis (42), we did not observe this phenomenon in UVA- and cycloheximide-treated cells.

c-Fos was implicated as a primary component in the AP-1 DNA binding complex, and its expression was induced at both the transcriptional and translational levels upon UVA stimulation. Other minor complex components included c-Jun, JunB, JunD and Fra-2. Djavaheri-Mergny *et al.* (19) reported the presence of c-Jun and c-Fos in the AP-1 DNA complexes induced with 190 kJ/m² UVA irradiation in NCTC 2544 human keratinocytes. However, other Fos and Jun family member antibodies were not tested for their ability to supershift the AP-1 DNA-binding complex.

UVA induction of AP-1 complex proteins, AP-1 DNA binding and AP-1 transactivation occurred more rapidly than induction by UVB in HaCaT cells. Whereas UVA-induced AP-1 transactivation and protein level changes in c-Fos, c-Jun and Fra-1 occurred between 2 and 4 h after irradiation, UVB induction of AP-1 activation occurred maximally between 12 and 24 h after irradiation (36). Time kinetic differences for UVA- and UVB-induced apoptosis (43), cell cycle arrest (44) and DNA damage repair (45) have also been reported. Therefore, the signaling pathways that are activated in response to UVA and UVB insult leading to AP-1 transactivation may differ as well.

c-Fos, c-Jun and Fra-1 protein accumulation paralleled the induction of AP-1 transactivation by UVA irradiation. Additionally, the unaltered expression of JunB, JunD and FosB implicated these proteins as possible contributors to the detectable basal levels of AP-1 activity. The actual protein complexes formed in these irradiated and unirradiated human keratinocytes have not been fully elucidated. Although Fra-2 protein expression was detected in both irradiated and unirradiated cells, the slight induction of the faster migrating

form at later time points suggests a possible role for this protein in UVA-induced AP-1 activity as well.

Induction of c-fos mRNA levels and transcriptional activation of the c-fos gene promoter by UVA suggest that *de novo* transcription of c-fos occurs in these keratinocytes. Interestingly, c-jun mRNA levels were also induced upon UVA irradiation but peaked at a later time point, appeared to be less sensitive to the stress of treatment conditions and remained upregulated for an extended period of time when compared with UVA-induced c-fos expression. The sustained induction of c-jun RNA levels may be a consequence of c-Jun's ability to positively autoregulate its own transcription through an AP-1 binding site in its promoter region (46,47). This autoactivation of c-jun mRNA may first require the posttranslational modification of existing c-Jun proteins that we observed at 15 and 30 min after UVA irradiation (47).

Immediate early gene products are frequently posttranslationally modified to induce their transcriptional activator potential in response to extracellular stimuli (30). The apparent Fra-1 and Fra-2 protein shifts detected after PP1 treatment are testament to the posttranslational phosphorylation of these proteins. In fact, Gruda *et al.* (48) reported that Fra-1 and Fra-2 proteins were highly phosphorylated in serum-stimulated, asynchronously growing 3T3 cells and that their phosphorylation caused dramatic shifts in the electrophoretic mobility of the proteins. The inability of PP1 treatment to produce significant shifts for c-Fos and c-Jun suggested that these proteins may not be suitable substrates for PP1 activity. PP1 is a serine-threonine phosphatase that may not be able to recognize the phosphorylation sites of these proteins. Recognition and cleavage of only a few key sites may not change the mobility of the proteins dramatically enough to be detected by Western blot analyses.

c-Fos can be phosphorylated by protein kinase A (PKA), PKC, MAPK, p34^{cdc2}, DNA protein kinase, glycogen synthase kinase-3 (GSK-3) and rsk at multiple sites in the regulatory regions of the protein (49,50). We detected a distinct reduction in c-Fos mobility upon induction of the protein by UVA irradiation. Distinct conformational alterations and charge effects that change the electrophoretic mobility of c-Fos have been reported previously in *in vitro* phosphorylation assays with p34^{cdc2}, PKA and PKC (50). Because c-Fos is known to be extensively phosphorylated on serine and threonine residues in the nucleus (50), we attempted phosphate cleavage with another serine-threonine phosphatase, PP2A, which appears to be the major kinase phosphatase responsible for the downregulation of activated protein kinases (51). Although protein bands for the PP2A enzyme itself were also detected with the c-Fos antibody, dramatic shifts in c-Fos protein migration were detected with this phosphatase. The predominant shifted band migrated at approximately 40 kDa and was more pronounced in the UVA-irradiated lysates. Barber and Verma (52) demonstrated that most, if not all, c-Fos phosphate groups were in the form of phosphoesters. Hydrolysis of these phosphoesters caused a dramatic increase in the electrophoretic mobility of c-Fos, with extreme shifts resulting in a 15 kDa molecular mass difference.

c-Jun is preferentially dephosphorylated by purified preparations of PP2A in okadaic acid-treated cells, and its activ-

ity can be regulated by this phosphatase. The site of PP2A-catalyzed dephosphorylation of c-Jun has been mapped to the amino acid serine at position 63 (53,54). PP2A treatment shifted the slower migrating form of c-Jun in the UVA-irradiated cells at 15 and 30 min after irradiation to a faster migrating form. The phospho-form of c-Jun serine 73 was detected between 2 and 4 h after irradiation, but there was a concomitant lack of PP1- or PP2A-induced band shifting at these time points. Serine 73 may not be a target for PP1 or PP2A dephosphorylation. Additionally, c-Jun contains repressive serine-threonine phosphorylation sites near the basic region that holds c-Jun in an inactive state (24,55). GSK-3 has been shown to phosphorylate these sites and modulate the DNA-binding activity of c-Jun (41). Therefore, c-Jun requires a delicate balance of phosphorylation-dephosphorylation events to achieve maximal transactivation potential.

Although most studies of UV-induced signal transduction pathways leading to altered gene expression have focused on UVB and UVC radiations, UVA effects on signal transduction and activation of stress response genes are current topics of great interest. The oxidative stress induced by UVA irradiation is primarily mediated through reactive oxygen intermediates and has been found to induce the expression or activation of several key signal transduction genes, such as JNK, p38 and c-Fos in human skin fibroblasts (12,13,56). Intracellular glutathione depletion reduced the intracellular redox equivalents and significantly increased the expression of c-Fos and c-Jun in UVA-irradiated human skin fibroblasts (57). UVA-induced NF- κ B activation in human skin fibroblasts was correlated with membrane damage (20). In human keratinocytes, UVA radiation activated STAT1 (18), AP-1 (19), AP-2 (11), PKC (17) and the MAPK (ERK, JNK and p38) (14) but decreased NF- κ B DNA-binding activity (58). In mouse epidermal cells, phosphorylation and activation of STAT3, p70^{STAT3} and p90^{STAT3} after UVA exposure have also been reported (21-23).

This study further characterized the role of AP-1 activation in UVA-irradiated human keratinocytes and implicated key components that are activated in response to this oxidative stress. Taken together, these results demonstrated that UVA irradiation induces AP-1 DNA binding and AP-1 activation in the human keratinocyte cell line HaCaT. Accumulation of c-fos mRNA and protein may play a critical role in the response of these cells to UVA irradiation. c-Fos has poor affinity to DNA and cannot transactivate without a jun family member (24,41). Therefore, the combined effects of other AP-1 family members whose expression is induced (c-Jun, Fra-1, Fra-2) or that bind to the AP-1 site in response to UVA irradiation (c-Jun, JunB, JunD, Fra-2) are also important to ultimately achieve AP-1 induction in these keratinocytes.

Acknowledgements—We thank Barbara G. Grant of UVR Research Institute for measuring the spectral irradiance of our UVA irradiation system. This work was supported, in part, by the National Cancer Institute-funded grant R25CA78447 through the Cancer Prevention and Control Program at the Arizona Cancer Center, Tucson, AZ. This work was also supported by the National Institutes of Health grants CA27502 and CA23074.

REFERENCES

1. Urbach, P. (1997) Ultraviolet radiation and skin cancer of humans. *J. Photochem. Photobiol. B: Biol.* **40**, 3-7.

2. Madronich, S. (1993) The atmosphere and UV-B radiation at ground level. In *Environmental UV Photobiology* (Edited by A. R. Young, L. O. Björn, J. Moan and W. Nultsch), pp. 1-39. Plenum Press, New York.
3. de Laat, A., J. C. van der Leun and F. R. de Gruijl (1997) Carcinogenesis induced by UVA (365-nm) radiation: the dose-time dependence of tumor formation in hairless mice. *Carcinogenesis* **18**, 1013-1020.
4. Berg, R. J., F. R. de Gruijl and J. C. van der Leun (1993) Interaction between ultraviolet A and ultraviolet B radiations in skin cancer induction in hairless mice. *Cancer Res.* **53**, 4212-4217.
5. Sierenberg, H. J. and J. C. van der Leun (1990) Tumorigenesis by a long wavelength UV-A source. *Photochem. Photobiol.* **51**, 325-330.
6. Kligman, L. H. (1991) The hairless mouse and photoaging. *Photochem. Photobiol.* **54**, 1109-1118.
7. Keltjens, G., F. R. de Gruijl and J. C. van der Leun (1991) Tumorigenesis by short-wave ultraviolet A: papillomas versus squamous cell carcinomas. *Carcinogenesis* **12**, 1377-1382.
8. Bender, K., C. Blattner, A. Knebel, M. Iordanov, P. Herrlich and H. J. Rahmsdorf (1997) UV-induced signal transduction. *J. Photochem. Photobiol. B: Biol.* **37**, 1-17.
9. Grether-Beck, S., G. Bonizzi, H. Schmitt-Brenden, I. Felsner, A. Timmer, H. Sies, J. P. Johnson, J. Pielte and J. Krutmann (2000) Non-enzymatic triggering of the ceramide signalling cascade by solar UVA radiation. *EMBO J.* **19**, 5793-5800.
10. Tyrrell, R. M. (1991) UVA (320-380 nm) as an oxidative stress. In *Oxidative Stress: Oxidants and Antioxidants* (Edited by H. Sies), pp. 57-83. Academic Press, London.
11. Grether-Beck, S., S. Olazola-Horn, H. Schmitt, M. Grewe, A. Jahnke, J. P. Johnson, K. Briviba, H. Sies and J. Krutmann (1996) Activation of transcription factor AP-2 mediates UVA radiation- and singlet oxygen-induced expression of the human intercellular adhesion molecule 1 gene. *Proc. Natl. Acad. Sci. USA* **93**, 14586-14591.
12. Klotz, L. O., K. Briviba and H. Sies (1997) Singlet oxygen mediates the activation of JNK by UVA radiation in human skin fibroblasts. *FEBS Lett.* **408**, 289-291.
13. Klotz, L. O., C. Pellieux, K. Briviba, C. Pierlot, J. M. Aubry and H. Sies (1999) Mitogen-activated protein kinase (p38-, JNK-, ERK-) activation pattern induced by extracellular and intracellular singlet oxygen and UVA. *Eur. J. Biochem.* **260**, 917-922.
14. Maziere, C., M. A. Conte, L. Lchorgne, T. Levade, W. Hornebeck, R. Santus and J. C. Maziere (2001) UVA radiation stimulates ceramide production: relationship to oxidative stress and potential role in ERK, JNK, and p38 activation. *Biochem. Biophys. Res. Commun.* **281**, 289-294.
15. Zhang, Y., P. Maltjes, P. C. Schmid, Z. Dong, S. Zhong, W. Y. Ma, R. E. Brown, A. M. Bode and H. H. Schmid (2001) Involvement of the acid sphingomyelinase pathway in UVA-induced apoptosis. *J. Biol. Chem.* **276**, 11775-11782.
16. Tyrrell, R. M. (1996) UV activation of mammalian stress proteins. In *Stress-inducible Cellular Responses* (Edited by U. Feige, R. I. Morimoto, I. Yahara and B. S. Polla), pp. 255-271. Birkhauser Verlag, Boston.
17. Matsui, M. S., N. Wang, D. MacFarlane and V. A. DeLeo (1994) Long-wave ultraviolet radiation induces protein kinase C in normal human keratinocytes. *Photochem. Photobiol.* **59**, 53-57.
18. Maziere, C., F. Dantini, F. Daboies, R. Santus and J. Maziere (2000) Biphasic effect of UVA radiation on STAT1 activity and tyrosine phosphorylation in cultured human keratinocytes. *Free Radic. Biol. Med.* **28**, 1430-1437.
19. Djavaheri-Mergny, M., J. L. Mergny, P. Bertrand, R. Santus, C. Maziere, I. Dubertret and J. C. Maziere (1996) Ultraviolet-A induces activation of AP-1 in cultured human keratinocytes. *FEBS Lett.* **384**, 92-96.
20. Vile, G. F., A. Tanew-Ilitschew and R. M. Tyrrell (1995) Activation of NF-kappa B in human skin fibroblasts by the oxidative stress generated by UVA radiation. *Photochem. Photobiol.* **62**, 463-468.
21. Zhang, Y., S. Zhong, Z. Dong, N. Chen, A. M. Bode and W.

310 Amy L. Silvers and G. Timothy Bowden

- Ma (2001) UVA induces Scr381 phosphorylation of p90RSK/MAPKAP-K1 via ERK and JNK pathways. *J. Biol. Chem.* **276**, 14572-14580.
22. Zhang, Y., Z. Dong, M. Nomura, S. Zhong, N. Chen and A. M. Bode (2001) Signal transduction pathways involved in phosphorylation and activation of p70S6K following exposure to UVA irradiation. *J. Biol. Chem.* **276**, 20913-20923.
 23. Zhang, Y., G. Liu and Z. Dong (2001) MSK1 and JNKs mediate phosphorylation of STAT3 in UVA-irradiated mouse epidermal JB6 cells. *J. Biol. Chem.* **276**, 42534-42542.
 24. Angel, P. and M. Karin (1991) The role of Jun, Fos and the AP-1 complex in cell-proliferation and transformation. *Biochim. Biophys. Acta* **1072**, 129-157.
 25. Briata, P., F. D'Anna, A. T. Franzì and R. Gherzi (1993) AP-1 activity during normal human keratinocyte differentiation: evidence for a cytosolic modulator of AP-1/DNA binding. *Exp. Cell Res.* **204**, 136-146.
 26. Domann, F. E., J. P. Levy, M. J. Birrer and G. T. Bowden (1994) Stable expression of a c-JUN deletion mutant in two malignant mouse epidermal cell lines blocks tumor formation in nude mice. *Cell Growth Differ.* **5**, 9-16.
 27. Bernstein, L. R. and N. H. Colburn (1989) AP1/jun function is differentially induced in promotion-sensitive and resistant JB6 cells. *Science* **244**, 566-569.
 28. Greenhalgh, D. A., D. J. Welty, A. Player and S. H. Yuspa (1990) Two oncogenes, v-fos and v-ras, cooperate to convert normal keratinocytes to squamous cell carcinoma. *Proc. Natl. Acad. Sci. USA* **87**, 643-647.
 29. Suez, E., S. F. Rutberg, E. Mueller, H. Oppenheim, J. Smoluk, S. H. Yuspa and B. M. Spiegelman (1995) c-fos is required for malignant progression of skin tumors. *Cell* **82**, 721-732.
 30. Sachsenmaier, C., A. Radler-Pohl, R. Zinck, A. Nordheim, P. Herrlich and H. J. Rahmsdorf (1994) Involvement of growth factor receptors in the mammalian UVC response. *Cell* **78**, 963-972.
 31. Huang, C., W. Ma, G. T. Bowden and Z. Dong (1996) Ultraviolet B-induced activator protein-1 activation does not require epidermal growth factor receptor but is blocked by a dominant negative PKC λ hda1/ota. *J. Biol. Chem.* **271**, 31262-31268.
 32. Shah, G., R. Ghosh, P. A. Amstad and P. A. Cerutti (1993) Mechanism of induction of c-fos by ultraviolet B (290-320 nm) in mouse JB6 epidermal cells. *Cancer Res.* **53**, 38-45.
 33. Nakano, H., F. P. Gasparro and J. Uitto (2001) UVA-340 as energy source, mimicking natural sunlight, activates the transcription factor AP-1 in cultured fibroblasts: evidence for involvement of protein kinase-C. *Photochem. Photobiol.* **74**, 274-282.
 34. Hong, J. T., E. J. Kim, K. S. Ahn, K. M. Jung, Y. P. Yun, Y. K. Park and S. H. Lee (2001) Inhibitory effect of glycolic acid on ultraviolet-induced skin tumorigenesis in SKH-1 hairless mice and its mechanism of action. *Mol. Carcinog.* **31**, 152-160.
 35. Huang, C., W. Y. Ma, D. Hanenberger, M. P. Cleary, G. T. Bowden and Z. Dong (1997) Inhibition of ultraviolet B-induced activator protein-1 (AP-1) activity by aspirin in AP-1-luciferase transgenic mice. *J. Biol. Chem.* **272**, 26325-26331.
 36. Chen, W., A. H. Borchers, Z. Dong, M. B. Powell and G. T. Bowden (1998) UVB irradiation-induced activator protein-1 activation correlates with increased c-fos gene expression in a human keratinocyte cell line. *J. Biol. Chem.* **273**, 32176-32181.
 37. Dignam, J. D., R. M. Lebovitz and R. G. Roeder (1983) Accurate transcription initiation by RNA polymerase II in a soluble extract from isolated mammalian nuclei. *Nucleic Acids Res.* **11**, 1475-1489.
 38. Rittling, S. R., C. W. Gibson, S. Ferrari and R. Baserga (1985) The effect of cycloheximide on the expression of cell cycle dependent genes. *Biochem. Biophys. Res. Commun.* **132**, 327-335.
 39. Cochran, B. H., J. Zullo, I. M. Verma and C. D. Stiles (1984) Expression of the c-fos gene and of an fos-related gene is stimulated by platelet-derived growth factor. *Science* **226**, 1080-1082.
 40. Karin, M., Z. Liu and E. Zandi (1997) AP-1 function and regulation. *Curr. Opin. Cell Biol.* **9**, 240-246.
 41. Woodgett, J. R. (1990) Fos and jun: two into one will go. *Semin. Cancer Biol.* **1**, 389-397.
 42. Jordanov, M. S., D. Pribnow, J. L. Magun, T. H. Dinh, J. A. Pearson and B. E. Magun (1998) Ultraviolet radiation triggers the ribotoxic stress response in mammalian cells. *J. Biol. Chem.* **273**, 15794-15803.
 43. Godar, D. E. and A. D. Lucas (1995) Spectral dependence of UV-induced immediate and delayed apoptosis: the role of membrane and DNA damage. *Photochem. Photobiol.* **62**, 108-113.
 44. de Laat, A., M. van Tilburg, J. C. van der Leun, W. A. van Vloten and F. R. de Gruij (1996) Cell cycle kinetics following UVA irradiation in comparison to UVB and UVC irradiation. *Photochem. Photobiol.* **63**, 492-497.
 45. Lehmann, J., D. Pollet, S. Peker, V. Steinkraus and U. Hoppe (1998) Kinetics of DNA strand breaks and protection by antioxidants in UVA- or UVB-irradiated HaCaT keratinocytes using the single cell gel electrophoresis assay. *Mutat. Res.* **407**, 97-108.
 46. Angel, P., K. Hattori, T. Smeal and M. Karin (1988) The jun proto-oncogene is positively autoregulated by its product, Jun/AP-1. *Cell* **55**, 875-885.
 47. Trejo, J., J. C. Chambard, M. Karin and J. H. Brown (1992) Biphasic increase in c-jun mRNA is required for induction of AP-1-mediated gene transcription: differential effects of muscarinic and thrombin receptor activation. *Mol. Cell Biol.* **12**, 4742-4750.
 48. Cruda, M. C., K. Kovary, R. Metz and R. Bravo (1994) Regulation of Fra-1 and Fra-2 phosphorylation differs during the cell cycle of fibroblasts and phosphorylation in vitro by MAP kinase affects DNA binding activity. *Oncogene* **9**, 2537-2547.
 49. Curran, T., C. Abate, S. Baker, T. Kerppola and S. Xanthopoulos (1993) The regulation of c-fos: too much is never enough. *Adv. Second Messenger Phosphoprotein Res.* **28**, 271-277.
 50. Abate, C., D. R. Marshak and T. Curran (1991) Fos is phosphorylated by p34cdc2, cAMP-dependent protein kinase and protein kinase C at multiple sites clustered within regulatory regions. *Oncogene* **6**, 2179-2185.
 51. Millward, T. A., S. Zolnierowicz and B. A. Hemmings (1999) Regulation of protein kinase cascades by protein phosphatase 2A. *Trends Biochem. Sci.* **24**, 186-191.
 52. Barber, J. R. and I. M. Verma (1987) Modification of fos proteins: phosphorylation of c-fos, but not v-fos, is stimulated by 12-tetradecanoyl-phorbol-13-acetate and serum. *Mol. Cell Biol.* **7**, 2201-2211.
 53. Zolnierowicz, S. (2000) Type 2A protein phosphatase, the complex regulator of numerous signaling pathways. *Biochem. Pharmacol.* **60**, 1225-1235.
 54. Al-Murrani, S. W., J. R. Woodgett and Z. Damuni (1999) Expression of 12PP2A, an inhibitor of protein phosphatase 2A, induces c-Jun and AP-1 activity. *Biochem. J.* **341**, 293-298.
 55. Boyle, W. J., T. Smeal, L. H. Defize, P. Angel, J. R. Woodgett, M. Karin and T. Hunter (1991) Activation of protein kinase C decreases phosphorylation of c-Jun at sites that negatively regulate its DNA-binding activity. *Cell* **64**, 573-584.
 56. Bose, B., M. Soriani and R. M. Tyrrell (1999) Activation of expression of the c-fos oncogene by UVA irradiation in cultured human skin fibroblasts. *Photochem. Photobiol.* **69**, 489-493.
 57. Soriani, M., V. Hejnadi and R. M. Tyrrell (2000) Modulation of c-jun and c-fos transcription by UVB and UVA radiations in human dermal fibroblasts and KB cells. *Photochem. Photobiol.* **71**, 551-558.
 58. Djavaheri-Mergny, M., M. P. Gras, J. L. Mergny and L. Dubertret (1999) UV-A-induced decrease in nuclear factor-kappaB activity in human keratinocytes. *Biochem. J.* **338**, 607-613.

FGH52352

CI-06862319-8

FGH52352

CISTI ICIST

CI-06862319-8

Document Delivery Service
in partnership with the Canadian Agriculture LibraryService de fourniture de Documents
en collaboration avec la Bibliothèque canadienne de l'agriculture**THIS IS NOT AN INVOICE / CECI N'EST PAS UNE FACTURE**LYNN BRAZIL
LIBRARIANHELLER EHRMAN WHITE & MCAULIFFE
275 MIDDLEFIELD RD
MENLO PARK, CA 94025
UNITED STATES

ORDER NUMBER:	CI-06862319-8
Account Number:	FGH52352
Delivery Mode:	F31
Delivery Address:	650/324-6034
Submitted:	2007/05/14 17:18:09
Received:	2007/05/14 17:18:09
Printed:	2007/05/15 00:13:21

Direct	Periodical	OPENURLOPAC	UNITED STATES
--------	------------	-------------	---------------

Client Number: 39780-7000 CD

Title: EUROPEAN JOURNAL OF CANCER = JOURNAL EUROPEEN DE CANCEROLOGIE =
EUROPAISCHE ZEITSCHRIFT FUR CANCEROLOGIE.

DB Ref. No.: IRN10096425

ISSN: ISSN00142964

Vol./Issue: 39/5

Date: 2003

Pages: 691-7

Article Title: A EXPRESSION OF DEOXYCYTIDINE KINASE IN LEUKAEMIC CELLS COMPARED WITH SOLID
TUMOUR CELL LINES, LIVER METASTASES AND NORMAL LIVER."

Article Author: VAN DER WILT, C.L., ET AL

Report Number: IRN10096425

Publisher: PERGAMON PRESS,

Estimated cost for this 7 page document: \$12.5 document supply fee +
\$32 copyright = \$44.5

The attached document has been copied under license from Access Copyright/COPIBEC or other
rights holders through direct agreements. Further reproduction, electronic storage or electronic transmission,
even for internal purposes, is prohibited unless you are independently licensed to do so by the rights holder.

Phone/Téléphone: 1-800-668-1222 (Canada - U.S./E.-U.) (613) 998-8544 (International)

www.nrc.ca/cisti

Fax/Télécopieur: (613) 993-7619

www.cnrc.ca/icist

info.cisti@nrc.ca

info.icist@nrc.ca

National Research
Council CanadaConseil national
de recherches Canada

Page

1 / 1



PERGAMON

European Journal of Cancer 39 (2003) 691-697

**European
Journal of
Cancer**

www.ejconline.com

Expression of deoxycytidine kinase in leukaemic cells compared with solid tumour cell lines, liver metastases and normal liver

C.L. van der Wilt^{a,1}, J.R. Kroep^a, W.J.P. Loves^a, M.G. Rots^{a,b,2},
C.J. Van Groenigen^a, G.J. Kaspers^b, G.J. Peters^{a,*}

^aDepartment of Medical Oncology, VU University Medical Center, Amsterdam, The Netherlands

^bDepartment of Pediatric Haematology/Oncology, VU University Medical Center, Amsterdam, The Netherlands

Received 20 May 2002; received in revised form 21 October 2002; accepted 3 December 2002

Abstract

Deoxycytidine kinase (dCK) is required for the phosphorylation of several deoxyribonucleoside analogues that are widely employed as chemotherapeutic agents. Examples include cytosine arabinoside (Ara-C) and 2-chlorodeoxyadenosine (CdA) in the treatment of acute myeloid leukaemia (AML) and gemcitabine to treat solid tumours. In this study, expression of *dCK* mRNA was measured by a competitive template reverse transcriptase polymerase chain reaction (CT RT-PCR) in seven cell lines of different histological origin, 16 childhood and adult AML samples, 10 human liver samples and 11 human liver metastases of colorectal cancer origin. The enzyme activity and protein expression levels of dCK in the cell lines were closely related to the mRNA expression levels ($r=0.75$, $P=0.026$ and $r=0.86$, $P=0.007$). In AML samples, *dCK* mRNA expression ranged from 1.16 to 35.25 ($\times 10^{-3} \times dCK/\beta\text{-actin}$). In the cell line panel, the range was 2.97–56.9 ($\times 10^{-3} \times dCK/\beta\text{-actin}$) of *dCK* mRNA expression. The enzyme activity in liver metastases was correlated to *dCK* mRNA expression ($r=0.497$, $P=0.05$). In the liver samples, these were not correlated. *dCK* mRNA expression showed only a 36-fold range in liver while a 150-fold range was observed in the liver metastases. In addition, dCK activity and mean mRNA levels were 2.5-fold higher in the metastases than in the liver samples. Since dCK is associated with the sensitivity to deoxynucleoside analogues and because of the good correlation between the different dCK measurements in malignant cells and tumours, the CT-RT PCR assay will be useful in the selection of patients that can be treated with deoxycytidine analogues.

© 2003 Published by Elsevier Science Ltd.

Keywords: Deoxycytidine kinase; Solid tumours; AML; Gemcitabine; Ara-C

1. Introduction

Deoxycytidine kinase (dCK) (EC 2.7.1.74) is a pyrimidine salvage enzyme that phosphorylates deoxycytidine, deoxyadenosine and deoxyguanosine. Furthermore, it is responsible for the phosphorylation of several deoxynucleoside analogues, which are widely used as anticancer and antiviral agents, such as 1- β -D-arabinosyl cytosine (cytarabine, Ara-C), 2',2'-difluorodeoxycytidine (gemcitabine, dFdC) and

2-chlorodeoxyadenosine (cladribine, CdA). The activity of dCK shows a wide variation in normal and malignant cells and tissues [1,2].

The level of dCK activity has been reported to be closely related to sensitivity to deoxynucleoside analogues such as CdA [3], Ara-C and dFdC [4–9]. A deficiency of dCK leads to a resistance to deoxycytidine and deoxyadenosine analogues [10,11], therefore pretreatment measurements of dCK might be of predictive value [5]. However, relative large cell numbers or tumour biopsy specimens are required for measurements of activity. The use of the polymerase-chain reaction (PCR) enables us to use small biopsy specimens or a small number of cells. Therefore, we applied reverse transcriptase (RT)-PCR techniques to develop a sensitive assay for the expression of *dCK* mRNA. In order to quantify the expression, we used competitive templates

* Corresponding author. Tel.: +31-20-444-2633; fax: +31-20-444-3844.

E-mail address: gj.peters@vumc.nl (G.J. Peters).

¹ Present address: Comprehensive Cancer Centre (IKA), Amsterdam, The Netherlands.

² Present address: University Centre for Pharmacy, University of Groningen, The Netherlands.

(CTs) for *dCK* mRNA which were included in the same reaction mixture.

In this study, *dCK* mRNA expression was compared with *dCK* activity and protein expression in a panel of solid tumour and leukaemia cell lines, as well as in samples from adult and paediatric leukaemia patients, and from liver and liver metastases from patients with colorectal cancer.

2. Materials and methods

2.1. Materials

[8-³H]-2-Chloro-2'-deoxyadenosine (24.2 Ci/mmol) was obtained from Moravek, Brea, CA, USA. RNazol was purchased from Campro Scientific (Veenendaal, The Netherlands); Moloney Murine Leukemia Virus Reverse Transcriptase (M-MLV-RT) and RNase inhibitor (25 IU/μl) were obtained from Promega (Madison, WI, USA). Deoxyribonucleotides (dNTPs), random hexamers, and Taq polymerase (5 IU/μl) were purchased from Amersham/Pharmacia Biotech (Roosendaal, The Netherlands). Primers were from Isogen (Maarssen, The Netherlands). RESponse Research agarose was obtained from Biozym (Landgraaf, The Netherlands). The rabbit anti-human *dCK* polyclonal antibody was produced and tested at the Institute of Molecular Biology and Biotechnology at Crete by the group of Dr I. Talianidis [12].

2.2. Cells

The cancer cell lines BxPC3 (pancreas), UMSCC14C (head and neck) A2780 (ovarian), H322 (non-small cell lung), CCRF CEM (T-cell acute lymphoid leukaemia), U937 (histiocytic lymphoma) and HL60 (acute myeloid leukaemia (AML)) were used to measure *dCK* expression and activity. The variants AG6000 (A2780 resistant to gemcitabine), CCRF CEM-*dCK*⁻ (CCRF CEM resistant to AraC) were included to set the lowest level of *dCK* activity. The solid tumour cell lines were cultured in Dulbecco's modification of Eagles medium (Bio Whittaker Europe, Verviers, Belgium) supplemented with 5% fetal calf serum (FCS) (Gibco, Paisly, UK). The others were cultured in Roswell Park Memorial Institute (RPMI) medium (Bio Whittaker) with 10% FCS. Subconfluent flasks with cells were harvested and counted. The cell pellets were frozen at -70 °C until further analysis.

2.3. Acute myeloid leukaemia samples

Mononuclear blast cells were derived after informed consent from 4 adult and 12 paediatric patients with acute myeloid leukaemia as previously described in Ref.

[13] and isolated by density gradient methods. Contaminating non-leukaemic cells were removed by immunomagnetic beads resulting in a percentage of leukaemic cells above 80%, as morphologically determined by May-Grünwald-Giemsa staining of the cytopins.

2.4. Liver and liver metastases

Biopsies of liver metastasis and normal liver of patients with histologically-proven colorectal cancer were used to study *dCK* in solid tumours and normal tissue. Samples were immediately frozen in liquid nitrogen and subsequently stored at -80 °C. Frozen tissues were pulverised using a microdismembrator [1], powdered tissue could be stored for the different *dCK* assays.

2.5. Deoxycytidine kinase activity

dCK activity in each of the cell lines was determined using ³H-CdA as a substrate, since CdA is a better and more specific substrate than deoxycytidine, which can also be phosphorylated by thymidine kinase 2. The assay was based on a method described by Arnér and colleagues in Ref. [14]. Cell pellets (at least 1.5 × 10⁷) were resuspended in 50 mM Tris(hydroxymethyl)-ammonium buffer (TRIS)/HCl buffer (pH 7.4), containing 4 mM dithiothreitol (DTT), at a concentration of 30 × 10⁶ cells/ml and kept on ice. Frozen tissue was suspended in 50 mM TRIS/HCl buffer (0.33 g/ml). Cells were disrupted by sonification and the suspension was centrifuged for 15 min at 7000g. The supernatant was used for the enzyme assay and protein determination. We used 25 μl of supernatant (6-126 μg protein) and added 10 μl 50 mM MgATP/100 mM NaF, 10 μl 250 μM [8-³H]-CdA (specific activity 0.19 μCi/nmol) and 5 μl TRIS/HCl buffer. This mixture was incubated at 37 °C. The assay was stopped by heating the samples to 90 °C, then 10 μl of 10 mM CdA was added to enable its localisation by ultraviolet (UV) absorbance on the PEI thin layer sheets. The samples were centrifuged in order to spin down the protein and subsequently 5 μl was spotted onto polyethyleneimine (PEI) cellulose thin-layer chromatography sheets. The sheets were developed with water to separate substrate and product. The different spots were cut and put into a vial with 750 μl of 0.1 M HCl/0.2 M KCl to enable elution of radioactivity from the PEI cellulose, during 2 h of shaking. After addition of liquid scintillation fluid, radioactivity was counted. Enzyme activity was expressed as pmol CdA-MP formed per h per mg protein.

2.6. Competitive template RT-PCR

The isolation of RNA was performed with RNazol as previously described in Ref. [13]. Cell pellets were

suspended in an aliquot of 200 μ l of RNazol per 10^6 cells. Twenty micrograms of the isolated RNA was used for reverse transcription into cDNA. Random hexamers were used as primers for M-MLV-RT at a concentration of 0.045 μ g/ μ l. After a brief incubation at 56 °C to remove secondary structures, samples were quickly cooled down on ice and annealing of the hexamers also took place on ice. The extension of the primers was at 42 °C using M-MLV-RT. The reaction was terminated by heating at 95 °C for 5 min. cDNA samples were stored at -20 °C until further use.

The design of the primers and the CT was based on the method described by Willey and colleagues in Refs. [13,15,16]. One forward (A) and two reverse primers (BC and C) were selected by Oligo software requiring an optimal annealing temperature of 58 °C, absence of hairpins and no predictable stable primer-dimer formations.

A: 5'-GAAGGGAACATCGCTGCAGG
C: 5'-TGGCCAAATTGGTTATTCATCC
BC: 5'-TGGCCAAATTGGTTATTCATCCTTGAG-
CTTGCCATTCAGAGAGG

The primers A and C were used to amplify a native template of 425 bp covering exons 2, 3 and part of 4 of *dCK*. The primers A and BC were selected for the construction of the CT. The B sequence is upstream of C and amplification with A and BC resulted in a shorter product of 294 bp. This product was the CT linked by the A and C sequence, which was further purified and quantified as described in Refs. [13,15]. The β -actin gene was used as a reference gene and the previously published construction of the β -actin CT was used [16].

CTs of β -actin and *dCK* were mixed in a ratio of 10, 100 and 1000 (10^{-12} M/ 10^{-13} M; 10^{-12} M/ 10^{-14} M; 10^{-12} M/ 10^{-15} M) based on preliminary experiments. One single master mix was prepared for every cDNA sample containing PCR buffer (1 \times), $MgCl_2$ (1.5 mM), dNTPs (200 μ M), Taq polymerase (5 μ l, final concentration 0.02 U/ μ l), sample cDNA and CT mix in a total volume of 46 μ l. *dCK* and β -actin primers (4 μ l, final concentration 4 ng/ μ l of each primer) were added to different tubes, which already contained certain aliquots of the master mix. Reaction mixtures were overlaid with mineral oil and cycled in a MJ Research PTC-200 (Biozym, Landgraaf, The Netherlands). A semi-hot start from ice to 94 °C was performed and with 1-min steps of denaturation at 94 °C, primer annealing at 58 °C and elongation at 72 °C the PCR reaction continued for 35 cycles.

PCR products were separated by electrophoresis on 2% agarose gels containing 0.1 μ g/ml ethidium bromide. Quantification was by digital image analysis using Scion Software. The concentration of native template molecules in the cDNA samples was calculated by the ratio of the intensity of native template/CT and the

molarity of the CT mixture as previously described in Refs. [13,15,16]. Normalisation of the *dCK* expression to the expression of β -actin was based on data obtained from assays with the same master mixture.

The *dCK* expression in the cell lines was determined at least three times on different cDNA samples of one cell line. The expression in the AML samples was measured once, because these samples were also used for several other assays. Levels of expression were reported as units *dCK* mRNA β -actin mRNA $\times 10^{-3}$ molecules.

2.7. Western blotting

Western blots were produced according to a published method in Ref. [12]. Protein extracts (30 μ g) were electrophoresed on 12.5% sodium dodecyl sulphate (SDS)-polyacrylamide gels and transferred by electroblotting to nitrocellulose membranes (Hybond ECL membranes, Amersham, Buckinghamshire, UK). After overnight incubation in blocking buffer (5% bovine serum albumin in TRIS-buffered saline with 0.1% Tween 20), the blot was probed with rabbit anti-human *dCK* polyclonal antibody (1:5000, 1 h at room temperature) and goat anti-rabbit secondary antibody conjugated to horseradish peroxidase (1:40,000, 1 h at room temperature). Purified recombinant *dCK* (10 ng), extracts of AG6000 cells lacking *dCK* and parental A2780 ovarian cancer cells were tested on every blot to identify the *dCK* band. Levels of relative expression were determined by densitometric scanning (Imaging Densitometer, model GS-690, Biorad of the X-ray films (Hyperfilm ECL). *dCK* protein levels were expressed as ng *dCK* per mg total protein.

2.8. Statistics

The Spearman correlation test was used to quantify the relationship between *dCK* activity and *dCK* expression at the mRNA and protein level. Student's *t*-test was used for comparison of paired and unpaired samples.

3. Results

The panel of cell lines had a 10-fold variation in *dCK* activity. The lower level was set by CCRF-CEM/*dCK*⁻ and AG6000 (1.2 and 1.4 pmol/h per mg protein, respectively). The mRNA expression showed a 19-fold variation for the cell lines (Table 1). No *dCK* mRNA could be detected in CCRF-CEM/*dCK*⁻. AG6000 showed a normal and a truncated mRNA product as has been previously published [6], this complicated accurate quantification and this cell line was excluded from the mRNA expression evaluation (Fig. 1). The reproducibility of the CT-RT-PCR assay in the cell lines is given in Table 1 as the relative standard deviation.

Table 1
dCK mRNA expression in cell lines and AML samples^a

Sample	<i>dCK</i> mRNA expression	Relative standard deviation
Cell line	Ratio $10^{-3} \times dCK/\beta\text{-actin}$	(%)
CCRF CEM	38.0 ± 17.3	33
HL60	56.3 ± 19.9	26
U937	56.9 ± 6.60	7
A2780	6.06 ± 6.76	15
UMSCC14C	4.73 ± 0.38	10
BxPC3	2.97 ± 0.16	9
H322	5.97 ± 1.54	6
AML		
0438*	4.24	
4695*	1.87	
4779	3.12	
6250*	10.79	
7470	26.30	
7578	35.23	
7621	19.40	
7747	1.16	
7985	2.77	
8019	12.27	
8051	9.88	
8069	3.52	
8196	26.17	
8400*	11.39	
8773	3.00	
8774	4.40	

AML, acute myeloid leukaemia.

^a mRNA expression is the mean ± standard error of the mean (S.E.M.) of at least three measurements on different samples for the cell lines. The relative standard deviation (S.D.) is based on 2-3 measurements on the same sample. (*) Indicates adult AML samples, the others are from childhood AML; not enough clinical material was available to measure enzyme activity. No expression was measured in the Ara-C- and gemcitabine-resistant cell lines.

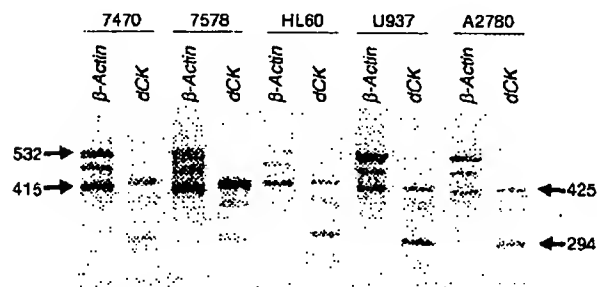


Fig. 1. Representative X-ray photos of $\beta\text{-actin}$ and *dCK* gene and competitive template (CT) products of the cell lines and 2 AML samples (7470 and 7578). The blots show three bands for both *dCK* and $\beta\text{-actin}$: 532 and 425 are the number of the basepairs encoded by the forward and reverse primers for the native cDNA of $\beta\text{-actin}$ and *dCK*, respectively; 415 and 294 are the number of basepairs encoded by the competitive templates for $\beta\text{-actin}$ and *dCK*, respectively. The intermediate band is a heterodimer (HD) which can be formed between the native cDNA and the competitive template. The contribution of the HD was calculated as previously described in Refs. [13,16]. The bands were scanned and the optical density (OD) was used to calculate a ratio between the native cDNA and CT of each target, thereafter these ratios were used to calculate the ratio for *dCK* and $\beta\text{-actin}$.

The AML samples had a 30-fold range of *dCK* mRNA expression that overlapped with that of the cell lines, although the high level of expression in the cell lines HL60 and U937 was not seen in the patient samples.

Liver metastases contained a mean 2.5-fold higher *dCK* enzyme activity than the surrounding normal liver samples (10.1 ± 1.9 and 4.0 ± 0.4 nmol/h/mg protein, respectively, $P=0.004$, Student's *t*-test for paired data) (Fig. 2). The range of *dCK* activities in the liver metastases was about 17-fold (1.4–23.8 nmol/h per protein), while that in the liver ranged only 3-fold (2.0–6.7). The *dCK* mRNA expression showed a wide variation for these samples: a 150-fold difference (0.53–80.4). The subgroup of liver samples had a 36-fold range (0.63–22.7) in *dCK* mRNA expression levels.

The correlation between *dCK* activity and *dCK* mRNA levels in the cell lines is depicted in Fig. 3a. The correlation coefficient determined by Spearman rank correlation was $r=0.75$ ($P=0.026$). The correlation between

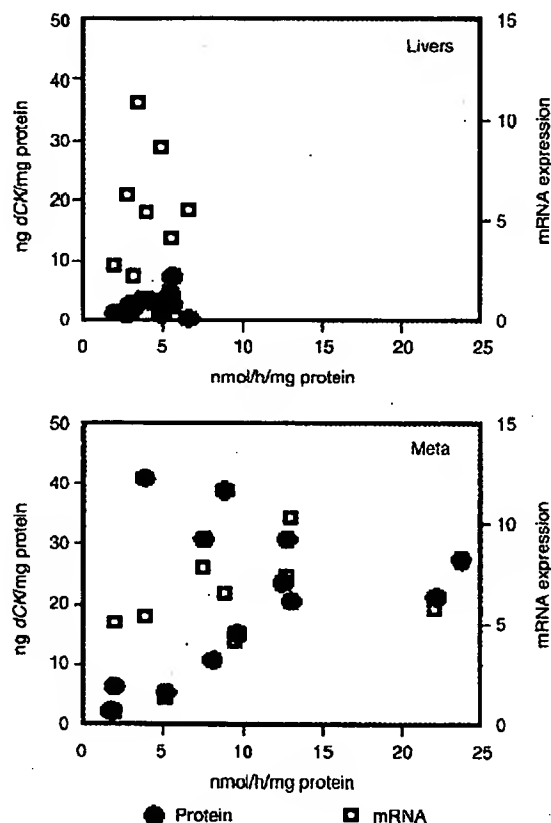


Fig. 2. Activity of *dCK*, amount of *dCK* protein and *dCK* mRNA expression in normal livers and liver metastases (meta) from colorectal cancer. The *dCK* activity in liver metastases was significantly higher than in livers ($P=0.004$). In livers, no correlation was found between *dCK* activity and *dCK* mRNA, while *dCK* activity was related to *dCK* protein ($r=0.59$; $P=0.013$). However, in liver metastases, *dCK* activity was correlated with *dCK* mRNA ($r=0.497$; $P=0.05$), but not to *dCK* protein. One liver metastasis sample is not shown having 72.9 ng *dCK*/mg protein and 80.4 as *dCK* mRNA expression. One liver sample had a *dCK* mRNA of 22.7 and a *dCK* activity of 5 nmol/h/mg protein.

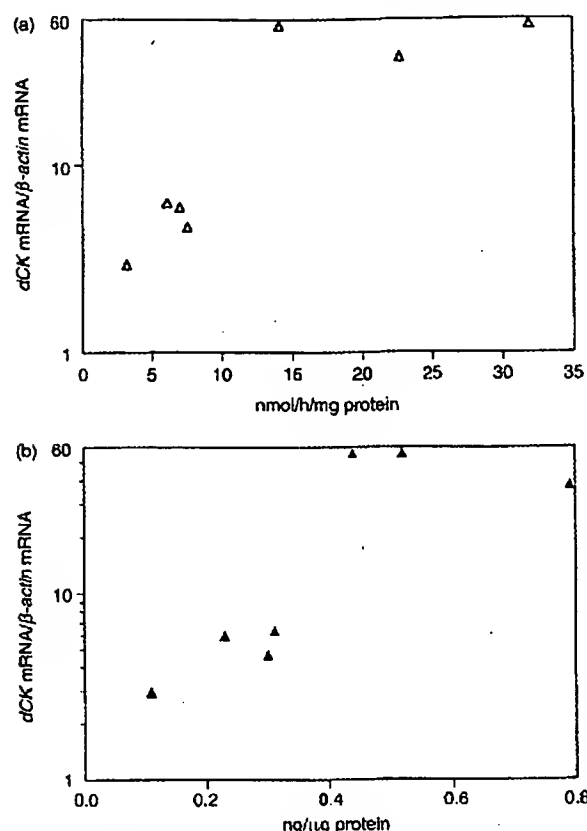


Fig. 3. (a) Correlation between mRNA expression and dCK activity in a panel of seven cell lines of different origin. Correlation coefficient $r = 0.75$ ($P = 0.026$). (b) Correlation between mRNA expression and dCK protein expression in a panel of seven cell lines of different origin. Correlation coefficient $r = 0.79$ ($P = 0.018$).

these dCK measurements in pooled liver and liver metastases is $r = 0.416$ ($P = 0.024$). The correlation was also observed for liver metastases only (Fig. 2) ($r = 0.497$, $P = 0.050$), but not for the subgroup of livers.

The dCK protein expression in the cell line panel (Figs. 3b and 4) varied about 7.2-fold. The correlation with dCK mRNA (Fig. 3b) was $r = 0.85$ ($P = 0.007$), as determined by Spearman rank correlation. In addition, the correlation coefficient of protein expression and activity was significant ($r = 0.79$, $P = 0.018$, Spearman).

In the liver metastases, dCK protein levels were clearly higher and had a broader range compared with the normal liver samples (5.3–72.9 and 0.5–7.4 ng dCK/mg protein, respectively) (Fig. 2). A correlation between

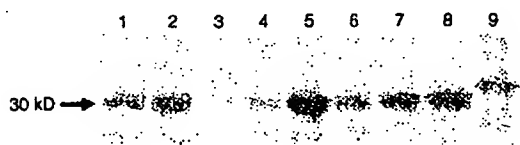


Fig. 4. Western blot of dCK protein in the different cell lines (1, 14C; 2, A2780; 3, AG6000; 4, BxPC3; 5, CEM; 6, H322; 7, HL60; 8, U937; 9, dCK-HIS).

dCK activity and protein was found in the liver samples ($r = 0.59$, $P = 0.013$), but not in the metastases. There was no correlation between dCK mRNA and protein expression in these samples.

4. Discussion

The expression of dCK mRNA in a panel of solid tumour cell lines and leukaemia and lymphoma cell lines was closely correlated to the activity of this enzyme. This relationship had already been established for a panel of six leukaemia cell lines by Kawasaki and colleagues in Ref. [17]. For solid tumour cells from different histological origin such a relationship had not yet been established. Any such correlation is of major interest because of the important role of some novel deoxynucleoside analogues, such as gemcitabine, in the treatment of solid tumours. Our panel is a mixture of both leukaemic and solid tumour cells, and if we considered only the four solid tumour cell lines, the relationship was weaker. The correlation between dCK activity and dCK mRNA expression in liver metastases was also weaker and its statistical significance was borderline ($P = 0.05$).

The substrate CdA, which we used, is also a substrate for deoxyguanosine kinase (dGK), albeit with a much higher K_m (85 μM) and lower efficiency than for dCK (5 μM) [18,19]. The cell lines CCRF-CEM-dCK⁻ and AG6000 have some CdA phosphorylating capacity, but they do not show a dCK protein band in western blotting. The activity measured here is most likely due to dGK activity, which is also present in the cell extract. The positive relationship between dCK enzyme activity and protein expression has also been observed in studies of Kawasaki [20] and Spasokoukotskaja [21]. The variation in the dCK mRNA expression in the AML samples (30-fold) is somewhat lower than that found in a study with 13 childhood AML samples (50-fold) [22] and 35 childhood ALL and AML samples [23] in which samples from relapsed leukaemic cells had a lower dCK expression. In addition, for the enzyme activities, a comparable range in dCK levels was found [24].

The relationship between dCK activity and response to treatment with deoxynucleoside analogues has been investigated in several malignancies. Hairy cell leukaemia, which is very sensitive to CdA showed both high dCK and dGK activity. The degree of total CdA phosphorylation correlated with the response to CdA treatment of both hairy cell leukaemias and chronic lymphocytic B-cell leukaemias, although other factors also seemed to be involved [3,25]. In AML, dCK activity correlated with the response to Ara-C treatment in 21 patients [26]. ALL patients more often relapsed when dCK expression was low or absent [27]. Transfection experiments with dCK and other deoxynucleoside kinase [28] genes has underlined the important role of

dCK in the antitumour activity of deoxynucleoside analogues. Increased expression of *dCK* gene by transfection restored and enhanced the sensitivity to deoxynucleoside analogues that are activated by dCK [8,9,29], both *in vitro* and *in vivo*.

Most of the AML samples were derived from childhood AMLs [13], which are always treated with an Ara-C-containing protocol. The large range of *dCK* mRNA expression, which overlapped with the expression of the cell lines, indicates that this disease in general has an intrinsic sensitivity to Ara-C, but that individual differences in sensitivity to Ara-C exist. Moreover, this has been reported and has prognostic significance [30,31]. Recently, a clinical protocol including Ara-C was started in which dCK expression will be evaluated prospectively.

Gemcitabine is currently being used for the treatment of many solid malignancies. Single agent gemcitabine shows little activity in colorectal cancer, but it is not clear whether this is due to a low dCK expression. Therefore, we designed this study to determine dCK expression in liver metastases. No information is currently available on the relationship between response and dCK activity in patients. In cell lines, we previously reported a relationship between gemcitabine sensitivity and dCK activity [6,7], while in xenografts [5], we also observed a relationship between gemcitabine sensitivity and dCK activity. *dCK* gene transfer enhanced the antitumour effect of gemcitabine on tumour xenografts [9], confirming the relationship between dCK and gemcitabine activity. It is remarkable that the dCK activity in the liver samples in our study showed relatively small variations and did not exceed a level of 5 nmol/h/mg protein. In contrast, protein and mRNA expression levels showed more variation. In liver metastases, both activity and mRNA varied considerably and correlated with one another. This would give an advantage for liver metastases compared with liver in selectively activating deoxynucleoside analogues in liver metastases. A high dose of gemcitabine is expected to lead to selective activation in metastases, and when given via a hepatic artery infusion would not leak to the systemic circulation as livers have a high deaminase activity. The much smaller range of dCK activity in the liver samples compared with the liver metastases also indicated that in the liver a posttranslational regulation mechanism exists, which seems to be deregulated in the liver metastases. It has been reported that dCK activity can be regulated by its phosphorylation [32,33]. dCK purified from leukaemic blasts can be phosphorylated by Protein Kinase C (PKC), resulting in a 100% increase in enzyme activity [32]. However, recombinant dCK is a poor substrate for PKC, but is effectively phosphorylated by protein kinase A, and this is not accompanied by an increase in enzyme activity [33]. An enhanced dCK activity could be eliminated by protein phosphatase treatment of lymphoid cells, supporting a secondary modification of the

dCK protein [34]. In addition, the promoter for *dCK* contains several potential regulatory transcription factor sites [35,36], although it is not yet clear whether this regulation is tissue-specific or deregulated in tumours.

For the enzyme activity assays and western blotting, relatively large pieces of tissue or many cells are required, and these are not always available. The current PCR assay detects a wide range of *dCK* mRNA levels. CT-RT-PCR can be performed with any PCR equipment, and does not need the requirement of an expensive Taq man or light cycler apparatus. In addition, results from this type of assay shows a high inter- and intralaboratory agreement [37]. Measurement of *dCK* mRNA expression offers the possibility for larger-scale studies, in patients with solid tumours and leukaemia, to determine a relationship between dCK expression and response to either gemcitabine or Ara-C. This data should be followed by a prospective study to select patients for deoxynucleoside analogue treatment based on their dCK activity.

Acknowledgements

This work was supported by European Union Grant BIOMED BMH4-CT96-0479.

References

1. Ruiz van Haperen VWT, Veerman G, Braakhuis BJM, et al. Deoxycytidine kinase and deoxycytidine deaminase activities in human tumour xenografts. *Eur J Cancer* 1993; 29A, 2132-2137.
2. Eriksson S, Arnér E, Spasokoukotskaja T, et al. Properties and levels of deoxynucleoside kinases in normal and tumor cells: implications for chemotherapy. *Adv Enzyme Regul* 1994; 34, 13-25.
3. Kawasaki H, Carrera CJ, Piro LD, Saven A, Kipps TJ, Carson DA. Relationship of deoxycytidine kinase and cytoplasmic 5'-nucleotidase to the chemotherapeutic efficacy of 2-chlorodeoxyadenosine. *Blood* 1993; 81, 597-601.
4. Kroep JR, Van Moorsel CJ, Veerman G, et al. Role of deoxycytidine kinase, thymidine kinase 2, and deoxycytidine deaminase in the antitumor activity of gemcitabine. *Adv Exp Med Biol* 1998; 431, 657-660.
5. Kroep JR, Loves WJP, Van der Wilt CL, et al. Pretreatment deoxycytidine kinase levels predict *in vivo* gemcitabine sensitivity. *Mol Cancer Ther* 2002; 1, 371-376.
6. Ruiz van Haperen VWT, Veerman G, Eriksson S, et al. Development and molecular characterization of a 2',2'-difluorodeoxycytidine-resistant variant of the human ovarian carcinoma cell line A2780. *Cancer Res* 1994; 54, 4138-4143.
7. Ruiz van Haperen VWT, Veerman G, Verwooten JB, Pinedo HM, Peters G. Regulation of phosphorylation of deoxycytidine and 2',2'-difluorodeoxycytidine (gemcitabine): effects of cytidine 5'-triphosphate and uridine 5'-triphosphate in relation to chemosensitivity for 2',2'-difluorodeoxycytidine. *Biochem Pharmacol* 1996; 51, 911-918.
8. Hapke DM, Stegmunn AP, Mitchell BS. Retroviral transfer of deoxycytidine kinase into tumor cell lines enhances nucleoside toxicity. *Cancer Res* 1996; 56, 2343-2347.

9. Blackstock AW, Lightfoot H, Case I.D, et al. Tumor uptake and elimination of 2', 2'-difluoro 2' deoxycytidine (gemcitabine) after deoxycytidine kinase gene transfer: correlation with in vivo tumor response. *Clin Cancer Res* 2001; 7, 3263-3268.
10. Peters GJ, Jansen G. Resistance to antimetabolites. In Schilsky RL, Milano GA, Ratain MJ, eds. *Principles of Antineoplastic Drug Development and Pharmacology*. New York: Marcel Dekker, 1996.
11. Bergman AM, Pinedo HM, Peters GJ. Determinants of resistance to 2',2'-difluorodeoxycytidine (gemcitabine). *Drug Res Update* 2002; 5, 19-33.
12. Hatzis P, Said Al-Madhoon A, Jullig M, Petrakis TG, Eriksson S, Talianidis I. The intracellular localization of deoxycytidine kinase. *J Biol Chem* 1998; 273, 30239-30243.
13. Rots MG, Willey JC, Jansen G, et al. mRNA expression levels of methotrexate resistance related proteins in childhood leukemia as determined by a competitive template based RT-PCR method. *Leukemia* 2000; 14, 2166-2175.
14. Arner E, Spasokoukotskaja T, Eriksson S. Selective assays for thymidine kinase 1 and 2 and deoxycytidine kinase and their activities in extracts from human cells and tissues. *Biochem Biophys Res Commun* 1992; 188, 712-718.
15. Willey JC, Coy EL, Frampton MS, et al. Quantitative RT-PCR measurement of cytochromes p450 1A1, 1B1, and 2B7, microsomal epoxide hydrolase and NADPH oxidoreductase expression in lung cells of smokers and nonsmokers. *Am J Resp Cell Mol Biol* 1997; 17, 114-124.
16. Willey JC, Crawford EL, Jackson CM, et al. Expression measurement of many genes simultaneously by quantitative RT-PCR using standardized mixtures of competitive templates. *Am J Resp Cell Mol Biol* 1998; 19, 6-17.
17. Kawasaki H, Shindou K, Higashigawa M, et al. Deoxycytidine kinase mRNA levels in leukemia cells with competitive polymerase chain reaction assay. *Leuk Res* 1996; 20, 677-682.
18. Arner ESJ, Eriksson S. Mammalian deoxynucleoside kinases. *Pharm Ther* 1995; 67, 155-186.
19. Eriksson S, Kicrduszuk B, Munch-Petersen B, Oberg B, Johansson MG. Comparison of the substrate specificities of human thymidine kinase 1 and 2 and deoxycytidine kinase toward antiviral and cytostatic nucleoside analogs. *Biochem Biophys Res Commun* 1991; 176, 586-592.
20. Kawasaki H, Carrera CJ, Carson DA. Quantitative immunoassay of human deoxycytidine kinase in malignant cells. *Anal Biochem* 1992; 207, 193-196.
21. Brosio O, Spasokoukotskaja T, Arner ES, et al. Expression of deoxycytidine kinase and phosphorylation of 2-chlorodeoxyadenosine in human normal and tumour cells and tissues. *Eur J Cancer* 1995; 31A, 202-208.
22. Kakiyama T, Fukuda T, Tanaka A, et al. Expression of deoxycytidine kinase (dCK) gene in leukemic cells in childhood: decreased expression of dCK gene in relapsed leukemia. *Leuk Lymphoma* 1998; 31, 405-409.
23. Mansson E, Lilienmark E, Soderhall S, Gustafsson G, Eriksson S, Albertioni F. Real-time quantitative PCR assays for deoxycytidine kinase, deoxyguanosine kinase and 5'nucleotidase mRNA measurement in cell lines and in patients with leukemia. *Leukemia* 2002; 31, 386-392.
24. Jacobsson B, Albertioni F, Eriksson S. Deoxynucleoside anabolic enzyme levels in acute myelocytic leukemia and chronic lymphocytic leukemia cells. *Cancer Lett* 2001; 165, 195-200.
25. Arner E. On the phosphorylation of 2-chlorodeoxyadenosine (CdA) and its correlation with clinical response in leukemia treatment. *Leuk Lymphoma* 1996; 21, 225-231.
26. Colly LP, Peters WG, Richel D, Arentsen-Honders MW, Starrenburg CW, Willemze RH. Deoxycytidine kinase and deoxycytidine deaminase values correspond closely to clinical response to cytosine arabinoside remission induction therapy in patients with acute myelogenous leukemia. *Semin Oncol* 1987; 14(Suppl. 1), 257-261.
27. Stamm G, Zintl F, Sauerbrey A, Volm M. Deoxycytidine kinase mRNA expression in childhood acute lymphoblastoid leukemia. *Anti-Cancer Drugs* 1997; 8, 517-521.
28. Zheng X, Johansson M, Karlsson A. Retroviral transduction of cancer cell lines with the gene encoding drosophila melanogaster multisubstrate deoxyribonucleoside kinase. *J Biol Chem* 2000; 275, 39125-39129.
29. Stegmann AP, Honders WH, Willemze R, Ruiz van Haperen VWT, Landegent JF. Transfection of wildtype deoxycytidine kinase (dCK) cDNA into Ara-C and DAC-resistant rat leukemic cell line of clonal origin fully restores drug sensitivity. *Blood* 1995; 85, 1188-1194.
30. Kaspers GJ, Zwaan CM, Pieters R, Veerman AJ. Cellular drug resistance in childhood acute myeloid leukemia. A mini-review with emphasis on cell culture assays. *Adv Exp Med Biol* 1999; 457, 415-421.
31. Zwaan CM, Kaspers GJ, Pieters R, et al. Different drug sensitivity profiles of acute myeloid and lymphoblastic leukemia and normal peripheral blood mononuclear cells in children with and without Down syndrome. *Blood* 2002; 99, 245-251.
32. Wang LM, Kucera GL. Deoxycytidine kinase is phosphorylated in vitro by protein kinase C alpha. *Biochim Biophys Acta* 1994; 1224, 161-167.
33. Spasokoukotskaja T, Csapo Z, Sasvari-Szekely M, et al. Effect of phosphorylation on deoxycytidine kinase activity. *Adv Exp Med Biol* 2000; 486, 281-285.
34. Csapo Z, Sasvari-Szekely M, Spasokoukotskaja T, Talianidis I, Eriksson S, Staub M. Activation of deoxycytidine kinase by inhibition of DNA synthesis in human lymphocytes. *Biochem Pharmacol* 2001; 61, 191-197.
35. Johansson M, Norda A, Karlsson A. Conserved gene structure and transcription factor sites in the human and mouse deoxycytidine kinase genes. *FEBS Letters* 2000; 487, 209-212.
36. Chen EH, Johnson EE 2nd, Vetter SM, Mitchell BS. Characterization of the deoxycytidine kinase promoter in human lymphoblast cell lines. *J Clin Invest* 1995; 95, 1660-1668.
37. Crawford EL, Peters GJ, Noordhuis P, et al. Standardized RT (StarT)-PCR provides a common language for gene expression. *Mol Diagn* 2001; 6, 217-225.

Adiposity Elevates Plasma MCP-1 Levels Leading to the Increased CD11b-positive Monocytes in Mice*

Received for publication, September 5, 2003
Published, JBC Papers in Press, September 16, 2003, DOI 10.1074/jbc.M309895200

Kazuhiko Takahashi, Shinji Mizuarai, Hiromitsu Araki, Satoshi Mashiko, Akane Ishihara, Akio Kanatani, Hiraku Itadani, and Hidehito Kotani†

From the Banyu Tsukuba Research Institute in collaboration with Merck Research Laboratories, Tsukuba, Ibaraki 300-2611, Japan

Obesity is currently considered as an epidemic in the western world, and it represents a major risk factor for life-threatening diseases such as heart attack, stroke, diabetes, and cancer. Taking advantage of DNA microarray technology, we tried to identify the molecules explaining the relationship between obesity and vascular disorders, comparing mRNA expression of about 12,000 genes in white adipose tissue between normal, high fat diet-induced obesity (DIO) and D-Trp³⁴ neuropeptide Y-induced obesity in mice. Expression of monocyte chemoattractant protein-1 (MCP-1) mRNA displayed a 7.2-fold increase in obese mice as compared with normal mice, leading to substantially elevated MCP-1 protein levels in adipocytes. MCP-1 levels in plasma were also increased in DIO mice, and a strong correlation between plasma MCP-1 levels and body weight was identified. We also showed that elevated MCP-1 protein levels in plasma increased the CD11b-positive monocyte/macrophage population in DIO mice. Furthermore, infusion of MCP-1 into lean mice increased the CD11b-positive monocyte population without inducing changes in body weight. Given the importance of MCP-1 in activation of monocytes and subsequent atherosclerotic development, these results suggest a novel role of adiposity in the development of vascular disorders.

Obesity is now considered epidemic throughout the western world and represents a major risk factor for a variety of life-threatening diseases, such as heart attack, stroke, diabetes, and cancer (1–4). According to current estimates, about 30% of adults in the United States are classified as obese, roughly double the number from 20 years ago. Obesity increases the risk of developing type 2 diabetes 10-fold, cardiovascular diseases 2-fold, and colon cancer 1.6-fold. Although recent progress in understanding the molecular basis of obesity may well open new opportunities to combat this epidemic, the molecular mechanisms underlying the relationship between obesity and obesity-related comorbidities remain unclear and are currently the focus of intense investigation.

Hypercholesterolemia has been considered to represent the critical factor in the development of atherosclerosis. However, a growing body of evidence suggests the importance of inflammatory processes in the pathogenesis of vascular diseases. Inflammatory processes are orchestrated by the recruitment of

mononuclear leukocytes and the migration, growth, and activation of cells within atherosclerotic lesions (5, 6). Attraction of circulating leukocytes to target sites is controlled by various chemokines, the presence of which is well documented in atherosclerotic lesions (7, 8). After attachment to the vessel wall, monocytes migrate into the subendothelial space, differentiating into macrophages and lipid-laden foam cells (5). These steps are likewise controlled by chemotactic cytokines; in particular, expression of monocyte chemoattractant protein-1 (MCP-1)¹ is enhanced in macrophages, endothelial cells, and vascular smooth muscle cells in the atheromatous plaque (9). MCP-1 is the member of the C-C chemokine β subfamily and is predominantly expressed in endothelial cells (10, 11). In hypercholesterolemic mice, genetic disruption of MCP-1 or its receptor, CCR2, results in markedly decreased occurrence of atheroma and the presence of fewer monocytes in vascular lesions (12–14). In apolipoprotein E-deficient mice, local infusion of MCP-1 induces CD11b expression on peripheral monocytes and increased formation of collateral arteries (15). MCP-1 is thus considered as a chemokine regulating inflammation in atherosclerotic lesions, and manipulation of the MCP-1/CCR2 interaction may modify the pathogenetic course of such lesions.

Adipose tissue is reportedly second only to lymphatic tissue in the secretion of signaling molecules (16). The biological significance of these molecules is largely unknown, but the inflammation compartment of vascular injury or regulation of insulin resistance may be affected. Proteins that are reportedly secreted and functional in atherosclerosis include IL-6 (17), tumor necrosis factor- α (18), resistin (19), adiponectin (20), PAI-1 (21), and leptin (22, 23).

The present study identified the molecular factors explaining the relationship between obesity and atherosclerosis, with a focus on adipose tissue. The mRNA expression of epididymal white adipose tissue (EWAT) was compared among obese mice, revealing that expression of MCP-1 mRNA is increased in obese mice, leading to elevated levels of plasma MCP-1 protein. Furthermore, the higher levels of MCP-1 protein in plasma were found to increase the CD11b-positive monocyte/macrophage population among peripheral blood cells, suggesting a role for elevated MCP-1 in the vascular inflammatory process during atherosclerosis.

MATERIALS AND METHODS

Animals—C57BL/6N mice (6 weeks old, CLEA Japan, Tokyo, Japan) were housed in individual cages. Mice were maintained under conditions of controlled temperature ($23 \pm 2^\circ\text{C}$) and light (07:00–19:00).

* The costs of publication of this article were defrayed in part by the payment of page charges. This article must therefore be hereby marked "advertisement" in accordance with 18 U.S.C. Section 1734 solely to indicate this fact.

† To whom correspondence should be addressed: Tel.: 81-029-877-2202; Fax: 81-029-877-2027; E-mail: kotanihh@banyu.co.jp.

¹ The abbreviations used are: MCP-1, monocyte chemoattractant protein-1; DIO, diet-induced obesity; WAT, white adipose tissue; EWAT, epididymal WAT; PBS, phosphate-buffered saline; NPY, neuropeptide Y; ELISA, enzyme-linked immunosorbent assay; CCR, C-C chemokine receptor.

Water and food (CA-1, CLEA Japan) were available *ad libitum* unless otherwise noted. For microarray analysis, 18-week-old mice were changed to an MHF diet (Oriental Bioservice, Kyoto, Japan) for 6 months to establish diet-induced obesity (DIO). The MHF diet provides 52.4% energy as carbohydrate, 15% as protein, and 32.6% as fat (4.41 kcal/g). For measurements of MCP-1 levels in plasma, normal diet was changed to the MHF diet when the mice were 9 weeks old. In food restriction experiments, body-weight changes in DIO mice were monitored after caloric intake was limited for 21 h and after food intake was restricted to a short, 3-h period for 7 days. All animal procedures complied with National Institutes of Health guidelines and were approved by the Banyu Animal Care and Usage Committee.

Surgical Procedure—D-Trp³⁴ neuropeptide Y (D-Trp³⁴NPY, a Y5 agonist) was synthesized at Banyu Tsukuba Research Institute. Mice were anesthetized using sodium pentobarbital (80 mg/kg, intraperitoneal, Dainabot, Tokyo, Japan), and a sterile brain infusion cannula (28 gauge, Alzet, Palo Alto, CA) was stereotactically implanted into the right lateral ventricle. The stereotaxic coordinates used were 0.4 mm posterior to the bregma, 0.8 mm lateral to the midline, and 2.0 mm from the surface of the skull, using a flat skull position. Cannulae were fixed to the skull using dental cement. The infusion cannula was connected to an osmotic minipump (model no. 2002, Alzet) filled with 10 mM phosphate-buffered saline (PBS) containing 0.05% bovine serum albumin via polyvinylchloride tubing. Pumps were implanted subdermally on the backs of mice, and antibiotic (Cefamedine A, 50 mg/kg, Fujisawa, Tokyo, Japan) was injected subcutaneously. Mice were divided into three groups, matched for average body weight: vehicle (PBS)-infused; D-Trp³⁴NPY-infused and fed *ad libitum* (*ad libitum*-fed group); and D-Trp³⁴NPY infused and pair-fed (pair-fed group). After 7–14 days of recovery following surgery, pumps were replaced with D-Trp³⁴NPY-(5 µg/day) or vehicle-containing pumps. The D-Trp³⁴NPY-pair-fed group was provided with the same amount of food as the vehicle group. Pair feeding was performed as described previously (24).

Microarray Analysis—In respective model mice, total RNA was extracted from EWAT using Trizol reagents (Invitrogen) and repurified with an RNeasy purification kit (Qiagen, Hilden, Germany). To determine expression changes between models, 10 µg of RNA was utilized for microarray analysis (MG-U74U74A chip, Affymetrix, Santa Clara, CA) of ~12,000 genes. For analysis of microarray data, GeneChip software (Affymetrix) was utilized. Appropriate control mice were used to provide baseline values for the experimental groups, and genes displaying values of $p < 0.05$ were identified using the Mann-Whitney test.

Measurement of MCP-1 Expression by Quantitative PCR—Total RNA was extracted from EWAT as described in the previous section. Reverse transcription was performed for 500 ng of total RNA, and obtained cDNA was applied to TaqMan PCR for quantification of MCP-1 mRNA expression. Data were collected and analyzed using an ABI PRISM 7700 sequence detector system (Applied Biosystems, Warrington, UK). MCP-1 expression data were normalized to β -actin expression levels in each sample. Primers and TaqMan probes used were as follows: TaqMan probe for MCP-1, 5'-CCA CTC ACC TGC TGC TAC TCA TTC ACC A-3'; PCR forward primer for MCP-1, 5'-TCA GCC AGA TGC AGT TAA CGC-3'; PCR reverse primer for MCP-1, 5'-TGA TCC TCT TGT AGC TCT CCA GC-3'; TaqMan probe for β -actin, 5'-CCT GAG GCT CTT TTC CAG CCT TCC TTC T-3'; PCR forward primer for β -actin, 5'-TAT TGG CAA CGA GCG GTT C-3'; PCR reverse primer for β -actin, 5'-ATG CCA CAG GAT TCC ATA CCC-3'.

Laser Microdissection—Ovarian white adipose tissues were excised, embedded in OCT compound (Sakura Finetek USA, Torrance, CA), frozen in cold hexan, and stored at -80 °C. Frozen sections were cut at 10-µm thickness and mounted on foil-covered microscope slides (Leica, Wetzlar, Germany). Sections were subsequently fixed in ethanol/acetic acid (19:1) for 1 min, stained using 0.05% toluidine blue solution (WAKO, Osaka, Japan) for 50 s, and air-dried for 30 min. Laser microdissection was performed using an AS LMD laser microdissection system (Leica) to collect either adipocytes or non-adipocyte cells. Total RNA was extracted from each fraction, and TaqMan PCR was performed as described above.

Measurement of MCP-1—Concentrations of MCP-1 in plasma and EWAT were determined using an ELISA kit (R&D Systems, Minneapolis, MN). EWAT was removed and homogenized in 2 volumes of ice-cold PBS with protease inhibitor mixture tablets (Roche Diagnostics). The homogenate was centrifuged at 2000 × *g* for 10 min at 4 °C. The supernatant was then used for MCP-1 ELISA.

Analysis of CD11b Expression Using Flow Cytometry—MCP-1 (R&D Systems) was infused subcutaneously for 2 weeks using an osmotic pump (Alzet) at a dose of 10 ng/0.5 µl/h. Flow cytometric analysis was performed to determine the monocyte/macrophage population among

whole blood cells. Whole blood samples from control, DIO, and MCP-1-treated mice were collected from the tail vein using heparinized capillaries. Blood cells were centrifuged at 300 × *g* for 5 min and incubated using fluorescein isothiocyanate-labeled anti-mouse CD11b (BD Biosciences) at room temperature for 15 min. To control non-specific binding, samples were incubated using rat IgG2b isotype. After washing stained cells with PBS, red blood cells were lysed using a lysing buffer for 5 min at room temperature. Cells were then washed with PBS and suspended in PBS containing 0.5% formaldehyde. Flow cytometry was performed using an EPICS Elite flow cytometer (Beckman Coulter) to identify the monocyte population, which was determined using fluorescence and scatter light characteristics. In all samples, 40,000 white blood cells were counted and analyzed.

Evaluation of Data and Statistical Analysis—All data were expressed as mean ± S.E. Statistics were performed using a two-tailed unpaired Student's *t* test (StatView, SAS Institute, Cary, NC).

RESULTS

Gene Expression Profiles of Adipocyte in Obesity Models—Two models of mice obesity were employed to examine expression changes in EWAT. These comprised the high fat DIO model and the D-Trp³⁴NPY-induced obesity model (*ad libitum*- and pair-fed groups). In the DIO model, mice were fed high fat chow (32.6% energy as fat, 52.4% as carbohydrate, and 15.0% as protein) for 6 months. Body weights of DIO mice had stabilized by 6 months, at 44.7 ± 2.6 g (mice fed regular chow, 31.1 ± 1.1 g). The other model utilized D-Trp³⁴NPY-induced obesity. D-Trp³⁴NPY is known to represent an appetite stimulant acting on the NPY Y5 receptor. Administration of this neuropeptide is known to increase food intake and body weight, with changes in body weight accompanied by increased fat weight (24). Treatment with D-Trp³⁴NPY not only increases food intake but also decreases energy expenditure (24), so that D-Trp³⁴NPY-treated mice pair-fed with a PBS-treated control group also displayed increased adiposity.

EWAT was excised, and total RNA was extracted, labeled, and hybridized to a DNA microarray. GeneChip Murine U74A arrays (Affymetrix) were used for DNA microarrays, and data were analyzed using GeneChip software comparison (Table I). Expressions of seven genes were increased in both DIO and D-Trp³⁴NPY-treated mice (*ad libitum*- and pair-fed group) comparisons, whereas expressions of nine genes were decreased. Some affected genes are known to display associations with increased adiposity, including: leptin; fatty acid-binding protein 5; and low density lipoprotein receptor-related protein 2. In addition, significant changes were observed in genes displaying roles in immune processes, such as: complement component 1q; complement component 2; and MCP-1. Both leptin and MCP-1 comprise secreted proteins with trans-acting signal transduction capabilities.

MCP-1 mRNA and Plasma Protein Levels—Changes in the expression of MCP-1 in EWAT were confirmed using quantitative TaqMan PCR methods in all obese mouse models. Results from DNA microarrays and quantitative TaqMan PCR coordinated well (Fig. 1A). White adipose tissues comprise various cell types, including adipocytes, vascular endothelial cells, smooth muscle cells, fibroblasts, mast cells, and macrophages (25). With the exception of mast cells, all other cell types reportedly display MCP-1 expression, so laser microdissection was used to confirm adipocyte-selective MCP-1 induction in high fat DIO mice. Each histological section of adipose tissues was stained, adipocytes and non-adipocyte cells were collected separately using laser microdissection, and TaqMan PCR was performed. Induction of adipocyte-selective MCP-1 mRNA (5.3-fold induction as compared with control lean mice) was observed in obese mice (Fig. 1B).

Next, we assessed whether increased levels of MCP-1 mRNA translated to increased levels of MCP-1 protein in EWAT. Adipose tissue from DIO mice was excised, homogenized, and

TABLE I
Common signature genes with EWAT in DIO and D-Trp³⁴NPY-treated mice

This table lists whose expression levels were either increased in both obese models or decreased in both obese models: DIO and D-Trp³⁴NPY-treated mice (free-fed (FF) and pair-fed (PF)). Fold change values represent ratios of mean expression levels for the two obese mice models compared with mean for each controls. For down-regulated genes fold changes represent inverse ratios and are denoted with minus signs.

Probe ID	Accession	Symbol	Name	Fold change		
				DIO	D-Trp ³⁴ NPY-FF	D-Trp ³⁴ NPY-PF
Up						
100436_at	M27008	Orm1	Orosomucoid 1	1.6	3.9	2.4
102736_at	M19681	MCP-1	Monocyte chemoattractant protein-1	7.2	6.3	4.9
99623_s_at	D78265	Olfm 1	Olfactomedin 1	1.7	3.4	2.0
160544_at	AJ223066	Fabp5	Fatty acid-binding protein 5, epidermal	2.8	9.0	3.7
101753_s_at	X51547	Lzp-s	P lysozyme structural	2.2	2.4	2.0
96020_at	M22531	C1qb	Complement component 1, q subcomponent, β -polypeptide	2.8	1.8	1.7
98443_at	A1882416	Lep	Leptin	2.3	3.1	1.8
Down						
94223_at	AJ010045	Net1	Neuroepithelial cell transforming gene 1	-3.9	-4.6	-2.6
102207_at	AW123249	MGC12117	Hypothetical protein MGC12117	-2.3	-5.0	-1.6
103673_at	M57891	C2	Complement component 2 (within H-2S)	-3.1	-5.9	-2.4
96146_at	D83745	Btg3	B-cell translocation gene 3	-1.8	-2.4	-2.5
160085_at	U35741	Tst	Thiosulfate sulfurtransferase, mitochondrial	-3.7	-2.0	-1.9
103377_at	AW259788	Lrp2	Low density lipoprotein receptor-related protein 2	-2.9	-2.9	-1.8
100629_at	U24428	Gstm5	Glutathione S-transferase, μ 5	-3.3	-2.1	-1.5
101676_at	U13705	Gpx3	Glutathione peroxidase 3	-2.5	-2.9	-1.8
100068_at	M74570	Aldh1a1	Aldehyde dehydrogenase family 1, subfamily A1	-2.0	-2.2	-1.6

centrifuged, yielding supernatants used for ELISA measurement of MCP-1 protein (Fig. 1C). An ~5-fold increase in tissue levels of MCP-1 protein was observed in DIO mice as compared with regular diet-fed control C57/BL6 mice, in good agreement with the observed mRNA changes. Calculated to a per WAT base, the change was more significant, at 17.6-fold (DIO, 655.4 pg of MCP-1/WAT *versus* control, 37.20 pg of MCP-1/WAT).

If increases in MCP-1 message/protein levels in WAT could affect functions in distant organs, plasma MCP-1 protein levels should be altered according to protein levels in WAT. Evaluation of plasma MCP-1 levels using ELISA confirmed this hypothesis (Fig. 1D). In DIO mice, plasma levels of MCP-1 were significantly increased as compared with regular diet-fed control mice.

Plasma MCP-1 Levels and Body Weight—Since increased plasma MCP-1 levels were observed in DIO mice, we evaluated whether plasma MCP-1 levels correlated with body weight in DIO mice. Forty mice were fed high fat diet for various periods (1–18 weeks), and blood was collected from these mice for MCP-1 ELISA. When plasma MCP-1 levels were plotted against body weight in these mice (Fig. 2A), correlations between plasma MCP-1 levels and body weight were highly significant ($r = 0.834$). These results indicated that EWAT-derived MCP-1 changes circulating levels according to body weight, probably as a result of increased adiposity.

To confirm a causal relationship between adiposity and plasma MCP-1 levels, the time course of DIO treatments as compared with plasma MCP-1 levels was also investigated. Mice were fed a high fat diet from the time they were 9 weeks old, and blood was collected at 2, 4, 10, and 20 weeks after initiation of treatment (Fig. 2B). As expected, plasma MCP-1 levels increased according to increased body weight, and increases were even observed in aged regular diet-fed mice, although these changes were relatively small as compared with mice fed the high fat diet. Since adiposity is known to increase with age in rodents, it is encouraging to see that MCP-1 increases in mice at the time they are 20 weeks old.

The effect of fasting on plasma MCP-1 levels was also evaluated. Dietary restriction represents a simple model for decreased fat storage in rodents, and we utilized DIO mice fed with 80% of the calories needed to maintain their body weight. Within 7 days, a 25% reduction in body weight was observed, in addition to decreased plasma MCP-1 levels (Fig. 2C). These

results confirmed a strong causal relationship between adiposity and plasma MCP-1 levels.

Plasma MCP-1 Levels and CD11b-positive Monocyte—MCP-1 is part of the C-C chemokine β subfamily, members of which bind to several CCR receptors to transmit signals. The interaction of MCP-1 with CCR2 has been well characterized (26), and genetic manipulation of the interaction is known to affect the pathological course of atherosclerosis. In this process, MCP-1 displays particular involvement in the activation and recruitment of monocytes to the atherosclerotic lesion. Changes to MCP-1 levels in the plasma of obese subjects may therefore produce functional consequences in the development of increased neointimal formations, and we decided to further characterize the significance of systemic increases in levels of MCP-1. Flow cytometric analysis was performed on mice in which plasma MCP-1 levels were raised by high fat diet treatment for 17–19 weeks (95.7 ± 7.1 pg/ml for DIO, 40.5 ± 2.4 pg/ml for regular diet). The results indicated that the CD11b (Mac 1, a member of the integrin family)-positive fraction of monocytes was increased significantly among DIO mice as compared with regular diet-fed control mice ($607.4 \pm 38.8/40,000$ white blood cells for DIO, *versus* $416.4 \pm 58.6/40,000$ white blood cells for regular diet, Fig. 3, A–C). This result suggests that effects such as elevation of plasma MCP-1 levels induced by a high fat diet could cause these changes in cell populations.

Since high fat diet treatments could have altered parameters other than MCP-1 plasma concentrations, which could in turn lead to the changes in the CD11b-positive monocyte population, we decided to test the direct effects of MCP-1 administration on CD11b-positive monocyte population. Recombinant murine MCP-1 was infused subcutaneously into C57/BL6 mice under regular diet conditions. Flow cytometric analysis was then performed after 2 weeks of treatment (Fig. 3, D–F). Under these experimental conditions, plasma MCP-1 levels increased about 2-fold as compared with saline-infused controls (209.3 ± 23.4 pg/ml for MCP-1 *versus* 93.5 ± 10.7 pg/ml for saline), comparable with the levels achieved with the high fat diet. Circulating CD11b-positive monocytes increased 1.7-fold, in good agreement with our study of mice on a high fat diet. Taken together, these results strongly suggest that changes in the CD11b-positive monocyte population in DIO mice are correlated with increases in plasma MCP-1 levels.

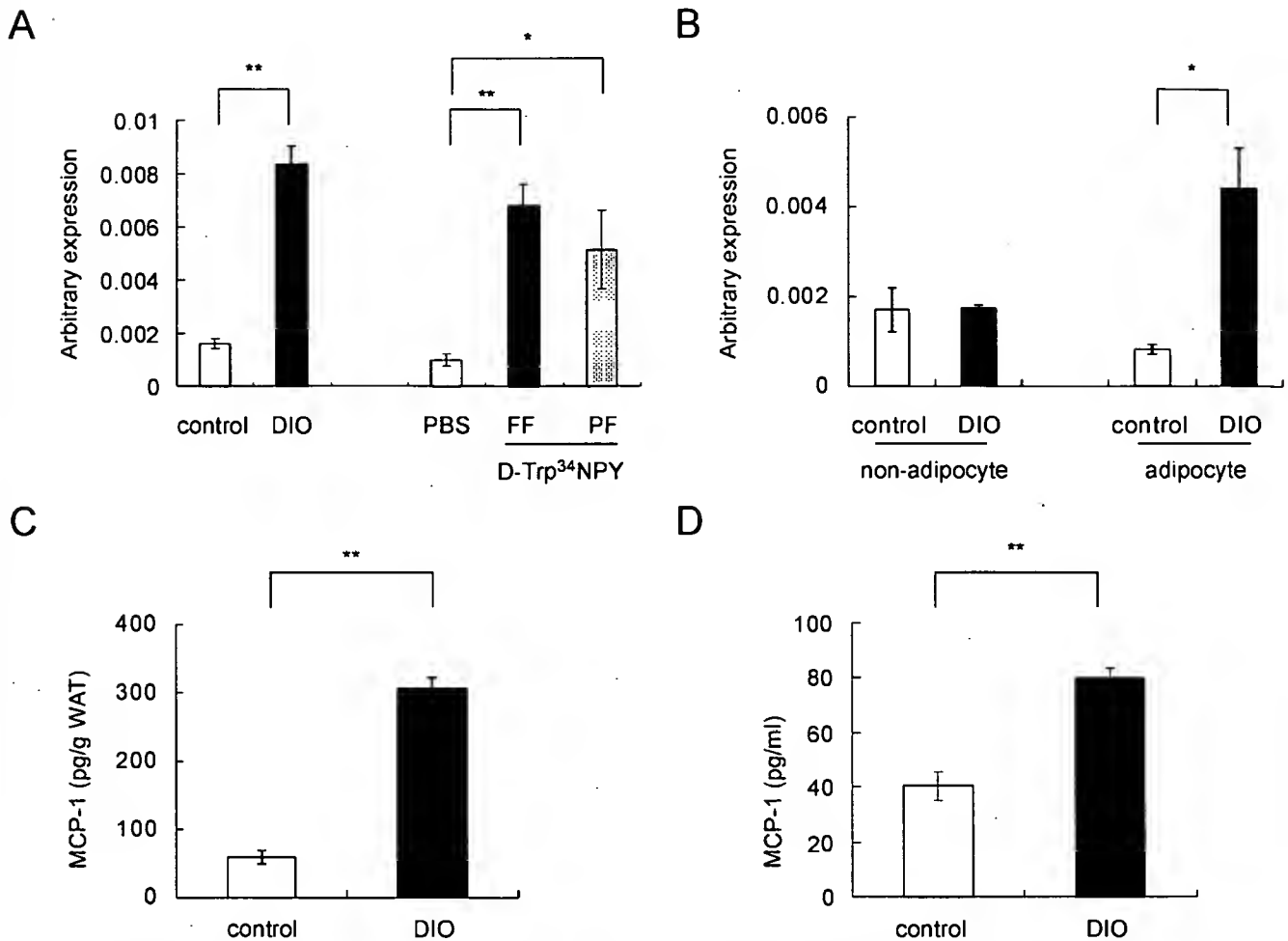


FIG. 1. MCP-1 mRNA expression and plasma MCP-1 protein level. A, MCP-1 mRNA expression in EWAT in two obese model mice. Expression of MCP-1 was determined in EWAT from male control and DIO mice ($n = 3$; **, $p < 0.01$) or PBS-infused, D-Trp³⁴NPY-treated free-fed (FF), D-Trp³⁴NPY-treated pair-fed (PF) mice ($n = 3$; *, $p < 0.05$; **, $p < 0.01$) using real-time TaqMan reverse transcriptase-PCR. Data were normalized to expression of β -actin. Control and PBS-treated mice are indicated by white bars, DIO, D-Trp³⁴NPY-treated FF mice are indicated by black bars, and D-Trp³⁴NPY-treated PF mice are indicated by gray bars. B, MCP-1 mRNA expression in adipocytes and non-adipocyte cells. Expression of MCP-1 was determined in ovarian white adipose tissue from 42-week-old DIO mice ($n = 3$; *, $p < 0.05$) and control mice using real-time TaqMan reverse transcriptase-PCR. Data were normalized to expression of β -actin. Control mice are indicated by white bars, and DIO mice are indicated by black bars. C, MCP-1 protein level in EWAT. MCP-1 was determined using ELISA in age-matched male controls and DIO mice after 10 weeks ($n = 3$; **, $p < 0.01$). Data were normalized to grams of EWAT. D, MCP-1 protein level in plasma. Blood was withdrawn from tail veins of age-matched male controls and DIO mice after 15 weeks ($n = 6$; **, $p < 0.01$). Plasma MCP-1 levels were determined using ELISA. Control mice are indicated by white bars, and DIO mice are indicated by black bars. Error bars represent S.E.

DISCUSSION

Obesity is well known as a risk factor for developments of atherosclerosis (1–3). Recent progress in our understanding of the complex pathogenesis underlying obesity has led to the term “syndrome X,” also known as metabolic cardiovascular syndrome or insulin resistance syndrome (27). However, the molecular pathophysiology of syndrome X has not been elucidated in any great detail, and the genes underpinning each phenotype are under active investigation.

The present study attempted to identify one such gene by focusing on secreted proteins generated from adipocytes since increased adiposity represents both the most notable change in obesity and a known risk factor for vascular disease. In addition, our interest in secreted proteins stems from the fact that such proteins have a strong potential for acting on distant tissues. DNA microarray techniques are well suited for mass analysis of gene expression, and using such expression profiling, we were able to identify two secreted proteins from the two murine models of obesity examined, namely DIO and D-Trp³⁴NPY-treated mice. All changes observed in D-Trp³⁴NPY-treated pair-fed models were included in the changes noted in D-Trp³⁴NPY-treated *ad libi-*

tum-fed models (data not shown). D-Trp³⁴NPY-treated pair-fed models were used to focus on genes whose expression changed with increased adiposity. Surprisingly, MCP-1 protein changed expression levels in obese adipocytes, as did only one other protein, leptin. Our observation is in good agreement with a recent report that MCP-1 mRNA is elevated in the adipose tissue of *ob/ob* obese mice (28). Observations were further extended to protein levels in EWAT and circulating plasma. Analysis of the correlation between body weight and plasma MCP-1 levels revealed a very strong association, reaching similar levels to that displayed by the correlation between body weight and plasma leptin levels (29). Moreover, plasma MCP-1 levels increased when body weight increased, and decreased when body weight decreased through fasting. These observations strongly suggest that changes in adipose weight associated with obesity/fasting are the direct cause of alterations in plasma levels of MCP-1.

In an effort to confirm the functional consequences of changes to plasma MCP-1 levels in obese mice, we measured CD11b-positive monocytes in circulating blood using flow cytometric analysis. MCP-1 reportedly induces CD11b expression on monocytes and adhesion of monocytes to blood vessels (15,

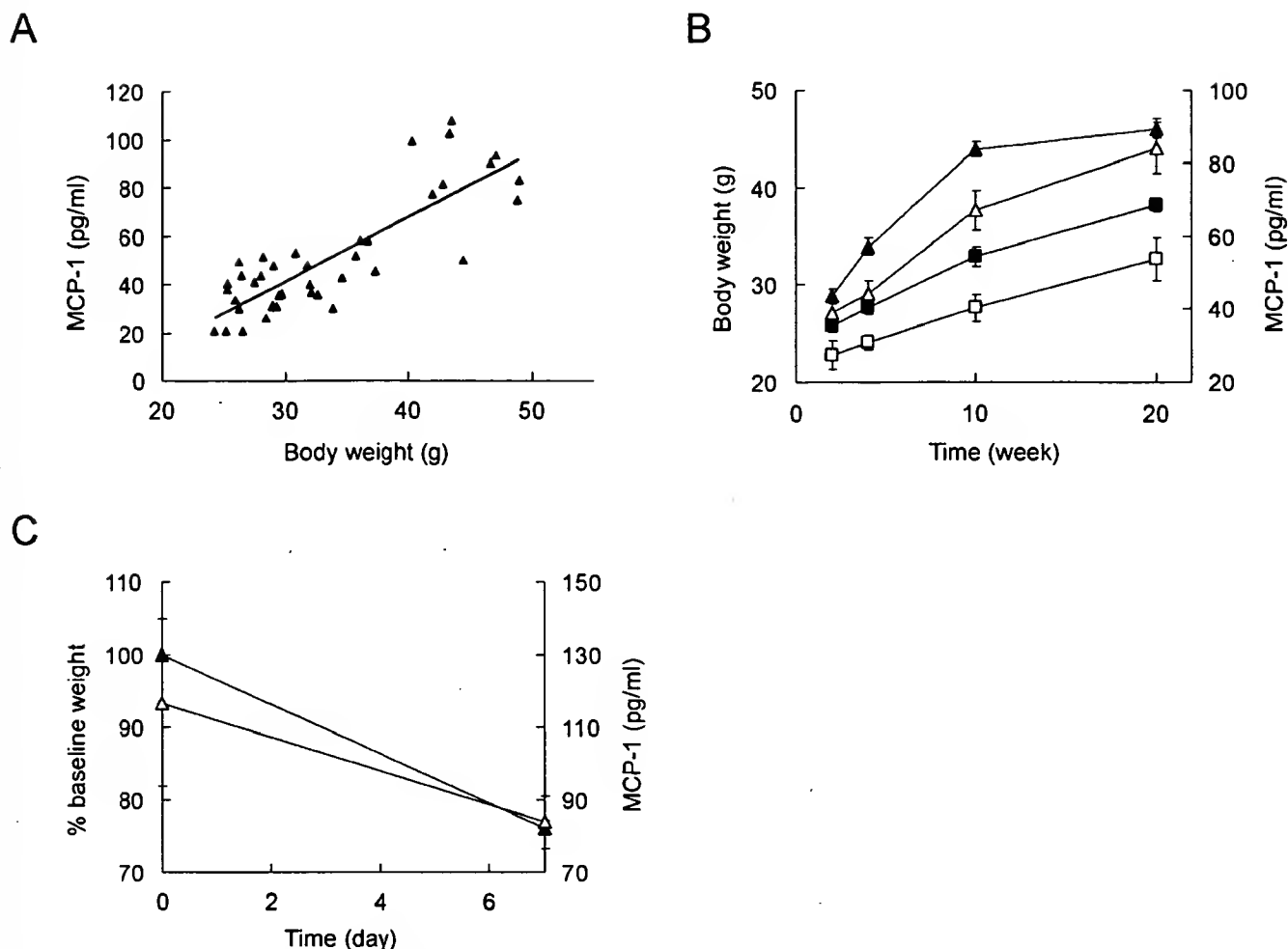


FIG. 2. Change of plasma MCP-1 level in obese model mice. *A*, Plasma MCP-1 levels and body weights in DIO mice. Male DIO mice ($n = 40$) at various periods (1–18 weeks) were used. *B*, time course for body weight and plasma MCP-1 levels in male control and DIO mice. Mice fed a normal diet until 9 weeks old were then fed MHF diet. Control mice are indicated by filled squares (body weight) and open squares (MCP-1), and DIO mice are indicated by filled triangles (body weight) and open triangles (MCP-1). *C*, change in body-weight and plasma MCP-1 levels in food-restricted male DIO mice ($n = 5$). Body weight was measured after 21 h of food restriction in DIO mice after 19 weeks. Plasma MCP-1 levels were determined on the indicated time points. Changes in body weight are indicated by filled triangles, and changes in MCP-1 are indicated by open triangles.

30). CD11b antigens are expressed when premature monocytes are activated to become differentiated monocytes and represent the best molecular marker of the macrophage lineage (31). In our analysis, circulating CD11b-positive monocytes increased in obese DIO mice as compared with regular diet-fed control mice, indicating that increased MCP-1 in obese mice affects the CD11b-positive monocyte population in obese mice. In fact, a suggestive report has been published regarding a study in humans in which the number of monocytes increased by about 10% in obese subjects (body mass index ≥ 30) and overweight subjects (body mass index 25–30) (32). Although that study did not evaluate CD11b-positive monocytes, this change could represent the result of increased CD11b-positive monocytes. An increase in CD11b-positive monocyte was also observed following direct administration of MCP-1 in regular diet-fed mice. Since MCP-1 was directly infused into mice to the same physiological levels observed in DIO mice, the possibility that increased CD11b-positive monocytes were caused by unknown obesity-related factors other than MCP-1 can be excluded. We therefore concluded that systemic increases in MCP-1 lead to changes in the CD11b-positive monocyte population in circulating blood. However, our study did not address the sites of monocyte activation. Current models of monocyte activation posit the attachment and rolling of monocyte to the MCP-1

secreted surface. Whether any local sites display high concentrations of MCP-1 protein in obese mice and the possibility of alternative activation pathways for monocyte to macrophages would represent interesting avenues of investigation. A recent report on the effect of systemic administration of MCP-1 on atherosclerotic development also supports our hypothesis (15). That study reported that MCP-1 infusion in mice causes accumulation of MOMA-2-positive monocytes in collateral arteries and increases neointimal formations. The increased macrophages in obese mice described in the present manuscript could thus lead to the stimulation of inflammatory processes in atheromatous plaque, contributing to the development of atherosclerotic lesions.

From the data presented, we infer that obesity in mice increases MCP-1 mRNA expressions in EWAT and MCP-1 plasma protein levels, both of which are well correlated with changes in body weight. In addition, these changes lead to increases in the population of CD11b-positive monocytes in circulating blood. We therefore propose MCP-1 protein as one of the molecular factors connecting obesity and atherosclerosis. A test of whether differences exist in response to pharmacological manipulation of MCP-1 between obese and normal subjects in terms of atherosclerotic developments would be of interest.

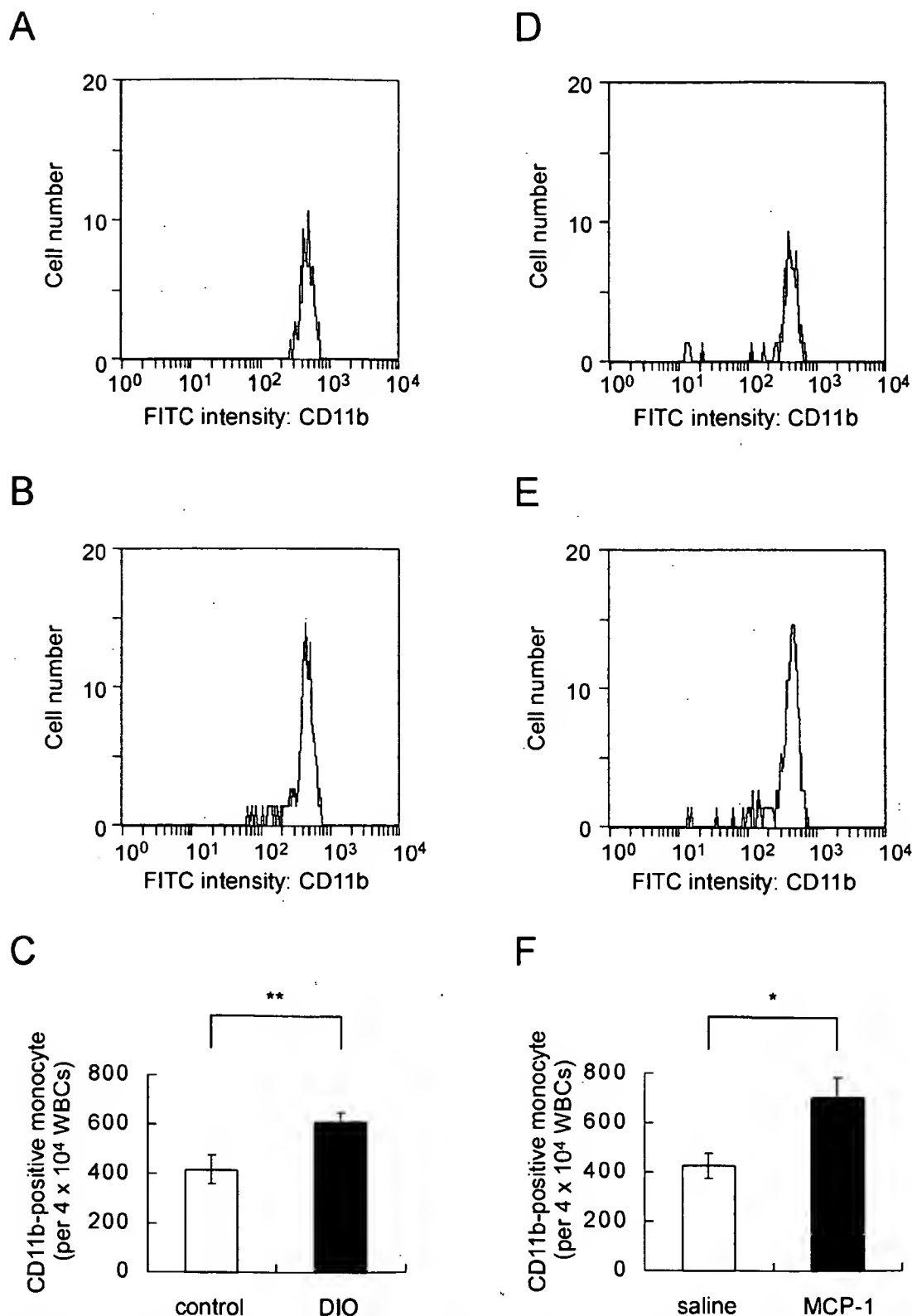


FIG. 3. Analysis of CD11b-positive monocyte using flow cytometry. Flow cytometric analysis was used to determine CD11b expression on circulating monocytes. Peripheral blood cells from each mouse model were stained using anti-CD11b monoclonal antibody conjugated with fluorescein isothiocyanate (FITC) and applied to flow cytometric analysis. A–C, CD11b-positive monocytes in control and DIO mice. Representative flow cytometric histograms of CD11-positive monocytes from control (A) and DIO mouse (B) are shown. C, mean number of CD11b-positive monocytes in control and DIO mice ($n = 10-14$; $**$, $p < 0.01$). Control mice are indicated by the white bar, and DIO mice are indicated by the black bar. WBCs, white blood cells. D–F, effects of MCP-1 treatment on CD11b expression on circulating monocytes. MCP-1 or saline was infused into normal female C57BL/6 mice ($n = 4-5$) for 2 weeks using an osmotic pump at a dose of $10 \text{ ng}/0.5 \mu\text{l}/\text{h}$. Representative flow cytometric histograms of saline-infused (D) or MCP-1-infused mice (E) are shown. F, mean number of CD11b-positive monocytes in saline- or MCP-1-infused mice ($n = 4-5$; $*$, $p < 0.05$). Saline-infused mice are indicated by white bars, and MCP-1-infused mice are indicated by black bars. Monocyte population was determined from fluorescence and light scatter characteristics. In all samples, 40,000 white blood cells were counted and analyzed. Error bars represent S.E.

REFERENCES

1. Zimmet, P., Alberti, K. G., and Shaw, J. (2001) *Nature* **414**, 782-787
2. Ginsberg, H. N. (2000) *J. Clin. Invest.* **106**, 453-458
3. Kopelman, P. G. (2000) *Nature* **404**, 635-643
4. Calle, E. E., Rodriguez, C., Walker-Thurmond, K., and Thun, M. J. (2003) *N. Engl. J. Med.* **348**, 1625-1638
5. Gerrity, R. G. (1981) *Am. J. Pathol.* **103**, 181-190
6. Ross, R. (1993) *Nature* **362**, 801-809
7. Rollins, B. J. (1997) *Blood* **90**, 909-928
8. Baggiolini, M. (1998) *Nature* **392**, 565-568
9. Yla-Herttuala, S., Lipton, B. A., Rosenfeld, M. E., Sarkioja, T., Yoshimura, T., Leonard, E. J., Witztum, J. L., and Steinberg, D. (1991) *Proc. Natl. Acad. Sci. U. S. A.* **88**, 5252-5256
10. Strieter, R. M., Wiggins, R., Phan, S. H., Wharram, B. L., Showell, H. J., Remick, D. G., Chensue, S. W., and Kunkel, S. L. (1989) *Biochem. Biophys. Res. Commun.* **162**, 694-700
11. Rollins, B. J., Yoshimura, T., Leonard, E. J., and Pober, J. S. (1990) *Am. J. Pathol.* **136**, 1229-1233
12. Boring, L., Gosling, J., Cleary, M., and Charo, I. F. (1998) *Nature* **394**, 894-897
13. Gu, L., Okada, Y., Clinton, S. K., Gerard, C., Sukhova, G. K., Libby, P., and Rollins, B. J. (1998) *Mol. Cell* **2**, 275-281
14. Gosling, J., Slaymaker, S., Gu, L., Tseng, S., Zlot, C. H., Young, S. G., Rollins, B. J., and Charo, I. F. (1999) *J. Clin. Invest.* **103**, 773-778
15. van Royen, N., Hoefer, I., Bottinger, M., Hua, J., Grundmann, S., Voskuil, M., Bode, C., Schaper, W., Buschmann, I., and Piek, J. J. (2003) *Circ. Res.* **92**, 218-225
16. Loskutoff, D. J., and Samad, F. (1998) *Arterioscler. Thromb. Vasc. Biol.* **18**, 1-6
17. Yudkin, J. S., Kumari, M., Humphries, S. E., and Mohamed-Ali, V. (2000) *Atherosclerosis* **148**, 209-214
18. Hotamisligil, G. S., Arner, P., Caro, J. F., Atkinson, R. L., and Spiegelman, B. M. (1995) *J. Clin. Invest.* **95**, 2409-2415
19. Steppan, C. M., Bailey, S. T., Bhat, S., Brown, E. J., Banerjee, R. R., Wright, C. M., Patel, H. R., Ahima, R. S., and Lazar, M. A. (2001) *Nature* **409**, 307-312
20. Yamauchi, T., Kamon, J., Waki, H., Terauchi, Y., Kubota, N., Hara, K., Mori, Y., Ide, T., Murakami, K., Tsuboyama-Kasaoka, N., Ezaki, O., Akanuma, Y., Gavrilova, O., Vinson, C., Reitman, M. L., Kagechika, H., Shudo, K., Yoda, M., Nakano, Y., Tobe, K., Nagai, R., Kimura, S., Tomita, M., Froguel, P., and Kadowaki, T. (2001) *Nat. Med.* **7**, 941-946
21. Juan-Vague, I., and Alessi, M. C. (1999) *Thromb. Haemostasis* **82**, 832-836
22. Friedman, J. M. (2000) *Nature* **404**, 632-634
23. Kahn, B. B., and Flier, J. S. (2000) *J. Clin. Invest.* **106**, 473-481
24. Mashiko, S., Ishihara, A., Iwaasa, H., Sano, H., Oda, Z., Ito, J., Yumoto, M., Okawa, M., Suzuki, J., Fukuroda, T., Jitsuoka, M., Morin, N. R., Macneil, D. J., Van der Ploeg, L. H. T., Ihara, M., Fukami, T., and Kanatani, A. (2003) *Endocrinology* **144**, 1793-1801
25. Wasserman, F. (1965) in *Handbook of Physiology* (Renold, A. E., and Cahill, G. F., eds) pp. 87-100, American Physiology Society, Washington, D. C.
26. Boring, L., Gosling, J., Monteclaro, F. S., Lysis, A. J., Tsou, C. L., and Charo, I. F. (1996) *J. Biol. Chem.* **271**, 7551-7558
27. Hansen, B. C. (1999) *Ann. N. Y. Acad. Sci.* **892**, 1-24
28. Sartipy, P., and Loskutoff, D. J. (2003) *Proc. Natl. Acad. Sci. U. S. A.* **100**, 7265-7270
29. Ahren, B., Mansson, S., Gingerich, R. L., and Havel, P. J. (1997) *Am. J. Physiol.* **273**, R113-R120
30. Vaddi, K., and Newton, R. C. (1994) *J. Immunol.* **153**, 4721-4732
31. Leenen, P. J. M., de Bruijn, M. F. T. R., Voerman, J. S. A., Campbell, P. A., and van Ewijk, W. (1994) *J. Immunol. Methods* **174**, 5-19
32. Kullo, I. J., Hensrud, D. D., and Allison, T. G. (2002) *Am. J. Cardiol.* **89**, 1441-1443

Circulation

JOURNAL OF THE AMERICAN HEART ASSOCIATION

American Heart
Association® 
Learn and Live™

**Augmented Expression of Neuronal Nitric Oxide Synthase in the Atria
Parasympathetically Decreases Heart Rate During Acute Myocardial Infarction
in Rats**

Yoshihito Takimoto, Takeshi Aoyama, Koichi Tanaka, Reiko Keyamura, Yoshiki Yui
and Shigetake Sasayama

Circulation 2002;105:490-496

DOI: 10.1161/hc0402.102662

Circulation is published by the American Heart Association, 7272 Greenville Avenue, Dallas, TX 72514
Copyright © 2002 American Heart Association. All rights reserved. Print ISSN: 0009-7322. Online
ISSN: 1524-4539

The online version of this article, along with updated information and services, is
located on the World Wide Web at:

<http://circ.ahajournals.org/cgi/content/full/105/4/490>

Subscriptions: Information about subscribing to *Circulation* is online at
<http://circ.ahajournals.org/subscriptions/>

Permissions: Permissions & Rights Desk, Lippincott Williams & Wilkins, a division of Wolters
Kluwer Health, 351 West Camden Street, Baltimore, MD 21202-2436. Phone: 410-528-4050. Fax:
410-528-8550. E-mail:
journalpermissions@lww.com

Reprints: Information about reprints can be found online at
<http://www.lww.com/reprints>

Augmented Expression of Neuronal Nitric Oxide Synthase in the Atria Parasympathetically Decreases Heart Rate During Acute Myocardial Infarction in Rats

Yoshihito Takimoto, MD; Takeshi Aoyama, MD, PhD; Koichi Tanaka, PhD; Reiko Keyamura, MD; Yoshiki Yui, MD, PhD; Shigetake Sasayama, MD, PhD

Background—Nitric oxide (NO) synthesized within sinoatrial cells recently has been shown to participate in the autonomic control of heart rate. We hypothesized that NO in the neuronal cells in the heart was increased and parasympathetically regulated heart rate after myocardial infarction (MI).

Methods and Results—We examined heart rate dynamics and neuronal NO synthase (nNOS) expression and activities in the atria of rats with MI 1, 3, 7, and 14 days after MI ($n=7$ to 22 for each group). Both the mRNA levels of nNOS in the atria determined by competitive reverse transcriptase–polymerase chain reaction and the protein levels determined by Western blotting were significantly increased compared with controls 1, 3, and 7 days after MI. nNOS activity in the atria 1 day after infarction was also increased in MI rats. nNOS immunoreactivity was observed in nerve fibers in the atria. After infusion of a specific inhibitor of nNOS and iNOS, 1-(2-trifluoromethylphenyl) imidazole (TRIM) (50 mg/kg IV), heart rate was significantly ($P<0.01$) increased in MI rats compared with controls 1, 3, and 7 days after MI. The iNOS-specific inhibitor, 1400W (10 mg/kg SC), did not significantly affect the heart rate in rats with MI. The effect of TRIM was abolished by pretreatment with L-arginine (25 mg/kg IV) or by parasympathetic blockade with atropine but not by propranolol. There was a strong correlation ($r=0.837$, $P<0.0001$) between the nNOS protein expression and heart rate change after TRIM infusion.

Conclusions—These results indicate that increased nNOS parasympathetically decreased heart rate via the production of NO in rats with acute MI. (*Circulation*. 2002;105:490-496.)

Key Words: nitric oxide synthase ■ heart rate ■ myocardial infarction

Neuronal nitric oxide synthase (nNOS), first identified in the cerebella, has also been detected in the heart. nNOS immunoreactivity has been demonstrated in the ganglia and nerve fibers in the heart.^{1,2} Recently, several lines of evidence have demonstrated that nitric oxide (NO) synthesized from nNOS is one of the modulators of autonomic activities and decreases the heart rate in intact mammals.³⁻⁹ However, the role of nNOS in the autonomic control of heart rate is controversial. Moreover, its role in pathological conditions remains to be determined.

We recently reported that nNOS expression was increased in the ventricle during acute myocardial infarction (MI) in rats.¹⁰ We hypothesized that nNOS expression in the atria might also be increased and parasympathetically play a role in heart-rate regulation during acute MI. We examined nNOS expression and heart-rate dynamics using a rat MI model and found that nNOS expression was significantly increased and that augmented expression of nNOS parasympathetically attenuated the heart rate during acute MI.

Methods

Rat Myocardial Infarction Model

We performed animal experiments in accordance with the Declaration of Helsinki, and these were approved by our institutional ethics committee for animal experiments. MI was surgically induced in 8-week-old male Sprague-Dawley (IGS) rats (Charles River Japan Inc, Yokohama, Japan) weighing 280 to 320 g by ligation of the left anterior descending coronary artery, as described previously.¹¹ Transthoracic echocardiography (Hewlett-Packard) was performed at each time point with a 7.5-MHz sector scan probe.¹² At 1, 3, 7, and 14 days after the procedure, rats were sacrificed. Three thin transverse slices were cut from the apex to the base, and the infarct size was determined as described previously.^{11,13}

Quantitative Competitive Reverse Transcriptase–Polymerase Chain Reaction

Total cellular RNA was extracted from the atria using the acid guanidinium thiocyanate-phenol-chloroform method and was reverse-transcribed into cDNA according to the method described previously.¹¹ The cDNA samples were subjected to polymerase chain reaction (PCR) amplification using primers complementary to

Received August 15, 2001; revision received October 31, 2001; accepted November 5, 2001.

From the Department of Cardiovascular Medicine (Y.T., T.A., R.K., Y.Y., S.S.), Graduate School of Medicine, Kyoto University, Kyoto, Japan, and Department of Anatomy (K.T.), Hyogo College of Medicine, Hyogo, Japan.

Correspondence to Takeshi Aoyama, MD, Department of Cardiovascular Medicine, Graduate School of Medicine, Kyoto University, 54 Kawaracho, Shogoin, Sakyo-ku, Kyoto 606-8507, Japan. E-mail taoyama@kuhp.kyoto-u.ac.jp

© 2001 American Heart Association, Inc.

Circulation is available at <http://www.circulationaha.org>

TABLE 1. Systolic Blood Pressure, Heart Rate, Body Weight, Heart Weight, Left Ventricular Dimension, and Fractional Shortening of Rats With Myocardial Infarction and of Sham-Operated Controls

Time After Infarction, days	0	1	3	7	14
Systolic BP, mm Hg					
MI	129±1	111±2*	109±1*	115±1*	124±1*
Sham	127±2	124±2	119±2	135±2	135±1
HR, beats/min					
MI	371±2	479±3*	419±5*	397±4*	379±2
Sham	366±5	402±8	375±2	377±6	380±2
BW, g					
MI	312±6	285±7	270±7	287±10	316±10
Sham	309±18	270±3	278±7	284±13	317±8
HW, mg					
MI	...	898±28	920±16†	854±26	936±29
Sham	...	818±25	831±39	846±48	957±27
HW/BW, mg/g					
MI	...	3.15±0.12	3.41±0.11†	2.98±0.05	2.96±0.04
Sham	...	3.03±0.04	2.99±0.06	2.98±0.08	3.02±0.04
LV0d, mm					
MI	6.1±0.1	6.9±0.1*	7.3±0.1*	7.7±0.1*	8.3±0.1*
Sham	6.0±0.1	6.0±0.1	6.0±0.1	6.1±0.1	6.4±0.1
LV0s, mm					
MI	3.3±0.1	5.3±0.1*	5.8±0.1*	6.2±0.1*	6.4±0.1*
Sham	3.4±0.1	3.4±0.1	3.5±0.1	3.6±0.1	3.7±0.1
FS, %					
MI	45.7±0.6	22.1±0.5*	21.3±0.6*	20.1±0.4*	19.9±0.7*
Sham	44.6±0.4	42.6±0.9	41.4±1.0	41.1±0.8	42.2±0.5
MI size, %					
MI	...	52.2±3.1	50.1±4.8	48.3±2.1	47.3±1.0
No. of rats					
MI	22	22	15	13	11
Sham	12	12	11	8	7

Values are mean±SEM.

BP indicates blood pressure; HR, heart rate; BW, body weight; HW, heart weight; LV0d, left ventricular diastolic dimension; LV0s, left ventricular systolic dimension; and FS, fractional shortening.

* $P<0.01$; † $P<0.05$ for the infarct group compared with the respective noninfarcted control group at each time point.

positions 2416 to 3033 of the rat nNOS cDNA sequence (sense, 5'-GTC TTC CAC CAG GAG ATG -3'; antisense, 5'-AAA GGC ACA GAA GTG GGG GTA -3').¹⁴ The PCR amplification of the constitutively expressed GAPDH cDNA was used as a measure of the amount of input RNA. DNA fragments that shared the same primer template sequence with the target cDNA but contained a completely different smaller intervening sequence were prepared and used as DNA internal standards (mimics).¹⁵ Aliquots of sample cDNA mixed together with 6 serial dilutions of DNA mimics were coamplified as templates in the presence of primer pairs. PCR was performed as described previously.¹¹ The PCR reaction products (20 μ L) were analyzed via electrophoresis through 1.5% agarose gels containing 0.5 μ g/mL ethidium bromide, and the results were quantified by scanning densitometry using the NIH Image computer software.

Western Blot Analysis

Lysates (60 μ g) from rat atria were separated by 7.5% SDS-PAGE, and Western blotting was performed with anti-nNOS antibody (NOS1, R-20, Santa Cruz Biotechnology, Inc) according to the method described previously.¹¹

Determination of NOS Activity

Total NOS activity was measured using a NOS Assay Kit (Cayman Chemical Co), [³H]-L-arginine (Amersham Pharmacia), and 10 mmol/L *N*-monomethyl-L-arginine (Wako Chemical) according to the manufacturer's instructions. NOS activity in the presence of ethylene diamine tetra acetic acid (1 mmol/L) (Wako Chemical), an nNOS- and inducible NOS (iNOS)-specific inhibitor, 1-(2-trifluoromethylphenyl) imidazole (TRIM) (100 μ mol/L) (Tocris Cookson Inc), or iNOS-specific inhibitor 1400W (2 μ mol/L) (Cal-

biochem) was also determined. Each NOS isoform activity was calculated from these measures.

Immunohistochemistry

The rats were reanesthetized and perfused through the left ventricle with 100 mL of 4% paraformaldehyde in 0.1 mol/L phosphate buffer (pH 7.4). Two blocks of the atrium known to contain ganglionic cell bodies were removed. One was the region around the sinoatrial node and the other near the pulmonary veins and the atrioventricular node. After rinsing with phosphate buffered saline (PBS), they were stored in 20% sucrose in PBS for 2 hours. Free-floating sections of 40- μ m thickness were preincubated with PBS containing 10% normal donkey serum, 0.2% BSA, and 0.3% Triton X-100 for 60 minutes at room temperature. The nNOS antibody was applied at a dilution of 1:500 in PBS containing 0.2% BSA and 0.1% Triton X-100 for 48 hours at 4°C. After rinsing with PBS, the sections were incubated with Cy3-conjugated anti-rabbit IgG produced in donkey (Jackson) diluted 1:500 in PBS for 90 minutes at room temperature. The tissue was viewed with an Olympus AX-80 fluorescence microscope using a filter with an excitation range of 560 to 596 nm and an emission range of 610 to 655 nm.

Heart-Rate Dynamics and Autonomic Blockade

The basal heart rate and systolic blood pressure of each animal were measured by a tail-cuff method in the fully conscious drug-free state. Rats with MI or sham operation received atropine 0.5 mg/kg IP or 1 mg/kg propranolol IV, and heart rate and blood pressure were measured every 2 minutes for 30 minutes 1 and 14 days after infarction. We used TRIM or 1400W to determine the effect of nNOS or iNOS on the heart rate regulation. After the measurement of baseline heart rate and blood pressure, rats received TRIM 50 mg/kg IV or 1400W 10 mg/kg SC, and heart rate and blood pressure were measured every 2 minutes for 1 hour 1, 3, 7, and 14 days after the operation. After the administration of L-arginine (25 mg/kg IV) or the autonomic blockade with atropine or propranolol, rats also received TRIM to determine the effect of nNOS on the autonomic heart-rate regulation.

Statistics

Values are presented as mean \pm SEM. The measurements from rats with MI were compared with those of sham-operated rats by the Student's unpaired *t* test. The significance of difference among the means of various groups was analyzed by one-way ANOVA with post-hoc comparisons by the Tukey-Kramer test. Relationships between 2 variables were tested by linear regression analysis. Significance was taken as $P < 0.05$.

Results

Heart Weight, Body Weight, and Echocardiographic Study

The heart weight and the heart-weight-to-body-weight ratio of the myocardial infarction group 3 days after infarction, by which time inflammation and edema had developed within the infarct, were significantly increased ($P < 0.05$) compared with those of the sham-operated control group. The heart weights of MI rats 7 days after infarction were decreased because of the shrinkage of infarcted tissue. All animals developed large MIs, with an infarct size ranging from 38.9% to 62.5% of the left ventricle's circumference. Left ventricular diastolic and systolic dimensions were rapidly increased during the acute phase of MI, and additional changes were observed by 2 weeks ($P < 0.01$ at each time point compared with sham-operated rats). Fractional shortening was rapidly decreased during the acute phase of MI because of akinesis of the anterior wall and then gradually decreased during the

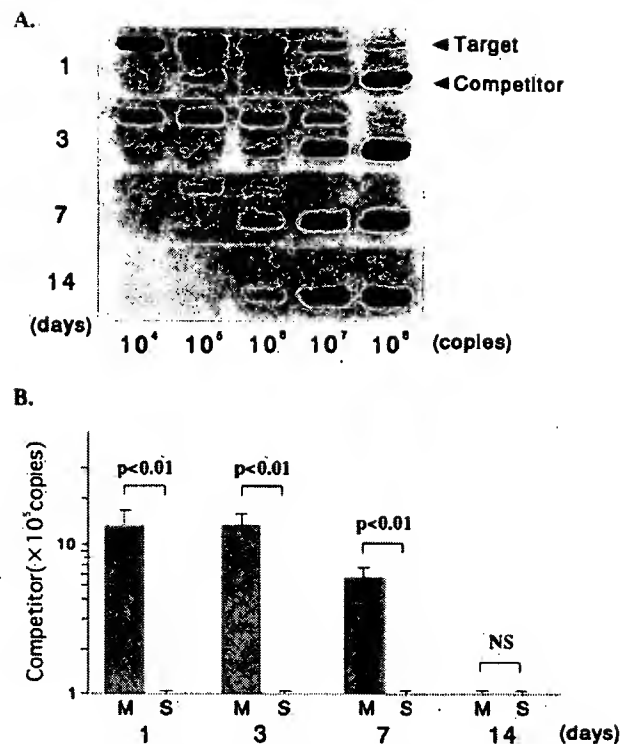


Figure 1. A, Representative competitive reverse transcriptase-PCR of nNOS. B, Densitometric analyses of the PCR bands show that nNOS mRNA expression was increased in the atria in rats with MI 1, 3, and 7 days after infarction.

chronic phase ($P < 0.01$ at each time point compared with sham-operated rats) (Table 1).

Quantitative Reverse Transcriptase-PCR of nNOS mRNA

The mRNA levels of nNOS were 13.4×10^5 , 13.3×10^5 , and 5.8×10^5 copies 1, 3, and 7 days after infarction in rats with

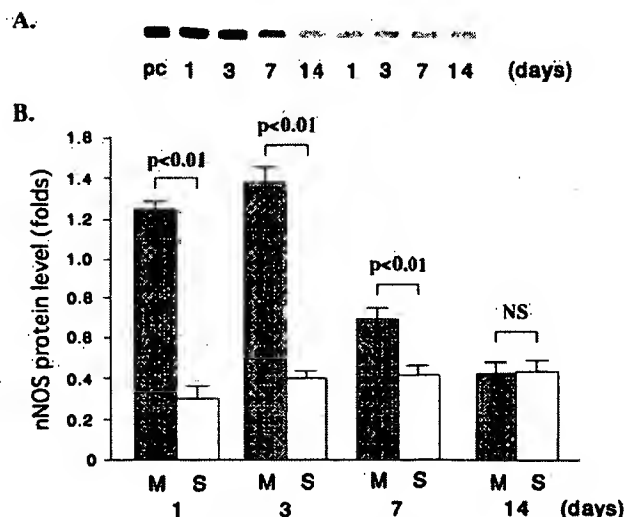


Figure 2. A, Representative Western blotting of nNOS. B, nNOS protein expression was significantly increased in the atria during acute MI. PC indicates positive control; M, rats with MI; and S, sham-operated rats.

TABLE 2. NOS Activity in the Atria

	MI (n=6)	Sham (n=6)
Total, nmol/g per min	1.43±0.04*	0.56±0.10
nNOS, nmol/g per min	0.86±0.13†	0.14±0.09
eNOS, nmol/g per min	0.45±0.19	0.38±0.07
iNOS, nmol/g per min	0.12±0.03	0.04±0.02

Values are mean±SEM.

* $P<0.01$; † $P<0.05$ for the infarct group compared with the noninfarcted control group.

MI, respectively, and $<1 \times 10^5$ in rats 14 days after MI and sham-operated rats (Figure 1). There was no difference in the expression levels of GAPDH in each group (data not shown). Thus, the nNOS mRNA expression level was significantly increased during acute MI.

Western Blotting of nNOS

Western blotting showed 160-kDa bands in the atria of rats with MI and in the sham-operated rats. No other minor bands were observed. As a positive control for nNOS, 20 μ g of lysates of rat cerebellar tissues were used in each experiment (Figure 2A). nNOS protein levels were expressed as the fold increase compared with positive controls. The protein levels of nNOS were 1.2-, 1.3-, 0.7-, and 0.4-fold compared with positive controls in the rats with MI and 0.3-, 0.4-, 0.4-, and 0.4-fold in the sham-operated rats 1, 3, 7, and 14 days after infarction, respectively. Protein expression of nNOS was significantly ($P<0.01$) increased in the rats with MI 1, 3, and 7 days after infarction compared with the sham-operated rats (Figure 2B).

NOS Activity

Total and nNOS activities were significantly increased in the atria of rats with MI 1 day after infarction compared with

those in sham-operated rats. NOS activity in the presence of TRIM but not 1400W was significantly decreased in the atria of rats with MI (data not shown). Endothelial NOS (eNOS) and iNOS activity did not change in the atria after MI (Table 2).

Immunohistochemistry of nNOS

There were nNOS immunoreactive nerve fibers in the region around the sinoatrial node and the region near the pulmonary veins and the atrioventricular node. The number of nNOS immunoreactive nerve fibers was increased compared with sham-operated rats (data not shown). Cardiomyocytes were not stained with nNOS antibody (Figure 3).

Effects of TRIM and 1400W on Heart Rate

Rats with MI had a significantly ($P<0.01$) higher basal heart rate compared with sham-operated rats 1, 3, and 7 days after the procedure (Table 1). Heart rate changes after the infusion of TRIM were 66 ± 12 , 59 ± 4 , 32 ± 3 , and 6 ± 2 bpm in rats with MI and 8 ± 4 , 6 ± 3 , 6 ± 2 , and 4 ± 3 bpm in sham-operated rats 1, 3, 7, and 14 days after the procedure, respectively (Figure 4A). Compared with the effect of TRIM on heart rate in sham-operated rats, the infusion of TRIM led to significantly ($P<0.01$) larger changes in rats with MI 1, 3, and 7 days after infarction. After the administration of L-arginine, the heart rate was changed from 466 ± 10 to 477 ± 21 in rats with MI and from 401 ± 15 to 404 ± 9 in controls 1 day after infarction. The heart rate was not significantly increased in infarcted rats (from 477 ± 21 to 490 ± 27) or in sham-operated rats (from 404 ± 9 to 401 ± 9) after the additional injection of TRIM. Thus, the effect of TRIM was abolished by the previous administration of L-arginine (Figure 4B). There was no significant heart rate change after the administration of 1400W in rats with MI or sham-operated rats 1 day after the procedure (Figure 4B).

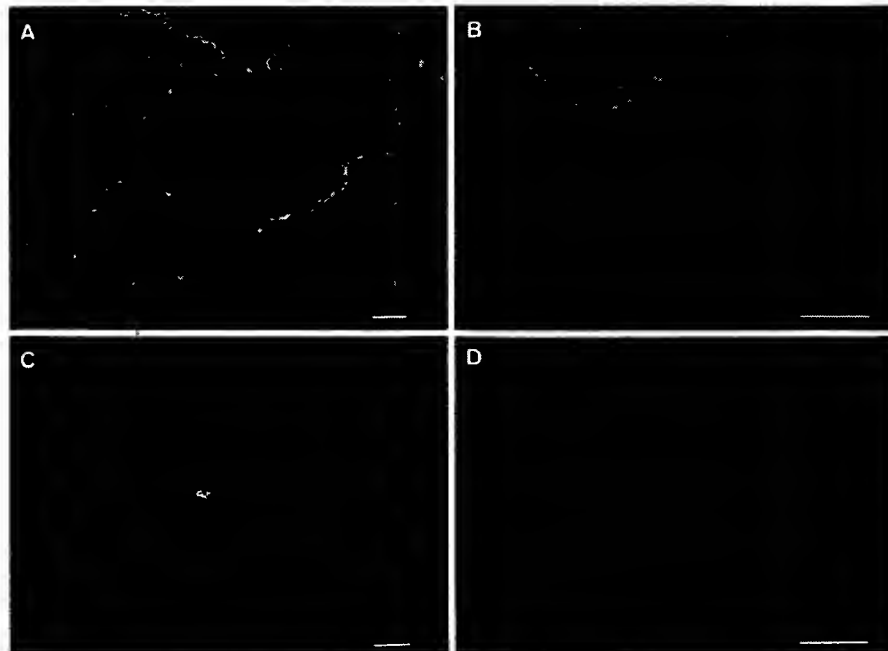


Figure 3. Immunohistochemistry of nNOS. There were nNOS immunoreactive nerve fibers in the region around the sinoatrial node (A and B) and the bundle of nerve fibers in the region near the pulmonary veins and the atrioventricular node (C and D). Cardiomyocytes were not stained with nNOS antibody. Bars=50 μ m.

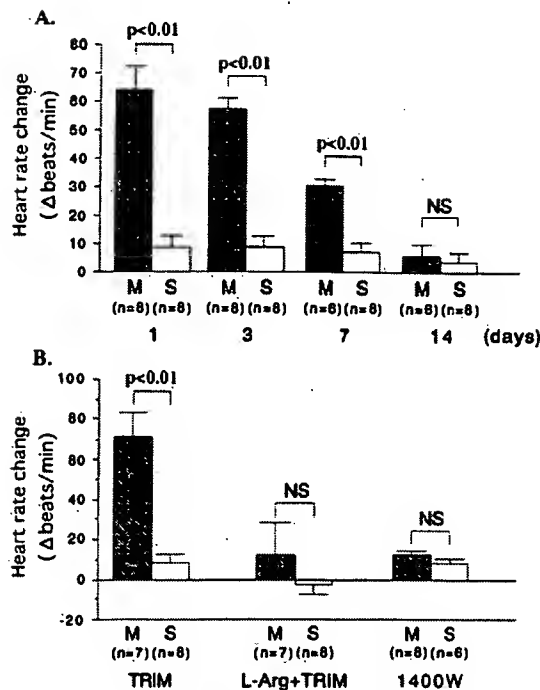


Figure 4. A, Heart rate change after the administration of TRIM. Heart rate was significantly increased after the administration of TRIM in rats with MI (M) compared with that of sham-operated rats (S) 1, 3, and 7 days after the procedure. B, Previous administration of L-arginine (L-Arg) abolished the effect of TRIM on heart rate 1 day after infarction. 1400W did not affect the heart rate in rats with MI and controls.

Autonomic Blockade

Administration of atropine led to a similar increase in heart rate; 118 ± 14 and 106 ± 9 bpm in rats with MI and 117 ± 13 and 101 ± 13 bpm in sham-operated rats 1 and 14 days after the procedure, respectively (Figure 5A). Propranolol administration also led to a similar heart rate change; -95 ± 11 and -67 ± 4 bpm in infarcted rats and -101 ± 7 and -77 ± 2 bpm in sham rats 1 and 14 days after infarction, respectively (Figure 5B). There was no significant difference in the heart rate change after autonomic blockade with atropine or propranolol between rats with MI and sham-operated rats in either the acute or the chronic phase of MI.

After the parasympathetic blockade with atropine, TRIM was infused into rats, and the heart rate was not significantly increased either in rats with MI (7 ± 5 bpm) or controls (0 ± 4 bpm) 1 day after infarction (Figures 5C and 5E). Administration of TRIM with pretreatment of propranolol led to a significant ($P < 0.01$) heart rate increase in rats with MI (55 ± 3 bpm) compared with sham-operated rats (14 ± 3 bpm) 1 day after infarction (Figures 5D and 5E).

Correlation of the Amount of nNOS Protein and the Effect of TRIM on Heart Rate

We plotted the relationships between the nNOS protein level and the heart rate change after TRIM infusion for each animal. As shown in Figure 6, there was a strong correlation ($Y = 69.263X - 14.338$, $r = 0.837$, $P < 0.0001$) between these two measures.

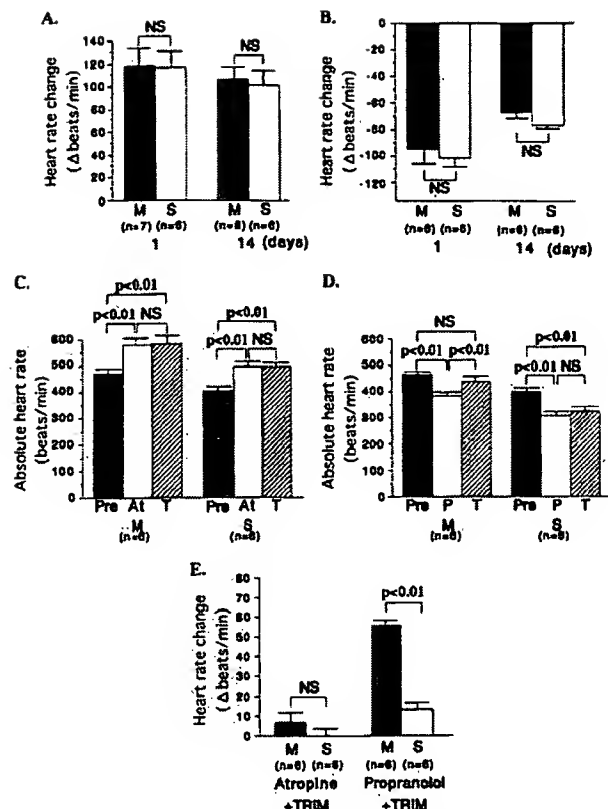


Figure 5. Heart rate change after parasympathetic blockade with atropine (A) or sympathetic blockade with propranolol (B). There was no significant difference between rats with MI (M) and controls (S). Absolute changes in heart rate (C and D) and heart rate change (E) after the administration of atropine (At) or propranolol (P) and TRIM (T). After the parasympathetic blockade with atropine, TRIM was infused into rats and heart rate was not significantly increased in either rats with MI or controls 1 day after infarction. Pre indicates preadministration of the drugs.

Discussion

We found that nNOS expression in both mRNA and protein levels and its activity were increased in the atria of the rat during the acute phase of MI. This is the first in vivo model in which nNOS expression was increased in the atria. We analyzed the effect of nNOS on heart rate using this novel model of rat MI. The administration of TRIM, but not 1400W, increased the heart rate, and this effect of TRIM was

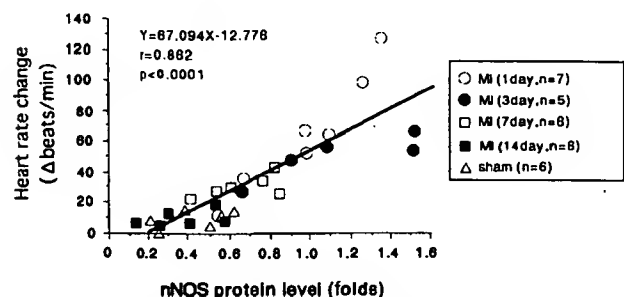


Figure 6. Relationships between the nNOS protein levels and the heart rate change after TRIM infusion for each animal. There was a strong correlation ($Y = 67.094X - 12.776$, $r = 0.862$, $P < 0.0001$) between these two measures.

abolished by the pretreatment with L-arginine. The heart rate was not increased additionally by the treatment of TRIM after parasympathetic blockade with atropine. This evidence suggests that nNOS parasympathetically decreased the heart rate via the production of NO in rats with acute MI.

It has been reported that the muscarinic control of heart rate is attenuated by inhibitors of the NO/cGMP pathway. Han et al¹⁶ reported that muscarinic regulation of L-type calcium current in cardiac myocytes is absent in mice deficient in eNOS. In contrast, the chronotropic responses to both β -adrenergic and muscarinic agonist were not altered in isolated cardiac tissue preparations in a study using the same mice.¹⁷ Thus, the role of eNOS in the muscarinic regulation of L-type calcium current is controversial. Tanaka et al¹ reported that the parasympathetic preganglionic nerve fibers originating from the vagus nerve contained nNOS in the guinea pig heart. Several lines of evidence suggest that endogenous NO synthesized from nNOS in the heart decreases heart rate.³⁻⁹ As to the mechanism of heart rate reduction by nNOS, there are two possibilities. First, Sears et al⁴ reported that specific inhibition of nNOS with TRIM significantly enhanced the magnitude of the change in heart rate with sympathetic nerve stimulation. Choate et al⁵ reported that NO inhibited the positive chronotropic response evoked by cardiac sympathetic nerve stimulation via a cGMP-dependent pathway in the isolated guinea pig double atrial/right stellate ganglion preparation. These studies suggest that endogenous NO plays an inhibitory role in cardiac sympathetic neurotransmission. Second, Conlon et al⁶ reported that vagally evoked frequency-dependent bradycardia was significantly attenuated by infusion of TRIM. Sears et al⁷ also demonstrated that the NO precursor significantly enhanced the decrease in heart rate seen with right vagal nerve stimulation. These results suggest that NO in the heart parasympathetically decreases the heart rate. On the other hand, Elvan et al⁸ reported that NO played a stimulating role in mediating vagal neurotransmission and an inhibitory role in mediating sympathetic neurotransmission using open-chest dogs. The quantitative differences among these studies may result from the effects of endogenous nitric oxide on the vagal control of heart rate being critically dependent on the availability of nNOS. However, the expression level of nNOS was not determined in these studies. In the present study, we measured the expression level and activity of nNOS in the atria and showed that they were increased in the atria during acute MI, whereas they were low in control rats. Administration of TRIM, but not 1400W, increased the heart rate in rats with acute MI. After parasympathetic blockade with atropine, the heart rate was increased and no additional heart rate increase was observed by TRIM. In contrast, after β -adrenergic blockade with propranolol, TRIM increased the heart rate to the same degree as TRIM infusion without autonomic blockade. Our findings strongly suggest the latter possibility that NO synthesized from nNOS facilitates vagal chronotropic actions on the heart in vivo and are compatible with the findings of the study of Jumrussirikul et al⁹ that NO within sinoatrial cells participates in the cholinergic control of heart rate using mice deficient in nNOS.

Immunohistochemical analyses showed that nNOS immunoreactivity was observed in the nerve fibers in the region around the sinoatrial node and the region near the pulmonary veins and the atrioventricular node. Because ganglia in these region were not stained with nNOS antibody and the administration of atropine blocked the effects of TRIM, nNOS immunoreactive nerve fibers seem to be preganglionic fibers of the vagal nerve. It has been reported that nNOS existed in the nerve fibers and cardiomyocytes in the heart.^{1,18} In the present study, we observed nNOS immunoreactivity only in the nerve fibers. This evidence suggested that nNOS in the parasympathetic nerve plays an important role in heart rate regulation after MI.

NO in the central nervous system is also responsible for the autonomic regulation of the cardiovascular system. Despite possibly different modes of action of NO in different brain regions, the overall sympathoinhibitory role of NO observed by several studies in vivo seems to be predominant at least under physiological conditions.¹⁹ Although we did not determine the nNOS levels in the central nervous system, inhibition of nNOS in the brain by TRIM could activate sympathetic tone, resulting in an increased heart rate. However, in the present study we showed that nNOS protein expression in the atria has a strong correlation with the heart rate changes after the administration of TRIM. Furthermore, atropine administration abolished the effects of TRIM on heart rate. Thus, TRIM seems to inhibit the activity of nNOS in the atria, but not in the brain, and increases the heart rate.

Acknowledgments

This study was supported by grants-in-aid for scientific research from the Ministry of Education, Science, Sports and Culture, Japan, and a grant from the Japan Cardiovascular Research Foundation. We express our appreciation to Daniel Mrozek for help with preparation of this manuscript.

References

1. Tanaka K, Chiba T. The vagal origin of preganglionic fibers containing nitric oxide synthase in the guinea-pig heart. *Neurosci Lett*. 1998;252:135-138.
2. Hassall CJS, Saffrey MJ, Hoyle CHV. Nitric oxide synthase immunoreactivity and NADPH-diaphorase activity in a subpopulation of intrinsic neurones of the guinea-pig heart. *Neurosci Lett*. 1992;143:65-68.
3. Han X, Shimoni Y, Giles WR. An obligatory role for nitric oxide in autonomic control of mammalian heart rate. *J Physiol*. 1994;476:309-314.
4. Sears CE, Choate JK, Paterson DJ. Effect of nitric oxide synthase inhibition on the sympathetic-vagal control of heart rate. *J Auton Nerv Syst*. 1998;73:63-73.
5. Choate JK, Paterson DJ. Nitric oxide inhibits the positive chronotropic and inotropic responses to sympathetic nerve stimulation in the isolated guinea-pig atria. *J Auton Nerv Syst*. 1999;75:100-108.
6. Conlon K, Kidd C. Neuronal nitric oxide facilitates vagal chronotropic and dromotropic actions on the heart. *J Auton Nerv Syst*. 1999;75:136-146.
7. Sears CE, Choate JK, Paterson DJ. NO-cGMP pathway accentuates the decrease in heart rate caused by cardiac vagal nerve stimulation. *J Appl Physiol*. 1999;86:510-516.
8. Elvan A, Rubart M, Zipes D. NO modulates autonomic effects on sinus discharge rate and AV nodal conduction in open-chest dogs. *Am J Physiol*. 1997;272:H263-H271.
9. Jumrussirikul P, Dinerman J, Dawson TM, et al. Interaction between neuronal nitric oxide synthase and inhibitory G protein activity in heart rate regulation in conscious mice. *J Clin Invest*. 1998;102:1279-1285.

10. Takimoto Y, Aoyama T, Inoue R, et al. Differential expression of three types of nitric oxide synthetase in both the infarcted and non-infarcted left ventricle after myocardial infarction in the rat. *Int J Cardiol*. 2000; 76:135-145.
11. Aoyama T, Takimoto Y, Pennica D, et al. Augmented expression of cardiotrophin-1 and its receptor component, gp130, in both left and right ventricles after myocardial infarction in the rat. *J Moll Cell Cardiol*. 2000;32:1821-1830.
12. Litwin SE, Katz SE, Morgan JP, et al. Serial echocardiographic assessment of left ventricular geometry and function after large myocardial infarction in the rat. *Circulation*. 1994;89:345-354.
13. Pfeffer JM, Pfeffer MA, Fletcher PJ, et al. Progressive ventricular remodeling in rat with myocardial infarction. *Am J Physiol*. 1991;260: H1406-H1414.
14. Bredt DS, Hwang PM, Glatt CE, et al. Cloned and expressed nitric oxide synthase structurally resembles cytochrome P-450 reductase. *Nature*. 1991;351:714-718.
15. Nishida Y, Knudson CB, Nietfeld JJ, et al. Antisense inhibition of hyaluronan synthase-2 in human articular chondrocytes inhibits proteoglycan retention and matrix assembly. *J Biol Chem*. 1999;274: 21893-21899.
16. Han X, Kubota I, Feron O, et al. Muscarinic cholinergic regulation of cardiac myocyte I_{Ca-L} is absent in mice with targeted disruption of endothelial nitric oxide synthase. *Proc Natl Acad Sci U S A*. 1998;95: 6510-6515.
17. Vandecasteele G, Eschenhagen T, Scholz H, et al. Muscarinic and β -adrenergic regulation of heart rate, force of contraction and calcium current is preserved in mice lacking endothelial nitric oxide synthase. *Nat Med*. 1999;5:331-334.
18. Xu KY, Huso DL, Dawson TM, et al. Nitric oxide synthase in cardiac sarcoplasmic reticulum. *Proc Natl Acad Sci U S A*. 1999;96:657-662.
19. Lo W, Jan C, Wu S, et al. Cardiovascular effects of nitric oxide and adenosine in the nucleus tractus solitarii of rats. *Hypertension*. 1998;32: 1034-1038.

Differential Upregulation of Cellular Adhesion Molecules at the Sites of Oxidative Stress in Experimental Acute Pancreatitis¹

Géza Telek, M.D.,* Robert Ducroc, M.D.,* Jean-Yves Scoazec, M.D.,† Catherine Pasquier, M.D.,‡ Gérard Feldmann, M.D.,† and Claude Rozé, M.D.*

*INSERM U 410, †INSERM U 327, and ‡INSERM U 479, Faculté de Médecine Xavier Bichat, Université Paris 7 Denis Diderot, 75870 Paris, France

Submitted for publication August 10, 2000; published online January 19, 2001

Background. Severe acute pancreatitis (AP) is associated with exaggerated leukocyte adherence and activation. Endothelial cellular adhesion molecules (CAMs) can be induced by cytokines, but also directly by oxygen free radicals (OFRs), mediated by nuclear factor kappa-B (NF- κ B). We investigated the behavior of inducible CAMs in relation to pancreatic oxidative stress. Our novel modification of cerium capture histochemistry (reaction of OFRs with cerium produces laser reflective Ce perhydroxide precipitates) combined with reflectance confocal laser scanning microscopy (CLSM) allows the histological codemonstration of *in vivo* OFR production and immunolabeled CAMs, or NF- κ B.

Methods. Taurocholate AP was induced in rats; sham operated and normal animals served as controls. To achieve *in situ*, *in vivo* reaction of cerium with OFRs, animals were perfused with CeCl₃ solution at different time points (1, 2, 8, 24 h) and then sacrificed. E-selectin, P-selectin, ICAM-1, VCAM, and NF- κ B p65 were labeled by immunofluorescence (IF) on frozen sections of cerium perfused pancreata. IF and Ce perhydroxide reflectance were simultaneously detected by CLSM. Pancreatic gene expression of the same CAMs was quantified by competitive RT-PCR (MIMIC internal control).

Results. Control pancreata showed negligible reflectance and minimal CAM expression. Early (1, 2 h) AP samples were characterized by intense, heterogeneous acinar OFR production, strong P-selectin, and increasing ICAM expression, with nuclear translocation of p65, histologically all colocalizing with the areas of acinar oxidative stress. Adherent polymorphonuclear leukocytes (PMNs) displayed weak OFR formation.

Later (8, 24 h), a slowly declining P-selectin, but persisting ICAM-1 expression, was paralleled by widespread adherence of PMNs producing surprisingly large amounts of OFRs. VCAM and E-selectin showed a mild increase at 24 h. CAM gene activation was in good correlation with the protein expression.

Conclusion. The early acinar oxidative stress is colocalized with NF- κ B activation, preferential P-selectin, and ICAM upregulation in this AP model. Subsequently, adherent, activated PMNs become the major source of OFRs, thereby contributing to tissue damage. © 2001 Academic Press

INTRODUCTION

Severe necrotizing acute pancreatitis (AP)² is recognized to be a multiple-stage disease where the pathological events at the acinar cell level are paralleled by an exaggerated local and systemic inflammatory response [1]. Excessive release of oxygen derived free radicals (OFRs) and destructive microbicid enzymes by activated leukocytes—predominantly polymorphonuclear (PMN) cells—aggravate the local and AP associated multiorgan injury.

The recruitment of leukocytes to inflammatory sites is mediated by the "adhesion cascade" of cellular adhesion molecules (CAMs) [2]. Selectins are responsible for

² Abbreviations used: AP, acute pancreatitis; CAM, cellular adhesion molecule; CLSM, confocal laser scanning microscopy; FITC, fluorescein isothiocyanate; ICAM-1, intercellular adhesion molecule; IF, immunofluorescence; LRS, lactated Ringer's solution; NF- κ B, nuclear transcription factor-kappaB; OFR, oxygen free radical; PAF, platelet activating factor; PBD, pancreatobiliary duct; PECAM, platelet endothelial cell adhesion molecule; PMN, polymorphonuclear leukocyte; PMSF, phenylmethylsulfonyl fluoride; RT-PCR, reverse transcriptase polymerase chain reaction; VCAM, vascular cell adhesion molecule.

¹ This study was supported in part by grants from IRMAD Foundation France, Solvay Pharmaceuticals France, and Charles Debray Foundation, France.



the initial leukocyte rolling along the vessel walls. In response to proinflammatory stimuli, OFRs [3], and hypoxia [4], preformed P-selectin can be translocated within minutes to the endothelial cell surface from the cytoplasmic Weibel-Palade bodies. Subsequently, a *de novo* synthesis of E- and P-selectin is initiated. The firm adhesion of PMNs is predominantly a result of interactions between leukocyte integrins and the constitutively expressed, or newly synthesized, endothelial ICAM-1. Requirements for the transmigration of PMNs include platelet-endothelial cell adhesion molecule-1 (PECAM-1) [5] and vascular cell adhesion molecule-1 (VCAM-1) [6].

The precise role and source of oxidative stress in AP is the subject of continued debate. Acinar cell xanthine oxidase [7-9] and activated leukocytes, principally PMNs [10-12], are thought to be the major OFR producers. OFRs have diverse detrimental effects [13-15]; furthermore, recent evidence suggests that they may function as second messengers by activating certain gene transcription factors, notably the nuclear transcription factor-kappa B (NF- κ B) [16, 17]. The induction of certain adhesion molecules (e.g. ICAM-1, VCAM, P- and E-selectin) and cytokines is mediated by NF- κ B [18], therefore acinar cell derived OFRs may promote the activation of the above proinflammatory factors in AP.

In the present study we have examined the behavior of endothelial adhesion molecules—with special attention to their potential correlation with local oxidative stress—in sodium taurocholate induced acute necrotizing pancreatitis in rats. The pancreatic tissue expression of CAM proteins, as well as the localization of NF- κ B (p65 element), was evaluated by indirect immunofluorescence (IF), combined with a novel histological demonstration of local OFR production by *in vivo* cerium capture. Reaction of cerium ions with OFRs forms stable, insoluble cerium perhydroxide [$\text{Ce}^{\text{III}}(\text{OH})_2\text{OOH}$ or $\text{Ce}^{\text{IV}}(\text{OH})_2\text{OOH}$] precipitates. Robinson and Batten [19], as well as Halhuber *et al.* [20], have shown that these transparent deposits can be directly visualized by taking advantage of their strong laser reflective properties, employing the *reflectance mode* of confocal laser scanning microscopy (CLSM). We have applied this concept, and by improving and clarifying certain technical details we have recently demonstrated the evolution of oxidative stress in experimental AP [21].

In the present study experimental animals were intravascularly perfused with cerium chloride immediately before sacrifice to achieve *in situ*, *in vivo* reaction of cerium with OFRs in the pancreas. Multichannel CLSM on cryostat sections of the cerium perfused pancreata allowed the codemonstration of OFR-derived cerium perhydroxide deposits together with immunolabeled CAMs or NF- κ B. The gene activation of E- and P-selectins, ICAM-1, and VCAM was quantified by

competitive reverse transcriptase polymerase chain reaction (RT-PCR).

MATERIALS AND METHODS

The Sodium Taurocholate Induced Acute Pancreatitis Model and Control Animals

Male Wistar rats (280–320 g) were fasted for 12 h prior to the experiments, but had free access to water. The animals were treated in accordance with the European Community Standards concerning the care and use of laboratory animals (INSERM and Ministère de l'Agriculture et de la Forêt, France, Authorization No. 02249). All animals were anesthetized by intraperitoneal injection of 50 mg/kg sodium pentobarbital (Sanofi, Libourne, France). After a small right paramedian laparotomy the pancreas was exteriorized, and the pancreaticobiliary duct (PBD) was temporarily closed at the liver hilum with a soft microvascular clamp to prevent reflux of the infused material into the liver. A cannula was inserted into the distal PBD in a transpapillary fashion through the duodenum and fixed exteriorly by a temporary ligature. This was followed by a slow, retrograde injection (100 μ l/100 g body wt, pressure 40 cm H_2O) of lactated Ringer's solution (LRS, Fresenius, Louviers, France) containing 5% sodium taurocholate (Sigma Chemical Co., St. Louis, MO) into the PBD. All reagents were filtered through a 0.2- μ m filter (Schleicher & Schuell France SARL, Ecqueville, France) to remove particles that might cause artifactual reflectance signals. After the removal of all devices, the laparotomy was closed in two layers.

The following control animals were included: normal controls, in which animals underwent laparotomy with cerium perfusion only (see below), and sham operated animals, which underwent the following procedure: laparotomy, temporary clamping of the PBD at the hilum of the liver, transpapillary cannulation of the PBD, but no fluid infusion into the pancreas [22].

Cerium Chloride Perfusion and Pancreas Sampling

At different time points (1, 2, 8, 24 h) after acute pancreatitis induction or sham operation the animals ($n = 5$ at each time point) underwent relaparotomy under pentobarbital anesthesia. The distal segment of the abdominal aorta was cannulated and then 50 ml of cerium^{III}chloride solution (Sigma, 20 mmol/L, dissolved in LRS) was slowly injected into the aorta. The inferior caval vein was immediately punctured for the release of the perfusate-blood mixture. In such a manner the entire aortic vascular bed was "washed through" with CeCl_3 solution. Samples of pancreas were rapidly collected, immediately snap frozen in liquid nitrogen, and stored at -80°C until processing. Normal control animals ($n = 5$) underwent this procedure only. For RT-PCR analysis of CAM gene expression, pancreata from identical animal groups were collected under similar conditions, but without cerium chloride infusion, and treated as below.

Processing of Pancreatic Tissue for Histology

For routine histology, formalin-fixed and frozen sections of pancreata were stained with hematoxylin-eosin. For IF studies 10- μ m-thick cryostat sections were cut from the cerium-perfused pancreas samples on 3-aminopropyltriethoxysilane-coated (Sigma) glass slides and then fixed for 5 min at -20°C in methyl alcohol (or paraformaldehyde in cases of E-selectin labeling), supplemented with 1 mmol/L of the protease inhibitor phenylmethylsulfonyl fluoride (PMSF, Sigma).

Indirect IF was performed as below. The following washing fluid was used: LRS supplemented with 1% bovine serum albumin (Sigma), protease inhibitors PMSF (0.1 mmol/L), aprotinin (Trasylol, Bayer, Zurich, Switzerland) (200 μ g/ml). Briefly, the sections were rehydrated with the washing fluid and then incubated with primary

TABLE 1

The Sequences Used as Endothelial Cellular Adhesion Molecule and β -Actin Specific Primers

Primers (Acc. No.)	Upstream primer	Downstream primer	Product size	MIMIC size
P-selectin (L23088)	5'-CCCAATAACAAGAGGAAC-3'	5'-GCTGGCACTCAAATTTAC-3'	541 bp	445 bp
ICAM-1 (D00913)	5'-TTCCTTCTCTATTACCCC-3'	5'-GTGAGCGTCCATATTTAG-3'	517 bp	347 bp
VCAM (X63722)	5'-CATGTAACCTCTGGGAAAC-3'	5'-ATTCACCTCCTTCACACAC-3'	593 bp	410 bp
E-selectin (L25527)	5'-GTGTGACCAAGTTCTGACCTGC-3'	5'-ATTGGCATCACAGGTCACAGC-3'	450 bp	347 bp
β -actin (V01217)	5'-ATTGGCCACCACACTTTCTACAAT-GAGCTGCG-3'	5'-GCAGATGTGGATCAGCAAGCA-GGAGTACGATG-3'	838 bp	613 bp

antibodies for 60 min. After being washed repeatedly, the fluorescein isothiocyanate (FITC)-conjugated secondary antibodies were applied for 60 min. The following primary antibodies were used; *P-selectin*: rabbit anti-human *P-selectin* (09361 A, PharMingen, San Diego, CA) which reacts with the human, rat, and mouse epitope. *E-selectin*: monoclonal anti-rat *E-selectin* 14G2 [23], kind gift of Dr. Barry A. Wolitzky (Hoffmann-La Roche Inc., Nutley, NJ) and RME-1 [24], a generous gift of Dr. Andrew C. Issekutz (Dalhousie University, Halifax, Canada). *ICAM-1*: monoclonal mouse anti-rat *ICAM-1* (BSA-1, R&D Systems, Abingdon, UK). *VCAM*: monoclonal mouse anti-rat *VCAM* (5F-10, Berkely Antibody Co., Richmond, CA). *NF- κ B p65*: rabbit anti-human p65 (sc-109, rat cross-reactive, Santa Cruz Biotechnology Inc., Santa Cruz, CA; kind gift of Dr. David Malka IN-SERM U315, Marseille, France). The corresponding FITC-conjugated secondary antibodies were obtained from Jackson ImmunoResearch Inc. (West Grove, PA). Nuclei were colored with 50 μ g/ml propidium iodide (Sigma), and the preparation was mounted in glycerol gelatin (Sigma) supplemented with 50 mg/ml anti-fading agent 1,4-diazabicyclo-[2.2.2]-octane (Sigma). Omission of primary antibody served as the negative control.

Confocal Microscopy and Digital Image Processing

Observations were performed with CLSM (Leica TCS 4D, Leica Lasertechnik GmbH, Heidelberg, Germany) using multichannel detection. In the cases of fluorescence and transmission detection channels the system's default excitation-detection settings were used, and photomultiplier sensitivities were adjusted according to the actual signal intensities. In contrast, the parameters of the reflectance channel (detecting OFR reaction derived cerium perhydroxide) were always set to the same previously defined values throughout the acquisition sessions: dual laser wavelengths of 488 + 567 nm, power: 100 (arbitrary value), photomultiplier sensitivity: 420. To further exclude operator bias, observations were performed on coded samples in a blinded fashion.

In each image series nine optical sections were recorded per channel, scanning a horizontal tissue area of 100 μ m² (final magnification: 570 \times), and a vertical tissue thickness of 5 μ m. The images of the consecutive optical layers were then digitally reconstructed using the microscope system's "pseudo-3D" object volume reconstruction algorithm (Simulated Fluorescence Process, Leica). Cerium reflectance signals were digitally colored in "glow," (See Fig. 2: color scale 1), FITC-derived IF signals in green (Fig. 2: color scale 2), and nuclei in red (Fig. 2: color scale 3). The tissue structure background obtained by transmission mode was represented in grayscale (Fig. 2: color scale 4). The images of the four detection channels were Gauss filtered and then digitally superposed to give a composite picture (Adobe Photoshop 5.0 software, Adobe Systems Inc., San Jose, CA). No digital enhancements were made that would alter the information content of the original images.

For comparative purposes the CAM protein expression was semi-quantitatively evaluated by counting the IF-positive microvessels on 10 randomly chosen 40 \times power microscopic fields per pancreas sam-

ple, and the results were represented as means \pm SEM. In the case of *P-selectin*, only endothelium associated, linearly shaped fluorescence signals were counted, whereas collections of bright, dot-like foci (corresponding to adherent platelets) were excluded.

Quantification of Cellular Adhesion Molecule mRNA Expression by Competitive RT-PCR Analysis

Preparation of pancreatic total RNA and reverse transcription to cDNA. Pancreata were quickly dissected and immediately frozen in liquid nitrogen. Pancreatic total RNA was extracted in 5 mol/L guanidium thiocyanate and purified through a cesium gradient [25]. RNA quality was verified by a better than 1:1 ethidium bromide staining of rRNA bands on denaturing agarose gel. Total RNA was precipitated and resuspended in diethylpyrocarbonate-treated sterile H₂O, quantified by spectrophotometry (A_{260}/A_{280} ratio >1.8), and diluted to the concentration of 1.0 μ g/ μ L. Equal aliquots (1 μ g) of each RNA stock were reverse-transcribed into cDNA by the random hexanucleotide method using Moloney murine leukemia virus reverse transcriptase (Promega, Charbonnières, France). Working stocks were stored at -80°C until required.

Quantitative competitive PCR analysis of pancreatic CAM specific mRNA content. To quantify changes in mRNA expression of adhesion molecules during the course of AP, we applied quantitative competitive PCR using the MIMIC system (Clontech Laboratories, Palo Alto, CA). PCR MIMIC constructs are nonhomologous, irrelevant DNA sequences that are engineered to possess on both ends the same priming sites as the endogenous (CAM-specific) message and designed to be slightly different in size from the cDNA of interest. Decreasing known concentrations of these MIMIC constructs are added to PCR amplification reactions, where they compete with the same sample's target message derived cDNA for the same primers and thus serve as internal standards. Comparison of band intensities produced by the endogenous CAM message, and by the known concentration of PCR MIMICs, allowed the accurate quantification of cDNA derived from the respective CAM mRNA. Values were normalized to those of an internal control housekeeping gene product (β -actin mRNA), determined similarly in the same sample.

Nonlooping nonoverlapping oligonucleotide primer pairs from separate exons were designed from published sequences for each gene studied and purchased from Gibco BRL (Life Technologies, Paisley, UK). The sequences used as endothelial CAM and β -actin specific primers are shown in Table 1. PCR MIMICs were constructed to harbor the respective specific primer sequences for each of the adhesion molecules studied, or for β -actin. Two-microliter aliquots of cDNA were used as target for separate competitive PCR reactions in the presence of 0.5 units of Taq DNA polymerase (Promega, Charbonnières, France), 50 μ mol/L of a primer pair, specific for the particular adhesion molecule (or β -actin), and decreasing amounts of the corresponding MIMIC constructs. The reaction fluid also contained 10 mmol/L Tris-HCl, (pH 8.3), 2.5 mmol/L MgCl₂, 50 mmol/L KCl, and 250 μ mol/L deoxynucleoside triphosphates. Amplification

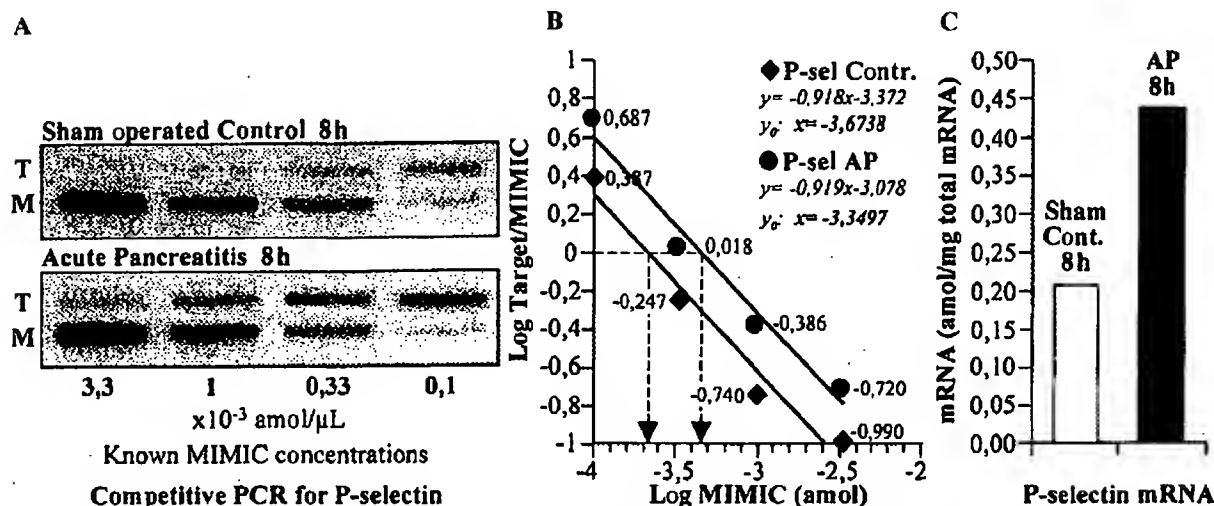


FIG. 1. Quantification of pancreatic adhesion molecule mRNA expression by competitive RT-PCR. (A) Representative gels showing P-selectin specific (T = target) and corresponding MIMIC competitor control (M) PCR products from the pancreas of a sham operated control (at 8 h) and a taurocholate induced acute pancreatitis (AP) (at 8 h) animal. Constant amounts of cDNA (prepared from 1 μ g total RNA of each pancreas) were coamplified using P-selectin specific primers in the presence of sequential 1:3 dilutions of P-selectin-MIMIC. The resulting PCR products were resolved on ethidium-bromide-stained agarose gel and band intensities were measured by densitometry. (B) After correction for the differences in size (T = 541 and M = 445 bp), the logarithm of the density ratios (log T/M) was plotted against the logarithm of the initial amounts of MIMIC added to the PCR reactions. The lines represent a linear regression analysis of data points (yielding slopes of approximately -1.0). (C) The absolute amounts of P-selectin specific cDNA were extrapolated from the target-MIMIC equivalence points (log T/M = 0). Subsequently, these values were normalized to the expression of β -actin (determined identically) in the same pancreata, and the actual abundance of P-selectin specific mRNA was expressed in attomoles (amol) per milligram of total RNA.

cycles were carried out in a DNA thermal cycler (Perkin-Elmer Corp., Norwalk, CT) under the following conditions: initial incubation for 2 min at 94°C, followed by repeated amplification cycles of 1 min at 94°C, 45 s at 50°C (E-selectin) or 56°C (P-selectin, VCAM, ICAM-1, β -actin), and 1 min at 72°C. Experiments were performed in duplicates. The specificity of products amplified at the expected sizes was verified by restriction enzyme analysis with the use of at least two different restriction enzymes. Control PCRs were performed by omitting reverse transcription during the DNA synthesis and by substituting water for cDNA during PCR experiments. The amplified PCR products were run on 1.6% agarose gels stained with ethidium bromide to resolve the proportion of sample and competitor cDNAs. The intensities of gene specific bands were photographed in UV light, and subsequent to image digitalization (Fig. 1A), the density ratios of target to mimic bands were determined by digital image analysis (NIH Image 1.61 program, NIH, Washington, DC, public domain). The amount of specific mRNA of interest was determined from the competition curve obtained by plotting the logarithm of the density ratios of the target to mimic PCR products (after correction for the difference in size) as a function of the logarithm of the amount of MIMIC added to the reaction (Fig. 1B). The total amount of adhesion molecule mRNA in the sample was calculated from the mimic values at the equivalence point (log density ratio = 0, Fig. 1C). To allow comparison between different RNA samples and experimental conditions, the CAM specific mRNA concentration values were further normalized to the expression level of β -actin mRNA, and these normalized values were used in the final data analysis. The amount of a specific RNA was expressed in attomoles (amol) per milligram of total RNA.

Statistical analysis. Data are expressed as means \pm SEM and compared using the nonparametric Kruskal-Wallis test to analyze the global differences in gene expression between the groups and the non parametric Wilcoxon test to identify individual differences between groups. In all statistical analyses, the difference was considered significant when $P < 0.05$.

RESULTS

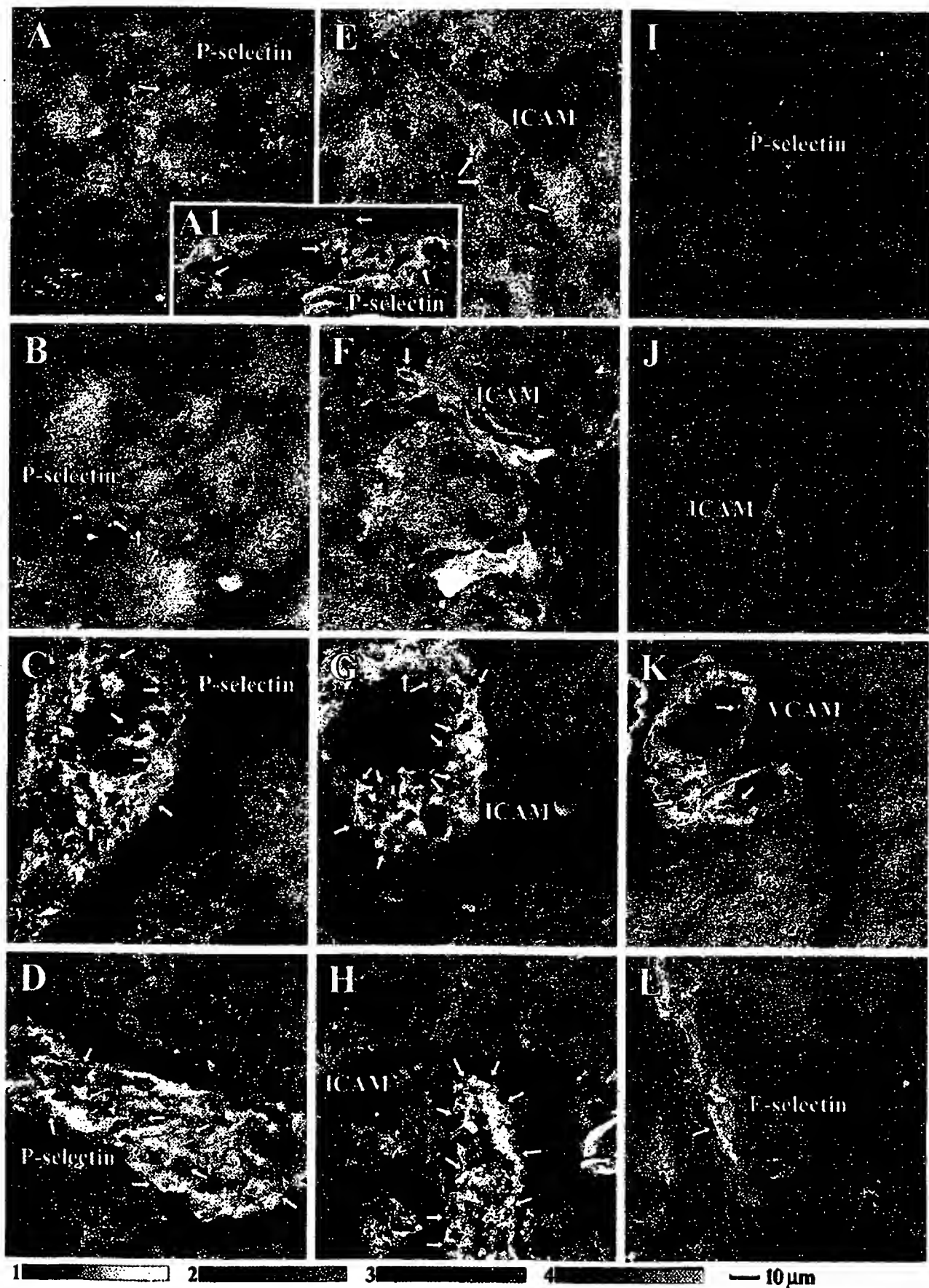
Macroscopic Lesions and Routine Histology

Normal control pancreata were macroscopically intact, with normal histological structure. Sham operated animals developed small increases of peritoneal fluid and laparotomy wound edema. The pancreata had normal appearance with a mild leukocyte presence at the peritoneal surfaces seen in certain cases. Neither acinar cell vacuolization nor necrosis was noted upon routine histology.

All sodium taurocholate treated animals developed classic [26] severe acute necrotizing pancreatitis. Histologically acinar cell vacuolization and heterogeneous necrosis were detected, adherent leukocytes were seen as early as 1 h, evolving into a leukocytic infiltration from 2 h. No mortality was observed in any of the animal groups sacrificed during the 1- to 24-h observation period.

Oxidative Stress and Adhesion Molecule Expression in Control Animals

Normal control pancreata showed low levels of acinar cell cerium reflectance at our standardized confocal microscopy settings, with practically no adherent or infiltrating leukocytes (Fig. 2I). Occasionally present adherent platelets and a few capillaries were focally positive for P-selectin, and some postcapillary venules showed weak constitutive ICAM-1 immunofluores-



cence. E-selectin and VCAM stained samples were negative.

Laparotomized controls showed a modest increase of acinar cerium reflectance signals in heterogeneous distribution, especially 1 h after laparotomy, subsiding at later time points. At 8 and 24 h the laparotomized control pancreata showed similar amounts and distribution of reflectance as the normal controls. One hour after laparotomy some capillaries and postcapillary venules presented occasional P-selectin positivity, which was partly associated with endothelial cells, but mostly with adherent platelets. A slight increase in ICAM-1 immunoreactivity was observed at 2 and 8 h (Fig. 2J) with rare, focal E-selectin and VCAM positivity (1–2 venules per slide preparation). The increases in CAM protein expression detected by IF in sham operated controls paralleled the results of the quantitative evaluation of the gene expression of the respective adhesion molecules.

Oxidative Stress and Adhesion Molecule Expression in Acute Pancreatitis

At 1 h after AP induction, strong cytoplasmic reflectance signals were detected over the pancreatic acini and occasionally intravascularly in the periacinar capillaries. Islets of Langerhans and small pancreatic ducts were free of cerium deposits. This strongly suggests that at this early time point, OFR production was mainly located within the acinar cells. Heterogeneously distributed, strong P-selectin expression was observed on the pancreatic capillary endothelial cell surfaces and postcapillary venules, most frequently in the close neighborhood of acini presenting intense reflectance signals (Fig. 2A). Aggregates of adherent P-selectin positive platelets were also frequently seen. Figure 2A1 shows a P-selectin positive venule with few adherent and transmigrating PMNs. It is noteworthy

that at this early phase PMNs can apparently adhere to each other by interposed P-selectin positive platelets. These leukocytes present low levels of cerium derived reflectance in comparison with those imaged at later time points of AP (Fig. 2D). Compared to controls, a mildly increased ICAM-1 protein expression was noted on capillary and postcapillary venular endothelial surfaces, with a higher incidence at the sites of oxidative stress (Fig. 2E). E-selectin and VCAM expression were negligible at this early phase. Leukocyte margination, however, was relatively rare, comprising mainly PMNs adhering to P-selectin and ICAM-1 positive vessel walls. Their OFR production was found to be weak, with few, mostly intracellular, cerium deposits.

At 2 h after AP induction the acinar cerium reflectance persisted, but additionally, the small capillaries/venules were frequently engorged with cerium perhydroxide deposits (Fig. 2F), whereas the arterioles were free of reflectance. We have also observed capillary endothelial surfaces thinly covered by cerium deposits, which may suggest OFR production by the endothelial cells themselves. Several capillaries/venules showed adherent PMNs, with the occasional appearance of extracellular cerium deposits around the leukocytes. P-selectin and ICAM-1 expression were found to be further increased, with a preponderance at the perinecrotic regions (Figs. 2B and 2F, respectively). E-selectin and VCAM IF were observed only occasionally.

At 8 h after AP induction there are important changes. The samples were characterized histologically by large numbers of adherent and transmigrating PMNs evolving into a strong periacinar leukocytic infiltration. A decrease in acinar reflectance signals was noted, whereas the OFR production by PMNs increased considerably, represented by the high intensity

FIG. 2. Multi-channel confocal microscopy images codemonstrating oxidative stress (histochemically detected by the cerium capture method, as described in the text) and cellular adhesion molecules (immunolocalized by IF) in cryostat sections prepared from cerium perfused pancreata of acute pancreatitis and control animals. The detection channels were color coded using the color scales 1–4, where the stronger signals correspond to brighter colors. (1) "Glow": oxidative stress, detected by cerium derived laser reflectance signals. (2) Green: immunolabeled cellular adhesion molecules (P-selectin: A–D and I, ICAM-1: E–H, and J, VCAM: K, E-selectin: L). (3) Red: propidium-iodide-stained nuclei. (4) Grayscale: tissue background obtained in transmission mode. Arrows point at adherent, or transmigrating, leukocytes. (A and E) Pancreata 1 h after acute pancreatitis induction. Strong cerium deposition derived reflectance signals are apparent in the pancreatic acinar cells representing active OFR production. Capillaries are positive for P-selectin (A) and ICAM-1 (E) in the close neighborhood of OFR producing acini, with few adherent PMNs. The lack of reflectance signals in these PMNs suggests low levels of activation. (A1) P-selectin positive postcapillary venule with numerous adherent and transmigrating PMNs presenting low levels of cerium reflectance. Some PMNs apparently adhere to each other by interposed P-selectin positive platelets (arrows). (B and F) AP at 2 h, showing persisting OFR production in acinar cells with perifocal P-selectin (B) expression. Some ICAM-1 positive capillaries are filled with cerium deposits (F, arrows) suggesting release of OFRs into the vascular space. Few adherent PMNs are visible in the venules. (C, G, and K) Acute pancreatitis at 8 h. Consecutive sections of the same region with a venule immunopositive for P-selectin (C), ICAM-1 (G), and VCAM (K). Reflectance signals are somewhat decreased over the acini, whereas numerous adherent and transmigrating PMNs (arrows) are surrounded by strongly reflective cerium deposits. (D, H, and L) Images of AP at 24 h, at this time point acinar reflectance signals are considerably diminished, and the principal sources of OFRs are the adherent, or already transmigrated (H, arrows) PMNs. Sections were characterized by persisting P-selectin (D) and ICAM-1 (H) and modestly increased E-selectin (L) and VCAM expression. (I and J) Control pancreata showed minimal oxidative stress, occasional, weak CAM expression, and negligible leukocyte adherence. (I) Normal control pancreas stained for P-selectin, (J) control pancreas 2 h after sham operation, showing focal ICAM-1 expression. (Original magnification: 570 \times . Scale bar: 10 μ m).

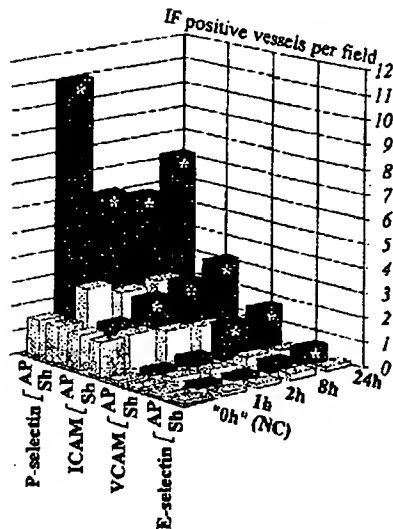


FIG. 3. Semi-quantitative evaluation of CAM protein expression in normal control (NC, gray columns), sham operated (Sh, nonfilled columns), and AP animals (dark columns). Adhesion molecules were labeled by indirect immunofluorescence (IF) on frozen sections of pancreata. In each pancreas sample IF positive microvessels (capillaries, postcapillary venules, and venules) were counted on 10 randomly chosen 40 \times power microscopic fields, and the results were represented as means. In case of P-selectin, only endothelium associated, linearly shaped fluorescence signals were counted (platelets were excluded). Normal control animals (NC) were considered time point "0 h" in the statistical analyses. * $P < 0.05$ versus control.

intra- and extracellular reflectance signals. P-selectin and ICAM-1 expression continued to be widespread, moreover, the incidence of E-selectin and VCAM positive vessels was focally augmented. In several instances the same postcapillary venules were positive for P-selectin, ICAM-1, and VCAM on consecutive sections (Figs. 2C, 2G, and 2K, respectively).

A similar histological picture was seen 24 h after AP induction, with aggravation of pancreas destruction and leukocyte infiltration. In general, the acinar OFR production was reduced, although due to the spreading nature of pancreatic inflammatory process the peri- or nonnecrotic areas still presented strong reflectance signals. By this time the major producers of oxidative stress appeared to be the leukocytes (morphologically mostly PMNs). These cells were shining with cerium reflectance, especially after their transmigration through the capillary walls (Fig. 2H, arrow). The high expression of P-selectin (Fig. 2D) and ICAM-1 (Fig. 2H) proteins persisted, and the vast majority of leukocyte adherence and transmigration appeared to be localized to microvessels positive for these two molecules. E-selectin (Fig. 2L) and VCAM IF were also noted with higher frequencies than those observed at earlier time points, but interestingly, it was rarely associated with considerable leukocytic adherence or infiltration. A summary of these findings is provided in Fig. 3, showing a semi-quantitative comparison of CAM IF positive

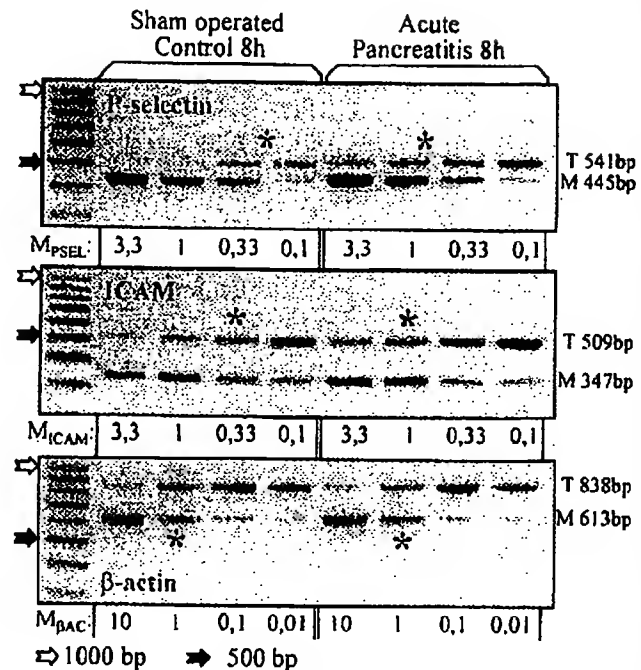


FIG. 4. Representative gels showing P-selectin (top), ICAM-1 (middle), and β -actin (bottom) mRNA expression as determined by competitive RT-PCR in pancreata of sham operated control (8 h) and AP (8 h) animals. The reaction products were at the expected sizes. (T = target, M = MIMIC, arrows point at the DNA ladder: 1000 bp, 500 bp). The approximate target-MIMIC concentration equivalence is marked by asterisks. M_{PSEL} , M_{ICAM} : initial MIMIC concentrations ($\times 10^{-3}$ amol/ μ L) added to the reaction tubes in the cases of P-selectin and ICAM-1. Adhesion molecule mRNA values were normalized to the expression of β -actin, determined by the same method in each respective pancreas. M_{BAC} : initial β -actin MIMIC concentrations (amol/ μ L).

microvessels (capillaries and postcapillary venules) in pancreata of the different animal groups. IF positive vessels per 40 \times microscopic field were counted, the columns represent the means of 10 fields per animal ($n = 5$).

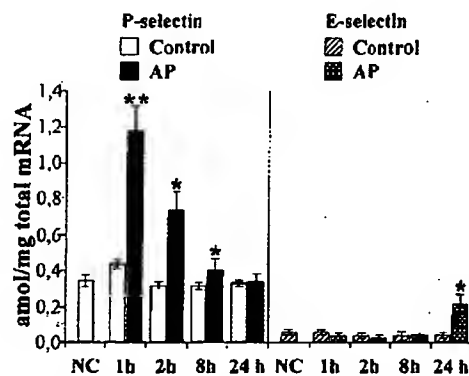


FIG. 5. P-selectin and E-selectin mRNA expression as measured by competitive RT-PCR in normal control (NC) and at different time points in sham operated and AP animals. Data are expressed as means \pm SEM. **Significantly different from control with $P < 0.01$; *significantly different from control with $P < 0.05$.

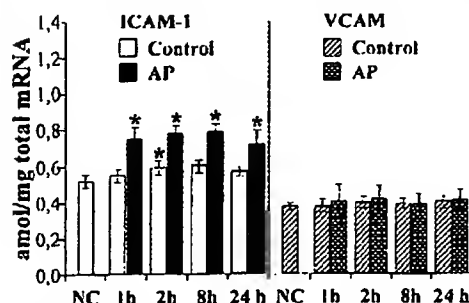


FIG. 6. Expression of ICAM-1 and VCAM mRNA in normal control (NC) and in sham operated versus AP animals, as measured by competitive RT-PCR. Data are represented as means \pm SEM. *Significantly different from control at $P < 0.05$.

Cellular Adhesion Molecule mRNA Expression in the Pancreata

Quantitative evaluation of CAM induction was obtained by measuring their gene expression by competitive RT-PCR using the MIMIC internal control method. The results were normalized to β -actin, a constitutively expressed housekeeping gene product, detected in the same sample. The level of β -actin in the pancreas samples showed minimal variance (mean $3.7 \pm 0.3 \times 10^3$ amol/mg total RNA), with no significant difference between the animal groups studied.

CAM specific mRNA concentrations were first quantified in pancreata of normal control rats. Low levels of constitutive P-selectin, ICAM-1, and VCAM mRNA expression were detectable with mean values of 0.34 ± 0.04 , 0.51 ± 0.04 , and 0.37 ± 0.02 amol/mg total RNA, respectively. In contrast, E-selectin mRNA remained undetectable in most of the control samples, even when twice as much total RNA ($2 \mu\text{g}$) was reverse-transcribed to cDNA. A representative series of competitive RT-PCR gels is shown in Fig. 4. As shown in Figs. 5 and 6, sham operation had no significant effect on P-selectin and VCAM specific mRNA expression. We observed a mild increase in ICAM-1 gene expression at 2 and 8 h after sham operation compared to untreated animals. E-selectin mRNA remained barely detectable.

Within 1 h after AP induction P-selectin mRNA expression peaked at 1.17 ± 0.09 amol/mg total RNA ($P < 0.01$), followed by a tendency to decline after 2 and 8 h, and by 24 h it returned to a level not different from the controls (Fig. 5). In contrast to the early and strong (2.7-fold) elevation of P-selectin gene expression after AP induction, E-selectin specific mRNA concentrations showed a modest increase only after 24 h (0.21 ± 0.06 amol/mg total RNA, Fig. 6). Moreover, AP also generated a rapid, significant upregulation of the ICAM-1 gene activity, resulting in a 25–36% increase in specific mRNA concentrations (Fig. 6). This rise was less pronounced than that of P-selectin, but remained significant and sustained up until 24 h. In contrast, VCAM gene expression showed no significant modification

during the early course (first 24 h) of the disease (Fig. 6).

Evaluation of NF- κ B Activation by Immunofluorescence

The p65 element of NF- κ B was labeled by IF, and NF- κ B was considered activated, if p65 was translocated from the cytoplasm to the nuclei on CLSM images. We detected p65 positivity colocalizing with nuclei on high-resolution confocal optical sections as early as 1 h post AP induction, where numerous pancreatic acinar cell (Figs. 7A, 7C, and 7D, arrows) and capillary endothelial cell nuclei (Fig. 7D, arrow) showed p65 fluorescence in a heterogeneous distribution. Similarly to CAM protein expression, evidence of NF- κ B activation was frequently found in acinar groups presenting strong OFR derived reflectance signals. Control samples were characterized by cytoplasmic p65 positivity with undetectable nuclear translocation, and low levels of cerium derived reflectance (Figs. 7B and 7E).

DISCUSSION

Cumulating evidence supports the pathogenic role of CAMs in uncontrolled leukocyte adherence and activation contributing to tissue damage in AP [27]. Experimental administration of antibodies against CD11a/CD18 and ICAM-1 attenuated superoxide anion release by PMNs and their accumulation in the lungs of rats with AP [28]. AP associated ascites fluid from rats induced NF- κ B activation together with ICAM and VCAM, but not E-selectin expression in human vascular endothelial cells [29]. ICAM-1-deficient knock-out mice showed less pancreatic and lung injury with decreased neutrophil sequestration [30]. Recently, CAMs were studied in different AP models using radiolabeled monoclonal antibodies. In the mouse choline-deficient/ethionine-supplemented diet AP model Lundberg *et al.* demonstrated widespread P-selectin induction in the pancreas, spleen, liver, and lung [31], as well as upregulation of pulmonary E-selectin, ICAM-1, and VCAM-1 [32]. In rat taurocholate AP Folch *et al.* have found increases in pancreatic and pulmonary P-selectin expression, whereas ICAM-1 was unchanged. Immunoneutralization of P-selectin or ICAM-1 or inhibition of OFR producing xanthine oxidase prevented the neutrophil infiltration in the lung [33]. Indeed, besides the unquestionable role of cytokines in CAM induction, the local and systemic oxidative stress may exert a similar effect via NF- κ B activation.

However, the *in situ*, *in vivo* detection of OFR production is practically impossible with the traditional methods. Using our novel modification of cerium based free radical histochemistry (combined with reflectance CLSM) we have recently described the *in vivo* evolu-

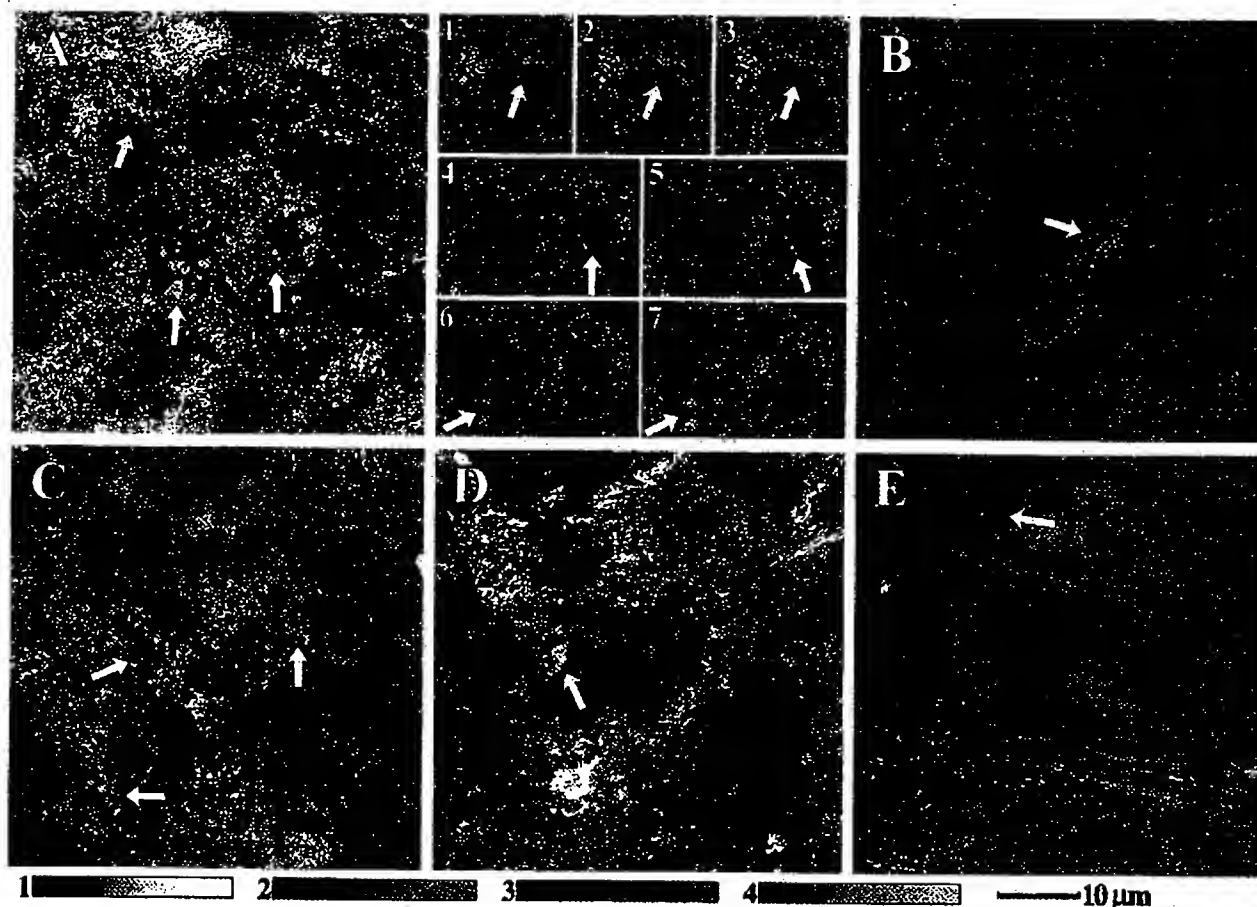


FIG. 7. Localization of the immunolabeled NF- κ B p65 element as detected by CLSM in the pancreas 1 h after AP induction (A, C, D), in normal control (B), and 1 h after sham operation (E). (A) Acinar cytoplasmic regions present strong reflectance signals, and p65 is translocated into the nuclei in certain cells (arrows), consistent with NF- κ B activation. (1-3) Separate confocal optical section images of the cell marked with yellow arrow on (A). (4-7) Separate confocal optical sections of the cells marked with white arrows on (A). (C) Arrows point at nuclei positive for p65. (D) Arrow points at an endothelial cell of a postcapillary venule with p65 translocated into the nucleus. (B and E) Control images showing cytoplasmic p65 immunopositivity (arrows). (Final magnification: 1140 \times , scale bar: 10 μ m.)

tion of OFR production at a histological level in the taurocholate AP model. We have shown an apparent OFR source switch in the pancreas from acinar cells—dominating the early period—to leukocytes as the disease progressed. In addition, we observed a generalized, time-dependent OFR production by blood and ascites derived PMNs [21].

In this study we demonstrate the differential up-regulation of the inducible endothelial CAMs at the sites of oxidative stress in the taurocholate AP model. Measurement of CAM protein expression by antibody techniques suffers from several drawbacks. Quantification of immunofluorescence is not reliable; antibodies can bind to necrotic tissues in a nonspecific manner; adherent platelets express P-selectin. Therefore, radio-labeled antibody binding studies may overestimate CAM expression in the lack of histological control. Although activation of a CAM gene does not necessarily mean the downstream increase in protein expression, measurements of gene activation using competitive

RT-PCR may add useful information to our current knowledge. Due to MIMIC internal standards, this procedure is suitable for the reliable quantification of small amounts of gene transcripts [34, 35]. Similarly to previous studies, we have normalized the CAM gene expression measurements to the sample's β -actin gene expression ("housekeeping" gene). Recently, Yuan *et al.* [36] showed significant β -actin gene upregulation in the supramaximal cerulein stimulation AP model and suggested that this gene may not be appropriate as RNA-loading controls for Northern blot analysis of pancreatic tissue. In the taurocholate induced AP we did not find such changes as detected by competitive RT-PCR, which may be explained in part by the different pathomechanism of this model. Our RT-PCR data were in good correlation with the CAM protein expression semi-quantitatively evaluated by counting CAM IF positive microvessels on cryostat sections.

Our choice of AP model and controls deserves further comments. The mechanism of taurocholate induced AP

model is based on the additive effects of retrograde fluid injection (elevating intraductal pressure), the detergent properties of sodium taurocholate, and the potential presence of bacteria, resulting in a severe inflammation comparable to human biliary pancreatitis. Due to its necrotizing nature, this model is less appropriate for evaluating the initial acinar intracellular events, however, it seems to be very suitable for studying the local and systemic inflammatory reaction. With our careful, minimally invasive surgical technique we could render this model highly reproducible with negligible surgical artifacts, as confirmed by the sham operated controls. Another problem is the sham operation, which traditionally includes retrograde intraductal injection of saline instead of taurocholate. The pancreas seems to respond to noxious events in a uniform manner, and it has been shown recently by Lüthen *et al.* [22] that this latter procedure provokes specific pancreatic damage with significant pancreatic enzyme elevation in the serum, consistent with low-grade acute pancreatitis. Moreover, these authors have observed a significant reduction in the intrapancreatic glutathione content, which is an indirect sign of oxidative stress. In agreement with these data, our preliminary experiments showed that retrograde saline injection modestly, but rapidly, increases intrapancreatic OFR production, as detected by the cerium method. Consequently, to exclude such specific pancreatogenic injury in our sham operated control animal group, the intraductal saline injection was omitted.

Our results demonstrate that this AP model is characterized by a strong and rapid P-selectin, as well as ICAM, upregulation, whereas only a modest and delayed augmentation of E-selectin and VCAM expression occurs. Similarly to other pathologies [37], this specific CAM combination may play a role in the preferential accumulation of PMNs in the AP tissue samples.

The early nature of leukocyte adherence was also remarkable. Presynthesized P-selectin can be translocated from endothelial Weibel-Palade bodies to the cell surface within minutes, and *de novo* synthesis supplies new molecules in case of prolonged inflammatory stimuli. This could be the explanation for the particularly rapid and persisting P-selectin immunopositivity observed over the time course of our experiments. P-selectin not only mediates the low-energy rolling phenomenon, but also has a juxtacrine anchoring function, thereby facilitating the binding of platelet-activating factor (PAF) to PAF receptors on the surface of PMNs. This results in the activation of CD11/CD18 leukocyte integrins, which then support the firm adhesion of PMNs to ICAM on the surface of endothelium [38]. Apparently, H_2O_2 produced by xanthine oxidase promotes this interaction as intermediate [39]. We have observed large numbers of platelets adhering to

pancreatic endothelial surfaces, but also to leukocytes in the pancreatitis samples, whereas this phenomenon was negligible in control pancreata. Activated platelets also express P-selectin and PAF on their surfaces and, once adherent to PMNs [40], platelets use these molecules to activate the leukocyte integrins in a similar fashion [41].

The potential pathogenic role of OFRs in the induction of exaggerated inflammatory response is supported by our observation that the strong upregulation of CAM expression colocalized with oxidative stress. Previously, in cases of single, isolated leukocytes we could successfully quantify OFR production by image analysis of Ce reflectance signals [21]. On the contrary, we felt that due to certain factors (temporal, spatial, and cellular heterogeneity of OFR production, complexity of pancreatic histology, and multichannel CLSM imaging) a meaningful, unbiased quantification of OFR derived reflectance signals in relation to CAM expression in a tissue environment is not resolved at present. Therefore we were obliged to omit the statistical evaluation by image analysis of tissue CAM expression versus local oxidative stress. Our conclusion of apparent colocalization is based on the review of large numbers of image series. At 1 and 2 h after AP induction, large acinar areas presented strong reflectance signals, consistent with intense OFR production. The majority of P-selectin and ICAM expression could be observed in the close proximity of these acini. At 2 h, besides the sustained acinar OFR production, a high prevalence of intracapillary and intravenular Ce deposits suggested the presence of OFRs in the bloodstream. OFR production by liberated xanthine oxidase [42] or by endothelial cells could be considered. Later, after 8 and 24 h, large numbers of activated PMNs adherent to P-selectin and ICAM-1 positive endothelial surfaces (or already transmigrated into the pancreatic tissue) showed strong reflectance signals.

The rapid CAM upregulation (appearing earlier than *de novo* synthesized cytokines could be expected as inducers [43]) could be explained by the direct activation of NF- κ B by OFRs as signal transmitters [16]. Using electrophoretic mobility shift assays, early NF- κ B activation has been demonstrated in different AP models by several recent reports [44–47]. We have found nuclear translocation (consistent with activation) of NF- κ B p65 element at the sites of oxidative stress as early as 1 h post AP induction. Therefore, the initial acinar OFR production may play an important role in the induction of the inflammatory reaction by mobilizing P-selectin and, in parallel, by activating the genes of several cytokines and adhesion molecules through NF- κ B. To our knowledge this has been the first morphological observation of nuclear translocation of the NF- κ B p65 element at the sites of strong oxidative stress in AP.

In conclusion, our results support the hypothesis that early pancreatic acinar oxidative stress may play an important role in the rapid and extensive activation of the proinflammatory machinery in the taurocholate model of acute pancreatitis, and the inadequate up-regulation of the adhesion molecule cascade could serve as an attractive target for future therapeutic interventions.

ACKNOWLEDGMENTS

This study was supported by grants from IRMAD Foundation France, Solvay Pharmaceuticals France, and Charles Debray Foundation, France. Confocal microscopy and image treatment facilities were kindly provided by INSERM Institut Fédératif de Recherches 02. The authors thank Dr. Andrew C. Issekutz, Dr. David Malka, and Dr. Barry A. Wolitzky for their generous gift of antibodies.

REFERENCES

- Norman, J. G. New approaches to acute pancreatitis: Role of inflammatory mediators. *Digestion* 60(S1): 57, 1999.
- Panes, J., and Granger, D. N. Leukocyte-endothelial cell interactions: Molecular mechanisms and implications in gastrointestinal disease. *Gastroenterology* 114: 1066, 1998.
- Gong, J. G., Bevilacqua, M. P., Moore, K. L., McIntyre, T. M., Prescott, S. M., Kim, J. M., Bliss, G. A., Zimmerman, G. A., and McEver, R. P. Rapid neutrophil adhesion to activated endothelium mediated by GMP-140. *Nature* 343: 757, 1990.
- Pinsky, D. J., Naka, Y., Liao, H., Oz, M. C., Wagner, D. D., Mayadas, T. N., Johnson, R. C., Hynes, R. O., Heath, M., Lawson, C. A., and Stern, D. M. Hypoxia-induced exocytosis of endothelial cell Weibel-Palade bodies. A mechanism for rapid neutrophil recruitment after cardiac preservation. *J. Clin. Invest.* 97: 493, 1996.
- Chosay, J. G., Fisher, M. A., Farhood, A., Ready, K. A., Dunn, C. J., and Jaeschke, H. Role of PECAM-1 (CD31) in neutrophil transmigration in murine models of liver and peritoneal inflammation. *Am. J. Physiol.* 274: G776, 1998.
- Essani, N. A., Bajt, M. L., Farhood, A., Vonderfecht, S. L., and Jaeschke, H. Transcriptional activation of vascular cell adhesion molecule-1 gene in vivo and its role in the pathophysiology of neutrophil-induced liver injury in murine endotoxin shock. *J. Immunol.* 158: 5941, 1997.
- Closa, D., Bulbena, O., Hotter, G., Rosello-Catafau, J., Fernandez-Cruz, L., and Gelpi, E. Xanthine oxidase activation in caerulein- and taurocholate-induced acute pancreatitis in rats. *Arch. Int. Physiol. Biochim. Biophys.* 102: 167, 1994.
- Nordback, I. H., and Cameron, J. L. The mechanism of conversion of xanthine dehydrogenase to xanthine oxidase in acute pancreatitis in the canine isolated pancreas preparation. *Surgery* 113: 90, 1993.
- Wisner, J. R., and Renner, I. G. Allopurinol attenuates caerulein induced acute pancreatitis in the rat. *Cut* 29: 926, 1988.
- Ito, T., Nakao, A., Kishimoto, W., Nakano, M., and Takagi, H. The involvement and sources of active oxygen in experimentally induced acute pancreatitis. *Pancreas* 12: 173, 1996.
- Tsuji, N., Watanabe, N., Okamoto, T., and Niitsu, Y. Specific interaction of pancreatic elastase and leucocytes to produce oxygen radicals and its implication in pancreatitis. *Cut* 35: 1659, 1994.
- Inagaki, H., Nakao, A., Kurokawa, T., Nonami, T., Harada, A., and Takagi, H. Neutrophil behavior in pancreas and liver and the role of nitric oxide in rat acute pancreatitis. *Pancreas* 15: 304, 1997.
- Lévy, P., Lettéron, F., Molas, G., Guimont, M. C., Pessayre, D., Bernades, P., and Rozé, C. Lipid peroxidation in different experimental models of acute pancreatitis: An in vivo assessment. *Pancreas* 14: 350, 1997.
- Reinheckel, T., Prause, J., Nedelev, B., Augustin, W., Schulz, H. U., Lippert, H., and Halangk, W. Oxidative stress affects pancreatic proteins during the early pathogenesis of rat caerulein pancreatitis. *Digestion* 60: 56, 1999.
- Heller, B., Burkle, A., Radons, J., Fengler, E., Jalowy, A., Muller, M., Burkart, V., and Kolb, H. Analysis of oxygen radical toxicity in pancreatic islets at the single cell level. *Biol. Chem. Hoppe Seyler* 375: 597, 1994.
- Schmidt, K. N., Amstad, P., Cerutti, P., and Baeuerle, P. A. The roles of hydrogen peroxide and superoxide as messengers in the activation of transcription factor NF-kappa B. *Chem. Biol.* 2: 13, 1995.
- Cominacini, L., Garbin, U., Fratta Pasini, A., Paulon, T., Davoli, A., Campagnola, M., Marchi, E., Pastorino, A. M., Gaviraghi, G., and Lo Cascio, V. Lacidipine inhibits the activation of the transcription factor NF-kappa B and the expression of adhesion molecules induced by pro-oxidant signals on endothelial cells. *J. Hypertens.* 15: 1633, 1997.
- Ghosh, S., May, M. J., and Kopp, E. B. NF-kappa B and Rel proteins: Evolutionarily conserved mediators of immune responses. *Annu. Rev. Immunol.* 16: 225, 1998.
- Robinson, J. M., and Batten, B. E. Localization of cerium-based reaction products by scanning laser reflectance confocal microscopy. *J. Histochem. Cytochem.* 38: 315, 1990.
- Halbhuber, K. J., Scheven, C., Jirinkowski, G., Feuerstein, H., and Ott, U. Reflectance enzyme histochemistry (REH): Visualization of cerium-based and DAB primary reaction products of phosphatases and oxidases in cryostat sections by confocal laser scanning microscopy. *Histochem. Cell. Biol.* 105: 239, 1996.
- Telek, G., Scazecz, J. Y., Chariot, J., Ducroc, R., Feldmann, G., and Rozé, C. Cerium based histochemical demonstration of oxidative stress in taurocholate-induced acute pancreatitis in rats. A confocal laser scanning microscopy study. *J. Histochem. Cytochem.* 47: 1201, 1999.
- Lüthen, R., Grendell, J. H., Niederau, C., and Häussinger, D. Trypsinogen activation and glutathione content are linked to pancreatic injury in models of biliary acute pancreatitis. *Int. J. Pancreatol.* 24: 193, 1998.
- Olofsson, A. M., Arfors, K. E., Ramezani, L., Wolitzky, B. A., Butcher, E. C., and von Andrian, U. H. E-selectin mediates leukocyte rolling in interleukin-1-treated rabbit mesentery venules. *Blood* 84: 2749, 1994.
- Walter, U. M., Ayer, L. M., Manning, A. M., Frenette, P. S., Wagner, D. D., Hynes, R. O., Wolitzky, B. A., and Issekutz, A. C. Generation and characterization of a novel adhesion function blocking monoclonal antibody recognizing both rat and mouse E-selectin. *Hybridoma* 16: 355, 1997.
- Chomczynski, P., and Sacchi, N. Single-step method of RNA isolation by acid guanidinium thiocyanate-phenol-chloroform extraction. *Anal. Biochem.* 162: 156, 1987.
- Banerjee, A. K., Galloway, S. W., and Kingsnorth, A. N. Experimental models of acute pancreatitis. *Br. J. Surg.* 81: 1096, 1994.
- Kaufmann, P., Demel, U., Tilz, G. P., and Krejs, G. J. Time course of plasma soluble intercellular adhesion molecule-1 (sICAM-1) is related to severity of acute pancreatitis. *Hepato-gastroenterology* 46: 2585, 1999.

TELEK ET AL.: ADHESION MOLECULES AND OXIDATIVE STRESS IN ACUTE PANCREATITIS

67

28. Inoue, S., Nakao, A., Kishimoto, W., Murakami, H., Harada, A., Nonami, T., and Takagi, H. LFA-1 (CD11a/CD18) and ICAM-1 (CD54) antibodies attenuate superoxide anion release from polymorphonuclear leukocytes in rats with experimental acute pancreatitis. *Pancreas* 12: 183, 1996.
29. Masamune, A., Shimosegawa, T., Kimura, K., Fujita, M., Sato, A., Koizumi, M., and Toyota, T. Specific induction of adhesion molecules in human vascular endothelial cells by rat experimental pancreatitis-associated ascitic fluids. *Pancreas* 18: 141, 1999.
30. Frossard, J. L., Saluja, A., Bhagat, L., Lee, H. S., Bhatia, M., Hofbauer, B., and Sleer, M. The role of ICAM-1 and neutrophils in acute pancreatitis and pancreatitis-associated lung injury. *Gastroenterology* 116: 694, 1999.
31. Lundberg, A. H., Granger, D. N., Russell, J., Sabek, O., Henry, J., Gaber, L., Kotb, M., and Gaber, A. O. Quantitative measurement of P- and E-selectin adhesion molecules in acute pancreatitis: Correlation with distant organ injury. *Ann. Surg.* 231: 213, 2000.
32. Lundberg, A. H., Granger, N., Russell, J., Callicutt, S., Gaber, L. W., Kotb, M., Sabek, O., and Gaber, A. O. Temporal correlation of tumor necrosis factor-alpha release, upregulation of pulmonary ICAM-1 and VCAM-1, neutrophil sequestration, and lung injury in diet-induced pancreatitis. *J. Gastrointest. Surg.* 4: 248, 2000.
33. Fulch, E., Salas, A., Panes, J., Gelpi, E., Rosello-Catafau, J., Anderson, D. C., Navarro, S., Pique, J. M., Fernandez-Cruz, L., and Closa, D. Role of P-selectin and ICAM-1 in pancreatitis-induced lung inflammation in rats: Significance of oxidative stress. *Ann. Surg.* 230: 792, 1999.
34. Takada, M., Nadeau, K. C., Shaw, G. D., Marquette, K. A., and Tilney, N. L. The cytokine-adhesion molecule cascade in ischemia/reperfusion injury of the rat kidney. Inhibition by a soluble P-selectin ligand. *J. Clin. Invest.* 99: 2682, 1997.
35. Sternberg, L. R., Byrd, J. C., Yunker, C. K., Dudas, S., Hoon, V. K., and Bresalier, R. S. Liver colonization by human colon cancer cells is reduced by antisense inhibition of MUC2 mucin synthesis. *Gastroenterology* 116: 363, 1999.
36. Yuan, S., Rosenberg, L., Ilieva, A., Agapitos, D., and Duguid, W. P. Early changes of gene expression during cerulein supra-maximal stimulation. *Pancreas* 19: 45, 1999.
37. Mizgerd, J. P., Quinlan, W. M., LeBlanc, B. W., Kutkoski, G. J., Bullard, D. C., Beaudet, A. L., and Doerschuk, C. M. Combinatorial requirements for adhesion molecules in mediating neutrophil emigration during bacterial peritonitis in mice. *J. Leukocyte Biol.* 64: 291, 1998.
38. Lorant, D. E., Patel, K. D., McIntyre, T. M., McEver, R. P., Prescott, S. M., and Zimmerman, G. A. Coexpression of GMP-140 and PAF by endothelium stimulated by histamine or thrombin: A juxtacrine system for adhesion and activation of neutrophils. *J. Cell. Biol.* 115: 223, 1991.
39. Terada, L. S., Hybertson, B. M., Connelly, K. G., Weill, D., Piermattei, D., and Ropinc, J. E. XO increases neutrophil adherence to endothelial cells by a dual ICAM-1 and P-selectin-mediated mechanism. *J. Appl. Physiol.* 82: 866, 1997.
40. Kirchhofer, D., Riederer, M. A., and Baumgartner, H. R. Specific accumulation of circulating monocytes and polymorphonuclear leukocytes on platelet thrombi in a vascular injury model. *Blood* 89: 1270, 1997.
41. Ostrovsky, L., King, A. J., Bond, S., Mitchell, D., Lorant, D. E., Zimmerman, G. A., Larsen, R., Niu, X. F., and Kubes, P. A juxtacrine mechanism for neutrophil adhesion on platelets involves platelet-activating factor and a selectin-dependent activation process. *Blood* 91: 3028, 1998.
42. Folch, E., Gelpi, E., Rosello-Catafau, J., and Closa, D. Free radicals generated by xanthine oxidase mediate pancreatitis-associated organ failure. *Dig. Dis. Sci.* 43: 2405, 1998.
43. Pan, J., Xia, L., Yao, J., and McEver, R. P. Tumor necrosis factor-alpha- or lipopolysaccharide-induced expression of the murine P-selectin gene in endothelial cells involves novel kappaB sites and a variant activating transcription factor/cAMP response element. *J. Biol. Chem.* 273: 10068, 1998.
44. Dunn, J. A., Li, C., Ha, T., Kao, R. L., and Browder, W. Therapeutic modification of nuclear factor kappa B binding activity and tumor necrosis factor-alpha gene expression during acute biliary pancreatitis. *Am. Surg.* 63: 1036, 1997.
45. Gukovsky, I., Gukovskaya, A. S., Blinnman, T. A., Zaninovic, V., and Pandol, S. J. Early NF-kappa B activation is associated with hormone-induced pancreatitis. *Am. J. Physiol.* 275: G1402, 1998.
46. Satoh, A., Shimosegawa, T., Fujita, M., Kimura, K., Masamune, A., Koizumi, M., and Toyota, T. Inhibition of nuclear factor-kappa B activation improves the survival of rats with taurocholate pancreatitis. *Gut* 44: 253, 1999.
47. Steinle, A. U., Weidenbach, H., Wagner, M., Adler, G., and Schmid, R. M. NF-kappaB/Rel activation in cerulein pancreatitis. *Gastroenterology* 116: 420, 1999.

seminars in CELL BIOLOGY, Vol 6, 1995: pp 13-19

Myotonic dystrophy: an unstable CTG repeat in a protein kinase gene

Luba Timchenko*, Darren G. Monckton* and C. Thomas Caskey*†‡

Myotonic dystrophy (DM) is caused by the amplification of CTG repeats in the 3' untranslated region of a gene encoding a protein homologous to serine/threonine protein kinases. In DM patients the CTG repeats are extremely unstable, varying in length from patient to patient and generally increasing in length in successive generations. There is a strong correlation between the size of the repeats and the age of onset and severity of the disease. The molecular basis of the effect of the CTG expansion on the development of the DM phenotype continues to be investigated. The first working hypothesis of the molecular mechanism of DM was a reduction in steady-state myotonin-protein kinase (Mt-PK) mRNA and protein levels. However, although the consensus finding is that the Mt PK mRNA and protein levels are decreased in DM patients, it is still not clear if this reduction leads directly to the DM phenotype. In this short review we discuss the molecular aspects of CTG instability and the expression of the myotonin-protein kinase gene in normal and DM populations.

Key words: myotonic dystrophy; CTG repeat; myotonin-protein kinase

MYOTONIC DYSTROPHY (DM) is an autosomal dominant disease characterized by muscle weakness, myotonia, endocrine abnormalities, cataracts and electrocardiographic defects.¹ The global incidence of DM is around 1 in 8000, although it is much higher in some populations, such as the French Canadians, and extremely rare in others, such as African blacks.² The symptoms expressed and the age of onset are extremely variable from patient to patient, both within and between families. DM is one of an apparently increasing number of disorders that displays the unusual phenomenon of genetic anticipation, that is an earlier age of onset and increasingly severe symptoms in succeeding generations.^{3,4} Fre-

quently, DM pedigrees will only be identified when a severely affected child with the congenital form of DM is born. Congenital DM (CDM) is characterized by severe hypotonia (so-called 'floppy babies') and respiratory distress. Further analysis of the families with CDM children often reveals early signs of the classic adult onset form of the disease in one of the parents. The classic adult onset form of the disease usually begins in mid-life, around 20- to 40-years-old, and is characterized by progressive myotonia and muscular atrophy. Detailed analysis of the grandparents in affected pedigrees will usually only reveal the existence of minor symptoms such as cataracts that appear late in life. Prior to the identification of the molecular defect underlying DM, it was unclear whether anticipation was a true phenomenon or an artifact of ascertainment bias in the collection of pedigrees.⁵ However, since the DM gene was cloned a molecular basis for the symptom variability and genetic anticipation have become apparent as products of a region of unstable repeated DNA.

Unstable DNA in the myotonic dystrophy gene

Early in 1992, after the region containing the DM gene had been narrowed down to a small area on the long arm of chromosome 19, a probe from this region was shown to detect enlarged and apparently unstable DNA fragments specific to DM patients.⁵⁻⁷ Soon after, it was demonstrated that the enlarged fragments seen in patients were the result of the expansion of a CTG repeat in the 3' untranslated region (UTR) of a gene showing homology to serine/threonine protein kinases, termed myotonin protein kinase (Mt-PK)⁸⁻¹⁰ (see Figure 1). The CTG repeat in the 3' UTR of the Mt-PK gene is polymorphic in normal individuals with an observed heterozygosity of ~80%. The most common alleles observed contain less than 20 copies of the CTG repeat, although rarer alleles up to ~40 repeats have been seen in normal individuals. In DM patients the CTG repeat array has expanded beyond the length usually observed in the normal population.

*From the Department of Molecular and Human Genetics, †Howard Hughes Medical Institute and ‡Human Genome Center, Baylor College of Medicine, Texas Medical Center, Houston, TX, 77030, USA

©1995 Academic Press Ltd

1043-4682/95/010013 + 07\$8.00/0

L. Timchenko *et al*

DM chromosomes have expanded CTG arrays carrying from 50 up to many 1000s of repeats. There is a direct correlation between the length of the CTG expansion and the age of onset of the disease and the severity of the symptoms.⁵⁻¹⁹ DM individuals who carry alleles in the range of 50 to 200 repeats are generally either asymptomatic or only mildly affected with a late age of onset of symptoms. Patients carrying expansions greater than 200 repeats are generally more severely affected with an earlier age on onset. CDM children are affected at birth and inherit the largest DM alleles, usually containing more than 700 repeats. However, these correlations are by no means absolute and large variations in phenotype still exist between individuals carrying similar sized expansions. Thus, although the size of the expansion has a major influence on age of onset and disease severity, the exact prognosis for any one patient appears to be related to other, as yet undetermined, genetic and/or environmental factors.

As mentioned above, DM families usually display the unusual feature of genetic anticipation. Once the CTG expansion in the DM gene had been identified an explanation for this unusual phenomenon became apparent. Typing of the blood DNA of patients within families revealed that the CTG repeat was not transmitted in a stable fashion and that the size of the expansion appeared to increase in succeeding generations, correlating directly with the observed clinical anticipation.^{5-10,19-16,20-27} The observed levels of intergenerational instability are remarkably high and frequently approach 100% of all transmissions. The observed intergenerational differences may also be very large, such that CTG repeat alleles with less than

100 repeats in asymptomatic or minimally affected grandparents, may expand to large alleles containing many thousands of repeats in congenitally affected grandchildren. The size of the observed intergenerational difference is dependent on both the initial size of the expansion and the sex of the transmitting parent. DM pedigrees contain an excess of transmitting grandfathers and consistent with this observation it has been demonstrated that smaller DM alleles are more unstable and more likely to expand when transmitted by a male than by a female. A dramatic example of germline instability in a male has been revealed by analysis of an asymptomatic DM male whose sperm showed a 98% bias toward expansion of the CTG repeat and an estimated >80% risk of fathering an overtly affected child (D.G. Monckton *et al*, unpublished observations). However, once the CTG array expands beyond several hundred repeats it appears to lose the dramatic expansion bias observed for smaller alleles in the male germline. Only a few cases of paternally transmitted CDM have been reported^{28,29} and direct sperm analysis has not revealed the presence of expanded alleles greater than 1000 repeats in the male germline.³⁰ (D.G. Monckton *et al*, unpublished observations). In contrast, transmission of expanded alleles through the female germline may frequently generate the very large alleles associated with CDM.¹⁵ However, allele size does not appear to be the only factor in the development of CDM. Children who inherit the DM chromosome from their mother are at greater risk of expressing the CDM phenotype than if they had inherited a similar sized allele from their father.³¹ This suggests that children inheriting larger alleles

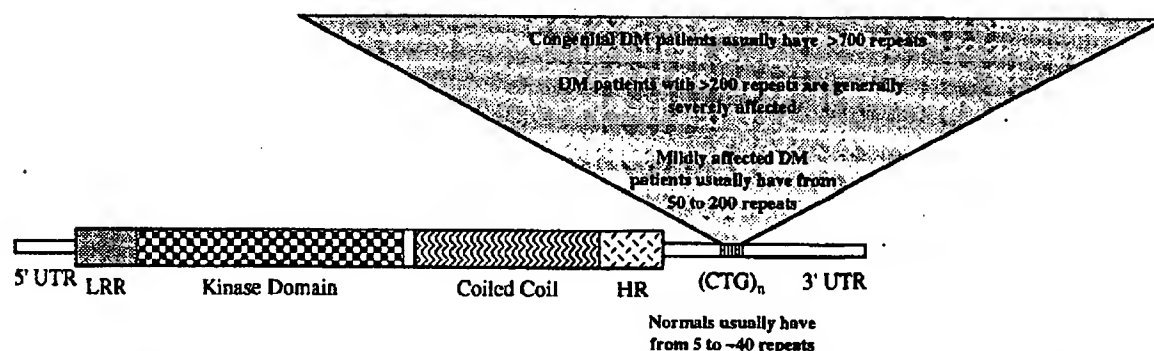


Figure 1. Schematic representation of the myotonin protein kinase gene product. The unfilled narrow rectangles represent the 3' and 5' untranslated regions (UTR). The coding sequence is shown as a broad rectangle with the leucine rich region (LRR), kinase domain, coiled coil domain and hydrophobic region (HR) indicated, as defined by Wieringa.⁵⁵ The position of the (CTG) in repeats in the 3'UTR that are polymorphic in normal individuals and expanded in DM patients is also shown.

from their father are protected *in utero* by a normal mother, or alternatively, that the affected status of DM mothers has an adverse *in utero* effect on their children.

Although the intergenerational differences in allele size observed are generally increases, reductions in allele size are occasionally detected.^{13,14,21-24,26} Comparison of parent and child allele sizes in blood DNA has revealed that approximately 7% of transmissions appear to involve a reduction in allele length.²¹ The frequency of such reductions is higher in male than in female transmission (~10% versus 3%) and in sibs who already have a sib carrying a reduced allele.²¹ Rarely, these reductions can occasionally generate alleles that fall back within the normal allele size range, although only four such reversions have been observed during pedigree analysis and all were transmitted by the father.^{14,24,26} Direct sperm analysis indicates that considerably less than 1% of gametes from affected males carry revertant alleles (D.G. Monckton *et al*, unpublished observation).

The high mutability of expanded DM alleles is not confined to the germline with high levels of somatic instability having also been observed. In fact, somatic instability may be so high that gel electrophoresis based size analysis of expanded alleles in somatic tissue usually results not in a discrete band, but a heterogeneous smear of multiple unresolved fragments.⁵⁻¹⁰ Direct comparison of the level of somatic heterogeneity between different tissues from the same person has shown that somatic instability is tissue specific.³⁰ Most interestingly, the expansion size seen in muscle is consistently larger than that observed in blood.^{11,32} The relevance of this observation to the mainly muscle related phenotype associated with DM is currently not clear. Recently, detailed analyses of the levels of repeat heterogeneity present in blood DNA has revealed that instability is positively correlated with patient age and repeat size.³³ Moreover, there appears to be a considerable bias toward continuous expansion of the repeats throughout adult life³³ (D.G. Monckton *et al*, unpublished observations). Once again, it is currently unclear whether this age related expansion bias is relevant to the increasingly severe symptoms associated with DM. It does, however, seem likely that since both patient age and tissue sample type can dramatically influence the expansion size measured, somatic instability may have sullied attempts to precisely associate disease prognosis with repeat size.

Reported intergenerational differences have been generally determined by comparison of allele size in

the blood DNA of parent and child and the differences detected assumed to reflect germline instability. However, the demonstration of considerable somatic instability, in particular the age related expansion bias, is likely to have confounded attempts to reconcile the observed clinical anticipation with increasing intergenerational allele length. As mentioned previously, approximately 7% of DM transmissions apparently involve a contraction of the DM repeat. Paradoxically though, the majority of these cases do not result in a later age of onset.²¹ However, recent results have indicated that some apparent 'contractions' may actually be artifacts of age-limited expansion in the children and that the DM allele is even more biased toward germline expansion than previously thought (D.G. Monckton *et al*, unpublished observations).

The Mt-PK gene and the pathogenesis of DM

Although the Mt-PK gene was discovered over two years ago, the molecular mechanisms that relay the CTG expansion to the observed phenotype of DM are still not known. The strong correlation between the size of repeats and severity of DM disease prompted us, and other laboratories, to investigate the DM gene structure and its expression in normal and DM population, as well as to study the Mt-PK protein structure and enzymatic activity.

The main features of the structural organization of the Mt-PK mRNA, deduced from the cDNA and genomic DNA nucleotide sequence of the Mt-PK gene, are presented in Figure 1. The N-terminal part of Mt-PK contains a leucine-rich sequence, which may participate in protein-protein interactions. The central portion of Mt-PK is the protein kinase domain, which by homology to other known kinases, particularly to cAMP-dependent kinases, would suggest that Mt-PK is a serine/threonine kinase. The C-terminal region of Mt-PK contains both a helical coiled-coil domain and a possible transmembranous hydrophobic domain. Presently, the structure of the 5' region of the Mt-PK mRNA is still unclear and it is not known from which start codon(s) the active Mt-PK gene product is translated. Tissue specific alternatively spliced Mt-PK transcripts have been observed,³⁴⁻³⁶ suggesting the existence of a number of different Mt-PK isoforms.

The CTG expansion is situated in the 3' untranslated region of the Mt-PK gene and is not translated into a protein product. However, expansion of the repeat may influence either the efficiency of Mt-PK

mRNA transcription or the regulation of messenger RNA stability, either of which could lead to changes in message level for the Mt-PK gene. Analysis of the steady-state level of Mt-PK mRNA by different groups has, however, revealed contradictory data.³⁶⁻⁴¹ Our group has demonstrated, using quantitative reverse transcription-polymerase chain reaction, and in agreement with three other groups, that the level of Mt-PK transcripts in skeletal muscle from adult DM patients is reduced, suggesting that DM may be the result of a simple reduction in steady state Mt-PK levels.³⁶ In contrast, Sabounin *et al*³⁹ found an apparent increase in the amount of the Mt-PK transcript in a congenital DM patient and postulated that elevated Mt-PK levels are responsible for the dominant pattern of DM pathogenesis. These contradictory results in the quantitative analysis of the Mt-PK expression could possibly be explained by a number of factors, including the use of different methods for Mt-PK mRNA detection and differences in DM muscle biopsies resulting from secondary pathological alterations in atrophied muscles. To resolve some of these technical controversies we have analyzed the expression of Mt-PK mRNA by northern blot hybridization, in addition to RT-PCR, in primary muscle cell cultures from DM patients. Our data demonstrate that the level of the expanded transcript in a DM homozygote, and additional DM heterozygous patients, is significantly reduced relative to the normal transcript (L. Timchenko *et al*, unpublished observations). These data confirm the reduction in levels of the enlarged transcript from the expanded allele, as was previously observed.³⁶

Direct information about the structure and function of the Mt-PK protein is very limited, with most progress having been made in immunological studies of Mt-PK. A number of polyclonal antipeptide antibodies to the predicted protein sequence of Mt-PK were developed, all recognizing a 52-55 kDa protein in muscle extracts.^{36,42-44} One antiserum also recognized a major 42 kDa protein in brain.⁴³ However, the exact size of the primary translation product of Mt-PK mRNA is unknown. The Mt-PK mRNA contains five in-frame AUG codons, none of which possesses a favorable 'Kozak' sequence^{45,46} for the initiation of translation. It is possible that leaky initiation could produce alternative protein isoforms. The size of the immunologically determined Mt-PK (55 kDa) corresponds to a protein initiated from the third AUG codon. To search for the full-length Mt-PK isoform a number of different antibodies were also tested. Two species of antibodies recognized a 72 kDa isoform of Mt-PK that is presumed to be the full-length Mt-PK

protein (L. Timchenko *et al*, unpublished observations). The 52-55 kDa protein may be an alternative translation product of the Mt-PK mRNA, or a product of post-translational maturation. The identification of two isoforms raises several questions. Which isoform(s) of Mt-PK is involved in DM pathogenesis? What is the steady state level of the full-length isoform in DM patients? To try and answer some of these questions, Mt-PK mRNA and protein expression were analyzed in muscle and fibroblasts cell lines derived from a homozygous DM patient. Reduction of the full-length (72 kDa) isoform was observed, correlating with the level of Mt-PK mRNA (L. Timchenko *et al*, unpublished observations).

To determine which Mt-PK isoform is active *in vivo*, human fibroblasts were grown with ³²P-phosphate. Analysis of the phosphorylated proteins with antibodies against Mt-PK revealed the phosphorylation *in vivo* of the full-length (72 kDa) Mt-PK isoform, but not the 55 kDa isoform (L. Timchenko *et al*, unpublished observations).

By homology with other kinases, Mt-PK is predicted to be a cAMP-dependent serine/threonine kinase.^{8-10,34} Two groups simultaneously and independently expressed the Mt-PK as a fusion protein in bacterial cells and demonstrated the ability of Mt-PK to autophosphorylate itself *in vitro*.^{47,48} Autophosphorylation is a common feature of many kinases and may be involved in the autoregulation of Mt-PK activity. The substrate specificity of Mt-PK has been investigated using synthetic peptides. These studies revealed that recombinant Mt-PK was able to phosphorylate serine containing peptides *in vitro* (L. Timchenko *et al*, unpublished observations). Dunne *et al* have also demonstrated serine/threonine specificity of Mt-PK in an *in vitro* assay with histone H1 as a substrate, in addition to autophosphorylation activity.⁴⁷ Taken together, these data show that Mt-PK, in agreement with its amino acid homology to other kinases, displays specificity for serine and threonine residues. The enzymatic properties of Mt-PK have also been investigated using Mt-PK immunoprecipitated from human muscle tissue.⁴⁴ The authors demonstrated the phosphorylation of a tyrosine containing peptide. These results suggest that Mt-PK is a kinase with dual activity, specific for serine/threonine and tyrosine residues, possibly mediated by different Mt-PK isoforms.

The *in vivo* biological substrates for Mt-PK are currently not known. Since DM is a muscle disease with defects in muscle excitability, ion channels that are involved in the regulation of muscle activity would

appear to be good candidates for biological substrates for Mt-PK. In addition to DM, several other disorders are also characterized by defects in muscle membrane hyperexcitability and for most of these diseases specific point mutations in ion channel genes have been found. Point mutations in the chloride ion channel gene have been identified in both Thomsen's disease⁴⁹ and for recessive generalized myotonia.⁵⁰ For paramyotonia congenita and hyperkalemic periodic paralysis, specific point mutations have been found in the sodium channel gene,⁵¹⁻⁵³ whilst hypokalemic periodic paralysis has been associated with mutations in the $\alpha 1$ subunit of the calcium voltage-dependent release channel or dihydropyridine receptor (DHPR).⁵⁴ Our group investigated the *in-vitro* phosphorylation by recombinant Mt-PK of one of these candidate substrates, DHPR. Mt-PK was shown to be capable of phosphorylating the β -subunit of the calcium ion channel *in vitro*.⁴⁸ However, the biological and/or pathogenic relevance of this phosphorylation *in vivo*, as well as the phosphorylation of other ion channels, remains to be determined.

Conclusions

DM is associated with the expansion of an unstable CTG repeat in the 3' UTR of the Mt-PK gene. The instability of the repeats appears to account for many of the unusual features of DM including the extremely variable phenotype and the clinical anticipation. However, the molecular mechanisms that are responsible for triplet repeat expansions remain obscure.

Although the general consensus is now that the expansion probably leads to a reduction in steady state Mt-PK mRNA and protein levels, it is unclear whether this reduction is the only factor involved in DM pathogenesis. To understand the molecular basis of DM, all components of the signal transduction pathway that include Mt-PK should be identified. It has been demonstrated in other signal transduction pathways that small perturbations in the early stages of the pathway can lead to very large differences further down the cascade. If, however, DM were really a simple 50% loss of activity of Mt-PK we might expect to find other inactivating mutations in the Mt-PK gene. Although apparent DM phenocopies without expansions do exist, no additional Mt-PK mutations have so far been reported. It is possible that in some non-expansion DM patients other genes encoding other proteins in the Mt-PK cascade, including possible substrates for Mt-PK, may carry deleterious muta-

tions. It is also possible that other genes close to Mt-PK may also be influenced by expansion of the repeat and much remains to be done to resolve the many uncertainties surrounding the pathogenesis of DM.

Acknowledgements

D.G.M. is the Muscular Dystrophy Association Sammy Davis Jr Neuromuscular Disease Research Fellow and C.T.C. is a Howard Hughes Medical Institute Investigator.

References

1. Harper PS (1989) Myotonic Dystrophy. 2nd edn. WB Saunders Co. London
2. Ashizawa T, Epstein HF (1991) Ethnic distribution of myotonic dystrophy gene. *Lancet* 338:642-643
3. Harper PS, Harley HG, Reardon W, Shaw DJ (1992) Anticipation in myotonic dystrophy: new light on an old problem. *Am J Hum Genet* 51:10-16
4. Ashizawa T, Dunne CJ, Dubel JR, Perryman MB, Epstein HF, Boerwinkle E, Hejmancik JF (1992) Anticipation in myotonic dystrophy. *Neurology* 42:1871-1877
5. Buxton J, Shelbourne P, Davies J, Jones C, Tongeren TV, Aslanidis C, de Jong P, Jansen G, Anvret M, Riley B, Williamson B, Johnson K (1992) Detection of an unstable fragment of DNA specific to individuals with myotonic dystrophy. *Nature* 355:547-548
6. Harley HG, Brook JD, Rundle SA, Crow S, Reardon W, Buckler AJ, Harper PS, Housman D, Shaw DJ (1992) Expansion of an unstable DNA region and phenotypic variation in myotonic dystrophy. *Nature* 355:545-546
7. Aslanidis C, Jansen G, Amemiya C, Shutter G, Mahadevan M, Tsilfidis C, Chen C, Alleman J, Wormskamp NGM, Vooijs M, Buxton J, Johnson K, Smets HJM, Lemmon GG, Carrazo AV, Korneluk RG, Wieringa B, de Jong PJ (1992) Cloning of the essential myotonic dystrophy region and mapping of the putative defect. *Nature* 355:548-550
8. Brook JD, McCurrach ME, Harley HG, Buckler AJ, Church D, Aburatani H, Hunter K, Stanton VP, Thirion J-P, Hudson T, Sohn R, Zemelman B, Snell RG, Rundle SA, Crow S, Davies J, Shelbourne P, Buxton J, Jones C, Juvonen V, Johnson K, Harper PS, Shaw DJ, Housman DE (1992) Molecular basis of myotonic dystrophy: expansion of a trinucleotide (CTG) repeat at the 3' end of a transcript encoding a protein kinase family member. *Cell* 68:799-808
9. Fu YH, Pizzuti A, Fenwick RG, King J, Rajnarayan S, Dunne PW, Dubel J, Nasser GA, Ashizawa T, de Jong P, Wieringa B, Korneluk R, Perryman MB, Epstein HF, Caskey CT (1992) An unstable triplet repeat in a gene related to myotonic muscular dystrophy. *Science* 255:1256-1258
10. Mahadevan M, Tsilfidis C, Sabourin I, Shutter G, Amemiya C, Jansen G, Neville C, Narang M, Barcelo J, O'Hoy K, (1992) Myotonic dystrophy mutation: an unstable CTG repeat in the 3' untranslated region of the gene. *Science* 255:1253-1255
11. Ashizawa HG, Dubel JR, Harai Y (1993) Somatic instability of CTG repeat in myotonic dystrophy. *Neurology* 43:2674-2678
12. Harley HG, Rundle SA, MacMillan JC, Myring J, Brook JD, Crow S, Reardon W, Fenton I, Shaw DJ, Harper PS (1993) Size of the unstable CTG repeat sequence in relation to phenotype and parental transmission in myotonic dystrophy. *Am J Hum Genet* 52:1164-1174

13. Reduan JB, Fenwick RG, Fu YH, Pizzuti A, Caskey CT (1993) Relationship between parental trinucleotide GCT repeat length and severity of myotonic dystrophy in offspring. *J Am Med Assoc* 269:1960-1965
14. Shelbourne P, Winquist R, Kunert E, Davies J, Leisti J, Thiele H, Bachmann H, Buxton J, Williamson B, Johnson K (1992) Unstable DNA may be responsible for the incomplete penetrance of the myotonic dystrophy phenotype. *Hum Mol Genet* 1:467-473
15. Tsilfidis C, MacKenzie AE, Mettler G, Barcelo J, Korneluk RG (1992) Correlation between CTG trinucleotide repeat length and frequency of severe congenital myotonic dystrophy. *Nature Genet* 1:192-195
16. Ashizawa T, Dunel JR, Dunne PW, Dunne CJ, Fu YH, Pizzuti A, Caskey CT, Coerwinkel E, Perryman MB, Epstein HF, Hejtmancik JF (1992) Anticipation in myotonic dystrophy. II. Complex relationships between clinical findings and structure of the GCT repeat. *Neurology* 42:1877-1883
17. Hunter A, Tsilfidis C, Mettler G, Jacob P, Mahadevan M, Surh L, Korneluk RG (1992) The correlation of age of onset with CTG trinucleotide repeat amplification in myotonic dystrophy. *J Med Genet* 29:774-779
18. Novelli G, Gennarelli M, Menegazzo E, Mostacciolo ML, Pizzuti A, Fattorini C, Tessarolo D, Tomelleri G, Giacomelli M, Danieli GA, Rizzuto N, Caskey CT, Angelini C, Dallapiccola B (1993) (CTG) in triplet mutation and phenotype manifestations in myotonic dystrophy patients. *Biochem Med Met Biol* 50:85-92
19. Reardon W, Harley HG, Brook JD, Rundle SA, Crow S, Harper PS, Shaw DJ (1992) Minimal expression of myotonic dystrophy: a clinical and molecular analysis. *J Med Genet* 29:770-773
20. Ashizawa T, Dunne PW, Ward PA, Seltzer WK, Richards CS (1994) Effects of sex of myotonic dystrophy patients on the unstable triplet repeat in their affected offspring. *Neurology* 44:120-122
21. Ashizawa T, Anvret M, Baiget M, Barcelo JM, Brunner H, Cobo AM, Dallapiccola B, Fenwick Jr. RG, Grandell U, Harley H, Junien C, Koch MC, Korneluk RG, Lavedan C, Miki T, Mulley JC, Lopez de Munain A, Novelli G, Roses AD, Seltzer WK, Shaw DJ, Smets H, Sutherland GR, Yamagata H, Harper PS (1994) Characteristics of intergenerational contractions of the CTG repeat in myotonic dystrophy. *Am J Hum Genet* 54:414-423
22. Barcelo JM, Mahadevan MS, Tsilfidis C, MacKenzie AE, Korneluk RG (1993) Intergenerational stability of the myotonic dystrophy protomutation. *Hum Mol Genet* 2:705-709
23. Brunner HG, Bruggenwirth HT, Nillesen W, Jansen G, Hamel CJ, Hoppe RJE, de Die CEM, Howeler CJ, van Oost BA, Wieringa B, Ropers HH, Smets HJM (1993) Influence of sex of the transmitting parent as well as of parental allele size on the CTG expansion in myotonic dystrophy (DM). *Am J Hum Genet* 53:1016-1023
24. Brunner HG, Jansen G, Nillesen W, Nelen MR, de Die CEM, Howeler C, van Oost BA, Wieringa B, Ropers HH, Smets HJM (1993) Reverse mutation in myotonic dystrophy. *New Eng J Med* 328:476-480
25. Lavedan C, Hofmann-Radvanyi H, Shelbourne P, Rabes J-P, Duros C, Savoy D, Dehaupas I, Luce S, Johnson K, Junien C (1993) Myotonic dystrophy: size- and sex-dependent dynamics of CTG meiotic instability, and somatic mosaicism. *Am J Hum Genet* 52:875-883
26. O'Hoy KL, Tsilfidis C, Mahadevan MS, Neville CE, Barcelo J, Hunter AGW, Korneluk RG (1993) Reduction in size of the myotonic dystrophy trinucleotide repeat mutation during transmission. *Science* 259:809-812
27. Hunter AGW, Jacob J, O'Hoy K, MacDonald I, Mettler G, Tsilfidis C, Korneluk RG (1993) Decrease in size of the myotonic dystrophy CTG repeat during transmission from parent to child: implications for genetic counselling and genetic anticipation. *Am J Med Genet* 45:401-407
28. Nakagawa M, Yamada H, Higuchi I, Kaminishi Y, Miki T, Johnson K, Osame M (1994) A case of paternally inherited congenital myotonic dystrophy. *J Med Genet* 31:397-400
29. Bergoffen J, Kant J, Sladky J, McDonald-McGinn D, Zacki FH, Fischbeck KH (1994) Paternal transmission of congenital myotonic dystrophy. *J Med Genet* 31:518-520
30. Jansen G, Willems P, Coerwinkel M, Nillesen W, Smets H, Vits L, Howeler C, Brunner H, Wieringa B (1994) Gonosomal mosaicism in myotonic dystrophy patients: involvement of mitotic events in (CTG) variation and selection against extreme expansion in sperm. *Am J Hum Genet* 54:575-585
31. Barcelo JM, Pluscauskas M, MacKenzie AE, Tsilfidis C, Narang M, Korneluk RG (1994) Additive influence of maternal and offspring DM-kinase gene CTG repeat lengths in the genesis of congenital myotonic dystrophy. *Am J Hum Genet* 54:1124-1125
32. Anvret M, Ahlberg G, Grandell U, Hedberg B, Johnson K, Edstrom L (1993) Larger expansions of the CTG repeat in muscle compared to lymphocytes from patients with myotonic dystrophy. *Hum Mol Genet* 2:1397-1400
33. Wong L-JC, Ashizawa T, Monckton DG, Caskey CT, Richards CS (1995) Somatic heterogeneity of the CTG repeat in myotonic dystrophy is age and size dependent. *Am J Hum Genet* 56:114-122
34. Jansen G, Mahadevan M, Amemiya C, Wormskamp N, Segers B, Hendriks W, O'Hoy K, Baird S, Sabourin L, Lennon G, Jap PI, Iles D, Coerwinkel M, Hofker M, Carrano AV, de Jong PJ, Korneluk RG, Wieringa B (1992) Characterization of the myotonic dystrophy region predicts multiple protein isoform-encoding mRNAs. *Nature Genet* 1:261-266
35. Mahadevan MS, Amemiya C, Jansen G, Sabourin L, Baird S, Neville CE, Wormskamp N, Segers B, Batzer M, Lamerding J, de Jong P, Wieringa B, Korneluk RG (1993) Structure and genomic sequence of the myotonic dystrophy (DM kinase) gene. *Hum Mol Genet* 2:299-304
36. Fu YH, Friedman DL, Richards S, Pearlman JA, Gibbs RA, Pizzuti A, Ashizawa T, Perryman MB, Scarlato G, Fenwick Jr RG, Caskey CT (1993) Decreased expression of myotonin-protein kinase messenger and protein in adult form of myotonic dystrophy. *Science* 260:235-238
37. Hofmann-Radvanyi H, Lavedan C, Rabes J-P, Savoy D, Duros C, Johnson K, Junien C (1993) Myotonic dystrophy: absence of CTG enlarged transcript in congenital forms, and low expression of the normal allele. *Hum Mol Genet* 2:1263-1266
38. Novelli G, Gennarelli M, Zelano G, Pizzuti A, Fattorini C, Caskey CT, Dallapiccola B (1993) Failure in detecting mRNA transcripts from the mutated allele in myotonic dystrophy muscle. *Biochem Mol Biol Int* 29:291-297
39. Sabourin LA, Mahadevan MS, Narang M, Lee DSC, Surh LC, Korneluk RG (1993) Effect of the myotonic dystrophy (DM) mutation on mRNA levels of the DM gene. *Nature Genet* 4:233-238
40. Hofmann-Radvanyi H, Junien C (1993) Myotonic dystrophy: over-expression or/and under-expression? A critical review on a controversial point. *Neuromusc Dis* 3:497-501
41. Carango P, Noble JE, Marks HG, Funanage VL (1993) Absence of myotonic dystrophy protein kinase (DMPK) mRNA as a result of a triplet expansion in myotonic dystrophy. *Genomics* 18:340-348
42. van der Ven PFM, Jansen G, van Kuppevelt THMSM, Perryman MB, Lupa M, Dunne PW, ter Laak HJ, Jap PIK, Veerkamp JH, Epstein HF, Wieringa B (1993) Myotonic dystrophy kinase is a component of neuromuscular junctions. *Hum Mol Genet* 2:1889-1894
43. Brewster BS, Jeal S, Strong PN (1994) Identification of a protein product of the myotonic dystrophy gene using peptide specific antibodies. *Biochem Biophys Res Commun* 194:1256-1260

Myotonic dystrophy

44. Etongue-Mayer P, Faure R, Bouchard J-P, Thibault M-C, Puymirat J (1994) The myotonin-protein kinase phosphorylates tyrosine residues in normal human skeletal muscle. *Biochem Biophys Res Commun* 199:89-92
45. Kozak M (1986) Point mutations define a sequence flanking the AUG initiator codon that modulates translation by eukaryotic ribosomes. *Cell* 44:283-292
46. Kozak M (1989) The scanning model for translation: an update. *Cell Biol* 108:229-241
47. Dunne PW, Walch ET, Epstein HF (1994) Phosphorylation reactions of recombinant human myotonic dystrophy protein kinase and their inhibition. *Biochemistry* 33:10809-10814
48. Timchenko L, Pizzuti A, Caskey CT (1993) Identification of an *in vitro* substrate for recombinant myotonin protein kinase. *Am J Hum Genet* 53:A734
49. George Jr AL, Crackower MA, Abdalla JA, Hudson AJ, Ebers GC (1993) Molecular basis of Thomsen's disease (autosomal dominant myotonia congenita). *Nature Genet* 3:305-310
50. Koch MC, Steinmeyer K, Lorenz C, Ricker K, Wolf F, Otto M, Zoll B, Lehmann-Horn F, Grzeschik K-H, Jentsch TJ (1992) The skeletal muscle chloride channel in dominant and recessive human myotonia. *Science* 257:797-800
51. McClatchey AJ, den Bergh PV, Pericak-Vance MA, Raskind W, Verellen C, McKenna-Yasck D, Rao K, Haines JL, Bird T, Brown Jr RH, Gusella JF (1992) Temperature-sensitive mutations in the III-IV cytoplasmic loop region of the skeletal muscle sodium channel gene in paramyotonia congenita. *Cell* 68:769-774
52. Ptacek LJ, George Jr AL, Barchi RL, Griggs RC, Riggs JE, Robertson M, Leppert MF (1992) Mutations in an S1 segment of the adult skeletal sodium channel cause paramyotonia congenita. *Neuron* 8:891-897
53. Rojas CV, Wang J, Schwartz LS, Hoffman EP, Powell BR, Brown Jr RH (1991) A Met-to-Val mutation in the skeletal muscle Na⁺ channel α -subunit in hyperkalaemic periodic paralysis. *Nature* 354:387-389
54. Ptacek LJ, Tawil R, Griggs RC, Engel AG, Layzer RB, Kwiecinski H, McManis PG, Santiago L, Moore M, Fouad C, Bradley P, Leppert MF (1994) Dihydropyridine receptor mutations cause hypokalemic periodic paralysis. *Cell* 77:863-868
55. Wieringa B (1994) Myotonic dystrophy reviewed: back to the future. *Hum Mol Genet* 3:1-7

Chem.-Biol. Interactions, 88 (1992) 107-119
Elsevier Scientific Publishers Ireland Ltd.

107

INDUCTION OF CLASS 3 ALDEHYDE DEHYDROGENASE IN THE MOUSE HEPATOMA CELL LINE HEPA-1 BY VARIOUS CHEMICALS

RITTA TÖRRÖNEN^a, MERJA KORKALAINEN^b and SIRPA O. KÄRENLAMPI^b

^aDepartment of Physiology and ^bDepartment of Biochemistry and Biotechnology, University of Kuopio, P.O. Box 1627, SF-70211 Kuopio (Finland)

(Received November 25th, 1991)

(Revision received March 27th, 1992)

(Accepted March 31st, 1992)

SUMMARY

The mouse hepatoma cell line Hepa-1 was shown to express an aldehyde dehydrogenase (ALDH) isozyme which was inducible by TCDD and carcinogenic polycyclic aromatic hydrocarbons. The induced activity could be detected with benzaldehyde as substrate and NADP as cofactor (B/NADP ALDH). As compared with rat liver and hepatoma cell lines, the response was moderate (maximally 5-fold). There was an apparent correlation between this specific form of ALDH and aryl hydrocarbon hydroxylase (AHH) in the Hepa-1 wild-type cell line — in terms of inducibility by several chemicals. However, the magnitude of the response was clearly smaller for ALDH than for AHH. Southern blot analysis showed that a homologous gene (class 3 ALDH) was present in the rat and mouse genome. The gene was also expressed in Hepa-1 and there was a good correlation between the increase of class 3 ALDH-specific mRNA and B/NADP ALDH enzyme activity after exposure of the Hepa-1 cells to TCDD. It is concluded that class 3 ALDH is inducible by certain chemicals in the mouse hepatoma cell line, although the respective enzyme is not inducible in mouse liver *in vivo*.

Key words: Aldehyde dehydrogenase — Induction — Mouse — Hepa-1 — Cell line — Hepatoma

INTRODUCTION

Aldehyde dehydrogenase (aldehyde:NAD⁺ oxidoreductase, EC 1.2.1.3, ALDH) occurs in most mammalian tissues, where it catalyses the oxidation of

Correspondence to: R. Törrönen, Department of Physiology, University of Kuopio, P.O. Box 1627, SF-70211 Kuopio, Finland.

0009-2797/92/\$05.00

© 1992 Elsevier Scientific Publishers Ireland Ltd.

Printed and Published in Ireland

aldehydes to carboxylic acids. It thus has a detoxicative function. There are several isozymes of ALDH. Induction of two distinct isozymes in rat liver is well documented. Phenobarbital was first discovered to enhance ALDH activity [1]. Mirex and DDT are phenobarbital-type inducers, which increase cytoplasmic ALDH activity characterized by preferentially catalysing the metabolism of propionaldehyde or phenylacetaldehyde in the presence of NAD as cofactor [2]. TCDD (2,3,7,8-tetrachlorodibenzo-*p*-dioxin) [2-4], polychlorinated biphenyls [2,5] and the polycyclic aromatic hydrocarbons β -naphthoflavone [2,6], 3-methylcholanthrene [2,4-7], benzo[*a*]pyrene [4-7], chrysene [4,5,7] and benzo[*a*]anthracene [5,7] induce another ALDH isozyme, which differs from the phenobarbital-type enzyme, e.g. in its ability to oxidize benzaldehyde in the presence of NADP (B/NADP ALDH). The endogenous function of these inducible forms of ALDH is not known.

Besides rat liver, ALDH is inducible by phenobarbital and several polycyclic aromatic hydrocarbons also in primary cultures of rat hepatocytes [8-10]. 3-Methylcholanthrene and benzo[*a*]pyrene strongly induce B/NADP ALDH activity also in the rat hepatoma cell lines H4-II-EC3 and McA-RH7777 with intermediate or low basal activities [11]. On the other hand, certain rat hepatoma cell lines express high constitutive B/NADP ALDH activity which is only marginally induced by these compounds [11,12].

In addition to a short-term exposure to various xenobiotics, also hepatocarcinogenesis increases B/NADP ALDH activity in the rat [13-15]. The genes for the rat liver tumour-associated [16] and TCDD-inducible [17] cytoplasmic ALDHs have been cloned and shown to be identical [18]. These ALDH isozymes are referred to as class 3 ALDHs (ALDH3) according to the new nomenclature [19].

As in the rat, B/NADP ALDH is also expressed in chemically-initiated mouse liver tumours [20,21]. However, in contrast to the rat, the induction of ALDH by TCDD or polycyclic aromatic hydrocarbons has not been convincingly shown in the mouse [3,22]. In the present report we describe the induction of B/NADP ALDH in the mouse hepatoma cell line Hepa-1 after a short-term exposure to these chemicals. Evidence is also given to show that the induced form of ALDH belongs to class 3 ALDHs.

MATERIALS AND METHODS

Cell culture

A subclone Hepa-1c1c7 of the mouse hepatoma cell line Hepa-1 [23] and the rat hepatoma cell line HTC [24] were obtained from Dr. D.W. Nebert, University of Cincinnati Medical Center, Cincinnati, Ohio. The cells were grown as monolayers in α -MEM supplemented with 5% foetal calf serum (irradiated), 100 units/ml penicillin and 0.1 mg/ml streptomycin. The cell culture medium, foetal calf serum and antibiotics were purchased from Gibco (Paisley, UK). For ALDH enzyme activity and mRNA studies, 1.3×10^6 cells were plated on an 85-mm dish in 10 ml of the medium. The inducers were dissolved in dimethyl sulphoxide (DMSO). The final concentration of DMSO in the culture medium never exceeded 0.5%.

ALDH and AHH assays

To assay ALDH or aryl hydrocarbon hydroxylase (AHH) the cells were harvested 24, 48 or 72 h after the initiation of exposure to the inducers. Following removal of the medium, the cell surface was washed twice with 5 ml of cold Dulbecco's phosphate buffered saline without calcium or magnesium (1% NaCl, pH 7.2). The cells were scraped and collected as pellets to be stored at -80°C . The cell pellets were thawed and sonicated briefly in 1 ml of ice-cold 33 mM potassium phosphate buffer (pH 7.5) containing 0.25 M sucrose. ALDH activities were assayed at 37°C by monitoring the reduction of NAD(P) at 340 nm. The assay mixture (final volume 1 ml) for non-specific ALDH activity (P/NAD ALDH) contained 70 mM sodium pyrophosphate buffer (pH 8.0), 1 mM pyrazole to inhibit alcohol dehydrogenase, 1 mM NAD as cofactor and 5 mM propionaldehyde (dissolved in water) as substrate. For B/NADP ALDH activity 2.5 mM NADP was used as cofactor, 0.1 mM benzaldehyde (dissolved in methanol, final concentration 1%) as substrate and pyrazole was omitted. The blanks containing no aldehyde were run for every sample. The activities were calculated as nmol of NAD(P)H formed/min per mg protein. In ten different experiments carried out during a 1-year period, the B/NADP ALDH activity of DMSO-treated (control) Hepa-1 cell cultures ranged from 2.9 to 13.4 (mean 6.8) nmol NADPH min^{-1} mg protein $^{-1}$. The highest activities were detected with freshly prepared benzaldehyde solutions. Therefore, some of the variations in the basal B/NADP ALDH activities can probably be explained by slight variations in the assay conditions. However, despite the differences in the control levels, the relative response to the inducers was stable from one experiment to another.

AHH activity was assayed using a method originally described by Nebert and Gelboin [25], with some modifications. The method is based on the hydroxylation of benzo[a]pyrene to its 3-hydroxy derivative, which is measured fluorometrically. Cell suspensions were incubated at 37°C for 15 min in a mixture (final volume 1 ml) containing 25 mM potassium phosphate buffer (pH 7.5), 3.6 mM magnesium chloride, 0.36 mM NADPH, 0.42 mM NADH, 675 μg of albumin and 80 μM benzo[a]pyrene (dissolved in acetone, final concentration 5%). The reaction was stopped by the addition of 1 ml of ice-cold acetone and 3.25 ml of hexane. After vigorous shaking (vortex) a 2.5-ml sample of the organic phase was taken and extracted with 2 ml of 1 M sodium hydroxide. The fluorescence of 3-OH-benzo[a]pyrene in the alkali phase was determined at the excitation and emission wavelengths of 391 and 517 nm, respectively. The assay was calibrated with 3-OH-benzo[a]pyrene and quinine sulphate. The activity is expressed as pmol of 3-OH-benzo[a]pyrene formed/min per mg protein. Protein was assayed by the method of Bradford [26] with Coomassie Brilliant Blue G-250 dye (Bio-Rad, Richmond, California) and using bovine serum albumin as standard.

Southern blot hybridization

DNA was isolated from the cultured Hepa-1 and HTC cells using phenol extraction [27]. Digestions were carried out under standard conditions. Hybridization was performed with the nick-translated probe p12x. p12x was a 1.150 bp cDNA clone specific for the TCDD-inducible rat liver ALDH [17] and was a gift from Dr. T.J. Dunn, McArdle Laboratory for Cancer Research, University of Wisconsin, Wisconsin.

Analysis of RNA

RNA was isolated from the cultured cells as previously described [28]. The purity of RNA was assessed by measuring the ratio between the absorbance readings at 260 nm and 280 nm. The concentration of RNA was determined at 260 nm. For slot blot hybridization analysis, 7.5 or 15 μ g of total RNA was diluted in $10 \times$ SSC. The mixture was applied on a nylon filter through a filtration manifold. RNA was fixed by UV light (254 nm, 5 min). The filters were prehybridized for about 4 h at 42°C in 15 ml of a solution containing $5 \times$ Denhardt's solution, $6 \times$ SSC, 0.5% SDS, 100 μ g/ml denatured salmon sperm DNA and 50% formamide. The hybridization mixture also contained 0.01 M EDTA and the p12x probe. In every experiment a duplicate filter was hybridized to a cDNA probe for hamster CAD (carbamyl-P synthetase, aspartate transcarbamylase, dihydroorotase) gene [29]. CAD was obtained from Dr. W. Liao, Stanford University Medical Center, Stanford, California and was used for the standardization of the amount of ALDH mRNA bound to the filter during slot blot hybridization analysis. The probes were nick-translated to a specific activity of $\sim 3 \times 10^8$ counts/min per μ g DNA and added to the hybridization mixture. The mRNA-DNA hybridization was carried out for 18–24 h at 42°C. Following the hybridization, the filters were washed three times with $2 \times$ SSC plus 0.1% SDS at room temperature and twice with $1 \times$ SSC plus 0.1% SDS at 60°C. The filters were then autoradiographed (Kodak X-Omat AR-5 film). The relative amounts of ALDH mRNA were obtained by densitometric scanning (500 nm) of the X-ray films and by integrating the surface areas of the peaks.

RESULTS

Induction of ALDH by various chemicals

Hepa-1 mouse hepatoma cell culture was exposed to several compounds known to be inducers of either ALDH or the microsomal cytochrome P-450 system. The concentrations of several compounds were chosen based on their ability to maximally induce AHH in Hepa-1 [28,30]. The non-specific ALDH activity was assayed with propionaldehyde as substrate and NAD as cofactor (P/NAD ALDH). Benzaldehyde and NADP were used to assay the ALDH form (B/NADP ALDH) which is inducible, e.g. by TCDD and carcinogenic polycyclic aromatic hydrocarbons in rat liver. Among the ten chemicals tested, TCDD (1 nM), 3-methylcholanthrene (1 μ M), benz[a]anthracene (13 μ M) and chrysene (25 μ M) were able at least to double P/NAD ALDH activity (Table I). In addition to these chemicals, B/NADP ALDH activity was also elevated by benzo[a]pyrene (1 μ M), α - and β -naphthoflavone (10 μ M) and CPBT (100 μ M). Under the conditions used, chrysene, benz[a]anthracene and TCDD were the most potent inducers of ALDH activities. Anthracene was not an inducer. Mirex (5–100 μ M) and DDT (20 μ M) had no effect on either ALDH activity.

The time course of induction of ALDHs in Hepa-1 were studied for TCDD (1 nM), 3-methylcholanthrene (1 μ M) and β -naphthoflavone (10 μ M). Maximal activities were reached after a 1- or 2-day-exposure of the cells to 3-methylcholanthrene or β -naphthoflavone and after a 2- or 3-day-exposure to TCDD.

TABLE I

EFFECTS OF VARIOUS COMPOUNDS ON ALDH ACTIVITIES IN HEPA-1 CELL LINE

Chemical ^a	P/NAD ALDH ^b	B/NADP ALDH ^b
Control (0.5%DMSO)	11.8	13.4
TCDD (1 nM)	28.3 2.4 ×	59.7 4.4 ×
3-Methylcholanthrene (1 μM)	23.6 2.0 ×	48.6 3.6 ×
Benzo[a]pyrene (1 μM)	18.3 1.5 ×	37.5 2.8 ×
Benz[a]anthracene (13 μM)	29.9 2.5 ×	60.6 4.5 ×
Chrysene (25 μM)	28.2 2.4 ×	70.5 5.3 ×
Anthracene (100 μM)	9.4 0.8 ×	12.5 0.9 ×
α-Naphthoflavone (10 μM)	18.2 1.5 ×	30.9 2.3 ×
β-Naphthoflavone (10 μM)	15.2 1.3 ×	34.8 2.6 ×
Phenobarbital (2 mM)	14.7 1.2 ×	22.6 1.7 ×
CPBT ^c (100 μM)	21.3 1.8 ×	49.9 3.7 ×

^aThe cells were exposed for 24 h to the compounds dissolved in DMSO. The final concentrations are given in parentheses.

^bThe specific activities (nmol NAD(P)H × min⁻¹ × mg protein⁻¹) and the fold-inductions (×) compared with the controls are given. Each value represents the mean of duplicate dishes of cells.

^c2-(4'-chlorophenyl)benzothiazole.

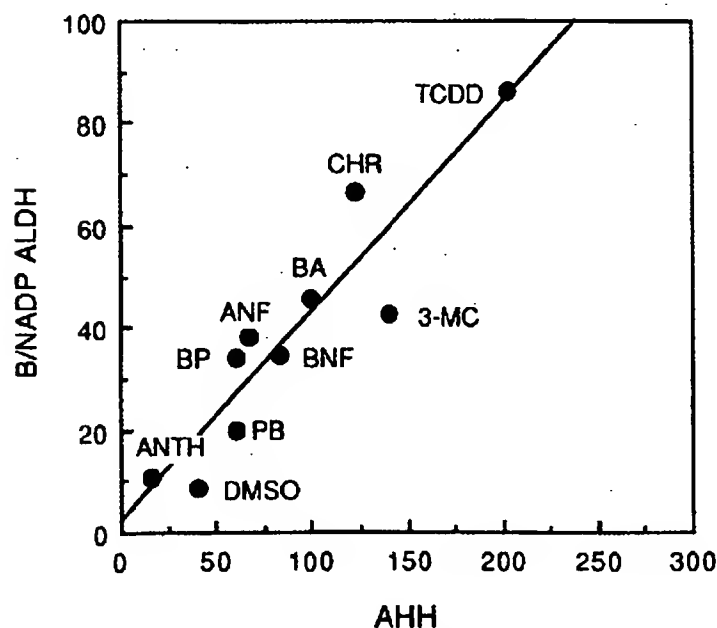


Fig. 1. Correlation of B/NADP ALDH and AHH activities in Hepa-1 cell line exposed to the compounds presented in Table I (except CPBT) for 24 h (AHH, pmol × min⁻¹ × mg protein⁻¹) or 48 h (B/NADP ALDH, nmol NADPH × min⁻¹ × mg protein⁻¹). Each point represents the mean of duplicate dishes of cells. The abbreviations used are: ANF, α-naphthoflavone; ANTH, anthracene; BA, benz[a]anthracene; BNF, β-naphthoflavone; BP, benzo[a]pyrene; CHR, chrysene; DMSO, dimethyl sulphoxide; 3-MC, 3-methylcholanthrene; PB, phenobarbital; TCDD, 2,3,7,8-tetrachlorodibenzo-p-dioxin.

112

Correlation between ALDH and AHH induction

In Fig. 1 the B/NADP ALDH activities are plotted against the AHH activities for the compounds presented in Table I (CPBT excluded). The best correlation between these enzyme activities was drawn from data obtained when Hepa-1 cells were exposed to these compounds for 24 h for AHH activity and for 48 h for ALDH activities. The correlation coefficients were 0.95 and 0.92 for P/NAD and B/NADP ALDH activities, respectively.

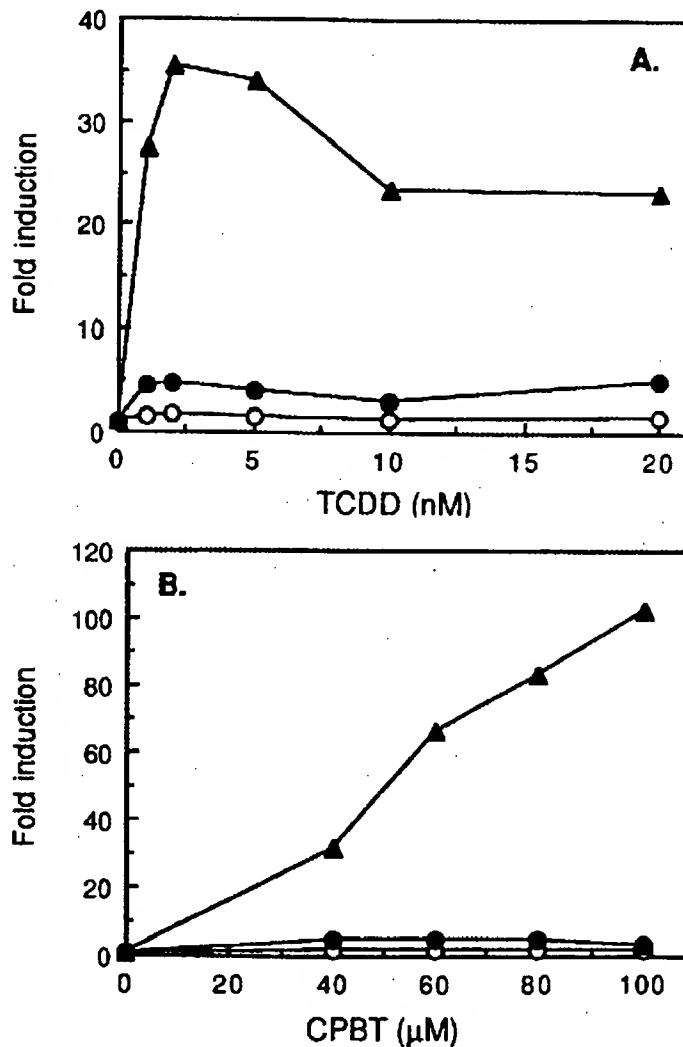


Fig. 2. Dose response of ALDH and AHH induction by TCDD (A) and CPBT (B) in Hepa-1 cell line. The cells were exposed to the chemicals for 24 h. The results are expressed as fold induction calculated by giving the value 1 to DMSO-treated control cells. Each point represents the mean of duplicate dishes of cells. ○, P/NAD ALDH; ●, B/NADP ALDH; ▲, AHH.

The dose response curves for TCDD and CPBT induction of ALDH and AHH are presented in Fig. 2. Maximal P/NAD ALDH, B/NADP ALDH and AHH activities were obtained with 2 nM TCDD. The maximal-fold inductions were: 1.7 for P/NAD ALDH, 4.7 for B/NADP ALDH and 35 for AHH. Maximal P/NAD ALDH and B/NADP ALDH activities were obtained with 60 μ M CPBT, the fold-inductions being 1.8 for P/NAD ALDH and 4.8 for B/NADP ALDH. The maximal AHH activity inducible by CPBT was apparently not reached at the concentration range used. With the highest CPBT concentration used (100 μ M), the fold-induction was as great as 102.

Induction of ALDH by polycyclic aromatic hydrocarbons of different carcinogenic potency

The non-carcinogenic polycyclic aromatic hydrocarbons anthracene and phenanthrene did not increase either P/NAD ALDH or B/NADP ALDH activities at the concentration range of 5–100 μ M. The weak or moderate carcinogens chrysene and benz[a]anthracene increased both P/NAD ALDH and B/NADP ALDH (Fig. 3) activities. Maximal activities were reached with 10–25 μ M inducer. Chrysene up to 50 μ M and benz[a]anthracene up to 25 μ M were not toxic to the cells. The potent carcinogens benzo[a]pyrene and 3-methylcholanthrene increased both P/NAD ALDH and B/NADP ALDH activities. However, at concentrations higher than 5 μ M the activities started to decrease due to toxicity of the compounds to the cells.

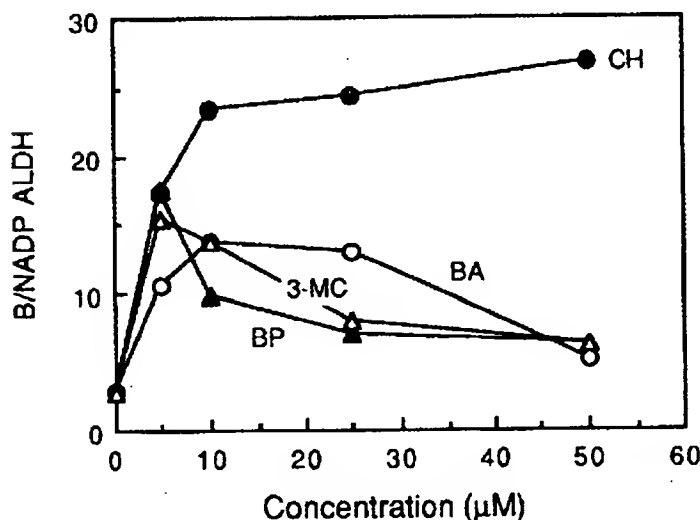


Fig. 3. Dose response of B/NADP ALDH induction by polycyclic aromatic hydrocarbons in Hepa-1 cell line. The cells were exposed to various concentrations of benz[a]anthracene (BA), benzo[a]pyrene (BP), chrysene (CH) and 3-methylcholanthrene (3-MC) for 24 h. Each point represents the mean of duplicate dishes of cells.

114

Correlation of ALDH3 mRNA levels with B/NADP ALDH enzyme activities in Hepa-1

Southern blot analysis was conducted in order to find out whether DNA homologous to the rat TCDD-inducible class 3 ALDH-specific cDNA probe was present in Hepa-1. One or two bands for genomic DNAs digested with either *Eco*RI, *Bam*HI, *Hind* III or *Pst* I were observed for both Hepa-1 and HTC cell lines. HTC was chosen as the positive control, because the cDNA probe used has

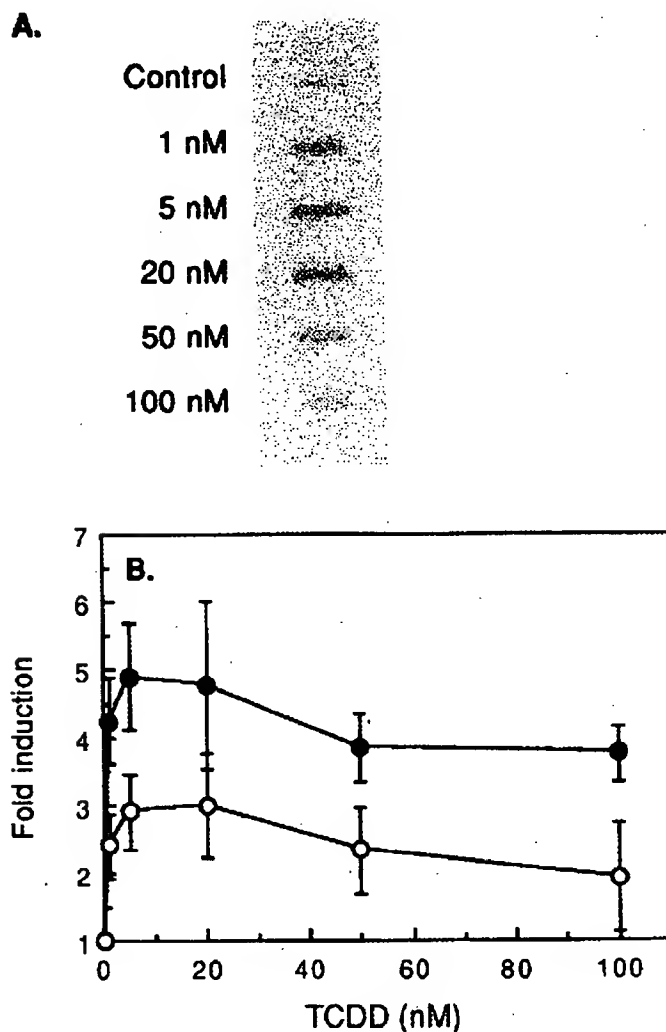


Fig. 4. (A) Slot blot analysis of ALDH3 mRNA in Hepa-1 cell line. (B) Dose-dependent induction of ALDH3 mRNA (O) and B/NADP ALDH activity (●). The cells were exposed to various concentrations of TCDD for 24 h. The results are expressed as fold inductions. Each point represents the mean (\pm S.E.) of three independent experiments.

been shown to be identical with ALDH3 in HTC [17]. Only one band in the Southern blot strongly suggested that there was a very specific binding of the probe to only one gene. This also allowed us to use the slot blot analysis instead of Northern analysis in the quantitation of class 3 ALDH-specific mRNA in Hepa-1. In order to compare the amounts of total RNA bound to the filters, a duplicate filter was hybridized to a cDNA probe for hamster CAD gene [29]. The results were similar with or without correcting the data by CAD mRNA.

The time-dependent induction of ALDH3 mRNA and B/NADP ALDH activity in the Hepa-1 cell line by TCDD showed that the maximal mRNA level was reached at 24 h. The enzyme activity was delayed by several hours and the maximal activity was reached after 48 h. The dose-dependent induction of ALDH3 mRNA and B/NADP ALDH activity correlated well (the correlation coefficient was 0.93). The maximal-fold inductions were obtained with 5–20 nM TCDD (Fig. 4). These data show that the amount of enzymatic activity is concordant with the specific mRNA levels.

DISCUSSION

In the present study, an inducible B/NADP ALDH is described in the mouse hepatoma cell line Hepa-1. A preliminary report has been published earlier [31]. The inducers included TCDD, carcinogenic polycyclic aromatic hydrocarbons, α - and β -naphthoflavone and CPBT. With the exception of α -naphthoflavone and CPBT, these compounds are known inducers of the B/NADP ALDH type isozyme in rat liver [2–7]. A peculiarity in the present observation is that, unlike in the rat, the normal mouse liver cytosolic P/NAD or B/NADP ALDH has not been found to be inducible by TCDD [3] or 3-methylcholanthrene [22].

The induction kinetics and magnitude of induction of B/NADP ALDH seen in the mouse Hepa-1 cell line was different from that previously observed in rat hepatoma cell lines. The fold-induction by 3-methylcholanthrene or benzo[a]pyrene was 3–17-times smaller in Hepa-1 than that reported for the rat hepatoma cell lines H4-II-EC3 or McA-RH7777 [11]. It should be noted, however, that Lin et al. [11] used very high inducer concentrations (1 mM) which according to our experiences would have been extremely toxic to the cells. In Hepa-1, maximal induction of B/NADP ALDH was seen after 1–2 days of exposure to 3-methylcholanthrene, whereas in H4-II-EC3 it is not reached until after 4 days [11].

In rat liver, the induction of B/NADP ALDH appears to correlate well with the carcinogenic potency of the polycyclic aromatic hydrocarbon inducers [7]. In Hepa-1, a similar correlation was not obvious. No induction of ALDH by the non-carcinogenic polycyclic aromatic hydrocarbons anthracene and phenanthrene was observed. However, the weak or moderate carcinogens chrysene and benz[a]anthracene gave maximal ALDH activities as high or even higher than those obtained by the potent carcinogens benzo[a]pyrene and 3-methylcholanthrene. Maximal activities were, however, reached by lower concentrations of benzo[a]pyrene and 3-methylcholanthrene than of benz[a]anthracene and chrysene. A problem was that benzo[a]pyrene and 3-methylcholanthrene are

more or less toxic to the cells, manifested as a rapid decline of the activities as the inducer concentration was increased. This toxicity of the more potent carcinogens makes the comparison of the inducing effects of the four polycyclic aromatic hydrocarbons rather difficult.

In the present study, no induction of ALDH by Mirex or DDT and only a marginal induction by phenobarbital was observed in Hepa-1. Because Mirex and DDT are phenobarbital-type inducers of ALDH [2], the results suggest that there is practically no induction of phenobarbital-type ALDH in Hepa-1.

Associations between the induction of ALDH and of the microsomal cytochrome *P*-450 system by phenobarbital [1,32-34] or TCDD [3,17] have been studied in rats and mice, but no relationship has been found. However, Nebert and coworkers suggest that ALDH may be under Ah receptor control [35]. Hepa-1 possesses an inducible AHH [28,30] and offers thus a model to study the associations. There was a good correlation between AHH and B/NADP ALDH inducibility by various chemicals. The only exception was CPBT which induced ALDH and AHH by 4- and over 100-fold, respectively, as compared with 4- and 45-fold by TCDD. CPBT has been observed to induce AHH exceptionally strongly [30]. However, the same does not seem to be true for B/NADP ALDH. Furthermore, the apparent correlation between AHH and B/NADP ALDH detected in the present study is questioned by our preliminary results with AHH-deficient mutant cell lines of Hepa-1 which possess variable B/NADP ALDH activities [31]. Those results are in concordance with the results of Dunn et al. [17] showing a lack of coordination in the regulation of the TCDD-inducible ALDH and cytochrome *P*-450c in the rat. They observed that the induction of rat liver ALDH by TCDD differs from that of cytochrome *P*-450c (expressed as AHH) with regard to dose response relationship, induction kinetics and tissue specificity. However, the possibility that Ah locus has some role in the induction of ALDH (especially B/NADP ALDH) cannot be ruled out conclusively and additional factors may be needed to explain the final responses.

In the rat, identity of the liver cytosolic ALDH induced by 3-methylcholanthrene, the tumour-associated ALDH and stomach ALDH has been suggested [36]. A very similar enzymatic species is found in normal rat urinary bladder [37] and cornea [38]. A similar constitutive or inducible B/NADP ALDH is also present in certain rat hepatoma cell lines [11,12,39]. As in the rat, B/NADP ALDH is expressed in chemically initiated mouse liver tumours [20,21]. Among the several constitutive murine ALDHs known [40], AHD-4 which occurs in mouse stomach and eye tissue [41,42], can with certainty be referred to as B/NADP ALDH and is therefore also a possible candidate for an analogous enzyme to the inducible B/NADP ALDH in Hepa-1 cells. Conclusive evidence on the identity between rat and mouse B/NADP ALDH cannot, however, be drawn on enzymatic basis, especially because mouse liver cytosolic B/NADP ALDH seems not, unlike the rat enzyme, to be induced by TCDD [3] or 3-methylcholanthrene [22].

The best way to study relationships between different ALDH isozymes is to work at the DNA and mRNA levels. The cDNAs for the tumour-associated B/NADP ALDH (from the rat hepatoma cell line HTC) and TCDD-inducible

B/NADP ALDH (from rat liver) appear to be identical belonging to class 3 ALDHs [16-19]. In the present study, the identity of the putative analogous enzyme in the mouse Hepa-1 cells with these class 3 ALDHs was studied. The clone p12x isolated from a cDNA library prepared from the liver of a TCDD-induced rat [17], corresponding to the middle two-thirds of the full-length cDNA, was shown to detect specific DNA sequences in Hepa-1. Although there is a ten amino acid residue segment which is invariant in all ALDH structures thus far known [18] (the nucleotide sequences do not have a perfect match), the specificity of the probes for class 3 ALDH has also been proven in the rat [16,17]: the probes recognize no sequences in normal or phenobarbital-induced rat liver. A further evidence for the identity of B/NADP ALDH in Hepa-1 with rat class 3 ALDH was that there was a clear induction of class 3 ALDH-specific mRNA in Hepa-1. The time course of induction of the enzyme and the corresponding mRNA correlated well. The same good correlation was also seen in the dose response curve.

The tumour-specific and stomach ALDH seem to be the same in the rat and mouse. The only clear difference between the rat and mouse is the inducibility of ALDH by compounds like TCDD and 3-methylcholanthrene. How does one then explain the inducible B/NADP ALDH in the mouse hepatoma cell line Hepa-1 when the same induction is not seen in mouse liver *in vivo*? The system presented here may offer an interesting model to study the regulation of class 3 ALDHs.

ACKNOWLEDGEMENTS

The skillful technical assistance of Ms. Raisa Malmivuori and Ms. Riitta Venäläinen is gratefully acknowledged. Mr. Harri Kokko is thanked for his help in some experiments.

REFERENCES

- 1 R.A. Deitrich, Genetic aspects of increase in rat liver aldehyde dehydrogenase induced by phenobarbital, *Science*, 173 (1971) 334-336.
- 2 R.A. Deitrich, P. Bludeau, M. Roper and J. Schmuck, Induction of aldehyde dehydrogenases, *Biochem. Pharmacol.*, 27 (1978) 2343-2347.
- 3 R.A. Deitrich, P. Bludeau, T. Stock and M. Roper, Induction of different rat liver supernatant aldehyde dehydrogenases by phenobarbital and tetrachlorodibenzo-*p*-dioxin, *J. Biol. Chem.*, 252 (1977) 6169-6176.
- 4 M. Marselos, R. Törrönen, T. Koivula and M. Koivusalo, Comparison of phenobarbital- and carcinogen-induced aldehyde dehydrogenases in the rat, *Biochim. Biophys. Acta*, 583 (1979) 110-118.
- 5 M. Marselos and V. Vasiliou, Effect of various chemicals on the aldehyde dehydrogenase activity of the rat liver cytosol, *Chem.-Biol. Interact.*, 79 (1991) 79-89.
- 6 E. Ritter and L.C. Eriksson, Kinetics of induction of cytosolic benzaldehyde: NADP and propionaldehyde: NAD aldehyde dehydrogenase activities in rat livers from male Wistar rats, *Carcinogenesis*, 12 (1991) 751-758.
- 7 R. Törrönen, U. Nousiainen and O. Hänninen, Induction of aldehyde dehydrogenase by polycyclic aromatic hydrocarbons in rats, *Chem.-Biol. Interact.*, 36 (1981) 33-44.

- 8 M. Marselos and G. Michalopoulos, Phenobarbital enhances the aldehyde dehydrogenase activity of rat hepatocytes in vitro and in vivo, *Acta Pharmacol. Toxicol.*, 59 (1986) 403-409.
- 9 M. Marselos, S.C. Strom and G. Michalopoulos, Enhancement of aldehyde dehydrogenase activity of human and rat hepatocyte cultures by 3-methylcholanthrene, *Cell Biol. Toxicol.*, 2 (1986) 257-269.
- 10 M. Huang and R. Lindahl, Effects of hepatocarcinogenic initiators on aldehyde dehydrogenase gene expression in cultured rat hepatic cells, *Carcinogenesis*, 11 (1990) 1059-1065.
- 11 K.-H. Lin, A.L. Winters and R. Lindahl, Regulation of aldehyde dehydrogenase activity in five rat hepatoma cell lines, *Cancer Res.*, 44 (1984) 5219-5226.
- 12 K.-H. Lin, M.F. Leach, A.L. Winters and R. Lindahl, Characteristics and aldehyde dehydrogenase activity of four rat hepatoma cell lines produced by diethylnitrosamine-phenobarbital treatment, *In Vitro Cell. Dev. Biol.*, 22 (1986) 263-272.
- 13 R. Lindahl, S. Evces and W.-L. Sheng, Expression of the tumor aldehyde dehydrogenase phenotype during 2-acetylaminofluorene-induced rat hepatocarcinogenesis, *Cancer Res.*, 42 (1982) 577-582.
- 14 S.M. Wischusen, S. Evces and R. Lindahl, Changes in aldehyde dehydrogenase activity during diethylnitrosamine- or 2-acetylaminofluorene-initiated rat hepatocarcinogenesis, *Cancer Res.*, 43 (1983) 1710-1715.
- 15 E. Ritter and I.C. Eriksson, Aldehyde dehydrogenase activities in hepatocyte nodules and hepatocellular carcinomas from Wistar rats, *Carcinogenesis*, 6 (1985) 1683-1687.
- 16 D.E. Jones, Jr., M.D. Brennan, J. Hempel and R. Lindahl, Cloning and complete nucleotide sequence of a full-length cDNA encoding a catalytically functional tumor-associated aldehyde dehydrogenase, *Proc. Natl. Acad. Sci. USA*, 85 (1988) 1782-1786.
- 17 T.J. Dunn, R. Lindahl and H.C. Pitot, Differential gene expression in response to 2,3,7,8-tetrachlorodibenzo-p-dioxin (TCDD). Noncoordinate regulation of a TCDD-induced aldehyde dehydrogenase and cytochrome P-450c in the rat, *J. Biol. Chem.*, 263 (1988) 10878-10886.
- 18 J. Hempel, K. Harper and R. Lindahl, Inducible (class 3) aldehyde dehydrogenase from rat hepatocellular carcinoma and 2,3,7,8-tetrachlorodibenzo-p-dioxin-treated liver: distant relationship to the class 1 and 2 enzymes from mammalian liver cytosol/mitochondria, *Biochemistry*, 28 (1989) 1160-1167.
- 19 Anonymous, Nomenclature of mammalian aldehyde dehydrogenases, in: H. Weiner and G.T. Flynn (eds.), *Enzymology and Molecular Biology of Carbonyl Metabolism 2. Aldehyde Dehydrogenase, Alcohol Dehydrogenase and Aldo-Keto Reductase*, Alan R. Liss, Inc., New York, 1989, pp. xix-xxi.
- 20 R.E. Richmond and M.A. Pereira, Aldehyde dehydrogenase as a marker for chemically initiated mouse liver tumours, *Cancer Lett.*, 31 (1986) 205-211.
- 21 R.E. Richmond, A.B. Deangelo, F.B. Daniel and R. Lindahl, Immunohistochemical detection of tumour-associated aldehyde dehydrogenase in formalin-fixed rat and mouse normal liver and hepatomas, *Histochem. J.*, 22 (1990) 526-529.
- 22 V. Vasilou, R. Törrönen, M. Malamas and M. Marselos, Inducibility of liver cytosolic aldehyde dehydrogenase activity in various animal species, *Comp. Biochem. Physiol.*, 94C (1989) 671-675.
- 23 H.P. Bernhard, G.J. Darlington and F.H. Ruddle, Expression of liver phenotypes in cultured mouse hepatoma cells: Synthesis and secretion of serum albumin, *Dev. Biol.*, 35 (1973) 83-96.
- 24 E.B. Thompson, G.M. Tomkins and J.F. Curran, Induction of tyrosine α -ketoglutarate transaminase by steroid hormones in a newly established tissue culture cell line, *Proc. Natl. Acad. Sci. USA*, 56 (1966) 296-303.
- 25 D.W. Nebert and H.V. Gelboin, Substrate-inducible microsomal aryl hydroxylase in mammalian cell culture. I. Assay and properties of induced enzyme, *J. Biol. Chem.*, 243 (1968) 6242-6249.
- 26 M.M. Bradford, A rapid and sensitive method for the quantitation of microgram quantities of protein utilizing the principle of protein-dye binding, *Anal. Biochem.*, 72 (1976) 248-254.
- 27 J. Sambrook, E.F. Fritsch and T. Maniatis, *Molecular Cloning: A Laboratory Manual*, Cold Spring Harbor Laboratory Press, Cold Spring Harbor, NY, 1989.
- 28 S.O. Kärenlampi, K. Tuomi, M. Korkalainen and H. Raunio, Induction of cytochrome P450IA1 in mouse hepatoma cells by several chemicals, *Biochem. Pharmacol.*, 38 (1989) 1517-1525.

- 29 G.M. Wahl, R.A. Padgett and G.R. Stark, Gene amplification causes overproduction of the first three enzymes of UMP synthesis in *N*-(phosphonacetyl)-*L*-aspartate-resistant hamster cells, *J. Biol. Chem.*, 254 (1979) 8679-8689.
- 30 S.O. Kärenlampi, K. Tuomi, M. Korkalainen and H. Raunio, 2-(4'-Chlorophenyl)benzothiazole is a potent inducer of cytochrome P450IA1 in a human and a mouse cell line. Anomalous correlation between protein and mRNA induction, *Eur. J. Biochem.*, 181 (1989) 143-148.
- 31 R. Törrönen and S. Kärenlampi, Associations of aldehyde dehydrogenase with aryl hydrocarbon hydroxylase in mouse hepatoma cells, in: I. Schuster (ed.), *Cytochrome P450: Biochemistry and Biophysics*, Taylor and Francis, London, 1989, pp. 519-522.
- 32 R.A. Deitrich, A.C. Collins and V.G. Erwin, Genetic influence upon phenobarbital-induced increase in rat liver supernatant aldehyde dehydrogenase activity, *J. Biol. Chem.*, 247 (1972) 7232-7236.
- 33 M. Marselos, Genetic variation of drug-metabolizing enzymes in the Wistar rat, *Acta Pharmacol. Toxicol.*, 39 (1976) 186-197.
- 34 T.J. Dunn, A.J. Koleske, R. Lindahl and H.C. Pitot, Phenobarbital-inducible aldehyde dehydrogenase in the rat. cDNA sequence and regulation of the mRNA by phenobarbital in responsive rats, *J. Biol. Chem.*, 264 (1989) 13057-13065.
- 35 D.W. Nebert, D.D. Petersen and A.J. Fornace, Cellular responses to oxidative stress: the [Ah] gene battery as a paradigm, *Environ. Health Perspect.*, 88 (1990) 13-25.
- 36 M. Koivusalo, M. Aarnio, M. Baumann and P. Rautoma, NAD(P)-linked aromatic aldehydes preferring cytoplasmic aldehyde dehydrogenases in the rat. Constitutive and inducible forms in liver, lung, stomach and intestinal mucosa, in: H. Weiner and G.T. Flynn (eds.), *Enzymology and Molecular Biology of Carbonyl Metabolism 2. Aldehyde Dehydrogenase, Alcohol Dehydrogenase and Aldo-Keto Reductase*, Alan R. Liss, Inc., New York, 1989, pp. 19-33.
- 37 R. Lindahl, Identification of hepatocarcinogenesis-associated aldehyde dehydrogenase in normal rat urinary bladder, *Cancer Res.*, 46 (1986) 2502-2506.
- 38 S. Evces and R. Lindahl, Characterization of rat cornea aldehyde dehydrogenase, *Arch. Biochem. Biophys.*, 274 (1989) 518-524.
- 39 R. Lindahl, D.W. Baggett and A.L. Winters, Characterization of aldehyde dehydrogenase from HTC rat hepatoma cells, *Biochim. Biophys. Acta*, 843 (1985) 180-185.
- 40 C.L. Manthey, G.J. Landkamer and N.E. Sladek, Identification of the mouse aldehyde dehydrogenases important in aldophosphamide detoxification, *Cancer Res.*, 50 (1990) 4991-5002.
- 41 E.M. Algar and R.S. Holmes, Purification and properties of mouse stomach aldehyde dehydrogenase. Evidence for a role in the oxidation of peroxidic and aromatic aldehydes, *Biochim. Biophys. Acta*, 995 (1989) 168-173.
- 42 R.S. Holmes, R.A. Popp and J.L. VandeBerg, Genetics of ocular NAD⁺-dependent alcohol dehydrogenase and aldehyde dehydrogenase in the mouse: evidence for genetic identity with stomach isozymes and localization of Ahd-4 on chromosome 11 near trembler, *Biochem. Genet.*, 26 (1988) 191-205.